Acta Chemica Scandinavica A 29 (1975) 1—6

The Crystal Structure of Magnesium Tetrametaphosphate, $Mg_2P_4O_{12}$

ANDERS G. NORD and K. BÖRJE LINDBERG

Department of Inorganic and Structural Chemistry, Arrhenius Laboratory, University of Stockholm, S-104 05 Stockholm 50, Sweden

The crystal structure of $Mg_2P_4O_{12}$ has been determined by means of direct methods and refined from three-dimensional X-ray diffractometer data ($R=6.0$ % for 781 independent reflections). $Mg_2P_4O_{12}$ crystallizes in the monoclinic space group $C2/c$ with $Z=4$. The cell constants are $a=11.756(2)$, $b=8.285(1)$, $c=9.917(1)$ Å, $\beta=118.96(2)°$, $V=845$ Å^3. The calculated density is 2.865 g/cm^3. The PO_4 tetrahedra in the structure are linked together in a ring to form $P_4O_{12}^{4-}$ ions with P—O—P angles of 134.2 and 138.8°. The magnesium ions are always six-coordinated.

The phase diagram of the system $MgO-P_2O_5$ was published in 1958 by Berak.[1] The crystal structures for three of the four compounds occurring in this system were determined some years ago, *viz.* α-$Mg_2P_2O_7$,[2] β-$Mg_2P_2O_7$[3], and $Mg_3(PO_4)_2$.[4] The structure of the remaining compound, magnesium metaphosphate, has been unknown to date. However, on the basis of spectroscopic measurements[5] and paper-chromatographic analysis[6,7] it has earlier been postulated that magnesium metaphosphate contains tetrametaphosphate ($P_4O_{12}^{4-}$) ions. Furthermore, it has been known since about 1956 that $Mg_2P_4O_{12}$ belongs to a family of isomorphous tetrametaphosphates $M^{II}_2P_4O_{12}$ with M=Mg, Co, Ni, Mn, Zn (α-phase), Cd (α-phase).[6,7] In order to establish the crystal structure of these compounds, a crystallographic study of $Mg_2P_4O_{12}$ was undertaken.

EXPERIMENTAL

A sample of $Mg_2P_4O_{12}$ was prepared by mixing $MgCO_3$ and $(NH_4)_2HPO_4$ in the molar ratio 1:2. The mixture was then slowly heated to 900 °C. A quantitative analysis by means of X-ray fluorescence spectroscopy, with MgO and Li_3PO_4 as standards, confirmed the empirical formula $Mg(PO_3)_2$. The d-values and relative intensities obtained from a Guinier powder photograph also agreed with those reported earlier in the literature for magnesium metaphosphate.[7–9] Good single crystals were then prepared in a sealed thin-walled platinum tube from the melt (m.p. 1165 °C)[1] allowed to solidify very slowly during a period of two weeks. An almost spherically shaped ($r=0.050\pm0.004$ mm) single crystal was selected from the sample. With this, the unit cell dimensions were determined and refined by an PW1100 automatic diffractometer on the basis of 25 strong but distinct reflections. The cell constants are: $a=11.756(2)$, $b=8.285(1)$, $c=9.917(1)$ Å, $\beta=118.96(2)°$, $V=845$ Å^3. $Z=4$ gives a calculated density of 2.865 g/cm^3. This is in agreement with values published by Beucher and Grenier.[8] The PW1100 diffractometer (graphite monochromator; Cu$K\alpha$ radiation, $\lambda=1.5405$ Å) was also used for the collection of single-crystal data. 786 independent non-extinct reflections were measured up to $\theta=70°$. Of these 52 reflections had $\sigma(I)/I>\frac{1}{2}$ and might be regarded as "insignificant". Nevertheless they were included in all the following calculations. The net

Table 1. Basic set used for solving the triple relations.

hkl	*E*	Sign	Comment
022	2.92	−	variable
$3\bar{5}\bar{7}$	2.87	+	def. of origin
$9\bar{1}\bar{4}$	2.65	+	def. of origin
$\bar{4}\bar{4}\bar{4}$	2.58	+	variable
044	1.94	+	from $\sum_1$ relations

Table 2. Fractional atomic coordinates and thermal parameters from the isotropic refinement of $Mg_2P_4O_{12}$. The estimated standard deviations (within parentheses) refer to the last digit of the respective values.

Atom	x	y	z	B
Mg(1)	0[a]	0.0513(2)	¼[a]	0.36(4)
Mg(2)	¼[a]	¼[a]	½[a]	0.38(4)
P(1)	0.0089(1)	0.2627(1)	−0.0242(1)	0.33(3)
P(2)	0.1967(1)	0.4915(1)	0.1968(1)	0.34(3)
O(1)	0.2329(3)	0.4198(4)	0.3469(3)	0.77(5)
O(2)	0.2988(3)	0.5809(4)	0.1765(3)	0.48(5)
O(3)	0.0779(3)	0.6102(4)	0.1554(3)	0.81(5)
O(4)	0.1421(3)	0.3589(4)	0.0643(3)	0.73(5)
O(5)	−0.0491(3)	0.2410(4)	0.0811(3)	0.56(5)
O(6)	0.0316(3)	0.1200(4)	−0.0952(3)	0.79(5)

[a] Parameter fixed by symmetry.

intensities were corrected for Lorentz, polarization, and absorption ($\mu = 104$ cm^{-1}) effects. The latter correction was performed assuming the crystal to be spherical with $r = 0.050$ mm.

DETERMINATION AND REFINEMENT OF THE STRUCTURE

The systematic extinctions, confirmed by diffractometer measurements as well as from Weissenberg photographs, are: hkl, $h+k \neq 2n$; $h0l$, $l \neq 2n$; and $0k0$, $k \neq 2n$. The distribution of the $|E|$ values and some statistical tests applied, *e.g.* the $N(z)$ test,[10] indicated space group $C2/c$ rather than Cc, and the former symmetry was indicated throughout the work.

The structure was solved by means of direct methods utilizing a program system developed by Norrestam [11] based on the variance-weighted phase-sum formula for phase determination. The 113 highest $|E|$ values ($|E| > 1.4$) were used to generate 591 triple relations. As a basic set five reflections were selected (see Table 1). The E map based on 112 determined phases revealed almost all atomic positions. The structure determination was then completed by Fourier methods and least-squares refinements.

The refinements were performed with a local modification of the full-matrix least-squares program LALS. The atomic scattering factors applied were those for Mg^{2+}, P^0, and O^- from the *International Tables for X-Ray Crystallography*,[12] with the real part of the anomalous dispersion included. The 52 "insignificant" reflections with $\sigma(I)/I > \frac{1}{2}$ were given zero weight, while Hughes' weighting function [13] (with $h = 4$ and $F_{o,min} = 8$) was applied to the other reflections. Initially all 786 reflections were used in the refinements, but prior to the final refinements, five strong low-angle reflections (022, 220, 310, 400, $\bar{2}02$) were omitted as severely suffering from extinction effects. The R value, defined as $R = \sum||F_{obs}| - |F_{calc}||/\sum|F_{obs}|$, fell to 6.0 % for the isotropically- and to 5.5 % for the anisotropically-refined structure (781 reflections). Since the atomic positional parameters obtained in these two final refinements are very similar and the anisotropic vibrations seem to be small, only the results of the 6.0 % isotropic refinement are considered below. The parameters obtained in this refinement are given in Table 2.

A three-dimensional difference Fourier synthesis calculated with the parameters in Table 2 at points 0.2 Å apart showed no maxima or minima greater than 15 % of the average oxygen peak in the electron density map. The observed and calculated structure factors from the isotropic refinement are shown in Table 3. The reflections with $\sigma(I)/I > \frac{1}{2}$ are marked with an asterisk.

Two summary papers of the crystallographic programs used in this work have been published at this institute.[14,15]

DISCUSSION

The crystal structure of magnesium tetrametaphosphate consists of PO_4 tetrahedra and

Table 3. Observed and calculated structure factors from the isotropic refinement of $Mg_2P_4O_{12}$. Reflections with $\sigma(I)/I > \frac{1}{2}$ are marked with an asterisk.

H	K	L	|FO|	FC	H	K	L	|FO|	FC	H	K	L	|FO|	FC	H	K	L	|FO|	FC	H	K	L	|FO|	FC
2	0	0	36.3	40.4	-7	5	1	49.2	48.9	-7	5	2	46.4	-43.7	-8	6	3	8.7	-6.3	0	6	4	22.3	-20.8
6	0	0	65.4	69.4	-5	5	1	78.5	-76.1	-5	5	2	47.2	44.5	-6	6	3	4.0*	-2.9	2	6	4	23.2	-23.9
8	0	0	27.3	26.4	-3	5	1	6.7	0.2	-3	5	2	23.1	-19.6	-4	6	3	0.0*	0.5	4	6	4	110.4	-126.4
10	0	0	69.6	69.3	-1	5	1	119.4	-120.1	-1	5	2	38.3	-34.7	-2	6	3	27.5	28.6	6	6	4	8.4	10.7
12	0	0	16.7	16.1	1	5	1	11.6	11.1	1	5	2	12.7	9.3	0	6	3	38.3	-38.3	-9	7	4	48.6	-49.3
1	1	0	13.8	-16.8	3	5	1	28.7	-28.8	3	5	2	117.0	-130.6	2	6	3	29.9	-28.1	-7	7	4	29.2	27.2
5	1	0	12.3	10.0	5	5	1	25.4	-26.2	5	5	2	22.6	23.9	4	6	3	11.7	10.5	-5	7	4	9.7	7.9
7	1	0	64.4	67.0	7	5	1	4.2*	0.6	7	5	2	40.1	-40.8	6	6	3	14.7	-16.2	-3	7	4	16.9	-17.2
9	1	0	6.6	5.2	9	5	1	11.0	10.3	9	5	2	25.4	-24.9	-9	7	3	19.7	18.9	-1	7	4	31.2	32.4
11	1	0	4.1*	-2.4	-10	6	1	0.0*	-3.8	-10	6	2	14.7	-11.4	-7	7	3	51.5	-51.3	1	7	4	24.5	-21.9
0	2	0	3.5*	-0.5	-8	6	1	48.6	-48.5	-8	6	2	21.8	-18.6	-5	7	3	2.0*	-0.0	3	7	4	41.3	44.2
4	2	0	46.7	-44.4	-6	6	1	78.2	-80.9	-6	6	2	37.9	37.2	-3	7	3	37.7	-38.4	5	7	4	17.4	-16.5
6	2	0	8.9	9.3	-4	6	1	64.4	-62.9	-4	6	2	117.4	-125.0	-1	7	3	19.8	-19.7	-8	8	4	42.5	43.5
8	2	0	89.1	-98.5	-2	6	1	61.0	-57.5	-2	6	2	41.0	40.1	1	7	3	15.6	16.4	-6	8	4	75.9	-79.6
10	2	0	61.6	63.6	0	6	1	20.0	-17.8	0	6	2	89.4	-89.8	3	7	3	6.3	5.0	-4	8	4	54.9	55.6
12	2	0	59.6	-54.8	2	6	1	36.5	-35.5	2	6	2	60.1	-58.6	5	7	3	3.9*	2.5	-2	8	4	75.7	-78.1
1	3	0	25.3	22.1	4	6	1	6.6	3.3	4	6	2	25.1	-26.1	-8	8	3	22.5	22.7	0	8	4	32.5	29.7
3	3	0	47.2	46.0	6	6	1	6.5	7.6	6	6	2	81.1	-89.3	-6	8	3	38.6	41.7	2	8	4	9.0	8.0
5	3	0	68.1	-62.4	8	6	1	27.9	-27.6	8	6	2	7.0	-5.8	-4	8	3	13.1	13.4	4	8	4	15.3	15.0
7	3	0	75.4	78.4	-9	7	1	34.8	-35.1	-9	7	2	32.5	31.0	-2	8	3	50.9	51.5	-5	9	4	62.1	-62.6
9	3	0	13.8	15.0	-7	7	1	39.2	-39.5	-7	7	2	13.4	-13.4	0	8	3	22.1	21.7	-3	9	4	52.8	-55.2
11	3	0	3.9*	-4.5	-5	7	1	7.9	-3.4	-5	7	2	81.4	85.4	2	8	3	20.0	22.3	-1	9	4	8.4	-5.9
0	4	0	84.2	82.6	-3	7	1	45.6	-42.8	-3	7	2	26.5	26.2	4	8	3	0.0*	-0.2	1	9	4	76.5	-79.6
2	4	0	0.0*	3.3	-1	7	1	3.6*	-2.1	-1	7	2	8.5	5.6	-5	9	3	0.0*	11.7	-13	1	5	10.2	9.9
4	4	0	115.8	122.2	1	7	1	77.5	-80.3	1	7	2	87.8	93.2	-3	9	3	66.4	68.8	-11	1	5	60.2	59.2
6	4	0	62.3	59.9	3	7	1	6.8	5.4	3	7	2	2.4*	-2.0	-1	9	3	43.5	-44.3	-9	1	5	45.4	45.0
8	4	0	14.4	14.1	5	7	1	42.3	-43.2	5	7	2	73.2	80.3	1	9	3	57.3	60.1	-7	1	5	67.8	67.9
10	4	0	66.8	67.2	7	7	1	19.3	21.2	7	7	2	1.9*	5.3	-12	0	4	0.0*	-0.6	-5	1	5	77.3	78.7
1	5	0	43.0	-39.3	-6	8	1	18.6	19.6	-8	8	2	41.0	41.3	-10	0	4	81.6	82.7	-3	1	5	78.6	84.7
3	5	0	23.2	20.6	-4	8	1	0.0*	0.2	-6	8	2	29.4	30.0	-8	0	4	81.9	85.1	-1	1	5	51.5	-48.0
5	5	0	107.2	-117.4	-2	8	1	28.4	-28.4	-4	8	2	11.9	13.0	-6	0	4	16.2	-15.2	1	1	5	40.4	39.1
7	5	0	6.4	3.8	0	8	1	30.8	31.5	-2	8	2	84.8	90.4	4	0	-4	7.2	4.1	3	1	5	11.2	-7.3
9	5	0	24.7	-24.2	2	8	1	7.6	-4.9	0	8	2	60.0	63.1	-2	0	4	9.7	-9.5	5	1	5	55.3	52.4
0	6	0	102.4	-107.9	4	8	1	23.5	-24.4	2	8	2	38.7	36.0	0	0	4	26.4	28.7	7	1	5	14.1	-11.3
2	6	0	74.6	-72.7	6	8	1	4.9	-6.8	4	8	2	103.1	113.3	2	0	4	66.1	65.4	-12	2	5	47.8	-47.7
4	6	0	100.3	-110.0	-5	9	1	13.6	-14.8	6	8	2	14.8	15.1	4	0	4	106.7	112.8	-10	2	5	30.5	-28.3
6	6	0	16.1	16.6	-3	9	1	15.5	16.1	-5	9	2	0.0*	-0.9	6	0	4	126.5	144.2	-8	2	5	55.2	-53.9
8	6	0	74.1	-78.2	-1	9	1	10.5	7.3	-3	9	2	40.6	-41.1	8	0	4	76.4	74.5	-6	2	5	73.1	-67.7
1	7	0	16.0	-17.0	1	9	1	18.5	-19.7	-1	9	2	21.2	-22.5	-13	1	4	29.9	28.4	-4	2	5	78.9	-75.9
3	7	0	81.3	86.3	3	9	1	3.7*	1.6	1	9	2	38.6	42.0	-11	1	4	62.7	63.2	-2	2	5	8.9	-9.5
5	7	0	31.4	-31.6	-12	0	2	52.5	51.3	3	9	2	26.7	-29.0	-9	1	4	89.8	-89.9	0	2	5	25.4	23.8
7	7	0	39.4	38.9	-10	0	2	116.0	-133.2	-13	1	3	20.7	19.8	-7	1	4	64.5	63.3	2	2	5	3.8*	4.8
0	8	0	108.5	125.0	-8	0	2	78.8	78.8	-11	1	3	86.2	88.7	-5	1	4	21.5	-20.5	4	2	5	54.4	-53.5
2	8	0	18.8	17.4	-6	0	2	88.8	-80.6	-9	1	3	41.8	38.7	-3	1	4	20.2	-19.4	6	2	5	24.8	23.4
4	8	0	41.0	40.8	-4	0	2	10.2	-9.8	-7	1	3	70.0	67.4	-1	1	4	79.0	87.8	8	2	5	23.7	-21.5
6	8	0	24.2	24.6	0	0	2	31.5	32.8	-5	1	3	69.8	65.6	1	1	4	44.1	-45.1	-13	3	5	48.0	-45.7
1	9	0	51.3	-53.4	2	0	2	84.3	95.1	-3	1	3	108.8	121.9	3	1	4	59.2	57.7	-11	3	5	104.5	-111.9
3	9	0	3.2*	0.5	4	0	2	68.5	74.4	-1	1	3	53.9	54.7	5	1	4	2.6*	-3.4	-9	3	5	51.8	-48.9
5	9	0	63.0	-65.8	6	0	2	62.2	60.8	1	1	3	9.4	-6.0	7	1	4	32.1	-28.6	-7	3	5	148.6	-163.4
-11	1	1	69.9	71.2	8	0	2	110.5	121.5	3	1	3	20.5	18.4	9	1	4	93.8	90.4	-5	3	5	34.1	-34.5
-9	1	1	26.2	25.8	10	0	2	13.7	-11.1	5	1	3	49.7	47.4	-12	2	4	72.7	-71.6	-3	3	5	125.7	-138.3
-7	1	1	62.4	60.8	-13	1	2	24.3	-24.4	7	1	3	3.9*	-5.3	-10	2	4	40.7	39.7	-1	3	5	71.0	-73.7
-5	1	1	111.8	-110.1	-11	1	2	39.5	-39.9	9	1	3	42.4	38.8	-8	2	4	37.6	-34.6	1	3	5	58.2	-60.7
-3	1	1	103.5	102.7	-9	1	2	30.3	29.5	-12	2	3	19.4	17.9	-6	2	4	24.7	20.4	3	3	5	12.1	-10.5
-1	1	1	54.8	-44.0	-7	1	2	143.9	-155.1	-10	2	3	20.1	-19.4	-4	2	4	16.9	14.2	5	3	5	4.3*	0.1
1	1	1	52.7	48.6	-5	1	2	20.3	17.6	-8	2	3	39.6	35.1	-2	2	4	4.2*	-5.4	7	3	5	14.5	-11.2
3	1	1	9.2	-4.1	-3	1	2	107.4	-111.0	-6	2	3	62.4	54.1	0	2	4	59.0	-58.4	-12	4	5	20.1	-18.3
5	1	1	33.6	34.4	-1	1	2	98.6	-109.5	-4	2	3	54.4	-46.1	2	2	4	25.7	27.0	-10	4	5	14.8	15.3
7	1	1	40.2	-40.8	1	1	2	71.9	79.2	-2	2	3	14.6	-12.0	4	2	4	112.5	-122.2	-8	4	5	31.3	-31.0
9	1	1	29.3	-29.6	3	1	2	7.9	-8.4	0	2	3	92.4	93.7	6	2	4	15.2	12.7	-6	4	5	30.9	-29.7
11	1	1	35.3	-35.1	5	1	2	6.2	3.7	2	2	3	53.8	51.3	8	2	4	82.8	-81.6	-4	4	5	9.2	6.4
-12	2	1	14.5	-14.7	7	1	2	13.5	-12.3	4	2	3	57.4	58.9	-13	3	4	11.1	-11.9	-2	4	5	14.5	-14.7
-10	2	1	39.0	-38.4	9	1	2	60.1	-58.3	6	2	3	22.6	21.8	-11	3	4	43.6	45.6	0	4	5	14.3	-15.1
-8	2	1	8.9	8.9	-12	2	2	3.2*	-3.6	8	2	3	25.6	24.4	-9	3	4	6.6	-6.2	2	4	5	27.5	25.2
-6	2	1	44.9	37.0	-10	2	2	80.7	-83.9	-13	3	3	47.5	-43.6	-7	3	4	102.0	100.2	4	4	5	35.4	-34.7
-4	2	1	83.8	75.3	-8	2	2	30.8	-30.2	-11	3	3	61.4	-61.9	-5	3	4	5.7	3.1	6	4	5	14.2	13.3
-2	2	1	63.1	-57.0	-6	2	2	23.9	-20.5	-9	3	3	46.1	-43.4	-3	3	4	38.8	36.0	-11	5	5	45.2	41.8
0	2	1	17.1	-14.7	-4	2	2	132.6	-138.0	-7	3	3	103.9	-100.7	-1	3	4	113.8	118.4	-9	5	5	34.5	33.6
2	2	1	21.0	-19.0	-2	2	2	26.1	23.1	-5	3	3	76.9	68.7	1	3	4	50.5	-49.5	-7	5	5	75.7	77.1
4	2	1	52.3	-49.5	2	2	2	56.1	-56.2	-3	3	3	14.6	-14.4	3	3	4	69.2	70.3	-5	5	5	24.8	21.1
6	2	1	34.0	-33.7	4	2	2	125.9	-150.6	-1	3	3	156.3	172.6	5	3	4	36.9	37.7	-3	5	5	32.6	31.6
8	2	1	27.6	27.7	6	2	2	97.4	-108.5	1	3	3	52.6	-49.5	7	3	4	11.7	-8.6	-1	5	5	20.8	20.2
10	2	1	31.6	-30.8	8	2	2	42.4	-42.8	3	3	3	80.6	84.6	-12	4	4	18.3	19.3	1	5	5	21.4	22.5
-11	3	1	55.5	-55.1	10	2	2	58.4	-54.8	5	3	3	25.9	-24.1	-10	4	4	18.0	18.2	3	5	5	57.1	-57.2
-9	3	1	30.9	-29.6	-11	3	2	20.7	-19.0	7	3	3	25.0	24.9	-8	4	4	57.8	57.5	5	5	5	13.7	13.0
-7	3	1	23.5	-22.7	-9	3	2	55.7	54.5	9	3	3	9.4	-6.1	-6	4	4	45.1	-41.8	-10	6	5	13.4	-10.8
-5	3	1	85.7	-79.9	-7	3	2	36.5	-32.2	-12	4	3	49.7	48.8	-4	4	4	167.9	185.2	-8	6	5	11.1	-13.1
-3	3	1	77.1	64.3	-5	3	2	69.2	62.0	-10	4	3	21.3	20.9	-2	4	4	45.3	-44.1	-6	6	5	26.7	-25.2
-1	3	1	17.6	14.4	-3	3	2	13.7	-13.7	-8	4	3	40.7	38.2	0	4	4	125.6	139.2	-4	6	5	7.7	7.9
1	3	1	9.3	-10.5	-1	3	2	8.4	6.8	-6	4	3	46.6	42.8	2	4	4	81.0	84.8	-2	6	5	56.4	-58.0
3	3	1	31.8	29.1	1	3	2	24.0	24.3	-4	4	3	27.4	24.9	4	4	4	15.1	14.3	0	6	5	66.4	-71.4
5	3	1	94.1	-100.6	3	3	2	119.8	-131.0	-2	4	3	62.5	59.6	6	4	4	74.2	73.1	2	6	5	28.7	-29.0
7	3	1	7.7	-6.3	5	3	2	32.7	31.3	0	4	3	39.1	39.3	8	4	4	42.1	39.3	4	6	5	44.0	-44.6
9	3	1	68.8	-71.6	7	3	2	0.0*	-0.3	2	4	3	26.4	26.2	-11	5	4	24.7	23.1	-9	7	5	60.9	-62.4
11	3	1	18.1	18.1	9	3	2	37.8	-34.4	4	4	3	67.8	71.7	-9	5	4	22.9	-23.9	-7	7	5	64.1	-62.8
-10	4	1	8.1	-7.9	-12	4	2	98.3	99.3	6	4	3	2.2*	1.8	-7	5	4	48.3	46.6	-5	7	5	48.9	-52.5
-8	4	1	8.4	6.8	-10	4	2	5.9	-3.9	8	4	3	18.0	14.3	-5	5	4	21.9	-19.3	-3	7	5	72.7	-74.0
-6	4	1	32.8	-30.8	-8	4	2	56.2	54.6	-11	5	3	81.0	82.1	-3	5	4	42.4	-39.0	-1	7	5	14.0	14.1
-4	4	1	25.7	24.1	-6	4	2	31.5	26.7	-9	5	3	62.3	61.9	-1	5	4	21.1	18.8	1	7	5	57.9	-62.0
-2	4	1	24.7	-20.5	-4	4	2	8.6	7.5	-7	5	3	96.8	98.9	1	5	4	71.4	-73.3	3	7	5	3.5*	0.5
0	4	1	30.8	-25.7	-2	4	2	59.1	53.5	-5	5	3	55.5	53.3	3	5	4	31.1	31.8	-8	8	5	45.4	44.6
2	4	1	61.1	-56.3	0	4	2	47.3	42.7	-3	5	3	6.8	3.8	5	5	4	14.4	-12.8	-6	8	5	2.5*	2.2
4	4	1	24.3	-22.3	2	4	2	82.2	78.9	-1	5	3	12.8	11.6	7	5	4	20.9	-22.0	-4	8	5	22.9	22.1
6	4	1	30.7	-29.1	4	4	2	127.7	146.6	1	5	3	49.1	48.7	-10	6	4	1.1*	-0.7	-2	8	5	0.5*	-0.2
8	4	1	19.5	-19.5	6	4	2	60.4	-61.7	3	5	3	11.2	-11.5	-8	6	4	11.6	-11.6	0	8	5	11.1	13.6
10	4	1	32.2	-35.1	8	4	2	85.8	89.9	5	5	3	32.7	34.8	-6	6	4	84.4	-86.7	2	8	5	5.1	7.8
-11	5	1	31.6	29.9	-11	5	2	2.1*	-3.6	7	5	3	22.5	23.6	-4	6	4	51.3	50.6	-5	9	5	7.8	8.7
-9	5	1	43.5	-40.9	-9	5	2	7.0	4.8	-10	6	3	3.2*	-1.4	-2	6	4	60.0	-57.9	-3	9	5	32.8	37.0

Table 3. Continued.

H	K	L	|FO|	FC	H	K	L	|FO|	FC	H	K	L	|FO|	FC	H	K	L	|FO|	FC	H	K	L	|FO|	FC
-1	9	5	17.0	17.7	1	5	6	29.6	28.6	2	4	7	25.4	23.4	1	3	8	6.3	0.6	-3	5	9	41.6	38.9
-14	0	6	44.9	-44.5	3	5	6	11.4	12.3	4	4	7	35.5	35.1	3	3	8	5.6	3.3	-1	5	9	46.8	45.7
-12	0	6	37.1	37.4	5	5	6	38.2	-38.1	-11	5	7	39.2	42.5	-12	4	8	0.0*	0.7	-8	6	9	45.1	-43.3
-10	0	6	52.7	54.2	-10	6	6	5.4	2.8	-9	5	7	53.2	54.2	-10	4	8	44.8	-47.0	-6	6	9	39.2	-40.3
-8	0	6	21.6	-22.4	-8	6	6	58.7	-60.5	-7	5	7	109.6	122.1	-8	4	8	74.0	76.5	-4	6	9	28.2	-27.2
-6	0	6	33.1	-30.4	-6	6	6	62.2	64.1	-5	5	7	31.8	32.4	-6	4	8	36.2	-36.9	-2	6	9	15.1	-15.2
-4	0	6	19.6	-18.6	-4	6	6	70.5	-75.1	-3	5	7	126.8	151.6	-4	4	8	7.4	7.0	0	4	9	0.0*	-0.7
-2	0	6	76.0	-74.8	-2	6	6	62.7	65.3	-1	5	7	48.6	51.7	-2	4	8	3.9*	-3.2	-12	0	10	71.9	-72.9
0	0	6	69.3	67.2	0	6	6	43.0	-43.9	1	5	7	79.5	80.2	0	4	8	4.5*	4.0	-10	0	10	4.5*	0.3
2	0	6	114.0	-120.5	2	6	6	23.1	-22.2	3	5	7	22.8	20.0	2	4	8	45.9	41.9	-8	0	10	68.7	-73.8
4	0	6	102.1	105.3	4	6	6	1.3*	1.0	-10	6	7	10.5	8.3	-11	5	8	36.9	37.8	-6	0	10	30.3	29.3
6	0	6	46.3	-42.4	-9	7	6	41.2	40.0	-8	6	7	21.6	-19.8	-9	5	8	38.9	-38.8	-4	0	10	28.7	25.8
-13	1	6	10.8	10.4	-7	7	6	15.7	14.8	-6	6	7	20.0	22.7	-7	5	8	28.6	-29.3	-2	0	10	52.4	-51.4
-11	1	6	61.4	-62.7	-5	7	6	15.0	12.5	-4	6	7	3.6*	1.5	-5	5	8	39.5	43.5	0	0	10	35.2	32.2
-9	1	6	19.0	19.4	-3	7	6	42.9	45.7	-2	6	7	2.9*	-2.0	-3	5	8	40.9	-43.1	-11	1	10	32.0	-32.6
-7	1	6	15.6	-16.1	-1	7	6	14.8	-12.8	0	6	7	21.9	22.3	-1	5	8	27.9	25.2	-9	1	10	31.7	-32.7
-5	1	6	20.9	-21.9	1	7	6	51.5	52.9	2	6	7	13.7	10.8	1	5	8	14.2	-14.8	-7	1	10	25.0	25.2
-3	1	6	10.4	8.9	3	7	6	27.5	24.9	-7	7	7	44.6	-46.8	-8	6	8	17.4	-14.5	-5	1	10	64.5	-64.9
-1	1	6	123.7	-140.2	-6	8	6	38.3	38.9	-5	7	7	1.6*	-0.0	-6	6	8	24.7	-25.2	-3	1	10	22.5	21.5
1	1	6	18.7	17.1	-4	8	6	9.5	-10.4	-3	7	7	25.6	-25.4	-4	6	8	35.7	-36.7	-1	1	10	19.9	17.9
3	1	6	74.7	-75.7	-2	8	6	29.7	30.0	-1	7	7	12.5	-13.3	-2	6	8	11.8	12.0	1	1	10	33.6	-31.1
5	1	6	48.3	-44.6	0	8	6	31.6	30.7	1	7	7	33.6	-33.8	0	6	8	65.0	-61.4	-10	2	10	77.6	80.8
7	1	6	33.5	29.0	-13	1	7	38.0	38.1	-6	8	7	38.1	38.9	-7	7	8	7.4	-7.6	-8	2	10	58.0	-60.7
-12	2	6	30.0	-28.0	-11	1	7	76.0	84.2	-4	8	7	11.4	8.7	-5	7	8	25.0	25.1	-6	2	10	33.6	33.9
-10	2	6	8.7	0.9	-9	1	7	21.4	21.8	-2	8	7	25.7	25.7	-3	7	8	54.8	-57.1	-4	2	10	35.7	-34.5
-8	2	6	112.3	-121.8	-7	1	7	93.1	104.3	-12	0	8	55.1	59.4	-1	7	8	38.9	34.8	-2	2	10	36.9	-35.6
-6	2	6	38.3	36.8	-5	1	7	28.9	29.1	-10	0	8	55.5	-58.5	-13	1	9	20.1	19.2	0	2	10	3.2*	3.2
-4	2	6	96.4	-105.1	-3	1	7	100.5	110.6	-8	0	8	114.4	139.5	-11	1	9	54.1	56.9	-11	3	10	16.3	-17.2
-2	2	6	19.9	-18.8	-1	1	7	9.6	5.5	-6	0	8	42.0	-43.3	-9	1	9	9.4	-9.3	-9	3	10	31.8	-32.9
0	2	6	2.3	-3.5	1	1	7	90.6	93.9	-4	0	8	128.6	150.5	-7	1	9	57.3	59.4	-7	3	10	19.6	19.5
2	2	6	82.1	-82.1	3	1	7	33.7	33.0	-2	0	8	66.2	65.8	-5	1	9	50.6	51.1	-5	3	10	52.9	-52.8
4	2	6	14.5	-15.2	5	1	7	28.6	27.2	0	0	8	28.5	-27.3	-3	1	9	61.0	59.1	-3	3	10	8.8	11.3
6	2	6	77.1	-73.6	-12	2	7	19.3	-17.2	2	0	8	62.5	60.6	-1	1	9	54.2	52.3	-1	3	10	41.9	-39.9
-13	3	6	5.5	5.7	-10	2	7	16.0	-15.0	4	0	8	12.0	-9.2	1	1	9	67.3	63.4	-10	4	10	9.7	-7.2
-11	3	6	55.7	-56.5	-8	2	7	9.7	11.4	-13	1	8	8.9	-9.4	3	1	9	19.5	17.3	-8	4	10	29.0	-29.9
-9	3	6	40.2	39.3	-6	2	7	7.1	-5.0	-11	1	8	53.3	55.3	-12	2	9	7.4	-4.7	-6	4	10	44.7	-44.0
-7	3	6	58.4	-57.7	-4	2	7	14.4	-15.2	-9	1	8	34.9	35.8	-10	2	9	6.2	5.6	-4	4	10	27.4	24.3
-5	3	6	49.2	-48.0	-2	2	7	22.4	24.2	-7	1	8	33.2	32.7	-8	2	9	16.8	14.9	-2	4	10	57.0	-52.7
-3	3	6	72.3	73.5	0	2	7	19.1	-20.3	-5	1	8	65.8	67.9	-6	2	9	26.5	-27.8	-7	5	10	47.5	48.1
-1	3	6	42.9	-43.4	2	2	7	39.9	-38.7	-3	1	8	50.8	-50.2	-4	2	9	26.2	-25.4	-5	5	10	38.2	-37.2
1	3	6	45.8	45.4	4	2	7	0.7*	1.6	-1	1	8	64.8	65.2	-2	2	9	33.7	-31.8	-3	5	10	32.9	31.0
3	3	6	10.8	11.8	-13	3	7	24.5	20.2	1	1	8	8.0	8.0	0	2	9	32.4	-31.7	-11	1	11	28.1	26.7
5	3	6	13.0	-9.2	-11	3	7	25.7	-24.8	3	1	8	4.7*	2.5	2	2	9	47.5	-43.3	-9	1	11	28.8	29.4
-12	4	6	30.8	30.3	-9	3	7	30.3	-29.9	-12	2	8	28.0	29.3	-11	3	9	27.4	-27.1	-7	1	11	65.5	64.2
-10	4	6	33.8	-32.3	-7	3	7	50.2	-51.4	-10	2	8	24.6	-25.7	-9	3	9	47.5	-50.2	-5	1	11	44.4	42.1
-8	4	6	0.0*	-1.6	-5	3	7	94.3	-102.7	-8	2	8	52.6	56.2	-7	3	9	78.6	-82.5	-3	1	11	59.7	56.3
-6	4	6	88.1	89.0	-3	3	7	60.9	-62.4	-6	2	8	36.0	-35.4	-5	3	9	21.7	-20.2	-10	2	11	35.8	36.2
-4	4	6	13.7	-12.2	-1	3	7	74.9	-78.3	-4	2	8	4.5*	-1.3	-3	3	9	112.7	-121.8	-6	2	11	14.2	-13.0
-2	4	6	7.1	5.0	1	3	7	29.1	-27.6	-2	2	8	53.0	52.2	-1	3	9	32.1	-29.1	-4	2	11	22.3	22.7
0	4	6	50.3	51.5	3	3	7	18.5	16.0	0	2	8	62.3	-61.1	1	3	9	103.4	-100.9	-2	2	11	16.2	12.8
2	4	6	26.2	-27.4	5	3	7	37.8	-36.5	2	2	8	78.2	75.8	-10	4	9	12.4	-11.3	-9	3	11	28.6	29.2
4	4	6	85.9	84.2	-12	4	7	33.5	35.3	4	2	8	58.0	-53.6	-8	4	9	14.2	13.8	-7	3	11	20.1	-16.7
6	4	6	11.0	11.2	-10	4	7	28.6	26.7	-11	3	8	43.6	44.6	-6	4	9	4.2*	2.0	-5	3	11	28.0	23.8
-11	5	6	44.9	-45.2	-8	4	7	22.8	22.9	-9	3	8	27.0	-25.4	-4	4	9	4.9	-4.0	-3	3	11	41.8	-37.2
-9	5	6	42.8	43.3	-6	4	7	49.5	49.7	-7	3	8	37.3	-38.3	-2	4	9	20.2	-18.0	-6	4	11	23.2	24.3
-7	5	6	38.3	-37.7	-4	4	7	32.5	32.8	-5	3	8	54.2	56.8	-9	5	9	1.9*	1.0	-6	0	12	17.6	-16.6
-5	5	6	45.2	-44.3	-2	4	7	34.8	35.5	-3	3	8	25.9	-24.9	-7	5	9	22.1	21.3	-8	2	11	3.4*	0.0
-3	5	6	35.5	37.0	0	4	7	26.3	23.5	-1	3	8	42.9	44.4	-5	5	9	17.3	20.3	-7	1	12	30.4	-30.8
-1	5	6	35.7	-37.1																				

Table 4. Interatomic distances (Å) and angles (°) in the tetrametaphosphate ion. The standard deviations are ±0.003 Å for the P—O distances, ±0.005 Å for the O—O distances, and ±0.5° for the angles.

P(1)—O(3)	1.599	P(2)—O(3)	1.591
—O(4)	1.590	—O(4)	1.590
—O(5)	1.510	—O(2)	1.505
—O(6)	1.464	—O(1)	1.461
Average:	1.541	Average:	1.537
O(3)—O(4)	2.459	O(1)—O(2)	2.550
—O(5)	2.523	—O(3)	2.463
—O(6)	2.503	—O(4)	2.520
O(4)—O(5)	2.530	O(2)—O(3)	2.513
—O(6)	2.473	—O(4)	2.455
O(5)—O(6)	2.563	O(3)—O(4)	2.526
O(3)—P(1)—O(4)	100.9	O(1)—P(2)—O(2)	118.6
O(3)—P(1)—O(5)	108.5	O(1)—P(2)—O(3)	107.6
O(3)—P(1)—O(6)	109.5	O(1)—P(2)—O(4)	111.3
O(4)—P(1)—O(5)	109.4	O(2)—P(2)—O(3)	108.6
O(4)—P(1)—O(6)	108.1	O(2)—P(2)—O(4)	104.9
O(5)—P(1)—O(6)	119.0	O(3)—P(2)—O(4)	105.2
P(1)—O(3)—P(2)	138.8		
P(1)—O(4)—P(2)	134.2		

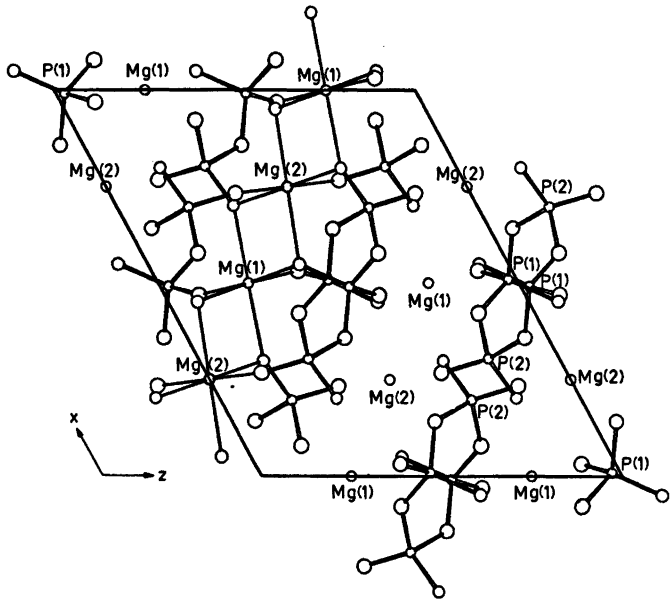

Fig. 1. Projection of the $Mg_2P_4O_{12}$ structure down the *b* axis.

MgO_6 octahedra which share corners forming a three-dimensional framework. An ORTEP [16] plot of the structure is shown in Fig. 1.

Most metaphosphate compounds have been found to have their PO_4 tetrahedra linked together in infinite chains. In $Mg_2P_4O_{12}$ four PO_4 tetrahedra are linked together in a ring to form $P_4O_{12}^{4-}$ ions, in accordance with the previously-mentioned postulations.[5,6,7] Only few metaphosphate structures with such anions have been found and determined to date.[17–20] The first of these structures was $Al_4(P_4O_{12})_3$, determined by Pauling and Sherman.[17]

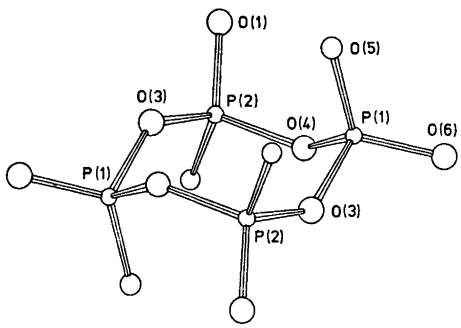

Fig. 2. The tetrametaphosphate ion.

Table 5. Interatomic distances (Å) in the magnesium-oxygen coordination octahedra. The e.s.d. of each Mg—O distance is ±0.003 Å.

Mg(1)—O(6)	(×2)	1.990
—O(2)	(×2)	2.125
—O(5)	(×2)	2.161
Average		2.092
Mg(2)—O(1)	(×2)	2.007
—O(2)	(×2)	2.094
—O(5)	(×2)	2.095
Average:		2.065

The $P_4O_{12}^{4-}$ ions in $Mg_2P_4O_{12}$ have a crystallographically imposed $\bar{1}$ symmetry. (*Cf.* Fig .2.) The shortest oxygen-oxygen distance between two different anions is 2.737 Å. Some interatomic distances and angles of the anion are given in Table 4. The PO_4 tetrahedra are fairly regular with O—O distances ranging from 2.455 to 2.563 Å. The bridging P—O distances (1.590—1.599 Å) are significantly longer than the terminal P—O distances (1.461—1.510 Å). The two different P—O—P angles are 134.2 and 138.8°, respectively. The tetrametaphosphate

ion dimensions (distances and angles) found in $Mg_2P_4O_{12}$ are in good agreement with those published for other tetrametaphosphates, *e.g.* $(NH_4)_4P_4O_{12}$,[18] $Na_4P_4O_{12}4H_2O$,[19] and $SrK_2P_4O_{12}$.[20] However, the configuration of the anions are different. In $Al_4(P_4O_{12})_3$ [17] as well as in $SrK_2P_4O_{12}$ [20] the anions have $\bar{4}$ point symmetry. In the ammonium phosphate the anion symmetry is $2/m$,[18] whereas in the sodium phosphate the P_4O_{12} rings, besides having point symmetry $\bar{1}$, show strong pseudosymmetry $2/m$.[19]

The magnesium ions in $Mg_2P_4O_{12}$ are always surrounded by six oxygen atoms thus forming rather regular MgO_6 octahedra of two different types: one with 2 point symmetry (around Mg(1)], the other with $\bar{1}$ symmetry [around Mg(2)]. The Mg—O distances range from 1.990 to 2.161 Å. Some interatomic distances for the magnesium-oxygen coordination octahedra are given in Table 5.

Octahedral coordination is the most common coordination for magnesium ions and it also occurs in the three previously mentioned magnesium phosphates.[2–4] However, two of these structures, α-$Mg_2P_2O_7$[2] and $Mg_3(PO_4)_2$[4] also contain magnesium ions with the quite unusual coordination number of five.

Acknowledgements. The authors sincerely thank Professor Peder Kierkegaard for his valuable guidance throughout the work. They are also most grateful to Dr. Donald F. Koenig who carefully revised the English of this article. This work has been financially supported by the Swedish Natural Science Research Council and the Tri-Centennial Fund of the Bank of Sweden.

REFERENCES

1. Berak, J. *Rocz. Chem. 32* (1958) 17.
2. Calvo, C. *Acta Crystallogr. 23* (1967) 289.
3. Calvo, C. *Can. J. Chem. 43* (1965) 1139.
4. Nord, A. G. and Kierkegaard, P. *Acta Chem. Scand. 22* (1968) 1466.
5. Steger, E. *Z. Anorg. Allg. Chem. 294* (1958) 146.
6. Grunze, I., *Diss.*, Humboldt-Universität, Berlin 1956.
7. Thilo, E. and Grunze, I. *Z. Anorg. Allg. Chem. 290* (1957) 209.
8. Beucher, M. and Grenier, J. C. *Mater. Res. Bull. 3* (1968) 643.
9. Sarver, J. F. *ASTM X-Ray Powder Data File*, Card 11—41.
10. Howells, E. R., Phillips, D. C. and Rogers, D. *Acta Crystallogr. 3* (1950) 210.
11. Norrestam, R. *Acta Crystallogr. A 28* (1972) 303.
12. *International Tables for X-Ray Crystallography* Kynoch Press, Birmingham 1968, Vol. III.
13. Hughes, E. W. *J. Amer. Chem. Soc. 63* (1941) 1737.
14. Brandt, B. G. and Nord, A. G. *Chem. Commun. Univ. Stockholm* (1970) No. 5.
15. Nord, A. G. *Chem. Commun. Univ. Stockholm* (1973) No. 15.
16. Johnson, C. K. *AEC Accession No. 33516*, ORNL-3794, Oak Ridge 1965.
17. Pauling, L. and Sherman, J. *Z. Kristallogr. 96* (1937) 481.
18. Romers, C., Ketelaar, J. A. A. and McGillavry, C. H. *Acta Crystallogr. 4* (1951) 114.
19. Ondik, H. M., Block, S. and McGillavry, C. H. *Acta Crystallogr. 14* (1961) 555.
20. Tordjman, I., Martin, C. and Durif, A. *Bull. Soc. Fr. Min. Crist. 90* (1967) 293.

Received August 9, 1974.

Acta Chemica Scandinavica A 29 (1975) 7—13

X-Ray Crystallographic Determination of the *cis* Form and ^{1}H NMR Investigation of the *cis* and *trans* Forms of (5*S*)-2-*t*-Butyl-5-carboxymethyl-1,3-dioxolan-4-one

MARTIN VAHL GABRIELSEN

The Royal Danish School of Pharmacy, Chemical Laboratory C, DK-2100 Copenhagen, Denmark

Synthesis and high resolution ^{1}H NMR investigation of *cis* and *trans* (5S)-2-*t*-butyl-5-carboxymethyl-1,3-dioxolan-4-one are described. An X-ray crystallographic investigation of the (2*S*,5*S*)-form of the compound has been performed. Long range coupling between the two ring protons is found to be stronger for the *trans* form (2*R*,5*S*), than for the *cis* form (2*S*,5*S*), the values are 1.8 and 1.25 Hz, respectively.

Crystals of (2*S*,5*S*)-2-*t*-butyl-5-carboxymethyl-1,3-dioxolan-4-one are monoclinic space group $P2_1$, $a=5.775(3)$, $b=8.534(2)$, $c=10.276(3)$ Å, $\beta=91.27(5)°$, $Z=2$. The structure has been solved by direct methods using X-ray diffraction data and has been refined by full-matrix least-squares method to a final R value of 0.071. The molecules adopt an O_1-envelope conformation (E_0) in the crystalline state.

2,5-Disubstituted 1,3-dioxolan-4-ones contain a ring with two asymmetric carbon atoms; one pair of enantiomers, with the hydrogen atoms to the same side of the mean ring plane, constitutes the *cis* forms and the other pair of enantiomers the *trans* forms. The possibility of being able to discriminate between the two forms on the basis of ^{1}H NMR data has been discussed by several authors.[1–5] When spectra of both the *cis* and the *trans* forms have been available it has been shown that the chemical shift of the ring protons are different for the two forms.[1–5] In some cases chemical shift differences have also been observed for protons attached to carbon atoms in the substituents.[1]

High resolution ^{1}H NMR spectroscopy has shown that long range coupling between the two ring protons is present in many, 2,5-disubstituted 1,3-dioxolan-4-ones.[2–6] In most cases where both forms have been investigated the coupling is stronger for the form, which is believed to be *trans*.

The coupling mechanism has been regarded [1,6] as similar to that in 2,5-dihydrofurans; this requires that the lactone function is approximately planar, *i.e.* the 1,3-dioxolan-4-ones which show long range coupling should adopt an O_1-envelope conformation.

RESULTS AND DISCUSSION

(5*S*)-2-*t*-Butyl-5-carboxymethyl-1,3-dioxolan-4-one (I) (Fig. 1) was synthesized by condensation of L-malic acid and 2,2-dimethylpropanal using a slight modification of the general method given by Salomaa and Sallinen.[7]

Heating of I at a temperature just above the melting point caused partial isomerization to II.

An X-ray analysis proved I to be the *cis* form; as it is reasonable to assume that no inversion takes place at C(2) in L-malic acid during the preparation of I, the absolute configuration of I is (2*S*,5*S*). The numbering of I [given as O(1), O(2), C(3) *etc.*] appears from Fig. 3.

The ^{1}H NMR spectrum of I consists of five groups of lines (Table 1). The ring proton H(51) and the two geminal methylene protons in the carboxymethyl substituent constitute an ABX system. The two ring protons H(51) and H(71) couple weakly; thus the signal from H(71) is a doublet, while the X part of the ABX system is further split to a total of eight lines.

Table 1. Chemical shift and coupling constants in *cis* and *trans* (5*S*)-2-*t*-butyl-5-carboxymethyl-1,3-dioxolan-4-one (Fig. 1).

Compound	Chemical shift (δ)						Coupling constants (Hz)[b]	
	COO*H*	*H*(71) (ring)	*H*(51) (ring)	C−C*H*$_2$−COOH		C−(C*H*$_3$)$_3$	Long range	ABX system (−CH−CH$_2$−)
cis (I)	9.88	5.19	4.66	3.01	2.83	1.01	1.25	$\|J_{AB}\| = 17.19$ $J_{AX} = \pm 3.67$ $J_{BX} = \pm 7.38$
trans (II)[a]	9.88	5.34	<4.66			1.01	1.8	

[a] Data on the *trans* form were obtained from a (5:1) mixture of the *cis* and the *trans* form. Chemical shifts and coupling constants are only given where assignment of frequencies were unambiguous. [b] Probable errors on coupling constants are 0.02 for the *cis* form and 0.07 for the *trans* form.

Table 2. Final positional and thermal (Å^2) parameters for non-hydrogen atoms. The estimated standard deviations of positional ($\times 10^4$) and thermal ($\times 10$) parameters are given in parentheses. The temperature expression is of the form: $\exp\{-2\pi^2\ h^2a^{*2}U_{11} + k^2b^{*2}U_{22} + \ldots + 2klb^*c^*U_{23}\}$.

	x/a	y/b	z/c	$U_{11}\times 100$	$U_{22}\times 100$	$U_{33}\times 100$	$U_{12}\times 100$	$U_{13}\times 100$	$U_{23}\times 100$
O(1)	0.9783(7)	0.5211(8)	0.9702(4)	3.9(2)	9.9(4)	5.1(3)	−0.5(2)	0.5(2)	1.3(3)
O(2)	0.8195(7)	0.4005(8)	1.1386(4)	4.9(2)	8.2(3)	6.6(3)	0.5(3)	−0.1(2)	2.5(3)
C(3)	0.8143(10)	0.4906(9)	1.0337(5)	4.5(3)	5.0(3)	3.5(3)	0.3(3)	−0.4(3)	−0.8(3)
C(4)	0.5736(9)	0.5500(9)	1.0040(5)	4.6(3)	4.9(4)	3.4(3)	−0.1(3)	0.3(2)	−0.2(3)
C(5)	0.5177(8)	0.5542(8)	0.8596(4)	3.6(3)	3.6(3)	3.8(3)	0.2(3)	0.3(2)	−0.1(3)
O(6)	0.5468(5)	0.3997(6)	0.8055(3)	4.0(2)	3.4(2)	3.5(2)	−0.7(2)	0.9(2)	0.0(2)
C(7)	0.6165(9)	0.4219(9)	0.6752(5)	3.8(3)	3.7(3)	3.5(3)	0.1(3)	0.5(2)	0.1(3)
O(8)	0.7389(6)	0.5682(6)	0.6751(3)	4.9(2)	3.8(2)	5.0(2)	−0.5(2)	1.7(2)	0.3(2)
C(9)	0.6805(9)	0.6524(8)	0.7803(6)	3.2(3)	4.0(3)	4.9(4)	0.1(3)	−0.7(3)	0.6(3)
O(10)	0.7440(7)	0.7823( )	0.7993(4)	5.9(3)	3.6(2)	6.8(3)	−1.2(2)	0.6(2)	0.1(2)
C(11)	0.7608(9)	0.2886(10)	0.6275(5)	4.2(3)	4.3(3)	3.8(3)	−0.4(3)	1.2(3)	0.4(3)
C(12)	0.8256(13)	0.3211(9)	0.4864(7)	11.7(6)	5.9(5)	6.5(4)	1.3(4)	4.8(4)	0.0(4)
C(13)	0.6176(13)	0.1403(9)	0.6318(6)	8.1(5)	4.9(4)	6.0(4)	0.5(4)	1.8(4)	−0.9(3)
C(14)	0.9758(11)	0.2663(10)	0.7143(7)	5.5(4)	8.0(5)	10.6(6)	3.4(4)	−0.7(4)	−2.7(5)

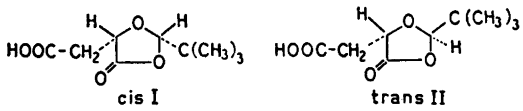

Fig. 1. cis and *trans* (5*S*)-2-*t*-Butyl-5-carboxymethyl-1,3-dioxolan-4-one.

The data on the *cis* form were obtained by iteration on all observed lines. The final RMS error was 0.052 Hz.

As no separation of I and II was attempted it was only possible to determine reasonably accurate frequencies for a few lines in the spectrum of II (Table 1). The signal from the proton H(71) (doublet) and two of the signals from the X part of the ABX system gave rise to fully resolved peaks. The rest of the signals originating in the *trans* form were more or less obscured (the ratio of the *cis* to the *trans* form was 5:1). It was, however, evident that the spectra of I and II had the same general characteristics. Inspection of the X-parts of the ABX systems showed that absorption for H(51) in the spectrum of the *trans* form was at slightly lower field than for the corresponding proton in the spectrum of the *cis* form. The absorption for H(71) shows the opposite effect.

The numerical value of the long-range coupling constant is greatest for the *trans* form. If it is assumed that long range coupling is most effective for a planar lactone function, a rationalization based on molecular models can be offered. For the *trans* form both of the two possible O_1-envelopes can be regarded as favourable conformations while only one, with both substituents pseudo-equatorial, is favourable for the *cis* form. For both forms only one of the two possible half chair conformations is favourable. Thus the contribution of the O_1-envelope conformation to the time average might be expected to be greatest for the *trans* form, giving rise to the strongest long-range coupling.

The X-ray structure determination of (2*S*,5*S*)-2-*t*-butyl-5-carboxymethyl-1,3-dioxolan-4-one (I) gave the result that in the crystalline state the conformation of the five-membered ring is an almost perfect O_1-envelope. The flap of the envelope O(6) is above the mean ring plane (Fig. 2) making the two bulky substituents pseudo-equatorial. The angle between the two planes of the envelope is 154°. The atoms

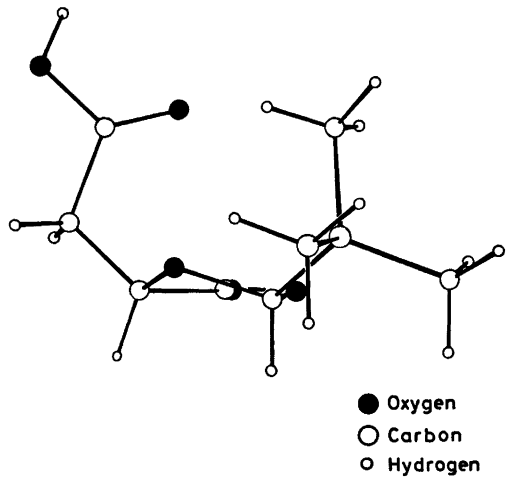

Fig. 2. Conformation of (2*S*,5*S*)-2-*t*-butyl-5-carboxymethyl-1,3-dioxolan-4-one. Molecule seen with the $-C-CO-O-$ plane perpendicular to the plane of the paper.

H(51), C(5), C(7), and H(71) form an almost planar system, which bisects the obtuse angle of the envelope. Distances of some atoms from the least-squares plane defined by all five ring atoms (plane 2) are given in Table 5 which also lists the distances of some atoms from the least-squares plane defined by the carbonyl group C(9)−O(10) and the attached carbon, C(5) and oxygen, O(8) atoms (plane 1). It is seen that the carbon atom C(7) is about 0.1 Å out of this plane, while the distance to the oxygen atom O(6) is more than 0.3 Å.

Fig. 2 illustrates the conformation of the molecule and values of torsion angles are listed in Table 5.

The rotations round all carbon-carbon sp_3-sp_3 bonds correspond to staggered conformations. It seems likely that the conformation of the molecule is determined by *intra*- rather than *inter*-molecular forces, apart from the carbonyl group which is involved in an *inter*-molecular hydrogen bond.

The crystal structure of (2*S*,5*S*)-2-*t*-butyl-5-carboxymethyl-1,3-dioxolan-4-one is depicted in Fig. 4. The molecules related by screw axis through origo are connected by a hydrogen bond between the carbonyl oxygen O(10) and the oxygen atom O(2) in the carboxy group forming infinite chains in the *b*-direction. The length of the hydrogen bond is 2.776(6) Å.

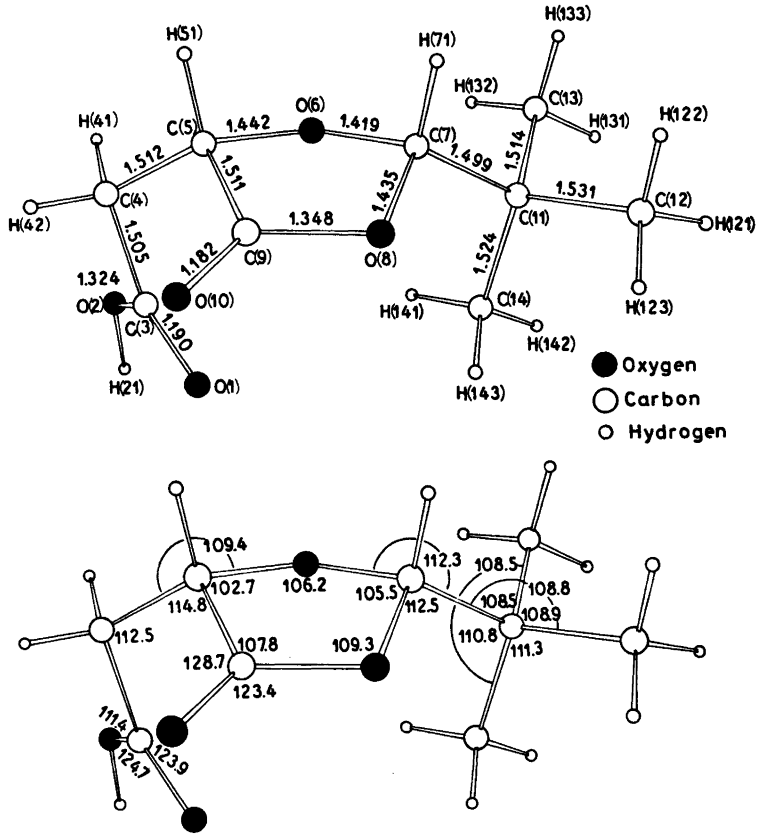

Fig. 3. Bond lengths (Å) and valency angles (°) for (2*S*,5*S*)-2-*t*-butyl-5-carboxymethyl-1,3-dioxolan-4-one.

Bond distances and valency angles for the molecule are given in Tables 3 and 4, the geometry is further illustrated by Fig. 3.

The bond lengths are close to normally accepted values and the valency angles in the ring system show no significant deviations from previously reported values.[8]

EXPERIMENTAL

Melting points were determined with a hot stage microscope (Mikroskop Heiztisch Ernst Leitz G.m.b.H., Wetzlar). The computations were performed on a GIER and an IBM 370/165 computer using *INDIFF*,[9] a local version of *The N.R.C. 2A Picker Data Reduction Program*,[10]

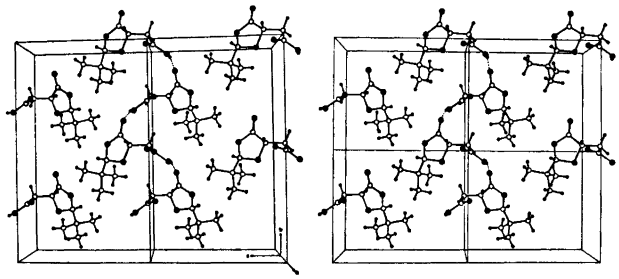

Fig. 4. Stereoscopic pair showing the crystal structure as seen from the direction of the *a*-axis. Hydrogen bonds are indicated by dotted lines.

Table 3. Intramolecular distances (Å) and valency angles (°). The estimated standard deviations are given in parenthesis.

O(1) – C(3)	1.190(7)	C(7) – O(8)	1.435(8)
O(2) – C(3)	1.324(8)	C(7) – C(11)	1.499(10)
C(3) – C(4)	1.505(8)	O(8) – C(9)	1.348(7)
C(4) – C(5)	1.512(7)	C(9) – O(10)	1.182(7)
C(5) – O(6)	1.442(9)	C(11) – C(12)	1.531(9)
C(5) – C(9)	1.511(8)	C(11) – C(13)	1.514(11)
O(6) – C(7)	1.419(6)	C(11) – C(14)	1.524(8)
O(1) – C(3) – O(2)	124.7(6)	C(7) – O(8) – C(9)	109.3(4)
O(1) – C(3) – C(4)	123.9(6)	C(5) – C(9) – O(8)	107.8(5)
O(2) – C(3) – C(4)	111.4(5)	C(5) – C(9) – O(10)	128.7(5)
C(3) – C(4) – C(5)	112.5(4)	O(8) – C(9) – O(10)	123.4(5)
C(4) – C(5) – O(6)	109.4(5)	C(7) – C(11) – C(12)	108.8(6)
C(4) – C(5) – C(9)	114.8(5)	C(7) – C(11) – C(13)	108.5(5)
O(6) – C(5) – C(9)	102.7(4)	C(7) – C(11) – C(14)	110.8(5)
C(5) – O(6) – C(7)	106.2(5)	C(12) – C(11) – C(13)	108.9(5)
O(6) – C(7) – O(8)	105.5(5)	C(12) – C(11) – C(14)	111.3(5)
O(6) – C(7) – C(11)	112.3(5)	C(13) – C(11) – C(14)	108.5(6)

Table 4. Hydrogen atoms: Positional and thermal parameters, bond distances and valency angles. Parameters for hydrogen atoms are not refined. For the *t*-butyl and methylene groups the values were determined by fitting a tetrahedral model with distances to hydrogen atoms *ca.* 0.96 Å to the difference fouriers.

Positional and thermal (Å²) parameters

	x/a	*y/b*	*z/c*	$U \times 100$
H(21)	0.9691	0.3884	1.1604	6
H(41)	0.4644	0.4825	1.0453	4
H(42)	0.5598	0.6542	1.0382	4
H(51)	0.3526	0.5880	0.8359	4
H(71)	0.4713	0.4392	0.6222	3
H(121)	0.8858	0.2274	0.4481	6
H(122)	0.6905	0.3546	0.4377	6
H(123)	0.9409	0.4020	0.4852	6
H(131)	0.7066	0.0550	0.5985	6
H(132)	0.5767	0.1187	0.7201	6
H(133)	0.4790	0.1535	0.5795	6
H(141)	0.9313	0.2575	0.8032	7
H(142)	1.0560	0.1733	0.6887	7
H(143)	1.0754	0.3557	0.7046	7

Bond distances (Å)

O(2) – H(21)	0.89
C(5) – H(51)	1.02
C(7) – H(71)	1.00

Valency angles (deg.)

C(3) – O(2) – H(21)	106
C(4) – C(5) – H(51)	115
O(6) – C(5) – H(51)	106
C(9) – C(5) – H(51)	108
O(6) – C(7) – H(71)	106
O(8) – C(7) – H(71)	106
C(11) – C(7) – H(71)	114

The X-Ray System,[11] and *ORTEP*.[12] The X-ray atomic scattering factors used were those listed in International Tables for X-Ray Crystallography (1962).

Synthesis. To a solution of 5.5 g (75 mmol) of 2,2-dimethylpropanal in 75 ml of benzene were added 6.6 g (50 mmol) of L-malic acid, 0.4 g of *p*-toluenesulfonic acid and 20 g of molecular sieve (Union Carbide 3A). After refluxing for 3 h the benzene was decanted and the residue refluxed for further 10 min with 50 ml of benzene. The combined benzene phases were filtered and concentrated *in vacuo* to give a yellow oil, which was then dissolved in benzene. After slow evaporation of the benzene at room temperature colourless plate shaped crystals were obtained. Yield 1 g, m.p. 102–103 °C. Recrystallization of 0.1 g from diethyl ether-ligroin (1:1) resulted in the formation of short thick monoclinic needles of (2*S*,5*S*)-2-*t*-butyl-5-carboxymethyl-1,3-dioxolan-4-one (proved by X-ray analysis) m.p. 103 °C. Some of the crude product was heated at 120 °C for 1 h, cooled and recrystallized from diethyl ether-ligroin (1:1). Long thin colourless needles were obtained. From ^{1}H NMR investigations it could be concluded, that the latter crystals were a 5:1 mixture of *cis* and *trans* (5*S*)-2-*t*-butyl-5-carboxymethyl-1,3-dioxolan-4-one.

^{1}H NMR spectra. ^{1}H NMR spectra were recorded in a Varian HA 100 spectrometer[13] operating at 31 °C in frequency sweep mode. The sample was dissolved in $CDCl_3$, and TMS was added as internal standard. The concentrations of the sample of the pure *cis* form and the sample of the mixture (5:1) of the *cis* and *trans* forms were 5 and 20 W/V %, respectively, Coupling constants were obtained from spectra recorded with 1 Hz/cm. Simulation and itera-

Table 5. Conformation of (2*S*,5*S*)-2-*t*-butyl-5-carboxymethyl-1,3-dioxolan-4-one.

Distances of atoms from least squares planes in the dioxolane ring			
Atom	Deviation	Atom	Deviation
Plane 1			
C(5)	−0.004	O(8)	−0.004
O(6)[a]	0.326	C(9)	0.014
C(7)[a]	−0.099	O(10)	−0.006
Plane 2			
C(5)	−0.126	C(4)[a]	0.811
O(6)	0.171	C(11)[a]	0.679
C(7)	−0.145	O(10)[a]	0.091
O(8)	0.061	H(51)[a]	−1.12
C(9)	0.039	H(71)[a]	−1.13

Equation in direct (unit cell) space for the dioxolane ring:

Plane 1. $4.479x - 3.090y + 5.135z = 5.024$
Plane 2. $4.807x - 2.612y + 4.555z = 5.083$

Torsion angles (deg.)			
O(1)−C(3)−C(4)−C(5)	+38.4	O(6)−C(7)−C(11)−C(14)	−58.1
O(2)−C(3)−C(4)−C(5)	−141.6	H(71)−C(7)−C(11)−C(14)	−178.7
C(3)−C(4)−C(5)−H(51)	+176.7	O(8)−C(7)−C(11)−C(14)	+60.7
C(3)−C(4)−C(5)−O(6)	+57.2	O(6)−C(7)−C(11)−C(12)	+179.2
C(3)−C(4)−C(5)−C(9)	−57.7	O(6)−C(7)−C(11)−C(13)	+61.0
C(9)−C(5)−O(6)−C(7)	−26.6	H(121)−C(12)−C(11)−C(7)	−167
C(5)−O(6)−C(7)−O(8)	+29.1	H(131)−C(13)−C(11)−C(7)	+178
O(6)−C(7)−O(8)−C(9)	−19.8	H(141)−C(14)−C(11)−C(7)	−53

[a] The coordinates did not contribute to the least squares matrix.

tion on the spin system were performed using *LAOCOON III*.[14]

Crystal data. (2*S*,5*S*)-2-*t*-Butyl-5-carboxymethyl-1,3-dioxolan-4-one, $C_9H_{14}O_5$, M = 202.21. Monoclinic, space group $P2_1$, $a = 5.775(3)$, $b = 8.534(2)$, $c = 10.276(3)$ Å, $\beta = 91.27(5)°$ $V = 506.3$ Å^3, $D_m = 1.31$ g cm^{-3}, $Z = 2$, $D_c = 1.33$ g cm^{-3}, linear absorption coefficient (λ(Mo$K\alpha$) = 0.7107 Å) $\mu = 1.2$. The unit-cell dimensions were determined from least-squares refinement of diffractometer measured theta values for 43 reflections. The crystal density was measured by flotation in an aqueous KI solution.

X-Ray data collection. The intensity data were obtained from a single crystal with approximate dimensions 0.3 × 0.2 × 0.2 mm mounted on a Nonius three-circle automatic diffractometer using graphite monochromatized Mo$K\alpha$ radiation (λ = 0.7107 Å). The crystal was mounted with the crystal *a*-axis along the ϕ-axis of the goniometer, the ω-scan technique with a fixed scan range of 1.0° and a scan speed of 1.2 deg. min^{-1} was employed, background intensity was measured for half the scanning time at the scan range limits. The intensity of one reference reflection was measured for every 25th reflection.

Out of the 1567 independent reflections in the range $2.5 \leq \theta \leq 30.0°$, 910 had an intensity greater than 1.5 times the estimated standard deviation, and were considered observed. The data were corrected for Lorentz and polarization effects.

STRUCTURE DETERMINATION

Normalized structure amplitudes, $|E(h,k,l)|$, were calculated using the results from application of Wilson statistics. The structure was solved by direct methods. Preliminary symbolic addition by hand suggested eight likely combinations of phases for a starting set consisting of eight structure factors. These starting sets were then expanded and refined by application of the tangent formula to the 150 largest E values($|E(h,k,l)| \geq 1.56$). Due to the few strong interactions involving reflections with k-index equal to one, the position of the origin on the screw-axis was fixed by assigning the phase $\pi/4$ to $E(24\bar{1})$ and restricting the phase of $E(212)$ to the range $0 < \phi \leq \pi/2$.

Parts of the structure (9 of the total 14 non-hydrogen atoms) were found in an E-map based on the solution with the lowest R-value

($R = \sum(|E_o| - |E_c|)/\sum|E_o|$). The five remaining non-hydrogen atoms of the molecule appeared clearly in a subsequent electron density map.

Full-matrix least-squares refinements (minimizing $\sum w(|F_o| - |F_c|)^2$, with weights equal to unity) using individual isotropic temperature factors converged at $R = 0.12$. Anisotropic thermal parameters were then introduced for the oxygen atoms and the carbon atoms in the terminal methyl groups. After three cycles of least-squares refinement, a difference Fourier was calculated using structure factors in the range $\sin\theta/\lambda \leq 0.35$. In the difference map the fourteen largest maxima were found in regions where hydrogen atoms would be expected to contribute.

As the small number of observed reflections made least-squares refinement on the parameters of the hydrogen atoms impossible, it was decided to determine the positions of the hydrogen atoms in the *t*-butyl and methylene groups by fitting a tetrahedral model with carbon-hydrogen bond distances of 0.96 Å to the corresponding positive regions. The parameters for the three remaining hydrogen atoms were taken directly from the difference map.

Individual isotropic thermal parameters, approximately equal to those calculated for the corresponding heavier atoms, were assigned to the hydrogen atoms. Refinement on the positional and individual anisotropic thermal parameters for all non-hydrogen atoms converged at $R = 0.071$ (weighted $R = 0.050$; values of average and maximum shift/error were 0.01 and 0.05, resp.). On the last cycles empirical weights were introduced in order to make $w(|F_o| - |F_c|)^2$ independent of $|F_o|$ and $\sin\theta$. The weight scheme chosen was: $w = 1/(1 + |(|F_o| - b)/a|^2)$, with $a = 3.0$ and $b = 12.0$.

The final atomic parameters are listed in Tables 2 and 4; tables of the structure factors are available on request.

Acknowledgement. The author wishes to thank Dr. M. Bàron, Facultad de Ciencias y Naturales, Buenos Aires, for his interest in this work. Thanks are also due to the staff of the Chemical Laboratory C, Royal Danish School of Pharmacy, and Dr. K. Schaumburg, University of Copenhagen, for fruitful discussions.

REFERENCES

1. Farines, M. and Soulier, J. *Bull. Soc. Chim. Fr.* (1970) 332.
2. Cort, L. A. and Stewart, R. A. *J. Chem. Soc. C* (1971) 1386.
3. Brettle, R. *J. Chem. Soc. Perkin Trans. 1* (1972) 611.
4. Baron, M. *J. Mol. Struct. 12* (1972) 71.
5. Brettle, R. and Logan, I. D. *J. Chem. Soc. Perkin Trans. 2* (1973) 687.
6. Asano, R., Moritani, I., Fujiwara, Y. and Teranishi, S. *Bull. Chem. Soc. Jap. 46* (1973) 663.
7. Salomaa, P. and Sallinen, K. *Acta Chem. Scand. 19* (1965) 1054.
8. Haagensen, C. O. and Danielsen, J. *Acta Chem. Scand. 18* (1964) 581.
9. Sørensen, A. M. *INDIFF, An Algol Nonius Three Circle Diffractometer Input Data Program*, Chemical Laboratory C, The Royal Danish School of Pharmacy, DK-2100 Copenhagen 1968.
10. Ahmed, F. R. *N.R.C. Crystallographic Program System*, National Research Council, Ottawa, Canada 1968.
11. Stewart, J. M., Kruger, C. J., Ammon, H. L., Dickinson, C. and Hall, S. R. *X-Ray 72 Crystal Structure Calculation System*, Computer Science Center, University of Maryland, June 1972.
12. Johnson, C. K. *ORTEP: A Fortran Thermal Ellipsoid Plot Program for Crystal Structure Illustrations*, Oak Ridge National Laboratory, Oak Ridge 1965.
13. Gillein, D. and Schaumburg, K. *Rev. Sci. Instrum. 39* (1968) 262.
14. Manschen, O. H. *Thesis*, University of Copenhagen, Copenhagen 1971.

Received July 5, 1974.

Acta Chemica Scandinavica A 29 (1975) 14—20

The Crystal and Molecular Structure of Tellurium Di(methylxanthate)

HALVOR GRAVER and STEINAR HUSEBYE

Department of Chemistry, University of Bergen, N-5014 Bergen-Universitetet, Norway

The structure of tellurium di(methylxanthate), $Te(CH_3OCS_2)_2$ has been determined by three-dimensional X-ray crystallography. The unit cell dimensions are $a = 4.2341(5)$ Å, $b = 14.202(2)$ Å, $c = 17.299(2)$ Å, $\beta = 92.99(2)°$ and $z = 4$. The crystals are monoclinic, space group $C_{2h}^5 - P2_1/c$. Data were collected by means of a Siemens AED-1 diffractometer. The final conventional R-value is 2.96 %.

The structure consists of monomeric molecules in which the central tellurium atoms are coordinated to all four sulfur atoms in a trapezoid planar configuration. The Te – S bond lengths are: Te – S1 = 2.510(1) Å, Te – S2 = 2.841(1) Å, Te – S3 = 2.499(1) Å and Te – S4 = 2.846(1) Å. The corresponding bond angles are: ∠S1 – Te – S2 = 66.20(4)°, ∠S1 – Te – S3 = 85.18(4)°, ∠S3 – Te – S4 = 66.33(4)° and ∠S2 – Te – S4 = 142.29(3)°. Weak intermolecular Te···S2 interactions of 3.51 Å tie the molecules into pairs across centres of symmetry.

Previous work on structures of divalent tellurium with bidentate dithio ligands, has shown its preference for a trapezoid planar configuration in complexes with such ligands.[1–4] The same preference has also been demonstrated for divalent selenium [5–8] and in one case such a structure has been found for a divalent sulfur compound.[8]

Two classes of trapezoid planar compounds can be distinguished. Class I consists of essentially monomeric molecules where the central selenium or tellurium atoms are bonded to all four sulfur atoms in the molecule. Class II consists of polymeric networks, where the central atom is strongly bonded to two sulfur atoms in the molecule proper and weakly to two sulfur atoms belonging to different neighbour molecules.

The structure of tellurium di(ethylxanthate) [8] belongs to class I, however, the structures of selenium di(methylxanthate) and its sulfur isomorph both belong to class II.[8] For comparison with the latter two compounds, it was felt worthwhile to undertake the present investigation. Also the high quality of the experimental data obtained here, enabled us to get the most accurate structure determination obtained so far for this type of complex.

EXPERIMENTAL

The preparation of crystals and their space group and unit cell dimensions have been reported earlier.[8] By recrystallization from methanol, deep red crystals are obtained with $a = 4.2341(5)$ Å, $b = 14.202(2)$ Å, $c = 17.299(2)$ Å, $\beta = 92.99(2)°$, $z = 4$ and space group $C_{2h}^5 - P2_1/c$. The observed and calculated densities are 2.18 and 2.19 g/cm³ respectively.

The crystals are relatively unstable, especially when exposed to X-rays. Small crystals were found to disintegrate in the beam, but crystals with cross sections of 0.1×0.1 mm² gave satisfactory intensity data in spite of some decomposition which was evidenced by darkening of crystals during exposure to X-rays.

The intensity measurements were made on a crystal mounted along c, using a Siemens off-line automatic AED-1 diffractometer and Mo$K\alpha$ radiation. Reflections out to $2\theta = 56°$ were collected using the "five value" measurement [9] and the $\theta - 2\theta$ scan technique with scan speed 2.5° per min. with automatic setting of greater speed for strong reflections. An automatic attenuation filter insertion mechanism reduced counting losses. The reflections were scanned between $\theta_1 = \theta - 0.50°$ and $\theta_2 = \theta + 0.50°$ where θ is the Bragg angle for the α_1 peak. Two reference reflections were

measured at intervals of 50 reflections. Out of 2521 reflections measured, 2163 had intensities greater than twice the standard deviations based on counting statistics, only the latter were labelled as observed.

Accurate cell dimensions were determined by least squares methods based on measurements of 20 strong high-order reflections.

The intensities were corrected for Lorentz and polarization effects as well as for absorption ($\mu = 36.7$ cm^{-1}).[10] Crystal dimensions measured as distances from a common origin to crystal faces were: 0.154 mm for $\bar{1}00$, 0.066 mm for $0\bar{1}0$, 0.070 mm for $01\bar{1}$ and $0\bar{1}1$, 0.062 mm for 011 and $0\bar{1}\bar{1}$, and 0.132 mm for 120.

The UV spectrum of tellurium di(methylxanthate) in hexane shows the following four absorption bands: I 360 nm, II 297 nm, III 248 nm and IV 212 nm. For comparison, the corresponding disulfide, dimethyldixanthogen gives three absorptions at 361 nm, 278 nm and 240 nm. These latter bands are due to $n \rightarrow \pi^*$, $\pi \rightarrow \pi^*$ and $n \rightarrow \sigma^*$ transitions, respectively, on the ligands.[11]

An IR spectrum was obtained using the KBr disc technique. The following absorption bands have been tentatively assigned: Two strong bands at ν 1220 and 1161 cm^{-1} to stretching vibrations of the O–C–O moiety; a strong band at 1044 cm^{-1} and a weak at 943 cm^{-1} to stretching vibrations in short and long C–S bonds, respectively. The assignments have been done by comparison with the IR spectra of a series of xanthate compounds,[12-14] the corresponding tellurium bis(diethyldithiocarbamate),[15] and the analogous tellurium di(benzylxanthate). The latter compound was from oscillation and Weissenberg films found to be monoclinic with space group $P2_1/c$ and $a = 8.35(5)$ Å, $b = 5.70(2)$ Å, $c = 38.19(4)$ Å, $\beta = 91.8(2)°$ and $Z = 4$.

DETERMINATION AND REFINEMENT OF THE STRUCTURE

The solution of the structure was accomplished by application of a Patterson synthesis which gave the heavy atom position. The positions of the other atoms except hydrogen were then found by successive Fourier syntheses.

The structure was refined by means of a full-matrix least squares program which

Table 1. Atomic coordinates for $[Te(CH_3OCS_2)_2]$. Standard deviations except for hydrogen in brackets.

	x	y	z
Te	0.33961(6)	0.14848(2)	0.05250(2)
S1	0.3099(3)	0.12768(9)	0.19602(7)
S2	0.0933(3)	−0.02884(8)	0.09587(6)
S3	0.5685(3)	0.30643(9)	0.08587(7)
S4	0.4901(3)	0.25692(9)	−0.07896(7)
O1	0.0798(8)	−0.0241(2)	0.2478(2)
O2	0.7456(8)	0.4131(2)	−0.0207(2)
C1	0.1479(10)	0.0184(3)	0.1819(2)
C2	−0.0698(14)	−0.1155(4)	0.2428(3)
C3	0.6118(10)	0.3310(3)	−0.0102(3)
C4	0.7958(13)	0.4436(4)	−0.0996(3)
H1	−0.130	−0.138	0.301
H2	0.096	−0.167	0.219
H3	−0.283	−0.113	0.205
H4	0.914	0.386	−0.130
H5	0.577	0.462	−0.130
H6	0.959	0.504	−0.097

Table 2. Components of atomic vibration tensors for Te, S, N, O, C ($U \times 10^4$ and H ($U \times 10^3$), in Å^2 with standard deviations, referred to crystallographic axes. The expression used for the Te, S, N, O, and C atoms is $\exp\{-2\pi^2[h^2a^{-2}U_{11} + \cdots + 2hka^{-1}b^{-1}U_{12}\cdots]\}$, while the expression used for hydrogen is $\exp[-8\pi^2 U(\sin^2\theta/\lambda)]$.

	U_{11}	U_{22}	U_{33}	U_{12}	U_{23}	U_{13}		U
Te	490(2)	463(2)	464(2)	7(1)	−25(1)	61(1)	H1	107(24)
S1	904(9)	578(8)	454(6)	128(6)	−115(5)	86(6)	H2	168(31)
S2	777(8)	514(7)	408(5)	−91(6)	−29(5)	28(5)	H3	71(20)
S3	720(8)	508(6)	494(6)	−68(6)	−107(5)	98(5)	H4	58(18)
S4	897(9)	524(7)	482(6)	−123(6)	−44(5)	16(6)	H5	73(20)
C1	495(23)	530(24)	384(20)	69(19)	1(18)	72(17)	H6	84(21)
C2	1064(46)	678(35)	579(31)	−219(32)	147(26)	61(30)		
C3	537(24)	412(23)	536(24)	21(18)	−18(18)	37(19)		
C4	895(38)	617(31)	689(31)	−93(29)	150(26)	149(28)		
O1	975(26)	641(22)	422(16)	−94(18)	41(15)	123(16)		
O2	892(24)	481(18)	650(20)	−134(17)	2(16)	117(17)		

Table 3. Bond lengths (Å) with standard deviations in parentheses. The last column contains RBM corrected bond lengths.

Te – S1	2.510(1)	2.528
Te – S2	2.841(1)	2.849
Te – S3	2.499(1)	2.516
Te – S4	2.846(1)	2.855
C1 – S1	1.709(4)	1.719
C1 – S2	1.638(4)	1.656
C1 – O1	1.335(5)	1.340
C3 – S3	1.717(4)	1.728
C3 – S4	1.650(4)	1.668
C3 – O2	1.314(5)	1.318
C2 – O1	1.445(7)	1.453
C4 – O1	1.458(6)	1.466
C2 – H1	1.092	
C2 – H2	1.103	
C2 – H3	1.088	
C4 – H4	1.103	
C4 – H5	1.070	
C4 – H6	1.105	

Some short intramolecular contacts (Å)

$C_2 - S_2$	2.939(5)	$S_1 - O_1$	2.547(4)
$C_4 - S_4$	2.980(6)	$S_3 - O_2$	2.530(4)
$S_1 - S_2$	2.936(2)		
$S_1 - S_3$	3.390(2)		
$S_3 - S_4$	2.939(2)		

minimizes the quantity $r = \sum w(|F_o| - K|F_c|)^2$. K is a scale factor and w, the weight of a reflection, is the inverse of the variance of F_o. Non-observed reflections with $K|F_c|$ larger than the observable limit are included in the refinement with F_o put equal to the limit. With anisotropic temperature factors for all atoms, the conventional R factor reached a value of 3.4 %. At this stage of refinement, a difference map revealed the positions of the six hydrogen atoms, and they were included in the refinement with isotropic temperature factors. However, the hydrogen atoms did not refine satisfactorily and their coordinates were fixed at values based on the difference map and a model of the molecule. The final R-value is 2.96 %. A difference map based on the final structure factors revealed no spurious features, the largest peak at 0.6 e/Å^3 occurred close to the tellurium atomic position. The observed and calculated structure factors can be obtained from the author Steinar Husebye upon request. Atomic scattering factors were taken from the International Tables [16] and those for tellurium and sulfur were corrected for anomalous dispersion according to Cromer.[17]

Final coordinates and temperature parameters are found in Tables 1 and 2, respectively. Two sets of bond lengths, one uncorrected and the other corrected for rigid-body motion considering the whole molecule as a rigid unit, are found in Table 3. Uncorrected values are used in the discussions throughout this article, because all comparisons are with uncorrected bond lengths. Bond angles are listed in Table 4. Some short intermolecular contacts are listed in Table 5, and some least squares planes through parts of the molecule are shown in Table 6.

Table 4. Bond angles with standard deviations, in degrees.

∠S1 – Te – S2	66.20(4)	∠C3 – O2 – C4	118.7(3)
∠S1 – Te – S3	85.18(4)	∠S1 – Te – S2′	127.92(4)
∠S1 – Te – S4	151.51(4)	∠S2 – Te – S2′	65.14(3)
∠S2 – Te – S3	151.37(4)	∠S3 – Te – S2′	141.63(3)
∠S2 – Te – S4	142.29(3)	∠S4 – Te – S2′	78.93(3)
∠S3 – Te – S4	66.33(4)	∠O1 – C2 – H1	109.58
∠Te – S1 – C1	90.3(1)	∠O1 – C2 – H2	109.10
∠Te – S2 – C1	80.8(2)	∠O1 – C2 – H3	110.32
∠Te – S3 – C3	91.1(1)	∠H1 – C2 – H2	109.10
∠Te – S4 – C3	81.0(2)	∠H1 – C2 – H3	109.71
∠S1 – C1 – S2	122.6(2)	∠H2 – C2 – H3	109.01
∠S1 – C1 – O1	113.1(3)	∠O2 – C4 – H4	108.18
∠S2 – C1 – O1	124.3(3)	∠O2 – C4 – H5	111.11
∠S3 – C3 – S4	121.6(2)	∠O2 – C4 – H6	108.24
∠S3 – C3 – O2	112.5(3)	∠H4 – C4 – H5	110.84
∠S4 – C3 – O2	125.9(3)	∠H4 – C4 – H6	107.42
∠C1 – O1 – C2	118.0(3)	∠H5 – C4 – H6	110.92

Table 5. Some short intermolecular interatomic distances (Å) with standard deviations in parentheses. The distances are from atoms in the original molecule to atoms in molecules whose transformations are given in the last column.

Te – Te	4.2341(4)	$(x+1,y,z)$
Te – S2	3.513(1)	$(-x,-y,-z)$
Te – S2	3.985(1)	$(1-x,-y,-z)$
Te – S2	4.103(1)	$(x+1,y,z)$
S2 – S2	4.234(2)	$(-x,-y,-z)$
S4 – S2	4.075(2)	$(-x,-y,-z)$

RESULTS AND DISCUSSION

The tellurium di(methylxanthate) molecule is shown in Fig. 1. Except for the hydrogen atoms, the molecule is nearly planar, the maximum deviation of any non-hydrogen atom from the least squares plane based on all atoms in the molecule except hydrogen, is 0.068 Å. Other corresponding deviations are 0.026, 0.009 and 0.016 Å for the least squares planes through ligands 1 (S1, S2), 2 (S3, S4) and the central TeS_4 group, respectively. Tellurium is coordinated to all four sulfur atoms in the molecule, just as in the corresponding ethylxanthate complex. The Te – S bond lengths are: Te – S1 = 2.510(1) Å, Te – S2 = 2.841(1) Å, Te – S3 = 2.499(1) Å and Te – S4 = 2.846(1) Å. Only one of the corresponding bond lengths is significantly different in the less accurately determined tellurium ethylxanthate complex.[2] As in the latter, there is a weak intermolecular Te···S2 bond across a centre of symmetry, being 3.513(1) Å in the present investigation,

Table 6. Least squares planes through parts of the molecule.

a. Atoms defining planes.

Plane 1: Te – S1 – S2 – S3 – S4 – C1 – C2 – C3 – C4 – O1 – O2
2: S1 – S2 – C1 – C2 – O1
3: S3 – S4 – C3 – C4 – O2
4: Te – S1 – S2 – S3 – S4

b. In the general equation for a plane, $A_iX + B_iY + C_iZ - D_i = 0$ where i is the number of the plane, the following constants were calculated:

i	1	2	3	4
A	3.8628	3.8419	3.7997	3.8972
B	−5.7650	−5.8435	−6.2237	−5.5166
C	0.1127	0.6667	0.0715	−0.0660
D	0.4692	0.5855	0.2591	0.5052

c. Interplanar angles in degrees.

1 – 2	1.871	2 – 4	2.834
1 – 3	2.045	3 – 4	3.169
1 – 4	1.245		
2 – 3	2.587		

d. Distances from planes in Å.

Plane No.	Te	S1	S2	S3	S4	C1
1	−0.0074	0.0140	0.0681	−0.0284	−0.0672	0.0173
2	−0.1133	−0.0102	0.0052	−0.1331	−0.2577	−0.0027
3	0.1110	0.1379	0.2815	0.0017	−0.0027	0.2021
4	−0.0041	−0.0146	0.0110	0.0161	−0.0083	−0.0416

Plane No.	C2	C3	C4	O1	O2
1	−0.0473	−0.0154	0.0444	0.0049	0.0169
2	−0.0185	−0.1760	−0.1783	0.0261	−0.1588
3	0.2102	0.0047	0.0049	0.2109	−0.0086
4	−0.1580	0.0539	0.1640	−0.0788	0.1131

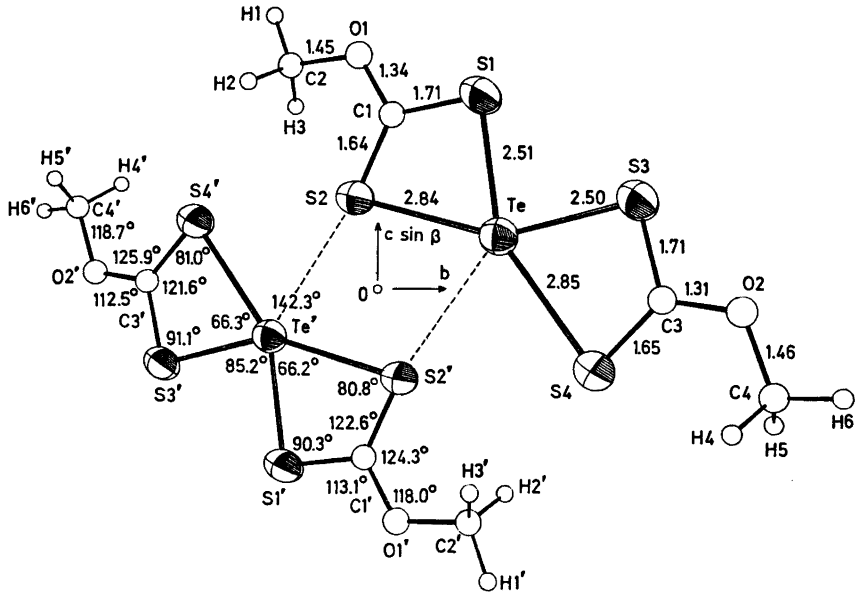

Fig. 1. A pair of molecules related by a center of symmetry as seen along *a*. The heavy atoms are indicated by 50 % probability thermal ellipsoids, and bond lengths (Å) and angles are indicated.

and also here bisecting the wide S2 – Te – S4 angle. However, while this bond in tellurium di(ethylxanthate) was 0.1 Å longer and only 0.65 Å above the TeS_4 plane, it is 1.10 Å above that plane in tellurium di(methylxanthate). This tendency to five-coordination is a feature found in all class I complexes of divalent tellurium whose structures are known, *i.e.* tellurium xanthates and dithiocarbamates. This weak association is probably a result of a nucleophilic interaction between non-bonded electron pairs on S2 and the central tellurium atom in a neighbour molecule. Assuming the two lone pairs of electrons on tellurium to be located on both sides of the molecular plane, the interaction is expected to be strongest near the molecular plane in the direction of the large interligand angle S2 – Te – S4 where the screening of the small, positive charge on the tellurium atom has its minimum.

Similar but stronger interactions are observed in several complex salts, for example in some with xenon fluoride cations.[18–19]

The molecules have nearly C_{2v} symmetry, bond lengths and angles in the two halves of the molecule are hardly significantly different. The Te-S bonding in the molecules is of the same type as in the corresponding ethylxanthate [2] and in dialkyldithiocarbamates of divalent selenium and tellurium,[4,6,7] probably being of the three-center four-electron type.[23,24] As in those compounds the two three-center systems S1 – Te – S4 and S3 – Te – S2 are not linear, the deviations from linearity are in both cases close to 28.5°. Their average total length is 5.35 Å, in excellent agreement with corresponding values found in the analogous tellurium(II) compounds above,[2,4] and in linear three-center systems in *trans* square planar complexes of divalent tellurium with monodentate thio ligands.[24]

A Mössbauer spectral investigation of tellurium di(methylxanthate) is in progress in order to see if tellurium *s* electrons participate in the bonding.[20] Contribution of orbitals other than two of the *5p*'s on tellurium in such non-linear three-center systems has earlier been assumed to explain the deviation from linearity.[21–23] In other divalent tellurium compounds with bidentate dithio ligands (diethyldithiocarbamate and dimethyldithiophosphate), a small *s*-contribution is indicated from Mössbauer spectra.[20]

The asymmetry in the Te – S bonds is

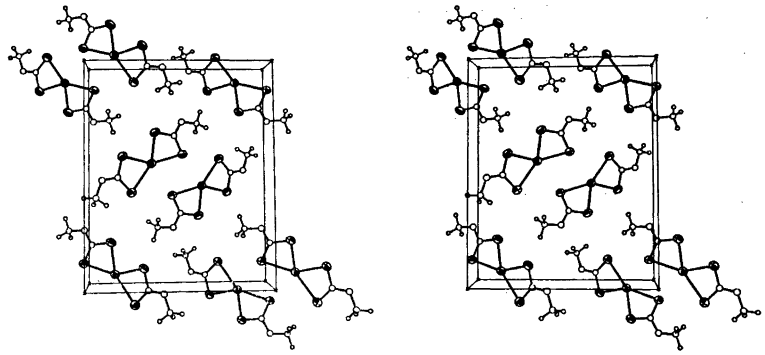

Fig. 2. A stereoscopic view of the structure of $Te(CH_3OCS_2)_2$ showing the unit cell packing. The *b*-axis is horizontal, the *c*-axis is vertical (pointing up along the paper) and the *a*-axis points up from the paper.

reflected in the S–C bonds; a short Te–S bond results in a long S–C bond, and *vice versa*, thus preserving the bond order on the sulfur atoms. In each ligand there is a short and a long C–S bond, the bond lengths being: C1–S1 = 1.709(4) Å, C1–S2 = 1.638(4) Å, C3–S3 = 1.717(4) Å and C3–S4 = 1.650(4) Å. Compared to a C–S single bond of 1.81 Å, they all have some double bond character as found in most xanthate complexes, and more so than in the corresponding dialkyldithiocarbamates,[23] indicating that the resonance form 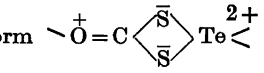 is of less importance than the resonance form 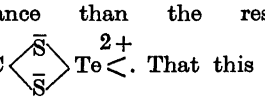 . That this is the case has earlier been shown by spectral work.[25] This may explain why the corresponding selenium di(methylxanthate) complex has a structure quite different from its tellurium analogue.[8] The former has a class II structure while the structure of the latter belongs to class I. In four-coordinate, planar complexes, divalent tellurium is a better acceptor than divalent selenium. When the donor capacity of the ligands decrease (xanthate less effective than dithiocarbamate as indicated by resonance above), there is a switch from the intramolecular, stronger four-coordination (class I) found in selenium dithiocarbamates, to partly intermolecular, weak four-coordination (class II) found in selenium di(methylxanthate). The stronger acceptor capacity of tellurium delays this switch from class I to II for tellurium complexes so that it occurs between the xanthate and dithiophosphate complexes.[8]

The asymmetry in C–S bond strength is also reflected in the S–C–O angles, in agreement with the VSEPR [26] theory which postulates that electrons in a double bond have greater repulsion effect than electrons in a single bond. Also the $C(sp^2)-O$ bonds show appreciable double bond character, as is usual for xanthates,[11] C1–O1 and C3–O2 being 1.340(5) and 1.318(5) Å, respectively. Other bond lengths and angles have normal values.

The packing of the molecules is indicated on Fig. 2. There are several short intermolecular contacts in addition to Te···S2 between the centrosymmetrically related pairs of molecules; these are shown in Table 4. As the *a*-axis is only 4.2341(5) Å, the Te···Te intermolecular non-bonded contacts in the *x* direction will have the same value. This indicates that the Pauling–van der Waals radius for tellurium, 2.20 Å, [27] is too large.

REFERENCES

1. Husebye, S. *Acta Chem. Scand. 20* (1966) 24.
2. Husebye, S. *Acta Chem. Scand. 21* (1967) 42.
3. Husebye, S. *Acta Chem. Scand. 23* (1969) 1389.
4. Husebye, S. *Acta Chem. Scand. 24* (1970) 2198.
5. Husebye, S. and Helland-Madsen, G. *Acta Chem. Scand. 23* (1969) 1398.
6. Husebye, S. and Helland-Madsen, G. *Acta Chem. Scand. 24* (1970) 2273.

7. Anderson, O. and Husebye, S. *Acta Chem. Scand. 24* (1970) 3141.
8. Brøndmo, N. J., Esperås, S., Graver, H. and Husebye, S. *Acta Chem. Scand. 27* (1973) 713.
9. Troughton, P. G. H. *Siemens Rev.* XXXVII (1970) Fourth Special Issue, p. 9.
10. Coppens, P., Leiserowitz, L. and Rabinovich, D. *Acta Crystallogr. 18* (1965) 1035.
11. Rao, S. R. *Xanthates and Related Compounds*, Dekker, New York 1971, p. 153.
12. Little, L. H., Poling, G. W. and Leja, J. *Can. J. Chem. 39* (1961) 745.
13. Agarwala, U., Lakshmi and Rao, P. B. *Inorg. Chim. Acta 2* (1968) 337.
14. Sceney, C. G. and Magee, R. J. *Chem. Scr. 6* (1974) 47.
15. Nikolov, G. S., Jordanov, N. and Havezov, I. *J. Inorg. Nucl. Chem. 33* (1971) 1055.
16. *International Tables for X-Ray Crystallography*, Kynoch Press, Birmingham 1962, Vol. III, p. 204.
17. Cromer, D. T. *Acta Crystallogr. 18* (1965) 17.
18. McKee, D. E., Zalkin, A. and Bartlett, N. *Inorg. Chem. 12* (1973) 1713.
19. Leary, K., Zalkin, A. and Bartlett, N. *Inorg. Chem. 13* (1974) 775.
20. Jones, C. H. W. *Private communication.*
21. Bartell, L. S. *Inorg. Chem. 5* (1966) 1635.
22. Wiebenga, E. H. and Kracht, D. *Inorg. Chem. 8* (1969) 738.
23. Husebye, S. *Compounds of Divalent Selenium and Tellurium with Bidentate Ligands. Their Preparation Structure and Bonding*, Diss., University of Bergen, Bergen 1970.
24. Foss, O. In Andersen, P., Bastiansen, O. and Furberg, S., Eds., *Special Topics in Structure Chemistry*, Universitetsforlaget, Oslo 1967, p. 145.
25. Chatt, J., Duncanson, L. A. and Venanzi, L. M. *Suom. Kemistilehti B 29* (1956) 75.
26. Gillespie, R. J. *J. Chem. Educ. 47* (1970) 18.
27. Pauling, L. *The Nature of the Chemical Bond*, 3rd. Ed., Cornell University Press, Ithaca, New York 1960, p. 257.

Received July 8, 1974.

Acta Chemica Scandinavica A 29 (1975) 21—28

Kinetics of the Ni/Ni(II) Electrode in Acid Chloride Solution

TOR HURLEN and HARALD A. DÅSNES*

Department of Chemistry, University of Oslo, Blindern, Oslo 3, Norway

From stationary potential/rate curves and galvanostatic transients for either reaction direction of the solid Ni/Ni(II) electrode in aqueous solutions of various pH (0 – 3), chloride ion molarity (1 – 3) and nickel(II) molarity (0 – 1) at 25 °C, and from comparisons to previous results, it appears that the charge transfer of this electrode occurs in two consecutive steps with Ni(I) as intermediate, that neither hydroxyl nor chloride ions participate noticeably in the transfer reactions, and that the ion-transfer step Ni/Ni(I) mostly occurs directly at kink sites, whereas the electron-transfer step Ni(II)/Ni(I) is independent of such sites. On this basis, the data suggest some simple functions for the dependence of the kink concentration on the overvoltage and on the reversible potential.

In spite of the Ni/Ni(II) electrode being a frequently studied solid metal/metal-ion electrode, its reaction mechanism under active conditions is not well clarified and understood (recent reviews in Refs.[1,2]). It is thus not yet clear whether its charge transfer occurs in two consecutive steps with Ni(I) as intermediate [2,3] or in one step with divalent nickel ion as charge carrier.[4,5] Nor is it clear whether its reactions are pH-dependent [2–4] or not.[5,7] Unexplained is also the possible participation by chloride and other anions [1,2] and the role played by crystal growth and demolition.[4] The liquid Ni(Hg)/Ni(II) electrode has recently been found to exhibit both a two-step and a one-step charge-transfer mechanism (the former dominating at low and the latter at high numerical overvoltage) and to be essentially free from direct participation by hydroxyl and chloride ions.[8]

In the present work, the above questions are pursued through determinations of stationary potential/rate curves and galvanostatic transients for solid nickel anodes and cathodes in acidified chloride solutions at 25°C (most previous work is at higher temperatures). The rate measurements (by weight change) allow for simultaneous hydrogen evolution [9] and, hence, give improved polarization data and extend the pH-region for access to such data. The transients yield further information, particularly on the interplay by crystal growth and demolition.

EXPERIMENTAL

All experiments were performed at 25 °C in a 100 ml cell and with equipment essentially as previously described.[8] High-purity (99.998 %) nickel rods (Koch-Light and Johnson, Matthey) were used as test electrodes with exposed surface area near 5 cm^2. Immediately before use and re-use the rods were degreased with chloroform, etched for 1 – 3 min in boiling nitric acid solution (15 %), immersed for about 30 min in hot 2 M HCl, washed with double-distilled water, dried with ethanol, and weighed. All chemicals mentioned as well as acid (HCl) and salts (KCl and $NiCl_2$) for test solutions were of p.a. quality. All solutions were made with double-distilled water, de-aerated with purified nitrogen, and stored and used under nitrogen atmosphere.

The experiments include determinations of the corrosion rate of nickel at open circuit in the solutions applied. In experiments with applied current, corrections were made on this basis for corrosion occurring during currentless periods. For stabilization purposes, the test electrode was generally immersed for about half an hour in the test solution prior to application of current.

In anodic runs, the average dissolution rate over the whole period of applied current was generally determined from the weight loss. In

* This paper comprises part of Harald A. Dåsnes' thesis for the academic degree at the University of Oslo 1972.

some cathodic cases (especially at low pH and low current density), the steady deposition rate reached after some time of electrolysis had to be determined from the weight change as a function of time by a series of comparable runs of various duration at the same current density. All weighings were performed on a Sartorius 2404 Semi-Micro Balance. These reaction rates have been transformed to current densities with a charge equivalent of 2F/mol nickel.

Single-step galvanostatic experiments were performed by means of a three-level fast electronic galvanostat (constructed and built at our institute [10]) combined with a Tektronix Type 564B Storage Oscilloscope with type 3A9 differential amplifier and type 3B4 time base for potential/time recording.

RESULTS

Figs. 1 and 2 give examples of potential/time curves obtained at various anodic and cathodic current densities, respectively. Noted on the curves are also the gravimetrically obtained average anodic dissolution rate (Fig. 1) and final steady deposition rate (Fig. 2). For construction of stationary polarization curves, these rates have been combined with the minimum usually exhibited by anodic potential/time curves (Fig. 1) and with the stationary potential finally reached in cathodic runs (Fig. 2), respectively. This implies the assumption that the minimum mentioned is nearest to representing the stationary anodic polarization of completely active nickel.

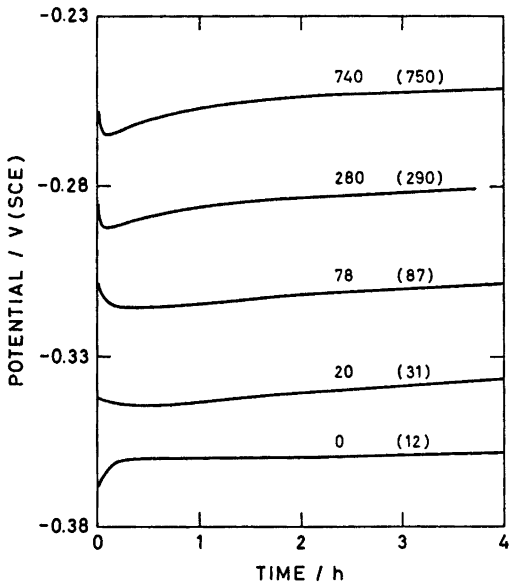

Fig. 1. Anodic potential/time curves in 1 M HCl + 1 M KCl at various applied currents (and average dissolution rates) in μA cm^{-2}.

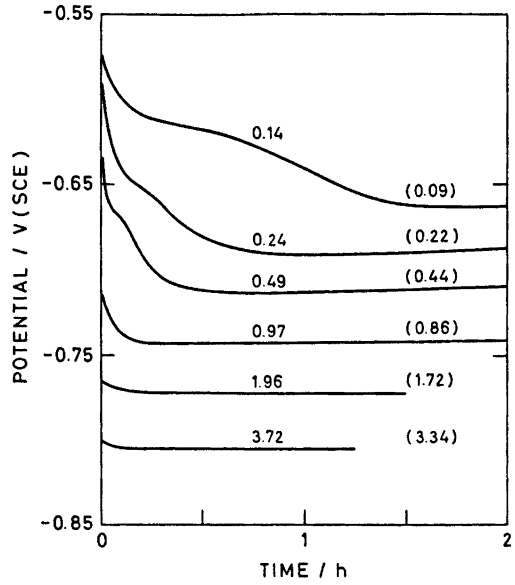

Fig. 2. Cathodic potential/time curves in 0.5 M $NiCl_2$ + 1 M (H+K)Cl of pH about 2 at various applied currents (and final deposition rates) in mA cm^{-2}.

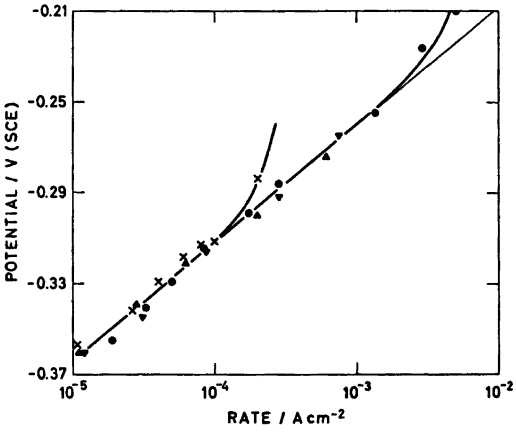

Fig. 3. Potential/rate data for dissolution in (●) 1 M HCl, (▲) 1 M HCl + 1 M KCl, (▼) 1 M HCl + 2 M KCl, and (×) 0.5 M $NiCl_2$ + 1 M (H+K)Cl of pH 2.8.

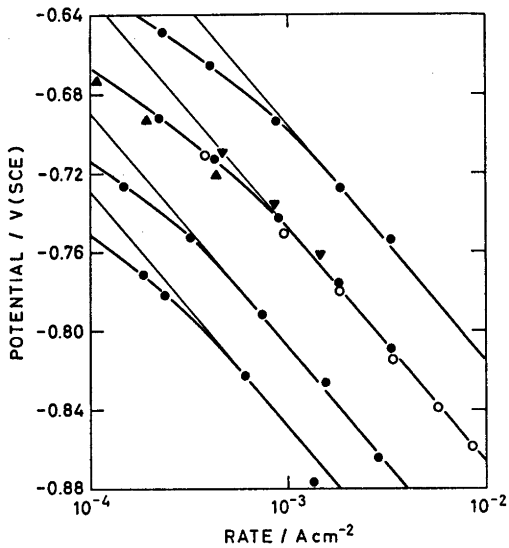

Fig. 4. Potential/rate data for deposition from 2 M chloride solutions of various Ni(II) molarity (1.0, 0.5, 0.2, and 0.1 from top to bottom curve) and pH (▼) 1, (● ○) 2, and (▲) 3; (▼ ●▲) no stirring; (○) stirring.

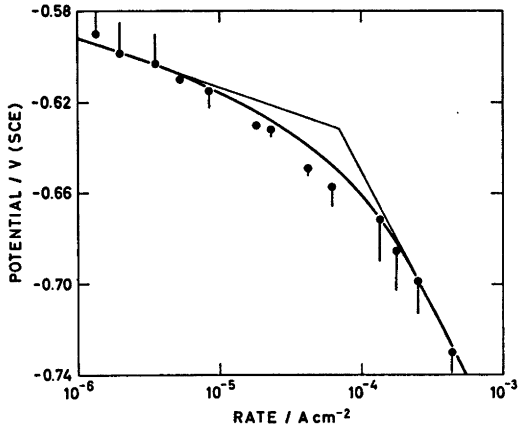

Fig. 5. Potential/rate data for deposition from 0.5 M $NiCl_2$ + 1 M (H+K)Cl of pH 2.8. The curve is calculated (see Interpretations). Corresponding dissolution data in Fig. 3.

Stationary polarization. Fig. 3 gives quasi-stationary polarization data obtained for dissolution of nickel in a number of differently composed chloride solutions. In spite of appreciable differences in pH (0 to 3), in chloride ion molarity (1 to 3) and in nickel(II) molarity (0 to 0.5) for these solutions, the polarization data essentially give one and the same Tafel line for stationary dissolution of active nickel, but show variations in deviations from this line at higher dissolution rates. The line in Fig. 3 has been drawn with a slope of 50 mV per rate decade.

Fig. 4 gives stationary polarization data obtained for deposition of nickel from 2 M chloride solutions of various pH (1 to 3) and nickel(II) molarity (0.1 to 1.0). Also these data appear to be essentially independent of pH. At sufficiently high cathodic overvoltages, the deposition obeys the Tafel law with slope near −120 mV per rate decade and essentially is first order in nickel(II) dependence. At lower cathodic overvoltages, distinct deviations occur from these relationships towards lower Tafel slope and higher nickel(II) dependence.

Fig. 5 gives results of long-time experiments in which the latter deviations are pursued to lower overvoltages and rates in a suitable solution (0.5 M $NiCl_2$ + 1 M (K + H)Cl of pH 2.8). It is suggested that a transition occurs from a Tafel line with slope about −120 mV at high to one with slope −21 mV at low cathodic overvoltages. The latter line intersects with the anodic Tafel line of Fig. 3 at −0.535 V (SCE) and 3×10^{-9} A cm^{-2}. The former line extrapolates to a rate of 7×10^{-6} A cm^{-2}, at the potential mentioned. The two rates may be connected to Ni/Ni(I) and Ni(II)/Ni(I) exhange (see Interpretations).

Galvanostatic transients. Fig. 6 gives examples of the response in potential to a sharp jump in anodic current from a given stationary anodic starting state. A transient superpolarization or potential overshoot clearly follows such a current step and gives a peak in the potential/time curve. In Fig. 7, values obtained for such peak potentials, when starting at one or the other of two different stationary anodic states, are presented in a Tafel diagram. The peak potentials essentially lie on nearly inter-parallel Tafel lines going through the respective starting points and having slopes between 70 and 75 mV per decade.

Analogous studies were performed also on the deposition reaction. A peak (or hump) was then obtained when stepping from a point on

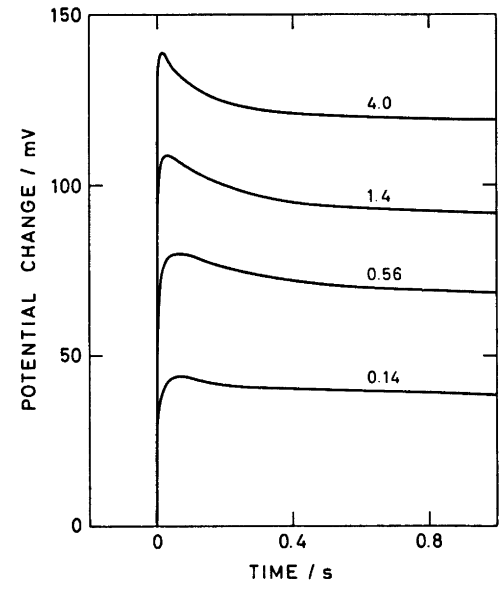

Fig. 6. Potential transients following sharp steps in anodic current to various densities (mA cm^{-2}) from a stationary dissolution rate of 0.04 mA cm^{-2} in 1 M HCl + 1 M KCl.

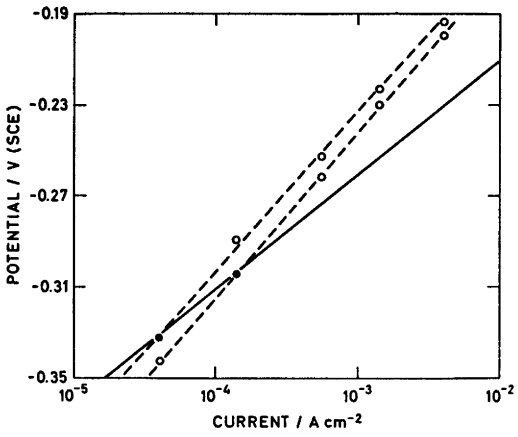

Fig. 7. Anodic peak polarization (○) with one or the other of two different stationary starting states (●) in 1 M HCl + 1 M KCl. The stationary line (fully drawn) is from Fig. 3.

the higher sloped Tafel line to a point on the lower sloped one, but essentially not when stepping reversely to this, nor when stepping between points on the former line. Except for these brief notes, observations on transients are reserved for a more thorough, separate treatment.

INTERPRETATIONS

The stationary polarization data suggest that the charge transfer of the Ni/Ni(II) electrode occurs in two consecutive steps with Ni(I) as intermediate. Together with the transient data, they further suggest that the ion-transfer step Ni/Ni(I) both controls and utilizes kink sites in exposed atom rows, and that the electron transfer step Ni(I)/Ni(II) is independent of such sites. These suggestions shall here be pursued. Attempts of interpretation by several other mechanisms (*e.g.* divalent ion transfer, surface diffusion) have failed.

The above suggestions lead to the following basic rate equations:

$$i_1 = i_{01}(s/s_r)[\exp(\alpha_1 f\eta) - (x/x_r)\exp(-(1-\alpha_1)f\eta)] \quad (1)$$

$$i_2 = i_{02}[(x/x_r)\exp(\alpha_2 f\eta) - \exp(-(1-\alpha_2)f\eta)] \quad (2)$$

for the Ni/Ni(I) step (assuming direct transfer at kinks) and the Ni(I)/Ni(II) step, respectively. In these equations, f means F/RT, x means the appropriate Ni(I) activity, s means the surface concentration of kinks, the subscript r refers to equilibrium conditions, the other symbols have their usual meaning, and signs are chosen so as to make anodic rates positive and cathodic ones negative.

Stationary polarization. If side reactions of Ni(I) can be neglected, steady-state requirements are:

$$i_1 = i_2 = i/2 \quad (3)$$

Provided $i_{01} \ll i_{02}$, eqns. (1) – (3) yield the following stationary Tafel relationships:

$$i = 2i_{01}(s/s_r)\exp(\alpha_1 f\eta) \quad (4)$$

$$i = -2i_{01}(s/s_r)\exp(-(2-\alpha_1)f\eta) \quad (5)$$

$$i = -2i_{02}\exp(-(1-\alpha_2)f\eta) \quad (6)$$

at anodic, moderate cathodic, and high cathodic overvoltages, respectively. Eqn. (5) implies that $x/x_r = \exp(-f\eta)$ at moderate cathodic overvoltages, which means that the Ni(II)/Ni(I) step there exhibits essentially reversible behaviour.

With $\alpha_2 = 0.5$, eqn. (6) shows the Tafel slope observed at high cathodic overvoltages (Figs. 4 and 5). This favours the proposed mechanism. Eqns. (4) and (5) are more involved. Both of them contain the relative surface-concentration of kinks (s/s_r) as a rate factor, and this factor is not yet well known. Good fit is obtained to the observed polarization behaviour, however, if one assumes that the stationary kink concentration obeys an overvoltage relationship of the kind:

$$s/s_r = \tfrac{1}{2}[\exp(\alpha_1' f\eta) + (x/x_r)\exp(-(1-\alpha_1')f\eta)] \quad (7)$$

With this relationship, eqns. (4) and (5) yield $\eta/\ln i$ slopes of $RT/(\alpha_1+\alpha_1')F$ and $-RT/(4-\alpha_1-\alpha_1')F$ at anodic and cathodic overvoltages, respectively. With $\alpha_1 + \alpha_1' = 1.2$, these slopes show the observed values (Figs. 3 and 5). The curve drawn in Fig. 5 has been calculated from the more complete eqns. (1) – (3) with (7) by use of $\alpha_1 = \alpha_1' = 0.6$ and best suiting values for i_{01} and i_{02} (see below).

Reversible exchange and activity effects. From eqns. (4), (5), and (7), it is expected that the stationary anodic Tafel line should intersect with the low-sloped cathodic one at the reversible potential of the Ni/Ni(II) electrode (E) and the exchange current of its Ni/Ni(I) step (i_{01}). The results in 0.5 M $NiCl_2$ + 1 M (H + K)Cl of pH 2.8 (Figs. 3 and 5) accordingly give -0.535 V(SCE) and 3×10^{-9} A cm^{-2} for E and i_{01} in this solution. This E-value is about 40 mV below the standard Ni/Ni(II) potential, which is acceptable enough (considering uncertainties in Ni(II) activity and liquid-junction potential) to satisfy the above expectation. Also this supports the reaction mechanism proposed. Applying eqn. (6) to the high-sloped cathodic Tafel line of Fig. 5, one obtains 3.5×10^{-6} A cm^{-2} for i_{02} in the above solution. This justifies the qualification $i_{01} \ll i_{02}$.

From ordinary electrode kinetics, the proposed reaction mechanism should yield:

$$i_{01} = I_{01}(s_r/s_0)(a/a_0)^{\alpha_1/2} = I_{01}(s_r/s_0)\exp[\alpha_1 f(E-E^\circ)] \quad (8)$$

$$i_{02} = I_{02}(a/a_0)^{(1+\alpha_2)/2} = I_{02}\exp[(1+\alpha_2)f(E-E^\circ)] \quad (9)$$

where a/a_0 is the dimensionless Ni(II) activity (unity at standard conditions) and I_{01}, I_{02}, and s_0 are the values of i_{01}, i_{02}, and s at standard equilibrium of the Ni/Ni(II) electrode. Eqn. (8) will fit observations, provided

$$s_r/s_0 = (x_r/x_0)^{\alpha_1'} = (a/a_0)^{\alpha_1'/2} = \exp[\alpha_1 f(E-E^\circ)] \quad (10)$$

where the latter two equalities follow from thermodynamics.

With eqns. (8) – (10), eqns. (4) – (7) may be transformed to the following stationary Tafel relationships (using $\eta = U - E$):

$$i = I_{01}\exp[(\alpha_1+\alpha_1')f(U-E^\circ)] \quad (11)$$

$$i = -I_{01}(a/a_0)^2\exp[(-(4-\alpha_1-\alpha_1')f(U-E^\circ)] \quad (12)$$

$$i = -I_{02}(a/a_0)\exp[(-(1-\alpha_2)f(U-E^\circ)] \quad (13)$$

at anodic, moderate cathodic, and high cathodic overvoltages, respectively. Eqns. (11) and (13) agree with the experimental results in Figs. 3 and 4, respectively, and their application yields

$$I_{01} = 2 \times 10^{-8} \text{ A cm}^{-2} \quad (14)$$

$$I_{02} = 3 \times 10^{-5} \text{ A cm}^{-2} \quad (15)$$

when -0.495 V (SCE) is used for E°. The activity dependence shown by eqn. (12) has not been tested in the present work, but it agrees with previous results in perchlorate solutions [4] (see below). It moreover must be as written to make eqn. (12) coincide with the confirmed eqn. (11) for $U = E$.

Galvanostatic transients. The occurrence of a peak in a galvanostatic transient is to be expected from the above reaction model when the changes required in s and/or x are slow compared to the double-layer charging. From studies on the Ni(Hg)/Ni(II) electrode,[3] where s is not involved, it appears that changes in x are fast enough and consume little enough current to essentially maintain obedience all the time to the steady-state requirements (3). This makes s the decisive factor, which allows peaks to occur in transients to states obeying eqn. (4) or (5), but not in transients to states obeying eqn. (6). This agrees with the experimental results above.

At a peak ($d\eta/dt = 0$), there is no capacitive current, and the whole current is faradaic. For anodic transients, the current/potential relationship for peaks (the superpolarization) should then be as given by eqn. (4) with s-values between those of the initial and the

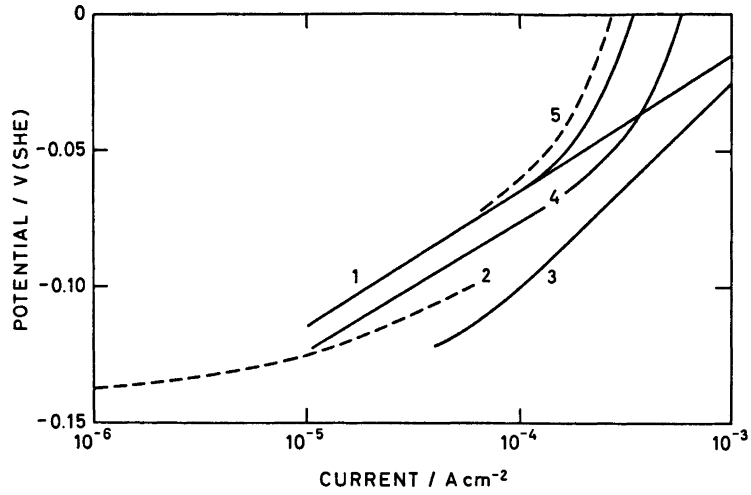

Fig. 8. Anodic polarization data for nickel in various solutions. (1) present work, 1 – 3 M Cl^-, pH 0 – 2.8, 25 °C; (2) Ref. 4, 2 M ClO_4^-, pH 2.5, 65 °C; (3) Ref. 2, 3 M Cl^-, pH 2.1, 60 °C; (4) Ref. 7, 0.5 – 4 M Cl^-, pH 0.6 – 3.0, 55 °C; (5) Ref. 3, 0.5 M SO_4^{2-}, pH 2.75, 40 °C.

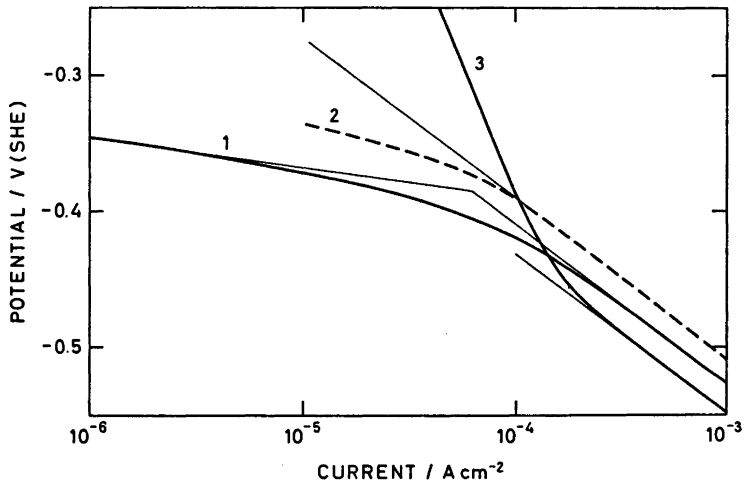

Fig. 9. Cathodic polarization data for nickel in various solutions at 25 °C. (1) present work, 0.5 M $NiCl_2$ + 1 M (H+K)Cl, pH 2.8; (2) Ref. 4, 1 M $Ni(ClO_4)_2$, pH 5.3; (3) Ref. 2, 0.5 M $NiCl_2$ + 2 M NaCl + HCl, pH 2.1.

final steady state concerned. This agrees with Fig. 7.

The present interpretation of the transients implies that the surface concentration of kinks changes appreciably already in the pre-peak period. This concentration is the product of the line density of kinks in crystal steps and the line density of such steps in the surface. The former density should not need much charge to change appreciably and most likely is the one changing in the pre-peak period. This adds to the general appearance of the functions (7) and (10) for s in suggesting that the line density of kinks in crystal steps is an important variable (not merely a temperature-dependent constant).

COMPARISONS

In Figs. 8 and 9, some present and previous quasi-stationary polarization data for nickel electrodes in chloride (solid curves), perchlorate, and sulfate solutions are reproduced for comparison. The standard hydrogen scale has been used, and data from the present work (curves 1) have been transformed to this scale by addition of 0.245 V to values measured on the saturated calomel scale.

Only curves 1 and 4 represent experimentally determined rates of nickel dissolution (Fig. 8) and nickel deposition (Fig. 9). The other curves are ordinary potential/current polarization curves and include some mixing with hydrogen electrode reactions. This particularly applies to curve 2 at low anodic current (Fig. 8) and curve 3 at low cathodic current (Fig. 9). In the former case, a too low Tafel slope and a too high pH-dependence may wrongly be ascribed to the nickel dissolution reaction (see below). In the latter case, hydrogen evolution may well be the main reaction occuring.[5,9]

Anodic data. The anodic data in Fig. 8 apply to various temperatures (25 – 65 °C). A high temperature is often preferred as a means of keeping nickel electrodes active. In the present work at 25 °C, compensations have been sought in the pre-treatment (activation by final etching in hot hydrochloric acid was indispensable), in the experimental procedure, and in the way of choosing representative potentials from potential/time curves. Some previous data [2] for nickel in acid chloride solution at 25 °C are clearly affected by partial passivation even at open circuit (the open-circuit potential reported being positive to the reversible hydrogen potential in the same solution) and are not comparable to the data in Fig. 8. This to some extent applies also to some previous data [3] in acid sulfate solution.

The data in Fig. 8 largely support the conclusions that the stationary dissolution of active nickel has an $U/\ln i$ slope near RT/F and does not involve much participation by hydroxyl and chloride ions. From data like curve 2, however, Heusler and Gaiser [4] derive a lower slope ($RT/2F$) and a second-order hydroxyl-ion interaction, but this may be due to a poor separation of nickel dissolution data from the mixed reaction data actually measured.

Cathodic data. The cathodic data in Fig. 9 all apply to 25 °C. These data combine well in showing that the quasi-stationary deposition of nickel at high current density (or numerical overvoltage) has an $U/\ln i$ slope near $-2RT/F$ and essentially is governed by a pH- and anion-independent first-order reaction of Ni(II). They partly further show that there is a transition to a lower Tafel slope at lower current density in perchlorate as well as in chloride solution. These high-current observations agree with data also at higher temperatures in chloride [5,7] and sulfate [5] solutions, and the low-current ones with data at various temperatures in perchlorate solution.[4] The latter data [4] show that the low-slope region expands with increasing temperature, and that the reaction in this region exhibits a stationary $U/\ln i$ slope between $-RT/3F$ and $-RT/2F$, a transient slope about twice as high, a second-order dependence on Ni(II), but no clear pH-dependence. This agrees with the results and interpretations of the present work [see eqn. (12) above].

DISCUSSION

From the above studies it appears that the charge transfer of the Ni/Ni(II) electrode in the solutions concerned, and within the potential region covered, mostly occurs in two consecutive steps with Ni(I) as intermediate, that neither hydroxyl nor chloride (or perchlorate or sulfate) ions participate specifically in these transfer reactions, and that the ion-transfer step Ni/Ni(I) mostly occurs directly at crystal-growth and -demolition sites, whereas the electron-transfer step Ni(II)/Ni(I) is independent of such sites.

The above mechanism fits both the present and previous results, when due regard is made of simultaneous hydrogen evolution and of partial passivation, and it reconciles much previous controversies on the matter (see Introduction). These controversies, therefore, are not due to conflicting results (as claimed by some authors [11]), but to conflicting interpretations. In subsequent work,[12] the two-step mechanism *via* Ni(I) has been confirmed by stirring, ring-disc, and galvanostatic double-pulse experiments, but the mono-chloro-com-

plex of Ni(II) has been found to enter as electroactive oxidant besides the pure aqua-complex at higher chloride activity and lower water activity than in the present work.

With the above interpretation, the stationary polarization data suggest two relationships, eqns. (7) and (10), which may be combined into the single one:

$$s/s_0 = \tfrac{1}{2}\{[\exp(\alpha_1' f(U-E^\circ)] + (x/x_0)\exp[-(1-\alpha_1')f(U-E^\circ)]\} \quad (16)$$

for the potential and activity dependence of the kink concentration under stationary conditions. This relationship clearly violates the usual assumption of thermal equilibrium of kinks in crystal steps. It rather suggests that kinks are being formed and controlled by electrochemical reactions. To the authors' knowledge, no hitherto treated model directly gives eqn. (16), but some ideas in this direction have been presented.[6,12] More theoretical work is needed on this matter.

With increasing overvoltage, the transfer of divalent nickel ions should be favoured and subsequently gain predominance, as is observed for the liquid Ni(Hg)/Ni(II) electrode.[8] No sign of divalent ion transfer is seen in the present work, however, but the overvoltage region covered is smaller than in the previous amalgam work. The specific rate of electron uptake by Ni(II) appears to be about the same at the solid nickel electrode as at the liquid amalgam electrode. The ion-transfer step Ni/Ni(I) generally is faster than the corresponding Ni(Hg)/Ni(I) step, but not very much so at equilibrium conditions (extrapolated exchange rates). The latter comparison is hampered, however, by Ni(Hg) being in equilibrium with $NiHg_x$ and not with Ni. A striking contrast is the essential absence at solid nickel and clear presence at liquid amalgam of kinetic stimulation by chloride ion adsorption (especially at anodic overvoltages). For both these electrodes, the zero-charge potential lies between most of the actual anodic and cathodic measuring regions.[13]

In closing this discussion, let us briefly consider uni- and divalent ions of the iron-group metals and their immediate neighbours. In weak octahedral ligand fields, the outer electron configurations of these ions and their difference are as given in Table 1.

Table 1. Outer electron configurations.

Metal	M^+	M^{2+}	Diff.
Mn	$t_{2g}^4 e_g^2$	$t_{2g}^3 e_g^2$	t_{2g}
Fe	$t_{2g}^5 e_g^2$	$t_{2g}^4 e_g^2$	t_{2g}
Co	$t_{2g}^6 e_g^2$	$t_{2g}^5 e_g^2$	t_{2g}
Ni	$t_{2g}^6 e_g^3$	$t_{2g}^6 e_g^2$	e_g
Cu	$t_{2g}^6 e_g^4$	$t_{2g}^6 e_g^3$	e_g

The difference shows the type of orbital which accommodates the extra electron of M^+ over M^{2+}. For Mn, Fe, and Co, this is a nonbonding t_{2g} orbital. For Ni and Cu, however, it is an antibonding e_g orbital. The extra electron hence weakens metal-ligand bonds more effectively in the latter cases than in the former ones, and this may correspondingly favour the path via M^+. Such a path does not seem to be used in Fe(Hg)/Fe(II) and Co(Hg)/Co(II) reactions.[14,15]

REFERENCES

1. Erdey-Gruz, T. *Kinetics of Electrode Processes*, Hilger, London 1972, p. 330.
2. Piatti, R. C. V., Arvia, A. J. and Podesta, J. J. *Electrochim. Acta 14* (1969) 541.
3. Sato, N. and Okamoto, G. *J. Electrochem. Soc. 111* (1964) 897.
4. Heusler, K. E. and Gaiser, L. *Electrochim. Acta 13* (1968) 59.
5. Yeager, J., Cels, J. P., Yeager, E. and Hovorka, F. *J. Electrochem. Soc. 106* (1959) 328.
6. Wiart, R. *Oberfläche-Surface 9* (1968) 213, 241 and 275; Epelboin, P. and Wiart, R. *J. Electrochem. Soc. 118* (1971) 1577.
7. Ovari, F. and Rotinyan, A. L. *Elektrokhimiya 6* (1970) 528.
8. Hurlen, T., Eriksrud, E. and Jørgensen, S. *J. Electroanal. Chem. 43* (1973) 339.
9. Dorsch, R. K. *J. Electroanal. Chem. 21* (1969) 495.
10. Grimnes, S. *Chem. Instrum. 5* (1973–74) 141.
11. Davison, W. and Harrison, J. A. *J. Electroanal. Chem. 44* (1973) 431.
12. Hurlen, T. *Electrochim. Acta 7* (1962) 653; *11* (1966) 1205; *20* (1975). *In press.*
13. Perkins, R. S. and Andersen, T. N. In Bockris, J. O'M. and Conway, B. E., Eds., *Modern Aspects of Electrochemistry, No. 5*, Butterworths, London 1969, p. 203.
14. Hurlen, T. and Breiland, B. *J. Electroanal. Chem. 48* (1973) 25.
15. Eriksrud, E. and Hurlen, T. *J. Electroanal. Chem. 36* (1972) 311.

Received July 10, 1974.

Acta Chemica Scandinavica A 29 (1975) 29—37

Reaction Rate Studies of the Acid Hydrolysis of Some Chromium(III) Complexes. V. Identification of Reaction Products of the Perchloric Acid Hydrolysis of the *cis*- and of the *trans*-Diaquabis(1,2-ethanediamine)- and of the Tris(1,2-ethanediamine)chromium(III) Ions

L. MØNSTED and O. MØNSTED

Chemistry Department I, Inorganic Chemistry, H.C. Ørsted Institute,'University of Copenhagen, Universitetsparken 5, DK-2100 Copenhagen Ø, Denmark

The title ions have been hydrolyzed in 1 M perchloric acid in the dark and the resulting mixtures of chromium(III) complexes have been separated by ion exchange chromatography. Large amounts of complexes coordinated with monoprotonated 1,2-ethanediamine ligand were found in the hydrolysis mixtures. Two new isomeric triamines and one pentaamine coordinated with one 2-aminoethylammonium ion ligand, and a diamine coordinated with two of these ligands were isolated in solution. Also a mixture of tetraamines, each coordinated with two 2-aminoethylammonium ion ligands was obtained in solution. By analogy with results for the chromium(III) ammonia system, *trans*-tetraamines and -diamines are not found as reaction products. Also from *trans*-tetraamine only *mer*-triamine is formed. Racemization of the *cis*-diaquabis(1,2-ethanediamine)chromium(III) ion has been observed, in contrast to the behaviour of the tris(1,2-ethanediamine)chromium(III) ion where no racemization could be detected.

As a continuation of our earlier studies of reactions of the ammineaquachromium(III) complexes,[1] it was of interest to us to investigate which effects would be observed for the chromium(III) amine bond breaking and isomerization reactions on introduction of a higher degree of stereochemical rigidity in the amine ligands studied. Therefore reactions of chromium(III) complexes coordinated with aliphatic amines were of particular interest, and as an introduction to this work we report here some initial results for the reactions of chromium(III) complexes coordinated with 1,2-ethanediamine.

Quantitative experiments on the acid hydrolysis of chromium(III) complexes of 1,2-ethanediamine were first carried out by Schläfer and coworkers, who studied the hydrolysis of the tris(1,2-ethanediamine)chromium(III)[2] and the *cis*-diaquabis(1,2-ethanediamine)chromium(III)[3] ions by spectrophotometric measurements, and of the optically active tris(1,2-ethanediamine)chromium(III)[4] ion by optical rotation experiments. The conclusions they reached about the initial stages of the tris(1,2-ethanediamine)chromium(III) hydrolysis reaction were later questioned by Jørgensen and Bjerrum,[5] who gave evidence for the production of the (2-aminoethylammonium)aquabis(1,2-ethanediamine)chromium(III) ion. Later the tetraaqua(1,2-ethanediamine)chromium(III) ion, postulated as an intermediate by Schläfer *et al.* was isolated in solution free of other chromium species by Garner *et al.*[6] who also investigated the aquation of this ion in an acid perchlorate medium, and were able to characterize the intermediate (2-aminoethylammonium)pentaaquachromium(III) ion. Our experience with the ammonia complexes of chromium(III) combined with the apparent robustness of the monoprotonated 1,2-ethanediamine ligand, questions the reported simplicity of the aquation

reactions of 1,2-ethanediamine complexes of chromium(III). Therefore we have undertaken a reinvestigation of this system and report here the characterization of reaction products from the acid hydrolysis of tris(1,2-ethanediamine)- and of the *cis*- and *trans*-diaquabis(1,2-ethanediamine)chromium(III) cations.

EXPERIMENTAL

*Chemicals.** $[Cr(en)_3]Cl_3$,[7] $(+)_D$-$[Cr(en)_3]Cl_3$,[8] *cis*-$[Cr(en)_2Cl_2]Cl$,[7] $(-)_D$*cis*-$[Cr(en)_2(aq)_2]Br_3$,[9] *trans*-$[Cr(en)_2(aq)OH](ClO_4)_2$,[9] *fac*-$[Cr(en)(enH)Cl_3]Cl$,[10] $[Cr(en)(aq)_2Cl_2]Cl$,[11,12] $[Cr(O_2)_2(aq)(en)]$,[12] and $[Cr(en)(a)(aq)Cl_2]Cl$ [13] were all prepared by literature methods. Other chemicals, the Dowex 50 W X8 and the SP Sephadex C-25 ion exchange resins have been described earlier.[14] The chloride salts of racemic and optically active tris(1,2-ethanediamine)chromium(III) were converted into perchlorate salts by reprecipitation twice from water with 70 % perchloric acid. Solutions of the tris(1,2-ethanediamine)- and the *trans*-diaquabis(1,2-ethanediamine)-chromium(III) ions were made by directly dissolving the perchlorate salts in dilute perchloric acid. Mercury(II) accelerated chloride ligand hydrolysis in acid solution was used to generate aqua complexes from chlorido complexes. Such solutions were purified as follows: an amount of solution containing about 0.5 mequiv. of chromium(III) complex was charged onto a column (2 cm × 10 cm) packed with Sephadex ion exchange resin. Excess mercury(II) was removed by elution with 0.1 M sodium chloride solution and the chromium(III) complex left at the column top was next displaced with 1 M sodium perchlorate solution.

Separation of hydrolysis mixtures. The technique employed for isolation of the chromium(III) complexes from the hydrolysis mixtures was based upon a combination of ion exchange methods in acid and basic solution.

By elution upon Sephadex columns (2 cm × 10 cm) at about 20 °C with sodium perchlorate solution made 1 mM acid with perchloric acid complete separation between amineaqua species of different charges was obtained. A definite but incomplete separation between species of equal charges was seen. For such species the elution took place more readily the greater the number of coordinated water molecules, as was likewise observed for the ammonia complexes. Also, as with the ammonia complexes, *trans* isomers were eluted prior to corresponding *cis* isomers and *mer* isomers prior to corresponding *fac* isomers.

By elution upon Sephadex columns (2 cm × 10 cm) at about 20 °C with ammonium ion-ammonia buffer solutions the tri-, di-, and monopositively charged cations could be separated from each other, and from uncharged or anionic species not retained by the cation exchanger. Contrary to the acid elution where all species are stable in the time necessary for the elution to take place, some rather fast reactions proceed in basic solution. The most notable of these are the chelation reactions of the triamines and the pentaamine, where the tetraamine is formed within a few minutes at room temperature from the triamines, and the hexaamine, also significantly but substantially slower, is formed from the pentaamine.

The individual chromium(III) complexes were isolated from mixtures prepared by hydrolysis in the dark in 1 M perchloric acid as follows.

Tris(1,2-ethanediamine)chromium(III). This ion was eluted free of other chromium(III) species by elution with acid 0.5 M sodium perchlorate solution after removal of other chromium(III) species by elution with an 0.1 M ammonium chloride – 0.05 M ammonia buffer solution. In order to avoid contamination with rechelated pentaamine, however, only the column band of tripositive species from an acid 0.5 M sodium perchlorate elution was subjected to the basic elution. In a typical experiment optically active hexaamine was boiled for 5 min and the unhydrolyzed hexaamine recovered with unchanged optical activity.

(2-Aminoethylammonium)aquabis(1,2-ethanediamine)chromium(III). Basic elution with an 0.1 M ammonium chloride – 0.01 M ammonia buffer solution was used to remove all anionic, neutral, or monopositively charged species. The pentaamine and hexaamine remaining at the column top were next separated by acid 0.5 M sodium perchlorate solution. In a typical experiment pentaamine ion was isolated from hexaamine solution boiled for 1 min.

cis-*Diaquabis(1,2-ethanediamine)chromium-(III).* After an acid 0.5 M sodium perchlorate elution, to isolate the tripositive ions, recovery of monopositively charged species in a basic 0.1 M ammonium chloride – 0.05 M ammonia buffer solution elution allowed the isolation of tetraamminediaqua ions. In one experiment pure *cis* isomer was isolated in this way from the hexaamine which had been boiled for 5 min. In another experiment active *cis* isomer maintained at 60 °C for 1.35 and 3.17 h was recovered with 48 % and 15 %, respectively, of the initial optical activity.

For the remaining cations described below acid sodium perchlorate elution only was employed for their isolation. In all cases fractionation of the column eluate was used to confirm

* All chemicals are written without water of crystallization since this may vary with the history of the compound. The following ligand abbreviations are used in chemical formula throughout the paper: a = ammonia, aq = water, en = 1,2-ethanediamine, enH = 2-aminoethylammonium ion.

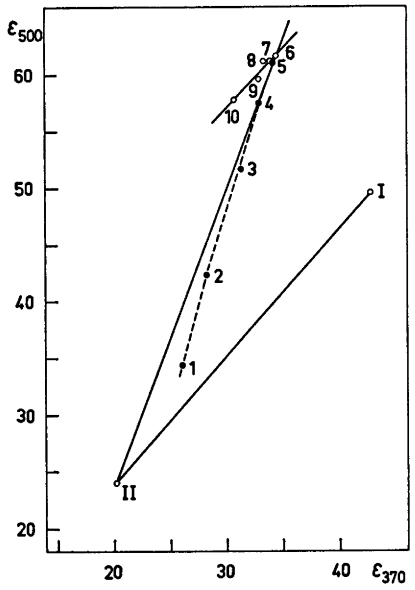

Fig. 1. Fractionation of hydrolysis mixture obtained by boiling tris(1,2-ethanediamine)-chromium(III) ions in 1 M perchloric acid for 3 min. The molar extinction coefficient at 500 nm for ten succesive fractions eluted after the main portion of tetrapositive pentaamine is plotted as a function of the molar extinction coefficient at 370 nm for these same fractions. Points I and II are the pure pentaamine and pure pentapositive diamine, inserted for comparative purposes. Incomplete separation mainly between pentapositive tetraamine and diamine is seen, but since the points, depicted by filled circles, are not situated on a straight line that passes through the pure pentapositive diamine, also some pentaamine must be present, mainly in the first fractions. The marked difference in fractionation behaviour before and after fraction 6 makes it likely that this fraction is free of pentapositive diamine. Constant spectra of successive fractions were, however, not obtained as depicted by the open circles. Complete visible absorption spectra of the first and the last pure tetraamine fraction, points 6 and 10 respectively, are given in Fig. 4.

the isomeric purity of the species.

Bis(2-aminoethylammonium)diaqua(1,2-ethanediamine)chromium(III). Results of a fractionation experiment of the band of pentapositively charged species formed by boiling a hexaamine solution for 3 min are exhibited in Fig. 1. In order to get measurable amounts of the tetraamines, hexaamine hydrolyzate was charged onto a Sephadex column (2 cm × 15 cm) until the yellow hexaamine colour was mainly

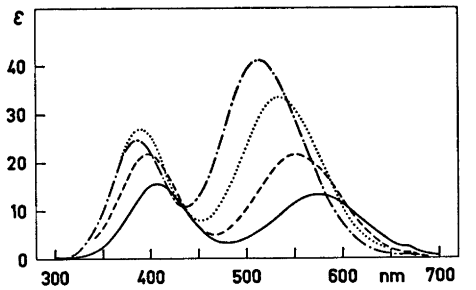

Fig. 2. Visible absorption spectra of compounds prepared as described in the text. ———, $[Cr(aq)_6]^{3+}$; - - -, $[Cr(enH)(aq)_5]^{4+}$; ···, *cis*-$[Cr(enH)_2(aq)_4]^{5+}$; — · —, $[Cr(en)(aq)_4]^{3+}$.

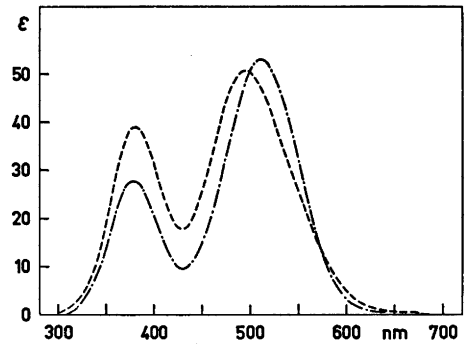

Fig. 3. Visible absorption spectra of compounds prepared as descibed in the text. - - -, *mer*-$[Cr(en)(enH)(aq)_3]^{4+}$; — · —, *fac*-$[Cr(en)(enH)(aq)_3]^{4+}$.

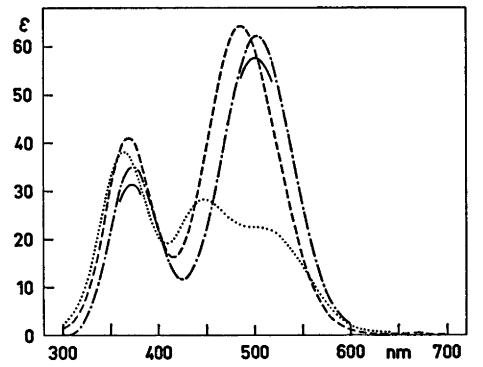

Fig. 4. Visible absorption spectra of compounds prepared as described in the text. · · ·, *trans*-$[Cr(en)_2(aq)_2]^{3+}$; - - -, *cis*-$[Cr(en)_2(aq)_2]^{3+}$; — · —, first; and ———, last fraction of the $[Cr(en)(enH)_2(aq)_2]^{5+}$ mixture. (Points 6 and 10 of Fig. 1, respectively).

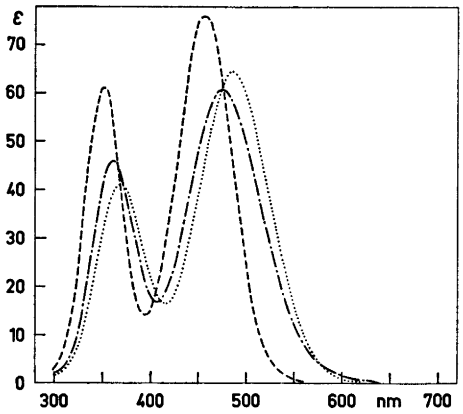

Fig. 5. Visible absorption spectra of compounds prepared as described in the text. · · ·, *cis*-$[Cr(en)_2(aq)_2]^{3+}$; — · —, $[Cr(en)_2(enH)(aq)]^{4+}$; - - -, $[Cr(en)_3]^{3+}$.

concentrated at the column bottom. The adsorbed species were then eluted with acid 1 M sodium perchlorate solution. The large amounts of chromium(III) species present account for the incomplete separation between tetrapositive and pentapositive species.

fac-*(2-Aminoethylammonium)triaqua(1,2-ethanediamine)chromium(III)*. Due to the limited column lengths necessitated by the instability of some of the chromium(III) species, this ion was never isolated pure in solution from the hydrolysis mixture of tetrapositive ions. Chloride ligand hydrolysis of crude impure *fac*-$[Cr(en)(enH)Cl_3]Cl$ generated, however, a mixture of the *fac* triamine ion and the tetraaqua(1,2-ethanediamine)chromium(III) ion which were easily separated from each other by acid 0.5 M sodium perchlorate elution.

mer-*(2-Aminoethylammonium)triaqua(1,2-ethanediamine)chromium(III)*. This ion was the only triamine hydrolysis product of the *trans*-diaquabis(1,2-ethanediamine)chromium(III)ion. In one experiment the *trans* tetraamine was boiled for a few seconds then rapidly cooled to room temperature. This treatment generated the *mer* triamine as the only tetrapositive cation, which consequently was readily obtained pure in solution by elution with acid 0.5 M sodium perchlorate solution.

Tetraaqua(1,2-ethanediamine)chromium(III). This ion was only with difficulty separated from other tripositive cations in the hydrolysis mixtures, although Dowex columns operated with 2 M sulfuric acid or Sephadex columns operated with acid 0.1 M sodium sulfate were able to affect this separation. Hydrolysis of the *cis* tetraamine gave always mixtures of tripositive cations, whereas the *trans* tetraamine isomer when boiled for 10 min formed the pure diamine ion, indistinguishable from the one produced both from $[Cr(en)(aq)_2Cl_2]Cl$ and from $[Cr(O_2)_2(aq)(en)]$.

Bis(2-aminoethylammonium)tetraaqua- and (2-aminoethylammonium)pentaaquachromium-(III) ions. These two cations are the only pentapositive and tetrapositive species produced by hydrolysis of the *cis*-diaquabis(1,2-ethanediamine)- and the tetraaqua(1,2-ethanediamine)chromium(III) ions, respectively. Therefore they were readily prepared pure in solution by acid 0.5 M sodium perchlorate elution upon Sephadex. Typical reaction times at the boiling point of the solution were about 10 min for production of substantial amounts of the diamine and 3 h for production of the monoamine.

Visible absorption spectra of the compounds prepared and purified as described above are given in Figs. 2 – 5.

RESULTS AND DISCUSSION

All aqua(1,2-ethanediamine)chromium(III) isomers with the diamine as a chelate ligand have previously been characterized in solution. As the displacement of the bidentate diamine ligand takes place in two distinct steps, with monoprotonated unchelated diamine complex as intermediate in acid solution, tetra-, penta-, and hexapositive cations are possible aquation products of the initial tripositive cations.

Sodium perchlorate solution is an effective eluting agent for the separation of chromium(III) amine species of different charges upon SP Sephadex C-25 cation exchange resins. With hydrolyzed solutions of both tetraaqua(1,2-ethanediamine)chromium(III) and *trans*-diaquabis(1,2-ethanediamine)chromium(III) ions only column bands indicative of tri- and tetrapositive species, respectively, are observed, whereas with hydrolyzed solutions of both *cis*-diaquabis(1,2-ethanediamine)chromium(III) and tris(1,2-ethanediamine)chromium(III) ions, also a column band indicative of pentapositive species appears. Evidence for the production of hexapositive species was never obtained, but in view of the very limited amounts of tetraamine with two nonchelated diamine ligands present in solu-

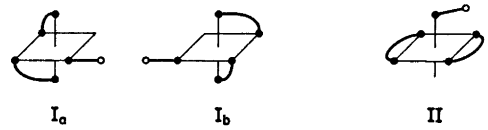

Fig. 6. Possible pentaamineaquachromium(III) isomers.

tions of hydrolyzed tris(1,2-ethanediamine)chromium(III), this is readily understood.

The two geometrical isomers of the (2-aminoethylammonium)aquabis(1,2-ethanediamine)-chromium(III) ion, one of which exists in optically active forms are shown in Fig. 6. Hydrolysis of optically active tris(1,2-ethanediamine)chromium(III) ions yields optically active pentaamine, of which different column eluates are indistinguishable as judged from the visible absorption spectra. Consequently, either pentaamine isomer II is not present in significant amounts, or elution behaviour or visible absorption spectra of the two isomers are almost identical. These latter possibilities seem unlikely from a comparison with the fractionation experiments with the bis(2-aminoethylammonium)diaqua(1,2-ethanediamine)chromium(III) mixtures, and therefore the pentaamine solution isolated is believed not to contain appreciable amounts of isomer II (see Fig. 6). Also the reaction mechanism, previously postulated by us [1] which rationalizes the chromium(III) ammine hydrolysis and isomerization reactions by assuming that these reactions takes place *via* an intermediate of increased coordination number with an approximately pentagonal bipyramidal structure, predicts that pentaamine isomer II cannot be formed directly from the tris(1,2-ethanediamine)chromium(III) ion but only by an isomerization reaction of the pentaamine isomer I.

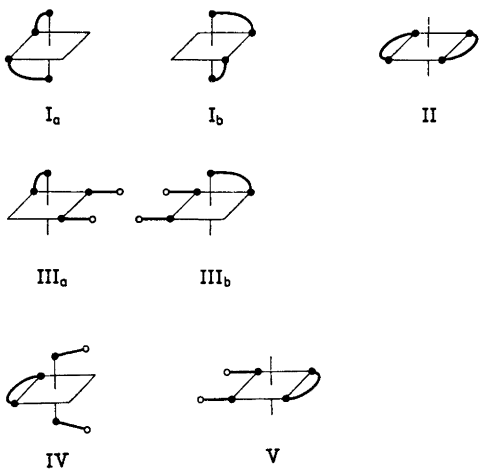

Fig. 7. Possible tetraaminediaquachromium(III) isomers.

Two geometrical isomers of diaquabis(1,2-ethanediamine)chromium(III) and three geometrical isomers of bis(2-aminoethylammonium)diaqua(1,2-ethanediamine)chromium(III) are possible. Two of these five tetraamine ions exist in optically active forms as shown in Fig. 7. In the hydrolysis experiments the *cis*-diaquabis(1,2-ethanediamine)chromium(III) ion is the only tripositive tetraamine species observed. From optically active tris(1,2-ethanediamine)-chromium(III) this tetraamine is produced optically active, but with reduced optical activity compared to that of the pure optical isomer, whereas the optical activity of the unhydrolyzed tris(1,2-ethanediamine)chromium(III) ion remains unchanged. Again the observations are consistent with the proposed substitution mechanism, which cannot account for racemization of the tris(1,2-ethanediamine)chromium(III) ion except by diamine rechelation, but leaves a number of posibilities for production of partly racemized *cis*-diaquabis(1,2-ethanediamine)-chromium(III) ions.

One of these possibilities was investigated further: optically active *cis*-diaquabis(1,2-ethanediamine)chromium(III) ions were kept in 1.0 M perchloric acid at 60 °C, and the optical activity of the isolated unhydrolyzed *cis*-tetraamine measured as a function of time. Since the *trans*-tetraamine has never been found in hydrolyzed solutions of the *cis* isomer, and is also known to hydrolyze appreciably faster than the *cis* isomer, the *trans*-tetraamine ion cannot be of importance as an intermediate for the $(-)_D$-*cis* to $(+)_D$-*cis* racemization reaction. We have therefore interpreted our preliminary kinetic data as showing that the reaction:

$$(-)_D\text{-}cis[Cr(en)_2(aq)_2]^{3+} \underset{k}{\overset{k}{\rightleftharpoons}} (+)_D\text{-}cis[Cr(en)_2(aq)_2]^{3+}$$

occurs in acid solution at 60 °C and has a rate constant, k, of about 8×10^{-5} s^{-1}.

Only small amounts of tetraamines with two unchelated diamines are present in hydrolyzed solutions of tris(1,2-ethanediamine)chromium-(III) ions. In Fig. 1 results of a fractionation experiment with the column band of pentapositive species are exhibited. Because of the very large amounts of hydrolyzed tris(1,2-ethanediamine)chromium(III) ion solution em-

Table 1. Comparison with literature values of spectral characteristics of compounds prepared and purified as described in the text.

Complex	Medium	λ_1 max (nm)	ε_1 max [l/(mol cm)]	λ_2 max (nm)	ε_2 max [l/(mol cm)]	ε_1 max/ ε_2 max	Ref.
$[Cr(en)_3]^{3+}$	1.0 M HCl	457	75.8	351	60.8	1.25	*b*
	1 M $NaNO_3$	457	76.5	351	60.7		15
$[Cr(en)_2(enH)(aq)]^{4+}$	0.5 M $HClO_4$ + 1.0 M $NaClO_4$	474	60.8	361	45.7	1.33	*b*
cis-$[Cr(en)_2(aq)_2]^{3+}$	0.25 M $HClO_4$ + 1.0 M $NaClO_4$	486	64.2	368	41.2	1.56	*b*
	1 M $NaNO_3$	484	67.0	367	42.5		15
?-$[Cr(en)(enH)_2(aq)_2]^{5+}$ [a]	0.5 M $HClO_4$ + 1.0 M $NaClO_4$	502	62.1	372	34.9	1.78	*b*
trans-$[Cr(en)_2(aq)_2]^{3+}$	1.0 M $HClO_4$	447	28.2	364	38.1	0.74	*b*
	1 M $NaNO_3$	442	29.3	361	39.2		15
fac-$[Cr(en)(enH)(aq)_3]^{4+}$	0.25 M $HClO_4$ + 1.0 M $NaClO_4$	511	52.9	378	27.8	1.90	*b*
mer-$[Cr(en)(enH)(aq)_3]^{4+}$	0.25 M $HClO_4$ + 1.0 M $NaClO_4$	495	50.7	380	38.9	1.30	*b*
$[Cr(en)(aq)_4]^{3+}$	0.25 M $HClO_4$ + 1.0 M $NaClO_4$	512	41.3	387	24.7	1.67	*b*
	0.1 – 3 M $HClO_4$	512	41.7	385	24.3		6
cis-$[Cr(enH)_2(aq)_4]^{5+}$	0.5 M $HClO_4$ + 1.0 M $NaClO_4$	534	33.3	391	26.8	1.23	*b*
$[Cr(enH)(aq)_5]^{4+}$	0.25 M $HClO_4$ + 1.0 M $NaClO_4$	551	21.5	397	21.4	1.01	*b*
	3 M $HClO_4$	549	22.2	396	21.5		6

[a] See legend to Fig. 1. [b] This work.

Table 2. Comparison between chromium(III) complexes equivalently coordinated with ammonia and 2-aminoethylammonium ions.

Complex	λ_1 max (nm)	ε_1 max [l/(mol cm)]	λ_2 max (nm)	ε_2 max [l/(mol cm)]
$[Cr(a)(aq)_5]^{3+}$	547	19.9	396	18.6
$[Cr(enH)(aq)_5]^{4+}$	551	21.5	397	21.4
cis-$[Cr(a)_2(aq)_4]^{3+}$	526	27.0	386	21.3
cis-$[Cr(enH)_2(aq)_4]^{4+}$	534	33.3	391	26.8
mer-$[Cr(en)(a)(aq)_3]^{3+}$	491	41.3	378	33.1
mer-$[Cr(en)(enH)(aq)_3]^{4+}$	495	50.7	380	38.9

ployed in order to get measurable amounts of these tetraamines, incomplete separation between the eluted chromium(III) species is seen to have occurred. The fractions of pentapositive species are seen to consist of at least two components in addition to the *cis*-bis(2-aminoethylammonium)tetraaquachromium(III) ion. The latter fractions of pentapositive species had spectra typical of *cis*-tetraaminediaquachromium(III) species. As the elution progresses the maximum of the first spin-allowed band is shifted towards the blue from the 502 nm of the first fraction believed to be free of the *cis*-diamine. This makes it less plausible that hexapositive triamines are eluted after the pentapositive species, as from Table 2 it seems to be a general feature that the position of the first spin-allowed band of 2-aminoethylammonium complexes of chromium(III) is shifted towards the red compared to complexes equivalently coordinated with ammonia, and first spin-allowed band positions of 502 and 513 nm for the *mer*- and *fac*-triamminetriaquachromium(III) ions, respectively, are observed.

The structure of the *cis*-tetraaminediaquachromium(III) isomers III and IV (Fig. 7) accounts well for both visible absorption spectra and elution behaviour of the pentapositive tetraamine species isolated from tris(1,2-ethanediamine)chromium(III) hydrolyzates. Since the maximum of the first spin-allowed band of the tetraamine fractions is shifted towards the red compared to that of the *mer*-(2-aminoethylammonium)triaqua(1,2-ethanediamine)chromium(III) ions, and substitution of water with an amine nitrogen donor atom is expected to be accompagnied by a blue shift, the first tetraamine fractions are tentatively assumed to contain most of the *cis*-tetraamine not derivable from the *mer*-triamine, by exchange of a coordinated water molecule with a 1,2-aminoethylammonium ion ligand, *i.e.* isomer IV. Tetraamine isomer III should in principle be expected to be produced optically active from the active tris(1,2-ethanediamine)chromium(III) ion. However, such dilute column eluates of this tetra-

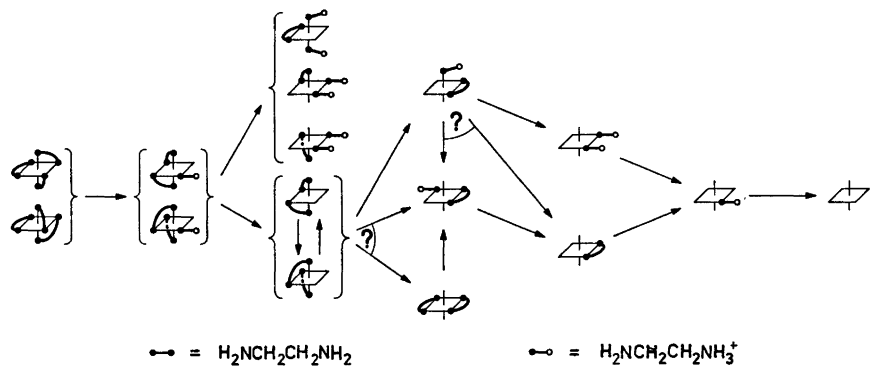

Fig. 8. Reaction scheme for the acid hydrolysis of 1,2-ethanediamine complexes of chromium(III).

amine were always obtained, that measurements of well defined rotations could not be performed, which is as would be expected even with a molar rotation of the active tetraamine comparable to that of the tris(1,2-ethanediamine)chromium(III) ion.

Significant amounts of tetrapositive triamines are present in hydrolyzed tris(1,2-ethanediamine)chromium(III) ion solutions even after comparatively short reaction times. The inconsistency between this fairly rapid production and the somewhat slower appearance of these same triamine ions from the main isolated tetraamine reaction product [the *cis*-diaquabis-(1,2-ethanediamine)chromium(III) ion] indicate that a significant amount of the triamines are formed *via* other tetraamines than this latter tetraamine species. In the chromium(III) ammine system the *trans*-diaqua species is not formed in detectable amounts.[1] If this holds true also for the chromium(III) 1,2-ethanediamine system tetraamine isomers II and V should not be expected to play any important role in the aquation reactions. Therefore, although always present in small amounts tetraamine isomers III and IV are formed in quantities comparable to the *cis*-diaquabis(1,2-ethanediamine)chromium(III) ion but removed substantially faster by the subsequent aquation.

The minor amounts of pentapositive tetraamine ions present in solution of hydrolyzed tris(1,2-ethanediamine)chromium(III) ions and the tedious procedure for the preparation of only very dilute solutions of mixtures of these tetraamine ions prevented the investigation of the further reactions of these species. Reaction products with fewer than three diamines coordinated were more conveniently studied by hydrolyzing the *cis*- and *trans*-diaquabis(1,2-ethanediamine)chromium(III) ions, since far less complicated reaction mixtures were obtained by hydrolysis of these two cations than by hydrolysis of the tris(1,2-ethanediamine)chromium-(III) ion.

Two tetrapositive triamine ions are possible, and these may be labelled *mer* and *fac*, respectively, if the coordinated water is considered. From the *trans* tetraamine ion one of these triamine ions is produced fairly rapidly compared to the speed at which a mixture of the two triamines are produced from the *cis* tetraamine ion. For this latter tetraamine ion the complexity of the tetrapositive column band is further enhanced by the fact that the initial tetraamine ion is so robust that further aquation produces the tetrapositive monoamine ion, (2-aminoethylammonium)pentaaquachromium-(III), within reaction times suitable for production of significant amounts of triamine ions. Although the triamine ion produced from the *trans* tetraamine ion was easily isolated free of other chromium species in solution, the mixture of tetrapositive species produced by hydrolysis of the *cis* tetraamine isomer was not easily converted into solutions of pure substances. Therefore solutions of the triaminetriaqua ion obtained by mercury(II) accelerated chloride hydrolysis of the (2-aminoethylammonium)trichlorido(1,2-ethanediamine)chromium(III) ion was examined. Such solutions contained one pure triamine ion, different from the one isolated from the *trans* tetraamine ion hydrolyzates, and less readily eluted on ion exchange columns than this latter triamine ion. From the positions and shapes of the first spin-allowed absorption bands given in Table 1 and Fig. 3, the elution behaviour, and their mode of formation if comparisons with the chromium(III) ammine system are valid, a *mer* triaqua structure is assigned to the triamine isomer obtained from the *trans* tetraamine ion, and to the other triamine isomer a *fac* triaqua structure is assigned.

By the further aquation the *cis*-tetraaqua-(1,2-ethanediamine)chromium(III) ion appears from both these triamine ions. From the *fac* triamine, however, also a pentapositive diamine can be isolated. The visible absorption spectrum and the mode of formation of this ion indicated a *cis* diamine structure, wherefore it must be the *cis*-bis(2-aminoethylammonium)tetraaquachromium(III) ion. Only the monoamine ion, (2-aminoethylammonium)pentaaquachromium-(III), is a possible aquation product of both diamine ions, and from the monoamine ion only the hexaaquachromium(III) ion is a possible reaction product in acid solution.

A summary of all these qualitative results is given in Fig. 8. Two question marks are seen in this kinetic scheme. These are caused by the considerably faster reactions of the *trans* than of the *cis*-diaquabis(1,2-ethanediamine)chromium(III) and the likewise faster reaction of the *mer*- than of the *fac*-(2-aminoethylammonium)-

triaqua(1,2-ethanediamine)chromium(III) ions, which do not allow distinction to be made between direct slow aquation or slow isomerization followed by rapid aquation. The eventual kinetic importance of undetected species and other reaction pathways in this system must await a complete quantitative investigation. The semiquantitative results reported here seem, however, to make doubtful the quantitative conclusions reached in some earlier works within this field.

REFERENCES

1. Mønsted, L. and Mønsted, O. *Acta Chem. Scand. A 28* (1974) 569.
2. Schläfer, H. L. and Kling, O. *Z. Phys. Chem. (Frankfurt am Main) 16* (1958) 14.
3. Schläfer, H. L. and Kollrack, R. *Z. Phys. Chem. (Frankfurt am Main) 18* (1958) 348.
4. Schläfer, H. L. and Seidel, H. *Z. Phys. Chem. (Frankfurt am Main) 16* (1958) 1.
5. Jørgensen, E. and Bjerrum, J. *Acta Chem. Scand. 13* (1959) 2075.
6. Childers, Jr., R. F., Vander Zyl, Jr., K. G., House, D. A., Hughes, R. G. and Garner, C. S. *Inorg. Chem. 7* (1968) 749.
7. Pedersen, E. *Acta Chem. Scand. 24* (1970) 3362.
8. Parry, R. W., Ed., *Inorg. Syntheses*, XII, New York 1970 p. 274.
9. Glerup, J. *To be published.*
10. Kauffman, G. B. *Chymia 12* (1967) 217; 221.
11. Weinmann, E. *Thesis*, E.T.H., Zürich 1919.
12. House, D. A. and Garner, C. S. *Inorg. Chem. 5* (1966) 840.
13. House, D. A., Hughes, R. G. and Garner, C. S. *Inorg. Chem. 6* (1967) 1077.
14. Mønsted, L. and Mønsted, O. *Acta Chem. Scand. 27* (1973) 2121.
15. Woldbye, F. *Acta Chem. Scand. 12* (1958) 1079.

Received July 19, 1974.

Acta Chemica Scandinavica A 29 (1975) 38—44

Crystal Structure of Cycloheptasarcosyl Hydrate

P. GROTH

Department of Chemistry, University of Oslo, Oslo 3, Norway

The crystals belong to the monoclinic system with space group $P2_1/c$ and cell dimensions $a=28.725(5)$ Å, $b=11.048(1)$ Å, $c=11.036(1)$ Å, $\beta=132.52(1)°$. The phase problem was solved by direct methods, and the R-value arrived at for 2250 observed reflections was 6.9 % ($R_w=4.9$ %. The conformation is *cis,cis,cis,cis,trans,trans,trans*. Water molecules form hydrogen bond bridges linking molecules to endless chains along [001]. Bond distances and angles are compared with those of cyclopentasarcosyl, cyclooctasarcosyl, and cycloalanyltetrasarcosyl.

Cyclic oligopeptides of sarcosine of the general formula (I) have been studied by Dale and Titlestad.[1-3] To account for the relatively high observed resistance to ring inversion,

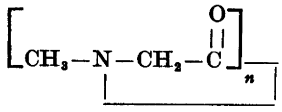

$n=2,3,\cdots,8$ (I)

transannular interactions between N and C (carbonyl) were suggested. Recent findings [4-6] do not support this assumption, and the explanation must be sought in the intrinsic conformation of the peptide chain itself.[2] For the case $n=7$ the NMR-spectrum is complex with broad methylene and N-methyl lines which do not become simpler on cooling to −70 °C. Benzene addition resolves seven main N-methyl signals together with several less intense signals, indicating that one major conformation is present. The crystal conformation which is obtained by dissolution in $CHFCl_2$ at −80 °C, shows three N-methyl lines (intensity 9:9:3) and seven partially resolved quartets. In order to settle the conformational problem, and to obtain detailed information of the molecular geometry, and X-ray crystallographic investigation of cycloheptasarcosyl has been carried out.

The crystals belong to the monoclinic system and the systematic absences lead to the space group $P2_1/c$. The cell parameters measured by means of a four circle diffractometer, and their estimated standard deviations are:
$a=28.725(5)$ Å, $b=11.048(1)$ Å, $c=11.036(1)$ Å, $\beta=132.52(1)°$
The unit cell contains four $C_{21}O_7N_7H_{35}.H_2O$ formula units.

With $2\theta_{max}=50°$ and Mo$K\alpha$-radiation 4575 independent reflections were measured on an automatic four-circle diffractometer. Using an observed unobserved cutoff at $2.0\sigma(I)$, 2250 were recorded as observed. No corrections have been made for absorption on secondary extinction effects.

The structure was solved by direct methods [7] and refined by full-matrix least squares technique.[8,*] Hydrogen atom positions were calculated and the positional parameters only were refined. Anisotropic temperature factors were introduced for O, N, and C-atoms, and weights in least squares were calculated from the standard deviations in intensities, $\sigma(I)$, taken as

$$\sigma(I)=[C_T+(0.02C_N)^2]^{\frac{1}{2}}$$

where C_T is the total number of counts and C_N net count (peak minus background). The conventional R-value arrived at was 6.9 % (weighted value $R_w=4.9$ %) for 2250 observed reflections. The form factors were those of Hanson *et al.*[9] except for hydrogen.[10] The final fractional coordinates and thermal vibration parameters are given in Table 1. The expression for anisotropic vibration is:

$$\exp[-(B11h^2+B22k^2+B33l^2+B12hk+B13hl+B23kl)]$$

* All programs used are included in this reference.

Table 1. Final fractional coordinates and anisotropic thermal vibration parameters with estimated standard deviations (multiplied by 10^5 for non-hydrogens and 10^4 for hydrogens). The symbols CC, CM, and OW are used for carbonyl carbons, methyl carbons, and water oxygen, respectively. Hmn is bonded to Cm, HMmn to CMm, and HW to OW.

ATOM	X	Y	Z	B	B11	B22	B33	B12	B13	B23
OW	22986(24)	63964(38)	-5195(62)		343(12)	851(48)	1852(74)	-167(37)	1008(52)	-122(92)
O1	29984(19)	30710(35)	25258(48)		319(12)	672(37)	2310(82)	-207(36)	1156(55)	-810(93)
O2	12689(18)	34963(36)	11709(46)		229(10)	1081(43)	1849(72)	-322(35)	893(49)	247(91)
O3	-1295(17)	46993(37)	-33321(48)		148(10)	1284(47)	2898(79)	-284(36)	449(48)	-662(103)
O4	15893(18)	75289(34)	12803(45)		285(11)	889(40)	1196(64)	-249(35)	662(47)	-198(88)
O5	27396(16)	83998(34)	16178(46)		183(10)	948(42)	1873(74)	43(33)	634(47)	-1174(91)
O6	37588(17)	81549(33)	57259(46)		279(11)	888(40)	2167(77)	150(35)	1286(51)	471(93)
O7	44775(18)	58478(34)	64716(45)		315(12)	790(41)	1634(73)	79(36)	928(51)	579(88)
N1	22578(28)	42332(48)	28744(53)		167(12)	857(48)	1142(76)	-197(39)	510(55)	-133(98)
N2	9208(19)	44288(39)	-15982(50)		164(11)	703(45)	1101(74)	-75(36)	508(52)	-283(93)
N3	7772(19)	71577(37)	-14257(50)		179(11)	644(43)	1079(75)	-84(37)	538(52)	-22(96)
N4	19671(28)	95720(38)	10382(52)		136(10)	503(39)	1286(73)	76(34)	492(49)	-134(90)
N5	36968(19)	96605(38)	42223(48)		143(10)	622(41)	1097(74)	-15(36)	434(49)	144(95)
N6	47087(19)	69497(40)	63186(51)		172(11)	736(45)	1072(75)	65(38)	552(51)	237(96)
N7	36037(20)	46955(40)	31560(50)		186(11)	667(44)	1518(82)	52(39)	745(54)	-286(100)
C1	27483(26)	49186(52)	31316(70)		163(14)	612(52)	1225(93)	15(44)	457(62)	-371(114)
C2	15536(28)	46801(59)	-943(64)		192(14)	855(57)	989(87)	-231(47)	513(63)	252(118)
C3	5071(28)	61740(57)	-12237(78)		177(14)	837(60)	1866(118)	-62(48)	834(78)	-73(134)
C4	14815(26)	88871(51)	-4598(65)		162(14)	564(51)	1281(93)	38(43)	535(65)	176(115)
C5	30598(27)	99819(57)	35208(72)		171(14)	715(54)	1105(89)	-45(45)	468(62)	-514(116)
C6	44997(26)	80747(53)	54048(72)		160(14)	640(53)	1510(101)	-92(45)	684(66)	-192(119)
C7	38158(26)	59179(52)	37659(69)		180(14)	593(51)	1388(95)	-82(44)	673(65)	-39(117)
CC1	31331(25)	41336(50)	29360(61)		173(14)	678(54)	989(86)	1(48)	419(61)	-273(118)
CC2	16842(26)	48621(49)	13971(73)		203(15)	446(48)	1400(99)	-109(44)	715(69)	-171(113)
CC3	4059(25)	60236(58)	-21410(65)		151(14)	766(57)	1447(99)	-115(48)	626(66)	-22(127)
CC4	12519(24)	78058(47)	-1273(65)		156(14)	612(55)	1058(92)	108(45)	415(64)	6(121)
CC5	25714(24)	92291(50)	19720(62)		158(14)	682(56)	1139(91)	-3(45)	517(62)	-146(117)
CC6	39497(23)	86311(46)	51386(62)		134(13)	558(50)	1033(91)	-105(43)	435(59)	-443(109)
CC7	43619(25)	59304(51)	56349(66)		177(14)	715(56)	1364(100)	-15(47)	746(69)	-187(125)
CM1	24378(34)	35385(69)	42366(79)		307(18)	1171(71)	1254(103)	-113(64)	765(77)	93(142)
CM2	8375(36)	32943(66)	-23938(91)		331(19)	902(64)	1969(120)	-42(59)	1315(84)	-593(147)
CM3	4469(33)	74813(64)	-31152(75)		234(16)	944(62)	1199(98)	-149(52)	525(68)	-134(133)
CM4	17640(36)	105198(68)	14958(99)		260(17)	811(60)	2518(136)	318(54)	1394(85)	-342(148)
CM5	38981(31)	101206(68)	33858(83)		199(15)	1008(65)	1497(101)	-94(51)	577(70)	366(134)
CM6	51693(33)	78594(69)	80829(74)		259(17)	1202(71)	1240(101)	-15(58)	618(72)	-355(141)
CM7	39923(37)	39942(69)	30259(90)		365(20)	1126(69)	1964(122)	247(61)	1305(89)	152(151)
HM11	3843(22)	5222(41)	4386(58)	4.0						
HM12	2568(21)	5697(44)	2421(56)	4.0						
HM21	1575(24)	4663(50)	575(61)	4.0						
HM22	1651(22)	5506(44)	-35(57)	4.0						
HM31	95(22)	6324(41)	-1639(56)	4.0						
HM32	730(21)	5989(41)	-91(58)	4.0						
HM41	1668(20)	8606(41)	-929(54)	4.0						
HM42	1130(22)	9502(42)	-1228(55)	4.0						
HM51	3812(21)	10862(44)	3328(55)	4.0						
HM52	3020(22)	9807(42)	4332(57)	4.0						
HM61	4380(21)	7917(42)	4348(58)	4.0						
HM62	4849(22)	8665(42)	5974(55)	4.0						
HM71	3481(22)	6430(42)	3547(56)	4.0						
HM72	3976(21)	6334(42)	3254(54)	4.0						
HM11	2128(22)	3115(44)	4887(55)	4.0						
HM12	2655(22)	4814(42)	5235(59)	4.0						
HM13	2783(22)	2906(44)	4693(56)	4.0						
HM21	487(22)	3291(42)	-3592(59)	4.0						
HM22	914(21)	2558(44)	-1690(57)	4.0						
HM23	1135(21)	3166(44)	-2457(56)	4.0						
HM31	685(21)	8012(45)	-3288(54)	4.0						
HM32	4(23)	7615(42)	-3800(56)	4.0						
HM33	449(22)	6802(45)	-3656(57)	4.0						
HM41	2047(22)	11028(44)	2513(58)	4.0						
HM42	1520(24)	10443(48)	1507(65)	4.0						
HM43	1605(23)	11120(45)	888(58)	4.0						
HM51	4354(23)	10243(43)	4152(57)	4.0						
HM52	3741(21)	10973(46)	3029(56)	4.0						
HM53	3686(22)	9728(44)	2365(59)	4.0						
HM61	5299(22)	6332(44)	8517(56)	4.0						
HM62	5008(21)	7380(44)	8530(56)	4.0						
HM63	5523(23)	7586(43)	8459(55)	4.0						
HM71	3768(22)	3305(45)	2371(56)	4.0						
HM72	4398(23)	3817(42)	4095(58)	4.0						
HM73	4059(22)	4371(44)	2440(58)	4.0						
HW1	2048(22)	6725(47)	-1454(58)	4.0						
HW2	2438(23)	7004(44)	-126(62)	4.0						

The principal axes of the thermal vibration ellipsoids for oxygen, nitrogen, and carbon atoms were calculated from the temperature parameters of Table 1. Maximum root mean squares amplitudes range from about 0.22 Å for ring atoms to about 0.33 Å for methyl carbon atoms and the water oxygen. Due to the size of the molecule, no rigid-body analysis of translational, librational, and screw motion has been carried out. A comparison between observed and calculated structure factors is presented in Table 2.

Interatomic distances, bond angles and dihedral angles are given in Table 3. The standard deviations, given in parentheses, are estimated from the correlation matrix of the last least

Table 2. Observed and calculated structure factors on 10 times absolute scale.

K=	0,L=12		10	1151	1207	11	84	7	11	550	535	13	210	203	7	79	54	6	291	287	16	90	76
11	183	163	11	428	435	12	91	132	12	262	282	14	152	149	9	142	157	8	544	524	17	160	145
12	96	57	12	343	345	13	208	195	14	242	231	15	390	384	12	121	108	9	277	265	19	112	122
19	138	157	13	74	47	23	181	193	15	400	388	18	116	126	18	89	100	10	351	362	20	118	107
20	90	88	14	622	619	25	223	230	16	371	373	19	145	163	20	166	183	12	365	357	K=	2,L=	1
24	93	93	15	232	232	26	147	148	18	292	289	20	103	121	21	147	167	13	256	248	0	1343	1328
26	92	104	16	361	352	28	141	142	19	219	221	K=	1,L=	2	23	177	186	14	127	126	1	530	535
28	89	8	17	218	240	29	88	67	23	96	117	0	440	416	24	212	210	15	569	558	3	194	210
29	93	54	18	79	95	30	95	67	24	129	119	1	310	326	25	164	157	16	638	635	4	489	511
K=	0,L=10		21	113	84	32	90	45	25	161	150	2	536	515	26	110	87	17	230	221	5	712	706
7	115	97	22	255	248	33	110	79	26	86	104	3	614	637	27	127	127	18	184	140	6	967	957
8	132	130	23	367	350	34	138	75	27	134	127	5	109	139	29	106	94	19	244	248	7	411	393
11	181	190	K=	0,L=	0	K=	1,L=	8	30	114	77	6	284	268	30	100	60	20	195	206	8	220	202
13	171	155	2	359	368	1	81	105	K=	1,L=	3	7	104	90	32	124	104	21	116	117	10	193	170
15	250	244	3	193	215	2	103	73	1	1000	994	8	146	181	K=	2,L=	8	23	122	145	11	237	218
18	133	152	4	564	575	7	83	107	3	371	352	9	145	168	1	83	47	26	356	356	12	84	58
20	134	125	5	261	267	9	85	131	4	706	665	11	331	334	4	92	93	27	166	141	13	108	98
24	96	81	6	341	350	10	107	94	5	519	507	12	272	262	5	136	131	28	135	128	14	143	150
25	168	183	7	365	361	11	86	87	7	85	84	16	98	113	6	131	97	K=	2,L=	3	15	179	177
26	113	108	8	447	452	12	121	135	8	711	725	19	113	101	7	80	64	1	906	895	16	131	118
27	193	215	9	717	750	13	382	374	9	583	580	K=	1,L=	3	8	182	189	2	88	108	17	192	193
29	189	180	10	308	323	14	165	159	10	410	409	0	856	864	11	143	147	3	491	506	18	108	108
31	198	208	11	291	304	16	208	216	11	511	497	2	690	701	13	209	219	4	288	263	20	88	64
K=	0,L=	8	12	558	565	19	125	132	13	407	395	3	105	78	14	194	191	5	300	319	K=	2,L=	2
1	159	167	13	743	739	21	83	85	15	140	81	4	210	203	15	186	195	6	760	724	0	493	506
2	81	107	15	210	208	25	119	141	16	108	120	5	606	593	16	120	104	7	822	800	1	819	782
3	299	294	16	141	130	26	204	205	17	111	68	6	148	145	17	100	97	8	289	298	2	492	492
4	369	370	17	226	241	33	117	111	18	193	191	7	304	305	18	266	269	9	913	909	3	217	223
6	181	173	22	108	112	K=	1,L=	7	20	142	148	9	160	163	19	190	186	10	869	870	4	487	475
7	345	334	23	152	145	1	84	71	21	169	177	11	305	281	21	159	171	11	399	408	5	514	519
8	151	166	25	149	138	2	267	272	23	421	411	13	102	96	22	173	172	12	357	347	6	240	244
10	121	119	K=	0,L=	2	4	77	73	24	146	136	15	119	120	25	157	141	13	139	112	7	110	107
11	193	215	0	836	851	5	152	150	25	89	111	K=	1,L=	4	26	85	17	14	131	85	9	283	276
13	151	119	2	600	614	6	74	69	K=	1,L=	2	0	188	193	29	145	179	16	307	311	11	327	328
16	258	250	3	926	929	7	314	318	1	1562	1554	1	569	591	K=	2,L=	7	17	134	117	14	215	221
17	266	261	4	647	659	8	106	119	2	132	135	2	395	411	1	347	342	19	95	70	16	89	95
20	108	120	5	537	551	10	76	103	3	460	486	3	128	124	3	193	200	20	157	157	18	176	165
21	227	242	6	959	949	11	278	244	4	730	751	4	231	228	4	177	186	24	124	127	20	90	73
22	403	420	7	488	483	12	484	491	5	357	347	7	221	222	5	124	103	25	188	206	K=	2,L=	3
23	269	294	9	88	98	13	100	106	7	500	488	10	250	255	6	189	178	27	91	71	0	84	114
24	117	117	10	110	131	14	201	210	8	408	410	11	136	114	8	234	237	28	110	102	2	273	258
26	101	89	12	256	246	15	229	222	10	307	298	12	117	133	9	266	265	29	104	98	3	303	306
27	246	250	13	140	147	17	90	77	11	172	151	14	106	56	11	127	124	K=	2,L=	2	4	276	289
28	102	87	14	414	430	19	118	119	12	301	279	15	125	108	12	403	402	1	805	586	5	216	238
31	89	86	15	129	146	20	389	375	13	250	239	K=	1,L=	5	14	263	284	2	802	841	7	114	113
K=	0,L=	6	K=	0,L=	4	21	82	79	14	608	588	0	155	177	19	119	102	3	1001	1012	10	86	105
1	328	334	0	850	848	23	379	398	16	173	164	1	124	112	20	296	292	4	869	863	11	115	113
2	111	116	1	149	175	24	376	394	17	290	298	2	217	213	21	227	231	5	128	156	13	214	246
3	186	193	2	82	87	25	146	136	18	139	138	3	271	274	28	162	198	6	298	301	17	109	96
4	379	390	3	228	221	27	170	167	19	177	162	6	174	206	29	184	186	7	82	97	K=	2,L=	4
5	121	108	4	87	123	29	123	117	20	233	231	7	78	43	33	90	98	8	1056	1058	0	186	197
6	307	305	6	293	302	K=	1,L=	6	21	94	91	8	126	113	K=	2,L=	8	9	1387	1402	1	71	70
7	147	146	7	105	72	1	98	132	22	133	127	9	97	80	1	116	130	10	366	346	3	138	109
9	696	716	8	97	99	2	120	107	23	141	134	11	86	47	3	77	67	11	865	857	4	176	174
10	346	351	9	379	396	3	372	362	K=	1,L=	1	12	97	105	5	214	200	12	585	594	5	267	271
11	235	251	11	430	424	4	443	437	1	182	191	K=	1,L=	6	6	297	273	13	205	197	6	83	33
12	649	685	14	128	146	5	178	180	2	349	338	0	855	864	8	126	129	15	253	261	7	92	118
13	80	51	16	150	142	6	133	140	3	256	262	1	144	167	9	109	102	18	120	135	9	161	145
14	225	235	K=	0,L=	6	8	390	371	4	831	837	2	115	128	10	260	264	19	89	101	10	306	311
15	105	92	0	400	400	10	97	92	5	1018	1026	3	181	200	11	277	273	21	182	194	11	260	273
16	353	344	1	485	490	11	96	85	7	849	842	5	141	149	13	605	617	22	314	301	12	128	105
17	117	168	2	401	398	15	146	135	8	393	374	6	218	221	14	106	118	23	207	210	14	141	136
22	116	135	3	149	141	16	237	224	10	466	456	7	96	104	15	208	204	24	109	114	16	110	94
25	330	318	4	220	211	18	138	136	11	124	125	K=	1,L=	7	17	102	104	K=	2,L=	1	K=	2,L=	5
26	171	165	5	275	288	21	195	235	12	313	326	0	163	179	18	99	93	1	344	325	0	133	127
27	138	159	7	199	229	22	295	301	13	429	438	2	156	163	20	205	198	2	1542	1500	1	152	177
K=	0,L=	4	K=	0,L=	8	23	221	229	16	153	134	K=	1,L=	9	22	84	116	3	311	325	4	245	240
2	923	922	1	110	124	24	164	182	17	115	155	1	104	92	23	89	84	4	1076	1064	5	222	223
3	1100	1118	2	135	192	26	166	169	18	281	295	K=	2,L=	13	24	204	206	5	412	420	6	112	107
4	562	566	3	134	118	K=	1,L=	5	19	302	309	23	189	181	25	219	236	6	928	933	7	104	100
5	456	453	5	115	108	1	298	293	20	193	190	K=	2,L=	12	27	142	153	7	107	117	9	266	248
7	102	87	K=	1,L=	12	2	255	231	22	97	69	13	118	83	28	83	21	8	355	357	11	133	130
9	574	570	19	159	154	3	413	399	23	116	142	14	83	24	30	100	119	9	108	123	K=	2,L=	6
10	307	308	22	116	108	5	385	373	K=	1,L=	0	16	87	57	K=	2,L=	5	10	183	194	0	174	180
11	71	62	28	106	127	6	357	376	1	588	572	18	84	52	2	338	332	11	423	438	2	90	122
12	414	429	K=	1,L=	11	7	96	93	3	921	921	23	98	121	3	367	358	12	535	526	3	144	140
13	115	72	14	146	146	8	467	445	4	347	341	K=	2,L=	11	5	88	49	13	83	86	5	150	116
14	471	474	17	131	111	9	494	488	5	509	513	18	104	109	6	212	198	14	258	263	6	169	165
15	143	160	19	115	126	12	218	206	6	447	466	22	107	117	7	174	158	15	141	139	7	196	206
16	134	139	22	208	203	13	100	112	8	330	311	26	101	40	9	177	169	16	127	110	8	82	14
17	114	166	23	108	99	14	166	155	9	714	693	27	123	106	10	600	576	17	102	101	K=	2,L=	7
19	135	153	25	127	120	15	234	264	10	330	322	K=	2,L=	10	11	78	62	18	128	112	0	91	63
20	180	162	K=	1,L=	10	17	482	479	11	170	174	2	102	102	12	88	68	21	140	127	1	85	88
21	130	163	8	140	114	19	472	490	13	337	332	7	141	146	13	179	161	23	149	137	2	106	81
22	102	97	15	146	164	20	170	145	16	315	304	10	163	160	14	82	96	24	112	111	5	82	41
23	88	129	16	145	144	21	375	370	17	135	116	11	124	134	15	620	644	25	131	109	K=	2,L=	8
26	202	191	19	129	138	22	353	366	18	118	113	12	174	177	16	271	285	K=	2,L=	0	0	105	127
27	218	216	20	84	107	24	148	159	22	117	96	14	87	84	18	278	284	0	962	943	3	88	89
29	92	68	21	82	75	26	83	33	K=	1,L=	1	15	92	49	22	239	234	1	249	259	K=	2,L=	9
30	92	15	24	292	280	27	86	38	1	248	248	16	107	90	23	104	110	2	708	739	0	120	121
31	132	116	27	87	85	K=	1,L=	4	2	650	671	18	102	67	24	130	99	3	745	745	K=	3,L=	12
K=	0,L=	2	28	99	97	1	139	114	3	604	608	19	164	152	25	287	290	4	157	199	22	90	23
1	529	560	K=	1,L=	9	2	337	321	4	651	639	21	97	131	26	117	83	5	1219	1212	K=	3,L=	11
2	550	583	2	88	106	3	103	114	5	453	444	23	102	92	31	96	74	6	285	281	9	100	84
3	1450	1451	3	82	9	4	432	426	6	72	78	25	186	199	K=	2,L=	4	7	132	149	10	134	114
5	829	816	5	92	78	5	503	494	7	130	129	26	140	144	1	610	600	8	135	133	14	161	152
6	1394	1389	6	152	143	6	307	310	9	565	541	27	143	121	2	144	155	10	171	139	15	127	120
7	1644	1747	7	170	164	7	274	263	10	219	205	29	105	102	3	429	420	11	442	425	19	125	144
8	739	770	8	93	81	9	220	214	11	352	358	31	95	45	4	451	452	14	88	91	22	118	128
9	1021	1035	10	232	246	10	608	608	12	135	116	K=	2,L=	9	5	388	385	15	299	284	24	159	156

Table 2. Continued.

26	132	137	26	154	124	6	101	75	9	373	363	24	169	158	7	100	89	8	316	310	9	239	226
28	93	91	28	171	187	7	394	410	11	247	251	25	124	141	8	80	14	9	125	130	12	253	238
K=	3,L=	10	30	112	100	8	160	164	12	281	291	27	107	99	9	116	109	10	270	271	13	257	272
8	89	72	K=	3,L=	4	9	355	363	13	95	103	28	107	100	12	140	112	11	269	269	14	210	204
10	286	281	1	180	168	11	113	110	14	142	126	K=	4,L=	2	13	172	196	12	100	79	15	239	231
12	151	121	3	290	267	12	126	149	16	115	114	1	92	71	K=	4,L=	5	14	89	51	16	148	135
13	185	160	4	167	185	14	125	138	17	135	149	3	185	181	0	437	440	15	267	260	17	288	278
20	93	67	5	388	380	15	405	424	18	164	178	4	989	981	1	213	213	16	141	137	K=	5,L=	2
21	91	74	6	655	652	16	202	200	19	113	135	6	373	381	2	313	325	17	113	82	0	338	323
22	113	77	7	300	287	18	155	151	23	100	132	7	440	440	6	203	214	18	93	56	1	362	371
23	99	67	8	608	618	20	132	131	24	185	170	8	180	194	7	82	68	19	206	202	2	220	187
24	85	12	9	109	122	21	147	137	26	86	61	9	301	287	9	103	124	20	167	197	3	448	428
25	96	102	10	390	377	22	128	115	27	96	105	10	421	447	K=	4,L=	6	22	191	196	4	152	170
28	89	45	11	424	395	K=	3,L=	2	32	123	112	11	203	211	0	285	299	23	91	93	5	176	181
32	107	47	12	179	170	0	312	310	K=	4,L=	7	12	367	365	1	86	62	27	145	118	7	88	85
K=	3,L=	9	13	816	803	2	261	249	1	209	210	17	196	193	10	93	96	29	120	118	8	253	261
4	132	92	14	296	304	3	301	287	4	177	180	18	149	171	K=	4,L=	7	K=	5,L=	4	9	122	103
5	102	118	15	200	210	4	238	206	6	190	202	19	134	123	1	108	90	1	368	372	11	150	146
6	241	233	16	160	153	5	340	324	7	177	172	20	180	184	3	105	99	2	82	79	13	138	145
8	119	145	17	135	130	6	179	181	8	96	106	22	141	151	5	90	72	3	266	279	16	126	125
9	137	139	21	145	137	7	249	245	9	307	306	K=	4,L=	1	K=	4,L=	8	5	174	174	K=	5,L=	3
10	244	258	23	162	165	8	225	215	10	131	145	1	585	561	2	97	92	6	279	257	0	88	78
12	114	94	30	92	20	9	90	102	11	121	96	2	243	236	3	148	145	7	310	301	1	72	55
13	211	211	K=	3,L=	3	10	307	302	12	78	96	3	83	67	K=	4,L=	9	8	137	115	2	99	86
15	92	95	2	272	258	13	156	176	14	320	333	4	96	42	0	121	127	9	208	244	3	331	327
16	87	82	3	866	859	14	147	151	15	216	214	5	360	342	K=	5,L=	12	10	448	468	5	114	110
17	189	202	4	248	246	15	104	87	16	157	156	6	551	537	18	128	107	12	120	146	6	77	8
18	115	102	5	537	521	17	159	161	17	247	244	7	296	274	K=	5,L=	11	13	220	200	7	261	275
19	90	85	6	498	504	18	158	149	21	194	197	9	424	420	14	140	147	14	150	188	9	97	87
20	91	120	7	728	706	19	103	100	24	152	152	10	273	267	17	122	106	15	256	271	10	438	452
21	147	163	8	269	272	K=	3,L=	3	26	116	100	12	132	92	22	155	131	17	188	169	11	304	314
22	189	209	10	135	113	0	261	265	32	105	17	13	150	140	25	95	47	18	172	185	14	134	95
23	260	242	11	333	341	1	835	840	K=	4,L=	6	14	422	439	K=	5,L=	10	19	191	175	K=	5,L=	4
27	146	137	12	166	155	2	94	93	1	119	117	15	100	51	7	88	66	20	95	73	0	233	224
28	87	92	13	91	74	4	312	313	2	188	179	16	125	115	14	136	144	21	181	170	2	86	90
29	86	81	14	334	343	5	301	297	3	221	229	18	116	122	21	155	105	24	215	208	3	230	228
K=	3,L=	8	15	178	198	6	336	343	4	106	102	19	98	103	23	137	127	K=	5,L=	3	4	359	379
2	294	299	16	80	87	7	119	133	6	79	69	20	137	129	24	100	3	1	192	159	5	179	174
3	109	104	17	182	162	9	176	184	8	122	138	21	338	346	K=	5,L=	9	2	246	226	7	127	125
4	333	335	20	92	103	10	249	251	12	293	287	24	94	28	4	134	124	3	100	130	8	91	119
5	203	191	23	150	124	12	210	194	13	406	404	K=	4,L=	0	6	84	58	4	237	219	11	81	11
6	364	372	24	172	187	13	146	170	14	169	151	0	362	360	9	89	83	5	292	283	12	180	172
9	114	118	26	107	80	14	253	256	18	257	272	1	150	145	10	206	207	6	651	641	K=	5,L=	5
11	135	114	K=	3,L=	2	15	96	57	21	119	146	2	631	656	11	86	73	7	288	278	0	108	105
14	118	122	1	899	939	16	150	148	22	121	116	3	221	238	14	90	79	8	209	198	1	148	159
15	227	220	3	93	81	17	116	91	K=	4,L=	5	5	231	244	15	129	120	9	101	136	2	274	274
18	85	87	4	535	534	K=	3,L=	4	1	192	179	6	640	650	16	179	174	10	276	276	3	244	254
23	103	112	5	434	438	0	422	430	2	254	261	7	123	122	18	137	128	11	454	458	4	272	286
27	126	109	6	1578	1615	1	324	345	3	135	131	8	292	288	22	121	133	13	200	193	5	122	101
K=	3,L=	7	7	395	414	2	502	507	4	224	246	9	82	42	23	97	111	14	198	183	6	188	191
2	151	170	8	230	223	6	97	60	7	287	264	10	103	74	K=	5,L=	8	15	262	258	11	144	141
3	292	294	9	910	921	7	190	191	9	180	179	11	358	354	4	92	83	16	194	188	K=	5,L=	6
5	205	205	10	427	408	8	108	121	10	128	121	12	219	221	8	198	200	17	153	154	1	259	269
6	121	139	11	182	137	10	147	140	11	646	664	14	149	152	10	112	123	18	113	103	2	84	44
7	104	115	12	546	540	11	111	117	12	95	93	15	97	100	13	276	279	19	256	261	4	105	136
8	209	211	13	187	200	15	125	110	13	108	73	16	178	166	15	342	346	23	107	82	K=	5,L=	7
10	256	276	16	104	109	K=	3,L=	5	14	85	75	19	92	71	16	119	124	K=	5,L=	2	0	264	264
11	158	150	18	143	137	1	379	390	15	132	137	K=	4,L=	1	17	174	180	1	317	329	5	89	95
12	188	177	19	168	181	2	145	140	17	219	213	0	206	201	18	115	136	3	232	218	K=	5,L=	8
13	110	104	20	140	140	3	127	118	19	118	97	1	141	145	20	100	102	4	285	281	2	94	101
15	119	118	23	111	106	9	169	160	20	408	404	2	319	307	21	270	259	5	140	137	K=	6,L=	11
16	287	277	24	119	96	10	96	95	22	89	102	3	287	290	23	93	63	8	176	131	16	109	120
17	182	191	25	208	206	13	117	83	23	102	125	4	552	550	K=	5,L=	7	9	343	352	K=	6,L=	10
19	344	343	K=	3,L=	1	K=	3,L=	6	25	100	104	5	709	692	1	95	96	10	145	145	11	135	96
24	150	149	1	353	349	0	329	317	28	120	115	6	134	121	2	134	153	11	461	458	13	150	132
25	129	122	3	337	332	1	334	334	K=	4,L=	4	7	332	325	3	162	155	12	389	386	14	111	76
26	194	187	4	396	377	2	196	210	1	517	491	10	291	273	4	99	100	14	199	206	15	100	107
28	131	140	6	319	319	3	196	205	2	175	172	11	201	213	7	126	102	17	199	166	20	85	66
31	120	98	8	108	84	5	112	97	3	431	424	14	241	256	9	229	223	18	128	117	24	90	70
K=	3,L=	6	9	215	211	K=	3,L=	7	4	220	222	15	122	125	10	84	102	20	170	147	26	89	14
1	116	102	10	304	298	1	143	154	6	211	201	16	232	237	12	365	375	21	187	208	K=	6,L=	9
3	83	76	11	443	440	2	105	78	7	166	160	17	106	95	14	138	155	22	80	42	6	90	73
4	89	49	12	516	506	3	140	140	8	294	299	22	93	59	15	120	135	K=	5,L=	1	8	122	130
6	135	126	13	117	97	K=	4,L=	11	10	339	348	K=	4,L=	2	17	126	129	1	594	585	10	165	178
7	263	257	14	225	225	12	95	86	11	214	248	0	539	506	18	103	129	2	106	88	13	258	255
8	164	178	15	449	429	13	90	68	12	162	170	1	83	73	20	100	69	3	324	316	15	86	80
9	264	237	18	92	75	20	106	92	13	510	480	2	425	427	21	116	124	4	123	134	22	140	151
10	286	269	19	372	361	21	102	95	15	221	216	3	127	144	22	90	83	5	127	137	K=	6,L=	8
11	260	251	20	159	164	23	123	112	16	158	149	4	294	308	23	122	137	6	219	208	2	112	107
12	291	99	22	97	68	24	164	157	17	217	235	5	275	282	24	116	115	8	131	123	3	98	88
14	90	106	23	109	103	K=	4,L=	10	18	203	198	7	196	199	26	48	143	11	80	24	6	106	116
15	90	67	26	112	126	10	215	203	20	130	161	8	98	108	K=	5,L=	6	12	355	339	8	179	166
16	110	90	K=	3,L=	0	13	230	250	22	168	158	11	221	241	1	192	197	13	179	174	9	202	221
17	203	202	1	589	592	14	209	208	23	104	100	12	284	273	2	176	173	15	90	42	11	231	244
20	150	137	2	856	854	16	85	59	24	167	181	16	100	91	3	120	135	17	123	121	12	213	194
21	189	186	3	460	469	18	138	138	29	97	85	17	110	130	4	212	212	20	102	97	14	140	140
22	127	144	5	472	473	19	129	140	K=	4,L=	3	19	149	138	5	110	107	21	136	142	15	85	62
23	196	194	6	228	224	21	154	163	1	620	611	K=	4,L=	3	6	81	94	K=	5,L=	0	16	128	122
29	108	160	7	139	138	22	210	199	2	458	459	0	74	65	7	284	297	1	155	160	18	162	195
K=	3,L=	5	8	139	110	K=	4,L=	9	3	429	432	2	296	265	9	101	107	2	447	453	19	179	175
1	233	229	9	96	62	2	103	94	4	280	263	4	324	322	10	395	389	3	228	222	23	153	148
2	121	154	11	199	214	8	162	156	5	207	203	5	170	170	12	278	288	4	169	160	24	133	144
3	147	145	12	235	239	9	111	70	6	616	623	7	241	238	13	138	124	6	146	131	29	94	70
4	524	535	13	104	126	10	134	125	7	227	205	8	112	98	14	86	66	9	145	176	K=	6,L=	7
7	85	109	14	175	151	13	115	144	8	306	307	9	82	69	15	168	157	10	215	242	2	117	113
8	516	523	16	137	139	14	164	159	9	620	634	11	142	129	17	107	75	12	116	115	3	149	137
9	516	518	17	174	190	18	194	204	10	209	198	12	258	255	20	192	193	13	125	129	9	290	266
10	445	433	18	128	109	19	95	89	11	365	346	13	147	159	23	116	102	14	134	127	10	160	184
11	564	565	21	211	225	21	148	143	12	172	154	16	94	10	24	146	165	15	138	141	11	211	218
12	434	424	22	131	131	24	131	127	13	79	65	17	88	94	26	152	141	16	139	120	16	92	58
17	257	235	K=	3,L=	1	25	151	153	14	239	237	K=	4,L=	4	K=	5,L=	8	17	352	363	18	191	226
18	187	205	0	426	399	27	87	73	15	289	301	0	222	225	1	280	290	23	112	143	19	118	150
20	138	126	1	480	475	K=	4,L=	8	16	525	529	1	86	67	2	212	216	K=	5,L=	1	22	127	84
21	84	140	2	711	704	1	84	70	17	94	123	2	186	188	4	79	73	0	308	314	25	109	27
22	256	256	3	427	425	3	147	146	20	108	96	3	287	294	5	83	108	3	560	559	K=	6,L=	6
23	81	63	4	498	507	7	229	255	21	156	171	4	135	124	6	245	233	4	578	567	1	120	132
24	244	253	5	775	775	8	95	109	23	298	298	5	145	153	7	84	54	5	177	169	5	273	275

Table 2. Continued.

7	311	331	3	400	403	16	154	158	1	102	125	11	135	166	2	102	76	10	229	230	1	212	203
9	192	181	4	245	232	18	210	220	2	377	410	12	145	113	3	101	79	13	161	151	2	189	210
11	86	58	5	205	193	19	90	100	3	91	106	13	83	24	6	104	69	K=	9,L=	2	3	133	128
12	312	308	7	90	90	21	112	130	4	123	130	14	373	379	K=	8,L=	6	2	89	121	5	99	95
14	291	308	8	119	151	22	135	153	5	168	187	15	109	138	3	111	101	3	106	115	8	205	201
15	258	273	10	88	60	23	152	145	7	226	223	16	126	88	K=	9,L=	9	4	92	100	10	123	78
16	90	100	11	206	222	24	105	109	8	205	211	21	115	145	11	87	28	6	166	176	11	143	140
17	139	126	12	369	389	27	95	89	10	240	248	22	92	79	19	109	78	7	196	196	K=	10,L=	3
18	239	253	15	89	72	K=	7,L=	5	11	133	158	K=	8,L=	3	21	94	47	8	88	63	0	123	134
20	148	175	K=	6,L=	1	2	322	318	12	335	353	1	140	133	K=	9,L=	8	9	136	140	3	133	126
24	305	309	0	149	126	4	105	104	13	96	75	2	167	163	12	137	117	10	102	101	4	103	106
K=	6,L=	5	1	348	357	6	144	142	K=	7,L=	2	3	79	96	13	112	90	K=	9,L=	3	5	101	8
1	113	113	2	154	126	8	251	265	0	181	201	4	131	132	21	137	136	0	179	190	6	141	138
3	130	128	3	127	123	11	250	268	1	95	93	5	190	177	22	92	74	1	104	131	7	97	89
4	138	148	6	158	156	12	166	136	2	195	202	6	108	86	K=	9,L=	7	3	128	113	10	100	88
5	137	167	7	205	226	13	86	97	4	132	156	7	273	266	6	123	98	5	96	65	K=	10,L=	4
6	290	281	8	108	75	14	174	157	7	186	208	8	176	171	9	100	70	6	185	173	8	116	126
7	467	486	9	116	113	15	204	200	8	175	178	9	97	108	10	94	62	7	99	75	K=	10,L=	5
8	164	178	10	139	158	20	100	105	9	144	142	10	347	347	11	84	13	12	95	21	3	100	74
9	288	293	11	140	151	21	87	118	10	103	138	12	180	185	13	96	68	K=	9,L=	4	K=	10,L=	6
10	284	286	12	305	306	26	109	68	11	218	223	14	86	83	21	103	83	0	86	99	0	92	26
12	147	152	13	185	186	K=	7,L=	4	16	107	88	16	299	307	23	94	65	1	116	131	K=	11,L=	7
13	192	190	18	111	100	1	239	249	K=	7,L=	3	20	91	80	K=	9,L=	6	2	255	248	11	115	100
14	146	160	K=	6,L=	2	2	78	36	3	163	155	K=	8,L=	2	2	144	154	4	153	162	K=	11,L=	6
15	80	44	3	340	354	3	137	142	4	91	86	1	132	121	5	174	182	K=	9,L=	6	10	122	69
16	165	148	5	112	127	4	80	66	5	121	111	2	97	72	13	261	245	0	146	137	K=	11,L=	9
18	96	80	6	99	103	5	168	183	6	96	108	5	223	234	15	199	166	K=	10,L=	8	9	147	144
19	140	135	8	294	299	7	146	174	8	94	78	6	195	226	16	128	102	15	137	101	11	112	93
20	102	93	11	264	257	8	99	80	10	86	60	7	95	88	17	190	224	K=	10,L=	7	12	172	153
22	138	144	13	204	198	9	141	153	11	117	99	8	81	39	18	106	104	6	94	60	13	146	124
23	130	136	K=	6,L=	3	13	181	206	12	122	141	10	317	320	K=	9,L=	5	9	92	31	18	96	26
25	140	154	0	173	176	14	134	144	13	93	82	11	219	248	1	90	78	12	99	119	K=	11,L=	4
26	93	73	1	198	227	15	185	185	14	133	100	12	262	243	3	152	167	K=	10,L=	6	4	187	179
K=	6,L=	4	2	142	163	20	193	210	K=	7,L=	4	13	106	132	12	237	236	3	99	69	16	108	71
1	176	196	3	143	158	21	90	93	0	83	93	14	146	160	13	84	86	17	120	120	K=	11,L=	3
2	113	119	4	97	120	23	123	140	1	93	29	16	113	113	19	96	75	K=	10,L=	5	2	141	130
3	101	99	5	137	147	K=	7,L=	3	4	96	103	18	84	73	20	86	24	5	124	103	5	187	218
5	108	99	6	117	161	1	153	140	5	83	96	K=	8,L=	1	K=	9,L=	4	6	91	59	9	175	175
8	255	266	7	222	225	2	248	247	6	121	134	2	365	368	1	113	106	7	153	124	10	178	162
8	141	170	8	92	85	5	115	115	11	144	174	3	97	106	3	84	75	8	113	119	16	112	82
9	77	52	9	105	97	6	284	293	K=	7,L=	5	4	220	228	5	143	111	10	119	124	K=	11,L=	2
10	220	197	K=	6,L=	4	7	117	130	0	93	103	6	104	95	7	252	253	12	146	158	1	144	264
11	308	297	1	207	208	9	114	117	1	112	107	7	139	159	9	99	100	14	118	134	4	86	36
12	304	311	3	160	165	10	140	134	3	111	98	8	162	189	10	146	140	K=	10,L=	4	8	101	83
13	118	121	4	293	260	11	321	333	K=	7,L=	6	9	173	195	11	392	388	1	245	241	12	127	115
14	123	108	5	151	140	14	154	176	3	150	132	10	130	127	12	360	373	2	233	243	K=	11,L=	1
15	345	337	8	224	229	15	100	80	5	89	59	11	125	113	14	129	132	3	82	64	1	207	213
16	110	90	9	283	265	16	240	227	6	117	82	12	318	340	15	236	254	5	100	56	5	100	97
20	113	128	10	85	66	18	135	146	7	112	115	13	223	237	18	172	166	7	84	77	6	200	187
21	137	144	13	92	21	19	187	190	K=	7,L=	7	14	172	183	20	136	134	8	103	138	10	102	77
23	132	119	K=	6,L=	5	20	178	171	4	123	125	16	125	119	23	98	94	13	166	212	K=	11,L=	0
24	144	103	1	217	221	23	101	81	K=	7,L=	8	K=	8,L=	0	K=	9,L=	3	14	152	159	2	105	114
K=	6,L=	3	3	250	255	K=	7,L=	2	0	100	100	1	157	140	1	120	130	15	121	92	3	141	172
1	210	188	4	82	57	1	225	222	K=	8,L=	9	2	116	109	2	167	152	18	94	105	8	172	166
4	224	217	11	103	22	2	125	106	7	96	30	3	115	88	4	94	109	K=	10,L=	3	K=	11,L=	1
5	493	476	K=	6,L=	6	3	84	129	14	102	66	5	144	134	5	149	145	1	170	155	2	124	99
7	94	101	1	163	188	4	253	252	16	151	154	7	196	219	7	109	90	2	231	222	9	105	100
8	166	157	3	122	108	6	290	292	K=	8,L=	8	9	137	136	9	160	178	5	89	92	10	105	97
10	149	152	4	110	132	7	269	283	10	96	81	10	229	225	11	103	123	9	93	103	K=	11,L=	2
11	329	334	5	183	196	8	193	169	16	124	113	11	318	324	16	99	104	10	200	193	0	125	109
12	106	114	K=	6,L=	7	9	84	95	17	110	121	12	105	82	17	111	130	11	152	122	2	89	64
13	130	115	3	115	137	10	237	235	K=	8,L=	7	18	101	113	K=	9,L=	2	12	154	171	9	128	134
15	239	237	5	105	90	11	130	126	5	192	195	K=	8,L=	1	1	158	142	13	113	113	K=	11,L=	3
17	135	130	K=	7,L=	10	12	297	309	7	118	89	0	153	150	5	104	110	15	88	93	1	95	88
18	329	343	9	103	86	13	104	105	9	109	93	1	224	229	6	100	116	16	110	91	6	219	258
21	210	219	19	91	75	14	156	125	11	190	194	5	141	169	7	197	212	19	107	68	K=	11,L=	4
22	140	154	K=	7,L=	9	15	164	172	12	116	126	7	139	104	9	306	289	20	89	58	4	87	56
K=	6,L=	2	5	118	73	17	113	115	15	173	163	8	159	161	10	101	125	K=	10,L=	2	K=	12,L=	5
1	169	181	12	201	210	19	92	111	16	169	172	9	119	160	14	179	187	2	88	23	10	97	62
2	392	388	15	162	173	21	138	128	18	113	113	11	106	95	16	103	111	4	204	219	K=	12,L=	4
3	245	235	27	116	77	K=	7,L=	1	K=	8,L=	6	12	206	194	17	101	81	5	113	124	1	91	96
5	419	424	K=	7,L=	8	1	149	143	1	145	170	13	148	141	K=	9,L=	1	8	275	261	4	116	65
6	290	271	5	143	143	2	195	186	3	115	96	16	112	103	1	143	165	9	194	188	7	141	154
7	503	503	8	144	154	4	157	155	6	138	126	K=	8,L=	2	3	81	41	10	87	133	12	95	70
8	188	174	9	120	31	7	206	206	7	194	193	0	123	133	4	133	169	12	101	108	K=	12,L=	3
9	118	113	10	139	139	8	77	71	8	133	111	1	196	214	7	263	250	14	226	231	8	149	113
10	115	110	12	143	153	9	118	115	9	263	255	2	347	363	8	143	135	K=	10,L=	1	K=	12,L=	2
14	250	237	14	151	145	11	512	509	10	127	120	3	200	178	9	203	174	5	85	94	2	128	129
15	88	82	22	120	129	13	119	97	11	103	81	7	96	87	10	111	105	7	267	270	9	148	150
16	237	231	27	149	138	14	278	270	12	303	312	8	143	142	12	226	224	10	88	126	11	93	111
19	119	121	K=	7,L=	7	15	189	180	13	184	190	9	108	105	13	111	108	11	86	55	K=	12,L=	1
21	158	150	6	160	169	16	242	233	14	106	91	12	95	76	14	132	119	17	101	36	1	108	68
K=	6,L=	1	8	275	283	17	201	221	20	108	98	13	112	110	15	122	99	18	92	50	3	96	42
1	473	474	9	208	192	19	88	49	24	117	122	K=	8,L=	3	K=	9,L=	0	K=	10,L=	0	4	97	93
2	428	422	11	160	153	23	101	72	26	126	121	0	236	251	1	154	162	0	129	173	8	140	122
3	187	155	15	198	198	K=	7,L=	0	K=	8,L=	5	1	87	90	2	103	104	1	297	289	11	131	97
4	169	181	16	106	129	1	150	155	1	104	81	2	230	237	3	172	201	2	156	150	K=	12,L=	0
5	509	486	18	150	166	2	437	434	2	164	177	4	110	91	6	125	151	3	87	104	7	153	134
6	84	97	19	101	70	3	235	226	3	107	80	5	113	122	7	178	168	5	143	139	9	107	35
7	239	244	21	109	139	4	210	209	5	85	56	8	101	109	8	102	125	7	93	137	K=	12,L=	1
8	70	43	22	114	96	5	164	167	7	128	125	9	127	135	9	176	192	8	106	153	0	84	56
10	257	250	24	114	60	6	153	148	12	256	271	10	92	95	10	164	155	12	102	113	4	120	99
11	155	142	27	115	114	8	215	234	14	373	390	11	121	118	11	142	145	13	127	123	K=	12,L=	2
13	222	228	K=	7,L=	6	11	297	293	17	188	184	K=	8,L=	4	12	164	142	16	93	47	0	166	180
14	363	356	1	156	141	12	195	205	19	90	60	0	128	113	16	96	73	K=	10,L=	1	1	91	66
18	272	276	4	155	154	15	88	105	K=	8,L=	4	1	89	54	K=	9,L=	1	2	232	237	3	112	94
19	126	115	5	280	264	16	118	95	1	98	35	2	127	149	2	156	144	4	231	234	K=	12,L=	3
21	131	155	6	315	330	17	103	81	2	77	24	4	110	122	3	228	214	6	120	137	0	101	68
22	92	77	9	176	179	18	92	102	3	192	184	10	119	116	4	228	230	7	102	110	K=	13,L=	1
K=	6,L=	0	10	322	338	20	106	115	5	134	141	K=	8,L=	5	5	99	111	11	117	114	4	94	59
0	360	355	11	115	111	K=	7,L=	1	7	235	253	0	109	70	6	79	56	K=	10,L=	2	K=	13,L=	0
1	399	383	14	267	260	0	211	217	8	362	357	1	172	170	8	156	151	0	114	112	1	97	48
2	82	65	15	89	91																		

Table 3. Interatomic distances, bond angles and dihedral angles with estimated standard deviations.

DISTANCE	(Å)	DISTANCE	(Å)	DISTANCE	(Å)
O1 - CC1	1.223(6)	O2 - CC2	1.214(6)	O3 - CC3	1.219(5)
O4 - CC4	1.225(5)	O5 - CC5	1.218(6)	O6 - CC6	1.223(6)
O7 - CC7	1.224(6)	CC1 - N7	1.352(6)	CC2 - N1	1.333(6)
CC3 - N2	1.335(6)	CC4 - N3	1.336(6)	CC5 - N4	1.342(6)
CC6 - N5	1.357(6)	CC7 - N6	1.347(6)	CC1 - C1	1.531(7)
CC2 - C2	1.525(8)	CC3 - C3	1.525(8)	CC4 - C4	1.524(7)
CC5 - C5	1.530(7)	CC6 - C6	1.523(7)	CC7 - C7	1.531(7)
C1 - N1	1.449(7)	C2 - N2	1.436(6)	C3 - N3	1.438(7)
C4 - N4	1.461(6)	C5 - N5	1.467(6)	C6 - N6	1.450(6)
C7 - N7	1.446(6)	N1 - CM1	1.438(7)	N2 - CM2	1.454(7)
N3 - CM3	1.454(7)	N4 - CM4	1.438(7)	N5 - CM5	1.455(7)
N6 - CM6	1.440(7)	N7 - CM7	1.444(8)	Ow - O5	2.833(6)
Ow - O4	2.864(6)				

ANGLE	(°)	ANGLE	(°)
O1 - CC1 - C1	121.2(5)	O2 - CC2 - C2	120.1(5)
O3 - CC3 - C3	119.9(5)	O4 - CC4 - C4	120.8(5)
O5 - CC5 - C5	120.3(5)	O6 - CC6 - C6	120.1(5)
O7 - CC7 - C7	121.1(5)	O1 - CC1 - N7	122.3(5)
O2 - CC2 - N1	123.7(6)	O3 - CC3 - N2	123.0(5)
O4 - CC4 - N3	122.8(5)	O5 - CC5 - N4	123.6(5)
O6 - CC6 - N5	123.0(5)	O7 - CC7 - N6	121.5(5)
CM1 - N1 - C1	117.4(5)	CM2 - N2 - C2	115.3(5)
CM3 - N3 - C3	115.6(5)	CM4 - N4 - C4	117.8(5)
CM5 - N5 - C5	117.1(5)	CM6 - N6 - C6	116.8(5)
CM7 - N7 - C7	116.8(5)	CM1 - N1 - CC2	118.4(5)
CM2 - N2 - CC3	118.3(5)	CM3 - N3 - CC4	123.5(5)
CM4 - N4 - CC5	123.7(5)	CM5 - N5 - CC6	121.1(5)
CM6 - N6 - CC7	118.9(5)	CM7 - N7 - CC1	118.8(5)
N7 - CC1 - C1	116.4(5)	N1 - CC2 - C2	116.2(5)
N2 - CC3 - C3	117.1(5)	N3 - CC4 - C4	117.1(5)
N4 - CC5 - C5	116.8(5)	N5 - CC6 - C6	116.9(5)
N6 - CC7 - C7	117.4(5)	C1 - N1 - CC2	123.2(5)
C2 - N2 - CC3	125.3(5)	C3 - N3 - CC4	120.4(5)
C4 - N4 - CC5	118.2(4)	C5 - N5 - CC6	116.6(5)
C6 - N6 - CC7	121.7(4)	C7 - N7 - CC1	124.5(5)
CC1 - C1 - N1	112.1(5)	CC2 - C2 - N2	110.1(4)
CC3 - C3 - N3	114.1(5)	CC4 - C4 - N4	111.8(5)
CC5 - C5 - N5	109.4(4)	CC6 - C6 - N6	111.7(5)
CC7 - C7 - N7	111.2(5)	Ow - O5 - CC5	143.6(4)
Ow - O4 - CC4	139.2(4)	O5 - Ow - O4	103.8(2)

DIHEDRAL ANGLE	(°)	DIHEDRAL ANGLE	(°)
CC1 - C1 - N1 - CC2	86.7(6)	C1 - N1 - CC2 - C2	1.4(8)
N1 - CC2 - C2 - N2	179.6(5)	CC2 - C2 - N2 - CC3	-82.8(7)
C2 - N2 - CC3 - C3	-9.5(8)	N2 - CC3 - C3 - N3	-68.7(7)
CC3 - C3 - N3 - CC4	134.4(5)	C3 - N3 - CC4 - C4	175.9(5)
N3 - CC4 - C4 - N4	-175.7(4)	CC4 - C4 - N4 - CC5	-87.4(6)
C4 - N4 - CC5 - C5	-179.8(5)	N4 - CC5 - C5 - N5	168.7(5)
CC5 - N4 - N5 - CC6	63.8(7)	C5 - N5 - CC6 - C6	-161.2(4)
N5 - CC6 - C6 - N6	177.1(4)	CC6 - C6 - N6 - CC7	-72.1(6)
C6 - N6 - CC7 - C7	-13.2(7)	N6 - CC7 - C7 - N7	-163.5(5)
CC7 - C7 - N7 - CC1	-92.4(6)	C7 - N7 - CC1 - C1	-8.6(7)
N7 - CC1 - C1 - N1	179.9(5)		

Table 4.

Distance (Å)	(I)	(II)	(III)	Cycloheptasarcosyl
CC—C	1.527	1.530	1.525	1.534
CC—N	1.344	1.345	1.346	1.343
CC—O	1.228	1.232	1.224	1.221
C—N	1.456	1.453	1.454	1.449
CM—N	1.483	1.487	1.466	1.446

Table 5.

Angle (°)	(I)	(II)	(III)	Cycloheptasarcosyl
(CM—N—CC) *cis*	118.7	118.6	117.9	118.6
(CM—N—CC) *trans*	123.9	123.5	123.8	122.8
(C—N—CC) *cis*	123.8	122.8	123.5	123.7
(C—N—CC) *trans*	117.2	117.5	116.1	118.4

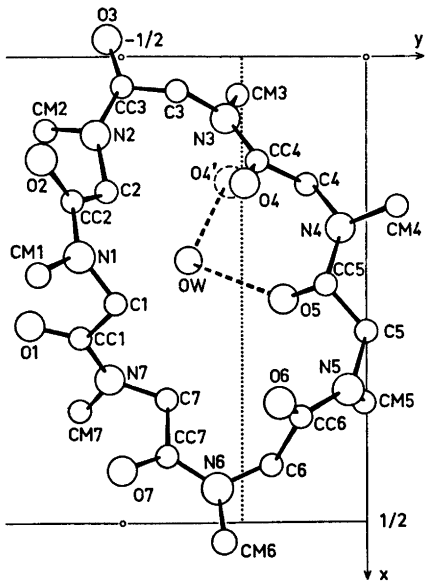

Fig. 1.

squares refinement cycle. Fig 1 shows the molecule viewed along [001].

By averaging bond distances of Table 3, and comparing with the results of the corresponding pentameric [6] (I) and octameric [5] (II) compounds, and with cycloalanyltetrasarcosyl [11] (III), no significant differences are observed (Table 4). The somewhat longer CM—N distances of (I) and (II) are possibly connected with the fact that for these compounds, methyl hydrogens were not included in the calculations. The geometry of the *cis* and *trans* *N*-methyl amide groups, respectively, is also roughly the same (Table 5).

Fig. 1 shows that the ring conformation is *cis,cis,cis,cis,trans,trans,trans*, quite unexpectedly a widely different conformation from that of cyclooctasarcosyl [5] (*cis,cis,trans,trans,cis,cis,trans,trans*).

The water molecules link glide plane equivalent molecules to endless chains along [001]. The two O···O distances are approximately equal (OW···O_5=2.833 Å; OW···O_4'=2.864 Å) and the angle O_5···OW···$O^{3'}$ is 103.8°.

Since the shortest CC···N distance across the ring is longer than 3.5 Å, no direct transannular contact can be held responsible for the rigidity of this 21-membered ring. As in earlier findings,[4–6,11] the explanation must be sought in the intrinsic conformation of the peptide chain itself.[2]

Apart from the hydrogen bonds, there are no short inter-molecular contacts.

Acknowledgement. The author thanks Cand. real. K. Titlestad for preparing the crystals.

REFERENCES

1. Dale, J. and Titlestad, K. *Chem. Commun.* (1969) 656.
2. Titlestad, K., Groth, P. and Dale, J. *Chem. Commun.* (1973) 346.
3. Titlestad, K., Groth, P. and Dale, J. *Chem. Commun.* (1973) 646.
4. Groth, P. *Acta Chem. Scand. 24* (1970) 780.
5. Groth, P. *Acta Chem. Scand. 27* (1973) 3117.
6. Groth, P. *Acta Chem. Scand. 27* (1973) 3419.
7. Germain, G., Main, P. and Woolfson, M. M. *Acta Crystallogr. A 27* (1971) 368.
8. Groth, P. *Acta Chem. Scand. 27* (1973) 1837.
9. Hanson, H. P., Herman, F., Lea, J. D. and Skillman, S. *Acta Crystallogr. 17* (1964) 1040.
10. Stewart, R. F., Davidson, E. R. and Simpson, W. T. *J. Chem. Phys. 43* (1965) 3175.
11. Groth, P. *Acta Chem. Scand. A 28* (1974) 449.

Received June 19, 1974.

Acta Chemica Scandinavica A 29 (1975) 45—50

The Structure of *N*-[3-Phenyl-5-(1,2,3,4-oxatriazolio)]-phenylamide at 105 K

T. OTTERSEN,[a] C. CHRISTOPHERSEN[b] and S. TREPPENDAHL[c]

[a] Department of Pharmacy, University of Oslo, Oslo 3, Norway, [b] Department of General and Organic Chemistry, University of Copenhagen, The H. C. Ørsted Institute, DK-2100 Copenhagen, Denmark and [c] Institute for Chemistry, Faculty of Medicine, University of Copenhagen, Rådmandsgade 71, DK-2200 Copenhagen, Denmark

The crystal and molecular structure of the *meso*-ionic title compound, $C_{13}H_{10}N_4O$, have been determined by X-ray methods using 2667 reflections above background level collected by counter methods at 105 K. The crystals are monoclinic, space group $P2_1/c$, with cell dimensions: $a=5.233(2)$ Å; $b=18.846(6)$ Å; $c=11.643(2)$ Å, $\beta=105.71°(2)$, with 4 molecules per unit cell. The structure model was refined to an *R*-factor of 0.047. In order to reduce the influence of the valence electrons all reflections with $\sin\theta/\lambda < 0.5$ Å^{-1} were excluded in the last stages of the refinement procedure (leaving 1658 F_o's, $R=0.058$). The central five-membered ring is found to be planar and the bond lengths within this ring indicate a resonance stabilized system, as has been found for sydnones. The planes of the two benzene rings are tilted 11.7 and 8.0°, respectively, with respect to the plane of the central oxatriazolio-ring.

meso-Ionic structures have recently attracted considerable interest because of their marked pharmacological activity associated with certain members of this group of organic compounds.[1] Among these compounds *O*-3-alkyl-5-(1,2,3,4-oxatriazolio)oxides have been shown to exhibit a marked hypotensive effect.[2] Molecular orbital calculations have been performed on the latter systems and a successful correlation between the predicted charge densities in these compounds and the isoelectronic sydnones, and their hypotensive potency has been obtained.[2]

Several structure investigations of sydnones have been reported.[3,4] These five-membered rings are found to be planar with bond lengths indicating a conjugated system, except for the relatively long intraring CO distance (1.40—1.42 Å). Hope and Thiessen [4] have therefore proposed I as the best single formula representation of a sydnone. This structure is in agreement with experimental evidence that the sydnone ring is aromatic and emphasize that the exocyclic C—O bond is of normal double bond length, whereas representation II [5] reflects the low bond order found for this bond by molecular orbital calculations using a normal σ-skeleton (see Ref. 2 and references therein).

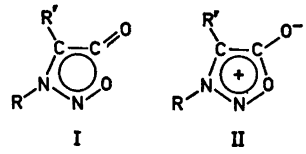

I II

The related 3-substituted *N*-[5-(1,2,3,4-oxatriazolio)]amides have attracted less interest, undoubtedly because until recently only one example of this class of compounds was recorded under this formula in the literature. However, it has been shown that a compound isolated by Busch and Becker [6] in 1896 and analogous compounds isolated by Busch and Schmidt [7] in 1929 first described as "isotetrazolon" and later as "azo-1,3-endoxy-hydrazomethylen" are 3-substituted *N*-[5-(1,2,3,4-oxatriazolio)]amides.[8] As a synthetic method for these compounds is now available [9] a systematic investigation of the structural, pharmacological, and physico-chemical properties of these compounds may be carried out.

In order to establish the constitution rigorously and to investigate the geometry of this

meso-ionic system a crystal structure investigation was undertaken. It is of interest to see if this five-membered ring system has the same structural properties as the sydnones and to get evidence about the "best" structural formula representation. These structural parameters may be helpful in the investigations of other properties of this class of compounds.

EXPERIMENTAL

The title compound [8] was recrystallized by very slow cooling of a saturated (at boiling point) solution in benzene:*cyclo*-hexane 1:2 to −20 °C.

Oscillation, Weissenberg and precession photographs indicated monoclinic symmetry; all reflections ($h0l$) for l odd and ($0k0$) for k odd, were systematically absent. This uniquely defines the space group as $P2_1/c$.

A computer-controlled Syntex-$P\bar{1}$ four-circle diffractometer with graphite-monochromatized Mo$K\alpha$ radiation and equipped with an Enraf-Nonius liquid nitrogen cooling device (modified by H. Hope) was utilized for preliminary experiments and for the measurement of diffraction intensities. The work was carried out using a crystal of dimensions $0.53 \times 0.18 \times 0.10$ mm. Unit cell parameters were determined by a least-squares treatment of the angular coordinates of fifteen symmetri-independent reflections with 2θ-values from 30 to 40°. The temperature at crystal site was 105 K.

Three-dimensional intensity data were recorded using the $\omega - 2\theta$ scanning mode with scan speed variable from 2 to 12° min^{-1}, depending on the peak intensity of the reflections. Background counting time was equal to 0.7 × scan time. Reflections with 2θ-values larger than 50° which had integrated counts of less than 8 cps, determined in a 2 s scan over the reflection, were not measured. The variations in the intensities of three standard reflections which were remeasured after every hundred reflections were random and less than three times their standard deviations. Accordingly no corrections were applied for these variations.

The estimated standard deviations were taken as the square root of the total counts with a 2 % addition for experimental uncertainties. Of the 3196 symmetry-independent reflections measured ($2\theta_{max} = 80°$), 2667 had intensities larger than twice their standard deviations. These were regarded as "observed" reflections, and the remaining reflections were excluded from further calculations. The intensities were corrected for Lorentz and polarization effects. The computer program used, as well as programs subsequently employed, is part of a local assembly of computer programs for CYBER-74 and is described in Ref. 10.

The atomic scattering factors used were those of Doyle and Turner [11] for carbon, oxygen and nitrogen, and of Stewart *et al.*[12] for hydrogen.

CRYSTAL DATA

N-[3-Phenyl-5-(1,2,3,4-oxatriazolio)]phenylamide, $C_{13}H_{10}N_4O$, monoclinic. Cell dimensions at 105 K:

$a = 5.233(.002)$ Å; $b = 18.846(.006)$ Å;
$c = 11.643(.002)$ Å; $\beta = 105.71(.02)°$.

Figures in parentheses are estimated standard deviations.

$V = 1105.2$ Å^3, $M = 238.2$ amu; $Z = 4$;
$D_{calc} = 1.431$ g/cm^3; $F(000) = 496$.

Absent reflections: ($h0l$) for l odd; ($0k0$) for k odd; space group $P2_1/c$.

STRUCTURE DETERMINATION AND REFINEMENTS

The phase problem was solved by a computer procedure [13] based on direct methods utilizing tangent refinement.

The structure model was refined to a conventional R of 0.11. At this point the hydrogen

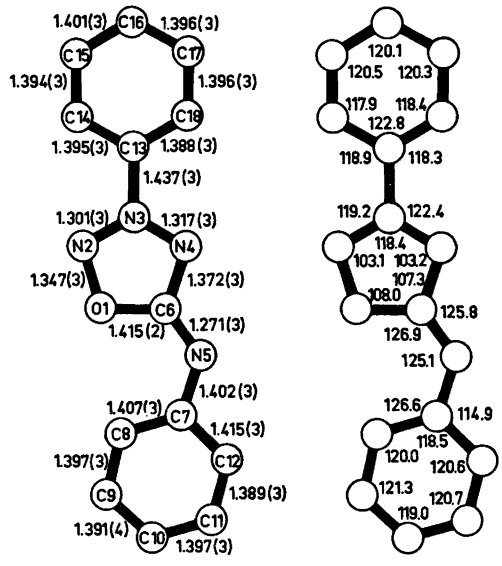

Fig. 1. Bond lengths (Å) with estimated standard deviations (Å × 10^3 in parentheses), and bond angles (°). E.s.d.'s in bond angles are 0.2°. Structure model obtained using high-angle data only in the refinement.

Table 1. Fractional atomic coordinates and thermal parameters with estimated standard deviations ($\times 10^5$) for non-hydrogen atoms. The temperature factor is given by $\exp -(B_{11}h^2+B_{22}k^2+B_{33}l^2+B_{12}hk+B_{13}hl+B_{23}kl)$. Results from the refinement using high-angle data only.

Atom	x	y	z	B_{11}	B_{22}	B_{33}	B_{12}	B_{13}	B_{23}
O1	33817(41)	94083(10)	88797(16)	1821(58)	128(4)	196(10)	236(25)	257(37)	3(10)
N2	13470(38)	98861(10)	87737(14)	1935(61)	126(4)	218(9)	183(24)	274(37)	−16(10)
N3	3033(45)	99225(11)	76263(16)	1659(64)	89(5)	180(10)	15(28)	299(38)	−11(11)
N4	13630(37)	95395(10)	69274(14)	1649(55)	108(4)	203(9)	183(25)	282(34)	2(9)
N5	50464(43)	87727(11)	74440(16)	1829(61)	120(4)	216(10)	287(27)	387(38)	42(10)
C6	34146(46)	91961(12)	77179(18)	1619(66)	103(4)	210(10)	103(27)	269(40)	32(11)
C7	71146(41)	84188(11)	82632(17)	1436(62)	92(4)	250(11)	32(26)	395(41)	42(11)
C8	76142(47)	84185(13)	95127(19)	1629(68)	137(5)	256(11)	104(31)	266(43)	36(13)
C9	97660(50)	80378(13)	102138(19)	1821(69)	117(5)	277(12)	−57(31)	66(46)	39(12)
C10	114545(48)	76578(13)	97022(22)	1578(67)	109(5)	363(14)	−15(30)	−104(48)	20(13)
C11	109822(49)	76615(13)	84626(21)	1690(68)	113(5)	374(14)	120(30)	242(49)	−5(13)
C12	88418(46)	80319(13)	77474(19)	1654(70)	109(5)	303(12)	117(30)	318(46)	0(12)
C13	−19048(41)	103906(11)	71654(17)	1339(59)	81(4)	216(10)	−17(24)	252(38)	−7(10)
C14	−32013(46)	106844(12)	79533(18)	1576(64)	106(5)	252(11)	75(28)	466(42)	−18(11)
C15	−53141(47)	111445(12)	74898(21)	1598(69)	115(5)	343(13)	146(29)	502(48)	−10(13)
C16	−61185(47)	112943(13)	62662(21)	1531(67)	106(5)	342(13)	130(29)	313(46)	13(12)
C17	−47805(48)	109906(13)	55017(19)	1726(70)	110(5)	267(11)	142(29)	163(44)	18(12)
C18	−26419(44)	105344(12)	59506(17)	1571(64)	103(5)	218(11)	35(27)	312(41)	0(11)

Table 2. Fractional atomic coordinates ($\times 10^3$) and isotropic thermal parameters with estimated standard deviations for hydrogen atoms. Results from the refinement using all observed data.

Atom	x	y	z	B
H19	643(4)	868(1)	987(2)	2.6(5)
H20	1012(4)	805(1)	1105(2)	2.4(4)
H21	1292(4)	741(1)	1018(2)	2.1(4)
H22	1218(4)	742(1)	810(2)	2.1(4)
H23	843(4)	802(1)	690(2)	2.7(5)
H24	−254(4)	1058(1)	877(2)	2.3(4)
H25	−614(4)	1136(1)	799(2)	2.4(4)
H26	−762(4)	1160(1)	598(2)	1.9(4)
H27	−533(4)	1109(1)	467(2)	2.5(4)
H28	−163(4)	1033(1)	544(2)	2.3(4)

atoms were placed in calculated positions and anisotropic thermal parameters for all nonhydrogen atoms were introduced. Full-matrix least-squares refinement of all positional parameters, anisotropic thermal parameters for nonhydrogen atoms and isotropic thermal parameters for hydrogen atoms using all observed reflections converged to a weighted R_w of 0.047 and a conventional R of 0.054.

Earlier structure determinations [14–16] have indicated that structural parameters found for molecular systems like the present one are significantly influenced by the asphericity of the valence electron densities. By a systematic variation of the lower sin θ/λ cutoff for reflections used in the refinement, it was found that this asphericity had little or no effect when all reflections with sin $\theta/\lambda < 0.5$ were excluded from the refinements. This is in agreement with earlier results.[16,17] Least-squares refinement of all parameters (s) involving non-hydrogen atoms using the 1658 observed reflections (m) with sin $\theta/\lambda > 0.5$ resulted in a conventional R of 0.058, an R_w of 0.055, and an R-factor for the total data set of 0.063. The "goodness of fit" $(\{\sum w(F_o - |F_c|)^2/(m-s)\}^{\frac{1}{2}})$ is 1.20. Atomic parameters for non-hydrogen atoms, obtained in this refinement are listed in Table 1, and parameters for hydrogen atoms, from the refinement using all observed reflections, are given in Table 2. A listing of observed and calculated structure factors is available from the authors upon request.*

* Also available from Department of Chemistry, University of Oslo, Oslo 3, Norway.

Standard deviations in molecular parameters were calculated from the correlation matrix ignoring standard deviations in cell parameters.

The r.m.s. difference between the observed U_{ij}'s and those calculated from the "rigid body" model [24] is 0.0014 Å^2. However, the corrections in atomic positional parameter for the librational motion are extremely small, giving maximum corrections in bond lengths of 0.001 Å; these corrections are, therefore, not included.

Table 3. Deviations (Å $\times 10^3$) from least-squares planes through the three ring systems. The deviations for those atoms used to define the plane are given in italicized figures.

Atom	Deviations (Å $\times 10^3$) Plane A	Plane B	Plane C
O1	*5*	−291	
N2	*−5*		−262
N3	*2*		−9
N4	*2*	−103	197
N5	−34	−1	
C6	*−6*	−115	
C7	−25	*2*	
C8		*−3*	
C9		*1*	
C10		*3*	
C11		*−4*	
C12		*2*	
C13	−28		*1*
C14			*4*
C15			*−6*
C16			*3*
C17			*2*
C18			*−3*

Angle between plane A and plane B: 8.0°
Angle between plane A and plane C: 11.7°

Table 4. Selected dihedral angles (°) with estimated standard deviations. The angles are positive in a right-hand screw.

Dihedral angle	(°)
C7−N5−C6−O1	1.6(4)
C7−N5−C6−N4	−179.2(2)
C6−N5−C7−C8	5.8(4)
C6−N5−C7−C12	−173.8(2)
N4−N3−C13−C18	−11.3(3)
N2−N3−C13−C14	−12.6(3)

DISCUSSION

Bond lengths and bond angles are given in Fig. 1, where the numbering of the atoms is indicated. Deviations from least-squares planes through the three rings are listed in Table 3 and some selected dihedral angles in Table 4.

The central oxatriazolio ring is planar while the two atoms (N5 and C7) bonded to this ring deviate significantly from the least-squares plane through the five ring atoms. The planes of the two phenyl groups are twisted only 8.0° (C7—C12) and 11.7° (C13—C18) with respect to the central ring. However, the two bonds C7—N5 and C13—N3 which connect the two phenyl groups with the central *meso*-ionic system are relatively long (1.402 Å and 1.437 Å, respectively) and may indicate that there is only a small, if any, coupling between the conjugation in the two phenyl rings and in the central ring system. Furthermore there is the "pure" C6—N5 double bond.

The N—N, N—C, and N—O bonds in the central ring indicate a conjugated system. They may be compared with the N—N bond in pyridazine (1.330 Å) [18] and *s*-tetrazine (1.321 Å),[19] the C—N bonds in a series of 3,6-pyridazindiones [14–16,20] (1.345—1.374 Å), and the N—O bond in 1,2,5-oxadiazole (1.380 Å).[21] However, the C—O bond of 1.415 Å is very much longer than that in furan [22] (1.36 Å), while the exocyclic C=N distance (1.271 Å) is close to the pure C—N double bond of 1.278 Å.[23] A similar situation is found for the sydnones [3,4] and in these compounds are the exocyclic ∠C—C—O opened to about 135—137°. An opening of the corresponding ∠N4—C6—N5 is not found in the present oxatriazolio-amide. The ∠O1—C6—N5 and the ∠N4—C6—N5 are almost equal (126.9 and 125.8°, respectively). Further, the angles in the central ring deviate significantly from the corresponding angles in the sydnones,[3,4] *e.g.* the angle at O1 is 108° while it is 111° in the latter structures.

Although the angles around C6 are not distorted in the same manner as in sydnones, the long O1—C6 distance and the pure N5=C6 double bond imply an electronic structure close to that of the sydnones. The "best" single formula representation of the oxatriazolioamide system is probably III in agreement to that proposed for sydnones [4] (I). This representation

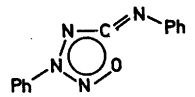

III

is only meant to emphasize that the C=N bond is of normal double bond length. A formula representation similar to II will be in sharp contradiction to this observation.

As was pointed out by Hope and Thiessen,[4] a literal interpretation of this formula (III) will give a net positive charge of 0.8 e on N3 and an equal negative charge distributed over the other ring atoms.

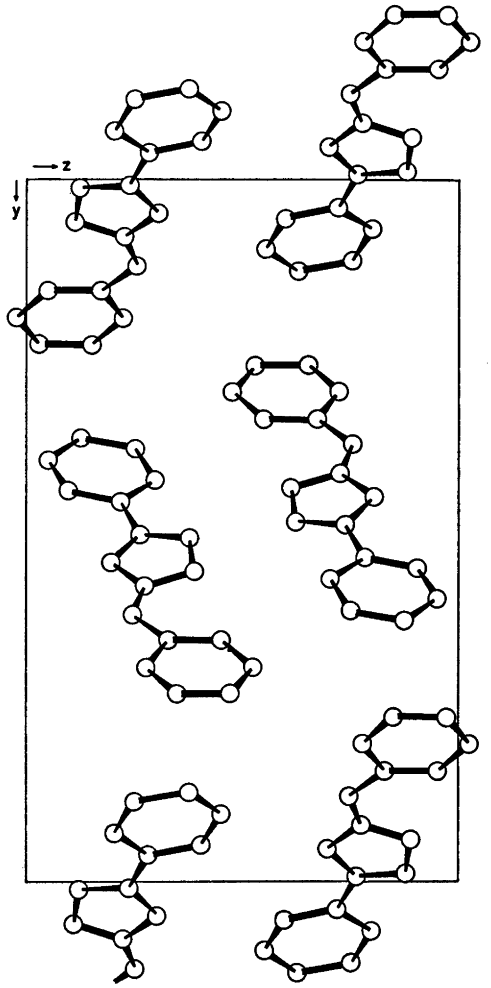

Fig. 2. The crystal structure as seen along the *a*-axis.

The C7—C12 phenyl ring has a mean bond length of 1.399 Å with an r.m.s. deviation of 0.009 Å. The two bonds C7—C8 and C7—C12 are slightly longer than this (1.407 and 1.415 Å, respectively) and may indicate a distortion around C7 caused by the amide group. The opening of ∠N5—C7—C8 to 126.6° is probably caused by repulsion between the hydrogen bonded to C8 (H19) and O1. The other phenyl ring is normal, mean bond length 1.395 Å with an r.m.s. deviation of 0.004 Å.

A view of the molecular packing in the crystal is given in Fig. 2. The packing is dominated by van der Waals forces with many short intermolecular contacts.

REFERENCES

1. Thomas, T. L., Fedorchuk, M., Shetty, B. V. and Anderson, F. E. *J. Med. Chem. 13* (1970) 196.
2. Kier, L. B., Al-Shamma, A., Hahn, R. and Tye, A. *J. Pharm. Sci. 55* (1966) 1467.
3. Bärnighausen, H., Jellinek, F., Munnik, J., and Vos, A. *Acta Crystallogr. 16* (1962) 471.
4. Hope, H. and Thiessen, W. *Acta Crystallogr. B 25* (1969) 1237.
5. Baker, W., Ollis, W. D. and Poole, V. D. *J. Chem. Soc.* (1949) 307.
6. Busch, M. and Baker, J. *Ber. Deut. Chem. Ges. 29* (1896) 1686.
7. Busch, M. and Schmidt, W. *Ber. Deut. Chem. Ges. 62* (1929) 1449.
8. Christophersen, C. and Treppendahl, S. *Acta Chem. Scand. 25* (1971) 625.
9. Christophersen, C. and Treppendahl, S. *Acta Chem. Scand. 26* (1972) 858.
10. Groth, P. *Acta Chem. Scand. 27* (1973) 1837.
11. Doyle, P. A. and Turner, P. S. *Acta Crystallogr. A 24* (1968) 390.
12. Stewart, R. F., Davidson, E. R. and Simpson, W. T. *J. Chem. Phys. 42* (1965) 3175.
13. Germaín, G., Main, P. and Woolfsoon, M. M. *Acta Crystallogr. A 27* (1971) 368.
14. Ottersen, T. *Acta Chem. Scand. 27* (1973) 797.
15. Ottersen, T. *Acta Chem. Scand. A 28* (1974) 661.
16. Ottersen, T. *Acta Chem. Scand. A 28* (1974) 666.
17. Ottersen, T. *Acta Chem. Scand. A 28* (1974) 1145.
18. Werner, W., Dreizler, D. and Rudolph, H. O. *Z. Naturforsch. 22a* (1967) 531.
19. Bertinotti, F., Giacomello, G. and Liquori, A. M. *Acta Crystallogr. 9* (1956) 510.
20. Ottersen, T. *Acta Chem. Scand. 27* (1973) 835.
21. Saegebarth, E. and Cox, A. P. *J. Chem. Phys. 43* (1965) 166.
22. Bak, B., Christensen, D., Dixon, W. B., Hansen-Nygaard, L., Rastrup-Andersen, J. and Schoffländer, M. *J. Mol. Spectrosc. 9* (1962) 124.
23. Fischers-Hjalmars, I, and Sundbom, M. *Acta Chem. Scand. 22* (1968) 2237.
24. Shoemaker, V. and Trueblood, K. N. *Acta Crystallogr. B 24* (1968) 63.

Received July 29, 1974.

Acta Chemica Scandinavica A 29 (1975) 51—59

The Crystal Structure of Thallium(I) Diisobutyldithiocarbamate

HELGA ANACKER-EICKHOFF, PER JENNISCHE and ROLF HESSE

Institute of Chemistry, University of Uppsala, Box 531, S-751 21 Uppsala, Sweden.

The crystal structure of thallium(I) diisobutyldithiocarbamate, $Tl(I)S_2CN(C_4H_9)_2$, has been determined from three-dimensional X-ray data. The crystals are triclinic, space group $P\bar{1}$. Unit cell parameters:

$a=7.866(2)$ Å, $b=13.945(3)$ Å, $c=6.218(2)$ Å, $\alpha=89.27(1)°$, $\beta=93.06(1)°$, $\gamma=103.29(2)°$.

There are two formula units per elementary cell. The structure may be regarded as consisting of dimers with the composition $[TlS_2CN(C_4H_9)_2]_2$ linked by thallium-sulfur coordination in linear strings in the c direction. The thallium-sulfur coordination is five-fold. The metal-metal distance within the dimer is 3.678(2) Å, whereas the shortest distance between metal atoms in different dimers is 5.193(2) Å. The metal atom arrangement thus consists of distinct pairs. The dimeric unit is rather similar to that of thallium diisopropyldithiocarbamate, but the orientation of the dimers in the strings and the metal atom arrangement are quite different. The difference between the structures is discussed with respect to the space requirement of the alkyl ligands.

The structures of several thallium(I) dialkyldithiocarbamates have been determined by the present research group.[1–5] All of these compounds may be considered as built from dimeric molecules linked by thallium-sulfur coordination. The nature of the linkage is, however, rather different, apparently depending on the length of the alkyl ligands. The resulting metal atom arrangement changes from a two-dimensional network of metal atoms in the methyl compound to chains in the two propyl compounds. The coordination numbers also decrease in the series. Since it could be expected that this process would continue with still larger ligands the present compound has been investigated.

UNIT CELL AND SYMMETRY

Formula unit: $Tl(I)S_2CN(C_4H_9)_2$
Crystal system: triclinic
Unit cell parameters:
$a=7.866\pm0.002$ Å, $b=13.945\pm0.003$ Å,
$c=6.218\pm0.002$ Å, $\alpha=89.27\pm0.01°$
$\beta=93.06\pm0.01°$ $\gamma=103.29\pm0.02°$
Volume of unit cell: 662.8 Å^3
Density (measured): 2.034 g cm^{-3}
Number of formula units per unit cell: 2
Density (calculated): 2.049 g cm^{-3}
Space group: $P\bar{1}$

EXPERIMENTAL

Crystals of thallium(I) diisobutyldithiocarbamate were prepared according to the method published by Åkerström.[6] They were crystallized from acetone and benzene (1:1) as long pale yellow needles with the needle axis parallel to the c axis. Their density was determined by the flotation method using an aqueous solution of K_2HgI_4. The unit cell dimensions were determined from a Guinier-Hägg powder photograph taken with $CrK\alpha_1$ radiation ($\lambda=2.2896$ Å) with silicon ($a=5.4305$ Å) [7] as internal standard.

For the intensity data, $CuK\alpha$ radiation was used. The X-ray reflections were recorded on equi-inclination Weissenberg photographs using the multiple film technique (five films). With the crystal rotating about the needle axis the layers $0\leq l\leq 4$ were recorded. The crystals were found to decompose slowly in the X-ray beam, and for that reason four crystals were used for the exposures. Details of the crystals are given in Table 1. In all 1409 independent reflections were recorded.

The relative intensities of the reflections were measured with an automatic film scanner SAAB AFS MK II,[8,9] connected on-line to an IBM 1800 processor controller at this Institute. They were corrected for Lorentz and polarisation effects but not for absorption and extinction.

Table 1. Crystals used for the exposures.

Crystal	Dimensions in mm			Layers recorded	Number of reflections
1	0.038	0.045	0.150	*hk*0, *hk*1	547
2	0.050	0.060	0.154	*hk*2, *hk*3	613
3	0.038	0.033	0.108	*hk*4	222
4	0.020	0.028	0.108	interlayer scaling	81

The usual orientation of the film, with the central line parallel to the scanning direction, allows an interval of 185° to be measured. In order to obtain sufficient overlap for the scaling of the two halves of each layer from the triclinic crystal it was necessary to increase the scanning area. By scanning the film with the central line normal to the scanning direction, *i.e.* parallel to the drum axis, it was possible to measure the entire recorded area, corresponding to a crystal rotation of 220°. The indexing was then performed by hand. For the calculation of the integrated intensities the computer programs written by Werner [9] were used. The parameters for the integration procedure were the same as those used in a previous determination at this Institute.[1] A correction factor (FK = 0.5) for the intensities of the strong reflections was applied as suggested by Werner [10] from a study of film factors. The area of integration for each reflection was large enough to include both the α_1 and the α_2 component. The film factors were initially calculated using standard methods, but they differed somewhat from those usually obtained. After the determination of the atomic positions the film factors were therefore systematically varied as will be described later.

Interlayer scale factors were obtained by exposing reflections from all the layers on the same film set. Only small changes in these values were noticed when the individual scale factors were included in the final refinement.

DETERMINATION OF THE ATOMIC POSITIONS

The approximate positions of the thallium and sulfur atoms were found from three-dimensional Patterson syntheses. The coordinates of these atoms were refined by the method of least squares. The nitrogen and carbon atoms were located in a three-dimensional difference synthesis. No attempt was made to locate the hydrogen atoms.

Table 2. Atomic coordinates and thermal parameters, listed as isotropic B or anisotropic b_{ij}. The anisotropic temperature factor is defined as $\exp(-b_{11}hh - 2b_{12}hk \cdots)$. The standard deviation corresponding to the last digit is shown in parentheses.

Atom	x	y	z	B (Å^2)
Tl	0.1897(1)	−0.01149(7)	−0.1499(2)	
S_1	0.1014(7)	0.1834(4)	−0.0441(10)	
S_2	0.1790(8)	0.0604(4)	0.3218(11)	
C_0	0.2099(23)	0.1742(13)	0.1995(37)	2.2(3)
N	0.3237(19)	0.2525(11)	0.2865(30)	2.2(3)
C_{11}	0.3479(26)	0.3505(14)	0.1868(37)	3.9(4)
C_{21}	0.4292(26)	0.2436(15)	0.4870(40)	2.8(4)
C_{12}	0.2078(28)	0.4047(16)	0.2418(43)	3.2(4)
C_{22}	0.5925(27)	0.2042(15)	0.4434(41)	2.9(4)
C_{13}	0.2381(38)	0.5037(21)	0.1312(52)	4.8(6)
C_{23}	0.6876(47)	0.1914(27)	0.6606(65)	6.8(8)
C_{14}	0.2000(37)	0.4176(21)	0.4891(53)	5.0(6)
C_{24}	0.7136(35)	0.2728(20)	0.2888(51)	4.6(6)

Atom	b_{11}	b_{22}	b_{33}	b_{12}	b_{13}	b_{23}
Tl	0.0140(2)	0.00370(5)	0.0135(37)	0.00071(5)	0.0009(1)	−0.0015(1)
S_1	0.0171(10)	0.0068(3)	0.0068(43)	−0.0004(4)	−0.0047(11)	−0.0001(5)
S_2	0.0208(12)	0.0025(2)	0.0084(44)	−0.0018(4)	−0.0075(11)	−0.00002(50)

Table 3. Observed and calculated structure amplitudes. Reflections marked with an asterisk were not included in the refinement.

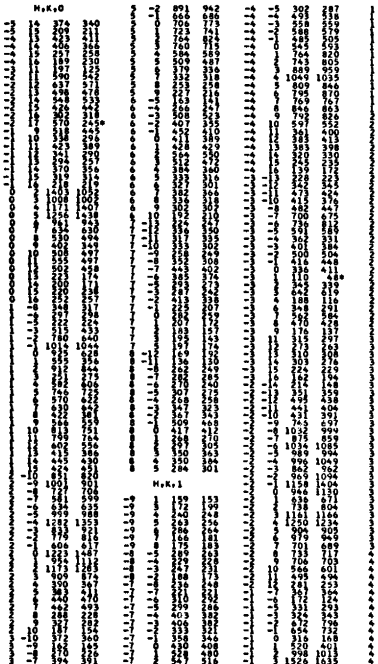

The coordinates and isotropic temperature factors of all but the hydrogen atoms were refined by the method of least squares using a full matrix program. In the expression minimized, $\sum\omega(|F_o|-|F_c|)^2$, the weights, ω, were calculated according to the equation suggested by Cruickshank *et al.*[11] $\omega=1/(a+|F_o|+c|F_c|^2+d|F_o|^3)$. The constants used were $a=40.0$, $c=0.0154$, $d=0.0$. Atomic scattering factors for the neutral elements obtained from Hanson *et al.*[12] were used with addition of the real part of the dispersion correction.[13] The discrepancy index $R=\sum(|F_o|-|F_c|)/\sum|F_o|$, was then 0.114. The nine scale factors and the anisotropic temperature factors for the thallium and sulfur atoms were then included in the refinement. The imaginary part of the dispersion correction for thallium was then applied.[13] The least-squares calculations were continued until the shifts on the parameters were less than one percent of

Table 3. Continued.

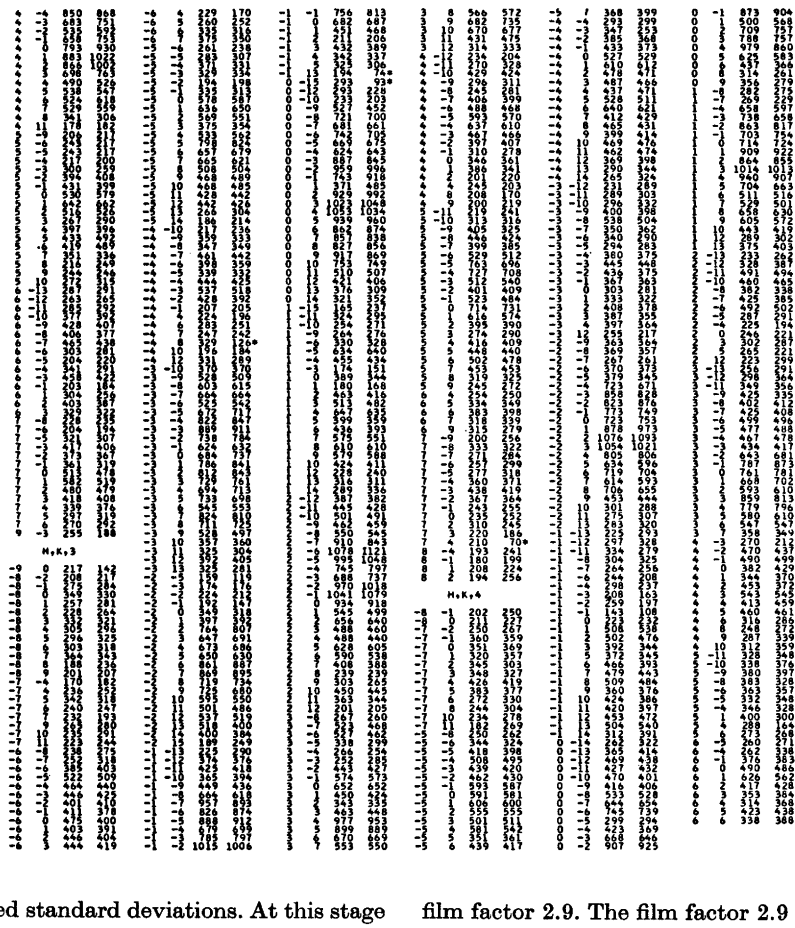

the estimated standard deviations. At this stage of the refinement the discrepancy index R was 0.087.

As mentioned above the film factors seemed to be somewhat lower than those usually observed, *e.g.* 2.3 for the zero layer. The errors appeared to be associated with a systematic underestimation of the intensities of the strong reflections. New sets of observed intensities were calculated using the film factors 2.5, 2.7, 2.9, 3.1 for the zero layer. The film factors for the layers $l=1,2,3$ were determined by interpolation between the selected value for $l=0$ and the film factor for $l=4$ which was held constant at the observed value 3.25. For each of these sets of intensities three additional cycles of refinement were run. The R value decreased continuously to 0.063 for the zero-layer film factor 3.1 but was only sligthly higher, 0.065, for the film factor 2.9. The film factor 2.9 which agrees well with the published value 2.93 for the film used,[14] Ilford Industrial G, was then selected as the final value. Changes in the atomic coordinates were negligible.

The final atomic and thermal parameters are shown in Table 2. The observed and calculated structure amplitudes are listed in Table 3 and the interatomic distances and angles in Table 4.

DESCRIPTION AND DISCUSSION OF THE STRUCTURE

General features. The structure consists of centrosymmetric dimeric molecules $[TlS_2CN(C_4H_9)_2]_2$. There is one such molecule in the unit cell. The molecule is shown in Fig. 1 which also shows the notation of the atoms. The arrangement of the molecules is illustrated in Fig. 2.

Table 4. Distances and angles. The notation used is shown in Fig. 1. Atoms which have been transformed according to the centrosymmetry are denoted by a bar. An asterisk represents the translation −**c**.

(a) Metal-metal distance

Atoms	Distance(Å)
$Tl-\overline{Tl}$	3.678(2)

(b) Distances and angles of coordination.

Atoms	Distance(Å)	Atoms	Angle(°)	Atoms	Angle(°)
$Tl-S_1$	3.043(5)	$S_1-Tl-\overline{S}_1$	107.6(1)	$S_2-Tl-\overline{S}_2$	105.7(2)
$Tl-\overline{S}_1$	3.184(5)	S_1-Tl-S_2	57.2(2)	$\overline{S}_1-Tl-\overline{S}_2$	57.3(2)
$Tl-S_2$	3.123(6)	$\overline{S}_1-Tl-S_2$	77.8(2)	$S_1-Tl-\overline{S}_2$	82.5(2)
$Tl-\overline{S}_2$	2.966(6)	S_1-Tl-S_2*	86.6(2)	$\overline{S}_1-Tl-S_2*$	123.2(2)
$Tl-S_2*$	3.424(7)	S_2-Tl-S_2*	143.5(2)	$\overline{S}_2-Tl-S_2*$	71.5(2)

(c) Distances and angles in the dithiocarbamate ligand

Atoms	Distance(Å)	Atoms	Angle(°)	Atoms	Angle(°)
S_1-C_0	1.72(2)	$Tl-S_1-C_0$	85.4(6)	$Tl-\overline{S}_1-C_0$	83.0(6)
S_2-C_0	1.72(2)	$Tl-S_2-C_0$	82.8(8)	$Tl-\overline{S}_2-C_0$	89.9(7)
C_0-N	1.34(2)	$S_1-C_0-S_2$	118(1)	S_1-C_0-N	121(2)
$N-C_{11}$	1.47(3)	S_2-C_0-N	121(2)	C_0-N-C_{11}	121(2)
$N-C_{21}$	1.48(3)	C_0-N-C_{21}	121(2)	$C_{11}-N-C_{21}$	117(2)
$C_{11}-C_{12}$	1.53(3)	$N-C_{11}-C_{12}$	113(2)	$N-C_{21}-C_{22}$	112(2)
$C_{12}-C_{13}$	1.51(4)	$C_{11}-C_{12}-C_{13}$	111(2)	$C_{11}-C_{12}-C_{14}$	112(2)
$C_{12}-C_{14}$	1.56(4)	$C_{13}-C_{12}-C_{14}$	110(2)		
$C_{21}-C_{22}$	1.55(3)	$C_{21}-C_{22}-C_{23}$	108(2)	$C_{21}-C_{22}-C_{24}$	112(2)
$C_{22}-C_{23}$	1.54(5)	$C_{23}-C_{22}-C_{24}$	112(2)		
$C_{22}-C_{24}$	1.55(4)				

(d) Intermolecular distances less than 4.0 Å. The relation of the second atom to the coordinates x,y,z of Table 2 is shown.

Atoms		Distance (Å)
Tl	$S_2(x,y,z-1)$	3.424
S_1	$C_{23}(x-1,y,z-1)$	3.674
S_2	$S_2(-x,-y,1-z)$	3.750
S_2	$C_{23}(1-x,-y,1-z)$	3.887
C_{12}	$C_{24}(x-1,y,z)$	3.924
C_{11}	$C_{11}(x,y,z-1)$	3.950
C_{13}	$C_{13}(-x,1-y,-z)$	3.984

It follows from the triclinic space group that all of the molecules are parallel. The central parts of the molecules are located close to the *ca* plane. The bulky organic ligands project from both sides of this plane to completely exclude any other interaction than van der Waals forces between dimers in different planes. In these planes the dimers are linked together by metal-sulfur interaction to form linear strings running in the *c* direction.

The dimer. The distances and angles in the dimeric unit are presented in Table 4. The two formula units are related by a centre of symmetry. The thallium and sulfur atoms in the central part of the dimer can be described as a bipyramid with a sulfur parallelogram as the common basis. This parallelogram has nearly rectangular shape; the corner angles are 87.9 and 92.1°, and the length of the edges 3.96 and 2.95 Å. The shorter edge corresponds to the sulfur-sulfur distances within the dithiocarbamate ligand. The distances from each metal

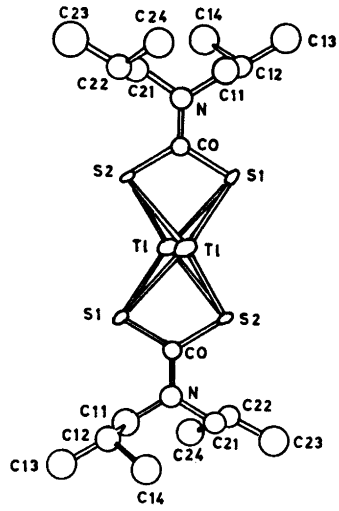

Fig. 1. The dimeric molecule in thallium(I) diisobutyldithiocarbamate. The sulfur plane coincides with the paper plane. The atomic notation is shown.

atom to the four sulfur atoms are 2.966(6), 3.043(5), 3.123(6), and 3.184(5) Å. (see Table 4b and Fig. 3). The line connecting the two thallium atoms is nearly perpendicular to the plane of the sulfur atoms (angle plane-line 87.7°). The metal-metal distance in the dimer is 3.678(2) Å.

The central part (S_1, S_2, C_0, N, C_{11}, C_{21}) of the dithiocarbamate ligand is almost planar; none of the atoms deviates more than 0.05 Å from the calculated least-squares plane (see Table 5). This plane is inclined by 6.6° (dihedral angle) to the central sulfur plane of the dimer. It passes close (0.23 Å) to the centre of the dimer. As is seen from Table 5 the outer parts of the isobutyl groups are situated on opposite sides of the central ligand plane. The nitrogen atom and the atoms C_{11}, C_{12}, C_{13} and C_{21}, C_{22}, C_{23}, respectively, form almost planar zig-zag chains (see also Fig. 1). The dihedral angles between these planes and the central ligand plane are almost equal, 83.3 and 82.5°, respectively.

Coordination. The metal atoms have five-fold sulfur coordination. The coordination poly-

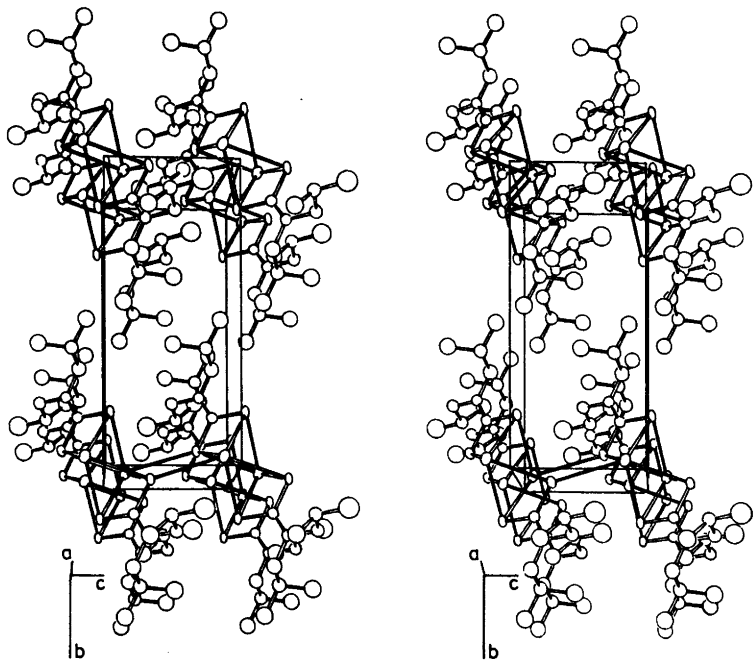

Fig. 2. Stereoscopic illustration of the unit cell. Eight dimers are shown. The linkage is indicated by solid lines between one pair of dimers.

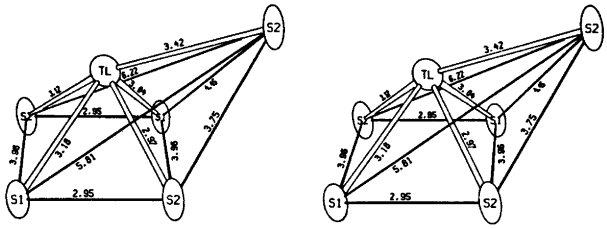

Fig. 3. Stereoscopic illustration of the coordination polyhedron.

hedron is a skew tetragonal pyramid as shown in Fig. 3. The four sulfur atoms in the dimer form the basal plane. The more distant fifth atom belongs to another dimer which is related by a unit translation in the *c* direction. All other sulfur atoms are more than 5.7 Å away. The coordination is such that more than half of the coordination sphere of the thallium atom is empty.

The irregular coordination environments known for a number of thallium(I) compounds have been associated with the outer pair of *s*-electrons ($6s^2$).[15] Mixed *s-p* metal orbitals may give stabilisation energy in antisymmetric environments. One example is salicylato-(1,10-phenanthroline)thallium(I) [16] where the metal coordination in the dimeric molecules is five-fold, and the coordinated atoms are all situated in one half sphere around the metal atom. The large region free from coordination was attributed to the presence of a stereochemically active $6s^2$ electron pair. This compound is similar to thallium(I) diisobutyldithiocarbamate as to the presence of large ligands.

It is interesting to note that the coordination number increases in the dialkyldithiocarbamates of thallium(I) as the length of ligands decreases. The coordination numbers are thus six and seven, respectively, in the ethyl and methyl compounds. Also the coordinated atoms become more regularly disposed in space. The shorter ligands allow the metal atoms to coordinate sulfur atoms from other dimeric molecules more easily. This group of compounds evidently represents a case where the irregular coordination environment of thallium(I) may not be attributed solely to the inert electron pair. The packing characteristics of the dimeric molecules strongly influence the structure as will be shown below.

The metal atom arrangement and the linking of the dimers. As mentioned above, the distances between the two thallium atoms in the dimeric unit is 3.68 Å, which is somewhat longer than the interatomic distance in metallic thallium (3.41 Å).[17] There are no other metal-metal distances shorter than 5 Å in the present compound. The metal arrangement thus consists of distinct pairs of thallium atoms.

The thallium dialkyl dithiocarbamates investigated by this research group all contain dimers with similar central parts.[1–5] It is then interesting to find that the arrangements of the metal atoms are quite different. Of the compounds studied the pair arrangement observed in thallium diisobutyldithiocarbamate apparent-

Table 5. Deviations from the least squares planes I, II and III defined by the atoms S_1, S_2, C_0, N, C_{11}, C_{21} (I); N, C_{11}, C_{12}, C_{13} (II); N, C_{21}, C_{22}, C_{23} (III).

Plane I		Plane II		Plane III	
Atoms	Dev. (Å)	Atoms	Dev. (Å)	Atoms	Dev. (Å)
S_1	0.047	N	0.007	N	0.022
S_2	−0.027	C_{11}	−0.007	C_{21}	0.023
N	−0.004	C_{12}	−0.006	C_{22}	0.019
C_0	−0.026	C_{13}	0.006	C_{23}	−0.020
C_{11}	−0.038				
C_{21}	0.049				

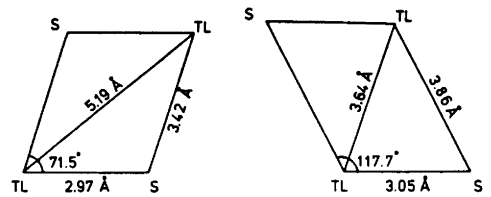

Fig. 4. The linking parallelograms in thallium(I) diisobutyldithiocarbamate (left) and thallium(I) diisopropyldithiocarbamate (right).

ly represents an end point in a breaking-up process starting with the two-dimensional net arrangement found in thallium dimethyldithiocarbamate.[1] The zig-zag chains found in the ethyl,[2] propyl,[3] and the isopropyl [4] compounds are intermediate steps in this process. The metal atom arrangement in these compounds is thus found to change in a consistent way with the length of the alkyl ligands. Apparently the orientation of the dimers with respect to each other is strongly influenced by the ligands.

An interesting comparison can be made between the isopropyl and the isobutyl compounds. In both cases the dimers are related by translation to form strings along the *c*-axis. Each thallium atom is coordinated to one sulfur atom in an adjacent dimer at a distance of 3.86 Å in the isopropyl and 3.42 Å in the isobutyl compound. Although the distances between the centres of the dimers are nearly the same, 6.31 Å in the isopropyl and 6.22 Å in the isobutyl compound, the thallium-thallium distances are quite different, 3.64 Å and 5.19 Å, respectively, as shown in Fig. 4. The parallelograms in the figure comprise the two thallium and two sulfur atoms involved in the linkage of each pair of dimers. The edges are similar, but the thallium-thallium distances are considerably different. The difference in orientation of the dimers within the strings is associated with the different space requirements of the ligands as is illustrated by Fig. 5 (a–d). Two mutually perpendicular projections of the isopropyl string are shown in Fig. 5 *c* and *d*. The sulfur parallelograms of the dimers are normal to the paper plane in *d* and the two figures show that the string makes only a small angle (12°) with that plane. The string of isobutyl dimers is shown in Fig. 5 *a* and *b* in the same orientation as *c* and *d*, respectively. Here the string makes a large angle (49°) with the paper plane of *b*. This change in direction of the string with respect to the dimers allows the ligands to slide on top of one another. The same molecular separation, the *c*-axis, as in the isopropyl string is then maintained despite the larger space requirement of the isobutyl ligands. The inclination of the string results in the skew coordination pyramid around the metal atom, Fig. 3, in the isobutyl compound. The coordination pyramid in the isopropyl compound is straight and the bond to the apical sulfur atom is almost normal to the sulfur parallelogram. This clearly demonstrates the connection between molecular packing and metal coordination in this group of compounds.

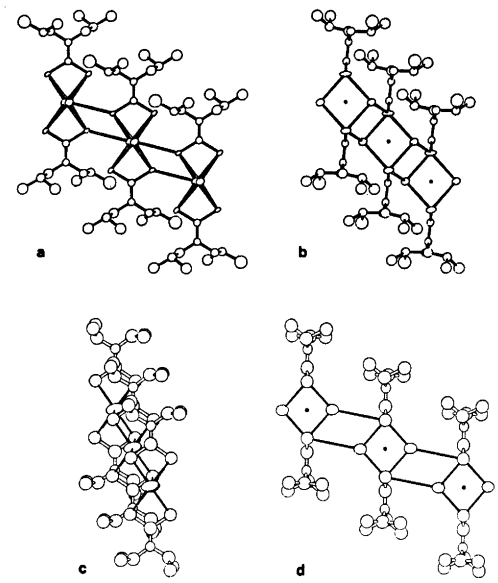

Fig. 5. The strings of dimers in thallium(I) diisobutyldithiocarbamate (a,b) and thallium(I) diisopropyldithiocarbamate (c,d). The sulfur planes are parallel to the paper in the left figures (a,c) and normal to the paper in the right figures (b,d).

Acknowledgements. We wish to express our gratitude to Professor Ivar Olovsson, the Head of this Department, for all the facilities placed at our disposal. We also wish to thank Dr. Åke Olin for valuable instruction and many stimulating discussions.

This work has been supported finanically by grants from the Swedish Natural Science Research Council which are gratefully acknowledged.

REFERENCES

1. Jennische, P. and Hesse, R. *Acta Chem. Scand. 27* (1973) 3531.
2. Pritzkow, H. and Jennische, P. *Acta Chem. Scand. A 29* (1975) 60.
3. Nilson, L. and Hesse, R. *Acta Chem. Scand. 23* (1969) 1951.
4. Jennische, P., Olin, Å. and Hesse, R. *Acta Chem. Scand. 26* (1972) 2799.
5. Anacker-Eickhoff, H., Elfwing, E., Jennische, P. and Hesse, R. *To be published.*
6. Åkerström, S. *Ark. Kemi 24* (1965) 495.
7. Parrish, W. *Acta Crystallogr. 13* (1960) 838.
8. Abrahamsson, S. *J. Sci. Instrum. 43* (1966) 931.
9. Werner, P.-E. *Ark. Kemi 31* (1969) 505.
10. Werner, P.-E. *Acta Chem. Scand. 25* (1971) 1297.
11. Cruickshank, D. W. J., Pilling, D. E., Bujosa, A., Lovell, F. M. and Truter, M. R. *Computing Methods and Phase Problems in X-Ray Analysis*, Pergamon, Oxford 1961, p. 32.
12. Hanson, H. P., Herman, F., Lea, J. D. and Skillman, S. *Acta Crystallogr. 20* (1966) 1040.
13. *Int. Tabl.* Vol. III pp. 214—215.
14. Morimoto, H. and Uyeda, R. *Acta Crystallogr. 11* (1963) 1107.
15. Lee, A. G. *Coord. Chem. Rev. 8* (1972) 289.
16. Hudges, D. L. and Truter, M. R. *J. Chem. Soc.* (1972) 2214.
17. Pearson, W. B. *Handbook of Lattice Spacings and Structures of Metals*, Pergamon, Oxford 1967, Vol. 2, p. 90.

Received July 24, 1974.

Acta Chemica Scandinavica A 29 (1975) 60—70

Molecular Packing and Metal Coordination in the Crystal Structure of Thallium(I) Diethyldithiocarbamate

HANS PRITZKOW[a] and PER JENNISCHE[b]

[a] Institute of Inorganic Chemistry, University of Heidelberg, 69 Heidelberg 1, Im Neuenheimer Feld 7, Germany and [b] Institute of Chemistry, University of Uppsala, Box 531, S-751 21 Uppsala, Sweden

The crystal structure of thallium(I) diethyldithiocarbamate, $Tl(I)S_2CN(C_2H_5)_2$, has been determined from three-dimensional X-ray data collected on a 2-circle Weissenberg diffractometer. The crystals are triclinic, space group $P\bar{1}$, with four formula units in the cell. Unit cell parameters are $a=11.353(3)$ Å, $b=14.735(4)$ Å, $c=5.997(2)$ Å, $\alpha=99.80(3)°$, $\beta=103.50(3)°$ and $\gamma=91.22(3)°$. The final R-value is 0.037.

The structure consists of dimeric molecules with four-fold Tl—S coordination which are linked in chains by weaker Tl—S bonds. The six coordinated sulfur atoms form elongated trigonal prisms. There are only van der Waals forces between the chains.

The dimeric molecules are similar to those in the methyl, propyl and isopropyl homologues, but the metal-ligand linkage between the dimers is quite different. The relation between metal coordination and molecular packing is discussed using packing surfaces obtained from a computer simulation program.

The crystal structures of the dipropyl-, diisopropyl- and dimethyldithiocarbamates of thallium(I) [1-3] were determined as part of a systematic investigation of compounds with the composition AX. The structures contain dimeric molecules which are linked by Tl—S coordination. Layers are formed in the methyl compound and chains in the propyl and isopropyl compounds. The central parts of the molecules are the same so that the type of linkage is determined by the alkyl groups. The determination of the structure of thallium(I) diethyldithiocarbamate was undertaken to increase the understanding of these structures.

EXPERIMENTAL

The sample was prepared by Dr. S. Åkerström. Colourless needles were obtained from benzene with [001] as principal axis. Weissenberg and precession photographs showed that most of the crystals were twinned. The crystals decomposed slowly, turning yellow after exposure to light or X-rays. The density was measured by flotation in aqueous K_2HgI_4. The cell parameters were determined from single crystal photographs and refined to fit a Guinier-Hägg powder photograph taken with $CuK\alpha_1$ radiation and silicon for calibration ($a=5.4305$ Å).[5] Crystal data are given in Table 1.

Three crystals were used because of the decomposition and they were all cut from a long crystal needle (cross section 0.15×0.16 mm^2) to a length of appr. 0.3 mm. The crystals were mounted in identical orientation and were used for two layers each.

The STOE Weissenberg diffractometer was controlled by a PDP 8/E computer and equipped with a graphite monochromator for $MoK\alpha$ radiation. The equatorial layer was measured in $\omega-2\theta$ scan, the higher layers in ω scan. The

Table 1. Crystal data.

Formula unit: $Tl(I)S_2CN(C_2H_5)_2$
Diffraction symmetry: $\bar{1}$
Crystal system: triclinic
Unit cell parameters:
$a=11.353(3)$ Å, $b=14.735(4)$ Å, $c=5.997(2)$ Å,
$\alpha=99.80(3)°$, $\beta=103.50(3)°$, $\gamma=91.22(3)°$
Cell volume: 959 Å^3
Density, measured: 2.41 g cm^{-3}.
Number of formula units: 4
Density, calculated: 2.44 g cm^{-3}
Space group: $P\bar{1}$
Linear absorption coefficient ($MoK\alpha$):
173.6 cm^{-1}

background was counted before and after the scan and the scanning speed was 0.6°/min. The scanning interval was constant in the two lowest layers, $\Delta\omega = 1.3$ and 1.6°, and calculated as $\Delta\omega = A + B \sin\mu \tan(v/2)$ in the higher layers (μ is the equi-inclination angle and v the counter angle). A and B were determined for each layer from the intensity profiles of a few reflections. Pre-scans were performed to determine if the reflections should be skipped or measured with attenuation filters. Two test reflections were measured in each layer after every twenty reflections. Their densities decreased by about 5 % during the two days needed for the layer.

1900 reflections with θ less than 20° (sin $\theta/\lambda = 0.48$ Å^{-1}) were measured in the layers $hk0$ to $hk5$ and 440 reflections at higher angles in the two highest layers. The intensities were corrected for Lorentz and polarization effects, including monochromator polarization, and for absorption. 180 of the 2340 reflections were excluded since their intensities were less than the estimated standard deviations, $\sigma_I = (N + 0.05^2 I^2)^{\frac{1}{2}}$. Approximate relative scale factors were obtained from measurements of certain $hk0$ reflections for each crystal.

DETERMINATION OF THE STRUCTURE

The thallium positions were determined from a three-dimensional Patterson synthesis. A difference synthesis revealed the positions of the remaining atoms except the hydrogens and the

Table 2. Atomic coordinates and thermal parameters, B or β_{ij}. The anisotropic temperature factor is defined as $\exp(-h^2\beta_{11} - 2hk\beta_{12} - \cdots)$.

Atom	x	y	z	B(Å^2)
Dimer A				
Tl	−0.06677(4)	0.04093(3)	0.24175(7)	
S1	0.2078(3)	0.0136(2)	0.2757(6)	
S2	0.0307(2)	−0.1477(2)	0.1376(5)	
C1	0.1765(8)	−0.1014(7)	0.2644(15)	4.2(2)
N1	0.2630(7)	−0.1547(5)	0.3442(13)	4.6(2)
C2	0.2393(12)	−0.2568(9)	0.3294(22)	7.1(3)
C3	0.3908(10)	−0.1191(8)	0.4439(19)	5.9(2)
C4	0.2502(15)	−0.3082(12)	0.0969(29)	9.8(4)
C5	0.4204(15)	−0.0957(12)	0.7153(27)	9.5(4)
Dimer B				
Tl	0.42802(4)	0.46184(3)	0.19590(7)	
S1	0.2951(3)	0.5065(2)	0.5838(6)	
S2	0.4483(2)	0.3470(2)	0.5735(5)	
C1	0.3136(8)	0.3934(6)	0.6004(15)	4.1(2)
N1	0.2250(7)	0.3395(6)	0.6365(14)	5.0(2)
C2	0.2325(12)	0.2385(9)	0.6348(21)	6.7(3)
C3	0.1084(11)	0.3769(9)	0.6743(20)	6.6(3)
C4	0.2902(13)	0.2170(10)	0.8773(23)	7.6(3)
C5	0.0197(17)	0.3691(13)	0.4409(33)	11.0(5)

Atom	β_{11}	β_{22}	β_{33}	β_{12}	β_{13}	β_{23}
Dimer A						
Tl	0.01266(5)	0.00793(3)	0.0419(2)	0.00487(3)	0.00845(7)	0.00507(5)
S1	0.0098(3)	0.0035(2)	0.064(1)	0.0007(2)	0.0004(4)	0.0026(3)
S2	0.0069(3)	0.0050(2)	0.060(1)	0.0005(2)	0.0023(4)	0.0046(3)
Dimer B						
Tl	0.01135(5)	0.00693(3)	0.03916(2)	−0.00209(3)	0.00395(6)	0.00185(5)
S1	0.0089(2)	0.0038(1)	0.064(1)	0.0013(1)	0.0089(5)	0.0037(4)
S2	0.0073(3)	0.0048(2)	0.062(1)	0.0012(2)	0.0068(4)	0.0044(3)

Table 3. Observed and calculated structure amplitudes. Reflections marked with an asterisk were not included in the refinement.

H	K	10FO	10FC
L = 0			
2	0	1261	1295
3	0	254	249
4	0	271	259
5	0	326	320
6	0	1499	1480
7	0	190	186
8	0	1059	1090
9	0	33*	37
10	0	154	176
-10	1	56	53
-9	1	655	662
-8	1	102	103
-7	1	1438	1456
-6	1	356	346
-5	1	612	630
-4	1	590	578
-3	1	473	444
-2	1	517	523
2	1	630	668
3	1	390	370
4	1	778	845
5	1	571	565
6	1	577	590
7	1	1362	1389
8	1	217	218
9	1	434	423
10	1	184	180
-10	2	39*	97
-9	2	34*	38
-8	2	1134	1088
-7	2	293	302
-6	2	1202	1172
-5	2	1094	1022
-4	2	512	469
-3	2	1645	1489
-2	2	1536	1404
-1	2	1125	1130
1	2	1002	1035
2	2	1249	1205
3	2	1610	1593
4	2	596	555
5	2	1131	1140
6	2	937	951
7	2	341	357
8	2	746	737
9	2	180	166
10	2	123	130
-10	3	274	260
-9	3	153	186
-8	3	79	86
-7	3	1295	1233
-6	3	756	724
-5	3	714	685
-4	3	1339	1348
-3	3	355	362
-2	3	1179	1203
-1	3	1645	1620
0	3	56	29
1	3	1593	1650
2	3	1130	1171
3	3	228	226
4	3	1347	1405
5	3	526	539
6	3	653	627
7	3	959	914
8	3	58	51
9	3	84	54
10	3	394	401
-10	4	155	165
-9	4	376	369
-8	4	610	581
-7	4	154	171
-6	4	865	856
-5	4	1092	1086
-4	4	368	345
-3	4	1753	1750
-2	4	124	129
-1	4	984	917
0	4	1120	1119
1	4	704	648
2	4	180	146
3	4	1477	1528
4	4	125	155
5	4	872	893
6	4	669	661
7	4	46	48
8	4	270	283
9	4	414	407
-10	5	466	494
-9	5	97	62
-8	5	405	394
-7	5	708	666
-6	5	374	371
-5	5	507	475
-4	5	1513	1457
-3	5	255	263
-2	5	1465	1468
-1	5	957	910
0	5	171	194
1	5	732	740
2	5	1243	1259
3	5	41	47
4	5	1401	1404
5	5	351	328
6	5	449	441
7	5	380	383
8	5	282	291
9	5	83	93
-9	6	556	537
-8	6	162	159
-7	6	97	96
-6	6	336	312
-5	6	982	953
-4	6	30*	62
-3	6	1725	1725
-2	6	44*	34
-1	6	385	421
0	6	706	742
1	6	227	267
2	6	109	116
3	6	1591	1607
4	6	28*	54
5	6	909	910
6	6	191	196
7	6	90	79
8	6	30*	30
9	6	307	323
-9	7	16*	123
-8	7	371	352
-7	7	142	129
-6	7	365	357
-5	7	127	167

H	K	10FO	10FC
-4	7	1763	1702
-3	7	140	155
-2	7	1309	1349
-1	7	112	131
0	7	158	188
1	7	88	97
2	7	1133	1163
3	7	342	367
4	7	1508	1553
5	7	111	104
6	7	387	376
7	7	103	97
-9	8	332	329
-8	8	163	184
-7	8	76	40
-6	8	208	224
-5	8	1078	1061
-4	8	33*	20
-3	8	1353	1362
-2	8	552	535
-1	8	700	652
0	8	134	146
1	8	630	574
2	8	728	716
3	8	1201	1244
4	8	37*	76
5	8	868	882
6	8	160	168
7	8	14*	20
8	8	313	296
-8	9	174	171
-7	9	265	280
-6	9	268	274
-5	9	444	438
-4	9	1186	1174
-3	9	572	554
-2	9	830	823
-1	9	706	725
0	9	18*	9
1	9	927	923
2	9	652	688
3	9	664	659
4	9	869	887
5	9	268	281
6	9	71	67
7	9	275	280
-7	10	207	191
-6	10	494	508
-5	10	374	363
-4	10	133	113
-3	10	850	813
-2	10	783	809
-1	10	209	230
0	10	883	849
1	10	92	122
2	10	875	893
3	10	660	667
4	10	95	101
5	10	34*	86
6	10	356	355
-7	11	416	420
-6	11	177	177
-5	11	442	445
-4	11	313	292
-3	11	477	475
-2	11	174	185
-1	11	680	695
0	11	58	46
1	11	782	800
2	11	237	225
3	11	434	419
4	11	65	79
5	11	286	284
6	11	202	227
-6	12	442	476
-5	12	159	171
-4	12	249	220
-3	12	184	171
-2	12	497	501
-1	12	35*	23
0	12	505	502
1	12	35*	40
2	12	594	577
3	12	57	110
4	12	137	139
-4	13	38*	21
-3	13	107	70
-2	13	54	58
-1	13	309	312
0	13	36*	31
1	13	370	389
2	13	65	13
3	13	80	103
L = 1			
-2	-14	294	300
-1	-14	77	36
0	-14	160	134
1	-14	40*	54
2	-14	480	484
-4	-13	156	123
-3	-13	430	427
-2	-13	21*	31
-1	-13	99	119
0	-13	290	292
1	-13	507	496
3	-13	509	507
4	-13	87	62
-5	-12	134	102
-4	-12	460	458
-3	-12	56	61
-2	-12	379	389
-1	-12	395	400
0	-12	222	232
1	-12	253	250
2	-12	578	584
3	-12	71	82
4	-12	477	474
5	-12	223	190
6	-12	108	129
-6	-11	330	316
-5	-11	458	434
-4	-11	36*	45
-3	-11	334	348
-2	-11	156	175
-1	-11	131	97
0	-11	676	655
1	-11	599	576
2	-11	145	141
3	-11	460	467
4	-11	240	228
5	-11	326	334
6	-11	516	471

H	K	10FO	10FC
-7	-10	443	448
-6	-10	421	405
-5	-10	219	236
-4	-10	346	370
-3	-10	158	133
-2	-10	376	369
-1	-10	738	733
0	-10	245	239
1	-10	424	435
2	-10	722	688
3	-10	319	303
4	-10	345	379
5	-10	540	529
6	-10	396	405
7	-10	555	553
-8	-9	468	461
-7	-9	444	423
-6	-9	405	425
-5	-9	372	371
-4	-9	176	154
-3	-9	558	528
-2	-9	568	543
-1	-9	102	118
0	-9	1313	1323
1	-9	432	457
2	-9	90	93
3	-9	545	531
4	-9	484	459
5	-9	568	593
6	-9	752	746
7	-9	272	272
8	-9	391	398
-8	-8	265	261
-7	-8	711	722
-6	-8	653	663
-5	-8	293	305
-4	-8	381	375
-3	-8	213	220
-2	-8	307	291
-1	-8	1454	1473
0	-8	332	346
1	-8	1118	1364
2	-8	384	378
3	-8	279	273
4	-8	470	461
5	-8	678	666
6	-8	518	536
7	-8	956	954
8	-8	244	216
-9	-7	224	221
-8	-7	741	756
-7	-7	433	425
-6	-7	594	582
-5	-7	473	475
-4	-7	70	68
-3	-7	33*	13
-2	-7	1234	1268
-1	-7	443	413
0	-7	2212	2213
1	-7	341	312
2	-7	653	657
3	-7	91	65
4	-7	306	308
5	-7	423	428
6	-7	1061	1063
7	-7	258	272
8	-7	678	701
9	-7	160	148
-9	-6	574	575
-8	-6	310	315
-7	-6	1004	1013
-6	-6	288	286
-5	-6	96	103
-4	-6	313	299
-3	-6	913	935
-2	-6	213	234
-1	-6	2429	2518
0	-6	28*	23
1	-6	1717	1682
2	-6	598	584
3	-6	123	118
4	-6	453	439
5	-6	763	734
6	-6	143	128
7	-6	1038	1048
8	-6	183	156
9	-6	349	375
-10	-5	319	325
-9	-5	152	153
-8	-5	912	906
-7	-5	34*	75
-6	-5	706	694
-5	-5	588	582
-4	-5	233	226
-3	-5	949	933
-2	-5	1535	1563
-1	-5	403	363
0	-5	2415	2490
1	-5	691	648
2	-5	944	885
3	-5	1365	1321
4	-5	318	303
5	-5	524	508
6	-5	1083	1088
7	-5	43*	49
8	-5	615	624
9	-5	306	283
-10	-4	291	276
-9	-4	580	569
-8	-4	74	63
-7	-4	902	907
-6	-4	576	571
-5	-4	199	175
-4	-4	1665	1578
-3	-4	802	788
-2	-4	743	761
-1	-4	1877	1966
0	-4	639	574
1	-4	1072	1343
2	-4	1714	1663
3	-4	252	215
4	-4	1535	1498
5	-4	793	764
6	-4	193	204
7	-4	638	663
8	-4	156	163
9	-4	151	159
-10	-3	190	181
-9	-3	151	138
-8	-3	615	642
-7	-3	114	123
-6	-3	753	756
-5	-3	1477	1658
-4	-3	226	241

H	K	10FO	10FC
-3	-3	1756	1802
-2	-3	534	594
-1	-3	556	555
0	-3	1359	1290
1	-3	903	946
2	-3	103	106
3	-3	2245	2225
4	-3	274	268
5	-3	868	839
6	-3	733	687
7	-3	256	219
8	-3	216	227
9	-3	524	494
10	-3	67	34
-10	-2	443	430
-9	-2	155	185
-8	-2	134	135
-7	-2	593	593
-6	-2	778	767
-5	-2	276	249
-4	-2	2099	2242
-3	-2	203	175
-2	-2	885	944
-1	-2	371	387
0	-2	379	353
1	-2	721	632
2	-2	1831	1824
3	-2	241	223
4	-2	1694	1703
5	-2	129	128
6	-2	94	110
7	-2	438	418
8	-2	416	410
9	-2	108	88
10	-2	587	590
-10	-1	103	57
-9	-1	475	468
-8	-1	434	434
-7	-1	80	95
-6	-1	60	42
-5	-1	1560	1598
-4	-1	146	167
-3	-1	1877	2071
-2	-1	895	864
-1	-1	79	100
0	-1	47	44
1	-1	835	829
2	-1	116	112
3	-1	2440	2500
4	-1	35*	9
5	-1	699	685
6	-1	44	2
7	-1	287	273
8	-1	34*	33
9	-1	567	566
10	-1	23*	36
-11	0	40*	29
-10	0	554	557
-9	0	15*	7
-8	0	356	332
-7	0	29*	22
-6	0	566	575
-5	0	189	184
-4	0	2215	2454
-3	0	269	251
-2	0	1052	1076
-1	0	143	174
0	0	235	268
1	0	58	83
2	0	1935	2065
3	0	188	156
4	0	1806	1818
5	0	221	235
6	0	165	170
7	0	118	146
8	0	391	385
9	0	44*	41
10	0	516	503
-11	1	597	566
-10	1	37*	24
-9	1	432	422
-8	1	237	212
-7	1	194	169
-6	1	373	378
-5	1	1927	1959
-4	1	406	427
-3	1	2022	2244
-2	1	814	835
-1	1	84	100
0	1	252	245
1	1	1201	1152
2	1	820	791
3	1	2339	2501
4	1	573	555
5	1	913	929
6	1	455	471
7	1	32*	34
8	1	327	311
9	1	331	348
10	1	130	98
-10	2	431	414
-9	2	266	264
-8	2	93	78
-7	2	594	550
-6	2	822	830
-5	2	715	672
-4	2	2203	2269
-3	2	724	707
-2	2	1223	1213
-1	2	776	774
0	2	175	187
1	2	1460	1492
2	2	1879	1914
3	2	195	202
4	2	1728	1738
5	2	690	719
6	2	263	244
7	2	674	667
8	2	114	117
9	2	357	352
-10	3	310	318
-9	3	120	119
-8	3	731	712
-7	3	179	191
-6	3	924	904
-5	3	1548	1520
-4	3	481	440
-3	3	1622	1630
-2	3	1798	1788
-1	3	326	365
0	3	2010	2154
1	3	802	812
2	3	1153	1159
3	3	1522	1572

H	K	10FO	10FC
4	3	311	309
5	3	397	390
6	3	849	871
7	3	46*	66
8	3	656	675
9	3	306	302
-10	4	356	327
-9	4	633	661
-8	4	67	82
-7	4	938	948
-6	4	293	253
-5	4	489	473
-4	4	1383	1309
-3	4	1046	1022
-2	4	414	415
-1	4	2364	2308
0	4	142	165
1	4	1778	1071
2	4	774	760
3	4	541	528
4	4	443	461
5	4	894	873
6	4	302	282
7	4	839	856
8	4	163	162
9	4	467	443
-10	5	477	473
-9	5	205	197
-8	5	872	882
-7	5	413	406
-6	5	904	960
-5	5	137	151
-4	5	269	239
-3	5	353	337
-2	5	1741	1730
-1	5	114	114
0	5	2160	2253
1	5	135	130
2	5	1005	1028
3	5	251	259
4	5	396	393
5	5	440	456
6	5	819	863
7	5	338	341
8	5	567	573
9	5	198	186
-10	6	216	201
-9	6	640	653
-8	6	378	392
-7	6	998	990
-6	6	451	461
-5	6	653	634
-4	6	116	75
-3	6	729	698
-2	6	286	279
-1	6	1736	1746
0	6	220	212
1	6	1282	1327
2	6	113	88
3	6	25*	31
4	6	409	427
5	6	614	638
6	6	511	504
7	6	625	638
8	6	145	133
-9	7	141	128
-8	7	758	747
-7	7	571	560
-6	7	866	861
-5	7	422	448
-4	7	409	381
-3	7	283	287
-2	7	858	807
-1	7	400	409
0	7	1253	1279
1	7	506	515
2	7	416	410
3	7	164	151
4	7	398	424
5	7	587	586
6	7	639	652
7	7	154	168
8	7	298	296
-9	8	369	367
-8	8	99	132
-7	8	828	793
-6	8	588	590
-5	8	677	676
-4	8	267	257
-3	8	202	201
-2	8	769	725
-1	8	944	949
0	8	312	285
1	8	754	744
2	8	275	273
3	8	159	165
4	8	366	355
5	8	443	456
6	8	396	384
7	8	417	427
-8	9	508	487
-7	9	336	352
-6	9	612	596
-5	9	268	295
-4	9	281	279
-3	9	672	676
-2	9	580	571
-1	9	368	372
0	9	693	713
1	9	365	386
2	9	238	248
3	9	330	332
4	9	320	329
5	9	483	485
6	9	389	409
-7	10	446	421
-6	10	434	447
-5	10	324	316
-4	10	569	547
-3	10	131	130
-2	10	667	689
-1	10	634	618
0	10	68	111
1	10	357	385
2	10	527	509
3	10	47*	60
4	10	429	436
5	10	365	369
6	10	376	352
-7	11	306	296
-6	11	326	294
-5	11	483	487
-4	11	55	44
-3	11	732	688

H	K	10FO	10FC
-2	11	249	246
-1	11	322	328
0	11	363	362
1	11	502	514
2	11	37*	27
3	11	475	472
4	11	163	172
5	11	525	523
-5	12	126	116
-4	12	505	505
-3	12	71	33
-2	12	674	646
-1	12	61	77
0	12	231	238
1	12	95	44
2	12	415	444
3	12	168	159
-3	13	476	489
-2	13	124	137
-1	13	202	183
0	13	185	156
1	13	334	364
L = 2			
-3	-14	76	17
-2	-14	345	352
-1	-14	35*	11
0	-14	364	369
1	-14	103	91
2	-14	38*	24
3	-14	36*	20
-4	-13	28*	84
-3	-13	402	384
-2	-13	36*	27
-1	-13	606	603
0	-13	25*	57
1	-13	404	411
2	-13	88	99
3	-13	95	58
-6	-12	90	118
-5	-12	159	188
-4	-12	298	297
-3	-12	248	243
-2	-12	693	686
-1	-12	17*	40
0	-12	657	659
1	-12	178	169
2	-12	302	313
3	-12	408	407
4	-12	233	229
5	-12	90	110
-7	-11	289	294
-6	-11	118	131
-5	-11	121	102
-4	-11	655	640
-3	-11	648	632
-2	-11	69	79
-1	-11	776	758
0	-11	61	74
1	-11	509	508
2	-11	828	790
3	-11	13*	28
4	-11	361	379
5	-11	354	368
6	-11	74	53
-8	-10	232	247
-7	-10	101	121
-6	-10	136	120
-5	-10	713	711
-4	-10	393	378
-3	-10	636	632
-2	-10	504	496
-1	-10	77	89
0	-10	472	478
1	-10	568	556
2	-10	213	227
3	-10	1044	1056
4	-10	197	171
5	-10	177	191
6	-10	271	289
7	-10	124	144
-9	-9	192	194
-8	-9	31*	12
-7	-9	189	184
-6	-9	581	576
-5	-9	119	116
-4	-9	1155	1131
-3	-9	260	256
-2	-9	313	306
-1	-9	258	251
0	-9	441	430
1	-9	126	124
2	-9	1056	1077
3	-9	31*	27
4	-9	812	813
5	-9	162	175
6	-9	231	200
7	-9	121	128
8	-9	219	245
-9	-8	51	66
-8	-8	79	99
-7	-8	73	99
-6	-8	36*	18
-5	-8	1161	1149
-4	-8	148	126
-3	-8	691	670
-2	-8	147	89
-1	-8	28*	31
0	-8	53	41
1	-8	781	785
2	-8	32*	59
3	-8	1255	1299
4	-8	73	55
5	-8	146	159
6	-8	97	63
7	-8	272	251
8	-8	102	101
-10	-7	273	292
-9	-7	71	57
-8	-7	70	79
-7	-7	190	187
-6	-7	623	603
-5	-7	164	169
-4	-7	1289	1291
-3	-7	8*	15
-2	-7	270	257
-1	-7	335	303
0	-7	323	330
2	-7	1358	1383
3	-7	176	176
4	-7	747	766
5	-7	307	304
6	-7	144	128

H	K	10FO	10FC
7	-7	73	33
8	-7	385	374
-10	-6	69	66
-9	-6	208	198
-8	-6	175	158
-7	-6	221	221
-6	-6	365	343
-5	-6	1212	1202
-4	-6	89	98
-3	-6	1095	1079
-2	-6	211	228
-1	-6	129	138
0	-6	343	332
1	-6	958	939
2	-6	86	64
3	-6	1369	1410
4	-6	483	465
5	-6	321	339
6	-6	424	415
7	-6	114	126
8	-6	50	29
9	-6	353	373
-10	-5	233	251
-9	-5	200	191
-8	-5	142	137
-7	-5	552	543
-6	-5	753	751
-5	-5	395	404
-4	-5	1431	1436
-3	-5	212	191
-2	-5	325	294
-1	-5	895	894
0	-5	409	393
1	-5	290	295
2	-5	1558	1608
3	-5	281	301
4	-5	1035	1043
5	-5	804	788
6	-5	239	250
7	-5	422	439
8	-5	181	164
-10	-4	70	85
-9	-4	93	48
-8	-4	642	626
-7	-4	516	516
-6	-4	652	669
-5	-4	1339	1377
-4	-4	52	70
-3	-4	1178	1179
-2	-4	1301	1267
-1	-4	42	57
0	-4	1368	1423
1	-4	1019	1028
2	-4	184	163
3	-4	1424	1433
4	-4	581	599
5	-4	461	473
6	-4	938	917
7	-4	194	171
8	-4	301	328
9	-4	226	226
-11	-3	38*	44
-10	-3	46	59
-9	-3	601	596
-8	-3	352	362
-7	-3	816	823
-6	-3	749	773
-5	-3	251	225
-4	-3	1228	1222
-3	-3	1119	1135
-2	-3	286	269
-1	-3	1958	2143
0	-3	327	336
1	-3	1489	1521
2	-3	1103	1071
3	-3	371	341
4	-3	644	624
5	-3	912	910
6	-3	179	186
7	-3	1027	1016
8	-3	45*	27
9	-3	147	177
-11	-2	194	183
-10	-2	369	384
-9	-2	234	220
-8	-2	1130	1132
-7	-2	146	160
-6	-2	591	586
-5	-2	705	731
-4	-2	338	298
-3	-2	277	247
-2	-2	2216	2564
-1	-2	28*	43
0	-2	2205	2545
1	-2	290	205
2	-2	494	501
3	-2	517	476
4	-2	658	633
5	-2	63	71
6	-2	1174	1198
7	-2	33*	25
8	-2	568	569
9	-2	107	100
-11	-1	144	162
-10	-1	32*	8
-9	-1	906	910
-8	-1	140	113
-7	-1	989	968
-5	-1	119	121
-4	-1	113	153
-3	-1	1343	1381
-2	-1	203	175
0	-1	355	314
1	-1	1225	1271
2	-1	353	347
3	-1	39	45
4	-1	409	378
5	-1	1077	1099
6	-1	362	367
7	-1	803	837
8	-1	120	90
9	-1	146	150
-11	0	34*	53
-10	0	498	498
-9	0	43*	14
-8	0	1019	1037
-7	0	512	504
-6	0	798	811
-5	0	407	403
-4	0	346	339
-3	0	770	779
-2	0	1747	1831
0	0	1071	2184
1	0	867	914

Table 3. Continued.

H	K	10FO	10FC
2	0	374	319
3	0	500	516
4	0	673	669
5	0	631	644
6	0	1017	1018
7	0	31*	6
8	0	369	365
9	0	138	121
-11	1	33*	30
-10	1	106	93
-9	1	704	706
-8	1	284	275
-7	1	1138	1147
-6	1	864	846
-5	1	405	394
-4	1	661	631
-3	1	567	559
-2	1	986	996
-1	1	1876	2092
0	1	1006	1011
1	1	678	685
2	1	730	735
3	1	294	301
4	1	813	857
5	1	768	781
6	1	216	213
7	1	529	543
8	1	222	229
9	1	98	86
-11	2	251	237
-10	2	190	199
-9	2	147	153
-8	2	923	910
-7	2	543	537
-6	2	652	647
-5	2	838	824
-4	2	158	168
-3	2	1094	1096
-2	2	1157	1182
-1	2	244	236
0	2	1251	1186
1	2	1100	1095
2	2	110	112
3	2	896	894
4	2	440	441
5	2	615	604
6	2	735	744
7	2	196	199
8	2	68	85
9	2	343	347
-11	3	100	107
-10	3	491	476
-9	3	453	466
-8	3	32*	32
-7	3	713	712
-6	3	788	784
-5	3	502	524
-4	3	1272	1272
-3	3	511	484
-2	3	940	994
-1	3	958	954
0	3	638	670
1	3	596	586
2	3	1033	1046
3	3	219	224
4	3	778	776
5	3	500	517
6	3	94	101
7	3	340	321
8	3	367	377
9	3	33*	57
-10	4	76	16
-9	4	415	426
-8	4	541	536
-7	4	526	513
-6	4	330	317
-5	4	1101	1083
-4	4	35*	18
-3	4	1360	1369
-2	4	796	775
-1	4	119	137
0	4	650	670
1	4	1069	1066
2	4	38	39
3	4	1217	1211
4	4	224	219
5	4	654	648
6	4	293	314
7	4	227	239
8	4	71	42
-10	5	484	472
-9	5	154	113
-8	5	36*	51
-7	5	185	200
-6	5	990	996
-5	5	89	67
-4	5	1375	1396
-2	5	911	913
-1	5	570	594
0	5	620	592
1	5	53	55
2	5	1309	1340
3	5	107	49
4	5	1042	1021
5	5	178	155
6	5	198	182
8	5	267	292
-10	6	123	157
-9	6	326	327
-7	6	565	586
-6	6	72	63
-5	6	1265	1282
-4	6	251	233
-3	6	1250	1280
-2	6	106	80
-1	6	87	64
0	6	209	222
1	6	1114	1106
2	6	425	415
3	6	1125	1142
4	6	69	48
5	6	530	535
6	6	120	94
7	6	166	174
-9	7	178	206
-8	7	88	61
-7	7	199	206
-6	7	791	785
-4	7	1137	1127
-3	7	644	629
-2	7	611	643
-1	7	322	330
0	7	503	487
1	7	800	774
2	7	965	949
3	7	111	85
4	7	742	750
5	7	182	177
6	7	32*	10
7	7	314	300
-9	8	304	294
-8	8	278	291
-7	8	188	201
-6	8	293	287
-5	8	753	757
-4	8	528	532
-3	8	787	756
-2	8	750	743
-1	8	54	60
0	8	762	735
1	8	564	593
2	8	585	574
3	8	515	524
4	8	263	248
5	8	43*	79
6	8	255	250
-8	9	238	238
-7	9	414	418
-6	9	275	267
-5	9	93	39
-4	9	426	420
-3	9	640	637
-2	9	460	458
-1	9	694	663
0	9	309	292
1	9	726	732
2	9	266	281
3	9	126	113
4	9	119	122
5	9	335	336
6	9	204	199
-7	10	120	117
-6	10	462	474
-5	10	102	79
-4	10	299	313
-3	10	306	323
-2	10	491	499
-1	10	82	39
0	10	625	612
1	10	184	187
2	10	334	319
3	10	49	46
4	10	250	263
5	10	94	90
-6	11	105	117
-5	11	259	242
-4	11	185	145
-3	11	356	354
-2	11	71	72
-1	11	382	383
0	11	74	96
1	11	493	480
2	11	9*	96
3	11	96	88
4	11	142	105
-5	12	111	88
-3	12	35*	28
-2	12	306	294
-1	12	51	42
0	12	366	369
1	12	64	81
2	12	178	167
-2	13	62	49
-1	13	293	281
L = 3			
-4	-14	331	315
-3	-14	35*	18
-2	-14	32*	15
-1	-14	158	165
0	-14	179	183
1	-14	26*	8
2	-14	403	393
-6	-13	87	82
-5	-13	359	344
-4	-13	50	49
-3	-13	138	156
-2	-13	179	183
-1	-13	104	105
0	-13	113	121
1	-13	311	330
2	-13	105	98
3	-13	309	332
4	-13	140	136
-7	-12	217	209
-6	-12	301	293
-5	-12	114	120
-4	-12	273	283
-3	-12	76	55
-2	-12	29*	59
-1	-12	360	359
0	-12	300	291
1	-12	68	69
2	-12	375	393
3	-12	196	189
4	-12	260	272
5	-12	310	303
-8	-11	286	286
-7	-11	234	226
-6	-11	188	197
-5	-11	405	464
-4	-11	85	77
-3	-11	250	223
-2	-11	441	430
-1	-11	148	138
0	-11	273	285
1	-11	427	435
2	-11	198	195
3	-11	414	441
4	-11	331	321
5	-11	207	226
6	-11	367	369
-8	-10	309	301
-7	-10	338	335
-6	-10	369	362
-5	-10	81	80
-4	-10	437	42[illegible]
-3	-10	332	325
-2	-10	410	92
-1	-10	836	827
0	-10	150	147
1	-10	86	109
2	-10	551	542
3	-10	237	222
4	-10	280	325
5	-10	511	522
6	-10	269	258
7	-10	341	342
-9	-9	240	225
-8	-9	520	505
-7	-9	338	343
-6	-9	188	175
-5	-9	354	340
-4	-9	194	195
-3	-9	105	83
-2	-9	1094	1095
-1	-9	68	77
0	-9	868	841
1	-9	256	247
2	-9	94	93
3	-9	288	308
4	-9	443	434
5	-9	238	250
6	-9	661	678
7	-9	178	152
-10	-8	179	165
-9	-8	586	565
-8	-8	234	227
-7	-8	370	359
-6	-8	193	197
-5	-8	114	99
-4	-8	31*	33
-3	-8	946	929
-2	-8	61	68
-1	-8	1425	1431
0	-8	31*	32
1	-8	485	491
2	-8	62	48
3	-8	197	201
4	-8	83	64
5	-8	683	685
6	-8	68*	85
7	-8	495	531
8	-8	147	123
-10	-7	356	355
-9	-7	198	188
-8	-7	648	640
-7	-7	47	41
-6	-7	96	95
-5	-7	159	158
-4	-7	453	463
-3	-7	366	362
-2	-7	1474	1475
-1	-7	90	105
0	-7	1086	1090
1	-7	547	562
2	-7	80	57
3	-7	288	270
4	-7	455	459
5	-7	110	121
6	-7	737	733
7	-7	195	187
8	-7	153	192
-10	-6	164	149
-9	-6	571	571
-8	-6	123	130
-7	-6	495	488
-6	-6	426	398
-5	-6	118	120
-4	-6	642	633
-3	-6	856	865
-2	-6	235	233
-1	-6	1364	1390
0	-6	605	567
1	-6	395	378
2	-6	711	729
3	-6	238	225
4	-6	456	454
5	-6	659	686
6	-6	61	38
7	-6	366	369
8	-6	246	230
-11	-5	151	143
-10	-5	321	321
-9	-5	86	87
-8	-5	617	613
-7	-5	427	407
-6	-5	189	184
-5	-5	814	775
-4	-5	323	315
-3	-5	701	698
-2	-5	984	967
-1	-5	277	285
0	-5	719	698
1	-5	943	961
2	-5	90	85
3	-5	834	846
4	-5	371	365
5	-5	147	155
6	-5	471	487
7	-5	259	258
8	-5	107	98
-11	-4	65	64
-10	-4	259	244
-9	-4	428	438
-8	-4	76	60
-7	-4	445	450
-6	-4	829	836
-5	-4	25*	16
-4	-4	1040	1017
-3	-4	359	359
-2	-4	421	426
-1	-4	958	951
0	-4	769	814
1	-4	84	85
2	-4	1137	1144
3	-4	55	72
4	-4	532	535
5	-4	490	482
6	-4	231	223
7	-4	166	175
8	-4	400	385
9	-4	56	15
-11	-3	366	356
-10	-3	181	185
-9	-3	219	219
-8	-3	446	446
-7	-3	471	457
-6	-3	86	75
-5	-3	1193	1196
-4	-3	68	55
-3	-3	863	833
-2	-3	688	663
-1	-3	167	161
0	-3	358	343
1	-3	1063	1053
2	-3	55	62
3	-3	1063	1075
4	-3	77	83
5	-3	154	149
6	-3	323	309
7	-3	340	329
8	-3	34*	19
9	-3	371	373
-11	-2	76	31
-10	-2	367	379
-9	-2	259	254
-8	-2	58	63
-7	-2	35*	25
-6	-2	1060	1075
-5	-2	78	87
-4	-2	1272	1297
-3	-2	271	265
-2	-2	447	450
-1	-2	361	338
0	-2	931	930
1	-2	82	85
2	-2	1425	1460
3	-2	119	123
4	-2	741	758
5	-2	50	3
6	-2	178	192
7	-2	66	89
8	-2	335	353
9	-2	25*	12
-11	-1	374	375
-9	-1	259	234
-8	-1	81	62
-7	-1	666	665
-6	-1	305	278
-5	-1	1492	1543
-4	-1	151	137
-3	-1	1028	1033
-2	-1	173	168
0	-1	53	51
1	-1	1377	1397
2	-1	226	229
3	-1	1324	1318
4	-1	263	308
5	-1	353	350
6	-1	66	45
7	-1	257	254
8	-1	174	157
9	-1	311	310
-11	0	121	106
-10	0	298	300
-9	0	32*	58
-8	0	291	300
-7	0	438	455
-6	0	1159	1156
-5	0	23*	24
-4	0	1493	1517
-3	0	540	523
-2	0	240	226
-1	0	361	375
0	0	800	756
1	0	615	639
2	0	1513	1590
3	0	390	405
4	0	749	743
5	0	353	359
6	0	85	65
7	0	271	277
8	0	260	278
-11	1	256	257
-10	1	253	256
-9	1	92	95
-8	1	437	416
-7	1	633	654
-6	1	415	421
-5	1	1332	1320
-4	1	709	721
-3	1	966	1004
-2	1	795	783
-1	1	309	294
0	1	1140	1126
1	1	1209	1237
2	1	245	232
3	1	1010	1009
4	1	493	480
5	1	185	187
6	1	533	505
7	1	200	206
8	1	343	333
-11	2	277	287
-10	2	218	193
-9	2	470	477
-8	2	140	92
-7	2	534	509
-6	2	831	825
-5	2	174	144
-4	2	851	839
-3	2	1285	1356
-2	2	405	407
-1	2	1143	1152
0	2	559	553
1	2	987	1030
2	2	667	643
3	2	297	299
4	2	313	308
5	2	563	588
6	2	130	135
7	2	459	477
8	2	210	211
-11	3	251	259
-10	3	419	442
-9	3	189	200
-8	3	593	616
-7	3	93	83
-6	3	475	491
-5	3	560	572
-4	3	821	799
-3	3	417	416
-2	3	1383	1408
-1	3	53	43
0	3	1280	1299
1	3	416	424
2	3	306	275
3	3	185	190
4	3	670	681
5	3	203	207
6	3	524	515
7	3	184	190
8	3	323	317
-11	4	301	317
-10	4	275	275
-9	4	543	539
-8	4	277	275
-7	4	742	751
-6	4	47	37
-5	4	77	75
-4	4	267	265
-3	4	981	952
-2	4	144	155
-1	4	1229	1221
0	4	60	44
1	4	728	729
2	4	178	82
3	4	287	301
4	4	214	218
5	4	498	508
6	4	223	229
7	4	398	400
8	4	136	116
-10	5	402	421
-9	5	255	253
-8	5	632	644
-7	5	238	238
-6	5	613	627
-5	5	29*	51
-4	5	399	401
-3	5	98	76
-2	5	1027	1026
-1	5	45	32
0	5	907	923
1	5	155	143
2	5	85	69
3	5	191	181
4	5	508	534
5	5	274	268
6	5	373	391
7	5	65	71
-10	6	46*	56
-9	6	471	472
-8	6	277	305
-7	6	756	744
-6	6	223	224
-5	6	239	253
-4	6	198	177
-3	6	609	599
-2	6	169	171
-1	6	876	875
0	6	164	155
1	6	463	449
2	6	106	86
3	6	313	323
4	6	299	303
5	6	447	446
6	6	160	144
7	6	247	247
-10	7	284	278
-9	7	102	80
-8	7	530	526
-7	7	277	277
-6	7	513	522
-5	7	278	289
-4	7	296	289
-3	7	441	443
-2	7	628	617
-1	7	84	83
0	7	626	634
1	7	223	230
2	7	30*	14
3	7	318	311
4	7	351	375
5	7	239	237
6	7	263	288
-9	8	290	284
-8	8	180	185
-7	8	450	468
-6	8	335	356
-5	8	172	167
-4	8	482	470
-3	8	521	527
-2	8	315	313
-1	8	448	504
0	8	303	292
1	8	352	366
2	8	342	334
3	8	332	344
4	8	391	374
5	8	255	274
-8	9	262	252
-7	9	341	385
-6	9	302	287
-5	9	467	460
-4	9	207	213
-3	9	482	480
-2	9	306	303
-1	9	90	75
0	9	289	297
1	9	416	426
2	9	58	50
3	9	390	378
4	9	255	267
5	9	308	304
-7	10	243	247
-6	10	386	386
-5	10	17*	43
-4	10	571	579
-3	10	113	133
-2	10	210	198
-1	10	101	112
0	10	319	331
1	10	34*	38
2	10	435	452
3	10	189	194
4	10	378	365
-6	11	204	199
-5	11	420	416
-4	11	57	26
-3	11	374	378
-2	11	69	79
-1	11	48*	97
0	11	61	37
1	11	323	329
2	11	122	116
-4	12	317	324
-3	12	163	131
-2	12	160	167
-1	12	214	184
L = 4			
-4	-13	143	144
-3	-13	361	368
-2	-13	36*	21
-1	-13	381	374
0	-13	168	172
1	-13	77	99
2	-13	221	217
-6	-12	81	76
-5	-12	304	315
-4	-12	237	236
-3	-12	135	137
-2	-12	365	374
-1	-12	128	109
0	-12	198	200
1	-12	418	408
2	-12	36*	9
3	-12	263	261
-8	-11	77	75
-7	-11	11*	41
-6	-11	357	352
-5	-11	106	109
-4	-11	378	369
-3	-11	203	214
-2	-11	63	65
-1	-11	246	267
0	-11	295	289
1	-11	65	48
2	-11	518	523
3	-11	67	33
4	-11	92	94
5	-11	162	192
-8	-10	129	126
-7	-10	251	259
-6	-10	65	93
-5	-10	552	547
-4	-10	74	69
-3	-10	166	147
-2	-10	230	212
-1	-10	144	162
1	-10	563	561
2	-10	65	53
3	-10	363	371
4	-10	57	39
5	-10	126	99
6	-10	86	101
-9	-9	65	88
-8	-9	50	45
-7	-9	69	52
-6	-9	540	544
-5	-9	106	89
-4	-9	421	422
-3	-9	71	48
-2	-9	81	58
-1	-9	137	150
0	-9	450	455
1	-9	75	23
2	-9	630	655
3	-9	140	139
4	-9	139	162
5	-9	45	41
6	-9	198	172
-10	-8	81	62
-9	-8	80	65
-8	-8	69	71
-7	-8	360	373
-6	-8	177	185
-5	-8	685	665
-4	-8	51	23
-3	-8	278	262
-2	-8	64	49
-1	-8	277	294
0	-8	32*	21
1	-8	674	656
2	-8	142	122
3	-8	527	535
4	-8	215	203
5	-8	57	31
6	-8	34*	37
7	-8	145	160
-10	-7	68	78
-9	-7	33*	33
-8	-7	163	165
-7	-7	315	319
-6	-7	709	710
-5	-7	33*	68
-4	-7	609	605
-3	-7	138	120
-2	-7	33*	11
-1	-7	179	201
0	-7	584	578
1	-7	111	94
2	-7	857	865
3	-7	328	326
4	-7	293	309
5	-7	238	224
6	-7	35*	31
7	-7	98	55
-10	-6	122	120
-9	-6	75	110
-8	-6	308	296
-7	-6	485	491
-6	-6	288	283
-5	-6	802	807
-4	-6	311	332
-3	-6	280	268
-2	-6	436	422
-1	-6	265	252
0	-6	365	340
1	-6	878	891
2	-6	160	151
3	-6	609	596
4	-6	450	440
5	-6	176	191
6	-6	247	240
7	-6	101	92
-11	-5	145	125
-10	-5	28*	27
-9	-5	313	303
-8	-5	313	343
-7	-5	415	415
-6	-5	693	680
-5	-5	143	136
-4	-5	580	577
-3	-5	760	764
-2	-5	40*	73
-1	-5	858	861
0	-5	533	520
1	-5	307	322
2	-5	689	660
3	-5	437	440
4	-5	252	255
5	-5	527	509
6	-5	21*	49
7	-5	276	291
-11	-4	49	37
-10	-4	330	334
-9	-4	125	122
-8	-4	454	463
-7	-4	329	330
-6	-4	181	155
-5	-4	549	543
-4	-4	701	682
-3	-4	179	202
-2	-4	1149	1186
-1	-4	78	77
0	-4	829	831
1	-4	487	482
2	-4	119	113
3	-4	295	292
4	-4	576	568
5	-4	34*	42
6	-4	518	523
7	-4	64	67
-11	-3	259	269
-10	-3	5*	10
-9	-3	540	542
-8	-3	41*	40
-7	-3	396	408
-6	-3	259	268
-5	-3	246	248
-4	-3	144	129
-3	-3	1244	1255
-2	-3	29*	37
-1	-3	1148	1139
0	-3	32*	36
1	-3	381	368
2	-3	152	130
3	-3	483	471
4	-3	116	135
5	-3	587	578
6	-3	22*	2
7	-3	323	336
8	-3	10	31
-11	-2	73	37
-10	-2	444	444
-9	-2	81	94
-8	-2	524	528
-7	-2	85	71
-6	-2	255	298
-5	-2	27*	26
-4	-2	704	731
-3	-2	91	89
-1	-2	175	172
0	-2	906	957
1	-2	189	200
2	-2	136	150
3	-2	151	145
4	-2	564	563
5	-2	207	203
6	-2	484	477
7	-2	36*	76
8	-2	94	87
-11	-1	255	252
-10	-1	34*	33
-9	-1	536	559
-8	-1	300	312
-7	-1	563	560
-6	-1	163	145
-5	-1	131	138
-4	-1	353	385
-3	-1	895	908
-1	-1	1016	1008
0	-1	397	386
1	-1	248	215
2	-1	253	259
3	-1	423	414
4	-1	256	259
5	-1	474	486
6	-1	31*	16
7	-1	227	227
-11	0	120	111
-10	0	403	392
-9	0	78	95
-8	0	609	625
-7	0	319	315
-6	0	334	335
-5	0	355	333
-4	0	447	400
-3	0	490	537
-2	0	994	1027
-1	0	329	330
0	0	577	523
1	0	409	418
2	0	96	50
3	0	415	426
4	0	546	541
5	0	143	128
6	0	287	286
7	0	190	182
-11	1	208	184
-10	1	167	151
-9	1	411	401
-8	1	251	246
-7	1	514	534
-6	1	493	502
-5	1	60	52
-4	1	583	569
-3	1	648	636
-2	1	142	148
-1	1	716	716
0	1	609	641
1	1	278	283
2	1	433	419
3	1	331	355
4	1	378	367
5	1	356	363
6	1	118	110
7	1	145	140
-11	2	304	296
-10	2	242	249
-9	2	34*	14
-8	2	410	418
-7	2	492	485
-6	2	234	240
-5	2	697	718
-4	2	439	466
-3	2	620	626
-2	2	561	512
-1	2	372	362
0	2	433	429
1	2	666	654
2	2	169	182
3	2	578	584
4	2	290	272
5	2	145	129
6	2	182	178
7	2	223	212
-11	3	37*	34
-10	3	228	217
-9	3	187	209
-8	3	329	335
-7	3	206	214
-6	3	690	681
-5	3	12*	11
-4	3	811	824
-3	3	363	355
-2	3	124	128
-1	3	321	326
0	3	665	659
1	3	106	95
2	3	759	769
3	3	184	178
4	3	474	454

Table 3. Continued.

H	K	10FO	10FC
5	3	137	154
6	3	103	96
7	3	37*	17
-10	4	35*	8
-9	4	51	36
-8	4	102	88
-7	4	619	640
-6	4	98	101
-5	4	836	845
-4	4	53	61
-3	4	527	532
-2	4	73	59
-1	4	419	425
0	4	53	26
1	4	785	773
2	4	120	116
3	4	624	613
4	4	33*	52
5	4	140	136
6	4	59	58
-10	5	189	190
-9	5	73	63
-8	5	310	326
-7	5	36*	56
-6	5	645	656
-5	5	160	149
-4	5	736	757
-3	5	176	165
-2	5	61	94
-1	5	235	232
0	5	581	573
1	5	212	204
2	5	627	644
3	5	33*	41
4	5	349	343
5	5	151	136
6	5	120	136
-10	6	166	163
-8	6	133	142
-7	6	407	412
-6	6	102	95
-5	6	588	606
-4	6	359	368
-3	6	406	400
-2	6	353	344
-1	6	267	259
0	6	381	356
1	6	487	501
2	6	96	85
3	6	344	342
4	6	107	123
5	6	34*	2
-9	7	204	222
-8	7	103	87
-7	7	87	96
-6	7	353	350
-5	7	203	196
-4	7	456	466
-3	7	417	411
-2	7	86	94
-1	7	419	412
0	7	337	340
1	7	323	318
2	7	232	233
3	7	88	92
4	7	74	80

H	K	10FO	10FC
5	7	192	192
-8	8	265	268
-7	8	119	96
-6	8	37*	24
-5	8	241	228
-4	8	296	300
-3	8	314	336
-2	8	402	398
-1	8	153	173
0	8	369	355
1	8	135	137
2	8	88	61
3	8	91	113
4	8	190	182
-7	9	274	270
-6	9	55	71
-5	9	120	88
-4	9	218	217
-3	9	299	292
-2	9	44*	23
-1	9	370	372
0	9	163	174
1	9	187	169
2	9	54	32
3	9	71	103
-6	10	138	131
-5	10	55	42
-4	10	132	139
-3	10	37*	107
-2	10	319	327
-1	10	98	102
0	10	252	252
1	10	49*	60
-4	11	39*	42
-3	11	242	243
-2	11	44*	43
	L = 5		
-3	-14	88	50
-2	-14	33*	35
-1	-14	37*	33
0	-14	158	151
-5	-13	183	181
-4	-13	70	57
-3	-13	35*	15
-2	-13	114	118
-1	-13	147	134
0	-13	34*	24
1	-13	226	232
2	-13	126	117
-7	-12	118	126
-6	-12	229	234
-5	-12	26*	13
-4	-12	89	87
-3	-12	198	196
-2	-12	56	53
-1	-12	173	179
0	-12	205	204
1	-12	38*	29
2	-12	254	249
3	-12	180	172
-8	-11	168	173
-7	-11	191	190
-6	-11	35*	29
-5	-11	155	158

H	K	10FO	10FC
-4	-11	230	222
-3	-11	20*	25
-2	-11	419	423
-1	-11	73	70
0	-11	111	116
1	-11	232	226
2	-11	122	120
3	-11	132	145
4	-11	249	262
-8	-10	112	122
-7	-10	109	110
-6	-10	166	155
-5	-10	130	156
-4	-10	33*	23
-3	-10	493	494
-2	-10	13*	53
-1	-10	421	421
0	-10	16*	58
1	-10	34*	16
2	-10	111	121
3	-10	253	233
4	-10	40*	46
5	-10	308	303
-9	-9	77	71
-8	-9	181	172
-7	-9	44*	21
-6	-9	32*	16
-5	-9	54	17
-4	-9	424	435
-3	-9	107	119
-2	-9	576	565
-1	-9	163	168
0	-9	271	280
1	-9	33*	17
2	-9	135	142
3	-9	34*	33
4	-9	307	299
5	-9	35*	40
-10	-8	84	62
-9	-8	261	285
-8	-8	68	65
-7	-8	124	116
-6	-8	88	55
-5	-8	206	201
-4	-8	192	194
-3	-8	578	605
-2	-8	60	64
-1	-8	461	455
0	-8	250	244
1	-8	32*	34
2	-8	121	127
3	-8	259	257
4	-8	93	89
5	-8	299	303
5	-8	109	109
-10	-7	238	241
-9	-7	43*	63
-8	-7	239	241
-7	-7	154	146
-6	-7	44	6
-5	-7	248	261
-4	-7	354	344
-3	-7	136	120
-2	-7	501	502
-1	-7	261	251
0	-7	248	236

H	K	10FO	10FC
1	-7	300	310
2	-7	109	96
3	-7	170	171
4	-7	274	295
5	-7	79	30
6	-7	163	182
-10	-6	99	110
-9	-6	256	272
-8	-6	199	181
-7	-6	149	165
-6	-6	299	302
-5	-6	135	163
-4	-6	361	367
-3	-6	440	434
-2	-6	68	102
-1	-6	360	362
0	-6	428	451
1	-6	31*	51
2	-6	317	312
3	-6	191	199
4	-6	98	92
5	-6	232	223
6	-6	186	178
-11	-5	172	165
-10	-5	195	206
-9	-5	8	22
-8	-5	210	213
-7	-5	341	328
-6	-5	53	22
-5	-5	438	428
-4	-5	268	277
-3	-5	241	239
-2	-5	407	395
-1	-5	345	340
0	-5	166	165
1	-5	461	463
2	-5	21*	40
3	-5	297	305
4	-5	205	209
5	-5	70	74
6	-5	137	116
-11	-4	113	125
-10	-4	133	141
-9	-4	142	149
-8	-4	244	243
-7	-4	45	49
-6	-4	520	550
-5	-4	121	126
-4	-4	477	487
-3	-4	273	259
-2	-4	85	106
-1	-4	226	238
0	-4	545	555
1	-4	69	71
2	-4	531	543
3	-4	33*	58
4	-4	149	138
5	-4	119	119
6	-4	192	171
7	-4	90	52
-11	-3	203	196
-10	-3	83	87
-9	-3	34*	42
-8	-3	1	39
-7	-3	524	542
-6	-3	50	62

H	K	10FO	10FC
-5	-3	598	619
-4	-3	99	105
-3	-3	280	297
-2	-3	196	210
-1	-3	481	495
0	-3	14*	3
1	-3	661	657
2	-3	48	24
3	-3	474	473
4	-3	32*	4
5	-3	62	48
6	-3	13	17
7	-3	181	168
-11	-2	7	3
-10	-2	98	71
-9	-2	13*	21
-8	-2	367	368
-7	-2	111	127
-6	-2	642	676
-5	-2	94	101
-4	-2	495	513
-3	-2	23*	48
-1	-2	111	124
0	-2	654	662
1	-2	83	66
2	-2	621	615
3	-2	149	156
4	-2	249	240
5	-2	68	63
6	-2	127	141
7	-2	92	86
-11	-1	181	162
-10	-1	65	60
-9	-1	134	130
-8	-1	191	212
-7	-1	522	537
-6	-1	78	76
-5	-1	635	691
-4	-1	257	236
-3	-1	231	227
-2	-1	319	349
-1	-1	455	442
0	-1	255	237
1	-1	654	669
2	-1	61	69
3	-1	386	360
4	-1	238	238
5	-1	69	9
6	-1	175	145
-11	0	132	142
-10	0	107	95
-9	0	198	205
-8	0	313	311
-7	0	128	127
-6	0	489	472
-5	0	316	316
-4	0	455	486
-3	0	467	467
-2	0	103	102
-1	0	470	465
0	0	479	466
1	0	145	168
2	0	386	375
3	0	251	254
4	0	123	122
5	0	269	258

H	K	10FO	10FC
6	0	119	142
-11	1	178	179
-10	1	230	230
-9	1	19*	29
-8	1	269	277
-7	1	279	280
-5	1	390	398
-4	1	556	597
-3	1	220	236
-2	1	566	560
-1	1	245	255
0	1	458	472
1	1	277	262
2	1	151	171
3	1	130	134
4	1	295	283
5	1	78	77
6	1	241	228
-11	2	155	192
-10	2	152	160
-9	2	325	332
-8	2	69	47
-7	2	205	214
-6	2	200	197
-5	2	300	286
-4	2	284	288
-3	2	581	572
-2	2	48	16
-1	2	555	570
0	2	169	194
1	2	127	110
2	2	72	64
3	2	252	260
4	2	12*	43
5	2	281	273
6	2	113	114
-10	3	296	289
-9	3	102	90
-8	3	377	381
-7	3	52	25
-6	3	81	50
-5	3	69	79
-4	3	423	412
-3	3	120	122
-2	3	592	605
-1	3	60	87
0	3	346	335
1	3	29*	21
2	3	119	123
3	3	52	23
4	3	284	282
5	3	92	98
6	3	183	197
-10	4	91	115
-9	4	359	353
-8	4	30*	79
-7	4	325	326
-5	4	162	155
-4	4	57	24
-3	4	505	519
-2	4	39*	10
-1	4	470	467
0	4	18*	8
1	4	76	70
2	4	87	71
3	4	257	266

H	K	10FO	10FC
4	4	103	98
5	4	230	211
-10	5	262	255
-9	5	89	99
-8	5	380	361
-7	5	119	120
-6	5	78	86
-5	5	130	130
-4	5	298	309
-3	5	81	57
-2	5	472	464
-1	5	37*	26
0	5	267	254
1	5	118	114
2	5	114	131
3	5	155	130
4	5	250	242
5	5	83	85
-9	6	281	268
-8	6	118	122
-7	6	264	259
-6	6	225	232
-5	6	149	141
-4	6	168	172
-3	6	357	359
-2	6	33*	8
-1	6	349	349
0	6	173	164
1	6	46	18
2	6	201	189
3	6	216	211
4	6	140	123
-8	7	247	240
-7	7	246	235
-6	7	77	62
-5	7	255	247
-4	7	233	231
-3	7	99	133
-2	7	242	247
-1	7	141	140
0	7	152	161
1	7	250	223
2	7	121	145
3	7	219	210
-7	8	149	157
-6	8	307	297
-5	8	110	67
-4	8	242	232
-3	8	108	119
-2	8	27*	28
-1	8	119	128
0	8	224	230
2	8	257	242
-6	9	97	78
-5	9	303	291
-4	9	75	49
-3	9	100	73
-2	9	36*	16
-1	9	112	110
0	9	62	32
1	9	265	260
-4	10	194	167
-3	10	65	61

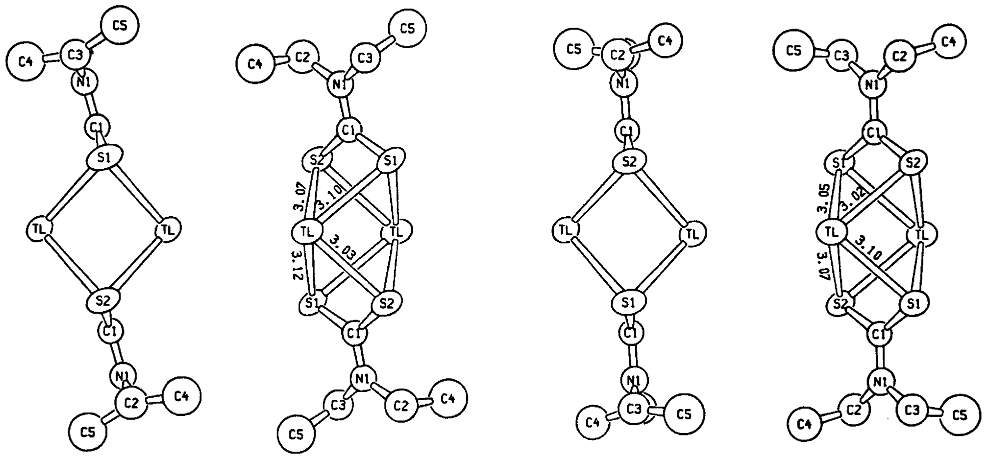

a b c d

Fig. 1 a–d. The dimeric molecules in thallium(I) diethyldithiocarbamate; *a* and *b* show molecule A, *c* and *d* molecule B. In *a* and *c* the sulfur plane is normal to the paper plane, in *b* and *d* it is inclined by 45°.

Table 4. Interatomic distances and angles in the dimeric molecules. Atoms which have been transformed according to the centrosymmetry are denoted by a bar.

Atoms	Distances (Å) in dimer A	Distances (Å) in dimer B
Tl—$\overline{\text{Tl}}$	3.619(1)	3.602(1)
Tl—S1	3.115(3)	3.047(3)
Tl—$\overline{\text{S1}}$	3.101(3)	3.104(3)
Tl—S2	3.034(3)	3.020(3)
Tl—$\overline{\text{S2}}$	3.073(3)	3.069(3)
S1—S2	2.954(4)	2.954(4)
S1—C1	1.71(1)	1.70(1)
S2—C1	1.72(1)	1.72(1)
C1—N1	1.32(1)	1.35(1)
N1—C2	1.51(2)	1.49(2)
N1—C3	1.48(2)	1.50(2)
C2—C4	1.50(2)	1.54(2)
C3—C5	1.56(2)	1.51(2)

Atoms	Angles (°) in dimer A	Angles (°) in dimer B
S1—C1—S2	118.6(4)	119.5(3)
S1—C1—N1	120.9(5)	121.3(5)
S2—C1—N1	120.4(5)	119.2(5)
C1—N1—C2	122.3(9)	123.5(9)
C1—N1—C3	122.4(8)	121.8(9)
C2—N1—C3	115.3(9)	114.6(9)
N1—C2—C4	110.1(11)	112.3(10)
N1—C3—C5	111.6(10)	108.5(11)

terminal carbons. Scattering factors published by Hanson *et al.*[6] were used to calculate F_c. Atomic coordinates, isotropic temperature factors and interlayer scale factors were refined by full matrix least squares minimizing $\sum\omega(|F_o|-|F_c|)^2$. The weight of a reflection, ω, was σ_F^{-2} where $\sigma_F=\sigma_I k/(4LpI)^{\frac{1}{2}}$ (k is the absolute scale factor, L the Lorentz and p the polarization factor). The discrepancy index, $R=\sum||F_o|-|F_c||\sum|F_o|$, was 0.126. With anisotropic temperature factors for thallium and sulfur R decreased to 0.059. Corrections for anomalous dispersion by thallium [7] decreased R further to 0.057. The remaining four carbon atoms were located in a difference synthesis. The refinement was continued to $R=0.037$ ($R_w=0.050$). The shifts in the last cycle were less than one tenth of the estimated standard deviations. The difference synthesis showed no significant maxima.

The final atomic parameters are given in Table 2 and the observed and calculated structure amplitudes in Table 3.

DESCRIPTION OF THE STRUCTURE

General features. The crystal is built from centrosymmetrical dimeric molecules, $[TlS_2CN(C_2H_5)_2]_2$. The two molecules in the unit cell are independent and have their centres

Table 5. Least squares planes through central parts of ligands defined by the equation $Ax+By+Cz+D=0$ where x,y,z are triclinic fractional coordinates. The distances of the defining points from the planes are shown. Unit weights were used for the first plane in each ligand, weights based on the estimated standard deviations of the coordinates for the second plane.

a. Plane parameters.

	A	*B*	*C*	*D*
Ligand A	4.933398	−0.564609	−5.741099	0.570082
	4.999688	−0.588242	−5.731134	0.549958
Ligand B	−1.650597	−0.683955	−5.412206	4.037951
	−1.482710	−1.009860	−5.414187	4.115935

b. Distance (Å).

	S1	S2	C1	N1	C2	C3
Ligand A	0.005	0.015	−0.020	−0.021	0.005	0.017
	0.001(3)	0.002(3)	−0.023(9)	−0.017(8)	0.010(13)	0.030(11)
Ligand B	0.045	−0.043	0.002	−0.011	0.055	−0.048
	0.006(3)	−0.004(3)	0.003(9)	−0.007(8)	0.093(12)	−0.076(12)

at 0,0,0 (A) and $\frac{1}{2},\frac{1}{2},\frac{1}{2}$ (B). Each molecule is linked by Tl—S bonds to two neighbours of its own kind so that two independent chains are formed. The chains run in the *c*-direction and are separated by the alkyl groups of the ligands.

The dimers. The dimeric molecules are similar to those found in the methyl,[3] propyl,[1] and isopropyl [2] homologues. Dimers have also been found in solutions.[4] The ethyl compound is the first case where there are two independent molecules in the structure. The molecules A and B are very similar; Fig. 1 and Table 4. The central parallelograms of sulfur atoms have corner angles 88.4°(A) and 89.1°(B). The short edges, *i.e.* the S—S bite in the ligands, are 2.95 Å in both dimers. The long edges are 4.02 Å (A) and 3.97 Å (B). Since the Tl—S bonds are in the close range 3.02 to 3.12 Å, the Tl—Tl vectors are normal to the sulfur planes (within 2°). The angles and distances in the dithiocarbamate ligands are in good agreement with the values in other dithiocarbamates. The SSCNCC groups are planar as usual. The fit of the least squares plane is somewhat better in A than in B; Table 5.

The linkage. Each dimer is linked to two identical neighbours, Fig. 2. The Tl—S networks of the two chains are strikingly similar, Fig. 3. The intramolecular Tl—S bonds are in the range 3.71 to 3.89 Å. Although rather long, these

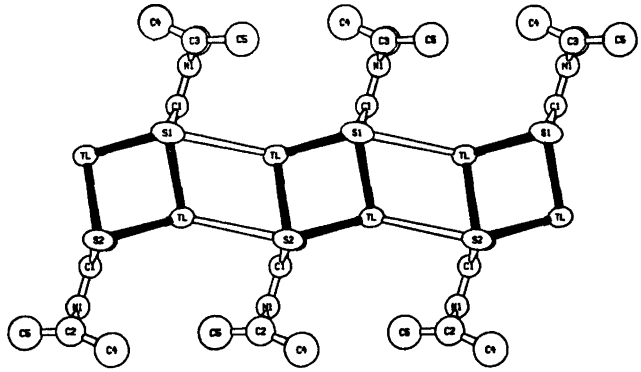

Fig. 2. Chains A. All the thallium atoms are situated in the paper plane.

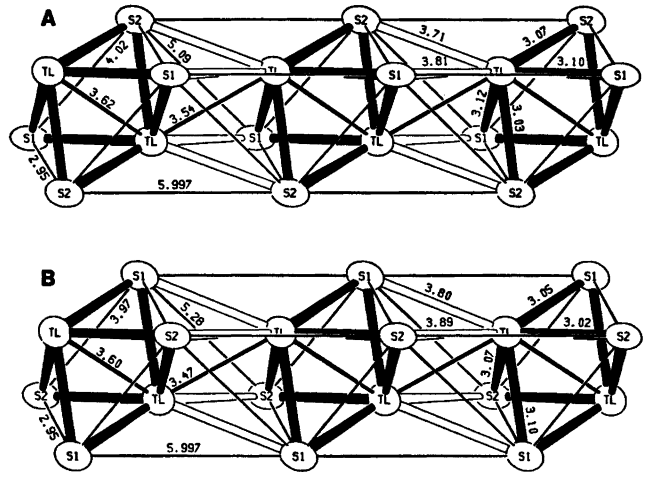

Fig. 3. The thallium sulfur arrangement within the chains of molecules; chain A above and chain B below. Tl—S bonds in the molecules are black.

Table 6. Interatomic distances in Å shorter than 4 Å between atoms in different dimers. The relation of the second atom to the coordinates x,y,z of Table 2 is shown. Distances between atoms in different chains are set in italics.

Distances from atoms in dimer A				Distances from atoms in dimer B			
Atom 1	Atom 2	Dist.		Atom 1	Atom 2	Dist.	
Tl(A)	Cl(A)	3.462	$-x,-y,-z+1$	Tl(B)	Cl(B)	3.466	$x,y,z-1$
Tl(A)	Tl(A)	3.536	$-x,-y,-z+1$	Tl(B)	Tl(B)	3.474	$-x+1,-y+1,-z$
S1(A)	C2(B)	*3.598*	x,y,z	C2(B)	S1(A)	*3.598*	x,y,z
C4(A)	S2(B)	*3.641*	$-x+1,-y,-z+1$	S2(B)	C4(A)	*3.641*	$-x+1,-y,-z+1$
Tl(A)	S2(A)	3.710	$-x,-y,-z+1$	Tl(B)	N1(B)	3.738	$x,y,z-1$
S2(A)	C4(B)	*3.739*	$-x,-y,-z+1$	C4(B)	S2(A)	*3.739*	$-x,-y,-z+1$
C2(A)	S2(B)	*3.766*	$-x+1,-y,-z+1$	S2(B)	C2(A)	*3.766*	$-x+1,-y,-z+1$
Tl(A)	S1(A)	3.806	$-x,-y,-z+1$	Tl(B)	S1(B)	3.803	$x,y,z-1$
C3(A)	S2(B)	*3.854*	$-x+1,-y,-z+1$	S2(B)	C3(A)	*3.854*	$-x+1,-y,-z+1$
C4(A)	C5(B)	*3.857*	$-x,-y,-z$	C5(B)	C4(A)	*3.857*	$-x,-y,-z$
S2(A)	C2(B)	*3.865*	$-x,-y,-z+1$	C5(B)	C5(B)	*3.857*	$-x,-y+1,-z+1$
C4(A)	S1(B)	*3.888*	$x,y-1,z-1$	C2(B)	S2(A)	*3.865*	$-x,-y,-z+1$
Tl(A)	N1(A)	3.907	$-x,-y,-z+1$	Tl(B)	S2(B)	3.888	$x,y,z-1$
C2(A)	C5(B)	*3.968*	$-x,-y,-z+1$	S1(B)	C4(A)	*3.888*	$x,y+1,z+1$
				Tl(B)	C4(B)	3.890	$x,y,z-1$
				C5(B)	C2(A)	*3.968*	$-x,-y,-z+1$

Table 7. Distances of coordination. The relation of the sulfur atoms to the coordinates x,y,z of Table 2 is shown.

Dimer A			Dimer B		
Atom	Dist. (Å)		Atom	Dist. (Å)	
S2	3.034(3)	x,y,z	S2	3.020(3)	x,y,z
S2	3.073(3)	$-x,-y,-z$	S1	3.047(3)	x,y,z
S1	3.101(3)	$-x,-y,-z$	S2	3.069(3)	$-x+1,-y+1,-z+1$
S1	3.115(3)	x,y,z	S1	3.104(3)	$-x+1,-y+1,-z+1$
S2	3.710(3)	$-x,-y,-z+1$	S1	3.803(3)	$x,y,z,-1$
S1	3.806(3)	$-x,-y,-z+1$	S2	3.888(3)	$x,y,z-1$

bonds are strong enough to maintain the similarity of the chains under the influence of the packing forces in the crystal.

The interatomic distances between different molecules are listed in Table 6. The Tl—Cl distance, 3.46 Å (A) and 3.47 Å (B), are substantially smaller than the sum of the van der Waals radii given by Bondi,[8] 3.73 Å (Tl: 1.96 Å; aromatic C: 1.77 Å). The Tl—C contacts are evidently compressed by the Tl—S bonds; Fig. 2. The shorter Tl—S distances in chains A, average 3.76 Å *vs.* 3.85 Å in B, are possible because of the larger angle between the ligand and the central sulfur plane in A, 16.2° *vs.* 5.1° in B; Fig. 1 *a* and *c*.

The coordination. The Tl—S distances are listed in Table 7. The metal coordination is trigonal prismatic, Fig. 3. Two of the quadrangular faces are shared with neighbours. The largest face is left unshared with the bulk of the ligands outside.

The metal coordination number is seven in the corresponding methyl compound,[3] six and five in the propyl compound,[1] and five in the isopropyl compound.[2] The consistency of the series [9] is confirmed by the coordination number six in the ethyl compound. The decrease in the number of coordinated atoms with the bulk of the ligands is associated with the increasing difficulty of obtaining molecular packings which are suitable for coordination.

The metal atom arrangement. The thallium atoms form planar zigzag chains, Table 8. The Tl—Tl distances in the molecules are similar to those found in the isopropyl compound,[2] 3.58 Å. The longer distances in the methyl [1] and

Table 8. Distances and angles in metal atom chains.

	Distances (Å)		Angle (°)
Chain A	3.536(1)	3.619(1)	113.87(5)
Chain B	3.474(1)	3.603(1)	115.84(5)

propyl [2] compounds, 3.85 and 4.00 Å, show that these molecules are deformed in the crystal structures.

The structure of the dimeric molecule suggests that the thallium atoms are held in contact, 3.6 Å apart, by the bridging sulfur atoms.[2] Shorter Tl—Tl distances occur between the molecules in the ethyl compound, 3.47 Å. The radius of Tl^+, which is a highly polarizable ion,[10] apparently depends not only on the bonding conditions but also on the direction.

The Tl—Tl distances in the dithiocarbamates are not much longer than the interatomic distances in metallic thallium, 3.408 Å.[11] Short distances are observed in other compounds *e.g.* $Tl_2Ti_4O_9$ (3.25 Å),[12] $Tl_4(OCH_3)$ (3.84 Å),[13] $Tl^{I}Tl^{III}S_2$ (3.40 Å),[14] Tl_3VS_4 (3.75 Å),[15] and $TlX.4(NH_2)_2CS$ (4.13 Å) [16] ($X=H_2PO_4^-$ ClO_3^-, ClO_4^-, NO_3^-). The Tl—Tl distances in the sulfur containing compounds are not related to the number of Tl—S—Tl bridges.

Table 9. Minimum distances used in the calculation of the packing surface. No tests were made for Tl—S distances. C_M represents methyl and methylene carbon atoms.

Atoms	Dist. (Å)	Atoms	Dist. (Å)
Tl—Tl	3.41	S—C_M	3.52
Tl—N	3.25	N—N	3.10
Tl—C	3.40	N—C	3.25
Tl—C_M	3.49	N—C_M	3.33
S—S	3.48	C—C	3.40
S—N	3.29	C—C_M	3.48
S—C	3.44	C_M—C_M	3.57

The packing of the chains. The packing of the flat chains running in the *c*-direction is shown in Fig. 4. Distances between atoms in different chains are shown in Table 6. The absence of metal-ligand interactions between the chains results in the parquet-like packing which is also found in some long chain hydrocarbons.[17]

THE RELATION BETWEEN THE METAL COORDINATION AND MOLECULAR PACKING

When molecules consisting of metal atoms and ligands form a crystal, the metal atoms may increase their coordination numbers by employ-

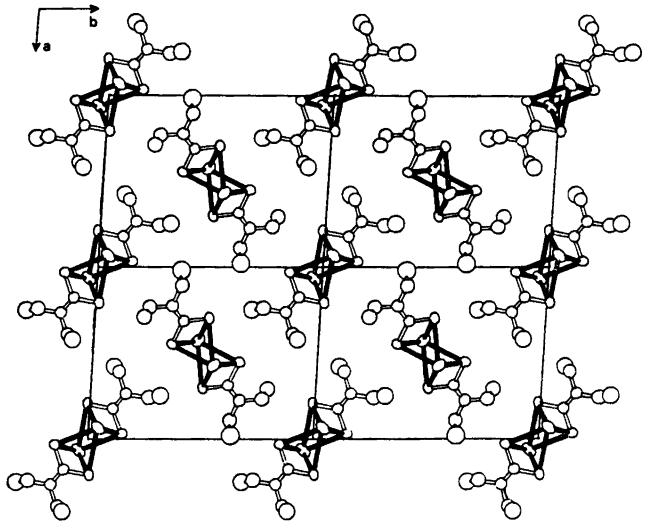

Fig. 4. Projection of the arrangement of the chains on a plane normal to **c**. The figure shows nine chains of molecules A ($z=0$) and four chains of molecules B ($z=\frac{1}{2}$).

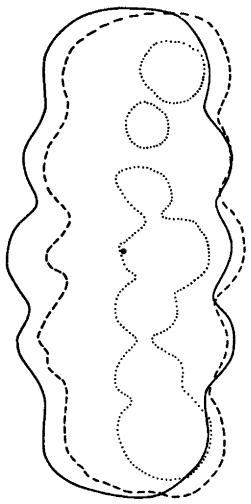

Fig. 5. The surface of parallel packing at three levels corresponding to 0.0 Å (full line), 3.2 Å (broken line) and 6.4 Å (dotted line) above the paper plane. The calculation was performed with molecule B in the orientation shown in Fig. 1c with the molecular centre in the paper plane.

ing donor atoms from suitably oriented molecules in the vicinity. The fundamental importance of the packing characteristics of the molecules for the coordination geometry in the crystal will be illustrated by a molecular packing program related to PACK.[2]

The program simulates the packing of two parallel molecules. One of the molecules is kept stationary. The other one is translated in small steps keeping the parallel orientation. The positions in scan are marked as allowed if all the interatomic distances exceed minimum values, otherwise as forbidden. This hard spheres approach is justified by the rapid increase in the repulsion between two atoms when their separation drops below a certain value.

The generated three-dimensional body of forbidden positions defines the *surface of parallel packing*. The parallel case is of particular interest in crystallography but similar packing surfaces may be calculated for other orientations. The set of positions which is inside the packing surfaces of all orientations defines the *surface of closest packing*. This surface cannot be penetrated by another molecule in any orientation.

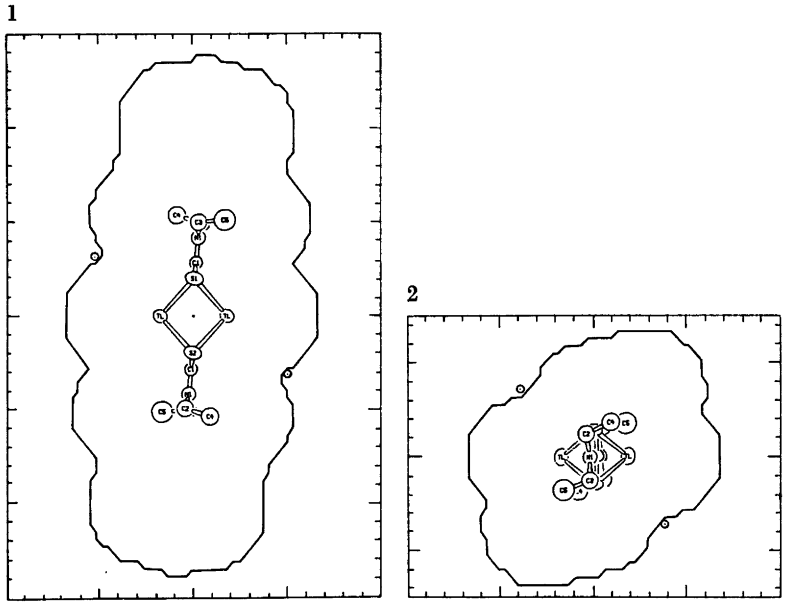

Fig. 6. Two sections of the packing surface of molecule B. The stationary molecule shows the orientation used: thallium atoms in the paper, the paper being normal to the short edge of the sulfur parallelogram in case 1 and to the long edge in case 2. Each thallium atom in the stationary molecule has two sulfur atoms in the moving molecule at equal distance. The minimum distances are obtained at the indicated points. An Ångström scale is shown in the frame.

The surface of parallel packing has been calculated for thallium(I) diethyldithiocarbamate. The molecule B was used as a model in the calculations, Fig. 1. The minimum distances, Table 9, were computed from the van der Waals radii defined by Bondi.[8] The thallium radius, 1.96 Å, assessed by Bondi with reservation, is rather long considering the observed distances. The radius in the metal,[11] 1.71 Å, was then selected as appropriate for minimum distances. The methyl and methylene groups were assigned radii as entities, 1.78 Å, since no hydrogen positions had been determined. The contact distances between carbon atoms in crystals of hydrocarbons [17,18] are usually around 3.9 Å but the distances may be as short as 3.57 Å if the packing is successful.[8] No tests were made for Tl—S distances which represent attractions.

Fig. 5 shows the surface obtained at a resolution of 0.4 Å. It is composed of intersecting contact spheres between pairs of atoms. Only surface positions close to the centre may involve Tl—S bonds between the two molecules. Positions close to the ends involve methyl-methyl contacts only.

The thallium coordination geometry varies with the position of the neighbour molecule on the packing surface. The highest possible coordination number is six since Tl—Tl contacts prevent the formation of more than two new Tl—S bonds from each metal atom. There are two planar regions on the surface where two sulfur atoms are at equal distances from the thallium atom, Fig. 6. In case 1 the sulfur atoms belong to the same ligand, in case 2 to different ligands. The shortest distances are obtained at the indicated points. They are equal within the resolution, 3.7 Å in case 1 and 3.6 Å in case 2. The coordination is trigonal prismatic in both cases but the metal atom is situated inside the faces of the prism in case 1 and slightly outside one of the faces in case 2.

Case 1 is observed in the structure of the ethyl compound. The neighbour molecule is found at the indicated point of minimum Tl—S distances. A map with twice as fine a grid also reproduces the actual position within the grid step.

Case 2 is observed in a somewhat deformed version in the methyl compound [3] where a seventh sulfur atom from a third molecule completes the coordination. The metal atom is again well inside the coordination polyhedron.

Acknowledgements. We wish to thank Dr. Rolf Hesse for many valuable and inspiring discussions. We are grateful to Dr. Stig Åkerström for the supply of sample. One of us (H.P.) thanks the Swedish Institute for a grant. The work has been supported by a grant from the Swedish Natural Science Research Council which is gratefully acknowledged.

REFERENCES

1. Nilson, L. and Hesse, R. *Acta Chem. Scand. 23* (1969) 1951.
2. Jennische, P., Olin, Å. and Hesse, R. *Acta Chem. Scand. 26* (1972) 2799.
3. Jennische, P. and Hesse, R. *Acta Chem. Scand. 27* (1973) 3531.
4. Åkerström, S. *Ark. Kemi 24* (1965) 495.
5. Parrish, W. *Acta Crystallogr. 13* (1960) 838.
6. Hanson, H. P., Herman, F., Lea, J. D. and Skillman, S. *Acta Crystallogr. 17* (1964) 1040.
7. *International Tables for X-Ray Crystallography*, Kynoch Press, Birmingham 1962, Vol. III.
8. Bondi, A. *J. Phys. Chem. 68* (1964) 441.
9. Jennische, P. and Hesse, R. *Paper presented to the First European Congress of Crystallography*, Bordeaux 1973.
10. Lee, A. G. *Coord. Chem. Rev. 8* (1972) 289.
11. Pearson, W. B. *Handbook of Lattice Spacings and Structures of Metals*, Pergamon, Oxford 1967, Vol. 2, p. 90.
12. Verbaere, A. and Tournoux, M. *Bull. Soc. Chim. Fr.* (1973) 1237.
13. Dahl, L. F., Davis, G. L., Wampler, D. L. and West, R. J. *J. Inorg. Nucl. Chem. 24* (1962) 357.
14. Müller, D., Eulenberger, G. and Hahn, H. *Z. Anorg. Allg. Chem. 398* (1973) 207.
15. Crevecoeur, C. *Acta Crystallogr. 17* (1964) 757.
16. Boeyens, J. C. A. and Herbstein, F. H. *Inorg. Chem. 6* (1967) 1408; Verhoef, L. H. W. and Boeyens, J. C. A. *Acta Crystallogr. B 24* (1968) 1262; Verhoef, L. H. W. and Boeyens, J. C. A. *Ibid. B 25* (1969) 607; Mitchell, J. and Boeyens, J. C. A. *Ibid. B 26* (1970) 1121.
17. Teare, P. W. *Acta Crystallogr. 12* (1959) 294.
18. Shearer, H. M. M. and Vand, V. *Acta Crystallogr. 9* (1956) 379.

Received July 24, 1974.

Acta Chemica Scandinavica A 29 (1975) 71—75

Studies on Polythionates. IV. The Action of the Cyanide Ion on the Selenotrithionate Ion and the Diselenotetrathionate Ion in Acetonitrile

TOR AUSTAD

Chemical Institute, University of Bergen, N-5000 Bergen, Norway

The reactions of the selenotrithionate ion and the diselenotetrathionate ion with ionic cyanide have been studied in acetonitrile. Kinetic studies showed both of the reactions to be of second order, first order in each of the reactants. Reaction mechanisms have been worked out that conform favourably with each other.

The electrophilic nature of divalent selenium and sulfur toward ionic cyanide is discussed by comparing the activation parameters.

As part of our work concerning polythionates in dipolar aprotic solvents, this paper reports a kinetic study on the selenotrithionate-cyanide reaction and the diselenotetrathionate-cyanide reaction in acetonitrile. Previous work has shown that ionic cyanide reacts with the tetrathionate ion, but it does not react with the trithionate ion even in boiling acetonitrile.[1]

With regard to the cyanide ion as the nucleophilic agent, it is further known that the activation energy for nucleophilic attack at divalent selenium is lower than the activation energy for nucleophilic substitution at the corresponding sulfur compound.[2] The purpose of this work was therefore to get some more knowledge about nucleophilic substitution at divalent selenium and to determine the reaction mechanisms of the two reactions mentioned above.

The reactions are studied in acetonitrile to prevent hydrolysis of the reaction intermediates. In this way the study of the mechanisms became easier, and one was able to detect some of the reaction intermediates. Tetraphenylarsonium salts of the polythionates were used as the substrates, and tetraphenylphosphonium cyanide was used as the nucleophilic agent.

To understand the reaction mechanisms, it appears necessary to present some notes dealing with the sulfite ion and the selenosulfate ion in dipolar aprotic solvents.

Notes on the sulfite ion and the selenosulfate ion. In aqueous solution, ionic sulfite is slowly oxidized to ionic sulfate, which makes quantitative determinations by means of iodometric titrations difficult. In acetonitrile, however, tetraphenylarsonium sulfite is nearly immediately oxidized to the corresponding sulfate salt, probably due to traces of oxygen in the solvent. Therefore, when working with ionic sulfite in acetonitrile, the solvent has to be carefully flushed with nitrogen prior to use.

In protic solvents ionic sulfite reacts with elemental selenium, and the equilibrium (1) is set up.

$$SO_3^{2-} + Se \rightleftharpoons SeSO_3^{2-} \qquad (1)$$

The reaction between the sulfite ion and sulfur S_8 has been formulated as an initial attack on the sulfur ring with ring opening followed by a series of displacements of ionic thiosulfate by the sulfite ion.[3] In view of the similarity of the sulfite–selenium reaction and the sulfite–sulfur reaction, it seems reasonable to assume that the mechanism is the same in both cases.

In acetonitrile free from oxygen, the sulfite ion reacts with elemental selenium in a way different from the one depicted by eqn. (1). The products were found to be ionic diselenotetrathionate and probably some unidentified polyselenide ions, Se_x^{2-}, eqn. (2).

$$SO_3^{2-} + Se \xrightarrow{MeCN} {}^-O_3S-Se-Se-SO_3^- + Se_x^{2-} \quad (2)$$

The second step of the sulfite – selenium reaction in acetonitrile probably is different from what happens in aqueous solution, where the selenosulfate ion appears to be the leaving group.

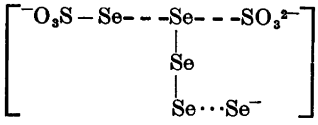

(I)

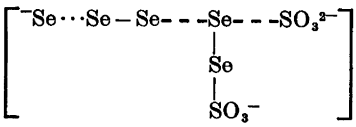

(II)

With regard to the two transition states visualized by (I) and (II), the transition state (I) thus appears to be favoured in the protic solvents, while the transition state (II) probably is more favourable in acetonitrile. The poor solvation of the sulfonate group by acetonitrile may explain this change in the leaving group when going from a protic to a dipolar aprotic solvent.

No liberation of red selenium is observed when tetraphenylarsonium selenosulfate is dissolved in acetonitrile. However, the solution turned yellowish-green, and ionic diselenotetrathionate, sulfate and probably some polyselenide ions were formed.[4] The reaction may take place as depicted schematically in eqn. (3).

$$SeSO_3^{2-} \xrightarrow{MeCN} SO_3^{2-} + Se \xrightarrow[O_2]{MeCN} {}^-O_3S-Se-Se-SO_3^- + SO_4^{2-} + Se_x^{2-} \quad (3)$$

The selenotrithionate-cyanide reaction. The selenotrithionate ion was found to react very slowly with ionic cyanide in acetonitrile. The rate of this reaction was followed by measuring the formation of ionic selenocyanate by means of IR. The reaction was observed to be of second order, first order in each of the reactants. Furthermore, the kinetic plots indicate that 1 mol of ionic selenotrithionate consumes 5 mol of cyanide ions to give 1 mol of ionic selenocyanate. On these observations the following stoichiometry is postulated, eqn. 4.

$$SeS_2O_6^{2-} + 5CN^- \xrightarrow{MeCN} 2SO_3^{2-} + (CN)_4^{2-} + SeCN^- \quad (4)$$

Due to traces of oxygen in the acetonitrile solution, the sulfite ion is, however, immediately oxidized to ionic sulfate.

With regard to the mechanism of the reaction, it appears likely that the first step involves a nucleophilic attack by the cyanide ion at the selenium atom, displacing the sulfite ion, eqn. 5.

$$^-O_3S-Se-SO_3^- + CN^- \xrightarrow{slow} {}^-O_3S-SeCN + SO_3^{2-} \quad (5)$$

The selenocyanato sulfonate ion, $^-O_3S-SeCN$, is then susceptible to nucleophilic attack by a second cyanide ion. The electrophilic centre appears to be the selenium atom, and ionic sulfite is displaced, eqn. 6.

$$^-O_3S-SeCN + CN^- \xrightarrow{fast} SO_3^{2-} + Se(CN)_2 \quad (6)$$

It is further known that selenium dicyanide reacts rapidly with 3 mol of cyanide ions in acetonitrile, probably according to eqn. 7.[5]

$$Se(CN)_2 + 3CN^- \xrightarrow{fast} SeCN^- + (CN)_4^{2-} \quad (7)$$

This reaction mechanism is consistent with the mole ratio of the reactants observed in the kinetic runs. The second order rate constants and the activation parameters are presented in Table 1.

The reaction mechanism outlined above gains support from a study of the diselenotetrathionate – cyanide reaction.

The diselenotetrathionate-cyanide reaction. Potassium diselenotetrathionate was synthesized

Table 1. Second order rate constants and activation parameters for the selenotrithionate-cyanide reaction in acetonitrile ($\mu = 6.0 \times 10^{-2}$).

$k_2 \times 10^5$ (M^{-1} s^{-1})		
20 °C	3.42	3.33
30 °C	7.15	6.85
45 °C	10.1	9.70
ΔH^* (kcal/mol)	9.2	
ΔS^* (cal/mol deg.)	−47	
ΔF^* (kcal/mol)	23.3	

Table 2. Verification of the stoichiometry of the diselenotetrathionate-cyanide reaction in acetonitrile.

$Se_2S_2O_6^{2-} + nCN^- \rightleftharpoons mSeCN^- + Products$

n	m	Rate
1	½	fast
2	1	fast
6	2	1st mol fast, 2nd mol slow

for the first time by Janickis and co-workers in 1954.[6] The compound was made by oxidation of selenosulfate (K_2SeSO_3) with iodine or hydrogen peroxide. In this work, tetraphenylarsonium diselenotetrathionate has been synthesized by the action of the sulfite ion on elemental selenium in acetonitrile, which was carefully flushed with nitrogen prior to use.

The reaction between ionic diselenotetrathionate and the cyanide ion was very fast in acetonitrile. The stoichiometry of the reaction was examined by varying the cyanide concentration, and measuring the formation of ionic selenocyanate by means of IR. The results are listed in Table 2.

According to Table 2, the diselenotetrathionate ion consumes 2 mol of cyanide ions to give 1 mol of ionic selenocyanate in a very fast reaction. On the addition of more ionic cyanide, a second mol of ionic selenocyanate started to form. However, this second mol of selenocyanate ion was formed at a much slower rate than the first mol, and furthermore, the concentration of the cyanide ions had to be six times the concentration of ionic diselenotetrathionate to give 2 mol of ionic selenocyanate quantiatively. According to these observations, the reaction in Scheme 1 may be written.

$$^-O_3S-Se-Se-SO_3^- + CN^- \xrightarrow{k_2'} {}^-O_3S-SeCN + SeSO_3^{2-}$$

$$k_2''' \downarrow CN^- \qquad k_2'' \downarrow CN^-$$

$$SO_3^{2-} + Se(CN)_2 \qquad SeCN^- + SO_3^{2-}$$

$$\text{Fast} \downarrow 3CN^-$$

$$SeCN^- + (CN)_4^{2-}$$

Scheme 1.

The first step probably involves a nucleophilic substitution at one of the selenium atoms of the polythionate ion, and ionic selenosulfate is displaced. Due to the instability of the selenosulfate ion in acetonitrile, it reacts immediately with a second cyanide ion to give ionic sulfite and selenocyanate. An approximate value of the second order rate constant of the first step, k_2', has been obtained using the stopped-flow technique. The rate was followed at $\lambda = 300$ nm, and the results are presented in Table 3. The fact that 1 mol of each of the reactants gave ½ mol of ionic selenocyanate, Table 2, appears to justify that $k_2' \ll k_2''$.

The selenocyanatosulfonate ion, $^-O_3SSeCN$, formed in the first step, consumes 4 mol of cyanide ions at a rate that is much slower than the rate of the first step. The rate of the selenocyanatosulfonate-cyanide reaction was followed by measuring the formation of the second mol of ionic selenocyanate by means of IR. When analysing the rate according to the assumption that 1 mol of ionic selenocyanatosulfonate reacts with 4 mol of cyanide ions, the kinetic plots showed excellent second order kinetics, up to three half lives, Table 3.

DISCUSSION

The reaction mechanism postulated for the selenotrithionate-cyanide reaction appears to be supported by the rate experiments of the diselenotetrathionate-cyanide reaction. From the rate constants presented in Tables 1 and 3 it is seen that $k_2(SeS_2O_6^{2-} + CN^-) \ll k_2(^-O_3SSeCN + CN^-) \ll k_2(Se_2S_2O_6^{2-} + CN^-)$ which is in ac-

Table 3. Second order rate constants between different substrates and the cyanide ion in acetonitrile at 25 °C.
Substrate + CN^- → Products

Substrate	k_2 M^{-1} s^{-1}	μ
$^-O_3S-Se-Se-SO_3^-$	2500	6.28×10^{-3}
$^-O_3S-S-S-SO_3^-$	2.90×10^{-3} [a]	2.55×10^{-2} [a]
$^-O_3S-SeCN$	1.92×10^{-1}	9.0×10^{-3}
	2.01×10^{-1}	9.0×10^{-3}
$^-O_3S-SCN$	2.95×10^{-2} [b]	1.7×10^{-2} [b]

[a] Ref. 1. [b] Ref. 2; 30 °C.

cordance with the reaction mechanisms outlined above.

A first step involving nucleophilic attack at one of the sulfonyl sulfur atoms of the selenotrithionate ion, displacing ionic selenosulfate, can hardly be made to fit the stoichiometry of the reactants that was experimentally observed.

In acetonitrile the thiocyanatosulfonate ion, $^{-}O_3SSCN$, which is believed to be an intermediate in other polythionate-cyanide reactions, probably is attacked by ionic cyanide at the sulfonyl sulfur in an S_N2 reaction to displace ionic thiocyante,[2] Table 3. With regard to the corresponding step of the selenocyanatosulfonate-cyanide reaction, the nucleophilic attack has to take place at the divalent selenium atom, otherwise the mol ratio of the reactants will not be in accordance with the experiments.

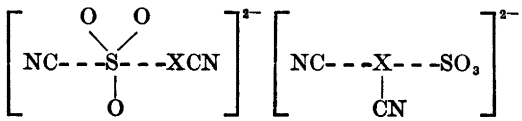

(III) (IV)

The transition state (III) for the intermediate step is thus believed to be the most favourable one for X = S, and the transition state (IV) for X = Se. The energy of activation for nucleophilic substitution at divalent selenium by the cyanide ion is found to be much lower than the energy of activation for the analogous reaction at divalent sulfur.[2] The change of the electrophilic positions in the thiocyanatosulfonate ion and the selenocyanatosulfonate ion thus appears reasonable. Furthermore, the more negative charge probably found on the sulfonate group of the selenocyanatosulfonate ion relative to that of the thiocyanatosulfonate ion, may lower the electrophilic nature of the sulfonyl sulfur of the former.

The activation parameters of the selenotrithionate-cyanide reaction are presented in Table 1. From the activation parameters of the selenopentathionate-cyanide reaction previously obtained ($\Delta H^* = 1.7$ kcal/mol, $\Delta S^* = -48$ cal/mol deg.),[2] it is seen that the difference in the enthalpy of activation is responsible for the large difference in the rate constants, by a factor of 10^6.

The accumulation of three negative charges in a small volume near the reactive position may be responsible for the relatively large value of ΔH^* in the selenotrithionate-cyanide reaction. The electrostatic repulsion between the two negatively charged sulfonate groups may work against the formation of the T-shaped transition state. The relatively smaller ability of the sulfenyl sulfur to participate in a three-centre four-electron bonding system appears to explain why the trithionate ion does not react with the cyanide ion in acetonitrile, while selenotrithionate reacts, albeit slowly. (The value of the enthalpy of activation probably is too high).

With regard to the diselenotetrathionate-cyanide reaction, it is seen from Table 3 that this reaction is about 10^6 times faster than the analogous tetrathionate-cyanide reaction in acetonitrile. Due to the low accuracy of the rate constant of the diselenotetrathionate-cyanide reaction, activation parameters of this reaction have not been calculated. However, previous work [2] indicates that the great difference in the rate constants is caused by a relatively lower energy of activation of the diseleno-tetrathionate – cyanide reaction.

EXPERIMENTAL

Acetonitrile and tetraphenylphosphonium cyanide were purified as reported.[1]

Tetraphenylarsonium selenotrithionate was precipitated from an aqueous solution of potassium selenotrithionate [7] by means of tetraphenylarsonium chloride in nearly quantitative yield. The product was recrystallized from acetonitrile by adding acetone. Dec. 245 °C. (Found: C 56.54; H 3.86; S 6.63. Calc. for $C_{48}H_{40}O_6S_2SeAs_2$: C 57.34; H 3.98; S 6.38.)

Tetraphenylarsonium sulfite 10.5 g (2.06×10^{-2} mol) of tetraphenylarsonium iodide was dissolved in 150 ml absolute methanol. 7.0 g freshly prepared dry silver sulfite was added, and the reaction mixture was left stirring at room temperature for 2 h. After filtration, the solvent was removed *in vacuo*. The residue was dissolved in 30 ml methanol and once more filtered to remove traces of elemental silver. On the addition of about 250 ml diethyl ether, an oily precipitate appeared. On standing in a refrigerator over night the product crystallized. Yield, 7.0 g or 82 %, based on the amount of tetraphenylarsonium iodide used.

Iodometric analysis of tetraphenylarsonium sulfite showed 3.9 % smaller value than the theoretical one.[2] If, however, the composition of the salt is $(Ph_4As)_2SO_3 \cdot 2H_2O$, the iodometric results agree with the theoretical value.

Oxidation of ionic sulfite in acetonitrile. 0.0480 g tetraphenylarsonium sulfite was dissolved in

6 ml of acetonitrile. After standing for 5 min in an open beaker, iodometric analysis showed that the solution did not contain any ionic sulfite. The only product isolated was tetraphenylarsonium sulfate.

Tetraphenylarsonium diselenotetrathionate. To a mixture containing 2.0 g grey selenium and 20 ml acetonitrile, which was carefully flushed with dry nitrogen, was added 2.0 g of tetraphenylarsonium sulfite. The temperature was raised to 50 °C and the reaction mixture acquired a deep green colour. After stirring for about 1 h, excess selenium was filtered off. The solvent was removed *in vacuo* and the residue was washed with 20 ml acetone. Most of the colour then transferred to the mother liquor. Afterwards the product was dissolved in 10 – 15 ml of acetonitrile and 100 ml of acetone was added to this yellowish – green solution, whereupon the salt crystallized. The yield was 0.70 g, or 59 % based on the amount of tetraphenylarsonium sulfite used.

Pure material was finally obtained by recrystallization from 10 ml warm acetonitrile. Yield, 0.35 g. Dec. 230 °C. (Found: C 52.41; H 3.54; S 6.48. Calc. for $C_{48}H_{40}O_6S_2Se_2As_2$: C 52.70; H 3.66; S 5.88.)

Kinetic experiments

The rate of the selenotrithionate-cyanide reaction was followed by measuring the formation of ionic selenocyanate applying IR. The kinetic plots were calculated by means of the rate equation:

$$dx/dt = k_2 (a-x)(b-5x)$$

where x is the concentration of ionic selenocyanate, and a and b are the concentrations of ionic selenotrithionate and cyanide, 8.0×10^{-3} and 4.0×10^{-2} M, respectively.

The rate of the first step of the diselenotetrathionate-cyanide reaction was determined by stopped-flow measurements. Due to absorption of the onium ion, the rate constant could only be approximately determined by measuring the disappearance of the absorption of the diselenotetrathionate ion at $\lambda = 300$ nm. Solutions containing 1.0×10^{-3} M of substrate and 9.56×10^{-3} M of the nucleophile were used.

The rate of the selenocyanatosulfonate-cyanide reaction was determined by measuring the rate of formation of the second mol of ionic selenocyanate formed in the reaction between the diselenotetrathionate ion and the cyanide ion, applying the initial concentrations of ionic diselenotetrathionate and cyanide, 2.0×10^{-3} and 1.2×10^{-2} M, respectively. The kinetic plots were analysed according to the equation:

$$x/[a(a-x)] = 4\, k_2'''t$$

where x is the concentration of the second mol of ionic selenocyanate and a is the initial concentration of the selenocyanato sulfonate ions, 2.0×10^{-3} M.

The rate constants of the selenotrithionate-cyanide reaction and the selenocyanatosulfonate-cyanide reaction were reproduced with an accuracy better than ± 5 %.

The IR measurements were performed on a SP 200 G Infrared Spectrophotometer applying 0.1 cm liquid cells, and the stopped-flow measurements were performed with a Durrum Stopped-Flow Model D-110.

Acknowledgement. The author is indebted to The Norwegian Research Council for Science and the Humanities for a grant.

REFERENCES

1. Austad, T. *Acta Chem. Scand. A 28* (1974) 693.
2. Austad, T. *Acta Chem. Scand. A 28* (1974) 935.
3. Foss, O. *Organic Sulfur Compounds*, Pergamon, London 1961, p. 83.
4. Austad, T. *Unpublished data.*
5. Austad, T. and Esperås, S. *Acta Chem. Scand. A 28* (1974) 892.
6. Janickis, J. *Accounts Chem. Res. 2* (1969) 316.
7. Foss, O. *Acta Chem. Scand. 3* (1949) 435.

Received July 25, 1974.

Acta Chemica Scandinavica A 29 (1975) 76—88

The Molecular and Crystal Structures of $[Ni_2Cl_2(C_2H_6O_2)_4]Cl_2$ and $[Co_2Cl_2(C_2H_6O_2)_4]Cl_2$, Two Isostructural Compounds Containing {Di-μ-chlorobis[di(1,2-ethanediol)metal(II)]} Cations

BRITT-MARIE ANTTI

Department of Inorganic Chemistry, University of Umeå, S-901 87 Umeå, Sweden

The crystal structures of the isostructural compounds $[Ni_2Cl_2(C_2H_6O_2)_4]Cl_2$ (I) and $[Co_2Cl_2(C_2H_6O_2)_4]Cl_2$ (II) have been determined and refined using three-dimensional X-ray diffraction data. The crystals are monoclinic, space group $C2/m$, with unit cell dimensions and corresponding standard deviations (the values in square brackets refer to the Co-compound), $a=12.445(1)$ Å [12.428(1) Å], $b=11.375(1)$ Å [11.456(1) Å], $c=9.258(1)$ Å [9.347(1) Å], and $\beta=133.086(4)°$ [133.017(7)°]. There are two formula units in the unit cell. The intensity materials were collected with the linear diffractometer PAILRED using Mo$K\alpha$-radiation. Both structures were solved by Patterson and heavy-atom Fourier methods and refined by full-matrix least-squares techniques.

With anisotropic temperature factors for all non-hydrogen atoms and isotropic temperature factors for the hydrogen atoms the refinements converged at R-values of 0.046 and 0.032 for structures I and II, respectively. The refinements were based on 1394 independent reflexions for structure I and 2041 for structure II.

The structures consist of dinuclear cations $[Me_2Cl_2(C_2H_6O_2)_4]^{2+}$ and chloride ions. In the cation, the metal ions are coupled together through two chlorine atoms forming a bridge. Oxygen atoms from the glycol* molecules complete an octahedral arrangement around each metal ion. These cations are linked through the chloride ions by means of hydrogen bonds of the type $Cl^-\cdots H-O$, to form layers. Between these layers there are only van der Waals contacts. The Me—Me distances are 3.458 and 3.470 Å, the Me—Cl distances 2.383 and 2.417 Å and the average Me—O distances 2.067 and 2.104 Å in the Ni- and Co-compounds, respectively.

* Throughout this paper 1,2-ethanediol will be referred to as glycol or ethylene glycol.

Crystal structure investigations of complexes between ethylene glycol and divalent transition metal ions are in progress at this department. Their aim is to elucidate the coordination changes within the series Mn^{2+}, Fe^{2+}, Co^{2+}, Ni^{2+}, Cu^{2+} and Zn^{2+}, particularly when sulfate and chloride are used as anions. The first two papers in this series, the crystal structures of $[Cu(C_2H_6O_2)_3]SO_4$[1] and $[MnCl_2(C_2H_6O_2)_2]$[2] have recently been published. A compilation of compounds prepared hitherto together with some characteristics of crystals of them, is presented in Table 1. The structure determinations of the isostructural compounds $[Co_2Cl_2(C_2H_6O_2)_4]Cl_2$ and $[Ni_2Cl_2(C_2H_6O_2)_4]Cl_2$ are presented here. In a recent report by Knetsch and Groeneveld[3] the preparation and properties of two crystalline compounds, to which the formulas $Ni(C_2H_6O_2)_2Cl_2$ and $Co(C_2H_6O_2)_2Cl_2$ were assigned, were carefully described. From visible, UV and IR spectra and magnetic susceptibility measurements it was concluded that glycol in these compounds acts as a bidentate ligand and has *gauche* conformation while the coordination around the metal ion is octahedral or pseudo-octahedral. From X-ray powder data, the two compounds were seen to be isostructural. A comparison of IR spectra of our compounds with the spectra published by Knetsch and Groeneveld shows that the compounds are identical.

EXPERIMENTAL

Crystal preparation and analyses. The Ni- and Co-compounds were prepared similarly. The

Table 1. A compilation of compounds prepared hitherto and some characteristics of crystals of them.

Compound	a (Å)	b (Å)	c (Å)	β (°)	Space group	Z	D_m(g/cm³)
$[Co(C_2H_6O_2)_3]SO_4$[a]	8.818(1)	7.585(1)	19.238(1)	99.357(5)	$P2_1/c$	4	1.77
$[Ni(C_2H_6O_2)_3]SO_4$[b]	10.32	9.03	15.04	116.4	$P2_1/c$	4	1.81
$[Cu(C_2H_6O_2)_3]SO_4$	10.166(1)	9.013(1)	15.365(1)	115.666(6)	$P2_1/c$	4	1.82
$[Zn(C_2H_6O_2)_3]SO_4$[c]	9.544(1)	14.198(1)	9.180(1)		$Ac2a$	4	1.84
$[MnCl_2(C_2H_6O_2)_2]$	9.491(1)	7.223(1)	14.213(1)	92.229(7)	$P2_1/c$	4	1.68
$[Co_2Cl_2(C_2H_6O_2)_4]Cl_2$	12.428(1)	11.456(1)	9.347(1)	133.017(7)	$C2/m$	2	1.71
$[Ni_2Cl_2(C_2H_6O_2)_4]Cl_2$	12.445(1)	11.375(1)	9.258(1)	133.086(4)	$C2/m$	2	1.75
$CuCl_2(C_2H_6O_2)$[d]	7.424	10.939	7.518	95.67	$P2_1/c$	4	2.14
$[CuCl_2(C_2H_6O_2)]\frac{1}{2}H_2O$[e]	10.198(1)	18.769(1)	7.043(1)		$Pcnb$	8	2.04

[a] Structure determined and refined (present R-value 0.038). To be published. [b] Isostructural with $[Cu(C_2H_6O_2)_3]SO_4$; X-ray data not yet collected. [c] Structure determined and refined (present R-value 0.047). To be published. [d] Structure determined and refined (present R-value 0.059). To be published. [e] X-Ray data just collected.

hexahydrates of the Ni(II)- and Co(II)-dichlorides were dissolved in glycol (molar ratio 1:2) by heating on a waterbath. The decanted solutions were then placed in a desiccator over sulfuric acid; crystals in the form of distorted tabular hexagons formed after some time. The Ni-containing crystals were pale green while the Co-containing crystals were deep violet. The crystals were analysed for metal and chlorine and the following results (in weight-%) were obtained: Found in crystal I Ni 23.0; Cl 27.1 and in crystal II Co 23.1; Cl 27.2. Calc. for $[Ni_2Cl_2(C_2H_6O_2)_4]Cl_2$: Ni 23.1; Cl 27.9 and for $[Co_2Cl_2(C_2H_6O_2)_4]Cl_2$: Co 23.2; Cl 27.9. The IR-spectra showed that no water was present. The densities of the crystals as determined by the flotation method using bromoform and xylene are 1.75 ± 0.01 and 1.71 ± 0.02 g/cm³ for the Ni- and Co-compounds, respectively. Calculated for $[Me_2Cl_2(C_2H_6O_2)_4]Cl_2$ with $Z=2$ gave the corresponding values of 1.76 and 1.73 g/cm³.

Crystal data and space group. From rotation photographs and corresponding Weissenberg photographs (zero and first layers) taken from crystals mounted around their b- and c-axis, it was concluded that the crystals are monoclinic. The unit cell parameters determined using these photographs were refined from powder photographs taken with a camera of Guinier-Hägg type, with Cu$K\alpha$-radiation, and with Si ($a=5.43054$ Å) as internal standard. (For the Co-compound Cu-foil was used to avoid fluorescence). The accurate cell parameters and their estimated standard deviations are listed in Table 1. Systematic extinctions of intensities were found for hkl when $h+k=2n+1$, which is characteristic for the three space groups $C2$ (No. 5), Cm (No. 8), and $C2/m$ (No. 12).[4] Of these only $C2/m$ is centrosymmetric.

Intensity data. The diffracted intensities from single crystals of I and II were collected and measured with the automatic linear diffractometer PAILRED using graphite-monochromated Mo$K\alpha$-radiation. As the crystals were hygroscopic they were enclosed in capillaries of Lindeman glass during the data collection. Both were rotated around their b-axis and intensities for $h0l-h15l$ were measured ($\sin\theta\leq 0.63$ for I and ≤ 0.67 for II). Reflexions for which the total number of counts during one scan interval was less than 4 000 were measured again. For the crystal of I the half scan interval for $h0l$ reflexions was 1.2 for $\theta\geq 20°$ (Ω_1) and 1.9 for $\theta\leq 20°$ (Ω_2). These half scan intervals were gradually increased for each layer up to 1.3 and 2.2, respectively, for $h15l$. The corresponding values for the crystal of II were 1.4 and 2.1 for $h0l$ and 1.6 and 2.5 for $h15l$. The scan speed was 1°/min. Background intensities were measured for 40 s (t_B) before and after each scan. The net intensity I for a reflexion was calculated from the measured total intensity TI (peak+background) by subtracting the two background counts B_1 and B_2 according to the relation.

$$I=TI/N-[t_T/(t_B/60)]\,(B_1+B_2)$$

where t_T is total scanning time [$\Omega_{1\text{ or }2}$/(scan speed/min)] and N is the number of times the reflexion was measured. 2238 independent intensities were measured from the crystal of I and 2442 from the crystal of II. From these 1394 and 2041, respectively, were significantly above background at the 95 % level, *i.e.* they had $\Delta I/I\leq 0.5$.[3] These were used in the refinements. Because of difficulties in obtaining large crystals of the Ni-compound the crystal of II was much larger than that of I ($V_I=0.449\times10^{-3}$ mm³, $V_{II}=0.859\times10^{-3}$ mm³). Thus there are more significant reflexions for II. Besides the normal correction for Lorentz

and polarization factors, absorption correction was also made. For the crystal of I the linear absorption coefficient was 25.3 cm^{-1} and the transmission factors varied from 0.84 to 0.92. Corresponding values for the crystal of II were 23.1 cm^{-1} and 0.63 to 0.76. When the refinements were terminated, structure factors for all the unobserved reflexions were calculated. These all had amplitudes equal to or lower than the corresponding threshold values.

The diffractometer data correction program is a modified version of a program originally written by Ivarsson and Lundberg.[5] The other computer programs used were those described by Antti and Lundberg.[6]

STRUCTURE DETERMINATION AND REFINEMENT

Structure I. The space group was initially assumed to be $C2/m$. From a three-dimensional Patterson synthesis the positions of the nickel and chlorine atoms were located, Ni on the twofold axis (4*g*) and Cl(1) and Cl(2) in the mirror plane (4*i*). The positions of the oxygen and carbon atoms were found in general eightfold positions, using heavy-atom Fourier methods.

After two cycles of full matrix least-squares refinement of the atomic positional parameters the R-value was 0.22 (R is defined as $[\sum||F_o|-|F_c||]/\sum|F_o|$). When atomic isotropic temperature factors were added as parameters the R-value decreased to 0.11 after one cycle. At this point anisotropic temperature factors for all atoms were introduced and after further refinement the R-value decrease to 0.056. A difference Fourier synthesis was calculated and probable positions for the hydrogen atoms were found. When they were included and refined with isotropic temperature factors the refinement converged at an R-value of 0.046. During the refinement the observations were weighted according to the function suggested by Cruickshank;[7] $w=1/(a+|F_o|+c|F_o|^2+d|F_o|^3)$, using the constants $a=250$, $c=-0.015$, and $d=0.00005$. The atomic scattering factors for Ni^{2+}, Cl^-, O, and C were those given by Cromer and Waber [8] and account was taken of the real part of the dispersion correction for Ni^{2+} and Cl^-.[9] (The scattering curve for Ni^+ [8] was also tested but there was no improvement neither in the least-squares refinements nor in a final difference Fourier synthesis). The scattering factors for the hydrogen atoms were those proposed by Stewart, Davidson and Simpson.[10]

Attempts were made to refine the structure in both of the noncentrosymmetrical space groups $C2$ and Cm. The very strong correlation (± 1.0) found between the parameters that are symmetry-related in space group $C2/m$ indicated that the structure in fact has a centre of symmetry.

Structure II. The two structures were assumed to be isostructural so the atomic positional parameters from structure I were used for the first cycle of least squares refinement of structure II. The R-value after this cycle was 0.22 and when isotropic temperature factors for all atoms were included the R-value decreased to 0.11. The refinement then proceeded in the same way as for structure I to a final R-value of 0.032.

Cruickshank constants used were; $a=175$, $c=-0.015$, and $d=0.0006$. The atomic scattering factors for Co^{2+} were those proposed by Cromer and Waber [8] and account was taken of the real part of the dispersion correction. Atomic scattering factors for the other atoms were as for structure I. Final positional and thermal parameters for the two structures are listed in Tables 2 and 3. The corresponding observed and calculated structure amplitudes are listed in Tables 4 and 5. For some of the strongest reflexions (those with $\sin\theta<0.2$) F_o is considerably less than F_c. This was noticed at the beginning of the refinements and as the intensities were believed to be affected by secondary extinction, attempts were made to introduce an isotropic extinction coefficient to correct the whole data. These were unsuccessful so the strong reflexions were excluded from further refinements. When the refinement had converged they were introduced again and were seen to have no significant effect on the atomic positional and thermal parameters. As the reflexions were measured with an Ω-scan there is a possibility that the chosen scan interval was too small for strong broad reflexions with low $\sin\theta$-values and hence that the intensities measured are too low.

DESCRIPTION AND DISCUSSION OF THE STRUCTURES

The structures consist of discrete dinuclear $[Me_2Cl_2(C_2H_6O_2)_4]^{2+}$-cations and Cl^--ions. They

Table 2. Atomic positional and thermal parameters for $[Ni_2Cl_2(C_2H_6O_2)_4]Cl_2$. For the non-hydrogen atoms all parameters have been multiplied by 10^4. The anisotropic temperature factors have been calculated according to the formula $\exp[-(h^2\beta_{11}+k^2\beta_{22}+l^2\beta_{33}+2hk\beta_{12}+2hl\beta_{13}+2kl\beta_{23})]$. For the hydrogen atoms the positional parameters have been multiplied by 10^3. The labelling of atoms is shown in Fig. 3. (Standard deviations for the last significant figure are given in parentheses).

	x/a	y/b	z/c	$\beta_{11}(B)$	β_{22}	β_{33}	β_{12}	β_{13}	β_{23}
Ni	0	1520(1)	0	55(1)	34(0.5)	90(1)	0	49(1)	0
Cl(1)	2563(2)	5000	1793(3)	127(2)	48(1)	317(5)	0	177(3)	0
Cl(2)	1649(2)	0	2232(2)	74(2)	44(1)	96(2)	0	33(2)	0
O(1)	3970(3)	3236(3)	988(4)	85(3)	63(3)	159(6)	18(2)	94(4)	18(3)
O(2)	1342(3)	2797(3)	2187(4)	88(3)	52(2)	153(6)	−13(2)	86(4)	−13(3)
C(1)	4905(5)	2684(5)	2906(6)	112(6)	82(4)	149(9)	15(4)	106(6)	17(5)
C(2)	680(5)	3295(4)	2842(7)	98(5)	59(4)	156(9)	−13(9)	86(6)	−30(4)
H(1)	357(6)	369(6)	105(9)	5(2)					
H(2)	168(5)	322(5)	200(7)	2(1)					
H(3)	60(5)	165(5)	398(7)	3(1)					
H(4)	428(5)	233(5)	310(7)	3(1)					
H(5)	500(6)	110(6)	200(8)	4(1)					
H(6)	147(5)	359(4)	415(6)	2(1)					

Table 3. Atomic positional and thermal parameters for $[Co_2Cl_2(C_2H_6O_2)_4]Cl_2$. Legend as for Table 2.

	x/a	y/b	z/c	$\beta_{11}(B)$	β_{22}	β_{33}	β_{12}	β_{13}	β_{23}
Co	0	1515(0.3)	0	64(0.3)	38(0.2)	99(0.5)	0	57(0.3)	0
Cl(1)	2567(1)	5000	1798(1)	140(1)	51(0.5)	336(2)	0	191(1)	0
Cl(2)	1716(1)	0	2231(1)	81(1)	46(0.4)	101(1)	0	32(1)	0
O(1)	3984(2)	3225(1)	1036(2)	93(1)	67(1)	169(3)	21(1)	101(2)	22(1)
O(2)	1337(2)	2819(1)	2203(2)	101(2)	56(1)	170(3)	−19(1)	99(2)	−19(1)
C(1)	4903(3)	2668(2)	2914(3)	127(3)	86(2)	155(4)	17(2)	114(3)	21(2)
C(2)	667(2)	3311(2)	2848(3)	116(2)	62(2)	162(4)	−15(2)	97(3)	−32(2)
H(1)	355(3)	361(3)	101(4)	4.1(7)					
H(2)	167(3)	323(2)	204(3)	2.1(4)					
H(3)	55(3)	170(3)	389(4)	4.4(6)					
H(4)	432(3)	236(3)	318(3)	3.3(5)					
H(5)	493(3)	108(3)	189(4)	3.7(6)					
H(6)	139(3)	369(3)	409(4)	3.9(6)					

are shown in Fig. 1. The ions are linked together by hydrogen bonds of the type $Cl^-\cdots H-O$, forming layers parallel to the *ab*-plane. These layers are separated by *c*, the contacts between them being solely of van der Waals type. Part of the coupling of the layers is shown in Fig. 2.

The $[Me_2Cl_2(C_2H_6O_2)_4]^{2+}$*-cation.* In the $[Me_2Cl_2(C_2H_6O_2)_4]^{2+}$-cation the two metal ions are coupled through two chlorines forming a bridge and the four oxygens from two bidentate coordinated glycol ligands complete the octahedral arrangement around each metal ion. The bridging arrangement

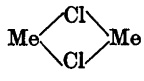

is nearly square. The angles Cl—Me—Cl are 87.0 and 88.2°, the distances Me—Me 3.458(1) and 3.470(1) Å and the distances Me—Cl 2.383(1) and 2.417(1) Å for the Ni- and Co-compounds, respectively. These distances agree well with earlier reported values. Since the glycol molecules are coordinated to the metal ion as bidentate chelates, puckered five-membered rings are obtained. The dimensions

Table 4. Observed and calculated structure amplitudes (×10) for $[Ni_2Cl_2(C_2H_6O_2)_4]Cl_2$.

L	H		
K=	0		
-2	16	129	123
-3	16	161	167
-4	16	179	163
-5	16	198	186
-6	16	288	299
-7	16	275	277
-10	16	163	177
-11	16	222	272
-12	16	220	237
-13	16	184	220
-15	14	133	134
-14	14	248	262
-13	14	224	214
-10	14	348	339
-9	14	361	380
-8	14	272	283
-7	14	279	301
-6	14	286	265
-5	14	247	255
-4	14	335	329
-3	14	287	287
-4	12	141	117
1	12	233	241
0	12	337	319
-1	12	162	152
-3	12	238	227
-4	12	257	242
-5	12	294	291
-6	12	615	625
-7	12	658	661
-8	12	311	316
-9	12	272	279
-10	12	350	339
-11	12	208	210
-12	12	141	181
-13	12	239	234
-13	10	189	184
-12	10	187	189
-11	10	298	293
-10	10	493	506
-9	10	507	506
-8	10	468	447
-7	10	601	578
-6	10	361	365
-5	10	105	-94
-4	10	258	245
-3	10	813	798
-2	10	628	618
-1	10	184	175
0	10	161	179
1	10	369	371
2	10	329	310
3	10	147	141
7	8	140	119
4	8	228	223
3	8	248	250
2	8	136	131
1	8	191	199
0	8	639	637
-1	8	1010	1026
-2	8	764	761
-3	8	193	200
-4	8	253	245
-5	8	966	955
-6	8	1019	1020
-7	8	257	224
-8	8	121	-120
-9	8	316	309
-10	8	594	576
-11	8	364	353
-12	8	171	170
-13	8	183	181
-14	8	152	166
-14	6	123	162
-13	6	240	251
-12	6	149	156
-10	6	177	198
-9	6	564	555
-8	6	616	597
-7	6	182	184
-5	6	928	906
-4	6	1857	1886
-3	6	1465	1481
-2	6	472	474
-1	6	280	285
0	6	613	607
1	6	531	522
2	6	236	213
3	6	166	188
4	6	362	355
5	6	370	352
6	6	166	167
7	4	256	250
6	4	492	485
5	4	335	329
4	4	199	188
3	4	508	507
2	4	881	881
1	4	810	820
0	4	424	419
-1	4	210	193
-2	4	445	421
-3	4	1162	1141
-4	4	955	939
-5	4	534	521
-6	4	924	912
-7	4	1079	1066

L	H		
-8	4	542	536
-11	4	231	250
-12	4	201	212
-13	4	139	97
-11	2	247	243
-10	2	377	364
-9	2	151	185
-8	2	229	235
-7	2	697	676
-6	2	838	823
-5	2	417	423
-4	2	162	161
-3	2	535	520
-2	2	843	776
-1	2	1601	1636
0	2	944	904
1	2	193	-196
2	2	1096	1087
3	2	1828	1874
4	2	844	856
5	2	157	-130
7	2	408	412
8	2	279	269
10	0	250	241
9	0	350	319
8	0	260	245
7	0	181	177
6	0	212	217
5	0	649	663
4	0	1037	1041
3	0	240	228
2	0	840	-854
1	0	1650	1765
K=	1		
-2	15	185	180
-3	15	157	142
-6	15	189	198
-7	15	312	308
-8	15	204	214
-12	15	150	160
-13	15	135	147
-11	13	161	154
-10	13	318	329
-9	13	260	276
-6	13	274	274
-5	13	446	459
-4	13	261	243
-3	13	106	-18
-1	13	164	150
2	11	129	85
1	11	169	177
0	11	168	186
-1	11	111	137
-2	11	177	169
-3	11	253	266
-4	11	198	194
-7	11	436	455
-8	11	569	572
-9	11	249	254
-12	11	161	188
-12	9	141	143
-11	9	311	325
-10	9	305	308
-9	9	148	133
-7	9	222	227
-6	9	259	243
-5	9	276	263
-4	9	395	407
-3	9	410	402
-2	9	287	286
-1	9	179	164
0	9	128	137
1	9	193	210
2	9	255	262
3	9	177	154
4	7	303	289
3	7	274	257
0	7	387	378
-1	7	793	789
-2	7	660	655
-3	7	350	348
-4	7	192	176
-5	7	236	247
-6	7	490	490
-7	7	367	364
-8	7	168	157
-9	7	178	169
-10	7	235	220
-11	7	167	126
-13	7	129	111
-13	5	148	123
-12	5	116	104
-9	5	235	249
-8	5	280	274
-7	5	128	154
-6	5	202	192
-5	5	669	652
-4	5	1257	1242
-3	5	968	951
-2	5	274	-284
-1	5	314	-298
0	5	550	554
1	5	752	749
2	5	252	263
4	5	158	163
5	5	309	289
6	5	155	180
7	3	212	198

L	H		
6	3	197	195
5	3	120	144
4	3	259	269
3	3	546	545
2	3	608	608
1	3	187	193
-1	3	516	490
-2	3	1318	1300
-3	3	672	662
-4	3	296	-293
-6	3	684	659
-7	3	653	652
-8	3	214	220
-11	3	167	149
-10	1	199	213
-9	1	271	255
-6	1	349	334
-5	1	632	642
-4	1	443	440
-2	1	137	119
1	1	1051	1046
2	1	775	776
3	1	543	539
4	1	335	343
5	1	151	130
6	1	97	22
7	1	164	156
8	1	246	260
9	1	141	145
K=	2		
-3	16	118	-43
-9	16	179	-190
-10	16	209	-205
-13	16	127	-89
-14	16	172	-171
-15	14	113	39
-13	14	129	-164
-12	14	132	-90
-7	14	206	-215
-6	14	191	-173
-5	14	116	-100
-4	14	124	-152
-1	12	136	79
-2	12	155	-182
-3	12	351	-351
-5	12	225	223
-7	12	350	-357
-8	12	230	-220
-9	12	139	-152
-10	12	171	-162
-11	10	206	-177
-10	10	375	-367
-8	10	253	255
-7	10	205	-191
-6	10	619	-622
-5	10	231	-240
-4	10	240	245
-3	10	208	211
-2	10	111	-130
-1	10	357	-360
0	10	252	-270
2	10	124	47
5	8	140	-117
1	8	271	-269
0	8	255	-242
-2	8	113	-119
-3	8	619	-613
-4	8	627	-605
-6	8	344	304
-7	8	136	131
-8	8	225	-228
-9	8	367	-359
-10	8	131	-147
-11	8	121	46
-13	8	126	-156
-12	6	144	-101
-11	6	140	-150
-9	6	166	145
-7	6	393	-379
-6	6	441	-445
-5	6	259	-241
-4	6	336	-305
-3	6	436	-418
-2	6	235	-246
-1	6	130	-121
0	6	171	-163
1	6	210	-200
2	6	150	-155
6	6	146	-148
4	4	314	-314
3	4	571	-566
2	4	268	-254
1	4	245	217
0	4	249	239
-2	4	338	-333
-3	4	720	-685
-4	4	409	-395
-6	4	234	-238
-7	4	274	-274
-8	4	132	-129
-9	4	130	-113
-10	4	145	-149
-8	2	179	-169
-7	2	282	-280
-6	2	209	-225
-5	2	158	-190
-4	2	254	-240
-3	2	231	214

L	H		
-2	2	882	844
-1	2	515	-478
0	2	1552	-1596
1	2	514	-495
2	2	117	123
3	2	191	-176
4	2	296	-308
5	2	246	-226
6	2	146	-150
7	0	282	-272
5	0	273	270
4	0	206	-185
3	0	800	-788
2	0	338	-332
1	0	180	-155
K=	3		
-3	15	128	-143
-4	15	283	-284
-5	15	381	-371
-6	15	265	-260
-9	15	204	-226
-10	15	234	-240
-11	15	159	-168
-12	15	140	-158
-13	15	138	-160
-14	15	140	-133
-16	13	129	-128
-14	13	139	-107
-13	13	145	-165
-12	13	192	-213
-11	13	143	-124
-9	13	220	-226
-8	13	521	-525
-7	13	580	-582
-6	13	349	-368
-5	13	171	-156
-4	13	128	-143
-3	13	236	-247
-2	13	236	-255
-1	13	167	-130
2	13	127	-144
3	11	171	-188
2	11	162	-175
1	11	172	-145
0	11	270	-270
-1	11	333	-343
-2	11	159	-163
-3	11	122	-86
-4	11	367	-368
-5	11	573	-568
-6	11	403	-396
-7	11	225	-219
-8	11	220	-266
-9	11	450	-457
-10	11	537	-530
-11	11	356	-343
-12	11	131	-101
-15	11	121	-129
-14	9	132	-154
-13	9	242	-237
-12	9	249	-233
-11	9	224	-221
-10	9	236	-248
-9	9	406	-403
-8	9	612	-611
-7	9	551	-525
-6	9	104	-94
-5	9	103	-90
-4	9	532	-528
-3	9	529	-539
-2	9	417	-424
-1	9	553	-558
0	9	562	-566
1	9	262	-264
3	9	139	-126
4	9	180	-177
5	9	119	-132
7	7	163	-150
6	7	224	-216
3	7	159	-170
2	7	383	-380
1	7	536	-536
0	7	386	-385
-1	7	187	-195
-2	7	569	-566
-3	7	1311	-1323
-4	7	1115	-1104
-5	7	341	-343
-6	7	426	-412
-7	7	506	-497
-8	7	225	-221
-10	7	279	-283
-11	7	330	-344
-12	7	233	-237
-13	7	173	-151
-11	5	187	-207
-10	5	332	-335
-7	5	731	-738
-6	5	1237	-1229
-5	5	688	-677
-4	5	235	-222
-3	5	833	-825
-2	5	1159	-1159
-1	5	1021	-1029
0	5	370	-365
1	5	139	111
2	5	168	-180
3	5	623	-642

L	H		
4	5	541	-552
5	5	143	-149
7	5	231	-221
8	5	171	-174
9	3	192	-173
8	3	138	-154
6	3	161	-156
5	3	555	-550
4	3	634	-641
3	3	310	-313
2	3	560	-552
1	3	1412	-1428
0	3	1343	-1358
-1	3	298	273
-2	3	627	607
-3	3	582	-575
-4	3	1243	-1255
-5	3	1099	-1108
-6	3	517	-514
-7	3	217	-208
-8	3	358	-365
-9	3	503	-502
-10	3	277	-264
-13	3	142	-140
-12	1	137	-155
-11	1	133	-131
-9	1	168	-195
-8	1	465	-463
-7	1	605	-606
-6	1	359	-363
-5	1	114	71
-3	1	1027	-1031
-2	1	1491	-1485
1	1	1529	-1569
2	1	1406	-1423
3	1	542	-530
4	1	244	-251
5	1	485	-488
6	1	452	-451
7	1	189	-186
10	1	199	-198
11	1	172	-151
K=	4		
-4	16	162	-182
-5	16	151	-151
-8	16	202	-233
-9	16	244	-242
-12	16	125	-76
-14	16	129	-148
-15	14	126	-102
-12	14	265	-252
-11	14	268	-259
-8	14	195	-201
-7	14	324	-324
-6	14	292	-285
-5	14	205	-213
-4	14	144	-144
1	14	144	-102
2	12	176	-153
0	12	123	-41
-1	12	163	-151
-2	12	253	-290
-3	12	267	-264
-4	12	187	-213
-5	12	178	-201
-6	12	156	-168
-7	12	210	-213
-8	12	310	-336
-9	12	345	-355
-10	12	236	-252
-11	12	191	-174
-15	12	159	-144
-14	10	120	-106
-13	10	148	-134
-12	10	172	-176
-11	10	191	-194
-10	10	229	-238
-9	10	308	-309
-8	10	181	-210
-7	10	179	-153
-6	10	486	-483
-5	10	634	-636
-4	10	245	-254
-2	10	182	-184
-1	10	432	-442
0	10	361	-354
4	10	160	-136
6	8	138	-132
5	8	137	-175
2	8	308	-317
1	8	387	-395
-2	8	497	-504
-3	8	860	-860
-4	8	680	-674
-5	8	161	-189
-7	8	254	-254
-8	8	642	-649
-9	8	428	-419
-12	8	225	-249
-13	8	169	-160
-12	6	188	-205
-11	6	289	-299
-10	6	148	-166
-8	6	132	-110
-7	6	470	-461
-6	6	930	-903
-5	6	774	-753
-4	6	83	-20

L	H		
-2	6	912	-904
-1	6	830	-832
0	6	167	-180
1	6	154	-158
2	6	439	-450
3	6	317	-317
6	6	185	-183
7	6	160	-157
8	4	188	-176
5	4	223	-208
4	4	482	-483
3	4	552	-557
2	4	313	-322
0	4	419	-410
-1	4	942	-938
-2	4	491	-488
-3	4	142	-170
-4	4	858	-837
-5	4	1006	-982
-6	4	332	-317
-8	4	286	-302
-9	4	444	-427
-10	4	208	-222
-9	2	262	-245
-8	2	485	-468
-7	2	259	-265
-6	2	153	-147
-5	2	596	-598
-4	2	845	-849
-3	2	365	-354
-2	2	185	167
-1	2	427	-416
0	2	1228	-1233
1	2	1346	-1352
2	2	556	-550
3	2	168	142
4	2	204	-210
5	2	613	-620
6	2	377	-397
9	2	187	-155
11	0	114	-155
8	0	191	-212
7	0	408	-422
6	0	321	-323
4	0	86	-71
3	0	935	-960
2	0	1581	-1620
1	0	490	-478
K=	5		
-2	15	111	111
-5	15	119	-93
-6	15	128	94
-7	15	164	187
-10	15	151	-136
-13	13	124	-72
-10	13	194	201
-8	13	157	-174
-7	13	128	-147
-6	13	174	166
-5	13	307	297
-4	13	108	65
-3	13	160	-154
1	11	109	86
-5	11	205	-189
-6	11	141	-159
-7	11	184	181
-8	11	330	329
-9	11	114	128
-10	11	99	-89
-11	11	125	-94
-11	9	184	166
-10	9	105	135
-8	9	96	-89
-6	9	144	-112
-5	9	170	-160
-4	9	111	124
-3	9	221	216
-1	9	110	-77
1	9	101	92
2	9	138	137
4	7	114	138
3	7	128	125
2	7	222	-214
1	7	317	-316
-1	7	401	416
-2	7	344	357
-3	7	107	107
-4	7	215	-204
-5	7	166	-148
-6	7	207	220
-7	7	134	151
-8	7	188	-172
-9	7	94	-106
-10	7	102	83
-5	5	338	338
-4	5	651	657
-3	5	230	232
-2	5	636	-618
-1	5	475	-457
0	5	256	254
1	5	274	254
2	5	141	-132
3	5	151	-149
5	5	142	129
4	3	96	92
3	3	156	157
2	3	102	93
0	3	153	-127

Table 4. Continued.

L	H			L	H			L	H			L	H			L	H			L	H		
				-7	4	446	448	-6	5	97	87	3	2	288	303	-9	12	208	-220	-7	9	191	-192
K=	5			-8	4	411	416	-5	5	462	469	4	2	123	121	-8	12	195	-208	-8	9	189	-199
				-9	4	159	128	-4	5	964	936	5	2	124	-133	-7	12	219	-201	-9	9	106	-125
-1	3	103	-94	-11	4	144	142	-3	5	840	831	7	2	176	162	-6	12	137	-142	-13	9	94	-102
-2	3	159	159	-12	4	132	175	-2	5	136	157	8	2	115	138	-5	12	113	-101	-8	7	137	-128
-3	3	115	100	-11	2	119	151	0	5	435	432	5	0	348	365	-4	12	151	-176	-7	7	181	-188
-4	3	387	-374	-10	2	148	177	1	5	830	835	4	0	291	300	-3	12	269	-265	-6	7	142	-140
-5	3	253	-254	-9	2	170	186	2	5	486	485	3	0	157	-168	-2	12	244	-224	-4	7	131	-144
-6	3	272	265	-8	2	341	285	4	5	133	108	2	0	303	-318	-1	12	131	-105	-3	7	197	-211
-7	3	322	326	-7	2	369	369	5	5	308	302	1	0	149	148	2	10	99	-53	-1	7	107	90
10	1	117	101	-6	2	341	350	6	5	240	215					0	10	229	-237	1	7	232	-239
-7	1	137	-129	-5	2	323	322	10	3	126	50	K=	9			-1	10	271	-286	2	7	217	-230
-5	1	153	144	-4	2	283	284	8	3	109	125					-2	10	160	-178	4	7	90	17
-3	1	160	-122	-3	2	468	430	7	3	235	224	-2	13	145	-127	-4	10	151	-186	4	5	135	-125
-2	1	290	-284	-2	2	722	698	6	3	208	210	-3	13	162	-149	-5	10	387	-379	3	5	249	-243
1	1	499	522	-1	2	691	678	5	3	122	135	-7	13	298	-299	-6	10	420	-407	1	5	124	105
2	1	349	369	0	2	185	171	4	3	231	217	-8	13	381	-383	-7	10	220	-214	0	5	145	-156
3	1	103	104	1	2	293	275	3	3	545	563	-9	13	104	-112	-8	10	125	-90	-1	5	505	-510
4	1	97	-28	2	2	962	954	2	3	670	679	-10	13	122	104	-9	10	168	-168	-2	5	378	-368
5	1	133	-135	3	2	930	924	1	3	162	165	-11	13	99	-38	-10	10	226	-233	-4	5	173	162
6	1	143	-130	4	2	351	360	-1	3	824	797	-12	13	168	-176	-11	10	150	-158	-6	5	230	-241
				7	2	198	224	-2	3	1381	1369	-11	11	238	-246	-12	10	103	-96	-7	5	149	-166
K=	6			8	2	129	149	-3	3	584	582	-10	11	220	-216	-10	8	109	-137	-10	5	137	-148
				10	0	150	139	-4	3	175	-156	-9	11	147	-139	-9	8	276	-294	-11	5	95	-107
-3	16	153	132	9	0	236	221	-5	3	148	178	-8	11	114	-107	-8	8	367	-381	-9	3	90	-139
-4	16	158	137	8	0	171	195	-6	3	657	648	-7	11	141	-113	-7	8	258	-257	-8	3	100	-83
-5	16	155	114	6	0	193	203	-7	3	575	585	-6	11	211	-213	-5	8	158	-160	-7	3	87	73
-6	16	160	157	5	0	456	458	-8	3	218	215	-5	11	265	-262	-4	8	469	-459	-6	3	94	93
-7	16	236	232	4	0	426	424	-10	3	151	125	-2	11	143	-152	-3	8	558	-533	-5	3	269	-272
-11	16	216	235	3	0	139	130	-11	3	194	204	-1	11	211	-196	-2	8	270	-260	-4	3	565	-552
-12	16	232	257	2	0	949	931	-12	3	147	128	2	11	113	-122	0	8	133	-161	-3	3	182	-186
-13	16	169	172	1	0	989	984	-10	1	218	220	4	9	117	-112	1	8	265	-265	-2	3	206	194
-14	16	111	80					-9	1	274	271	3	9	125	-68	2	8	183	-192	-1	3	108	-109
-14	14	154	163	K=	7			-6	1	427	434	0	9	289	-275	4	8	107	-94	0	3	494	-493
-11	14	129	122					-5	1	838	831	-1	9	400	-384	6	6	121	-128	1	3	287	-287
-10	14	187	196	-1	15	120	102	-4	1	513	504	-2	9	208	-209	4	6	104	-110	4	3	114	-102
-9	14	175	204	-2	15	115	149	-2	1	312	325	-4	9	146	-169	3	6	243	-236	5	3	113	-132
-8	14	227	219	-3	15	147	113	1	1	582	641	-5	9	178	-188	2	6	269	-279	7	1	136	-124
-7	14	218	223	-5	15	116	111	2	1	409	407	-6	9	103	-86	1	6	212	-224	6	1	227	-247
-6	14	195	198	-6	15	144	174	3	1	507	497	-7	9	137	-144	0	6	275	-261	5	1	117	-133
-5	14	181	193	-7	15	243	241	4	1	505	506	-8	9	262	-259	-1	6	405	-406	3	1	67	-112
-4	14	182	181	-8	15	257	264	5	1	285	290	-9	9	174	-205	-2	6	422	-424	2	1	104	-125
-3	14	162	161	-9	15	165	170	6	1	105	72	-10	9	118	-122	-3	6	209	-219	1	1	93	-96
-2	14	161	147	-13	15	174	149	7	1	158	154	-12	9	148	-102	-4	6	106	-117	-2	1	287	-299
1	12	156	146	-15	13	123	106	8	1	303	292	-12	9	114	-133	-5	6	338	-326	-3	1	457	-466
0	12	229	248	-13	13	120	101	9	1	183	200	-10	7	107	-92	-6	6	546	-531	-4	1	164	-173
-1	12	165	192	-12	13	143	142					-9	7	133	-128	-7	6	405	-396	-5	1	142	124
-4	12	149	170	-11	13	192	183	K=	8			-8	7	190	-183	-8	6	99	-125	-7	1	240	-272
-5	12	381	387	-10	13	241	247					-5	7	320	-313	-10	6	163	-181	-8	1	103	-125
-6	12	420	413	-9	13	294	310	-6	16	119	111	-4	7	636	-625	-11	6	196	-213	-10	1	91	14
-7	12	287	287	-8	13	170	183	-7	16	139	119	-3	7	477	-463	-12	6	116	-136				
-8	12	229	225	-6	13	174	178	-12	16	102	84	0	7	204	-210	-10	4	199	-205	K=	12		
-9	12	230	252	-5	13	375	377	-16	14	93	3	1	7	321	-327	-9	4	265	-259				
-10	12	209	218	-4	13	390	388	-10	14	149	147	2	7	164	-177	-8	4	183	-182	-2	10	120	129
-11	12	136	156	-1	13	162	154	-9	14	172	172	3	7	101	-7	-7	4	114	-123	-3	10	248	252
-12	12	123	131	0	13	159	148	-2	14	113	79	5	7	144	-106	-6	4	237	-243	-4	10	115	109
-12	10	154	211	2	11	140	128	1	12	92	35	4	5	205	-202	-5	4	416	-404	-5	10	99	-75
-11	10	123	147	1	11	145	164	-4	12	89	97	3	5	276	-272	-4	4	453	-434	-7	10	83	84
-10	10	209	188	0	11	122	145	-5	12	147	154	2	5	173	-192	-3	4	386	-369	-8	10	175	174
-9	10	463	458	-1	11	179	194	-12	12	106	89	-1	5	339	-332	-2	4	405	-396	-9	10	158	151
-8	10	533	528	-2	11	314	310	-8	10	172	164	-2	5	628	-609	-1	4	487	-471	-10	10	98	61
-7	10	229	241	-3	11	329	326	-7	10	155	153	-3	5	365	-369	0	4	389	-365	-10	8	97	98
-4	10	333	323	-4	11	203	196	-6	10	210	241	-5	5	156	-166	1	4	182	-189	-7	8	84	90
-3	10	542	536	-5	11	105	84	-3	10	333	351	-6	5	458	-449	2	4	200	-217	-6	8	272	275
-2	10	369	372	-6	11	196	181	-2	10	113	100	-7	5	377	-372	3	4	391	-379	-5	8	155	161
1	10	303	304	-7	11	468	462	-1	10	111	-121	-8	5	104	-130	4	4	327	-331	-2	8	222	226
2	10	255	244	-8	11	516	499	0	10	95	-93	-9	5	97	-37	5	4	100	-119	-1	8	207	217
4	8	115	94	-9	11	184	183	2	10	101	90	-10	5	109	-87	7	4	111	-99	-1	6	80	101
3	8	187	176	-11	11	157	167	3	8	154	149	-11	5	114	-110	6	2	257	-254	-2	6	113	107
2	8	209	208	-12	11	240	255	0	8	120	106	-9	3	232	-230	5	2	345	-345	-3	6	152	166
0	8	246	233	-13	11	111	146	-1	8	187	208	-8	3	151	-140	4	2	236	-226	-4	6	256	263
-1	8	663	655	-15	9	115	127	-3	8	212	-212	-6	3	283	-285	2	2	200	-211	-5	6	185	196
-2	8	693	686	-12	9	158	152	-4	8	131	-131	-5	3	514	-513	1	2	662	-642	-8	6	99	116
-3	8	162	152	-11	9	322	319	-5	8	200	220	-4	3	367	-350	0	2	754	-735	-9	6	127	145
-5	8	575	566	-10	9	324	309	-6	8	439	460	-3	3	134	-143	-1	2	329	-333	-8	4	118	122
-6	8	650	646	-9	9	209	207	-7	8	226	257	-1	3	94	-77	-2	2	119	-109	-7	4	155	159
-7	8	232	214	-8	9	131	132	-8	8	112	-108	0	3	322	-320	-3	2	384	-372	-6	4	131	131
-9	8	139	150	-7	9	190	205	-10	8	137	141	1	3	508	-505	-4	2	548	-535	-5	4	162	168
-10	8	224	244	-6	9	451	433	-10	6	112	119	2	3	321	-323	-5	2	353	-357	-4	4	159	164
-11	8	288	294	-5	9	549	545	-9	6	217	236	3	3	149	-154	-6	2	168	-175	-1	4	70	82
-12	8	226	226	-4	9	373	367	-8	6	179	178	4	3	225	-257	-7	2	224	-223	0	4	169	173
-13	8	129	92	-3	9	243	245	-6	6	191	-175	5	3	234	-233	-8	2	283	-270	1	4	187	194
-15	8	136	97	-2	9	349	347	-5	6	97	-85	6	3	135	-105	-9	2	145	-159	2	4	128	134
13	6	132	141	-1	9	307	298	-4	6	249	243	6	1	167	-162	1	0	254	-272	4	2	124	104
-9	6	428	447	0	9	152	153	-3	6	208	216	5	1	292	-305	2	0	668	-666	3	2	332	338
-8	6	394	384	1	9	153	167	-2	6	118	-113	4	1	164	-187	3	0	628	-619	2	2	235	249
-6	6	171	159	2	9	218	239	0	6	255	263	3	1	144	-156	4	0	232	-234	-1	2	139	147
-5	6	792	774	3	9	140	181	1	6	157	175	2	1	392	-393	5	0	82	-72	-2	2	198	207
-4	6	865	859	5	7	143	159	3	6	88	55	1	1	394	-398	6	0	237	-229	-3	2	141	161
-3	6	591	576	4	7	280	294	4	6	153	153	-2	1	594	-582	7	0	316	-325	-4	2	74	82
-2	6	573	570	3	7	183	216	6	4	120	115	-3	1	203	-195	8	0	160	-174	-7	2	141	129
-1	6	466	447	1	7	118	125	3	4	140	-152	-5	1	85	-117					1	0	222	244
0	6	188	181	0	7	437	438	2	4	80	55	-6	1	176	-203	K=	11			2	0	94	-82
1	6	140	162	-1	7	651	649	1	4	391	406	-7	1	209	-209					4	0	156	169
2	6	235	232	-2	7	416	421	0	4	303	331	-8	1	189	-212	-2	13	108	-122	5	0	111	130
3	6	181	202	-3	7	187	193	-2	4	149	148	-9	1	116	-122	-3	13	132	-139				
4	6	261	237	-4	7	384	387	-3	4	231	236					-7	13	178	-173	K=	13		
5	6	243	242	-5	7	548	534	-5	4	130	-134	K=	10			-12	13	97	-80				
6	4	342	337	-6	7	375	369	-6	4	116	115					-13	13	106	-92	-1	11	105	103
5	4	319	323	-7	7	253	251	-7	4	179	176	-3	14	128	-106	-10	11	204	-190	-3	11	188	189
3	4	228	228	-8	7	347	360	-9	4	107	-45	-4	14	131	-114	-8	11	127	112	-4	11	180	167
2	4	544	537	-9	7	356	347	-11	4	108	78	-5	14	136	-144	-6	11	162	-177	-6	11	102	100
1	4	518	508	-10	7	234	207	-12	4	96	78	-6	14	206	-207	-5	11	216	-236	-7	11	202	192
0	4	412	406	-13	7	120	121	-6	2	163	168	-7	14	202	-218	-4	11	144	-152	-8	11	218	218
-1	4	478	464	-14	7	132	130	-7	2	344	374	-8	14	151	-140	1	9	106	-85	-9	11	142	149
-2	4	208	208	-12	5	161	178	-2	2	554	572	-10	14	136	-121	0	9	122	-112	-10	9	129	146
-3	4	204	203	-11	5	121	116	-1	2	193	183	-11	14	145	-173	-3	9	145	-158	-9	9	110	104
-4	4	652	639	-9	5	288	282	0	2	259	-274	-12	14	178	-170	-4	9	101	-128	-8	9	89	114
-5	4	745	729	-8	5	452	453	1	2	232	-232	-11	12	162	-147	-5	9	72	-69	-7	9	198	184
-6	4	507	488	-7	5	239	241	2	2	108	110	-10	12	222	-213	-6	9	120	-118	-6	9	179	200

Table 4. Continued.

L	H			L	H			L	H			L	H			L	H		
				-7	5	126	124	-7	1	125	99	-9	8	75	49	1	4	240	244	-4	7	89	-116
K= 13				-6	5	119	107	-6	1	199	207	-7	8	152	149	2	4	154	154	-7	5	87	-90
				-5	5	254	246	-5	1	284	284	-6	8	270	269	4	2	150	144	-6	5	126	-139
-5	9	178	185	-4	5	421	408	-4	1	307	295	-5	8	222	216	3	2	247	248	-4	5	84	94
-4	9	235	233	-3	5	294	289	-3	1	233	216	-1	8	185	188	2	2	135	157	-2	5	109	-136
-3	9	263	246	0	5	315	322	-2	1	137	147	0	8	124	134	-1	2	232	239	-1	5	97	-115
-2	9	163	149	1	5	363	347	1	1	275	275	3	6	82	70	-2	2	378	375	1	5	100	90
0	9	106	95	2	5	155	172	2	1	236	228	2	6	88	70	-3	2	192	197	1	3	113	-147
1	9	118	136	4	5	114	118	3	1	247	244	1	6	170	168	-4	2	59	46	0	3	134	-147
3	7	169	164	5	3	111	100	4	1	214	197	0	6	195	188	-5	2	127	137	-1	3	79	70
0	7	185	190	4	3	123	137	5	1	124	121	-3	6	199	205	-6	2	204	186	-2	3	144	151
-1	7	291	293	3	3	224	224	6	1	115	116	-4	6	235	240	-7	2	86	68	-4	3	135	-153
-2	7	260	260	2	3	234	232	7	1	151	141	-7	6	76	64	-6	0	99	100	-5	3	102	-107
-3	7	148	154	1	3	149	154					-8	6	166	174	-5	0	274	277	-5	1	85	88
-5	7	149	164	0	3	192	187	K= 14				-9	6	179	189	-4	0	220	220	-3	1	98	-111
-6	7	286	275	-1	3	343	322					-7	4	171	170	-2	0	57	-33	-2	1	108	-128
-7	7	256	247	-2	3	442	426	-2	10	133	120	-6	4	143	141	-1	0	170	201	1	1	67	-76
-8	7	153	145	-3	3	350	337	-3	10	178	194	-4	4	62	67					2	1	71	-79
-9	7	110	131	-4	3	98	107	-4	10	156	156	-3	4	238	214	K= 15							
-10	7	138	153	-6	3	243	239	-7	10	155	140	-2	4	214	203								
-9	5	158	160	-7	3	285	294	-8	10	130	136	-1	4	83	112	-1	7	70	89				
-8	5	153	163	-8	3	127	125	-10	8	130	126	0	4	161	169	-3	7	139	-147				

of these rings are given in Tables 6 and 7. All the Me—O distances are approximately the same so the five-membered rings are very symmetrical. The average Me—O distance is 2.067(3) Å in the Ni-compound and 2.104(2) Å in the Co-compound.

The glycol oxygens taking part in the Me—O bonds have three neighbours each, one hydrogen atom, one carbon atom, and one Me^{2+}-ion (Fig. 3). The arrangement around each of these oxygens can be considered as being tetrahedral, although distorted, if a lone pair of electrons is assumed to complete each tetrahedron.

The glycol ligands. As mentioned above the glycol molecule acts as a bidentate ligand in its coordination to the metal ion. It has a *gauche* conformation with dihedral angles of 52.39 and 52.12° for the Ni- and Co-compounds, respectively. [The dihedral angle is defined as the angle between the planes O(1)—C(1)—C(2) and O(2)—C(2)—C(1)]. These dihedral angles are in good agreement with the mean value of 52.2° found in $[MnCl_2(C_2H_6O_2)_2]$.[2] In $[Cu(C_2H_6O_2)_3]SO_4$[1] this angle varies between 45.9 and 55.3°. *Gauche* conformation of glycol molecules (dihedral angle 65°) has also been reported in (1-phenylbutane-1,3-dionato)-(ethyleneglycol) sodium,[11] where the glycol molecules act as bridging ligands.

Bastiansen [12] found by the method of electron diffraction on the free glycol molecule a single O···O distance of 2.96(2) Å which reflects a dihedral angle of $\approx 75°$ if normal values are assumed for the other parameters. There was no indication of a *trans* isomer. Infrared spectra of liquid, gaseous, and crystalline ethylene glycol, measured and discussed by Buckley and Giguère, also seem to indicate that the molecule exists only as *gauche* isomer.[13] These authors claim that the *gauche*-form should be more stable than the *trans*-form because of intramolecular hydrogen bonding and that the structure of the molecule should be fairly rigid because of energy barriers to rotation around C—C and C—O, respectively.

From the above discussion it may be concluded that the dihedral angle of the glycol molecule decreases as it changes from being free to acting as bridging ligand and bidentate ligand, respectively.

There are no significant differences between the values obtained for the C—C and C—O distances in the Ni- and Co-compounds, respectively. They also agree well with previously reported distances.[1,2] The intramolecular angles, *i.e.* the O—C—C angles, are significantly smaller than the tetrahedral angle; for $[Ni_2Cl_2(C_2H_6O_2)_4]Cl_2$ there is a mean value of 106.5(4)° and for $[Co_2Cl_2(C_2H_6O_2)_4]Cl_2$ 106.6(2)°. These values are similar to those reported for $[MnCl_2(C_2H_6O_2)_2]$.[2]

The C—H and O—H distances in these structures are not significantly different from other reported values obtained using X-ray data.

The hydrogen bonds. As mentioned above the hydrogen bonds are in layers parallel to the *ab*-plane. A drawing showing a layer and with hydrogen bonds marked (dashed lines) is given in Fig. 1. All hydrogen bonds are of the $Cl^-\cdots H-O$ type. Around each Cl^- there are four such hydrogen bonds. The four oxygen atoms taking part in this arrangement form a nearly square plane; in the middle of this

Table 5. Observed and calculated structure amplitudes ($\times 10$) for $[Co_2Cl_3(C_2H_6O_2)_4]Cl_2$.

L	H			L	H			L	H			L	H			L	H			L	H		
K=	0			-13	6	228	222	-2	13	47	47	4	1	313	313	2	4	265	-264	-10	9	270	-269
				-12	6	146	143	-4	13	169	169	3	1	524	514	1	4	271	257	-9	9	367	-372
				-11	6	62	59	-5	13	386	389	2	1	781	752	0	4	302	295	-8	9	539	-546
0	16	74	70	-10	6	214	216	-6	13	278	280	1	1	1033	1008	-1	4	69	4	-7	9	512	-507
-1	16	64	61	-9	6	515	509	-8	13	198	207	-2	1	163	125	-2	4	400	-393	-6	9	141	-136
-2	16	88	77	-8	6	522	513	-10	13	296	302	-4	1	403	403	-3	4	697	-688	-5	9	104	-72
-3	16	138	134	-7	6	132	136	-11	13	182	170	-5	1	625	619	-4	4	324	-317	-4	9	400	-411
-4	16	158	159	-5	6	871	858	-14	13	82	85	-6	1	337	334	-5	4	70	-73	-3	9	438	-447
-5	16	173	170	-4	6	1710	1777	-15	13	105	108	-8	1	68	53	-6	4	278	-275	-2	9	408	-412
-6	16	236	231	-3	6	1353	1372	-16	13	61	67	-9	1	233	233	-7	4	282	-282	-1	9	548	-555
-7	16	208	207	-2	6	475	465	-14	11	83	79	-10	1	193	194	-8	4	78	-74	0	9	486	-494
-8	16	46	46	-1	6	306	310	-13	11	153	150					-9	4	57	-66	1	9	176	-179
-10	16	158	158	0	6	556	553	-12	11	140	143	K=	2			-10	4	144	-146	3	9	120	-127
-11	16	223	223	1	6	422	417	-9	11	264	262					-11	4	57	-48	4	9	157	-168
-12	16	213	216	2	6	167	161	-8	11	517	517	-3	16	53	-38	-14	4	59	-62	5	9	102	-99
-13	16	228	223	3	6	206	207	-7	11	382	384	-4	16	68	-70	-13	2	53	-47	7	9	49	-29
-14	16	162	157	4	6	360	355	-6	11	52	55	-5	16	79	-82	-10	2	44	-53	7	7	110	-107
-15	16	62	72	5	6	303	299	-4	11	193	187	-7	16	56	52	-9	2	71	-76	6	7	186	-191
-16	16	71	76	6	6	117	118	-3	11	188	187	-8	16	52	22	-8	2	153	-151	5	7	138	-142
-17	16	80	83	7	6	49	46	-2	11	120	116	-9	16	145	-154	-7	2	254	-248	4	7	77	-62
-17	14	95	103	8	6	95	92	-1	11	156	150	-10	16	184	-186	-6	2	216	-224	3	7	110	-109
-16	14	86	105	9	6	97	102	0	11	202	201	-11	16	47	20	-5	2	227	-225	2	7	310	-310
-15	14	116	114	10	4	121	113	1	11	139	140	-12	16	86	90	-4	2	250	-251	1	7	509	-506
-14	14	234	227	7	4	193	194	5	11	78	71	-13	16	76	-75	-3	2	284	276	0	7	383	-385
-13	14	216	216	6	4	445	434	7	9	67	68	-14	16	138	-146	-2	2	916	911	-1	7	146	-142
-10	14	265	264	5	4	319	318	6	9	71	85	-15	16	71	-61	-1	2	508	-463	-2	7	451	-441
-9	14	311	315	4	4	167	169	3	9	102	99	-17	14	74	-72	0	2	1476	-1522	-3	7	1212	-1239
-8	14	264	267	3	4	443	438	2	9	246	242	-15	14	48	36	1	2	487	-474	-4	7	1063	-1078
-7	14	288	290	2	4	820	814	1	9	223	229	-14	14	63	-57	2	2	181	160	-5	7	328	-328
-6	14	224	221	1	4	820	819	0	9	119	116	-13	14	162	-162	3	2	182	-162	-6	7	321	-318
-5	14	176	180	0	4	447	451	-1	9	82	83	-12	14	74	-76	4	2	286	-290	-7	7	409	-407
-4	14	276	272	-1	4	146	132	-2	9	228	231	-7	14	155	-154	5	2	214	-205	-8	7	209	-209
-3	14	280	272	-2	4	324	305	-3	9	427	430	-6	14	163	-164	6	2	122	-124	-9	7	144	-148
-2	14	146	137	-3	4	1094	1111	-4	9	430	427	-5	14	134	-125	8	2	51	47	-10	7	281	-284
-1	14	77	61	-4	4	985	981	-5	9	201	196	-4	14	129	-133	9	2	64	-68	-11	7	300	-304
0	14	51	61	-5	4	528	529	-6	9	165	161	-3	14	47	-46	10	2	93	-98	-12	7	215	-216
1	14	67	63	-6	4	849	852	-7	9	230	227	-2	14	60	63	12	0	47	-24	-13	7	150	-150
2	14	69	75	-7	4	970	988	-8	9	146	148	0	14	93	-92	11	0	92	-91	-14	7	95	-87
3	14	76	74	-8	4	486	486	-9	9	141	140	1	14	59	-59	10	0	79	-80	-15	5	78	-83
5	12	57	58	-10	4	61	55	-10	9	262	261	2	12	110	-112	8	0	68	-62	-14	5	114	-111
4	12	100	103	-11	4	213	218	-11	9	291	285	1	12	96	-91	7	0	276	-270	-13	5	83	-91
3	12	80	76	-12	4	186	195	-12	9	139	143	-1	12	110	108	6	0	58	-51	-12	5	75	-75
2	12	53	54	-13	4	86	99	-15	9	58	59	-2	12	136	-137	5	0	303	292	-11	5	202	-202
1	12	175	168	-11	2	209	216	-15	7	66	58	-3	12	343	-342	4	0	157	-148	-10	5	301	-300
0	12	270	266	-10	2	325	321	-14	7	104	106	-4	12	75	-68	3	0	786	-767	-9	5	94	-89
-1	12	179	178	-9	2	145	148	-13	7	85	86	-5	12	230	227	2	0	327	-307	-8	5	63	-61
-2	12	103	104	-8	2	209	209	-12	7	56	55	-7	12	330	-330	1	0	165	-134	-7	5	695	-699
-3	12	150	143	-7	2	672	669	-11	7	147	149	-8	12	250	-244	K=	3			-6	5	1159	-1169
-4	12	155	153	-6	2	827	824	-10	7	229	225	-9	12	147	-147					-5	5	597	-596
-5	12	301	294	-5	2	401	397	-9	7	126	124	-10	12	109	-107					-4	5	183	-178
-6	12	649	643	-4	2	135	136	-8	7	119	115	-13	12	58	-57	0	15	79	-80	-3	5	831	-834
-7	12	599	599	-3	2	540	507	-7	7	393	390	-16	12	69	-69	-1	15	91	-90	-2	5	1130	-1172
-8	12	225	224	-2	2	755	741	-6	7	516	515	-17	12	53	-55	-2	15	71	-71	-1	5	906	-926
-9	12	214	222	-1	2	1359	1541	-5	7	179	175	-11	10	187	-181	-3	15	95	-90	0	5	270	-267
-10	12	328	328	0	2	875	845	-4	7	58	54	-10	10	355	-355	-4	15	223	-215	1	5	114	115
-11	12	191	197	1	2	202	-203	-3	7	335	336	-8	10	271	272	-5	15	333	-336	2	5	210	-213
-12	12	145	145	2	2	1106	1082	-2	7	695	707	-9	10	227	-220	-6	15	254	-253	3	5	600	-608
-13	12	201	201	3	2	1759	1806	-1	7	751	761	-6	10	642	-642	-7	15	50	-52	4	5	458	-469
-14	12	113	114	4	2	756	745	0	7	283	279	-5	10	204	-200	-9	15	165	-177	5	5	109	-111
-16	12	103	108	5	2	178	-177	1	7	133	-130	-4	10	313	310	-10	15	230	-240	6	5	73	-87
-17	12	115	118	6	2	69	64	2	7	39	-25	-3	10	218	210	-11	15	172	-182	7	5	203	-202
-16	10	103	97	7	2	394	390	3	7	270	271	-2	10	179	-177	-12	15	135	-140	8	5	140	-140
-15	10	62	51	8	2	237	240	4	7	251	250	-1	10	338	-346	-13	15	184	-187	10	3	79	-73
-14	10	85	94	9	2	47	56	5	7	46	37	0	10	189	-193	-14	15	119	-123	9	3	159	-159
-13	10	183	183	10	2	52	53	7	7	73	66	3	10	104	-102	-15	15	122	-137	8	3	151	-146
-12	10	156	148	11	2	97	93	8	7	98	88	4	10	90	-89	-16	15	103	-122	6	3	100	-105
-11	10	213	210	10	0	220	216	9	5	65	71	5	10	46	14	-17	13	74	-77	5	3	482	-487
-10	10	465	472	9	0	313	300	6	5	146	138	5	8	116	-114	-16	13	104	-108	4	3	601	-609
-9	10	543	546	8	0	250	237	5	5	283	280	4	8	71	-80	-15	13	113	-114	3	3	299	-300
-8	10	469	454	7	0	172	167	4	5	181	185	3	8	76	66	-14	13	123	-120	2	3	508	-494
-7	10	491	483	6	0	202	202	2	5	192	190	2	8	44	36	-13	13	171	-174	1	3	1316	-1353
-6	10	281	285	5	0	627	613	1	5	697	687	1	8	223	-228	-12	13	190	-188	0	3	1274	-1307
-5	10	49	-47	4	0	992	978	0	5	592	591	0	8	268	-269	-11	13	71	-74	-1	3	272	259
-4	10	287	273	3	0	187	183	-1	5	264	-253	-1	8	54	-25	-9	13	220	-222	-2	3	640	628
-3	10	708	705	2	0	945	-929	-2	5	349	-338	-2	8	75	-57	-8	13	486	-491	-3	3	504	-507
-2	10	494	490	1	0	1531	1709	-3	5	850	839	-3	8	510	-506	-7	13	482	-489	-4	3	1204	-1225
-1	10	135	140					-4	5	1207	1235	-4	8	609	-598	-6	13	277	-286	-5	3	1109	-1120
0	10	203	201	K=	1			-5	5	701	704	-5	8	101	-73	-5	13	151	-157	-6	3	520	-522
1	10	346	347					-6	5	176	175	-6	8	340	324	-4	13	161	-166	-7	3	161	-163
2	10	241	239	-3	17	69	55	-7	5	68	74	-7	8	199	197	-3	13	204	-202	-8	3	308	-309
3	10	82	80	-6	17	112	111	-8	5	229	225	-8	8	217	-207	-2	13	169	-168	-9	3	457	-461
4	10	55	49	-5	17	129	120	-9	5	255	260	-9	8	397	-396	-1	13	89	-95	-10	3	230	-240
5	10	75	80	-6	17	50	56	-10	5	128	127	-10	8	167	-169	0	13	82	-85	-12	3	58	-42
6	10	59	79	-9	17	116	111	-12	5	88	86	-11	8	68	65	1	13	112	-120	-13	3	129	-127
8	8	84	82	-10	17	163	167	-13	5	112	120	-13	8	143	-148	2	13	101	-102	-14	3	86	-88
7	8	117	114	-11	17	125	132	-14	5	59	59	-14	8	78	-71	3	11	149	-153	-13	1	56	-68
6	8	71	68	-12	17	94	88	-12	3	86	90	-13	6	53	-48	2	11	169	-172	-12	1	130	-136
5	8	57	55	-13	17	53	63	-11	3	133	130	-12	6	109	-114	1	11	134	-134	-11	1	114	-106
4	8	161	158	-14	17	48	45	-10	3	78	75	-11	6	134	-139	0	11	199	-199	-9	1	174	-178
3	8	236	224	-16	17	58	64	-8	3	213	218	-9	6	152	149	-1	11	269	-266	-8	1	446	-443
2	8	151	153	-17	17	55	48	-7	3	628	626	-7	6	371	-368	-2	11	166	-164	-7	1	574	-579
1	8	176	172	-16	15	65	65	-6	3	631	614	-6	6	350	-351	-3	11	119	-118	-6	1	352	-346
0	8	519	515	-15	15	63	62	-4	3	258	-255	-5	6	164	-156	-4	11	321	-321	-5	1	86	79
-1	8	887	896	-14	15	84	80	-3	3	706	700	-4	6	378	-342	-5	11	447	-455	-4	1	37	-41
-2	8	747	745	-13	15	156	153	-2	3	1213	1258	-3	6	495	-484	-6	11	348	-348	-3	1	992	-982
-3	8	228	227	-12	15	170	166	-1	3	419	394	-2	6	201	-201	-7	11	254	-253	-2	1	1387	-1410
-4	8	265	196	-11	15	47	44	0	3	75	-71	-1	6	45	-31	-8	11	271	-275	1	1	1474	-1547
-5	8	835	816	-10	15	66	-54	1	3	242	237	0	6	135	-137	-9	11	374	-387	2	1	1358	-1373
-6	8	919	924	-9	15	46	39	2	3	611	601	1	6	218	-227	-10	11	440	-447	3	1	452	-447
-7	8	268	249	-8	15	232	225	3	3	492	489	2	6	164	-156	-11	11	309	-312	4	1	176	-186
-8	8	75	-79	-7	15	272	274	4	3	211	215	3	6	41	-13	-12	11	90	-101	5	1	448	-446
-9	8	288	288	-6	15	131	135	5	3	127	130	4	6	65	54	-14	11	107	-100	6	1	423	-425
-10	8	533	526	-3	15	141	141	6	3	194	193	6	6	152	-150	-15	11	115	-119	7	1	164	-167
-11	8	345	341	-2	15	132	133	7	3	178	177	7	6	99	-101	-16	11	70	-83	8	1	51	-50
-12	8	171	180	-1	15	46	34	11	3	70	78	8	4	89	-99	-16	9	48	-32	9	1	122	-119
-13	8	157	162	2	15	61	53	12	1	57	66	7	4	94	-91	-15	9	48	-50	10	1	177	-182
-14	8	125	126	3	13	65	70	9	1	134	134	6	4	53	43	-14	9	135	-138	11	1	123	-132
-15	8	85	82	2	13	57	36	8	1	249	249	5	4	63	58	-13	9	190	-190				
-16	8	56	62	0	13	94	86	7	1	152	148	4	4	282	-286	-12	9	181	-186	K=	4		
-4	6	144	147	-1	13	136	138	5	1	106	101	3	4	572	-571	-11	9	221	-218				

Table 5. Continued.

L	H			L	H			L	H			L	H			L	H			L	H		
				-3	6	96	-91	-8	9	47	-34	-7	14	215	212	-5	4	716	701	-6	9	358	355
K=	4			-2	6	800	-819	-6	9	167	-165	-6	14	154	161	-6	4	420	406	-5	9	486	483
				-1	6	700	-719	-5	9	206	-201	-5	14	122	130	-7	4	400	392	-4	9	386	380
-1	16	71	-65	0	6	150	-154	-4	9	134	140	-4	14	145	143	-8	4	399	395	-3	9	262	260
-2	16	78	-72	1	6	199	-197	-3	9	244	249	-3	14	165	158	-9	4	115	111	-2	9	270	277
-3	16	93	-87	2	6	433	-442	-1	9	126	-127	-2	14	138	133	-11	4	128	119	-1	9	205	215
-4	16	130	-127	3	6	253	-258	1	9	116	119	-1	14	76	66	-12	4	160	166	0	9	123	131
-5	16	111	-111	5	6	79	-86	2	9	125	131	1	14	57	29	-13	4	67	70	1	9	167	175
-6	16	58	-47	6	6	177	-182	4	9	107	-100	2	14	59	67	-12	2	93	50	2	9	214	214
-7	16	80	-80	7	6	136	-131	5	9	48	-45	3	14	63	63	-11	2	141	138	3	9	138	131
-8	16	180	-187	8	6	50	-35	6	9	49	45	4	12	71	80	-10	2	150	146	5	9	44	42
-9	16	185	-190	9	4	108	-100	8	7	46	49	3	12	63	56	-9	2	140	136	6	9	74	79
-10	16	116	-128	8	4	166	-164	7	7	51	33	1	12	97	93	-8	2	252	253	7	9	68	67
-11	16	105	-99	7	4	77	-77	6	7	73	-60	0	12	206	203	-7	2	368	370	8	7	73	83
-12	16	71	-68	5	4	153	-152	5	7	68	-63	-1	12	196	198	-6	2	356	350	5	7	112	112
-13	16	71	-65	4	4	428	-431	4	7	118	113	-2	12	42	54	-5	2	294	286	4	7	257	255
-14	16	116	-128	3	4	544	-554	3	7	140	144	-3	12	54	-45	-4	2	238	245	3	7	222	222
-15	16	118	-132	2	4	325	-335	2	7	180	-171	-4	12	104	101	-3	2	405	392	2	7	52	63
-16	16	50	-54	1	4	64	-50	1	7	348	-342	-5	12	366	364	-2	2	689	686	1	7	76	82
-17	14	44	-49	0	4	330	-329	-1	7	415	411	-6	12	423	416	-1	2	641	626	0	7	361	362
-16	14	48	-63	-1	4	907	-927	-2	7	413	422	-7	12	258	251	0	2	120	106	-1	7	588	594
-15	14	102	-97	-2	4	531	-529	-3	7	83	91	-8	12	155	160	1	2	240	233	-2	7	420	424
-14	14	82	-76	-3	4	161	-165	-4	7	300	-298	-9	12	197	204	2	2	919	913	-3	7	182	185
-13	14	83	-85	-4	4	768	-773	-5	7	181	-182	-10	12	201	203	3	2	873	878	-4	7	297	301
-12	14	205	-206	-5	4	916	-921	-6	7	254	252	-11	12	147	142	4	2	306	299	-5	7	455	454
-11	14	225	-231	-6	4	306	-306	-7	7	156	162	-12	12	97	103	6	2	94	96	-6	7	366	366
-10	14	79	-84	-7	4	45	-3	-8	7	209	-208	-13	12	92	98	7	2	208	207	-7	7	279	279
-9	14	48	-27	-8	4	270	-273	-9	7	133	-131	-14	12	97	94	8	2	155	155	-8	7	324	326
-8	14	147	-148	-9	4	365	-374	-10	7	89	96	-15	12	71	75	9	2	56	61	-9	7	288	291
-7	14	249	-254	-10	4	197	-199	-11	7	41	47	-16	12	56	57	11	2	72	64	-10	7	205	197
-6	14	256	-263	-11	4	83	-77	-14	7	50	45	-16	10	69	68	10	0	133	124	-11	7	132	135
-5	14	208	-217	-12	4	62	-53	-13	5	58	58	-15	10	45	48	9	0	219	211	-12	7	95	93
-4	14	127	-125	-13	4	68	-64	-11	5	79	-82	-14	10	50	39	8	0	179	180	-13	7	96	95
-3	14	53	-59	-14	4	82	-83	-9	5	81	81	-13	10	123	126	7	0	86	95	-14	7	114	112
-2	14	51	-60	-13	2	90	-86	-8	5	97	-92	-12	10	181	182	6	0	178	187	-15	7	59	73
-1	14	90	-91	-12	2	127	-125	-7	5	190	-179	-11	10	91	96	5	0	438	435	-13	5	114	116
0	14	98	-105	-11	2	42	-45	-6	5	36	24	-10	10	164	153	4	0	397	390	-12	5	155	151
1	14	82	-77	-9	2	229	-225	-5	5	416	403	-9	10	476	462	3	0	52	63	-11	5	107	105
3	12	81	-68	-8	2	432	-433	-4	5	666	667	-8	10	528	524	2	0	168	155	-10	5	85	95
2	12	134	-135	-7	2	234	-239	-3	5	142	142	-7	10	187	186	1	0	942	951	-9	5	274	273
1	12	96	-108	-6	2	163	-139	-2	5	679	-650	-6	10	77	-63					-8	5	411	404
-1	12	97	-91	-5	2	599	-596	-1	5	421	-405	-5	10	46	43	K=	7			-7	5	207	200
-2	12	235	-234	-4	2	824	-838	0	5	274	276	-4	10	341	331					-6	5	75	71
-3	12	273	-273	-3	2	301	-294	1	5	223	215	-3	10	473	466	1	15	46	51	-5	5	456	455
-4	12	225	-226	-2	2	202	203	2	5	166	-170	-2	10	280	282	0	15	57	35	-4	5	891	897
-5	12	148	-150	-1	2	450	-441	3	5	149	-142	-1	10	55	55	-1	15	65	62	-3	5	756	753
-6	12	98	-95	0	2	1170	-1234	4	5	82	86	0	10	130	127	-2	15	113	108	-2	5	104	110
-7	12	181	-188	1	2	1258	-1285	5	5	128	134	1	10	274	275	-3	15	107	110	-1	5	78	-72
-8	12	346	-355	2	2	477	-475	6	5	45	33	2	10	185	182	-4	15	70	84	0	5	446	449
-9	12	330	-340	3	2	177	161	8	5	43	-27	5	10	67	75	-5	15	86	78	1	5	773	779
-10	12	191	-194	4	2	216	-209	9	5	48	26	6	10	65	66	-6	15	119	117	2	5	399	401
-11	12	126	-132	5	2	578	-589	9	3	75	-67	7	8	80	84	-7	15	210	211	4	5	110	120
-12	12	96	-97	6	2	341	-348	8	3	68	-48	6	8	55	69	-8	15	250	264	5	5	277	280
-13	12	71	-72	9	2	155	-150	7	3	61	55	4	8	55	55	-9	15	163	158	6	5	172	169
-14	12	108	-110	10	2	129	-137	6	3	50	58	3	8	151	153	-11	15	70	66	9	5	71	76
-15	12	110	-120	12	0	81	-81	4	3	53	53	2	8	210	208	-12	15	154	154	8	3	91	101
-16	12	57	-67	11	0	145	-139	3	3	120	123	1	8	106	104	-13	15	147	151	7	3	205	202
-16	10	45	-49	10	0	68	-76	2	3	125	115	0	8	158	156	-14	15	108	109	6	3	201	201
-15	10	79	-84	8	0	183	-192	0	3	155	-144	-1	8	557	563	-15	15	82	77	5	3	110	118
-14	10	77	-85	7	0	394	-400	-1	3	178	-162	-2	8	639	651	-17	13	44	47	4	3	155	168
-13	10	96	-100	6	0	313	-316	-2	3	109	102	-3	8	157	154	-16	13	75	73	3	3	495	497
-12	10	173	-172	4	0	50	-49	-3	3	129	128	-5	8	481	471	-15	13	106	104	2	3	638	644
-11	10	206	-210	3	0	885	-907	-4	3	365	-331	-6	8	583	584	-14	13	85	82	1	3	174	178
-10	10	219	-214	2	0	1485	-1561	-5	3	267	-257	-7	8	229	227	-13	13	68	74	0	3	54	-43
-9	10	236	-237	1	0	474	-458	-6	3	238	236	-8	8	66	68	-12	13	144	140	-1	3	742	729
-8	10	166	-175					-7	3	314	312	-9	8	128	124	-11	13	199	197	-2	3	1294	1321
-7	10	191	-191	K=	5			-8	3	57	60	-10	8	215	208	-10	13	226	223	-3	3	567	578
-6	10	494	-500					-9	3	75	-65	-11	8	294	289	-9	13	232	232	-4	3	159	-155
-5	10	552	-564	-1	15	55	-21	-10	3	41	-27	-12	8	228	223	-8	13	148	145	-5	3	128	135
-4	10	158	-162	-2	15	88	77	-10	1	86	91	-13	8	64	66	-7	13	57	61	-6	3	609	603
-3	10	48	41	-3	15	82	82	-9	1	102	99	-15	8	83	85	-6	13	177	176	-7	3	559	548
-2	10	214	-223	-4	15	53	-48	-7	1	125	-111	-15	6	76	64	-5	13	309	305	-8	3	193	198
-1	10	400	-412	-5	15	92	-95	-6	1	36	30	-14	6	91	91	-4	13	221	213	-9	3	39	27
0	10	262	-266	-6	15	57	50	-5	1	140	128	-13	6	114	119	-3	13	84	79	-10	3	108	107
1	10	92	-88	-7	15	163	164	-3	1	154	-137	-12	6	135	127	-2	13	91	93	-11	3	183	184
2	10	62	-59	-8	15	60	62	-2	1	288	-291	-11	6	63	61	-1	13	139	138	-12	1	114	119
3	10	109	-108	-9	15	105	-114	1	1	494	505	-10	6	113	121	0	13	101	103	-13	1	45	44
4	10	112	-107	-10	15	152	-150	2	1	376	372	-9	6	387	382	1	13	55	60	-11	1	57	62
5	10	48	-46	-11	15	46	-35	3	1	87	85	-8	6	332	329	2	13	49	59	-10	1	198	197
6	8	97	-97	-12	15	87	78	4	1	81	-58	-7	6	67	-51	3	13	57	63	-9	1	245	244
5	8	166	-166	-13	15	67	66	5	1	149	-152	-6	6	132	130	5	11	63	67	-8	1	60	63
4	8	68	-75	-16	15	45	31	6	1	139	-132	-5	6	746	743	4	11	48	57	-6	1	403	411
2	8	233	-233	-15	13	49	52	8	1	90	95	-4	6	799	789	3	11	48	42	-5	1	801	800
1	8	337	-337	-14	13	55	25					-3	6	500	493	2	11	80	77	-4	1	489	471
0	8	149	-153	-13	13	90	-80	K=	6			-2	6	530	530	1	11	130	127	-2	1	291	301
-1	8	99	-99	-12	13	116	-119					-1	6	451	468	0	11	153	151	1	1	495	489
-2	8	409	-417	-10	13	179	183	1	16	60	45	0	6	145	148	-1	11	191	191	2	1	371	371
-3	8	718	-728	-8	13	194	-190	-2	16	63	52	1	6	96	95	-2	11	249	250	3	1	469	464
-4	8	633	-647	-7	13	118	-115	-3	16	105	103	2	6	188	192	-3	11	259	253	4	1	478	477
-5	8	242	-245	-6	13	186	180	-4	16	132	130	3	6	199	203	-4	11	184	181	5	1	253	259
-6	8	90	86	-5	13	246	252	-5	16	107	103	4	6	226	230	-5	11	129	108	7	1	144	145
-7	8	180	-181	-3	13	134	-140	-6	16	112	116	5	6	201	204	-6	11	168	172	8	1	281	283
-8	8	589	-598	-2	13	49	-52	-7	16	173	177	6	6	70	73	-7	11	392	391	9	1	174	176
-9	8	432	-432	3	11	48	-39	-8	16	114	111	8	6	67	75	-8	11	436	430				
-10	8	75	-74	2	11	45	-31	-9	16	48	-39	9	6	76	80	-9	11	179	174	K=	8		
-11	8	90	-89	1	11	57	66	-11	16	193	198	10	4	81	79	-11	11	149	149				
-12	8	212	-210	0	11	115	116	-12	16	226	226	9	4	52	49	-12	11	224	218	-2	14	77	82
-13	8	136	-141	-2	11	98	-102	-13	16	118	120	8	4	43	-12	-13	11	130	128	-3	14	56	52
-15	8	62	-52	-3	11	42	-25	-14	16	78	75	7	4	72	77	-14	11	70	66	-7	14	46	-24
-15	6	82	-80	-5	11	140	-135	-15	16	76	73	6	4	296	295	-15	11	89	85	-8	14	55	54
-13	6	46	-40	-6	11	146	-147	-16	16	45	54	5	4	303	299	-16	11	60	65	-9	14	144	147
-12	6	199	-206	-7	11	134	132	-16	14	74	75	4	4	85	99	-16	9	67	64	-10	14	118	127
-11	6	268	-271	-8	11	292	298	-15	14	144	147	3	4	179	184	-15	9	114	107	-14	14	39	25
-10	6	124	-129	-9	11	141	146	-14	14	151	144	2	4	495	496	-14	9	71	71	-14	12	41	45
-9	6	59	-53	-10	11	82	-76	-13	14	64	58	1	4	502	486	-12	9	142	141	-13	12	71	65
-8	6	140	-144	-11	11	126	-119	-12	14	48	39	0	4	391	391	-11	9	287	278	-12	12	71	69
-7	6	421	-423	-13	11	74	67	-11	14	110	110	-1	4	403	401	-10	9	265	264	-11	12	78	86
-6	6	791	-796	-11	9	139	138	-10	14	144	150	-2	4	142	142	-9	9	199	196	-10	12	54	57
-5	6	686	-696	-10	9	100	99	-9	14	155	160	-3	4	195	195	-8	9	158	156	-8	12	78	-83
-4	6	87	-64	-9	9	59	-51	-8	14	204	201	-4	4	648	658	-7	9	190	190	-6	12	112	113

Table 5. Continued.

L	H		
K=	8		
-5	12	152	159
-4	12	53	66
-3	12	39	-37
-1	12	98	104
0	12	95	100
2	12	43	-40
2	10	67	69
1	10	70	74
0	10	58	-51
-1	10	126	-132
-2	10	54	47
-3	10	320	334
-4	10	258	277
-5	10	57	-56
-6	10	107	-115
-7	10	104	108
-8	10	160	170
-9	10	36	40
-13	10	64	58
-14	10	39	49
-11	8	84	94
-10	8	108	108
-9	8	104	-110
-8	8	88	-93
-7	8	279	297
-6	8	435	453
-5	8	161	164
-4	8	140	-143
-3	8	142	-145
-2	8	42	34
-1	8	146	152
0	8	48	55
1	8	53	-50
2	8	50	55
3	8	135	143
4	8	42	47
6	6	51	-57
4	6	150	158
3	6	75	76
2	6	42	-43
1	6	121	128
0	6	252	260
-2	6	84	-79
-3	6	148	156
-4	6	191	189
-5	6	42	-45
-6	6	96	-102
-8	6	133	141
-9	6	211	221
-10	6	126	134
-13	6	41	45
-12	4	66	67
-11	4	63	62
-8	4	35	33
-7	4	151	150
-6	4	83	90
-5	4	103	-104
-4	4	26	13
-3	4	214	210
-2	4	NA	92
-1	4	46	55
0	4	350	375
1	4	389	414
2	4	53	20
3	4	159	-174
4	4	75	-71
5	4	69	74
6	4	105	115
7	4	44	41
8	2	112	119
7	2	164	168
5	2	116	-124
4	2	103	104
3	2	287	296
2	2	126	129
1	2	202	-208
0	2	263	-277
-1	2	162	155
-2	2	543	570
-3	2	379	409
-4	2	29	22
-5	2	35	27
-6	2	138	142
-7	2	33	27
-8	2	71	-75
-10	2	79	84
-11	2	43	55
1	0	150	141
2	0	288	-295
3	0	128	-129
4	0	291	307
5	0	326	342
6	0	56	60
7	0	45	-48
8	0	54	47
9	0	72	78
K=	9		
1	13	77	-81
0	13	41	-31
-2	13	78	-75
-3	13	126	-121
-4	13	107	-98
-7	13	247	-248
-8	13	355	-350
-9	13	110	-101
-10	13	127	112
-12	13	153	-155
-13	13	94	-92
-13	11	49	46
-12	11	87	-82
-11	11	236	-228
-10	11	174	-176
-9	11	90	-90
-8	11	103	-96
-7	11	132	-130
-6	11	185	-186
-5	11	195	-190
-4	11	81	-73
-2	11	145	-146
-1	11	139	-145
2	11	124	-114
3	11	84	-89
4	9	103	-105
3	9	78	-68
0	9	240	-234
-1	9	382	-365
-2	9	193	-192
-4	9	102	-111
-5	9	175	-175
-6	9	98	-105
-7	9	129	-127
-8	9	209	-207
-9	9	182	-181
-10	9	143	-134
-11	9	118	-111
-12	9	70	-64
-13	9	61	-57
-14	9	73	-82
-13	7	79	-77
-12	7	122	-117
-11	7	115	-113
-10	7	78	-83
-9	7	133	-137
-8	7	182	-180
-7	7	33	-36
-6	7	52	38
-5	7	285	-280
-4	7	631	-609
-3	7	426	-422
-1	7	54	45
0	7	210	-211
1	7	306	-308
2	7	126	-130
5	7	105	-109
6	7	111	-105
7	5	99	-101
6	5	59	-54
5	5	49	-50
4	5	155	-158
3	5	247	-249
2	5	197	-197
1	5	31	-12
0	5	67	56
-1	5	272	-267
-2	5	605	-595
-3	5	371	-368
-4	5	32	22
-5	5	88	-95
-6	5	421	-412
-7	5	370	-362
-8	5	103	-100
-10	5	70	-71
-11	5	104	-113
-12	5	78	-71
-13	3	102	-107
-9	3	204	-203
-8	3	104	-97
-6	3	275	-279
-5	3	511	-505
-4	3	328	-316
-3	3	86	-93
-2	3	25	-32
-1	3	78	-78
0	3	301	-293
1	3	461	-452
2	3	274	-274
3	3	131	-135
4	3	237	-235
5	3	198	-194
8	3	92	-96
9	3	78	-83
8	1	58	-46
6	1	140	-145
5	1	275	-270
4	1	146	-147
3	1	103	-110
2	1	354	-353
1	1	369	-364
-2	1	531	-519
-3	1	165	-165
-4	1	53	37
-5	1	93	-106
-6	1	177	-175
-7	1	188	-188
-8	1	201	-202
-9	1	111	-107
K=	10		
0	14	103	-94
-1	14	79	-75
-2	14	50	-55
-3	14	72	-64
-4	14	92	-91
-5	14	140	-139
-6	14	192	-188
-7	14	169	-168
-8	14	98	-99
-9	14	83	-83
-10	14	128	-128
-11	14	149	-151
-12	14	139	-134
-13	14	111	-105
-14	14	81	-73
-14	12	104	-103
-13	12	99	-101
-12	12	83	-79
-11	12	116	-112
-10	12	184	-180
-9	12	222	-209
-8	12	211	-202
-7	12	170	-166
-6	12	90	-90
-5	12	67	-71
-4	12	179	-174
-3	12	261	-250
-2	12	184	-176
-1	12	59	-64
0	12	52	-55
1	12	96	-99
2	12	98	-91
3	10	77	-87
2	10	53	-54
1	10	75	-72
0	10	173	-172
-1	10	253	-246
-2	10	188	-187
-3	10	84	-82
-4	10	122	-129
-5	10	330	-322
-6	10	406	-391
-7	10	222	-214
-8	10	57	-59
-9	10	124	-125
-10	10	221	-209
-11	10	150	-149
-12	10	93	-88
-13	10	108	-106
-14	10	103	-101
-13	8	132	-126
-12	8	104	-103
-11	8	62	-60
-10	8	134	-132
-9	8	292	-285
-8	8	347	-339
-7	8	213	-212
-6	8	73	-70
-5	8	171	-166
-4	8	421	-417
-3	8	458	-449
-2	8	216	-212
-1	8	66	-69
0	8	151	-154
1	8	227	-220
2	8	143	-143
3	8	78	-72
4	8	94	-95
5	8	123	-115
6	6	108	-116
5	6	71	-67
4	6	75	-80
3	6	193	-195
2	6	262	-258
1	6	218	-217
0	6	235	-230
-1	6	344	-347
-2	6	369	-371
-3	6	194	-201
-4	6	97	-103
-5	6	293	-279
-6	6	487	-471
-7	6	379	-368
-8	6	120	-129
-9	6	62	-66
-10	6	159	-154
-11	6	195	-190
-12	6	127	-127
-13	6	51	-55
-12	4	46	-43
-11	4	94	-93
-10	4	197	-192
-9	4	229	-225
-8	4	152	-151
-7	4	109	-109
-6	4	219	-221
-5	4	376	-368
-4	4	394	-384
-3	4	338	-329
-2	4	386	-374
-1	4	454	-449
0	4	336	-331
1	4	141	-143
2	4	183	-190
3	4	359	-354
4	4	297	-291
5	4	84	-83
7	4	84	-91
8	4	113	-115
9	2	95	-93
8	2	47	-47
7	2	88	-89
6	2	227	-228
5	2	322	-315
4	2	203	-202
3	2	30	-19
2	2	149	-157
1	2	616	-598
0	2	717	-710
-1	2	296	-291
-2	2	66	-59
-3	2	351	-343
-4	2	542	-530
-5	2	330	-329
-6	2	128	-135
-7	2	195	-192
-8	2	254	-246
-9	2	144	-143
-10	2	54	-48
-11	2	55	-55
-1	0	231	-232
-2	0	646	-623
3	0	613	-594
4	0	207	-208
6	0	215	-212
7	0	319	-310
8	0	151	-152
9	0	49	-25
10	0	56	-66
K=	11		
0	13	41	-39
-1	13	40	-38
-2	13	85	-88
-3	13	122	-119
-5	13	50	52
-6	13	42	-45
-7	13	135	-134
-8	13	82	-87
-9	13	47	-44
-10	13	60	-51
-11	13	37	-48
-12	13	65	-72
-13	13	94	-94
-14	13	54	-44
-14	11	64	-52
-13	11	53	-59
-12	11	42	-28
-11	11	69	-70
-10	11	161	-158
-9	11	69	-71
-8	11	94	88
-7	11	31	24
-6	11	153	-152
-5	11	181	-189
-4	11	131	-134
-3	11	90	-94
-2	11	63	-64
-1	11	54	-52
0	11	42	-40
4	9	74	-87
1	9	56	-51
0	9	102	-103
-1	9	57	-64
-2	9	66	-67
-3	9	114	-113
-4	9	97	-98
-5	9	82	-87
-6	9	134	-140
-7	9	164	-173
-8	9	146	-157
-9	9	101	-102
-11	9	39	30
-12	9	43	-46
-13	9	90	-87
-12	7	52	-59
-11	7	72	-72
-10	7	53	-62
-9	7	79	-75
-8	7	129	-132
-7	7	156	-156
-6	7	106	-111
-5	7	80	-90
-4	7	167	-176
-3	7	190	-191
-1	7	102	95
0	7	38	-56
1	7	234	-242
2	7	190	-194
3	7	38	-30
5	7	41	-48
6	7	68	-67
7	5	60	-68
5	5	53	37
4	5	89	-87
3	5	209	-222
2	5	82	-92
1	5	91	88
0	5	110	-118
-1	5	433	-458
-2	5	368	-372
-3	5	27	9
-4	5	172	163
-5	5	31	-28
-6	5	226	-227
-7	5	176	-185
-8	5	40	-42
-9	5	45	-46
-10	5	127	-129
-11	5	93	-99
-10	3	77	-88
-9	3	127	-131
-8	3	75	-70
-7	3	70	66
-6	3	79	74
-5	3	247	-254
-4	3	483	-501
-3	3	154	-165
-2	3	170	169
-1	3	119	-126
0	3	449	-461
1	3	246	-247
3	3	44	41
3	3	32	11
4	3	110	-113
5	3	114	-121
6	3	42	-45
8	1	49	41
7	1	100	-103
6	1	233	-235
5	1	134	-141
4	1	43	-51
3	1	90	-99
2	1	115	-118
1	1	92	-95
-2	1	279	-290
-3	1	438	-445
-4	1	151	-160
-5	1	120	115
-6	1	63	-68
-7	1	240	-245
-8	1	100	-106
-9	1	36	34
K=	12		
1	12	42	36
0	12	95	95
-1	12	57	66
-3	12	47	-45
-5	12	121	123
-6	12	147	147
-7	12	59	51
-9	12	54	59
-10	12	91	92
-13	12	43	43
-14	12	49	44
-13	10	59	58
-12	10	38	41
-10	10	49	40
-9	10	155	153
-8	10	168	171
-7	10	43	52
-6	10	86	-86
-5	10	73	-67
-4	10	109	121
-3	10	214	222
-2	10	75	81
-1	10	62	-56
1	10	114	118
2	10	48	63
4	8	37	13
3	8	62	62
2	8	66	65
-1	8	157	166
-2	8	209	218
-4	8	104	-92
-5	8	103	104
-6	8	240	246
-7	8	98	106
-8	8	51	-46
-10	8	69	73
-11	8	101	103
-12	8	64	64
-10	6	50	53
-9	6	121	125
-8	6	68	78
-7	6	60	-51
-5	6	176	184
-4	6	202	210
-3	6	105	110
-2	6	84	91
-1	6	104	112
0	6	48	52
1	6	64	69
3	6	99	110
5	6	60	68
8	4	39	-28
6	4	106	107
5	4	97	100
2	4	84	98
1	4	174	187
0	4	167	182
-1	4	46	55
-2	4	62	-55
-3	4	29	32
-4	4	164	174
-5	4	145	153
-6	4	82	85
-7	4	117	123
-8	4	104	107
-11	4	48	43
-12	4	39	52
-11	2	41	51
-10	2	56	50
-8	2	56	64
-7	2	120	127
-6	2	66	71
-4	2	61	73
-3	2	150	161
-2	2	171	183
-1	2	100	105
0	2	43	-30
1	2	29	-10
2	2	213	226
3	2	291	299
4	2	64	67
5	2	89	-85
7	2	95	100
10	0	40	38
9	0	53	59
8	0	56	60
7	0	37	38
5	0	95	106
4	0	139	147
3	0	29	-17
2	0	113	-103
1	0	193	208
K=	13		
1	11	71	73
0	11	130	119
-1	11	104	98
-2	11	93	90
-3	11	143	140
-4	11	151	146
-5	11	91	86
-6	11	90	84
-7	11	155	150
-8	11	188	182
-9	11	140	133
-11	11	64	55
-11	11	45	42
-12	11	94	95
-12	9	86	87
-11	9	131	125
-10	9	126	116
-9	9	89	85
-8	9	111	110
-7	9	168	163
-6	9	165	156
-5	9	157	153
-4	9	234	222
-3	9	242	227
-2	9	110	107
-1	9	34	35
0	9	83	78
1	9	134	125
2	9	116	111
3	9	55	64
4	7	130	133
3	7	156	151
2	7	67	65
1	7	38	38
0	7	146	148
-1	7	257	255
-2	7	247	240
-3	7	134	130
-4	7	48	53
-5	7	128	130
-6	7	273	261
-7	7	251	234
-8	7	120	116
-9	7	104	104
-10	7	145	142
-11	7	107	100
-11	5	70	64
-10	5	125	118
-9	5	161	155
-8	5	143	141
-7	5	94	93
-6	5	86	84
-5	5	230	223
-4	5	384	373
-3	5	253	245
-1	5	59	69
0	5	306	302
1	5	325	311
2	5	134	134
3	5	50	57
4	5	111	105
5	5	122	121
6	5	54	69
7	3	104	103
6	3	118	113
5	3	88	81
4	3	109	105
3	3	184	187
2	3	195	199
1	3	138	138
0	3	146	144
-1	3	288	277
-2	3	414	400
-3	3	333	320
-4	3	69	78
-6	3	217	211
-7	3	271	259
-8	3	108	107
-10	3	87	77
-9	1	99	96
-8	1	39	37
-7	1	78	77
-6	1	203	196
-5	1	273	264
-4	1	260	251
-3	1	185	179
-2	1	129	132
1	1	235	231
2	1	194	191
3	1	216	211
4	1	182	178
5	1	105	109

Table 5. Continued.

L	H			L	H			L	H			L	H			L	H		
				-11	10	55	56	-3	6	163	169	6	4	100	99	-2	0	54	-39
K=	13			-11	8	75	75	-4	6	208	207	7	2	109	108	-1	0	175	188
				-10	8	109	102	-5	6	74	79	5	2	29	3				
6	1	93	95	-9	8	30	36	-7	6	59	54	4	2	126	126	K=	15		
7	1	120	116	-7	8	148	144	-8	6	161	152	3	2	234	235				
8	1	116	118	-6	8	250	245	-9	6	174	173	2	2	148	151	0	7	24	-16
				-5	8	190	183	-10	6	85	84	1	2	59	-39	-1	7	98	101
K=	14			-4	8	37	36	-10	4	37	36	0	2	44	-37	-2	7	41	45
				-2	8	59	66	-9	4	47	43	-1	2	213	223	-3	7	112	-125
1	10	47	50	-1	8	154	156	-8	4	89	91	-2	2	356	359	-4	7	100	-119
-1	10	34	21	0	8	100	101	-7	4	156	148	-3	2	177	178	-6	7	27	27
-2	10	88	87	2	8	55	59	-6	4	122	120	-4	2	29	33	-7	5	73	-85
-3	10	174	166	3	8	98	98	-4	4	58	66	-5	2	118	121	-6	5	101	-116
-4	10	154	154	4	6	93	[illegible]	-3	4	195	192	-6	2	169	168	-5	5	31	41
-5	10	54	56	3	6	66	66	-2	4	173	176	-7	2	58	60	-4	5	94	105
-6	10	34	32	2	6	51	55	-1	4	92	98	-9	2	50	48	-3	5	21	-28
-7	10	102	107	1	6	135	135	0	4	152	158	-8	0	53	60	-2	5	110	-132
-8	10	122	123	0	6	170	170	1	4	231	226	-6	0	79	81	-1	5	67	-82
-9	10	60	64	-1	6	55	64	2	4	138	134	-5	0	266	257	0	5	32	35
-10	10	49	42	-2	6	31	38	5	4	63	65	-4	0	215	212	1	5	78	80

L	H			L	H		
2	5	26	-1				
3	3	30	25				
2	3	28	29				
1	3	93	-113				
0	3	106	-126				
-1	3	60	58				
-2	3	123	136				
-4	3	99	-121				
-5	3	77	-96				
-5	1	76	79				
-4	1	54	51				
-3	1	74	-88				
-2	1	89	-106				
1	1	50	-60				
2	1	45	-53				
3	1	28	30				
4	1	28	24				

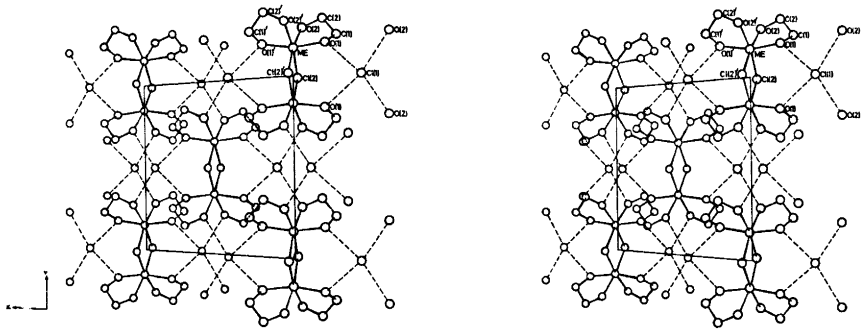

Fig. 1. A stereoscopic illustration of the *ab*-plane of the unit cell, showing the dinuclear $[Me_2Cl_2(C_2H_6O_2)_4]^{2+}$-ions, the Cl^--ions and the hydrogen bonds between these.

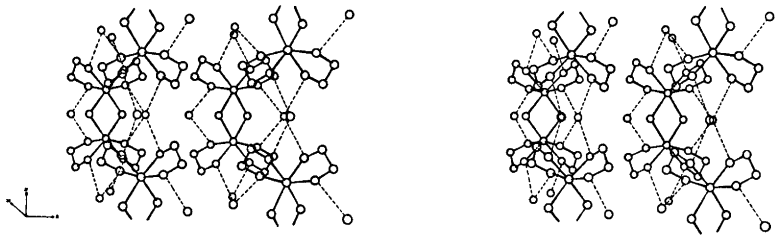

Fig. 2. A stereoscopic view of the layers which repeat themselves with displacement *c*. For the sake of clarity only half the unit cell in the *a*-direction is illustrated.

plane and a little below it (0.088 and 0.075 Å for the Ni- and Co-compounds, respectively) the chloride ion is situated. The mean Cl···O distance is 3.075 and 3.080 Å for the Ni- and Co-compounds, respectively.

In Fig. 3 the positions of the hydrogen atoms between the oxygen and chlorine atoms are shown. The O—H and Cl—H distances are quite reasonable and are given in Table 8. The angles Cl—H—O vary between 162

Table 6. Interatomic distances and angles in the two compounds. The roman figures I and II refer to the Ni- and Co-compounds respectively. (Standard deviations for the last significant figure are given in parentheses).

Atoms	I d/Å	II d/Å	Atoms	I angle/°	II angle/°
Me—Me	3.458(1)	3.470(1)	Cl(2)—Me—Cl(2)′	86.97(5)	88.22(2)
Me—O(1)	2.040(3)	2.071(1)	Cl(2)—Me—O(1)	98.24(9)	99.24(4)
Me—O(2)	2.093(3)	2.137(2)	Cl(2)—Me—O(1)′	93.14(9)	92.66(4)
Me—Cl(2)	2.383(1)	2.417(1)	Cl(2)—Me—O(2)	91.10(9)	91.27(4)
O(1)—O(2)	2.617(4)	2.612(2)	Cl(2)—Me—O(2)′	171.16(9)	169.14(4)
O(1)—C(1)	1.442(6)	1.434(3)	O(1)—Me—O(1)′	164.3 (2)	163.4 (1)
O(2)—C(2)	1.432(6)	1.436(3)	O(1)—Me—O(2)	78.6 (1)	76.7 (1)
C(1)—C(2)	1.501(7)	1.497(3)	O(1)—Me—O(2)′	90.5 (1)	91.6 (1)
Cl(1)—O(1)	3.071(3)	3.075(2)	O(2)—Me—O(2)′	92.1 (2)	91.2 (1)
Cl(1)—O(2)	3.079(3)	3.084(2)	Me—Cl(2)—Me	93.03(5)	91.78(2)
			Me—O(1)—C(1)	112.7 (3)	113.9 (1)
			Me—O(2)—C(2)	112.0 (3)	112.7 (1)
			O(1)—C(1)—C(2)	105.9 (4)	106.3 (2)
			O(2)—C(2)—C(1)	107.1 (4)	106.8 (2)
			Me—O(1)—Cl(1)	131.1 (1)	129.9 (1)
			Me—O(2)—Cl(1)	125.6 (1)	125.0 (1)

Table 7. Interatomic distances and angles involving hydrogen atoms. The roman figures I and II refer to the Ni- and Co-compounds respectively. (Standard deviations for the last significant figure are given in parentheses).

Atoms	I d/Å	II d/Å	Atoms	I angle/°	II angle/°
O(1)—H(1)	0.75(6)	0.68(3)	Me—O(1)—H(1)	127(5)	127(3)
O(2)—H(2)	0.73(5)	0.70(2)	Me—O(2)—H(2)	116(4)	116(2)
C(1)—H(3)	1.06(5)	1.00(3)	C(1)—O(1)—H(1)	103(5)	106(2)
C(1)—H(4)	1.00(5)	0.98(2)	C(2)—O(2)—H(2)	116(4)	115(2)
C(2)—H(5)	0.94(6)	1.00(3)	O(1)—C(1)—H(3)	107(3)	105(2)
C(2)—H(6)	0.96(4)	0.96(3)	O(1)—C(1)—H(4)	109(3)	111(1)
			C(2)—C(1)—H(3)	115(3)	116(2)
			C(2)—C(1)—H(4)	108(3)	110(2)
			H(3)—C(1)—H(4)	111(4)	108(2)
			O(2)—C(2)—H(5)	113(3)	109(2)
			O(2)—C(2)—H(6)	106(3)	111(2)
			C(1)—C(2)—H(5)	110(3)	110(2)
			C(1)—C(2)—H(6)	110(3)	113(2)
			H(5)—C(2)—H(6)	111(5)	107(2)

Table 8. Hydrogen bond distances (Å) and angles (°). The roman figures I and II refer to the Ni- and Co-compounds respectively. (Standard deviations for the last significant figure are given in parentheses.)

	Cl(1)···H(1)—O(1)		Cl(1)···H(2)—O(2)	
	I	II	I	II
Cl—H	2.32 (6)	2.41 (3)	2.37 (5)	2.40 (3)
O—H	0.75 (6)	0.68 (3)	0.73 (5)	0.70 (2)
Cl—O	3.071(3)	3.075(2)	3.079(3)	3.084(2)
∠Cl—H—O	171 (6)	166 (3)	162 (5)	164 (3)

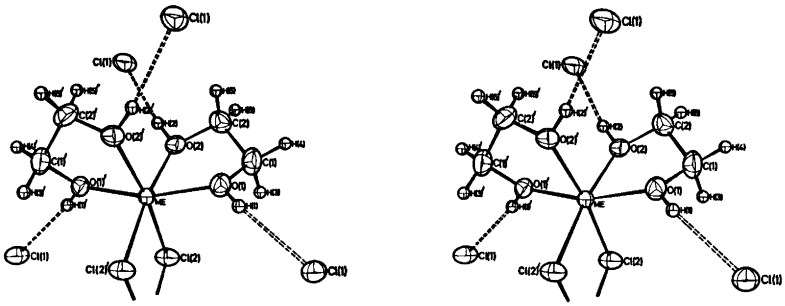

Fig. 3. A stereoscopic illustration, showing the coordination around the metal ion and four adjacent chloride ions. Thermal ellipsoids for the nonhydrogen atoms are scaled to enclose 50 % probability.

and 171° for the two compounds but there is no significant difference between these values.

Acknowledgements. I wish to express my sincere thanks to Professor Nils Ingri for much valuable advice and for all the facilities placed at my disposal. I also thank Dr. Britt Hedman for much valuable help with computational problems. The English of this paper has been corrected by Dr. Michael Sharp. This work forms part of a program supported by the Swedish Natural Science Research Council.

REFERENCES

1. Antti, B.-M., Lundberg, B. K. S. and Ingri, N. *Acta Chem. Scand. 26* (1972) 3984.
2. Antti, B.-M. *Acta Chem. Scand. 27* (1973) 3513.
3. Knetsch, D. and Groeneveld, W. L. *Inorg. Chim. Acta 7* (1973) 81.
4. *International Tables for X-Ray Crystallography*, Kynoch Press, Birmingham 1965, Vol. I.
5. Ivarsson, G., Lundberg, B. K. S. and Ingri, N. *Acta Chem. Scand. 26* (1972) 3005.
6. Antti, C.-J. and Lundberg, B. K. S. *Acta Chem. Scand. 25* (1971) 1758.
7. Cruickshank, D. W. J. *Computing Methods in Crystallography*, Pergamon, London 1965, p. 114.
8. Cromer, D. T. and Waber, J. T. *Acta Crystallogr. 18* (1965) 104.
9. *International Tables for X-Ray Crystallography*, Kynoch Press, Birmingham 1962, Vol. III.
10. Stewart, R. F., Davidson, E. R. and Simpson, W. T. *J. Chem. Phys. 42* (1965) 3175.
11. Bright, D., Milburn, G. H. W. and Truter, M. R. *J. Chem. Soc. A* (1971) 1582.
12. Bastiansen, O. *Acta Chem. Scand. 3* (1949) 415.
13. Buckley, P. and Giguère, P. A. *Can. J. Chem. 45* (1967) 397.

Received May 21, 1974.

Acta Chemica Scandinavica A 29 (1975) 89—92

Spin Probe Studies on the Dynamic Structure of Dimethyl Sulfoxide—Water Mixtures

IVAN BULLA,* PERTTI TÖRMÄLÄ and J. JOHAN LINDBERG

Department of Wood and Polymer Chemistry, University of Helsinki, Malminkatu 20, SF-00100 Helsinki 10, Finland

The rotational diffusion data of free nitroxyl radicals in dimethyl sulfoxide (DMSO) indicated two transition temperatures at which changes in intermolecular arrangement occurred: There was first a steep decrease in the rotational correlation time (τ) beginning at the melting point 18.5 °C. Then a steep decrease in τ at 55 °C. The latter was deduced to arise from the dissociation reaction of the DMSO ordered structure.

When τ was plotted as a function of the molar composition of the DMSO—water mixture at constant temperature, ($T = 60$ °C) two τ-maxima were found: one at a DMSO—water ratio of 1:2 and another at a ratio of about 1:1. The very weak nature of the association complexes of DMSO with water seems to be in agreement with the experimental results obtained.

Several opinions have been given regarding the structure and kind of the bonds that are established between water and dimethyl sulfoxide (DMSO). Thus, Cowie and Toporowski assumed the formation of a stoichiometric adduct $(H_2O)_2$.DMSO,[1] whereas Kenttämaa and Lindberg and co-workers[2,3] proposed the presence of non-specific dipole-dipole or ionic type bonds rather than definite complexes. From NMR-studies Drinkard and Kivelson concluded in favour of mixed hydrogen and dipolar bonding.[4] Later Rallo *et al.*[5] inferred from calorimetric measurements an interaction without the formation of stoichiometric compounds. Recent NMR-chemical shift and Raman-spectroscopic measurements[6,7] seem to support the non-stoichiometric structural model.

Furthermore, the measurements of Salonen,[8] among others, of the infrared spectra of DMSO containing traces of water indicate that the water molecules are subjected to strong forces tending to straighten the molecules and the transverse motion of the molecules is markedly hindered. In addition a polymer chain structure of DMSO seems to be prevalent.[2,9] From Raman-spectra of DMSO—water mixtures Scherer and co-workers[7] have deduced a simple structural model in which it is assumed that water can be separated into two major species: one is symmetrically hydrogen bonded and the other asymmetrically hydrogen bonded.

Such a structural model presents several unsolved problems, especially with regard to the formation, breaking, and rotation of secondary valence bonds. In a previous report Lindberg and Hakalax[10] calculated an approximate dielectric relaxation time τ_d equal to 7×10^{-12} s for DMSO-benzene mixtures. From viscosity data[11] the relaxation time was estimated to be 3×10^{-11} s, in rough agreement with the value above.

The above data indicate that there should be a relaxational motion of DMSO—water mixtures in the microwave region. As the recently developed spin probe method seems to be especially suitable for accurate resolution of dynamic and microviscometric problems in this region, the present authors have studied the DMSO—water system by using stable nitroxyl radicals as labels and their ESR spectra as sensitive indicators of environmental effects.

* Present address: Pulp and Paper Research Institute, Bratislava, Czechoslovakia.

EXPERIMENTAL

3-Carbamoyl-2,2,5,5-tetramethylpyrroline-1-oxyl (I) was prepared by the method of Rozantsev *et al.*[12] Commercial DMSO was purified by distillation *in vacuo* and repeated recrystallization to a melting point of 18.52 °C.[13] Freshly distilled water was used as such.

The binary mixtures were made by weighing and traces of radical I were added. At the concentration of probe used, (8×10^{-4} M), the spin-spin exchange was absent. All measurements were made in a time interval very short as compared to the decay time of the radicals in solution.

The ESR spectra were obtained on a Varian E-4 spectrometer operating at a microwave frequency of 9.5 GHz, *i.e.* about 3.2 cm. The magnetic field was modulated with an amplitude less than one sixth of the line-width. The microwave power was 1 mW to avoid saturation effects. The measurements were made, where possible, in the temperature range 223–423 K, a Varian E-257 variable temperature accessory with an accuracy of ±2 K, calibrated with an iron/constantan thermocouple, was employed.

RESULTS

It has been found that under conditions where intermolecular interactions between radicals are eliminated, the rotational frequencies of radicals of small molecules as indicated by ESR spectra are affected by the motions of the surrounding molecules.[14,15]

In Fig. 1 are given some typical examples of the ESR spectra of free radicals intermixed with DMSO–water solutions at different temperatures. At room temperature the motion is so rapid that an isotropic spectrum is obtained.

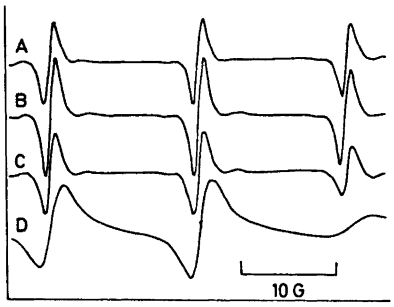

Fig. 1. ESR spectra of pyrroline nitroxyl radicals (I) in DMSO–water solution ($x_{DMSO} = 0.25$) at different temperatures. (A) T = 55 °C; (B) T = 27 °C; (C) T = 0 °C; (D) T = −50 °C.

However, with decreasing temperature and increasing viscosity it goes gradually over to a non-isotropic spectral pattern. A marked change in spectral behaviour is observed only at the respective melting points in pure DMSO and water.

DISCUSSION

A more quantitative picture of the results was obtained by estimating the rotational correlation times (τ) of the radicals from the ESR spectra. Here it is significant that the values of τ also are related to the microviscosity of the surroundings of the spin probe. In the region of rapid rotations ($\sim 5 \times 10^{-9} - 5 \times 10^{-11}$ s), τ could be calculated by the alternative eqns. (1) and (2) which are based on Kivelson's theory.[16–17]

$$\tau_1 = 8.7 W_0[(h_0/h_1)^{\frac{1}{2}} - (h_0/h_{-1})^{\frac{1}{2}}] \times 10^{-10} \text{ s} \quad (1)$$

$$\tau_2 = 7.9 W_0[(h_0/h_1)^{\frac{1}{2}} + (h_0/h_{-1})^{\frac{1}{2}} - 2] \times 10^{-10} \text{ s} \quad (2)$$

Here W_0 is the line width (Gauss) of the centre line in the ESR spectrum and h_1, h_0 and h_{-1} are the intensities of the low, centre, and high field components. In general a mean value of τ_1 and τ_2 is used.[17] The numerical parameters are dependent on the magnetic field and on the $\bar{g}$ and $\bar{T}$ tensors for which values given by Ohnishi *et al.* were used.[18] The difference between the two values of τ was, as a rule, less than 10 % and they can be roughly explained as the time required for a nitroxyl radical to turn a complete rotation around its axis. The calculation of τ is reviewed more thoroughly elsewhere.[19,20] A relative accuracy of about ±2 % was achieved, as deduced from the variation in the experimental data.

Although there is still not found any simple physical connection between the correlation times obtained by spin relaxation measurements and macroscopically observed viscosities, it is evident that the rotation of the spin probe must be strongly influenced also by the viscous behaviour of neighbour molecules.[19,25] This is also manifested by the approximate validity of the Stokes-Einstein relation,

$$\tau = 4\pi\eta r^3/3kT \quad (3)$$

for the tumbling probe in a viscous medium. Therefore it is possible, at least qualitatively,

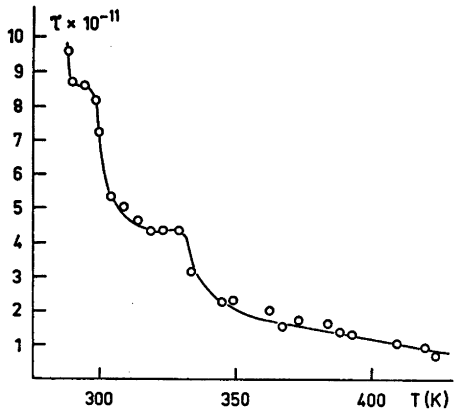

Fig. 2. Rotational correlation time τ or radicals in DMSO *vs.* temperature.

to correlate structural changes in the surrounding medium with changes in correlation times of the spin probes. A similar correlation has also been observed between δ and γ relaxations and spin label and probe data.[26,27]

A closer inspection of the results presented reveals therefore the following details regarding the dynamic (microviscosimetric) structure and thus also the structural changes of the surroundings of the probe.

Pure DMSO. In Fig. 2 the correlation time τ in pure DMSO is plotted as a function of temperature in the range 285—425 K (*i.e.* from +10 to +150 °C). The curve obtained shows a steep decrease beginning at the melting point, 18.5 °C, and ending in a plateau at about 40 °C. There is another steep decrease at about 55 °C, again followed by a linear, slow decrease in the whole last part of the region investigated, *i.e.* 60—150 °C.

One may interpret the first transition region from 18.5 °C onwards as corresponding to the breaking up of the ordered network into an assembly of free DMSO chains. Such a breaking up is also indicated by dipole and calorimetric measurements.[2,9]

The similarity of the intermolecular frequencies in the neutron elastic scattering spectra of solid and liquid DMSO [21] suggests that the degree of association arising from dipole interactions in liquid DMSO is high and that there is a quasisolid ordering in liquid DMSO. From IR spectra of solutions of DMSO in carbon tetrachloride, Figueroa, Roig and Szmant [22] concluded that dimethyl sulfoxide exists primarily in the form of cyclic dimers in the concentration range from 0.1 to 0.3 M, but may exist in the form of chains at higher concentrations. These conclusions are in accordance with the data of Lindberg, Kenttämaa and Nissema.[9] It seems evident therefore that the second transition region mentioned above corresponds to a dissociation reaction of the DMSO ordered structure and that above 60 °C DMSO is chiefly present as a monomolecular species, which also is manifested by a smaller microviscosity.

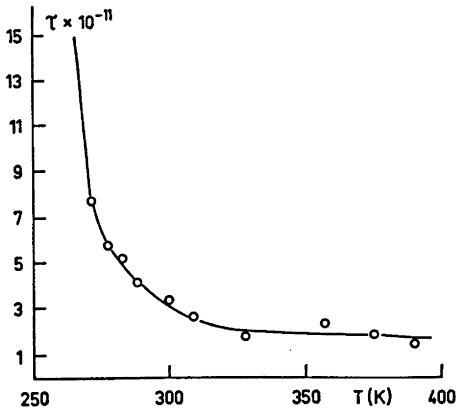

Fig. 3. τ of radicals in H_2O *vs.* temperature.

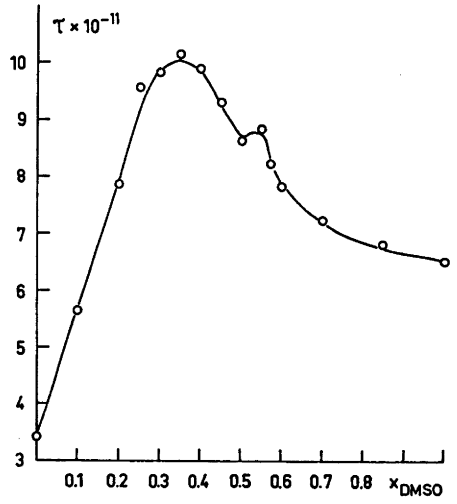

Fig. 4. τ of radicals in DMSO—water solutions of different molar compositions.

Pure water. In Fig. 3 the correlation time τ for pure water is plotted as a function of temperature in the range from −50 to +117 °C. It is evident that the steep decrease in τ sets in at the melting point. It is directly followed by the uniform liquid region up to the boiling point. The structure of water has been reported by previous authors [23,24] and is, as expected, markedly different from that of pure DMSO. The three-dimensional hydrogen bond network of H_2O gives the substance quite other dynamic properties than does the stiff chain structure of DMSO, which is also deduced from spectral data.[3,7-8]

DMSO—water mixtures. The correlation times in DMSO—water mixtures of various molar composition were measured at −50, −17, +15, +27, +40, +55, +84, +103, and +117 °C. In Fig. 4, by way of example, the correlation times in DMSO—water mixtures of various molar composition at 27 °C are plotted. From the curves it was found that at all temperatures investigated a marked relaxation time maximum is observed in the region of 1:2 DMSO—water molar composition. In addition, a corresponding maximum at about 1:1 DMSO—water molar composition is observed at lower temperatures. The intensity of the latter maximum in respect to the former decreases rapidly with increasing temperature and is only slightly observable at higher temperatures, *i.e.* > 60 °C. Therefore, the above result also indicates the weakness and instability of the latter complex in respect to the former.

Acknowledgement. The authors are grateful to the National Research Council for Sciences and to the Finnish Society of Science for financial aid.

REFERENCES

1. Cowie, J. M. G. and Toporowski, P. M. *Can. J. Chem. 39* (1961) 2240.
2. Lindberg, J. J. and Kenttämaa, J. *Suom. Kemistilehti B 33* (1960) 104.
3. Lindberg, J. J. and Majani, C. *Acta Chem. Scand. 17* (1963) 1477.
4. Drinkard, W. and Kivelson, D. *J. Phys. Chem. 62* (1968) 1494.
5. Rallo, F., Rodante, F. and Silvestroni, P. *Thermochim. Acta 1* (1970) 311.
6. Köhler, W. and Radeglia, R. *Z. phys. Chem. (Leipzig) 243* (1970) 127.
7. Scherer, J. R., Go, M. K. and Kint, S. *J. Phys. Chem. 77* (1973) 2108.
8. Salonen, A. K. *Ann. Acad. Sci. Fenn. Ser. A VI Physica 67* (1961).
9. Lindberg, J. J., Kenttämaa, J. and Nissema, A. *Suom. Kemistilehti B 34* (1961) 156.
10. Lindberg, J. J. and Hakalax, R. *Finska Kemistsamfundets Medd. 71* (1962) 97.
11. Lindberg, J. J. *Finska Kemistsamfundets Medd. 71* (1962) 77.
12. Rozantsev, E. G. and Krinitskaya, L. A. *Tetrahedron 21* (1965) 491.
13. Kenttämaa, J. and Lindberg, J. J. *Suom. Kemistilehti B 33* (1960) 98.
14. Wasserman, A. M., Buchachenko, A. L., Kovarskii, A. L. and Neiman, M. B. *Eur. Polym. J. 5* (1969) 473.
15. Gross, S. C. *J. Polym. Sci. (A-1) 9* (1971) 3327.
16. Kivelson, D. *J. Chem. Phys. 33* (1960) 1094.
17. Waggoner, A. S., Griffith, O. H. and Christensen, C. R. *Proc. Nat. Acad. Sci US 57* (1967) 1198.
18. Ohnishi, S., Boeyens, J. C. A. and McConnell H. M. *Proc. Nat. Acad. Sci US 56* (1966) 809.
19. Griffith, O. H. and Waggoner, A. S. *Accounts Chem. Res. 2* (1969) 17.
20. Törmälä, P., Brotherus, J. and Lindberg, J. J. *Finska Kemistsamfundets Medd. 81* (1972) 11.
21. Safford, G. J., Schaffer, P. C., Leung, P. S., Doebbler, G. F., Brady, G. W. and Lyden, E. F. X. *J. Phys. Chem. 50* (1969) 2140.
22. Figueroa, R. H., Roig, E. and Szmant, H. H. *Spectrochim. Acta 22* (1966) 587.
23. Pimentel, G. C. and McClellan, A. L. *The Hydrogen Bond*, San Francisco and London 1960 and the numerous references cited there.
24. Horne, R. A., Ed., *Water and Aqueous Solutions*, New York 1972.
25. Rozantsev, E. G. *Free Nitroxyl Radicals*, Plenum, New York 1970.
26. Bullock, A. T., Cameron, G. G. and Smith, P. M., *J. Polym. Sci., Polym. Phys. Ed. 11* (1973) 1263.
27. Törmälä, P. *Polymer 15* (1974) 124.

Received May 25, 1974.

Acta Chemica Scandinavica A 29 (1975) 93—104

The Crystal Structures of the Isomorphous Methylxanthates of Divalent Sulfur and Selenium

NILS JOHAN BRØNDMO, STEINAR ESPERÅS and STEINAR HUSEBYE

Chemical Institute, University of Bergen, N-5014 Bergen, Norway

The crystals of sulfur and selenium di(methylxanthate) are isomorphous, space group $I2/c$ and have the unit cell dimensions $a=13.580(5)$ Å, $b=8.243(3)$ Å, $c=18.429(4)$ Å, $\beta=92.80(4)°$ and $a=13.640(6)$ Å, $b=8.299(3)$ Å, $c=18.409(14)$ Å, $\beta=93.56(6)°$, respectively. In both cases, the unit cell contains eight molecules.

Their structures have been determined by means of three-dimensional X-ray methods based on 712 reflection intensities above background, collected by photographic methods for the sulfur compound, and on 386 reflection intensities above background measured on a diffractometer for the selenium analogue. Least squares refinements of their structures have given conventional R-values of 0.109 and 0.052, respectively, for the former and latter compound.

In the molecules, the central sulfur and selenium atoms are bonded to two sulfur atoms, one from each of the two ligands. In addition, each central atom is weakly bonded to two sulfur atoms, one from each of two different neighbour molecules, resulting in a trapezoid planar configuration around the central atoms. Some relevant bond lengths and angles are: S0—S1=2.045(7) Å, S0—S3=2.059(6) Å, S0···S2=3.625(6) Å, S0···S4=3.709(8) Å and ∠S1—S0—S3=104.2(3)° for sulfur di(methylxanthate); and Se—S1=2.205(6) Å, Se—S3=2.170(9) Å, Se···S2=3.501(9) Å, Se···S4=3.595(7) Å and ∠S1—Se—S3=100.8(3)° for the selenium analogue.

During our study of structures of divalent sulfur, selenium, and tellurium with bidentate dithio and related ligands,[1–11] three classes of structures have been found, as indicated by the three first examples in Fig. 1. Class I contains trapezoid planar four-coordinated complexes, where the central atom to ligand bonds are all intramolecular. To this class belong the structures of selenium and tellurium bis(diethyldithiocarbamate),[6,12] and selenium and tellurium bis(4-morpholinecarbodithioate),[7,9] and the ethyl- and methylxanthates of tellurium.[6,10] Also arsenic and bismuth with phenyl substituents will bind to bidentate ligands forming class I structures.[13,14] To class II, where the trapezoid planar four-coordinated structure is based on two intramolecular and two very weak intermolecular central atom to ligand bonds, belong the structures of selenium bis(diethyldiselenophosphinate),[5] tellurium bis(dimethyldithiophosphate),[2] and tellurium bis(diethylthioselenophosphinate.[4] Structures of distorted square planar *cis*-complexes of divalent tellurium with monodentate ligands, and structures found for some positive polyhalogens also belong to this class.[15,16] Only one compound in the present study belongs to class III, which represents the trichalcogenide structure. It is the bis(dithiocarbamate) of divalent sulfur, bis(4-morpholinethiocarbonyl) trisulfide.[17] For comparison, two other structural classes are listed in Fig. 1. Structural work on *trans* square planar tellurium complexes with monodentate thio ligands as thiourea, shows that their structures belong to class IV.[15] In the last class, V, one finds the square planar structures of transition metals such as Ni(II), with bidentate dithio ligands.[18]

Of the structures of divalent selenium and tellurium complexes with bidentate dithio ligands, none belong to classes III—V. Steric reasons prevent them from forming complexes of class IV. However, if they were to adopt structures of class V with all four M—S bonds and all four C—S bonds being equal, both types of bonds having lengths being the average of corresponding lengths in the class I compounds above, the following angles would be found:

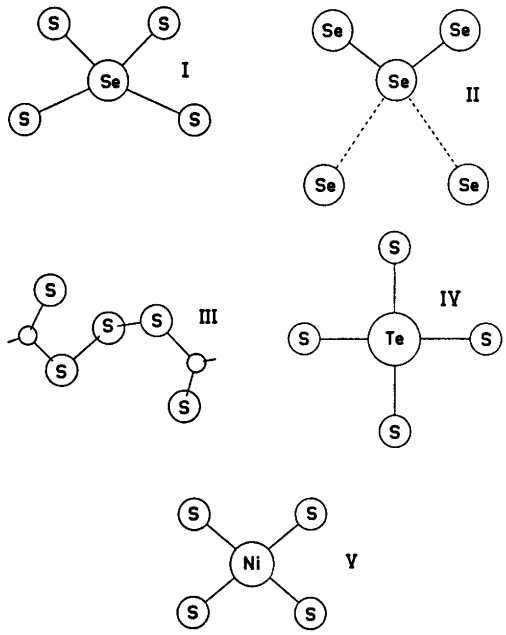

Fig. 1. Examples of the five classes of compounds I–V. Only the central atoms and their environments are shown. As representatives of the classes are chosen I: $(Et_2NCS_2)_2Se$,[8] II: $(Et_2PSe_2)_2Se$,[5] III: $OC_4H_8NC(S)S_3(S)NC_4H_8O$,[17] IV: $Te(SC(NH_2)_2)_4Cl_2.2H_2O$[15] and V: $(EtOCS_2)_2Ni$.[18] The small circles in the class III compound represent carbon atoms.

∠S–M–S intraligand with M=Se *ca.* 71°, with M=Te *ca.* 67°. ∠S–M–S interligand, with M=Se *ca.* 109°, with M=Te *ca.* 113°. In both cases, the C–S–M angles would be around 86–87°. In this discussion the S–C–S angle is assumed to be *ca.* 118°. Steric considerations, *i.e.* a combination of the small S–S bite of 2.94 Å in the ligand and the large S–M bond prevent a type IV structure being formed, and also seem to make a type V structure less likely, probably because of the two large interligand angles it would require.

In the group I compounds, the "inner" parts of the ligand sulfur *p* orbitals pointing into the S–C–S angle, overlap with *p* orbitals on the same central atom, forming a mononuclear complex.[11] The deviation from linearity and the asymmetry of the three-center four-electron S–M–S systems do not seem to influence the average S–M bond length relative to that found for the linear, symmetric three-center systems of group VI.[15] This is not expected and implies that other orbitals, probably *s*-orbitals on tellurium, also contribute to the bonding.[11] Quite recently, Mössbauer spectra have been measured for tellurium bis(dimethyldithiophosphate) and tellurium bis(diethyldithiocarbamate), and the data are interpreted as evidence for some incorporation of the tellurium *5s* electrons in the bonding scheme.[19] For the compounds in group II, it is the "outer" part of the ligand *p* orbitals that overlap with *p* orbitals on the central atoms. Each ligand thus forms one intramolecular bond to the central atom in the molecule proper, and in addition one intermolecular weak bond to the central atom of a neighbour molecule. The three-center systems are here nearly linear and the average ligand to central atom bonds are longer than those in groups I and IV. This is expected on basis of the asymmetry in the strength of the two bonds in the linear three-center systems.[15,20]

Whether the divalent sulfur, selenium and tellurium compounds above adopt a class I, II, or III structure, seems to depend on two factors — the stronger the donor capacity of the ligand and the stronger the acceptor capacity of the central atom, the lower the group number to which the structure of the resulting compound belongs.[10]

The fact that the selenium and sulfur methylxanthates are isomorphous,[10] for the first time makes it possible to find a tendency to planar four-coordination for divalent sulfur. They are also the first xanthates of these elements whose structures have been solved.

EXPERIMENTAL

Selenium di(methylxanthate), $Se(MeOCS_2)_2$, was first made by Foss by nucleophilic substitution on the central atom of the selenopentathionate ion.[21] By an analogous procedure, we prepared sulfur di(methylxanthate), $S(MeOCS_2)_2$, from potassium pentathionate. For the present investigation, the selenium compound was made by a procedure similar to that used to prepare the diethyldithiocarbamate analogue.[8] An aqueous solution of potassium methylxanthate was added with stirring to selenious acid dissolved in 2 N hydrochloric acid in the molar ratio 4:1. The resulting oil consisting of equimolecular amounts of selenium di(methylxanthate) and the corresponding disulfide was then recrystallized from ethyl

acetate. Attempts to prepare crystals of other alkylxanthates of divalent selenium failed; in all cases the results were oily substances. Selenium di(methylxanthate) crystallized as yellow prisms, elongated along *c*, while the disulfide stayed in solution. The sulfur analogue gave colourless crystals of a similar shape upon recrystallization from ethyl acetate.

Crystals of the two compounds are isomorphous. From systematic extinctions, the possible space groups are *I*2/*c* or *Ic*. (*C*2/*c* or *Cc* if a face-centered group is preferred). The successful refinement shows that the crystals belong to the space group *I*2/*c* with the eight general positions: $\pm(x,y,z;\ \bar{x},y,\frac{1}{2}-z;\ \frac{1}{2}+x,\ \frac{1}{2}+y,\ \frac{1}{2}+z;\ \frac{1}{2}-x,\ \frac{1}{2}+y,\bar{z})$. There are eight formula units per cell. The following unit cell dimensions were found for the methylxanthate of sulfur: $a=13.580(5)$ Å, $b=8.243(3)$ Å, $c=18.429(4)$ Å and $\beta=92.80(4)°$.[10] Those for the selenium analogue are $a=13.640(6)$ Å, $b=8.299(3)$ Å, $c=18.409(14)$ Å and $\beta=93.56(6)°$.[10]

The intensity data for the sulfur compound were collected by means of the multiple-film, equi-inclination Weissenberg technique, employing Ni-filtered Cu$K\alpha$ radiation. The crystals were unstable, and decomposed upon prolonged exposure to X-rays, even when kept in capillaries. The crystals therefore had to be changed for each layer, and the exposure time was maximum 8 h for each layer. Out of 1281 0*kl*, 1*kl* and *h*0*l* through *h*3*l* reflections with $\sin\theta<0.98$, only 712 were observed. The intensities of unobserved reflections were set equal to the threshold value on the visual scale.

The intensities for the selenium compound were obtained by using a Siemens AED-1 punched paper-tape-controlled single crystal diffractometer. The diffractometer was operated as a three-circle instrument using Nb-filtered Mo$K\alpha$ radiation. Due to the rapid decomposition of the crystals as evidenced by a colour change from yellow to red, it was difficult to obtain a satisfactory set of reflection intensities. Three sets of data were taken with three different crystals. Only one of the sets, taken from a crystal mounted in a glass capillary with the *c* axis parallel to the spindle axis, could be used. However, out of 974 reflections with sin $\theta<20°$, only the first 472 were later during the refinement and by comparison with short exposure films, found to be correctly measured. The final refinement of the structure is based on these reflections only. Of the latter reflections, only 386 were observed. The intensities were collected using "five-value" measurements and the $\theta-2\theta$ scan technique with minimum scan speed 5° per min [22] with automatic setting of greater speed for the strongest reflections. Attenuation filters were automatically inserted for strong reflections to reduce counting losses. The reflections were scanned between $\theta_1=\theta-0.5°$ and $\theta_2=\theta+0.5°$ where θ is the Bragg angle for the α_1 peak. Two reference reflections were measured at intervals of 50 reflections and reflections with intensities less than twice the standard deviation based on counting statistics, were labelled as unobserved.

Lorentz and polarization corrections were applied to the intensity data for both compounds. No correction for secondary extinction or absorption ($\mu=95.4$ cm^{-1}) was applied to the sulfur di(methylxanthate) data, but the selenium di(methylxanthate) data was corrected for absorption ($\mu=46.2$ cm^{-1}) by means of a program based on the Gaussian grid technique.[23] The crystal used in the latter case had the following dimensions measured as distances from a common origin to the crystal faces: 0.117 mm for 001 and 00$\bar{1}$, 0.020 mm for 110 and $\bar{1}10$ and 0.039 mm for $\bar{1}10$ and 1$\bar{1}$0. The correction was made on basis of a $8\times6\times14$ grid.

The cell dimensions for the sulfur compound were determined from NaCl-calibrated zero-layer Weissenberg films, while those for the selenium compound were calculated on basis of diffractometer measurements of a set of high-order reflections.

STRUCTURE DETERMINATIONS

The structure of the selenium compound was first to be solved. Overall scale and temperature factors were computed from a Wilson plot [24] and used in calculation of normalized structure factors for all reflections, using a program written by Shiono.[25] The resulting *E* statistics were slightly in favour of a centrosymmetric space group.

Phase determination for 150 reflections with $E>1.40$ was then carried out using Long's computer program based on reiterative application of Sayre's equation.[26] The three initial reflections (10,0,4; 7,2,5; 7,4,3) produced eight possible sign sets. Two sets had a consistency index, *C*, equal to 1.000. $C=(|E_A\Sigma E_B E_C|)/(|E_A|\Sigma|E_B||E_C|)$ where the sum is over all terms in the Sayre equations. One of the two resulting *E* maps revealed most of the non-hydrogen atomic positions. All atomic positions, except those for hydrogen, were then found by a Fourier synthesis based on structure factors with contributions from the atoms above.

Since the crystals of selenium and sulfur di(methylxanthate) are isomorphous, the structure of the latter was found by assuming as a first approximation that corresponding atoms have identical coordinates in the two compounds.

Table 1. Final coordinates, in fractions of cell edges with standard deviations in parentheses.

	x	y	z
	$S(MeOCS_2)_2$		
S0	0.0903(3)	0.3542(6)	0.1464(2)
S1	0.0167(3)	0.5548(7)	0.1075(2)
S2	0.0451(3)	0.8155(7)	0.0100(3)
S3	0.1423(3)	0.4211(7)	0.2489(2)
S4	0.3159(4)	0.5623(8)	0.3182(2)
O1	0.1788(8)	0.5904(16)	0.0402(6)
O2	0.2946(7)	0.4927(15)	0.1782(5)
C1	0.0889(11)	0.6578(23)	0.0470(8)
C2	0.2459(13)	0.6709(30)	−0.0096(10)
C3	0.2597(10)	0.4988(22)	0.2447(7)
C4	0.3974(13)	0.5539(25)	0.1704(9)
	$Se(MeOCS_2)_2$		
Se	0.0876(1)	0.3371(2)	0.1464(2)
S1	0.0122(3)	0.5574(6)	0.1059(5)
S2	0.0429(4)	0.8174(6)	0.0080(5)
S3	0.1459(3)	0.4173(7)	0.2526(5)
S4	0.3214(4)	0.5638(8)	0.3189(6)
O1	0.1708(8)	0.5853(15)	0.0377(11)
O2	0.2911(9)	0.4954(14)	0.1793(14)
C1	0.0868(11)	0.6511(21)	0.0478(15)
C2	0.2391(14)	0.6647(26)	−0.0124(17)
C3	0.2632(14)	0.4967(22)	0.2473(21)
C4	0.3903(13)	0.5659(25)	0.1635(16)

STRUCTURE REFINEMENT

The structures were both refined by a full-matrix least squares program which minimizes the quantity $r=\sum w(|F_o|-K|F_c|)^2$. Here K is a scale factor and w, the weight of a reflection, is the inverse of the variance of F_o.

Table 2. Isotropic thermal parameters $U\times10^4$, in Å^2, with standard deviations in parentheses. The expression used is exp $[-8\ \pi^2U(\sin^2\theta/\lambda^2)]$.

	$S(MeOCS_2)_2$	$Se(MeOCS_2)_2$
O1	617(33)	558(42)
O2	577(30)	539(43)
C1	535(45)	412(54)
C2	793(63)	708(68)
C3	464(40)	458(61)
C4	740(57)	720(73)

Observed reflections with $K|F_c|$ larger than the observable limit, are included in the refinement with F_o put equal to the limit. Hydrogen atoms were not located and therefore not included in the refinements of the two structures (Table 1).

For selenium di(methylxanthate) the factor $R=\sum||F_o|-|F_c||/\sum|F_o|$ converged to the value 0.20 based on all 971 reflections and isotropic temperature factors for all atoms (Table 2). At this stage of refinement, the error in the intensity data was found, and the subsequent refinements were based on the remaining 472 (including 86 unobserved) reflections. After introducing anisotropic temperature factors (Table 3) for the selenium and sulfur atoms, the R factor converged to a value of 0.054. A difference map based on the final atomic parameters gave no peaks larger than 0.5 e/Å^3.

The observed structure factors for sulfur di(methylxanthate) were brought to the same

Table 3. Anisotropic thermal parameters (Å$^2\times10^4$) in the form exp $[-2\pi^2(h^2a^{-2}U_{11}+...+2hka^{-1}b^{-1}U_{12}+...)$ with standard deviations in parentheses.

	U_{11}	U_{22}	U_{33}	U_{12}	U_{23}	U_{13}
$S(MeOCS_2)_2$						
S0	489(22)	549(39)	642(24)	−63(29)	80(26)	66(18)
S1	450(21)	665(42)	695(25)	41(29)	57(27)	78(18)
S2	685(28)	652(44)	752(29)	170(36)	114(32)	89(23)
S3	533(25)	820(46)	525(21)	−37(28)	88(27)	114(18)
S4	836(33)	1058(57)	547(23)	−20(37)	−77(30)	−48(22)
$Se(MeOCS_2)_2$						
Se	362(10)	418(13)	732(67)	−13(11)	32(22)	−45(17)
S1	443(26)	581(34)	522(133)	61(26)	72(53)	27(38)
S2	716(33)	453(35)	1429(151)	164(28)	142(54)	−30(49)
S3	467(29)	698(39)	935(159)	4(29)	39(57)	88(50)
S4	718(37)	896(49)	1194(193)	−112(36)	−80(69)	−198(58)

scale by means of comparison of common reflections for the different layers. The refinement was then started by using the same coordinates and temperature factors found for corresponding atoms in the selenium compound. The four strong reflections $20\bar{4}$, $20\bar{6}$, $40\bar{2}$, and $60\bar{6}$ had consistently much higher observed than calculated intensities. This effect cannot be explained, and the reflections were given zero weight in the final refinement cycles, but they were included in the R-factor. The R-factor reached a final value of 0.109. A final difference map revealed no peaks above 0.7 e/Å^3.

The atomic scattering factor curves used were taken from the *International Tables*.[27] Those for sulfur and selenium were corrected for anomalous dispersion, using $\Delta f'$ and $\Delta f''$ values compiled by Cromer,[28] and letting f equal the magnitude of the complex scattering factor. The calculations were carried out on an IBM 360/50H computer, using a program library made available by the Weizman Institute of Science, Rehovoth, Israel, and modified for use on the IBM computer by Dr. D. Rabinovich. The programs used to produce steering tape for the diffractometer and to produce structure factors from the output tape, were made by Mr. K. Maartmann-Moe of this Institute.

RESULTS AND DISCUSSION

The structures of the sulfur and selenium xanthate molecules are seen in Figs. 2. 3, and

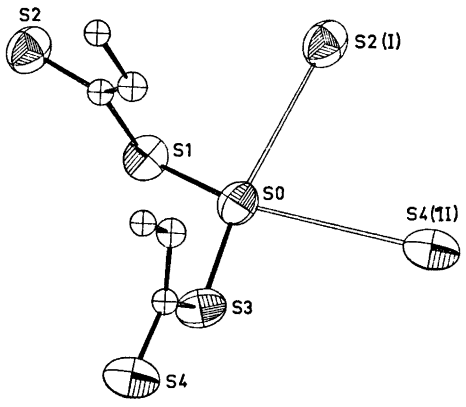

Fig. 2. The structure of $S(MeOCS_2)_2$ and the coordination around the central atom as seen along the a axis.

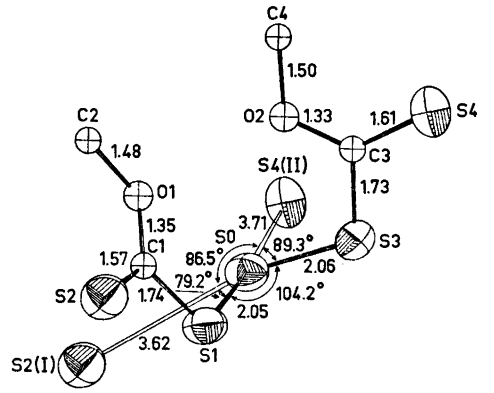

Fig. 3. The structure of $S(MeOCS_2)_2$ and the coordination around the central atom as seen along the b axis.

4. Weak intermolecular sulfur to central atom bonds are indicated by weaker lines. By inspection of the figures, it is seen that the structures belong to class II, mentioned above. The arrangement around the central atoms closely resembles that found around the selenium and tellurium atoms in selenium bis(diethyldiselenophosphinate) and tellurium bis(diethylthioselenophosphinate), respectively.[4,5] Thus, in the present investigation it is found that both sulfur and selenium as central atoms are bonded to four sulfur atoms in a trapezoid planar configuration. Two of these bonds are intramolecular: S0—S1=2.045(7) Å and S0—S3=2.059(6) Å for the sulfur compound: Se—S1=2.205(6) and Se—S3=2.170(9) Å for the selenium compound. These values agree well with the sum of the respective covalent radii which are 2.08 and 2.21 Å for S—S and Se—S single bonds, respectively. This indicates that the intermolecular central atom to ligand sulfur interactions *trans* to these essentially covalent bonds, must be very weak. For the sulfur compound, the lengths of these weak S0···S bonds are 3.625(6) and 3.709(8) Å. The corresponding Se—S lengths for the selenium compound are 3.501(9) and 3.595(7) Å. They may be compared to the sum of Pauling's van der Waals radii which are 3.70 and 3.85 Å for S···S and Se···S contacts, respectively.[29] From the above, it is clear that in the sulfur compound, the intermolecular S0···S interactions are of the same order of magnitude as a van der Waals contact.

Table 4. Bond lengths (Å) with standard deviations in parentheses.

$S(MeOCS_2)_2$		$Se(MeOCS_2)_2$	
S0—S1	2.045(7)	Se—S1	2.205(6)
S0—S3	2.059(6)	Se—S3	2.170(9)
S1—C1	1.74(2)	S1—C1	1.71(2)
S2—C1	1.57(2)	S2—C1	1.66(2)
S3—C3	1.73(2)	S3—C3	1.74(2)
S4—C3	1.61(2)	S4—C3	1.60(3)
C1—O1	1.35(2)	C1—O1	1.29(2)
O1—C2	1.48(2)	O1—C2	1.50(3)
C3—O2	1.33(2)	C3—O2	1.33(5)
O2—C4	1.50(2)	O2—C4	1.52(2)
S0—S2(I)	3.625(6)	Se—S2(I)	3.501(9)
S0—S4(II)	3.709(8)	Se—S4(II)	3.595(7)

Table 5. Some nonbonded intramolecular distances (Å) with standard deviations in parentheses.

S1—S2	2.839(8)	S1—S2	2.859(10)
S3—S4	2.873(7)	S3—S4	2.887(9)
S1—S3	3.238(6)	S1—S3	3.370(11)
C2—C4	3.94(2)	C2—C4	3.82(4)
O1—O2	3.03(2)	O1—O2	3.08(3)

Table 6. Bond angles (°) with standard deviations in parentheses.

$S(MeOCS_2)_2$		$Se(MeOCS_2)_2$	
S1—S0—S3	104.2(3)	S1—Se—S3	100.8(3)
S0—S1—C1	109.7(6)	Se—S1—C1	107.8(7)
S0—S3—C3	109.3(5)	Se—S3—C3	110.6(13)
S1—C1—S2	117.9(8)	S1—C1—S2	116.3(9)
S3—C3—S4	118.7(7)	S3—C3—S4	119.9(17)
S1—C1—O1	113.5(11)	S1—C1—O1	117.7(13)
S2—C1—O1	128.6(11)	S2—C1—O1	125.9(14)
C1—O1—C2	117.3(13)	C1—O1—C2	119.5(15)
S3—C3—O2	113.7(9)	S3—C3—O2	111.6(17)
S4—C3—O2	127.6(9)	S4—C3—O2	128.5(15)
C3—O2—C4	116.8(11)	C3—O2—C4	119.2(18)
S1—S0—S2(I)	79.2(2)	S1—Se—S2(I)	80.0(2)
S3—S0—S2(I)	166.2(2)	S3—Se—S2(I)	169.5(2)
S1—S0—S4(II)	165.6(2)	S1—Se—S4(II)	167.6(2)
S3—S0—S4(II)	89.3(2)	S3—Se—S4(II)	91.2(2)
S2(I)—S0—S4(II)	86.5(2)	S2(I)—Se—S4(II)	87.6(2)
C3(II)—S4(II)—S0	89.5(7)	C3(II)—S4(II)—Se	88.4(7)
C1(I)—S2(I)—S0	101.1(6)	C1(I)—S2(I)—Se	101.8(8)

For the selenium compound, the two intermolecular Se···S distances are on the average 0.3 Å shorter than the sum of the van der Waals radii. However, the direction of the bonds and the planarity of the trapezoid MS_4 group, strongly indicate a secondary bonding interaction.[30] Least squares planes through the central SOS_4 and SeS_4 groups, show that they are planar to within 0.17 and 0.14 Å, respectively (Table 8).

The difference between the structures of the methylxanthates of divalent sulfur and selenium on one side, and that of tellurium di(methyl-

Table 7. Some intermolecular contacts (Å) with standard deviations in parentheses.

	$S(MeOCS_2)_2$	$Se(MeOCS_2)_2$	Transform.
S1—C1	3.58(2)	3.51(2)	$-x,1-y,-z$
S2—S2	3.293(8)	3.255(8)	$-x,2-y,-z$
S2—S4	3.744(7)	3.718(12)	$\frac{1}{2}-x,\frac{3}{2}-y,\frac{1}{2}z$
S4—C1	3.59(2)	3.58(2)	
S1—S3	3.655(6)	3.672(11)	$-x,y,\frac{1}{2}-z$

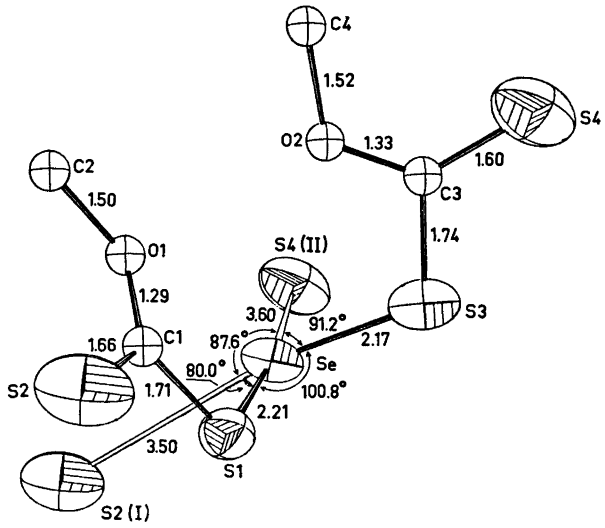

Fig. 4. The structures of $Se(MeOCS_2)_2$ and the coordination around the central atom as seen along the *b* axis.

xanthate)[10] on the other, is pronounced. The first two belong to class II, while the latter which contains a TeS_4 group where all four Te—S bonds are intramolecular, belong to class I. As the ligand is the same for the three compounds, the difference in structure must be due to the difference in the acceptor capacity (electrophilicity) of the central atom. Thus, the compound with the best acceptor as central atom, here tellurium, belongs to the class with the lowest number. Divalent tellurium complexes change structural type from I to II when going from xanthate to dithiophosphate ligands, while this change for the weaker acceptor selenium, takes place between the stronger donors dithiocarbamate and xanthate.[10] Sulfur gives here for the first time a compound where there is a tendency to planar SS_4 four coordination. A similar sulfur dithiocarbamate compound does not give a class II(or I) structure, but a trisulfide or class III structure.[17] The reason for this may be that with such a poor acceptor as sulfur, the tendency to four-coordination is so weak that packing effects play a large role in determining the structure.

The molecular structures of sulfur and selenium di(methylxanthate) also differ from those of the other molecules having class II structures. If one looks at the two central C—S1—M—S3—C chains in the present investigation, they both have a *cis* configuration, *i.e.* the S1—C and S3—C bonds point to the

Table 8. Least squares planes.

Equations [a]

$S(MeOCS_2)_2$
Plane 1: $4.630x+4.591y+13.634z-4.085=0$
Plane 2: $-4.867x+7.544y-3.075z-1.730=0$
Plane 3: $11.284x+1.883y-10.087z-0.062=0$

$Se(MeOCS_2)_2$
Plane 1: $4.947x+4.490y+13.526z-3.994=0$
Plane 2: $-5.425x+7.505y-2.386z-1.725=0$
Plane 3: $11.427x+1.874y-10.093z-0.039=0$

Distances from planes (Å)

Plane 1						
Atom [b]	S1	S2	C1	O1	C2	
$S(MeOCS_2)_2$	0.005	0.004	−0.013	0.001	0.003	(S0= −0.045)
$Se(MeOCS_2)_2$	0.002	−0.030	0.005	−0.010	0.006	(Se= −0.067)
Plane 2						
Atom [b]	S3	S4	C3	O2	C4	
$S(MeOCS_2)_2$	−0.011	−0.004	0.018	0.006	−0.009	(S0=0.053)
$Se(MeOCS_2)_2$	0.013	0.002	−0.015	−0.014	0.014	(Se= −0.020
Plane 3						
Atom [b]	S0	Se	S1	S3	S2(I)	S4(II)
$S(MeOCS_2)_2$	0.147	—	0.087	−0.174	−0.123	0.064
$Se(MeOCS_2)_2$	—	0.116	0.076	−0.140	−0.106	0.054

Interplanar angles (°)

	∠1.2	∠1.3	∠2.3
$S(MeOCS_2)_2$	75.66	88.49	89.72
$Se(MeOCS_2)_2$	76.83	87.20	92.99

[a] The equations are referred to the unit cell axes. The coefficients are adjusted so that insertion of atomic coordinates given in fractions of cell edges gives the atom's distance from the plane in Å. [b] Atoms defining plane.

same side of the plane defined by S1MS3. This is clearly seen by looking at Figs. 3 and 4. Taking selenium bis(diethyldiselenophosphinate)[5] as a representative of the other compounds with class II structures, the corresponding central P—Se—Se—Se—P chain has a *trans* configuration with Se—P bonds pointing to opposite sides of the plane defined by the three selenium atoms. Both types of analogous chains are formed by the five sulfur atoms in pentathionates.[31] The reason why the *trans* structure is preferred for selenium diselenophosphinate, is that steric repulsions between ethyl groups on the two end phosphorus atoms in the chain are much reduced relative to a *cis* structure. In the methylxanthates, with only a methoxy group on each end atom of the chain, the steric repulsion in a *cis* structure is lessened, and both *cis* and *trans* configurations may be found. In both sulfur and selenium bis(methylxanthate), the ligands are planar to within 0.02 Å, and their planes make angles close to 90° with the central MS_4 group. The angles between the ligand planes in a molecule is near

Table 9. Some data on divalent S, Se, and Te three-centre systems. Lengths in Å, angles in degrees. M—L and M···L represent central atom to ligand bonds in the asymmetric L—M···L three-centre systems. $\Delta 1$ is the difference between these bond lengths, $\Delta 2$ and $\Delta 3$ are the differences between a single covalent bond and M—L and M···L, respectively.

Class	Compound	M—L	M···L	$\Delta 1$	$\Delta 2$	$\Delta 3$	∠L—M···L
II	$Te((MeO)_2PS_2)_2$[2]	2.440(7)	3.306(7)	0.87	0.07	0.93	173.0(3)
II	$Te(Et_2P(S)Se)_2$[4]	2.501(3)	3.654(5)	1.26[a]		1.28	164.4(3)
I	$Te(MeOCS_2)_2$[10]	2.510(1)	2.846(1)	0.34	0.14	0.47	151.51(4)
		2.499(1)	2.841(1)	0.34	0.13	0.47	151.37(4)
I	$Te(EtOCS_2)_2$[6]	2.486(13)	2.857(16)	0.37	0.11	0.48	149.8(4)
		2.480(15)	2.897(19)	0.42	0.11	0.52	149.0(3)
I	$Te(OC_4H_8NCS_2)_2$[9]	2.498(7)	2.834(9)	0.34	0.12	0.46	147.4(2)
		2.530(6)	2.856(8)	0.33	0.16	0.48	147.6(2)
I	$Te(Et_2NCS_2)_2$[12]	2.519(4)	2.893(4)	0.37	0.15	0.52	145.5(1)
		2.518(4)	2.830(3)	0.31	0.14	0.46	146.4(1)
II	$Se(Et_2PSe_2)_2$[5]	2.352(2)	3.679(4)	1.33	0.01	1.34	160.8(3)
II	$Se(MeOCS_2)_2$[10]	2.205(6)	3.501(9)	1.30		1.30	167.6(2)
		2.170(9)	3.595(7)	1.43		1.39	169.5(2)
I	$Se(OC_4H_8NCS_2)_2$[7]	2.282(6)	2.791(6)	0.51	0.07	0.59	155.0(2)
		2.314(6)	2.782(5)	0.47	0.11	0.58	155.1(2)
I	$Se(Et_2NCS_2)_2$[8]	2.312(5)	2.779(5)	0.47	0.11	0.58	157.7(2)
		2.332(4)	2.719(5)	0.39	0.13	0.52	158.5(2)
I	$Se(C_4H_8NCSe_2)_2$[34]	2.451(1)	2.863(1)	0.41	0.11	0.52	161.37(3)
		2.449(1)	2.870(1)	0.42	0.11	0.53	161.95(3)
II	$S(MeOCS_2)_2$[10]	2.045(7)	3.625(6)	1.58		1.55	165.6(2)
		2.059(6)	3.709(8)	1.65		1.63	166.2(2)

[a] M—L supposed to be a covalent Te—S bond

76° in both compounds. The bond lengths and angles found in the xanthate ligands are quite normal.[32] Each ligand sulfur atom strongly bonded to the central atom, forms a long S—C bond, ranging from 1.71—1.74 Å in the two compounds. The other S—C bonds have a higher degree of double bond character, their lengths are found between 1.57 and 1.66 Å. The O···C bond lengths range between 1.29 and 1.35 Å, demonstrating a mesomeric shift of electron density from oxygen towards the ligand sulfur atoms.

The angles on oxygen and on carbon bonded to the sulfur atoms correspond to sp^2 hybridization on these atoms. The large difference in the two S—C—O angles on sp^2 hybridized carbon, found in most xanthates may be explained on basis of VSEPR theory.[33] The average M—S—C angle is 109.4°, a relatively high value, but such high values are found in several other sulfur-containing compounds.[17]

In Table 9, structural data from structures of compounds of divalent sulfur, selenium, and tellurium with bidentate ligands belonging to the structure classes I and II are listed. For class I compounds, the three-centre L—M···L systems are more linear for M=Se than for M=Te. The average angles are 158.2° [156.6° excluding $Se(C_4H_8NCSe_2)_2$ [34]] and 148.6°, respectively, and can in part be explained by the difference in size of the two central atoms.[8] From the table, it is seen that the asymmetry in bond length in a three-centre system is smaller for M=Te than for M=Se, $\Delta 1$ on the average being 0.35 and 0.45 Å, respectively, for the compounds listed. If it is assumed that the compounds are essentially two-coordinate in solution with the ligands monodentate, then the new and weaker bonds forming in the solid state will be stronger for the stronger acceptor — in this case tellurium. This will thus have a weakening effect on the original strong bond *trans* to it, most so in the tellurium compounds. The $\Delta 2$ and $\Delta 3$ values tend to confirm this. $\Delta 2$, which lists the elongation of the stronger M—S bond relative to a covalent bond has as average value of 0.13 Å for M=Te and 0.11 Å for M=Se while the average $\Delta 3$ values, which

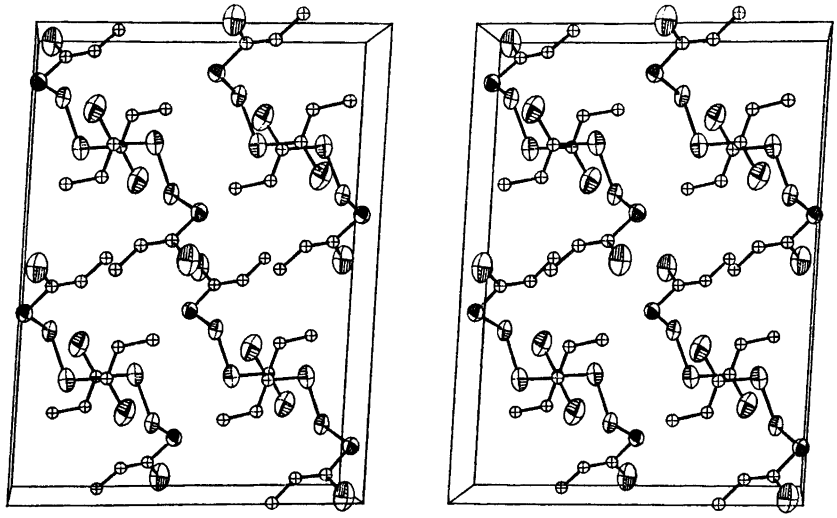

Fig. 5. A stereoscopic drawing showing the packing of $S(MeOCS_2)_2$ molecules as seen along the *b* axis.

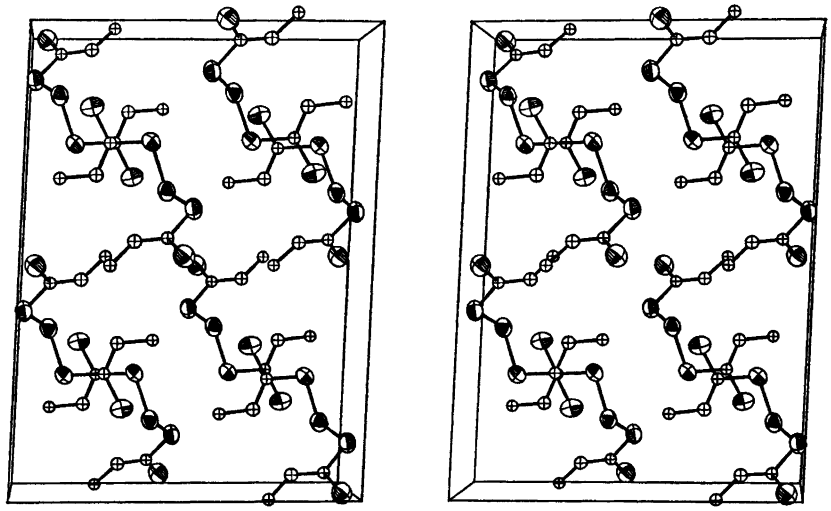

Fig. 6. A stereoscopic drawing showing the packing of $Se(MeOCS_2)_2$ molecules as seen along the *b* axis.

represent differences in length between weak bonds and covalent bonds are 0.48 and 0.55 Å, respectively.

Comparison between class I and class II structures, show that the latter are more linear, the L—M···L angles for the latter vary between 160.8 and 173.0°. In most class II compounds, the M···L bond is so weak that it hardly effects the strong M—L bond *trans* to it. The latter therefore is hardly significantly different from a covalent single bond, except perhaps in $Te[(MeO)_2PS_2]_2$.[2] Thus the $\Delta 1$ values are about 0.8 Å larger in the class II than in the class I selenium and tellurium compounds.

Why do these class I and II complexes adopt a trapezoid planar configuration and not a

more symmetric one like a class V complex? The two three-centre systems, based mainly on p-orbitals require a near planar complex. When there are no restrictions on the S···S distances between donor atoms as found in tellurium complexes with monodentate thio-ligands, a square planar geometry of the central MS_4 group is preferred.[15] The same is found for ICl_4^- and XeF_4,[35,36] and the reason is that the bonding in the three isoelectronic (valence electrons) cases is based essentially on two three-centre four-electron systems at right angles to each other where only p-orbitals are involved.[15,37–40] In the bidentate dithio ligands used, the S—S bite near 2.94 Å combined with a long average M—S bond require intraligand S—Te—S and S—Se—S angles near 66 and 70° in the class I compounds. If the resulting complex is to be symmetric, then interligand S—Se—S and S—Te—S angles of 109 and 113°, respectively, will be the result. Obviously, this configuration is not an energetically favourable one. However, with dithio ligands with larger S···S spacing, where the S—M—S intraligand angle will be permitted to reach a value close to 90°, symmetric square-planar complexes will probably be found. For the class II complexes with more linear three-centre systems, a symmetric complex require formation of a more strongly bound polymer, as found for polymeric Cu(II) complexes.[41] But with such strong bonding, it is more likely that a class I structure is adopted.

The packing of the molecules in the unit cells are vizualized in Figs. 5 and 6. There is one remarkably short intermolecular distance in both compounds, namely from S2 in the original molecule to S2 in a molecule whose transformation from the original one is $\bar{x},2-y,\bar{z}$. This short distance, which is 3.293(8) and 3.255(8) Å in the sulfur and selenium compound, respectively, is significantly shorter than a van der Waals contact of 3.70 Å.[29] The easy decomposition of the crystals of both compounds may be caused by disulfide formation across this short contact, followed by reduction of the central atoms to the respective elements.

REFERENCES

1. Husebye, S. *Acta Chem. Scand. 19* (1965) 1045.
2. Husebye, S. *Acta Chem. Scand. 20* (1966) 24.
3. Husebye, S. *Acta Chem. Scand. 20* (1966) 2007.
4. Husebye, S. *Acta Chem. Scand. 23* (1969) 1389.
5. Husebye, S. and Helland-Madsen, G. *Acta Chem. Scand. 23* (1969) 1398.
6. Husebye, S. *Acta Chem. Scand. 21* (1967) 42.
7. Husebye, S. *Acta Chem. Scand. 24* (1970) 2198.
8. Husebye, S. and Helland-Madsen, G. *Acta Chem. Scand. 24* (1970) 2273.
9. Anderson, O. and Husebye S. *Acta Chem. Scand. 24* (1970) 3141.
10. Brøndmo, N. J., Esperås, S., Graver, H. and Husebye, S. *Acta Chem. Scand. 27* (1973) 713.
11. Husebye, S. *Compounds of Divalent Selenium and Tellurium with Bidentate Ligands; Their Preparation, Structure and Bonding*, Diss., University of Bergen, Bergen 1969.
12. Fabiani, C., Spagna, R., Vaciago, A. and Zambonelli, L. *Acta Crystallogr. B 27* (1971) 1499.
13. Bally, R. *Acta Crystallogr. 23* (1967) 295.
14. Curry, J. D. and Jandacek, R. J. *J. Chem. Soc. Dalton Trans.* (1972) 1120.
15. Foss, O. In Andersen, P., Bastiansen, O. and Furberg, S., Eds., *Selected Topics in Structure Chemistry*, Universitetsforlaget, Oslo 1967, p. 145.
16. Vonk, C. G. and Wiebenga, E. H. *Rec. Trav. Chim. Pays-Bas 78* (1959) 913.
17. Husebye, S. *Acta Chem. Scand. 27* (1973) 756.
18. Franzini, M. *Z. Kristallogr. 118* (1963) 393.
19. Jones, C. H. W. *Private communication.*
20. Foss, O. *Acta Chem. Scand. 16* (1962) 779.
21. Foss, O. *Acta Chem. Scand. 3* (1949) 1385.
22. Troughton, P. G. H. *Siemens Rev. XXXVII* (1970), Fourth Special Issue, p. 9.
23. Coppens, P., Leiserowitz, L. and Rabinovich, D. *Acta Crystallogr. 18* (1965) 1035.
24. Wilson, A. J. C. *Nature (London) 150* (1942) 151.
25. Shiono, R. *Normalized Structure Factors Program*, The Crystallography Laboratory, University of Pittsburgh, Pittsburgh 1966.
26. Long, R. E. *Ph. D. Diss.*, University of California at Los Angeles 1965.
27. *International Tables for X-Ray Crystallography*, Kynoch Press, Birmingham 1962, Vol. III, p. 204.
28. Cromer, D. T. *Acta Crystallogr. 18* (1965) 17.
29. Pauling, L. *The Nature of the Chemical Bond*, Cornell University Press, Ithaca 1960, p. 257.
30. Alcock, N. W. *Advan. Inorg. Chem. Radiochem. 15* (1972) 2.
31. Foss, O. *Advan. Inorg. Chem. Radiochem. 2* (1960) 237.
32. Rao, S. R. *Xanthates and Related Compounds*, Marcel Dekker, New York 1971, p. 189.
33. Gillespie, R. J. *J. Chem. Educ. 47* (1970) 18.

34. Esperås, S., Husebye, S. and Rolandsen, Å. *To be published.*
35. Elema, R. J., de Boer, J. L. and Vos, A. *Acta Crystallogr. 16* (1963) 243.
36. In Hyman, H. H., Ed., *Noble-Gas Compounds*, Part 6, Chapters by Templeton, D. H. *et. al.* and Burns, J. H. *et al.*, The University of Chicago Press, Chicago 1963.
37. Havinga, E. E. and Wiebenga, E. H. *Rec. Trav. Chim. Pays-Bas 78* (1959) 724.
38. Wiebenga, E. H., Havinga, E. E. and Boswijk, K. H. *Advan. Inorg. Chem. Radiochem. 3* (1961) 133.
39. Rundle, R. E. *J. Amer. Chem. Soc. 85* (1963) 112.
40. Coulson, C. A. *J. Chem. Soc.* (1964) 1442.
41. Cotton, F. A. and Wilkinson, G. *Advanced Inorganic Chemistry*, 3rd. Ed., Interscience, London 1972, p. 903.

Received May 29, 1974.

Acta Chemica Scandinavica A 29 (1975) 105—110

On the Crystal Structures of the High-temperature Forms of Strontium and Barium Carbonate and Structurally Related Compounds

K. O. STRØMME

Department of Chemistry, Blindern, Oslo 3, Norway

The crystal structures of the orientationally disordered rhombohedral and cubic high-temperature phases of strontium and barium carbonate are discussed. Approximate values of the configurational entropies are calculated from structural models of the disordered phases and compared with entropy changes observed in the corresponding phase transitions, involving changes in orientational disorder. The structure of the rhombohedral phases is probably more complex than the kind of model proposed previously for disordered rhombohedral phases such as $NaNO_3$-I, in accordance with observations made on other disordered structures.

Calcium, strontium and barium carbonate belong to a structural family,[1] the members of which transform into structurally closely related, disordered rhombohedral or cubic phases at higher temperatures.[1] Structural models have previously been proposed for both kinds of high-temperature phase.[2,3] These were used as basis in the present configurational entropy calculations to be discussed in the next two sections. The oxygen positions can hardly be obtained from standard X-ray or neutron diffraction data because of the strong positional overlap and the small number of observable reflections,[4] *etc.*

Crystallographic data for the room and high-temperature forms of barium and strontium carbonate are shown along with calorimetric data in Table 1.[4–8] Some of the high-temperature data were measured at elevated CO_2-pressures to avoid dissociation of the salt. The room temperature phases are of the ordered aragonite-type [8] (KNO_3-II). Crystal data for $SrCO_3$-I, stable above 1413 °C,[7] are not known. The phase is probably isostructural with the face-centered, cubic form of $BaCO_3$.[7]

The heat of transition in solid calcium carbonate and the unit cell dimensions of the rhombohedral high-temperature phase of this compound have not been measured, probably because of experimental difficulties due to dissociation of the salt. The transition temperature is reported to be 970 °C.[9]

On the structure of the rhombohedral phases. Average atomic positions and the shortest, statistical intermolecular distances based on standard calcite- and aragonite-like O-positions [2] in space group $R\bar{3}m$ of the rhombohedral phases, are listed in Table 2.

The metal-oxygen contact distances are somewhat shorter than the sum of the ionic radius reported for barium or strontium,[12] and the oxygen contact radius of 1.40 Å.[12] Two of the listed, inequivalent O—O distances implied statistically, are considerably shorter than the normal O—O contact distance of 2.80 Å in the case of $SrCO_3$, while only one such distance is found in the other case. Assuming the corresponding relative positions of the carbonate groups to be inaccessible and assigning a common probability to the remaining, accessible configurations for simplicity, approximate configurational entropy values were derived as outlined for $NaNO_3$-I [2] and others. The results are shown plotted in Fig. 1, a and b. The fraction of anions occupying the two types of position is not known. The III→II

Table 1. (a) Crystallographic and (b) calorimetric data for strontium and barium carbonate.

	$SrCO_3$	$BaCO_3$
(a) Crystallographic data [a]		
Orthorhombic (III); 4 molec./cell		
a (r.t.)	5.08 Å	5.30 Å
b (r.t)	8.36	8.88
c (r.t.)	6.00	6.42
Rhombohedral (II); 3 molec./cell		
a_{hex}	5.092 (920 °C)	5.205 (830 °C)
c_{hex}	9.53 (920 °C)	10.55 (830 °C)
a_{hex} [b]	5.106 (965 °C)	
c_{hex} [b]	9.516 (965 °C)	
Cubic face centered; 4 molec./cell		
a [c]		6.96 (960 °C)
(b) Calorimetric data [d]		
ΔH(III→II) (kcal/mol)	4.70	4.49
t(III→II) (°C)	924	806
	930 [e]	779 [e]
	912 [f]	803 [f]
ΔH(II→I) (cal/mol)	800 [g]	730
t(II→I) (°C)	1413 [g]	968
		976 [f]

[a] Data from Ref. 4, if not otherwise stated. [b] Ref. 5. [c] Super-cooled sample. [d] Data from Ref. 6, if not otherwise stated. [e] Ref. 8. [f] Ref. 4. [g] Ref. 7.

entropy changes [ΔS(III→II)] obtained for $SrCO_3$ and $BaCO_3$ from Table 1, are 3.94 and 4.17 cal/mol K, respectively. Configurational changes are generally found to predominate in order-disorder transitions,[13,14] The rather large discrepancy between observed and calculated entropy terms (Fig. 1) indicates therefore that the configurational entropy of the rhombohedral phases is probably actually considerably greater than the maximum values indicated in Fig. 1, a and b. This may be achieved by assuming additional equilibrium orientations of the anions to be accessible in the rhombohedral phases. Similar findings were also obtained for $AgNO_3$-I [15] and $RbNO_3$-II,[3] in which cases possible alternative positions were actually discussed.

The structure of the face-centred cubic phase. The II→I transition resembles the II→I transition in $RbNO_3$.[3] The entropy changes are small. The values obtained for $SrCO_3$ and $BaCO_3$ from Table 1, are 0.42 and 0.55 cal/mol K, respectively which are close to the ΔS(II→I) values of 0.42 [14] and 0.55 (0.01) cal/mol K [16] available for $RbNO_3$ (e.s.d. in parentheses). The hexagonal unit cell axes of $BaCO_3$ change from $a=5.205$ Å and $c=10.55$ Å in phase II to $a=4.921$ Å and $c=12.06$ Å in phase I (Table 1) at the experimental temperatures, respectively. The hexagonal c-axis thus increases, whereas the a and b axes decrease in the transition, as obtained for $RbNO_3$. The molecular volume changes from 82.5 Å^3 in phase II to 84.3 Å^3 in phase I, *i.e.* only by 2.2 %.

Phase I is probably isostructural [1,7] with $RbNO_3$-I.[3] The carbonate groups are accordingly assumed to be centred about the

Table 2. (a) Average atomic positions and (b) statistical intermolecular distances in phase II according to space group $R\bar{3}m$.[2] Hexagonal unit cell dimensions from Table 1.[4] $d(C-O)=1.285$ Å (ass.) [10,11] in planar carbonate group. Metal ions in $(00\frac{1}{2})$ *etc.*[2] Molecular three-fold axes along hexagonal *c*-axes.

(a)	Calcite-type positions (C)	Aragonite-type positions (A)
$SrCO_3$	Carbon: $x=y=z=0$ Oxygen: $x=0.252$, $y=z=0$	$x=y=0$, $z=z$ (oxygen) $x=2y=0.291$, $z=0.031$ (0.004)
$BaCO_3$	Carbon: $x=y=z=0$ Oxygen: $x=0.247$, $y=z=0$	$x=y=0$, $z=z$ (oxygen) $x=2y=0.285$, $z=0.026$ (0.004)

z_A is calculated on the assumption that the $Me-O_A$ contact distance $=Me-O_C$ contact distance. Assuming roughly an error of 0.03 Å in the $Me-O_A$ contact distance leads to the estimated errors in the parentheses. Errors in unit cell dimensions and the CO bond length expected to be small and are ignored.

(b) Atomic positions	$SrCO_3$ Distance (Å) (920 °C)	$BaCO_3$ Distance (Å) (830 °C)
$O_C(x\ 0\ 0)-Me(2/3\ 1/3-1/6)$	2.505	2.662
$O_A(x\ \frac{1}{2}\ x\ z)-Me(2/3\ 1/3-1/6)$	» (0.030) (ass.)	» (0.030) (ass.)
$O_A(x\ \frac{1}{2}\ x\ z)-Me(1/3\ 2/3\ 1/6)$	2.86 (0.02)	3.00 (0.02)
$O_C(x\ 0\ 0)-O_C(1-x,0,0)$	2.52	2.63
$O_C(x\ 0\ 0)-O_C(2/3-x,1/3-x,1/3)$	3.26	3.60
$O_C(x\ 0\ 0)-O_A(2/3-x,1/3-\frac{1}{2}x,1/3-z)$	3.00 (0.04)	3.36 (0.04)
$O_A(x\ \frac{1}{2}\ x\ z)-O_C(1-x,0,0)$	2.785 (0.004)	2.892 (0.004)
$O_A(x\ \frac{1}{2}\ x\ z)-O_A(2/3-x,1/3-x,1/3-z)$	2.61 (0.06)	3.00 (0.06)
$O_A(x\ \frac{1}{2}\ x\ z)-O_A(1-\frac{1}{2}x,\ \frac{1}{2}x,\ z)$	2.87 (0)	2.98 (0)

three-fold axes (space diagonals) in either calcite and/or aragonite-type equilibrium positions.[3] There are statistically 8 positions of each kind per anion. Each oxygen atom makes close contact with two metal ions when the anion is in a calcite-type position, whereas one short distance and two intermediate metal-oxygen separations are formed for each O atom when an aragonite-like orientation is occupied. Average atomic positions and statistical intermolecular distances based on space group $Fm3m$ are listed for $BaCO_3$-I in Table 3. The metal-oxygen contact distance is somewhat larger than the corresponding values obtained for $BaCO_3$-II. A complete set of inequivalent O—O distances less than 2.80 Å is also contained in Table 3 together with some equivalent O—O distances. The corresponding number of statistical anion positions less than 2.80 Å from a given anion in either the calcite- or aragonite-like orientation [2] are listed as a function of associated lattice site in Table 4.

These relative positions of two and two carbonate groups were assumed to be blocked in the subsequent configurational entropy calculation, while the remaining, accessible configurations were assigned a common weight factor. The approximate entropy values, Fig. 1, c, were obtained as outlined for $RbNO_3$,[3] using the information contained in Table 4. Comparison of graph b and c, Fig. 1, indicates that $S_c(I)$ is considerably higher than $S_c(II)+\Delta S(II\rightarrow I)$. $\Delta S(II\rightarrow I)$ is given above and $Sc(II)$ denotes the configurational entropy corresponding to the simple calcite- and aragonite-type positional disorder [2] discussed in the preceding section. (The change $x_A(II)\sim 0.6$ to $x_A(I)\sim 1$ is seen to produce a relatively small configurational entropy change. This implies that calcite-like orientations are practically blocked in phase I but not in II, which seems unreasonable in view of the structural resemblance of the two phases.) It appears therefore, in agreement with the result of the

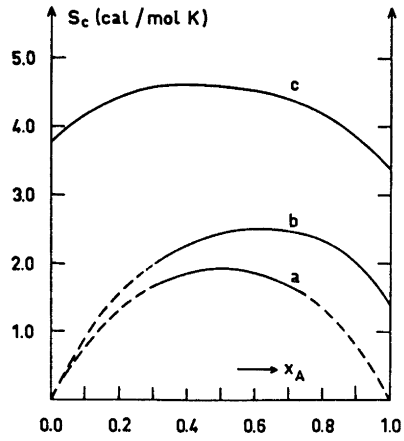

Fig. 1. Calculated configurational entropy values derived from calcite- and aragonite-like anion disorder,[2,3] as a function of average fraction, x_A, of molecules in argaonite-type positions. Molecular threefold axes aligned along the three-fold axes of either the rhombohedral or cubic lattice. Broken lines are used when the computed values are more uncertain because of the computational approximations involved. (Nearly) zero configurational entropy is evident from mere inspection of structural model, however.
a: $SrCO_3$-II, b: $BaCO_3$-II and c: $BaCO_3$-I.

preceding section, that the actual configurational entropy of phase II is probably considerably higher than that based on the simple calcite- and aragonite-type positional disorder. A similar way of showing this holds probably also for $SrCO_3$. An alternative explanation of the indicated discrepancies is difficult to see.

Possible, additional equilibrium positions of the anions in the rhombohedral phases. Fig. 2, a shows the two types of average equilibrium anion orientation proposed previously for $NaNO_3$-I and others and used in the preceding configurational entropy analysis of the rhombohedral phases. Possible, additional average equilibrium positions of the anions are indicated in Fig. 2, b. $BaCO_3$-II is used as model. The arrangement of positive ions in Fig. 2, b is somewhat contracted in the vertical direction in the paper plane and somewhat lengthened in the direction perpendicular to this plane compared with the rhombohedral arrangement of the positive ions in Fig. 2, a. The aragonite-like position in Fig. 2, b may be adjusted by translation in the mirror plane and rotated about an axis perpendicular to

Table 3. (a) Average atomic positions and (b) intermolecular statistical distances in $BaCO_3$-I according to space group $Fm3m$. $a=6.96$ Å (Table 1).[4] $d(C-O)=1.285$ Å (ass.)[10,11] in planar carbonate group. Metal ions in $(\frac{1}{2}00)$ *etc.*[3] Threefold axis of anion, centred about the origin, along the [111]-direction.

(a) Calcite-type positions (C)	Aragonite-type positions (A)
Carbon: $x=y=z=0$	$x=y=z=-0.019$ (0.004)
Oxygen: $x=0$, $y=-z=-0.130(5)$	$x=y=-0.094(0.004)$, $z=0.132(0.004)$

z_A is calculated on the assumption that the Me$-O_A$ contact distance=Me$-O_C$ contact distance. Assuming roughly an error 0.03 Å in the Me$-O_A$ contact distance leads to the estimated errors in the parentheses. Errors in the a-axis and the C$-$O bond length expected to be relatively small and are ignored.

(b) Atomic positions	Distance (Å) (960 °C)
$O_C(0\ \bar{z}\ z)-Me(0\ 0\ \frac{1}{2})$	2.727
$O_A(x\ x\ z)-Me(0\ 0\ \frac{1}{2})$	2.727 (0.030) (ass.)
$O_A(x\ x\ z)-Me(-\frac{1}{2}\ 0\ 0)$	3.04 (0.03)
$O_C(0\ \bar{z}\ z)-O_C(0,-\frac{1}{2}+z,\frac{1}{2}-z)$	2.35
$O_C(0\ \bar{z}\ z)-O_A(x,-\frac{1}{2}+z,\frac{1}{2}+x)$	2.61 (0.03)
$O_C(0\ \bar{z}\ z)-O_A(-x,-\frac{1}{2}+z,\frac{1}{2}+x)$	2.61 (0.03)
$O_C(0\ \bar{z}\ z)-O_A(x,-\frac{1}{2}-x,\frac{1}{2}-z)$	2.61 (0.03)
$O_C(0\ \bar{z}\ z)-O_A(-x,-\frac{1}{2}-x,\frac{1}{2}-z)$	2.61 (0.03)
$O_A(x\ x\ z)-O_A(-\frac{1}{2}+z,x,\frac{1}{2}+x)$	2.69 (0.04)
$O_A(x\ x\ z)-O_A(x,-\frac{1}{2}-x,\frac{1}{2}-z)$	2.72 (0.04)

Table 4. The number of calcite (C)- and aragonite (A)-type anion positions at neighbour sites, L, less than 2.80 Å from a central anion, S, in either the calcite- or aragonite-type position defined in Table 3, which contains the necessary information for the present derivation along with the molecular and space group symmetry.

		L lattice site:											
S	L	$(\frac{1}{2}\frac{1}{2}0)$	$(0\frac{1}{2}\frac{1}{2})$	$(\frac{1}{2}0\frac{1}{2})$	$(\frac{1}{2}\bar{\frac{1}{2}}0)$	$(0\frac{1}{2}\bar{\frac{1}{2}})$	$(\bar{\frac{1}{2}}0\frac{1}{2})$	$(\bar{\frac{1}{2}}\frac{1}{2}0)$	$(0\bar{\frac{1}{2}}\frac{1}{2})$	$(\frac{1}{2}0\bar{\frac{1}{2}})$	$(\bar{\frac{1}{2}}\bar{\frac{1}{2}}0)$	$(0\bar{\frac{1}{2}}\bar{\frac{1}{2}})$	$(\bar{\frac{1}{2}}0\bar{\frac{1}{2}})$
C	C				1	1	1						
C	A				4	4	4						
A	C				1	1	1				1	1	1
A	A				1	1	1				1	1	1

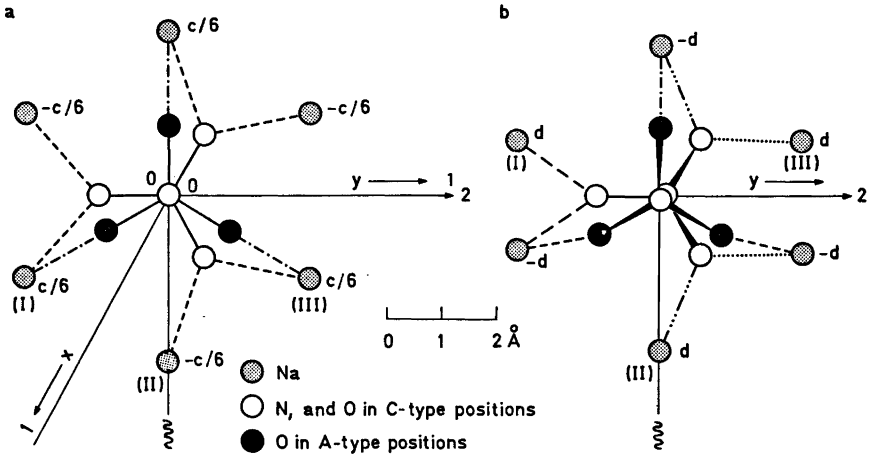

Fig. 2. Orientational disorder in the rhombohedral phases. Crystal and molecular data for $BaCO_3$-II are used. Hexagonal indexing.
a. The arrangement of positive ions in the rhombohedral phase, as viewed along the hexagonal c-axis. One of the two standard aragonite (A)- and one of the two standard calcite (C)-type anion orientations [2] used in the preceding calculations are also shown. Molecular threefold axes along the threefold axes of the lattice.
b. The corresponding arrangement of positive ions as viewed perpendicular to the plane containing the positive ions denoted by (I), (II) and (III) in Fig. 2, a. The hexagonal c-axis, in the symmetry plane, makes an angle of 113.1° with the (downwards) normal to the plane of (I), (II) and (III), as compared with 109°28′ for a cubic crystal. Distance from origin to plane containing (I), (II) and (III), $d=2.07$ Å, compared with $c/6=1.76$ Å (Fig. 2, a). An *alternative* "calcite-like" and an alternative "aragonite-like" anion positions are indicated. A symmetry plane of the latter grouping coincide with a symmetry plane of the space groups ($R\bar{3}m$), while a two-fold axis of the former position coincides with a two-fold axis of the space group. Two orientations of each kind are obtained through the operation of the space group symmetry elements shown.

this plane ("three degrees of freedom" as compared with one for the A-type positions in Fig. 2, a), while the calcite-like position may be translated along and rotated about the two-fold axis "two degrees of freedom,, as compared to none for the C-type position in Fig. 2, a). Three oxygen-metal contacts of lengths similar to the metal-oxygen contacts in Fig. 2, a, are obtained by a small adjustment of the A-like position in Fig. 2, b from a position where the carbonate group is parallell with the plane of these three nearest neighbour metal ions at the same distance as in Fig. 2, a, and the C atom is situated on the normal to this plane through the inversion centre (origin). Similarly, four short and two somewhat longer metal-oxygen positions, for instance, may be obtained by adjusting the

C-like position in Fig. 2, b. (The latter kind of position may seem to be somewhat less probable than the former.) Two and two of the intermolecular metal-oxygen distances (except one) are crystallographically equivalent, as indicated in Fig. 2, b.

Three equivalent configurations of the Fig. 2, b-type are obtained through the operation of the three-fold symmetry axis. There are altogether six anion positions of each kind shown in Fig. 2, b. On transforming to the cubic phase, the Fig. 2, b-type configurations change with relatively small positional adjustments into the Fig. 2, a-type, which become representative of the cubic structure, showing the two kinds of anion orientation mentioned in the preceding section. The anion positions shown in Fig. 2, a and b are thus rather closely related to those of the cubic phase.

Obviously, simple spatial considerations as used in the present section are by themselves only indicative of actual equilibrium positions, which will ultimately have to be confirmed in other ways. On the other hand, the anion positions shown in Fig. 2 appear to be the only kinds of orientation that satisfy reasonably well general, qualitative, spatial requirements necessary to define an anion-orientationel potential minimum in a given frame of positive ions. Furthermore, arguments in favour of an extended model of disorder have already been advanced for the rhombohedral phase. Thus a relatively small number of anions in either or both kinds of molecular orientation shown in Fig. 2, b is required in addition to those in Fig. 2, a-type positions to remove the previously mentioned discrepancies between observed transition and calculated configurational entropy values.

Inspection shows further that Fig. 2, b-type anion positions may also represent (permanent or temporary) equilibrium positions bounded by potential barriers in the rhombohedral phases of $SrCO_3$, $RbNO_3$, $AgNO_3$ and KNO_3. The need of additional orientational disorder has previously been stressed for $SrCO_3$-II, $RbNO_3$-II [8] and $AgNO_3$-I.[15] Some additional configurational disorder may similarly be possible in KNO_3-I, but probably not in $NaNO_3$-I, considering the differences between the transition and configurational entropy data quoted for these compounds.[2,17]

REFERENCES

1. Muller, O. and Roy, R. *The Major Ternary Structural Families*, Springer, New York 1974.
2. Strømme, K. O. *Acta Chem. Scand. 23* (1969) 1616.
3. Strømme, K. O. *Acta Chem. Scand. 25* (1971) 211.
4. Lander, J. J. *J. Chem. Phys. 17* (1949) 892.
5. Moreau, R. *Bull. Soc. Franc. Mineral. Crist. 87* (1964) 547.
6. Kelley, K. K. *Bull. 584, Bureau of Mines* (1960) 23 and 180.
7. Baker, E. H. *J. Chem. Soc.* (1962) 2525.
8. Rapoport, E. and Pistorius, C. W. F. T. *J. Geophys. Res. 12* (1967) 6353.
9. Boeke, H. E. *Neues Jahrb. Mineral, Geol. und Paläontologie 1* (1912) 91.
10. Felty, E. J. *Diss. Abstr. 24* (1964) 4423.
11. Chessin, H., Hamilton, W. C. and Post, B. *Acta Crystallogr. 18* (1965) 689.
12. Slater, J. C. *J. Chem. Phys. 41* (1964) 3199.
13. Darmon, I. and Brot, C. *Molecular Crystals 2* (1967) 301.
14. Newns, D. M. and Staveley, L. A. K. *Chem. Revs. 66* (1966) 267.
15. Strømme, K. O. *Acta Chem. Scand. 24* (1970) 1477.
16. Strømme, K. O. *Unpublished results.*
17. Strømme, K. O. *Acta Chem. Scand. 23* (1969) 1625.

Acta Chemica Scandinavica A 29 (1975) 111—116

Microwave Spectrum and Structural Parameters of 4-Chlorobuten-3-yne

FRED KARLSSON, MATS GRANBERG and RAGNAR VESTIN

Department of Physical Chemistry, Arrhenius Laboratory, University of Stockholm, S-104 05 Stockholm, Sweden

The microwave spectra of the two natural species of 4-chlorobuten-3-yne: $CH_2CHCC^{35}Cl$ and $CH_2CHCC^{37}Cl$ together with the three possible monodeuterated species: $CDHCHCC^{35}Cl$, $CHDCHCC^{35}Cl$ and $CH_2CDCC^{35}Cl$, have been measured and assigned in the region 34 000—40 000 MHz. The rotational constants A, B and C for the ground state as well as the centrifugal distortion constants D_J and D_{JK} were determined. The centrifugal distortion constants were also calculated from a simple estimated valence force field.

The positions of the chlorine atom and the three hydrogen atoms in the principal axis system of the molecule $CH_2CHCC^{35}Cl$ were obtained with Kraitchman equations from the change in moments of inertia due to isotopic substitution. The nuclear quadrupole coupling constant χ_{aa} was calculated for the $CH_2CHCC^{35}Cl$ and $CH_2CHCC^{37}Cl$ species from the hyperfine splittings of the rotational lines.

The substance 4-chlorobuten-3-yne was first described by Carothers *et al.*[1] Recently we have confirmed this identification with NMR, IR and mass spectroscopy,[2] and in order to obtain a detailed structure we have also started to investigate 4-chlorobuten-3-yne with microwave spectroscopy and electron diffraction in gas phase. The configuration with the chlorine atom in line with three of the four carbon atoms is very suitable for a study of the molecular structure with the electron diffraction method. However, since the hydrogen atoms have a low nuclear charge, their accurate positions in the molecule are sometimes very hard to determine by electron diffraction. Therefore it was convenient to substitute the different hydrogen atoms by deuterium and obtain their positions with Kraitchman's equations[3] from the changes in moments of inertia on isotopic substitution as recommended by Costain.[4] The moments of inertia were obtained from the rotational constants measured by microwave spectroscopy.

4-Chlorobuten-3-yne is an important member of the series of highly unsaturated chlorohydrocarbons which we have been studying for some time.[5–8].

EXPERIMENTAL

4-Chlorobuten-3-yne was prepared by treating butenyne with hypochlorite solution:[1]

$$CH_2{=}CH{-}C{\equiv}CH + ClO^- \rightarrow CH_2{=}CH{-}C{\equiv}CCl + OH^-$$

The sample was isolated by distillation *in vacuo* and finally gas-liquid chromatography at a temperature of 100 °C. The column was packed with diethylhexylsebacete (15 %) absorbed on Chromosorb. Pure 4-chlorobuten-3-yne is unstable to polymerization but could be stored at −70 °C.

A mixture containing about 10 % of each of the three possible monodeuterated species of 4-chlorobuten-3-yne was obtained in the following way. We used the fact that acetylene is a very weak acid and prepared a mixture of normal and deuterated acetylene: C_2H_2, C_2HD and C_2D_2 by leading ordinary acetylene free from acetone from a steel flask through a strong alkaline solution of KOH dissolved in a mixture of H_2O and D_2O. The D/H-ratio was held at 1/3 in this solution. The partly deuterated acetylene leaving the washing flask was then dimerized to butenyne in a liquid Cu(I) catalyst according to Nieuwland *et al.*[9]

$$2\,HC{\equiv}CH \rightarrow CH_2{=}CH{-}C{\equiv}CH$$

The partly deuterated butenyne was purified by distillation *in vacuo* and used to synthesize

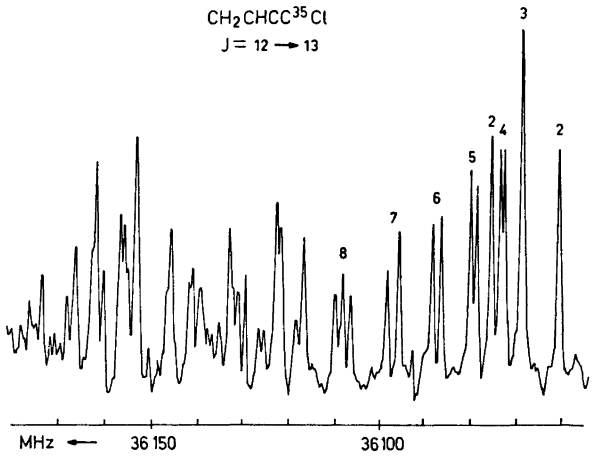

Fig. 1. Bandhead of the $J=12\rightarrow13$ transitions of $CH_2CHCC^{35}Cl$ near 36 100 MHz. Sweep rate 0.5 MHz/s.

4-chlorobuten-3-yne as described above. The amount of double and triple deuterated species of 4-chlorobuten-3-yne in this sample was found to be negligible. The rate of deuteration on acetylene and butenyne was controlled by IR-spectroscopy.

The microwave spectra were recorded on a Hewlett-Packard model 8460A R-band microwave spectrometer with a phase stabilized source oscillator. The upper part of the R-band (34 000—40 000 MHz) was used due to the better performance of the spectrometer in that region. The precision of the measured transitions was estimated to be 0.05 MHz.

MICROWAVE SPECTRUM

Most of the lines in the spectrum are gathered in bands at intervals of approximately 2770 MHz. Each band begins abruptly on the low frequency side and continues for 300—400 MHz with decreasing intensity. A characteristic bandhead is shown in Fig. 1. The line abundance of the bands and the repeated structure within the bands indicates the existence of several low lying excited vibrational modes, presumably states in which the skeletal bending modes are excited.

4-Chlorobuten-3-yne is expected to be an almost prolate symmetric rotor with the dipole moment lying close to the principal axis a: see Fig. 2. Therefore the microwave spectrum is expected to consist of R-branch a-type transitions with $\Delta J=+1$ and $\Delta K_{-1}=0$. Consequently, the regions of dense absorption are assigned to the transitions with $K_{-1}\geq2$. The remaining transitions with $K_{-1}=0$ and $K_{-1}=1$ are found outside the bands and identified on the basis of their characteristic second order (but unresolved) Stark effects.

The individual transitions within the bands were identified by their relative intensities and nuclear quadrupole hyperfine splitting: see Table 1. This observable nuclear quadrupole splitting is due to transitions with $\Delta F=+1$. The splitting increases with K_{-1}. Thus for low values of K_{-1}, the four nuclear quadrupole components merge into one single peak. As K_{-1} increases the peak splits into two, and

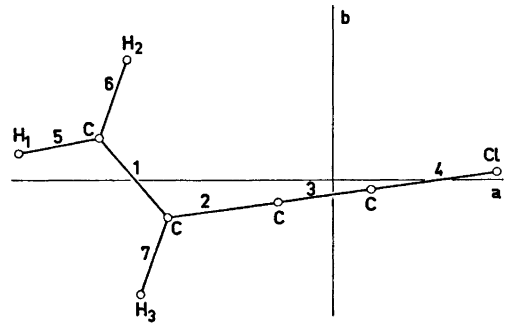

Fig. 2. Assumed structure of 4-chlorobuten-3-yne with principal axes of inertia.

Table 1. Observed rotational transitions and nuclear quadrupole hyperfine splitting in MHz for $CH_2CHCC^{35}Cl$ and $CH_2CHCC^{37}Cl$.

Transition						$CH_2CHCC^{35}Cl$		$CH_2CHCC^{37}Cl$	
J	K_{-1}	K_{+1}	J	K_{-1}	K_{+1}	ν_{obs}	Δ_{Qobs}	ν_{obs}	$\Delta\nu_{Qobs}$
13	1	13	12	1	12	35753.07		34926.75	
13	0	13	12	0	12	36045.52		35206.64	
13	2	12	12	2	11	36060.91		35220.86	
13	3	11	12	3	10	36068.88	0.42	35228.39	
13	4	10	12	4	9	36073.26	0.87	35232.74	0.66
13	2	11	12	2	10	36075.64		35234.31	
13	5	9	12	5	8	36079.60	1.31	35238.94	1.04
13	6	8	12	6	7	36087.56	1.93	35246.76	1.54
13	7	7	12	7	6	36097.09	2.56	35256.07	2.06
13	8	6	12	8	5	36108.06	3.40	35266.88	2.73
13	1	12	12	1	11	36361.73		35508.29	
14	1	14	13	1	13	38502.49		37612.68	
14	0	14	13	0	13	38815.51		37912.33	
14	2	13	13	2	12	38834.22		37929.59	
14	3	12	13	3	11	38843.55		37938.44	
14	4	11	13	4	10	38848.12	0.66	37942.93	0.48
14	2	12	13	2	11	38852.62		37946.41	
14	5	10	13	5	9	38854.87	1.07	37949.56	0.82
14	6	9	13	6	8	38863.42	1.52	37957.95	1.21
14	7	8	13	7	7	38873.63	2.08	37967.96	1.62
14	8	7	13	8	6	38885.49	2.64	37979.53	2.14
14	1	13	13	1	12	39157.94		38238.93	

Table 2. Observed rotational transition in MHz for the three monodeuterated species of 4-chlorobuten-3-yne.

Transition						$CDHCHCC^{35}Cl$[a]	$CHDCHCC^{35}Cl$[b]	$CH_2CDCC^{35}Cl$
J	K_{-1}	K_{+1}	J	K_{-1}	K_{+1}	ν_{obs}	ν_{obs}	ν_{obs}
13	1	13	12	1	12	34202.70	34893.54	35023.66
13	0	13	12	0	12	34472.51	35222.95	
13	2	12	12	2	11	34486.15	35244.57	35372.80
13	3	11	12	3	10	34493.63	35253.98	35381.37
13	4	10	12	4	9	34498.37	35256.51	35382.81
13	2	11	12	2	10	34498.71	35267.67	35395.55
13	5	9	12	5	8	34504.97	35260.88	35385.66
13	6	8	12	6	7	34513.28		
13	7	7	12	7	6	34523.17		
13	1	12	12	1	11	34762.86	35588.43	35715.70
14	1	14	13	1	13	36832.94	37576.42	37716.61
14	0	14	13	0	13	37121.92		
14	2	13	13	2	12	37138.39	37954.80	38093.00
14	3	12	13	3	11	37147.08	37966.09	38103.32
14	4	11	13	4	10	37152.03	37968.64	38104.60
14	2	12	13	2	11	37154.07	37983.65	38121.40
14	5	10	13	5	9	37159.09	37973.25	38107.53
14	6	9	13	6	8	37168.00	37979.25	38111.78
14	7	8	13	7	7	37178.65	37986.76	
14	1	13	13	1	12	37436.15	38324.83	38461.90

[a] Deuterium *trans* to the chloroacetylene group. [b] Deuterium *cis* to the chloroacetylene group.

Table 3. Observed rotational constants in MHz for five isotopic species of 4-chlorobuten-3-yne.

	A	B	C
$CH_2CHCC^{35}Cl$	41927.±50	1410.388±0.004	1363.563±0.004
$CH_2CHCC^{37}Cl$	41907.±50	1377.027±0.004	1332.289±0.004
$CDHCHCC^{35}Cl$[a]	41705.±50	1347.939±0.004	1304.846±0.004
$CHDCHCC^{35}Cl$[b]	35145.±50	1382.398±0.006	1328.929±0.006
$CH_2CDCC^{35}Cl$	35341.±60	1387.239±0.008	1333.992±0.008

[a] Deuterium *trans* to the chloroacetylene group. [b] Deuterium *cis* to the chloroacetylene group.

finally into four, observable peaks. Only splitting into doublets was observed since the transitions with $K_{-1} \geq 9$ were obscured by the very dense vibrational satellite bands: see Fig. 1. The observable splitting is mainly determined by only one nuclear quadrupole coupling constant χ_{aa}.[6] For ^{35}Cl in $CH_2CHCC^{35}Cl$ this value was determined to be $\chi_{aa} = -76.9 \pm 0.4$ MHz and for ^{37}Cl in $CH_2CHCC^{37}Cl$ $\chi_{aa} = -60.9 \pm 0.4$.

The assignment of the microwave transitions from the three possible monodeuterated species: $CDHCHCC^{35}Cl$, $CHDCHCC^{35}Cl$ and $CH_2CDCC^{35}Cl$, was very complicated for two of them due to band overlapping with the more abundant $CH_2CHCC^{37}Cl$ species. The lines outside with $K_{-1} = 1$ were weaker than expected due to incomplete Stark modulation. The problem was solved by making high resolution sweeps at low pressure and low temperature of the $J = 12 \rightarrow 13$ and $J = 13 \rightarrow 14$ bands from the $CH_2CHCC^{37}Cl$ molecules in samples with and without deuterated species. A close comparison between these spectra revealed the contributions from the deuterated species. Once these bandheads were found it was rather easy to find the $K_{-1} = 1$ transitions outside the bands: see Table 2.

Corresponding lines in the spectra of the deuterated species $CDHCHCC^{35}Cl$, $CHDCHCC^{35}Cl$ and $CH_2CDCC^{35}Cl$ showed the same nuclear quadrupole hyperfine structure as the $CH_2CHCC^{35}Cl$ species. The rotational constants A, B and C for the natural and deuterated species of 4-chlorobuten-3-yne are given in Table 3.

Table 4. Measured and calculated centrifugal distortion constants for five isotopic species of 4-chlorobuten-3-yne in kHz.

		Observed	Calculated
$CH_2CHCC^{35}Cl$	D_J	0.12±0.01	0.12
	D_{JK}	−28.55±0.02	−26.43
$CH_2CHCC^{37}Cl$	D_J	0.11±0.01	0.12
	D_{JK}	−27.94±0.02	−25.93
$CDHCHCC^{35}Cl$[a]	D_J	0.13±0.01	0.12
	D_{JK}	−29.65±0.02	−27.44
$CHDCHCC^{35}Cl$[b]	D_J	0.13±0.02	0.13
	D_{JK}	−21.05±0.03	−19.74
$CH_2CDCC^{35}Cl$	D_J	0.13±0.02	0.11
	D_{JK}	−14.85±0.05	−13.25

[a] Deuterium *trans* to the chloroacetylene group. [b] Deuterium *cis* to the chloroacetylene group.

CENTRIFUGAL DISTORTION

It was necessary to include the centrifugal distortion terms D_J and D_{JK} in the least squares fit of the rotational constants A, B and C to the observed spectra. The term D_{JK} makes an important contribution and reverses the normal order of the K_{-1} values. However, these centrifugal distortion constants could be adequately predicted with theoretical calculations from a simple estimated diagonal force field:[10] see Table 4. In fact these calculations turned out to be a very valuable aid in the assignment of the overlapped deuterium spectral bands. The bandheads of the species $CH_2CDCC^{35}Cl$ were in the most dense regions of the vibrational satellites from another deuterated species $CHDCHCC^{35}Cl$ as well as from the natural

Table 5. The absolute values of the coordinates for the chlorine atom and the hydrogen atoms calculated with Kraitchman's equations and the distances between these atoms. Conversion factor 505 376 (MHz) (auÅ²).

Kraitchman's coordinates (Å)		
Atom	$\|a\|$	$\|b\|$
Cl	2.1090	0.1000
H_1	4.0858	0.2731
H_2	2.6988	1.5582
H_3	2.4429	1.5141

Chlorine-hydrogen and hydrogen-hydrogen distances (Å).			
Cl—H_1	6.197	H_1—H_2	1.891
Cl—H_2	5.024	H_1—H_3	2.428
Cl—H_3	4.830	H_2—H_3	3.083

species $CH_2CHCC^{37}Cl$, but the general appearance of the bandheads from $CH_2CDCC^{35}Cl$ were well predicted from the theoretical calculation of the D_{JK} distortion constant. This D_{JK}-value turned out to be considerable less than the values obtained from the other species: see Table 4.

The following symbols are used for the force constants.[11] K_i is the force constant for the stretching of the bond i, K_{ij} is the bending of the angle between the bonds i and j, ϱ_k^{ij} is the bending of the bond k out of the plane spanned by the bonds i and j, χ_{kl}^{ij} finally is the torsion between the planes spanned by the bonds i and j, and k and l, respectively. The values for the constants are, with the bond numbers of Fig. 2: $K_5=K_6=5.53$, $K_7=5.38$, $K_1=7.69$, $K_2=7.12$, $K_3=16.49$, $K_4=5.16$, $K_{12}=1.08$, $K_{15}=K_{16}=0.59$, $K_{17}=0.42$, $K_{23}=0.32$, $K_{34}=0.28$, $\delta_1^{27}=0.273$, $\delta_1^{56}=0.223$ and $\chi_{56}^{27}=0.577$ in mdyn/Å and mdyn Å for stretching and bending constants, respectively. We have assumed the same force constants for bending in plane and out of plane for the acetylenic group. The agreement between measured and calculated centrifugal distortion parameters is of course no direct proof of the validity of this simple force field.

MOLECULAR STRUCTURE

The measured inertial defect for $CH_2CHCC^{35}Cl$ is 0.25 ± 0.02 au Å² which can be compared with the value 0.29 au Å² obtained from theoretical calculations using the previous mentioned valence force field assuming planar configuration.[10,12] Thus there is no reason to expect the molecular structure to deviate from planarity.

The absolute values of the Cartesian coordinates for the chlorine atom and the hydrogen atoms were calculated in the principal axis system of the $CH_2CHCC^{35}Cl$ molecule from the changes in the moments of inertia I_b and I_c on isotopic substitution:[3,4] see Table 5. We have also calculated the distances between these atoms to combine with later information from electron diffraction measurements. However, great care must be taken in the use of these structural parameters due to several sources of uncertainties. Primarily, these uncertainties arise from the vibrational effects. It was not possible to obtain the moments of inertia I_a accurate enough so we used I_b and I_c assuming no change in inertial defect due to substitution. However, theoretical calculations for the different isotopic species with the force field above suggest that the inertial defect increases by as much as 0.01 au Å² for the hydrogens H_2 and H_3. This alone leads to an uncertainty in the b-coordinates of H_2 and H_3 of about 0.005 Å.

There is also the well known effect of change in effective bond length with isotopic substitution especially for the hydrogen-deuterium substitution.[10,13] This effect might be of the magnitude 0.01 Å for the hydrogen-hydrogen distances and 0.005 Å for the hydrogen-chlorine distances.

If an atom is close to a principal axis there is a corresponding uncertainty in the obtained distance to that axis. Therefore the b-coordinate of the chlorine atom is rather uncertain due to its position near the a-axis: see Fig. 2. However, even if we assume such a large error as 0.1 Å in this coordinate the error in the Cl—H_1 distance becomes only 0.004 Å and in the Cl—H_2 and Cl—H_3 distances 0.03 Å. From this discussion we expect the deviation of the r_s-distances obtained to be about ±0.005 Å for the hydrogen-chlorine distances and about ±0.01 Å for the hydrogen-hydrogen distances. The best determined value is probably the molecular length given by the distance Cl—H_1 to 6.197 Å.

The distance parameters from the substitution structure r_s are actually not directly com-

parable with the distances obtained with electron diffraction due to vibrational effect.[12,14] However, both methods are comparable in the average structure r_z and this can be calculated from the effective parameters obtained by microwave spectroscopy.[12,15] We have done that using the force field given above but the magnitude of these corrections falls within the uncertainty of the r_s-distances. Moreover, even for the average structure the deuterium substitution causes an error in the coordinates.[13] However, if the effective principal moments of inertia are to be used directly for a comparison with the principal moments of inertia calculated from an average structure it would be advisable to calculate the correction from effective to average parameters. Using the force field above the effective moments of inertia $I_b^0 = 358.324$ and $I_c^0 = 370.629$ au Å^2 for $CH_2CHCC^{35}Cl$ were transformed to the corresponding average parameters $I_b^z = 358.486$ and $I_c^z = 370.595$ au Å^2. No attempts were made to look for ^{13}C-substituted species in natural abundance due to the frequent occurrence of vibrational satellites in the expected spectral regions.

Acknowledgements. We thank all those who have contributed to this paper and especially Dr. Stig Ljunggren, Dr. Allan Rupprecht and Dr. Harald Møllendal for pleasant cooperation and valuable discussions.

REFERENCES

1. Carothers, W. H., Jacobson, R. A. and Berechet, G. J. *J. Amer. Chem. Soc. 55* (1933) 4665.
2. Granberg, M., Karlsson, F. and Vestin, R. *Acta Chem. Scand. B 28* (1974) 580.
3. Kraitchman, J. *Amer. J. Phys. 21* (1953) 17.
4. Costain, C. C. *J. Chem. Phys. 29* (1958) 864.
5. Karlsson, F., Borg, A. and Vestin, R. *Acta Chem. Scand. 26* (1972) 3394.
6. Karlsson, F. and Vestin, R. *Acta Chem. Scand. 27* (1973) 3033.
7. Karlsson, F., Granberg, M. and Vestin, R. *Acta Chem. Scand. A 28* (1974) 201.
8. Karlsson, F., Granberg, M. and Vestin, R. *Acta Chem. Scand. A 28* (1974) 206.
9. Nieuwland, J. A. and Vogt, R. *The Chemistry of Acetylene*, New York 1945.
10. Gordy, W. and Cook, R. L. *Microwave Molecular Spectra*, Interscience, New York 1970.
11. Gribov, L. A. *Vvedenie v teoriyu i raschet kolebatelnykh spektrov mnogoatomnykh molecul*, Istadelstvo Leningradskogo Universita, 1965.
12. Herschbach, D. R. and Laurie, V. W. *J. Chem. Phys. 37* (1962) 1668.
13. Laurie, V. W. and Herschbach, D. R. *J. Chem. Phys. 37* (1962) 1687.
14. Morino, Y., Kuchitsu, K. and Oka, T. *J. Chem. Phys. 36* (1962) 1108.
15. Oka, T. and Morino, Y. *J. Mol. Spectrosc. 8* (1962) 300.

Received August 12, 1974.

Acta Chemica Scandinavica A 29 (1975) 117—124

Phthalic Acid as a Reagent in Inorganic Qualitative Analysis of Metal Ions. Part III. Thermodynamics of the Protonation of Phthalate Ion in Aqueous Sodium Perchlorate Solutions

PAAVO LUMME and ESKO KARI

Department of Chemistry, University of Jyväskylä, Jyväskylä Finland

The protonation constants of phthalate ion were determined potentiometrically as functions of the ionic strength in aqueous sodium perchlorate solutions within the temperature range from 15 to 35 °C. The thermodynamic values ($K°_n$) of the protonation constants were evaluated by fitting the experimental data to semi-theoretical equations. The values of the free energies, enthalpies, entropies, and heat capacities of the protonation equilibria were calculated on the basis of the thermodynamic values of the protonation constants. On the basis of the obtained data and our experience, phthalic acid was concluded to be well suited for use as a group reagent and a buffering agent, within wide ionic strength and temperature limits, for solutions in the inorganic qualitative analysis of metal ions.

The protonation of the phthalate ion in aqueous solutions has been studied several times before,[1–12] but generally the protonation constants were evaluated at one ionic strength and temperature only. An exception from this general tendency is the work of Hamer *et al.*[9–10] where the thermodynamic quantities were also considered.

In the present paper the protonation of the phthalate ion was studied potentiometrically in aqueous sodium perchlorate solutions. The determination of the protonation constants at different temperatures made it possible to estimate the thermodynamic quantities as well.

EXPERIMENTAL

Reagents and solutions. Phthalic acid was a product of E. Merck, designed for use in chromatography. The acid was dried in a desiccator. By potentiometric titration with a known sodium hydroxide solution its alkalimetric purity was found to be 99.64 %. Potassium biphthalate, sodium chloride, sodium hydroxide, mercurous chloride, mercury, and perchloric acid were all guaranteed reagents of E. Merck. Potassium biphthalate was dried in a desiccator and sodium chloride at 150 °C. Sodium perchlorate was an anhydrous product of G. Frederic Smith Chemical Co. The salt was dissolved in water. pH of the solution was adjusted with sodium hydroxide to 7. The solution was allowed to stand one day and filtered through a glass-sinter (G4). The filtrate was made neutral with perchloric acid so that it consumed no sodium hydroxide against phenolphthalein. The concentration of the solution (~4 M) was determined by evaporating 5 ml aliquots to dryness at 140 °C and, on the other hand, using cation exchanger (Ionentauscher E. Merck) and titrating the obtained perchloric acid solution with sodium hydroxide. The water used was distilled, deionized and carbon dioxide-free.

About 0.1 M sodium hydroxide solution was prepared diluting a Titrisol solution (E. Merck) under nitrogen atmosphere in a carbon dioxide tight titration equipment from Pyrex-glass. The concentration of the solution was determined by potentiometric titrations of weighed amounts of potassium biphthalate.

A dilute (0.1 M) perchloric acid solution was prepared from conc. acid (70 %) and its concentration was determined by potentiometric titrations with the known sodium hydroxide solution. The obtained solution was used to prepare the reference buffer solutions of 0.005 M.

The concentrations of the stock solutions are given in Table 1. The compositions of the solutions used in connection with the titrations are given in Table 2.

Sodium chloride was added as solid, the other reagents as stock solutions to the solutions

Table 1. The concentrations of the stock solutions used (20 °C). $[HClO_4]=0.1003$ M.

I	M $NaClO_4$	M NaOH
0.040	4.013	0.09945
0.250	4.013	0.09943
0.500	4.013	0.09961
1.000	4.013	0.09971
2.000	6.437	0.10038

prepared. In the preparation of the solutions at 20 °C guaranteed measuring flasks, burettes and pipettes were used. The temperature expansion of the solutions was assumed to be that of pure water and relative density values of water were used [13] to correct the volumes to the desired temperature.

Apparatus. The titration vessels (200 ml) were of Pyrex glass with gas tight covers equipped with inlets for glass and reference electrodes, burette and nitrogen gas. The nitrogen gas was washed and thermostated before inlet to the titration vessel. The water thermostat, where the titrations were performed, was held constant within ±0.01 °C. The titrated solution was stirred magnetically. The glass electrode was a Beckman type, No. 41260 and the reference calomel electrode of the immersion type. The potentiometer was a Radiometer PHM 4. The potentials were read to ±0.2 mV.

Measurements. For both protonation equilibria the measurements were made at eleven points of the titration curve. For K_2 the potentials were measured from 4 to 6 ml and for K_1 from 14 to 16 ml of 0.01 M sodium hydroxide added in increments of 0.2 ml. At least two titrations were performed at each temperature and the results were combined to calculate the K_n values. The system was checked against a perchloric acid solution (0.005 M in $HClO_4$) at the beginning and at the end of every titration. The starting volume of the titrated solutions was 100 ml at 20 °C. The pH (= $-\log[H^+]$) values were calculated from the measured potentials.[14] To minimize the possible diffusion potentials the cell system used in the potentiometric titrations was of the type:[15]

Glass electrode	100 ml 0.01 M $C_8H_6O_4$ 0.01 M NaCl $(I-0.01)$ M $NaClO_4$	‖
0.01 M NaCl $(I-0.01)$ M $NaClO_4$		Hg_2Cl_2, Hg

RESULTS AND DISCUSSION

The protonation equilibria of the phthalate ion in aqueous solutions may be briefly expressed as follows:

$$L^{2-}+H_3O^+ \rightleftharpoons HL^- + H_2O \quad (1)$$

$$HL^-+H_3O^+ \rightleftharpoons H_2L + H_2O \quad (2)$$

The corresponding protonation constants

$$K_1=[HL^-]/[L^{2-}]\,[H^+] \quad (3)$$

$$K_2=[H_2L]/[HL^-]\,[H^+] \quad (4)$$

were calculated by iteration from the equations:

$$\log K_1=\mathrm{pH}-\log\{(Y-C+[H^+]YK_2)/(2C-Y)\} \quad (5)$$

$$\log K_2=\mathrm{pH}-\log\{Y/[C-Y+(2C-Y)/K_1[H^+]]\} \quad (6)$$

where $Y=C_B+[H^+]$ and C and C_B are the total concentrations of phthalic acid and the added sodium hydroxide, respectively, in the titrated solutions. The expressions are easily derived by taking into account the total concentrations and neglecting $[OH^-]$.

The equations consider the effect of the overlapping of the protonation equilibria.

Table 2. The compositions of the solutions used in connection with the titrations (20 °C).

Titrant 0.1 M NaOH 0.01 M NaCl M $NaClO_4$	I	Reference electrode 0.01 M NaCl M $NaClO_4$	Reference buffer 0.005 M $HClO_4$ 0.01 M NaCl M $NaClO_4$	Studied solution 0.01 M $C_8H_6O_4$ 0.01 M NaCl M $NaClO_4$
0.030	0.040	0.030	0.025	0.030
0.240	0.250	0.240	0.235	0.240
0.490	0.500	0.490	0.485	0.490
0.990	1.000	0.990	0.985	0.990
1.990	2.000	1.990	1.985	1.990

Table 3. The potentiometric titration data of phthalic acid in aqueous sodium perchlorate solutions at 15 and 20 °C.

Titrant ml	pH 15 °C					20 °C				
4.00	2.807	2.778	2.774	2.796	2.849	2.803	2.780	2.773	2.782	2.859
4.20	2.826	2.796	2.791	2.817	2.872	2.824	2.800	2.793	2.804	2.880
4.40	2.847	2.820	2.818	2.837	2.895	2.846	2.822	2.816	2.823	2.900
4.60	2.868	2.840	2.839	2.858	2.919	2.867	2.844	2.837	2.847	2.926
4.80	2.892	2.872	2.861	2.884	2.944	2.890	2.866	2.859	2.870	2.948
5.00	2.914	2.894	2.884	2.904	2.968	2.914	2.888	2.881	2.893	2.973
5.20	2.937	2.917	2.907	2.928	2.991	2.937	2.911	2.906	2.919	2.996
5.40	2.961	2.940	2.931	2.952	3.016	2.962	2.936	2.930	2.941	3.020
5.60	2.984	2.963	2.955	2.977	3.042	2.985	2.962	2.957	2.967	3.045
5.80	3.007	2.987	2.978	3.003	3.068	3.010	2.986	2.976	2.990	3.070
6.00	3.031	3.012	3.005	3.030	3.093	3.037	3.012	3.003	3.015	3.099
14.00	4.790	4.637	4.565	4.533	4.599	4.808	4.627	4.557	4.524	4.601
14.20	4.823	4.670	4.599	4.565	4.631	4.841	4.662	4.592	4.555	4.636
14.40	4.859	4.701	4.630	4.596	4.663	4.876	4.694	4.625	4.587	4.664
14.60	4.891	4.735	4.661	4.626	4.695	4.912	4.727	4.657	4.622	4.697
14.80	4.925	4.769	4.691	4.658	4.730	4.946	4.760	4.691	4.654	4.729
15.00	4.962	4.799	4.726	4.691	4.762	4.978	4.795	4.726	4.685	4.763
15.20	4.996	4.833	4.759	4.721	4.795	5.013	4.827	4.759	4.718	3.793
15.40	5.030	4.868	4.790	4.756	4.830	5.047	4.862	4.795	4.752	4.827
15.60	5.065	4.902	4.824	4.794	4.864	5.080	4.897	4.826	4.785	4.862
15.80	5.100	4.936	4.860	4.824	4.897	5.115	4.930	4.862	4.820	4.898
16.00	5.137	4.973	4.895	4.858	4.936	5.153	4.965	4.896	4.856	4.932
Approx. *I*	0.05	0.25	0.50	1.00	2.00	0.05	0.25	0.50	1.00	2.00

Table 4. The potentiometric titration data of phthalic acid in aqueous sodium perchlorate solutions at 25 and 35 °C.

Titrant ml	pH 25 °C					35 °C				
4.00	2.801	2.785	2.776	2.788	2.856	2.808	2.793	2.786	2.804	2.883
4.20	2.820	2.806	2.797	2.807	2.878	2.829	2.814	2.805	2.826	2.903
4.40	2.841	2.828	2.818	2.828	2.900	2.851	2.834	2.825	2.846	2.925
4.60	2.863	2.849	2.839	2.851	2.924	2.874	2.857	2.845	2.865	2.945
4.80	2.886	2.871	2.862	2.874	2.948	2.897	2.876	2.867	2.887	2.967
5.00	2.910	2.894	2.885	2.897	2.968	2.919	2.901	2.889	2.909	2.991
5.20	2.932	2.918	2.908	2.921	2.995	2.942	2.924	2.910	2.932	3.014
5.40	2.955	2.942	2.931	2.945	3.016	2.968	2.945	2.935	2.955	3.038
5.60	2.979	2.964	2.955	2.970	3.045	2.992	2.969	2.959	2.978	3.063
5.80	3.005	2.989	2.980	2.994	3.071	3.018	2.994	2.982	3.002	3.090
6.00	3.032	3.016	3.005	3.019	3.098	3.044	3.019	3.006	3.027	3.117
14.00	4.789	4.622	4.556	4.523	4.597	4.812	4.625	4.556	4.525	4.611
14.20	4.823	4.653	4.591	4.556	4.629	4.847	4.658	4.589	4.558	4.642
14.40	4.857	4.690	4.625	4.587	4.662	4.881	4.693	4.622	4.592	4.675
14.60	4.889	4.723	4.658	4.620	4.693	4.914	4.724	4.656	4.623	4.706
14.80	4.922	4.757	4.690	4.653	4.727	4.943	4.759	4.689	4.657	4.739
15.00	4.958	4.790	4.724	4.686	4.760	4.980	4.791	4.722	4.690	4.772
15.20	4.991	4.824	4.756	4.718	4.792	5.013	4.825	4.754	4.723	4.805
15.40	5.025	4.856	4.791	4.752	4.826	5.048	4.860	4.788	4.758	4.838
15.60	5.059	4.891	4.827	4.787	4.861	5.082	4.892	4.822	4.791	4.872
15.80	5.095	4.924	4.860	4.820	4.894	5.116	4.925	4.857	4.824	4.908
16.00	5.128	4.962	4.895	4.856	4.930	5.150	4.960	4.889	4.859	4.942
Approx. *I*	0.05	0.25	0.50	1.00	2.00	0.05	0.25	0.50	1.00	2.00

Table 5. The calculated protonation constants of the phthalate ion at different ionic strengths and temperatures.

t °C	I	Mean log K_1	I	Mean log K_2
15	0.0573	4.967	0.0459	2.705
20	0.0572	4.985	0.0459	2.704
25	0.0570	4.963	0.0457	2.697
35	0.0569	4.984	0.0456	2.710
15	0.2675	4.804	0.2562	2.674
20	0.2672	4.796	0.2560	2.672
25	0.2668	4.791	0.2556	2.680
35	0.2661	4.791	0.2548	2.685
15	0.5177	4.722	0.5064	2.665
20	0.5173	4.720	0.5060	2.663
25	0.5166	4.719	0.5053	2.666
35	0.5150	4.715	0.5038	2.672
15	1.0182	4.682	1.0069	2.702
20	1.0173	4.677	1.0060	2.682
25	1.0160	4.677	1.0047	2.688
35	1.0129	4.681	1.0016	2.705
15	2.0193	4.724	2.0076	2.789
20	2.0175	4.745	2.0058	2.796
25	2.0150	4.733	2.0034	2.795
35	2.0090	4.743	1.9973	2.823

Table 6. The results of the fitting of the data in Table 5 to eqns. (7) and (8) at 25 °C.

I	A	α_1	B_1	Obs. log K_1	Calc. eqn. (7) log K_1
0.2668				4.791	4.792
0.5166				4.719	4.716
1.0160	0.5115[16]	1.4127	0.1690	4.677	4.679
2.0150				4.733	4.732
I	A	α_2	B_2	Obs. log K_2	Calc. eqn. (8) log K_2
0.2556				2.680	2.680
0.5053				2.666	2.665
1.0047	0.5115[16]	1.5875	0.1563	2.688	2.689
2.0034				2.795	2.795

log $K°_1 = 5.358$; log $K°_2 = 2.927$.

The experimental data of the determinations of the protonation constants are given in Tables 3 and 4 and the values of the constants calculated from these, in Table 5.

The data in Table 5 were fitted by the method of least squares to the semiempirical equations:

$$\log K_1 = \log K°_1 - \frac{4A\sqrt{I}}{1+\alpha_1\sqrt{I}} + B_1 I \qquad (7)$$

$$\log K_2 = \log K°_2 - \frac{2A\sqrt{I}}{1+\alpha_2\sqrt{I}} + B_2 I \qquad (8)$$

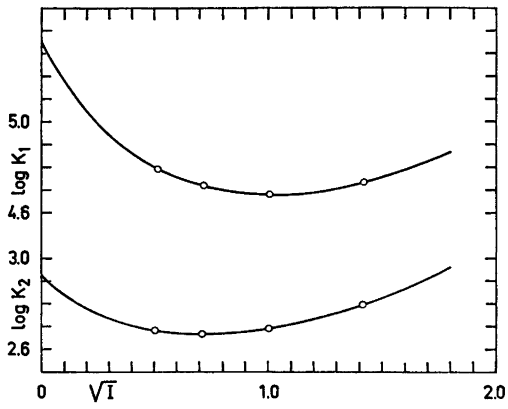

Fig. 1. The log K_1 and log K_2 values of the protonation constants of the phthalate ion in aqueous sodium perchlorate solutions as functions of the square root of the ionic strength at 25 °C.

at 25 °C only. The values of the constants of eqns. (7) and (8) obtained at 25 °C are given in Table 6 with the experimental and calculated values of the protonation constants. The constants at 25 °C were used to calculate the thermodynamic values of the protonation constants from eqns. (7) and (8) at the other temperatures. The results of these calculations are given in Table 7. In fitting the curve the values of the protonation constants at the lowest ionic strengths were disregarded, due to errors caused by diffusion potentials.

The log K_1 and log K_2 values of the protonation constants are represented as functions of the square roots of the ionic strength at 25 °C in Fig. 1.

As regards earlier studies of the protonation equilibria of the phthalate ion only the work of Hamer *et al.*[9,10] was carried out at different temperatures. The temperature range was from 0 to 60 °C and the ionic strength varied from about 0 to 0.55. Cells without liquid junctions were used. Further, Topp and Davies [2] evaluated the protonation constants at zero ionic strength. The results obtained by different workers are compared in Table 8.

In general the values of the protonation constants obtained by different workers are of the same order of magnitude. However, the present values are generally a little lower. This may be due to the liquid junction potentials in the measuring cells, if we assume the glass electrode to have functioned normally and that the error due to the potential measurements in log K_n values was about ± 0.003 units. The determinations were made as consistent duplicate measurements and the stabilization of the systems at different titration points and temperatures was good.

The present thermodynamic values of the protonation constants showed so little variation

Table 7. The thermodynamic values of the protonation constants of the phthalate ion calculated from eqns. (7) and (8) at different ionic strengths and temperatures.

t °C	A[16]	I	log $K°_1$	Mean log $K°_1$	I	log $K°_2$	Mean log $K°_2$
15	0.5028	0.2675	5.360		0.2562	2.916	
		0.5177	5.352	5.348	0.5064	2.922	2.917
		1.0182	5.347		1.0069	(2.934)	
		2.0193	5.333		2.0076	2.914	
20	0.5070	0.2672	5.357		0.2560	2.916	
		0.5173	5.356		0.5060	2.922	
		1.0173	5.348	5.356	1.0060	2.917	2.920
		2.0175	5.362		2.0058	2.924	
25	0.5115	0.2668–2.0150	–	5.358	0.2556–2.0034	–	2.927
35	0.5211	0.2661	5.368		0.2548	2.937	
		0.5150	5.371		0.5038	2.941	
		1.0129	5.376	5.375	1.0016	2.951	2.948
		2.0090	5.387		1.9973	2.965	

Table 8. Comparison of the protonation constants of the phthalate ion determined by different workers.

°C	Ionic strength added salt	log K_1	log K_2	Method	Reference
15	→0	5.405	2.937	H, Ag–AgCl	9,10
15	→0	5.348	2.917	Glass electrode	This work
20	→0	5.405	2.943	H, Ag–AgCl	9,10
20	→0	5.356	2.920	Glass electrode	This work
25	→0	5.40	3.14	Conductivity	2
25	→0	5.408	2.950	H, Ag–AgCl	9,10
25	→0	5.358	2.927		This work
25	0.1 (KNO_3)	4.92	2.76		3
25	0.1	4.92	2.76		4
25	0.1 ($NaClO_4$)	4.928	2.728		This work
25	0.15 ($NaClO_4$)	5.13	2.91		12
25	0.15 ($NaClO_4$)	4.871	2.705		This work
25	1.0 (KNO_3)	4.73	2.67	Glass electrode	5
25	1.0 (KNO_3)	4.73	2.63		6
25	1.0 ($NaClO_4$)	4.679	2.688		This work
25	3.0 ($NaClO_4$)	4.89	3.05		7
25	3.0 ($NaClO_4$)	4.837	2.923		This work
35	→0	5.427	2.967	H, Ag–AgCl	9,10
35	→0	5.375	2.948	Glass electrode	This work

with temperature that the dependence was assumed to be linear according to the equation:

$$\log K^\circ_n = a + bT \quad (9)$$

On the basis of this assumption the thermodynamic quantities, the free energies, enthalpies, entropies, and heat capacities of the protonation equilibria of the phthalate ion were calculated from the following expressions:

$$\Delta G^\circ = -2.303\ R(aT + bT^2) \quad (10)$$

$$\Delta H^\circ = 2.303\ RbT^2 \quad (11)$$

$$\Delta S^\circ = 2.303\ R(a + 2bT) \quad (12)$$

$$\Delta C^\circ_p = 4.606\ RbT \quad (13)$$

where $R = 8.31433$ J K^{-1} mol^{-1} and T is the absolute temperature.

Fitting the mean values of log K°_1 and log K°_2 at different temperatures from Table 7 with the method of least squares to eqn. (9) gave for the constants a and b the following values:

	a	$b \times 10^3$
log K°_1	4.967	1.320
log K°_2	2.450	1.611

The values of the free energies, enthalpies and entropies were then calculated from eqns. (10)–(12). These are given for the first protonation equilibrium in Table 9 and for the second in Table 10.

The mean values of log K°_1 and log K°_2 from Table 7 are represented as functions of the absolute temperature in Fig. 2.

The effect of temperature on the protonation of the phthalate ion is very weak (Fig. 2, Table 7). The values of both protonation constants increase only slightly with temperature.

For both protonation reactions ΔH° is positive, which indicates endothermic processes (Tables 9 and 10). The values of ΔS° are also positive and increase almost unobservably with increasing temperature within the tem-

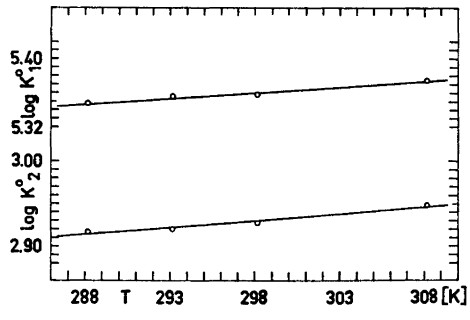

Fig. 2. The thermodynamic values log K°_1 and log K°_2 of the protonation constants of phthalate ion as functions of the absolute temperature.

Table 9. The calculated thermodynamic quantities of the first protonation equilibrium of the phthalate ion.

t °C	log $K°_1$ (eqn. (7))	log $K°_1$ (eqn. (9))	$-\Delta G°$ (kJmol^{-1})	$\Delta H°$ (kJmol^{-1})	$\Delta S°$ (JK^{-1}mol^{-1})	$\left\lvert\frac{10^2 T\Delta S°}{\Delta G°}\right\rvert$
15	5.348	5.347	29.50	2.10	110	107
20	5.356	5.354	30.05	2.17	110	107
25	5.358	5.360	30.60	2.25	110	107
35	5.375	5.374	31.71	2.40	111	108
Mean at 15–35 °C			30.47 ± 0.70	2.23 ± 0.1	110 ± 1	107

Table 10. The calculated thermodynamic quantities of the second protonation equilibrium of the phthalate ion.

t °C	log $K°_2$ (eqn. (8))	log $K°_2$ (eqn. (9))	$-\Delta G°$ (kJ mol^{-1})	$\Delta H°$ (kJ mol^{-1})	$\Delta S°$ (J K^{-1}mol^{-1})	$\left\lvert\frac{10^2 T\Delta S°}{\Delta G°}\right\rvert$
15	2.917	2.914	16.08	2.56	64.8	116
20	2.920	2.922	16.40	2.65	64.8	116
25	2.927	2.930	16.73	2.74	65.3	116
35	2.948	2.946	17.39	2.93	66.1	117
Mean at 15–35 °C			16.65 ± 0.41	2.72 ± 0.1	65.3 ± 0.5	116

Table 11. The thermodynamic quantities of the protonation reactions of the phthalate ion previously obtained at the present temperatures.

t °C	$-\Delta G°$ (kJ mol^{-1})	$\Delta H°$ (kJ mol^{-1})	$\Delta S°$ (J K^{-1} mol^{-1})	$\Delta C°p$ (J K^{-1} mol^{-1})	Ref.
The first protonation reaction					
15	29.812	−0.810	100.6	283.5	10
20	30.327	0.620	105.5	288.5	10
25	30.867	2.074	110.5	293.4	10
25	29.884	2.075	87.9	292.9	8
35	32.021	5.056	120.3	303.2	10
The second protonation reaction					
15	16.198	1.780	61.4	87.0	9
20	16.513	2.219	63.9	88.5	9
25	16.836	2.666	65.4	90.0	9
35	17.505	3.581	68.4	93.0	9

perature range used. These changes are in agreement with the opinion that the protonation of the phthalate ion is favored by temperature increase although the enthalpy changes are against this, because the increase of the entropy values due to the liberation of hydration water molecules of the reaction species. The values of $\Delta C°_p$ are also positive and increase with increasing temperature, but are very inaccurate and are not given.[17]

Hamer *et al.*[9,10] and Banerjee *et al.*[8] have determined previously the thermodynamic quantities of the protonation reactions of the phthalate ion. The latter evaluated the thermodynamic quantities of the first protonation reaction at 25 °C by extrapolation from potentiometric measurements in mixtures of ethylene glycol and water at different temperatures (5–45 °C). The results of these studies in

the temperature range 15—35 °C are compared in Table 11.

Comparing our results in Tables 9 and 10 with the earlier ones in Table 11, they may be said to be of the same order of magnitude. The error in log K_n values when working with a glass electrode and a system with minimized liquid junction potentials may, however, easily be of the order of ± 0.02 unit. This means estimated inaccuracies of about ± 0.2 kJ mol^{-1} in $\Delta G°$, ± 3 kJ mol^{-1} in $\Delta H°$ and ± 10 J K^{-1} mol^{-1} in $\Delta S°$ values or better.

On the basis of Table 8 and Fig. 1 and 2 it may be concluded that, within the temperature range of 15 to 35 °C, the protonation equilibria of the phthalate ion are fairly independent both of the nature of the neutral salts present, and of ionic strength in solution. This means that phthalic acid is, in these respects, well suited for use as a group reagent and a buffering agent in the usual precipitation conditions prevailing in the inorganic qualitative analysis of metal ions.[18]

Acknowledgements. The authors are indebted to Mr. M. Peacock, M. A., for correcting the English of this paper and to Mr. I. Laitinen and R. Vähälä for valuable cooperation in preparing the computer programs for IBM 1130 and Honeywell 1642 computers. Financial support from the National Research Council for Sciences (Finland) is also gratefully acknowledged.

REFERENCES

1. Sillén, L. G. and Martell, A. E. *Stability Constants of Metal-Ion Complexes*, Special Publ. No. 17, p. 564 and No. 25, p. 534, The Chemical Society, London 1964 and 1971.
2. Topp, N. E. and Davies, C. W. *J. Chem. Soc.* (1940) 87.
3. Yasuda, M., Suzuki, K. and Yamasaki, K. *J. Phys. Chem. 60* (1956) 1649.
4. Yasuda, M., Yamasaki, K. and Ohtaki, H. *Bull. Chem. Soc. Jap. 33* (1960) 1067.
5. Rajan, K. S. *Diss.*, Illinois Institute of Technology, Chicago 1964.
6. Rajan, K. S. and Martell, A. E. *J. Inorg. Nucl. Chem. 29* (1967) 523.
7. Palmæus, R. and Kierkegaard, P. *Acta Chem. Scand. 18* (1964) 2226.
8. Banerjee, S. K., Kundu, K. K. and Das, M. N. *J. Chem. Soc. A* (1968) 139.
9. Hamer, W. J., Pinching, G. D. and Acree, S. F. *J. Res. Nat. Bur. Stand. 35* (1945) 539.
10. Hamer, W. J. and Acree, S. F. *J. Res. Nat. Bur. Stand. 35* (1945) 381.
11. Krishnamurthy, M. and Prasad, N. S. K. *Indian J. Chem. 4* (1966) 316.
12. de Bruin, H. J., Kaitis, D. and Temple, R. B. *Aust. J. Chem. 15* (1962) 457.
13. *Handbook of Chemistry and Physics*, 45th Ed., Chemical Rubber, Ohio 1964, p. F-4.
14. Bates, R. G. *Determination of pH*, Wiley, New York 1965, p. 403.
15. Lumme, P. and Tummavuori, J. *Acta Chem. Scand. 19* (1965) 617; Lumme, P., Lahermo, P. and Tummavuori, J. *Ibid.* p. 2175; Sallavo, K. and Lumme, P. *Suom. Kemistilehti B 40* (1967) 155; Tummavuori, J. and Lumme, P. *Acta Chem. Scand. 22* (1968) 2003; Lumme, P. and Virtanen, P. *Suom. Kemistilehti B 42* (1969) 333.
16. *Ref.* 14, p. 406.
17. Timimi, B. A. *Electrochim. Acta 19* (1974) 149.
18. Lumme, P. and Tummavuori, J. *Acta Chem. Scand. 27* (1973) 851 and 2287.

Received May 17, 1974.

Acta Chemica Scandinavica A 29 (1975) 125—135

Phthalic Acid as a Reagent in Inorganic Qualitative Analysis of Metal Ions. Part IV. Thermodynamics of the Complexation of Phthalate Ion with Divalent Copper, Nickel, and Cobalt Ions in Aqueous Sodium Perchlorate Solutions

PAAVO LUMME and ESKO KARI

Department of Chemistry, University of Jyväskylä, Jyväskylä, Finland

The complex formation of the phthalate ion with divalent copper, nickel, and cobalt ions was studied potentiometrically. The stability constants β_1 were evaluated for the three complexes as functions of the ionic strength at 25 °C. At a lower ionic strength the measurements were performed at 15 and 35 °C also. The second stability constant β_2 was derived for the copper complex only. The thermodynamic values of the stability constants were obtained by fitting the experimental data to semitheoretical equations and the thermodynamic quantities, the free energies, enthalpies, and entropies were calculated from these values.

The different precipitation behaviour of the copper(II) phthalate and benzoate complexes in the course of the qualitative analysis of metal ions is discussed.

In the previous parts of this series [1-3] we have discussed the application of phthalic acid in the inorganic qualitative analysis of metal ions,[1] the composition and structure of certain basic metal complexes [2] and the protonation equilibria of the phthalate ion.[3] To obtain a more comprehensive picture of the complex formation ability of the phthalate ion with metal ions we report in the present paper the results of our potentiometric studies on the complexation tendency of the phthalate ion with divalent copper, nickel and cobalt ions in aqueous sodium perchlorate solutions.

EXPERIMENTAL

Reagents and solutions. In addition to the reagents mentioned in the previous paper [3] the following reagents were used: copper(II) carbonate (Analyzed reagent, J. T. Baker), nickel(II) perchlorate, and cobalt(II) perchlorate (G. Frederick Smith Chemical Co.).

The copper(II) perchlorate solution was prepared by dropping conc. perchloric acid into a copper(II) carbonate water mixture and stirring well. The addition of the acid was ceased before all the carbonate had reacted. The solution was filtered through a glass-sinter (G4), made slightly acid (pH ~ 3) with a dilute perchloric acid and warmed to release the carbon dioxide. The solution was diluted with carbon dioxide-free water, and analyzed for copper electroanalytically in acidified conditions and for perchlorate by cation exchange.

The nickel(II) perchlorate solution was prepared by dissolving the salt in water, allowing the solution to stand for several days and filtering. The nickel concentration was determined gravimetrically with dimethylglyoxime and the perchlorate concentration as above.

The cobalt(II) perchlorate solution was made as the nickel(II) salt solution and analyzed for cobalt electroanalytically and for perchlorate as mentioned.

The preparation, rinsing and analyses of the other stock solutions were described in the previous part.[3] The concentrations of the stock solutions used were (20 °C): 5.440 M $NaClO_4$, 0.1738 M $Cu(ClO_4)_2$, 0.3716 M $Ni(ClO_4)_2$, 0.3897 M $Co(ClO_4)_2$, 0.1003 M $HClO_4$ and 0.09994—0.1004 M NaOH. The compositions of the solutions used in connection with the titrations are presented in Table 1.

The titrated solutions were prepared in a water thermostat at 20 °C. Sodium chloride and phthalic acid were weighed into the measuring flasks and allowed to dissolve into a small quantity of water. Sodium and metal perchlorate were then added as stock solutions, and the flask was filled with water to the mark.

Table 1. The composition of the solutions used in connection with the potentiometric titrations (20 °C). All studied solutions contained 0.01 M phthalic acid. The figures, except those for the ionic strengths, give the concentrations of $NaClO_4$ in mol/l (M).

Titrant	I	References		Studied solutions		
0.1 M NaOH		Electrode 0.01 M NaCl	Buffer 0.005 M $HClO_4$	0.005 M $Cu(ClO_4)_2$	0.01 M $Ni(ClO_4)_2$	0.01 M $Co(ClO_4)_2$
0.250	0.250	0.240	0.245	0.235	0.220	0.220
0.500	0.500	0.490	0.495	0.485	0.470	0.470
1.000	1.000	0.990	0.995	0.985	0.970	0.970
2.000	2.000	1.990	1.995	1.985	1.970	1.970

The temperature expansion of the solutions was assumed to be the same as that of pure water.[3]

Apparatus. These were described in the preceding part of this series.[3]

Measurements. To find the optimum conditions of the complex formations and the metal—ligand relations, several titrations were performed varying the metal ion concentrations and keeping the ligand concentration constant, and *vice versa*. The obtained titration curves were compared with that of phthalic acid alone at the same ionic strength.

Corresponding metal perchlorate solutions, containing no phthalic acid, were titrated at an ionic strength of 0.5 M to correct for the excess perchlorate anion concentration observed in the metal perchlorate solutions. The amount of sodium hydroxide needed to neutralize the solution was deduced from the sodium hydroxide consumption at the ordinary titration. The excesses of perchlorate anion found were the same as those obtained by cation exchange analyses of the stock solutions. The amounts of sodium perchlorate formed by the neutralization of the perchlorate anion excesses were in all cases, however, so small that they did not affect the ionic strengths of the titration solutions.

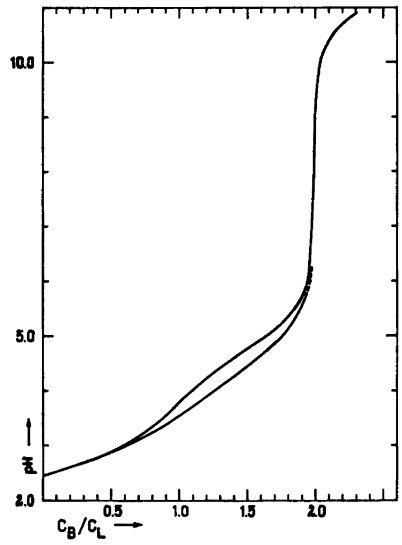

Fig. 1. The potentiometric titration curve of a solution 0.01 M in phthalic acid and 0.005 M in $Cu(ClO_4)_2$ at the ionic strength 0.5 and at 25 °C (the lower curve). The upper curve represents the titration of a solution 0.01 M in phthalic acid under the same conditions.

The ordinary complex titrations were performed at four ionic strengths at 25 °C. Titrations were also made at 15 and 35 °C to find the effect of the temperature variation, but only at the ionic strength of 0.5 M. The added increments of the sodium hydroxide solutions were 0.2 ml. The emf of the titrated solution was generally stabilized in 2 min. The titration was continued until the formation of metal hydroxide began. At the beginning and end of every titration, reference measurements were made with the reference buffer solution. If a difference greater than the potential reading accuracy (± 0.2 mV) was observed a new titration was performed.

The type of titration cell was the following:

Glass electrode	100 ml 0.01 M $C_8H_6O_4$ X M $M(ClO_4)_2$ $(I-3X)$ M $NaClO_4$	‖	
0.01 M NaCl $(I-0.01)$ M $NaClO_4$		|	Hg_2Cl_2, Hg

With this arrangement we attempted to minimize the diffusion potentials.

RESULTS AND DISCUSSION

Several titrations were done at ionic strength 0.5 M by varying the metal—ligand relation from tenfold excess of the metal ions to tenfold excess of the ligand ions in respect of each

others to find the optimum complex formation conditions and the corresponding metal—ligand relations. According to the calculations the best results for copper(II) complexes were obtained when the solution was 0.01 M in phthalic acid and 0.005 M in copper(II) perchlorate. Both β_1 and β_2 could be calculated from the measurements. In the first case a complex containing one and in the latter case two seven membered chelate rings are formed. A typical titration curve is presented in Fig. 1. In the case of a dicarboxylic ligand, the formation of dinuclear metal complexes may be suspected. However, the formation of the complexes of the form $(M_2L)^{2+}$ was found to be negligible, although a tenfold excess of the metal ion with respect to the ligand concentration was used. A complex of the type M_2L_2 is yet more unlikely at low conc. of copper(II) ions.

The complex formation tendency of nickel(II) and cobalt(II) ions with the phthalate ion is still weaker than that of copper(II) ion. No positive value of β_2 was obtained for these metals. However, comparable values for β_1 were obtained using 0.01 M solutions at the metal—ligand ratio 1:1. From Fig. 1 it is also seen that the formation of complexes of the form $(MHL)^+$ is slight, because the difference between the titration curves in Fig. 1 is not generally observed until the vicinity of the first equivalent point of phthalic acid is reached.

The assumed complex formation equilibria of phthalate ion ($C_8H_4O_4^{2-}=L^{2-}$) with divalent metal ions prevailing in aqueous solutions may therefore be presented as follows:

$$M^{2+}+L^{2-}\rightleftharpoons ML \quad (1)$$

$$ML+L^{2-}\rightleftharpoons ML_2^{2-} \quad (2)$$

The corresponding consecutive complex formation constants are

$$k_1=[ML]/[M^{2+}][L^{2-}] \quad (3)$$

$$k_2=[ML_2^{2-}]/[ML][L^{2-}] \quad (4)$$

and the gross stability constants

$$\beta_1=k_1 \quad (5)$$

$$\beta_2=[ML_2^{2-}]/[M^{2+}][L^{2-}]^2=\beta_1 k_2 \quad (6)$$

On the basis of the total concentrations of the phthalate ion (C_L), the metal ion (C_M), and the hydrogen ion (C_H) of the solution, and the equations (5) and (6) the concentration of the free ligand and the constants β_n may be calculated from the equations:

$$[L^{2-}]=(2C_L-C_B-[H^+])/P \quad (7)$$

$$\sum_{n=1}^{2}\{\beta_n[L^{2-}]^{n-1}(C_L-nC_M-Q[L^{2-}])\}+ \\ +(C_L/[L^{2-}])-Q=0 \quad (8)$$

where C_B is the total concentration of the added sodium hydroxide in the titrated solution and

$P=K_1[H^+]+2K_1K_2[H^+]^2$

$Q=1+K_1[H^+]+K_1K_2[H^+]^2$

and in which K_1 and K_2 are the first and second protonation constants of the phthalate ion determined in the previous part of this series.[3] Because of the low values of pH the hydroxyl ion concentration was neglected in the equations. The values of β_n were calculated by the method of least squares from eqn. (8).

The experimental results of the complex titrations and values of β_n calculated from eqn. (8) are given in Tables 2—7.

The values of the stability constants determined could be expressed as functions of the ionic strength by the semitheoretical equation:

$$\log \beta_n=\log \beta^\circ_n-\frac{8A\sqrt{I}}{1+\alpha\sqrt{I}}+BI \quad (9)$$

The values of $\log \beta_1$ in Tables 2—7 were fitted by the method of least squares with eqn. (9). The results for the three complexes studied are given at 25 °C in Table 8. Rough values of β_2 could be calculated only for the copper(II) phthalate complex. On the basis of the obtained values it can merely be said that $\log \beta^\circ_2$ of the copper(II) phthalate complex is of the order of 5.3 ± 0.3 at 25 °C, showing a weak tendency to form the complex CuL_2^{2-}. A corresponding tendency was not found for nickel(II) and cobalt(II) ions. The $\log \beta_1$ values showed the stability of the first complexes to decrease in the order: Cu > Ni > Co. The approximate thermodynamic values at 15 and 35 °C were extrapolated on the basis of eqn. (9) of the first complexes and are presented with the values of $\log \beta^\circ_1$ of the complexes at 25 °C in Table 9.

The values of $\log \beta_1$ of the first complexes are presented as functions of the square root of the ionic strength at 25 °C in Fig. 2.

Table 2. Potentiometric determination of the gross stability constants β_1 and β_2 of copper(II) phthalate complexes at 25 °C. Mean values of the constants are represented.

C_M $\times 10^3$	C_L $\times 10^3$	$[H^+]$ $\times 10^5$	$[L^{2-}]$ $\times 10^3$	C_M $\times 10^3$	C_L $\times 10^3$	$[H^+]$ $\times 10^5$	$[L^{2-}]$ $\times 10^3$
$I=0.2507$				$I=1.0018$			
4.358	8.716	4.906	1.468	4.358	8.716	4.646	1.991
4.350	8.701	4.486	1.550	4.350	8.701	4.298	2.075
4.343	8.686	4.102	1.634	4.343	8.686	3.945	2.177
4.335	8.670	3.721	1.733	4.335	8.670	3.635	2.270
4.328	8.655	3.389	1.827	4.328	8.655	3.324	2.381
4.320	8.640	3.075	1.929	4.320	8.640	3.051	2.482
4.313	8.626	2.801	2.025	4.313	8.626	2.790	2.592
4.305	8.611	2.551	2.119	4.305	8.611	2.541	2.710
4.298	8.596	2.314	2.221	4.298	8.596	2.324	2.814
4.291	8.581	2.100	2.321	4.291	8.581	2.116	2.926
4.283	8.566	1.890	2.437	4.283	8.566	1.920	3.043
				4.276	8.552	1.728	3.178
				4.269	8.537	1.556	3.305
$\log \beta_1 = 2.976 \pm 0.005$				$\log \beta_1 = 2.698 \pm 0.008$			
$\log \beta_2 = 4.448 \pm 0.018$				$\log \beta_2 = 3.731 \pm 0.071$			
$I=0.5024$				$I=2.0017$			
4.373	8.746	5.471	1.675	4.381	8.762	5.241	1.728
4.366	8.731	5.041	1.759	4.373	8.746	4.849	1.811
4.358	8.716	4.628	1.852	4.366	8.731	4.486	1.896
4.350	8.701	4.248	1.947	4.358	8.716	4.150	1.981
4.343	8.686	3.899	2.042	4.350	8.701	3.839	2.067
4.335	8.670	3.565	2.147	4.343	8.686	3.538	2.161
4.328	8.655	3.260	2.253	4.335	8.670	3.273	2.247
4.320	8.640	2.969	2.369	4.328	8.655	3.016	2.340
4.313	8.626	2.715	2.474	4.320	8.640	2.779	2.433
4.305	8.611	2.473	2.589	4.313	8.626	2.551	2.533
4.298	8.596	2.244	2.711	4.305	8.611	2.324	2.652
4.291	8.581	2.035	2.832	4.298	8.596	2.125	2.758
4.283	8.566	1.840	2.959	4.291	8.581	1.928	2.882
4.276	8.552	1.656	3.093	4.283	8.566	1.756	2.990
4.269	8.537	1.485	3.232	4.276	8.552	1.580	3.128
$\log \beta_1 = 2.795 \pm 0.007$				$\log \beta_1 = 2.633 \pm 0.014$			
				$\log \beta_2 = 4.144 \pm 0.050$			

The complex formation of phthalate ions with transition metal ions has been studied intensively as seen from Table 10, where a part of the results obtainable from the literature is represented for comparison. Systematic studies on the effects of the ionic strength and temperature are, however, fewer.

When inspecting the results in Table 10 the diversity of the stability constant values is observed to be rather high. For the copper(II) phthalate complexes our values of log β_1 are in best agreement with those of Yamasaki *et al.*[7] The difference between our values and those reported by Ghosh and Nair [9] is obviously at least partly due to the fact that these authors have taken into consideration the formation of $CuHL^+$ complexes which was disregarded in the present case as described above. A log β_1 value of about 0.97 at 25 °C was found [9] for the complex $CuHL^+$, which shows its weak stability and low tendency of formation.

By assuming the difference between the titration curves (Fig. 1) to be wholly due to the formation of MHL^+ complexes at the C_B/C_L values from zero to one we calculated from the titration curves at 25 °C the following maximum values of log β_1 for the MHL^+ complexes: 1.2 ± 0.4 (Cu), $I=0.473$; 0.72 ± 0.1 (Ni), $I=0.494$; 1.28 ± 0.04 (Co), $I=0.493$. Their effect in the pH ranges used in Tables 2–7 is negligible.

Table 3. Potentiometric determination of the gross stability constants β_1 and β_2 of copper(II) phthalate complexes at 15 and 35 °C. Mean values of the constants are represented.

$I=0.5034$, 15 °C				$I=0.5014$, 35° C			
C_M $\times 10^3$	C_L $\times 10^3$	$[H^+]$ $\times 10^5$	$[L^{2-}]$ $\times 10^3$	C_M $\times 10^3$	C_L $\times 10^3$	$[H^+]$ $\times 10^5$	$[L^{2-}]$ $\times 10^3$
4.367	8.734	4.461	1.903	4.349	8.699	4.887	1.748
4.359	8.719	4.083	2.006	4.342	8.684	4.482	1.840
4.352	8.704	3.736	2.111	4.334	8.669	4.110	1.933
4.344	8.688	3.433	2.208	4.327	8.654	3.755	2.035
4.337	8.673	3.130	2.324	4.319	8.639	3.443	2.129
4.329	8.658	2.876	2.420	4.312	8.624	3.122	2.249
4.322	8.643	2.632	2.526	4.304	8.609	2.863	2.343
4.314	8.629	2.380	2.662	4.297	8.594	2.596	2.463
4.307	8.614	2.161	2.786	4.290	8.579	2.380	2.552
4.299	8.599	1.977	2.883	4.282	8.565	2.142	2.688
4.292	8.584	1.781	3.024	4.275	8.550	1.942	2.800
4.285	8.569	1.604	3.159	4.267	8.535	1.741	2.939
				4.260	8.521	1.567	3.061
$\log \beta_1 = 2.764 \pm 0.007$				$\log \beta_1 = 2.849 \pm 0.008$ $\log \beta_2 = 3.569 \pm 0.136$			

Table 4. Potentiometric determination of the constant β_1 of nickel(II) phthalate complex at 25 °C. $C_M = C_L$. C_M was the same in all series.

$I=0.2492$			$I=0.5009$		$I=1.002$		$I=2.002$	
C_M $\times 10^3$	$[H^+]$ $\times 10^5$	$[L^{2-}]$ $\times 10^3$	$[H^+]$ $\times 10^5$	$[L^{2-}]$ $\times 10^3$	$[H^+]$ $\times 10^5$	$[L^{2-}]$ $\times 10^3$	$[H^+]$ $\times 10^5$	$[L^{2-}]$ $\times 10^3$
8.689	2.332	2.957	2.323	3.518	2.305	3.830	2.133	3.689
8.674	2.166	3.058	2.149	3.652	2.125	3.989	1.958	3.861
8.658	1.988	3.194	1.988	3.783	1.958	4.147	1.811	4.002
8.643	1.832	3.317	1.832	3.927	1.804	4.303	1.656	4.190
8.629	1.688	3.437	1.695	4.051	1.656	4.472	1.538	4.307
8.614	1.556	3.553	1.562	4.186	1.520	4.637	1.417	4.453
8.599	1.428	3.679	1.434	4.331	1.401	4.776	1.306	4.592
8.584	1.311	3.798	1.316	4.469	1.286	4.924	1.194	4.759
8.569	1.199	3.924	1.190	4.670	1.171	5.100	1.096	4.898
8.555	1.096	4.040	1.088	4.805	1.063	5.285	0.998	5.063
8.540	0.998	4.160	0.987	4.963	0.968	5.431	0.902	5.254
8.525	0.902	4.299	0.859	5.104	0.868	5.645	0.806	5.492
8.511	0.809	4.454	0.806	5.263	0.778	5.835	0.734	5.601
8.496	0.726	4.589	0.717	5.458	0.698	5.995	0.656	5.791
8.482	0.646	4.733	0.636	5.644	0.614	6.235	0.572	6.089
8.468	0.568	4.900	0.542	6.019	0.546	6.353	0.507	6.251
$\log \beta_1 = 1.892 \pm 0.009$			1.719 ± 0.023		1.560 ± 0.011		1.631 ± 0.020	

The formation of the complex CuL_2^{2-} is so weak and highly dependent on the metal—ligand ratio in the experiments that the deviations between the log β_2 values are not surprising (Table 10).

Bobtelsky and Bar-Gadda [13] determined spectrophotometrically, using Job's method, the value 3.55 of log k_2 for the second stepwise stability constant of the complex CuL_2^{2-} at the ionic strength about 0.4 and 18—25 °C. From our values of log β_2—log β_1 we obtain an approximate value of 1.2 for log k_2. The value of 3.55 must be too high.

For the nickel(II) phthalate complex the

Table 5. Potentiometric determination of the stability constant β_1 of nickel(II) phthalate complex at 15 and 35 °C. $C_M = C_L$.

$I=0.5020$, 15 °C			$I=0.500$, 35 °C		
$C_M \times 10^3$	$[H^+] \times 10^5$	$[L^{2-}] \times 10^3$	$C_M \times 10^3$	$[H^+] \times 10^5$	$[L^{2-}] \times 10^3$
8.707	2.134	3.794	8.672	2.301	3.555
8.691	1.953	3.981	8.657	2.126	3.694
8.676	1.824	4.084	8.642	1.972	3.817
8.661	1.710	4.165	8.627	1.822	3.951
8.646	1.565	4.343	8.612	1.683	4.082
8.632	1.438	4.501	8.597	1.544	4.239
8.617	1.316	4.670	8.582	1.416	4.390
8.602	1.200	4.853	8.567	1.298	4.535
8.587	1.094	5.026	8.553	1.186	4.686
8.572	0.993	5.209	8.538	1.079	4.845
8.558	0.905	5.355	8.524	0.989	4.951
8.543	0.819	5.525	8.509	1.055	4.323
8.529	0.731	5.740	8.494	0.802	5.295
8.514	0.661	5.857	8.480	0.721	5.429
8.499	0.591	6.008	8.466	0.637	5.634
8.485	0.517	6.237	8.451	0.563	5.799
$\log \beta_1 = 1.550 \pm 0.023$			$\log \beta_1 = 1.650 \pm 0.125$		

Table 6. Potentiometric determination of the stability constant β_1 of cobalt(II) phthalate complex at 25 °C. $C_M = C_L$. C_M was the same in all series.

	$I=0.2505$		$I=0.5028$		$I=1.003$		$I=2.0012$	
$C_M \times 10^3$	$[H^+] \times 10^5$	$[L^{2-}] \times 10^3$	$[H^+] \times 10^5$	$[L^{2-}] \times 10^3$	$[H^+] \times 10^5$	$[L^{2-}] \times 10^3$	$[H^+] \times 10^5$	$[L^{2-}] \times 10^3$
8.709	2.397	3.040	2.369	3.648	2.444	3.817	2.270	3.658
8.694	2.217	3.163	2.183	3.809	2.261	3.969	2.084	3.838
8.679	2.043	3.299	2.035	3.924	2.100	4.104	1.935	3.972
8.664	1.883	3.435	1.876	4.084	1.935	4.269	1.790	4.119
8.649	1.742	3.555	1.742	4.208	1.790	4.415	1.650	4.281
8.634	1.612	3.671	1.605	4.362	1.643	4.592	1.538	4.387
8.619	1.485	3.798	1.468	4.547	1.514	4.747	1.412	4.557
8.604	1.368	3.920	1.342	4.727	1.390	4.913	1.291	4.741
8.589	1.256	4.051	1.242	4.844	1.271	5.091	1.190	4.880
8.575	1.148	4.190	1.144	4.968	1.158	5.280	1.088	5.048
8.560	1.050	4.320	1.034	5.180	1.058	5.435	0.998	5.184
8.546	0.957	4.455	0.942	5.337	0.960	5.617	0.895	5.430
8.531	0.865	4.611	0.851	5.519	0.868	5.802	0.815	5.575
8.516	0.778	4.768	0.760	5.747	0.778	6.010	0.728	5.810
8.502	0.698	4.923	0.687	5.881	0.693	6.238	0.653	5.997
8.487	0.626	5.050	0.607	6.121	0.614	6.456	0.584	6.175
$\log \beta_1 = 1.754 \pm 0.011$			1.492 ± 0.023		1.449 ± 0.020		1.498 ± 0.023	

agreement between the log β_1 values is on the other hand better (Table 10). In the case of the cobalt(II) phthalate complex our value of log β_1 agrees best with the previously reported value [10] at 35 °C.

In this context it is interesting to notice that Evans and Monk [14] in connection with their studies on association constants of zinc dicarboxylates in water have pointed out that owing to the formation of metal chloride com-

Table 7. Potentiometric determination of the stability constant β_1 of cobalt(II) phthalate complex at 15 and 35 °C. $C_M = C_L$.

$I=0.5039$, 15 °C			$I=0.5018$, 35 °C		
$C_M \times 10^3$	$[H^+] \times 10^5$	$[L^{2-}] \times 10^3$	$C_M \times 10^3$	$[H^+] \times 10^5$	$[L^{2-}] \times 10^3$
8.727	2.370	3.604	8.693	2.417	3.575
8.712	2.196	3.744	8.677	2.233	3.724
8.697	2.042	3.866	8.662	2.063	3.872
8.682	1.876	4.036	8.647	1.913	4.003
8.667	1.731	4.186	8.632	1.768	4.147
8.652	1.584	4.370	8.617	1.633	4.287
8.637	1.456	4.532	8.603	1.509	4.422
8.622	1.343	4.669	8.588	1.389	4.567
8.607	1.229	4.837	8.573	1.274	4.721
8.593	1.121	5.016	8.558	1.164	4.885
8.578	1.026	5.163	8.544	1.063	5.038
8.563	0.935	5.316	8.529	0.971	5.175
8.548	0.852	5.449	8.514	0.877	5.355
8.534	0.767	5.628	8.500	0.793	5.513
8.519	0.686	5.826	8.485	0.713	5.666
8.505	0.613	5.993	8.471	0.640	5.807
$\log \beta_1 = 1.505 \pm 0.011$			$\log \beta_1 = 1.434 \pm 0.014$		

Table 8. The values of $\log \beta_1$ of the copper(II), nickel(II) and cobalt(II) phthalate complexes calculated from eqns. (8) and (9) at different ionic strengths and at 25 °C. The constants α and B of eqn. (9) are also given.

Copper			Nickel			Cobalt		
I	$\log \beta_1$ eqn. (8)	$\log \beta_1$ eqn. (9)	I	$\log \beta_1$ eqn. (8)	$\log \beta_1$ eqn. (9)	I	$\log \beta_1$ eqn. (8)	$\log \beta_1$ eqn. (9)
0.2507	2.976	2.971	0.2492	1.892	1.901	0.2505	1.754	1.735
0.5024	2.795	2.810	0.5009	1.719	1.699	0.5028	1.492	1.533
1.0018	2.698	2.687	1.0020	1.560	1.574	1.0029	1.449	1.419
2.0017	2.633	2.636	2.0002	1.631	1.627	2.0012	1.498	1.504
$\alpha=1.879$, $B=0.1096$			$\alpha=1.204$, $B=0.3375$			$\alpha=1.144$, $B=0.3869$		

plexes in solutions there is obviously no preference in precision to use the H_2,Pt—Ag,AgCl electrode system (without liquid junction potentials) with emf measurement readings to ± 0.01 mV compared with the glass electrode—saturated calomel electrode system (with liquid junction potentials) with emf read to ± 0.1 mV when doing the stability constant determinations of metal complexes. The chloride complex formation tendency of copper(II), nickel(II), and cobalt(II) ions is likewise of about the same order as that of the zinc(II) ions.[15]

The thermodynamic values of the stability constants were assumed to depend on the absolute temperature according to the equation:

$$\log \beta^\circ_n = a + b/T \qquad (10)$$

where a and b are parameters obtained by fitting the data from Table 9 to the equation. The values of the constants are:

Complex	a	$-b \times 10^2$
Copper	5.9199	5.7279
Nickel	5.3695	6.9761
Cobalt	2.6967	−0.6037

The dependence of the experimental values of $\log \beta^\circ_1$ of the copper(II) phthalate complex on $1/T$ seems to be almost linear (Fig. 3). For

Table 9. The thermodynamic values of the stability constants of the first copper(II), nickel(II), and cobalt(II) phthalate complexes calculated from eqn. (9) at different temperatures. The values [4] of the constant A of eqn. (9) are also represented.

°C	A	Cu log β°_1	Ni log β°_1	Co log β°_1
15	0.5028	3.932	2.918	2.886
25	0.5115	3.999	3.093	2.941
35	0.5211	4.061	3.073	2.871

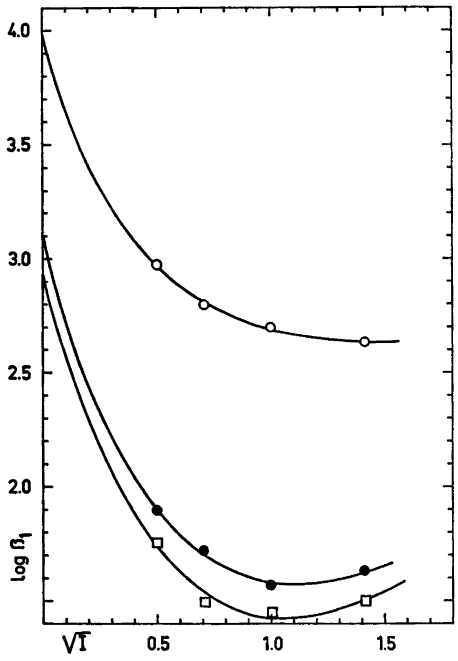

Fig. 2. The values of log β_1 of the copper(II), nickel(II), and cobalt(II) phthalate complexes represented as functions of the square root of the ionic strength at 25 °C. Curve: ○, copper; ●, nickel; □, cobalt.

nickel(II) and cobalt(II) phthalate complexes the dependence of log β°_1 on temperature is more uncertain.

The thermodynamic quantities, free energies, enthalpies, and entropies of the complex formation equilibria were calculated on the basis of the constants a and b from eqns. (11)–(13):

$$\Delta G^\circ = -2.303\, R(aT+b) \quad (11)$$

$$\Delta H^\circ = -2.303\, Rb \quad (12)$$

$$\Delta S^\circ = (\Delta H^\circ - \Delta G^\circ)/T \quad (13)$$

where R is the general gas constant 8.31433 J K^{-1} mol^{-1} and T the absolute temperature. The results are given in Table 11.

The thermodynamics of the formation of the copper(II), nickel(II), and cobalt(II) phthalate complexes has been studied by Nair *et al.*[9,10,16] only. Their values of the thermodynamic quantities at 25 °C (?) were converted to SI units [17] by assuming them to be expressed in thermochemical calories (factor 4.184). The converted values are given for comparison in Table 12.

By comparing the present results in Table 11 with those of Nair *et al.* in Table 12 they can be said to be only roughly of the same order of magnitude, except for ΔG° and the copper(II) complex. It is interesting to observe that the data (Table 12) for the copper(II) complex are from the later calorimetric studies of Parthasarathy and Nair [16] who did not take into account the formation of $CuHL^+$ (*cf.* Table 10 and above), whereas the data for the cobalt(II) and nickel(II) complexes were obtained by Desai and Nair [10] from the temperature coefficient measurements performed with a H,Pt—Ag,AgCl electrode system.

The formations of the copper(II) and nickel(II) phthalate complexes are endothermic reactions; the enthalpy changes (ΔH) are positive and unfavorable from the viewpoint of complex formation and the stability of the complex (*cf.* Table 11). The entropy effects (ΔS), however, are also positive (and dominating) which implies free release of water molecules of hydration in the complex formation and obviously makes this possible and increases the stability of the complexes. The stabilities of the complexes increase only slightly with the increasing temperature.

In the case of the cobalt(II) phthalate complex ΔH is not so unfavorable for complex formation as in the former cases, but the entropy change (ΔS) is lower and means lower liberation of water molecules of hydration and therefore also lower stability of the complex.

Hamm *et al.*[18] concluded on the basis of their kinetic measurements (at 25 °C) on the formation of chromium(III) complexes with dicar-

Table 10. Comparison of the values of log β_n of the copper(II), nickel(II), and cobalt(II) complexes of the phthalate ion determined by different workers.

Metal ion	°C	Ionic strength (added salt)	log β_1	log β_2	Method	Ref.
Cu^{2+}	18	0.01		4.51	glass el.	5
	25	→0		4.06	glass el.	6
	25	0.1 (KNO_3)	3.10		glass el.	7
	25	0.1($NaClO_4$)	3.20		glass el.	this work
	25	→0	3.98		glass el.	7
	25	→0	4.00	5.34±0.3	glass el.	this work
	—	→0	3.46	4.83	spectrophotom.	8
	25	0 corr.	3.10		glass el., Ag−AgCl	9
	25	0 corr.	4.038		calorimetric	16
	25	0 corr.	3.14		solubility	9
	35	0 corr.	3.50		solubility	9
	35	→0	4.06		glass. el	this work
Ni^{2+}	15	0 corr.	2.911		H,Ag-AgCl	10
	15	→0	2.92		glass el.	this work
	25	0.1 (KNO_3)	2.14		glass el.	7
	25	0.1 ($NaClO_4$)	2.19		glass el.	this work
	25	→0	3.09		glass el.	this work
	25	0 corr.	2.95		H,Ag−AgCl	10
	35	0 corr.	2.996		H,Ag−AgCl	10
	35	→0	3.07		glass el.	this work
Co^{2+}	15	0 corr.	2.795		H,Ag−AgCl	10
	15	→0	2.89		glass el.	this work
	25	0 corr.	2.83		H,Ag−AgCl	10
	25	→0	2.94		glass el.	this work
	25	0 corr.	2.76±0.06	3.66±0.1	ion exchange	11
	25	0 corr.	2.86±0.02		glass el.	12
	35	→0	2.87		glass el.	this work
	35	0 corr	2.885		H,Ag−AgCl	10

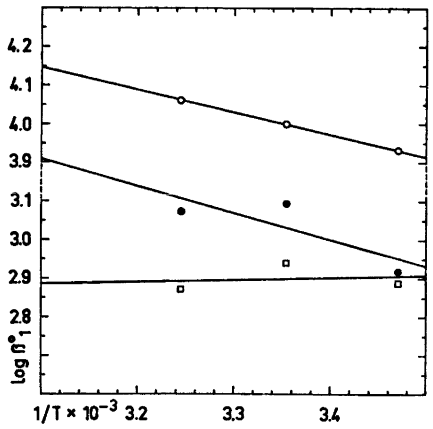

Fig. 3. The values of log β°_1 of the copper(II), nickel(II), and cobalt(II) phthalate complexes represented as functions of the reciprocal absolute temperature. Curve: ○, copper; ●, nickel; □, cobalt.

boxylic anions, among others with phthalate ion, that the escape of a hydration water molecule is the slowest and rate determining step in the complex formation. Possibly we can assume the situation to be the same with the other metal phthalate complexes and so the liberation tendency of the hydration water molecules is parallel with the complex formation tendency, the complex stability and the entropy effect.

Because we do not know exactly the hydration degree of the species in eqns. (1) or (2) and the numbers of the liberated water molecules in the complex formation reactions and the inaccuracy of the present data a further going consideration [19,20] of the thermodynamic quantities would be inappropriate.

When considering the analytical method [1] and the application of benzoic acid [21] instead of phthalic acid, the observed difficulties with

Table 11. The values of log β°_1 calculated from eqn. (10) and the values of the free energy, enthalpy, and entropy calculated from the relations (11)–(13) and for the first complexation equilibria of the phthalate ion with the divalent copper, nickel, and cobalt ions.

°C	log β°_1	$-\Delta G^\circ$ (kJ mol^{-1})	ΔH° (kJ mol^{-1})	ΔS° (J K^{-1} mol^{-1})	
Copper(II) phthalate complex					
15	3.932	21.70		113	
25	3.999	22.83	11.0	113	
35	4.061	23.96		113	
Nickel(II) phthalate complex					
15	2.949	16.3		103	
25	3.030	17.3	13.4	103	
35	3.106	18.3		103	
Cobalt(II) phthalate complex					
15	2.906	16.0		52	
25	2.899	16.6	−1.2	52	
35	2.893	17.1		52	
	±0.03	±0.2	±2	±10	Mean accuracy or better

Table 12. The thermodynamic quantities of the first copper(II), nickel(II), and cobalt(II) phthalate complexes converted from the literature [9,10,16] at 25 °C (?).

Complex (ML)	$-\Delta G^\circ$ (kJ mol^{-1})	ΔH° (kJ mol^{-1})	ΔS° (J K^{-1} mol^{-1})	ΔC_p° (J K^{-1} mol^{-1})
Copper	23.05	8.41	105.4	—
Nickel	16.84±0.02	7.38±0.21	81.2±1.3	285±84
Cobalt	16.15±0.02	7.82±0.21	80.3±0.8	213±63

benzoic acid as a reagent,[1] may obviously be explained now. The copper(II) benzoate complex [7] is about half as stable (log $\beta_1 = 1.6$ at 25 °C and $I = 0.1$) as the corresponding phthalate complex (*cf.* Table 10), but the enthalpy (ΔH) of the formation of the copper(II) benzoate complex is about zero [22] and the entropy change (ΔS) about one third lower [22] in the temperature range 25–35 °C.

On the other hand the solubility products (K_s) of the copper(II) bisbenzoate and copper(II) oxalate may be calculated to be 3.5×10^{-8} (20 °C) and 2.53×10^{-8} (18 °C), respectively, in the saturated water solutions of the salts on the bases of the given solubility data.[23] The solubility product of the copper(II) diphthalato compound is not known, but may be expected to be higher than the above values because the solubility product of the copper(II) tetrachlorophthalate is $< 7.5 \times 10^{-6}$ and those of the copper(II) salts of the *ortho*-derivatives of benzoic acid are in general considerably higher at 25 °C (Ref. 23, p. 917). Therefore the higher complexation tendency of the phthalate ions with the copper(II) ions (*cf.* Table 10, although in general the formation tendency of the lower complexes increases the insolubility of the solid higher complexes [24]), the higher solubility and the property of the copper(II) diphthalato complex to form highly supersaturated solutions [5] (broken with a strong alkali [1] when precipitating the copper(II) ions as $Cu(OH)_2$ ($pK^\circ_s = 19.66$ (25 °C), Refs 15 and 23, p. 959) in the fourth cation group [1]) are obviously due to the fact that the copper(II) diphthalato complex does not separate as a precipitate in the course of the qualitative analysis of metal ions [1] in the second and further in the fifth group (the

phthalate ions obviously have a greater ability than the benzoate ions to prevent copper(II) hydroxide to go as colloidal (soluble hydroxy complexes) into the fifth group [1]) depending still on the salt composition and pH of the solution, as does the copper(II) benzoate. For precipitation of different forms of the copper(II) and cobalt(II) phthalate compounds; *cf.* Refs. 5, 25—27 and 28.

The opinions presented above are also in agreement with the idea that the bonds between the metal and the ligand (M—O) in the complexes are mainly ionic by nature, because the precipitated iron(III) and chromium(III) phthalate complexes showed strong bands at 1530—1540 cm^{-1} due to the asymmetric CO_2^- stretching band.[2]

Acknowledgements. The authors are indebted to Mr. M. Peacock, M. A. for correcting the English of this paper and to Mr. I. Laitinen and R. Vähälä for valuable cooperation in preparing the computer programs for IBM 1130 and Honeywell 1642 computers. Financial support from the National Research Council for Sciences (Finland) is also gratefully acknowledged.

REFERENCES

1. Lumme, P. and Tummavuori, J. *Acta Chem. Scand. 27* (1973) 851.
2. Lumme, P. and Tummavuori, J. *Acta Chem. Scand. 27* (1973) 2287.
3. Lumme, P. and Kari, E. *Acta Chem. Scand. 29* (1975) 117.
4. Bates, R. G. *Determination of pH*, Wiley, 1965, p. 406.
5. Riley, H. L. *J. Chem. Soc.* (1929) 1307.
6. Peacock, J. M. and James, J. C. *J. Chem. Soc.* (1951) 2233.
7. Yasuda, M., Suzuki, K. and Yamasaki, K. *J. Phys. Chem. 60* (1956) 1649.
   Yasuda, M., Yamasaki, K. and Ohtaki, M. *Bull. Chem. Soc. Jap. 33* (1960) 1067.
8. Graddon, D. P. *J. Inorg. Nucl. Chem. 5* (1958) 219.
9. Ghosh, R. and Nair, V. S. K. *J. Inorg. Nucl. Chem. 32* (1970) 3033.
10. Desai, I. R. and Nair, V. S. K. *J. Chem. Soc.* (1962) 2360.
11. Seys, R. G. and Monk, C. B. *J. Chem. Soc.* (1965) 2452.
12. Monk, C. B. *J. Chem. Soc.* (1965) 2456.
13. Bobtelsky, M. and Bar-Gadda, I. *Bull. Soc. Chim. Fr.* (1953) 276.
14. Evans, C. E. and Monk, C. B. *Trans. Faraday Soc. 66* (1970) 1491.
15. Sillén, L. G. and Martell, A. E. *Stability Constants of Metal-Ion Complexes*, Special Publ. Nos. 17 and 25, The Chemical Society, London 1964 and 1971.
16. Parthasarathy, S. and Nair, V. S. K. *Thermochim. Acta 2* (1971) 69.
17. McGlashan, M. L. *Pure Appl. Chem. 21* (1970) 1.
18. Hamm, R. E., Johnson, R. L., Perkins, R. H. and Davis, R. E. *J. Amer. Chem. Soc. 80* (1958) 4469.
19. Nancollas, G. H. *Interactions in Electrolyte Solutions*, Elsevier, Amsterdam 1966.
20. Anderegg, G. *Helv. Chim. Acta 51* (1968) 1856.
21. West, P. W. and Vick, M. M. *Qualitative Analysis and Analytical Chemical Separations*, 2nd Ed., MacMillan, New York 1959.
22. May, R. M. and Jones, M. M. *J. Inorg. Nucl. Chem. 24* (1962) 511.
23. Seidell, A. and Linke, W. F. *Solubilities of Inorganic and Metal-Organic Compounds*, Vol. I, 4th Ed., American Chemical Society, Washington 1958, pp. 916 and 924.
24. Lumme, P. *Ann. Acad. Sci. Fenn. Ser. A 2*, No. 68 (1955) pp. 12 and 67.
25. Schimizu, I., Tsuchiya, R. and Kyuno, E. *Bull. Chem. Soc. Jap. 40* (1967) 1162.
26. Cingi, M. B., Guastini, C., Muratti, A. and Nardelli, M. *Acta Crystallogr. B 25* (1969) 1833.
27. Prout, C. K., Carruthers, J. R. and Rossotti, F. J. C. *J. Chem. Soc. A* (1971) 3350.
28. Acheson, R. J. and Galwey, A. K. *J. Inorg. Nucl. Chem. 30* (1968) 2383.

Received May 17, 1974.

Acta Chemica Scandinavica A 29 (1975) 136—140

The Crystal and Molecular Structure of 2-Methyl-6a-thiathiophthene

LEIF J. SÆTHRE AND ASBJØRN HORDVIK*

Department of Chemistry, University of Bergen, N-5000 Bergen, Norway

2-Methyl-6a-thiathiophthene crystallizes in the monoclinic space group $P2_1/c$ with four molecules in a unit cell of dimensions: $a=5.9558(9)$, $b=7.8563(8)$, $c=16.014(4)$ Å, and $\beta=91.31(2)°$.

The structure was solved by direct methods and refined by full matrix least squares.

Unequal S—S distances occur in the linear three sulphur sequence of the molecule, *i.e* S(1)—S(6a)=2.4311(16) and S(6a)—S(6)= 2.3076(17) Å, as predicted by the results from CNDO/2 calculations.

The 6a-thiathiophthene system is almost planar, and other bond lengths in the molecule are, S(1)—C(2) = 1.698(4), S(6a)—C(3a) = 1.763(5), S(6)—C(5)=1.681(5), C(2)—C(3)= 1.362(7), C(3)—C(3a)=1.408(6), C(3a)—C(4)= 1.428(7), C(4)—C(5)=1.367(7), and C(2)—C(6)= 1.526(8) Å. The S—S, S—C, and C—C bond lengths have been corrected for libration.

CNDO/2 calculations on 6a-thiathiophthene (I) and on its mono-methyl derivatives have been carried out,[1] *cf.* Fig. 1. The change in CNDO/2 total energy as a function of the S(1)—S(6a) bond length shows that a 2-methyl group causes a lengthening of the S(1)—S(6a) bond, and that a 3-methyl group causes a shortening of this bond relative to the symmetric structure of the unsubstituted compound.

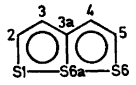

(I)

The present structure study of 2-methyl-6a-thiathiophthene has been carried out in order to test the CNDO/2 predictions.

* Present address: University of Tromsø, Box 790, N-9001 Tromsø, Norway.

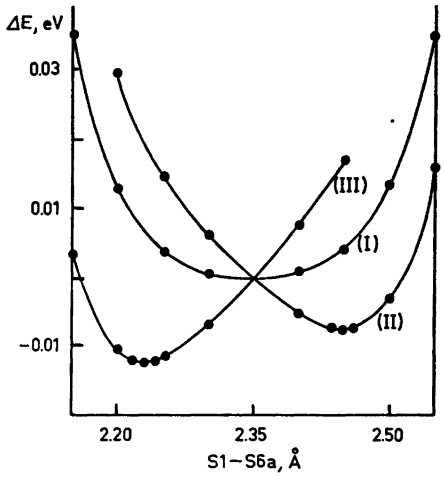

Fig. 1. The change ΔE in CNDO/2 total energy for 6a-thiathiophthene (I), 2-methyl-6a-thiathiophthene (II), and 3-methyl-6a-thiathiophthene (III) as a function of the S(1)—S(6a) bond length.

STRUCTURE ANALYSIS AND REFINEMENT

A brief account of the structure analysis has been reported,[2] and a more detailed description is given here.

Crystals of 2-methyl-6a-thiathiophthene from cyclohexane are orange red plates with {001} predominant.

CRYSTAL DATA

$C_6H_6S_3$ M.w.=174.31

Monoclinic, systematic extinctions: *h0l* when $l=2n+1$;

Table 1. Atomic coordinates in fractions of corresponding cell edges. The standard deviations given in parentheses refer to the last digits of the respective values.

Atom	x	y	z
S(1)	0.22743(18)	0.05761(19)	0.38631(7)
S(6a)	0.04167(18)	0.05576(16)	0.25001(8)
S(6)	−0.12664(19)	0.06320(19)	0.11928(7)
C(2)	0.4320(7)	0.1880(6)	0.3533(3)
C(3)	0.4300(8)	0.2372(6)	0.2721(3)
C(3a)	0.2585(7)	0.1871(5)	0.2158(3)
C(4)	0.2494(9)	0.2368(7)	0.1304(3)
C(5)	0.0750(8)	0.1851(6)	0.0801(3)
C(6)	0.6129(11)	0.2495(11)	0.4146(4)
H(3)	0.536(6)	0.319(4)	0.2531(27)
H(4)	0.363(7)	0.305(6)	0.1166(29)
H(5)	0.064(6)	0.224(5)	0.0240(24)
H(61)	0.667(11)	0.169(9)	0.444(4)
H(62)	0.751(9)	0.278(7)	0.388(4)
H(63)	0.558(9)	0.340(8)	0.442(4)

$0k0$ when $k=2n+1$
Space group $P2_1/c$ with $Z=4$
$a=5.9558(9)$ Å, $b=7.8563(8)$ Å, $c=16.014(4)$ Å,
$\beta=91.31(2)°$
$V=749.1$ Å^3
$D_{calc}=1.545$ g/cm^3, $D_{exp}=1.54$ g/cm^3
$\mu_{MoK\alpha}=8.56$ cm^{-1}

The crystal used for all X-ray measurements had the shape of a rectangular prism, and the dimensions were $0.15\times0.17\times0.05$ mm along [110], [$\bar{1}$10], and [001], respectively.

Unit cell dimensions and intensity data were measured on a paper-tape controlled Siemens AED diffractometer using Mo$K\alpha$ radiation.

A least squares procedure on the 2θ values of 16 high order reflections, measured at 20 °C, gave the cell dimensions quoted above.

The intensities were collected by means of the five-value scan technique.[3] 790 independent reflections, measured within $\theta=27°$, and for which the net count was greater than 2.5 times the respective standard deviation in the net count, were accepted as observed. Unobserved reflections were neglected in order to save computing time.

Lp corrections and absorption corrections were applied, the latter according to a procedure of Coppens, Leiserowitz and Rabinovich.[4] A grid of $12\times14\times4$ points along a, b, and c, respectively, was used.

Observed structure factors were put on an absolute scale [5] and converted to normalized structure factors by means of a program written by Shiono.[6] The scattering factors used for sulfur and carbon were those given in the

Table 2. Temperature parameters U_{ij} (Å^2) for sulfur and carbon, and U (Å^2) for hydrogen. The expressions used are exp $\{-2\pi^2(h^2a^{*2}U_{11}+\cdots2hka^*b^*U_{12}+\cdots)\}$ and exp $\{-8\pi^2U(\sin^2\theta/\lambda^2)\}$. All values are multiplied by 10^4. Standard deviations in parentheses refer to the last digits of the respective values.

Atom	U_{11}	U_{22}	U_{33}	U_{12}	U_{23}	U_{13}
S(1)	467(7)	431(7)	384(7)	−43(7)	37(8)	43(5)
S(6a)	356(5)	338(6)	459(6)	−38(8)	8(9)	65(5)
S(6)	444(7)	510(8)	479(7)	−37(8)	−33(9)	−68(5)
C(2)	343(28)	348(26)	422(29)	63(20)	27(23)	14(24)
C(3)	402(31)	333(29)	402(30)	−80(25)	24(23)	25(25)
C(3a)	303(27)	280(26)	432(30)	−28(20)	−89(23)	112(24)
C(4)	433(29)	426(30)	377(30)	−58(25)	−9(23)	108(24)
C(5)	570(36)	467(30)	401(31)	69(24)	100(27)	−54(28)
C(6)	446(38)	689(45)	578(39)	−62(36)	−65(37)	−76(33)

Atom	U	Atom	U	Atom	U
H(3)	300(110)	H(5)	420(130)	H(62)	740(210)
H(4)	490(150)	H(61)	1240(300)	H(63)	920(240)

Table 3. Librational tensor L, from the rigid-body analysis of 2-methyl-6a-thiathiophthene.

Eigenvalues		Eigenvectors		
L	37.5 (°) [a]	4131	864	9066
	9.3	8160	−4770	−3264
	8.6	4043	8746	−2676

[a] Direction cosines × 10^4 relative to *a*, *b*, and *c**, respectively.

Table 4. Bond lengths (*l*) in 2-methyl-6a-thiathiophtene. The values (*l'*) have been corrected for rigid-body libration. Standard deviations in parentheses refer to the last digits of the respective values.

Bond	*l'* (Å)	*l* (Å)
S(1)−S(6a)	2.4311	2.4244(16)
S(6a)−S(6)	2.3076	2.3012(17)
S(1)−C(2)	1.698	1.686(4)
S(6a)−C(3a)	1.763	1.750(5)
S(6)−C(5)	1.681	1.670(5)
C(2)−C(3)	1.362	1.356(7)
C(3)−C(3a)	1.408	1.403(6)
C(3a)−C(4)	1.428	1.422(7)
C(4)−C(5)	1.367	1.362(7)
C(2)−C(6)	1.526	1.520(8)
C(3)−H(3)		0.96(4)
C(4)−H(4)		0.89(5)
C(5)−H(5)		0.95(4)
C(6)−H(61)		0.85(7)
C(6)−H(62)		0.96(6)
C(6)−H(63)		0.90(6)

International Tables.[7] For hydrogen, the scattering factor given by Stewart *et al.*[8] was used.

The structure was solved by direct methods [9] and refined by full matrix least squares procedure (see for example Ref. 10). With anisotropic temperature factor coefficients for all atoms except hydrogen, the final *R* factor is 0.035.

Final atomic coordinates from the least squares refinement are listed in Table 1, and the temperature parameters are listed in Table 2. The final list of structure factors is available on request.

An analysis of the thermal parameters of the S and C atoms, assuming the molecule to be a rigid body, was carried out according to the method by Schomaker and Trueblood.[11] The librational tensor arrived at is given in Table 3. The r.m.s. difference between observed and calculated U_{ij}' s was found to be 0.0032 Å^2 as compared with the value 0.0041 Å^2 for the e.s.d. of U_{ij}. The S−S, S−C, and C−C bond lengths have been corrected for rigid body libration.[12]

All the calculations mentioned above were carried out on an IBM 360/50H computer. The programs, with a few exceptions, originate from the Weizmann Institute of Science, Rehovoth, Israel, and have been modified for the 360 by D. Rabinovich, L. M. Milje and K. Åse. The diffractometer programs have been written by K. Maartmann-Moe.

Table 5. Bond angles ∠(ijk) in 2-methyl-6a-thiathiophthene. The standard deviations given in parentheses refer to the last digits of the respective values.

i	j	k	∠(ijk)°	i	j	k	∠(ijk)°
S(1)	S(6a)	S(6)	177.77(6)	C(3a)	C(4)	C(5)	119.9(4)
S(1)	S(6a)	C(3a)	87.32(16)	C(2)	C(3)	H(3)	120(3)
S(6a)	S(6)	C(5)	93.12(18)	H(3)	C(3)	C(3a)	118(3)
C(2)	S(1)	S(6a)	92.25(16)	C(3a)	C(4)	H(4)	113(3)
C(3a)	S(6a)	S(6)	90.55(16)	H(4)	C(4)	C(5)	127(3)
S(1)	C(2)	C(6)	119.8(4)	C(4)	C(5)	H(5)	120(3)
S(1)	C(2)	C(3)	118.9(3)	H(5)	C(5)	S(6)	120(3)
S(6a)	C(3a)	C(3)	119.8(3)	C(2)	C(6)	H(61)	112(5)
S(6a)	C(3a)	C(4)	116.8(3)	C(2)	C(6)	H(62)	113(3)
S(6)	C(5)	C(4)	119.6(4)	C(2)	C(6)	H(63)	108(4)
C(6)	C(2)	C(3)	121.3(4)	H(61)	C(6)	H(62)	96(6)
C(2)	C(3)	C(3a)	121.7(4)	H(62)	C(6)	H(63)	111(5)
C(3)	C(3a)	C(4)	123.5(4)	H(61)	C(6)	H(63)	117(6)

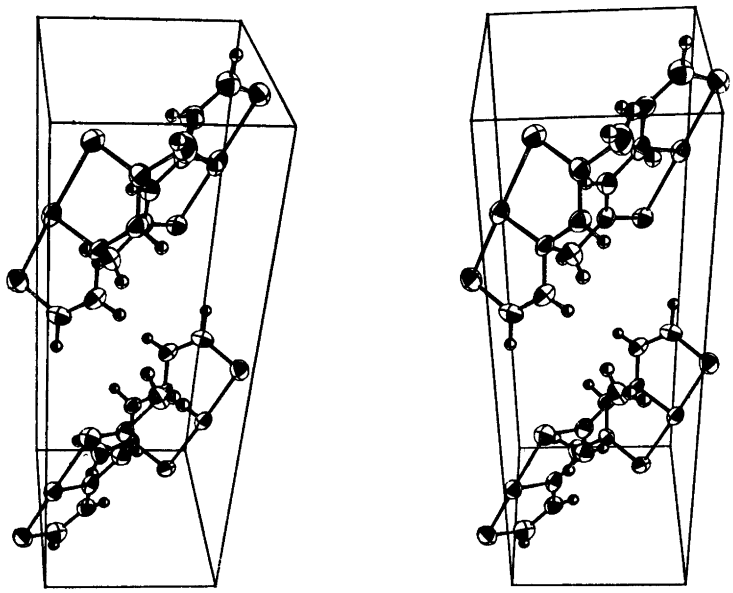

Fig. 2. A stereoscopic view of the arrangement of 2-methyl-6a-thiathiophthene molecules in the unit cell.

DESCRIPTION AND DISCUSSION OF THE STRUCTURE

Bond lengths and angles in the 2-methyl-6a-thiathiophthene molecule, as calculated from the positional parameters in Table 1, are listed in Table 4 and 5, respectively. Bond lengths which have been corrected for rigid-body libration are listed in the first column of Table 4.

The standard deviations given for bond lengths and angles are based on the standard deviations in positional parameters from the least squares refinement. According to Hamilton and Abrahams [13] a more realistic estimate of the standard deviations would probably be obtained by multiplying those given by a factor of two.

Deviations from a least squares plane for the atoms of the 6a-thiathiophthene system, with triple weight on sulfur, are, S(1) −0.007; S(6a) −0.010; S(6) 0.015; C(2) 0.035; C(3) 0.010; C(3a) −0.005; C(4) −0.022; C(5) −0.013; and C(6) 0.116 Å. One notes that the methyl carbon, C(6), lies slightly out of the plane.

The S(1)−S(6a) bond in the present compound is 2.4311(16) Å and thus longer than the S(6a)−S(6) bond of 2.3076(17) Å. This agrees with the CNDO/2 prediction. The C−S and C−C bond lengths, *cf.* Table 4, are compatible with those usually found in 6a-thiathiophthenes.[14]

A stereoscopic view of the arrangement of 2-methyl-6a-thiathiophthene molecules in the unit cell is given in Fig. 2.[15]

Acknowledgements. We thank Dr. D. H. Reid, Department of Chemistry, The University, St. Andrews, Scotland, for a sample of 2-methyl-6a-thiathiophthene.

REFERENCES

1. Hansen, L. K., Hordvik, A. and Sæthre, L. J. *Chem. Commun.* (1972) 222.
2. Hordvik, A. and Sæthre, L. J. *Acta Chem. Scand. 26* (1972) 1729.
3. Troughton, P. G. H. *Siemens Review XXXVII* (1970), Fourth Special Issue: X-Ray and Electron Microscopy News.
4. Coppens, P., Leiserowitz, L. and Rabinovich, D. *Acta Crystallogr. 18* (1965) 1035.
5. Wilson, A. J. C. *Nature 150* (1942) 151.
6. Shiono, R. *Normalized Structure Factors Program*, The Crystallography Laboratory, University of Pittsburgh, Pittsburgh 1966.
7. *International Tables for X-Ray Crystallography*, Kynoch Press, Birmingham 1968, Vol. III, p. 202.

8. Stewart, R. F., Davidson, E. R. and Simpson, W. T. *J. Chem. Phys. 42* (1965) 3175.
9. Main, P., Woolfson, M. M. and Germain, G. *MULTAN-A Computer Program for the Automatic Solution of Crystal Structures*, Department of Physics, University of York, York, England, May 1971.
10. Hordvik, A. and Sæthre, L. J. *Acta Chem. Scand. 26* (1972) 3114.
11. Schomaker, V. and Trueblood, K. N. *Acta Crystallogr. B 24* (1968) 63.
12. Cruickshank, D. W. J. *Acta Crystallogr. 9* (1956) 757; *14* (1961) 896.
13. Hamilton, W. C. and Abrahams, S. C. *Acta Crystallogr. A 26* (1970) 18.
14. Hansen, L. K. and Hordvik, A. *Acta Chem. Scand. 27* (1973) 411.
15. Johnson, C. K. *A Fortran Thermal Ellipsoid Plot Program for Crystal Structure Illustrations*, ORNL-3794, Oak Ridge National Laboratory, Tennessee 1965.

Received July 22, 1974.

Acta Chemica Scandinavica A 29 (1975) 141—148

The Crystal Structure of the Monoclinic Form of *trans*-Tetrachlorobis(tetramethylthiourea)tellurium(IV). An Example of Structural Change in the Solid State

STEINAR ESPERÅS, JOHN W. GEORGE,* STEINAR HUSEBYE and ØYVIND MIKALSEN

Chemical Institute, University of Bergen, N-5014 Bergen-Universitetet, Norway

Monoclinic *trans*-tetrachlorobis(tetramethylthiourea)tellurium(IV), $TeCl_4(C_5H_{12}N_2S)_2$, forms dark, red prismatic crystals, elongated along *c*, with $a = 14.009(3)$ Å, $b = 14.708(3)$ Å, $c = 10.053(2)$ Å, $\beta = 90.37(2)°$ and $Z = 4$. Data were collected by counter methods and the structure solved by a Patterson synthesis and refined by least-squares methods to a conventional *R* value of 3.5 %. The molecules are monomeric and the coordination around the central tellurium atom is distorted octahedral. Some relevant bond lengths and angles are: Te – S1 = 2.726(1) Å, Te – S2 = 2.649(1) Å, Te – Cl1 = 2.455(1) Å, Te – Cl2 = 2.530(2) Å, Te – Cl3 = 2.601(1) Å, Te – Cl4 = 2.544(2) Å, and ∠S1 – Te – Cl3 = 105.9°.

Conversion of the originally orthorhombic crystals to the monoclinic form is very slow, and takes place in the solid state. It is accompanied by small changes in cell dimensions, by significant changes in some bond lengths and angles and by rather large changes in the packing of the molecules. Also, the stereochemically inert lone pair on tellurium may have become stereochemically active during the transformation.

The solution of this structure is part of a study of the stereochemical role of the lone electron pair in complexes with central atoms possessing an $(n-1)d^{10}\ ns^2$ electronic configuration.[1–7] During our work on the structure of orthorhombic *trans*-tetrachlorobis(tetramethylthiourea)tellurium(IV), it was found that a several years old sample contained mostly monoclinic crystals, whereas the crystals were orthorhombic in fresh samples.[1] During exposure to X-rays, some orthorhombic crystals were transformed during a couple of weeks and the transformation could be followed as shifts and intensity changes of the reflections on Weissenberg films.

This structure investigation was undertaken to see which changes had taken place in the crystals and if they could be related to any stereochemical activity of the lone pair of electrons on the tellurium atom.[1,4,8–11]

Table 1. Unit cell dimensions of *trans*-$TeCl_4(tmtu)_2$ before and after transformation.

Orthorhombic form – *Pbca*	Monoclinic form – $P2_1/n$ (present investigation)
b (Å) 13.87(3)	*a* 14.009(3)
a (Å) 14.74(3)	*b* 14.708(3)
c (Å) 10.06(2)	*c* 10.053(2)
β (°) 90	90.37(2)
Vol (Å³) 2058	2069
Z 4	4

EXPERIMENTAL

The crystals used were taken from the same sample as were the crystals used for determining the structure of the orthorhombic form of tetrachlorobis(tetramethylthiourea)tellurium(IV).[1] During the intervening four and a half years, most of the crystals had become monoclinic.

For data recording, a Siemens papertape-controlled single crystal diffractometer (AED-1) was used. The diffractometer was operated as a three-circle instrument, using Mo$K\alpha$ radiation.

* Present address: Dept. of Chemistry, University of Massachusetts, Amherst, Mass. 01002, USA.

Table 2. Atomic coordinates for monoclinic *trans*-tetrachlorobis(tetramethylthiourea)tellurium(IV) in fractions of cell edges. Standard deviations in brackets.

	x	*y*	*z*
Te	0.00104(2)	0.23600(2)	0.19402(3)
S1	0.15607(9)	0.25791(10)	0.03470(13)
S2	−0.15671(8)	0.20313(9)	0.32973(12)
Cl1	−0.02828(11)	0.10722(10)	0.04384(14)
Cl2	−0.09265(12)	0.33767(12)	0.03779(16)
Cl3	0.01023(11)	0.36590(10)	0.36910(15)
Cl4	0.10261(11)	0.13725(11)	0.34707(14)
C1	−0.2209(3)	0.1139(3)	0.2560(4)
C2	−0.1153(7)	−0.0013(7)	0.3520(11)
C3	−0.2195(3)	−0.0405(4)	0.1624(6)
C4	−0.3892(6)	0.0735(6)	0.2142(10)
C5	−0.3285(5)	0.2252(5)	0.1539(9)
C6	0.2399(3)	0.3096(3)	0.1373(4)
C7	0.1635(6)	0.4594(5)	0.1151(8)
C8	0.2643(6)	0.4239(5)	0.3114(7)
C9	0.4121(5)	0.3129(7)	0.1858(8)
C10	0.3297(5)	0.1674(5)	0.1568(8)
N1	−0.1911(3)	0.0288(3)	0.2615(4)
N2	−0.3055(3)	0.1335(3)	0.2009(4)
N3	0.2267(3)	0.3943(3)	0.1824(5)
N4	0.3210(3)	0.2650(3)	0.1673(4)
H1	−0.101(6)	0.038(6)	0.416(8)
H2	−0.054(6)	−0.011(5)	0.305(8)
H3	−0.130(5)	−0.050(5)	0.387(7)
H4	−0.157(5)	−0.061(4)	0.134(6)
H5	−0.247(7)	−0.007(7)	0.080(9)
H6	−0.263(6)	−0.079(5)	0.195(8)
H7	−0.440(7)	0.115(7)	0.259(10)
H8	−0.410(6)	0.052(5)	0.135(8)
H9	−0.378(5)	0.023(5)	0.270(8)
H10	−0.359(5)	0.254(5)	0.217(7)
H11	−0.367(5)	0.221(4)	0.071(7)
H12	−0.272(5)	0.254(5)	0.129(7)
H13	0.146(5)	0.434(5)	0.024(8)
H14	0.202(5)	0.518(5)	0.113(7)
H15	0.113(6)	0.469(5)	0.167(7)
H16	0.216(5)	0.450(4)	0.366(6)
H17	0.315(5)	0.469(5)	0.302(6)
H18	0.291(4)	0.368(5)	0.354(6)
H19	0.433(5)	0.305(5)	0.275(8)
H20	0.404(5)	0.373(5)	0.165(7)
H21	0.455(6)	0.294(5)	0.117(8)
H22	0.266(5)	0.139(5)	0.168(7)
H23	0.369(5)	0.153(5)	0.082(7)
H24	0.380(5)	0.156(5)	0.236(7)

Intensity data were collected using a scintillation counter, the "five-value" measurement, and $\theta-2\theta$ scan technique.[12] Reflections out to $2\theta=56°$ were scanned with scan speed 2.5° per min with automatic setting of greater speed for strong reflections. Attenuation filters were automatically inserted in the beam to reduce counting losses. The reflections were scanned between $\theta_1=\theta-0.41°$ and $\theta_2=\theta+0.41°$, where θ is the Bragg angle for the α_1 peak. Two reference reflections were measured at intervals of 50 reflections. Of the 4958 reflections measured, 4028 had intensities greater than twice the standard deviations and were labelled as observed. The very strong reflection $\bar{1}\bar{1}\bar{1}$ was not recorded due to an error occurring during data collection.

The intensities were corrected for Lorentz and polarization effects and for absorption ($\mu=21.9$ cm^{-1}).[13] The crystal used for data collection had the following dimensions measured as distances from a common origin to crystal faces: 100 and $\bar{1}00$; 37 μ, 010 and $0\bar{1}0$; 42 μ, 001; 17 μ, $\bar{2}21$, $2\bar{2}1$, $\bar{2}\bar{2}1$ and 221; 78 μ.

Accurate unit cell dimensions were based on measurements of 20 high-order reflections and determined by a least-squares procedure. The calculated and observed densities are 1.71 and 1.70 g/cm^3, respectively.

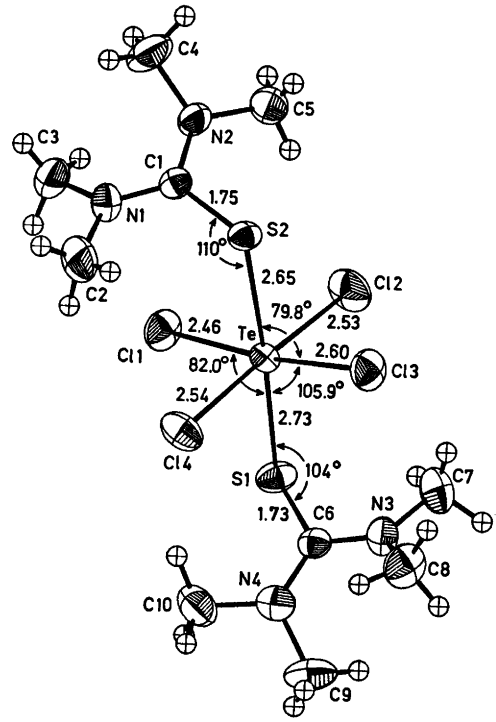

Fig. 1. Monoclinic *trans*-tetrachlorobis(tetramethylthiourea)tellurium(IV) as seen along the *c*-axis. Distances are in Å, and unlabelled spheres represent hydrogen atoms. The other atoms are represented by 50 % probability thermal ellipsoids.

Table 3. Components of atomic vibration tensors, $U \times 10^3$, in Å^2, with standard deviations, referred to crystallographic axes. For hydrogen, the expression used is $\exp[-8\pi^2 U(\sin^2\theta/\lambda^2)]$. For the other atoms, the expression is $\exp[-2\pi^2(h^2a^2U_{11}+\cdots+2hka^{-1}b^{-1}U_{12}+\cdots)]$.

Te	30.22(0.15)	32.13(0.16)	28.11(0.15)	(U_{11}, U_{22}, U_{33})
	4.68(0.13)	−0.56(0.13)	−0.58(0.10)	(U_{12}, U_{23}, U_{13})
S1	35.6(0.6)	59.6(0.9)	38.0(0.6)	
	−7.4(0.6)	−9.4(0.6)	8.3(0.5)	
S2	30.3(0.6)	41.2(0.7)	35.3(0.6)	
	−1.7(0.5)	−8.1(0.5)	4.6(0.5)	
Cl1	61.2(0.9)	48.3(0.8)	48.2(0.8)	
	−6.8(0.7)	−16.7(0.6)	3.6(0.6)	
Cl2	62.4(1.0)	66.8(1.0)	60.8(0.9)	
	16.2(0.8)	25.4(0.8)	−9.4(0.8)	
Cl3	62.0(0.9)	45.7(0.8)	54.0(0.8)	
	0.7(0.7)	−14.1(0.6)	−5.2(0.7)	
Cl4	52.8(0.9)	64.4(0.9)	46.4(0.8)	
	19.2(0.7)	11.0(0.7)	−7.2(0.6)	
C1	35.0(2.6)	36.2(2.6)	30.8(2.4)	
	−2.92(2.0)	3.4(1.9)	1.1(2.0)	
C2	75.3(5.6)	48.2(4.9)	82.7(6.5)	
	10.8(4.1)	23.1(4.8)	−17.7(4.9)	
C3	58.1(2.1)	44.1(2.8)	76.3(3.7)	
	−9.7(1.9)	−10.5(2.5)	3.1(2.2)	
C4	51.8(4.4)	72.0(5.1)	84.7(6.1)	
	−26.8(3.8)	13.7(4.7)	−19.4(4.2)	
C5	49.5(3.8)	50.5(3.9)	81.6(5.5)	
	2.3(3.2)	8.5(3.8)	−25.0(3.8)	
C6	32.2(2.5)	40.1(2.7)	31.6(2.4)	
	−2.4(2.0)	7.9(2.0)	3.3(1.9)	
C7	74.4(5.2)	43.8(3.7)	68.6(4.8)	
	12.1(3.6)	11.2(3.2)	−2.5(4.1)	
C8	71.6(4.9)	62.1(4.5)	51.6(3.3)	
	−7.4(3.9)	−17.9(3.3)	−3.8(3.4)	
C9	35.4(3.4)	101.1(6.5)	54.5(4.3)	
	−8.5(3.6)	6.7(4.1)	−8.0(3.0)	
C10	58.6(4.1)	56.9(3.9)	80.9(5.2)	
	18.3(3.2)	15.9(3.4)	22.3(3.8)	
N1	52.5(2.8)	32.5(2.4)	45.6(2.6)	
	2.2(2.0)	3.9(1.9)	−1.6(2.1)	
N2	38.7(2.4)	39.0(2.0)	55.1(2.7)	
	−6.9(1.7)	5.0(1.8)	−12.0(2.0)	
N3	53.7(2.9)	34.7(2.4)	46.0(2.6)	
	−0.6(2.1)	−0.2(2.0)	−5.1(2.1)	
N4	43.2(2.2)	54.1(2.6)	38.2(2.2)	
	1.4(2.0)	6.1(2.0)	0.2(1.7)	

H1	56(33)	H7	101(37)	H13	49(22)	H19	53(24)
H2	84(28)	H8	50(25)	H14	51(22)	H20	42(21)
H3	50(23)	H9	47(23)	H15	44(23)	H21	67(26)
H4	21(17)	H10	40(20)	H16	24(18)	H22	45(20)
H5	136(34)	H11	39(19)	H17	31(18)	H23	52(23)
H6	41(26)	H12	34(23)	H18	37(18)	H24	54(20)

STRUCTURE ANALYSIS

The structure was solved by conventional heavy atom methods. Full-matrix least-squares refinement was performed by using a program which minimizes the expression $r = \sum W(|F_o| - K|F_c|)^2$. K is a scale factor and W, the weight of a reflection, is the reciprocal of the variance of F_o. With isotropic temperature factors for all atoms (hydrogen not included) the R-factor, $R = \sum||F_o| - K|F_c||/\sum|F_o|$ reached a value of 0.08. With anisotropic temperature factors for the heavier atoms the R factor became 0.047. From a model and a difference

Table 4. Intramolecular bond lengths (Å) based on the coordinates of Table 1. Standard deviations in brackets.

Te – S1	2.726(1)	C6 – N3	1.338(5)
Te – S2	2.649(1)	C6 – N4	1.345(6)
Te – Cl1	2.455(1)	N1 – C2	1.462(10)
Te – Cl2	2.530(2)	N1 – C3	1.478(6)
Te – Cl3	2.601(1)	N2 – C4	1.474(9)
Te – Cl4	2.544(2)	N2 – C5	1.464(8)
S1 – C6	1.734(5)	N3 – C7	1.466(8)
S2 – C1	1.752(5)	N3 – C8	1.464(7)
C1 – N1	1.321(5)	N4 – C9	1.468(9)
C1 – N2	1.337(6)	N4 – C10	1.444(8)

map, all hydrogen positions were found. With anisotropic temperature factors for all atoms except hydrogen (isotropic), the structure was refined to its final R-value of 0.036. No spurious peaks were found in the final difference map.

Observed and calculated structure factors following the last refinement cycle can be obtained from the author St. Husebye upon request. Atomic scattering factors were taken from the *International Tables.*[14] Those for tellurium, sulfur and chlorine were corrected for anomalous dispersion, using the expression $f=[(f_o+\Delta F')^2+(\Delta f'')^2]^{\frac{1}{2}}$, where the values of $\Delta f'$ and $\Delta f''$ were taken from Cromers calculations.[15] Final atomic coordinates are listed in Table 2 and components of atomic vibration tensors in Table 3. Interatomic distances and angles are found in Tables 4 – 7.

RESULTS AND DISCUSSION

Molecular shape. The structure of one molecule of monoclinic *trans*-tetrachlorobis-(tetramethylthiourea)tellurium(IV) is shown in Fig. 1. The central tellurium atom is bonded to the two sulfur atoms of the tetramethylthiourea groups and to the four chlorine atoms in a distorted octahedral configuration. The bond lengths and bond angles (excluding hydrogen) are shown in Tables 4 and 5. The main deviations from a perfect octahedral structure are apparent in two of the pairs of ligand-tellurium bonds *trans* to each other, and in three bond angles on tellurium deviating considerably from 90°. These bonds and angles are Te – S1 = 2.726(1)Å and Te – S2 = 2.649(1) Å; Te – Cl1 = 2.455(1) Å and Te – Cl3 = 2.601 Å and ∠S1 – Te – Cl3 = 105.95(5)°, ∠S1 – Te – Cl1 = 81.99(5)° and ∠S2 – Te – Cl3 = 79.82(4)°. Also the interplanar angle, $TeCl_4$/TeCl2Cl4S1S2, is only 80.7°.

Comparison with the orthorhombic modification. The structure of orthorhombic *trans*-tetrachlorobis(tetramethylthiourea)tellurium-(IV) has been solved earlier in this laboratory.[1] The conversion of the crystals from an orthorhombic to a monoclinic form is accompanied by certain changes in unit cell parameters, molecular structure and in the packing of the molecules in the crystals. However, there appears to be no change in the shape of the crystals.

The unit cell parameters for the two modifications A (Orthorhombic) and B (Monoclinic) are

Table 5. Intramolecular bond angles (°), with standard deviations in brackets.

∠S1 – Te – S2	174.06(0.04)	∠Te – S2 – C1	110.3(0.2)
∠S1 – Te – Cl1	81.99(0.05)	∠S2 – C1 – N1	122.1(0.3)
∠S1 – Te – Cl2	88.71(0.05)	∠S2 – C1 – N2	117.7(0.3)
∠S1 – Te – Cl3	105.94(0.05)	∠C1 – N1 – C2	122.8(0.4)
∠S1 – Te – Cl4	88.76(0.04)	∠C1 – N1 – C3	122.8(0.3)
∠S2 – Te – Cl1	92.24(0.05)	∠C2 – N1 – C3	113.7(0.4)
∠S2 – Te – Cl2	89.80(0.05)	∠C1 – N2 – C4	122.5(0.5)
∠S2 – Te – Cl3	79.82(0.04)	∠C1 – N2 – C5	121.7(0.4)
∠S2 – Te – Cl4	92.84(0.04)	∠C4 – N2 – C5	114.0(0.5)
∠Cl1 – Te – Cl2	89.44(0.05)	∠C6 – N3 – C7	122.4(0.4)
∠Cl1 – Te – Cl3	172.07(0.05)	∠C6 – N3 – C8	121.8(0.4)
∠Cl1 – Te – Cl4	91.28(0.05)	∠C7 – N3 – C8	115.3(0.4)
∠Cl2 – Te – Cl3	90.53(0.05)	∠C6 – N4 – C9	121.8(0.5)
∠Cl2 – Te – Cl4	177.24(0.05)	∠C6 – N4 – C10	122.7(0.4)
∠Cl3 – Te – Cl4	89.14(0.05)	∠C9 – N4 – C10	114.3(0.5)
∠Te – S1 – C6	104.0(0.2)		

Table 6. Some short intramolecular distances in Å.

Te – Cl	3.647(5)	S2 – Cl2	3.656(2)
Te – C6	3.566(5)	S2 – Cl3	3.368(2)
S1 – Cl1	3.405(2)	S2 – Cl4	3.763(2)
S1 – Cl2	3.677(2)	Cl1 – C2	3.508(2)
S1 – Cl3	4.232(2)	Cl – Cl4	3.575(2)
S1 – Cl4	3.688(2)	Cl2 – Cl3	3.645(2)
S2 – Cl1	3.681(2)	Cl3 – Cl4	3.611(2)

listed in Table 1. From photographic data, the axes *a*, *b*, *c* in B corresponds to axes *b*, *a*, $-c$, respectively, in A. The only significant changes in unit cell parameters are thus found in the β angle and the *a* axis (B). They are both larger than the corresponding unit cell dimensions in A. Also the cell volume is larger in the more stable modification, B.

The changes in molecular structure is more striking. First, the center of symmetry observed in the molecules of the orthorhombic form, A, is not preserved during conversion to the monoclinic form, B. The average lengths of the Te – Cl and Te – S bonds change very little, being 2.528 and 2.669 Å, respectively, for A, as compared to 2.533 and 2.688 Å, respectively, for B. However, whereas the three linear three-center S – Te – S and Cl – Te – Cl systems are symmetric and exactly linear in A, two of them are quite asymmetric in B, both with regard to bond lengths and bond angles, although their overall lengths are not significantly different from the corresponding

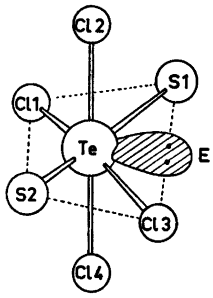

Fig. 2. The possible location of the lone pair of electrons, E, in the complex.

lengths found in A. In the monoclinic form of *trans*-tetrachlorobis(tetramethylthiourea)tellurium(IV), (B), the difference in bond lengths are 0.077 and 0.145 Å, respectively, for the bond pairs constituting the S1 – Te – S2 and Cl1 – Te – Cl3 three-center systems. It is probable that the two bonds that are elongated, Te – S1 and Te – Cl3, are the same that make up one of the two very large bond angles of 98.5° in A. One of these two, ∠S1 – Te – Cl3(B), upon transformation to the monoclinic form B, increases with 7.4°, whereas the other decreases with 6.5°. Another significant change is found in the Te – S – C angles. These are both 109.0(8)° in A, whereas ∠Te – S1 – C6 = 103.97(2)° and ∠Te – S2 – Cl = 110.3(2)° in B.

The large difference between the two sulfur valency angles may be a consequence of the changes in the Te – S bonds. The increase in

Table 7. Some short intermolecular distances in Å.

S1 – S2	$\frac{1}{2}+x$,	$\frac{1}{2}-y$,	$-\frac{1}{2}+z$	3.395(2)
S1 – H10		»		3.20(7)
S2 – C6	$-\frac{1}{2}+x$,	$\frac{1}{2}-y$,	$\frac{1}{2}+z$	3.428(5)
Cl1 – Cl1	$-x$,	$-y$,	$-z$	3.371(2)
Cl1 – H18	$-\frac{1}{2}+x$,	$\frac{1}{2}-y$,	$-\frac{1}{2}+z$	3.18(6)
Cl1 – H19		»		3.04(8)
Cl2 – H14	$-x$,	$1-y$,	$-z$	3.02(8)
Cl2 – H24	$-\frac{1}{2}+x$,	$\frac{1}{2}-y$,	$-\frac{1}{2}+z$	3.05(8)
Cl3 – H8	$-\frac{1}{2}-x$,	$\frac{1}{2}+y$,	$\frac{1}{2}-z$	3.07(8)
Cl3 – H8	$\frac{1}{2}+x$,	$\frac{1}{2}-y$,	$\frac{1}{2}+z$	3.14(8)
Cl3 – H11		»	$\frac{1}{2}+z$	2.93(7)
Cl3 – H23	$-\frac{1}{2}+x$,	$\frac{1}{2}-y$,	$\frac{1}{2}+z$	2.95(7)
Cl4 – H17	$\frac{1}{2}-x$,	$-\frac{1}{2}+y$,	$\frac{1}{2}-z$	3.11(6)
Cl4 – H3	$-x$,	$-y$,	$1-z$	2.99(7)
Cl4 – H11	$\frac{1}{2}+x$,	$\frac{1}{2}-y$,	$\frac{1}{2}+z$	3.10(7)
H5 – H16	$-\frac{1}{2}+x$,	$\frac{1}{2}-y$,	$-\frac{1}{2}+z$	2.36(12)
H7 – H24	$-1+x$,	y,	z	2.58(12)

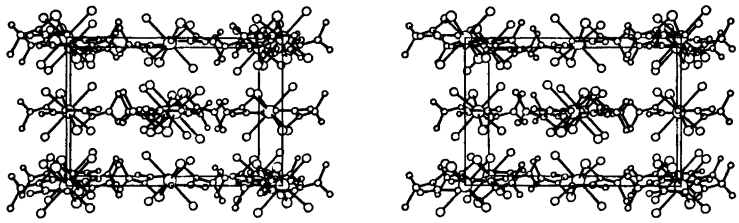

Fig. 3. A stereoscopic view of the structure of orthorhombic *trans*-tetrachlorobis(tetramethylthiourea)tellurium(IV) showing the unit cell packing. The *a* axis is horizontal, the negative *c* axis is vertical and the *b* axis points up from the paper.

the Te – S1 bond length lessens the repulsion between the tetramethylthiourea methyl groups and the chlorine atoms, thus the Te – S1 – C6 angle decreases relative to the corresponding angle in A. The opposite holds for the Te – S2 – C angle.

Lone pair activity and bonding. The seventh valency electron pair on tetravalent tellurium has previously been shown to be stereochemically inert in octahedral complexes.[9–11] This was also assumed to be the case for the orthorhombic form of *trans*-tetrachlorobis(tetramethylthiourea)tellurium(IV), (A), and has recently been indicated also from Mössbauer spectra.[16] Thus the deviation from perfect octahedral symmetry found in A, demonstrated by the S′ – Te – Cl2 and S – Te – Cl2′ angles of 98.5°,[1] probably is due to packing effects. The Mössbauer data also indicate that the bonding in the three linear S – Te – S and Cl – Te – Cl systems in A is of the three-center four-electron type, involving *p*-orbitals only on the central tellurium atom.[16]

The increased distortion from octahedral symmetry in B as compared to A may possibly be due to packing effects. But there is a characteristic feature that indicates lone pair activity, namely the aforementioned lengthening of the two bonds that constitute the large S1 – Te – Cl3 angle in B. This fact can be explained if one assumes that the lone pair of valency electrons on tellurium in form A more or less squeezes through one of the two "cracks" in the valency shell presented by the large S – Te – Cl angles in direction of the corresponding S – Cl octahedral edge. According to VSEPR theory,[9] the lone pair-bond pair repulsions would then tend to increase the Te – S1 and Te – Cl3 bond lengths and at the same time increase the S1 – Te – Cl3 angle when going from A to B. This situation is indicated in Fig. 2. Such an AB_6E structure with idealized C_{2v} symmetry has only slightly higher energy than the C_{3v} structure with the lone pair above the center of one of the octahedral faces.[17] As a result of the bond elongations, one finds a corresponding contraction of bonds *trans* to the two elongated ones. Such *trans* effects are earlier found in *cis*-square-planar complexes of divalent tellurium and interpreted as a result of one ligand atom orbital overlapping more effectively with a

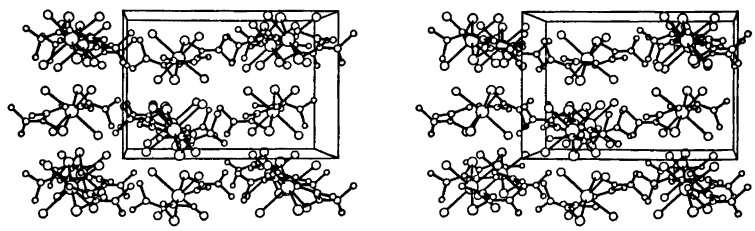

Fig. 4. A stereoscopic view of the structure of monoclinic *trans*-tetrachlorobis(tetramethylthiourea)tellurium(IV) showing the unit cell packing. The *b* axis is horisontal, the *c* axis is vertical and the *a* axis points up from the paper.

Table 8. Least squares planes through parts of the molecule. (Weights; Te:6, S and Cl:3, C and N:1).

No. of plane	Atoms defining plane	Equation of plane
1	TeCl1Cl2Cl3Cl4	$11.780x + 4.183y - 4.684z = 0.052$
2	TeCl1Cl3S1S2	$7.298x - 8.770y + 6.106z = -0.890$
3	TeCl2Cl4S1S2	$3.202x + 11.725y + 5.603z = 3.820$
4	S1C6N3N4	$-6.326x - 5.580y + 8.147z = -2.142$
5	S2C1N1N2	$-6.639x - 2.162y + 8.759z = 3.487$

No. of plane	Distances of atoms from planes in Å				
1	Te: 0.038,	Cl1: −0.142,	Cl2: 0.092,	Cl3: −0.133,	Cl4: 0.106
2	Te: 0.012,	Cl1: 0.010,	Cl3: 0.008,	S1: −0.021,	S2: −0.022
3	Te: 0.037,	Cl2: 0.055,	Cl4: 0.065,	S1: −0.102,	S2: −0.092
4	S1: −0.002,	C6: 0.017,	N3: −0.006,	N4: −0.006,	
5	S2: 0.002,	C1: −0.025,	N1: 0.010,	N4: 0.009	

Interplanar angles (°):
1 − 2 = 90.7, 1 − 3 = 80.7, 2 − 3 = 90.9, 2 − 4 = 61.0, 2 − 5 = 68.2.

common *p*-orbital on the central atom than the one *trans* to it.[18,19]

Mössbauer spectra have later been obtained for the monoclinic form of *trans*-tetrachlorobis-(tetramethylthiourea)tellurium(IV), (B), to find out if they can be interpreted in terms of some tellurium *s*-orbital character in the tellurium-ligand bonds in agreement with the above.[20] However, the bonding also here is mainly of the three-center four-electron type. In a recent structure determination of the compound $TeCl_4.PCl_5$, the tellurium atoms were found to be coordinated to six chlorine atoms in a distorted octahedral configuration.[21] Two of the ligands are bridging with an average Te − Cl bond length of 2.79 Å. For the bonds between tellurium and terminal chlorines, the average length is 2.43 Å. Thus the lone pair is here probably located on the octahedral edge between the two bridging chlorines. The Te − Cl bonds *trans* to the long ones are significantly shorter than the other bonds from tellurium to terminal chlorines. The lone pair activity is also reflected in the tellurium bond angles.

Molecular packing. The packing of the complex molecules both in the orthorhombic modification and the monoclinic one are shown as stereo pairs in Figs. 3 and 4, respectively. It can clearly be seen that there are great changes in the packing as a result of the transformation from one form to the other, in spite of the small changes in cell dimensions. The A molecules have the tellurium atom at a center of symmetry and are related through screw axes and glide planes whereas the B molecules are interrelated through screw axes, glide planes and centers of symmetry.

In both cases, the normal to the $TeCl_4$ plane is roughly parallel (makes an angle below 30°) to the viewing direction, and along *c* the molecules are stacked so that every other one is one half axis length above or below the next one. For the A molecules, the twofold screw axis parallel to *b* prevents near contacts between thiourea sulfur atoms on neighbour molecules (Min. S···S contact is 5.59 Å). For the B molecules, there is no screw axis in the corresponding direction; also the molecular S − Te − S axis in the B molecules is tilted nearly the same angle relative to the *bc* plane. This makes possible a short intermolecular S···S approach of only 3.40 Å in the *c*-direction.

The change in packing can also be visualized by looking at the positions of the central tellurium atoms in the four molecules in the unit cells. In A, the tellurium atoms are situated at 0,0,0; 0,½,½; ½,½,0; ½,0,½. In B, after moving the origin to the tellurium position in the asymmetric unit and interchanging *b* and *a*

plus c and $-c$, one gets 0,0,0; 0.028,½,½; ½,0.498,−0.112; 0.528,0.002,0.388 as coordinates for the tellurium atoms, referred to the original A-cell. Thus the center of the molecules are moved very little in the a and b directions during the conversion, but every other molecule has moved 1.1 Å in the c direction.

Such solid state transformations have been observed earlier, especially in organic compounds, but they usually occur at elevated temperatures.[22]

Other distances and angles. The C−S distances in the two tetramethylthiourea groups in monoclinic *trans*-tetrachlorobis(tetramethylthiourea)tellurium(IV) are not significantly different, C6−S1 and C1−S2 being 1.734(5) and 1.752(5) Å, respectively. These values are normal for complexes containing tetramethylthiourea ligands.[1,19] However, the shorter bond corresponds to a long S−Te bond and *vice versa*, so the difference may be real. The C−N partial double bond lengths vary between 1.321 and 1.345 Å with 1.335 Å as the average, while the C−N single bonds from nitrogen to methyl carbon vary in length between 1.444 and 1.478 Å with 1.465 Å as the average. The above values are normal for tetramethylthiourea ligands.

All twentyfour hydrogen atoms refined satisfactorily. The C−H bond lengths vary between 0.82 and 1.07 Å with standard deviations ranging from 0.07 to 0.10 Å. Their average length is 0.96 Å.

The angles on the nitrogen atoms correspond to sp^2 hybridization on these atoms, the same do the angles on C1 and C6.

The tetramethylthiourea groups have a roughly planar SCN_2 skeleton (Table 8), but the carbon atoms in methyl groups bonded to the nitrogen atoms, are located above or below the SCN_2 plane, in order to minimize steric repulsion. Each nitrogen atom is bonded to three carbon atoms and the resulting NC_3 groups are all nearly planar. The interplanar angles for neighbouring NC_3 groups have an average value of 130.7° and the interplanar NC_3/SCN_2 angles on the same ligand have an average value of 153.5°.

REFERENCES

1. Husebye, S. and George, J. W. *Inorg. Chem. 8* (1969) 313.
2. Esperås, S., Husebye, S. and Sværen, S. E. *Acta Chem. Scand. 25* (1971) 3539.
3. Esperås, S. and Husebye, S. *Acta Chem. Scand. 26* (1972) 3293.
4. Husebye, S. and Sværen, S. E. *Acta Chem. Scand. 27* (1973) 763.
5. Esperås, S. and Husebye, S. *Acta Chem. Scand. 27* (1973) 706.
6. Esperås, S., George, J. W., Husebye, S. and Mikalsen, Ø. *Acta Chem. Scand. 27* (1973) 1089.
7. Esperås, S. and Husebye, S. *Acta Chem. Scand. 27* (1973) 1827.
8. Urch, D. S. *J. Chem. Soc.* (1964) 5775.
9. Gillespie, R. J. *J. Chem. Educ. 47* (1970) 18.
10. Cox, J. J. and Whiston, C. D. *Educ. Chem. 7* (1970) 234.
11. Wynne, K. J. *J. Chem. Educ. 50* (1973) 328.
12. Troughton, P. G. H. *Siemens Rev.* XXXVII (1970), Fourth Special Issue, p. 9.
13. Coppens, P., Leiserowitz, L. and Rabinovich, D. *Acta Crystallogr. 18* (1965) 1035.
14. *International Tables for X-Ray Crystallography*, Kynoch Press, Birmingham 1962, Vol. III, p. 204.
15. Cromer, D. T. *Acta Crystallogr. 18* (1965) 17.
16. Cheyne, B. M., Jones, C. H. W. and Vasudek, P. *Can. J. Chem. 50* (1972) 3677.
17. Cotton, F. A. and Wilkinson, G. *Advanced Inorganic Chemistry*, 3rd Ed., Interscience, New York 1972, p. 140.
18. Foss, O. *Acta Chem. Scand. 16* (1962) 779.
19. Foss, O. In Andersen, P., Bastiansen, O. and Furberg, S., Eds., *Selected Topics in Structure Chemistry*, Universitetsforlaget, Oslo 1967, p. 145.
20. Jones, C. H. W. *Private communication.*
21. Krebs, B., Buss, B. and Berger, W. *Z. Anorg. Allg. Chem. 397* (1973) 1.
22. Paul, I. C. and Curtin, D. Y. *Accounts Chem. Res. 6* (1973) 217.

Received July 8, 1974.

Acta Chemica Scandinavica A 29 (1975) 149—156

Short Communications

On the Peak Broadening in Chromatography

HANS VINK

Institute of Physical Chemistry, University of Uppsala, Box 532, S-751 21 Uppsala, Sweden

In a recent article by Sørensen [1] on the mechanisms behind peak broadening in gel chromatography, some earlier work in the field was critically reviewed. In this connection a comment concerning the present author's work was somewhat misleading, which occasions the following clarifying remarks.

According to the author's theory peak broadening is expressed in terms of the variance $\mu_2(t)$ for the concentration profile in the mobile phase within the column. The expression was derived in Ref. 2 and was developed further in Refs. 3, 4. It may be written as follows:

$$\mu_2(t)=\mu_2(0)+2Dt \qquad (1)$$

where t is the time (with an arbitrary zero point), and D is the generalized diffusion coefficient:*

$$D=D_1'w_1+D_2w_2+\frac{v^2V_2^2w_1^2(1-w_1)}{2D_2} \qquad (2)$$

Here w_1 and w_2 are the amounts of solute in the mobile and stationary phases, respectively, expressed as fractions of the total amount of solute in the column. In Sørensen's terminology

$$w_1=\frac{1}{1+K} \qquad (3)$$

In eqn. (2) D_1' is a composite diffusion coefficient characterizing axial diffusion in the mobile phase. It represents two different effects, the Brownian diffusion and eddy diffusion. If the effects are separated we may write for moderate flow rates [4]

$$D_1'=D_1+kv \qquad (4)$$

where D_1 is the ordinary diffusion coefficient, k the eddy diffusion coefficient and v the translational velocity of the mobile phase.

Although most investigators seem to favor this (linear) form of velocity dependence of the eddy diffusion effect, its validity may be questioned. Eqn. (4) is obviously not invariant with respect to flow reversal (as it should be if the conditions in the column are identical in both flow directions, and eqn. (1) is valid). A quadratic dependence of eddy diffusion on velocity may therefore be more appropriate. It is also possible that in a rigorous treatment of eddy diffusion the simple form of eqn. (1) cannot be retained. In any case, eqn. (4) should be considered as an approximation.

The second term in eqn. (2) represents axial Brownian diffusion in the stationary phase. In most columns this term should be omitted (as explicitly stated in Ref. 4). However, it has to be retained if the stationary phase has large unbroken dimensions in the axial direction of the column. As examples we may consider a column filled with threadlike gel particles, ordered coaxially in the column, or a column having the form of a capillary tubing, with its walls coated with absorbing material.

Finally, the third term in eqn. (2) represents the "chromatographic dispersion", which is due to non-equilibrium in the process of mass transfer between the mobile and stationary phases. This term is essentially identical to the corresponding term in Sørensen's equation.

With eqns. (2) and (3) in mind we may thus conclude that the results obtained by Sørensen and the author are substantially in agreement. It should be noted that results very similar to those discussed here have also been obtained by Giddings and Mallik.[5]

1. Sørensen, T. S. *Acta Chem. Scand. A 28* (1974) 753.
2. Vink, H. *J. Chromatogr. 20* (1965) 305.
3. Vink, H. *J. Chromatogr. 25* (1966) 71.
4. Vink, H. *J. Chromatogr. 52* (1970) 205.
5. Giddings, J. C. and Mallik, K. L. *Anal. Chem. 38* (1966) 997.
6. Vink, H. *Makromol. Chem. 116* (1968) 241.

Received November 25, 1974.

* Unfortunately, eqn. (2) was incorrectly reproduced in Ref. 6.

Reactions of Diphenylditelluride with Halogens in Presence of Substituted Thioureas as Ligands

OLAV VIKANE

Department of Chemistry, University of Bergen, N-5014 Bergen-Univ., Norway

In a recent paper, the preparation of several benzenetellurenyl halide complexes with ligands containing sulfur or selenium as donor atoms was reported.[1] The present work discusses the preparation of a series of analogous divalent tellurium compounds with ethylenethiourea (etu), trimethylenethiourea (trtu), and tetramethylthiourea (tmtu) as ligands.

The reaction used in the preparation is:

$$C_6H_5TeTeC_6H_5 + X_2 + 2L = 2C_6H_5Te(L)X \quad (1)$$

where X_2 is chlorine or bromine, and L is a substituted thiourea. The same type of compound can also be prepared from phenyltellurium trichloride and thiourea, as follows:[2]

$$C_6H_5TeCl_3 + 3SC(NH_2)_2 = C_6H_5Te[SC(NH_2)_2]Cl + [SC(NH_2)_2]_2^{2+} + 2Cl^-$$

When chlorine is used in reaction (1), and the thiourea is in excess, the following equilibrium seems to be established:

$$C_6H_5Te(L)Cl + L \rightleftharpoons [C_6H_5Te(L)_2]^+ + Cl^- \quad (2)$$

With ethylenethiourea as ligand, the bis-ethylenethiourea complex was isolated in fairly good yield. When, on the other hand, tetramethylthiourea or trimethylenethiourea were used as ligands, only the complexes $C_6H_5Te(L)Cl$ were isolated.

Space groups and unit cell dimensions were determined from single-crystal oscillation and Weissenberg photographs using Cu$K\alpha$ radiation. The unit cell dimensions are believed to be accurate to within 0.5 %. Densities were determined by flotation. Melting points are corrected.

Diphenylditelluride was prepared by the method of Haller and Irgolic.[3]

Bromo(ethylenethiourea)phenyltellurium(II), $C_6H_5Te(etu)Br$. 1.25 mmol (0.5 g) of diphenylditelluride and 2.5 mmol (0.255 g) of ethylenethiourea were dissolved in 10 ml of warm methanol. 1.25 mmol of bromine dissolved in 2.6 ml of methanol was added. The resulting orange red solution was filtered while hot. Orange red crystals started to separate almost immediately. After about 10 min also a yellow form started to crystallize.

The pure yellow form was later obtained on seeding with the yellow crystals, but the orange red form could not be obtained pure on seeding with the orange red crystals, in the latter case both orange red and yellow crystals deposited.

Yield of the pure yellow form, 0.97 g (83 %). M.p. 142–143 °C. (Found: C 28.02; H 3.02; N 7.33; S 8.35; Br 20.71. Calc. for $C_9H_{11}N_2STeBr$: C 27.94, H 2.85, N 7.24; S 8.28; Br 20.67).

The yellow crystals are monoclinic plates, with $a = 15.54$ Å, $b = 9.09$ Å, $c = 19.03$ Å, $\beta = 114.77°$. There are eight formula units per unit cell; density, calc. 2.10, found 2.11 g/cm³. The space group, from systematic absences, is Cc (No. 9) or $C2/c$ (No. 15).

The orange red crystals could be picked out and separated from the yellow ones under a microscope. M.p. 143–144 °C. (Found: C 28.06; H 2.98; N 7.28; S 8.39, Br 20.64).

The orange red crystals are monoclinic prisms extended along the a axis, with $a = 7.05$ Å, $b = 12.78$ Å, $c = 14.47$ Å, $\beta = 102.3°$. There are four formula units per unit cell; density, calc. 2.01, found 2.02 g/cm³. The space group, from systematic absences, is $P2_1/c$ (No. 14).

Chloro(ethylenethiourea)phenyltellurium(II), $C_6H_5Te(etu)Cl$, was prepared in a similar way as the bromide, from 1.25 mmol (0.5 g) of diphenylditelluride and 2.5 mmol (0.255 g) of ethylenethiourea dissolved in 8 ml of warm methanol, by adding 1.25 mmol of chlorine dissolved in 1.92 ml of tetrachloromethane. The resulting orange red solution was filtered while hot. After 12 h in a refrigerator, the orange red crystals which had deposited were filtered off, washed with small amounts of cold methanol, then with ether, and dried. Yield, 0.68 g (79 %). M.p. 133–136 °C. (Found: C 31.61; H 3.28; N 8.05; S 9.25; Cl 10.42. Calc. for $C_9H_{11}N_2STeCl$: C 31.56; H 3.21; N 8.18; S 9.35; Cl 10.36).

The crystals are isomorphous with those of the orange red form of the bromide, and have the same colour and morphology. The unit cell dimensions are, $a = 7.03$ Å, $b = 12.38$ Å, $c = 14.39$ Å, $\beta = 102.25°$, and the space group, from systematic absences, is $P2_1/c$ (No. 14). Density, calc. 1.87, found 1.87 g/cm³.

Ethylenethiourea(phenyl)thiocyanatotellurium-(II), $C_6H_5Te(etu)SCN$. To a solution of 2.5 mmol (0.255 g) of ethylenethiourea and 3.1 mmol (0.3 g) of potassium thiocyanate in 8 ml of warm water, 1.25 mmol (0.5 g) of diphenylditelluride dissolved in 8 ml of warm methanol and 1.25 mmol of chlorine dissolved in 2.1 ml of methanol were added. The resulting clear orange yellow solution was placed in a refrigerator for 12 h. Yield, 0.64 g (70 %). M.p. 111–113 °C. (Found: C 32.84; H 3.13; N 11.69; S 17.52. Calc. for $C_{10}H_{11}N_3S_2Te$: C 32.88; H 3.01; N 11.51; S 17.54).

The crystals are yellow orthorhombic needles extended along the c axis, with $a = 11.58$ Å, $b = 16.97$ Å, $c = 6.83$ Å. There are four formula units per unit cell; density, calc. 1.80, found 1.80 g/cm³. The space group, from systematic absences, is $P2_12_12$ (No. 18).

The compound was also prepared by adding

a solution of 2.06 mmol (0.2 g) of potassium thiocyanate in 5 ml of warm water to a solution of 1 mmol (0.34 g) of ethylenethiourea-benzenetellurenyl chloride in 5 ml of warm methanol. The resulting clear orange yellow solution was placed in a refrigerator for 12 h. Yield, 0.32 g (88 %). M.p. 112–113 °C. The compound was identified by its melting point and by X-ray photographs.

Chlorobis(ethylenethiourea)phenyltellurium-(II), $C_6H_5Te(etu)_2Cl$. 1.25 mmol (0.5 g) of diphenylditelluride and 5.88 mmol (0.6 g) of ethylenethiourea were dissolved in 10 ml of warm methanol. 1.25 mmol of chlorine dissolved in 1.92 ml of tetrachloromethane was added. The resulting orange yellow solution was filtered while hot, and placed in a refrigerator for 6 h. Yield, 0.89 g (80 %). M.p. 166–167 °C. (Found: C 32.46; H 3.93; N 12.53; S 14.56; Cl 8.01. Calc. for $C_{12}H_{17}N_4S_2TeCl$: C 32.42; H 3.83; N 12.61; S 14.41; Cl 7.98).

The compound forms yellow tetragonal crystals, with $a=b=10.30$ Å, $c=32.42$ Å. There are eight formula units per unit cell; density, calc. 1.72, found 1.71 g/cm³. The space group, from systematic absences, is $P4_12_12$ (No. 92) or $P4_32_12$ (No. 96).

The compound was also prepared by adding a solution of 1 mmol (0.34 g) of ethylenethiourea-benzenetellurenyl chloride in 5 ml of warm methanol to a solution of 2.94 mmol (0.3 g) of ethylenethiourea in 5 ml of warm water and 2 drops of conc. hydrochloric acid. The resulting clear orange yellow solution was placed in a refrigerator for 8 h. Yield, 0.43 g (97 %). M.p. 166–167 °C. The compound was identified by its melting point and by X-ray photographs.

Bromo(phenyl)trimethylenethioureatellurium-(II), $C_6H_5Te(trtu)Br$, was prepared using 1.25 mmol (0.5 g) of diphenylditelluride and 2.58 mmol (0.3 g) of trimethylenethiourea dissolved in 10 ml of warm methanol. 1.25 mmol of bromine dissolved in 2.6 ml of methanol was added. The resulting clear orange yellow solution was placed at room temperature for 4 h. Yield, 0.86 g (86 %). M.p. 159–160 °C. (Found: C 30.06; H 3.38; N 6.82; S 8.07; Br 20.01. Calc. for $C_{10}H_{13}N_2STeBr$: C 29.96; H 3.25; N 6.99; S 7.99; Br 19.95).

The compound forms yellow monoclinic crystals, with $a=9.09$ Å, $b=15.81$ Å, $c=10.48$ Å, $\beta=120.2°$. There are four formula units per unit cell; density, calc. 2.04, found 2.04 g/cm³.The space group, from systematic absences, is $P2_1/c$ (No. 14).

Chloro(phenyl)trimethylenethioureatellurium-(II), $C_6H_5Te(trtu)Cl$, was prepared in the same way as the bromide, using 1.25 mmol (0.5 g) of diphenylditelluride and 2.58 mmol (0.3 g) of trimethylenethiourea dissolved in 9 ml of warm methanol. 1.25 mmol of chlorine dissolved in 1.92 ml of tetrachloromethane was added to the warm solution. The resulting orange red solution was filtered while hot, and placed in a refrigerator for 8 h. Yield, 0.63 g (71 %). M.p. 165–166 °C. (Found: C 33.81; H 3.73; N 8.01; S 9.07; Cl 9.93. Calc. for $C_{10}H_{13}N_2STeCl$: C 33.70; H 3.65; N 7.86; S 8.99; Cl 9.96).

The crystals are orange red monoclinic plates, with $a=7.40$ Å, $b=10.76$ Å, $c=8.74$ Å, $\beta=114.8°$. There are two formula units per unit cell; density, calc. 1.87, found 1.86 g/cm³. The space group, from systematic absences, is $P2_1$ (No. 4) or $P2_1/m$ (No. 11).

Bromo(phenyl)tetramethylthioureatellurium-(II), $C_6H_5Te(tmtu)Br$, was prepared using 1.25 mmol (0.5 g) of diphenylditelluride and 2.5 mmol (0.33 g) of tetramethylthiourea dissolved in 15 ml of warm methanol. 1.25 mmol of bromine dissolved in 2.6 ml of methanol was added to the solution. The resulting orange red solution was filtered while hot, and placed in a refrigerator for 12 h. Yield, 0.6 g. The volume of the mother liquor was reduced to half its volume. After 12 h in a refrigerator, an additional 0.25 g of the compound was isolated. Total yield, 0.85 g (82 %). M.p. 115–116 °C. (Found: C 31.66; H 4.10; N 6.67; S 7.67; Br 19.23. Calc. for $C_{11}H_{17}N_2STeBr$: C 31.69; H 4.08; N 6.72; S 7.69; Br 19.19).

The compound forms orange red monoclinic crystals, with $a=7.76$ Å, $b=12.77$ Å, $c=15.90$ Å, $\beta=108°$. There are four formula units per unit cell; density, calc. 1.88, found 1.87 g/cm³. The space group, from systematic absences, is $P2_1/c$ (No. 14).

Chloro(phenyl)tetramethylthioureatellurium-(II), $C_6H_5Te(tmtu)Cl$, was prepared as described for the bromide, using 1.25 mmol (0.5 g) of diphenylditelluride and 2.5 mmol (0.33 g) of tetramethylthiourea dissolved in 10 ml of warm methanol, and 1.25 mmol of chlorine dissolved in 1.92 ml of tetrachloromethane. The resulting clear orange red solution was placed in a refrigerator for 8 h. Yield, 0.59 g (63 %). M.p. 111–113 °C. (Found: C 35.49; H 4.54; N 7.55; S 8.52; Cl 9.55. Calc. for $C_{11}H_{17}N_2STeCl$: C 35.46; H 4.57; N 7.52; S 8.60; Cl 9.52).

The crystals are isomorphous with those of the bromide and have the same colour and morphology. The unit cell dimensions are, $a=7.70$ Å, $b=12.54$ Å, $c=15.85$ Å, $\beta=109.2°$, and the space group, from systematic absences, is $P2_1/c$ (No. 14). Density, calc. 1.71, found 1.71 g/cm³.

The tetramethylthiourea complexes were examined in solution by NMR spectroscopy. The NMR spectra were recorded at ambient probe temperature (*ca.* 30 °C) on a JEOL-C-60H spectrometer. TMS was used as internal reference and lock signal. The spectra were recorded at 54 Hz sweep width. Chemical shifts were determined using a frequency counter. The chemical shifts are accurate to within ±0.1 Hz.

The methyl groups of tetramethylthiourea in the free ligand as well as in the complexes,

are equivalent on the NMR time scale. For tetramethylthiourea itself, the chemical shift was δ 3.08 in chloroform and δ 3.03 in dichloromethane. For $C_6H_5Te(tmtu)Br$ upfield shift to δ 3.05 in chloroform and δ 3.02 in dichloromethane were observed, while $C_6H_5Te(tmtu)Cl$ displayed shifts of δ 3.04 in chloroform and δ 3.01 in dichloromethane.

Addition of tetramethylthiourea to freshly prepared solutions of the two complexes resulted in one sharp peak of intermediate chemical shift. An exchange, rapid on the NMR time scale, between coordinated and free tetramethylthiourea evidently takes place.

1. Hauge, S. and Vikane, O. *Acta Chem. Scand. 27* (1973) 3596.
2. Foss, O. and Hauge, S. *Acta Chem. Scand. 13* (1959) 2155.
3. Haller, W. S. and Irgolic, K. J. *J. Organometal. Chem. 38* (1972) 97.

Received October 10, 1974.

Reactions of Diphenylditelluride with Halogens in Presence of Substituted Selenoureas as Ligands

OLAV VIKANE

Department of Chemistry, University of Bergen, N-5014 Bergen-Univ., Norway

Three-coordinated complexes of divalent tellurium containing thioureas as ligands are well known.[1-3] Far less known are the analogous complexes of divalent tellurium containing selenoureas as ligands.

The present paper discusses the preparation of some complexes of divalent tellurium with the formula $C_6H_5Te(L)X$ where L is ethyleneselenourea (esu), tetramethylselenourea (tmsu), or trimethyleneselenourea (trsu), and X is chlorine or bromine; also a complex $C_6H_5Te(esu)_2Cl$ has been prepared.

The selenourea complexes were prepared in the same way as the thiourea analogoues,[1,2] from diphenylditelluride, chlorine or bromine and the suitable selenourea. Diphenylditelluride was prepared by the method of Haller and Irgolic.[4] Tetramethylselenourea, ethyleneselenourea, and trimethyleneselenourea were prepared as described by Klayman and Griffin,[5] using the corresponding thiourea, iodomethane, selenium, and sodium borohydride in methanol. The crude products were recrystallized as described in the literature.[5,6]

Space groups and unit cell dimensions were determined from single-crystal oscillation and Weissenberg photographs, using Cu$K\alpha$ radiation. The unit cell dimensions are believed to be accurate to within 0.5 %. Densities were determined by flotation. Melting points are corrected.

Bromo(phenyl)tetramethylselenoureatellurium-(II), $C_6H_5Te(tmsu)Br$. 1.25 mmol (0.5 g) of diphenylditelluride and 2.5 mmol (0.45 g) of tetramethylselenourea were dissolved in 30 ml of warm methanol. 1.25 mmol of bromine dissolved in 2.58 ml methanol was added. After filtering, the resulting clear orange red solution was placed at room temperature over night. Yield, 0.92 g (80 %). M.p. 162 – 163 °C. (Found: C 28.44; H 3.72; N 6.11; Br 17.31. Calc. for $C_{11}H_{12}N_2SeTeBr$: C 28.51; H 3.67; N 6.04; Br 17.24).

The compound forms orange-red monoclinic prisms extended along the a axis, with $a = 7.71$ Å, $b = 13.06$ Å, $c = 16.17$ Å, $\beta = 108.2°$. There are four formula units per unit cell; density, calc. 1.99, found 1.99 g/cm³. The space group, from systematic absences, is $P2_1/c$ (No. 14). The crystals are isomorphous with the corresponding tetramethylthiourea complex, and shows the same colour and morphology.[3]

Chloro(phenyl)tetramethylselenoureatellurium-(II), $C_6H_5Te(tmsu)Cl$, was prepared in the same way as the bromide, using 1.25 mmol (0.5 g) of diphenylditelluride and 2.5 mmol (0.45 g) of tetramethylselenourea dissolved in 15 ml warm methanol and adding 1.25 mmol of chlorine dissolved in 2.35 ml tetrachloromethane. The mixture was filtered while hot and the resulting clear orange-red solution was placed at room temperature for 12 h. Yield, 0.77 g (73 %). M.p. 151 – 152 °C. (Found: C 31.52; H 3.98; N 6.59; Cl 8.52. Calc. for $C_{11}H_{17}N_2SeTeCl$: C 31.48; H 4.05; N 6.68; Cl 8.46).

The crystals are isomorphous with those of the bromide, and shows the same colour and morphology. The unit cell dimensions are, $a = 7.69$ Å, $b = 12.80$ Å, $c = 15.93$, $\beta = 109.2°$. Density, calc. 1.88, found 1.87 g/cm³.

Bromo(ethyleneselenourea)phenyltellurium-(II), $C_6H_5Te(esu)Br$, was prepared in a similar way as the compounds mentioned above, using 1.25 mmol (0.5 g) of diphenylditelluride and 2.5 mmol (0.37 g) of ethyleneselenourea dissolved in 10 ml warm methanol, adding 1.25 mmol of bromide dissolved in 2.58 ml methanol. The resulting clear orange-red solution was placed at room temperature for 3 h. Yield, 0.87 g (80 %). M.p. 163 – 164 °C. (Found: C 24.87; H 2.61; N 6.39; Br 18.51. Calc for $C_9H_{11}N_2SeTeBr$: C 24.92; H 2.54; N 6.46; Br 18.43).

The compound forms orange-red monoclinic prisms extended along the a axis, with $a = 7.20$

are equivalent on the NMR time scale. For tetramethylthiourea itself, the chemical shift was δ 3.08 in chloroform and δ 3.03 in dichloromethane. For $C_6H_5Te(tmtu)Br$ upfield shift to δ 3.05 in chloroform and δ 3.02 in dichloromethane were observed, while $C_6H_5Te(tmtu)Cl$ displayed shifts of δ 3.04 in chloroform and δ 3.01 in dichloromethane.

Addition of tetramethylthiourea to freshly prepared solutions of the two complexes resulted in one sharp peak of intermediate chemical shift. An exchange, rapid on the NMR time scale, between coordinated and free tetramethylthiourea evidently takes place.

1. Hauge, S. and Vikane, O. *Acta Chem. Scand. 27* (1973) 3596.
2. Foss, O. and Hauge, S. *Acta Chem. Scand. 13* (1959) 2155.
3. Haller, W. S. and Irgolic, K. J. *J. Organometal. Chem. 38* (1972) 97.

Received October 10, 1974.

Reactions of Diphenylditelluride with Halogens in Presence of Substituted Selenoureas as Ligands

OLAV VIKANE

Department of Chemistry, University of Bergen, N-5014 Bergen-Univ., Norway

Three-coordinated complexes of divalent tellurium containing thioureas as ligands are well known.[1-3] Far less known are the analogous complexes of divalent tellurium containing selenoureas as ligands.

The present paper discusses the preparation of some complexes of divalent tellurium with the formula $C_6H_5Te(L)X$ where L is ethyleneselenourea (esu), tetramethylselenourea (tmsu), or trimethyleneselenourea (trsu), and X is chlorine or bromine; also a complex $C_6H_5Te(esu)_2Cl$ has been prepared.

The selenourea complexes were prepared in the same way as the thiourea analogoues,[1,2] from diphenylditelluride, chlorine or bromine and the suitable selenourea. Diphenylditelluride was prepared by the method of Haller and Irgolic.[4] Tetramethylselenourea, ethyleneselenourea, and trimethyleneselenourea were prepared as described by Klayman and Griffin,[5] using the corresponding thiourea, iodomethane, selenium, and sodium borohydride in methanol. The crude products were recrystallized as described in the literature.[5,6]

Space groups and unit cell dimensions were determined from single-crystal oscillation and Weissenberg photographs, using Cu$K\alpha$ radiation. The unit cell dimensions are believed to be accurate to within 0.5 %. Densities were determined by flotation. Melting points are corrected.

Bromo(phenyl)tetramethylselenoureatellurium-(II), $C_6H_5Te(tmsu)Br$. 1.25 mmol (0.5 g) of diphenylditelluride and 2.5 mmol (0.45 g) of tetramethylselenourea were dissolved in 30 ml of warm methanol. 1.25 mmol of bromine dissolved in 2.58 ml methanol was added. After filtering, the resulting clear orange red solution was placed at room temperature over night. Yield, 0.92 g (80 %). M.p. 162 – 163 °C. (Found: C 28.44; H 3.72; N 6.11; Br 17.31. Calc. for $C_{11}H_{12}N_2SeTeBr$: C 28.51; H 3.67; N 6.04; Br 17.24).

The compound forms orange-red monoclinic prisms extended along the a axis, with $a = 7.71$ Å, $b = 13.06$ Å, $c = 16.17$ Å, $\beta = 108.2°$. There are four formula units per unit cell; density, calc. 1.99, found 1.99 g/cm³. The space group, from systematic absences, is $P2_1/c$ (No. 14). The crystals are isomorphous with the corresponding tetramethylthiourea complex, and shows the same colour and morphology.[3]

Chloro(phenyl)tetramethylselenoureatellurium-(II), $C_6H_5Te(tmsu)Cl$, was prepared in the same way as the bromide, using 1.25 mmol (0.5 g) of diphenylditelluride and 2.5 mmol (0.45 g) of tetramethylselenourea dissolved in 15 ml warm methanol and adding 1.25 mmol of chlorine dissolved in 2.35 ml tetrachloromethane. The mixture was filtered while hot and the resulting clear orange-red solution was placed at room temperature for 12 h. Yield, 0.77 g (73 %). M.p. 151 – 152 °C. (Found: C 31.52; H 3.98; N 6.59; Cl 8.52. Calc. for $C_{11}H_{17}N_2SeTeCl$: C 31.48; H 4.05; N 6.68; Cl 8.46).

The crystals are isomorphous with those of the bromide, and shows the same colour and morphology. The unit cell dimensions are, $a = 7.69$ Å, $b = 12.80$ Å, $c = 15.93$, $\beta = 109.2°$. Density, calc. 1.88, found 1.87 g/cm³.

Bromo(ethyleneselenourea)phenyltellurium-(II), $C_6H_5Te(esu)Br$, was prepared in a similar way as the compounds mentioned above, using 1.25 mmol (0.5 g) of diphenylditelluride and 2.5 mmol (0.37 g) of ethyleneselenourea dissolved in 10 ml warm methanol, adding 1.25 mmol of bromide dissolved in 2.58 ml methanol. The resulting clear orange-red solution was placed at room temperature for 3 h. Yield, 0.87 g (80 %). M.p. 163 – 164 °C. (Found: C 24.87; H 2.61; N 6.39; Br 18.51. Calc for $C_9H_{11}N_2SeTeBr$: C 24.92; H 2.54; N 6.46; Br 18.43).

The compound forms orange-red monoclinic prisms extended along the a axis, with $a = 7.20$

Å, $b=12.88$ Å, $c=14.34$ Å, $\beta=101.5°$. There are four formula units per unit cell; density, calc. 2.23, found 2.23 g/cm^3. The space group, from systematic absences, is $P2_1/c$ (No. 14). The crystals are isomorphous with those of the corresponding ethylenethiourea compound.[2]

Bromo(phenyl)trimethyleneselenoureatellurium(II), $C_6H_5Te(trsu)Br$, was prepared using 1.25 mmol (0.5 g) of diphenylditelluride and 2.5 mmol (0.41 g) of trimethyleneselenourea dissolved in 10 ml of warm methanol. 1.25 mmol of bromine dissolved in 2.58 ml of methanol was added. The resulting clear orange red solution was placed at room temperature for 2 h. Yield, 0.83 g (74 %). M.p. 152 – 153 °C. (Found: C 26.86; H 2.84; N 6.19; Br 17.91. Calc. for $C_{10}H_{13}N_2SeTeBr$: C 26.80; H 2.90; N 6.25; Br 17.85).

The compound forms yellow monoclinic prisms and plates, the prisms are extended along the *a* axis. The unit cell dimensions are $a=9.04$ Å, $b=15.99$ Å, $c=10.53$ Å, $\beta=120.8°$, and there are four formula units per unit cell; density, calc. 2.27, found 2.25 g/cm^3. The space group, from systematic absences, is $P2_1/c$ (No. 14).

Chlorobis(ethyleneselenourea)phenyltellurium(II), $C_6H_5Te(esu)_2Cl$, was prepared from 1.25 mmol (0.5 g) of diphenylditelluride and 5.4 mmol (0.8 g) of ethyleneselenourea dissolved in 15 ml warm methanol, adding 1.25 mmol of chlorine dissolved in 2.25 ml of tetrachloromethane. The resulting clear orange-red solution was placed at room temperature for 4 h. Yield, 0.93 g (68 %). M.p. 190 – 191 °C (dec.). (Found: C 26.71; N 10.32; Cl 6.67. Calc. for $C_{12}H_{17}N_4Se_2TeCl$: C 26.75; H 3.16; N 10.40; Cl 6.59).

The crystals are orange-red orthorhombic prisms extended along the *c* axis, with $a=13.56$ Å, $b=15.43$ Å, $c=8.52$ Å. There are four formula units per unit cell; density, calc. 2.01, found 2.02 g/cm^3. The space group, from systematic absences, is $P2_12_12_1$ (No. 19).

1. Hauge, S. and Vikane, O. *Acta Chem. Scand. 27* (1973) 3596.
2. Vikane, O. *Acta Chem. Scand. A 29* (1975) 150.
3. Foss, O. and Hauge, S. *Acta Chem. Scand. 13* (1959) 2155.
4. Haller, W. S. and Irgolic, K. J. *J. Organometal. Chem. 38* (1972) 97.
5. Klayman, D. L. and Griffin, T. S. *J. Amer. Chem. Soc. 95* (1973) 197.
6. Klayman, D. L. and Shine, R. J. *J. Org. Chem. 34* (1969) 3549.

Received December 6, 1974.

Distribution of Tritium Labeling between Alternative Sites in Carbon Compounds

ALPO KANKAANPERÄ, LEENA OINONEN and PENTTI SALOMAA

Department of Chemistry, University of Turku, SF-20500 Turku 50, Finland

The tritium labeling of carbon compounds leads usually to more than one product. Specific labeling is possible only if the replaceable protons differ greatly by their acidities. In other cases, however, an analysis of the products would be highly desirable but suitable methods for this kind of analysis have not been available. This paper reports a method which is based on the formal kinetics of the detritiation reactions. Labeled phenyl-2-propanone (I) was

$$C_6H_5-\overset{a}{CH_2}-\overset{\overset{O}{||}}{C}-\overset{b}{CH_3} \quad (I)$$

chosen as an example. Preliminary experiments indicated that the nonaromatic hydrogens of this compound were acidic enough to display isotope exchange reactions even in slightly alkaline solutions. In addition, the difference between the rates of the exchange reactions occurring at the two nonequivalent reaction sites was sufficient to make the kinetic analysis possible.

Tritiation of phenyl-2-propanone (Fluka) took place as follows. A mixture of 10^{-5} m^3 of the ketone, 3×10^{-5} m^3 of 100 mol m^{-3} sodium hydroxide, and 10^{-9} m^3 of tritiated water (this amount of water had an activity of about 10^7 s^{-1}) were vigorously agitated at room temperature for 20 h, and the ketone was then extracted into diethyl ether. The ether was subsequently distilled off, and the remaining ketone was distilled under reduced pressure, b.p. 344 K at 0.40 kPa. The purity of the product (denoted by A) was ascertained by NMR spectroscopy. Its activity was 7.5×10^{11} s^{-1} m^{-3}. As will be shown later, about 57 % of the labeling was at the methylene group. The higher labeling of the methylene hydrogens must be the result of kinetic control, these hydrogens being obviously more acidic than those of the methyl group. In the case of thermodynamic control, at the final equilibrium, only 40 % of the labeling would be at the methylene hydrogens. This suggested that even higher labeling at the methylene group might be achieved by shortening the reaction time. Accordingly, the product (denoted by B) obtained after only 2 h reaction time gave an activity of 5×10^{11} s^{-1} m^{-3} with about 90 % of the label at the methylene group. When 3×10^{-6} m^3 of product A was stirred at room

Å, $b = 12.88$ Å, $c = 14.34$ Å, $\beta = 101.5°$. There are four formula units per unit cell; density, calc. 2.23, found 2.23 g/cm³. The space group, from systematic absences, is $P2_1/c$ (No. 14). The crystals are isomorphous with those of the corresponding ethylenethiourea compound.[2]

Bromo(phenyl)trimethyleneselenoureatellurium(II), $C_6H_5Te(trsu)Br$, was prepared using 1.25 mmol (0.5 g) of diphenylditelluride and 2.5 mmol (0.41 g) of trimethyleneselenourea dissolved in 10 ml of warm methanol. 1.25 mmol of bromine dissolved in 2.58 ml of methanol was added. The resulting clear orange red solution was placed at room temperature for 2 h. Yield, 0.83 g (74 %). M.p. 152–153 °C. (Found: C 26.86; H 2.84; N 6.19; Br 17.91. Calc. for $C_{10}H_{13}N_2SeTeBr$: C 26.80; H 2.90; N 6.25; Br 17.85).

The compound forms yellow monoclinic prisms and plates, the prisms are extended along the *a* axis. The unit cell dimensions are $a = 9.04$ Å, $b = 15.99$ Å, $c = 10.53$ Å, $\beta = 120.8°$, and there are four formula units per unit cell; density, calc. 2.27, found 2.25 g/cm³. The space group, from systematic absences, is $P2_1/c$ (No. 14).

Chlorobis(ethyleneselenourea)phenyltellurium(II), $C_6H_5Te(esu)_2Cl$, was prepared from 1.25 mmol (0.5 g) of diphenylditelluride and 5.4 mmol (0.8 g) of ethyleneselenourea dissolved in 15 ml warm methanol, adding 1.25 mmol of chlorine dissolved in 2.25 ml of tetrachloromethane. The resulting clear orange-red solution was placed at room temperature for 4 h. Yield, 0.93 g (68 %). M.p. 190–191 °C (dec.). (Found: C 26.71; N 10.32; Cl 6.67. Calc. for $C_{12}H_{17}N_4Se_2TeCl$: C 26.75; H 3.16; N 10.40; Cl 6.59).

The crystals are orange-red orthorhombic prisms extended along the *c* axis, with $a = 13.56$ Å, $b = 15.43$ Å, $c = 8.52$ Å. There are four formula units per unit cell; density, calc. 2.01, found 2.02 g/cm³. The space group, from systematic absences, is $P2_12_12_1$ (No. 19).

1. Hauge, S. and Vikane, O. *Acta Chem. Scand. 27* (1973) 3596.
2. Vikane, O. *Acta Chem. Scand. A 29* (1975) 150.
3. Foss, O. and Hauge, S. *Acta Chem. Scand. 13* (1959) 2155.
4. Haller, W. S. and Irgolic, K. J. *J. Organometal. Chem. 38* (1972) 97.
5. Klayman, D. L. and Griffin, T. S. *J. Amer. Chem. Soc. 95* (1973) 197.
6. Klayman, D. L. and Shine, R. J. *J. Org. Chem. 34* (1969) 3549.

Received December 6, 1974.

Distribution of Tritium Labeling between Alternative Sites in Carbon Compounds

ALPO KANKAANPERÄ, LEENA OINONEN and PENTTI SALOMAA

Department of Chemistry, University of Turku, SF-20500 Turku 50, Finland

The tritium labeling of carbon compounds leads usually to more than one product. Specific labeling is possible only if the replaceable protons differ greatly by their acidities. In other cases, however, an analysis of the products would be highly desirable but suitable methods for this kind of analysis have not been available. This paper reports a method which is based on the formal kinetics of the detritiation reactions. Labeled phenyl-2-propanone (I) was

$$\overset{a}{C_6H_5}-\overset{}{CH_2}-\overset{O}{\overset{\|}{C}}-\overset{b}{CH_3} \quad (I)$$

chosen as an example. Preliminary experiments indicated that the nonaromatic hydrogens of this compound were acidic enough to display isotope exchange reactions even in slightly alkaline solutions. In addition, the difference between the rates of the exchange reactions occurring at the two nonequivalent reaction sites was sufficient to make the kinetic analysis possible.

Tritiation of phenyl-2-propanone (Fluka) took place as follows. A mixture of 10^{-5} m³ of the ketone, 3×10^{-5} m³ of 100 mol m^{-3} sodium hydroxide, and 10^{-9} m³ of tritiated water (this amount of water had an activity of about 10^7 s^{-1}) were vigorously agitated at room temperature for 20 h, and the ketone was then extracted into diethyl ether. The ether was subsequently distilled off, and the remaining ketone was distilled under reduced pressure, b.p. 344 K at 0.40 kPa. The purity of the product (denoted by A) was ascertained by NMR spectroscopy. Its activity was 7.5×10^{11} s^{-1} m^{-3}. As will be shown later, about 57 % of the labeling was at the methylene group. The higher labeling of the methylene hydrogens must be the result of kinetic control, these hydrogens being obviously more acidic than those of the methyl group. In the case of thermodynamic control, at the final equilibrium, only 40 % of the labeling would be at the methylene hydrogens. This suggested that even higher labeling at the methylene group might be achieved by shortening the reaction time. Accordingly, the product (denoted by B) obtained after only 2 h reaction time gave an activity of 5×10^{11} s^{-1} m^{-3} with about 90 % of the label at the methylene group. When 3×10^{-6} m³ of product A was stirred at room

Table 1. Detriatiation of phenyl-2-propanon at 298.15 K in aqueous sodium hydroxide. k_a and k_b are the rate coefficients for detritiation from the methylene and methyl groups, respectively, and x is the fraction of tritium labeling initially present at the methylene group. The errors given are standard errors.

Sample	$k_a/10^{-5}$ mol^{-1} m^3 s^{-1}	$k_b/10^{-6}$ mol^{-1} m^3 s^{-1}	x
A	8.16	3.85	0.570±0.003
	8.51	3.90	0.574±0.002
B	8.27	3.84	0.909±0.002
	8.87	4.39	0.899±0.003
C	8.41	3.78	0.441±0.002
	9.52	3.83	0.438±0.002
D = 2B + 1C	7.88	3.65	0.759±0.002
	7.62	3.67	0.759±0.002
E = 1B + 2C	8.28	3.84	0.610±0.002
	8.14	3.84	0.608±0.002
	av. 8.37±0.17	3.86±0.06	

temperature with 10^{-5} m^3 of 100 mol m^{-3} sodium hydroxide for 2 h the product (denoted by C) thus obtained gave a total activity of 5×10^{11} s^{-1}m^{-3} with only 44 % methylene labeling. Higher activity at the less acidic site at the expense of the labeling at the more acidic site could thus be effected by partial detritiation of the labeled product.

The kinetic measurements were made at 298.15±0.05 K in 100 mol m^{-3} aqueous sodium hydroxide. The aliquots, 5×10^{-6} m^3, withdrawn from the reaction mixture were run into 2×10^{-6} m^3 of 300 mol m^{-3} sulfuric acid. The sample solution were saturated with sodium phosphate and the ketone was extracted into 10^{-5} m^3 of anisole. The samples, 5×10^{-6} m^3, were then pipetted from the organic layer and transferred to vials containing 10^{-5} m^3 of the scintillation liquid (0.25 g of *p*-bis(*o*-methylstyryl)benzene and 10 g of diphenyloxazole in 2.5×10^{-3} m^3 of toluene). The analysis was performed on a Wallac 81000 scintillation counter. In these runs the first 4 – 5 samples were taken as fast as possible in order to extrapolate the count rates to the zero time. Thereafter, about thirty samples were taken during the progress of the reaction. The final samples were taken after the slower detritiation reaction had continued for about ten half lives.

Since two parallel reactions are involved, the apparent first-order rate coefficients decrease with time. In order to calculate the true rate coefficients of the individual reactions and the radiochemical composition of the substrate, the experimental data were fitted to eqn. (1), where N_0 is the activity at the beginning

$$(N_0 - N_t)/(N_0 - N_\infty) = x[1 - \exp(-k_a't)] + (1-x)[1 - \exp(-k_b't)] \quad (1)$$

of the reaction, N_t is the activity at time t, and N_∞ is the final activity. A similar equation has previously been used for the determination of the isomeric composition of certain cyclic compounds.[1] In eqn. (1) k_a' is the first-order rate coefficient for the detritiation from carbon *a* (see I) and k_b' the corresponding rate coefficient for the detritiation from carbon *b*. The fraction of the labeling at carbon atom *a* at the beginning of the reaction is denoted by x. The parameters x, k_a', and k_b' with standard errors were calculated from the experimental data on a Univac 1108 computer using the method of least squares.[2] Kinetic data for phenyl-2-propanone are collected in Table 1. In addition to the labeled samples A, B, and C (see above), two mixtures of B and C were also studied.

The results from the kinetic study can be summarized as follows: The measured rate coefficients k_a and k_b (coefficients k_a' and k_b' divided by the hydroxide ion concentration) are independent of the tritium distribution in the sample analyzed. The standard errors of the mean values of k_a and k_b are less than 2 %, and thus their effect on the x-values cannot be significant. Accordingly, parallel experiments are seen to give almost equal x-values. Finally, the x-values measured for mixtures D and E, which were mixed up of products B and C, are in good agreement with the known compositions of the mixtures. The calculated x-value for the mixture D is 0.749, which is only 1.3 % lower than the directly measured value shown in Table 1, and that for mixture E is 0.594, which is 2.5 % lower than the measured value.

The present data clearly indicate that the kinetic method described can be applied for the determination of the relative tritium activities at separate sites in certain carbon compounds. However, it is obviously not applicable in cases in which the labeling is at more than two sites, as the increased number of parameters

makes their experimental evaluation impossible. On the other hand, the acid strengths of the hydrogens in question cannot be a limiting factor; for less acidic compounds more basic media can be used in the kinetic measurements involved.

Acknowledgement. Financial aid from the Finnish Academy, Division of Sciences, is gratefully acknowledged.

1. Salomaa, P. and Sallinen, K. *Acta Chem. Scand. 19* (1965) 1054.
2. The computer program was written in this laboratory by Mr. M. Hotokka, B.Sc.

Received November 5, 1974.

Electrolytic Nitrogen Fixation in a Molten Salt

BJÖRN ÅKERMARK and MATS ALMEMARK

Department of Organic Chemistry, Royal Institute of Technology, S-100 44 Stockholm 70, Sweden

Electrolytic reduction of nitrogen in the presence of transition metal complexes has recently been reported.[1,2] In the most successful version, a solution of titanium tetraisopropoxide, aluminium isopropoxide, naphthalene and tetrabutylammoniumchloride in 1,2-dimethoxyethane was electrolysed under an atmosphere of nitrogen. Up to 6.1 mol NH_3 was produced per mol titanium.[1b]

In the early electrolytic experiments it was evident that the solvent (tetrahydrofuran, THF) was partially decomposed, giving tarry deposits on the electrodes. In addition to being ideal solvents for electrolytic reactions, molten salts should generally be more stable than most organic solvents. We have therefore investigated the electrolytic reduction of molecular nitrogen in a molten mixture of aluminium chloride, potassium chloride, and sodium chloride containing titanium chloride. Quantitative data from two representative experiments are given in Table 1.

The electrolysis cell was equipped with a platinum cathode and an aluminium anode. In order to avoid chemical reduction by aluminium metal (*cf.* Ref. 3) the electrode compartments were separated by two consecutive glass filters. During electrolysis, approximately the required amount of aluminium was dissolved at the anode (Table 1). No chlorine was evolved. When molecular nitrogen was bubbled through the cell during the electrolysis, reduction occurred as evidenced by the formation of ammonia on hydrolysis of the electrolyte. No ammonia was detected if the electrolysis was performed under helium or if titanium tetrachloride was omitted. Hydrazine could not be detected by qualitative tests. Reduction of molecular nitrogen to the ammonia stage started when approximately 2 F per mol of titanium had been passed through the cell. This is in accordance with van Tamelen's suggestion that titanium(II) is the active catalytic species.[4] A maximum yield of ammonia (0.25 mol/mol Ti) was obtained at 4–6 F per mol titainum, then the yield decreased slowly. Electrolytic deposition of titanium on the cathode is insufficient to explain the relatively low maximum yield. A possible explanation for the observed maximum yield of ammonia is that titanium metal separates from the molten phase due to the equilibrium (I) which is strongly displaced towards Ti(0).[5]

$$3\ \mathrm{Ti(II)} \rightleftharpoons 2\ \mathrm{Ti(III)} + \mathrm{Ti(0)} \qquad (1)$$

Another possible but hypothetical explanation is that the reduced titanium-nitrogen species is in equilibrium with molecular nitrogen according to eqn. (2). The existence

$$2\ \text{"TiN"} \overset{\mathrm{Al(III)}}{\rightleftharpoons} 2\ \text{"Ti"} + 2\ \mathrm{AlN} \rightleftharpoons N_2 + 2\mathrm{Al(0)} \qquad (2)$$

of such an equilibrium is indicated by a rough calculation using Volpin's data on the titanium catalysed reduction of molecular nitrogen by aluminium metal in molten aluminium bromide[3] (see Table 2). Reduction of nitrogen to ammonia and of titanium(IV) to titanium(0) does not account for all the current consumed. A reasonable explanation would be cathodic reduction of aluminium(III). However, no aluminium was deposited on the cathode during the electrolysis.

Table 1. Experimental data.

Exp. No.	$TiCl_4$ mmol	Current mF	NH_3 found after hydrolysis, mmol	Current yield for the oxidation of Al at the anode %
1	19	131	4.6	82
2	21	274	4.1	75

makes their experimental evaluation impossible. On the other hand, the acid strengths of the hydrogens in question cannot be a limiting factor; for less acidic compounds more basic media can be used in the kinetic measurements involved.

Acknowledgement. Financial aid from the Finnish Academy, Division of Sciences, is gratefully acknowledged.

1. Salomaa, P. and Sallinen, K. *Acta Chem. Scand. 19* (1965) 1054.
2. The computer program was written in this laboratory by Mr. M. Hotokka, B.Sc.

Received November 5, 1974.

Electrolytic Nitrogen Fixation in a Molten Salt

BJÖRN ÅKERMARK and MATS ALMEMARK

Department of Organic Chemistry, Royal Institute of Technology, S-100 44 Stockholm 70, Sweden

Electrolytic reduction of nitrogen in the presence of transition metal complexes has recently been reported.[1,2] In the most successful version, a solution of titanium tetraisopropoxide, aluminium isopropoxide, naphthalene and tetrabutylammoniumchloride in 1,2-dimethoxyethane was electrolysed under an atmosphere of nitrogen. Up to 6.1 mol NH_3 was produced per mol titanium.[1b]

In the early electrolytic experiments it was evident that the solvent (tetrahydrofuran, THF) was partially decomposed, giving tarry deposits on the electrodes. In addition to being ideal solvents for electrolytic reactions, molten salts should generally be more stable than most organic solvents. We have therefore investigated the electrolytic reduction of molecular nitrogen in a molten mixture of aluminium chloride, potassium chloride, and sodium chloride containing titanium chloride. Quantitative data from two representative experiments are given in Table 1.

The electrolysis cell was equipped with a platinum cathode and an aluminium anode. In order to avoid chemical reduction by aluminium metal (*cf.* Ref. 3) the electrode compartments were separated by two consecutive glass filters. During electrolysis, approximately the required amount of aluminium was dissolved at the anode (Table 1). No chlorine was evolved. When molecular nitrogen was bubbled through the cell during the electrolysis, reduction occurred as evidenced by the formation of ammonia on hydrolysis of the electrolyte. No ammonia was detected if the electrolysis was performed under helium or if titanium tetrachloride was omitted. Hydrazine could not be detected by qualitative tests. Reduction of molecular nitrogen to the ammonia stage started when approximately 2 F per mol of titanium had been passed through the cell. This is in accordance with van Tamelen's suggestion that titanium(II) is the active catalytic species.[4] A maximum yield of ammonia (0.25 mol/mol Ti) was obtained at 4–6 F per mol titainum, then the yield decreased slowly. Electrolytic deposition of titanium on the cathode is insufficient to explain the relatively low maximum yield. A possible explanation for the observed maximum yield of ammonia is that titanium metal separates from the molten phase due to the equilibrium (I) which is strongly displaced towards Ti(0).[5]

$$3\ \mathrm{Ti(II)} \rightleftharpoons 2\ \mathrm{Ti(III)} + \mathrm{Ti(0)} \qquad (1)$$

Another possible but hypothetical explanation is that the reduced titanium-nitrogen species is in equilibrium with molecular nitrogen according to eqn. (2). The existence

$$2\ \text{"TiN"} \overset{\mathrm{Al(III)}}{\rightleftharpoons} 2\ \text{"Ti"} + 2\ \mathrm{AlN} \rightleftharpoons N_2 + 2\mathrm{Al(0)} \qquad (2)$$

of such an equilibrium is indicated by a rough calculation using Volpin's data on the titanium catalysed reduction of molecular nitrogen by aluminium metal in molten aluminium bromide[3] (see Table 2). Reduction of nitrogen to ammonia and of titanium(IV) to titanium(0) does not account for all the current consumed. A reasonable explanation would be cathodic reduction of aluminium(III). However, no aluminium was deposited on the cathode during the electrolysis.

Table 1. Experimental data.

Exp. No.	$TiCl_4$ mmol	Current mF	NH_3 found after hydrolysis, mmol	Current yield for the oxidation of Al at the anode %
1	19	131	4.6	82
2	21	274	4.1	75

Table 2. Nitrogen reduction in the system $TiCl_4-Al-AlBr_3$. Data from Ref. 3.

$TiCl_4$:Al:$AlBr_3$	$NH_3/TiCl_4$	Mol fractions of AlN	Al^{3+}	N^{3-}	Activity of AlN
1:12:16	6.44	0.286	0.960	0.110	0.106
1:12:33	10.7	0.236	0.979	0.0943	0.092
1:150:200	95	0.320	0.995	0.136	0.135
1:600:1000	284	0.221	1.00	0.0864	0.087

In conclusion, titanium catalysed electrolytic reduction of molecular nitrogen is possible in a molten salt. The reduction is inefficient, probably due to precipitation of titanium metal according to eqn. (1). Other catalysts should therefore be investigated.

Experimental. The electrolysis cell consisted of a 100 ml four-necked flask into which a filtering tube with a ground glass joint could be fitted. This tube served as anode chamber. The anode was a sheet of aluminium which dissolved during the electrolysis (anodes of platinum and carbon were found to disintegrate rapidly during the electrolysis). The cathode was a sheet of platinum and the current was supplied by a stabilized DC-power supply. All chemicals used were dry and free from ammonia as determined with Nessler's reagent.

The eutectic mixture (about 150 g) of $AlCl_3$ (63.5 mol %), KCl (16.5 mol %), and NaCl (20.0 mol %), m.p. 89 °C [6] was placed in the reaction flask which was heated to 100 °C in a thermostated oil bath. Titanium (IV) chloride was added and the electrolysis started. The current was kept at 0.25 A. An atmosphere of nitrogen was maintained in the flask during these operations. At intervals, samples were taken and analysed for ammonia with Nessler's reagent. Tests for hydrazine in the melt were negative. After the electrolysis, the total amount of reduced nitrogen was determined as ammonia by Kjeldahl analysis. Maximum yields of about 0.25 mol NH_3/mol Ti were obtained at 4–6 F/mol Ti. If the electrode compartments were not rigorously separated, up to 1.5 mol NH_3/mol Ti were obtained, probably due to reduction by aluminium metal.

During the electrolysis, small amounts of titanium were deposited on the cathode, as indicated by an analysis of the surface of the cathode (0.00 % Al, 3.24 % Ti) (a few mg of the outer surface were removed by scraping).

In the calculation using Volpin's data the mol fractions of aluminium ions and nitride ions in the melt were calculated from the reported compositions of the melt and the reported yields of ammonia. The activity of aluminium nitride was then taken as the product of these two mol fractions.[7] This product was roughly constant as required by eqn. (2) at a constant nitrogen pressure.

Acknowledgements. This work has been supported by the C.B. Nathorst Foundation for Science.

1. a. van Tamelen, E. E. and Åkermark, B. *J. Amer. Chem. Soc. 90* (1968) 4492; b. van Tamelen, E. E. and Seeley, D. A. *Ibid. 91* (1969) 5194.
2. Haight, G. P. and Scott, R. *J. Amer. Chem. Soc. 86* (1964) 743.
3. Volpin, M. E., Ilatovskaya, M. A., Kozyakova, L. B. and Shur, V. B. *Chem. Commun.* (1968) 1074.
4. van Tamelen, E. E., Boche, G., Ela, S. W. and Fechter, R. B. *J. Amer. Chem. Soc. 89* (1967) 5707.
5. Rossokin, B. G., Smirnov, M. V. and Loginov, N. A. *Electrochemistry of Molten and Solid Electrolytes 4* (1967) 17.
6. Gordon, J. E. In Denney, D. B., Ed., *Techniques and Methods of Organic and Organometallic Chemistry*, Dekker, New York and London 1969, Vol. 1, p. 51.
7. Bloom, H. *The Chemistry of Molten Salts*, Benjamin, New York and Amsterdam 1967, p. 44.

Received January 2, 1975.

Acta Chemica Scandinavica A 29 (1975) 157—162

Formylcamphor Condensed with Amines. The Structure in Solution as Obtained by NMR, UV Absorption, and Circular Dichroism Spectroscopy

H. P. JENSEN [a] and ERIK LARSEN [b]

[a]Chemistry Department A, Building 207, Technical University of Denmark, DK-2800 Lyngby, Denmark and [b]Chemistry Department I, The H. C. Ørsted Institute, Universitetsparken 5, DK-2100 Copenhagen Ø, Denmark

The condensation products of diamines and two molecules of formylcamphor have been investigated by means of nuclear magnetic resonance, UV absorption, and circular dichroism spectroscopy. It is shown that the configuration of the ketoenamine depends strongly on the choice of solvent. Thus in chloroform these molecules have dominantly a *syn* structure with intramolecular hydrogen bonding. The condensation product of the stereochemically rigid *trans*-1,2-cyclohexanediamine is used to demonstrate that the exciton theory can be used to rationalize the absorption and circular dichroism spectra of chloroform solutions. Then for derivatives of less rigid diamines the exciton model has been used to study the rotational conformation of the diamine bridge. The spectra obtained from methanol solutions where the *anti* structure of the ketoenamines dominates are discussed and it is tentatively suggested that a "chelating solvation" is the reason for the observed very big Cotton effects.

During many years Schiff bases or enamines of β-diketones and diamines and also their transition metal complexes have enjoyed study by a variety of techniques. Dudek and Holm [1] studied by ^{1}H NMR the equilibrium composition for the tautomers of bis(acetylacetone)ethylenediimine, and related compounds and concluded that these compounds were largely in the ketoenamine form. In this tautomer form the "acetylacetoneimine" unit is presumed to be planar as found experimentally in a large number of copper(II) complexes (see Baker, Hall, and Waters [2] and references therein). The "acetylacetoneimine" units have been treated as weakly (*i.e.* electrostatically) interacting chromophores (having $\pi \rightarrow \pi^*$ transitions polarized approximately in the N—O direction) and the average structure in solution has thus been determined for (*R*)-propylene-bis(acetylacetoneimine) using the exciton theory to interpret UV-absorption and circular dichroism spectra.[3] The same method has been used to discuss the structure in solution for VO^{2+}, Ni^{2+}, and Cu^{2+} complexes of this and related ligands.[4] The results were shown to be in accordance with ^{1}H NMR for the ligands and the diamagnetic nickel(II) complexes.[5]

The use of the exciton model for the complexes must necessarily be crude since it considers only the two acetylacetoneimine parts as weakly coupled chromophores and thus ignores the presence of the metal ion. This model has been valuable in explaining electronic spectra of many organic molecules [6] but when used for tris *o*-phenanthroline and tris α,α'-bipyridyl complexes to assign absolute configuration it has been the source of much controversy.[7]

Most of the difficulty in the application of exciton theory to such complexes seems to arise from charge transfer transitions of energies close to the internal ligand $\pi \rightarrow \pi^*$ transitions. The oxovanadium(IV) and copper(II) Schiff base complexes investigated by us earlier have the internal ligand $\pi \rightarrow \pi^*$ transitions well isolated from charge transfer bands and are, therefore, suited for an investigation of the usefulness of exciton theory for metal complexes. The predictions arrived at should preferably be checked by independent means. For

the complex Cu R-pn(acac)$_2$ it was found that in solution the two acetylacetonate parts deviate considerably (some 40°) from being coplanar.[4] However, absorption and circular dichroism spectra of this compound in the crystalline state dispersed in pressed KBr plates indicate [8] a smaller but still significant deviation from planarity. A crystal structure determination for this compound has shown that the two planes form a dihedral angle of 10°.[8]

The absolute configuration of the complex defined as the chirality of a pair of non-crossing, non-parallel lines representing the oxygen-nitrogen directions within the ligand was found [8] by the X-ray structure analysis to be that arrived at by means of the exciton model.[4] Thus we feel it worthwhile to pursue the more delicate problems presented by the stereochemically varied Schiff bases of diamines with formylcamphor. Recently a paper [9] has occurred in the literature dealing with this subject. However, as shown below, experimental insufficiencies render the derived conclusions unreliable when the free ligands are considered.

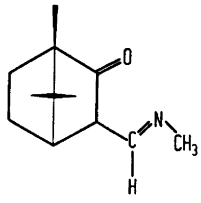

I

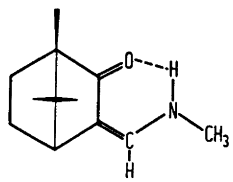

II

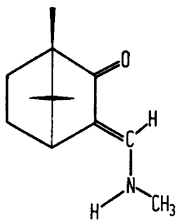

III

The complexity of the stereo-chemistry for condensation products between formylcamphor and primary amines is demonstrated by the various possibilities of ma(fmcH) (for abbreviations see the experimental section) shown by structure I – III. When the condensation products of diamines are considered, *e.g.* en(fmcH)$_2$, evidently the number of possibilities increases. In this paper these structural possibilities have been considered and NMR spectroscopy has been used to obtain information on the tautomer distribution. This distribution has been found to vary with the solvent, with temperature and for chloroform solutions also with time. The spectra reported by Ugo *et al.*[9] are in some cases recorded during the transformation of one tautomer to the other before equilibrium between the tautomers was established.

It seems natural first to answer the question why are the condensation products of formylcamphor much more complicated than the formally analogous enamines of acetylacetone? The working hypothesis for us has been that the presence of two conjugated double bonds on the camphor skeleton (II and III) is not completely energetically favourable relative to the Schiff base form (I). A small population of the latter tautomer (I) in dynamic equilibrium with the enamines serves as a "catalyst" in the *syn-anti* rearrangement. A similar situation has been examined for bis(*anti*-camphorquinonedioximato)nickel(II) which rearranges to the complexes of the *amphi* ligands.[10] For the enamine system the relative concentrations of the tautomers in the equilibrium may be determined by the competition between *inter* and *intra*-molecular hydrogen bonding. The rate of conversion of *anti* ketoamine to the *cis* form can be accelerated by acid in qualitatively the same way as for the oximes.[10]

EXPERIMENTAL

Formylcamphor was prepared by formylation of natural $(+)_D$-camphor.[11]

(*R*)-1,2-Propanediamine and (*R,R*)-1,2-cyclohexanediamine were obtained from the racemic diamines by resolution with natural tartaric acid.[12,13] 1,3-Butanediamine was prepared from acetonitrile [14] and resolved with tartaric acid.[15] 2,3-Butanediamine was prepared from dimethylglyoxime and the two isomers separated through the different solubilities of the hydrochlorides in methanol.[16] The racemic diamine was resolved with tartaric acid.[9]

Schiff bases were prepared according to Pfeiffer *et al.*[17] and recrystallized from methanol. The identity of the compounds was established through chemical analyses and NMR spectra.

Ultraviolet spectra were measured with a Cary 14 spectrophotometer and the circular dichroism spectra with a Roussel-Jouan dichrograph II. ^{13}C NMR spectra were recorded at

22.63 MHz with a Bruker WH 90 and ^{1}H NMR spectra at 90 MHz with a Bruker HX-90E.

Abbreviations. Amines: ma = methylamine, en = 1,2-ethanediamine, R-pn = (*R*)-(−)$_D$-1,2-propanediamine, R-2,3-bn = (*R,R*)-(−)$_D$-2,3-butanediamine, R-1,3-bn = (*R*)-(−)$_D$-1,3-butanediamine, R-chxn = *trans*-(*R,R*)-1,2-cyclohexanediamine, tn = 1,3-propanediamine. Dioxo-compounds: acacH = acetylacetone, fmcH = formylcamphor obtained from natural (+)$_D$-camphor. ma(fmcH) *etc.* symbolizes the condensation product of an amine and a dioxocompound.

RESULTS AND DISCUSSION

During the process of the spectral investigation of the formyl derivatives very strong solvent dependence and spectral changes with time in some solvents were observed. In attempting to correlate UV absorption and circular dichroism measurements with ^{1}H NMR results it became clear that the relatively simple behaviour observed for acetylacetone derivatives was not found for the analogous formylcamphor products. In the following we shall try to use NMR data to establish which isomers, tautomers, or rotamers are present in chloroform and methanol solutions and this knowledge is then correlated with UV absorption and circular dichroism spectra.

Garbisch [18] has investigated the enolization of formyl derivatives of cyclic ketones including formylcamphor. In tetrachloromethane formylcamphor was found to exist mainly in the s-*cis* or *syn*-hydroxymethylene form stabilized by intramolecular hydrogen bonds together with 5 – 30 % of the s-*trans* or *anti* form and 5 – 10 % of the two ketoaldehyde forms. The 90 MHz proton NMR data for ma(fmcH) in $CDCl_3$ is listed in Table 1. The spectrum recorded soon after preparing the solution is different from spectra obtained later. After 10 h no change in the spectrum is observed. The assignments indicated in Table 1 are similar to those of Garbisch when appropriate. The spectrum obtained at first in $CDCl_3$ shows that an *anti* conformation of the enamine is dominant and, therefore, this isomer probably is the species which builds up the crystalline material used. This is also the configuration which is likely to be most abundant in strongly hydrogen bonding solvents as was also shown by Garbisch introducing DMSO into CCl_4 solutions of formylcamphor.[17] In $CDCl_3$ after 24 h the ratio of *syn*/*anti* is approximately 6:1 as obtained from integration of the vinyl proton signals. The spectrum of ma(fmcH) in CD_3OD shows that the same ratio in methanol solution is 1:3. In benzene and acetone solutions the *anti* form III is dominant. There is not enough of the Schiff base forms (I) to allow their detection.

The coupling constant between the vinyl proton and the NH proton is the same for the forms II and III, *i.e.* 12 – 13 Hz (Table 1). This magnitude is characteristic for a *trans* coupling of *vic.* protons and thus we conclude that the carbon-nitrogen bond CH – $NHCH_3$ has some double bond character and that the two hydrogen atoms are *trans* also in III.

Table 1. Proton magnetic resonance data (90 MHz) for some of the protons of ma(fmcH) in deuterated chloroform, methanol, benzene, and acetone. For the signals from chloroform solution it is indicated how these vary the first hours after dissolution and for all solvents the equilibrium ratio between the isomers II and III are given. δ is measured from TMS as an internal standard.

Protons of structure		$CDCl_3$ δ	Variation with time	(J Hz)	CD_3OD δ	(J Hz)	C_6D_6 δ	(J Hz)	CD_3COCD_3 δ	(J Hz)
N – H···O = C	II	7.39	increases				7.55			
N – H	III	4.25	decreases				3.71		5.54	
= CHN	III	7.00	decreases	(12.6)	7.09		7.00	(12.6)	6.88	(12.7)
= CHN	II	6.29	increases	(12.6)	6.51		5.85	(12)	6.41	(12)
CH_3N	III	2.94	decreases	(5.0)	2.96		2.11		2.93	(4.8)
CH_3N	II	2.91	increases	(5.0)	2.93		2.34	(3.5)		
CH	III	2.48	decreases	(3.6)	2.63	(3.6)			2.65	(4)
CH	II	2.30	increases	(3.7)	2.33	(3.6)				
The ratio of II:III after 24 h		6:1			1:3		changing from 1:10 to 10:1 during 24 h		~1:20	

Table 2. Wave-length of absorption maxima and the associated molar absorptivity to the left and corresponding circular dichroism data to the right.

Compound	Absorption spectra Solvent	λ nm	$\varepsilon_{mol} \times 10^{-4}$	λ nm	$\varepsilon_{mol} \times 10^{-4}$	Circular dichroism spectra λ nm	$\Delta\varepsilon_{mol}$	λ nm	$\Delta\varepsilon_{mol}$
ma(fmcH)	CH_3OH	314	2.2			295	10.6		
ma(fmcH)	$CHCl_3$, aged	313	1.3[a]			298	7.6	338	−3.5
tn(fmcH)$_2$	CH_3OH	322	4.3			295	19.0		
tn(fmcH)$_2$	$CHCl_3$, aged	310	2.8[a]			298	17.3	330	−3.7
R-chxn(fmcH)$_2$	CH_3OH	300	4.1	326	1.9	298	−51.6	333	60.8
R-chxn(fmcH)$_2$	$CHCl_3$, aged	293	2.9	312	2.2	300	44.7	340	−46.5
R-pn(fmcH)$_2$	CH_3OH	298	3.6	326	2.4	295	−24.3	333	35.7
R-pn(fmcH)$_2$	$CHCl_3$, aged	298	2.3	311	2.5	296	23.1	333	−30.0
en(fmCH)$_2$	CH_3OH	298	3.3	326	2.9	297	−4.7	335	24.0
en(fmcH)$_2$	$CHCl_3$, aged	292[b]	2.5	311	2.8	308	19.6	344	−2.1
	$CHCl_3$, aged, at −60 °C					297	−9.9	324	23.8
						332	20.7	337	22.0

[a] shoulder on low energy side. [b] shoulder.

^{13}C NMR is consistent with the above results. However, this method is a less accurate measure of the isomer distribution and will, therefore, not be discussed here.

For the *trans*-(−)$_D$-(*R*,*R*)-1,2-cyclohexanediamine derivative, R-chxn(fmcH)$_2$, the same kind of *syn-anti* isomerization is noticed in the ^1H NMR spectra of $CDCl_3$ solutions. Intergration of the vinyl proton signals gives a ratio of *syn*/*anti* of *ca.* 10:1 in aged $CDCl_3$ solution. For other formylcamphor derivatives used in this work a similar analysis has been carried out to ensure that in aged chloroform solutions the major constituents are the *syn* isomers.

The optical properties vary with the choice of solvent in accordance with the isomer distribution. Absorption and circular dichroism data for methanol and aged chloroform solutions are shown in Table 2. The monomeric ma(fmcH) in methanol has a much more intense absorption than it has in chloroform after 4 h whereas there is little change in the band position. This is in perfect agreement with the usual behaviour for $\pi \rightarrow \pi^*$ transitions in systems having conjugated double bonds either s-*trans* or s-*cis*. Two small Cotton effects are found under this absorption band, for methanol and chloroform solutions. The larger CD maximum is found at 298 − 295 nm for the two solvents, *i.e.* significantly displaced from the absorption maximum at 314 − 313 nm. This leads us to attribute the Cotton effect not to the $\pi \rightarrow \pi^*$ transition but to the magnetically allowed $n \rightarrow \pi^*$ transition. This may be supported by the fact that the sign of the Cotton effect is the same as for camphor.

The dimeric molecules formed by condensation of diamines and formylcamphor will then have two reasons to exhibit Cotton effects, *i.e.* the inherent Cotton effect from the presumed $n \rightarrow \pi^*$ transition and the Cotton effects produced by the coupling of the two $\pi \rightarrow \pi^*$ transitions. Only when very intense Cotton effects are observed can they be assigned as arising from exciton coupling. This can be illustrated by tn(fmcH)$_2$ and R-chxn(fmcH)$_2$. The former molecule has CD bands in $CHCl_3$ having $\Delta\varepsilon$ approximately twice that of ma(fmcH) while the latter has two large Cotton effects of opposite sign (Fig. 1) associated with the exciton split transitions. The insignificant electronic coupling during excitation between two formylcamphor groups attached to a bridge of three carbons is further demonstrated by the fact that R-(1,3)-bn(fmcH)$_2$ exhibits exactly the same UV absorption and circular dichroism as tn(fmcH)$_2$.

The analyses of the exciton transitions for R-chxn(fmcH)$_2$ follows closely the treatment outlined earlier.[3] It is gratifying to notice that in solutions where the *syn* forms are the

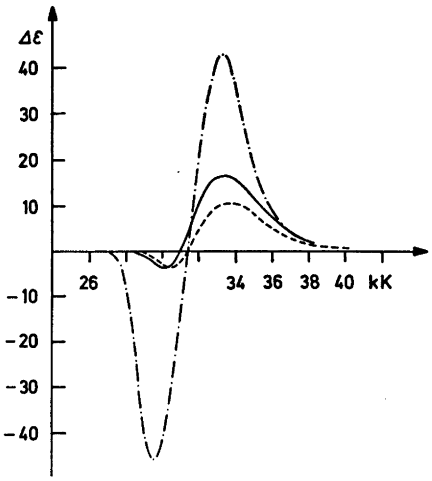

Fig. 1. Circular dichroism spectra of aged (24 h) chloroform solutions of ma(fmcH) - - - -, tn(fmcH)$_2$ ———, and R-chxn(fmcH)$_2$ —.—.—.

dominant the geometry of the set of lines defined by the N—O directions within the π system is the same as for R-chxn(acacH)$_2$. The exciton splitting for R-chxn(fmcH)$_2$ is *ca.* 2.0 kK and therefore, the two split components show considerable circular dichroism in spite of partial cancellation.

The absorption and circular dichroism of R-chxn(fmcH)$_2$ in methanol (Fig. 3 of Ref. 3) is very different from the spectra in aged chloroform. The general characteristics for exciton coupled transitions are present and realizing that only *ca.* 2/3 of the sample is in the *anti* configuration the rotatory strengths are very high indeed. The energy separation of the two transitions is found to be ~2.6 kK and for exciton coupling it is calculated as

$$\Delta E = 2\frac{D_{\text{monomer}}}{r^3_{\text{AB}}}(\cos\theta - 3\cos\phi_{\text{A}}\cos\phi_{\text{B}})$$

with symbols explained in Ref. 3. Considering the length of a O=C—C=C—N chromophore in the *trans* configuration we must conclude that in order for ΔE to be larger than for the *cis* isomer the value in the parenthesis must be larger. Therefore, we tentatively suggest that the solvation in methanol is of a special nature, *e.g.* such that one solvent molecule coordinates to both nitrogen atoms forcing ϕ_{A} and ϕ_{B} to be close to 90°.

In order to verify that the *syn-anti* equilibrium is established in methanol the following experiments were performed. Aged solutions of R-chxn(fmcH)$_2$ in $CHCl_3$ were evaporated, and when the residue was redissolved in $CHCl_3$ it showed immediately the CD spectrum characteristic for aged $CHCl_3$ solutions. However, when dissolved in methanol it took several hours before the CD-spectrum had reached the normal shape for CH_3OH solutions.

When $CHCl_3$ is used without purification or when HCl is added to the solvent the change with time in the spectra is accelerated, probably because the *anti/syn* interconversion is sensitive to acid catalysis. The effect is only of a catalytic nature since the same final results are obtained for pure and acidified solvents.

Condensation products of 1,2-ethanediamine and 1,2-propanediamine with formylcamphor have low barriers for rotation around the C—C bond of the diamine. If equal amounts of the two *gauche* isomers exist in equilibrium with the *trans* isomer for en(fmcH)$_2$ then the circular dichroism is expected to be similar to that of ma(fmcH) but twice as intense. The extremum values from Table 2 show that in $CHCl_3$ this is not too far from being the case at room temperature.

However, at lower temperatures aged chloroform solutions of en(fmcH)$_2$ exhibit circular dichroism curves which gradually approach the characteristic shape for exciton bands of dimers. At −60 °C the circular dichroism spectrum is still rather far from the supposed final band shape (Table 2). The dichroism variation with temperature is explained as a displacement of the equilibrium between the three rotamers towards the most stable rotamer. This should be the one having the opposite absolute configuration of R-chxn(fmcH)$_2$ as judged from the CD spectrum. R-chxn(fmcH)$_2$ does not exhibit a similar variation of CD with temperature consistent with the non-existance of rotamers.

As expected there is some stabilisation of one *gauche* rotamer over the other for R-pn(fmcH)$_2$ in $CHCl_3$. However, the methyl group of the diamine interacts much less with the camphor group than with the methyl group of acetylacetone in R-pn(acacH)$_2$, and, therefore, the circular dichroism is small compared to that of R-pn(acacH)$_2$ and also smaller than that of R-chxn(fmcH)$_2$. For an aged chloroform solu-

tion of R-pn(fmcH)$_2$ a small (5 – 10 %) increase of the circular dichroism on cooling to – 60 °C was observed. This effect is smaller for R-2,3-bn(fmcH)$_2$ where the intensity enhancement is very close to that caused by contraction of the solution. These findings could be explained in several ways, *e.g.* as due to the *syn*, *anti* equilibrium. The ^{1}H-NMR is not sensitive enough to exclude such an explanation but one would then be left with the problem of why R-chxn(fmcH)$_2$ has no temperature dependent Cotton effects in aged chloroform. Therefore, it is assumed that the variable temperature circular dichroism reflects the rotamer equilibrium and it follows as expected that the derivatives of 1,2-ethanediamine, 1,2-propanediamine, and 2,3-butanediamine have increasing barriers towards rotation.

The above illustrates that the stereochemistry of the condensation products between diamines and formylcamphor can be understood. These molecules are unfortunately not well suited for a quantitative investigation of the exciton coupling mechanism and as here demonstrated mistakes were introduced if one relied on the exciton theory alone.

REFERENCES

1. Dudek, G. O. and Holm, R. H. *J. Amer. Chem. Soc. 83* (1961) 209.
2. Baker, E. N., Hall, D. and Waters, T. N. *J. Chem. Soc. A* (1970) 400.
3. Larsen, E. *Acta Chem. Scand. 23* (1969) 2158.
4. Jensen, H. P. and Larsen, E. *Acta Chem. Scand. 25* (1971) 1439.
5. Larsen, E. and Schaumburg, K. *Acta Chem. Scand. 25* (1971) 962.
6. Murrell, J. N. *The Theory of Electronic Spectra of Organic Molecules*, Methuen, London 1963, Chapter 7.
7. Hawkins, C. J. *Absolute Configuration of Metal Complexes*, Wiley, Interscience, New York, Chapter 5.
8. Larsen, S., Larsen, E., Røen, S. and Watson, K. J. *To be published.*
9. Gullotti, M., Pasini, A., Fantucci, P., Ugo, R. and Gillard, R. D. *Gazz. Chim. Ital. 102* (1972) 855.
10. Pedersen, S. B. and Larsen, E. *Acta Chem. Scand. 27* (1973) 3291.
11. Bishop, A. W., Claisen, L. and Sinclair, W. *Justus Liebigs Ann. Chem. 281* (1894) 314.
12. Dwyer, F. P., Garvan, F. L. and Schulman, A. *J. Amer. Chem. Soc. 81* (1959) 290.
13. Asperger, R. G. and Liu, C. F. *Inorg. Chem. 4* (1965) 1492.
14. Strack, E. and Schwaneberg, H. *Ber. Deut. Chem. Ges. 67* (1934) 39.
15. Balieu, E., Boll, P. and Larsen, E. *Acta Chem. Scand. 23* (1969) 2191.
16. Dickey, F. H., Fickett, W. and Lucas, H. J. *J. Amer. Chem. Soc. 74* (1952) 994.
17. Pfeiffer, P., Chisteleit, W., Hesse, T., Pfitzner, H. and Thielert, H. *J. Prakt. Chem. NF 150* (1938) 261.
18. Garbish, E. W. *J. Amer. Chem. Soc. 85* (1963) 1696.

Received October 4, 1974.

Acta Chemica Scandinavica A 29 (1975) 163—169

The Crystal Structure of Cesium Triselenocyanate

SVERRE HAUGE

Chemical Institute, University of Bergen, N-5014 Bergen, Norway

The crystal structure of cesium triselenocyanate, $Cs(SeCN)_3$, has been determined by X-ray methods, and refined by full-matrix least squares procedures. The crystals are monoclinic, space group $C2/c$ (No. 15). with $a=7.969(4)$ Å, $b=21.156(10)$ Å, $c=5.593(4)$ Å, and $\beta=98.84(6)°$, and four formula units per unit cell.

The triselenocyanate ion possesses by space group requirements a twofold axis of symmetry; the middle selenocyanate group is located on this axis. The three-selenium sequence of the triselenocyanate ion is very nearly linear, with Se—Se—Se bond angle 178.31(10)°, and Se—Se bond lengths of 2.650(3) Å, which is 0.31 Å longer than single covalent selenium-selenium bonds.

The middle selenocyanate group, located on a twofold axis, is exactly linear, and the terminal selenocyanate groups are linear within error. A least squares plane through a terminal selenocyanate group and the middle selenium atom makes an angle of 43.9° with the plane through the middle selenocyanate group and the terminal selenium atoms.

Cesium triselenocyanate, $Cs(SeCN)_3$, was first prepared in 1925 by Birckenback and Kellermann.[1]

The crystal structures of the triselenocyanate ion in the potassium and rubidium salts, both hemihydrates, have been determined.[2,3] In the potassium salt, no molecular symmetry is required. In the rubidium salt, the triselenocyanate ion lies across a crystallographic mirror plane, with the middle selenocyanate group in the plane. In the cesium salt, the present work, the middle selenocyanate group is located on a crystallographic twofold axis.

CRYSTAL DATA

Preparative and crystallographic data, and a short note of the crystal structure of cesium triselenocyanate have been reported earlier.[4,5]

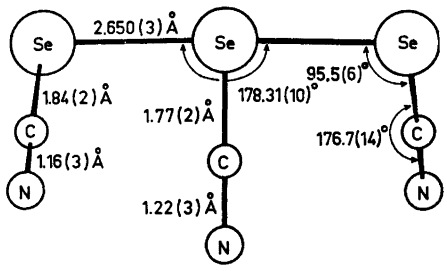

Fig. 1. The triselenocyanate ion in $Cs(SeCN)_3$, as seen normal to the plane through the middle selenocyanate group and the terminal selenium atoms.

The salt, $Cs(SeCN)_3$, forms brown monoclinic prisms extended along the c axis, with $a=7.969(4)$ Å, $b=21.156(10)$ Å, $c=5.593(4)$ Å, and $\beta=98.84(6)°$. The unit cell dimensions were determined from zero-layer Weissenberg photographs around the three axis; 32 observations were measured and evaluated by means of a least squares program.

There are four formula units per unit cell; density, calc. and found 3.18 g/cm³. The space group, from systematic absences and subsequent structure analysis, is $C2/c$ (No. 15).

Intensities were estimated visually from integrated Weissenberg photographs around the a and c axes, taken with Cu$K\alpha$ radiation using the multi-film technique. The three-dimensional refinement was based on the $0kl-2kl$ and $hk0-hk3$ data. In all 637 out of 842 independent reflections accessible with Cu$K\alpha$ radiation were observed with measurable intensities. Three different crystals were used; the crystal used for collection of $0kl-2kl$ data had the following dimensions, from an arbitrarily chosen origin to crystal faces: to (010) and $(0\bar{1}0)$, 0.037 mm; to $(2\bar{1}0)$ and $(\bar{2}10)$, 0.058 mm; to $(01\bar{2})$ and $(0\bar{1}2)$, 0.070 mm. The dimensions of the crystal used for $hk0-hk2$ data were: to $(\bar{1}00)$ and (100), 0.025 mm; to $(0\bar{1}0)$ and (010), 0.040 mm; to $(\bar{1}2\bar{1})$ and $(12\bar{1})$, 0.070 mm. The dimensions of the crystal used for $hk3$ data were:

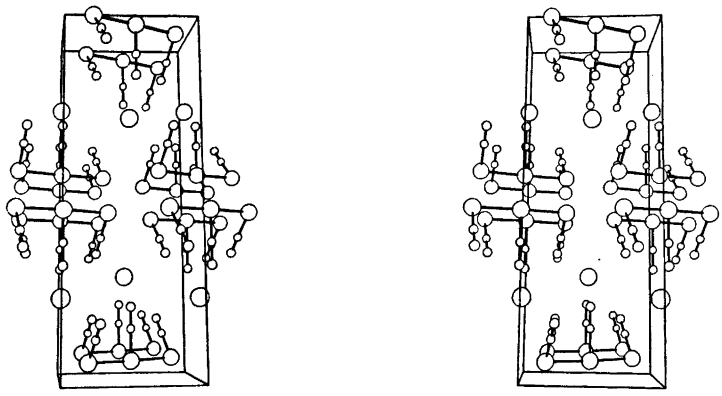

Fig. 2. A stereoscopic pair of drawings showing the content of the unit cell.

to (010) and (0$\bar{1}$0), 0.019 mm; to (110) and ($\bar{1}$10), 0.023 mm; to (12$\bar{1}$) and ($\bar{1}\bar{2}$1), 0.043 mm. The linear absorption coefficient, μ=456.8 cm^{-1}.

The intensities were corrected for absorption by the method of Coppens *et al.*[6] The subdivisions in Gaussian points along the *a*, *b*, and *c* axes were, respectively: for the crystal used for collection of $0kl-2kl$ data, 10, 6, and 10; for the crystal used for collection of $hk0-hk2$ data, 8, 10, and 8; and for the crystal used for collection of $hk3$ data, 8, 8, and 10.

Later the structure factors were corrected for secondary extinction, using the method of Zachariasen,[7] neglecting the absorption term: $F_{corr}=KF_o(1+\beta CI_o)$, where $\beta=2(1+\cos^4 2\theta)/(1+\cos^2 2\theta)^2$. C was found to be 3.2×10^{-6}, 3.3×10^{-6}, and 2.5×10^{-6}, for the $0kl-2kl$, $hk0-hk2$, and $hk3$ data, respectively. The intensities of reflections that occurred more than once in the data set were then averaged, and such reflections thereafter included only once.

THE STRUCTURE ANALYSIS

With four cesium ions and four triselenocyanate ions in the unit cell, the space group, $C2/c$, if correct, would demand that the ions lie in special positions. From the $hk0$ and $0kl$ Patterson maps it was found that both the cesium ion and the middle selenocyanate group in the triselenocyanate ion were located on a crystallographic twofold axis.

The approximate y coordinate of the cesium ion was found from the $hk0$ and $0kl$ Patterson maps. The selenium atoms were placed partly on the basis of subsequent $hk0$ and $0kl$ Fourier maps and partly on the basis of the two Patterson maps. The positions of the carbon and nitrogen atoms were found from a three-dimensional Fourier map based on the determined positions of the cesium and selenium atoms, and from known dimensions of the triselenocyanate group.

The three-dimensional refinement was carried out on the IBM 360/50H computer using a full-matrix least squares program minimizing the function

$$r = \sum W(|F_o|-K|F_c|),^2$$

where K is the scale factor and

$$W=1/[(Ka_1)^2+(a_2F_o)^2/4W_o+(a_3F_o)].$$

The weight W_o is based on the estimated reliability of the film readings. The constant a_1, a_2, and a_3 were given the values 0.8, 0.15, and 0.004, respectively. Unobserved reflections with calculated structure factors, $|F_c|$, greater than threshold value, F_t, were included in the refinement with F_o equal to F_t.

The final refinement, with anisotropic temperature factors for all atoms, brought the reliability index, R, down to 0.062, with unobserved reflections included if $|F_c|$ exceeds the observable limit, F_t.

A three-dimensional Fourier difference map based on the data of Table 3 showed no higher peak than 1.4 e Å^{-3}.

Most computer programs were made available by the Chemical Department of X-Ray Crystallography, Weizmann Institute of Science, Rehovoth, Israel, and modified for use on the IBM 360/50H computer by Dr. D. Rabinovich. The programs used for secondary extinction corrections and Fourier summations were written by K. Åse, and the programs used for calculating distances and angles, and least squares planes, were written by K. Maartmann-Moe, both of this Institute.

Table 1. Atomic coordinates for cesium triselenocyanate in fractions of monoclinic cell edges, with origin on a center of symmetry. Standard deviations from least squares are given in parentheses.

	x	y	z
Cs	0	0.22063(7)	1/4
Se_1	0.1850(3)	0.05816(8)	0.0356(4)
Se_2	½	0.05631(10)	1/4
C_1	0.222(3)	0.1196(8)	−0.185(3)
C_2	½	0.1400(11)	1/4
N_1	0.246(3)	0.1603(9)	−0.314(4)
N_2	½	0.1978(9)	1/4

Table 2. Anisotropic temperature parameters (Å²) in the form $\exp -[B_{11}(h^2/4a^2)+...+B_{23}(kl/4bc+...]$.

	B_{11}	B_{22}	B_{33}	B_{23}	B_{13}	B_{12}
Cs	5.68(12)	3.44(5)	3.32(6)	0	−0.95(7)	0
Se_1	3.39(9)	3.84(7)	5.42(10)	0.31(6)	−0.32(8)	−0.24(7)
Se_2	3.77(13)	2.57(8)	4.29(11)	0	−0.48(11)	0
C_1	3.8(8)	5.0(8)	3.8(7)	−0.1(6)	−1.5(8)	−0.5(7)
C_2	10.9(26)	3.4(9)	4.7(12)	0	0.0(16)	0
N_1	6.1(12)	6.9(9)	8.3(12)	1.9(9)	−0.7(11)	1.5(10)
N_2	8.3(18)	2.5(7)	6.1(12)	0	2.1(13)	0

The calculated structure factors were based on atomic scattering factors given in *International Tables* (Ref. 8, Table 3.3.1A). The scattering factors for cesium and selenium were corrected for anomalous dispersion, real and imaginary parts (Ref. 8, Table 3.3.2A), by taking the amplitude of f as the corrected value.

The final atomic coordinates and temperature factors are listed in Tables 1 and 2, and structure factors in Table 3.

RESULTS

Bond lengths and angles in the triselenocyanate ion, based on the atomic coordinates in Table 1 are listed in Table 4. The uncertainties in cell dimensions are taken into account in the given standard deviations. In Tables 4 and 5 a prime denotes an atom located at $1-x,y,\frac{1}{2}-z$ relative to the unprimed one.

In the triselenocyanate ion, the symmetry of a twofold axis makes the two Se—Se bonds equal. The Se—Se bond length is 2.650(3) Å. The three-selenium sequence is very nearly linear, with Se—Se—Se bond angle of 178.31(10)°. The middle selenocyanate group, located on a twofold axis, is exactly linear and bisects the Se—Se—Se angle. The terminal selenocyanate group is linear within error; the Se—C—N angle is 176.7(14)°. The Se—Se—C bond angle is 89.15(7)° at the central selenium atom, and 95.5(6)° at the terminal selenium atom.

Due to the twofold axis, the atoms of the middle selenocyanate group and the terminal selenium atoms of the three-selenium sequence are exactly coplanar. The atoms of a terminal selenocyanate group and the central selenium atom are approximately coplanar, the largest deviation of an atom from a least squares plane being 0.03 Å. The angle between the two least squares planes is 87.8°, and the angle between one of the least squares planes, and the plane through the middle selenocyanate group and the two terminal selenium atoms, is one half of this value, 43.9°.

This is the third crystal structure reported of a salt of the triselenocyanate ion. The triseleno-

Table 3. Observed and calculated structure factors. Unobserved reflections are indicated by a minus sign on $F(O)$.

H	K	L	F(O)	F(C)
0	2	0	45	49
0	4	0	113	107
0	6	0	206	-211
0	8	0	241	-244
0	10	0	187	-184
0	12	0	166	-157
0	14	0	148	148
0	16	0	56	50
0	18	0	177	183
0	20	0	15	13
0	22	0	19	16
0	24	0	54	-52
0	26	0	45	-46
0	2	1	142	-140
0	4	1	36	-31
0	6	1	288	-305
0	8	1	131	131
0	10	1	78	-77
0	12	1	176	178
0	14	1	42	40
0	16	1	38	35
0	18	1	-10	6
0	20	1	60	-56
0	22	1	12	-12
0	24	1	60	-58
0	26	1	26	25
0	0	2	161	-162
0	2	2	218	220
0	4	2	80	-74
0	6	2	-8	3
0	8	2	70	-65
0	10	2	67	-64
0	12	2	63	61
0	14	2	55	-53
0	16	2	88	88
0	18	2	45	-42
0	20	2	43	39
0	22	2	32	-28
0	24	2	-7	1
0	26	2	-4	-1
0	2	3	40	33
0	4	3	94	-94
0	6	3	105	101
0	8	3	91	-95
0	10	3	95	93
0	12	3	62	-60
0	14	3	30	26
0	16	3	12	-11
0	18	3	24	-19
0	20	3	21	15
0	22	3	19	-17
0	24	3	40	32
0	0	4	171	155
0	2	4	20	-16
0	4	4	70	75
0	6	4	76	-79
0	8	4	75	-72
0	10	4	47	-47
0	12	4	61	-66
0	14	4	58	61
0	16	4	-10	-2
0	18	4	81	74
0	20	4	9	-3
0	22	4	16	16
0	2	5	79	-78
0	4	5	26	-25
0	6	5	91	-101
0	8	5	33	37
0	10	5	24	-24
0	12	5	80	80
0	14	5	25	23
0	16	5	21	21
0	18	5	-6	-2
0	0	6	52	-52
0	2	6	28	31
0	4	6	31	-33
0	6	6	23	22
0	8	6	-10	9
0	10	6	-9	0
0	12	6	19	20
0	14	6	23	-26
0	2	7	10	12
0	4	7	15	-20
1	3	0	87	-86
1	5	0	113	120
1	7	0	130	-137
1	9	0	164	164
1	11	0	87	-88
1	13	0	82	86
1	15	0	49	-48
1	17	0	-10	-8
1	19	0	-10	5
1	21	0	49	-49
1	23	0	42	36
1	25	0	25	-23
1	27	0	21	24
1	1	1	101	-101
1	3	1	59	56
1	5	1	206	-215
1	7	1	29	24
1	9	1	36	32
1	11	1	-11	-4
1	13	1	112	114
1	15	1	55	-53
1	17	1	67	68
1	19	1	81	-83
1	21	1	26	22
1	23	1	23	-21
1	25	1	-7	6
1	1	2	68	61
1	3	2	112	109
1	5	2	130	-132
1	7	2	67	66
1	9	2	154	-163
1	11	2	47	44
1	13	2	83	-84
1	15	2	63	63
1	17	2	42	36
1	19	2	-11	6
1	21	2	47	44
1	23	2	37	-37
1	25	2	14	13
1	1	3	39	40
1	3	3	246	-248
1	5	3	84	-86
1	7	3	137	-139
1	9	3	-12	7
1	11	3	147	141
1	13	3	65	57
1	15	3	121	122
1	17	3	46	-41
1	19	3	16	14
1	21	3	85	-79
1	23	3	31	-27
1	1	4	69	-68
1	3	4	76	-77
1	5	4	85	93
1	7	4	22	-18
1	9	4	113	125
1	11	4	20	-14
1	13	4	49	47
1	15	4	56	-55
1	17	4	45	-39
1	19	4	15	-12
1	21	4	29	-27
1	1	5	55	-63
1	3	5	44	43
1	5	5	44	-42
1	7	5	25	21
1	9	5	-12	5
1	11	5	28	-23
1	13	5	37	32
1	15	5	31	-30
1	17	5	32	29
1	1	6	-12	-6
1	3	6	19	18
1	5	6	31	-33
1	7	6	41	41
1	9	6	31	-31
1	11	6	25	25
1	13	6	24	-24
1	1	-1	48	42
1	3	-1	449	-411
1	5	-1	145	-141
1	7	-1	167	-170
1	9	-1	-12	10
1	11	-1	151	161
1	13	-1	94	94
1	15	-1	172	184
1	17	-1	61	-61
1	19	-1	17	13
1	21	-1	94	-104
1	23	-1	44	-35
1	25	-1	23	-21
1	1	-2	179	186
1	3	-2	164	148
1	5	-2	138	-129
1	7	-2	39	-26
1	9	-2	299	-294
1	11	-2	-21	-5
1	13	-2	50	-51
1	15	-2	96	101
1	17	-2	76	76
1	19	-2	45	44
1	21	-2	53	49
1	23	-2	60	-53
1	1	-3	93	-98
1	3	-3	109	111
1	5	-3	64	-60
1	7	-3	23	22
1	9	-3	-13	9
1	11	-3	27	-23
1	13	-3	40	33
1	15	-3	68	-70
1	17	-3	56	55
1	19	-3	41	-38
1	21	-3	34	32
1	23	-3	-7	-6
1	1	-4	44	42
1	3	-4	22	-23
1	5	-4	44	41
1	7	-4	94	-93
1	9	-4	57	55
1	11	-4	62	-63
1	13	-4	34	36
1	15	-4	-13	-6
1	17	-4	20	16
1	19	-4	13	13
1	21	-4	27	-25
1	3	-5	43	41
1	5	-5	74	-77
1	7	-5	-13	7
1	9	-5	31	-29
1	11	-5	-13	-7
1	13	-5	28	27
1	15	-5	-13	-3
1	17	-5	48	49
1	19	-5	26	-24
1	21	-5	18	19
1	1	-6	38	32
1	3	-6	35	36
1	5	-6	36	-34
1	7	-6	-12	3
1	9	-6	64	-65
1	11	-6	-10	5
1	13	-6	15	-17
1	1	-7	14	-17
1	3	-7	28	32
2	2	0	193	-194
2	4	0	154	164
2	6	0	52	-56
2	8	0	31	23
2	10	0	63	61
2	12	0	74	-74
2	14	0	74	72
2	16	0	80	-80
2	18	0	47	43
2	20	0	35	-31
2	22	0	40	35
2	24	0	-9	-10
2	26	0	-6	-6
2	2	1	284	-277
2	4	1	58	-54
2	6	1	240	-258
2	8	1	77	73
2	10	1	55	-53
2	12	1	160	147
2	14	1	67	66
2	16	1	59	59
2	18	1	-11	-4
2	20	1	77	-76
2	22	1	28	-19
2	24	1	54	-55
2	26	1	14	19
2	0	2	322	-356
2	2	2	43	-35
2	4	2	148	-146
2	6	2	159	171
2	8	2	171	178
2	10	2	116	115
2	12	2	108	110
2	14	2	111	-116
2	16	2	34	-27
2	18	2	119	-127
2	20	2	14	-10
2	22	2	22	-20
2	24	2	37	43
2	2	3	96	91
2	4	3	47	-39
2	6	3	119	120
2	8	3	84	-80
2	10	3	77	71
2	12	3	88	-86
2	14	3	-14	0
2	16	3	25	-23
2	18	3	-12	-4
2	20	3	39	33
2	22	3	11	-9
2	0	4	61	59
2	2	4	98	-103
2	4	4	55	58
2	6	4	-12	-14
2	8	4	31	30
2	10	4	37	32
2	12	4	39	-34
2	14	4	43	37
2	16	4	62	-55
2	18	4	31	26
2	20	4	23	-22
2	2	5	31	-32
2	4	5	29	27
2	6	5	64	-64
2	8	5	47	45
2	10	5	42	-43
2	12	5	45	43
2	14	5	-10	-6
2	16	5	12	12
2	0	6	86	-84
2	2	6	17	11
2	4	6	32	-30
2	6	6	34	34
2	8	6	27	25
2	10	6	23	18
2	12	6	30	30
2	2	-1	83	84
2	4	-1	199	-211
2	6	-1	66	65
2	8	-1	104	-113
2	10	-1	132	141
2	12	-1	46	-41
2	14	-1	62	60
2	16	-1	13	-10
2	18	-1	31	-26
2	20	-1	17	11
2	22	-1	39	-34
2	24	-1	32	28
2	26	-1	16	-15
2	0	-2	238	-263
2	2	-2	40	33
2	4	-2	126	-125
2	6	-2	123	115
2	8	-2	105	95
2	10	-2	58	52
2	12	-2	101	97
2	14	-2	83	-84
2	16	-2	-12	6
2	18	-2	92	-91
2	20	-2	-12	0
2	22	-2	28	-25
2	24	-2	31	26
2	2	-3	171	-165
2	4	-3	87	-83
2	6	-3	206	-212
2	8	-3	50	46
2	10	-3	22	-14
2	12	-3	151	156
2	14	-3	63	63
2	16	-3	45	44
2	18	-3	-12	-5
2	20	-3	63	-60
2	22	-3	29	-24
2	24	-3	35	-44
2	0	-4	135	138
2	2	-4	39	-35
2	4	-4	55	52
2	6	-4	59	-54
2	8	-4	40	-35
2	10	-4	24	-18
2	12	-4	45	-47
2	14	-4	52	51
2	16	-4	-13	-10
2	18	-4	52	49
2	20	-4	12	-10
2	22	-4	9	10
2	2	-5	-14	8
2	4	-5	53	-49
2	6	-5	39	37
2	8	-5	43	-44
2	10	-5	39	41
2	12	-5	20	-21
2	14	-5	21	20
2	16	-5	-10	-2
2	18	-5	9	-8
2	0	-6	46	-42
2	2	-6	34	29
2	4	-6	22	-21
2	6	-6	-13	12
2	8	-6	-13	-3
2	10	-6	-12	-4
2	12	-6	19	20
2	14	-6	16	-16
2	2	-7	15	-17
2	4	-7	-7	-1
3	0	0	104	96
3	1	0	224	-244
3	3	0	168	-164
3	5	0	165	161
3	7	0	67	59
3	9	0	283	296
3	11	0	43	37
3	13	0	67	64
3	15	0	119	-117
3	17	0	102	-101
3	19	0	49	-54
3	21	0	43	-47
3	23	0	44	54
3	25	0	15	13
4	0	0	197	226
4	2	0	71	-69
4	4	0	64	63
4	6	0	61	-55
4	8	0	45	-39
4	10	0	33	-28
4	12	0	76	-70
4	14	0	61	58
4	16	0	25	-23
4	18	0	71	73
4	20	0	-20	-9
4	22	0	19	18
4	24	0	13	-14
5	1	0	64	67
5	3	0	26	-22
5	5	0	44	36
5	7	0	105	-98
5	9	0	42	34
5	11	0	78	-73
5	13	0	44	39
5	15	0	-24	-1
5	17	0	27	20
5	19	0	24	18
5	21	0	17	-22
5	23	0	12	13
6	0	0	171	171
6	2	0	37	35
6	4	0	62	64
6	6	0	85	-90
6	8	0	95	-96
6	10	0	64	-64
6	12	0	56	-55
6	14	0	59	57
6	16	0	27	25
6	18	0	59	64
6	20	0	-13	7
6	22	0	7	8
7	1	0	59	-50
7	3	0	38	-40
7	5	0	44	44
7	7	0	-21	0
7	9	0	70	73
7	11	0	-20	7
7	13	0	31	26
7	15	0	26	-26
7	17	0	24	-26
7	19	0	12	-15
8	0	0	-19	2
8	2	0	49	-48
8	4	0	-19	14
8	6	0	-18	6
8	8	0	29	25
8	10	0	25	22
8	12	0	-15	-7
8	14	0	-12	5
8	16	0	22	-26
9	1	0	32	-29
9	3	0	28	-27
9	5	0	22	16
9	7	0	19	16
9	9	0	43	46
9	11	0	-10	5
10	0	0	35	37
10	2	0	12	12
10	4	0	-8	11
3	1	1	71	-68
3	3	1	264	259
3	5	1	96	87
3	7	1	126	122
3	9	1	-25	-11
3	11	1	128	-119
3	13	1	57	-50
3	15	1	138	-135
3	17	1	51	49
3	19	1	-28	-18
3	21	1	68	77
3	23	1	25	25
3	25	1	-13	17
4	2	1	33	29
4	4	1	146	134
4	6	1	66	-56
4	8	1	107	102
4	10	1	102	-104
4	12	1	-30	18
4	14	1	63	-56
4	16	1	-30	-4
4	18	1	-28	23
4	20	1	-25	3
4	22	1	28	27
4	24	1	17	-24
5	1	1	34	-36
5	3	1	145	147
5	5	1	-26	20
5	7	1	73	63
5	9	1	-29	3
5	11	1	75	-69
5	13	1	-31	-20
5	15	1	83	-77

Table 3. Continued.

H	K	L	F(o)	F(c)	H	K	L	F(o)	F(c)	H	K	L	F(o)	F(c)	H	K	L	F(o)	F(c)	H	K	L	F(o)	F(c)
5	17	1	35	32	5	21	-1	-18	-17	5	21	2	24	30	6	4	-2	-29	-31	6	16	3	-10	-6
5	19	1	-22	-13	5	23	-1	-12	6	6	0	2	53	-53	6	6	-2	-30	-1	7	1	3	-17	16
5	21	1	39	47	6	2	-1	40	31	6	2	2	55	46	6	8	-2	-30	-33	7	3	3	64	-72
5	23	1	10	10	6	4	-1	46	-41	6	4	2	51	-52	6	10	-2	-31	-33	7	5	3	25	-26
6	2	1	109	-114	6	6	-1	47	45	6	6	2	-31	24	6	12	-2	-30	20	7	7	3	28	-33
6	4	1	65	-66	6	8	-1	39	-40	6	8	2	-31	7	6	14	-2	-29	-12	7	9	3	-14	5
6	6	1	128	-130	6	10	-1	37	36	6	10	2	-31	-3	6	16	-2	36	34	7	11	3	37	36
6	8	1	-27	22	6	12	-1	34	-33	6	12	2	34	28	6	18	-2	-21	-7	7	13	3	19	16
6	10	1	-27	-7	6	14	-1	-26	13	6	14	2	38	-31	6	20	-2	-16	14	8	1	-3	68	-67
6	12	1	103	103	6	16	-1	-23	-7	6	16	2	30	27	7	1	-2	36	31	8	3	-3	79	79
6	14	1	48	48	6	18	-1	-20	-6	6	18	2	25	-26	7	3	-2	29	29	8	5	-3	40	-33
6	16	1	36	37	6	20	-1	-16	13	7	1	2	-28	-12	7	5	-2	40	-34	8	7	-3	52	52
6	18	1	-19	-5	7	1	-1	-25	1	7	3	2	-28	10	7	7	-2	-28	-1	8	9	-3	-15	9
6	20	1	40	-44	7	3	-1	108	-112	7	5	2	37	-27	7	9	-2	52	-49	8	11	-3	42	-40
7	1	1	59	-55	7	5	-1	74	-72	7	7	2	52	45	7	11	-2	-27	2	8	13	-3	24	22
7	3	1	-25	4	7	7	-1	68	-65	7	9	2	32	-26	7	13	-2	-25	-16	8	15	-3	31	-33
7	5	1	44	-43	7	9	-1	-25	10	7	11	2	33	26	7	15	-2	-21	24	8	17	-3	30	24
7	7	1	-25	3	7	11	-1	67	68	7	13	2	-22	-20	7	17	-2	-17	18	8	19	-3	34	-35
7	9	1	-24	5	7	13	-1	52	45	7	15	2	-18	5	7	19	-2	-10	7	8	21	-3	28	30
7	11	1	-23	2	7	15	-1	53	58	7	17	2	-11	-2	8	0	-2	79	-76	8	23	-3	-8	8
7	13	1	32	35	7	17	-1	-16	-11	8	0	2	103	-98	8	2	-2	-26	-21	4	2	-3	24	-17
7	15	1	-18	-15	7	19	-1	-12	-5	8	2	2	25	-22	8	4	-2	26	-22	4	4	-3	64	64
7	17	1	18	17	8	2	-1	-23	11	8	4	2	23	-21	8	6	-2	31	33	4	6	-3	43	-42
8	2	1	28	-28	8	4	-1	-23	-9	8	6	2	45	43	8	8	-2	51	45	4	8	-3	61	61
8	4	1	-22	-1	8	6	-1	27	26	8	8	2	48	48	8	10	-2	34	35	4	10	-3	59	-59
8	6	1	43	-40	8	8	-1	-21	-17	8	10	2	38	37	8	12	-2	28	22	4	12	-3	26	24
8	8	1	-20	20	8	10	-1	-20	21	8	12	2	27	29	8	14	-2	23	-20	4	14	-3	25	-21
8	10	1	-19	-13	8	12	-1	-18	-15	9	1	2	-16	6	9	1	-2	-21	-14	4	16	-3	-16	2
8	12	1	30	29	8	14	-1	-15	-1	9	3	2	-16	18	9	3	-2	-20	2	4	18	-3	-14	7
8	14	1	-13	4	9	1	-1	-19	16	9	5	2	-14	-12	9	5	-2	-19	-3	4	20	-3	-12	-8
9	1	1	-17	6	9	3	-1	-18	-5	9	7	2	-12	4	9	7	-2	-18	19	4	22	-3	-8	14
9	3	1	65	63	9	5	-1	22	19	1	25	-2	-18	-8	9	9	-2	-16	-3	5	1	-3	-16	-9
9	5	1	34	35	9	7	-1	-17	3	3	1	-2	72	-70	9	11	-2	-13	12	5	3	-3	134	130
9	7	1	27	29	9	9	-1	-15	-3	3	3	-2	-24	16	10	2	-2	-11	3	5	5	-3	66	61
9	9	1	-13	-1	9	11	-1	-13	-3	3	5	-2	71	-69	3	1	3	103	104	5	7	-3	96	96
9	11	1	26	-32	10	2	-1	27	25	3	7	-2	134	138	3	3	3	61	-59	5	9	-3	-17	-8
3	1	-1	65	94	10	4	-1	25	26	3	9	-2	-27	-22	3	5	3	84	81	5	11	-3	62	-61
3	3	-1	146	-149	3	1	2	37	-36	3	11	-2	84	85	3	7	3	-17	-5	5	13	-3	42	-43
3	5	-1	20	21	3	3	2	36	32	3	13	-2	72	-65	3	9	3	-18	-15	5	15	-3	61	-58
3	7	-1	85	-85	3	5	2	69	-69	3	15	-2	-32	7	3	11	3	-19	1	5	17	-3	22	21
3	9	-1	-23	3	3	7	2	128	126	3	17	-2	-31	-21	3	13	3	55	-54	5	19	-3	-11	2
3	11	-1	76	77	3	9	2	89	-88	3	19	-2	-30	-26	3	15	3	54	51	5	21	-3	33	42
3	13	-1	-27	-14	3	11	2	77	76	3	21	-2	-26	26	3	17	3	47	-45	6	2	-3	37	-34
3	15	-1	76	82	3	13	2	59	-51	3	23	-2	-21	-16	3	19	3	42	44	6	4	-3	-17	0
3	17	-1	57	-51	3	15	2	-36	16	3	25	-2	28	28	3	21	3	19	-18	6	6	-3	56	-56
3	19	-1	43	37	3	17	2	-35	-12	4	0	-2	196	-225	4	2	3	105	100	6	8	-3	20	18
3	21	-1	41	-50	3	19	2	-32	-12	4	2	-2	-26	5	4	4	3	62	58	6	10	-3	18	-17
3	23	-1	-21	-6	3	21	2	-27	32	4	4	-2	64	-66	4	6	3	172	163	6	12	-3	38	37
3	25	-1	-15	-9	3	23	2	32	-23	4	6	-2	74	83	4	8	3	48	-42	6	14	-3	-14	8
4	2	-1	151	160	4	0	2	131	-146	4	8	-2	86	90	4	10	3	-19	17	6	16	-3	-12	14
4	4	-1	138	129	4	2	2	77	85	4	10	-2	65	59	4	12	3	115	-122	6	18	-3	-10	0
4	6	-1	236	246	4	4	2	60	-55	4	12	-2	69	60	4	14	3	38	-38	7	1	-3	30	-26
4	8	-1	55	-51	4	6	2	45	38	4	14	-2	68	-68	4	16	3	32	-31	7	3	-3	-17	1
4	10	-1	-26	8	4	8	2	-36	0	4	16	-2	-32	-9	4	18	3	-14	-1	7	5	-3	32	-31
4	12	-1	170	-172	4	10	2	-37	-6	4	18	-2	72	-77	4	20	3	38	44	7	7	-3	-16	1
4	14	-1	88	-84	4	12	2	58	55	4	20	-2	-26	0	5	1	3	38	40	7	9	-3	-15	3
4	16	-1	45	-49	4	14	2	45	-45	4	22	-2	-21	-9	5	3	3	99	-98	7	11	-3	-14	1
4	18	-1	-27	8	4	16	2	49	34	4	24	-2	21	24	5	5	3	-18	-8	7	13	-3	20	21
4	20	-1	58	64	4	18	2	59	-53	5	1	-2	78	86	5	7	3	52	-50	7	15	-3	-11	-6
4	22	-1	32	33	4	20	2	-26	20	5	3	-2	75	76	5	9	3	-18	-3	7	17	-3	13	11
4	24	-1	35	50	4	22	2	-19	-17	5	5	-2	58	-56	5	11	3	54	54	8	2	-3	36	-32
5	1	-1	66	70	5	1	2	112	121	5	7	-2	-31	-21	5	13	3	-17	5	8	4	-3	30	-26
5	3	-1	54	-53	5	3	2	116	109	5	9	-2	148	-141	5	15	3	52	55	8	6	-3	36	-39
5	5	-1	66	63	5	5	2	95	-87	5	11	-2	-33	-10	5	17	3	23	-25	8	8	-3	-13	7
5	7	-1	-26	-9	5	7	2	51	-46	5	13	-2	-33	-29	5	19	3	14	16	8	10	-3	-12	1
5	9	-1	-26	-16	5	9	2	172	-171	5	15	-2	51	46	6	2	3	-18	9	8	12	-3	29	32
5	11	-1	-29	1	5	11	2	-35	-20	5	17	-2	46	41	6	4	3	59	-58	8	14	-3	17	18
5	13	-1	38	-35	5	13	2	46	-38	5	19	-2	35	27	6	6	3	22	16	9	1	-3	-12	-2
5	15	-1	50	44	5	15	2	74	69	5	21	-2	26	28	6	8	3	43	-44	9	3	-3	22	23
5	17	-1	-27	-30	5	17	2	62	64	6	0	-2	-29	-10	6	10	3	48	52	9	5	-3	13	12
5	19	-1	35	34	5	19	2	37	33	6	2	-2	69	69	6	12	3	-15	-9	9	7	-3	15	12
															6	14	3	18	22	9	9	-3	-7	0

cyanate ion has in all three salts been found to have a nearly linear three-selenium sequence. In the potassium salt [2] no molecular symmetry is required, and the three-selenium sequence is asymmetric with Se—Se bonds of 2.689(4) Å and 2.648(4) Å. In the rubidium salt [3] the three-selenium sequence is symmetric and the Se—Se bond length is 2.656(3) Å, which is within the error equal to the Se—Se bond length in the present structure.

In the crystal structures of salts of the triiodide ion the total length of the three-center system increases with increasing asymmetry.[9] The same trend is found in the structures of the triselenocyanate ion.

In the potassium and rubidium salts of the triselenocyanate ion, the terminal selenocyanate groups and the central selenium atom are approximately coplanar. In the present structure, the cesium salt, the triselenocyanate ion is fanshaped.

In the middle selenocyanate group the Se—C bond length is 1.77(2) Å and the C—N bond length is 1.22(3) Å. In the terminal group the lengths are 1.84(2) and 1.16(3) Å, respectively. Within the accuracy of the analysis these values

Table 4. Dimensions of the triselenocyanate ion. Bond lengths (Å) and angles (°). Standard deviations are given in parentheses.

Se_1-Se_2	2.650(3)	$\angle Se_1-Se_2-Se_1'$	178.31(10)
Se_1-C_1	1.84(2)	$\angle Se_1-C_1-N_1$	176.7(14)
Se_2-C_2	1.77(2)	$\angle Se_2-C_2-N_2$	180
C_1-N_1	1.16(3)	$\angle Se_1-Se_2-C_2$	89.15(7)
C_2-N_2	1.22(3)	$\angle Se_2-Se_1-C_1$	95.5(6)

Table 5. Equations of planes and distances (Å) from least squares planes. The equations of the least squares planes were calculated with the selenium coordinates given six times the weight of the carbon and nitrogen coordinates. The equations refer to the axes of the unit cell, with coordinates X, Y, and Z in Å.

Plane through Se_1, Se_2 C_2 N_2, and Se_1'
$-0.44937\ X+0.94048\ Z+0.47536=0$
The atoms are exactly coplanar.

Plane through Se_1 C_1 N_1 and Se_2
$-0.31512\ X+0.69370\ Y+0.68057\ Z-0.52248=0$
Se_1 0.002; C_1 −0.028; N_1 0.017; Se_2 0

Table 6. Distances (Å) from the cesium ion to neighbouring nitrogen atoms. Standard deviations are given in parentheses.

$Cs\cdots N_{1A}$	3.23(2)	$Cs\cdots N_{2A}$	3.286(10)
$Cs\cdots N_{1B}$	3.23(2)	$Cs\cdots N_{2B}$	3.286(10)
$Cs\cdots N_{1C}$	3.20(2)		
$Cs\cdots N_{1D}$	3.20(2)		

are the same as found in the corresponding potassium and rubidium salts,[2,3] and in potassium selenocyanate.[10]

In potassium and rubidium triselenocyanate, each selenium atom has two selenium-selenium contacts to atoms in adjacent triselenocyanate ions. The Se···Se distances are in the range 3.467 to 3.602 Å. One of the selenium atoms involved in these contacts approaches the fourth coordination site of a square-planar four-coordination at the central selenium atom. There is no such approach in the present structure. The shortest non-bonding distances are from the central selenium atom, Se_2, to Se_2'' $(1-x,\bar{y},\bar{z})$ and to Se_2''' $(1-x,\bar{y},1-z)$; both are 3.674(3) Å. The angles $C_2-Se_2\cdots Se_2''$ and $C_2-Se_2\cdots Se_2'''$ are both 130.43(4)°.

The cesium ion lies on the twofold axis at $(0,y,1/4)$. The closest contacts of the ion are listed in Table 6. In the table a subscript A denotes an atom located at $(\frac{1}{2}-x,\frac{1}{2}-y,\bar{z})$, B at $(x-\frac{1}{2},\frac{1}{2}-y,z+\frac{1}{2})$, C at $(x,y,z+1)$, and D at $(\bar{x},y,\bar{z}-\frac{1}{2})$, where x, y, z are the atomic coordinates of Table 1. The cesium ion is surrounded by six nitrogen atoms at distances from 3.20 to 3.29 Å. The sum of the ionic radii of cesium and nitrogen is 3.40 Å.[11] The shape of the resulting polyhedron is a rather irregular trigonal prism.

Each of the nitrogen atoms has close contacts to two cesium ions. Those involving the nitrogen atom of the middle selenocyanate group occur in the a plane at $x=\frac{1}{2}$ and are to the cesium atoms at $(\frac{1}{2}-x,\frac{1}{2}-y,\bar{z})$ and $(\frac{1}{2}-x,\frac{1}{2}-y,1-z)$. The N···Cs distances are 3.29 Å and the Cs···N···Cs angle is 116.7°. The nitrogen atom of the terminal selenocyanate group has close contacts to Cs_A and Cs_D. The N···Cs distances are 3.23 and 3.20 Å, the Cs···N···Cs angle is 95.3, and the C—N···Cs angles are 130.0 and

131.3°. The carbon atom, the nitrogen atom, and the two cesium ions are almost coplanar.

REFERENCES

1. Birckenback, L. and Kellermann, K. *Ber. Deut. Chem. Ges. 58* (1925) 2377.
2. Hauge, S. and Sletten, J. *Acta Chem. Scand. 25* (1971) 3094.
3. Hauge, S. *Acta Chem. Scand. 25* (1971) 3103.
4. Hauge, S. *Acta Chem. Scand. 25* (1971) 3081.
5. Hauge, S. *Acta Chem. Scand. 25* (1971) 1134.
6. Coppens, P., Leiserowitz, L. and Rabinovich, D. *Acta Crystallogr. 18* (1965) 1035.
7. Zachariasen, W. H. *Acta Crystallogr. 16* (1963) 1139.
8. *International Tables for X-Ray Crystallography*, Kynoch Press, Birmingham 1962, Vol. III.
9. Mooney Slater, R. C. L. *Acta Crystallogr. 12* (1959) 187.
10. Swank, D. D. and Willett, R. D. *Inorg. Chem. 4* (1965) 499.
11. Pauling, L. *The Nature of the Chemical Bond*, 3rd. Ed., Cornell University Press, Ithaca 1960.

Received August 7, 1974.

Acta Chemica Scandinavica A 29 (1975) 170—174

Crystal Structure of the 1:1 Addition Compound between *p*-Xylene and Hexafluorobenzene

TOR DAHL

Institute of Mathematical and Physical Sciences, University of Tromsø, Box 790, 9001 Tromsø, Norway

The 1:1 addition compound between *p*-xylene and hexafluorobenzene crystallizes in the triclinic space group $P\bar{1}$ with cell parameters $a = 6.844$ Å, $b = 7.327$ Å, $c = 7.318$ Å, $\alpha = 102.42°$, $\beta = 98.13°$, $\gamma = 102.86°$. The crystals show a great tendency to form twins. The partner molecules are stacked alternately in infinite columns. An angle of 5.3° has been found between the molecular planes, whose mean separation within the stack is 3.55 Å. The benzene rings of the partner molecules are twisted 30° relative to each other.

The crystal structures of the 1:1 addition compounds of hexafluorobenzene (HFB) with mesitylene and hexamethylbenzene show considerable differences in interplanar distances and relative orientations of the molecules.[1] As the structure of the mesitylene compound is less similar to typical charge-transfer complexes, the differences may be explained from the higher ionisation potential of the "donor" in this compound.

To test the tenability of this reasoning, the structure of the addition compound between HFB and *p*-xylene, whose ionisation potential is still higher, was investigated.

DESCRIPTION OF THE CRYSTALS. CRYSTAL DATA

X-Ray diagrams taken at room temperature show that most of the crystals are twins of the pseudo-merohedral type.[2] The single crystals obtained were transformed into twins when exposed to the X-ray beam for a few hours.

The crystals are triclinic and the following cell parameters were found: $a = 6.844 \pm 0.008$ Å, $b = 7.327 \pm 0.007$ Å, $c = 7.318 \pm 0.009$ Å, $\alpha = 102.42 \pm 0.10°$, $\beta = 98.13 \pm 0.06°$, $\gamma = 102.86 \pm 0.10°$. Assuming one molecule of each kind in the cell calculated density is 1.42 g/cm³. The twin plane is $(1\bar{1}0)$ and the obliquity is 4.5°.

EXPERIMENTAL

Needle-shaped crystals were obtained by mixing equimolecular amounts of the two components, followed by crystallization and sublimation.

The crystals whose melting point is 27.4 °C,[3] are unstable at room temperature even when kept in sealed capillaries and are completely destroyed due to sublimation after a few days' exposure to the X-ray beam. When cooled below room temperature the crystals are damaged. The intensity data were therefore collected at room temperature and several crystals had to be used.

Cu$K\alpha$-radiation was used for all the diagrams. Cell dimensions were determined from oscillation diagrams which could be indexed, taken about the *c*-axis and using NaCl ($a = 5.6395$ Å) as calibrating substance, and from precession diagrams of the $0kl$- and $h0l$-zone.

The intensity data were collected from Wesisenberg diagrams taken about the *c*-axis. To avoid overlap of reflections from different individuals of the twin crystals and also to decrease the exposure time non-integrated diagrams were used. The precession diagrams mentioned above and oscillation diagrams taken about the *c*-axis were used to calculate interlayer scale factors. All the 329 observed reflections were measured visually, and the intensities of those having important spot-elongation were corrected for this effect.[4] All the crystals used were so small that absorption correction was found to be unimportant and was not performed.

Table 1. Observed and calculated structure factors, ten times the absolute values. The columns listed are *h*, *k*, *l*, F_o and F_c. Unobserved reflections have F_o-values like 1/2 F_{min} and are marked with asterisks.

h	k	l	F_o	F_c	
0	1	0	312.	304.	
0	2	0	172.	-176.	
0	3	0	82.	-81.	
0	4	0	78.	-75.	
0	5	0	47.	47.	
0	6	0	18.	11.	
1	-5	0	8.	1.	*
1	-4	0	49.	-36.	
1	-3	0	68.	57.	
1	-2	0	112.	-115.	
1	-1	0	232.	244.	
1	0	0	288.	283.	
1	1	0	89.	-97.	
1	2	0	43.	35.	
1	3	0	131.	-129.	
1	4	0	18.	-19.	
1	5	0	48.	53.	
2	-6	0	22.	22.	
2	-5	0	16.	*	
2	-4	0	62.	-51.	
2	-3	0	61.	-55.	
2	-2	0	115.	-106.	
2	-1	0	100.	-90.	
2	0	0	169.	-166.	
2	1	0	5.	-6.	*
2	2	0	6.	26.	*
2	3	0	68.	-66.	
3	-5	0	19.	21.	
3	-4	0	24.	-6.	
3	-3	0	87.	-85.	
3	-2	0	69.	-72.	
3	-1	0	48.	46.	
3	0	0	57.	-49.	
3	1	0	130.	-128.	
3	2	0	70.	-57.	
3	4	0	24.	19.	
4	-5	0	19.	20.	
4	-4	0	48.	51.	
4	-3	0	8.	5.	*
4	-2	0	58.	-51.	
4	-1	0	49.	-40.	
4	0	0	58.	-50.	
4	1	0	17.	7.	
4	2	0	36.	42.	
4	3	0	19.	17.	
5	-3	0	19.	27.	
5	-2	0	9.	8.	*
5	-1	0	8.	2.	*
5	0	0	29.	29.	
5	1	0	44.	46.	
5	3	0	18.	-6.	
-5	1	1	8.	10.	*
-5	2	1	8.	-1.	*
-5	3	1	9.	-7.	*
-5	4	1	9.	6.	*
-4	-4	1	36.	-38.	
-4	-2	1	34.	28.	
-4	-1	1	36.	40.	
-4	0	1	20.	19.	
-4	1	1	38.	-40.	
-4	2	1	15.	14.	
-4	3	1	19.	20.	
-4	4	1	8.	-6.	*
-3	-5	1	19.	-21.	
-3	-3	1	29.	28.	
-3	-2	1	44.	-39.	
-3	-1	1	44.	46.	
-3	0	1	50.	-52.	
-3	1	1	116.	-133.	
-3	2	1	47.	41.	
-3	3	1	44.	52.	
-3	4	1	16.	11.	
-3	5	1	19.	-27.	
-3	6	1	19.	-20.	
-2	-4	1	36.	32.	
-2	-3	1	71.	-74.	
-2	-2	1	138.	-136.	
-2	-1	1	99.	100.	
-2	0	1	31.	43.	
-2	1	1	127.	151.	
-2	2	1	30.	-34.	
-2	3	1	112.	-106.	
-2	4	1	15.	14.	
-2	5	1	18.	-18.	
-1	-4	1	46.	48.	
-1	-3	1	36.	38.	
-1	-2	1	113.	123.	
-1	-1	1	91.	-96.	
-1	0	1	103.	-126.	
-1	1	1	143.	149.	
-1	2	1	118.	-105.	
-1	3	1	56.	-53.	
-1	4	1	37.	33.	
-1	5	1	8.	-6.	*
0	-4	1	41.	39.	
0	-3	1	28.	-26.	
0	-2	1	40.	39.	
0	-1	1	89.	-99.	
0	0	1	201.	-204.	
0	2	1	144.	116.	
0	3	1	95.	97.	
0	4	1	16.	16.	
0	6	1	19.	27.	
1	-5	1	8.	11.	*
1	-4	1	46.	-47.	
1	-3	1	167.	-178.	
1	-2	1	126.	117.	
1	-1	1	176.	188.	
1	0	1	102.	99.	
1	1	1	64.	43.	
1	2	1	178.	-166.	
1	3	1	17.	12.	
1	4	1	21.	11.	
2	-3	1	47.	51.	
2	-2	1	5.	-12.	*
2	-1	1	161.	-153.	
2	0	1	89.	95.	
2	1	1	75.	-68.	
2	2	1	102.	-85.	
2	3	1	46.	44.	
2	4	1	22.	-26.	
3	-3	1	64.	59.	
3	-2	1	85.	-75.	
3	-1	1	81.	-79.	
3	0	1	83.	84.	
3	1	1	48.	41.	
3	2	1	50.	44.	
3	3	1	42.	-38.	
3	4	1	45.	-50.	
4	-2	1	16.	10.	
4	-1	1	28.	27.	
4	0	1	8.	6.	*
4	1	1	5.	*	*
4	2	1	9.	-7.	*
4	3	1	24.	-30.	
5	-3	1	18.	-19.	
5	-2	1	28.	-23.	
5	-1	1	9.	-9.	*
5	1	1	19.	24.	
-5	-2	2	21.	28.	
-5	2	2	9.	-4.	*
-4	-2	2	38.	-33.	
-4	-1	2	57.	-59.	
-4	0	2	6.	-1.	*
-4	1	2	8.	-14.	*
-4	2	2	45.	-47.	
-4	3	2	9.	-3.	*
-4	4	2	9.	20.	*
-3	-3	2	30.	-22.	
-3	-2	2	19.	-17.	
-3	-1	2	51.	-54.	
-3	0	2	33.	-35.	
-3	1	2	53.	-56.	
-3	2	2	60.	-65.	
-3	3	2	44.	-41.	
-3	4	2	9.	-14.	*
-2	-5	2	21.	22.	
-2	-4	2	45.	-46.	
-2	-3	2	24.	-22.	
-2	-2	2	6.	-6.	*
-2	-1	2	53.	-59.	
-2	0	2	36.	43.	
-2	1	2	43.	-44.	
-2	2	2	6.	6.	*
-2	3	2	16.	-9.	
-2	4	2	31.	-25.	
-2	5	2	10.	15.	*
-1	-6	2	21.	25.	
-1	-4	2	79.	-82.	
-1	-3	2	67.	-65.	
-1	-2	2	64.	-67.	
-1	-1	2	480.	533.	
-1	0	2	523.	664.	
-1	1	2	60.	-51.	
-1	2	2	66.	-64.	
-1	3	2	84.	-70.	
-1	4	2	8.	-3.	*
-1	5	2	31.	27.	
0	-5	2	26.	-20.	
0	-4	2	7.	-2.	*
0	-3	2	6.	-19.	*
0	-2	2	19.	13.	
0	-1	2	422.	576.	
0	0	2	182.	207.	
0	1	2	104.	-80.	
0	2	2	64.	-58.	
0	3	2	111.	-112.	
0	4	2	48.	53.	
0	5	2	24.	25.	
1	-5	2	21.	-22.	
1	-4	2	16.	-19.	
1	-3	2	68.	-70.	
1	-2	2	65.	-63.	
1	-1	2	76.	-76.	
1	0	2	140.	-135.	
1	1	2	117.	108.	
1	2	2	70.	-48.	
1	3	2	56.	-46.	
1	4	2	41.	45.	
2	-4	2	60.	-58.	
2	-3	2	87.	-103.	
2	-2	2	6.	-8.	*
2	-1	2	24.	-17.	
2	0	2	87.	-96.	
2	1	2	101.	-92.	
2	2	2	75.	-72.	
2	3	2	22.	18.	
3	-3	2	63.	-47.	
3	-2	2	50.	-45.	
3	-1	2	60.	-60.	
3	0	2	76.	-85.	
3	1	2	8.	-5.	*
3	2	2	29.	35.	
3	3	2	32.	25.	
4	-2	2	8.	-16.	*
4	-1	2	8.	-1.	*
4	0	2	46.	56.	
4	1	2	49.	59.	
5	-2	2	24.	22.	
-5	2	3	16.	6.	
-4	0	3	51.	-46.	
-4	1	3	7.	-15.	*
-4	2	3	26.	28.	
-4	3	3	8.	13.	*
-3	-3	3	55.	-48.	
-3	-2	3	13.	-11.	
-3	-1	3	25.	14.	
-3	0	3	6.	*	*
-3	1	3	35.	34.	
-3	2	3	26.	-20.	
-3	3	3	7.	-6.	*
-3	4	3	8.	-8.	*
-2	-5	3	16.	18.	
-2	-2	3	30.	32.	
-2	-1	3	54.	-58.	
-2	0	3	46.	44.	
-2	1	3	23.	24.	
-2	2	3	75.	-91.	
-2	3	3	13.	-1.	
-2	4	3	7.	-2.	*
-1	-5	3	18.	22.	
-1	-4	3	17.	18.	
-1	-3	3	25.	28.	
-1	-2	3	30.	-33.	
-1	-1	3	140.	-160.	
-1	0	3	21.	20.	
-1	1	3	47.	51.	
-1	2	3	38.	41.	
-1	3	3	43.	43.	
-1	4	3	7.	-7.	*
0	-4	3	52.	-62.	
0	-3	3	33.	-34.	
0	-2	3	63.	74.	
0	-1	3	66.	72.	
0	0	3	103.	91.	
0	1	3	23.	-19.	
0	2	3	4.	-7.	*
0	3	3	18.	11.	
0	4	3	7.	6.	*
0	5	3	19.	27.	
1	-4	3	14.	-13.	
1	-3	3	33.	35.	
1	-2	3	4.	- *	*
1	-1	3	9.	11.	
1	0	3	35.	31.	
1	1	3	126.	-122.	
1	2	3	29.	-22.	
1	3	3	7.	9.	*
1	5	3	16.	11.	
2	-4	3	33.	39.	
2	-3	3	12.	5.	
2	-2	3	117.	-117.	
2	-1	3	5.	4.	*
2	0	3	67.	56.	
2	1	3	12.	7.	
2	2	3	15.	19.	
2	3	3	45.	-52.	
2	4	3	19.	-21.	
3	-4	3	8.	8.	*
3	-3	3	13.	-2.	
3	-2	3	6.	-3.	*
3	-1	3	37.	33.	
3	0	3	6.	5.	*
3	1	3	7.	8.	*
3	2	3	24.	-29.	
3	3	3	32.	-38.	
4	-3	3	18.	-19.	
4	-2	3	15.	-13.	
4	-1	3	8.	-4.	*
4	0	3	7.	15.	*
4	1	3	16.	24.	
5	-3	3	18.	-21.	
5	0	3	22.	27.	
-4	-2	4	27.	-23.	
-4	0	4	17.	-17.	
-4	1	4	33.	-29.	
-3	-4	4	23.	-17.	
-3	-3	4	20.	-12.	
-3	-2	4	30.	-21.	
-3	-1	4	20.	-18.	
-3	0	4	21.	-18.	
-3	1	4	20.	-17.	
-3	3	4	18.	-17.	
-2	-4	4	34.	-35.	
-2	-3	4	36.	-28.	
-2	-2	4	43.	39.	
-2	-1	4	182.	198.	
-2	0	4	92.	96.	
-2	1	4	22.	-17.	
-2	2	4	35.	-29.	
-2	3	4	25.	-23.	
-1	-3	4	20.	-12.	
-1	-2	4	141.	162.	
-1	-1	4	270.	276.	
-1	0	4	36.	32.	
-1	1	4	41.	-44.	
-1	2	4	56.	-62.	
-1	4	4	19.	32.	
0	-3	4	37.	-31.	
0	-2	4	39.	48.	
0	-1	4	9.	-6.	
0	0	4	27.	-16.	
0	1	4	23.	19.	
0	2	4	53.	-58.	
0	3	4	9.	19.	*
1	-5	4	25.	-20.	
1	-4	4	52.	-53.	
1	-3	4	39.	-43.	
1	-2	4	6.	-15.	*
1	-1	4	65.	-60.	
1	0	4	39.	-29.	
1	1	4	64.	-58.	
1	2	4	33.	-32.	
1	3	4	26.	28.	
2	-4	4	23.	-19.	
2	-3	4	34.	-31.	
2	-2	4	41.	-38.	
2	-1	4	75.	-71.	
2	0	4	65.	-62.	
2	1	4	17.	-14.	
2	2	4	26.	30.	
3	-3	4	22.	-12.	
3	-2	4	27.	-23.	
3	-1	4	9.	- *	*
3	0	4	39.	44.	
3	1	4	41.	39.	
4	-3	4	19.	21.	
4	0	4	28.	22.	
-4	1	5	13.	8.	
-3	-1	5	11.	-10.	
-3	0	5	17.	18.	
-3	1	5	15.	-10.	
-3	2	5	18.	-15.	
-2	-2	5	56.	-40.	
-2	-1	5	31.	-18.	
-2	0	5	29.	23.	
-2	2	5	16.	11.	
-1	-4	5	18.	-14.	
-1	-2	5	12.	4.	
-1	-1	5	46.	38.	
-1	0	5	18.	29.	
-1	2	5	12.	11.	
-1	4	5	14.	16.	
0	-3	5	23.	22.	
0	-2	5	22.	21.	
0	-1	5	28.	26.	
0	0	5	20.	-15.	
0	1	5	35.	-33.	
0	2	5	8.	-5.	
1	-4	5	14.	16.	
1	-3	5	16.	-16.	
1	-2	5	39.	-33.	
1	-1	5	15.	16.	
1	0	5	8.	-5.	
1	2	5	14.	-10.	
1	3	5	24.	-20.	
2	-3	5	12.	-19.	
2	-1	5	22.	18.	
2	2	5	28.	-33.	
2	3	5	12.	-18.	
3	-3	5	14.	-13.	
3	0	5	19.	17.	
4	-3	5	16.	-16.	
4	-1	5	22.	22.	
4	0	5	22.	26.	

STRUCTURE DETERMINATION

As both the partner molecules may have centres of symmetry, the space group $P\bar{1}$ was assumed. Expecting one of the mirror planes of each molecule to coincide approximately with the twin plane, the possible orientations of the molecules were limited, and the correct orientations could be found from a sharpened three-dimensional Patterson synthesis. The HFB molecule and the *p*-xylene molecule were placed in $(0,0,\frac{1}{2})$ and (0,0,0), respectively. Structure factors based on the F-and C-atoms were calculated, giving an *R*-value of 33 %, and least squares refinement was started.

During the least squares refinement, some restrictions were put on the geometry of the molecules. Straight lines were assumed to run along the C–F bonds and the $C-CH_3$ bonds through the centres of the molecules. The quotient between the length of each of these bonds and the distance of the corresponding ring C-atom from the centre of the molecule was kept constant with a value of 1.326/1.394

Table 2. Coordinates and anisotropic thermal parameters according to the expression: $\exp -(B_{11}h^2+B_{22}k^2+B_{33}l^2+B_{12}hk+B_{13}hl+B_{23}kl)$, with estimated standard deviations in parentheses.

	x	y	z	B_{11}	B_{22}	B_{33}	B_{12}	B_{13}	B_{23}
F1	0.2543(21)	−0.2289(19)	0.5279(17)	0.1012(58)	0.0938(55)	0.0998(50)	0.107(9)	0.061(8)	0.067(8)
F2	0.3867(17)	0.1557(17)	0.6872(14)	0.0619(38)	0.1074(52)	0.0557(30)	−0.029(7)	−0.009(5)	0.029(6)
F3	0.1358(19)	0.3819(16)	0.6676(15)	0.1313(62)	0.0496(31)	0.0662(35)	−0.018(7)	0.034(7)	−0.006(5)
C1	0.1303(11)	−0.1173(10)	0.5143(9)	0.0670(78)	0.0632(74)	0.0406(45)	0.061(12)	0.028(9)	0.047(9)
C2	0.1982(9)	0.0797(9)	0.5959(7)	0.0639(82)	0.0569(62)	0.0296(43)	−0.011(12)	0.006(9)	0.031(8)
C3	0.0696(10)	0.1957(8)	0.5859(7)	0.0889(92)	0.0498(75)	0.0302(45)	0.014(13)	0.025(10)	0.021(9)
C4	0.3324(28)	0.3445(27)	0.1886(19)	0.0910(86)	0.0758(72)	0.0471(49)	−0.067(14)	0.000(10)	0.000(9)
C5	0.1911(24)	−0.0163(34)	0.0540(19)	0.0515(59)	0.0688(69)	0.0266(37)	0.037(13)	0.007(7)	0.034(9)
C6	0.1594(13)	0.1652(13)	0.0904(9)	0.0636(79)	0.0530(65)	0.0229(35)	0.013(13)	0.013(8)	0.020(8)
C7	−0.0394(54)	0.1815(23)	0.0348(21)	0.0651(65)	0.0456(51)	0.0332(37)	0.015(11)	0.004(8)	0.015(7)

for the HFB molecule [5] and 1.52/1.40 for the *p*-xylene molecule.

Positional and anisotropic thermal parameters were varied for the F- and C-atoms. H-atoms with positions calculated assuming disorder due to rotation of the methyl groups were also included in the structure factor calculations.

For reflections with $F_o > \sim 3|F|_{min}$ the weight factors chosen were $A(F_o)^{-0.7}$ where A is constant. For the weaker reflections a constant weight was chosen.

55 unobserved low-angle reflections were given values of 1/4 I_{min} for I_o and included in the first cycles of the least squares refinement. In the last cycles only observed reflections were included. During the refinement it became obvious that the observed intensities of the 3 strongest reflections, $\bar{1}\bar{1}2$, $0\bar{1}2$, and $\bar{1}02$ were much too low. This may be due to secondary extinction, but may just as well be due to poorly estimated scale factors between the weakest diagrams of the second layer. It was considered that deleting these reflections from the refinement was more correct than performing corrections for secondary extinction.

In the last refinement cycles 326 reflections were thus included, and 79 independent parameters were varied. The conventional R-value arrived at was 10.8 % ($R_w = 13.2$ %).

A difference synthesis gave no indications neither of the positions of the H-atoms nor of any disorder in the positions of the F- and C-atoms.

All programs used are described in Ref. 6, and the atomic form factors are given in Ref. 7.

DISCUSSION

Observed and calculated structure factors are given in Table 1, positional and thermal parameters in Table 2, bond distances and angles in Table 3, and principal axes of the vibration ellipsoids in Table 4. The orientation and the packing of the molecules and intermolecular distances are shown in Fig. 1.

Rigid-body analysis of the thermal parameters gave r.m.s. discrepancies between observed and calculated amplitudes of vibration of 0.0117 Å for the HFB molecule and 0.0067 Å for the *p*-xylene molecule. In view of the large amplitudes these values seem reasonable. The direc-

Table 3. Bond distances (Å) and angles (°). Estimated standard deviations are from 0.01 to 0.02 Å for the distances, and approximately 1° for the angles. Bond distances corrected for libration are given in parentheses.

C3′–C1	1.39(1.41)	C3′–C1–C2	119.3
C1–C2	1.38(1.40)	C1–C2–C3	120.8
C2–C3	1.36(1.38)	C2–C3–C1′	119.8
C1–F1	1.31(1.31)	F1–C1–C3′	120.2
C2–F2	1.30(1.30)	F1–C1–C2	120.5
C3–F3	1.31(1.31)	F2–C2–C1	119.9
C7′–C5	1.37(1.39)	F2–C2–C3	119.2
C5–C6	1.37(1.40)	F3–C3–C2	120.0
C6–C7	1.40(1.42)	F3–C3–C1′	120.2
C6–C4	1.52(1.52)	C7′–C5–C6	123.4
		C5–C6–C7	118.0
		C6–C7–C5′	118.6
		C4–C6–C5	121.6
		C4–C6–C7	120.4

Table 4. Principal axes of the thermal vibration ellipsoids.

	R.m.s. amplitudes	Components of the r.m.s. amplitudes (Å)		
	Å	$U(x)$	$U(y)$	$U(z)$
F1	0.531	0.401	0.425	0.344
	0.477	0.146	0.149	−0.391
	0.368	−0.242	0.229	0.012
F2	0.577	−2.002	0.503	0.068
	0.405	0.171	0.097	−0.322
	0.311	0.277	0.173	0.207
F3	0.585	0.526	−0.157	0.113
	0.435	0.119	0.129	−0.364
	0.311	0.143	0.306	0.185
C1	0.418	0.323	0.371	0.168
	0.339	−0.223	0.157	0.161
	0.282	0.073	−0.099	0.236
C2	0.454	−0.288	0.289	0.076
	0.315	0.261	0.266	0.098
	0.260	0.017	−0.022	0.255
C3	0.457	0.433	−0.084	0.041
	0.343	0.152	0.358	0.079
	0.268	0.008	0.016	0.272
C4	0.602	0.392	−0.377	0.014
	0.384	0.146	0.123	−0.301
	0.279	0.202	0.222	0.193
C5	0.408	0.107	0.432	0.104
	0.339	0.322	0.002	−0.069
	0.240	0.083	0.004	0.238
C6	0.401	−0.293	0.216	0.013
	0.343	0.253	0.311	0.055
	0.235	0.028	0.027	0.243
C7	0.396	−0.358	0.088	0.060
	0.336	0.117	0.323	−0.051
	0.283	0.113	0.109	0.290

tion of the largest axis of libration is approximately perpendicular to the molecular plane for the HFB molecule and approximately along *c* for the *p*-xylene molecule. Bond distances corrected for libration are given in Table 3.

The largest deviation of the atoms from least squares planes through the molecules is 0.019 Å for the HFB molecule and 0.003 Å for the *p*-xylene molecule not including the H-atoms. These deviations from planarity are not significant. The angle between the *c*-axis and the plane normal of the molecular plane is 16.8° for the HFB molecule and 11.6° for the *p*-xylene molecule. The angle between the molecular planes is 5.3°. This non-parallelism has the effect of increasing the distance from the HFB molecule of the methyl group situated approximately above this molecule (Fig. 1).

The mean separation between the molecular planes is 3.55 Å, not significantly shorter than the separation of 3.56 Å found in the compound between mesitylene and HFB.[8] The twisting of the benzene rings of approximately 30° relative to each other was found also in the mesitylene compound. As distinct from that observed in the mesitylene compound, no distances shorter than 3.59 Å (shown in Fig. 1) between F-atoms and methyl C-atoms of different stacks are present in this structure.

Assuming rotation of the methyl groups, the smallest distances possible were calculated between methyl H-atoms and the adjacent HFB molecule within the stack. These distances were compared with van der Waals distances, using a van der Waals radius of 1.55 Å for the F-atoms in directions approximately perpendicular to the C–F-bonds.[9] It was found that no distances could possibly be within the van der Waals distance neither in the *p*-xylene compound nor in the mesitylene compound. Similar calculations of the distances in the triclinic form of the addition compound between HFB and hexamethylbenzene show several distances from methyl H-atoms within the van der Waals distance both to F-atoms and to the benzene ring of HFB. In this compound the benzene rings have a nearly parallel orientation, and the mean separation between the molecular planes is 3.43 Å.[1]

The relative orientations of the molecules, the distances between the molecular planes, and the results of the more detailed analysis of the

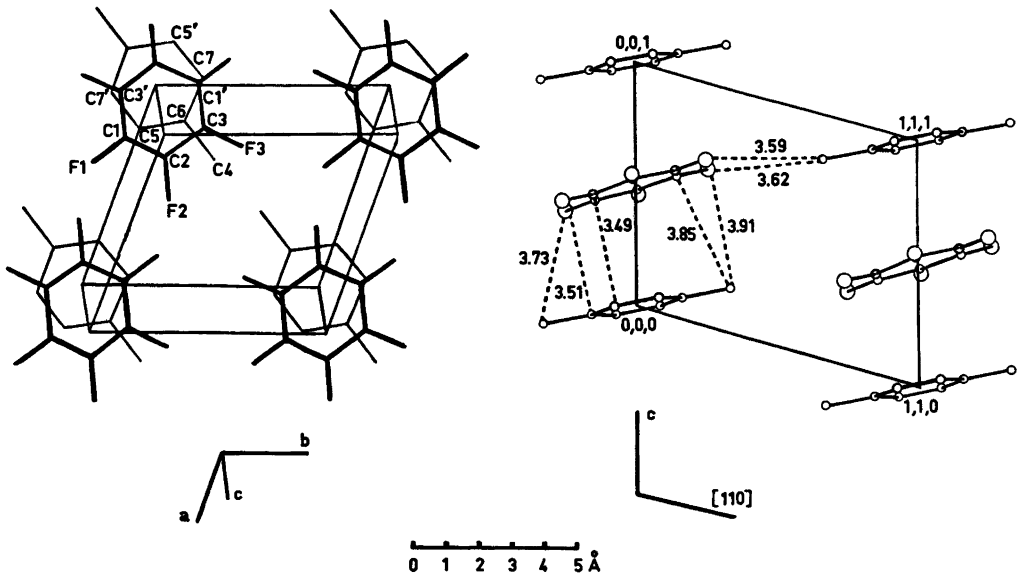

Fig. 1. The packing and the orientation of the molecules viewed perpendicular to the plane of the *p*-xylene molecule (left) and perpendicular to (1$\bar{1}$0) (right). Intermolecular distances, including the shortest ones, within the stack and between different stacks, are given.

intermolecular distances indicate that the intermolecular forces are of a similar kind in the *p*-xylene compound and the mesitylene compound, and that charge-transfer forces contribute little or nothing to these forces. The additional methyl groups in the hexamethylbenzene compound, however, seem to result in charge-transfer forces with considerable effect on the structure. Further informations on how the structure of these compounds varies with varying number of methyl groups were found to be of great interest, and a structure determination of the addition compound between HFB and durene is now going on. The distance between the molecular planes and the relative orientation of the molecules has been found to be something between that found in the hexamethylbenzene compound and that found in the two other addition compounds investigated. A full report of this structure will be published very soon.

REFERENCES

1. Dahl, T. *Acta Chem. Scand. 27* (1973) 995.
2. Cahn, R. W. *Advan. Phys. 3* (1954) 363.
3. Duncan, W. A. and Swinton, F. L. *Trans. Faraday Soc. 62* (1966) 1082.
4. Phillips, D. C. *Acta Crystallogr. 9* (1956) 819.
5. Almenningen, A., Bastiansen, O., Seip, R. and Seip, H. M. *Acta Chem. Scand. 18* (1964) 2115.
6. Groth, P. *Acta Chem. Scand. 27* (1973) 1837.
7. Hanson, H. P., Herman, F., Lea, J. D. and Skillman, S. *Acta Crystallogr. 17* (1964) 1040.
8. Dahl, T. *Acta Chem. Scand. 25* (1971) 1031.
9. Nyburg, S. C. and Szymanski, J. T. *Chem. Commun.* (1968) 669.

Received September 14, 1974.

Acta Chemica Scandinavica A 29 (1975) 175—178

The Raman Spectra of Some Halogen Gas Hydrates

J. W. ANTHONSEN

Department of Chemistry, University of Odense, DK-5000 Odense, Denmark

The Raman spectra of Br_2, Cl_2, and BrCl gas hydrates have been recorded at −196 °C in the range ~20 − 600 cm^{-1}. The spectra indicate remarkably little interaction between the "guest" and "host" molecules in bromine and chlorine gas hydrates and a little more pronounced interaction in bromine chloride gas hydrate. The isotope effect observed in the spectra is in fair agreement with the expected. Bands observed below 200 cm^{-1} are tentatively assigned to translational vibrations of the host molecules.

A clathrate compound may be described as a group of molecules called "guest" molecules, which are enclosed in the cavities in a crystal lattice called the "host" lattice. In the cases where water forms the lattice and where the guest molecules have a diameter less than approximately 5.9 Å, the compound is designated a "gas hydrate".

The first known gas hydrate was that of chlorine, which was discovered by Davy [1] in 1811. The number of guest molecule species, which take part in the formation of gas hydrates, has since turned out to be large.[2–5]

Though it is difficult exactly to predict which molecular species are able to form gas hydrates, the following conditions must in general be fulfilled:[5] The molecule must have a size, which fits in the cavities of the lattice; it must not form hydrogen bonds to the solvent (low solubility in water) and the van der Waals forces in the given molecular species must not be too large (b.p. < ~60 °C).

The structures of these compounds have been described by several authors.[2–6] According to these investigations all such compounds crystallize in one of two cubic structures called type I and type II. The guest molecules are trapped in the cavities formed by a network of hydrogen bonded water molecules. The number and size of these cavities are different in the two structures. As all compounds described in the present investigation belong to type I, type II will not be further discussed.

The unit cell in structure I contains 46 water molecules which form two smaller and six larger cavities. The smaller cavities are very nearly spherical and have a free diameter of approximately 5.2 Å. The larger cavities are slightly oblate with a free diameter of approximately 5.9 Å.

The "empty" host lattice itself is thermodynamically unstable, but becomes stabilized by inclusion of guest molecules.

The difference in chemical potentials $\Delta\mu$ between the stable phase (ice) and the empty type I hydrate has been calculated by van der Waals and Platteeuw [9] at 0 °C to be 167 cal/mol. Though the difference is small, it may explain why the "open ice" host lattice has never been prepared in absence of guest molecules to stabilize it.

The compositions of the compounds investigated here has been determined to be $Cl_2.7.27H_2O$,[10] $Br_2.8.47H_2O$,[11] and $BrCl.4H_2O$.[12]

It is believed that the enclosed guest molecules interact only weakly with the surrounding host molecules. By comparing the wavenumbers of the vibrations of a given molecular species enclosed in the cavities of the lattice with the wavenumbers observed in other phases, it is possible to form an impression of the sizes of these forces.

Chassonneau *et al.*[13] have reported an NMR investigation on some type II hydrates. Until now no spectroscopic investigation on type I gas hydrates have been reported.

EXPERIMENTAL

Chlorine gas hydrate has been prepared by bubbling chlorine gas through a 5 % aqueous $CaCl_2$ solution at 0 °C. The "feathery" crystals, which separated, were filtered off in a cold room at 0 °C. The compound was greenish yellow.

Bromine chlorine gas hydrate was prepared according to the method reported by Anwar-Ullah.[12] Chlorine was bubbled into a layer of bromine under water at 0 °C until a large crop of crystals had separated. The water and crystals were decanted from the bromine and warmed until all crystals were dissolved. The solution was then cooled and inocculated with a few crystals, which had been kept. The crystals, which then precipitated out of solution, were orange-red. The compound were filtered off in a cold room at 0 °C.

In order to prepare bromine gas hydrate, liquid bromine was purified as described by D'Ans and Höfer.[14] The purified bromine was added to distilled water and the mixture then kept agitated for four days at 0 °C in a cold room. The compound was brought to crystallize out of solution by cooling under vigorous stirring. The crystals were filtered off in a cold room at 0 °C. The red gas hydrate was recrystallized once from water.

Instrumental

The Raman spectra were recorded with a spectrometer equipped with a Jarrell-Ash model 25–101 double grating monochromator. The exciting lines used were 6471 Å and 6764 Å obtained from a Spectra-Physics model 165–01 Krypton-ion laser.

The spectra were recorded at −196 °C in the range from the exciting line up to 600 cm^{-1}.

The spectral resolution in any scan is better than 3 cm^{-1}. The spectrometer was calibrated using standard Krypton lines and the wavenumbers are believed to be accurate to within ±1 cm^{-1}.

The compounds were placed at the bottom of a little dewar vessel and cooled directly from the top with liquid nitrogen.

RESULTS

The spectra above 200 cm^{-1}

(i) *Cl_2 gas hydrate.* Above 200 cm^{-1} three bands have been observed in this compound at 538, 545, and 554 cm^{-1}, with a relative intensity ratio at about 1:6:9, respectively. These bands are assigned to the stretching vibration in $^{37}Cl^{37}Cl$, $^{37}Cl^{35}Cl$ and $^{35}Cl^{35}C$, respectively. The isotope shift between $^{35}Cl^{35}Cl$ and $^{37}Cl^{37}Cl$ has been calculated to about 8 cm^{-1} and between $^{35}Cl^{35}Cl$ and $^{37}Cl^{37}Cl$ to about 15 cm^{-1}. The relative intensity ratio $^{37}Cl^{37}Cl$:$^{37}Cl^{35}Cl$:$^{35}Cl^{35}Cl$ has been calculated to about 1:6:9. Both the observed isotope shift and relative intensity ratio are in very good agreement with the calculated values. The wavenumbers are given in Table 1 and for comparison the wavenumbers of the fundamental in other phases are also given.

(ii) *BrCl gas hydrate.* In this range three bands at 317, 414, and 424 cm^{-1} are observed in the Raman spectrum. The two latter, which have a relative intensity ratio at about 1:3.5, are assigned to the stretching vibration in bromine chloride. The isotope shift between $^{79}Br^{35}Cl$ and $^{81}Br^{35}Cl$ is small (calculated to ~2 cm^{-1}) and the band at 424 cm^{-1} is assigned to the fundamental in these two isotropic species. The isotope shift between $^{79}Br^{37}Cl$ and $^{81}Br^{37}Cl$ is

Table 1. Wavenumbers of the stretching vibrations in diatomic halogens (cm^{-1}).

Species	Phase gas hydrate	gas	liquid	solid	matrix	Ref.
$^{35}Cl^{35}Cl$	554	554	548	540	546	16,19,15,20
$^{35}Cl^{37}Cl$	545	547	541	532	539	16,19,15,20
$^{37}Cl^{37}Cl$	538	~540	533	524	–	16,19,15,20
$^{79}Br^{35}Cl$	424	440	–	–	–	16
$^{81}Br^{35}Cl$	424	440	–	–	–	16
$^{79}Br^{37}Cl$	414	432	–	–	–	16
$^{81}Br^{37}Cl$	414	432	–	–	–	16
$^{79}Br^{79}Br$	318	318	306	~300	305	16,17,15,18
$^{79}Br^{81}Br$	318	318	306	~300	305	16,17,15,18
$^{81}Br^{81}Br$	318	318	306	~300	305	16,17,15,18

small as well (calculated to ~ 1 cm^{-1}) and the band at 414 cm^{-1} is assigned to the fundamental of these two isotopic species. The isotope shift between these two pairs is calculated to be approximately 8 cm^{-1} and the relative intensity ratio to be about 1:3. Although the observed isotope shift is larger than expected, the calculated data are in fair agreement with the observed values. The wavenumbers are given in Table 1 together with the wavenumbers in other phases.

The band at 317 cm^{-1} is assigned to the fundamental in bromine, as it is very likely that the bromine chlorine compound contains some bromine gas hydrate. Furthermore the observed wavenumber is very close to the gas-phase value of the stretching vibration in bromine and it is also in accordance with the wavenumber of a far more intense band found in pure bromine gas hydrate.

(iii) *Br_2 gas hydrate.* In bromine gas hydrate the bromine stretching vibration is observed as a relatively broad band at 318 cm^{-1}. No isotope shift was observed in this case, probably because of instrumental conditions. The band center at 318 cm^{-1} is assigned to $^{79}Br^{81}Br$. The isotope shift for $^{79}Br^{79}Br$ and $^{81}Br^{81}Br$ has been calculated to about ± 2 cm^{-1}, respectively. The relative intensity ratio between $^{81}Br^{81}Br$: $^{81}Br^{79}Br$:$^{79}Br^{79}Br$ should be approximately 1:2:1. It is therefore very reasonable that the line broadening is due to overlap of the three bands mentioned above. The wavenumber is given in Table 1 together with the wavenumbers in other phases.

It can be seen from the table, that the stretching vibration wavenumbers in both bromine- and chlorine gas hydrate are very close to the gas-phase values, whereas the matrix values are close to the liquid-phase wavenumbers. This indicates remarkably little interaction between the guest molecules and the surrounding host molecules, far smaller than is the case in a "normal" matrix. Because the enclosed molecules behave very nearly as in the gas-phase it indicates, that there is only trapped one guest molecule in each cavity.

There is a more pronounced deviation between the gas-phase and gas hydrate wavenumbers for the fundamental in bromine chloride, than is the case for the two former mentioned compounds. It is possibly due to the fact that bromine chloride has a small permanent dipole moment, which can interact with the surrounding water lattice. However, there cannot be any doubt about the existence of bromine chloride as a gas hydrate. It should be mentioned that bromine chloride trapped as a gas hydrate was stable several weeks, when stored in a refrigerator, although bromine chloride itself is an unstable compound.

The spectra below 200 cm^{-1}

Bands observed in this region may be due to external vibrations of the water lattice together with translational and hindered rotational motions of the guest molecules in the cavities. In each of the three compounds there has only been observed one band below 200 cm^{-1} at 103 cm^{-1} (s), 88 cm^{-1} (s), and 130 cm^{-1} (m,br) in chlorine, bromine chloride, and bromine gas hydrates, respectively.

The band observed in each compound can hardly be due to a translational or "rattling" motion of the guest molecules, because it then would have been expected that the wavenumber decreased as the mass of the enclosed molecule increased. Furthermore the translational motions should not be active in the Raman spectrum according to the point group symmetry of the free guest molecules, unless the interaction with the lattice has violated the selection rules.

The rotational constants of the free molecules are in each case small ($B < 0.3$ cm^{-1}). This means that the rotational Raman spectrum must be very close to the exciting line in the free unhindered case. As the interaction between guest and host molecules is supposed to be strongest in the case of bromine chloride one would expect, that a band due to a hindered rotational motion would have been observed at higher wavenumber in this compound than in the two other gas hydrates. Because this is not the case, it is unlikely that the bands are due to rotational motions. Furthermore the potential barriers should be relatively high to make the bands appear at a wavenumber as high as observed and this is not in accordance with the small interaction suggested above.

It seems therefore most reasonable to assign these bands to lattice vibrations, although the wavenumbers deviate somewhat from com-

pound to compound. According to Taylor and Whalley [21] in most of the ice modifications only one band – sometimes two – is observed in the low frequency Raman spectrum. This band is observed between 150 and 225 cm^{-1} and is assigned to a translational motion of the water lattice. The observation of only one band also in the gas hydrates is in accordance with the Raman spectra of the pure water modifications. The shift towards lower wavenumber in the gas hydrates could be due to an increasing interaction between the guest molecules and the lattice in the order $BrCl > Cl_2 > Br_2$. This order is in accordance with the spectra above 200 cm^{-1} and the bands below 200 cm^{-1} are therefore tentatively assigned to translational vibrations of the lattice.

Acknowledgement. The author is greatly indebted to Professor C. Knakkergaard Møller for many stimulating discussions and unfailing interest in this work.

REFERENCES

1. Davy, H. *Phil. Trans. Roy. Soc. 101* (1811) 1.
2. von Stackelberg, M. *Fortschr. Mineral. 26* (1947) 122.
3. von Stackelberg, M. *Naturwissenschaften 36* (1949) 327.
4. von Stackelberg, M. and Müller, H. R. *J. Chem. Phys. 19* (1951) 1319.
5. von Stackelberg, M. and Müller, H. R. *Z. Elektrochem. 58* (1954) 25.
6. Claussen, W. F. *J. Chem. Phys. 19* (1951) 259.
7. Claussen, W. F. *J. Chem. Phys. 19* (1951) 1425.
8. Pauling, L. and Marsh, R. E. *Proc. Nat. Acad. Sci. U.S. 38* (1952) 112.
9. van der Waals, J. H. and Platteeuw, J. C. *Advan. Chem. Phys. 2* (1959) 1.
10. Allen, K. W. *J. Chem. Soc.* (1959) 4131.
11. Mulders, E. M. J. *Ph. D. Thesis*, University of Delft, Netherlands 1937.
12. Anwar-Ullah, S. *J. Chem. Soc.* (1932) 1176.
13. Chassonneau, M. A., Dufourcq, J. and Lemanceau, B. *C. R. Acad. Sci. C 273* (1971) 793.
14. D'Ans, J. and Höfer, P. *Angew. Chem. 47* (1934) 71.
15. Cahill, J. E. and Leroi, G. *J. Chem. Phys. 51* (1969) 4514.
16. Holzer, W., Murphy, W. F. and Bernstein, J. H. *J. Chem. Phys. 52* (1970) 399.
17. Stammreich, H. and Forneris, R. *J. Chem. Phys. 22* (1954) 1624.
18. Boal, D. H. and Ozin, G. A. *J. Chem. Phys. 55* (1971) 3598.
19. Stammreich, H. and Forneris, R. *Spectrochim. Acta 17* (1961) 775.
20. Clarke, M. R. and Mamantov, G. *Inorg. Nucl. Chem. Lett. 7* (1971) 993.
21. Taylor, M. J. and Whalley, E. *J. Chem. Phys. 40* (1964) 1660.

Received September 7, 1974.

Acta Chemica Scandinavica A 29 (1975) 179—184

The Raman Spectra of Some Guest Molecules in β-Quinol Clathrates

J. W. ANTHONSEN

Department of Chemistry, University of Odense, DK-5000 Odense, Denmark

The Raman spectra of some β-quinol clathrates together with "empty" β-quinol and α-quinol have been recorded at low-temperature in the range ~20 – 3300 cm^{-1}. The spectra indicates, that some of the enclosed molecular species are able to rotate in the host cavities. Bands below 200 cm^{-1} due to the guest molecules are tentatively assigned to translational motions.

In continuation of an earlier investigation on the clathrate compounds of HCHO, CH_3CHO, CH_3OH, CH_2CH_2, HCOOH, and HCl together with "empty" β-quinol and α-quinol at room temperature,[1] is here reported an investigation of the same compounds at low temperature. Furthermore tha Raman spectra of the guest molecules H_2S and HCN have been recorded both at room temperature and low temperature in the region ~20 – 3300 cm^{-1}.

EXPERIMENTAL

The preparation of all compounds except hydrogen cyanide clathrate has been described before.[1,2] The clathrate of hydrogen cyanide was prepared by adding liquid hydrogen cyanide to a saturated solution of quinol in diethylether. The compound precipitated out of solution as the volatile components evaporated.

The Raman spectra were recorded with a spectrometer equipped with a Jarrell-Ash model 25 – 101 double grating monochromator. The exciting lines used were 4880 and 5145 Å obtained from a Spectra-Physics model 165 – 00 Argon-ion laser and 6471 and 6764 Å from a Spectra-Physics model 165 – 01 Krypton-ion laser.

The spectral resolution in any scan is better than 2.7 cm^{-1} below 200 cm^{-1} and above 1000 cm^{-1} better than 4.2 cm^{-1} depending on the exciting line used. The wavenumbers are believed to be accurate to within ± 1.5 cm^{-1}.

THE GUEST SPECTRA ABOVE 200 cm^{-1}

The wavenumbers, half-widths and relative intensities of the bands assigned to the guest molecules in the eight clathrate compounds at room-temperature and approximately 93 K are given in Table 1. Furthermore the wavenumbers of the liquid- and gas-phase are given for comparison. The Raman spectra at room temperature of all the compounds except hydrogen cyanide have been previously reported.[1–4] It should be mentioned that all observed bands except 2948 cm^{-1} in methanol and 2970 cm^{-1} in acetaldehyde belong to the totally symmetric species in the point groups of the free molecules.

At low temperature the population in the higher rotational energy levels is diminished, which will give rise to reduced half-widths of the bands in the Raman spectrum.

If the trapped guest molecules are able to rotate more or less hindered in the cavities, it will be expected, that bands with a big half-width at room-temperature must have a considerably diminished half-width at 93 K.

In the clathrates of hydrogen chloride, formaldehyde, methanol, formic acid, and acetaldehyde several relatively broad bands are observed at room temperature. At low temperature there is observed a considerably decrease in the half-widths of the broad bands of the three first mentioned compounds, which indicates that these molecules can rotate in the host cavities. Davies and Child [17] have investigated the infrared spectrum of methanol clathrate and suggested that the enclosed molecules rotate in the cavities. This suggestion is supported by the Raman spectrum. It is also

Table 1. Guest bands in the Raman spectra above 200 cm^{-1}.

Guest Species	$T \sim 300$ K Wave-number cm^{-1}	Rel. int. [a]	Half-width cm^{-1}	$T \sim 93$ K Wave-number cm^{-1}	Rel. int. [a]	Half-width cm^{-1}	(Gas) Wave-number cm^{-1}	(Liquid) Wave-number cm^{-1}
HCl	2806	w	16	2804	m	8	2886 [5]	2758 [6]
HCN	2091	m	3	2093	m	3	2095 [7]	2096 [8]
H_2S	2585	w	5	2582	w	5	2611 [5]	2574 [5]
CH_2CH_2	1350	w	8	1354	vw	8	1342 [9]	1339 [10]
CH_3OH	3630	w	13	3619	m	7	3682 [11]	3340 [2]
	2948	w	14	2948	w	8	2977	2946
	2839	w	14	2844	m	10	2844	2837
	1033	w	11	1030	w	7	1034	1038
HCOOH	3484	vw	–	3470	w	13	3570 [12]	3110 [13]
	2948	w	8	2949	m	7	2943	2960
	1747	vw	–	1747	vw	–	1770	1654
	–	–	–	1379	vw	19	1387	1398
	1111	w	28	1116	m	25	1105	1208
HCHO	2790	w	17	2790	m	8	2780 [14]	–
	1732	w	8	1728	m	7	1748	–
	1499	w	9	1500	vw	–	1507	–
CH_3CHO	2970	w	23	2976	w	–	2971 [15]	– [16]
	2922	m	12	2926	m	10	2918	2918
	2859	w	18	2866	vw	18	2844	–
	1729	m	9	1733	m	8	1721	1721

[a] w = weak; vw = very weak; m = medium.

possible that the formic acid molecules rotate in the cavities because a new band, not observed at room temperature, is observed at low temperature and because the band at 3470 cm^{-1} has sharpened so much that the half-width has become measurable. The half-widths of the bands in the acetaldehyde compound do not change essentially, which indicates stronger interaction in this case. In the other clathrates, where the half-widths of the bands at room temperature are small, there is, as expected, not observed any essential changes and it is not possible in these cases to conclude anything about rotation from these experiments.

The observed bands in the clathrate compounds do not show any regular shift relative to the gas-phase wavenumbers as a function of temperature.

THE SPECTRA BELOW 200 cm^{-1}

(i) The quinol spectra. The bands assigned to the β-quinol lattice vibrations are observed at approximately 69, 80, and 99 cm^{-1} at room temperature; furthermore a weak band at approximately 186 cm^{-1} is observed in most of the compounds. The intensity and wavenumber of each line vary from compound to compound. This is believed to be caused by different interaction between the host and the guest molecules. The variation in intensity could also be caused by overlap with bands due to the enclosed molecules.

In a recent communication Fukushima [18] has reported the Raman spectrum of the acetonitrile clathrate. The three bands below 100 cm^{-1} mentioned above are also observed by Fukushima, but he has assigned the band at highest wavenumber (96 cm^{-1}) to the guest molecules. Fukushima has not investigated further clath-

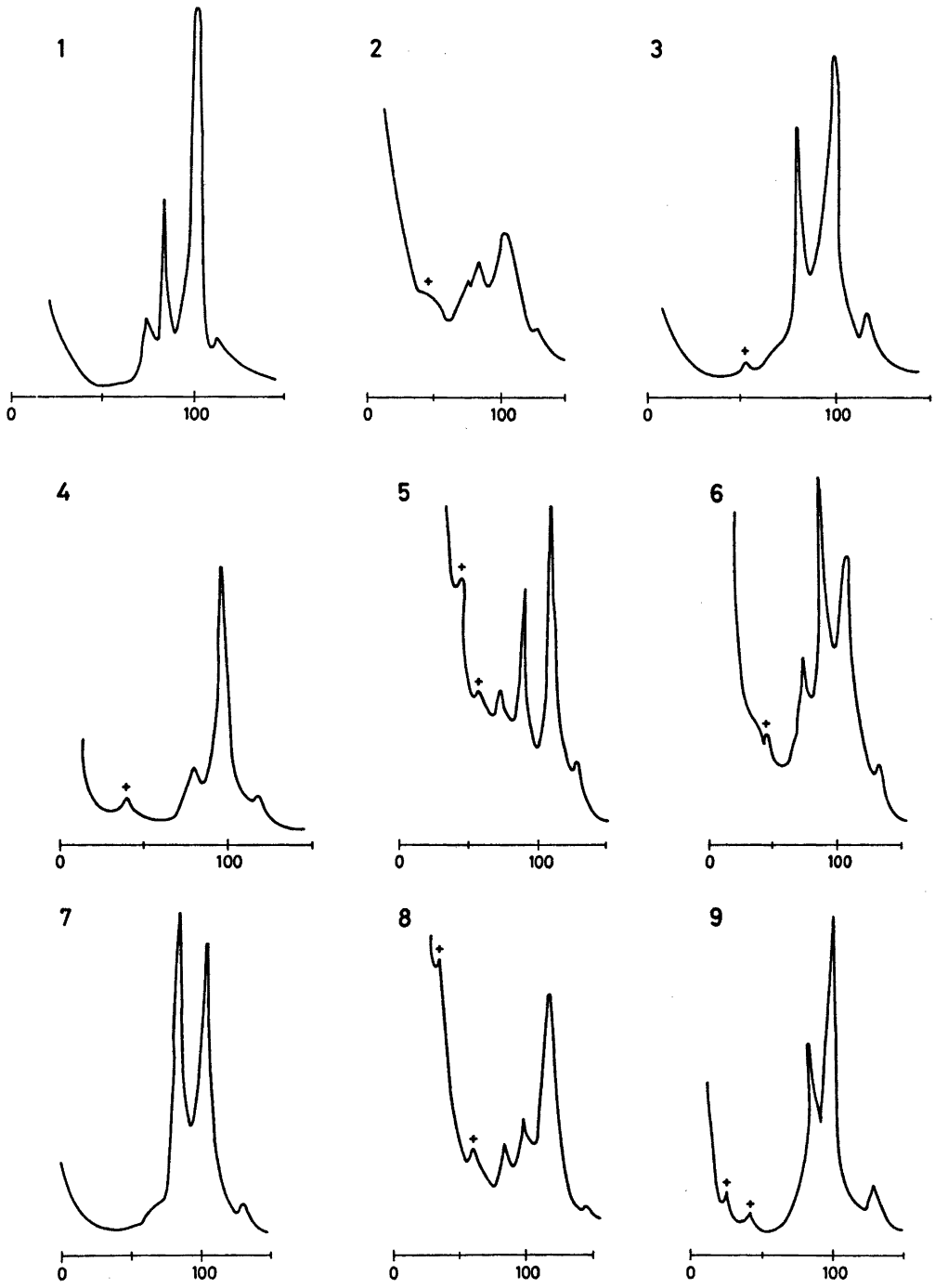

Fig. 1. The Raman spectra below 150 cm^{-1} of (1) "empty" β-quinol, (2) HCl-, (3) HCN-, (4) H_2S-, (5) CH_3CH_2-, (6) CH_3OH-, (7) HCOOH-, (8) HCHO-, and (9) CH_3CHO clathrate. (+): Bands assigned to the guest molecules. Abscissa unit: cm^{-1}.

rates nor "empty" β-quinol. In the present investigation it has become apparent that this band is observed in all clathrate compounds and in "empty" β-quinol. It is therefore most likely that the band should be assigned as a host lattice vibration and not to a rotational motion of the guest molecules.

In "empty" β-quinol at approximately 93 K the following bands are observed: 75(m), 86(s), 102(vs), 121(w), and 190 cm^{-1}(w). Those bands, which also are observed at room-temperature, show a shift towards higher wavenumber at low-temperature as expected. The bands mentioned above are also observed in the clathrates and show variation in intensity and wavenumber from compound to compound just as at room temperature. The spectra below 150 cm^{-1} are sketched in Fig. 1.

At room temperature the α-quinol spectrum is far more complex than the β-quinol spectrum as mentioned in Ref. 1. The bands of the former observed at room-temperature are given in Ref. 1. At 93 K the following ten bands are observed: 33(w), 48(w), 57(w), 67(s), 88(vs), 96(w), 107(vs), 124(w), 140(w), and 161 cm^{-1}(vw). This complex spectrum in comparison with the β-quinol spectrum reflects the lower symmetry of the α-modification.[19]

(ii) The guest spectra. In the region below 200 cm^{-1} bands due to translational and hindered rotational motions of the molecules enclosed in the cavities are expected.

As mentioned in Ref. 1 no bands due to the enclosed molecules are observed below 200 cm^{-1} at room temperature in the six investigated clathrates. The same is valid for the hydrogen sulfide and hydrogen cyanide clathrates.

At 93 K the population will be considerable in not only the rotational level $J=0$, but in several of the lower levels. Transitions from these levels will be comparable in intensity and it is expected that this will give rise to very broad bands, which cannot be discerned.

According to the point group symmetry of the free guest molecules the translational motions should be active in the Raman spectrum of all

Table 2. Guest bands below 200 cm^{-1}.

Guest Species	Raman [a] wave-number cm^{-1}	Temp. K	FIR wave-number cm^{-1}	Temp. K	Assignment [b]
	51	93	52	1.2 [22]	trans.
HCl	–	–	39	90 – 300 [20]	rot.
	–	–	25	1.2 [22]	rot.
	–	–	20 – 90	90 [20]	rot.
HCN	55	93	–	–	trans.
	–	–	74	18 [23]	trans.
H_2S	–	–	57	18 [23]	trans.
	45	93	–	–	trans.
CH_2CH_2	52	93	–	–	trans.
	43	93	–	–	trans.
CH_3OH	–	–	73	80 [23]	trans.
	49	93	–	–	trans.
HCOOH	–	–	–	– [24]	–
HCHO	55	93	–	–	trans.
	29	93	–	–	trans.
CH_3CHO	43	93	–	–	trans.
	27	93	–	–	trans.

[a] This work. [b] trans. = translational motion; rot. = rotational motion.

compounds except ethylene.

The bands observed below 200 cm^{-1} at 93 K, which are assigned to the guest molecules, are given in Table 2. For comparison FIR data, found in the literature, are also given. The spectra below 150 cm^{-1} are sketched in Fig. 1. The bands assigned to the enclosed molecules are all very weak and may possibly in some cases be questionable.

Because the rotational motions are believed to give rise to very broad bands, all observed bands are tentatively assigned as translational motions. It should be noted that also the bands observed in the ethylene compound have been assigned as translational motions, as it is likely that interaction with the host lattice may break down the selection rules.

When the mass of the enclosed molecules increases, one would expect that the wavenumber of the translational motions decreases. By comparing the wavenumbers of the translational motions given in Table 2 with the wavenumbers of the translational motions for a larger number of clathrate compounds found in the literature (N_2, O_2, NO, CO, SO_2, CO_2) [20,21] it can be seen, that such a dependence does not appear to exist.

As for the clathrates of ethylene, formaldehyde, and acetaldehyde no comparison between FIR and Raman data can be made because FIR investigations are lacking.

The FIR spectrum of hydrogen chloride clathrate was first investigated by Allen.[22] He observed two bands at 52 cm^{-1} and approximately 25 cm^{-1} due to the enclosed molecules. The wavenumber of the latter band was found to be dependent on temperature and HCl concentration. It was shown that the band at 52 cm^{-1} was not altered by isotopic substitution (DCl) whereas the band at 25 cm^{-1} was considerably diminished. On the basis of these observations Allen assigned the band at 52 cm^{-1} to a translational and the band at 25 cm^{-1} to a rotational motion. A weak shoulder observed at 51 cm^{-1} in the Raman spectrum is in agreement with the FIR investigation assigned to a translational motion of the trapped molecules.

No bands due to the enclosed molecules are observed neither in the FIR nor Raman spectrum of formic acid clathrate.

Davies [20] has reported that the FIR spectrum of hydrogen cyanide clathrate is very complex. In the Raman spectrum only one band at 55 cm^{-1}, assigned to the enclosed molecules, is observed in this region.

Barthel *et al.*[23] have observed two bands at 74 and 57 cm^{-1} due to the enclosed molecules in the FIR spectrum of hydrogen sulfide clathrate. Both bands are assigned to translational motions. In the Raman spectrum none of these bands have been observed, the former presumably because of overlap with a quinol band. Only one band at 45 cm^{-1}, assigned to the guest molecules, has been observed in the Raman spectrum.

The band at 49 cm^{-1} in the Raman spectrum of methanol clathrate has not been observed in the FIR spectrum.[23] The band at 73 cm^{-1} in the FIR spectrum cannot be found in the Raman spectrum possibly because of overlap with a quinol band. Fukushima [24] has also recorded the FIR spectrum of methanol clathrate, but he has not reported any band at all due to the guest molecules in the range below 100 cm^{-1}.

Acknowledgement. I acknowledge my gratitude to professor C. Knakkergaard Møller for his unfailing interest in this work.

REFERENCES

1. Anthonsen, J. W. *J. Mol. Struct. 23* (1974) 468.
2. Davies, J. E. D. *J. Chem. Soc. Dalton* (1972) 1182.
3. Davies, J. E. D. *Chem. Commun.* (1971) 270.
4. Davies, J. E. D. *J. Mol. Struct. 9* (1971) 483.
5. Herzberg, G. *Molecular Spectra and Molecular Structure*, Van Nostrand, New York 1945.
6. Wang, C. H. and Fleury, P. A. *J. Chem. Phys. 53* (1970) 2243.
7. Douglas, E. and Sharma, D. *J. Chem. Phys. 21* (1953) 448.
8. Pézolet, M. and Savoie, R. *Can. J. Chem. 47* (1969) 3041.
9. Bhagavantam, S. *Nature (London) 138* (1936) 1096.
10. Glockler, G. and Renfrew, M. M. *J. Chem. Phys. 6* (1938) 170.
11. Barnes, J. A. and Hallam, H. E. *Trans. Faraday Soc. 66* (1970) 1920.
12. Millikan, R. C. and Pitzer, K. S. *J. Chem. Phys. 27* (1957) 1305.
13. Tomlinson, G. E., Curnutteand, B. and Hathaway, C. E. *J. Mol. Spectrosc. 36* (1970) 26.
14. Chapput, A. and Roussel, B. *J. Raman Spectrosc. 1* (1973) 507.

15. Morris, J. C. *J. Chem. Phys. 11* (1943) 230.
16. Gerding, H., Nijveld, W. J. and Rijnders, G. W. A. *Rec. Trav. Chim. Pays-Bas 60* (1941) 25.
17. Davies, M. and Child, W. C. *Spectrochim. Acta 21* (1965) 1195.
18. Fukushima, K. *Chem. Lett.* (1973) 617.
19. Palin, D. E. and Powell, H. M. *J. Chem.* (1948) 571.
20. Davies, P. R. *Discuss. Faraday Soc. 48* (1969) 181.
21. Burgiel, J. C., Meyer, H. and Richards, P. L. *J. Chem. Phys. 43* (1965) 4291.
22. Allen, S. J. *J. Chem. Phys. 44* (1966) 394.
23. Barthel, C., Gerbeaux, X. and Hadni, A. *Spectrochim. Acta A 26* (1970) 1183.
24. Furushima, K. *J. Mol. Struct. 18* (1973) 277.

Received September 24, 1974.

Acta Chemica Scandinavica A 29 (1975) 185—194

The Crystal and Molecular Structure of an Eight-coordinated Tellurium(IV) Complex

STEINAR ESPERÅS and STEINAR HUSEBYE

Chemical Institute, University of Bergen, N-5014 Bergen, Norway

Tetrakis(4-morpholinecarbodithioato)tellurium-(IV), $[Te(OC_4H_8N.CS_2)_4]$, crystallizes from benzene-ethanol mixtures with three benzene molecules per molecule of complex. The yellow to orange crystals belong to the space group $P2_1/c$, with $a=15.445(4)$ Å, $b=13.565(4)$ Å, $c=26.591(10)$ Å and $\beta=122.23(4)°$. With four formula units, $[Te(OC_4H_8N.CS_2)_4]3C_6H_6$, in the cell, the density is calc. 1.43, found 1.45 g/cm³.

The structure analysis is based on 2721 intensities above background, collected with a Siemens AED-1 diffractometer using Mo$K\alpha$ radiation. Patterson and Fourier syntheses were used to solve the structure, and full-matrix least squares refinement has given a conventional R-value of 0.094.

In the complex molecule, the central tellurium atom is bonded to all eight sulfur atoms in a slightly distorted dodecahedral D_{2d} configuration. The Te—S bond lengths vary between 2.672 and 2.824 Å, the average being 2.737 Å.

During the study of compounds of divalent selenium and tellurium with bidentate dithio and related ligands, it was generally found that the ligands upon reaction with Se(IV) and Te(IV) reduced the elements to the divalent state.[1,2] Thus the reaction could be used to prepare complexes of divalent selenium and tellurium. The other part of the redox process taking place is the oxidation of two ligands to a disulfide molecule.[1,3] With diethyldithiocarbamate as ligand, the tetravalent selenium and tellurium complexes are initially formed,[4,5] and the tellurium(IV) complex is stable enough to be isolated in the crystalline state,[6,7] before conversion to divalent complex and disulfide takes place. The general reaction between tetravalent element and bidentate dithio ligand is then (L is ligand, L_2 is disulfide)[7]:

$$M(IV)+4L^- \rightleftharpoons ML_4 \rightleftharpoons ML_2+L_2$$

Only with M=Te and L=dialkyldithiocarbamate has ML_4 been stable enough to be isolated. The structure of both ML_4, ML_2 and L_2 are known for L=diethyldithiocarbamate and M=Te,[7-9] and there are several common features in the manner in which the ligands are coordinated to the central atom in ML_4 and ML_2. In ML_2 the TeS_4 coordination is trapezoid planar, in ML_4 the TeS_8 coordination is dodecahedral, and may be described by two planar TeS_4 trapezoids at right angles to each other fused together at the tellurium atom.[7]

Unlike tetrakis(diethyldithiocarbamato)tellurium(IV), $[Te(dtc)_4]$, tetrakis(4-morpholinecarbodithioato)tellurium(IV), $[Te(mtc)_4]$, which is also a dithiocarbamate complex, is remarkably resistent to conversion to divalent complex and disulfide when heated in solution.

This structure investigation was partly undertaken to see if the difference in behaviour of the two complexes is due to some structural feature, and partly to investigate further the stereochemical role of the lone pair of electrons in highly coordinated tellurium(IV) compounds.

A lone pair of electrons has so far been shown to be stereochemically inert in complexes of several ions in the lower right hand corner of the periodic table with a $(n-1)d^{10}ns^2$ electron configuration. Examples are octahedral complexes of Se(IV), Te(IV), Sb(III), Bi(III), Pb(II).[10-14] Also for $[Te(dtc)_4]$,[7] the lone pair is found to be stereochemically inert. Several explanations have been given for this behaviour, one delocalizing the lone pair mainly on the ligands,[15,16] another using the three-center

four-electron description,[17] and a third explaining it in terms of steric repulsions.[18,19]

EXPERIMENTAL

The preparation of crystals of tetrakis(4-morpholinecarbodithioato)tellurium(IV) with three benzene molecules of crystallization per molecule of complex, $[Te(mtc)_4].3C_6H_6$, is reported elsewhere.[20] The crystals consisted of flat yellow to orange plates and prisms. Tiny red prisms were also seen adhering to nearly all of the larger crystals; these were probably crystals of the corresponding divalent complex, $[Te(mtc)_2]$.[21] Upon standing, the crystals slowly become covered by a yellow powder.

For recording of intensity data, a Siemens AED-1 tape-controlled single crystal diffractometer and Mo$K\alpha$ radiation were used. A small crystal, with dimensions $0.18 \times 0.13 \times 0.09$ mm^3, was mounted along the c axis. After measuring the angles θ, χ, and ψ for three non-coplanar reciprocal vectors, approximate setting angles for all reflections were calculated.

Accurate cell dimensions were based on measurements of accurate setting angles for 20 high order reflections, and determined by least squares methods. They are $a=15.445(4)$ Å, $b=13.565(4)$ Å, $c=26.591(10)$ Å and $\beta=122.23(4)°$. There are four formula units in the cell. The observed and calculated densities are 1.45 and 1.43 g/cm^3, respectively. Based on systematic extinctions $h0l$ for $l=2n+1$ and $0k0$ for $k=2n+1$, the space group is $P2_1/c$.

After determination of accurate setting angles, intensity data were collected using a scintillation counter and $\theta-2\theta$ scan technique. The scan speed was 2.50° per min, with automatic setting of greater speed for strong reflections. Attenuation filters were used to avoid counting losses. The reflections were scanned between $\theta_1=\theta-0.40°$ and $\theta_2=\theta+0.40°$, where θ is the Bragg angle for the α_1 peak.

The scan was performed by going from θ to θ_1, then from θ_1 to θ_2 and finally from θ_2 to θ. The intensities for all three scans and their sum I_t were recorded. Likewise, background was measured for one half the total scan time at both θ_1 and θ_2, and the respective intensities and their sum I_b were recorded. The net intensity for a reflection, I_N, was put equal to I_t-I_b.

Two reference reflections were measured at intervals of 50 reflections and the intensity variations for these reflections were used to scale the net intensities of the recorded reflections. The standard deviation in net intensity is defined as the square root of the sum of I_b and I_t. Reflections with net intensities less than twice the standard deviation were regarded as unobserved and assigned intensities equal to this lower intensity limit. Out of 5800 measured reflections only 2721 were observed. This is

Table 1. Final coordinates for the atoms in the asymmetric unit in fractions of cell edges.

	x	y	z
Te	0.11791(11)	0.23045(9)	0.15583(6)
S1	0.2399(5)	0.0589(4)	0.1981(2)
S2	0.0877(5)	0.1145(4)	0.2274(3)
S3	0.2868(5)	0.3074(4)	0.2501(2)
S4	0.0814(5)	0.3732(4)	0.2158(2)
S5	0.0866(5)	0.3879(4)	0.0878(2)
S6	0.2457(4)	0.2443(4)	0.1101(2)
S7	−0.0909(4)	0.2434(4)	0.1004(2)
S8	0.0111(5)	0.1122(4)	0.0600(2)
O1	0.3178(14)	−0.1460(13)	0.3804(7)
O2	0.3397(14)	0.6155(12)	0.3766(7)
O3	0.3004(14)	0.5553(12)	0.0142(7)
O4A	−0.3762(25)	0.0635(24)	−0.0920(13)
O4B	−0.3684(30)	0.0172(25)	−0.0658(16)
N1	0.2163(14)	−0.0347(13)	0.2771(8)
N2	0.2549(13)	0.4487(12)	0.3063(7)
N3	0.2174(15)	0.4144(13)	0.0537(8)
N4	−0.1909(17)	0.1205(15)	0.0092(9)
C11	0.1865(15)	0.0391(14)	0.2387(8)
C21	0.1699(19)	−0.0533(16)	0.3118(10)
C31	0.2557(20)	−0.0669(18)	0.3777(11)
C41	0.3673(21)	−0.1283(17)	0.3507(12)
C51	0.2858(19)	−0.1147(18)	0.2813(10)
C12	0.2112(16)	0.3826(13)	0.2623(8)
C22	0.3680(18)	0.4560(14)	0.3529(9)
C32	0.3980(21)	0.5652(18)	0.3577(11)
C42	0.2284(19)	0.6168(17)	0.3290(10)
C52	0.1876(18)	0.5129(16)	0.3217(9)
C13	0.1841(16)	0.3555(14)	0.0804(8)
C23	0.2914(22)	0.3833(19)	0.0361(11)
C33	0.3648(23)	0.4723(22)	0.0476(12)
C43	0.2396(23)	0.5888(20)	0.0373(12)
C53	0.1600(18)	0.5083(16)	0.0232(9)
C14	−0.0987(17)	0.1551(14)	0.0520(9)
C24	−0.2859(23)	0.1599(19)	0.0008(11)
C34A	−0.3689(35)	0.1475(32)	−0.0580(20)
C34B	−0.2674(47)	−0.0128(37)	−0.0492(23)
C44A	−0.2839(40)	0.0404(33)	−0.0877(20)
C44B	−0.3440(34)	0.0785(32)	−0.0093(18)
C54	−0.1953(30)	0.0464(27)	−0.0324(16)
C101	−0.0030(18)	0.1831(17)	0.3346(10)
C102	0.0003(19)	0.2781(22)	0.3234(11)
C103	−0.0002(20)	0.3530(19)	0.3619(11)
C104	−0.0067(19)	0.3203(18)	0.4123(10)
C105	−0.0040(21)	0.2224(24)	0.4236(12)
C106	−0.0047(18)	0.1491(16)	0.3832(10)
C201	0.2890(20)	0.2319(21)	0.3901(11)
C202	0.2911(21)	0.2886(20)	0.4348(12)
C203	0.3865(24)	0.3005(19)	0.4911(12)
C204	0.4711(19)	0.2515(19)	0.4983(10)
C205	0.4745(22)	0.1940(20)	0.4557(13)
C206	0.3755(23)	0.1853(18)	0.4003(11)
C301	0.5328(29)	0.0749(29)	0.2750(14)
C302	0.5287(28)	0.1806(30)	0.2762(14)
C303	0.6140(30)	0.2454(26)	0.2954(14)
C304	0.7058(22)	0.1942(22)	0.3141(11)
C305	0.7026(22)	0.0969(23)	0.3085(11)
C306	0.6235(29)	0.0342(22)	0.2902(13)

Table 2. Components of atomic vibration tensors, $U \times 10^3$, in Å^2 with standard deviations, referred to crystallographic axes. For Te and S the expression is $\exp\{-2\pi^2(h^2a^{-2}U_{11}+k^2b^{-2}U_{22}+l^2c^{-2}U_{33}+2hka^{-1}b^{-1}U_{12}+2klb^{-1}c^{-1}U_{23}+2hla^{-1}c^{-1}U_{13})\}$. For O, N, and C, the expression is $\exp\{-8\pi^2U \times (\sin^2\theta/\lambda^2)\}$.

	U_{11}	U_{22}	U_{33}	U_{12}	U_{23}	U_{13}
Te	51.9(1.0)	40.0(0.7)	50.1(0.8)	5.7(0.9)	1.2(0.9)	30.9(0.7)
S1	74.3(5.0)	59.1(3.8)	76.1(4.2)	16.2(3.5)	12.2(3.2)	51.6(4.0)
S2	73.5(5.4)	54.7(3.7)	68.7(4.1)	11.4(3.5)	13.5(3.2)	48.0(4.0)
S3	64.4(4.8)	60.7(3.8)	79.5(4.3)	8.2(3.4)	−20.4(3.2)	37.8(3.9)
S4	65.1(5.2)	51.5(3.7)	64.4(4.1)	6.4(3.5)	−6.6(3.1)	37.1(3.9)
S5	57.1(4.6)	56.2(3.7)	81.5(4.4)	18.8(3.5)	20.8(3.4)	45.1(3.9)
S6	79.0(4.6)	56.5(4.1)	87.1(4.0)	23.3(3.7)	22.2(3.4)	56.4(3.7)
S7	63.2(4.5)	53.3(3.9)	65.8(3.4)	−2.4(3.5)	−9.3(2.9)	37.2(3.4)
S8	52.1(4.5)	74.2(4.2)	61.4(3.9)	7.6(3.7)	−15.6(3.4)	28.8(3.6)

	U		U		U		U
O1	113.9(6.3)	C51	93.1(8.2)	C34A	67.6(14.4)	C203	112.4(10.0)
O2	105.6(5.8)	C12	49.7(5.8)	C34B	86.1(17.2)	C204	87.7(8.1)
O3	105.3(6.0)	C22	66.1(6.7)	C44A	67.5(14.7)	C205	109.9(10.1)
O4A	74.5(10.0)	C32	97.2(8.7)	C44B	70.1(13.7)	C206	102.9(9.1)
O4B	72.1(12.2)	C42	88.3(8.0)	C54	148.6(14.1)	C301	166.1(13.8)
N1	72.4(5.6)	C52	75.3(7.5)	C101	88:3(7.8)	C302	169.7(14.1)
N2	61.7(5.1)	C13	54.4(6.1)	C102	116.6(8.9)	C303	162.6(12.5)
N3	76.2(5.9)	C23	113.8(9.6)	C103	95.0(9.1)	C304	109.3(9.5)
N4	92.8(6.6)	C33	125.4(10.8)	C104	90.9(8.2)	C305	110.6(9.7)
C11	50.5(5.9)	C43	114.8(10.0)	C105	126.6(10.1)	C306	130.8(11.3)
C21	86.4(8.2)	C53	74.6(7.3)	C106	86.7(7.6)		
C31	91.7(8.5)	C14	60.3(6.4)	C201	99.6(8.4)		
C41	105.1(9.1)	C24	102.8(9.1)	C202	109.1(9.4)		

Table 3. Dodecahedral parameters for some complexes with approximate D_{2d} symmetry. The unit of length for a, b, g, and m is in each case equal to the average central atom to ligand bond length.

Compound	ϕ_A	ϕ_B	MA/MB	a	b	g	m
$[Te(mtc)_4]$	37.4	77.8°	1.04	1.24	1.42	1.29	1.07
$[Te(dtc)_4]$ [7]	35.0	79.9	1.02	1.16	1.42	1.31	1.07
$[Ti(dtc)_4]$ [27]	35.1	77.5	1.03	1.17	1.42	1.29	1.11
$[V(dta)_4]$ [28]	35.4	77.0	1.02	1.17	1.44	1.27	1.11
"Best" values [25]	35.2	73.5	1.03	1.17	1.49	1.24	1.17

partly due to a yellow powder appearing on the surface of the crystal during exposure. The powder probably consists of crystal material from which the benzene molecules have escaped. This effect is probably also the cause of the reduction in the net intensities of the standard reflections with about 30 % during the data collection.

STRUCTURE ANALYSIS

Three-dimensional Patterson and Fourier syntheses revealed the positions of all non-hydrogen atoms in the asymmetric unit, except those of oxygen and two of its neighbour carbon atoms in one of the morpholyl groups.

This part of the ring was later found to be disordered.

Full-matrix least squares refinement was then started using a program (BDLS) which minimizes the expression $r=\sum W(|F_o|-K|F_c|)^2$. Here K is a scale factor and W, the weight of a reflection, is the inverse of the variance of F_o: $\sigma^2(F_o)=F_o^2\{I_t+I_b+k^2(I_t-I_b)^2\}/4(I_t-I_b)^2$, where k may be interpreted as the relative standard deviation in the scaling curve based on the variation in the net intensities of the reference reflections.

Non-observed reflections with $K|F_c|$ larger than the observable limit, were included in the refinement with F_o put equal to the limit.

Based on anisotropic temperature factors for sulfur and tellurium and isotropic temperature factors for oxygen, nitrogen and carbon atoms, the factor $R=(||F_o|-|F_c||)/\sum|F_o|$ converged to a final value of 0.094. Hydrogen atoms were excluded from the calculations and in the morpholyl group with disorder, the ring was given two orientations, A and B, corresponding to a rotation of 180° around the N4—C14 bond and sp^3 hybridization on N4. The disordered atoms in the two configurations were given extra indices A and B and occupancy factors equal to 0.5. A final difference map revealed no spurious peaks.

In the third benzene ring, the temperature factors are very high, especially for the atoms C301, C302, C303. This may be due to the fact that these atoms make very few van der Waals contacts (Table 7); also it could perhaps indicate that not all such benzene positions are occupied.

Table 4. Bond lengths with standard deviations, in Å.

Te—S1	2.824(6)	S7—C14	1.72(2)
Te—S2	2.694(8)	S8—C14	1.68(3)
Te—S3	2.684(5)	C11—N1	1.33(3)
Te—S4	2.752(7)	C12—N2	1.34(2)
Te—S5	2.672(6)	C13—N3	1.34(3)
Te—S6	2.824(8)	C14—N4	1.36(3)
Te—S7	2.744(6)	N1—C21	1.46(4)
Te—S8	2.702(5)	N1—C51	1.49(3)
S1—C11	1.69(3)	N2—C22	1.51(3)
S2—C11	1.73(2)	N2—C52	1.57(4)
S3—C12	1.71(3)	N3—C23	1.51(5)
S4—C12	1.71(2)	N3—C53	1.52(3)
S5—C13	1.68(3)	N4—C24	1.46(4)
S6—C13	1.73(2)	N4—C54	1.47(5)

Table 5. Bond angles with standard deviations, in degrees.

S1—Te—S2	64.41(23)
S3—Te—S4	65.34(20)
S5—Te—S6	64.56(20)
S7—Te—S8	65.16(20)
S1—Te—S6	75.78(21)
S4—Te—S7	73.82(18)
S2—Te—S5	155.27(23)
S3—Te—S8	155.75(23)
Te—S1—C11	86.3(7)
Te—S2—C11	89.9(8)
Te—S3—C12	89.3(6)
Te—S4—C12	87.0(8)
Te—S5—C13	91.2(7)
Te—S6—C13	85.1(10)
Te—S7—C14	86.8(8)
Te—S8—C14	88.9(7)
S1—C11—N1	121.6(1.7)
S2—C11—N1	119.5(1.8)
S3—C12—N2	119.3(1.5)
S4—C12—N2	122.2(1.5)
S5—C13—N3	121.9(1.5)
S6—C13—N3	119.2(1.6)
S7—C14—N4	119.0(1.8)
S8—C14—N4	121.8(1.7)
S1—C11—S2	118.8(1.0)
S3—C12—S4	118.4(1.0)
S5—C13—S6	118.9(1.2)
S7—C14—S8	119.1(1.0)
C11—N1—C21	122.1(1.9)
C11—N1—C51	123.2(2.2)
C21—N1—C51	113.8(1.9)
C12—N2—C22	125.8(1.7)
C12—N2—C52	120.4(1.6)
C22—N2—C52	112.7(1.5)
C13—N3—C23	124.5(1.8)
C13—N3—C53	120.3(2.0)
C23—N3—C53	113.1(2.0)
C14—N4—C24	121.9(2.0)
C14—N4—C54	118.1(2.4)
C24—N4—C54	119.8(2.1)

Table 6. Some non-bonded S—S distances (Å) in the $Te(mtc)_4$ molecule.

S1—S2	2.943(12)	S6—S8	3.600(9)
S3—S4	2.935(10)	S4—S2	3.520(8)
S5—S6	2.937(9)	S4—S5	3.454(11)
S7—S8	2.933(10)	S7—S2	3.484(7)
S1—S6	3.468(9)	S7—S5	3.528(10)
S4—S7	3.301(7)	S5—S3	3.892(7)
S1—S3	3.568(8)	S5—S8	3.869(8)
S1—S8	3.557(7)	S3—S2	3.833(9)
S6—S3	3.531(10)	S8—S2	3.948(9)

Table 7. Intermolecular distances less than 4.0 Å. The left column represents distances from an atom in the original molecule (Table 1) to an atom in a molecule whose transformation from the original one is listed in the next column.

C101 – S2	x	y	z	3.90(3)
– C201	x	y	z	3.98(4)
– C42	$-x$	$-\frac{1}{2}+y$	$\frac{1}{2}-z$	3.96(3)
C102 – S4	x	y	z	3.90(4)
– C201	x	y	z	3.87(4)
– C202	x	y	z	3.84(3)
– N1	$-x$	$\frac{1}{2}+y$	$\frac{1}{2}-z$	3.90(3)
– C21	$-x$	$\frac{1}{2}+y$	$\frac{1}{2}-z$	3.87(3)
C103 – C202	x	y	z	3.93(4)
– C11	$-x$	$\frac{1}{2}+y$	$\frac{1}{2}-z$	3.69(3)
– N1	$-x$	$\frac{1}{2}+y$	$\frac{1}{2}-z$	3.74(3)
C104 – S8	x	$\frac{1}{2}-y$	$\frac{1}{2}+z$	3.90(3)
C105 – C304	$-1+x$	y	z	3.85(4)
– C13	x	$\frac{1}{2}-y$	$\frac{1}{2}+z$	3.74(3)
– N3	x	$\frac{1}{2}-y$	$\frac{1}{2}+z$	3.81(3)
C106 – C304	$-1+x$	y	z	3.87(4)
– C305	$-1+x$	y	z	3.91(4)
– S5	$-x$	$-\frac{1}{2}+y$	$\frac{1}{2}-z$	3.97(3)
– C53	x	$\frac{1}{2}-y$	$\frac{1}{2}+z$	3.85(3)
C201 – S3	x	y	z	3.85(3)
– C12	x	y	z	3.58(3)
– N2	x	y	z	3.55(3)
– C22	x	y	z	3.60(4)
C202 – N2	x	y	z	3.83(4)
– C22	x	y	z	3.75(4)
– C52	x	y	z	3.97(3)
– C23	x	$\frac{1}{2}-y$	$\frac{1}{2}+z$	3.56(5)
C203 – O4B	$-x$	$\frac{1}{2}+y$	$\frac{1}{2}-z$	3.64(5)
– C44B	$-x$	$\frac{1}{2}+y$	$\frac{1}{2}-z$	3.90(5)
– C34B	$-x$	$\frac{1}{2}+y$	$\frac{1}{2}-z$	3.90(8)
– O2	$1-x$	$1-y$	$1-z$	3.96(3)
– C23	x	$\frac{1}{2}-y$	$\frac{1}{2}+z$	3.42(5)
C204 – C41	$1-x$	$-y$	$1-z$	3.80(3)
– O1	$1-x$	$-y$	$1-z$	3.44(3)
– O2	$1-x$	$1-y$	$1-z$	3.54(3)
– C23	x	$\frac{1}{2}-y$	$\frac{1}{2}+z$	3.88(5)
– C33	x	$\frac{1}{2}-y$	$\frac{1}{2}+z$	3.99(5)
– C24	$1+x$	$\frac{1}{2}-y$	$\frac{1}{2}+z$	3.91(5)
– C34A	$1+x$	$\frac{1}{2}-y$	$\frac{1}{2}+z$	3.76(7)
– C44B	$1+x$	$\frac{1}{2}-y$	$\frac{1}{2}+z$	3.76(6)
C205 – C33	$1-x$	$-\frac{1}{2}+y$	$\frac{1}{2}-z$	3.93(5)
– O3	$1-x$	$-\frac{1}{2}+y$	$\frac{1}{2}-z$	3.65(4)
– O1	$1-x$	$-y$	$1-z$	3.85(3)
– C24	$1+x$	$\frac{1}{2}-y$	$\frac{1}{2}+z$	3.78(4)
– C34A	$1+x$	$\frac{1}{2}-y$	$\frac{1}{2}+z$	3.40(7)
– C44B	$1+x$	$\frac{1}{2}-y$	$\frac{1}{2}+z$	3.93(5)
C206 – S3	x	y	z	3.84(3)
– C31	x	y	z	3.78(4)
– C22	x	y	z	3.86(3)
C301 – S1	x	y	z	3.85(4)
C302 – S3	x	y	z	3.82(5)
C303 – C51	$1-x$	$\frac{1}{2}+y$	$\frac{1}{2}-z$	3.68(6)
– O4A	$1+x$	$\frac{1}{2}-y$	$\frac{1}{2}+z$	3.90(5)
– C44A	$1+x$	$\frac{1}{2}-y$	$\frac{1}{2}+z$	3.92(6)
C304 – C51	$1-x$	$\frac{1}{2}+y$	$\frac{1}{2}-z$	3.68(4)
– C43	$1-x$	$-\frac{1}{2}+y$	$\frac{1}{2}-z$	3.85(4)
C305 – N2	$1-x$	$-\frac{1}{2}+y$	$\frac{1}{2}-z$	3.99(4)
– C32	$1-x$	$-\frac{1}{2}+y$	$\frac{1}{2}-z$	3.85(4)
– C43	$1-x$	$-\frac{1}{2}+y$	$\frac{1}{2}-z$	3.70(5)
– C53	$1-x$	$-\frac{1}{2}+y$	$\frac{1}{2}-z$	3.98(3)
C306 – S3	$1-x$	$-\frac{1}{2}+y$	$\frac{1}{2}-z$	3.76(4)
– C32	$1-x$	$-\frac{1}{2}+y$	$\frac{1}{2}-z$	3.79(5)
– C13	$1-x$	$-\frac{1}{2}+y$	$\frac{1}{2}-z$	3.95(3)
– N3	$1-x$	$-\frac{1}{2}+y$	$\frac{1}{2}-z$	3.88(3)
– C43	$1-x$	$-\frac{1}{2}+y$	$\frac{1}{2}-z$	3.97(4)
S1 – C44A	$-x$	$-y$	$-z$	3.61(6)
S2 – C52	$-x$	$-\frac{1}{2}+y$	$\frac{1}{2}-z$	3.97(3)
S4 – C21	$-x$	$\frac{1}{2}+y$	$\frac{1}{2}-z$	3.68(3)
S5 – C53	$-x$	$1-y$	$-z$	3.63(2)
S6 – C44A	$-x$	$-y$	$-z$	4.00(5)
– C34B	$-x$	$-y$	$-z$	3.63(6)
S7 – C31	$-x$	$\frac{1}{2}+y$	$\frac{1}{2}-z$	3.88(3)
– C42	$-x$	$-\frac{1}{2}+y$	$\frac{1}{2}-z$	3.90(3)
– C43	$-x$	$1-y$	$-z$	3.86(3)
S8 – C54	$-x$	$-y$	$-z$	3.94(5)
C31 – O3	x	$\frac{1}{2}-y$	$\frac{1}{2}+z$	3.32(4)
C41 – C42	x	$-1+y$	z	3.95(4)
– O2	x	$-1+y$	z	3.61(3)
– C33	$1-x$	$-\frac{1}{2}+y$	$\frac{1}{2}-z$	3.79(4)
O1 – C42	x	$-1+y$	z	3.48(3)
– O2	x	$-1+y$	z	3.26(2)
– O3	x	$\frac{1}{2}-y$	$\frac{1}{2}+z$	3.91(3)
C22 – O4A	$1+x$	$\frac{1}{2}-y$	$\frac{1}{2}+z$	3.41(5)
– C34A	$1+x$	$\frac{1}{2}-y$	$\frac{1}{2}+z$	3.72(5)
– O4B	$1+x$	$\frac{1}{2}-y$	$\frac{1}{2}+z$	3.46(5)
C32 – O4A	$1+x$	$\frac{1}{2}-y$	$\frac{1}{2}+z$	3.47(5)
– O4B	$1+x$	$\frac{1}{2}-y$	$\frac{1}{2}+z$	3.25(5)
O2 – C24	$-x$	$\frac{1}{2}+y$	$\frac{1}{2}-z$	3.82(4)
– C44B	$-x$	$\frac{1}{2}+y$	$\frac{1}{2}-z$	3.53(6)
C43 – C24	$-x$	$1-y$	$-z$	3.73(4)
– C34A	$-x$	$1-y$	$-z$	3.99(5)
O3 – C24	$-x$	$1-y$	$-z$	3.88(3)

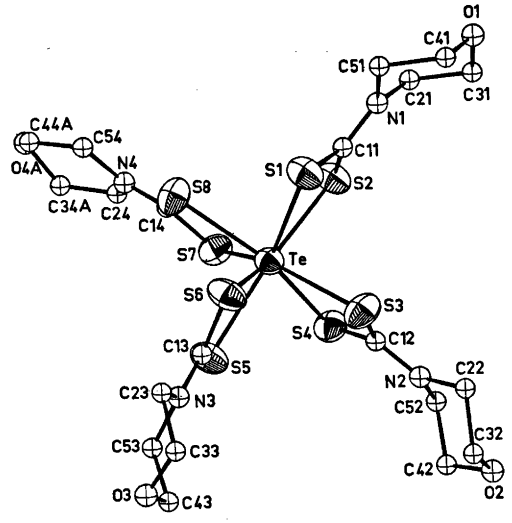

Fip. 1. The molecule as seen along the a axis after rotation $+12°$ around the c^* axis.

Table 8. Least squares planes through groups of atoms in the tetrakis(4-morpholinecarbodithioato)tellurium(IV) molecule. The first row lists atoms defining a plane, the next its equation. (Input coordinates from Table 1 gives distance from plane in Å). The next rows list atoms and their distance in Å from the plane.

Plane 1. TeS1S2S5S6

$4.696X+6.877Y+13.830Z-4.311=0$

Te	S1	S2	S5	S6	C11	N1	C21	C51
−0.017	−0.040	0.034	−0.023	0.045	0.136	0.299	0.434	0.133

C13	N3	C23	C53
0.111	0.304	0.194	0.258

Plane 2. TeS3S4S7S8

$5.805X+9.662Y-18.665Z=0$

Te	S3	S4	S7	S8	C12	N2	C22	C52
0.002	−0.032	0.050	−0.049	0.029	0.026	0.098	−0.045	0.040

C14	N4	C24	C54
−0.040	−0.115	−0.131	−0.081

Plane 3. S1S2C11N1C21C51

$5.819X+7.680Y+11.149Z-4.014=0$

Te	S1	S2	C11	N1	C21	C51
0.179	0.042	−0.089	0.033	0.068	0.042	−0.096

Plane 4. S3S4C12N2C22C52

$6.224X+9.539Y-18.891Z-0.005=0$

Te	S3	S4	C12	N2	C22	C52
−0.016	−0.011	−0.015	0.003	0.076	−0.031	−0.022

Plane 5. S5S6C13N3C23C53

$3.958X+6.291Y+15.444Z-4.194=0$

Te	S4	S5	C13	N3	C23	C53
0.129	−0.056	0.015	0.013	0.104	−0.072	−0.005

Plane 6. S7S8C14N4C24C54

$5.227X+9.703Y-18.553Z-0.027=0$

Te	S7	S8	C14	N4	C24	C54
−0.065	−0.002	0.007	0.002	−0.025	0.015	0.003

Some interplanar angles:

Angle				
1—2	90.2°	4—6	4.0
1—3	6.8	3—4	83.1
1—5	4.4	3—6	85.2
2—4	1.7	5—4	93.9
2—6	2.4	5—6	95.7
3—5	11.2		

Observed and calculated structure factors can be obtained from the author S.H. upon request.

The scattering factors were taken from the *International Tables* [22] and those for sulfur and tellurium were corrected for anomalous dispersion according to Cromer.[23] The intensity data were corrected for Lorentz and polarization effects but not for secondary extinction and absorption ($\mu = 10.3$ cm^{-1}). Final atomic coordinates are listed in Table 1 and components of atomic vibration tensors in Table 2. Interatomic distances and angles are listed in Tables 4—7, while least squares planes through groups of atoms are listed in Table 8.

RESULTS AND DISCUSSION

The contents of the asymmetric unit as seen along the *a* axis, with atoms labelled, are shown in Fig. 1. As can be seen from the figure, all eight sulfur atoms in the tetrakis(4-morpholinecarbodithioato)tellurium(IV) molecule are bonded to the central tellurium atom.

The configuration around the central tellurium atom is slightly distorted from dodecahedral D_{2d} symmetry. This corresponds to the energetically most favourable distribution of only the eight bonding electron pairs in the valency shell of tellurium.[7,18] Thus the lone pair is again stereochemically inert in the sense that it does not occupy a position in the coordination polyhedron. A square antiprismatic configuration is also energetically favourable for eight coordination. For complexes with four bidentate ligands, the choice between the two configurations may depend on the ligand "bite" which is defined by Blight and Kepert as the distance between the donor atoms in a ligand divided by the donor atom to central atom bond length.[24] The bite in the present investigation is 1.07 ($=m$ in Table 3), making the two configurations about Te equally probable.[24]

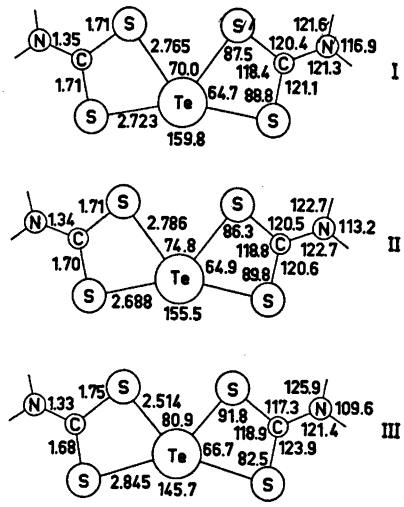

Fig. 2. The average tellurium coordination within a trapezoid for $Te(Et_2NCS_2)_4$ (I), $Te(OC_4H_8NCS_2)_4$ (II), and $Te(OC_4H_8NCS_2)_2$ (III).

A regular dodecahedron can be vizualized as two interleaving planar trapezoids at right angles to each other.[24] In[$Te(mtc)_4$], the two trapezoids are defined by S1, S2, S5, S6 and by S3, S4, S7, S8, respectively, and their interplanar angle is 89.8°. In [$Te(dtc)_4$] with a similar structure,[7] the angle is 88.5°, but then its structure is more distorted from D_{2d} symmetry than the structure of [$Te(mtc)_4$].

The average coordination within a trapezoid is shown in Fig. 2. The least squares planes through the TeS_4 groups in the two trapezoids (Table 8) show them to be nearly planar. They are also somewhat similar to the TeS_4 group in the corresponding divalent complex, [$Te(mtc)_2$],[21] shown in Fig. 2. In this respect, [$Te(mtc)_4$] does not differ from [$Te(dtc)_4$]. In addition, the structure of the trisulfide, [$(mtc)_2S$] is now known.[26]

Dodecahedral and square antiprismatic eight coordination have been studied in some detail by several workers.[24,25] The eight corners in a dodecahedral configuration are not equivalent, there being four corners of type A and four of type B. In [$Te(mtc)_4$] as in [$Te(dtc)_4$], the chelation is along edges *m*. Atoms S1, S4, S6, and S7 are located at A positions, while the other sulfur atoms are at the B positions.

Among the parameters used to describe a dodecahedron are θ_A, θ_B, MA/MB.[25] θ_A (θ_B) represents the angle between bonds MA(MB) from the central atom, M, to ligand atoms of type A(B), and the unique axis. In the present structure as well as for [$Te(dtc)_4$], the "unique axis" in the distorted dodecahedron is taken as the line joining the midpoint of the A—A(B—B) contacts in the two trapezoids with the tellurium atom. The average θ_A and θ_B angles

were then calculated on this basis.

In Table 3, values are given for the various dodecahedral parameters for $[Te(mtc)_4]$, and for comparison, those of $[Te(dtc)_4]$,[7] $[Ti(dtc)_4]$ [27] and $[V(dta)_4]$,[28] all with approximate D_{2d} symmetry. In addition, the parameters for the energetically most "favourable" dodecahedron are included.[25]

From the table, it can be seen that the structural parameters for the four eight-coordinated dithiocarbamates are similar. Since Ti(IV) and V(IV) have smaller radii than Te(IV), the ligand bite as defined above, corresponding to m in the table, is smallest for the tellurium complexes. However, $[Te(mtc)_4]$ is significantly different from the other complexes with respect to a. The parameter a is equal to the average S_A-S_A distance within the two trapezoids of the dodecahedron, divided with the average M—S bond length. The average S_A-S_A distance in a trapezoid is 3.39 Å for $[Te(mtc)_4]$ as compared to 3.17 Å for $[Te(dtc)_4]$.[7] This is reflected in the larger average S_A-Te-S_A angle of 74.8° in $[Te(mtc)_4]$ as compared to 70.0° for the corresponding angle in $[Te(dtc)_4]$. The S_B-Te-S_B angles then vary in the opposite manner due to the planarity of the trapezoids and the constancy of the intrachelate S_A-Te-S_B angles.

A possible mechanism suggested for the breakdown of tetrakis(diethyldithiocarbamato)-tellurium(IV) into divalent tellurium complex and tetraethylthiuram disulfide, involved formation of disulfide by means of a S_A-S_A bond being formed and the four Te—S bonds within one trapezoid being broken. The other trapezoid, with some adjustment of bond lengths and angles gives the divalent tellurium complex.[7]

According to the above, the S_A-S_A distance in a trapezoid should be of major importance for the stability of such eight-coordinated tellurium complexes. Thus, the greater this S_A-S_A distance, the more difficult the S_A-S_A bond formation, and the more stable the complex should be. The fact that the minimum S_A-S_A distance in $[Te(mtc)_4]$ is 0.14 Å greater than the corresponding distance in $[Te(dtc)_4]$ is in accord with the greater stability of the former complex. However, the difference in the S_A-S_A distances may partly be due to packing effects, and thus may not fully account for the difference in stability found in solution.

The $Te-S_A$ and $Te-S_B$ bond lengths range from 2.74 to 2.82 and from 2.67 to 2.70 Å, respectively, and the average Te—S bond length is 2.737 Å. This latter value is very close to 2.744 Å, the corresponding bond length found for $[Te(dtc)_4]$.[7] Thus the dodecahedral radius of Te(IV) seems to be close to 1.70 Å. This may be compared to the octahedral radius of Te(IV) of 1.55 Å and the radius of 1.64 Å found for Te(II) in planar four-coordinated complexes.[29]

This large dodecahedral radius may in part be due to the antibonding nature of the lone pair, and to steric crowding. In favour of the latter effect is the structure of $[TeI_6]^{2-}$,[30] where Te(IV) has a larger radius than in the chlorine and bromine analogs.[10,31] Also attempts made at this laboratory to prepare crystals of dialkyldithiocarbamates of tetravalent selenium has so far been unsuccessful.

Recent MO calculations on IF_7, BrF_5, AsF_5, PF_5 and nuclear quadruple measurements on $[TeCl_6]^{2-}$ have indicated that d-orbitals only make minor contributions to the bonding in these compounds.[32–34] It is therefore possible that they also for $[Te(mtc)_4]$ and related compounds make but a small contribution. Full contribution of high energy d-orbitals on tellurium to the tellurium-sulfur bonds, will, however, also have a bond lengthening effect.

The ligands are nearly planar (Table 8) and the average C—S and C—N bond lengths of 1.71 and 1.34 Å, respectively, are normal, both corresponding to π-bond orders near 0.3. All bond lengths in the benzene rings and in the morpholyl groups, except for the disordered one, are in the expected range.

The packing of the molecules in the unit cell is shown in Fig. 3. The benzene rings are stacked in pairs across twofold screw axes and centres of symmetry and thus form long rows parallel with the b axis. They make normal van der Waals contacts (Table 7) with each other, but there are several short contacts to the S1—S2 and S5—S6 ligands in the complex molecules. These short contacts may explain why the S_A-S_A distance in the trapezoid defined by these ligands is 0.17 Å larger than the corresponding distance in the other trapezoid. There is however, no tendency

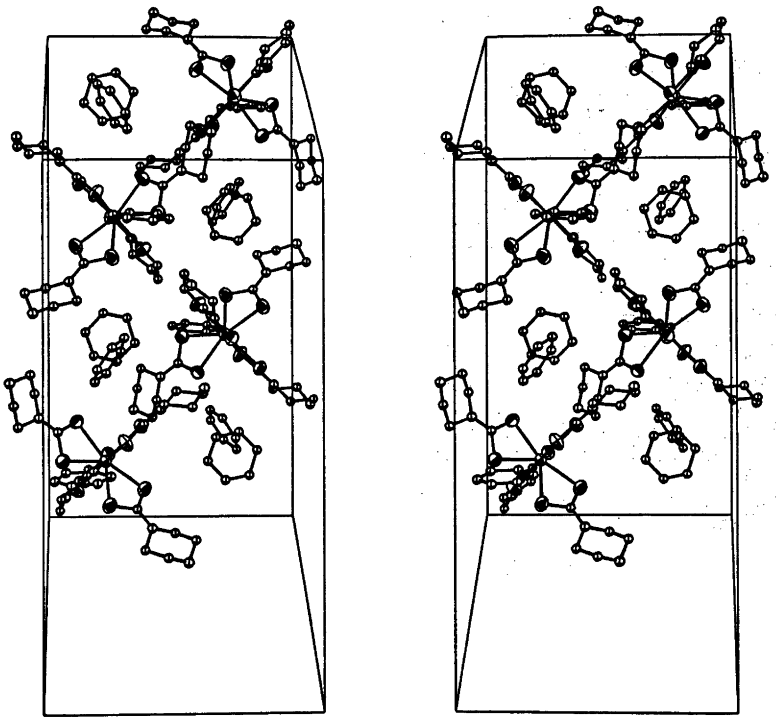

Fig. 3. A stereoscopic drawing showing the packing of molecules as seen along the a^* axis.

to adduct formation. The tetrakis(4-morpholinecarbodithioato)tellurium(IV) molecules themselves make normal van der Waals contacts with each other.

REFERENCES

1. Husebye, S. *Acta Chem. Scand. 19* (1965) 1045.
2. Husebye, S. *Diss.* University of Bergen, 1969.
3. Busev, A. I. *Talanta 11* (1964) 485.
4. Russel, W. F. *U. S. Pat.* 2.347.128 (1944).
5. Foss, O. *Acta Chem. Scand. 7* (1953) 226.
6. Nikolov, G. St., Jordanov, N. and Havezov, I. *J. Inorg. Nucl. Chem. 33* (1970) 1059.
7. Husebye, S. and Sværen, S. E. *Acta Chem. Scand. 27* (1973) 763.
8. Fabiani, C., Spagna, R., Vaciago, A. and Zambonelli, L. *Acta Crystallogr. B 27* (1971) 1499.
9. Karle, I. L., Estlin, J. A. and Britts, K. *Acta Crystallogr. 22* (1967) 273.
10. Hazell, A. C. *Acta Chem. Scand. 20* (1966) 165.
11. Engel, G. *Z. Kristallogr. 90* (1935) 341.
12. Vonk, C. G. and Wiehenga, E. H. *Acta Crystallogr. 12* (1959) 859.
13. Morss, L. R. and Robinson, W. R. *Acta Crystallogr. B 28* (1972) 653.
14. Goldberg, I. and Herbstein, F. H. *Acta Crystallogr. B 28* (1972) 400.
15. Urch, D. S. *J. Chem. Soc.* (1964) 5775.
16. Couch, D. A., Wilkins, C. J., Rossman, G. R. and Gray, H. B. *J. Amer. Chem. Soc. 92* (1970) 307.
17. Cotton, F. A. and Wilkinson, G. *Advanced Inorganic Chemistry*, 3rd. Ed., Interscience, London 1972, p. 142.
18. Gillespie, R. J. *J. Chem. Educ. 47* (1970) 18.
19. Gillespie, R. J. *Molecular Geometry*, Van Nostrand Reinhold, London 1972, p. 158.
20. Esperås, S. and Husebye, S. *Acta Chem. Scand. 27* (1973) 706.
21. Husebye, S. *Acta Chem. Scand. 24* (1970) 2198.
22. *International Tables for X-Ray Crystallography*, Kynoch Press, Birmingham 1962, Vol. III, p. 204.
23. Cromer, D. T. *Acta Crystallogr. 18* (1965) 17.
24. Blight, D. G. and Kepert, D. L. *Inorg. Chem. 11* (1972) 1556.
25. Hoard, J. L. and Silverton, J. V. *Inorg. Chem. 2* (1963) 235.

26. Husebye, S. *Acta Chem. Scand. 27* (1973) 756.
27. Colapietro, M., Vaciago, A., Bradley, D. C., Hursthouse, M. B. and Rendall, I. F. *J. Chem. Soc. Dalton Trans.* (1972) 1052.
28. Fanfani, L., Nunzi, A., Zanazzi, P. F. and Zanzari, A. R. *Acta Crystallogr. B 28* (1972) 1298.
29. Foss, O. In Andersen, P., Bastiansen, O. and Furberg, S., Eds., *Selected Topics in Structure Chemistry*, Universitetsforlaget, Oslo 1967, p. 145.
30. Soyama, S., Osaki, K. and Kusanagi, S. *Inorg. Nucl. Chem. Lett. 8* (1972) 181.
31. Das, A. K. and Brown, I. D. *Can. J. Chem. 44* (1966) 939.
32. Oakland, R. L. and Duffey, G. H. *J. Chem. Phys. 46* (1967) 19.
33. Benny, R. S., Tamres, M. T., Ballhausen, C. J. and Johansen, H. *Acta Chem. Scand. 22* (1968) 231.
34. Nakamura, D., Ito, K. and Kubo, M. *J. Amer. Chem. Soc. 84* (1962) 163.

Received June 26, 1974.

Acta Chemica Scandinavica A 29 (1975) 195—200

The Crystal and Molecular Structure of 2,5-Diphenyl-3,4-trimethylene-6a-thiathiophthene

BJØRN BIRKNES, ASBJØRN HORDVIK* and LEIF J. SÆTHRE

Department of Chemistry, University of Bergen, N-5000 Bergen, Norway

2,5-Diphenyl-3,4-trimethylene-6a-thiathiophthene crystallizes in the monoclinic space group $P2_1/c$ with four molecules in a unit cell of dimensions $a=6.882(1)$ Å, $b=12.871(1)$ Å, $c=19.049(1)$ Å, and $\beta=94.98(2)°$.

The structure was solved by three-dimensional Patterson synthesis, and refined by full-matrix least squares to an R of 0.037.

C(8) and C(10), bonded to C(3) and C(4), lie near the plane of the 6a-thiathiophthene system, and the 2- and 5-phenyl groups are twisted 47.3 and 54.3° about the respective connecting bonds.

S(1)—S(6a) and S(6a)—S(6) are 2.329(1) and 2.288(1) Å, respectively, with the angle S(1)—S(6a)—S(6)=179.28(4)°. Other bond lengths in the central ring system are, S(1)—C(2)=1.710(2), S(6a)—C(3a)=1.755(2), S(6)—C(5)=1.709(2), C(2)—C(3)=1.381(3), C(3)—C(3a)=1.426(3), C(3a)—C(4)=1.425(3), and C(4)—C(5)=1.378(3) Å.

The present structure investigation of 2,5-diphenyl-3,4-trimethylene-6a-thiathiophthene (I) has been carried out in order to find the degree to which a 3,4-trimethylene bridge shortens the sulfur-sulfur bonds there relative to those in 2,5-diphenyl-6a-thiathiophthene II.[1] Structure studies on the 6a-selenaselenophthenes III [2] and IV [3] show that a 3,4-trimethylene bridge has a shortening effect on the Se—Se bonds. Furthermore, we wanted to test whether the phenyl substituents would affect the S—S bonds in accordance with theoretical predictions.[4]

STRUCTURE ANALYSIS

A brief account of the structure determination has been reported,[5] and a more detailed description is given here.

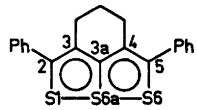

(I)

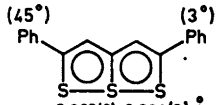

(II)

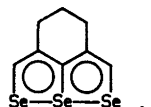

(III)

(IV)

A sample of I was generously supplied by M. Stavaux.[6] The crystals are dark red.

Crystal data

$C_{20}H_{16}S_3$ M.w.=352.54
Space group $P2_1/c$
$a=6.8824(8)$ Å, $b=12.8711(4)$ Å, $c=19.049(11)$ Å, $\beta=94.98(2)°$
$V=1680.9$ Å^3
$D_c=1.391$ g/cm^3, D_m(flotation)$=1.38$ g/cm^3
$Z=4$
$\mu=38.2$ cm^{-1} (Cu$K\alpha$)

All the X-ray measurements were carried out on a paper-tape controlled Siemens AED diffractometer using Cu$K\alpha$ radiation ($\lambda=1.5418$ Å).

The unit cell dimensions were determined from the 2θ values of 12 high order reflections measured at room temperature, $t=22$ °C, $\lambda\alpha_1=1.5404$ Å. A least squares procedure gave the values quoted above.

* Present address: Chemistry Section, University of Tromsø, P.O. Box 790, N-9001 Tromsø, Norway.

The intensities of the reflections were measured by means of the five-value scan technique.[7] Reflections for which the net count was greater than two times the respective standard deviation in the net count, were accepted as observed. With this criterion 2546 independent reflections were observed within $\theta = 71°$; the unobserved reflections were neglected in order to save computer time.

Lp corrections and absorption corrections [8] were applied. The dimensions of the crystal were $0.2 \times 0.4 \times 0.07$ mm in the three axial directions; a grid of $16 \times 8 \times 4$ points was used.

The scattering factors for sulfur and carbon were taken from the *International Tables*.[9] For hydrogen, the scattering factor curve given by Stewart *et al.*[10] was used.

Approximate coordinates for the sulfur atoms were found from a three-dimensional Patterson synthesis, and the positions of the carbon atoms were found from a subsequent Fourier map; hydrogen positions were calculated. The atomic parameters were refined by full matrix least squares (see for example Ref. 11) to an R of 0.037.

Final atomic coordinates and temperature parameters are listed in Tables 1 and 2, respectively. The final structure factor list is available on request.

Rigid body analyses for the entire molecule as well as for certain parts of the molecule have been carried out according to the method of Schomaker and Trueblood.[12] The parts of the molecule treated in this way are, the three central rings plus C(7) and C(11), the 2-phenyl group plus C(2), and the 5-phenyl group plus C(5), cf. Fig. 1. The corresponding librational tensors, $\mathbf{L}_1$, $\mathbf{L}_2$, and $\mathbf{L}_3$, are given in Table 3. One notes from the values there that the libration is rather anisotropic in either case.

The calculations mentioned above were carried out on an IBM 360/50H computer. The programs, with some exeptions, originates from the Weizmann Institute of Science, Rehovoth, Israel, and have been modified for the 360 by D. Rabinovich, L. M. Milje, K. Maartmann-Moe and K. Åse.

DISCUSSION

Bond lengths and angles with standard deviations, calculated from the values in Table 1, are listed in Tables 4 and 5, respectively. A more realistic estimate of the standard deviations might probably be obtained by multiplying those given by a factor of two.[13]

The S—S, C—S, and C—C bond lengths have been corrected [14] for rigid-body libration according to the libration tensors given in Table 3. The corrections which give the l' values are based on the libration tensor L, and the corrections leading to the l'' values are based on

Table 1. Atomic coordinates in fractions of corresponding cell edges. The standard deviations given in parentheses refer to the last digits of the respective values.

Atom	x	y	z
S(1)	0.13658(11)	0.38796(5)	0.25399(4)
S(6a)	0.41424(10)	0.39356(4)	0.32917(4)
S(6)	0.69494(11)	0.39799(5)	0.40671(4)
C(2)	0.13425(36)	0.25623(17)	0.24082(12)
C(3)	0.28201(36)	0.20239(18)	0.28556(12)
C(3a)	0.42892(36)	0.25834(16)	0.32700(13)
C(4)	0.58586(36)	0.20837(18)	0.36724(12)
C(5)	0.71937(36)	0.26671(18)	0.40819(13)
C(7)	−0.02645(36)	0.21024(18)	0.20120(13)
C(8)	0.28780(50)	0.08470(20)	0.28620(18)
C(9)	0.40753(54)	0.04149(22)	0.34859(18)
C(10)	0.60259(50)	0.09178(21)	0.36009(18)
C(11)	0.88521(37)	0.22514(18)	0.45519(12)
C(12)	0.85509(43)	0.15319(20)	0.50828(15)
C(13)	1.00906(51)	0.11950(22)	0.55357(15)
C(14)	1.19584(47)	0.15674(24)	0.54689(16)
C(15)	1.22673(45)	0.22825(27)	0.49563(18)
C(16)	1.07174(42)	0.26247(23)	0.44973(15)
C(17)	−0.21615(42)	0.24588(23)	0.20446(15)
C(18)	−0.36673(44)	0.20771(28)	0.15833(18)
C(19)	−0.32898(50)	0.13536(25)	0.10800(16)
C(20)	−0.14040(50)	0.09955(21)	0.10372(15)
C(21)	0.00881(42)	0.13641(21)	0.15015(15)
H(12)	0.7193(37)	0.1317(19)	0.5105(13)
H(13)	0.9974(43)	0.0685(21)	0.5899(15)
H(14)	1.3291(39)	0.1362(18)	0.5762(14)
H(15)	1.3629(47)	0.2566(24)	0.4878(17)
H(16)	1.0914(40)	0.3164(20)	0.4147(14)
H(17)	−0.2441(40)	0.2994(20)	0.2392(14)
H(18)	−0.5069(43)	0.2371(22)	0.1622(15)
H(19)	−0.4413(45)	0.1075(22)	0.0758(16)
H(20)	−0.1155(52)	0.0515(26)	0.0626(18)
H(21)	0.1262(33)	0.1160(18)	0.1471(13)
H(81)	0.3465(52)	0.0594(25)	0.2426(18)
H(82)	0.1535(48)	0.0548(23)	0.2830(16)
H(91)	0.3490(63)	0.0500(31)	0.3931(20)
H(92)	0.4282(50)	−0.0410(29)	0.3430(17)
H(101)	0.6686(59)	0.0712(29)	0.3179(20)
H(102)	0.6858(46)	0.0665(22)	0.4012(16)

Table 2. Temperature parameters U_{ij} (Å²) for sulfur and carbon, and U (Å²) for hydrogen. The expressions used are $\exp[-2\pi^2(h^2a^{*2}U_{11}+\cdots 2hka^*b^*U_{12}+\cdots)]$ and $\exp[-8\pi^2U(\sin^2\theta/\lambda^2)]$. All values are multiplied by 10^4. Standard deviations in parentheses refer to the last digits of the respective values.

Atom	U_{11}	U_{22}	U_{33}	U_{12}	U_{23}	U_{13}
S(1)	575(5)	352(3)	626(4)	90(3)	29(3)	−91(4)
S(6a)	544(4)	277(3)	543(4)	7(3)	21(3)	7(3)
S(6)	604(5)	350(3)	650(5)	−69(3)	17(3)	−116(4)
C(2)	432(15)	388(13)	438(13)	13(11)	29(11)	68(12)
C(3)	425(15)	341(12)	490(14)	2(11)	16(10)	2(12)
C(3a)	438(14)	295(11)	451(13)	18(11)	13(10)	59(11)
C(4)	437(15)	355(13)	497(15)	34(11)	−22(10)	−6(12)
C(5)	422(15)	407(13)	462(14)	−7(11)	10(11)	55(12)
C(7)	426(15)	424(13)	449(14)	−12(11)	103(11)	29(12)
C(8)	672(22)	312(14)	841(23)	−8(14)	21(14)	−245(19)
C(9)	814(25)	335(14)	953(25)	−51(15)	54(15)	−357(21)
C(10)	673(21)	346(14)	910(24)	85(14)	−48(15)	−295(18)
C(11)	429(15)	429(13)	433(14)	7(12)	−48(11)	21(12)
C(12)	530(17)	445(14)	553(16)	−15(13)	3(12)	−9(14)
C(13)	750(22)	504(16)	542(17)	45(16)	28(13)	−113(16)
C(14)	587(20)	704(20)	611(19)	115(16)	−82(16)	−143(16)
C(15)	427(17)	885(23)	685(20)	4(17)	−97(18)	8(16)
C(16)	445(16)	723(20)	536(17)	−22(15)	0(14)	59(14)
C(17)	446(17)	681(19)	547(17)	32(15)	110(14)	50(14)
C(18)	436(18)	877(24)	671(20)	−31(16)	218(18)	23(18)
C(19)	681(23)	640(19)	625(19)	−200(17)	220(16)	−178(17)
C(20)	730(21)	474(16)	586(17)	−45(16)	62(14)	−117(16)
C(21)	511(17)	437(14)	544(16)	19(13)	29(12)	−21(14)

Atom	U	Atom	U	Atom	U
H(12)	610(134)	H(18)	903(167)	H(2)	993(193)
H(13)	849(167)	H(19)	947(158)	H(91)	1566(298)
H(14)	667(130)	H(20)	1390(229)	H(92)	1330(201)
H(15)	1130(198)	H(21)	434(122)	H(101)	1459(284)
H(16)	716(155)	H(81)	1172(239)	H(102)	958(205)
H(17)	691(151)				

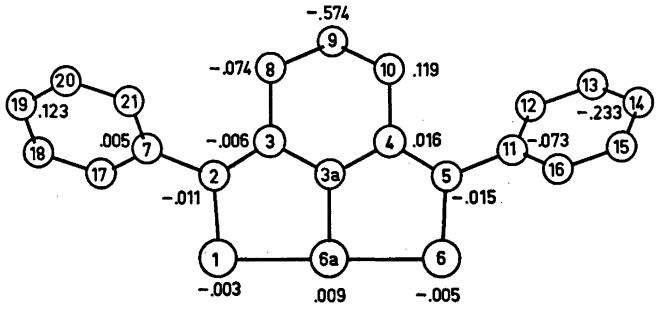

Fig. 1. The 2,5-diphenyl-3,4-trimethylene-6a-thiathiophthene molecule, with numbering of carbon and sulfur atoms. Deviations (Å) from a least squares plane through the atoms of the 6a-thiathiophthene system are given.

Table 3. Rigid body libration tensors for the entire molecule (**L**), the three central rings plus C(7) and C(11) ($\mathbf{L}_1$), the 2-phenyl group plus C(2) ($\mathbf{L}_2$), and the 5-phenyl group plus C(5) ($\mathbf{L}_3$).

	Eigenvalues	Eigenvectors		[a]
L	37.30 (°)[2]	−6631	−112	−7501
	2.25	−6720	−4355	5989
	0.86	−3333	9002	2804
$\mathbf{L}_1$	38.50	−7110	−309	−7025
	2.72	−6841	−2004	7013
	−0.38	−1625	9792	1212
$\mathbf{L}_2$	37.91	−5700	−1252	−8121
	12.87	−2231	−9276	2996
	2.82	−7902	3520	5008
$\mathbf{L}_3$	35.37	6565	−2415	7146
	15.86	1156	−9039	−4118
	5.66	7454	3529	−5656

[a] Direction cosines × 10^4 relative to *a*, *b*, and *c**, respectively.

Table 4. Bond lengths (*l*) in 2,5-diphenyl-3,4-trimethylene-6a-thiathiophthene. Standard deviations in parentheses. Bond lengths (*l'*) and (*l''*) with corrections for rigid-body libration are given for the S−S, S−C, and C−C bonds. The corrections in (*l'*) are based on the libration tensor one arrives at by treating the whole molecule as a rigid body, and the corrections in (*l''*) are based on the libration tensors one gets when the three central rings and each of the phenyl groups are treated separately. For further explanation see the test.

Bond	*l''* (Å)	*l'* (Å)	*l* (Å)
S(1)−S(6a)	2.288	2.289	2.287(1)
S(6a)−S(6)	2.329	2.330	2.328(1)
S(1)−C(2)	1.710	1.710	1.699(2)
S(6a)−C(3a)	1.755	1.754	1.744(2)
S(6)−C(5)	1.709	1.708	1.698(2)
C(2)−C(3)	1.381	1.381	1.378(3)
C(3)−C(3a)	1.426	1.426	1.423(3)
C(3a)−C(4)	1.425	1.425	1.423(3)
C(4)−C(5)	1.378	1.378	1.375(3)
C(3)−C(8)	1.525	1.525	1.515(4)
C(8)−C(9)	1.496	1.496	1.494(5)
C(9)−C(10)	1.494	1.494	1.489(5)
C(10)−C(4)	1.522	1.521	1.512(4)
C(2)−C(7)	1.487	1.485	1.482(3)
C(5)−C(11)	1.492	1.490	1.488(3)
C(7)−C(17)	1.399	1.396	1.390(4)
C(17)−C(18)	1.393	1.391	1.389(4)
C(18)−C(19)	1.386	1.385	1.377(5)
C(19)−C(20)	1.396	1.392	1.386(5)
C(20)−C(21)	1.384	1.382	1.380(4)
C(21)−C(7)	1.405	1.403	1.396(4)
C(11)−C(12)	1.408	1.407	1.400(4)
C(12)−C(13)	1.381	1.379	1.377(4)
C(13)−C(14)	1.397	1.394	1.388(5)
C(14)−C(15)	1.380	1.379	1.372(5)
C(15)−C(16)	1.395	1.392	1.391(4)
C(16)−C(11)	1.392	1.389	1.383(4)
C(12)−H(12)			0.98(3)
C(13)−H(13)			0.96(3)
C(14)−H(14)			1.07(3)
C(15)—H(15)			1.03(3)
C(16)−H(16)			0.98(3)
C(17)−H(17)			0.99(3)
C(18)−H(18)			1.04(3)
C(19)−H(19)			1.01(3)
C(20)−H(20)			1.02(3)
C(21)−H(21)			0.86(2)
C(8)−H(81)			1.01(4)
C(8)−H(82)			1.00(3)
C(9)−H(91)			0.98(4)
C(9)−H(92)			1.08(4)
C(10)−H(101)			0.99(4)
C(10)−H(102)			0.98(3)

$\mathbf{L}_1$, $\mathbf{L}_2$, and $\mathbf{L}_3$. There is close agreement between the *l'* and *l''* values in this case, *cf.* Table 4, and one should note in this connection that the axes of maximum libration for $\mathbf{L}_1$, $\mathbf{L}_2$, and $\mathbf{L}_3$, *cf.* Table 3, are roughly parallel. In cases where this is not so, see for example Ref. 1, there will be a difference between the *l'* and *l''* values.

The numbering of C and S atoms in the 2,5-diphenyl-3,4-trimethylene-6*a*-thiathiophthene molecule is shown in Fig. 1. Deviations from a least squares plane through the atoms of the thiathiophthene-system are given on the figure. The 2-phenyl group is twisted 47.3° about the C(2)−C(7) bond. This twist angle was taken as the angle between the normal to the plane through C(2), C(7), C(17), and C(21), and the normal to the plane through C(2), C(7), C(3), and S(1). Similarly, the twist angle of the 5-phenyl group about C(5)−C(11) is 54.3°.

From Table 4 the sum of the S−S bond lengths in the present compound is 4.617(1) Å as compared with the value 4.666(3) Å for the sum of the S−S bond lengths in II. Thus, the 3,4-trimethylene bridge in I causes a shortening of the three-sulfur sequence there relative that in II. This agrees with the results from the structure studies on the analogous selenium compounds mentioned in the introduction. In compounds III and IV the sums of the Se−S bond lengths are 5.122(3) and 5.165(3) Å,

Table 5. Bond angles ∠(ijk) in 2,5-diphenyl-3,4-trimethylene-6a-thiathiophthene. The standard deviations given in parentheses refer to the last digits of the respective values.

i	j	k	∠(ijk)°
S(1)	S(6a)	S(6)	179.28(4)
C(2)	S(1)	S(6a)	94.35(8)
C(3)	C(2)	S(1)	117.7(2)
C(3a)	C(3)	C(2)	119.3(2)
S(6a)	C(3a)	C(3)	118.6(2)
S(1)	S(6a)	C(3a)	90.04(8)
C(3a)	S(6a)	S(6)	89.59(8)
C(4)	C(3a)	S(6a)	118.8(2)
C(5)	C(4)	C(3a)	119.8(2)
S(6)	C(5)	C(4)	118.3(2)
S(6a)	S(6)	C(5)	93.54(8)
C(3)	C(2)	C(7)	126.1(2)
S(1)	C(2)	C(7)	116.2(2)
C(11)	C(5)	C(4)	125.8(2)
C(11)	C(5)	S(6)	115.9(2)
C(4)	C(3a)	C(3)	122.7(2)
C(10)	C(4)	C(3a)	117.4(2)
C(5)	C(4)	C(10)	122.7(2)
C(4)	C(10)	C(9)	111.7(2)
C(10)	C(9)	C(8)	112.5(2)
C(9)	C(8)	C(3)	113.0(2)
C(3a)	C(3)	C(8)	119.0(2)
C(8)	C(3)	C(2)	121.6(2)
C(2)	C(7)	C(17)	119.7(2)
C(2)	C(7)	C(21)	121.7(2)
C(7)	C(17)	C(18)	120.5(2)
C(17)	C(18)	C(19)	120.3(3)
C(18)	C(19)	C(20)	120.0(3)
C(19)	C(20)	C(21)	119.8(3)
C(20)	C(21)	C(7)	121.1(2)
C(21)	C(7)	C(17)	118.5(2)
C(5)	C(11)	C(16)	119.9(2)
C(5)	C(11)	C(12)	121.2(2)
C(11)	C(12)	C(13)	120.5(2)
C(12)	C(13)	C(14)	120.1(2)
C(13)	C(14)	C(15)	119.9(3)
C(14)	C(15)	C(16)	120.1(3)
C(15)	C(16)	C(11)	120.6(2)
C(16)	C(11)	C(12)	118.7(2)
C(3)	C(8)	H(81)	109(2)
C(3)	C(8)	H(82)	111(2)
C(9)	C(8)	H(81)	108(2)
C(9)	C(8)	H(82)	110(2)
H(81)	C(8)	H(82)	105(3)
C(81)	C(9)	H(91)	114(2)
C(8)	C(9)	H(92)	111(2)
C(10)	C(9)	H(91)	105(2)
C(10)	C(9)	H(92)	109(2)
H(91)	C(9)	H(92)	105(3)
C(4)	C(10)	H(101)	112(2)
C(4)	C(10)	H(102)	107(2)
C(9)	C(10)	H(101)	104(2)
C(9)	C(10)	H(102)	115(2)
H(101)	C(10)	H(102)	106(3)
C(11)	C(16)	H(16)	119(2)
C(15)	C(16)	H(16)	121(2)
C(16)	C(15)	H(15)	117(2)
C(14)	C(15)	H(15)	123(2)
C(15)	C(14)	H(14)	111(1)
C(13)	C(14)	H(14)	129(1)
C(14)	C(13)	H(13)	116(2)
C(12)	C(13)	H(13)	124(2)
C(11)	C(12)	H(12)	115(1)
C(13)	C(12)	H(12)	125(1)
C(7)	C(17)	H(17)	120(2)
C(18)	C(17)	H(17)	120(2)
C(17)	C(18)	H(18)	118(2)
C(19)	C(18)	H(18)	122(2)
C(18)	C(19)	H(19)	119(2)
C(20)	C(19)	H(19)	121(2)
C(19)	C(20)	H(20)	118(2)
C(21)	C(20)	H(20)	122(2)
C(20)	C(21)	H(21)	120(2)
C(7)	C(21)	H(21)	119(2)

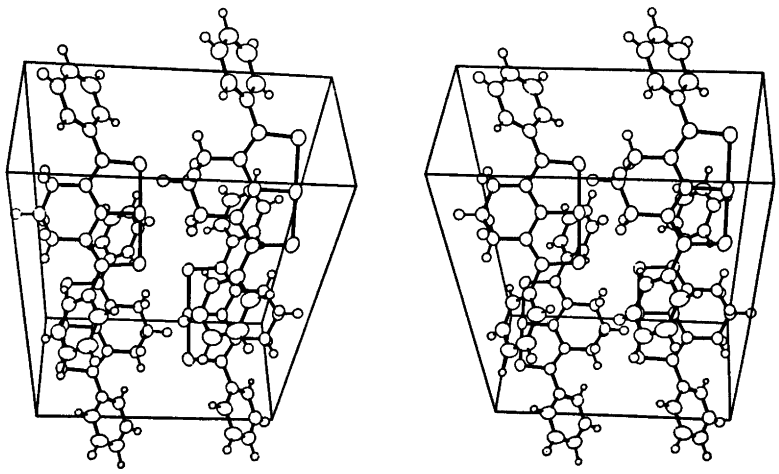

Fig. 2. Stereoview of the molecular packing.

respectively.[2,3] It should be mentioned in this connection that the Se—Se bond lengths in IV have not been corrected for libration, and the latter value is therefore probably somewhat too low.

The results from CNDO/2 calculations on mono-phenyl substituted 6a-thiathiophthenes show that a phenyl group in 2-position has a lengthening effect on the S(1)—S(6a) bond which varies with the twist angle of the phenyl group,[4] being negligible at twist angle 0° and most pronounced at 90°. As the twist angles of the 2- and 5-phenyl groups in the present structure deviate by 7° only, one might, in accordance with the CNDO/2 results, expect the S—S bond lengths to be almost equal. It is interesting, however, that the S(1)—S(6a) bond of 2.288(1) Å corresponds to twist angle 47.3°, while the S(6a)—S(6) bond of 2.329(1) Å corresponds to twist angle 54.3°.

CNDO/2 studies on 3,4-trimethylene-6a-thiathiophthene show that the trimethylene bridge does not affect the symmetry of the sulfur sequence.[15] This agrees with the results from the present study.

A stereoscopic view [16] of the molecular packing in the unit cell is given in Fig. 2. There are no intermolecular contacts shorter than corresponding van der Waals distance.

Acknowledgements. We thank Dr. M. Stavaux, Département de Chimie, Université de Caen, France, for a sample of 2,5-diphenyl-3,4-trimethylene-6a-thiathiophthene.

REFERENCES

1. Hordvik, A. *Acta Chem. Scand. 22* (1968) 2397; *25* (1971) 2507.
2. Hordvik, A. and Porten, J. A. *Acta Chem. Scand. 27* (1973) 485.
3. Hordvik, A. and Julshamn, K. *Acta Chem. Scand. 25* (1971) 2507.
4. Hansen, L. K., Hordvik, A. and Sæthre, L. J. *Chem. Commun.* (1972) 222.
5. Birknes, B., Hordvik, A. and Sæthre, L. J. *Acta Chem. Scand. 26* (1972) 2140.
6. Stavaux, M. and Lozac'h, N. *Bull. Soc. Chim. Fr.* (1967) 2082.
7. Throughton, P. G. H. *Siemens Review XXXVII* (1970), Fourth Special Issue: X-Ray and Electron Microscopy News.
8. Coppens, P., Leiserowitz, L. and Rabinovich, D. *Acta Crystallogr. 18* (1965) 1035.
9. *International Tables for X-Ray Crystallography*, Kynoch Press, Birmingham 1968, Vol. III, p. 202.
10. Stewart, R. F., Davidson, E. R. and Simpson, W. T. J. *Chem. Phys. 42* (1965) 3175.
11. Hordvik, A. and Sæthre, L. J. *Acta Chem. Scand. 26* (1972) 3114.
12. Schomaker, V. and Trueblood, K. N. *Acta Crystallogr. B 24* (1968) 63.
13. Hamilton, W. C. and Abrahams, S. C. *Acta Crystallogr. A 26* (1970) 18.
14. Cruickshank, D. W. J. *Acta Crystallogr. 9* (1956) 757; *14* (1961) 896.
15. Birknes, B. *Structure and Bonding in 6a-Thiathiophthenes with 3,4-Trimethylene and 3,4-Dimethylene Bridges*, Thesis, Department of Chemistry, University of Bergen, 1973.
16. Johnson, C. K. *A Fortran Thermal Ellipsoid Plot Program for Crystal Structure Illustrations*, ORNL-3794, Oak Ridge National Laboratory, Tennessee 1965.

Received July 22, 1974.

Acta Chemica Scandinavica A 29 (1975) 201—211

Conformational Analysis. VIII. The Molecular Structure, Torsional Oscillations, and Conformational Equilibrium of Gaseous 1,1,2,2,3,3,3-Heptachloropropane ($CHCl_2—CCl_2—CCl_3$) as Determined by Electron Diffraction and Compared with Semi-empirical (Molecular Mechanics) Calculations

JAN PETTER JOHNSEN and REIDAR STØLEVIK

Department of Chemistry, University of Oslo, Blindern, Oslo 3, Norway

Gaseous 1,1,2,2,3,3,3-heptachloropropane (HCP) has been studied by electron diffraction at a nozzle temperature of 80 °C. *Gauche* and *anti* conformers are possible for HCP. The conformer with the H atom *anti* to the CCC group was not present in detectable amounts, however, a small percentage (< 10 %) can not be ruled out. According to the semi-empirical calculations the percentage of *anti* should be less than 0.5 % at 80 °C.

Results are presented with error limits (2σ). The following values for bond lengths (r_g) and bond angles ($\angle_\alpha$) were obatined. Average parameters within the C—C—C group: r(C—C) = 1.603(12) Å and $\angle$CCC = 117.6°(3.8), average parameters within the $-CCl_3$ and $-CHCl_2$ groups: r(C—Cl) = 1.779(12) Å and $\angle$CCCl = 110.3°(1.2), average parameters within the $>CCl_2-$ group: r(C—Cl) = 1.767(28) Å and $\angle$CCCl = 108.3°(1.2). The deviations from an exact all-staggered (1:2) *gauche* conformation are statistically significant, but quite small [*ca.* 8°(2)].

It has been demonstrated, that for the *gauche* conformer an average torsional force constant can be estimated from the electron-diffraction data, if the remainder of the force field is approximately known. Within the experimental error limits, the values of the torsional force constants predicted by the energy model, agree with the experimental value.

To a large extent the structural parameters predicted by the molecular mechanics calculations reasonably agree with the experimental findings.

I. INTRODUCTION

This work is part of a systematic conformational study of halogenated propanes, by electron diffraction in the gas phase. Results for the following molecules have recently been published: $BrH_2C-CHBr-CH_2Br$,[1] $BrH_2C-CH_2-CH_2Br$,[2] $ClH_2C-CHCl-CH_2Cl$,[3] $Cl_3C-CCl_2-CCl_3$;[4] also molecules with $-CH_2X$ (X=Cl or H) groups bonded to the central C atom of a C—C—C skeleton have been studied: $C(CH_2Cl)_4$,[5] $(CH_3)_2C(CH_2Cl)_2$,[6] and $(CH_3)C(CH_2Cl)_3$.[7]

General information [8] relevant to this investigation and to the electron-diffraction method [9] is found in Refs. 8 and 9.

Some of the symbols which are used in this paper need a few comments. HCP is used for the compound itself. Capital letters A/G combined as AA, AG and GG indicate *anti*/*gauche* relations of a Z···Y distance in a Z—C—C—C—Y fragment, while small letters a/g indicate *anti*/*gauche* Z···Y distance in a Z—C—C—Y fragment (see Table 7).

Chlorinated propanes have been extensively studied by Dempster, Price and Sheppard using IR and NMR spectroscopy. The principal results obtained from such studies in the liquid phase, are found in Refs. 10, 11, and 12. In heavily chlorinated propanes many staggered confor-

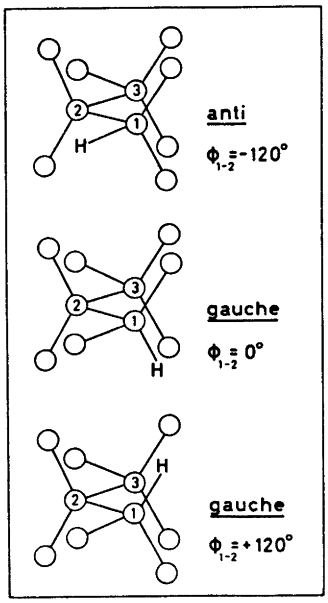

Fig. 1. The staggered conformers which are possible in 1,1,2,2,3,3,3-heptachloropropane. The two *gauche* forms are spectroscopically indistinguishable.

mers have parallel C—Cl bonds on the same side of the carbon skeleton [parallel (1:3) Cl···Cl interaction].[10] Conformers which possess parallel (1:3) Cl···Cl interactions, are energetically less stable than conformers without such interactions.[10]

Assuming all-staggered (1:2) conformations, only two spectroscopically distinguishable forms are possible for HCP. The conformers and their names are shown in Fig. 1. The two *gauche* forms are not spectroscopically distinguishable. If the torsion angles of a *gauche* conformer have to be specified, then the one with $\phi_{1-2}=\phi_{2-3}=0°$ in staggered positions will be mentioned. Both of the staggered conformers possess parallel (1:3) Cl···Cl interactions.

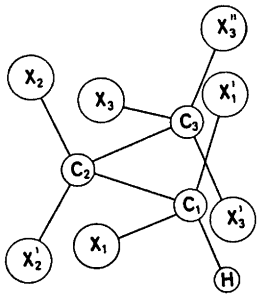

Fig. 2. The numbering of atoms in the *gauche* conformer of 1,1,2,2,3,3,3-heptachloropropane.

The liquid and crystal IR spectra, obtained near room temperature, show no indication of more than one conformer.[11] It is likely that the *gauche* conformer, which has one parallel (1:3) Cl···Cl interaction less than the *anti* conformer, is the most stable one energetically. It is also likely that the C—C bonds and the CCC angles in both conformers have unusual values, in accordance with the experimental findings for octachloropropane.[4] Most probably, *gauche* conformers have torsion angles somewhat different from staggered values.

II. CALCULATION OF CONFORMATIONAL ENERGIES, GEOMETRIES, BARRIERS AND TORSIONAL FORCE CONSTANTS

The semi-empirical energy model corresponds to simple molecular mechanics calculations, including atom-atom potentials and valence force constants as described in Ref. 1.

Energy parameters (a, b, c, d and V_0) were taken from the paper by Abraham and Parry,[13] and the diagonal force constants of Table 5 were used. In minimizing the energy, the geometry was constrained in the same way as described in Sect. V-A.

The structural parameters of the conformers are presented in Table 1.

Conformational energies are found in Table 2. According to the present energy model, *gauche* is the conformer of lowest potential energy. The energy minimum of *gauche* is somewhat displaced from an exact staggered conformation, leading to a lower conformational energy. For *anti* the energy minimum corresponds to an exact staggered conformation with $\phi_{1-2}=-120°$ and $\phi_{2-3}=0°$.

Torsional barriers may be estimated from the energy values of Table 3. Each energy value in Table 3 corresponds to a conformer having all structural parameters adjusted, except for one or two torsion angles (ϕ) being kept at constant values. Eclipsed conformers correspond to values of ϕ being $\pm 60°$ or $\pm 180°$. The actual

Table 1. Calculated structural parameters in the stable conformers of 1,1,2,2,3,3,3-heptachloropropane. In minimizing the energy the geometry was constrained as described in Sect. V-A.

Type of parameter r(Å), ∠(°), X=Cl	Normal value	*gauche*	*anti*
Average parameters in the CCC group:			
r(C–C)	(1.513)	1.597	1.582
∠CCC	(110.0)	114.8	120.7
Average parameters in the $-CX_3$ and $-CHX_2$ groups:			
r(C–X)	(1.760)	1.779	1.776
∠CCX	(109.47)	113.6	113.9
r(C–H)	(1.094)	1.093	1.095
∠CCH	(109.47)	109.1	109.0
Average parameters in the $\angle CX_2$ group:			
r(C–X)	(1.760)	1.797	1.793
∠CCX	(109.47)	109.2	107.9
Torsion angles:			
$\angle\phi_{1-2}(-C_1-C_2)$	(60)[a]	+6.6[b]	−120.0
$\angle\phi_{2-3}(-C_2-C_3)$	(60)[a]	−7.2[b]	±0.0

[a] $\phi_0 = 60°$ in eqn. (1) in Ref. 1. [b] $\phi_{1-2} = \phi_{2-3} = 0°$ for exact staggered positions (Fig. 1). Conventional designation of ϕ values would be $\phi_{1-2} = \pm 60°$ *(gauche)* and $\phi_{1-2} = 180°$ *(anti)*.

Table 2. Calculated conformational energies in 1,1,2,2,3,3,3-heptachloropropane. Details about the energy expression are found in Ref. 1. The zero-point vibrational energies of the conformers are not included.

Type of energy (kcal/mol)	*gauche*	*anti*	Δ(g−a)
E(bonded)	9.2	12.3	−3.1
E(van der Waals)	7.5	6.7	+0.8
E(polar: Cl···H)	−3.8	−3.5	−0.3
E(polar: Cl···Cl)	32.4	33.0	−0.6
E(total)	45.3	48.5	−3.2

values of the geometry variables are not shown in Table 3, however, the values of the torsion angles ϕ_{1-2} and ϕ_{2-3} are approximately those given in parenthesis. Details about the stable conformers are found in Table 1 and Table 2. The stable conformers correspond to well defined minima of the potential-energy surface. The lowest barrier is as high as 9.3 kcal/mol.

Table 3. Calculated conformational energies and torsional barriers in 1,1,2,2,3,3,3-heptachloropropane.

ϕ_{2-3} (°)	ϕ_{1-2} (°) −180 +180 −60	−120	0 +120	+60
−60 +60	44.8	18.7	16.9	28.5
0	14.5	*anti*= 3.2[a]	"*gauche*"= 1.4[a] min (=0)	9.3

[a] Details about the conformational minima are given in Tables 1 and 2. The energy values here are relative to the *gauche* value. See also explanations in the text.

Table 4. Calculated torsional force constants in conformers of 1,1,2,2,3,3,3-heptachloropropane.

(mdyn Å (rad)$^{-2}$)	*gauche*	*anti*
$F_\phi(1-2)^a = \delta^2E/\delta\phi_{1-2}^2$	0.57	0.47
$F_\phi(2-3)^a = \delta^2E/\delta\phi_{2-3}^2$	0.67	0.68
$F_{\phi\phi'}{}^b = \delta^2E/\delta\phi_{1-2}\delta\phi_{2-3}$	−0.35	−0.44

[a] Diagonal force constant. [b] Interaction force constant (non-diagonal element).

Torsional force constants were computed according to their definitions (Table 4). The derivatives were calculated numerically at the potential-energy minima.

III. CALCULATION OF VIBRATIONAL QUANTITIES

Infrared and Raman frequencies and schematic assignments for liquid and crystalline HCP have been published by Sheppard *et al.*[11] However, the low frequencies (< *ca.* 550 cm^{-1}), which are the most important ones for an electron-diffraction study, have not been published.

Therefore, valence force constants, except for the torsional part, were taken from the work of Schachtschneider and Snyder.[14] Certain compromises between force-constant values had to be made. The final values selected for HCP are given in Table 5.

Table 5. Valence force constants for 1,1,2,2,3,3,3-heptachloropropane (X=Cl).

Stretch (mdyn Å^{-1})		Bend (mdyn Å (rad)$^{-2}$)			
C—C	4.39	CCC	0.90	HCX	0.79
C—H	4.89	CCH	0.69	XCX	1.13
C—X	2.76	CCX	1.17	—	

Stretch/stretch (mdyn Å^{-1}), C common
C—X/C—X 0.49; C—X/C—C 0.73; C—C/C—C 0.064

Stretch/bend (mdyn (rad)$^{-1}$)
C—C common: C—C/CCX 0.29; C—C/CCC 0.35; C—C/CCH 0.25
C—X common; C—X/CCX 0.55; C—X/HCX 0.33; C—X/XCX 0.41
C common: C—X/XCX 0.38

Bend/bend (mdyn Å (rad)$^{-2}$)
C—X common: XCX/XCX −0.13; CCX/XCX −0.12
C common: CCX/XCX −0.06
C—H common: HCX/HCX 0.09; CCH/HCX 0.10
C—C common (dihedral angles in parenthesis)
CCC/CCX +0.04 (CCC/CCX 180°)
CCC/CCX −0.02 (CCC/CCX 60°)
CCX/CCX −0.09 (CCX/CCX 180°)
CCX/CCX +0.07 (CCX/CCX 60°)
CCX/CCH +0.07 (CCX/CCH 180°)
CCX/CCH −0.04 (CCX/CCH 60°)
CCH/CCC −0.06 (CCH/CCC 60°)
Torsion [a] (mdyn Å (rad)$^{-2}$)
$F_\phi(1-2)=F_\phi(2-3)=0.54$ (see Sect. V-B),[b] $F_{\phi\phi'}=0$

[a] The torsional force constants have been defined in the following way: each fragment of type A′—C_i—C_3—A″ (A=C, Cl, or H) has been assigned an equal torsional force constant. The total force constant (F_ϕ) for the torsional coordinate ϕ_{i-3} (i=1,3) is thus sum of *nine* equal contributions. The input to Gwinn's normal-coordinate program demands a separate specification for each torsion fragment. [b] This value was estimated from the electron-diffraction data as described in Sect. V-B.

Table 6. Fundamental vibrational frequencies (cm^{-1}) in the *gauche* conformer of 1,1,2,2,3,3,3-heptachloropropane. The force constants in Table 5 and the cartesian coordinates in Table 8 were used in calculating these frequencies.

Torsional oscillations:[a]	67 and 77
Bending vibrations:[b]	93, 144, 169, 177, 192, 210, 228, 254, 266, 298, 331, 345, 408
C—Cl stretching:[c]	565, 653, 700, 774, 776, 845, 879
C—C stretching:[d]	904 and 1173
C—H deformation:[e]	1234 and 1255
C—H stretching:	2995

[a] The two modes are roughly described as follows: 67 cm^{-1} ($\Delta\phi_{1-3}=+\Delta\phi_{2-3}$) and 77 cm^{-1} ($\Delta\phi_{1-2}\simeq-\Delta\phi_{2-3}$), where $\Delta\phi$ represents the torsion-angle deformation. [b] Modes largely corresponding to mixed CCX, XCX, and CCC angle deformations. [c] Largely C—X stretching, but mixed with angle deformations. [d] Largely C—C stretching. [e] Deformations in CCH and HCX angles.

The normal-coordinate program described by Gwinn [15] was used in computing vibrational frequencies. Their values are shown in Table 6. The agreement between these values and those observed by Sheppard *et al.*[11] is quite good. The C—Cl stretching frequencies were assigned to observations between 578 and 872 cm^{-1}. The average relative deviation between observed and calculated values is less than 2 % for C—Cl stretching modes, while the average deviation for the remaining modes is *ca.* 5 %.

Mean amplitudes of vibration (u) and vibrational correction terms (K and D) were calculated as explained in Ref. 16. Their values are found in Table 7.

According to the semi-empirical model (Table 4), the value of the torsional interaction constant ($F_{\phi\phi'}$) is negative and in magnitude comparable to the value of the diagonal elements. The values of the torsional frequencies depend on the value of $F_{\phi\phi'}$. However, it has been shown [4]

Table 7. Mean amplitudes of vibration (u) and vibrational correction terms, $K-(u^2/r)$, for the *gauche* conformer of 1,1,2,2,3,3,3-heptachloropropane at 80 °C. The force constants in Table 5 and the cartesian coordinates in Table 8 were used in calculating these quantities. The correction term corresponds to $r_a-r_\alpha=K-(u^2/r)= -D$.

Dist. type (X=Cl)	u-Value (Å)	$K-(u^2/r)$ (Å)	Dist. type (X=Cl)	u-Value (Å)	$K-(u^2/r)$ (Å)
C_1-C_2	0.0544	0.0020	$X_1'\cdots H$	0.1093	0.0115
C_2-C_3	0.0550	0.0013	$X_1\cdots H$	0.1093	0.0120
C_1-X_1'	0.0574	0.0087	$X_1\cdots X_1'$	0.0735	0.0129
C_1-X_1	0.0575	0.0085	$X_3'\cdots X_3''$	0.0757	0.0076
C_3-X_3'	0.0570	0.0056	$X_3\cdots X_3''$	0.0757	0.0086
C_3-X_3''	0.0570	0.0060	$X_3\cdots X_3'$	0.0757	0.0079
C_3-X_3	0.0570	0.0062	$X_2\cdots X_2'$	0.0743	0.0036
C_2-X_2	0.0590	0.0032	$C_1\cdots X_3'$(g)	0.1301	−0.0007
C_2-X_2'	0.0589	0.0032	$C_1\cdots X_3''$(g)	0.1301	−0.0008
C_1-H	0.0778	0.0124	$C_3\cdots X_3$(g)	0.1297	0.0004
$C_2\cdots H$	0.1099	0.0058	$C_1\cdots X_3$(a)	0.0765	0.0011
$C_2\cdots X_1'$	0.0725	0.0064	$C_3\cdots X_1$(a)	0.0766	0.0021
$C_2\cdots X_1$	0.0724	0.0063	$C_3\cdots H$(g)	0.1503	±0.0000
$C_2\cdots X_3'$	0.0728	0.0038	$X_1'\cdots X_2'$(a)	0.0759	0.0049
$C_2\cdots X_3''$	0.0727	0.0039	$X_3'\cdots X_2$(a)	0.0762	0.0020
$C_2\cdots X_3$	0.0725	0.0047	$X_3''\cdots X_2'$(a)	0.0762	0.0022
$C_1\cdots C_3$	0.0741	0.0002	$X_2\cdots H$ (a)	0.1044	0.0058
$C_1\cdots X_2$	0.0735	0.0026	$X_2'\cdots H$ (g)	0.1515	0.0015
$C_1\cdots X_2'$	0.0733	0.0025	$X_1'\cdots X_2$(g)	0.1383	0.0013
$C_3\cdots X_2$	0.0735	0.0018	$X_3'\cdots X_2'$(g)	0.1344	±0.0000
$C_3\cdots X_2'$	0.0736	0.0019	$X_3''\cdots X_2$(g)	0.1344	−0.0001
$X_1\cdots X_2$(g)	0.1414	0.0069	$X_1'\cdots X_3'$(GG)	0.1996	−0.0056
$X_1\cdots X_2'$(g)	0.1370	0.0071	$X_1'\cdots X_3''$(GG)	0.2193	−0.0051
$X_3\cdots X_2$(g)	0.1371	0.0004	$X_1'\cdots X_3$(AG)	0.1334	−0.0009
$X_3\cdots X_2'$(g)	0.1373	0.0003	$X_1\cdots X_3'$(AG)	0.1344	−0.0004
$X_3'\cdots H$(GG)	0.2159	−0.0040	$X_1\cdots X_3''$(AG)	0.1343	−0.0008
$X_3''\cdots H$(GG)	0.1954	−0.0032	$X_1\cdots X_3$(AA)	0.1130	0.0001
$X_3\cdots H$(AG)	0.1499	0.0001	—	—	—

Table 8. Cartesian coordinates (x,y,z) and the root-mean-square displacements of atoms in the *gauche* conformer of 1,1,2,2,3,3,3-heptachloropropane (at 80 °C).

x (Å) (see Fig. 2)[a]	y (Å)	z (Å)	Atom	$\langle\Delta x^2\rangle^{\frac{1}{2}}$ (in Å units)[b]	$\langle\Delta y^2\rangle^{\frac{1}{2}}$	$\langle\Delta z^2\rangle^{\frac{1}{2}}$
0	0	0	C_2	0.0422	0.0698	0.0632
1.3947	0.7843	0	C_1	0.0570	0.0550	0.0635
1.4619	1.4332	−0.9227	H	0.1543	0.1420	0.1272
1.5179	1.8071	1.4396	X_1'	0.1171	0.1017	0.1202
2.7401	−0.3663	0	X_1	0.0685	0.0866	0.1188
−1.3947	0.7843	0	C_3	0.0486	0.0486	0.0509
−1.5179	1.8071	−1.4396	X_3'	0.1005	0.0885	0.0739
−1.5179	1.8071	1.4396	X_3''	0.1175	0.0968	0.0741
−2.7401	−0.3663	0	X_3	0.0736	0.0707	0.1092
0	−1.0743	1.4062	X_2	0.0786	0.0872	0.0743
0	−1.0748	−1.4062	X_2'	0.0786	0.0846	0.0740

[a] These values of the cartesian coordinates were used in the calculations of all vibrational quantities (staggered model). [b] The r.m.s. quantities were computed according to formulas given in Ref. 16.

Table 9. Vibrational quantities in the *gauche* conformer of 1,1,2,2,3,3,3-heptachloropropane, calculated with different values of the average torsional force constant ($\bar{F}_\phi$). See also explanations given in the Tables 5, 6, 7, and 8. $\bar{F}_{\phi\phi'}$ was fixed at zero value.

$\bar{F}_\phi$(mdyn Å (rad)$^{-2}$)	0.36	0.54[a]	0.81
Mean amplitudes u(X···X), X=Cl	u (Å) at 80 °C		
X···X(*anti*)[b]	0.076	0.076	0.076
X···X(*gauche*)[b]	0.147	0.138	0.130
$X_1'\cdots X_3'$(GG)	0.225	0.200	0.180
$X_1'\cdots X_3''$(GG)	0.231	0.219	0.210
X···X (AG)[b]	0.140	0.134	0.129
X···X (AA)	0.113	0.113	0.113
Low frequencies[c]	ω cm^{-1})		
ω_1(torsion)	55	67	81
ω_2(»)	66	77	84
ω_3(bend)	89	92	101
ω_4(»)	140	144	151
ω_5(»)	167	169	171
ω_6(»)	177	177	178
ω_7(»)	192	192	193
ω_8(»)	210	210	211

[a] The best value as determined in Sect. V-B. [b] Average value for several X···X distances of this type. See also Table 7. [c] All frequencies, calculated with $\bar{F}_\phi = 0.54$, have been shown in Table 6.

that the u and K values are much less dependent on the $F_{\phi\phi'}$ value.

Values of the cartesian coordinates (x,y,z) and the vibrational quantities $\langle\Delta x^2\rangle^{\frac{1}{2}}$, $\langle\Delta y^2\rangle^{\frac{1}{2}}$, $\langle\Delta z^2\rangle^{\frac{1}{2}}$ have been given in Table 8. The coordinate values in Table 8 were used in all calculations involving vibrational quantities. The r.m.s. quantities were computed according to the formulas derived in Ref. 16.

According to the adjustments described in Sect. V-B, the most probable value of the average torsional force constant ($\bar{F}_\phi$) is expected in the range 0.36—0.81 mdyn Å (rad)$^{-2}$. In Table 9 are shown low vibrational frequencies and mean amplitudes of vibration corresponding to values of $\bar{F}_\phi$ in this range.

IV. EXPERIMENTAL AND DATA REDUCTION

HCP was obtained from "K&K" laboratories. The purity of the sample was better than 97 %.

Electron-diffraction photographs were made at a nozzle temperature of 80 °C in the Balzer [17] apparatus [18] under conditions summarized below.

Nozzle-to-plate distance (mm)	498.8	249.0
Electron wavelength (Å)	0.05856	0.05853
Number of plates	5	4
Range of data, in s(Å^{-1})	1.125—15.625	2.25—30.50
Data interval, Δs(Å^{-1})	0.125	0.25
Estimated uncertainty in s-scale (%)	0.14	0.14

The electron wavelength was determined by calibration against ZnO and corrected by an experiment with CO_2 giving a correction of +0.1 % in the s-scale. The data were reduced in the usual way [19] to yield an intensity curve for each plate.

Average curves for each set of distances were formed. A composite curve was then made by connecting the two average curves after scaling. The final experimental curve is shown in Fig. 3. The intensities have been modified [19] by $s|f'_{Cl}|^{-2}$. The scattering amplitudes were calculated by the partial-wave method,[20] using Hartree-Fock atomic potentials.[21]

The radial-distribution curve obtained by Fourier [19] transformation of the final experimental intensity is shown in Fig. 4.

V. STRUCTURE ANALYSIS

From the RD curves in Fig. 5 it is obvious that *gauche* is the most abundant conformer. The relative amount of the *anti* conformer has to be very small. If the conformational energies predicted by the semi-empirical model are correct, the presence of the *anti* conformer can not be detected at 80 °C [$\alpha(anti) < 0.5$ %].

In calculating theoretical intensities, it was decided not to consider contributions from the *anti* conformer. (See also Sect. VII).

A. *Least-squares refinements.*[19] HCP represents a complicated structural problem. Several assumptions about bond lengths and bond angles

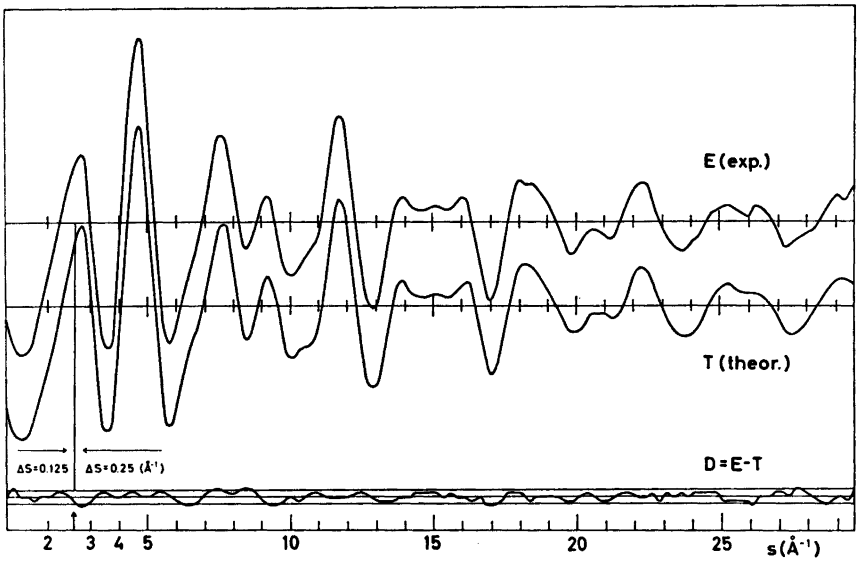

Fig. 3. Experimental (E) and theoretical (T) intensity curves for 1,1,2,2,3,3,3-heptachloropropane at 80 °C. The difference curve (D) is shown together with the experimental error limits of the intensities. All curves are on the same scale.

have to be made in constructing the molecular model to be used in the least-squares adjustments. The following assumptions were introduced (see Fig. 2).

(1) The plane of the CX_2 group is perpendicular to the plane of the C atoms and bisects the CCC angle,

(2) the $C-CX_3$ group possess C_{3v} symmetry,

(3) the $C-CHX_2$ group possess C_s symmetry, and the projection of the $X_1C_1X_1'$ angle on a plane perpendicular to the C_1-C_2 axis is 120,°

(4) the CCX angles in the $-CHX_2$ and $-CX_3$ groups are equal ($\angle CC_1X = \angle CC_3X$),

(5) all CCX angles of the $-CX_2-$ group are equal: $\angle CC_2X$,

(6) the C—X bond lengths of the $-CHX_2$ and $-CX_3$ groups are equal: $r(C_1-X)=r(C_3-X)$,

(7) the C—X bond lengths in the $-CX_2-$ group are equal: $r(C_2-X)$.

(8) the two C—C bond lengths are equal: $r(C-C)$.

Models were refined in terms of the following parameters: $r(C-C)$, $r(C_1-X)=r(C_3-X)$, $r(C_2-X)$, $r(C-H)$, $\angle CCC$, $\angle CC_1X=\angle CC_3X$, $\angle CC_2X$, and the torsion angles (ϕ_{1-2} and ϕ_{2-3}) of the *gauche* conformer (see Fig. 1). For the exact staggered conformation of *gauche* $\phi_{1-2}=\phi_{2-3}=0°$, corresponding to a coplanar arrangement of the atoms $X_1-C_1-C_2-C_3-X_3$.

Non-bonded internuclear distances were computed as dependent quantities, restricted under the constraints of geometrically consistent r_α parameters.[22,23]

Several of the bond distances which have been assigned equal *lengths* in the least-squares adjustments, are not *vibrationally* identical, as shown in Table 7. This fact has been allowed for when D values ($D=r_\alpha-r_a=(u^2/r)-K$) were assigned to the internuclear distances.

B. Determination of torsional force constants. Mean amplitudes of vibration (u) and perpendicular amplitude correction coefficients (K) are easily calculated if a reasonable force field is known for the molecule (see Sect. III). The values of the torsional force constants $F_\phi(1-2)$, $F_\phi(2-3)$, and $F_{\phi\phi'}$ for HCP had not been experimentally determined prior to this investigation.

If the interaction constant ($F_{\phi\phi'}$) is not considered (see discussion in sect. III), then two elements, $F_\phi(1-2)$ and $F_\phi(2-3)$, of different values ought to be adjusted. It is clear that $F_\phi(1-2)<F_\phi(2-3)$. According to the semi-empirical model $F_\phi(2-3)$ is *ca.* 20 % (Table 4) greater than $F_\phi(1-2)$.

Unfortunately the electron-diffraction data for HCP do not contain enough information for an independent determination of $F_\phi(1-2)$ and

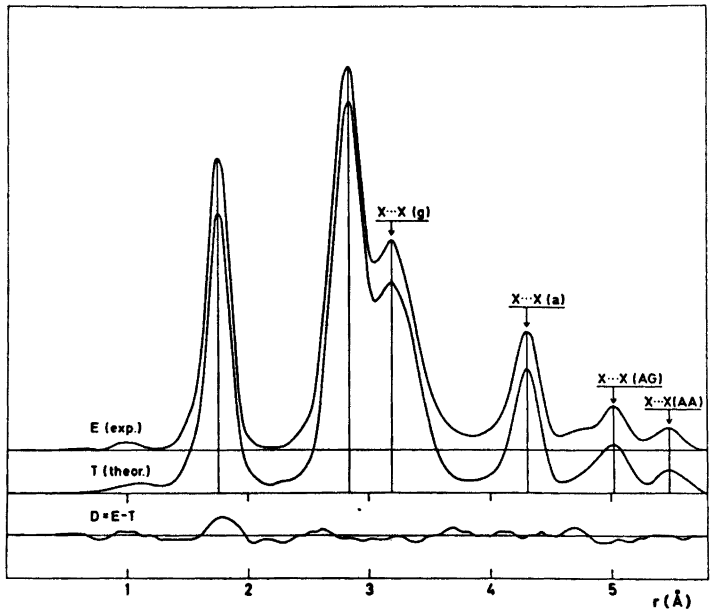

Fig. 4. Experimental (E) and theoretical (T) radial-distribution curves for 1,1,2,2,3,3,3-heptachloropropane at 80 °C and difference curve (D). The curves have been calculated by Fourier transformation of the intensities in Fig. 3, using an artificial damping constant equal to 0.0020 Å^2.

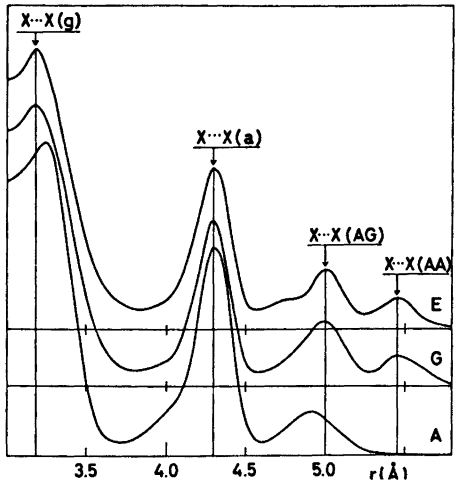

Fig. 5. Theoretical radial-distribution curves for the conformers *anti* (A) and *gauche* (G). The experimental curve (E) is also shown.

$F_\phi(2-3)$ simultaneously. It is, however, possible to estimate an average element $\bar{F}_\phi$ ($F_\phi(1-2)=F_\phi(2-3)=\bar{F}_\phi$).

The value of $\bar{F}_\phi$ was determined as follows: u and K values for different values of $\bar{F}_\phi$ were calculated and then included in the least-squarse refinements. The value of $\bar{F}\phi$ which lead to a minimum in the error sum (V'PV) was obtained. In each least-squares run all structural variables were refined simultaneously. The best value of $\bar{F}_\phi$ obtained in this way was: $\bar{F}_\phi = 0.54\ ^{+0.27}_{-0.18}$ mdyn Å (rad)$^{-2}$. The error limits are believed to be pessimistic; however, there is no objective way to estimate these limits. The most direct estimate, but subjective to a certain degree, is probably obtained by comparing experimental and calculated RD curves for a range of $\bar{F}_\phi$ values. Several types of *systematic* errors ought to be considered, as discussed in a previous paper.[4] The error limits here do not allow for systematic errors.

VI. FINAL RESULTS

Parameters from the least-squares refinements, and their standard deviations (σ) corrected for correlation [24] in the experimental data, are given in Table 10. The final parameters correspond to refinements with equal weights for all intensities. Data beyond $s=29.5$ Å^{-1} were not included in these refinements.

Table 10. Structural parameters in the *gauche* conformer of 1,1,2,2,3,3,3-heptachloropropane (X=Cl). Standard deviations are shown in parentheses. The uncertainty (0.14 %) in the *s*-scale has been included in the standard deviations for bond lengths. An experiment with CO_2 gave a correction of +0.1 % in the *s*-scale. The bond lengths are therefore 0.1 % longer than the least-squares estimates.

Bond lengths (Å)[a] (r_a-values)	Bond angles (°)[a] ($\angle_\alpha$-values)
r(C−C)=1.601(8)	∠CCC=117.6(1.9)
Average parameters in the $-CX_3$ and $-CHX_2$ groups:	
r(C−X)=1.777(6)	∠CCX=110.3(0.6)
Average parameters in the $>CX_2$ groups:	
r(C−X)=1.765(14)	∠CCX=108.3(0.6)
r(C−H)=1.05(9)[b]	∠CCH=(109.47)[c]
Torsion angles (assuming $\phi_{2-3}=-\phi_{1-2}$):	
$\phi_{1-2}=+7.8°(1.1)$[d] and $\phi_{2-3}=-7.8°(1.1)$[d]	

[a] The geometrical assumptions have been explained in Sect. V-A. [b] See Fig. 4. [c] Assumed value. [d] Staggered values: $\phi_{1-2}=\phi_{2-3}=0°$, see Fig. 1.

Non-bonded internuclear distances were restricted under the geometrical constraints of r_α parameters, by including correction terms $D=r_\alpha-r_a$ ($D=(u^2/r)-K$) for all distances (Sect. III).

Parameter-correlation coefficients (ϱ) are shown in Table 11.

The fit obtained between theoretical and experimental intensities, using the u and K values calculated with the force constants of Table 5 was generally quite satisfactory. It is important that the large number of u values do not have to be adjusted as individual parameters in the least-squares refinements. However, it ought to be kept in mind that the torsiondependent u and K values have been adjusted *simultaneously* by adjusting the diagonal torsional-force constants (Sect. V-B). The vibrationally consistent u values of Table 7, which combine information from both vibrational spectroscopy and electron diffraction, are considered more reliable than the individual u values obtained by direct least-squares refinements in the usual way.[19] The average relative standard deviation, $\langle\sigma/u\rangle$, of individually adjusted u values was *ca.* 10 %, while the average relative deviation between these u values and those of Table 7, $\langle|\Delta|/u\rangle$, was *ca.* 16 %. Only one u value, u(C−Cl)=0.037 Å and σ=0.004 Å, obtained by direct refinement, was significantly different from the value (*ca.* 0.058 Å) of Table 7. Most probably the low value of u(C−Cl) is caused by an error in the blackness correction. It is, however, unlikely that such an error is critical for the determination of the remaining u values.

In calculating the theoretical intensities of Fig. 3, the individually adjusted u-values were used. The theoretical intensities obtained with the u-values from Table 7 were only slightly different from those of Fig. 3.

VII. DISCUSSION

In comparing theoretical radial distribution curves with the experimental one, it was concluded that the smallest detectable amount of *anti* is *ca.* 10 % or more. The actual amount of *anti* could not be determined by least-squares refinements in this particular case. However, from the experimental data alone a small (< 10 %) of *anti* is not ruled out.

Assuming equal vibrational partition functions for the conformers *anti* and *gauche*, and the conformational energies of Table 2 (ΔE(a−g)=3.2 kcal/mol), then the percentage of *anti* should be less than 0.5 % at 80 °C. In order to get as much as *ca.* 10 % of the *anti* conformer at 80 °C, the value of ΔE(a−g) have to be *ca.* 1.1 kcal/mol. It is possible, but unlikely, that the calculated energy difference ΔE(a−g) (3.2 kcal/mol) is wrong by as much as *ca.* 2 kcal/mol. Therefore, in conclusion, the best estimate of the conformational energy difference is 3.2 kcal/mol in favour of *gauche*, as predicted by the semi-empirical model. This estimate is also consistent with the electron-diffraction data.

It seems natural to compare the structural parameters of HCP with those found in octachloropropane (OCP),[4] where *all* hydrogen positions in propane have been substituted with chlorine. The C−C bond lengths and the CCC bond angles of both molecules are very different from those in propane itself. The experimentally determined difference between the C−C bond

Table 11. Parameter correlation coefficients (100 ϱ).

		(1)	(2)	(3)	(4)	(5)	(6)	(7)	(8)	(9)	(10)	(11)
r(C−C)[a]	(1)	100										
r(C_2−X)	(2)	−37	100									
r(C_1−X)	(3)	6	−84	100								
r(C−H)	(4)	−10	6	3	100							
∠CCC	(5)	5	−48	54	10	100						
∠CC_1X	(6)	−62	82	−67	11	−32	100					
∠CC_2X	(7)	9	7	−10	0	−62	−27	100				
∠CCH	(8)	−41	19	−14	45	12	34	−3	100			
ϕ[b]	(9)	3	2	1	3	−38	−21	70	−2	100		
k(scale)	(10)	−32	−37	−26	20	−6	38	−1	34	7	100	
u(C−X)[c]	(11)	−18	−6	19	10	13	−5	4	12	9	54	100

[a] The geometrical assumptions are given in Sect. V-A. [b] Torsion angles: $\phi_{1-2}=\phi$ and $\phi_{2-3}=-\phi$. [c] All u(C−X) values were refined as one parameter.

lengths [r_a(OCP)−r(HCP)=1.655 Å−1.601 Å] is 0.054 Å, and the difference between the CCC angles (∠CCC(OCP)−∠CCC(HCP)=119.0°−117.6°) is 1.4°. According to the semi-empirical calculations the *anti* conformer of HCP should have a CCC bond angle even larger than the one in OCP. No significant deviations from an all-staggered (1:2) conformation were observed for OCP, while the deviations from an all-staggered (1:2) *gauche* conformation for HCP are statistically significant, but quite small.

To a large extent the values of the structural parameters predicted by the semi-empirical model (Table 1), reasonably agree with the experimental findings. Within the experimental error limits for HCP, the predicted parameters r(C−C), <CCC, and the torsion angles agree with the observed values. Although adjustments in the non-torsional force constants and the "normal" reference parameters (Table 1) would remove most of the remaining discrepancies, it was felt that results from additional molecules ought to be included before such corrections were considered.

It has been demonstrated that the average diagonal element of the torsional force field may be estimated from the electron-diffraction data. Although the torsional interaction force constant cannot be obtained in this way, the most probable values of the two torsional frequencies have been limited to the range 55−85 cm^{-1} (Table 9). For octachloropropane [4] this range was 45−65 cm^{-1}. The average torsional force constants were 0.54 and 0.36 mdyn Å $(rad)^{-2}$ for HCP and OCP, respectively. Within the experimental error limits (Sect. V-B) the calculated (Table 4) force constants agree with the experimental average value for HCP.

Acknowledgements. We are grateful to Kristen Brendhaugen for recording the diffraction photographs. Computer programs made available by Dr. H. M. Seip, Prof. W. D. Gwinn, and Cand.real. S. Rustad have been extensively used in this work. Financial support from Norges almenvitenskapelige forskningsråd is gratefully acknowledged.

REFERENCES

1. Stølevik, R. *Acta Chem. Scand. A 28* (1974) 299.
2. Farup, P. E. and Stølevik, R. *Acta Chem. Scand. A 28* (1974) 680.
3. Farup, P. E. and Stølevik, R. *Acta Chem. Scand. A 28* (1974) 871.
4. Fernholt, L. and Stølevik, R. *Acta Chem. Scand. A 28* (1974) 963.
5. Stølevik, R. *Acta Chem. Scand. A 28* (1974) 327.
6. Stølevik, R. *Acta Chem. Scand. A 28* (1974) 455.
7. Stølevik, R. *Acta Chem. Scand. A 28* (1974) 612.
8. Bastiansen, O., Seip, H. M. and Boggs, J. E. In Dunitz, J. D. and Ibers, J. A., Eds., *Perspectives in Structural Chemistry*, Wiley, New York 1971, Vol. IV.
9. Seip, H. M. In Sim, G. A. and Sutton, L. E., Eds, *Molecular Structure by Diffraction Methods*, Specialist Periodical Reports, The Chemical Society, London 1973, Vol. 1, Part 1, Chapter 1.
10. Dempster, A. B., Price, K. and Sheppard, N. *Spectrochim. Acta Part A 25* (1969) 1381.

11. Dempster, A. B., Price, K. and Sheppard, N. *Spectrochim. Acta Part A 27* (1971) 1563.
12. Dempster, A. B., Price, K. and Sheppard, N. *Spectrochim. Acta Part A 27* (1971) 1579.
13. Abraham, R. J. and Parry, K. J. *J. Chem. Soc. B* (1970) 539.
14. Schachtschneider, J. H. and Snyder, R G. *Vibrational Analysis of Polyatomic Molecules. IV.* (Force constants for the haloparaffins). Project No. 31450, Technical Report No. 122—63 of Shell Development Company.
15. Gwinn, W. D. *J. Chem. Phys. 55* (1971) 477.
16. Stølevik, R., Seip, H. M. and Cyvin, S. J. *Chem. Phys. Lett. 15* (1972) 263.
17. Zeil, W., Haase, J. and Wegmann, L. *Z. Instrumentenk. 74* (1966) 84.
18. Bastiansen, O., Graber, R. and Wegmann, L. *Balzer's High Vacuum Report 25* (1969) 1.
19. Andersen, B., Seip, H. M., Strand, T. G. and Stølevik, R. *Acta Chem. Scand. 23* (1969) 3224.
20. Peacher, J. and Willis, J. C. *J. Chem. Phys. 46* (1967) 4809.
21. Strand, T. G. and Bonham, R. A. *J. Chem. Phys. 40* (1964) 1686.
22. Morino, Y., Kuchitsu, K. and Oka, T. *J. Chem. Phys. 36* (1962) 1108.
23. Kuchitsu, K. *J. Chem. Phys. 49* (1968) 4456.
24. Seip, H. M. and Stølevik, R. In Cyvin, S. J., Ed., *Molecular Structures and Vibrations*, Elsevier, Amsterdam 1972.

Received August 5, 1974.

Acta Chemica Scandinavica A 29 (1975) 212—216

The Crystal and Molecular Structures of *cis* Square-planar Complexes of Tellurium Dichloride and Dibromide with Trimethylenethiourea

KJELL S. FREDIN, KJARTAN MARØY and SJUR SLOGVIK

Department of Chemistry, University of Bergen, N-5014 Bergen-Univ., Norway

The crystal and molecular structures of *cis*-dichloro- and *cis*-dibromobis(trimethylenethiourea)tellurium(II), $Te(trtu)_2Cl_2$ (I) and $Te(trtu)_2Br_2$ (II), have been determined by X-ray methods. The least squares refinement based on 933 observed reflections for I and 809 observed reflections for II converged at R values of 0.055 and 0.065, respectively.

The space group is $C2/c$ (No. 15), with $Z=4$, and unit cell, $a=16.492(5)$ Å, $b=7.606(4)$ Å, $c=14.515(6)$ Å, $\beta=120.20(3)°$ for I, and $I2/c$ (No. 15), with $Z=4$, and unit cell, $a=16.118(6)$ Å, $b=7.880(4)$ Å, $c=14.312(6)$ Å, $\beta=117.60(4)°$ for II.

The dimensions of the distorted square-planar *cis* TeS_2X_2 groups are: Te—S = 2.465(4) Å, Te—Cl = 2.964(4) Å in I, and Te—S = 2.499(5) Å, Te—Br = 2.994(2) Å in II.

The present structure determinations form part of the extensive studies on linear three-atom systems centered on divalent tellurium, selenium, and sulfur which are being carried out at this institute.[1,2]

The complexes of tellurium dichloride and dibromide with trimethylenethiourea, $Te(trtu)_2Cl_2$ and $Te(trtu)_2Br_2$, belong to the square-planar complexes where *cis-trans* isomerism is possible. When the configuration around tellurium is square-planar *trans*, the tellurium atoms usually lie in crystallographic centres of symmetry, whereas the tellurium atoms usually lie on crystallographic twofold axes when the arrangement is square-planar *cis*.[1] From a preliminary crystallographic investigation it was concluded that the present complexes belong to the latter type of configuration.[3]

EXPERIMENTAL

The crystals of $Te(trtu)_2Cl_2$ (I) and $Te(trtu)_2Br_2$ (II) used for the present studies were of samples prepared for the earlier investigations,[3] which had been kept in a refrigerator.

The unit cell dimensions were redetermined by means of a least squares program, using the diffraction angles of 82 reflections in I and 79 reflections in II, measured from zero-layer Weissenberg photographs around the b and c axes. The derived values are, $a=16.492(5)$ Å, $b=7.606(4)$ Å, $c=14.515(6)$ Å, $\beta=120.20(3)°$ for I, and $a=16.118(6)$ Å, $b=7.880(4)$ Å, $c=14.312(6)$ Å, $\beta=117.60(4)°$ for II.

The intensity data were collected by the multiple-film technique. Integrated zero-layer and equi-inclination photographs were taken with Cu$K\alpha$ radiation (Ni-filtered) for the $h0l-h3l$, $hk0$ and $hk1$ reflections. Out of 1001 attainable independent reflections for I, and 1003 for II, 933 and 809, respectively, were strong enough to be observed with measurable intensities; the unobserved reflections were set equal to the observable limit. The reflections were estimated visually on the upper and lower parts of the films. At high angles, only α_1 reflections were estimated, and the resulting intensities were increased by 2 — 50 %, according to an experimental scale.

Lorentz and polarization corrections were carried out, and absorption corrections were done by the method described by Busing and Levy [4] and modified by Coppens *et al.*[5] For I, $\mu=211$ cm^{-1} and for II, $\mu=241$ cm^{-1}. The crystals of I are monoclinic prisms extended along the b axis. Two crystals were used for collection of intensity data; the one rotated about the b axis was 0.24 mm long and had a cross section of 0.06×0.08 mm^2, and the one rotated about the c axis was cut such that the distances between the pairs of faces were 0.08 — 0.09 mm. Only one crystal of II was used; a monoclinic

plate (100) with distances between pairs of faces 0.07 mm. The number of grid points used for absorption corrections were in the range 5 – 600.

The observed structure factors were eventually corrected for secondary extinction according to Zachariasen.[6] The absorption term in the expression for F_{corr} was put equal to one, and C was found to be 0.88×10^{-7} and 0.63×10^{-7} for the crystals of I, rotated about the b and c axes, respectively, and 1.95×10^{-7} for the crystal of II.

The scattering factors used were those given in *International Tables for X-Ray Crystallography*,[7] Table 3.31B for Te and Br, and Table 3.3.1A for Cl, S, N, and C. The factors for Te, Br, Cl, and S were corrected for anomalous dispersion using the $\Delta f'$ and $\Delta f''$ values given by Cromer,[8] and taking the amplitude of f as the corrected value.

Least squares refinements were carried out with a full-matrix program, minimizing the function

$$r = \sum W(|F_o| - K|F_c|)^2$$

with $W = [(a_1K)^2 + (a_2F_o)^2/4W_o]^{-1}$. Here W_o is based on the reliability of the individual intensities, and the constants a_1 and a_2 were put equal to 5 and 1, respectively, for I, and 10 and 1, respectively, for II. Unobserved reflections were included with $|F_o|$ equal to the observable limit when $|F_c|$ exceeded this value.

The programs used for calculation of unit cell dimensions, film data processing, absorption corrections, two-dimensional Fourier summations, and least squares refinement were made available by the Chemical Department of X-Ray Crystallography, Weizmann Institute of Science, Rehovoth, Israel. The program used for drawing of illustrations is written by C. K. Johnson, Oak Ridge National Laboratory, Oak Ridge, Tennessee, U.S.A. The other programs used are written by K. Åse and K. Maartmann-Moe, both of this Department. The calculations were carried out on an IBM 360/50H computer.

THE STRUCTURE ANALYSES

The tellurium atoms in both crystals lie on twofold axes of symmetry $(0,y,\frac{1}{2})$ and their y coordinates were found from $hk0$ Patterson maps. The approximate positions of all atoms, except hydrogen, were evaluated from $h0l$ and $hk0$ electron density maps, starting with signs based on tellurium contributions only. One of the strongest reflections, 400, in both structures turned out to have sign opposite of the tellurium contribution.

The three-dimensional least squares refinements were started with coordinates derived from the projections. Isotropic thermal param-

Table 1. Atomic coordinates, in fractions of cell edges, and isotropic thermal parameters, in the form $\exp[-8\pi^2U(\sin^2\theta/\lambda^2)]$. Standard deviations are given in parentheses.

	x	y	z	U
Dichlorobis(trimethylenethiourea)tellurium(II)				
Te	0	0.1032(2)	1/4	
Cl	0.1304(2)	−0.1601(5)	0.2454(2)	
S	0.1216(2)	0.3238(6)	0.2848(2)	
N(1)	0.1275(6)	0.1822(18)	0.1195(7)	0.0521(23)
N(2)	0.1351(6)	0.4876(17)	0.1334(7)	0.0477(22)
C(1)	0.1283(6)	0.3319(21)	0.1677(8)	0.0410(23)
C(2)	0.1391(8)	0.1773(25)	0.0243(10)	0.0604(32)
C(3)	0.1055(8)	0.3501(22)	−0.0340(9)	0.0568(30)
C(4)	0.1479(8)	0.5098(23)	0.0405(9)	0.0581(31)
Dibromobis(trimethylenethiourea)tellurium(II)				
Te	0	0.1275(2)	1/4	
Br	0.1340(1)	−0.1261(3)	0.2400(1)	
S	0.1141(3)	0.3535(7)	0.2645(3)	
N(1)	0.1137(9)	0.2138(22)	0.0945(11)	0.0550(37)
N(2)	0.1250(9)	0.5133(22)	0.1092(11)	0.0519(37)
C(1)	0.1178(9)	0.3598(29)	0.1450(11)	0.0469(36)
C(2)	0.1221(11)	0.2241(28)	−0.0070(13)	0.0573(47)
C(3)	0.1834(10)	0.3739(26)	−0.0009(12)	0.0559(41)
C(4)	0.1413(11)	0.5335(28)	0.0158(13)	0.0547(43)

Table 2. Anisotropic thermal parameters expressed in the form $\exp[-2\pi^2(h^2a^{-2}U_{11}+\cdots+2hka^{-1}\times b^{-1}U_{12}+\cdots)]$. All values have been multiplied by 10^4. Standard deviations are given in parentheses.

	U_{11}	U_{22}	U_{33}	U_{12}	U_{23}	U_{13}
Dichlorobis(trimethylenethiourea)tellurium(II)						
Te	643(6)	321(8)	503(6)	0	0	345(5)
Cl	755(18)	300(19)	845(20)	51(16)	−15(22)	408(16)
S	1022(22)	412(24)	708(19)	−225(20)	−197(21)	608(18)
Dibromobis(trimethylenethiourea)tellurium(II)						
Te	621(9)	308(10)	485(8)	0	0	308(6)
Br	817(12)	364(13)	834(14)	121(13)	−28(18)	405(11)
S	859(27)	376(27)	567(22)	−220(30)	−144(33)	456(20)

eters were used for all atoms in the first refinement cycles, and then anisotropic parameters were introduced for Te, Br, Cl, and S. Secondary extinction corrections were carried out, and then additional least squares refinement until the maximum shift of a parameter was about one tenth of its standard deviation. The final R value ($\sum||F_o|-|F_c||/\sum|F_o|$) was 0.055 for I and 0.065 for II. Unobserved reflections are included when $|F_c|$ is greater than the observable limit.

Final three-dimensional difference electron density maps revealed the positions of some of the hydrogen atoms. An attempts was made to refine the coordinates of the hydrogen atoms bonded to nitrogen in the dichloro complex, but without success as the atoms were shifted to unreasonable positions.

The final atomic coordinates together with the isotropic thermal parameters of N and C are listed in Table 1, and the anisotropic parameters of the other atoms are listed in Table 2. Lists of observed and calculated structure factors are available from author K. M. on request.

RESULTS

Bond lengths and angles, from the atomic coordinates of Table 1, are given in Table 3 and Figs. 1 and 2. Views of the cell contents are shown in Figs. 3 and 4.

The two complexes, $Te(trtu)_2Cl_2$ (I) and $Te(trtu)_2Br_2$ (II), crystallize in unit cells of nearly the same dimensions when space group $I2/c$ is chosen for II instead of $C2/c$ for I. The compounds, though not isomorphous, are nearly

Table 3. Atomic distances (Å) and angles (deg.) of the trimethylenethiourea groups and the halogen-nitrogen approaches. X = Cl, Br. Standard deviations are given in parentheses.

	Dichloro complex	Dibromo complex		Dichloro complex	Dibromo complex
S−C(1)	1.758(13)	1.738(18)	∠Te−S−C(1)	105.4(4)	107.3(6)
C(1)−N(1)	1.333(20)	1.344(27)	∠S−C(1)−N(1)	119.3(10)	119.3(13)
C(1)−N(2)	1.312(20)	1.340(27)	∠S−C(1)−N(2)	117.3(9)	116.8(13)
N(1)−C(2)	1.487(20)	1.522(27)	∠N(1)−C(1)−N(2)	123.4(11)	123.9(15)
N(2)−C(4)	1.474(19)	1.485(27)	∠C(1)−N(1)−C(2)	122.5(12)	117.6(15)
C(2)−C(3)	1.509(23)	1.516(29)	∠C(1)−N(2)−C(4)	122.0(9)	121.6(15)
C(3)−C(4)	1.541(21)	1.499(30)	∠N(1)−C(2)−C(3)	108.4(12)	109.3(14)
			∠N(2)−C(4)−C(3)	109.2(12)	109.6(15)
			∠C(2)−C(3)−C(4)	112.6(10)	109.4(15)
N(1)···X	3.168(14)	3.315(17)	∠C(1)−N(1)···X	113.9(8)	112.8(11)
			∠C(2)−N(1)···X	122.9(9)	128.0(11)
N(2′)···X	3.156(13)	3.369(17)	∠C(1′)−N(2′)···X	122.8(8)	122.6(11)
			∠C(4′)−N(2′)···X	115.2(9)	115.4(11)

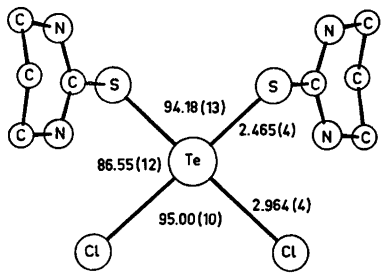

Fig. 1. The *cis*-dichlorobis(trimethylenethiourea)tellurium(II) molecule as seen normal to the plane of the TeS_2Cl_2 coordination group.

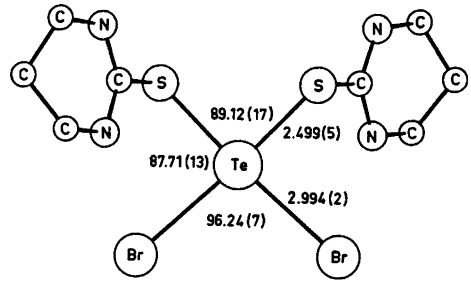

Fig. 2. The *cis*-dibromobis(trimethylenethiourea)tellurium(II) molecule as seen normal to the plane of the TeS_2Br_2 coordination group.

isostructural, as also indicated by the similarity of the *h0l* and *hk*0 zones of reflections.[3] As seen from the figures, the middle carbon atom of the trimethylene chain is moved out of the plane through the other non-hydrogen atoms of the thiourea group, towards Te in I and away from Te in II. This difference may be due to space requirements of the trimethylene groups and is connected with the different locations of the symmetry elements in the two unit cells.

The tellurium atoms are each bonded to two sulfur atoms and two halogen atoms in a distorted square-planar *cis* arrangement. The Te–X bonds are bent out of the TeS_2 plane, to opposite sides of the plane. The configuration is similar to that of the analogous thiourea complexes Te(tu)$_2$Cl$_2$ and Te(tu)$_2$Br$_2$.[9] The deviation from planarity is larger in the dichloro than in the dibromo complex, the angle between the TeS_2 and TeX_2 planes being 15.5° in I and 9.3° in II. The S–Te–X three-atom systems deviate from linearity as the angle at Te is 168.61(9)° in I and 172.41(11)° in II. When the present *cis* Te(trtu)$_2$Br$_2$ is compared to the *trans* Te(etu)$_2$Br$_2$,[10,11] where Te–S = 2.657(2) Å and Te–Br = 2.765(1) Å, one finds that the Te–S bonds are 0.158 Å shorter in the *cis* complex, whereas the Te–Br bonds are 0.229 Å longer. This illustrates the relative stronger *trans* bond lengthening effect of a thiourea group than of a halogen atom.[1]

In the *trans* square-planar complexes of Te(etu)$_2$Br$_2$ and Te(etu)$_2$I$_2$,[11] Te–Br = 2.765(1) Å and Te–I = 2.956(1) Å. The difference between these bond lengths is in accordance with the difference in single covalent bond radii of iodine and bromine, 0.19 Å.[12] The covalent bond radii of bromine and chlorine differ by 0.15 Å,[12] whereas the difference between the Te–Br and Te–Cl bond lengths in the present *cis*

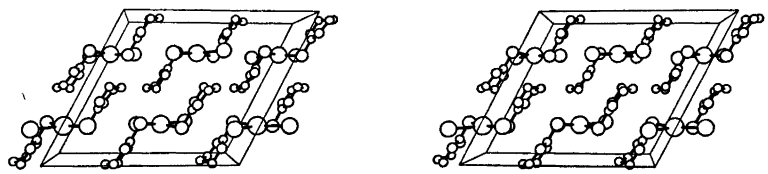

Fig. 3. A stereoscopic view of the cell packing in *cis*-Te(trtu)$_2$Cl$_2$ as seen normal to the *b* plane.

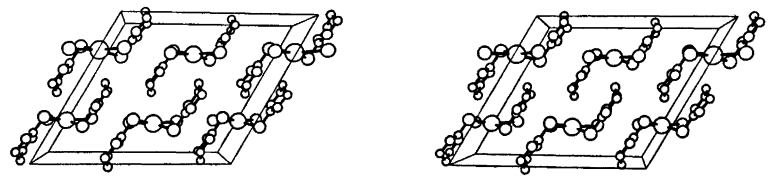

Fig. 4. A stereoscopic view of the cell packing in *cis*-Te(trtu)$_2$Br$_2$ as seen normal to the *b* plane.

complexes is only 0.03 Å. Bromine is thus more strongly bonded to tellurium than is chlorine, and this has a small but significant effect on the *trans*-positioned Te–S bond, which is 2.499(5) Å in the dibromo and 2.456(4) Å in the dichloro complex.

The bond lengths and angles of the trimethylene-thiourea ligands are, within the rather large standard deviations, in accordance with those of trimethylenethiourea.[13] The thioamide groups, SCN_2, are planar within the errors, and make angles of 70.6° with the TeS_2 plane in I and 66.8° in II. The least squares plane of N(1), N(2), C(2), and C(4) passes at a distance of 0.62 Å from C(3) in I and 0.68 Å in II, and at a distance of 0.03 Å from C(1) in I and 0.05 Å in II. In I, C(1) and C(3) are on opposite sides of the plane, whereas in II they are on the same side of the plane.

Each halogen atom seems to be hydrogen-bonded to two nitrogen atoms, one of the same molecule and one of the molecule with coordinates, x, $y-1$, z. In Table 3, primes are used to denote atoms of the latter molecule. The least squares planes of the two thioamide groups connected to the same halogen atom are thus parallel and the halogen atom is situated between the planes. The distance between the planes is 0.38 Å in I and 0.55 Å in II. The hydrogen positions derived from the difference electron density maps are in accordance with the assumed hydrogen bonds. The observed N–H···X angles are in the range 165–176°. The hydrogen bonds are directed out of the TeS_2 plane and may be the cause of the deviations from planarity of the TeS_2X_2 groups. If so, it may explain the greater distortion in the dichloro than in the dibromo complex, the hydrogen bonds in the former being stronger.

REFERENCES

1. Foss, O. In Andersen, P., Bastiansen, O. and Furberg, S. *Selected Topics in Structure Chemistry*, Universitetsforlaget, Oslo 1967, p. 145.
2. Foss, O. *Pure Appl. Chem. 24* (1970) 31.
3. Foss, O. and Marøy, K. *Acta Chem. Scand. 15* (1961) 1945.
4. Busing, W. R. and Levy, A. H. *Acta Crystallogr. 10* (1957) 180.
5. Coppens, P., Leiserowitz, L. and Rabinovich, D. *Acta Crystallogr. 18* (1965) 1035.
6. Zachariasen, W. H. *Acta Crystallogr. 16* (1963) 1139.
7. *International Tables for X-Ray Crystallography*, Kynoch Press, Birmingham 1962, Vol. III.
8. Cromer, D. T. *Acta Crystallogr. 18* (1965) 17.
9. Foss, O., Johnsen, K., Maartmann-Moe, K. and Marøy, K. *Acta Chem. Scand. 20* (1966) 113.
10. Foss, O., Kjøge, H. M. and Marøy, K. *Acta Chem. Scand. 18* (1965) 2349.
11. Foss, O. and Marøy, K. *To be published.*
12. Pauling, L. *The Nature of the Chemical Bond*, 3rd Ed., Cornell University Press, Ithaca, New York 1960.
13. Dias, H. W. and Truter, M. R. *Acta Crystallogr. 17* (1964) 937.

Received September 20, 1974.

Acta Chemica Scandinavica A 29 (1975) 217—219

^{121}Sb Mössbauer Studies on $NbSb_2$ and $TaSb_2$

L. BRATTÅS,[a] J. D. DONALDSON,[b] A. KJEKSHUS,[a] D. G. NICHOLSON[a] and J. T. SOUTHERN[b]

[a]Department of Chemistry, University of Oslo, Blindern, Oslo 3, Norway and [b]Department of Chemistry, Chelsea College, University of London, Manresa Road, London S.W.3, England

^{121}Sb Mössbauer spectra of $NbSb_2$ and $TaSb_2$ have been obtained at 4.2 K and are discussed in relation to their $NbAs_2$ type structure.

Our previous experience [1–5] in the use of ^{121}Sb Mössbauer spectroscopy as a tool in the exploration of the bonding properties of transition metal (T) antimonides has encouraged us to pursue this line further. Another intention has been to gain some insight into the influence of the stereochemical environment around the Sb atoms on the Mössbauer parameters. In the compounds studied so far the Sb environments take approximately C_{3v} symmetry with coordination SbT_3Sb [*e.g.* in the compounds with the FeS_2-*p* (*p* = pyrite), FeS_2-*m* (*m* = marcasite), and $CoSb_2$ (arsenopyrite, FeAsS) type structures [1]] or SbS_3 [as in the structure of berthierite ($FeSb_2S_4$) [2]], approximately C_{2v} symmetry with coordination SbT_2Sb_2 [*e.g.* in the compounds with the $CoAs_3$ (skutterudite) type structure [3,4]], and two different tetrahedral Sb sites with coordinations SbT_4 and SbT_3Sb [as in the structure(s) of Mo_3Sb_7 (and $Nb_3Sb_2Te_5$) [5]]. The analyses of the data for Mo_3Sb_7 and $Nb_3Sb_2Te_5$ were made possible through the use of the Fourier transform sharpening technique prior to the least squares refinements. This has in turn led us to examine $NbSb_2$ and $TaSb_2$ which are other compounds having two Sb sites. $NbSb_2$ [6–8] and $TaSb_2$ [9] are the only antimonides among eleven isostructural transition metal group VB compounds which belong to the $NbAs_2$ type structure.

EXPERIMENTAL

The experimental details concerning the purity of the elements, sample preparation and characterization (at and below room temperature), ^{121}Sb Mössbauer measurements, and data reduction have been presented in previous communications.[1,4,7,9,10]

RESULTS AND DISCUSSION

The ^{121}Sb Mössbauer spectra of $NbSb_2$ and $TaSb_2$ are very similar, that of $NbSb_2$ at 4.2 K being shown in Fig. 1. The sharpness of the spectra shows that the envelopes which must arise from the two different Sb sites must overlap almost exactly. In line with this the Fourier transform sharpened spectra (shown in Fig. 1 for $NbSb_2$) *do not* reveal the presence of more than one Sb site in these compounds. The curve through the experimental points on Fig. 1 represents a least squares fit with the parameters $\delta = -9.0 \pm 0.1$ mm/s, $eQV_{zz} = 9.0 \pm 0.5$ mm/s, $\Gamma = 2.9 \pm 0.2$ mm/s, and $A = 12$ % for $NbSb_2$, those for $TaSb_2$ being $\delta = -9.2 \pm 0.1$ mm/s, $eQV_{zz} = 6.4 \pm 0.5$ mm/s, $\Gamma = 3.8 \pm 0.2$ mm/s, and $A = 14$ %.

In order to appreciate the full impact of this result it is necessary to recapitulate on the essential details of the $NbAs_2$ type structure.[8] The structure contains two non-equivalent X atoms and the crystallographic formula is TX_IX_{II}. Each T is surrounded by six close X (four X_I and two X_{II}) at the corners of a triangular prism and by two other close X (X_I and X_{II}) outside the rectangular faces of the prism, interatomic distances and angles for $NbSb_2$ being given in Table 1. (In addition there is one relatively close T outside the third rectangular face of the prism.) The coordinations around the X atoms are illustrated in Fig. 2. The X_I atoms are surrounded by five near T in a distorted square pyramidal arrangement.

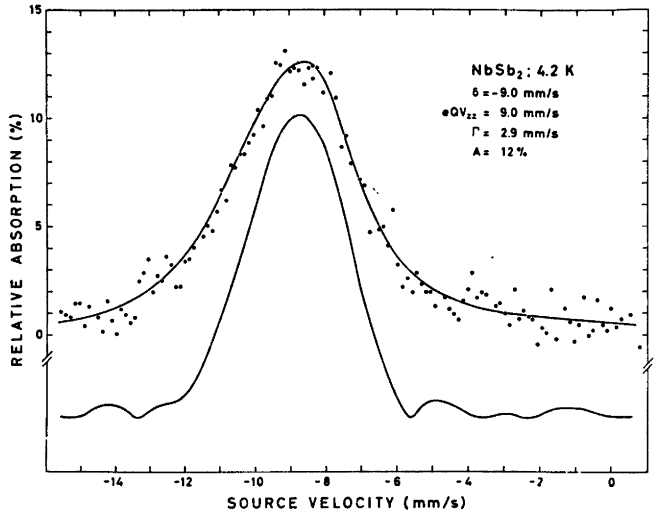

Fig. 1. ^{121}Sb Mössbauer spectrum of $NbSb_2$ with its Fourier transform shown below.

Each X_{II} is coordinated to three near T and one near X_{II} at the corners of a distorted tetrahedron, the X_{II} atoms forming $X_{II}-X_{II}$ pairs with a short interatomic distance. The distance within the $Sb_{II}-Sb_{II}$ pair in $NbSb_2$, which is shorter than those normally found in similar structures, is still in reasonable agreement with the corresponding expectation value for single Sb – Sb bonds.[11] The second shortest $Sb_{II}-Sb_{II}$ distance (being the next shortest Sb – Sb distance) is distinctly longer (3.06 Å) and any bonding interaction between these atoms is probably negligible.

Obviously, with such widely differing stereochemical environments at the two Sb sites, the observation of narrow single line ^{121}Sb Mössbauer spectra for both $NbSb_2$ and $TaSb_2$ requires an explanation. Since the structural data apply to the situation at room temperature and the Mössbauer spectra are taken at 4.2 K these findings could have been indicative of low temperature phase transitions to structures where all Sb atoms are equivalent. However, this explanation can be excluded since X-ray powder diagrams taken at 78 and 4.2 K show only reflections characteristic of the $NbAs_2$ type

Table 1. Bond distances (Å) and angles (°) in $NbSb_2$.

Nb – Sb_I	2.91	Nb – Sb_{II}	2.84
Nb – Sb_I	2.92	Nb – Sb_{II}	2.85
Nb – Sb_I	2.94	Nb – Sb_{II}	2.85
Nb – Sb_I	2.94	Sb_{II} – Sb_{II}	2.71
Nb – Sb_I	2.97		
Sb_I – Nb – Sb_I	67.5	Nb – Sb_I – Nb	76.3
Sb_I – Nb – Sb_I	68.1	Nb – Sb_I – Nb	77.1
Sb_I – Nb – Sb_I	76.3	Nb – Sb_I – Nb	112.1
Sb_I – Nb – Sb_I	77.0	Nb – Sb_I – Nb	112.1
Sb_I – Nb – Sb_{II}	89.9	Nb – Sb_I – Nb	133.6
Sb_I – Nb – Sb_{II}	89.9	Nb – Sb_I – Nb	133.6
Sb_I – Nb – Sb_{II}	93.1	Nb – Sb_{II} – Nb	79.3
Sb_I – Nb – Sb_{II}	93.4	Nb – Sb_{II} – Nb	114.8
Sb_I – Nb – Sb_{II}	135.2	Nb – Sb_{II} – Nb	114.8
Sb_{II} – Nb – Sb_{II}	79.3	Sb_{II} – Sb_{II} – Nb	114.5
Nb – Sb_I – Nb	67.2	Sb_{II} – Sb_{II} – Nb	114.5
Nb – Sb_I – Nb	67.2	Sb_{II} – Sb_{II} – Nb	114.5

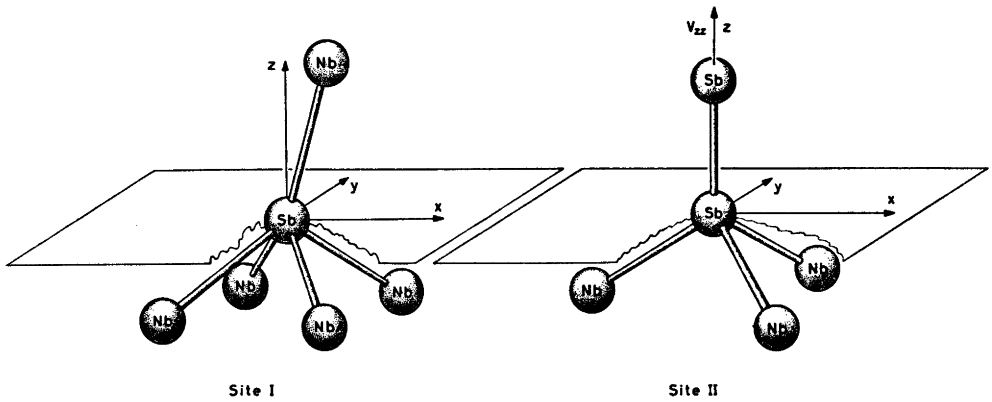

Fig. 2. Models showing the environments of the two Sb sites in $NbSb_2$ and $TaSb_2$.

structure and hence no evidence of low temperature phase transitions. In fact improbably large rearrangements would have been required below room temperature in order to accomplish crystallographic equivalence between the Sb atoms.

A more likely interpretation of the data seems to be that each spectrum consists of two overlapping peaks with similar Mössbauer parameters. To obtain approximately the same chemical shift for the two sites the total *s* electron density withdrawn from both kinds of Sb must be very similar. Since the four-coordinate Sb has a shorter average $Sb-T$ bond length than the five-coordinate Sb, this interpretation would not be inconsistent with the structural data. Similarly, the quadrupole splittings (eQV_{zz}), and consequently also the electric field gradients, at both sites would have to be relatively small in order to produce narrow Mössbauer spectra. Nevertheless, it is possible to envisage that eQV_{zz} differs appreciably for the two sites, the overall shape of the envelope being dominated by that with the larger quadrupole coupling constant. The Sb_{II} site, which has nearly perfect C_{3v} symmetry, would thus expectedly be responsible for the smallest eQV_{zz} value (*cf.*, *e.g.*, $eQV_{zz}=2.7$ mm/s in $PtSb_2$[1] where the Sb environment resembles that of Sb_{II} in the present compounds) whereas the Sb_I site with the more irregular environment might give rise to a larger eQV_{zz} value (*e.g.* eQV_{zz} has values of ~ 9.0 and 6.4 mm/s for Sb_I in $NbSb_2$ and $TaSb_2$, respectively).

It should be emphasized that the Mössbauer parameters presented above are derived for a single site fit to each of the absorption envelopes and that no attempt has been made to take account of the presence of the two Sb sites with individual characteristics. Further experiments on similar substances are being carried out in order to substantiate the above interpretation of the Mössbauer data for $NbSb_2$ and $TaSb_2$.

REFERENCES

1. Donaldson, J. D., Kjekshus, A., Nicholson, D. G. and Tricker, M. T. *Acta Chem. Scand. 26* (1972) 3215.
2. Donaldson, J. D., Kjekshus, A., Mukherjee, A. D., Nicholson, D. G. and Southern, J. T. *Acta Chem. Scand. 26* (1972) 4063.
3. Kjekshus, A., Nicholson, D. G. and Rakke, T. *Acta Chem. Scand. 27* (1973) 1315.
4. Kjekshus, A. and Nicholson, D. G. *Acta Chem. Scand. A 28* (1974) 469.
5. Donaldson, J. D., Kjekshus, A., Nicholson, D. G. and Southern, J. T. *Acta Chem. Scand. A 28* (1974) 866.
6. Furuseth, S. and Kjekshus, A. *Nature (London) 203* (1964) 512.
7. Furuseth, S. and Kjekshus, A. *Acta Chem. Scand. 18* (1964) 1180.
8. Furuseth, S. and Kjekshus, A. *Acta Crystallogr. 18* (1965) 320.
9. Furuseth, S., Selte, K. and Kjekshus, A. *Acta Chem. Scand. 19* (1965) 95.
10. Furuseth, S., Kjekshus, A. and Andresen, A. F. *Acta Chem. Scand. 23* (1969) 2325.
11. Furuseth, S., Selte, K. and Kjekshus, A. *Acta Chem. Scand. 19* (1965) 735.

Received October 1, 1974.

Acta Chemica Scandinavica A 29 (1975) 220—224

^{121}Sb Mössbauer Studies on Antimony(III) Chalcogenohalides

J. D. DONALDSON,[a] A. KJEKSHUS,[b] D. G. NICHOLSON[b] and J. T. SOUTHERN[a]

[a] Department of Chemistry, Chelsea College, University of London, Manresa Road, London S.W. 3, England and [b] Department of Chemistry, University of Oslo, Blindern, Oslo 3, Norway

^{121}Sb Mössbauer spectra of SbSBr, SbSeBr, SbSI, SbSeI, and SbTeI have been obtained at 4.2 K and are discussed in relation to available structural data. A remarkable feature of the iodides is that the quadrupole coupling constant decreases in the order SbSI > SbSeI > SbTeI, becoming negative for the latter.

Some one hundred years after Schneider [1] reported the first antimony(III) chalcogenohalide Dönges [2,3] showed that the compounds SbXY (X = S, Se, or Te; Y = Br or I) constitute an isostructural series. The fact that the compounds are composed of one element from each of three consecutive main groups arouses interest in their bonding characteristics. Moreover, the isostructural nature of the compounds permits systematic studies as to the variations in the properties within the series.

More recent investigations include *inter alia* measurements of their ferroelectric [4,5] and semiconducting [6,7] behaviours, improved structure determinations of SbSBr [8] and SbSI [9] (above and below the ferroelectric transition temperature), nuclear quadrupole resonance (NQR),[10,11] Mössbauer,[12,13] and IR/Raman [14–16] studies. The available ^{121}Sb Mössbauer data [12,13] are incomplete in several respects. We report here the results after least squares and Fourier transform data reduction for SbSBr, SbSeBr, SbSI, SbSeI, and SbTeI taken at 4.2 K.

EXPERIMENTAL

The SbXY compounds were prepared by heating stoichiometric quantities of Sb, X, and SbY_3 for one week in sealed, evacuated ampoules at 280 and 400 °C for Y = Br and I, respectively. $SbBr_3$ and SbI_3 were prepared by addition of the halogen to a suspension of freshly powdered Sb in refluxing anhydrous benzene under a nitrogen atmosphere. The resulting crystalline products of $SbBr_3$ and SbI_3 were purified by sublimation *in vacuo*.

X-Ray (Guinier) powder photographs were taken of the various SbXY samples using monochromatized Cu$K\alpha_1$ radiation (λ = 1.54050 Å) and KCl as internal standard. The least squares fitted unit cell dimensions confirm that the present samples match those previously documented.[2,3] The experimental details concerning the ^{121}Sb Mössbauer measurements and data reductions have been presented in previous communications.[17,18]

RESULTS AND DISCUSSION

Fig. 1 shows the ^{121}Sb Mössbauer spectra of SbSI, SbSeI, and SbTeI at 4.2 K, presented as typical examples of those obtained for all compounds. The corresponding Fourier transformed sharpened spectra confirm the presence of only one Sb site for all of the pure compounds.

The preparations of SbSBr yielded two products which, although clearly differing in appearance (orange and black), gave identical X-ray powder patterns. The preparative procedures for the two samples differed only slightly in that the reaction temperatures for $2Sb + 3S + SbBr_3 \rightarrow 3SbSBr$ were 250 and 280 °C for the black and orange samples, respectively. Whereas the orange sample gives a Mössbauer spectrum (Fig. 2) characteristic of a single Sb site the black material shows the presence of overlapping peaks. A least squares treatment of the composite spectrum revealed that one of the components is identical to that of the orange sample (*cf.* Table 1) and the other implies an impurity with a chemical shift (δ) of -11.9 ± 0.2 mm/s and line width (Γ =) 3.5 ± 0.2 mm/s; the quadrupole coupling constant (eQV_{zz}) con-

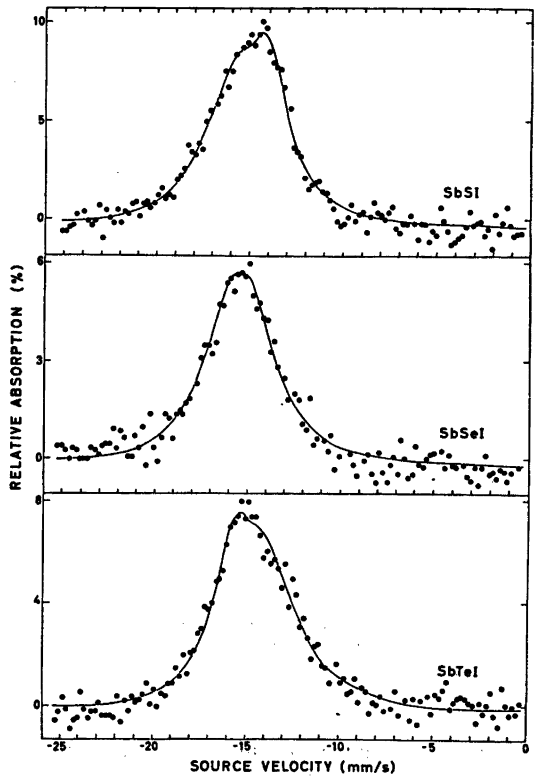

Fig. 1. ^{121}Sb Mössbauer spectra for SbSI, SbSeI, and SbTeI at 4.2 K. Curves show computer fitting to experimental points for parameters given in Table 1.

Table 1. ^{121}Sb Mössbauer (and NQR [11]) parameters for SbSBr, SbSeBr, SbSI, SbSeI, and SbTeI. Chemical shifts with respect to $Ba^{121}SnO_3$. ($Ca^{121}SnO_3$ and $^{121}SnO_2$ for data quoted from Refs. 12 and 13, respectively.) Probable experimental errors in present data are ± 0.1 mm/s in δ, ± 0.5 mm/s in eQV_{zz}, and ± 0.2 mm/s in Γ.

Compound	T (K)	δ (mm/s)	eQV_{zz} (mm/s)	Γ (mm/s)	η	A (%)	Ref.
SbSBr	4.2	−14.9	10.4	2.9	0.14	4.9	Present
SbSBr	77	–	11.2	–	0.139	–	11
SbSBr	77	−14.6	–	5.2	–	–	12
SbSBr	77	−15.5	–	4.5	–	–	13
SbSeBr	4.2	−14.5	10.6	4.0	0	5.0	Present
SbSeBr	77	−14.6	–	5.2	–	–	12
SbSI	4.2	−14.8	12.3	3.0	0.31	9.5	Present
SbSI	77	−15.1	10.3	3.0	0.31	4.6	Present
SbSI	77	–	10.41	–	0.31	–	11
SbSI	77	−15.2	–	4.3	–	–	12
SbSI	77	−14.2	–	4.0	–	–	13
SbSeI	4.2	−14.9	6.4	3.1	~1	5.7	Present
SbSeI	77	−17.4	–	4.1	–	–	13
SbTeI	4.2	−14.0	−12.0	3.0	0.2	7.5	Present
SbTeI	77	−14.7	–	3.5	–	–	13

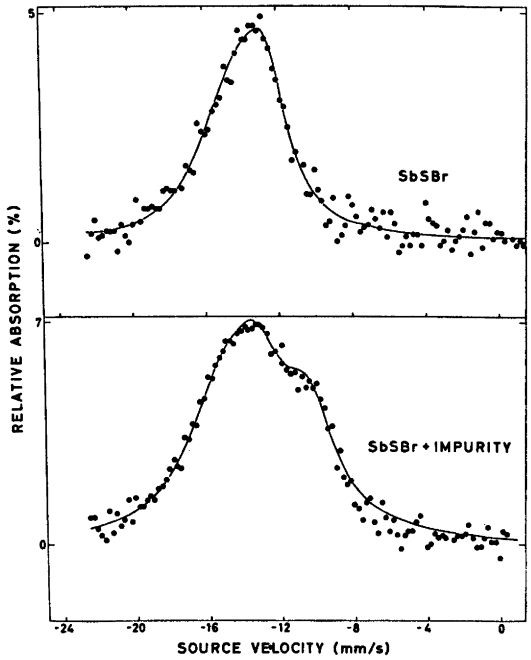

Fig. 2. ^{121}Sb Mössbauer spectra (at 4.2 K) of pure and impure SbSBr.

strained to zero. The latter parameters suggest that the impurity is antimony ($\delta = -11.5$ mm/s, $\Gamma = 2.85$ mm/s, and $eQV_{zz} = 0$ mm/s according to Ref. 19), *viz.* amorphous because its presence was undetected by X-ray diffraction. This illustrates the advantages of the Mössbauer technique in certain situations where impurity detection by other methods proves difficult.

The Mössbauer parameters [δ, eQV_{zz}, Γ, η (asymmetry parameter), and A (maximum absorption effect)] resulting from the least squares fittings are compiled in Table 1. Also included in the table are those values which have been previously reported from NQR and Mössbauer studies.

The crystal structures of the isostructural series SbXY, as typified by those reported [8,9] for SbSBr and SbSI, consist of Sb and X atoms arranged in pleated chains with Y atoms positioned outside. Fig. 3 depicts the coordination of Sb in SbXY based on data reported for SbSI above its ferroelectric transition temperature of 295 K. In the case of SbSI, at least, complicating features concern the structural changes below 295 K which destroy the centre of symmetry through displacements of the Sb and S atoms in the direction of the crystallographic axes. The effect of these displacements are clearly reflected in the temperature dependencies of the NQR determined quadrupole coupling constant and asymmetry parameter.[10] Additional complications in the description of the SbSI structure are caused by two further

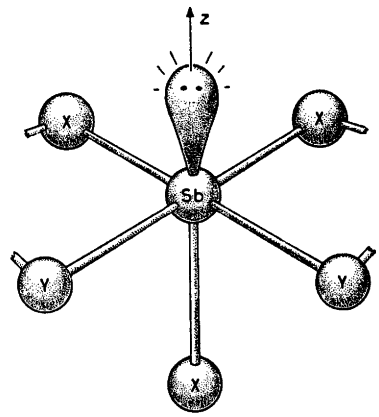

Fig. 3. Model showing the immediate environment of Sb in SbXY, the fully contented lone-pair pointing upwards.

anomalies recorded at 158 and 223 K in the NQR data. However, these presumably only concern finer structural details and because of the polymeric nature of SbSI it appears reasonable to suppose that the gross stereochemistry depicted in Fig. 3 represents a useful approximation at all temperatures. Thus, for the present purpose the immediate coordination symmetry of Sb in all compounds is taken to be C_s.

The chemical shifts for SbXY (Table 1) are of the same order of magnitude as those reported [20,21] for Sb_2X_3 and SbY_3, being in every case closest to the value for the corresponding chalcogenide. This indicates that the chalcogen atoms have a greater effect on the antimony valence electrons than the halogen atoms. Moreover, the δ values indicate relatively high total s electron densities at the Sb nuclei and suggest that the Sb(III) non-bonding electrons in these compounds have considerable s character.

The valence orbitals on Sb transform under the operations of point group C_s as the irreducible representations $a'(5s)$, $a'(5p_y)$, $a'(5p_z)$, and $a''(5p_x)$. The direction of the Sb $5p_z$ atomic orbital may not coincide with the direction of the lone pair which probably consists of a mixture of $5p_z$, $5p_y$, and $5s$ (all with a' symmetry). Information concerning the distribution of Sb $5p$ electron density is contained in the quadrupole coupling constants. Since eQ for ^{121}Sb is negative the sign of the principal component of the electric field gradient V_{zz} is known. Apart from SbTeI all the compounds under consideration have positive eQV_{zz}. This would be consistent with the direction (z) of the principal component of the field gradient being aligned along the direction of the lone pair which contains an excess of p electron density. For the SbXI compounds V_{zz} increases in the order SbSI < SbSeI < SbTeI becoming positive for X=Te. According to the crystal structures of SbSBr and SbSI the S–Sb–S bond angles should be close to 90° thus implying high p contributions to the Sb–S bonds. The Sb–S bond opposite to the lone pair is, however, considerably shorter than the others (*cf.* Ref. 9) which indicates a higher s contribution to this bond relative to the other two. The negative sign of V_{zz} for SbSI can be explained in terms of an excess of p electron density in the lone pair at Sb. As may have been expected, the replacement of S by Se and Te has a pronounced effect on the electron distribution around Sb. Replacement by Se reduced the magnitude of V_{zz} although its negative value shows that there is still an excess of p electron density along the z direction of the principal component of the field gradient. Replacement by Te, however, causes a change in sign of eQV_{zz}; the positive sign of V_{zz} arising from a p electron *deficiency* in some direction other than that of the lone pair. The lone pair must consequently have a p electron character similar to those found in some of the bond directions. It seems significant that the trend of decreasing eQV_{zz} follows the increase in size of X, which must have a major effect on the Sb–I bond because of the steric effect of the X atoms within the Sb–X chains. The presence of I together with a large chalcogen atom such as Te must also affect the nature of the Sb–X bonds particularly that opposite to the lone pair. The Sb–I bonds are long (*e.g.* 3.10 Å in the paraelectric *versus* 2.99 and 3.25 Å in the ferroelectric phase of SbSI) which may be indicative of considerable charge transfer. This suggestion would be in line with the small ^{127}I NQR determined [11] quadrupole coupling constant for SbSI. Such a charge transfer from Sb to I could be the cause of the deficiency of p-electron density of Sb in SbTeI and the decreasing ^{121}Sb coupling constant within the SbXI series. It seems likely, however, that the positive value of V_{zz} arises from a very long Sb–Te bond in the opposite direction to that of the lone pair. Such a bond would involve a relatively high use of Sb p electron density and produce a p electron deficiency in comparison with the other bond and lone pair directions. In the absence of complete structure determinations of SbSeI and SbTeI (now in progress) either of these interpretations must be regarded as tentative.

REFERENCES

1. Schneider, R. *Ann. Phys. (Pogg. Ann.) 110* (1860) 150.
2. Dönges, E. *Z. Anorg. Allg. Chem. 263* (1950) 112.
3. Dönges, E. *Z. Anorg. Allg. Chem. 263* (1950) 280.

4. Fatuzzo, E., Harbeke, G., Merz, W. J., Nitsche, R., Roelschi, H. and Ruppel, W. *Phys. Rev. 127* (1962) 2036.
5. Fridkin, F. M., Gerzanić, E. I., Grosik, I. I., and Ljachovickaja, V. A. *Zh. Exp. Teor. Fiz. 4* (1966) 201.
6. Nitsche, R. and Merz, W. J. *J. Phys. Chem. Solids 13* (1960) 154.
7. Horák, J., Kozáková, M. and Klazar, J. *Collect. Czech. Chem. Commun. 37* (1972) 2309.
8. Christofferson, G. D. and McCullough, J. D. *Acta Crystallogr. 12* (1959) 14.
9. Kikuchi, A., Oka, Y. and Sawaguchi, E. *J. Phys. Soc. Jap. 23* (1967) 337.
10. Popov, S. N., Krainik, N. N. and Mylnikova, I. E. *J. Phys. Soc. Jap. 28S* (1970) 120.
11. Semin, G. K. *Phys. Status Solidi 11* (1972) K61.
12. Khimich, T. A., Belov, V. F., Zhukov, O. K., Yurin, V. A., Korablin, L. N., Shipko, M. N., Lobachev, A. N. and Popolitov, V. I. *Soviet Phys. Solid State 13* (1971) 1265.
13. Aleksandrov, A. Yu., Baltrunas, D. I., Belyaev, L. M., Lyubutin, I. S. and Lyakhovitskaya, V. A. *Soviet Phys. Crystallogr. 17* (1972) 281.
14. Balkanski, M., Teng, M. K., Shapiro, S. M. and Ziolkiewicz, M. K. *Phys. Status Solidi B 44* (1971) 355.
15. Teng, M. K., Balkanski, M. and Massot, M. *Phys. Rev. B 5* (1972) 1031.
16. Teng, M. K., Balkanski, M., Massot, M. and Ziolkiewicz, M. K. *Phys. Status Solidi B 62* (1974) 173.
17. Donaldson, J. D., Kjekshus, A., Nicholson, D. G. and Tricker, M. T. *Acta Chem. Scand. 26* (1972) 3215.
18. Kjekshus, A. and Nicholson, D. G. *Acta Chem. Scand. A 28* (1974) 469.
19. Dokuzoguz, H. Z., Bowen, L. H. and Stadelmaier, H. H. *J. Phys. Chem. Solids 31* (1970) 1565.
20. Birchall, T. and Valle, B. D. *Chem. Commun.* (1970) 675.
21. Bowen, L. H., Stevens, J. G. and Long, G. G. *J. Chem. Phys. 51* (1969) 2010.

Received October 1, 1974.

Acta Chemica Scandinavica A 29 (1975) 225—230

The Crystal Structures of Tris(selenourea) Dichloride Hydrate and Tris(selenourea) Dibromide Hydrate

SVERRE HAUGE, DAVID OPEDAL and JON ÅRSKOG

Department of Chemistry, University of Bergen, N-5014 Bergen-Univ., Norway

The crystal structures of tris(selenourea) dichloride hydrate, $(su)_3Cl_2.H_2O$, and tris(selenourea) dibromide hydrate, $(su)_3Br_2.H_2O$, where $su = SeC(NH_2)_2$, have been determined by X-ray methods, and refined by full-matrix least squares procedures. The dichloride and the dibromide are isomorphous, space group *Pbca* (No. 61) with eight formula units per unit cell. The dichloride has the cell dimensions, $a = 12.202(5)$ Å, $b = 18.142(7)$ Å, $c = 12.232(5)$ Å. The cell dimensions of the dibromide are, $a = 12.604(5)$ Å, $b = 18.268(7)$ Å and $c = 12.512(5)$ Å.

The tris(selenourea) ion possesses a nearly linear three-selenium system with Se – Se – Se bond angle 173.8°, and Se – Se bond lengths from 2.597(2) Å to 2.717(2) Å.

The atoms in each selenourea group are co-planar, and the three selenourea groups of the ion are nearly parallel, with dihedral angles of 5° to 15°. The three selenium atoms and the carbon atoms of the two terminal selenourea groups are nearly co-planar, and so are the three selenium atoms and the carbon atom of the middle selenourea group. These two planes make an angle of about 75° with each other. The selenium-carbon bonds are nearly normal to the three-selenium sequence.

Tris(selenourea) dichloride hydrate, $(su)_3Cl_2.H_2O$, and the analogous dibromide, $(su)_3Br_2.H_2O$, were first prepared by Verneuil [1–3] by air oxidation of an aqueous solution of selenourea containing hydrochloric or hydrobromic acid, respectively. The cation may be regarded as the adduct of selenourea and its oxidative dimerization product, the formamidinium diselenide cation:

$$2\ SeC(NH_2)_2 = [SeC(NH_2)_2]^{2+} + 2\ e,\ E^\circ = 0.24\ V\ [4]$$

$$[SeC(NH_2)_2]_2^{2+} + SeC(NH_2)_2 = [SeC(NH_2)_2]_3^{2+}$$

The reaction is analogous to the formation reaction of the trihalide ions and the pseudo-trihalide ion, $(SeCN)_3^-$.[5,6]

Preparative and crystallographic data on the compounds have been reported earlier.[7]

CRYSTAL DATA

The crystals of tris(selenourea) dichloride hydrate, $(su)_3Cl_2.H_2O$, and of the analogous dibromide, $(su)_3Br_2.H_2O$, are isomorphous. Both crystallized as red brown orthorhombic prisms elongated along the *a* axis. The unit cell dimensions were determined from zero-layer Weissenberg photographs around the three axes. Seventy observations for each compound were measured and evaluated by means of a least squares program. Intensities were estimated visually from integrated Weissenberg photographs around the *a* and *c* axes, taken with $CuK\alpha$ radiation using the multi-film technique.

Data of $(su)_3Cl_2.H_2O$:
Space group *Pbca* (No. 61), $a = 12.202(5)$ Å, $b = 18.142(7)$ Å, $c = 12.232(5)$ Å, $Z = 8$. $D_m = 2.25$ g/cm³, $D_x = 2.26$ g/cm³.
Crystal I: $0.154 \times 0.096 \times 0.096$ mm³, $0kl - 7kl$,
Crystal II: $0.250 \times 0.144 \times 0.176$ mm³, $hk0 - hk1$,
number of reflections 1731 of 2129 possible, $\mu = 146$ cm⁻¹.

Data of $(su)_3Br_2.H_2O$:
Space group *Pbca* (No. 61), $a = 12.604(5)$ Å, $b = 18.268(7)$ Å, $c = 12.512(5)$ Å, $Z = 8$. $D_m = 2.52$ g/cm³, $D_x = 2.55$ g/cm³.
Crystal I: $0.132 \times 0.110 \times 0.086$ mm³, $0kl - 7kl$
Crystal II: $0.080 \times 0.110 \times 0.090$ mm³, $hk0 - hk1$
number of reflections 1701 of 2401 possible, $\mu = 177.8$ cm⁻¹.

Intensities were corrected for absorption [8] and extinction.[9]

THE STRUCTURE ANALYSES

The two structures were solved by Patterson and Fourier methods, and refined by full-matrix least-squares program minimizing the

function $r = \sum W(|F_o| - K|F_c|)$,[2] where K is the scale factor and $W = 1/[Ka_1 + (a_2F_o)^2/4W_o + (a_3F_o)^4]$. The weight W_o is based on the estimated reliability of the film readings. At the start of the refinement the values of a_1, a_2, and a_3 were chosen to be 0.8, 0.05, and 0.004, respectively, for both structures. Cruickshank[10] has suggested to check the weighting scheme by checking that $\sum W(\Delta F)^2/N$ is constant in groups of increasing $|F|$ or $\sin\theta/\lambda$. In this work the structure factors were divided into five groups with $\sin^3\theta_n - \sin^3\theta_{n-1}$ equal for all groups, and the weighting parameters were varied. In the structure of the dichloride the final choice of the parameters were: $a_1 = 0.8$, $a_2 = 0.15$, and $a_3 = 0.004$. The difference between the highest and the lowest value of $\sum W(\Delta F)^2/N$ was then 15 %. In the case of the dibromide the original weighting parameters seemed to fit well and were not changed. The difference between the highest and the lowest value of $\sum W(\Delta F)^2/N$ was 16 %.

The final refinements brought the reliability index, R, to 0.055 for the dichloride and to 0.062 for the dibromide. The difference map of the dibromide showed a peak of 4e/Å^3 at the position of one of the selenium atoms, Se_1. Apart from this peak, the peaks in both difference maps were 0.4 – 0.8 e/Å^3 and were found in positions expected for hydrogen atoms.

Computational procedures and programs used have been described earlier.[11]

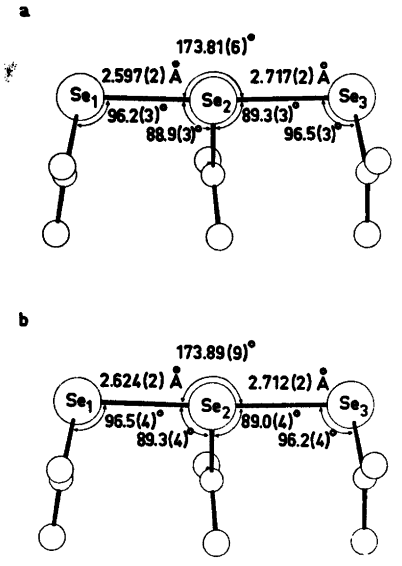

Fig. 1. The triselenourea ion in $(su)_3Cl_2.H_2O$ (a) and in $(su)_3Br_2.H_2O$ (b), as seen normal to the plane passing through Se_1, Se_3, and a point which is equidistant from C_2 and the middle point between C_1 and C_3.

Table 1. Atomic coordinates for tris(selenourea) dichloride hydrate and for tris(selenourea) dibromide hydrate, in fractions of orthorhombic cell edges, with origin at a centre of symmetry. Standard deviations from least squares are given in parentheses.

	x	y	z
$[SeC(NH_2)_2]_3Cl_2.H_2O$			
Se_1	0.28088(9)	0.27125(4)	0.16569(7)
Se_2	0.25241(8)	0.41281(5)	0.17943(6)
Se_3	0.24471(8)	0.56245(5)	0.18459(6)
Cl_1	0.06050(18)	0.10427(11)	0.47303(15)
Cl_2	0.05636(19)	0.39622(11)	0.46484(16)
C_1	0.1878(8)	0.2458(4)	0.2866(6)
C_2	0.3534(8)	0.4146(3)	0.3019(6)
C_3	0.1424(8)	0.5702(4)	0.3017(5)
N_1	0.0830(7)	0.2377(4)	0.2691(6)
N_2	0.2349(7)	0.2363(4)	0.3815(5)
N_3	0.4593(7)	0.4155(3)	0.2819(6)
N_4	0.3161(6)	0.4166(3)	0.4001(5)
N_5	0.0375(7)	0.5761(4)	0.2806(6)
N_6	0.1761(6)	0.5689(4)	0.4021(5)
O	0.4661(6)	0.2472(4)	0.4327(5)
$[SeC(NH_2)_2]_3Br.H_2O$			
Se_1	0.27860(13)	0.27396(7)	0.16532(10)
Se_2	0.25235(12)	0.41610(7)	0.17960(8)
Se_3	0.24599(12)	0.56445(7)	0.18479(9)
Br_1	0.06170(11)	0.10175(7)	0.47453(9)
Br_2	0.05851(11)	0.39559(7)	0.46983(9)
C_1	0.1895(11)	0.2486(5)	0.2842(9)
C_2	0.3526(11)	0.4181(5)	0.2980(9)
C_3	0.1447(11)	0.5718(5)	0.2973(8)
N_1	0.0871(11)	0.2425(6)	0.2667(9)
N_2	0.2333(9)	0.2392(5)	0.3757(7)
N_3	0.4547(9)	0.4184(5)	0.2766(8)
N_4	0.3179(9)	0.4190(5)	0.3957(7)
N_5	0.0419(9)	0.5770(5)	0.2762(8)
N_6	0.1769(9)	0.5703(5)	0.3978(7)
O	0.4576(8)	0.2494(5)	0.4233(7)

THE TRIS(SELENOUREA) ION

Bond lengths and angles in the tris(selenourea), ion, based on the atomic coordinates in Table 1, are given in Fig. 1 and Table 3. The uncertainties in cell dimensions are taken into account in the given standard deviations.

The tris(selenourea) ion, in both compounds, has an approximate linear three-selenium sequence with a Se – Se – Se bond angle of 173.8°. The Se – Se bond lengths in the dichloride are 2.597(2) Å and 2.717(2) Å, and in the dibromide 2.624(2) Å and 2.712(2) Å; the mean values of

Table 2. Anisotropic temperature parameters (Å²) in the form $\exp-[2\pi^2(U_{11}h^2a^{*2}+\cdots+2U_{23}klb^*c^*)+\cdots]$. The values are multiplied with 10^3. Standard deviations are given in parentheses.

	U_{11}	U_{22}	U_{33}	U_{12}	U_{23}	U_{13}
$[SeC(NH_2)]_3Cl_2.H_2O$						
Se_1	28.3(11)	37.5 (4)	25.3(4)	1.8(4)	−1.0(3)	3.2(4)
Se_2	12.3(10)	51.7(5)	17.3(4)	0.7(4)	1.5(3)	−0.4(4)
Se_3	19.3(11)	38.2(4)	24.4(4)	1.5(4)	0.6(3)	2.4(4)
Cl_1	20.2(15)	44.3(10)	26.3(9)	−5.0(9)	2.0(8)	6.0(10)
Cl_2	21.3(15)	49.4(11)	29.8(10)	1.1(10)	1.3(9)	5.9(11)
C_1	21(6)	32(3)	26(3)	−3(3)	2(3)	8(5)
C_2	11(6)	26(3)	27(4)	0(3)	3(3)	−7(4)
C_3	21(6)	23(3)	20(3)	1(3)	−2(3)	5(4)
N_1	20(5)	57(4)	44(4)	4(4)	−1(4)	6(5)
N_2	50(7)	42(4)	23(3)	−1(4)	12(3)	0(4)
N_3	25(5)	44(4)	29(3)	−1(3)	8(3)	2(4)
N_4	17(6)	50(4)	19(3)	3(3)	−1(3)	2(3)
N_5	26(5)	52(4)	31(4)	1(4)	−1(3)	−6(4)
N_6	15(5)	45(4)	28(3)	−3(3)	−5(3)	−2(4)
O	43(5)	61(4)	34(3)	−1(3)	1(3)	3(4)
$[SeC(NH_2)_2]_3Br_2.H_2O$						
Se_1	47.7(15)	44.7(7)	33.8(6)	1.9(6)	−1.8(5)	3.1(7)
Se_2	23.4(13)	54.2(7)	20.8(5)	0.7(5)	2.5(4)	−0.8(6)
Se_3	30.4(13)	44.1(6)	26.7(5)	0.9(5)	−1.0(5)	3.8(6)
Br_1	28.9(14)	50.6(7)	27.9(6)	−3.7(6)	−0.2(5)	4.2(6)
Br_2	29.7(14)	55.5(8)	32.3(6)	0.1(6)	2.4(5)	5.3(6)
C_1	37(9)	23(4)	35(5)	5(5)	−2(4)	0(7)
C_2	21(9)	38(6)	30(5)	−1(5)	5(4)	−9(7)
C_3	29(9)	31(5)	23(5)	3(5)	−2(4)	5(6)
N_1	41(8)	56(6)	51(6)	2(6)	−1(5)	0(7)
N_2	50(9)	49(6)	32(5)	1(5)	6(4)	2(5)
N_3	28(7)	51(6)	33(5)	3(5)	1(4)	−7(6)
N_4	23(8)	47(5)	22(4)	2(4)	−2(4)	−4(5)
N_5	29(8)	56(6)	35(5)	−1(5)	−3(4)	5(6)
N_6	27(7)	43(5)	27(4)	−3(4)	−2(4)	−3(5)
O	67(8)	53(5)	43(5)	1(5)	1(4)	−4(5)

Table 3. Dimensions of the selenourea groups. Bond lengths (Å) and angles (°). Standard deviations are given in parentheses.

	Dichloride	Dibromide		Dichloride	Dibromide
Se_1-C_1	1.921(8)	1.921(12)	$Se_1-C_1-N_1$	118.7(5)	117.7(8)
C_1-N_1	1.304(13)	1.341(19)	$Se_1-C_1-N_2$	117.1(6)	118.2(9)
C_1-N_2	1.308(11)	1.283(15)	$N_1-C_1-N_2$	124.2(7)	124.1(10)
Se_2-C_2	1.940(8)	1.947(12)	$Se_2-C_2-N_3$	118.7(5)	118.7(7)
C_2-N_3	1.315(13)	1.315(18)	$Se_2-C_2-N_4$	119.8(6)	119.9(8)
C_2-N_4	1.285(10)	1.298(14)	$N_3-C_2-N_4$	121.5(7)	121.4(10)
Se_3-C_3	1.905(8)	1.906(12)	$Se_3-C_3-N_5$	119.9(5)	120.8(7)
C_3-N_5	1.310(13)	1.325(18)	$Se_3-C_3-N_6$	120.3(6)	119.7(8)
C_3-N_6	1.295(10)	1.321(14)	$N_5-C_3-N_6$	119.9(7)	119.5(10)

the Se–Se bond lengths are 2.657 Å and 2.668 Å, respectively.

In the triiodide ion [12,13] the total length of the three-center system increases with increasing asymmetry, and there is a relationship between total length and the asymmetry of the system. The same trend has also been found in the three-selenium sequence in the triselenocyanate ion.[14] The ion is symmetrical in the rubidium and the cesium salts, with Se–Se bond lengths of 2.656(3) Å and 2.650(3) Å, respectively. In the potassium salt the ion is unsymmetrical, with bond lengths 2.689(4) Å and 2.648(4) Å, mean value 2.669 Å. In the structures of the tris(selenourea) ion the total length of the three-selenium sequence is largest in the dibromide salt, but the asymmetry of the ion is largest in the dichloride salt.

The Se–Se–Se angle in the triselenocyanate ion has been found to vary between 176.0(3)° in the potassium salt to 178.3(1) in the cesium salt. The bending occurs in a such way that the –CN groups are coming closer to each other. In the tris(selenourea) ion the bending of the

Table 4. Nitrogen-halide and nitrogen-oxygen distances (Å) and angles (°). Standard deviations are given in parentheses.

Distance	Length N···X	Angle C–N···X	Distance from plane
$[SeC(NH_2)_2]_3Cl_2.H_2O$			
$N_1\cdots Cl_{1A}$	3.487(8)	92.2(5)	−1.806
$N_1\cdots Cl_{2A}$	3.756(8)	83.9(5)	3.316
$N_1\cdots M$	2.473	93.1	0.755
$N_1\cdots O_G$	2.856(10)	128.6(6)	−0.133
$N_2\cdots Cl_{1A}$	3.393(8)	96.3(5)	−1.806
$N_2\cdots Cl_{2A}$	3.769(8)	83.3(5)	3.316
$N_2\cdots M$	2.417	90.7	0.755
$N_2\cdots O_A$	2.897(11)	127.7(5)	−0.071
$N_3\cdots Cl_{1B}$	3.262(7)	101.5(5)	−0.430
$N_3\cdots Cl_{2C}$	3.261(7)	121.9(5)	−0.288
$N_4\cdots Cl_{1B}$	3.384(8)	96.5(5)	−0.430
$N_4\cdots Cl_{2A}$	3.287(8)	124.3(5)	−0.360
$N_5\cdots Cl_{1D}$	3.363(8)	122.8(5)	0.446
$N_5\cdots Cl_{2E}$	3.356(8)	99.4(5)	0.346
$N_6\cdots Cl_{1F}$	3.391(8)	122.7(5)	0.917
$N_6\cdots Cl_{2E}$	3.331(8)	100.9(6)	0.346
$N_6\cdots Cl_{2A}$	3.540(7)	95.2(5)	−3.265
$[SeC(NH_2)_2]_3Br_2.H_2O$			
$N_1\cdots Br_{1A}$	3.672(11)	91.5(7)	−1.914
$N_1\cdots Br_{2A}$	3.796(11)	85.4(7)	3.288
$N_1\cdots M$	2.596	92.3	0.687
$N_1\cdots O_G$	2.886(15)	133.6(8)	−0.303
$N_2\cdots Br_{1A}$	3.537(11)	98.3(7)	−1.914
$N_2\cdots Br_{2A}$	3.795(11)	85.8(7)	3.288
$N_2\cdots M$	2.500	87.4	0.687
$N_2\cdots O_{1A}$	2.896(16)	126.5(8)	−0.038
$N_3\cdots Br_{1B}$	3.413(10)	101.6(7)	−0.433
$N_3\cdots Br_{2C}$	3.376(10)	124.4(7)	−0.374
$N_4\cdots Br_{1B}$	3.496(10)	98.0(8)	−0.433
$N_4\cdots Br_{2A}$	3.425(11)	125.1(8)	−0.417
$N_5\cdots Br_{1D}$	3.428(10)	124.4(6)	0.380
$N_5\cdots Br_{2E}$	3.457(10)	100.6(6)	0.346
$N_6\cdots Br_{1F}$	3.480(11)	123.4(8)	0.833
$N_6\cdots Br_{2E}$	3.454(10)	100.9(8)	0.346
$N_6\cdots Br_{2A}$	3.637(10)	97.4(7)	−3.320

M is the midpoint between Cl_{1A} and Cl_{2A}, and between Br_{1A} and Br_{2A}.

Se – Se – Se sequence is opposite, so that the $-C(NH_2)_2$ groups are coming further away from each other. The main reason for this and for the asymmetry of the Se – Se – Se sequence is probably an approach of a halide ion to the terminal selenium atom which has the longest bond to the central selenium atom. The $Se_3\cdots Cl_2'$ $(\frac{1}{2}-x,\ 1-y,\ z-\frac{1}{2})$ distance is 3.699(2) Å and the $Se_3\cdots Br_2'$ distance is 3.719(2) Å. The $C_3-Se_3\cdots Cl_2'$ angle is 164.0(2)° and the $C_3-Se_3\cdots Br_2'$ angle is 164.6(3)°. The angle between the central selenium atom, the terminal selenium atom and the chloride ion, $Se_2-Se_3\cdots Cl_2'$, is 99.38(4)° and the $Se_2-Se_3\cdots Br_2'$ is 99.16(5)°.

Each of the selenourea groups in both structures of the tris(selenourea) ion is planar within the error, the largest deviation of an atom from the least square plane of the group being 0.009 Å.

Bond lengths and angles in the selenourea groups do not deviate significantly from the values found in the crystals of selenourea.[15] As seen from Table 3 the differences in the individual Se – C bond lengths are not significant, nor are the differences in the individual C – N bond lengths. The mean value of the Se – C bond lengths is 1.92 Å, and the mean value of the C – N bond lengths is 1.30 Å. The N – C – N angles are from 119.5(9)° to 124.2(7)° and the Se – C – N angles are beteeen 117.1(6)° and 120.8(7)°.

Since the atoms in each selenourea group of the tris(selenourea) ion are co-planar, as in the structure of selenourea, and the bond lengths and angles have not changed, the oxydation:

$$3\ SeC(NH_2)_2 = [SeC(NH_2)_2]_3^{2+} + 2e$$

has not altered the dimensions of the selenourea groups.

Corresponding Se – Se – C angles in the two structures are equal within the error. The mean value of the angles at the central selenium atom, Se_2, is 89.1°, and the mean value of the angles at the terminal selenium atoms, Se_1 and Se_3, is 96.3°.

The three selenium atoms and the two carbon atoms of the terminal selenourea groups are approximately co-planar, the largest deviation of an atom from a least squares plane being 0.05 Å in the dichloride and 0.07 Å in the dibromide. So are the three selenium atoms and the carbon atom of the middle selenourea group, the largest deviation of an atom from a least squares plane being 0.09 Å in both compounds. The angle between these two planes is 74.9° in the dichloride and 76.3° in the dibromide.

The plane of the terminal selenourea groups, Se_1, and of the central selenourea group, Se_2, make an angle of 14.9° with each other in the dichloride and 14.6° in the dibromide. The dihedral angle between the planes of the Se_2 and the Se_3 groups is 5.4° in the dichloride and 5.3° in the dibromide.

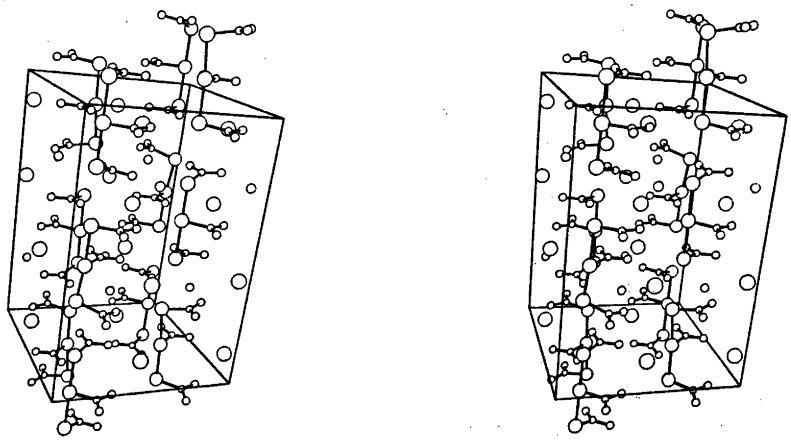

Fig. 2. A stereoscopic pair of drawing showings the content of the unit cell in $(su)_3Br_2.H_2O$.

THE PACKING IN THE CRYSTALS

The central selenium atom, Se_2, in the three-selenium sequence has a close contact to a halide ion. The $Se_2\cdots Cl_1''$ (x, $\frac{1}{2}-y$, $\frac{1}{2}+z$) distance is 3.457(3) Å and the $Se_2\cdots Br_1''$ (x, $\frac{1}{2}-y$, $\frac{1}{2}+z$) distance is 3.530(3) Å. Taking the difference in the ionic radii of the bromide ion and chloride ion to be 0.14 Å, the selenium atom should be more engaged in the contact to the bromide ion than to the chloride ion. The angle $C_2-Se_2\cdots Cl_1''$ is 174.6(2)° and the angle $C_2-Se_2\cdots Br_1''$ is 175.0(3)°. The distance from Cl_1'' to the least squares plane through Se_1, Se_2, Se_3, and C_2 is 0.523 Å. The distance from Br_1'' to the corresponding plane is 0.489 Å. From these data it appears that the halide ion approaches the fourth coordination site of square-planar four-coordination at Se_2. This is a tendency encountered also in other primarily three-coordinated complexes of selenium(II) [16,17] and of tellurium(II).[18,19]

The amino nitrogen atoms have short distances, probably involving hydrogen bonds, to halide ions and to water oxygen atoms. The nitrogen atoms are assumed to have a trigonal-planar bonding system, *i.e.*, the hydrogen atoms lie in or close to the planes through the selenourea groups. The interatomic distances and angles, and the distances of the halide ions and the oxygen atoms from the selenourea plane, are listed in Table 4. In the table an atom marked with A denotes an atom at (x, y, z), B at ($x+\frac{1}{2}$, $\frac{1}{2}-y$, $1-z$), C at ($x+\frac{1}{2}$, y, $\frac{1}{2}-z$), D at ($\bar{x}$, $y+\frac{1}{2}$, $\frac{1}{2}-z$), E at ($\bar{x}$, $1-y$, $1-z$), F at ($\frac{1}{2}-x$, $\frac{1}{2}+y$, z), and G at ($x-\frac{1}{2}$, y, $\frac{1}{2}-z$), where x, y, z are the atomic coordinates of Table 1. Since the halide ions X_{1A} and X_{2A} are rather far out of the selenourea plane, the N_1-H and the N_2-H bonds are probably directed not towards X_{1A} and X_{2A} but towards a point somewhere between X_{1A} and X_{2A}, probably closer to X_{1A} than X_{2A}. Something like this could also be the case with the N_6-H bonds.

Hydrogen bonds are also found from the water molecule to the halide ion. The $O\cdots Cl_{1B}$ distance is 3.149(7) Å and the $O\cdots Cl_{2B}$ is 3.091(7) Å. The $Cl\cdots O\cdots Cl$ angle is 116.2(2)°. The $O\cdots Br_{1B}$ is 3.278(10) Å and the $O\cdots Br_{2B}$ is 3.228(10) Å with $Br\cdots O\cdots Br$ angle of 111.2(2)°. The hydrogen atoms located in the difference electron density maps are in accordance with such hydrogen bonds.

The water molecule is surrounded by two nitrogen atoms, *cf.* Table 4, and, as mentioned above, by two halide ions. The arrangement is approximately tetrahedral. The angles are from 97.0° to 119.6° in the dichloride, and from 94.7° to 121.6° in the dibromide.

REFERENCES

1. Verneuil, A. *Ann. Chim. Phys.* [6] *9* (1886) 289.
2. Verneuil, A. *C. R. Acad. Sci. 99* (1884) 1154.
3. Verneuil, A. *C. R. Acad. Sci. 100* (1885) 1296.
4. Preisler, P. W. and Scortia, T. N. *J. Amer. Chem. Soc. 80* (1958) 2309.
5. Birckenbach, L. and Kellermann, K. *Ber. Deut. Chem. Ges. 58* (1925) 2377.
6. Hauge, S. *Acta Chem. Scand. 25* (1971) 3081.
7. Hauge, S., Opedal, D. and Aarskog, J. *Acta Chem. Scand. 24* (1970) 1107.
8. Coppens, P., Leiserowitz, L. and Rabinovich, D. *Acta Crystallogr. 18* (1965) 1035.
9. Zachariasen, W. H. *Acta Crystallogr. 16* (1963) 1139.
10. Rollett, J. S. *Computing Methods in Crystallography*, Pergamon, London 1965.
11. Hauge, S. *Acta Chem. Scand. A 29* (1975) 163.
12. Mooney, Slater, R. C. L. *Acta Crystallogr. 12* (1959) 187.
13. Brown, R. D. and Nunn, E. K. *Aust. J. Chem. 19* (1966) 1567.
14. Hauge, S. *Acta Chem. Scand. 25* (1971) 1134.
15. Rutherford, J. S. and Calvo, C. *Z. Kristallogr. 128* (1969) 229.
16. Hauge, S. and Sletten, J. *Acta Chem. Scand. 25* (1971) 3094.
17. Hauge, S. *Acta Chem. Scand. 25* (1971) 3103.
18. Foss, O., Husebye, S. and Marøy, K. *Acta Chem. Scand. 17* (1963) 1806.
19. Foss, O. and Marøy, K. *Acta Chem. Scand. 20* (1966) 123.

Received August 7, 1974.

Acta Chemica Scandinavica A 29 (1975) 231—235

Aqueous Chemistry of Protactinium(IV). 5. Benzoylacetone Complexes of Pa(IV) and Hf(IV)

ROBERT LUNDQVIST

Department of Nuclear Chemistry, Chalmers University of Technology, Fack, S-402 20 Göteborg 5, Sweden

The liquid-liquid distribution systems M-HBA in C_6H_6-1 M (Na,H)ClO_4, where M = Pa(IV) or Hf(IV) and HBA = benzoylacetone, were studied at 25 °C in the p*h* range 0 – 10. The experimental results indicated that $Pa(BA)_4$ and PaO^{2+} (or $Pa(OH)_2^{2+}$), and $Hf(BA)_4$ and HfO^{2+} (or $Hf(OH)_2^{2+}$) were the competing dominating species in aqueous phase. The extraction constants ($K_D(Pa) = [Pa(BA)_4(org)][H^+]^2[H_2O]/[PaO^{2+}][HBA(org)]^4$ or $[Pa(Ba)_4(org)]\ [H^+]^2\ [H_2O]^2/[Pa(OH)_2^{2+}]\ [HBA(org)]^4$) were found to be log $K_D(Pa) = -0.7 \pm 0.1$ and log $K_D(Hf) = 0.6 \pm 0.2$, for Pa(IV) and Hf(IV), respectively. The distribution constant ($\lambda_{4,-2} = [Hf(BA)_4(org)]/[Hf(BA)_4]$) for the hafnium benzoylacetone complex was determined to be log $\lambda_{4,-2} = 3.6 \pm 0.1$. The stability constant β_4' for the aqueous reaction $HfO^{2+} + 4BA^- + 2H^+ \rightleftharpoons Hf(BA)_4 + H_2O$ (or $Hf(OH)_2^{2+} + 4BA^- + 2H^+ \rightleftharpoons Hf(BA)_4 + 2H_2O$) was calculated to be log $\beta_4' = 41.8 \pm 0.2$.

Pa(IV) has been found to form different types of β-diketonate complexes; tetrakis thenoyltrifluoroacetone [1] (TTA) and bisacetylacetone [2] (HAA) complexes. The unexpected formation of only a twofold coordination of acetylacetone needs further information, *i.e.* the composition of other β-diketone complexes, in order to be understood. Benzoylacetone (HBA) is a β-diketone with a configuration rather close to acetylacetone and which might be looked upon as an intermediary between TTA and HAA. A liquid-liquid distribution study of the complex formation between Pa(IV) and HBA was therefore undertaken. In order to compare the aqueous chemistry of Pa(IV) with other tetravalent metals a re-investigation of the corresponding Hf(IV) system was also made. The hafnium(IV)-benzoylacetone extraction system has been the subject of a previous study.[3]

EXPERIMENTAL

Chemicals. A mixture of the isotopes ^{175}Hf (3.8 mCi) and ^{181}Hf (26.3 mCi) was supplied from R.C.C. Amersham as an 8.5 ml 2 M HCl solution, where [Hf] ~ 0.4 mg/ml. High resolution gamma spectroscopy with a Ge(Li)-detector showed that the hafnium was radiochemically pure. Benzene solutions of benzoylacetone (Merck, *p.a.*) of various concentrations up to saturation (~3 M HBA, yellowish solution) were prepared. The preparation of other chemicals used has been described elsewhere.[2,4]

Extraction procedure. The extraction procedure for Pa(IV) in presence of 0.01 M Cr^{3+} under continuous electrolysis was carried out as before.[2,4] Concerning Hf(IV), it was observed that no reproducible distribution values were obtained if the back extraction technique was not used (*i.e.* the hafnium was pre-extracted into the organic phase before equilibrating with fresh inactive aqueous phase). The back extraction technique was especially important in order to obtain the maximum distribution values. The organic phases were prepared by shaking 16 ml benzene solutions of benzoylacetone with 4 ml 1 M $NaClO_4$ + 20 µl 2 M HCl stock solution of $^{175,181}Hf$. Equal volumes of organic phase and 1 M (Na,H)ClO_4 were mixed in two different ways: either by shaking 1.29 ml phases in 5 ml glass tubes closed with polyethylene caps for 1 – 66 h at 23 ± 1 °C (batch experiments) or by stirring 15 ml phases 5 – 30 min at 25.0 °C in a glass vessel, the latter technique allowing investigation at different p*h* (= −log (H^+)] or [HBA] in the same run. The distribution of hafnium was calculated from the measured gamma activity, using a well type NaI(Tl) crystal, for equal samples (0.400 ml) of each

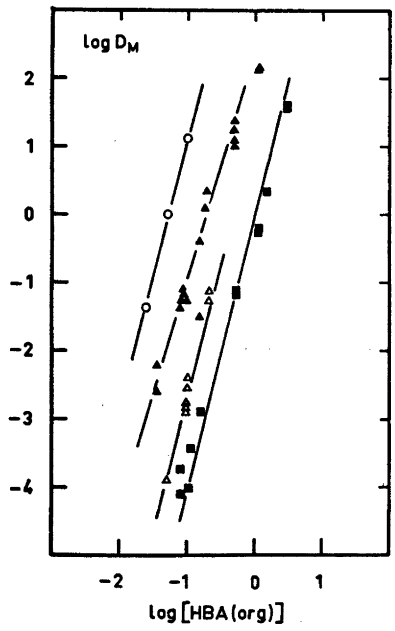

Fig. 1. The distribution of ^{233}Pa(IV) and ^{175,181}Hf(IV) between dilute solutions of benzoylacetone in benzene and 1 M (Na, H)ClO_4 as a function of the benzoylacetone concentration [HBA(org)] at 25 °C and different hydrogen ion concentrations. △Pa(IV), p*h* 1.03; ○Pa(IV), p*h* 3.00; ▲Hf(IV), p*h* 1.00; ■Hf(IV) p*h* 0.00.

phase. Normally about 400 000 cpm were measured for each pair of samples. The background was about 130 cpm.

EXTRACTION OF Pa(IV) AND Hf(IV) WITH BENZOYLACETONE

The distribution of ^{233}Pa(IV) and ^{175,181}Hf(IV) between dilute solutions of HBA in C_6H_6 and 1 M (Na,H)ClO_4 was studied at 25 °C. The influence of the concentration of HBA in the organic phase [HBA(org)] on the distribution D_M (M = Pa(IV) or Hf(IV)) was determined at different hydrogen concentrations, see Fig. 1.

Linear relationships between log D_M and log [HBA(org)] were found for the investigated p*h* ranges (1 – 3 for Pa(IV) and 0 – 1 for Hf(IV)). The slopes of the lines, $\partial \log D_M/\partial$ log [HBA(org)] were close to 4 indicating that four molecules of HBA per molecule of metal were involved in the extraction mechanism. To further examine the composition of the extracted species the p*h* dependence of the distribution was measured at 0.096 M [HBA(org)] for Pa(IV) and at 0.147 M [HBA(org)] for Hf(IV), see Fig. 2. Also here linear relationships were found. The slope of the lines $\partial \log D_M/\partial$ p*h* being +2. The extraction of Hf(IV) was somewhat higher than for Pa(IV) but, in all the behaviour of the two metals was similar. The highest p*h* investigated in the case of Pa(IV) was around 3 because Cr^{2+} (present for reduction of Pa) forms Cr-HBA complexes at higher p*h*. However, there was no such p*h* limit for Hf(IV) and therefore a more thorough investigation of the p*h* dependence of the distribution of Hf(IV) was undertaken at different concentrations of HBA, see Fig. 3. All extraction curves rise with p*h* (the limiting slope for decreasing p*h* being $\partial \log D_{Hf}/\partial$ p*h* = +2) and reach a plateau with a very high distribution factor (log D_{Hf} = 3.6). No decrease from this plateau value at p*h* up to 10 was found. The time for reaching equilibrium was studied by shaking or stirring for 5 min up to 66 h. The time needed for equilibrium seemed to be less than 5 min in most cases and was not found to depend on p*h*. However, a rather strong adsorp-

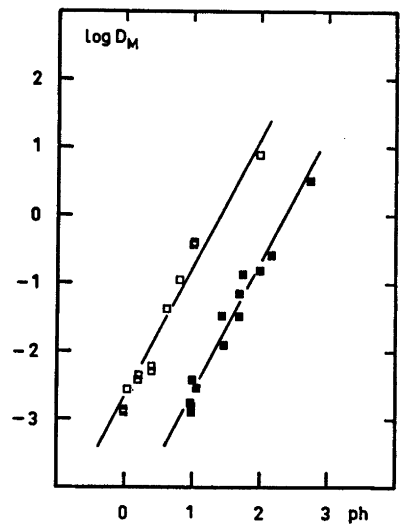

Fig. 2. The influence of the hydrogen ion concentration on the distribution of ^{233}Pa(IV) and ^{175,181}Hf(IV) between benzoylacetone in benzene and 1 M (Na,H)ClO_4 at 25 °C. ■Pa(IV) [HBA(org)] = 0.096 M; □Hf(IV) [HBA(org)] = 0.147 M.

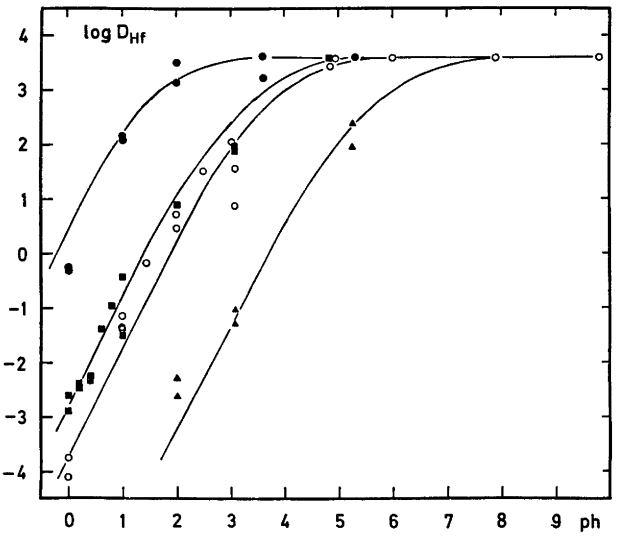

Fig. 3. The distribution of ^{175,181}Hf(IV) between benzene solutions of benzoylacetone and 1 M (Na,H)ClO_4 at 25 °C as a function of the hydrogen ion concentration at various benzoylacetone concentrations [HBA(org)]. [HBA(org)]: ●1.16 M, ■0.147 M, ○0.078 M, ▲0.0101 M.

tion of Hf on the glass walls was observed at ph 1 – 3 depending on the concentration of HBA. High concentrations reduced the adsorption and for lower and higher ph the adsorption was negligible. Similar observations concerning the adsorption of Th, in trace concentrations, on glass in the presence of acetylacetone has been made.[5] The distribution of Hf was not found to be affected by the adsorption.

The metal concentration was kept at trace levels; [Pa(IV)] $\approx 10^{-10}$ M and [Hf(IV)] $\approx 10^{-6}$ M. Changes of the metal concentrations did not influence the distribution.

EVALUATING THE EXTRACTION MECHANISM

The theory for extraction of a metal (M^{i+}) from an aqueous medium into an organic solvent in the presence of a chelating agent has been outlined in an earlier paper.[4] One can conclude from the partial derivatives ∂ log D_M/∂ log [H^+] = −2 and ∂ log D_M/∂ log $[HBA]_{org} = 4$ of the linear parts of the corresponding distribution functions for Pa(IV) and Hf(IV), that the metals are extracted with HBA according to the following formula:

$$M^{i+} + 4HBA(org) - 2H^+ \rightleftharpoons M(HBA)_4H_{-2}^{(i-2)+}(org)$$

Only one extractable species is indicated. The electroneutrality criterium for the extracted species requires that the charge of the metal ion is 2. M^{2+} is then to be identified with HfO^{2+} (or $Hf(OH)_2^{2+}$) or PaO^{2+} (or $Pa(OH)_2^{2+}$). The formation of benzoylacetone complexes of Pa(IV) and Hf(IV), respectively, in aqueous phase can then be described by the formation constants $\beta_{x,y}$ related to the equilibria

$$M^{2+} + x\,HBA - y\,H^+ \rightleftharpoons M(HBA)_xH_{-y}.$$

Possible values of x and y are listed in Table 1, taking Hf(IV) as an example.

The distribution of the metal may be written

$$D_M = \frac{\lambda_{4,-2}\beta_{4,-2}[HBA]^4[H^+]^{-2}}{\sum^{x,y}\beta_{x,y}[HBA]^x[H^+]^y}$$

where $\lambda_{4,-2}$ is the distribution constant for the extracted species $M(HBA)_4H_{-2}$. The distribution data of Hf(IV) was analysed using an iterative least squares method of the same type as had been used previously in determining the stability constants for Pa(V) acetylacetone complexes.[6] It turned out that within the accuracy of the primary data, the extraction

Table 1. Possible composition of the hafnium benzoylacetone complexes in aqeous phase. Negative complexes as well as adduct formation on charged complexes are neglected.

x values	Possible species	Derived y values
4	$Hf(BA)_4$, $HfO(BA)_2(HBA)_2$ (or $Hf(OH)_2(BA)_2(HBA)_2$)	−2
3	$Hf(BA)_3^+$, $HfO(BA)_2HBA$ (or $Hf(OH)_2(BA)_2(HBA)$, $Hf(OH)(BA)_3$)	−1, −2
2	$Hf(BA)_2^{2+}$, $HfO(BA)_2$ (or $Hf(OH)_2(BA)_2$, $Hf(OH)(BA)_2^+$)	0, −2, −1
1	$Hf(BA)^{3+}$, $HfO(BA)^+$ (or $Hf(OH)_2BA^+$), $Hf(OH)BA^{2+}$	1, −1, 0
0	HfO^{2+} (or $Hf(OH)_2^{2+}$)	0

system could be described with only the two species M^{2+} and $M(HBA)_4H_{-2}$. No reasonable reliable conclusions concerning the presence of intermediate complexes could be made.

Assuming M^{2+} and $M(HBA)_4H_{-2}$ to be the main species the distribution function is simplified to

$$D_M = \frac{\lambda_{4,-2}\beta_{4,-2}([HBA][H^+]^{-1/2})^4}{1+\beta_{4,-2}([HBA][H^+]^{-1/2})^4}$$

It is found that all data (different [HBA] and $[H^+]$) coincide within experimental scatter with a single curve when plotting log D as a function of log $[HBA][H^+]^{-1/2}$, see Fig. 4.

The distribution constant $\lambda_{4,-2}$ for the hafnium benzoylacetone complex was found to be log $\lambda_{4,-2} = 3.6 \pm 0.1$. The extraction constant, $K_D(M) = [M(HBA)_4H_{-2}\ (org)]\ [H^+]^2/[M^{2+}][HBA(org)]^4$, for Pa(IV) and Hf(IV) was calculated to be log $K_D(Pa) = -0.7 \pm 0.1$ and log $K_D(Hf) = 0.6 \pm 0.2$.

Using the value log $k_D = 2.97 \pm 0.06$ for the partition constant of HBA [7] (25 °C, 1 M $NaClO_4 - C_6H_6$, $[HBA(org)] = 0.01 - 0.1$ M) log $\beta_{4,-2}$ can be calculated to be 8.9 ± 0.2. The stability constant, log $\beta_4' = 41.8 \pm 0.2$, for the reaction $M^{2+} + 4BA^- + 2H^+ \rightleftharpoons M(HBA)_4H_{-2}$ for hafnium was obtained using literature data for the dissociation of benzoylacetone,[8] $pK_a = 8.24$.

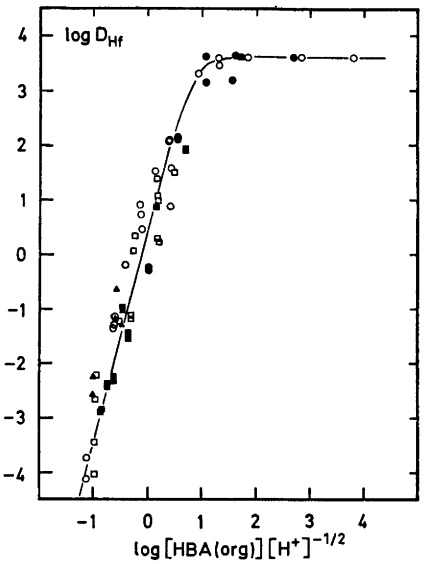

Fig. 4. The relationship between the distribution of $^{175,181}Hf(IV)$, between benzene solutions of benzoylacetone and 1 M $(Na,H)ClO_4$ at 25 °C, at various benzoylacetone [HBA(org)] and hydrogen ion concentrations, and the function $[HBA(org)][H^+]^{-1/2}$. The line is calculated from estimated stability constants. [HBA(org)]; ●1.16 M, ■0.147 M, ○0.078 M, ▲0.0101 M, □0.035 − 3.03 M.

DISCUSSION

From the present investigation it was concluded that Pa(IV) in trace concentrations exists as PaO^{2+} (or $Pa(OH)_2^{2+}$) in perchlorate media in conformity with several other observations.[9] Similar species were also found for Hf(IV). Further, no hydrolysis of the species was observed, in the presence of benzoylacetone, for ph up to at least 10. The distribution of the elements was not affected by changes in the concentration of the elements indicating that no polynuclear species were developed. Neither is this to be expected due to the low concentrations ($[Pa] \approx 10^{-10}$ M, $[Hf] \approx 10^{-6}$ M) used. The polymerisation of Pa(IV) or Hf(IV) in 1 M $HClO_4$ is reported to be negligible [10,3] for $[Pa] < 10^{-6}$ M or $[Hf] < 10^{-3}$ M. The mononuclear hydrolysis of Hf(IV) has been the subject of several in-

vestigations [11] but conflicting conclusions were reached. Reported values of the first hydrolysis constant are disparate. A recent investigation [11] using both solvent extraction and potentiometric measurements shows that the hydrolysis of Hf(IV) is not so severe as previously believed. Only one set of hydrolysis constants has been reported. The constants being calculated from a rather limited solvent extraction study [3] using benzoylacetone and acetylacetone as extrating agents. The results were interpreted as a stepwise hydrolysation of Hf^{4+}. The reported data for benzoylacetone agrees with the present investigation. Except for the highest D-values, which were too low because the back extraction technique was not used, all data (ph 0 – 3) fitted the function $\partial \log D_{Hf} = 2\ \partial ph$. A similar linear relationship between log D and ph was also obtained from the acetylacetone data and this suggests that the extent of hydrolysis of Hf(IV) was not changed. The similar chemical properties of Zr and Hf justifies a comparison of the results from studies of Zr. Using oxine as extracting agent [12] ZrO^{2+} (or $Zr(OH)_2^{2+}$) was assumed to dominate at ph 0.8 – 1.5. No further hydrolysis for ph less than 4 was observed. Another solvent extraction study [13] of Zr with acetylacetone and benzoylacetone indicated the existence of ZrO^{2+} (or $Zr(OH)_2^{2+}$.) By titration of zirconyl compounds in neutral solutions with potassium fluoride the number of OH groups displaced was determined and it was concluded that $Zr(OH)_2^{2+}$ rather than ZrO^{2+} existed.[14]

Pa(IV) and Hf(IV) are here shown to be extracted in a similar fashion. The extracted complex can be written in the general form $M(HBA)_4H_{-2}$. The formula for this species may be written in several equal forms. Taking Pa as an example: $Pa(BA)_4$ or $PaO(BA)_2(HBA)_2$ (or $Pa(OH)_2(BA)_2(HBA)_2$) which also can be written $Pa(BA)_4(H_2O)_n$, where $n = 0,1,2$. Complexes with benzoylacetone adducts are not expected according to the theory [15] of solvent extraction, as the maximum distribution ($D = \lambda_{4,-2}$) was not dependent on the HBA concentration ($[HBA]_{org} = 0.03 - 3$ M). On the other hand $Pa(BA)_4$ and $Hf(BA)_4$ are expected from the comparison with other β-diketonates of Zr(IV) and Hf(IV). Tetrakis diketonates [16] with acetylacetone, trifluoroacetylacetone, 2-furoylacetone, 2-furoyltrifluoroacetone, 2-thenoylacetone, 2-pyrroyltrifluoroacetone and 2-thenoyltrifluoroacetone have been prepared. Contradictory to this $ZrO(BA)_2$ has been prepared [17] in the excess of Zr relative to HBA, but in general Me(diket)^4 is expected to be formed.

Acknowledgement. Thanks are due to Professor Jan Rydberg and Dr. Jan-Olof Liljenzin for valuable advice and programming aid. I would also like to thank Dr. Wanda Mark for supplying some Hf compounds and for interesting discussions. This work has been supported by the Swedish Atomic Research Council which is gratefully acknowledged. The English was revised by Ph.D. Richard Warren.

REFERENCES

1. Guillaumont, R. *C. R. Acad. Sci. Paris 260* (1965) 1416.
2. Lundqvist, R. *Acta Chem. Scand. A 28* (1974) 243.
3. Peshkova, V. M. and Peng Ang *Russ. J. Inorg. Chem. 7* (1962) 1091.
4. Lundqvist, R. and Rydberg, J. *Acta Chem. Scand. A 28* (1974) 399.
5. Rydberg, J. and Rydberg, B. *Sv. Kem. Tidskr. 64* (1952) 200.
6. Liljenzin, J. O. *Acta Chem. Scand. 24* (1970) 1655.
7. Liljenzin, J. O. *Private communication.*
8. Peshkova, V. M., Mel'chakova, N. V. and Zhemchuzin, S. G. *Russ. J. Inorg. Chem. 6* (1961) 630.
9. Lundqvist, R. *Proceedings International Solvent Extraction Conference*, Lyon 8 – 14 Sept., 1974 Soc. Chem. Ind., London, p. 469
10. Guillaumont, R. *Bull. Soc. Chim. Fr.* (1968) 163.
11. Norén, B. *Acta Chem. Scand. 27* (1973) 1369.
12. Stary, J. *Anal. Chim. Acta 28* (1963) 132.
13. Stary, J. and Hladky, E. *Anal. Chim. Acta 28* (1963) 227.
14. Zaitsev, L. M. and Bochkarev, G. S. *Russ. J. Inorg. Chem. 7* (1962) 411.
15. Rydberg, J. *Ark. Kemi 8* (1954) 101.
16. Larsen, E. M., Terry, G. and Leddy, J. *J. Amer. Chem. Soc. 75* (1953) 5107.
17. Morgan, G. T. and Bowen, A. R. *J. Chem. Soc. 125* (1924) 1252.

Received August 29, 1974.

Acta Chemica Scandinavica A 29 (1975) 236—240

A Superstructure of Ni_6Se_5

GUNVOR ÅKESSSON and ERLING RØST

Kjemisk Institutt, Universitetet i Oslo, Blindern, Oslo, Norway

The crystal structure of Ni_6Se_5 quenched from 420 °C has been determined by X-ray methods using 1750 reflections recorded by counter methods. The crystal system is orthorhombic, space group $Pca2_1$ with lattice constants $a = 6.863 \pm 0.003$ Å; $b = 17.09 \pm 0.01$ Å; $c = 11.821 \pm 0.005$ Å. There are eight formula units per unit cell. The Se-atoms form a zig-zag pattern and the nickel atoms are situated in deformed tetrahedral, octahedral, or pyramidal positions in the selenium lattice. A number of possible nickel positions are vacant, so that the crystal lattice can be regarded as a superstructure of a ground cell with nickel atoms randomly distributed over some partly occupied nickel positions.

A compound Ni_6Se_5 which is stable between 400 and 670 °C was reported by Kuznecov *et al.*[1] The structure was found to be hexagonal with $a = 3.78$ Å and $c = 15.89$ Å. Grønvold, Møllerud and Røst [2] reported that the structure of Ni_6Se_5 is orthorhombic with $a = 3.437$ Å, $b = 11.86$ Å, and $c = 17.06$ Å. X-Ray high temperature measurements indicated that this phase is stable between 400 and 640 °C. The existence of Ni_6Se_5 with orthorhombic crystal structure has been confirmed by others.[3,4] In this phase tellurium can be partly substituted for selenium,[5] whereas a complete substitution of sulfur for selenium is possible.[6] Density measurements have been carried out on several ternary samples from the systems Ni – Se – Te [5] and Ni – S – Se.[6] In all cases the unit cells were found to contain 20 chalcogen atoms whereas the number of nickel atoms was found to vary within certain limits. A crystal structure determination of Ni_6Se_5 has been carried out by Røst and Haugsten.[7] The phase has, however, shown a tendency of superstructure formation and the structure determination concerned only the subcell of the structure. Some of the nickel positions were regarded as being only partly occupied. It was pointed out that some apparently short distances between nickel atoms could be due to an alternating occupancy of some nickel positions in a superstructure lattice. The crystal structure of Ni_7S_6, determined by Fleet,[8] seems to be isostructural to Ni_6Se_5 as far as the subcell is concerned.

EXPERIMENTAL

Samples of Ni_6Se_5 were prepared by melting calculated amounts of the elements in evacuated and sealed silica tubes. The samples were annealed at 600 °C and quenched in water. Single crystals were obtained by annealing crushed samples in long silica tubes in an oven with a temperature gradient. Small amounts of iodine were added as a transport agent. After an annealing time of two weeks at 600 °C, very small crystals of Ni_6Se_5 were found in the colder end of the tube. Several crystals were examined using Weissenberg X-ray cameras. Crystals which had been quenched from 600 °C showed weak and diffuse superstructure reflections corresponding to a doubling of two lattice constants. Crystals that had been slowly cooled to 420 °C and annealed at that temperature for two weeks showed, however, a second kind of superstructure corresponding to a doubling of only one lattice constant, the a-axis. In this case the superstructure reflections were sharp and relatively strong. A single crystal which had been quenched from 420 °C was used for further investigations. It was 0.07 mm long and had a cross section of 0.04 by 0.04 mm. The unit cell dimensions were calculated from measurements using a Picker manual single crystal diffractometer with Cu$K\beta$ radiation. The intensity data were recorded on an automatic Picker fourcircle diffractometer using Mo$K\alpha$ radiation. About 3600 reflections with $2\theta < 75°$ were measured using the $\omega - 2\theta$ scanning mode with 2θ scanning speed of 1° min^{-1}. Background counts were taken for 20 s at each of the scan range limits. 1750 reflections with intensities larger than $2\sigma(I)$ were considered to be observed.

Those with lower intensity were exlucded from the final refinement procedure.

The computer programmes used in the present analysis are described in Ref. 9. Intensity data were corrected for absorption and for Lorentz and polarization effects. Atomic form factors were those of Hanson *et al.*[10]

CRYSTAL DATA

Orthorhombic
Ni_6Se_5
$a = 6.863 \pm 0.003$ Å, $b = 17.09 \pm 0.01$ Å,
$c = 11.821 \pm 0.005$ Å
Unit cell volume = 1368.4 Å^3
Unit cell content: 40 Se and 48 Ni atoms.
Calculated density 7.16 g cm^{-3}.
Linear absorption coefficient = 4.40 cm^{-1}
Systematically absent reflections:
$0kl$ for $l = 2n+1$ and $h0l$ for $h = 2n+1$
Possible space groups: $Pca\ 2_1$ and $Pcmb$

STRUCTURE DETERMINATION

Preliminary crystal structure calculations were based on atomic parameters corresponding to the subcell structure of Ni_6Se_5.[7] In accordance with a unit cell content of 48 nickel and 40 selenium atoms the selenium atoms were arranged in ten fourfold positions, referring to the lowest symmetrical space group $Pca2_1$. The previous structure determination of the ground cell strongly indicated that six of the nickel positions are completely occupied. In the present investigation (Fig. 1) these correspond to the positions Ni1,2,7,8,9 and 12. The remaining 24 nickel atoms must be distributed over 12 fourfold positions. Both reduced occupancy of the nickel positions, and a successive distribution between occupied and vacant positions were tried as a basis for least squares calculations.

The calculations led to a crystal structure in which the nickel atoms are arranged in twelve completely occupied positions leaving the rest of the possible nickel positions empty. The final positional parameters assuming anisotropic temperature factors are given in Table 1. The corresponding conventional R-factor is 0.060 ($R_w = 0.053$). The R-factors found using isotropic temperature factors were 0.066 and 0.060, respectively. Further refinements assuming anomalous dispersion were also tried, but no significant improvement of the reliability factor was obtained.

This solution of the superstructure confirms a stoichiometric composition of Ni_6Se_5 with eight formula units per unit cell.

DESCRIPTION OF THE STRUCTURE AND DISCUSSION

A projection along the a-axis of Ni_6Se_5 is found in Fig. 1. Selenium and nickel atoms are

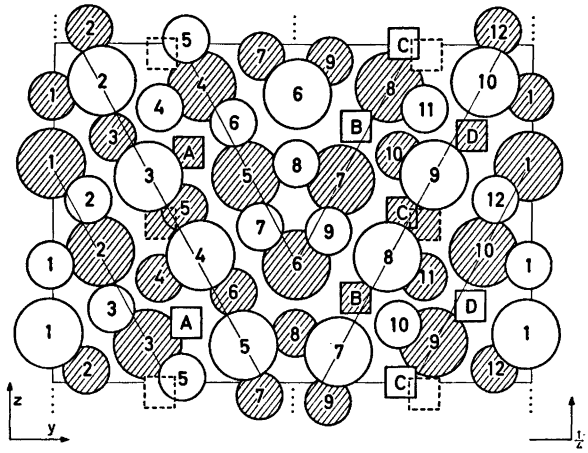

Fig. 1. A projection of the superstructure of Ni_6Se_5 along the x-axis. Large and small circles show selenium and nickel atoms, respectively, and the squares represent vacant nickel positions. Only the atoms and vacancies with x-parameter $\sim\frac{1}{8}$ and $\sim\frac{3}{8}$ are presented. Atoms and vacancies in the layer with $x \sim \frac{1}{8}$ are hatched. Glide planes along the x-direction and along the z-direction are indicated. The zig-zag pattern of the structure is indicated by thin lines.

shown as large and small circles, respectively. Vacancies corresponding to possible nickel positions are indicated as squares. The atoms are situated in layers perpendicular to the a-axis with x-parameters near 1/8, 3/8, 5/8, and 7/8. The deviations from these values are of the order of 0.1 Å. Only two of the layers, $x \sim 1/8$ and $x \sim 3/8$, are presented in the figure. Atoms and vacancies in the layer with $x \sim 1/8$ are hatched. The rest of the unit cell can be visualized using the glide plane along the x-direction, which is indicated on the figure at the edges of the unit cell.

The selenium atoms form a zig-sag pattern parallel to the bc plane. Each selenium atom is surrounded by 11 or 12 other selenium atoms at distances between 3.33 Å and 4.0 Å. The nickel atoms are situated in deformed tetrahedral, octahedral, or square pyramidal positions in the selenium lattice. In addition, the nickel atoms are bound also to other nickel atoms. The distances from the different nickel atoms to the adjacent atoms are given in Table 2.

The nickel positions which were regarded as completely filled in the subcell correspond to the atoms Ni1,2,7,8,9, and 12. These are all coordinated to five selenium atoms in a deformed square pyramidal arrangement at distances between 2.31 and 2.59 Å and, in addition, to two or three nickel atoms at distances between 2.5 and 2.8 Å. The rest of the nickel positions correspond to those which were regarded as partly occupied in the subcell. With respect to the surrounding selenium atoms, they can be divided into three kinds:

a: Ni5 and vacancy C are possible double positions, one on each side of the center of a deformed octahedron. The distance between the two positions is about 1.0 Å only and both of them can obviously not be occupied at the same time.

b: Ni3, Ni6, and vacancies B and D are surrounded by five selenium atoms in a deformed square pyramidal arrangement. The positions lie near the center of a deformed octahedron.

c: Ni4,10,11 and vacancy A are tetrahedrally surrounded by selenium.

In this superstructure of Ni_6Se_8 only one of the type a positions (Ni5) is occupied. It is obviously necessary that the nearest nickel position A must be empty as the distance from Ni5 would

Table 1. Positional and thermal parameters ($\times 10^4$) with estimated deviations. The temperature factor is given by $\exp -(B_{11}h^2+B_{22}k^2+B_{33}l^2+B_{12}hk+B_{13}hl+B_{23}kl)$.

Atom	x	y	z	B_{11}	B_{22}	B_{33}	B_{12}	B_{13}	B_{23}
Se 1	1272(9)	9911(2)	6440(0)	38(7)	5(1)	12(2)	4(6)	−2(10)	−1(2)
Se 2	1261(9)	956(2)	3869(4)	31(6)	6(1)	17(2)	−11(7)	18(10)	0(2)
Se 3	1411(8)	1989(2)	1124(5)	38(7)	5(1)	11(2)	−3(5)	−1(9)	−2(2)
Se 4	1314(9)	3085(2)	8743(4)	24(6)	9(1)	18(2)	1(6)	19(10)	−1(2)
Se 5	1407(8)	3999(2)	6124(4)	48(7)	7(1)	12(2)	11(5)	−29(7)	4(2)
Se 6	1247(11)	5058(2)	3483(2)	36(7)	10(1)	9(2)	4(5)	11(12)	1(2)
Se 7	1304(8)	5994(2)	5969(4)	28(6)	7(1)	11(2)	1(6)	3(9)	−3(2)
Se 8	1280(9)	7009(2)	8708(5)	28(6)	8(1)	12(2)	−12(5)	23(8)	1(2)
Se 9	1126(8)	7971(2)	1153(5)	67(8)	6(1)	12(2)	−5(5)	−27(9)	1(2)
Se 10	1168(9)	9006(2)	3890(5)	58(8)	6(1)	23(2)	11(7)	36(10)	−3(2)
Ni 1	1239(15)	9957(3)	8458(5)	55(10)	8(1)	10(2)	−5(6)	13(18)	5(3)
Ni 2	1311(11)	712(3)	360(5)	53(9)	5(1)	9(3)	6(9)	10(12)	−1(3)
Ni 3	1241(9)	1207(3)	7187(5)	76(10)	3(1)	20(3)	−3(7)	−3(12)	−0(3)
Ni 4	1415(11)	2200(2)	3089(4)	58(10)	5(1)	10(2)	4(7)	−21(10)	−1(2)
Ni 5	1283(8)	2726(2)	5109(4)	42(6)	10(1)	11(2)	0(6)	14(10)	6(2)
Ni 6	1263(10)	3751(3)	2670(5)	57(9)	10(1)	14(2)	−3(7)	15(11)	5(3)
Ni 7	1277(12)	4306(3)	9587(5)	45(9)	7(1)	10(2)	1(8)	4(12)	1(3)
Ni 8	1151(15)	5058(3)	1452(5)	42(11)	7(1)	10(2)	5(6)	−11(10)	−1(3)
Ni 9	1107(11)	5764(3)	9501(6)	58(12)	7(1)	20(3)	15(7)	−16(11)	6(3)
Ni10	1242(9)	7241(3)	6731(5)	40(8)	8(1)	16(2)	−6(7)	20(10)	−4(3)
Ni11	1081(10)	7752(3)	3127(5)	48(10)	8(1)	14(3)	−7(7)	−10(10)	1(4)
Ni12	1152(11)	9241(3)	400(5)	46(10)	6(1)	10(3)	3(7)	0(11)	−1(3)

Table 2. Nearest neighbour interatomic distances (<2.8 Å) from the nickel atoms with x-parameter $\sim \frac{1}{8}$. The standard deviations are of the order of 0.01 Å. Atoms with negative x-parameter ($\sim -\frac{1}{8}$) are marked with an asterisk.

Ni1 – Se1	2.29	Ni2 – Se1*	2.43	Ni3 – Se1	2.39	Ni4 – Se2	2.32	Ni5 – Se3	2.35	Ni6 – Se4	2.38
Se2*	2.37	Se1	2.50	Se2	2.66	Se3	2.35	Se4	2.39	Se5	2.47
Se2	2.47	Se2	2.46	Se3	2.44	Se4	2.31	Se5	2.49	Se6	2.43
Se10*	2.48	Se3	2.36	Se9*	2.47	Se8*	2.40	Se8*	2.46	Se7*	2.71
Se10	2.46	Se10*	2.48	Se10*	2.63	Ni3	2.57	Se9*	2.38	Se8*	2.50
Ni2	2.59	Ni1	2.59	Ni1	2.61	Ni5	2.55	Ni4	2.55	Ni8	2.66
Ni3	2.61	Ni12	2.52	Ni4	2.57	Ni6	2.70			Ni10*	2.66
Ni12	2.60			Ni11*	2.63						
				Ni12*	2.78						
Ni7 – Se4	2.31	Ni8 – Se5*	2.41	Ni9 – Se5*	2.61	Ni10 – Se3*	2.36	Ni11 – Se4*	2.30	Ni12 – Se1*	2.53
Se5	2.47	Se5	2.50	Se6*	2.46	Se7	2.31	Se8	2.32	Se1	2.44
Se6	2.50	Se6	2.40	Se6	2.49	Se8	2.37	Se9	2.36	Se2*	2.48
Se6*	2.43	Se7	2.44	Se7	2.51	Se9	2.30	Se10	2.33	Se9	2.35
Se7*	2.46	Se7*	2.53	Se8	2.33	Ni4*	2.61	Ni3*	2.63	Se10	2.59
Ni8	2.55	Ni6	2.66	Ni7	2.50	Ni6*	2.66	Ni10	2.62	Ni1	2.60
Ni9	2.50	Ni7	2.55	Ni8	2.60	Ni11	2.62			Ni2	2.52
		Ni9	2.60							Ni3*	2.78

be about 2.0 Å only. The distance to Ni4 (2.55 Å) is, however, acceptable. Around the completely vacant double position *C*, however, both the nearest nickel positions (Ni10 and Ni11) are occupied.

Compared to the subcell of Ni_6Se_5 the superstructure formation results in a doubling of the *a*-axis. Instead of a casual occupation of nickel positions a successive alternation between filled and empty sites is found. There are four such alternating pairs of positions in the *x*-direction: Vacancy *A* and Ni10; vacancy *B* and Ni6; vacancy *C* and Ni5; vacancy *D* and Ni3.

The atomic arrangements around the nickel atoms in Ni_6Se_5 may be compared with those found in the neighbouring nickel selenides NiSe of the millerite- and of the NiAs-type and in Ni_3Se_2. In millerite (NiS) nickel is coordinated to five sulfur atoms in a deformed square pyramidal arrangement, and in addition, to two nickel atoms.[11] In the high temperature NiAs-type phase of NiSe nickel is octahedrally coordinated to selenium. According to the lattice constants of $NiSe_{1.03}$ [12] the Ni – Se distances are 2.50 Å. In addition nickel is coordinated to two other nickel atoms at 2.68 Å. The Se – Se distances are 3.41 Å. In Ni_3Se_2 with rhombohedral crystal structure the nickel atoms are tetrahedrally surrounded by selenium at distances of 2.36 and 2.38 Å and, in addition, by four nickel atoms at about 2.60 Å. The shortest Se – Se distance in Ni_3Se_2 is 3.67 Å.[13,14]

In Ni_6Se_5 as well as in the nickel selenides referred to above there is no close Se – Se bonding contact. The shortest Se – Se distance in Ni_6Se_5 is 3.31 Å whereas a corresponding bonding distance as found for example in $NiSe_2$ [12] is 2.40 Å only. The shortest Ni – Ni distances found in Ni_6Se_5 correspond well to those found in nickel metal (2.49 Å). The shortest Ni – Se distance in Ni_6Se_5 (2.31 Å) is surprisingly short. This is, however, probably a consequence of the irregularity of the structure. Corresponding short metal-selenium distances are also observed in $(Fe_xNi_{1-x})_{22}Se_{16}$ [15] which also crystallizes in a kind of superstructure lattice.

The present superstructure of Ni_6Se_5 was found in samples quenched from 420 °C. As mentioned above quenching from temperatures around 600 °C results in another type of superstructure. This structure is, however, not necessarily stable at that temperature, but may be formed during the quenching procedure. The disorder in the atomic arrangement may possibly increase by increasing temperature, leading to a more casual occupation of some of the nickel positions. This will involve a possible variation in stoichiometry of the phase, just as has been observed for some ternary samples referred to above.[5,6]

Acknowledgement. The authors are indebted to Dr. Chr. Rømming for valuable discussions concerning the X-ray methods.

A copy of the intensity data from this investigation can be obtained from the authors.

REFERENCES

1. Kuznecov, V. G., Eliseer, A. A., Špak, Z. S., Palkina, K. K., Sokolova, M. A. and Dmitriev, A. V. *Vopr. Met. i Fiz. Poluprov. Akad. Nauk. SSSR, Tr. 4-go Soveshch.* (1961) 159.
2. Grønvold, F., Møllerud, R. and Røst, E. *Acta Chem. Scand. 20* (1966) 1997.
3. Stevels, A. L. N., Diss., Groningen, *Philips Res. Rep., Suppl. 9* (1969).
4. Komarek, K. L. and Wessely, K. *Monatsh. Chem. 103* (1972) 923.
5. Røst, E. and Vestersjø, E. *Acta Chem. Scand. 22* (1968) 2118.
6. Haugsten, K. and Røst, E. *Acta Chem. Scand. 23* (1969) 3599.
7. Røst, E. and Haugsten, K. *Acta Chem. Scand. 25* (1971) 3194.
8. Fleet, M. E. *Acta Crystallogr. B 28* (1972) 1237.
9. Dahl, T., Gram, F., Groth, P., Klewe, B. and Rømming, C. *Acta Chem. Scand. 24* (1970) 2232.
10. Hanson, H. P., Herman, F., Lea, J. D. and Skillman, S. *Acta Crystallogr. 17* (1964) 1040.
11. Jellinek, F. In Nickless, G., Ed., *Inorganic Sulphur Chemistry*, Elsevier, Amsterdam 1968, p. 669.
12. Grønvold, F. and Jacobsen, E. *Acta Chem. Scand. 10* (1956) 1440.
13. Agarwala, R. P. and Sinha, A. P. B. *Z. Anorg. Allg. Chem. 289* (1957) 203.
14. Hiller, J.-E. and Wegener, W. *Neues Jahrb. Mineral. 94* ((1960) 1147.
15. Røst, E. and Haugsten, K. *Acta Chem. Scand. 23* (1969) 1601.

Received September 23, 1974.

Acta Chemica Scandinavica A 29 (1975) 241—249

Studies on Polythionates. V. The Action of the Cyanide Ion on Aromatic Sulfinates of Divalent Sulfur and Selenium in Acetonitrile

TOR AUSTAD

Chemical Institute, University of Bergen, N-5014 Bergen-Universitetet, Norway

Aromatic sulfinates of divalent sulfur and selenium have been found to react quantitatively with ionic cyanide in acetonitrile. Reaction mechanisms have been suggested on the basis of experiments carried out by varying the concentration of the nucleophile and measuring the formation of the corresponding pseudohalide ion by means of IR. The reaction mechanisms conform favourably with each other. The results are discussed in relation to previous studies on the corresponding polythionates-cyanide reactions in acetonitrile.

A method for analysing sulfinates of divalent sulfur and selenium by means of ionic cyanide and IR has been described.

In previous papers [1–4] we have reported reactions between polythionates and ionic cyanide in the dipolar aprotic solvent acetonitrile. From kinetic studies the reaction mechanisms have been described. Aromatic sulfinates of divalent sulfur [5] and selenium [6] constitute another series of polythionic compounds that exhibits much the same chemical properties as do the polythionates. We have therefore found it of interest to study the action of ionic cyanide on these compounds.

In contrast to the polythionates, reactions concerning nucleophilic attack by ionic cyanide on sulfinates of divalent sulfur and selenium have not been studied earlier. The reason may be that these compounds are nearly insoluble in aqueous solution. Acetonitrile has been found to be a convenient solvent for studying these reactions, because in this solvent both the substrates and the nucleophilic reagent, tetraphenylarsonium cyanide, appear to be very soluble. Furthermore, no hydrolysis can take place, which facilitates the determination of the reaction mechanism.

The following substrates will be discussed in this paper:

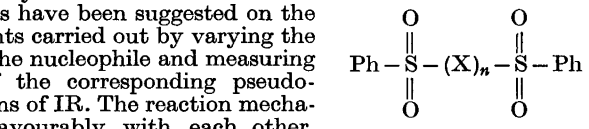

(X = S and Se, n = 1 and 2)

RESULTS

The stoichiometry of the reactions between the cyanide ion and the various sulfinates has been determined by changing the concentration of the nucleophile and measuring the formation of the corresponding pseudohalide ion by means of IR. Contrary to the polythionate-cyanide reactions, the reactions between the sulfinates and the cyanide ion appear to be very fast in acetonitrile, and no kinetic experiments applying IR could be performed.

During all the reactions examined, the nucleophilic reagent was always added to the substrate. The experimental data are collected in Table 1.

The sulfur disulfinate-cyanide reaction. From Table 1 it is seen that 1 mol of sulfur di(benzenesulfinate) consumes 2 mol of the nucleophile in order to form 1 mol of ionic thiocyanate. Upon mixing the reactants in the mol ratio of 1:1 only ½ mol of the pseudohalide ion was found, indicating that the reaction passes through two steps.

There are three potential electrophilic centres in the sulfur disulfinate molecule, *i.e.*, the divalent sulfur atom and both of the sulfonyl sulfur atoms. Considering the sulfonyl sulfur

Table 1. Determination of the stoichiometry of the reaction between the cyanide ion and different aromatic sulfinates of divalent sulfur and selenium in acetonitrile.

Reaction	Amount of XCN^- formed
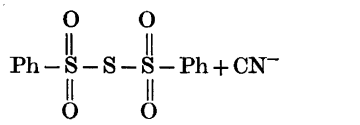	½ mol SCN^-
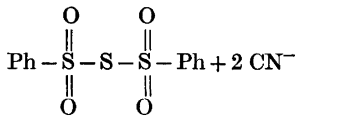	1 mol SCN^-
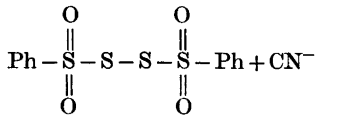	½ mol SCN^-
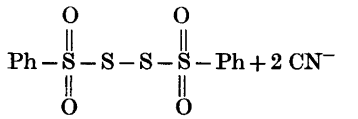	1 mol SCN^-
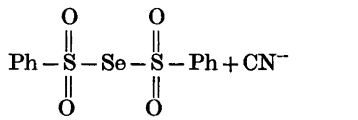	½ mol $SeCN^-$
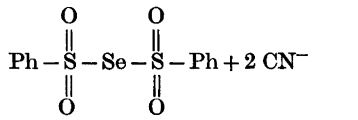	1 mol $SeCN^-$
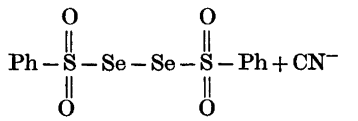	2/3 mol $SeCN^-$
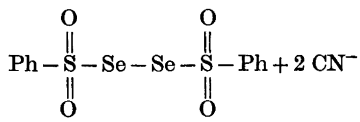	4/3 mol $SeCN^-$
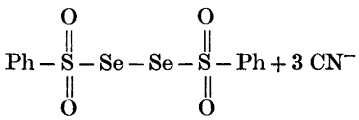	2 mol $SeCN^-$

atoms as the electrophilic centres, the stoichiometry with respect to ionic thiocyanate may be explained by a first step according to eqn. 1,

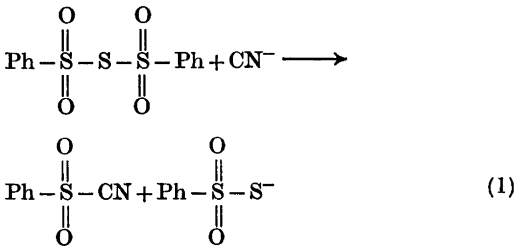

(1)

followed by a fast removal of a sulfur atom from the thiosulfinate ion by a second cyanide ion, eqn. 2.

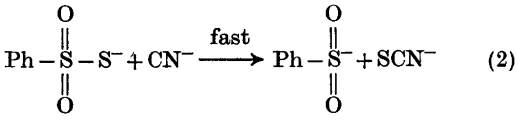

(2)

However, separate experiments proved that ionic benzenethiosulfonate did not react with the cyanide ion in a fast reaction in acetonitrile. After 2 h at room temperature no ionic thiocyanate could be detected using 5.0×10^{-3} M solutions of each of the reactants. From these observations the mechanism involving nucleophilic substitution at the sulfonyl atoms can be rejected as a possible first step in the sulfur di (benzenesulfinate)-cyanide reaction.

The electrophilic centre thus has to be the divalent sulfur atom, and the following two mechanisms are in agreement with the data of Table 1.

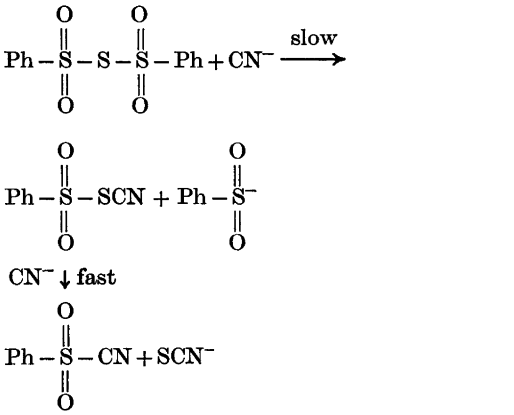

Scheme 1a.

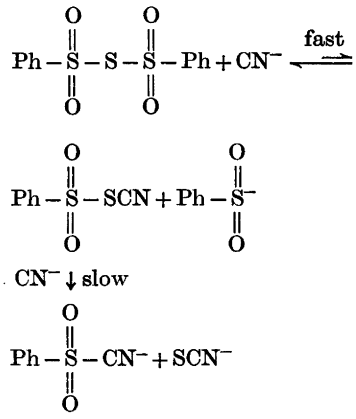

Scheme 1b.

Mechanism 1a involves a nucleophilic attack by the cyanide ion at the divalent sulfur atom to displace ionic benzenesulfinate in the rate determining step. The stoichiometry requires that the intermediate, benzenesulfonyl thiocyanate, once formed reacts with any additional cyanide ion, *i.e.*, the cyanide ion prefers the intermediate to the original reactant. Otherwise cyanide would be tied up in the intermediate and not quantitatively delivered as benzenesulfonyl cyanide and thiocyanate.

Mechanism 1b involves a fast reversible first step with a small equilibrium constant. Under these circumstances no appreciable accumulation of the intermediate can take place and the stoichiometry with respect to ionic thiocyanate will be the same. The second step is thought to be rate determining, irreversible, product formation.

In order to determine which of these two mechanisms really takes place, separate reactions between the intermediate, $PhSO_2SCN$, and ionic cyanide and ionic benzenesulfinate were carried out.

1 mol of benzenesulfonyl thiocyanate was found to react quantitatively with 1 mol of ionic cyanide to give ionic thiocyanate and benzenesulfonyl cyanide in a fast reaction, eqn. 3.

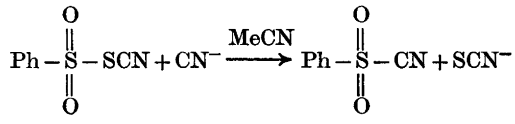

(3)

Experiments have also shown that the benzenesulfinate ion rapidly reacts with benzenesulfonyl thiocyanate in acetonitrile, giving quantitatively 1 mol of ionic thiocyanate and probably disulfon, eqn. 4.

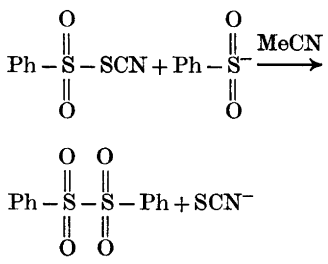

(4)

In both reactions, eqns. 3 and 4, the electrophilic centre of benzenesulfonyl thiocyanate thus appears to be the sulfonyl sulfur atom.

If the mechanism of the sulfur disulfinate-cyanide reaction is of the type 1b, reaction 4 has to pass through an equilibrium first-hand, eqn. 5.

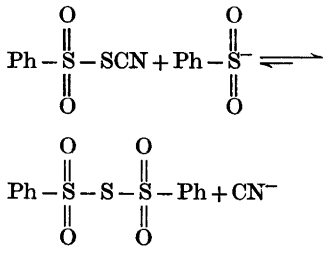

(5)

Since $PhSO_2SCN$ is present from the beginning in the reaction vessel, the reaction 3 would have converted part of the cyanide into $PhSO_2CN$, and hence the yield of ionic thiocyanate would not have been quantitative. This is not in agreement with the experimental results. Furthermore, the first step of the mechanism 1b predicts that the sulfinate ion is a better nucleophile towards divalent sulfur than the cyanide ion, contrary to what has been reported earlier.[7]

On the other hand, if the mechanism is of the type 1a, there may be a reaction path for the intermediate to react according to eqn. 4 at a rate which is inferior to the rate of reaction in the presence of ionic cyanide but still superior to the rate of the inversion of the first step. Hence, if no ionic cyanide is present, reaction 4 can give other products than the original reaction. When ionic cyanide is present, however, the second step, eqn. 3, represents the easiest path.

The sulfur di(benzenesulfinate)-cyanide reaction thus appears to follow the mechanism of the type 1a, and consequently the nucleophilicity of the cyanide ion towards sulfenyl sulfur and sulfonyl sulfur is much larger than the nucleophilicity of the benzenesulfinate ion towards the same substrates.

The disulfur disulfinate-cyanide reaction. Disulfur di(benzenesulfinate) has been found to react with ionic cyanide in the same mol ratio as sulfur di(benzenesulfinate), *i.e.* 1:2 (Table 1); 1 mol of ionic thiocyanate was formed. When the reaction was performed in the mol ratio of 1:1, only ½ mol of ionic thiocyanate was detected, indicating that the reaction passes through two steps.

Furthermore, the benzenethiosulfonate ion has been found to displace ionic thiocyanate quantitatively when reacted with benzenesulfonyl thiocyanate in acetonitrile. The reaction appeared to be fast, eqn. 6.

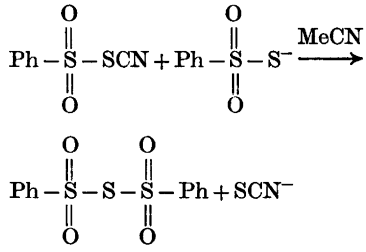

(6)

By applying the same kind of reasoning for the disulfur disulfinate-cyanide reaction as was made for the sulfur disulfinate-cyanide reaction, we arrive at the mechanism given in Scheme 2.

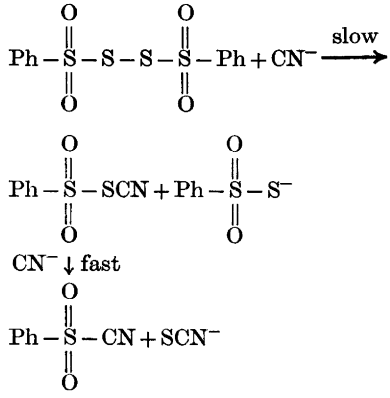

Scheme 2.

The first step is supposed to be a nucleophilic attack by the cyanide ion at one of the divalent sulfur atoms, displacing ionic benzenethiosulfonate. The second step, which appears to be much faster, is analogous to the second step of the sulfur disulfinate-cyanide reaction.

Hence, the cyanide ion is a better nucleophile towards sulfenyl sulfur and sulfonyl sulfur than is the benzenethiosulfonate ion.

The selenium disulfinate-cyanide reaction. With regard to nucleophilic substitution reactions on divalent sulfur and selenium in acetonitrile, ionic cyanide has been found to be far more reactive towards the latter.[2] From analogy with the sulfur di(benzenesulfinate)-cyanide reaction, nucleophilic attack at the sulfonyl sulfur atoms may then be rejected as a possible first step in the selenium disulfinate-cyanide reaction.

The difference in the stoichiometry with respect to ionic selenocyanate, Table 1, may indicate that selenium di(benzenesulfinate) reacts with ionic cyanide in an analogous way as the corresponding sulfur compound, Scheme 3.

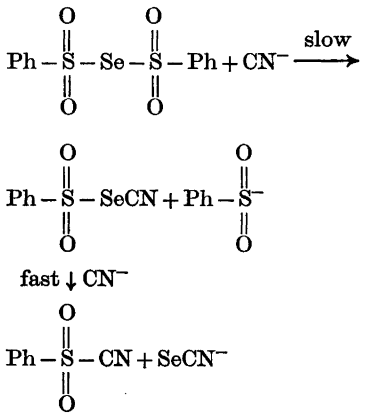

Scheme 3.

A fast reversible first step with a small equilibrium constant can hardly take place because the nucleophilicity of the cyanide ion towards divalent selenium in methanol is $\approx 10^3$ times greater than the nucleophilicity of the benzenesulfinate ion towards the same substrate.[8] In acetonitrile, however, the difference is believed to be even higher.[9]

Unfortunately, the second step of this reaction can not be separately studied since benzenesulfonyl selenocyanate has not yet been prepared.

The diselenium disulfinate-cyanide reaction. 1 mol of diselenium di(benzenesulfinate) was found to consume 3 mol of cyanide ions, giving 2 mol of ionic selenocyanate Table 1. Upon mixing the reactants in the mol ratio of 1:1, 2/3 mol of ionic selenocyanate was formed. This may indicate that the reaction passes through three steps.

Foss [6] has pointed out that in reactions of diselenium disulfinates with nucleophilic agents the sulfinate groups are the leaving groups. Nucleophiles like ionic ethylxanthate displace both of the sulfinate groups without breakdown of the selenium-selenium bond.[6] If ionic cyanide reacts in an analogous manner, selenocyanogen would be formed, eqn. 7.

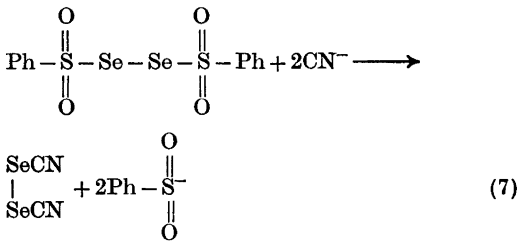

(7)

However, previous studies have shown that 1 mol of selenocyanogen consumes 4 mol of cyanide ions to give 2 mol of ionic selenocyanate, eqn. 8.[10]

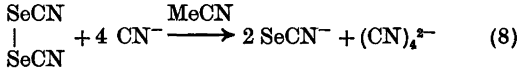

(8)

The stoichiometry of the diselenium disulfinate-cyanide reaction would thus be quite different from the one experimentally observed, Table 1.

Combining the present results, the work of Foss,[6] and applying the same reasoning as for the other reactions in this series, we arrive at a possible mechanism for the diselenium disulfinate-cyanide reaction as depicted by Scheme 4.

The leaving group in the slow step of the mechanism in Scheme 4 is the sulfinate ion. In a relatively much faster step a second cyanide ion attacks the intermediate. $Ph-S(O)_2-Se-SeCN$, to displace ionic selenocyanate. Benzenesulfonyl selenocyanate formed in the second

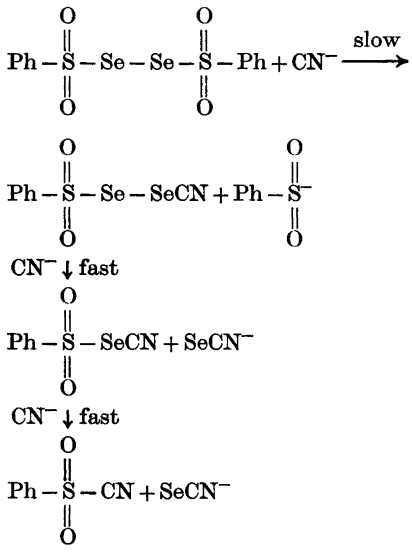

Scheme 4.

step is attacked by a third cyanide ion in a reaction similar to the second step of the selenium disulfinate-cyanide reaction.

Ionic selenocyanate is thus a better leaving group than the benzenesulfinate ion when considering nucleophilic substitution at divalent selenium in acetonitrile.

Analysis by means of ionic cyanide and IR. The cyanide method has occupied a central position in analysing polythionates in aqueous solution.[11] The amount of ionic thiosulfate formed is determined by iodometric titrations. With regard to the sulfinates of divalent sulfur and selenium studied in this work, the cyanide method may as well be applied. This may be done by reacting the sulfinate with excess ionic cyanide in acetonitrile and measuring by means of IR the amount of the corresponding pseudohalide ion formed.[12] The experimental values have been found to agree within $\pm 2-3$ % of the theoretical one.

Benzenesulfonyl cyanide which is one of the products in the reactions mentioned above is, however, attacked by excess of ionic cyanide. The electrophilic centre is the carbon atom, and ionic benzenesulfinate is displaced,[13] eqn. 9.

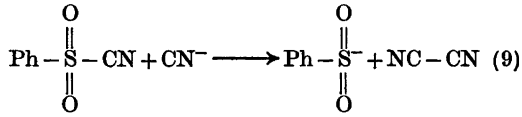

The cyanogen then rapidly adds 2 mol of cyanide ions and probably forms the diiminosuccinonitrile dianion, having strong absorption in IR at 2142 cm^{-1} and 2153 cm^{-1}, [14] eqn. 10.

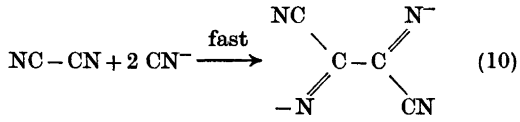

Separate experiments have shown that 1 mol of cyanide ions completely reacts with 1 mol of benzenesulfonyl cyanide, forming a yellowish solution that has a strong IR absorption at 2135 cm^{-1}. This may be explained by a reaction between the postulated diiminosuccinonitrile dianion and 2 mol of benzenesulfonyl cyanide according to eqn. 11.

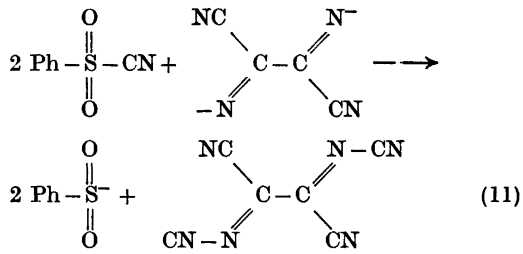

DISCUSSION

The rate of reaction between two negatively charged ions in many cases is largely depressed in a dipolar aprotic solvent relative to a protic solvent.[1] In aqueous solution aromatic thiosulfonates can be analysed by reacting them with ionic cyanide.[15] If, however, ionic benzenethiosulfonate at all reacts with ionic cyanide in acetonitrile, the reaction has to be very slow. After 2 h at room temperature no ionic thiocyanate could be detected when using 5.0×10^{-3} M of each of the reactants.

It is of particular interest to note that benzenesulfonyl thiocyanate is much more susceptible to nucleophilic attack by the cyanide ion in acetonitrile than is the thiocyanatosulfonate ion, $^{-}O_3SSCN$.[2] The electrophilic centre in both cased is the sulfonyl sulfur atom, and ionic thiocyanate is the leaving group.

Likewise, the cyanosulfonate ion appears to be unaffected by ionic cyanide in acetonitrile,[2] while benzenesulfonyl cyanide undergoes a fast nucleophilic attack at the carbon atom by the same anion, eqn. 9.

In contrast to the trithionate ion, $^{-}O_3SSSO_3^{-}$, which does not react with ionic cyanide even in boiling acetonitrile,[16] sulfur di(benzenesulfinate) reacts rapidly with ionic cyanide in the same solvent. The rate constants of the various steps of the latter reaction appear to follow the order:

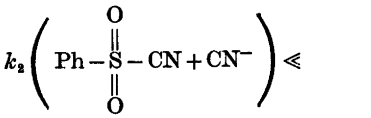

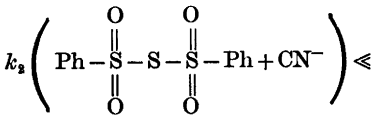

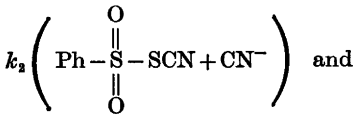

and

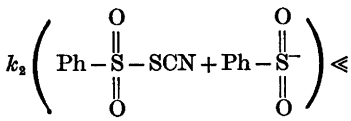

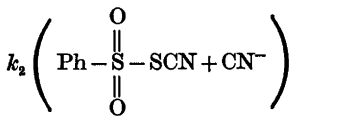

With regard to the disulfur di(benzenesulfinate), it appears to follow the same mechanism when reacted with ionic cyanide as does the tetrathionate ion, albeit the former reaction is much faster.[1] The sequence of the rate constants of the various steps is believed to be:

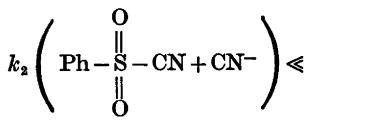

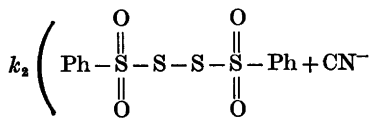

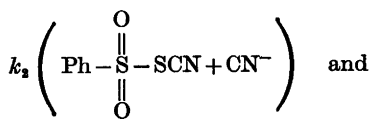

and

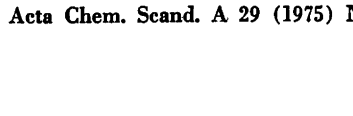

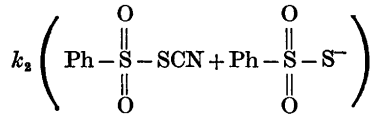

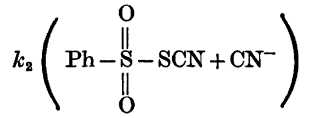

Benzenesulfonyl selenocyanate, which has been postulated to be the intermediate of the selenium di(benzenesulfinate)-cyanide reaction, has two potential electrophilic centres; the sulfur atom and the selenium atom. The selenocyanatosulfonate ion, $^{-}O_3SSeCN$, is supposed to be attacked by ionic cyanide at the selenium atom, displacing ionic sulfite in acetonitrile.[4] If, however, benzenesulfonyl selenocyanate undergoes a nucleophilic substitution by ionic cyanide in the same manner, selenium dicyanide would also here be formed, and would immediately consume 3 mol of cyanide ions to form 1 mol of ionic selenocyanate.[14] The stoichiometry of the reactants of the selenium di(benzenesulfinate)-cyanide reaction would then be different from what is experimentally found.

The mechanism of the selenium di(benzenesulfinate)-cyanide reaction, Scheme 3, is thus different from the mechanism of the selenotrithionate-cyanide reaction in acetonitrile which is believed to follow the mechanism pictured by eqns. 12 – 14.[4]

$$^{-}O_3S-Se-SO_3^{-}+CN^{-} \xrightarrow{\text{slow}} {}^{-}O_3S-SeCN+SO_3^{2-} \quad (12)$$

$$^{-}O_3S-SeCN+CN^{-} \xrightarrow{\text{fast}} Se(CN)_2+SO_3^{2-} \quad (13)$$

$$Se(CN)_2+3\ CN^{-} \xrightarrow{\text{fast}} SeCN^{-}+(CN)_4^{2-} \quad (14)$$

These findings support our previous statement that the negative charge on the sulfonyl group of the selenocyanatosulfonate ion probably prevents the cyanide ion from attacking at the sulfur atom.[4]

The first step in the reaction between the diselenotetrathionate ion, $^{-}O_3SSeSeSO_3^{-}$, and the cyanide ion in acetonitrile is supposed to involve nucleophilic substitution on one of the selenium atoms, followed by ionic scission of the selenium-selenium bond, eqn. 15.[4]

$$^{-}O_3S-Se-Se-SO_3^{-}+CN^{-} \longrightarrow {}^{-}O_3S-SeCN+SeSO_3^{2-} \quad (15)$$

However, in nucleophilic substitutions on diselenium di(benzenesulfinate) the sulfinate groups are the leaving groups.[6] The first step in these reactions is thus different from the first step of the diselenotetrathionate-cyanide reaction.

EXPERIMENTAL

Acetonitrile and tetraphenylarsonium cyanide were purified as reported previously.[2]

Sulfur di(benzenesulfinate) was prepared by oxidation of equivalent amounts of sodium benzenesulfinate and sodium benzenethiosulfonate by means of iodine in aqueous solution.[5] The compound was recrystallized from ethanol and it melted at 134 °C as reported in the literature.[5]

Disulfur di(benzenesulfinate) was prepared in the same way as described by Foss [6] for disulfur di(*p*-toluenesulfinate). The compound was recrystallized several times from benzene-petroleum ether (b.p. 40 – 60 °C). The substance melted at 76 °C as reported by Otto and Tröger.[5]

Selenium di(benzenesulfinate) was prepared from selenium tetrachloride and sodium benzenesulfinate as reported by Foss.[6]

Diselenium di(benzenesulfinate) was prepared and purified by the method of Foss.[6]

Benzenesulfonyl thiocyanate was prepared by the action of sodium benzenesulfinate on thiocyanogen in carbon tetrachloride.[17] The substance was recrystallized from petroleum ether (b.p. 40 – 60 °C) by cooling in dry ice-acetone mixture (m.p. 28 °C). IR showed a strong sharp peak at 2165 cm^{-1}, indicating that no iso form was present.

Benzenesulfonyl cyanide was prepared from sodium benzenesulfinate and chlorocyanogen as described by Cox and Ghosh.[18] The compound was crystallized from petroleum ether (b.p. 40 – 60 °C) by cooling in dry ice-acetone mixture. IR showed a strong sharp peak at 2188 cm^{-1}.

The benzenesulfonyl thiocyanate and the benzenesulfonyl cyanide were both stored in a refrigerator.

Tetraphenylarsonium benzenethiosulfonate was precipitated from an aqueous solution of sodium benzenethiosulfonate by means of tetraphenylarsonium chloride. The compound was recrystallized from acetonitrile by adding some ether. (Found: C 64.66; H 4.47; S 11.37. Calc. for $C_{30}H_{25}O_2S_2As$: C 64.80; H 4.50; S 11.50).

Tetraphenylarsonium benzenesulfinate was prepared from tetraphenylarsonium chloride and sodium benzenesulfinate in methanol. Upon mixing the solutions made by dissolving 5.0 g of tetraphenylarsonium chloride in 10 ml of methanol and 3.0 g of sodium benzenesulfinate dihydrate in 10 ml of methanol, sodium chloride was precipitated. The sodium salt was filtered off and the solvent was removed in vacuum. The residue was dissolved in acetonitrile that had been carefully flushed with nitrogen prior to use. Excess of sodium benzenesulfinate was filtered off and ether was added, whereupon tetraphenylarsonium benzenesulfinate crystallized. (Found: C 68.45; H 4.85; S 6.01. Calc. for $C_{30}H_{25}O_2SAs$: C 68.60; H 4.77; S 6.11).

The sulfinate-cyanide reactions were studied in the concentration range $2-5\times10^{-3}$ M of the substrate. The nucleophilic reagent was always added to the substrate, and the amount of pseudohalide ions formed was measured immediately after mixing the reactants by means of IR. All the reactions were performed at room temperature.

The reactions between benzenesulfonyl thiocyanate and the various nucleophiles (ionic cyanide, ionic benzenethiosulfonate, and ionic benzenesulfinate) were quantitatively studied by measuring the amount of formed ionic thiocyanate applying IR. The nucleophile was always added to the substrate.

The benzenesulfonyl cyanide-cyanide reaction was quantitatively studied by measuring the disappearance of the peak at 2188 cm^{-1} applying IR. When excess of ionic cyanide was added to the benzenesulfonyl cyanide solution, a yellowish-red solution immediately occurred, giving strong absorption in IR at 2142 cm^{-1} and 2153 cm^{-1}. This may be due to the postulated diiminosuccinonitrile dianion. Upon mixing the reactants in the mol ratio of 1:1 the peak of the benzenesulfonyl cyanide completely disappeared. The solution turned yellowish and gave strong IR absorption at 2135 cm^{-1}. This may be due to the formation of a polycyanic compound, eqn. 11.

The IR measurements were performed on a Unicam SP 200 G Infrared Spectrophotometer applying 0.1 cm liquid cells.

Acknowledgement. The author is indebted to the Norwegian Research Council for Science and Humanities for a grant.

REFERENCES

1. Austad, T. *Acta Chem. Scand. A 28* (1974) 693.
2. Austad, T. *Acta Chem. Scand. A 28* (1974). 935.
3. Austad, T. *Acta Chem. Scand. A 28* (1974) 927.
4. Austad, T. *Acta Chem. Scand. A 29* (1975) 71.
5. Otto, R. and Troeger, J. *Ber. Deut. Chem. Ges. 24* (1891) 1125.
6. Foss, O. *Acta Chem. Scand. 6* (1952) 508.
7. Footner, H. B. and Smiles, S. *J. Chem. Soc. 127* (1925) 2887.

8. Austad, T. *To be published.*
9. Austad, T., Engemyr, L. B. and Songstad, J. *Acta Chem. Scand. 25* (1971) 3535.
10. Austad, T. *Acta Chem. Scand. A 28* (1974) 806.
11. Kurtenacker, A. and Goldbach, E. *Z. Anorg. Allg. Chem. 166* (1927) 177.
12. Austad, T., Songstad, J. and Åse, K. *Acta Chem. Scand. 25* (1971) 331.
13. Van Leusen, A. M. and Jagt, J. C. *Tetrahedron Lett.* (1970) 967.
14. Austad, T. and Esperås, S. *Acta Chem. Scand. A 28* (1974). 892.
15. Gutmann, A. *Z. Anal. Chem. 47* (1908) 294.
16. Austad, T. *Unpublished results.*
17. Goerdeler, J. and Rosenthal, P. *Tetrahedron Lett.* (1964) 3665.
18. Cox, J. M. and Ghosh, R. *Tetrahedron Lett.* (1969) 3351.

Received July 25, 1974.

Acta Chemica Scandinavica A 29 (1975) 250—254

Cadmium—Imidazole Complex Formation in Aqueous Solutions. Stability Constants, Changes in Standard Free Energies, Enthalpies, Entropies, and Heat Capacities Accompanying the Complex Formation at 5, 15, 25, and 40 °C

JØRGEN BIRGER JENSEN

Fysisk-Kemisk Institut, DTH 206, DK-2800 Lyngby, Denmark

The over-all complexity constants, changes in standard values of free energy, enthalpy, and molar heat capacity of the equilibrium:

$$\mathrm{Cd\ aq}_x^{2+} + j\ \mathrm{im} \rightleftharpoons \mathrm{Cd\ aq}_y\mathrm{im}_j^{2+} + (x-y)\mathrm{aq}$$

have been determinated at 5, 15, 25, and 40 °C. The measurements were performed in aqueous solutions at pH 9.5 and ionic strength 1.0 established with sodium perchlorate. The complexity constants were obtained by means of the polarographic standard method, and the experimental results were fitted to a polynomium of the type:

$$\log K_{0j} = A_j + B_j/T + C_j/T^2$$

by application of a polynomium regression program. The enthalpies and entropies of the various steps show remarkable differences and it is concluded that structural changes occur, most probably, so that the cadmium ions are six-coordinated, when $j = 1$, 5, and 6, and only four-coordinated when $j = 2$, 3, and 4.

The over-all complexity constants, K_{0j}, of the complex equilibria:

$$\mathrm{Cd\ aq}_x^{2+} + j\ \mathrm{im} \rightleftharpoons \mathrm{Cd\ aq}_y\ \mathrm{im}_j^{2+} + (x-y)\mathrm{aq} \quad (1)$$

(im = imidazole, $C_3H_4N_2$; aq = water, H_2O)

are related to thermodynamic quantities by the equations:

$$-RT \ln K_{0j} = \Delta^\circ_{0j}G = \Delta^\circ_{0j}H - T\Delta^\circ_{0j}S \quad (2)$$

$$\partial \ln K_{0j}/\partial(1/T) = -\Delta^\circ_{0j}H/R \quad (3)$$

where $\Delta^\circ_{0j}G$, $\Delta^\circ_{0j}H$ and $\Delta^\circ_{0j}S$ indicate changes in standard free energy, enthalpy and entropy, respectively, accompanying reaction (1). From a knowledge of values of $\Delta^\circ_{0j}H$ the corresponding changes in standard molar heat capacity, $\Delta^\circ_{0j}C_p$, can be found:

$$\partial\Delta^\circ_{0j}H/\partial T = \Delta^\circ_{0j}C_p \quad (4)$$

In our previous studies [1,2] on cadmium-imidazole complex formation carried out at 25 °C, the complexity constants of reaction (1) were determined. The maximum value of j was found to be 6. In the present paper we shall report the measurements of the complexity constants at four different temperatures covering the range from 5 to 40 °C. The determinations were performed at constant ionic strength by a polarographic procedure described earlier,[1] and the values of the activity coefficients at 37 °C and at the freezing points of the imidazole solutions reported in the same paper will be utilized. Having determined the enthalpy and entropy changes connected to the complex formation we have some background to discuss whether structural changes may occur at various steps of the complex formation.[3-6]

EXPERIMENTAL

Chemicals. The cadmium perchlorate was prepared as described earlier.[1] All other chemicals were of analytical grade and were used without further purification.

Polarographic measurements. The equipment and experimental procedure in the polarographic measurements were the same as described

earlier.[1] In order to avoid precipitations of cadmium-imidazole complex compounds [2] the half wave potentials were determined with a total concentration of cadmium not exceeding 5×10^{-4} mol/kg but in no experiments it was necessary to go below 5×10^{-5} mol/kg. The concentration of imidazole was varied from 0.01 to 1.0 mol/kg in 15 steps. To ensure that the imidazole was present as unprotonated molecule, pH was kept constant at 9.5 and the ionic strength at 1.0 by addition of sodium perchlorate.

The temperature control. The temperature was continuously recorded and kept constant within ± 0.05 °C. All solutions were pre-cooled (pre-heated) before being added to the cell. In order to obtain better thermal stability at 5 °C and to avoid condensation, the experimental equipment was placed in a cold-storage room with a temperature a little below 5 °C. By means of a water bath the temperature in the cell was then kept at 5 ± 0.05 °C.

RESULTS

By application of the results from the polarographic measurements the over-all complexity constants, K_{0j} at ionic strength 1.0, were determined at 5, 15, 25, and 40 °C. The results are shown in Table 1. In order to obtain a correspondence in dimensions of the consecutive complexity constants the mean over-all complexity constants, $K_{0j}{}^{1/j}$ are compared, and for similar reasons the mean standard thermodynamic quantities: $\Delta^\circ_{0j}G/j$, $\Delta^\circ_{0j}H/j$, $\Delta^\circ_{0j}S/j$ and $\Delta^\circ_{0j}C_p/j$ are considered. The thermodynamic functions are then compared per mol of coordinated imidazole. In Fig. 1 the logarithm of the estimated values of the mean over-all complexity constants together with the standard deviations are plotted *versus* the reciprocal absolute temperature. The curves combining the estimated values have been determined by fitting a function of the type:

$$\log K_{0j} = A_j + B_j/T + C_j/T^2 \; (j = 1,2,3,4,5,6) \qquad (5)$$

The parameters A_j, B_j, and C_j were determined by application of a subroutine polynomium POLRG in the FORTRAN series. Knowing the values of these parameters the mean standard enthalpy and the mean standard molar heat capacity at 25 °C can be determined:

$$0.4343\ \Delta^\circ_{0j}H/R = -B_j - 2C_j/298 \qquad (6)$$

$$0.4343\ \Delta^\circ_{0j}C_p/R = 2C_j/298^2 \qquad (7)$$

When the standard enthalpy is independent of temperature within the temperature range covered here, the best curve describing the experimental results must be a straight line and $\Delta^\circ_{0j}C_p$ must be zero. Fig. 1 shows that this is the case for the first three steps whereas the last three steps are accompanied by a remarkable change in standard molar heat capacity. The results obtained for $\Delta^\circ_{0j}C_p$ together with other thermodynamic data are shown in Table 2. But although it must not be forgotten, that

Table 1. Logarithm of the over-all stability constants for the cadmium-imidazole system at four different temperatures. Ionic strength 1.0 by means of sodium perchlorate, pH 9.5. Standard deviations = ± 0.05.

j	5 °C	15 °C	25 °C	40 °C
1	3.08	2.95	2.70	2.48
2	5.48	5.26	5.10	4.85
3	7.30	7.00	6.63	6.30
4	8.35	8.11	7.60	6.70
5	8.30	8.30	8.18	7.74
6	9.90	9.48	8.95	7.92

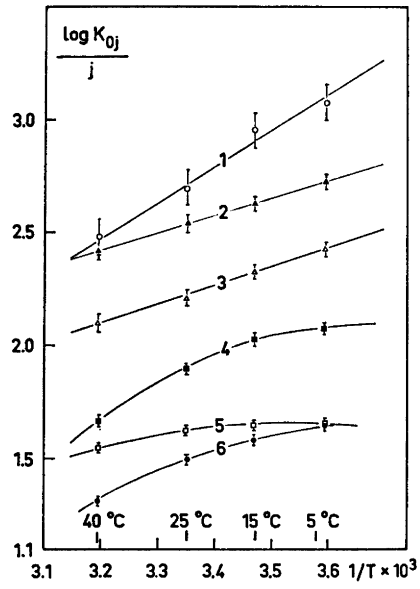

Fig. 1. Dependence of $(1/j)$ log K_{0j} for the Cd(II)-imidazole system *versus* the reciprocal absolute temperature for $j = 1$, 2, 3, 4, 5, and 6. Ionic strength 1.0 by means of sodium perchlorate, pH 9.5.

Table 2. Calculated values of changes in the over-all thermodynamic functions $\Delta^\circ_{0j}G$, $\Delta^\circ_{0j}H$, $\Delta^\circ_{0j}S$, and $\Delta^\circ_{0j}C_p$ at 25 °C for the cadmium-imidazole system. Ionic strength 1.0 by means of sodium perchlorate, pH 9.5.

j	$(\Delta^\circ_{0j}G/R)\times 10^{-3}$	$(\Delta^\circ_{0j}H/R)\times 10^{-3}$	$\Delta^\circ_{0j}S/R$	$\Delta^\circ_{0j}C_p/R$
1	-1.85 ± 0.03	-3.5 ± 0.3	-5.5 ± 0.2	0
2	-3.50 ± 0.03	-3.5 ± 0.3	0.0 ± 0.2	0
3	-4.55 ± 0.03	-5.7 ± 0.3	-3.8 ± 0.2	0
4	-5.22 ± 0.03	-11.0 ± 0.5	-19.4 ± 0.3	-380 ± 50
5	-5.62 ± 0.03	-4.4 ± 0.5	$+4.2\pm0.3$	-275 ± 50
6	-6.15 ± 0.03	-12.6 ± 0.5	-21.6 ± 0.3	-350 ± 50

$\Delta^\circ_{0j}C_p$-data obtained in this way may be defective to some extent due to accumulation of errors when first and second derivatives are calculated from experimental free energy data, the actual values agree reasonably well with those found for similar compounds, *i.e.* silver-imidazole complex compounds,[7] tetraamylammonium bromide [8,9] and tetrabutylphosphonium bromide,[10] all compounds containing organic nitrogen. Similar observations as described here for the last three complex compounds have been made for rare earth complexes,[11–13] a lot of weak organic acids,[14] and water.[15] Furthermore, when regarding Fig. 1 it is seen, that the temperature coefficients of $\log K_{0j}$ – and consequently the changes in standard enthalpies, $\Delta^\circ_{0j}H$ – are of the right order of magnitude and with the right sign as would be expected for a complex formation of the type investigated in this paper.[3,4,5] This suggests, that no serious experimental and systematic errors affect the results. The changes in free energies and entropies are calculated by application of eqn. (2). Fig. 2 summarizes the results. The values of $\Delta^\circ_{0j}G$, $\Delta^\circ_{0j}H$, and $\Delta^\circ_{0j}S$ were calculated at 25 °C and plotted *versus* j, where j indicates the step of reaction (1). The vertical lines indicate standard deviations. From the values shown in Table 2, the thermodynamic quantities $\Delta^\circ_{1-j,j}$ (G,H,S,C_p) corresponding to the step equilibria:

$$\mathrm{Cd\ aq}_x\ \mathrm{im}_{j-1}^{2+} + \mathrm{im} \rightleftharpoons \mathrm{Cd\ aq}_y\ \mathrm{im}_j^{2+} + (z-y)\mathrm{aq} \quad (8)$$

can be calculated by the equations:

$$\Delta^\circ_{j-1,j}(G,H,S,C_p) = \Delta^\circ_{0j}(G,H,S,C_p) - \Delta^\circ_{0,j-1}(G,H,S,C_p) \quad (9)$$

$$\log K_{j-1,j} = \log K_{0j} - \log K_{0,j-1} \quad (10)$$

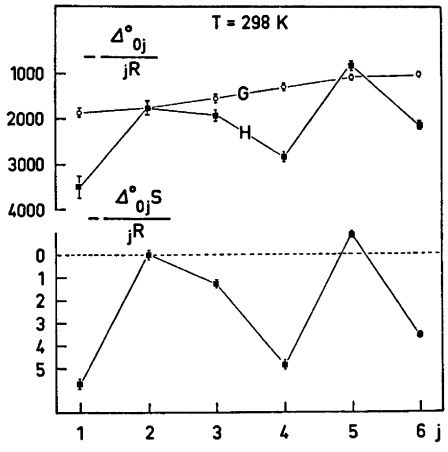

Fig. 2. Changes of the mean thermodynamic quantities, $-\Delta^\circ_{0j}G/jR$, $-\Delta^\circ_{0j}H/jR$ (upper part) and $-\Delta^\circ_{0j}S/jR$ (lower part) at 25 °C *versus* step number, j, in the Cd(II)-imidazole system.

DISCUSSION

Cadmium ions in aqueous solutions are generally suggested to be coordinated with six water molecules,[4] and likewise it seems reasonable to assume, that complexes with five and six imidazole ligands in aqueous solutions will have a similar, octahedral configuration.[16] The simplest reaction scheme of complex formation would be, that a water molecule from step to step was replaced by an imidazole molecule as visualized in (8) when $z-y = 1$. From Fig. 2 it is seen that for $j = 1$, 3, 4, and 6 the reduction in free energy is mainly governed by the enthalpy term and so the results in these three cases agree well with the simple reaction scheme. If, however, a sudden change in $\Delta^\circ_{0j}H$

towards positive values is observed, this may be caused by a sudden change in the coordination geometry.[4,5,17,18] The necessary increase in entropy can be explained by a change in the hydration shell belonging to the metal ions.[5,18,19] So, when structural changes occur, the contribution to the $-\Delta^\circ_{0j}G$ is mainly coming from a large gain in entropy, and the enthalpy change contributes only slightly. An example of such a case – given by Ahrland [4] is the complex formation between cadmium and halide ions. Similar effects in the cadmium-imidazole system are observed at the second and fifth step (Fig. 2). In the second step, $\Delta^\circ_{1,2}H$ was found $\cong 0$, *i.e.* the reduction in free energy is due to contribution from the entropy term. We therefore assume, that the coordination at this step changes from six to four, and the consecutive complex-equilibrium can be written:

$$\mathrm{Cd\,aq_5\,im^{2+} + im \rightleftharpoons Cd\,aq_2\,im_3^{2+} + 3aq} \qquad (11)$$

As seen from Fig. 2 the fourth coordinated cadmium-imidazole complex compound is characterized by very small values in both enthalpy and entropy indicating a relatively stable compound. This is in good agreement with the results observed by Bjerrum [20] in the case of cadmium-ammine complex formation. Based on these observations Bjerrum introduced the term "characteristic coordination number" besides the maximum coordination number, and he found these values to be 4 and 6, respectively, for the cadmium ion. The thermodynamic data shown in Fig. 2 seem to confirm the presence of such "characteristic" complex compounds also in the cadmium-imidazole system. Most likely the imidazole molecules are strongly bound in this characteristic form involving a change in the hydration shell. This effect might explain the contribution to the change in heat capacity observed at this step of the complex formation.

According to the above mentioned it is assumed, that the complex components at the fourth step exist in a four-coordinated form. In order to be able to end up as six-coordinated compounds a new coordination change must occur. The results shown in fig. 2 suggest this coordination change to occur at the fifth step in the complex formation, and therefore we propose the fifth complex equilibrium:

$$\mathrm{Cd\,im_4^{2+} + im + aq \rightleftharpoons Cd\,aq\,im_5^{2+}} \qquad (12)$$

Most likely the coordination change at the fifth step is accompanied by a formation of a new coordination geometry, which at this step is characterized by a lack of symmetry. The influence on the hydration shell is therefore weaker than that at the fourth step. This involves $\Delta^\circ_{45}C_p > 0$ in good agreement with the experimental results. In this six-coordinated form the high symmetry is re-established. From Table 1 it is seen that $\Delta^\circ_{56}C_p < 0$, in good agreement with the expected value.

Conclusions. Based on values of enthalpy changes, estimated from free energy data, we have tried to suggest a model by means of which we were able to describe the consecutive complex formation between Cd(II)-ions and uncharged imidazole molecules. According to this model it is assumed, that during the complex formation the Cd(II)-ions change their coordination number twice: at the second step from six to four and at the fifth step from four to six.

Acknowledgements. The author expresses his thanks to Professor Jørgen Koefoed for keen interest, advice, and encouraging discussions and to Mrs. Jette Klausen for skilled technical assistence.

REFERENCES

1. Jensen, J. B. *Acta Chem. Scand. 26* (1972) 4031.
2. Jensen, J. B. *Acta Chem. Scand. 27* (1973) 3563.
3. Ahrland, S. *Struct. Bonding (Berlin) 1* (1966) 207.
4. Ahrland, S. *Struct. Bonding (Berlin) 15* (1973) 167.
5. Schwarzenbach, G. *Pure Appl. Chem. 24* (1970) 307.
6. Pearson, R. G. *J. Amer. Chem. Soc. 85* (1963) 3533.
7. Datta, S. P. and Grzybowski, A. K. *J. Chem. Soc. A* (1966) 1059.
8. Mohanty, R. K., Sunder, S. and Ahluwalia, J. C. *J. Phys. Chem. 76* (1972) 2577.
9. Chawla, B. and Ahluwalia, J. C. *J. Phys. Chem. 76* (1972) 2582.
10. Sunder, S., Chawla, B. and Ahluwalia, J. C. *J. Phys. Chem. 78* (1974) 738.
11. Grenthe, I. and Ots, H. *Acta Chem. Scand. 26* (1972) 1217.
12. Grenthe, I. and Ots, H. *Acta Chem. Scand. 26* (1972) 1229.
13. Ots, H. *Acta Chem. Scand. 27* (1973) 2351.
14. Harned, H. S. and Embree, N. D. *J. Amer. Chem. Soc. 56* (1934) 1050.

15. Clever, H. L. *J. Chem. Educ. 45* (1968) 231.
16. Mighell, A. D. and Santoro, A. *Acta Crystallogr. B 27* (1971) 2089.
17. Williams, R. J. P. *J. Phys. Chem. 58* (1954) 121.
18. King, E. L. *J. Chem. Educ. 30* (1953) 71.
19. Prue, J. E. *J. Chem. Educ. 46* (1969) 12.
20. Bjerrum, J. *Metal Ammine Formation in Aqueous Solution*, Haase, Copenhagen 1941, p. 110.

Received August 26, 1974.

Acta Chemica Scandinavica A 29 (1975) 255—264

The Crystal Structure of Potassium Hexacyanovanadate(II), $K_4[V(CN)_6]$

SUSAN JAGNER *

Department of Inorganic Chemistry, University of Aarhus, DK-8000 Aarhus C, Denmark

The crystal structure of potassium hexacyanovanadate (II), $K_4[V(CN)_6]$, has been determined from X-ray single crystal diffractometer data. $K_4[V(CN)_6]$ crystallizes with a disordered structure characterised by the OD groupoid symbol:

Pma(b)

$\{c_2\ n_{2,\frac{1}{2}}\ (n_{\frac{1}{2},1})\}$

The unit cell of the ordered monoclinic form (MDO_2) has the dimensions: $a = 8.5770(6)$ Å, $b = 21.5271(26)$ Å, $c = 7.5270(8)$ Å, and $\beta = 106.55(1)°$ and belongs to space group $P2_1/a$, with $Z = 4$. Following a determination of the superposition structure, the MDO_2 structure was determined and refined to $R = 0.053$ ($R_w = 0.055$), using full-matrix least squares refinement based on 757 independent reflections, the positional and thermal parameters being constrained so as to comply with the partial symmetry operations of the OD groupoid symbol. The complex ion has octahedral symmetry with mean V—C and C—N bond lengths of 2.161(4) and 1.153(7) Å, respectively.

Variations in σ and π contributions to metal-ligand bonds in transition metal hexacyanides and cyanocomplexes have been the subject of much attention in recent years. It ought to be possible to clarify such variations by correlating the bond lengths and geometries of the complex ions, obtained from crystal structure determinations, and information concerning the charges on the central metal atoms and ligands, obtained from X-ray photoelectron spectra, with existing semi-empirical molecular orbital calculations.[1–5]

In connection with such an investigation, in progress at the Department of Inorganic Chemistry, University of Göteborg and Chalmers University of Technology, the crystal structures of the hexacyanovanadates were of interest. These complexes were originally thought to have the formulae $K_2[V(CN)_6]$, $K_3[V(CN)_6]$, and $K_4[V(CN)_6]$. $K_2[V(CN)_6]$ has, however, been shown [6] to be $K_3[VO(CN)_5]$, whose crystal structure has recently been determined.[7] It was suspected [2,6,8–11] that $K_3[V(CN)_6]$ was in fact $K_4[V(CN)_7].2H_2O$, final confirmation being provided by a crystal structure determination by Towns and Levenson.[12,13] The crystal structure of the last member of the series, $K_4[V(CN)_6]$, has now been determined. Although yellow crystals of potassium hexacyanovanadate(II) have been reported [8–11] to have the formula $K_4[V(CN)_6].3H_2O$, the compound studied in this investigation had the formula $K_4[V(CN)_6]$, which is in accordance with the findings of Bennett and Nicholls.[6]

PREPARATION AND ANALYSIS

Potassium hexacyanovanadate(II) was prepared according to a modification of the method described by Bennett and Nicholls.[6] VCl_3 (5.5 g) was dissolved in 0.01 M HCl (15 ml) and the solution was passed through a zinc reductor (20 mesh). The resulting violet solution was allowed to drop, under an atmosphere of hydrogen, into a saturated solution of potassium cyanide, at a rate of approximately 1 drop/s. The cyanide solution was stirred and cooled to 0 °C, a yellow powder being deposited. This was filtered off, washed with methanol, and dissolved in 3 M potassium cyanide, the solution then being set aside to crystallize in an argon-filled desiccator. After a few days, yellow, needle-shaped crystals of suitable size for single

* On leave from the Department of Inorganic Chemistry, University of Göteborg and Chalmers University of Technology, Fack, S-402 20 Göteborg 5, Sweden.

crystal X-ray work were deposited. Although aqueous solutions of potassium hexacyanovanadate(II) decompose rapidly on exposure to air, the solid substance can be stored for several weeks in dry air. X-Ray photoelectron spectroscopic studies suggest that the decomposition product is $K_3[VO(CN)_5]$.

The *potassium* and *vanadium* contents were determined by means of atomic absorption spectroscopy, using a Perkin Elmer 403 spectrometer. The *cyanide* content was determined by potentiometric titration with Ag^+. [Found: K 43.8; V 13.9; CN 43.1. Calc. for $K_4[V(CN)_6]$: K 43.0; V 14.0; CN 43.0].

The infra-red spectrum, registered with a Beckman IR 9 spectrophotometer, agreed well with that given by Bennett and Nicholls.[6] That the compound studied had the formula $K_4[V(CN)_6]$ and not $K_4[V(CN)_6].3H_2O$ is evident from the results of the crystal structure determination, the infra-red spectrum, and the chemical analysis.

OD STRUCTURE

Rotation photographs of crystals mounted along the *a* axis showed layer lines composed of discrete reflections for $A \approx 4.29$ Å and diffuse streaks corresponding to $a = 2A \approx 8.58$ Å. It was thus apparent that $K_4[V(CN)_6]$ crystallized with a disordered crystal structure of OD type,[14] *i.e.* a structure which consists of ordered, equivalent layers whose mode of stacking is disordered. Weissenberg photographs of diffuse layer lines showed that there were intensity maxima on the streaks with monoclinic symmetry which would necessitate a doubling of the *c* axis corresponding to the discrete reflections, *i.e.* $c_{app} = 2c \approx 28.86$ Å.

If the *c* direction is defined as that of non-periodicity, the conditions limiting possible reflection for $K_4[V(CN)_6]$ may be summarized:

(i) discrete reflections, hkl, for $h = 2H$; diffuse streaks, $hk\zeta$, for $h = 2H + 1$, where ζ can take any value

(ii) Hkl: $H + l = 2n$
(iii) $hk0$: $k = 2n$
(iv) $h0\zeta$: $h = 2n$

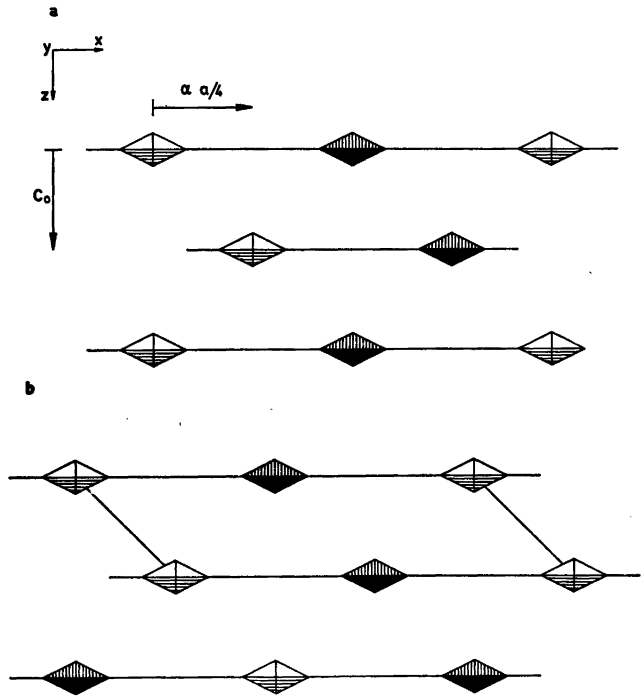

Fig. 1. Schematic representation of the stacking of layers in (a) the ordered orthorhombic structure (MDO_1) and (b) the ordered monoclinic structure (MDO_2). $\vec{c_0}$ is the unit vector perpendicular to the layers in the non-periodic direction, while α is a factor which can take the value +1 or −1. *Notation:* empty triangles: y; filled triangles: $-y$; vertically shaded triangles: $\frac{1}{2}-y$; and horizontally shaded triangles: $\frac{1}{2}+y$.

where *hkl* refer to an orthogonal unit cell with the approximate dimensions: $a = 8.58$ Å, $b = 21.53$ Å, and $c = 14.43$ Å.

According to reflection conditions (i) and (ii), the superposition structure,[14] corresponding to the family reflections, *Hkl*, has an a axis of one-half 8.58 Å and is B face-centred with $Bmmb$ or $B2_1mb$ as possible space groups [*cf.* also reflection condition (iii)].

According to reflection conditions (iii) and (iv), the minimum layer symmetry is $P2_1a(b)$. Owing to the high symmetry of the building units,[15–17] the layer symmetry has, however, been assumed to be $Pma(b)$. The B face-centring of the superposition structure requires that each layer be related to the next by a translation $\alpha\,\vec{a}/4 + \vec{c}_0$, where α can take the value ± 1 and $\vec{c}_0$ is the unit vector perpendicular to the layers in the non-periodic direction. This means that the symmetry elements converting a given layer, L_0, into the next, L_1, are ${}_{0,1}[c_2\ n_{2,\frac{1}{4}}\ (n_{\frac{1}{4},1})]$ or ${}_{0,1}[c_2\ n_{2,\frac{1}{4}}\ (n^{-}_{\frac{1}{4},1})]$. These symmetry elements are illustrated in Fig. 1.

$K_4[V(CN)_6]$ thus crystallizes as a family of structures characterized by the OD groupoid symbol:[14]

$Pma(b)$

$\{c_2\ n_{2,\frac{1}{4}}\ (n_{\frac{1}{4},1})\}$

this symbol giving the total symmetry of any pair of consecutive layers.

There are two ordered extreme structures, or "structures of maximum degree of order" (MDO).[14] One is orthorhombic, obtained by a zig-zag stacking of layers (α = alternately $+1$ and -1, *cf.* Fig. 1a), while the other is monoclinic, obtained by an oblique stacking of layers ($\alpha = +1$ or -1, only, *cf.* Fig. 1b). The orthorhombic structure (MDO_1) has a unit cell with the approximate dimensions: $a = 8.58$ Å, $b = 21.53$ Å, and $c = 14.43$ Å and belongs to space group $Pcab$, while the unit cell of the monoclinic structure (MDO_2) has the approximate dimensions: $a = 8.58$ Å, $b = 21.53$ Å, $c = 7.53$ Å, and $\beta = 106°$, the space group being $P2_1/a$.

Since the crystals studied showed streaks with intensity maxima of monoclinic symmetry, only, they must contain much larger regions of MDO_2-type structure than of MDO_1-type structure. The apparent doubling of the c axis ($c_{app} \approx 28.86$ Å) can be explained by the presence of regions corresponding to both the MDO_2 "twins", *i.e.* that with the stacking sequence given by $\alpha = +1$ and that with $\alpha = -1$.

The fictitious superposition structure, $\hat{\varrho}(x,y,z)$, which is related to the real structure, $\varrho(x,y,z)$ by

$$\hat{\varrho}(x,y,z) = \tfrac{1}{2}[\varrho(x,y,z) + \varrho(x+\tfrac{1}{2},y,z)]$$

has the approximate unit cell dimensions: $A = 4.29$ Å, $b = 21.53$ Å, $c = 14.43$ Å and belongs to space group $Bmmb$. The disorder in $K_4[V(CN)_6]$ is thus very similar to that found in $K_4[Mo(CN)_5NO]$, the superposition and MDO_1 structures of which have been solved.[18]

ACCURATE UNIT CELL DIMENSIONS

Powder photographs of $K_4[V(CN)_6]$ were taken in a Guinier focusing camera with $CuK\alpha_1$ radiation, using lead nitrate as an internal standard ($a = 7.8564$ Å).[19] Thirty-one family reflections were indexed and used to refine the unit cell dimensions of the superposition structure with the program Powder.[20] The following values were obtained (standard deviations, $\times 10^4$, in parentheses): $A = 4.2885(3)$ Å, $b = 21.5271(26)$ Å, and $c = 14.4308(16)$ Å. Observed and calculated $\sin^2\theta$ values are listed in Table 1. The calculated density corresponding to a cell content of four formula units is 1.81 g cm^{-3}. The experimental density, as determined by the method of flotation, using bromoform and carbon tetrachloride, is 1.83 g cm^{-3}.

The unit cell dimensions of the MDO_2 structure were derived from those of the superposition structure, the following values being obtained (standard deviations, $\times 10^4$ for a,b,c and $\times 10^2$ for β, in parentheses): $a = 8.5770(6)$ Å, $b = 21.5271(26)$ Å, $c = 7.5270(8)$ Å and $\beta = 106.55(1)°$. There are four formula units of $K_4[V(CN)_6]$ per unit cell of the MDO_2 structure.

DETERMINATION OF THE SUPERPOSITION AND MDO_2 STRUCTURES

A crystal of $K_4[V(CN)_6]$ with the approximate dimensions $0.055 \times 0.005 \times 0.015$ cm was mounted along the a axis, in a glass capillary, and the intensities of the family reflections (hkl, $h = 2H$) and of the streaks ($hk\zeta$, $h = 2H + 1$)

Table 1. X-Ray powder diffraction data for $K_4[V(CN)_6]$. Guinier camera, Cu$K\alpha_1$ radiation ($\lambda = 1.54050$ Å).

$H\ k\ l$	$10^5 \sin^2\theta_{obs}$	$10^5 \sin^2\theta_{calc}$	I_{calc} (relative scale)	I_{obs}
0 2 0	512	512	16	w
0 4 0	2046	2048	3	vw
0 3 2	2291	2292	14	w
0 4 2	3187	3188	21	m
1 0 1	3516	3511	3	vw
1 1 1	3641	3639	12	w
1 2 1	4024	4023	16	w
0 5 2	4342	4340	100	vs
0 0 4	4560	4558	16	w
1 3 1	4665	4663	20	m
0 6 2	5748	5748	59	s
1 1 3	5920	5918	49	m
1 2 3	6305	6302	151	vvs
1 5 1	6709	6711	2	vvw
1 3 3	6941	6942	92	vs
0 7 2	7411	7413	21	m
1 5 3	8996	8990	4	vw
1 7 1	9782	9784	16	w
1 8 1	11706	11704	51	s
1 7 3	12073	12063	3	vw
0 4 6	12301	12304	14	w
1 4 5	12403	12397	36	m
2 0 0	12908	12904	35	m
0 5 6	13456	13457	22	w
1 8 3	13984	13984	14	w
2 2 2	14557	14555	1	vvw
1 7 5	16627	16621	8	vw
2 5 2	17243	17244	21	m
2 0 4	17458	17462	6	vw
2 3 4	18614	18614	2	vw
2 7 2	20315	20316	3	vw

at the reciprocal lattice points corresponding to the MDO_3 "twins" were measured with an Arndt-Phillips linear diffractometer. Mo$K\alpha$ radiation was selected by a graphite monochromator and data were collected for layers $0kl - 10kl$, for $h = 2H$, and $1kl - 5kl$, for $h = 2H + 1$.

Symmetry-related family reflections were averaged and correction was made for Lorentz and polarisation effects, using the program G4,[21] assuming the graphite monochromator to behave as an ideal mosaic crystal. The intensities of the maxima on the streaks were processed with a function of the background *v.* $\sin\theta$, obtained from data collected for a "layer" midway between $0kl$ and $1kl$. This was achieved by modifying G4,[21] the averaging of symmetry related reflections being carried out in the same way as for the family reflections. A total of 757 independent reflections for which $F_o^2 > 3.0\sigma(F_o^2)$ according to counting statistics, *i.e.* 641 family reflections and 116 non-family reflections from the larger "twin", were used in the subsequent calculations. No correction was made for absorption (linear absorption coefficient for $K_4[V(CN)_6]$ in Mo$K\alpha$ radiation = 19.9 cm^{-1}).

The superposition structure of $K_4[V(CN)_6]$, ($A = 4.2885(3)$ Å, $b = 21.5271(26)$ Å, $c = 14.4308(16)$ Å, $Z = 4$, space group *Bmmb**) which proved to be isomorphous with that of $K_4[Mo(CN)_5NO]$,[18] was determined from a Patterson function and a subsequent electron density calculation (FORDAP) [21] based on the family reflections, *Hkl*. Positional and isotropic thermal parameters were refined with the full-

* Equipoints of general position of *Bmmb* (conventional setting,[19] No. 63, *Cmcm*): (0,0,0, $\frac{1}{2}$,0,$\frac{1}{2}$)± (x,y,z; $x,\bar{y},\bar{z}$; $x,\frac{1}{2}-y,z$; $x,\frac{1}{2}+y,\bar{z}$). Equipoints of general position of $P2_1/a$ (conventional, setting,[19] No.14, $P2_1/c$): ± (x,y,z, $\frac{1}{2}+x,\frac{1}{2}-y,z$).

Table 2. Atomic coordinates, expressed as fractions of the cell edges and isotropic thermal parameters (Å²) for the superposition structure of $K_4[V(CN)_6]$. Standard deviations ($\times 10^4$) and ($\times 10^2$), respectively, are given in parentheses.

Atom	Site	Occupation No.	x	y	z	B
K(1)	4*c*	1.0	0.5000	0.2500	0.1528(3)	2.76(7)
K(2)	8*f*	1.0	0.0000	0.0479(1)	0.1367(2)	2.13(4)
K(3)V	8*f*	1.0	0.0000	0.1390(1)	0.4067(2)	2.58(5)
N(1)	8*f*	1.0	0.0000	0.1699(6)	0.0564(9)	4.35(26)
N(2)	8*f*	1.0	0.5000	0.0746(6)	0.2650(9)	4.00(25)
N(3)	8*f*	0.5	0.0000	0.2532(30)	0.2877(11)	2.86(41)
N(4)	8*f*	0.5	0.0000	0.0140(11)	0.4885(18)	2.21(54)
C(1)	16*h*	0.5	0.3557(34)	0.1583(6)	0.5057(9)	1.68(21)
C(2)	16*h*	0.5	0.3552(36)	0.0930(6)	0.3145(10)	1.82(23)
C(3)	8*f*	0.5	0.0000	0.2116(10)	0.3330(16)	2.14(38)
C(4)	8*f*	0.5	0.0000	0.0337(12)	0.4781(18)	1.61(42)

matrix least squares program LINUS [21] to an R value of 0.090. The atomic scattering factors due to Cromer and Mann [22] were used for all atoms, mean values of the scattering factors for potassium and vanadium being used for the four potassium and four vanadium atoms occupying the same eight-fold site, *i.e.* K(3)V. Unit weights were assigned to all reflections. The resulting parameters are given in Table 2.

The positions of the atoms in the MDO_2 structure ($a = 8.5770(6)$ Å, $b = 21.5271(26)$ Å, $c = 7.5270(8)$ Å, $\beta = 106.55(1)°$, $Z = 4$, space group $P2_1/a^*$) were calculated from the atomic parameters of the superposition structure, best agreement being obtained for an origin corresponding to $\frac{1}{4}\ 0\ \frac{1}{4}$ in the superposition structure. Preliminary refinement of positional and anisotropic thermal parameters for the potassium and vanadium atoms and isotropic thermal parameters for the remaining atoms, together with a separate scale-factor for the non-family reflections yielded R values of between 0.08 and 0.09. The refinement was extremely unstable and did not converge satisfactorily, very poor agreement being obtained for the streak reflections. The factor scaling the latter reflections obtained, moreover, unrealistic values.

REFINEMENT OF THE MDO_2 STRUCTURE

As will be described elsewhere,[23] it would seem to be a logical consequence of OD theory to constrain positional and thermal parameters during the refinement of an MDO structure so as to comply with the partial symmetry elements of the OD groupoid symbol. The MDO_2 structure of $K_4[V(CN)_6]$, which contains a single layer only, was therefore constrained to have *Pma(b)* symmetry by the introduction of the following equivalent positions: $\pm(x,y,z;\ \frac{1}{2}+x,\ \frac{1}{2}-y,\ z;\ \frac{1}{4}+\frac{1}{2}z-x,y,z;\ \frac{3}{4}+\frac{1}{2}z-x,\ \frac{1}{2}-y,z)$. The z coordinates of the atoms situated on the mirror plane (*viz.* K(1), K(3), V, C(3), N(3), C(4), and N(4) were refined, while the x coordinates were reset according to $x = \frac{1}{8} + \frac{1}{2}z$. Similarly, the β_{12} and β_{13} parameters of these atoms were reset according to $\beta_{12} = \frac{1}{4}\beta_{23}$ and $\beta_{13} = \frac{1}{4}\beta_{33}$, respectively. The refinement became stable and converged to an R value of 0.053 ($R_w = 0.055$), the standard deviations of the parameters and the agreement for the non-family reflections being considerably improved compared with the previous refinement. The ratio between the scale factors for the non-family and family reflections attained a credible value, *i.e.* 1.84, with respect to film observations.

The constraints were then released. After three cycles of refinement, the R value dropped to 0.049 ($R_w = 0.051$), but several of the ligand atoms obtained negative temperature factors. The hypothesis that the constrained refinement (89 parameters) provided a more satisfactory model than the unconstrained refinement (155 parameters) was tested by means of an R factor ratio test,[24] using the approximation due to Pawley.[25] The R factor ratio ($R_{w,\text{constr.}}/R_{w,\text{unconstr.}} = 1.0734$) indicated that, although the hypothesis could be rejected at the 0.05 probability level ($\mathcal{R}_{66,602,0.05} = 1.0702$) it could

Table 3. Atomic coordinates, expressed as fractions of the cell edges, and mean square vibration amplitudes, U_{ij}, ($Å^2$) for the MDO_2 structure of $K_4[V(CN)_6]$. The estimated standard deviations of the parameters ($\times 10^4$) are given in parentheses.

Atom	x	y	z	U_{11}	U_{22}	U_{33}	U_{12}	U_{13}	U_{23}
K(1)	0.3265	0.2526(4)	0.8059(4)	0.0281(11)	0.0429(16)	0.0333(12)	0.0022	0.0095	0.0078(36)
K(2)	0.0689(8)	0.4522(1)	0.7736(2)	0.0237(17)	0.0322(8)	0.0248(7)	−0.0022(20)	0.0021(33)	−0.0006(6)
K(3)	0.2003	0.3596(2)	0.3013(11)	0.0338(17)	0.0170(20)	0.0267(22)	−0.0028	0.0076	−0.0098(19)
V	0.2054	0.1246(1)	0.3217(7)	0.0186(11)	0.0103(15)	0.0179(16)	0.0005	0.0051	0.0018(15)
N(1)	0.5021(18)	0.3299(4)	0.6108(12)	0.0369(116)	0.0394(40)	0.0354(37)	−0.0030(37)	0.0127(40)	0.0012(33)
N(2)	0.9013(35)	0.4252(4)	0.0292(12)	0.0508(145)	0.0423(40)	0.0409(38)	0.0084(54)	0.0183(65)	0.0117(34)
N(3)	0.1445	0.2569(9)	0.0780(16)	0.0365(52)	0.0207(78)	0.0349(47)	0.0020	0.0099	0.0070(74)
N(4)	0.2561	−0.0140(5)	0.5243(28)	0.0383(70)	0.0125(88)	0.0255(86)	0.0050	0.0073	0.0177(74)
C(1)	0.5728(11)	0.3430(3)	0.5100(12)	0.0285(43)	0.0110(34)	0.0222(38)	0.0013(32)	0.0075(38)	−0.0034(31)
C(2)	0.8349(11)	0.4064(4)	0.1295(12)	0.0224(43)	0.0213(40)	0.0262(41)	0.0034(33)	0.0049(35)	0.0032(32)
C(3)	0.1674	0.2108(6)	0.1698(18)	0.0258(72)	0.0291(67)	0.0246(58)	0.0006	0.0070	0.0020(55)
C(4)	0.2384	0.0353(7)	0.4536(32)	0.0152(64)	0.0275(88)	0.0212(88)	−0.0037	0.0060	−0.0132(84)

Table 4. Observed and calculated structure factors (×10) for the MDO_2 structure of $K_4[V(CN)_6]$.

K	L	FOBS	FCALC
* H= 0 *			
0	3	201	-192
0	4	713	712
0	6	341	341
0	7	329	-341
0	8	227	-216
0	9	283	285
1	2	217	227
1	3	246	-249
1	4	1281	-1312
1	5	238	270
1	6	649	652
1	7	326	-307
1	8	209	-146
2	2	106	-70
2	4	724	720
2	6	316	-332
2	8	253	258
2	9	330	309
3	1	632	-604
3	2	378	355
3	3	475	-454
3	4	526	-521
3	5	557	544
3	6	398	389
3	7	567	-566
3	8	252	-218
3	9	205	164
4	0	517	-520
4	1	939	817
4	3	1564	-1548
4	4	362	382
4	5	946	975
4	6	463	-457
4	7	369	-400
5	1	2248	2203
5	3	1988	-1936
5	6	236	212
5	7	144	172
5	8	323	-318
5	9	323	-292
6	0	511	-496
6	1	2010	-1904
6	2	517	511
6	3	413	383
6	5	503	-495
7	1	1411	1348
7	2	314	-320
7	3	245	-230
7	4	458	442
7	7	243	-238
7	8	190	-189
8	0	479	516
8	1	431	-421
8	2	405	-394
8	3	445	453
8	4	352	-317
8	5	756	-755
8	6	582	587
8	7	157	175
8	8	470	-481
9	2	1268	1248
9	3	207	-191
9	4	966	-977
9	5	229	171
9	6	596	602
9	7	243	-241
10	0	1712	-1786
10	1	174	159
10	2	1027	1011
10	3	233	232
10	4	733	-732
10	5	278	-278
10	6	171	142
10	7	428	439
11	1	894	-893
11	2	262	238
11	3	271	237
11	4	423	414
11	5	286	184
11	7	231	-218
11	8	195	192
12	0	373	-377
12	1	342	387
12	2	1134	1159
12	3	456	-465
12	4	332	-329
12	5	223	228
13	1	465	-486
13	2	688	-656
13	4	391	387
13	5	419	-406
13	7	430	424
14	0	282	-275
14	1	158	-96
14	2	286	279
14	3	505	527
14	5	441	-460
14	6	259	258
14	7	292	290
15	1	802	-795
15	2	465	-460
15	3	494	496
15	4	580	573
15	5	306	-274
15	6	336	-335
16	0	424	443
16	1	174	94
16	2	538	-553
16	3	455	451
16	8	317	-329
17	1	673	-709
17	2	376	384
17	3	293	287
17	4	336	-356
17	5	246	-285
18	0	190	-174
18	1	213	-158
18	3	191	-167
18	5	213	239
18	6	232	-211
18	7	210	-198
19	1	287	-262
19	3	360	347
19	6	261	-259
20	0	281	274
20	1	231	222
20	2	318	-309
20	3	583	-623
20	4	299	278
20	5	293	266
20	6	205	-230
21	1	378	373
21	2	181	-106
21	3	235	-185
22	0	255	226
22	2	448	-478
24	0	474	516
24	2	286	-275
25	3	174	-185
26	2	262	215
* H= 1 *			
5	-2	313	285
5	4	297	339
6	3	260	313
7	-1	347	-286
7	2	270	252
8	-2	387	-379
8	0	353	354
8	2	366	-395
9	-5	326	-359
9	-1	472	488
9	1	525	-486
10	-3	463	-435
10	-1	264	222
10	2	273	308
10	3	321	-396
12	-3	340	-301
12	-2	354	392
12	0	335	-391
12	1	344	-276
12	2	289	349
13	-2	417	482
13	-1	414	-424
13	1	522	505
13	2	413	-384
13	4	381	349
14	0	409	502
14	2	327	-245
17	-4	446	418
17	-2	515	-498
17	1	454	-493
17	2	316	254
17	3	349	359
18	-3	604	-643
18	2	578	512
18	3	538	-502
21	-2	413	389
21	-1	335	-333
21	1	373	428
21	4	369	356
22	-1	381	-334
22	0	488	548
25	1	458	-391
26	-3	388	-399
26	2	486	348
26	2	406	348
* H= 2 *			
0	3	608	-648
0	4	202	-187
0	5	1877	1898
0	6	221	-192
0	7	697	-719
0	8	385	379
0	9	248	280
1	2	501	-529
1	3	491	-501
1	4	472	484
1	5	286	283
1	6	142	-140
2	1	2196	2234
2	2	294	-308
2	3	656	-691
2	4	133	-93
2	5	511	548
2	6	226	265
2	8	252	-218
3	0	716	-751
3	1	1892	1895
3	2	1098	1111
3	3	368	-397
3	4	393	-400
3	5	151	-102
3	7	406	422
4	0	239	245
4	1	186	154
4	2	1683	-1716
4	3	519	548
4	4	502	504
4	5	385	-396
4	7	164	157
5	0	336	322
5	1	577	-576
5	2	804	810
5	3	332	319
5	4	801	-838
5	5	263	261
5	6	694	699
5	8	416	-419
6	0	146	152
6	2	231	214
6	3	150	-129
6	4	438	-441
6	5	185	155
6	6	151	156
7	0	926	-910
7	1	390	372
7	2	879	893
7	3	507	525
7	4	1029	-1059
7	5	244	-233
7	6	433	443
7	8	242	-251
8	0	1791	-1809
8	1	1046	-1045
8	2	742	760
8	3	155	147
8	4	278	-286
8	6	358	-367
8	8	325	329
9	0	830	-824
9	1	564	577
9	2	422	-421
9	3	684	-712
9	4	275	294
9	5	369	387
9	6	286	-272
10	0	219	-204
10	3	595	608
10	5	457	-452
10	7	408	431
11	0	419	-438
11	1	138	125
11	2	172	147
11	5	221	-209
11	6	298	-294
11	7	207	227
12	0	283	290
12	1	718	-735
12	2	245	-247
12	3	942	963
12	4	204	179
12	5	741	-763
12	7	377	404
13	0	879	911
13	1	757	-796
13	2	782	-794
13	3	412	418
13	5	161	134
13	6	189	144
13	7	185	-199
14	0	338	-339
14	2	498	516
15	0	433	431
15	1	242	-209
15	3	283	298
15	6	222	-281
16	0	479	-526
16	1	207	-216
16	2	210	219
16	5	295	284
17	0	309	298
17	2	462	-477
17	3	215	-234
17	4	686	738
17	5	263	257
17	6	452	-433
18	0	586	615
18	1	318	328
18	2	279	-257
18	3	260	-268
19	1	134	83
19	2	136	-96
19	3	195	213
19	4	179	170
19	5	173	-185
20	0	329	356
20	1	140	129
20	2	291	-295
20	3	191	-179
21	0	184	178
21	1	328	-371
21	3	172	141
22	1	370	404
22	3	332	-333
22	4	229	-191
22	5	250	266
23	0	161	-170
23	2	280	246
23	4	254	-287
24	3	165	-169
24	4	171	64
25	0	262	-242
25	1	263	256
25	3	196	-167
26	0	162	140
27	1	173	153
27	2	180	155
* H= 3 *			
2	2	526	-540
5	1	446	-501
5	3	372	383
6	2	301	344
8	-5	401	374
8	-2	246	-287
8	-1	218	254
8	0	230	-311
9	-2	531	510
9	0	281	-293
9	1	426	501
10	0	271	243
12	-1	297	-327
12	0	276	277
13	-5	377	-340
13	-2	476	-492
13	0	329	364
13	1	338	-448
14	-6	417	-413
14	-1	704	715
14	0	389	-391
14	5	377	406
16	0	395	-333
17	-5	369	389
17	-2	375	424
17	0	384	-368
18	-6	353	331
18	-4	338	-334
18	-1	420	-368
20	-3	334	292
20	1	313	399
21	-2	355	-386
21	0	434	426
22	-1	596	614
22	0	389	-355
25	-2	401	378
26	-3	389	400
* H= 4 *			
0	3	568	-547
0	4	178	-168
0	5	180	-165
0	6	277	280
0	7	341	326
0	8	318	-289
1	2	139	154
1	3	916	925
1	4	144	-142
1	5	489	-498
1	6	296	298
2	3	605	-617
2	5	262	259
2	6	180	149
2	7	230	-221
3	0	188	189
3	1	507	-511
3	2	192	175
3	3	408	396
3	4	357	-342
3	5	259	-241
3	6	531	515
3	8	226	-192
4	-1	91	-65
4	0	491	-491
4	1	195	-185
4	2	1337	1329
4	3	264	-275
4	4	648	-658
4	5	312	297
4	6	348	334
4	7	182	-176
5	0	1617	-1626
5	2	1282	1255
5	5	161	-152
5	6	162	-169
5	7	268	294
6	-1	371	349
6	0	713	688
6	1	168	-172
6	2	347	-332
6	3	288	258
6	4	367	365
6	6	205	-216
7	0	738	-740
7	1	365	360
7	2	336	343
7	3	386	-391
7	4	154	-155
7	5	178	-144
7	6	187	174
7	7	161	162
8	-1	468	-463
8	0	303	295
8	1	274	263
8	2	403	-393
8	3	288	256
8	4	587	579
8	5	468	-490
8	7	430	411
9	1	756	-752
9	2	240	245
9	3	736	748
9	4	196	-191
9	5	577	-582
9	6	208	200
10	-1	1310	1255
10	0	204	186
10	1	941	-922
10	2	167	-170
10	3	380	359
10	4	285	267
10	5	210	-182
10	6	235	-243
11	0	631	621
11	1	191	-145
11	2	238	-239
11	3	261	-259
11	4	186	-154
11	6	180	183
12	-1	658	640
12	0	269	-287
12	1	737	-746
12	2	233	223
12	3	255	258
12	4	281	-276
13	0	444	-455
13	1	349	331
13	3	316	-317
13	4	419	429
13	5	215	189
13	6	323	-328
13	7	227	-203
14	-1	209	221
14	1	164	-158
14	2	411	-422
14	3	148	84
14	4	362	365
14	5	191	-180
14	6	204	-298
15	0	570	563
15	1	306	-300
15	2	444	-433
15	3	493	-488
15	4	322	293
15	5	300	304
16	-1	608	-619
16	1	341	341
16	2	183	-169
16	5	207	-167
17	0	565	597
17	1	232	-226
17	2	257	-246
17	3	320	316
17	4	164	164
18	-1	169	158
18	4	217	-213
18	5	225	189
19	0	316	311
19	1	140	146
19	2	265	-228
19	3	146	-146
20	0	200	-215
20	1	313	314
20	2	402	403
20	3	240	-233
20	4	312	-334
20	5	235	259
21	0	305	-298
21	2	170	172
22	-1	226	-218
22	0	146	103
22	1	276	291
22	3	179	-201
24	-1	433	-433
24	1	248	245
25	1	190	-161
26	-1	193	167
* H= 5 *			
5	3	308	-266
6	-1	261	-261
7	1	274	-234
8	-3	249	287
8	-1	258	-221
8	1	265	301
9	-6	328	263
9	0	288	251
9	3	288	251
10	-4	348	362
10	-1	289	283
10	2	385	367
12	-1	314	272
12	0	392	252
13	-2	264	298
13	0	418	-322
13	1	328	292
13	3	311	-262
14	-1	346	-316
14	1	322	231
14	2	322	-298
16	-6	365	243
17	-3	397	419
17	0	361	389
18	-4	476	541
18	1	510	-449
18	2	418	401
21	-3	317	-352
21	0	436	-346
22	-1	410	-390
* H= 6 *			
0	3	180	144
0	4	883	-908
0	6	458	441
1	2	304	303
1	3	381	-393
1	4	181	-175
2	1	184	188
2	2	489	511
2	4	375	-368
2	5	255	-242
3	0	806	-826
3	1	625	-627
3	2	158	127
3	3	152	150
3	6	241	-230
4	-1	425	-457
4	0	83	-58
4	1	672	687
4	2	300	-291
4	3	361	-363
4	4	402	404
5	0	280	289
5	1	367	-361
5	2	282	-257
5	3	567	583
5	4	284	-198
5	5	467	-458
5	7	327	343
6	-1	129	90
6	0	360	-363
6	1	170	-137
6	2	115	-68
6	3	390	391
7	-1	301	304
7	0	151	-154
7	1	549	-558
7	2	157	-164
7	3	749	763
7	4	174	180
7	5	374	-371
8	-1	929	935
8	0	596	608
8	1	520	-509
8	2	134	-131
8	3	194	177
8	5	267	256
9	-1	274	263
9	0	437	-446
9	1	266	270
9	2	522	544
9	4	240	-236
9	5	151	127
9	6	161	-129
10	0	286	294
10	2	260	-236
10	3	138	-96
10	4	322	307
10	5	165	-101
10	6	300	-260
11	-1	282	276
11	0	170	-166
11	4	147	105
11	5	231	244
12	0	417	433
12	1	336	347
12	2	670	-661
12	4	429	441
12	6	328	-355
13	-1	463	-476
13	0	566	585
13	1	398	399
13	2	350	-353
13	3	132	-122
13	4	158	-117
13	6	234	225
14	-1	212	205
14	1	316	-313
14	3	139	131
15	-1	183	-196
15	0	202	204
15	2	225	-243
15	3	154	-136
15	5	199	139
16	-1	174	158
16	0	189	174
16	1	375	-384
16	2	152	170
17	-1	234	-233
17	1	405	414
17	2	206	197
17	3	454	-456
17	4	213	-180
17	5	352	326
18	-1	341	-353
18	0	324	-336
18	1	183	183
18	2	164	158
20	-1	212	-177
20	0	139	-102
20	1	312	346
20	3	182	-109
21	-1	175	-156
21	0	265	265
22	-1	172	-158
22	0	144	-117
22	2	328	343
23	-1	178	177
23	1	208	-199
25	-1	219	228
* H= 8 *			
0	3	148	137
0	5	202	-169
1	2	427	-459
1	3	121	82
1	4	291	278
1	5	211	-187
2	2	310	334
2	4	181	-164
3	0	308	316
3	2	226	-204
3	3	192	189
3	5	369	-335
4	-1	203	217
4	0	142	129
4	1	718	-728
4	2	141	148
4	3	383	361
4	4	191	-164
4	5	285	-204
5	-1	801	847
5	1	568	-579
6	-2	198	-194
6	-1	111	-128
6	0	86	67
6	1	204	203
6	2	193	-182
6	3	213	-215
6	5	202	185
7	-1	309	309
7	0	207	-187
7	1	281	-273
7	2	221	244
7	3	139	104
8	-2	317	297
8	-1	169	-145
8	0	143	-109
8	1	257	257
8	2	156	-161
8	3	318	-319
8	4	278	310
9	-1	113	-72
9	0	361	347
9	1	156	-178
9	2	429	-434
9	3	153	124
9	4	363	380
10	-2	637	-625
10	-1	176	-174
10	0	546	541
10	2	183	-152
10	3	180	-179
10	4	187	141
11	-1	320	-329
11	1	180	154
11	2	128	104
12	-2	547	-529
12	-1	186	187
12	0	337	343
12	2	141	-143
12	3	197	188
13	-1	269	255
13	2	228	200
13	3	302	-297
14	-2	175	-147
14	1	244	242
14	2	146	-111
14	3	224	-207
15	-1	275	-292
15	0	187	-169
15	1	287	282
15	2	293	315
15	3	247	-205
16	-2	488	450
16	0	179	-177
17	-1	344	-347
17	1	208	179
17	2	221	-204
18	-2	159	-104
19	-1	247	-246
20	-1	148	151
20	0	182	-196
* H= 10 *			
0	3	368	402
1	2	151	171
2	3	176	193
3	1	96	-113
3	2	129	-117
4	1	171	181
4	2	192	178
5	-1	84	-119
5	0	117	140
5	1	118	119
5	2	289	-319
6	-1	100	123
6	0	86	71
6	2	167	-119
7	-2	153	-172
7	0	303	319
7	2	383	-393
8	-2	407	-421
8	0	261	288
9	-2	142	-131
9	-1	222	242
9	0	125	-114
9	1	250	-226
10	0	92	38
10	1	139	156
11	-2	135	-125
11	-1	110	132
11	0	181	24
12	-1	200	-215
12	0	140	-141
12	1	363	331
13	-2	285	296
13	-1	308	-304
13	0	214	-199
14	-2	187	-69
15	-2	123	111
15	-1	179	-128

not be rejected at the 0.01 level ($\mathcal{R}_{66,602,0.01} = 1.0784$). The introduction of sixty-six extra parameters thus resulted in a barely significant improvement in the agreement between observed and calculated structure factors. The results of the constrained refinement were therefore considered to provide the more appropriate model.

All refinement was carried out with the full-matrix least squares program LINUS,[21] the reflections being assigned unit weights. Atomic scattering factors due to Cromer and Mann[22] were employed for all atoms.

An $F_o - F_c$ Fourier synthesis based on the final parameters, calculated with the program JIMDAP,[21] showed a maximum electron density of 0.7 e/Å^3. The final atomic parameters are listed in Table 3 and observed and calculated structure factors in Table 4. Distances and angles within the $[V(CN)_6]^{4-}$ complex ion, calculated with the program ORFFE,[21] are given in Table 5.

Table 5. Bond distances (Å) and angles (°) within the $[V(CN)_6]^{4-}$ complex ion. Standard deviations of the distances ($\times 10^3$) and the angles are given in parentheses.

Notation: no superscript, atom in x,y,z; ′, atom in $x-\frac{1}{2},\frac{1}{2}-y,z$; ″, atom in $\frac{3}{4}+\frac{1}{2}z-x,\frac{1}{2}-y,z$.

Distances			
V–C(1)″	2.169(10)	C(1)′–N(1)′	1.134(14)
V–C(2)″	2.165(10)	C(2)′–N(2)′	1.141(22)
V–C(3)	2.153(13)	C(3)–N(3)	1.194(20)
V–C(4)	2.146(17)	C(4)–N(4)	1.177(19)
Angles			
V–C(1)″–N(1)″	175.8(0.7)	C(2)′–V–C(2)″	89.4(0.5)
V–C(2)″–N(2)″	177.3(0.9)	C(3)–V–C(1)″	92.4(0.4)
V–C(3)–N(3)	176.8(1.1)	C(3)–V–C(2)″	86.6(0.4)
V–C(4)–N(4)	179.3(1.2)	C(3)–V–C(4)	175.8(0.7)
C(1)′–V–C(1)″	90.5(0.5)	C(4)–V–C(1)″	90.5(0.6)
C(1)′–V–C(2)″	90.0(0.3)	C(4)–V–C(2)″	90.4(0.6)
C(1)′–V–C(2)′	178.9(0.4)		

No attempt was made to scale and average the intensity data used in the above calculations with the data corresponding to the smaller MDO_2 "twin". Refinement based on the latter data yielded, however, substantially the same parameters as listed in Table 3, but with somewhat larger standard deviations.

DESCRIPTION OF THE STRUCTURE AND DISCUSSION

A stereoscopic projection of a unit cell of the MDO_2 structure of $K_4[V(CN)_6]$ along [010], drawn with the program ORTEP,[21] is shown in Fig. 2. The unit cell is composed of a single

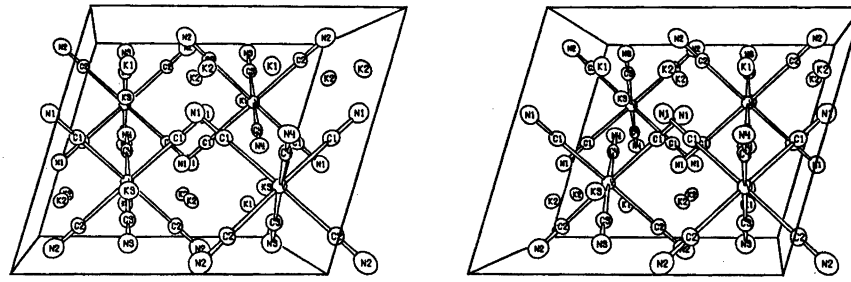

Fig. 2. Stereoscopic projection of a unit cell of the MDO_2 structure of $K_4[V(CN)_6]$ along [010]. The *a* axis is horizontal.

Table 6. A comparison of V–C and C–N bond distances in some cyanocomplexes of vanadium.

Compound	Formal Oxid. No.	Ground State Config.	Mean V–C (Å)	Mean C–N (Å)	Ref.
$K_3[V(CN)_5NO].2H_2O$	I	d^4	2.166(6)	1.142(8)	28
$K_4[V(CN)_6]$	II	d^3	2.161(4)	1.153(7)	present work
$K_4[V(CN)_7].2H_2O$	III	d^2	2.147(3)	1.145(4)	12, 13
$K_3[VO(CN)_5]$	IV	d^1	2.137(14)	1.154(21)	7

Table 7. Me–C and C–N bond lengths and infra-red stretching frequencies for some transition metal hexacyanides.

Compound	Ground State Config.	Mean Me–C (Å)	ν_5 (cm^{-1}) (Me–C stretch)	Mean C–N (Å)	ν_6 (cm^{-1}) (C–N stretch)	Ref.
$K_3[Cr(CN)_6]$	d^3	2.077(5)	339	1.136(7)	2128	11, 17, 32
$K_4[V(CN)_6]$	d^3	2.161(4)	328	1.153(7)	2080 (2065,2050)	6, 11, present work
$K_3[Mn(CN)_6]$	d^4	2.002(8)	361	1.142(12)	2112	11, 15, 32
$K_3[Fe(CN)_6]$	d^5	1.950(9)	389	1.143(14)	2118	11, 16, 32
$Na_4[Mn(CN)_6].10H_2O$	d^5	1.95(3)	386[a]	1.16(3)	2060[a]	11, 29
$K_3[Co(CN)_6]$	d^6	1.896(6)	416	1.154(9)	2129	11, 16, 32
$Na_4[Fe(CN)_6].10H_2O$	d^6	1.91(1)		1.17(1)		29
$K_4[Fe(CN)_6].3D_2O]$	d^6	1.925(1)	416[b]	1.167(1)	2044[b]	11, 30

[a] for $K_4[Mn(CN)_6].3H_2O$ [b] for $K_4[Fe(CN)_6].3H_2O$.

layer of the OD structure (*cf.* Fig. 1b). The superposition structure may be visualized by translating one-half of the unit cell in the *a* direction through $\vec{a}/2$ and superimposing it on the original arrangement.

As may be seen from Table 5, the $[V(CN)_6]^{4-}$ complex ion has almost regular octahedral symmetry, there being, however, significant deviation of a few angles from 90 or 180°. The V–C bond lengths do not differ from one another and the mean value, 2.161(4) Å, is in good agreement with V–C bond lengths found in other cyanocomplexes of vanadium (see Table 6). Nor is there any significant difference between the C–N bond lengths found in $K_4[V(CN)_6]$. The mean value, 1.153(7) Å, is also consistent with C–N distances determined for other cyanocomplexes (*cf.*, *e.g.*, Table 6). Although the V–C(2)–N(2), V–C(3)–N(3), and V–C(4)–N(4) linkages are linear, the V–C(1)–N(1) angle [175.8(0.7)°] would appear to differ from 180°. The unconstrained refinement also yielded a $[V(CN)_6]^{4-}$ ion with the same trend towards distortion, *i.e.* corresponding angles showed similar deviations from 90 or 180°.

A comparison of V–C and C–N bond lengths found in some cyanocomplexes of vanadium is given in Table 6. Although the comparison is obviously not strictly relevant, since vanadium is seven-coordinated in one of the complexes, and, although there is no significant difference between the V–C bond lengths found in the four compounds, there would, however, appear to be a slight trend towards shorter V–C distances the higher the formal oxidation state of vanadium, or the lower the number of *d* electrons in its ground-state configuration. Molecular orbital calculations [26,5] on $[V(CN)_7]^{4-}$ and $[V(CN)_5NO]^{3-}$ and X-ray photoelectron spectroscopic studies [27] on $[V(CN)_5NO]^{3-}$ indicate that the π contributions to the V–C bonds are slight in these complexes. This is in accordance with the observed trend in V–C bond lengths, which must simply just reflect the decrease in σ bond strength with decreasing formal oxidation state.

Crystal structure determinations of hexacyanoferrates [16,29,30] and hexacyanomanganates [15,29] and X-ray photoelectron spectra of the former [31] indicate, however, that π contributions to the Fe–C and Mn–C bonds increase with decreasing oxidation state. Bond lengths and infra-red stretching frequencies for some transition metal hexacyanides are given in Table 7. Molecular orbital calculations [1] for the d^6 configuration indicate that the decrease in carbon to metal σ bonding in going from Co(III) in $[Co(CN)_6]^{3-}$ to Fe(II) in $[Fe(CN)_6]^{4-}$ is largely compensated for by an increase in metal to carbon π bonding. This is supported by the similarity in Co(III)–C and Fe(II)–C bond lengths and infra-red stretching frequencies, and by the slight increase in C–N bond length and corresponding decrease in ν_6(C–N) from Co to Fe. It is apparent that there are similar trends for the d^5 (*cf.* also Ref. 2) and d^3 configurations. The somewhat larger discrepancy

between the Cr(III) – C and V(II) – C distances and stretching frequencies and the somewhat smaller drop in ν_6(C – N) from Cr to V would, however, appear to indicate that π contributions to the Me(II) – C bonds (Me = metal) are of less importance in $[V(CN)_6]^{4-}$ than in the corresponding Mn(II) and Fe(II) complexes. This is in contrast to $[Me(CN)_5NO]^{n-}$ where the π contribution to Me – N(NO) increases from iron to vanadium.[27] The observed decrease in the Me – C bond length in $[Me(CN)_6]^{4-}$ from vanadium to iron can thus be attributed to increases in both σ and π contributions.

The potassium-nitrogen contacts range from 2.908 – 3.274 Å for K(1) ($\sigma \sim 0.010$), from 2.766 – 3.119 Å for K(2) ($\sigma \sim 0.016$) and from 2.736 – 3.126 Å for K(3) ($\sigma \sim 0.016$). K(2) and K(3) are octahedrally coordinated, whereas K(1) is surrounded by a trigonal prism of nitrogen atoms. All three coordination polyhedra are severely distorted. Each potassium ion has six carbon contacts at distances only slightly longer than the K – N distances and can thus, alternatively, be regarded as being twelve-coordinated, *i.e.* octahedrally or trigonal prismatically coordinated by six cyanide ligands.

Acknowledgements. The author wishes to thank Professor N.-G. Vannerberg and Dr. R. G. Hazell for valuable discussions and Professor S. E. Rasmussen for facilities placed at her disposal. She is indebted to Fil. kand. E. Ljungström for preparation and chemical analysis of the crystals. A grant from the Swedish Natural Science Research Council (contract No. 2286 – 18) is gratefully acknowledged.

REFERENCES

1. Alexander, J. J. and Gray, H. B. *Coord. Chem. Rev. 2.* (1967) 29.
2. Alexander, J. J. and Gray, H. B. *J. Amer. Chem. Soc. 90* (1968) 4260.
3. Manoharan, P. T. and Gray, H. B. *Inorg. Chem. 5* (1966) 823.
4. Manoharan, P. T. and Gray, H. B. *J. Amer. Chem. Soc. 87* (1965) 3340.
5. Fenske, R. F. and DeKock, R. L. *Inorg. Chem. 11* (1972) 437.
6. Bennett, B. G. and Nicholls, D. *J. Chem. Soc. A* (1971) 1204.
7. Jagner, S. and Vannerberg, N.-G. *Acta Chem. Scand. 27* (1973) 3482.
8. Petersen, E. *Ber. Deut. Chem. Ges. 36* (1903) 1911.
9. Petersen, E. *Z. Anorg. Allg. Chem. 38* (1904) 342.
10. Chadwick, B. M. and Sharpe, A. G. *Advan. Inorg. Chem. Radiochem. 8* (1966) 83.
11. Griffith, W. P. and Turner, G. T. *J. Chem. Soc. A* (1970) 858.
12. Towns, R. L. R. and Levenson, R. A. *J. Amer. Chem. Soc. 94* (1972) 4345.
13. Towns, R. L. R. and Levenson, R. A. *Inorg. Chem. 13* (1974) 105.
14. Dornberger-Schiff, K. *Lehrgang über OD-Strukturen*, Akademie-Verlag, Berlin 1966.
15. Vannerberg, N.-G. *Acta Chem. Scand. 24* (1970) 2335.
16. Vannerberg, N.-G. *Acta Chem. Scand. 26* (1972) 2863.
17. Jagner, S., Ljungström, E. and Vannerberg, N.-G. *Acta Chem. Scand. A 28* (1974) 623.
18. Svedung, D. H. and Vannerberg, N.-G. *Acta Chem. Scand. 22* (1968) 1551.
19. *International Tables for X-Ray Crystallography*, Kynoch Press, Birmingham 1959.
20. Lindqvist, O. and Wengelin, F. *Ark. Kemi 28* (1967) 179.
21. Program library of Dept. of Inorg. Chem., University of Aarhus: G4 written by Hazell, R. G.; FORDAP by Zalkin, A.; LINUS by Hamilton, W. C. and Ibers, J. (modification of the Busing-Martin-Levy program ORFLS); JIMDAP by Zalkin, A.; ORFFE by Busing, W. R., Martin, K. O. and Levy, H. A. and ORTEP by Johnson, C. K.
22. Cromer, D. T. and Mann, J. B. *Acta Crystallogr. A 24* (1968) 321.
23. Hazell, R. G. and Jagner, S. *Acta Crystallogr. B 31* (1975). *In press.*
24. Hamilton, W. C. *Acta Crystallogr. 18* (1965) 502.
25. Pawley, G. S. *Acta Crystallogr. A 26* (1970) 691.
26. Levenson, R. A. *Chem. Phys. Lett. 22* (1973) 293.
27. Vannerberg, N.-G. and Jagner, S. *Chem. Scr. 6* (1974) 19.
28. Jagner, S. and Vannerberg, N.-G. *Acta Chem. Scand. 24* (1970) 1988.
29. Tullberg, A. and Vannerberg, N.-G. *Acta Chem. Scand. A 28* (1974) 551.
30. Taylor, J. C., Mueller, M. H. and Hitterman, R. L. *Acta Crystallogr. A 26* (1970) 559.
31. Vannerberg, N.-G. and Tullberg, A. *Chem. Scr. In press.*
32. Jones, L. H. *Inorg. Chem. 2* (1963) 777.

Received August 26, 1974.

Acta Chemica Scandinavica A 29 (1975) 265—272

Short Communications

Molecular Structure of Gaseous Tris(methylseleno)borane

S. LINDØY,[a] H. M. SEIP,[a] and W. SIEBERT[b]

[a]Department of Chemistry, University of Oslo, Oslo 3, Norway and [b]Fachbereich Chemie der Phillips-Universität, Marburg/Lahn, Germany

The tendency of boron to form partial double bonds with sulfur atoms seems now to be established both by experimental [1–6] and theoretical [7] methods. *Ab initio* calculations give a considerable barrier to rotation about the B–S bond in H_2BSH (about 20 kcal mol^{-1}) [7] and planar $\diagup B-S\diagdown$ arrangements have been found experimentally in a series of compounds. We have now extended these investigations to BSe compounds and report here the results of an electron-diffraction investigation of $B(SeCH_3)_3$.

The compound was synthesised by one of us (W.S.) and the electron-diffraction diagrams recorded with Balzers' eldigraph KD-G2 in Oslo.[8,9] The nozzle temperature was about 105 °C. Three sets of plates were obtained: Set 1 (4 plates, electron wavelength 0.05844 Å, nozzle-to-plate distance 578.82 mm), set 2 (5 plates, 0.05844 Å, 188.92 mm) and set 3 (4 plates, 0.05853 Å, 188.95 mm). Two average intensity curves were computed, one from the plates in set 1 covering the s-range 1.0 – 13.5 Å^{-1} and the other from the plates in set 2 and set 3 covering the s-range 3.25 – 40.0 Å^{-1}. The data were treated in the usual way [10] using the modification function $s/|f_B'||f_C|'$. The scattering amplitudes were calculated as described previously.[3]

The experimental radial distribution function (Fig. 1) calculated by Fourier inversion of a composite experimental intensity curve, showed that the heavy atom skeleton must be essentially planar and gave approximate values for the most important structural parameters. Least-squares refinements were then carried out assuming C_3 symmetry and no tilt of the methyl groups. The composite experimental intensity curve was used in some calculations, in others

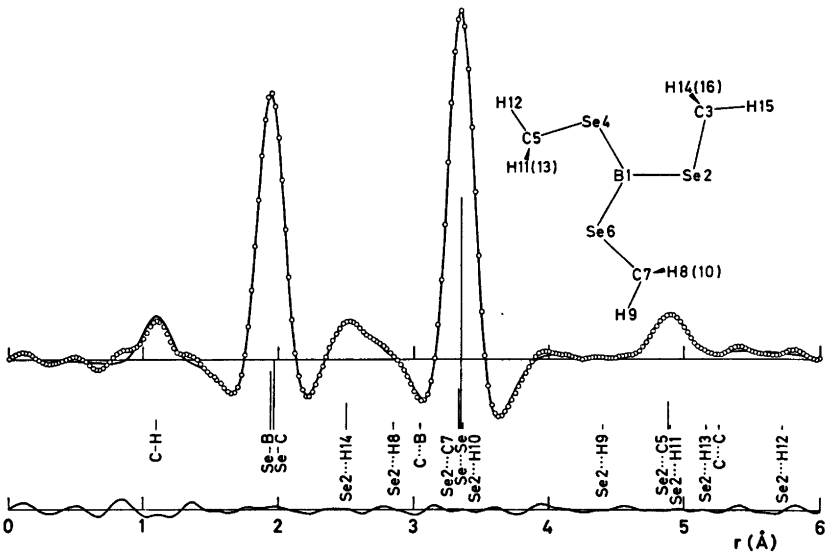

Fig. 1. Experimental (circles) and theoretical (full line) radial distribution functions for $B(SeMe)_3$ (artificial damping constant [10] $k = 0.002$ Å^2). The differences between experimental and theoretical values are also shown. The positions and approximate areas of the peaks corresponding to the most important interactomic distances are indicated.

Table 1. Bond distances, angles and mean amplitudes of vibration in tris(methylseleno)borane. The strandard deviations given in parentheses apply to the last digit given.

	r_a [16] (Å)	u (Å)	Angles (degrees)	
C–H[a]	1.102(15)	0.073(14)	∠SeCH	107.0(10)
Se–B[b]	1.936(2)	0.054 (5)	∠BSeC	102.5(5)
Se–C[b]	1.954(4)	0.051 (5)	ϕ(Se4B1Se2C3)[c]	2.0(171)
			ϕ(B1Se2C3H15)	165.0(65)

[a] All the C–H distances were assumed equal and an asymmetry constant $\varkappa = 0.00002$ Å^3 was used. [b] A shrinkage for the Se···Se distance equal to 0.003 Å was assumed;[4] if the shrinkage was neglected, 1.934 and 1.955 Å were obtained for the Se–B and Se–C distances. [c] See text for a discussion of the accuracy of this angle.

Table 2. The most important non-bonded distances and mean amplitudes of vibration.

	r_a (Å)	u (Å)	r_a (Å)	u (Å)	
Se···Se	3.350[a]	0.086(2)	Se2···H14	2.508	0.110(16)
Se2···C5	4.890	0.107(9)	Se2···H8	2.876	0.300
Se2···C7	3.336	0.178(40)	Se2···H9	4.415	0.230
C···C	5.253	0.213(50)	Se2···H10	3.330	0.300 [b]
C···B	3.034	0.170[b]	Se2···H11	4.906	0.270
			Se2···H12	5.731	0.200
			Se2···H13	5.159	0.270

[a] A shrinkage of 0.003 Å is included. [b] The value was not refined with the other parameters.

the two average intensity curves were used simultaneously without combining them. In the former case a diagonal weight matrix was assumed while in the latter a weight matrix with off-diagonal elements different from zero was used.[11] The data for $s > 33.25$ Å^{-1} were discarded in both cases.

Lack of the necessary spectroscopic information made it impossible to compute reliable mean amplitudes of vibration (u) and shrinkage effects from the force field. However, it seems likely that the values should be similar to those obtained for $B(SCH_3)_3$.[4] The results in Tables 1 and 2 are based on the values obtained in several least-squares refinements. Various weighting schemes were used, and various assumptions about the u-values which are difficult to refine, were tried. The results for the most important parameters, Se–B and Se–C bond lengths and ∠BSeC, were essentially the same in all the refinements. The standard deviations given include the effect of correlation between the intensity data as well as a 0.1 % uncertainty in the s-scale. The torsional angle, ϕ(Se4B1Se2C3), refines to a value close to zero, and the corresponding standard deviation becomes then unrealistically large. According to Hamilton's R-factor test [12] the torsional angle is less than 14° at the 99 % significance level. The planarity of the heavy atom skeleton is consistent with a non-negligible π-bond order in the B–Se bonds.

Pauling gives 0.81 Å for the covalent radius of boron.[13] If the modified Schomaker-Stevenson rule,[13]

$$D(X-B) = r_X + r_B - 0.08|x_X - x_B| \quad (1)$$

is used, the pure single B–S and B–Se bond lengths are estimated to 1.81 and 1.95 Å, respectively. As opposed to other evidence, the comparison of these values with the observed bond lengths for B–S (1.78–1.81 Å) and B–Se (1.94 Å), seems to indicate no significant double bond character. However, the estimates of the pure single bond lengths are rather uncertain. If the observed B–C bond length in $B(CH_3)_3$ (1.58 Å [14]) is used, eqn. (1) gives $r_B = 0.85$ Å. This value is in agreement with the B–B bond length in B_2Cl_4 [1.702 (0.035) Å [15]]. The estimates of the pure single bonds

become then $D(B-S) = 1.85$ Å and $D(B-Se) = 1.99$ Å, *i.e.* about 0.05 Å longer than the observed values in $B(SCH_3)_3$ and $B(SeCH_3)_3$ respectively. We conclude therefore that the π-bond order is non-negligible in $\diagdown B-Se \diagup$ as well as in $\diagdown B-S \diagup$ bonds.

Acknowledgement. The authors are grateful to K. Brendhaugen for recording the diffraction diagrams.

1. Seip, H. M., Seip, R. and Siebert, W. *Acta Chem. Scand. 27* (1973) 15.
2. Almenningen, A., Seip, H. M. and Vassbotn, P. *Acta Chem. Scand. 27* (1973) 21.
3. Brendhaugen, K., Nilssen, E. W. and Seip, H. M. *Acta Chem. Scand. 27* (1973) 2965.
4. Johansen, R., Nilssen, E. W., Seip, H. M. and Siebert, W. *Acta Chem. Scand. 27* (1973) 3015.
5. Kroner, J., Nölle, D. and Nöth, H. *Z. Naturforsh. B 28* (1973) 416.
6. Bock, H. and Ramsay, B. G. *Angew. Chem. 85* (1973) 773.
7. Gropen, O., Nilssen, E. W. and Seip, H. M. *J. Mol. Struct. 23* (1974) 289.
8. Zeil, W., Haase, J. and Wegmann, L. *Z. Instrumentenk. 74* (1966) 84.
9. Bastiansen, O., Graber, R. and Wegmann, L. *Balzers' High Vacuum Report 25* (1961) 1.
10. Andersen, B., Seip, H. M., Strand, G. T. and Stølevik, R. *Acta Chem. Scand. 23* (1969) 3224.
11. Seip, H. M., Strand, T. G. and Stølevik, R. *Chem. Phys. Lett. 3* (1969) 617.
12. Hamilton, W. C. *Acta Crystallogr. 18* (1965) 502.
13. Pauling, L. *The Nature of the Chemical Bond*, 3rd Ed., Cornell, Univ. Press, New York 1960.
14. Bartell, L. S. and Carroll, B. L. *J. Chem. Phys. 42* (1965) 3076.
15. Ryan, R. R. and Hedberg, K. *J. Chem. Phys. 50* (1969) 4986.
16. Kuchitsu, K. and Cyvin, S. J. In Cyvin, S. J., Ed., *Molecular Structures and Vibrations*, Elsevier, Amsterdam 1972, Chapter 12.

Received January 6, 1975.

Density and Surface Tension of Molten Manganese—Cesium Chloride Mixtures

LAILA EL-SAYED* and HARALD A. ØYE

Institutt for uorganisk kjemi, Norges tekniske høgskole, Universitetet i Trondheim, N-7034 Trondheim-NTH, Norway

Density and surface tension of molten $MnCl_2-CsCl$ were investigated to supplement absorption [1] and Raman spectroscopic [2] studies. The density and surface tension were determined from liquidostatic weighing and the pin detachment force, respectively. The principle and experimental details have been previously described.[3–5]

Anhydrous salts were obtained from $MnCl_2 \cdot xH_2O$ (*p.a.* Merck, Darmstadt, Germany) and

* Post doctoral fellow. Permanent Address: Chemistry Department, Faculty of Science, Alexandria University, Moharem Bay, Alexandria, Egypt.

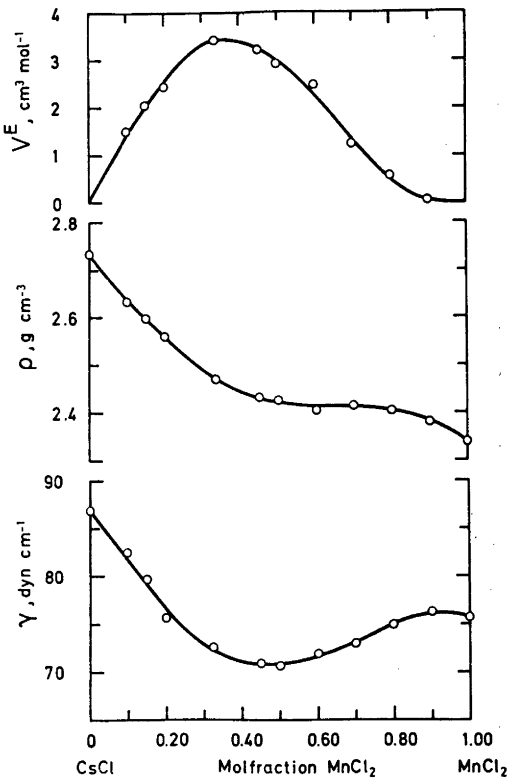

Fig. 1. Surface tension, γ; density, ϱ; and molar excess volume, V^E, for molten mixtures of CsCl and $MnCl_2$ at 700 °C.

become then $D(B-S) = 1.85$ Å and $D(B-Se) = 1.99$ Å, *i.e.* about 0.05 Å longer than the observed values in $B(SCH_3)_3$ and $B(SeCH_3)_3$ respectively. We conclude therefore that the π-bond order is non-negligible in $\diagdown B-Se \diagup$ as well as in $\diagdown B-S \diagup$ bonds.

Acknowledgement. The authors are grateful to K. Brendhaugen for recording the diffraction diagrams.

1. Seip, H. M., Seip, R. and Siebert, W. *Acta Chem. Scand. 27* (1973) 15.
2. Almenningen, A., Seip, H. M. and Vassbotn, P. *Acta Chem. Scand. 27* (1973) 21.
3. Brendhaugen, K., Nilssen, E. W. and Seip, H. M. *Acta Chem. Scand. 27* (1973) 2965.
4. Johansen, R., Nilssen, E. W., Seip, H. M. and Siebert, W. *Acta Chem. Scand. 27* (1973) 3015.
5. Kroner, J., Nölle, D. and Nöth, H. *Z. Naturforsh. B 28* (1973) 416.
6. Bock, H. and Ramsay, B. G. *Angew. Chem. 85* (1973) 773.
7. Gropen, O., Nilssen, E. W. and Seip, H. M. *J. Mol. Struct. 23* (1974) 289.
8. Zeil, W., Haase, J. and Wegmann, L. *Z. Instrumentenk. 74* (1966) 84.
9. Bastiansen, O., Graber, R. and Wegmann, L. *Balzers' High Vacuum Report 25* (1961) 1.
10. Andersen, B., Seip, H. M., Strand, G. T. and Stølevik, R. *Acta Chem. Scand. 23* (1969) 3224.
11. Seip, H. M., Strand, T. G. and Stølevik, R. *Chem. Phys. Lett. 3* (1969) 617.
12. Hamilton, W. C. *Acta Crystallogr. 18* (1965) 502.
13. Pauling, L. *The Nature of the Chemical Bond*, 3rd Ed., Cornell, Univ. Press, New York 1960.
14. Bartell, L. S. and Carroll, B. L. *J. Chem. Phys. 42* (1965) 3076.
15. Ryan, R. R. and Hedberg, K. *J. Chem. Phys. 50* (1969) 4986.
16. Kuchitsu, K. and Cyvin, S. J. In Cyvin, S. J., Ed., *Molecular Structures and Vibrations*, Elsevier, Amsterdam 1972, Chapter 12.

Received January 6, 1975.

Density and Surface Tension of Molten Manganese—Cesium Chloride Mixtures

LAILA EL-SAYED* and HARALD A. ØYE

Institutt for uorganisk kjemi, Norges tekniske høgskole, Universitetet i Trondheim, N-7034 Trondheim-NTH, Norway

Density and surface tension of molten $MnCl_2-CsCl$ were investigated to supplement absorption [1] and Raman spectroscopic [2] studies. The density and surface tension were determined from liquidostatic weighing and the pin detachment force, respectively. The principle and experimental details have been previously described.[3–5]

Anhydrous salts were obtained from $MnCl_2 \cdot xH_2O$ (*p.a.* Merck, Darmstadt, Germany) and

* Post doctoral fellow. Permanent Address: Chemistry Department, Faculty of Science, Alexandria University, Moharem Bay, Alexandria, Egypt.

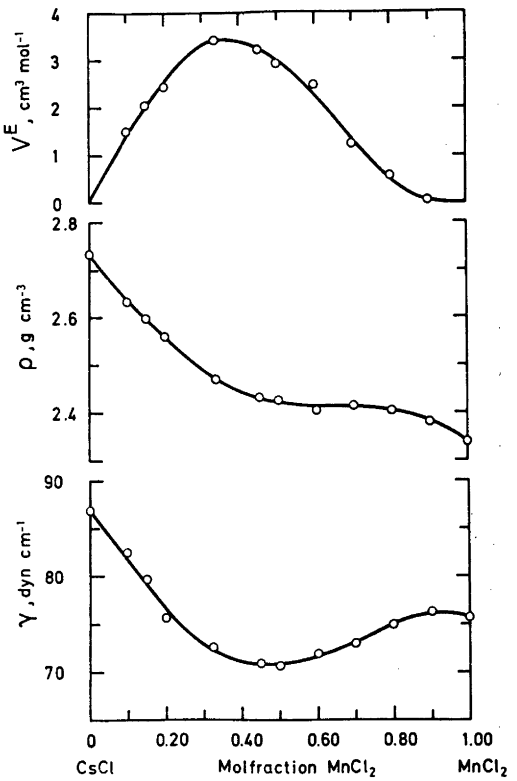

Fig. 1. Surface tension, γ; density, ϱ; and molar excess volume, V^E, for molten mixtures of CsCl and $MnCl_2$ at 700 °C.

Table 1. Density, ϱ, surface tension, γ, and excess molar volumes, V^E, for molten $CsCl-MnCl_2$ mixtures at 700 °C.

Mol fraction $MnCl_2$	ϱ g cm^{-3}	$\alpha \times 10^{-4}$ g cm^{-3} K^{-1}	γ dyn cm^{-1}	$-\alpha \times 10^2$ dyn cm^{-1}K^{-1}	V^E cm^3 mol^{-1}
0	2.735	10.7	86.9	8.4	0
0.10	2.635	10.0	82.5	5.9	1.497
0.15	2.534	10.0	73.7	6.8	2.047
0.20	2.560	9.3	75.6	6.3	2.429
0.33	2.470	7.7	72.6	6.0	3.434
0.45	2.435	8.4	70.9	6.4	3.202
0.50	2.426	8.4	70.6	5.3	2.935
0.60	2.404	7.2	71.8	5.6	2.482
0.70	2.414	8.3	72.9	5.9	1.248
0.80	2.401	7.5	74.9	5.3	0.566
0.90	2.380	6.4	76.3	3.5	0.047
1.00	2.337	4.8	75.6	0.6	0

CsCl (Analar, Hopkin and Williams, England) by standard procedures.[3]

The experiments were performed in the temperature range 660 – 740 °C, and least-squares programs were used for determination of the temperature coefficient. The average standard deviation for the fitting was 0.15 % for the surface tension and 0.03 % for the density, except for the 60 mol % $MnCl_2$ mixture, where the standard deviation of the density was 0.13 %.

Table 1 gives the surfaces tension, density and calculated excess molar volume at 700 °C and the determined temperature coefficients. Fig. 1 shows the concentration variation at 700 °C graphically. The density and surface tension data for the pure salts are in good agreement with those reported in the literature (ϱ for $CsCl = 2.734$,[3] from this work $\varrho = 2.735$. γ for $CsCl = 87.4$,[4] from this work $\gamma = 86.9$. ϱ for $MnCl_2 = 2.332$,[6] from this work $\varrho = 2.337$).

Excess molar volume as well as excess surface tension, defined as deviation from additivity, exhibit maxima near 33 mol % $MnCl_2$ (Cs_2MnCl_4), similar to observations made in the corresponding $CsCl-MgCl_2$ system.[3,4] This supports the existence of the spectroscopically detected $MnCl_4^{2-}$.[1,2]

The properties of pure $MnCl_2$ also show similarities to those of pure $MgCl_2$. The temperature coefficient of the surface tension for $MnCl_2$ is abnormally low compared with the mixtures with CsCl, and close to that of pure $MgCl_2$: 0.6×10^{-2} *versus* 0.4×10^{-2} dyn cm^{-1} K^{-1} for $MgCl_2$. The thermal expansion coefficient is also considerably lower than for CsCl, although not as low as for $MgCl_2$: 4.8×10^{-4} *versus* 2.9×10^{-4} g cm^{-3} K^{-1} for pure $MgCl_2$.

Consequently, the shape of the density and surface tension curves *versus* concentration shows great similarities to those of $RbCl-MgCl_2$ and $CsCl-MgCl_2$.[3,4] The curves (Fig. 1) are S-shaped, being convex upwards on the $MnCl_2$ side and concave on the CsCl side.

Apart from the existence of $MnCl_4^{2-}$ configurations in these melts, one cannot draw any other definite conclusion concerning the structure. The postulated octahedral coordination of Mn^{2+} in $MnCl_2$-rich mixtures is,[1] however, not contradicted by this study, as a change from octahedral to tetrahedral coordination is expected to be accompanied by volume expansion, in agreement with the positive excess molar volume having a maximum close to 33 mol % $MnCl_2$.

Acknowledgement. A grant to one of us (L.E.-S.) from the Norwegian Agency of International Development, and general support from The Norwegian Research Council for Science and the Humanities are gratefully acknowledged. We also thank Dr. T. Naterstad for advice on experimental procedure.

1. El-Sayed, L. and Øye, H. A. *To be published.*
2. Øye, H. A. and Bues, W. *To be published.*
3. Grjotheim, K., Holm, J. L., Lillebuen, B. and Øye, H. A. *Trans. Faraday Soc. 67* (1971) 640.
4. Grjotheim, K., Holm, J. L., Lillebuen, B. and Øye, H. A. *Acta Chem. Scand. 26* (1972) 2050.
5. Lillebuen, B. *Acta Chem. Scand. 24* (1970) 3287.
6. Janz, G. J., Dampier, F. W., Lakshminarayanan, G. R., Lorenz, P. K. and Tomkins, R. P. T. *Molten Salts*, Vol. I, Electrical Conductance, Density and Viscosity Data, NSRDS-NBS 15, Washington 1968.

Received January 2, 1975.

Tricenter Iron(II) dicobalt(III) Complexes with Two Cyanide Bridges

SVEN BAGGER and ÁGNES NÉMETH*

Chemistry Department A, The Technical University of Denmark, Building 207, DK-2800 Lyngby, Denmark

Owing to the ambidentate nature of cyanide it is in some cases possible to link metallic coordination centers together through cyano bridges. This represents a way of utilizing known metal complexes as units for building compounds with new properties.

Recently it was reported that strongly coloured species of notable stability containing the Co(III) – NC – Fe(II) – CN – Co(III) chain are formed in reactions between isomers of bis(histidinato)cobalt(III) and hexacyanoiron(II).[1] The aim of this work was to examine whether bis(histidinato)cobalt(III) generally combines with low-spin iron(II) complexes having two or more cyano ligands to give tricenter μ-cyano species.

Experimental. $Na_2[Fe(CN)_5(NO)].2H_2O$ was obtained from B.D.H. ("Analar" purity). The compounds $[Fe(CN)_2(bpy)_2].3H_2O$, $K_2[Fe(CN)_4(bpy)].3H_2O$, $Na_3[Fe(CN)_5(py)].1\frac{1}{2}H_2O$, $Na_3[Fe(CN)_2(NH_3)].3H_2O$, $Na_3[Fe(CN)_5(H_2O)].H_2O$, and $Na_4[Fe(CN)_5(NO_2)].10H_2O$ were prepared according to procedures given in Refs. 2, 3, 4, 5, 6, and 7, respectively. *trans*-Imidazole-[Co(L-his)$_2$]$ClO_4.1\frac{1}{2}H_2O$ and racemic all-*cis*-[Co(L-his)(D-his)]Br were prepared as previously.[1] (py = pyridine, bpy = 2,2′-bipyridine, his = histidinate).

All the spectrophotometric measurements were carried out under O_2-free conditions at 20.0 °C.

Results. Information obtained from the visible absorption spectra before and after mixing aqueous solutions of bis(histidinato)cobalt(III) isomers and cyanoiron(II) complexes is summarized in Table 1. In the four combinations of reactants with a plus sign in Table 1 a broad charge-transfer absorption band developed in the spectra of the mixtures, and a constant spectrum was reached after some hours. For illustration of the phenomenon the spectra from one of the experiments are shown in Fig. 1.

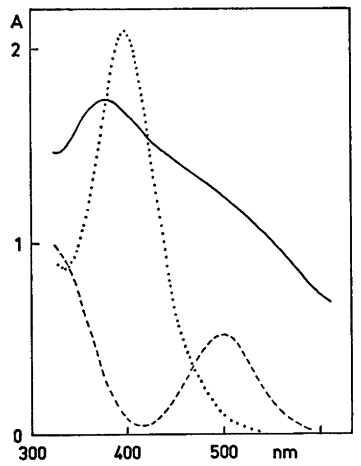

Fig. 1. Absorption spectra in aqueous solution (1 cm cells). – – –, 5.0 mM *trans*-imidazole-$[Co(his)_2]^+$; · · ·, 5.0 mM $[Fe(CN)_5(NH_3)]^{3-}$; and ———, the 1:1 mixture of these two solutions after 3 h.

In order to elucidate the stoichiometry of the four established reactions, Job's method of continuous variations was applied in the same way as previously.[1]

Job plots at three wavelengths for one of the reactions are shown in Fig. 2. All four reactions

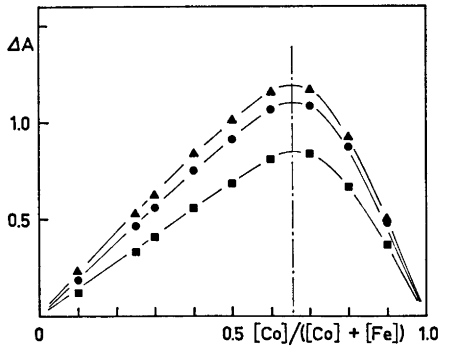

Fig. 2. Job plots for the *trans*-imidazole-$[Co(his)_2]^+$/$[Fe(CN)_5(NH_3)]^{3-}$ system with experimental points indicated. ▲, at 468 nm; ●, at 500 nm; ■, at 600 nm. The concentration of the two solutions used was 5.0 mM.

* On leave from Institute for Applied Chemistry, Technical University, Budapest, Hungary.

Table 1. Results from mixing experiments.

	$[Co(his)_2]^+$-isomer [a]	
	trans-imidazole	all-*cis*
$[Fe(CN)_5(NO)]^{2-}$	–	–
$[Fe(CN)_2(bpy)_2]$	–	–
$[Fe(CN)_4(bpy)]^{2-}$	–	–
$[Fe(CN)_5(py)]^{3-}$	+	+
$[Fe(CN)_5(NH_3)]^{3-}$	+	+

[a] A plus sign means that an additional broad band appeared in the spectrum of the mixed solution. A minus sign means that no evidence of interaction was found.

were found to show the same pattern with a maximum in the Job plot at a Co:Fe ratio of about 2:1.

Each of the complexes in Table 1 were found to follow Beer's law at concentrations used in the Job experiments. $[Fe(CN)_5(H_2O)]^{3+}$ and $[Fe(CN)_5(NO_2)]^{4-}$ also react with the two $[Co(his)_2]^+$ isomers to give brown species, but the behaviour of these two iron(II) complexes is more complicated since their solutions do not comply with Beer's law.

Conclusions. The experimental results suggest that two of the cyanoiron(II) complexes, $[Fe(CN)_5(py)]^{3-}$ and $[Fe(CN)_5(NH_3)]^{3-}$, form tricenter μ-cyano-iron(II)dicobalt(III) species with each of the two $[Co(his)_2]^+$ isomers. This is in analogy with the mode of reaction found for $[Fe(CN)_6]^{4-}$, which has been studied in more detail.[1]

Of the factors controlling the formation of a stable Co–NC–Fe–CN–Co chain the redox properties of the iron center and the charge of the iron(II) complex are likely to be important.

The standard redox potentials for the Fe(II)/Fe(III) couples [2–10] presumably decrease in the order

$[Fe(CN)_5(NO)]^{2-} > [Fe(CN)_2(bpy)_2] >$

$[Fe(CN)_4(bpy)]^{2-} > [Fe(CN)_5(py)]^{3-} >$

$[Fe(CN)_6]^{4-} > [Fe(CN)_5(NH_3)]^{3-}$

Our experiments have shown that only the three more reducing of these iron(II) complexes form μ-cyano species. The same three complexes are also the more favoured with regard to coulombic interaction with the positively charged cobalt(III) complexes.

The electrochemistry of the new tricenter compounds appears to be interesting. The Co(III)–NC–Fe(II)–CN–Co(III) moiety may undergo a one-electron oxidation as well as a two-electron reduction.

1. Bagger, S. and Gibson, K. *Acta Chem. Scand. 27* (1973) 3227.
2. Schilt, A. A. *Inorg. Syn. 12* (1970) 249.
3. Schilt, A. A. *J. Amer. Chem. Soc. 82* (1960) 3000.
4. Manchot, W. and Woringer, P. *Ber. Deut. Chem. Ges. 46* (1913) 3514.
5. Keeny, D. J., Flynn, T. P. and Gallini, J. B. *J. Inorg. Nucl. Chem. 20* (1961) 75.
6. Hofmann, K. A. *Justus Liebigs Ann. Chem. 312* (1900) 14.
7. Hofmann, K. A. *Z. Anorg. Allgem. Chem. 11* (1896) 279.
8. Latimer, W. M. *Oxidation Potentials*, 2nd Ed., Prentice-Hall, Englewood Cliffs 1952.
9. Schilt, A. A. *Anal. Chim. Acta 26* (1962) 134.
10. Toma, H. E. and Malin, J. M. *Inorg. Chem. 12* (1973) 1039.

Received January 6, 1975.

The Base Hydrolysis of Bis(2,2′-bipyridyl)platinum(II) Perchlorate

GWYNETH NORD

Chemistry Department I, Inorganic Chemistry, H. C. Ørsted Institute, University of Copenhagen, Universitetsparken 5, DK-2100 Copenhagen Ø, Denmark

The cation $[Pt(bipy)_2^{2+}]$ of the title compound reacts with aqueous acid and base as follows:

$$Pt(bipy)_2^{2+} + OH^- \xrightarrow{K_B} Pt(bipy)_2(OH)^+ \quad (1)$$

$$Pt(bipy)_2^{2+} \underset{(H_2O)}{\overset{k_A}{\rightleftharpoons}} Pt(bipy)(OH)(H_2O)^+ + bipyH^+ \quad (2)$$

$$Pt(bipy)_2(OH)^+ + H_2O \xrightarrow{k_B} Pt(bipy)(OH)(H_2O)^+ + bipy \quad (3)$$

These reactions are followed by fast proton equilibration of the products of the slow steps 2 and 3 and by the very slow dissociation of the second (bipy) ligand.

Equilibrium 1 is fast as is evidenced by the pH dependence of the compositions of the solutions, resulting in the changes of ultraviolet absorption which were reported by Gillard *et al.*[1–3] These authors envisage attachment of OH to a carbon atom of the ligand with no increase in the coordination number of the metal ion. Although we have, ourselves, shown [4,5] that the *oxidation* of OH^- by $Fe(bipy)_3^{3+}$ and related oxidising complexes occurs through "a highly reactive precursor complex $[Fe(bipy)_2R^{\cdot}\text{-}OH]^{2+}$ where $R^{\cdot}$-OH is probably the pseudo-base of a radical formed by addition of an electron to a ligand which approaches the structure of a quaternary cation" we consider it likely that $Pt(bipy)_2^{2+}$ in solution contains coordinated water. Such water would be acid and equilibrium 1 thus involve addition of OH^- to the metal ion. The fact that neither $Pt(py)_4^{2+}$ (py = pyridine) nor [6] $Pt(bipy)(py)_2^{2+}$ show pH dependent spectral behaviour similar to that of $Pt(bipy)_2^{2+}$ suggests to us that distorted square planar coordination is necessary for equilibria such as (1) and that this is a consequance of the *steric*, not of the chemical properties of the coordinated ligands. Two molecules of bipy, or of 1,10-phenanthroline, cannot form unstrained square planar complexes because of steric interaction between the H atoms at the 6,6′ and 2,9 positions, respectively. This strain may be relieved by distortion – as may easily be seen from models.

were found to show the same pattern with a maximum in the Job plot at a Co:Fe ratio of about 2:1.

Each of the complexes in Table 1 were found to follow Beer's law at concentrations used in the Job experiments. $[Fe(CN)_5(H_2O)]^{3+}$ and $[Fe(CN)_5(NO_2)]^{4-}$ also react with the two $[Co(his)_2]^+$ isomers to give brown species, but the behaviour of these two iron(II) complexes is more complicated since their solutions do not comply with Beer's law.

Conclusions. The experimental results suggest that two of the cyanoiron(II) complexes, $[Fe(CN)_5(py)]^{3-}$ and $[Fe(CN)_5(NH_3)]^{3-}$, form tricenter μ-cyano-iron(II)dicobalt(III) species with each of the two $[Co(his)_2]^+$ isomers. This is in analogy with the mode of reaction found for $[Fe(CN)_6]^{4-}$, which has been studied in more detail.[1]

Of the factors controlling the formation of a stable Co–NC–Fe–CN–Co chain the redox properties of the iron center and the charge of the iron(II) complex are likely to be important.

The standard redox potentials for the Fe(II)/Fe(III) couples [2–10] presumably decrease in the order

$[Fe(CN)_5(NO)]^{2-} > [Fe(CN)_2(bpy)_2] >$

$[Fe(CN)_4(bpy)]^{2-} > [Fe(CN)_5(py)]^{3-} >$

$[Fe(CN)_6]^{4-} > [Fe(CN)_5(NH_3)]^{3-}$

Our experiments have shown that only the three more reducing of these iron(II) complexes form μ-cyano species. The same three complexes are also the more favoured with regard to coulombic interaction with the positively charged cobalt(III) complexes.

The electrochemistry of the new tricenter compounds appears to be interesting. The Co(III)–NC–Fe(II)–CN–Co(III) moiety may undergo a one-electron oxidation as well as a two-electron reduction.

1. Bagger, S. and Gibson, K. *Acta Chem. Scand. 27* (1973) 3227.
2. Schilt, A. A. *Inorg. Syn. 12* (1970) 249.
3. Schilt, A. A. *J. Amer. Chem. Soc. 82* (1960) 3000.
4. Manchot, W. and Woringer, P. *Ber. Deut. Chem. Ges. 46* (1913) 3514.
5. Keeny, D. J., Flynn, T. P. and Gallini, J. B. *J. Inorg. Nucl. Chem. 20* (1961) 75.
6. Hofmann, K. A. *Justus Liebigs Ann. Chem. 312* (1900) 14.
7. Hofmann, K. A. *Z. Anorg. Allgem. Chem. 11* (1896) 279.
8. Latimer, W. M. *Oxidation Potentials*, 2nd Ed., Prentice-Hall, Englewood Cliffs 1952.
9. Schilt, A. A. *Anal. Chim. Acta 26* (1962) 134.
10. Toma, H. E. and Malin, J. M. *Inorg. Chem. 12* (1973) 1039.

Received January 6, 1975.

The Base Hydrolysis of Bis(2,2′-bipyridyl)platinum(II) Perchlorate

GWYNETH NORD

Chemistry Department I, Inorganic Chemistry, H. C. Ørsted Institute, University of Copenhagen, Universitetsparken 5, DK-2100 Copenhagen Ø, Denmark

The cation $[Pt(bipy)_2^{2+}]$ of the title compound reacts with aqueous acid and base as follows:

$$Pt(bipy)_2^{2+} + OH^- \xrightarrow{K_B} Pt(bipy)_2(OH)^+ \quad (1)$$

$$Pt(bipy)_2^{2+} \underset{(H_2O)}{\overset{k_A}{\rightleftharpoons}} Pt(bipy)(OH)(H_2O)^+ + bipyH^+ \quad (2)$$

$$Pt(bipy)_2(OH)^+ + H_2O \xrightarrow{k_B} Pt(bipy)(OH)(H_2O)^+ + bipy \quad (3)$$

These reactions are followed by fast proton equilibration of the products of the slow steps 2 and 3 and by the very slow dissociation of the second (bipy) ligand.

Equilibrium 1 is fast as is evidenced by the pH dependence of the compositions of the solutions, resulting in the changes of ultraviolet absorption which were reported by Gillard *et al.*[1–3] These authors envisage attachment of OH to a carbon atom of the ligand with no increase in the coordination number of the metal ion. Although we have, ourselves, shown [4,5] that the *oxidation* of OH^- by $Fe(bipy)_3^{3+}$ and related oxidising complexes occurs through "a highly reactive precursor complex $[Fe(bipy)_2R^{\cdot}\text{-}OH]^{2+}$ where $R^{\cdot}$-OH is probably the pseudo-base of a radical formed by addition of an electron to a ligand which approaches the structure of a quaternary cation" we consider it likely that $Pt(bipy)_2^{2+}$ in solution contains coordinated water. Such water would be acid and equilibrium 1 thus involve addition of OH^- to the metal ion. The fact that neither $Pt(py)_4^{2+}$ (py = pyridine) nor [6] $Pt(bipy)(py)_2^{2+}$ show pH dependent spectral behaviour similar to that of $Pt(bipy)_2^{2+}$ suggests to us that distorted square planar coordination is necessary for equilibria such as (1) and that this is a consequance of the *steric*, not of the chemical properties of the coordinated ligands. Two molecules of bipy, or of 1,10-phenanthroline, cannot form unstrained square planar complexes because of steric interaction between the H atoms at the 6,6′ and 2,9 positions, respectively. This strain may be relieved by distortion – as may easily be seen from models.

Thus, for bipy it is possible to retain the 4 N atoms of the ligands in a plane and distort the two rings about 30 degrees towards the *trans* configuration of the ligands, while for the more rigid 1,10-phenanthroline the steric interaction cannot be relieved in a structure with square plane coordination. Steric hindrance is also eliminated in *cis*-bis octahedral complexes (see Ref. 7 for discussion). Analogously, addition of a fifth (mono-dentate) ligand could also form a sterically unhindered five-coordinate Pt(II) complex similar to that well documented as the trigonal bipyramidal intermediate in substitutions at d^8 electron configuration metal ions. $Pt(bipy)_2(OH)^+$ formed according to equilibrium 1 would in this case be expected to be an intermediate in the base hydrolysis reaction and, by combining the value for $pK_B = 4.76$ (see experimental) with the kinetic data given in the table, we find that this is so. Changes in pK_B with temperature are, within the experimental error, equal to those due to the fast protonic equilibrium of the buffer. The loss of a proton from water loosely bound to the Pt in $Pt(bipy)_2^{2+}$ would also explain the specificity of equilibrium 1 to OH^-. The data in the table for k_B, using reaction rate theory, give $\Delta H^{\ddagger} = 22.1$ kcal/mol; $\Delta S^{\ddagger} = -13.5$ cal/(mol K).

We consider that the new experimental data reported here clearly demonstrate that the unified mechanism given in Ref. 2, which purports to explain unusual properties of all diimine complexes in basic solution in the terms of ligand reactions only, cannot be accepted.

Experimental. Solutions of $Pt(bipy)_2(ClO_4)_2$ (6×10^{-6} M to 5×10^{-5} M) were found to obey Beers Law (220 to 350 nm) in each of a series of buffers (pH 2 to 12) and also in 0.01 NaOH and in 0.01 M HCl. From data at 16 wavelengths and at an ionic strength of 0.1 M, pK_B for equilibrium 1 is 4.76 ± 0.01 at 25 °C.

The rate of appearance of free bipy according to reactions 2 and 3 was followed spectrophotometrically after extraction into chloroform. First order plots were obtained and the rate constants calculated from these agreed with those from the time dependence of the changes in the spectra of the reaction mixtures as illustrated in Fig. 1.

$Pt(py)_4Cl_2.3H_2O$ was a sample from the collection of S. M. Jørgensen. The other complexes were prepared by published methods. Extinction coefficients all agreed with the literature values.

Acknowledgements. Thanks are due to Karen Jørgensen for experimental assistance.

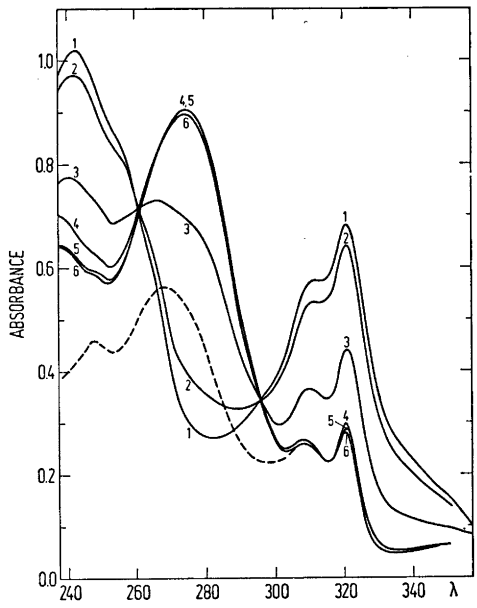

Fig. 1. Hydrolysis of 3.35×10^{-5} M $Pt(bipy)_2(ClO_4)_2$ in 0.01 M borax. Ionic strength 0.10 M, 60 °C. (Spectra measured at room temperature). ——— Absorption spectra of reaction solutions.

No.	1	2	3	4	5	6
Time (h)	0	4	23	95	119	265

- - - Absorption spectrum of aqueous phase of 5 after chloroform extraction. This is also the spectrum of 3.35×10^{-5} M $Pt(bipy)(OH)_2$ in the medium and this coincides with 5 above 305 nm. 5 minus - - - is the absorption spectrum of 3.35×10^{-5} dipy in the medium.

Table 1. Rate constants for hydrolysis of $Pt(bipy)_2^{2+}$ (k_A) and $Pt(bipy)_2(OH)^+$ (k_B). Ionic strength 0.10 M with NaCl.

Temp. °C	Medium 0.01 M	Constant [a] s^{-1}
25	NaOH	$10^7\ k_B = 4.0 \pm 0.1$
25	borax	$10^7\ k = 1.8 \pm 0.1$
25	borax	$10^7\ k$ calc.[b] $= 1.86$
45	NaOH	$10^6\ k_B = 4.50 \pm 0.08$
45	borax	$10^6\ k = 1.90 \pm 0.04$
60	NaOH	$10^5\ k_B = 2.3 \pm 0.3$
60	borax	$10^5\ k = 1.10 \pm 0.03$
60	HCl	$10^5\ k_A$[c] $= 0.058 \pm 0.002$

[a] $k = \alpha k_A + (1-\alpha) k_B$; $(1-\alpha)/\alpha = K_B[OH^-]$

[b] k calc. $= (1-\alpha) k_B$ using $pK_B = 4.76$ together with $\log [OH^-] = -4.82$ in medium.

[c] First half-life only.

1. Gillard, R. D. and Lyons, J. R. *Chem. Commun.* (1973) 585.

2. Gillard, R. D. *Inorg. Chim. Acta 11* (1974) L 21 received 1 August 1974.
3. Bielli, E., Gidney, P. M., Gillard, R. D. and Heaton, B. T. *J. Chem. Soc. Dalton Trans.* (1974) 2133.
4. Nord, G. and Wernberg, O. *J. Chem. Soc. Dalton Trans.* (1972) 866.
5. Nord, G. and Wernberg, O. *J. Chem. Soc. Dalton Trans. In press*, received 3 June 1974.
6. Lyons, J. R. *Private communication to M. P. Hancock and G. Nord.*
7. Andersen, P., Josephsen, J., Nord, G., Schäffer, C. E. and Tranter, R. L. *Chem. Commun.* (1969) 408.

Received December 20, 1974.

Acta Chemica Scandinavica A 29 (1975) 273—276

The Molecular Structure of Dimethylaminodichloroalane Dimer Determined by Gas Phase Electron Diffraction

THEODORE C. BARTKE, ARNE HAALAND and DAVID P. NOVAK

Department of Chemistry, University of Oslo, Blindern, Oslo 3, Norway

The molecular structure of $[Cl_2AlN(CH_3)_2]_2$ has been determined by gas phase electron diffraction. The scattering pattern is consistent with a model of D_{2h} symmetry with bridging $N(CH_3)_2$ groups. The main molecular parameters are Al−Cl = 2.106(4) Å, Al−N = 1.961(6) Å, N−C = 1.479(4) Å, ∠Cl−Al−Cl = 118.2(1.5)°, ∠Al−N−Al = 92.5(0.4)°.

Cl_2AlNMe_2 (Me = CH_3) is dimeric in boiling benzene [1] (by molecular weight) and in the gas phase [2] (by mass spectroscopy). Infrared absorption spectra show that association occurs through the NMe_2 group rather than through the Cl atoms.[2] As part of our study of associated aluminium compounds we have determined the molecular structure of the dimer for comparison with the molecular structures of the $AlCl_3$ dimer and dimeric Me_2AlNMe_2. The structure of the first of these compounds has been determined by gas phase electron diffraction by Hedberg and coworkers,[3] the structure of the second has been determined by X-ray crystallography by Hess and coworkers [4] and by Smith and coworkers.[5]

The Al−N bond distance in the addition complex Cl_3AlNMe_3[6,7] is about 0.14 Å shorter than in the complex Me_3AlNMe_3 [8] and the bridging Al−Cl bond in dimeric $AlCl_3$ is about 0.05 Å shorter than in $[Me_2AlCl]_2$.[9] Both shortenings are reasonably ascribed to the inductive effect of the terminal Cl atoms. It was therefore anticipated that the bridging Al−N bond in $[Cl_2AlNMe_2]_2$ would be found to be several hundredths of an Å unit shorter than in $[Me_2AlNMe_2]_2$.

Since the Me_2N group generally forms stronger bridges than the Cl atom, it was further anticipated that the terminal Al−Cl bond in $[Cl_2AlNMe_2]_2$ would be found to be longer than in $[AlCl_3]_2$.

EXPERIMENTAL AND CALCULATION PROCEDURE

The sample of $[Cl_2AlNMe_2]_2$, which had been prepared from $[Me_2AlNMe_2]_2$ and $AlCl_3$ in hexane,[10] was a gift from Dr. Heinz Hoberg. The electron scattering pattern was recorded on the Oslo electron diffraction unit [11] with a nozzle temperature of about 175 °C. Exposures were made with nozzle to photographic plate distances of about 48 and 26 cm. The optical densities of six plates from the first set were recorded at $\Delta s = 0.125$ Å^{-1} intervals, the optical densities of five plates from the second set were recorded at $\Delta s = 0.250$ Å^{-1} intervals and the

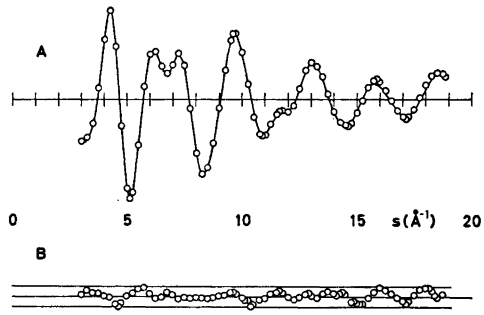

Fig. 1. A, O: Experimental modified molecular intensity points from $s = 3.00$ to 18.75 Å^{-1}. Only every other experimental point is shown. Full line: Theoretical intensity curve calculated for the best model. B, O: Difference points. The full lines indicate the estimated uncertainty (three standard deviations) of the experimental points. *Note:* The scale of B is twice that of A.

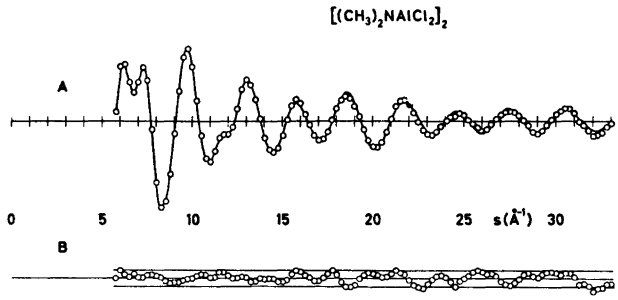

Fig. 2. A, O: Experimental modified molecular intensity points from $s = 5.75$ to 33.00 Å^{-1}. Full line: Theoretical intensity curve calculated for the best model. B, O: Difference points. The full lines indicate the estimated uncertainty (three standard deviations) of the experimental points. *Note:* The scale of B is twice that of A.

data processed as described by Andersen *et al.*[12]

Every other modified molecular intensity point obtained from the 48 cm plates is shown in Fig. 1A, while the modified molecular intensity points obtained from the 26 cm plates are shown in Fig. 2A.

Theoretical intensity curves were calculated from

$$I^{AlCl}(s) = \sum_{i \neq j} \frac{|f_i(s)||f_j(s)|}{|f_{Al}(s)||f_{Cl}(s)|} \cos[\eta_i(s) - \eta_j(s)] \times \frac{\sin(R_{ij}s)}{R_{ij}} \exp(-\tfrac{1}{2}l^2_{ij}s^2)$$

The sum extends over all atom pairs in the molecule. R_{ij} is the internuclear distance, l_{ij} the root mean square amplitude of vibration. $f_j(s) = |f_j(s)| \exp[i\eta_j(s)]$ is the complex atomic scattering factor of atom j.

The molecular structure was refined by least-squares calculations on the intensity data with a non-diagonal weight matrix and a separately refined scale factor for the two sets of intensity data.[13] The standard deviations obtained were expanded to take into account an estimated uncertainty of 0.1 % in the electron wavelength.

Radial distribution functions were calculated by Fourier inversion of experimental and theoretical modified molecular intensity curves after multiplication with the artificial damping function exp ($-ks^2$). The experimental intensity curves were then first spliced to each other and to the theoretical curve calculated for the best model below $s = 3.00$ Å^{-1}.

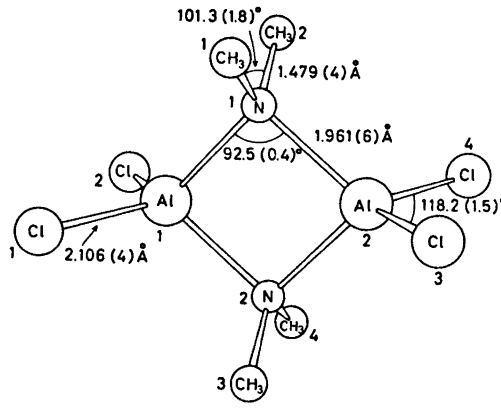

Fig. 3. Molecular model of $[Cl_2AlN(CH_3)_2]_2$.

STRUCTURE ANALYSIS

A molecular model of $[Cl_2AlNMe_2]_2$ is shown in Fig. 3. It was assumed that:

(i) The molecular symmetry is D_{2h}.

(ii) The Me groups have C_{3v} symmetry with the C_3 axes coinciding with the N–C bonds.

(iii) The angle of rotation of the Me groups about the C–N bonds is such that the H atoms are staggered with respect to the bonds radiating from the N atom.

The molcular structure is then determined by eight independent parameters, *e.g.* the four bond distances Al–Cl, Al–N, N–C, and C–H and the four valence angles ∠Cl–Al–Cl, ∠Al–N–Al, ∠C–N–C, and ∠N–C–H. In addition the shrinkages of the two longest intramolecular distances $Cl_1 \cdots Cl_3$ and $Cl_1 \cdots Cl_4$ were refined as independent parameters. All other shrinkages were neglected.

Simultaneous least squares refinement of these ten parameters and fourteen vibrational

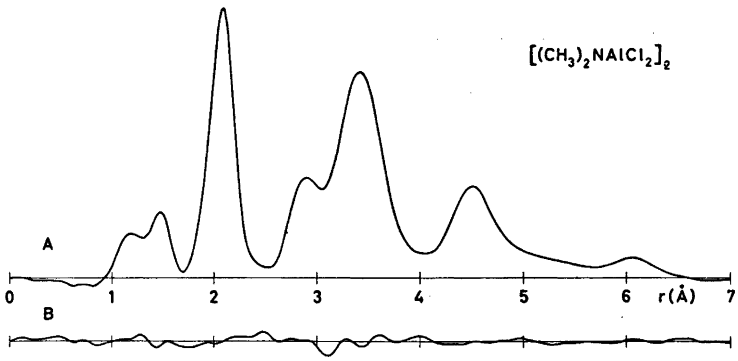

Fig. 4. A: Experimental radial distribution curve. Artificial damping constant $k = 0.0025$ Å^2. B: Difference between the experimental curve and a theoretical curve calculated for the best model.

Table 1. Internuclear distances, valence angles and root mean square vibrational amplitudes (l) of $[Cl_2AlNMe_2]_2$. (Estimated standard deviations in parentheses.) For numbering of the atoms consult Fig. 3. The distances are listed as r_a. The angles have not been corrected for shrinkage.

	R (Å)	l (Å)
Bond distances		
Al – Cl	2.106(4)	0.058(2)
Al – N	1.961(6)	0.088(7)
N – C	1.479(4)	0.058(4)
C – H	1.160(8)	0.075(8)
Nonbonded distances		
$Cl_1 \cdots Cl_2$	3.614(30)	0.192(34)
$Cl_1 \cdots Cl_3$	5.231(44)	0.427(43)
$Cl_1 \cdots Cl_4$	6.082(13)	0.197(10)
$Cl_1 \cdots Al_1$	4.312(14)	0.392(71)
$Cl_1 \cdots N_1$	3.368(8)	0.141(7)[a]
$Cl_1 \cdots C_1$	3.456(13)	0.141(7)[a]
$Cl_1 \cdots C_2$	4.496(7)	0.159(7)
$Al_1 \cdots Al_2$	2.833(13)	0.073(10)[b]
$Al_1 \cdots C_1$	2.929(8)	0.158(11)
$N_1 \cdots N_2$	2.713(16)	0.073(10)[b]
$N_1 \cdots C_3$	3.825(15)	0.232(64)
$C_1 \cdots C_2$	2.288(30)	0.083(17)
$C_1 \cdots C_3$	4.588(33)	0.350[c]
$C_1 \cdots C_4$	5.127(19)	0.300[c]
Shrinkages (Å)		
$Cl_1 \cdots Cl_3$	−0.234(51)	
$Cl_1 \cdots Cl_4$	0.085(22)	
Valence angles (deg)		
∠Cl – Al – Cl	118.2(1.5)	
∠Al – N – Al	92.5(0.4)	
∠C – N – C	101.3(1.8)	
∠N – C – H	104.1(3.4)	

[a] $l(Cl_1 \cdots N_1)$ and $l(Cl_1 \cdots C_1)$ were assumed equal.
[b] $l(Al_1 \cdots Al_2)$ and $l(N_1 \cdots N_2)$ were assumed equal.
[c] These amplitudes were not refined.

amplitudes converged to the values listed in Table 1. Attempts to refine the amplitudes of the distances $Cl_1 \cdots C_1$, $N_1 \cdots N_2$, $C_1 \cdots C_3$, and $C_1 \cdots C_4$ lead to divergence. These amplitudes were therefore constrained as indicated in the table. Since $l(C_1 \cdots C_3)$ and $l(C_1 \cdots C_4)$ were correlated with some of the parameters that were refined (in particular the correlation coefficient between $<C-N-C$ and $l(C_1 \cdots C_3)$ is 0.42) the standard deviations listed in the table are those obtained in a final least-squares cycle in which $l(C_1 \cdots C_3)$ and $l(C_1 \cdots C_4)$ were allowed to vary.

Modified molecular intensity curves calculated for the best model are shown in Figs. 1A and 2A. The difference between experimental and calculated intensities is shown in Figs. 1B and 2B. The agreement is satisfactory.

An experimental radial distribution function is shown in Fig. 4A, the difference between this curve and one calculated for the best model is shown in Fig. 4B.

DISCUSSION

Contrary to expectation the Al – N bond distance in $[Cl_2AlNMe_2]_2$ is found to be exactly equal to the Al – N bond distance found in $[Me_2AlNMe_2]_2$ by X-ray crystallography [4,5] (mean value 1.961). However, taking into consideration the combined uncertainties of the structure determinations as well as the fact that correction for thermal motion in the crystal would increase the bond distance in $[Me_2AlNMe_2]_2$, it is clear that a difference of 0.04 Å or less cannot be ruled out.

The Al–Cl bond distance in $[Cl_2AlNMe_2]_2$, 2.106(4) Å, is significantly longer than the terminal Al–Cl bonds in $[AlCl_3]_2$,[8] 2.065(2) Å, and significantly shorter than in Cl_3AlNMe_3,[7] 2.121(4) Å.

The other bond distances and valence angles fall in the expected range.

Acknowledgements. We are grateful to Dr. Heinz Hoberg of the Max-Planck-Institut für Kohlenforschung for a sample of $[Cl_2AlNMe_2]_2$ and to the Norwegian Research Council for Science and the Humanities and to the National Science Foundation (grant GP 24090) for financial support.

REFERENCES

1. Ruff, J. K. and Hawthorne, M. F. *J. Amer. Chem. Soc. 83* (1960) 1798.
2. Ehrlich, R. *Inorg. Chem. 9* (1970) 146.
3. Shen, M., Hagen, K. and Hedberg, K. *Personal communication.*
4. Hess, H., Hinderer, A. and Steinhauser, S. *Z. Anorg. Allg. Chem. 377* (1970) 1.
5. McLaughlin, G. M., Sim, G. A. and Smith, J. D. *J. Chem. Soc. Dalton Trans.* (1972) 2197.
6. Grant, D. F., Killean, R. D. G. and Lawrence, J. L. *Acta Crystallogr. B 25* (1969) 377.
7. Almenningen, A., Haaland, A., Haugen, T. and Novak, D. P. *Acta Chem. Scand. 27* (1973) 1821.
8. Anderson, G. A., Forgaard, F. R. and Haaland, A. *Acta Chem. Scand. 26* (1972) 1947.
9. Brendhaugen, K., Haaland, A. and Novak, D. P. *Acta Chem. Scand. A 28* (1974) 45.
10. Hoberg, H. and Mur, J. B. *Justus Liebigs Ann. Chem. 733* (1970) 141.
11. Bastiansen, O., Hassel, O. and Risberg, E. *Acta Chem. Scand. 9* (1955) 232.
12. Andersen, B., Seip, H. M., Strand, T. G. and Stølevik, R. *Acta Chem. Scand. 23* (1969) 3224.
13. Seip, H. M., Strand, T. G. and Stølevik, R. *Chem. Phys. Lett. 3* (1969) 617.

Received October 4, 1974.

Acta Chemica Scandinavica A 29 (1975) 277—281

Heterogeneous Nucleation of Calcium Phosphates. II. Inhibition by Cupric Ions

H. E. LUNDAGER MADSEN

Department of Inorganic Chemistry, Royal Veterinary and Agricultural University, Thorvaldsensvej 40, DK-1871 Copenhagen V, Denmark

Inhibition of nucleation of $Ca_4H(PO_4)_3$ on $CaHPO_4.2H_2O$ by Cu^{2+} has been studied. At low concentrations of copper a slight increase in incubation time and a slight decrease in precipitation rate was observed, whereas at higher concentrations the rate of precipitation was initially very low; after a lapse of time which increased with increasing $[Cu^{2+}]$ the rate increased strongly. The observations are explained in terms of sorption of Cu^{2+} in the adsorbed and surface layers of $CaHPO_4.2H_2O$ and by the subsequent transfer of Cu^{2+} to the interior of the crystals. There was no indication of a direct interference of Cu^{2+} with the crystal growth of $Ca_4H(PO_4)_3$.

In a previous paper[1] investigations on the hydrolysis of brushite ($CaHPO_4.2H_2O$) in pure water or dilute phosphoric acid were reported. The process which takes place under the existing conditions is

$$5CaHPO_4(s) \rightarrow Ca_4H(PO_4)_3(s) + Ca^{2+} + 2H_2PO_4^-$$

The crystallization of tetracalcium monohydrogen phosphate is accompanied by a pH drop from about 7 to below 6. The rate of crystallization was shown to depend strongly on pH of the initial solution saturated with respect to brushite.

It has long been known that this process is strongly sensitive to trace amounts of other substances, particularly copper.[2] For this reason, water of high purity, preferably glass-distilled, has to be used for the experiments.

In the present paper is reported a detailed examination of the influence of cupric ions on the heterogeneous nucleation of basic calcium phosphates on secondary calcium phosphate as substrate.

EXPERIMENTAL

In the following, only new procedures and changes from those applied in the previously reported investigation are described.

Apparatus. For pH measurements a Radiometer digital pH meter type 52 was used. Calibration was carried out using two standard buffers, 0.05 m potassium hydrogen phthalate and 0.025 m KH_2PO_4 + 0.025 m $Na_2HPO_4.2H_2O$. For pCu measurements at concentrations above 10^{-5} M a Radiometer ion-selective electrode type F 1112 Cu (sensing element: copper selenide single crystal) and a mercurous sulfate reference electrode were used. In this case, calibration was performed using various standard cupric nitrate solutions, which were 0.1 M with respect to potassium nitrate, as were the samples; in this way a constant liquid-junction potential was ensured.[3]

Precipitates were examined by X-ray powder diffraction using a General Electric diffractometer equipped with a Cu-anode X-ray tube and a scintillation counter, and by infrared spectrometry using a Perkin-Elmer spectrophotometer model 457. Samples for IR spectrometry were prepared as nujol mulls, and KBr windows were used.

Radioactive samples were counted on a Frieseke and Hoepfner counting equipment type 49 B using a well-type scintillation counter.

Materials. Stock solutions of $Cu(NO_3)_2$ were standardized by adding an excess of solid potassium iodide to an acidified sample and titrating the iodine liberated with sodium thiosulfate, which had previously been standardized against potassium iodate.

Radioactive copper (^{64}Cu) of high specific activity was obtained by a Szilard-Chalmers process.[4] A sample of copper-phthalocyanine (α form) was irradiated with thermal neutrons in the DR 2 reactor at Risø. The activity of the sample after irradiation was 20 mCi per g Cu-phthalocyanine. 50 mg was dissolved in 1 ml hot (80 − 100 °C) concentrated H_2SO_4.

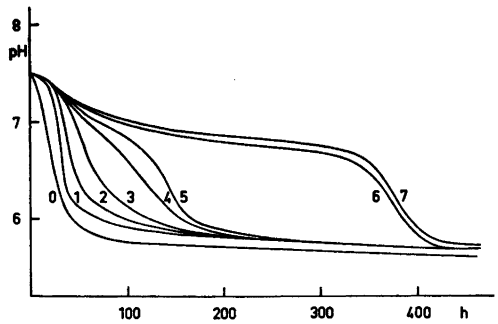

Fig. 1. pH variation as a function of time. Numbers on curves indicate cupric ion concentration in μM.

Subsequent dilution with 10 ml water caused complete precipitation of the Cu-phthalocyanine, which was filtered off. The filtrate, which contained most of the radioactive copper, was electrolyzed between platinum electrodes, until the solution was no longer radioactive. The cathode was rinsed in water and the copper dissolved in nitric acid, which was then evaporated under a heat lamp; the residue was finally dissolved in water, and this solution was used in the experiments. $[Cu^{2+}]$ was determined by solvent extraction of the diethyldithiocarbamate complex followed by spectrophotometery.[5] A specific activity of 36 Ci per g Cu was found, corresponding to an enrichment factor of 230. The retention was 11 %.

RESULTS

Unless otherwise stated, the experiments were carried out as described in the previous paper.[1] The initial solid/solution ratio was always 2 g to 1 litre.

Experiments with addition of calcium nitrate up to a concentration of 1 mM showed that the nitrate ion had no effect. When the initial phosphoric acid concentration was too low, no appreciable inhibition by cupric ions in the concentration range of interest was observed. For this reason an initial phosphoric acid concentration of 10^{-4} M was chosen in most of the experiments.

Fig. 1 shows the results of a series of experiments with $[Cu^{2+}]$ ranging from 0 to 7×10^{-6} M. The limiting value of pH as $t \rightarrow \infty$ was about 5.6 which corresponds to saturation with respect to $Ca_4H(PO_4)_3$. The lapse of time before the large pH drop showed variations up to ~20 %, but the same regular pattern was observed in all series of experiments with the pH drop always occurring in the order of increasing $[Cu^{2+}]$. A cupric ion concentration of about 4 μM appeared to be critical; below this, the incubation time was increased somewhat by the copper, and the rate of the process was altogether a little lower, whereas at higher concentrations there was a considerable delay. In the latter case, several stages of the process could be observed; first the initial incubation period, where pH was about 7.5; then a drop to about pH 7.0, followed by a very slow, but steady decrease of pH; finally, pH dropped to < 6 within a day or two. The time at which this occurred depended strongly on $[Cu^{2+}]$. The initial incubation time was the same at all cupric ion concentrations ≥ 2 μM within the same series of experiments, and above the critical concentration the rates of both the slow pH decrease and the final drop were virtually independent of $[Cu^{2+}]$.

Table 1 shows the results of a series of measurements of the second incubation time. The first incubation time was in this case about 20 h.

By X-ray diffractometry it was shown that the product of hydrolysis was a mixture of $CaHPO_4.2H_2O$ and $Ca_4H(PO_4)_3$, as was expected. In the microscope the crystals of $Ca_4H(PO_4)_3$ appeared as the caracteristic spherulites, and they were particularly well developed when precipitated at high Cu concentration. Before the final pH drop only brushite could be detected, even in an experiment with a cupric ion concentration as high as 1 mM. In the latter case the brushite had a distinct blue-green colour, and the lines in the diffractogram were slightly displaced, but changes of unit-cell dimensions did not exceed 0.01 Å in any direction; there was no change in the IR spectrum. When brushite was boiled with reflux for 4 h in a 2 mM cupric nitrate solution it was transformed mainly to monetite (anhydrous $CaHPO_4$); a small amount of $Ca_4H(PO_4)_3$ was also present. The monetite was

Table 1.

$[Cu^{2+}]$, μM	4.5	5.0	5.5
t_{i2}, h	87	151	213
6.0	6.5	7.0	7.5
248	257	297	407

blue-green, whereas the other compound was colourless. With pure water instead of cupric nitrate solution brushite is transformed completely to hydroxylapatite, $Ca_5(PO_4)_3OH$, presumably *via* $Ca_4H(PO_4)_3$, after a short time of boiling.

The reproducibility of results from experiments with radioactive copper was rather poor. Apparently, single-layer absorption corresponded to 0.6 ± 0.1 mmol Cu per kg $CaHPO_4 \cdot 2H_2O$; that is 1.2 ± 0.2 μmol from 1 litre of solution with 2 g solid. At a Cu^{2+} concentration of about 5 μM the amount in the solid phase increased strongly. This amount apparently depended on pH, although no regularity could be found, except that it increased with increasing pH.

Finally, an experiment was carried out in which brushite was added to a 1 mM solution of $Cu(NO_3)_2$. The suspension was stirred constantly, and $a(Cu^{2+})$ was monitored potentiometrically and was found to decrease by a factor of 100 within half an hour. When a similar experiment was carried out with tetracalcium monohydrogen phosphate instead of brushite no decrease in cupric ion activity could be measured, even after nearly 20 h.

DISCUSSION

It is obvious that precipitation of tetracalcium monohydrogen phosphate under the circumstances studied requires the presence of brushite as a substrate for nucleation; there is no evidence for homogeneous nucleation. The inhibiting action of cupric ions is due to their adsorption on the surface of the brushite crystals or to exchange of calcium and copper in the outermost atomic layers. The effect is a delay of crystallization of $Ca_4H(PO_4)_3$. No foreign solid phase could ever be detected, so it is reasonable to assume that only brushite and tetracalcium monohydrogen phosphate occur in the system. At 100 °C brushite is transformed to Cu-containing monetite; there is still a strong inhibition of precipitation of $Ca_4H(PO_4)_3$.

Brushite is seen to have a high affinity for Cu^{2+}, whereas there is no sign of cupric ion uptake by $Ca_4H(PO_4)_3$. It was hoped that the experiments with radioactive copper would reveal the details of copper uptake, but, as stated above, the results were subject to high uncertainty, presumably due to the difficulty of avoiding contamination by decomposition products of phthalocyanine; these may well be highly active surfactants. The pH dependence may be explained by an exchange equilibrium of the kind

$$Ca^{2+}(\text{in solid}) + Cu^{2+}(\text{in solution}) \rightleftharpoons Ca^{2+}(\text{in solution}) + Cu^{2+}(\text{in solid})$$

because the calcium ion concentration in solution decreases as pH increases. However, it was not possible to fit the experimental data to any particular hypothesis.

As a fast precipitation of $Ca_4H(PO_4)_3$ eventually sets in even at the highest Cu^{2+} concentration the cupric ions must somehow disappear from the surface of the brushite crystals. The only place where they can go is the interior of the crystals, and it may happen either by recrystallization or by solid-state diffusion. That the latter process is just as plausible as the former may be realized by the following argument. We assume that the decrease of surface concentration of copper due to inward diffusion follows an exponential rate law:

$$\Gamma = \Gamma_0 \exp(-t/\tau)$$

At a definite value of Γ, Γ^*, the copper in the surface, can no longer prevent nucleation of $Ca_4H(PO_4)_3$; the value Γ^* is reached after the incubation time t_i:

$$\Gamma^* = \Gamma_0 \exp(-t_i/\tau)$$

In this equation Γ_0 is the independent and t_i the dependent variable, whereas Γ^* and τ are constants. Taking the logarithm on both sides, we get

$$t_i = \tau(\ln \Gamma_i - \ln \Gamma^*)$$

Assuming that no copper is left in solution we may substitute the total amount of copper added for Γ_0, to which the former is proportional. Instead of Γ^* we then find the critical copper concentration c^* mentioned in the preceding section. A least-squares fit of the data in Table 1 yields

$$c^* = 3.8 \ \mu\text{M}$$
$$\tau = 543 \text{ h} = 1.95 \times 10^6 \text{ s}$$

The value of c^* agrees well with experiments. In order to see whether the value of τ is con-

sistent with the diffusion hypothesis, we make use of the equation [6]

$$1/\tau = \nu_0 \exp(-E_a/RT)$$

where ν_0 is the vibration frequency of positive ions in the crystal, and E_a is the activation energy for diffusion. With $\nu_0 = 3 \times 10^{12}$ s^{-1} (corresponding to a wavenumber of 100 cm^{-1}) we get $E_a = 111$ kJ/mol

No other determinations of this quantity have been carried out, but the order of magnitude is the same as for alkali halides and related ionic solids.[6]

In the rest of our discussion it will be advantageous to consider three different ranges of Cu^{2+} concentrations: (1) $0 < [Cu^{2+}] < 2$ μM, (2) $2\ \mu M \leq [Cu^{2+}] < 4\ \mu M$, and (3) $[Cu^{2+}] \geq 4\ \mu M$. In range 3 the precipitation of $Ca_4H(PO_4)_3$ takes place in two stages, the slow and the fast stage. The rate of precipitation in range 2 is almost equal to the rate at the fast stage in range 3. If we call this rate v_1, the rate at the slow stage in range 3, v_2, and the rate when $[Cu^{2+}] = 0$, v_0, the following approximate ratio of the three rates is found

$$v_0 : v_1 : v_2 = 1 : 0.45 : 0.0105$$

The rate of precipitation is presumably nearly proportional to the rate of nucleation. Hence the activation energy of nucleation is increased by the presence of copper (assuming the same frequency factor) by an amount, which in range 2 is equal to $-RT \ln 0.45 \simeq 2.1$ kJ/mol and in range 3, slow stage, equal to $-RT \ln 0.0105 \simeq 11.7$ kJ/mol.

In the previous paper [1] the nucleation mechanism was postulated to be composed of the four elementary reactions occurring at the

I. $Ca^{2+} + PO_4^{3-} \rightarrow CaPO_4^-$
II. $CaPO_4^- + Ca^{2+} \rightarrow Ca_2PO_4^+$
III. $Ca_2PO_4^+ + PO_4^{3-} \rightarrow Ca_2(PO_4)_2^{2-}$
IV. $Ca_2(PO_4)_2^{2-} + Ca^{2+} \rightarrow Ca_3(PO_4)_2$

surface of the brushite crystals, and with III as the rate-determining step. The encounter of calcium and phosphate ions presumably takes place in the mobile adsorbed layer, but the stationary surface layer of the crystal plays an important role in stabilization of the nucleus. In range 2 calcium ions in the adsorbed layer are displaced by cupric ions; before nucleation can take place, this exchange must be reversed, and the activation energy for exchange of ions between solution and the adsorbed layer – presumably the desorption energy of Cu^{2+} – must be added to the activation energy of nucleation to obtain the activation energy of the overall process. Hence we ascribe the value 2.1 kJ to the molar desorption energy of Cu^{2+}. In range 3 the calcium ions are also displaced from the surface layer, so that the stabilizing effect of this layer is missing. Hence an ion exchange in this layer must take place prior to nucleation, and the activation energy for exchange in this layer is considerably higher than in the adsorbed layer; we ascribe the value of 11.7 kJ/mol to this second activation energy or, maybe more correct, this value is equal to the sum of the two activation energies. These assignments are consistent with the theory of Giddings and Eyring for multibarrier kinetics.[7]

CONCLUSION

When a copper salt is added to a suspension of brushite in dilute phosphoric acid, the cupric ions are taken up by the brushite crystals, at low concentration only in the adsorbed layer, at higher concentrations also in the surface layer. As copper cannot replace calcium in $Ca_4H(PO_4)_3$ the nucleation of this compound is thereby hindered. Ion exchange in the adsorbed layer is relatively fast, and at low concentrations of copper only a slight inhibition is observed. Copper in the surface layer disappears by exchange with calcium either in solution or in the interior of the crystal; the latter is achieved by recrystallization or by solid-state diffusion. Exchange in the surface layer is much slower than in the adsorbed layer, so nucleation is slowed down considerably in this case. Eventually the inward transport of Cu^{2+} ions brings their surface concentration down to a level where nuclation of $Ca_4H(PO_4)_3$ is possible without prior exchange in the surface layer; then an increase in nucleation rate sets in.

Acknowledgements. The author wishes to thank Professor A. Tovborg Jensen for his interest and valuable advice. The equipment for radioactivity measurements has been purchased on a grant from the Carlsberg Foundation.

REFERENCES

1. Madsen, H. E. L. *Acta Chem. Scand. 24* (1970) 1677.
2. Rowles, S. R., quoted in: Bjerrum, N. *Kgl. Dan. Vidensk. Selsk. Mat.-Fys. Medd. 31* (1958) No. 7.
3. Madsen, H. E. L., Hansen, B. S. and Olafsson, S. A. *Kgl. Vet.- og Landbohøjsk. Årsskr.* (1974) 29.
4. Sharp, R. A., Schmitt, R. A., Suffredini, C. S. and Randolph, D. F. *USAEC report GA-910* (1959).
5. Henriksen, A. *Tidsskr. Planteavl 61* (1957) 685; *Arbejdsmetoder III, Fælles metoder til jordbundsanalyser*, Copenhagen 1966.
6. Frenkel, J. *Kinetic Theory of Liquids*, Oxford 1946, Chapter 1.
7. Giddings, J. C. and Eyring, H. *J. Phys. Chem. 62* (1958) 305.

Received September 12, 1974.

Acta Chemica Scandinavica A 29 (1975) 282—284

Crystal Structure of *trans*-3-(7-Dihydrothiazolo[2,3-*e*]-1,2,3-triazolyl)propenal

CHRISTIAN RØMMING

Department of Chemistry, University of Oslo, Oslo 3, Norway

The crystals are triclinic, space group $P\bar{1}$, with cell dimensions $a = 10.740(4)$ Å; $b = 4.055(1)$ Å; $c = 9.847(3)$ Å; $\alpha = 81.45(2)°$; $\beta = 75.66(3)°$; $\gamma = 72.85(3)°$, and two molecules in the unit cell. The structure was solved by the use of the program assembly MULTAN and refined by full-matrix least squares methods to an R-value of 0.054 (1697 reflections with $\sin\theta/\lambda$ larger than 0.3, recorded by counter techniques). Estimated standard deviations are 0.002 – 0.003 Å in distances and 0.2 – 0.3° in angles not involving hydrogen atoms.

The propenal side chain has a planar *trans* configuration. The atoms of the triazole ring are coplanar and the three substituent atoms are also situated near the ring plane. The dihydrothiazole ring has an envelope conformation with one carbon atom 0.4 Å out of the plane through the other ring atoms. The two S – C bond lengths are 1.729(2) and 1.840(2) Å, respectively.

Hagen, Ulsaker and Undheim have studied the nitro and diazonium activation in reactions of pyridinium derivatives.[1] Diazotisation of the 8-amino derivative of dihydrothiazolo[3,2-*a*]-pyridine

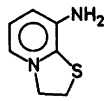

is followed by addition of a hydroxyl ion to the diazonium salt with subsequent re-arrangement to a product with the composition $C_7H_7N_3SO$. In order to identify this compound an X-ray structure determination was undertaken.

EXPERIMENTAL AND STRUCTURE DETERMINATION

The crystals are triclinic with space group $P\bar{1}$. The cell dimensions were determined from diffractometer measurements on 15 general reflections using Mo$K\alpha$ radiation ($\lambda = 0.71069$ Å) $a = 10.740(4)$ Å; $b = 4.055(1)$ Å; $c = 9.847(3)$ Å; $\alpha = 81.45(2)°$; $\beta = 75.66(3)°$; $\gamma = 72.85(3)°$
The volume of the unit cell, which contains two molecules, is 395.7(2) Å^3 giving a calculated density of 1.521 g cm^{-3}.

2347 reflections with $\sin\theta/\lambda < 0.7$ were measured with the use of an automatic four-circle diffractometer using Mo$K\alpha$ radiation (graphite monochromator) and $\omega - 2\theta$ scan technique. 1899 reflections were recorded as observed, the intensities being larger than 2.5 times their standard deviations. The data set was corrected for Lorentz and polarization effects; no corrections for absorption or secondary extinction have been applied.

The structure was solved by the program assembly MULTAN [2] and refined by full-matrix least-squares techniques.[3] Anisotropic temperature factor parameters were introduced for all non-hydrogen atoms. For hydrogen atoms positional parameters (calculated from stereochemical considerations) and isotropic thermal parameters were refined. The final least squares refinement included only reflections with $\sin\theta/\lambda > 0.3$; the function minimized was $\sum w\Delta F^2$. The weights were obtained from the variance in the intensities taken as $C_T + (0.05C_N)^2$ where C_T is the total number of counts and C_N the net count (peak minus background). The atomic form factors were those of Doyle and Turner [4] for carbon, nitrogen, oxygen, and sulfur and of Stewart *et al.*[5] for hydrogen.

The refinement converged to a final conventional R-factor of 0.054 for 1697 reflections ($R_W = 0.067$). The corresponding atomic parameters are listed in Tables 1 and 2. The structure factor list may be obtained from the author upon request. A rigid-body analysis showed that the thermal motion of the molecule could to a

Table 1. Fractional atomic coordinates and thermal parameters ($\times 10^4$) with estimated standard deviations. The temperature factor is given by exp $-(B_{11}h^2+B_{22}k^2+B_{33}l^2+B_{12}hk+B_{13}hl+B_{23}kl)$.

Atom	x	y	z	B_{11}	B_{22}	B_{33}	B_{12}	B_{13}	B_{23}
S	2854(1)	4374(1)	1156(1)	82(1)	677(5)	68(1)	−172(2)	−49(7)	113(2)
O	8206(2)	698(6)	1498(2)	82(2)	1149(19)	125(2)	−234(9)	−18(3)	22(10)
N1	1688(2)	1390(5)	3387(2)	69(2)	659(15)	68(2)	−140(7)	−37(2)	56(7)
N2	1747(2)	−777(6)	4566(2)	86(2)	834(15)	78(2)	−181(8)	−36(3)	155(8)
N3	3003(2)	−1919(6)	4619(2)	87(2)	811(15)	76(2)	−193(8)	−51(3)	135(8)
C1	2894(2)	1664(5)	2685(2)	70(2)	542(12)	59(2)	−126(7)	−35(3)	10(7)
C2	1106(2)	4412(7)	1317(2)	88(2)	712(17)	84(2)	−132(10)	−76(3)	68(10)
C3	529(2)	3559(7)	2863(2)	68(2)	713(16)	95(2)	−130(9)	−50(3)	52(10)
C4	3759(2)	−476(5)	3480(2)	75(2)	592(13)	62(2)	−128(8)	−46(3)	44(7)
C5	7398(2)	−625(7)	2292(3)	74(2)	787(17)	94(2)	−103(9)	−42(3)	−20(10)
C6	5184(2)	−1214(6)	3295(2)	77(2)	613(13)	71(2)	−102(8)	−58(3)	24(8)
C7	5984(2)	303(6)	2308(2)	75(2)	675(15)	81(2)	−113(8)	−50(3)	31(9)

Table 2. Fractional atomic coordinates ($\times 10^3$) and isotropic thermal parameters with estimated standard deviations for hydrogen atoms.

Atom	x	y	z	B
H1C2	106(5)	291(12)	78(5)	3.9(8)
H2C2	69(5)	631(13)	109(5)	5.2(8)
H1C3	14(3)	562(8)	340(3)	3.0(5)
H2C3	−9(4)	225(10)	305(4)	4.4(6)
HC5	770(4)	−256(10)	296(4)	4.9(7)
HC6	558(3)	−285(8)	398(3)	3.5(5)
HC7	565(4)	184(10)	163(4)	4.5(7)

Table 3. Selected interatomic distances and angles. For numbering of atoms, see Fig. 1.

Distance	Å	Corr.	Distance	Å	Corr.	Distance	Å
S−C1	1.729(2)	1.734	N3−C4	1.376(3)	1.379	C2−H2C2	0.80(5)
S−C2	1.840(2)	1.843	C1−C4	1.383(3)	1.386	C3−H1C3	0.98(3)
C2−C3	1.524(3)	1.529	C4−C6	1.439(3)	1.441	C3−H2C3	0.95(4)
C3−N1	1.458(3)	1.460	C6−C7	1.335(3)	1.339	C6−H6	0.96(3)
N1−C1	1.337(3)	1.340	C7−C5	1.450(3)	1.451	C7−HC7	0.91(4)
N1−N2	1.351(2)	1.354	C5−O	1.211(3)	1.213	C5−HC5	0.98(4)
N2−N3	1.302(3)	1.304	C2−H1C2	0.89(5)			

Angle	(°)	Angle	(°)	Angle	(°)
C1−S−C2	89.5(1)	C1−N1−N2	112.1(2)	C1−C4−C6	131.1(2)
S−C2−C3	107.7(1)	N1−N2−N3	106.4(2)	N3−C4−C6	121.6(2)
C2−C3−N1	103.4(2)	N2−N3−C4	109.8(2)	C4−C6−C7	126.0(2)
C3−N1−C1	118.0(2)	N3−C4−N1	107.3(2)	C6−C7−C5	119.5(2)
N1−C1−S	113.3(1)	N1−C1−C4	104.4(2)	C7−C5−O	125.4(2)
C3−N1−N2	129.7(2)	S−C1−C4	142.4(2)		

Atomic deviations (Å) from a plane through the 1,2,3-triazole ring.

N1	−0.001	C1	0.000	C2	−0.413	C7	0.173
N2	0.002	C4	0.002	C3	0.092	C5	0.245
N3	−0.002	S	−0.029	C6	0.036	O	0.438

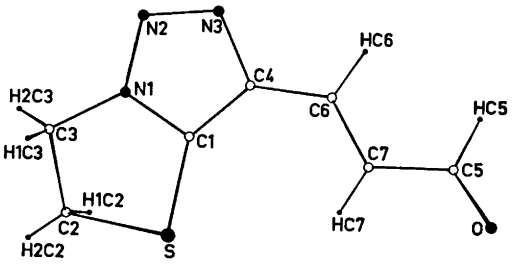

Fig. 1. Schematical drawing of the molecule as viewed normal to the 1,2,3-triazole ring.

fair approximation be interpreted in terms of translational and librational oscillations (r.m.s.-$\Delta U = 0.0017$ Å^2).

Bond lengths corrected for thermal libration are also listed. Standard deviations are calculated from the correlation matrix. The numbering of atoms may be seen from Fig. 1.

DISCUSSION

The structure of the molecule formed by rearrangement of the diazonium salt is visualized in Fig. 1. The addition of a hydroxyl ion to the carbon atom next to the ring nitrogen atom in the pyridyl diazonium part has been followed by a ring opening and the formation of a 1,2,3-triazole ring with a propenal side chain; the thiazole moiety remains unaltered. The reaction is discussed in some detail by Hagen, Ulsaker and Undheim.[1]

The 1,2,3-triazole ring is planar (*cf.* Table 3). The bond lengths indicate a high degree of aromaticity in this part of the molecule. The C1–N1 bond length (1.340 Å) is the same as that found in pyridine.[6] The lengths of the C1–C4 and N2–N3 bonds (1.386 and 1.304 Å, respectively) indicate only a slightly higher double bond character than that expected for an aromatic compound; the N1–N2 and N3–C4 bonds (1.354 and 1.379 Å, respectively) have correspondingly only slightly less double bond character than the aromatic value.[7]

In the thiazole ring four of the atoms are situated close to the plane of the 1,2,3-triazole ring whereas C2 is by 0.4 Å out of this plane. The geometry of the ring is comparable to that found for other thiazole compounds and of tetrahydrothiophene.[8]

The propenal side chain has the planar *trans* configuration with normal bond lengths and angles. The dihedral angles along the chain are as follows: C1–C4–C6–C7 −5.2°; C4–C6–C7–C5 182.5°; C6–C7–C5–O 175.9°. The external angle C1–C4–C6 at C4 is large, probably to relieve strain caused by the small S–HC7 separation (3.01 Å).

The intermolecular separations in the crystal are those to be expected for a packing determined by normal van der Waals' interactions.

Acknowledgement. The author would like to thank cand. real. G. A. Ulsaker for preparing the crystals.

REFERENCES

1. Hagen, S., Ulsaker, G. A. and Undheim, K. *Acta Chem. Scand. B 28* (1974) 523.
2. Germain, G., Main, P. and Woolfson, M. M. *Acta Crystallogr. A 27* (1971) 368.
3. Groth, P. *Acta Chem. Scand. 27* (1973) 1837.
4. Doyle, P. A. and Turner, P. S. *Acta Crystallogr. A 24* (1968) 390.
5. Stewart, R. F., Davidson, E. R. and Simpson, W. T. *J. Chem. Phys. 42* (1965) 3175.
6. Bak, B., Hansen-Nygaard, L. and Rastrup-Andersen, J. *J. Mol. Spectrosc. 2* (1958) 361.
7. Gropen, O. and Skancke, P. N. *Acta Chem. Scand. 24* (1970) 1768.
8. Groth, P. *Acta Chem. Scand. 25* (1971) 118.

Received October 28, 1974.

Acta Chemica Scandinavica A 29 (1975) 285—288

Activation Parameters for Inversion of 1-(1-Naphthyl)-isoquinoline. III.* Dependence on Acidity of the Rate of Inversion of 1-(1-Naphthyl)-isoquinolinium Chloride

JÖRGEN R. PEDERSEN

Department of Organic Chemistry, University of Göteborg and Chalmers University of Technology, Fack, S-402 20 Göteborg 5, Sweden

The rate of inversion of 1-(1-naphthyl)-isoquinolinium chloride has been determined at 20 °C in ethanol solutions of different H_0. The results give a limiting rate corresponding to a free energy of activation for inversion of 95.9 ± 0.3 kJ mol^{-1} at $H_0 \approx -0.8$. This is compared with the barrier to inversion of 1,1′-binaphthyl and interpreted as support for the assumption that the two systems undergo inversion through similar transition states.

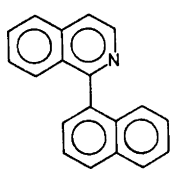

1

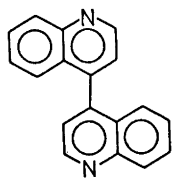

2

1-(1-Naphthyl)-isoquinoline *1* presents an interesting case of biphenyl-like atropisomerism in which the barrier to inversion partly consists of steric interaction between hydrogen and the lone electron pair on nitrogen. The successful resolution of *1* depends on the fact that its conjugate acid has a considerably higher barrier to inversion than has the free base.[1] Preliminary data on the racemization of (−)-1-(1-naphthyl)-isoquinolinium chloride show that, due to the rather low basicity of *1* ($pK_a \approx 3.8$ in 95 % v.v. aqueous ethanol), the rate of racemization is acidity dependent.[1] The measured rate of racemization appeared to be a composite of the rate of racemization *via* the cation and *via* the free base.

The protonation of *1* affects the rate of racemization in two ways, partly due to the assumed increase in steric interaction and partly due to an inductive effect similar to that found on protonation of 4,4′-biquinolyl *2*.[2] The latter effect probably changes the rate of racemization to a minor extent only. Crawford and Ingle [2] have shown that *monoprotonated 2* racemizes only 20 % slower than does the free base.

The rate of inversion of *1* compared to that of its conjugate acid could therefore be expected to yield a qualitative estimate of the difference in steric "size" between the lone pair and hydrogen. Contrary to the earlier comparison between the activation parameters for inversion of *1* and those for 1,1′-binaphthyl,[3] such a comparison would be independent of an assumed similarity between the latter molecule and *1*. On the other hand, the difference in charge between *1* and its conjugate acid is an inevitable fact tending to obscure the interpretation of the experimental evidence.

In order to measure separately the rate of racemization of the hydrochloride of *1*, the rate was studied as a function of H_0. The limiting rate of racemization of the hydrochloride at low H_0 values should yield the rate of racemization of the cation.

* For Part I and II of this series see Refs. 1 and 3.

EXPERIMENTAL

Kinetic runs were performed on a ZEISS OLD 5 polarimeter with digital output at the wave-length 436 nm. The polarimeter cell was a 10 cm microcell with vacuum windows custom-made by LKB-BECKMAN Instruments AB. The error in each reading determined on the pure H_0 solutions was $\pm 0.001°$. The temperature in the cells was measured using a calibrated thermistor and a Fluke 8300 A digital voltmeter with BCD outlet. The thermistor was calibrated against a Hewlett Packard 2801 A quartz thermometer to a precision of ± 0.1 K and was capable of measuring temperature changes of ± 0.0013 K. The constant-temperature medium was supplied by a Hetotherm Ultrathermostat 02 Pt 623 UO. The temperature setting was adjusted to 293.16 K using a mercury thermometer calibrated to ± 0.01 K. The polarimeter and the voltmeter were interfaced on-line to a Compucorp 425 Scientist programmable calculator providing automatic data collecting and statistical treatment of the data using the least squares method. In addition the highest and the lowest temperature in each run were recorded. The temperature fluctuation did not exceed ± 0.1 K in any run and in 87 % of the runs it was less than 0.03 K. The interface was custom-made by Scandia Metric.

The H_0 solutions were prepared from 99.5 % ethanol diluted to 95 % v.v. ethanol with distilled water using a stock solution of 12.5 M HCl in 95 % v.v. ethanol. The molarity of each solution was determined by titration with 0.1 M NaOH solution on a Radiometer Titrigraph automatic titrator. The H_0 of the solution was then calculated by interpolation using the data given in Refs. 4 and 5.

All attempts to obtain crystalline optically active 1-(1-naphthyl)-isoquinolinium chloride have failed as previously reported.[1] Solutions of (−)-1-(1-naphthyl)-isoquinolinium chloride at different H_0 were prepared in the following way: A methanolic solution of (−)-1-(1-naphthyl)-isoquinoline was prepared at −20 °C from (−)-1-(1-naphthyl)-isoquinolinium α-bromocamphor-π-sulfonate by the method previously described.[1,3] The solution was immediately added to a slight excess of HCl in absolute methanol kept at −80 °C and then quickly freeze-dried to a viscous yellow glass by means of a mercury diffusion pump and a vapor trap cooled with liquid nitrogen. Ethanolic HCl solution (5 ml), with the desired H_0 and kept at −80 °C, was then added, and the sample was kept at dry-ice temperature until used. Samples kept in this way were sufficiently optically stable for 3−5 days even in solutions of the highest H_0 used. In 81 % of the samples the absolute rotation was between 1.4 and 0.5°, only one sample had starting rotation below 0.3°. From each batch one run was followed until no further change in optical activity could be observed. This was done in order to check that no residual impurity due to optically active anion was present. All runs from batches with residual rotation were discarded.

The resulting H_0 of a batch was subject to small errors due to the method of preparation. Because of the tendency of the hydrochloride of *1* to form a glass on freeze-drying rather than crystals, complete removal of residual methanol was found to be impossible. The amount of residual methanol, however, is probably very small and certainly less than 1 % of the final volume of the batch. The freeze-drying was monitored by visual inspection and the H_0 solution was not added until the glass was too viscous to flow. In addition, the solutions of H_0 lower than −0.3 did not wet the polarimeter cell directly. In order to fill the cell without bubbles in the light-path, it was necessary to wet it first with ethanol and then wash it out a number of times with reference solution of the desired H_0. The error produced by this practice is also assumed to be quite small, and in view of the approximate character of the H_0 function, the total error in H_0 is certainly unimportant in the present context.

The racemization reactions appeared to follow strictly first-order kinetics, $\ln(\alpha_0/\alpha_t)$ plotted against time yielding straight lines with regression coefficients larger than 0.995 in 93 % of the

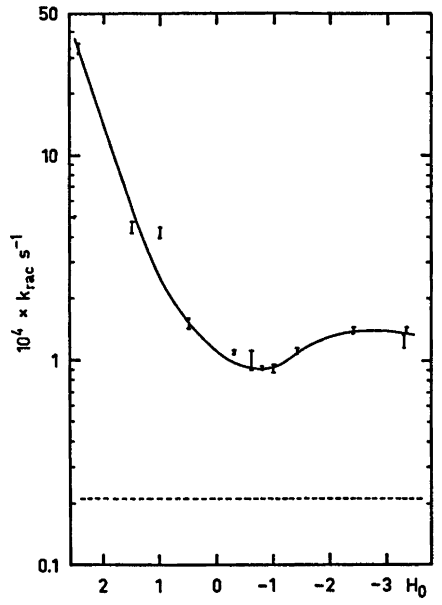

Fig. 1. Logarithmic plot of the rate of racemization of (−)-1-(1-naphthyl)-isoquinolinium chloride at 293.16 K as a function of H_0. (Uncertainty in H_0 not represented.) Dotted line shows rate of racemization of 1,1′-binaphthyl in DMF solution at the same temperature, computed from the activation parameters in Ref. 6.

Table 1. Kinetic data on the racemization of (−)-1-(1-naphthyl)-isoquinolinium chloride in solutions of different H_0.

H_0	No. of runs	$k_{rac} \times 10^4$ s^{-1}	S.D. of $k_{rac} \times 10^4$ s^{-1}	Largest deviation of $k_{rac} \times 10^4$ s^{-1}	Largest deviation of mean temperature of any run from 293.16 K. K
+2.43	7	33.0	1.8	2.9	0.01
+1.52	5	4.39	0.31	0.43	0.02
+1.04	7	4.15	0.27	0.29	0.01
+0.51	5	1.53	0.08	0.09	0.03
−0.27	5	1.10	0.03	0.05	0.01
−0.60	11	0.99	0.11	0.21	0.03
−0.79	7	0.91	0.01	0.02	0.01
−0.99	5	0.90	0.04	0.05	0.01
−1.38	6	1.08	0.05	0.07	0.04
−2.38	5	1.39	0.04	0.06	0.10
−3.26	4	1.23	0.10	0.21	0.10
−3.35	6	1.39	0.03	0.04	0.01

runs. Lower regression coefficients were generally connected with large deviations from the mean temperature of the run.

RESULTS AND DISCUSSION

The kinetic data were obtained for eleven values of H_0 between +2.43 and −3.35 with the greatest density of measurements in the region with limiting racemization rates. The results are listed in Table 1 along with the largest deviations of the mean temperatures of the runs from 293.16 K. The presence of residual impurity of the optically active anion was shown to alter the kinetic results but, as mentioned in the Experimental Section, each batch of (−)-1-(1-naphthyl)-isoquinolinium chloride solution was checked for residual rotation and runs from batches with permanent optical activity were discarded. This criterion of purity is quite sensitive since the specific rotation of sodium (+)-α-bromocamphor-π-sulfonate is above 200° at the wavelength 436 nm and the corresponding acid has an even higher specific rotation.

A few large interexperimental deviations occur, as can be seen from Table 1. In the region of interest, $H_0 \approx -0.2$ to -1.4, however, the mean value of k_{rac} varies only within an interval of 20 %, and the reproducibility appears to be satisfactory. The large deviation at $H_0 = -0.6$ is mainly due to a single large deviation from the mean; this is partially corrected for by a substantially larger number of measurements at this point.

The rate of racemization has been represented as a function of H_0 in the plot of Fig. 1. It can be seen that the rate of racemization goes through a shallow minimum at $k_{rac} = (1.0 \pm 0.1) \times 10^{-4}$ s^{-1} and increases slightly at very low H_0. The latter feature is similar to the behaviour of *2* which also shows a slight increase in the rate of racemization at very low H_0. Crawford and Ingle [2] suggest that this effect may be due to further protonation of diprotonated *2* at one of the pivot-bond carbons, resulting in a tetrahedral intermediate which can undergo inversion readily *via* rotation about the pivot bond which is then a true single bond. Another explanation may be that salt effects become very important at low H_0 values with the inevitable high ionic strength. Berntsson *et al.*[7] found a linear relation between ln k and the ionic strength in the racemization of the 2,2′-diiodo-4,4′-dicarboxybiphenyl dianion. They did not follow the relation further than to approximately $J = 1.5$ and it is unlikely that the relation remains linear at ionic strengths greater than that. The observed increase in the rate of racemization at low H_0 values, however, is rather small suggesting that erratic salt effects may interfere.

While rates of racemization are the quantities observed, the quantity of interest in this investigation is the free energy of activation for

inversion. This was calculated using the equations:[8]

$$k_{rac} = 2k_{inv}$$
$$\Delta G^{\ddagger} = RT[\ln(k/h) - \ln(k_{inv}T)]$$

The limiting free energy of activation for inversion of protonated *1* is thus found to be 95.9 ± 0.3 kJ mol^{-1}, close to that for 1,1′-binaphthyl which has been measured by two independent research teams.[6,9] From the data in Refs. 6 and 9 the barrier to inversion for 1,1′-binaphthyl in DMF solution at 293.16 K has been calculated to be 99.7 ± 1.5 kJ mol^{-1}, and 98.0 kJ mol^{-1}, respectively. Detailed analyses of bond lengths and angles in the rings of monoazanaphthalenes have not yet been published, but Crawford and Ingle [2] have argued that the non-bonded distances of importance should be slightly greater in *2* than in 1,1′-binaphthyl. Similar arguments imply that the same non-bonded distances in protonated *1* should also be slightly greater than in 1,1′-binaphthyl. This would presumably explain why the barrier to inversion of protonated *1* is lower than that for 1,1′-binaphthyl. One cannot exclude, of course, the possibility that the small difference in $\Delta G^{\ddagger}$ for inversion is due to a difference in $\Delta S^{\ddagger}$ for inversion. The entropies of activation for inversion of biphenyls and biphenyl-like compounds are known to range between +36 and −68 J mol^{-1} K^{-1}.[10]

The close similarity in molecular structure and barrier to inversion of protonated *1* and 1,1′-binaphthyl supports the reasonable assumption that the two systems undergo inversion through similar transition states. The suggestion that *1* and similar systems may be used to estimate the van der Waals volume of the lone electron pair in comparison to that of hydrogen [1] seems to be strongly supported by the present results.

A study of the temperature dependence of the limiting racemization rate was not undertaken for the following reason. The limiting racemization rate for protonated *1* has to be measured at high ionic strength in ethanol. Carter and Berntsson [7,11,12] have unambiguously shown the necessity of eliminating salt effects from the Eyring plot by extrapolating the rate constants to infinite dilution. It would be possible, of course, to do a temperature variation of the racemization rate at a specific H_0 value, *e.g.* $H_0 = -0.8$. The change in H_0 with temperature is probably not very large and the rates of racemization are not very sensitive to small changes in H_0, as can be seen from Fig. 1. The results could undoubtedly yield some information about changes in solvation and similar intermolecular changes as the molecule passes into the transition state for inversion. In the present context, however, only intramolecular changes are of interest, and it seems impossible to determine activation parameters for these separately.

Acknowledgement. A grant from Stiftelsen Bengt Lundquists Minne during part of this investigation is gratefully acknowledged. The use of the polarimeter, purchased partly on a grant from the Swedish Natural Science Research Council to Professor Lars Melander, is hereby acknowledged.

REFERENCES

1. Pedersen, J. R. *Acta Chem. Scand. 26* (1972) 929.
2. Crawford, M. and Ingle, R. B. *J. Chem. Soc.* (1971) 1907.
3. Pedersen, J. R. *Acta Chem. Scand. A 28* (1974) 213.
4. Rochester, C. H. *Acidity Functions*, Academic, New York 1970.
5. Nálovský, B. and Chvalovský, V. *Collect. Czech. Chem. Commun. 33* (1968) 3122.
6. Carter, R. E. and Dahlgren, L. *Acta Chem. Scand. 23* (1969) 504.
7. Berntsson, P., Wanger, M. and Carter, R. E. *Acta Chem. Scand. 21* (1967) 879.
8. Glasstone, S., Laidler, K. J. and Eyring, H. *The Theory of Rate Processes*, McGraw, New York 1941.
9. Cooke, A. S. and Harris, M. M. *J. Chem. Soc.* (1963) 2365.
10. Hall, M. and Harris, M. M. *J. Chem. Soc.* (1960) 490.
11. Berntsson, P. and Carter, R. E. *Acta Chem. Scand. 22* (1968) 2141.
12. Carter, R. E. and Berntsson, P. *Acta Chem. Scand. 23* (1969) 499.

Received October 12, 1974.

Acta Chemica Scandinavica A 29 (1975) 289—297

On the Interpretation of Conductance Data for Electrolyte Solutions

PER BERONIUS

Division of Physical Chemistry, University of Umeå, S-901 87 Umeå Sweden

For electrolytes subject to ion-pair formation the limiting molar conductivity, Λ_∞, the association constant, K_A, and the association distance, R, may be derived from conductance equations involving these quantities as adjustable parameters. Ordinarily that set of conductance parameters, Λ_∞, K_A, and R which minimizes $\sigma(\Lambda)$, the standard deviation between observed and computed Λ values, is adopted as the "best set".

In this investigation the equation of Fuoss and Hsia, in the form of Fernandez-Prini, has been applied to conductance data for numerous 1:1-electrolytes in pure and mixed solvents. By employing calculational methods involving the determination of those values of Λ_∞ and K_A which minimize $\sigma(\Lambda)$ for selected values of the distance parameter, R, it is shown that the "best set" of conductance parameters is frequently non-unique; almost equally good fits of the conductance equation to the experimental points are obtained for two significantly different values of the distance parameter.

By measurements of electrical conductance, Masterton and Bierly [1] investigated the 2:2-electrolyte, $[Co(NH_3)_5NO_2]SO_4$ in aqueous solution at 25 °C with respect to the equilibrium between free ions and ion-pairs. Their conductance data were subsequently reanalyzed by Hanna, Pethybridge, and Prue [2] using the conductance equation of Fuoss, Hsia, and Fernandez-Prini [3–5] ("FHFP" equation) in its form for associated electrolytes,

$$\Lambda = \alpha[\Lambda_\infty - S(c\alpha)^{1/2} + Ec\alpha\,{}^{10}\log(c\alpha) + J_1 c\alpha - J_2(c\alpha)^{3/2}] \quad (1)$$

together with the law of mass action for the equilibrium between free ions and ion-pairs and the Debye-Hückel equation for the mean activity coefficient of free ions.

In eqn. (1) Λ is the molar conductivity at the analytical concentration, c, of the electrolyte, α is the degree of dissociation of the ion-pairs, S and E are coefficients [6] which depend upon Λ_∞, ε, the permittivity of solvent, η, the viscosity of solvent, and T, the absolute temperature, while J_1 and J_2, according to Ref. 5, are also dependent upon the association distance, R. The last quantity is defined as the furthest distance of separation of the ions in the ion-pair; compare for instance Ref. 7.

One result of the aforementioned reanalysis [2] of the conductance data for the $[Co(NH_3)_5NO_2]SO_4$ system was that the "best set" of conductance parameters, *viz.* $\Lambda_\infty = 289.52$ cm^2 Ω^{-1} mol^{-1}, $K_A = 367$ M^{-1}, and $R = 12.5$ Å, giving a standard deviation, $\sigma(\Lambda) = 0.12$ cm^2 Ω^{-1} mol^{-1}, between experimental and calculated Λ values was not unique.* The insignificantly larger $\sigma(\Lambda) = 0.13$ was obtained for the set, $\Lambda_\infty = 289.42$, $K_A = 320$, and $R = 7.2$ Å.

Upon reanalyzing conductance data by means of the FHFP equation for numerous 1:1 electrolytes in pure and mixed solvents the present author observed similar behaviour for a not insignificant proportion of systems examined. The object of the present paper is to document and discuss some typical results for electrolyte systems showing behaviour of this kind.

CALCULATIONAL METHODS

Two calculational methods, the first according to Ref. 2, the second according to Ref. 8, were used to investigate the existence of non-unique

* These units are implied throughout the remaining text.

sets of conductance parameters. The first method permits $\sigma(\Lambda)$ to be determined for arbitrary combinations of Λ_∞ and R provided that these quantities do not differ too much from the "best set" parameters. In the second method one restricts oneself to establish the conditional minimum $\sigma(\Lambda)$ as a function of R (*i.e.* with implicit variation of Λ_∞ and K_A). Hence, the second method requires less computer time.

The values of ε and η used in the calculations are the same as adopted in the original publications.[9-15]

The computer programmes, which were prepared for use with a CDC 3300 computer, operate essentially as follows.

Method 1. For a selected pair of values of Λ_∞ and R, α values are iteratively calculated for all concentrations under investigation starting with $\alpha = \Lambda/\Lambda_\infty$ as a first approximation. Eqn. (1) is then repeatedly applied in the usual manner, *cf.* Ref. 16, until for all points the difference between successive α values falls below a predetermined limit, which was set equal to 1×10^{-7} in the present study. (Increasing this limit to 1×10^{-6} yielded practically identical results).

For each experimental point (c/Λ), an association constant is then calculated using the expression,

$$K_A = \frac{\Lambda_\infty - S(c\alpha)^{1/2} + Ec\alpha\,{}^{10}\log(c\alpha) + J_1 c\alpha - J_2(c\alpha)^{3/2} - \Lambda}{c\alpha\gamma^2\Lambda} \quad (2)$$

obtained from eqn. (1) and the law of mass action,

$$K_A = (1-\alpha)/(c\gamma^2\alpha^2) \quad (3)$$

for the equilibrium between free ions and ion-pairs.

In eqn. (3) γ is the mean molar activity coefficient of free ions, which is calculated from the Debye-Hückel equation,

$$^{10}\log\gamma \simeq -A(c\alpha)^{\frac{1}{2}}/[1 + BR(c\alpha)^{\frac{1}{2}}] \quad (4)$$

where A and B depend upon the solvent.[17]

The average value of K_A for the N experimental points is then computed and used together with the selected Λ_∞ and R to obtain calculated Λ values for the different concentrations investigated. The standard deviation between experimental and calculated Λ values is computed from the expression,

$$\sigma(\Lambda) = \left(\frac{\sum[\Lambda(\text{exp}) - \Lambda(\text{calc})]^2}{N-3}\right)^{\frac{1}{2}} \quad (5)$$

The calculations are repeated, as demonstrated below, for different combinations of Λ_∞ and R to establish the dependence of $\sigma(\Lambda)$ on these quantities.

Method 2. Preliminary figures for Λ_∞ and K_A are used, together with a pre-selected value of R, to start the calculations. Values of α are computed as above. For each experimental point the difference,

$$\Delta\Lambda = \Lambda(\text{exp}) - \Lambda(\text{calc}) \quad (6)$$

is then established.

The preliminary figures for Λ_∞ and K_A are improved by adding the $\Delta\Lambda_\infty$ and ΔK_A obtained upon solving the set of normal equations [8] derived from the expression,

$$\Delta\Lambda = \frac{\partial\Lambda}{\partial\Lambda_\infty}\Delta\Lambda_\infty + \frac{\partial\Lambda}{\partial K_A}\Delta K_A \quad (7)$$

cf. Ref. 16 and references therein. The improved values of Λ_∞ and K_A are used to start a second round of computation (with unchanged R value). This procedure is repeated until $\Delta\Lambda_\infty$ falls below a pre-selected limit, which was set equal to 1×10^{-7} in this study. The final Λ_∞ and K_A are used together with the selected R in calculating, according to eqn. (5), the standard deviation between experimental and computed Λ values, *i.e.* the conditional minimum $\sigma(\Lambda)$ for the R value chosen.

The calculational procedure outlined is repeated for several different values of R to establish the dependence of the conditional minimum $\sigma(\Lambda)$ on R over the desired range of the latter. In the present study the range $1-25$ Å was investigated using 0.2 Å increments in R. Repeated calculations with successively smaller increments were then performed near each minimum of the $\sigma(\Lambda) - R$ curve to determine the R value of the minimum with less than 0.01 Å uncertainty.

Applications. The use of the two calculational methods outlined will be demonstrated by their application to the conductance data of Evans and Gardam [9] for Bu_4NClO_4 in propanol at 25 °C.

Using Method 1 the dependence of $\sigma(\Lambda)$ on Λ_∞ was established for selected values of the distance parameter, R. Results for a few R values are shown graphically in Fig. 1.

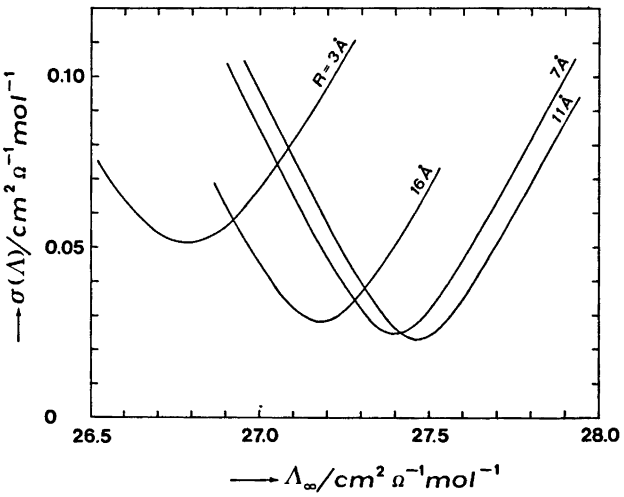

Fig. 1. Standard deviation of single Λ-value as a function of Λ_∞ (implicit variation of K_A) at different values of the distance parameter, R, for Bu_4NClO_4 in propanol [9] at 25 °C.

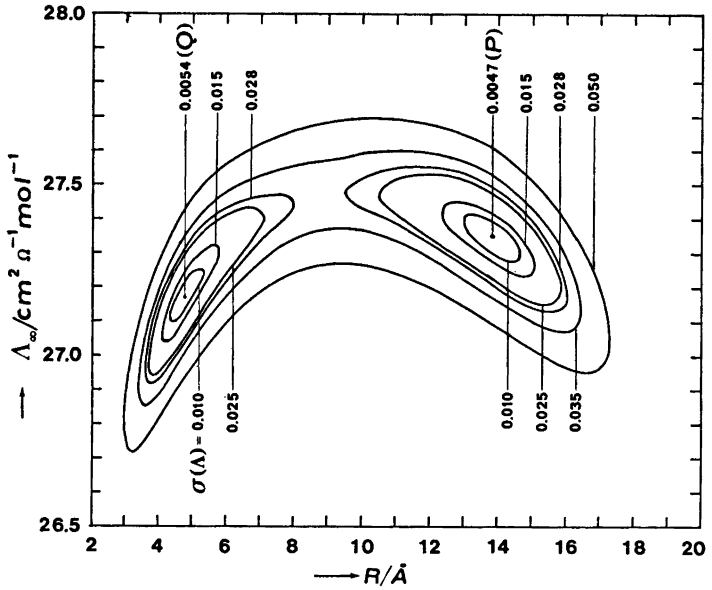

Fig. 2. Contour diagram for the same system as in Fig. 1. The contour lines, representing the different values of $\sigma(\Lambda)$ quoted in the diagram, illustrate how $\sigma(\Lambda)$ depends on different combinations of Λ_∞ and R. The points P and Q indicate minima.

By employing a large number of curves of the kind shown in Fig. 1 the contour diagram, Fig. 2, was constructed. The contour lines represent different values of $\sigma(\Lambda)$. Pertinent values of $\sigma(\Lambda)$ are attached to the contour lines.

The contour diagram for the system concerned exhibits two minima, in Fig. 2 denoted P and Q, respectively. The minimum at P, with $\sigma(\Lambda) = 0.0047$ cm² Ω^{-1} mol^{-1}, corresponds to the "best set" parameters, $\Lambda_\infty = 27.35$, $K_A = 905$, $R = 13.86$ Å, while the minimum at Q, with the insignificantly larger $\sigma(\Lambda) = 0.0054$, refers to

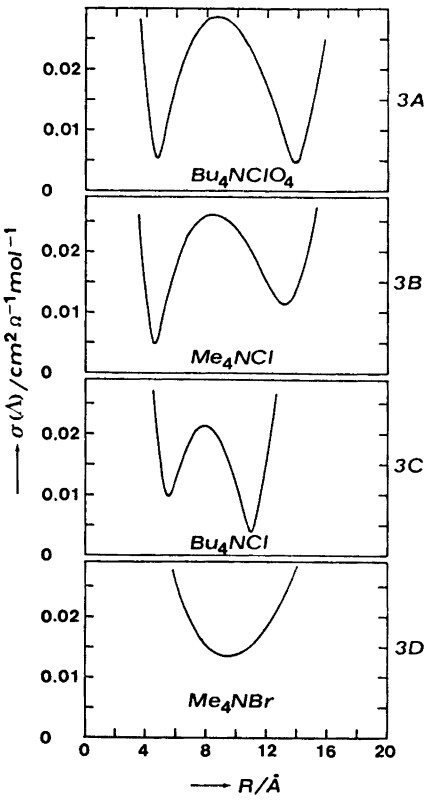

Figs. 3 A–D. Conditional minimum $\sigma(\Lambda)$ as a function of the distance parameter, R (implicit variation of Λ_∞ and K_A) for electrolytes in propanol [9] at 25 °C.

the set, $\Lambda_\infty = 27.17$, $K_A = 789$, $R = 4.75$ Å. The two minima, with almost identical values of $\sigma(\Lambda)$, appear thus at two significantly different association distances.

The contour diagram representation of $\sigma(\Lambda)$ in Fig. 2 for the Bu_4NClO_4–propanol system may be compared with the alternative representation in Fig. 3A in which the conditional minimum $\sigma(\Lambda)$, obtained by means of Method 2, has been plotted *vs.* association distance.

Three additional examples of $\sigma(\Lambda) - R$ curves, derived from the conductance data in Ref. 9 for quaternary ammonium salts in propanol, have been included in Fig. 3 to demonstrate a few different shapes of such curves.

RESULTS AND DISCUSSION

Evans and Gardam [9] report conductance data for twelve tetraalkylammonium salts in propanol at 25 °C. For ten* of these systems the present reanalysis (Method 2) yielded $\sigma(\Lambda) - R$ curves with double minima, *cf.* Figs. 3 A–C. A compilation of the values of Λ_∞, K_A, R, and $\sigma(\Lambda)$ corresponding to these minima is given in Table 1 ("FHFP" equation). For comparison the corresponding values derived in the original investigation [9] from the Fuoss-Onsager equation of 1957 ("FO-57" equation) have been included in this table. The considerably better fit of the FHFP equation to the experimental data as compared with the FO-57 equation is apparent from the $\sigma(\Lambda)$'s listed in the last column.

I has been claimed [7] that the distance parameter, R, should be identified with Bjerrum's critical distance,[18] $q = |z_+ z_-| e^2/(2\varepsilon kT)$, where z_+ and z_- are the valencies of the ions, e is the electronic charge, and k is Boltzmann's constant. Hence, it may be of interest to compare the association distances according to the FHFP equation in Table 1 with this critical distance, which for 1:1 salts in propanol ($\varepsilon = 20.45$) amounts to 13.70 Å. With the exception of Me_4NCl the association distance of the "best set" for each salt listed in this table is rather close to the critical Bjerrum distance though, as pointed out in a previous section, the $\sigma(\Lambda)$'s for Bu_4NClO_4 at 4.75 and 13.86 Å are almost identical.

The conductance data for two of the salts listed in Table 1 (Me_4NCl and He_4NI) have been previously treated in a different manner by Justice [7] using eqns. (1), (3), and (4). In his method the R parameter of the J_1 term in the FHFP equation and in the Debye-Hückel expression is set equal to Bjerrum's critical distance. The value of R in the J_2 term of the FHFP equation which minimizes $\sigma(\Lambda)$ is then evaluated. For comparison with the values of the parameters derived in the present study for these two salts in propanol the corresponding figures according to the Justice method, as reported in Ref. 7, are included in Table 1, in which the notation "FHFP-Bj" is used to denote that special case of the FHFP equation in which R in the J_1 term is set equal to the critical Bjerrum distance.

Reynolds and Kraus [10] report conductance data for fourteen salts in acetone at 25 °C. The

* For the remaining two salts, Et_4NI and Me_4NBr, $\sigma(\Lambda) - R$ curves with a single minimum, at 8.95 and 9.41 Å, respectively, were obtained.

Table 1. Conductance parameters for electrolytes in propanol [a] at 25 °C derived from conductance data of Evans and Gardam.[9] The two sets of Λ_∞, K_A, R, and $\sigma(\Lambda)$ quoted for each salt according to the FHFP equation correspond to the two minima in the $\sigma(\Lambda)-R$ curve, *cf.* Figs. 3 A–C. N = number of points (c,Λ).

Salt	N	Cond. equation	Λ_∞ cm² Ω⁻¹ mol⁻¹	K_A M⁻¹	R Å	$\sigma(\Lambda)$ cm² Ω⁻¹ mol⁻¹
Me_4NCl	7	FHFP	25.28	583	13.15	0.011
		FHFP	25.06	470	4.59	0.005
		FO-57	25.05	456	4.2	0.01
		FHFP-Bj	25.29	587	13.4	0.01
Bu_4NCl	8	FHFP	21.26	237	10.96	0.004
		FHFP	21.19	173	5.52	0.010
		FO-57	21.16	149	4.4	0.02
Et_4NBr	8	FHFP	27.30	436	9.28	0.0017
		FHFP	27.27	419	7.76	0.0021
		FO-57	27.19	373	5.0	0.01
Pr_4NBr	8	FHFP	24.66	369	10.35	0.0010
		FHFP	24.51	301	5.54	0.0079
		FO-57	24.42	270	4.4	0.02
Bu_4NBr	8	FHFP	23.06	355	10.88	0.0014
		FHFP	22.97	294	5.89	0.0068
		FO-57	22.92	266	4.6	0.01
Pr_4NI	8	FHFP	26.31	490	10.80	0.0013
		FHFP	26.17	423	5.81	0.0073
		FO-57	26.08	391	4.5	0.02
Bu_4NI	8	FHFP	24.76	510	11.21	0.0010
		FHFP	24.66	445	6.00	0.0055
		FO-57	24.60	415	4.7	0.01
i-Am_3BuNI	8	FHFP	24.12	552	11.87	0.0021
		FHFP	24.06	493	6.37	0.0061
		FO-57	24.02	462	4.9	0.01
He_4NI	8	FHFP	22.27	536	12.37	0.0025
		FHFP	22.21	469	6.16	0.0065
		FO-57	22.18	442	4.8	0.01
		FHFP-Bj	22.281	547	13.1	0.002
Bu_4NClO_4	8	FHFP	27.35	905	13.86	0.0047
		FHFP	27.17	789	4.75	0.0054
		FO-57	27.13	769	4.2	0.01

[a] $\eta = 1.952$ cP; $\varepsilon = 20.45$; Bjerrum's critical distance, $q = 13.70$ Å.

present reanalysis of their data yielded $\sigma(\Lambda)-R$ curves with double minima for eleven* systems, see Table 2.

* Two salts, Bu_4NI and Et_4NPi, yielded $\sigma(\Lambda)-R$ curves with a single minimum, at 7.00 and 9.11 Å, respectively. For Me_4NF no minimum was obtained in the 1–25 Å range. Calculations outside this range revealed one minimum at 0.44 Å (Λ_∞ = 182.43; $K_A = 1093$; $\sigma(\Lambda) = 0.15$) and another minimum at 32.70 Å ($\Lambda_\infty = 182.51$; $K_A = 1334$; $\sigma(\Lambda) = 0.17$).

Inspection of this table reveals that for all salts listed, with the exception of LiPi, one of the two minima in the $\sigma(\Lambda)-R$ curve appears close to Bjerrum's critical distance, which for 1:1-electrolytes in acetone at 25 °C ($\varepsilon = 20.47$) amounts to 13.69 Å, while the other minimum appears for association distances in the 4.8–7.5 Å range. It is noteworthy that for a large proportion of the salts listed in Table 2, *viz.* Bu_4NFBPh_3, Bu_4NPi, Bu_4NClO_4, Bu_4NBr,

Table 2. Conductance parameters for electrolytes in acetone [a] at 25 °C calculated by means of the FHFP equation from data of Reynolds and Kraus.[10] N = number of points (c,Λ).

Salt	N	Λ_∞ cm² Ω⁻¹ mol⁻¹	K_A M⁻¹	R Å	$\sigma(\Lambda)$ cm² Ω⁻¹ mol⁻¹
Bu_4NFBPh_3	6	134.35	107	14.20	0.047
		134.28	39	5.98	0.048
Bu_4NPi	6	152.43	104	15.68	0.12
		152.31	15	4.78	0.09
Bu_4NClO_4	6	182.93	128	11.85	0.15
		182.86	91	7.34	0.14
Bu_4NNO_3	6	187.31	217	13.65	0.074
		187.17	150	5.72	0.017
Bu_4NBr	6	183.42	328	12.62	0.0976
		183.35	285	7.26	0.0971
Me_4NFBPh_3	6	165.26	182	13.05	0.061
		165.18	131	6.80	0.046
LiPi	6	158.12	1023	24.92	0.025
		157.94	830	1.47	0.078
NaPi	6	163.85	763	13.54	0.043
		163.78	714	7.52	0.061
KPi	6	166.34	320	13.07	0.027
		166.28	270	6.90	0.073
KI	6	193.01	163	13.05	0.18
		192.83	100	5.81	0.11
KCNS	5	201.83	281	13.00	0.062
		201.77	235	7.15	0.022

[a] $\eta = 0.304$ cP; $\varepsilon = 20.47$; Bjerrum's critical distance, $q = 13.69$ Å.

Me_4NFBPh_3, and NaPi, almost equally good fits of the conductance equation to the experimental points are obtained for two quite different values of the association distance, *viz.* for $R \simeq q$ and $R \ll q$.

The series of conductance data according to Graham, Kell, and Gordon [11] for LiCl, NaCl, and KCl in ethanol at 25 °C, and according to Hawes and Kay [12] for CsCl in this solvent yielded all $\sigma(\Lambda) - R$ curves with double minima, *cf.* Table 3 in which data according to the Justice treatment [7] are included. For all these systems one minimum appears close to Bjerrum's critical distance, which for this solvent at 25 °C ($\varepsilon = 24.3$) and the charge type of salt concerned is equal to 11.53 Å. However, better fits are in fact obtained for R values of the order 4 – 5 Å, *i.e.* considerably below the Bjerrum distance. Noteworthy is also the better fit of the FHFP equation as compared with the FHFP-Bj equation.

Banewicz, Maguire, and Shih [13] report conductance data for Et_4NClO_4 in valeronitrile at four temperatures. Reanalysis of their data results in a similar pattern to that above, *i.e.* one minimum in the $\sigma(\Lambda) - R$ curve appears close to the Bjerrum q value, which for this solvent ($18.06 \leq \varepsilon \leq 20.03$) at the temperatures concerned varies from 13.99 to 14.31 Å, while another minimum, with approximately the same $\sigma(\Lambda)$, appears at $R = 3.9$ Å, see Table 4. Included in this table is also the set of conductance parameters at 25 °C evaluated according to the Justice method in Ref. 7.

Table 3. Parameters for electrolytes in anhydrous ethanol [a] at 25 °C calculated from conductance data of Graham, Kell, and Gordon [11] (LiCl, NaCl, KCl), and Hawes and Kay [12] (CsCl). N = number of points (c,Λ).

Salt	N	Cond. equation	Λ_∞ cm² Ω⁻¹ mol⁻¹	K_A M⁻¹	R Å	$\sigma(\Lambda)$ cm² Ω⁻¹ mol⁻¹
LiCl	6	FHFP	38.96	77	12.83	0.018
		FHFP	38.93	29	4.67	0.012
		FHFP-Bj	38.95	68	11.9	0.02
NaCl	6	FHFP	42.19	102	13.99	0.023
		FHFP	42.16	44	4.04	0.017
		FHFP-Bj	42.18	87	12.4	0.03
KCl	6	FHFP	45.43	142	12.80	0.018
		FHFP	45.41	98	5.05	0.012
		FHFP-Bj	45.43	134	11.8	0.02
CsCl	5	FHFP	48.54	205	9.71	0.0051
		FHFP	48.39	170	5.27	0.0021
		FHFP-Bj	48.58	215	10.7	0.008

[a] $\eta = 1.084$ cP; $\varepsilon = 24.3$; Bjerrum's critical distance, $q = 11.53$ Å.

Table 4. Conductance parameters for Et_4NClO_4 in valeronitrile [a] calculated from data reported by Banewicz, Maguire, and Shih.[13] N = number of points (c,Λ).

t °C	N	Cond. equation	Λ_∞ cm² Ω⁻¹ mol⁻¹	K_A M⁻¹	R Å	$\sigma(\Lambda)$ cm² Ω⁻¹ mol⁻¹	q Å
25	19	FHFP	88.64	310	14.16	0.14	13.99
		FHFP	88.11	189	3.89	0.17	13.99
		FHFP-Bj	88.49	302	14.0	0.15	13.99
30	16	FHFP	94.56	319	13.64	0.15	14.03
		FHFP	93.73	192	3.89	0.14	14.03
40	15	FHFP	106.81	336	14.15	0.19	14.18
		FHFP	106.08	206	3.90	0.18	14.18
50	17	FHFP	119.66	359	14.38	0.225	14.31
		FHFP	118.81	225	3.92	0.222	14.31

[a] $\eta = 0.6928$, 0.6485, 0.5719, and 0.5084 cP and $\varepsilon = 20.03$, 19.64, 18.81, and 18.06 at 25, 30, 40, and 50 °C, respectively.

For three * of the twelve salts in sulfolane at 30 °C ($\varepsilon = 43.33$; $q = 6.36$ Å) investigated by Fernandez-Prini and Prue [14] double minima with nearly identical $\sigma(\Lambda)$'s were obtained at two different values of the distance parameter, R, as can be seen from Table 5 in which the conductance parameters, evaluated in the original investigation from the Pitts' equation ("P" equation), are also listed.

Of the five series of conductance data for NaCl in propanol-water mixtures at 15 °C reported by Goffredi and Shedlovsky [15] three series yielded $\sigma(\Lambda) - R$ curves with double minima. Again, nearly identical $\sigma(\Lambda)$'s are observed at two quite different association distances, one of which appears at $R \simeq q$, see Table 6 which for comparison includes the values of the conductance parameters evaluated in the

* The remaining nine salts yielded $\sigma(\Lambda) - R$ curves with a single minimum at the following values of the association distance: $LiClO_4$, 5.87 Å; $NaClO_4$, 5.53 Å; $KClO_4$, 5.47 Å; $RbClO_4$, 10.49 Å; $CsClO_4$, 5.20 Å; LiI, 5.85 Å; Et_4NI, 3.35 Å; LiCl, 6.66 Å; KPF_6, 8.71 Å.

Table 5. Parameters for sulfolane [a] as solvent at 30 °C calculated from conductance data of Fernandez-Prini and Prue.[14] N = number of points (c,Λ).

Salt	N	Cond. equation	Λ_∞ cm² Ω⁻¹ mol⁻¹	K_A M⁻¹	R Å	$\sigma(\Lambda)$ cm² Ω⁻¹ mol⁻¹
NaI	14	FHFP	10.868	7.77	8.30	0.0031
		FHFP	10.867	0.34	3.12	0.0034
		P	10.865	4.7	5[b]	0.003
KI	12	FHFP	11.255	9.6	8.33	0.0062
		FHFP	11.253	1.3	2.74	0.0061
		P	11.253	6.5	5[b]	0.005
LiBr	13	FHFP	13.237	279	9.13	0.0063
		FHFP	13.235	270	2.95	0.0062
		P	13.250	278	5[b]	0.010

[a] $\eta = 10.29$ cP; $\varepsilon = 43.33$; Bjerrum's critical distance, $q = 6.36$ Å. [b] Arbitrarily chosen value for the distance parameter.[14]

Table 6. Conductance parameters for sodium chloride in aqueous propanol at 15 °C calculated from data of Goffredi and Shedlovsky.[15] N = number of points (c,Λ).

N	η cP	ε	Cond. equation	Λ_∞ cm² Ω⁻¹ mol⁻¹	K_A M⁻¹	R Å	$\sigma(\Lambda)$ cm² Ω⁻¹ mol⁻¹	q Å
6	3.805	38.60	FHFP	25.906	14.9	6.99	0.0025	7.51
			FHFP	25.899	9.7	4.65	0.0022	7.51
			FOS	25.894	6	3.1	0.002	7.51
5	3.310	28.19	FHFP	21.199	65	9.47	0.0013	10.28
			FHFP	21.159	40	4.52	0.0014	10.28
			FOS	21.144	31	3.19	0.003	10.28
6	2.881	24.50	FHFP	20.212	148	15.55	0.0054	11.83
			FHFP	20.196	83	4.08	0.0053	11.83
			FOS	20.19	76	3.2	0.006	11.83

original research from the Fuoss-Onsager-Skinner ("FOS") equation.

Several further examples of 1:1-electrolyte systems for which sets of conductance parameters with almost equal $\sigma(\Lambda)$'s are observed at two different values of the distance parameter might be listed. As stated in the introduction, however, the purpose of this paper is to cite only some typical examples. The examples here accounted for would suffice to give an idea of the frequent appearance of such non-unique sets of conductance parameters.

CONCLUSIONS

From the present reevaluation, by means of the FHFP equation, of a large body of conductance data for 1:1-electrolytes in pure and mixed solvents it follows that the "best set" of conductance parameters frequently refers to a value of the association distance coinciding within experimental errors with Bjerrum's critical distance, a result in accord with observations of Justice.[7] However, these observations provide no unequivocal support for a conclusion that the distance parameter, R, should be numerically identified with the Bjerrum q value because of the frequent observations that, for a given system, an equally good fit as for $R = q$ may be obtained for a value of the association distance deviating considerably from Bjerrum's critical distance.

In calculating activity coefficients for non-associated ions using the Debye-Hückel ap-

proximation, eqn. (4), the use of R values less than the Bjerrum q value is in poor consistency with approximations made in deriving the activity coefficient expression, *cf.* Ref. 19. Yet, the present treatment of experimental data reveals that an equally good fit as for $R=q$, or even a better fit, is frequently observed for an association distance value considerably less than Bjerrum's critical distance.

An extension of the present investigation to include other conductance equations, in particular the Pitts equation, *cf.* Ref. 20, is a matter for further research.

Acknowledgement. Financial support by the Swedish Natural Science Research Council is gratefully acknowledged.

REFERENCES

1. Masterton, W. L. and Bierly, T. *J. Phys. Chem. 74* (1970) 139.
2. Hanna, E. M., Pethybridge, A. D. and Prue, J. E. *J. Phys. Chem. 75* (1971) 291.
3. Fuoss, R. M. and Hsia, K.-L. *Proc. Nat. Acad. Sci. U.S. 57* (1967) 1550.
4. Fuoss, R. M. and Hsia, K.-L. *Proc. Nat. Acad. Sci. U.S. 58* (1968) 1818.
5. Fernandez-Prini, R. *Trans. Faraday Soc. 65* (1969) 3311.
6. Fuoss, R. M. and Accascina, F. *Electrolytic Conductance*, Interscience, New York 1959, Chapter XV.
7. Justice, J.-C. *Electrochim. Acta 16* (1971) 701.
8. Beronius, P. *Acta Chem. Scand. A 28* (1974) 77.
9. Evans, D. F. and Gardam, P. *J. Phys. Chem. 72* (1968) 3281.
10. Reynolds, M. B. and Kraus, C. A. *J. Amer. Chem. Soc. 70* (1948) 1709.
11. Graham, J. R., Kell, G. S. and Gordon, A. R. *J. Amer. Chem. Soc. 79* (1957) 2352.
12. Hawes, J. L. and Kay, R. L. *J. Phys. Chem. 69* (1965) 2420.
13. Banewicz, J. J., Maguire, J. A. and Shih, P. S. *J. Phys. Chem. 72* (1968) 1960.
14. Fernandez-Prini, R. and Prue, J. E. *Trans. Faraday Soc. 62* (1966) 1257.
15. Goffredi, M. and Shedlovsky, T. *J. Phys. Chem. 71* (1967) 2176.
16. Barthel, J. *Angew. Chem. Int. Ed. 7* (1968) 260.
17. Robinson, R. A. and Stokes, R. H. *Electrolyte Solutions*, Butterworths, London 1965, p. 230.
18. Bjerrum, N. *Kgl. Dan. Vidensk. Selsk. Mat.-Fys. Medd. 7* (1926) No. 9.
19. Robinson, R. A. and Stokes, R. H. *Electrolyte Solutions*, Butterworths, London 1965, Chapter 4.
20. Pitts, E., Tabor, B. E. and Daly, J. *Trans. Faraday Soc. 66* (1970) 693.

Received October 14, 1974.

Acta Chemica Scandinavica A 29 (1975) 298—300

The Molecular Structure in the Solid State of a Dimerisation Product of Benzo[c]thiopyrylium-4-oxide

P. GROTH

Department of Chemistry, University of Oslo, Oslo 3, Norway

The major product of the dimerisation $2C_9H_8OS \rightarrow (C_9H_6OS)_2$ belongs to the orthorhombic system with space group *Fdd*2 and cell dimensions $a = 7.722(2)$ Å, $b = 21.991(4)$ Å, $c = 17.267(5)$ Å. The unit cell contains eight molecules with two-fold axes of symmetry. The structure was solved by the heavy atom method and refined by full-matrix least squares technique to an R-value of 4.4 % ($R_w = 4.7$ %) for 1003 reflections recorded on an automatic four circle diffractometer. The isomer has the *syn* structure. One of the intramolecular C—C distances between overlying benzene rings is as short as 3.242(6) Å, and the C—C bridge bond is 1.577(5) Å, which is significantly longer than a normal C—C single bond.

Dimerisation of thiopyrylium-4-oxides are studied by Undheim *et al.*[1] by spectroscopic methods. For benzo[*c*]thiopyrylium-4-oxide the reaction scheme is:

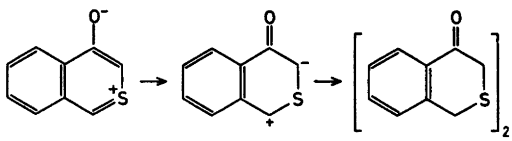

The product consists of two isomeric dimers. Weak indications from NMR- and UV-studies suggest that the major isomer has a *syn* structure (see Fig. 1). In order to settle the structural problem an X-ray crystallographic investigation has been carried out.

The crystals are orthorhombic with space group *Fdd*2, cell dimensions $a = 7.722(2)$ Å, $b = 21.991(4)$ Å, $c = 17.267(5)$ Å, and eight molecules in the unit cell. With 2θ-max = 60° and Mo$K\alpha$-radiation (graphite crystal monochromator), 1225 reflections were measured on an automatic four-circle diffractometer. With an observed-unobserved cutoff at $2.5\sigma(I)$, 1003 were recorded as observed. No corrections for absorption (crystal size 0.2 mm × 0.2 mm × 0.3 mm) or secondary extinction effects have been carried out.

The structure was solved by the heavy atom method and refined by full-matrix least squares technique.[2],* Anisotropic temperature factors were introduced for all non-hydrogens. Weights in least squares were obtained from the standard deviations in intensities, $\sigma(I)$, taken as where

$$\sigma(I) = [C_T + (0.02C_N)^2]^{\frac{1}{2}}$$

C_T is the total number of counts, and C_N the net count (peak minus background). The atomic form factors were those of Hanson *et al.*[3] except for hydrogen.[4] The R-value arrived at was 4.4 %

* All programs used are included in this reference.

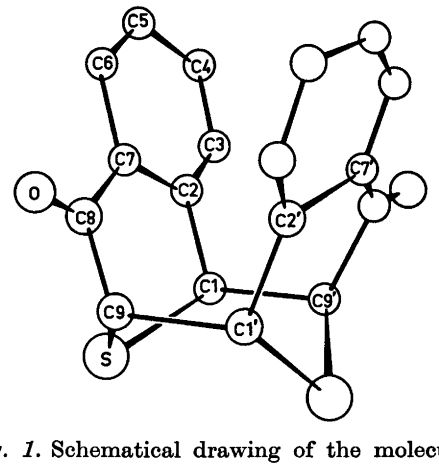

Fig. 1. Schematical drawing of the molecule.

Table 1. Final fractional coordinates and anisotropic thermal vibration parameters with estimated standard deviations (multiplied by 10^5 for non-hydrogens and 10^4 for hydrogen atoms). H*n* is bonded to C*n*.

ATOM	X	Y	Z	B	B11	B22	B33	B12	B13	B23
S	5489(13)	24589(4)	24970		1832(18)	164(2)	281(2)	-54(12)	-389(13)	-1(4)
O	-159(39)	35233(12)	41480(18)		2120(61)	159(6)	368(11)	255(29)	-48(45)	-78(12)
C1	15682(48)	18867(14)	30983(20)		1514(63)	112(6)	215(11)	-38(33)	-87(44)	-14(13)
C2	8738(42)	19126(14)	39145(21)		979(54)	141(7)	241(12)	-26(31)	-60(41)	2(14)
C3	6934(52)	13775(17)	43285(27)		1290(63)	147(7)	350(15)	-0(37)	91(52)	53(17)
C4	1149(53)	13795(20)	52858(31)		1359(64)	207(9)	377(17)	-61(38)	163(55)	169(22)
C5	-3322(55)	19241(22)	54354(28)		1676(88)	281(12)	284(15)	-108(47)	334(57)	66(21)
C6	-1791(64)	24584(20)	50327(31)		1456(72)	200(8)	292(12)	-2(36)	244(46)	-37(21)
C7	4836(43)	24628(15)	42688(22)		992(57)	144(7)	256(11)	2(30)	12(38)	-14(15)
C8	5518(44)	30622(16)	38625(22)		1175(56)	141(7)	257(12)	15(33)	-282(45)	-38(14)
C9	13923(48)	30867(15)	38654(28)		1575(67)	117(6)	211(11)	29(33)	-184(45)	39(14)
H1	1288(47)	1525(16)	2866(22)	2,5(,8)						
H3	962(52)	1019(18)	4095(23)	3,0(,8)						
H4	28(50)	1032(18)	5368(24)	2,8(,8)						
H5	-653(64)	1972(22)	5972(31)	4,5(1,1)						
H6	-483(58)	2826(24)	5236(30)	4,0(1,2)						
H9	996(56)	3422(18)	2718(26)	3,9(,9)						

(weighted valve $R_w = 4.7$ %) for 1003 observed reflections.

Final fractional coordinates and thermal parameters with estimated standard deviations are given in Table 1. The expression for anisotropic vibration is

$$\exp[-(B11h^2 + B22k^2 + B33l^2 + B12hk + B13hl + B23kl)]$$

The principal axes of the thermal vibration ellipsoids for sulfur, oxygen, and carbon atoms were calculated from the temperature parameters of Table 1. Maximum root mean squares amplitudes range from 0.19 to 0.27 Å. Rigid-body analysis of translational, librational, and screw motion [5] gave relatively large r.m.s. discrepancy between atomic vibration tensor components calculated from the thermal parameters of Table 1 and those calculated from the rigid-body parameters. By including the 22 non-hydrogen atoms the value obtained was 0.0039 Å^2, not strongly supporting the assumption of

Table 2. Bond distances and angles with estimated standard deviations.

DISTANCE	(Å)	DISTANCE	(Å)	DISTANCE	(Å)
S - C1	1,811(3)	S - C9	1,815(3)	C1 - C2	1,389(5)
C8 - C9	1,523(5)	C1 - C9′	1,377(5)	C2 - C7	1,402(5)
C7 - C8	1,399(5)	O - C8	1,209(4)	C2 - C3	1,384(5)
C3 - C4	1,382(7)	C4 - C5	1,385(7)	C5 - C6	1,370(6)
C6 - C7	1,394(6)				

ANGLE	(°)	ANGLE	(°)
C1 - S - C9	93,6(2)	S - C1 - C2	110,8(2)
S - C9 - C8	108,8(2)	S - C1 - C9′	112,8(2)
S - C9 - C1′	114,8(2)	C2 - C1 - C9′	112,8(3)
C8 - C9 - C1′	113,2(3)	C1 - C2 - C7	122,1(3)
C9 - C8 - C7	119,1(3)	C2 - C7 - C8	122,3(3)
C1 - C2 - C3	119,1(3)	C8 - C7 - C6	118,2(3)
O - C8 - C7	121,3(3)	O - C8 - C9	119,5(3)
C2 - C3 - C4	121,2(4)	C3 - C4 - C5	119,7(4)
C4 - C5 - C6	119,9(4)	C5 - C6 - C7	120,9(4)
C6 - C7 - C2	119,4(3)	C7 - C2 - C3	118,8(3)

DISTANCE	(Å)	DISTANCE	(Å)	DISTANCE	(Å)
C1 - H1	,92(4)	C9 - H9	1,00(4)	C3 - H3	,91(4)
C4 - H4	,91(4)	C5 - H5	,96(5)	C6 - H6	,91(5)

ANGLE	(°)	ANGLE	(°)
H1 - C1 - S	124,(2)	H1 - C1 - C2	111,(2)
H1 - C1 - C9′	105,(2)	H9 - C9 - S	97,(2)
H9 - C9 - C8	116,(3)	H9 - C9 - C1′	107,(3)
H3 - C3 - C2	119,(2)	H3 - C3 - C4	120,(2)
H4 - C4 - C3	122,(3)	H4 - C4 - C5	118,(3)
H5 - C5 - C4	125,(3)	H5 - C5 - C6	115,(3)
H6 - C6 - C5	123,(3)	H6 - C6 - C7	116,(3)

regarding the molecule as an oscillating rigid body. Further, since the maximum libration amplitude was only 3.1°, librational corrections were smaller than one e.s.d., and the coordinates are therefore given with their uncorrected values.

Bond distances and angles are given in Table 2, and Fig. 1 shows the molecule.

The C–S bond lengths of 1.811 and 1.815 Å correspond closely to the single bond (1.816 Å).[6]

The part of the molecule consisting of O,C1, . . . ,C9 is planar to within 0.1 Å with S 1.0 Å out of the plane. The angle between this plane and the one defined by C1,C9,C1′ is 67°. In spite of this tilt of the planar groups, the distance C8–C2′ of 2.763 Å, and even those of C8–C3′ (3.251 Å) and C7–C7′ (3.242 Å), are short and imply repulsions; a fact which is reflected in the bond length C9–C1′ (1.577 Å) which is significantly longer than the normal C–C single bond. Similar effects have been observed in cage molecules where C–C bonds are lengthened to 1.574(8), 1.572(7),[7] and 1.574(3) Å[8] by cage formation. However, in contradiction to such cases, where the internal strain is forced on the molecules by synthesis, one would, in view of the reaction scheme shown above, expect the *anti* form (I) to be the more stable structure.

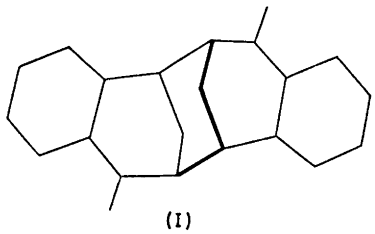

(I)

Other bond distances and angles are normal. No short *inter*-molecular contacts are observed. A list of observed and calculated structure factors is available by request to the author.

Acknowledgement. The author would like to thank S. Baklien for supplying the crystal.

REFERENCES

1. Undheim, K. and Baklien, S. *Personal communication.*
2. Groth, P. *Acta Chem. Scand. 27* (1973) 3131.
3. Hanson, H. P., Herman, F., Lea, J. and Skillman, S. *Acta Crystallogr. 17* (1964) 1040.
4. Stewart, R. F., Davidson, E. R. and Simpson, W. T. *J. Chem. Phys. 42* (1965) 3175.
5. Schomaker, V. and Trueblood, K. N. *Acta Crystallogr. B 24* (1968) 63.
6. Knobler, C., Baker, C., Hope, H. and McCullough, J. D. *Inorg. Chem. 10* (1971) 697.
7. Schwarzenbach, D. *Acta Crystallogr. B 24* (1968) 238.
8. Gilardi, R. D. *Acta Crystallogr. B 28* (1972) 742.

Received October 25, 1974.

Acta Chemica Scandinavica A 29 (1975) 301—306

Tris-[(±)$_D$-1-(2-pyridyl)ethylamine]cobalt(III) Complexes. Preparation and Partial Structural Assignment of Geometrical and Optical Isomers*

KIRSTEN MICHELSEN

Chemistry Department I (Inorganic Chemistry), University of Copenhagen, H. C. Ørsted Institute, Universitetsparken 5, DK-2100 Copenhagen Ø, Denmark

Tris-[(±)$_D$-1-(2-pyridyl)ethylamine]cobalt(III) chloride has been prepared and separated into five distinct, racemic fractions by column chromatography. Four of the racemates were separated into their catoptric forms by column chromatography using an optically active eluent.

X-Ray powder photographs, absorption spectra and CD spectra identified four of these new isomers as:

I(+): *fac*-Λ(+)$_D$-[Co{(*S*)(−)$_D$-$C_7H_{10}N_2$}$_3$]$^{3+}$,
I(−): *fac*-Δ(−)$_D$-[Co{(*R*)(+)$_D$-$C_7H_{10}N_2$}$_3$]$^{3+}$,
IV(+): *fac*-Λ(+)$_D$-[Co{(*R*)(+)$_D$-$C_7H_{10}N_2$}$_3$]$^{3+}$,
and
IV(−): *fac*-Δ(−)$_D$-[Co{(*S*)(−)$_D$-$C_7H_{10}N_2$}$_3$]$^{3+}$,

compounds that have been prepared recently using optically active amines as initial materials.

The physical measurements suggest the remaining four isomers to be:

II(+): *fac*-Λ(+)$_D$-[Co{(*S*)(−)$_D$-$C_7H_{10}N_2$}$_2$-{(*R*)(+)$_D$-$C_7H_{10}N_2$}]$^{3+}$,
II(−): *fac*-Δ(−)$_D$-[Co{(*R*)(+)$_D$-$C_7H_{10}N_2$}$_2$-{(*S*)(−)$_D$-$C_7H_{10}N_2$}]$^{3+}$,
III(+): *fac*-Λ(+)$_D$-[Co{(*S*)(−)$_D$-$C_7H_{10}N_2$}{(*R*)(+)$_D$-$C_7H_{10}N_2$}$_2$]$^{3+}$, and
III(−): *fac*-Δ(−)$_D$-[Co{*R*)(+)$_D$-$C_7H_{10}N_2$}{(*S*)(−)$_D$-$C_7H_{10}N_2$}$_2$]$^{3+}$.

Recently tris-diamine complexes of cobalt(III) and chromium(III) have been given considerable attention by this laboratory.[2–5] The present work represents an extension of this attention by including tris-complexes of cobalt(III) and the hitherto rather unknown bidentate ligand 1-(2-pyridyl)-ethylamine (Fig. 1b).

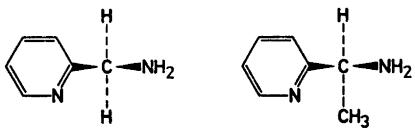

Fig. 1. a. (2-Pyridyl)methylamine (2-picolylamine). b. 1-(2-Pyridyl)ethylamine.

In a previous paper [1] tris-complexes of cobalt and the optically active ligands (−)$_D$- and (+)$_D$-1-(2-pyridyl)ethylamine were described. Because of geometrical and configurational isomerism, four isomers of each of the formulas [Co{(−)$_D$-$C_7H_{10}N_2$}$_3$]X_3 and [Co{(+)$_D$-$C_7H_{10}N_2$}$_3$]X_3 should be expected. We succeeded in isolating and assigning three different complexes with (−)$_D$-1-(2-pyridyl)ethylamine, namely two *facial* and one *meridional* isomer and the corresponding three enantiomers with the (+)$_D$-amine.

In this work concerning the tris-[(±)$_D$-1-(2-pyridyl)ethylamine]cobalt(III) system, we succeeded in isolating and identifying eight *facial* isomers. Analogously with the corresponding propylenediamine system [5] the racemic amine should, at least theoretically, give rise to eight *facial* isomers.

THE PREPARATIVE METHODS AND THE ASSIGNMENT OF THE ISOMERS

The racemic mixture of [Co{(±)$_D$-$C_7H_{10}N_2$}$_3$]Cl_3 was prepared from an ethanolic

* See Ref. 1.

solution of *trans*-dichlorotetrakis(pyridine)-cobalt(III) chloride and racemic amine.[3,6] The crude product was separated by column chromatography into four *facial* (I, II, III, IV) and one *meridional* fraction (V). The *facial* compounds were further resolved into their enantiomers on a column with a tartrate eluent. From fraction V it was possible to isolate one *meridional* compound, while another, the racemate of *mer*-$\Lambda(+)_D$-$[Co\{(S)(-)_D$-$C_7H_{10}N_2\}_3]^{3+}$ (abbrev. *mer*-ΛS_3) and *mer*-$\Delta(-)_D$-$[Co\{(R)(+)_D$-$C_7H_{10}N_2\}_3]^{3+}$ (abbrev, *mer*-ΔR_3), which was expected to be present in a very small amount, disappeared. As the yield of the remaining compound was small, and the first attempts at resolution were unsuccessful, further investigations of the *meridional* compounds were postponed.

As in the previous work [1] it is assumed to be correct that the $(-)_D$-form of the amine has the configuration *S*,[7,8] the $(+)_D$-form consequently the configuration *R*. It is also assumed that there is a relationship between the total (net) $d-d$ rotatory strength (or the sign of the algebraic sum of the $d-d$ CD band areas) and the absolute configuration of the complexes, the strength being positive for the Λ isomers.[9] The nomenclature is that proposed by IUPAC.[10]

EXPERIMENTAL

Reagents. The initial material *trans*-$[Copy_4Cl_2]Cl.6H_2O$ was prepared by a method developed by Glerup and Schäffer.[11] Racemic 1-(2-pyridyl)ethylamine was prepared as described before.[1] SP-Sephadex C-25 was purchased from Pharmacia, Uppsala, Sweden. All other chemicals were of reagent grade and were used without further purification.

Analyses. The cobalt analyses were performed on a Perkin Elmer 403 Atomic Absorption Spectrophotometer. The microanalytical laboratory of this institute carried out the carbon and the nitrogen analyses by standard methods.

Physical measurements. Absorption spectra were recorded on a Cary Model 14 spectrophotometer. The spectra are characterized by their maxima and minima (ε,λ), where the molar extinction coefficient ε is in units of 1 mol^{-1} cm^{-1} and λ is in nm. Circular dichroism was measured on a Roussel-Jouan Dichrographe I. The maxima are given below as $(\Delta\varepsilon,\lambda) = [(\varepsilon_l - \varepsilon_r),\lambda]$. Optical rotation was measured on a Perkin Elmer Model 141 polarimeter. In all cases the solvent was 0.1 M hydrochloric acid. The X-ray powder photographs were obtained on a camera of the Guinier type with Cu$K\alpha$ radiation. Silicium was used as standard.

Preparation of the cobalt complexes. 2.00 g of $[Copy_4Cl_2]Cl.6H_2O$ (3.39 mmol) was dissolved in 50 ml of ethanol (99 %). 1.25 ml of racemic amine ($\sim$ 10.2 mmol) was added. An immediate colour-shift from green to yellow-brown took place. After 10 min a yellow-brown solid was precipitated by addition of ether. Washing with ether.

Ion exchange separations. The crude product was dissolved in 0.1 M hydrochloric acid. The solution was poured on a column (length 60 cm, diameter 5 cm) of an SP-Sephadex C-25 cation exchanger (Sephadex was introduced for similar purposes by Yoshikawa and Yamasaki [12]), and the adsorbed bands were eluted with a solution that was 0.2 M in sodium dihydrogenorthophosphate and 0.02 M in disodium hydrogenorthophosphate (acid solutions were necessary in order to avoid destruction of the compounds). Four yellow and one orange band resulted. They were named I, II, III, IV, and V, following the order of their elution.

I: The first yellow fraction was a very small one. The eluate was diluted with an equal amount of water and poured on a small Sephadex column (length 20 cm, diameter 1.25 cm). Sodium and phosphate ions were removed by a subsequent elution with 0.1 M hydrochloric acid. When the eluate showed negative phosphate reaction, the complex was eluted with 0.5 M sulfuric acid. The concentrated solution weas evaporated to nearly dryness on a vacuum rotatory evaporator. The residue was dissolved in ethanol (99 %), the solution was cooled on ice, and the complex was precipitated with ether. The compound was redissolved in 2 M sulfuric acid and reprecipitated with ethanol and ether after filtering. Yield: 195 mg (8.0 %). (Found: Co 8.38; N 11.7. Calc. for $[Co(C_7H_{10}N_2)_3](HSO_4)$: Co 8.22; N 11.7). In another experiment the yield was 8.1 %. When sodium perchlorate was added to a concentrated solution of the complex, compact bright yellow crystals precipitated. They were filtered and washed with ice-cold water. (Found: Co 7.79; C 33.2; N 11.2; Cl 14.1. Calc. for $[Co(C_7H_{10}N_2)_3](ClO_4)_3.2H_2O$ Co 7.76; C 33.2; N 11.1; Cl 14.0). $(\varepsilon,\lambda)_{max}$: (149,461), (160,338). $(\varepsilon,\lambda)_{min}$: (15,388), (143,322). The X-ray powder photograph of this compound was identical with that of the perchlorate prepared in a similar manner from a solution of an equimolar mixture of the previously described compounds [1] assumed to be *fac*-ΛS_3 and *fac*-ΔR_3. (About the abbreviations: see Table 1).

II: The second yellow fraction was a large one. It was treated like fraction I with the exception that it was finally eluted with 1 M hydrochloric acid instead of sulfuric acid. The solution was evaporated on a vacuum rotatory evaporator, and the complex was precipitated by means of ethanol and ether. Yield:

Table 1. The *facial* isomers of $[Co\{(\pm)_D\text{-}C_7H_{10}N_2\}_3]^{3+}$.

Symbol	Formula	Abbrev.
I(+)	*fac*-$\Lambda(+)_D$-$[Co\{(S)(-)_D\text{-}C_7H_{10}N_2\}_3]^{3+}$	*fac*-ΛS_3
II(+)	*fac*-$\Lambda(+)_D$-$[Co\{(S)(-)_D\text{-}C_7H_{10}N_2\}_2\{(R)(+)_D\text{-}C_7H_{10}N_2\}]^{3+}$	*fac*-ΛS_2R
III(+)	*fac*-$\Lambda(+)_D$-$[Co\{(S)(-)_D\text{-}C_7H_{10}N_2\}\{(R)(+)_D\text{-}C_7H_{10}N_2\}_2]^{3+}$	*fac*-ΛSR_2
IV(+)	*fac*-$\Lambda(+)_D$-$[Co\{(R)(+)_D\text{-}C_7H_{10}N_2\}_3]^{3+}$	*fac*-ΛR_3
I(−)	*fac*-$\Delta(-)_D$-$[Co\{(R)(+)_D\text{-}C_7H_{10}N_2\}_3]^{3+}$	*fac*-ΔR_3
II(−)	*fac*-$\Delta(-)_D$-$[Co\{(R)(+)_D\text{-}C_7H_{10}N_2\}_2\{(S)(-)_D\text{-}C_7H_{10}N_2\}]^{3+}$	*fac*-ΔR_2S
III(−)	*fac*-$\Delta(-)_D$-$[Co\{(R)(+)_D\text{-}C_7H_{10}N_2\}\{(D)(-)_D\text{-}C_7H_{10}N_2\}_2]^{3+}$	*fac*-ΔRS_2
IV(−)	*fac*-$\Delta(-)_D$-$[Co\{(S)(-)_D\text{-}C_7H_{10}N_2\}_3]^{3+}$	*fac*-ΔS_3

757 mg (35 %). (Found: Co 9.19. Calc. for $[Co(C_7H_{10}N_2)_3]Cl_3.6H_2O$: Co 9.20). In another experiment the yield was 31 %. As the chloride inclined to deliquescence, it was converted into the perchlorate as described above. (Found: Co 8.13; C 34.8; N 11.7; Cl 14.9. Calc. for $[Co(C_7H_{10}N_2)_3](ClO_4)_3$: Co 8.14; C 34.9; N 11.6; Cl 14.7). $(\varepsilon,\lambda)_{max}$: (149,459.5), (155,336). $(\varepsilon,\lambda)_{min}$: (17,386), (146,324).

III: This relatively large, yellow fraction was isolated exactly like II. Yield: 525 mg (26 %). (Found: Co 9.83. Calc. for $[Co(C_7H_{10}N_2)_3]Cl_3.4H_2O$: Co 9.76). In another experiment the yield was 29 %. The perchlorate was prepared, as it was easier to handle in humid air. (Found: Co 7.84; C 33.3; N 11.2; Cl 14.4. Calc. for $[Co(C_7H_{10}N_2)_3](ClO_4)_3.1\frac{1}{2}H_2O$: Co 7.85; C 33.6; N 11.2; Cl 14.2). $(\varepsilon,\lambda)_{max}$: (150,459), (160,330). $(\varepsilon,\lambda)_{min}$: (17,386).

IV: The fourth yellow fraction was very small. It was isolated as a chloride and identified (see later) as a racemic mixture of the previously described compounds [1] assumed to be *fac*-ΔS_3 and *fac*-ΛR_3. Based on a comparison with their absorption spectra the yield was estimated to be 3.4 % (74 mg of $[Co(C_7H_{10}N_2)_3]Cl_3.6\frac{1}{2}H_2O$). In another experiment it was 3.8 %.

V: The fifth band was orange, indistinct, and probably consisted of two compounds, one of which was present only in a very small amount. From the eluate the most abundant compound was isolated and purified by recrystallization as described for fraction I. Yield: 183 mg of orange crystals (7.0 %). (Found: Co 7.67; C 32.8; N 10.9. Calc. for $[Co(C_7H_{10}N_2)_3](HSO_4)_3.3H_2O$: Co 7.65; C 32.3; N 10.9). $(\varepsilon,\lambda)_{max}$: (190,474), (221,337). $(\varepsilon,\lambda)_{min}$: (20,393), (218,329). In another experiment the yield was 5.3 %. "The impurity" that vanished during the recrystallization was presumably a racemic mixture of the two earlier desribed compounds [1] *mer*-ΛS_3 and *mer*-ΔR_3, as one should expect this racemic mixture to be formed, although in a small amount.

Resolution into enantiomers. Each of the four racemates was resolved on columns (length 60 cm, diameter 2.5 cm) of SP-Sephadex C-25. The compounds (in amounts ranging from 0.1 to 0.5 mmol) were absorbed to the columns from water solutions, and the bands were eluted with a solution that was 0.09 M in sodium $(+)_D$-tartrate and 0.04 M in sodium $(+)_D$-hydrogentartrate. The resolution was complete in the case of the compounds II, III, and IV, but only partial for I. In all cases the Λ-fraction was eluted first. The single fractions were treated in nearly the same way. They were absorbed on smaller columns. Sodium and tartrate ions were removed by a subsequent elution with 0.1 M hydrochloric acid, and finally the complexes were eluted with 1 M hydrochloric acid or 0.5 M sulfuric acid. Isolation of the solid chlorides or hydrogensulfates was performed as described above (see I and II).

I(+) and (−): In this case only, the separation was not complete, but the first fraction consisted mainly of the Λ-form, the last one of the Δ-form. As the racemate was identified by other means as an equimolar mixture of the earlier described [1] compounds *fac*-ΛS_3 and *fac*-ΔR_3, an attempt to accomplish the separation on a longer column was not considered worthwhile.

II(+) and (−): The column had exactly the right dimensions to give a complete separation. The enantiomers II(+) and II(−) were both isolated as chlorides. II(+): (Found: Co 9.36. Calc. for $[Co(C_7H_{10}N_2)_3]Cl_3.5\frac{1}{2}H_2O$: Co 9.34). $(\varepsilon,\lambda)_{max}$: (149,459.5), (146,337). $(\varepsilon,\lambda)_{min}$: (16,386), (130,322). $(\Delta\varepsilon,\lambda)_{max}$: (+2.16,470), (−0.46,340). $[M]_D^{25} = +653°$ ($c = 1.7$ mg/ml). II(−): (Found: Co 9.34. Calc. for $[Co(C_7H_{10}N_2)_3]Cl_3.5\frac{1}{2}H_2O$: Co 9.34). $(\varepsilon,\lambda)_{max}$: (150,459.5), (150,337). $(\varepsilon,\lambda)_{min}$: (17,386), (137,322). $(\Delta\varepsilon,\lambda)_{max}$: (−2.15,470), (+0.47,344). $[M]_D^{25} = -651°$ ($c =$ 1.7 mg/ml).

III(+) and (−): A smaller column (45 cm instead of 60 cm) would have sufficed to complete the separation. The enantiomers III(+) and III(−) were both isolated as the hydrogensulfates. III(+): (Found: Co 7.43. Calc. for $[Co(C_7H_{10}N_2)_3](HSO_4)_3.4H_2O$: Co 7.47). $(\varepsilon,\lambda)_{max}$: (150,459), (135,336.5). $(\varepsilon,\lambda)_{min}$: (17,385.5), (125,323). $(\Delta\varepsilon,\lambda)_{max}$: (+2.23,464),

Table 2. Electronic spectral parameters for $[Co\{C_7H_{10}N_2\}_3]^{3+}$. VI(+) is *mer*-$\Lambda$(+)$_D$-$[Co\{(S)(-)_D$-$C_7H_{10}N_2\}_3]Cl_3$.[1] δ is the half-width of the long-wavelength band.

Symbol	$\lambda_{max}(1)$ (nm)	$\varepsilon_{max}1)$	$\delta(1)$ cm^{-1}	$\lambda_{max}(2)$ (nm)	$\varepsilon_{max}(2)$
I(+)[a]	460.5	149	3327	338	156
I(+)	459.5	149	3335	337	146
III(+)	459	150	3363	336.5	135
IV(+)	459	156	3301	336	131
V	474	190	3575	337	221
VI(+)[a]	475	193	3526	341	209

[a] The measurements were carried out on previously prepared and described compounds.

(−0.61,343). $[M]_D^{25} = +542°$ (1.9 mg/ml). III(−): (Found: Co 7.20. Calc. for $[Co_7H_{10}N_2)_3](HSO_4)_3.5H_2O$: 7.31). $(\varepsilon,\lambda)_{max}$: (151,459), (137,336.5). $(\varepsilon,\lambda)_{min}$: (17,385.5), (128,323). $(\Delta\varepsilon,\lambda)_{max}$: (−2.22,464), (+0.63,344). $[M]_D^{25} = -543°$ (1.9 mg/ml).

IV(+) and (−): A column of only 30 cm would have been sufficiently large to ensure a complete separation. Both isomers were isolated as the hydrogensulfates. IV(+): (Found: Co 7.07. Calc. for $[Co(C_7H_{10}N_2)_3](HSO_4)_3.6H_2O$: Co 7.15). $(\varepsilon,\lambda)_{max}$: (156,459), (131,336). $(\varepsilon,\lambda)_{min}$: (20,385), (127,326). $(\Delta\varepsilon,\lambda)_{max}$: (+2.39,464), (−0.57,344). IV(−): (Found: Co 7.35. Calc. for $[Co(C_7H_{10}N_2)_3](HSO_4)_3.5H_2O$: Co 7.31). $(\varepsilon,\lambda)_{max}$: (154,459), (136,333). $(\varepsilon,\lambda)_{min}$: (17,385), (135,326). $(\Delta\varepsilon,\lambda)_{max}$: (−2.40,464), (+0.57,343). X-Ray powder photographs, absorption spectra and CD-spectra showed that IV(+) and IV(−) were identical with the hydrogensulfates of the earlier investigated compounds,[1] *fac*-ΛR_3 and *fac*-ΛS_3.

RESULTS AND DISCUSSION

Characterization and identification of the isomers. $[Co\{(\pm)_D$-$C_7H_{10}N_2\}_3]Cl_3$ was separated into five distinct fractions on a Sephadex column with a phosphate eluent. The fractions I−IV had the same yellow colour as the *facial* isomer of tris-[2-picolylamine]cobalt(III) bromide [3] [2-picolylamine = (2-pyridyl)methylamine], see Fig. 1a), while the orange fraction (V) had the same colour as the meridional isomer. This immediately suggests that I, II, III, and IV are *facial* isomers, while V is a *meridional* isomer. The assumption is supported by the data from the electronic absorption spectra (see later). Fraction I was partially and fractions II, III and IV were completely resolved into their enantiomers on a Sephadex column with a tartrate eluent. In all cases the Λ-form was eluted as the first one.

I: The X-ray powder photograph of the perchlorate of this compound was identical with that of the perchlorate prepared from an equimolar mixture of the previously described compounds [1] assumed to be *fac*-ΛS_3 and *fac*-ΛR_3 (as to the abbrev. see Table 1). I, therefore, can

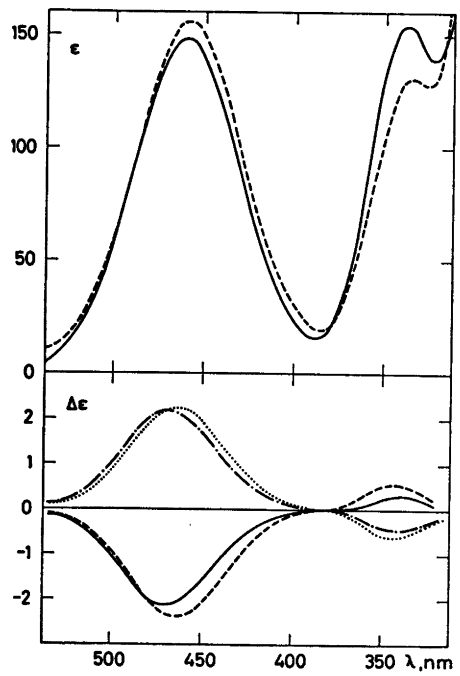

Fig. 2. The absorption spectra (top) of I [I(+), I(−)] (———) and IV [IV(+), IV(−)] (- - -) and the circular dichroism spectra (bottom) of I(−) (———), II(+) (−·−), III(+) (···) and IV(−) (- - -).

Table 3. Circular dichroim data for *fac*-$\Lambda(+)_D$-$[Co\{C_7H_{10}N_2\}_3]^{3+}$. In the same table the molar optical rotations at the Na_D-line are given as $[M]_D^{25}$.

Symbol	$\lambda_{max}(1)$ (nm)	$\Delta\varepsilon_{max}(1)$	$\lambda_{max}(2)$ (nm)	$\Delta\varepsilon_{max}$	$[M]_D^{25}$ (°)
I(+)[a]	470	+2.14	340	−0.36	+947
II(+)	470	+2.16	340	−0.46	+653
III(+)	464	+2.23	343	−0.61	+542
IV(+)	464	+2.39	344	−0.57	+566

[a] The measurements was carried out on a previously prepared and described compound.

be characterized as the racemate *fac*-(ΛS_3, ΔR_3).

IV: X-Ray powder photographs, absorption spectra and CD spectra proved that IV(+) and IV(−) were identical with the hydrogensulfates of the earlier investigated compounds *fac*-ΛR_3 and *fac*-ΔS_3.[1] IV, therefore, is characterized as the racemate *fac*-(ΛR_3,ΔS_3).

II and III: It is an obvious thought that the variation in the elution rate of the compounds I−IV is connected with a systematic variation in the structure of the compounds. This coherence is observed in the tris-[$(\pm)_D$-1,2-propanediamine]cobalt(III) system [5] and would imply that II is the racemate *fac*-(ΛS_2R,ΔR_2S) and III the racemate *fac*-(ΛSR_2,ΔRS_2). These suppositions are supported by the data from the absorption and CD spectra.

Electronic spectra. The electronic spectra of I [I(+), I(−)] and IV [IV(+), IV(−)] in the visible region are given in Fig. 1. The spectra of II [II(+), II(−)] and III [III(+), III(−)] are so similar to the former that they are situated between them. The resemblance between these four spectra (see Table 2) and that belonging to *fac*-tris-[2-picolylamine]cobalt(III) bromide,[3] ($(\varepsilon,\lambda)_{max}$: (130,462), (135,336.5). δ = 3360 cm^{-1}) supports the supposition that I−IV have *facial* structures. A comparison of the absorption spectra of V, of the previously described *mer*-$\Lambda(+)_D$-$[Co\{(S)(-)_D$-$C_7H_{10}N_2\}_3]Cl_3$ and of *mer*-tris-[2-picolylamine]cobalt(III) bromide,[3] ($(\varepsilon,\lambda)_{max}$: (155,471), (170,339). δ = 3450 cm^{-1}), shows that V is likely to be a *meridional* compound. Furthermore, the half-width of the long-wavelength band is greater for V than for the compounds of a higher symmetry I−IV. The variation, if any, in the λ and ε values, is systematic, going from I to IV (see Table 2).

Circular dichroism spectra. The CD spectra of II(+), III(+) and (to avoid coincidence) (I−) and IV(−) are shown in Fig. 2. The spectra are all very alike showing one CD band only corresponding to the first absorption band. As mentioned before, we use the sign of the algebraic sum of the $d-d$ CD band areas to assign the configuration Λ to the four compounds I(+)−IV(+), and the configuration Δ to the compounds I(−)−IV(−).[9]

As is appears from Table 3, the variation, if any, in the CD data is nearly systematic going from I(+) to IV(+). It is also noticeable that there is a strong mutual resemblance between the spectra of I(+) and II(+) and between III(+) and IV(+), respectively. This might be due to greater similarities in the composition of the compounds in question providing a further support to our suppositions about the systematic variation of the structure when going from I to IV.

Conclusion. The assignments of the eight obtainable *facial* isomers are summarized in Table 1, while the problems concerning the *meridional* isomers require further investigations. Another important question is so far unanswered: What are the conformations of the ligands? Are they fixed in preferred conformations, or are they flexible, the methyl-groups flapping between an equatorial and an axial position? The determination of the structure and absolute configuration of I(+) by X-ray analysis, presently being carried out at this laboratory, may perhaps throw some light upon this problem.

REFERENCES

1. This work represents a continuation of the earlier publication: Michelsen, K. *Acta Chem. Scand. A 28* (1974) 428.
2. Andersen, P., Galsbøl, F. and Harnung, S. E. *Acta Chem. Scand. 23* (1969) 3027.

3. Michelsen, K. *Acta Chem. Scand. 24* (1970) 2003.
4. Toftlund, H. and Pedersen, E. *Acta Chem. Scand. 26* (1972) 4019.
5. Harnung, S. E., Kallesøe, S., Sargeson, A. M. and Schäffer, C. E. *Acta Chem. Scand. A 28* (1974) 385.
6. Smirnoff, A. P. *Helv. Chim. Acta 3* (1920) 181.
7. Smith, H. E., Schaad, L. J., Banks, R. B., Wiant, C. J. and Jordan, C. F. *J. Amer. Chem. Soc. 95* (1973) 811.
8. Cervinka, O., Belovsky, O. and Rejmanova, P. *Z. Chem. 10* (1970) 69.
9. Schäffer, C. E. *Proc. Roy. Soc. London A 297* (1967) 96.
10. IUPAC *Inorg. Chem. 9* (1970) 1.
11. Glerup, J. and Schäffer, C. E. *Acta Chem. Scand. To be published.*
12. Yoshikawa, J. and Yamasaki, K. *Inorg. Nucl. Chem. Lett. 6* (1970) 523.

Received October 10, 1974.

Acta Chemica Scandinavica A 29 (1975) 307—311

Conformational Analysis. 1. The Temperature Effect on the Structure and Composition of the Rotational Conformers of 1,2-Dichloroethane as Studied by Gas Electron Diffraction. Additional Remarks.

KARI KVESETH

Department of Chemistry, University of Oslo, Blindern, Oslo 3, Norway

Gaseous 1,2-dichloroethane has been studied by electron diffraction at 2 °C. The ratio between the amounts of *anti* and *gauche* conformers is determined and the results compared with the values obtained in the previous investigation [1] of this compound.

The temperature dependency of the thermodynamical differences for the conformational equilibrium *anti*⇌*gauche*, ΔE and ΔS, is discussed in detail.

The temperature average of ΔS is determined fitting the best straight line to the $R \ln(1/K)$ *versus* $1/T$ data, and the slope gives ΔE. The results obtained in this investigation are $\Delta E =$ 1.05(.10) kcal mol^{-1} and $\Delta S = 0.90(.29)$ cal mol^{-1} deg^{-1}.

In the previous investigation on 1,2-dichloroethane,[1] some uncertainties were introduced because the observation at −13 °C did not seem to represent the conformational equilibrium at that temperature. The deviation from the best straight line fitted to the other observed (R ln $1/K$, $1/T$)-points was too large to originate from the temperature dependency of the thermodynamical terms, and was believed to be caused by some condensing phenomena in the nozzle, favouring the *anti* conformer.

Partly to check this, but also to present a more complete analysis of the temperature dependency of the thermodynamical quantities ΔE and ΔS, the molecule has been studied at 2 °C by gas electron diffraction.

EXPERIMENTAL AND STRUCTURE ANALYSIS

The sample of 1,2-dichloroethane was obtained from British Drug Houses (> 98.9 %) and used without further purification. Electron-diffraction photographs were obtained with the Balzer Eldigraph KDG-2 [2,3] unit, the experimental conditions being summarized in Table 1. The data corrections and analysis are performed as described in Ref. 1.

D and u values calculated from the force field [4] at 2 °C are given in Table 2, and the refined structure in Table 3. The distances are all R_a-values, the angles correspond to R_α-values.[5] The standard deviations, given in parentheses, are those calculated by the least-squares procedure, using off-diagonal elements in the applied weight matrix and adding 0.1 % as contribution from systematic errors in the wavelength.

RESULTS AND DISCUSSION

The structural parameters (Table 3) agree well with the previous results,[1] although the R(C−H) and CCH-angle are definitely smaller than the means in the latter (Table 4, column c of Ref. 1). The better values for u(C−C) and u(C−Cl), indicates that a more correct blackness correction has been used.

If R ln $(1/K)$ varies linearly with $1/T$ in the actual temperature interval, this means that R ln $(2Q_g/Q_a)$ is temperature independent, or at least that the temperature derivative of ln (Q_g/Q_a) is so small that it can be neglected in the calculations of ΔE and ΔS (eqn. 1)

Table 1. Experimental conditions and photographic plate data.

Temp (°C)	2	
Apparatus	Balzer	
Nozzle-to-plate distance (mm)	579.93	189.91
Electron wavelength (Å) [a]	0.058550	0.058534
Number of plates used	5	5
Range of data (s) [b]	1.125 – 13.500	5.500 – 32.250
Data interval (Δs)	0.125	0.250

[a] Determined in separate experiments by calibration to benzene. [b] $s = 4\pi/\lambda \sin\theta$; 2θ is the scattering angle.

Table 2. The difference, D, between R_a and R_α and vibrational amplitudes, u, calculated from valence force field for $t = 2$ °C.

	D (Å)	u (Å)
(C – C)	0.00008	0.052
(C – Cl)	– 0.00439	0.052
(C – H)	– 0.01123	0.078
$(C\cdots Cl)_a$ [a]	– 0.00291	0.068
$(C\cdots Cl)_g$	– 0.00035	0.068
$(C\cdots H)_a$	– 0.00192	0.109
$(C\cdots H)_g$	– 0.00523	0.109
$(Cl\cdots H)$	– 0.00713	0.109
$(H\cdots H)$	– 0.01133	0.128
$(Cl\cdots Cl)_a$	0.00100	0.066
$(Cl\cdots H)_{a,g}$	0.00055	0.163
$(Cl\cdots H)_{a,g}$	0.00055	0.163
$(H\cdots H)_{a,a}$	– 0.00246	0.128
$(H\cdots H)_{a,g}$	0.00162	0.178
$(H\cdots H)_{a,g}$	0.00162	0.178
$(Cl\cdots Cl)_g$	0.00614	0.144
$(Cl\cdots H)_{g,g}$	0.00263	0.159
$(Cl\cdots H)_{g,a}$	– 0.00218	0.102
$(H\cdots H)_{g,g}$	– 0.00354	0.170
$(H\cdots H)_{g,g}$	– 0.00520	0.174
$(H\cdots H)_{g,a}$	– 0.00686	0.129

[a] The suffix a and g refers to *anti* and *gauche* respectively. In the double suffix the first letter gives the conformation, the second the type of distance involved.

$$\Delta E = \Delta E^\circ + RT^2(\partial/\partial T)[\ln(Q_g/Q_a)] \quad (1)$$
$$\Delta S = R \ln 2 + R \ln(Q_g/Q_a) + RT(\partial/\partial T)[\ln(Q_g/Q_a)]$$

where Q is the vibrational-rotational partition function, ΔE° is the energy-difference between *gauche* and *anti* at the absolute zero point. $\Delta E = \Delta H$ and ΔS are the thermodynamical quantities for the reaction. The factor 2 is the statistical weight of the *gauche* form.

This usual assumption can be tested by calculating the partition functions from the moments of inertia and vibrational frequencies. Combined with the observed values of K, the thermodynamical quantities are calculated according to eqns. 1 and 2, and the results given in Tables 4 and 5.

$$K = \frac{n_g}{n_a} = \frac{2Q_g}{Q_a} e^{-\Delta E^\circ/RT} = e^{-(\Delta E - T\Delta S)/RT} \quad (2)$$

where n is the percentage of the conformers *gauche* (g) and *anti* (a).

The calculated values for ΔE° agree very well except the ΔE° value at – 13 °C which deviates significantly from the mean. Since this point

Table 3. Molecular parameters for 1,2-dichloroethane. Distance (R_a) and amplitudes (u) in Å, angles ($\angle\alpha$) in degrees.

Temp.	2 °C
R(C – C)	1.510 (6)[a]
R(C – Cl)	1.788 (2)
R(C – H)	1.081 (8)
∠CCCl	109.21(.28)
∠CCH	110.93(.43)
ϕ_a	72.36(3.05)
u(C – C)	0.052 (6)
u(C – Cl)	0.053 (2)
u(C···Cl)	0.080 (3)
u(Cl···H)	0.078 (9)
$u(Cl\cdots Cl)_a$	0.068 (3)
$u(Cl\cdots Cl)_g$	0.148 (30)
%-*anti*	81.4 (3.8)

[a] The distances are corrected for shrinkage. Standard deviations obtained from the refinement using off-diagonal elements in the weight-matrix, are given in parentheses.

Table 4. Thermodynamical terms calculated from measured equilibrium mol fractions (n_a) and calculated partition functions (Q).

Temp (°C)	(− 13)	2	40	140	140 B	300
%-*anti* [a]	89.4(4.4)	81.4(3.8)	78.7(3.4)	67.9(3.6)	67.0(5.1)	63.9(5.8)
R ln $(2Q_g/Q_a)$ (cal mol^{-1} deg^{-1}) [b]	1.453	1.437	1.395	1.313	1.313	1.228
RT $(\partial/\partial T)$[ln (Q_g/Q_a)] (cal mol^{-1} deg^{-1}) [b]	− 0.330	− 0.326	− 0.314	− 0.281	− 0.281	− 0.236
$\Delta E°$ (kcal mol^{-1})	1.48(.25)	1.26(.14)	1.25(.13)	1.16(.14)	1.12(.19)	1.35(.27)
ΔE (kcal mol^{-1})[c]	1.15	1.14	1.13	1.10	1.10	1.05
ΔS (cal mol^{-1} deg^{-1})	1.12	1.11	1.08	1.03	1.03	0.99

[a] Determined from electron diffraction in Ref. 1 and this investigation, standard deviations from the structure determination in parentheses (σn_a). [b] Calculated from the valence force field of Snyder and Schachtschneider [4] with torsional force constants $f_{t,g}=0.253$ ($\nu_{t,g}$ 117 cm^{-1}) and $f_{t,a}=0.174$ (mdyn Å rad^{-2}) ($\nu_{t,a}=125$ cm^{-1}), and products of principal moments $(I_A I_B I_C)_g = 2.954 \times 10^6$ and $(I_A I_B I_C)_g$ 2.109×10^6 (a.w.Å^2). [c] The mean of $\Delta E°$ is applied ($\Delta E° = 1.22$ kcal mol^{-1}). Standard deviations in $\Delta E°$, given in parentheses are calculated acccording to $[\partial(\Delta E°)]^2 = \left(\frac{\partial}{\partial n_a} \Delta E°\right) [\sigma(n_a)]^2$

Table 5. Thermodynamical quantities.

	I	II
ΔE (kcal mol^{-1})	1.11(.04)	1.05(.10)
$R \ln(2Q_g/Q_a)$ (cal mol^{-1} deg^{-1})	1.33	1.19 (.29)
$RT\,\partial/\partial T \ln(Q_g/Q_a)$ (cal mol^{-1} deg^{-1})	−0.29	−0.29
ΔS (cal mol^{-1} deg^{-1})	1.04	0.90(.29)

I. The results obtained applying K from electron diffraction and calculating the partition functions, when $\nu_{t,g} = 117$ cm^{-1} and $\nu_{t,a} = 125$ cm^{-1}. The values are the mean of those in Table 4, the standard deviation for ΔE in parenthesis, is calculated from the deviations from the mean.

II. The results obtained by fitting a straight line to the ($R \ln(1/K)$, $1/T$)-points. $\Delta S = 0.90$ corresponds to $\nu_{t,g}/\nu_{t,a} = 1.02$ (giving $\nu_{t,} = 128(20)$ cm^{-1}, if $\nu_{t,a}$ is kept at the experimental value 125 cm^{-1}). The standard deviations as obtained from the least squares fitting are given in parentheses. The observations at −13 °C are excluded in this treatment of the data.

also is off the line around which the other points are grouped (Fig. 1), this observation is excluded in the further treatment of the data.

Table 4 demonstrates quite clearly that $(\partial/\partial T)[\ln(Q_g/Q_a)]$ is *not* sufficiently small to be neglected in the calculations of ΔS, while considering ΔE as temperature independent, is sufficiently accurate within the experimental error limits. Still the least squares fitting of a straight line to $R \ln (1/K)$ *versus* $1/T$ seems to give a slope which is a reasonable good estimate of ΔE, and the temperature mean of $-\Delta S$ as

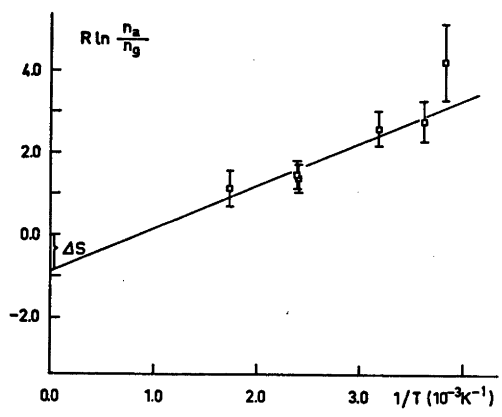

Fig. 1. $R \ln(1/K) = R \ln(n_a/n_g) = \Delta E/T - \Delta S$ as a function of $1/T$. $\Delta E = 1.05$ kcal mol^{-1} is the slope of the straight line drawn, $\Delta S = 0.90$ cal mol^{-1} deg^{-1} is the "constant". The standard deviations marked in each point by vertical lines are calculated from those obtained on n_a in the least squares refinement on the total structure.

the intersection of the $R \ln(1/K)$-axis (see Fig. 1). This can be demonstrated by applying the least squares method to theoretically calculated $R \ln(1/K)$-points. The determined coefficients in the assumed straight line then agree with the temperature average of ΔE and ΔS rather than $\Delta E°$ and $R \ln(2Q_g/Q_a)$ (see eqn. 2).

The best fitted straight line gave $\Delta S = 0.90(.29)$ cal mol^{-1} deg^{-1}, (Table 5, column II). If the usual assumption that the temperature derivative, $RT(\partial/\partial T)[\ln(Q_g/Q_a)]$, can be neglected, is applied, then $R \ln(2Q_g/Q_a) = \Delta S$ gives $\nu_{t,g} = 147$ cm^{-1} when $\nu_{t,a} = 125$ cm^{-1} is considered as the correct value (see below).

Even though $R \ln(2Q_g/Q_a)$ is temperature dependent, Table 4 shows that $RT(\partial/\partial T)[\ln (Q_g/Q_a)]$ is fairly temperature independent. The mean value of $R \ln(2Q_g/Q_a)$ can therefore be calculated from the least squares ΔS-value, substracting the average $RT(\partial/\partial T)[\ln(Q_g/Q_a)]$ calculated from the experimental frequencies (with $\nu_{t,g} = 117$ cm^{-1} and $\nu_{t,a} = 125$ cm^{-1}).

Table 5 demonstrates the excellent agreement between the results obtained from the electron diffraction data and the spectroscopic torsional frequencies. The least squares determined $R \ln(2Q_g/Q_a) = 1.19$ cal mol^{-1} deg^{-1} corresponds to a ratio of 1.02 between the torsional frequencies in *gauche* and *anti*, giving $\nu_{t,g} = 128(20)$ cm^{-1} if $\nu_{t,a} = 125$ cm^{-1} is considered as the correct value. The experimental frequencies are respectively 123 cm^{-1} and 125 cm^{-1}, with a reasonable liquid/gas shift in *gauche* down to 117 cm^{-1}, ratio 0.94, which agrees both with the above straight line approach and the u-value estimate at 300 °C

(Ref. 1). Very reliable torsional frequencies [6] have not yet been obtained in the gas phase. Within an uncertainty of 10 cm^{-1} in the frequency, the experimental $\nu_{t,g}/\nu_{t,a}$ ratio may be shifted to a value close to 1.02. Unfortunately this shift in frequency ratio does not change the u values significantly compared to the experimental refined results and error limits. On the other hand it is possible that the correction terms because of anharmonicity may be a bit larger in *gauche*, where the potential is much more asymmetric. This will move the calculated $\nu_{t,g}$ closer to $\nu_{t,a}$, more in accordance with the experiment, although the effect probably is small.

This uncertainty in the calculated partition functions has minor influence on the obtained ΔE value.

Since any changes in the torsional frequencies mainly will influence the $R \ln(2Q_g/Q_a)$ term $[RT(\partial/\partial T)[\ln(Q_g/Q_a)]$ does only change from -0.29 to -0.40 (cal mol^{-1} deg^{-1}) when $\nu_{t,g}/\nu_{t,a}$ goes from 0.93 to 1.18] the uncertainty in the thermodynamical estimate of ΔS originates only from the uncertainty of $R \ln(2Q_g/Q_a)$.

According to Table 5 this means that ΔS for the conformational equilibrium should be close to 0.9 cal mol^{-1} deg^{-1}. The two outlined procedures give in the case of 1,2-dichloroethane equally good estimates of ΔE and ΔS. Which one to apply depends on the quality of the experimental $R \ln(1/K)$-points on one hand, and the quality of the observed vibrational and torsional frequencies on the other. A combination of the two sets of information is a method to check the consistency of the obtained results.

Acknowledgement. I like to thank Siv.ing. R. Seip for recording the diffraction photographs, and Siv.ing. L. Fernholt for carrying out much of the computer work and data corrections. Dr. philos. H. M. Seip should also be thanked for many helpful discussions.

REFERENCES

1. Kveseth, K. *Acta Chem. Scand. A 28* (1974) 482, and the references cited therein.
2. Zeil, W., Haase, J. and Wegmann, L. *Z. Instrumentenk. 74* (1966) 84.
3. Bastiansen, O., Graber, R. and Wegmann, L. *Balzer's High Vacuum Report 25* (1969) 1.
4. Schachtschneider, J. H. and Snyder, R. G. *Vibrational Analysis of Polyatomic Molecules. IV. Shell Dev. Co. Tech. Report* No. 122–63.
5. Stølevik, R., Seip, H. M. and Cyvin, S. J. *Chem. Phys. Lett. 15* (1972) 263.
6. Shimanouchi, T. *Tables of Molecular Vibrational Frequencies. Part 1, NSRDS-NBS 6* (1967) 33.

Received October 18, 1974.

Acta Chemica Scandinavica A 29 (1975) 312—316

Magnetic Structures and Properties of $V_{1-t}Cr_tAs$

KARI SELTE,[a] HJALTE HJERSING,[a] ARNE KJEKSHUS[a] and ARNE F. ANDRESEN[b]

[a]Kjemisk Institutt, Universitetet i Oslo, Blindern, Oslo 3, Norway and [b]Institutt for Atomenergi, Kjeller, Norway

The pseudo-binary VAs-CrAs system has been investigated by X-ray and neutron diffraction and magnetic susceptibility measurements. VAs and CrAs are completely soluble in each other, and the structure of the ternary, random solid solution phase is of the MnP type at and below room temperature. Like CrAs, the Cr-rich samples undergo a transition from MnP to NiAs type structure at high temperatures. The double, helimagnetic *c* axis type ordering in CrAs extends only to $V_{0.05}Cr_{0.95}As$.

The purpose of the protracted research programme [1–15] of which the work described in this paper forms a part, is to elucidate the structural and magnetic properties of compounds with the NiAs and MnP type structures and, especially, the factors which govern the similarities and distinctions between the two classes. The present paper concerns $V_{1-t}Cr_tAs$, the properties of VAs and CrAs being relatively well documented through earlier work.[2,7,16,17] The quasi-binary system VAs – CrAs has previously been studied, among others, by Sobczak *et al.*[18] who, unfortunately, present only a brief account of their data. In view of the current knowledge of the magnetic properties [13] of compounds with the MnP type structure, the unusually high Néel temperatures reported by Sobczak *et al.* call for reexamination.

EXPERIMENTAL

Samples of VAs and CrAs were prepared by heating weighed quantities of the elements [99.5 % V (A.D. Mackay), 99.0 % Cr (powder crystals; Koch-Light Laboratories), and 99.9999 % As (Koch-Light Laboratories)] in evacuated, sealed silica tubes, as described in Refs. 2 and 7. Ternary $V_{1-t}Cr_tAs$ samples of desired compositions were prepared from appropriate proportions of VAs and CrAs, by 3 – 4 heat treatments of one week's duration at 950 °C, interrupted by intermediate crushings. The samples were finally cooled to room temperature over a period of two days.

Experimental details concerning X-ray and neutron diffraction (including data reduction) and magnetic susceptibility measurements have been reported earlier.[6]

RESULTS

(i) *Composition and chemical crystal structure.* Fig. 1 shows the room temperature unit cell dimensions of $V_{1-t}Cr_tAs$ as functions of the composition parameter *t*. The contin-

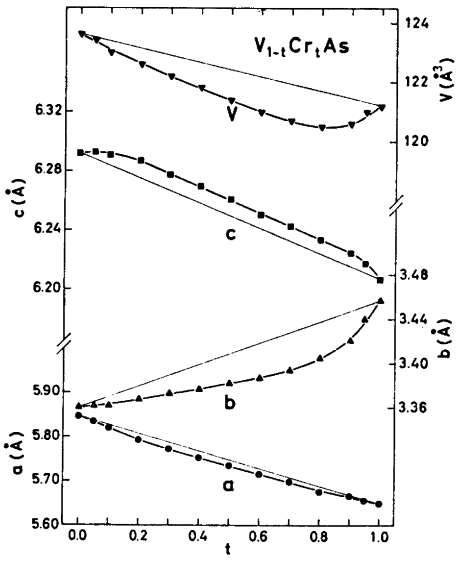

Fig. 1. Orthorhombic unit cell dimensions of ternary solid solution series VAs-CrAs as functions of composition.

Table 1. Unit cell dimensions and positional parameters with standard deviations for some $V_{1-t}Cr_tAs$ samples; space group *Pnma*, positions 4(*c*). (Overall profile reliability factors ranging between 0.027 and 0.056.)

t	T (K)	a (Å)	b (Å)	c (Å)	x_T	z_T	x_X	z_X
0.50	80	5.707(1)	3.368(1)	6.237(1)	0.0069(22)	0.1960(20)	0.1975(4)	0.5737(6)
	293	5.724(1)	3.382(1)	6.250(1)	0.0086(20)	0.1970(18)	0.1986(4)	0.5728(5)
0.75	4.2	5.661(1)	3.373(1)	6.215(1)	0.0066(14)	0.1966(12)	0.1980(6)	0.5733(5)
	80	5.663(1)	3.374(1)	6.215(2)	0.0060(11)	0.1982(9)	0.1982(4)	0.5739(5)
	293	5.678(1)	3.396(1)	6.225(1)	0.0057(12)	0.1987(10)	0.1990(4)	0.5746(5)
0.90	4.2	5.645(1)	3.375(1)	6.209(1)	0.0061(11)	0.1964(9)	0.1983(6)	0.5735(5)
	80	5.641(1)	3.376(1)	6.204(1)	0.0066(9)	0.1981(7)	0.1981(5)	0.5740(4)
	293	5.652(1)	3.411(1)	6.208(1)	0.0062(9)	0.2012(7)	0.1990(5)	0.5745(4)
0.93	4.2	5.638(1)	3.376(1)	6.205(1)	0.0073(10)	0.1989(8)	0.1981(6)	0.5733(5)
	80	5.646(1)	3.384(1)	6.213(1)	0.0079(9)	0.1997(8)	0.1976(5)	0.5742(5)
	293	5.656(1)	3.426(1)	6.216(1)	0.0056(8)	0.2012(7)	0.1988(5)	0.5744(4)
0.95	80	5.590(2)	3.564(2)	6.124(3)	0.0085(21)	0.2029(17)	0.2036(14)	0.5808(23)
	293	5.645(2)	3.447(1)	6.205(2)	0.0095(15)	0.2053(13)	0.1985(10)	0.5776(8)

uous variations in all unit cell dimensions with t demonstrate that VAs and CrAs are completely soluble in each other. According to earlier findings [3,7] VAs and CrAs are well defined, stoichiometric compounds. The possibility of an extension of the homogeneity range of $V_{1-t}Cr_tAs$ to metal/non-metal (atomic) ratios different from 1.00 has not been systematically studied for the ternary samples. It should be noted, however, that apart from the vanadium-rich samples ($0 \leqq t \leqq 0.2$), disengagement of small amounts of arsenic was observed in the capsules after the heat treatments. Weighing of the disengaged As shows that the implied non-metal deficiency corresponds to less than 1 % of the original As content. No attempts have been made to pursue this problem further, and the apparent non-stoichiometric nature of these samples may well originate from imperfections in the preparative procedure.

The X-ray data confirm an MnP type structural arrangement for $0 \leqq t \leqq 1$ at room temperature. The absence of additional superstructure reflections shows that the substituted atoms are randomly distributed over the metal sub-lattice. As seen from Fig. 1 the variations in unit cell dimensions with compositions do not follow Vegard's Law.

Samples with $t = 0.50$, 0.75, 0.90, 0.93, and 0.95 were prepared primarily for the purpose of studying the magnetic structures, but data collected in this connection were conveniently utilized to evaluate the variable positional parameters of the MnP type structure. The final values for the least squares, profile refined parameters at and below room temperature are listed in Table 1. Due to the generally small differences in positional parameters between VAs and CrAs and the relatively high, calculated values for the standard deviations given in Table 1, it is difficult to unveil the expected continuous changes in these variables with composition. Like CrAs,[2,16,17] $V_{0.05}Cr_{0.95}As$ undergoes a first order transition at 240 K (onset on cooling; accompanied by hysteresis) between two MnP type phases (associated with the magnetic transition; see section iii). This is reflected in the unit cell dimensions, but not in the positional parameters in Table 1.

Since CrAs also is known to undergo a second (or higher) order transformation to the NiAs type structure at a temperature of 1173 ± 20 K,[10] three representative samples with compositions $t = 0.80$, 0.90, and 0.95 were studied in the interval 293 – 1350 K. The temperature dependences of the unit cell dimensions (Fig. 2) demonstrate corresponding

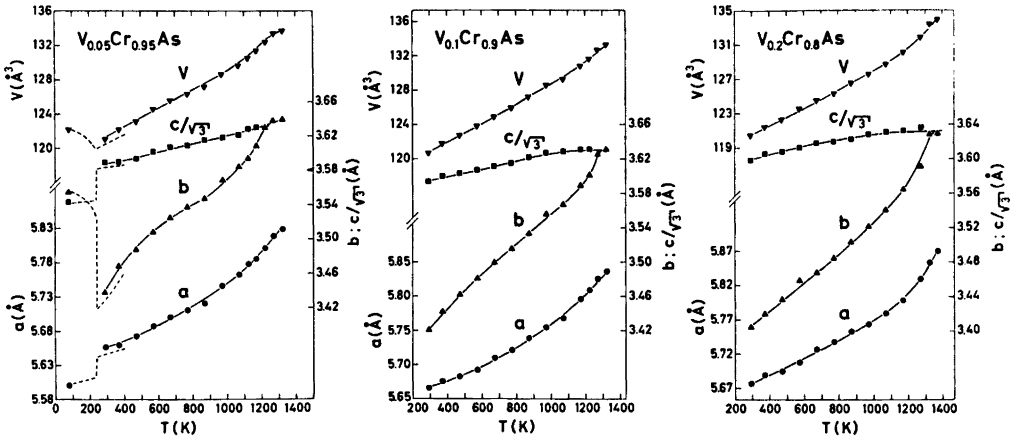

Fig. 2. Unit cell dimensions of three $V_{1-t}Cr_tAs$ samples *versus* temperature. Average relative expansion coefficients $\alpha_a\ [=(a_T - a_{T'})/a_{300}(T-T')]$, α_b, α_c multiplied by 10^6 K are 25, 52, 12; 28, 52, 13; and 28, 47, 14 for $V_{0.2}Cr_{0.8}As$, $V_{0.1}Cr_{0.9}As$, and $V_{0.05}Cr_{0.95}As$, respectively.

transitions at 1250 ± 50, 1300 ± 50, and 1350 ± 50 K for $V_{0.05}Cr_{0.95}As$, $V_{0.10}Cr_{0.90}As$, and $V_{0.20}Cr_{0.80}As$, respectively.

(ii) *Magnetic susceptibility.* The gradual change in the temperature dependence of the reciprocal magnetic susceptibility with composition parameter t of $V_{1-t}Cr_tAs$ is shown in Fig. 3. No field strength dependent susceptibilities were observed. In this respect the thermomagnetic curve for CrAs differs from that reported in Ref. 2, the difference being probably caused by slight impurities in the samples used in the earlier investigation. None of the samples within the entire composition range of the VAs-CrAs system satisfies the Curie-Weiss Law.

(iii) *Magnetic structure.* CrAs has previously [2,16,17] been found to exhibit helimagnetism, whereas no cooperative magnetic phenomenon

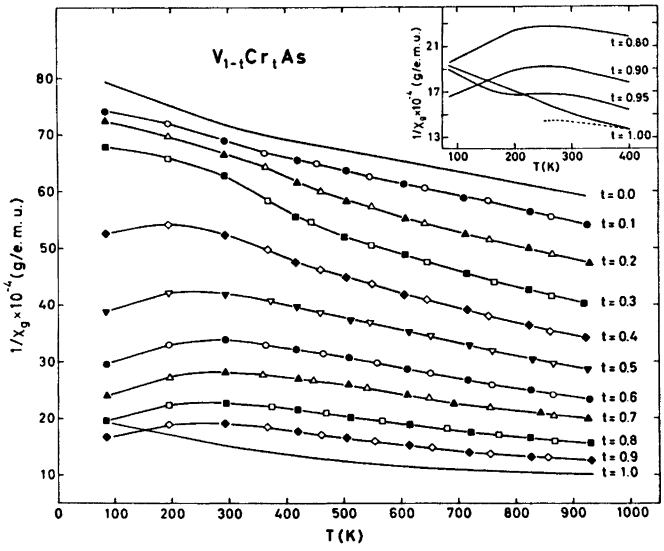

Fig. 3. Reciprocal magnetic susceptibility *versus* temperature for various $V_{1-t}Cr_tAs$ samples. Inset shows low temperature portions of $\chi_g^{-1}(T)$ curves for $0.80 \leqq t \leqq 1.00$; broken curve quoted from Ref. 2.

has been detected [7] for VAs down to 4.2 K. The double, helimagnetic *c* axis type ordering extends to a composition $t = 0.95$ of the $V_{1-t}Cr_tAs$ phase. The samples with $0.50 \leqq t \leqq 0.93$ gave no indication of reflections characteristic of the helimagnetic arrangement. Only small changes were experienced in all parameters specifying the spirals on going from CrAs to $V_{0.05}Cr_{0.95}As$, the values (at 80 K) being for CrAs $T_N = 261$ K (onset on cooling; followed by hysteresis), $\mu_T = 1.70 \pm 0.05$ μ_B, $\tau = 0.353 \times 2\pi c^*$, $\phi = -133 \pm 1°$, and for $V_{0.05}Cr_{0.95}As$ $T_N = 240$ K (onset on cooling; followed by hysteresis), $\mu_T = 1.70 \pm 0.05$ μ_B, $\tau = 0.360 \times 2\pi c^*$, $\phi = -115 \pm 1°$. As demonstrated in Figs. 4 and 5 the onset of the cooperative magnetic phenomenon in $V_{0.05}Cr_{0.95}As$ is accompanied by a marked hysteresis, resembling also in this respect CrAs. The pronounced similarity in temperature dependence of the integrated intensity of $000^{\pm}$ and 101^{-} suggests that the phase angle between the spirals in $V_{0.05}Cr_{0.95}As$ varies relatively little with temperature. Similarly, only minor variations are observed in the temperature dependence of the spiral turn angle ($\tau = 0.38 \times 2\pi c^*$ at 232 K).

Fig. 5 demonstrates that the magnetic ordering in $V_{0.05}Cr_{0.95}As$ is accompanied by a first order structural transformation. At first sight the transition in this substance seems to be somewhat peculiar, in that the reflection characteristic of the high temperature, paramagnetic phase does not completely vanish at low temperatures. However, there appears to be a very simple explanation of this observation, involving the imposition of the magnetic phase bondary at $t = 0.95$. The slight variation in composition which necessarily must be present in all samples of non-stoichiometric phases, would, on the assumption of the phase borderline being located at the composition of the investigated sample, account for the coexistence of (say) 10 % of the paramagnetic phase in admixture with the bulk of the sample in the low temperature, helimagnetic state.

The termination of the helimagnetic region of the $V_{1-t}Cr_tAs$ phase already at $t = 0.95$ is somewhat unexpected and provokes some discussion. The only omen of this result is perhaps brought out in Fig. 3, where a similarity in the low temperature portions of the $\chi^{-1}(T)$ curves for $t = 0.95$ and 1.00 is noted. Several possibilities are open for speculations.

On crossing the magnetic phase boundary at $t = 0.95$ the cooperative ordering could change from helimagnetism to ferromagnetism. However, if such an interpretation applies, the

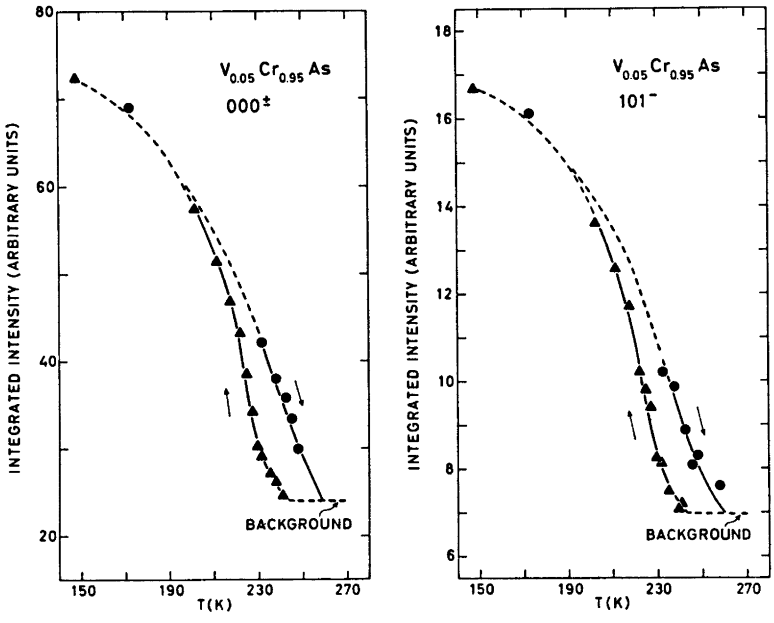

Fig. 4. Temperature dependencies of integrated intensities of $000^{\pm}$ and 101^{-} for $V_{0.05}Cr_{0.95}As$.

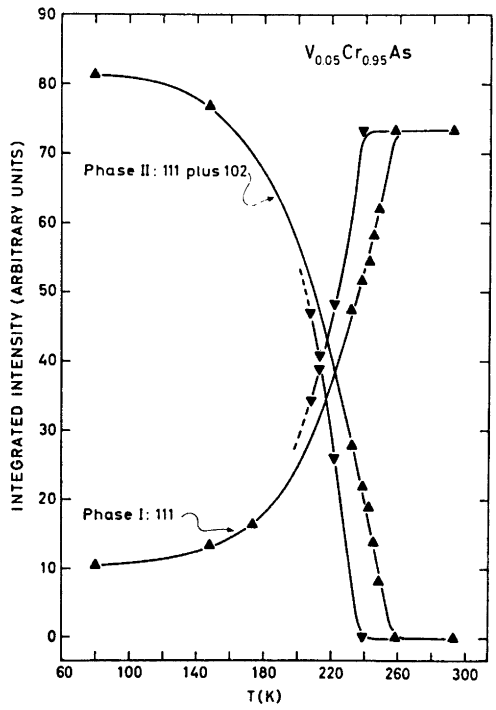

Fig. 5. Integrated intensities *versus* temperature of 111 for paramagnetic, high temperature phase (I) and 111 plus 102 for helimagnetic, low temperature phase (II) for $V_{0.05}Cr_{0.95}As$.

number of unpaired electrons would have to drop from 1.70 ± 0.05 in the helimagnetic mode to less than 0.5, which represents the detection limit for various models with different orientations of the assumed ferromagnetic moments. Considerations along this line are presented in Refs. 12, 13, 15, and 19, but it should be emphasized that the spiral parameters for $V_{0.05}Cr_{0.95}As$ (like those for $CrAs_{1-x}Sb_x$; $\sim 0.14 \leqq x \leqq \sim 0.50$ [19]) do not satisfy Kallel *et al.*'s [19] model for cooperative magnetism in phases with the MnP type structure. As pointed out by these authors the shortcomings may be mendable by increasing the number of exchange interactions.

It is feasible although not probable that the Néel temperature of the $V_{1-t}Cr_tAs$ phase exhibits an almost discontinuous drop at $t = 0.95$. In terms of the molecular field approximation this would require a correspondingly rapid decrease in the magnetic exchange parameters or their linear combinations.

Another variable which more likely could show a rapid change with composition, is the magnitude of the magnetic moment. An explanation along this line would be consistent with our present experience which shows that small substitutions of another metal in binary phases with MnP type structure seem to have a radical influence on their electronic band structures.

REFERENCES

1. Selte, K. and Kjekshus, A. *Acta Chem. Scand. 23* (1969) 2047.
2. Selte, K., Kjekshus, A., Jamison, W. E., Andresen, A. F. and Engebretsen, J. E. *Acta Chem. Scand. 25* (1971) 1703.
3. Kjekshus, A. and Jamison, W. E. *Acta Chem. Scand. 25* (1971) 1715.
4. Selte, K. and Kjekshus, A. *Acta Chem. Scand. 25* (1971) 3277.
5. Selte, K. and Kjekshus, A. *Acta Chem. Scand. 26* (1972) 1276.
6. Selte, K., Kjekshus, A. and Andresen, A. F. *Acta Chem. Scand. 26* (1972) 3101.
7. Selte, K., Kjekshus, A. and Andresen, A. F. *Acta Chem. Scand. 26* (1972) 4057.
8. Selte, K., Kjekshus, A. and Andresen, A. F. *Acta Chem. Scand. 26* (1972) 4188.
9. Selte, K. and Kjekshus, A. *Acta Chem. Scand. 27* (1973) 1448.
10. Selte, K. and Kjekshus, A. *Acta Chem. Scand. 27* (1973) 3195.
11. Selte, K., Kjekshus, A. and Andresen, A. F. *Acta Chem. Scand. 27* (1973) 3607.
12. Selte, K., Kjekshus, A. and Andresen, A. F. *Acta Chem. Scand. A 28* (1974) 61.
13. Selte, K. *Thesis*, University of Oslo, Oslo 1974.
14. Selte, K., Kjekshus, A. and Oftedal, T. A. *Acta Chem. Scand. A 28* (1974) 803.
15. Selte, K., Kjekshus, A., Oftedal, T. A. and Andresen, A. F. *Acta Chem. Scand. A 28* (1974) 957.
16. Kazama, N. and Watanabe, H. *J. Phys. Soc. Japan 30* (1971) 1319; *31* (1971) 943.
17. Boller, H. and Kallel, A. *Solid State Commun. 9* (1971) 1699.
18. Sobczak, R., Boller, H. and Bittner, H. *Monatsh. Chem. 99* (1968) 2227.
19. Kallel, A., Boller, H. and Bertaut, E. F. *J. Phys. Chem. Solids 35* (1974) 1139.

Received October 21, 1974.

Acta Chemica Scandinavica A 29 (1975) 317—325

Structures of Linear Multisulfur Systems. VIII. The Crystal and Molecular Structure of 3,5-Bis(*N*,*N*-diisopropylthiocarbamoylimino)-4-(4-nitrophenyl)-1,2,4-dithiazolidine, $C_{22}H_{32}N_6O_2S_4$

JORUNN SLETTEN

Department of Chemistry, University of Bergen, N-5014 Bergen, Norway

The structure of $C_{22}H_{32}N_6O_2S_4$ has been determined by X-ray crystallographic methods. 7456 independent reflections were measured on a diffractometer using the $\theta-2\theta$ scan technique and Mo$K\alpha$ radiation. The crystals are monoclinic, space group $P2_1/c$ with cell dimensions $a=12.643(6)$ Å, $b=24.365(6)$ Å, $c=27.147(6)$ Å, $\beta=99.67(4)°$. There are three molecules per asymmetric unit, giving a total of 12 formula units in the cell. The structure was solved by direct methods and refined by full-matrix least-squares to an R of 0.035. The three crystallographically independent molecules show only minor differences in their geometry. The four sulfur atoms in each molecule are approximately collinear, the average distances being S(1)–S(2) = 2.747 Å, S(2)–S(3) = 2.194 Å, S(3)–S(4) = 2.683 Å. Standard deviations in the individual S–S bond length are 0.001 Å.

The present structure determination was carried out as part of a program of X-ray crystallographic investigations of linear multisulfur compounds. In most of these compounds studied so far, the molecular skeleton connecting the sulfur atoms, has been made up of carbon atoms. Recently structure reports on similar compounds, where nitrogen atoms have been introduced into the frame, have been published.[1,2]

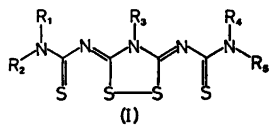

(I)

The present paper reports on the structure of a 1,2,4-dithiazolidine derivative, (I), where $R_1=R_2=R_4=R_5=$ isopropyl and $R_3=p$-nitrophenyl.

EXPERIMENTAL

A sample of the compound, consisting of orange, prismatic crystals was generously supplied by Goerdeler and Ulmen.[3] A single crystal of dimensions $0.25\times0.43\times0.42$ mm (along a, b, and c, respectively) mounted along the crystallographic b-axis, was used for all X-ray measurements. The experimental procedure for determination of cell dimensions and data collection are described elsewhere.[1] Standard deviations in intensities were calculated as $\sigma_I=[\sigma_c^2+(0.02N_{net})^2]^{\frac{1}{2}}$ where σ_c is the error due to counting statistics, and N_{net} is the net count of the reflections. Standard deviations in structure factors were evaluated as $\sigma_F=\sigma_I/2(I\,Lp)^{\frac{1}{2}}$. Out of a total of 7456 reflections with $2\theta\lesssim40°$ 1677 were less than $2\sigma_c$. These reflections were given a threshold value of $2\,\sigma_c$ and were later included in the refinement only if $|F_{calc}|>|F_{threshold}|$. Data were corrected for Lorentz and polarization effects according to standard procedures, and for absorption by the method described by Coppens *et al.*[4]

CRYSTAL DATA

$C_{22}H_{32}N_6O_2S_4$; M.W. = 540.80.
Crystal system monoclinic; space group $P2_1/c$; cell dimensions: $a=12.643(6)$ Å, $b=24.365(6)$ Å, $c=27.147(6)$ Å.

$\beta = 99.67(4)°$.
$V = 8244(1)$ Å^3; $D_x = 1.308$ g cm^{-3}; $D_m = 1.300$ g cm^{-3}.
$Z = 12$; $F_{000} = 3432$; $\mu_{MoK\alpha} = 3.7$ cm^{-1}.

STRUCTURE DETERMINATION AND REFINEMENT

The structure was solved by a symbolic addition procedure programmed by Long.[5] Signs for 360 reflections with $|E| \geq 1.70$ were derived by

Table 1. Atomic coordinates and thermal parameters for S, O, N, C with the corresponding standard deviations, referring to the last decimal places, listed in parentheses. Values for the coordinates are multiplied by 10^5, the thermal parameters by 10^4. $T_i = \exp[-2\pi^2(U_{11}h^2a^{*2} + U_{22}k^2b^{*2} + U_{33}l^2c^{*2} + 2U_{12}hka^*b^* + 2U_{23}klb^*c^* + 2U_{13}hla^*c^*)]$.

Atom	Molecule	x/a	y/b	z/c	U_{11}	U_{22}	U_{33}	U_{12}	U_{23}	U_{13}
S(1)	a	48790(8)	15023(5)	12514(4)	386(6)	813(9)	810(8)	-80(6)	254(7)	165(6)
	b	57677(8)	48030(5)	13882(4)	388(7)	987(10)	917(9)	0(6)	406(8)	189(6)
	c	52228(7)	80882(5)	12074(4)	350(6)	744(8)	718(8)	-74(5)	183(6)	134(5)
S(2)	a	67741(7)	10052(4)	16578(4)	441(6)	484(7)	634(7)	-79(5)	124(6)	177(5)
	b	76296(7)	43013(4)	18326(4)	402(6)	545(7)	574(7)	-67(5)	147(6)	142(5)
	c	70999(7)	75843(4)	16369(4)	373(6)	473(7)	567(7)	-81(5)	88(5)	150(5)
S(3)	a	83681(7)	6616(4)	19363(4)	501(6)	407(7)	552(7)	-38(5)	109(5)	170(5)
	b	91988(7)	39455(4)	21349(4)	451(6)	456(7)	459(6)	-28(5)	118(5)	146(5)
	c	86810(7)	72428(4)	19392(3)	427(6)	410(7)	495(6)	-56(5)	76(5)	149(5)
S(4)	a	103870(8)	3270(4)	22441(4)	618(7)	570(8)	621(7)	74(6)	207(6)	154(6)
	b	112125(8)	35768(4)	24446(4)	512(7)	668(8)	615(7)	44(6)	280(6)	94(6)
	c	106876(8)	69124(4)	22815(4)	517(7)	519(7)	483(6)	9(5)	141(5)	122(5)
O(1)	a	106382(27)	30982(14)	266(14)	1144(29)	1185(31)	1020(27)	-258(21)	315(24)	557(24)
	b	116322(25)	60935(14)	271(13)	1005(26)	1199(30)	750(24)	-234(20)	239(22)	418(21)
	c	111119(28)	94917(16)	-721(15)	1066(29)	1327(35)	1163(31)	-183(23)	432(27)	590(26)
O(2)	a	106970(28)	36250(15)	6658(14)	1189(29)	657(25)	1427(34)	-375(22)	186(24)	281(24)
	b	117580(31)	66682(17)	6236(14)	1548(37)	1086(32)	1107(31)	-766(28)	80(25)	397(25)
	c	112142(31)	100502(16)	5331(16)	1216(33)	794(29)	1693(41)	-384(24)	257(27)	547(27)
N(1)	a	52191(21)	23966(12)	7319(11)	395(18)	508(22)	594(21)	-14(16)	64(18)	113(16)
	b	61619(22)	55869(13)	7515(11)	390(19)	611(23)	616(22)	101(16)	152(19)	90(16)
	c	56184(21)	89737(13)	6865(11)	345(18)	607(23)	551(21)	58(16)	99(19)	118(15)
N(2)	a	67375(23)	19380(12)	10804(10)	355(20)	460(22)	489(20)	23(16)	50(17)	98(15)
	b	76520(23)	51401(12)	11583(11)	327(21)	508(22)	502(20)	49(16)	90(17)	76(16)
	c	71118(22)	84976(12)	10413(10)	319(21)	431(21)	470(20)	9(15)	27(16)	77(15)
N(3)	a	83705(22)	15546(11)	13898(10)	396(20)	357(20)	392(18)	-32(16)	78(15)	121(15)
	b	92578(22)	47716(11)	15141(10)	349(20)	409(20)	412(19)	-10(16)	102(16)	107(16)
	c	87214(21)	80989(11)	13529(10)	330(20)	356(20)	397(18)	-27(16)	50(15)	111(15)
N(4)	a	100596(25)	12359(11)	16726(10)	400(21)	426(20)	469(20)	55(16)	71(15)	136(16)
	b	109279(24)	44629(11)	18471(10)	314(20)	475(21)	445(19)	26(16)	79(16)	98(16)
	c	103949(24)	77857(11)	16668(10)	328(20)	409(20)	449(19)	14(16)	43(15)	102(15)
N(5)	a	118192(23)	9955(12)	19326(10)	453(21)	628(22)	545(21)	89(17)	87(17)	146(16)
	b	126742(23)	42559(12)	21763(10)	391(20)	633(22)	420(19)	34(16)	60(16)	63(15)
	c	121524(23)	75365(11)	19448(10)	404(21)	491(21)	490(20)	33(15)	102(15)	80(15)
N(6)	a	104402(27)	32022(17)	4409(17)	562(24)	654(31)	937(34)	-39(22)	249(29)	191(24)
	b	114626(27)	62365(18)	4322(15)	578(24)	834(34)	630(29)	-202(22)	208(27)	36(22)
	c	109074(29)	96280(19)	3296(18)	493(26)	855(36)	1022(37)	59(24)	411(34)	209(26)
C(1)	a	56381(29)	19675(15)	10086(13)	421(27)	489(28)	472(25)	-40(20)	-39(21)	130(19)
	b	65559(30)	51981(16)	10842(14)	434(29)	616(30)	536(27)	45(22)	53(22)	116(21)
	c	60070(29)	85443(15)	9667(13)	403(27)	494(29)	461(25)	-11(20)	-75(21)	122(20)
C(2)	a	72559(29)	15449(15)	13447(12)	415(26)	401(26)	395(23)	-80(20)	-29(20)	164(19)
	b	81437(29)	47819(15)	14652(13)	377(27)	460(27)	395(24)	-46(20)	9(20)	112(20)
	c	76077(28)	81055(15)	13117(12)	334(25)	390(26)	377(23)	-65(20)	-83(19)	109(18)
C(3)	a	90340(31)	11693(13)	16580(12)	497(28)	330(25)	351(22)	13(20)	-4(18)	144(19)
	b	99045(31)	44067(14)	18252(12)	454(27)	383(25)	377(24)	8(20)	-15(19)	142(20)
	c	93756(30)	77254(14)	16479(12)	393(26)	348(25)	377(23)	-18(20)	-14(19)	123(19)
C(4)	a	107858(31)	8766(15)	19362(13)	500(27)	511(28)	397(23)	31(22)	-29(20)	182(20)
	b	116317(30)	41233(15)	21460(12)	409(26)	589(28)	350(23)	23(22)	21(20)	97(20)
	c	111137(30)	74377(15)	19504(12)	406(26)	446(26)	383(23)	-12(21)	-46(19)	88(20)

Table 1. Continued.

C(5)	a	58758(35)	28169(18)	5253(17)	462(27)	483(29)	782(34)	9(24)	133(27)	-27(26)
	b	68542(35)	59495(18)	5019(16)	550(28)	510(30)	646(31)	46(25)	175(26)	38(25)
	c	63036(32)	93770(16)	4685(15)	428(25)	468(28)	656(30)	44(22)	103(25)	49(24)
C(6)	a	65959(56)	31419(26)	9246(30)	820(44)	551(41)	1156(56)	-115(35)	54(40)	-230(43)
	b	75696(51)	63196(25)	8574(25)	880(42)	567(39)	907(45)	-127(33)	-11(36)	-141(37)
	c	70286(45)	97054(24)	8614(23)	628(36)	584(39)	1017(45)	-47(31)	-10(35)	-100(35)
C(7)	a	64302(46)	25959(25)	1118(21)	632(36)	744(41)	863(42)	37(34)	298(34)	265(33)
	b	74394(48)	56368(26)	1459(21)	769(40)	852(44)	607(37)	11(36)	83(35)	246(34)
	c	68726(44)	91267(23)	748(20)	596(34)	730(38)	698(37)	96(31)	17(32)	246(31)
C(8)	a	40378(31)	24781(20)	6238(18)	405(26)	719(36)	829(38)	74(24)	144(30)	115(25)
	b	49894(35)	57155(25)	6601(21)	489(31)	961(45)	991(45)	170(30)	358(37)	183(30)
	c	44426(31)	90702(22)	5714(19)	417(27)	882(39)	821(38)	137(26)	265(32)	137(26)
C(9)	a	37227(60)	29952(40)	8747(34)	656(49)	1524(81)	1285(67)	347(55)	-371(57)	200(48)
	b	47916(84)	62466(64)	9170(36)	942(61)	2404(99)	1084(65)	979(84)	-400(68)	81(50)
	c	41499(58)	96136(38)	7874(27)	686(45)	1559(79)	819(49)	587(50)	-90(47)	97(37)
C(10)	a	36182(48)	24662(27)	638(22)	605(39)	784(46)	980(48)	23(32)	34(37)	-109(32)
	b	45091(48)	57324(28)	1057(25)	606(38)	781(44)	1148(54)	66(36)	44(41)	-164(35)
	c	40360(46)	90279(28)	127(23)	485(36)	920(47)	1007(49)	48(32)	-82(39)	-135(32)
C(11)	a	88608(25)	19918(15)	11443(14)	362(22)	411(28)	422(27)	-14(19)	59(23)	117(19)
	b	97880(25)	51607(16)	12302(14)	324(22)	421(29)	369(25)	-45(19)	88(22)	61(19)
	c	92301(25)	85136(15)	10843(14)	314(22)	402(28)	401(26)	2(19)	55(23)	90(19)
C(12)	a	92717(30)	24475(17)	14123(16)	544(27)	419(30)	473(29)	-66(21)	-32(26)	151(23)
	b	100222(29)	56767(18)	14134(15)	529(26)	522(34)	412(28)	-55(22)	-23(26)	147(21)
	c	96074(29)	89887(17)	13179(16)	529(26)	475(31)	425(28)	-81(22)	-38(26)	129(23)
C(13)	a	97718(32)	28466(19)	11752(19)	548(28)	379(31)	720(38)	-92(23)	-23(30)	101(25)
	b	105683(31)	60408(19)	11490(17)	580(28)	431(32)	606(33)	-124(24)	7(28)	116(24)
	c	101384(31)	93645(19)	10619(19)	517(28)	446(32)	727(37)	-107(24)	80(30)	102(25)
C(14)	a	98504(28)	27872(17)	6823(17)	407(24)	465(30)	574(31)	-49(21)	162(26)	130(22)
	b	108622(27)	58588(19)	7137(15)	390(24)	564(34)	420(28)	-82(22)	171(25)	96(20)
	c	102734(28)	92453(18)	5866(18)	339(24)	562(33)	671(34)	-42(22)	283(28)	160(23)
C(15)	a	94185(30)	23483(18)	4055(17)	469(26)	619(34)	496(30)	-24(23)	82(28)	147(23)
	b	106426(31)	53429(20)	5333(16)	507(28)	616(38)	384(29)	-46(24)	-13(29)	123(23)
	c	98631(31)	87831(20)	3419(17)	457(26)	669(35)	500(31)	0(24)	119(29)	175(23)
C(16)	a	89201(29)	19386(17)	6432(15)	501(25)	433(30)	502(31)	-89(22)	15(25)	150(21)
	b	100891(29)	49907(18)	7910(14)	526(26)	385(31)	378(28)	-90(22)	20(25)	83(21)
	c	93382(28)	84061(18)	5962(15)	381(24)	542(31)	447(30)	-41(21)	35(25)	119(21)
C(17)	a	121821(35)	14286(18)	16127(15)	407(28)	700(36)	563(31)	22(23)	52(24)	169(23)
	b	130834(33)	46545(18)	18346(14)	380(28)	770(38)	506(30)	-13(23)	50(24)	112(22)
	c	125478(31)	79980(16)	16633(14)	327(26)	562(32)	584(30)	6(20)	78(22)	121(21)
C(18)	a	120288(48)	20018(22)	18091(24)	698(40)	681(41)	841(44)	-60(30)	-50(33)	255(35)
	b	128384(51)	52423(22)	19398(26)	761(42)	655(43)	1011(50)	-135(32)	16(35)	335(35)
	c	123488(46)	85539(21)	18791(26)	609(37)	567(38)	1032(50)	-1(28)	-55(34)	260(34)
C(19)	a	117463(44)	13592(26)	10614(17)	612(36)	974(46)	528(34)	-81(31)	73(31)	224(28)
	b	127768(43)	44927(28)	12914(17)	556(35)	1101(52)	427(33)	48(32)	61(30)	110(27)
	c	121866(42)	79527(27)	11004(17)	492(33)	992(45)	548(34)	39(31)	140(31)	149(26)
C(20)	a	126754(36)	6598(21)	22337(19)	476(29)	844(38)	953(39)	166(27)	307(33)	73(29)
	b	135030(35)	39559(20)	25305(16)	454(28)	918(37)	573(30)	38(27)	204(29)	11(25)
	c	129939(35)	71877(20)	22400(18)	422(28)	800(36)	807(36)	14(26)	330(31)	44(27)
C(21)	a	134807(60)	10164(35)	25689(30)	891(50)	1632(71)	970(55)	123(50)	222(55)	-336(46)
	b	142399(69)	43611(40)	28483(27)	1013(57)	1746(81)	791(49)	-400(60)	411(54)	-481(47)
	c	135929(71)	75080(38)	26695(30)	1081(55)	1405(69)	958(53)	-21(56)	348(54)	-443(45)
C(22)	a	132023(66)	2974(33)	18804(35)	967(55)	988(57)	1631(74)	559(46)	72(57)	173(56)
	b	140617(99)	35347(54)	22579(39)	1310(77)	1803(94)	1203(73)	1004(74)	168(75)	155(70)
	c	136740(71)	69109(45)	19022(38)	1092(56)	1189(71)	1560(80)	824(58)	299(60)	306(51)

reiterative application of Sayres equation, starting with three origin determining reflections (1 3 $\bar{6}$, 3 6 $\bar{10}$, 5 12 $\bar{11}$) and three reflections with variable signs (0 3 4, 8 10 1, 0 9 12). The most probable set of phases had an internal consistency [5] of 0.87. The corresponding E-map revealed clearly only the twelve sulfur atoms, arranged in three almost parallel rows, separated by approximately 1/3 of a unit cell in the b-axis direction. A sub-cell with $b' = b/3$ is also indi-

Table 2. Coordinates and thermal parameters for hydrogen atoms with the corresponding standard deviations in parentheses. Values for coordinates are multiplied by a factor of 10^4, and thermal parameters by 10^3.

	Molecule	X/a	Y/b	Z/c	U
H(5)	a	5350(24)	3039(12)	384(11)	32(10)
	b	6370(24)	6177(12)	302(11)	32(10)
	c	5789(26)	9619(13)	272(11)	44(11)
H(61)	a	6174(42)	3250(22)	1189(20)	147(29)
	b	7147(42)	6509(23)	1131(20)	157(26)
	c	6534(34)	9884(18)	1091(16)	105(18)
H(62)	a	6833(37)	3398(20)	784(18)	93(22)
	b	7807(37)	6596(20)	723(18)	100(22)
	c	7375(35)	9999(19)	742(16)	101(19)
H(63)	a	7182(33)	2935(17)	1110(15)	86(16)
	b	8127(35)	6145(17)	1123(17)	102(18)
	c	7525(32)	9479(16)	1081(14)	78(15)
H(71)	a	5850(39)	2392(19)	-166(17)	123(20)
	b	6958(33)	5436(17)	-80(15)	89(18)
	c	6365(33)	8951(17)	-220(16)	95(17)
H(72)	a	6774(31)	2910(17)	-36(15)	85(15)
	b	7749(31)	5891(17)	-42(15)	80(16)
	c	7226(31)	9414(17)	-89(14)	83(15)
H(73)	a	6900(30)	2329(16)	194(14)	72(16)
	b	8038(38)	5373(20)	337(17)	119(19)
	c	7402(31)	8880(16)	212(15)	69(15)
H(8)	a	3764(28)	2143(16)	773(13)	73(13)
	b	4662(29)	5399(16)	758(14)	70(15)
	c	4114(30)	8781(16)	767(14)	85(15)
H(91)	a	3003(38)	2978(19)	850(16)	107(19)
	b	4095(43)	6254(21)	887(19)	119(22)
	c	3424(36)	9649(17)	727(15)	91(16)
H(92)	a	4070(39)	3256(19)	779(19)	85(24)
	b	5095(58)	6509(31)	884(30)	183(54)
	c	4491(45)	9916(23)	688(22)	129(33)
H(93)	a	4109(50)	2983(25)	1252(23)	182(31)
	b	5046(56)	6184(29)	1273(28)	215(39)
	c	4361(46)	9598(24)	1159(23)	175(29)
H(101)	a	2851(36)	2492(16)	3(15)	89(16)
	b	3702(45)	5762(21)	102(19)	147(23)
	c	3321(38)	9062(18)	-7(17)	108(19)
H(102)	a	3838(37)	2778(20)	-104(18)	103(22)
	b	4833(40)	6072(22)	-68(19)	146(23)
	c	4301(43)	9342(24)	-198(20)	158(27)
H(103)	a	3894(36)	2094(20)	-75(17)	115(19)
	b	4727(39)	5444(20)	-47(18)	113(23)
	c	4174(42)	8665(23)	-139(20)	158(27)
H(12)	a	9182(25)	2484(13)	1753(13)	51(12)
	b	9859(24)	5794(13)	1732(12)	52(12)
	c	9507(24)	9059(13)	1641(13)	44(11)
H(13)	a	10052(24)	3136(13)	1347(11)	36(12)
	b	10802(27)	6389(15)	1289(12)	59(13)
	c	10412(28)	9697(16)	1227(13)	65(14)
H(15)	a	9416(26)	2300(14)	39(14)	66(13)
	b	10826(22)	5227(12)	254(11)	30(10)
	c	9947(25)	8668(14)	-15(14)	61(12)
H(16)	a	8624(24)	1621(14)	469(11)	44(11)
	b	9946(20)	4623(12)	684(9)	14(9)
	c	9044(27)	8059(15)	428(13)	66(13)
H(17)	a	12902(27)	1376(13)	1632(12)	49(12)
	b	13848(25)	4611(11)	1927(10)	32(9)
	c	13305(26)	7975(12)	1726(10)	35(10)
H(181)	a	12387(33)	2051(18)	2148(16)	97(19)
	b	13038(38)	5366(20)	2274(18)	117(23)
	c	12636(36)	8591(19)	2247(18)	118(21)
H(182)	a	12392(37)	2250(19)	1611(17)	111(19)
	b	13203(33)	5509(18)	1749(15)	97(17)
	c	12641(39)	8794(21)	1685(19)	126(24)
H(183)	a	11290(35)	2062(16)	1827(15)	86(16)
	b	12075(36)	5335(18)	1916(15)	99(18)
	c	11601(33)	8644(15)	1847(13)	75(14)
H(191)	a	11833(38)	939(22)	940(19)	139(23)
	b	12975(40)	4116(22)	1257(19)	127(25)
	c	12421(38)	7602(20)	950(18)	127(22)
H(192)	a	12112(31)	1586(16)	865(15)	79(15)
	b	13120(33)	4669(17)	1066(16)	97(18)
	c	12542(36)	8236(19)	942(17)	112(19)
H(193)	a	10999(36)	1407(17)	955(15)	96(18)
	b	12013(33)	4531(16)	1159(14)	84(15)
	c	11465(31)	8014(14)	995(13)	67(14)
H(20)	a	12291(34)	391(18)	2444(16)	111(17)
	b	13086(25)	3759(12)	2732(11)	40(11)
	c	12568(28)	6938(15)	2383(13)	63(13)
H(211)	a	13971(41)	782(21)	2814(20)	133(21)
	b	14667(36)	4167(18)	3042(17)	87(18)
	c	14099(36)	7240(18)	2842(17)	100(17)
H(212)	a	13901(44)	1224(23)	2334(21)	156(29)
	b	14707(43)	4526(23)	2604(20)	149(26)
	c	13955(45)	7821(27)	2544(22)	150(30)
H(213)	a	13100(46)	1208(24)	2841(22)	165(30)
	b	13711(55)	4642(30)	2982(25)	208(44)
	c	13200(60)	7764(33)	2850(27)	213(49)
H(221)	a	13609(43)	64(22)	2090(19)	136(23)
	b	14480(44)	3347(23)	2515(21)	143(25)
	c	13960(42)	6657(22)	2065(19)	98(22)
H(222)	a	13555(48)	536(26)	1565(24)	198(32)
	b	14556(42)	3749(22)	2035(22)	149(27)
	c	14245(78)	7277(39)	1908(40)	230(50)
H(223)	a	12677(47)	96(24)	1696(22)	154(33)
	b	13621(57)	3368(33)	2064(28)	167(48)
	c	13439(57)	6835(31)	1497(30)	212(44)

cated by the precession 0*kl* photograph where the 0, 3*n*, *l* lines are appreciably stronger than the other lines. Structure factor calculation based on sulfur only, gave an R of 0.56 ($R = \sum||F_o| - |F_c||/\sum|F_o|$). All 102 non-hydrogen atoms were located in four subsequent Fourier maps. The structure was initially refined using 3700 low order reflections. Later all reflections were included, and anisotropic thermal parameters were introduced on all non-hydrogen atoms. The 92 hydrogen atoms were located from a difference map, and included in the refinement with isotropic temperature factors. The refinement converged at an R of 0.035, the weighted R is 0.034 and the standard deviation of an observation of unit weight, $([\sum w(F_o - F_c)^2/$

$(n-m)]^{\frac{1}{2}}$) is 1.61. The function minimized in the refinement was $\sum w(|F_o|-|F_c|)^2$, where $w = 1/\sigma_F^2$. At the end of the refinement the shifts in atomic parameters were less than 0.7σ. No indication of secondary extinction was observed. In a residual difference map no regions significantly above the noice level were found.

The scattering factors used were for sulfur, oxygen, and carbon those of Hanson *et al.*[6] and for hydrogen those of Stewart *et al.*[7] Final coordinates and thermal parameters are listed in Tables 1 and 2. Lists of observed and calculated structure factors may be obtained from the author.

THERMAL ANALYSIS

The thermal parameters of the 11 atoms of rings $A+B+C$ (Fig. 1) of each molecule were analyzed in terms of rigid body motion using

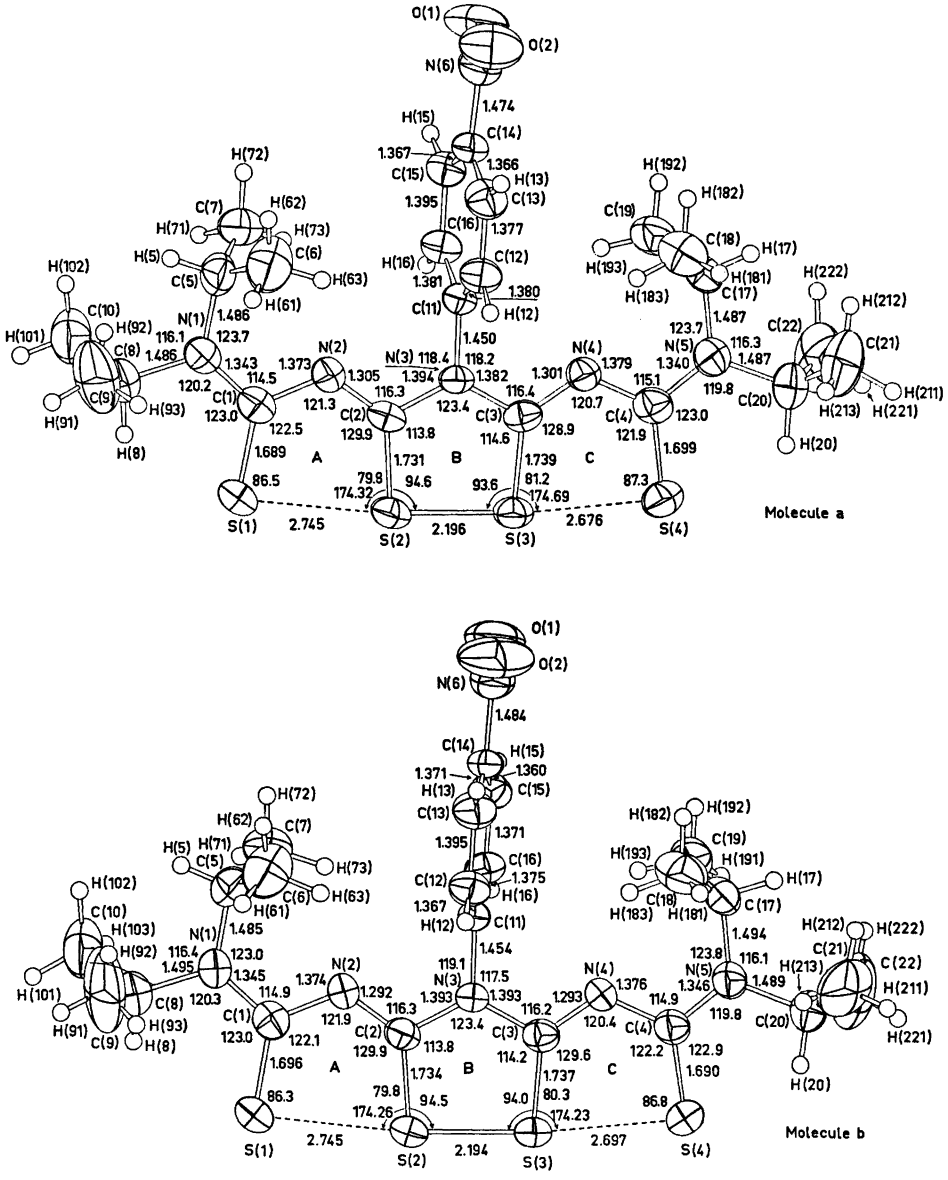

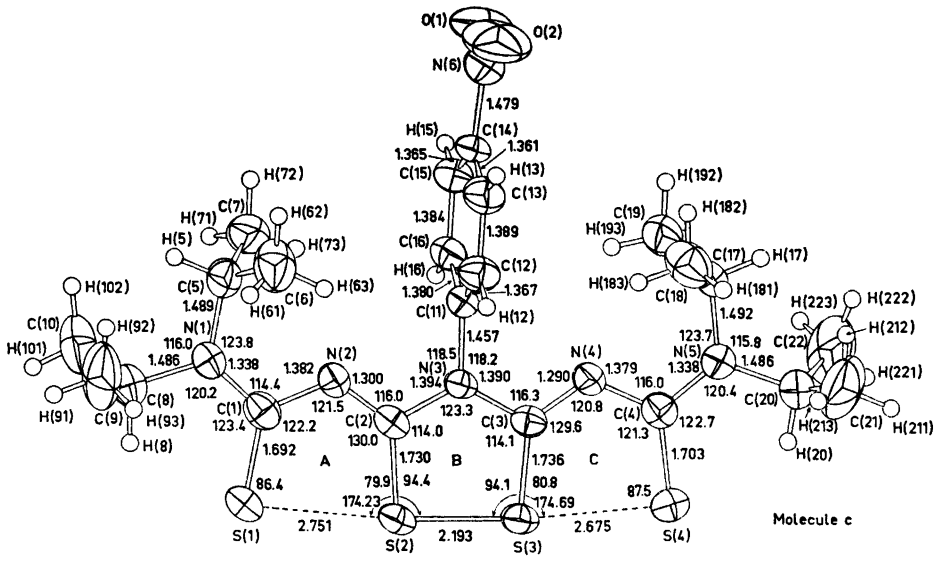

Fig. 1. Bond distances and angles in the three independent molecules (not corrected for rigid body motion). Standard deviations are 0.001 Å in S – S, 0.004 Å in S – C and 0.005 Å in N – C and C – C bonds. In the bond angles the standard deviations are 0.05° in S – S – S angles, 0.1° in S – S – C angles and 0.3° in the angles at C and N. For S, O, N, C the thermal ellipsoids are plotted at the 50 % probability level; H atoms are plotted with a fixed radius.

the method of Schomaker and Trueblood.[8] The observed mean-squares amplitude of vibration and the corresponding values calculated from the molecular **T**, **L**, **S** tensors, agree reasonably well, the r.m.s. ΔU being 0.0032, 0.0041, and 0.0026 Å^2 for molecules **a**, **b**, and **c**, respectively. In each case the axis of maximum libration was found to lie approximately parallel to the linear sulfur row, the angles of vibration being 7.3 (molecule **a**), 6.7 (**b**), and 6.7° (**c**). Corrections in bond distances were calculated according to Cruickshank's method.[9] The corrections are not significantly different in the three molecules, and amount to 0.004 Å in S – S, 0.012 – 0.014 Å in S – C, and 0.005 Å in C – N bond lengths.

RESULTS AND DISCUSSION

Bond distances and angles involving non-hydrogen atoms are shown in Fig. 1 and in

Table 3. Bond distances (Å) not shown in Fig. 1. Standard deviations in N – O distances are 0.006 Å and in C – C bonds of the isopropyl groups 0.010 Å.

Bond	Molecule **a**	Molecule **b**	Molecule **c**
N(6) – O(1)	1.219	1.207	1.209
N(6) – O(2)	1.214	1.204	1.201
C(5) – C(6)	1.516	1.506	1.513
C(5) – C(7)	1.519	1.517	1.513
C(8) – C(9)	1.517	1.511	1.519
C(8) – C(10)	1.524	1.516	1.521
C(17) – C(18)	1.519	1.503	1.513
C(17) – C(19)	1.515	1.513	1.523
C(20) – C(21)	1.519	1.522	1.498
C(20) – C(22)	1.536	1.508	1.517

Table 4. Bond angles (°) not shown in Fig. 1. Standard deviations are in the range 0.3 – 0.6°.

Angle	Molecule **a**	Molecule **b**	Molecule **c**
N(3) – C(11) – C(12)	120.1	119.9	120.3
N(3) – C(11) – C(16)	118.8	118.9	118.2
C(12) – C(11) – C(16)	121.1	121.2	121.5
C(11) – C(12) – C(13)	118.9	119.6	119.1
C(12) – C(13) – C(14)	119.8	117.9	118.8
C(13) – C(14) – C(15)	122.2	122.7	122.7
C(13) – C(14) – N(6)	119.2	118.6	118.5
C(15) – C(14) – N(6)	118.5	118.6	118.9
C(14) – C(15) – C(16)	118.4	119.0	118.7
C(15) – C(16) – C(11)	119.5	119.6	119.1
C(14) – N(6) – O(1)	117.7	118.3	117.9
C(14) – N(6) – O(2)	118.1	117.9	118.8
O(1) – N(6) – O(2)	124.2	123.8	123.3
N(1) – C(5) – C(6)	113.4	113.6	113.0
N(1) – C(5) – C(7)	113.0	112.3	113.0
C(6) – C(5) – C(7)	114.7	113.8	114.0
N(1) – C(8) – C(9)	110.7	109.8	110.9
N(1) – C(8) – C(10)	111.4	112.9	111.0
C(9) – C(8) – C(10)	113.0	111.3	112.4
N(5) – C(17) – C(18)	112.2	113.4	112.6
N(5) – C(17) – C(19)	113.6	112.1	112.9
C(18) – C(17) – C(19)	113.8	114.0	114.3
N(5) – C(20) – C(21)	111.6	110.2	110.1
N(5) – C(20) – C(22)	109.0	110.7	110.8
C(21) – C(20) – C(22)	112.7	115.3	116.0

Tables 3 and 4. The C – H distances all lie in region from 0.76 to 1.18 Å with a mean value of 0.97 Å both for C_{sp^2} – H and C_{sp^3} – H bonds. Standard deviations in the individual C – H distances range from 0.03 to 0.10 Å.

Corresponding bond distances in the three crystallographically independent molecules are identical within the experimental error, except for the S(3) – S(4) distance which is significantly longer in molecule **b** than in **a** and **c**. Molecule **b** also differs slightly, but significantly, from the two other molecules by showing a somewhat larger deviation from planarity in "rings" $A+B+C$ (Fig. 2.) The phenyl groups are oriented almost perpendicular to the main molecular planes. The twist angles in molecules **a** and **c** are 98 and 95° while the corresponding angle in **b** is 83°. There are short intramolecular contacts between the planes of the phenyl rings and the isopropyl groups (Table 5).

The asymmetry in the sulfur sequence of each molecule is reflected in different crystallographic

Table 5. Intramolecular contacts, distances in Å units. (ph···H) refers to the distance from a hydrogen atom to the plane of the phenyl group.

	Molecule **a**	Molecule **b**	Molecule **c**
S(1)···H(8)	2.34	2.49	2.38
S(4)···H(20)	2.38	2.41	2.35
ph···H(63)	2.89	2.56	2.85
ph···H(73)	2.73	2.83	2.75
ph···H(183)	2.70	2.85	2.72
ph···H(193)	2.92	2.66	2.85

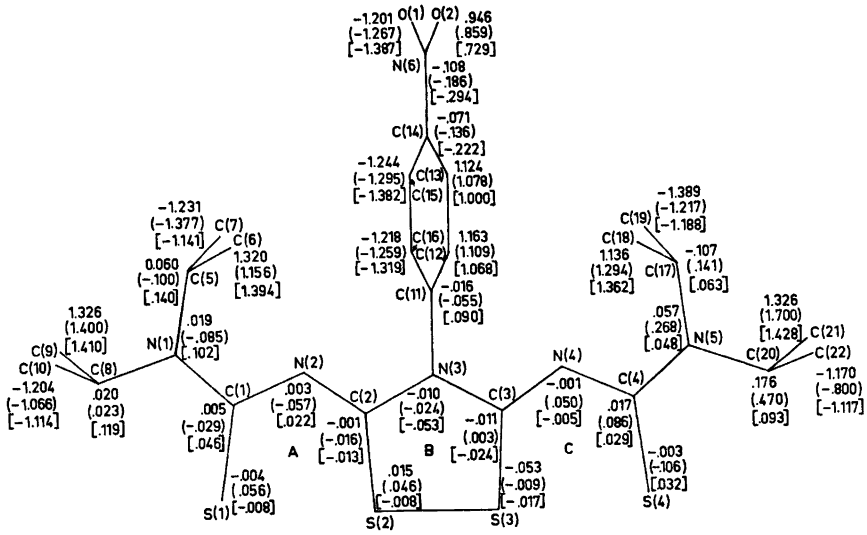

Fig. 2. Atomic deviations from the least-squares plane through rings $A+B+C$. Values for all three molecules are given; values for molecule **b** in parentheses, for molecule **c** in square brackets.

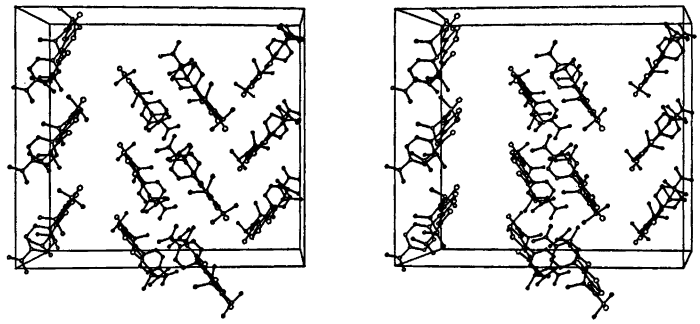

Fig. 3. Stereo drawing showing the packing of molecules in the crystal. The a^* axis is pointing towards the viewer, the b-axis is running top to bottom and the c-axis horisontally left to right. Hydrogen atoms have been omitted. Figs. 1 and 3 were drawn by computer using the ORTEP program.[14]

environment for atoms S(1) and S(4). This is best illustrated in the stereo drawing in Fig. 3. The molecules are arranged in columns running parallel to the crystallographic b-axis; molecules **a**, **b**, and **c** alternating through the column at a separation of approximately 1/3 unit cell. While there are no intermolecular short distances to S(1) of any molecule, the S(4) atoms have fairly short contacts to the molecules in the neighbouring stack related by a two-fold screw axis. S(4)**a** lies 3.40 Å above the molecular plane of molecule **b**′ (primed molecule at position $2-x$, $y-\frac{1}{2},\frac{1}{2}-z$); S(4)**b** is situated 3.25 Å above the plane of molecule **c**′; and S(4)**c** lies 3.35 Å from the plane of molecule **a**″ (double prime referring to position $2-x,y+\frac{1}{2},\frac{1}{2}-z$).

In one of the other dithiazolidine structures (II) determined, a similar asymmetry in the sulfur sequence is observed.[2] In two other analogous compounds (III, IV) the molecules possess a crystallographic twofold axis.[1,2]

In the present structure the central S–S bond is significantly longer than in molecules II, III, and IV. The sum of the three S–S

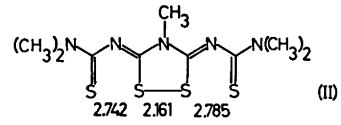

(II)

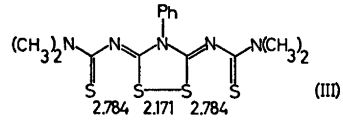

(III)

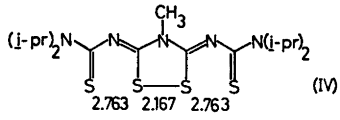

(IV)

bond lengths in each molecule is shorter in the present structure than in those previously studied; the values are 7.617, 7.636, and 7.619 Å for molecules **a**, **b**, and **c** respectively, compared to 7.688, 7.738, and 7.693 Å for II, III, and IV. The shorter overall S···S distances in the present compound may be caused by intramolecular strain; *i.e.* by repulsion between the *p*-nitrophenyl group and the closest isopropyl groups.

The sulfur–sulfur distances within each molecule are all in the region between single bond of 2.10 Å [10] and van der Waals distance. In other linear four-sulfur compounds (V and VI), however, the terminal S–S bonds have been found to be of the same length as those in isolated cyclic disulfides.[11,12] In these compounds (V, VI) the σ-bonding in the sulfur rows may be considered as four-centre four-electron bonding, giving two essentially localized bonds as the energetically most favourable arrangement. In the 1,2,4-dithiazolidine derivatives (I), where nitrogen atoms have been introduced into the ring system, the σ-bonding between the sulfur atoms may formally be regarded as four-centre six-electron bonding. The excess electrons populate non-bonding or weakly antibonding orbitals, resulting in partial σ-bonding between the sulfur atoms. Semi-empirical MO calculations on these systems will be published.

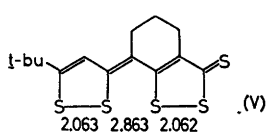

(V)

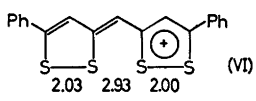

(VI)

Acknowledgement. Thanks are due to Dr. J. Goerdeler for supplying a crystalline sample of the compound.

REFERENCES

1. Sletten, J. *Acta Chem. Scand. 28* (1974) 989.
2. Flippen, J. L. *J. Amer. Chem. Soc. 95* (1973) 6073.
3. Goerdeler, J. and Ulmen, J. *Chem. Ber. 105* (1972) 1568.
4. Coppens, P., Leiserowitz, L. and Rabinovich, D. *Acta Crystallogr. 18* (1965) 1035.
5. Long, R. E. *Ph. D. Dissertation*, University of California, Los Angeles 1965.
6. Hanson, H. P., Hermann, F., Lea, J. D. and Skillman, S. *Acta Crystallogr. 17* (1964) 1040.
7. Stewart, R. F., Davidson, E. R. and Simpson, W. T. *J. Chem. Phys. 42* (1965) 3175.
8. Schomaker, V. and Trueblood, K. N. *Acta Crystallogr. B 24* (1968) 63.
9. Cruickshank, D. W. J. *Acta Crystallogr. 9* (1956) 757.
10. Hordvik, A. *Acta Chem. Scand. 20* (1966) 1885.
11. Sletten, J. *Acta Chem. Scand. 26* (1972) 873.
12. Hordvik, A. *Acta Chem. Scand. 19* (1965) 1253; Hordvik, A., Sletten, E. and Sletten, J. Paper given at the 6th Nordic Structure Chemistry Meeting, Århus, Denmark, Jan. 1967.
13. Johnson, C. K. *ORTEP, A Fortran Thermal Ellipsoid Plot Program for Crystal Structure Analysis*, Report ORNL-3794, Oak Ridge National Laboratory, Oak Ridge 1965.

Received October 22, 1974.

Acta Chemica Scandinavica A 29 (1975) 326—332

Studies on Cobalt(II) Halide Complex Formation. I. A Spectrophotometric Study of the Chloro Cobalt(II) Complexes in Strong Aqueous Chloride Solutions

JANNIK BJERRUM, A. S. HALONIN* and L. H. SKIBSTED**

Chemistry Department I, Inorganic Chemistry, H. C. Ørsted Institute, University of Copenhagen, DK-2100 Copenhagen Ø, Denmark

In this paper the stability constants for the chloro cobalt(II) complexes are estimated from spectrophotometric measurements on solutions of HCl, LiCl and $CaCl_2$. It was shown that in a certain wavelength range (610 – 690 nm), and for chloride concentrations higher than ≈ 5 M, the fraction of tetrachloro complex α_4 could be calculated from the relation $\alpha_4 = \varepsilon/\varepsilon_4$, where ε_4 is the limiting molar absorptivity for the most concentrated solutions of LiCl and HCl. Activity corrections were included semiquantitatively by introducing a one parameter activity function: $a_{Cl^-} = [Cl^-] \times 10^{B[Cl^-]-0.5}$ adjusted to the measurements and assumed to be valid for $[Cl^-] \geq 5$ M. On this basis the following values were obtained for the stability constants at 25 °C: $K_1(\text{l mol}^{-1}) = 10^{-1.05 \pm 0.38}$, $K_2 = 10^{-2.69 \pm 0.90}$, $K_3 = 10^{-1.54 \pm 0.89}$ $K_4 = 10^{-1.34 \pm 0.13}$ and β_4 (l^4 mol^{-4}) $= 10^{-6.62 \pm 0.24}$ from measurements of LiCl solutions with the activity parameter $B = 0.170 \pm 0.005$. The same stability constants could also be used for HCl, with $B = 0.185$, and for $CaCl_2$ solutions, with $B = 0.132$. The distribution of the complexes is shown graphically in Fig. 3.

The change in colour of cobalt(II) chloride solutions from red to blue with increasing temperature and chloride concentration has been the subject of numerous studies since the last century. Some of the early authors [1,2] assume that the colour change is caused by dehydration of the solvated cobalt(II) ion, others [3,4] that the colour change is caused by complex formation. It is now generally recognized that the octahedral hexaquo cobalt(II) ion at high chloride concentrations is more or less converted into a tetrahedral tetrachloro complex.[5–15] Some authors [6,10,13] do not find evidence for other chloro complexes than the tetra complex. Others [8,11,16–18] have estimated values for K_1 varying from 0.004 to 0.67 l mol^{-1}. The lowest of these values, $K_1 = 10^{-2.40}$, is estimated by Job,[16] who also estimates a value for β_3 of $10^{-5.92}$ l^3 mol^{-3} but wrongly assumes, as later do Cotton *et al.*,[19] that $CoCl_3(H_2O)^-$ is the dominating complex in concentrated aqueous hydrochloric acid solutions. Stability constants for all the chloro complexes have only been estimated by Zeltmann *et al.*[12] and Belousov *et al.*[15] Zeltmann *et al.* identify the species present in hydrochloric acid solutions by means of NMR methods and they correct for activity semiquantitatively simply by equating the chloride ion activity with the hydrochloric acid activity. Belousov *et al.*, on the other hand, estimate concentration constants in mixtures of HCl and $HClO_4$ at different high, but constant ionic strengths from spectrophotometric measurements. The findings of these authors are discussed in connection with the results obtained in this paper, in which the stability constants are computed from a spectrophotometric determination of the fraction of cobalt present as tetrachloro complex in dilute Co(II) solutions with chloride concentration higher than ≈ 5 M.

* On leave from Metallurgical Faculty, Kalinin's Polytechnical Institute, Leningrad, USSR.

** Present adddress: Chemistry Department, Royal Veterinary and Agricultural University, DK-1871 Copenhagen V, Denmark.

EXPERIMENTAL

Measurements of absorption spectra were performed with a Cary 14 recording spectrophotometer and in the case of measurements at selected wavelengths with a Beckman DU spectrophotometer. Both instruments were thermostatted to 25.0 ± 0.1 °C. Cobalt concentrations and cell lengths were chosen so that the absorbance was always in the well defined measuring range of the instrument.

Solutions of known molar concentration at 25 °C were made up from analyzed stock solutions of $CoCl_2$, HCl, LiCl, $CaCl_2$, and $HClO_4$ by weighing or pipetting the components into calibrated measuring flasks. Analytical reagents and redistilled water were used.

TREATMENT OF DATA

The characteristic absorption band between 600 and 700 nm which causes the blue colour of Co(II) in strong solutions of HCl, LiCl, and $CaCl_2$ is shown in Fig. 1. This band is due to the tetrachloro complex and it can be seen from Fig. 2 that the formation of this complex is nearly complete in concentrated HCl and LiCl solution. This figures (in which log ε for the two wavelengths 624 and 690 nm is plotted *versus* the total chloride concentrations) shows that the same limiting molar absorptivity is reached

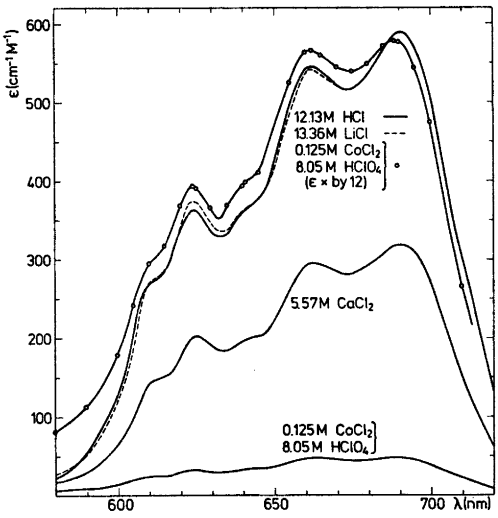

Fig. 1. Absorption spectra of 10^{-3} M $CoCl_2$ in aqueous 12.13 M HCl, 13.36 M LiCl, and 5.57 M $CaCl_2$, and of 0.125 M $CoCl_2$ in 8.05 M $HClO_4$. The spectrum of the $CoCl_2$,$HClO_4$ solution with the molar absorptivities multiplied by 12 is also shown.

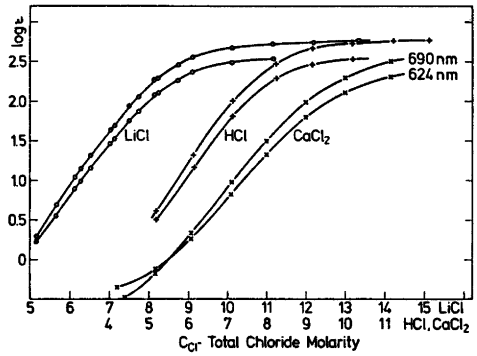

Fig. 2. Logarithm of molar absorptivity, at 624 and 690 nm, of Co(II) in solutions of HCl, LiCl, and $CaCl_2$ as a function of the total chloride concentration. Note the different scale division of the abscissa for HCl and $CaCl_2$ relative to that for LiCl.

for HCl concentrations higher than ≈ 11 M and LiCl concentrations higher than ≈ 13 M. Furthermore, it can be seen that the limiting absorptivity is not yet reached in saturated $CaCl_2$ solutions having $C_{Cl^-} \approx 12$ M. That the absorption between 600 and 700 nm is nearly exclusively due to the tetrachloro complex, even in solutions with a relatively small degree of formation of this complex, is demonstrated in Fig. 1, in which the low absorption band for a solution of the composition 0.125 M $CoCl_2$, 8.05 M $HClO_4$ is also given enlarged by a factor of 12. It is remarkable how closely the enlarged spectrum agrees, in details of maxima, minima, and shoulders, with that measured for the tetrachloro complex in concentrated HCl and LiCl solutions. Therefore, denoting the limiting molar absorptivity in these solutions by ε_4 it should be possible, down to a certain limit of chloride concentration, to calculate the degree of formation of the tetrachloro species from the relationship $\alpha_4 = \varepsilon/\varepsilon_4$. The result of such a calculation for 5 wavelengths between 610 and 690 nm (one for each maximum or shoulder) is given in Table 1. In the case of $CaCl_2$ solutions the value of ε_4 is taken to be the same as in the HCl and LiCl solutions. It is notable that the same degree of formation is found at all the wavelengths for values of $\varepsilon/\varepsilon_4$ higher than ≈ 0.05. In the range $\alpha_4 \approx 0.01 - 0.05$ there is a trend towards lower values for $\varepsilon/\varepsilon_4$ with increasing wavelength, but not more than that the *smallest* of the values may be assumed to be a

Table 1. Estimation of the degree of formation of the tetrachloro complex as $\alpha_4 = \varepsilon/\varepsilon_4$.

$CoCl_2 - LiCl - H_2O$

	ε_4	279	380	372	550	600		
C_{CoCl_2}	C_{LiCl}	610	624	641	662	690 nm	α_4 (exp)	α_4 calc)
0.1000	4.98	0.0053	0.0045	0.00435	0.0038	0.0033	0.003 ± 0.0005	0.0027
0.1016	5.24	0.0065	0.0059	0.0057	0.0034	0.0031	0.0028 ± 0.0005	0.0037
0.0503	5.60	0.0099	0.0094	0.00925	0.0087	0.0082	0.0077 ± 0.0005	0.0068
0.0504	5.75	0.0124	0.0119	0.0123	0.0112	0.0105	0.0105 ± 0.0005	0.0090
0.0402	6.05	0.0212	0.0207	0.0204	0.0194	0.0183	0.0176 ± 0.0007	0.0164
0.0251	6.25	0.0254	0.0256	0.0254	0.0253	0.0234	0.0225 ± 0.001	0.0213
0.0251	6.50	0.0372	0.0376	0.0374	0.0363	0.0350	0.034 ± 0.001	0.0327
0.00995	7.00	0.0742	0.0765	0.0750	0.0750	0.0730	0.072 ± 0.002	0.0718
0.0217	7.09	0.0855	0.0870	0.0868	0.0848	0.0818	0.081 ± 0.002	0.0860
0.01005	7.49	0.149	0.1485	0.149	0.146	0.147	0.147 ± 0.002	0.145
0.00303	7.73	0.192	0.192	0.192	0.188	0.190	0.190 ± 0.002	0.193
0.00300	8.12	0.317	0.318	0.317	0.311	0.315	0.315 ± 0.002	0.297
0.00203	8.23	0.328	0.324	0.328	0.322	0.325	0.325 ± 0.002	0.330
0.00201	8.74	0.485	(0.419)	0.484	0.480	0.483	0.483 ± 0.002	0.488
0.00155	9.09	0.609	0.610	0.610	0.602	0.610	0.610 ± 0.003	0.596
0.00101	10.11	0.800	0.799	0.798	0.791	0.797	0.797 ± 0.003	0.807
0.00102	11.17	0.899	0.902	0.900	0.895	0.899	0.899 ± 0.004	0.905
0.00102	12.20	0.955	0.955	0.952	0.951	0.954	0.954 ± 0.004	0.948
0.00101	13.36	0.985	0.986	0.985	0.983	0.985	0.985 ± 0.005	0.971

$CoCl_2 - HCl - H_2O$

	ε_4	279	380	380	560	610		
C_{CoCl_2}	C_{HCl}	610	624	641	662	690 nm	α_4 (exp)	α_4 (calc)[a]
0.0401	5.13	0.0087	0.0082	0.0078	0.0073	0.0067	0.006	0.0053
0.0201	6.10	0.038	0.038	0.037	0.036	0.0345	0.034	0.032
0.00595	7.12	0.167	0.170	0.171	0.169	0.164	0.166	0.163
0.00202	8.23	0.490	0.505	0.502	0.505	0.494	0.496	0.486
0.000100	9.17	0.755	0.770	0.765	0.775	0.765	0.765	0.764
0.000402	10.19	0.893	0.897	0.895	0.908	0.899	0.896	0.887
0.000396	11.24	0.951	0.912	0.940	0.960	0.949	0.950	0.944
0.000407	12.13	0.972	0.960	0.960	0.976	0.966	0.967	0.967

$CoCl_2 - CaCl_2 - H_2O$

	ε_4	279	380	372	550	600		
C_{CoCl_2}	C_{CaCl_2}	610	624	641	662	690 nm	α_4 (exp)	α_4 (calc)[a]
0.0999	2.000	0.00179	0.00116	0.00108	0.00069	0.00047	0.0004	0.0001
0.1007	2.495	0.00265	0.00195	0.00193	0.00138	0.00113	0.001	0.0006
0.0408	2.999	0.0056	0.0047	0.0046	0.0040	0.0036	0.003	0.0025
0.00964	3.538	0.0182	0.0175	0.0172	0.0165	0.0156	0.015	0.012
0.00302	4.001	0.0534	0.0545	0.0540	0.0530	0.0513	0.051	0.045
0.00149	4.503	0.162	0.167	0.167	0.165	0.162	0.162	0.136
0.00103	4.999	0.323	0.335	0.335	0.338	0.332	0.335	0.332
0.00103	5.567	0.512	0.535	0.535	0.540	0.533	0.536	0.568

[a] Calculated with the stability constants obtained for LiCl solutions, but with different values for the activity parameter B, 0.185 for HCl, and 0.132 for $CaCl_2$ compared to 0.170 for LiCl.

relatively good measure of the degree of formation of the tetrachloro complex. It can be seen directly from the lower part of the absorption curves for $CaCl_2$ solutions in Fig. 2 that there is some disturbance from other complexes for $C_{Cl^-} \leq 5$ M.

In order to calculate the stability constants in solutions of strongly varying concentrations of a single electrolyte, such as, *e.g.*, HCl, it is necessary to make some rough assumptions about the activity coefficients of the species involved. Zeltmann *et al.*[12] assume that the

ratio of activity coefficients for the chlorocobalt complexes is constant and introduce for the chloride ion activity the hydrochloric activity. As the uptake of a chloride ion is accompanied by a splitting-off of water molecules, these authors also correct for the change in the water activity. In the present paper, as in an earlier paper of one of the authors,[20] it has also been found necessary to assume that the ratio of the activity coefficients for the chloro complexes, $f(CoCl_{n-1}^{3-n})/f(CoCl_n^{2-n})$, is independent of $[Cl^-]$. Such an assumption is reasonable for concentrated electrolyte solutions in which the Coulombic attraction is of relatively little importance. However, instead of applying arbitrarily the mean activity of the complex-forming chloride electrolyte, a one parameter activity function adjusted to the measurements has been introduced. It is an empirical fact that $\log \gamma_{\pm}$ for solvated strong electrolytes increases linearly with the molar concentration for high concentrations of the salt.[20,21] Thus the following relationships are approximately valid for chloride concentrations higher than 3 to 5 M:

$$\log \gamma_{(HCl)}^{(C)} = -0.42 + 0.18\ C_{Cl^-}$$

$$\log \gamma_{(CaCl_2)}^{(C)} = -0.55 + 0.20\ C_{Cl^-}$$

($\gamma^{(C)}$ indicates molar concentration scale). The negative term in these expressions is of little importance for concentrated electrolyte solutions and the following one parameter activity expression:

$$a_{Cl^-} = [Cl^-] \times 10^{B[Cl^-]-0.5}$$

has therefore been assumed to be sufficiently accurate. This function for the chloride ion activity, with a value for B adjusted to suit the measurements, is furthermore assumed to include a correction for the change in the water activity. Expressed more precisely, the consecutive stability constants given by the expression:

$$K_n = \frac{[CoCl_n^{2-n}]}{[CoCl_{n-1}^{3-n}]a_{Cl^-}},\ n = 1,2,3,4$$

are assumed to be valid in the limited concentration range (5 – 12 M) in which it has been possible to obtain reliable values for the degree of formation of the tetrachloro complex. In the terminology of Marcus [21] a_{Cl^-} is the effective ligand activity, and the K_n's (denoted by an asterisk) are the effective stepwise formation constants. The latter are to be distinguished from, but are assumed to approximate to, the true activity formation constants.

CALCULATION OF STABILITY CONSTANTS

The stability constants were calculated by use of the values for the degree of formation of the fourth complex:

$$\alpha_4 = \beta_4 a_{Cl^-}^4 / \sum_0^4 \beta_n a^n{}_{Cl^-},\ \text{where}\ \beta_n = K_1 K_2 \cdots K_n$$

Since most of the determinations of α_4 were made for LiCl solutions these measurements were used in the calculation. A preliminary calculation was made by making the reasonable assumption that apart from the small fractions of tetrachloro complex mainly the aqua and monochloro complexes were present in the range of chloride concentrations from ≈5 to 8 M. K_1 was tentatively taken to be 0.1 l mol^{-1}, and values of β_4 calculated by means of the expression

$$\beta_4 \approx \alpha_4/(1-\alpha_1)a_{Cl^-}^4$$

with $1-\alpha_1$ inserted for α_0. In this way it was found by trial and error that the parameter B must be close to 0.17 in order to obtain constant values for β_4. β_4 itself was found to be $\approx 10^{-6.6}$ l^4 mol^{-4}, and K_4 was estimated to be $10^{-1.3}$ l mol^{-1} from the values of α_4 for chloride concentrations > 11 M, where $\alpha_4 \to 1$. The final calculation of the four stability constants was made by the method of least squares. With the preliminary estimated stability constants as starting values, the expression was minimized as a function of the four stability constants.

$$\sum_i \frac{[\alpha_4(calc)_i - \alpha_4(obs)_i]^2}{\sigma_i^2}$$

The σ_i are the tentatively assumed uncertainties in the values of α_4 shown in Table 1. No distinction was made between total and free chloride ion concentration and the activity parameter B was taken to be 0.170 ± 0.005. Minimization under these conditions gave the results shown in Table 3. A calculation in which the parameter B was taken to be 0.17 ± 0.02 gave unchanged values for the constants with nearly unchanged uncertainties in K_2 and K_3 but with somewhat higher uncertainties (about 60 %) in K_1, K_4,

Table 2. Results of calculations of the stability constants with different fixed values for the parameter B.

B	$\log K_1$	$\log K_2$	$\log K_3$	$\log K_4$	$\log \beta_4$
0.16	-1.33 ± 0.28	-2.40 ± 0.81	-1.64 ± 0.78	-1.17 ± 0.14	-6.54 ± 0.16
0.17	-1.05 ± 0.31	-2.73 ± 0.97	-1.49 ± 0.97	-1.33 ± 0.11	-6.60 ± 0.23
0.18	-0.82 ± 0.42	-2.71 ± 0.68	-1.65 ± 0.68	-1.46 ± 0.10	-6.63 ± 0.37

Table 3. Comparison of stability constants for the cobalt(II) chloride system.

Reference	$\log K_1$	$\log K_2$	$\log K_3$	$\log K_4$	$\log \beta_4$
This paper [a]	-1.05 ± 0.38	-2.69 ± 0.90	-1.54 ± 0.89	-1.34 ± 0.13	-6.62 ± 0.24
Zeltmann *et al.*[12] [b]	-0.77 ± 0.19	-2.77 ± 0.12	-2.51 ± 0.15	-2.06 ± 0.09	-8.11
Belousov *et al.*[15] [c]	$+0.64\pm0.03$	0.13	-0.01	-0.57	0.20 ± 0.12

[a] C_{LiCl} var., calc. with $a_{Cl^-}=[Cl^-]\times 10^{(0.170\pm0.005)[Cl^-]-0.5}$ [b] m_{HCl} var., calc. with $a_{Cl^-}=m_{HCl}\gamma_\pm(HCl)/a_{H_2O}$ [c] 9 M $H(ClO_4)$, calc. with $a_{Cl^-}=[Cl^-]$.

and β_4. Calculations with different fixed values for B of 0.16, 0.17, and 0.18, respectively, were also made (see Table 2).

Calculated values for α_4 corresponding to the constants, with B taken as 0.170 ± 0.005, are shown in Table 1 and it can be seen that the agreement with the experimental values is satisfactory. The values of α_4(calc) for HCl and $CaCl_2$, given in the same table, are calculated using the same constants but with B chosen to be 0.185 and 0.132, respectively.

DISCUSSION

A graphical picture of the distribution of the cobalt complexes, which shows the very small range of existence of the dichloro and trichloro complexes, is presented in Fig. 3. In this figure the fractions α_n of the various complexes are plotted *versus* the logarithm of the chosen chloride ion activity function. The full curves are calculated by the use of the stability constants obtained for the LiCl solutions. The experimental values of α_4 obtained for HCl and $CaCl_2$ solutions are also plotted in the figure. The latter are plotted *versus* the activity function based on the values for B used to compute α_4(calc) in Table 1. The points plotted (+ for HCl and × for $CaCl_2$) are seen to lie close to the full curve valid for LiCl solutions. This agreement (excellent for the HCl, and satisfactory for the $CaCl_2$

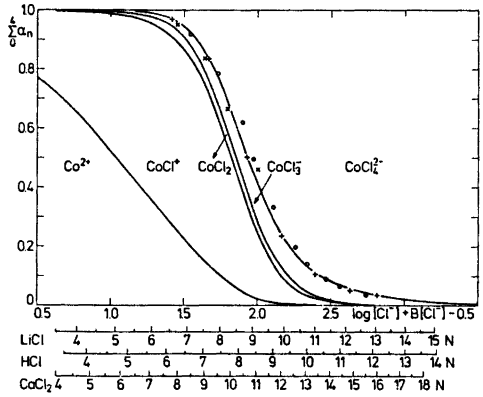

Fig. 3. Plots of the fractions α_n for various complexes $CoCl_n^{2-n}$ *versus* the logarithm of the chloride ion activity function: $a_{Cl^-}=[Cl^-]\times 10^{B[Cl^-]-0.5}$. The full curves show graphically the distribution of the complexes, calculated using the stability constants valid for LiCl solutions with the parameter $B=0.170$. The experimental values for α_4 (HCl, +; $CaCl_2$, ×) shown are plotted *versus* log a_{Cl^-} calculated using the values for B (HCl, 0.185; $CaCl_2$, 0.132), which give the best fit to the full curve for LiCl. Below the activity scale are given scales for the molar chloride concentrations which correspond to the stated values of the B parameter. For comparison purposes, connected values of α_4 and C_{HCl} from the paper of Zeltmann *et al.*[12] (converted from molal to molar concentrations) are indicated by O points in the figure.

solutions) shows directly that it is possible with some approximation, and by simply changing the value for the parameter B, to use the same set of stability constants for all three of the chloride electrolytes studied.

The composition of a given cobalt(II) chloride solution can be estimated from Fig. 3, which gives scales for the molar chloride concentrations corresponding to the activity function for the different chloride electrolytes. The scale for HCl makes possible a direct comparison with the values of α_4 obtained by Zeltmann *et al.*[12] These authors use molal HCl concentrations but their values converted for molar concentrations are plotted as O points. The figure shows how closely these values, obtained in a completely different way by means of NMR measurements with oxygen-17 and chlorine-35, follow our curve, and this agreement gives support to our assumption that the tetrachloro complex is nearly exclusively producing the absorbance in the wavelength range 600 – 700 nm in strong aqueous chloride solutions. On the other hand, measurements in non-aqueous solutions,[22–24] as well as the measurements of Zeltmann *et al.*,[12] provide evidence that the molar absorptivity of the trichloro complex may amount to as much as one third to more than one half of that of the tetrachloro complex in the stated wavelength range. It must, therefore, be the small range of existence of the trichloro complex in aqueous medium that is mainly responsible for the justification of the calculations made.

The stability constants obtained in this paper with $B = 0.170 \pm 0.005$ are compared in Table 3 with the activity-corrected constants obtained by Zeltmann *et al.*[12] and with the concentration constants estimated by Belousov *et al.*[15] for a 9 M perchloric acid medium. The constants obtained by Zeltmann *et al.* agree fairly well with ours but their values for K_4 and β_4 are most probably too high, considering the fine agreement between their values of α_4 and ours for HCl solutions of given molarity. The discrepancy can only be due to the fact that Zeltmann *et al.* arbitrarily introduce too strong an activity correction, and an activity correction derived from the measurements themselves, as in the present paper, is probably more realistic.

The concentration stability constants estimated by Belousov *et al.*[15] for 9 M and other strong perchloric acid solutions are, as should be expected (considering the high activity of hydrochloric acid in these solutions), much higher than our activity-corrected values but the relative magnitude of their constants is suspect. According to the ratio between the consecutive constants the dichloro and trichloro complexes have a rather large range of existence, in contradiction with our results. We find, in disagreement with Belousov *et al.*,[15] that the tetrachloro complex also in strong perchloric acid solutions is almost solely responsible for the absorption in the wavelength range 600 – 700 nm, even when it is present in only a few per cent. The spectrum of such a solution (0.125 M $CoCl_2$ in 8.05 M $HClO_4$) with $\alpha_4 = 0.078$ is, as already mentioned, shown in Fig. 1. Assuming that the distribution of the complexes for a given value of α_4 is the same as in Fig. 3, this solution is estimated to have $\alpha_0 = 0.2$, $[Cl^-] \cong 0.10$ M and $\beta_4 = \alpha_4/(\alpha_0[Cl^-]^4) \cong 10^{3.6}$. Another solution (0.050 M $CoCl_2$ in 8.99 M $HClO_4$) with $\alpha_4 \cong 0.027$ was estimated to have $\alpha_0 \cong 0.28$, $[Cl^-] \cong 0.057$ M and $\beta_4 \cong 10^4$. Using the constants given by Belousov *et al.* one calculated $\alpha_4 \sim 0.0006$ for the same solution. Such a value for α_4 is not even of the right order of magnitude and the constants given by these authors cannot therefore stand closer criticism.

According to our estimate, the concentration constant $\beta_4 = [CoCl_4^{2-}]/([Co^{2+}][Cl^-]^4)$ increases from $10^{-6.6}$ to 10^4 on going from water at ionic strength zero to 9 M $HClO_4$. This is perhaps too great an increase but not unreasonable considering that β_4 is a function of the fourth power of the chloride ion activity. The activity coefficient of hydrochloric acid in 9 M $HClO_4$ is not known but that of perchloric acid is estimated [25] to be ≈ 350. The fourth power of this figure for $\gamma_{\pm}^{(C)}$ is as high as 1.5×10^{10}, which supports our estimate of the value of β_4 in 9 M $HClO_4$.

REFERENCES

1. Jones, H. C. *Z. Physik. Chem. 74* (1910) 325.
2. Hantzsch, A. *Z. Anorg. Chem. 159* (1926) 273.
3. Gróh, J. and Schmid, R. *Z. Anorg. Chem. 162* (1927) 321.
4. Bassett, H. and Croucher, H. H. *J. Chem. Soc.* (1930) 1784.
5. Howell, O. R. and Jackson, A. *J. Chem. Soc.* (1936) 1268.

6. Kiss, A. v. and Gerendás, M. *Z. Phys. Chem. A 180* (1937) 117.
7. Dreisch, Th. and Trommer, W. *Z. Phys. Chem. B 37* (1937) 37.
8. Smithson, J. M. and Williams, R. J. P. *J. Chem. Soc.* (1958) 457.
9. Yatsimirskiĭ, K. B. and Korableva, V. D. *Izvest. Vyssh. Ucheb. Zavadeniĭ, Khim. Tekhn.* (1958) No. 4, 19.
10. Andreev, S. N. and Khaldin, V. G. *Dokl. Akad. Nauk. SSSR 134* (1960) 345.
11. Mizutani, K. and Sone, K. *Z. Anorg. Chem. 350* (1967) 216.
12. Zeltmann, A. H., Matwiyoff, N. A. and Morgan, L. O. *J. Phys. Chem. 72* (1968) 121.
13. Stankov, V., Jedináková, V. and Leleda, J. *Sbor. vysoké školy chem.-techn. Praze B 15* (1972) 165.
14. Kraus, U. and Lehmann, G. *Ber. Bunsenges. phys. Chem. 76* (1972) 1066.
15. Belousov, E. A., Bocharow, V. V. and Mironov, V. E. *Russ. J. Inorg. Chem. 17* (1972) 1717.
16. Job, P. *Ann. Chim. (Paris) 6* (1936) 97.
17. Trémillon, B. *Bull. Soc. Chim. Fr.* (1958) 1483.
18. Lister, M. W. and Rosenblum, P. *Canad. J. Chem. 38* (1960) 1827.
19. Cotton, F. A., Goodgame, D. M. L. and Goodgame, M. *J. Amer. Chem. Soc. 83* (1961) 4690.
20. Bjerrum, J. *Kgl. Dan. Vidensk. Selsk., Mat.-fys. Medd. 22* (1946) No. 18.
21. Marcus, Y. *Rec. Chem. Progr. 27* (1966) 105.
22. Magnell, K. R. and Reynolds, W. L. *Inorg. Chim. Acta 6* (1972) 571.
23. Schriver, A. *Bull. Soc. Chim. Fr.* (1973) 11.
24. Sawada, K. and Tanaka, M. *J. Inorg. Nucl. Chem. 36* (1974) 1971.
25. *Landolt-Börnstein Phys.-Chem. Tabellen*, 2. Erg. (1931) 260; 3. Erg. (1936) 2144.

Received October 31, 1974.

Acta Chemica Scandinavica A 29 (1975) 333—344

Studies on the Hydrolysis of Metal Ions. 62. The Plutonyl Ion in Sodium Perchlorate Medium

ULLA SCHEDIN

Department of Inorganic Chemistry, Royal Institute of Technology, S-100 44 Stockholm 70, Sweden, and Division of Materials Research, Research Institute of National Defence, S-172 04 Sundbyberg 4, Sweden

The hydrolysis equilibria of plutonyl ion in 3 M $(Na)ClO_4$ have been studied at 25 °C using a glass electrode. The concentration range for PuO_2^{2+} (B) was 10 – 150 mM and the average number of ligands, OH^-, bound per PuO_2^{2+} (Z) was 0 – 1.3. Fresh Pu(VI) solutions were always used, in which the concentration of other plutonium ions was less than one per cent.

About 20 species $(p,q) = (PuO_2)_q(OH)_p^{(2q-p)+}$ were tried in the LETAGROP "species selector".

For $Z < 0.3$, where the attainment of chemical equilibria could be proved by back titrations, all the data could be explained by (2,2), with the "best" equilibrium constant $\log {}^*\beta_{2,2} = -8.24 \pm 0.01$, where ${}^*\beta_{p,q}$ is the equilibrium constant for

$$q PuO_2^{2+} + p H_2O \rightleftharpoons (PuO_2)_q(OH)_p^{(2q-p)+} + p H^+.$$

For higher Z the data are uncertain as equilibrium could not be proved. The best fit is given by (2,2) and (7,4) with the equilibrium constant ${}^*\beta_{2,2} = -8.23 \pm 0.04$ and (${}^*\beta_{7,4} = -29.13 \pm 0.04$).

A short survey is also given of some properties of plutonium ions in aqueous solutions, as they might have affected this investigation.

It is well-known, that the plutonyl ion hydrolyzes in water solution, but there is still much uncertainty about what species that are formed upon hydrolysis. For this reason it was considered of great interest to try to get further information on this basic problem in plutonium chemistry.

Until recently very little has been published in the literature on this subject, as shown in Table 1. O'Connor [1] made an early investigation in 1944, and he found PuO_2OH^+, here called (1,1). Kraus and Dam [2] made potentiometric titrations in 1949. They worked at rather low concentrations (0.718 – 1.32 mM PuO_2^{2+}) and found the mononuclear complexes PuO_2OH^+ and $PuO_2(OH)_2$. Krevinskaya *et al.*[3] dissolved a known amount of a plutonium salt in a certain amount of nitric acid and measured pH with a glass electrode. They found five different complexes, some of which also contained nitrate. Their results must be considered unreliable as the accuracy obtained in this way is rather low. Moskvin *et al.*[4] made solubility investigations. Their experimental procedures are not recorded in detail. They dissolved a solid plutonium phase at different pH and measured $[H^+]$ potentiometrically. The solid phase was prepared by adding ammonia to a Pu(VI) solution and was considered to be ammonium diplutonate. However Cleveland [5] later found that a precipitate prepared in the same way mainly contained plutonium(VI) hydroxide. Recently, in 1972, Cassol *et al.*[6] reported potentiometric measurements of $[H^+]$ at 25 °C in 1 M $(Na)ClO_4$ containing plutonium in the concentration range 0.1 – 30 mM. They found PuO_2OH^+ in agreement with Kraus *et al.* and $(PuO_2)_2(OH)_2^{2+}$ in agreement with our earlier paper [7] and a new species $(PuO_2)_3(OH)_5^+$, which they considered a little uncertain. Their data seem to be the most reliable yet published and are complementary to our investigation, in which higher B values have mainly been studied.

Table 1. Hydrolysis of plutonyl ion. Complexes found in the literature and in our investigation. They are given as $-\log^*_{p,q}$, for the (p,q) values shown at the top of each column.

(1,1)	(2,1)	(2,2)	(3,2)	(5,2)	(5,3)	(7,4)	Ionic medium	*B* range mM	°C	Year	Ref.
5.30	–	–	–	–	–	–				1944	1
5.71	11.42	–	–	–	–	–	1 M $NaClO_4$	0.718 – 1.32		1949	2
3.33	7.38	–	–	–	–	–	0.186 mM HNO_3	0.001 – 0.01		1959	3
3.39	8.64	–	17.77	31.50	–	–		0.122 – 58.5		1962	4
–	–	8.21	–	–	–	–	3 M (Na)ClO_4	15 – 130	25	1971	7
5.97	–	8.51	–	–	22.16	–	1 M (Na)ClO_4	0.1 – 30	25	1972	6
–	–	8.24	–	–	–	(29.13)	3 M (Na)ClO_4	10 – 150	25	1974	[a]

[a] Present paper.

EXPERIMENTAL

All work where plutonium was involved in these experiments, was performed in glove boxes. The preparation of plutonium solutions was made in a special box in order to avoid acidic fumes during analysis and hydrolysis. The analytical determination of plutonium in solution took place in another box and was performed by a special staff. The titrations were performed in a third glove box.

All inactive reagents were prepared and stored outside the glove boxes, where necessary in rooms kept at 25.0 ± 1.5 °C.

Reagents and solutions

Sodium perchlorate stock solution was prepared by neutralization of concentrated $HClO_4$, Merck *p.a.*, with Na_2CO_3, Merck *p.a.* waterfree. To avoid some impurities, *e.g.* Fe, the solution was made slightly alkaline and allowed to stand for a week. It was filtered through a G4 Jena glass filter and recrystallized once and standardized by evaporation at about 120 °C. The reproducibility was within 0.1 %. This method of analysis had previously been checked against an ion exchange method used on another stock solution prepared in the same way. The agreement was better than 0.2 %.

Perchloric acid solutions were made by dilution of $HClO_4$, Merck *p.a.*, and standardized against recrystallized $KHCO_3$ with a reproducibility of 0.2 %. They were also checked against the NaOH stock solution, which gave the same result to within 0.2 %.

Sodium hydroxide was prepared as a 50 % solution from solid NaOH, EKA *p.a.* Na_2CO_3 was removed by filtering through a G4 Jena glass filter. The solution was diluted with boiled distilled water under an N_2 atmosphere and standardized against hydrazine sulfate with a reproducibility of 0.2 %.

Silver(II) oxide was prepared according to Hammer *et al.*[8] from $K_2S_2O_8$, N-free, Merck *p.a.* It was decanted three times from very dilute NaOH solutions, and washed several times with water during filtration.

Sodium chloride used was NaCl, Merck suprapur.

The *distilled water* used was always boiled to expel CO_2.

Plutonium solutions were prepared from plutonium metal. Two different castings were used. Their purity, which was examined by spectral analysis, was high (less than 0.02 % impurities).

Due to the autoreduction of Pu(VI) in solution it is important to use freshly prepared samples. A method was developed to prepare in one day a solution of PuO_2^{2+} with an accurately known concentration in 3 M (Na)ClO_4. A weighed piece of Pu metal was dissolved in a known aliquot of 5 M $HClO_4$. More dilute acid gave a black, insoluble precipitate, probably Pu(IV) oxide. The blue Pu(III) solution, formed during dissolution, was rapidly and completely oxidized to PuO_2^{2+} by a known amount of AgO(s). The silver(II) oxide was added in small portions under shaking, as some of it reacted with water with O_2 evolution. Thus AgO had to be added in excess; usually 50 % was used. The excess oxide was easily destroyed by heating to about 80 °C. At the same time the excess acid, added at the dissolution of Pu metal, was neutralized. Finally the proper amount of $NaClO_4$ was added. Excess Ag^+ was precipitated as AgCl by NaCl(s) and filtered off.

The determination of plutonium was performed according to Andersson, Baurén and Helleday[9] and in cooperation with these authors. The method used was potentiometric titration of Pu(VI) with Fe(II) after oxidation with AgO. This gave the total amount of plutonium. If we omitted the oxidation step, we got a slightly lower value of plutonium due to the autoreduction of Pu(VI). As the solutions, used in these experiments, were never more than one day old, it was assumed, following Rabideau,[10] that practically only Pu(V) had been formed. If this assumption was

Table 2. Hydrolysis of plutonyl ion in 3 M $(Na)ClO_4$. The result of the plutonium analysis. $[Pu_{tot}]$ and $[PuO_2^{2+}]$ are usually the mean of two determinations with the limits given.

Titration No.	$[Pu_{tot}]$ mM	$[PuO_2^{2+}]$ mM	$[PuO_2^{+}]$ mM	$\frac{[PuO_2^{+}]10^2}{[Pu_{tot}]}$
1	27.102 ± 0.004	26.32	0.78	1.4
2	40.69 ± 0.06	39.91 ± 0.02	0.78	2.0
3	56.66 ± 0.01	55.40 ± 0.00	1.26	2.2
4	79.20 ± 0.01	78.60 ± 0.01	0.60	0.78
5	129.94 ± 0.05	127.62 ± 0.05	2.32	1.8
6	223.94 ± 0.06	222.91 ± 0.04	0.82	0.36

correct, we could get a good value for $[PuO_2^{2+}]$ (*cf.* discussion below). The results are shown in Table 2. There are also given the amount of Pu(V) and the decrease of Pu(VI) in per cent of total Pu, which are both determined from a small difference between two large numbers and must be considered uncertain. On the average the decrease in the concentration of PuO_2^{2+} was 1.4 % per day. Other authors have given figures of the same order, *e.g.* Rabideau,[10] who found 1.5 % per day.

The agreement between the value calculated in advance for $[Pu_{total}]$ and that found by analysis was usually better than 1 %.

The isotopic composition of the plutonium used corresponded to the atomic weight 239.1.

Procedure

All experiments were carried out as potentiometric titrations with a glass electrode (GE) and a reference electrode (RE). The cell was:

$$-\text{GE} \mid \text{plutonyl solution} \parallel \text{RE} +$$

where

RE = Ag,AgCl/2.99 M Na^+, 0.01 M Ag^+, 3 M ClO_4^-.

The plutonyl solution in the titration vessel (S) had the general composition:

B M PuO_2^{2+}, H M H^+, (D M Ag^+), $(3-2B-H-D)$ M Na^+, (C M Cl^-), $(3-C)$ M ClO_4^-.

C and D are small amounts of Cl^- or Ag^+, one of which may remain after the precipitation of AgCl during the preparation of the plutonyl solution. Naturally the ideal case would be, where $C=D=0$, but this is impossible to achieve in practice without special precautions. Mostly there seemed to be a small excess of Ag^+, but neither Ag^+ nor Cl^- were considered of any harm because of the low concentrations of these species.

The solution in the buret (T) only contained NaOH (negative H) or $HClO_4$ and ionic medium. It had the general composition:

H M H^+, $(3-H)$ M Na^+, 3 M ClO_4^-.

It was impractical in this case to keep the total amount of plutonium (B) constant by adding it from a buret, which is the usual method. The composition of a plutonyl solution changes so rapidly that the content of PuO_2^{2+} and H^+ in solution T would be uncertain. The radiolytic reactions also produce $H_2(g)$ and $O_2(g)$ in small bubbles, which would give erratic values for the volume of solution added from the buret of at most a few per cent per day at the highest concentrations of plutonium studied.

The initial solution S was always acidic and NaOH was added from the buret. The first part of the titration was a neutralization of H^+ for the determination of better values of H and E_0. Then the hydrolysis started and the titration was continued during all day. Next day a back titration with $HClO_4$ was performed ending with the same neutralization part as in the beginning.

Using Nernst's formula it is possible to calculate the concentration of free H^+ (h) for each point on the titration curve:

$$E = E_0 + E_j + 59.16 \log h \qquad (1)$$

Following Biedermann and Sillén[11] it was assumed that $E_j = jh$. The j value was determined in solutions not containing plutonium. Then E_0 could be determined from the first part of the forward titrations and the last part of the back titrations, where no hydrolysis was involved. First a Gran plot[12] was made to get a better value of the analytical excess of H^+ (H), which in this part of the curve is equal to h. With knowledge of this and from a plot of $(E - 59.16 \log h)$ *versus* h, E_0 was obtained.

It was now possible to calculate Z, the average number of OH^- bound per Pu, which is defined as:

$$Z = (h - H)/B \qquad (2)$$

From the material balance equations for Pu(VI) and protons we get

$$B = b + \sum q^* \beta_{p,q} h^{-p} b^q \qquad (3)$$

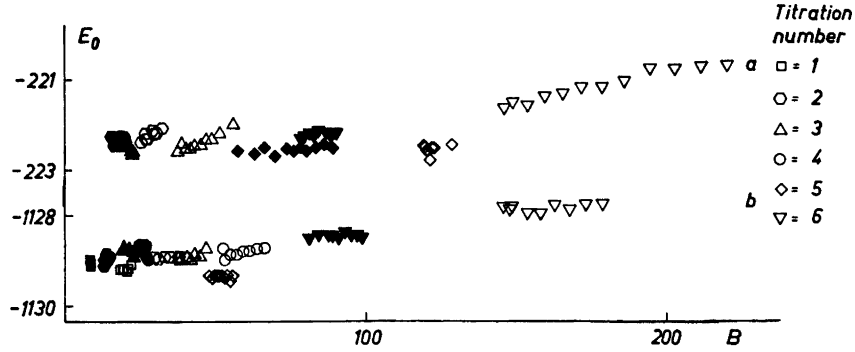

Fig. 1. Potentiometric titrations of plutonyl solutions. $E_0 = f(B)$ in the points before (open points) and after the hydrolysis (full points) in Titrations 1 – 6 for the two glass electrodes used. In Titrations a: Beckman 41 263 and in Titrations b: Jena Thalamid U 161.

$$BZ = \sum p\,{}^*\beta_{p,q} h^{-bq} \qquad (4)$$

where ${}^*\beta_{p,q}$ is the equilibrium constant for the reaction

$$q\mathrm{PuO_2^{2+}} + p\mathrm{H_2O} \rightleftharpoons (\mathrm{PuO_2})_q(\mathrm{OH})_p^{2(p-q)+} + p\mathrm{H^+} \qquad (5)$$

The H values obtained from the Gran plots did not agree for the forward and back titrations. An increase in H, probably due to radiolytic effects, was always found. A correction was added to all points under the assumption that the increase of H was direct proportional to time, though it might not be correct. The order of the change in H was about 0.001 mol per Pu and hour, which would give a correction in Z of at most 0.01 for a titration performed in one day.

E_0 seemed to vary with the plutonium content. In Fig. 1 ($E - E_j - 59.16$ log h) is plotted *versus* B ($= [\mathrm{Pu_{total}}]$). Another term of the type $E_B = kB$ or $E_B = kb$ should be necessary above $B = 150$ mM. For that reason titrations have only been performed for $B < 150$ mM.

Apparatus

When this work started very little plutonium was available. For that reason much attention was paid to the development of smaller titration assemblies as illustrated in an earlier paper.[13] Gradually more and more plutonium became available and in the final apparatus we worked with an initial volume of 10 ml.

The titration vessel was the Ingold Titration Vessel 604.[13]

The reference electrode was finally of the Wilhelm type,[14] but reduced in size and containing only 10 ml. It was also provided with some spherical joints to make it more flexible to minimize the risk of breakage in the glove box.

Many different glass electrodes were tried. Some makes, *e.g.* Ingold and Radiometer, were impossible to use in the glove box. They were too sensitive to static electricity built up by the gloves in the plexiglass box, or by people passing the apparatus, probably due to poor shielding. On the other hand the electrodes from Jena and Beckman were found to be very good. In the final experiments a Jena glass electrode, type Thalamid U 161, and Beckman glass electrodes, type 41 263 and 40 498, were used.

The burets used were Metrohm piston buret EA 902, volume 10 ml. The outlet was a rather long glass tube supplied with three spherical joints for flexibility, and a pointed tip, that fitted in the cap of the titration vessel.

The solution was stirred with a teflon covered rod by a magnetic stirrer.

All different parts were mounted on a stand to make it easy to handle. Two identical titration assemblies were placed in the glove box and used parallell to make the best use of the freshly prepared plutonium solutions. For example one apparatus could be used for the study of low and the other of high Z values.

The EMF was measured by two valve potentiometers pHM4 from Radiometer placed outside the box. They were calibrated against a Cambridge Vernier Potentiometer.

The whole glove box was thermostated as described earlier.[13] The temperature around the vessel was 25.0 ± 0.1 °C. The temperature of the solution was also checked sometimes and was within the same limits.

DATA

The experimental data are collected in Table 3 and shown in Fig. 2 as $Z = f(-\log h)$. Each curve corresponds to one titration, the values of B decreasing when Z increases due to dilution.

Table 3. Hydrolysis of plutonyl ion in 3 M (Na)ClO_4. The experimental data ($-\log h$, Z, B mM) are given together with their value of $1000(Z_{calc}-Z_{obs})$ found in the LETAGROP calculations using the "best" set of equilibrium constants. Two titrations (a and b) were performed simultaneously using the same initial solutions but in different titration assemblies.

Titration 1a. 3.200, 0.002, 17.21, −1; 4.089, 0.032, 16.88, −4; 4.224, 0.051, 16.77, −1; 4.351, 0.080, 16.61, +4; 4.440, 0.110, 16.45, +7; 4.527, 0.151, 16.25, +9; 4.618, 0.212, 15.96, +7; 4.728, 0.316, 15.48, +4; 4.882, 0.523, 14.63; +20; 4.985, 0.689, 14.01, +53; 5.063, 0.836, 13.50, +64.

Titration 1b. 3.210, 0.002, 17.19, −1; 4.102, 0.033, 16.86, −3; 4.353, 0.083, 16.57, +1; 4.537, 0.152, 16.23, +14; 4.719, 0.318, 15.47, −9; 4.866, 0.529, 14.60, −17; 4.992, 0.738, 13.83, +14; 5.107, 0.946, 13.14, +38; 5.228, 1.156, 12.51, +45; 5.369, 1.365, 11.94, +30.

Titration 2a. 3.335, 0.003, 26.27, −2; 3.999, 0.029, 25.92, 0; 4.214, 0.067, 25.59, +3; 4.393, 0.125, 25.11, +13; 4.544, 0.224, 24.34, +7; 4.653, 0.344, 23.48, −14; 4.723, 0.442, 22.82, −26.

Titration 2b. 2.811, 0.001, 26.60, −1; 3.123, 0.002, 26.34, −1; 3.724, 0.010, 26.08, −1; 4.699, 0.446, 22.80, −65; 4.768, 0.544, 22.16, −65; 4.833, 0.643, 21.56, −54; 4.888, 0.743, 20.99, −51; 4.951, 0.843, 20.45, −24; 5.007, 0.943, 19.94, −12; 5.063, 1.042, 19.46, −4; 5.132, 1.163, 18.90, −3.

Titration 3a. 4.266, 0.110, 35.05, +3; 4.440, 0.189, 34.21, +17; 4.576, 0.313, 32.98, +7; 4.687, 0.458, 31.66, 0; 4.812, 0.664, 29.93, +6; 4.983, 0.975, 27.71, +29.

Titration 3b. 2.877, 0.002, 36.68, −2; 3.216, 0.003, 36.44, −2; 3.938, 0.031, 35.96, −1; 4.158, 0.071, 35.50, +4; 4.334, 0.131, 34.83, +13; 4.530, 0.253, 33.56, +24; 4.616, 0.357, 32.57, +8; 4.757, 0.564, 30.76, +7; 4.870, 0.772, 29.14, +11; 4.980, 0.980, 27.68, +18.

Titration 4. 2.794, 0.001, 51.33, −1; 3.659, 0.013, 50.66, −1; 3.871, 0.031, 50.33, 0; 4.156, 0.091, 49.38, +7; 4.344, 0.172, 48.16, +18; 4.476, 0.274, 46.71, +16; 4.601, 0.437, 44.58, −9; 4.704, 0.601, 42.63, −14; 4.784, 0.744, 41.06, −11; 4.888, 0.951, 38.98, −17; 5.019, 1.177, 36.95, −7; 5.135, 1.361, 35.44, −22.

Titration 5a. 3.247, 0.000, 117.1, +4; 3.715, 0.036, 115.0, −2; 3.911, 0.076, 113.0, 0; 4.084, 0.136, 110.0, +7; 4.229, 0.214, 106.5, +14; 4.341, 0.315, 102.2, +1.

Titration 5b. 4.337, 0.301, 103.0, +12; 4.435, 0.421, 98.21, −7; 4.501, 0.523, 94.59, −25; 4.560, 0.624, 91.22, −39; 4.621, 0.724, 88.08, −37; 4.674, 0.825, 85.15, −43; 4.782, 1.028, 79.84, −48; 4.897, 1.231, 75.15, −55.

Titration 6a. 4.368, 0.385, 127.4, +9; 4.435, 0.486, 123.8, −10; 4.554, 0.683, 117.3, −22.

Titration 6b. 2.865, 0.003, 143.8, −2; 3.648, 0.034, 141.9, −3; 3.856, 0.072, 140.1, +2; 4.035, 0.133, 137.5, +10; 4.151, 0.192, 135.0, +16; 4.287, 0.290, 131.1, +23; 4.378, 0.389, 127.3, +18; 4.501, 0.587, 120.4, −14.

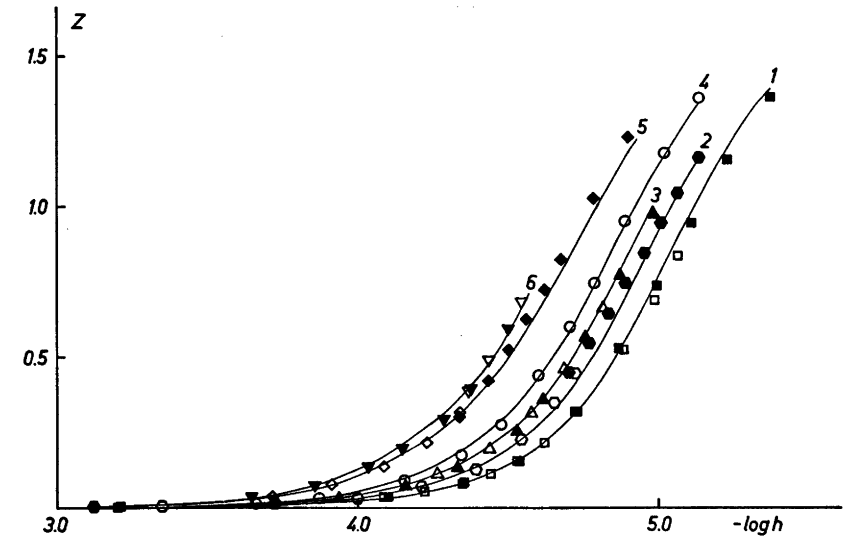

Fig. 2. Hydrolysis of plutonyl ion in 3 M (Na)ClO_4. Points are all experimental data $Z=f(-\log h)$ and curves are calculated with "best" values of $^*\beta_{2,2}$ and $^*\beta_{7,4}$. Open and full points of the same shape are from different titrations using identical solutions.

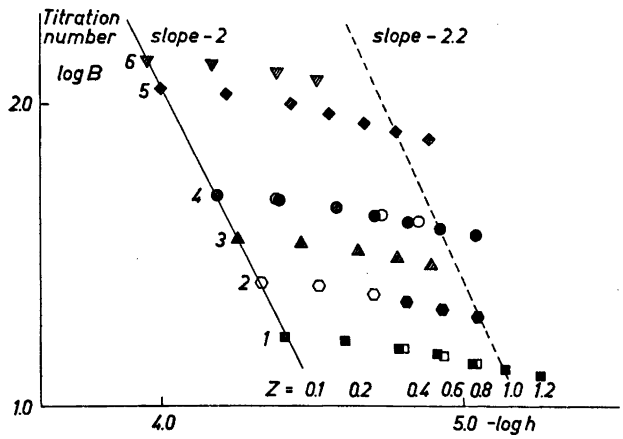

Fig. 3. Hydrolysis of plutonyl ion in 3 M (Na)ClO_4. Experimental data from Fig. 2 here transformed to $\log B = f(-\log h)_Z$. Points from the same titration have the same shape here as in Fig. 2 and shaded points mean coinciding full and open points. The full straight line is the "best" curve through the points with $Z = 0.1$. The broken curve is the "best" straight line through the points with $Z = 1.0$.

The concentration range for plutonium was 10 – 150 mM.

With the procedure used it was necessary to have exactly the same solutions when an experiment was to be repeated. As the starting material was a piece of plutonium metal this was hard to achieve quickly enough and was never done. For comparison the different Z-curves were transformed to $\log B = f(-\log h)_z$ (Fig. 3). The points seemed to fall on the same straight line for different experiments. This can be taken as an indication that the experiments were reproducible.

TREATMENT OF DATA

All calculations were made on the assumption, that the law of mass action was valid, which means that in every point the solution must have been in equilibrium. In this respect the data could be divided into two parts. One part includes the points with low Z ($Z < 0.3$), where chemical equilibrium could be proved by agreement between forward and back titrations. The rest of the data must be treated with some caution as no stable potentials could be achieved during the back titrations. It has been assumed, however, that the forward titrations correspond to equilibrium.

The computer program LETAGROP [15–19] was used for the analysis of data. Various sets of complexes (p,q) and rough values of their stability constants ${}^*\beta_{p,q}$ were given to the computer, which then calculated the error squares sum $U = \sum(Z_{calc} - Z_{obs})^2$. In this program the set of equilibrium constants is searched for, which gives the lowest U-value.

To speed up the search for plausible complexes the so called "species selector" of the LETAGROP program [19] was used. This means that beside the probable main complexes a pile of new species were given one by one. The new one was first varied alone to get a better value of ${}^*\beta_{p,q}$ and then together with the main complexes. The computer calculated ${}^*\beta_{p,q}$ and $\sigma({}^*\beta_{p,q})$ and also ${}^*\beta/\sigma$, which is called "sigfak". If the value of "sigfak" was smaller than a given value, the complex was rejected.

Our first trial was with the complexes found in the literature. The next step was to try species found in the uranyl system, which has many properties in common with plutonyl and has been thoroughly investigated. Finally those (p,q) combinations were tried, where size and charge were reasonable. Species with a higher charge than +3 were not considered. The 20 different (p,q) values tried are shown in Fig. 4.

If only the more accurate data with $Z < 0.3$ were used in the calculations the complex (2,2) alone gave an acceptable fit to the data (*cf.* Fig. 5). The result was:

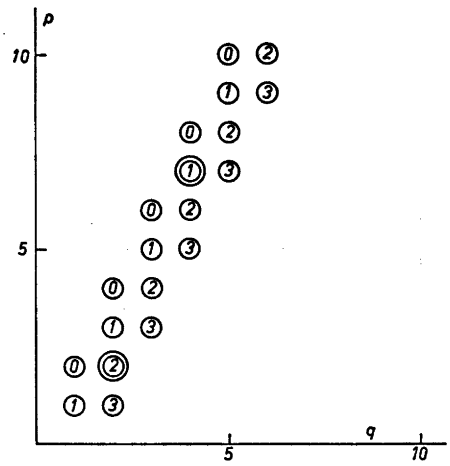

Fig. 4. Hydrolysis of plutonyl ion in 3 M (Na)ClO_4. (p,q) values tried in the LETAGROP calculations. The figures in the circles show the positive charge of the complex. The double circles show our two, most plausible complexes.

$^*\beta_{2,2} = (0.574 \pm 0.004)10^{-8}$ or $\log {}^*\beta_{2,2} = -8.24 \pm 0.01$ with $\sigma(Z) = \pm 0.0045$.

Including all experimental points, (2,2) alone could not explain the data. It gave $U_{min} = 0.330$ and $\sigma(Z) = 0.180$. Some higher complex had to be added as was pointed out in our earlier paper.[7] Every complex in Fig. 4 was passed through the "species selector" at least twice, using "*sigfak*" = 1.0 and 1.5. With these rather low values of "*sigfak*" the following higher complexes were retained at least once during the calculations: (3,2), (5,3), (7,4), (9,5), (4,3), (6,4), (8,5), and (10,6). Together with the well established (2,2) each of these species were given a new opportunity in an "ordinary" LETAGROP calculation (Rurik = 3) with the results given in Table 4. It should be mentioned that lower values than $U_{min} = 0.040$ and $\sigma(Z) = 0.021$ were never achieved during any of the calculations, even if several complexes were combined.

It is obvious from Fig. 3, that the data, transformed to $\log B = f(-\log h)$, give rather good straight lines with a slope of approximately -2. According to Sillén [20] this indicates the formation of "core and links" species with the general composition $B(A_2B)_n$. The five first in this serie are all to find among the retained complexes in Table 4, while the rest could be generally written $AB(A_2B)_n$.

If the data were used without any correction in H with time, the calculations seemed to give the same main species.

The computer program HALTAFALL [21] was used to calculate how the amounts of the different species vary with pH and B. In Fig. 6 α-curves are given for $B = 0.15$ M and $B = 0.01$ M, which are about the maximum and minimum values used in this work, and $B = 0.001$ M, which is about the concentration investigated by Kraus *et al.*[2] $B = 0.001$ M and $B = 0.01$ M are also in the lower and upper part of the concentration range studied by Cassol *et al.*[6] Four different stability constants were taken into consideration namely for (1,1) and (2,1) found by Kraus *et al.* and for (2,2) and (7,4) found in this investigation. α is the fraction of plutonium present in each species.

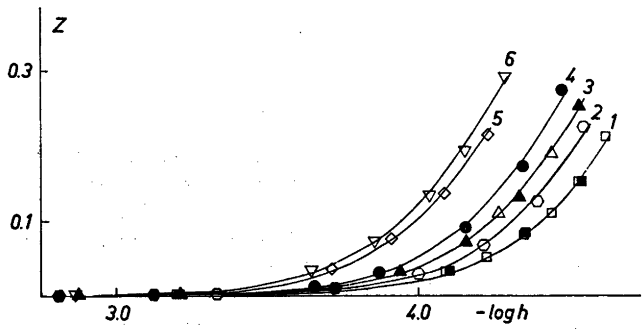

Fig. 5. Hydrolysis of plutonyl ion in 3 M (Na)ClO_4. Points are the same experimental data $Z = f(-\log h)$ as in Fig. 2 but limited to $Z < 0.3$. Curves are calculated with the "best" value of $^*\beta_{2,2}$.

Table 4. Hydrolysis of plutonyl ion in 3 M (Na)ClO_4. The "best" constants obtained in the LETAGROP calculations (Rurik = 3) assuming only two species: (2,2) and some of the higher species previously retained at least once by the "species selector" (Rurik = 17) using all data.

$*\beta_{2,2}$ 10^8		U_{min} $\times 10^3$	$\sigma(Z)$ $\times 10^3$
0.587 ± 0.017	$*\beta_{7,4} = (0.768 \pm 0.022)10^{-29}$	44.8	22.3
0.417 ± 0.021	$*\beta_{5,3} = (0.776 \pm 0.022)10^{-21}$	75.3	28.9
0.686 ± 0.022	$*\beta_{9,5} = (0.850 \pm 0.039)10^{-37}$	72.5	28.4
0.314 ± 0.038	$*\beta_{6,4} = (0.881 \pm 0.049)10^{-24}$	213	48.6
0.714 ± 0.408	$*\beta_{3,2} = (0.106 \pm 0.004)10^{-12}$	300	57.8
MIKO	$*\beta_{4,3} = (0.103 \pm 0.007)10^{-15}$	516	75.7
0.498 ± 0.026	$*\beta_{8,5} = (0.945 \pm 0.047)10^{-32}$	103	33.8
0.607 ± 0.023	$*\beta_{10,6} = (0.111 \pm 0.006)10^{-39}$	76.4	29.1
0.579 ± 0.072	$*\beta_{2,1} = (0.687 \pm 0.054)10^{-10}$	941	102

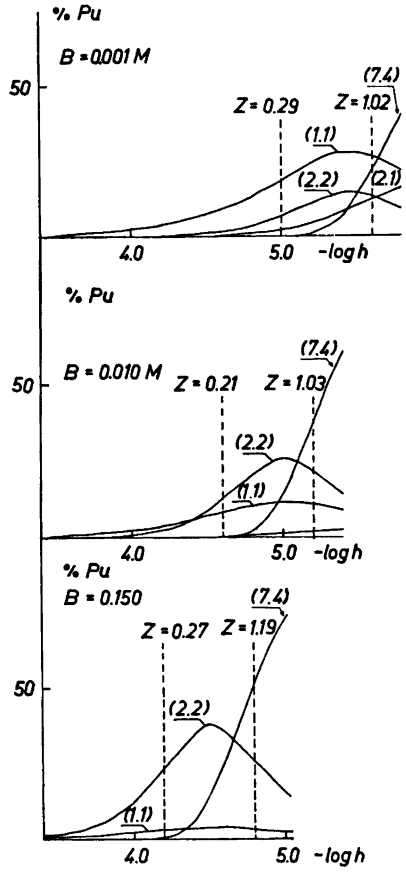

Fig. 6. Hydrolysis of plutonyl ion. α-curves or the fraction of total Pu present in the different complexes in per cent as a function of pH and B, calculated by HALTAFALL using the constants $*\beta_{1,1}$ and $*\beta_{2,1}$ found by Kraus *et al.*[2] and $*\beta_{2,2}$ and $*\beta_{7,4}$ found by us.

DISCUSSION

The complex chemical nature of plutonium and the effect of irradiation on aqueous solutions will be briefly discussed here, as they have affected the accuracy in this work.

Disproportionation. At least four different plutonium ions can exist together in aqueous solutions: Pu^{3+}, Pu^{4+}, PuO_2^+, and PuO_2^{2+}. In fact the oxidation potentials are such that coexistence is favoured.[22] PuO_2^+ and Pu^{4+} can both spontaneously disproportionate and give a mixture of all four oxidation states. For Pu(V) Connick [23] found two possible paths:

$$Pu(V) + Pu(V) \rightleftharpoons Pu(IV) + Pu(VI) \quad (6)$$

or if also Pu(III) is present:

$$Pu(V) + Pu(III) \rightleftharpoons 2Pu(IV) \quad (7)$$

Both these reactions involve the rupture of a chemical bond, when PuO_2^+ is reduced to Pu^{4+} and are rather slow reactions. Connick found reaction (6) to be the slowest. These rate-determining steps are followed by the rapid reversible equilibrium

$$Pu(V) + Pu(IV) \rightleftharpoons Pu(VI) + Pu(III) \quad (8)$$

which only requires the transfer of one electron. It is a fast reaction and can mostly be considered in completion. Rabideau [10] studied the kinetics of reaction (6), and Rabideau and Kline [24] the kinetics of reaction (8) and confirmed the mechanisms.

The mechanism for the disproportionation of Pu(IV) was suggested by Connick [23] to be the reverse of reaction (7) or (6):

$$Pu(IV) + Pu(IV) \rightleftharpoons Pu(V) + Pu(III) \quad (7a)$$

and if Pu(VI) is also present:

$$Pu(IV) + Pu(VI) \rightleftharpoons 2Pu(V) \quad (6a)$$

Again these must be the rate-determining steps, and he considered (7a) to be the fastest. They were also followed by the fast reaction (8). This discription was confirmed through kinetic studies by Rabideau [25] in $HClO_4$ and by Rabideau and Cowan [26] in HCl.

Irradiation ^{239}Pu, which was the main isotope in this work, is an α-emitter with a half-life of about 24 000 years and an energy of 5.15 MeV. The α-particles with their high energy are able to ionize molecules in their path. Water molecules are considered to be decomposed, possibly *via* activated molecules, into free radicals as $H^{\cdot}$, $^{\cdot}OH$, $HO_2^{\cdot}$, which then combine under formation of H_2, O_2 and H_2O_2 as described by Miner and Seed.[27] According to Rabideau *et al.*,[28] who studied the effect of radiolysis in perchlorate medium, the gas generated consisted of about 60 % O_2 and 40 % H_2. This does not correspond to the pure decomposition of water, which would give a much lower O_2 content.

The difference in H found in this work between the first and last Gran plot was also assumed to be a radiolytic effect. Considering that the formation of oxygen was greater than corresponded to the decomposition of water into hydrogen and oxygen, the over all reaction of the reduction of Pu(VI) and oxidation of water initiated by α-particles, might be:

$$2PuO_2^{2+} + H_2O \xrightarrow{\alpha} 2PuO_2^{+} + \tfrac{1}{2}O_2(g) + 2H^{+} \quad (9)$$

This would give an increase in H of the same order as the decrease in Pu(VI) of 1.5 % per day. In our work a somewhat higher value, 2.4 %, was observed, which might be explained by addition from some, other radiolytic reaction. The change in H could also be due to some irreversible protolytic reaction or analytical error, which must be of the order 1 – 1.5 % to explain the whole increase. Since analytical errors in H mostly are about 0.2 %, the latter explanation seems rather unlikely.

The irradiation causes a continuous reduction of a Pu(VI) solution. As mentioned above, Rabideau [10] found the decrease in the plutonyl concentration to be 1.5 % per day in perchlorate medium, and similar values have been obtained by others. The mechanism of this reduction seems not to be completely understood, but H_2O_2 is considered to take part as a reductant of PuO_2^{2+}. Rabideau found that no Pu(IV) could be detected after one day. His explanation was that in the beginning only Pu(V) was formed with the rate of 1.5 % per day. Then Pu(V) disproportionated according to the slow reaction (6) followed by the rapid reaction (8), when the concentration of Pu(IV) increased. If this is correct the amount of the undesirable Pu(IV) must have been very low in the fresh solutions used in our experiments.

Rabideau *et al.*[28] also found that the autoreduction was independent of many parameters such as the initial value of the mean oxidation number, pH and temperature, and that the steady state, reached after a couple of weeks, was just above a mean oxidation number of 3 (3.02 – 3.05).

The ionic medium seems to play an interesting role in the radiolysis reactions. In chloride medium no reduction was observed. The molecules of the ionic medium could also be decomposed. In perchlorate medium Cl^{-} was found. This was also observed during this work as a precipitate of AgCl in old solutions containing Ag^{+}.

The net result of disproportionation and radiolysis reactions in a Pu(VI) solution in $NaClO_4$ medium will in a few days be a solution containing an unknown amount of Pu(III), Pu(IV), Pu(V), Pu(VI), an unknown change in H^{+} concentration, decomposition products of the ionic medium as Cl^{-} beside $NaClO_4$. Of course all these reactions must have had influence on the accuracy of the data in the present investigation.

Hydrolysis of other Pu ions. Naturally it is of interest to know the hydrolytic behaviour of the other plutonium ions, as they might be present in small quantities in our solutions. Rather little seems to be known about Pu(III) and Pu(V). Kraus and Dam [29] made some experiments on Pu(III) and found its hydrolysis weak and to occur around pH = 7. They also studied Pu(V),[30] whose hydrolysis seems to start around the same pH. It is thus obvious that the presence of these two ions does not disturb the investigation of the hydrolysis of Pu(VI).

On the other hand the hydrolysis of Pu(IV)

starts at very low pH. The first hydrolytic product $PuOH^{3+}$ has been recognized by Rabideau [31] in a potentiometric study as well as spectrophotometrically by Rabideau and Kline.[32] On further alkalification the hydrolytic species grow and a rather stable colloid appears before the precipitation of hydroxide starts. This polymerization is an irreversible process, and the colloid may be extremely hard to dissolve. This colloid may easily appear, when a solution is diluted with water or whenever a local deficit of acid arises. It is obvious that Pu(IV) must be avoided and our efforts have been to keep its concentration as low as possible. In order to analyze for Pu(IV) some of the solutions were studied with a Cary 14 M recording spectrophotometer. No trace of Pu(IV) was ever seen after one day. However, the detection limit is rather high, about 1 % without special precautions. Also the possible presence of small amounts of colloidal Pu(IV) would not give the typical Pu(IV) peaks but only result in a slight increase of the background.

Chemical equilibrium. During the titrations some observations were made about the reaction rates and the time necessary to reach chemical equilibrium. When NaOH was added to the Pu(VI) solutions, it took a considerable time to get stable potentials for the first points, between 20 min and a couple of hours. It was also found that when the value of Z had increased to about $0.2-0.3$, the EMF seemed to be constant within 5 or 10 min. At the highest Z values studied the equilibration became slow again. The EMF was now instead increasing after each addition, and the titrations were interrupted here.

It was desirable to make back titrations with $HClO_4$ to check that the same curve was obtained and that chemical equilibrium had been reached, but it was very difficult to get stable potentials. The pH values achieved were too low and only slowly increased towards the values obtained in the forward titration, never actually reaching them. As Pu(VI) solutions are so quickly destroyed, it was impossible to wait for equilibrium to be reached. This has been a great dilemma during this work: on one side the desire to wait long enough to be sure of chemical equilibrium, on the other hand the wish to work fast enough to be certain of the composition of the Pu solutions.

If the forward titration was interrupted at a Z value of $0.2-0.3$ and the back titration was started from this point, stable potentials could be achieved, which fitted well on the forward curve. Here chemical equilibrium seems to have been attained and these data, for $Z<0.3$, must be considered reliable.

The change in EMF during the night between the forward and the back titration was $0.3-2.0$ mV measured at the highest value of Z. Probably the solutions were not too far from equilibrium, as the radiolysis must be taken into consideration, which causes a continuing change in the content of Pu(VI) and H.

CONCLUSIONS

The most important result of this investigation is the establishment of the dimer $(PuO_2)_2(OH)_2^{2+}$, which alone can explain all the points for $Z<0.3$, which we consider accurate and reliable. It is interesting to note that Cassol *et al.* probable unaware of our earlier results, also have found (2,2) to be one of the main species.

That at least one more higher complex must exist is quite clear. Its influence is greatest on the higher values of Z, where the data are less accurate and chemical equilibrium could not be proved. So unfortunately the composition of the higher complex must still be considered uncertain. From Table 4 it is obvious that (7,4) gave the best fit followed by (5,3) and (9,5). At the highest Pu concentrations (5,3) gave increasing deviations at the highest Z values (titrations 4 and 5), so it was excluded from the discussion. Assuming (2,2) and (7,4) we got the same "best" value of ${}^*\beta_{2,2}$ as was found in the region $Z<0.3$. As this combination also gave the lowest U_{min} and $\sigma(Z)$ it is considered the most plausible. However, the explanation might as well be the existence of a serie of higher complexes, *e.g.* of the type $AB(A_2B)_n$ or $B(A_2B)_n$ mentioned earlier, but that could not be deduced from the present data.

It is interesting to make a comparison between the observations made during the titrations regarding reaction rates and equilibration and the amount of the different species in Fig. 6, calculated by HALTAFALL. As can be

seen in Fig. 6 (2,2) predominates, where $Z < 0.3$ in both 0.01 and 0.15 M Pu(VI) solutions. When $Z > 0.3$ (7,4) grows and predominates at the highest Z, where (2,2) disappears. The slow, reversible reactions for $Z < 0.3$ thus coincide with the formation of (2,2). For higher Z values faster equilibration was noticed, and thus connected with the building up of (7,4) and the disappearence of (2,2).

Using the data of Kraus *et al.*[2] the amount of (2,1) in the B region examined in our investigation would be extremely small according to Fig. 6 and this complex was never found by us. (1,1) would however be possible to find at the lower B concentrations. Special calculations were performed using only Titration 1, which has the lowest B value, but (1,1) could not be established in this investigation even at this low concentration. However, it must be kept in mind that Kraus *et al.* used a different ionic medium than we did.

For $B = 0.001$ M the picture is quite different. Here (1,1) dominates for $Z < 1$, where (2,1) and (7,4) grow. The amount of (2,2) is never large. This may explain, why Kraus *et al.* found (1,1) and (2,1) in their investigation at $B = 0.718 - 1.32$ mM. Using LETAGROP on their data the following result was obtained:

$\log {}^*\beta_{1,1} = -5.58 \pm 0.05$, $\log {}^*\beta_{2,1} = -11.50 \pm 0.03$ with $\sigma(Z) = 0.038$.

Cassol *et al.*[6] suggested (1,1) (2,2), and (5,3) in their investigation at $B = 0.1 - 30$ mM. Unfortunately they have only published the data from one single titration at $B = 2 - 3$ mM. We made some LETAGROP calculations on that figures and found (2,1) to give a good fit together with (2,2):

$\log {}^*\beta_{2,1} = -11.24 \pm 0.02$, $\log {}^*\beta_{2,2} = -8.68 \pm 0.10$ with $\sigma(Z) = 0.017$.

Surprisingly (2,1) was never mentioned by Cassol *et al.* neither was (7,4). As long as their complete data are not available it is not possible to make any further conclusions about the existence of higher complexes.

Kraus *et al.* reported the same failure to get stable potentials during the back titrations as was found by us, while Cassol *et al.* mentioned nothing about that problem. The drift in pH during the back titrations went towards higher pH, which means that OH^- was liberated, and the new species must have contained less OH^-. One explanation may be that for some reason the breaking up of the large molecules, when *e.g.* (7,4) disintegrates into (2,2) and PuO_2^{2+} and OH^-, is a slower reaction than the reverse. If this is the case the forward curve would still be useful for obtaining information about the hydrolysis. Another explanation may be that the drift in EMF was caused by some impurity, *e.g.* Pu(IV), which reacted slowly. If this was the case, all the data for $Z < 0.3$ would be unreliable and useless, and (2,2) the only certain result.

Thus our "best" set of species and their equilibrium constants together with their standard deviations are considered to be:

${}^*\beta_{2,2} = (0.574 \pm 0.004)10^{-6}$, ${}^*\beta_{7,4} = (0.768 \pm 0.022)10^{-29}$ or $\log {}^*\beta_{2,2} = -8.23 \pm 0.01$, $\log {}^*\beta_{7,4} = -29.11 \pm 0.04$ with $\sigma(Z) = 0.022$.

Acknowledgements. Dr. Lennart W. Holm is gratefully thanked for his support and interest and the late Professor Lars Gunnar Sillén for much good advice under valuable discussions during this work. The author is also indebted to Mr. Eyvind Helleday, who skilfully performed the plutonium analysis, and to Dr. Derek Lewis, who kindly revised the English of this paper.

This work was mainly financed by the Research Institute of National Defence.

REFERENCES

1. O'Connor, P. R. *USAEC-CN-2088* 1944.
2. Kraus, K. A. and Dam, J. R. *Natl. Nuclear Energy Ser. IV-14B* (1949) 528.
3. Krevinskaya, M. E., Nikol'skii, V. D., Pozharskii, B. G. and Zastenker, E. E. *Radiokhimiya 1* (1959) 548.
4. Moskvin, A. I. and Zaitseva, V. P. *Radiokhimiya 4* (1962) 73.
5. Cleveland, J. M. *Inorg. Nucl. Chem. Lett. 6* (1970) 535.
6. Cassol, A., Magon, L., Portanova, R. and Tondello, E. *Radiochim. Acta 17* (1972) 28.
7. Schedin, U. *Acta Chem. Scand. 25* (1971) 747.
8. Hammer, R. N. and Kleinberg, J. *Inorg. Syn. 4* (1953) 12.
9. Andersson, L. H., Baurén, E. B. and Helleday, E. *FOA Reports, 4* (1970) No. 7.
10. Rabideau, S. W. *J. Amer. Chem. Soc. 79* (1957) 6350.
11. Biedermann, G. and Sillén, L. G. *Ark. Kemi 5* (1953) 425.
12. Gran, G. *Analyst 77* (1952) 661.

13. Schedin, U. and Frydman, M. *Acta Chem. Scand. 22* (1968) 115.
14. Forsling, W., Hietanen, S. and Sillén, L. G. *Acta Chem. Scand. 6* (1952) 901.
15. Sillén, L. G. *Acta Chem. Scand. 16* (1962) 159.
16. Ingri, N. and Sillén, L. G. *Acta Chem. Scand. 16* (1962) 173.
17. Sillén, L. G. *Acta Chem. Scand. 18* (1964) 1085.
18. Ingri, N. and Sillén, L. G. *Ark. Kemi 23* (1964) 97.
19. Sillén, L. G. and Warnqvist, B. *Ark. Kemi 31* (1969) 341.
20. Sillén, L. G. *Acta Chem. Scand. 8* (1954) 299.
21. Ingri, N., Kakolowicz, W., Sillén, L. G. and Warnqvist, B. *Talanta 14* (1967) 1261.
22. Wick, O. J. *Plutonium Handbook 1* (1968) 405.
23. Connick, R. E. *J. Amer. Chem. Soc. 71* (1949) 1528.
24. Rabideau, S. W. and Kline, R. J. *J. Phys. Chem. 62* (1958) 617.
25. Rabideau, S. W. *J. Amer. Chem. Soc. 75* (1953) 798.
26. Rabideau, S. W. and Cowan, H. D. *J. Amer. Chem. Soc. 77* (1955) 6145.
27. Miner, F. J. and Seed, J. R. *Chem. Rev. 67* (1967) 299.
28. Rabideau, S. W., Bradley, M. J. and Cowan, H. D. *LAMS-2236* (1958).
29. Kraus, K. A. and Dam, J. R. *Nat. Nuclear Energy Ser. IV-14B* (1949) 466.
30. Kraus, K. A. and Dam, J. R. *Ibid.* 478.
31. Rabideau, S. W. *J. Amer. Chem. Soc. 79* (1957) 3675.
32. Rabideau, S. W. and Kline, R. J. *J. Phys. Chem. 64* (1960) 680.

Received October 28, 1974.

Acta Chemica Scandinavica A 29 (1975) 345—349

A Study of the Thermo-oxidation of Fe(II) in $FeSO_4.7H_2O$

NAHED HASSANEIN* and O. ØRJASAETER**

Institute of Experimental Physics, NTH, University of Trondheim, Trondheim, Norway

The thermo-oxidation in air of Fe(II) and weight loss of $FeSO_4 \cdot 7H_2O$ has been measured as a function of time in the temperature range 43 to 170 °C. The analysis of the results suggests the following reaction mechanism: by heating, the heptahydrate looses water resulting in a mixture of the tetra- and monohydrate. Only the latter can be oxidized. The activation energy for oxidation is found to be about 3.5×10^4 J mol^{-1}.

I. INTRODUCTION

When $FeSO_4.7H_2O$ is heated in air two processes take place: thermal decomposition and oxidation. Kohler,[1] studying the thermal decomposition of $FeSO_4.7H_2O$ obtained the following hydrate phases when heating isobarially at 20 Torr: $FeSO_4.7H_2O$, $FeSO_4.4H_2O$, $FeSO_4.H_2O$, $FeSO_4$ at 22, 30, 165, and higher than 240 °C, respectively.

Safiullin,[2] using X-ray and IR spectroscopy found that in the 134 – 309 °C range the monohydrate is oxidized to $Fe(OH)SO_4$ by the reaction

$$FeSO_4.H_2O + \tfrac{1}{4}O_2 = Fe(OH)SO_4 + \tfrac{1}{2}H_2O$$

X-Ray analysis revealed the presence of both the basic salt and the anhydrous ferrous sulfate at 312 °C. On further heating they are oxidized to $Fe_2O(SO_4)_2$.

Gallagher,[3] using weight loss data in the region 150 to 500 °C concluded that in O_2 atmosphere, Fe(II) was converted to Fe(III) before the sulfate ion decomposed, whereas in N_2 atmosphere the conversion occurred simultaneously with the first step of the sulfate decomposition. Two pathways were suggested leading to the formation of $Fe_2O(SO_4)_2$.

Kamel,[4] using X-ray and chemical analysis investigated the intermediate products of the thermal decomposition of ferrous sulfate heptahydrate in a current of air. The monohydrate undergoes dehydration followed by oxidation, combined hydrolysis and oxidation to $Fe_2O(SO_4)$ and $Fe(OH)SO_4$, respectively.

Wanek and Knob [5] showed that the weight loss is strongly temperature dependent below 220 °C.

The purpose of the present work was to study in some detail the processes which take place when $FeSO_4.7H_2O$ is heated in air using weight loss and oxidation measurements.

II. EXPERIMENTAL PROCEDURE

1. Materials. "Mercks Reagenzien"-$FeSO_4.7H_2O$ crystalline powder with mean grain size 0.1 mm[3] and molecular weight 278.03, $FeSO_4.7H_2O$ crystals grown to about 100 mg, "standard solution" made of 0.8 N H_2SO_4 and 1 mM NaCl.[6] All chemicals were of grade *p.a.* For the temperature measurements a PYE scalamp galvanometer with copper-constantan thermocouple was used. The optical densities were measured using a "Carl Zeiss" spectrophotometer PMQII/M4QIII.

2. Procedure. Samples of $FeSO_4.7H_2O$ were carefully weighed ($X \approx 25$ mg), placed in open glass boats and heated in a copper tube furnace.[7] This furnace has a connection to the source of the desired gas (O_2, N_2 or air). The desired temperature was obtained by the use of a heating element, controlled by a thermo regulator. When air was not used, a stream of the desired gas was passed through the furnace for about 15 h at room temperature to get rid of undesired gases.

The sample was removed from the furnace, weighed and then dissolved in V ml of the standard solution. Values for the concentration

* Permanent address: Astronomy Dept., Faculty of Science, Cairo University, Cairo, Egypt.

** Present address: Svevegen 6, N-2830 Raufoss, Norway.

Table 1. Values and formulae used for the molar extinction coefficients in mol^{-1} cm^{-1}. The temperature of the measured solution, τ, in °C.

λ (nm)	ε_{III}	ε_{II}
304	$2121\{1+0.007(\tau-20)\}$	1
275	1830	1
224	$4565\{0.0015(\tau-25)+1\}$	20

of Fe(III) were obtained by the measurement of optical densities.

The optical density [8,9] (OD_{rel}) of the resulting solution relative to that of the standard solution is composed of the optical densities of the two components Fe(II) and Fe(III), *i.e.*

$$OD_{rel}=[\varepsilon_{II}\{Fe(II)\}+\varepsilon_{II}\{Fe(III)\}]d \quad (1)$$

where ε_{II} and ε_{III} are the molar extinction coefficients of Fe(II) and Fe(III), respectively, and $d=1$ cm, is the light path length in the solution. The concentration of Fe(III) is then given by:

$$\{Fe(III)\}=\frac{OD_{rel}-\{Fe(II)\}\varepsilon_{II}d}{d(\varepsilon_{III}-\varepsilon_{II})} \quad (2)$$

Here $\{Fe(II)\}_0=X/MV$, where M is the molecular weight of $FeSO_4.7H_2O$. Values and formulae used for the molar extinction coefficients in units of mol^{-1} cm^{-1} are given in Table 1,[10,11] where τ(°C) is the temperature of the measured solution. Uncertainties in measurements were: for relative concentration, $\pm(1.2\ \%+5\times10^{-4})$; for temperature, ±2 %; and for weighing, ±0.6 ‰.

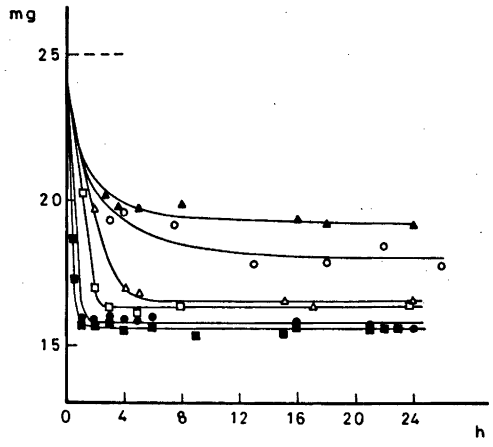

Fig. 1. The variation of the weight of the sample with time at various temperatures. ▲ 43 °C; ○ 54 °C; △ 67 °C; □ 77 °C; ● 85 °C; ■ 92 °C; × 170 °C.

Table 2. Average water concentration, per molecule and fraction monohydrate, $f=\{FeSO_4.H_2O\}_{t=0}\{Fe(II)\}_0$, at various temperatures, τ (°C).

τ (°C)	n (H_2O mol)	f
43	3.6	0.13
54	2.6	0.46
67	1.8	0.74
77	1.6	0.79
85	1.3	0.90
92	1.15	0.95
170	1.15	0.95

III. RESULTS AND DISCUSSION

The weight of the samples (normalized to 25 mg) at various temperatures in ordinary air is plotted *versus* time in Fig. 1. The figure shows that within a relative short time the weight reaches a limiting value. At 54 °C this time is about 3 h and it decreases with increasing temperature. This indicates that the composition of the crystals do not change appreciably after that time and within the time limit of the experiments. Assuming the weight-loss to be entirely due to H_2O, we estimated the values of the water concentration $\{H_2O\}$ to be those given in Table 2. X-Ray analysis shows the presence

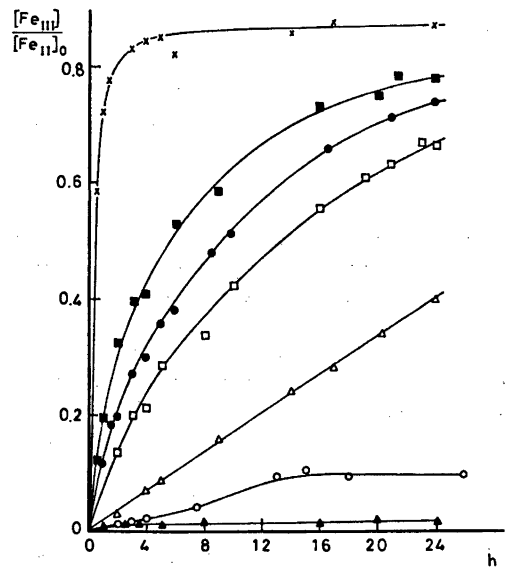

Fig. 2. Oxidation of Fe(II) with time at various temperatures. Symbols as in Fig. 1.

Table 3. Results from oxidation experiments, where $Y = [\{Fe(III)\}/\{Fe(II)\}_0] \times 10^3$.

Time h	Y	Time h	Y	Time h	Y	Time h	Y	Time h	Y	Time h	Y	Time h	Y
$\tau = 43$ °C		$\tau = 54$ °C		$\tau = 67$ °C		$\tau = 77$ °C		$\tau = 85$ °C		$\tau = 92$ °C		$\tau = 170$ °C	
1	4	2.1	14	2	32	2	139	1	114	0.25	23	0.5	587
2.5	12	3	17	4	73	3	201	1.5	185	0.5	122	1	722
3.5	12	4	20	5	87	4	213	2	200	1	196	1.5	778
5	9	7.5	43	9	158	5	282	3	270	2	325	3	833
8	17	13	92	14	241	8	339	4	301	3	395	4	846
16	11	15	105	17	280	10	423	5	357	4	409	5	852
20	19	18	93	20.25	340	16	555	6	383	6	528	6	824
24	15	26	98	24	400	19	610	8.5	482	9	582	14	861
						21	635	10	513	16	732	17	881
						23	673	16.5	660	20	750	24	873
						24	667	21	715	21.5	783		
								24	738	24	781		

of only tetrahydrate and monohydrate; consequently the fraction of the monohydrate at the beginning of oxidation was estimated and given in Table 2.

Results from the oxidation experiments are given in Table 3. In Fig. 2, values for the ratio $[\{Fe(III)\}/\{Fe(II)\}_0] \times 10^3$ with ordinary air as oxidant are plotted *versus* time for the temperatures 43, 54, 67, 77, 85, 92, and 170 °C.

The figure shows that (1) no oxidation takes place below 54 °C, and (2) at each temperature the oxidation yield increases with time and reaches an appearant limiting value which increases with increasing temperature.

In a separate experiment with a current of about 30 $dm^3\ h^{-1}$ of pure and wet N_2 instead of air we observed no oxidation to take place. Hence O_2 in the air must be the oxidant. The species which can be oxidized are $FeSO_4.7H_2O$, $FeSO_4.4H_2O$, and $FeSO_4.H_2O$ which have been shown to be present in the temperature range we are considering.

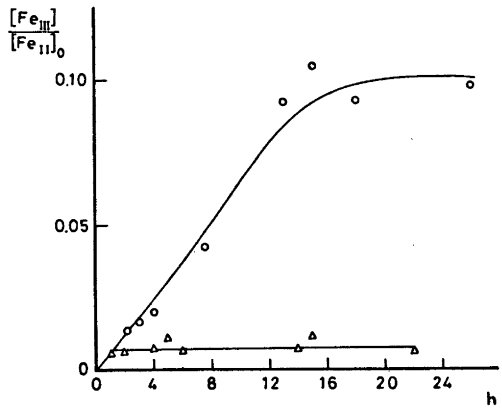

Fig. 3. Comparison between oxidation curves in ordinary air and in saturated air at $\tau = 54$ °C. ○ Ordinary air; △ saturated air.

To study the possibility of the heptahydrate oxidation, samples were heated at 54 °C in a current of 180 $dm^3\ h^{-1}$ of air saturated with H_2O, as obtained by passing the air through water at $\tau = 54$ °C. Under these conditions only the heptahydrate is present and no oxidation was shown to take place whereas in ordinary air heated to 54 °C the oxidation is not negligible. A comparison between the results from these two experiments is shown in Fig. 3.

That the crystals have to loose water before they can be oxidized was further substantiated by the fact that when large crystals were used, the oxidation rate remained low for a longer time than when smaller crystals were used as shown in Fig. 4.

According to weight loss measurements, Fig. 1 and Table 2, and the increase of the oxidation rate with increasing temperature, one suggests that neither tetrahydrate can be oxidized.

The oxidation of the monohydrate may proceed as follows:

$$FeSO_4.H_2O + \tfrac{1}{4}O_2 \underset{k_2}{\overset{k_1}{\rightleftharpoons}} Fe(OH)SO_4 + \tfrac{1}{2}H_2O \qquad (3)$$

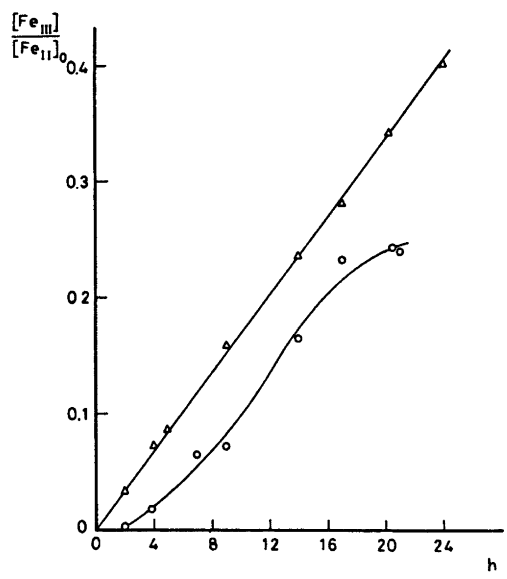

Fig. 4. Comparison between oxidation curves for ordinary powder and for bigger crystals at $\tau = 67$ °C. △ Ordinary powder, ○ crystal.

The oxidation rate is then given by:

$$\frac{d\{Fe(III)\}}{dt} = k_1\{O_2\}^{\alpha}\{FeSO_4.H_2O\}^{\beta} - k_2\{H_2O\}^{\gamma}\{Fe(OH)SO_4\}^{\delta} \quad (4)$$

where k_1 is the oxidation rate constant, k_2 is the rate of the reverse reaction; α, β, γ, and δ are the reaction orders relevant to the various species.

To study the reverse reaction, samples, which had been oxidized for 24 h at 92 °C were heated for another 24 h and at the same temperature in a current of 60 $dm^3\ h^{-1}$ of nitrogen saturated with water. The amount of Fe(III) did not change with time. Also X-ray analysis showed no variation in the composition with time. This suggests that the reverse reaction can be ignored. If this is the case, then, according to eqn. (4), all Fe(II) in the sample should be oxidized to Fe(III). However, according to Fig. 2, it is seen that only a fraction of Fe(II) is oxidized and this fraction increases with increasing temperature. One reason might be that the concentration $\{O_2\}$ in the crystals decreases to zero, *i.e.* the value of the rate constant for the diffusion of O_2 into the crystals goes to zero after a certain time. Such effect could be due to the formation of a crust of oxides on the surface of the crystals. This was shown to be the case by the following two sets of experiments:

(1) For a specimen heated and oxidized in ordinary air for 24 h. X-ray analysis revealed the presence of ferrous sulfate monohydrate and a mixture of oxides.

(2) Scanning microscopic examination of sections cut from a crystal heated to 85 °C for 24 h shows an outer crust around the original crystal. A comparison of the spectrum of the inner and outer layers indicates difference in the composition of these layers. Hence at the end of oxidation there is a crust of oxides around an inner layer of ferrous sulfate (mono- and tetrahydrate). The formation of such crust may affect the reaction rate constant; therefore to avoid complications we shall analyze the oxidation rate at the beginning of the process where $\{Fe(III)\}$ is negligible and $\{O_2\}$ may be assumed to be constant. Assuming first order reaction, we obtain.

$$\left(\frac{d\{Fe(III)\}}{dt}\right)_{t=0} = K\{FeSO_4.H_2O\}_{t=0} \quad (5)$$

where $\{FeSO_4.H_2O\}_{t=0}$ is the concentration of the monohydrate at the beginning of the oxidation (and after dehydration). The concentration of $FeSO_4.H_2O$ does in fact vary with time due to the following process:

$$FeSO_4.7H_2O = FeSO_4.H_2O + 6H_2O$$

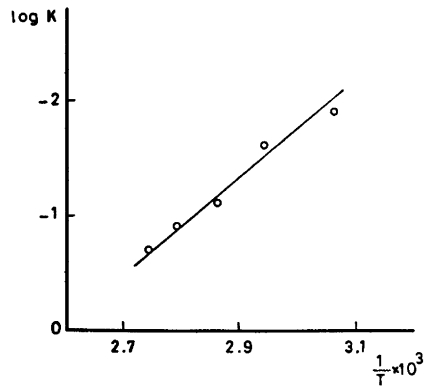

Fig. 5. Relationship between rate constant K, $(= k_1\{O_2\}^{1/4})$, and absolute temperature T.

However, according to the results obtained above from weightloss measurements this process is fast relative to the oxidation process except perhaps at $\tau = 54$ °C. To check the effect of dehydration during oxidation, an experiment was performed in which the samples were dehydrated for 3 h in an inert atmosphere (N_2) at the desired temperature before oxidation. No significant changes in the oxidation rate were observed.

We assume now the oxidation rate constant k_1 to be proportional to $e^{-E/RT}$, where E is the activation energy for oxidation, R is the universal gas constant; and T is the absolute temperature. Then since $\{O_2\}$ is a constant the parameter K, given by $\left(\frac{d\{Fe(III)\}}{dt}\right)_{t=0}/\{FeSO_4.H_2O_t\}_{=0}$ in eqn. (5), is also proportional to $e^{-E/RT}$.

Using the oxidation curves in Fig. 2, values of $(d\{Fe(III)\}/dt)_{t=0}$ have been determined by the slope of the curves at the beginning of the process and by applying $\{FeSO_4.H_2O\}_{t=0}$ values, illustrated in Table 2. The plot of log K *versus* $1/T$ is presented in Fig. 5. The slope of the curve corresponds to an activation energy of $(3.5 \pm 0.5) \times 10^4$ J mol^{-1}.

CONCLUSION

In this work we have measured the oxidation rate of Fe(II) in $FeSO_4.7H_2O$ in the temperature range $\tau = 43 - 170$ °C. At a certain temperature, the oxidation increases with time and reaches an apparent limiting value which increases with increasing temperature.

No oxidation take place below $\tau = 54$ °C, also no oxidation takes place when heating the sample neither in N_2 atmosphere nor in air saturated with H_2O.

Crystals have to loose water before they can be oxidized. The oxidation rate constant is proportional to $e^{-E/RT}$. The activation energy of oxidation is found to be 3.5×10^4 J mol^{-1}.

Acknowledgements. We are grateful to Professor T. Sikkeland for helpful consultations concerning the interpretation of these data. Our thanks are also due to J. Grønbeck for his help with the preparation of the graphs. We are also very grateful to NORAD for the financial support of this work.

REFERENCES

1. Kohler, K. and Zäske, P. *Z. Anorg. Allg. Chem. 331* (1964) 7.
2. Safiullin, N., Gitis, F. B. and Panasenko, N. M. *J. Appl. Chem. USSR 42* (1969) 1956; *32* (1959) 2230.
3. Gallagher, P. K., Johnson, D. W. and Schrey, F. J. *Amer. Ceram. Soc. Bull. 53* (1970) 666.
4. Kamel, A. E., Sawires, Z., Khalifa, H., Saleh, S. A. and Abdallah, A. M. J. *Appl. Chem. Biotechnol. 22* (1972) 591.
5. Wanek, W. and Knob, B. *Silikaty 6* (1962) 63.
6. Attix, F. H., Roesch, W. C. and Tochilin, E. *Radiation Dosimetry II*, Academic, New York 1966.
7. Ørjasæter, O. Diploma, Ch. IV, *An Experimental Study on the Thermo-oxidizing Effect in Iron Sulfate Hydrate*, Institute of Experimental Physics, NTH, Trondheim 1972.
8. Woods, R. J. and Spinks, J. W. *An Introduction to Radiation Chemistry*, Wiley, New York 1964.
9. Waggener, R. G., Hiatt, C. W. Rogers, L. F. and Zanca, P. *Radiation Res. 45* (1971) 244.
10. Donnell, J. and Sangster, D. *Principles of Radiation Chemistry*, London 1970.
11. Scarf, K. and Lee, R. M. *Radiation Res. 16* (1962) 115.

Received July 3, 1974.

Acta Chemica Scandinavica A 29 (1975) 350—358

Multicomponent Polyanions. 12. The Crystal Structure of $Na_6Mo_{18}P_2O_{62}(H_2O)_{24}$, a Compound Containing Sodiumcoordinated 18-Molybdodiphosphate Anions

ROLF STRANDBERG

Department of Inorganic Chemistry, University of Umeå, S-901 87 Umeå, Sweden

The crystal structure of $Na_6Mo_{18}P_2O_{62}(H_2O)_{24}$ has been determined from three-dimensional X-ray diffraction data collected with a PAILRED diffractometer using Mo$K\alpha$-radiation. The cell dimensions of the monoclinic ($C2/c$) unit cell are $a = 23.091(2)$ Å, $b = 13.481(1)$ Å, $c = 23.157(2)$ Å and $\beta = 100.35(1)°$, and it contains four formula units. Final refinement by least squares methods using anisotropic vibrational parameters gave an R-value of 0.040, based on 7260 independent reflexions.

The structure consists of $Mo_{18}P_2O_{62}^{6-}$-groups linked together by direct sodium bridges (O – Na – O) in the y- and z-directions forming layers parallel with the yz-plane. The layers are held together by O – Na – H_2O – Na – O linkages.

The Mo – Mo distances vary between 3.35 and 3.39 Å for edge-sharing MoO_6-octahedra and increase to 3.66 – 3.84 Å for corner-sharing octahedra. The Mo – O distances fall in four ranges, 1.67 – 1.70, 1.75 – 2.14, 2.31 – 2.36, and 2.37 – 2.40 Å, depending on the coordination number of the coordinated oxygen atom.

In equilibrium analysis involving H^+, MoO_4^{2-}, and HPO_4^{2-} a series of protonized enneamolybdomonophosphates, $(H^+)_{14}(MoO_4^{2-})_9(HPO_4^{2-})$, $(H^+)_{15}(MoO_4^{2-})_9(HPO_4^{2-})$, $(H^+)_{16}(MoO_4^{2-})_9(HPO_4^{2-})$, $(H^+)_{17}(MoO_4^{2-})_9(HPO_4^{2-})$, have been reported.[1] These emf-investigations also indicate the presence of a dimer of the 17,9,1 complex in the most acidic part of the pH-range investigated. In connection with these studies two crystalline phases have been obtained, $Na_3H_6Mo_9PO_{34}(H_2O)_{12-13}$ and $Na_6Mo_{18}P_2O_{62}(H_2O)_{24}$. The structure of the first has already been published [2,3] and the structure of the latter is the topic of the present report.

EXPERIMENTAL

Crystal preparation and analyses. In a typical preparation of the crystals, $Na_2MoO_4.2H_2O$ and $NaH_2PO_4.2H_2O$ were dissolved in $HClO_4$. The concentrations used were $[MoO_4^{2-}]_{tot} = 1.0$ M, $[HPO_4^{2-}]_{tot} = 0.11$ M and $[HClO_4]_{tot} = 1.78$ M. After one or a few days of evaporation at a temperature of about 40 °C, yellow prismatic crystals were formed. The crystals are not stable in air and during the X-ray exposures they were sealed together with part of the mother liquor in a capillary of Lindemann glass. The contents of Na, Mo, and P were determined by elemental analyses (carried out at the Department of Analytical Chemistry, University of Umeå). (Found weight-%: Na 4.2, Mo 50.2, P 1.8, Calc.: Na 4.1, Mo 51.5, P 1.8). The water content of the crystal was determined by thermogravimetric analysis as well as by simply heating (400 °C) a very big crystal (weight about 1.4 g). The results found here were 13.7 weight-% H_2O (Calc. 12.9).

Crystal data and space group. Rotation photographs around [100], [010], and [001] and the corresponding Weissenberg photographs (zero, first and second layer lines) taken with Cu$K\alpha$-radiation showed that the crystals are monoclinic. This was confirmed from precession photographs. Accurate cell dimensions were determined with a Guinier-Hägg camera using Si as internal standard. The cell parameters and their corresponding standard deviations are: $a = 23.091 \pm 0.002$ Å, $b = 13.481 \pm 0.001$ Å, $c = 23.157 \pm 0.002$ Å and $\beta = 100.35° \pm 0.01°$.

The density of the crystals as determined by flotation in a bromoform-diiodomethane solution was $d = 3.10$ g/cm^3 ($d_{calc} = 3.14$). The systematic extinctions of reflexions were: hkl, $h + k = 2n + 1$ and $h0l$, $l = 2n + 1$. This is characteristic for the two space groups $C2/c$ and Cc.

Collection and reduction of intensity data. Three-dimensional intensity data were collected,

at 25 °C, with a Philips PAILRED linear diffractometer using Mo$K\alpha$-radiation. A crystal of approximate dimensions 0.34 × 0.17 × 0.09 mm was mounted and rotated along the *c*-axis (parallel to the 0.34 mm-edge of the crystal). A total of 10 008 unique reflexions from the layers $hk0 - hk23$ were scanned. Data beyond a limit of sin $\theta = 0.5$ were left out. Reflections with a relative statistical error of $\Delta I_o/I_o$ greater than 0.5 were omitted, the final data set thus consisting of 7260 reflexions. The intensities were corrected for Lorentz and polarization effects and a correction was applied for absorption.

Computer programs. The computer programs used were based on the programs given in Ref. 4. With the exception of ORTEP the programs have been modified for a CDC 3300 computer by Dr. Britt Hedman, University of Umeå.

CRYSTAL DATA

$Na_6Mo_{18}P_2O_{62}(H_2O)_{24}$ F.W. = 3351.1
Monoclinic $C2/c$ $V = 7091$ Å^3
$a = 23.091(2)$ Å $Z = 4$
$b = 13.481(1)$ Å $d_{calc} = 3.14$ g cm^{-3}
$c = 23.157(2)$ Å) $d_{exp} = 3.10$ g cm^{-3}
$\beta = 100.35(1)°$ $\mu = 32.3$ cm^{-1} (Mo$K\alpha$)

STRUCTURE DETERMINATION AND REFINEMENT

The three-dimensional Patterson synthesis showed extremely strong overlapping of cross-vectors and attempts to solve it failed at first. Direct methods were then applied but these gave no useful information. From the elemental analysis, giving the ratio Mo/P = 9, as well as from the observations during the crystallization experiments, a heteropolyanion with 18 Mo and 2 P was assumed. This anion, if isostructural with $P_2W_{18}O_{62}^{6-}$,[5] should in a Patterson synthesis give a rather high peak, at a distance of about 3.7 Å, arising from the Mo – Mo vectors between the two zigzag rings (see below). On the basis of these assumptions six eight-fold Mo-positions could be found from the Patterson

Table 1. The fractional atomic coordinates and in parentheses their estimated standard deviations (referring to the last decimal place given). For the oxygen atoms indexed O(ij) or OP(ij) the (ij) means that the atom is bonded to the molybdenum atoms i and j. When the oxygen atoms are denoted Aq(ij) they are water oxygens and (ij) means that the atom is bonded to the sodium ions i and j.

	X	*Y*	*Z*
Mo1	0.81547(3)	0.75392(5)	0.33590(3)
Mo2	0.76889(2)	0.55495(5)	0.25075(3)
Mo3	0.84482(3)	0.52146(5)	0.38865(3)
Mo4	0.97687(3)	0.82944(5)	0.35101(3)
Mo5	0.87845(3)	0.82859(5)	0.20815(3)
Mo6	0.85794(3)	0.61696(5)	0.13156(3)
Mo7	0.88073(3)	0.38408(5)	0.21357(3)
Mo8	0.97277(3)	0.38087(5)	0.34301(3)
Mo9	0.99616(3)	0.61496(5)	0.42462(3)
P	0.42110(7)	0.10940(12)	0.28119(8)
O(1)	0.2272(2)	0.1546(4)	0.6447(3)
O(13)	0.3118(2)	0.1616(4)	0.3937(3)
O(14)	0.1120(2)	0.2009(4)	0.6401(2)
O(15)	0.1738(2)	0.1982(4)	0.7459(2)
O(12)	0.2526(2)	0.1733(4)	0.2833(2)
OP(123)	0.3620(2)	0.1089(3)	0.3047(2)
O(2)	0.2005(2)	0.0136(4)	0.2224(3)
O(23)	0.2798(2)	0.0035(4)	0.8327(2)
O(26)	0.2952(2)	0.0998(4)	0.1873(2)
O(27)	0.3187(2)	0.0697(4)	0.7408(2)
O(3)	0.3242(3)	0.0216(5)	0.9499(3)
O(38)	0.3936(2)	0.0700(4)	0.8699(2)
O(39)	0.4196(2)	0.0951(4)	0.4270(2)
O(4)	0.0273(2)	0.0580(4)	0.6184(3)
O(45)	0.0607(2)	0.1485(4)	0.7266(2)
O(54′)	0.0486(2)	0.1720(4)	0.8360(2)
O(49)	0.4939(2)	0.2561(4)	0.4232(2)
OP(49)	0.4673(2)	0.1624(3)	0.3261(2)
O(5)	0.1404(2)	0.0566(4)	0.8160(3)
O(56)	0.1583(2)	0.2442(4)	0.8589(2)
OP(56)	0.4107(2)	0.1640(3)	0.2219(2)
O(6)	0.3054(2)	0.0968(5)	0.0714(3)
O(67)	0.3771(2)	0.0137(4)	0.6577(2)
O(69′)	0.4215(2)	0.1351(4)	0.1009(2)
O(7)	0.3533(2)	0.2126(4)	0.6716(3)
O(78)	0.4172(2)	0.1836(4)	0.7821(2)
O(78′)	0.4645(2)	0.1347(4)	0.6894(2)
OP(78)	0.4385(2)	0.0014(3)	0.2736(2)
O(8)	0.4801(3)	0.2130(4)	0.8922(3)
O(89)	0.4966(2)	0.0106(4)	0.6097(2)
O(9)	0.4716(2)	0.0977(4)	0.0054(3)
Na1	0.2284(4)	0.0107(8)	−0.0033(4)
Na2	0.0932(17)	0.1315(27)	0.0996(10)
Na3	0.1011(11)	0.2014(18)	0.4100(9)
Aq1(1)	0.2270(12)	0.1645(15)	0.9618(6)
Aq2(1)	0.1150(12)	0.0740(22)	0.9512(12)
Aq3(1)	0.2690(6)	0.1465(12)	0.5337(6)
Aq(12)	0.1733(6)	0.0269(12)	0.0840(7)
Aq(13)	0.1916(4)	0.0912(8)	0.4068(5)
Aq1(2)	0.3716(7)	0.2430(10)	0.9714(7)
Aq2(2)	0.0186(13)	0.1048(12)	0.0227(9)
Aq3(2)	0.0864(5)	0.1099(7)	0.2080(8)
Aq4(2)	0.2979(5)	0.2378(8)	0.8459(5)
Aq1(3)	0.0516(10)	0.1067(13)	0.3443(18)
Aq2(3)	0.3913(5)	0.1415(11)	0.5464(5)
Aq3(3)	0.1074(12)	0.1515(19)	0.5111(9)

Table 2. Final anisotropic thermal parameters ($\times 10^4$) and their estimated standard deviations ($\times 10^4$) in parentheses. The parameters are calculated according to the formula $\exp[-(h^2\beta_{11}+k^2\beta_{22}+l^2\beta_{33}+2hk\beta_{12}+2hl\beta_{13}+2kl\beta_{23})]$.

	β_{11}	β_{22}	β_{33}	β_{12}	β_{13}	β_{23}
Mo1	7(0)	22(0)	8(0)	1(0)	3(0)	−1(0)
Mo2	5(0)	24(0)	8(0)	−1(0)	2(0)	−0(0)
Mo3	8(0)	24(0)	8(0)	0(0)	3(0)	2(0)
Mo4	8(0)	17(0)	7(0)	−1(0)	2(0)	−2(0)
Mo5	7(0)	18(0)	7(0)	3(0)	2(0)	2(0)
Mo6	7(0)	24(0)	6(0)	1(0)	1(0)	−0(0)
Mo7	7(0)	18(0)	8(0)	−1(0)	1(0)	−1(0)
Mo8	7(0)	18(0)	8(0)	−0(0)	2(0)	2(0)
Mo9	8(0)	23(0)	5(0)	−1(0)	1(0)	1(0)
P	5(0)	15(1)	5(0)	0(0)	2(0)	0(0)
O(1)	8(1)	31(3)	11(1)	2(1)	3(1)	−3(1)
O(13)	8(1)	24(3)	10(1)	−1(1)	4(1)	1(1)
O(14)	7(1)	27(3)	6(1)	1(1)	2(1)	−2(1)
O(15)	7(1)	22(3)	7(1)	1(1)	3(1)	1(1)
O(12)	8(1)	26(3)	10(1)	3(1)	2(1)	1(1)
OP(123)	5(1)	20(2)	7(1)	−1(1)	2(1)	0(1)
O(2)	9(1)	34(3)	11(1)	−2(1)	2(1)	−0(1)
O(23)	8(1)	22(3)	7(1)	0(1)	3(1)	−0(1)
O(26)	5(1)	24(3)	9(1)	1(1)	2(1)	−1(1)
O(27)	7(1)	23(3)	8(1)	−1(1)	2(1)	−0(1)
O(3)	13(1)	39(3)	9(1)	1(2)	5(1)	−4(2)
O(38)	6(1)	19(2)	9(1)	2(1)	1(1)	−3(1)
O(39)	10(1)	24(3)	6(1)	1(1)	3(1)	1(1)
O(4)	11(1)	27(3)	11(1)	−2(1)	3(1)	−5(1)
O(45)	10(1)	28(3)	7(1)	1(1)	3(1)	1(1)
O(54′)	7(1)	25(3)	7(1)	2(1)	2(1)	0(1)
O(49)	11(1)	20(3)	6(1)	−2(1)	3(1)	−0(1)
OP(49)	7(1)	15(2)	5(1)	0(1)	1(1)	−0(1)
O(5)	12(1)	26(3)	11(1)	2(1)	5(1)	3(1)
O(56)	6(1)	29(3)	7(1)	4(1)	1(1)	4(1)
OP(56)	7(1)	17(2)	6(1)	1(1)	2(1)	3(1)
O(6)	9(1)	37(3)	10(1)	2(1)	−0(1)	−0(2)
O(67)	6(1)	16(2)	8(1)	−2(1)	1(1)	−1(1)
O(69′)	7(1)	25(3)	8(1)	2(1)	2(1)	−1(1)
O(7)	6(1)	25(3)	16(1)	3(1)	2(1)	8(2)
O(78)	8(1)	17(2)	10(1)	2(1)	4(1)	−3(1)
O(78′)	6(1)	21(3)	8(1)	2(1)	1(1)	−3(1)
OP(78)	5(1)	17(2)	5(1)	1(1)	0(1)	2(1)
O(8)	13(1)	26(3)	13(1)	0(1)	4(1)	−8(1)
O(89)	8(1)	23(3)	7(1)	1(1)	2(1)	2(1)
O(9)	12(1)	37(3)	7(1)	3(1)	1(1)	−3(1)
Na1	60(3)	172(9)	31(2)	4(4)	−0(2)	−16(3)
Na2	324(21)	560(54)	61(7)	185(28)	67(9)	33(14)
Na3	175(11)	349(26)	76(6)	95(14)	62(7)	32(10)
Aq1(1)	163(13)	219(19)	16(3)	149(14)	−13(5)	−8(6)
Aq2(1)	105(10)	371(35)	64(10)	132(16)	16(7)	22(14)
Aq3(1)	44(4)	176(15)	34(4)	10(6)	17(3)	−7(6)
Aq(12)	46(4)	165(15)	45(4)	21(6)	0(3)	43(6)
Aq(13)	22(2)	83(7)	28(3)	−9(3)	4(2)	−5(3)
Aq1(2)	60(5)	106(10)	41(4)	36(6)	7(3)	−9(5)
Aq2(2)	158(15)	108(12)	36(5)	−6(11)	13(7)	6(6)
Aq3(2)	27(3)	38(5)	90(7)	7(3)	−10(3)	−4(5)
Aq4(2)	33(3)	85(8)	38(3)	28(4)	−8(2)	3(4)
Aq1(3)	78(7)	119(13)	260(22)	60(8)	118(11)	90(14)
Aq2(3)	24(2)	175(13)	22(3)	8(4)	2(2)	−13(5)
Aq3(3)	116(12)	323(28)	32(5)	−8(15)	31(6)	−42(10)

synthesis. A least squares refinement at this stage gave a conventional R-value of 0.52. A Fourier synthesis based on these atoms gave the positions of the remaining Mo-atoms and the R-value decreased to 0.26. In a second Fourier synthesis the positions of the phosphorus and oxygen atoms belonging to the $Mo_{18}P_2O_{62}^{6-}$-group could be located. The positions of the sodium and water oxygen atoms, were finally obtained from numerous successive Fourier and difference Fourier syntheses.

The positional parameters and anisotropic temperature factors for the atoms were refined by full-matrix least squares methods, a final R-value of 0.040 being obtained, $R = \sum||F_o| - |F_c||/\sum|F_o|$. The atomic scattering factors used for molybdenum were those given for Mo^{3+} by Cromer and Waber,[6] for phosphorus those given for P by Hanson, Herman, Lea and Skillman,[7] and for sodium and oxygen the values for Na^+ and O^- in International Tables. Account was taken of the real part of the dispersion correction. A weighting scheme according to Cruickshank was applied:
$\omega = 1/(a + |F_o| + c|F_o|^2 + d|F_o|^3)$ where the values of the constants were $a = 600$, $c = 0.0001$ and $d = 0$.

Final atomic coordinates, vibrational parameters, and corresponding standard deviations are given in Tables 1 and 2. The structure factor table is available from the author on request. The difference Fourier synthesis based on the listed parameters showed no anomalies. No attempts were made to locate hydrogen atoms.

DESCRIPTION AND DISCUSSION OF THE STRUCTURE

The structure is built up from $Mo_{18}P_2O_{62}^{6-}$-anions, Na^+-ions and H_2O-molecules. Two of the Na^+-ions act as links in O – Na – O-bridges between adjacent groups and in this way layers parallel to the yz-plane are formed. The third Na^+-ion connects these layers by O – Na – H_2O – Na – O linkages.

The $Mo_{18}P_2O_{62}^{6-}$-group. This group consists of two enneamolybdomonophosphate groups joined together by the sharing of six oxygen atoms. A detailed description of the Mo_9PO_{34}-group has been given in an earlier paper [2] and will only be outlined briefly here. It consists of

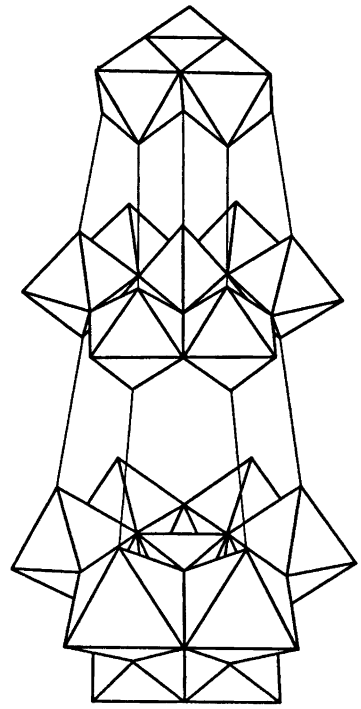

Fig. 1. The coupling of the eighteen MoO_6-octahedra and the two PO_4-tetrahedra in the $Mo_{18}P_2O_{62}^{6-}$-group. For clarity the figure is idealized.

a central PO_4-tetrahedron sharing corners with nine MoO_6-octahedra. Three of these octahedra form a compact group by sharing edges and the remaining six octahedra form a zigzag ring by alternately sharing edges and corners (Fig. 1). The six MoO_6-octahedra forming the ring have one unshared oxygen each pointing in approximately the same direction (perpendicular to the plane of the ring). On forming the $Mo_{18}P_2O_{62}^{6-}$-group, these oxygens are shared with the corresponding oxygens from another Mo_9PO_{34}-group as outlined in Fig. 1. Eighteen of the oxygen atoms in the group are unshared, one per octahedron. The symmetry in the group is a two-fold rotation axis (parallel to the b-axis) but the deviations from the symmetry $\bar{6}$ are rather small. Distances and angles between the Mo and P atoms in the group are given in Table 3. The Mo – Mo distances vary between 3.35 and 3.39 Å in edge-sharing MoO_6-octahedra. There is a significant difference between these distances in the compact group (3.386 – 3.388 Å)

Table 3. Distances (Å) and angles (degrees) within the $Mo_{18}P_2O_{62}^{6-}$-group. The designation of the atoms is explained in Table 1. The estimated standard deviations, given in parentheses, refer to the last decimal place given.

Mo, P			
Mo1 – Mo2	3.388(1)	P – Mo1	3.530(2)
Mo1 – Mo3	3.387(1)	P – Mo2	3.535(2)
Mo1 – Mo4	3.818(1)	P – Mo3	3.503(2)
Mo1 – Mo5	3.664(1)	P – Mo4	3.510(2)
Mo2 – Mo3	3.386(1)	P – Mo5	3.459(2)
Mo2 – Mo6	3.819(1)	P – Mo6	3.511(2)
Mo2 – Mo7	3.676(1)	P – Mo7	3.467(2)
Mo3 – Mo8	3.816(1)	P – Mo8	3.514(2)
Mo3 – Mo9	3.667(1)	P – Mo9	3.460(2)
Mo4 – Mo9	3.345(1)	P – P	4.154(3)
Mo4 – Mo5	3.662(1)	Mo1 – Mo2 – Mo3	60.01(2)
Mo4 – Mo5′	3.832(1)	Mo2 – Mo3 – Mo1	60.02(2)
Mo5 – Mo6	3.348(1)	Mo3 – Mo1 – Mo2	59.96(2)
Mo6 – Mo7	3.658(1)	Mo4 – Mo5 – Mo6	119.15(2)
Mo6 – Mo9′	3.823(1)	Mo5 – Mo6 – Mo7	117.57(3)
Mo7 – Mo8	3.349(1)	Mo6 – Mo7 – Mo8	119.00(2)
Mo7 – Mo8′	3.841(1)	Mo7 – Mo8 – Mo9	117.46(2)
Mo8 – Mo9	3.668(1)	Mo8 – Mo9 – Mo4	119.16(3)
		Mo9 – Mo4 – Mo5	117.51(2)

MoO_6-octahedra

	O(1)	O(13)	O(12)	O(14)	O(15)	OP(123)
Mo1	1.689(5)	1.841(6)	2.034(5)	1.775(5)	2.057(5)	2.404(5)
O(1)		2.730(8)	2.846(8)	2.717(7)	2.898(8)	
OP(123)		2.636(7)	2.633(7)	2.879(7)	2.911(7)	
O(12)		2.678(8)			2.599(7)	
O(14)		2.764(7)			2.603(7)	
O(1) – Mo1-		101.2(3)	99.3(2)	103.3(2)	100.9(2)	
OP(123) – Mo1-		75.5(2)	72.3(2)	85.7(2)	81.1(2)	
O(12) – Mo1-		87.3(2)			78.9(2)	
O(14) – Mo1-		99.7(2)			85.2(2)	

	O(2)	O(26)	O(12)	O(27)	O(23)	OP(123)
Mo2	1.691(5)	1.793(5)	1.832(5)	2.073(5)	2.027(5)	2.398(4)
O(2)		2.725(7)	2.732(8)	2.910(7)	2.872(8)	
OP(123)		2.878(7)	2.633(7)	2.907(7)	2.599(7)	
O(12)		2.771(8)			2.669(7)	
O(27)		2.610(7)			2.610(8)	
O(2) – Mo(2)-		102.9(3)	101.6(3)	100.8(2)	100.8(3)	
OP(123) – Mo2-		85.4(2)	75.7(2)	80.8(2)	71.4(2)	
O(12) – Mo2-		99.7(2)			87.4(2)	
O(27) – Mo2-		84.6(2)			79.1(2)	

	O(3)	O(13)	O(23)	O(39)	O(38)	OP(123)
Mo3	1.679(6)	2.048(5)	1.829(5)	2.051(5)	1.775(5)	2.366(5)
O(3)		2.781(8)	2.735(8)	2.833(8)	2.737(8)	
OP(123)		2.636(7)	2.599(7)	2.910(7)	2.869(7)	
O(23)		2.668(7)			2.763(7)	
O(39)		2.627(7)			2.603(7)	
O(3) – Mo3-		96.1(3)	102.4(3)	98.4(3)	104.8(3)	
OP(123) – Mo3-		72.9(2)	75.3(2)	82.1(2)	86.4(2)	
O(23) – Mo3-		86.8(2)			100.1(2)	
O(39) – Mo3-		79.7(2)			85.4(2)	

Table 3. Continued.

	O(4)	O(45)	O(14)	O(54′)	O(49)	OP(49)
Mo4	1.684(6)	1.874(6)	2.138(5)	1.752(5)	1.922(5)	2.325(5)
O(4)		2.768(8)	2.726(7)	2.685(7)	2.698(8)	
OP(49)		2.850(7)	2.806(7)	2.898(7)	2.557(7)	
O(14)		2.601(7)			2.680(7)	
O(54′)		2.617(8)			2.744(7)	
O(4)–Mo4-		102.0(3)	90.2(2)	102.8(3)	96.7(3)	
OP(49)–Mo4-		84.8(2)	77.8(2)	89.5(2)	73.3(2)	
O(14)–Mo4-		80.5(2)			82.4(2)	
O(54′)–Mo4-		95.9(2)			96.5(2)	
	O(5)	O(56)	O(15)	O(54′)	O(45)	OP(56)
Mo5	1.676(6)	1.902(5)	1.784(5)	2.122(5)	1.894(5)	2.344(5)
O(5)		2.721(8)	2.707(8)	2.735(7)	2.799(8)	
OP(56)		2.549(7)	2.888(7)	2.833(7)	2.823(7)	
O(15)		2.775(7)			2.655(7)	
O(54′)		2.677(7)			2.693(7)	
O(5)–Mo5-		98.8(3)	102.9(3)	91.4(2)	103.1(3)	
OP(56)–Mo5-		72.9(2)	87.7(2)	78.6(2)	82.8(2)	
O(15)–Mo5-		97.6(2)			92.4(2)	
O(54′)–Mo5-		83.2(2)			81.1(2)	
	O(6)	O(67)	O(26)	O(69′)	O(56)	OP(56)
Mo6	1.697(6)	1.889(5)	2.119(5)	1.758(5)	1.929(5)	2.311(5)
O(6)		2.787(8)	2.736(8)	2.695(7)	2.723(8)	
OP(56)		2.852(7)	2.780(7)	2.884(7)	2.549(7)	
O(26)		2.619(7)			2.671(7)	
O(69′)		2.699(7)			2.743(7)	
O(6)–Mo6-		101.9(3)	90.9(2)	102.5(3)	97.1(3)	
OP(56)–Mo6-		84.9(2)	77.6(2)	89.2(2)	73.3(2)	
O(26)–Mo6-		81.4(2)			82.4(2)	
O(69′)–Mo6-		95.4(2)			96.0(2)	
	O(7)	O(67)	O(27)	O(78′)	O(78)	OP(78)
Mo7	1.680(6)	1.882(5)	1.778(5)	2.123(5)	1.891(5)	2.356(5)
O(7)		2.767(7)	2.716(8)	2.736(7)	2.741(8)	
OP(78)		2.810(7)	2.897(7)	2.820(7)	2.556(7)	
O(27)		2.652(7)			2.767(7)	
O(78′)		2.595(7)			2.661(7)	
O(7)–Mo7-		101.8(3)	103.5(2)	91.3(2)	100.1(3)	
OP(78)–Mo7-		82.2(2)	87.8(2)	77.8(2)	73.1(2)	
O(27)–Mo7-		92.8(2)			87.8(2)	
O(78′)–Mo7-		80.5(2)			82.8(2)	
	O(8)	O(78)	O(38)	O(78′)	O(89)	OP(78)
Mo8	1.690(6)	1.934(5)	2.140(5)	1.759(5)	1.887(5)	2.322(5)
O(8)		2.727(8)	2.757(7)	2.681(8)	2.783(8)	
OP(78)		2.556(7)	2.794(7)	2.820(7)	2.848(7)	
OP(38)		2.679(7)			2.620(7)	
O(78′)		2.661(7)			2.691(7)	
O(8)–Mo8-		97.3(3)	91.3(2)	102.0(3)	102.0(3)	
OP(78)–Mo8-		73.2(2)	77.4(2)	89.6(2)	84.5(2)	
O(38)–Mo8-		82.1(2)			80.9(2)	
O(78′)–Mo8-		97.2(2)			95.1(2)	

Table 3. Continued.

	O(9)	O(49)	O(39)	O(69′)	O(89)	OP(49)
Mo9	1.674(6)	1.903(5)	1.799(5)	2.108(5)	1.891(5)	2.348(5)
O(9)		2.729(8)	2.710(8)	2.721(8)	2.794(8)	
OP(49)		2.557(7)	2.903(7)	2.834(7)	2.810(7)	
O(39)		2.778(7)			2.663(7)	
O(69′)		2.680(7)			2.605(7)	
O(9)–Mo9-		99.3(3)	102.6(3)	91.3(2)	103.1(3)	
OP(49)–Mo9-		73.1(2)	87.8(2)	78.8(2)	82.3(2)	
O(39)–Mo9-		97.2(2)			92.4(2)	
O(69′)–Mo9-		83.7(2)			81.1(2)	

PO_4-tetrahedron

	OP(49)	OP(56)	OP(78)	OP(123)
P	1.528(5)	1.538(5)	1.528(5)	1.557(5)
OP(49)		2.530(7)	2.517(6)	2.499(6)
OP(56)			2.525(7)	2.504(7)
OP(78)				2.489(6)
OP(49)–P-		111.2(3)	110.9(3)	108.2(3)
OP(56)–P-			110.8(3)	108.0(3)
OP(78)–P-				107.5(3)

and in the ring of six MoO_6-octahedra (3.345–3.349 Å). A similar difference was also found in the structure of $Na_3H_6Mo_9PO_{34}(H_2O)_{12-13}$. In corner-sharing there are four different types of Mo–Mo distance:

(i) 3.66–3.67 Å in the zigzag rings;
(ii) 3.66–3.68 Å between the Mo-atoms in the compact group and three of the Mo-atoms in the zigzag ring;
(iii) 3.82 Å between the Mo-atoms in the compact group and the remaining three Mo-atoms in the zigzag ring;
(iv) 3.82–3.84 Å between the two zigzag rings.

The Mo–P distances vary between 3.46 and 3.54 Å while the P–P distance is 4.15 Å. A stereoscopic view of the $Mo_{18}P_2O_{62}^{6-}$-group is given in Fig. 2.

The MoO_6-octahedra. The MoO_6-octahedra are somewhat distorted from an ideal octahedron and the Mo-O distances can be divided into four groups according to the number of atoms that the oxygen atoms is coordinated to:

(i) Coordinated to one Mo-atom; the distances vary between 1.67 and 1.70 Å;
(ii) coordinated to two Mo-atoms; the distances vary between 1.75 and 2.14 Å;
(iii) coordinated to P and to two Mo-atoms; the distances vary between 2.31 and 2.36 Å;
(iv) coordinated to P and to three Mo-atoms; the distances vary between 2.37 and 2.40 Å.

This trend of increasing distances with increasing coordination numbers has also been found in other structures.[3,4]

As mentioned above, the six MoO_6-octahedra

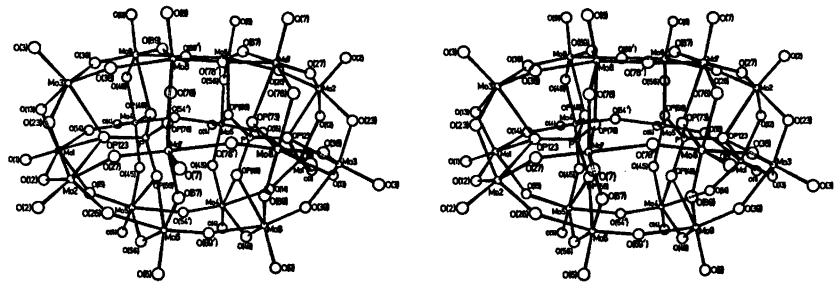

Fig. 2. Stereoscopic view of the $Mo_{18}P_2O_{62}^{6-}$-group.

forming a ring in the Mo_9PO_{34}-group have one unshared oxygen each with the Mo – O direction approximately perpendicular to the plane of the ring. In the structure of $Na_3H_6Mo_9PO_{34}(H_2O)_{12-13}$ the distances from the Mo-atoms to these oxygens were alternately short and long. The short distance given was 1.70 Å, which is a normal distance for Mo – O (unshared), while the long distance was 2.21 Å, the lengthening being ascribed to protonization of the oxygen atom (if two protons are attached we have a Mo-coordinated water molecule). In the $Mo_{18}P_2O_{62}$-group these distances are still alternately short and long but the difference is reduced and the mean values found here are 1.76 and 2.12 Å, respectively. In the dimerization reaction of the two Mo_9PO_{34} groups the oxygens with short Mo – O distances in one group approach the oxygens with long distances in the other group and vice versa. The six Mo – Mo distances are practically equal (3.82 – 3.84 Å).

The sodium ions and water molecules. In the structure there are three kinds of crystallographically different sodium ions, Na1, Na2, and Na3. Each of these ions is always coordinated to two $Mo_{18}P_2O_{62}^{6-}$-oxygens, Na1 and Na2 to oxygens in two different groups, and Na3 to oxygens in one and the same group (Table 4). The O – Na1 – O bridges connect symmetry related groups in the *z*-direction and in this way a zigzag chain is formed. These chains are then connected by O – Na2 – O bridges in the *y*-direction thus forming infinite layers parallel to the *yz*-plane. Finally the layers are coupled by O – Na3 – H_2O – Na1 – O-linkages. In all there are ten Na^+-ions coordinated to the group but since eight of these are shared between two groups this implies that the charge has been neutralized by the coordinated Na^+-ions.

Table 4. Sodium – oxygen distances (Å). The designation of the atoms is explained in Table 1. The estimated standard deviations are given in parentheses and refer to the last decimal place given.

Na1 – Aq1(1)	2.22(2)
Na1 – Aq2(1)	2.78(3)
Na1 – Aq3(1)	2.41(2)
Na1 – Aq(12)	2.58(2)
Na1 – Aq(13)	2.51(1)
Na1 – O(3)	2.64(1)
Na1 – O(6)	2.53(1)
Na2 – Aq1(2)	2.59(4)
Na2 – Aq2(2)	2.27(4)
Na2 – Aq3(2)	2.56(3)
Na2 – Aq4(2)	3.14(4)
Na2 – Aq(12)	2.40(4)
Na2 – O(4)	3.05(4)
Na2 – O(8)	2.72(4)
Na3 – Aq1(3)	2.15(4)
Na3 – Aq2(3)	2.34(3)
Na3 – Aq3(3)	2.42(3)
Na3 – Aq(13)	2.57(3)
Na3 – O(7)	2.60(2)
Na3 – O(8)	2.98(3)

Besides bonding to two group-oxygens each sodium ion is also surrounded by water oxygen atoms. In earlier determinations of similar structures the Na^+-ions have always coordinated six oxygen atoms but in this investigation seven coordination is also found.

Na3 has the ordinary octahedral oxygen coordination, while the seven oxygen atoms around Na1 and Na2 form no distinct polyhedron. Two of the water oxygens, Aq(13) and Aq(12) are shared between two Na^+-ions. All water molecules are sodium coordinated.

The PO_4-tetrahedron. It can be seen from the distances and angles in Table 3 that the PO_4-tetrahedron is not far from regular. The P – O distances are in the range 1.53 – 1.56 Å and the different O – P – O angles vary between 108 and 111°. It can also be seen that the oxygen OP(123), which is coordinated to three Mo-atoms gives the longest distance and is one of the oxygen atoms in the smallest angles. The values given above and the values of the O – O distances (2.49 – 2.53 Å) agree well with distances found in other compounds containing phosphate groups.

Acknowledgements. I thank Professor Nils Ingri for much valuable advice, for his great interest and for all the facilities placed at my disposal. Thanks are also due to Dr. Britt Hedman for computational help and to Ing. Ewa Lundström for valuable help in data collection. I also express my gratitude to Dr. Lage Pettersson for much valuable help. The English of the present paper has been corrected by Dr. Michael Sharp. The work forms part of a program supported by the Swedish Natural Science Research Council.

REFERENCES

1. Pettersson, L. *Chem. Scr. Accepted for publication.*

2. Strandberg, R. *Acta Chem. Scand. A 28* (1974) 217.
3. d'Amour, H. and Allmann, R. *Naturwissenschaften 61* (1974) 31.
4. Hedman, B. *Acta Chem. Scand. 27* (1973) 3335.
5. Dawson, B. *Acta Crystallogr. 6* (1953) 113.
6. Cromer, D. T. and Waber, J. T. *Acta Crystallogr. 18* (1965) 104.
7. Hanson, H. P., Herman, F., Lea, J. D. and Skillman, S. *Acta Crystallogr. 17* (1964) 1040.

Received September 26, 1974.

Acta Chemica Scandinavica A 29 (1975) 359—364

Multicomponent Polyanions. 13. The Crystal Structure of a Hydrated Dodecamolybdophosphoric Acid, $H_3Mo_{12}PO_{40}(H_2O)_{29-31}$

ROLF STRANDBERG

Department of Inorganic Chemistry, University of Umeå, S-901 87 Umeå, Sweden

In $H_3Mo_{12}PO_{40}(H_2O)_{29-31}$ the positions of the atoms in the $Mo_{12}PO_{40}$-groups have been determined from three-dimensional X-ray diffraction data collected with a PAILRED diffractometer using Mo$K\alpha$-radiation. The structure of this group was found to be of Keggin type. The $Mo_{12}PO_{40}$-groups are arranged in a three-dimensional network connected by water molecules through hydrogen bonds. Only six of the water oxygen atoms could be located and the explanation for this is probably that the remaining water molecules are not structural. No proposal for the positions of the protons can be given.

In edge-sharing MoO_6-octahedra the Mo—Mo distances are 3.42 Å, while in corner-sharing octahedra the distances increase to 3.70 Å. Mo—Mo distances fall into three ranges, depending on the coordination number of the coordinated oxygen atom, with the mean values 1.70, 1.92, and 2.43 Å.

The cell dimensions of the tetragonal ($I4_1/amd$) unit cell are $a = 16.473$ Å and $c = 23.336$ Å and it contains four formula units. The structure has been refined by least squares methods using anisotropic vibrational parameters, a final R-value of 0.047, based on 3114 reflexions being obtained.

Recent emf investigations of aqueous equilibria [1,2] involving the three components H^+, MoO_4^{2-}, and HPO_4^{2-} have shown that two series of complexes are formed, one including the pentamolybdodiphosphates $(H^+)_8(MoO_4^{2-})_6(HPO_4^{2-})_2$, $(H^+)_9(MoO_4^{2-})_5(HPO_4^{2-})_2$, and $(H^+)_{10}(MoO_4^{2-})_5(HPO_4^{2-})_2$ and another with the enneamolybdomonophosphates $(H^+)_{14}(MoO_4^{2-})_9(HPO_4^{2-})$, $(H^+)_{15}(MoO_4^{2-})_9(HPO_4^{2-})$, $(H^+)_{16}(MoO_4^{2-})_9(HPO_4^{2-})$, and $(H^+)_{17}(MoO_4^{2-})_9(HPO_4^{2-})$. In the most acidic part of the investigated pH-range, evidence for the formation of 18-molybdodiphosphate $(H^+)_{34}(MoO_4^{2-})_{18}(HPO_4^{2-})_2$ as well as dodecamolybdophosphate $(H^+)_{23}(MoO_4^{2-})_{12}(HPO_4^{2-})$ was found. In connection with these equilibrium investigations a number of crystalline phases corresponding to the mentioned complexes, with sodium as cation, were also prepared and X-ray investigated. By means of these X-ray investigations we were able to give reasonable structural interpretations for the proposed complexes. The pentamolybdodiphosphates were found to be built up of $Mo_5P_2O_{23}$-groups, the enneamolybdophosphates of Mo_9PO_{34}-groups and the 18-molybdodiphosphate of $Mo_{18}P_2O_{62}$-groups. Thus the above mentioned complexes would then be more properly written as $Mo_5P_2O_{23}^{6-}$, $HMo_5P_2O_{23}^{5-}$, $H_2Mo_5P_2O_{23}^{4-}$, $H_3Mo_9PO_{34}^{6-}$, $H_4Mo_9PO_{34}^{5-}$, $H_5Mo_9PO_{34}^{4-}$, $H_6Mo_9PO_{34}^{3-}$, and $Mo_{18}P_2O_{62}^{6-}$. For details of the structural arrangements in these groups the reader is referred to Refs. 3—6.

It has not been possible to prepare a sodium salt of the dodecamolybdomonophosphate. However, the corresponding acid can readily be obtained through crystallization from aqueous solutions, prepared by dissolving the commercial product known as dodecamolybdophosphoric acid (Ventron).

The aim of the present investigation was to perform a single crystal X-ray investigation of this dodecamolybdomonophosphoric acid, in order to obtain both arrangements and distances within the acid and also to try to elucidate how the protons and the water molecules are arranged in the crystal. In particular, it may be mentioned that a great number of different crystalline dodecamolybdophosphoric acids have been described in the literature. However, no complete single crystal X-ray investigation

seems to have been carried out. A compilation of earlier investigations (mostly based on analysis and X-ray powder data) are collected in the review by Evans.[7]

EXPERIMENTAL

The crystals were prepared by recrystallizing a commercial dodecamolybdophosphoric acid (Ventron). In a typical preparation, 15 g of the commercial acid were dissolved in 20 ml of water on a water bath. The solution was then filtered and placed at room temperature for slow evaporation. After a few days, bright-yellow, octahedronshaped crystals, were obtained. They were very unstable and decomposed in a few seconds in air. During the X-ray exposures they were enclosed together with part of the mother liquor in a sealed capillary of Lindemann glass. The contents of Mo and P were determined by elemental analysis (carried out at the Department of Analytical Chemistry, University of Umeå). (Found weight-%: Mo 49.1, P 1.4. Calc. (30 H_2O): Mo 48.7, P 1.3). The water content of the crystal was determined by thermogravimetric analysis. The result found was 29.9 water molecules per formula unit.

From rotation photographs around [100] and [001] and the corresponding Weissenberg photographs (zero, first and second layer lines) taken with Cu$K\alpha$-radiation it was concluded that the crystals are tetragonal. On account of the instability of the crystals the cell dimensions could not be refined from powder photographs; instead they were calculated from omega measurements on the diffractometer. It seems likely that the crystals lose some water and change their structure in air since indexing of the reflexions of the powder photographs (with the given tetragonal unit cell) is impossible although the photographs are relatively good. Triclinic as well as cubic phases of dodecamolybdophosphoric acid have been reported.[7] Systematic extinctions were found for hkl, $h+k+l=2n+1$; $hk0$, $h=2n+1$ and hhl, $2h+l=4n+1$ and the space group was uniquely determined as $I4_1/amd$ (No. 141). Precession photographs were taken as a check on the space group determination. The origin of the unit cell was chosen at the centre ($2/m$).

The density of the crystals was determined by flotation in a bromoform-xylene solution and found to be 2.42 g/cm³. (Calc. (30 H_2O) 2.48).

Three-dimensional intensity data were collected at 25 °C with a Philips PAILRED linear diffractometer using Mo$K\alpha$-radiation. The crystal, whose approximate dimensions were 0.27 × 0.40 × 0.40 mm, was mounted and rotated along the b-axis. A total of 7220 reflexions from the layers $h0l-h18l$ up to a limit of sin $\theta \approx 0.5$ were scanned. The intensities were corrected for Lorentz and polarization effects and a correction was applied for absorption. Reflexions with a relative statistical error of $\Delta I_0/I_0$ greater than 0.5 were omitted. In each level the reflexions h,l and $h,-l$ were equivalent within experimental errors. For these equivalent reflexions an arithmetic mean value was calculated, giving a final set of 3114 reflexions. The computer programs used were based on the programs given in Ref. 4.

CRYSTAL DATA

$H_3Mo_{12}PO_{40}(H_2O)_{29-31}$	F.W. = 2365.8 (30 H_2O)
Tetragonal, $I4_1/amd$	$Z=4$
$a=16.473$ (5) Å	$d_{calc}=2.48$ g cm^{-3}
$c=23.336$ (7) Å	$d_{exp}=2.42$ g cm^{-3}
$V=6332$ Å^3	$\mu=24.0$ cm^{-1} (Mo$K\alpha$)

STRUCTURE DETERMINATION AND REFINEMENT

From a three-dimensional Patterson synthesis the approximate coordinates for the Mo-atoms were found. The atom Mo1 was located in a general thirty-two-fold position and Mo2 in the special position 16(h). A refinement at this stage gave an R-value of about 0.25. From a Fourier synthesis based on these atoms, the coordinates of the remaining atoms in the $Mo_{12}PO_{40}$-group were determined. The R-value decreased to 0.11 using isotropic temperature factors. A second

Table 1. The fractional atomic coordinates and in parentheses their estimated standard deviations (referring to the last decimal place given). For the oxygen atoms indexed O(ij) or OP(ij) the (ij) means that the atom is bonded to the molybdenum atoms i and j.

	X	Y	Z
Mo1	0.38764(3)	0.35375(3)	0.01693(2)
Mo2	0.28386(4)	0.25	0.12068(3)
P	0.5	0.25	0.125
O(1)	0.3340(3)	0.0998(3)	0.2832(2)
O(2)	0.1833(3)	0.25	0.1327(3)
O(11″)	0.5	0.1220(4)	0.2691(2)
O(11′)	0.4024(3)	0.25	0.2529(2)
O1(12)	0.3234(2)	0.1709(2)	0.1739(2)
O2(12)	0.4197(2)	0.0419(2)	0.1889(2)
OP(11′2)	0.4236(3)	0.25	0.0868(2)
Aq1	0.5	0.75	0.1240(7)
Aq2	0.2489(6)	0.4989(6)	0.375

(Space group No. 141, origin at centre.)

Table 2. Final anisotropic thermal parameters ($\times 10^4$) and their estimated standard deviations ($\times 10^4$) in parentheses. The parameters are calculated according to the formula $\exp[-(h^2\beta_{11}+k^2\beta_{22}+l^2\beta_{33}+2hk\beta_{12}+2hl\beta_{13}+2kl\beta_{23})]$.

	β_{11}	β_{22}	β_{33}	β_{12}	β_{13}	β_{23}
Mo1	21(0)	20(0)	12(0)	−2(0)	−4(0)	5(0)
Mo2	13(0)	31(0)	11(0)	0	1(0)	0
P	15(1)	15(1)	8(1)	0	0	0
O(1)	28(2)	26(2)	15(1)	1(1)	10(1)	8(1)
O(2)	11(2)	49(3)	14(1)	0	1(1)	0
O(11″)	26(2)	22(2)	10(1)	0	0	4(1)
O(11′)	25(2)	20(2)	9(1)	0	1(1)	0
O1(12)	18(1)	22(1)	12(1)	−1(1)	1(1)	1(1)
O2(12)	24(2)	17(1)	13(1)	−4(1)	2(1)	2(1)
OP(11′2)	14(2)	17(2)	8(1)	0	−1(1)	0
Aq1	177(19)	44(7)	33(4)	0	0	0
Aq2	102(6)	102(6)	61(5)	−33(7)	41(4)	−41(4)

Fourier synthesis gave the positions of two water oxygen atoms. Considerable time was spent in locating the remaining water oxygen atoms, but without positive result. Oxygen atoms placed in positions corresponding to the highest peaks in the difference Fourier map or the remaining maxima in the Fourier synthesis, could not be refined (their temperature factors did not converge) and furthermore many of the peaks were too close to the oxygen atoms in the $Mo_{12}PO_{40}$-group. In the description and discussion of the structure the water content will be treated further. The positional parameters and anisotropic temperature factors for the atoms were refined by full-matrix least squares methods, a final R-value of 0.047 being obtained. $R=\sum||F_o|-|F_c||/\sum|F_o|$. The atomic scattering factors used for Mo^{3+} were those given by Cromer and Waber,[8] for P those given by Hanson, Herman, Lea and Skillman [9] and for O^- the values in International Tables. Account was taken of the real part of the dispersion correction. A weighting scheme according to Cruickshank was applied: $\omega=1/(a+|F_o|+c|F_o|^2+d|F_o|^3)$ where the values of the constants were $a=200$, $c=0.00002$ and $d=0.000001$.

The final difference Fourier synthesis showed no anomalies, the highest peaks being equivalent to an electron density of about 1.5 $e^-/Å^3$. In Tables 1 and 2 final atomic coordinates, vibrational parameters and corresponding standard deviations are given. The structure factor table is available from the author on request.

DESCRIPTION AND DISCUSSION OF THE STRUCTURE

The structure is built up of $Mo_{12}PO_{40}$-groups connected by water molecules. In this way

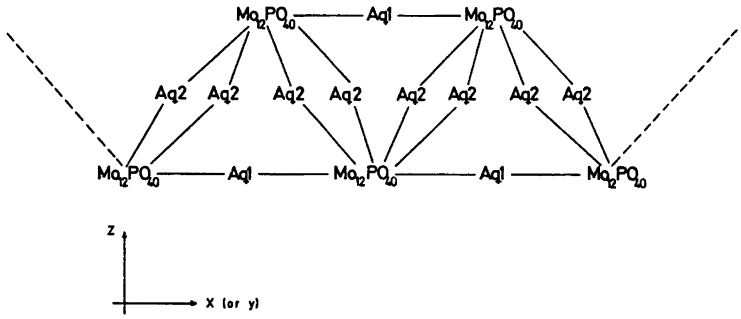

Fig. 1. The coupling O – Aq – O between the $Mo_{12}PO_{40}$-groups within the zigzag chains (schematically drawn).

zigzag chains are formed parallel to the x- and y-axes with the two-dimensional zigzag arrangement parallel to the xz- and yz-planes, respectively. The chains in the x-direction are linked to those in the y-direction thus forming a three-dimensional network. The two water-oxygen atoms located seem to provide the connecting links within the chains by forming O – Aq – O-bridges (Fig. 1). The shortest O – O distances between oxygens in adjacent groups within the chains are only 3.0 Å which means that the groups are quite close to each other.

The $Mo_{12}PO_{40}$-group. This group consists of a central PO_4-tetrahedron surrounded by twelve MoO_6-octahedra. The twelve octahedra may be subdivided into four Mo_3O_{13}-groups. In these groups each MoO_6-octahedron is linked to its neighbour on either side by a shared edge making one corner common to the three octahedra. The four groups are then linked to each other by sharing corners and to the PO_4-tetrahedron by the three-coordinated oxygen atoms. This structure is often named the Keggin-molecule. A stereoscopic view of the $Mo_{12}PO_{40}$-

Table 3. Distances (Å) and angles (degrees) within the $Mo_{12}PO_{40}$-group. The designation of the atoms is explained in Table 1. The estimated standard deviations given in parentheses refer to the last decimal place given.

Mo, P			
Mo1 – Mo1′	3.418(1)	Mo1 – Mo2′	3.706(1)
Mo1 – Mo1″	3.702(1)	Mo1 – P	3.565(1)
Mo1 – Mo2	3.421(1)	Mo2 – P	3.562(1)
MoO_6-octahedra			
Mo1 – O(1)	1.676(4)	O(1) – Mo1 – O(11″)	100.9(2)
Mo1 – O(11″)	1.922(2)	O(1) – Mo1 – O(11′)	102.9(2)
Mo1 – O(11′)	1.910(2)	O(1) – Mo1 – O1(12)	103.1(2)
Mo1 – O1(12)	1.910(4)	O(1) – Mo1 – O2(12)	101.1(2)
Mo1 – O2(12)	1.924(4)	OP(11′2) – Mo1 – O(11″)	72.6(2)
Mo1 – OP(11′2)	2.436(3)	OP(11′2) – Mo1 – O(11′)	83.7(2)
O(1) – O(11″)	2.779(5)	OP(11′2) – Mo1 – O1(12)	83.5(1)
O(1) – O(11′)	2.809(5)	OP(11′2) – Mo1 – O2(12)	72.5(2)
O(1) – O1(12)	2.812(6)	O(11″) – Mo1 – O(11′)	88.7(2)
O(1) – O2(12)	2.784(6)	O(11″) – Mo1 – O2(12)	86.9(2)
OP(11′2) – O(11″)	2.613(7)	O1(12) – Mo1 – O(11′)	86.0(2)
OP(11′2) – O(11′)	2.925(6)	O1(12) – Mo1 – O2(12)	88.5(2)
OP(11′2) – O1(12)	2.919(4)		
OP(11′2) – O2(12)	2.610(6)		
O(11″) – O(11′)	2.678(6)		
O(11″) – O2(12)	2.645(6)		
O1(12) – O(11′)	2.605(6)		
O1(12) – O2(12)	2.674(5)		
Mo2 – O(2)	1.680(6)	O(2) – Mo2 – O1(12)	103.2(2)
Mo2 – O1(12)	1.914(4)	O(2) – Mo2 – O2(12)	100.9(2)
Mo2 – O2(12)	1.923(4)	OP(11′2) – Mo2 – O1(12)	83.6(1)
Mo2 – OP(11′2)	2.433(5)	OP(11′2) – Mo2 – O2(12)	72.6(1)
O(2) – O1(12)	2.820(6)	O1(12) – Mo2 – O1(12)′	85.8(2)
O(2) – O2(12)	2.782(6)	O1(12) – Mo2 – O2(12)	88.7(2)
OP(11′2) – O1(12)	2.923(6)	O2(12) – Mo2 – O2(12)′	86.9(2)
OP(11′2) – O2(12)	2.610(6)		
O1(12) – O1(12)′	2.606(8)		
O1(12) – O2(12)	2.682(5)		
O2(12) – O2(12)′	2.645(8)		
PO_4-tetrahedron			
P – OP(11′2)	1.542(5)	OP(11′2) – P – OP(11′2)′	109.5(2)
OP(11′2) – OP(11′2)′	2.518(8)	OP(11′2) – P – OP(11′2)″	109.4(4)
OP(11′2) – OP(11′2)″	2.52(1)		

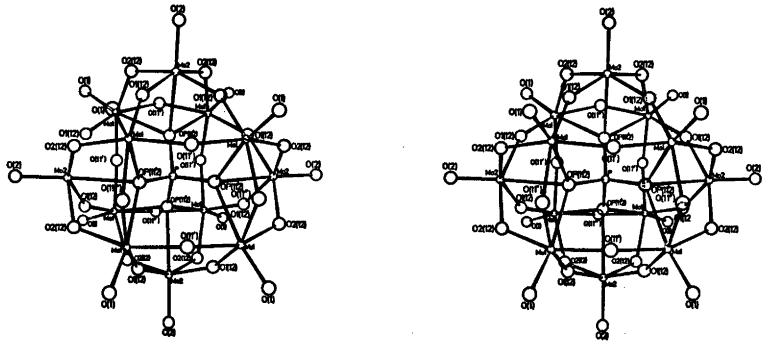

Fig. 2. Stereoscopic view of the $Mo_{12}PO_{40}$-group.

group is given in Fig. 2 and in Fig. 3 the coupling of the MoO_6-octahedra and the PO_4-tetrahedron is shown with idealized polyhedra.

Distances within the group are given in Table 3. It can be seen that for edge-sharing MoO_6-octahedra the Mo – Mo distances are 3.42 Å, while for corner-sharing octahedra the distances increase to 3.70 Å. These distances are in good agreement with those found in other structures.

The MoO_6-octahedra. As can be seen from the distances and angles in Table 3 the MoO_6-octahedra are somewhat distorted. The trend of increasing distances with increasing coordination numbers found in many other structures is also found in this investigation. The Mo – O distances can be divided into three groups according to the number of atoms that the oxygen atom is coordinated to:

(i) Coordinated to only one Mo-atom, the distances are 1.68 Å;
(ii) coordinated to two Mo-atoms, the distances vary between 1.91 and 1.92 Å;

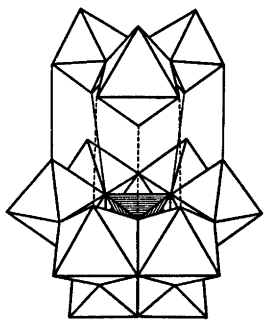

Fig. 3. The coupling of the twelve MoO_6-octahedra and the PO_4-tetrahedron in the $Mo_{12}PO_{40}$-group shown with idealized polyhedra.

(iii) coordinated to P and to three Mo-atoms, the distances are 2.43 and 2.44 Å.

These distances are in good agreement with those found in other heteropolyanions containing molybdenum and phosphorus. Perhaps it should be pointed out that in this $Mo_{12}PO_{40}$-group the two unique octahedra ($Mo(1)O_6$ and $Mo(2)O_6$) are very similar. The distances in the group (ii) are almost the same and independent of whether the oxygen atom is situated between edge-sharing or corner-sharing octahedra. The two distances to unshared oxygen atoms indicate that these oxygens are not protonized.

The PO_4-tetrahedron. This group is almost regular and the distances P – O = 1.54 Å and O – O = 2.52 Å are in good agreement with those found in other structures. The angles O – P – O are 109.5° and 109.4°, *i.e.* quite close to the tetrahedral angle.

The water molecules and the protons. Although much time was spent in attempting to locate the water oxygen atoms, only six atoms per formula unit, corresponding to two positions, could be found. These oxygen atoms, Aq1 and Aq2, seem to connect the $Mo_{12}PO_{40}$-groups in O – Aq – O bridges (Fig. 1). The oxygens connected in this way are the unshared oxygen atoms O(1) and O(2). The distances Aq1 – O(2) and Aq2 – O(1) are 3.02 and 3.03 Å, respectively, and these values indicate hydrogen bonds. With regard to the instability of the crystals and the positions of the anions in the unit cell (leaving unoccupied channels) it may be assumed that the remaining water molecules are not structural.

The protons must either be hydrated or

bonded to Mo-oxygen atoms. The Mo–O distances indicate that these oxygen atoms are not protonized. If this is the case then the protons must be hydrated. Examination of the environment of the water oxygen atoms located provided no information which could be used to resolve the question of whether these water molecules are, or are not, protonized.

Acknowledgements. I thank Professor Nils Ingri for much valuable advice, for his great interest and for all the facilities placed at my disposal. Thanks are also due to Dr. Britt Hedman for computational help and to Ing. Ewa Lundström for valuable help in data collection. I also express my gratitude to Dr. Lage Pettersson for much valuable help. The English text has been revised by Dr. Michael Sharp. The work forms part of a program supported by the Swedish Natural Science Research Council.

REFERENCES

1. Pettersson, L. *Acta Chem. Scand. 25* (1971) 1959.
2. Pettersson, L. *Chem. Scr. Accepted for publication.*
3. Strandberg, R. *Acta Chem. Scand. 27* (1973) 1004.
4. Hedman, B. *Acta Chem. Scand. 27* (1973) 3335.
5. Strandberg, R. *Acta Chem. Scand. A 28* (1974) 217.
6. Strandberg, R. *Acta Chem. Scand. A 29* (1975) 350.
7. Dunitz, J. D. and Ibers, J. A. *Perspectives in Structural Chemistry*, Wiley, New York 1971, Vol. IV, p. 1.
8. Cromer, D. T. and Waber, J. T. *Acta Crystallogr. 18* (1965) 104.
9. Hanson, H. P., Herman, F., Lea, J. D. and Skillman, S. *Acta Crystallogr. 17* (1964) 1040.

Received September 26, 1974.

Acta Chemica Scandinavica A 29 (1975) 365—373

Some Aspects of the Constant Ionic Medium Principle. Studies on the Iron(III) Fluoride and Tris(propylenediamine)cobalt(III) Iodide Systems

LARS JOHANSSON

Division of Inorganic Chemistry 1, Chemical Center, University of Lund, P.O. Box 740, S-220 07 Lund 7, Sweden

When a significant part of a monovalent ion of an inert medium is replaced by a polyvalent ion, either the total of ionic equivalents or the formal ionic strength can be kept constant. Determinations of the first stability constant of the $Fe^{3+} - HF$ and $Co\,pn_3^{3+} - I^-$ systems clearly indicate that a constant concentration of equivalents is the better choice. When the ionic strength was constant, the stability constant was dependent on the total metal ion concentration. This can be shown to be due to activity coefficient changes and, on the cobaltammine system, also to perchlorate association.

When equilibria are studied in electrolytic solutions, a constant ionic medium is commonly employed with the aim of keeping activity coefficients constant. Activity coefficients are generally found to be effectively independent of the concentrations of the reacting species, as long as these concentrations are low compared to that of the inert electrolyte. On the other hand, if a significant part of one of the medium ions is replaced with some other ion *of the same charge*, it is common experience [1–10] that the activity coefficients change. The studies by Biedermann and Sillén [3] on the effects of exchanging Na^+ by H^+ and by Ginstrup [5] who varied the anion (ClO_4^-, Cl^-, Br^-) as well as the cation (H^+, Na^+) are important in this respect. Occasionally, the activity coefficient variation is quite small, as when H^+ is substituted for Li^+ (Ref. 1) or when I^- is substituted for ClO_4^- (see discussion in Ref. 9).

When a significant amount of the medium is replaced with an ion *of different charge* the question arises of how the concept "constant ionic medium" should be defined. Several workers, including the present author, have successfully used a constant *total concentration of ionic equivalents*:

$$I_I = \tfrac{1}{2}\sum_i c_i|z_i| \qquad (1)$$

c_i and z_i being the concentrations and charges of the ions. Often, however, a constant *formal ionic strength* is preferred:

$$I_{II} = \tfrac{1}{2}\sum_i c_i z_i^2 \qquad (2)$$

I_I and I_{II} differ only when polyvalent ions are present in significant amounts. There is no theoretical ground for the use of the one principle or the other, except at very low concentrations ($I_{II} \ll 0.1$ M), where activity coefficients should depend on I_{II} only.[11] It is the aim of the present investigation to compare the two principles expressed by eqns. (1) and (2). On two model systems, β_1 for the 1:1 complex has been determined for various total concentrations of the (polyvalent) metal ion. Two series of experiment have been run for each system, one with I_I constant, the other with I_{II} constant.

As this question was raised in connexion with studies of outer-sphere cobaltamine halide complexes,[9,12–14] it has been natural to choose one such system for these experiments, namely the tris(propylenediamine)cobalt(III) iodide system.[14] However, the cobaltammine systems are

almost certainly complicated by perchlorate complexation,[15] a fact which, as shown below, tends to obscure the present issue. As discussed before,[15] the perchlorate ion is associated to Fe^{3+} to a much smaller degree, if at all. Therefore, the iron(III) fluoride system has been chosen as another model system. Under the conditions chosen, perchlorate association should, in this system, have no influence on the measurements.

Since the concentration of the trivalent ion should be varied as much as possible, some method of ligand measurement has been the natural choice. In the iron(III) fluoride solutions, $[F^-]$ has been measured with a fluoride ion sensitive electrode. The $Copn_3^{3+} - I^-$ system has been studied with the aid of a I^-, I_3^-/Pt electrode, employed previously.[14]

As shown,[14] the measured quantity – an emf difference – is roughly independent of the ligand concentration. The latter can thus be kept low enough to avoid the formation of higher complexes, without any adverse effects on the precision of the measurements. A low ligand concentration has the further advantage that the complex formation does not affect the composition of the medium.

It was felt desirable to perform the measurements over a range of I_I (and I_{II}) values. For the iron system, a lower limit is set by the necessity to suppress the hydrolysis of Fe^{3+}, by keeping the acidity high. The medium concentrations 1 M and 0.5 (acidities 0.4 M and 0.2 M), respectively, were chosen for this system. The ligand is then present mainly as HF. The cobaltammine iodide system was studied at $I_I(I_{II}) = 0.60$, 0.30, and 0.15 M, in addition to 1.0 M as already reported (I_I only [14]). All measurements have been performed at 25 °C.

EXPERIMENTAL

Chemicals. Analytical grade chemicals were used. Details of the preparation of $Co\,pn_3(ClO_4)_3$ have been given before.[14]

Measurements. For the $Fe^{3+} - HF$ system, the element was constituted as follows

$$\mathrm{RE}\;\left|\begin{array}{l|l} C_H\ HClO_4 & C_L\ HF \\ NaClO_4 & C_M\ Fe(ClO_4)_3 \\ & C_H\ HClO_4 \\ & NaClO_4 \end{array}\right|\;\mathrm{FME} \qquad (3)$$

Ag – AgCl electrodes were used as reference electrodes. $NaClO_4$ was added to give $I_I(I_{II}) = 0.5$ or 1.0 M throughout the element. When $I_I(I_{II}) = 0.5$ M, $C_L = 0.500 \times 10^{-3}$ M and 1.000×10^{-3} M, $0 \leq C_M \leq 0.0500$ M, $C_H = 0.2000$ M; when $I_I(I_{II}) = 1.0$ M, $C_L = 0.500 \times 10^{-3}$ M and 1.000×10^{-3} M, $0 \leq C_M \leq 0.1000$ M, $C_H = 0.400$ M. In the bulk of the experiments, C_M was successively increased in the test solution by titration, all other total concentrations being kept constant. All experiments were repeated at least twice. All acid fluoride solutions were handled and stored using plastic equipment only.

The fluoride membrane electrode (Orion Research Inc.) was shown to conform to Nernst's equation under the prevailing conditions. Stable potentials were normally reached within 10 min. The reproducibility (between titrations) was within 0.5 mV.

For the cobaltammine study, the following element was used

$$\mathrm{RE}\;\left|\begin{array}{l|l} NaClO_4 & \begin{array}{l} C_L\ NaI \\ C_T\ NaI_3 \\ C_M\ Co\,pn_3(ClO_4)_3 \\ NaClO_4 \end{array} \end{array}\right|\;\mathrm{Pt} \qquad (4)$$

The measurements have been described in detail earlier.[14] Titrations as well as batch measurements were performed. C_M ranged from 0 to 0.1 M, C_L from 0.01 to 0.1 M. C_T was ca. 2×10^{-3} M in all experiments. Emf's could normally be reproduced within 0.1 mV.

Elements were thermostated to 25 °C. All emf's were measured by a Radiometer PHM 52 potentiometer.

CALCULATIONS, RESULTS

Iron(III) fluoride system

Since F^- is protolyzed to HF in these acidic solutions, the reaction under study is

$$Fe^{3+} + HF \rightleftharpoons FeF^{2+} + H^+ \qquad (5)$$

with the stability constant

$$^*\beta_1 = [MF]h/[M][HF] \qquad (6)$$

where h is the free hydrogen ion concentration. Below, small correction terms are introduced to account for the formation of F^-

$$K_F = h[F^-]/[HF] \qquad (7)$$

and of $FeOH^{2+}$

$$K_{OH} = [MOH]h/[M] \qquad (8)$$

The values [16,17] $K_F = 1.11 \times 10^{-3}$ M ($I = 1$ M) and 1.24×10^{-3} ($I = 0.5$ M) and $K_{OH} = 1.6 \times 10^{-3}$ M

(both ionic strengths [17]) have been used.

The emf of element (3) may be written

$$E = E^\circ - k \log [F^-] \quad (9)$$

where E° is constant if activity coefficients and liquid junction potentials are constant, and $k = RTF^{-1} \ln 10$. The difference in emf between a solution with $C_M > 0$ and one with $C_M = 0$ (subscript "0") is then

$$E_L = E - E_0 = k \log [F^-]_0/[F^-] \quad (10)$$

Further

$$C_L = [HF] + [F^-] + [MF] = [HF]_0 + [F^-]_0 \quad (11)$$

$$C_M = [M] + [MF] + [MOH] \quad (12)$$

$$h = C_H + [MF] + [F^-] + [MOH] \quad (13)$$

Taking eqn. (11) into account, eqn. (13) may be written

$$h = C_H + C_L - [HF] + [MOH] \quad (14)$$

For the calculation of h, the approximations

$$[HF] \approx C_L([F^-]/[F^-]_0) \quad (15)$$

and

$$[MOH] \approx C_M K_{OH} C_H^{-1} \quad (16)$$

are completely satisfactory. $([F]/[F]_0)$ is obtained from eqn. (10). When $C_M = 0$, $h_0 = C_H$, effectively. To calculate $^*\beta_1$ [eqn. (6)] we further need accurate values of [HF] and of ([HF)] + [F]). The latter quantity may then be subtracted from C_L [eqn. (11)] to yield [MF], which in turn may be substratected from C_M [eqn. (12)] to yield ([M] + [MOH]).

Eqns. (7) and (11), combined, give

$$([HF] + [F^-]) = \frac{C_L (K_F + h)}{([F^-]_0/[F^-])(K_F + h_0)}$$

However, the error introduced by omitting the K_F's is completely negligible:

$$([HF] + [F^-]) = \frac{C_L h}{([F^-]_0/[F^-])h_0} \quad (17)$$

Further

$$[HF] = ([HF] + [F^-])h/(K_F + h) \quad (18)$$

Table 1. Experimental data on the *iron(III) fluoride system*. Series I: constant I_I; series II: constant I_{II}. I1 and III: $C_L = 1.000 \times 10^{-3}$ M; I2 and II2: $C_L = 0.500 \times 10^{-3}$ M.

	Series I1		Series I2		Series III1		Series II2	
$C_M \times 10^2$ / M	E_L / mV	$^*\beta_1$	E_L / mV	$^*\beta_1$	E_L / mV	$^*\beta_1$	E_L / mV	$^*\beta_1$
$I = 0.5$ M								
6.18	45.0	180.3	46.4	178.9	45.2	182.0	46.7	181.5
10.86	58.9	181.1	59.5	177.9	59.1	182.7	60.2	183.4
14.55	66.1	180.1	66.5	177.2	66.6	183.9	67.6	185.6
19.83	73.9	179.8	74.0	176.2	74.7	185.9	76.5	188.2
23.57	78.2	179.1	78.3	176.2	79.3	187.4	80.1	189.6
26.34	81.1	179.7	81.1	176.4	82.3	188.7	83.1	191.3
28.5	83.0	178.9	83.1	176.5	84.4	189.3	85.5	194.5
31.6	85.6	178.6	85.7	176.6	87.2	190.5	88.0	193.7
45.3	94.7	177.9	94.7	176.0	97.1	195.8	98.0	200.7
$I = 1.0$ M								
12.35	43.4	154.1	43.6	150.3	43.2	152.2	44.1	153.9
21.73	56.4	154.2	56.6	152.3	56.1	152.2	56.8	153.3
29.1	63.4	154.5	63.7	153.7	63.2	153.2	63.6	153.4
39.7	71.0	154.0	71.1	153.1	70.8	153.3	71.1	153.1
47.1	75.2	154.1	75.0	151.3	75.2	154.1	75.4	153.6
52.6	78.0	154.2	77.9	152.5	78.0	154.5	78.0	153.4
57.0	79.9	153.9	78.9	152.0	80.0	154.8	80.0	152.9
63.1	82.4	153.9	81.9	149.4	82.6	154.6	82.6	153.4
90.6	91.5	153.7			91.3	153.0		

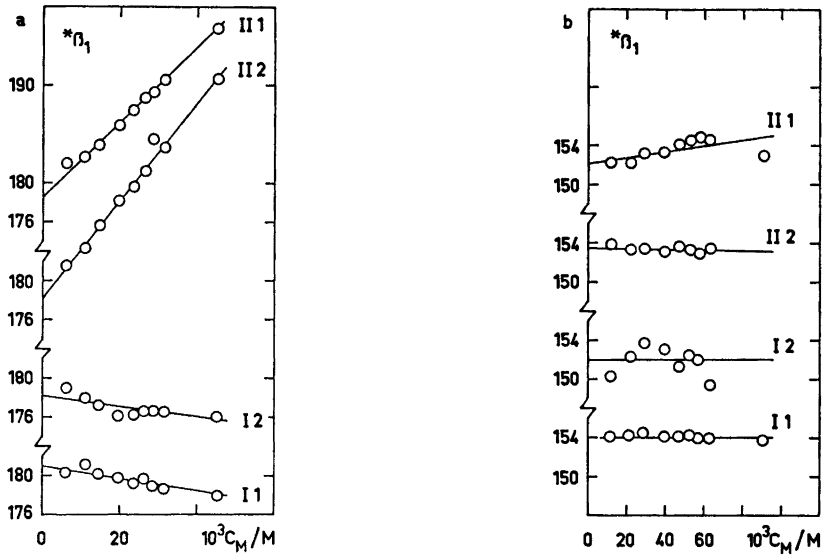

Fig. 1. Iron(III) fluoride system. $*\beta_1$ *vs.* C_M in 0.5 M (*a*) and 1.0 M medium (*b*). The series are labelled as in Table 1. For clarity the curves are successively displaced 10 units vertically, as indicated on the ordinate axes. Straight lines are drawn only to emphasize the trends.

Finally,

$$*\beta_1 = \frac{(C_L - ([HF]+[F^-]))h(1+K_{OH}\,h^{-1})}{(C_M - C_L + ([HF]+[F]))\,[HF]} \qquad (19)$$

These calculations were performed using a programmable desk calculator.

The experimental data are given in Table 1. In Fig. 1, $*\beta_1$ is plotted *vs.* C_M for the various I_I, I_{II}, and C_L.

It should be mentioned that although each experiment was run at least twice, only the mean values are given here, for brevity and clarity. As a consequence, most of the *slopes* of the plots in Fig. 1 appear to be accurate to within 1 – 2 units of $*\beta_1$ over the range of C_M. However, between single titrations (of the same experiment) the slopes normally differed 3 – 4 units of $*\beta_1$. Therefore, the only difference in Fig. 1 that can be considered significant is that between the $I_{II} = 0.5$ experiments, with a positive slope of ca. 20 units, on the hand, and, on the other, all other experiments, which have practically zero slope.

Tris(propylenediamine) cobalt(III) iodide system

Since the calculations have been described in detail before,[14] only the working equations will be given here. For the emf difference

$$E_L = 1.5k \log \delta C_L/[L] \qquad (20)$$

where δ is a correction for the slight dissociation of I_3^-:

$$\delta = \left(\frac{1-(K_{tri}[L])^{-1}}{1-(K_{tri}\,C_L)^{-1}}\right)^{\frac{1}{3}} \qquad (21)$$

Inspection of the literature [17,18] shows that K_{tri} does not vary much between $I = 0$ and $I = 1$. In the present context it is satisfactory to use $K_{tri} = 725$ M^{-1}. Then

$$\bar{n}/[L] = (C_L/[L] - 1)/C_M \qquad (22)$$

Normally, $\boldsymbol{\beta}_1$ is obtained from $\bar{n}/[L]$ by extrapolation [the bold-faced symbol is used to distinguish this observed constant from the "true" β_1; *cf.* eqn. (25) below]

$$\lim_{[L]\to 0} \bar{n}/[L] = \boldsymbol{\beta}_1 \qquad (23)$$

Table 2. Experimental data on the *Co* $pn_3^{3+} - I^-$ *system.* Series 1: $C_{L'} = 28 \times 10^{-3}$ M ($I = 0.15$ M and 0.30 M), $C_{L'} = 50 \times 10^{-3}$ M ($I = 0.60$ M); series 2: $C_{L'} = 13 \times 10^{-3}$ M ($I = 0.15$ M and 0.30 M), $C_{L'} = 25 \times 10^{-3}$ M ($I = 0.60$ M). The values of β_1 in the last column are extrapolated values ($I = 0.15$ M and 0.30 M) or averages ($I = 0.60$ M), respectively.

	Series 1		Series 2		β_1
$C_M \times 10^3$ / M	$E_{L'}$ / mV	β_1 / M^{-1}	$E_{L'}$ / mV	β_1 / M^{-1}	$(C_{L'} = 0)$ / M^{-1}
$I_I = 0.15$ M					
2.50	0.69	9.22	0.70	8.52	7.99
4.71	1.28	9.10	1.31	8.45	7.97
10.00	2.71	9.20	2.74	8.49	7.96
16.00	4.33	9.34	4.38	8.63	8.10
20.00	5.48	9.61	5.49	8.80	8.21
25.00	6.90	9.85	6.89	9.00	8.37
$I_{II} = 0.15$ M					
6.00	1.15	5.97	1.03	4.97	4.34
10.00	2.05	6.53	1.83	5.39	4.68
15.00	3.35	7.33	3.05	6.15	5.55
20.00	5.05	8.65	4.60	7.17	6.23
$I_I = 0.30$ M					
5.00	0.75	4.49	0.77	4.44	4.40
9.41	1.40	4.49	1.47	4.55	4.60
20.00	2.95	4.53	3.09	4.59	4.65
32.0	4.80	4.72	4.85	4.61	4.52
40.0	5.90	4.69	6.00	4.64	4.58
50.0	7.45	4.84	7.50	4.73	4.64
$I_{II} = 0.30$ M					
12.00	1.28	3.11	1.20	2.84	2.64
20.00	2.27	3.36	2.20	3.19	3.06
30.0	3.81	3.88	3.80	3.77	3.68
40.0	5.83	4.63	5.90	4.55	4.48
$I_I = 0.60$ M					
40.0	3.40	2.61	3.45	2.53	2.57
80.0	6.75	2.69	6.70	2.57	2.63
$I_{II} = 0.60$ M					
40.0	2.35	1.72	2.80	2.01	1.87
80.0	6.20	2.43	6.85	2.62	2.52

which eliminates the influence of higher complexes. Since these should be negligible under the present conditions, β_1 has instead been calculated directly for each data point

$$\beta_1 = 1/([L]/\bar{n} - [L]) \quad (24)$$

The results are given in Table 2; Fig. 2 shows β_1 plotted *vs.* C_M. The values of β_1 in Fig. 2 are those obtained by extrapolation to $C_{L'} = 0$ according to eqns. (27) or (30) below. When $I = 0.60$ M (and 1.00 M), an extrapolation was not meaningful, since the values for different $C_{L'}$ were equal within the limits of error. Averages have been plotted instead.

Effects of perchlorate association. Since the stability constant has been computed in the same way, in principle, for both systems, the following is valid for the iron system as well.

If ClO_4^- (denoted A) forms a complex MA, stability constant γ_1, it can be readily shown that the apparent β_1, as computed here, is related to the "true" β_1 by the relation (*cf.* Refs. 12, 15)

$$\beta_1 = \beta_1/(1 + \gamma_1[A]) \quad (25)$$

provided, of course, that activity coefficients are constant. When I_I is constant, we have, as a satisfactory approximation

$$[A] = I_I - C_{L'} \quad (26)$$

i.e.

$$\beta_1 = \frac{\beta_1}{1 + \gamma_1(I_I - C_{L'})} \quad (I_I \text{ constant}) \quad (27)$$

or, after extrapolation to $C_{L'} = 0$

$$\beta_1 = \beta_1/(1 + \gamma_1 I_I) \quad (28)$$

When I_{II} is constant

$$[A] = I_{II} - C_{L'} - 3C_M \quad (29)$$

hence

$$\beta_1 = \frac{\beta_1}{1 + \gamma_1(I_{II} - C_{L'} - 3C_M)} \quad (I_{II} \text{ constant}) \quad (30)$$

or, after extrapolation

$$\beta_1 = \frac{\beta_1}{1 + \gamma_1(I_{II} - 3C_M)} \quad (31)$$

Eqn. (31) shows, thus, that when perchlorate association occurs to a significant degree, β_1 would depend on C_M, even if activity coefficients were constant, when the formal ionic strength I_{II} is held constant.

Combined effect of perchlorate association and activity coefficient changes. In reality, of course,

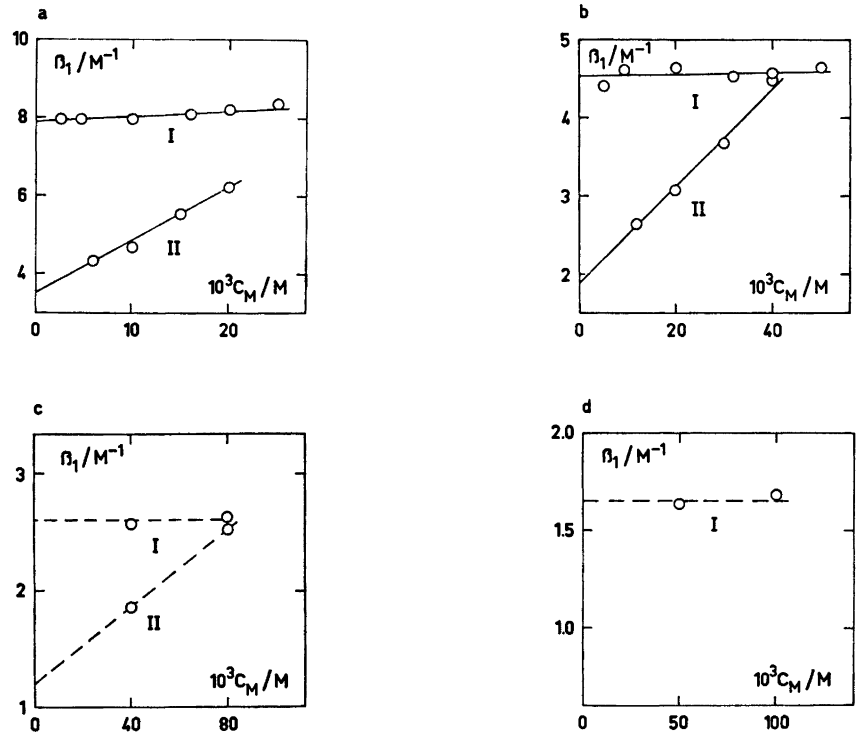

Fig. 2. Co $pn_3^{3+} - I^-$ system. β_1 ($C_L = 0$) *vs.* C_M in the media 0.15 M (*a*), 0.30 M (*b*), 0.60 M (*c*) and 1.00 M (*d*; data taken from Ref. 14).

both these factors should affect the results when I_{II} is constant. At first thought one might expect the effects of both factors to disappear for small C_M, thus giving, on extrapolation to $C_M = 0$, the same value of β_1 as when I_I is constant [*cf.* eqns. (28) and (31)]. However, a closer look reveals that if both factors affect this system one should expect β_1 to start at values *lower* than those obtained at constant I_I, and then increase with increasing C_M. This is exactly what is observed, Fig. 2.

DISCUSSION

In order to explain the variation of the stability constant with C_M in some of the present experiments, a number of factors may be discussed:

1. The formation of higher complexes.
2. Liquid junction potential changes.
3. Perchlorate association.
4. Activity coefficient changes.

As already mentioned, the possibility of keeping C_L low decreases the interference from higher complexes. Estimates based on known [14,17] stabilities of ML_n, $n \geq 2$, show that these can be safely neglected in the ranges of C_L and C_M studied, in both systems.

Estimates according to Henderson's equation,[19] however doubtful, indicate liquid junction potential changes to be very small in both systems when I_I is kept constant, in agreement with the experimental results. They may be of some significance when I_{II} is kept constant. However, regarding the iron system (Fig. 1), the fact that $^*\beta_1$ increases rather rapidly when $I_{II} = 0.5$ M, but hardly at all when $I_{II} = 1.0$ M is difficult to explain with liquid junction potential changes.

As regards perchlorate association, the data on the iron system when $I_{II} = 0.5$ M could indeed be explained using the hypothesis: constant activity factors, and perchlorate association. The required perchlorate association would

be of a quite reasonable magnitude. However, when $I_I = 0.5$ M, perchlorate association does not cause a change in $*\beta_1$ with C_M, according to eqn. (27). On the other hand, if the above hypothesis were correct, since I_{II} is *not* constant when I_I is, activity coefficients – and hence also $*\beta_1$ – should be expected to vary with C_M. Since no variation is observed, the data when $I_I = 0.5$ M do not support the hypothesis. Moreover, the stability constant of the perchlorate complex is expected to follow the general trend, *i.e.* it should be slightly, but not dramatically, smaller when $I_{II} = 1$ M. Thus, a significant increase of $*\beta_1$ with increasing C_M should be expected also when $I_{II} = 1$ M. The near constancy observed is strong evidence against perchlorate association as a major factor contributing to the trends found on the iron(III) fluoride system. In fact, from the data when $I_{II} = 1$ M, an upper limit of about 0.1 M^{-1} can be estimated for the stability constant of $FeClO_4^{2+}$.

In this connexion, reference may be made to the study by Olson and Simonson [15,20] on the hydrolysis of iron(III). They found that when Na^+ of the inert medium was exchanged for Ba^{2+} or La^{3+}, the light absorption by the hydrolyzed species was constant if the exchange was performed keeping the perchlorate concentration constant but changed if a constant ionic strength (I_{II}) was applied. The authors assumed that activity coefficients were constant in the former case but varied in the latter. Sykes,[21] however, interpreted the same results assuming constant activity coefficients when I_{II} was constant, the formation of $FeClO_4^{2+}$ being responsible for the observed spectral change. However, Sykes failed to realize that the constancy of the spectra when $[ClO_4^-]$ was constant is very difficult to rationalize from his assumptions. Thus, the best interpretation of these data seems to be that given by Olson and Simonson.[20] This is of special interest, since the ionic strength was very low, < 0.05 M.

In the present study of the $Fe^{3+} - F^-$ system, it may now be concluded that changing activity coefficients are the main cause of the changes of $*\beta_1$ observed. It may also be concluded, on the other hand, that the activity coefficients are practically constant when I_I is constant. In Fig. 3 the variation with I_I of $*\beta_1$, as determined by several workers [17,22] is shown. When

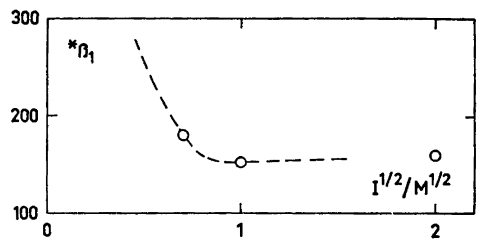

Fig. 3. $*\beta_1$ for $Fe^{3+} - HF$ *vs.* $I^{\frac{1}{2}}$. Data from the present work and from Refs. 17 and 22. For zero ionic strength, values of $*\beta_1 \approx 10^3$ are reported.[17]

I_I is decreased below 0.5 M, $*\beta_1$ increases rather rapidly. Thus, when $I_{II} = 0.5$ M (Fig. 1), an increase of C_M implies a decrease of I_I, and an increase of $*\beta_1$ should be expected. The observed increase is even of the right order of magnitude. Around $I_I = 1$ M the situation is quite different: $*\beta_1$ passes through a very flat minimum (Fig. 3). Even a substantial change in the medium will have little effect on $*\beta_1$, as observed (Fig. 1).

The trends observed in the series II experiments in the Co $pn_3^{3+} - I^-$ system, Fig. 2, can all be rationalized assuming perchlorate association and activity coefficients changes acting together, possibly with some contribution from liquid junction potential changes. It should be noticed, however, that the results cannot be explained by perchlorate association [eqn. (31)] and/or liquid junction potential changes alone. When I_I is constant, β_1 is constant, as expected, except at $I_I = 0.15$ M, where a slight increase occurs. This may be due to a variety of reasons. However, since the trend is more pronounced the higher the value of C_L (Table 2), it probably has its grounds in the slight decrease in the *actual* value of I_I in these solutions caused by the complex formation. The extrapolation according to eqn. (27) performed is probably inadequate in eliminating this trend completely. However, the value of β_1 approached at low C_M should be that valid at $I_I = 0.150$ M.

In conclusion, the present investigation shows quite convincingly that it is not the formal ionic strength I_{II} but rather the total concentration of ionic equivalents I_I that should be held constant. As shown in the cobaltammine system, this is especially important when the medium is not completely inert.

This conclusion is, in a way, a consequence of Brønsted's principle of specific interactions.[23] If the reacting species are predominantly positive [*cf.* eqn. (5)] their activity coefficients depend on the negative part of the medium; the composition of this part should be kept as constant as possible. In the example of the iron(III) fluoride system, $[ClO_4^-]$ should be kept constant. Conversely, with negative reacting species, a constant positive part of the medium is required. However, this is always equivalent to saying that I_I [eqn. (1)] should be constant. That this is true also when species of different charges react is indicated by the results on the Co $pn_3^{3+} - I^-$ system.

Support of this conclusion has been given earlier by Olson and Simonson,[20] as already mentioned, and also, *e.g.*, by Näsänen,[24] who stated that a pentavalent ion had about the same medium effect as five monovalent ions [not 25, as required by eqn. (2)]. Sillén and his coworkers have in fact used a constant medium as defined by eqn. (1) in their numerous studies on hydrolysis and other equilibria.[6,25-28] Leden,[29] studying the silver and cadmium sulfate systems, replaced ClO_4^- with SO_4^- according to eqn. (1) as well as to eqn. (2). The results were significantly different. Although no direct choice could be made from the results, it was inferred from various evidence that the exchange according to eqn. (1) was the better one.

Naturally, medium effects cannot be expected always to be completely eliminated even when I_I is kept constant. As well as when, *e.g.*, ClO_4^- is exchanged with Cl^-,[5] an effect could be expected when Na^+ is replaced by 1/3 M^{3+}, or ClO_4^- by 1/2 SO_4^{2-}, *etc.* This *qualitative* medium effect might be serious only when a substantial part of the medium is exchanged, and when there are reacting species of a charge opposite to that of the exchanging medium ions.

The present study also emphasizes (Fig. 3) the fact that there normally is a region where activity coefficients and hence also equilibrium constants are not very sensitive to the medium concentration (the *quantitative* medium effects are small). Of course it may be an advantage to work in this region. It should be clear, however, that the qualitative medium effects mentioned above are not eliminated in this region.

Finally, some comments will be made on the stability constants observed *per se*. As for $*\beta_1$ of the $Fe^{3+} - HF$ system, the values 180 ± 2 M^{-1} in 0.5 M medium and 153 ± 2 M^{-1} in 1.0 M medium are in good agreement with earlier determinations.[17] In the Co $pn_3^{3+} - I^-$ system, the observed stability constant β_1 decreases with increasing medium concentration, as expected both from activity coefficient changes and from the perchlorate association, eqn. (28). The constant obtained earlier [14] at $I_I = 1$ M conforms to the same pattern.

This work was supported by a grant from the Swedish Natural Science Research Council. The author is indebted to Professor I. Leden for an enlightening discussion. The skilful technical assistance of Mrs. Agneta Nilsson and Mrs. Christina Oskarsson is gratefully acknowledged.

REFERENCES

1. Harned, H. S. and Owen, B. B. *Physical Chemistry of Electrolytic Solutions*, 3rd Ed., Reinhold, New York 1967.
2. Leden, I. *Sv. Kem. Tidskr. 64* (1952) 249.
3. Biedermann, G. and Sillén, L. G. *Ark. Kemi 5* (1953) 425.
4. Nilsson, R. O. *Ark. Kemi 19* (1957) 363.
5. Ginstrup, O. *Acta Chem. Scand. 24* (1970) 875.
6. Ohtaki, H. and Biedermann, G. *Bull. Chem. Soc. Jap. 44* (1971) 1515.
7. Danielsson, I. and Stenius, P. In Högfeldt, E., Ed., *Coordination Chemistry in Solution*, Royal Institute of Technology, Stockholm 1972, p. 79.
8. Byé, J., Fischer, R., Krumenacker, L., Lagrange, J. and Vierling, F. *Ibid.*, p. 99.
9. Johansson, L. *Acta Chem. Scand. 27* (1973) 1637.
10. Ulmgren, P. and Wahlberg, O. *Chem. Scr. In press.*
11. Lewis, G. N. and Randall, M. *J. Amer. Chem. Soc. 43* (1921) 1140.
12. Johansson, L. *Acta Chem. Scand. 25* (1971) 3752.
13. Johansson, L. *Acta Chem. Scand. 27* (1973) 2335.
14. Johansson, L. *Acta Chem. Scand. A 28* (1974) 708.
15. Johansson, L. *Coord. Chem. Rev. 12* (1974) 241.
16. Ahrland, S. and Kullberg, L. *Acta Chem. Scand. 25* (1971) 3457.
17. Martell, A. E. and Sillén, L. G. *Stability Constants*, The Chemical Society, London 1964; *Suppl.* No. *1*, 1971.
18. Håkansson, Å. and Johansson, L. *Chem. Scr. 7* (1975). *In press.*

19. Henderson, P. *Z. Phys. Chem. (Leipzig) 59* (1907) 118; *63* (1908) 325.
20. Olson, A. R. and Simonson, T. R. *J. Chem. Phys. 17* (1949) 1322.
21. Sykes, K. W. *J. Chem. Soc.* (1959) 2473.
22. Norén, B. *Acta Chem. Scand. 21* (1967) 2435.
23. Brønsted, J. N. *J. Amer. Chem. Soc. 44* (1922) 877.
24. Näsänen, R. *Acta Chem. Scand. 11* (1957) 1308.
25. Högfeldt, E. *Coordination Chemistry in Solution*, Royal Institute of Technology, Stockholm 1972, p. XV (bibliography of L. G. Sillén).
26. Havel, J. and Högfeldt, E. *Acta Chem. Scand. 27* (1973) 3323.
27. Havel, J. and Högfeldt, E. *Chem. Scr. 5* (1974) 164.
28. Biedermann, G., Lagrange, J. and Lagrange, P. *Chem. Scr. 5* (1974) 153.
29. Leden, I. *Acta Chem. Scand. 6* (1952) 971.

Received October 30, 1974.

Acta Chemica Scandinavica A 29 (1975) 374—380

Short Communications

On the Crystal Structure of Cyclotetradecanone at −157 °C

P. GROTH

Department of Chemistry, University of Oslo, Oslo 3, Norway

By semiempirical calculations Dale [1] has found the rectangular diamond-lattice conformation of cyclotetradecane to be of lowest enthalpy. This is also the observed conformation in liquid and solution.[2]

The crystals of $C_{14}H_{26}O$ belong to the triclinic system with cell dimensions (for Dirichlet's reduced cell) $a = 5.391(2)$ Å, $b = 7.974(3)$ Å, $c = 8.404(4)$ Å, $\alpha = 64.23(3)°$, $\beta = 89.77(3)°$, $\gamma = 81.81(3)°$. There is one molecule in the unit cell, and the space group $P\bar{1}$ (determined on basis of statistical tests) demands the structure to be disordered.

771 observed reflections were measured on an automatic four circle diffractometer at −157 °C (Mo$K\alpha$-radiation). No corrections for absorption or secondary extinction were carried out (crystal size = (0.05 × 0.25 × 0.32) mm[3]).

The structure was solved by direct methods [3] and refined by full-matrix least squares technique.[4]* No disorder effects could be observed for the ring skeleton, and anisotropic temperature factors were introduced for carbon atoms. With a half-oxygen bonded to C1 (Fig. 1), the R-factor converged at about 15 %. A Fourier map based on the corresponding phases contained relatively large peaks in the vicinity of C3 and C4. Three oxygens were therefore introduced (at C1, C3, and C4) with multiplicity factors 0.250, 0.125, and 0.125, respectively. These were refined simultaneously together with isotropic temperature factors. The multiplicity factors of hydrogens, the positions of which had been calculated, were adjusted for those at C1, C3, C4. No hydrogen parameters were refined. The R-value dropped to 6.4 % (R_W = 6.0 %) for 771 observed reflections. The oxygen multiplicity factors arrived at were $G(O1) = 0.250$, $G(O3) = 0.100$, $G(O4) = 0.132$. Weights in least squares were obtained from the standard deviations in intensities $\sigma(I)$, taken as

$$\sigma(I) = [C_T + (0.02C_N)^2]^{\frac{1}{2}}$$

where C_T is the total number of counts, and C_N the net count.

Final fractional coordinates and thermal parameters with estimated standard deviations are given in Table 1. The principal axes of thermal vibration ellipsoids for carbon atoms were calculated from the temperature parameters of Table 1. Maximum r.m.s. amplitudes range from 0.182 to 0.197 Å (corresponding B-values 2.61 and 3.06 Å^2).

Interatomic distances, bond angles and dihedral angles for the ring skeleton are listed in Table 2. The rectangular diamond-lattice conformation of the ring is shown in Fig. 1, where the molecule is viewed along [100].

Mean value of C−C−C bond angles is 114.4° which corresponds closely to that of cycloundecanone [5] (114.6°). The average C−C bond distance is 1.526 Å, while the corresponding value for cycloundecanone is 1.528 Å.

The observed C−O bond lengths C1−O1 = 1.09 Å, C3−O3 = 1.05 Å, C4−O4 = 1.15 Å are greatly influenced by the methylene hydrogens and have no physical significance. Corresponding bond angles are:

C2−C1−O1 = 122°	C7−C1−O1 = 123°
C2−C3−O3 = 125°	C4−C3−O3 = 117°
C3−C4−O4 = 119°	C5−C4−O4 = 118°

* All programs used (except those for phase determination) are included in this reference.

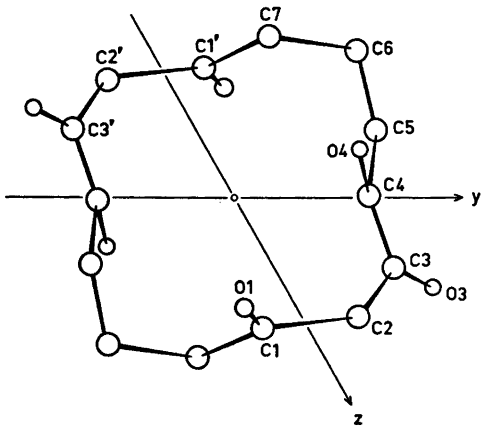

Fig. 1. The molecule viewed along [100].

Table 1. Final fractional coordinates and thermal parameters (multiplied by 10^5 for C and by 10^4 for O and H atoms). Expression for anisotropic vibration is: $\exp[-(B11h^2+B22k^2+B33l^2+B12hk+B13hl+B23kl)]$. Hn1 and Hn2 are bonded to Cn.

ATOM	X	Y	Z	B11	B22	B33	B12	B13	B23
C2	25479(59)	8938(44)	38124(39)	2477(138)	1276(76)	725(60)	-1065(163)	338(142)	-875(113)
C1	35591(63)	-8724(43)	28812(40)	1794(129)	1184(74)	874(62)	-382(154)	-346(140)	-755(112)
C3	581(63)	19343(43)	19928(42)	2287(133)	929(68)	817(60)	-315(153)	338(141)	-871(105)
C4	377(63)	25647(44)	-93(41)	2377(135)	1158(72)	875(60)	-1267(162)	358(147)	-774(108)
C5	-25687(58)	34489(42)	-9386(39)	2489(136)	950(68)	933(63)	-214(152)	110(147)	-997(110)
C6	-26979(61)	40141(43)	-29318(40)	2591(141)	1117(73)	832(61)	-413(160)	-199(146)	-713(112)
C7	-18739(57)	23944(42)	-34318(39)	2237(131)	1094(71)	815(59)	-935(154)	178(138)	-716(106)

ATOM	X	Y	Z	B	ATOM	X	Y	Z	B
O1	5438(18)	-1077(13)	2355(12)	3,3(,3)	H32	-1259	1088	2588	2,0
O3	-1423(40)	2588(30)	2461(28)	2,5(,7)	H41	578	1464	-179	2,0
O4	1754(29)	3130(21)	-751(28)	2,3(,5)	H42	1048	3568	-489	2,0
H11	3736	-449	1538	2,0	H51	-3255	4558	-737	2,0
H12	5110	-1399	3518	2,0	H52	-3748	2448	-392	2,0
H21	3839	1794	2463	2,0	H61	-1462	4948	-3443	2,0
H22	2513	586	4273	2,0	H62	-4388	4624	-3443	2,0
H31	-459	3088	2288	2,0	H71	-111	1784	-3415	2,0
					H72	-1933	2954	-4825	2,0

Table 2. Interatomic distances, bond angles and dihedral angles with estimated standard deviations for the ring skeleton.

DISTANCE	(Å)	DISTANCE	(Å)	DISTANCE	(Å)
C1 - C2	1,528(4)	C2 - C3	1,528(4)	C3 - C4	1,532(4)
C4 - C5	1,522(4)	C5 - C6	1,532(4)	C6 - C7	1,533(4)
C7 - C1′	1,526(4)				

ANGLE	(°)	ANGLE	(°)
C1 - C2 - C3	114,4(3)	C2 - C3 - C4	115,1(3)
C3 - C4 - C5	112,7(3)	C4 - C5 - C6	114,8(3)
C5 - C6 - C7	114,6(3)	C6 - C7 - C1′	114,2(3)
C7 - C1′ - C2′	115,0(3)		

DIHEDRAL ANGLE	(°)	DIHEDRAL ANGLE	(°)
C1 - C2 - C3 - C4	-57,8(4)	C2 - C3 - C4 - C5	174,9(3)
C3 - C4 - C5 - C6	-177,4(3)	C4 - C5 - C6 - C7	59,8(4)
C5 - C6 - C7 - C1′	64,8(4)	C6 - C7 - C1′ - C2′	-179,4(3)
C7 - C1′ - C2′ - C3′	68,7(4)		

Cyclotetradecanone has been studied by ^{13}C and ^{1}H nuclear magnetic resonance [6] with the following result: "The cmr spectra of cyclotetradecanone reveal the presence of at least two different kinds of conformations. At $-160°$, there are two carbonyl bands (intensity ratio 3:2) separated by 1.3 ppm, and the α-carbon resonance is complex".

No short inter-molecular contacts are observed.

A list of observed structure factors is available by request to the author.

Acknowledgement. The author would like to thank A. Aasen for technical assistance during data collection, and Cand.real. T. Ledaal for supplying the compound.

1. Dale, J. *Acta Chem. Scand. 27* (1973) 1115.
2. Borgen, G. and Dale, J. *Chem. Commun.* (1970) 1340.
3. Germain, G., Main, P. and Woolfson, M. M. *Acta Crystallogr. A 27* (1971) 368.
4. Groth, P. *Acta Chem. Scand. 27* (1973) 1837.
5. Groth, P. *Acta Chem. Scand. A 28* (1974) 294.
6. Anet, F. A. L., Cheng, A. K. and Krane, J. *J. Amer. Chem. Soc. 95* (1973) 7877.

Received February 5, 1975.

NMR Studies on Cyclic Arsenites. Geometric Isomerism in Methyl-substituted 2-Chloro- and 2-Methoxy-1,3,2-dioxarsenanes

DAGFINN W. AKSNES and SVEIN TØGERSEN

Department of Chemistry, University of Bergen, Allégaten 70, 5014 Bergen-The University, Norway

In two recent papers [1,2] the NMR spectra of several arsenanes have been studied. As a continuation of previous work we have prepared the following eight methyl-substituted 1,3,2-dioxarsenanes and investigated their NMR spectra:

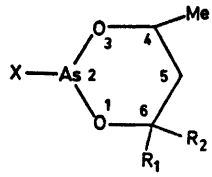

I: X = Cl, $R_1 = R_2 = H$
II: X = Cl, $R_1 = H$, $R_2 = CH_3$ (*cis* methyl)
III: X = Cl, $R_1 = CH_3$, $R_2 = H$ (*trans* methyl)
IV: X = Cl, $R_1 = R_2 = CH_3$
V: X = OCH_3, $R_1 = R_2 = H$
VI: X = OCH_3, $R_1 = H$, $R_2 = CH_3$ (*cis* methyl)
VII: X = OCH_3, $R_1 = CH_3$, $R_2 = H$ (*trans* methyl)
VIII: X = OCH_3, $R_1 = R_2 = CH_3$

The conformational preferences of external substituents on six-membered arsenites have received little attention.[3] The related methyl-substituted arsolanes are, however, configurationally stable about the arsenic atom in the sense that geometrical isomers have been observed.[5] Pairs of geometrical isomers have also been found for 2-methoxy- and 2-ethoxy-4-methyl-1,3,2-dioxaphosphorinane [6,7] and *cis*-2-methoxy-4,5-dimethyl-1,3,2-dioxaphosphorinane.[6,8] It seems, therefore, likely that the prepared arsenanes might exist as a mixture of two geometrical isomers.

Compounds I – IV were prepared according to a procedure of Kamai and Chadaeva,[9] from trichloroarsine and 1,3-butanediol, 2,4-pentanediol, and 2-methyl-2,4-pentanediol as appropriate, in ether solution using triethyl amine as base. The crystalline *cis*-2-chloro-4,6-dimethyl-1,3,2-dioxarsenane (II) was separated from the liquid *trans*-dimethyl form (III) in the racemic mixture by fractional distillation at 5.5 mmHg pressure.

Treatment of compounds I – IV with methanol in ether solution in the presence of excess triethylamine yielded the corresponding methoxy derivatives. All compounds were purified by vaccuum distillation. The boiling and melting points and refractive indices of the prepared compounds are listed in Table 1 together with the chemical shifts of the C – CH_3 protons.

A broadening and partial collapse of the NMR spectrum for a neat sample of III was observed. Dilution of the sample in benzene reduced the broadening considerably. We therefore believe in accord with previous conclusions,[5] that the broadening is due to intermolecular exchange of chlorine.

On basis of previous results on related systems [5–8] and the present NMR studies (*vide*

Table 1. Boiling points, melting points, refractive indices and chemical shifts in δ-values of the C – CH_3 protons in compounds I – VIII (unstable isomers).

Compound	B.p. °C 5.5 mmHg	M.p. °C	n_D^{20}	Chemical shifts δ[c] Me_{4e}	Me_{6e}	Me_{6a}
I	34 – 38[a]	20 – 21		1.25		
II	60	38 – 39		1.21	1.21	
III	66		1.5095	1.20		1.42
IV	45 – 47[b]		1.4958	1.33	1.38	1.59
V	43 – 44		1.4674	1.55		
VI	49 – 50		1.4613	1.05	1.05	
VII	52 – 53		1.4701	1.18		1.39
VIII	39 – 40[a]		1.4627	1.15	1.20	1.46

[a] 0.3 mmHg. [b] 0.05 mmHg. [c] From first-order analysis.

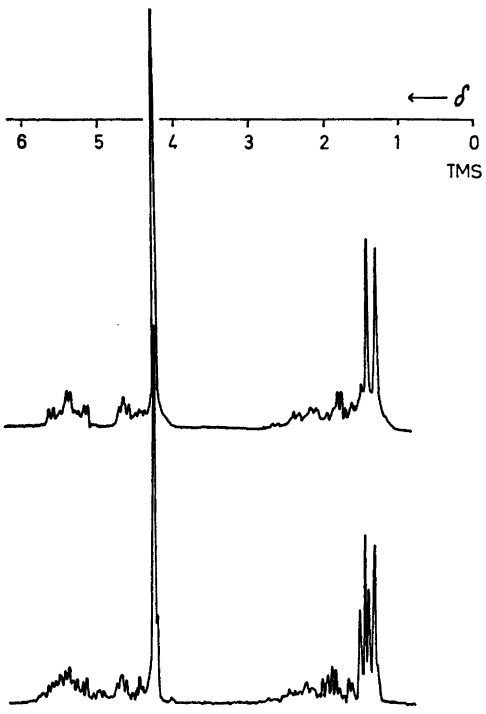

Fig. 1. The 60 MHz NMR spectrum of compound V in benzene solution (*ca.* 50 % v/v). Upper trace: a freshly prepared sample; lower trace: the same sample after about one month.

infra) we believe that the investigated molecules are a mixture of two principal chair forms A and B differing essentially in the orientation of the substituent on arsenic. On basis of 1,3-steric interactions the B structure would seem more probable than A; however, in the related phosphites [10,11] and sulfites [12,13] a strong preference for axial 2-substituents has been reported (anomeric effect). Hence, a possible contribution from the C conformer must also be considered.

When $R_1=CH_3$ and $R_2=H$ the A and C conformers are identical. In general, however, conformer A is certainly more stable than C which makes a negligible contribution when $R_2=CH_3$ owing to severe diaxial methyl-interactions. The 1,3-non-bonded interactions are probably greatly reduced in A compared to the analogous phosphorinane ring as previously explained.[8] The above evidence thus indicates that A is the thermodynamically more stable form.

The NMR spectra of compounds I–IV showed the presence of only one isomer. A large vicinal coupling constant (10–12 Hz) observed in compounds I, II, and IV is typical for an axial-axial coupling in a chair conformation. We therefore believe that these compounds are formed mainly in one preferred configuration which corresponds to the thermodynamically more stable form A. The low-field doublets at 1.42 ppm and 1.59 ppm have been assigned to the axial methyl hydrogens at the 6 position in III and IV, respectively. The remaining doublets at higher field are due to the equatorial methyl groups at the 4 and 6 positions. In particular, the high-field methyl signal at 1.25 ppm in I indicates a preference for an equatorial methyl group in accord with previous results for the corrresponding chlorophosphite.[14] The observation that the NMR signals of axial methyl protons appear at lower field than equatorial methyl signals agrees with previous results for related systems.[15]

The NMR spectra of freshly prepared samples of the methoxy derivatives showed that these molecules existed almost entirely in one form (Fig. 1). These compounds appeared to be unstable, however, since the presence of a new species was observed after some time. About 30 % of this new species was found for V (Fig. 1) whereas smaller amounts were observed for the other methoxy compounds. The rate of conversion into the new material also seemed to be acid catalyzed. These results are most readily explained by assuming that the methoxy compounds are a mixture of geometrical isomers A and B (possibly in equilibrium with C).

The preparation of V–VIII *via* the cyclic chloro-compounds is thus expected to give the unstable isomer B in nearly pure form. We believe, in accord with previous results for the related phosphites [6,7] that this process involves an inversion about the arsenic atom as a result of an S_N2 reaction.

The large axial-axial coupling constants (10.4–12.3 Hz) observed in the unstable forms of V, VI, and VIII again indicate measureable

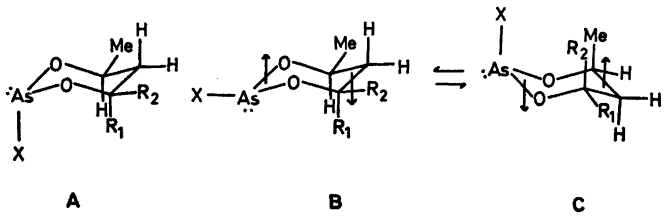

amounts of only one chair conformation. In VII, however, the vicinal coupling constants spanning from 3.1 to 8.4 Hz, appear to be time-averaged values resulting from an equilibrium between B and C in which C predominates.

Again the axial methyl proton signals appear at lower field than the corresponding equatorial methyl signals. The methyl signal of V (Fig. 1) clearly demonstrates that axial and equatorial methoxy substituents at arsenic give rise to different stereo-specific substituent effects.

Experimental. The 60 MHz NMR spectra of the eight compounds were examined in benzene solutions (*ca.* 50 % v/v for the liquid compounds). A small amount of TMS was added and used as internal standard and lock signal source. The spectra were run at ambient probe temperature (*ca.* 30 °C) on a JEOL-C-60H spectrometer.

1. Aksnes, D. W. and Vikane, O. *Acta Chem. Scand. 26* (1972) 4170.
2. Aksnes, D. W. *Acta Chem. Scand. A 28* (1974) 1175.
3. Samitov, Y. Y., Taceeva, N. K., Chadaeva, N. A. and Kamai, G. H. *Chem. Heterocycl. Compounds (USSR)* (1973) 457.
4. Aksnes, D. W. and Bjorøy, M. *Acta Chem. Scand. A 29* (1975). *In press.*
5. Aksnes, D. W. and Vikane, O. *Acta Chem. Scand. 27* (1973) 2135, and references therein.
6. Denney, D. Z. and Denney, D. B. *J. Amer. Chem. Soc. 88* (1966) 1830.
7. Aksnes, G., Eriksen, R. and Mellingen, K. *Acta Chem. Scand. 21* (1967) 1028.
8. Haemer, M., Ottinger, R., Zimmermann, D. and Reisse, J. *Tetrahedron 29* (1973) 3539.
9. Kamai, G. and Chadaeva, N. A. *Chem. Abstr. 47* (1953) 3792c–f, 10470c–h.
10. White, D. W., Bertrand, R. D., McEwen, G. K. and Verkade, J. G. *J. Amer. Chem. Soc. 92* (1970) 7125.
11. Bentrude, W. G. and Hargis, J. H. *J. Amer. Chem. Soc. 92* (1970) 7136.
12. Albriktsen, P. *Acta Chem. Scand. 26* (1972) 1783.
13. Buchanan, G. W., Stothers, J. B. and Wood, G. *Can. J. Chem. 51* (1973) 3746.
14. Bergesen, K. and Albriktsen, P. *Acta Chem. Scand. 26* (1972) 1680.
15. Maroni, P. and Gorrichon, J.-P. *Bull. Soc. Chim. Fr.* (1972) 785.

Received January 13, 1975.

Conformational Energies and Conversion Barriers for Cyclononane

STEINAR RUSTAD and HANS M. SEIP

Department of Chemistry, University of Oslo, Oslo 3, Norway

A novel approach to semiquantitative calculations of conformational energies of C_9-C_{16} cycloalkanes has been suggested by Dale.[1] The method is based on the reasonable assumptions that the bonding energies are of minor importance and that the main part of the non-bonded interactions can be included in the torsional potentials. According to Dale, cyclononane has three conformations which he denoted [333] (D_3 symmetry), [234] (C_1) and [12222] (C_2) *cf.* Fig. 1). He found [333] to be the most stable form, [234] and [12222] were found to be 1.4 and 2.8 kcal mol^{-1} less stable, respectively. We used these results as a starting point for the present, more accurate calculation. Results for an additional conformation with C_s symmetry considered by Bixon and Lifson,[2] are also included.

The conformational energies were calculated according to the method first applied by Westheimer,[3] and later used by many others in various versions.[4–8] A combination of the steepest-descent and the Newton-Raphson method was used to obtain the energy minima. The computer program was written by one of us (S.R.) in FORTRAN EXTENDED for CYBER 74. A subroutine for calculating the dependent structural parameters for the molecule must be provided.

For cyclononane we used the cartesian coordinates for the carbon atoms as independent parameters. The van der Waals energy was calculated as described by Eliel *et al.*[4] with the necessary constants from their book (p. 452). The intrinsic barrier to torsion about a CC bond was given the value 2.65 kcal mol^{-1}.[9] The CCC angle was assigned the normal value 112° and the bending force constant 1.086 mdyn Å rad^{-2}.[10] The normal value and the stretching force constant for a CC bond were taken as 1.535 Å and 4.534 mdyn Å^{-1}.[10] The CH bond lengths and the HCH angles were kept at the fixed values 1.113 Å and 112°. The planes through HCH were assumed perpendicular to the planes through CCC, bisecting the CCC angles. No symmetry restrictions were imposed on the models during the minimalization. The iteration procedure was terminated when the absolute value of the shifts in the independent parameters were less than 10^{-3} Å.

Table 1 gives the calculated conformational energies and the corresponding torsional angles and bond angles. Results obtained by Dale and by Bixon and Lifson are also included. The agreement is quite good. As in previous calcula-

amounts of only one chair conformation. In VII, however, the vicinal coupling constants spanning from 3.1 to 8.4 Hz, appear to be time-averaged values resulting from an equilibrium between B and C in which C predominates.

Again the axial methyl proton signals appear at lower field than the corresponding equatorial methyl signals. The methyl signal of V (Fig. 1) clearly demonstrates that axial and equatorial methoxy substituents at arsenic give rise to different stereo-specific substituent effects.

Experimental. The 60 MHz NMR spectra of the eight compounds were examined in benzene solutions (*ca.* 50 % v/v for the liquid compounds). A small amount of TMS was added and used as internal standard and lock signal source. The spectra were run at ambient probe temperature (*ca.* 30 °C) on a JEOL-C-60H spectrometer.

1. Aksnes, D. W. and Vikane, O. *Acta Chem. Scand. 26* (1972) 4170.
2. Aksnes, D. W. *Acta Chem. Scand. A 28* (1974) 1175.
3. Samitov, Y. Y., Taceeva, N. K., Chadaeva, N. A. and Kamai, G. H. *Chem. Heterocycl. Compounds (USSR)* (1973) 457.
4. Aksnes, D. W. and Bjorøy, M. *Acta Chem. Scand. A 29* (1975). *In press.*
5. Aksnes, D. W. and Vikane, O. *Acta Chem. Scand. 27* (1973) 2135, and references therein.
6. Denney, D. Z. and Denney, D. B. *J. Amer. Chem. Soc. 88* (1966) 1830.
7. Aksnes, G., Eriksen, R. and Mellingen, K. *Acta Chem. Scand. 21* (1967) 1028.
8. Haemer, M., Ottinger, R., Zimmermann, D. and Reisse, J. *Tetrahedron 29* (1973) 3539.
9. Kamai, G. and Chadaeva, N. A. *Chem. Abstr. 47* (1953) 3792c–f, 10470c–h.
10. White, D. W., Bertrand, R. D., McEwen, G. K. and Verkade, J. G. *J. Amer. Chem. Soc. 92* (1970) 7125.
11. Bentrude, W. G. and Hargis, J. H. *J. Amer. Chem. Soc. 92* (1970) 7136.
12. Albriktsen, P. *Acta Chem. Scand. 26* (1972) 1783.
13. Buchanan, G. W., Stothers, J. B. and Wood, G. *Can. J. Chem. 51* (1973) 3746.
14. Bergesen, K. and Albriktsen, P. *Acta Chem. Scand. 26* (1972) 1680.
15. Maroni, P. and Gorrichon, J.-P. *Bull. Soc. Chim. Fr.* (1972) 785.

Received January 13, 1975.

Conformational Energies and Conversion Barriers for Cyclononane

STEINAR RUSTAD and HANS M. SEIP

Department of Chemistry, University of Oslo, Oslo 3, Norway

A novel approach to semiquantitative calculations of conformational energies of C_9-C_{16} cycloalkanes has been suggested by Dale.[1] The method is based on the reasonable assumptions that the bonding energies are of minor importance and that the main part of the non-bonded interactions can be included in the torsional potentials. According to Dale, cyclononane has three conformations which he denoted [333] (D_3 symmetry), [234] (C_1) and [12222] (C_2) *cf.* Fig. 1). He found [333] to be the most stable form, [234] and [12222] were found to be 1.4 and 2.8 kcal mol^{-1} less stable, respectively. We used these results as a starting point for the present, more accurate calculation. Results for an additional conformation with C_s symmetry considered by Bixon and Lifson,[2] are also included.

The conformational energies were calculated according to the method first applied by Westheimer,[3] and later used by many others in various versions.[4–8] A combination of the steepest-descent and the Newton-Raphson method was used to obtain the energy minima. The computer program was written by one of us (S.R.) in FORTRAN EXTENDED for CYBER 74. A subroutine for calculating the dependent structural parameters for the molecule must be provided.

For cyclononane we used the cartesian coordinates for the carbon atoms as independent parameters. The van der Waals energy was calculated as described by Eliel *et al.*[4] with the necessary constants from their book (p. 452). The intrinsic barrier to torsion about a CC bond was given the value 2.65 kcal mol^{-1}.[9] The CCC angle was assigned the normal value 112° and the bending force constant 1.086 mdyn Å rad^{-2}.[10] The normal value and the stretching force constant for a CC bond were taken as 1.535 Å and 4.534 mdyn Å^{-1}.[10] The CH bond lengths and the HCH angles were kept at the fixed values 1.113 Å and 112°. The planes through HCH were assumed perpendicular to the planes through CCC, bisecting the CCC angles. No symmetry restrictions were imposed on the models during the minimalization. The iteration procedure was terminated when the absolute value of the shifts in the independent parameters were less than 10^{-3} Å.

Table 1 gives the calculated conformational energies and the corresponding torsional angles and bond angles. Results obtained by Dale and by Bixon and Lifson are also included. The agreement is quite good. As in previous calcula-

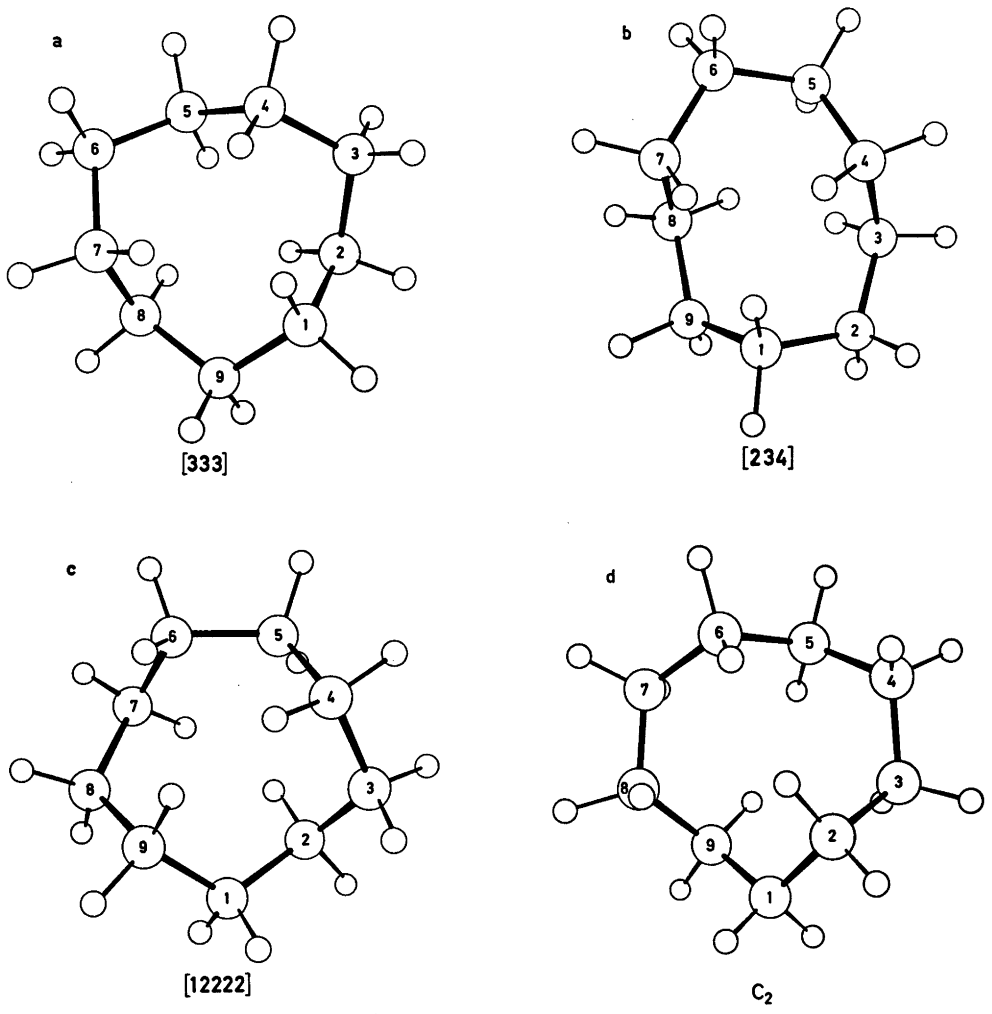

Fig. 1. The conformations found for cyclononane.[14]

tions [1,2,5] we get the lowest energy for the [333] form. Our results indicate that the [12222] form is slightly more stable than the [234] form, while Dale obtained a lower energy for the [234] form. The ^{13}C NMR spectrum of cyclononane is consistent with D_3 symmetry for the most stable form,[11] and evidence for small amounts of other conformers has also been obtained.[12]

In a second paper [13] Dale has dealt with interconversions in cycloalkanes. The reasonable path for the interconversion of [333] forms is [333]→[234]→[234] (mirror image)→[333].

The corresponding energy profile was computed. The path linking [333] and [234] was obtained by letting the torsional angle ϕ_{2-3} pass through zero. Similarly, going from [234] to its mirror image implies that ϕ_{5-6} passes through zero. The energies and structural parameters corresponding to the transition states [1233] and [1323] are included in Table 1. The energies are seen to be in good agreement with those calculated by Dale, though there are considerable differences in torsional angles and bond angles.

Table 1. Conformational energies (kcal mol^{-1}) and corresponding torsional and CCC bond angles (degrees) in cyclononane. The CC bond lengths obtained were in the range 1.538–1.554 Å.

	[333]	Ref. 1	[234]	Ref. 1	[12222]	Ref. 1	C_s	Ref. 2	[1233]	Ref. 1	[1323]	Ref. 1
1–2 [a]	128	135	58	65	68	75	−65	−63	92	110	64	80
2–3	−57	−55	51	50	−73	−85	120	121	0	0	52	45
3–4	−57	−55	−131	−140	−48	−45	−74	−77	102	−95	−137	−150
4–5	128	135	110	115	105	110	87	86	122	145	82	95
5–6	−57	−55	−41	−40	−92	−100	−123	−120	−47	−65	0	0
6–7	−57	−55	−50	−55	105	110	87	86	−48	−40	−82	−95
7–8	128	135	137	150	−48	−45	−74	−74	140	130	137	150
8–9	−57	−55	−52	−45	−43	−85	120	121	−67	−55	−52	−45
9–1	−57	−55	−70	−85	68	75	−65	−67	−60	−60	−64	−80
9–1–2 [b]	113.7	[c]	116.9	[c]	118.2	[c]	113.8	113	120.8	[c]	117.5	[c]
1–2–3	113.7		117.3		116.1		113.0	113	120.4		115.0	
2–3–4	114.9		115.1		117.6		114.8	114	113.4		113.3	
3–4–5	113.7		113.1		115.2		114.6	115	114.6		118.2	
4–5–6	113.7		114.7		115.4		114.6	115	114.3		118.2	
5–6–7	114.9		115.4		115.4		114.6	116	113.6		113.3	
6–7–8	113.7		113.9		115.2		114.6	115	112.2		114.9	
7–8–9	113.7		114.3		117.6		114.8	115	114.2		117.5	
8–9–1	114.9		117.4		116.1		113.0	113	114.1		116.7	
E_r [d]	0.15		0.22		0.17		0.08		0.28		0.26	
E_θ [e]	1.06		2.85		4.24		1.15		4.16		4.26	
E_ϕ [f]	7.72		8.32		7.29		10.91		11.46		8.81	
E_v [g]	−5.49		−4.57		−5.38		−6.29		−4.76		−4.46	
E_{tot} [h]	3.43		6.82		6.31		5.85		11.14		8.87	
ΔE [i]	0.0	0.0	3.39	1.4	2.89	2.8	2.42	3.11	7.71	8.6	5.44	5.6

[a] Torsional angles. [b] CCC bond angles. [c] Dale assumed tetrahedral bond angles. [d] Bond stretching energies. [e] Bond angle strain energies. [f] Torsional strain energies. [g] Van der Waals energies. [h] Total energies. [i] Conformational energies above the value for the [333] form.

1. Dale, J. *Acta Chem. Scand. 27* (1973) 1115.
2. Bixon, M. and Lifson, S. *Tetrahedron 23* (1967) 769.
3. Westheimer, F. H. In Newman, M. S, Ed., *Steric Effects in Organic Chemistry*, Wiley, New York 1956.
4. Eliel, E. L., Allinger, N. L., Angyal, S. J. and Morrison, G. A. *Conformational Analysis*, Interscience, New York 1965.
5. Hendrickson, J. B. *J. Amer. Chem. Soc. 83* (1961) 4537; *84* (1962) 3355; *86* (1964) 4854.
6. Allinger, N. L., Miller, M. A., Van-Catledge, F. A. and Hirsch, J. A. *J. Amer. Chem. Soc. 89* (1967) 4345.
7. Allinger, N. L., Hirsch, J. A., Miller, M. A., Tyminski, I. J. and Van-Catledge, F. A. *J. Amer. Chem. Soc. 90* (1968) 1199.
8. Boyd, R. H. *J. Chem. Phys. 49* (1968) 2574.
9. Abraham, R. J. and Parry, K. J. *J. Chem. Soc. B* (1970) 539.
10. Schachtschneider, J. H. and Snyder, R. G. *Vibrational Analysis of Polyatomic Molecules* IV (Force Constants for the Haloparaffins) Project No. 31450, Technical Report No. 122–63 of Shell Development Company.
11. Anet, F. A. L. and Wagner, J. J. *J. Amer. Chem. Soc. 93* (1971) 5266.
12. Anet, F. A. L. and Krane, J. *Unpublished results.*
13. Dale, J. *Acta Chem. Scand. 27* (1973) 1130.
14. Johnson, C. K. (1965) *ORTEP, Report ORNL-3795*, Oak Ridge National Laboratory, Oak Ridge.

Received December 9, 1975.

Acta Chemica Scandinavica A 29 (1975) 381—390

Equilibrium Studies of Chromium(III) Complexes. I. The Complex Formation between Chromium(III) and Ethylenediamine in Aqueous Solution

PETER ANDERSEN, TORSTEN BERG and JENS JACOBSEN

Chemistry Department I, Inorganic Chemistry, H. C. Ørsted Institute, University of Copenhagen, DK-2100 Copenhagen Ø, Denmark

A new method is described whereby it is possible to establish equilibrium in aqueous solution between chromium(III) and different amine ligands (here ethylenediamine) within 3 – 5 days at room temperature as far as mononuclear complexes are concerned. The catalyst used is charcoal in combination with small amounts of chromium(II). A constant chromium(II) concentration is maintained by electrolytic reduction of chromium(III).

The hitherto unknown ion, Cr $en_2en^*(OH)^{2+}$ (en≡ethylenediamine, en*≡en as a monodentate ligand) is one of the equilibrium species, and it was isolated in solution.

The stability constants for the formation of Cr en_3^{3+} and Cr $en_2(enH)(H_2O)^{4+}$ from *cis*-Cr $en_2(H_2O)_2^{3+}$ were determined in 1 M chloride medium (NaCl) at 24 °C to be $10^{6.43}$ and $10^{0.0}$ M^{-1}, and the acid dissociation constants of Cr $en_2(enH)(H_2O)^{4+}$ to be $10^{-4.4}$ and $10^{-8.8}$ M. The gross stability constant for Cr en_3^{3+} was found to be $10^{19.5}$ M^{-3} and the ratio between *cis*- and *trans*-Cr $en_2(OH)_2^{+}$ to be 5.

The equilibrated solutions contain several polynuclear species among which are the ions $[en_2Cr(OH)_2Cr\ en_2]^{4+}$ and the new $[Cr\{(OH)_2Cr\text{-}en_2\}_3]^{6+}$ which we isolated as various salts. The latter is the chromium analogue of Werner's brown cobalt salt.

Attempts to study equilibria between chromium(III) and ligands in aqueous solution are complicated by the robustness of chromium(III) complexes. Therefore very little has been published in this field. Cobalt(III) complexes are in many ways analogous to those of chromium(III), and cobalt(III) likewise exhibits this robust behaviour. Bjerrum [1] showed, however, that it is possible to obtain equilibrium between cobalt(III) and ammonia if charcoal is used as a catalyst, a method which has later been used with other ligands, among them ethylenediamine.[2]

It has been shown that charcoal reduces a little of the cobalt(III) to cobalt(II).[3–5] Charcoal alone does not seem to have any catalytic effect on chromium(III) but if chromium(II) is added as well, the robustness is strongly reduced.[6–8] This has been used in attempts to establish equilibrium between chromium(III) and ammonia by adding charcoal to concentrated ammonium chloride solutions containing different amounts of ammonia and all the chromium initially as chromium(II).[8] Chromium(II) alone, like charcoal alone, does not establish equilibrium in such solutions. When both are present, charcoal, besides its catalytic effect on chromium(III), also catalyzes the oxidation of chromium(II) by the medium:

$$Cr(II) + H(I) \xrightarrow{C} Cr(III) + H(0) \qquad (I)$$

This has the disadvantage that all chromium(II) may disappear before equilibrium is reached.

We present here a new method based on the same catalyst, *i.e.* chromium(II) and charcoal. By electrolytic reduction of chromium(III) to chromium(II) it is possible to maintain a constant concentration of chromium(II) because a steady state is reached when the amount of chromium(II) removed by reaction I equals the amount generated by electrolysis. In this way it is possible to choose a suitable catalyst

concentration and keep it for days without any changes in the medium, except for a small H(I) consumption due to the continuous reduction.

We have applied the method to several chromium(III) complex equilibria. This paper concerns the equilibria between chromium(III) and ethylenediamine. Such equilibria have been studied before mainly by Woldbye,[9] who determined the ratio between *cis*- and *trans*-$[Cr\ en_2(OH)_2]^+$ (en≡ethylenediamine) and measured the acid dissociation constants for the diaqua and hydroxo aqua tetramine complexes.

EXPERIMENTAL

Procedure. A typical experiment was carried out as follows. A 100 ml flask was equipped with an inlet and outlet for nitrogen gas freed from oxygen by a washing-flask with Cr(II)-solution. At the bottom of the 100 ml flask were two mercury electrodes which could be filled with pure mercury from outside. One mercury electrode served as cathode in combination with a platinum anode separated from the cathode chamber (containing the chromium(III) solution) by the membrane of a Radiometer K 401 calomel electrode. The other mercury electrode, together with a saturated calomel electrode, registered the emf of the solution. Furthermore, the flask was provided with a thermometer, a valve for taking out samples without letting in oxygen, and a magnetic stirrer. The gas outlet ended under water or ethanol so that with a calibrated gas burette it was possible to measure the volume of hydrogen evolved.

The 50 – 100 ml solutions containing chromium(III) and ligands were placed in the cathode chamber. The compositions of such solutions are given in Fig. 1 and Table 1. In the anode chamber we used 2 M H_2SO_4, so that the current through the membrane was mainly established by hydrogen ions, in order to make the pH-change in the chromium solution as small as possible. After addition of charcoal and after removal of oxygen a voltage of about 10 V was applied, giving rise to a current of 5 – 15 mA. After 0.5 – 1 h the emf dropped to *ca.* – 1.1 V and a distinct change in the solution had then taken place. The hydrogen evolved, now equivalent to the current, maintained a slight overpressure in the flask, which was kept like this, *i.e.* with $[Cr(II)]/[Cr(III)] \simeq 0.01$, for 3 – 5 days. At this time equilibrium was reached and the current was switched off. The solution was analyzed when the small amount of chromium(II) had been oxidized to chromium(III) by the medium. The robustness of chromium(III) facilitated the further investigations of such solutions.

All the experiments were carried out at (24 ± 1) °C. The amount of charcoal and the current could be varied within wide limits, but the use of 1 – 2 g of charcoal *per* l and the above-mentioned conditions were found to produce the best catalytic effect.

Analysis of the medium and of the distribution of chromium(III) complexes in the equilibrium solutions. The solutions were analyzed for the total content of chloride, nitrogen (Kjeldahl) and chromium (atomic absorption spectrophotometry) before and after equilibration; the pH of the solutions was measured with a glass electrode and the amount of basic components was determined by titration with 0.1 M hydrochloric acid. The amounts of different chromium(III) species were determined by atomic absorption spectrophotometry after separation by cation-exchange chromatography on columns of Sephadex SP-C-25. No significant changes in the medium were observed. Initial difficulties with some solutions losing chromium during the reaction were overcome by thorough rinsing of the equipment. The most important results of these analyses are given in Fig. 1 and in Tables 1 and 2.

Table 1. The composition of the solutions having $[Cl^-] = 1.0$ M (NaCl). The determination of the concentrations of free enH_2^{2+}, enH^+, and en are based on a total nitrogen analysis (Kjeldahl), a correction for coordinated en, on our determination of the acid dissociation constants of enH_2^{2+} (Table 3), pH_{exp}, and on a determination of basic components by titration with 0.1 M HCl. "tris" and "bis" refer to $[Cr\ en_3]Cl_3.3H_2O$ and *trans*-$[Cr\ en_2Cl_2]Cl.H_2O$, respectively.

Experiment No.	1	2	3	4	5	6	7	8	9	10
Final pH_{exp}	8.54	9.01	9.16	9.71	9.71	9.76	9.78	9.78	10.48	10.49
Total conc. of N (M)	1.05	1.17	1.10	1.03	1.13	1.02	1.04	1.02	2.88	2.92
$[enH_2^{2+}]$ (mM)	44	16	11							
$[enH^+]$ (mM)	456	517	476	367	404	353	355	348	461	460
[en] (mM)	10.9	36.6	47.6	130	143	141	148	145	964	983
C_{Cr} (mM)	10.65	15.76	10.25	13.7	9.82	13.30	11.45	13.7	6.2	15.9
Initial Cr(III)-comp.	tris	bis	tris	tris	bis	tris	bis	bis	tris	tris

Table 2. The content, in mol-%, of the mononuclear complexes relative to the total chromium(III) content. CrN_4O_2 refers to the sum of *cis-* and *trans*-Cr $en_2(OH)_2^+$ and *cis-* and *trans*-Cr $en_2(OH)(H_2O)^{2+}$; CrN_5O is the sum of Cr $en_2en^*(OH)^{2+}$ and Cr $en_2(enH)(OH)^{3+}$. The hydrolysis constants for reactions II and III are given at the bottom of the table. ( ) denote analyses repeated after one year.

Exp. No.	1	2	3	4	5	6	7	8	9	10
% CrN_4O_2	58	79	87(84)	93	92	93	93	95	100	98
% *cis*-Cr $en_2(OH)_2^+$	46.0	64.7	71.7	77.5	76.7	77.5	77.5	79.2	83.3	81.7
% CrN_5O	4.0	2.8	3.0(3.1)	1.83	2.8	2.1	3.1	1.76	1.06	1.5
% Cr $en_2en^*(OH)^{2+}$	1.42	1.73	2.06	1.63	2.49	1.89	2.81	1.59	1.04	1.47
% Cr en_3^{3+}	8.8	5.9	3.1(3.0)	0.99	1.0	1.0	1.0	1.0		
$K_{h6}/_{cis4}$ (M) [a]	100	80	112	81	88	69	66	66		
$K_{h5}/_{cis4}$ (M) [b]	14.8	19.3	16.5	17.4	12.5	14.5	9.8	17.3	36.9	25.6
$K_{h6}/_{trans4}$ (M)	Average: 16.6									
$K_{h5}/_{trans4}$ (M)	Average: 3.7									

[a] Average 83. [b] Average 18.5.

The separations on cation-exchange columns of Sephadex SP-C-25 are described in the following in more detail. The separations were made in acid as well as in basic solution on columns 1.2 cm in diameter and *ca.* 5 cm long, protected from light when necessary. During the separation solutions were cooled in ice to prevent further reaction and separations were carried out as fast as possible ($\frac{1}{2}-1$ h).

For the acid separation 5 ml of the equilibrium solution ($C_{Cr} = 0.01-0.02$ M) were diluted with water (0 °C) to 100 ml and acidified with hydrochloric acid to pH $\simeq 3$. This solution was applied to the column with 0.5 – 1 atm overpressure and eluted with sodium chloride solutions of concentrations increasing from 0.2 to 2.0 M (pH $\simeq 3$). This divided the chromium mixture into several bands of cations with increasing charge, at least as regards mononuclear complexes. The first contained *cis-* and *trans*-Cr $en_2(H_2O)_2^{3+}$ and Cr en_3^{3+}, the second Cr $en_2(enH)(H_2O)^{4+}$ (see later) and en_2 Cr$(OH)_2$-Cr en_2^{4+}. In the following 4 – 5 violet bands it was not possible to identify any mononuclear complexes. These bands are therefore assumed to contain polynuclear complexes exclusively.

For the basic separation 5 ml of the equilibrium solution were diluted with water (0 °C) to 75 ml. After application to the column it was eluted with an ammonium chloride-ammonia buffer with $[NH_3] = 0.1$ M and $[NH_4^+]$ increasing from 0.15 to 2.0 M. This divided the mixture into the following bands of mononuclear complexes with increasing charge: A first band containing *cis-* and *trans*-Cr $en_2(OH)_2^+$, a second containing Cr $en_2en^*(OH)^{2+}$ (see later), and a third one containing Cr en_3^{3+}. At the bottom of this band was a band of en_2Cr$(OH)_2$Cr en_2^{4+} mixed with another unidentified polynuclear complex. The subsequent violet bands (up to four) contained polynuclear species. In this basic separation a few per cent of the chromium remained on the column, even after elution with 2 M NH_4Cl.

From these two methods of separation and a combination of them it was possible, by chromium atomic absorption spectrophotometry, to determine the amounts of most of the different chromium species in the equilibrated solutions.

Identifications of the chromium(III) complexes. Several methods were used to identify the chromium species and to verify that the separate bands did not contain significant amounts of undetcected species. Visible spectrophotometry and analyses of the molar ratio between chromium and nitrogen after removal of nitrogen not bound to chromium were performed directly on the eluates. It was possible to obtain eluates rather concentrated with respect to chromium by applying a less concentrated eluate to a new short column after this less concentrated eluate had been diluted further 5 – 10 times. By eluting this short column with a concentrated (2 – 4 M) electrolyte we obtained eluates with $[Cr(III)] \simeq 0.1-0.2$ M. These eluates were very suitable for precipitations of salts and in this way we isolated, among others, salts of Cr en_3^{3+} and some of the polynuclear complexes (see later) which could then be further analyzed.

The eluates with high chromium concentrations were also suitable for ESR spectroscopy. Such eluates were diluted × 2 with glycerol and cooled to – 130 °C within 1 – 2 min, after which the ESR spectrum of the frozen glass was taken. Such spectra appeared to be good fingerprints which could be compared with those of known chromium(III) complexes, and they also served as a convenient means to determine the ratio between *trans-* and *cis*-Cr $en_2(H_2O)_2^{3+}$ (see Fig. 3).

Other properties, in addition to the methods mentioned above, contributed to the identification of the complexes, among them the acid-

Table 3. Relevant acid dissociation constants determined by glass electrode measurements. pK_{S2pen} for Cr $en_2(enH)(H_2O)^{4+}$ was determined on the basis of elution rates (see Fig. 5).

Acid (abbr.)	pK_{S1}	pK_{S2}	Medium	Reference
	7.52	10.16	1 M Cl^- (NaCl)	This work
enH_2^{2+}	7.49	10.17	1 M KNO_3	Poulsen & Bjerrum [23]
	7.44	10.06	1 M KCl	Pecsok & Bjerrum [14]
Cr $en_2(enH)(H_2O)^{4+}$	4.4		1 M NaCl	This work
(pen)		8.8	0.25 M NH_4Cl	This work
cis-Cr $en_2(H_2O)_2^{3+}$ (*cis*)	4.80	7.17	1 M $NaNO_3$	Woldbye [9]
trans-Cr $en_2(H_2O)_2^{3+}$ (*trans*)	4.08	7.49	1 M $NaNO_3$	Woldbye [9]

base properties (see Table 3) and the elution rates which, as mentioned above, gave an indication of the charge.

Determination of the chromium(II) content during the equilibration. This and other investigations [8,10] show that it is possible to use mercury as an inert electrode in order to measure the potential in solutions such as the equilibrium mixtures described here. With a mercury electrode it was possible to follow the potential during equilibration, and when equilibrium was obtained it was possible to measure the potential and at the same time determine the chromium(II) concentration (see Fig. 4) by one of the following methods.

The content of chromium(II), $[Cr(II)]_0$, in the steady state, where the amount of chromium(II) generated by electrolysis equals that removed by the charcoal-catalyzed oxidation to chromium(III), was determined by measuring the volume of hydrogen evolved, according to eqn. I, after stopping the electrolysis.

$[Cr(II)]_0$ was also determined by measuring the current, I, in the steady state and $(\partial E/\partial t)_0$ after stopping the electrolysis (see Fig. 4). From $E = E' + (RT/F) \ln [Cr(III)]/[Cr(II)]$, assumed to be valid under our conditions for the total concentration of Cr(III) and Cr(II), one finds by differentiation with respect to time, t, and substituting $[Cr(III)] = C_{Cr} - [Cr(II)]$:

$$\frac{\partial E}{\partial t} = -\frac{RT}{F} \frac{C_{Cr}}{[Cr(II)]\{C_{Cr} - [Cr(II)]\}} \frac{\partial [Cr(II)]}{\partial t}$$

The rate of oxidative removal of chromium(II) at $t=0$ is thus $(\partial[Cr(II)]/\partial t)_0 = -(F/RT)[Cr(II)]_0(\partial E/\partial t)_{t\to 0+}$ (when $C_{Cr} \gg [Cr(II)]$), which in the steady state equals the rate at which chromium(II) is generated by electrolysis, *i.e.* $I/(FV_{sol})$ where V_{sol} is the volume of the solution.

Thus $[Cr(II)]_0 = \dfrac{RTI}{F^2 V_{sol}(\partial E/\partial t)_0} =$

$$0.0158 \frac{I}{V_{sol} \cdot (\partial E/\partial t)_0} \text{ at } 24\ ^\circ C,$$

where I is in mA, V_{sol} in ml and $(\partial E/\partial t)_0$ in mV/min.

We have several reasons to believe that all the current is used for the reduction of chromium(III) to chromium(II) namely the good agreement between the two methods, and the

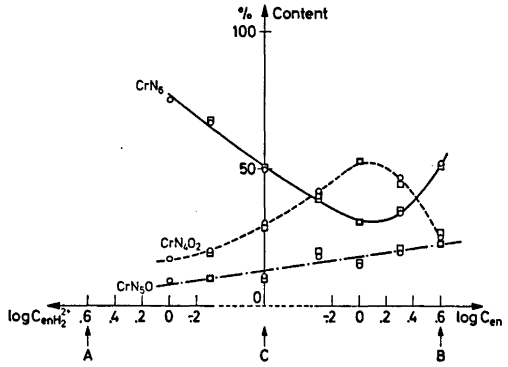

Fig. 1. The content, in mol per cent, of Cr en_3^{3+} (——— CrN_6), Cr $en_2en^*(OH)^{2+}$ + Cr $en_2enH(OH)^{3+}$ (— · — CrN_5O), and Cr $en_2(OH)_2^+$ (- - CrN_4O_2) as a function of log C_{en} and log $C_{en.2HCl} \cdot C_{Cr} = 0.05$ M and $C_{en.HCl} = 4$ M. The distance AB is set to 2.6 log units, *i.e.* the difference between the acid dissociation constants pK_{S2enH_2} and pK_{S1enH_2} found by pH-measurements in the neighbourhood of the point C referring to a solution of 4 M ethylenediamine hydrochloride. [Cr en_3]$Cl_3.3H_2O$ (□) and *trans*-[Cr en_2Cl_2]$Cl.H_2O$ (○) were used as starting materials.

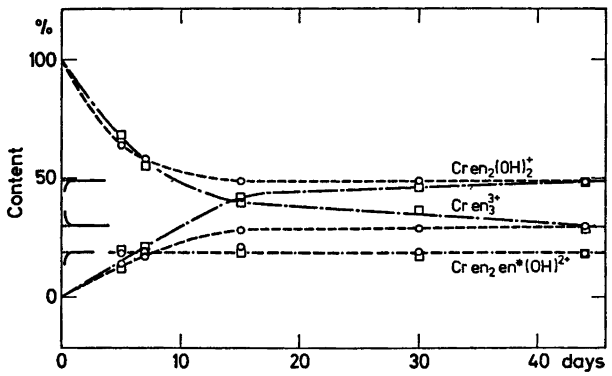

Fig. 2. The content, in mol per cent, of Cr en_3^{3+}, Cr $en_2en^*(OH)^{2+}$ and Cr $en_2(OH)_2^+$ as a function of time. $C_{Cr} = 0.05$ M, $C_{en,HCl} = 4$ M, and $C_{en} = 2$ M.
– · – □: Uncatalyzed starting with $[Cr\ en_3]Cl_3 \cdot 3H_2O$;
– – – ○: uncatalyzed starting with *trans*-$[Cr\ en_2Cl_2]Cl.H_2O$;
———: catalyzed starting with $[Cr\ en_3]Cl_3.3H_2O$;
· · ·: catalyzed starting with *trans*-$[Cr\ en_2Cl_2]Cl \cdot H_2O$.

fact that the hydrogen evolution, when starting with [Cr(II)] = 0, increases slowly until the steady state is reached, whereas no hydrogen is evolved when there is no charcoal present. Finally, addition of known amounts of chromium(II) sulfate confirmed the validity of both methods.

Chemicals and apparatus. All chemicals used were reagent grade or analyzed by us. $[Cr\ en_3]Cl_3.3H_2O$,[11] *trans*-$[Cr\ en_2Cl_2]Cl.H_2O$,[12] *cis*-$[Cr\ en_2(H_2O)_2]Br_3$,[13] and *trans*-$[Cr\ en_2(OH)(H_2O)]Br_2.H_2O$ [12] were prepared according to or analogously to the reference methods and were analyzed for Cr, N, and halogen. All analyses agreed within 1 – 2 % (relative) with the given formulae. The charcoal used was a Norit W product.

Visible spectra were taken on a Cary 14 or a Bausch and Lomb Spectronic 505 recording spectrophotometer, and ESR spectra on a Jeol JES-ME-1X. A Perkin-Elmer 403 Atomic Absorption Spectrophotometer was used for chromium analysis. All emf and pH measurements were performed with a Radiometer PHM 52, the G 202 C glass electrodes used being tested in the relevant media according to Bjerrum.[1]

RESULTS

Equilibria studied. We have studied the following hydrolysis equilibria:

$$Cr\ en_3^{3+} + en + 2\ H_2O \rightleftharpoons Cr\ en_2(OH)_2^+ + 2\ enH^+ \quad (II)$$

$$Cr\ en_2en^*OH^{2+} + H_2O \rightleftharpoons Cr\ en_2(OH)_2^+ + enH^+ \quad (III)$$

and in addition to these the *cis-trans* equilibrium:

$$trans\text{-}Cr\ en_2(OH)_2^+ \rightleftharpoons cis\text{-}Cr\ en_2(OH)_2^+$$

These are equilibria between well known species with the exception of $Cr\ en_2en^*OH^{2+}$, where en* denotes en binding as a monodentate ligand. A more detailed description of the properties of this complex, which is able to take up two protons, is given later in this section.

Fig. 1 gives the results of equilibration in 4 M ethylenediamine hydrochloride. In this medium the predominant complexes are the three mononuclear ones shown. No hydrolysis constants are given as the medium is far from constant, especially at high $[enH_2^{2+}]$ and high [en]. The ratio between *cis-* and *trans*-$Cr\ en_2(OH)_2^+$ was found to be *ca.* 10 by ESR measurements (see later).

Equilibrium was also achieved without catalysis in solutions with the same initial composition as those in Fig. 1 with log $C_{en} = 0.3$. Fig. 2 shows these catalyzed and uncatalyzed equilibrations and gives an impression of the increase of rate due to the catalyst. It is seen that the same final composition is reached independent of the choice of initial chromium compound and of whether the catalyst is used or not.

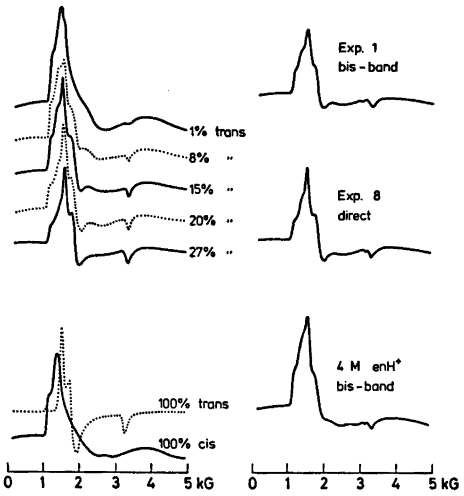

Fig. 3. First derivative ESR spectra of frozen glasses (−130 °C) at 9.3 GHz. The medium was a 1:1 mixture of glycerol and 2 M LiCl (exp. 8: 1 M NaCl) with $[H^+] \simeq 0.001 - 0.01$ M and $C_{Cr} = 0.01 - 0.1$ M.

Left: Mixtures of *cis*- and *trans*-Cr $en_2(H_2O)_2^{3+}$ from *cis*-[Cr $en_2(H_2O)_2]Br_3$ and *trans*-[Cr en_2-$(OH)(H_2O)]Br_2.H_2O$, respectively (% = mol per cent).

Right: Spectra of the acid ion-exchange bands from exp. 1 (Tables 1 and 2) and from a 4 M enH^+-exp. (Fig. 1), containing *cis*-and *trans*-Cr $en_2(H_2O)_2^{3+}$, eluted with 2 M LiCl. In the middle is shown the spectrum of the unseparated equilibrium solution from exp. 8 after addition of hydrochloric acid.

In order to determine the stability constants for chromium(III) and ethylenediamine we made a series of experiments in a constant ionic medium where the chloride concentration was kept at 1 M with sodium chloride. The compositions of the solutions in this series are given in Table 1. During the equilibration the pH varied at most 0.1 pH-unit. When analysis showed that there had been no change in the amounts of the different chromium complexes for a day or two the catalysis was stopped. The results of a final analysis of the content of Cr en_3^{3+}, CrN_5O, and CrN_4O_2 are given in Table 2.

The ratio between *cis*- and *trans*-CrN_4O_2 was determined from ESR spectra of frozen glasses of the CrN_4O_2-eluate and also of solutions Nos. 7 – 10 without preceding separation (Fig. 3). We did not succeed in separating *cis*- and *trans*-CrN_4O_2 by ion-exchange chromatography but the ESR spectra enabled us to detect even small amounts of *trans* in *cis*, as shown in Fig. 3. The content of *trans* in CrN_4O_2 was measured to be between 15 and 19 % in the series, corresponding to

$q_2 = [cis\text{-Cr } en_2(OH)_2^+]/[trans\text{-Cr } en_2(OH)_2^+] = 5$

in good agreement with Woldbye's result.[9]

We determined the acid dissociation constants of enH_2^{2+} and of Cr $en_2(enH)(H_2O)^{4+}$ in media similar to those used in exp. 1 – 10. The results are given in Table 3 together with relevant constants determined by other workers.

With $q_2 = 5$ and with the aid of Table 3 it is possible to calculate the equilibrium amounts of Cr $en_2(enH)(OH)^{3+}$ and of Cr $en_2en^*(OH)^{2+}$ comprising the CrN_5O-eluates, as well as the amounts of *cis*- and *trans*-Cr $en_2(OH)H_2O^{2+}$ and *cis*- and *trans*-Cr $en_2(OH)_2^+$ comprising the CrN_4O_2-eluates. This is done in Table 2.

From the analytical results in Tables 1 and 2 it is now possible to calculate the hydrolysis constants for reactions II and III, that is

$$K_{h6/cis_4} = \frac{[cis\text{-Cr } en_2(OH)_2^+][enH^+]}{[Cr\ en_3^{3+}][en]}$$

and the analogous $K_{h6/trans_4}$ and

$$K_{h5/cis_4} = \frac{[cis\text{-Cr } en_2(OH)_2^+][enH^+]}{[Cr\ en_2en^*(OH)^{2+}]}$$

and the analogous $K_{h5/trans_4}$.

These constants for the exp. 1 – 10 are given in Table 2.

The 3rd consecutive stability constant, K_3, for the reaction Cr $en_2(H_2O)_2^{3+} + en \rightleftharpoons Cr\ en_3^{3+} + 2H_2O$ is derived from Tables 2 and 3:

$$K_{3cis} = \frac{[Cr\ en_3^{3+}]}{[cis\text{-Cr } en_2(H_2O)_2^{3+}][en]} = \frac{K_{S1cis}\, K_{S2cis}}{K_{S2enH2}\, K_{h6/cis4}}$$

giving $K_{3cis} = 10^{6.43}$ M^{-1} and analogously $K_{3trans} = 10^{7.53}$ M^{-1}.

K_5' for the reaction

Cr $en_2(H_2O)_2^{3+} + enH^+ \rightleftharpoons$ Cr $en_2(enH)(H_2O)^{4+} + H_2O$

is also derived from Tables 2 and 3:

$$K'_{5cis} = \frac{[Cr\ en_2(enH)(H_2O)^{4+}]}{[cis\text{-Cr } en_2(H_2O)_2^{3+}][enH^+]} = \frac{K_{S1cis}\, K_{S2cis}}{K_{h5/cis4}\, K_{S1pen}\, K_{S2pen}}$$

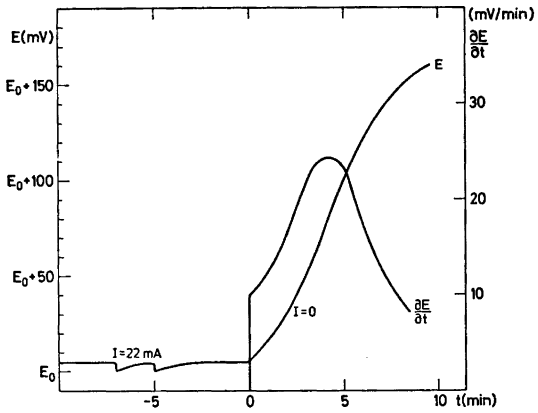

Fig. 4. The electrode potential, measured between a mercury electrode and a saturated calomel electrode, for a typical experiment as a function of time, and its first derivative.

giving $K'_{5cis} = 10^{0.0}$ M^{-1} and analogously $K'_{5trans} = 10^{1.1}$ M^{-1}.

The gross stability constant from emf-measurements. During the equilibration period the electrode potential, E, between a mercury electrode and a saturated calomel electrode was followed continuously. Typical behaviour is shown in Fig. 4. The solution was at the final state of equilibration, and at -7 and -5 min a pure mercury surface was established by addition of new mercury to the electrode. E in the steady state, E_0, was measured as the lower points at -7 and -5 min, and [Cr(II)] at $t=0$ was calculated from $(\partial E/\partial t)_0 = 10$ mV/min (see exp. section) to be 0.35 mM. Measurement of the volume of hydrogen evolved between $t=0$ and $t=10$ min (0.42 ml) gave [Cr(II)] = 0.34 mM. Table 4 shows the measurements on solutions 1 – 3 in their final state of equilibration. From these data one can estimate the stability constant β_{2cis} for the reaction $Cr(H_2O)_6^{3+} + 2en \rightleftharpoons cis\text{-}Cr\ en_2(H_2O)_2^{3+} + 4H_2O$:

$$\log \beta_{2cis} = \log \beta_2^{II} + pK_{S1cis} + pK_{S2cis} - 2pK_{S2enH_2} - (E_0 + 652)/59 + \log \frac{[cis\text{-}Cr\ en_2(OH)_2^+][enH^+]^2}{[en]^2[Cr(II)]}$$

where β_2^{II} is the gross stability constant for the uptake of 2 en by Cr^{2+}. $\log \beta_2^{II}$ has been determined to be 9.19 in 1 M KCl,[14] and nearly all the Cr(II) will be present as $Cr\ en_2^{2+}$ in exp. 1 – 10. "652" is the sum of the standard potentials of the $Cr^{2+} - Cr^{3+}$ couple and of the saturated calomel electrode (410 mV [15] and 242 mV, respectively). The pK_S values are given in Table 3. Table 4 gives the values of $\log \beta_{2cis}$ as found from the emf-measurements.

The gross stability constant for Cr^{3+} binding 3 en is then given by $\beta_3 = \beta_{2cis} K_{3cis} = 10^{19.5}$ M^{-3}.

Table 4. $\log \beta_{2cis}$ determined from measurements of [Cr(II)] and the electrode potential E_0 between a mercury and a saturated calomel electrode in solutions 1 – 3 at their final state of equilibration.

Exp. No.	$-E_0$ (mV)	[Cr(II)] (mM)	$\log \beta_{2cis}$	
	1133	0.39	13.32	
	1139	0.91	13.06	
1	1187	1.92	13.55	13.38
	1139	0.35	13.47	
	1140	0.34	13.50	
	1128	0.35	12.67	
	1145	0.47	12.83	
	1160	0.80	12.85	
2	1134	0.50	12.61	12.74
	1160	0.55	13.01	
	1135	0.68	12.50	
	1150	0.69	12.74	
	1166	0.31	12.92	
3	1175	0.37	12.99	
	1142	0.150	12.83	12.99
	1120	0.025	13.23	
		Average of exp. Nos. 1 – 3:		13.04

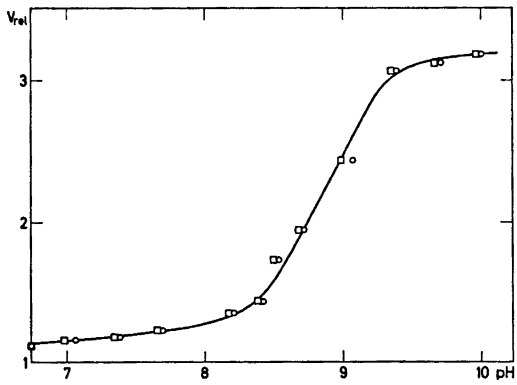

Fig. 5. The elution rate on Sephadex SP-C-25, V_{rel}, of Cr $en_2(enH)(OH)^{3+}$ + Cr $en_2en^*(OH)^{2+}$ relative to that of Cr en_3^{3+} as a function of pH. The eluting agent was 0.25 M NH_4Cl with varying concentrations of NH_3. pH was measured with a glass electrode (tested in this same medium according to Bjerrum [1]) before (○) and after (□) elution.

The Cr $en_2(enH)(H_2O)^{4+}$ ion and its deprotonated forms. This ion, believed to be an intermediate in the acid hydrolysis of Cr en^{3+} [16] and recently found as such in this laboratory,[17] is, in its two basic forms, among the mononuclear complexes present in the equilibrium solutions dealt with above. As it has not been described in the literature so far, we shall give here a few details. The acid dissociation constants of the protonated ion are given in Table 3. Owing to the lower robustness in basic solution pK_{S2} was determined from the elution rate relative to that of Cr en_3^{3+}, using 0.25 M NH_4Cl with varying concentrations of ammonia as eluent (Fig. 5), because we found that robustness of many of the complex ions is significantly higher when bound to the resin. A similar magnitude of pK_S for enH^+ bound to chromium(III) has been found for $(NH_3)_5Cr(OH)(NH_3)_4enH^{6+}$, namely 8.42 in 0.1 M KCl at 20 °C.[18]

The visible spectra of the ions are shown in Fig. 6. The visible spectrum and the ESR spectrum of Cr $en_2(enH)(H_2O)^{4+}$ are identical with those of the acid hydrolysis product of Cr en_3^{3+}.[17] Attempts to isolate salts of the ions resulted only in an amorphous, hygroscopic powder, most of which changed within hours into Cr en_3^{3+} salt. Thus, out of the two possible isomers we believe that we are dealing mainly with the one having enH^+ (en*) and H_2O (OH) *cis* to each other.

Polynuclear complexes. It appears that the mononuclear complexes quoted in Table 2 only form part of the total chromium(III) content. The ion-exchange separations showed at least five other bands, presumably all consisting of polynuclear complexes. It has not yet been possible to determine any equilibrium constants involving polynuclear complexes owing to the difficulties in separating and identifying them. Similar investigations with ammonia as ligand show [10] that equilibrium is established much more slowly, if at all, among the polynuclear than for the mononuclear complexes.

While the visible spectra of the polynuclear species isolated in solution by ion-exchange chromatography only show small differences, the ESR spectra of their frozen glasses have served as a very useful means of identification and recognition as they are often very different. The content of polynuclear species increases with increasing [Cr(III)] and increasing $[H^+]$ and two of them have been identified, *viz.* the diol, $en_2Cr(OH)_2Cr\,en_2^{4+}$, which was isolated as the iodide, and $Cr\{(OH)_2Cr\,en_2\}_3^{6+}$, the chromium analogue of the tetranuclear cobalt(III) complex

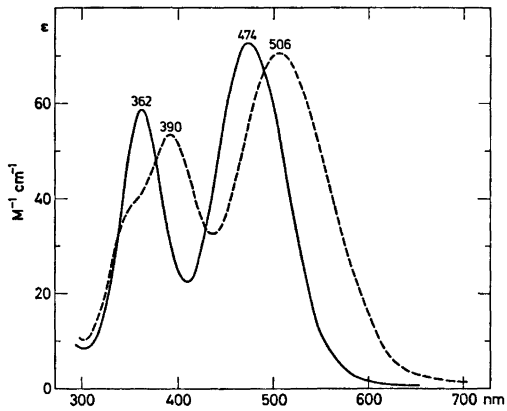

Fig. 6. The visible spectra of Cr $en_2(enH)(H_2O)^{4+}$ (———) and Cr $en_2en^*(OH)^{2+}$ (- - -) in 2 M LiCl. The former spectrum was measured directly on a 2 M LiCl eluate of Cr $en_2(enH)(H_2O)^{4+}$ from Sephadex SP-C-25, and the latter after addition of 12 M NH_3 to give $[NH_3] = 0.5$ M. Both spectra were measured twice with an interval of 5 min, and no changes were observed.

Table 5. Comparison of stability constants for Cr(III), Co(III), and Ni(II) with en.

	$\log K_1$	$\log K_2$	$\log K_3$	$\log \beta_3$	Ref.
Cr(III)			6.4 ≤ 6.2	19.5	This work Woldbye [9]
Co(III)			13.3	48.7	Bjerrum & Rasmussen [2] Woldbye [9]
Ni(II)	7.51	6.35	4.42	18.3	Poulsen & Bjerrum [23]

often referred to as Werner's brown salt.[19] We discovered this tetranuclear ion through its hydrolysis products in concentrated perchloric acid, and isolated the nitrate and iodide.[20] A more detailed report of our investigations of polynuclear chromium(III) complexes will be published later.[10]

DISCUSSION

From the results obtained we conclude that equilibrium among the mononuclear chromium(III) ethylenediamine complexes is indeed achieved by this catalytic procedure. We emphasize, in support of this conclusion, that the necessary condition is fulfilled that no further change is observed after some time. The final distribution of mononuclear complexes is independent of the initial chromium(III) compounds used and no difference in distribution is observed if the catalyst is not used at all (Fig. 2). Table 2 shows in addition a repeated analysis of the solution from exp. 3 after a year without catalyst. The differences from the first analysis are within the experimental error. Finally, the law of mass action is well obeyed, permitting the determination of the stability constants described in the previous section. The mercury electrode used for emf-measurements seems to work satisfactorily. This has been confirmed by similar investigations with, among others, ammonia and EDTA as ligands.[7,10] The high overvoltage of mercury towards hydrogen prevents the evolution of hydrogen in all these cases.

Fig. 2 illustrates the catalytic effect of Cr(II) and charcoal in 4 M ethylendiamine hydrochloride. Woldbye's investigation of the ethylenediamine system [9] shows that in a solution very similar to exp. 6 – 8 (NO_3^- instead of Cl^-) equilibrium is not reached within 50 days starting with Cr en_3^{3+}, whereas the present method requires only 3 – 5 days. The *cis-trans* equilibrium is established without catalysis within a few days according to Woldbye.[9]

Table 5 compares the equilibrium constants resulting from this investigation with other relevant constants. Chromium(III) is intermediate in stability between nickel(II) and cobalt(III), lying nearer to nickel(II). This same behaviour is observed with ammonia or EDTA as ligand.[10]

Our value of $K_3\left(\frac{1}{K_3} = \frac{1}{K_{3cis}} + \frac{1}{K_{3trans}}\right)$

agrees reasonably well with Woldbye's estimate [9] of $K_3 \leq 10^{6.2}$ (owing to a calculation error the reference quotes $K_3 \leq 10^{10.2}$), which is based on the assumption that there is less than 0.5 % Cr en_3^{3+} in his solutions. We find, using $K_3 = 10^{6.4}$, that there is 0.8 %.

If one considers the equilibria

cis-Cr $en_2(OH)(H_2O)^{2+} + en \rightleftharpoons$
Cr $en_2en^*(OH)^{2+} + H_2O$ and

cis-Cr $en_2(OH)(H_2O)^{2+} + enH^+ \rightleftharpoons$
Cr $en_2(enH)(OH)^{3+} + H_2O$

with the stability constants K_α and K_β, respectively, then the stability ratio between en* and enH^+ is $K_\alpha/K_\beta = K_{S2pen}/K_{S2enH_3} = 10^{1.4}$ (Table 3). Assuming this same ratio for en* and enH^+ binding to *cis*-Cr $en_2(H_2O)_2^{3+}$, one finds the stability constant for the reaction

cis-Cr $en_2(H_2O)_2^{3+} + en \rightleftharpoons$
Cr $en_2en^*(H_2O)^{3+} + H_2O$

$K_5'' = K'_{5cis}K_\alpha/K_\beta = 10^{1.4}$ M^{-1}, that is nearly the same magnitude as we find for chromium-

(III) and ammonia [10] ($K_5 = 10^{1.6}$ M^{-1}). Also, for silver(I) [21] and mercury(II) [22] it has been found that the stability of the complexes with ammonia and with monodentate ethylenediamine is of the same magnitude.

As mentioned above the method has been applied to other chromium(III) systems and we have, in this way, established equilibrium with, among others, ammonia, EDTA and 1,2-propanediamine.[10] However, the method seems to fail with glycine and non-amine ligands such as oxalate and thiocyanate, where we have so far been unable to build up a steady state with constant chromium(II) concentration, and equilibrium has not been obtained in these cases.

Acknowledgements. The authors are grateful to J. Bjerrum and C. E. Schäffer for valuable discussions and suggestions and to K. Jørgensen for her help in the analytical work.

REFERENCES

1. Bjerrum, J. *Metal Ammine Formation in Aqueous Solution*, Haase, Copenhagen 1941. Reprinted 1957.
2. Bjerrum, J. and Rasmussen, S. E. *Acta Chem. Scand. 6* (1952) 1265.
3. Schilow, N. and Nekrassow, B. *Z. Phys. Chem. 118* (1925) 84.
4. Bjerrum, J. *Quad. Chim. Cons. Naz. Ric. (Italy)*, Roma 1964, 3.
5. Mureinik, R. J., Feltham, A. M. and Spiro, M. *J. Chem. Soc. Dalton Trans.* (1972) 1981.
6. Schäffer, C. E. *Advances in the Chemistry of the Coordination Compounds*, MacMillan, New York 1961, p. 628.
7. Andersen, P., Bjerrum, J. and Schäffer, C. E. *Proc. of the 7th I.C.C.C., Stockholm 1962*, p. 325.
8. Schäffer, C. E. and Andersen, P. *Proc. Symp. Theory and Structure of Complex Compounds*, Wroclaw, Poland 1962, Pergamon, Oxford 1964, p. 571.
9. Woldbye, F. *Acta Chem. Scand. 12* (1958) 1079.
10. Andersen, P., Berg, T. and Jacobsen, J. *To be published.*
11. Pedersen, E. *Acta Chem. Scand. 24* (1970) 3362.
12. Glerup, J., Josephsen, J., Michelsen, K., Pedersen, E. and Schäffer, C. E. *Acta Chem. Scand. 24* (1970) 247.
13. Springborg, J. *Private Communication.*
14. Pecsok, R. L. and Bjerrum, J. *Acta Chem. Scand. 11* (1957) 1419.
15. Grube, G. and Breitinger, G. *Z. Elektrochem. 33* (1927) 112.
16. Jørgensen, E. and Bjerrum, J. *Acta Chem. Scand. 13* (1959) 2075.
17. Mønsted, L. and Mønsted, O. *Acta Chem. Scand. A 28* (1974).
18. Schwarzenbach, G. and Magyar, B. *Helv. Chim. Acta 45* (1962) 1454.
19. Werner, A. *Ber. Deut. Chem. Ges. 40* (1907) 2103.
20. Andersen, P. and Berg, T. *Chem. Commun.* (1974) 600.
21. Schwarzenbach, G., Ackermann, H., Maissen, B. and Anderegg, G. *Helv. Chim. Acta 35* (1952) 2337.
22. Bjerrum, J. and Larsen, E. *Experientia Suppl. 9* (1964) 39.
23. Poulsen, I. and Bjerrum, J. *Acta Chem. Scand. 9* (1955) 1407.

Received October 24, 1974.

Acta Chemica Scandinavica A 29 (1975) 391—394

Crystal Structures of Condensation Products of Malononitrile. V. 2,4-Diamino-3,5-dicyano-6-cyanomethylpyridine*

AGNAR AASEN, ERIK GRØNN IVERSEN and BERNT KLEWE

Department of Chemistry, University of Oslo, Oslo 3, Norway

2,4-Diamino-3,5-dicyano-6-cyanomethylpyridine, a trimer of malononitrile, crystallizes in space group $P\bar{1}$ with lattice parameters $a=4.947(1)$, $b=9.546(2)$, $c=10.675(2)$ Å, $\alpha=69.91(2)$, $\beta=80.94(2)$, $\gamma=76.36(2)°$. 770 X-ray reflections were recorded as observed on an automatic four-circle diffractometer. The structure was refined by full-matrix least squares methods ($R_w=6.0$ %, $R=5.8$ %). The molecule is essentially planar apart from the cyano group and hydrogen atoms of the $CH_2(CN)$ group; the dihedral N−C−C−(CN) angle is 53°. The hydrogen atoms of the amino groups are engaged in hydrogen bonding to cyano nitrogen atoms and the ring nitrogen atom of neighbouring molecules, the N···N contacts ranging from 3.00 to 3.16 Å.

Three trimers of malononitrile, called I, II, and III, were described by Schenk and Finken [1] in 1928 and several structures for the trimers have since then been proposed. Trimer II, obtained by the reaction of malononitrile with gaseous ammonia in benzene, has been shown independently by Atkinson and Johnson [2] and Taguchi and Matsuura [3] to be ammonium 2-cyanomethyl-1,1,3,3-tetracyanopropenide and the crystal structure of the corresponding potassium salt has been determined.[4] Trimer I was synthesized by reaction of malononitrile with sodium ethanolate. From considerations based on IR-, NMR-, and mass spectra Taguchi and Matsuura [3] and Takeshima *et al.*[5] proposed the structure to be 2,4-diamino-3,5-dicyano-6-cyanomethylpyridine, a finding which is confirmed by the present X-ray investigation. Trimer III which is obtained by pyrolysis of II, shows close chemical similarity to I. The formula 2,6-diamino-3,5-dicyano-4-cyanomethylpyridine seemed reasonable from IR- and NMR-spectra [5] and an X-ray structure investigation of this compound has been initiated in our laboratory.

Ducker and Gunter [7] have recently discussed and summarized different structures postulated earlier for the three trimers. According to Ducker and Gunter an unambiguous distinction between such complex structures cannot be made on the spectral evidence reported. By performing alternative syntheses they have shown that trimer I and III are in fact 2,4-diamino-3,5-dicyano-6-cyanomethylpyridine and 2,6-diamino-3,5-dicyano-4-cyanomethylpyridine, respectively.

EXPERIMENTAL

Trimer I was synthesized as described by Schenk and Finken [1] and crystallized from water as transparent brown platy needles. The crystals showed a curved appearance and the reflections on Weissenberg diagrams (Laue symmetry $\bar{1}$) were elongated. It was found difficult to obtain crystals suitable for an investigation of high accuracy and accordingly a rapid data collection routine was applied. Several crystals were rejected when examined in the X-ray beam. Finally, a crystal cut to a rhomb shaped plate ($0.35\times0.14\times0.05$ mm^3) and mounted in a general orientation on a Syntex $P\bar{1}$ diffractometer gave narrow peaks by ω scan for several reflections. This crystal was used for all measurements.

Intensity data were collected using graphite-monochromated Mo$K\alpha$ radiation and utilizing the ω scan technique with a scan range of 1° and a scan speed of 2° min^{-1}. Background counts were registered for a total time of 0.5 of the integration time ± 1° off the peak position. Three standard reflections were monitored after every 50 reflections and their intensities showed no decrease with time. One half of the reciprocal sphere was examined out to $2\theta=45°$. All data

* Part IV: *Acta Chem. Scand. 26* (1972) 317.

Table 1. Final atomic parameters. Fractional coordinates ($\times 10^4$), thermal parameters ($\times 10^4$), and the principal values for the r.m.s. amplitudes of vibration (Å $\times 10^2$) are listed for the heavy atoms. The temperature factor is given by $\exp-(B11h^2+B22k^2+B33l^2+B12hk+B13hl+B23kl)$. Fractional coordinates ($\times 10^3$) and isotropic temperature factors (Å^2) are listed for the hydrogen atoms. For numbering of atoms, see Fig. 1.

	x	y	z	B11(B)	B22	B33	B12	B13	B23	u1,u2,u3
C1	1864(10)	7600(5)	1142(5)	495(32)	97(8)	84(7)	-24(23)	-172(24)	-80(11)	26,19,16
C2	3339(10)	6106(5)	1786(4)	450(29)	72(7)	66(6)	-6(21)	-77(22)	-60(10)	24,18,16
C3	5185(9)	5887(5)	2715(5)	339(27)	75(7)	81(6)	-3(22)	-55(21)	-54(11)	21,20,16
C4	5348(10)	7166(5)	3048(5)	397(28)	90(7)	90(6)	-8(22)	-125(22)	-79(11)	24,18,18
C5	3734(11)	8573(5)	2421(5)	525(32)	79(8)	128(7)	5(24)	-229(27)	-95(12)	29,20,16
C6	2955(10)	4869(6)	1412(5)	386(29)	96(8)	76(6)	-54(22)	-38(21)	-47(12)	22,20,19
C7	7227(11)	7009(5)	4013(5)	440(29)	77(7)	111(7)	5(22)	-117(26)	-81(11)	25,21,16
C8	3799(14)	9951(6)	2809(7)	604(39)	111(8)	197(11)	99(29)	-384(33)	-167(15)	36,20,18
C9	933(16)	10684(6)	3160(6)	828(48)	97(8)	135(9)	24(33)	-354(34)	-93(14)	35,20,19
N1	2083(9)	8800(4)	1485(4)	600(28)	84(6)	127(6)	35(19)	-315(22)	-94(10)	31,18,17
N2	187(11)	7883(5)	186(5)	778(33)	85(7)	125(7)	17(24)	-364(25)	-84(10)	34,19,17
N3	2622(10)	3885(5)	1110(4)	788(33)	111(7)	112(6)	-185(23)	-73(21)	-101(11)	30,24,18
N4	6716(10)	4516(5)	3290(5)	487(29)	91(7)	123(7)	54(22)	-192(21)	-81(11)	28,21,17
N5	8776(10)	6829(5)	4769(5)	563(30)	148(8)	144(7)	39(23)	-287(25)	-112(12)	32,23,19
N6	-1290(13)	11260(6)	3408(6)	796(41)	150(9)	213(9)	32(29)	-164(30)	-201(14)	35,30,21
H1	-83(11)	891(6)	-20(5)	4.9(0.7)						
H2	0(11)	728(6)	-14(5)	"						
H3	662(11)	370(6)	304(5)	"						
H4	794(11)	439(6)	374(5)	"						
H5	511(14)	984(7)	355(7)	8.7(1.3)						
H6	524(14)	1069(8)	207(6)	"						

Table 2. Bond distances, bond angles, hydrogen bond distances, and hydrogen bond angles.

BOND DISTANCES (A)

N1-C1	1.348(6)	C5-N1	1.318(5)	C3-N4	1.338(6)	C8-C9	1.478(10)	N4-H3	0.92(5)
C1-C2	1.426(6)	C1-N2	1.332(6)	C4-C7	1.441(7)	C9-N6	1.143(7)	N4-H4	0.79(5)
C2-C3	1.383(6)	C2-C6	1.430(7)	C7-N5	1.143(6)	N2-H1	0.97(5)	C8-H5	1.06(6)
C3-C4	1.406(6)	C6-N3	1.144(6)	C5-C8	1.517(7)	N2-H2	0.80(6)	C8-H6	1.14(7)
C4-C5	1.391(6)								

BOND ANGLES (°)

C5-N1-C1	118.6(4)	C2-C3-C4	117.1(4)	C4-C5-C8	120.1(4)	C1-N2-H1	120(3)
N1-C1-C2	121.2(4)	C2-C3-N4	121.7(4)	C8-C5-N1	116.3(4)	C1-N2-H2	126(4)
N1-C1-N2	116.6(4)	N4-C3-C4	121.3(4)	C5-C8-C9	110.2(5)	H2-N2-H1	114(5)
N2-C1-C2	122.1(4)	C3-C4-C5	119.5(4)	C2-C6-N3	179.3(5)	C3-N4-H3	120(3)
C1-C2-C3	119.8(4)	C3-C4-C7	119.6(4)	C4-C7-N5	177.1(5)	C3-N4-H4	123(4)
C1-C2-C6	118.8(4)	C7-C4-C5	120.9(4)	C8-C9-N6	178.8(6)	H4-N4-H3	116(5)
C6-C2-C3	121.3(4)	C4-C5-N1	123.6(4)				

HYDROGEN BOND LENGTHS (A)				HYDROGEN BOND ANGLES (°)		EQUIV. POS.
N2···N1(1)	3.09	H1···N1(1)	2.15	N2-H1···N1(1)	163	1: -x,2-y,-z
N2···N3(2)	3.16	H2···N3(2)	2.42	N2-H2···N3(2)	155	2: -x,1-y,-z
N4···N6(3)	3.00	H3···N6(3)	2.24	N4-H3···N6(3)	139	3: 1+x,-1+y,z
N4···N5(4)	3.03	H4···N5(4)	2.28	N4-H4···N5(4)	160	4: 2-x,1-y,1-z

were collected within 24 h. 770 of the 1204 independent reflections were recorded as observed ($I_{count} > 2\sigma(I_{count})$). A 4 % uncertainty because of experimental fluctuations was included in the estimated standard deviations in the net intensities; the uncertainties calculated from the standard reflections were 1.1, 0.6, and 3.5 %. No absorption correction was applied.

The cell dimensions were obtained by a least squares calculation based upon the 2θ values of 24 reflections. The computations have been carried out on a CYBER 74 with programs described elsewhere.[8] Figures have been prepared by ORTEP.[9] Atomic form factors were those of Doyle and Turner [10] except for hydrogen.[11] $\lambda(MoK\alpha) = 0.71069$ Å.

CRYSTAL DATA

2,4-Diamino-3,5-dicyano-6-cyanomethylpyridine, $C_9H_6N_6$, M.W. 198.0
Space group $P\bar{1}$, $Z = 2$, $F(000) = 204$.
$a = 4.947(1)$, $b = 9.546(2)$, $c = 10.675(2)$ Å, $\alpha = 69.91(2)$, $\beta = 80.94(2)$, $\gamma = 76.36(2)°$, $U = 458.5$ Å^3, $D_x = 1.434$ g cm^{-3}, a is the needle axis.

STRUCTURE DETERMINATION AND REFINEMENT

The reflections recorded as unobserved were scaled assuming the space group to be $P\bar{1}$. The N(Z) plot and the Wilson ratio showed a hypercentric intensity distribution and the Wilson plot was far from linear. An assumed value of 3.0 Å^2 for the temperature factor was used in deriving the unitary structure factors. Application of symbolic addition procedures did only reveal molecular fragments. An essentially planar molecule was indicated by the high U-value of $(10\bar{2})$ (0.86) and from inspection of a sharpened Patterson map. The peaks close to the origin gave a good fit to the molecule, which was assumed to be the substituted pyridine as proposed from spectroscopical studies.[3,5] By moving the planar part of the molecule through the cell, and calculating the R value for 40 low-order reflections for each step, an R minimum of 42 % was obtained. The remaining cyano group was located by Fourier techniques.

Full-matrix least squares refinement of $M = \sum w\Delta F^2$ with $w = 1/\sigma^2(F_o)$ proceeded to an R_w index of 6.0 % for the observed reflections ($R = 5.8$ %). Initial positions of the hydrogen atoms were calculated from geometrical considerations; positional parameters and a common thermal parameter for the amino and the methylene hydrogen atoms, respectively, were refined. The weight analysis indicated that the estimated standard deviations for the low angle data ($\sin\theta/\lambda < 0.3$) might have been slightly underestimated.

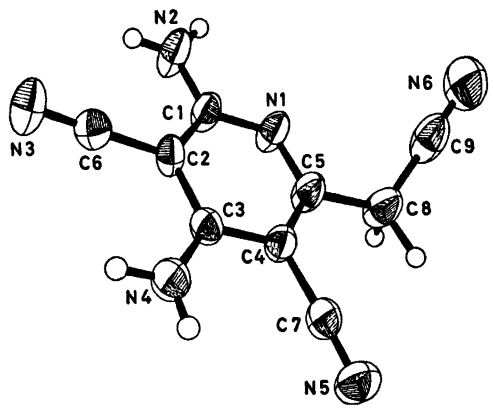

Fig. 1. A drawing of the molecule (50 % probability thermal motion ellipsoids for the heavy atoms).

The final atomic parameters together with the eigenvalues of the vibration tensors are listed in Table 1. The numbering of the atoms may be seen from Fig. 1. Bond distances and angles are given in Table 2. The standard deviations have been calculated from the correlation matrix of the last refinement cycle. The observed and calculated structure factors are available from the authors upon request.

DISCUSSION

Molecular orbital calculation of π-electron densities of 2,4-diamino-3,5-dicyanopyridine has been carried out by Lofthus, using a method [12] based on extended HMO theory. The calculated π-bond orders for the bonds within the ring starting from N1 – C1 were as follows: 0.488, 0.543, 0.548, 0.491, 0.673, and 0.571. If these values are applicable for the present molecule one would expect asymmetry within the ring. However, the accuracy of this investigation prevents a detailed discussion of the bond length values. By a conservative estimation of the standard deviations given in Table 2 all distances must be considered as normal.

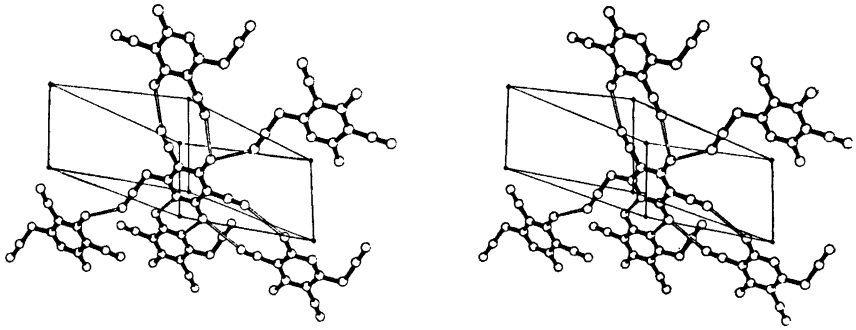

Fig. 2. One molecule and its hydrogen bonded neighbours. (The origin at the upper left corner; right handed crystal system; the *a* axis parallel to the plane of the paper.)

Table 3. Deviations (in Å) of atoms from a least squares plane through the ring. The distances from this plane to the centres of symmetry between hydrogen bonded neighbours are also given.

Atoms defining the plane		Other atoms and centres of symmetry			
C1	−0.015	N2	−0.051	C8	0.088
C2	0.028	C6	0.062	C9	1.217
C3	−0.018	N3	0.097	N6	2.078
C4	−0.005	N4	−0.049	$0,\frac{1}{2},0$	0.205
C5	0.019	C7	−0.047	0,1,0	−0.325
N1	−0.007	N5	−0.100	$1,\frac{1}{2},\frac{1}{2}$	−0.188

The crystal packing is presented in Fig. 2. All hydrogen atoms of the amino groups are engaged in hydrogen bonding (Table 2). Three pairs of hydrogen bonds between molecules related by centres of symmetry result in an infinite roughly planar arrangement of molecules in the $(10\bar{2})$ planes. The fourth hydrogen atom links translational related molecules of parallel layers by forming a bond to the nitrogen atom of the cyanomethyl group. The torsion of the cyanomethyl group is probably determined by these forces. The dihedral angle N1 – C5 – C8 – C9 is 52.9(7)°. The hydrogen bond lengths to the cyano nitrogen atoms are quite typical, as is the bond to the nitrogen atom of the ring (Refs. 13 – 16 and references therein).

The deviations of atoms from the least squares plane through the ring is presented in Table 3. The slight indication of a boat shaped ring becomes pronounced if the atom of the substituents are considered. The parallel planes are 3.46 Å apart and form an angle of 6.4° with $(10\bar{2})$ ($d_{10\bar{2}} = 3.32$ Å). The shortest *inter*-molecular contacts between heavy atoms are C···C of 3.32 Å and C···N of 3.22 Å.

REFERENCES

1. Schenk, R. and Finken, H. *Justus Liebigs Ann. Chem. 462* (1928) 267.
2. Atkinson, J. D. and Johnson, M. C. *J. Chem. Soc. C* (1969) 2182.
3. Taguchi, M. and Matsuura, K. *Yuki Gosei Kagaku Kyokai Shi 27* (1969) 1230.
4. Klewe, B. *Acta Chem. Scand. 25* (1971) 1975.
5. Takeshima, T., Yokoyama, M., Fukada, N. and Akano, M. *J. Org. Chem. 35* (1970) 2438.
6. Iversen, E. G. *Thesis*, University, Oslo 1973, p. 45.
7. Ducker, J. W. and Gunter, M. J. *Aust. J. Chem. 26* (1973) 2567.
8. Groth, P. *Acta Chem. Scand. 27* (1973) 1837.
9. Johnson, C. K. *ORTEP*, Report ORNL-3795, Oak Ridge National Laboratory, Oak Ridge 1965.
10. Doyle, P. A. and Turner, P. S. *Acta Crystallogr. A 24* (1968) 390.
11. Stewart, R. F., Davidson, E. R. and Simpson, W. T. *J. Chem. Phys. 42* (1965) 3175.
12. Lofthus, A. *Mol. Phys. 2* (1959) 367.
13. Klewe, B. *Acta Chem. Scand. 25* (1971) 1999.
14. Chieh, P. C. and Trotter, J. *J. Chem. Soc. A* (1970) 184.
15. Kvick, Å. and Backeus, M. *Acta Crystallogr. B 30* (1974) 474.
16. Larson, A. C. and Cromer, D. T. *J. Chem.* Phys. *60* (1974) 185.

Received November 20, 1974.

Acta Chemica Scandinavica A 29 (1975) 395—403

Electron-diffraction Studies of Chlorobutatriene and Chlorobutenynes. I. Molecular Structure of Gaseous Chlorobutatriene

ARNE ALMENNINGEN,[a] GRETE GUNDERSEN,[a] ASTRID BORG,[b] MATS GRANBERG[b] and FRED KARLSSON[b]

[a] Department of Chemistry, University of Oslo, Oslo 3, Norway and [b] Department of Physical Chemistry, University of Stockholm, Arrhenius Laboratory, Fack, S-104 05 Stockholm, Sweden

Chlorobutatriene has been studied by gas phase electron diffraction. An assumed force field was used to supply correction terms to be used in the r_α-refinements and amplitudes of vibration that could not be determined from the electron diffraction data. The important structural parameters obtained from r_α-refinements on a coplanar model with a linear carbon atom chain and equal terminal C=C bonds are: C=C-($sp-sp$) = 1.260(10) Å, C=C($sp-sp^2$) = 1.326(5) Å, C–Cl = 1.733(5) Å, ∠CCCl = 122.2(0.8)°; the r_a-values are given, and the parenthesized values are 2σ with systematic uncertainties included. Different assumptions regarding the CCH-angles did not cause significant changes in the other structural parameters. Determination of the difference between the two terminal C=C bonds was not possible.

Some years ago Vestin *et al.*[1] studied the kinetics and mechanisms of the aliphatic acetylene dimerization in a liquid Cu(I) catalyst. The product of this reaction is vinylacetylene, but by introducing a small flow of O_2 in the entering gas, formation of diacetylene was expected. However, they observed, as it turned out Finlay (du Pont) [2] had done previously, that instead a chlorohydrocarbon was formed:

$$2C_2H_2 + \tfrac{1}{2}O_2 + HCl \rightarrow C_4H_3Cl + H_2O$$

Finlay had suggested that the product was 2-chlorobuten-3-yne, and Vestin *et al.* confirmed this by mass spectroscopy and IR- and NMR-spectroscopy.

As an alternative route for preparation of this chlorobutenyne Vestin *et al.*[1] also studied the dehydrochlorination of 1,4-dichloro-2-butyne by alkali. While the end product of this reaction is diacetylene, Canadian [3] and Russian [4] chemists claimed to have isolated 2-chlorobuten-3-yne as an intermediate. Vestin *et al.*[1] discovered, however, that in fact three C_4H_3Cl-isomers could be isolated, neither of which being identical to the product of the dimerization reaction described above. Two of these were found to be the chlorobutenynes, *trans*- and *cis*-1-chlorobuten-3-yne, the identification being based upon mass spectroscopy, IR-spectroscopy and their relative delay in gas liquid chromatography.[1] Using mass spectroscopy and UV-, IR-, and NMR-spectroscopy the third compound was identified as chlorobutatriene.[5]

We have recently become interested in the molecular structure of the four described C_4H_3Cl compounds as well as the remaining chlorobutenyne, 4-chlorobuten-3-yne.[6] Since the molecular structures of the corresponding hydrocarbons butatriene [7] and buten-3-yne [8] are known, determination of the molecular structure of the C_4H_3Cl-compounds should reveal to which extent monochloro substitution results in significant changes of the carbon skeleton. Also determination of the carbon-chlorine bond length for the varying hybridization state of the carbon atom was of some interest.

The Vestin group initiated studies of the microwave spectra of the compounds,[9–13] and the above identifications were confirmed by assignments of the rotational spectra of the substances. Due to low natural ^{13}C-concentration, the high cost of ^{13}C enriched samples, and the many steps and very low yields of the reactions, complete structure determinations by

microwave spectroscopy was regarded as unrealistic, and only three structure dependent parameters could therefore at the best be obtained from these investigations. It was therefore decided to carry out concurrent electron diffraction studies of the compounds, the result of which we shall now report.

EXPERIMENTAL AND CALCULATION PROCEDURES

The reaction mixture from the dehydrochlorination of 1,4-dichloro-2-butyne by alkali in alcohol was fractionated by gas liquid chromatography at a temperature of 100 °C. The chromatograph column was packed with diethylhexyl sebacate (15 %) absorbed on Chromosorb. Pure chlorobutatriene as well as pure *trans*- and *cis*-1-chlorobuten-3-yne was obtained in this way. Due to extremely low stability toward polymerization, chlorobutatriene had to be stored at low temperatures (−70 °C) and hydroquinone was used as stabilizer. Electron-diffraction photographs were made in the Oslo Apparatus [14] using 48 cm and 28 cm nozzle-to-plate distances. In order to reach a sufficient vapour pressure the sample reservoir was maintained at about −10 °C during the experiment. Simultaneous polymerization was then unavoidable and substantial loss of sample was experienced. Two plates of good quality for the long camera distance and four for the shorter distance were obtained and used in the structure determination. The electron wavelength was 0.06464 Å as calibrated against the diffraction patterns of gaseous benzene.[15]

The photographic plates were analyzed and the data reduced in routine fashion [16] to yield the experimental intensity and radial distribution curves shown in Figs. 1 and 2, respectively. The background corrections were carried out on the individual levelled intensity curves and the resulting curves were transformed to the modified form. The modification function $s/|f'|_{C}|f'|_{Cl}$ was applied. The modified electron scattering amplitudes, $|f'|_i$, and the phase factors, η_i, were computed for 35 kV electrons by the partial wave method [17] based upon analytical HF potentials for the C- and Cl-atoms [18] and using the best electron density of bonded hydrogen for H.[19] The deduction of trial models was based upon interpretation of the radial distribution curve, while the structure refinement was carried out by the method of least squares based upon the modified intensity data. The procedure involves the fitting of theoretical curves simultaneously to the two experimental ones by adjustments of geometrical and vibrational parameters and two separate scale factors. To account for correlation among the data [20] off-diagonal elements were included in the weight matrix. The standard deviations thus obtained from the least squares refinement, σ_{LS}, should be corrected for systematic uncertainties in the distance parameters, $\sigma = (\sigma_{LS}^2 + (0.001\ r)^2)^{\frac{1}{2}}$.

Closely spaced distances, large number of vibrational parameters, and neglect of shrinkage effects often make the least-squares results ambiguous. However, a modified [21] program by Gwinn,[22] computes root-mean-square amplitudes of vibration (l-values) and perpendicular amplitude correction coefficients (K-values) in addition to vibrational frequencies, from assumed force fields. This provides an important supplement to the electron diffraction investigations, as l-values may be kept fixed at calculated values, and introduction of the correction term $D = l^2/r - K$, in the distance parameters ($r_\alpha = r_a + D$) allows for refinements on a geometrically consistent model (r_α), the problem of shrinkage effects being accounted for.[21] Even when observed fundamentals are lacking, such calculations by adopting force constants from similar molecules, have proven to be of great value as the l-values and to some extent the K-values, are not too sensitive to the force field chosen. Also, the knowledge of the r_α rather than the r_a-values makes it possible to calculate moments of inertia which are compatible with those obtained from microwave investigations when a similar force field is used to transform r_0 into r_z-values.[10]

Table 1. Force field for chlorobutatriene, C_4H_3Cl[a].

$K_1 = K_2 = 9.4$	$K_{34} = K_{35} = 0.56$	$\varrho_4^{35} = \varrho_5^{34} = \varrho_6^{17} = 0.20$
$K_2 = 10.1$	$K_{16} = 0.50$	$\varrho_7^{16} = 0.30$
$K_4 = K_5 = 5.5$	$K_{17} = 0.85$	$\chi_{16}^{43} = \chi_{17}^{53} = 0.08$
$K_6 = 5.6$	$K_{45} = 0.25$	$\chi_{17}^{43} = \chi_{16}^{53} = 0.07$
$K_7 = 3.8$	$K_{67} = 0.40$	
	$K_{12} = K_{23} = 0.35$[b]	

[a] For numbering of the bonds, see Fig. 3. The meaning of the symbols:[21] K_i, stretching of bond i; K_{ij}, bending of angle between bonds i and j; ϱ_k^{ij}, bending of bond k out of ij-plane; χ_{kl}^{ij}, torsion between the ij- and kl-planes. The force constants are given in md/Å and md Å/(rad)^2. [b] Identical force constants for bending in plane and out of plane are assumed.

Table 2. Refinement conditions for chlorobutatriene.

Curve (camera dist.), cm	48	28
Data range		
s_{min}	2.25	6.00
s_{max}	15.00	30.00
Data interval (Δs)	0.125	0.25
Constants of the weight scheme [16,20]		
s_1	6.00	6.00
s_2	15.00	22.00
w_1	0.05	0.05
w_2	0.01	0.02
p_2	−0.64	−0.60
p_3	0.146	0.125
w	1.0	1.0

CALCULATIONS AND REFINEMENTS

Restricting all the atoms to one plane and adopting a linear carbon chain, the molecule is described by eight geometrical parameters when all the CH-bond distances are assumed equal and when $\angle CCH_5 = \angle CCH_6$. The parameters used were: r_{CH}, $r_{C_3C_4}$, $r_{C_1C_2}$, $\Delta r_t = r_{C_1C_2} - r_{C_3C_4}$, r_{CCl}, $\angle CCH_5 = \angle CCH_6$, $\angle CCH_7$, and $\angle CCCl$. See Fig. 3 for the numbering of the atoms.

Taking support in force constants from similar molecules the force field given in Table 1 was designed for chlorobutatriene, and the resulting *l*- and *D*-values are given in Table 3.

Table 3. Computed *D*- and *l*-values, and r_a-structure for chlorobutatriene.[a]

Parameters [b]		*D*-values	*l*-values	r_a-structure [c]
C−H	4,5	−0.0194	0.074	
	4,6	−0.0226	0.074	1.096(10)
	1,7	−0.0131	0.074	
C=C	2,3	−0.0047	0.039_8	1.262(4)
	1,2	−0.0053	0.040_4	1.326(2)
	3,4	−0.0116	0.040_5	
C−Cl	1,8	−0.0033	0.047	1.734(2)
C···C	1,3	−0.0072	0.048	2.588(3)
	2,4	−0.0086	0.048	
	1,4	−0.0020	0.054	3.914(3)
C···Cl	2,8	−0.0035	0.066	2.676(3)
	3,8	+0.0005	0.096	3.793(4)
	4,8	+0.0028	0.128	5.041(5)
Cl···H	7,8	−0.0068	0.106	2.424(9)
	5,8	+0.0062	0.235	5.436(7)
	6,8	−0.0027	0.130	5.918(10)
C···H	2,7	−0.0121	0.096	
	3,5	−0.0187	0.097	2.127(8)
	3,6	−0.0246	0.097	
	3,7	−0.0046	0.113	
	2,5	−0.0123	0.114	3.309(9)
	2,6	−0.0172	0.114	
	4,7	−0.0004	0.129	
	1,5	−0.0042	0.130	4.597(8)
	1,6	−0.0060	0.130	
H···H	5,6	−0.0305	0.124	1.850(17)
	7,6	+0.0015	0.216	5.092(12)
	7,5	−0.0046	0.145	5.417(12)
$\angle CCH_5 = \angle CCH_6$		−	−	[1.225]
$\angle CCH_7$		−	−	[122.5]
$\angle CCCl$		−	−	121.5(0.3)
R_W[d] (%)		−	−	8.6

[a] Correction terms (*D*-values), amplitudes (*l*-values) and distances (r_a) in Å; angles in degrees. The r_a-structure gives the result of r_a-refinement (no *D*-value correction) using the calculated *l*-values. Quantities in brackets are assumed values. [b,c,d] See corresponding comments under Table 4.

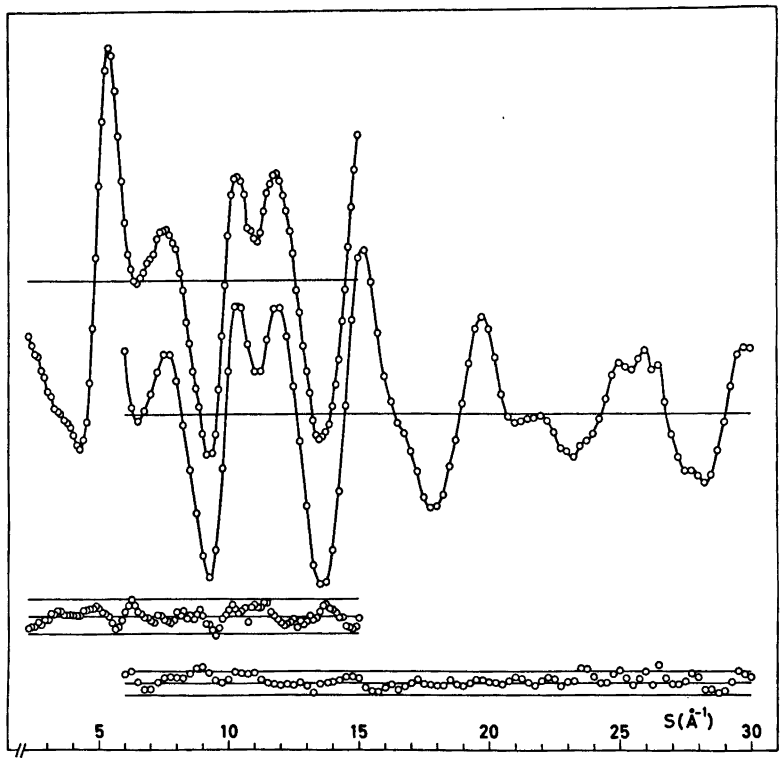

Fig. 1. Experimental intensity data for chlorobutatriene from the 48 cm ($\Delta s = 0.125$ Å^{-1}) and 28 cm ($\Delta s = 0.25$ Å^{-1}) camera distances, and the corresponding difference between the experimental intensities and the theoretical ones computed according to the parameter values of model IV (Table 4). The full lines given along with the difference points indicate the estimated uncertainties (three standard deviations) of the experimental intensity points.

The calculation was carried out using coordinates consistent with the r_a-model also given in Table 3. Only a diagonal force field was used since the designing of a more sophisticated force field was, in the absence of observed fundamentals, judged meaningless. The calculated l-values for the distance types that also occur in butatriene are in fair agreement with those calculated for this molecule.[24]

The interpretation of the main features of the radial distribution curve was straight forward as indicated by the approximate positions of the important interatomic distances (*cf.* Table 3) shown in Fig. 2.

Least squares refinements of the model were carried out under conditions given in Table 2.

Comparison of the r_a- and r_α-structure for the molecule was carried out for $\Delta r_t = 0$ and $\angle CCH_5 = \angle CCH_6 = \angle CCH_7 = 122.5°$. The results of r_a-refinements using the calculated l-values are given in Table 3, while model I in Table 4 is the result of the corresponding r_α-refinement where the D-values are used to obtain a geometrically consistent model. The results of further r_α-refinements on models where $\Delta r_t = 0$ are also given in Table 4, where quantities in brackets are assumed values and indicate different restrictions on the vibrational parameters and the CCH angles. The goodness of the least-squares fit for the four models of Table 4 is demonstrated by the agreement-factors given in the table and by the difference between experimental and theoretical radial distribution curves shown in Fig. 2. The correlation matrix for the less restricted model (IV) is given in Table 5, and the corresponding differences in observed and calculated intensity points are shown in Fig. 1.

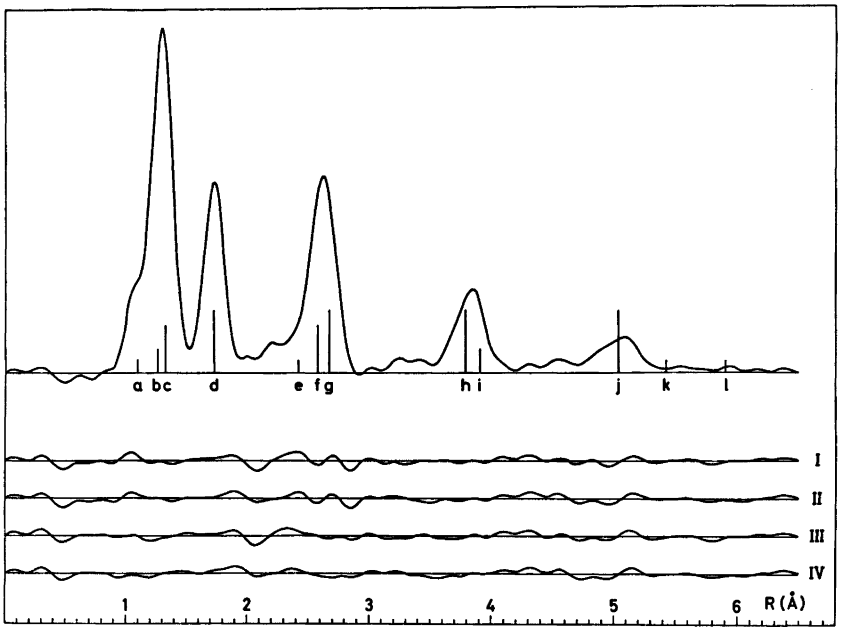

Fig. 2. Experimental radial distribution curve for chlorobutatriene calculated for the artificial damping constant $k = 0.0015$ Å^2. The approximate positions of the important interatomic distances are indicated: a, C−H; b, C=C (central); c, C=C (terminal); d, C−Cl; e, Cl···H_7; f, C_1···C_3; g, C_2···Cl; h, C_3···Cl; i, C_1···C_4; j, C_4···Cl; k, Cl···H_5; l, Cl···H_6. The differences between the experimental and theoretical radial distribution curves are shown for models I−IV, Table 4.

The amplitudes of vibration for the group of C=C distances could not be determined and they were kept at the calculated values after checking that assignments to smaller or larger values did not improve the least-squares fit. In particular it should be mentioned than in order to obtain a $sp-sp^2/sp-sp$ bond distance splitting comparable to the one found in butatriene the amplitudes had to be increased by about 0.007 Å.

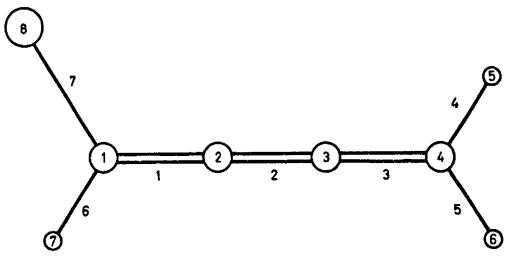

Fig. 3. Numbering of the atoms and bonds in chlorobutatriene, C_4H_3Cl.

Chlorine substitution is known to cause a slight lengthening of the C=C bond in ethylenes.[25-27] We could, however, not determine the difference between the two terminal bonds (Δr_t) in chlorobutatriene. Introduction of Δr_t equal to small positive values (0.01, 0.02 Å) made the least-squares fit poorer while negative values improved it. Refinements of this parameter resulted in one $sp-sp^2$ double bond longer than the sp^2-sp^2 double bond in ethylene ($\Delta r_t < -0.04$ Å), but this did not cause significant changes in the central C=C bond length nor in the CCH angles.

Finally, models with non-linear carbon chains were considered. Two models with *cis*- and two with *trans*-configuration were tested, neither of which improved the least-squares fit nor refined to models significantly different from the linear ones.

The r_a-values given for the four models in Table 4 were transformed to r_α-values, using the D-correction terms of Table 3. The corresponding moments of inertia, I_a, I_b, and I_c,

Table 4. Important parameter values and corresponding moments of inertia for chlorobutatriene.[a]

Parameters [b]		Model I r_a[c]	l[c]	Model II r_a[g]	l[c]	Model III r_a[g]	l[c]	Model IV r_a[g]	l[c]
C–H		1.106(10)	[0.074]	1.099(11)	[0.074]	1.089(9)	0.067(9)	1.082(10)	0.064(9)
$C_2=C_3$		1.268(4)	[0.039_3]	1.267(4)	[0.039_3]	1.263(5)	[0.039_3]	1.260(5)	[0.039_3]
$C_1=C_2$, $C_3=C_4$		1.327(2)	{[0.040_4] [0.040_5]}	1.327(2)	{[0.040_4] [0.040_5]}	1.326(2)	{[0.040_4] [0.040_5]}	1.326(2)	{[0.040_4] [0.040_5]}
C–Cl		1.734(2)	[0.047]	1.734(2)	[0.047]	1.733(2)	0.048(3)	1.733(2)	0.050(3)
C···C	1,3; 2,4	2.587(3)	[0.048]	2.586(3)	[0.048]	2.581(2)	0.058(6)	2.578(4)	0.052(7)
	1,4	3.902(3)	[0.054]	3.900(3)	[0.054]	3.895(4)	0.053(8)	3.892(5)	0.056(8)
C···Cl	2,8	2.679(3)	[0.066]	2.681(3)	[0.066]	2.676(5)	0.057(5)	2.682(4)	0.053(6)
	3,8	3.793(4)	[0.096]	3.796(5)	[0.096]	3.786(5)	0.107(7)	3.792(5)	0.106(7)
	4,8	5.029(5)	[0.128]	5.033(5)	[0.128]	5.021(4)	0.146(9)	5.028(6)	0.140(8)
Cl···H	7,8	2.420(9)	[0.106]	2.455(32)	[0.106]	2.408(10)	[0.106]	2.433(33)	[0.106]
	5,8	5.419(7)	[0.235]	5.592(47)	[0.235]	5.402(8)	[0.235]	5.580(47)	[0.235]
	6,8	5.900(10)	[0.130]	5.996(26)	[0.130]	5.878(10)	[0.130]	5.977(26)	[0.130]
$\angle CCH_5 = \angle CCH_6$		[122.5]		133.2(3.1)		[122.5]		133.4(3.0)	
$\angle CCH_7$		[122.5]		119.4(3.0)		[122.5]		119.5(2.6)	
$\angle CCCl$		121.9(0.3)		122.1(0.3)		121.8(0.4)		122.2(0.4)	
R_W[d] (%)		8.44		8.17		7.82		7.70	
I_a[e](−)[10]		20.6		20.2		20.5		20.1	
I_b (326.01)		324.1		326.8		322.9		325.8	
I_c (346.20)		344.8		347.0		343.4		345.8	

[a] Results of r_α-refinements (the distances given are r_a-values), where Δr for the terminal C=C distances is zero. Quantities in brackets are assumed values and the brackets indicate the different restrictions on the vibrational parameters and the CCH angles in Models I–IV. Distances, r_a, amplitudes, l, in Å; angles in degrees; moment of inertia, I, in u Å^2. [b] See Fig. 3 for numbering of the atoms. [c] Parenthesized values are standard deviations obtained from the least-squares refinement (σ_{LS}) and they refer to the last digit given. For the distance parameters they should be corrected for systematic uncertainties according to $\sigma=(\sigma_{LS}{}^2+(0.001\ r)^2)^{\frac{1}{2}}$. [d] Agreement factor $R_W=[\sum w_i \Delta_i{}^2/\sum w_i I_i{}^2(\text{obs})]^{\frac{1}{2}}$ where $\Delta_i = I_i(\text{obs})-I_i(\text{th})$. [e] Moments of inertia (r_α-values); parenthesized values are microwave results (r_z-values). See text for estimates of uncertainties.

Table 5. Correlation matrix for parameters of chlorobutatriene (Model IV).

$r_{C_1C_2}$	$r_{C_2C_3}$	r_{CH}	$\angle CCH_5$	r_{C-Cl}	$\angle CCCl$	$\angle CCH_7$	l_{CH}	$l_{C_1C_2}$	$l_{C_1C_4}$	l_{C_4Cl}	l_{C_3Cl}	l_{C_1Cl}	l_{C-Cl}	Scale Long	Middle
1.0															
−0.49	1.0														
−0.08	0.58	1.0													
−0.02	−0.13	−0.18	1.0												
0.02	−0.02	0.06	−0.11	1.0											
−0.25	−0.28	−0.19	0.37	−0.40	1.0										
0.03	−0.26	−0.26	−0.27	0.18	−0.13	1.0									
0.17	0.07	0.16	−0.06	−0.02	−0.10	−0.08	1.0								
0.09	0.48	0.22	−0.25	−0.06	−0.65	−0.16	0.06	1.0							
−0.01	−0.05	−0.07	0.09	−0.05	0.30	−0.03	−0.00	−0.19	1.0						
0.02	−0.06	−0.10	0.01	−0.01	0.07	−0.10	−0.02	−0.01	0.04	1.0					
−0.09	−0.39	−0.38	−0.08	0.00	0.02	0.17	−0.12	−0.18	0.05	0.07	1.0				
0.13	0.50	0.26	−0.22	−0.04	−0.56	−0.13	0.12	0.77	−0.10	−0.01	−0.24	1.0			
0.17	−0.31	−0.26	0.05	−0.02	0.10	0.16	−0.05	−0.10	0.07	0.03	0.17	−0.05	1.0		
0.20	−0.41	−0.39	−0.06	−0.12	0.06	0.18	−0.17	0.06	0.12	0.09	0.31	0.04	0.35	1.0	
0.45	−0.59	−0.44	0.17	−0.08	0.13	0.14	−0.07	−0.07	0.14	0.07	0.28	−0.01	0.47	0.43	1.0

were calculated using a program written by H. Møllendal. The results are given in Table 4 along with the values calculated from microwave data.[10] The program did not estimate the standard deviations. However, a change of 0.1 % for all the distance parameters (systematic uncertainty) resulted in about 0.2 % changes in the moments of inertia, while addition of $\sigma_{L,S}$ to the geometrical parameters caused changes of 0.1 – 0.3, 0.6 – 1.1, and 0.6 – 1.1 %. Models with Δr_t about – 0.04 Å gave I_b and I_c values 0.3 – 0.4 % higher than the corresponding $\Delta r_t = 0$ models of Table 4.

DISCUSSION

The agreement-factors given in Table 4 and the difference curves shown in Figs. 1 and 2 demonstrate that the four models are in fair agreement with the experimental data. The refined amplitudes agree within two standard deviations with those calculated from the assumed force field.

The values obtained for the important structural parameters ($C_1 = C_2$, $C_2 = C_3$, and C – Cl bond distances, and $\angle$CCCl) do not differ significantly in the four models given in Table 4, although there is a trend towards a somewhat shorter central C = C bond in the models where the amplitudes are refined. Model IV is chosen to represent the final results of this investigation. The CCH-angles are unreasonable, but if one choses not to believe in these, the other structural parameters would not be different (model III). It shall be mentioned that similar problems with the determination of the CCH-angles and the fit in the 2.0 – 2.5 Å region appear to have been encountered in the electron diffraction investigations of chloro-[27] and *cis*-1,2-dichloro-ethylene.[26]

It was hoped that the moments of inertia obtained from the microwave investigation [10] would supply the additional information needed to make a clear choice between different models obtained from the electron diffraction study. However, the I_b- and I_c-values obtained from the electron diffraction data are probably associated with uncertainty limits of about 1 %. Therefore, although comparisons with the microwave results tend to favour models which gave the better least-squares fit, but which were considered unacceptable (unreasonable CCH angles and $\Delta r_t = -0.04$ Å), this support is not significant and it will not reverse our previous judgements.

The carbon chlorine bond which is adjacent to a $sp^2 - sp$ double bond, is found to be 1.733(5) Å which is within the range usually found for C(sp^2) – Cl bonds adjacent to $sp^2 - sp^2$ double bonds. For example, electron diffraction studies of chloro-,[27] *cis*-1,2-dichloro-,[26] and tetrachloroethylene,[25] 2,3-dichloro-,[28] and hexachloro-1,3-butadiene,[29] have given the following results: 1.728(7), 1.718(7), 1.718(3), 1.747(3), and 1.715(2) Å, respectively. The variations in the bond length could be due to small deviations from sp^2-hybridization of the carbon atom and to different amount of double bond character in the C – Cl bond. It is interesting to note that in chlorobutatriene the C···Cl non-bonded interaction across one bond angle is 2.682(4) Å, which conforms to the 2.67 – 2.70 Å values usually found for such distances.

The average carbon-carbon bond lengths in chlorobutatriene and butatriene [7] are in good agreement. The results of r_a-refinements on a linear model for butatriene gave the following parameter values: $C_1 = C_2 = 1.327$ Å, $C_2 = C_3 = 1.257$ Å, C – H = 1.083 Å and $\angle$CCH = 122.5°, while due to shrinkage effects the best values for the carbon-carbon bonds were estimated to 1.318 and 1.283 Å, respectively. This means that the chlorine substitution has not resulted in any significant change in the total length of the carbon chain. However, while the r_a-models for the two molecules also are in agreement with respect to the individual C = C bonds, this is not the case for the models where attempts to account for the shrinkage effects were made. To which extent this difference is real and caused by the chlorine substitution, or related to improper treatment of the shrinkage effect for either molecule has to be considered.

The D-values used in the r_α-refinements for chlorobutatriene were based upon an assumed force field. A complete spectroscopic investigation of chlorobutatriene upon which a rigorous normal coordinate analysis could be based would clarify the effect of this assumption. However, in our judgement, the small differences in the parameter values obtained in this investigation for corresponding r_a- (Table 3) and r_α-models (Table 4, model I) suggest that this effect would be small.

The method of D-value correction was not available when butatriene was investigated,[7] and the shrinkage problem could only be handled in a round-about manner. We feel that the differences between the parameter values of the r_a-model and those cited as the final results are larger than usually encountered. A reanalysis of the electron diffraction data for butatriene, utilizing the D-value correction method and the results of a new normal coordinate analysis now available,[24] is therefore planned by one of us (G.G.) in cooperation with the earlier investigators.

The $sp-sp^2$ double bonds in chlorobutatriene and in butatriene are both longer than the corresponding bond in allene [1.312(1) Å].[30] A similar trend is observed for the terminal $sp-sp$ triple bonds in diacetylene [1.218(1) Å][31] as compared to acetylene. At the first sight the short $sp-sp$ double bond found in chlorobutatriene was surprising. However, we feel that more information about such bonds is needed before a possible effect from the substituted chlorine atom should be discussed. It was found to be beyond the capability of the method to determine a possible difference between the two terminal double bonds in chlorobutatriene. The attempts to refine the Δr_t parameter, however, indicated that abnormal bonding conditions might be present. This suggests that also further studies on the bonding in chlorobutatriene would be worthwhile.

Acknowledgement. We are grateful to Professor Otto Bastiansen and Professor Ragnar Vestin for their stimulating interest in this project. We wish to express our gratitude to Dr. Hans M. Seip for helpful discussions and suggestions regarding the manuscript.

REFERENCES

1. Vestin, R., Borg, A. and Lindblom, T. *Acta Chem. Scand. 22* (1968) 687.
2. Finlay, J. B. (du Pont) *U.S. pat. 2.999.887*, 1961.
3. Georgiett, K. K. and Richard, V. *Can. J. Chem. 36* (1958) 1280.
4. Shostakovskii, M. F. and Khomenko, A. *Kh. Izv. Akad. Nauk. SSSR. Otd. Khim. Nauk.* (1958) 519; (1960) 1098.
5. Vestin, R., Borg, A. and Lindblom, T. *Acta Chem. Scand. 22* (1968) 685.
6. Granberg, M., Karlsson, F. and Vestin, R. *Acta Chem. Scand. B 28* (1974) 580.
7. Almenningen, A., Bastiansen, O. and Trætteberg, M. *Acta Chem. Scand. 15* (1961)1557.
8. Fukuyama, T., Kuchitsu, K. and Morino, Y. *Bull. Chem. Soc. Jap. 42* (1969) 379.
9. Karlsson, F., Vestin, R. and Borg, A. *Acta Chem. Scand. 26* (1972) 3394.
10. Karlsson, F., Grandberg, M. and Vestin, R. *Acta Chem. Scand. A 28* (1974) 201.
11. Karlsson, F. and Vestin, R. *Acta Chem. Scand. 27* (1973) 3033.
12. Karlsson, F., Granberg, M. and Vestin, R. *Acta Chem. Scand. A 28* (1974) 206.
13. Karlsson, F., Granberg, M. and Vestin, R. *Acta Chem. Scand. A 29* (1975) 111.
14. Bastiansen, O., Hassel, O. and Risberg, F. *Acta Chem. Scand. 9* (1955) 232.
15. Fernholt, L. and Seip, R. *Unpublished results.*
16. Andersen, B., Seip, H. M., Strand, T. G. and Stølevik, R. *Acta Chem. Scand. 23* (1969) 3224.
17. Peacher, J. L. and Wells, J. G. *J. Chem. Phys. 46* (1967) 4809.
18. Strand, T. G. and Bonham, R. A. *J. Chem. Phys. 40* (1964) 1686.
19. Stewart, R. F., Davidson, E. R. and Simpson, W. T. *J. Chem. Phys. 42* (1965) 3175.
20. Seip, H. M., Strand, T. G. and Stølevik, R. *Chem. Phys. Lett. 3* (1969) 617.
21. Stølevik, R., Seip, H. M. and Cyvin, S. *J. Chem. Phys. Lett. 15* (1972) 263.
22. Gwinn, W. D. *J. Chem. Phys. 55* (1971) 477.
23. Gribov, L. A. *Vvedenie v teoriyu i rachet kolebatel nyjkh spectrov mnogoatomnyjkh molekul*, Izdatel stvo Leningradskogo Universiteta, Leningrad 1965.
24. Cyvin, S. J. and Hagen, G. *Acta Chem. Scand. 23* (1969) 2037.
25. Strand, T. G. *Acta Chem. Scand. 21* (1967) 2111.
26. Davis, M. I. and Hanson, H. P. *J. Phys. Chem. 69* (1965) 4091.
27. Ivey, R. C. and Davis, M. I. *J. Chem. Phys. 57* (1972) 1909.
28. Gundersen, G., Hedberg, K. and Neisess, J. A. *To be published.*
29. Gundersen, G. *J. Amer. Chem. Soc. In press.*
30. Almenningen, A., Bastiansen, O. and Trætteberg, M. *Acta Chem. Scand. 13* (1959) 1699.
31. Tanimoto, M., Kuchitsu, K. and Morino, Y. *Chem. Soc. Jap. 44* (1971) 386.

Received November 29, 1974.

Acta Chemica Scandinavica A 29 (1975) 404—408

Structural Effects of Vanadium Substitution in $Mo_{17}O_{47}$

NOROBU YAMAZOE,* THOMMY EKSTRÖM and LARS KIHLBORG

Department of Inorganic Chemistry, Arrhenius Laboratory, University of Stockholm, S-104 05 Stockholm, Sweden

A crystal of the composition $(Mo_{1-x}V_x)_{17}O_{47}$, $x \approx 0.07$, prepared by thermal decomposition of $(Mo,V)_5O_{14}$, has been studied by X-ray diffraction. The structure, obtained by least squares refinement, has been compared with that of unsubstituted $Mo_{17}O_{47}$. The main change is an increased off-center displacement of the metal atoms within the polyhedra in the direction of the short c axis. About 2/3 of the vanadium is substituting in two particular sites, while the rest seems more or less statistically distributed over the remaining seven positions. A short metal-metal distance, likely to indicate a metal-metal bond, has increased only very slightly, and this leads to the conclusion that only a part of the formally available valence electrons are engaged in this bond.

$Mo_{17}O_{47}$ and Mo_5O_{14} are two molybdenum oxides which form only at rather low temperatures.[1] It has been shown that their formation temperature can be markedly increased by a partial substitution of titanium, tungsten, or vanadiumgroup metals for molybdenum.[2–5] For example, while pure $Mo_{17}O_{47}$ forms only below 560 °C and has been observed to decompose at 630 °C, a corresponding vanadium containing phase is obtained at temperatures as high as 760 °C as a product of the thermal decomposition of $(Mo,V)_5O_{14}$.[2] Even more striking stabilization effects have been reported for Mo_5O_{14}.

The crystal structures of $Mo_{17}O_{47}$[6] and Mo_5O_{14}[7] have MoO_6 octahedra and MoO_7 pentagonal bipyramids as building units, forming networks which are rather complicated in two dimensions. The MoO_7 pentagonal bipyramids share their equatorial edges with five octahedra and by connection to the corners of identical polyhedra above and below form characteristic units which have been called "pentagonal columns".[8,9] In $Mo_{17}O_{47}$ these pentagonal columns are pairwise connected by component octahedra sharing edges, with a very short metal-metal distance across the shared edge (Fig. 1).

In view of these features it was considered very interesting to learn how the substituting metal atoms are distributed and how the ternary structures have changed compared to those of the unsubstituted phases. This paper is concerned with $Mo_{17}O_{47}$ in which Mo was partly substituted by V. A similar study of $(Mo,Ta)_5O_{14}$ will be presented elsewhere.

EXPERIMENTAL

The crystal used in this study could be assumed to have a composition close to $(Mo_{0.93}V_{0.07})_{17}O_{47}$, which will be abbreviated $(Mo,V)_{17}O_{47}$ in the following. It had been prepared by thermal decomposition of a monophasic sample of $(Mo_{0.93}V_{0.07})_5O_{14}$ by heating at 780 °C for a short time and subsequently annealed for three weeks at 760 °C. The thermal treatment was done in a sealed, evacuated silica tube. The parent phase had been prepared from appropriate amounts of MoO_3, MoO_2, and V_2O_5 and its composition could be assumed the same as that of the reaction mixture since it formed as a single phase in a closed system.[2] The vanadium content was supposed to remain essentially unchanged during the decomposition since only trace amounts of a second phase, *viz.* Mo_8O_{23}, were observed in the product. A precise knowledge of the vanadium content was not essential for the present study, however.

X-Ray powder patterns were recorded by means of a Guinier-Hägg focusing camera using $CuK\alpha_1$ radiation ($\lambda = 1.54051$ Å) and KCl ($a = 6.2930$ Å) as internal standard. The lattice constants of $(Mo,V)_{17}O_{47}$ were found to be significantly different from those of the binary $Mo_{17}O_{47}$ (Table 1). The relative differences given in Table 1 are nearly the same as those observed

* On leave from Department of Applied Chemistry, Kyushu University, Fukuoka City, Japan.

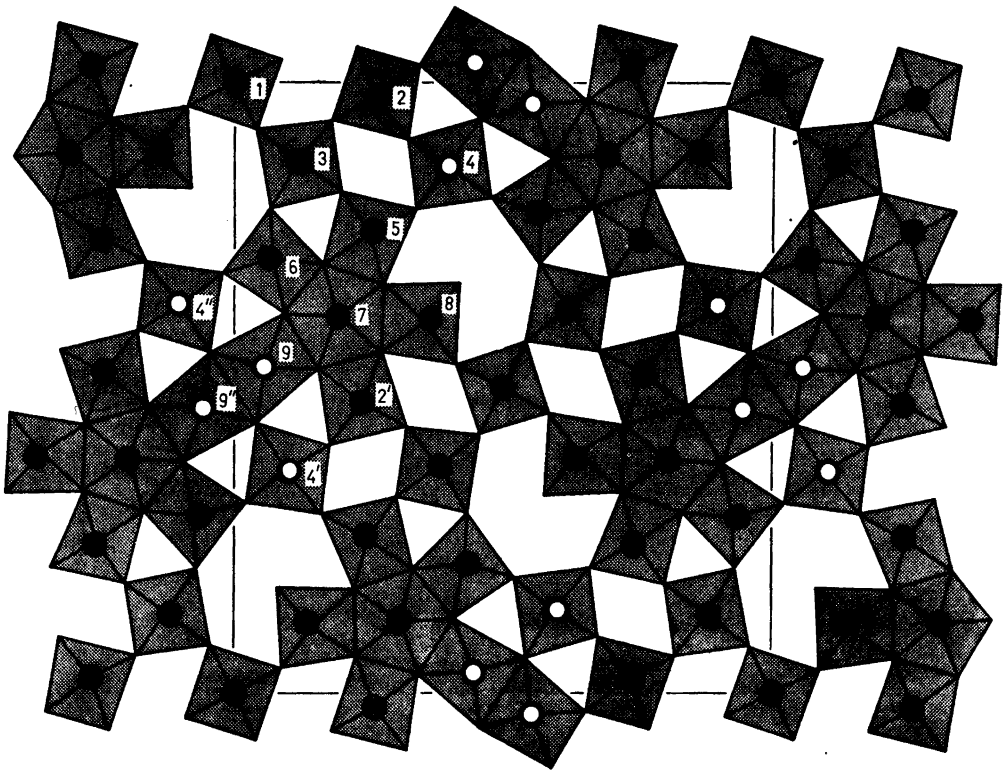

Fig. 1. The structure of $(Mo,V)_{17}O_{47}$ in projection along [001]. The unit cell is outlined; the *a* axis is vertical, *b* horizontal. MO_6 octahedra and MO_7 pentagonal bipyramids are shown with (filled and open) circles indicating the metal atom positions. The open circles indicate the positions where most of the vanadium substituates.

for $(V_{0.05}Mo_{0.95})_5O_{14}$ with respect to pure Mo_5O_{14}.

A needle-like crystal with the size 10 μm × 10 μm × 250 μm (elongated along the *c* axis) was selected for the single crystal X-ray study. The Weissenberg photographs were very similar to those of $Mo_{17}O_{47}$ and the space group was therefore assumed to be the same, *Pba2* (No. 32). X-Ray diffraction data were collected with a Siemens AED diffractometer using Mo$K\alpha$ radiation. The lattice parameters of the crystal were in good agreement with those of the powder. Out of about 2000 reflections with $\theta < 26.6°$, measured within one octant, 985 reflections had $\sigma(I)/I < 0.35$ and were used for the structure refinement. Corrections for Lorentz-polarization and absorption effects were applied. All calculations were carried out on an IBM 360/75 computer, using programs which have been described elsewhere.[10,11] The full matrix program FALFA [11] was used for the least squares refinement. The atomic scattering

Table 1. Lattice parameters of $(Mo_{0.93}V_{0.07})_{17}O_{47}$ and $Mo_{17}O_{47}$.

	$(Mo_{0.93}V_{0.07})_{17}O_{47}$	$Mo_{17}O_{47}$	Difference %
a (Å)	21.531 ± 0.004	21.615	−0.389
b (Å)	19.534 ± 0.004	19.632	−0.499
c (Å)	4.001 ± 0.001	3.9515	+1.253
Cell volume (Å^3)	1682.8	1676.8	+0.358

Table 2. Analysis of the weighting scheme used. w = weighting factor, $\Delta = |F_{obs} - F_{calc}|$.

Interval F_{obs}	Number of reflections	$\overline{w\Delta^2}$ (normalized)	Interval sin θ	Number of reflections	$\overline{w\Delta^2}$ (normalized)
0 – 82	155	1.42	0.0 – 0.214	166	0.96
82 – 88	71	1.48	0.214 – 0.269	138	0.85
88 – 96	96	1.08	0.269 – 0.308	129	0.78
96 – 106	99	0.81	0.308 – 0.339	110	0.75
106 – 118	94	0.82	0.339 – 0.365	88	0.92
118 – 134	123	0.78	0.365 – 0.388	95	0.93
134 – 153	98	0.78	0.388 – 0.408	101	1.18
153 – 180	85	0.83	0.408 – 0.427	72	1.88
180 – 229	80	0.77	0.427 – 0.494	62	1.38
> 229	84	1.11	0.444 – 0.460	24	1.01

Table 3. The refined parameters for $(Mo_{0.93}V_{0.07})_{17}O_{47}$. Space group: *Pba*2 (No. 32). Equivalent positions: x,y,z; $\bar{x},\bar{y},z$; $\frac{1}{2}-x,\frac{1}{2}+y,z$; $\frac{1}{2}+x,\frac{1}{2}-y,z$ (Mo1 and O1 in 2-fold positions). Parameters without standard deviations (within parentheses) were kept fixed.

	$x(\sigma)$	$y(\sigma)$	$z(\sigma)$	$B(\sigma)$	Occupancy factor (σ)
Mo1	0	0	0.579	0.22(15)	2 × 0.453(18)
Mo2	0.02427(16)	0.26120(23)	0.5789(32)	0.12(10)	0.921(30)
Mo3	0.12948(19)	0.11753(21)	0.4006(29)	0.26(11)	0.903(29)
Mo4	0.13558(20)	0.40039(27)	0.4117(32)	0.36(12)	0.823(28)
Mo5	0.24223(18)	0.25749(23)	0.5626(36)	0.43(11)	0.946(30)
Mo6	0.28823(18)	0.06502(23)	0.5773(34)	0.30(10)	0.929(30)
Mo7	0.38259(20)	0.19341(21)	0.4062(30)	0.09(10)	0.917(29)
Mo8	0.38568(25)	0.36643(26)	0.4096(29)	1.31(13)	0.946(32)
Mo9	0.46517(20)	0.05591(25)	0.5619(33)	0.39(12)	0.846(28)
O1	0	0	0.020(19)	1.9(11)	
O2	0.0227(16)	0.2640(21)	0.026(14)	2.0(8)	
O3	0.1286(18)	0.1219(19)	0.994(12)	1.9(8)	
O4	0.1331(14)	0.4025(18)	0.998(8)	0.7(6)	
O5	0.2459(16)	0.2571(18)	−0.010(10)	1.2(7)	
O6	0.2867(14)	0.0685(17)	−0.002(9)	0.8(6)	
O7	0.3829(17)	0.1957(19)	0.993(10)	1.4(7)	
O8	0.3879(13)	0.3584(15)	0.992(9)	0.2(6)	
O9	0.4635(14)	0.0565(18)	0.992(10)	0.8(7)	
O10	0.0746(15)	0.0447(16)	0.491(10)	0.6(6)	
O11	0.0588(14)	0.1782(15)	0.503(9)	0.4(6)	
O12	0.0875(13)	0.3215(16)	0.543(13)	0.8(6)	
O13	0.0575(18)	0.4577(21)	0.494(13)	2.2(9)	
O14	0.2037(16)	0.0672(19)	0.496(11)	1.5(7)	
O15	0.1773(16)	0.1986(19)	0.486(11)	1.5(8)	
O16	0.2062(14)	0.3396(16)	0.479(9)	0.5(6)	
O17	0.1869(19)	0.4758(22)	0.550(20)	2.9(9)	
O18	0.2950(12)	0.1692(15)	0.501(8)	0.0(5)	
O19	0.3322(13)	0.2808(17)	0.481	0.4(6)	
O20	0.3291(19)	0.4241(23)	0.465(14)	2.7(10)	
O21	0.3798(17)	0.0940(19)	0.518(11)	1.5(7)	
O22	0.4683(14)	0.1558(17)	0.499(11)	0.9(7)	
O23	0.4381(15)	0.2719(18)	0.480(11)	1.2(7)	
O24	0.4577(19)	0.4116(23)	0.496(13)	2.6(10)	

factors for neutral atoms given by Cromer and Waber [12] were used with the anomalous dispersion corrections published by Cromer.[13]

Starting from the positional parameters reported for $Mo_{17}O_{47}$ [6] the least squares refinement was carried out in several steps with successively increasing number of variables. A compound scattering curve formed from 93 % Mo and 7 % V were used for all metal positions and occupancy factors were introduced as additional variables to simulate any uneven vanadium distribution. An isotropic secondary extinction parameter was introduced and refined in the last few least squares cycles. The refinement was terminated when the shifts of the variables became less than 5 % of the corresponding standard deviations. The discrepancy index $R = \sum||F_{obs}| - |F_{calc}||/\sum|F_{obs}|$ was then 0.064. Hughes' weighting scheme was found appropriate for the refinement and a weight analysis obtained in the last cycle is given in Table 2. A list of observed and calculated structure factors may be obtained from this laboratory on request.

RESULTS

The final positional parameters and isotropic temperature factors for all atoms are listed in Table 3 together with the occupancy factors for the metal positions. The atomic coordinates are very close to the corresponding ones in $Mo_{17}O_{47}$.

The occupancy factors should reveal any deviation of the V/Mo distribution from the average composition at the particular site. The mean value of the occupancy factors is expected to come out as unity if there are no vacancies on the metal sites and if a correct value for the gross composition was used in the formation of the compound scattering factor curve. In the present case the mean value is only 0.904. Metal vacancies are not very likely for structural reasons, and it was not believed that the gross V/Mo ratio, assumed to be 0.07/0.93, was so much in error as this figure would indicate (V/Mo = 0.28/0.72). The occupancy factors are, however, strongly correlated with the scale factor (correlation coefficients ranging from −0.67 to −0.80) and are dependent on the particular scattering factor curves used for the three kinds of atoms. This latter was demonstrated by a test calculation in which the scattering curves of the ionized atoms Mo^{5+}, V^{5+} and O^{-} were used instead of those for neutral atoms. This refinement gave an average occupancy of 0.957, with only insignificant changes in the positional parameters. The deficiency of the average occupancy is thus thought to be essentially a computational artifact and for the evaluation of the vanadium distribution it seemed justified to normalize the occupancy factors on the condition that their sum (taking the site multiplicity into account) should be equal to the number of metal atoms in the unit cell. The normalized occupancy factors are listed in Table 4.

The normalized occupancy factor A for a position is related to the actual statistical vanadium content, x, at that position by the

$$A = (f_{Mo}/f_M)(1-x) + (f_V/f_M)x$$

equation where f_{MO} and f_V are the atomic scattering factors of Mo and V, respectively, and f_M is that used in the refinement and equal to $0.93\ f_{Mo} + 0.07\ f_V$. Since f_{Mo}/f_M vary only

Table 4. Some quantities calculated to metal atoms.

Metal atom	Normalized occupancy factor	Calc. content of V (%)	Asymmetry of O−*M*−O bonds along [001] $d_1 - d_2$ (Å) $(Mo,V)_{17}O_{47}$	$Mo_{17}O_{47}$
Mo 1	0.502	6 ± 7	0.48 ± .15	0.36
Mo 2	1.02	3 ± 6	0.43 ± .12	0.47
Mo 3	1.00	7 ± 6	0.77 ± .10	0.24
Mo 4	0.91	24 ± 6	0.61 ± .08	0.50
Mo 5	1.05	−2 ± 6	0.57 ± .08	0.57
Mo 6	1.03	2 ± 6	0.65 ± .08	0.64
Mo 7	1.01	4 ± 6	0.69 ± .08	0.46
Mo 8	1.05	−2 ± 6	0.69 ± .09	0.26
Mo 9	0.94	20 ± 5	0.57 ± .08	0.44
Average		6.9	0.607	0.436

slightly with sin θ/λ approximate values of x can be calculated by this equation, choosing an adequate value for sin θ/λ. This was done for sin $\theta/\lambda = 0.30$ and the resulting x values are listed in the third column of Table 4.

Although the accuracy is rather poor, the conclusion can be drawn that the larger amount of vanadium, accounting for about 2/3 of the total, is located at the two sites $M(4)$ and $M(9)$. As seen in Fig. 1 these positions are in the octahedra which lie in the middle of a pair of pentagonal columns, including the octahedra which form the bridge with the short metal-metal separation.

As mentioned above, the effects of the substitution on the crystal structure are rather small. The main changes are in the z parameters. The metal atoms form puckered layers by displacements from the centers of the polyhedra, giving rise to considerable divergence in the Mo – O bond lengths in the c direction. This puckering is more pronounced in $(Mo,V)_{17}O_{47}$ than in $Mo_{17}O_{47}$, which is reflected in the increase in the length of the c axis (Table 1). The average asymmetry $|d_n - d_{n'}|$, where d_n and $d_{n'}$ are the bond lengths $M_n - O_n$ and $M_n - O_{n'}$ approximately parallel to c, is 0.61 Å in $(Mo,V)_{17}O_{47}$ compared to 0.44 Å in $Mo_{17}O_{47}$. The values for the individual metal atoms are given in Table 4. It is seen that these values are not significantly different and, for instance, no enhanced asymmetry can be observed for the two sites with high vanadium content.

The changes in the rest of the $M - O$ bond lengths, those approximately parallel to the ab plane, are very small; the average difference compared to $Mo_{17}O_{47}$ is 0.036 Å, which is the same value as the average standard deviation. The differences seem to be of random nature and no particular pattern can be recognized.

It has been proposed [5,9] that non-bonding valence electrons destabilize structures containing pentagonal columns. Such structures will then be more stable if the extra electrons are engaged in localized bonding, indicated by short metal-metal distances, or if the number of electrons is reduced by substitution.

The formal number of extra electrons per slice, one polyhedron thick, of a pentagonal column is 4 in $Mo_{17}O_{47}$ and this number is reduced to 3.4 by the vanadium substitution. As mentioned above, the structure contains short metal-metal separations Mo(9) – Mo(9″). If the extra valence electrons are forming metal-metal bonds, one should expect that this interaction should be weaker in the vanadium substituted phase, resulting in a lengthening of the metal-metal distance. The Mo(9) – Mo(9″) distance is in fact longer, but only slightly: 2.649 ± 0.010 Å in $(Mo,V)_{17}O_{47}$ compared to 2.626 ± 0.007 Å in $Mo_{17}O_{47}$.

From the smallness of this effect it can be concluded that only part of the available valence electrons are engaged in the metal-metal interaction, and it is mainly the number of electrons not involved in this which is reduced by the substitution. In MoO_2, which has similar metal-metal pairs and where the formal number of electrons per pair is 4, the separation is only 2.5106 ± 0.0005 Å.[14] The present values, however, are closer to the corresponding distance in VO_2, 2.6191 ± 0.0004 Å,[15] with half as many electrons per pair.

Acknowledgements. This investigation forms a part of a research program supported by the Swedish Natural Science Research Council. One of us (N.Y.) acknowledges a scholarship from the Japan-Sweden Foundation, Tokyo.

REFERENCES

1. Kihlborg, L. *Ark. Kemi 21* (1963) 471.
2. Ekström, T. and Nygren, M. *Acta Chem. Scand. 26* (1972) 1827.
3. Ekström, T. and Nygren, M. *Acta Chem. Scand. 26* (1972) 1836.
4. Ekström, T. *Acta Chem. Scand. 26* (1972) 1843.
5. Ekström, T. *Mater. Res. Bull. 7* (1972) 19.
6. Kihlborg, L. *Acta Chem. Scand. 14* (1960) 1612; *17* (1963) 1485.
7. Kihlborg, L. *Ark. Kemi 21* (1963) 427.
8. Lundberg, M. *Chem. Commun. Univ. Stockholm* (1971) No. XII.
9. Ekström, T., Kihlborg, L. and Lundberg, M. *Acta Crystallogr. A 28* (1972) S57.
10. Brandt, B. G. and Nord, A. G. *Chem. Commun. Univ. Stockholm* (1970) No. V.
11. Nord, A. G. *Chem. Commun. Univ. Stockholm* (1973) No. XV.
12. Cromer, D. T. and Waber, J. T. *Acta Crystallogr. 18* (1965) 104.
13. Cromer, D. T. *Acta Crystallogr. 18* (1965) 17.
14. Brandt, B. G. and Skapski, A. C. *Acta Chem. Scand. 21* (1967) 661.
15. Longo, J. M. and Kierkegaard, P. *Acta Chem. Scand. 24* (1970) 420.

Received November 6, 1974.

Acta Chemica Scandinavica A 29 (1975) 409—413

The Crystal and Molecular Structure of the Diacetone Adduct of the Copper(II) Complex of 1-Nitroso-2-naphthol: $[Cu(C_{10}H_6NO_2)_2].2(CH_3)_2CO$

HEIKKI SAARINEN and JORMA KORVENRANTA

Department of Inorganic Chemistry, University of Helsinki, SF-00100 Helsinki 10, Finland

The crystal and molecular structure of the diacetone adduct of the copper(II) complex of 1-nitroso-2-naphthol (⇌1,2-naphthoquinone-1-oxime) has been determined from three-dimensional X-ray data. The crystals are dark brown, $P2_1/c$, with cell dimensions, $a = 8.001(5)$ Å, $b = 13.806(11)$ Å, $c = 11.012(18)$ Å, $\beta = 98.0(1)°$, and $Z = 2$. The structure was solved by the heavy atom method and refined by least-squares procedures. The final R-value, based on 1282 observed reflections, is 0.077.

The chelate rings in the complex are five-membered and the nearest positions around copper are occupied by two oxime nitrogen atoms (Cu—N, 1.988 Å) and two naphtholic oxygen atoms (Cu—O, 1.951 Å), forming an approximately square-planar configuration. The approximate octahedral arrangement around Cu is completed by two acetone oxygens at distances of 2.651 Å. The bond lengths in the complex suggest a resonance structure between bis(1-nitroso-2-naphtholato)copper(II) and bis-(1,2-naphthoquinone-1-oximato)copper(II).

1-Nitroso-2-naphthol was apparently the first organic substance found to form precipitates with metal ions.[1] Until recently, this reagent, its 2-nitroso-1-naphthol isomer, and their water-soluble sulfonic acid derivatives have been used for the determination of several metal ions, especially the microdetermination of cobalt. Even though the complexes were discovered long time ago, their structure has been repeatedly debated.

It is well known that 1,2-nitrosonaphthols (and 1,2-nitrosophenols) can tautomerise to the corresponding quinonemonoximes. On the basis of infrared data it is mostly concluded that *o*-nitrosophenols, including 1-nitroso-2-naphthol, exist in their respective oxime forms in the solid state.[2] This is supported by the X-ray studies on β-5-propoxy-*o*-quinone-2-oxime and α-5-(2′-chloroethoxy)-*o*-quinone-2-oxime.[3,4] On the other hand, absorption spectra [4] and the effect of substituents on the protolysis of the compounds [5] suggest the existence of a nitrosophenol structure in solution.

The indefinite structure of the ligand is reflected in the various interpretations given for the structure of *o*-nitrosophenol complexes. Because of the complexity of the complexes, unambiguous conclusions can hardly be drawn from the known mass spectrometric, infrared or electronic spectral, or magnetic susceptibility data. Particularly the size of the chelate ring has remained in doubt. Several authors have interpreted the infrared spectra of the copper(II) complexes of 1-nitroso-2-naphthol as indicating the presence of six-membered chelate rings (*i.e.* coordination through naphtholic oxygen and oxime oxygen atoms, structure I).[6,7] However, a recent re-examination of the published IR data by Chakravorty, led to the conclusion that the five-membered ring structure II (*i.e.* coordination through naphtholic oxygen and oxime nitrogen atoms) could satisfy the IR data equally well.[8]

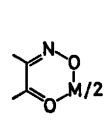

I

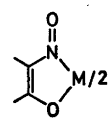

II

Table 1. Fractional atomic coordinates ($\times 10^4$) and thermal parameters [a] ($\times 10^3$). Estimated standard deviations are given in parentheses.

Atom	X/a	Y/b	Z/c	U_{11}	U_{22}	U_{33}	$2U_{12}$	$2U_{23}$	$2U_{13}$
C(1)	818(9)	−438(4)	2509(6)	35(4)	27(3)	30(3)	0(6)	5(5)	17(5)
C(2)	−335(8)	−1153(4)	1942(5)	39(4)	31(3)	27(3)	2(5)	5(5)	18(5)
C(3)	−865(9)	−1936(4)	2656(6)	53(5)	28(3)	36(4)	0(6)	7(5)	31(6)
C(4)	−234(9)	−1996(5)	3863(6)	52(5)	41(4)	41(4)	22(7)	30(6)	41(7)
C(5)	1466(10)	−1375(6)	5751(6)	47(5)	72(5)	37(4)	29(8)	15(8)	23(7)
C(6)	2563(10)	−697(6)	6348(6)	55(5)	74(5)	33(4)	28(8)	12(7)	4(7)
C(7)	3125(11)	77(6)	5693(6)	54(6)	74(5)	34(4)	34(9)	16(8)	−7(7)
C(8)	2588(10)	189(5)	4425(6)	54(5)	50(4)	34(4)	6(7)	−10(6)	−1(6)
C(9)	1454(9)	−498(5)	3811(6)	37(4)	41(4)	26(3)	12(6)	0(5)	12(5)
C(10)	930(9)	−1285(5)	4476(5)	46(5)	44(4)	23(3)	12(6)	6(6)	13(5)
C(11)	−3889(11)	1461(6)	11(8)	60(6)	55(5)	65(5)	2(8)	24(9)	39(8)
C(12)	−4770(14)	1128(11)	−1197(9)	76(8)	158(12)	59(6)	70(15)	−19(14)	−33(10)
C(13)	−4714(14)	2230(8)	680(11)	90(8)	72(6)	103(8)	44(11)	−12(13)	82(13)
N(1)	1164(7)	232(3)	1690(5)	39(4)	21(2)	31(3)	−2(4)	3(4)	19(5)
O(1)	2179(7)	914(3)	1987(4)	63(4)	36(3)	45(3)	−30(5)	5(4)	2(5)
O(2)	−924(6)	−1105(3)	788(4)	57(3)	32(2)	26(2)	−21(4)	1(4)	5(4)
O(3)	−2532(7)	1116(4)	466(5)	64(4)	73(4)	58(3)	30(6)	5(6)	7(6)
Cu	0000	0000	0000	69(1)	40(1)	33(1)	−18(1)	5(1)	12(1)

[a] The anisotropic thermal parameters are of the form exp $[-2\pi^2(h^2a^{*2}U_{11}+k^2b^{*2}U_{22}+l^2c^{*2}U_{33}+2hka^*b^*U_{12}+2klb^*c^*U_{23}+2hla^*c^*U_{13}]$.

X-Ray studies on the metal complexes of the nitrosonaphthol type are scarce. McPartlin [9] reports that the 1:1 pyridine adduct of bis(4-methyl-1-quinone-2-oximato)copper(II) complex has a square planar structure with five-membered chelate rings and ligands of predominantly quinonoid form. The crystal structure of tris(4-chloro-1-quinone-2-oximato)nickelate(II) anion, reported by Carreck *et al.*,[10] is essentially similar. A third complex of this ligand class is ferroverdin (an iron-containing pigment isolated from an unidentified species of *Streptomyces*).[11] In this complex, too, the chelate rings are five-membered, but the bond distances suggest considerable contribution from the nitrosophenol structure.

The present study of a copper(II) complex of 1-nitroso-2-naphthol has been carried out in order to obtain further information about the structure of such compounds.

EXPERIMENTAL

Crystal preparation and analysis. 1-Nitroso-2 naphthol (Merck AG, "zur Synthese", 2 mol) was dissolved in 1:1 acetic acid, after which copper nitrate solution (1 mol) was added. The precipitated bis complex was washed with water and dried in air. The crude product was first recrystallized from chloroform. Well-developed lustrous crystals were obtained, but on standing in air they soon lost their luster and disintegrated. When recrystallized from acetone, crystals containing two molecules of acetone were formed within a few days. They proved to be sufficiently stable for X-ray studies. Anal. (air-dried material): Calc. for $C_{26}H_{24}O_6N_2Cu$: C 59.59; H 4.62; O 18.32; N 5.35. Found: C 59.57; H 4.39; O 18.54; N 5.54. Thermogravimetric analysis showed that acetone was smoothly lost between 80 °C and 120 °C (weight loss 22 %, calc. 22.2 %). After the acetone had escaped, the crystals were stable to about 275 °C, at which temperature they decomposed explosively. The IR spectra of the complex (KBr pellet and Nujol mull) indicated a strong ν(C=O) stretching vibration of acetone at 1700 cm^{-1} which disappeared when the material was dried at 120 °C.

The formation of the 1:2 acetone adduct of the complex was unexpected in view of the earlier observations: it is precipitated from aqueous solution as monohydrate, forms an anhydrous 1:1 adduct with pyridine, but fails to form adducts with several other strong donors, such as methyl cyanide, triethylamine, and dimethyl sulfoxide.[12]

Crystal data. Rotation photographs and Weissenberg photographs, taken with Cu$K\alpha$ radiation (1.5418 Å), show that the crystals are monoclinic. The space group, from systematic absences, is $P2_1/c$.

Unit cell dimensions were found from powder photographs taken with a Hägg-Guinier camera,

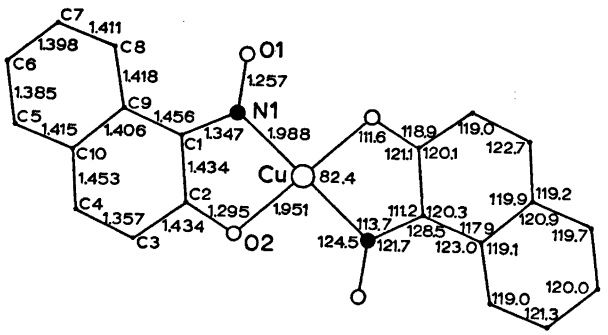

Fig. 1. Schematic representation of the complex showing bond lengths and angles. The e.s.d.'s in bond lengths are: Cu–O, 0.004 Å; Cu–N, 0.005 Å; N–O, 0.007 Å; C–O, 0.008 Å; C–N, 0.008 Å; C–C, 0.009–0.012 Å. The e.s.d.'s in angles are in the range 0.2–0.7°.

using Cu$K\alpha$ radiation with calcium fluoride ($a = 5.4630$ Å) as internal standard. There are two formula units in the cell; the calculated density is 1.44 g cm^{-3}, and the density found by flotation is 1.4 g cm^{-3}. The crystal data (calculated by least-squares procedures) are:

$a = 8.001(5)$ Å	$V = 1204.6$ Å^3
$b = 13.806(11)$ Å	FW = 524.03
$c = 11.012(18)$ Å	$Z = 2$
$\beta = 98.0(1)°$	Space group $P2_1/c$

Intensity data. A crystal with approximate dimensions 0.2 × 0.2 × 0.3 mm was used for the intensity measurements. Ni-filtered Cu radiation (Cu$K\alpha$, $\lambda = 1.5418$ Å) and a Stoe-Güttinger diffractometer equipped with a scintillation counter and pulse height analyser were used to measure the intensities of 1807 reflections from the levels $0kl - 6kl$. The background-peak-background technique was used. Only 1282 reflections had intensities greater than twice the standard deviations calculated from counting statistics. The data were corrected for Lorentz and polarization effects. No correction for absorption was applied (μ(Cu$K\alpha$) = 16.9 cm^{-1}).

Structure determination. The structure was solved by the heavy atom method. The copper atom was placed at the origin and the approximate positions of the naphthalene carbons were found from a three-dimensional Patterson map. Three-dimensional Fourier syntheses were used to locate the other nonhydrogen atoms. The atomic scattering factors for Cu^{2+}, O, N, and C were taken from International Tables for X-Ray Crystallography.[13]

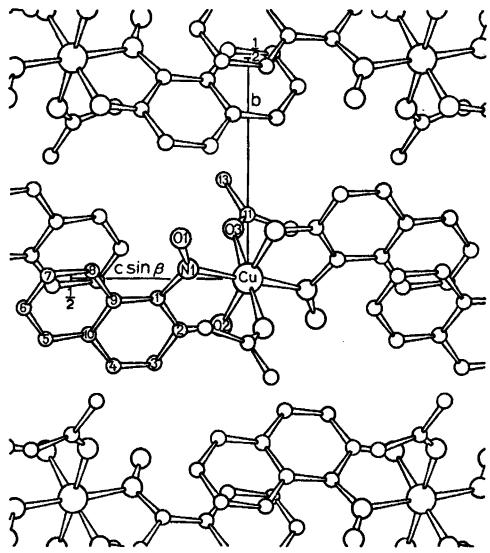

Fig. 2. Projection of the structure along the *a* axis.

Table 2. The bond lengths (Å) and angles (°) of the acetone molecule with their standard deviations.

C(11)–C(12)	1.488(15)	C(11)–O(3)–Cu	143.4(6)
C(11)–C(13)	1.497(14)	C(12)–C(11)–C(13)	118.2(9)
C(11)–O(3)	1.227(10)	C(12)–C(11)–O(3)	121.8(8)
Cu–O(3)	2.651(6)	C(13 –C(11)–O(3)	120.0(8)
		N(1)–Cu–O(3)	89.8(2)
		O(2)–Cu–O(3)	91.2(2)

Table 3. The least-squares plane defined by the naphthalene carbon ring. Deviations (Å) of different atoms from the plane are given. X', Y', and Z' are orthogonal axes related to X, Y, and Z by $X'=X+Z\cos\beta$, $Y'=Y$, and $Z'=Z\sin\beta$.

Plane C(1)–C(10): $-0.8121X'+0.5454Y'+0.2074Z'-0.0202=0$

Atom	Distance	Atom	Distance	Atom	Distance	Atom	Distance
C(1)	−0.002	C(5)	0.008	C(9)	−0.004	N(1)	−0.013
C(2)	0.010	C(6)	0.016	C(10)	−0.023	O(1)	−0.051
C(3)	0.015	C(7)	0.003	Cu	0.020	O(2)	0.024
C(4)	−0.016	C(8)	−0.008				

The refinement of the structure was carried out by block-diagonal least-squares procedures in which the function $\sum w(|F_o|-|F_c|)^2$ was minimized. After 7 cycles of refinement with isotropic thermal parameters, the R-index $\sum||F_o|-|F_c||/\sum|F_o|$ was 0.12. The refinement was then continued with anisotropic thermal parameters, and the final R-value is 0.077 for 1282 reflections.

The final atomic coordinates and thermal parameters together with their estimated standard deviations are given in Table 1. A list of the observed and calculated structure factors is obtainable on request from the authors. All calculations were carried out on an Elliott 803 B computer using programmes of Daly, Stephens, and Wheatley.[14]

RESULTS AND DISCUSSION

The bond lengths and bond angles of the complex are presented in Fig. 1, and the dimensions of the acetone molecule are given in Table 2. A projection of the structure along the *a* axis is shown in Fig. 2. It can be seen, that the Cu^{2+} ion is bonded to the ligand anions through the oxime nitrogen and naphtholic oxygen atoms, thus confirming the correctness of the five-membered chelate ring alternative. The ligands are in *trans*-position giving rise to a nearly planar structure (Table 3). Within the limits of experimental error, the naphthalene planes do not deviate from the coordination plane of Cu^{2+} ion, and even the oxime oxygens can be included in this plane.

Table 4. The least-squares plane defined by the acetone molecule. The equation and the deviations of the atoms are given as in Table 3.

Plane C(11)–C(13), O(3):
$-0.5471X'-0.7016Y'+0.4566Z'-0.2976=0$

Atom	Distance	Atom	Distance
C(11)	−0.004	C(13)	0.001
C(12)	0.001	O(3)	0.001

Table 5. Intermolecular distances (Å; below 3.5 Å). Roman numerals refer to the following equivalent positions: I $\bar{x},\frac{1}{2}+y,\frac{1}{2}-z$; II $x,-\frac{1}{2}-y,-\frac{1}{2}+z$; III $1-x,\bar{y},1-z$.

O(1)–C(3)^{I}	3.191
O(1)–C(4)^{I}	3.349
O(3)–C(4)^{I}	3.433
O(2)–C(4)^{II}	3.464
C(8)–C(7)^{III}	3.470

Judging from the bond lengths in the complex there is contributions from the nitrosonaphthol as well as the quinone oxime structure. The observed C(1)–N distance (1.35 Å) is somewhat greater than the corresponding bond length in several typical oximates (*e.g.* in *vic*-dioximates the average value is 1.30 Å) but shorter than could be expected for nitrosonaphthalene compounds, 1.44 Å (*cf.* 1.42 Å in ferroverdin).[8,11,15] The N–O distance in oximates (1.34 Å, av.) is greater than the one found here (1.26 Å).[8] Furthermore, the C(2)–O bond (1.30 Å) cannot be described as a single nor as a double bond; *e.g.* the equivalent bond in salicylaldoxime [16] and salicylaldehyde [17] complexes varies from 1.31 Å to 1.36 Å and, on the other hand, the C–O double bond in naphthoquinones (1.22 Å) [18] can alter on complex formation. Moreover, as C(3)–C(4) is the only carbon-carbon bond with pronounced double bond character, the distribution of longer or shorter bonds in the naphtha-

lene nucleus does not unambiguously indicate the quinonoid form. This being the case, the complex cannot be categorically labelled as bis(1-nitroso-2-naphtholato)copper(II) nor bis-(1,2-naphthoquinone-1-oximato)copper(II).

It is of interest to note that the N–O and C(2)–O distances in the present complex are approximately equal to the corresponding distances in ferroverdin, in the 1:1 pyridine adduct of bis(4-methyl-1-quinone-2-oximato)copper(II), as well as in the tris(4-chloro-1-quinone-2-oximato)nickelate(II) anion (naming of the complexes is from the original authors).[9,10,11] As a whole, the main difference between the nitrosophenolate groupings in all these complexes is the lengthened C–N bond of ferroverdin.

The acetone oxygen atoms complete the distorted octahedral arrangement around the Cu^{2+} ion. The distance between copper and acetone oxygen (2.651 Å) indicates a relatively weak interaction which seems to have practically no influence on the planarity of the acetone molecule (*cf.* Table 4) or its bond lengths and bond angles.

There are only weak interactions between separate complex units, *cf.* Table 5, and the structure is therefore monomeric. This differs from the complexes $Cu(qo)_2$ and $Ni(qo)_2$ (qoH = 1-nitroso-2-naphthol or *o*-nitrosophenol derivative) for which polymeric or dimeric structure has been proposed.[19]

REFERENCES

1. Feigl, F. *Chemistry of Specific, Selective and Sensitive Reactions*, Academic, New York 1949, pp. 251–280.
2. Hadzi, D. *J. Chem. Soc.* (1956) 2725.
3. van Oijen, J. W. L. and Romers, C. *Acta Crystallogr. 20* (1966) 169.
4. Romers, C. *Acta Crystallogr. 17* (1964) 1287.
5. Saarinen, H. *Ann. Acad. Sci. Fenn. A II 170* (1973).
6. Gurrieri, S. and Siracusa, G. *Inorg. Chim. Acta 5* (1971) 650.
7. Janowski, A. and Cukrowski, J. *J. Mol. Struct. 7* (1971) 185.
8. Chakravorty, A. *Coord. Chem. Rev. 13* (1974) 1.
9. McPartlin, M. *Inorg. Nucl. Chem. Lett. 9* (1973) 1207.
10. Carrek, P. W., Charalambous, J., Kensett, M. J., McPartlin, M. and Sims, R. *Inorg. Nucl. Chem. Lett. 10* (1974) 749.
11. Candeloro, S., Grdenic, D., Taylor, N., Thomson, B., Viswamitra, M. and Hodgin, D. C. *Nature (London) 224* (1969) 589.
12. Charalambous, J., Frazer, M. J. and Taylor, F. B. *J. Chem. Soc. A* (1969) 2787.
13. *International Tables for X-Ray Crystallography*, Kynoch Press, Birmingham 1952, Vol. III.
14. Daly, J. J., Stephens, F. S. and Wheatley, P. J. *MRSA* Final Report No 52.
15. Prout, C. K., Cameron, T. S., Dunn, R. M. A., Hodder, O. J. R. and Viterbo, D. *Acta Crystallogr. B 27* (1971) 1310.
16. Srivastava, R. C., Lingafelter, E. C. and Jain, P. C., *Acta Crystallogr. 22* (1967) 922.
17. Hall, D., McKinnon, A. J. and Waters, T. N. *J. Chem. Soc.* (1965) 425.
18. Gaultier, P. J. and Hauw, C. *Acta Crystallogr. 18* (1965) 179.
19. Charalambous, J., Frazer, M. J. and Taylor, F. B. *J. Chem. Soc. A* (1971) 602.

Received November 11, 1974.

Acta Chemica Scandinavica A 29 (1975) 414—418

^{1}H NMR Analysis of 1,3,2-Oxadithiolan-2-oxide, 3-Phenyl-1,2,3-oxathiazolidin-2-oxide and 2,5-Dimethyl-1,2,5-thiadiazolidin-1-oxide

PER ALBRIKTSEN* and MALVIN BJORØY

Department of Chemistry, University of Bergen, N-5014 Bergen, Norway

Three analogues of ethylene sulfite, containing oxygen, sulfur or nitrogen as ring heteroatoms in positions 1 and 3 have been prepared, and their NMR data are reported and discussed. The NMR spectra of the compounds have been fully analysed on the basis of ABXY and $[AB]_2$ spin systems. Interpretation of the ^{1}H spectra of the compounds in this series suggests the existence of a single conformation for each of these compounds.

Recently NMR investigations on ethylene sulfite [1] and the various isomers of 4,5-dimethylethylene sulfite [2] have been reported. It is assumed that ethylene sulfites [1,2] exist in a twist-envelope conformation or pseudorotate between twist-envelope conformations with the S=O bond pseudoaxial. Various phosphorus-substituted 1,3,2-dioxaphospholanes [1,3] and 1,3,2-oxathiaphospholanes [4,5] have been carefully studied by NMR. A significant change in the conformation is found upon substitution of a ring oxygen atom in the dioxaphospholanes with a sulfur atom. In order to investigate the effect of ring heteroatoms other than oxygen in ring positions 1 and 3 of ethylene sulfite, the following molecules have been synthesized: 1,3,2-oxadithiolan-2-oxide (I), 3-phenyl-1,2,3-oxathiazolidin-2-oxide (II), and 2,5-dimethyl-1,2,5-thiadiazolidin-1-oxide (III).

EXPERIMENTAL

1,3,2-Oxadithiolan-2-oxide (I) was prepared from thionyl chloride and 2-hydroxy-ethanethiol in diethyl ether using triethylamine as base: b.p.$_{0.1}$ 58 °C; yield 30 %.

3-Phenyl-1,2,3-oxathiazolidin-2-oxide (II) was prepared from 2-phenylaminoethanol according to the method used for compound I; b.p.$_{0.5}$ 122 °C; yellow crystals, m.p. 34–35 °C; yield 45 %.

2,5-Dimethyl-1,2,5-thiadiazolidin-1-oxide (III) was prepared as above from *N,N'*-dimethylethylenediamine; b.p.$_{0.5}$ 52 °C; yield 10 %.

The spectra were recorded on 50 % solutions of compounds I–III in deuterioacetone, deuteriochloroform, or benzene in 5 mm O.D. NMR sample tubes, using a small amount of added TMS as reference and locking substance. The spectra were recorded on a JEOL JNM–C–60H NMR instrument, operating at 60 MHz in internal lock mode with frequency sweep. The spectra for the NMR analysis were obtained with a chart expansion of 1.2 Hz cm^{-1}. The line positions were taken as an average of several spectra, and are assumed to be correct to about 0.05 Hz. The computation was carried out using an UNIVAC 1110 computer and graphical output was obtained using a Calcomp Plotter.

SPECTRAL ANALYSIS

The NMR spectra of compounds I and II consist of two regions with the separation between the two signal groups larger than any of the coupling constants involved.

The signals at the higher frequency (I and II) are assigned to the protons, A and B, at the carbon attached to the ring oxygen atom and the signals at lower frequency to the protons, X and Y, on the carbon adjacent to the sulfur (I) or the nitrogen (II) atom. The higher

* Present address: Rafinor A/S & Co., N-5154 Mongstad, Norway.

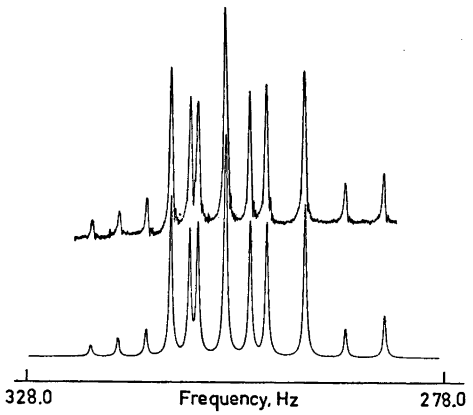

Fig. 1. 60 MHz spectrum of the AB protons in 2-oxo-1,3,2-oxathiasulfolane. Upper: Observed spectrum. Lower: Calculated spectrum.

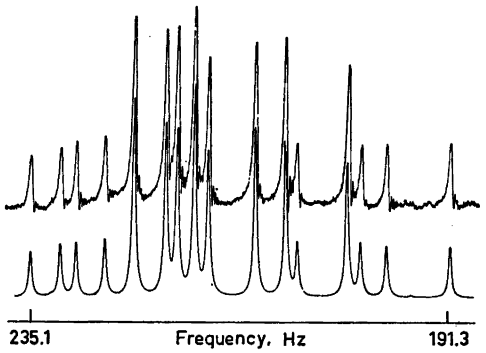

Fig. 2. 60 MHz spectrum of the XY protons in 2-oxo-1,3,2-oxathiasulfolane. Upper: Observed spectrum. Lower: Calculated spectrum.

frequency shift of the AB protons as compared to the XY protons is due to the larger deshielding effect of an adjacent ring oxygen atom as compared to a sulfur or a nitrogen atom.[11] The spectra of compounds I and II were analysed on the basis of an ABXY spin system,[6] and a good correlation between the theoretical and the experimental spectrum was obtained (Figs. 1 and 2). In the analysis of the proton signals in the spectrum of compound II, the protons of the phenyl group have been neglected since coupling to the protons of the parent ring is negligible. The spectrum of III consists of a symmetrical band of signals and can be fully analysed as an $[AB]_2$ spin system. The chemical shift difference between the A and B parts is larger when the compound is dissolved in benzene rather than in deuterioacetone.

The iterative computations for compounds I and II were performed using the computer programme LAOCN3,[7] while compound III was analysed with the aid of the computer programme LACX.[8] The spectral parameters are listed in Table 1. The final RMS values obtained were 0.06 Hz or less when all parameters were allowed to vary. The probable errors in the parameters were less than 0.02 Hz when 32 theoretical transitions were assigned to 29 observed lines for compounds I and II. The probable errors in the parameters of compound III are 0.2 Hz or less when 26 theoretical transitions are assigned.

DISCUSSION

The detailed spectral analysis of compound III was carried out successfully on the basis of an $[AB]_2$ spin system. This implies that this five-membered ring (III) is; (a) planar, or (b) in an envelope form with the sulfur as the "flap" atom, or most likely (c) that intramolecular processes interconvert non-planar forms at a rate that is large on the NMR time scale, but that the inversion at sulfur is either slow on this time scale or does not occur.

The spectral analysis of compounds I and II were carried out on the basis of an ABXY spin system (Figs. 1 and 2). It is, however, not possible to be certain which intramolecular motion, if any, does occur for these compounds, I and II. All the coupling constants obtained are within the expected range for the various coupling paths. The geminal coupling constant of the CH_2-O moiety of compound I is more negative than in compounds II, III, and ethylene sulfite.[1] The values of the geminal coupling constant [9] of the CH_2-X group is sensitive to the electronegativity of X as well as the H–C–H angle. The change in electronegativity of substituents on the methylene group attached to the ring oxygen in compounds I, II, and ethylene sulfite, cannot account for the variation in J_{gem}, −9.71 Hz (I), −8.51 Hz (II), and −8.59 Hz (ethylene sulfite).[1] This change in J_{gem}, as regards I, might be due to different H–C–H angles of I as compared to II and ethylene sulfite. The magnitude of

Table 1. NMR parameters for the compound I, II, and III.[a]

	δ_A	δ_B	δ_X	δ_Y	$^2J_{AB}$	$^2J_{XY}$	$^3J_{AY}$	$^3J_{AX}$	$^3J_{BY}$	$^3J_{BX}$	$^3J_{AA'}$	$^3J_{BB'}$	$J_{AB'}$	Reference
I[h]	5.141	4.970	3.441	3.738	−9.71	−10.85	2.61	5.85	4.71	10.65				This work
II[h]	4.518	4.870	3.709	3.485	−8.51	−8.62	4.28	6.96	6.49	8.38				This work
2-*t*-Butyl-1,3-oxathiolane	4.330	3.643	2.903	2.809	−9.03	−9.76	2.21	5.77	5.02	9.92				Ref. 11
2-*t*-Butyl-2-methyl--1,3-oxathiolane	4.248	3.916	2.925	2.797	−9.06	−9.56	3.21	5.35	4.38	9.63				»
2-Ethyl-2-methyl 1,3-oxathiolane	4.109	4.030	2.969	2.951	−9.40	−9.86	4.08	6.47	6.02	7.18				»
2-Phenyl-1,3-oxathiolane	3.96	3.39	2.56	2.73	−8.59	−9.31	2.79	6.72	6.51	8.39				Ref. 17
III	3.37[b]		3.27[c]			−9.1[d,e]					8.8[e]	8.8[e]	5.9[e,f]	This work
	3.094[b]		2.842[c]			−8.72[d]					6.92	7.23	6.06[g]	

[a] Chemical shifts are ±0.005 p.p.m. Errors in coupling constants are ±0.05 Hz. [b] $\nu_A=\nu_{A'}$. [c] $\nu_B=\nu_{B'}$. [d] $J_{AB}=J_{A'B'}$. [e] Errors in coupling constants are ±0.1 Hz. [f] Deuterioacetone. [g] Benzene. [h] Deuteriochloroform.

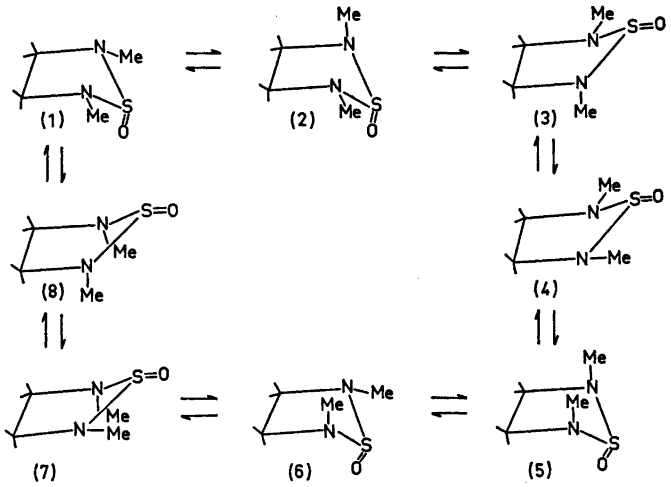

Scheme 1.

^2J is, however, within the limits expected in 1,3-oxathiolanes.[10,11] The geminal coupling constants in II and III are better understood when compared with values obtained for 1,3-oxazolidines. The more the nitrogen lone pair bisects the X–C–Y angle, the more negative is the coupling constant.[12]

The inequality of $^3J_{AA'}$ and $^3J_{BB'}$ of compound III is of interest, since it appears to be detectable only when the compound is dissolved in benzene. This may be due to a long range effect of the lone pair of the sulfur atom and the nitrogen atom on ^3J.[12] It is, however, not possible at present to be certain which of these groups gives the major contribution to this inequality in ^3J. Moreover, a similar observation has been made by Haake *et al.*[1] on ethylenesulfite where $^3J_{AA'}$ and $^3J_{BB'}$ are equal when the compound is studied as neat liquid, whereas when it is dissolved in benzene, the two coupling constants are different.

Scheme 1 clearly indicates that in the present case it is not possible to neglect the possibility of nitrogen inversion in compounds II and III.[13,14] Forms with both N–Me groups pseudoaxial may be omitted. Enantiomers with the S=O bond and one N–Me group pseudoaxial and forms with a pseudoequatorial S=O bond may contribute appreciably. Accordingly, it is reasonable to expect that under certain conditions an $[AB]_2$ type spectrum is obtained for III where $^3J_{AA'} \neq {}^3J_{BB'}$.

Inversion at the sulfoxide sulfur atom is shown not to occur in the case of the cyclic trimethylene sulfites.[15,16] Accordingly it is not likely that such an inversion should occur in the compounds I, II, and III. Hence it is reasonable to assume that the S=O bond adopts only one position with respect to the ring. It has been suggested [1,2] for 1,3-dioxa-ring compounds that the high frequency resonance, A, is due to protons *cis* to the substituent at the heteroatom in ring position 2. It is not possible from the available data of compounds I, II, and III, to be certain whether the S=O bond adopts a pseudo axial or equatorial position. The swopping of chemical shifts for the A and B nuclei in compound II, relative to I, is not clearly understood, but it might indicate that the compounds exist in a fixed conformation. It is, however, not possible to arrive at any certain conclusion about the conformation from the available data (Table 1).

REFERENCES

1. Haake, P., McNeal, J. P. and Goldsmith, E. *J. Amer. Chem. Soc. 90* (1968) 715.
2. Albriktsen, P. *Acta Chem. Scand. 26* (1972) 3671.
3. Bergesen, K. and Vikane, T. *Acta Chem. Scand. 26* (1972) 2153.
4. Bergesen, K., Bjorøy, M. and Gramstad, T. *Acta Chem. Scand. 26* (1972) 2156.

5. Bergesen, K. and Bjorøy, M. *Acta Chem. Scand. 27* (1973) 357.
6. Diehl, P. and Chuck, R. J. *Mol. Phys. 13* (1972) 417.
7. Castellano, S. and Bothner-By, A. A. *J. Phys. Chem. 41* (1964) 3863.
8. Haigh, C. W. *Private communication.*
9. Pople, J. A. and Bothner-By, A. A. *J. Chem. Phys. 42* (1965) 1339.
10. Keskinen, R., Nikkila, A. and Pihlaja, K. *J. Chem. Soc. Perkin Trans. 2* (1973) 1376.
11. Pasto, D. J., Klein, F. M. and Doyle, T. W. *J. Amer. Chem. Soc. 89* (1967) 4368.
12. Cohill, R., Cookson, R. C. and Crabb, T. A. *Tetrahedron 25* (1969) 4681.
13. Simmons, H. E. and Park, C. H. *J. Amer. Chem. Soc. 90* (1968) 2428.
14. Hutchin, R. O., Kopp, L. D. and Eliel, E. L. *J. Amer. Chem. Soc. 90* (1968) 7174.
15. Albriktsen, P. *Acta Chem. Scand. 25* (1971) 478.
16. Albriktsen, P. *Acta Chem. Scand. 26* (1972) 1783.
17. Wilson, G. E., Jr., Huang, M. G. and Bovey, F. A. *J. Amer. Chem. Soc. 92* (1970) 5907.

Received November 25, 1974.

Acta Chemica Scandinavica A 29 (1975) 419—426

Concurrent Carbon and Oxygen Protonation in the Hydrolytic Decomposition of β-Acetyl Substituted Vinyl Ethers

ALPO KANKAANPERÄ and MARJA MATTSÉN

Department of Chemistry, University of Turku, 20500 Turku 50, Finland

The acid-catalyzed decomposition of β-acetyl substituted vinyl ethers was studied kinetically in light water-heavy water and in dimethyl sulfoxide-water mixtures. Some measurements were also performed in various buffer solutions in order to study the nature of the acid catalysis. The kinetic data reveal that the hydrolytic decomposition of 4-ethoxy-3-penten-2-one proceeds through two different routes. In the first route the carbonyl oxygen is protonated in a pre-equilibrium process followed by the rate-limiting attack of water (*A*-2 mechanism). In the second route the proton attack at the β-position of the carbon-carbon double bond occurs in the rate-limiting step of the reaction (*A*-S_E2 mechanism). The contributions of these reactions were estimated on the basis of the deuterium solvent isotope effect. The third possible route, the pre-equilibrium protonation of the β-carbon atom followed by attack of water at the protonated substrate, could be excluded in the present case.

It is well known that the rate-limiting step in the acid-catalyzed hydrolysis of vinyl ethers is the transfer of the proton at the β-position of the carbon-carbon double bond.[1,2] Although in some cases alternative mechanisms have been suggested for vinyl ether hydrolysis,[3–6] the experimental evidence for these conclusions seems to be inconclusive. Stamhuis *et al.*[3] proposed that in the hydrolytic decomposition of some furans, which are closely related to vinyl ethers, the rate-limiting proton transfer takes place at the α-position of the carbon-carbon double bond. In contradiction to this proposal it has been found [4–7] that furan and 2-methylfuran exchange α-hydrogens in aqueous solution at rates which are markedly higher than the rates of the subsequent reactions. Thus no arguments can be found for the assumption of Unverferth *et al.*[4] that the rate-limiting proton transfer at the β-position could be excluded in the hydrolysis of furans on the basis of the kinetic results obtained for the hydrogen exchange reactions. Recently [8] it was shown that all these kinetic results could, at least in the case of 2-methylfuran, best be explained in terms of a rate-limiting protonation of the β-carbon. Vitullo *et al.*[5] assumed on the basis of buffer experiments that in the hydrolysis of a cyclic vinyl ether the rate-limiting step changes with the change in the buffer concentration. It seems, however, evident that this apparent anomaly is only due to the changes in the hydronium ion concentration of the used buffer mixtures in which the pH has been kept constant; experimental evidence for this kind of changes in different buffer systems is available.[9] The proposed mechanistic change can also be criticized on the basis of previous kinetic data for the hydrolysis of related cyclic vinyl ethers.[10] Recently Loudon *et al.*[6a] assumed on the basis of structural effects that the hydrolytic decomposition of 1-methoxy-1-(*p*-methoxyphenyl)ethene does not proceed through the *A*-S_E2 mechanism. Later Loudon *et al.*[6b] have, however, neglected this concept of the exceptional reaction mechanism of vinyl ether hydrolysis.

There is, however, a particular case of vinyl ether hydrolysis, namely the hydrolysis of alkyl β-alkoxyvinyl ketones, in which the catalysis by Brønsted acids, typical of the *A*-S_E2 mechanism has not been observed.[11] The kinetic data for these derivatives have been interpreted in terms of a mechanism in which the protonation of the carbonyl oxygen is a pre-equilibrium process followed by the ratelimiting attack of

water at carbon 4 (eqn. 1). Thus the reaction

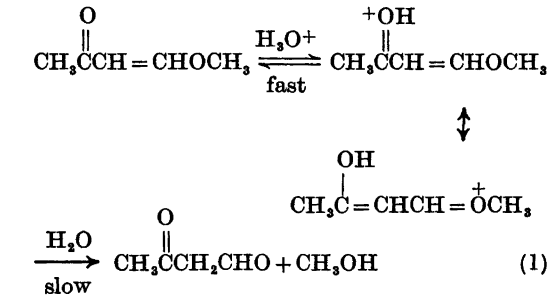

(1)

had no characteristics typical of vinyl ether hydrolysis in spite of the structural similarity, since the acid-catalyzed decomposition proceeded through the alternative oxygen protonation.

Although it is likely that the reaction proposed by Fedor *et al.*[11] is operating in the hydrolysis of 4-methoxy-3-buten-2-one, another mechanism, a pre-equilibrium protonation of the β-position of vinyl ether and the subsequent attack of water in the rate-limiting stage of the reaction (eqn. 2) might also be in accordance with the kinetic data. In the hydrolysis of 4-methoxy-3-buten-2-one structural factors favor the proton abstraction from the oxocarbenium ion. If this structural effect is sufficient then $k_{-1} \gg k_2$ as is the case in reaction (2). Therefore the hydrolysis of 4-methoxy-3-buten-2-one (I) was subjected to a thorough kinetic study. In addition the kinetics of the hydrolysis of 4-ethoxy-3-penten-2-one (II) was studied since this compound can be assumed to be more favorable for carbon protonation than is compound I due to the electropositive methyl group attached to the carbenium ion formed during the hydrolytic decomposition.

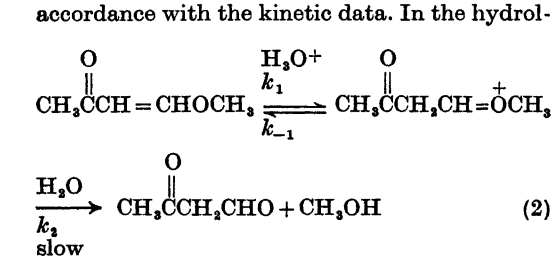

(2)

EXPERIMENTAL

Materials. 4-Methoxy-3-buten-2-one was a product of EGA-Chemie and was purified by distillation. The purity of the compound was checked by NMR spectroscopy (10 % solution in carbon tetrachloride with tetramethyl silane as internal standard): δ 2.13 (3 H, s), 3.72, (3 H, s), 5.52 (1 H, d), and 7.56 (1 H, d). The coupling constant $J_{3H,4H}$ 13.2 Hz reveals that the product has the *trans* configuration (see Ref. 12). No peaks from the *cis* isomer could be detected.

A fraction of 4-ethoxy-3-penten-2-one used in the kinetic measurements was a gift by E. Taskinen.[13] The *trans* configuration of this sample was verified by the following NMR data: δ 1.34 (3 H, t), 2.05 (3 H, s), 2.20 (3H, s), 3.84 (2H, q), and 5.38 (1 H, s).[13]

Kinetic measurements. Most of the kinetic measurements were performed on a Unicam SP 800 spectrophotometer. The progress of the reaction was followed by checking the disappearance of the absorption at 260 nm. In some cases the reactions were followed on a Perkin-Elmer 46 BCD spectrophotometer. The concentration of the substrate varied in the kinetic measurements from 3×10^{-5} to 3×10^{-4} mol dm^{-3}. The cell-housing block of the spectrophotometer was adjusted to the desired temperature with water circulation from a Lauda thermostat.

Perchloric acid was used as catalyst in the lyonium ion-catalyzed reactions. When the effect of the acid concentration was studied in 0.002 – 0.1 mol dm^{-3} perchloric acid solutions the second-order rate coefficients were found to be independent of the acid concentration. Deuterium oxide, used in the measurements in heavy water and in light water-heavy water mixtures, was a product of New England Nuclear. The catalysis by Brønsted acids was studied in formic acid-sodium formate and in monochloroacetic acid-sodium monochloroacetate buffers. In both cases the ratio of the concentration of the acid to the base was 1 to 1. The concentration of the undissociated acid varied between 0.1 and 0.0167 mol dm^{-3}. The ionic strength was kept constant at 0.1 mol dm^{-3} with sodium chloride. The rate coefficients k_{HA} for the reactions catalyzed by formic acid and monochloroacetic acid were calculated from the slopes of the plots of k_{obs} *versus* [HA] by the method of least squares.

Some measurements were also performed in dimethyl sulfoxide (DMSO)-water mixtures. The applied DMSO was purified by distillation under reduced pressure from calcium hydride and the pressure was adjusted so that the temperature did not exceed 363 K. In the experiments in solvent mixtures the perchloric acid concentration was 0.1 mol dm^{-3}. In the case of the hydrolysis of 4-ethoxy-3-penten-2-one the measurements in water-DMSO mixtures were performed by spectrophotometry. When the hydrolytic decomposition of 4-methoxy-3-buten-2-one was studied the spectrophotometric method could be applied only in solutions in which the mol fraction of DMSO was lower than 0.3 .For higher

Table 1. Kinetic data for the hydronium ion-catalyzed hydrolysis of 4-methoxy-3-buten-2-one (I) and 4-ethoxy-3-penten-2-one (II) in water at different temperatures. The thermodynamic functions of activation are given at 298.15 K.

Compound	Temp./K	k/mol^{-1} dm^3 s^{-1}	$\Delta G^{\ddagger}$/kJ mol^{-1}	$\Delta S^{\ddagger}$/J K^{-1} mol^{-1}	$\Delta H^{\ddagger}$/kJ mol^{-1}	k_{298}/mol^{-1} dm^3 s^{-1}
I	298.6	0.198 ± 0.001				
		0.215 ± 0.001				
	298.2	0.421 ± 0.002				
		0.435 ± 0.001				
	298.4	0.437 ± 0.004				
		0.440 ± 0.006				
		0.427 ± 0.002	75.15 ± 0.03	−79 ± 2	51.6 ± 0.7	0.424 ± 0.004
	308.3	0.857 ± 0.008				
		0.798 ± 0.002				
		0.872 ± 0.007				
	317.8	1.653 ± 0.008				
		1.653 ± 0.006				
		1.66 ± 0.01				
II	297.8	0.1469 ± 0.0008				
		0.1517 ± 0.0004				
	298.1	0.138 ± 0.002				
		0.134 ± 0.001				
		0.139 ± 0.002				
	298.2	0.149 ± 0.001	77.76 ± 0.05	−57 ± 4	60.8 ± 1.1	0.143 ± 0.003
		0.1577 ± 0.0007				
		0.1452 ± 0.0009				
	308.1	0.359 ± 0.003				
		0.358 ± 0.006				
		0.337 ± 0.003				
	317.6	0.726 ± 0.005				
		0.717 ± 0.004				
	327.9	1.371 ± 0.008				
		1.51 ± 0.01				

mol fractions of DMSO the progress of the reaction was followed by NMR from the disappearance of the peaks at δ 5.52 and 7.56. The practical performance of the kinetic runs took place as follows: 10 cm^3 of perchloric acid solution (0.02 mol dm^{-3}) was thermostated to the desired temperature. The mixture contained about 5 vol. % of chloroform as internal standard. After 2 cm^3 of the substrate had been added, the reaction mixture was shaken vigorously. At suitable intervals 1 cm^3 samples were withdrawn from the reaction mixture and transferred to an equivalent amount of sodium hydroxide to stop the reaction. The samples were analyzed on a 60 MHz Perkin-Elmer Model R 10 NMR spectrometer. When the first-order rate coefficients were calculated, the ratio of the peak heights of the doublets at δ 5.52 and 7.56 to the peak height of the internal standard, chloroform, was used as a quantitative measure of the progress of the reaction.

RESULTS AND DISCUSSION

The kinetic data for the hydronium ion-catalyzed hydrolysis of 4-methoxy-3-buten-2-one (I) and 4-ethoxy-3-penten-2-one (II) are collected in Table 1. If both of the studied compounds were hydrolyzed through the A-S_E2 mechanism, the ratio of the rate coefficients of (II) and (I) should be of the magnitude 10^3 due to the electropositive methyl group in (II) attached to the center of the intermediate carbenium ion.[2] This is, however, in contradiction to the kinetic data, since the rate coefficients for the hydronium ion-catalyzed hydrolysis of I and II are seen to be almost equal and the small difference which can be observed is even in favor of compound (I) which should be hydrolyzed slower by the A-S_E2 mechanism. In reaction (1) the total structural effect may remain relatively low: the electropositive methyl group favors the pre-equilibrium protonation,

Table 2. The acid-catalyzed hydrolysis of 4-methoxy-3-buten-2-one (I) and 4-ethoxy-3-penten-2-one (II) in buffer solutions. The molar ratio of the acid HA to the base A^- is 1 to 1. The ionic strength has been adjusted at 0.1 mol dm^{-3} with sodium chloride.

HA/ mol dm^{-3}	k/ mol^{-1} dm^3 s^{-1}	k_{HA}/ mol^{-1} dm^3 s^{-1}
I; 298.3 K; HA = $ClCH_2COOH$		
0.100	1.12 ± 0.02	
	1.124 ± 0.009	
	1.017 ± 0.004	
0.0833	1.09 ± 0.01	
	1.146 ± 0.006	
0.0667	1.134 ± 0.005	
	1.087 ± 0.005	
	1.100 ± 0.004	
0.0500	1.028 ± 0.005	
	1.069 ± 0.008	
0.0333	0.974 ± 0.005	
	1.068 ± 0.006	
	1.095 ± 0.006	$(1.3 \pm 0.4) \times 10^{-3}$
	1.02 ± 0.01	corr.coeff. 0.655
0.0167	0.973 ± 0.004	
	0.979 ± 0.016	
II; 298.2 K; HA = $ClCH_2COOH$		
0.100	0.394 ± 0.003	
	0.400 ± 0.004	
0.0833	0.393 ± 0.003	
	0.363 ± 0.003	
0.0667	0.369 ± 0.003	
	0.371 ± 0.002	
0.0500	0.334 ± 0.003	
	0.327 ± 0.002	
0.0333	0.326 ± 0.001	
	0.327 ± 0.004	
	0.321 ± 0.001	$(1.4 \pm 0.1) \times 10^{-3}$
0.0167	0.284 ± 0.003	corr.coeff. 0.962
	0.281 ± 0.002	
	0.273 ± 0.001	
II; 327.5 K; HA = $ClCH_2COOH$		
0.100	4.18 ± 0.05	
	4.28 ± 0.04	
0.0833	3.94 ± 0.02	
	4.06 ± 0.03	
0.0667	3.69 ± 0.03	
	3.97 ± 0.03	
0.0500	3.55 ± 0.02	
	3.67 ± 0.03	
0.0333	3.25 ± 0.02	$(1.6 \pm 0.1) \times 10^{-2}$
	3.39 ± 0.03	corr.coeff. 0.971
0.0167	2.88 ± 0.02	
	2.86 ± 0.02	
II; 346.7; HA = HCOOH		
0.100	3.08 ± 0.02	
	3.35 ± 0.01	
	3.30 ± 0.03	
0.0800	2.82 ± 0.02	
	2.72 ± 0.01	
0.0600	2.52 ± 0.02	
	2.57 ± 0.02	
0.0400	2.12 ± 0.02	$(1.6 \pm 0.1) \times 10^{-2}$
	2.23 ± 0.02	corr.coeff. 0.978
0.0200	1.90 ± 0.01	
	2.05 ± 0.02	

but this substitution similarly reduces the nucleophilic attack of water at the carbenium ion center. Thus the only conclusion which can be drawn on the basis of structural effects is that at least one of the studied compounds hydrolyzes through the A-S_E2 mechanism. Additional kinetic data are required to get information of the possible reaction routes.

The activation entropies for the studied reactions, −79 and −57 J K^{-1} mol^{-1} for the hydrolysis of I and II, respectively, are slightly smaller than generally observed for the A-S_E2 hydrolysis of vinyl ethers.[1,2] The magnitude of the activation entropy, however, can be considered as a poor criterion of the reaction mechanism since in the hydrolysis of vinyl ethers the value of $\Delta S^{\ddagger}$ has been observed to vary remarkably with the structure of the substrate.[14] In this context it is more important to note that in the hydrolytic decomposition of 4-ethoxy-3-penten-2-one (II) $\Delta S^{\ddagger}$ is about 20 J K^{-1} mol^{-1} higher than in the hydrolysis of compound (I). As compounds I and II are closely related, the observed difference may reflect a definite change in the reaction mechanism. Although the A-S_E2 mechanism cannot be excluded on the basis of the magnitude of the activation entropy, it must be remembered, that the calculated $\Delta S^{\ddagger}$ values are in accordance with a mechanism in which pre-equilibrium protonation of the oxygen atom is followed by the rate-limiting attack of water at the carbenium ion center (A-2 mechanism).[15]

General acid catalysis. As shown above the choice between the A-S_E2 mechanism and the A-2 mechanism cannot be made on the basis of structural effects and the temperature dependence of the rate coefficients, but additional kinetic data are required. In this context buffer experiments might be informative, since in the reaction proceeding through the A-S_E2 mechanism general acid catalysis should by detected in contrast to the alternative reaction (A-2

Table 3. The hydronium ion-catalyzed hydrolysis of 4-methoxy-3-buten-2-one (I) and 4-ethoxy-3-penten-2-one (II) in dimethyl sulfoxide-water mixtures at 298 K.

Compound	x_{DMSO}	k/mol^{-1} dm^3 s^{-1}
	0.000	0.428 [a]
I	0.119	0.480 ± 0.003
		0.476 ± 0.001
		0.465 ± 0.002
	0.214	0.501 ± 0.003
		0.473 ± 0.002
	0.299	0.419 ± 0.003
		0.425 ± 0.001
		0.442 ± 0.001
		0.439 ± 0.002
	0.733	0.192 ± 0.002
		0.191 ± 0.003
	0.769	0.166 ± 0.005
		0.171 ± 0.004
	0.846	0.129 ± 0.008
		0.125 ± 0.007
	0.000	0.144 [a]
II	0.214	0.0701 ± 0.0005
		0.0695 ± 0.0007
	0.414	0.0307 ± 0.0003
		0.0298 ± 0.0002
	0.615	0.0180 ± 0.0002
		0.0180 ± 0.0002
	0.791	0.0128 ± 0.0001
		0.0124 ± 0.0002
		0.0108 ± 0.0002
	0.926	0.00539 ± 0.00003
		0.00574 ± 0.00004

[a] The average from Table 1.

mechanism), which is catalyzed only be the hydronium ion. Kinetic measurements were therefore performed both in monochloroacetic acid-sodium monochloroacetate and in formic acid-sodium formate buffers. The obtained rate coefficients are collected in Table 2. When the first-order rate coefficients for the hydrolytic decomposition of 4-ethoxy-3-penten-2-one (II) were plotted against the concentration of the undissociated acid, a linear correlation (eqn. 3) was obtained the correlation coefficients being

$$k_{obs} = k_{HA}[HA] + \text{constant} \quad (3)$$

0.962 and 0.978 in the case of monochloroacetic acid and formic acid, respectively. The catalytic coefficients k_{HA} were calculated from the experimental data by the method of least squares (Table 2).

In the hydrolysis of 4-methoxy-3-buten-2-one (I) the general acid catalysis is less probable due to the fact that the observed first-order rate coefficients are almost independent of the concentration of the undissociated acid. When the first-order rate coefficients determined in monochloroacetic acid-sodium monochloroacetate buffer are plotted against the concentration of the undissociated acid (eqn. 3) the correlation coefficient of the plot is found to be only 0.65. Thus the contribution of the A-S_E2 reaction must be relatively small in the hydrolytic decomposition of 4-methoxy-3-buten-2-one. Fedor *et al.*[11] have previously studied the hydrolysis of 4-methoxy-3-buten-2-one in formic acid-sodium formate buffer and a general acid catalysis could not be observed.

Solvent effects. Since the kinetic measurements in solvent mixtures have been found to be an excellent method to distinguish between the A-S_E2 and A-2 mechanisms,[16-17] the hydrolysis of 4-methoxy-3-buten-2-one and 4-ethoxy-3-penten-2-one was subjected to kinetic studies in water-dimethyl sulfoxide mixtures. The measured first-order rate coefficients are collected in Table 3. To illustrate the solvent effects in the

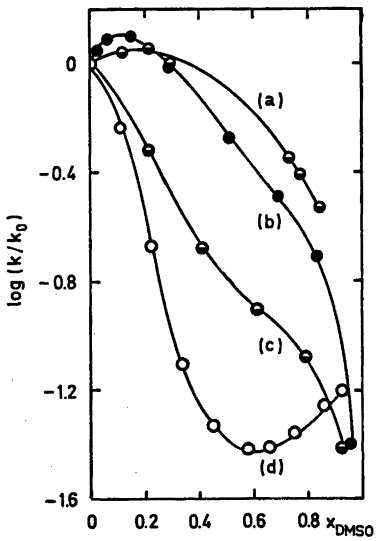

Fig. 1. The dependence of the rate coefficients on the solvent composition: (a) the hydrolysis of 4-methoxy-3-buten-2-one, (b) the A-2 hydrolysis of ethyl acetate,[18] (c) the hydrolysis of 4-ethoxy-3-penten-2-one, and (d) the A-S_E2 hydrolysis of 2-methyl-4-methylene-1,3-dioxolane.[17]

Table 4. The lyonium ion-catalyzed hydrolysis of 4-methoxy-2-buten-3-one (I) and 4-ethoxy-3-penten-2-one (II) in the mixture of light and heavy water. Temperature 298.2 K.

Deuterium atom fraction	$k_{L_3O^+}$/ mol^{-1} dm^3 s^{-1}	k_n/k_H
I		
0.000	0.428 [a]	1.000
0.199	0.485 ± 0.001	
	0.491 ± 0.001	1.140
0.399	0.564 ± 0.001	
	0.528 ± 0.002	1.276
0.599	0.633 ± 0.001	
	0.637 ± 0.003	1.484
0.799	0.736 ± 0.003	
	0.731 ± 0.003	1.715
0.998	0.903 ± 0.007	
	0.875 ± 0.003	2.078
0.998 [b]	0.871 ± 0.004	
	0.847 ± 0.003	
II		
0.000	0.144 [a]	
0.199	0.1478 ± 0.0009	
	0.1527 ± 0.0006	1.047
0.399	0.169 ± 0.001	
	0.165 ± 0.001	1.160
0.599	0.1771 ± 0.0004	
	0.1780 ± 0.0008	1.237
0.799	0.191 ± 0.001	
	0.201 ± 0.001	1.365
0.998	0.2181 ± 0.0007	
	0.212 ± 0.001	
	0.205 ± 0.002	
	0.204 ± 0.003	
	0.221 ± 0.002	1.499
0.998 [c]	2.11 ± 0.02	
	2.02 ± 0.02	
	2.09 ± 0.04	

[a] The average from Table 1. [b] Temperature 298.4 K. [c] Temperature 327.3 K.

studied reactions the logarithms of the relative rate coefficients were plotted against the mol fraction of dimethyl sulfoxide (Fig. 1). The observed effect for the hydrolysis of 4-methoxy-3-buten-2-one (plot a) is seen to be typical of the A-2 mechanism since the rate dependence is almost equal to that observed in the A-2 hydrolysis of ethyl acetate (plot b).[18]

The measured solvent effect in the hydrolysis of 4-ethoxy-3-penten-2-one is shown in plot c in Fig. 1. For comparison the logarithms of the rate coefficients of a model A-S_E2 reaction, the hydrolysis of 2-methyl-4-methylene-1,3-dioxolane,[17] are plotted in Fig. 1 as well (plot d). The form of plot c as compared with plots b and d reflects the existence of concurrent A-S_E2 and A-2 reactions in the hydrolysis of 4-ethoxy-3-penten-2-one. In solutions in which the mol fraction of dimethyl sulfoxide is lower than 0.4 a remarkable rate decrease can be observed with increasing DMSO content of the solvent. As shown in plot d this trend is typical of the A-S_E2 mechanism. The effect of the possible A-2 route remains negligible under these conditions, since the rate of the A-2 reaction is almost independent of the solvent composition in solutions in which x_{DMSO} is less than 0.4 (plot b).

If the hydrolysis of 4-ethoxy-3-penten-2-one proceeds, at least partially, through the A-2 route, its contribution should be increased with increasing DMSO content of the solvent while the rate of the A-S_E2 reaction is decreased. In Fig. 1 it can be seen that this is really the case. In solutions in which the mol fraction of DMSO is higher than 0.6, plot c for the hydrolysis of 4-ethoxy-3-penten-2-one is similar to that for the A-2 hydrolysis of ethyl acetate (plot b). Thus in solutions in which the mol fraction of DMSO is higher than 0.6 the contribution of the A-S_E2 reaction in the hydrolysis of 4-ethoxy-3-penten-2-one must be negligible, since otherwise, especially at the lowest water concentrations, the effect of the A-S_E2 reaction should also be observed.

Although the kinetic data determined in dimethyl sulfoxide-water mixtures reveal that the hydrolysis of 4-ethoxy-3-penten-2-one proceeds through concurrent A-S_E2 and A-2 reactions the contributions of the different routes remain still undetermined. This analysis can be performed from kinetic data determined in mixtures of light and heavy water.

Deuterium solvent isotope effects. The kinetic data for the hydrolysis of 4-methoxy-3-buten-2-one (I) and 4-ethoxy-3-penten-2-one (II) in mixtures of light and heavy water are collected in Table 4. In the hydrolysis of the former compound the observed deuterium solvent isotope effect, $k_{D_3O^+}/k_{H_3O^+} = 2.08$, is in contradiction to the A-S_E2 hydrolysis of vinyl ethers, since a reverse isotope effect, $k_{D_3O^+}/k_{H_3O^+} = 0.3 - 0.5$, was to be expected.[1,2] The measured isotope effect is also in excellent agreement with the value obtained by Fedor *et al.*[11] Thus the A-S_E2 mechanism can be excluded in the hydrolysis of 4-methoxy-3-buten-2-one, especially in

view of the fact that catalysis by general acids could not be detected (see above). The measured deuterium solvent isotope effect is, however, in accordance with the A-2 mechanism, since in this case $k_{D_3O^+}/k_{H_3O^+}$ values higher than unity are to be expected.[19] Thus the mechanism proposed by Fedor *et al.*[11] (eqn. 1) seems to be the most probable one when considering the present kinetic data. However, the mechanism given in eqn. 2 cannot be excluded on the basis of the kinetic data discussed above. Therefore additional measurements were performed in heavy water in order to study the possible deuteriation of the α-hydrogen of the vinyl ether which would be the case in the hydrolytic decomposition through reaction (2). When the disappearance of the α- and β-hydrogens was followed, it was found that these rates were equal within the limits of the experimental error. In addition it was found that the coupling of the α-hydrogens remained unaltered during the protolytic reaction. These results can be understood only if the deuteriation does not take place during the progress of the hydrolytic decomposition. Thus reaction (2) can be excluded in the hydrolysis of 4-methoxy-3-buten-2-one.

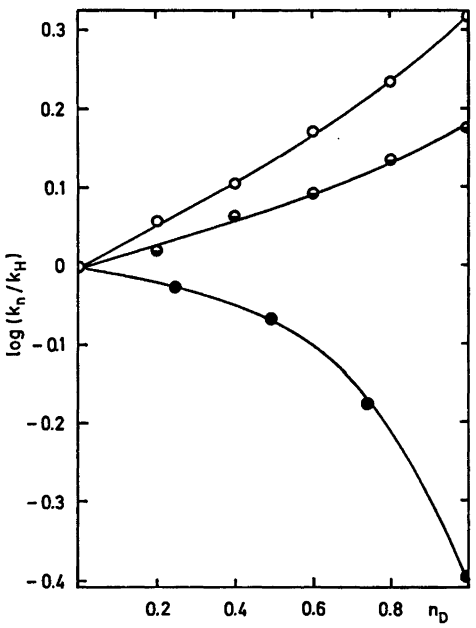

Fig. 2. The logarithms of the rate coefficients in the hydrolysis of vinyl ethers as a function of the deuterium mol fraction of the solvent. Notation: 4-methoxy-3-buten-2-one (open circles), 4-ethoxy-3-penten-2-one (half-filled circles), and 2-chloroethyl vinyl ether (filled circles).[2]

In the hydrolytic decomposition of 4-ethoxy-3-penten-2-one the deuterium solvent isotope effect is found to be 1.50 (Table 4) which is slightly lower than that for the hydrolysis of 4-methoxy-3-buten-2-one but markedly higher than the deuterium solvent isotope effect in the A-S_E2 hydrolysis of vinyl ethers. This situation could be explained if the hydrolysis of 4-ethoxy-3-penten-2-one took place through concurrent A-S_E2 and A-2 reactions. This conclusion was also drawn on the basis of the solvent effects (see above).

Let us denote by k' the rate coefficient for the reaction proceeding through the A-2 mechanism (oxygen protonation) and by k'' the rate coefficient for the A-S_E2 reaction (carbon protonation). In the mixture of light and heavy water, in which the deuterium mol fraction is n, the total rate coefficient can be expressed by eqn. (4). In the particular cases when $n=0$ and $n=1$ the observed rate coefficient can be

$$k_n = k_n' + k_n'' \tag{4}$$

expressed by eqn. (5). As discussed above 4-methoxy-3-buten-2-one (I) hydrolyzes mainly through the A-2 mechanism. As I is closely

$$\begin{aligned} k_{0.0} &= k_{0.0}' + k_{0.0}'' \\ k_{1.0} &= k_{1.0}' + k_{1.0}'' \end{aligned} \tag{5}$$

related to II it can be assumed that in the A-2 hydrolysis of compounds I and II the $k_{D_3O^+}/k_{H_3O^+}$ values are almost equal. Thus the value $k_{1.0}'/k_{0.0}' = 2.078$, obtained for the hydrolysis of 4-methoxy-3-buten-2-one, can also be applied to the hydrolysis of 4-ethoxy-3-penten-2-one proceeding through the A-2 route. The deuterium solvent isotope effect in the A-S_E2 hydrolysis of 4-ethoxy-3-penten-2-one can be estimated on the basis of the kinetic data for vinyl ether hydrolysis. If β-chloroethyl vinyl ether is chosen as the model compound, since its hydrolysis has been studied thoroughly in H_2O-D_2O mixtures,[2] then $k_{1.0}''/k_{0.0}'' = 0.397$. When the deuterium solvent isotope effects given above and the observed rate coefficients for the hydrolysis of 4-ethoxy-3-penten-2-one (Table 4) are substituted into eqn. 5, the following partial rate

coefficients are obtained in light water; $k_{0.0}'' = 0.051$ mol^{-1} dm^3 s^{-1} (carbon protonation) and $k_{0.0}' = 0.092$ mol^{-1} dm^3 s^{-1} (oxygen protonation). Thus the contribution of the carbon protonation is about 35 % in light water, but in heavy water it decreases to 10 % as can be estimated on the basis of the kinetic data.

The existence of concurrent A-2 and A-S_E2 reactions in the hydrolysis of 4-ethoxy-3-penten-2-one (II) is apparent also on the basis of the kinetic data in the mixtures of light and heavy water. From Fig. 2 it can be seen that in all solvent mixtures the deuterium solvent isotope effect in the hydrolysis of compound II is an intermediate between those of A-2 and A-S_E2 reactions. When the rate coefficients of the hydrolysis of 4-ethoxy-3-penten-2-one are calculated from the partial rate coefficients $k_{0.0}'$ and $k_{0.0}''$ given above and from the ratios $k_n'/k_{0.0}'$ and $k_n''/k_{0.0}''$ obtained from plots b and c in Fig. 2, it is found that the calculated values are in excellent agreement with the experimental data, since the difference between the measured and calculated values is in all cases lower than 3 %.

From the kinetic data obtained in the present study it can thus be concluded that the protonation of the β-carbon atom is not a pre-equilibrium process in the hydrolysis of β-acetyl substituted vinyl ethers. The hydrolysis of 4-methoxy-3-buten-2-one proceeds mainly through oxygen protonation. Although in the hydrolysis of 4-ethoxy-3-penten-2-one some evidence for carbon protonation could be observed the general acid catalysis reveals that proton transfer takes place in the rate-limiting step of this reaction.

Acknowledgements. Grants for support of this work from the Finnish Academy, Division of Sciences, are gratefully acknowledged.

REFERENCES

1. Kresge, A. J. and Chiang, Y. *J. Chem. Soc. B* (1967) 53; 58.
2. Salomaa, P., Kankaanperä, A. and Lajunen, M. *Acta Chem. Scand. 20* (1966) 1790.
3. Stamhuis, E. J., Drenth, W. and van der Berg, H. *Rec. Trav. Chim. Pays-Bas 83* (1964) 167.
4. Unverferth, K. and Schwetlick, K. *J. Prakt. Chem. 312* (1970) 882.
5. Cooper, J. D., Vitullo, V. P. and Whalen, D. L. *J. Amer. Chem. Soc. 93* (1971) 6294.
6. a. Loudon, G. M., Smith, C. K. and Zimmerman, S. E. *J. Amer. Chem. Soc. 96* (1974) 465; b. Loudon, G. M. and Berke, C. *J. Amer. Chem. Soc. 96* (1974) 4508.
7. Kankaanperä, A. and Kleemola, S. *Acta Chem. Scand. 23* (1969) 3607.
8. Salomaa, P., Kankaanperä, A., Nikander, E., Kaipainen, K. and Aaltonen, R. *Acta Chem. Scand. 27* (1973) 153.
9. Salomaa, P., Lahti, M. and Kankaanperä, A. *Unpublished results from this laboratory.*
10. Kankaanperä, A. *Acta Chem. Scand. 23* (1969) 1465.
11. a. Fedor, L. R. and McLaughlin, J. *J. Amer. Chem. Soc. 91* (1969) 3594; b. Fedor, L. R., De, N. C. and Gurwara, S. K. *J. Amer. Chem. Soc. 95* (1973) 2905.
12. Taskinen, E. and Liukas, P. *Acta Chem. Scand. B 28* (1974) 114.
13. Taskinen, E. *Unpublished results from this laboratory.*
14. Matesich, M. A. *J. Org. Chem. 32* (1967) 1258.
15. Schaleger, L. L. and Long, F. A. *Advan. Phys. Org. Chem.* (1963) 1.
16. Kreevoy, M. M. and Williams, Jr., J. M. *J. Amer. Chem. Soc. 90* (1968) 6809.
17. Kankaanperä, A. and Merilahti, M. *Acta Chem. Scand. 26* (1972) 685.
18. Tommila, E. and Murto, E. L. *Acta Chem. Scand. 17* (1963) 1957.
19. Salomaa, P., Schaleger, L. L. and Long, F. A. *J. Amer. Chem. Soc. 86* (1964) 1.

Received November 5, 1974.

Acta Chemica Scandinavica A 29 (1975) 427—435

Spectroscopic Studies of 1,1-Dichloro-, *cis*-1,4-Dichloro-, and *cis*-1-Bromo-2-chlorocyclohexane

HANS T. HORNTVEDT and PETER KLÆBOE

Department of Chemistry, University of Oslo 3, Norway

The IR spectra of the three title compounds as liquids, in the solid state at −70 or −180 °C and at ambient temperature under high pressure were recorded in the region 4000 – 200 cm^{-1}. Correspondingly, Raman spectra of the liquids, including semi-quantitative polarization measurements of the dichloro compounds, and spectra of the low temperature solids were recorded.

The spectra of 1,1-dichloro- and *cis*-1,4-dichlorocyclohexane were interpreted in terms of C_s symmetry; the fundamentals were assigned and compared with those of *trans*-1,4-dichlorocyclohexane.

cis-1-Bromo-2-chlorocyclohexane consisted of two conformers (Br(*e*), Cl(*a*) and Br(*a*), Cl(*e*) in the liquid state (at low temperature and under high pressure). Presumably, the two conformers can be simultaneously present in a 1:1 ratio in the crystallographic unit cell.

As a continuation of our spectral studies of halogenated cyclohexanes,[1] we have now investigated 1,1-dichloro-, *cis*-1,4-dichloro-, and *cis*-1-bromo-2-chlorocyclohexane, later to be called 1,1-DCC, 1,4-DCC, and 1,2-BCC, respectively, in this paper. Obviously, 1,1-DCC and 1,4-DCC are transferred into their mirror images upon conversion of the cyclohexane ring, leading to spectra of one single conformation. It was our goal to interpret the IR and Raman spectra of these compounds and compare them with those of related molecules, notably chlorocyclohexane [2–4] and *trans*-1,4-dichlorohexane.[5] Later, we intend to derive force fields for the chlorinated cyclohexanes, partly transferred from the thorough work recently published for cyclohexane itself.[6]

The third compound 1,2-BCC was expected to give more complicated spectra because of the non-identical conformers. These are distinguished by an interchange of the two halogens, Br(*e*), Cl(*a*) and Br(*a*), Cl(*e*), thought to be of nearly equal abundance. We have previously studied the crystalline solids of various *trans*-1,2-dihalocyclohexanes [1,7] (dichloro, dibromo, 1-chloro-2-bromo, 1-chloro-2-iodo, and 1-bromo-2-iodo), revealing a preference for the *aa* conformer with bulky halogens. In 1,2-BCC we wanted particularly to decide which of the two very similar conformers existed in the crystalline state.

EXPERIMENTAL

The sample of 1,1-DCC was prepared from cyclohexanone and phosphorus pentachloride, and was steam distilled, dried and purified by repeated fractional distillation (b.p. 172 °C, n_D (20 °C) 1.4790) according to well known methods.[8] 1,4-DCC was prepared by reacting 1,4-cyclohexandiol with HCl, and separated from the *trans* compound by fractional crystallization.[9] The sample was purified by distillation and subsequent preparative gas liquid chromatography (m.p. 18 °C, n_D (20 °C) 1.4942) and the NMR spectrum found identical with that reported.[10] The sample of 1,2-BCC was prepared by adding hypobromous acid to cyclohexene giving *trans*-2-bromocyclohexanol. This material reacted with thionylchloride in the presence of pyridine. Since this reaction proceeds with inversion [8,11] 1,2-BCC was formed, and separated from the less volatile *trans*-1-bromo-2-chlorocyclohexane by distillation under reduced pressure in a column having 30 theoretical plates. After three times fractionation the sample was better than 99 % pure as checked by gas chromatography (n_D (20 °C) = 1.4982).

The IR and Raman spectrometers, cryostats,

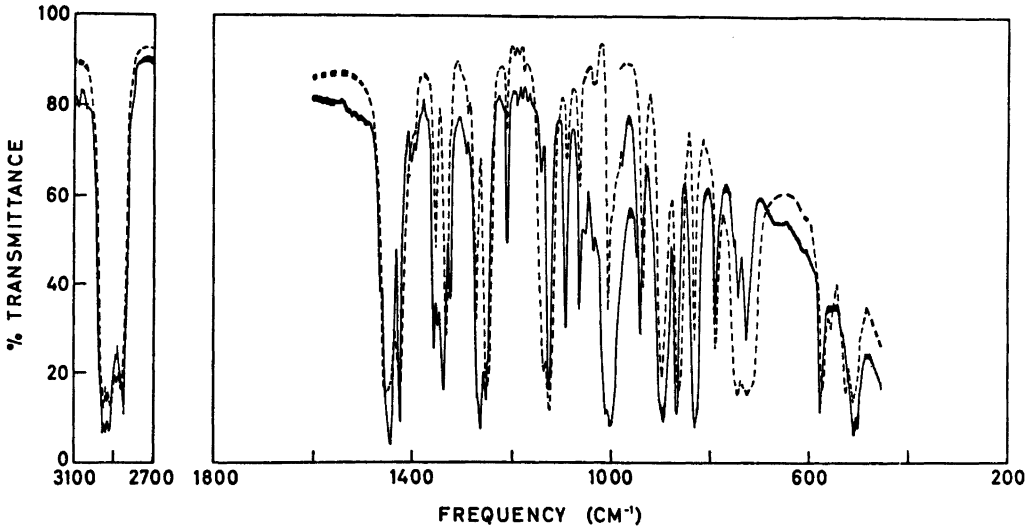

Fig. 1. The IR spectrum of a single crystal of 1,1-dichlorocyclohexane (20 kbar, 50 °C), using planar polarized radiation.

high pressure diamond cell, and general experimental procedure have been described in detail elsewhere.[4,5,7]

RESULTS AND DISCUSSION

With 18 atoms in the molecule 1,1-DCC and 1,4-DCC should have 48 fundamentals whereas 1,2 BCC should have still richer IR and Raman spectra because of the simultaneous presence of two conformers with non-identical vibrational modes. The spectral results were in good agreement with these predictions as seen from Tables 1 (1,1-DCC), 2 (1,4-DCC), and 4 (1,2-DBC). As an illustration of our high pressure technique,[7] the high pressure crystalline solids of the three compounds are given in Figs. 1, 2 and 3, respectively. For 1,1-DCC, a single crystal was prepared and an IR spectrum revealing the dichroism is shown in Fig. 1.

Obviously, 1,1-DCC as well as 1,4-DCC both belong to point group C_s and the 48 fundamentals divide themselves between 27 A' and 21 A''. The IR vapour contours were poorly resolved and therefore not useful for classifying the vibrations into the symmetry species. However, like other chlorinated or brominated cyclohexanes [1,5,7] the present compounds had intense Raman spectra and most of the fundamentals could be assigned with reasonable confidence from the polarization measurements. The resemblance with cyclohexane,[6] chlorocyclohexane,[2-4] and *trans*-1,2-dichlorocyclohexane [1,7] was of considerable help for the interpretations. Most of all, the striking similarity between the spectra of 1,1-DCC and 1,4-DCC with *trans*-1,4-dichlorocyclohexane was of special significance because of the very complete data recently obtained [5] for the latter molecule.

1,1-Dichlorocyclohexane. Our tentative assignments for this molecule are given in Table 1 and for the sake of brevity only some very short comments will be given. The 10 C–H stretching modes (6 $A'+4\,A''$) partly coincided into out-of-phase (above 2900 cm^{-1}) and in-phase (below 2900 cm^{-1}) CH_2 stretches, making the interpretations somewhat ambiguous. Five CH_2 scissoring modes (3 $A'+2\,A''$) were assigned around 1420 cm^{-1} of which ν_9 and ν_{23} presumably overlapped. The corresponding CH_2 wagging modes were found between 1350 and 1250 cm^{-1}. Below, vibrations classified as CH_2 twisting (5) and rocking (5) mixed with six ring stretching modes were observed between 1250 and 530 cm^{-1}.

Particular interest is focused on the C–Cl stretching frequencies since these modes are generally regarded as group frequencies, sensitive to conformational changes in open chain and cyclic compounds.[12] In 1,1-DCC the C–Cl

Table 1. Infrared and Raman spectral data[a] of 1,1-dichlorocyclohexane.

Liquid IR	Raman		Solid Pressure 20 kbar IR		Assignments	
2950 s,sd[b]	2953 m,sd	P	2945 vs[c]		A'	ν_1
2940 s,sd	2941 s	P			A',A''	ν_2, ν_{28}
2920 s,sd	2918 m	D	2920 vs		A',A''	ν_3,ν_{29}
2899 m	2903 m	P	2900 m		A'	ν_4
2860 s	2862 m	P	2862 s		A',A''	ν_5, ν_{30}
2844 m,sd	2842 w	P	2845 m,sd		A',A''	ν_6,ν_{31}
1460 m	1459 w	P?	1462 m		A'	ν_7
1448 s	1449 vs[d]		1449 s		A''	ν_{32}
1444 s,sd	1442 s[d]		1441 s	∥	A'	ν_8
1427 m	1428 m	D	1422 s	∥	A',A''	ν_9, ν_{33}
1397 vw			1399 w	∥		$\nu_{23}+\nu_{41}$
1353 m	1352 w	P	1352 s	⊥	A'	ν_{10}
1345 m,sd	1347 w,sd	D	1347 m	∥	A''	ν_{34}
1336 m	1336 m	P	1333 s		A'	ν_{12}
1317 w	1319 w	D	1322 w	∥	A''	ν_{35}
1268 m	1267 s	P	1269 s	∥	A'	ν_{12}
1260 m,sd			1260 m,sd			$\nu_{23}+\nu_{44}$
1246 s	1247 w	P	1249 vs	∥	A'	ν_{13}
1205 vw	1205 w	D	1209 m	∥	A''	ν_{36}
1136 m	1136 w	P?	1138 m	⊥	A'	ν_{14}
1124 s	1124 m	D	1123 s	⊥	A''	ν_{37}
1082 w	1082 w	D?	1087 m	∥	A''	ν_{38}
1067 vw	1066 m	D	1062 m	∥	A''	ν_{39}
1044 vw	1045 vw		1048 w	∥		$\nu_{21}+\nu_{22}$
1027 w	1027 s	D	1030 m		A''	ν_{40}
1018 w,sd			1018 w,s[d]	∥		$\nu_{22}+\nu_{23}$
1004 vs	1004 s	P	1005 s	∥	A'	ν_{15}
944 vw			945 w,sd			$\nu_{20}+\nu_{46}$
929 w	929 vw		934 m			$\nu_{21}+\nu_{45}$
897 m,sd	897 w,sd	D	896 m,sd[d]		A''	ν_{41}
890 s	890 s	D	889 vs[d]	∥	A''	ν_{42}
864 s	864 s	P	863 vs		A'	ν_{16}
825 s	825 vs	P	829 s	∥	A'	ν_{17}
820 s	820 m,sd	D	819 w,sd		A''	ν_{43}
779 w	781 w	D	784 s	⊥	A''	ν_{44}
766 w,bd			772 w,sd			$\nu_{23}+\nu_{26}$
737 vs	737 m	P	739 s	⊥	A'	ν_{18}
720 vs	721 s	P	722 s	⊥	A'	ν_{19}
570 s	572 vs	P	572 vs	∥	A'	ν_{20}
535 w,sd	535 w	P?	545 w		A'	ν_{21}
521 s	522 s	P	521 s	⊥	A'	ν_{22}
500 s	502 vs	P	503 vs	∥	A'	ν_{23}
460 w	458 w	P	460 w			$2\,\nu_{47}$
389 w	389 w	D?	394 w		A''	ν_{45}
374 m	375 s	D	382 m		A''	ν_{46}
354 m	354 vs	P	355 s		A'	ν_{24}
302 m	303 s	P	310 m		A'	ν_{25}
267 s	270 vs	P	272 s		A'	ν_{26}
234 w	234 w	D	243 w		A''	ν_{47}
207 w	209 vs	P	215 m		A'	ν_{27}
	179 m	D			A''	ν_{48}

[a] Very weak bands in the region 4000–3000 and 2700–1500 cm^{-1} were omitted. [b] Abbreviations: s, strong; m, medium; w, weak; v, very; sd, shoulder, bd, broad, P, polarized; D, depolarized; ∥ and ⊥, dichroic measurements. [c] Intensities obtained by ordinary infrared radiation, contrary to Fig. 1. [d] Bands observed at −170 °C.

Table 2. Infrared and Raman spectral data [a] of *cis*-1,4-dichlorocyclohexane.

Liquid IR	Raman		Solid (−70 °C) IR	Assignment
2956 vs[b]	2961 s	D	2977 s	A'' ν_{28}
			2938 s	A', A' ν_1,ν_2
2912 s	2910 s	P	2911 vs	A', A'' ν_3,ν_4,ν_{29}
2869 s	2872 s	P	2870 s	A',A'' ν_5,ν_{30}
2846 s	2845 s	P	2846 m	A', A'' ν_6,ν_{31}
1460 s	1460 m	D?		
1457 s,sd	1456 m,sd		1458 s	A' ν_7
1442 vs	1442 s	D	1442 s	A'' ν_{32}
1437 s,sd	1434 s	P	1435 s	A' ν_8
1430 s	1430 m	D	1426 m,sd	A'' ν_{33}
1358 m	1356 s	P	1358 s	A' ν_9
1351 s,sd	1349 s	P	1351 s	A' ν_{10}
1345 s	1345 m	D	1347 s	A'' ν_{34}
1318 w	1320 w	D	1318 w	A'' ν_{35}
1301 vw	1300 w		1300 w	$\nu_{17}+\nu_{46}$
1290 vw	1290 w	P?	1290 w	$\nu_{17}+\nu_{24}$
1276 vs	1276 s	P	1277 s	A' ν_{11}
1265 s	1266 m	D?	1266 s	A'' ν_{36}
1238 s	1238 m	P	1238 s	A' ν_{12}
1218 w,sd	1216 w	P	1218 w	$\nu_{18}+\nu_{24}$
1191 s	1191 m	D	1188 s	A'' ν_{37}
1141 m	1141 m	P	1142 m	A' ν_{13}
1121 w	1121 w	D	1121 w	A'' ν_{38}
1095 vw	1096 vw	P	1095 w	A' ν_{14}
1080 m	1081 m	D	1080 s	A'' ν_{39}
1075 m	1076 m	D	1074 s	A'' ν_{40}
1054 w,sd	1055 w,sd	P	1054, w,sd	A' ν_{15}
1024 m	1024 s	D	1024 s	A'' ν_{41}
995 vs	997 s	P	996 s	A' ν_{16}
972 m,sd	970 w	P?	972 m,sd	A' ν_{17}
955 vw			953 vw	$\nu_{23}+\nu_{45}$
932 m	930 m	D	935 vw	A'' ν_{42}
897 s			899 m	A' ν_{18}
876 vs	876 m	D	875 s	A'' ν_{43}
839 w,sd			838 w	$\nu_{23}+\nu_{25}$
827 vs	828 s	P	827 s	A' ν_{19}
805 w			806 w	$\nu_{21}+\nu_{48}$
780 m	775 vs	P	778 s	A' ν_{20}
771 s	771 m,sd		765 s	A'' ν_{44}
756 w,sd	756 w,sd		756 m	$\nu_{23}+\nu_{27}$
715 m	714 s	P	715 w	A' ν_{21}
683 vs	685 s	P	680 s	A' ν_{22}
661 w,sd	662 vw	D?	660 m	$\nu_{24}+\nu_{26}$
588 w,sd	590 w,sd	P	590 w	$2\ \nu_{25}$
566 s	566 vs	P	560 s	A' ν_{33}
470 w	467 w	D	470 w	$\nu_{26}+\nu_{47}$
438 w	437 w	D	439 w	$\nu_{27}+\nu_{47}$
390 m	390 vs	D	385 s	A'' ν_{45}
350 w,sd			348 w	$\nu_{47}+\nu_{48}$
341 m	341 m	D	341 m	A'' ν_{46}
326 s	325 vs	P	326 s	A' ν_{24}
301 vw	300 w,sd	P	302 w	A' ν_{25}
277 vw	279 w	D	278	$\nu_{27}+\nu_{48}$
257 m	257 s	D	261 m	A'' ν_{47}
212 m	213 m	P	216 m	A' ν_{26}
	197 m	P		A' ν_{27}
	94 vs	D		A'' ν_{48}

[a] Very weak bands in the regions 4000–3000 and 2700–1500 cm^{-1} were omitted. [b] For abbreviations, see footnotes to Table 1.

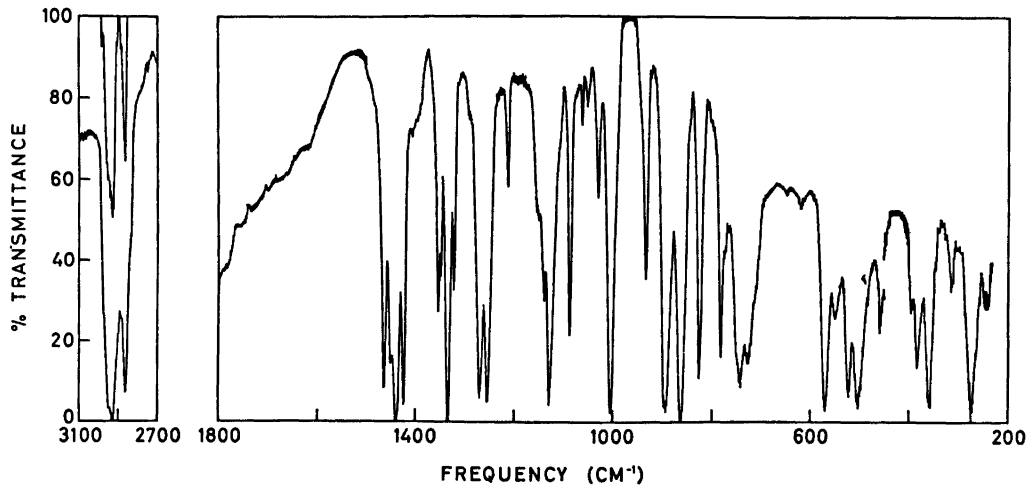

Fig. 2. The IR spectrum of polycrystalline *cis*-1,4-dichlorocyclohexane (20 kbar, 50 °C).

stretching frequencies were tentatively attributed to the intense bands at 737 and 720 cm^{-1}, although the small separation between them seemed surprising. Thus, in the related 2,2-dichloropropane the geminal C–Cl stretching modes were found [13] at 669 and 562 cm^{-1}, suggesting the 570 cm^{-1} band as another possible choice in 1,1-DCC. As apparent from Table 3, however, no C–Cl stretch as low as 570 cm^{-1} has to our knowledge been suggested in cyclohexanes. This leaves us with the 737 and 720 cm^{-1} bands supporting the notion that more than one chlorine on a carbon raises the C–Cl stretching frequency.[14]

Ten additional fundamentals (6 $A'+4$ A'') connected with ring bend and CCX bends are expected, and as apparent from Table 1 they fit nicely in with the experimental data. Only a few weak IR and Raman bands were not assigned as fundamentals and they can easily be interpreted as binary combination bands.

As apparent from Fig. 1 and Table 1, the dichroic ratios (symbolized with $\parallel$ and $\perp$ in Table 1) bear no simple correlation to the symmetry species A' and A''. In order to derive this relationship the orientation of the high pressure single crystal in the diamond cell and the crystallographic space group should be known.

cis-*1,4-Dichlorocyclohexane.* We expect mostly the same number of fundamentals in the respective regions for 1,4-DCC as for 1,1-DCC. The structural differences: four methylene and two methine groups (1,4-DCC) contra five methylene groups (1,1-DCC) will result in slight differences in the various CH_2 stretching and bending

Table 3. Carbon-chlorine stretching vibrations in cyclohexanes.

Compound	Equatorial	Axial
Chlorocyclohexane [a]	731	684
1,1-Dichlorocyclohexane [b]	737	720
cis-1,4-Dichlorocyclohexane [b]	780	683
trans-1,4-Dichlorocyclohexane [c]	782	756
	726	648
trans-1,2-Dichlorocyclohexane [d]	743	695
	736	616

[a] Ref. 4. [b] This work. [c] Ref. 5. [d] Refs. 7 and 12.

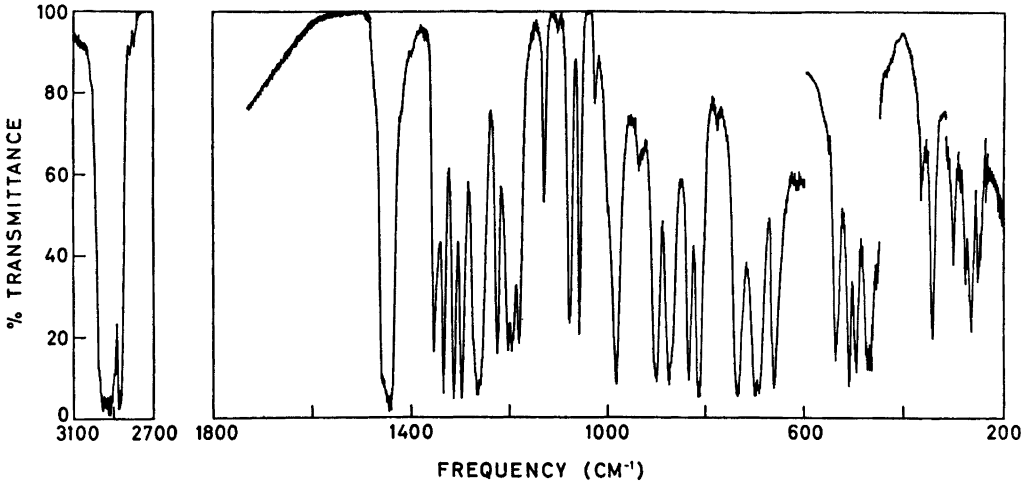

Fig. 3. The IR spectrum of polycrystalline *cis*-1-bromo-2-chlorocyclohexane at ambient temperature (*ca.* 20 kbar pressure).

regions. Also the widely separated heavy chlorine atoms will lead to considerably lower CCCl bending frequencies in 1,4-DCC compared to 1,1-DCC.

The 10 C–H stretching vibrations overlapped considerably as found for cyclohexanes,[5,6] 1,4-dioxan and related compounds.[15] As apparent from Table 2, the various methylene and C–H deformation frequencies appear in the expected regions below 1500 cm^{-1}. The intense bands at 1024 and 995 cm^{-1} in 1,4-DCC (1027 and 1004 cm^{-1} for 1,1-DCC) previously [7] considered as ring stretching modes have diagnostic value for evaluating conformational equilibria in halogenated cyclohexanes.

The bands at 780 and 683 cm^{-1} were interpreted as the C–Cl stretching modes, the former very intense in Raman, the latter in IR. The fundamentals assigned to the "C–Cl stretching modes" (undoubtedly mixed with C–C stretch and CH_2 deformations) for various chlorinated cyclohexanes are shown in Table 3.

Ten additional fundamentals (6 $A'+4$ A'') mainly involving ring bend and CCCl bend were expected below the C–Cl stretching modes and were assigned to distinct IR and Raman bands. The lowest vibrational modes were found at 257, 212, 197 and 94 cm^{-1} in good agreement with the results for *trans*-1,4-dichlorocyclohexane.

cis-*1-Bromo-2-chlorocyclohexane.* Like the other dihalocyclohexanes 1,2-BCC should have approximately 34 fundamentals (CH_2 stretch and scissor excluded) below 1400 cm^{-1} for each conformer. From the IR and Raman frequencies (Table 4) it can be seen that close to 50 bands were observed in this region. Although some of the lines in BCC can be combination bands or overtones the data clearly demonstrate that both conformers Br(*e*), Cl(*a*) and Br(*a*), Cl(*e*) were present. Moreover, the IR and Raman spectra of 1,2-BCC are very similar to those of the *trans*-1,2-dihalocyclohexane [7] and to *trans*-1-bromo-2-chlorocyclohexane [7,16] in particular. This compound had a few additional bands compared to 1,2-BCC which can be explained as additional cases of overlapping bands belonging to both conformers in the latter spectra. It is actually surprising that the two conformers of 1,2-BCC, considering their similarity, have so comparatively few coinciding conformer bands.

As apparent from Table 4 the low temperature IR and Raman spectra of solid 1,2-BCC were practically identical to those of the liquid. No significant cases of bands vanishing in the solid were observed, in spite of several attempts in various cryostats and prolonged annealing just below the melting point. Since we would expect only one conformer in crystalline 1,2-BCC like in other halogenated cyclohexanes, it seemed possible that the low temperature solid was

Table 4. Infrared and Raman spectral data of *cis*-1-bromo-2-chlorocyclohexane.

Liquid IR[a]	Raman	Solid IR High press. (*ca.* 20 kbar)	Low temp [a] (−70 °C)	Raman Low temp (−170 °C)
				2987 w
2959 m[b]	2957 m		2959 m	2955 s
2944 vs	2945 s	2940 vs, bd	2944 vs	2945 vs
	2911 m			2921 m
2902 m,sd	2903 s		2901 m,sd	2903 s
2871 vs			2872 vs	
	2866 s	2867 vs		2860 s
2863 vs			2863 vs	
2850 m,sd	2849 m		2850 m,sd	
1460 s	1458 w,sd	1460 m,sd	1460 s	1457 w
1448 vs	1446 s		1443 vs	1442 m
		1441 vs		
1436 s	1436 m		1434 s	
1356 m	1355 m,sd	1353 m	1356 m	
1346 m	1345 m	1346 m,sd	1346 m	1347 m,sd
1335 m	1334 m	1332 s	1334 s	1336 m
1311 s	1311 m	1311 s	1313 s	1311 m
1298 s	1297 m	1298 s	1297 s	1301 m
1272 s	1271 m	1272 s,bd	1272 m	1275 m
1268 m,sd			1268 m,sd	
1263 vs	1262 s	1260 s	1261 s	1260 s
1224 m	1224 m	1223 s	1224 s	
1203 s	1203 m	1204 s	1204 s	
1196 s	1195 m	1194 s	1195 s	1193 m
1190 w,sd			1191 m,sd	
1180 s	1183 m	1179 s	1181 s	1182 w
1130 m	1131 w	1129 m	1129 s	1130 s
1103 vw		1102 w	1101 w	
1080 m	1080 m	1079 m	1080 m	1082 m
1076 m	1077 m,sd	1074 m	1075 m	1077 w
1056 w	1056 m	1058 m	1057 m	1058 m
			1054 w	
1025 w	1025 m	1027 m	1027 w	1027 m
984 vs	982 s	982 vs	986 vs	986 vs
980 m,sd			981 m	981 m
935 vw	935 vw	938 w	935 w	
904 s	906 m		906 s	908 w
899 m,sd	899 m	901 s	899 s	899 w
877 s	875 s	877 s	877 s	877 vs
870 s	869 s	871 s	871 s	870 s,sd
832 s	832 s	833 s	832 s	834 s
816 s	815 m	817 m	815 s	811 m
809 m	810 m	811 m,sd	810 m	807 w
780 vw		778 w	782 w	
763 vw			761 w	
740 s	739 s	737 s	739 s	732 s
701 s	700 vs	701 s	701 s	698 vs
697 s	694 vs	693 s	694 s	693 s
662 s	662 vs	662 s	662 s	659 s
648 w,sd			647 w	
539 s	539 s	537 s	537 s	532 s
510 m	509 vs	510 s	509 s	509 m
496 m	496 s	496 s	495 m	495 m
473 s	472 s	470 s,bd	473 s	468 vs
465 m,sd			465 m,sd	

Table 4. Continued.

392 vw			390 vw	
369 w	368 w,sd	390 vw	364 w	368 w,sd
		365 m		
357 m	358 m		357 w,sd	359 m
342 s	343 vs	343 s	342 s	341 s
				310 m,sd
299 m	300 s	300 m	299 m	300 s
275 s	276 m,sd	277 m	276 s	279 w
264 s	265 vs	265 s	263 s	264 vs
247 m	248 s	250 m	248 m	244 s
	182 m			180 m
	179 m			174 m
	152 m,sd			
	143 s			147 s
	114 s			118 s
				104 w

[a] Very weak IR bands in the regions 4000 – 3000 cm^{-1} and 2700 – 1500 cm^{-1} are omitted. [b] For abbreviations, see footnotes to Table 1.

amorphous and not truly crystalline. However, the IR and Raman bands were narrow and "looked" crystalline although only few cases of correlation splitting were observed.

The IR spectrum of the high pressure crystal of BCC is shown in Fig. 3. From this curve as well as from the frequencies of Table 3 it can be concluded that no liquid IR bands vanished in the high pressure solid either. Because of the small sample size and low IR signal, large slits were employed in the high pressure recordings and close bands were not always resolved. It is highly significant, however, that the crystallinity of the high pressure solid was ascertained by visual observation in a polarization microscope. Therefore it has to be concluded that the high pressure (probably also the low temperature) crystals contained both conformers. Presumably, the extreme similarity of the conformers in 1,2-BCC makes a mixed crystal consisting of Br(*e*), Cl(*a*) and Br(*a*), Cl(*e*) feasible.

No variations in relative band intensities between the liquid, low temperature or high pressure solids were observed. Moreover, separate recordings of the liquid spectra at −10, 30 and 100 °C did not reveal any relative intensity variations with temperature, indicating a negligible enthalpy difference (ΔH) between the conformers. This is entirely as expected when assuming additive contributions from bromo- and chloro-cyclohexane each having practically the same ΔG values.[17] Therefore, nearly equal concentrations of each conformer seem present in the solids as well as in liquid 1,2-BCC. If the low temperature and high pressure crystals consist of molecules of Br(*a*), Cl(*e*) and Br(*e*), Cl(*a*) conformers of 1:1 ratio in the crystal lattice or if a solid solution of the two conformers are present, cannot be decided.

Both conformations of 1,2-BCC have C_1 symmetry and the vibrational bands therefore all belong to the same symmetry species. Accordingly no information can be extracted from IR vapour band contours or Raman polarization measurements. The spectral region around 1000 cm^{-1} was not as straightforward as for other halogenated cyclohexanes.[5,7] Two bands at 1025 and 984 cm^{-1} can possibly be assigned to one of the conformers and those at 1056 and 980 cm^{-1} to the other, corresponding to 1032 and 1000 cm^{-1} (*aa*) and 1048 and 976 cm^{-1} (*ee*) in *trans*-1-bromo-2-chlorocyclohexane.[7] The close spacing between the bands at 984 and 980 cm^{-1} in 1,2-BCC contrasts the *trans*-1,2-dihalocyclohexanes where the spacing is approximately 25 cm^{-1}.[7]

Extensive studies of the C–hal stretching vibrations in open chains have been reported[11] and successfully applied to cyclohexanes by Altona *et al.*[12] The atom situated *anti* to the halogen influences the C–hal stretching frequency significantly, resulting in equatorial halogens having higher stretching frequencies than axial. Applying suggested values for these frequencies in cyclohexanes,[11,12] the following frequencies were derived: 742 and 660 cm^{-1} for

Br(*a*) Cl(*e*) and 686 and 685 cm*a*[1] for Br(*e*) Cl(*a*). As apparent from Table 4, four bands of high intensity in IR as well as in Raman were observed at 740, 701, 697, and 662 cm^{-1} presumably connected with the C–hal stretching modes. Accordingly, these frequencies can tentatively be assigned as the C–Cl(*e*), C–Br(*e*), C–Cl(*a*), and C–Br(*a*) stretches, respectively, the high and low frequency bands belonging to conformer Br(*a*), Cl(*e*) and the doublet at 701 and 697 cm^{-1} belonging to Br(*e*), Cl(*a*). The extremely close spacing of the doublet ($\Delta\nu \sim 5$ cm^{-1}) is very surprising for two fundamentals of the same molecule and might suggest very little vibrational interaction between the two stretching movements.

Acknowledgement. The authors are very grateful to the late Kaare Lunde of this department for many helpful discussions and for preparing the three samples. Financial support from NAVF is acknowledged.

REFERENCES

1. Hornvedt, H. T. and Klæboe, P. *Acta Chem. Scand. 26* (1972) 3797 and earlier references cited.
2. Kozima, K. and Sakashita, K. *Bull. Chem. Soc. Jap. 31* (1958) 796.
3. Remizov, A. B. and Sverdlov, L. M. *Izv. Vyssh. Ucheb. Zaved. Fiz. 11* (1968) 150.
4. Klæboe, P. *Acta Chem. Scand. 23* (1969) 2641.
5. Ellestad, O. H. and Klæboe, P. *J. Mol. Struct. 26* (1975) 25.
6. Wiberg, K. B. and Shrake, A. *Spectrochim. Acta A 27* (1971) 1139; *A 29* (1973) 567, 583.
7. Klæboe, P. *Acta Chem. Scand. 25* (1971) 695.
8. Carrol, B., Kubler, D. G., Davis, H. W. and Whaley, A. M. *J. Amer. Chem. Soc. 73* (1951) 5382.
9. Kwestroo, W., Meijer, F. A. and Havings, E. *Rec. Trav. Chim. Pays-Bas T 73* (1954) 717.
10. Wood, G. and Woo, E. P. *Can. J. Chem. 45* (1967) 2477.
11. Stevens, H. C. and Grummit, O. *J. Amer. Chem. Soc. 74* (1952) 4876.
12. Altona, C. *Tetrahedron Lett.* (1968) 2325; Altona, C., Hageman, H. J. and Havinga, E. *Spectrochim. Acta A 24* (1968) 633.
13. Klæboe, P. *Spectrochim. Acta A 26* (1970) 977; Green, J. H. S. and Harrison, D. J. *Spectrochim. Acta A 27* (1971) 1217.
14. Colthup, N. B., Daly, L. H. and Wiberley, S. E. *Introduction to Infrared and Raman Spectroscopy*, Academic, New York 1964.
15. Ellestad, O. H., Klæboe, P. and Hagen, G. *Spectrochim. Acta A 27* (1971) 1025; *A 29* (1973) 1247.
16. Hornvedt, H. T. and Klæboe, P. *Acta Chem. Scand. 25* (1971) 772.
17. Jensen, F. R., Bushweller, C. H. and Beck, B. H. *J. Amer. Chem. Soc. 91* (1969) 344.

Received November 26, 1974.

Acta Chemica Scandinavica A 29 (1975) 436—442

Structures of Linear Multisulfur Systems. IX. The Crystal and Molecular Structure of 2,6-Bis(*p*-methoxyphenyl-1,2-dithiole-3-ylidene)cyclohexanethione Carbon Disulfide Solvate, $C_{26}H_{22}O_2S_5 \cdot \frac{1}{2}CS_2$

JORUNN SLETTEN

Department of Chemistry, University of Bergen, N-5014 Bergen, Norway

Crystals of the title compound, $C_{26}H_{22}O_2S_5 \cdot \frac{1}{2}CS_2$, are triclinic, space group $P\bar{1}$, with $Z=2$ in a unit cell of dimensions $a=9.871(5)$ Å, $b=11.705(2)$ Å, $c=10.918(1)$ Å, $\alpha=90.84(1)°$, $\beta=94.32(1)°$, $\gamma=90.58(1)°$. 5760 unique reflections were recorded on an off-line four-circle diffractometer. The structure was solved by Patterson synthesis, and refined by full-matrix least-squares technique to an R of 0.049. The sulfur atoms of the 5-sulfur molecule are approximately collinearly arranged. The S—S bonds are all partial bonds with bond lengths in the region between a single bond and van der Waals distance. Although the molecule is symmetrically substituted, the sulfur row shows a pronounced deviation from twofold symmetry with distances: S(1)—S(2) = 2.113 Å, S(2)—S(3) = 2.626 Å, S(3)—S(4) = 2.396 Å, S(4)—S(5) = 2.271 Å. The carbon disulfide molecule is disordered around a centre of symmetry.

In a symmetrically substituted thiathiophthene the S—S bonds are expected to be of equal length according to the simple valence bond resonance.

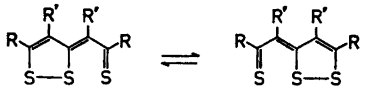

(Ia) (Ib)

A linear five-sulfur compound may be considered as two fused thiathiophthene molecules. Using the same simple valence bond formalism as above, the two central S—S bond lengths would be expected to be longer than the terminal ones.

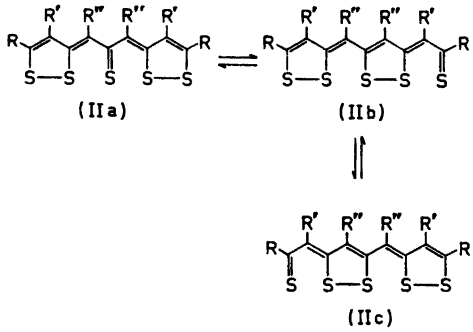

(IIa) (IIb) (IIc)

It might be interesting to find out if the overall length of the five-sulfur sequence is equal to twice the chain length in thiathiophthenes, and if any of the three canonical forms are predominant.

Previously the structure of one symmetrically substituted five-sulfur compound has been determined.[1] The sulfur sequence of the molecule is symmetrical within experimental error. A comparison of the S—C bond lengths indicates that IIa is the more dominant resonance form. Furthermore, half the overall chainlength of 4.76 Å is significantly longer than the S···S···S length in any of the thiathiophthene structures reported.

EXPERIMENTAL

The compound was synthesized by Stavaux and Lozac'h.[2,3] Very dark bluish crystals grew from a carbon disulfide solution by slow

Table 1a. Atomic coordinates and anisotropic thermal parameters with the corresponding standard deviations, referring to the last decimal places, listed in parentheses. Values for coordinates are multiplied by 10^5, thermal parameters by 10^4. The anisotropic temperature factors are defined by: $T_i = \exp\ [-2\pi^2(U_{11}h^2a^{*2} + U_{22}k^2b^{*2} + U_{33}l^2c^{*2} + 2U_{12}hka^*b^* + 2U_{23}klb^*c^* + 2U_{13}hla^*c^*)]$.

Atom	X/a	Y/b	Z/c	U_{11}	U_{22}	U_{33}	U_{12}	U_{23}	U_{13}
S(1)	−6845(7)	70421(6)	4786(6)	392(4)	541(4)	351(3)	146(3)	69(3)	94(3)
S(2)	1567(6)	61541(6)	20211(6)	310(3)	487(4)	314(3)	87(3)	21(3)	76(2)
S(3)	12616(7)	51144(7)	39582(6)	329(3)	637(5)	317(3)	144(3)	25(3)	104(3)
S(4)	22169(6)	42872(6)	58184(6)	306(3)	561(4)	295(3)	64(3)	−7(3)	88(2)
S(5)	31572(7)	35064(7)	75703(6)	328(4)	712(5)	315(3)	105(3)	65(3)	61(3)
O(1)	2225(25)	83394(20)	−52971(18)	841(16)	701(15)	401(11)	86(12)	185(10)	33(11)
O(2)	83465(22)	3081(20)	96249(20)	615(14)	778(16)	616(13)	281(12)	176(12)	−12(11)
C(1)	5914(25)	67070(22)	−4601(22)	335(13)	398(14)	314(12)	−14(11)	−10(10)	52(10)
C(2)	15834(25)	60389(23)	444(22)	320(13)	483(15)	318(12)	32(11)	−3(11)	75(10)
C(3)	15662(24)	56591(22)	12826(21)	304(12)	403(14)	303(12)	10(10)	−27(10)	65(10)
C(4)	25561(24)	49842(22)	18570(21)	296(12)	441(14)	282(12)	28(11)	−34(10)	56(9)
C(5)	25530(24)	46808(22)	31178(21)	283(12)	421(14)	302(12)	12(10)	−38(10)	74(9)
C(6)	36050(24)	40579(21)	37403(21)	295(12)	404(14)	310(12)	30(10)	−21(10)	63(10)
C(7)	35769(24)	38318(21)	49913(21)	303(12)	383(14)	320(12)	23(10)	−23(10)	57(10)
C(8)	46100(25)	32238(23)	56761(22)	334(13)	500(16)	334(13)	79(12)	11(11)	54(10)
C(9)	45516(25)	29911(23)	68874(22)	315(13)	463(15)	349(13)	5(11)	5(11)	40(10)
C(10)	4893(26)	71604(21)	−17145(22)	368(13)	363(14)	343(13)	−17(11)	31(10)	35(10)
C(11)	−6160(28)	77983(27)	−21405(26)	412(15)	668(20)	434(15)	117(14)	110(14)	104(12)
C(12)	−7477(31)	82116(28)	−33277(28)	515(18)	630(20)	488(17)	125(15)	159(14)	2(14)
C(13)	2456(32)	79906(24)	−41092(25)	612(19)	420(16)	361(14)	−25(14)	59(12)	55(13)
C(14)	13746(32)	73708(26)	−36971(25)	585(18)	587(19)	384(15)	108(15)	64(13)	149(13)
C(15)	14869(29)	69546(25)	−25219(25)	468(16)	544(17)	386(14)	119(13)	70(12)	98(12)
C(16)	−10004(40)	88228(32)	−58065(30)	874(27)	749(24)	512(19)	−32(20)	198(17)	−116(18)
C(17)	37283(24)	45817(24)	11461(21)	312(13)	639(18)	277(12)	92(12)	−11(12)	65(10)
C(18)	43610(27)	35118(25)	16753(23)	399(14)	588(17)	344(13)	132(13)	−72(12)	88(11)
C(19)	47786(26)	36534(25)	30350(23)	370(14)	595(17)	323(12)	163(13)	25(12)	94(10)
C(20)	55489(26)	23120(23)	76234(22)	347(13)	450(15)	341(12)	6(11)	9(11)	11(10)
C(21)	52846(29)	19513(26)	87864(25)	411(15)	581(18)	387(14)	92(13)	63(13)	86(12)
C(22)	61828(32)	12751(28)	94876(27)	527(18)	634(20)	407(15)	102(15)	150(14)	63(13)
C(23)	73836(30)	9579(25)	90284(26)	473(16)	461(16)	469(15)	84(13)	35(13)	−30(13)
C(24)	76776(31)	13251(28)	78697(28)	407(16)	689(21)	519(17)	144(15)	69(15)	78(13)
C(25)	67883(29)	19981(28)	71947(26)	395(15)	675(20)	386(14)	88(14)	96(14)	75(12)
C(26)	81662(45)	49(36)	108528(36)	730(26)	540(22)	618(22)	119(20)	170(18)	−80(18)

Table 1b. Coordinates and isotropic thermal parameters for CS_2 and hydrogen atoms with corresponding standard deviations in parentheses. Values for coordinates are multiplied by a factor of 10^4, and thermal parameters by 10^3. Temperature factors are defined by $T_i = \exp[-8\pi^2 U(\sin^2\theta)/\lambda^2]$.

Atom	X/a	Y/b	Z/c	U	Atom	X/a	Y/b	Z/c	U
S(61)	4372(6)	9549(4)	6440(5)	150(2)	H(172)	4418(27)	5259(23)	1184(23)	44(8)
S(62)	5678(5)	10309(4)	4150(5)	144(2)	H(181)	3726(27)	2843(23)	1506(24)	46(8)
C(27)	5081(14)	9883(11)	5357(9)	79(3)	H(182)	5169(26)	3277(22)	1214(23)	42(7)
H(2)	2285(27)	5788(22)	−380(23)	44(8)	H(191)	5116(26)	2963(22)	3374(23)	40(7)
H(8)	5389(28)	2895(23)	5253(24)	47(8)	H(192)	5533(30)	4337(25)	3199(27)	59(9)
H(11)	−1313(31)	7940(26)	−1620(27)	60(9)	H(21)	4466(31)	2186(25)	9127(26)	49(8)
H(12)	−1563(31)	8675(26)	−3528(27)	63(9)	H(22)	5937(36)	995(30)	10256(33)	78(11)
H(14)	2040(27)	7196(23)	−4256(24)	47(8)	H(24)	8602(32)	1112(26)	7595(27)	53(8)
H(15)	2323(31)	6487(26)	−2312(27)	60(9)	H(25)	7086(30)	2294(25)	6429(28)	54(9)
H(161)	−1222(33)	9472(29)	−5451(30)	74(10)	H(261)	8112(41)	554(36)	11405(37)	87(14)
H(162)	−886(42)	8960(35)	−6634(38)	107(14)	H(262)	8954(42)	−523(35)	11092(35)	99(13)
H(163)	−1832(41)	8352(35)	−5749(36)	105(14)	H(263)	7331(40)	−479(34)	10921(33)	83(13)
H(171)	3425(28)	4456(23)	311(24)	48(8)					

evaporation at 5 °C. The crystal used throughout the data collection had dimensions 0.69 mm × 0.41 mm × 0.16 mm and was mounted along its longest dimension which is parallel to the [101] vector. Weissenberg and precession photographs showed that the space group was triclinic. Unit cell dimensions were derived from diffractometer measurement of 2θ values for 21 reflections using Mo$K\alpha$ radiation ($\lambda_{\alpha 1}$ = 0.70926 Å). The density as measured by flotation in a KI-water solution is 1.47 g cm^{-3}. This does not agree with the density calculated for two $C_{26}H_{22}O_2S_5$ molecules (later referred to as "5S" molecules) per unit cell. It is likely that CS_2 has cocrystallized. The density calculated for two "5S" molecules and one CS_2 molecule per unit cell is 1.49 g cm^{-3}.

5760 unique reflections with $2\theta \leqslant 55°$ were measured according to the experimental procedure described elsewhere.[4] No significant deterioration was detected during the course of data collection. The crystals do, however, disintegrate over a period of approximately six months at room temperature.

947 of the reflections were less than twice the estimated error in measurement, these reflections were given the threshold value of $2\sigma_c$ and were not included in the refinement unless $|F_c| > |F_{threshold}|$. Standard deviations in intensities were calculated as $\sigma_I = k[\sigma_c^2 + (0.02\ N_{net})^2]^{\frac{1}{2}}$, where k is the appropriate scale factor, σ_c is the estimated error due to counting statistics and N_{net} is the net count, ($N_{scan} - N_{background}$), of the reflection. Standard deviations in structure factors were calculated as $\sigma_F = \sigma_I/2(I\ Lp)^{\frac{1}{2}}$. The data were corrected for Lorentz and polarization effects according to standard procedures and for absorption using the method of Coppens *et al.*[5]

CRYSTAL DATA

$C_{26}H_{22}O_2S_5 \cdot \frac{1}{2}CS_2$; M.W. = 564.95. Crystal system triclinic, space group $P\bar{1}$ (or $P1$). Cell dimensions: $a = 9.871(5)$ Å, $b = 11.705(2)$ Å, $c = 10.918(1)$ Å, $\alpha = 90.84(1)°$, $\beta = 94.32(1)°$, $\gamma = 90.58(3)°$.

$V = 1258$ Å^3, $Z = 2$.

$D_x = 1.492$ g cm^{-3}, $D_m = 1.47$ g cm^{-3}.

$\mu_{MoK\alpha} = 4.9$ cm^{-1}.

Table 2. Bond angles, not involving hydrogen atoms, with the corresponding standard deviations, referring to the last demical places, in parentheses.

Angle	(°)	Angle	(°)
S(2) – S(1) – C(1)	95.63(9)	C(7) – C(8) – C(9)	122.7(2)
S(1) – S(2) – S(3)	177.91(3)	S(5) – C(9) – C(8)	116.1(2)
S(1) – S(2) – C(3)	94.55(8)	S(5) – C(9) – C(20)	118.8(2)
S(3) – S(2) – C(3)	85.17(8)	C(8) – C(9) – C(20)	125.1(2)
S(2) – S(3) – S(4)	175.61(3)	C(1) – C(10) – C(11)	121.1(2)
S(2) – S(3) – C(5)	89.49(8)	C(1) – C(10) – C(15)	121.5(2)
S(4) – S(3) – C(5)	93.95(8)	C(11) – C(10) – C(15)	117.4(2)
S(3) – S(4) – S(5)	179.05(3)	C(10) – C(11) – C(12)	122.0(2)
S(3) – S(4) – C(7)	87.66(8)	C(10) – C(12) – C(13)	119.5(2)
S(5) – S(4) – C(7)	91.50(8)	C(12) – C(13) – C(14)	119.6(2)
S(4) – S(5) – C(9)	94.12(9)	C(12) – C(13) – O(1)	124.9(2)
S(1) – C(1) – C(2)	115.5(2)	C(14) – C(13) – O(1)	115.6(2)
S(1) – C(1) – C(10)	117.7(2)	C(13) – C(14) – C(15)	120.4(2)
C(2) – C(1) – C(10)	126.7(2)	C(10) – C(15) – C(14)	121.1(2)
C(1) – C(2) – C(3)	121.2(2)	C(13) – O(1) – C(16)	117.1(2)
S(2) – C(3) – C(2)	113.1(2)	C(4) – C(17) – C(18)	112.0(2)
S(2) – C(3) – C(4)	122.8(2)	C(17) – C(18) – C(19)	111.8(2)
C(2) – C(3) – C(4)	124.1(2)	C(6) – C(19) – C(18)	111.4(2)
C(3) – C(4) – C(5)	122.6(2)	C(9) – C(20) – C(21)	120.8(2)
C(3) – C(4) – C(17)	119.4(2)	C(9) – C(20) – C(25)	122.3(2)
C(5) – C(4) – C(17)	118.0(2)	C(21) – C(20) – C(25)	117.0(2)
S(3) – C(5) – C(4)	119.8(2)	C(20) – C(21) – C(22)	122.2(2)
S(3) – C(5) – C(6)	116.9(2)	C(21) – C(22) – C(23)	119.4(2)
C(4) – C(5) – C(6)	123.3(2)	C(22) – C(23) – C(24)	119.3(2)
C(5) – C(6) – C(7)	120.7(2)	C(22) – C(23) – O(2)	125.1(2)
C(5) – C(6) – C(19)	119.0(2)	C(24) – C(23) – O(2)	115.7(2)
C(7) – C(6) – C(19)	120.4(2)	C(23) – C(24) – C(25)	120.6(3)
S(4) – C(7) – C(6)	120.9(2)	C(20) – C(25) – C(24)	121.4(2)
S(4) – C(7) – C(8)	115.6(2)	C(23) – O(2) – C(26)	118.2(3)
C(6) – C(7) – C(8)	123.5(2)		

STRUCTURE DETERMINATION AND REFINEMENT

The intensity distribution clearly suggested a centrosymmetric structure, thus the space group was assumed to be $P\bar{1}$ rather than $P1$. The sulfur atoms of the "5S" molecule were localized from a three dimensional Patterson synthesis. Structure factor calculation based on five sulfur atoms gave an R of 0.57 ($R = \sum||F_o| - |F_c||/\sum|F_o|$). The remaining non-hydrogen atoms of the "5S" molecule were found in two subsequent Fourier maps. An elongated region of electron density with centre of gravity in $(\frac{1}{2},1,\frac{1}{2})$ indicated the presence of a three-atomic molecule with the central atom in the centre of symmetry. Tentatively half a CS_2 molecule was included in the asymmetric unit. During the course of refinement these atoms got abnormal temperature parameters. A difference map indicated that a disordered model would be more appropriate. The model arrived at is one where the CS_2 molecule is slightly displaced from the centre of symmetry, and is situated on alternate sides of the centre in different unit cells throughout the crystal. The occupancy factors of the CS_2 atoms were refined; the values arrived at did not deviate significantly from 0.5. The CS_2 atoms were refined with isotropic, and the remaining atoms with anisotropic thermal parameters in the full-matrix least-squares refinement, minimizing the function $\sum w(|F_o| - |F_c|)^2$, where $w = 1/\sigma_F$. Hydrogen atoms were located from a difference map and were included in the refinement with isotropic temperature factors.

At the end of the refinement it was found that a few strong, low order reflections clearly suffered from extinction. A correction for secondary extinction was thus carried out according to the method of Zachariassen.[6] The extinction coefficient arrived at is 0.89×10^{-6}, the maximum correction in F_{obs} amounting to 26 %.

The refinement converged at a conventional R of 0.049, and a weighted R of 0.050. The standard deviation of an observation of unit weight, $[\sum w(|F_o| - |F_c|)^2/(m-n)]^{\frac{1}{2}}$, is 3.88. Atomic scattering factors used were for sulfur, oxygen, and carbon those of Hanson *et al.*[7] and for hydrogen those of Stewart *et al.*[8]

The final atomic positional and thermal parameters with standard deviations as estimated from the inverse least-squares matrix, are listed in Tables 1 and 2. Lists of observed and calculated structure factors may be obtained from the author.

THERMAL MOTION

The thermal parameters were analyzed in terms of rigid body motion according to the method of Schomaker and Trueblood.[9] The thermal motions of the 14 atoms in "rings" A, B, C, D (Fig. 1) are described reasonably well by the r.b.m. approximation; the r.m.s. difference between observed and calculated U_{ij}'s being 0.0020 Å^2. The axis of largest libration is approximately parallel to the row of sulfur atoms, the angle of libration being 5.4°. Bond distances corrected for rigid body motion were calculated according to

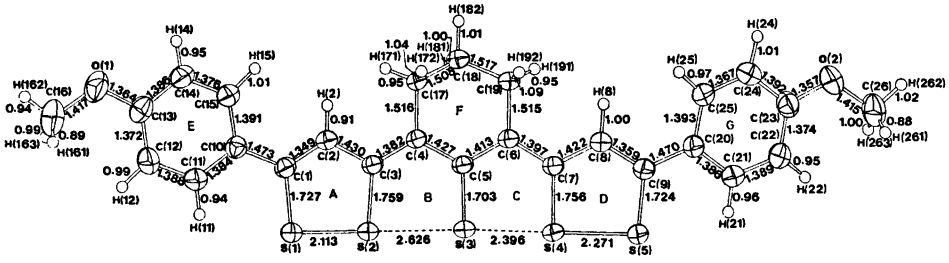

Fig. 1. Bond distances (not corrected for thermal motion) in the „5S" molecule. Standard deviations in S–S, S–C, C–C(O) and C–H bonds are 0.001, 0.003, 0.004, and 0.04 Å, respectively. The thermal ellipsoids are plotted at the 50 % probability level; H atoms are drawn with a fixed radius.

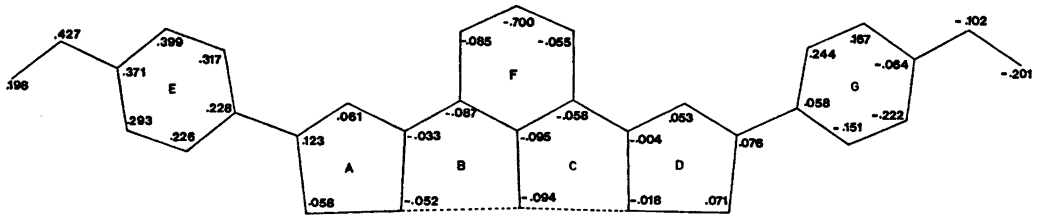

Fig. 2. Atomic deviations from the least-squares plane through rings A+B+C+D.

Cruickshank's method.[10] The corrections in S−S bond lengths amount to only 0.001 Å, and are thus not significant, corrections in C−S bonds are 0.008 Å, while C−C bond length corrections in rings A, B, C, D are in the range 0.001−0.002 Å.

RESULTS AND DISCUSSION

Bond distances are shown in Fig. 1, and the bond angles except those involving hydrogen atoms are listed in Table 2. The five sulfur atoms are almost collinearly arranged, the angles S(1)−S(2)−S(3), S(2)−S(3)−S(4) and S(3)−S(4)−S(5) being 177.91, 175.31, and 179.05°, respectively. Each of the five-membered rings, A, B, C, and D (Fig. 2) is approximately planar. The molecule is, however, slightly but significantly bent around the S(3)−C(5) bond, the angle between the planes through A+B and C+D being 4.4°. A similar geometry has also been observed in the two other five-sulfur compounds studied.[1,11] The four intramolecular sulfur-sulfur distances are all significantly longer than single bonds of 2.10 Å,[12] suggesting partial bonding between all sulfur atoms. The σ-bonding in the sulfur sequence may be formally considered as a 5-centre-6-electron system delocalized across the five atoms. This is quite analogous to the 3-centre-4-electron delocalized σ-bonding proposed for the thia-thiophthenes.[13]

In the linear five-sulfur compounds studied previously the feature of partial bonding between the sulfur atoms is also obvious, III, IV.

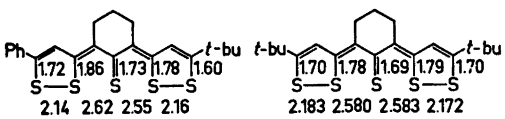

In the unsymmetrically substituted compound (III) the sulfur sequence shows a small deviation from twofold symmetry; while in the symmetrically substituted compound (IV) the S···S row has twofold symmetry within the experimental error. In the present compound however, the deviation from symmetry in the sulfur sequence is pronounced, although the molecule is symmetrically substituted. There is a sligth difference in conformation between the two halves of the molecule, as the plane of the phenyl group E is twisted 2.5° relative to the plane of ring A; while phenyl group G, is twisted around the C(9)−C(20) bond and bent out of the plane of ring D by 12.0°. It is unlikely, however, that this small difference in twist angles may account for the observed asymmetry in the S···S sequence. On the other hand the intermolecular environment of the two halves of the molecule is quite different. Dithiole ring A is sandwiched between the corresponding ring A′ of a centrosymmetrically related molecule $(-x,1-y,-z)$, and the phenyl group G″ of the molecule in position $1-x,1-y,1-z$. The distances between the partially overlapping rings are in the range 3.4−3.5 Å. Dithiole ring D, is partially overlapping the saturated ring F″, the interplanar spacing being 3.7 Å [excluding atom C(18)″]. The central sulfur atom S(3) is situated above the centre of phenylgroup E′ at a distance of 3.65 Å. Furthermore there are intermolecular S···S contacts in the range 3.361 to 3.537 Å between molecules related by a centre of symmetry, $-x,1-y,1-z$. One may notice that while S(1) has only one such contact, S(1)···S(5)‴= 3.420 Å, S(5) has two contacts, S(5)···S(1)‴= 3.420 Å and S(5)···S(2)‴=3.361 Å.

The mutual interaction between the π-systems of the aromatic rings A, A′, and G″, and between phenyl group E′ and S(3) may produce an overall shift of electron density

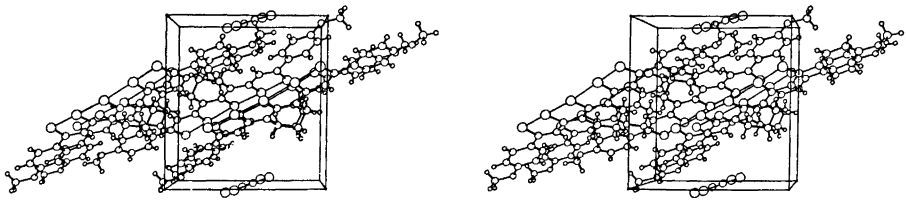

Fig. 3. Stereodrawing showing the packing of molecules in the crystal lattice. CS_2 molecules are drawn at both of the fractional sites. The a^*-axis is pointing towards the viewer, the b-axis is running vertically, top to bottom, and c horisontally, left to right. Figs. 1 and 3 were drawn by use of the ORTEP program.[17]

in the sulfur sequence from S(1) towards S(5). Theoretical calculations have shown that such a redistribution of charge is consistent with a shortening of S(1)–S(2) and a lengthening of S(4)–S(5).[14]

The variation in S–S bond lengths in the molecule is consistent with a predominance of the canonical form IIa. The asymmetry indicates that resonance form IIb is energetically more favourable than IIc due to intra- and intermolecular forces. The overall chain length is significantly shorter in this five-sulfur compound than in the two previous ones (III, IV). However, the shortening is mainly concentrated in the S(3)···S(5) portion of the chain.

There are no short contacts between the "5S" molecule and the cocrystallized CS_2 molecule. Due to the disorder, the dimensions in CS_2 are not accurately determined, C(27)–S(61) = 1.47(2) Å, C(27)–S(62) = 1.57(2) Å, ∠S–C–S = 173(1)°. The average C–S distance agrees reasonably well with the distance of 1.553 Å as determined by IR and microwave spectroscopy.[15,16]

The packing of the molecules in the unit cell is illustrated in the stereodrawing, Fig. 3.

Acknowledgement. The author is indebted to Dr. M. Stavaux for supplying a sample of the compound.

REFERENCES

1. Kristensen, R. and Sletten, J. *Acta Chem. Scand. 27* (1973) 2517.
2. Stavaux, M. and Lozac'h, N. *Bull. Soc. Chim. Fr.* (1968) 4273.
3. Stavaux, M. *Bull Soc. Chim. Fr.* (1971) 4429.
4. Sletten, J. *Acta Chem. Scand. 28* (1974) 989.
5. Coppens, P., Leiserowitz, L. and Rabinovich, D. *Acta Crystallogr. 18* (1965) 1035.
6. Zachariassen, W. H. *Acta Crystallogr. 16* (1963) 1139.
7. Hanson, H. P., Hermann, F., Lea, J. D. and Skillmann, S. *Acta Crystallogr. 17* (1964) 1040.
8. Stewart, R. F., Davidson, E. R. and Simpson, W. T. *J. Chem. Phys. 42* (1965) 3175.
9. Schomaker, T. and Trueblood, K. N. *Acta Crystallogr. B 24* (1968) 63.
10. Cruickshank, D. W. J. *Acta Crystallogr. 9* (1956) 757.
11. Sletten, J. *Acta Chem. Scand. 24* (1970) 1464.
12. Hordvik, A. *Acta Chem. Scand. 20* (1966) 1885.
13. Gleiter, R. and Hoffman, R. *Tetrahedron 24* (1968) 5899.
14. Sletten, J. *To be published.*
15. Allen, H. C., Plyler, E. K. and Blaine, L. R. *J. Amer. Chem. Soc. 78* (1956) 4843.
16. Guenther, A. H., Wiggins, T. A. and Rank, D. H. *J. Chem. Phys. 28* (1958) 682.
17. Johnson, C. K. *ORTEP, A Fortran Thermal Ellipsoid Plot Program for Crystal Structure Analysis*, Report ORNL-3794, Oak Ridge National Laboratory, Oak Ridge, Tennessee 1970.

Received December 6, 1974.

Acta Chemica Scandinavica A 29 (1975) 443—452

Compounds with the Marcasite Type Crystal Structure. XI. High Temperature Studies of Chalcogenides

ARNE KJEKSHUS and TROND RAKKE

Kjemisk Institutt, Universitetet i Oslo, Blindern, Oslo 3, Norway

High temperature investigations by X-ray diffraction, DTA, and quenching experiments have been performed for FeS_2, $FeSe_2$, $FeTe_2$, $CoTe_2$, and $CuSe_2$, and syntheses and characterizations of $OsTe_2$ are reported. The transition properties of these compounds are discussed in relation to the FeS_2-*m versus* FeS_2-*p* type structure.

Despite all endeavours already devoted to studies of the relationship between the FeS_2-*p* (*p* = pyrite) and FeS_2-*m* (*m* = marcasite) type structures (*cf.* Ref. 1 and references therein), mostly speculative thoughts rather than decisive facts have been accumulated. In all, eight binary dichalcogenides have so far been reported (see Ref. 1) to take both of these structure types, *viz.* NaO_2, FeS_2, $FeSe_2$, $FeTe_2$, $OsTe_2$, $CoSe_2$, $CoTe_2$, and $CuSe_2$. Of these, $CoSe_2$ is in a special position in that its FeS_2-*m* type modification refers [2] to a poorly characterized mineral sample whose existence may be stabilized by smaller or larger amounts of impurities (*e.g.* Fe).

The FeS_2-*p* type modifications of $FeSe_2$, $FeTe_2$, $CoTe_2$, and $CuSe_2$ have hitherto only been generated by high pressure/high temperature syntheses,[3] whereas their FeS_2-*m* type modifications are easily obtained by the conventional sealed silica capsule technique.[4,5] For FeS_2 an opposite situation prevails in that its FeS_2-*m* modification appears to require hydrothermal conditions.[6]

The existence of two modifications of $OsTe_2$ has only rather recently been discovered [7] and the *pure* FeS_2-*m* variant of this compound has not yet been obtained. However, our prior knowledge [5] strongly suggests that the FeS_2-*m* type modification of $OsTe_2$ can be obtained in the pure form by syntheses at temperatures $< 500\,^{\circ}C$, whereas the pure FeS_2-*p* type phase is obtained at temperatures $\geqq 550\,^{\circ}C$. The implied question of the FeS_2-*m* and FeS_2-*p* type modifications as low and high temperature forms of $OsTe_2$ has its parallel for FeS_2; a discussion which has been carried on for many years (*cf.*, *e.g.*, Refs. 8, 9).

NaO_2 occupies a particular position among these compounds in undergoing reversible transformations between the FeS_2-*m*, FeS_2-*p*, and *random* FeS_2-*p* type structures as a function of temperature.[10]

The object of this paper is to report results of high temperature studies of FeS_2, $FeSe_2$, $FeTe_2$, $CoTe_2$, and $CuSe_2$, including some preliminary data for $OsTe_2$.

EXPERIMENTAL

The natural *marcasite* sample used in this study originated from Joplin (U.S.A.) and was obtained from Mineralogisk-Geologisk Museum, Universitetet i Oslo; analytical data being included in Ref. 4. The syntheses of $FeSe_2$, $FeTe_2$, $CoTe_2$, and $CuSe_2$ were performed as described in Refs. 4, 5. Samples with compositions on both sides of the stoichiometric ratio were made for $FeSe_2$ and $CuSe_2$ by heating the stoichiometric samples with lower selenides or excess selenium in evacuated, sealed silica capsules.

As a continuation of the synthetical work described in Ref. 4, numerous further attempts were made to prepare FeS_2 in its FeS_2-*m* modification. However, all endeavours were in vain, the FeS_2-*p* modification being obtained as the only reaction product above 350 °C. FeS_2-*p* is also obtained below this temperature, but, in

variable amounts (*viz.* incomplete reactions) depending on temperature, heating period, and number of intermediate crushings.

Samples of $OsTe_2$ were prepared by heating stoichiometric quantities of the elements [99.999 % Os (Johnson, Matthey & Co.) and 99.999 % Te (Koch-Light Laboratories)] in evacuated, sealed silica capsules. A variety of different reaction and annealing temperatures (400 – 950 °C) were tried. Below ~500 °C, the reaction rate is extremely slow, above ~650 °C the annealing of the samples leads to crystallization of the silica, but this does not become a serious problem until ~750 °C.

The temperature of the furnaces surrounding the specimens was kept constant to within ±0.5 °C during the annealing processes using Getrosist (Philips) temperature regulators and a Frigistor reference chamber for the cold points of the Pt/Pt-Rh thermocouples (0.00 ± 0.02 °C). The recorded annealing temperatures were measured separately with a calibrated Pt/Pt-Rh thermocouple. The silica capsules were made as short as possible in order to minimize effects of thermal gradients in the furnaces, and thin-walled ampoules were utilized for quenching experiments in order to ensure fast cooling rates. Following the conventional quenching technique, care was taken in initial experiments to drop the ampoules into ice-water without shattering. In the course of the study, the technique was modified to almost instantaneous mechanical shattering of the ampoules when brought in contact with ice-water. The overall gain in quenching rate on turning to the latter procedure is estimated to be a factor of about ten, but, apart from for the decomposition results, this improvement had no detectable influence.

The DTA data were collected with a Mettler Recording Vacuum Thermoanalyzer, using ~60 mg samples in sealed silica crucibles. The heating rate was generally 2 °C/min and Pd powder was used as reference. The X-ray powder diffraction techniques applied at ambient and higher temperatures are described in Ref. 11.

In an attempt to eliminate possible, arbitrary effects of inhomogeneity, impurity, non-stoichiometry, *etc.*, all results described in this paper for the (nominally) stoichiometric samples (except some of those for $OsTe_2$) refer to specimens taken from one and the same batch of each compound.

RESULTS

The scope of the present study is determined by the availability of FeS_2 in its FeS_2-*p* and FeS_2-*m* forms, $OsTe_2$ in one pure and one impure modification, and $FeSe_2$, $FeTe_2$, $CoTe_2$, and $CuSe_2$ only in their FeS_2-*m* type modifications. These distinctions in starting points are reflected in the subsequent presentation of our findings.

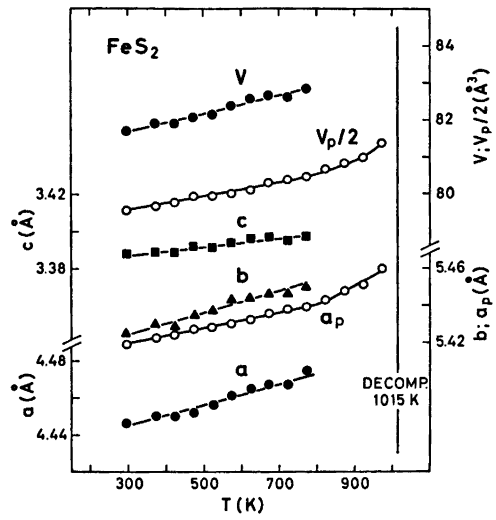

Fig. 1. Unit cell dimensions for *natural* FeS_2-*m* (*a*, *b*, *c*, *V*) and *synthetic* FeS_2-*p* (a_p, V_p) *versus* temperature. (Calculated standard deviations do not exceed size of symbols; correspondingly in Figs. 3 and 4.)

(i) *FeS_2-m versus FeS_2-p*. In line with earlier findings,[8,9] the FeS_2-*m*→FeS_2-*p* transition is induced by heat treatments, the transformation rate being extremely susceptible to the experimental conditions, notably the temperature. It was therefore, not surprising to find that this transition could not be detected by DTA. In fact, the DTA curves were featureless apart from endothermic peaks due to sample decomposition at 745 °C independent of whether FeS_2-*m* or FeS_2-*p* was used as the starting material. In order to establish the decomposition temperature more accurately, samples were heated at various temperatures between 730 and 760 °C until thermal equilibrium was achieved, and then quenched. Using this procedure on various samples of FeS_2-*m* and FeS_2-*p*, the decomposition temperature was established as 742 ± 6 °C, where the uncertainty refers to the reproducibility between different runs. This result was verified by high temperature X-ray diffraction.

An advantage of the sluggish FeS_2-*m*→FeS_2-*p* transition is that the former modification can

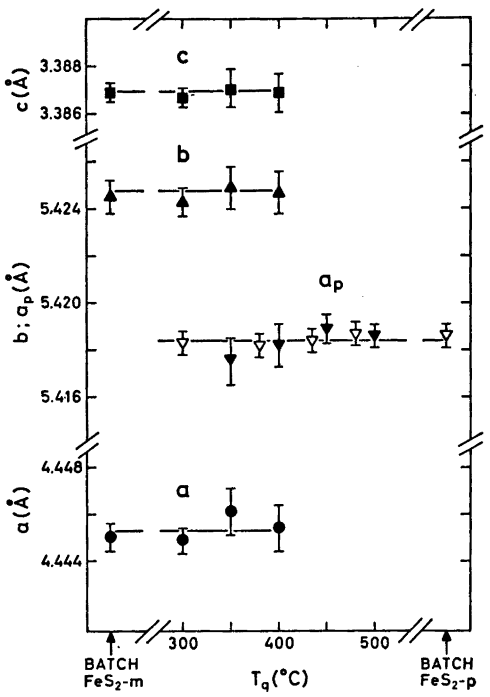

Fig. 2. Unit cell dimensions and corresponding standard deviations (as determined at room temperature) for samples (originally) of *natural* FeS_2-*m* (filled symbols) and *synthetic* FeS_2-*p* (open symbols), quenched from various temperatures (T_q).

be followed up to ~500 °C on high temperature X-ray diagrams. Hence, Fig. 1 shows the temperature dependence of the unit cell dimensions of FeS_2-*m* between 22 and 500 °C. Up to 450 °C, only reflections characteristic of FeS_2-*m* could be seen on the diagrams, whereas at 500 °C a mixture of FeS_2-*m* and FeS_2-*p* had emerged. For the purpose of comparison, the temperature variation of the FeS_2-*p* cell (synthetic sample) is also included in Fig. 1. Since the unit cell dimension of the synthetic FeS_2-*p* sample matches (within experimental error) that obtained from the transformed FeS_2-*m* sample at ≧500 °C, there can apparently not be any significant distinction in composition between the two lots of FeS_2.

In fact, this result was further substantiated by quenching experiments. As is evident from Fig. 2, the unit cell dimensions (as derived from room temperature Guinier photographs) of FeS_2-*m* and FeS_2-*p* are independent of the temperature (T_q) from which the samples were quenched.

The quenching experiments also showed that the onset of the reaction FeS_2-*m*→FeS_2-*p* under steady state conditions, takes place at a much lower temperature than the 500 °C found by high temperature X-ray diffraction. At ≦300 °C, heat treatments up to 14 months did not induce any changes in FeS_2-*m* samples, whereas an increase to 350 °C resulted in mixtures of FeS_2-*m* and FeS_2-*p* after the same annealing period. A further increase to 400 °C produced mixtures of the two modifications after annealing for only 1 month, and at this temperature, the FeS_2-*m*→FeS_2-*p* conversion was found to be completed within 4 months. At still higher temperatures, the conversion goes even more quickly to completion, *e.g.*, ≦1 month, ≦2 weeks, and ≦1 h at 450, 500, and 700 °C, respectively. The quenching experiments further emphasize the gradual nature of the FeS_2-*m*→FeS_2-*p* conversion, thus explaining why this reaction escapes DTA detection.

(ii) *Preliminary report on* $OsTe_2$. As briefly reported in an earlier communication,[5] the FeS_2-*p* type modification of $OsTe_2$ is easily synthesized above 550 °C. The upper preparation temperature is limited by the decomposition of $OsTe_2$ at 890 ± 10 °C, as presently determined by DTA and quenching experiments. The unit cell dimension is 6.3985(4) Å at room temperature and its temperature dependence is shown in Fig. 3.

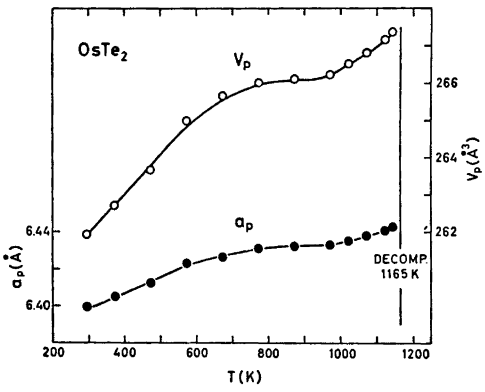

Fig. 3. Thermal expansion of the FeS_2-*p* type unit cell of $OsTe_2$.

Once the FeS_2-*p* type modification has been generated by a reaction above 550 °C it remains invariant to subsequent annealings at lower temperatures. However, on lowering both the preparation and annealing temperatures, a different situation arises. Thus, heat treatments at 480 – 500 °C (still complete reactions $Os + 2Te \rightarrow OsTe_2$) gave mixtures of the FeS_2-*p* and FeS_2-*m* type [$a = 5.280(2)$, $b = 6.402(3)$, $c = 4.048(2)$ Å] modifications in roughly equal amounts. Prolongation of the annealing period for such samples at these or lower temperatures did not result in detectable changes in the relative amounts of the two modifications. If, on the other hand, the same samples are subjected to subsequent annealings at $\geqq 550$ °C, the FeS_2-*p* type modification is obtained as the ultimate reaction product.

It should be emphasized that the above results refer to samples which were subjected to comparatively long term annealings (for $t \leqq 600$ °C, not less than 4 and up to 10 months). At higher temperatures (> 600 °C) equilibrium is attained much faster (*e.g.*, within 2 h at 850 °C; in complete accordance with the findings of Meijer [12]). At first sight, these results appear to contradict those of Sutarno *et al.*[7], who report preparation of mixtures of the FeS_2-*m* and FeS_2-*p* type modifications of $OsTe_2$ at 700 °C. However, these authors used only a one day reaction period which, according to the present results, is too short. The small amounts of the FeS_2-*m* type modification formed during the gradual heating in the furnace need about 3 days annealing at 700 °C for complete conversion into the FeS_2-*p* type modification.

Since reactions at 480 – 500 °C produced mixtures of the two $OsTe_2$ modifications and determination of relative yields as a function of temperature was not intended, the intervals $440 < t < 480$ °C and $500 < t < 550$ °C were not tried.

At temperatures $\leqq 440$ °C the reaction rate for $Os + 2Te \rightarrow OsTe_2$ is incredibly low and reaction periods up to 10 months have resulted mainly in unreacted reactants. However, the sample treated at 440 °C contained a measurable amount of $OsTe_2$, notably in its FeS_2-*m* type modification and without any detectable trace of its FeS_2-*p* type variant. This promising result suggests that the FeS_2-*m* type modification of $OsTe_2$ can be obtained in pure form by prolonged heat treatments at (say) 440 °C. Our continued engagement on the properties of $OsTe_2$ will undoubtedly be rather time consuming, which appears to justify presentation of some preliminary results here.

(iii) *On thermal properties of $FeSe_2$, $FeTe_2$, $CoTe_2$, and $CuSe_2$.* The findings for FeS_2 and $OsTe_2$ could lead one to believe that it would be worthwhile to search systematically for the FeS_2-*p* type modifications of $FeSe_2$, $FeTe_2$, $CoTe_2$, and $CuSe_2$ at high temperatures (*viz.* preparational procedures which would make their expensive, high pressure/high temperature syntheses unnecessary), and this was in fact the original intention for the whole investigation. If this working hypothesis is rooted in realities, the conversions between the FeS_2-*m* and FeS_2-*p* type modifications of these compounds would most likely occur in relatively narrow regions below their decomposition temperatures, where, moreover, optimum conversion rates are to be expected.

The decomposition temperatures for $FeSe_2$, $FeTe_2$, and $CoTe_2$ as determined by DTA, quenching experiments, and high temperature X-ray diffraction show excellent mutual agreement, numerical values being 582 ± 3, 648 ± 3, and 767 ± 4 °C, respectively. The decomposition temperature of ~ 330 °C obtained by DTA for $CuSe_2$, differs appreciably from the value 285 ± 4 °C found by quenching experiments and high temperature X-ray diffraction. The former value matches that similarly derived from DTA by Gattow,[13] although it should be noted that the present DTA results for $CuSe_2$ showed variation with heating rates. The fairly slow sample decomposition encountered in this case, accounts for the distinction of the DTA results from those obtained under steady state conditions.

High temperature X-ray diffraction data (Fig. 4) show that the FeS_2-*m* type modifications of $FeSe_2$, $FeTe_2$, $CoTe_2$, and $CuSe_2$ persist right up to sample decompositions. None of the many X-ray photographs taken just below their decomposition temperatures contained any reflections characteristic of the FeS_2-*p* type modifications. In order to exclude the possibility that the hypothetical conversions between FeS_2-*m* and FeS_2-*p* type modifications may be extremely sluggish, samples were an-

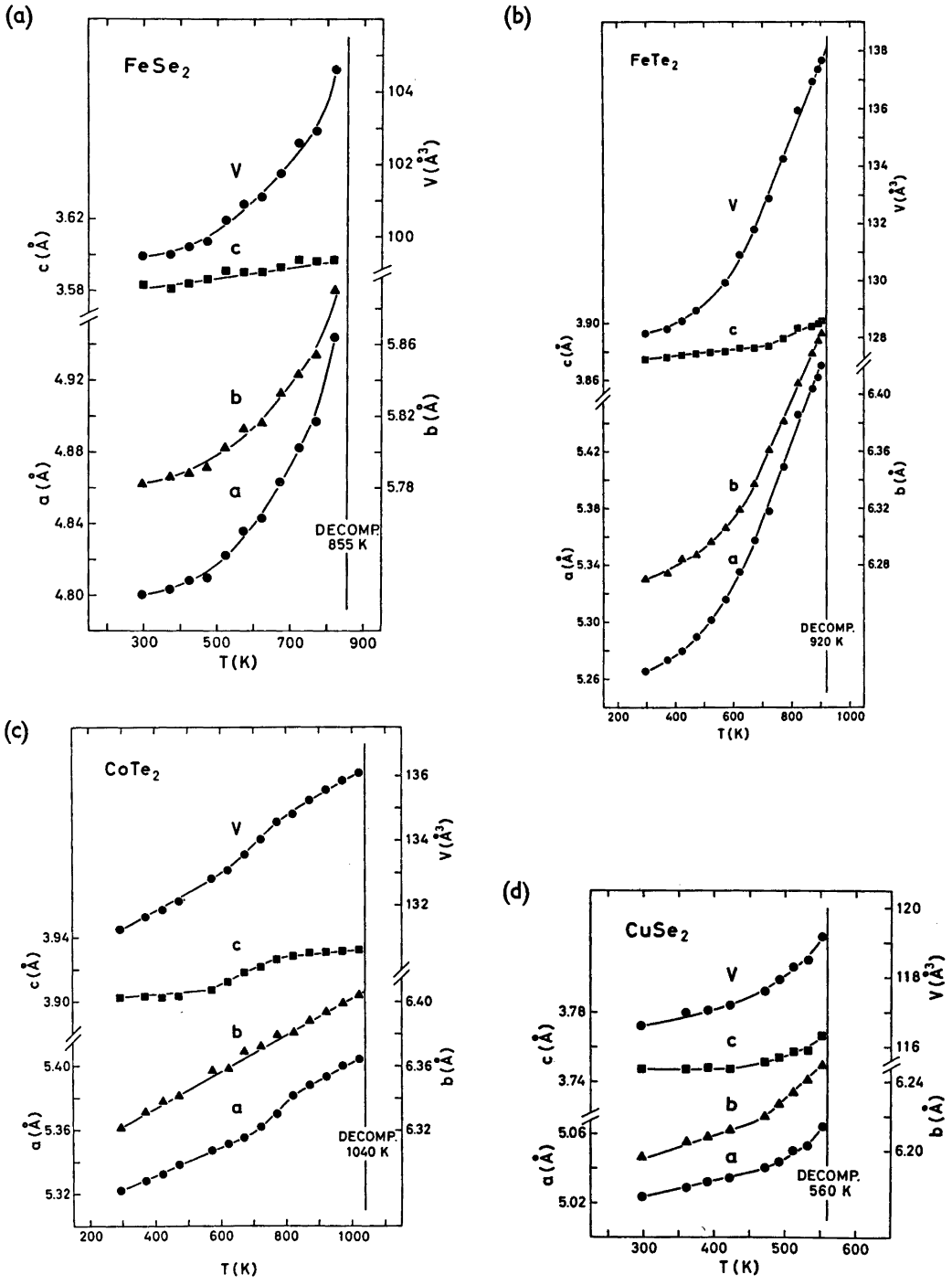

Fig. 4. Unit cell dimensions of: (a) $FeSe_2$, (b) $FeTe_2$, (c) $CoTe_2$, and (d) $CuSe_2$ as functions of temperature.

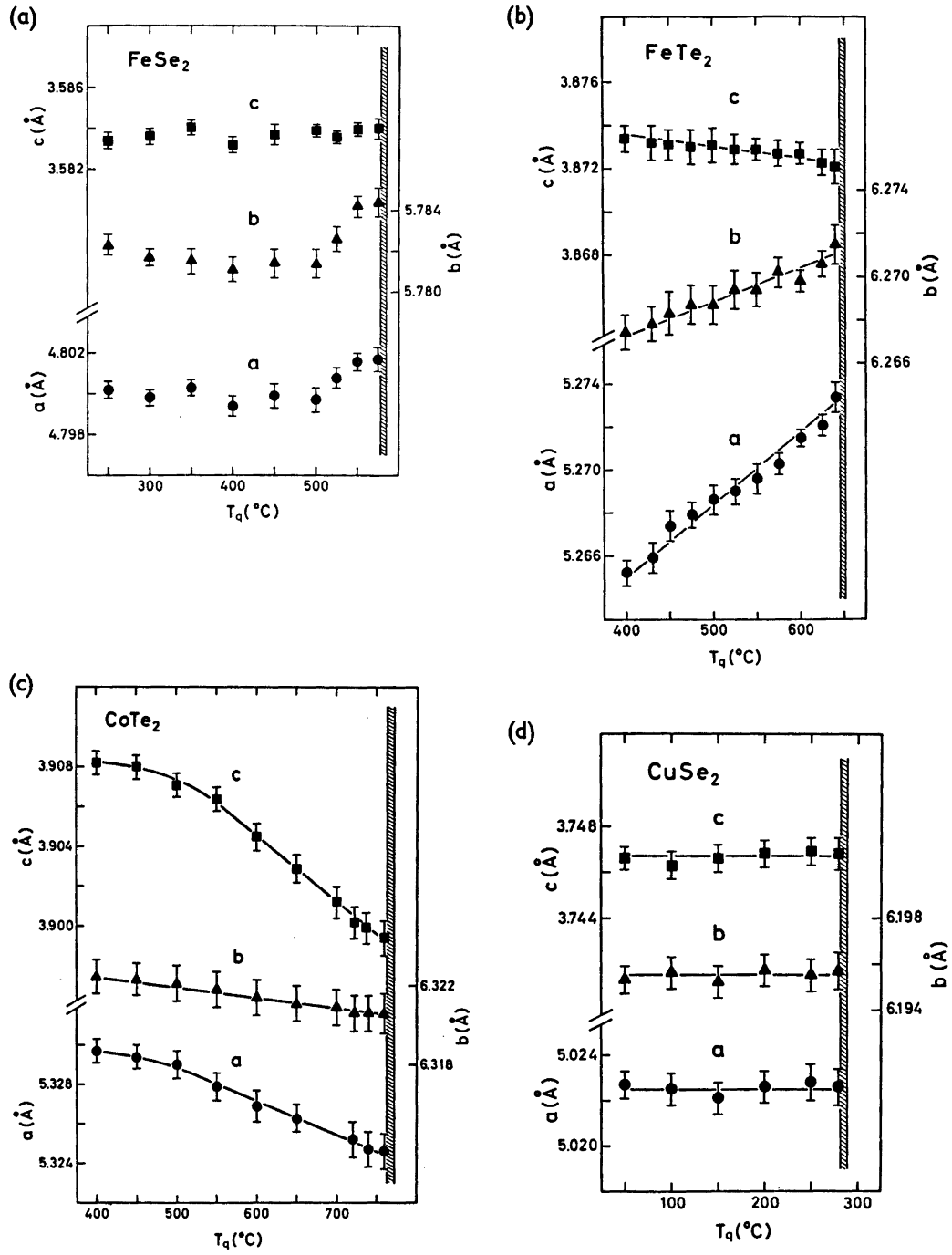

Fig. 5. Room temperature unit cell dimensions (with standard deviations) for samples of: (a) $FeSe_2$, (b) $FeTe_2$, (c) $CoTe_2$, and (d) $CuSe_2$ quenched from various temperatures (T_q).

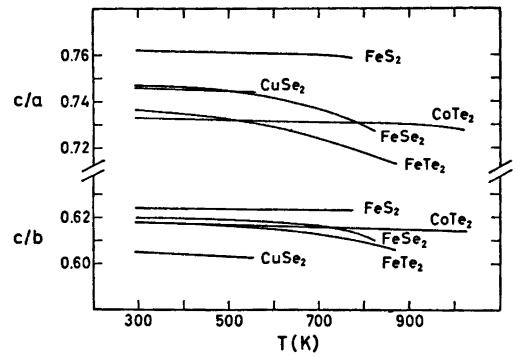

Fig. 6. Axial ratios *versus* temperature for FeS_2, $FeSe_2$, $FeTe_2$, $CoTe_2$, and $CuSe_2$.

nealed below their decomposition temperatures for up to 14 months and then quenched. The results of the quenching experiments (Fig. 5) unequivocally confirm that the FeS_2-*p* type modifications of these compounds are unobtainable through the conventional sealed capsule technique.

The variation in unit cell dimensions of $FeSe_2$, $FeTe_2$, $CoTe_2$, and $CuSe_2$ with quenching temperature (Fig. 5) also shed some light on the question of stoichiometry/non-stoichiometry of these compounds. The invariance in unit cell dimensions with T_q for $CuSe_2$ (Fig. 5d) together with similar results for samples with different initial compositions, show that $CuSe_2$ exhibits no appreciable range of homogeneity. Earlier findings [14] suggest that $FeSe_2$ takes a slight homogeneity range on the Fe-rich side of the stoichiometric ratio. Although the present results for stoichiometric (Fig. 5a) and non-stoichiometric $FeSe_2$ samples are not entirely conclusive, the homogeneity range for this compound appears to be more narrow than proposed in Ref. 14. The non-stoichiometric nature of $Fe_{1-u}Te_2$ ($0 \leqq u \leqq 0.03$; 450 °C) and $Co_{1-u}Te_2$ ($0 \leqq u \leqq 0.13$; 450 °C) is already well established.[4] The data presented in Fig. 5 b, c merely show that the metal-rich phase limit shifts from $u = 0.00$ at $\leqq 450$ °C to 0.01 and 0.06 for $Fe_{1-u}Te_2$ and $Co_{1-u}Te_2$, respectively, in the vicinity of their decomposition temperatures.

The present thermal expansion data are also relevant in relation to the use of unit cell proportions for classification of compounds with the FeS_2-*m* type structure. It is seen from Fig. 6 that the axial ratios for FeS_2, $CoTe_2$, and $CuSe_2$ are practically independent of temperature, as opposed to those for $FeSe_2$ and $FeTe_2$. Although, as pointed out in Ref. 1, the unit cell proportions are not even approximately constant from compound to compound within each class, but vary systematically, the marked temperature variations for $FeSe_2$ and $FeTe_2$ show that *c/a* and *c/b* may even not be entirely characteristic parameters for a given compound.

Similar *c/a* and *c/b* variations to those in Fig. 6 are observed [4] for $Fe_{1-u}Te_2$ as functions of the compositional parameter *u*, whereas the axial ratios for $Co_{1-u}Te_2$ are approximately independent of *u*. Due to the only slight temperature dependence of the Fe-rich phase limit in $Fe_{1-u}Te_2$ inferred above, the *c/a* and *c/b* *versus* *T* relationships (Fig. 6) cannot be attributed to compositional changes alone. For $FeSe_2$ no such explanation is appropriate.

DISCUSSION

The formation of and transformation modes between the FeS_2-*m* and FeS_2-*p* type structures for the eight MX_2 (M = metal, X = chalcogen) compounds which take both of these types, appear to suggest that they divide into four categories.

NaO_2:

$m \rightleftharpoons p$ reversible at −77 °C (Ref. 10).

$OsTe_2$:

$m \rightarrow p$ at $> \sim 480$ °C.

$p \rightarrow m$ unknown; requires complete decomposition (Os + 2Te) and anewed synthesis at $< \sim 440$ °C.

FeS_2:

$m \rightarrow p$ at $> \sim 300$ °C.

$p \rightarrow m$ unknown; a feasible path appears to involve dissolution and subsequent hydrothermal synthesis under slightly acidic conditions.[6]

$FeSe_2$, $FeTe_2$, $CoTe_2$, and $CuSe_2$:

$m \rightarrow p$ actually unknown, but since the *p* type modifications have been made by direct syntheses from the elements,[3] $m \rightarrow p$ can probably be generated under high temperature/high pressure conditions.

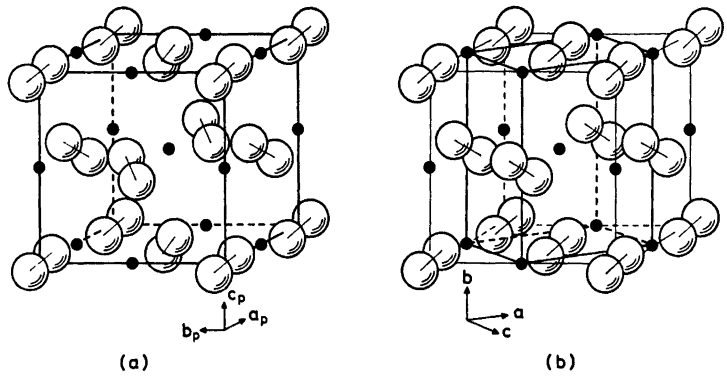

Fig. 7. Models for the (a) FeS_2-*p* and (b) FeS_2-*m* type structures.

p→*m* unknown; experience from other high temperature/high pressure induced syntheses (*cf.*, *e.g.*, Ref. 15) indicates conversion by conventional heat treatments in evacuated, sealed capsules.

The similarities and differences between the FeS_2-*p* and FeS_2-*m* type structures may be seen from Fig. 7. For a detailed discussion of these structure types and their mutual relationships, the reader is referred to Ref. 1.

The reversible nature of the FeS_2-*m*⇌FeS_2-*p* type transition in NaO_2 may be attributed to features of its $X-X$ pairs and bonding characteristics. The $X-X$ pairs in NaO_2 differ in at least two respects from those of the other compounds under consideration, *viz.* in size relative to M as well as in its more nearly spherical shape. Within this class of compounds, NaO_2 almost certainly distinguishes itself in having a more extreme charge distribution between M and $X-X$, *viz.* less directional character of the $M-X$ bonds. (It should be emphasized that the questions of size and shape of the $X-X$ pair are interrelated with bonding characteristics, thus making a distinction between cause and effect somewhat arbitrary.) These features of the $X-X$ and $M-X$ bonds facilitate the FeS_2-*m*⇌ FeS_2-*p* type *solid state* transition. This is compatible with the fact that NaO_2 also undergoes a further FeS_2-*p*⇌*random* FeS_2-*p* type transition at -50 °C. Neither of these transitions in NaO_2 are accompanied by any detectable changes in cell volume (per formula unit).

At the FeS_2-*m*→FeS_2-*p* type transition in $OsTe_2$, an appreciable volume contraction [$\Delta V/V=(V_p/2-V)/V=-0.041$] takes place. The volume change and irreversible nature of the transition distinguish $OsTe_2$ from NaO_2 and suggest that the transition in the former is not of the solid state type. On the contrary, the reaction is more likely to involve the vapour phase, through

$$\underset{(FeS_2\text{-}m\ \text{type})}{OsTe_{2(s)}} \rightleftharpoons Os_{(s)} + Te_{2(g)} \rightleftharpoons \underset{(FeS_2\text{-}p\ \text{type})}{OsTe_{2(s)}}$$

without taking an attitude to the actual molecular species of Te present in the vapour. The observed coexistence of the FeS_2-*m* and FeS_2-*p* type modifications over a range of temperatures, together with the irreversible nature of the transition, would thus demand approximately equal equilibrium partial pressures of Te for the two modifications as well as rather small Te total pressures.

It is natural to suspect that the *m*→*p* transition in FeS_2 should be governed by a mechanism similar to that proposed for $OsTe_2$. The sluggish nature of the transition as well as the accelerating effect [8] of added sulfur, support this assumption. In this case, however, one is faced with the puzzling question of why not even trace amounts of FeS_2-*m* have been obtained by the sealed silica capsule technique. The answer appears to be that the reaction rate for the synthesis of FeS_2 is too low at $t < \sim 300$ °C. The thus suggested similarity between FeS_2 and $OsTe_2$ is subject to future verification through long-term (say, several years) annealings. The volume contraction at the FeS_2-*m*→FeS_2-*p* transition amounts to $\Delta V/V=-0.026$.

Disconnected from the above discussion is the definite distinction in formation and transformation modes of FeS_2 and $OsTe_2$ on the one hand, and $FeSe_2$, $FeTe_2$, $CoTe_2$, and $CuSe_2$ on the other. Provided that this distinction is thermodynamical in origin, it is expected to be reflected also in structural parameters, *viz.* bond distances and angles. Since structure determinations have been carried out [4,5,16] for all FeS_2-*m* type modifications except $OsTe_2$, the implications are that the hitherto undetermined FeS_2-*p* type structures of $FeSe_2$, $FeTe_2$, $CoTe_2$, and $CuSe_2$ carry a secret. (It is of little help in this connection that the structures of both modifications of FeS_2 have been explored in detail. [16,17])

Awaiting the results of the structure determinations advertised for, unit cell dimensions or proportions might be suspected to reflect some structural details. However, apart from the c/a ratio where NaO_2 ($c/a = 0.801$), FeS_2 ($c/a = 0.762$), and $OsTe_2$ ($c/a = 0.767$) take higher values than the others ($c/a \leqq 0.747$), no significant distinction could be traced. In view of the averaging effects operative in unit cell dimensions and proportions, this disappointing result is hardly unexpected.

The unit cell volume is an even more averaged parameter and as such, more featureless in the structural sense. Nevertheless, volume frequently enters into pressure considerations. The volume contractions $\Delta V/V$ are -0.026 for both FeS_2 and $FeTe_2$, -0.042 and -0.019 for $CoTe_2$ and $CuSe_2$, respectively. Thus, the lack of correlation is seen from the fact that the contractions for $FeSe_2$ and $FeTe_2$ are identical with that for FeS_2, and the contraction for $CoTe_2$ almost matches that for $OsTe_2$.

The whole discussion contains an inherent weakness in taking for granted that the high pressure induced modifications of $FeSe_2$, $FeTe_2$, $CoTe_2$, and $CuSe_2$ are replicas of the products searched in more conventional syntheses, *e.g.* evacuated, sealed capsule conditions. The effect of hydrostatic pressure on solids is visualized as a compression of the atomic electron clouds. For a given pressure the extent of the compression depends on the individual atoms as well as on their bonding situations. Thus, the various constituents of a compound may respond differently to applied pressure, which in turn may lead to smaller or larger structural rearrangements. When this pressure is released the atomic size and/or some structural details may not be fully relaxed. In other words, it is suggested that for a given structure type, the structural parameters, pressure, and free energy relationship may have more than one minimum. [The high pressure induced PdS_2(II) modification [18] may be a relevant example, and moreover, the situation has its probable parallel in structural rearrangements caused by the additional internal stress associated with paramagnetic→cooperative magnetic transitions.] The only way of proving or disproving such a hypothesis requires the synthesis of the FeS_2-*p* type modifications for at least one of $FeSe_2$, $FeTe_2$, $CoTe_2$, or $CuSe_2$, by means other than high temperature/high pressure methods, and the subsequent comparison of structural details between this and the corresponding high pressure product. It would, however, be interesting and almost equally decisive to subject the more conventionally synthesized FeS_2-*p* type modifications of:

NaO_2, MgO_2, $MgTe_2$, MnS_2, $MnSe_2$, $MnTe_2$, FeS_2, RuS_2, $RuSe_2$, $RuTe_2$, OsS_2, $OsSe_2$, $OsTe_2$, CoS_2, $CoSe_2$, $RhSe_2$, $RhTe_2$, NiS_2, $NiSe_2$, ZnO_2, CdO_2, $PdAs_2$, $PdSb_2$, PtP_2, $PtAs_2$, $PtSb_2$, $PtBi_2$, and SiP_2

(*cf.* Ref. 1 and references therein) to high temperature/high pressure treatment, followed by detailed structural analyses. Knowledge about what happens to the high pressure induced FeS_2-*p* type modifications of:

$FeSe_2$, $FeTe_2$, $CoTe_2$, $NiTe_2$, CuS_2, $CuSe_2$, $CuTe_2$, ZnS_2, $ZnSe_2$, CdS_2, $CdSe_2$, IrS_2, NiP_2, $NiAs_2$, and $SiAs_2$

(*cf.* Refs. 3, 19 – 21) when exposed to annealings in evacuated, sealed capsules at successively higher temperatures, would also contribute greatly to a better understanding of these problems.

REFERENCES

1. Kjekshus, A. and Rakke, T. *Struct. Bonding (Berlin) 19* (1974) 85.
2. Ramdohr, P. and Schmitt, M. *Neues Jahrb. Mineral., Monatsh.* (1955) 133.
3. Bither, T. A., Bouchard, R. J., Cloud, W. H., Donohue, P. C. and Siemons, W. J. *Inorg. Chem. 7* (1968) 2208.

4. Brostigen, G. and Kjekshus, A. *Acta Chem. Scand. 24* (1970) 1925.
5. Kjekshus, A., Rakke, T. and Andresen, A. F. *Acta Chem. Scand. A 28* (1974) 996.
6. Kullerud, G. *Carnegie Inst. Wash. Year Book 1965–1966*, p. 352.
7. Sutarno, Knop, O. and Reid, K. I. G. *Can. J. Chem. 45* (1967) 1391.
8. Kullerud, G. and Yoder, H. S. *Econ. Geol. 54* (1959) 533.
9. Schubert, E. *Beitr. Mineral. Petrogr. 6* (1959) 388.
10. Carter, G. F. and Templeton, D. H. *J. Amer. Chem. Soc. 75* (1953) 5247.
11. Furuseth, S., Kjekshus, A. and Andresen, A. F. *Acta Chem. Scand. 23* (1969) 2325.
12. Meijer, W. O. J. G. *Amer. Mineral. 40* (1955) 646.
13. Gattow, G. *Z. Anorg. Allgem. Chem. 340* (1965) 312.
14. Svendsen, S. R. *Acta Chem. Scand. 26* (1972) 3757.
15. Bjerkelund, E., Kjekshus, A. and Meisalo, V. *Acta Chem. Scand. 22* (1968) 3336.
16. Brostigen, G., Kjekshus, A. and Rømming, C. *Acta Chem. Scand. 27* (1973) 2791.
17. Brostigen, G. and Kjekshus, A. *Acta Chem. Scand. 23* (1969) 2186.
18. Munson, R. A. and Kasper, J. S. *Inorg. Chem. 8* (1969) 1199.
19. Munson, R. A. *Inorg. Chem. 7* (1968) 389.
20. Donohue, P. C., Bither, T. A. and Young, H. S. *Inorg. Chem. 7* (1968) 998.
21. Donohue, P. C., Siemons, W. J. and Gillson, J. L. *J. Phys. Chem. Solids 29* (1968) 807.

Received December 2, 1974.

Acta Chemica Scandinavica A 29 (1975) 453—456

Crystal Structures of two Dimerisation Products of 5-Methylthiopyrylium-3-oxide

P. GROTH

Department of Chemistry, University of Oslo, Oslo 3, Norway

Both isomers of the dimerisation product $(C_6H_6OS)_2$ belong to the monoclinic system with space group $P2_1/c$ and four molecules in the unit cell. The cell dimensions for the *anti* and *syn* isomer, respectively, are
$a = 6.692(1)$ Å, $b = 14.113(3)$ Å, $c = 13.087(3)$ Å, $\beta = 112.15(1)°$
$a = 7.715(3)$ Å, $b = 7.582(2)$ Å, $c = 20.496(4)$ Å, $\beta = 108.25(2)°$
Intensities were recorded on an automatic four circle diffractometer. The structures were solved by direct methods and refined by full-matrix least squares technique:
anti: $R = 4.8$ % ($R_w = 4.2$ %) for 1442 observed reflections;
syn: $R = 4.4$ % ($R_w = 5.7$ %) for 1848 observed reflections.
The results are compared with those of the major dimerisation product of benzo[*c*]thiopyrylium-4-oxide.

Dimerisation of thiopyrylium-4-oxide derivates are studied by Undheim *et al.*[1] In the case of benzo[*c*]thiopyrylium-4-oxide a recent crystal structure investigation [2] revealed that the major product has the *syn* structure. The reaction scheme may be written as in I.

To the minor product (for which no good single crystals yet have been obtained) it seems

(I)

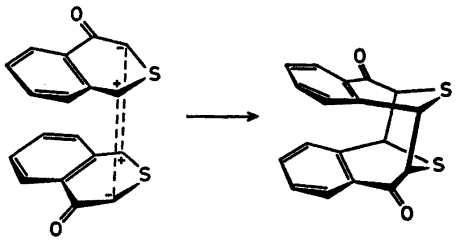

(II)

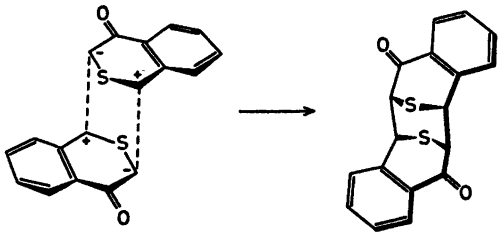

reasonable to assign the *anti* structure with the dimerisation II.

Also in the case of 5-methylthiopyrylium-3-oxide two products are obtained, and it was expected that the dimerisation followed the analogous scheme (III).

(III)

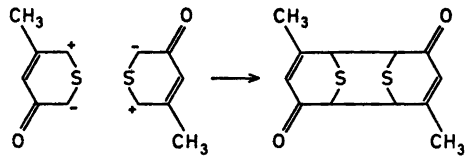

However, the crystal structure determinations presented in this paper show that the scheme for dimerisation of 5-methylthiopyry-

(IV)

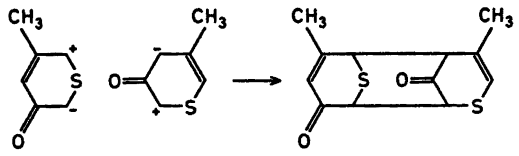

Table 1. Final fractional coordinates and thermal parameters with estimated standard deviations (multiplied by 10^5 for non-hydrogens and 10^4 for hydrogens) for the *anti* isomer. For numbering of atoms, see Fig. 1. Hn is bonded to Cn and Hm,n is bonded to CMm.

ATOM	X	Y	Z	B11	B22	B33	B12	B13	B23
S1	38218(19)	43244(8)	7334(11)	2513(37)	369(7)	699(18)	518(27)	83(32)	-181(15)
S2	75281(17)	32455(8)	6834(9)	2112(31)	381(7)	467(8)	-98(25)	658(28)	115(13)
O1	33688(44)	22112(23)	23178(23)	2569(94)	609(22)	591(25)	-674(75)	1137(83)	-64(37)
O2	36575(50)	12281(23)	-6661(27)	3379(107)	533(21)	695(28)	-415(81)	175(92)	-371(41)
C1	51697(71)	46701(34)	19423(39)	2439(138)	313(27)	793(43)	-164(104)	788(129)	-270(57)
C2	66127(63)	41422(31)	26836(34)	1674(122)	422(29)	543(36)	-238(94)	781(113)	-260(50)
C3	66818(59)	38752(30)	25841(32)	1743(111)	484(28)	348(30)	30(87)	486(97)	67(45)
C4	43489(60)	27115(29)	19452(32)	1766(116)	323(24)	434(32)	-48(85)	789(101)	-156(45)
C5	34134(64)	38464(30)	7516(33)	1657(117)	420(27)	431(31)	-176(92)	344(105)	-19(46)
C6	61323(63)	26906(29)	20191(33)	1533(117)	387(26)	424(32)	-220(89)	388(104)	50(47)
C7	79833(59)	16263(29)	19345(33)	1664(118)	387(26)	585(33)	288(91)	816(103)	97(49)
C8	65384(68)	11779(33)	10592(35)	2554(134)	382(28)	545(35)	42(108)	918(115)	-74(51)
C9	49366(64)	16598(31)	1838(34)	2178(128)	387(26)	473(32)	-84(99)	797(107)	-121(51)
C10	48548(64)	27427(31)	1178(33)	2142(126)	420(27)	388(31)	178(93)	328(103)	183(47)
CM1	83437(90)	45588(43)	36788(46)	2832(174)	685(41)	679(47)	-943(129)	788(147)	-368(66)
CM2	94183(83)	10918(41)	29285(42)	2387(152)	580(35)	653(42)	247(111)	544(134)	388(61)

ATOM	X	Y	Z	B	ATOM	X	Y	Z	B
H1	5211(61)	5338(30)	1999(33)	4,2(1,0)	H11	8252(62)	5263(33)	3659(34)	5,1(1,1)
H3	6958(62)	2761(28)	3272(33)	3,0(1,0)	H12	9940(70)	4415(28)	3742(33)	6,0(1,0)
H5	1998(64)	2788(28)	414(34)	2,1(1,0)	H13	8189(64)	4361(30)	4294(37)	5,6(1,1)
H6	9581(59)	2891(28)	2462(33)	1,3(1,0)	H21	9186(63)	436(31)	2904(34)	5,4(1,1)
H8	6391(61)	519(30)	1047(33)	2,7(1,1)	H22	9881(65)	1267(30)	3563(36)	5,4(1,1)
H10	4267(60)	3013(27)	-581(34)	2,9(1,0)	H23	10922(69)	1244(29)	3859(32)	5,0(1,0)

Table 2. Final fractional coordinates and thermal parameters with estimated standard deviations (multiplied by 10^5 for nonhydrogens and 10^4 for hydrogens) for the *syn* isomer. For numbering of atoms, see Fig. 2. Hn is bonded to Cn and Hm,n to CMm.

ATOM	X	Y	Z	B11	B22	B33	B12	B13	B23
S1	15575(11)	41865(9)	38989(4)	2524(19)	1193(13)	288(2)	257(23)	165(10)	145(8)
S2	3940(9)	95285(9)	41730(3)	1757(15)	1480(13)	253(2)	378(20)	718(8)	-8(7)
O1	-19404(25)	66108(27)	27588(10)	1502(38)	2289(44)	293(6)	-183(64)	116(25)	145(26)
O2	28873(33)	63808(33)	55162(11)	2816(55)	3441(58)	254(6)	-870(92)	349(29)	657(33)
C1	26393(38)	49718(38)	33159(15)	1678(55)	1645(53)	294(8)	612(98)	163(34)	-376(36)
C2	23575(32)	64696(33)	29662(12)	1224(44)	1663(49)	215(7)	-38(75)	243(28)	-370(31)
C3	10576(30)	78326(31)	36816(12)	1271(42)	1364(42)	157(6)	143(69)	227(25)	188(26)
C4	-5365(33)	68396(31)	31915(12)	1423(46)	1238(43)	213(7)	-208(72)	392(31)	-62(27)
C5	-649(35)	59497(33)	38898(13)	1486(48)	1470(47)	253(7)	-664(78)	348(30)	235(30)
C6	19736(33)	91387(31)	36985(12)	1601(49)	1117(41)	283(6)	-184(72)	567(29)	12(27)
C7	38116(32)	85465(32)	41571(12)	1341(46)	1696(47)	191(6)	-714(75)	388(27)	-292(28)
C8	40285(35)	76107(38)	47247(13)	1416(51)	2069(57)	285(7)	-244(86)	193(30)	-182(32)
C9	25349(36)	69749(35)	49713(12)	1888(54)	1679(48)	181(7)	-597(84)	354(31)	18(29)
C10	5867(34)	72794(34)	44942(13)	1593(49)	1788(49)	214(7)	-242(80)	665(31)	198(30)
CM1	32725(50)	68855(64)	24312(19)	1993(78)	3259(91)	318(10)	-377(129)	847(43)	-631(52)
CM2	54454(44)	91136(61)	39684(17)	1628(59)	3438(98)	269(9)	-1756(123)	621(38)	-435(49)

ATOM	X	Y	Z	B	ATOM	X	Y	Z	B
H1	3481(48)	4141(37)	3256(15)	6,1(,6)	H11	3251(84)	7961(82)	2229(34)	19,3(1,8)
H3	609(38)	8489(35)	2677(15)	3,6(,6)	H12	2981(83)	6394(73)	2152(32)	16,1(1,7)
H5	-998(45)	5378(58)	3954(18)	3,5(,8)	H13	4465(91)	6438(73)	2513(32)	16,7(1,8)
H6	2196(52)	10351(55)	3513(20)	1,2(1,0)	H21	6574(63)	8667(50)	4354(22)	8,5(1,0)
H8	5249(42)	7228(36)	5852(15)	3,7(,6)	H22	5426(60)	10418(67)	3846(24)	9,5(1,2)
H10	-188(66)	7255(52)	4749(23)	4,0(1,0)	H23	5433(58)	8683(53)	3555(24)	8,7(1,0)

Table 3. Bond distances and angles for the *anti* isomer.

DISTANCE	(Å)	DISTANCE	(Å)	DISTANCE	(Å)
S1 - C1	1,759(5)	S1 - C5	1,821(4)	S2 - C10	1,804(4)
S2 - C6	1,816(4)	O1 - C4	1,186(4)	O2 - C9	1,211(4)
C1 - C2	1,312(6)	C2 - C3	1,511(6)	C3 - C4	1,515(5)
C4 - C5	1,522(5)	C2 - CM1	1,499(6)	C7 - CM2	1,496(6)
C3 - C6	1,569(5)	C5 - C10	1,551(6)	C6 - C7	1,507(5)
C7 - C8	1,346(5)	C8 - C9	1,472(6)	C9 - C10	1,530(6)

ANGLE	(°)	ANGLE	(°)
C1 - S1 - C5	101,4(2)	C6 - S2 - C10	93,0(2)
O1 - C4 - C5	122,1(3)	O1 - C4 - C3	124,5(4)
O2 - C9 - C10	119,7(4)	O2 - C9 - C8	122,3(4)
C1 - C2 - CM1	122,1(4)	C3 - C2 - CM1	116,3(4)
C6 - C7 - CM2	115,9(4)	C8 - C7 - CM2	121,4(4)
S1 - C1 - C2	129,2(4)	C1 - C2 - C3	121,6(4)
C2 - C3 - C4	110,9(3)	C3 - C4 - C5	113,4(3)
C4 - C5 - S1	108,8(3)	S2 - C6 - C7	112,0(3)
C6 - C7 - C8	122,5(4)	C7 - C8 - C9	124,4(4)
C8 - C9 - C10	118,0(4)	C9 - C10 - S2	111,3(3)
S1 - C5 - C10	112,5(3)	C4 - C5 - C10	111,6(3)
C2 - C3 - C6	113,7(3)	C4 - C3 - C6	108,4(3)
S2 - C10 - C5	113,1(3)	C9 - C10 - C5	108,4(3)
S2 - C6 - C3	110,9(3)	C7 - C6 - C3	110,0(3)

Table 4. Bond distances and angles for the *syn* isomer.

DISTANCE	(Å)	DISTANCE	(Å)	DISTANCE	(Å)
S1 - C1	1.748(3)	S1 - C5	1.831(3)	S2 - C10	1.817(3)
S2 - C6	1.818(2)	O1 - C4	1.178(3)	O2 - C9	1.186(3)
C1 - C2	1.325(4)	C2 - C3	1.509(3)	C3 - C4	1.518(3)
C4 - C5	1.528(3)	C2 - CM1	1.511(4)	C7 - CM2	1.502(4)
C3 - C6	1.576(3)	C5 - C10	1.554(4)	C6 - C7	1.509(3)
C7 - C8	1.329(4)	C8 - C9	1.471(4)	C9 - C10	1.532(4)

ANGLE	(°)	ANGLE	(°)
C1 - S1 - C5	102.8(1)	C6 - S2 - C10	93.6(1)
O1 - C4 - C5	122.4(2)	O1 - C4 - C3	123.9(2)
O2 - C9 - C10	121.8(2)	O2 - C9 - C8	122.5(2)
C1 - C2 - CM1	122.5(3)	C3 - C2 - CM1	117.1(3)
C6 - C7 - CM2	116.5(2)	C8 - C7 - CM2	128.4(3)
S1 - C1 - C2	128.7(2)	C1 - C2 - C3	120.5(2)
C2 - C3 - C4	107.8(2)	C3 - C4 - C5	113.2(2)
C4 - C5 - S1	106.7(2)	S2 - C6 - C7	111.1(2)
C6 - C7 - C8	123.1(2)	C7 - C8 - C9	125.6(2)
C8 - C9 - C10	116.5(2)	C9 - C10 - S2	109.8(2)
S1 - C5 - C10	115.8(2)	C4 - C5 - C10	112.6(2)
C2 - C3 - C6	113.5(2)	C4 - C3 - C6	112.2(2)
S2 - C10 - C5	110.5(2)	C9 - C10 - C5	114.8(2)
S2 - C6 - C3	108.8(2)	C7 - C6 - C3	114.5(2)

lium-3-oxide is as in IV, and that the major product (as in the case of benzo[*c*]thiopyrylium-4-oxide) has the *syn* structure.

Both isomers belong to the monoclinic system with space group $P2_1/c$ and four molecules in the unit cell. The cell dimensions for the *anti* and *syn* isomer, respectively, are: $a=6.692(1)$ Å, $b=14.113(3)$ Å, $c=13.087(3)$ Å, $\beta=112.15(1)°$, $a=7.715(3)$ Å, $b=7.582(2)$ Å, $c=20.496(4)$ Å, $\beta=108.25(2)°$. With $2\theta(\max)=50°$ and Mo$K\alpha$-radiation, about 2000 independent reflections were measured on an automatic four circle diffractometer for each crystal. Using an observed unobserved cutoff at $2.0\sigma(I)$, 1442 were recorded as observed for the *anti* isomer and 1848 for the *syn* isomer. No corrections have been made for absorption or secondary extinction effects.

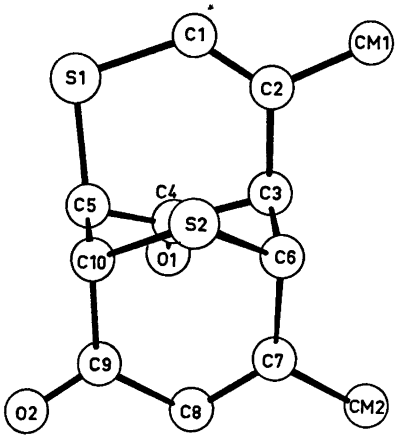

Fig. 1. Schematical drawing of the *anti* isomer.

The structures were solved by direct methods [3] and refined by full-matrix least squares technique.[4],* Hydrogen atom positions were calculated. Anisotropic temperature factors were introduced for S, O, and C atoms, and weights in least squares were calculated from the standard deviations in intensities, $\sigma(I)$, taken as

$$\sigma(I)=[C_T+(0.02C_N)^2]^{\frac{1}{2}}$$

where C_T is the total number of counts and C_N the net count (peak minus background). The form factors were those of Hanson *et al.*[5] except for hydrogen.[6] The final R-values arrived at were:

anti: $R=4.8$ % ($R_w=4.2$ %) for 1442 observed reflections;

syn: $R=4.4$ % ($R_w=5.7$) % for 1848 observed reflections.

Final fractional coordinates and thermal vibration parameters are given in Tables 1 and 2. The expression for anisotropic vibration is:

$$\exp[-(B11h^2+B22k^2+B33l^2+B12hk+B13hl+B23kl)]$$

Principal axes of the thermal vibration ellipsoids for sulfur, oxygen, and carbon atoms were calculated from the temperature parameters of Tables 1 and 2. Maximum root mean square

* All programs used (except those for phase determination) are included in this reference.

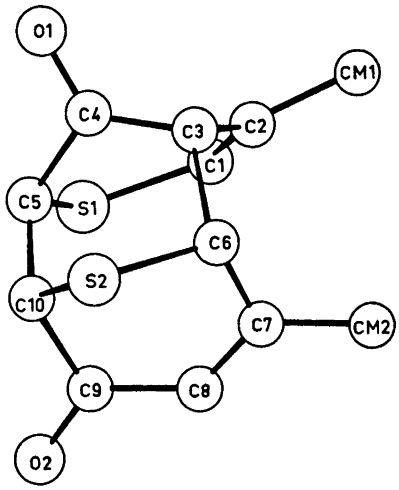

Fig. 2. Schematical drawing of the *syn* isomer.

amplitudes range from 0.20 to 0.35 Å. Rigid-body analyses of translational, librational, and screw motion [7] gave relatively large r.m.s. discrepancies between atomic vibration tensor components calculated from the thermal parameters of Tables 1 and 2, and those calculated from the rigid-body parameters. By including all 16 non-hydrogen atoms, the values obtained for the *anti*- and *syn* isomer, respectively, were 0.0040 and 0.0036 Å^2. These numbers do not strongly support the assumption of regarding the molecules as oscillating rigid-bodies, and the coordinates were therefore not corrected for librational motion.

Interatomic distances and bond angles are given in Tables 3 and 4. The standard deviations (in parentheses) are estimated from the correlation matrix of the last least squares refinement cycle. Figs. 1 and 2 are schematical drawings of the molecules.

From Tables 1 and 2 it may be seen that the only possibly significant difference in bond length is that of O2 – C9 which is 0.025 Å longer for the *anti* isomer. The S1 – C1 bonds as well as the other sulfur carbon bond distances correspond closely to normal values for S – C(sp^2) and S – C(sp^3), respectively.[8,9] The C3 – C6 bonds seem to be somewhat longer than C5 – C6 (and significantly longer than a normal C – C single bond). This effect has also been observed in the case of the major dimerisation product of benzo[*c*]thiopyrylium-4-oxide [2] (C – C = 1.577 Å).

When comparing the angles of Table 3 with those of Table 4 some differences may be observed. C2 – C3 – C6, C3 – C6 – C7, S1 – CS – C10, and C5 – C10 – C9 are somewhat larger for the *syn* isomer, possibly due to repulsions between the methyl groups which are separated by a distance of only 3.49 Å. The angles C6 – S2 – C10 have approximately the same value as that of the major dimerisation product of benzo[*c*]thiopyrylium-4-oxide [2] (93.6°), while the C1 – S1 – C5 angles correspond to the three C – S – C angles in a cyclisation product of 6-chloropyrid-2-thione [9] (102.4, 101.0, 101.8°). The ring angles at the carbonyl group C4 = O1 may be compared with values found in the crystals of cyclohexane-1,4-dione,[10] and the latter are seen to be about four degrees larger (117.5, 117.3°).

C – H distances range from 0.90 to 1.05 Å. Except for a close contact (3.55 Å) between centrosymmetrically related CM1-atoms of the *anti* isomer no short *inter*-molecular distances are observed.

Lists of observed and calculated structure factors are available by request to the author.

REFERENCES

1. Undheim, K. and Baklien, S. *J. Chem. Soc. Perkin Trans. 1. In press.*
2. Groth, P. *Acta Chem. Scand. A 29* (1975) 298.
3. Germain, G., Main, P. and Woolfson, M. M. *Acta Crystallogr. A 27* (1971) 368.
4. Groth, P. *Acta Chem. Scand. 27* (1973) 1837.
5. Hanson, H. P., Herman, F., Lea, J. D. and Skillman, S. *Acta Crystallogr. 17* (1964) 1040.
6. Stewart, R. F., Davidson, E. R. and Simpson, W. T. *J. Chem. Phys. 43* (1965) 3175.
7. Schomaker, V. and Trueblood, K. N. *Acta Crystallogr. B 24* (1968) 63.
8. Groth, P. *Acta Chem. Scand. 25* (1971) 118.
9. Groth, P. *Acta Chem. Scand. 27* (1973) 5.
10. Groth, P. and Hassel, O. *Acta Chem. Scand. 18* (1964) 923.

Received November 25, 1974.

Acta Chemica Scandinavica A 29 (1975) 457—467

Conformational Analysis. IX. The Molecular Structure, Torsional Oscillations, and Conformational Equilibrium of Gaseous 1,1,3,3,3-Pentachloropropane ($CHCl_2$—CH_2—CCl_3) as Determined by Electron Diffraction and Compared with Semi-empirical (Molecular Mechanics) Calculations

JAN PETTER JOHNSEN and REIDAR STØLEVIK

Department of Chemistry, University of Oslo, Blindern, Oslo 3, Norway

Gaseous $CHCl_2-CH_2-CCl_3$ (PCP) has been studied by electron diffraction at a nozzle temperature of 80 °C. *Gauche* and *anti* conformers are possible for PCP. The conformer with the terminal H atom *anti* to the CCC group was not present in detectable amounts.

Results are presented with error limits (2σ). The following values for bond lengths (r_g) and bond angles ($\angle_\alpha$) were obtained: $r(C-C)=1.547(12)$ Å, $r(C-Cl)=1.774(4)$ Å, $\angle CCC=115.7°$ (2.8), and $\angle CCCl=109.9°$ (0.6). The deviations from an exact all-staggered (1:2) *gauche* conformation are large [$\phi_{1-2}=+14.1°$ (3.0) and $\phi_{2-3}=-22.5°$ (2.2); with $\phi_{1-2}=\phi_{2-3}=0°$ for the exact staggered form].

An average torsional force constant was estimated from the electron-diffraction data. Within the experimental error limits, the values of the diagonal torsional force constants predicted by the semi-empirical model, agree with the experimental value. The fundamental frequencies, 56 cm^{-1} and 77 cm^{-1}, corresponding to torsional oscillations in the *gauche* conformer, have been estimated.

Experimental and calculated results for $CHX_2-CH_2-CX_3$, $CHX_2-CX_2-CX_3$, and $CX_3-CX_2-CX_3$ (X = Cl) have been compared.

I. INTRODUCTION

This work is part of a systematic conformational study of halogenated propanes by electron diffraction in the gas phase. Results for the following molecules have recently been published:

$BrH_2C-CHBr-CH_2Br$,[1] $BrH_2C-CH_2-CH_2Br$,[2] $ClH_2C-CHCl-CH_2Cl$,[3] $Cl_3C-CCl_2-CHCl_2$,[4] $Cl_3C-CCl_2-CCl_3$.[5] Molecules with $-CH_2X$ groups (X = Cl or H) bonded to the central C atom of a C—C—C skeleton have also been investigated: $C(CH_2Cl)_4$,[6] $(CH_3)_2C(CH_2Cl)_2$,[7] and $(CH_3)C(CH_2Cl)_3$.[8]

General information [9] relevant to this investigation and to the electron diffraction method [10] is found in Refs. 9 and 10.

Chlorinated propanes were extensively studied by Sheppard *et al.* using vibrational and NMR spectroscopy. The principal results obtained by these methods, in the liquid phase, are found in Refs. 11, 12, and 13. Conformers which possess parallel C—Cl bonds on the same side of the carbon skeleton (parallel (1:3) Cl···Cl interaction), are energetically less stable than conformers without such interactions.[11]

Assuming all-staggered (1:2) conformations, only two spectroscopically distinguishable forms are possible for PCP. The conformers and their names are shown in Fig. 1. The two *gauche* forms are not spectroscopically distinguishable. If the torsion angles of a *gauche* conformer have to be specified, then the one with $\phi_{1-2}=\phi_{2-3}=0°$ in staggered positions will be ment. Both *anti* and *gauche* conformers involve parallel (1:3) Cl···Cl interactions, but the *gauche* ones have one such interaction less than the *anti* conformer.

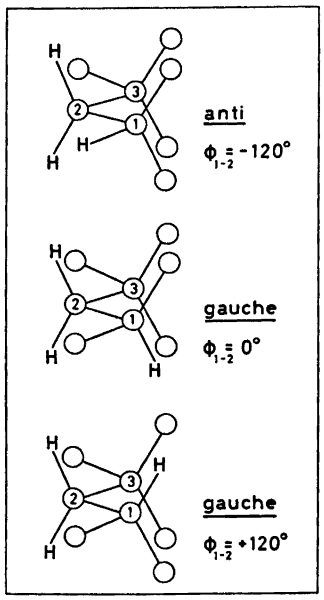

Fig. 1. The staggered conformers in $HCCl_2-CH_2-CCl_3$. The value of the torsion angle ϕ_{2-3} is 0° for exact staggered forms.

Based on vibrational and NMR spectra Sheppard *et al.*[12] concluded that only one type of conformer (*gauche*) is present in the liquid in any quantity.

Some symbols which are used in this paper need a few comments. PCP is used for the compound itself. Capital letters A/G combined as AA, AG, and GG indicate *anti/gauche* relations (of a Z···Y distance) in a Z–C–C–C–Y, fragment, while small letters a/g indicate *anti/gauche* relations in a Z–C–C–Y fragment. The symbols are then combined with the symbols for the internuclear Z···Y distance (see Table 7).

II. CALCULATION OF STRUCTURAL PARAMETERS, CONFORMATIONAL BARRIERS, TORSIONAL BARRIERS, AND TORSIONAL FORCE CONSTANTS

The semi-empirical energy model corresponds to simple molecular-mechanics calculations, including atom-atom potentials and valence force constants, as described in Ref. 1. Energy parameters (a,b,c,d, and Vo) were taken from the work of Abraham and Parry.[14] The diagonal valence force constants in Table 5 were used. In minimizing the energy, the geometrical model was constrained as described in Sect. V-A.

Table 1. Calculated structural parameters in the stable conformers of $C(1)HX_2-C(2)H_2-C(3)X_3$. The structural parameters were constrained as described in Sect. V-A.

Type of parameter r(Å), ∠(°), X=Cl	Normal value	*gauche*	*anti*
$r(C-C)^a$	(1.513)	1.543	1.552
$r(C-X)^b$	(1.760)	1.768	1.769
$r(C_2-H)$	(1.094)	1.096	1.096
$r(C_1-H)$	(1.094)	1.093	1.094
∠CCC	(110.0)	116.1	123.3
$\angle CCX^c$	(109.47)	111.1	112.1
$\angle C_2C_1H$	(109.47)	108.6	106.8
$\angle C_1C_2H$	(109.47)	110.4	108.9
$\angle\phi_{1-2}(-C_1-C_2-)$	$(60)^d$	+32.3	−102.0
$\angle\phi_{2-3}(-C_2-C_3-)$	$(60)^d$	+1.9	+17.0

[a] Average C–C parameter. [b] Average C–X parameter for $-CHX_2$ and $-CX_3$. [c] Average ∠CCX parameter for $C-CHX_2$ and $C-CX_3$. [d] $\phi = 60°$ corresponds $V_\phi = 0$; see Ref. 1.

Table 2. Calculated conformational energies in $C(1)HX_2-C(2)H_2-C(3)X_3$, X=Cl. The energy expression was explained in Ref. 1. Zero-point energies for the conformers are not included.

Type of energy (kcal/mol)	*gauche*	*anti*	Δ(g-a)
E(bonded)	3.76	7.87	−4.11
E(van der Waals)	3.42	3.30	+0.12
E(polar: Cl···H)	−10.80	−9.89	−0.91
E(polar: Cl···Cl)	10.36	11.79	−1.43
E(total)	6.74	13.07	−6.33

The structural parameters in Table 1 correspond to the minima found by minimizing the energy. It is clear that large deviations from all-staggered (1:2) conformations are likely for both *gauche* and *anti*. Moreover, the ∠CCC values of the conformers are quite different.

The calculated conformational energies which are given in Table 2, show that *gauche* is energetically more stable than *anti* by as much as 6.33 kcal/mol.

Torsional barriers may be estimated from the energy values in Table 3. The details about the three minima have been shown in Tables 1 and

Table 3. Calculated conformational energies and torsional barriers in $C(1)HX_2-C(2)H_2-C(3)X_3$, X = Cl. Approximative values of the torsion angles are those in parentheses (ϕ_{1-2} and ϕ_{2-3}; see also Fig. 1). All energy values are relative to the *gauche* minimum.

ϕ_{2-3}	ϕ_{1-2} $-180°$ $-60°$ $+180°$	$-120°$	$0°$ $+120°$	$+60°$
$+60°$ $-60°$	29.7	11.3	8.1	11.3
		"anti"	*"gauche"*	
$0°$	10.3	7.4[a] min: 6.33	3.6[b] min: 0	0.7

[a] Energy of the exact staggered *anti* form ($\phi_{1-2}=-120°$ and $\phi_{2-3}=0°$). Details about the *minimum* are given in Tables 1 and 2. [b] Energy of the exact staggered *gauche* forms ($\phi_{1-2}=\phi_{2-3}=0°$). Details about the *gauche* minimum are given in Tables 1 and 2. See also explanation in text.

2. All energy values are relative to the *gauche* minima. The values of the torsion angles (ϕ_{1-2} and ϕ_{2-3}) are approximately those given in parentheses. Each energy value was obtained by adjusting all geometry variables except for values of ϕ being $-180°$, $-60°$, $+60°$, and $+180°$. The energy value 8.1 kcal/mol thus corresponds to a form with $\phi_{2-3}=+60°$ (or $-60°$), while the value of ϕ_{1-2} is approximately equal to 0°. The actual values of the remaining structural variables are not shown in Table 3 in order to save space.

Between the two *gauche* minima is a low barrier of *ca.* 0.7 kcal/mol, corresponding to values of ϕ_{1-2} and ϕ_{2-3} being $+60°$ and 0°, respectively. The barrier separating *anti* and *gauche* minima is considerably higher.

Table 4. Calculated torsional force constants in Conformers of $C(1)HX_2-C(2)H_2-C(3)X_3$, X = Cl. These values were *numerically* computed according to the definitions given.

(mdyn Å (rad)$^{-2}$)	*gauche*	*anti*
$F_\phi(1-2)=\partial^2E/\partial\phi_{1-2}{}^2$	0.20	0.38
$F_\phi(2-3)=\partial^2E/\partial\phi_{2-3}{}^2$	0.27	0.44
$F_{\phi\phi'}=\partial^2E/\partial\phi_{1-2}\partial\phi_{2-3}$	-0.07	0.02

The *exact* all-staggered (1:2) forms clearly do not correspond to minima of the energy function. (7.4[a] and 3.6[b] in Table 3).

The torsional force constants of Table 4 were calculated at the conformational minima. It is noteworthy that the magnitude of the interaction constant ($F_{\phi\phi'}$) is quite small for both conformers.

III. CALCULATION OF VIBRATIONAL QUANTITIES

Vibrational frequencies for PCP (liquid) have been published by Sheppard *et al.*[12] However, the low frequencies (< ca. 570 cm^{-1}) which are the most important ones for an electron diffraction study, have not been published. Therefore, valence force constants, except for the torsional part, were taken from the work of Schachtschneider and Snyder.[15] Certain compromises between force constant values had to be made. The final values selected for PCP are given in Table 5.

According to the semi-empirical model (Table 4) the value of the torsional interaction constant ($F_{\phi\phi'}$) is much smaller in magnitude than the diagonal element. $F_{\phi\phi'}$ has been given zero value in this work.

According to the semi-empirical model, a low barrier (0.7 kcal/mol) separates the two *gauche* conformers. If the calculated value of this barrier is correct, then the usual approximation assuming small vibrational amplitudes (SVA) is not valid, in calculating mean amplitudes of vibration for the *gauche* conformer. It is, however, possible that the calculated value is too low. With a barrier value of *ca.* 1.5 kcal/mol, or higher, the SVA approximation is valid at 60 °C. It was decided to apply the SVA approximation. The validity of that approximation then has to be judged by the final results (see Sect. VII).

The normal-coordinate program described by Gwinn [16] was used in computing vibrational frequencies. Their values are shown in Table 6. The agreement between these values and those observed by Sheppard *et al.*[12] is quite satisfactory. The average relative deviation between observed and calculated values is *ca.* 3 % for C–Cl stretching modes.

Mean amplitudes of vibration (u) and vibrational correction terms (K and D) for the

Table 5. Valence force constants for $C(1)HX_2-C(2)H_2-C(3)X_3$, X = Cl.

Stretch (mdyn Å^{-1})

C–C: 4.39
C–H: 4.89
C–X: 2.76

Bend (mdyn Å(rad)$^{-2}$)

CCC: 0.90
CCH: 0.69
CCX: 1.17
HCX: 0.79
XCX: 1.13
HCH: 0.54

Stretch/bend (mdyn(rad)$^{-1}$)

C–X/CCX: 0.55 (C–X common)
C–X/HCX: 0.33 (C–X common)
C–C/CCX: 0.29 (C–C common)
C–C/CCC: 0.35 (C–C common)
C–C/CCH: 0.26 (C–C common)
C–X/XCX: 0.41 (C–X) common)
C–X/XCX: 0.38 (C common)

Stretch/stretch (mdyn Å^{-1}) (C common)

C–X/C–X: 0.49
C–X/C–C: 0.73
C–C/C–C: 0.064
C–H/C–H: 0.06

Bend/bend (mdyn Å(rad)$^{-2}$)

HCX/HCX: 0.09 (C–H common)
XCX/XCX: −0.13 (C–X common)
CCX/XCX: −0.12 (C–X common)
CCX/XCX: −0.06 (C common)
CCH/HCX: 0.10 (C–H common)
CCH/CCC: −0.12 (C–C common)

Bend/bend (C–C common and dihedral angle *anti* or *gauche*)

CCC/CCX: 0.04 (*anti*) and −0.02 (*gauche*)
CCH/CCC: – (*anti*) and −0.06 (*gauche*)
CCH/CCH: 0.10 (*anti*) and −0.03 (*gauche*)

Torsion [a] (mdyn Å(rad)$^{-2}$)

$F_\phi(1-2) = F_\phi(2-3) = \bar{F}_\phi{}^b = 0.32_{-0.16}{}^{+0.18}$ ($F_{\phi\phi'} = 0$)

[a] The torsional force constants were defined as follows: each fragment $A'-C_i-C_2-A''$ (A = C, Cl, H) has been assigned an equal torsional force constant. The total force constant (F_ϕ) for the torsion coordinate ϕ_{i-2} (i = 1,3) is thus the sum of *nine* equal contributions. Gwinn's normal-coordinate program [16] demands a separate specification for each torsion fragment. [b] This value was derived from the electron-diffraction data as described in Sect. V-B.

Table 6. Fundamental vibrational frequencies, ω(cm^{-1}), in the *gauche* conformer of $C(1)HX_2-C(2)H_2-C(3)X_3$, (X = Cl). The force constants of Table 5 were used. Experimental (average of liquid IR and Raman) values from Ref. 12 are shown in parentheses.

Torsion: 56 ($\Delta\phi_{1-2} \simeq +\Delta\phi_{2-3}$)[a] and 77 ($\Delta\phi_{1-2} \simeq -\Delta\phi_{2-3}$)[a]

Bend[b] (CCX, XCX, CCC): 110, 197, 214, 252, 262, 313, 369, 394, 478
C–X (stretch)[c]: 566, 640, 702, 758, 855 (577, 640, 716, 734, 831)
CH_2-rock: 998 (971)
CH_2-twist: 1197 (1204)
CH_2-wag: 1421 (1347)
C–C (stretch):[d] 1007, 1083, (1026, 1069)
Def.[e] (CCH, HCX): 1229, 1320 (–)[f]
Def.[e] (HCH): 1475 (1419)
C–H (stretch): 2991, 2997, 3001 (2943, 2982, 3003)

[a] Deformations in torsional angles ($\Delta\phi$) have been indicated. [b] Modes involving deformations in angles as indicated, mixed with a certain amount of C–X stretching. [c] Modes involving C–X stretching mixed with bending of CCX, HCX, and CCC angles. [d] Modes involving C–C stretching mixed with deformations of CCH angles. [e] Modes involving deformations of angles as indicated. [f] Experimental values in this range are: 1218, 1248, 1300.

Table 7. Mean amplitudes of vibration (u) and vibrational correction terms, $K-(u^2/r)$, for $C(1)HX_2-C(2)H_2-C(3)X_3$ at 60 °C. The force constants in Table 5 and the Cartesian coordinates in Table 9 were used in calculating these quantities. The correction terms correspond to $r_a-r_\alpha = K-(u^2/r) = -D$.

Dist. type (X=Cl)	u-Value (Å)	$K-(u^2/r)$ (Å)	Dist. type (X=Cl)	u-Value (Å)	$K-(u^2/r)$ (Å)
C_1-C_2	0.0523	0.0038	$X_1'\cdots H_1$	0.1090	0.0176
C_2-C_3	0.0529	0.0024	$X_1\cdots H_1$	0.1090	0.0139
C_1-X_1'	0.0572	0.0128	$X_1\cdots X_1'$	0.0718	0.0177
C_1-X_1	0.0571	0.0094	$X_3'-X_3''$	0.0740	0.0081
C_3-X_3'	0.0563	0.0073	$X_3\cdots X_3''$	0.0740	0.0084
C_3-X_3''	0.0563	0.0082	$X_3\cdots X_3'$	0.0740	0.0068
C_3-X_3	0.0563	0.0076	$H_2\cdots H_2'$	0.1292	0.0109
C_2-H_2	0.0778	0.0110	$C_1\cdots X_3'$(g)	0.1323	−0.0001
C_2-H_2'	0.0778	0.0111	$C_1\cdots X_3''$(g)	0.1299	−0.0010
C_1-H_1	0.0778	0.0152	$C_3\cdots X_1'$(g)	0.1329	0.0026
$C_2\cdots H_1$	0.1089	0.0101	$C_1\cdots X_3$(a)	0.0792	0.0010
$C_2\cdots X_1'$	0.0702	0.0112	$C_3\cdots X_1$(a)	0.0756	0.0020
$C_2\cdots X_1$	0.0701	0.0072	$C_3\cdots H_1$(g)	0.1541	0.0022
$C_2\cdots X_3'$	0.0705	0.0048	$X_1'\cdots H_2'$(a)	0.1053	0.0133
$C_2\cdots X_3''$	0.0704	0.0054	$X_3'\cdots H_2$(a)	0.1052	0.0061
$C_2\cdots X_3$	0.0704	0.0056	$X_3''\cdots H_2'$(a)	0.1081	0.0068
$C_1\cdots C_3$	0.0716	0.0011	$H_2\cdots H_1$(a)	0.1275	0.0136
$C_1\cdots H_2$	0.1074	0.0075	$H_2'\cdots H_1$(g)	0.1647	0.0085
$C_1\cdots H_2'$	0.1068	0.0074	$X_1'\cdots H_2$(g)	0.1561	0.0080
$C_3\cdots H_2$	0.1071	0.0109	$X_3'\cdots H_2'$(g)	0.1448	0.0036
$C_3\cdots H_2'$	0.1070	0.0112	$X_3''\cdots H_2$(g)	0.1539	0.0036
$X_1\cdots H_2$(g)	0.1515	0.0054	$X_1'\cdots X_3'$(GG)	0.2342	−0.0093
$X_1\cdots H_2'$(g)	0.1518	0.0053	$X_1'\cdots X_3''$(GG)	0.2343	−0.0042
$X_3\cdots H_2$(g)	0.1468	0.0045	$X_1'\cdots X_3$(AG)	0.1230	−0.0008
$X_3\cdots H_2'$(g)	0.1521	0.0050	$X_1\cdots X_3'$(AG)	0.1542	−0.0022
$X_3'\cdots H_1$(GG)	0.2187	0.0004	$X_1\cdots X_3''$(AG)	0.1278	−0.0021
$X_3''\cdots H_1$(GG)	0.2035	−0.0041	$X_1\cdots X_3$(AA)	0.1165	0.0005
$X_3\cdots H_1$(AG)	0.1703	−0.0004	–	–	–

internuclear distances were calculated according to the formulas in Ref. 17. Their values are found in Table 7.

According to the adjustments described in Sect. V-B, the most probable value of the average torsional force constant ($\overline{F}_\phi$) is expected in the range 0.16 − 0.50 mdyn Å(rad)$^{-2}$. In Table 8 are shown low frequencies and important mean amplitudes of vibration corresponding to values of $\overline{F}_\phi$ in that range.

Values of the Cartesian coordinates (x,y,z) have been given in Table 9. The coordinate values in Table 9 were used in all calculations of vibrational quantities. The location of the Cartesian-coordinate system should be clear from the x, y, and z values in Table 9 (origin at the atom C_2).

IV EXPERIMENTAL AND DATA REDUCTION

PCP was obtained from "K&K" laboratories. The purity of the sample was better than 98 %.

Electron-diffraction photographs were made at a nozzle temperature of 60 °C in the Oslo apparatus [18] under conditions summarized below.

Nozzle-to-plate distance (mm)	481.8	201.8
Electron wavelength (Å)	0.06452	0.06452
Number of plates	6	6
Range of data, in s (Å^{-1})	1.375 − 19.375	7.25 − 43.25
Data interval, ΔS (Å^{-1})	0.125	0.25
Estimated uncertainty in s-scale %)	0.14	0.14

Table 8. Vibrational quantities in the *gauche* conformer of $C(1)HX_2-C(2)H_2-C(3)X_3$, (X = Cl), calculated for different values of the average torsional force constant ($\overline{F}_\phi$) at 60 °C.

$\overline{F}_\phi$ (mdyn Å(rad)$^{-2}$)	0.16[a]	0.32	0.50[a]
$u(X\cdots X)$[b] values (Å)			
$X_1\cdots X_3$ (AA)	0.125	0.117	0.113
$X_1'\cdots X_3$ (AG)	0.137	0.123	0.117
$X_1\cdots X_3'$ (AG)	0.171	0.154	0.147
$X_1\cdots X_3''$(AG)	0.144	0.128	0.121
$X_1'\cdots X_3''$ (GG)	0.277	0.234	0.215
$X_1\cdots X_3$ (GG)	0.303	0.234	0.204
$u(C\cdots X)$[b] values (Å)			
$C_1\cdots X_3$ (a)	0.083	0.079	0.078
$C_3\cdots X_1$ (a)	0.077	0.076	0.075
$C_1\cdots X_3'$ (g)	0.148	0.136	0.131
$C_1\cdots X_3''$ (g)	0.152	0.130	0.120
$C_3\cdots X_1'$ (g)	0.155	0.133	0.124
Frequencies,[c] ω (cm^{-1})			
Torsion (++)	40	56	69
Torsion (+−)	62	77	85
Bend (CCX/XCX/CCC)	107	110	113
	197	198	197
	213	214	215
	250	252	254
	260	262	264
	311	313	316
	356	369	377
	394	394	394
	452	478	499

[a] Except for these values, the force fields in Table 5 were used. [b] Mean amplitudes of vibration for torsion dependent X···X and C···X distances. See also Table 7. [c] Low vibrational frequencies (<500 cm^{-1}). See also Table 6.

Table 9. Cartesian coordinates from atoms in the *gauche* conformer of $C(1)HX_2-C(2)H_2-C(3)X_3$. These coordinate values were used in the calculations of all vibrational quantities (non-staggered model).

x (Å)	y (Å)	z (Å)	Atom[a] (X = Cl)
0	0	0	C_2
1.3137	0.8089	0	C_1
1.2493	1.6209	−0.7581	H_1
1.5757	1.5153	1.5903	X_1'
2.6629	−0.2504	−0.3931	X_1
−1.3137	0.8089	0	C_3
−1.1358	2.2299	−1.0226	X_3'
−1.6965	1.3192	1.6401	X_3''
−2.6251	−0.1890	−0.6175	X_3
0	−0.7106	0.8628	H_2
0	−0.7106	−0.8628	H_2'

[a] *Cf.* Fig. 2.

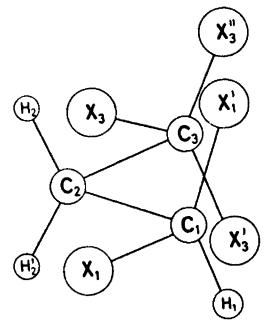

Fig. 2. Numbering of atoms (X = Cl) in the *gauche* conformer ($\phi_{1-2}=\phi_{2-3}=0°$) of $HCX_2-CH_2-CX_3$.

The electron wavelength was determined by calibration against gold and corrected by an experiment with CO_2 giving a correction of +0.1 % in the s-scale. The data were reduced in the usual way [19] to yield an intensity curve for each plate.

Average curves for each set of distances were formed. A composite curve was then made by connecting the two average curves after scaling. The final experimental curve is shown in Fig. 3. The intensities have been modified [19] by $s|f_{Cl'}|^{-2}$. Scattering amplitudes were calculated by the partial-wave method,[20] using Hartree-Fock atomic potentials.[21]

The radial-distribution curve [19] obtained by Fourier transformation of the final experimental intensity is shown in Fig. 4.

V. STRUCTURE ANALYSIS

The presence of the large peak in the experimental RD-curve (Fig. 4) at 5.0 − 5.5 Å shows that *gauche* is the predominating conformer.

According to the semi-empirical model, the conformational energy difference between *gauche* and *anti* is 6.3 kcal/mol in favour of *gauche*. If this value is approximately correct, then *anti* can not be present in detectable amounts at *ca.* 60 °C. Therefore, the *anti* conformer has not been included in the structural analysis. The validity of this assumption has to be judged by the final results (see also Sect. VII).

A. *Least-squares refinements.*[19] Several assumptions about bond lengths and bond angles had to be made in constructing the molecular model for the least-squares refinements. The following assumptions were introduced: (see Fig. 2; X = Cl)

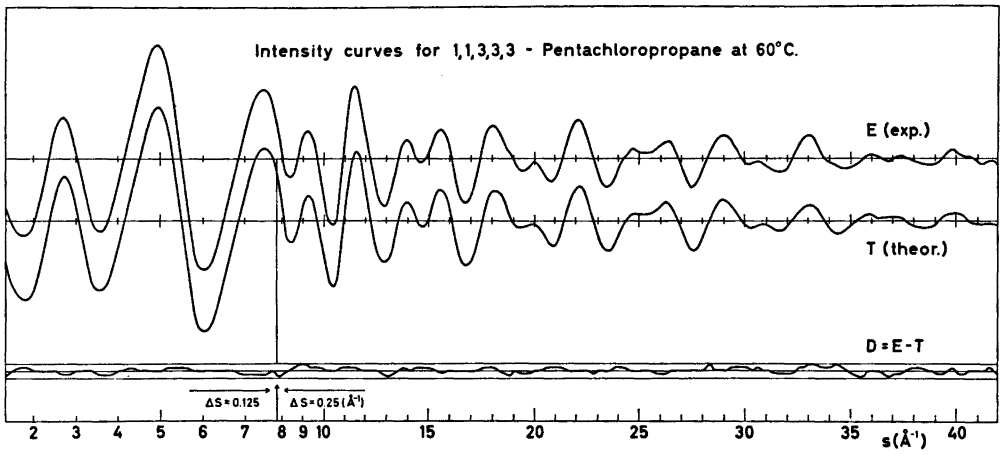

Fig. 3. Experimental (E) and theoretical (T) intensity curves, and D = E − T, corresponding to the final least-squares parameters. The straight lines give the experimental uncertainties (± 3 × experimental standard deviation).

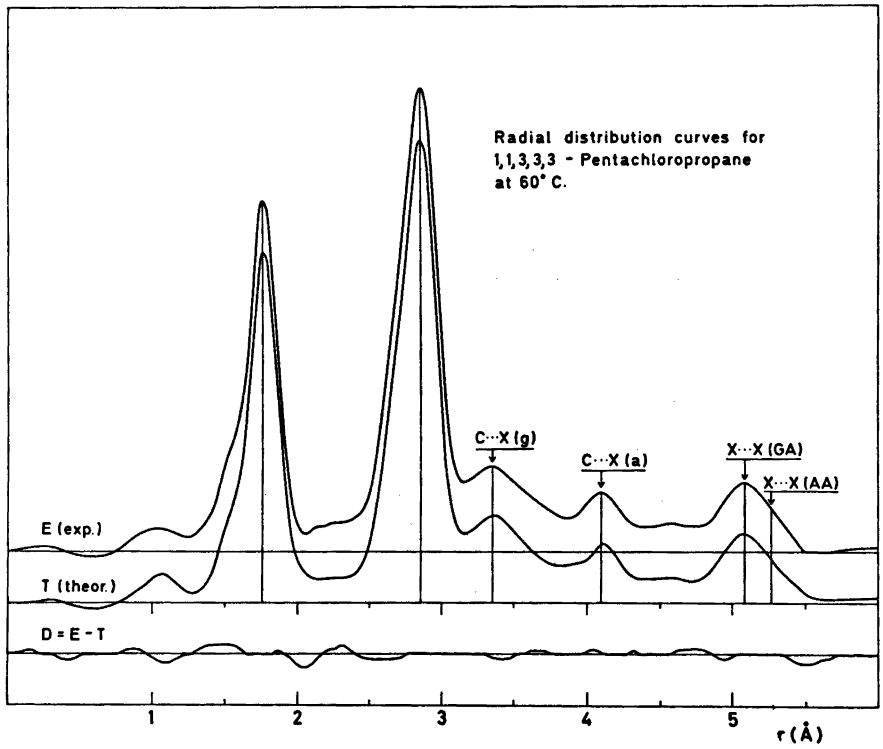

Fig. 4. Experimental (E) and theoretical (T) radial distribution curves, and D = E − T. The curves were calculated from the intensity curves in Fig. 3 with an artificial damping constant of 0.0020 Å^2. Some of the peaks corresponding to non-bonded internuclear distances have been indicated; see also Tables 12 and 7.

(1) the plane of the CH_2 group is perpendicular to the plane of the C atoms and bisects the CCC angle, (2) the $C-CX_3$ group possess C_{3v} symmetry, (3) the $C-CHX_2$ group possess C_s symmetry, and the projection of the $X_1C_1X_1'$ angle on a plane perpendicular to the C_1-C_2 axis is 120°, (4) all CCX angles are equal, (5) all CCH angles of the $>CH_2$ group are equal: $\angle CC_2H$, (6) all C–X bond lengths are equal: $r(C-X)$, (7) the C–H bond lengths in the $>CH_2$ group are equal: $r(C_2-H)$, (8) the two C–C bond lengths are equal: $r(C-C)$.

Models were refined in terms of the following parameters: $r(C-C)$, $r(C-X)$, $r(C_1-H)$, $r(C_2-H)$, $\angle CCC$, $\angle CCX$, $\angle CC_2H$, $\angle C_2CH$, and the torsion angles (ϕ_{1-2} and ϕ_{2-3}) of the *gauche* conformer (see Fig. 1). For the exact all-staggered (1:2) conformation of *gauche* $\phi_{1-2}=\phi_{2-3}=0°$, corresponding to a coplanar arrangement of the atoms $X_1-C_1-C_2-C_3-X_3$ (Fig. 2).

Non-bonded internuclear distances were computed under the constraints of geometrically consistent r_α parameters.[22,23]

Several of the bond distances which have been assigned equal *lengths* are *not vibrationally* identical, as shown in Table 7. This fact has been allowed for when D values ($D=r_\alpha-r_a=(u^2/r)-K$) were included for the internuclear distances.

B. *Determination of torsional force constants.* Mean amplitudes of vibration (u) and perpendicular amplitude correction coefficients (K) are easily calculated if a reasonable force field is known for the molecule (Sect. III). The values of the torsional force constants $F_\phi(1-2)$, $F_\phi(2-3)$, and $F_{\phi\phi'}$ had not been experimentally determined previous to this investigation.

If the value of the interaction constant ($F_{\phi\phi'}$) is assumed to be zero (see Table 4), then two elements, $F_\phi(1-2)$ and $F_\phi(2-3)$, of different values ought to be adjusted. According to the semi-empirical model (Table 4) the two diagonal constants have approximately equal value, ($F_\phi(2-3)$ being a little greater than $F_\phi(1-2)$.

Unfortunately, the electron-diffraction data for PCP do not contain enough information for an independent determination of both $F_\phi(1-2)$ and $F_\phi(2-3)$. It is, however, possible to estimate an average element $\overline{F}_\phi$, with $F_\phi(1-2)=F_\phi(2-3)=\overline{F}_\phi$.

The value of $\overline{F}_\phi$ was determined as follows: u and K values for different values of $\overline{F}_\phi$ were calculated and then included in the least-squares refinements. The value of $\overline{F}_\phi$ which lead to a minimum in the error sum (**VPV**)[19] was obtained. In each least-squares run all structural parameters, except for $r(C-H)$ and $\angle CCH$, were refined simultaneously. The best value of $\overline{F}_\phi$ obtained in this way was: $\overline{F}_\phi=0.32\ {}_{-0.16}{}^{+0.18}$ mdyn Å(rad)$^{-2}$. The error limits are believed to be pessimistic, however, there is no straight forward way to estimate these limits. The most direct estimate, but subjective to a certain degree, is obtained by comparing experimental and calculated RD curves for a range of $\overline{F}_\phi$ values. Several types of systematic errors ought to be considered, as discussed in a previous paper.[5] The error limits here do not allow for systematic errors.

VI. FINAL RESULTS

Parameters from the least-squares refinements,[19] and their standard deviations (σ) corrected for correlation [24] in the experimental data, are given in Table 10. The final parameters correspond to refinements with equal weights [19] for all intensities.

Table 10. Structural parameters in the *gauche* conformer of $C(1)HX_2-C(2)H_2-C(3)X_3$ (X = Cl). Standard deviations are shown in parentheses. The uncertainty (0.14 %) in the s-scale has been included in the standard deviations for bond lengths. An experiment with CO_2 gave a correction of +0.1 % in the s-scale. The bond lengths are therefore 0.1 % longer than the least-squares estimates.

Bond lengths (Å)[a] (r_a-values)	Bond angles (°)[a] ($\angle_\alpha$-values)
$r(C-C)=1.545(6)$	$\angle CCC=115.7(1.4)$
$r(C-X)=1.772(2)$	$\angle CCX=109.9(0.3)$
$r(C-H)=1.05(-)^b$	$\angle CCH=109.47)^c$
Torsion angles	
$\phi_{1-2}=+14.1°$ (1.5)[d] and $\phi_{2-3}=-22.5°(1.2)^d$	

[a] The geometrical assumptions were explained in Sect. V-A. [b] Not refined; estimated from the RD curve in Fig. 4. [c] Assumed value; see Table 1. [d] Staggered values: $\phi_{1-2}=\phi_{2-3}=0°$; see Fig. 1.

Table 11. Correlation coefficients (100ϱ).

X = Cl[a]		(1)	(2)	(3)	(4)	(5)	(6)	(7)	(8)
r(C−C)	(1)	100							
r(C−X)	(2)	−22	100						
∠CCC	(3)	−32	8	100					
∠CCX	(4)	−66	39	28	100				
ϕ_{1-2}	(5)	6	6	−22	−18	100			
ϕ_{2-3}	(6)	1	14	58	9	40	100		
u(C−X)[b]	(7)	−18	1	8	−3	4	−4	100	
scale[c]	(8)	−28	6	12	−15	13	−5	49	100

[a] The parameter assumptions are given in Sect. V-A. [b] All u(C−X) values were refined as one parameter; see also Table 7. [c] Scale-factor [19] between experimental and theoretical intensities.

Table 12. Refined and calculated mean amplitudes (u) of vibration for the *gauche* conformer of C(1)HX_2−C(2)H_2−C(3)X_3 at 60 °C. Standard deviations are given in parentheses.

Type of distance (r) (see Fig. 2; X = Cl)	r (Å) (see Fig. 4)	Refined u-value (Å)	Calculated[a] u-value (Å)
C−X (bond dist.)	(1.772)	0.044(2)	0.056
C···X (in CCX)	(2.71)	0.071(5)	0.070
X···X (in XCX)	(2.88)	0.065(2)	0.072
$C_1\cdots X_3'$ (g)	(2.99)	0.113(41)[b]	0.132
$C_1\cdots X_3''$(g)	(3.46)	0.112(41)[b]	0.130
$C_3\cdots X_1'$ (g)	(3.36)	0.114(41)[b]	0.133
$C_1\cdots X_3$ (a)	(4.10)	0.075(15)[b]	0.079
$C_3\cdots X_1$ (a)	(4.13)	0.071(15)[b]	0.076
$X_1'\cdots X_3'$ (GG)	(3.80)	0.197(24)	0.234
$X_1'\cdots X_3''$ (GG)	(3.27)	(0.234)(−)[c]	0.234
$X_1'\cdots X_3$ (AG)	(5.04)	0.143(20)[b]	0.123
$X_1\cdots X_3'$ (AG)	(4.56)	0.168(20)[b]	0.154
$X_1\cdots X_3''$ (AG)	(5.06)	0.146(20)[b]	0.128
$X_1\cdots X_3$ (AA)	(5.30)	(0.117(−)[c]	0.117

[a] Calculated in Sect. III. [b] Refined as one parameter. [c] Not refined.

Non-bonded internuclear distances were restricted under the geometrical constraints of r_α parameters,[22,23] by including correction terms $D = r_\alpha - r_a$, with $D = (u^2/r) - K$, for all distances (Sect. III)

The r(C−H) and ∠CCH parameters did not refine to reasonable values. All r(C−H) values were fixed at 1.05 Å as suggested by the C−H peak in the experimental RD curve (Fig. 4). All values of ∠CCH were fixed at 109.47° (see Table 1).

Parameter-correlation [19] coefficients (ϱ) are shown in Table 11.

It is important that the great number of u values (Table 7) do not have to be adjusted as individual parameters in the least-squares refinements. However, it ought to be kept in mind that the torsion-dependent u and K values have been adjusted simultaneously by adjusting the torsional force constant (Sect. V-B).

For internuclear distances between heavy atoms, several mean amplitudes of vibration were refined as individual parameters [19] together with the geometry variables. These u values, and the corresponding values calculated in Sect. III, have been compared in Table 12. Generally the agreement between the two sets of u values is reasonable, but unfortunately the standard

Table 13. Comparison of results for $C(1)HX_2-C(2)H_2-C(3)X_3=PCP$, $C(1)HX_2-C(2)X_2-C(3)X_3=HCP$, and $C(1)X_3-C(2)X_2-C(3)X_3=OCP$ as determined by electron diffraction and semi-empirical calculations.

X: chlorine	Experimental values PCP	HCP[a]	OCP[b]	Calculated values PCP	HCP[a]	OCP[b]
r_a(C−C) in Å	1.545(6)	1.601(8)	1.655(15)	1.543	1.597	1.594
$\angle_\alpha$ CCC in deg.	115.7(1.4)	117.6(1.9)	119.0(2.0)	116.1	114.8	120.0
Deviations of torsion angles from all-staggered (1:2) form:						
$\Delta\phi_{1-2}$ in deg.	+14.1(1.5)	+7.8(1.1)	±0.0[c]	+32.3	+6.6	±0.0
$\Delta\phi_{2-3}$ in deg.	−22.5(1.2)	−7.8(1.1)	±0.0[c]	+1.9	−7.2	±0.0
Average torsional force constant, $\overline{F}_\phi=F_\phi(1-2)=F_\phi(2-3)$:[d]						
$\overline{F}_\phi$(mdyn Å(rad)$^{-2}$)	$0.32^{+0.18}_{-0.16}$	$0.54^{+0.27}_{-0.18}$	$0.36^{+0.14}_{-0.07}$	–	–	–
$F_\phi(1-2)$	–	–	–	0.20	0.57	0.69
$F_\phi(2-3)$	–	–	–	0.27	0.67	0.69
Fundamental frequencies (ω) corresponding to torsional oscillations of $-CHX_2$ and $-CX_3$ groups:						
$\omega(++)$[e] in cm^{-1}	56	67	48	–	–	–
$\omega(+-)$[e] in cm^{-1}	77	77	62	–	–	–

[a] Parameters for the *gauche* conformer; for further details see Ref. 4. [b] For further details see Ref. 5. [c] No deviation from an all-staggered (1:2) conformer detected. [d] The experimental values were determined as explained in Sect. V-B. [e] Deformations in the torsion angles have been indicated; see also Table 6.

deviations for the torsion-dependent u values are very large. However, since the refined u values for torsion-dependent distances are consistent with those calculated in Sect. III, it is likely that the approximation assuming small vibrational amplitudes is valid for the *gauche* conformer of PCP at 60 °C (see also discussion in Sect. III).

Except for the u(C−X) value, the u values in Table 7 were used in calculating the final theoretical functions shown in Figs. 3 and 4. The vibrationally consistent set of u values in Table 7, which combine information from both spectroscopy and electron diffraction, are considered the final ones for PCP.

VII. DISCUSSION

The agreement between the experimental data and the theoretical functions (Figs. 3 and 4) is quite satisfactory. It is thereby shown that *gauche* is the predominating conformer of PCP in the gas phase at 60 °C. Although the *anti* conformer was not included in the least-squares refinements, the percentage of *anti* (< 0.5 %) corresponding to the conformational energies in Table 2, is consistent with the electron-diffraction data. A few percent (< 10 %) of *anti* is, however, not ruled out by the experimental data alone. Our result agrees with the conclusion drawn by Sheppard *et al.*[12] who studied PCP in the liquid phase.

According to the semi-empirical model a low torsional barrier (*ca.* 0.7 kcal/mol) separates the two *gauche* conformers (Table 3). The approximation assuming small vibrational amplitudes was discussed in Sects. III and VI. In conclusion, the barrier between the *gauche* conformers is probably not as low as 0.7 kcal/mol, but the value of the barrier was not determined in this work.

It seems natural to compare the results obtained for PCP with the results for HCP-($HCCl_2-CCl_2-CCl_3$)[4] and OCP($CCl_3-CCl_2-CCl_3$).[5] Experimental and calculated results for PCP, HCP, and OCP are found in Table 13. The results of the semi-empirical model to a large extent reasonably agree with the experimental findings; however, some shortcomings

of the model are obvious from the parameter values in Table 13. Although adjustments in the non-torsional force constants and the "normal" reference parameters (Table 1) could remove most of the discrepancies, it was decided that results from additional molecules ought to be included, before such corrections were considered.

Acknowledgements. We are grateful to cand. real. A. Almenningen for recording the diffraction photographs. Computer programs made available by Dr. H. M. Seip, Prof. W. D. Gwinn, and cand.real. S. Rustad have been extensively used in this work. Financial support from Norges almenvitenskapelige forskningsråd is gratefully acknowledged.

REFERENCES

1. Stølevik, R. *Acta Chem. Scand. A 28* (1974) 299.
2. Farup, P. E. and Stølevik, R. *Acta Chem. Scand. A 28* (1974) 680.
3. Farup, P. E. and Stølevik, R. *Acta Chem. Scand. A 28* (1974) 871.
4. Johnsen, J. P. and Stølevik, R. *Acta Chem. Scand. A 29* (1975) 201.
5. Fernholt, L. and Stølevik, R. *Acta Chem. Scand. A 28* (1974) 963.
6. Stølevik, R. *Acta Chem. Scand. A 28* (1974) 327.
7. Stølevik, R. *Acta Chem. Scand. A 28* (1974) 455.
8. Stølevik, R. *Acta Chem. Scand. A 28* (1974) 612.
9. Bastiansen, O., Seip, H. M. and Boggs, J. E. In Dunitz, J. D. and Ibers, J. A., Eds., *Perspectives in Structural Chemistry*, Wiley, New York 1971, Vol. IV.
10. Seip, H. M. In Sim, G. A. and Sutton, L. G., Eds., *Molecular Structure by Diffraction Methods*, (Specialist Periodical Reports), The Chemical Society, London 1973, Vol. 1, Part 1, Chapter 1.
11. Dempster, A. B., Price, K. and Sheppard, N. *Spectrochim. Acta A 25* (1969) 1381.
12. Dempster, A. B., Price, K. and Sheppard, N. *Spectrochim. Acta A 27* (1971) 1563.
13. Dempster, A. B., Price, K. and Sheppard, N. *Spectrochim. Acta A 27* (1971) 1579.
14. Abraham, R. J. and Parry, K. J. *J. Chem. Soc. B* (1970) 539.
15. Schachtschneider, J. H. and Snyder, R. G. *Vibrational Analysis of Polyatomic Molecules.* IV. (Force constants for the haloparaffins). Project No. 31450, Technical Report No. 122-63 of Shell Development Company.
16. Gwinn, W. D. *J. Chem. Phys. 55* (1971) 477.
17. Stølevik, R., Seip, H. M. and Cyvin, S. J. *Chem. Phys. Lett. 15* (1972) 263.
18. Bastiansen, O., Hassel, O. and Risberg, E. *Acta Chem. Scand. 9* (1955) 232.
19. Andersen, B., Seip, H. M., Strand, T. G. and Stølevik, R. *Acta Chem. Scand. 23* (1969) 3224.
20. Peacher, J. and Willis, J. C. *J. Chem. Phys. 46* (1967) 4809.
21. Strand, T. G. and Bonham, R. A. *J. Chem. Phys. 40* (1964) 1686.
22. Morino, Y., Kuchitsu, K. and Oka, T. *J. Chem. Phys. 36* (1962) 1108.
23. Kuchitsu, K. *J. Chem. Phys. 49* (1968) 4456.
24. Seip, H. M. and Stølevik, R. In Cyvin, S. J., Ed., *Molecular Structures and Vibrations*, Elsevier, Amsterdam 1972.

Received December 9, 1974.

Acta Chemica Scandinavica A 29 (1975) 468—474

Short Communications

Synthesis and Characterisation of *cis*-Tetraammine Rhodium(III) Complexes

MARTIN PAUL HANCOCK

Chemistry Department I (Inorganic Chemistry), University of Copenhagen, H.C. Ørsted Institute, Universitetsparken 5, DK-2100 Copenhagen Ø, Denmark

Although the *trans*-isomer of the tetraammine-dichlororhodium(III) cation was first prepared many years ago [1] and increasingly efficient methods for the synthesis of *trans*-$[RhX_2(NH_3)_4]^+$ (X = Cl, Br or I) have subsequently been devised,[2,3] there appears to have been no report in the literature of the synthesis of any rhodium(III) complexes containing the *cis*-tetraammine moiety. This is rather surprising in view of the fact that cobalt(III) complexes of both the *trans*- and *cis*-tetraammine series have been known since the time of Werner.[4] This communication reports the synthesis and characterisation of the tetraammineoxalato-rhodium(III) cation, $[Rh(ox)(NH_3)_4]^+$, and the ready conversion of the latter to the *cis*-tetra-amminedichloro and dibromo complexes in high yield.

The synthesis of $[Rh(ox)(NH_3)_4]^+$ involves the reaction of the easily-prepared [5,6] complex $[RhCl(NH_3)_5]^{2+}$ (as the chloride salt) with oxalate ion, in the presence of one proton per complex ion, in water at 120 °C for 24 h in an autoclave. Addition of perchloric acid to the resulting, cooled solution results in the rapid crystallisation of the sparingly soluble crude perchlorate salt of the desired complex. Pure $[Rh(ox)(NH_3)_4]ClO_4.H_2O$ is then obtained in *ca.* 55 % yield on recrystallisation.

The *cis*-dihalo complexes, *cis*-$[RhX_2(NH_3)_4]X.\frac{1}{2}H_2O$ (X = Cl or Br), may be isolated in high yield from the solutions obtained by boiling the oxalato complex in the appropriate strong aqueous hydrohalic acid. Further purification is readily achieved by recrystallisation from hot aqueous hydrohalic acid. No evidence was obtained for any *cis*→*trans* isomerisation during the above procedures. The sparingly soluble, pure crystalline dithionate salts of *cis*-$[RhX_2(NH_3)_4]^+$ (X = Cl or Br) are readily obtained by addition of sodium dithionate to concentrated aqueous solutions of the halide salts.

The reactions involved in the synthesis of the new *cis*-tetraammine complexes are summarized in Scheme 1.

$$[RhCl(NH_3)_5]^{2+} + ox^{2-} + H^+ \xrightarrow[120\,°C]{H_2O} [Rh(ox)(NH_3)_4]^+ + Cl^- + NH_4^+ \quad (1)$$

$$[Rh(ox)(NH_3)_4]^+ + 2H^+ + 2X^- \xrightarrow[\text{boil}]{H_2O} \textit{cis}\text{-}[RhX_2(NH_3)_4]^+ + H_2ox \quad (2)$$

Scheme 1. ox^{2-} = oxalate dianion, $C_2O_4^{2-}$; X = Cl or Br.

Oxalato complexes of the type formed in reaction (1) are established for bis(diamine)rhodium-(III) systems [7–9] and are known to undergo conversion to the corresponding *cis*-dichloro and dibromo species, under the same conditions as employed in reaction (2) here, with retention of geometric configuration.[8,9]

A comparison of the Guinier powder photographs of *cis*-$[MCl_2(NH_3)_4]Cl.\frac{1}{2}H_2O$ (M = Co or Rh) showed the two complexes to be isomorphous, thereby demonstrating the *cis*-configuration of the rhodium(III) complex. The IR spectra (4000 – 400 cm^{-1}) of the two compounds are extremely similar to one another. The IR spectra of $[M(ox)(NH_3)_4]ClO_4.H_2O$ (M = Co or Rh) are also very similar, although the Guinier powder photographs indicate these congeners to be non-isomorphous. Further evidence concerning the nature of the new rhodium(III) complexes is provided by their ligand-field spectra, which are very similar to those of the well-characterised [2,7,8] bis(ethylenediamine)rhodium(III) analogues (Table 1). Data for the *trans*-dichloro and *trans*-dibromo isomers of the tetraammine and bis(ethylenediamine)rhodium-(III) complexes are also included in Table 1 for comparison purposes. It can be seen that the longer-wavelength absorption maxima for the *cis*-tetraammine complexes occur at somewhat lower energy than those for the *cis*-bis-(ethylenediamine) analogues, as is also the case for the *trans*-dihalo complexes of the two systems.

Further work on the *cis*-tetraammine rhodium(III) system will be described in a subsequent publication.[9]

Table 1. Ligand-field spectra.

Complex	λ_{max}	ε_{max}	Ref.
$[Rh(ox)(NH_3)_4]^+$	333	167	This work
$[Rh(ox)(en)_2]^+$	325	260	7
cis-$[RhCl_2(NH_3)_4]^+$	360, 295	126, 108	This work
cis-$[RhCl_2(en)_2]^+$	352, 295	155, 180	2
cis-$[RhBr_2(NH_3)_4]^+$	377, *ca.* 275(sh)	170, *ca.* 940	This work
cis-$[RhBr_2(en)_2]^+$	362, 276(sh)	210, 900	2
trans-$[RhCl_2(NH_3)_4]^+$	412, —	66, —	2
	415, 293	74, 85	3
trans-$[RhCl_2(en)_2]^+$	406, 286	75, 130	2
trans-$[RhBr_2(NH_3)_4]^+$	441, *ca.* 280(sh)	111, *ca.* 2700	3
trans-$[RhBr_2(en)_2]^+$	425, 276	100, 1800	2

Experimental. Materials. $[RhCl(NH_3)_5]Cl_2$ and $[CoCO_3(NH_3)_4]ClO_4$ were kindly provided by Dr. Erik Pedersen and Dr. Claus Schäffer, respectively, of this department. The *cis*-$[CoCl_2(NH_3)_4]^+$ ion was prepared essentially as in Ref. 10, starting from $[CoCO_3(NH_3)_4]ClO_4$, and purified as the dithionate salt according to Ref. 4. The pure chloride salt was then prepared from the dithionate by a modification of Werner's original method,[4] involving the use of ice-cold conc. hydrochloric acid in place of an ammonium chloride solution. The fine blue-violet crystals were washed with ice-cold conc. hydrochloric acid and then 96 % ethanol, and air-dried. (Found: N 22.57; H 5.34; Cl 44.25. Calc. for *cis*-$[CoCl_2(NH_3)_4]Cl.\frac{1}{2}H_2O$: N 23.08; H 5.40; Cl 43.90). $[Co(ox)(NH_3)_4]ClO_4.H_2O$ was prepared by boiling an aqueous solution containing *cis*-$[CoCl_2(NH_3)_4]Cl.\frac{1}{2}H_2O$ and a slight excess of oxalic acid, treating the carmine-red solution with lithium perchlorate and cooling it in ice. The crimson-red crystals were then recrystallised from hot water by addition of lithium perchlorate, washed with 96 % ethanol and air-dried. (Found: C 7.24; N 16.98; H 4.32; Cl 10.61. Calc. for $[Co(ox)(NH_3)_4]ClO_4.H_2O$: C 7.22; N 16.84; H 4.24; Cl 10.67). The visible absorption spectrum agreed with that published previously.[11]

All other chemicals were of reagent grade and were used without further purification.

Spectra. Absorption spectra in the region 600 – 250 nm were recorded using a Cary Model 14 spectrophotometer. Data for absorption maxima or shoulders (sh) in Table 1 are given as λ_{max} and ε_{max} with the wavelength λ in nm and the molar absorbance ε in 1 mol^{-1} cm^{-1}. Medium: water.

Preparation of new complexes. 1. Tetraammine-oxalatorhodium(III) perchlorate monohydrate, $[Rh(ox)(NH_3)_4]ClO_4.H_2O$. A mixture of $[RhCl(NH_3)_5]Cl_2$ (2.0 g, 6.8 mmol), disodium oxalate (0.91 g, 6.8 mmol), oxalic acid (0.43 g, 3.4 mmol) and water (70 ml) was placed in a stainless-steel autoclave (volume *ca.* 300 ml). The autoclave was tightly closed and heated in an oven at 120 °C for 24 h, after which it was allowed to cool to about 50 °C and opened. The contents were filtered and the autoclave rinsed with water (10 ml). The washings were filtered and added to the bulk solution which was then allowed to cool to room temperature. 70 % perchloric acid (2.5 ml) was added to the pale-yellow solution, whereupon crystals of the crude product began to form. After cooling and agitating the mixture in an ice-bath for 20 min the crystals were isolated by filtration, washed with a little ice-cold 2 M perchloric acid and then methanol, and air-dried. Yield 1.6 g. The crude product was purified by dissolving in the minimum volume of hot (90 °C) water, and adding activated charcoal (0.1 g) to the solution. The solution was then filtered through a fine sintered glass funnel, treated with a hot solution of lithium perchlorate (2.0 g) in water (10 ml) and cooled in ice. The pale-yellow crystals were recrystallised once more from hot water by adding lithium perchlorate as before and allowing the solution to cool overnight. They were isolated by filtration, washed with methanol and air-dried. Yield 1.4 g (55 %). (Found: C 6.24; N 14.87; H 3.98; Cl 9.44. Calc. for $[Rh(ox)(NH_3)_4]ClO_4.H_2O$: C 6.37; N 14.87; H 3.74; Cl 9.43).

2. cis*-Tetraamminedichlororhodium(III) chloride hemihydrate*, *cis*-$[RhCl_2(NH_3)_4]Cl.\frac{1}{2}H_2O$. $[Rh(ox)(NH_3)_4]ClO_4.H_2O$ (1.32 g, 3.5 mmol) was boiled for 1 min with 6 M hydrochloric acid (40 ml). The clear, bright-yellow solution was then cooled in ice for 10 min, when a good yield of bright-yellow crystals was obtained. Precipitation was completed by addition of methanol (40 ml) and further cooling. The crystals were isolated by filtration, washed with methanol and air-dried. Yield 0.98 g. The product was then recrystallised by dissolving in hot (95 °C) 3 M hydrochloric acid (25 ml), filtering the solution and allowing it to cool to room temperature. After further cooling at 0 °C overnight the bright-yellow needles were filtered off,

washed well with methanol and air-dried. Yield 0.89 g (91 %). (Found: N 19.34; H 4.60; Cl 36.62. Calc. for *cis*-$[RhCl_2(NH_3)_4]Cl.\frac{1}{2}H_2O$: N 19.54; H 4.57; Cl 37.16).

3. cis-*Tetraamminedibromorhodium(III) bromide hemihydrate, cis*-$[RhBr_2(NH_3)_4]Br.\frac{1}{2}H_2O$. $[Rh(ox)(NH_3)_4]ClO_4.H_2O$ (0.70 g, 1.86 mmol) was boiled with 5 M hydrobromic acid (30 ml) until all the complex had dissolved (*ca.* 2 – 3 min). The resulting orange solution was allowed to cool to room temperature and then kept in a freezer at – 15 °C overnight. The product was isolated by filtration, washed with 96 % ethanol and air-dried. Yield 0.68 g. Recrystallisation was performed as for the *cis*-dichloro chloride (prep. 2), using 3 M hydrobromic acid (30 ml) in place of hydrochloric acid. The orange crystals were filtered off, washed with 96 % ethanol and air-dried. Yield 0.60 g (77 %). (Found: N 13.48; H 3.08; Br 57.25. Calc. for *cis*-$[RhBr_2(NH_3)_4]Br.\frac{1}{2}H_2O$: N 13.33; H 3.12; Br 57.10).

4. cis-*Tetraamminedichlororhodium(III) dithionate, cis*-$[RhCl_2(NH_3)_4]_2S_2O_6$. $[RhCl_2(NH_3)_4]Cl.\frac{1}{2}H_2O$ (0.25 g, 0.87 mmol) was dissolved in water (20 ml) at room temperature and the solution filtered. A solution of sodium dithionate dihydrate (0.5 g, 2.1 mmol) in water (10 ml) was added, whereupon crystals of the desired product began to form immediately. After cooling the solution overnight at 0 °C the fine pale-yellow crystals were isolated by filtration, washed well with ice-cold water and then 96 % ethanol, and air-dried. Yield 0.21 g (75 %). (Found: N 17.58; H 3.45; S 9.88. Calc. for *cis*-$[RhCl_2(NH_3)_4]_2S_2O_6$: N 17.39; H 3.76; S 9.93).

5. cis-*Tetraamminedibromorhodium(III) dithionate, cis*-$[RhBr_2(NH_3)_4]_2S_2O_6$. This complex was prepared in the same way as the *cis*-dichloro dithionate (prep. 4), using *cis*-$[RhBr_2(NH_3)_4]Br.\frac{1}{2}H_2O$ (0.30 g, 0.71 mmol) dissolved in water (25 ml). The shiny orange crystals were filtered off, washed with ice-cold water and 96 % ethanol, and air-dried. Yield 0.23 g (78 %). (Found: N 13.78; H 2.83; S 7.89. Calc. for *cis*-$[RhBr_2(NH_3)_4]_2S_2O_6$: N 13.63; H 2.94; S 7.80).

1. Lebedinskii, W. W. *Izv. Inst. Izuch. Platiny Drugikh. Blagorod. Metal. Akad. Nauk SSSR 12* (1935) 67.
2. Johnson, S. A. and Basolo, F. *Inorg. Chem. 1* (1962) 925.
3. Poë, A. J. and Twigg, M. V. *Can. J. Chem. 50* (1972) 1089.
4. Werner, A. *Ber. Deut. Chem. Ges. 40* (1907) 4817.
5. Addison, A. W., Dawson, K., Gillard, R. D., Heaton, B. T. and Shaw, H. *J. Chem. Soc. Dalton Trans.* (1972) 589.
6. Osborn, J. A., Thomas, K. and Wilkinson, G. *Inorg. Syn. 13* (1972) 213.
7. Dasgupta, T. P., Milburn, M. M. and Damrauer, L. *Inorg. Chem. 9* (1970) 2789.
8. Addison, A. W., Gillard, R. D., Sheridan, P. S. and Tipping, L. R. H. *J. Chem. Soc. Dalton Trans.* (1974) 709.
9. Hancock, M. P. *To be published.*
10. Werner, A. *Justus Liebigs Ann. Chem. 386* (1912) 103.
11. Shimura, Y. and Tsuchida, R. *Bull. Chem. Soc. Jap. 28* (1955) 572.

Received February 20, 1975.

On the Structure of Deuterated Squaric Acid, $C_4D_2O_4$, at Room Temperature

DAG SEMMINGSEN

Department of Chemistry, University of Oslo, Oslo 3, Norway

The crystal structure of 3,4-dihydroxy-3-cyclobutene-1,2-dione (Squaric acid, hereafter denoted H_2SQ) as determined by X-ray diffraction has been reported previously.[1] Interest in this compound developed recently due to the discovery of a continuous phase transition in both H_2SQ ($T_C = 97$ °C) and D_2SQ ($T_C = 243$ °C).[2] The magnitude of the isotope effect in the transition temperatures of these compounds suggests that the hydrogen bonds are essential to the dynamics of the transition. Since the length of the hydrogen bonds in H_2SQ lie in the range where isotope effects in these bonds are to be expected, it was considered of importance to acquire exact information of the crystal structure of D_2SQ.

Squaric acid (H_2SQ) has also been independently examined by X-ray and neutron diffraction.[3] However, there are some points of disagreement between that work and our X-ray study.[2] In our X-ray study squaric acid crystals were found almost invariably to be twinned, and it was only after considerable effort that an untwinned sample could be found. Such difficulties were apparently not encountered in the combined X and N study.[3] A high degree of consistency was obtained between chemically equivalent but crystallographically independent bonds in our X-ray study,[1] but not in the combined study.[3] In the latter study poor agreement was also obtained for certain bond distances between the X-ray and neutron results. The X-ray structure determination of D_2SQ was therefore also undertaken in order to establish the validity of our previous X-ray work.[1]

washed well with methanol and air-dried. Yield 0.89 g (91 %). (Found: N 19.34; H 4.60; Cl 36.62. Calc. for *cis*-$[RhCl_2(NH_3)_4]Cl.\frac{1}{2}H_2O$: N 19.54; H 4.57; Cl 37.16).

3. cis-*Tetraamminedibromorhodium(III) bromide hemihydrate, cis*-$[RhBr_2(NH_3)_4]Br.\frac{1}{2}H_2O$. $[Rh(ox)(NH_3)_4]ClO_4.H_2O$ (0.70 g, 1.86 mmol) was boiled with 5 M hydrobromic acid (30 ml) until all the complex had dissolved (*ca.* 2 – 3 min). The resulting orange solution was allowed to cool to room temperature and then kept in a freezer at – 15 °C overnight. The product was isolated by filtration, washed with 96 % ethanol and air-dried. Yield 0.68 g. Recrystallisation was performed as for the *cis*-dichloro chloride (prep. 2), using 3 M hydrobromic acid (30 ml) in place of hydrochloric acid. The orange crystals were filtered off, washed with 96 % ethanol and air-dried. Yield 0.60 g (77 %). (Found: N 13.48; H 3.08; Br 57.25. Calc. for *cis*-$[RhBr_2(NH_3)_4]Br.\frac{1}{2}H_2O$: N 13.33; H 3.12; Br 57.10).

4. cis-*Tetraamminedichlororhodium(III) dithionate, cis*-$[RhCl_2(NH_3)_4]_2S_2O_6$. $[RhCl_2(NH_3)_4]Cl.\frac{1}{2}H_2O$ (0.25 g, 0.87 mmol) was dissolved in water (20 ml) at room temperature and the solution filtered. A solution of sodium dithionate dihydrate (0.5 g, 2.1 mmol) in water (10 ml) was added, whereupon crystals of the desired product began to form immediately. After cooling the solution overnight at 0 °C the fine pale-yellow crystals were isolated by filtration, washed well with ice-cold water and then 96 % ethanol, and air-dried. Yield 0.21 g (75 %). (Found: N 17.58; H 3.45; S 9.88. Calc. for *cis*-$[RhCl_2(NH_3)_4]_2S_2O_6$: N 17.39; H 3.76; S 9.93).

5. cis-*Tetraamminedibromorhodium(III) dithionate, cis*-$[RhBr_2(NH_3)_4]_2S_2O_6$. This complex was prepared in the same way as the *cis*-dichloro dithionate (prep. 4), using *cis*-$[RhBr_2(NH_3)_4]Br.\frac{1}{2}H_2O$ (0.30 g, 0.71 mmol) dissolved in water (25 ml). The shiny orange crystals were filtered off, washed with ice-cold water and 96 % ethanol, and air-dried. Yield 0.23 g (78 %). (Found: N 13.78; H 2.83; S 7.89. Calc. for *cis*-$[RhBr_2(NH_3)_4]_2S_2O_6$: N 13.63; H 2.94; S 7.80).

1. Lebedinskii, W. W. *Izv. Inst. Izuch. Platiny Drugikh. Blagorod. Metal. Akad. Nauk SSSR 12* (1935) 67.
2. Johnson, S. A. and Basolo, F. *Inorg. Chem. 1* (1962) 925.
3. Poë, A. J. and Twigg, M. V. *Can. J. Chem. 50* (1972) 1089.
4. Werner, A. *Ber. Deut. Chem. Ges. 40* (1907) 4817.
5. Addison, A. W., Dawson, K., Gillard, R. D., Heaton, B. T. and Shaw, H. *J. Chem. Soc. Dalton Trans.* (1972) 589.
6. Osborn, J. A., Thomas, K. and Wilkinson, G. *Inorg. Syn. 13* (1972) 213.
7. Dasgupta, T. P., Milburn, M. M. and Damrauer, L. *Inorg. Chem. 9* (1970) 2789.
8. Addison, A. W., Gillard, R. D., Sheridan, P. S. and Tipping, L. R. H. *J. Chem. Soc. Dalton Trans.* (1974) 709.
9. Hancock, M. P. *To be published.*
10. Werner, A. *Justus Liebigs Ann. Chem. 386* (1912) 103.
11. Shimura, Y. and Tsuchida, R. *Bull. Chem. Soc. Jap. 28* (1955) 572.

Received February 20, 1975.

On the Structure of Deuterated Squaric Acid, $C_4D_2O_4$, at Room Temperature

DAG SEMMINGSEN

Department of Chemistry, University of Oslo, Oslo 3, Norway

The crystal structure of 3,4-dihydroxy-3-cyclobutene-1,2-dione (Squaric acid, hereafter denoted H_2SQ) as determined by X-ray diffraction has been reported previously.[1] Interest in this compound developed recently due to the discovery of a continuous phase transition in both H_2SQ ($T_C = 97$ °C) and D_2SQ ($T_C = 243$ °C).[2] The magnitude of the isotope effect in the transition temperatures of these compounds suggests that the hydrogen bonds are essential to the dynamics of the transition. Since the length of the hydrogen bonds in H_2SQ lie in the range where isotope effects in these bonds are to be expected, it was considered of importance to acquire exact information of the crystal structure of D_2SQ.

Squaric acid (H_2SQ) has also been independently examined by X-ray and neutron diffraction.[3] However, there are some points of disagreement between that work and our X-ray study.[2] In our X-ray study squaric acid crystals were found almost invariably to be twinned, and it was only after considerable effort that an untwinned sample could be found. Such difficulties were apparently not encountered in the combined X and N study.[3] A high degree of consistency was obtained between chemically equivalent but crystallographically independent bonds in our X-ray study,[1] but not in the combined study.[3] In the latter study poor agreement was also obtained for certain bond distances between the X-ray and neutron results. The X-ray structure determination of D_2SQ was therefore also undertaken in order to establish the validity of our previous X-ray work.[1]

Table 1. Fractional atomic coordinates and thermal parameters with estimated standard deviations ($\times 10^5$), isotropic temperature factor and positional parameters ($\times 10^4$) for the deuterium atoms. The anisotropic temperature factor is given by $\exp-(B_{11}h^2+B_{22}k^2+B_{33}l^2+B_{12}hk+B_{13}hl+B_{23}kl)$.

ATOM	X	Y	Z	B	B11	B22	B33	B12	B13	B23
O1	11398(8)	25000(0)	-9234(8)		795(9)	2532(24)	548(8)	0(0)	-214(13)	0(0)
O2	-8493(8)	25000(0)	39140(8)		539(8)	2544(24)	809(10)	0(0)	178(13)	0(0)
O3	39328(8)	25000(0)	59650(8)		864(10)	2374(24)	574(9)	0(0)	-228(14)	0(0)
O4	60539(8)	25000(0)	11080(8)		557(8)	2363(23)	855(10)	0(0)	143(13)	0(0)
C1	20859(9)	25000(0)	9895(9)		581(9)	1558(22)	562(10)	0(0)	-47(14)	0(0)
C2	10834(9)	25000(0)	30799(9)		555(9)	1577(23)	599(10)	0(0)	-11(14)	0(0)
C3	32237(9)	25000(0)	41073(10)		617(9)	1536(22)	564(10)	0(0)	-33(14)	0(0)
C4	42136(9)	25000(0)	18711(9)		558(9)	1534(22)	618(10)	0(0)	-19(15)	0(0)
D1	2318(22)	2500(0)	-2060(27)	5.7(.4)						
D2	-2043(25)	2500(0)	2730(28)	6.5(.5)						

A single crystal with the dimensions $0.4 \times 0.1 \times 0.4$ mm was cut from a larger specimen and thoroughly examined by optical methods, before and after collection of intensity data. Details of the crystallization procedure will be published later. Scans along 2θ and ω on a four circle diffractometer for several highorder reflections revealed only $\alpha_1-\alpha_2$ splitting,[1b] confirming the absence of twinning. Intensity data were collected at room temperature (19 ± 1 °C) on a SYNTEX P$\bar{1}$ diffractometer with graphite monochromated Mo$K\alpha$ radiation ($\lambda = 0.71069$ Å) in two steps. One hemisphere of the reciprocal lattice ($h, \pm k, \pm l$) was examined with $2\theta \leq 55°$ and one quadrant ($h,k, \pm l$) was recorded with $55° < 2\theta \leq 110°$. In the latter shell, an instrumental threshold value was applied to avoid measurements of reflections with intensities less than $3\sigma(I)$. A total of 2271 reflections were measured, of which 146 had intensities less than $2\sigma(I)$ and were classified as unobserved. Equivalent reflections were averaged to yield about 1720 independent reflections. The average disagreement between equivalent reflections was 2.0 % [$Rc = \sum|F_o^2 - F^2|/\sum F_o^2$]. The average disagreement between pseudo-equivalent reflections, *i.e.* (hkl) and ($lk\bar{h}$) pairs was 10 %. The conditions for systematically absent reflections indicate the space group to be $P2_1$ or $P2_1/m$ in agreement with the previous X-ray determination. The cell dimensions were determined by a least-squares adjustment of 30 high-angle reflections giving:

$a = 6.152(1)$, $b = 5.269(1)$, $c = 6.165(1)$ Å, $\beta = 89.92(1)°$

The atomic parameters of the non-hydrogen atoms from the H_2SQ investigation [1b] were used as the starting point in full-matrix least-squares refinements, assuming the space group to be $P2_1/m$. The D atoms were included in the final cycles with a variable isotropic temperature factor. The weights used were those from counting statistics including a 2 % uncertainty in instrument stability. The final values for the residuals are $R = 0.041$ and $R_w = 0.051$. The positional and thermal parameters are given in Table 1. Tables of measured and calculated structure amplitudes are available from the author, on request.

The molecular geometry of D_2SQ is shown in Fig. 1, together with that of H_2SQ.[1b] Hydrogen bond distances and angles are given in Table 2.

The e.s.d. in bond distances between heavy atoms as calculated from the correlation matrix from the final L.S.R. refinement are 0.0008 Å or less. Crystallographically independent, but chemically equivalent bonds differ by a maximum of 0.0017 Å. The results from the previous X-ray determination are fully confirmed. The independent study of H_2SQ by neutron and X-ray diffraction [3] has therefore probably been carried out on twinned crystals.

H_2SQ and D_2SQ are closely isostructural. Thus the conclusions previously drawn for H_2SQ [1] in general also apply to D_2SQ: The deuterium atoms are asymmetrically located in

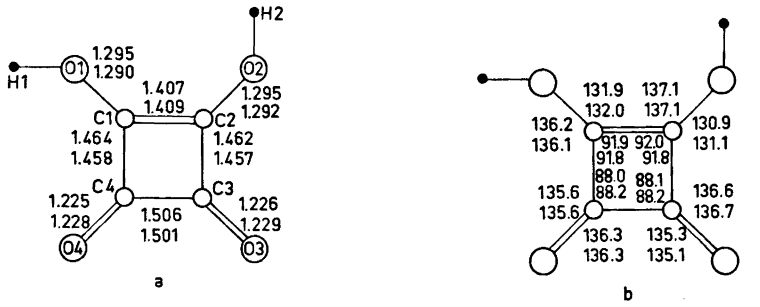

Fig. 1. Bond distances (a) and angles (b) uncorrected for thermal motion (upper values D_2SQ, lower values H_2SQ).

Table 2. Hydrogen bond distances and angles.

Bond lengths (Å)		Bond angles (°)	
O1···O3	2.5731(7)	O1–D1···O3	174.0(1.0)
O2···O4	2.5751(7)	O2–D2···O4	176.0(2.0)
O3···D1	1.56(2)	C1–O1–D1	110.4(0.8)
O4···D2	1.54(2)	C1–O1···O3	113.8(0.1)
O1–D1	1.01(2)	C2–O2–D2	111.8(0.9)
O3–D2	1.04(2)	C2–O2···O4	114.4(0.1)
		C3–O3···D1	119.5(0.5)
		C3–O3···O1	117.3(0.1)
		C4–O4···D2	117.0(0.6)
		C4–O4···O2	115.2(0.1)

the hydrogen bonds (Fig. 2). Each C_4O_4 unit is thus surrounded by two close and two distant deuterium atoms. The structure is built up from two-dimensional hydrogen-bonded layers perpendicular to the unique (*b*) axis. The stacking sequence may be described by a translation $\frac{1}{2}(\mathbf{a}+\mathbf{b}+\mathbf{c})$ of a layer with respect to that below or above. However, the directions of hydrogen bonds in neighbouring layers are opposite each other. The crystal structure is therefore pseudo-body-centered tetragonal with approximate fourfold rotation and screw (4_2) axes.

The O···O distances found in this study (2.575(1) and 2.573(1) Å) are longer than those found in the H_2SQ crystal (2.548(1) and 2.549(1) Å) by an average amount of 0.025 Å. This is highly significant, and is comparable with the figure (0.03 Å) estimated from expansions of the *a* and *c* axis (0.023 and 0.025 Å) on deuteration. According to calculations [4] an increase in the O···O distance is to be expected if the potential energy function is of the symmetric or asymmetric double minimum type. It has been suggested [5] that this isotope effect is at maximum for hydrogen bonds at a range (2.50–2.56 Å) closely centered around the values found in H_2SQ. Isotope effects of comparable magnitudes have previously been found in single crystal studies of $NaHC_2O_4.H_2O$ (0.022 Å) [6] and $(COOH)_2.2H_2O$ (0.012 Å).[7] These structures are, however, rather complicated in comparison to the H_2SQ structure, so that secondary effects may also be of importance.[6,7] In the $(COOH)_2.2H_2O$ structure [7] large isotope effects are even found in the weaker hydrogen bonds, which are not in agreement with predictions from the theory.[4,5] In the layers of molecules in D_2SQ and H_2SQ the intermolecular approaches are almost entirely dominated by the attractive hydrogen-bonding forces, whereas interplanar forces are predominantly of van der Waals nature and presumably much weaker, as is shown by the prominent cleavage along (010).[2]

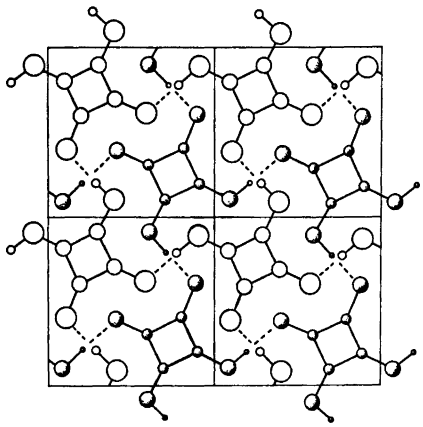

Fig. 2. The content of four unit cells of D_2SQ as viewed along the *b*-axis. Open circles: molecules at $y = 1/4$. Shaded circles: molecules at $y = 3/4$.

A very interesting feature in the H_2SQ [1b] and D_2SQ structures is that isotope effects in the hydrogen bonds seem to be transmitted to the molecule itself. Although differences in the corresponding bond distances in the two structures are of marginal significance, there appears to be slightly less delocalization of π-bonding in the deuterated material. This is in keeping with the results from the H_2SQ investigation [1b] where the high degree of conjugation found in the molecule was judged to be partly due to the strong hydrogen bonding.

The standard deviations and systematic errors in the parameters of the light atoms, (H and D) in X-ray determinations are large, and a full discussion of the hydrogen bond geometry and isotope effects will be given in a forthcoming neutron diffraction analysis.

Finally, an additional striking isotope effect in this material which is worth mentioning, is the large observed difference in domain wall mobility in H_2SQ and D_2SQ. Crystals of H_2SQ and D_2SQ show ferroelastic twinning,[8] and samples of H_2SQ have been successfully detwinned by application of uniaxial stress along the *a* and *c* axes. The motion of the domain walls is easily followed under a polarizing microscope. Similar attempts with D_2SQ have so far resulted in breakdown of the crystal before detwinning occurs.

Acknowledgements. The author is indebted to S. C. Abrahams at Bells Laboratories for his suggestion that the twinning in squaric acid crystals could be of ferroelastic origin.

1. a. Semmingsen, D. *Tetrahedron Lett.* (1973) 807; b. Semmingsen, D. *Acta Chem. Scand. 27* (1973) 3961.
2. Semmingsen, D. and Feder, J. *Solid State Commun. 15* (1974) 1369.

3. Wang, Y., Stucky, G. D. and Williams, J. M. *J. Chem. Soc. Perkin Trans. 2* (1974) 35.
4. Singh, T. R. and Wood, J. L. *J. Chem. Phys. 50* (1969) 3572.
5. Rundle, R. E. *J. Phys. Radium 25* (1964) 487.
6. Tellgren, R. and Olovsson, I. *J. Chem. Phys. 54* (1971) 127.
7. Delaplane, R. G. and Ibers, J. A. *Acta Crystallogr. B 25* (1969) 2423.
8. Abrahams, S. C. *Mater. Res. Bull. 6* (1971) 881.

Received March 19, 1975.

On the Formation of Phosgene and Trichloroacetyl Chloride in the Non-sensitized Photo-oxidation of Perchloroethylene in Air

HANS F. ANDERSSON, JAN ANDERS DAHLBERG and RUNE WETTSTRÖM

Uddeholms AB, Chemicals Division, Research Laboratory, S-663 00 Skoghall, Sweden

The non-sensitized photo-oxidation of trichloroethylene (tri) and 1,1,1-trichloroethane in the gas phase have earlier been reported.[1,2] In this paper the non-sensitized photo-oxidation of perchloroethylene (per) at low vapour pressures in air is described. The experimental technique has been described in the paper on photo-oxidation of trichloroethylene by Dahlberg.[1]

In the tri case the initiating step was shown to be a reaction between one tri molecule in the excited state and one in the ground state in competition with a pseudo first-order deactivation step.[1] However, for perchloroethylene we have shown that the initiating step is a dissociation of a per molecule upon light absorption. It is further shown that phosgene is probably formed not only according to the scheme by Huybrecht *et al.*[3] for the chlorine-sensitized photo-oxidation, but also by a parallel chain mechanism.

The results of the kinetic measurements are shown in Figs. 1 and 2. Obviously there are linear relationships between the rates of formation (v) of trichloroacetyl chloride (TCAC) and phosgene, respectively, and the absorbed light (I_{abs}). Thus all measurements made at the oxygen pressure 0.2 atm and at I_{abs} above 8.5×10^{-13} einstein/s fit well to the following equations calculated by the method of least squares:

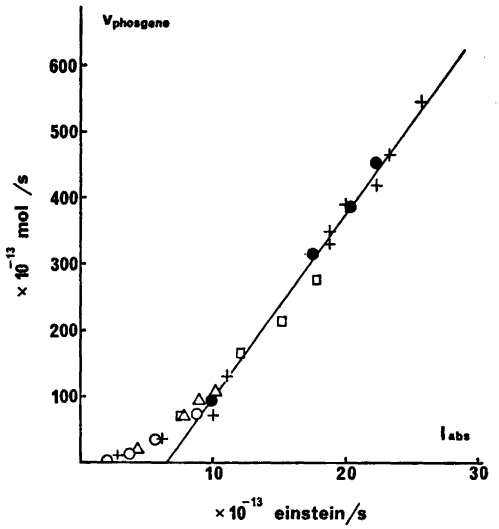

Fig. 1. $v_{phosgene}$ (measured) plotted *vs.* I_{abs} at different p_{per}. ○, $p_{per} = 5$ Pa; △, $p_{per} = 10$ Pa; □, $p_{per} = 30$ Pa; ●, $p_{per} = 50$ Pa; +, $p_{per} = 100$ Pa.

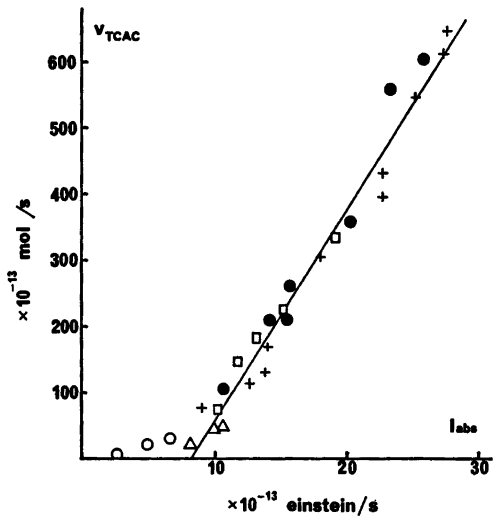

Fig. 2. v_{TCAC} (measured) plotted *vs.* I_{abs} at different p_{per}. ○, $p_{per} = 5$ Pa; △, $p_{per} = 10$ Pa; □, $p_{per} = 30$ Pa; ●, $p_{per} = 50$ Pa; + $p_{per} = 100$ Pa.

$$v_{TCAC} = 31.9\ I_{abs} - 263 \times 10^{-13} \text{ mol s}^{-1}$$
$$v_{phosgene} = 27.6\ I_{abs} - 177 \times 10^{-13} \text{ mol s}^{-1}$$

The slopes of these lines, *i.e.* the quantum yields, seem to be independent of the per pres-

3. Wang, Y., Stucky, G. D. and Williams, J. M. *J. Chem. Soc. Perkin Trans. 2* (1974) 35.
4. Singh, T. R. and Wood, J. L. *J. Chem. Phys. 50* (1969) 3572.
5. Rundle, R. E. *J. Phys. Radium 25* (1964) 487.
6. Tellgren, R. and Olovsson, I. *J. Chem. Phys. 54* (1971) 127.
7. Delaplane, R. G. and Ibers, J. A. *Acta Crystallogr. B 25* (1969) 2423.
8. Abrahams, S. C. *Mater. Res. Bull. 6* (1971) 881.

Received March 19, 1975.

On the Formation of Phosgene and Trichloroacetyl Chloride in the Non-sensitized Photo-oxidation of Perchloroethylene in Air

HANS F. ANDERSSON, JAN ANDERS DAHLBERG and RUNE WETTSTRÖM

Uddeholms AB, Chemicals Division, Research Laboratory, S-663 00 Skoghall, Sweden

The non-sensitized photo-oxidation of trichloroethylene (tri) and 1,1,1-trichloroethane in the gas phase have earlier been reported.[1,2] In this paper the non-sensitized photo-oxidation of perchloroethylene (per) at low vapour pressures in air is described. The experimental technique has been described in the paper on photo-oxidation of trichloroethylene by Dahlberg.[1]

In the tri case the initiating step was shown to be a reaction between one tri molecule in the excited state and one in the ground state in competition with a pseudo first-order deactivation step.[1] However, for perchloroethylene we have shown that the initiating step is a dissociation of a per molecule upon light absorption. It is further shown that phosgene is probably formed not only according to the scheme by Huybrecht *et al.*[3] for the chlorine-sensitized photo-oxidation, but also by a parallel chain mechanism.

The results of the kinetic measurements are shown in Figs. 1 and 2. Obviously there are linear relationships between the rates of formation (v) of trichloroacetyl chloride (TCAC) and phosgene, respectively, and the absorbed light (I_{abs}). Thus all measurements made at the oxygen pressure 0.2 atm and at I_{abs} above 8.5×10^{-13} einstein/s fit well to the following equations calculated by the method of least squares:

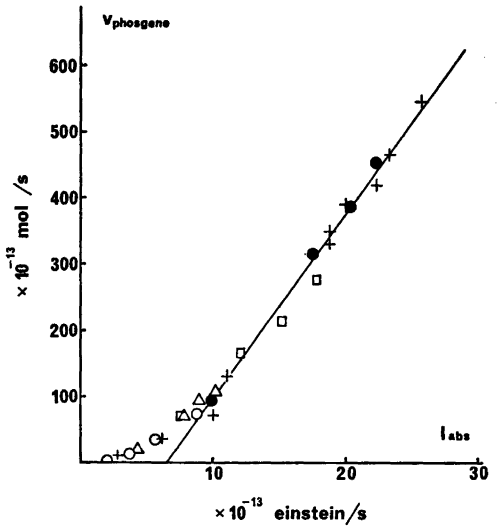

Fig. 1. $v_{phosgene}$ (measured) plotted *vs.* I_{abs} at different p_{per}. ○, $p_{per} = 5$ Pa; △, $p_{per} = 10$ Pa; □, $p_{per} = 30$ Pa; ●, $p_{per} = 50$ Pa; +, $p_{per} = 100$ Pa.

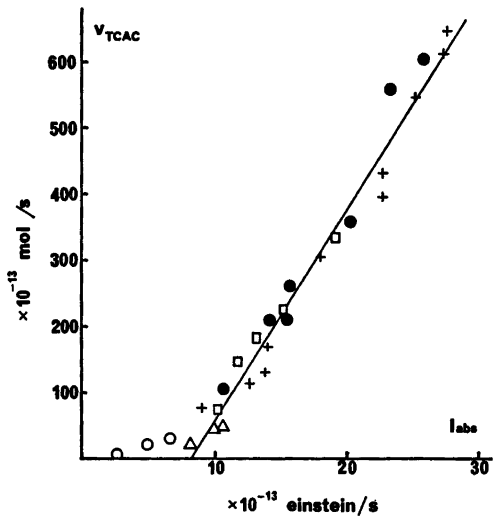

Fig. 2. v_{TCAC} (measured) plotted *vs.* I_{abs} at different p_{per}. ○, $p_{per} = 5$ Pa; △, $p_{per} = 10$ Pa; □, $p_{per} = 30$ Pa; ●, $p_{per} = 50$ Pa; + $p_{per} = 100$ Pa.

$$v_{TCAC} = 31.9\ I_{abs} - 263 \times 10^{-13} \text{ mol s}^{-1}$$
$$v_{phosgene} = 27.6\ I_{abs} - 177 \times 10^{-13} \text{ mol s}^{-1}$$

The slopes of these lines, *i.e.* the quantum yields, seem to be independent of the per pres-

sure, which suggests other absorption and chain-initiating steps than in the tri case. Hence, we assume in agreement with Horowitz and Rajbenbach [4] that absorption of UV light in this region causes dissociation of the per molecule according to the formula:

$$C_2Cl_4 + h\nu \rightarrow C_2Cl_3 + Cl \quad (1)$$

Now, the chlorine atom may initiate the chain mechanism proposed by Huybrecht *et al.*[3] for the chlorine-sensitized oxidation:

$$Cl + C_2Cl_4 \rightarrow C_2Cl_5 \quad (2)$$

$$C_2Cl_5 + O_2 \rightarrow C_2Cl_5O_2 \quad (3)$$

$$C_2Cl_5O_2 \rightarrow C_2Cl_5 + O_2 \quad (4)$$

$$2C_2Cl_5O_2 \rightarrow 2C_2Cl_5O + O_2 \quad (5)$$

$$C_2Cl_5O \rightarrow C_2Cl_4O + Cl \quad (6)$$

The terminating steps are:

$$2C_2Cl_5 \rightarrow \text{stable products} \quad (7)$$

$$C_2Cl_5 + C_2Cl_5O_2 \rightarrow C_2Cl_5O_2C_2Cl_5 \quad (8)$$

$$2C_2Cl_5O_2 \rightarrow O_2 + C_2Cl_5O_2C_2Cl_5' \quad (9)$$

The C_2Cl_4O formed in step 6 is either TCAC or perchloroethylene epoxide.

According to Huybrecht *et al.*[3] phosgene is formed by cleavage of C_2Cl_5O and further oxidation of the CCl_3 radical. As to the fate of the C_2Cl_3 radical we have detected dichloroacetylene as a photolysis product of perchloroethylene by gas chromatography contrary to Horowitz and Rajbenbach.[4] We thus propose the following step:

$$C_2Cl_3 \rightarrow C_2Cl_2 + Cl \quad (10)$$

The C_2Cl_3 radical might also give rise to an alternative route to phosgene:

$$C_2Cl_3 + O_2 \rightarrow C_2Cl_3O_2 \quad (11)$$

$$C_2Cl_3O_2 \rightarrow COCl_2 + COCl \quad (12)$$

$$COCl + C_2Cl_4 \rightarrow COCl_2 + C_2Cl_3 \quad (13)$$

This chain would terminate by step 10 and by:

$$C_2Cl_3O_2 \rightarrow C_2Cl_2 + Cl + O_2 \quad (14)$$

This also implies a switch-over to the TCAC-forming chain.

If we assume that k_4 is much greater than $k_8\,[C_2Cl_5] + 2(k_5 + k_9)[C_2Cl_5O_2]$ a stationary state treatment of the TCAC-forming chain gives the kinetic equation

$$v_{TCAC} = I_{abs} \times 2k_5/A$$
where $A = k_4k_8/k_3[O_2] + k_7k_4^2/k_3^2[O_2]^2 + k_9$

Likewise a stationary state treatment of the phosgene-forming chain gives the equation:

$$v_{phosgene} = I_{abs}\,\frac{2k_{12}k_{11}[O_2]}{k_{12}k_{10} + k_{10}k_{14} + k_{14}k_{11}[O_2]}$$

The derived equations are both compatible with the fact that the quantum yields are independent of I_{abs} and the per pressure. The phosgene route proposed above could thus afford an explanation to the high phosgene/TCAC ratio – about 1 in this reaction compared to about 1/3 in the chlorine-sensitized one. Contrary to this, the ratios of the corresponding reactions of trichloroethylene are almost equal. However, in this connection one shall also take into consideration the formation of epoxides isomeric to the acetyl chlorides. The results of measurements of epoxides are given in Table 1. The values in the last column are calculated assuming a [phosgene]/[TCAC] ratio = 28/32. Obviously the $[COCl_2]/[C_2Cl_4O]$ ratio is still rather high compared to the corresponding value of the chlorine-sensitized reaction. This suggests a contribution to the phosgene formation from the chain proposed above, *i.e.* steps 11 – 13.

Table 1. Relationship between phosgene and TCAC + epoxide formation.

Exp. No.	$n_{phosgene}$ 10^{-10} mol	$n_{epoxide}$ 10^{-10} mol	Phosgene/ TCAC + epoxide
1	416	368	0.49
2	367	368	0.47
3	376	350	0.48

An objection against the dissociative absorption step may be that all chemical evidence in the trichloroethylene case favours a non-dissociative absorption process.[1] The perchloroethylene molecule, however, has a much greater symmetry, which might afford an explanation to this problem. A result of this greater symmetry should thus be that the number of vibrational modes is rather strongly diminished in the excited state in comparison with trichloroethylene. The chance that the excitation energy will concentrate in a CCl-bond should therefore be greatly enhanced. The probability that the N→V transition will cause dissociation of a CCl bond would thus increase when going from tri- to perchloroethylene.

The authors wish to thank Drs. K. Sandros and C. Åqvist for valuable discussions. The research has been sponsored by the Swedish Board for Technical Development and Uddeholms AB.

1. Dahlberg, J. A. *Acta Chem. Scand. 23* (1969) 3081.
2. Christiansen, V. O., Dahlberg, J. A. and Andersson, H. F. *Acta Chem. Scand. 26* (1972) 3319.
3. Huybrecht, G., Olbregts, J. and Thomas, K. *Trans. Faraday Soc. 63* (1967) 1647.
4. Horowitz, A. and Rajbenbach, L. A. *J. Amer. Chem. Soc. 90* (1968) 4105.

Received January 27, 1975.

Acta Chemica Scandinavica A 29 (1975) 475—480

An NMR Investigation of the Acetylene—Cu(I)—π-Complex in Homogeneous Aqueous Solution

A. BORG, T. LINDBLOM and R. VESTIN

Department of Physical Chemistry, Arrhenius Laboratory, University of Stockholm, Fack, S-104 05 Stockholm, Sweden

^{1}H NMR and ^{13}C NMR spectra of the π-complexes acetylene – Cu(I) and ethylene – Cu(I) are recorded. The solutions used contain the systems $HCl - CuCl - C_2H_2$ and $DCl - CuCl - C_2H_4 - D_2O$, prepared in specially designed devices for gas saturation of air-sensitive NMR-samples. The chemical exchange between complexed and dissolved hydrocarbon is rapid and only one narrow peak is seen in the spectrum, and the ^{1}H NMR frequency of the pure complex is determined by means of extrapolation. The acetylene resonance is shifted 2.6 ppm to lower field from its uncomplexed frequency in ^{1}H NMR, the ethylene 0.77 ppm to higher field. In ^{13}C NMR the acetylene resonance is shifted 1.1 ppm, the ethylene 31.1 ppm. Since shift of the acetylene resonance on complexing is restricted to protons, the molecule is believed to be bent, *cis* or *trans*, in the complex.

Our studies of the ^{1}H NMR properties of π-complexes between olefines and Ag(I) and olefines and acetylenes and Cu(I) have shown that, in some cases, the resonance frequencies of the hydrocarbons are shifted considerably on complex formation. Measured shifts are listed in Table 1, where ΔK symbolizes the coordination shift according to $\Delta K = \Delta$(uncomplexed) – Δ(complexed). The ethylene shows a quite normal behaviour with a change of 0.77 ppm to higher field, but the large shift of the acetylenic protons on complex formation with Cu(I) is quite exceptional [1] and therefore submitted to more careful studies in order to clarify its causes.

Table 1. ^{1}H NMR coordination shifts of some olefines and acetylenes
$\Delta K = \Delta$(uncomplexed) – Δ(complexed).

Ligand	Central atom	ΔK (ppm)
Ethylene	Ag^+	−0.1
Vinyl acetate	Ag^+	−0.09
Ethylene	Cu^+	+0.77
Acetylene	Cu^+	−2.62
Propyne	Cu^+	−2.4

For the determination of the ^{1}H NMR shift of the Cu(I) – π-complex with acetylene, two series of measurements have been carried out in homogeneous systems with the components $H_2O - HCl - CuCl - C_2H_2$, where the acetylene is distributed between physically dissolved and complexed to Cu(I). One of the series contains samples where the total concentration of CuCl, $CuCl_t$, is varied, and is called the $CuCl_t$ series. In the other series the acetylene resonance is studied at varied acetylene pressures, P_A, and otherwise constant conditions, and is called the P_A series. The equilibria in these systems, where the acetylenic components are mainly $C_2H_2.CuCl$ and $C_2H_2.CuCl_2^-$, have been carefully studied by Vestin and Löfman.[2] Water has been chosen as solvent instead of the normally preferred D_2O for two reasons. Firstly, we have found that a chemical exchange takes place between the protons, which in deuteriated solution leads to a decrease in the intensity of the acetylene signal until an equilibrium mixture between the two deuteriated species is established. Secondly, the water signal in these strongly acidic solutions (8 – 9 m) is shifted so far downfield as to remain outside the region of interest. Moreover, the results of the measurements can be evaluated using the relations be-

tween the components of the systems which have been found by Vestin and Löfman.[2] For comparison, a series of ^{1}H NMR measurements of the corresponding ethylene – Cu(I) – π-complex was performed. (Unfortunately an acetylene series with silver is impossible because the acetylide formation predominates.) The samples of this series contain the system $DCl - C_2H_4 - CuCl - D_2O$, where the total concentration of the copper(I) chloride is varied but the ethylene partial pressure, P_E, and the deuterium chloride concentration are kept constant. In this series it is necessary to use deuteriated water and acid because otherwise the strong proton signal interferes with the rather weak ethylene signal, and it is this time possible because we have not found any evidence of an exchange between ethylene and water protons. The series is called the ethylene $CuCl_t$-series.

Ordinary ^{1}H NMR standard substances cannot be used in these solutions, because they either form complexes with Cu(I), like DMSO, or they are insoluble in water, like TMS. Instead in the $CuCl_t$ series the water signal was used as a shift reference and acetic acid as a concentration reference, CH_3OH in the P_A series, and DSS in the ethylene $CuCl_t$ series. Since CuCl is very sensitive to oxidation, especially when moist, and since trace of paramagnetic contamination produces a deleterious effect upon the spectra (line broadening), the samples have been prepared with the help of the devices for preparation and gas saturation at atmospheric and higher pressures of air sensitive samples, which have been developed in this laboratory.[3] In these devices the addition of the solvent and the saturation by the gas at atmospheric pressure is performed in an argon atmosphere ('Sondett') and addition of gas to higher pressures is carried out after evacuation in special sample tubes equipped with valves ('Bombett'). CuCl is, on the other hand, stable enough in the dry state to allow its weighing without any special precautions.[4]

EXPERIMENTAL

Preparation of the acetylene $CuCl_t$ series (constant P_A). CuCl of a very high degree of purity was weighed into well dried, ordinary NMR sample tubes. These were placed in the Sondett, and 0.500 ml of a stock solution, containing 8.42 m HCl and 0.0369 m CH_3COOH in water, was added with the help of an all-glass syringe ('Agla'), which allows accurate volume readings. The solutions were afterwards saturated with acetylene, free from acetone, according to the instructions for the device. The tubes were closed and the NMR spectra were recorded immediately.

Preparation of the acetylene P_A series (constant $CuCl_t$). 0.0605 g CuCl (purity as above) was weighed into a high pressure NMR sample tube of wall thickness 0.6 mm, with the valve device removed. The tube was placed in the Sondett. 0.500 ml of a stock solution, containing 8.1 m HCl and 0.273 m CH_3OH, was added as described above. The valve was fitted and the tube connected to the Bombett and evacuated. Acetylene was added to the required pressures under simultaneous equilibration by vibrating the tube in a thermostatic bath at 25 °C.

Preparation of the ethylene $CuCl_t$ series (constant P_E). The CuCl was weighed into well dried NMR sample tubes, which were afterwards placed in the Sondett. An amount of 0.500 ml of a stock solution of 8.95 m DCl and 0.0142 m trimethylsilylpropanesulfonic acid (DSS) dissolved in D_2O was added, and finally the solution was saturated with ethylene. ^{1}H NMR measurement was made directly after closing the tube.

Measurement of the spectra. The ^{1}H NMR spectra were recorded at 25 °C on a Varian A60-A spectrometer, and the resonance frequencies were read in Hz directly from the spectrum. However, the spectrometer is such that it does not allow more accurate determination of the frequencies than 1 Hz, due to drifting of the scale during the recording. The accuracy of the integral peak is limited by the reproducibility of the integral, which, according to the specifications of the instrument, is approximately 98 %. The height of the integral peak has been read from the mm scale of the chart paper. The ^{13}C NMR spectra were recorded on a Varian XL 100 spectrometer at about 40 °C.

RESULTS

The ^{1}H NMR spectra of the individual samples of the $CuCl_t$-series and the P_A series contain three peaks; Fig. 1. The largest peak at 6.5 ppm is water, then follows acetylene at 4.25 ppm and CH_3 protons at 3.1 ppm. The appearance of one single, unbroadened peak of acetylene indicates a rapid exchange between the two acetylenic species in the solution. Its resonance frequency, $\nu(C_2H_2)$, is determined by

$$\nu(C_2H_2) = Q[\nu(C_2H_2)_{Cu} - \nu(C_2H_2)_{aq}] \quad (1)$$

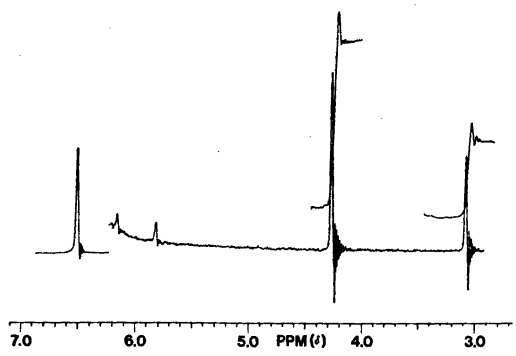

Fig. 1. ^{1}H NMR spectrum of the acetylene-Cu(I) complex. The peak at 6.5 ppm is water, the acetylene protons at 4.25 ppm, and CH_3COOH at 3.1 ppm. The two small peaks at 6.2 and 5.85 ppm are second sideband due to rotation and a 50 Hz perturbation; 25 °C.

where $\nu(C_2H_2)_{Cu}$ is the resonance frequency of the pure complex, $\nu(C_2H_2)_{aq}$ is the resonance frequency of the acetylene protons in absence of copper(I) chloride, and

$$Q = [C_2H_2]_{Cu}/[C_2H_2]_t$$

where $[C_2H_2]_{Cu}$ is the concentration of the Cu(I) bound acetylene, and $[C_2H_2]_t$ is the total concentration of acetylene in the solution.

During the course of the $CuCl_t$ series, the acetylene peak undergoes a negative coordination shift as the $CuCl_t$ is increased; $\nu(C_2H_2) =$ 157.2 Hz is the largest frequency measured downfield from $\nu(C_2H_2)_{aq}$. The difference $[\nu(C_2H_2) - \nu(C_2H_2)_{aq}]$ is later on referred to as $\Delta\nu(C_2H_2)$. Table 2, Fig. 2a.

Table 2. Data for the acetylene $CuCl_t$ series. HCl_t const. = 8.42 m, P_A const. = 0.96 atm.

$CuCl_t$	$\nu(H_2O) - \nu(C_2H_2)$ Hz	I	$[C_2H_2]_t$ m	Q
0	278.4	–	–	–
0.050	249.2	0.72	0.046	0.216
0.118	219.2	1.23	0.059	0.356
0.180	204.2	1.44	0.072	0.500
0.272	188.2	1.77	0.100	0.602
0.423	171.4	1.53	0.120	0.701
0.724	154.8	3.85	0.180	0.801
0.995	145.0	5.42	0.233	0.847
2.010	126.6	9.86	0.434	0.918
2.736	121.2	13.53	0.558	0.938

Table 3. Data for the acetylene P_A series. HCl_t const. = 8.1 m, $CuCl_t$ const. = 1.52 m.

P_A	$\nu(C_2H_2) - \nu(CH_3)$ Hz	I	$[C_2H_2]_t$ m	$Q(I)$	$Q(P_A)$
–	– 63.2	–	–	–	–
1.42	75.6	1.47	0.600	0.878	0.888
3.90	65.4	2.49	1.018	0.829	0.843
5.31	61.4	2.79	1.143	0.810	0.820
5.42	61.7	2.84	1.163	0.807	0.818
7.04	58.9	2.98	1.219	0.797	0.793
7.64	53.8	3.31	1.354	0.772	0.784
8.91	56.6	3.00	1.229	0.795	0.765

In the P_A series the acetylene frequency is neither constant nor shifted further downfield but is shifted towards higher field by a comparatively small amount upon increasing the P_A. See Table 3 and Fig. 2b.

Ethylene is only slightly soluble in water, and thus the ratio of copperbound to total ethylene approaches unity already at very low CuCl concentrations. The resonance frequency of the ethylene peak is dependent on the concentrations of the two ethylenic species in the solution according to the formula (1) but with C_2H_4 inserted instead of C_2H_2. During the course of the experiments the peak moves 46.0 Hz towards higher field; see Table 4.

The individual concentrations of the copperbound resp. physically dissolved acetylene species are calculated with the help of the relations found by Vestin and Löfman,[6] and are, for the $CuCl_t$ series,

$$[C_2H_2]_{aq} = 0.0357 \text{ m}$$
$$[C_2H_2]_{Cu} = CuCl_t \times 0.1982$$

and

$$Q = \frac{CuCl_t \times 0.1982}{CuCl_t \times 0.1982 + 0.0357}$$

In Fig. 3 $\Delta\nu(C_2H_2)$ is plotted against Q. The function is linear until $Q = 0.8$, whereafter the curve becomes concave upwards, with $d\Delta/dQ$ approaching 2.4×10^2, compared to 1.5×10^2 in the lower part of the curve.

For the P_A series, where the $CuCl_t$ is constant and the acetylene pressure varied, the Q-values are calculated according to

$$Q(P_A) = \frac{1.0047}{P_A \times 0.0242 + 1.0969}$$

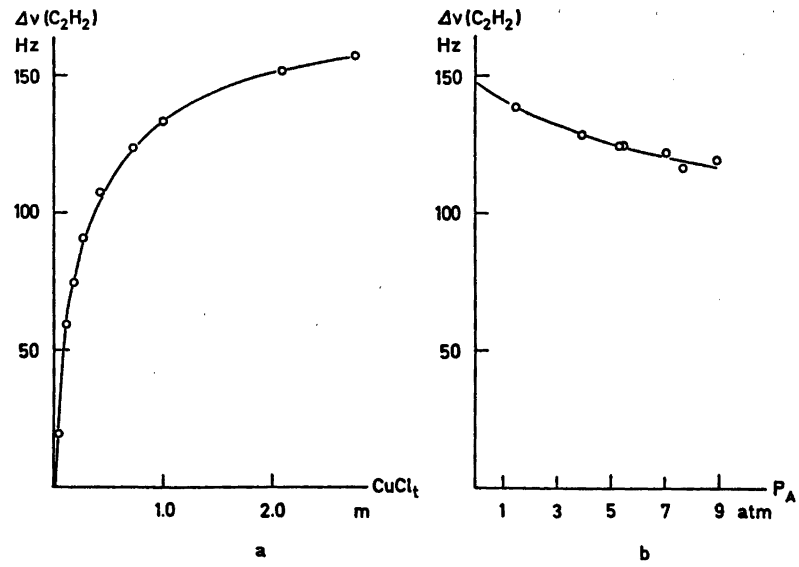

Fig. 2. Acetylene frequency as a function of (a), the cuprous chloride concentration (P_A const. = 0.96 atm., HCl_t const. = 8.42 m); (b), the acetylenic pressure ($CuCl_t$ const. = 1.52 m, HCl_t const = 8.1 m).

However, into the P_A-term there might enter uncertainties because of insufficient equilibration, defectiveness of the manometer *etc.*, which would affect the Q-values computed in the described manner. Therefore the total concentration of acetylene of the sample is also calculated from the integral peak of the spectrum, according to

$$[C_2H_2]_t = [-CH_2] \times \tfrac{2}{3} \times I$$

I is the quotient between the two integral peaks, and $[-CH_2] = 0.273$ m. With the help of a calibration curve, $[C_2H_2]_t = f(Q)$, constructed from a set of P_A values chosen to fit the region of interest, the Q-values corresponding to the $[C_2H_2]_t$ values from the integral measurements can be read. These Q-values are called $Q(I)$ and are listed in Table 3. From this table it is evident that the reason why the acetylene protons are shifted towards higher field upon increasing the acetylene pressure is that the physically dissolved portion increases more rapidly than the complexed, and the ratio of complexed to total acetylene decreases in the pressure region used. In Figs. 4a and b the $\Delta\nu(C_2H_2)$ of the series are plotted against $Q(P_A)$ and $Q(I)$, resp. These functions are linear too, but the slope $d\Delta/dQ = 2.2 \times 10^2$ differs from that of the lower part of the graph in Fig. 3 and is rather in accordance with the slope of the upper part, where the $CuCl_t$ values are high. This result may be interpreted as the indication of a species with two Cu atoms, which would be formed at high CuCl concentrations.

Table 4. Data for the ethylene $CuCl_t$ series. DCl const. = 8.95 m, P_E const. = 1 atm.

$CuCl_t$ m	C_2H_4 m	Q	$\nu(C_2H_4)$ Hz
0	0.0054	–	328.0
0.0133	0.0187	0.711	293.0
0.0953	0.1007	0.946	282.7
0.243	0.2486	0.978	282.0

Extrapolation of the lower part of the graph in Fig. 3 to $Q = 1$ gives $\Delta\nu(C_2H_2) = 153.3$ Hz, which is the resonance frequency for the 1:1 complex.

The lack of reliable data on the equilibria in the *ethylene $CuCl_t$ series* and the low solubility of the hydrocarbon add up to a less accurate series of measurements. The concentrations of the species are calculated exclusively from the experimental values and listed in Table 4. The $\Delta\nu(C_2H_4)$, *e.g.* the frequencies of the

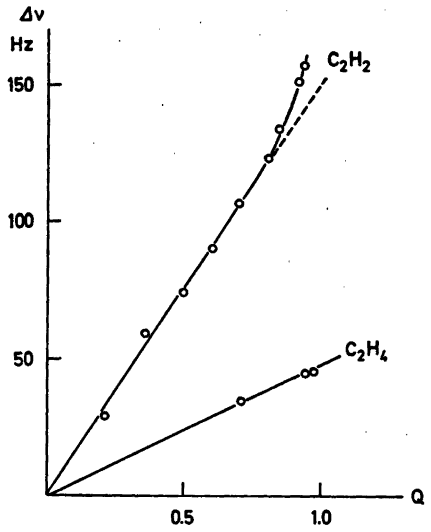

Fig. 3. Acetylene and ethylene frequencies as functions of the copperbound to total hydrocarbon ratio in the $CuCl_t$ series.

ethylene protons in solutions with Cu(I) measured relative to the ethylene frequency in solution with Cu(I) absent, are plotted against the quotient copperbound to total ethylene in the lower part of Fig. 3. ΔK for the ethylene complex amounts to +47.5 Hz, or 0.97 ppm.

^{13}C NMR spectra of acetylene and ethylene samples with and without univalent copper were recorded in the respective solvents. The large proton NMR shift of acetylene is not reflected in the ^{13}C NMR spectra, the measured ΔK being only +1.1 ppm, the copperbound to total acetylene ratio being close to unity. For ethylene, on the other hand, ΔK amounts to +31.1 ppm, but the signal remains in the region of olefinic ^{13}C shifts.[5,6]

DISCUSSION

Acetylene holds an exclusive position in ^1H NMR contexts, in that the resonance frequency for ethane is 0.96 ppm, ethylene 5.84 ppm, but for acetylene 2.88 ppm. The high shielding of the protons in acetylene may be qualitatively explained by considering the anisotropy of the magnetic susceptibility in the triple bond.[7]

It is now generally accepted [8] that when disubstituted acetylenes enter into complexes, their linear geometry is abandoned in favour of a preferably *cis*-bent structure, with the substituents bent away from the central atom. In a preliminary wide band ^1H NMR measurement of the solid addition compound $C_2H_2(CuCl)_3$ we have measured an intranuclear H – H distance of 2.3 Å, which indicates a bent structure. We cannot, however, tell if it is *cis* or *trans*, only that the protons remain equal. It therefore seems reasonable to seek an explanation for the large negative coordination shift of acetylene on π-complex formation with Cu(I) in a change of the acetylene geometry which involves diminished shielding of the protons.

The theory of the nature of the bonding of this type of metal-olefine and metal-acetylene π-complexes is that a σ-bond is formed by the

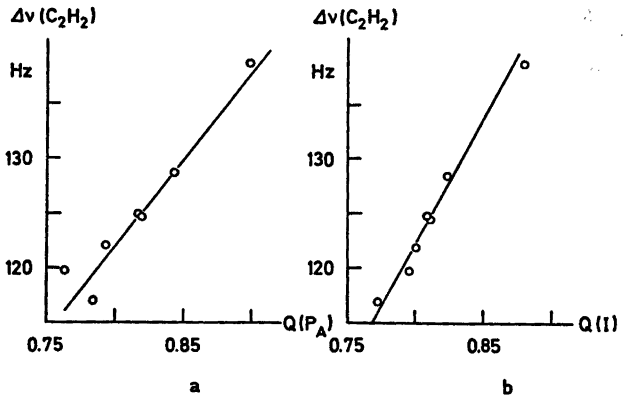

Fig. 4. Acetylene frequency as function of the copperbound to total acetylene ratio in the P_A series: (a), calculated from P_A; (b), calculated from I.

overlapping of the empty 4*s* or 5*s* orbital of the metal by the filled bonding molecular π-orbital of the olefine (two in acetylene). One additional bond is formed by the overlapping by a lower filled *d* orbital of the metal with the empty anti-bonding π^*-orbital of the olefine or one of the empty π^*-orbitals of acetylene. As regards the acetylene it is difficult to find unambiguous proof for the formation of these π-bonds. Modified CNDO-calculations [9] show that a *cis* or *trans* bent structure would lead to a change of the electron density such that the triple bond on coordination takes the character of a double bond, which leads to less ^{1}H NMR shielding. This investigation shows that the acetylene protons remain magnetically equivalent on the π-complex formation, but the ^{1}H NMR shift is changed with a sufficiently large amount to make a deviation from the linear geometry look probable. The ^{13}C NMR spectrum confirms that the change of geometry is restricted to the protons, and comparison with the corresponding ethylene complex shows that the effect cannot be attributed to the copper atom. Therefore the ^{1}H NMR behaviour can be rationalized in terms of a bending of the C≡C−H angle.

REFERENCES

1. Keller, H. J. *NMR Untersuchungen an Komplexverbindungen* Vol. 2, *NMR Basic Principles and Progress*, Berlin 1970, p. 21.
2. Vestin, R. and Löfman, C. *Acta Chem. Scand. 7* (1953) 398.
3. Lindblom, T. *Chem. Scr. 4* (1973) 103.
4. Vestin, R. *Sv. Kem. Tidskr. 66* (1954) 65.
5. Stothers, J. B. *Carbon-13-NMR-Spectroscopy*, Academic, New York 1972.
6. Beverwijk, C. D. M. and van Dongen, J. P. C. M. *Tetrahedron Lett. 42* (1972) 4291.
7. Pople, J. A. *Proc. Roy. Soc. Ser. A. 239* (1957) 541.
8. Glanville, J. O., Stewart, J. M. and Grim, S. O. *J. Organometal. Chem. 7* (1967) 9.
9. Blizzard, A. C. and Santry, D. P. *J. Amer. Chem. Soc. 90* (1968) 5749.

Received December 3, 1974.

Acta Chemica Scandinavica A 29 (1975) 481—488

The Crystal and Molecular Structure of Bis(thiosemicarbazide)-cadmium(II) Sulfate

ERIK LARSEN and PER TRINDERUP*

Chemistry Department I, The H. C. Ørsted Institute, Universitetsparken 5, DK-2100 Copenhagen Ø, Denmark

The crystal structure of bis(thiosemicarbazide)-cadmium(II) sulfate has been determined by single crystal X-ray diffraction methods. The crystals are monoclinic with the space group $C2/c$, $Z=8$, and the cell dimensions $a=27.962(14)$ Å; $b=6.564(3)$ Å; $c=15.908(9)$ Å and $\beta=126°6'(6)$. The diffraction data were collected on an automatic four circle diffractometer. The structure was determined from three-dimensional Patterson and Fourier functions.

1915 reflections were used to solve and refine the structure for all non-hydrogen atoms. Final unit weighted and weighted residuals of 0.042 and 0.034, respectively, were obtained.

The asymmetric unit contains two independent formula units. Both cadmium complexes have octahedral configuration with sulfate oxygens taking up axial coordination sites such that sulfate ions function as bridges. The remaining four coordination sites are taken up by two unsymmetric bidentate chelate thiosemicarbazides, in one complex in a *trans* configuration and in the other in a *cis* configuration.

The present crystal structure analysis is part of a study on the chemistry of thiosemicarbazide complexes. For a series of alkyl-substituted thiosemicarbazides potentiometric measurements have led to stability constants for the cadmium(II) complexes.[1] The results show that the mono and bis("thiosemicarbazide")cadmium(II) complexes are formed with stability constants varying significantly for differently substituted thiosemicarbazides. This is not unexpected and the trends have been rationalized semi-quantitatively in terms of the electronegativity of the substituents. Nørlund Christensen and Rasmussen [2] found that the stability of the tris(thiosemicarbazide)cadmium-(II) ion is low and proposed to explain this as a stereochemical change from a tetrahedrally coordinated bis complex to an octahedrally coordinated tris complex. The series of substituted ligands gives tris complexes with stability constants identical within the experimental uncertainty and thus confirms Nørlund Christensen and Rasmussen's proposal. The present structure determination of the bis(thiosemicarbazide)cadmium(II) sulfate was initiated in an attempt to obtain further knowledge on the stereochemistry of the bis complex.

EXPERIMENTAL

Bis(thiosemicarbazide)cadmium(II) sulfate ($Cd(tscH)_2SO_4$) was precipitated by mixing a 0.05 M aqueous solution of cadmium sulfate and a 0.1 M aqueous solution of thiosemicarbazide in a test tube. Crystals suitable for the X-ray structure determination developed within 24 h. Analysis: Calc.: C 6.15; H 2.58; N 21.51; O 16.30; S 24.62. Found: C 6.10; H 2.57; N 21.61; S 24.42.

Preliminary Weissenberg and precession film data for space group determination was obtained using Cu$K\alpha$ radiation. 12 reflections in the region of 2θ from 40.3 to 47.4 were used in least squares refinement of the unit cell dimensions and the orientation matrix. The density of the crystals were measured by flotation in a mixture of $CHBr_3$ and CCl_4.

Intensity data were collected on a Picker FACS 1 diffractometer using Mo$K\alpha$ radiation from a graphite monochromator.

A crystal with the dimensions $0.11 \times 0.11 \times 0.11$ mm^3 was used for the data collection. A total of 2029 symmetry-independent reflections were collected up to a maximum $\sin\theta/\lambda=0.5946$ by the $\theta-2\theta$ scan technique with

* Present address: Chemistry Department A, Technical University of Denmark, DK-2800 Lyngby, Denmark.

a 1° min^{-1} scan speed. Backgrounds were measured for 20 s on each side of the peak and 3 standard reflections were monitored for every 40 measurements to check for decomposition of the crystal. At the end of the data collection the intensity of the standard reflections had dropped by 14 % and the colour of the crystal had changed from colourless to light yellow. The decrease in intensity of the standard reflections was used to place the data on a uniform scale. The data was corrected for Lorentz and polarization effects but not for absorption.

The X-ray atomic scattering factors used in the calculations [3] were for Cd from Cromer and Mann [4] and for the remaining atoms from *International Tables*.[5] Anomalous dispersion corrections were made for the cadmium and sulfur atoms only.[6]

All computations were performed on an IBM 370/165 computer using a set of crystallografic programs by Stewart *et al.*[3] and for illustrations ORTEP II.[7]

CRYSTAL DATA

Bis(thiosemicarbazide)cadmium(II) sulfate, $C_2H_{10}N_6O_4S_3Cd$, M = 390.8. Monoclinic (*b* unique), $a = 27.962(14)$ Å, $b = 6.564(3)$ Å, $c = 15.908(9)$ Å, $\beta = 126°6'(6)$; $V = 2293.7$ Å^3; $Z = 8$; $d_{obs} = 2.24$ g/cm^3, $d_{calc} = 2.251$ g/cm^3; $F(000) = 1536$; $\mu = 11.99$ cm^{-1}.

Systematically absent reflections: $l = 2n+1$ for $k = 0$ and $h+k = 2n+1$ for all reflections. Possible space groups *Cc* or *C*2/*c* (No. 9, C_s^4 or No. 15, C_{2h}^6).

STRUCTURE DETERMINATION

The statistical distribution of the calculated *E*-values did not indicate whether the compound crystallizes in the centric space group *C*2/*c* with one formula unit in the asymmetric unit or in the acentric *Cc* with two formula units in the asymmetric unit. In the computed Patterson function high density was found on the line $(0,v,\frac{1}{2})$ and in the plane $(u,0,w)$ indicating that the correct space group is *C*2/*c*.

Assuming a general eight fold position for cadmium the fractional coordinates for this atom were found from the Patterson map to be (1/8,1/4,7/8).

The fourier map phased from the Cd atom showed a larger number of peaks than expected and among these six peaks had a density obviously higher than the rest. Four of these peaks were in bonding distance from the Cd atom. Attempts to interpret these peaks as S and N atoms gave Fourier maps without clear

Table 1. Final atomic coordinates in fractions for the heavier atoms in bis(thiosemicarbazide)-cadmium(II) sulfate, standard deviations $\times 10^5$ in parentheses. The general equivalent positions are (x,y,z), $(\bar{x},\bar{y},\bar{z})$, $\bar{x},y,\frac{1}{2}-z)$, $(x,\bar{y},\frac{1}{2}+z)$, $(\frac{1}{2}+x,\frac{1}{2}+y,z)$, $(\frac{1}{2}-x,\frac{1}{2}-y,\bar{z})$, $(\frac{1}{2}-x,\frac{1}{2}+y,\frac{1}{2}-z)$, $(\frac{1}{2}+x,\frac{1}{2}-y,\frac{1}{2}+z)$.

	x/a	*y/b*	*z/c*
Cd1	0.00000(0)	0.69552(7)	0.25000(0)
C1	0.06239(17)	0.65348(65)	0.12793(29)
N11	0.03701(16)	0.94088(54)	0.19091(28)
N21	0.05080(16)	0.85340(57)	0.12476(28)
N31	0.08112(19)	0.59373(64)	0.07080(30)
S1	0.05516(5)	0.47485(16)	0.19834(8)
Cd2	0.25000(0)	0.25000(0)	0.00000(0)
C2	0.24071(20)	0.13525(70)	0.36338(34)
N12	0.31312(15)	0.96160(57)	0.04402(27)
N22	0.20759(18)	0.66714(62)	0.04198(30)
N32	0.22605(25)	0.27494(79)	0.29027(36)
S2	0.30861(5)	0.43959(21)	0.16990(9)
O1	0.18723(13)	0.10096(55)	0.05472(26)
O2	0.10897(17)	0.15710(53)	0.07931(26)
O3	0.40592(13)	0.22842(48)	0.07807(22)
O4	0.40667(15)	0.58965(48)	0.04726(26)
S3	0.12047(4)	0.10948(15)	0.00151(7)

Table 2. Thermal parameters for the non-hydrogen atoms in $Cd(tscH)_2SO_4$. The temperature factors, U_{ij}, are in unit of $Å^2 \times 10^{-2}$. The estimated standard deviation from the least squares refinement are given in parentheses in unit of the last significant figure in the parameter value.

	$U(11)$	$U(22)$	$U(33)$	$U(12)$	$U(13)$	$U(23)$
Cd1	1.93(2)	2.52(3)	2.05(2)	0.00(0)	1.40(2)	0.00(0)
C1	1.59(18)	2.48(20)	1.95(18)	−0.17(16)	1.06(16)	−0.04(16)
N11	2.68(18)	1.89(17)	3.54(19)	−0.20(14)	2.23(16)	−0.21(15)
N21	2.88(18)	2.38(18)	3.10(18)	0.10(15)	2.25(16)	0.44(15)
N31	4.35(22)	3.66(22)	3.30(20)	0.34(18)	3.08(19)	0.31(17)
S1	3.81(6)	1.82(5)	3.06(5)	0.37(4)	2.67(5)	0.36(4)
Cd2	3.19(3)	3.00(3)	3.38(3)	0.22(2)	1.52(2)	−1.13(2)
C2	3.12(23)	2.68(22)	2.97(22)	0.07(18)	2.17(19)	0.43(18)
N12	2.22(17)	2.69(19)	2.50(17)	−0.14(15)	1.26(15)	−0.06(15)
N22	3.08(20)	2.94(21)	3.11(20)	0.93(16)	1.50(17)	−0.07(17)
N32	6.65(33)	4.73(28)	3.63(24)	−1.19(24)	2.78(24)	1.12(21)
S2	2.34(5)	4.26(7)	3.07(6)	0.91(5)	0.44(5)	−1.14(5)
O1	1.62(14)	4.20(20)	3.97(18)	0.68(13)	1.41(14)	1.16(15)
O2	5.48(21)	3.50(18)	3.70(18)	0.27(16)	3.93(17)	0.26(15)
O3	2.16(15)	2.98(16)	2.15(15)	−0.19(12)	0.85(13)	0.90(12)
O4	3.90(18)	2.12(16)	3.97(18)	−0.27(13)	2.36(15)	−0.17(14)
S3	1.74(5)	2.04(5)	1.88(5)	0.26(4)	1.19(4)	0.42(4)

features of the rest of the structure and the R-factor never decreased to less than 0.40. Instead, the six stronger peaks around each Cd-atom were identified as the two pairs of coordinating sulfurs and sulfur in sulfate ions using the space group *Cc*.

From chemical arguments these peaks were separated between the two independent Cd-atoms. The structure factor calculation from two Cd-atoms and six S-atoms gave $R = 0.25$ and the Fourier map phased from this partial structure showed the positions of the rest of the non-hydrogen atoms in the structure. The positional parameters and isotropic temperature factors for all these atoms were varied in a unit weighted full matrix least squares refinement using the 1915 reflections with intensities greater than their standard deviation. Convergence was obtained at $R = 0.087$.

After advice from R. G. Hazell it was realized that this structure could also be described in the space group *C2/c* with the two Cd-atoms in special positions. In the *cis* complex the Cd-atom has the site symmetry of the twofold axis and in the *trans* complex Cd is in the special position (1/4,1/4,0) with a center of symmetry. Full matrix refinement of the atomic parameters, positional and anisotropic temperature factors corresponding to this structure using the 1915 reflections converged rapidly. The weights used in the least squares refinement were of the form $w = \{1 + [(F - 45)/55]^2\}^{-1}$ as this function gave a mean value of $w(F_o - F_c)^2$ that showed little variation with F. For the last refinement cycle no parameter shifted more than 0.6 σ and the average shift was 0.01σ. The corresponding residuals were $R = 0.042$ and $R_w = 0.034$. The position of the hydrogen atoms were not clearly indicated from the final difference Fourier map, therefore, no attempts were made to locate these atoms.

The resulting coordinates are shown in Table 1 while the thermal parameters are listed in Table 2. A list of the observed and calculated structure factors is available from the authors upon request.

DESCRIPTION AND DISCUSSION OF THE STRUCTURE

The crystals of *bis*(thiosemicarbazide)-cadmium(II) sulfate contains two independent sets of complex ions. They both have octahedral coordination with two oxygens from sulfate groups as axial ligands. The chelating thiosemicarbazide groups are coordinating in the

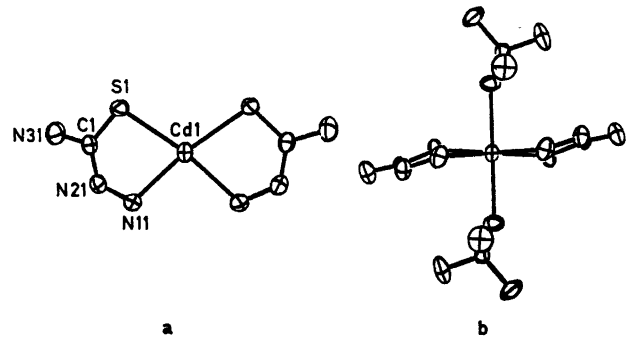

Fig. 1. The *cis*-bis(thiosemicarbazide)cadmium(II) ion viewed perpendicular (a) and parallel (b) to the 2-fold axis of the molecule. The thermal ellipsoids are scaled to include 74 % probability.

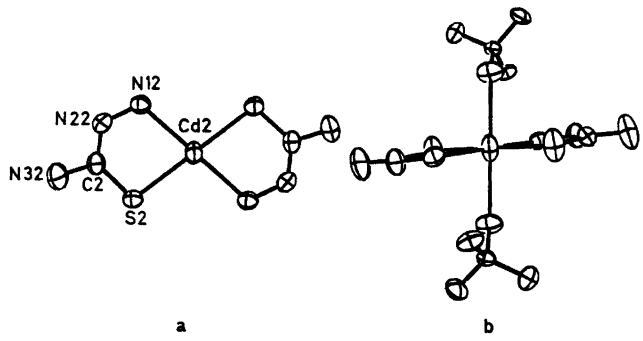

Fig. 2. The *trans*-bis(thiosemicarbazide)cadmium(II) ion viewed parallel (a) and perpendicular (b) to the O – O axis. The molecule is centrosymmetric about the cadmium atom. The thermal ellipsoids are scaled to include 74 % probability.

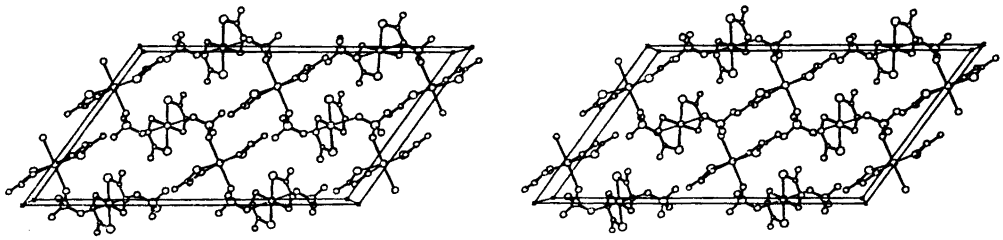

Fig. 3. An ORTEP stereo drawing of a full unit cell as viewed down the *b*-axis (parallel to the 2-fold symmetry axis of the cell).

plane *cis* in one complex (Fig. 1) and *trans* in the other (Fig. 2). Each sulfate group uses two oxygens for coordination, one to each type of cadmium in such a way that chains are formed through the crystal (Fig. 3). Although it was not possible from the final difference Fourier map to locate the hydrogen atoms with certainty, it is indicated from the interatomic distances that the remaining oxygens in the sulfate groups are used for hydrogen bonding to the thiosemicarbazides. In this way the individual chains in the crystal are bound together in a very efficient network which accounts well for the high density and the insolubility of the crystals.

A few examples of structures where two geometric isomers crystallize together are previously reported in the literature.[8–11] Among

Table 3. Bond lengths (in Å) and some angles (in degrees) in $Cd(tscH)_2SO_4$. The estimated standard deviations are given in parentheses in units of the last significant figure of the parameter values.

cis	
Cd1–S1	2.545(2)
Cd1–O3	2.413(3)
Cd1–N11	2.367(5)
S1–C1	1.711(5)
C1–N31	1.336(8)
C1–N21	1.344(6)
N21–N11	1.429(7)
Cd1–S1–C1	97.9(2)
S1–C1–N31	118.7(3)
S1–C1–N21	125.4(4)
C1–N21–N11	121.5(4)
N21–N11–Cd1	112.1(3)
N11–Cd1–S1	77.9(1)
N11–Cd1–N11	94.3(2)
S1–Cd1–S1	110.6(1)
O3–Cd1–O3	169.7(1)
S1–Cd1–N11	170.0(2)
trans	
Cd2–S2	2.514(2)
Cd2–O1	2.525(5)
Cd2–N12	2.367(4)
S2–C2	1.700(5)
C2–N32	1.344(8)
C2–N22	1.339(5)
N22–N12	1.413(6)
Cd2–S2–C2	98.9(2)
S2–C2–N32	117.9(3)
S2–C2–N22	125.5(4)
C2–N22–N12	123.4(4)
N22–N12–Cd2	112.7(2)
N12–Cd2–S2	79.2(1)
Sulfate	
S3–O1	1.484(4)
S3–O2	1.478(5)
S3–O3	1.476(3)
S3–O4	1.477(3)
O1–S3–O2	108.7(2)
O1–S3–O3	109.2(2)
O1–S3–O4	109.3(2)
O2–S3–O3	109.3(2)
O2–S3–O4	109.9(3)
O3–S3–O4	110.3(2)

these is the so-called β-form of bis(thiosemicarbazide)nickel(II) sulfate,[8] which contains planar *cis*- and *trans*-complexes held together by hydrogen bonding between the complex ions and the sulfate ions. Both forms of the nitrate have also been investigated by X-ray structure analysis.[12]

The final bond lengths and angles with their estimated standard deviations for bis(thiosemicarbazide)cadmium(II) sulfate are listed in Table 3. The two independent chelate rings in the asymmetric unit have virtually the same bond distances and angles. The Cd–O bonds are significantly different, with the *cis* complex having the shortest length of 2.413(3) Å compared to 2.525(5) Å in the *trans* complex.

Table 4 gives the bond distances of the metal chelate rings for some thiosemicarbazide complexes for comparison.

Mean planes were calculated for groups of atoms using the coordinates in Table 1. The equations defining these planes and the distance of the atoms to the planes are listed in Table 5.

Both in the *cis* and the *trans* isomers of $Cd(tscH)_2^{2+}$ the thiosemicarbazide skeleton (N–N–C–S) of the chelate rings are planar, with the amide nitrogen a little out of the plane. The *cis* isomer is significantly distorted from an ideal planar arrangement of the ligators and the cadmium ion (Fig. 1). Both a small tetrahedral distortion of the ligating atoms in tscH and a bent configuration is present. This leads to a 0.65 Å displacement of Cd from the plane defined by the atoms in the tscH part of the chelate rings (Table 5).

The S–S distances observed for *cis*-bis(thiosemicarbazide) complexes of nickel and copper are *ca.* 3.1 and 3.4 Å, respectively.[8,12,13] This is considerably shorter than twice the estimated van der Waals radius, 3.7 Å. For such complexes the S–M–S angles are close to 90°. For the *cis*-bis(thiosemicarbazide)cadmium(II) complex the S–S distance is 4.19 Å and S–Cd–S angle is 110.7°. This marked difference between thiosemicarbazide complexes of the transition metals and cadmium illustrates the tendency shown by the former group to maximize the overlap between the empty or partly filled *d*-orbitals and the ligand orbitals.

The number of structures published on cadmium complexes containing sulfur donor atoms are rather limited. They fall in two

Table 4. Some interatomic distances in the thiosemicarbazide ligand in various complexes compared to these found from the present investigation.

	Ref.	M–S	S–C	C–N(3)	C–N(2)	N(2)–N(1)	N(1)–M
cis-Ni(tscH)$_2$(NO$_3$)$_2$	12	2.15 2.15	1.77 1.72	1.29 1.27	1.30 1.31	1.44 1.42	1.95 1.96
trans-Ni(tscH)$_2$(NO$_3$)$_2$	12	2.19	1.71	1.32	1.32	1.43	1.92
trans-Ni(tscH)$_2$(NO$_3$)$_2$.2H$_2$O	20	2.41	1.69	1.35	1.34	1.42	2.05
cis-Ni(tscH)$_2$SO$_4$	8	2.15	1.73	1.32	1.33	1.43	1.93
trans-Ni(tscH)$_2$SO$_4$	8	2.17	1.72	1.32	1.32	1.43	1.92
trans-Ni(tscH)$_2$SO$_4$.3H$_2$O	21	2.16	1.75	1.29	1.33	1.44	1.90
trans-Pt(tscH)$_2$SO$_4$.3H$_2$O	23	2.34	1.74	1.34	1.38	1.46	2.06
cis-Cd(tscH)$_2$SO$_4$	this work	2.55	1.71	1.34	1.34	1.43	2.37
trans-Cd(tscH)$_2$SO$_4$	this work	2.51	1.70	1.34	1.34	1.41	2.37

classes, one containing discrete (usually tetrahedrally coordinated) cadmium(II) ions and another with 6 coordinated Cd(II) obtained as a result of bridge formation of one or more of the ligands. Examples of the former class are for example the structures of bis(thiourea)-cadmium(II) chloride [14] and tetrakis(thiourea)-cadmium(II) tetrakis(thiocyanato)zincate(II).[15] Examples of the second class are more numerous. These are ,*e.g.*, thiourea-cadmium(II) sulfate dihydrate (with sulfate ions and sulfur in thiourea as bridges [16] and bis(ethylenethiourea)cadmium(II) thiocyanate (with two SCN bridges).[17] The structure of tris(thiourea)-cadmium(II) sulfate is described as a binuclear complex built either of distorted octahedrons [18] or of intermediate forms between a square pyramid and a trigonal bipyramid.[19]

The reported cadmium-sulfur bond distances for these complexes are far from being constant. They vary from 2.45 Å in bis(thiourea)-cadmium(II) chloride [14] to 2.73 Å in bis-(ethylenethiourea)cadmium(II) thiocyanate.[17]

Several structures of metal complexes containing thiosemicarbazide (tscH) or similar ligands are reported in the literature: *cis*- and *trans*-Ni(tscH)$_2$(NO$_3$)$_2$,[12] Ni(tscH)$_2$(NO$_3$)$_2$.2H$_2$O,[20] Ni(tscH)$_2$SO$_4$,[8] Ni(tscH)$_2$SO$_4$.3H$_2$O,[21] Ni(tsc)$_2$,[22]

Table 5. Least square planes calculated for some characteristic groups of atoms (marked with an asterisk) in Cd(tscH)$_2$SO$_4$ and the distance from such planes to selected atoms. Symmetry related atoms are marked with a prime. Equation for the planes in direct space is $Px+Qy+Rz=S$.

Cd1	−0.653		Cd1	0.000	
C1 *	0.028		N11 *	−0.134	
N11 *	0.013	I	N11′ *	0.134	II
N21 *	−0.030		S1 *	0.111	
N31	0.126		S1′ *	−0.111	
S1 *	−0.012		C1	−0.417	
Cd2	0.151		Cd2	0.000	
C2 *	0.001		N12 *	0.000	
N12 *	0.001	III	N12′ *	0.000	IV
N22 *	−0.002		S2 *	0.000	
N32	−0.047		S2′ *	0.000	
S2 *	−0.001		C2	0.108	

Plane	P	Q	R	S
I	17.9588	0.8062	3.3266	2.0449
II	9.9814	0.0000	8.5142	2.1285
III	21.6256	−3.6343	−10.6207	−2.4782
IV	22.5094	−3.1967	−11.3321	−2.4363

$Cu(tscH)_2SO_4$,[13] $Pt(tscH)_2SO_4.3H_2O$,[23] $Zn(tscH)Cl_2$,[24] Ag(tscH)Cl,[25] catena-μ-thiocyanato-bis-thiosemicarbazide)silver(I),[26] *cis*- and *trans*-bis(thioacethydroximato)nickel(II),[27,28] acetone thiosemicarbazone zinc(II) chloride,[29] bis-(acetonethiosemicarbazone)nickel(II) chloride monohydrate,[30] bis(thioacethydrazidato)nickel-(II),[31] and bis(ethylenedithiocarbazato)nickel-(II).[32] The crystal structure of the free thio-semicarbazide is also known.[33,34] No crystal structure with Cd^{2+} as the central metal ion with this type of ligands has apparently been reported.

It is an accepted fact that one should be careful, deducing the geometrical structure of labile metal complexes in solution from the structures in the crystalline state. The bis(thio-semicarbazide)cadmium(II) ion is believed [1,2] to have a tetrahedral structure in solution as found indirectly by potentiometric determinations of stability constants while its sulfate salt here is shown to be of octahedral coordination.

As discussed above cadmium complexes can exist in the crystalline state as four as well as six coordinated species. For a long time it has been suspected that this is also the case in solution.[35] Thermochemical studies of cadmium(II) halide complex formation in aqueous and dimethyl sulfoxide solutions have more recently been interpreted in terms of a change in coordination from a supposed hexa-solvate complex to a final tetrahedral tetrahalide complex.[36–38] Moreover, recent X-ray studies of cadmium-aqua and cadmium-iodide solutions have shown that the species $Cd(H_2O)_6^{2+}$ and CdI_4^{2-} indeed are present in the respective solutions and the interatomic distances have been calculated, assuming octahedral and tetrahedral symmetry.[39,40] Thus it is concluded that to a large degree the structure of cadmium complexes is determined by non-bonded interactions between the ligand atoms.

Acknowledgements. The authors are grateful to F. Hansen and K. J. Watson for collection data on the diffractometer made available by The Danish Science Research Council. Help during the structure solution and many fruitful discussions with S. Larsen are gratefully acknowledged.

Computations were performed at NEUCC, The Technical University, Lyngby.

REFERENCES

1. Trinderup, P. *Acta Chem. Scand. To be published.*
2. Christensen, A. N. and Rasmussen, S. E. *Acta Chem. Scand. 17* (1963) 1315.
3. Stewart, J. M., Kundell, F. A. and Baldwin, J. S. *The X-Ray System*, Computer Science Center, University of Maryland.
4. Cromer, D. T. and Mann, J. B. *Acta Crystallogr. A 24* (1968) 321.
5. *International Tables for X-Ray Crystallography*, Kynoch Press, Birmingham 1962, Vol. III, p. 202, Table 3.3.1A.
6. Cromer, D. T. *Acta Crystallogr. 18* (1965) 17.
7. Johnson, C. K. *ORTEP: A Fortran Ellipsoid Plot Program for Crystal Structure Illustrations*, Report, ORNL-3794, Oak Ridge National Laboratory, Oak Ridge 1970. Second Rev.
8. Hazell, R. G. *Acta Chem. Scand. 22* (1968) 2171.
9. Smith, G. S. and Alexander, L. E. *Acta Crystallogr. 16* (1963) 1015.
10. Nyburg, S. C. and Wood, J. S. *Inorg. Chem. 3* (1964) 468.
11. Kilbourn, B. T., Powell, H. M. and Darbyshire, J. A. C. *Proc. Chem. Soc. London* (1963) 207.
12. Hazell, R. G. *Acta Chem. Scand. 26* (1972) 1365.
13. Villa, A. C., Manfredotti, A. G. and Guastini, C. *Cryst. Struct. Commun. 1* (1972) 125.
14. Nardelli, M., Cavalca, L. and Braibanti, A. *Gazz. Chim. Ital. 87* (1957) 137.
15. Korczynski, A. *Rocz. Chem. 41* (1967) 1197.
16. Cavalca, L., Domiano, P., Fava Gasparri, G. and Boldrini, P. *Acta Crystallogr. 22* (1967) 878.
17. Cavalca, L., Nardelli, M. and Fava, G. *Acta Crystallogr. 13* (1960) 125.
18. Cavalca, L., Chiesi Villa, A., Mangia, A. and Palmieri, C. *Inorg. Chim. Acta 4* (1970) 463.
19. Corao, E. and Baggio, S. *Inorg. Chim. Acta 3* (1969) 617.
20. Hazell, R. G. *Acta Chem. Scand. 22* (1968) 2809.
21. Grønbæk, R. and Rasmussen, S. E. *Acta Chem. Scand. 16* (1962) 2325.
22. Cavalca, L., Nardelli, M. and Fava, G. *Acta Crystallogr. 15* (1962) 1139.
23. Gastaldi, L. and Forta, P. *Cryst. Struct. Commun 1* (1972) 353.
24. Cavalca, L., Nardelli, M. and Branchi, G. *Acta Crystallogr. 13* (1960) 688.
25. Nardelli, M., Fava Gasparri, G., Giraldi Battistini, G. and Musatti, A. *Chem. Commun.* (1965) 187.
26. Capdacchi, L. C., Fava Gasparri, G., Ferrari, M. and Nardelli, M. *Chem. Commun.* (1968) 910.
27. Sato, T. Tsukuda, Y., Shiro, M. and Koyama, H. *J. Chem. Soc.* (1969) 125.

28. Sato, T., Shiro, M. and Kyama, H. *J. Chem. Soc.* (1968) 989.
29. Mathew, M. and Palenik, J. *Inorg. Chim. Acta 5* (1971) 349.
30. Mathew, M. and Palenik, G. J. *J. Amer. Chem. Soc. 91* (1969) 4923.
31. Larsen, E., Trinderup, P., Olsen, B. and Watson, K. J. *Acta Chem. Scand. 24* (1970) 261.
32. Gastaldi, L. and Porta, F. *Cryst. Struct. Commun. 3* (1973) 467.
33. Andreetti, G. D., Domiano, P., Gasparri, G. F., Nardelli, M. and Sgarabotto, P. *Acta Crystallogr. B 26* (1970) 1005.
34. Hansen, F. and Hazell, R. G. *Acta Chem. Scand. 23* (1969) 1359.
35. Bjerrum, J. *Metal Ammine Formation in Solution*, Haase, Copenhagen 1941.
36. Gerding, P. *Acta Chem. Scand. 20* (1966) 79.
37. Ahrland, S. *Struct. Bonding (Berlin) 15* (1973) 167.
38. Ahrland, S. and Björk, N. O. *Private communication.*
39. Bol, W., Gerrits, G. J. A. and Eck, C. L. v. P. v. *J. Appl. Crystallogr. 3* (1970) 486.
40. Ohtaki, H. Maeda, M. and Ito, S. *Bull. Chem. Soc. Jap. 47* (1974) 2217.

Received December 11, 1974.

Acta Chemica Scandinavica A 29 (1975) 489—498

Coordination and Bridge Formation in Molten Gallium(III)-Cesium Chloride Mixtures from Raman Spectroscopy

HARALD A. ØYE and WERNER BUES

Institute of Inorganic Chemistry, The Technical University of Norway, N-7034 Trondheim, Norway, and Institute of Inorganic Chemistry, The Technical University of Clausthal, Clausthal-Zellerfeld, German Federal Republic, D-3392

The Raman spectra of molten and solid mixtures of $GaCl_3$ and CsCl, as well as $CsAlGaCl_7$, have been investigated. The data are interpreted in terms of the successive formation of $GaCl_4^-$, $Ga_2Cl_7^-$, $Ga_nCl_{3n+1}^-$, $n \geq 3$, and Ga_2Cl_6 upon addition of $GaCl_3$ to CsCl. The data for $GaCl_4^-$ have been analyzed by the **FG** matrix method. Experimental evidence for strong bridge bonds in $Ga_2Cl_7^-$ and $Al_2Cl_7^-$ has been obtained. The frequencies of the aluminium and gallium chloride species are compared.

Although halogen bridges might be more common in inorganic chemistry than generally anticipated, few attempts have been made to characterize them. The present study of $GaCl_3-CsCl$ mixtures is part of a general study of chlorine bridges, which started with an investigation of molten $AlCl_3-KCl$.[1,2] This work has now been extended to include mixtures with LiCl and CsCl as well.[3] Bridge formations in $AlCl_3-MCl$ and $GaCl_3-MCl$ systems are accompanied by a very strong variation in acid-base characteristics, which make the mixtures suitable reaction media for inorganic as well as organic reactions.

In contrast to the $AlCl_3$-containing system, the present $GaCl_3$-CsCl system has the advantage of being completely miscible,[4] and a full study over the whole concentration range can be performed. The vibrational force constants of $GaCl_4^-$ are also rather similar to those of $AlCl_4^-$, as demonstrated by the close identity of frequencies for the two vibrational modes where the central atom is not moving.[2,5]

A brief account of some preliminary results on $GaCl_3-CsCl$ liquid mixtures has been published previously.[6]

EXPERIMENTAL

Apparatus. A Coderg PH 1 Raman spectrometer with a pulsed ruby laser, exciting line 6943 Å, was used. The time average power of the laser was between 500 and 150 mW, depending on the applied voltage and the operating time of the activating Philips 1000 W high pressure mercury pulse lamp. The detector was an EMI Electronics photomultiplier, type 9558 A. The Raman spectrometer apparatus is described in more detail by Bues, Brockner and Grünewald.[7] The partly circular and partly plane polarized ruby laser light is passed through a horizontal polarizer before reaching the sample. The 90° emitted Raman light is then passed through a horizontal polarizer (non-polarization spectra) or a vertical polarizer (polarization spectra), in front of the instrument's monochromator. The purpose of the horizontal polarizer in front of the monochromator for the non-polarization spectra was to reduce stray light.

Each sample was contained in a sealed cylindrical quartz cell, inner diameter 4 mm and length 20 mm, fitted with a side arm (Hellma, Müllheim Baden).[8] Independent experiments showed that the cells could withstand pressures up to 80 atm at 600 °C.

The optical cell (A) was contained in a stainless steel tube (B). These were both heated in a small furnace fitted to a Coderg multiple reflection Unit (M.R.) (Fig. 1). The scattered Raman light was observed through an opening in the furnace (C) perpendicular to the incident laser beam. On the opposite side of the Raman spectrophotometer was a mirror, which reflected the scattered light in this direction back to the spectrometer. The furnace was insulated with fire bricks (D) and water-cooled on the outside (E).

The temperature was controlled with four heating elements (F), two end elements, a middle element, and a top element. The two end elements were coupled in series. Each of

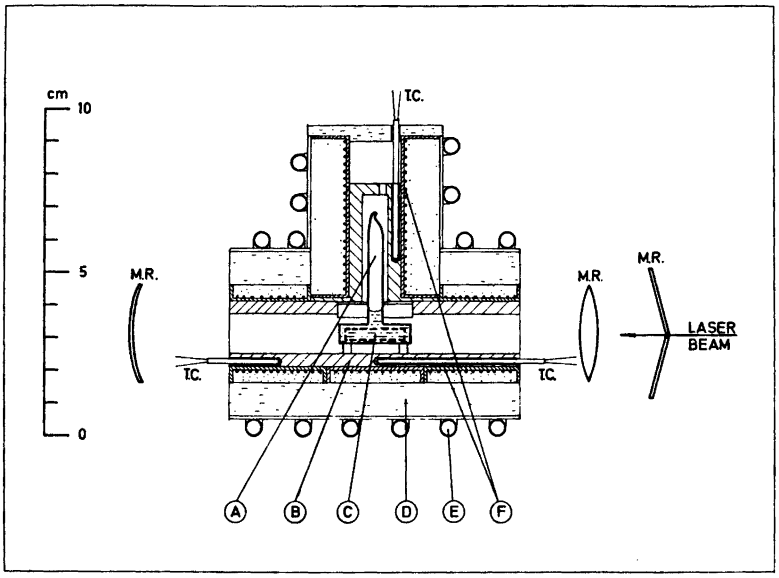

Fig. 1. Furnace with sample. A. Optical quartz cuvette with sample. B. Stainless steel tube. C. Opening for observation and back reflection. D. Fire bricks. E. Cooling coils. F. Kanthal heating wires. M. R. Coderg multiple reflection unit. T. C. Pt/Pt10Rh thermocouples.

the three heating circuits was regulated independently using a Pt/Pt10Rh thermocouple (T.C.) and proportional controllers, (PID+SCR, Eurotherm, Worthing, Sussex, England).

As the furnace had openings for the incident laser beam as well as for the scattered Raman light, temperature gradients in the sample were hard to avoid. To minimize cooling at the end windows, the end elements were kept 20°C above the middle element. Nevertheless, temperature gradients within the sample of $\pm 5°$ were observed by solidification experiments. Fortunately, the temperature was found not to be a sensitive parameter in the present investigation.

Chemicals. Anhydrous $GaCl_3$, 99,99 % was obtained in 10 g ampules from Schuchardt, München. Cesium chloride, *p.a.*, was obtained from Merck, Darmstadt. The CsCl was further purified by dissolution and re-crystallization in water and drying under vacuum at 400 °C. The salt was then melted and filtered through a quartz frit.

Procedure. In an N_2-filled glove-box (moisture content < 20 ppm) a calculated amount of $GaCl_3$ was transferred to a quartz tube above a quartz frit. The tube was evacuated to < 0.1 Torr and sealed off. (The poor vacuum was due to the relatively high vapour pressure of $GaCl_3$ at room temperature). The salt was then sublimed through the frit and condensed on the other side as large crystals. Small pieces of glass from the broken ampule remained on the frit. They were later weighed and their weight subtracted.

The optical cell was fused to a tube with a quartz frit. In the glove-box, a calculated amount of CsCl was added, together with the $GaCl_3$ and the tube connected to a vacuum-line and sealed.

The salts were melted and mixed in a Kanthal-wound quartz furnace. When the salts were thoroughly mixed, the temperature was suddenly raised and the furnace tilted. The sudden increase in vapour pressure pushed the melt through the frit and down into the optical cell. The optical cell was sealed off and was then ready for use.

RESULTS

The Raman spectra of liquid $GaCl_3-CsCl$ mixtures, retraced directly from the spectrometer charts, are shown in Figs. 2a and 2b, Fig. 2b giving polarization spectra for some selected compositions. See the experimental section for a description of the optical arrangement. The spectral slit width for the melt spectra was 8 cm^{-1} and the scanning rate was 30 cm^{-1}/min.

The given composition corresponds to the weighed-in amount of salt. Great care was

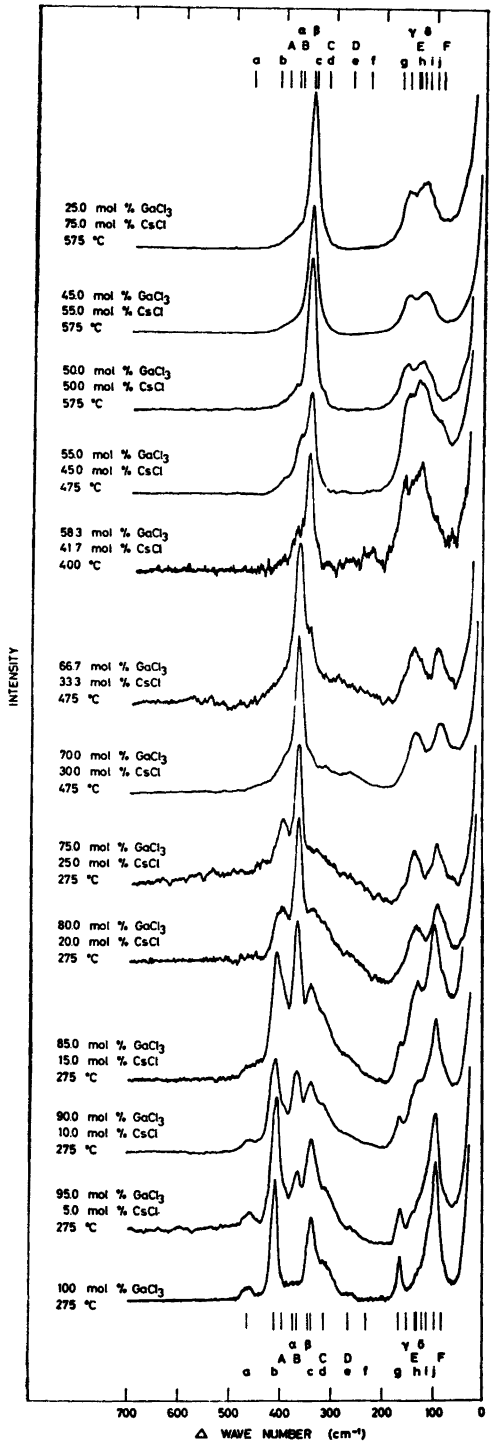

Fig. 2a. Raman spectra of liquid $GaCl_3-CsCl$ mixtures.

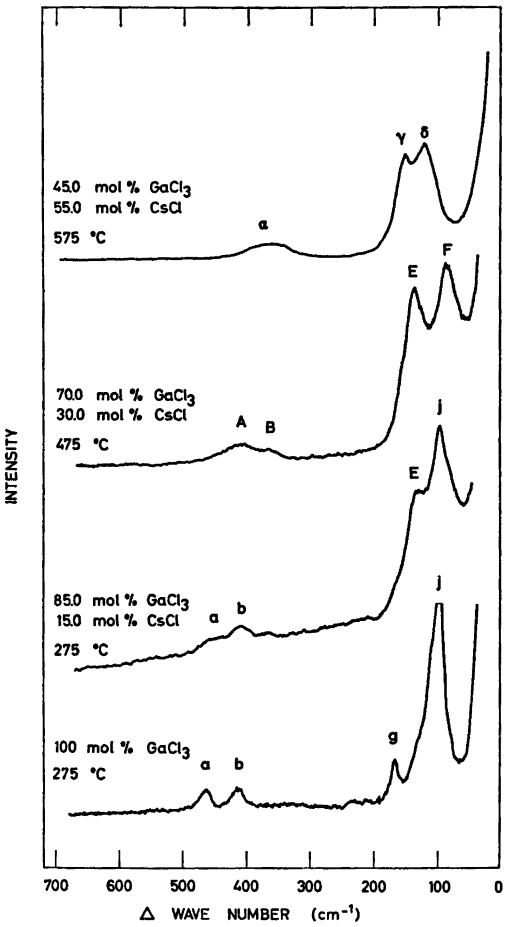

Fig. 2b. "Polarized" Raman spectra of some selected liquid mixtures of $GaCl_3-CsCl$.

taken to avoid evaporation losses, consequently no chemical analysis was performed after the experiments.

Because of the high vapour pressure of $GaCl_3$, it was not desirable to carry out the investigation isothermally. Fig. 2a gives the spectra as a function of composition in isothermal steps.

The Raman vibrational frequencies of molten $GaCl_3-CsCl$, solid $GaCl_3$ and solid $CsGaCl_4$ are listed in Table 1. Each value given is the average for all spectra recorded at the specific composition and temperature. The frequency was measured as the middle of the peak at 3/4 its maximum height. The standard deviation

Table 1. Raman vibration frequencies of molten $GaCl_3$–CsCl, solid $GaCl_3$ and solid $CsGaCl_4$ (cm^{-1}).[a]

$GaCl_4^-$ / $Ga_nCl_{3n+1}^-$, $n \leq 2$ / Ga_2Cl_6		a	b(p)	A	α	B(p)	β(p) c(p)	C d(p)	D e	f	γ g	E	δ h	i	j	F	k
Mol % $GaCl_3$	Temp. °C																
25.0	575				(374)		342				151		121				
45.0	575				(370)		343				153		120				
50.0	575				(375)		344				154		122				
55.0	475			(396)		(364)	344				(151)	(134)	(118)			(88)	
58.3	400					(367)	346				(153)	(137)	(125)			(90)	
66.7	475					365	(342)					136				89	
70.0	475			(393)		366	(344)	316	266			140				90	
75.0	275			394		365						135			(94)	(83)	
80.0	275			401		365	(335)	(306)	(262)		(166)	134			(94)	(80)	
85.0	275	(457)	409	(396)		367	338	(313)	(266)		(166)	133			97	(77)	
90.0	275	463	411	(392)		367	341	(313)	(266)		167	(136)			98	(78)	
95.0	275	464	411			368	342	(318)	267		168		(134)	(114)	98		
100.0	275	464	411				340	(320)	267	230	166		(130)	(110)	98		
$GaCl_3$(s)	30	457	406				(348)	329	243		167		125	115	102		43
															98		35
$CsGaCl_4$(s)	35				(382)		354				157		126				

[a] Shoulders are given in parenthesis.

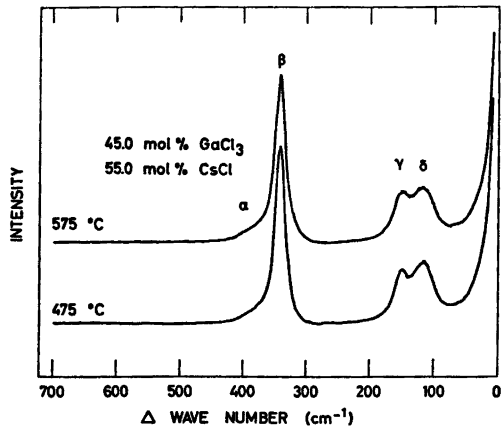

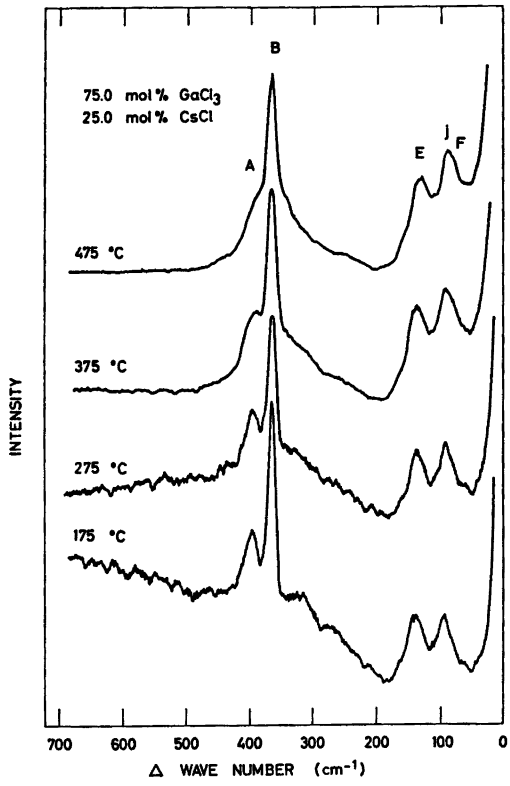

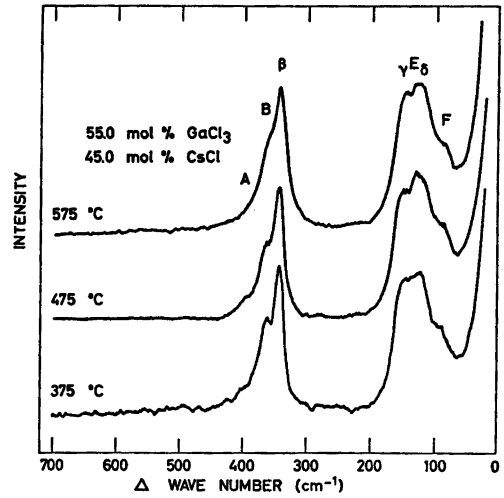

Fig. 3. Raman spectra of liquid $GaCl_3-CsCl$ mixtures as a function of temperature: (a) 45 mol % $GaCl_3$, (b) 55 mol % $GaCl_3$; (c) 75 mol % $GaCl_3$.

was ± 2 cm^{-1}. The recorder was calibrated using CCl_4. The polarization features of the bands are, in many cases, difficult to establish. Only peaks that are polarized with certainty are marked accordingly. Table 1 gives the assignment of the different lines to $GaCl_4^-$, $Ga_nCl_{3n+1}^-$, $n \geq 2$, and Ga_2Cl_6.

Figs. 3a, 3b and 3c demonstrate the influence of temperature on the Raman spectra of the liquid mixture $GaCl_3-CsCl$ at three compositions: (a) 45, (b) 55, and (c) 75 mol % $GaCl_3$.

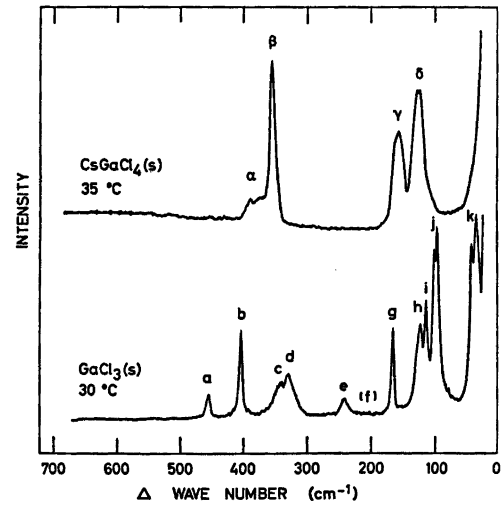

Fig. 4. Raman spectra of the solid compounds $CsGaCl_4$ and $GaCl_3$.

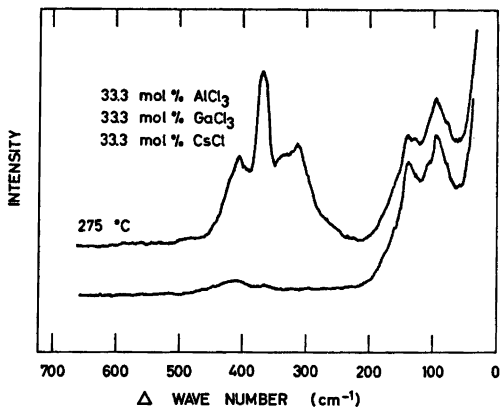

Fig. 5. Raman spectra of the liquid mixtures corresponding to the stoichiometry $CsAlGaCl_7$.

Fig. 4 gives the spectra of the solid compounds, $GsGaCl_4$ and $GaCl_3$. The latter was measured using a slit width of 2 cm^{-1}. Repeated attempts to obtain the spectra of the reported peritectic compound $CsGa_2Cl_7$[4] gave only background scattering and a featureless spectrum.

In order to obtain additional information about the bond structure in the Ga – Cl polymers, a spectrum of the mixture 33 mol % $GaCl_3$, 33 mol % $AlCl_3$ and 33 mol % CsCl was measured. This corresponds to the stoichiometry of $CsAlGaCl_7$. The results are given in Fig. 5.

DISCUSSION

Species formation. Upon inspection of Figs. 2a and 3a – c, it becomes apparent that the spectral contrasts between the different mixtures are not characterized by a gradual shift of the frequencies of the Raman bands. The spectral changes are, however, well described by Raman bands having definite frequencies. The relative intensities then change with composition and temperature. These indicate the presence of species equilibria in the melt mixtures, rather than gradual structural changes. The Raman frequencies in Table 1 have been interpreted accordingly.

The assignments have been performed as follows:

The spectral bands present in liquid mixtures with $X_{GaCl_3} \leq 0.50$, Fig. 2a, have been attributed to the tetrahedral $GaCl_4^-$ (Ref. 5) and marked $\alpha - \delta$. The relative intensities of these bands decrease with increasing $GaCl_3$ content above 50 mol % $GaCl_3$, corresponding to the stoichiometric composition of $CsGaCl_4$. The bands $\alpha - \delta$ correlate closely with the bands observed for the solid compound $CsGaCl_4$, Fig. 4.

The spectral bands in pure liquid $GaCl_3$, Fig. 2a, have been attributed to a double bridged Ga_2Cl_6, symmetry D_{2h}, and marked a – j. The relative peak intensities of these bands decrease with decreasing $GaCl_3$ content. The bands correspond closely to those of a previous investigation by Beattie and Horder,[8] and to those of solid $GaCl_3$ (Fig. 4), which is known to consist of Ga_2Cl_6 entities.[9]

Our spectrum of solid $GaCl_3$ agrees closely with that of Balls *et al.*[10] We obtained better resolution below 150 cm^{-1} which showed band splittings and new low-lying bands, probably caused by Ga_2Cl_6 rocking modes, (Table 1).

The bands not assigned to $GaCl_4^-$ or Ga_2Cl_6 have been attributed to polymers of the form $Ga_nCl_{3n+1}^-$, $n \geq 2$, and marked A – F.

Polymerization mechanisms. $Ga_2Cl_7^-$ in the form of two tetrahedra sharing one edge with a single chlorine bridge, is assumed to be one of the species present in the molten $GaCl_3 - CsCl$ mixture. This is inferred from the similarity between the Raman spectroscopic bands assigned to $Al_2Cl_7^-$ and to $Ga_2Cl_7^-$,[6] and the presence of the solid compound $GsGa_2Cl_7$.[4] The double tetrahedron $Ga_2Cl_7^-$ also provides the natural structural link between the isolated $GaCl_4^-$ tetrahedrons for 50 mol % $GaCl_3$, and the Ga_2Cl_6 double-bridged tetrahedron for pure $GaCl_3$. Taylor has obtained the Raman spectra of solid Ga_2Cl_7 and KGa_2Cl_7.[11] Although the spectral details are somewhat different, the same strong band around 342 cm^{-1} is observed.

Species with a chlorine/gallium ratio lower than 3, for example $GaCl_2^+$, appear very unlikely in view of the strong chlorine affinity of gallium(III) chloride and the lack of evidence for dissociation of Ga_2Cl_6 into its monomers. An octahedral complex like $GaCl_6^{3-}$ can also be ruled out, since no Raman evidence for octahedral coordination is found at compositions corresponding to Cs_3GaCl_6, *i.e.* 25 mol % $GaCl_3$ (Fig. 2a). The radius ratio is also unfavourable for $GaCl_6^{3-}$.

Table 2. Integrated peak intensities in molten $GaCl_3-CsCl$ mixtures given in percentages of the band envelope between 250 and 800 cm^{-1} (from Fig. 2a).

Mol % $GaCl_3$	t °C	α	β	B	
25.0	575	13	87		
45.0	575	13	87		
50.0	575	13	79		
55.0	475	11	57	28	
58.3	475		59	21	
66.7	475	6	12	53	
70.0	475	15	9	50	
75.0	275	19		36	
80.0	275	19		36	
85.0	275	5	17	26	26
90.0	275	5	18	22	25
95.0	275		24	19	33
100.0	275		29		32
		A	c		b

The scattering of the Raman light is very sensitive to small changes in the experimental arrangement and the physical state of the sample. It is only with difficulty that the intensity of a Raman band can be used as a direct measure of species concentration. The relative intensities of the Raman bands for a certain species in the liquid state, however, are insensitive to changes in the environmental structure and temperature. This is demonstrated by $GaCl_4^-$ in the three upper curves in Fig. 2a and in Fig. 3a.

Table 2 lists the relative intensities of some of the more prominent Raman bands for the $GaCl_3-CsCl$ mixtures. The integrated peak intensities are determined from Fig. 2a as peak areas after dividing the total peak area between the different peaks, and are given as the percentage of the total peak intensity of the band envelope between 250 and 500 cm^{-1}. There is no established theoretical basis for this normalization, but the figures obtained by this method are more easily read than those found if only peak intensities, relative to other peak intensities, are tabulated. A fairly large margin of error must be allowed, due to the difficulties involved in separating overlapping peaks and subtracting the background scattering. The numbers in Table 2 may nevertheless have some physical meaning as demonstrated by the variation with increasing content of $GaCl_3$. A monotonic decrease in the peak assigned to $GaCl_4^-$ and an increase in the c and b peak assigned to Ga_2Cl_6, were observed. The most important feature of Table 2 is the relative variation of the band intensities of A and B. The intensity of A increases relative to B upon the addition of $GaCl_3$ beyond 66.7 mol % ($CsGa_2Cl_7$). A maximum around 75 mol % is observed, which corresponds to the stoichiometry of $CsGa_3Cl_{10}$. This is contrary to indications of the preliminary studies.[6] Hence $Ga_2Cl_7^-$ cannot be the only polymer present, but higher polymers, $Ga_nCl_{3n+1}^-$, $n \geq 3$, are formed.

The temperature variation of the Raman spectra supports also the assumption of the stepwise formation of $GaCl_4^-$, $Ga_2Cl_7^-$, Ga_nCl_{3n+1}, $n=3$, $n>3$? Fig. 3a, as previously mentioned, demonstrates the temperature insensitivity of the spectra for the mixture 45 mol % $GaCl_3-55$ mol % CsCl. Fig. 3b shows, for the mixture 55 mol % $GaCl_3-45$ mol % CsCl, that the peaks B and A, assigned to $Ga_2Cl_7^-$ and $Ga_nCl_{3n+1}^-$, $n \geq 3$, respectively, become less prominent with increasing temperature. Fig. 3c shows for the mixture 75 mol % $GaCl_3-25$ mol % CsCl that peak B increases relative to peak A with increasing temperature, *i.e.* the polymer $Ga_nCl_{3n+1}^-$, $n \geq 3$, becomes less prominent. This tendency toward a decrease in polymerization degree with increasing temperature is expected from statistical thermodynamic considerations.

The technique developed for calculating the equilibrium constant for the dissociation of $2Al_2Cl_7^- = 2AlCl_4^- + Al_2Cl_6$[2] can also be applied to this system. The species assumed to be present are $GaCl_4^-$, $Ga_2Cl_7^-$, $Ga_3Cl_{10}^-$ and Ga_2Cl_6. The many equilibrium data required and the difficulties in determining reliable relative intensities, however, make such a calculation impracticable and prone to uncontrollable errors. Our conclusions, therefore, are more qualitative in nature.

In the $GaCl_3-CsCl$ systems a stepwise formation of the species Ga_2Cl_6, $Ga_3Cl_{10}^-$ ($Ga_nCl_{3n+1}^-$, $n \geq 3$), $Ga_2Cl_7^-$, and $GaCl_4^-$ upon addition of CsCl to $GaCl_3$ is observed. A reasonable stoichiometric condition is that each species is at a maximum concentration at the

corresponding bulk composition.

The corresponding composition as a function of the number of Ga atoms in the complex, n, is then given by $X_{GaCl_3}=n/(n+1)$. From Fig. 2 it can, however, be seen that $Ga_2Cl_7^-$ or $Ga_3Cl_{10}^-$ is not exclusively present at the respective mol fractions 0.67 and 0.75. Therefore, the equilibrium constants for the following dissociations are not negligible:

$$2Ga_2Cl_7^- = GaCl_4^- + Ga_3Cl_{10}^- \quad (1)$$

$$2Ga_3Cl_{10}^- = 2Ga_2Cl_7^- + Ga_2Cl_6 \quad (2)$$

The results found in the $GaCl_3-CsCl$ system closely parallel those recently found in $AlCl_3-CsCl$ mixtures.[3] In the $GaCl_3-CsCl$ system, however, there is only one band that can be assigned with certainty to higher polymers. In view of the general features of the Raman bands in Fig. 2, it is possible that the additional bands might be hidden, since despite the structural differences of $GaCl_4^-$, $Ga_2Cl_7^-$, and Ga_2Cl_6, the spectra have the same general features: A collection of bands containing the strongest polarizable peak is found between 380 and 450 cm^{-1}, and between 100 and 180 cm^{-1} another band envelope appears which contains the strongest depolarizable bands.

Gallium tetrachloride ion ($GaCl_4^-$). The observed Raman frequencies for $GaCl_4^-$ closely resemble those found by Woodward and Nord [5] for $GaCl_3$ dissolved in aqueous hydrochloric acid. The difference is less than 6 %.

For determining the vibrational force constants, the Wilson **FG**-matrix method is applied.[12] A modified valence force field and T_d symmetry are used,[13] setting non-diagonal **F**-matrix elements equal to zero.

$$F_{11}(A_1) = f_r + 3f_{rr}$$
$$F_{22}(E) = f_\alpha - 2f_{\alpha\alpha}$$
$$F_{33}(T_2) = f_r - f_{rr}$$
$$F_{44}(T_2) = f_\alpha$$

The calculation yields in mdyn/Å: $f_r=1.842$, $f_{rr}=0.210$, $f_\alpha=0.147$, and $f_{\alpha\alpha}=0.045$. The corresponding force constants (mdyn/Å) for $AlCl_4^-$ in $CsAlCl_4$ are: $f_r=1.651$, $f_{rr}=0.273$, $f_\alpha=0.187$, and $f_{\alpha\alpha}=0.044$.[3]

The close similarity in **F** matrix elements of $GaCl_4^-$ and $AlCl_4^-$ means that the difference in Ga–Cl and Al–Cl vibrations are mainly due to the mass difference between Al and Ga.

Digallium heptachloride ion ($Ga_2Cl_7^-$). The frequencies B, C, D, E, and F are assigned to $Ga_2Cl_7^-$. For the corresponding ion $Al_2Cl_7^-$ a double tetrahedral model with the sharing of one Cl and with symmetry D_{3d}[2] was previously assumed. The Al–Cl–Al bridge was assumed weak.[3]

The assumption of a weak bridge for $Al_2Cl_7^-$ was tested experimentally in the present work by obtaining the spectrum of $CsAlGaCl_7$ (Fig. 5) and comparing it with the spectra of $CsAl_2Cl_7$ and $CsGa_2Cl_7$. If the bridge force constant is very weak, the bridge would act as a vibrational insulator and the spectra of $AlGaCl_7^-$ should be superimposed on the spectra of $Al_2Cl_7^-$ and $Ga_2Cl_7^-$. This is not the case. In addition to the strong peaks at 311 and 366 cm^{-1}, corresponding to the strongest peaks for $Al_2Cl_7^-$ and Ga_2Cl_7, a strong polarizable peak at 405 cm^{-1} is observed, rendering a weak bridge model highly unlikely.

Recent structural work on crystals of $Pd_2(Al_2Cl_7)_2(C_6H_6)_2$,[14] $Te_4(Al_2Cl_7)_2$,[15] as well as KAl_2Br_7,[16] all give a bent Al–X–Al bridge (X = Cl, Br), the angle being close to the tetrahedral angle and the bridge bond length being only slightly larger than the terminal Al–X bond length.

The Raman spectrum of $CsAlGaCl_7$, the apparent stability of $Ga_2Cl_7^-$ and $Al_2Cl_7^-$, as well as the similarities in bond length between the Al–X bridge and the terminal Al–X in solid crystals, all point to a strong bridge force constant in the $Al_2Cl_7^-$ and $Ga_2Cl_7^-$ ions.

The bent Al–Xl–Al bridge found in solid crystals does not necessarily imply a bent bridge for $Al_2Cl_7^-$ and $Ga_2Cl_7^-$ in liquid mixtures. In spite of the good quality Raman-spectra of the $GaCl_3-CsCl$ liquid mixtures, no more than 5 Raman active frequencies have been detected, compared with a minimum of 21 expected for a bent bridge. A calculation based on a D_{3d} model, not given here, also gives a reasonable explanation of the spectra.

Nevertheless, a bent bridge structure in the melt with, for instance, C_{2v} symmetry cannot be excluded, as it may give the same general spectrum as a D_{3d} model, having two major band envelopes around 350 and 100 cm^{-1}, the fine structure being blurred by thermal movements. As a conclusion we will, however,

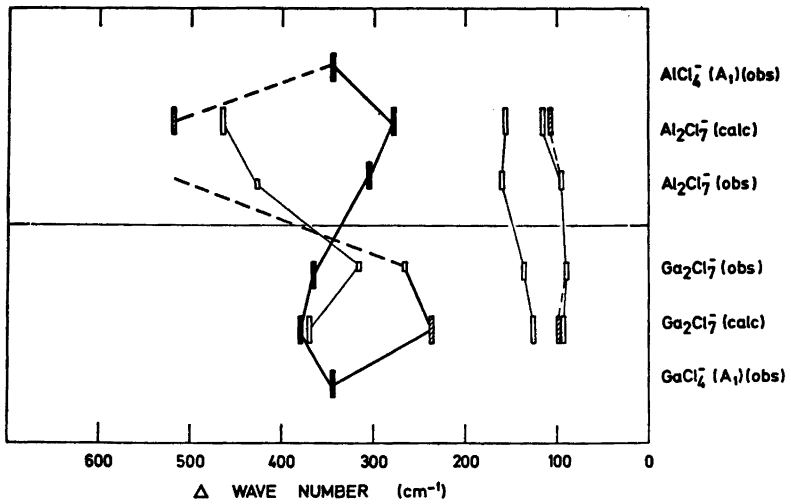

Fig. 6. Correlation diagram. Diagram illustrating the connection between calculated and observed Raman-active frequencies for $Al_2Cl_7^-$ and $Ga_2Cl_7^-$, D_{3d} and the "cross over" of $Al_2Cl_7^-$ and $Ga_2Cl_7^-$ modes. A strong chlorine bridge is assumed. Filled columns: Vibrational modes involving stretching of r. Hatched columns: Other total symmetric modes.

emphasize that the present melt studies do not give any positive evidence for such a structure.

A correlation diagram for observed frequencies for $Al_2Cl_7^-$ and $Ga_2Cl_7^-$ is given in Fig. 6. The valence stretch frequencies for $AlCl_4^-$ and $GaCl_4^-$ are also shown. In the present correlation diagram frequencies with similar vibrational characteristics have been joined together, and differs somewhat from the diagram given in the preliminary publication.[6]

The symmetric stretching frequencies of $AlCl_4^-$ and $GaCl_4^-$ are independent of the mass of the central ion, and are found to be approximately equal. In view of this fact, it might seem surprising that the strongest polarized frequency of $Ga_2Cl_7^-$ is at a higher frequency than for $Al_2Cl_7^-$, as a mass effect would predict the opposite trend.

This is considered due to the fact that the mass of Cl is intermediate between Al and Ga. The valence stretch frequency of $MeCl_4^-$ can for $Me_2Cl_7^-$ be considered split up in an end and bridge frequency, and a "cross over" is obtained when going from $Al_2Cl_7^-$ to $Ga_2Cl_7^-$.

This "cross over" for $Me_2Cl_7^-$ can be explained qualitatively from a **GF** matrix calculation where for simplicity a D_{3d} model was chosen. Assuming a bridge stretch force constant being 90 % of the terminal force constant and assigning the different vibrational modes according to the potential energy distribution,[17,18] the observed shifts in the A_g stretching modes for $Al_2Cl_7^-$ relative to $Ga_2Cl_7^-$ were reproduced. A parallel phenomenon is described by Sicbert [19] for XCN molecules. For X being very much lighter or very much heavier than C the CN frequency was about the same. For intermediate masses of X the CN frequency was shifted to lower frequencies for X lighter than N, and to higher frequencies for X heavier than N, with a similar "cross-over".

Acknowledgement. We gratefully acknowledge grants for instruments and materials from Volkswagenstiftung and experimental assistance from Mr. D. Grünewald and Mr. M. Sørlie. We appreciate the use of the computer programs of Dr. S. J. Cyvin. H. A. Ø. is thankful for support from Norges almenvitenskapelige forskningsråd.

REFERENCES

1. Cyvin, S. J., Klæboe, P., Rytter, E. and Øye, H. A. *J. Chem. Phys. 52* (1970) 2776.
2. Øye, H. A., Rytter, E., Klæboe, P. and Cyvin, S. J. *Acta Chem. Scand. 25* (1971) 559.

3. Rytter, E., Øye, H. A., Cyvin, S. J., Cyvin, B. N. and Klæboe, P. *J. Inorg. Nucl. Chem. 35* (1973) 1185.
4. Fedorov, P. J. and Tsimbalist, V. V. *Russ. J. Inorg. Chem. 9* (1964) 908.
5. Woodward, L. A. and Nord, A. A. *J. Chem. Soc.* (1965) 3721.
6. Øye, H. A. and Bues, W. *Inorg. Nucl. Chem. Lett. 8* (1972) 31.
7. Bues, W., Brockner, W. and Grünewald, D. *Spectrochim. Acta A 28* (1972) 1519.
8. Beattie, I. R. and Horder, J. R. *J. Chem. Soc. A* (1969) 2655.
9. Wallwork, S. C. and Worral, I. J. *J. Chem. Soc.* (1965) 1816.
10. Balls, A., Downs, A. J., Greenwood, N. N. and Straughan, B. P. *Trans. Faraday Soc. 62* (1966) 521.
11. Taylor, M. J. *J. Chem. Soc. A* (1970) 2812.
12. Wilson, E. B., Decius, J. C. and Cross, P. C. *Molecular Vibrations*, McGraw Hill, New York 1955.
13. Cyvin, S. J. *Molecular Vibrations and Mean Square Amplitude*, Universitetsforlaget, Oslo 1968, p. 121.
14. Allegra, G., Casogrande, G. T., Immirzi, A., Porri, L. and Vitulli, G. *J. Amer. Chem. Soc. 92* (1970) 289.
15. Cough, T. W., Lokken, D. A. and Corbett, J. D. *Inorg. Chem. 11* (1972) 357.
16. Rytter, E., Rytter, B. E. D., Øye, H. A. and Krogh-Moe, J. *Acta Crystallogr. B 29* (1973) 1541.
17. Morino, Y. and Kuchitsu, K. *J. Chem. Phys. 20* (1952) 1809.
18. Nakamoto, K. *Infrared Spectra of Inorganic and Coordination Compounds*, 2nd Ed., Wiley, New York 1970, p. 68.
19. Siebert, H. *Anwendungen der Schwingungsspektroskopie in der Anorganische Chemie*, Springer, Berlin 1966, p. 11.

Received December 13, 1974.

Acta Chemica Scandinavica A 29 (1975) 499—504

The Crystal Structure of *trans*-Dichlorobis(ethylenediamine)-platinum(IV) Tetrachlorocuprate(II) Monohydrate

KARL PEDER LARSEN,[a,*] RITA GRØNBÆK HAZELL,[a] HANS TOFTLUND,[b] POUL RASMUS ANDERSEN,[a] POUL BISGÅRD,[a] KAJ EDLUND,[a] MOGENS ELIASEN,[a] CARSTEN HERSKIND,[a] THOMAS LAURSEN,[a] and POUL MØLLER PEDERSEN[a]

[a] Department of Inorganic Chemistry, Aarhus University, DK-8000 Aarhus C, Denmark and [b] Department of Chemistry, Odense University, DK-5000 Odense, Denmark

trans-Dichlorobis(ethylenediamine)platinum-(IV) tetrachlorocuprate(II) monohydrate, *trans*-$Pt[(en)_2Cl_2][CuCl_4].H_2O$, is monoclinic, $P2/c$ with $a = 7.788(6)$ Å, $b = 7.369(7)$ Å, $c = 15.080(20)$ Å, $\beta = 114.4(1)°$, and $Z = 2$. The structure has been solved by Patterson and Fourier methods from three dimensional X-ray data and refined by the method of least squares to an R-value of 0.051. The refinement was based on 1359 independent reflections. The coordination around Pt is nearly octahedral with an average Pt—N distance of 2.081(8) Å; the Pt—Cl distance is 2.313(4) Å. The $[CuCl_4]^{2-}$ configuration is a strongly distorted tetrahedron with Cu—Cl distances of 2.239(5) and 2.276(4) Å; the dihedral angle is 35.7(2)°. The strong deformation may in part be due to hydrogen bonding.

Complex ions of the type $[CuCl_n]^{(n-2)-}$, $n = 3$, 4, and 5, have received much interest recently,[1-7] mainly because of the variety of coordination polyhedra they exhibit. However, isolated $[CuCl_n]^{(n-2)-}$ complexes with $n = 6$, the most frequent coordination number in 3*d*-transition metal complexes, have not been reported in the literature.

In $[Cr(NH_3)_6][CuCl_5]$ the uncommon $CuCl_5^{3-}$ ion is stabilised by the large $[Cr(NH_3)_6]^{3+}$ cation.[8] This suggests that a suitable cation, *i.e.* with respect to size and charge, might facilitate the existence of an isolated $CuCl_6^{4-}$ complex. $[Pt(en)_3]^{4+}$ was chosen as cation and the reaction assumed to take place was

$$[Pt(en)_3]Cl_4 + CuCl_2 \rightarrow [Pt(en)_3][CuCl_6]$$

However, this attempt led to the formation of *trans*-$[Pt(en)_2Cl_2][CuCl_4].H_2O$, exclusively. For $n = 4$, at least three distinct coordination polyhedra are known of which examples are given in Table 1. The present compound contains $[CuCl_4]^{2-}$ complexes of type 1, but a strong distortion of the tetrahedron brings it close to type 2.

EXPERIMENTAL

Chemistry. $[Pt(en)_3]Cl_4.3H_2O$: A modification of Smirnoff's method [9] was used to prepare this compound. (Found: C 12.35; H 4.11; N 14.49; Calc. for $[Pt(C_2H_8N_2)_3]Cl_4.3H_2O$: C 12.61; H 4.25; N 14.71). *trans*-$[Pt(en)_2Cl_2][CuCl_4].H_2O$: A mixture of 0.3 g $[Pt(en)_3]Cl_4.3H_2O$ in 1.5 ml water was added dropwise to a solution of 2.0 g LiCl and 0.2 g $CuCl_2.2H_2O$ in a mixture of 2 ml ethanol and 3 ml 4 M hydrochloric acid. A brown salt precipitated after a few seconds. Recrystallization from hot conc. HCl gave grass-green prismatic crystals. Yield 0.2 g. (Found: C 7.57; H 2.89; N 8.79; Cl 34.48. Calc. for $[Pt(C_2H_8N_2)_2Cl_2][CuCl_4].H_2O$: C 7.88; H 2.98; N 9.19; Cl 34.89). The density of the crystals was determined by flotation in a mixture of CCl_4 and $CHBr_3$.

X-Ray technique. Lattice parameters and space group were determined from Weissenberg and precession photographs using Cu and Mo radiation ($\lambda_{Cu} = 1.5418$ Å, $\lambda_{Mo} = 0.7109$ Å). Preliminary intensity data were collected in the $h0l$ plane from Weissenberg photographs using the multiple film technique and visual intensity estimation. Ni-filtered Cu radiation was employed, and the crystal, which was bounded by {100}, {001}, and {010}, had the linear dimensions $0.11 \times 0.10 \times 0.30$ mm³. Three

* Author to whom correspondence is to be addressed.

Table 1.

	Type	Compound	Coordination polyhedron	Ref.
	1	$[(C_2H_5)_3NH]_2[CuCl_4]$	flattened tetrahedron	4
	2	$[(C_6H_5)C_2H_4NH_2(CH_3)]_2[CuCl_4]$	square plane [a]	7
	3	$[(C_6H_5)NH_3]_2[CuCl_4]$	elongated octahedron	6

[a] Room temperature modification.

dimensional intensity data were obtained by means of a semi-automatic Supper diffractometer controlled by an *RC4000* computer. This computer was also used for the data reduction. Graphite monochromatized Mo$K\alpha$ radiation was used and data were collected out to sin $\theta/\lambda = 0.7$ Å^{-1}, yielding 1570 independent reflections. No correction was applied for absorption.

CRYSTAL DATA

Crystal system: monoclinic (b-axis unique).
Unit cell: $a = 7.788(6)$ Å, $b = 7.369(7)$ Å, $c = 15.080(20)$ Å, $\beta = 114.4(1)°$, $Z = 2$, $d_{obs} = 2.54$ g/cm^3, $d_{calc} = 2.56$ g/cm^3, $\mu_{MoK\alpha} = 116.8$ cm^{-1}.
Systematic absences: $h0l$. $l = 2n + 1$.
Space group: $P2/c$ (or Pc).

STRUCTURE DETERMINATION

A Patterson function based on the $h0l$ film data confirmed that the platinum and copper atoms were in special positions. The position of the three chlorine atoms could also be determined, whereas the lighter atoms were undetectable both in Patterson and Fourier maps. The R-value at this stage was 0.21, ($R = (\sum||F_{obs}| - k|F_{calc}||)/\sum|F_{obs}|$). This part of the structure analysis constituted an undergraduate course in X-ray crystallography.

The three dimensional data confirmed the positions of the heavy atoms and the ethylenediamine molecule was easily found from a Fourier map. The structure was refined by the full matrix least squares program LINUS.[10] An R-value of 0.065 based on all reflections was obtained when anisotropic thermal parameters were included. A difference Fourier map showed the oxygen atom of the water molecule and to some extent the hydrogen atoms. The criterion $F_{obs}^2 \leq 3\sigma(F_{obs}^2)$ was then applied and reflections with $k^2 + l^2 \leq 8$ were deleted due to the diffractometer geometry. This reduced the number of reflections to 1359 and they were in the further refinement weighted by $w = 1/[\mu(F)]^2$, where $\mu(F) = [\sigma(F^2)_{count} + 1.03F_{obs}^2]^{\frac{1}{2}} - |F_{obs}|$. Hydrogen atoms were inserted in fixed calculated positions with constant B-values of 4.0. The scattering factors used for Pt, Cu, Cl, N, C, and O were those given by Cromer and Mann,[11] and for hydrogen the scattering curve

Table 2. Atomic coordinates with standard deviations $\times 10^4$ in parentheses. Calculated hydrogen positions under the assumption of sp^3 hybridized atoms and N–H = 1.00 Å, C–H = 1.05 Å, O–H = 0.95 Å.

Atom	x	y	z	Atom	x	y	z
Pt	0.0000	0.0000	0.0000	H_1	0.192	−0.235	0.131
Cu	0.5000	0.2955(3)	0.2500	H_2	0.327	−0.060	0.139
Cl_1	0.2043(6)	0.2194(5)	−0.0092(3)	H_3	0.104	−0.071	−0.140
Cl_2	0.2715(6)	0.4966(7)	0.2301(3)	H_4	−0.080	−0.196	−0.155
Cl_3	0.3566(6)	0.0759(6)	0.3014(3)	H_5	0.396	−0.358	0.073
N_1	0.2328(18)	−0.1453(17)	0.0930(9)	H_6	0.413	−0.158	0.019
N_2	0.0435(19)	−0.1497(16)	−0.1064(8)	H_7	0.092	−0.411	−0.045
C_1	0.3209(23)	−0.2451(22)	0.0338(13)	H_8	0.232	−0.356	−0.105
C_2	0.1704(24)	−0.3067(21)	−0.0590(12)	H_9	0.095	−0.248	0.245
O	0.0000	−0.1717(33)	0.2500				

Table 3. Thermal parameters with standard deviations in parentheses, both $\times 10^4$. The u_{ij} are defined by exp $[-2\pi^2(u_{11}a^{*2}h^2 + \cdots 2u_{12}a^*b^*hk + \cdots)]$.

Atom	u_{11}	u_{22}	u_{33}	u_{12}	u_{13}	u_{23}
Pt	287 (3)	162(16)	214(3)	0(5)	135(2)	23(5)
Cu	423(15)	241(19)	384(14)	0	216(12)	0
Cl_1	445(21)	244(21)	535(23)	21(16)	300(19)	−64(19)
Cl_2	652(24)	338(21)	643(24)	105(30)	369(21)	81(27)
Cl_3	454(22)	341(22)	380(19)	16(16)	240(17)	38(15)
N_1	451(76)	270(58)	357(64)	33(54)	195(60)	35(50)
N_2	514(78)	293(55)	281(58)	10(54)	259(59)	−23(58)
C_1	345(82)	414(84)	506(93)	108(68)	208(76)	86(71)
C_2	567(101)	309(74)	447(87)	30(69)	355(82)	−24(67)
O	652(140)	742(169)	1404(224)	0	570(152)	0

given by Stewart, Davidson and Simpson [12] was used. A final R-value of 0.051 was obtained; no attempt has been made to use the non-centrosymmetric space group Pc. Atomic coordinates are listed in Table 2 and anisotropic thermal parameters in Table 3; a list of observed and calculated structure factors is available on request.

DISCUSSION

Chemistry. The compound *trans*-[Pt(*en*)$_2$Cl$_2$]-[CuCl$_4$].H$_2$O is prepared according to the following overall reaction scheme:

$$[Pt(en)_3]^{4+} + [CuCl_4]^{2-} + 2H^+ + 2Cl^- \rightarrow [Pt(en)_2Cl_2]^{2+} + [CuCl_4]^{2-} + enH_2^{2+}$$

This is a rather unusual reaction because the ion $[Pt(en)_3]^{4+}$ is normally kinetically inert. The formation of the *trans* isomer suggests a mechanism involving the planar $[Pt(en)_2]^{4+}$ ion as a simple splitting off of one *en* molecule would lead to the *cis* isomer. It is possible [9] that the starting material $[Pt(en)_3]Cl_4.3H_2O$ contained small amounts of $[Pt(en)_2]Cl_2$; furthermore, it is known [13] that chlorocomplexes of Cu(II) are able to oxidize Pt(II) to Pt(IV). It is therefore suggested that the dark brown salt isolated first contains both Cu(I) and Cu(II); salts of this type have been described by Mori.[14] When this salt is recrystallized from hydrochloric acid, copper(I) is reoxidized to copper(II) by molecular oxygen, and $[Pt(en)_3]^{4+}$ is converted to *trans*-$[Pt(en)_2Cl_2]^{2+}$. It is presumed that Cu(I) here acts as a catalyst. The details of this last reaction are under further investigation.

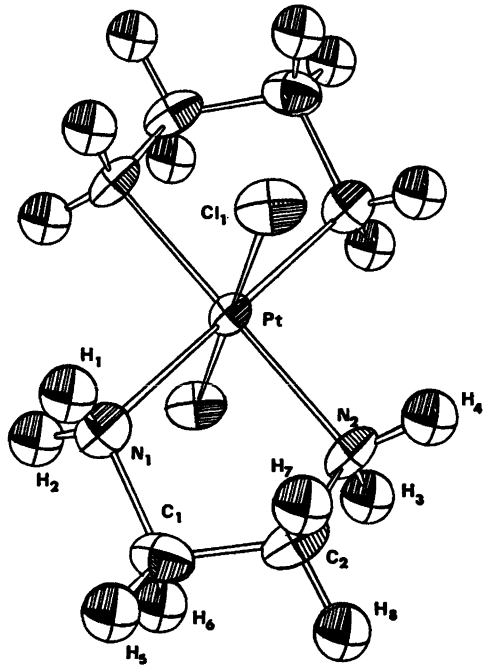

Fig. 1. Perspective drawing of *trans*-[Pt(*en*)$_2$-Cl$_2$]$^{2+}$ in *trans*-[Pt(*en*)$_2$Cl$_2$][CuCl$_4$].H$_2$O. Thermal ellipsoids enclose 50 % probability (ORTEP II).[15]

Structure. The platinum atom lies at a centre of symmetry which causes the four nitrogen atoms and the platinum to be exactly in a plane and the chlorines to be in *trans* position (Fig. 1). The two Pt−N distances (Table 4) are equal within one standard deviation, and apart from the N_1-Pt-N_2 angle only slight devia-

Table 4. Interatomic angles and distances in *trans*-$[Pt(en)_2Cl_2][CuCl_4].H_2O$ calculated with the program ORFFE [16] including variance-covariance matrix and cell parameter errors. Standard deviations in parentheses.[a]

Angle	Degrees	Distance	Å
$N_1-Pt-Cl_1$	88.3(4)	$Pt-Cl_1$	2.313(4)
$N_2-Pt-Cl_1$	89.4(3)	$Pt-N_1$	2.074(12)
N_1-Pt-N_2	82.7(5)	$Pt-N_2$	2.087(11)
$Pt-N_1-C_1$	109.4(9)	N_1-C_1	1.522(20)
$N_1-C_1-C_2$	109.3(1.2)	C_1-C_2	1.478(23)
$C_1-C_2-N_2$	108.9(1.2)	C_2-N_1	1.497(20)
C_2-N_1-Pt	109.0(9)		
$Cl_2-Cu-Cl_2'$	97.1(3)	$Cu-Cl_2$	2.239(5)
$Cl_3-Cu-Cl_3'$	89.4(2)	$Cu-Cl_3$	2.276(4)
$Cl_2-Cu-Cl_3$	92.4(2)		
$Cl_2-Cu-Cl_3'$	154.1(2)		
Dihedral angle $(Cl_2-Cu-Cl_2')-(Cl_3-Cu-Cl_3')$ 35.7(2)°.			

[a] (') Symmetry operation $\bar{x},y,\frac{1}{2}-z$.

tions from pseudo octahedral symmetry are observed. Several papers [17–21] report Pt – Cl and Pt – N distances and they all lie in the ranges 2.30 – 2.34 Å and 2.01 – 2.10 Å, respectively. The structure of *cis*-$[Pt(en)_2Cl_2]Cl_2$ (Ref. 22) contains two independent Pt – Cl distances with an average value of 2.306(5) Å, and this value is within one standard deviation of the distance found in the present study. The average Pt – N distance in the *cis* complex is 2.057(12) Å as compared with 2.081(8) Å in the present complex. The geometry of the ethylenediamine molecule, which is quite similar in the two isomers, shows only slight deviations from the expected configuration. The water molecule lies on the two-fold axis through $(x,z)=(0,1/4)$ and from the calculated hydrogen positions there seems to be weak hydrogen bonding between the water molecule and the ethylenediamine moiety, *cf.* Table 5.

The $[CuCl_4]^{2-}$ ion (Fig. 2a,b) is situated on the two-fold axis through $(x,z)=(1/2, 1/4)$. The two independent Cu – Cl distances (Table 4) seem to be significantly different, but they agree with previously obtained values [1–4,6,7,23,24] which normally lie in the range 2.20 – 2.34 Å. The Cl – Cu – Cl angles, *cf.* Table 4, show a large distortion of the $[CuCl_4]^{2-}$ ion from tetrahedral towards square planar configuration. The deformation, expressed by the dihedral angle as defined in Table 4, seems to be the most pronounced so far reported. Table 6 shows a selection of dihedral angles in distorted $[CuCl]_4^{2-}$ ions along with the extreme cases, *i.e.* the tetrahedral and the square planar configurations.

Theoretical calculations [5,30–32] on the geometry of the $[CuCl_4]^{2-}$ ion predict the flattened tetrahedron (approx. D_{2d} symmetry) to be the most stable coordination polyhedron. However,

Table 5. Probable hydrogen bonds in *trans*-$[Pt(en)_2Cl_2][CuCl_4].H_2O$.[a]

A···B	Distance (Å)	H···B	Distance (Å)
$N_1\cdots Cl_3'$	3.35(1)	$H_2\cdots Cl_3'$	2.46
$N_1\cdots Cl_3$	3.31(1)	$H_2\cdots Cl_3$	2.55
$N_2\cdots Cl_2$	3.50(1)	$H_4\cdots Cl_2$	2.63
$N_2\cdots O$	3.13(2)	$H_3\cdots O$	2.35

[a] (') Symmetry operation $\bar{x},y,\frac{1}{2}-z$.

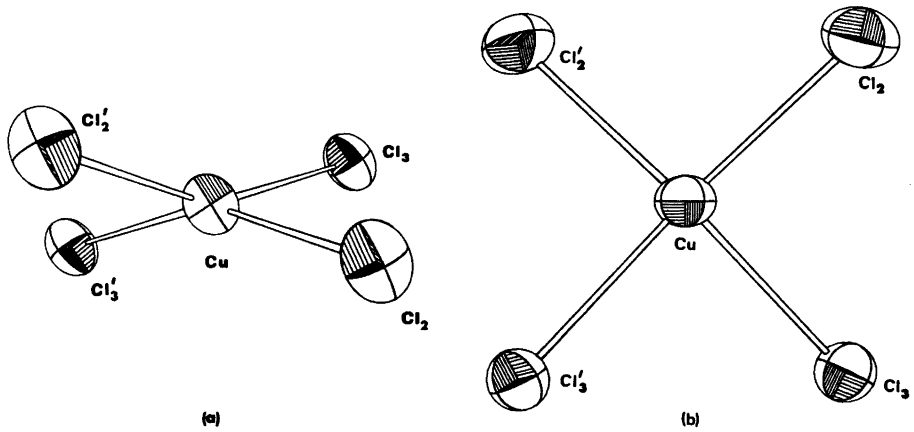

Fig. 2. Perspective drawing of $[CuCl_4]^{2-}$ in *trans*-$[Pt(en)_2Cl_2][CuCl_4].H_2O$. a. Viewed along the twofold axis. b. Viewed perpendicular to the twofold axis. Thermal ellipsoids enclose 50 % probability.

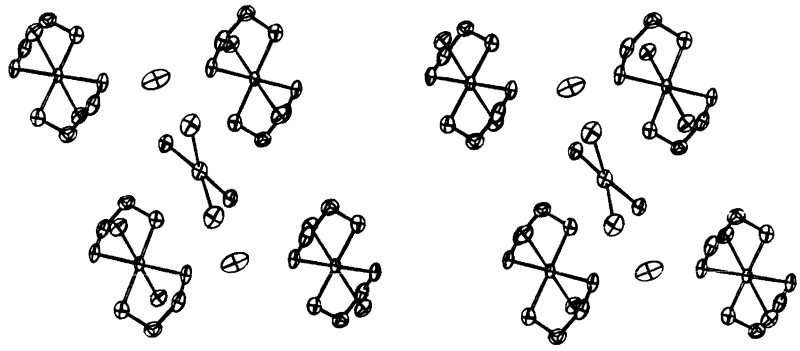

Fig. 3. Stereoscopic drawing of the *b*-projection in *trans*-$[Pt(en)_2Cl_2][CuCl_4].H_2O$. Hydrogen atoms have been omitted for clarity.

Table 6. Dihedral angles in $[CuCl_4]^{2-}$ ions.

Compound	Angle (degrees)	Ref.
Tetrahedron	90.0	
$[(C_6H_5)C_2H_4NH_2(CH_3)]_2[CuCl_4]$[a]	80.0	7
Cs_2CuCl_4	73.6	25
$[(CH_3)_4N]_2[CuCl_4]$	68.6	26
$[(C_5H_4NCH_3)_2][CuCl_4]$	67.6	27
$[(C_6H_5)CH_2N(CH_3)_3]_2[CuCl_4]$	66.6	28
$[(C_2H_5)_3NH]_2[CuCl_4]$	63.7	4
$[C_{13}H_{19}N_3OS]_2[CuCl_4]$	49.5	29
$[Pt(en)_2Cl_2][CuCl_4].H_2O$	35.7	
Square plane	0.0	

[a] High temperature modification.

in many of the structures solved so far, hydrogen bonding seems to be of importance in determining the final geometry of the $[CuCl_4]^{2-}$ ion. This is so also in the present compound where several short distances which may correspond to hydrogen bonds are found, *cf.* Table 5. The interaction between $[CuCl_4]^{2-}$ and $[Pt(en)_2Cl_2]^{2+}$ through hydrogen bonds might be taken as an explanation of the stronger distortion towards square planar configuration in the present compound than in the other compounds in Table 6. Further evidence for the importance of hydrogen bonds in this type of compounds is given by the complex $[(C_6H_5)C_2H_4NH_2(CH_3)]_2[CuCl_4]$ which exists in two modifications.[7] At room temperature the configuration of the $[CuCl_4]^{2-}$ ion is a square plane with substantial hydrogen bonding, while the modification at 80 °C, *i.e.* at higher thermal energy, contains $[CuCl_4]^{2-}$ as a flattened tetrahedron. This seems to indicate that with weak hydrogen bonding or completely without, as is the case in Cs_2CuCl_4 (Refs. 25, 33), the most favourable geometry of the $[CuCl_4]^{2-}$ ion is in fact the moderately flattened tetrahedron as predicted by theory. It is therefore likely that the strong deformation of the $[CuCl_4]^{2-}$ ion in the present compound is due only to packing forces and hydrogen bonding and not to any inherent feature of the $[CuCl_4]^{2-}$ ion itself.

Acknowledgement. The authors wish to thank cand. scient. L. Kryger, this department, for the program system used in data collection and data processing.

REFERENCES

1. Willett, R. D. and Chow, C. *Acta Crystallogr. B 30* (1974) 207.
2. Ferguson, G. L. and Zaslov, B. *Acta Crystallogr. B 27* (1971) 849.
3. Hodgson, D. J., Hale, P. K. and Hatfield, W. E. *Inorg. Chem. 10* (1971) 1061.
4. Lamotte-Brasseur, J., Dupond, L. and Dideberg, O. *Acta Crystallogr. B 29* (1973) 241.
5. Demuynck, J., Veillard, A. and Wahlgren, U. *J. Amer. Chem. Soc. 95* (1973) 5563.
6. Larsen, K. P. *Acta Chem. Scand. A 28* (1974) 194.
7. Harlow, R. L., Wells, W. J., III, Watt, G. W. and Simonsen, S. H. *Inorg. Chem. 13* (1974) 2106.
8. Raymond, K. N., Meek, D. W. and Ibers, J. A. *Inorg. Chem. 7* (1968) 1111.
9. Basolo, F. and Bailar, J. C. *J. Amer. Chem. Soc. 72* (1950) 2433.
10. Coppens, P. and Hamilton, W. C. *Acta Crystallogr. A 26* (1970) 71.
11. Cromer, D. T. and Mann, J. B. *Acta Crystallogr. A 24* (1968) 321.
12. Stewart, R. F., Davidson, E. R. and Simpson, W. T. *J. Chem. Phys. 42* (1965) 3175.
13. Kurnakoff, N. S. *Z. Anorg. Allg. Chem. 17* (1898) 207.
14. Mori, M. *Bull. Chem. Soc. Jap. 33* (1960) 985.
15. Johnson, C. K. *ORTEP* Report ORNL-3794, Oak Ridge National Laboratory, Oak Ridge 1965. Revised 1971, ORTEP II.
16. Busing, W. R., Martin, K. O. and Levy, H. A. *ORFFE* Report ORNL-TM 306, Oak Ridge National Laboratory, Oak Ridge 1964.
17. Atoji, H., Richardson, J. W. and Rundle, R. E. *J. Amer. Chem. Soc. 79* (1957) 3017.
18. Alderman, P. R. H., Owston, P. G. and Rowe, J. M. *Acta Crystallogr. 13* (1960) 149.
19. Milburn, G. H. W. and Truter, M. R. *J. Chem. Soc. A* (1966) 1609.
20. Anderson, J. S., Carmichael, J. W. and Cordes, A. W. *Inorg. Chem. 9* (1970) 143.
21. Keeton, M., Mason, R. and Russel, D. R. *J. Organometal Chem. 33* (1971) 259.
22. Liu, C. F. and Ibers, J. A. *Inorg. Chem. 9* (1970) 773.
23. Willet, R. D. *J. Chem. Phys. 44* (1966) 39.
24. Steadman, J. P. and Willet, R. D. *Inorg. Chim. Acta 4* (1970) 367.
25. Helmholz, L. and Kruh, R. F. *J. Amer. Chem. Soc. 74* (1952) 1176.
26. Morosin, B. and Lingafelter, E. C. *J. Phys. Chem. 65* (1961) 50.
27. Russel, J. H. and Wallwork, S. C. *Acta Crystallogr. B 25* (1969) 1691.
28. Bonamico, M., Dessy, G. and Vaciago, A. *Theor. Chim. Acta 7* (1967) 367.
29. Bonamartini, A., Nardelli, M., Palmieri, C. and Pelizzi, C. *Acta Crystallogr. B 27* (1970) 1775.
30. Ros, P., Van der Avoird, A. and Schuit, G. G. A. *Coord. Chem. Rev. 2* (1967) 77.
31. Lohr, L. L. and Lipscomb, W. N. *Inorg. Chem. 2* (1963) 911.
32. Felsenfeld, G. *Proc. Roy. Soc. A 236* (1956) 506.
33. McGinnety, J. A. *J. Amer. Chem. Soc. 94* (1972) 8406.

Received December 4, 1974.

Acta Chemica Scandinavica A 29 (1975) 505—512

The Oxidation of Thiosulfate by the Tetramminegold(III) Ion in Aqueous Solution

GWYNETH NORD, L. H. SKIBSTED* and A. S. HALONIN**

Chemistry Department I, Inorganic Chemistry, H. C. Ørsted Institute, University of Copenhagen, DK-2100 Copenhagen Ø, Denmark

The stoicheiometry of the oxidation of $S_2O_3^{2-}$ by $Au(NH_3)_4^{3+}$ in acid solution is

$$Au(NH_3)_4^{3+} + 4S_2O_3^{2-} + 4H^+ \rightarrow Au(S_2O_3)_2^{3-} + S_4O_6^{2-} + 4NH_4^+$$

Reaction kinetic and equilibrium studies of the above system are interpreted in terms of the following consecutive reactions:

$$Au(NH_3)_4^{3+} + S_2O_3^{2-} \xrightarrow[H^+]{k_s} Au(NH_3)_3S_2O_3^+ + NH_4^+$$

$$Au(NH_3)_3S_2O_3^+ + 2S_2O_3^{2-} \xrightarrow[H^+, H_2O]{\text{fast}} Au(S_2O_3)_3H_2O^{3-} + 3NH_4^+$$

$$Au(S_2O_3)_3H_2O^{3-} + S_2O_3^{2-} \xrightarrow{k_r} Au(S_2O_3)_2^{3-} + S_4O_6^{2-} + H_2O$$

$k_s = 195\ M^{-1}s^{-1}$, $\Delta H^{\neq} = 11.4$ kcal/mol at 25.0 °C and an ionic strength 1.0 M ($NaNO_3$).
$k_r = 1.5 \times 10^{-2}\ M^{-1}s^{-1}$, $\Delta H^{\neq} = 8.4$ kcal/mol at 25.0 °C in 0.333 M $Na_2S_2O_3$.

Changes in the rate of the reduction reaction in weakly alkaline solutions accord with the reactant being the weak acid $Au(S_2O_3)_3H_2O^{3-}$ with $pK_a = 9.96$ at 25.0 °C at an ionic strength of 1.0 M. This same reactant is produced by addition of $S_2O_3^{2-}$ to solutions prepared by dissolving $NaAuCl_4.2H_2O$ in water.

Complexes of Au(III) have been much less studied than have those of Pt(II)/which is the classic example of a square planar tetracoordinated d^8 configuration metal ion, because they are more labile and also because they are more strongly oxidising. The composition of solutions prepared from Au(III) complexes is often unknown — a consequence of the increased proton acidity of the hydrolysis products. We have chosen the $Au(NH_3)_4^{3+}$ cation as reactant because it was possible, using the recent work of Skibsted and Bjerrum,[1] to choose conditions where hydrolysis was negligible.

We found that the rate of substitution of NH_3 in $Au(NH_3)_4^{3+}$ by $S_2O_3^{2-}$ was amenable to study by stopped flow spectrophotometry and was much faster than the rate of oxidation of $S_2O_3^{2-}$ by the intermediate product, a thiosulfato Au(III) complex. It then became possible to deduce the composition of this intermediate, and thus the stoicheiometry of the consecutive reaction steps from the pH changes during the reactions together with the pH dependence of the reduction rate in a series of buffers. The reduction reactions are slow enough for measurement by conventional spectrophotometry.

The general rate law for substitution in complexes of Au(III) is also that well established for those of Pt(II),

$$\text{Rate} = k_1[\text{complex}] + k_2[\text{complex}][\text{substituent}] \quad (1)$$

where the first term represents solvent attack on the complex, the second term represents direct attack by the substituent, and the k_1 term is usually of much less importance for Au(III) than it is for Pt(II) complexes. The detailed mechanism of such reactions is generally accepted.[2,3] The subsequent reductions or "reductive elimination" [3] reactions,

* Chemistry Department, Royal Veterinary and Agricultural University, DK-1871 Copenhagen V, Denmark.
** On leave from Metallurgical Faculty, Kalinin's Polytechnical Institute, Leningrad, USSR.

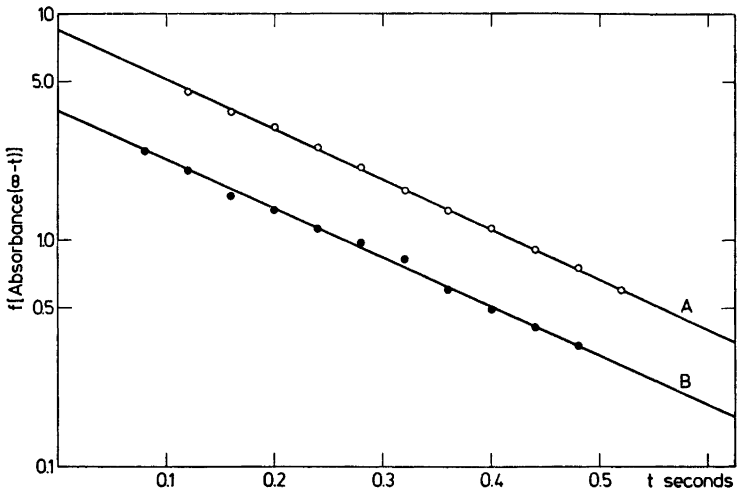

Fig. 1. Pseudo first order plots for the reaction

$$Au(NH_3)_4^{3+} + S_2O_3^{2-} \xrightarrow[H^+]{k_s} Au(NH_3)_3S_2O_3^{+} + NH_4^{+}$$

Plot of data read from stopped flow traces.
$\lambda = 480$ nm, $t = 25.0$ °C, ionic strength 1.0 M with $NaNO_3$.
A: $C_{Au(NH_3)_4^{3+}} = 1.13$ mM, $C_{S_2O_3^{2-}} = 0.025$ M, $C_{H^+} = 5.6$ mM.
B: $C_{Au(NH_3)_4^{3+}} = 0.55$ mM, $C_{S_2O_3^{2-}} = 0.025$ M, $C_{H^+} = 5.0$ mM.

analogous to that which occurs in the present system, have however been very little studied. In the present work we combine our results with those from one earlier investigation [4] which we find pertinent, and attempt to evaluate the usefulness of two alternative mechanisms as tools for predicting further definitive experiments.

EXPERIMENTAL

$[Au(NH_3)_4](NO_3)_3$ was prepared as in Ref. 1. All other chemicals were analytical grade. Water was doubly distilled in an all quartz apparatus. $Na_2S_2O_3$ solutions were used immediately after preparation.

The stopped flow apparatus was that described in Ref. 5 and the other measurements were made with a thermostatted Cary 14 recording spectrophotometer and with a digital pH meter (PH M 52 Radiometer) fitted with a glass electrode (Radiometer Type G202C).

All pH measurements and calculations were based on concentration standards in the actual media.

RESULTS

Substitution reaction. The rate of formation of the yellow-brown colour which appeared on mixing solutions of $[Au(NH_3)_4](NO_3)_3$ and of $Na_2S_2O_3$ was measured at 410 nm and at 480 nm by the stopped flow technique. The reaction was investigated in weakly acid

Table 1. Rate constant for the reaction [a]

$$Au(NH_3)_4^{3+} + S_2O_3^{2-} \xrightarrow[H^+]{k_s} Au(NH_3)_3S_2O_3^{+} + NH_4^{+}.$$

t °C	k_s $M^{-1}s^{-1}$	Number of runs
21.0	148 ± 5	3
25.0	195 ± 5	13[b]
30.0	272 ± 10	5

[a] C_{HNO_3} 5.0 to 7.0 mM. $C_{Au(NH_3)_4^{3+}}$ 0.55 to 1.13 mM. $C_{S_2O_3^{2-}}$ 0.025 to 0.050 M. Ionic strength 1.0 M, adjusted with $NaNO_3$. [b] Two pseudo first order plots are given in Fig. 1.

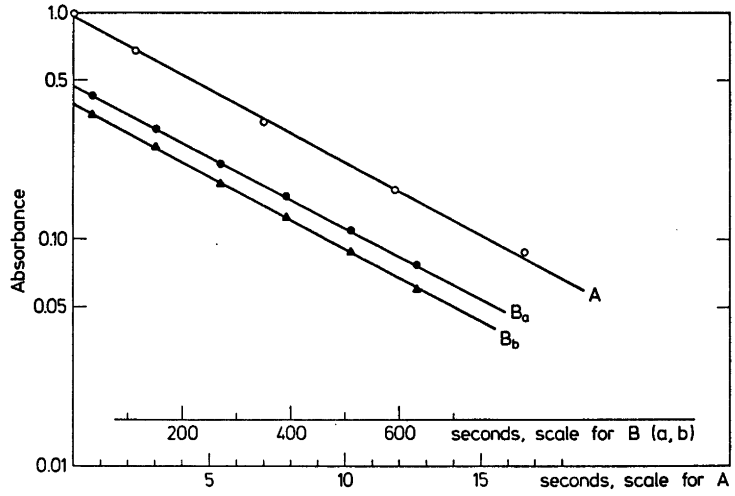

Fig. 2. Pseudo first order plots for the formation of $Au(S_2O_3)_2^{3-}$.
A: $C_{Au(NH_3)_4^{3+}} = 3.43$ mM, $C_{S_2O_3^{2-}} = 0.25$ M, pH = 10.75, $\lambda = 410$ nm, $t = 25.0$ °C, ionic strength 1.0 M with $NaNO_3$. Zero time in the plot corresponds to about five seconds after mixing.
B: $C_{Au(NH_3)_4^{3+}} = 8.57$ mM, $C_{S_2O_3^{2-}} = 0.10$ M, pH = 4.8, $t = 25.0$ °C, ionic strength 1.0 M with $NaNO_3$.
B_a: $\lambda = 410$ nm, B_b: $\lambda = 390$ nm.

Table 2. pH dependence of rate of formation of $Au(S_2O_3)_2^{3-}$. Ionic strength 1.0 M (Na_2SO_4), 25.0 °C.[a]

$C_{Au(NH_3)_4^{3+}}$ M	$C_{S_2O_3^{2-}}$ M	pH	$k_{obs} \times 10^3$ s^{-1}	pK_a
0.00111	0.200	3.90	2.96	
0.00111	0.200	4.53	3.06	
0.00111	0.200	4.86	3.00	
0.00111	0.200	5.52	2.96	
0.00111	0.200	6.97	3.20	(9.82)
0.00111	0.200	7.29	3.49	(9.78)
0.00111	0.200	8.30	6.62	9.94
0.00111	0.200	8.80	13.9	9.90
0.00111	0.200	8.88	15.4	9.91
0.00111	0.200	9.03	18.5	9.96
0.00111	0.200	9.10	20.1	9.98
0.00111	0.200	9.12	21.3	9.97
0.00444 [b]	0.167	9.88	71.2	9.94
0.00343 [b]	0.100	10.66	128	
0.00343 [b]	0.150	10.71	157	
0.00343 [b]	0.200	10.75	150	
0.00343 [b]	0.250	10.75	144	

[a] $pK_a = pH + \log(\alpha/(1-\alpha))$,

$$\alpha = \frac{[Au(S_2O_3)_3H_2O^{3-}]}{[Au(S_2O_3)_3H_2O^{3-}] + [Au(S_2O_3)_3OH^{4-}]} = (k_{obs} - k_b)/(k_a - k_b).$$

$10^3 k_b = 150$ s^{-1}; $10^3 k_a = 15[S_2O_3^{2-}]$ s^{-1}. [b] In 1.0 M $NaNO_3$.

Table 3. Rate laws used in interpretation of the rate of the reductive elimination reaction, *cf.* Scheme 1.[a]

$$-d([Au(S_2O_3)_3H_2O^{3-}]+[Au(S_2O_3)_3OH^{4-}])/dt = k_{obs}[Au(S_2O_3)_3H_2O^{3-}]$$

pH range studied	Rate law
3.9 – 6.5	$k_{obs} = k_a^{\circ} + k_a[S_2O_3^{2-}]$
7.0 – 9.9	$k_{obs} = \alpha k_a^{\circ} + \alpha k_a[S_2O_3^{2-}] + (1-\alpha)k_b$ $\alpha/(1-\alpha) = [H^+]/K_a$ $pK_a = 9.96 \pm 0.01$
10.6 – 10.8	$k_{obs} \approx k_b$

[a] Experimental values at 25.0 °C in 1.0 M medium:

$k_a^{\circ} = 2 \times 10^{-4}$ s^{-1} (corrected to 2nd order: 4×10^{-6} M^{-1} s^{-1}.)
$k_a = 1.5 \times 10^{-2}$ M^{-1} s^{-1}
$k_b = 0.15$ s^{-1} (corrected to 2nd order: 2.7×10^{-3} M^{-1} s^{-1}.)

Table 4. $C_{S_2O_3^{2-}}$ dependence of rate of formation of $Au(S_2O_3)_2^{3-}$ at constant pH near 9.0. Ionic strength 1.0 M with Na_2SO_4. 25.0 °C. $C_{Au(NH_3)_4^{3+}} = 1.11$ mM.[a]

$C_{S_2O_3^{2-}}$ M	pH	$10^3 k_{obs}$ s^{-1}	$10^3 k_{calc}$ s^{-1}
0.333	8.95	20.4	20.0
0.250	8.97	18.8	18.8
0.167	8.99	18.7	18.7
0.0833	9.01	17.6	17.7
0.0333	9.01	16.2	16.2

[a] $k_{calc} = \alpha(k_a^{\circ} + k_a[S_2O_3^{2-}]) + (1-\alpha)k_b$; $k_a^{\circ} = 2 \times 10^{-4}$ s^{-1}; $k_a = 1.5 \times 10^{-2}$ M^{-1}s^{-1}; $k_b = 0.15$ s^{-1}.

solution to ensure that the tetrammine and not an amido complex was the reactant. At thiosulfate/gold(III) ratios lower than 4 the product solutions gave a precipitate and were not investigated further. At ratios $\geqslant 4$, pseudo first order plots were linear throughout with no interference from the subsequent reduction (see Fig. 1).

The reaction was first order in each of the reactants and no solvent path corresponding to the k_1 term of eqn. 1 could be detected. We assume that reaction (2) is rate determining. This assumption is based on the known substitution behaviour of all similar complexes and is also the simplest way of interpreting the data.

$$Au(NH_3)_4^{3+} + S_2O_3^{2-} \xrightarrow[H^+]{k_s} Au(NH_3)_3S_2O_3^{+} + NH_4^{+} \quad (2)$$

The data for k_s in Table 1 give a good linear Arrhenius plot. From this, and using reaction rate theory, we calculate that $\Delta H^{\ddagger} = 11.4$ kcal/mol and $\Delta S^{\ddagger} = -10$ cal/mol K.

pH Measurements and stoicheiometry. The experiments were performed with different concentrations of nitric acid, the final pH ranging from 3 to 9. For the acid solutions pK_a of $HS_2O_3^-$ was taken as 1.01 in the 1 M media.[6] The pH of solutions of the substitution product was always found to be that calculated for liberation of all four ammonia molecules from the metal complex.

Reaction (2) is thus followed by

$$Au(NH_3)_3S_2O_3^{+} + 2S_2O_3^{2-} + H_2O \xrightarrow[H^+]{\text{fast}} Au(S_2O_3)_3H_2O^{3-} + 3NH_4^{+} \quad (3)$$

The visible spectrum of this intermediate product is a broad band, $\lambda_{max} \approx 410$ nm, $\varepsilon_{max} \approx 600$ cm^{-1} M^{-1}. The pH of all solutions remained constant during the fading of this yellow-brown colour which was used to follow the rate of the reductive elimination reaction. This confirmed negative tests for SO_4^{2-} and together with the presence of the colourless thermodynamically very stable[7] $Au(S_2O_3)_2^{3-}$ as a product gave the overall stoichiometry as

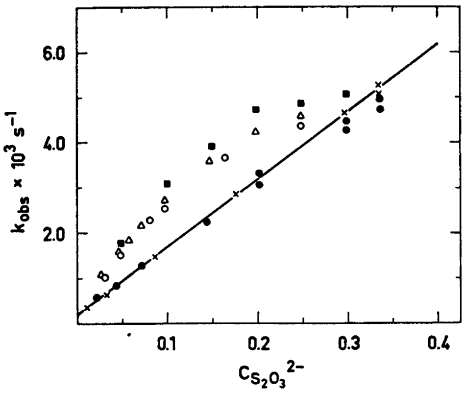

Fig. 3. Pseudo first order rate constants for the reductive elimination reaction

$$Au(S_2O_3)_3H_2O^{3-} + S_2O_3^{2-} \xrightarrow{k_{obs}} Au(S_2O_3)_2^{3-} + S_4O_6^{2-} + H_2O$$

at pH = 6.3 and 25.0 °C as a function of $C_{S_2O_3^{2-}}$. The reactant $Au(S_2O_3)_3H_2O^{3-}$ is produced from $Au(NH_3)_4^{3+}$ (●, ○, ■) or from $AuCl_n(OH)_m(H_2O)_{4-n-m}^{(3-n-m)+}$ (×, △). Ionic strength is in all experiments 1.0 M, adjusted with Na_2SO_4 (×, ●), $NaNO_3$ (△, ○) or with $NaClO_4$ (■). The straight line represents the experiments in the $Na_2(SO_4,S_2O_3)$ medium where C_{Na^+} as well as ionic strength are constant. All experiments with $C_{S_2O_3^{2-}} = 0.333$ M correspond to a pure $Na_2S_2O_3$ medium.

$$Au(NH_3)_4^{3+} + 4\ S_2O_3^{2-} \xrightarrow[H^+]{} Au(S_2O_3)_2^{3-} + 4\ NH_4^+ + S_4O_6^{2-}$$

Reductive elimination reaction. The rate of this reaction and the order in thiosulfate was found to be pH dependent, but was in all cases first order in complex. The kinetic experiments were performed with excess of thiosulfate giving experimental first or pseudo first order conditions (see Fig. 2). The reaction was followed at each 10 nm in the wavelength range 370 to 450 nm and no wavelength dependence on rate was found. The compositions of some of the solutions together with the pseudo first order rate constants are given in Tables 2 and 4. The pH of the solutions was adjusted either with nitric acid or with small concentrations of ammonium nitrate and ammonia, potassium hydrogen phthalate, sodium hydrogen orthophosphate, borax, or sodium acetate and acetic acid, buffers. The pH of the reaction mixture was measured in all experiments. The buffer component did not affect the rates.

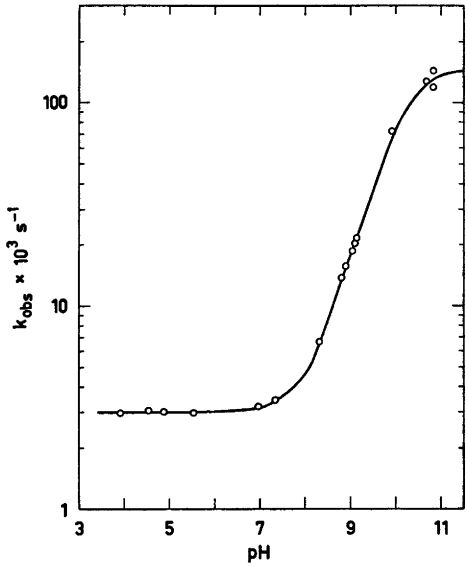

Fig. 4. pH dependence of rate of formation of $Au(S_2O_3)_2^{3-}$ at ionic strength 1.0 M and 25.0 °C. Experimental points from Table 2. Calculated line from rate laws given in Table 3.

The rate of reduction is independent of hydrogen ion concentration in the pH range 3 to 6.5. Below pH ~ 3 the decomposition of thiosulfate excludes further investigation. Fig. 3 gives the pseudo first order constants at 25.0 °C and ionic strength 1.0 M with pH adjusted to 6.3 as a function of thiosulfate concentration. Salt effects are large, but in a

Table 5. Temperature dependence of the reductive elimination reaction

$$Au(S_2O_3)_3H_2O^{3-} + S_2O_3^{2-} \rightarrow Au(S_2O_3)_2^{3-} + S_4O_6^{2-} + H_2O$$

Experiments under pseudo first order conditions in 0.333 M $Na_2S_2O_3$ at pH = 6.3. $C_{Au(NH_3)_4^{3+}} = 1.20$ mM.

t °C	k_{obs} $s^{-1} \times 10^3$
19.5	3.37
21.7	3.76
24.2	4.44
26.2	4.92
28.0	5.42
31.1	6.30
34.4	7.02

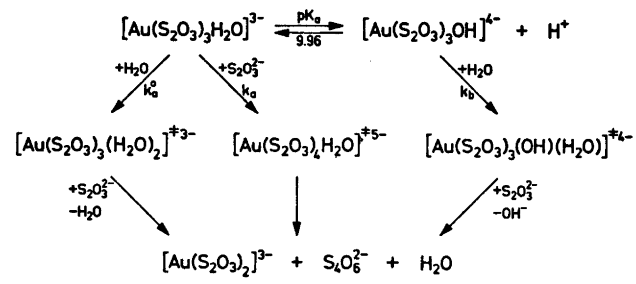

Scheme 1.

sodium sulfate thiosulfate medium where the ionic strength as well as the sodium ion concentration are constant the reactions are first order in both complex and (excess) thiosulfate. Fig. 3 also illustrates that the same behaviour is found with solutions prepared from $NaAuCl_4$ and thiosulfate. It should be noted that as the $AuCl_4^-$ is hydrolysed in water, the aquo thiosulfato gold(III) reactant is, in these solutions, produced by substitution of $S_2O_3^{2-}$ in $AuCl_n(OH)_m(H_2O)_{4-n-m}^{(3-n-m)+}$ complexes.*

Fig. 4 is a semilogarithmic plot of the pH profile for the observed rate of reduction at constant thiosulfate concentration. At the highest pH studied (10.60 – 10.75) there is a limiting rate, within experimental error independent of thiosulfate concentration. The pH dependence and the dependence on thiosulfate concentration on the observed rate fit the rate law given in Table 3. Table 4 illustrates the accuracy with which the thiosulfate dependence at intermediate and constant pH can be reproduced. The activation parameters for the k_a path (see Tables 3 and 5 and Scheme 1) in 0.333 M $Na_2S_2O_3$ are: $\Delta H^{\ddagger} = 8.4$ kcal/mol, $\Delta S^{\ddagger} = -46$ cal/mol K. In calculating these we did not correct for the effect of the small, poorly defined, intercept in Fig. 3.

*Preliminary experiments with $NaAuCl_4$ in weakly acid 1 M NaCl and with $KAuBr_4$ in weakly acid 1 M NaBr, where the gold(III) is almost exclusively present as the tetrahalogenidoaurate(III) ion, showed that reduction is rapid and that no intermediate yellowbrown thiosulfato gold(III) complex was detectable.

In completely hydrolysed gold(III) solutions where $Au(OH)_4^-$ and polymers dominate, we find that the rate of substitution of the first thiosulfate is of the same order of magnitude as the reductive elimination.

DISCUSSION

The rate of substitution of NH_3 in $Au(NH_3)_4^{3+}$ by $S_2O_3^{2-}$ is much faster than is the solvent substitution. This is in accordance with the well known increased nucleophilic character of the substitution. The bimolecular substitution can be supposed to take place through a five coordinate trigonal bipyramidal reactive complex as suggested for other d^8 systems. The rate and activation parameters for this reaction thus supplement the rather sparse earlier data for cationic Au(III) complexes.

The mechanism of the reductive elimination reaction is more speculative in that, firstly, measurements could only be made in an excess of $S_2O_3^{2-}$ so that the composition of the reactant complex could not be directly determined and secondly, it cannot be assumed that the reaction path for reductive elimination is analogous to that for substitution.

We believe that the reactant is $Au(S_2O_3)_3H_2O^{3-}$ on the following grounds.

From the lack of pH change during reduction

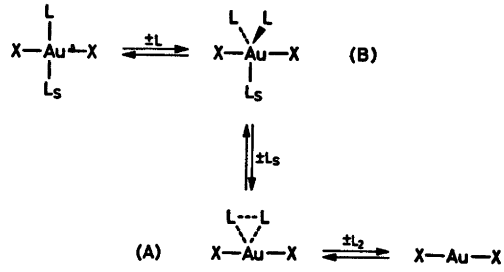

Fig. 5. Mechanism 1: Three centred AuL_3 and a trigonal bipyramid. Would explain:
1. The gold(III) – thiosulfate reaction. $L_s = H_2O$, $X = L = S_2O_3^{2-}$.
2. The iodide catalysed formation of *trans*-$Au(CN)_2I_2^-$. $X = CN^-$, $L = L_s = I^-$.

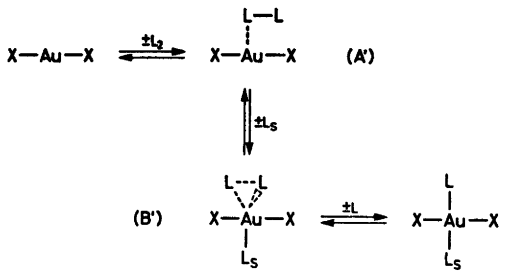

Fig. 6. Mechanism 2: Oxidation is attack on electron pair of Au(I) by L_2; back reaction is attack by L^- on L coordinated to Au(III). Would explain *trans* product and solvent dependence of $Au(CN)_2I_2^-$ formation and, for $L_S = I^-$, also the I^- catalysed path. For the thiosulfate reduction this means rate determining attack by $S_2O_3^{2-}$ on coordinated $S_2O_3^{2-}$.

and the initial pH changes before reduction then no NH_3 is present. This is confirmed by the fact that the same species is produced from chlorohydroxo Au(III) complexes.

Changes in the rate of reduction with pH show that the reactant is a weak acid, $pK_a = 9.96$. We think that the alternative formulation as $Au(S_2O_3)_4H^{4-}$ is (in view of the strength [6] of uncomplexed $HS_2O_3^-$) very unlikely and that, therefore, the acid ligand is a water molecule. The reduction rate in acid solution is first order in $[S_2O_3^{2-}]$ and the overall stoicheiometry $4S_2O_3^{2-} + 1Au(III)$. From the charge repulsion of the reactants successive additions of $S_2O_3^{2-}$ should proceed with progressively slower rates unless other factors are involved.

The following extra experimental facts are in accord with this interpretation, but are not definitive. Thus, the kinetic ionic strength effect is large and positive but the media used are outside the theoretically predictable range. Similarly, the large negative $\Delta S^{\neq}$ and the large kinetic specific Na^+ effect also would be expected but cannot be used quantitatively.

Our interpretation of the reaction paths necessary to explain the complete reduction rates is given in Scheme 1.

Experimental data such as that reported here, and for one system alone, cannot profitably be used to deduce the detailed mechanism of the reductive elimination. We find, however, that one other Au(III) – Au(I) system has been subjected to detailed study and discuss this below, together with our results, chiefly in order to attempt to define the problems needing to be solved and to suggest experiments which may aid in the solution of these problems.

Ford-Smith *et al.*[4] studied the oxidative-*addition* reaction $Au(CN)_2^- + I_2 \rightarrow$ *trans*-$Au(CN)_2I_2^-$ and found the following two term rate law:

$$d[Au(CN)_2I_2^-]/dt = k_2[Au(CN)_2^-][I_2] + k_3[Au(CN)_2^-][I_2][I^-]$$

They also found that the rate of reduction of $Au(CN)_2I_2^-$ is dependent on [X] where X is an organic substance known to react with I_2. We suggest that either of the following two mechanisms depicted in Figs. 5 and 6 which incorporate ideas of earlier workers [2,3] for similar reactions of metal complexes but involving a $d^6 - d^8$ electronic configuration change, could explain the above limited data presently available for $d^8 - d^{10}$ complexes.

In Fig. 5 (Mechanism I) the formation of a three centred AuL_2 and a trigonal bipyramid would explain

1. the $Au(III) - S_2O_3^{2-}$ reaction, $L_S = H_2O$, $X = L = S_2O_3^{2-}$;
2. the I^- catalysed formation of *trans*-$Au(CN)_2I_2^-$, $X = CN^-$, $L = I^-$.

In Fig. 6 (Mechanism II) oxidation occurs by attack on an electron pair of Au(I) by L_2 while the back reaction is attack by L^- on L coordinated to Au(III). This would explain *trans*-product and solvent dependence of $Au(CN)_2I_2^-$ formation, and, for $L_S = I^-$, also the I^- catalysed path. For the thiosulfate reduction this means rate determining attack by $S_2O_3^{2-}$ on the S atom of the coordinated $S_2O_3^{2-}$. Whether such direct attack on the coordinated S of the ligand does occur may possibly be tested experimentally by examining the magnitude of the changes in activation enthalpy with changes of the coordinated axial ligands. The present work does show, however, that when these axial ligands are Cl^- or NH_3 then no reduction occurs. Direct attack on coordinated S would thus be less than the substitution rate. The trigonal bipyramidal intermediate of the substitution reaction is included in both mechanisms. The linear

X–Au–X group remains effectively unchanged during the reactions. It would seem probable that the extent to which the transition state for the rate determining step resembles the extreme forms B and A′ (in Figs. 5 and 6) depends on the degree of metal bonding to the extra ligand depicted in Figs. 5 and 6 as L_s.

We have confined the above discussion to the two reactions giving the rate constants (k_s and k_a in tables) which we have studied in detail and over a range of temperature. The reduction reaction of the conjugate base will be the subject of a further study.

REFERENCES

1. Skibsted, L. H. and Bjerrum, J. *Acta Chem. Scand. A 28* (1974) 740.
2. Basolo, F. and Pearson, R. G. *Mechanisms of Inorganic Reactions*, 2nd Ed., Wiley, New York 1967.
3. Cattalini, L. In Emeléus, H. J., Ed., *M. T. P. International Review of Science. Inorganic Chemistry, 9*, Butterworth, London 1972, p. 269.
4. Ford-Smith, M. H., Habeeb, J. J. and Rawsthorne, J. H. *J. Chem. Soc. Dalton Trans.* (1972) 2116.
5. Nord, G. and Wernberg, O. *J. Chem. Soc. Dalton Trans.* (1972) 867.
6. Page, F. M. *J. Chem. Soc.* (1953) 1719.
7. Pouradier, J. and M.-C. Gadet. *J. Chim. Phys. 66* (1969) 109.

Received December 18, 1974.

Acta Chemica Scandinavica A 29 (1975) 513—516

On the Structure of Gaseous 3-Bromotetrahydrofuran

Z. SMITH,[a] H. M. SEIP,[a] B. NAHLOVSKY [b] and D. A. KOHL [b]

[a] Department of Chemistry, University of Oslo, Oslo 3, Norway and [b] Department of Chemistry, The University of Texas at Austin, Austin, Texas 78712, U.S.A.

Gaseous 3-bromotetrahydrofuran has been studied by electron diffraction and its conformational energies have been calculated by the Westheimer-Hendrickson method. The best agreement between theoretical and experimental electron diffraction data is obtained when one assumes that the ring undergoes nearly free pseudorotation. The bond distances (r_a) and standard deviations determined are: r(CO) = 1.428(0.005) Å, r(CC) = 1.527(0.008) Å, and r(CBr) = 1.954(0.008) Å. The low energy difference between different conformations, calculated to be about 0.5 kcal mol^{-1}, confirms the results obtained by electron diffraction.

In the previous papers of this series [1-6] the influence of heteroatoms on the pseudorotation of five-membered saturated rings was studied. It appeared that a heteroatom in the ring tends to restrict the ring pseudorotation and to stabilize the conformation with C_2 symmetry, the effect increasing with the size of the heteroatom.

Several studies have been made [7-9] to determine the effect of halogens on the conformational arrangement of the five-membered rings. Reisse *et al.*[7] calculated the barrier for pseudorotation of chloro- and bromocyclopentane to be only 1.1 kcal mol^{-1} which would allow the presence of all pseudorotational conformations in the gas and liquid phases. From a temperature study of the Raman spectra, Durig *et al.*[8] estimated the enthalpy difference between the axial and the equatorial orientations of the halogen atom in chloro- and bromocyclopentane to be 0.34 and 0.61 kcal mol^{-1}, respectively. From an IR study [8] they concluded that both molecules exist in a mixture of the different conformers and suggested that the barrier to pseudorotation is smaller than 4 kcal mol^{-1}. 3-Halotetrahydrofurans,[9] however, were reported to be less flexible, despite the fact that tetrahydrofuran itself undergoes pseudorotation. Buys *et al.*[9] interpreted infrared spectra and dipole-moment measurements of 3-halotet-

Table 1. Structural parameters with standard deviations referring to the last digit given for 3-bromotetrahydrofuran.[a]

Distances	r^b (Å)	u (Å)
C—O	1.428 (5)	0.040 (5)
C—C	1.527 (8)	0.045 (5)
C—Br	1.954 (8)	0.052 (5)
C—H	1.105 (8)	0.080 (8)

[a] Standard deviations include estimate of systematic errors. [b] r_a values.[13]

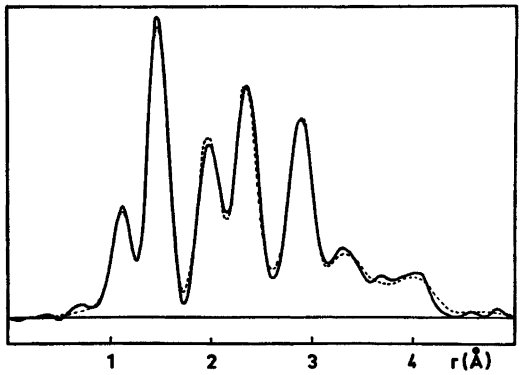

Fig. 1. The experimental (———) and calculated (— — —) radial distribution function for 3-bromotetrahydrofuran (data in the s-ranges 2.0—15.5 Å^{-1} and 7.0—30.0 Å^{-1} were used for nozzle-to-plate distance of 50 cm and 25 cm, respectively). The damping constant used was $k = 0.0015$ Å^2. The calculated radial distribution function for model 6 (see text for definition) was used.

Table 2. Conformational energies E (in kcal mol^{-1}) and the corresponding angle parameters (in degrees) in 3-bromotetrahydrofuran. Constants used in the calculations: (k is given in kcal mol^{-1} degree^{-2} and V° in kcal mol^{-1}). Bond distances: $r(C-O)=1.428$ Å, $r(C-C)=1.527$ Å, $r(C-Br)=1.951$ Å, $r(C-H)=1.10$ Å, $\angle HCBr=107°$, and $\angle HCH=110°$. $\theta^{\circ}_{COC}=109°$, $\theta^{\circ}_{OCC}=\theta^{\circ}_{CCC}=112°$; $k_{COC}=k_{OCC}=k_{CCC}=0.030$, $k_{CC(Br)C}=0.035$; $V^{\circ}_{CO}=2.0$, $V^{\circ}_{CC}=2.9$; $V^{\circ}_{CC(Br)}=3.1$ (Set I),[14] $V^{\circ}_{CC(Br)}=3.6$ (Set II).[15]

Δ[a]	Set I $\angle C_5O_1C_5$	$\angle O_1C_2C_3$	$\angle C_2C_3C_4$	$\phi(O_1-C_2)$	$\phi(O_1-C_5)$	E	Set II E
0	108.0	107.2	101.2	12.5	13.0	9.57	9.97
36	107.8	107.9	102.1	0.5	24.0	9.67	10.21
72	107.0	108.0	103.2	−12.5	34.0	9.78	10.50
108	105.9	107.7	103.9	−22.6	40.0	9.87	10.77
144	105.1	105.5	104.9	−36.5	44.0[b]	9.94	10.89
180	103.5	104.7	104.0	−43.0	43.0[b]	9.85	10.73
216	104.2	103.7	103.3	−43.5	35.0	9.72	10.40
252	105.6	103.5	102.2	−40.5	25.0	9.65	10.11
288	106.9	104.2	101.2	−34.1	13.0	9.60	9.96
324	107.7	105.5	100.8	−24.8	0.0	9.55	9.89
360	107.9	106.7	101.2	−13.3	−13.0	9.55	9.93
396	107.7	107.3	101.9	−4.0	−22.0	9.61	10.16
432	106.9	107.7	103.2	11.1	−34.0	9.80	10.55
468	105.9	107.6	103.9	21.5	−40.0	9.93	10.83
504	104.0	106.0	104.9	36.0	−45.0[b]	10.00	10.89
540	103.2	104.6	104.0	43.0	−42.0	9.82	10.77
576	104.2	103.8	103.2	43.6	−35.0	9.69	10.37
612	105.6	103.7	102.1	40.4	−25.0	9.60	10.07
648	106.9	104.5	101.1	33.9	−13.0	9.54	9.91
684	107.7	105.8	100.7	24.4	0.0	9.52	9.87

[a] Approximate phase angle of pseudorotation. [b] Not optimized.

rahydrofurans in the liquid phase as favouring the presence of only one conformer, the halogen atom being in an axial position on the most puckered part of the ring.

Due to the presence of the bromine, which is a strong scatterer, one would expect the possible multiple conformers in 3-bromotetrahydrofuran to be detectable by electron diffraction. Therefore an investigation of this compound was undertaken, and the electron-diffraction study was complemented by calculations (Westheimer-Hendrickson method) of the conformational energies and by recording IR spectra. The nozzle temperature was about 75 °C; further experimental details are given in Ref. 10.

Altona *et al.*[9,11] have described the pseudorotation by

$$\phi_j=\phi_m \cos(\Delta/2+j\times 144°),\ j=0,\ 1,\ 2,\ 3,\ 4$$

where ϕ_j is the torsional angle around the j-th bond in the ring, ϕ_m is a constant equal to the maximum possible torsional angle, and Δ is called "the phase angle of pseudorotation" (see also Ref. 12). In order to estimate the barrier to pseudorotation, the energy of the conformer as a function of the phase angle must be calculated. The phase angle increment chosen was 36°, and the modified Westheimer-Hendrickson method [1] was used to calculate the conformation energies. The bond lengths were obtained from this electron-diffraction experiment (see Table 1). The planes through the atoms HCH and HCBr were assumed to be perpendicular to the planes through XCC (where X is O or C) and to bisect the XCC angle. Dipole-dipole interactions were not included in the calculations since the effect was expected to be small.

The conformational energies were calculated for two sets of parameters and the differences between maxima and minima were about 0.5 kcal mol^{-1} in set I and 1.0 kcal mol^{-1} in set II (see Table 2). In both sets the minima were found at phase angles 324 and 684°, both conformers having "nearly" C_s symmetry (neglecting the difference between CH_2 and O) with the "plane of symmetry" passing through

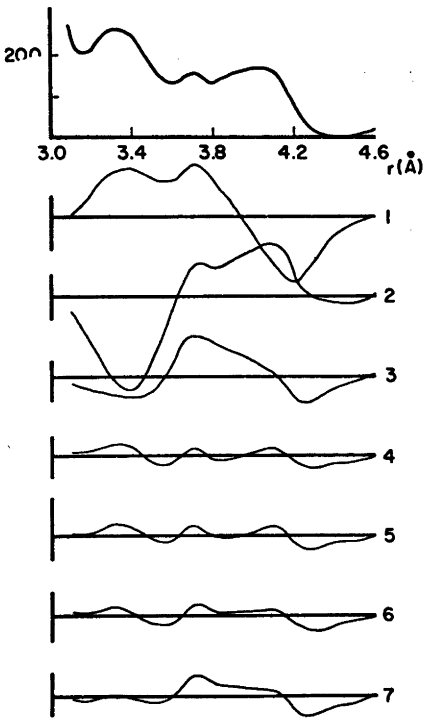

Fig. 2. Comparison of the experimental and calculated radial distribution functions in the region which exhibits the conformational effects. The top curve is the experimental function, the lower curves are differences between experimental and theoretical curves. The numbers correspond to the models defined in the text.

the carbon atom to which the bromine is bonded. The bromine is in the equatorial position at 324° and axial position at 684°. At both maxima the ring has "nearly" C_2 symmetry, with the axis of symmetry passing through the brominated carbon. The results of these calculations show that the most favourable conformations are those with maximum puckering on the brominated carbon. When the puckering moves away from this carbon the energy of the conformers increases until it reaches a maximum when the puckering is on the opposite side of the ring.

Buys *et al.*[9] calculated the barrier to be considerably higher, 2.9 kcal mol^{-1}, considering only torsional energy contributions. These authors [9] used a value for the barrier to rotation of $V^{\circ}_{CO} = 1.07$ kcal mol^{-1} in comparison to 2.00 kcal mol^{-1} used in the present calculations and also kept the maximum torsional angle constant at 39°, while in this work all torsional angles were varied. As can be seen from the calculations,[10] the contributions of the bending energy have just the opposite trend from the torsional energy, and this tends to cancel the energy differences between the conformations.

The experimental radial distribution function is shown in Fig. 1 (the solid line). All bond angles and torsional angles in the ring constantly change so that any refinement of angles from electron-diffraction data is impossible. Except for the bond lengths and amplitudes of vibrations, all of the structural parameters for different models were obtained from the calculations. These models were used to construct radial distribution functions for comparison with the experimental function. The agreement for the outer part of the radial distribution function, which is most sensitive to the conformational arrangement, is shown in Fig. 2 for the following models:

1. The conformation with a phase angle of 324° of set I, which corresponds to a minimum on the potential curve.
2. The conformation with a phase angle 684° of set I, which corresponds to a minimum on the potential curve,
3. The 1:1 mixture of models 1 and 2.
4. An equally-weighted mixture of all 20 conformers with parameters from set I.
5. An equally-weighted mixture of all 20 conformers with parameters from set II.

6,7. A mixture of all 20 conformers, each conformer weighted by the Boltzmann factor $f_i = \exp(E_{min} - E_i)/RT$, where E_i is the energy of i-th conformer, E_{min} is the energy minimum, R is the gas constant, and T is the temperature. Model 6 uses the angles and energies of set I, model 7 of set II.

From Fig. 2 one can see that the best agreement between the experimental and the calculated radial distribution functions is obtained with models 4, 5, and 6. The radial distribution function for model 6 is shown in Fig. 1 (dashed line).

Despite the lack of perfect agreement between the calculated and experimental molecular intensity, it is clear that 3-bromotetra-

hydrofuran undergoes hindered pseudorotation. The location of the bromine and the barrier to pseudorotation are less certain, but it appears that bromine prefers to be on the puckered part of the ring and that the barrier is about 0.5 kcal mol^{-1}.

The electron diffraction results are contradictory to those reported in the IR and Raman study of liquid 3-halotetrahydrofurans;[9] IR spectra of *gaseous* 3-bromotetrahydrofuran were therefore recorded at three different temperatures, namely 72, 85, and 105 °C. The C-Br stretching frequencies for the axial and the equatorial bromine were previously assigned to 535 and 728 cm^{-1}, respectively. The infrared spectra of the gaseous sample showed the presence of both bands with the intensity of the peaks about equal. This is consistent with a small energy difference between the two forms having equatorial and axial bromine. However, two peaks would also be consistent with the picture of free or slightly-hindered interchange of conformations by pseudorotation in the gas-phase.

Acknowledgement. We are indebted to Mr. K. Brendhaugen for recording the diffraction patterns. We wish to thank the Robert A. Welch Foundation and the Norwegian Research Council for Science and the Humanities for financial support.

REFERENCES

1. Seip, H. M. *Acta Chem. Scand. 23* (1969) 2741.
2. Almenningen, A., Seip, H. M. and Willadsen, T. *Acta Chem. Scand. 23* (1969) 2748.
3. Almenningen, A., Kolsaker, P., Seip, H. M. and Willadsen, T. *Acta Chem. Scand. 23* (1969) 3398.
4. Nahlovska, Z., Nahlovsky, B. and Seip, H. M. *Acta Chem. Scand. 23* (1969) 3534.
5. Nahlovska, Z., Nahlovsky, B. and Seip, H. M. *Acta Chem. Scand. 24* (1970) 1903.
6. Seip, H. M. *J. Chem. Phys. 54* (1971) 440.
7. Reisse, J., Nagels, L. and Chiurdoglu, G. *Bull. Soc. Chim. Belges 74* (1965) 162.
8. Harris, W. C., Karriker, J. M. and Durig, J. R. *J. Mol. Struct. 9* (1971) 139.
9. Buys, H. R., Altona, C. and Havinga, E. *Tetrahedron 24* (1968) 3019.
10. Smith, Z. *Dissertation*, The Univ. of Texas at Austin 1973.
11. Altona, C., Geise, H. J. and Romers, C. *Tetrahedron 24* (1968) 13.
12. Bastiansen, O., Seip, H. M. and Boggs, J. E. In Dunitz, J. D. and Ibers, J. A., Eds., *Perspectives in Structural Chemistry*, Wiley, New York 1971, Vol. IV.
13. Kuchitsu, K. *Bull Chem. Soc. Jap. 40* (1967) 498.
14. Scott, R. A. and Scheraga, H. A. *J. Chem. Phys. 42* (1965) 2209.
15. Lide, D. R. *J. Chem. Phys. 30* (1959) 37.

Received December 19, 1974.

Acta Chemica Scandinavica A 29 (1975) 517—522

The Crystal Structure of Bis(*o*-nitrobenzeneselenenyl) Sulfide

ROLF ERIKSEN*

Chemical Institute, University of Bergen, N-5000 Bergen, Norway

Bis(*o*-nitrobenzeneselenenyl) sulfide, $C_{12}H_8N_2O_4SSe_2$ is known to occur as monoclinic and orthorhombic crystals. The modification investigated here crystallizes in the orthorhombic space group $P2_12_12$ (No. 18), with $a = 13.809(5)$ Å, $b = 12.298(4)$ Å, $c = 4.196(2)$ Å. There are two formula units per unit cell. The sulfur atom is situated on a two-fold axis. The two symmetrically related halves of the molecule are nearly planar. The divalent selenium atom of each half molecule occurs as the central atom in a practically planar three-coordinated system, with sulfur and oxygen as *trans* ligand atoms and a benzene carbon atom as the third ligand atom. The bond lengths from the selenium atom to the sulfur, oxygen, and carbon atoms are 2.202(2), 2.574(8), and 1.918(8) Å, respectively. A loose five-membred ring is thus formed by the selenium atom, two carbon atoms of the benzene ring and the nitrogen atom and one oxygen atom of the nitro group.

The investigated bis-(*o*-nitrobenzeneselenenyl) sulfide (I) was prepared by a conversion of a thiourea adduct of *o*-nitrobenzeneselenenyl thiocyanate (II). The structure of the latter compound has been solved,[1] and the conversion procedure described earlier.[2] The *o*-nitrobenzeneselenenyl-sulfur system occurs in both compounds and the present structure determination was undertaken in order to collect more information about this system, with special regard to the coordination around selenium.

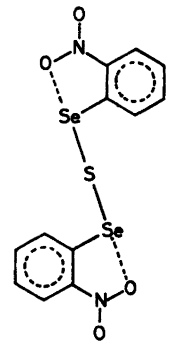

I

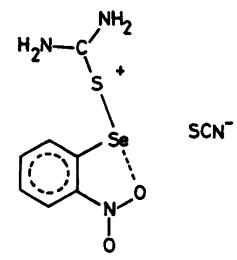

II

EXPERIMENTAL

The space group and preliminary cell dimensions were determined from Weissenberg photographs.[2] Final cell dimensions were obtained by a least squares treatment of the θ-settings of 18 reflections on the diffractometer, a Siemens automatic, offline, single-crystal diffractometer (AED-1). Nb-filtered Mo$K\alpha$ radiation was used ($\lambda = 0.70926$ Å). Density was determined by flotation in a $ZnCl_2$ solution.

Crystal data.

$C_{12}H_8N_2O_4SSe_2$, molecular weight 434.19.

Cell dimensions: $a = 13.809(5)$ Å, $b = 12.298(4)$ Å, $c = 4.196(2)$ Å, $V = 712.5$ Å^3.

Space group $P2_12_12$ (from systematic absences).

$Z = 2$.

Density, calc. 2.02, found 2.01 g/cm^3.

$\mu = 57.45$ cm^{-1}.

* Present address: Department of Biochemistry, University of Bergen, N-5000 Bergen, Norway.

Intensity values for 1049 unique reflections with $\theta < 28°$ were collected with a scintillation counter, by scanning with $\theta - 2\theta$-technique. The peaks were scanned twice between $\theta - 0.27° - 0.15°\text{tg}\ \theta$ and $\theta + 0.25° + 0.25°\text{tg}\ \theta$, starting at the Bragg angle θ. The scanning speed for each reflection was selected such that it gave all sufficiently high intensities approximately the same accuracy. The background intensity was measured on both sides of each peak, the counting time being equal to the scanning time. None of the reflections were strong enough to make attenuation necessary.

With a maximum measuring time set to 0.24 s per 0.01°, 147 of the possible reflections were coded unobserved, *i.e.* $I_t - I_b < 2\sqrt{I_t + I_b}$. Here I_t and I_b are the total count numbers of the scan and the background, respectively.

Two reference reflections were measured after every 50 reflections and the intervening periods thus became 2 – 3 h. The intensities showed a general decrease of about 16 % during the period of data collection. A more random fluctuation was superimposed on this tendency, resulting in a maximum variation of 4 % for two subsequent reference measurements. In order to obtain the data on a common scale each intensity value was multiplied with a scale factor which was a linear function of the time between the reference measurements, and which brought all the reference intensities to the same initial value.

The crystal used for data collection was prism-formed. From an arbitrarily chosen origin to the faces, the crystal had the following dimensions: to (100) and ($\bar{1}00$): 0.0405 mm, to ($\bar{1}10$) and ($1\bar{1}0$): 0.0410 mm, to (230) and ($\bar{2}\bar{3}0$): 0.0412 mm, to (001) and ($00\bar{1}$): 0.0700 mm. The observed intensities were corrected for absorption by the method of Coppens *et al.*[3] Subdivisions of 4, 6, and 10 Gaussian points were used along the *a*, *b*, and *c* axes, respectively.

The intensity values were given weights, W, according to the formula $W = (I_t - I_b)^2/[(I_t + I_b) + k^2(I_t - I_b)^2]$, were $k = 0.08$ is the estimated relative standard deviation in the time-dependent scale factor described above. These weights were used in the refinement of atomic positions and temperature factors by a full-matrix least squares procedure. The function minimized was $r - W(|F_o| - K|F_c|)^2$, where K is a scale factor. The unobserved reflections were included in the refinement when the scaled, calculated structure factors exceeded the limiting value. In such cases F_o was given a value equal to the limit.

Atomic scattering factors for all elements except hydrogen were taken from the *International Tables*.[4] The scattering factors for selenium and sulfur were adjusted with the real part of the anomalous dispersion correction term using the values for $\Delta f'$ given by Cromer.[5] The scattering factors published by Stewart *et al.* were used for hydrogen.[6]

The calculations were carried out on an IBM 360/50 H computer, except for the plotting procedures, for which a UNIVAC 1110 was used. Both machines were at the University of Bergen. The program used for the least squares procedure was made available by the Chemical Department of X-Ray Crystallography, Weizmann Institute of Science, Rehovoth, Israel, and modified for use on the IBM computer by Dr. D. Rabinowitch. The illustrations were plotted by means of the program OR TEP.[7] The remaining programs were written by K. Åse and K. Maartman-Moe of the Chemical Institute, University of Bergen.

STRUCTURE DETERMINATION

The space group $P2_12_12$ requires that the sulfur atom lies on a two-fold axis. Approximate values for the sulfur z-coordinate and the selenium coordinates were found from a Patterson synthesis. These values gave phase to 133 reflections used in a subsequent three-dimentional Fourier synthesis. This established the position of one oxygen atom. Two successive sequences of one refinement cycle of atomic positions followed by Fourier synthesis revealed the positions of all atoms except hydrogen. Refinement of these positions and isotropic temperature factors brought the reliability index $R = \sum||F_o| - |F_o||/\sum|F_o|$ down to 0.12. Introducing anisotropic temperature factors for the sulfur and selenium atoms and re-

Table 1. Fractional coordinates with standard deviations from least squares in parantheses.

	x	y	z
Se	0.13059(7)	0.02220(7)	0.0617(3)
S	0.00000	0.00000	0.3558(8)
C_1	0.1207(6)	0.1723(6)	−0.058(3)
C_2	0.1901(6)	0.2228(8)	−0.248(3)
C_3	0.1831(9)	0.3301(9)	−0.347(4)
C_4	0.1043(8)	0.3899(8)	−0.260(3)
C_5	0.3346(7)	0.3424(8)	−0.065(4)
C_6	0.0405(7)	0.2359(7)	0.016(3)
N	0.2776(6)	0.1636(7)	−0.340(2)
O_1	0.2884(5)	0.0714(6)	−0.231(2)
O_2	0.3353(6)	0.2069(7)	−0.517(3)
H_1	0.225(9)	0.355(9)	−0.49(4)
H_2	0.093(6)	0.466(8)	−0.35(2)
H_3	−0.011(7)	0.389(7)	0.00(2)
H_4	−0.004(6)	0.206(7)	0.14(2)

Table 2. Thermal parameters (Å²) with their standard deviations in parentheses. Anisotropic temperature factors are given by the form $\exp[-2\pi^2(U_{11}h^2a^{*2}+\cdots+2U_{12}hka^*b^*+\cdots)]$ and isotropic temperature factors by the form $\exp(-8\pi^2U\sin^2\theta/\lambda^2)$. The parameters for non-hydrogen atoms are multiplied by 10^3, those for hydrogen atoms by 10^2.

	U_{11}	U_{22}	U_{33}	U_{12}	U_{23}	U_{13}
Se	42.4(5)	34.3(4)	54.4(6)	3.1(4)	1.8(5)	4.8(5)
S	58(2)	45(2)	40(2)	−9(2)	—	—
C_1	31(4)	35(4)	52(6)	−3(4)	−7(5)	0(6)
C_2	30(5)	40(5)	62(7)	−3(4)	−10(6)	−6(5)
C_3	55(7)	44(6)	66(10)	−19(5)	−8(6)	10(6)
C_4	60(7)	33(5)	80(9)	1(5)	3(6)	−9(7)
C_5	47(6)	40(5)	71(8)	8(5)	−6(7)	11(6)
C_6	37(5)	40(5)	57(8)	−2(4)	−1(6)	−1(5)
N	35(5)	64(6)	60(7)	0(5)	−13(6)	10(5)
O_1	50(4)	56(4)	94(6)	12(4)	−7(5)	5(5)
O_2	52(5)	109(7)	151(12)	−1(5)	26(9)	50(6)

	U		U		U		U	
H_1	10(5)	H_2	7(3)	H_3	6(3)	H_4	4(3)	

fining one cycle resulted in an R-value of 0.085. Anisotropic temperature factors were then assigned to the remaining non-hydrogen atoms, and $R=0.079$ was obtained.

The average calculated C – C bond distance of the benzene ring was 1.418 Å at this stage. This high value was assumed to be the result of refinement of the carbon atoms to positions a little too close to the neighbouring hydrogen atoms, since these were at this stage not included in the calculations. However, the positions of the latter were clearly revealed

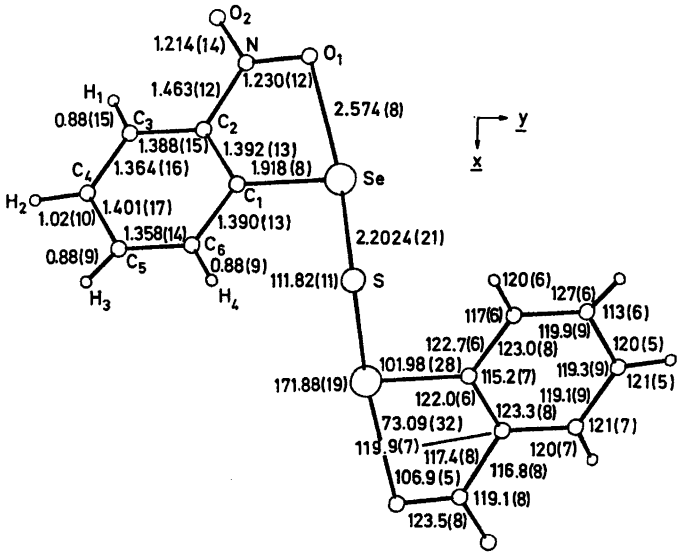

Fig. 1. Bond lengths and angles. The molecule is shown in (001) projection.

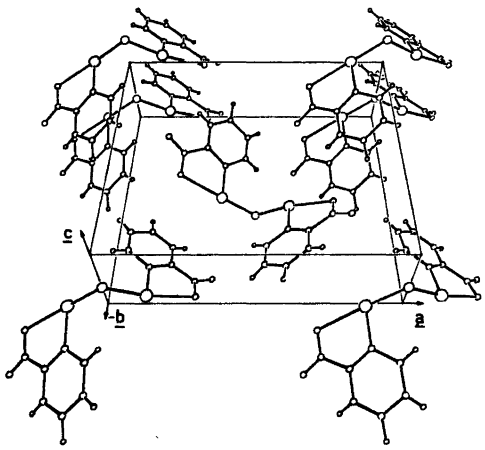

Fig. 2. Perspective drawing of molecular packing as viewed perpendicular to the x-axis.

in a difference map. Mainly to improve the apparent dimensions of the benzene ring, the four hydrogen atoms were now included in the refinement. Although their final calculated isotropic temperature factors were high, and the accuracy of their positions low, their inclusion seems justified by the obtained average C–C bond length of 1.382 Å. The final R-value was 0.051.

The calculated atomic parameters are given in Tables 1–2.

Observed and calculated structure factors can be obtained from the author upon request.

RESULTS AND DISCUSSION

The bond lengths and angles are given in Fig. 1. The arrangement of the molecules in the unit cell is illustrated by Figs. 2 and 3.

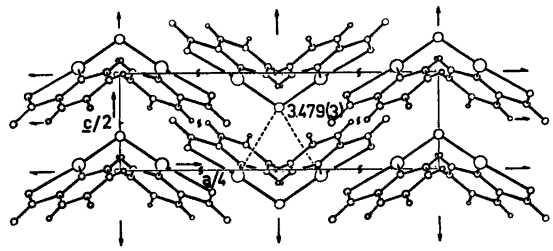

Fig. 3. Packing of the molecules shown in (010) projection. The intermolecular contact between a sulfur atom of one molecule and the two selenium atoms of another is indicated. (Distance in Å).

Table 3. Least squares planes and dihedral angles. The plane equation refer to orthorombic coordinates X, Y and Z in Å.

Plane through all atoms, except hydrogen, of one half molecule:

$6.5026\ X + 3.7285\ Y + 3.4765\ Z - 1.2227 = 0$
Distances (Å) of atoms from this plane:

S	Se	O_1	O_2	N	C_1
0.014	−0.076	0.115	−0.069	0.011	0.003
C_2	C_3	C_4	C_5	C_6	
−0.016	−0.009	0.007	0.045	−0.024	

Angle between this plane and the corresponding plane of the other half molecule, related by the two-fold axis: 68.12°
Dihedral angle $C_1SeSSe' = 79.67°$
Se′ is related to Se by the two-fold axis.

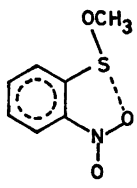

III (Ref. 8)

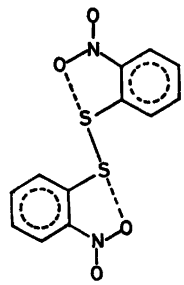

IV (Ref. 9)

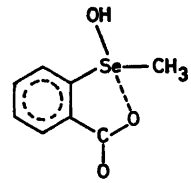

V (Ref. 10)

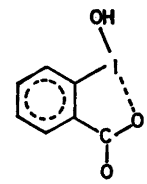

VI (Ref. 11)

Both the present compound (I) and its precursor (II) contain the *o*-nitrobenzeneselenenyl sulfur system in approximately the same linear arrangement. A five-membered ring is formed by the loose interaction between an oxygen atom of the nitro group and the selenium atom in the *ortho* position. In both compounds the selenium atom is further linked to a benzene carbon atom and a sulfur atom which is *trans* to the loosely bonded oxygen atom.

The planarity of the *o*-nitrobenzeneselenenyl sulfur system in the diselenenyl sulfide (I) is illustrated in Table 3. The largest distance of a relevant non-hydrogen atom from a least squares plane through one of the symmetrically related halves of the molecules is 0.115 Å. The angle between the least squares planes of the two molecular halves is 68.1°.

A ring closure by *ortho* substituents of benzene similar to the present case, and II, is characteristic of several compounds (III–VI) investigated by X-ray crystallography.[8–11] The compounds all contain an approximately linear sequence of three atoms, corresponding to the sequence O···Se–S of the present compound. The central atoms are either sulfur. selenium, or iodine, and the loosely connected atoms are oxygen atoms of carbonyl or nitro groups.

Referring to the three-center four-electron model of linear three-atoms systems, one would be inclined to expect that a reduction of one bond length should be accompanied by a lengthening of the bond in the *trans* position.[12–13] In contrast, the present molecule shows slightly increased bond lengths for both the O···Se and Se–S bonds relative to the corresponding bonds in the thiourea adduct (II). The O···Se bond lengths are 2.574(8) and 2.505(8) Å, and the Se–S bond lengths are 2.202(2) and 2.188(3) Å, respectively. However, these variations seem reasonable when regarding the different charge distributions of the two compounds. In the thiourea adduct (II) the *o*-nitrobenzeneselenenyl sulfur system is part of a cation with the charge formally located on the thiourea group, whereas the dieselenenyl sulfide (I) is a neutral molecule. The positive charge in II must be expected to reduce the electron density on the selenium atom to some extent, and thus facilitate the approach of the oxygen donor atom in the formation of a coordinate O···Se bond. Also the same positive charge may affect the π-electron system that probably has some importance for the bonds of the selenium atom. The course of this influence is hard to predict, but the nearly insignificant increase of the Se–C distance of II relative to I seems to be consistent with a higher π-bond order of the Se–S bond in II.

The O···Se bond length of 2.378(3) Å reported for *o*-carboxybenzene methyl selenium oxide (V) is considerably shorter than those of I and II. This is consistent with the charge distribution of V. When disregarding the O···Se interaction, the selenium atom formally carries one unit positive charge and the neighbouring carboxyl group one unit negative charge. Both with respect to charge separation and to O···Se bond length, the thiourea adduct (II) represents a situation between I and V.

The structures of bis(*o*-nitrobenzene) disulfide [14] and its *ortho* isomer (IV) [9] reported by Ricci and Bernal seem to indicate a small *trans*-bond lengthening effect by one oxygen atom

of the nitro group on the S–S bond in IV. The S–S bond lengths of the *ortho* and *para* isomers are 2.045(3) and 2.019(5) Å, respectively. *trans*-Bond lengthening effects of a similar magnitude can hardly be excluded for the analogous O···Se interactions on the basis of the available observations.

Besides the bond distances discussed so far, there are no significant differences between corresponding values of I and II. Among the pairs of corresponding bond angles there is a significant difference only for the $S-Se-C_1$ angle, which is 102.0(3)° in I and 99.9(3)° in II.

The closest intermolecular contact of the present compound exists between the selenium atoms of one molecule and the sulfur atom of another, related to the first by one unit cell translation along *z*; see Fig. 3. The distance is 3.479(3) Å, which is approximately the sum of the van der Waals radii. The compound II has a hydrogen bond in a direction roughly corresponding to this van der Waals contact.

REFERENCES

1. Eriksen, R. and Hauge, S. *Acta Chem. Scand. 26* (1972) 3153.
2. Eriksen, R. *Acta Chem. Scand. 26* (1972) 1274.
3. Coppens, P.,Leiserowitz, L. and Rabinovich, D. *Acta Crystallogr. 18* (1965) 1035.
4. *International Tables for X-Ray Crystallography*, Kynoch Press, Birmingham 1962, Vol. III, Table 3.3.1.
5. Cromer, D. T. *Acta Crystallogr. 18* (1965) 17.
6. Stewart, R. F., Davidson, E. R. and Simpson, W. T. *J. Chem. Phys. 42* (1965) 3175.
7. Johnson, C. K. *ORTEP: A Fortran Thermal-Ellipsoid Plot Program For Crystal Structure Illustrations*, 2nd Revision, Oak Ridge National Laboratory, Oak Ridge 1970.
8. Hamilton, W. C. and La Plaza, S. *J. Amer. Chem. Soc. 86* (1964) 2289.
9. Ricci, J. S. and Bernal, I. *J. Chem. Soc. B* (1970) 806.
10. Dahlén, B. *Acta Crystallogr. B 29* (1973) 595.
11. Shefter, E. and Wolf, W. *J. Pharm. Sci. 54* (1965) 104.
12. Foss, O. *Acta Chem. Scand. 16* (1962) 779.
13. Foss, O. In Andersen, P., Bastiansen, O. and Furberg, S. *Selected Topics in Structure Chemistry*, Universitetsforlaget, Oslo 1967, p. 145.
14. Ricci, J. S. and Bernal, I. *J. Amer. Chem. Soc. 91* (1969) 4078.

Received December 2, 1974.

Acta Chemica Scandinavica A 29 (1975) 523—527

The Crystal Structure of the Cesium Salt of 1-(2-Thienyl)-4,4,4-trifluoro-1,3-butanedione

H. SOLING

Chemistry Department B, Technical University of Denmark, DK-2800 Lyngby, Denmark

The crystal structure of the title compound, $CsC_8H_4F_3O_2S$, has been determined from 2410 independent, non-zero X-ray reflections collected with a counter diffractometer. The compound crystallizes in the space group $A2/a$ (No. 15) with 8 formula units in a unit cell of dimensions $a=16.55(1)$ Å, $b=4.969(6)$ Å, $c=27.73(9)$ Å and $\beta=108.0(2)°$. The crystal densities are $D_x=2.17$ g cm^{-3} and $D_m=2.17$ g cm^{-3}. The structure was solved by the heavy atom method and refined by the full matrix least squares procedure to a final value of $R=0.040$. The structure consists of infinite $(CsC_8H_4F_3O_2S)_n$ chains running in the direction of the b axis. Within each chain pairs of cesium atoms alternate with pairs of β-diketonate residuals, which roughly may be represented as planes inclined 42, 125 and 70° to the axes of the *abc** reference system. The chains are connected by a 2.73(2) Å F···H contact and two F···Cs contacts of 3.26(2) and 3.43(2) Å. Two of the fluorine atoms involved in these contacts are disordered. The observed bond lengths and angles agree well with those given in the literature for a wide range of acetylacetonates.

The present work is the first of a series of crystal structure studies of metal compounds formed with the unsymmetrical ligand 1-(2-thienyl)-4,4,4-trifluoro-1,3-butanedione (trivial name thenoyltrifluoracetone), henceforth referred to as HTTA; Fig. 1.

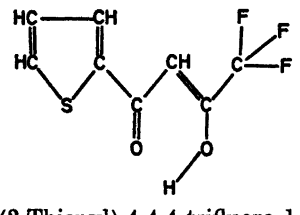

Fig. 1. 1-(2-Thienyl)-4,4,4-trifluoro-1,3-butanedione.

As far as the author is aware, this is the first crystal structure determination of a β-diketonate of an alkali metal. A crystal structure analysis of $NH_4Pr(TTA)_4.H_2O$ has been published by Lalancette *et al.*[1]

EXPERIMENTAL

Preparation and analysis. 5.00 g of powdered Cs_2CO_3 (Merck) was suspended in 50 ml of ethanol and saturated with CO_2. 6.80 g of the purified β-diketone (Merck) dissolved in 50 ml of ethanol was added slowly, while a stream of CO_2 was passed through the mixture. The yellowish, impure crystalline residue obtained by evaporation of the solvent was rinsed with benzene and recrystallized from nitromethane. The yield of colourless crystals was 1.1 g. Cs was determined microgravimetrically as Cs_2SO_4. A few milligrams of the substance were moistened with a mixture of nitric acid and sulfuric acid, taken to fumes by gentle heating and then ignited until constant weight. (Found: Cs 37.36. Calc. for $CsC_8H_4F_3O_2S$: 37.53).

The thin crystal needles are very easily split along the direction of the needle axis. Only completely transparent crystals showing perfect extinction in polarized light were selected for the structure analysis.

Collection and treatment of intensity data. A nearly cylindrical crystal of 0.01 cm cross section was mounted with the needle axis (b-axis) in the direction of the spindle on a semiautomatic STOE Weissenberg diffractometer, which was run in the ω-scan mode. Monochromatized (LiF) MoKα radiation ($\lambda=0.71069$ Å) was applied. Intensities diffracted from all unique planes within a sin θ/λ range from 0.06 to 0.70 Å^{-1} were measured by means of a scintillation detector provided with a pulse height analysator. The stability of the crystal and the diffractometer system was monitored by frequent remeasurement of a standard reflection of medium strength. The observed intensities

were converted to relative structure factors and standard deviations by the formulas,

$$F_o = (I_o/\mathrm{Lp})^{\frac{1}{2}} \text{ and}$$

$$\sigma(F_o) = \left(\frac{[I+\sigma(I)]^2 - I^2}{\mathrm{Lp}}\right)^{\frac{1}{2}},$$

where Lp is the usual Lorents and polarization correction factor, neglecting prepolarization. The latter calculation, and all other calculations necessary for the solution of the structure, were performed by means of the X-RAY system of crystallographic programs.[2] Corrections for absorption were omitted ($\mu R = 0.183$). 675 reflections having $F_o < 2\sigma(F_o)$ were rejected as not observable, leaving 2410 reflections for the structure analysis, *i.e.* more than 14 observations per adjustable parameter

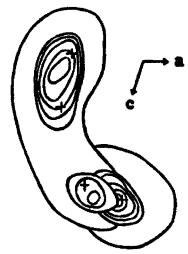

Fig. 2. Composite projection on the *ac* plane of the difference Fourier map showing the positive electron density in the vicinity of the disordered fluorine atoms. Contours are at 0.5 e Å^{-3} intervals, beginning at 0.5 e Å^{-3}. The final half atom sites are shown by +.

CRYSTAL DATA

Formula weight for $CsC_8H_4F_3O_2S$ is 354.1, monoclinic (*b* axis unique). Unit cell at 22 °C: $a = 16.55(1)$ Å, $b = 4.969(6)$ Å, $c = 27.73(9)$ Å, $\beta = 108.0(2)°$. $V = 2169$ Å^3. $F(000) = 1238$. D_x $(Z = 8) = 2.17$ g cm^{-3}, D_m(flot.) $= 2.17$ g cm^{-3}, $\mu(\mathrm{Mo}K\alpha) = 36.6$ cm^{-1}.

The unit cell dimensions are average values from several independent precession photographs. The space groups $A2/a$ (No. 15) or Aa (No. 9) were indicated by the systematic absences, hkl for $h+l$ odd and $h0l$ for h odd. The structure analysis was based on space group $A2/a$: $(0,0,0;\ 0,\frac{1}{2},\frac{1}{2}) \pm (x,y,z;\ \frac{1}{2}+x,\bar{y},z)$. The choice of the centrosymmetric space group was confirmed by the solution and successful refinement of the structure.

SOLUTION AND REFINEMENT OF THE STRUCTURE

The structure was solved for all non-hydrogen atoms by the heavy atom method. Atomic form factors for Cs^+, given by Cromer and Waber [3] were used. The correction for the anomaleous dispersion of cesium as well as the form factors for the light atoms were taken from International Tables for X-Ray Crystallography.[4] The refinement by full matrix least squares calculations proceeded well except for the fluorine atoms F(1) and F(3), Fig. 4. They were substituted by pairs of half atoms F(11), F(12) and F(31), F(32), as suggested by the difference Fourier map, shown in part on Fig. 2.

Then, the refinement was reassumed and continued until all shifts were less than 1/10 of the estimated standard deviation. The R value was 0.042. The hydrogen atoms H(1), H(2), and H(6) now showed up clearly on a new difference map. They were assigned an (invariant) isotropic temperature factor corresponding to that of the carrier atom, and refined by two more cycles of least squares calculations. The site of the hydrogen atom H(3), however, remained obscure. During the later stages of refinement an empirical weight function $w^{\frac{1}{2}} = 1/\sigma = [F/(25 + 0.00015F^2)]^{\frac{1}{2}}$ was used. The final R value was 0.040, and the value of the error of fit function, $[\sum w(\Delta F)^2/(n-m)]^{\frac{1}{2}}$, was 1.06. The fractional coordinates of the observed atoms and the thermal parameters are listed in Table 1. A list of the observed and calculated structure factors may be obtained from this institute.

RESULTS AND DISCUSSION

The characteristic feature of the structure is illustrated in Fig. 3. Irregular Cs_2O_4 octahedra sharing two opposite faces form an infinite chain running in the direction of the *b* axis. The complete chain is made up of pairs of cesium atoms alternating with pairs of the TTA moiety. Roughly, the interleaving TTA pairs (except the fluorine atoms) may be regarded as planes inclined 42, 125, and 70° to the axes of the orthogonal reference system abc^*. The six unique Cs–O distances shown on Fig. 3 range from 3.031(6) to 3.391(6) Å.

Table 1. CsTTA. Fractional atomic coordinates and anisotropic thermal parameters. Standard deviations are in parentheses. The form of the temperature factor is exp $[-2\pi^2\sum_{ij}h_ih_ja_i^*a_j^*U_{ij}]$. For labelling of the atoms see Fig. 4. *=half atom sites.

Atom	x	y	z	U or U_{11}	U_{22}	U_{33}	U_{12}	U_{13}	U_{23}
Cs^+	0.10636(2)	0.21891(6)	0.02515(1)	0.0397(2)	0.0322(2)	0.0492(2)	−0.0037(1)	0.0176(1)	−0.0041(1)
S	0.1591(1)	1.0549(5)	0.1610(1)	0.065(1)	0.070(1)	0.065(1)	−0.014(1)	0.012(1)	−0.011(1)
O(1)	0.0630(3)	0.6980(9)	0.0803(2)	0.061(3)	0.042(3)	0.043(2)	−0.006(2)	−0.028(2)	−0.009(2)
O(2)	−0.0694(3)	0.2796(9)	0.0432(2)	0.054(3)	0.043(2)	0.050(2)	−0.005(2)	0.023(2)	−0.007(2)
C(1)	0.1659(7)	1.2035(19)	0.2162(4)	0.095(7)	0.056(5)	0.068(5)	−0.004(5)	0.024(5)	−0.011(4)
C(2)	0.1045(8)	1.1282(24)	0.2344(4)	0.123(9)	0.082(7)	0.049(4)	0.009(6)	0.017(5)	−0.022(4)
C(3)	0.0464(4)	0.9503(13)	0.2048(2)	0.057(3)	0.051(3)	0.029(2)	−0.005(3)	0.021(2)	−0.006(2)
C(4)	0.0723(4)	0.8798(12)	0.1599(2)	0.054(3)	0.035(2)	0.031(2)	0.006(2)	0.007(2)	−0.017(2)
C(5)	0.0326(4)	0.6987(11)	0.1163(2)	0.044(3)	0.031(2)	0.036(2)	0.004(2)	0.013(2)	0.001(2)
C(6)	−0.0402(4)	0.5479(13)	0.1177(2)	0.051(3)	0.044(3)	0.044(3)	−0.008(2)	0.024(3)	−0.003(2)
C(7)	−0.0840(4)	0.3632(12)	0.0820(2)	0.041(3)	0.036(3)	0.037(3)	0.006(2)	0.014(2)	0.004(2)
C(8)	−0.1654(5)	0.2538(16)	0.0907(2)	0.049(4)	0.065(5)	0.061(4)	−0.013(3)	0.017(3)	−0.012(3)
*F(11)	−0.2281(11)	0.408(4)	0.0808(10)	0.056(9)	0.089(9)	0.209(26)	0.031(7)	0.074(16)	0.024(15)
*F(12)	−0.2302(11)	0.380(6)	0.0528(8)	0.032(6)	0.147(15)	0.125(14)	0.020(7)	0.011(8)	0.011(13)
F(2)	−0.1887(4)	0.0158(13)	0.0685(3)	0.085(4)	0.076(4)	0.182(7)	−0.025(3)	0.064(4)	−0.013(4)
*F(31)	−0.1524(9)	0.140(4)	0.1358(6)	0.071(7)	0.122(12)	0.083(8)	−0.14(7)	0.042(6)	0.038(9)
*F(32)	−0.1832(12)	0.331(6)	0.1296(7)	0.101(13)	0.268(27)	0.098(12)	−0.107(15)	0.082(11)	−0.075(16)
H(1)	0.209(9)	1.315(19)	0.223(4)	0.090					
H(2)	0.098(8)	1.221(26)	0.226(3)	0.106					
H(6)	−0.052(5)	0.564(13)	0.151(2)	0.058					

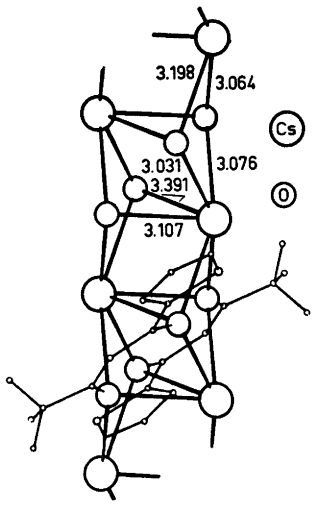

Fig. 3. The Cs – O chain and one centrosymmetric pair of TTA ligands, viewed approximately along the c^* axis. Cs – O distances are given in Å, the estimated standard deviation is 0.006 Å.

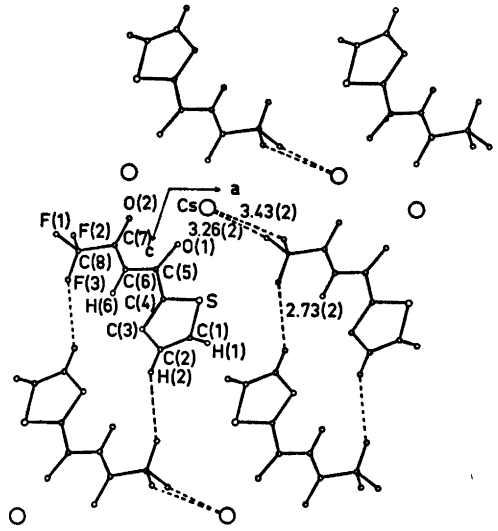

Fig. 4. Projection of the CsTTA structure on the *ac* plane. Short interchain distances *F*···*H* and *F*···*Cs* are shown as broken lines.

Fig. 4 shows the packing of the chains. Only three short interchain distances less than 3.5 Å have been found, *viz* the 2.73(2) Å F(3)···H(2) distance, which is approximately equal to the sum of the van der Waals radii, the 3.26(2) Å F(1)···Cs+ distance, and the 3.43(2) Å F(2)···Cs+ distance. They are indicated by broken lines. These contacts provide the weak interchain cohesion which explains the extreme ease with which the crystals are split along the *b* direction. Two of the fluorine atoms F(1) and F(3) involved in these contacts are considered to be disordered. Computationally they have been represented by pairs of half atoms. The distances quoted above refer to the center of gravity of the respective half-atom pairs.

Table 2. CsTTA, bond lengths and angles of the ligand with estimated standard deviations.

Bond lengths in Å		Angles in degrees	
S – C(4)	1.679(7)	C(1) – S – C(4)	93.1(5)
S – C(1)	1.676(12)	S – C(1) – C(2)	112.8(8)
C(1) – C(2)	1.318(19)	C(1) – C(2) – C(4)	115.7(9)
C(2) – C(3)	1.375(13)	C(2) – C(3) – C(4)	108.9(8)
C(3) – C(4)	1.480(10)	C(3) – C(4) – S	109.4(4)
C(4) – C(5)	1.487(8)	C(3) – C(4) – C(5)	131.2(6)
C(5) – C(6)	1.427(9)	C(5) – C(4) – S	119.3(5)
C(6) – C(7)	1.380(8)	C(4) – C(5) – O(1)	117.8(6)
C(7) – C(8)	1.538(11)	C(4) – C(5) – C(6)	117.4(6)
C(5) – O(1)	1.247(9)	C(6) – C(5) – O(1)	124.8(5)
C(7) – O(2)	1.243(9)	C(5) – C(6) – C(7)	126.1(6)
C(8) – F(1)[a]	1.268(11)	C(6) – C(7) – O(2)	130.1(6)
C(8) – F(2)	1.334(11)	C(6) – C(7) – C(8)	114.4(6)
C(8) – F(3)[a]	1.182(11)	C(8) – C(7) – O(2)	115.5(5)
C(1) – H(1)	0.88(14)	C(7) – C(8) – F(2)	112.5(7)
C(2) – H(2)	1.04(14)		
C(6) – H(6)	1.00(9)		

[a] Distance to the center of gravity of the half atoms.

The observed bond lengths and bond angles of the ligand are listed in Table 2. In general they agree well with those reported in the literature for a wide range of acetylacetonates,[5] and with those found in the $NH_4Pr(TTA)_4.H_2O$ compound.[1] The C(7) – C(8) bond is a single bond, 1.54(1) Å. The C(1) – C(2), bond, 1.32(2) Å, is a double bond. The remaining C – C bonds are of intermediate order.

The non-hydrogen atoms of the thiophene ring are coplanar ($\chi^2 = 3.0$). The C_{2v} symmetry found in the free thiophene molecule,[6] however, is destroyed. A similar distortion of the ring has been observed in 2-chloro- and the 2-bromothiophene.[7]

It is noteworthy, that the two C – O bonds are identical, *viz.* 1.247(9) and 1.243(9) Å, in this compound where no benzenoid chelate ring is formed. The C – O bonds are the shortest observed in a β-diketonate, probably due to the ionic character of the Cs – O bond. The intraligand distance O(1) to O(2), 2.962(7) Å, the so-called bite of the ligand, is the longest observed.

The shape of the ligand has been analyzed in terms of several best planes. The dihedral angle between the thiophene plane and the best plane through the atoms C(4) to C(8) is only 2.3°. The O – C – C – C – O arc is twisted; the dihedral angle between the planar groups O(1) – C(4 – 6) and O(2) – C(6 – 8) is 8.1°.

All crystallographic calculations have been performed at the Northern Europe University Computing Center (NEUCC). DK-2800 Lyngby. The drawings, Figs. 3 and 4, have been made be means of the ORTEP II program; of C. K. Johnson.[8]

REFERENCES

1. Lalancette, R. A., Cefola, M., Hamilton, W. C. and La Placa, S. J. *Inorg. Chem. 6* (1967) 2127.
2. X-RAY *Program System for X-Ray Crystallography 1967*, Computer Science Center, University of Maryland.
3. Cromer, D. T. and Waber, J. T. *Acta Crystallogr. 18* (1965) 104.
4. *International Tables for X-Ray Crystallography*, Kynoch Press, Birmingham 1962, Vol. III.
5. Lingafelter, E. C. and Braun, R. L. *J. Amer. Chem. Soc. 88* (1966) 2951.
6. Bak, B., Christensen, D. and Hansen-Nygaard, L. *J. Mol. Spectrosc. 7* (1961) 58.
7. Harshbarger, W. R. and Bauer, S. H. *Acta Crystallogr. B 26* (1970) 1010.
8. Johnson, C. K. *ORTEP*, Report ORNL 3794, Oak Ridge National Laboratory, Oak Ridge 1965.

Received January 22, 1975.

Acta Chemica Scandinavica A 29 (1975) 528—536

Conformational Spectroscopic Studies of Cyano- and Isocyanatocyclohexane

HANS T. HORNTVEDT and PETER KLÆBOE

Department of Chemistry, University of Oslo, Oslo 3, Norway

The IR spectra of cyano- and isocyanatocyclohexane as liquids, in solution and as solids at −175 °C were recorded in the region 4000−200 cm^{-1}. Spectra of the high pressure crystals were obtained with the aid of a high pressure cell having diamond windows. Raman spectra of the compounds as liquids and low temperature solids were recorded.

Both compounds form a mixture of *e*- and *a*-conformers in the liquid state and in solution. At low temperature isocyanatocyclohexane crystallizes in the *e*-conformer whereas both conformers were present in solid cyanocyclohexane probably as a result of incomplete crystallization. When pressurized to *ca.* 20 kbar at ambient temperature both compounds crystallize in the *a*-conformation as observed for certain dihalocyclohexanes. The vibrational spectra have been discussed and compared with those of other monosubstituted cyclohexanes.

We have for a long time been interested in the vibrational spectra of halogenated cyclohexanes and various monohalo- and *trans*-1,2-dihalocyclohexanes have been investigated. The purpose of this work was to study the conformational equilibria in the liquid state (and possibly in the vapour) and particularly to decide which conformer was present in the crystal. For this purpose we have successfully utilized high pressure crystallization at ambient temperature in addition to low temperature crystallization under atmospheric pressure. The low temperature and the high pressure crystals most often consist of molecules in the same conformation. However, when the enthalpy difference between the conformers is small, intermolecular crystal forces may become the deciding factors and the low temperature and the high pressure crystals can have molecules in different conformations.[1,2] These cases are intrinsically interesting, and besides, they offer excellent opportunities for interpreting the vibrational spectra in detail and assigning the bands to one or the other conformers.

The studies have now been extended to other substituted cyclohexanes, and in the present communication we will present our results for cyanocyclohexane ($C_6H_{11}CN$) and isocyanatocyclohexane ($C_6H_{11}NCO$), later called CCN and CNCO, respectively. The conformational equilibria for CCN and CNCO in solution have previously been investigated by NMR technique,[3,4] further by equilibration measurements [5,6] of the *cis* and *trans* isomers of 4-*t*-butylcyclohexylcyanide. To our knowledge, no vibrational spectral studies of these compounds have been reported, nor have they ever been investigated as pure liquids or in the crystalline state.

EXPERIMENTAL

The samples of CCN and CNCO were commercial products from the K & K laboratories and from Koch-Light, respectively. They were fractionated three times under reduced pressure. When checked by gas chromatography CCN was found to be better than 99.5 % pure, whereas CNCO had *ca.* 11 % impurities. Therefore, CNCO was treated by preparative gas chromatography, after which 10 IR bands present in the impure sample disappeared.

The IR and Raman spectrometers and the high pressure diamond cell [7] have been described.[8] The low temperature Raman spectra were obtained by 90° illumination technique using a cryostat [9] with a cold copper tip.

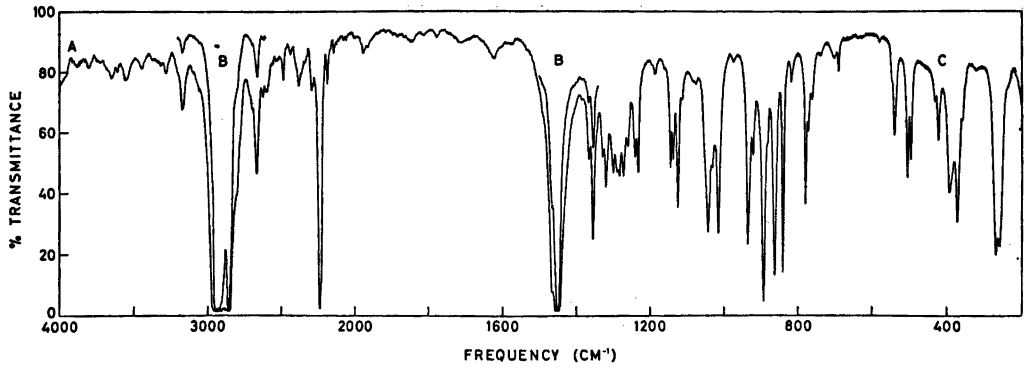

Fig. 1. The IR spectrum of liquid cyanocyclohexane. A, 0.1 mm KBr cell; B, 0.025 mm KBr cell, and C, 0.2 mm polyethylene cell.

RESULTS AND DISCUSSION

Cyanocyclohexane

The IR spectra of CCN in the liquid state and as high pressure crystal are shown in Figs. 1 and 2, respectively, while the IR and Raman frequencies are listed in Table 1. With 19 atoms, CCN should have 51 fundamental frequencies for each conformer out of which *ca.* 35 should appear below 1400 cm^{-1}. Since *ca.* 45 strong or medium intense IR or Raman bands were observed in this region an estimated 25 bands may be attributed to overlapping fundamentals for both conformers with *ca.* 20 vibrational modes appearing as distinct bands for each conformer.

Low temperature solid. As apparent from Table 1 no significant simplification of the IR or Raman spectra were observed upon cooling to a solid in contradiction to the results previously obtained for mono [10,11] and dihalogenated [1,8,12–14] cyclohexanes. Several attempts were made to anneal the sample just below the melting point before cooling down to −175 °C, but no apparent changes were observed in the spectra. It is well known that certain cyclohexanes, *e.g.* fluoro- and chlorocyclohexane as well as *trans*-1,4-dichlorocyclohexane,[15] solidify into a disordered, rotating phase consisting of both conformers before reaching a transition temperature and converting into an anisotropic

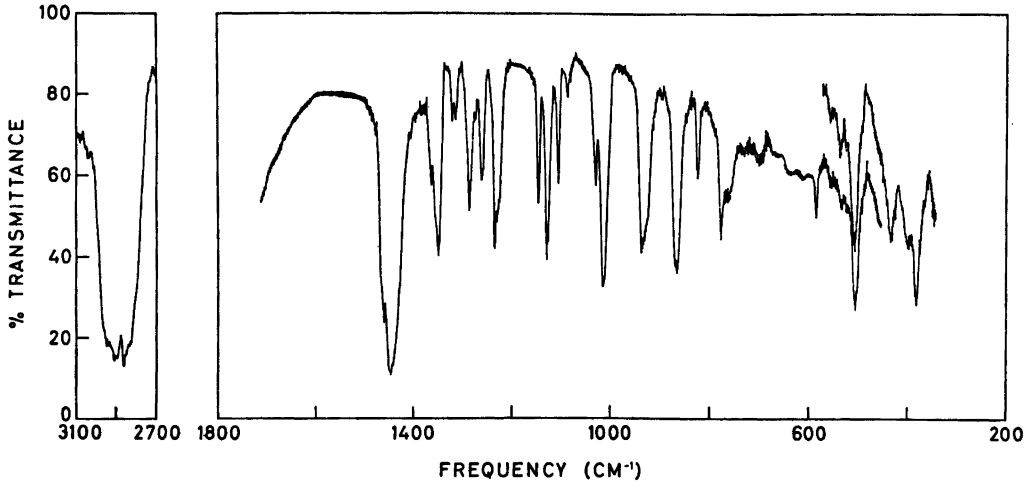

Fig. 2. The IR spectrum of polycrystalline cyanocyclohexane at ambient temperature (*ca.* 20 kbar pressure).

Table 1. Infrared [a] and Raman spectral data of cyanocyclohexane.

Liquid		Solid			Conformer[b]
		IR		Raman	
IR	Raman	Low temp. (−175 °C)	High press. (~20 kbar)	Low temp. (−175 °C)	
3171 w[c]		3170 w	3170 w		
2948 s,sd	2947 vs	2950 s,sd		2948 s	
2928 vs	2928 s,sd	2929 vs		2930 m	
			2900 vs,bd		
2903 s,sd	2904 s	2904 s,sd		2902 m	
2859 vs	2861 vs	2860 vs		2860 s	
2800 w,sd		2801 w,sd			
2663 m		2665 m	2668 m		
2291 vw		2290 wv			
2240 vs	2241 vs	2240 s		2240 s	*a, e*
2235 s,sd	2236 m,sd	2234 m,sd		2236 m,sd	
2183 vw	2184 vw	2182 vw			
1490 vw,sd					
1465 s,sd	1464 m,sd P	1465 m	1465 s,sd		*a, e*
1450 vs,bd	1448 vs D	1450 vs	1450 vs,bd	1448 s	*a, e*
1364 m,sd	1364 m P	1362 w	1363 w,sd		*a, e*
		1353 m			
1352 s	1354 m D		1352 vs	1360 w,bd	*a, e*
		1349 m			
1326 m	1328 m	1328 w,sd	1325 m	1327 w	*a*
1317 m	1319 w,sd	1320 m	1316 m	1320 vw	*a, e*
1297 m	1298 s D	1298 m	*[d]	1298 s	*e*
1286 w,sd		*			*a*
			1286 s		
1281 m		1281 m			*a, e*
1270 m	1272 vs D	1270 m	*	1271 s	*e*
1258 m	1260 s D	1260 m	1261 s	1260 s	*a, e*
1239 m	1239 m P	1239 m	1239 vs	1239 w	*a, e*
1231 m	1232 w,sd	1230 m	1230 m		*a*
1185 w	1186 m D	1185 w	*	1186 w	*e*
1143 m	1143 w,sd	*	1144 s		*a*
1136 m	1137 s P	1136 m	*	1138 m	*e*
1123 s	1124 m D	1126 m	1128 s		*a*
1112 w	1112 vw	1110 w	1110 m		*a, e*
1082 vw	1082 w,sd	1085 w,bd	1086 w		*a, e*
1074 vw	1075 m D	1074 vw	*	1077 w	*e*
1042 s	1044 s P	1043 s	*	1045 s	*e*
1031 w,sd	1032 vs D	1033 m	1031 m,sd	1033 vs	*a, e*
1013 s		1015 m	1015 vs		*a*
		937 w			
935 s	933 s P		937 s,bd	932 m	*a, e*
		930 m			
920 m	920 w	922 vw	925 w,sd		*a, e*
892 s	893 w D	894 vs	*	891 w	*e*
882 w,sd	881 m D	882 w	*	884 m	*e*
862 s	862 w	865 s	867 s		*a*
840 s	840 s P	842 s	*	843 m	*e*
817 w	817 s P	829 w	820 m	821 m	*a*
779 s	779 vs P	780 s	778 s	780 vs	*a, e*
771 m,sd	772 s D	773 w,sd			*a, e*
762 w,sd		760 w,sd	758 w,sd		*a, e*
739 vw		745 vw			
701 vw		702 vw	707 vw		
689 w		689 w	*		*e*
580 vw		582 vw	582 m		*a, e*
547 w,sd		547 w,sd	549 w		*a, e*

Table 1. Continued.

540 m	541 s P	540 m	*	543 s	*e*
505 m	506 m P	509 s	*	508 w	*e*
496 m	496 m	499 w	501 s		*a*
431 w	431 m D	431 w	*	430 m	*e*
422 m	422 w,sd	421 w	430 m		*a*
391 m	391 w,sd D	392 w,sd	397 m, sd	390 vw	*a*
386 w,sd	387 w	388 m	*		*e*
371 s	372 m D	375 m	378 s		*a, e*
359 w,sd	359 m P	360 w		362 m	*a, e*
267 s	268 s D	272 vs		270 w	*e*
258 s	260 s P	258 vw,sd			*a*
	160 s D			162 w	*a, e*
	125 m P			132 w	*a, e*

[a] Very weak IR bands in the regions 4000–3200, 2600–2300 and 2200–1500 cm^{-1} were omitted. [b] *a*, axial and *e*, equatorial. [c] Abbreviations: s, strong; m, medium; w, weak; v, very; sd, shoulder, bd, broad; P, polarized and D, depolarized. [d] Bands with an asterisk are absent in the solid state.

crystalline solid. However, differential thermal analysis (DTA) of CCN gave only one discontinuity in the temperature range −100 to 25 °C corresponding to the melting point. Thus, it seems likely that in spite of the annealing our low temperature sample was merely a glass as indicated by the lack of correlation field splitting in the IR and Raman spectra.

High pressure solid. In contrast to the low temperature, the high pressure IR spectrum was highly simplified compared to that of the liquid (Figs. 1 and 2). Evidently, only one conformer was present in the high pressure crystal, and various criteria were employed to decide if this conformer was the *e* or the *a*. IR spectra of liquid CCN were recorded at elevated temperatures (*ca.* 150 °C) and at low temperature (−10 °C) and compared with those at ambient temperature (30 °C). Significant intensity variations of certain bands were observed with temperature. Measurements of band areas or absorbance values revealed that the bands present in the high pressure spectrum were enhanced at higher temperatures compared to those vanishing in the high pressure spectrum.

The following pairs of bands were investigated: 1136/1231, 1136/1123, 1136/1143, 1042/1013, 892/862, 840/862, 840/817, 505/496, 540/496, 432/422, and 267/258 cm^{-1}. The thermodynamic functions (ΔG) for the $e \rightleftharpoons a$ conversion reveal a preference of the equatorial conformer for nearly all monosubstituted cyclohexanes. The enthalpy terms (ΔH) are known for fewer systems, but when investigated,[16] the equatorial conformers appear the more stable. Applied to CCN, a negative ΔH_{e-a} would therefore lead to

Table 2. Some characteristic vibrations in monosubstituted cyclohexanes in the region around 850 cm^{-1}.

Conf.	CN	NC[a]	NCO	Cl[b]	Br[b]	I[b]
e,a	920 m	913 s	905 s	921 w	919 w	915 w
e	892 s	895 s	893 s	889 vs	885 vs	883 s
e	882 w	887 w	881 s	858 s	852 s	848 m
a	862 s	865 m	863 m	868 s	864 m	862 m
				852 m		
e	840 s	843 m	839 s	817 vs	810 vs	806 s
a	817 w	817 w	815 m	807 m	804 m	

[a] Data from Ref. 17, no conformations known. DMS card No. 6357. [b] Data from Ref. 11, distinction between *e* and *e* + *a* uncertain.

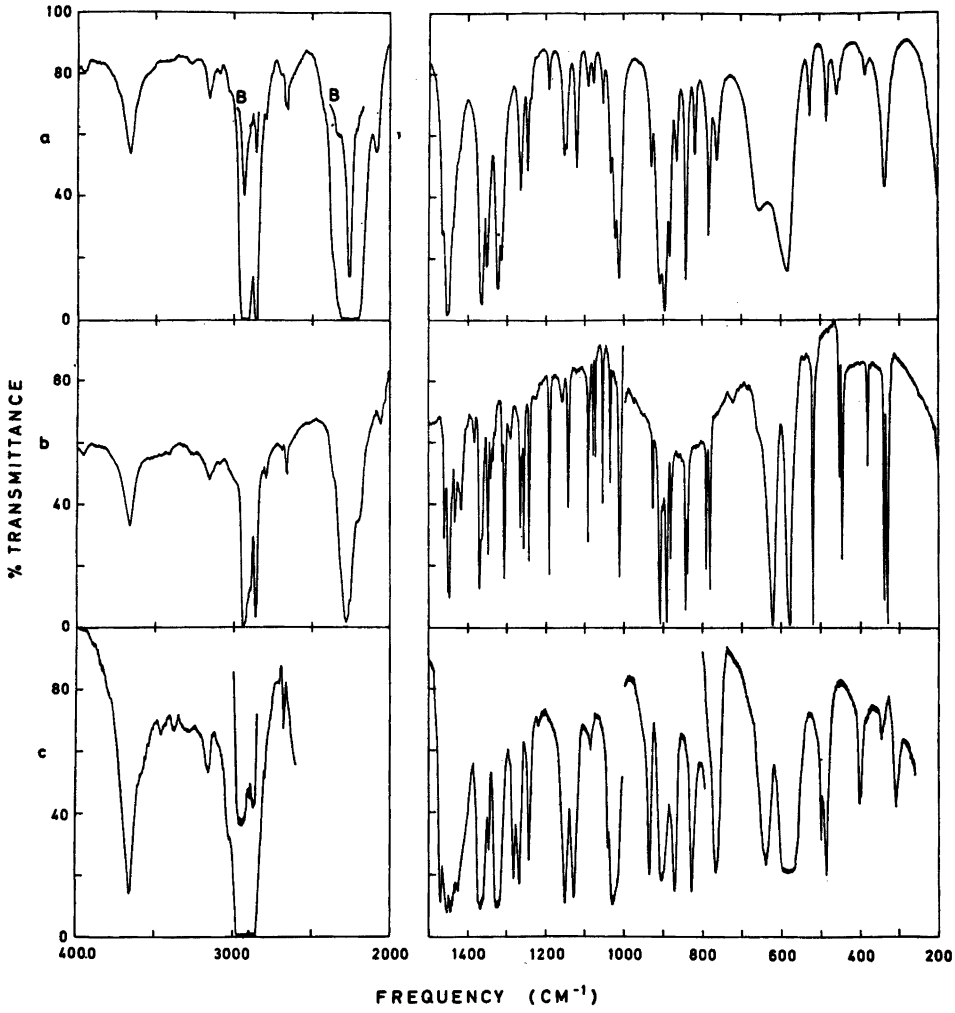

Fig. 3. The IR spectra of isocyanatocyclohexane: a. (upper curve) A, 0.05 mm. CsI cell and B, *ca.* 25 % CCl_4 solution in 0.025 mm. KBr cell; b. (middle curve) polycrystalline solid at −175 °C, and c. (lower curve) polycrystalline solid at ambient temperature (*ca.* 20 kbar pressure).

the high pressure conformer being *a*. However, when extrapolated from the 4-*t*-butylcyclohexylcyanide, a ΔH close to zero ($\Delta H = 0.042 \pm 0.095$ kcal/mol) was suggested [6] for CCN, whereas calculations [5] based upon the van der Waals repulsions indicate that the *a*-conformer should be 0.46 kcal/mol less stable than the *e*-conformer.

Since the *e*- and *a*-conformers of CCN should have nearly the same dipole moment, no displacement of the conformational equilibrium with solvent polarity would be expected (and none was found). A close comparison between the IR and Raman spectra of CCN with other related cyclohexanes might give a clue to the spectral attributions. The C – C stretching region around 1000 cm^{-1}, found to be of diagnostic value [8] for the halogenated cyclohexanes (and for CNCO, see later) did not fall into this regular pattern, probably because of the additional exocyclic C – (CN) stretching mode falling into the same region for CCN. However, a remarkable similarity between the vibrational spectra of CCN, CNCO, and cyclohexylisocya-

Table 3. Infrared[a] and Raman spectral data for isocyanatocyclohexane.

Liquid IR	Raman	Solid IR High press. (~20 kbar)	Low temp. (−175 °C)	Raman Low temp. (−175 °C)	Conformer[b]
3665 m[c]		3660 m	3642 w		
3160 w		3160 w	3160 vw		
				2954 m, sd	
2934 vs, bd	2943 vs	2940 vs,bd	2933 vs	2944 vs	
				2935 m,sd	
2913 m,sd			2913 s		
	2900 m			2902 m	
			2894 s	2894 m	
			2861 s	2861 vs	
2857 vs	2858 vs	2862 vs, bd			
			2852 s	2854 m,sd	
2795 w			2799 w		
2670 w	2672 vw,sd	2671 w	2669 w	2670 vw, sd	
2660 w	2663 vw	2660 vw	2663 w	2663 vw	
2350 m,sd			2350 w,sd		
2255 vs,bd	2254 vw		2282 vs,bd		
			2259 s,sd		
2210 s			2208 m,sd		
2090 m			2090 m		
1465 m,sd	1465 w,sd	1469 s	1461 m	1466 vw	
1453 vs			1451 s,sd	1450 vs	
		1452 s			
1449 vs			1448 s		
1437 m,sd	1443 vs	1442 s	1433 m	1443 vs	
1420 w,sd	1425 m,sd	1424 s	1417 m	1419 s	
			1383 w		
		1370 s,sd	1369 s		
1363 s	1365 w,sd			1369 w	*a, e*
		1361 s	1363 w,sd		
1349 s	1348 m	1349 m	1348 s	1347 s,bd	*a, e*
			1341 w		
			1336 w		
1321 s	1322 w	1323 s,bd	*[d]	*	*a*
			1312 w		
1311 s	1308 m	*		1308 s	*e*
			1307 s		
			1291 w,bd		
1267 m,sd	1265 s	1282 s	1265 m	1267 vs	*a, e*
1262 s		1267 s	1257 s	1257 w	*a, e*
1245 s	1245 m		1243 s	1244 m	*a, e*
		1243 s			
1236 w,sd	1236 w,sd		*	*	*a*
1190 w	1190 w	*	1191 s	1193 m	*e*
1151 s		1150 s	*	*	*a*
1145 s	1145 m		1143 m	1145 s	*a, e*
1120 s	1120 vw	1127 s	*	*	*a*
1090 w		*	1091 m		*e*
1076 w	1076 w	1083 w	1078 m	1077 s	*a, e*
			1073 m		
1052 w	1052 m	*	1054 m	1054 m	*e*
1032 m	1030 s	1040 m	1035 m	1030 vs	*a, e*
			1029 vw		
1020 s		1028 s,bd	*		
1010 s	1012	*	1011 s	1012 s	*e*
928 m	926 vw	935 s	928 m	926 vw	*a, e*
905 s		905 s,bd	909 s	912 vw	*a, e*

Table 3. Continued.

893 s	893 w	*	893 s	894 vw	*e*
881 s	880 w	*	881 s	882 w	*e*
863 m		870 s	*		*a*
			843 s		
839 s	838 s	*		843 s	*e*
			839 s		
815 m	815 s	827 s,sh	*	*	*a*
			790 s		
780 s	780 vs	*		781 vs	*e*
			780 s		
759 m	761 s	767 s	*	*	*a*
650 s,bd	652 vw	641 vs	621 vs	644 w	*a, e*
598 m,sd	597 w		*	*	*a*
		580 s,bd			
580 s,bd	579 w,sd		579 vs	579 m	*a, e*
523 m	524 m	*	520 vs	523 m	*e*
		497 m,sd			
482 m	482 w	484 s	*	*	*a*
	459 m	*	453 m	456 s	*e*
455 w,bd					
	450 w,sd	*	445 s	448 m,sd	*e*
382 w	382 w	397 m	381 m	380 m	*a, e*
335 s	337 m	340 w	340 s	335 vs	*a, e*
			331 sv		
		308 m			
	175 w			175 w	*a, e*
				132 w	*a, e*

[a] Very weak IR bands in the regions 4000–3000 and 2000–1500 cm^{-1} were omitted. [b] *a*, axial and *e* equatorial. [c] Abbreviations, see footnotes to Table 1. [d] Bands with an asterisk are absent in the solid state.

nide [17] was observed in the region 900–800 cm^{-1}. As apparent from Table 2, the corresponding frequencies between CCN and CNCO fall within 2 cm^{-1} and the band intensities show corresponding similarities. With the CNCO bands attributed to the *e* or *a* conformers (see below) the CCN bands were assigned correspondingly. Preliminary measurements indicate that also cyclohexylisocyanide bands follow the same pattern. Thus, the spectral relations also support the high pressure crystal to be in the *a*-conformer and the observed bands of Table 1 have been attributed accordingly. Only the *e*-bands can be attributed with certainty whereas the bands present in the high pressure solid can be *a*-bands or they are common to both conformers.

The IR band at 2240 cm^{-1} was assigned as the C≡N stretching modes for both conformers since this frequency always seems independent of conformational changes. A weaker satellite at 2235 cm^{-1} corresponds with the isotopic shift of the $^{13}C\equiv^{14}N$ stretch.

Isocyanatocyclohexane

The IR spectra of CNCO in the liquid, low temperature solid and high pressure solid are shown together in Fig. 3, whereas the IR and Raman frequencies are listed in Table 3. Having an additional atom, CNCO should have one more fundamental below 1400 cm^{-1} than CCN. Because the CNC angles in isocyanates and isothiocyanates are different from 180°, rotational conformers might exist,[18,19] although no conformations were detected in alkylisocyanate.[18] The very low barrier to internal rotation around the C–N bonds, equal to 83 ± 15 cal/mol in methylisocyanate [20] should indicate free or nearly free rotation, as recently discussed [21] for allylisocyanate and allylisothiocyanate. Although rotational conformers in CNCO cannot be completely ruled out, our data can be best interpreted in terms of a conformational equilibrium, derived from the cyclohexane ring conversion only.

Low temperature solid. When CNCO was cooled

Table 4. Some characteristic skeletal vibrations in monosubstituted cyclohexanes around 1000 cm^{-1}.

Substituent	Axial IR	Raman	Equatorial IR	Raman
Cl[a]	1029 m	1028 vs	1029 m	1028 vs
	1014 s	1013 w	993 vs	993 s
Br[a]	1028 w	1028 s	1028 w	1028 s
	1010 m	1010 w	988 s	989 s
I[a]	1021 w	1023 s	1030 m	1032 s
	1006 s	1008 vw	988 s	988s
NCO	1032 m	1030 s	1032 m	1030 s
	1020 s		1010 s	1012 m

[a] Data from Ref. 8.

below the freezing point several IR or Raman bands diminished in intensity and disappeared completely after annealing (Fig. 3). The number of IR or Raman bands in the low temperature crystal agree with one conformer.

In order to decide if the low temperature solid had crystallized as *e*- or *a*-conformers, spectra were recorded of liquid CNCO at 150, 30 and −20 °C. Significant intensity variations were observed, interpreted as a shift in the conformational equilibrium. The following pairs of bands were suitable for measurements: 1010/1020, 893/863, 881/863, 839/815, and 780/759 cm^{-1}, and in each case these intensity ratios became smaller at higher temperatures. Since the IR bands in the nominators were present and those of the denominations absent in the solid spectra, the low temperature crystal should therefore consist of molecules in the more stable conformer. As discussed previously, the *e*-conformation generally has the lower ΔH value for monosubstituted cyclohexanes. For CNCO, NMR measurements [4] at 35 and at −75 °C clearly demonstrated a negative enthalpy difference (ΔH) and the low temperature crystal will therefore consist of molecules in the *e*-conformer in agreement with the halocyclohexanes.[11]

Our attributions of the bands present in the low temperature crystal as *e* were further supported by the spectral features of the ring stretching region around 1000 cm^{-1}. The IR and Raman bands in this region are listed in Table 4 together with those of chloro-, bromo-, and iodocyclohexane.[11] It can be seen that the CNCO bands correspond particularly with those of the chloro- and bromocyclohexanes. The high frequency band is attributed to both conformers in CNCO as well as in the chloro- and bromo-compound, but not for iodocyclohexane [11] or the dihalocyclohexanes.[8] The *e*-bands are invariably situated at lower frequencies and for several halo- [11] and dihalocyclohexanes [8] they appear weak in the Raman spectra.

High pressure solid. When crystallized under *ca.* 20 kbar pressure in the diamond cell, the IR spectrum of CNCO was drastically different from that of the low temperature solid. Thus, the high pressure crystal will consist of molecules in the *a*-conformation as concluded for CCN. In addition to *trans*-1-bromo-2-chlorocyclohexane,[1] also *trans*-1,4-dichloro- and dibromocyclohexane [22] have been found to crystallize in the *ee* and *aa* conformations upon cooling and pressurizing, respectively. Obviously, several factors, including the molar volume and intermolecular forces in the "axial" and "equatorial" crystals, the enthalpy (ΔH) and the entropy (ΔS) difference as well as the barrier between the conformers are some of the deciding factors. Probably, the molar volume of the axial conformers was smaller than for the equatorial, thus favouring the *a* conformations under high pressure.

Spectral features. For CNCO we were able to attribute the IR and Raman bands with considerable certainty. Bands present in the low temperature crystal and absent in the high pressure crystal should be *e*, with *a* bands the other way around. On the other hand, bands present in both the crystals should be common to the conformers. It can be seen from Table 3 that approximately 12 *e*-bands, 10 *a*-bands, and 16 *a*+*e* bands were attributed below 1400 cm^{-1}.

This indicates that some fundamentals have remained unobserved or they are hidden by other fundamentals. Correlation splitting of 5 – 10 cm^{-1} was observed for certain bands in the low temperature IR spectrum, while the resolution might not have been sufficient in the high pressure IR or the low temperature Raman spectra in which larger slits were employed.

Because of the many atoms and low symmetry (C_s or C_1) the fundamental frequencies for both conformers should be highly mixed and attributions to specific vibrational motions very approximate. Comparison of CNCO and CCN with the monohalocyclohexanes,[11] reveals close similarities in the spectra, regarding positions and intensities of the bands. In CNCO, the very strong IR band at 2255 cm^{-1} with a very weak Raman counterpart is undoubtedly the N=C=O asymmetric stretch. Due to incomplete data (diamond absorption, low Raman intensity) it cannot be ascertained if this band is common to both conformers. The symmetric N=C=O stretching mode, expected[17] around 1450 cm^{-1}, will be mixed with the CH_2 scissoring frequencies. The bands at 780 and 759 cm^{-1} are tentatively assigned as the C–N stretches and as observed for the halocyclohexanes, the *e*-band is at higher frequency than the *a*-band.

Alkyl isocyanates[17] have characteristic N=C=O bending modes and the bands at 650 and 580 cm^{-1} are assigned as the out-of-plane and the in-plane N=C=O bending mode, respectively, both common to the *e* and *a* conformers.

Acknowledgement. We are grateful to K. Ruzicka and Gerd Teien who purified the samples. Financial support from NAVF is acknowledged.

REFERENCES

1. Horntvedt, H. T. and Klæboe, P. *Acta Chem. Scand. 25* (1971) 772.
2. Thorbjørnsrud, J., Ellestad, O. H., Klæboe, P. and Torgrimsen, T. *J. Mol. Struct. 15* (1973) 61.
3. Jensen, F. R., Bushweller, C. H. and Beck, B. H. *J. Amer. Chem. Soc. 91* (1969) 344.
4. Corfield, G. C. and Crawshaw, A. *J. Chem. Soc. B* (1969) 495.
5. Allinger, N. L. and Szkrybalo, W. *J. Org. Chem. 27* (1962) 4601.
6. Rickborn, B. and Jensen, F. R. *J. Org. Chem. 27* (1962) 4606.
7. Whatley, L. S., Lippincott, E. R., Valkenburg, A. V. and Weir, C. *Science 144* (1964) 968.
8. Klæboe, P. *Acta Chem. Scand. 25* (1971) 695.
9. Levin, I. W. *Spectrochim. Acta A 25* (1969) 1157.
10. Klæboe, P., Lothe, J. J. and Lunde, K. *Acta Chem. Scand. 10* (1956) 1465.
11. Klæboe, P. *Acta Chem. Scand. 23* (1969) 2641; Rey-Lafon, M., Rouffi, C., Camiade, M. and Forel, M. *J. Chim. Phys. 67* (1970) 2030.
12. Klæboe, P., Lothe, J. J. and Lunde, K. *Acta Chem. Scand. 11* (1957) 1677.
13. Horntvedt, H. T. and Klæboe, P. *Acta Chem. Scand. 26* (1972) 3797.
14. Thorbjørnsrud, J. and Klæboe, P. *Acta Chem. Scand. 25* (1971) 781.
15. Dahl, T., Hassel, O. and Rømming, C. *Acta Chem. Scand. 18* (1964) 2280.
16. Eliel, E. L., Allinger, N. L., Angyal, S. J. and Morrison, G. A. *Conformational Analysis*, Interscience, New York 1966.
17. Ugi, I. and Meyer, R. *Chem. Ber. 93* (1960) 239.
18. Hirschmann, R. P., Krisley, R. N. and Fassel, V. A. *Spectrochim. Acta 21* (1965) 2125.
19. Knisley, R. N., Hirschmann, R. P. and Fassel, V. A. *Spectrochim. Acta A 23* (1967) 109.
20. Lett, R. G. and Flygare, W. H. *J. Chem. Phys. 47* (1967) 4730.
21. Torgrimsen, T., Klæboe, P. and Nicolaisen, F. *J. Mol. Struct. 20* (1974) 213.
22. Ellestad, O. H. and Klæboe, P. *J. Mol. Struct. 26* (1975) 25.

Received November 25, 1974.

Acta Chemica Scandinavica A 29 (1975) 537—544

The Electrical Conductance of Rubidium Iodide in Water-Acetonitrile Solvent Mixtures at 25 °C

A. E. MAHGOUB * and AXEL LASSON

Institut for uorganisk kjemi, Norges tekniske högskole, Universitetet i Trondheim, Trondheim-NTH, Norway

The conductance of rubidium iodide in the concentration range 10^{-2} to 10^{-3} M has been measured in water-acetonitrile solvent mixtures. The solvent compositions covered the whole range from pure water to pure acetonitrile. The viscosities and the densities of the solvent mixtures were also determined.

The data were analysed according to the Fuoss-Onsager conductance equation. A graph of the limiting molar conductance, $\Lambda°$, *versus* solvent composition showed a pronounced minimum at about 20 mol percent acetonitrile, while the viscosity, η, had a maximum at about 10 mol percent. The Walden product, $\Lambda°\eta$, decreased steadily when going from pure water to pure acetonitrile.

The study of transport processes in general, and of conduction and diffusion in particular, is one of the many approaches to elucidate the structure of electrolyte solutions. This has been extensively used for aqueous solutions for which a large body of experimental data is available.

Classical theory tended to regard the solvent as merely providing the viscous and dielectric medium for the movement of the ions and for the long range ion-ion interactions. The interaction between the ions and the solvent molecules was often neglected. If there had been no such interaction — *i.e.* if the model of the ion as a charged sphere in a continuous medium had been valid — the Walden product (the limiting conductance times the viscosity of the solvent) for any given ion should be constant. This, however, is very often not the case. It is found to vary from solvent to solvent and also in the same solvent at different temperatures. In water, for instance, the Walden product for a given salt or ion varies considerably with temperature, having a positive temperature coefficient for some ions and a negative one for others, the latter being the most usual for simple ions. This has been interpreted in terms of the effect of the ions on the hydrogen bond structure of water. This interpretation is supported by the observation that in acetonitrile, which can be regarded as a non structural liquid, there seems to be very little variation in the Walden product with temperature for any given ion.[1]

In this respect, then, acetonitrile is close to an ideal solvent, while water is highly non-ideal. This raises the question of mixtures of water and acetonitrile. To the authors' knowledge no conductance data in these solvent mixtures have been reported. A project has therefore been started in these laboratories to investigate the conductances of the alkali- and the halide ions in water-acetonitrile mixtures. The measurements reported in this paper are part of this project.

Acetonitrile (methyl cyanide, CH_3CN, abbreviated, MeCN) is a non-associated liquid with a relatively high dielectric constant, 36.0 at 25 °C, due to the high dipole moment of the acetonitrile molecule (3.9 Debye in the gas phase, 3.4 – 3.5 in solutions).[2] For water the high dielectric constant, 78.5 at 25 °C, is, to a large extent, due to its associated structure through hydrogen bonds. The dipole moment of the water molecule is 1.8 D.

* Assistant Professor. Permanent address: Chemistry Department, Faculty of Science, University of Cairo, Egypt.

Conductance data for salts in mixed solvents also provide a test of the extended conduction equations commonly used. The data presented in this paper have been analyzed according to the Fouss-Onsager equation.[3,4] For completely dissociated electrolytes it has the form

$$\Lambda = \Lambda^\circ - Sc^{\frac{1}{2}} + Ec \log c + Jc \qquad (1)$$

S, the limiting Onsager slope, and E are given by

$$S = \alpha\Lambda^\circ + \beta \text{ and } E = E_1\Lambda^\circ - E_2$$

where α, β, E_1 and E_2 are constants depending on solvent properties only (dielectric constant and viscosity), and on temperature.

The coefficient of the linear term, J, is similarly given by

$$J = \sigma_1\Lambda^\circ + \sigma_2$$

where σ_1 and σ_2 are functions of the ion size parameter a (the distance of closest approach or the mean ionic diameter), in addition to viscosity, dielectric constant and temperature.

At 25 °C the constants in the conduction equation are given by

$$\alpha = 159.35/D^{3/2}$$
$$\beta = 4.7779/\eta D^{1/2}$$
$$E_1 = 2.5559 \times 10^5/D^3$$
$$E_2 = 1122.3/\eta D^2$$
$$\sigma_1 = 0.4343E_1(7.133 \times 10^5 aD + 1.274 \times 10^{11}a^2D^2 - 1.137 \times 10^{16}a^3D^3 + 3.953 - \ln D + 2 \ln 10^8 a)$$
$$\sigma_2 = \alpha\beta + 12.757 \times 10^8 a - 0.4343E_2(4.172 - \ln D + 2 \ln 10^8 a)$$

The extended conduction equation (1) is the well-known Onsager limiting equation $\Lambda = \Lambda^\circ - Sc^{\frac{1}{2}}$, to which have been added the terms $Ec \log c$ and Jc. These represent mainly the higher terms of the relaxation effect, the leading term of which is $\alpha\Lambda^\circ$.

A convenient way to analyse the data is to use the function Λ' defined by

$$\Lambda' = \Lambda + Sc^{\frac{1}{2}} - Ec \log c \qquad (2)$$

It follows from eqns. (1) and (2) that

$$\Lambda' = \Lambda^\circ + Jc \qquad (3)$$

A plot of Λ' *versus* concentration should give a straight line with intercept Λ° and slope J.

In order to calculate the value of Λ' for each concentration, one must, however, know the value of Λ° (to find S and E). A simple procedure is to find a preliminary value of Λ° – usually by a straight line extrapolation by hand of a Λ *versus* $c^{\frac{1}{2}}$ plot – and to use this to calculate preliminary values of S and E. An extrapolation of the Λ' *versus* c plot to zero concentration then gives a more accurate value of Λ°, which in turn is used to calculate more accurate values of S and E. This procedure is then repeated until one gets no further change in Λ°. Usually two iterations are sufficient.

If the electrolyte is associated, an additional term – the association term – must be added to the conduction equation:

$$\Lambda = \Lambda^\circ - Sc_i^{\frac{1}{2}} + Ec_i \log c_i + Jc_i - K_A\Lambda f_\pm^2 c_i \qquad (4)$$

Here K_A is the association constant. $f_\pm$ is the mean ionic activity coefficient, and it can be calculated from the Debye-Hückel theory: $\log f_\pm^2 = -708.85\ c^{\frac{1}{2}}/D^{3/2}$. c_i is the concentration of ions: $c_i = \gamma c$ where γ is the degree of dissociation. K_A and γ are related through $K_A = (1-\gamma)/c\gamma^2 f_\pm^2$. When the degree of association is small, one can approximate c_i by c.

The need to include an association term in the conduction equation is indicated by the Λ' plot becoming curved upwards. A graph of Λ'' *versus* c_i, however, should be linear when Λ'' is defined by

$$\Lambda'' = \Lambda + Sc_i^{\frac{1}{2}} - Ec_i \log c_i + K_A\Lambda f_\pm^2 c_i \quad (= \Lambda^\circ + Jc_i) \qquad (5)$$

Fitting the experimental data to these conduction data is most conveniently done by computer. A program was developed that is essentially a modified version of the one suggested by Kay.[5] By a least squares method the data were first fitted to the three parameter eqn. (5), and then, if the association constant is small, to the two parameter eqn. (1) From the values of the root mean square deviations one could then see which of the two conduction equations gave the better fit.

EXPERIMENTAL

Materials. Acetonitrile. Baker's reagent grade acetonitrile with a maximum water content of 0.2 % was stored over calcium hydride of mixed mesh for at least one day with intermittent shaking. After refluxing it was distilled onto phosphorus pentoxide, from which it was redistilled at once. The middle fraction of a final distillation gave a constant boiling product with a density of 0.7768 g/cm³ and a specific conductivity in the range $(0.3-1)\times10^{-7}$ ohm^{-1} cm^{-1}.

Water. After distillation and deionising, the water used had a specific conductivity of $(0.8-1)\times10^{-6}$ ohm^{-1} cm^{-1}.

The salts. Merck's suprapure rubidium iodide and potassium chloride were used without further purification, except for drying at about 400 °C in a stream of dry nitrogen.

Bridge and accessories. The bridge was a Tinsley, LCRF, type 4725 conventional a.c. bridge with an accuracy of better than 0.1 %, with a separate Wagner earth device. The signal generator (Hewlett Packard model 201 oscillator with continuous frequency control) and the oscilloscope, used as a null detector, were connected so as to display the signal as an ellipse for easy distinction between capacitative and resistive imbalance.

The cells were of pyrex glass and of conventional design.

Experimental procedure. The electrodes were of bright platinum which made the resistance markedly frequency dependent. Frequencies between 770 and 10 000 Hz were used. Plots of resistance *versus* frequency^{-1} were rectilinear and could easily be extrapolated to infinite frequency. This extrapolated resistance was used to calculate the conductivity of the solution. Correction was made for the conductivity of the pure solvent, which for the solvent mixtures was about 10^{-6} ohm^{-1} cm^{-1}.

Calibration of the cells was made with aqueous potassium chloride solutions in the concentration range 0.002 to 0.01 M. The conductivities of these solutions were calculated using the equation given by Lind, Zwolenik and Fuoss,[6]

$$\Lambda = 149.93 - 94.65c^{\frac{1}{2}} + 58.71\ c \log c + 198.4c$$

All solutions were made up by weight reduced to vacuum. The concentrations in mol/liter were calculated, assuming the densities of the solutions to be that of the pure solvent.

The densities of the solvent mixtures were determined by the conventional pycnometer method, and the viscosities by measuring the

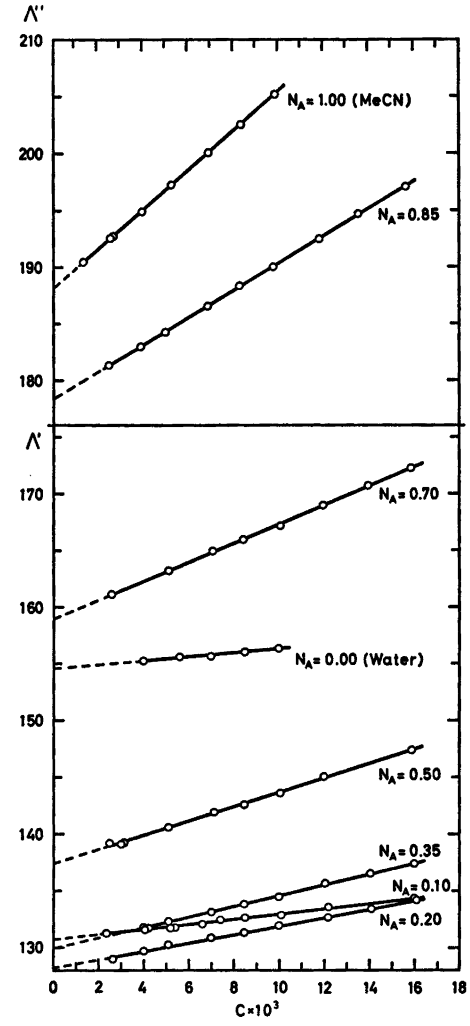

Fig. 1. Λ' and Λ'' versus c for RbI in water–acetonitrile mixtures.

Table 1. The dielectric constant (D), the viscosity (η) and the density (d) of water-acetonitrile mixtures at 25 °C.

N_A	0.00	0.10	0.20	0.35	0.50	0.70	0.85	1.00
D	78.5	70.6	62.2	53.2	47.0	41.5	38.5	36.0
η (cp)	0.890	0.970	0.864	0.698	0.552	0.431	0.371	0.347
d (g/cm³)	0.9971	0.9611	0.9232	0.8791	0.8445	0.8080	0.7905	0.7768

Table 2. The equivalent conductance of RbI in water-acetonitrile mixtures. c in mol/l, Λ in ohm^{-1} cm^2.

$N_A = 0.00$		$N_A = 0.35$		$N_A = 0.85$	
10^3c	Λ	10^3c	Λ	10^3c	Λ
2.5847	149.70	3.9739	121.00	2.5384	160.38
3.9740	148.68	5.1023	119.97	3.9519	156.01
5.5665	147.75	7.0317	118.39	5.0577	153.16
7.0328	146.76	8.4642	117.48	6.9328	149.31
8.5037	146.16	9.9614	116.55	8.4040	146.77
10.027	145.57	12.065	115.70	9.9331	144.31
		14.072	114.82	12.005	141.50
		15.982	114.06	13.770	139.56
				15.922	137.25
$N_A = 0.10$		$N_A = 0.50$		$N_A = 1.00$	
10^3c	Λ	10^3c	Λ	10^3c	Λ
2.3559	126.32	2.5370	127.79	1.4264	172.31
4.0631	124.95	2.9894	126.61	2.6559	166.60
4.2571	124.94	3.1644	126.44	2.7987	165.98
5.1723	124.14	5.1086	123.84	4.0428	161.71
5.4212	124.03	7.0778	121.86	5.3745	158.13
6.6328	123.55	8.4653	120.43	7.1170	154.09
7.3824	123.29	10.060	119.18	8.6520	151.13
8.5146	122.75	11.999	118.13	10.156	148.85
10.086	122.06	15.920	115.81		
12.210	121.55				
16.004	120.48				
$N_A = 0.20$		$N_A = 0.70$			
10^3c	Λ	10^3c	Λ		
2.6285	122.54	2.6070	144.74		
4.0042	121.63	5.1230	139.23		
5.0722	121.08	7.0761	136.15		
6.9983	120.00	8.4379	134.14		
8.4583	119.25	10.066	132.03		
9.9940	118.73	11.988	130.15		
12.184	117.91	14.035	128.25		
14.051	117.43	15.912	126.62		
16.101	116.95				

flow time in an Ostwald viscometer. In both cases water was used for calibration. The density and viscosity of pure water at 25 °C were taken to be 0.9971 g/cm^3 and 0.890 centipoise, respectively.[7]

The temperature was kept at 25.0 ± 0.01 °C.

For each solvent composition, 8 to 12 solutions of different concentrations of RbI were used. These were made up from three independently prepared stock solutions. Only six different solutions were used in water, for which published data for the conductance of RbI were available. Our measurements in pure water were made as a quick check on the apparatus and experimental procedure.

RESULTS AND DISCUSSION

The dielectric constant, D, the viscosity, η, and the density, d, of the eight solvents used are shown in Table 1. The solvent composition is given in terms of N_A – the mol fraction of acetonitrile. The values of the dielectric constants have been interpolated from a large scale graph of the data of Douhéret and Morénas.[8] Our density data agree well with the ones reported by Maslan and Stoddard Jr.[9] No viscosity data at 25 °C could be found in the literature.

The results of the conductance measurements of rubidium iodide in the eight solvents used

Table 3. Values of the parameters in the conduction equations for RbI in water–acetonitrile mixtures.

N_A	0.00	0.10	0.20	0.35	0.50	0.70	0.85	1.00
Λ°	154.56±0.09	130.68±0.06	128.24±0.09	129.99±0.06	137.39±0.09	158.98±0.07	178.31±0.16	188.02±0.16
J	181±13	232±7	371±9	464±5	629±11	832±7	1199±31	1735±66
a(Å)	2.82±0.19	3.31±0.11	3.98±0.10	3.28±0.04	3.01±0.06	2.43±0.02	2.57±0.07	3.02±0.14
K_A	–	–	–	–	–	–	2.3±0.7	6.2±1.1
$\sigma\Lambda$	0.08	0.09	0.12	0.06	0.14	0.08	0.06	0.07

are given in Table 2. These data were analysed by the methods outlined in the introduction. For solvents with mol fraction of acetonitrile 0.70 or less, conduction eqn. (1), *i.e.* without association, gave the best fit. The Λ' plots for these systems are rectilinear and are shown in Fig. 1. For $X_A = 0.85$ and 1.00, the Λ' plots showed a slight upward curvature. The deviations from straight lines were within the estimated limits of experimental errors, approximately 0.1 %, but they were systematic with positive deviations at high and low concentrations, and negative in the middle range. For these two systems, then, the data were fitted to the three parameter conduction eqn. (4), and it is the Λ'' plot that is shown on Fig. 1.

The values of Λ°, J, a, and K_A and their standard deviations are given in Table 3. The last row of the table gives the root mean square deviation defined by $\sigma\Lambda = (\sum d_i^2/n-2)^{\frac{1}{2}}$ and $\sigma\Lambda = (\sum d_i^2/n-3)^{\frac{1}{2}}$, respectively, according to whether the data have been fitted to the two parameter or to the three parameter conduction equation. Here d_i is the difference between the observed Λ and the calculated Λ and n is the number of experimental points. It is seen that the $\sigma\Lambda$'s are 0.03 to 0.10 % of the values of Λ°. This shows that the self-consistency of the data is satisfactory. But there may be systematic errors (in viscosity, density, dielectric constant, bridge resistance, cell constant, *etc.*) in addition to the random errors that are reflected in the values of the root mean square deviations.

The only Λ° value which can be compared with previously reported data is the one in pure water. Robinson and Stokes [7] have compiled a table of the most reliable (up to 1959) values of single ion conductances in water at 25 °C. From their values of 77.8_1 and 76.8_4 for λ° of

Table 4. Values for the terms in the conduction equations for RbI in water-acetonitrile mixtures.

$N_A = 0.10$	$\Lambda^\circ = 130.68$	$S = 93.74$	$E = 71.7$	$J = 231.5$	
10^3c (mol/l)	2.3559	5.1723	8.5146	12.210	16.004
Λ(ohm^{-1} cm^2)	126.32	124.14	122.75	121.55	120.48
$Sc^{\frac{1}{2}}$	4.55	6.74	8.65	10.36	11.86
$-Ec \log c$	0.44	0.85	1.26	1.68	2.06
Jc	0.54	1.20	1.97	2.83	3.71
d_i	+0.09	−0.15	+0.01	+0.08	+0.01
$N_A = 0.70$	$\Lambda^\circ = 158.98$	$S = 266.98$	$E = 417.2$	$J = 832$	
10^3c (mol/l)	2.6070	5.1230	8.4379	11.988	15.912
Λ(ohm^{-1} cm^2)	144.74	139.23	134.14	130.15	126.62
$Sc^{\frac{1}{2}}$	13.63	19.11	24.52	29.23	33.68
$-Ec \log c$	2.81	4.90	7.30	9.61	11.94
Jc	2.17	4.27	7.02	9.98	13.25
d_i	+0.03	−0.01	−0.04	+0.03	+0.01
$N_A = 1.00$	$\Lambda^\circ = 188.02$	$S = 368.1$	$E = 780.5$	$J = 1735$	$K_A = 6.2$
10^3c (mol/l)	1.4264	2.7987	5.3745	7.1170	10.156
Λ(ohm^{-1} cm^2)	172.31	165.98	158.13	154.09	148.85
$Sc^{\frac{1}{2}}$	13.86	19.36	26.74	30.70	36.58
$-Ec_i \log c_i$	3.15	5.52	9.38	11.71	15.46
Jc_i	2.46	4.80	9.16	12.07	17.13
$K_A\Lambda f_{\pm}c_i^2$	1.15	1.93	3.01	3.56	4.33
d_i	−0.01	+0.03	+0.08	−0.03	+0.07

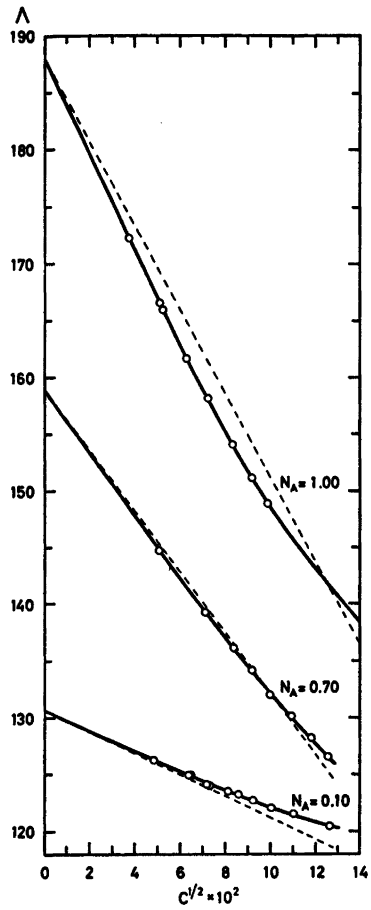

Fig. 2. Λ versus $c^{\frac{1}{2}}$ for RbI in water-acetonitrile mixtures. (---) Onsager limiting tangent. (———) Calculated from the conduction equation. (O) Experimental point.

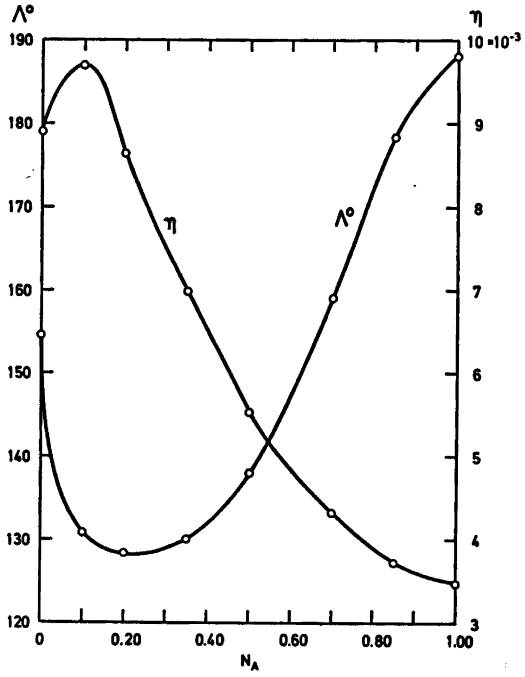

Fig. 3. Λ° for RbI and viscosity of solvent *versus* mol fraction of acetonitrile in water–acetonitrile solvent mixtures.

Rb^+ and I^-, one gets $\Lambda^\circ_{RbI} = 154.6_6$ as compared with our 154.56. The excellent agreement – to within 0.06 % – is probably fortuitous since our measurements in water were made just as a quick check on the apparatus and experimental procedure. The value for Λ°_{RbI} as calculated from Kay's table,[5] and the one reported by Fabry and Fuoss,[10] are lower (about 154.1_5 and 154.0).

It is of interest to consider the magnitudes of the individual terms in the conduction eqns. (1) and (4). This is done in Table 4 for three solvent compositions, 10, 70, and 100 % acetonitrile. The first two of these have been chosen because they clearly show the effect of the higher terms, *i.e.* the logarithmic and the linear terms, in the conduction eqn. (1). Of these terms, the logarithmic is negative while the linear is positive. At very low concentrations $Ec \log c$ will be numerically larger than Jc. This will be the case when $c < 10^{-J/E}$. The points on a Λ *versus* $c^{\frac{1}{2}}$ plot will then lie below the Onsager limiting tangent represented by the line $\Lambda = \Lambda^\circ - Sc^{\frac{1}{2}}$. For $c > 10^{-J/E}$ the points will lie above this line (see Fig. 2).

For the solvent mixture containing 10 % acetonitrile, we have $E_1 = 0.7263$, $E_2 = 23.22$, and $E = E_1\Lambda^\circ - E_2 = 71.70$. J was found to be 232. The concentration at which the Λ crosses the Onsager limiting tangent is then $10^{-232/71.70} = 5.8 \times 10^{-4}$ M. This is below the concentration range covered in this investigation. It becomes difficult to get accurate conductance data as one comes down to such low concentrations, because of the uncertainty in the correction for the conductivity of the pure solvent. For this solvent composition, then, all the experimental points lie above the Onsager limiting tangent.

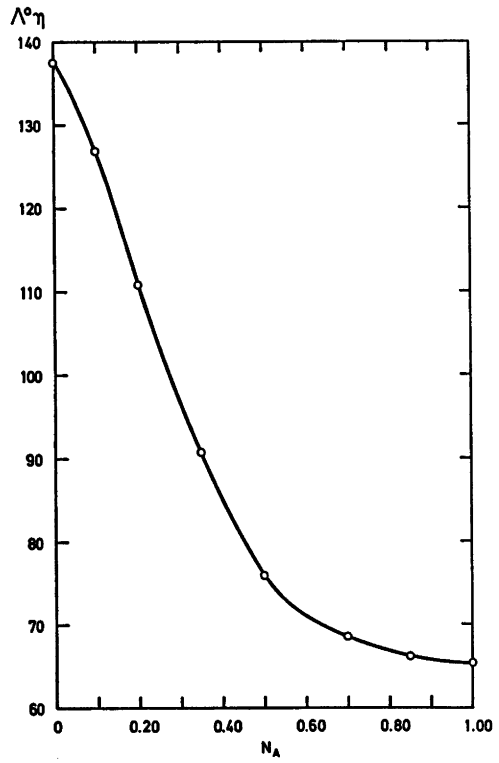

Fig. 4. $\Lambda^\circ\eta$ for RbI *versus* mol fraction of acetonitrile in water – acetonitrile mixtures.

For 70 % acetonitrile, however, the situation is different. Because of the lower dielectric constant and viscosity, the value of E is larger: $E = 417.2$. J was found to be 832 and the "crossing" concentration is then $10^{-832/417.2} = 1.0 \times 10^{-2}$ M, which is well within the actual working range. Fig. 2 clearly shows the difference between the 10 % and the 70 % acetonitrile mixtures in this respect.

For pure acetonitrile, a small association term had to be added to the conduction equation to get the best fit. The "crossing" concentration is still higher than in 70 % acetonitrile.

Fig. 3 shows how Λ° for rubidium iodide varies with solvent composition. The Λ° has a conspicuous minimum at about 20 mol percent acetonitrile, while the viscosity, shown in the same figure, has a maximum at about 10 mol percent. There is, then, no obvious direct relationship between Λ° and viscosity. The Walden product, $\Lambda^\circ\eta$, is plotted *versus* solvent composition in Fig. 4. It decreases monotonically from pure water to pure acetonitrile. This shows that the model on which Stoke's law, and hence Walden's rule, is based – the sphere in a continuous viscous medium – is not valid for this system. The sharp decrease in the Walden product as acetonitrile is added to water, reflects a corresponding increase in the solute-solvent interaction (solvation). In terms of Stoke's law, the rubidium and/or the iodide ions (or rather the spheres that are hydrodynamically equivalent to these), become larger as the acetonitrile content increases. There is, however, no a priori reason why the mobilities of the two ions should be affected to the same extent by the change in solvent composition. In fact, known single ion conductances in pure water and pure acetonitrile [11] indicate that the rubidium ion is more affected than the iodide ion. Further comments on specific ion-solvent interaction will, however, have to wait until single ion conductances in this solvent system have been determined. Work on this is now in progress in this laboratory.

Acknowledgement. We express our gratitude to the Norwegian Agency of International Development which made this work possible through a research fellowship to one of us (A.E. Mahgoub). We also want to thank Professor Harald A. Øye for his encouragement and support.

REFERENCES

1. Evans, D. F. and Broadwater, T. L. *J. Phys. Chem. 72* (1968) 1037.
2. Smyth, C. P. *Dielectric Behaviour and Structure*, McGraw Hill, New York 1955.
3. Fuoss, R. M. and Onsager, L. *J. Phys. Chem. 61* (1957) 668; *Ibid. 62* (1958) 1339.
4. Fuoss, R. M. and Accascina, F. *Electrolytic Conductance*, Interscience, New York 1959.
5. Kay, R. L. *J. Amer. Chem. Soc. 82* (1960) 2099.
6. Lind, J. E., Zwolenik, J. J. and Fuoss, R. M. *J. Amer. Chem. Soc. 81* (1959) 1557.
7. Robinson, R. A. and Stokes, R. H. *Electrolyte Solutions*, Butterworths, London 1959.
8. Douhéret, G. and Morénas, M. *C. R. Acad. Sci. Ser. C 264* (1967) 729.
9. Maslan, F. D. and Stoddard, Jr., E. A. *J. Phys. Chem. 60* (1956) 1147.
10. Fabry, T. L. and Fuoss, R. M. *J. Phys. Chem. 68* (1964) 974.
11. Cunningham, G. P., Evans, D. F. and Kay, R. L. *J. Phys. Chem. 70* (1966) 3998.

Received September 5, 1974.

Acta Chemica Scandinavica A 29 (1975) 545—552

Electron-diffraction Studies of Chlorobutatriene and Chlorobutenynes. II. Molecular Structures of Gaseous *cis*- and *trans*-1-Chlorobutenynes

ARNE ALMENNINGEN,[a] GRETE GUNDERSEN,[a] ASTRID BORG,[b] MATS GRANBERG[b] and FRED KARLSSON[b]

[a] Department of Chemistry, University of Oslo, Oslo 3, Norway and [b] Department of Physical Chemistry, University of Stockholm, Arrhenius Laboratory, Fack, S-104 05 Stockholm, Sweden

The molecular structure of *cis*- and *trans*-1-chlorobuten-3-yne have been investigated by electron diffraction from the vapour. Normal coordinate calculations based upon assumed force fields supplied amplitudes of vibration which could not be determined from the electron-diffraction data, and correction terms which were used in geometrically consistent r_α-refinements. The final bond distances (r_a-values; Å) and valence angles (°) are:

	cis	*trans*
C(*sp*)−H	1.068(17)	1.090(15)
C(sp^2)−H	1.095(17)	1.117(15)
C≡C	1.212(6)	1.220(8)
C=C	1.345(7)	1.356(7)
C−C	1.426(6)	1.436(6)
C−Cl	1.716(5)	1.717(4)
∠C=C−C	123.9(0.6)	120.7(1.0)
∠C≡C−C	178.0(2.2)	180.2(2.4)
∠C=C−Cl	123.9(0.6)	121.1(0.8)
∠C=C_1−H	119.2(4.4)	124.7(4.2)
∠C=C_2−H	122.0 (assumed)	122.0 (assumed)
∠C≡C−H	180.0 (assumed)	180.0 (assumed)

Parenthesized values are 2σ where systematic uncertainties are included.

Electron-diffraction studies of *cis*- and *trans*-1-chlorobuten-3-yne were carried out as a part of the determination of the molecular structures of gaseous C_4H_3Cl isomers.[1]

EXPERIMENTAL AND CALCULATION PROCEDURES

Pure *cis*- and *trans*-1-chlorobuten-3-yne were obtained and prevented from polymerization as described for chlorobutatriene.[1] Some, but not severe loss of sample due to polymerization during the experiment was experienced. Electron diffraction photographs were made in the Oslo Apparatus [2] at nozzle-to-plate distances of 48 and 28 cm, keeping the sample reservoirs at about −12 and −15 °C, respectively for the two compounds. The electron wavelength was 0.06464 Å as calibrated against diffraction patterns of gaseous benzene. The scattering functions for the 35 kV electrons were those computed for chlorobutatriene. Three plates made at each of the two camera distances were used in the investigation for both compounds. The plates were handled and the data reduced in routine fashion [3] to yield the experimental modified intensities and radial distribution curves shown respectively in Figs. 1 and 3, and Figs. 2 and 4 for the two compounds. The structure analysis and supporting calculations were carried out using the standard procedures and computer programs [3–5] as outlined elsewhere.[1]

CALCULATIONS AND REFINEMENTS

Planar models of 1-chlorobutenyne are described by thirteen geometrical parameters; see Fig. 5. In this investigation the following restrictions were introduced: ∠C≡C−H = 180°, $r_{C_1-H} = r_{C_3-H} = r_{C_4-H} + 0.027$ Å $= r_{C-H}$. The ten parameters to be adjusted were then: r_{C-H}, $r_{C\equiv C}$, $r_{C=C}$, r_{C-C}, r_{C-Cl}, ∠C=C−Cl, ∠C=C−C, ∠C≡C−C (*trans* to the C=C−C angle), ∠C=C_1−H, and ∠C=C_2−H.

Force constants for similar molecules were used to design a diagonal force field for *cis*- and *trans*-chlorobutenyne; see Table 1. Normal coordinate calculations were then carried out

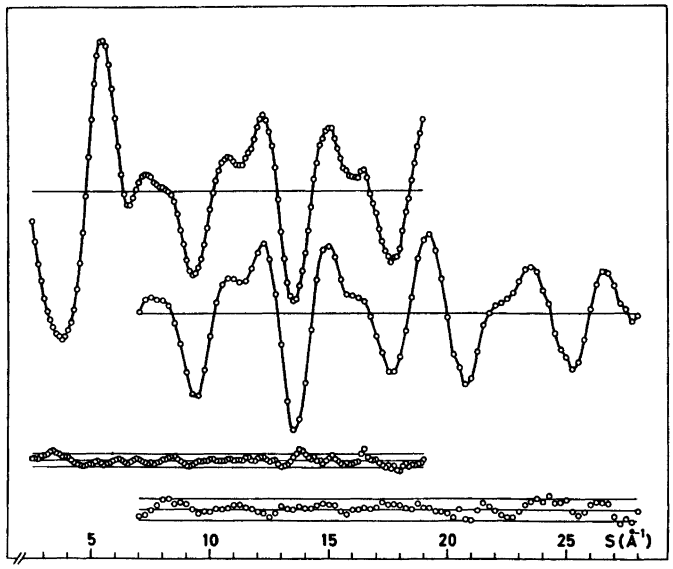

Fig. 1. Experimental intensity data for *cis*-1-chlorobutenyne from the 48 cm ($\Delta s = 0.125$ Å^{-1}) and 28 cm ($\Delta s = 0.25$ Å^{-1}) camera distances. Theoretical curves are not shown, but the corresponding differences between experimental and theoretical intensities calculated according to the parameter values of Table 4, are given. The full lines given along with the differences indicate the estimated uncertainties (three standard deviations) of the experimental intensity points.

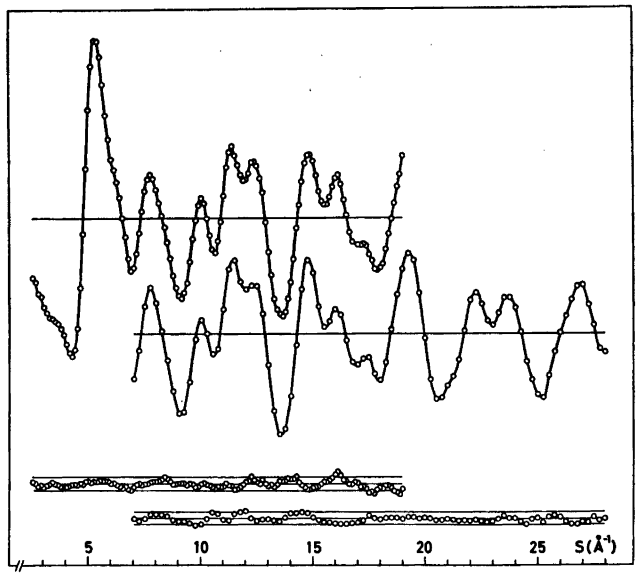

Fig. 2. Experimental intensity data for *trans*-1-chlorobutenyne from the 48 cm ($\Delta s = 0.125$ Å^{-1}) and 28 cm ($\Delta s = 0.25$ Å^{-1}) camera distances. Theoretical curves are not shown, but the corresponding differences between experimental and theoretical intensities calculated according to the parameter values of Table 4, are given. The full lines given along with the differences indicate the estimated uncertainties (three standard deviations) of the experimental intensity points.

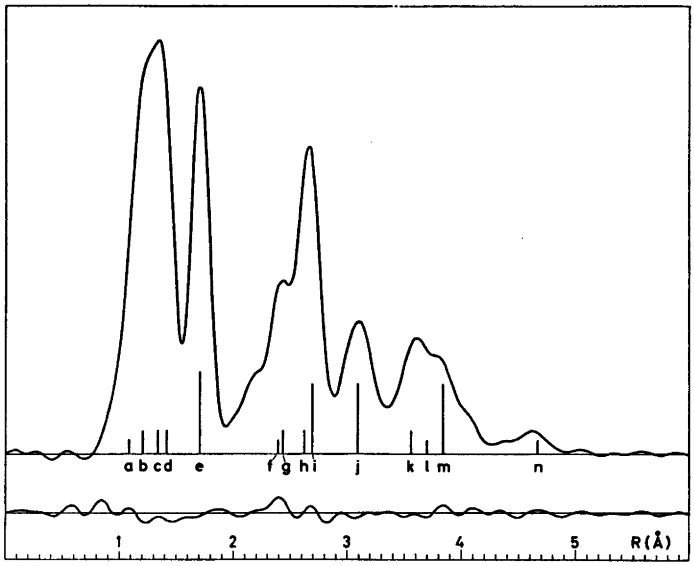

Fig. 3. Experimental radial distribution curve for *cis*-1-chlorobutenyne, calculated for the artificial damping constant $k = 0.0015$ Å^2. The approximate positions of the important interatomic distances are indicated: a, C(sp^2) – H and C(sp) – H; b, C≡C; c, C=C; d, C–C; e, C–Cl; f, Cl···H_7; g, C_1···C_3; h, C_2···C_4; i, C_2···Cl; j, C_3···Cl; k, C_1···C_4; *l*, Cl···H_6; m, C_1···Cl; n, Cl···H_5. The difference between the experimental and theoretical radial distribution curves calculated according to the parameter values in Table 4 is also shown.

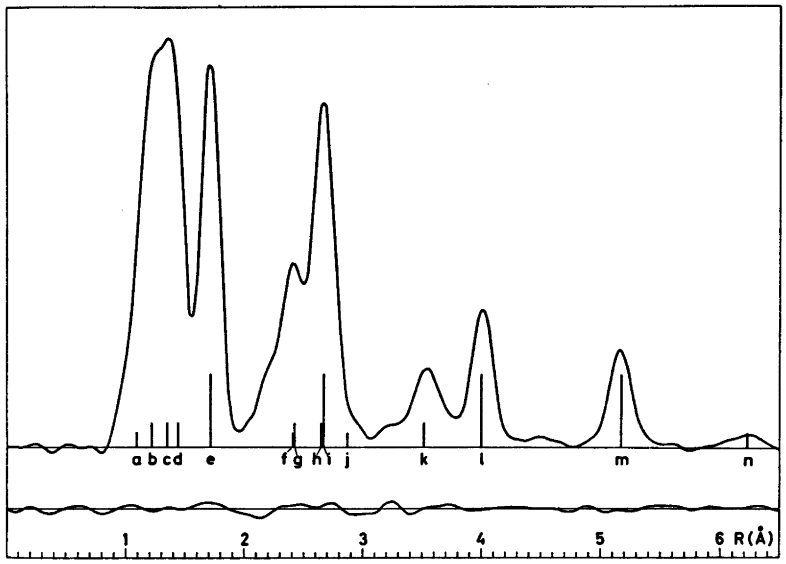

Fig. 4. Experimental radial distribution curve for *trans*-1-chlorobutenyne calculated for the artificial damping constant $k = 0.0015$ Å^2. The approximate positions of the important interatomic distances are indicated: a, C(sp^2) – H and C(sp) – H; b, C≡C; c, C=C; d, C–C; e, C–Cl; f, Cl···H_7; g, C_1···C_3; h, C_2···C_4; i, C_2···Cl; j, Cl···H_6; k, C_1···C_4; l, C_3···Cl; m, C_4···Cl; n, Cl···H_5. The difference between the experimental and theoretical radial distribution curves calculated according to the parameter values in Table 4 is also shown.

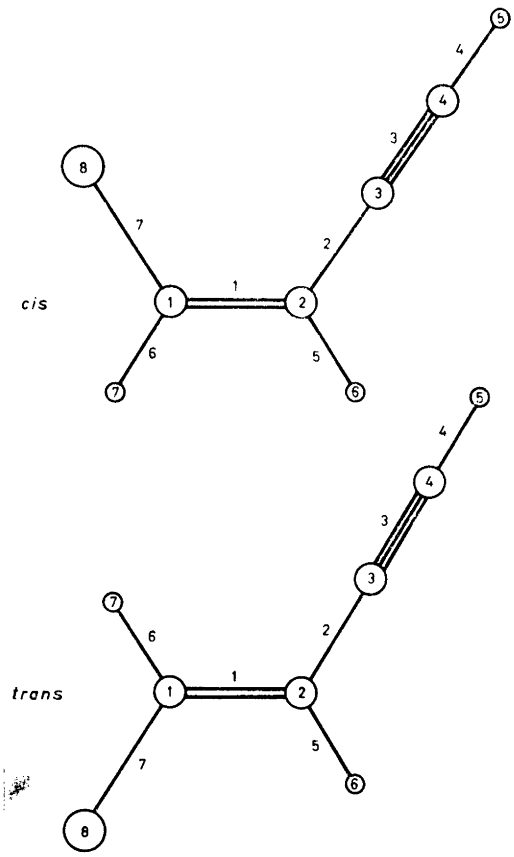

Fig. 5. Numbering of atoms and bonds in *cis*- and *trans*-1-chlorobutenyne, C_4H_3Cl.

Table 1. Force field for *cis*- and *trans*-1-chlorobuten-3-yne.[a]

$K_1 = 9.1$	$K_{16} = 0.50$	$\varrho_7^{16} = 0.30$
$K_2 = 4.6$	$K_{17} = 0.85$	$\varrho_6^{17} = 0.20$
$K_3 = 15.7$	$K_{67} = 0.25$	$\varrho_5^{12} = 0.20$
$K_4 = 6.3$	$K_{15} = 0.53$	$\varrho_2^{15} = 0.25$
$K_5 = 5.4$	$K_{25} = 0.25$	$\chi_{12}^{16} = \chi_{15}^{18} = 0.12$ (0.14)[c]
$K_6 = 5.6$	$K_{12} = 0.84$	$\chi_{15}^{16} = \chi_{12}^{18} = 0.14$ (0.12)[c]
$K_7 = 3.9$	$K_{23}^{b} = 0.32$	
	$K_{34}^{b} = 0.23$	

[a] For numbering of the bonds, see Fig. 3. The meaning of the symbols: K_i, stretching of bond i; K_{ij}, bending of angle between bonds i and j; ϱ_k^{ij}, bending of bond k out of ij-plane; χ_{kl}^{ij}, torsion between the ij- and kl-planes. The force constants are given in mdyn/Å and mdynÅ/(rad)². [b] Identical force constants for bending in plane and out of plane are assumed. [c] Parenthesized values for *trans*.

using coordinates consistent with the models given in Table 3 where also the resulting D and l-values [5] are given. The obtained l-values agree well with those calculated for corresponding distances in butenyne.[6]

The interpretation of the main features of the experimental radial distribution curves was straightforward as indicated by the approximate positions of the important interatomic distances (*cf.* Table 3) shown in Figs. 2 and 4, respectively, for *cis*- and *trans*-chlorobutenyne. Least-squares refinements were carried out under conditions given in Table 2. The results of r_a-refinements where the amplitudes of vibration were fixed at the calculated values and where $\angle C = C_2 - H = 122.0°$ are given in Table 3. Corresponding r_α-refinements where the D-values in Table 3 were used to obtain the geometrically consistent models [5] did not result in significant changes in the parameter values nor in the least-squares fits. Attempts were now made to include the amplitudes of vibration in the least-squares refinements, except those corresponding to the C···H and H···H non bonded interactions. Amplitudes for overlapping distances were refined in groups. The group containing the C,C bond distances refined, however, to unreasonable values for both molecules, as was also the case for the C,H bond distances in *cis*-chlorobutenyne. These amplitudes were therefore restricted to the calculated values, which finally also was the case for the amplitudes associated with the two longest Cl···H distances. The results of a refinement using these restrictions on the amplitudes are given in Table 4 for *trans*-chlorobutenyne. A corresponding refinement for *cis*-chlorobutenyne revealed additional problems. The amplitudes for the two groups of amplitudes corresponding to interatomic distances at about 2.4 and 2.6 Å both refined to unacceptable low values ($l_{C_1C_3} = 0.043$, $l_{C_2C_4} = 0.037$), and they were consequently also fixed at the calculated values. The result of this final refinement for *cis*-chlorobutenyne is given in Table 4. The least-squares fit was better for the less restricted refinement ($R = 6.37$ %), but only the values for the C – C single bond (1.417(3) Å) and the C = C – C angle (124.7(0.3)°) differed from those of the final model by as much as two standard deviations. Non-planar models (torsion about the C = C bond and bending

Table 2. Refinement conditions for *cis*- and *trans*-1-chlorobuten-3-yne.

	Curve	Data range		Data interval	Constants of the weightscheme [4,5]						
	(camera dist.)	s_{min}	s_{max}	Δs	s_1	s_2	w_1	w_2	p_1	p_2	W
cis-	48 cm	2.50	19.50	0.125	6.00	15.00	0.05	0.01	−0.64	0.146	1.0
	28 cm	7.00	28.00	0.25	7.00	22.00	0.05	0.02	−0.60	0.125	0.5
trans-	48 cm	2.50	19.00	0.125	6.50	15.00	0.05	0.01	−0.64	0.146	1.0
	28 cm	7.00	28.00	0.25	8.00	22.00	0.05	0.02	−0.60	0.125	0.5

Table 3. Computed *D*- and *l*-values, and r_a-structure for *cis*- and *trans*-chlorobutenyne.[a]

Parameters [b]		*cis* *D*-values	*l*-values	r_a-structure [c]	*trans* *D*-values	*l*-values	r_a-structure [c]
C−H	4,5	−0.0329	0.072	1.069(8)	−0.0348	0.072	1.083(7)
	2,6	−0.0103	0.075	1.096(8)	−0.0095	0.075	1.110(7)
	1,7	−0.0117	0.074		−0.0106	0.074	1.110(7)
C≡C	3,4	−0.0104	0.036	1.210(3)	−0.0121	0.036	1.220(3)
C=C	1,2	−0.0025	0.041	1.344(3)	−0.0010	0.041	1.355(3)
C−C	2,3	−0.0024	0.048	1.423(3)	−0.0027	0.048	1.437(3)
C−Cl	1,8	−0.0027	0.047	1.716(2)	−0.0053	0.047	1.716(1)
C...C	2,4	−0.0039	0.052	2.633(4)	−0.0059	0.052	2.657(4)
	1,3	−0.0015	0.066	2.446(5)	−0.0009	0.067	2.419(5)
	1,4	−0.0002	0.086	3.574(7)	−0.0028	0.090	3.521(4)
C···Cl	2,8	−0.0005	0.067	2.699(3)	−0.0018	0.067	2.674(3)
	3,8	+0.0036	0.126	3.098(7)	−0.0005	0.069	4.013(3)
	4,8	+0.0085	0.188	3.856(14)	+0.0009	0.081	5.180(3)
Cl···H	8,7	−0.0055	0.110	2.404(27)	−0.0081	0.109	2.408(26)
	8,6	−0.0032	0.097	3.716(8)	+0.0026	0.151	2.869(6)
	8,5	+0.0053	0.259	4.687(22)	−0.0081	0.118	6.233(7)
C···H	3,5	−0.0291	0.077	2.279(9)	−0.0327	0.077	2.303(8)
	2,5	−0.0158	0.085	3.703(10)	−0.0195	0.085	3.740(8)
	1,5	−0.0081	0.127	4.605(12)	−0.0135	0.131	4.550(8)
	1,6	−0.0057	0.098	2.138(8)	−0.0033	0.098	2.159(7)
	3,6	−0.0044	0.108	2.118(8)	−0.0042	0.106	2.190(10)
	4,6	−0.0024	0.127	3.228(11)	−0.0024	0.124	3.338(10)
	2,7	−0.0076	0.098	2.127(23)	−0.0041	0.099	2.180(23)
	3,7	−0.0058	0.098	3.437(18)	+0.0011	0.147	2.716(44)
	4,7	−0.0023	0.105	4.610(15)	+0.0005	0.189	3.559(42)
H···H	6,7	−0.0038	0.165	2.488(35)	−0.0060	0.119	3.169(19)
	5,6	−0.0110	0.158	4.250(18)	−0.0119	0.154	4.389(16)
	5,7	−0.0072	0.134	5.659(19)	−0.0088	0.241	4.456(41)
∠C=C−C		–	–	124.2(0.4)	–	–	120.0(0.5)
∠C≡C−C		–	–	178.9(1.2)	–	–	181.9(1.1)
∠C=C−Cl		–	–	123.3(0.3)	–	–	120.7(2.2)
∠C=C_1−H		–	–	120.9(2.1)	–	–	124.1(0.3)
∠C=C_2−H		–	–	[122.0]	–		[122.0]
R_w [d] (%)		–	–	8.23			7.24

[a] Correction terms (*D*-values), amplitudes (*l*-values) and distances (r_a) in Ångströms; angles in degrees. The r_a-structure gives the result of r_a-refinement (no *D*-value correction) using the calculated *l*-values. [b,c,d] See corresponding comments under Table 4.

Table 4. Important parameter values and corresponding moments of inertia for *cis*- and *trans*-1-chlorobutenyne.[a]

Parameters [b]		*cis*- r_a [c]	l [c]	*trans*- r_a [c]	l [c]
C–H	4,5	1.068(8)	[0.072]	1.090(7)	0.071(10)′
	2,6	1.095(8)	[0.075]	1.117(7)	0.074(10)′
	1,7	1.095(8)	[0.074]	1.117(7)	0.074(10)′
C≡C	3,4	1.212(3)	[0.036]	1.220(3)	[0.036]
C=C	1,2	1.345(3)	[0.041]	1.356(3)	[0.041]
C–C	2,3	1.426(3)	[0.048]	1.436(3)	[0.048]
C–Cl	1,8	1.716(2)	0.051(3)	1.717(1)	0.047(2)
C···C	2,4	2.629(5)	[0.052]	2.646(5)	0.046(3)″
	1,3	2.442(4)	[0.066]	2.424(5)	0.053(5)‴
	1,4	3.565(6)	0.082(8)	3.531(4)	0.076(7)
C···Cl	2,8	2.703(3)	[0.067]	2.678(4)	0.061(3)″
	3,8	3.098(4)	0.110(5)	4.013(2)	0.064(3)
	4,8	3.857(12)	0.184(10)	5.177(3)	0.076(3)
Cl···H	8,7	2.412(28)	[0.110]	2.397(27)	0.095(5)‴
	8,6	3.710(10)	[0.097]	2.873(8)	[0.151]
	8,5	4.669(20)	[0.257]	6.215(8)	[0.118]
∠C=C–C		123.9(0.3)		120.7(0.5)	
∠C≡C–C		178.0(1.1)		180.1(1.2)	
∠C=C–Cl		123.9(0.3)		121.1(0.4)	
∠C=C_1–H		119.2(2.2)		124.7(2.1)	
∠C=C_2–H		[122.0]		[122.0]	
R_w [d] (%)		7.52		6.58	
I_a [e]		(56.60)[g]	56.2	(–)[f]	11.1
I_b		(196.86)	196.6	(334.88)	333.5
I_c		(253.40)	252.8	(345.33)	344.6

[a] Results of r_α-refinements (the distances given are r_a-values). Distances, r_a, amplitudes, l, in Ångströms; angles in degrees; moment of inertia, I, in u Å^2. [b] See Fig. 3 for numbering of the atoms. [c] Parenthesized values are standard deviations obtained from the least-squares refinement (σ_{LS}) and they refer to the last digits given. For the distance parameters they should be corrected for systematic uncertainties according to $\sigma=[\sigma_{LS}^2+(0.001\ r)^2]^{\frac{1}{2}}$. Quantities in brackets are assumed values and primed amplitudes are refined in groups. [d] Agreement factor $R_w=[\sum w_i\Delta_i^2/\sum w_i I_i^2(\text{obs})]^{\frac{1}{2}}$ where $\Delta_i=I_i(\text{obs})-I_i(\text{th})$. [e] Moments of inertia (r_α-values); parenthesized values are microwave results (r_z-values). See text for estimates of uncertainties.

of the C–Cl bond out of the plane) did not reduce these problems, and such models were therefore discarded. The elements of the correlation matrices for the final refinements are given in Tables 5 and 6, respectively. The differences between the experimental and theoretical intensities and radial distribution curves calculated according to the final results given in Table 4, are shown in Figs. 1–4.

The r_a-values given in Table 4 were transformed to the corresponding r_α-values using the D-values of Table 3. The moments of inertia were calculated according to these values and the results are given in Table 4. The program employed, did not estimate the standard deviations in the calculated moments. However, increments of about 0.2 % to the distance parameters (the standard deviation due to systematic uncertainties in the electron wavelength is usually estimated to 0.1 %) caused changes in the moments of inertia of about 0.4 %. Changes in the parameter values according to the standard deviations obtained from the least-squares procedure revealed, however, that the error limits for *cis*-chlorobutenyne should be at least 1 %, while 0.5 % should be a corresponding estimate for *trans*-chlorobutenyne.

DISCUSSION

The agreement factors given in Table 4 and the difference curves shown in Figs. 1–4

Table 5. Correlation matrix for parameters of *cis*-1-chlorobutenyne.

$r_{C\equiv C}$	r_{C-C}	$r_{C=C}$	$\angle C=C-C$	r_{CH}	r_{C-Cl}	$\angle C=C-Cl$	$\angle C=C_1-H$	l_{ClC_4}	l_{C_4Cl}	l_{C_3Cl}	l_{C-Cl}	Scale 48 cm	Scale 28 cm
1.0													
−0.03	1.0												
0.59	−0.15	1.0											
0.12	−0.28	0.06	1.0										
0.24	−0.09	0.16	0.55	1.0									
0.53	−0.02	0.47	0.06	0.18	1.0								
−0.04	0.02	−0.10	0.24	0.07	0.01	1.0							
−0.43	0.08	−0.55	−0.56	−0.26	−0.30	−0.33	1.0						
−0.13	−0.09	−0.06	0.60	0.28	−0.19	0.15	−0.35	1.0					
−0.17	−0.01	−0.16	0.06	0.00	−0.23	0.02	0.03	0.21	1.0				
0.08	0.00	0.06	−0.05	−0.10	0.19	0.05	−0.01	−0.02	0.32	1.0			
−0.17	0.02	−0.09	−0.01	−0.15	−0.23	−0.04	−0.03	0.14	−0.01	−0.14	1.0		
−0.26	−0.02	−0.10	−0.20	−0.16	−0.36	−0.07	0.21	0.03	0.22	0.06	0.21	1.0	
−0.47	0.11	−0.34	−0.15	−0.18	−0.54	−0.07	0.31	0.12	0.14	−0.04	0.30	0.52	1.0
−0.34	0.10	0.18	−0.29	−0.23	−0.43	−0.14	0.29	0.00	0.20	0.02	0.35	0.67	0.48	1.0

demonstrate that the final structures are in fair agreement with the experimental data. The refined amplitude of vibration agree well with those calculated from the assumed force field (*cf.* Tables 3 and 4), and the moments of inertia obtained from the electron diffraction data are as compared to the estimated error limits in reasonable agreement with the microwave results.[7,8] The model for *cis*-chlorobutenyne where a linear C≡C−C chain was assumed, yielded moments of inertia in an overall poorer agreement with the microwave values.

The carbon-chlorine bond lengths are found to be 1.716(5) and 1.717(4) Å, respectively, for the *cis*- and *trans*-configuration; the parenthesized values correspond to 2σ where σ is corrected for systematic uncertainties (*cf.* Table 4, comment c). These are both in agreement with the C(sp^2)−Cl bonds found in tetrachloroethylene [9] (1.718(3) Å) and in *cis*-1,2-dichloroethylene [10] (1.718(7) Å), while they seem to differ significantly from the corresponding bond in the monosubstituted ethylene where this bond is found to be 1.728(7) Å.[11] The C=C−Cl angles in *cis*- and *trans*-1-chlorobutenyne are found to be 123.9(0.6) and 121.1(0.8)° and they confirm respectively to the C=C−Cl angles in *cis*-dichloroethylene (123.8(0.5)°) [10] and chloroethylene (121.1(0.9)°).[11] This correspondence seems reasonable as the environment with respect to steric strain should be quite similar in each pair of molecules. Differences in steric environment for the C=C−C angles in *cis*- and *trans*-chlorobutenyne may also be used to account for the observed difference in this angle for the two compounds (123.9(0.6)° and 120.7(1.0)°, respectively). However, the C=C−C angle in the unsubstituted hydrocarbon [6] is 123.1(0.5)°, and the explanation for the decrease in this angle by chlorine substitution in the *trans* position appears far less obvious. The C≡C−C chain in butenyne appears to be slightly bent [6] (∠C≡C−C= 177.9(1.2)°). Significant deviations from linearity are, however, not observed in *cis*- and *trans*-1-chlorobutenyne (178.0(2.2)° and 180.2(2.4)°, respectively) although one might argue that there is a similar trend in the *cis*-compound. The C−C bond distances in the two chlorobutenynes deviate slightly in a non-systematic manner from those in butenyne (C≡C = 1.215(3) Å, C=C = 1.344(4) Å, C−C = 1.434(3) Å),

Table 6. Correlation matrix for parameters of *trans*-1-chlorobutenyne.

$r_{C\equiv C}$	r_{C-C}	$r_{C=C}$	$\angle C=C-C$	$\angle C=C-C$	r_{CH}	$\angle C=C_1-H$	r_{C-Cl}	$\angle C=C-Cl$
1.0								
0.16	1.0							
0.48	−0.14	1.0						
0.04	−0.49	−0.07	1.0					
0.62	−0.04	0.28	0.64	1.0				
0.34	−0.12	0.48	−0.04	0.20	1.0			
0.16	0.01	0.08	0.63	0.57	−0.14	1.0		
−0.16	0.00	−0.06	−0.12	−0.11	0.00	−0.01	1.0	
−0.59	−0.29	−0.58	−0.11	−0.50	−0.17	−0.54	−0.22	1.0
−0.77	−0.11	−0.21	−0.11	−0.50	−0.22	−0.15	0.17	0.39
0.18	0.48	−0.21	−0.22	0.00	−0.37	0.12	−0.07	−0.18
−0.04	0.14	−0.15	−0.06	−0.05	−0.17	0.00	−0.03	0.03
0.29	0.09	0.20	−0.37	−0.04	0.31	−0.43	−0.32	0.11
−0.06	0.13	−0.14	0.03	−0.01	−0.25	0.14	−0.07	−0.02
−0.08	0.08	−0.17	0.01	−0.04	−0.31	0.11	−0.04	0.02
−0.07	−0.03	−0.12	0.15	0.04	−0.38	0.23	−0.05	−0.01
−0.29	0.20	−0.33	0.00	−0.16	−0.53	0.20	−0.05	0.08
−0.06	0.19	−0.25	0.06	0.00	−0.48	0.26	−0.12	−0.03
							Scales	
l_{CH}	$l_{C_3C_4}$	$l_{C_1C_4}$	$l_{C_3C_1}$	l_{C_4Cl}	l_{C_3Cl}	l_{CCl}	48 cm	28 cm
1.0								
−0.21	1.0							
0.04	0.25	1.0						
−0.22	−0.05	−0.02	1.0					
0.04	0.33	0.11	−0.11	1.0				
0.00	0.28	0.14	−0.16	0.26	1.0			
0.00	0.32	0.20	−0.31	0.37	0.28	1.0		
0.21	0.43	0.16	−0.25	0.34	0.38	0.49	1.0	
−0.03	0.61	0.29	−0.22	0.51	0.46	0.65	0.54	1.0

while there seems to be a significant trend towards longer bond distances in the *trans*-isomer as compared to *cis*-chlorobutenyne. A discussion of the carbon skeleton in mono-chloro-substituted butenynes will be given and related to the unsubstituted butenyne in more detail in the last paper in this series.

Acknowledgement. We are grateful to Professor Otto Bastiansen and Professor Ragnar Vestin for their stimulating interest in this project and we wish to express our gratitude to Dr. Hans M. Seip for helpful discussions and suggestions regarding the manuscript.

REFERENCES

1. Almenningen, A., Gundersen, G., Borg, A., Granberg, M. and Karlsson, F. *Acta Chem. Scand. A 29* (1975) 395.
2. Bastiansen, O., Hassel, O. and Risberg, F. *Acta Chem. Scand. 9* (1955) 232.
3. Andersen, B., Seip, H. M., Strand, T. G. and Stølevik, R. *Acta Chem. Scand. 23* (1969) 3224.
4. Seip, H. M., Strand, T. G. and Stølevik, R. *Chem. Phys. Lett. 3* (1969) 617.
5. Stølevik, R., Seip, H. M. and Cyvin, S. J. *Chem. Phys. Lett. 15* (1972) 263.
6. Fukuyama, T., Kuchitsu, K. and Morino, Y. *Bull. Chem. Soc. Jap. 42* (1969) 379.
7. Karlsson, F. and Vestin, R. *Acta Chem. Scand. 27* (1973) 3033.
8. Karlsson, F., Granberg, M. and Vestin, R. *Acta Chem. Scand. A 29* (1975). *In press.*
9. Strand, T. G. *Acta Chem. Scand. 21* (1967) 2111.
10. Davis, M. I. and Hanson, H. P. *J. Phys. Chem. 69* (1965) 4091.
11. Ivey, R. C. and Davis, M. I. *J. Chem. Phys. 57* (1972) 1909.

Received December 16, 1974.

Acta Chemica Scandinavica A 29 (1975) 553—557

Radiolysis of Aqueous Aniline Solutions

IVAN P. KARAIVANOV [a] and HILBERT C. CHRISTENSEN [b]

[a] Institute of Nuclear Research and Nuclear Energy, Bulgarian Academy of Sciences, Sofia, Bulgaria and [b] AB Atomenergi, Studsvik, Fack, S-611 01 Nyköping, Sweden

Aqueous aniline solutions have been irradiated with ^{60}Co γ-rays. In N_2O-saturated solutions the following products are formed: 2-aminophenoxazine-3-one ($G=0.24$), hydrazobenzene ($G=0.2$), hydrogen ($G=0.36$), and ammonia ($G=0.9$). Furthermore, traces of azobenzene, *o*-aminophenol, diphenylamine, 2-aminobiphenyl, *N*-phenyl-*o*-phenylenediamine, and phenol ($G=0.01$) are formed. After irradiation N_2O-saturated solutions are considerably more coloured than are the corresponding Ar- and air-saturated solutions. The yield of aniline decomposition [$G(-A)$] is also higher in N_2O-saturated [$G(-A)=3.3$] than in Ar-saturated solutions [$G(-A)=0.5$]. In the reaction mechanism presented in the report, the lower yield in Ar-saturated solutions is accounted for by back reactions between oxidized and reduced aniline radicals. A study of model compounds indicates that 2-aminophenoxazine-3-one can be formed in irradiated aniline solutions by reactions of *o*-aminophenol.

1. INTRODUCTION

Information about the end products formed by the radiolysis of aniline is scarce: Knight [1] irradiated pure aniline with ^{137}Cs β-rays to a dose of 4×10^{21} eV/g and identified the products by means of gas chromatography. He identified 2,2-diaminobiphenyl, diphenylamine, 3,3- and 2,4-diaminobiphenyl, and hydrogen [$G(H_2)=0.11$] as final products. He did not find ammonia.

The only information about the end products from the radiolysis of aqueous solutions is given by Kumagai.[2] He identified the following products: phenol, diphenylamine, and nitrosobenzene and also traces of nitrobenzene and ammonia.

It is known that the aromatic amines are easily oxidized: If solutions of sodium metavanadate, sulfuric acid and aniline are mixed the initial products give a yellow-green colour after which an intense blue-green colour is developed.[3] Oxidation of aniline with five-valence vanadate yields products which absorb light at 410 – 425 nm. The absorption has been assigned to intermediate products with the structures of the anilino radical and quinoline.

During the oxidation of aqueous aniline solutions with potassium persulfate Geverkian *et al.*[4] found that azobenzene is formed when aniline is present in excess while aniline black is formed with aniline in deficit.

Udenfriend *et al.*[5] have pointed out that the Fenton reagent oxidizes aniline to aminophenol. Aniline is transformed into *p*-aminophenol in the organism.[6]

The aim of the present study was to obtain additional information about the end products formed by the radiolysis of aqueous aniline solutions and to study the reaction mechanism.

2. EXPERIMENTAL

2.1. Material. Triple distilled water was used for the preparation of solutions. Aniline was purified by distillation under vacuum in the presence of zinc dust. Ar and N_2O were purified by distillation, N_2O furthermore by bubbling through solutions of hydroquinone.

2.2. Preparation of samples and irradiation. The samples were prepared in ampoules by successive evacuations and saturations under shaking. After saturation the ampoules were sealed and irradiated in a Gammacell 220 (Atomic Energy of Canada Ltd) charged with ^{60}Co. The dose rate was about 16 000 rad/min. Doses were normally in the range of 50 – 200 krad. The irradiation temperature was about 30 °C.

2.3. Analysis. Absorption spectra were recorded with a Beckman model B spectrophotometer. Ammonia was identified by Nessler's reagent using a Conway cell.[7]

A Perkin Elmer model 800 gas chromatograph was used for the quantitative analysis of (1) hydrogen using a column with molecular sieve, (2) phenol using a trixylenyl phosphate column at 180 °C and *o*-cresol as internal standard, (3) the decomposition of aniline using the trixylenyl phosphate column at 115 °C and *o*-cresol and benzyl alcohol as internal standards. Qualitative and quantitative analysis of the products extracted into ether was made by gas chromatography using a 2 m Apiezon-L column at 180 °C.

In order to verify the products samples were also analyzed by thin layer chromatography using Al_2O_3 or SiO_2 plates. The spots on the plates were analyzed by mass spectrometry.

3. RESULTS

3.1. Absorption spectra. The irradiated solutions were coloured from yellow to yellow-brown with the N_2O saturated solutions yielding a higher intensity. At higher doses a precipitate was formed in N_2O-saturated solutions.

Most of the coloured products can be extracted with ether. Under the influence of light and air extractable coloured products are reformed in the aqueous phase undoubtedly by autoxidation of the radiolytic products. Of the products likely to be formed both hydrazobenzene and aminophenols are easily oxidized. While *m*-aminophenol is stable the *o*- and *p*-aminophenols become rapidly dark in the presence of air and light.[6] Autoxidation of concentrated aqueous solutions of *p*-aminophenol yields a precipitate of black crystals. The absorption spectrum of the precipitate dissolved in alcohol is shown in Fig. 1.

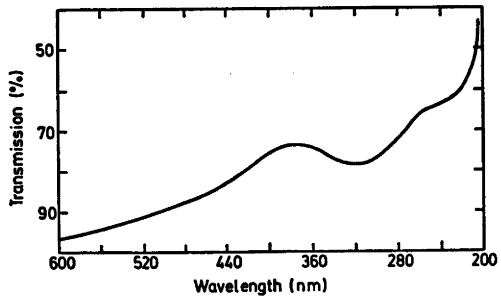

Fig. 1. Absorption spectrum of the *p*-aminophenol oxidation product dissolved in ethanol The product was obtained after exposure of an aqueous solution of *p*-aminophenol to air and day light at room temperature for 2 d.

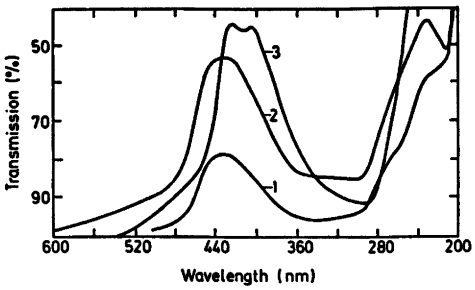

Fig. 2. Absorption spectrum of the *o*-aminophenol oxidation product. Solvents: 1 = water, 2 = ethanol and 3 = ether. The product was obtained after exposure of an aqueous solution of *o*-aminophenol to air and day light at room temperature for 2 d.

Autoxidation of fairly concentrated aqueous solutions of *o*-aminophenol yields a brown precipitate which is appreciably soluble in water, methanol, ethanol and ether. The spectra of the precipitate in different solvents are compared in Fig. 2. In ethanol and methanol absorption maxima are found at 238 and 440 nm with an extinction coefficient of 23 500 M^{-1} cm^{-1} at 440 nm. It is known that 2-aminophenoxazine-3-one is obtained as an inter-

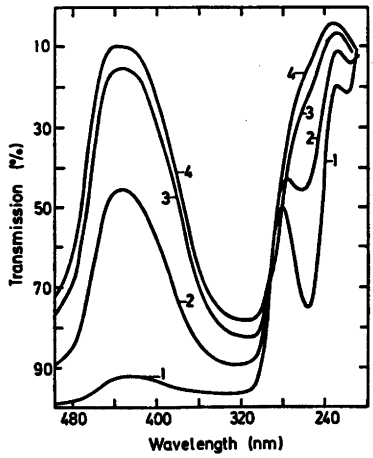

Fig. 3. Photolysis of an aerated 10^{-4} M solution of *o*-aminophenol at room temperature. Absorption spectra of the oxidation product dissolved in water; (1) Within 1 h from dissolution of the *o*-aminophenol in water. (2) 1 d after dissolution. (3) 4 d after dissolution. (4) 5 d after dissolution. The only light source was day light.

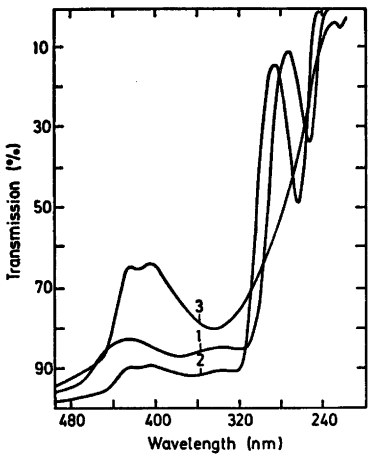

Fig. 4. Absorption spectra of (1) an irradiated aqueous aniline solution, (2) the products extracted from this solution into ether, and (3) the *o*-aminophenol oxidation product dissolved in ether.

mediate product during the oxidation of *o*-aminophenol by cytochromoxidase,[8] lead dioxide,[9] and *p*-benzoquinone.[10]

The spectrum of the oxidation product obtained in this investigation is similar to that of 2-aminophenoxazine-3-one given in the literature.[8,11,12] Clearly the autoxidation of *o*-aminophenol in aqueous solutions leads to the formation of 2-aminophenoxazine-3-one. At lower concentrations no precipitate is formed, the solution turns yellow, the spectrum of the solution is identical to that of 2-aminophenoxazine-3-one and the kinetics of the oxidation can be observed. The kinetics of the oxidation of 10^{-4} M solutions of *o*-aminophenol are indicated in Fig. 3. It can be seen that the main product is 2-aminophenoxazine-3-one; after five days about 90 % of the *o*-aminophenol has been transformed into 2-aminophenoxazine-3-one. This compound is also formed by the irradiation of N_2O-saturated, 10^{-2} M aniline solutions. In Fig. 4 the spectra of the irradiated aqueous solution and its ether extract are compared with that of 2-aminophenoxazine-3-one. It can be seen that close to 420 nm the spectrum of the product agrees with that of phenoxazine. The wave-length range below 320 nm is dominated by aniline. However, following the removal of aniline by repeated evaporations with ether, it also becomes possible to observe the spectrum of the products below 320 nm. The spectrum of an aqueous solution of the dry residue prepared in this way is shown in Fig. 5. The maximum at 290 nm probably belongs to the spectrum of *o*-aminophenol since the oxidation of the extract demonstrates kinetics similar to that of *o*-aminophenol (Fig. 3). The extinction coefficient of *o*-aminophenol is 2.2×10^3 M^{-1} cm^{-1}.[13]

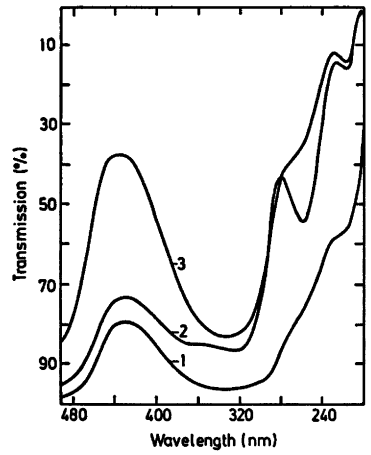

Fig. 5. Absorption spectra of aqueous solutions of (1) the *o*-aminophenol oxidation product, (2) the product isolated from 10^{-2} M aniline solution irradiated at 1000 krad, and (3) solution (2) after two days of exposure to air and day light at room temperature.

3.2 Gas chromatographic analysis. The irradiated solutions were extracted with ether and the extracts analysed by gas chromatography. The following products were identified with the aid of their retention times: azobenzene, hydrazobenzene, diphenylamine, 2-aminobiphenyl, and *N*-phenyl-*o*-phenylenediamine.

Measurement of G(Phenol) gave 0.01 in N_2O-saturated solutions after a dose of 1000 krad, while $G(H_2)$ was 0.36, a little less than the molecular yield, and $G(-\text{aniline})$ was 0.5 and 3.3 in Ar- and N_2O-saturated solutions, respectively. $G(-\text{aniline})$ was 1.2 in acid (pH = 2), Ar-saturated solutions.

3.3 Ammonia. The measured $G(NH_3)$ was 0.9 in both air- and N_2O-saturated solutions. In Ar-saturated solutions the yield was low (< 0.1).

4. DISCUSSION

Radiolysis of aqueous aniline solutions yields hydrogen, ammonia, 2-aminophenoxazine-3-one, and hydrazobenzene. Phenol, diphenylamine, 2-aminobiphenyl, and *N*-phenyl-*o*-phenylenediamine are found in trace amounts.

Our results disagree to some extent with those of Kumagai [2] who found phenol, diphenylamine and nitrosobenzol as the main products.

We have studied Ar-, N_2O-, and air-saturated solutions. The following reactions may take place with rate constants expressed in M^{-1} s^{-1} printed after the reactions.[14]

$H_2O \rightarrow e_{aq}^-$, H, OH, H_2, H_2O_2 (0)

$e_{aq}^- + N_2O \rightarrow OH + OH^- + N_2$ 5.6×10^9 (1)

$e_{aq}^- + O_2 \rightarrow O_2^-$ 1.9×10^{10} (2)

$H + O_2 \rightarrow HO_2$ 1.9×10^{10} (3)

In neutral water the G-values of the primary products are:[15] OH: 2.65; e_{aq}^-: 2.6; H: 0.55; H_2: 0.45; H_2O_2: 0.7.

The yields in water saturated with Ar, N_2O or O_2 are

Saturated with	G(OH)	$G(e_{aq}^-)$	G(H)	$G(O_2^-)$
Ar	2.65	2.6	0.55	–
O_2	2.65	–	–	3.15
N_2O	5.25	–	0.55	–

It can be seen that the sum of the oxidizing radicals (O_2^-, HO_2, and OH) is almost the same in the systems saturated with air and with N_2O.

Aniline (A) reacts with e_{aq}, H, and OH radicals with the rate constants 2.6×10^7, 2.9×10^9, and 1.4×10^{10} M^{-1} s^{-1}, respectively.[16]

Since $k(A + e_{aq}^-)$ is small hydrated electrons will not react with aniline in N_2O-saturated solutions; e_{aq}^- is transformed instead into OH radicals through reaction 1. Thus the H and OH adducts of aniline will be initially formed according to the reactions:[16]

$C_6H_5NH_2 + OH \rightarrow (C_6H_5NH_2)OH$ (4)

$C_6H_5NH_2 + H \rightarrow (C_6H_5NH_2)H$ (5)

The coloured products are formed with the highest yield in solutions saturated with N_2O, probably as a result of reactions between aniline and OH radicals. The radicals H, e_{aq}, O_2^-, and HO_2 either form colourless products or participates in back reactions with the reformation of aniline.

In Ar-saturated solutions the low yield of coloured products is probably due to the occurrence of back reactions. This is confirmed by the low yield for the decomposition of aniline in these solutions, $G(-A) = 0.5$.

Due to the comparatively low value of the rate constant for the reaction between hydrated electrons and aniline, the back reaction probably follows the scheme:

$C_6H_5NH_2 + OH \rightarrow (C_6H_5NH_2)OH$ (4)

$(C_6H_5NH_2)OH) + e_{aq}^- \rightarrow C_6H_5NH_2 + OH^-$ (6)

A similar reaction has been observed by Nakken [17] in aqueous solutions of *p*-aminobenzoic acid (PABA) saturated with nitrogen. Since in this instance $k(e_{aq}^- + PABA)$ is high (2.1×10^9 M^{-1} s^{-1}) the reaction follows the scheme:

$PABA + e_{aq}^- \rightarrow PABA^-$ (7)

$PABA + OH \rightarrow (PABA)OH$ (8)

$(PABA)OH + PABA^- \rightarrow 2PABA + OH^-$ (9)

If one OH radical were responsible for the transformation of one molecule of aniline the decomposition yield $G(-A)$ in N_2O-saturated solutions would be about 5. The measured $G(-A)$ of 3.3 obtained here indicates either the occurrence of reactions which lead back to aniline or the participation of OH radicals in secondary reactions. *o*-Aminophenol and 2-aminophenoxazine-3-one could be formed in such reactions:

$(C_6H_5NH_2)OH + (C_6H_5NH_2)OH \rightarrow$
$NH_2C_6H_4OH + C_6H_5NH_2 + H_2O$ (10)

$NH_2C_6H_4OH + OH \rightarrow$
2-aminophenoxazine-3-one (11)

We have verified that 2-aminophenoxazine-3-one is formed by reaction between *o*-aminophenol and OH radicals, during the irradiation of aqueous, N_2O-saturated solutions of *o*-aminophenol. The irradiation of aniline solutions yielded *o*-aminophenol only at high doses (500 krad) whereas at doses of 200 krad or less only 2-aminophenoxazine-3-one was found.

This indicates that the latter product may be formed without the participation of *o*-aminophenol as an intermediate product.

Hydrazobenzene is formed by recombination of anilino radicals:

$$C_6H_5NH + C_6H_5NH \rightarrow C_6H_5NHNHC_6H_5 \quad (12)$$

The formation of anilino radicals in these systems has been demonstrated by means of flash photolysis [18] and pulse radiolysis.[16]

Ammonia and phenol might be formed according to the reactions 4, 5, and 13.

$$(C_6H_5NH_2)OH + (C_6H_5NH_2)H \rightarrow C_6H_5OH + C_6H_5NH_2 + NH_3 \quad (13)$$

The measured $G(H_2)$ of 0.36 obtained in Ar-saturated solutions is a little lower than the molecular yield. This shows that hydrogen is not formed by the abstraction of H atoms from aniline.

4. CONCLUSION

Irradiation of aqueous aniline solutions yields coloured products, mainly as a result of attack by OH radicals. The participation of the radicals H, e_{aq}^- and O_2^- in the reactions leads to a decrease in the yield of coloured products. In Ar-saturated solutions the decrease is probably due to the participation of hydrated electrons in back reactions. Of the products identified the following are the most important: 2-aminophenoxazine-3-one (0.24), *o*-aminophenol, hydrazobenzene (0.2), ammonia (0.9) and phenol (0.01), the yields in N_2O-saturated solutions being given in parenthesis. The yields of hydrogen and phenol and the aniline decomposition yield have also been determined. Molecular hydrogen is not formed by the abstraction of H atoms from aniline.

REFERENCES

1. Knight, J. A., Jr., AEC rep. ORO-3519-3 (1969).
2. Kumagai, H. *Nippon Igaku Hoshasen Gakkai Zasshi 21* (1962) 971.
3. Yatsimirskii, K. B. and Nikolov, G. S. *Zh. Fiz. Khim. 44* (1970) 1400.
4. Gevorkyan, M. G., Beileryan, N. M. and Chaltykyan, O. A. *Arm. Khim. Zh. 22* (1969) 288.
5. Udenfriend, S., Clark, C. T., Axelrod, J. and Brodie, B. B. *J. Biol. Chem. 208* (1954) 731.
6. Kirk, R. E. and Othmer, D. F., Ed., *Encyclopedia of Chemical Technology*, Interscience Encyclopedia, New York 1948, Vol. 2, p. 229.
7. Borsok, H. and Dubnoff, J. W. *J. Biol. Chem. 131* (1939) 163.
8. Nagasawa, H. T., Gutmann, H. R. and Morgan, M. A. *J. Biol. Chem. 234* (1959) 1593.
9. Fischer, R. and Jonas, O. *Ber. Deut. Chem. Ges. 27* (1894) 2782.
10. Abdel-Megud, O. and Ismail, B. *J. Amer. Chem. Soc. 82* (1960) 1607.
11. Gerber, N. N. and Lechevalier, M. P. *Biochemistry 3* (1964) 598.
12. *UV Atlas of Organic Compounds*, Butterworth, London 1966, No. 71.
13. Bol'shakov, G. F., Vatago, V. S. and Agrest, F. B. *Ultrafioletovie spektri heteroorganicheskij soedinenii*, Izd. Khimiya, Leningradskoe otdelenie 1969.
14. Anbar, M. and Neta, P. *Int. J. Appl. Radiat. Isotopes 18* (1967) 493.
15. Dorfman, L. M. and Matheson, M. S. *Progr. React. Kinet. 3* (1965) 237.
16. Christensen, H. C. *Int. J. Radiat. Phys. Chem. 4* (1972) 311.
17. Nakken, K. F. *Radiat. Res. 21* (1964) 446.
18. Land, E. J. and Porter, G. *Trans. Faraday Soc. 59* (1963) 2027.

Received December 19, 1975.

Acta Chemica Scandinavica A 29 (1975) 558—562

Effects of Dihedral Angle and Substitution on S—S Bond Lengths. A CNDO/2 Molecular Orbital Study of Simple Disulfides

LEIF J. SÆTHRE

Department of Chemistry, University of Bergen, N-5014 Bergen-Univ., Norway

The relationship between dihedral angle and bond length in HSSH has been studied by the CNDO/2 molecular orbital method. The results are in better qualitative agreement with experimental data when sulfur 3*d* orbitals are included in the basis set. Calculations on simple disulfides, XSSX, where X = H, CH_3, Cl, and F show that relative changes in S—S bond lengths are fairly well reproduced.

From a survey of experimental bond lengths between divalent sulfur atoms, Hordvik [1] suggested that the sulfur-sulfur bond length varies with the dihedral angle.

Dihedral angle = 0° Dihedral angle = 90°

In non-cyclic and saturated cyclic compounds the smallest S—S bond lengths were found for dihedral angles of about 90° while smaller dihedral angles gave longer bond lengths. A more recent investigation [2] supports this contention, but the relationship is not obvious in other cases.[3]

The purpose of this paper is to study the above mentioned relationship from a theoretical point of view. To the author's knowledge this has not been done before, although the barriers to internal rotation in disulfides have been investigated in great detail by numerous workers.[4] The semiempirical CNDO/2 method [5] is used in the calculations presented here. The HSSH molecule was chosen as the geometrical model for a general disulfide. The reason for this choice is that in the accurately determined molecular structure, the S—S bond length (2.055 Å) is comparable with those in a number of organic disulfides.[1-3] Furthermore, the molecule has no bulky substituents that may cause sterical hindrance problems in twisted configurations (as is the case, *e.g.*, with the methyl groups in CH_3SSCH_3).

Experimental data indicate that the S—S bond length also depends on the electronegativities of the disulfide substituents.[6] This dependence is demonstrated for the molecules HSSH, CH_3SSCH_3, ClSSCl, and FSSF, where the sulfur-sulfur bond lengths are found to decrease with increasing electronegativity of the substituents. The S—S bond lengths for these molecules have therefore been calculated and the optimized values compared in order to evaluate how well the CNDO/2 method can reproduce the experimentally observed trends.

The calculations were done both with and without sulfur and chlorine 3*d* orbitals in the basis set. The program CNINDO distributed by the Quantum Chemistry Program Exchange [7] was used.

RESULT AND DISCUSSION

I. *Calculations on HSSH.* The CNDO/2 total energy [8] was calculated for HSSH as a function of the S—S bond length for dihedral angles between (and including) 0 and 180°. The S—H bond length and S—S—H bond angle were held fixed at the experimental values.[9]

Fig. 1 shows the S—S bond length corresponding to minimum energy as a function of dihedral angle. The results are compared with Hordvik's empirical curve,[1] which is also

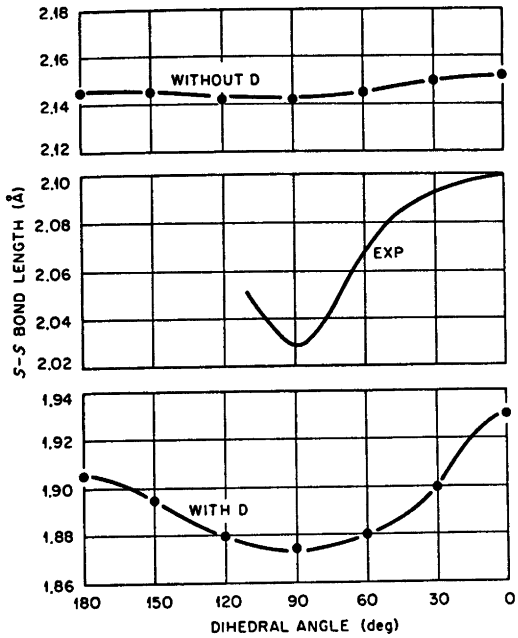

Fig. 1. Calculated S – S bond length as a function of dihedral angle compared with the experimental curve derived by Hordvik (*cf.* Ref. 1). The calculations are performed both with and without sulfur 3*d* orbitals.

shown in Fig. 1. As can be seen from the figure, the calculated S – S bond length decreases when the dihedral angle is varied from 180 to 90°, and increases to a maximum value for 0°. The same qualitative trends are obtained both with and without sulfur 3*d* orbitals. However, the results are in better qualitative agreement with the experimental curve when *d* orbitals are included in the basis set (*spd* approximation). The dependence is far less pronounced when *d* orbitals are excluded (*sp* approximation).

On the other hand, the calculated S – S bond lengths at 90° are far from the experimental value (2.055 Å) with both basis sets. However, the CNDO/2 method seems to be able to reproduce the relative changes reasonably well. The difference between the calculated S – S bond lengths for HSSH at 0 and 90° is 0.055 Å in the *spd* approximation. Adding this value to the experimental value for HSSH (2.055 Å), one obtains 2.110 Å which is close to the S – S single bond length (2.10 Å) suggested by Hordvik for a *cis* planar disulfide group.[1]

The present study for HSSH indicates that 3*d* orbitals may be important for the description of the geometry of disulfides, at least within the CNDO/2 framework. The importance of *d* orbital participation to the bonding in HSSH may be understood from an analysis of the electron density-bond order matrix, $P_{\mu\nu} = 2\sum_{i}^{occ} C_{\mu i}C_{\nu i}$, where $C_{\mu i}$ are LCAO coefficients and the summation being over all occupied molecular orbitals. Since the sign of the bond-order matrix elements are defined according to the coordinate system, it was decided to multiply all bond-orders, $P_{\mu\nu}$, with the *sign* of the corresponding overlap integral, $S_{\mu\nu}$. In this way bonding and antibonding interactions are given positive and negative values, respectively.[10]

The atomic orbitals and dihedral angle θ are defined according to the coordinate system in Fig. 2. The redistribution of electron density is discussed by inspecting the atomic orbitals (AOs) on H^A and S^A. The two sulfur atoms (S^A and S^B) are, of course, identical, and have the same electron densities. However, since the atoms H^A and S^A are stationary when the dihedral angle is varied, the AO's on these atoms will not change their nature, *e.g.*, the sulfur p_z AO on atom A (Sp_z^A) will remain perpendicular to the $H_A - S_A - S_B$ plane. At $\theta = 90°$ this orbital will be equivalent to Sp_y^B. Similarly Sd_{xy}^A is equivalent to Sd_{xz}^B at $\theta = 90°$, and these orbitals as well as the S*p* orbitals mentioned have π symmetry with respect to the $S^A - S^B$ axis.

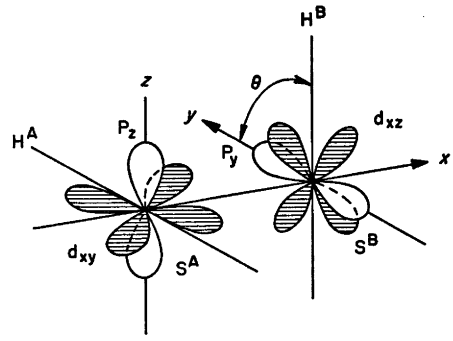

Fig. 2. Definition of the coordinate system axes.

One finds the greatest changes of the electron densities with dihedral angle for Sp_z^A and Sd_{xy}^A, *cf.* Table 1. The electron densities of the other 3*d* orbitals are small and do not change much with θ. The minimum value for Sp_z^A at about 90° corresponds to a maximum value for Sd_{xy}^A. The variation of bond orders with θ are all relatively small except for those involving the AO's mentioned above. Table 1 shows that the $Sp_z^A - Sp_z^B$ bond order is slightly antibonding at 0 and 180° but becomes fairly bonding at 90°. More important is the strong increase in bond order for $Sd_{xy}^A - Sp_y^B$ with a maximum value at about 90°. This strong increase in bond character is also reflected in the "bond index", $W(A-B) = \sum_{\mu}^{A}\sum_{\nu}^{B} P_{\mu\nu}^2$, indroduced by Wiberg [11] as a measure of the bond strength between atoms A and B.

The interaction between S and H on the other hand, do not change very much. Both the $Sp_y^A - Hs^A$ bond order and the $W(S^A - H^A)$ bond index remain almost constant. This is also true for the Hs^A electron density, which has a small maximum at 90°. The net charge on the S atom will, of course, follow the opposite trend, being −0.03e and −0.04e, respectively, at 0 and 180°, and 0.01e only at 90°. The net charges on the atoms at 90° are therefore close to zero. This is in agreement with a recent *ab initio* calculation [12] on HSSH.

The major effect of changing the dihedral angle from 0 to 90° is therefore an internal redistribution of electron density from the lone-pair $p\pi$ orbital and into the $3d\pi$ orbital. This back donation of electrons is mainly accomplished by the interaction between the $p\pi$ lone pair on one sulfur atom with the corresponding $3d\pi$ orbital on the other. At 90° two such π bonds are established ($Sd_{xy}^A - Sp_y^B$ and $Sp_z^A - Sd_{xz}^B$). The difference in S−S bond lengths at 0 and 90° can therefore be explained (according to the CNDO/2 results), to be partly due to lone pair repulsion at 0°, and partly due to π bonding which is most pronounced at 90°.

The discussion so far has been confined to the *spd* approximation, mainly because this basis set gave best agreement with experimental data. In the *sp* approximation there are only small changes in the electron density-bond order matrix when the dihedral angle is varied. The $Sp_x^A - Sp_x^B$ bond order is essentially independent of the dihedral angle (as in the *spd* approximation). There is a small π bond order (0.08) between Sp_z^A and Sp_z^B at 90°, while the corresponding bond order is zero at 0 and 180°. The increase in π bond-order is, however, (according to CNDO) too small to affect the S−S bond length.

II. *The S−S bond length in simple disulfides*, XSSX. The results in Fig. 1 show that the S−S

Table 1. Electron densities, bond-orders,[a] and bond indices [b] for HSSH as a function of dihedral angle at optimum S−S bond lengths. Sulfur 3*d*-orbitals are included.

Dihedral angle (°)	0	30	60	90	120	150	180
Electron densities							
Sp_z^A	1.87	1.78	1.70	1.68	1.71	1.79	1.86
Sd_{xy}^A	0.06	0.13	0.19	0.21	0.19	0.12	0.07
Hs^A	0.97	0.99	1.00	1.01	1.00	0.98	0.96
Bond orders [a]							
$Sp_z^A - Sp_z^B$	−0.4	0.07	0.16	0.20	0.17	0.04	−.05
$Sd_{xy}^A - Sp_y^B$	0.25	0.38	0.53	0.60	0.53	0.37	0.26
$Sp_y^A - Hs^A$	0.88	0.87	0.86	0.86	0.86	0.86	0.86
Bond indices [b]							
$W(S^A - S^B)$	1.66	1.82	1.97	2.03	1.96	1.83	1.75
$W(S^A - H^A)$	0.94	0.94	0.94	0.93	0.93	0.92	0.92

[a] Defined as the product of the bond order matrix element, $P_{\mu\nu}$, and the *sign* of the corresponding overlap integral, $S_{\mu\nu}$. [b] Bond indices according to Wiberg (Ref. 11), $W(A-B) = \sum_{\mu}^{A}\sum_{\nu}^{B} P_{\mu\nu}^2$.

Table 2. Calculated S–S bond lengths in simple disulfides compared with experimental results. All values are given in Å.

Molecule	Exp	With D[a] Calc	Diff	Without D[a] Calc	Diff
HSSH	2.055 [b]	1.875	0.18	2.14	−0.085
CH_3SSCH_3	2.022 [c]	1.84	0.18	2.14	−0.12
ClSSCl	1.931 [d]	1.80	0.13	2.13	−0.20
FSSF	1.888 [e]	1.79	0.10	2.12	−0.23

[a] Calculations were performed both with and without sulfur and chlorine *3d*-orbitals. [b] Ref. 9. [c] Ref. 13. [d] Ref. 6. [e] Ref. 14.

bond length for HSSH is too short in the *spd* approximation and too long in the *sp* approximation. The differences between observed and calculated values at 90° are 0.18 and −0.09 Å, respectively. However, we have shown above that the CNDO/2 method is able to reproduce relative bond length differences. In order to test this assumption further, the S–S bond lengths of the molecules CH_3SSCH_3, ClSSCl, and FSSF were optimized in the CNDO/2 scheme. In each case the remaining bonds and angles were fixed at the experimental values (Refs. 13, 6, and 14, respectively). The S–S bond lengths determined in this way are compared with the observed values in Table 2.

The experimental S–S bond lengths in Table 2 are seen to vary considerably with the disulfide substituents. Both basis sets are, however, able to reproduce the relative change in bond lengths fairly well, as is seen from the differences between observed and calculated values.

Kiers and Vos [15] have performed similar calculations in the *sp* approximation both for disulfides and oxy-disulfides. Although no specific compound is mentioned, the calculated bonds are found to be 0.10 to 0.13 Å longer than the observed values, in agreement with the results presented here.

The results obtained may now be discussed with reference to the calculated electronic properties. The electron density-bond order matrix for the molecules HSSH, CH_3SSCH_3, ClSSCl, and FSSF have been analysed and some relevant elements are given in Table 3. The dihedral angle is 90° for all compounds in order to facilitate comparison, and in each case the data refer to the optimized S–S bonds in Table 2.

For the *spd* approximation it is seen that when X gets increasingly more electronegative there is a pronounced decrease of electron density

Table 3. Bonding properties in simple disulfides at their optimum S–S bond length. Dihedral angle is 90°.

	HSSH	CH_3SSCH_3	ClSSCl	FSSF
With D				
Electron densities				
Sp_z^A	1.68	1.52	1.28	1.13
Sd_{xy}^A	0.21	0.33	0.42	0.43
S_{tot}^A	5.99	6.04	5.91	5.78
Bond orders [a]				
$Sp_x^A - Sp_x^B$	0.83	0.80	0.79	0.79
$Sp_z^A - Sp_z^B$	0.20	0.29	0.42	0.56
$Sd_{xy}^A - Sp_y^B$	0.60	0.64	0.64	0.59
Bond indices [a]				
$W(S^A - S^B)$	2.03	2.25	2.49	2.76
$W(S^A - X^A)$	0.93	1.07	1.33	1.17
Without D				
Electron densities				
Sp_z^A	1.99	1.98	1.98	1.97
S_{tot}^A	6.03	6.04	5.90	5.78
Bond orders [a]				
$Sp_x^A - Sp_x^B$	0.92	0.90	0.89	0.88
$Sp_z^A - Sp_z^B$	0.08	0.07	0.13	0.16
Bond indices [a]				
$W(S^A - S^B)$	1.01	0.99	1.01	1.03
$W(S^A - X^A)$	0.99	1.01	0.98	0.94

[a] Bond orders and bond indices are defined as in Table 1.

in the Sp_z^A "lone-pair" orbital (see Fig. 2). The electron density is partly back donated into the Sd_{xy}^A orbital and partly transferred to the substituents. This is accompanied by a net increase in $Sp_z^A - Sp_z^B$ bond order. The $Sd_{xy}^A - Sp_y^B$ bond order is substantial, but does not change much with substituents. The same is noted for the $Sp_x^A - Sp_x^B$ bond order. Thus the shortening of the S–S bond length in these molecules (according to CNDO/2) may be explained almost entirely in terms of a net increase in $p-p$ π bonding due to delocalization of the lone-pair electrons.

In the *sp* approximation the decrease of the Sp_z^A orbital is less pronounced. There is, however, an increase in $Sp_z^A - Sp_z^B$ bond order, and this seems to be responsible for the decrease in bond lengths. In both basis sets the increase in π bonding is reflected in the $W(S^A - S^B)$ bond index.

The discrepancies between observed and calculated bond lengths in Table 2, may in part be due to the choice of 3*d* orbital exponents given to the Slater-type orbitals used here. The CNDO treatment depends markedly on the values assigned to overlap integrals, and hence on the orbital exponents.[16] In the *spd* approximation the 3*d* orbital exponents are taken to be identical to those of 3*s* and 3*p* orbitals and regarded as being maximally contracted. The *sp* approximation is equivalent to setting the exponents to zero. Thus the importance of 3*d* orbitals are most probably over-emphasized in these calculations. The results in Table 1, for example, indicate quite substantial 3*d* orbital contribution in HSSH, while large basis set *ab initio* calculations show only modest occupation of sulfur 3*d* orbitals.[12]

CONCLUSIONS

CNDO/2 calculations on the dihedral angle/bond length dependence in HSSH give results in better qualitative agreement with experimental data when sulfur 3*d* orbitals are included in the basis set. This is mainly because of $p-d$ π bonding which is most pronounced when the dihedral angle is 90°.

Calculations on simple disulphides, XSSX, where X=H, CH_3, Cl, and F, show that the relative decrease in S–S bond length is reproduced fairly well. The shortening observed in these molecules is explained to be due to increasing $p-p$ π bonding. The bond lengths are, however, calculated to be too short when 3*d* orbitals are used and too long when they are omitted. Sulfur 3*d* orbitals may, therefore, be important for the description of the geometry of disulfides, but they are most probably over-emphasized in the conventional CNDO/2 parametrization.

Acknowledgement. The author wishes to thank Professor Asbjørn Hordvik for encouragement and helpful discussions.

REFERENCES

1. Hordvik, A. *Acta Chem. Scand. 20* (1966) 1885.
2. Lee, J. D. and Bryant, M. W. R. *Acta Crystallogr. B 25* (1969) 2094.
3. Shefter, E. *J. Chem. Soc. B* (1970) 903; Lee, J. D. *Naturwissenschaften 59* (1972) 36.
4. See, for example, Boyd, D. B. *Theor. Chim. Acta 30* (1973) 137, and references cited therein.
5. Pople, J. A. and Beveridge, D. L. *Approximate Molecular Orbital Theory*, McGraw-Hill, New York 1970.
6. Beagley, B., Eckersley, G. H., Brown, D. P. and Tomlinson, D. *Trans. Faraday Soc. 65* (1969) 2300.
7. Quantum Chemistry Program Exchange, No. 141, Chemistry Department, Indiana University, Bloomington, Indiana 47401, U.S.A.
8. Santry, D. P. and Segal, G. H. *J. Chem. Phys. 47* (1967) 158.
9. Winnewisser, G., Winnewisser, M. and Gordy, W. *J. Chem. Phys. 49* (1968) 3465.
10. Ehrenson, S. and Seltzer, S. *Theor. Chim. Acta 20* (1971) 17.
11. Wiberg, K. B. *Tetrahedron 24* (1968) 1083.
12. Veillard, A. and Demuynck, J. *Chem. Phys. Lett. 4* (1970) 476.
13. Beagley, B. and McAloon, K. T. *Trans. Faraday Soc. 67* (1971) 3216.
14. Kuczkowski, R. L. *J. Amer. Chem. Soc. 86* (1964) 3617.
15. Kiers, C. Th. and Vos, A. *Rec. Trav. Chim. Pays-Bas 91* (1972) 126.
16. Clark, D. T. In Reid, D. H., Ed., *Organic Compounds of Sulphur, Selenium, and Tellurium*, Specialist Periodic Reports, The Chemical Society, London 1970, Vol. 1, Chapter 1.

Received January 16, 1975.

Acta Chemica Scandinavica A 29 (1975) 563—568

Short Communications

A Neutron Diffraction Investigation on Single Crystals of Titanium Carbide, Titanium Nitride, and Zirconium Nitride

A. NØRLUND CHRISTENSEN

Department of Inorganic Chemistry, University of Aarhus, DK-8000 Aarhus C, Denmark

Single crystals of titanium carbide, TiC, titanium nitride, TiN, and zirconium nitride, ZrN, have been prepared using the floating zone technique. [1] The carbide was grown in helium, and the nitrides were grown in nitrogen. The experimental crystal growth conditions for the samples used in the neutron diffraction investigation are listed in Table 1. The unit cell parameters of the compounds were determined from Guinier powder patterns using $CuK\alpha_1$ radiation, $\lambda = 1.54051$ Å, with NaCl, $a = 5.6389$ Å, as an internal standard. The values obtained are: TiC: $a = 4.328(2)$ Å, TiN: $a = 4.235(2)$ Å, and ZrN: $a = 4.585(2)$ Å. The densities of the compounds were measured using the method of Archimedes, and the values found are: TiC: $\varrho = 4.87(1)$ g/cm³, TiN: $\varrho = 5.02(1)$ g/cm³, and ZrN: $\varrho = 7.29(1)$ g/cm³. Chemical analyses of the metals in the three compounds were made. Titanium in TiC was determined spectrophotometrically as the peroxy titanium ion, and titanium and zirconium in the nitrides were determined gravimetrically by combustion of the nitrides in oxygen at 1 000 °C to TiO_2 and ZrO_2. The results of the chemical analysis are listed in Table 2, where the chemical formulae corresponding to the results of the chemical analysis are listed. The neutron diffraction data were measured at an automatic four-circle diffractometer at DR3, Risø, using 1.07 Å neutrons, and the standard $\omega - 2\theta$ scan technique.[2] A single crystal of TiC with a volume of 0.027 mm³ and linear dimensions in the range 0.17 to 0.55 mm was used in measuring a total of 96 reflections. The diffraction data were reduced using a standard procedure,[3] yielding a total of 16 independent reflections. The single crystal of TiN had the linear dimensions $2.5 \times 2.5 \times 0.8$ mm. A total of 445 reflections was measured. After data reduction the number of independent reflections was 16. The single crystal of ZrN had a volume of 5 mm³ and linear dimensions in the range 1.5 to 3.0 mm. The number of measured reflections was reduced from 337 to 16 independent reflections in the data reduction.

Table 1. Experimental conditions for the growth of TiC, TiN, and ZrN. A: Starting material(s). B: Gas, pressure in atm. C: Length of zone melted specimen in mm. D: Growth rate mm h^{-1}. E: Gear.

Compound	A	B	C	D	E
TiC	TiC	He 17.5	72	7.5	1:1.2
TiN	$Ti + N_2$	N_2 20.4	29	25	none
ZrN	$Zr + N_2$	N_2 15.5	60	7.5	none

Table 2. Densities of crystals and chemical formulae. Standard deviations in parentheses.

Compound	Densities in g/cm³ Obs.	Calc. [a]	Composition from chemical analysis	Composition from neutron diffraction
TiC	4.87(1)	4.908	$Ti_{1.00}\ C_{1.0}$	$Ti_{0.98(3)}\ C_{1.0}$
TiN	5.02(1)	5.394	$Ti_{0.72}\ N_{1.0}$	$Ti_{0.76(4)}\ N_{1.0}$
ZrN	7.26(1)	7.304		
ZrN	7.29(1)	7.304	$Zr_{1.0}\ N_{0.97}$	$Zr_{1.00(1)}\ N_{1.0}$

[a] From unit cell parameters and assuming stoichiometric composition.

Table 3. Results from neutron diffraction. Standard deviations in parentheses.

	Site	Occupancy	B (Å^2)
TiC, $R = 3.8$ %			
Ti	4*a*	0.98(3)	0.24(14)
C	4*b*	1.0	0.36(07)
TiN, $R = 3.7$ %			
Ti	4*a*	0.76(4)	0
N	4*b*	1.0	0
ZrN, $R = 3.9$ %			
Zr	4*a*	1.00(1)	0
N	4*b*	1.0	0

The three compounds are isostructural with sodium chloride, space group $Fm3m$, No. 225. The metal atoms are placed in the site 4*a*, and the non-metal atoms are placed in the site 4*b*. Observed and calculated structure factors were compared using the least squares program LINUS.[4] The neutron scattering lengths used for Ti, Zr, C, and N were -0.335, 0.714, 0.6648, and 0.940, all in units of 10^{-12} cm.[5] The variable parameters for each refinement were a scale factor, isotropic temperature factors for the metal and the non-metal atoms, and an occupancy factor for the metal atom or for the non-metal atom. The results of the refinements are listed in Table 3. A list of observed and calculated structure factors can be obtained from the author at request.

The result of the neutron diffraction investigation is that the investigated specimens of the titanium carbide and zirconium nitride were stoichiometric within experimental errors, and that the titanium nitride investigated is clearly non-stoichiometric with the 4*a* site only partly occupied. The formation of metal atom vacancies should, according to Brager,[6] result in a reduction of the unit cell parameter from 4.235 Å for the N/Ti ratio 1.00 to 4.220 Å for the N/Ti ratio 1.10. Such a reduction of the unit cell parameter has not been observed in the present investigation, as the unit cell parameter for the crystal investigated is 4.235 Å and the N/Ti ratio is 1.30(06).

The temperature factors for the atoms in TiC have been found to have the very small values listed in Table 3. These values are comparable with the temperature factors for the atoms in sodium chloride measured at 4.2 K, B_{Na^+}: 0.35(08) Å, and B_{Cl^-}: 0.27(04) Å,[7] and the low temperature factors for TiC reflect the hardness of the compound. The temperature factors of the atoms in TiN and ZrN are also very small, but become negative values in the least squares refinements. As the numerical values of the temperature factors were from 2 to 4 times the corresponding standard deviations on the temperature factors, the values for the temperature factors were set to zero as listed in Table 3.

Formation of stoichiometric TiC by a zone melting technique is in conflict with previously published phase diagrams for the TiC-system which shows that the maximum in the liquidus curve for TiC is not found for the stoichiometric composition but rather for a compound with the composition $TiC_{0.77}$.[8]

1. Christensen, A. N. *J. Crystal Growth* (submitted).
2. Lehmann, M. S., Larsen, F. K., Poulsen, F. R., Christensen, A. N. and Rasmussen, S. E. *Acta Chem. Scand. 24* (1970) 1662.
3. Lehmann, M. S. and Larsen, F. K. *Acta Crystallogr. A 30* (1974) 580.
4. Busing, W. R., Martin, K. O., and Levy, H. A. (1962). *ORFLS, A Fortran Crystallographic Least Squares Program*, Oak Ridge National Laboratory Report, ORNL-TM-305. *LINUS* is a 1971 version of *ORFLS*.
5. Shull, C. G. *Coherent Neutron Scattering Amplitudes*, Massachusetts Institute of Technology, Cambridge, Mass. 1972.
6. Brager, A. *Acta Physicochim. URSS 11* (1939) 617. (Referred to in Ref. 8, p. 27).
7. Butt, N. M., Cheetham, A. K. and Willis, B. T. M. *Acta Crystallogr. A 29* (1973) 727.
8. Toth, L. E. *Transition Metal Carbides and Nitrides*, Academic, New York 1971.

Received May 20, 1975.

Raman Spectra of Molten Mixtures Containing Aluminium Fluoride. II. Dissociation of AlF_6^{3-}

ERLING RYTTER [a]
and SIGNE KJELSTRUP RATKJE [b]*

[a] The University of Trondheim, Norwegian Institute of Technology, Division of Inorganic Chemistry, N-7034 Trondheim-NTH, Norway and [b] The University of Trondheim, Department of Chemistry, NLHT-Rosenborg, N-7000 Trondheim, Norway

Both ideal [1-4] and regular solution models [5] have been adapted to explain the thermodynamic data of the alkali fluoride-aluminium fluoride melts. In the sodium system Grjotheim [1] found that the dissociation reaction

$$AlF_6^{3-} \rightleftharpoons AlF_4^- + 2F^- \quad (1)$$

gave the best description of the cryolite peak in the phase diagram of NaF and AlF_3. The same result was found for the corresponding lithium system.[2,3] Holm [4] interpreted the total value of ΔH_{mix} in the system NaF-AlF_3 as due to the dissociation of the cryolite anion into AlF_3 and F^- in the composition range $0 < X_{AlF_3} < 0.25$. Dewing [5] found that NaF-$NaAlF_4$ mixtures may be described for all values of X_{AlF_3} as a regular solution the two ions F^- and AlF_4^-. Deviations near the $NaAlF_4$ composition were explained by the formation of $Al_2F_7^-$.

All these calculations, however, are based on model assumptions and are as such only indirect indications of melt species. In a previous investigation [6] we reported the ion AlF_6^{3-} as the main complex in the system LiF-Li_3AlF_6. In order to test the existence of other species proposed in the cryolite melts, compositions in the system Li_3AlF_6-AlF_3 should be investigated. In this paper we report the results of a Raman spectroscopic investigation of the Li_3AlF_6-AlF_3 eutectic melt. After completion of the present work we became aware of a Raman investigation of the sodium system.[7,8]

Results. The experiments were performed according to a procedure previously described.[6] The only change in the experimental design was the introduction of a cylindric platinum liner in the Raman cell in order to increase the Raman intensity. The spectrum obtained at 730 °C for the molten Li_3AlF_6-AlF_3 eutectic mixture, LiF + 35.5 mol % AlF_3,[9] is presented in Fig. 1. Two peaks at 545 ± 10 and 620 ± 10 cm^{-1} were found by subtraction of the background and by resolution of the band complex into two approximate Gaussian curves. The band positions were determined from six spectra. There were signs of additional bands at ~ 220 and ~ 350 cm^{-1}. For comparison, the spectrum of the LiF-Li_3AlF_6 eutectic mixture [6] also is given in Fig. 1. The ratio of the peak intensities I_{545}/I_{620} was calculated from the average of four spectra to be 1.0 ± 0.1. Uncertainties in melt compositions are included in this limit.

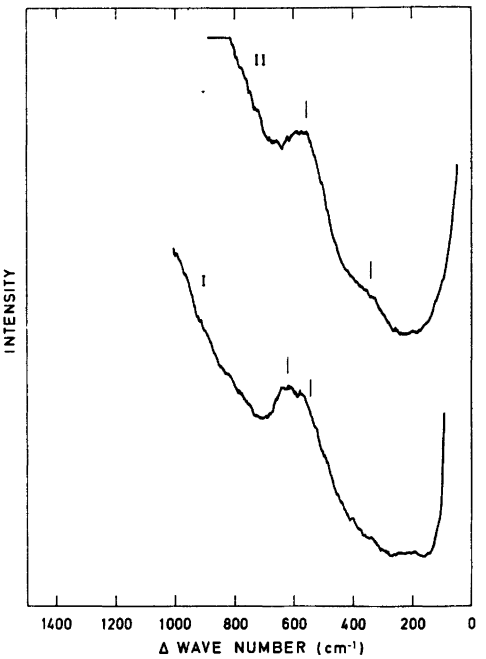

Fig. 1. The Raman spectra of the molten $Li_3AlF_6 - AlF_3$ (I) and LiF-Li_3AlF_6 (II) eutectic mixtures at 730 °C. The band widths were 20 cm^{-1} (curve I) and 25 cm^{-1} (curve II). Sensitivity: 1000 cps. Scan speed: 0.2 cm^{-1}/s. Period: 50 s.

Discussion. The 620 cm^{-1} band is assigned to the ν_1 frequency of the AlF_4^- tetrahedron. The frequency agrees well with 630 ± 20 cm^{-1} estimated in our previous publication.[6] The band at 545 ± 10 cm^{-1} is attributed to the totally symmetric stretching frequency of AlF_6^{3-}. This result is within the uncertainty limits of our first value, 556 ± 5 cm^{-1}. In NaF-AlF_3 mixtures,[7,8] the corresponding frequencies were found to be 622 and 555 cm^{-1}.

Since no definite sign of species other than AlF_6^{3-} and AlF_4^- was found, the dissociation (1) is used in a description of the melt mixtures in the composition range LiF-$LiAlF_4$. Thus the melt is considered as being composed of a cation mixture and a mixture of the anionic entities AlF_6^{3-}, AlF_4^- and F^-. This represents a Temkin model, but not necessarily an ideal one.

* To whom correspondence should be addressed.

The following expression then is valid for the stoichiometric dissociation constant K of reaction (1) in the system $LiF\text{-}AlF_3$:

$$K = \frac{[(1+P) - X_{AlF_3}^{\circ}\,(2+4P)]^2}{P[(1+P) - X_{AlF_3}^{\circ}\,(1+3P)]^2} \quad (2)$$

where P is the ratio between the concentrations of AlF_6^{3-} and AlF_4^-. The equation is derived by a procedure similar to that described for $KCl - AlCl_3$ melts.[10,11] For pure cryolite, Li_3AlF_6, P is related to the dissociation degree α_0 of AlF_6^{3-} through

$$P = \frac{X_{AlF_6^{3-}}}{X_{AlF_4^-}} = \frac{1-\alpha_0}{\alpha_0} \quad (3)$$

Combination of eqns (2) and (3) and introduction of $X_{AlF_3}^{\circ} = 1/4$ yield

$$K = 4\alpha_0^3/(1+2\alpha_0)^2(1-\alpha_0) \quad (4)$$

At a constant temperature, the relationship between P, α_0 and $X_{AlF_3}^{\circ}$ is given by eqns. (2) and (4) provided the activity coefficient term is constant. This assumption is not as rigid as the ideal mixture approximation. The value α_0 at a temperature T may be used as a frame of reference for the function $P = P\,(X_{AlF_3})$.

According to Wolkenstein's bond polarizability theory, the mean molecular polarizability derivative is a bond property (see Chantry [12]). It follows that the mol fraction ratio may be calculated from [10–12]

$$\frac{X_{AlF_6^{3-}}}{X_{AlF_4^-}} = k\frac{I_{AlF_6^{3-}}}{I_{AlF_4^-}} = P \quad (5)$$

with $k = 1/1.9$. The value $k = 4/6$ was used by Solomons *et al.*,[13] but they did not take the difference in ν_1 frequencies between the two species into account. The Al – F bonds in the two species are assumed similar. Gilbert *et al.*[8] found that the coefficient k should be between 1/2.0 and 1/2.1 in the $NaF\text{-}AlF_3$ system. By using the value $k = 1/2.0$ and inserting 1.0 for the intensity ratio $I_{AlF_6^{3-}}/I_{AlF_4^-}$ at $X_{AlF_3}^{\circ} = 0.355$, the result $P = 0.5$ is obtained. This gives $K = 3.4 \times 10^{-2}$ from eqn. (2) and $\alpha_0 = 0.24$ from eqn. (4) at 730 °C. This result is consistent with previous investigations of the $LiF\text{-}Li_3AlF_6$ eutectic mixture [6,8] which gave no sign of AlF_4^-. By taking into consideration the uncertainty of the observed intensity ratio, the uncertainty of α_0 is calculated to be ± 0.06. It is a linear relationship between α_0 and P at $X_{AlF_3}^{\circ} = 0.355$ and therefore the upper and lower limits are equal.

The effect of changing the temperature from 730 °C to the melting temperature of lithium cryolite, 782 °C,[2] may be estimated by using the value $\Delta H = 50.3$ J/mol at 700 °C which Holm and Holm [9] have calculated for the dissociation $AlF_6^{3-} = AlF_3 + 3F^-$. Van't Hoff's equation then leads to an increase in α_0 of about 10 % when the undercooled liquid is heated to the melting point.

The obtained value of α_0 is in reasonable agreement with the thermodynamic values $\alpha_0 = 0.35$ and $\alpha_0 = 0.40$ reported by Malinovsky and Vrebenska [2,14] and with $\alpha_0 = 0.20$ given by Jenssen.[3] The thermodynamic values refer to 782 °C. Good correspondence with thermodynamic results also are found in the recent Raman investigations by Gilbert *et al.*[7,8] of $NaF\text{-}AlF_3$ melts. They found $K = 3 \times 10^{-3}$ at 780 °C.

To conclude, the dissociation of AlF_6^{3-} in cryolite melts is found to follow the equilibrium reaction $AlF_6^{3-} \rightleftharpoons AlF_4^- + 2F^-$ with $K = 3 \times 10^{-2}$ and $\alpha = 0.24 \pm 0.06$ at 730 °C in the lithium system. These values are based on a Temkin melt model and a scattering efficiency (ν_1) of AlF_6^{3-} two times greater than of AlF_4^-.

Acknowledgement. The authors wish to thank Dr. K. Larsson for the use of a Cary 82 Raman spectrometer. The financial support of Elkem-Spigerverket A/S, Royal Norwegian Council for Scientific and Industrial Research, and the Norwegian Research Council for Science and the Humanities is gratefully acknowledged.

1. Grjotheim, K. *Kgl. Nor. Vidensk. Selsk. Skr.* (1956) No. 5.
2. Malinovsky, M. and Vrebenska, J. *Collect. Czech. Chem. Commun. 36* (1971) 567.
3. Jenssen, B. *Fase- og strukturforhold for noen komplekse alkali- aluminiumfluorider*, Lic. techn. thesis, Institutt for uorganisk kjemi, Norges Tekniske Høgskole, Universitetet i Trondheim, Trondheim 1969.
4. Holm, J. L. *Inorg. Chem. 12* (1973) 2062.
5. Dewing, E. *Met. Trans. 3* (1972) 495.
6. Ratkje, S. K. and Rytter, E. *J. Phys. Chem. 78* (1974) 1499.
7. Gilbert, B., Mamantov, G. and Begun, G. M. *Inorg. Nucl. Chem. Lett. 10* (1974) 1123.
8. Gilbert, B., Mamantov, G. and Begun, G. M. *J. Chem. Phys. In press.*
9. Holm, J. L. and Holm, B. J. *Thermochim. Acta 6* (1973) 375.
10. Øye, H. A., Rytter, E., Klæboe, P. and Cyvin, S. J. *Acta Chem. Scand. 25* (1971) 559.
11. Rytter, E. *Aluminium, Gallium and Indium Halide Complexes*, Lic. techn. thesis 26, Institutt for uorganisk kjemi, Norges Tekniske Høgskole, Universitetet i Trondheim, Trondheim 1974.
12. Chantry, G. In Anderson, A., Ed., *The Raman Effect*, Dekker, New York 1973.
13. Solomons, C., Clarke, J. H. R. and Bockris, J. O'M. *J. Chem. Phys. 49* (1968) 445.
14. Vrebenska, J. and Malinovsky, M. *Collect. Czech. Chem. Commun. 38* (1973) 659.

Received May 27, 1975.

Analysis of the High Resolution ^{1}H NMR Spectra of 2-Phenyl-1,3,2-dithiaphosphorinane

KNUT BERGESEN

Department of Chemistry, University of Bergen, Allégaten 70, N-5014 Bergen-Univ., Norway

^{1}H NMR studies of 1,3,2-dioxaphosphorinanes with tervalent phosphorus atom have received much attention the last years.[1–5] Most of the six-membered ring phosphites show no change of the NMR spectra over the temperature range −90 to +160 °C. This observation indicates anancomeric ring structure of the compounds and is therefore well suited to NMR analysis. NMR studies have also confirmed that the compounds have chair-structure and that the ring phosphites exist predominantly in one conformation with the group attached to the phosphorus atom in axial position. This paper reports the ^{1}H NMR analysis of 2-phenyl-1,3,2-dithiaphosphorinane, I, where the conformation

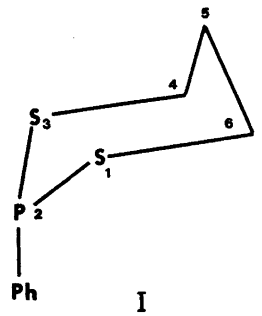

I

Table 1. 100 MHz spectral parameters (in Hz) of 2-phenyl-1,3,2-dithiaphosphorinane.

Chemical shift[a]		Coupling constants			
ν	Hz	J	Hz	J	Hz
4a	275.22	4a4e	−14.09	4e6a	0.06
4e	235.58	5a5e	−17.11	4a6a	0.01
5a	212.79	4a5a	12.01	P4a	2.36
5e	172.95	4e5a	2.52	P4e	−0.08
		4e5e	5.60	P5a	2.68
		4a5e	2.19	P5e	2.52
		4e6e	1.02		

[a] Downfield from TMS.

is discussed on the basis of spectral properties. The iterated spectral parameters of I are listed in Table 1.

The ^{1}H NMR spectrum of I was analyzed as an AA'BB'CDP spin system by means of the computer programs LAOCN3 [6] and KOMBIP.[7] The latter sub-routine generated "stick"- and Lorentzian line-shape plots.

The 100 MHz ^{1}H NMR spectrum of I, Fig. 1. shows a more complex pattern as compared to the dioxa analog which was divided into four well resolved bands. However, the splitted triplet observed in the lower field region of the spectrum indicates that there is a coupling of nearly the same magnitude as the geminal coupling, together with a smaller coupling. The larger coupling is assumed to be the vicinal *trans* (J_{aa}) coupling, and the smaller coupling to the *equatorial* proton in position 5. The low field part is therefore assigned to the axial protons at carbon 4 and 6. As a consequence the *equatorial* protons at C(4) and C(6) are therefore shifted to higher field compared to the axial protons. This relative shift position is the reversed as observed in cyclohexane derivatives,[8] but the same as reported for 1,3,2-dioxaphosphorinanes [3] and cyclic sulfites.[9–10] Apparently, this reversed or larger down field shift of axial protons at carbon 4 and 6, as compared to the geminal proton, indicates an axial position of the P−Ph group. The high field part of the spectrum is very complex and is due to the equatorial protons at carbon 4 and 6 and the protons at carbon 5.

It has been found that the axial proton at carbon 5 in trimethylenesulfide,[9] 2-chloro-, 2-methoxy- and 2-phenoxy-1,3,2-dioxaphosphorinane,[3] 2-chloro-1,3,2-dithiarsenane,[11] and also now 2-phenyl-1,3,2-dithiaphosphorinane (I) is always observed at lower field than the corresponding geminal equatorial proton. These compounds resemble the dioxanes with respect to relative shift positions of geminal protons at carbon 5, which also show this reversed relative position.[12] The reason for this observation is probably an interaction between H_{5e} and the *p*-orbitals of the ring oxygen and ring sulfur atoms.[13]

The vicinal coupling constants, J_{4a5a} and J_{4e5e}, found for 2-phenyl-1,3,2-dithiaphosphorinane are in the expected ranges [14] and are also consistent with a chair conformation of the ring. The rather large value of J_{4e5e} in I and 2-chloro-1,3,2-dithiarsenane [11] probably indicates a high ring puckering of the C(4)−C(5)−C(6) moiety of the ring.[15] In dioxanes, where the ring is assumed to be somewhat "flattened", J_{5e4a} is observed to be greater than J_{5e4e}.[12,16]

The geminal coupling constants in six-membered rings [17] are in the ranges −13 to −14 Hz and −12 to −18 Hz in C−CH_2−S− and C−CH_2−C, moieties, respectively. The observed values for I are in the expected range, and the magnitude of J_{4a4e} is close to the cor-

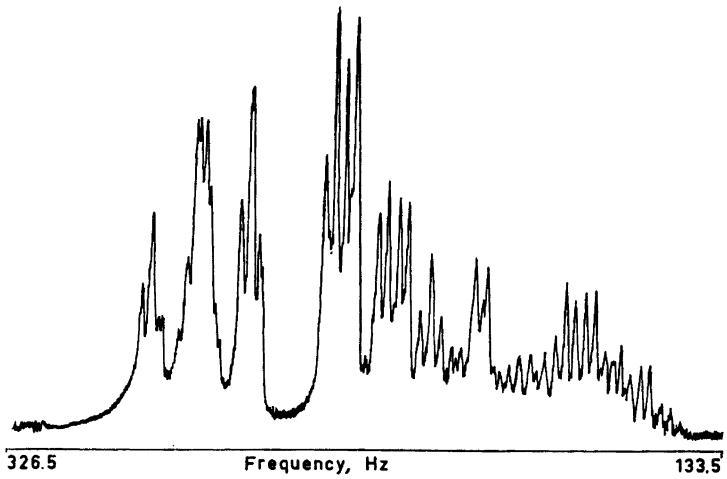

Fig. 1. Experimental 100 MHz spectrum of compound I in benzene solution.

responding coupling constant in 2-phenyl-5-*tert*-butyl-1,3,2-dithiaphosphorinane [18] and 2-chloro-1,3,2-dithiarsenane.[11]

The four-bond coupling of 1.02 Hz between the equatorial protons in 4 and 6 positions is an expected value for this type.[18]

The dihedral angle in the carbon part of the 1,3,2-dithiaphosphorinane is calculated using the vicinal proton-proton coupling constants according to the method of Buys.[19] The calculated ring torsion angle of the fragment $-CH_2-CH_2-$ is found to be 59°, which indicates that the carbon part exists in nearly staggered conformation.

Further analysis of ring substituted 1,3,2-dithiaphosphorinanes are in progress in this laboratory.

Experimental. 2-Phenyl-1,3,2-dithiaphosphorinane (I), was prepared from propanedithiol and dichlorophenyl-phosphine in benzene solution using triethylamine as base. B.p. 100 °C/0.5 mm Hg.

The NMR spectrum was recorded on a 100 MHz, Varian HA-100 spectrometer at 28 °C in 50 % solution of I in benzene. The spectrum was analysed on the basis of AA'BB'CDP spin system using the iterative computer program LAOCN3 [6] with some modification. Line positions was taken by averaging the data of four spectra. The computations were carried out on an UNIVAC 1110 computer. The r.m.s. deviation of 197 experimental and calculated transitions were less than 0.1, and the probable errors of the coupling constants are 0.02 to 0.03 Hz.

1. Hargis, J. H. and Bentrude, W. G. *Tetrahedron Lett.* (1968) 5365.
2. Albrand, J. P., Sagnaire, D. and Robert, J. B. *Bull. Soc. Chim. Fr.* (1969) 3496.
3. Bergesen, K. and Albriktsen, P. *Acta Chem. Scand. 25* (1971) 2257.
4. Bergesen, K. and Albriktsen, P. *Acta Chem. Scand. 26* (1972) 1680.
5. Bentrude, W. G. and Hargis, J. H. *J. Amer. Chem. Soc. 92* (1970) 7136.
6. Castellano, S. and Bothner-By, A. A. *J. Phys. Chem. 41* (1964) 3863.
7. Aksnes, D. W. *KOMBIP*, Quantum Chemistry Program Exchange, Chemistry Department, Indiana University, Indiana, USA.
8. Emsley, J. W., Feeney, J. and Sutcliffe, L. H. *High Resolution NMR Spectroscopy*, Vol. 2, 696–703.
9. Albriktsen, P. *Acta Chem. Scand. 25* (1971) 478.
10. Albriktsen, P. *Acta Chem. Scand. 26* (1972) 1783.
11. Aksnes, D. W. *Acta Chem. Scand. 26* (1972) 4170.
12. Pihlaja, K. and Äyräs, P. *Acta Chem. Scand. 24* (1970) 204, 531.
13. Anteunis, M., Travernier, D. and Borremans, F. *Bull. Soc. Chim. Belg. 75* (1966) 396.
14. See, for example, Thomas, W. A. *Annu. Rev. NMR Spectrosc. 1* (1968) 43.
15. Lambert, J. B. *Accounts Chem. Res. 4* (1971) 87.
16. Ramey, K. C. and Messick, J. *Tetrahedron Lett.* (1965) 4423.
17. Cahill, R., Cookson, R. C. and Crabb, T. A. *Tetrahedron 25* (1969) 4681, 4711.
18. Hutchins, R. O. and Maryanoff, B. E. *J. Amer. Chem. Soc. 94* (1972) 3266.
19. Buys, H. R. and Eliel, E. L. *Tetrahedron Lett.* (1970) 2779.

Received April 16, 1975.

Acta Chemica Scandinavica A 29 (1975) 569—579

Metal Complexes with Mixed Ligands. 10. A Potentiometric Study of Nickel(II) Imidazoles and Nickel(II) Hydroxo-imidazoles in 3.0 M (Na)ClO_4 and 3.0 M (Na)Cl

WILLIS FORSLING and STAFFAN SJÖBERG

Department of Inorganic Chemistry, University of Umeå, S-901 87 Umeå, Sweden

Three component equilibria between nickel(II), imidazole ($C_3H_4N_2$) and OH^- have been studied by means of emf titrations at 25 °C in two media 3.0 M (Na)ClO_4 and 3.0 M (Na)Cl using a glass electrode. The total nickel, B, and the total imidazole, C, have been varied within the limits $0.0025 \leq B \leq 0.090$ M and $0.0035 \leq C \leq 0.270$ M and the ratios C/B between $0.25 \leq C/B \leq 12$. At the highest C/B-ratios, data can be explained solely with stepwise metal complexes $Ni(C_3H_4N_2)_n^{2+}$, $n = 1,2,3,4$ and the following log ($\beta \pm 3\sigma$) could be determined: log $\beta_1 = 3.344 \pm 0.005$, log $\beta_2 = 6.087 \pm 0.008$, log $\beta_3 = 8.31 \pm 0.01$ and log $\beta_4 = 9.92 \pm 0.03$ in 3.0 M (Na)ClO_4 and log $\beta_1 = 3.250 \pm 0.004$, log $\beta_2 = 5.852 \pm 0.006$ log $\beta_3 = 7.86 \pm 0.02$ and log $\beta_4 = 9.08 \pm 0.06$ in 3.0 M (Na)Cl. At the lowest C/B-ratios also a ternary hydroxo-imidazole $Ni(OH)C_3H_4N_2^+$ with log K ($Ni^{2+} + C_3H_4N_2 \rightleftharpoons Ni(OH)C_3H_4N_2^+ + H^+$) $= -5.85 \pm 0.05$ in 3.0 M (Na)ClO_4 and -6.04 ± 0.04 in 3.0 M (Na)Cl seems to be formed.

In part 7 of this series Sjöberg [7] investigated the three component equilibria in the system copper(II)-imidazole-OH^- in 3.0 M (Na)ClO_4, 3.0 M (Na)Cl, and 5.0 M (Na)Cl using a glass electrode at 25° C. It was found that at $C/B > 8$ (B and C are the total copper and imidazole concentrations, respectively) only stepwise metal complexes were formed. At the lower C/B-ratios, data indicated that hydroxo-imidazoles must also be formed and the complexes $Cu_2(OH)_2(C_3H_4N_2)_2^{2+}$, $Cu_2(OH)_2(C_3H_4N_2)_4^{2+}$, and $Cu(OH)C_3H_4N_2^+$ were proposed. In equilibrium solutions of these lower C/B-ratios the binary hydroxo complexes $Cu_2(OH)_2^{2+}$ and $CuOH^+$ are also present. It therefore seems likely that the hydroxo-imidazoles formed result from complex formation between these ions and imidazole molecules.

The purpose of the present investigation is to determine whether similar behaviour is obtained in the nickel(II)-imidazole-OH^- system. The binary hydroxo complexes are in this case $Ni_4(OH)_4^{4+}$, Ni_2OH^{3+} and $NiOH^+$. One would then expect hydroxo-imidazoles of the types $Ni_4(OH)_4(C_3H_4N_2)_x^{4+}$, $Ni_2(OH)(C_3H_4N_2)_y^{3+}$ and $NiOH(C_3H_4N_2)_z^+$. Previous studies of nickel(II)-imidazole complexes indicate that solely $Ni(C_3H_4N_2)_n^{2+}$-complexes with $n = 1, \cdots 6$, should be formed (see Table 1). However, these conclusions are based on rather few data with small variations in concentrations and no experimental attempts seem to have been made to try to find hydroxo-imidazoles.

EXPERIMENTAL

Chemicals and analysis. Stock solutions of *sodium perchlorate* were prepared by neutralizing concentrated perchloric acid (Merck *p.a.*) with solid Na_2CO_3 (Merck *p.a.*) After the acid had been neutralized, a slight excess of sodium carbonate was added. This slightly alkaline solution ($pH \approx 8$) was then allowed to stand for about a week. If Fe-, Al-, and Si-impurities were present, they usually precipitated during this time as silicates or hydroxides. These precipitated impurities were filtered off, using a Jena G4 glass filter. The filtered solution was acidified with a slight excess of perchloric acid and then boiled to expel the carbonate as CO_2. After boiling, the solution was neutralized to $pH \approx 6$. Neither Cl^- nor CO_3^{2-} or Fe^{3+} could be detected in the solution prepared in this

Table 1. Earlier studies on nickel(II) imidazoles.

Ref.	Temp	Medium	Method	pK_a	log K_1	log K_2	log K_3	log K_4	log K_5	log K_6
13	25	0.135M KCl	pot.	7.09	2.94	2.41	1.99	1.3		
14	25	0.15M KNO_3	pol., pot.	7.12	3.27	2.68	2.15	1.65	1.12	0.52
16	25	0.16M KNO_3	pot.	7.11	3.09	2.47	2.00	1.54	1.1	0.5
15	25	0.5M NH_4NO_3	pot., pol.		2.933	2.27	1.82	0.76	0.97	
	Present work									
	25	3M (Na)Cl	pot.	7.637	3.25	2.60	2.01	1.22		
	25	3M $(Na)ClO_4$	pot.	7.913	3.34	2.75	2.22	1.61		

way. The sodium perchlorate stock was analysed for $NaClO_4$ by evaporating a known weight of solution at 120° C and then drying to constant weight.

The dilute *perchloric acids* and *hydrochloric acids* were standardized against tris(hydroxymethyl)aminomethane (TRISMA-base).

Dilute *sodium hydroxide* was prepared from "oljelut" (50 % NaOH and 50 % H_2O) and standardized against acid or hydrazine sulfate.

Imidazole, $C_3H_4N_2$, (Merck *p.a.*) with melting point 88 – 90 °C (lit. 90 °C) was used without further purification after drying. In some stock solutions it was, however, recrystallized from benzene.

Stock solutions of $C_3H_5N_2^+$ were prepared by dissolving $C_3H_4N_2$ in $HClO_4$ or HCl. The $C_3H_5N_2^+$-content was determined potentiometrically using the Gran [3] extrapolation method. The titrated amount was always a little higher than that expected from the weighed amount (~0.4 %). The value from titration has been assumed to be correct.

Stock solutions of *nickel perchlorate* were prepared by dissolving solid $NiCO_3$ (Baker, Reagent Grade) in perchloric acid, boiling and recrystallizing as $Ni(ClO_4)_2.6H_2O$ from distilled water several times.

Nickel chloride $NiCl_2.6H_2O$ (Baker, Reagent Grade) was recrystallized from water and dissolved in distilled water in order to prepare a stock solution of nickel chloride.

The Ni(II)-content (≈0.75 – 0.9 M) of the stock solutions was determined by precipitation with dimethylglyoxime according to Vogel [2] and by indirect titration with EDTA-$Pb(NO_3)_2$ (Indicator: Xylenolorange). The difference in $[Ni^{2+}]$ obtained by the two methods was less than 0.2 %.

The different Ni^{2+}-solutions used in the titrations were prepared from different stock solutions in order to detect possible systematic errors caused by impurities and analytical errors.

Stock solutions of *sodium chloride* were prepared by drying solid NaCl (Merck *p.a.*) for one day at about 200 °C in an electric oven, weighing and then dissolving in distilled water. All solutions were prepared using distilled water.

Apparatus. All emf measurements were carried out at 25.00 ± 0.05 °C. The salt bridge was of the "Wilhelm" type, described by Forsling, Hietanen and Sillén.[5] The cell arrangement was immersed in an oil thermostat (The oil thermostat and the burettes with NaOH- and Ni(II)-solutions were kept in a thermostated room at 25.0 ± 0.2 °C.)

During the experiments a stream of nitrogen was bubbled through the solution for stirring and for maintaining an inert atmosphere. Nitrogen from a cylinder was purified from acid and alkaline impurities by bubbling through solutions of 10 % NaOH and 10 % H_2SO_4. Finally, before the gas came into contact with the equilibrium solution, it was passed through pure ionic medium.

The potentiometric titrations were performed with an automatic system for precise emf titrations, a system constructed and built at this institute by O. Ginstrup.[6] The Ag, AgCl electrodes were prepared according to Brown.[10] Glass electrodes, Beckman type 40498 and Ingold type 201-NS were employed, giving constant and reproducible potentials within ± 0.2 mV.

The free H^+-concentration, h, was determined by measuring the emf of the cell

(A) $-$Re||equilibrium solution |GE+

where GE denotes a glass electrode and RE = Ag, AgCl|3 M NaCl saturated with AgCl||3 M NaCl and RE = Ag, AgCl/0.01 M NaCl, 2.99 M $NaClO_4$||3 M $NaClO_4$ respectively. The emf of cell (A) can be written at 25 °C as

$$E = E^\circ + 59.157 \log h + E_j \quad (1)$$

where E° is a constant determined at each titration in the acidic range ($-\log h < 3$) where h is known from a Gran [3] plot. For the liquid junction potentials we have used in 3.0 M (Na)Cl $E_j = -17.0h + 8.0k_w h^{-1}$ mV and in 3.0 M (Na)ClO_4 $E_j = -16.3\ h + 8.0\ k_w\ h^{-1}$ mV where $k_w = 9.33 \times 10^{-15}$ M^2 and $k_w = 6.03 \times 10^{-15}$ M^2 are the ionic products of water in 3.0 M (Na)Cl and 3.0 M (Na)ClO_4, respectively. However, in most of our titrations the correction for the E_j terms could be neglected.

METHOD

The titration procedures used were similar to those earlier described by Sjöberg.[7] During the titrations the total concentrations of nickel, B, and imidazole, C, were kept either constant or varied. In general each titration was performed at a constant C/B-ratio. The free hydrogen ion concentration, h, was varied by adding hydroxide ions or hydrogen ions, and was measured with a glass electrode. In order to avoid activity coefficient variations, a constant ionic medium of 3.0 M (Na)ClO_4 or 3.0 M (Na)Cl was used. The reproducibility and reversibility of equilibria were tested by performing both forward (increasing $-\log h$) and backward (decreasing $-\log h$) titrations. Dilution experiments at constant Z-values were also carried out to test the reversibility, especially at low C/B-quotients. Special efforts were made to cover as great part of the concentration range as possible and at the same time to try to cover the most interesting C/B ratios as well as possible. Due to the formation of precipitates, the available $-\log h$ range was restricted to an upper limit of 6.5 – 9. The crystalline precipitate with a composition of $Ni(C_3H_4N_2)_6(ClO_4)_2$ in 3.0 M (Na)ClO_4 has been X-ray investigated by Ivarsson. [21] However, at $C/B < 4$ a voluminous nickel-hydroxoprecipitate was always formed. The total concentrations (initial concentrations) of B and C were varied within the limits $0.0025 \leq B \leq 0.090$ M and $0.0035 \leq C \leq 0.270$ M. The following quotients C/B were thereby studied: 0.25, 0.5, 1, 1.4, 2, 3, 4, 5, 8, 10, and 12.

Most of the titrations were started with a calibration of the glass electrode (determination of E° and E_j) using those acidic points where hydrolysis and complex formation can be neglected. In the range of complex formation the $[H^+] = h$ can then be obtained for each point from the measured emf using eqn. 1. Since B, C, and H are known from analysis we can calculate for each point in a titration either

$$Z_B = (h - H)/B \quad (2)$$

or

$$Z_C = (h - H)/C \quad (3)$$

which are the average numbers of OH^- reacted per B and C, respectively. The experiments thus provide sets of data Z_B (log h) and/or Z_C (log h) at constant B, C or C/B.

We will assume the presence of three component equilibria of the general type

$$pH^+ + qNi^{2+} + rC_3H_5N_2^+ \rightleftharpoons H_pNi_q(C_3H_5N_2)_r^{(p+2q+r)+} \quad (4)$$

Applying the law of mass action to these equilibria the conditions for the total concentrations then give:

$$B = b + \sum_{pqr} q\beta_{pqr} h^p b^q c^r \quad (5)$$

$$C = c + K_a h^{-1} c + \sum_{pqr} r\beta_{pqr} h^p b^q c^r \quad (6)$$

$$H = h - K_a h^{-1} c + \sum_{pqr} p\beta_{pqr} h^p b^q c^r \quad (7)$$

where $b = [Ni^{2+}]$ and $c = [C_3H_5N_2^+]$. The calculational problem is then to find the model (sets of pqr and β_{pqr}) that best can explain the experimental data. The search for "best" model was performed by using the least squares computer program LETAGROPVRID [11] (version ETITR [12]). As "best" model or models we will consider those giving the lowest error squares sum $U = \sum[Z_C - Z_C(\text{calc})]^2$. The Letagrop calculations also give standard deviations $\sigma(Z_C)$, $\sigma(\beta_{pqr})$ and/or $\sigma(\log \beta_{pqr})$. For the definitions of these errors the reader is referred to the Letagrop paper I.[18]

Concerning the binary proton imidazole equilibrium

$$C_3H_5N_2^+ \rightleftharpoons C_3H_4N_2 + H^+ \quad (8)$$

we will make use of the result obtained by Sjöberg [7] and for binary hydrolysis equilibria

$$pH^+ + qNi^{2+} \rightleftharpoons Ni_qH_p^{(p+2q)+} \quad (9)$$

the results obtained by Ohtaki-Biedermann [8] (3 M (Na)Cl) and Burkov-Sillén [17] (3 M $(Na)ClO_4$). For reaction (3), Sjöberg [7] reported log $(K_a \pm 3\sigma)$ to be -7.637 ± 0.001 in 3 M (Na)Cl and -7.913 ± 0.002 in 3 M $(Na)ClO_4$. Concerning equilibria (4) the investigations both of Ohtaki-Biedermann and of Burkov-Sillén clearly show that the main species in a hydrolyzed Ni^{2+} solution is a tetramer $Ni_4(OH)_4^{4+}$ and the following log β_{-404} values were reported -28.5 (3.0 M (Na)Cl) and -27.37 (3.0 M $(Na)ClO_4$). Only minor amounts of the complexes $NiOH^+$ and Ni_2OH^{3+} were found in the concentration ranges studied.

From separate experiments the results of these binary equilibria were carefully tested and we found excellent agreement with the result earlier reported. We will therefore assume these binary equilibria to be exactly known, and all effects above this level will be treated as being caused by ternary species. Note that complexes $Ni(C_3H_4N_2)_n^{2+}$ in the following will be regraded as ternary species, where $p = -r$.

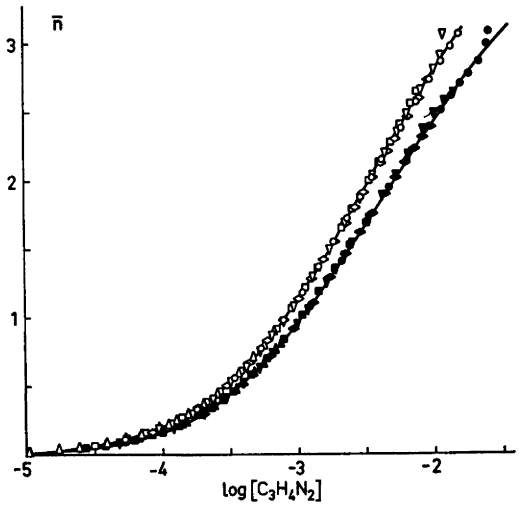

Fig. 1. Experimental data plotted as curves $\bar{n}(\log [C_3H_4N_2])$ for C/B ratios 1,2,3,4,8 and high B/C concentrations. Open symbols mark titrations in 3 M $(Na)ClO_4$ and dark symbols 3 M (Na)Cl. The figure also gives a comparison between the strength of complexation in the two media. The symbols stand for the following B and C in mM (start concentrations). ○●, 10 – 80; ◇◆, 10 – 40; △▲, 40 – 40; ▽▼, 20 – 80; □, 90 – 270; ■, 80 – 160. In order to make the figure clear only a few titrations have been plotted. The full curves have been calculated with the set of proposed constants in Table 3.

DATA, CALCULATIONS AND RESULTS

The mathematical analysis of data was started by making a Bjerrum plot, $\bar{n}(\log [C_3H_4N_2])$. The plot is shown in Fig. 1. It is seen from the plot that for quotients $C/B > 4$ and $B > 0.01$ M the function $\bar{n}(\log[C_3H_4N_2])$ seems to be independent of B and C thus indicating formation of a series of stepwise mononuclear complexes $Ni(C_3H_4N_2)_n^{2+}$. Data fulfilling these conditions will in the following be denoted Data 0.

However, at quotients $C/B < 4$ and $C < 0.01$ M the function $\bar{n}(\log[C_3H_4N_2])$ is not independent of B and C (Fig. 2a, b). This would indicate that ternary hydrolytic species of the type $Ni_q(OH)_p(C_3H_4N_2)_r^{(2q-p)+}$ are probably formed. These data will below be denoted as Data 1. It may be mentioned that data at very high C/B-ratios. $12 < C/B < 80$, have also been collected. These $\bar{n}(\log[C_3H_4N_2])$ functions are dependent on B and C as well.

A preliminary analysis of these data indicates formation of acidic ternary complexes of the type $Ni(C_3H_4N_2)_x(C_3H_5N_2)_y^{(2+y)+}$. However, the results and discussion of these complexes will be given in a forthcoming paper.

Data 0. A Letagrop analysis showed that these data could well be explained with the complexes $Ni(C_3H_4N_2)^{2+}$, $Ni(C_3H_4N_2)_2^{2+}$, $Ni(C_3H_4N_2)_3^{2+}$, and $Ni(C_3H_4N_2)_4^{2+}$ for both the NaCl and for the $NaClO_4$ media. The analysis ended at a $\sigma(Z)$ of 0.003 in 3.0 M $(Na)ClO_4$ and a $\sigma(Z) = 0.002$ in 3.0 M (Na)Cl, which must be considered as a very good explanation. The data included in the analysis consist of around 350 experimental points distributed over 15 BC-combinations. The "best" equilibrium constants with corresponding standard deviations obtained in these analyses, are given in Table 3, calculation denoted 1. The residuals $\Delta Z = Z_C - Z_C(\text{calc})$ after "best" fit are given together with experimental data in Table 5.

Data 1. These data cover the ranges

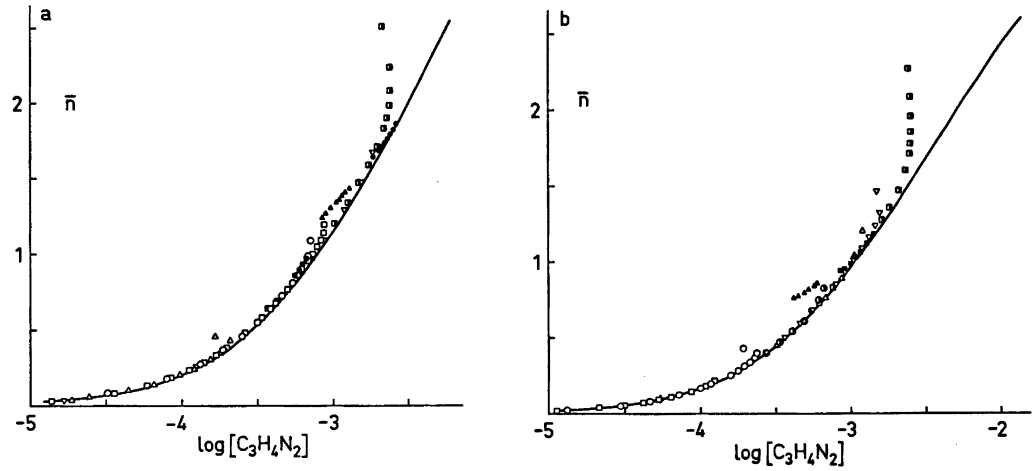

Fig. 2. Experimental data plotted as curves $\bar{n}(\log [C_3H_4N_2])$ for C/B ratios 0.25, 0.5, 1, 1.4, 2, 4 and low B,C concentrations. Dark symbols mark back titrations with pure ionic media. The symbols stand for the following B and C in mM (start concentrations). *a.* 3 M $(Na)ClO_4$-medium. ○, 4.5 – 6.5; □, 9 – 13; △, 10 – 15; ▽, 10 – 20; ◹, 2.5 – 10; ■, 4.2 – 6; ●, 4.2 – 12; ▲, 4.6 – 9.2. *b.* 3 M (Na)Cl-medium. ○, 26.8 – 12.1; □, 53.6 – 12.1; △, 2.5 – 5; ▽, 5 – 10; ◑, 10 – 10; ◹, 2.5 – 10; ■; 3.3 – 6.6; ▲, 6.4 – 6.6. Only a few titrations have been plotted. The full curves have been calculated with the set of proposed constants (not $-\log \beta_{-2,1,1}$) in Table 3.

$0.0025 \leq B \leq 0.08$ M, $0.003 \leq C < 0.08$ M, $1 \leq -\log h \leq 9$ and the quotients $C/B \leq 5$. The C/B-ratios studied were, in 3.0 M $(Na)ClO_4$, 0.5, 1, 1.4, 2, 3, and 4 in 3.0 M (Na)Cl, 0.25, 0.5, 1, 2, 5.

In the search for the ternary hydrolytic species it was assumed that the binary complexes were known and that the equilibrium constants had the values given above. The search was started with a *pqr*-analysis (systematic testing of different *pqr*-complexes). The result of the analysis is given in Fig. 3 and Table 3. It is seen from these calculations that the lowest error squares sum, in both media, is obtained for the complex $Ni(OH)C_3H_4N_2^+$. In 3 M (Na)Cl medium data could be fairly well explained by the complex $NiOH^+$. However, the value of the formation constant obtained, $\log \beta_{11} = -9.22$, is quite different from the value -10.5, obtained and proposed by Ohtaki-Biedermann in their binary investigation, and therefore an explanation with the ternary complex $Ni(OH)C_3H_4N_2^+$ appears more likely. Furthermore, in the

Table 2. The material, which has been used in the LETAGROP calculations, 73 points, is chosen to cover the range where the amount of the ternary complex is high.

Number of points	$\sigma(Z)$	$\log K_a \pm 3\sigma$	$\log \beta_{-211} \pm 3\sigma$	U
73	0.003	-6.52 ± 0.03 [a]	–	444
73	0.002	–	-13.68 ± 0.02	259
73	0.0003	-7.44 ± 0.16 [b]	-13.44 ± 0.02	11

[a] The amount of the impurity acid was about 0.1 mM. [b] The impurity acid obtained negative concentrations.

Table 3. Results of the final covariations of binary and ternary constants in the two media investigated. When no $3\sigma(\log \beta_{pqr})$ is given the formation constant has not been varied. To illustrate the difficulties in determining formation constants of complexes in the buffer range of imidazole, we have shown the change of $\log \beta_{-313}$ and $\log \beta_{-414}$ when $\log \beta_{-101}$ is changed 0.02 logarithmic units. The variation in $\log \beta_{-414}$ is big, but the change in $\log \beta_{-313}$ is negligible (as the change in $\log \beta_{-212}$ and $\log \beta_{-111}$).

	Method	Medium	Number of points	$\log \beta_{-101}$	$\sigma(z)$	$\log \beta_{-111}$ $\pm 3\sigma$	$\log \beta_{-212}$ $\pm 3\sigma$	$\log \beta_{-313}$ $\pm 3\sigma$	$\log \beta_{-414}$ $\pm 3\sigma$	$\log \beta_{-211}$ $\pm 3\sigma$
1	Emf.	3M(Na)Cl	353	−7.637	0.002	−4.387 ±0.004	−9.422 ±0.006	−15.053 ±0.018	−21.469 ±0.056	
2	Emf.	3M(Na)Cl	327	−7.637 −7.657	0.004	−4.387 −4.387	−9.422 −9.422	−15.053 −15.050 ±0.013	−21.469 −21.236 ±0.037	−13.684 ±0.035
1	Emf.	3M(Na)ClO_4	326	−7.913	0.003	−4.569 ±0.005	−9.739 ±0.008	−15.429 ±0.012	−21.728 ±0.032	
2	Emf.	3M(Na)ClO_4	387	−7.913	0.005	−4.569	−9.739	−15.429	−21.728	−13.763 ±0.048

3 M (Na)ClO_4 medium it was not possible to explain data with $NiOH^+$.

In order to visualize the amounts of $Ni(OH)C_3H_4N_2^+$ at some typical concentrations and C/B-ratios, we have calculated a set of distribution diagrams, which are shown in Fig. 4. It can be seen from the diagrams that the maximum amounts of $Ni(OH)C_3H_4N_2^+$ are obtained at around $-\log h = 8.5$, where about 5 – 10 % of the total nickel is present as $Ni(OH)C_3H_4N_2^+$. However, the total concentrations of the species are always rather low, mainly due to the fact that the necessary $-\log h$ values can be reached solely at low total nickel concentrations. Since the $Ni(OH)C_3H_4N_2^+$ concentrations are obviously rather low, it seems worthwhile to test whether the complex can be explained equally well with an impurity acid. A Letagrop calculation showed, however, that the "$Ni(OH)C_3H_4N_2^+$-effect" could not be explained with an impurity acid. The results of these calculations are collected in Table 2. Thus there appears to be good evidence that the complex $Ni(OH)C_3H_4N_2^+$ really exists. As stated in the introduction we had hoped to find some polynuclear complexes related to the species $Ni_4OH_4^{4+}$, but no indications in this direction could be found. This finding was tested and settled by performing experiments at constant Z, where hydrolyzed solutions of nickel chloride were titrated with nickel imidazole solutions. No effects due to complexes other than those given in Table 3 were found.

For complex formation in the chloride medium, the formation of chloro complexes must be taken into consideration. Many workers have reported that nickel(II) ions

Table 4. "Conditional stability constants" β'_{pqr} defined according to $pH^+ + qNi^{2+} + rC_3H_4N_2 \rightleftharpoons (H^+)_p(Ni^{2+})_q(C_3H_4N_2)_r$ and calculated from the relation $\beta'_{pqr} = \beta_{pqr}(1 + \beta_{010})^q$. The values of β_{pqr} are calculated from constants given in Table 1. Approximate values of β_{010} have been calculated (see eqn. 10) by assuming $\log K(NiCl^+) = -0.48$ and $[Cl^-] = 3$ M.

Medium	NiL^{2+} $\log \beta'_{011}$	NiL_2^{2+} $\log \beta'_{012}$	NiL_3^{2+} $\log \beta'_{013}$	NiL^{2+} $\log \beta'_{014}$	$Ni(OH)L^+$ $\log \beta'_{-111}$
3.0 M (Na)Cl	3.55	6.15	8.16	9.38	−5.64
3.0 M (Na)ClO_4	3.34	6.09	8.31	9.94	−5.85

form weak complexes with chloride ions. The dominating complex seems to be $NiCl^+$ and formation constants of other complexes are so small and erroneous that only this species is taken into account in the following discussion.

Assuming the equilibrium $Ni^{2+} + Cl^- \rightleftharpoons NiCl^+$ to be known with $\log K_1 = -0.48$ (an average value) it is possible to calculate a new conditional constant β'_{pqr} which is corrected for the equilibrium through the relation

Table 5. Experimental data Z ($\log h$) at different B and C concentrations (initial concentrations) (3.0 M $(Na)ClO_4$ medium). For each point the quantities, H (in mM), $\log h$, Z, ΔZ_0 and ΔZ_1 are given. ΔZ is the residual $(Z_{exp} - Z_{calc}) \times 1000$ and the indices 0 and 1 refer to the assumptions 0, Binary complexes $Ni(C_3H_4N_2)_n^{2+}$ only with constants given in Table 3 together with hydrolysis species $Ni_4OH_4^{4+}$ with constants proposed by Burkov *et al.*;[17] 1, Binary complexes and proposed ternary complex with equilibrium constants given in Table 3.

SATS 1 B = 0.01000 C = 0.01000

H	log h	Z	ΔZ_0	ΔZ_1
-0.38	-5.084	0.033	2.88	2.07
-0.71	-5.485	0.076	3.64	3.61
-0.91	-5.612	0.098	4.31	4.27
-1.50	-5.888	0.164	5.97	5.86
-1.70	-5.960	0.186	6.48	6.33
-1.89	-6.028	0.207	6.71	6.51
-2.08	-6.090	0.229	7.17	6.93
-2.27	-6.148	0.251	7.64	7.35
-2.45	-6.204	0.273	7.77	7.42
-2.64	-6.258	0.295	8.04	7.63
-3.18	-6.406	0.361	9.16	8.51
-3.72	-6.544	0.426	9.72	8.76
-4.23	-6.679	0.492	9.57	8.18
-4.74	-6.811	0.558	10.06	8.12
-5.23	-6.948	0.623	10.05	7.35
-5.71	-7.092	0.689	9.84	6.03
-6.18	-7.250	0.754	9.82	4.33
-6.48	-7.369	0.798	9.88	2.68
-6.63	-7.435	0.820	9.87	1.51
-6.78	-7.506	0.842	9.87	0.05
-6.93	-7.584	0.864	9.88	-1.84
-7.08	-7.671	0.886	10.12	-4.12

SATS 2 B = 0.02000 C = 0.04000

H	log h	Z	ΔZ_0	ΔZ_1
-0.23	-4.283	0.009	-0.15	-0.15
-0.95	-4.830	0.029	0.29	0.29
-1.64	-5.095	0.051	0.59	0.58
-2.31	-5.274	0.073	0.98	0.97
-2.96	-5.415	0.095	1.20	1.18
-3.59	-5.532	0.117	1.29	1.26
-4.20	-5.634	0.138	1.43	1.38
-4.79	-5.725	0.160	1.43	1.36
-5.36	-5.807	0.182	1.65	1.56
-5.92	-5.884	0.204	1.78	1.66
-6.46	-5.957	0.226	1.78	1.64
-6.99	-6.025	0.248	1.68	1.51
-7.50	-6.090	0.270	1.85	1.65
-8.00	-6.153	0.292	2.03	1.79
-8.48	-6.213	0.314	2.06	1.78
-8.96	-6.274	0.336	1.35	1.03
-9.42	-6.333	0.357	0.79	0.42
-9.86	-6.390	0.379	0.49	0.07
-10.30	-6.445	0.401	0.58	0.11
-10.72	-6.500	0.423	0.40	-0.13
-11.14	-6.554	0.445	0.18	-0.42
-11.54	-6.608	0.467	-0.09	-0.76
-11.94	-6.662	0.489	-0.42	-1.16
-12.32	-6.715	0.511	-0.27	-1.08
-12.70	-6.768	0.533	-0.42	-1.32
-13.06	-6.822	0.555	-0.43	-1.43

SATS 3 B = 0.01000 C = 0.02000

H	log h	Z	ΔZ_0	ΔZ_1
-0.39	-4.896	0.023	3.45	3.45
-2.43	-5.823	0.137	8.34	8.26
-4.43	-6.206	0.253	11.12	10.86
-6.40	-6.500	0.368	11.09	10.55
-8.34	-6.762	0.483	10.79	9.84
-10.24	-7.022	0.599	8.99	7.44
-12.11	-7.303	0.714	6.55	3.96
-13.95	-7.646	0.830	4.80	-0.23
-15.75	-8.212	0.945	5.87	-10.81

SATS 4 B = 0.01976 C = 0.01977

H	log h	Z	ΔZ_0	ΔZ_1
-0.21	-4.459	0.014	0.36	0.36
-1.06	-5.166	0.063	0.44	0.43
-1.87	-5.469	0.113	0.33	0.30
-2.63	-5.676	0.164	0.28	0.21
-3.37	-5.841	0.214	0.33	0.20
-4.06	-5.979	0.265	1.81	1.60
-4.73	-6.106	0.316	2.12	1.81
-5.37	-6.223	0.366	3.00	2.56
-5.98	-6.336	0.417	3.06	2.45
-6.56	-6.444	0.467	3.60	2.80
-7.12	-6.551	0.518	3.85	2.79
-7.66	-6.659	0.569	4.29	2.90
-8.17	-6.769	0.619	4.73	2.92
-8.67	-6.883	0.670	4.85	2.48
-9.14	-7.005	0.720	5.22	2.07
-9.60	-7.139	0.771	5.11	0.83
-9.75	-7.187	0.788	5.48	0.71
-10.04	-7.292	0.822	5.19	-0.86
-10.33	-7.409	0.855	5.55	-2.35
-10.47	-7.477	0.872	5.24	-3.96

SATS 5 B = 0.004189 C = 0.005960

H	log h	Z	ΔZ_0	ΔZ_1
-4.73	-7.648	0.794	15.97	6.29
-4.58	-7.650	0.791	16.04	6.32
-4.31	-7.653	0.786	15.73	5.91
-4.06	-7.655	0.780	15.42	5.53
-3.83	-7.656	0.774	15.40	5.47
-3.63	-7.657	0.768	15.01	5.03
-3.44	-7.657	0.762	14.77	4.78
-3.27	-7.657	0.756	14.47	4.46
-3.11	-7.656	0.750	14.31	4.32
-2.97	-7.654	0.745	14.47	4.52
-2.84	-7.652	0.739	14.35	4.43

SATS 6 B = 0.009081 C = 0.01292

H	log h	Z	ΔZ_0	ΔZ_1
-1.81	-5.890	0.151	5.60	5.50
-2.97	-6.195	0.249	6.52	6.23
-4.12	-6.433	0.346	6.47	5.89
-5.26	-6.648	0.444	4.59	3.57
-6.39	-6.850	0.542	4.35	2.71
-7.51	-7.054	0.640	6.33	3.76
-8.62	-7.284	0.738	5.77	1.56
-9.72	-7.556	0.835	9.20	1.62

SATS 7 B = 0.009081 C = 0.01292

H	log h	Z	ΔZ_0	ΔZ_1
0.14	-3.804	0.002	0.40	0.40
-0.27	-5.027	0.026	3.39	3.38
-0.68	-5.460	0.063	5.63	5.61
-1.09	-5.701	0.100	6.86	6.81
-1.49	-5.875	0.138	7.54	7.45
-1.89	-6.014	0.176	8.27	8.12
-2.29	-6.136	0.213	7.90	7.67
-2.68	-6.240	0.251	8.82	8.50
-3.07	-6.336	0.288	9.22	8.79
-3.45	-6.427	0.326	9.42	8.86
-3.83	-6.512	0.363	9.69	8.98
-4.21	-6.592	0.401	10.92	10.04
-4.59	-6.671	0.439	11.24	10.17
-5.33	-6.828	0.514	11.63	10.08
-5.70	-6.907	0.551	10.87	9.00
-6.07	-6.986	0.589	10.92	8.68
-6.43	-7.066	0.627	11.25	8.59
-6.79	-7.149	0.664	11.56	8.38
-7.14	-7.236	0.702	11.39	7.54
-7.50	-7.328	0.739	11.33	6.64
-7.85	-7.427	0.777	11.49	5.70
-8.19	-7.536	0.815	11.59	4.27
-8.54	-7.659	0.852	11.88	2.29
-8.88	-7.807	0.890	12.01	-1.22
-9.22	-7.992	0.927	12.83	-7.02

SATS 8 B = 0.005000 C = 0.01000

H	log h	Z	ΔZ_0	ΔZ_1
-0.65	-5.718	0.068	3.55	3.51
-2.13	-6.385	0.226	6.96	6.60
-3.59	-6.778	0.384	8.16	7.14
-5.04	-7.117	0.542	8.70	6.60
-6.47	-7.470	0.699	8.04	3.91
-7.88	-7.901	0.857	15.13	5.30

SATS 9 B = 0.004155 C = 0.01254

H	log h	Z	ΔZ_0	ΔZ_1
-10.59	-8.108	0.858	2.15	-3.92
-10.30	-8.115	0.858	2.02	-4.25
-10.02	-8.121	0.858	2.04	-4.40
-9.76	-8.127	0.858	1.93	-4.71
-9.51	-8.133	0.858	1.90	-4.92
-9.27	-8.139	0.858	1.86	-5.14
-9.05	-8.145	0.858	1.69	-5.50
-8.83	-8.150	0.858	1.61	-5.77
-8.63	-8.155	0.858	1.71	-5.84
-8.43	-8.160	0.858	1.72	-6.00
-8.25	-8.164	0.858	1.92	-5.97
-8.07	-8.169	0.858	1.91	-6.16
-7.90	-8.173	0.858	2.00	-6.24
-7.73	-8.178	0.858	1.96	-6.45
-7.58	-8.182	0.858	2.03	-6.54
-7.43	-8.186	0.858	2.03	-6.72
-7.28	-8.189	0.858	2.22	-6.69
-7.14	-8.193	0.858	2.30	-6.77
-7.01	-8.196	0.858	2.43	-6.79
-6.88	-8.200	0.858	2.55	-6.83
-6.75	-8.203	0.858	2.64	-6.90
-6.63	-8.206	0.858	2.84	-6.84
-6.52	-8.209	0.858	2.94	-6.91
-6.40	-8.212	0.858	3.14	-6.85
-6.30	-8.215	0.858	3.28	-6.85
-6.19	-8.218	0.858	3.41	-6.88
-6.09	-8.220	0.858	3.65	-6.78
-5.99	-8.223	0.858	3.69	-6.89
-5.90	-8.226	0.858	3.85	-6.87
-5.81	-8.229	0.858	3.72	-7.16
-5.72	-8.232	0.858	3.89	-7.12
-5.63	-8.234	0.858	4.14	-7.01
-5.55	-8.236	0.858	4.24	-7.05
-5.47	-8.239	0.858	4.32	-7.11
-5.39	-8.241	0.858	4.43	-7.13
-5.31	-8.244	0.858	4.26	-7.47
-5.23	-8.246	0.858	4.44	-7.42
-5.16	-8.248	0.858	4.74	-7.24

SATS10 B = 0.004505 C = 0.01802

H	log h	Z	ΔZ_0	ΔZ_1
-11.48	-7.557	0.637	1.37	0.52
-11.17	-7.563	0.637	1.33	0.44
-10.87	-7.570	0.637	1.27	0.35
-10.58	-7.576	0.637	1.26	0.31
-10.32	-7.582	0.637	1.10	0.12
-10.06	-7.588	0.637	0.87	-0.15
-9.82	-7.594	0.637	0.77	-0.28

Table 5. Continued.

-9.59	-7.600	0.637	0.67	-0.41
-9.37	-7.605	0.637	0.44	-0.68
-9.16	-7.611	0.637	0.42	-0.73
-8.96	-7.616	0.637	0.35	-0.84
-8.76	-7.621	0.637	-0.06	-1.29
-8.58	-7.626	0.637	0.11	-1.15
-8.40	-7.631	0.637	-0.13	-1.42
-8.23	-7.636	0.637	-0.34	-1.67
-8.07	-7.640	0.637	-0.39	-1.75
-7.91	-7.644	0.637	-0.41	-1.80
-7.76	-7.648	0.637	-0.47	-1.90
-7.62	-7.652	0.637	-0.43	-1.90
-7.48	-7.656	0.637	-0.29	-1.78
-7.34	-7.659	0.637	-0.11	-1.64
-7.21	-7.662	0.637	0.18	-1.38
-7.09	-7.666	0.637	0.07	-1.52
-6.96	-7.670	0.637	0.07	-1.56
-6.85	-7.673	0.637	0.26	-1.40
-6.73	-7.676	0.637	0.34	-1.35
-6.63	-7.679	0.637	0.25	-1.48
-6.52	-7.683	0.637	0.27	-1.49

SATS11 B = 0.005000 C = 0.02000

H	log h	Z	ΔZ_0	ΔZ_1
-2.47	-6.126	0.132	2.71	2.59
-3.63	-6.381	0.195	2.75	2.54
-4.78	-6.587	0.258	3.19	2.87
-5.92	-6.768	0.321	3.76	3.33
-7.05	-6.938	0.384	2.93	2.41
-8.18	-7.096	0.448	3.02	2.43
-9.29	-7.252	0.511	1.70	1.05
-10.39	-7.405	0.574	0.84	0.10
-11.48	-7.557	0.637	1.33	0.48

SATS12 B = 0.004598 C = 0.009196

H	log h	Z	ΔZ_0	ΔZ_1
-7.88	-7.901	0.857	15.10	5.27
-7.61	-7.911	0.857	15.35	5.24
-7.36	-7.921	0.857	15.39	4.99
-7.13	-7.930	0.857	15.51	4.83
-6.91	-7.938	0.857	15.76	4.82
-6.70	-7.946	0.857	15.96	4.76
-6.51	-7.954	0.857	16.12	4.65
-6.33	-7.961	0.857	16.53	4.82
-6.15	-7.969	0.857	16.58	4.60
-5.99	-7.975	0.857	16.78	4.56
-5.83	-7.983	0.857	16.87	4.39
-5.69	-7.989	0.857	17.04	4.32
-5.54	-7.996	0.857	17.14	4.17
-5.41	-8.001	0.857	17.71	4.54
-5.28	-8.006	0.857	18.03	4.65
-5.16	-8.012	0.857	18.16	4.54
-5.05	-8.017	0.857	18.42	4.59
-4.94	-8.022	0.857	18.64	4.59
-4.73	-8.033	0.857	18.84	4.33
-4.54	-8.044	0.857	18.96	4.01
-4.36	-8.053	0.857	19.26	3.90
-4.20	-8.062	0.857	19.62	3.86
-4.05	-8.070	0.857	19.99	3.85
-3.98	-8.078	0.857	20.19	3.65
-3.65	-8.093	0.857	20.70	3.42
-3.43	-8.108	0.857	20.96	2.96
-3.23	-8.120	0.857	21.38	2.70
-3.05	-8.132	0.857	21.74	2.41

SATS13 B = 0.008841 C = 0.008841

H	log h	Z	ΔZ_0	ΔZ_1
-6.69	-7.234	0.757	6.66	1.37
-6.53	-7.239	0.755	6.61	1.26
-6.24	-7.248	0.752	6.43	0.96
-5.97	-7.257	0.749	6.38	0.81
-5.71	-7.264	0.746	6.35	0.69
-5.48	-7.272	0.743	6.23	0.48
-5.27	-7.279	0.740	6.25	0.41
-5.06	-7.284	0.737	6.34	0.43
-4.88	-7.290	0.734	6.32	0.34
-4.70	-7.296	0.731	6.27	0.22
-4.54	-7.300	0.728	6.34	0.23
-4.38	-7.305	0.725	6.26	0.09
-4.24	-7.309	0.722	6.18	-0.05
-4.10	-7.313	0.719	6.11	-0.17
-3.97	-7.317	0.716	6.13	-0.19
-3.85	-7.321	0.713	6.02	-0.34
-3.73	-7.324	0.710	5.88	-0.52
-3.62	-7.327	0.707	5.78	-0.66
-3.51	-7.330	0.704	5.65	-0.83
-3.41	-7.332	0.701	5.64	-0.86
-3.32	-7.335	0.698	5.54	-0.99
-3.23	-7.337	0.695	5.36	-1.20
-3.14	-7.339	0.692	5.39	-1.18
-3.06	-7.340	0.689	5.34	-1.25
-2.98	-7.342	0.686	5.22	-1.39
-2.90	-7.344	0.683	4.94	-1.68
-2.83	-7.345	0.680	4.98	-1.65

SATS14 B = 0.008181 C = 0.01164

H	log h	Z	ΔZ_0	ΔZ_1
-9.72	-7.556	0.835	9.17	1.61
-9.39	-7.562	0.834	9.24	1.56
-9.09	-7.567	0.832	9.41	1.61
-8.80	-7.572	0.830	9.68	1.78
-8.52	-7.577	0.828	9.74	1.74
-8.27	-7.582	0.827	9.82	1.72
-8.02	-7.587	0.825	9.75	1.55
-7.79	-7.592	0.823	9.65	1.34
-7.37	-7.600	0.820	9.52	1.04
-6.98	-7.608	0.817	9.21	0.55
-6.63	-7.615	0.813	9.08	0.25
-6.31	-7.622	0.810	8.75	-0.23
-6.02	-7.627	0.806	8.42	-0.70
-5.75	-7.632	0.803	8.29	-0.95
-5.51	-7.636	0.800	8.33	-1.01
-5.28	-7.640	0.796	8.13	-1.31
-4.97	-7.644	0.791	7.99	-1.57
-4.69	-7.648	0.786	7.78	-1.90

SATS15 B = 0.04000 C = 0.02000

H	log h	Z	ΔZ_0	ΔZ_1
-0.64	-4.609	0.038	-0.12	-0.13
-1.58	-5.031	0.092	0.64	0.63
-2.48	-5.275	0.146	1.17	1.14
-3.34	-5.458	0.201	1.26	1.20
-4.17	-5.607	0.256	1.76	1.66
-4.97	-5.740	0.310	1.85	1.69
-5.73	-5.861	0.365	1.97	1.73
-6.70	-6.011	0.438	2.56	2.19
-7.48	-6.122	0.493	1.95	1.45
-8.07	-6.232	0.548	1.89	1.20
-8.72	-6.343	0.602	2.09	1.17
-9.34	-6.458	0.657	2.40	1.17
-9.94	-6.582	0.712	2.29	0.60
-10.52	-6.719	0.767	2.20	-0.15
-11.09	-6.876	0.822	2.70	-0.73
-11.45	-6.998	0.858	3.60	-0.97
-11.63	-7.069	0.876	3.82	-1.57
-11.81	-7.148	0.895	3.85	-2.63
-11.98	-7.237	0.913	4.15	-3.80
-12.16	-7.336	0.931	4.64	-5.35
-12.33	-7.438	0.949	6.23	-6.34

SATS16 B = 0.02000 C = 0.01000

H	log h	Z	ΔZ_0	ΔZ_1
-0.45	-4.987	0.049	1.25	1.24
-1.05	-5.397	0.114	3.10	3.07
-1.63	-5.640	0.179	4.57	4.49
-2.20	-5.825	0.245	5.43	5.27
-2.76	-5.981	0.310	5.65	5.38
-3.12	-6.075	0.354	6.43	6.06
-3.30	-6.120	0.376	6.79	6.37
-3.48	-6.164	0.398	6.91	6.43
-3.65	-6.207	0.420	7.14	6.59
-3.83	-6.250	0.442	7.14	6.52
-4.34	-6.378	0.507	6.92	6.01
-5.08	-6.546	0.595	7.84	6.40
-5.48	-6.680	0.660	7.81	5.77
-5.96	-6.824	0.726	8.32	5.40
-6.42	-6.988	0.792	8.71	4.35
-6.72	-7.119	0.836	8.41	2.47
-6.86	-7.193	0.857	8.25	1.17
-7.01	-7.277	0.879	7.99	-0.61
-7.16	-7.371	0.901	8.05	-2.63
-7.30	-7.478	0.923	8.28	-5.37
-7.45	-7.590	0.945	9.85	-7.73

SATS17 B = 0.01000 C = 0.005000

H	log h	Z	ΔZ_0	ΔZ_1
-0.15	-5.024	0.033	4.58	4.58
-0.36	-5.438	0.075	6.55	6.53
-0.57	-5.674	0.119	7.49	7.43
-0.78	-5.845	0.162	7.66	7.55
-0.98	-5.982	0.206	7.75	7.56
-1.18	-6.100	0.250	7.73	7.44
-1.38	-6.204	0.293	7.68	7.26
-1.58	-6.300	0.337	7.68	7.10
-1.78	-6.390	0.381	7.54	6.77
-1.98	-6.475	0.425	7.94	6.93
-2.17	-6.558	0.468	8.46	7.17
-2.36	-6.640	0.512	8.58	6.95
-2.55	-6.722	0.556	8.85	6.80
-2.74	-6.806	0.600	9.08	6.51
-2.93	-6.892	0.644	9.16	5.93
-3.11	-6.982	0.687	9.54	5.48
-3.29	-7.079	0.731	9.58	4.41
-3.48	-7.186	0.775	9.44	2.75
-3.66	-7.305	0.819	9.80	0.90
-3.83	-7.443	0.862	10.66	-1.65
-4.01	-7.611	0.906	12.33	-5.80
-4.19	-7.791	0.950	19.40	-7.79

SATS18 B = 0.004541 C = 0.006460

H	log h	Z	ΔZ_0	ΔZ_1
-0.82	-6.111	0.140	10.87	10.71
-1.26	-6.371	0.215	10.67	$10\cdot3_0$
-1.69	-6.570	0.290	10.83	10.12
-2.12	-6.744	0.365	9.77	8.59
-2.54	-6.901	0.440	10.31	8.54
-2.96	-7.055	0.515	9.79	7.21
-3.37	-7.206	0.590	10.34	6.67
-3.79	-7.361	0.665	12.00	6.81
-4.20	-7.532	0.740	13.08	5.54
-4.60	-7.728	0.815	15.27	3.72
-5.00	-7.973	0.890	19.42	-0.32

SATS19 B = 0.002500 C = 0.01000

H	log h	Z	ΔZ_0	ΔZ_1
-0.06	-4.891	0.009	3.50	3.50
-0.59	-6.066	0.074	7.92	7.86
-1.11	-6.441	0.141	8.73	8.52
-1.61	-6.694	0.207	8.80	8.37
-2.09	-6.896	0.274	9.25	8.56
-2.56	-7.073	0.341	8.60	7.66
-3.02	-7.234	0.408	7.93	6.71
-3.24	-7.310	0.441	7.66	6.30
-3.47	-7.384	0.474	7.44	5.92
-3.68	-7.457	0.508	7.38	5.70
-3.90	-7.529	0.541	7.50	5.63
-4.11	-7.608	0.574	7.90	5.82
-4.31	-7.672	0.608	8.19	5.88
-4.52	-7.745	0.641	8.36	5.76
-4.72	-7.819	0.675	9.04	6.09
-4.92	-7.896	0.708	9.60	6.22
-5.12	-7.976	0.741	10.49	6.57
-5.31	-8.061	0.775	11.30	6.68
-5.50	-8.151	0.808	12.50	6.96
-5.69	-8.252	0.841	13.57	6.74

SATS20 B = 0.004550 C = 0.01351

H	log h	Z	ΔZ_0	ΔZ_1
-0.13	-4.848	0.012	3.75	3.75
-0.98	-5.885	0.083	5.63	5.58
-1.82	-6.248	0.155	5.21	5.03
-2.64	-6.501	0.227	4.38	4.01
-3.45	-6.708	0.299	3.53	2.94
-4.24	-6.893	0.370	2.32	1.47
-5.02	-7.064	0.442	1.62	0.48
-5.79	-7.228	0.514	1.19	-0.27
-6.55	-7.392	0.586	0.93	-0.92
-7.29	-7.558	0.658	1.33	-1.06
-8.02	-7.735	0.730	2.46	-0.75
-8.74	-7.934	0.802	4.61	-0.02
-9.45	-8.175	0.874	8.13	0.58
-10.14	-8.535	0.946	12.64	-3.47

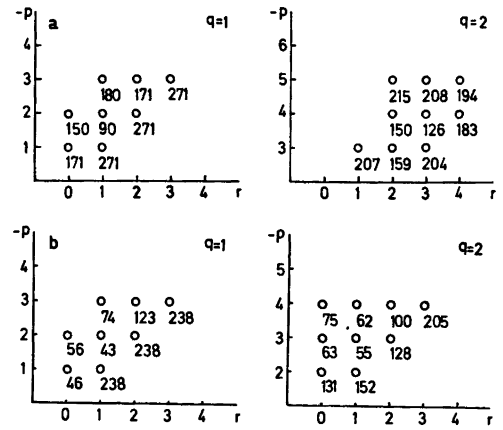

Fig. 3. LETAGROP-search for ternary $H_pNi_q(C_3H_5N_2)_r^{(2q+p+r)}$-complexes. The diagrams give error square sums $U(pr)_q \times 10^{-2}$ assuming only one complex. In the calculations the species $Ni_4OH_4^+$, $Ni(C_3H_4N_2)_n^{2+}$, $(n = 1, 2, 3, 4)$ have been assumed to be known. a, shows the calculations in 3 M ($NaClO_4$ (387 points) and b, shows the calculations in 3 M (Na)Cl (327 points).

$$\beta'_{pqr} = \beta_{pqr}(1 + \beta_{010})^q \quad (10)$$

where $$\beta_{010} = K_1[Cl^-], \quad (11)$$

β_{010} is constant provided $[Cl^-]$ remains constant during the titration.

The values of β'_{pqr} from the chloride medium are given in Table 4. As is seen from this table the values of the β'_{pqr} constants are (usually) greater than those in the perchlorate medium indicating that $(H^+)_p(Ni^{2+})_q(C_3H_5N_2^+)_r(Cl^-)_s$ complexes are also formed.

DISCUSSION

The present emf investigation has given clear evidence for the existence of a hydrolyzed nickel imidazole complex. $Ni(OH)C_3H_4N_2^+$, together with a series of stepwise metal complexes $Ni(C_3H_4N_2)_n^{2+}$, $n = 1,2,3,4$. No evidence for the formation of any polynuclear ternary complexes $Ni_q(OH)_p(C_3H_4N_2)_r^{(2q-p)+}$ was found.

The logarithms of the formation constants could be determined with an accuracy (3σ) greater than 0.02 for the stepwise complexes and greater than 0.05 for the hydrolyzed complex.

The behaviour of the nickel system differs a little from the corresponding copper system due to the fact that in the copper system polynuclear complexes are formed whereas in the nickel system no such complexes could be detected. However, in both systems a ternary hydrolyzed complex of the type

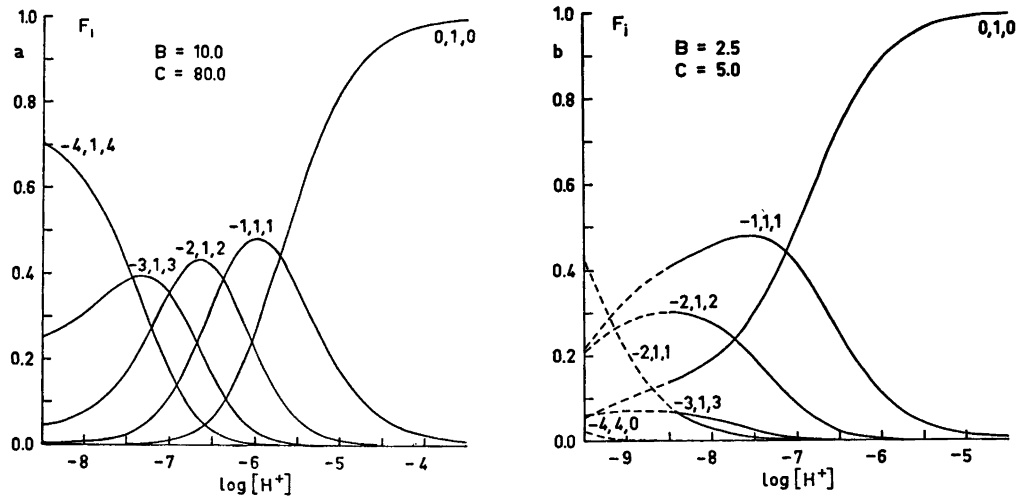

Fig. 4. Distribution diagrams F_i (log $[H^+])_{B,C}$. F_i is defined as the ratio between nickel(II) in a species and total nickel(II). The calculations have been performed using a version of the computer program SOLGAS [20] valid for equilibria in solution and equipped with a plotting procedure (Gunnar Eriksson, to be published). Broken lines denote ranges where no measurements have been performed due to precipitation (extrapolated range).

$Me(OH)C_3H_4N_2^+$ seems to be formed in a not negligible amount.

The logarithms of the formation constants are in 3 M $(Na)ClO_4$ $\log \beta_{-211}(Ni(OH)C_3H_4N_2^+) = -13.76$ and $\log \beta_{-211}$ $(Cu(OH)C_3H_4N_2^+) = -10.44$. Thus the ternary complex in the copper system is more easily formed than the corresponding complex in the nickel system. Furthermore the chloride media seem to increase the stability in both systems.

The reason that no polynuclear complexes can be detected in the nickel system is probably due to the fact that at high B concentrations, the available $-\log h$ range is too restricted to permit polynuclear complexes to be formed. The precipitated nickel hydroxoperchlorate and nickel hydroxochloride seem to be less soluble than the corresponding copper compounds.

By means of the present investigation it has also become possible to compare the acidities (tendency to hydrolyze) of the species $Ni(H_2O)_x^{2+}$ and $Ni(H_2O)_y(C_3H_4N_2)^{2+}$. For both the perchlorate and chloride media it was found that $\log K_a(NiC_3H_4N_2^{2+}) > \log K_a(Ni^{2+})$. The actual values of $\log K_a$ are -9.19 [3 M $(Na)ClO_4$] and -9.30 [3 M (Na)Cl]. (*Cf.* $\log K_a(Ni^{2+}) \leq -10.5$.) It seems that the introduction of an imidazole ligand increases the acidity of the nickel ion. The same effect is observed by Sjöberg in the copper(II) imidazole system.

With regard to the complexes in the $Ni(C_3H_4N_2)_n^{2+}$ series we found that they could be well explained with a two-parameter approximation of the following type:

$$Ni(C_3H_4N_2)_n^{2+} + C_3H_4N_2 \rightleftharpoons Ni(C_3H_4N_2)_{n+1}^{2+}, \quad n = 0, \cdots 3 \tag{12}$$

$$K_{n+1} = \frac{[Ni(C_3H_4N_2)_{n+1}^{2+}]}{[Ni(C_3H_4N_2)_n^{2+}][C_3H_4N_2]} \tag{13}$$

$K_{n+1} = K_0 K^n$ where $K_0 = 10$ exp (3.34) M and $K = 10$ exp (-0.55) in 3 M $(Na)ClO_4$ and $K_0 = 10$ exp (3.25) M and $K = 10$ exp (-0.59) in 3 M (Na)Cl, respectively.

This two-parameter behaviour was also found in the copper imidazole system by Sjöberg and in 3 M $(Na)ClO_4$ he found $K_0 =$ 10 exp (4.66) M and $K = 10$ exp (-0.67).

By comparing the two systems we can see that the higher tendency for complex formation in the copper system is reflected in a greater value of K_0 whereas the value of K is greater in the nickel system, but, however, of the same order of magnitude.

In 3 M $(Na)ClO_4$, as well as in 3 M (Na)Cl medium, the following equilibrium could be established:

$$NiOH^+ + C_3H_4N_2 \rightleftharpoons NiOH(C_3H_4N_2)^+ \tag{14}$$

with $\log K = 4.65$ in 3 M $(Na)ClO_4$ and $\log K = 4.56$ in 3 M (Na)Cl.

Comparing these values with $\log k$ for the following equilibrium

$$Ni^{2+} + C_3H_4N_2 \rightleftharpoons NiC_3H_4N_2^{2+} \tag{15}$$

with $\log K_1 = 3.34$ in 3 M $(Na)ClO_4$ and $\log K_1 = 3.25$ in 3 M (Na)Cl, we find that the hydrolyzed nickel ion is a stronger complexing agent than the corresponding hydrated nickel ion.

Acknowledgements. We thank Professor Nils Ingri for much valuable advice, for his great interest and for all the facilities placed at our disposal. The English of the present paper has been corrected by Dr. Michael Sharp. The work forms part of a program financially supported by the Swedish Natural Science Research Council.

REFERENCES

1. Sillén, L. G. and Martell, A. E. (compilers), *Stability Constants, Chem. Soc. London Spec. Publ. No. 17* (1964) and *No. 25* (1971).
2. Vogel, I. *Quant. Inorg. Analysis*, pp. 479–481.
3. Gran, G. *Acta Chem. Scand. 4* (1950) 559.
4. Sjöberg, S. *Acta Chem. Scand. 27* (1973) 3721.
5. Forsling, W., Hietanen, S. and Sillén, L. G. *Acta Chem. Scand. 6* (1952) 901.
6. Ginstrup, O. *Chem. Instrum. 4* (3) (1973) 141.
7. Sjöberg, S. *Acta Chem. Scand. 25* (1971) 2149.
8. Ohtaki, H. and Biedermann, G. *Bull. Chem. Soc. Jap. 44* (1971) 1822.
9. Ingri, N., Kakalowics, W., Sillén, L. G. and Warnqvist, B. *Talanta 14* (1967) 1261.
10. Brown, A. S. *J. Amer. Chem. Soc. 56* (1934) 646.
11. Ingri, N. and Sillén, L. G. *Ark. Kemi 23* (1964) 97.
12. Arnek, R., Sillén, L. G. and Wahlberg, O. *Ark. Kemi 31* (1969) 353; Brauner, P., Sillén, L. G. and Whiteker, R. *Ark. Kemi 31* (1969) 365.

13. Michel, B. L. and Andrews, A. C. *J. Amer. Chem. Soc. 77 (1955) 5291.*
14. Li, N. C., T. L., Fuji, C. T. and White, J. M. *J. Amer. Chem. Soc. 77* (1955) 859.
15. Berthon, G. and Luca, C. *Chim. Anal. (Paris) 53* (1971) Oct. 10.
16. Sklenskaya, E. V. and Karapet'yants, M.Kh. *Russ. J. Inorg. Chem. 11* (1966) 1102 (2061).
17. Burkov, K. A., Lilič, L. S. and Sillén, L. G. *Acta Chem. Scand. 19* (1965) 14.
18. Sillén, L. G. *Acta Chem. Scand. 16* (1962) 159. Sillén, L. G. and Warnqvist, B. *Ark. Kemi 31* (1969) 341.
19. Forsling, W. *To be published.*
20. Eriksson, G. *Acta Chem. Scand. 25* (1971) 2651.
21 Ivarsson, G. and Forsling, W. *To be published.*

Received January 14, 1975.

Acta Chemica Scandinavica A 29 (1975) 580—582

Empirical Correlation of CNDO/2 and Extended Hückel Ionization Energies for the Azines

BJØRN BIRKNES and KNUT FÆGRI, JR.

Department of Chemistry, University of Bergen, N-5014 Bergen-University, Norway

Empirical corrections to orbital energies from CNDO/2 and Extended Hückel calculations for benzene are used in an attempt to calculate ionization energies of the azines. Some experimental tendencies are reproduced but the results are markedly inferior to those obtained by the same technique using *ab initio* wavefunctions.

Koopmans' theorem makes possible relatively simple calculations of molecular ionization energies but does not always give sufficient accuracy for the assignment of photoelectron spectra. For the azines, Koopmans' theorem seems to give the wrong ordering of ionization energies for n and π orbitals. Almlöf *et al.*[1] have performed *ab initio* calculations for benzene and the azine series adding empirical corrections to the calculated energies. These corrections were obtained for each orbital with a photoelectron line of definite assignment, in general from the benzene assignment by Lindholm *et al.*[2] With a "topological" classification of the orbital symmetries these corrections could be transferred also to the other molecules. The resulting assignment of the azines was in essential agreement with the work of Gleiter *et al.*[3]

It is well known that semi-empirical MO methods often introduce additional inaccuracies to those caused by Koopmans' theorem, and in their standard versions they are not accurate enough for the direct assignment of the azines.[4,5] Still, one may ask whether the procedure of Almlöf *et al.*, gauged to the benzene photoelectron spectrum might not give useful results for the azines. The present note shows this not to be the case using standard CNDO/2 and Extended Hückel wavefunctions.

Thus, we have first estimated the differences between experimental and calculated ionization energies for benzene using Koopmans' theorem and the assignment by Lindholm and coworkers.[2] We have then classified the orbitals of the azines according to the topological scheme of Almlöf *et al.* and assumed that the same corrections to Koopmans' theorem apply for each orbital in the azines as in benzene.

The classification scheme of Almlöf *et al.* is based upon an idealized cylinder symmetry ($D_{\infty h}$). Orbital labels are of the form nA_p, where n is a "principal quantum number" describing node planes encircling the cylinder symmetry axis ($n=1$, no node plane; $n=2$, one plane, *etc.*), and A is an "angular" quantum number used for nodes passing through the cylinder axis (orbitals with 0, 1, 2, and 3 such planes are labelled S, P, D, and F). The subscript indicates inversion symmetry (g for symmetric and u for antisymmetric orbitals).

Apart from benzene, the molecules considered are all nitrogen heterocycles which may be notionally derived from benzene by the successive replacement of CH-groups by nitrogen: pyridine has one N-atom, pyridazine, pyrimidine, and pyrazine two N-atoms, 1,3,5-triazine three N-atoms and 1,2,4,5-tetrazine four N-atoms. All molecules are planar and have 30 valence electrons and consequently 15 occupied valence molecular orbitals, counting degenerate orbitals separately.

RESULTS

Table 1 shows the calculated and the observed ionization energies for benzene. For CNDO/2 [6]

Table 1. Experimental and calculated (Koopmans' theorem) ionization energies of benzene (eV).

Orbital	Experimental	CNDO/2	Diff.	Extended Hückel	Diff.
σ orbitals					
$1S_g$	25.9	51.2	−25.3	26.9	−1.0
$1P_u'$, $1P_u''$	22.7	38.0	−15.3	23.7	−1.0
$1D_g'$, $1D_g''$	19.1	30.5	−11.4	18.9	0.2
$2S_g$	16.9	29.3	−12.4	16.2	0.7
$1F_u'$	14.9	21.7	−6.8	13.7	1.2
$1F_u''$	15.6	20.0	−4.4	16.5	−0.9
$2P_u'$, $2P_u''$	14.1	19.3	−5.2	14.4	−0.3
$2D_g'$, $2D_g''$	11.8	14.4	−2.6	12.8	−1.0
π orbitals					
$1S_u$	12.2	23.6	−11.4	13.9	−1.7
$1P_g'$, $1P_g''$	9.3	14.1	−4.8	12.3	−3.0

the difference between these quantities is greatest for the innermost orbitals. This is to be expected from the known errors of Koopmans' theorem but is due mainly to the choice of parameters as may be seen by comparison with the *ab initio* calculations of Almlöf *et al.*[1] For the Extended Hückel method[7] ionization energy corrections are much smaller, especially for the σ orbitals.

The ionization energies from CNDO/2 calculations using Koopmans' theorem change relatively little with increasing nitrogen content, a result which is unchanged by the empirical corrections taken from benzene. The photoelectron spectra, however, show increasing ionization energies with nitrogen substitution. After correction the deviations between observed and calculated ionization energies using CNDO/2 lie within 1.1 eV for pyridine, within 1.8 eV for the diazines and within 2.2 eV for 1,3,5-triazine. Exceptions are found for one level each of pyridazine, pyrazine, and 1,3,5-triazine. Even larger deviations are obtained for 1,2,4,5-tetrazine.

With the Extended Hückel method the agreement between orbital energies and ionization energies is better and the same is true for the results after correction. With one or two exceptions for each molecule the results are within 0.6 eV for pyridine, and within 1.3 eV

Table 2. Calculated and experimental ionization energies of pyridine and pyrazine. The calculated results are obtained using Koopmans' theorem corrections for benzene (eV).

	Pyridine CNDO/2	EH	AI	Exp.	Pyrazine CNDO/2	EH	AI	Exp.
$1S_g$	26.4	28.3	29.2	–	26.6	28.9	30.7	–
$1P_u'$	22.2	22.7	23.2	23.3	21.7	22.7	24.0	24.0
$1P_u''$	24.0	24.1	24.8	24.2	25.2	27.0	28.6	–
$1D_g'$	19.1	19.4	19.6	19.6	19.0	19.7	20.5	20.6
$1D_g''$	19.7	19.5	19.8	20.0	20.2	20.2	21.2	21.0
$2S_g$	16.3	16.8	17.0	17.1	15.4	17.0	17.2	17.1
$1F_u'$	15.6	16.1	15.8	15.7	16.2	16.5	17.0	17.0
$1F_u''$	16.0	15.6	15.7	15.7	16.6	15.5	16.4	16.2
$2P_u'$	13.7	14.0	14.5	14.4	13.4	13.9	15.0	15.0
$2P_u''$	13.1	14.2	13.8	13.7	11.7	14.1	11.4	11.7
$2D_g'$	12.1	12.1	12.6	12.5	12.6	13.1	13.6	13.3
$2D_g''$	10.7	11.3	9.6	9.7	10.1	11.0	9.4	9.4
$1S_u$	12.4	13.4	12.9	13.2	12.4	13.7	13.9	14.0
$1P_g'$	9.3	9.2	9.5	9.7	9.3	9.2	10.0	10.2
$1P_g''$	9.9	10.1	10.4	10.5	10.3	11.7	11.8	11.4

for the diazines. For 1,3,5-triazine and 1,2,4,5-tetrazine the deviations are within 1.9 eV.

The order of ionization energies, after correction, is in essential agreement with experiment and with the *ab initio* calculations for the inner valence orbitals. This is an expected result since it is also obtained with the Extended Hückel method directly.[8] Notable deviations, however, are obtained for the outermost orbitals. Even after correction the semiempirical wavefunctions fail to predict the correct ordering of σ and π states. The lowest σ ionization energy, conventionally related to a nitrogen lone-pair is systematically stabilized relative to the π orbitals, leading to erroneous assignements for the first ionization energy for all azines except, possibly, for pyridine. Representative results for pyridine and pyrazine are given in Table 2. The *ab initio* results as well as the experimental assignments are from Almlöf *et al.*,[1] the latter in essential agreement with the work of Gleiter *et al.*[3]

The systematic increase of the deviations with increasing nitrogen substitution may be interpreted as due to non-optimal nitrogen parameters relative to those of carbon and hydrogen. A reparametrization might therefore give some improvement.

The conclusion of the present study is that the utility of the approach of Almlöf *et al.* in assigning photoelectron spectra of series of similar molecules with conventional semi-empirical wavefunction is limited.

Acknowledgements. This work was supported by a grant from the Norwegian Research council for Science and the Humanities. Thanks are due to professor Rolf Manne who instigated this project.

REFERENCES

1. Almlöf, J., Johansen, H., Roos, B. and Wahlgren, U. *J. Electron Spectrosc. Relat. Phenom. 2* (1973) 51.
2. Jonsson, B. Ö., Lindholm, E. and Skerbele, A. *Int. J. Mass Spectrom. Ion Phys. 8* (1972) 101.
3. Gleiter, R., Heilbronner, E. and Hornung, V. *Helv. Chim. Acta 55* (1972) 255.
4. Ellis, R. L., Jaffé, H. H. and Masmamdes, C. A. *J. Amer. Chem. Soc. 96* (1974) 2623.
5. Palmer, M. H., Gaskell, A. J. and Findlay, R. H. *Tetrahedron Lett. 47* (1973) 4659.
6. Pople, J. A. and Segal, G. A. *J. Chem. Phys. 44* (1966) 3289.
7. Hoffmann, R. *J. Chem. Phys. 39* (1963) 1397.
8. Friedh, C., Åsbrink, L., Jonsson, B. Ö. and Lindholm, E. *Int. J. Mass. Spectrom. Ion Phys. 8* (1972) 101.

Received February 10, 1975.

Acta Chemica Scandinavica A 29 (1975) 583—589

The Crystal Structure of Silver(I) Cyclohexanethiolate

SAM-HYO HONG, ÅKE OLIN and ROLF HESSE

Institute of Chemistry, University of Uppsala, P.O.B. 531, S-751 21 Uppsala

The crystal structure of silver(I) cyclohexanethiolate, $AgSC_6H_{11}$, has been determined from three-dimensional X-ray data. The crystals are triclinic, space group $P\bar{1}$. The unit cell contains twelve formula units and has the dimensions $a = 14.827$ Å, $b = 15.747$ Å, $c = 11.218$ Å, $\alpha = 103.68°$, $\beta = 107.71°$, and $\gamma = 91.79°$.

The structure consists of infinite silver-sulfur frameworks extending in the *c*-direction. These frameworks are shielded from each other by the surrounding cyclohexane rings. Both two- and three-coordinated silver atoms are present.

The silver(I) alkanethiolates belong to the same groups of compounds, $(AX)_n$, as the polymeric mono- and dithiocarbamates of Cu(I),[1,2] Ag(I),[3,4] Au(I),[5] and Tl(I)[6] which have been studied in this laboratory. These studies have shown the existence of a close relationship between the degree of association n (= 2, 4, or 6) of these substances in inert solvents and in their crystal structures. The preparation and properties of many silver(I) alkanethiolates, Ag(I) S*R*, has been reported by Åkerström.[7] Cryoscopic and ebullioscopic molecular weight determinations in benzene and chloroform of most of these compounds showed that they were associated in these solvents. With the sulfur atom bound to a tertiary carbon atom, the degree of association was found to be 8. When the sulfur atom was associated with a secondary carbon atom, n in most cases was close to 12. When *R* was unbranched, the compounds tended to be so insoluble that molecular weight determinations could not be performed.

X-Ray crystal structure investigations of silver(I) thiolates have been started to obtain information about the structures of polymers with high degree of association in solutions. It was then found that only a few of the thiolates yielded crystals of sufficiently good quality for single-crystal diffraction studies. In most cases the crystals showed severe disorder or twin formation. We here report our results on silver(I) cyclohexanethiolate. For this compound, which is rather insoluble, a value of $n = 25$ was found by Åkerström. This value is thus larger than for most other *sec*-thiolates, which have $n = 12$.

EXPERIMENTAL

A sample of silver(I) cyclohexanethiolate was kindly supplied by Dr. S. Åkerström. The unit cell parameters were determined from a powder photograph taken with a Guinier-Hägg focussing camera using Cr$K\alpha_1$ radiation ($\lambda = 2.2896$ Å) and silicon ($a = 5.4305$ Å) as an internal standard. The crystal data are presented in Table 1. Using [001] as the rotation axis, equi-inclination photographs were recorded up to $l = 9$ with nickel-filtered Cu$K\alpha$ radiation at room

Table 1. Crystal data.

Formula unit: $AgSC_6H_{11}$		
Crystal system: triclinic		
Space group: $P\bar{1}$		
Unit cell parameters:[a]		
$a = 14.827(3)$	$b = 15.747(3)$	$c = 11.218(1)$ Å
$\alpha = 103.68(1)$	$\beta = 107.71(1)$	$\gamma = 91.79(1)°$
Formula weight: 223.09		
Cell volume: 2409 Å^3		
Number of formula units per unit cell: 12		
Density(measured): 1.85(1) g cm^{-3}		
Density(calculated:) 1.845 g cm^{-3}		
Linear absorption coefficient for Cu$K\alpha$: 221 cm^{-1}		

[a] Here and elsewhere in this paper estimated standard deviations given within parentheses refer to the least significant digits.

temperature. The cross section of the crystal needles averaged 0.04×0.05 mm^2. The multiple film technique with 5 films was used, and 2154 independent reflexions were collected. The relative intensities were estimated visually.

The crystals decomposed rather rapidly in the X-ray beam, and each crystal was used for the recording of only one layer. Inter-layer scale factors were determined from small range Weissenberg photographs of the layers recorded on the same film. When the scale factors were later refined in the least-squares treatment of the data, only small changes were observed. The intensity data have been corrected for

Table 2. The final atomic coordinates and thermal parameters with their e.s.d.'s. in parentheses. The anisotropic thermal parameters of the silver and sulfur atoms are given in Table 3.

Atom	x	y	z	B Å^2
Ag(1)	−0.0166(2)	0.2354(2)	0.1330(3)	
Ag(2)	0.0969(2)	0.0311(2)	0.1961(3)	
Ag(3)	0.0399(2)	0.1775(2)	0.3785(3)	
Ag(4)	−0.0065(3)	−0.1694(2)	0.1335(3)	
Ag(5)	0.0230(2)	−0.1199(2)	0.4287(3)	
Ag(6)	−0.1171(2)	0.0705(2)	0.1416(3)	
S(A)	0.0860(7)	0.3162(7)	0.3407(10)	
S(B)	−0.0987(8)	−0.2237(8)	0.2474(10)	
S(C)	0.1360(7)	−0.1579(7)	0.0603(9)	
S(D)	0.0898(6)	0.0270(6)	0.4065(8)	
S(E)	0.1186(6)	0.0698(6)	0.0096(8)	
S(F)	−0.1391(7)	0.1299(7)	0.3500(9)	
C(A1)	0.210(3)	0.325(3)	0.338(4)	7(1)
C(A2)	0.274(3)	0.369(3)	0.473(4)	6(1)
C(A3)	0.380(4)	0.376(4)	0.473(5)	10(2)
C(A4)	0.387(4)	0.427(4)	0.368(5)	10(2)
C(A5)	0.321(3)	0.385(3)	0.239(5)	8(1)
C(A6)	0.212(3)	0.375(3)	0.227(4)	8(1)
C(B1)	−0.065(4)	−0.336(4)	0.265(5)	10(1)
C(B2)	−0.046	−0.383	0.139	
C(B3)	0.015	−0.459	0.160	
C(B4)	−0.038	−0.522	0.214	
C(B5)	−0.057	−0.477	0.339	
C(B6)	−0.111(5)	−0.397(5)	0.320(7)	20(2)
C(C1)	0.214(4)	−0.247(4)	0.094(5)	10(1)
C(C2)	0.177(5)	−0.293(5)	0.175(6)	12(2)
C(C3)	0.264(5)	−0.368(4)	0.194(6)	11(2)
C(C4)	0.363(5)	−0.326(5)	0.246(7)	13(2)
C(C5)	0.395(5)	−0.279(5)	0.171(7)	13(2)
C(C6)	0.317(5)	−0.200(4)	0.131(6)	12(2)
C(D1)	0.211(3)	0.046(3)	0.519(3)	5(1)
C(D2)	0.275(3)	−0.030(3)	0.471(3)	5(1)
C(D3)	0.376(4)	−0.013(3)	0.564(5)	8(1)
C(D4)	0.426(4)	0.083(4)	0.587(5)	9(1)
C(D5)	0.360(3)	0.153(3)	0.623(4)	7(1)
C(D6)	0.262(3)	0.137(3)	0.531(4)	7(1)
C(E1)	0.243(3)	0.112(2)	0.065(3)	5(1)
C(E2)	0.279(3)	0.106(3)	−0.051(4)	8(1)
C(E3)	0.387(4)	0.147(3)	−0.002(5)	8(1)
C(E4)	0.440(4)	0.089(4)	0.075(5)	10(1)
C(E5)	0.410(4)	0.106(4)	0.201(6)	11(2)
C(E6)	0.306(4)	0.066(3)	0.155(5)	8(1)
C(F1)	−0.189(4)	0.236(4)	0.343(5)	9(1)
C(F2)	−0.202(7)	0.269(6)	0.454(9)	18(3)
C(F3)	−0.234(7)	0.378(6)	0.443(9)	18(3)
C(F4)	−0.339(5)	0.352(4)	0.363(6)	12(2)
C(F5)	−0.335(7)	0.304(7)	0.228(10)	20(3)
C(F6)	−0.298(6)	0.203(6)	0.255(8)	16(3)

Table 3. The anisotropic thermal parameters ($\times 10^4$) for silver and sulfur atoms. The temperature factor is expressed as $\exp[-(\beta_{11}h^2+\beta_{22}k^2+\beta_{33}l^2+2\beta_{12}hk+2\beta_{13}hl+2\beta_{23}kl)]$.

Atom	β_{11}	β_{22}	β_{33}	β_{12}	β_{13}	β_{23}
Ag(1)	78(2)	79(2)	116(12)	1(2)	20(2)	44(3)
Ag(2)	64(2)	81(2)	72(12)	−2(2)	28(2)	24(2)
Ag(3)	68(2)	72(2)	103(12)	1(1)	26(2)	33(2)
Ag(4)	103(3)	81(2)	126(12)	4(2)	58(3)	40(3)
Ag(5)	91(2)	79(2)	100(12)	2(2)	40(2)	30(3)
Ag(6)	67(2)	108(3)	102(12)	−18(2)	28(2)	−9(3)
S(A)	69(7)	60(6)	124(17)	5(5)	30(7)	18(7)
S(B)	76(8)	92(8)	114(18)	−12(6)	24(8)	40(8)
S(C)	65(7)	71(7)	97(16)	13(5)	27(7)	43(7)
S(D)	52(6)	41(6)	72(16)	8(4)	24(6)	8(6)
S(E)	41(5)	63(6)	73(15)	2(4)	16(6)	32(7)
S(F)	75(7)	78(7)	86(16)	9(6)	32(7)	43(7)

Lorentz and polarization effects but not for absorption or extinction.

Determination of the structure. The space group was assumed to be $P\bar{1}$. The position vectors r_i of the silver atoms were determined from the corresponding interatomic vectors $2r_i$ in the three-dimensional Patterson function. The vectors $2r_i$ were identified by systematic addition and subtraction of Pattersson vectors using the relations: $(r_n+r_m)+(r_n-r_m)=2r_n$ and $(r_n+r_m)-(r_n-r_m)=2r_m$.

The silver atom coordinates were next refined by Fourier and least-squares calculations. Data up to $\sin\theta/\lambda=0.35$ were included and the reliability index, $R=\sum||F_o|-|F_c||/\sum|F_o|$, became 0.17 after 3 cycles. The positions of the sulfur and carbon atoms were located from consecutive difference syntheses alternating with least-squares refinements. The electron densities of some of the carbon atoms were quite low, and the positions of C(B2)–C(B5) were roughly determined by geometrical considerations.

In the concluding least-squares refinement the expression $\sum w(|F_o|-|F_c|)^2$ was minimized using a full-matrix program.[8] The weights, w, which in the previous computations had been unity, were now calculated from the formula suggested by Cruickshank $w=1/(a+|F_o|+c|F_o|^2+d|F_o|^3)$ with $a=20.0$, $c=0.0057$, and $d=0.00005$ as final values. Atomic scattering factors for silver and sulfur were taken from Hanson *et al.*[9] and carbon from International Tables of X-Ray Crystallography, Vol. 3 (1962). Correction for dispersion was applied to silver. 18 very weak reflections, which lay outside the range $0.5<|F_o/F_c|<2.0$, were excluded. When the positional parameters and an individual isotropic temperature factor for each atom were refined together with an overall scale factor, R became 0.110. When anisotropic temperature factors for the silver and sulfur atoms were introduced, R decreased to 0.084. The largest change in a silver or sulfur coordinate was 0.0014, when the anisotropic temperature factors were introduced. When the nineteen inter- and intra-layer scale factors and the atomic parameters were refined together, the value of R decreased to 0.080. The final values of the atomic parameters are presented in Tables 2 and 3. The observed and calculated structure factors can be obtained from the authors on request.

DESCRIPTION AND DISCUSSION OF THE STRUCTURE

Notation. The silver atoms are denoted Ag(1)–Ag(6), and the ligands A–F. In each of the cyclohexane rings the carbon atoms are numbered 1 to 6. The carbon atom 1 is bonded to the sulfur atom. For example the carbon atom C(D1) is bonded to S(D) in the ligand D. Atoms related by a center of symmetry to those given in Table 2 are marked with a bar.

In the figures the silver atoms were denoted by the numbers 1 to 6 and the sulfur atoms by A–F.

General features. The metal atoms and ligands are linked together by Ag–S bonds to form unlimited polymer chains running parallel to the crystallographic c-axis. Fig. 1 gives an illustration of a part of a chain. The silver and sulfur atoms form the central core which is surrounded and shielded by the cyclohexyl groups of the ligands. The only contacts between atoms in different chains occur among the cyclohexyl groups and are of the van der

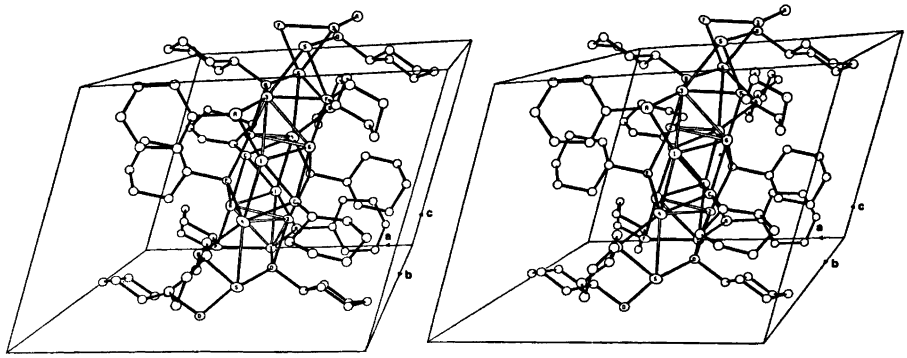

Fig. 1. A stereoscopic view of the unit cell. Silver atoms situated to a distance less than 3.3 Å from each other are connected by open lines. The silver-sulfur coordination (Ag−S < 2.9 Å) is marked by filled lines.

Waals type. The shortest interligand distances are given in Table 4.

The silver-sulfur arrangement. The framework of the silver and sulfur atoms can be seen in Fig. 1. The interatomic distances are given in Table 5. The silver atoms form two parallel chains, $-Ag(\bar{5})-Ag(\bar{4})-Ag(1)-Ag(3)-Ag(\bar{5})-$ and $-Ag(\bar{3})-Ag(\bar{1})-Ag(4)-Ag(5)-Ag(\bar{3})-$, which are related by a centre of symmetry and crosslinked through the atoms Ag(2), Ag(6), Ag($\bar{2}$) and Ag($\bar{6}$). The metal-metal distances range from 2.91 to 3.11 Å in the chains and from 3.03 to 3.29 Å in the cross links. These intermetallic distances are slightly longer than those in the metallic phase of silver (2.89 Å).[10] Comparable Ag−Ag distances have been reported in $[(C_3H_7)_2NCS_2Ag]_6$,[3] $[(C_3H_7)_2NCOSAg]_6$,[4] $Ag[SC(NH_2)_2]_2Cl$,[11] Ag_3AsS_3,[12] Ag_5SbS_4,[13] and also in a number of other silver compounds.

Eight of the silver atoms of the unit cell have three-fold, almost planar coordination, while four of them have two-fold, nearly linear coordination. The structure accordingly can be described as a framework of coordination triangles and almost linear S−Ag−S segments. Fig. 2 shows the schematic representation of the triangles and segments which will be used in the following treatment. The coordination triangles are arranged in two groups, each comprising four triangles. The triangles share vertices in such a way that in each case a central parallelogram is formed. The centres of the parallelograms are also centres of sym-

Table 4. Interligand distances shorter than 4 Å. The coordinates of the second atom in each pair are related to those given in Table 2 (x,y,z) by the operations (a−j).

a:	x,y,z		f:	$1-x,-y,1-z$	
b:	$x,1+y,z$		g:	$-x,1-y,1-z$	
c:	$1+x,y,z$		h:	$1-x,1-y,1-z$	
d:	$1-x,-y,-z$		i:	$-x,-1-y,-z$	
e:	$-x,-y,1-z$		j:	$-x,-1-y,1-z$	
C(A2)−C(B6)	e	3.80(18)	C(B5)−C(B5)	j	3.74
−C(D6)	a	3.87(6)	C(C2)−C(F2)	e	3.99(11)
−C(F3)	g	3.99(11)	C(C5)−C(D4)	f	3.88(9)
C(A4)−C(A4)	h	3.95(11)	−C(D5)	f	3.83(8)
C(A6)−C(B3)	b	3.99	C(D3)−C(D4)	f	3.88(7)
C(B2)−C(B3)	i	3.83	C(E4)−C(E4)	d	3.71(11)
−C(C2)	a	3.42	−C(F6)	c	3.94(10)
C(B3)−C(B3)	i	3.40			
−C(C2)	a	3.43			
−C(C3)	a	3.79			

Table 5. Interatomic distances (Å) with their estimated standard deviations in parentheses.

Ag(1) – Ag(3)	2.992(5)	Ag(5) – Ag(3)	2.911(5)
– Ag(4)	3.020(5)	– Ag(4)	3.106(5)
– Ag(6)	3.025(5)	– S(B)	2.64(1)
– S(A)	2.36(1)	– S(D)	2.58(1)
– S(C)	2.40(1)	– S(F)	2.60(1)
Ag(2) – Ag(3)	3.025(5)	Ag(6) – Ag(1)	3.025(5)
– Ag(4)	3.287(5)	– Ag(2)	3.154(4)
– Ag(6)	3.154(4)	– Ag(3)	3.032(5)
– S(D)	2.41(1)	– S(C)	2.87(1)
– S(E)	2.42(1)	– S(E)	2.44(1)
		– S(F)	2.43(1)
Ag(3) – Ag(1)	2.992(5)		
– Ag(2)	3.025(5)	S(A) – C(A1)	1.85(4)
– Ag(5)	2.911(5)	S(B) – C(B1)	1.90(6)
– Ag(6)	3.032(5)	S(C) – C(C1)	1.88(6)
– S(A)	2.44(1)	S(D) – C(D1)	1.83(4)
– S(D)	2.57(1)	S(E) – C(E1)	1.81(4)
– S(F)	2.64(1)	S(F) – C(F1)	1.86(6)
Ag(4) – Ag(1)	3.020(5)		
– Ag(2)	3.286(5)		
– Ag(5)	3.106(5)		
– S(B)	2.40(1)		
– S(C)	2.50(1)		
– S(E)	2.75(1)		

metry in the structure with the coordinates 0,0,0 and 0,0,1/2. There are striking similarities in shape between the groups. In both cases the obtuse angle of the parallelograms is 118° (117.5 and 117.7°). The sides and short diagonals of the two parallelograms are almost equal in length (3.75, 4.02, 4.04 and 3.77, 3.98, 4.01 Å). Thus the parallelograms resemble fractions of a layer of closed-packed sulfur atoms. Since the distances are only slightly longer than those commonly expected for sulfur contacts (3.7 Å), sterical restrictions in the packing of the sulfur atoms can be of importance for the formation of the parallelogram configurations. Similar restrictions probably are also reflected in the short silver-silver distances. The groups are linked together by sharing the vertices B, $\overline{B}$, $\overline{F}$, and F which leads to the infinite arrangement illustrated in Fig. 3. The four linear S – Ag – S bridges have also been included in this figure.

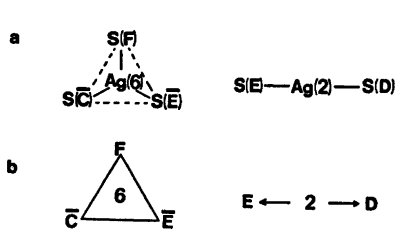

Fig. 2. Schematic representation (a) and notation (b) used for the silver-sulfur coordination.

The coordination. Distances and angles of coordination are given in Table 5 and Fig. 4. For the three-coordinated silver atoms the silver-sulphur arrangement is almost planar. The distance from a silver atom to the plane defined by the three sulfur atoms is 0.13 Å for Ag(3), 0.05 Å for Ag(4), 0.16 Å for Ag(5), and 0.20 Å for Ag(6). Therefore, the coordination figure may be described as a much flattened pyramid. This configuration is a common feature for three-coordinated silver and is present in the structure of $AgS_2CN(C_3H_7)_2$,[3] $AgSOCN(C_3H_7)_2$,[4] $Ag[SC(NH_2)_2]_2Cl$,[11] and Ag_3AsS_3.[12] The two-fold silver coordination is almost linear, with the S – Ag – S angles equal to 167 and 169°, which means that the silver atom in each case is at a distance of 0.25 Å from the line joining the sulfur atoms. Similar deviations from linearity for two-fold silver coordination have been reported by Lindqvist [14] for AgSCN (S – Ag – N = 165°) and by Strickler [15] for $Pt[S-C_2H_4-P(C_2H_5)_2]_2.AgNO_3$ (S – Ag – S = 171°).

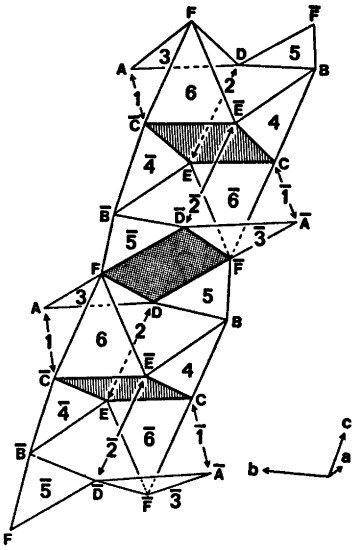

Fig. 3. A part of the infinite linkage of the coordination triangles and (linear) S–Ag–S segments.

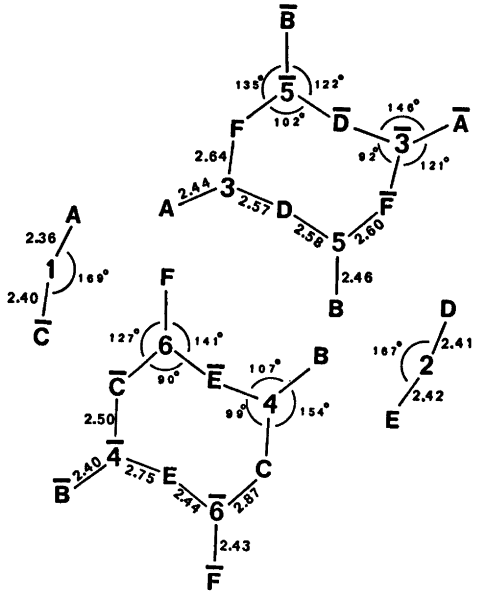

Fig. 4. Details of the coordination showing bond distances (Å) and bond angles (°).

The Ag–S distance is on the average 2.40 Å for two-fold and 2.56 Å for three-fold coordination of silver. The deviations from the average are small in the first group of distances, and the mean value given above (2.40 Å) is equal to that reported for $Pt[S-C_2H_4-P(C_2H_5)_2]_2.AgNO_3$ [15] and AgCuS.[16] For the three-coordinated silver atoms, more pronounced variations are observed in the distances which lie between 2.40 Å and 2.87 Å. Ag–Ag distances within this range are found in a number of compounds, for instance in Ag_5SbS_4 [3] and $AgSCN.P(C_3H_7)_3$.[17] The S–Ag distance is on the average 2.41 Å for two-fold and 2.55 Å for three-fold coordination of sulfur.

In the following list the Ag–S distances (in Å) are grouped according to the coordination numbers of the silver and sulfur atoms:

Ag 2, S 2
2.36
Ag 2, S 3
2.40, 2.41, 2.42 (av. 2.41)
Ag 3, S 2
2.40, 2.44, 2.46 (av. 2.43)
Ag 3, S 3
2.43, 2.44, 2.50, 2.57, 2.57, 2.58
2.60, 2.64, 2.75, 2.87 (av 2.60)

One observes that all distances are short (≤ 2.46 Å) when one of the atoms involved is two-coordinated. In fact the shortest distance is found for the case where both atoms are two-coordinated. The longest distances, 2.75 and 2.87 Å, occur when the two atoms both are three-coordinated.

The ligands. The structural properties of cyclohexane and its derivatives are well-known from other investigations (see for instance Hassel and Viervoll [18]). Because of the presence of heavy atoms and since the number of structural parameters is high, the present compound is not very well suited for obtaining exact carbon positions. This is reflected in the high standard deviations of the atomic coordinates of the carbon atoms (Table 2). However, the positions are accurate enough to clearly show that the cyclohexyl rings are in the chair conformation (see also Fig. 1). One also observes that the carbon-sulfur bonds are oriented equatorially with respect to the cyclohexyl rings in all the ligands. The average value of the carbon-sulfur distance is 1.86 Å. Hassel and Viervoll [18] obtained a value of 1.87 Å in cyclohexanethiol by electron diffraction investigations. Some recently reported

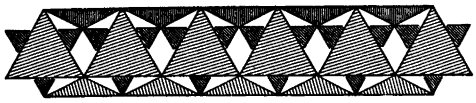

Fig. 5. Tubular arrangement of AX_3-groups sharing vertices.

values [19,20] for the single bonded carbon-sulfur distance range between 1.86 and 1.90 Å.

In a number of other silver (I) alkanethiolates studied by this group severe disorder effects have been observed. The high B-values in the temperature factors of the carbon atoms indicate that such effects are also of importance in the present compound.

In AgX compounds the coordination number of silver is 2 or 3 when X contains a bulky organic group. With two-fold coordination only, a structure can be realized from rings or unlimited chains for an AX compound. The latter alternative has been found in the structure of silver(I) 2,3-dimethylbutane-2-thiolate.[21] AX_3 groups have been found to be joined to a tetrahedron in some copper(I) dithiocarbamates and to an octahedron in silver(I) dithiocarbamates. Arrangements based on (A)X_3 triangles connected by sharing edges can apparently not be realized for the silver(I) thiolates. If the Ag–S distance is assumed to be 2.5 Å, one finds an Ag–Ag distance 0.3 Å shorter than in metallic silver, even if the height of the silver atom above the S_3-plane is as large as 0.5 Å. Arrangements of triangles sharing only corners yield longer metal-metal distances. Such arrangements can be constructed in a variety of ways. One example is given in Fig. 5. It contains the same group of four triangles as illustrated in Fig. 3. The fact that the present structure is not solely built from AgS_3-groups sharing corners is probably caused by steric hindrances from the ligands.

Acknowledgements. Professor Ivar Olovsson is thanked for the facilities put at our disposal and Dr. Stig Åkerström for supplying the sample.

This work has been supported by a grant from the Swedish Natural Science Research Council.

REFERENCES

1. Hesse, R. *Ark. Kemi 20* (1963) 481.
2. Hesse, R. and Aava, U. *Acta Chem. Scand. 24* (1970) 1355.
3. Hesse, R. and Nilsson, L. *Acta Chem. Scand. 23* (1969) 825.
4. Jennische, P. and Hesse, R. *Acta Chem. Scand. 25* (1971) 423.
5. Hesse, R. and Jennische, P. *Acta Chem. Scand. 26* (1972) 3855.
6. Jennische, P. and Hesse, R. *Acta Chem. Scand. 27* (1973) 3531.
7. Åkerström, S. *Ark. Kemi 24* (1965) 505.
8. Lundgren, J.-O. *Crystallographic Computer Programs*, University of Uppsala, Uppsala, Sweden, UUIC-B13-04-2, (1975).
9. Hanson, H. P., Herman, F., Lea, J. D. and Skillman, S. *Acta Crystallogr. 17* (1964) 1040.
10. Pearson, W. B. *A Handbook of Lattice Spacings and Structure of Metals and Alloys*, Pergamon, Oxford 1967, Vol. II.
11. Viggini, E. A., Taylor, I. F. and Amma, I. L. *Inorg. Chem. 7* (1968) 1351.
12. Engel, P. and Nowacki, W. *Acta Crystallogr. B 24* (1968) 77.
13. Ribar, B. and Nowacki, W. *Acta Crystallogr. B 26* (1970) 201.
14. Lindqvist, I. *Acta Crystallogr. 10* (1957) 29.
15. Strickler, P. *Helv. Chim. Acta 52* (1969) 270.
16. Frueh, A. J. *Z. Kristallogr. 106* (1955) 299.
17. Panattoni, C. and Frasson, E. *Acta Crystallogr. 16* (1963) 1258.
18. Hassel, O. and Viervoll, H. *Acta Chem. Scand. 1* (1947) 149.
19. Fridrichson, J. and Mathieson, A. McL. *Acta Crystallogr. 23* (1967) 439.
20. Weber, H. P. *Acta Crystallogr. B 28* (1972) 2945.
21. Hong, S.-H., Olin, Å. and Hesse, R. *To be published.*

Received December 4, 1974.

Acta Chemica Scandinavica A 29 (1975) 590—598

The Crystal Structure of $Sn_3O(OH)_2SO_4$

SIV GRIMVALL

Department of Inorganic Chemistry, Chalmers' University of Technology and the University of Göteborg, P.O. Box, S-402 20 Göteborg 5, Sweden

The crystal structure of $Sn_3O(OH)_2SO_4$ has been determined. The compound crystallizes in the orthorhombic system with $a = 13.045 \pm 0.002$ Å, $b = 4.9383 \pm 0.0014$ Å, $c = 12.140 \pm 0.002$ Å. The space group is $Pca2_1$. There are four formula units in the unit cell.

The positions of the tin, sulfur, and oxygen atoms were obtained from Patterson and Fourier syntheses. Full matrix least-squares refinement, based on 452 independent reflexions, gave a final R-value of 6.9 %. The tin and oxygen atoms form infinite chains connected by distorted sulfate groups. Two tin atoms are four-coordinated by oxygen while the third is three-coordinated. The Sn—O bonding distances vary within the range 2.01—2.51 Å with a standard deviation of 0.003 Å. The shortest tin—tin distances are 3.523, 3.578, and 3.580 Å with a mean standard deviation of 0.0004 Å.

Thermogravimetric and differential thermal analyses of $Sn_3O(OH)_2SO_4$ show that one water molecule per formula unit is expelled endothermically. The remaining substance is rearranged in an exothermic reation and then endothermically decomposed.

The present work was part of a series of investigations on structures and bonding in tin(II) compounds.

In 1882, Ditte [1] prepared a basic tin(II) sulfate to which he assigned the formula $Sn_3O_2SO_4(H_2O)_n$, where $n = 1.5-3$. In 1967, Davies and Donaldson [2] formulated this compound as $Sn_3O(OH)_2SO_4$, basing their suggestion on a potentiometric investigation of the hydrolysis of tin(II) compounds in aqueous solution by Tobias.[3] Tobias showed that the dominating polynuclear ion in aqueous solution was $Sn_3(OH)_2^{2+}$, or $Sn_3O(OH)_2^{2+}$, since he was not able to determine the number of water molecules in the complex. From Mössbauer measurements, Davies and Donaldson [4] were able to show the presence of both tin-oxide and tin-hydroxide bonds.

EXPERIMENTAL

The basic stannous sulfate crystals were prepared according to the method of Davies and Donaldson [2] except that no special precautions were taken in order to prevent oxidation of tin(II) to tin(IV). The shapes of the crystals varied from rectangular plates to needles. A plate ($0.162 \times 0.052 \times 0.034$ mm) was used in this investigation. An X-ray rotation photograph around [010] and two sets of Weissenberg equi-inclination photographs ($h0l$, $h1l$ and $h2l$) were taken. The multiple film technique was used and six films were obtained from each exposure. The first Weissenberg data set was the basis for a short communication on the

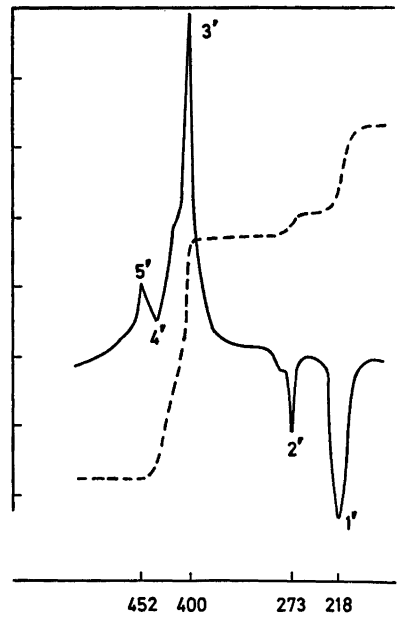

Fig. 1. Thermogravimetric and differential thermal analysis of $Sn_3O(OH)_2SO_4$ in 100 % argon. (– – – TG, ——— DTA. TG range 10 mg, DTA range 100 μV, heating rate 4°/min).

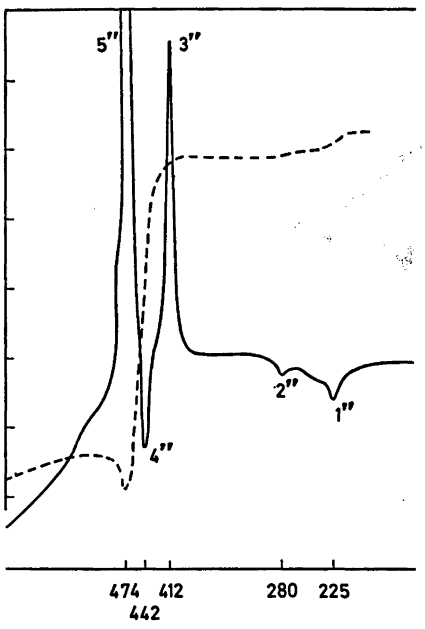

Fig. 2. Thermogravimetric and differential thermal analysis of $Sn_3O(OH)_2SO_4$ in an atmosphere of 20 % oxygen in argon. (– – – TG, ——— DTA. TG range 10 mg, DTA range 100 μV, heating rate 4°/min).

structure of $Sn_3O(OH)_2SO_4$.[5] Mean values from the two sets were used for the present publication. Using Cu$K\alpha$-radiation, 452 independent reflexions were recorded and estimated visually. Accurate cell parameters were obtained from a Guinier photograph.

Thermogravimetric (TG) and differential thermal analysis (DTA) were carried out both in an inert (100 % argon) and in an oxidizing (20 % oxygen in argon) atmosphere. A Mettler Recording Thermoanalyzer was used with Al_2O_3 as reference. The curves are shown in Figs. 1–2. Fig. 1 shows the water analysis. There are two or three endothermic reactions (*cf.* the DTA curve) below 300 °C. The weight loss as indicated in the TG curve for these reactions is 3.6 % of the total amount. This corresponds to the loss of one water molecule per formula unit, which is in agreement with the formula proposed by Davies and Donaldson.[2]

UNIT CELL AND SPACE GROUP

Crystals of $Sn_3O(OH)_2SO_4$ are orthorhombic. The cell parameters were determined from photographs taken with Guinier focusing camera using Cu$K\alpha_1$-radiation ($\lambda = 1.5405$ Å) and potassium chloride ($a = 6.2921$ Å at 21 °C) [6]

Table 1. Powder photograph of $Sn_3O(OH)_2SO_4$. Lines with $10^5 \sin^2\theta$ (obs) up to 27759 are listed. The max. value for indexed lines is 42675. Cu$K\alpha_1$-radiation. $\lambda = 1.5405$ Å.

h	k	l	$10^5 \sin^2\theta$ obs	$10^5 \sin^2\theta$ calc	I obs	d(calc) Å
0	0	2	1584	1610	vs	6.070
2	0	1	1803	1797	s	5.746
0	1	0	2422	2433	s	4.938
1	1	0	2773	2782	m	4.618
2	0	2	3023	3005	vw	4.443
1	1	1	3179	3184	m	4.317
2	1	0	3833	3827	vs	3.937
0	1	2	4042	4043	m	3.831
2	1	1	4239	4230	m	3.745
1	1	2	4397	4392	w	3.675
2	0	3	5039	5018	w	3.439
2	1	2	5449	5438	vs	3.303
4	0	1	5981	5981	vs	3.150
0	0	4	6434	6441	vvs	3.035
3	1	2	7163	7181	vvw	2.874
4	0	2	7208	7188	s	2.873
2	1	3	7477	7451	m	2.822
4	1	1	8411	8413	w	2.656
3	1	3	9223	9194	w	2.540
4	0	3		9201		2.539
4	1	2	9645	9621	vw	2.483
0	2	0	9712	9732	s	2.469
1	2	0	10067	10080	w	2.426
2	1	4	10291	10269	m	2.404
1	2	1	10466	10483	s	2.379
0	2	2	11343	11342	m	2.287
2	0	5	11531	11459	w	2.275
2	2	1		11529		2.269
4	1	3	11661	11634	vvw	2.258
1	2	2		11691		2.253
6	0	0	12531	12550	m	2.174
3	2	1	13267	13272	w	2.114
1	2	3	13729	13704	vw	2.081
2	1	5	13915	13892	vw	2.067
0	0	6	14474	14493	w	2.023
6	1	0	15003	14983	m	1.990
6	1	1	15362	15386	vw	1.964
4	0	5	15669	15642	m	1.948
4	2	1	15728	15712	w	1.943
0	2	4	16195	16173	s	1.915
6	0	3				
3	2	3	16506	16993	vw	1.897
1	2	4		16522		1.895
4	2	2	16913	16920	vw	1.873
0	1	6		16926		1.872
2	2	4	17584	17568	vvw	1.838
2	1	6	18298	18320	m	1.800
4	0	6	20066	20071	m	1.719
1	2	5		20145		1.716
6	1	4	21445	21425	w	1.664
5	2	3	22075	22070	vvw	1.640
1	3	1	22717	22648	vvw	1.619
6	2	1		22685		1.617
8	0	1		22714		1.616

Table 1. Continued.

h k l	$10^5 \sin^2\theta$ obs	$10^5 \sin^2\theta$ calc	I obs	d(calc) Å
8 1 1	25329	25147	vw	1.536
3 1 7		25297		1.531
0 0 8	25753	25765	w	1.517
1 3 3		25868		1.514
8 1 2	26378	26355	vvw	1.500
2 3 3	26969	26914	vvw	1.485
4 1 7	27759	27737	vvw	1.463

as an internal standard. The resulting cell parameters, calculated with the program POWDER,[7] are:

$a = 13.045 \pm 0.002$ Å
$b = 4.9383 \pm 0.0014$ Å
$c = 12.140 \pm 0.002$ Å
$V = 782.04 \pm 0.28$ Å^3

Observed and calculated $\sin^2\theta$ values are listed in Table 1. The results are in good agreement with the cell parameters published earlier by Davies and Donaldson.[2] The a and b axes are, however, interchanged.

The systematically absent reflexions are:

$h0l$ with $h = 2n+1$
$0kl$ with $l = 2n+1$

which is characteristic for space groups *Pcam* (No. 57) and $Pca2_1$ (No. 29).[8] Analysis of the tree-dimensional Patterson function showed the correct space group to be $Pca2_1$.

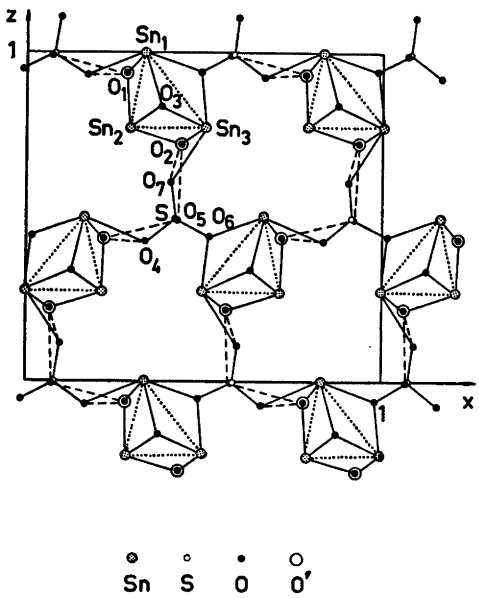

Fig. 3. Projection of the structure of $Sn_3O(OH)_2SO_4SO_4$ on the xz plane. Tin triangles are marked with dotted lines, coordinated atoms are connected by full lines and O – O distances indicating possible hydrogen bonds are dashed. O′ corresponds to an oxygen atom in the next unit cell above or below. The z coordinates are changed compared to Ref. 5.

STRUCTURE DETERMINATION

The estimated intensity values were corrected for Lorentz and polarisation effects using the program DATAP2.[9] Correction for absorption was carried out with the same program but not until an approximate structure had been derived. The linear absorption coefficient for $Sn_3O(OH)_2SO_4$ is 788 cm^{-1}.

A three-dimensional Patterson synthesis $P(uvw)$ was calculated with the program DRF.[9] It showed no vector set concentrations[10] in the planes $(u0w)$ and $(\frac{1}{2}vw)$ which would be required for *Pcam*. It thus became clear that the correct space group was $Pca2_1$.

In $Pca2_1$ all atoms occupy fourfold positions. The first tin atom position (Sn_1) was obtained from $P(uvw)$ and was then refined with a few cycles of least squares refinement using the block diagonal approximation program, BLOCK.[9] The z parameter for Sn_1 had to be kept constant to define the origin.

An electron density function $\varrho(xpz)$, based on the F_{h0l} signs obtained from the Sn_1 parameters, was then calculated. This Fourier synthesis yielded the second tin atom position (Sn_2), the x and z parameters of which were then also refined. By means of subsequent Fourier syntheses and refinements the remaining atoms (Sn_3, S, $O_1 - O_7$) were located. Atomic scattering factors for Sn, S and O were taken from the International Tables.[11] To obtain the y parameters, the three-dimensional intensity data set was used. Successive least-squares refinements (using BLOCK[9]) and electron density calculations using all the data, were then carried out. Atomic parameters and scale factors from these least-squares refinements yielded an R value of 11.3 %. At this stage the preliminary data were replaced by absorp-

Table 2. Observed and calculated structure factors. The columns are l, F_o and $|F_c|$, respectively.

0	0	L
2	233	177
4	538	480
6	219	231
8	231	241
10	155	151
12	151	135
14	137	131
2	0	L
1	160	149
2	78	79
3	92	85
4	28	28
5	143	125
6	35	38
7	67	71
8	32	36
9	65	66
11	20	20
12	46	44
13	62	51
4	0	L
0	113	127
1	325	258
2	374	321
3	164	163
4	136	134
5	252	250
6	256	248
7	57	52
8	151	149
9	192	187
10	138	120
11	14	18
12	112	102
13	107	97
14	36	39
6	0	L
0	192	195
1	85	101
2	67	71
3	94	90
4	146	156
5	91	99
6	75	76
7	99	88
8	100	100
9	41	42
10	55	54
11	47	45
12	54	56
13	26	26
14	48	50
8	0	L
1	149	171
2	116	132
3	159	180
4	63	65
5	90	91
6	85	86
7	191	181
8	63	63
10	55	50
11	121	109
12	56	54
13	18	18
10	0	L
0	101	117
1	34	33
2	141	160
3	42	44
4	108	96
5	43	37
6	144	141
7	56	51
8	86	81
10	69	78
11	37	35
12	54	63
12	0	L
0	96	90
1	49	47
2	83	84
3	49	50
4	74	75
5	30	32
6	62	61
7	30	31
8	49	47
9	26	25
10	53	55
14	0	L
0	97	92
1	49	43
2	95	92
3	54	53
4	74	77
5	21	21
6	77	76
7	38	41
8	46	54
16	0	L
1	34	31
2	36	33
3	28	29
0	1	L
2	163	156
4	62	64
6	105	108
8	47	48
10	72	76
12	34	33
14	45	46
1	1	L
2	107	115
3	86	81
4	34	36
5	92	90
6	85	84
7	32	32
8	56	53
9	48	50
10	46	43
11	33	29
12	40	40
13	22	22
14	21	21
2	1	L
0	261	226
1	175	160
2	342	353
3	193	191
4	194	179
5	119	108
6	275	261
7	145	149
8	139	151
9	41	37
10	148	130
11	101	88
12	118	107
13	25	26
14	50	54
15	42	47
3	1	L
0	67	73
1	87	89
2	55	55
3	106	112
4	19	17
5	71	69
6	36	32
7	125	127
8	18	19
10	23	16
11	66	61
12	21	23
14	12	13
15	26	30
4	1	L
0	19	17
1	124	122
2	96	95
3	117	126
4	23	21
5	78	76
6	71	68
7	127	125
8	49	49
9	24	25
10	39	34
11	90	82
12	42	39
5	1	L
0	107	118
1	37	37
2	47	43
3	88	95
4	48	51
5	68	73
7	34	32
8	14	15
9	79	77
10	19	18
11	29	25
12	17	19
13	22	23
14	21	22
6	1	L
0	248	268
1	150	154
2	61	56
3	127	136
4	192	212
5	108	116
6	97	90
7	97	97
8	132	115
9	84	73
10	95	83
11	59	56
12	51	52
13	42	44
14	59	64
7	1	L
1	92	104
2	54	57
3	74	71
4	36	34
5	84	82
6	29	26
9	69	63
10	19	19
12	18	18
13	35	38
8	1	L
0	93	111
1	95	104
2	124	144
3	68	73
4	83	86
5	91	96
6	130	112
7	35	32
8	78	63
9	85	76
10	72	63
12	43	48
13	48	48
9	1	L
0	20	22
1	54	63
2	24	25
3	58	66
5	19	19
7	46	44
8	14	14
10	19	20
11	30	29
10	1	L
0	20	19
1	105	104
2	48	46
3	71	70
4	36	31
5	111	114
6	39	36
7	26	25
8	37	33
9	90	87
12	22	28
11	1	L
0	66	62
1	34	33
2	34	37
3	34	34
4	52	48
5	32	31
6	34	29
7	33	29
8	32	30
9	23	22
10	25	24
11	13	17
12	1	L
0	175	155
2	72	65
4	132	128
6	84	73
8	81	87
9	13	14
10	48	55
13	1	L
0	30	30
1	18	18
2	35	33
3	31	30
4	23	25
5	20	20
6	13	11
7	20	20
8	18	17
9	17	20
14	1	L
0	27	24
1	33	33
2	13	15
3	45	45
4	23	21
5	18	20
6	13	11
7	33	38
8	16	18
15	1	L
0	11	8
1	19	17
2	27	25
3	33	28
5	9	10
6	18	21
16	1	L
0	38	36
1	43	40
2	58	62
3	32	35
0	2	L
2	161	160
4	234	247
6	112	118
8	152	161
10	125	113
12	72	65
14	53	52
1	2	L
2	71	75
3	120	116
4	103	103
5	136	143
6	53	53
7	45	47
8	65	65
9	100	100
10	48	46
12	47	41
13	61	56
14	33	35
2	2	L
0	84	89
1	112	105
2	24	22
3	77	81
4	94	92
5	105	102
6	22	19
7	26	26
8	60	60
9	100	87
10	28	29
12	27	23
13	48	48
14	14	17
3	2	L
0	23	23
1	154	136
2	34	34
3	156	168
4	32	35
5	65	59
6	29	28
7	139	125
8	38	34
10	18	19
11	78	77
12	11	13
13	24	24
14	11	14
4	2	L
0	116	130
1	155	135
2	157	164
3	98	95
4	97	103
5	102	110
6	107	107
7	63	60
8	78	68
9	68	67
10	70	64
11	26	27
12	48	49
13	49	44
14	30	36
5	2	L
0	82	93
1	116	119
2	84	86
3	128	117
4	78	75
5	117	119
6	68	70
7	59	59
8	62	53
9	106	99
10	48	46
11	32	32
12	34	37
13	44	48
6	2	L
0	110	120
1	76	91
2	23	22
3	86	94
4	104	107
5	69	67
6	45	47
7	57	57
8	80	72
9	56	51
10	55	50
11	41	42
12	29	29
13	31	30
7	2	L
0	49	51
1	50	52
2	77	82
3	54	56
4	68	66
5	69	72
6	75	63
7	14	12
8	55	50
9	65	61
10	34	37
11	15	11
12	37	38
13	24	26
8	2	L
1	76	86
2	23	25
3	112	116
5	72	61
6	25	26
7	85	72
8	20	16
9	49	49
11	56	54
12	11	11
9	2	L
0	31	37
1	85	92
2	38	38
3	110	112
5	44	42
6	45	40
7	109	103
8	21	21
10	15	15
11	70	66
12	16	19
10	2	L
0	63	57
1	59	59
2	112	116
3	64	63
4	63	58
5	26	26
6	90	82
7	55	47
8	50	51
10	48	49
11	32	37
11	2	L
0	52	51
1	49	46
2	38	36
3	38	41
4	42	44
5	72	60
6	33	31
7	17	18
8	24	23
9	45	49
10	26	26
12	2	L
1	23	23
2	25	29
3	22	21
5	27	28
6	31	33
7	18	17
9	18	22
13	2	L
1	45	42
2	59	56
3	31	34
4	15	13
5	45	47
6	38	40
7	14	13
8	22	25
14	2	L
0	48	42
1	35	32
2	70	67
3	36	36
4	45	42
5	14	16
6	48	54
15	2	L
0	15	14
1	47	39
3	51	50
4	11	11

tion corrected values. A few least-squares cycles then caused the R value to decrease to 10.4 %. A correction for extinction was also included with the program LINUS.[9] The R value then converged to 8.0 % after three cycles of refinement. Finally, anisotropic temperature factors for the tin atoms were introduced, together with constant scale factors, the isotropic thermal parameters being retained for all the remaining atoms. A weighting scheme according to Cruickshank's formula $w=(a+F_o+cF_o^2+dF_o^3)^{-1}$, with $a=10.0$, $c=0.04$, and $d=0.00$ was used. After a final series of least-squares refinements using the LINUS program [9] the R value converged to 6.9 % and R_w to

Table 3. Final atomic coordinates and their standard deviations.

Atom	x	y	z
Sn_1	0.3344(2)	0.0803(9)	1.000(–)
Sn_1	0.2884(2)	0.5211(8)	0.7714(4)
Sn_3	0.5057(2)	0.0786(9)	0.7757(3)
S	0.4188(5)	0.2923(35)	0.4964(8)
O_1	0.2838(17)	0.7010(93)	0.9317(21)
O_2	0.4352(19)	0.6946(90)	0.7238(19)
O_3	0.3746(19)	0.2176(86)	0.8406(21)
O_4	0.3324(14)	0.2181(90)	0.4286(16)
O_5	0.4277(21)	0.5827(106)	0.4912(26)
O_6	0.5094(16)	0.1422(82)	0.4423(23)
O_7	0.4041(23)	0.1706(104)	0.6042(27)

Table 4. Final thermal parameters and their standard deviations. The temperature coefficient is expressed as $\exp[-(h^2\beta_{11}+k^2\beta_{22}+l^2\beta_{33}+2hkB_{12}+2hl\beta_{13}+2kl\beta_{23})]$ for the tin atoms.

Atom	$\beta_{11}\times 10^5$ or β	$\beta_{22}\times 10^5$	$\beta_{33}\times 10^5$	$\beta_{12}\times 10^5$	$\beta_{13}\times 10^5$	$\beta_{23}\times 10^5$
Sn_1	460(13)	2589(414)	354(12)	−90(38)	−2(11)	−7(77)
Sn_2	421(12)	2117(402)	459(15)	94(33)	−41(13)	97(52)
Sn_3	337(11)	3613(448)	455(16)	−3(35)	44(11)	136(74)
S	1.868(110)					
O_1	2.716(433)					
O_2	2.856(431)					
O_3	2.811(469)					
O_4	1.636(342)					
O_5	3.203(575)					
O_6	2.285(449)					
O_7	3.997(572)					

8.5 %. The final value of the isotropic extinction parameter was $g=(0.91\pm 0.07)\times 10^4$.

A three-dimensional electron difference density calculation was performed with the program FFT.[9] Its maximum electron density was 2.1 e/Å^3 which probably can be attributed to termination errors, since the peak was observed near a tin atom.

A list of observed and calculated structure factors is given in Table 2. Final positional parameters and temperature factors are given with their standard deviations in Tables 3 and 4. Selected interatomic distances and angles, together with their standard deviations, calculated with the program DISTAN,[9] are given in Table 5.

HYDROGEN BONDS

The final refinement from $R=13.3$ %[5] to 6.9 % changed the coordination of the atoms O_2, O_6, O_7 and Sn_3. The oxygen atom O_7 moved towards Sn_3 to within a coordination distance (*cf.* Ref. 5). This means that the layers parallel to the *xy* plane are held together even without hydrogen bonds. There are, however, short O−O distances (O_2-O_5, O_2-O_7) outside the Sn_3 group (see Fig. 4). Ref. 12 shows that the angle Sn−O−O for hydrogen bonded hydroxide groups varies from 90 to 135°. According to this fact (*cf.* Table 5) the most probable position for a hydrogen atom bonded to O_2 ought to be between the oxygen atoms O_2 and O_5. The position can nevertheless be influenced by the slightly longer distance between O_5 and O_7.

A similar situation holds for the other hydrogen atom bonded to O_1'' (see Fig. 5). From the angles it ought to be found between O_1'' and O_5. However, the O−O-distances (see Table 5) are contradictory. An explanation might be that a bifurcated bond $O_1''-O_4$, O_5 is formed. The analysis of the TG curve discussed later, supports this explanation.

The hydrogen atom positions could not be determined directly from the X-ray data, since the tin atoms dominate the scattering to too great an extent.

DESCRIPTION AND DISCUSSION OF THE STRUCTURE

The structure of $Sn_3O(OH)_2SO_4$ is non-centrosymmetric. The tin atoms lie in groups, three and three, forming triangles. The Sn−Sn distances within such a group are 3.52, 3.58, and 3.58 Å (*cf.* Table 5). The triangles are joined together to form a zig-zag chain (*cf.* Fig. 6), the distances from Sn_2 in one triangle to Sn_1 and Sn_3 in the triangle in the next unit cell being 3.96 and 4.02 Å, respectively.

A projection of the structure of $Sn_3O(OH)_2SO_4$ down the short *y* axis is shown in Fig. 3. Two OH^- ions and one O^{2-} ion are coordinated to the Sn triangle. The Sn_1 and Sn_2 atoms are both coordinated to O_1, Sn_1 being coordinated to an O_1 atom in the unit cell below, while Sn_2 is coordinated to an O_1 atom in the same unit cell. Similar coordination relations exist for Sn_2, Sn_3, and the oxygen atom O_2. The complex $Sn_3O(OH)_2^{2+}$ corresponds to one

Table 5. Interatomic distances (Å) and angles (°) with their standard deviations in paranthesis. * indicates atoms in the unit cell above or below.

Between the tin atoms:

Sn_1-Sn_3	3.523(3)
Sn_1-Sn_2	3.578(5)
Sn_2-Sn_3	3.580(4)
Sn_1-Sn_2*	3.961(5)
Sn_1-Sn_3*	4.021(4)

Within the Sn_1 coordination group:

Sn_1-O_3	2.116(28)	O_1*$-Sn_1-O_3$	90.1(1.3)
Sn_1-O_1*	2.152(42)	O_1*$-Sn_1-O_4''$	80.4(1.3)
Sn_1-O_6'*	2.419(27)	O_1*$-Sn_1-O_6'$*	75.6(1.1)
Sn_1-O_4''	2.439(21)	$O_3-Sn_1-O_4''$	78.9(0.9)
		$O_3-Sn_1-O_6'$*	70.8(1.2)
		$O_4''-Sn_1-O_6'$*	140.9(0.9)

Within the Sn_2 coordination group:

Sn_2-O_1	2.140(31)	$O_1-Sn_2-O_2$	95.9(1.1)
Sn_2-O_2	2.177(28)	$O_1-Sn_2-O_3$	86.9(1.3)
Sn_2-O_3	2.054(36)	$O_2-Sn_2-O_3$	85.1(1.3)

Within the Sn_3 coordination group:

Sn_3-O_2*	2.200(40)	O_2*$-Sn_3-O_3$	92.9(1.3)
Sn_3-O_3	2.005(28)	O_2*$-Sn_3-O_6'$*	78.9(1.1)
Sn_3-O_6'*	2.306(31)	O_2*$-Sn_3-O_7$	72.4(1.4)
Sn_3-O_7	2.509(33)	$O_3-Sn_3-O_6'$*	75.2(1.2)
		$O_3-Sn_3-O_7$	79.2(1.1)
		O_6'*$-Sn_3-O_7$	140.2(1.1)

Within the sulfate group:

$S-O_4$	1.442(23)	O_4-S-O_5	106.9(2.2)
$S-O_5$	1.441(55)	O_4-S-O_6	103.5(1.8)
$S-O_6$	1.542(30)	O_4-S-O_7	107.8(1.9)
$S-O_7$	1.453(38)	O_5-S-O_6	113.5(1.9)
		O_5-S-O_7	117.5(2.5)
		O_6-S-O_7	106.6(2.2)

$Sn-O_3-Sn$ bond angles:

$Sn_1-O_3-Sn_2$	118.2(1.3)
$Sn_1-O_3-Sn_3$	117.5(1.6)
$Sn_2-O_3-Sn_3$	123.8(1.5)

Short $O-O$ distances outside the coordination groups and corresponding $Sn-O-O$ angles:

$O_1''-O_4$	2.826(56)
$O_1''-O_5$	2.911(38)
O_2-O_5	2.879(41)
O_2-O_7	2.994(62)
$Sn_1''-O_1''-O_4$	154.6(1.2)
$Sn_1''-O_1''-O_5$	111.7(1.5)
$Sn_2''-O_1''-O_4$	69.7(1.2)
$Sn_2''-O_1''-O_5$	99.7(1.3)
$Sn_2-O_2-O_3$	98.9(1.2)
$Sn_2-O_2-O_7$	70.7(1.2)
$Sn_3-O_2-O_5$	117.4(1.6)
$Sn_3-O_2-O_7$	160.2(1.2)

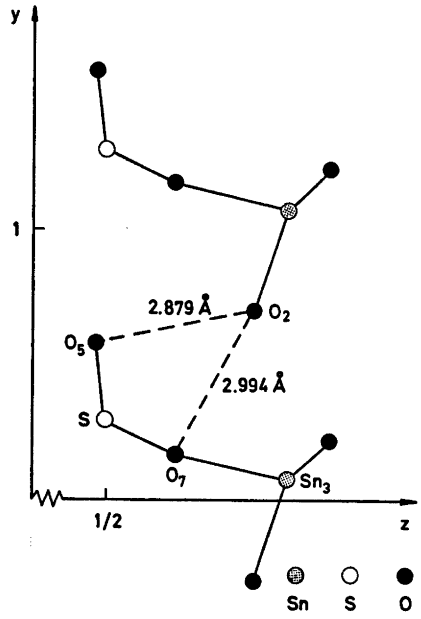

Fig. 4. One environment with O – O distances indicating hydrogen bonds. Coordinated atoms are connected by full lines and O – O distances corresponding to possible hydrogen bonds are dashed.

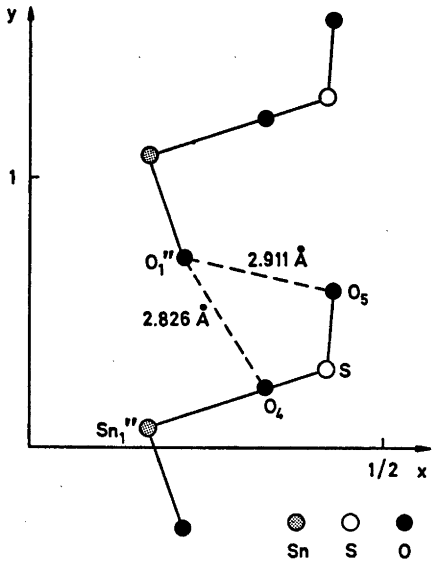

Fig. 5. Another environment with short O – O distances indicating hydrogen bonds. Coordinated atoms are connected by full lines and O – O distances corresponding to possible hydrogen bonds are dashed.

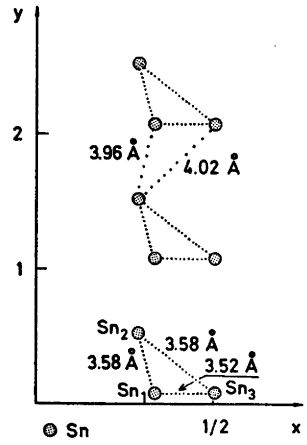

Fig. 6. The tin atom arrangement. Short distances are marked with dotted lines and larger distances within the chain are marked with more sparsely dotted lines in the upper part of the figure.

formula unit. There are, however, no discrete $Sn_3O(OH)_2^{2+}$ ions but infinite tin-oxygen chains which can be formulated $(Sn_3O(OH)_2)_n^{2n+}$. Similar chains, of general formula $(Pb_2O)_n^{2n+}$, are present in the structure of Pb_2OSO_4.[13] It that compound, the chains are connected to each other by sulfate ions only, whereas in $Sn_3O(OH)_2SO_4$ the chains are held together by sulfate groups and hydrogen bonds.

Two of the tin atoms (Sn_1 and Sn_3) have similar oxygen coordination polyhedra, while the third (Sn_2) is coordinated in a different way. Sn_1 has four oxygen neighbours at distances of 2.12, 2.15, 2.42, and 2.44 Å (*cf.* Table 5). The sulfate oxygen atoms O_4'' and O_6'* are at a longer distance than the chain building ones O_1* and O_3. Since the next oxygen atom it at a distance of 3.24 Å, Sn_1 would appear to be four-coordinated. The configuration can be described as a seriously distorted octahedron, in which two adjacent positions are empty.

Sn_2 has three oxygen neighbours at distances of 2.05, 2.14, and 2.18 Å, respectively, and a fourth one at a distance of 2.89 Å. Sn_2 may thus be considered to be three-coordinated. The O – Sn – O angles are equal to the corresponding ones published for SnS which is described as a chain structure [14] in which Sn has three nearest neighbours.

The Sn_3 coordination group shows approxi-

mately the same angles as the Sn_1 group (*cf.* Table 5). It has one short Sn – O distance (2.01 Å), two intermediate values (2.20 and 2.31 Å) and a large distance (2.51 Å), giving four-coordination. Again the sulfate oxygen atoms are the most remote and the next nearest oxygen atom is at a distance of 3.17 Å.

The Sn – O, OH distances vary from 2.01 to 2.20 Å and the $Sn - O_{SO_4}$ distances range from 2.31 to 2.51 Å. The oxygen atom, O_3, which is coordinated to three tin atoms, gives bonding distances ranging from 2.01 to 2.12 Å. These values are shorter than those published previously.[15,16] Wernfors [17] has given Sn – O distances varying from 2.12 to 2.36 Å for an oxygen atom bonded to four tin atoms in a tetrahedron. When three metal atoms, lying in a triangle, are the sole atoms coordinated to an oxygen atom outside the triangle plane, it is natural for the oxygen atom to be drawn towards the plane. The result ought to be close linkage as observed. The Sn – O – Sn bond angles are 118.2, 117.5, and 123.8° (*cf.* Table 5). The rest of the oxygen atoms (*i.e.* OH^- ions forming hydrogen bonds) give Sn – O distances of 2.14 – 2.21 Å while the sulfate oxygen atoms give Sn – O distances of 2.31 – 2.51 Å, all in good agreement with values obtained previously.[15–17] The Sn – Sn distances are also within known limits [18,19] but considerably shorter than those reported by Davies and Donaldson.[20] Fig. 3 indicates apart from the chain building that the O – 3Sn group is the fundamental unit in this substance as in Ref. 19 and not the O – 4Sn tetrahedron as in Sn_2OSO_4.[17]

The infinite oxygen chains are connected by sulfate groups each of which is coordinated to three tin atoms (*cf.* Fig. 3). The sulfate ions also take part in hydrogen bonds. The sulfate oxygen atom O_6'* is connected to Sn_1 as well as to Sn_3. These contacts result in the long $S - O_6$ bonding distance of 1.54 Å (*cf.* Table 5), whereas the remaining $S - O_{SO_4}$ distances are normal.[11] In addition to O_6'*, the sulfate oxygen atom $O^{4''}$ is also included in the Sn_1 coordination group and O_7 in the Sn_3 coordination group. The sulfate ion angles are within normal limits [11] with the exception of $O_4 - S - O_6$, which is too small, and $O_5 - S - O_6$ and $O_5 - S - O_7$ which are too large. The anomalous angles involving O_6 can be explained through the tin atom contact. The O_7 angle deviation is more difficult to account for, but it could be a result of the hydrogen bond. As many strong bonding forced act upon the sulfate group the result is a somewhat distorted tetrahedron.

It is apparent from Fig. 3 that there are tunnels between the $(Sn_3O(OH)_2)_n^{2n+}$ chains running parallel to the [010] direction. However, as is shown in Ref. 21, the lone pair electrons of a metal atom, *e.g.* tin, would require space.

INTERPRETATION OF THE TG AND DTA CURVES

Figs. 1 and 2 show that different environments give distinctly different curve forms. Small lateral shifts too can be detected. The peaks 1′, 2′ (in Fig. 1) and 1″, 2″ (in Fig. 2) are endothermic and should correspond to a reaction during which water is expelled from the substance. However, if atmospheric oxygen is present, the endothermic peaks have a flatter form, caused by the simultaneous exothermic oxidation (*cf.* peak 5′, 5″) of tin(II) to tin(IV). The weight loss, when water leaves, is partly compensated for by the uptake of oxygen, as shown by the TG curve in Fig. 2. Originally [5] it was supposed that the difference in size between the peaks 1″ and 2″ was caused by a more effective oxidation at the higher temperature. Fig. 1 shows that this assumption is wrong. The weight loss according to the TG curve in Fig. 1, corresponds to $\frac{3}{4}$ H_2O for 1′ and $\frac{1}{4}$ H_2O for 2′. The water molecules thus seem to leave the substance in two steps, forming an intermediate compound. It may, hoever, be observed, that one hydroxide oxygen, O_2, is coordinated mainly to O_5, covering $\frac{1}{2}$ H_2O from $\frac{3}{4}$. The remaining H_2O ($2 \times \frac{1}{4}$ H_2O) gives two possibilities equally frequented for the hydrogen atom bonded to O_1''. The bond is probably bifurcated. One of the two possibilities seems to be very similar to the coordination of the first hydroxide group (O_2), as the water molecules leave at the same time (peak 1′, 1″). Davies and Donaldson [2] explained incorrectly peak 2′, 2″ as an oxidation of tin(II) to tin(IV) which should have given a weight increase through oxygen uptake. The oxidation, which actually occurs at 440 – 480 °C (peak 5′, 5″) is, of course, also exothermic.

Fig. 2 shows that the exothermic peak 3″ (3′)

must correspond to a rearrangement of $Sn_3O_2SO_4$ since no change in weight can be detected. The peak 4″ (4′) indicates an endothermic reaction with a weight decrease (*cf.* the TG curves) corresponding to the decomposition of $Sn_3O_2SO_4$ and loss of SO_2(g). As the decomposition proceeds, oxidation of tin(II) to tin(IV) gradually commences.

When the atmosphere contains oxygen (Fig. 2) the oxidation reaction is revealed by the exothermic peak 5″. The TG curve also shows a weight increase caused by final oxidation.

Acknowledgements. The author wishes to thank Professor Georg Lundgren for valuable discussions and encouragement. She is also indebted to Fil.dr. Inge Svedung for manipulating the Mettler Recording Thermoanalyser and to Fil.lic. Ove Lindgren for help concerning the computer programs. Many thanks are also due to Fil.dr. Susan Jagner for revising the English text of this paper.

This work has been supported by the Swedish Natural Science Research Council (Contract No. 2318) and by Chalmers' University of Technology, which supplied a grant to cover the costs of the computer work.

REFERENCES

1. Ditte, A. *Ann. Chim. Phys. 27* (1882) 159.
2. Davies, C. G. and Donaldson, I. D. *J. Chem. Soc. A* (1967) 1790.
3. Tobias, R. S. *Acta Chem. Scand. 12* (1958) 198.
4. Davies, C. G. and Donaldson, I. D. *J. Chem. Soc. A* (1968) 946.
5. Grimvall, S. *Acta Chem. Scand. 27* (1973) 1447.
6. Hambling, P. G. *Acta Crystallogr. 6* (1953) 98.
7. Lindqvist, O. and Wengelin, F. *Ark. Kemi 28* (1967) 179.
8. *International Tables for X-Ray Crystallography*, 2nd Ed., Kynoch Press, Birmingham 1952, Vol. I.
9. Modified programs in use at this Department. *DATAP2* was originally written by Coppens, P., Leiserowitz, L. and Rabinowich, D., *DRF* by Zalkin, A. *BLOCK* was written locally by Lindgren, O. and *LINUS* by Busing, W. R., Martin, K. O. and Levy, I. A. *FFT* was originally written by Sande, G. and extended to three dim. by Ten Eyck, L. *DISTAN* was written by Zalkin, A.
10. Buerger, M. I. *Vector space*, Wiley, New York 1967, p. 203.
11. *International Tables for X-Ray Crystallography*, 2nd Ed., Kynoch Press, Birmingham 1962, Vol. III.
12. Pimental, G. and McClellan, A. *The Hydrogen Bond*, Freeman, San Francisco 1960, p. 232.
13. Sahl, K. *Naturwissenschaften 56* (8) (1969) 414.
14. Rundle, R. E. and Olsson, D. H. *Inorg. Chem. 3* (1964) 596.
15. Donaldson, J. D. *Progr. Inorg. Chem. 8* (1967) 287.
16. Jelen, A. and Lindqvist, O. *Acta Chem. Scand. 23* (1969) 3071.
17. Wernfors, G. *On the Crystal Structures of Basic Tin(II) Salts*, Thesis, Department of Inorganic Chemistry, Göteborg 1970.
18. Wernfors, G. *Acta Chem. Scand. 15* (1961) 1007.
19. Johansson, G. and Ohtaki, H. *Acta Chem. Scand. 27* (1973) 643.
20. Davies, C. G. and Donaldson, I. D. *Acta Crystallogr. A 25* (1969) 122. XIIth IUCr Suppl.
21. Åström, A. *Det ensamma elektronparets stereokemiska effekt i vissa fasta oxider, oxidfluorider och fluorider*, Thesis, Institute of Inorganic Chemistry 2, Chemical Centre, Lund 1972.

Received January 2, 1975.

Acta Chemica Scandinavica A 29 (1975) 599—607

Equilibrium Studies of Chromium(III) Complexes. II. The Complex Formation between Chromium(III) and Ammonia in Aqueous Solution

PETER ANDERSEN, TORSTEN BERG and JENS JACOBSEN

Chemistry Department I, Inorganic Chemistry, H. C. Ørsted Institute, University of Copenhagen, DK-2100 Copenhagen Ø, Denmark

Equilibrium has been obtained between $Cr(NH_3)_6^{3+}$, $Cr(NH_3)_5OH^{2+}$, *cis*-$Cr(NH_3)_4(OH)_2^+$, and *trans*-$Cr(NH_3)_4(OH)_2^+$ in aqueous solutions with $C_{NH_4Cl}=4.5$ M, $C_{NH_3}=2-10$ M, and $C_{Cr(III)}=0.05$ M. Equilibrium was established within 5 days at room temperature due to the combined catalytic effect of chromium(II) and charcoal.

The hydrolysis constants of the reactions

$Cr(NH_3)_6^{3+}+H_2O \rightleftharpoons Cr(NH_3)_5(OH)^{2+}+NH_4^+$

and $Cr(NH_3)_5(OH)^{2+}+H_2O \rightleftharpoons Cr(NH_3)_4(OH)_2^+ + NH_4^+$

are found to be 195 M and 3.16 M, respectively, and the ratio between *cis*- and *trans*-$Cr(NH_3)_4(OH)_2^+$ to be 4.9. The fifth and sixth consecutive stability constants are calculated to be $K_5=10^{1.6}$ M^{-1} and $K_6=10^{1.5}$ M^{-1}, and on the basis of emf measurements the gross stability constant, β_6, can be estimated to be 10^{13} M^{-6}.

The equilibrium solutions, with $[NH_3]=9$ M, contain *ca.* 5 % of polynuclear chromium(III) species and this amount increases with decreasing ammonia concentration, but equilibrium has only been demonstrated between the mononuclear complexes mentioned above.

In a recent paper [1] we introduced a new method of obtaining equilibrium between chromium(III) and different amine ligands in aqueous solution. The method was applied to the ethylenediamine system and is based on the catalytic effect of charcoal and chromium(II), both of which must be present in the solutions to be equilibrated. During the 3 – 5 days of equilibration a steady state with a constant, small concentration of chromium(II) is maintained by electrolytic reduction of chromium(III) to chromium(II). In this steady state the amount of chromium(II) generated by electrolysis equals the amount removed due to the charcoal-catalyzed oxidation by the medium:

$$Cr(II)+H(I) \xrightarrow{C} Cr(III)+H(0) \qquad (I)$$

This paper concerns the application of the method to the chromium(III) – ammonia system.

It is necessary to keep a high ammonium-ion concentration in the ammonia solutions in order to prevent the formation of basic chromium(III) precipitates. Several reactions in such ammonia-ammonium chloride buffers with all chromium initially present as chromium(II) have been described. Rhodo chloride, $[(NH_3)_5CrOHCr(NH_3)_5]Cl_5.H_2O$, is formed if such solutions are oxidized by air.[2] If the solutions are kept in an inert atmosphere, Jørgensen [3] found that luteo chloride, $[Cr(NH_3)_6]Cl_3.H_2O$, was formed as well as some rhodoso chloride,[3,4]

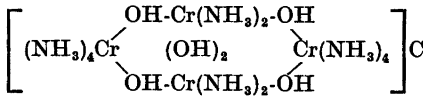

$Cl_5.4H_2O$.[5]

Later attempts to prepare the hexammine in this way have been futile unless one adds small amounts of, preferably group VIII, metals or metal ions.[6] These metals have the effect that the small rate of oxidation of chromium(II) to chromium(III) under hydrogen evolution, which

is observed when no catalyst is present (reagent grade chemicals), is increased so that one obtains rates of oxidation and yields of hexammine similar to those observed by Jørgensen. Addition of charcoal likewise increases the rate of oxidation but the yield of hexammine is negligible. On the other hand addition of chromium(II) to such ammonia-ammonium chloride buffers containing hexammine and charcoal has the effect that the hexammine disappears within a few minutes.[6] These observations led to equilibration experiments with the catalyst charcoal + chromium(II). In these experiments all the chromium was initially present as chromium(II) [7,8] which, however, involved the difficulty that the chromium(II) might disappear according to reaction (I) before equilibrium was reached. With the new method by which it is possible continuously to keep part of the chromium as chromium(II) this problem has been solved, and we present here the results of an investigation of the complex formation under these circumstances in 4.5 M ammonium chloride with the ammonia concentration varying between 2 and 10 M.

EXPERIMENTAL

Procedure. The procedure and equipment has been described in a similar investigation with ethylenediamine.[1] All experiments were carried out at (24 ± 1) °C using $C_{Cr} = 0.05$ M, $C_{NH_4Cl} = 4.5$ M, and $C_{NH_3} = 2-10$ M. 2 g charcoal *per* l were used and the solutions were equilibrated for 3 – 10 days with a current of *ca.* 10 mA giving a chromium(II) concentration of *ca.* 10^{-3} M. The equilibration was followed by taking out samples which were analyzed as described below. Pairs of experiments with the same ammonia concentration, but different initial chromium(III) compound, within 3 – 5 days gave an identical distribution of at least the mononuclear complexes, and further equilibration did not change this distribution. Changes in $[NH_3]$ and $[NH_4^+]$ during the equilibration were negligible when 2 M H_2SO_4 was used in the anode chamber and the gas outlet was under ammonia of the same concentration as in the cathode chamber.

During the equilibration the emf was measured with a mercury electrode *vs.* a saturated calomel electrode and the Cr(II) content was determined in the same way as in the ethylenediamine system.[1]

Analysis of the composition of the equilibrium solutions. $[NH_3]$ was determined by potentiometric titration with 0.1 M HCl. The distribution of the chromium(III) complexes was determined by atomic absorption spectrophotometry after separation of the complexes by cation-exchange chromatography on columns of Sephadex SP-C-25. The robustness of the chromium(III) complexes, after removal of the catalyst, made this analytic procedure possible. The results of these analyses for a series of experiments, exp. 1 – 12, are given in Table 1.

The basic and acid chromatographic separations were very similar to those described for the ethylenediamine complexes.[1] A basic elution with an NH_4Cl/NH_3 buffer with $[NH_3] = 0.1$ M and $[NH_4^+]$ increasing from 0.5 to 2.0 M divided the mixture into the following bands of mononuclear complexes with increasing charge: A first band containing *cis-* and *trans-* $Cr(NH_3)_4(OH)_2^+$, a second one containing $Cr(NH_3)_5OH^{2+}$, and a third one containing $Cr(NH_3)_6^{3+}$. Four bands followed the $Cr(NH_3)_6^{3+}$ band. None of these purple species could be identified as mononuclear complexes and are therefore assumed to be polynuclear ones. A few per cent of the chromium remained on the column, even after elution with 2 M NH_4Cl. The first polynuclear band was at the end of the $Cr(NH_3)_6^{3+}$-band but subsequent acid chromatography (0.7 M NH_4Cl, 10^{-3} M HCl) easily separated these two species.

The acid elution with 0.5 M NH_4Cl or NaCl ($pH \simeq 2-3$) did not result in a complete separation of the mononuclear complexes, now having the same charge, but gave a check on the sum of these. We were able to separate the remaining polynuclear species in up to four bands by increasing the concentration of the eluting agent to 1 – 2 M.

Identification of the chromium(III) complexes. The same methods were used to identify the chromium species as were used for the ethylenediamine system.[1] The elution rates gave an indication of the charge and the visible spectra and the ESR spectra of the eluates, which, when necessary, were concentrated on separate columns, identified the well known mononuclear complexes. Analysis of the molar ratio between chromium and nitrogen in the eluates after removal of nitrogen not bound to chromium was used in attempts to identify the polynuclear species. Furthermore, the crystalline iodide of the chromium species in the third polynuclear band was isolated and analyzed.

As mentioned above we were not able to separate *cis-* and *trans-* $Cr(NH_3)_4(OH)_2^+$ completely by ion-exchange chromatography but the visible spectra and the ESR spectra of the diaqua complexes showed that they are both present, and from analysis of the spectra it was possible to determine the ratio between them.

Chemicals and apparatus. All chemicals used were reagent grade or analyzed by us. $[Cr(NH_3)_6]Cl_3$,[6] *cis*-$[Cr(NH_3)_4Cl(H_2O)]Cl_2$,[9] *cis*-$[Cr(NH_3)_4(H_2O)_2](ClO_4)_3$,[10] *trans*-$[Cr(NH_3)_4(OH)H_2O](ClO_4)_2$,[11] *trans*-$[Cr(NH_3)_4(H_2O)_2](ClO_4)_3$,[11], and *cis*-$[Cr(NH_3)_2Cl_2(H_2O)_2]Cl$ [9]

Table 1. The composition of the solutions from experiments 1 to 12. $C_{NH_4Cl} = 4.5$ M. a_6 is $[Cr(NH_3)_6]Cl_3$, *cis*-a_2 is *cis*-$[Cr(NH_3)_2Cl_2(H_2O)_2]\cdot Cl.H_2O$, *cis*-$a_4$ is *cis*-$[Cr(NH_3)_4Cl(H_2O)]Cl_2$, and *trans*-a_4 is *trans*-$[Cr(NH_3)_4(OH)H_2O](ClO_4)_2$. The content of mononuclear complexes are in mol % relative to the total chromium(III) content. ( ) denote analyses repeated after six months. The equilibrium constants of the reactions II, III, and IV are given in the last three columns.

Exp. No.	$[NH_3]$ (M)	C_{Cr} (mM)	Initial Cr-comp.	% $Cr(NH_3)_6^{3+}$	% $Cr(NH_3)_5OH^{2+}$	% $Cr(NH_3)_4(OH)_2^{+}$	$K_{h6/5}$ (M)	$K_{h5/4}$ (M)	$10^2 \times K_{disp}$
1	2.60	48.2	a_6	1.00	36.5	21.8	164	2.69	1.64
	(2.61)			(0.55)	(20.5)	(12.6)	(168)	(2.77)	(1.65)
2	2.42	48.0	*cis*-a_2	0.92	36.1	21.0	177	2.62	1.48
3	3.78	48.7	a_6	1.40	47.7	23.1	153	2.18	1.42
4	3.62	49.5	*cis*-a_4	1.50	47.4	23.6	142	2.24	1.57
5	4.66	50.1	a_6	1.83	55.1	24.7	135	2.02	1.49
6	4.77	49.3	*cis*-a_4	1.78	54.6	24.2	138	1.99	1.44
7	6.64	49.4	a_6	2.48	64.6	24.2	117	1.69	1.44
8	6.55	50.2	*trans*-a_4	2.39	65.3	23.7	123	1.63	1.32
9	8.19	50.3	a_6	3.22	71.1	21.3	99.3	1.35	1.36
10	8.24	50.9	*cis*-a_2	3.01	71.8	20.9	107	1.31	1.23
11	9.27	48.2	a_6	4.04	74.4	17.1	82.8	1.03	1.24
12	9.18	50.1	*trans*-a_4	3.97	74.1	17.6	84.0	1.07	1.27
	(9.21)			(3.57)	(68.8)	(16.0)	(86.7)	(1.05)	(1.21)

were prepared according to or analogously to the reference methods and were analyzed for Cr, N, and chloride. All analyses agreed within 1 – 2 % (relative) with the given formulae. The charcoal used was a Norit W product.

Visible spectra were taken on a Cary 14 or a Bausch and Lomb Spectronic 505 recording spectrophotometer and ESR spectra of frozen glasses (diluted × 2 with glycerol) on a Jeol JES-ME-1X at −130 °C and 9.3 GHz. The emf and pH measurements were performed with a Radiometer PHM 52, the G 202 C glass electrodes being tested in the relevant media according to Bjerrum.[12]

RESULTS

Equilibria. We have studied the following hydrolysis reactions:

$$Cr(NH_3)_6^{3+} + H_2O \rightleftharpoons Cr(NH_3)_5(OH)^{2+} + NH_4^+ \quad (II)$$

and

$$Cr(NH_3)_5(OH)^{2+} + H_2O \rightleftharpoons Cr(NH_3)_4(OH)_2^+ + NH_4^+ \quad (III)$$

which can be combined in the disproportionation reaction

$$2Cr(NH_3)_5OH^{2+} \rightleftharpoons Cr(NH_3)_6^{3+} + Cr(NH_3)_4(OH)_2^+ \quad (IV)$$

$Cr(NH_3)_4(OH)_2^+$ exists in a *cis-* and a *trans-*form and the equilibrium between these forms was also studied.

The composition of the equilibrium solutions are given in Table 1 for the series of experiments 1 – 12. Each solution was equilibrated *ca.* 5 days after which no further changes could be observed. Solutions with the same ammonia concentration but different initial chromium(III) compound had then attained the same distribution of mononuclear species. This distribution of $Cr(NH_3)_6^{3+}$, $Cr(NH_3)_5(OH)^{2+}$, and $Cr(NH_3)_4(OH)_2^+$ (*cis-* and *trans-*) are given in Table 1, and at the end of the table are the calculated values of the hydrolysis constants of reactions II and III, *i.e.* $K_{h6/5}$ and $K_{h5/4}$, respectively, together with the disproportionation constant K_{disp} of reaction IV.

The ratio $q_2 = [cis\text{-}Cr(NH_3)_4(OH)_2^+]/[trans\text{-}Cr(NH_3)_4(OH)_2^+]$ was determined in two ways, the results of which are given in Table 2. Both methods are based on analyses of the mixed *cis-* and *trans-*tetrammine eluates in 1 M perchloric acid.

Table 2. $q_2 = [cis\text{-}Cr(NH_3)_4(OH)_2^+]/[trans\text{-}Cr(NH_3)_4(OH)_2^+]$ determined in the tetrammine eluates (1 M $HClO_4$) from visible spectra (method A) and ESR spectra (method B).

Exp. No.	q_2 A	B
1	5.2	6
3	4.1	4
6	4.6	5
7	4.3	4
10	5.0	6
11	5.3	6
Average	4.9	

By method A, the visible spectra of the eluates and of the pure components were used for the calculation of the composition of the eluates, according to Mønsted.[10]

By method B, the ESR spectra of the frozen glasses of the eluates were used in a manner similar to the one by which we determined the equilibrium ratio between *cis-* and *trans-*Cr $en_2(OH)_2^+$.[1] As shown in Fig. 1 the ESR spectrum of *trans*-$Cr(NH_3)_4(H_2O)_2^{3+}$, unlike *trans*-Cr $en_2(H_2O)_2^{3+}$, does not contain any narrow bands so that the method is not particularly well suited in this respect. It has, however, the advantage that the solutions are cooled rapidly to −130 °C so that further reaction is prevented.

From these results it is possible to calculate the 5th and 6th consecutive stability constants, K_5 and K_6, respectively. This is done in Table 3. The acid dissociation constants of the pentammine and tetrammines have been measured by other workers in 1 M salt medium [13,14] and are in Table 3 estimated to be 0.7 pK units higher in 4.5 M NH_4Cl. This is the increase that one finds when extrapolating the measurements, by Bjerrum, of $pK_{S\,pen}$ for $Co(NH_3)_5(H_2O)^{3+}$ in ammonium salt media with $[NH_4^+]$ varying between 0.25 and 2.0 M.[12]

The variation of $K_{h6/5}$ and $K_{h5/4}$ and the small variation of K_{disp} with the ammonia concentration are shown in Fig. 2. The values of $K_{h6/5}$ and $K_{h5/4}$ used in Table 3 are those obtained from extrapolation to $[NH_3] = 0$.

Estimation of the gross stability constant, β_6, from emf-measurements. The electrode potential, E, was measured with a mercury electrode (saturated calomel as reference electrode) and

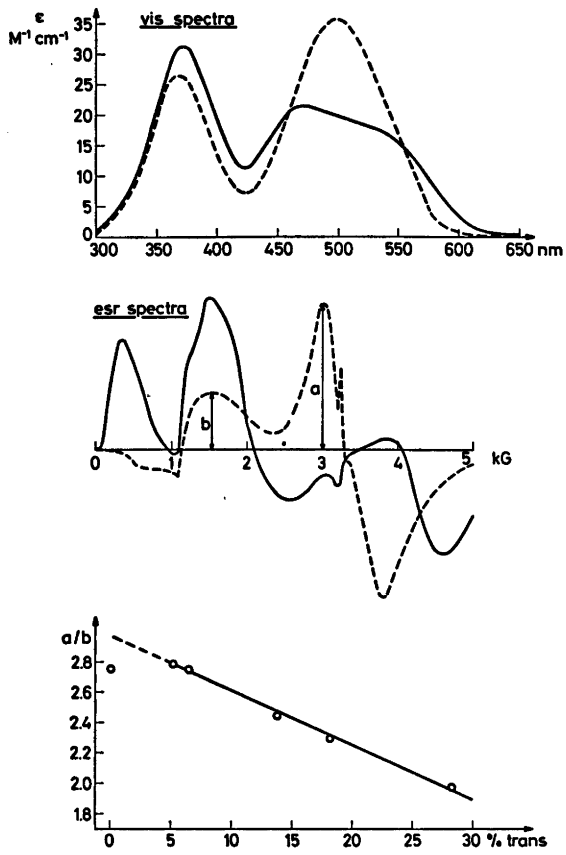

Fig. 1. Visible spectra and first derivative ESR spectra of *cis*-$Cr(NH_3)_4(H_2O)_2^{3+}$ (– – –) and *trans*-$Cr(NH_3)_4(H_2O)_2^{3+}$ (——). The ESR spectra were measured of frozen glasses of 1:1 mixtures of glycerol and aqueous 1 M $HClO_4$ solutions of the perchlorates at −130 °C and 9.3 GHz.
The lowest figure gives the ratio between the peak heights a and b plotted as a function of mol per cent *trans*-$Cr(NH_3)_4(H_2O)_2^{3+}$ relative to the sum of *cis* and *trans*, in different known mixtures of *cis*- and *trans*-tetrammine. In method B (Table 2) this plot was used to find q_2 in the tetrammine eluates from some of the exp. 1 – 12.

simultaneously [Cr(II)] was determined in similar ways to those described in our investigation with ethylenediamine as ligand.[1] Table 4 shows such measurements from exp. 1 – 12 when the solutions were at their final state of equilibration. It is possible, from these data, to make an estimate of the gross stability constant, β_6, for the reaction $Cr(H_2O)_6^{3+} + 6NH_3 \rightleftharpoons Cr(NH_3)_6^{3+} + 6H_2O$:

$$\log \beta_6 = \log \beta_4^{II} - (E + 652)/59 + \log \frac{[Cr(NH_3)_6^{3+}]}{[Cr(NH_3)_4^{2+}][NH_3]^2}$$

$\beta_4^{II} = \dfrac{[Cr(NH_3)_4^{2+}]}{[Cr(H_2O)_4^{2+}][NH_3]^4}$ can be estimated to be 10^5 M^{-4} by comparison with the chromium(II) – ethylenediamine system [15] and with other metal ammine and ethylenediamine systems (mainly copper(II)).[12,15] "652" is the sum of the standard potentials of the $Cr^{2+} - Cr^{3+}$ couple and of the saturated calomel electrode (410 mV [16] and 242 mV, respectively). Under our conditions all chromium(II) is likely to be present as $Cr(NH_3)_4^{2+}$. We determined $\bar{n}$ to be 4, within the experimental error, in solutions

Table 3. Calculation of the stability constants K_6, $K_{5\,cis}$, $K_{5\,trans}$ and K_5 in 4.5 M NH_4Cl.

$$K_6 = \frac{[Cr(NH_3)_6^{3+}]}{[Cr(NH_3)_5(H_2O)^{3+}][NH_3]} = \frac{K_{S\,pen}}{K_{h6/5}\cdot K_{S\,NH_4^+}} = 10^{1.5}\ M^{-1}$$

$$K_{5\,cis} = \frac{[Cr(NH_3)_5(H_2O)^{3+}]}{[cis\text{-}Cr(NH_3)_4(H_2O)_2^{3+}][NH_3]} = \frac{K_{S1\,cis}\cdot K_{S2\,cis}}{K_{h5/4\,cis}\cdot K_{S\,pen}\cdot K_{S\,NH_4^+}} = 10^{1.6}\ M^{-1}$$

$$K_{5\,trans} = \frac{[Cr(NH_3)_5(H_2O)^{3+}]}{[trans\text{-}Cr(NH_3)_4(H_2O)_2^{3+}][NH_3]} = \frac{K_{S1\,trans}\cdot K_{S2\,trans}}{K_{h5/4\,trans}\cdot K_{S\,pen}\cdot K_{S\,NH_4^+}} = 10^{2.5}\ M^{-1}$$

$$K_5 = \frac{[Cr(NH_3)_5(H_2O)^{3+}]}{\{[cis\text{-}Cr(NH_3)_4(H_2O)_2^{3+}] + [trans\text{-}Cr(NH_3)_4(H_2O)_2^{3+}]\}[NH_3]} = \frac{K_{5\,cis}\cdot K_{5\,trans}}{K_{5\,cis} + K_{5\,trans}} = 10^{1.6}\ M^{-1}$$

From Fig. 2: $K_{h6/5} = 195$ M and $K_{h5/4} = 3.16$ M. $q_2 = 4.9$

$$K_{h5/4\,cis} = \frac{q_2}{1+q_2} \times K_{h5/4} = 2.62\ \text{M}, \quad K_{h5/4\,trans} = \frac{1}{1+q_2} \times K_{h5/4} = 0.54\ \text{M}$$

Acid dissociation constant for			NH_4^+	$K_{S\,NH_4^+}$	$= 10^{-9.8}$ M [12]
»	»	»	$Cr(NH_3)_5(H_2O)^{3+}$	$K_{S\,pen}$	$= 10^{-6.0}$ M [13]
»	»	constants	*cis*-$Cr(NH_3)_4(H_2O)_2^{3+}$	$K_{S1\,cis}$	$= 10^{-5.7}$ M, $K_{S2\,cis} = 10^{-8.1}$ M [13,14]
»	»	»	*trans*-$Cr(NH_3)_4(H_2O)_2^{3+}$	$K_{S1\,trans}$	$= 10^{-5.1}$ M, $K_{S2\,trans} = 10^{-8.5}$ M [14]

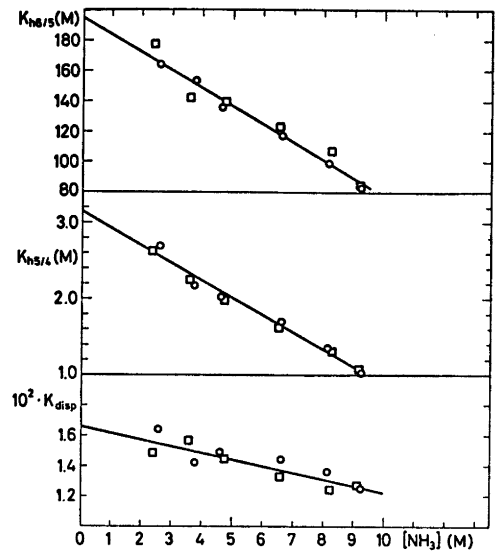

Fig. 2. The hydrolysis constants $K_{h6/5}$ and $K_{h5/4}$ and the disproportionation constant $K_{disp}=K_{h5/4}/K_{h6/5}$ as a function of $[NH_3]$, with $[Cr(NH_3)_6]Cl_3$ (○) and lower ammine complexes (□) as initial Cr(III) compound (exp. 1–12).

Table 4. $\log \frac{\beta_6}{\beta_4^{II}} \left(= -(E+652)/59 + \log \frac{[Cr(NH_3)_6^{3+}]}{[Cr(II)][NH_3]^2} \right)$

determined from measurements of [Cr(II)] and the electrode potential, E, between a mercury and a saturated calomel electrode in solutions 1 to 12 at their final state of equilibration.

Exp. No.	$-E$ (mV)	[Cr(II)] (mM)	$\log \frac{\beta_6}{\beta_4^{II}}$
1	1126	0.25	7.5
2	1140	0.31	7.7
3	1181	0.54	7.9
4	1201	1.0	8.1
5	1155	0.35	7.6
6	1120	0.10	7.5
7	1182	0.37	7.9
8	1162	0.28	7.6
9	1210	0.97	7.9
10	1150	0.21	7.5
11	1230	2.3	7.8
12	1205	0.52	8.0
		Average:	7.7_5

with $C_{NH_4Cl}=4.5$, $C_{Cr(II)}=0.25$ M and with $[NH_3]$ varying between 1.1 and 2.3 M. These measurements were made with a glass electrode according to Bjerrum.[12] The calculated values of $\log (\beta_6/\beta_4^{II})$ in exp. 1–12 are given in Table 4, giving an estimated value of $\beta_6=10^{13}$ M^{-6}.

Polynuclear complexes. From Table 1 the mononuclear complexes comprise nearly 100 % of the total chromium content at high ammonia concentrations. The content of polynuclear complexes increases as the ammonia concentration decreases. From the separations by ion-exchange chromatography we know that there are at least four different polynuclear species in the solutions but we have not yet been able to identify any of these. Analyses show that the molar ratio between Cr and N is 1:3 for the polynuclear species in the first three bands. We isolated the third polynuclear species as the iodide and this crystalline salt analyzed as $\{Cr_2(NH_3)_6(OH)_3I_3(H_2O)_4\}_n$ (Found: Cr 14.62; I 53.21; N 12.18. Calc.: Cr 14.64; I 53.62; N 11.84).

DISCUSSION

We conclude from the results given in the previous section that equilibrium has been obtained among the mononuclear ammines mentioned, just as we found when using the catalyst with the ethylenediamine system. Part of the equilibrium solutions from exp. 1–12 was filtered after the equilibration and kept in glass ampoules for six months after which they were reanalyzed. The results of such repeated analyses are given in Table 1 and show that the molar ratio between the mononuclear complexes is unchanged. The total amount of mononuclear complexes has, however, decreased at the expense of polynuclear complexes, especially at low ammonia concentration.

Table 1 shows that the amount of polynuclear species is highest at low ammonia concentrations. This is what one would expect from the equilibria when ammonia and hydroxide ions are the only ligands bound to chromium(III) [8] as ammonia is released when OH-bridges are formed, *e.g.*

$$2Cr(NH_3)_5OH^{2+} \rightleftharpoons (NH_3)_4Cr(OH)_2Cr(NH_3)_4^{4+} + 2NH_3$$
diol

Table 5. Comparison of stability constants, at room temperature, for Cr(III), Co(III), and Ni(II) with ammonia (extrapolated values) and ethylenediamine (en).

	NH_3			en	
	$\log K_5$	$\log K_6$	$\log \beta_6$	$\log K_3$	$\log \beta_3$
Cr(III) [1]	1.6	1.5	13	6.4	19.5
Co(III) [12,20,21]	5.5	4.9	38	13.3	48.7
Ni(II) [12,22]	0.9	0.2	10	4.4	18.3
Medium	4.5 M NH_4Cl			1 M 1:1 salt	

The analyses, repeated after six months, show, however, that equilibria involving polynuclear complexes are attained much more slowly, if at all. We are at present continuing our investigations of these complexes.

The change in the water activity is probably the main reason why $K_{h6/5}$ and $K_{h5/4}$ decrease with increasing ammonia concentration as shown in Fig. 2. K_{disp} for the reaction involving the complex ions only is less dependent on the ammonia concentration in the investigated interval. At very high ammonia concentrations and correspondingly low water concentrations one would expect equilibrium II to be displaced in favour of $Cr(NH_3)_6^{3+}$.

This was confirmed by an experiment with $C_{NH_4Cl} = 4.5$ M, $C_{NH_3} = 15$ M (continuous NH_3-gas flow) and $C_{Cr} = 0.10$ M (initially as *cis*-$[Cr(NH_3)_4Cl(H_2O)]Cl_2$), which after equilibration gave 12.4 % $Cr(NH_3)_6^{3+}$.[17]

The results of this work are summerized in Table 5 which, for comparison, also shows the corresponding stability constants for the chromium(III) ethylenediamine system and also those for Co(III) and Ni(II). The stability constants for chromium(III) and ammonia are intermediate between those for Ni(II) and Co(III) and closer to Ni(II) as we have found for ethylenediamine [1] and EDTA.[9] Stability constants for complexes of ammonia are very close to those with ethylenediamine when bound as a monodentate ligand [1] ($10^{1.6}$ and $10^{1.4}$, respectively, for Cr(III)), as it has been found also for Ag(I) [18] and Hg(II).[19]

The determination of the gross stability constant is only an estimate because β_4^{II} is based on an estimate. β_3 for Cr en_3^{3+} seems a little low when compared to β_3 for Ni en_3^{3+}. Any small error in the emf due to the Cr(III)/Cr(II) couple as measured in this way with the mercury electrode will most probably be in the direction which would give low gross stability constants, because possible formation of hydrogen at the mercury surface will tend to make the initial (very negative) potentials less negative. We have, however, investigated the reliability of the mercury electrode more thoroughly in connection with a similar determination of the stability constant between chromium(III) and EDTA [9] and found that in this EDTA case the mercury electrode does work satisfactorily.

Acknowledgements. The authors are grateful to J. Bjerrum and C. E. Schäffer for valuable discussions and suggestions and to K. Jørgensen for her help in the analytical work.

REFERENCES

1. Andersen, P., Berg, T. and Jacobsen, J. *Acta Chem. Scand. A 29* (1975) 381.
2. Jørgensen, S. M. *J. Prakt. Chem. 25* (1882) 321.
3. Jørgensen, S. M. *J. Prakt. Chem. 30* (1884) 1.
4. Jørgensen, S. M. *J. Prakt. Chem. 45* (1892) 260.
5. Bang, E. *Acta Chem. Scand. 22* (1968) 2671.
6. Schäffer, C. E. *Advances in the Chemistry of the Coordination Compounds*, MacMillan, New York 1961, p. 628.
7. Andersen, P., Bjerrum, J. and Schäffer, C. E. *Proc. of the 7th I.C.C.C., Stockholm 1962*, p. 325.
8. Schäffer, C. E. and Andersen, P. *Proc. of Symp. on "Theory and Structure of Complex Compounds", Wroclaw, Poland 1962*, Pergamon, Oxford 1964, p. 571.
9. Andersen, P., Berg, T. and Jacobsen, J. *To be published.*
10. Mønsted, L. and Mønsted, O. *Acta Chem. Scand. A 28* (1974) 23.
11. Glerup, J. *To be published.*
12. Bjerrum, J. *Metal Ammine Formation in Aqueous Solution*, Haase, Copenhagen 1941. Reprinted 1957.
13. Sillén, L. G. *Stability Constants of Metal-Ion Complexes. Special Publication No. 17.* The Chemical Society, London 1964, p. 49.
14. Mønsted, L. and Mønsted, O. *Acta Chem. Scand. To be published.*
15. Pecsok, R. L. and Bjerrum, J. *Acta Chem. Scand. 11* (1957) 1419.
16. Grube, G. and Breitinger, G. *Z. Elektrochem. 33* (1927) 112.
17. Andersen, P. *Proc. 14de Nordiska Kemistmötet, Umeå 1971*, p. 158.

18. Schwarzenbach, G., Ackermann, H., Maissen, B. and Anderegg, G. *Helv. Chim. Acta 35* (1952) 2337.
19. Bjerrum, J. and Larsen, E. *Experientia Suppl. 9* (1964) 39.
20. Bjerrum, J. and Rasmussen, S. E. *Acta Chem. Scand. 6* (1952) 1265.
21. Woldbye, F. *Acta Chem. Scand. 12* (1958) 1079.
22. Poulsen, I. and Bjerrum, J. *Acta Chem. Scand. 9* (1955) 1407.

Received January 15, 1975.

Acta Chemica Scandinavica A 29 (1975) 608—614

The Crystal and Molecular Structure of Selenium Bis(1-pyrrolidinecarbodiselenoate)

STEINAR ESPERÅS, STEINAR HUSEBYE and ÅGE ROLANDSEN

Department of Chemistry, University of Bergen, N-5014 Bergen-Univ., Norway

The structure of selenium bis(1-pyrrolidinecarbodiselenoate), $Se(C_4H_8NCSe_2)_2$, has been determined by three-dimensional X-ray crystallographic methods. The crystals are monoclinic with unit cell dimensions $a = 15.800(3)$ Å, $b = 6.590(1)$ Å, $c = 15.152(2)$ Å, $\beta = 100.42(2)°$ and $Z = 4$. The space group is $P2/c$. Reflection intensities were measured by means of a Siemens AED-1 diffractometer. The structure was solved by the symbolic addition procedure and refined by full-matrix least-squares methods to an R-value of 0.041. There are two types of crystallographically independent molecules in the unit cell, both being very similar to each other and both with the central selenium atom situated on a twofold rotation axis. The monomeric compounds can be regarded as four-coordinated trapezoid planar selenium(II) complexes with two bidentate diselenocarbamate ligands. Average bond lengths from the central selenium atoms to the ligand selenium atoms are 2.445(1) and 2.867(1) Å, respectively, for the short and long bonds which are *trans* to each other.

The average interbond angle in this system of two *trans* bonds, is 161.66(3)°.

In our studies of complexes of divalent selenium and tellurium with bidentate dithio-, thioseleno-, or diseleno ligands,[1–5] the central atom has always been found to be bonded to four ligand sulfur and/or selenium atoms in a trapezoid planar configuration. Two classes of such complexes have been found.[4] Class I consists of essentially monomeric molecules where the central selenium or tellurium atoms are coordinated to all four ligand donor atoms in the molecule with two relatively strong bonds and two relatively weak ones. Class II compounds are built up of essentially polymeric networks, where the central atom is strongly bonded to two ligand atoms in the parent molecule and weakly to two ligand atoms belonging to different neighbouring molecules. The only complex with a diseleno ligand whose structure has previously been solved in this laboratory, is selenium bis(diethyldiselenophosphinate),[1,6] which has a class II structure. With diselenocarbamate ligands, it was from analogy with tellurium and selenium dithiophosphinates and dithiocarbamates [1–4,7–9] thought more likely that both divalent selenium and tellurium would give class I complexes.

Diselenocarbamates have been prepared by several workers and metal complexes with such ligands have been prepared and characterized.[10–27] So far, only a few structures of such compounds seem to have been solved.[13,22,23,27]

EXPERIMENTAL

A sample of crystalline selenium(II) bis(1-pyrrolidinecarbodiselenoate), $Se(C_4H_8NCSe_2)_2$, was kindly supplied by Dr. L. Henriksen at the H. C. Ørsted Institute, University of Copenhagen, Denmark. The ligand itself was first made by Shankaranarayana.[19] Such diselenocarbamate ligands are easily oxidized to the corresponding diselenides which disproportionate into mono- and triselenides,[10–12] the latter may alternatively be termed selenium bis(diselenocarbamates).

For data recording, a Siemens off-line automatic AED-1 diffractometer was used. The diffractometer was operated as a three-circle instrument and Mo$K\alpha$ radiation was used.

Intensity data were collected using a scintillation counter, the "five-value" measurement, and the $\theta - 2\theta$ scan technique.[28] Reflections out to $2\theta = 56°$ were scanned with scan speed 2.5° per min, but with automatic setting of greater speed for strong reflections. An automatic

Table 1. Atomic coordinates in fractions of cell edges. Standard deviations in parentheses.

	x	y	z
Molecule I			
Se1	½	0.4535(1)	¼
Se2	0.41167(6)	0.6570(1)	0.09250(5)
Se3	0.44401(6)	0.1869(1)	0.14254(5)
C1	0.4011(5)	0.3881(9)	0.0559(5)
N1	0.3664(4)	0.3303(8)	−0.0233(4)
C2	0.3635(6)	0.1139(11)	−0.0544(5)
C3	0.3435(6)	0.1405(12)	−0.1581(5)
C4	0.2928(6)	0.3339(11)	−0.1773(5)
C5	0.3336(5)	0.4783(11)	−0.0975(5)
Molecule II			
Se4	0	0.6262(1)	¼
Se5	0.08431(6)	0.4248(1)	0.40926(6)
Se6	0.05891(6)	0.8947(1)	0.35536(5)
C6	0.0979(5)	0.6935(9)	0.4420(4)
N2	0.1351(4)	0.7545(8)	0.5221(4)
C7	0.1445(5)	0.9743(11)	0.5473(5)
C8	0.1931(6)	0.9714(12)	0.6449(5)
C9	0.1720(7)	0.7661(12)	0.6822(5)
C10	0.1655(5)	0.6167(11)	0.5987(5)

attenuation filter insertion mechanism reduced counting losses, and the reflections were scanned between $\theta_1 = \theta - 0.41°$ and $\theta_2 = \theta + 0.41°$, where θ is the Bragg angle for the α_1 peak. Two reference reflections were measured twice at intervals of 50 reflections. Of the 3680 reflections measured, 2183 had intensities greater than twice the standard deviations, σ_C, based on counting statistics and were labelled as observed.[29] Unobserved reflections were given intensities equal to $2\sigma_C$.

The intensities were corrected for Lorentz and polarization effects and for absorption ($\mu = 126.5$ cm^{-1}).[30] The crystal used for data collection had the following dimensions measured as distances from a common origin to crystal faces: 100 and $\bar{1}00$; 0.043 mm, 010 and $0\bar{1}0$; 0.089 mm, 011, $0\bar{1}1$, $01\bar{1}$ and $0\bar{1}\bar{1}$, 0.097 mm.

Accurate cell dimensions were based on measurements of 20 high-order reflections and calculated using a least squares procedure. The crystals are monoclinic with $a = 15.800(3)$ Å, $b = 6.590(1)$ Å, $c = 15.152(2)$ Å, $\beta = 100.42(2)°$ and $Z = 4$. Based on systematic absences, the space group is either $P2/c$ or Pc. The calculated and observed (flotation) densities are 2.40 and 2.39 g/cm^3, respectively.

STRUCTURE ANALYSIS

The structure factors were converted to normalized structure factors using a program written by Shiono.[31] The resulting E statistics clearly indicated that the space group was centric, *i.e.* $P2/c$. This was later confirmed by the successful structure refinement. Reflections with E values greater than 2.0 (196 of the reflections with $2\theta < 48°$), were used as input in program package MULTAN.[32,33] The correct

Table 2. Components of atomic vibration tensors, $U \times 10^4$, in Å^2 with standard deviations, referred to the crystallographic axes. The expression used is $\exp[-2\pi^2(h^2a^{-2}U_{11} + \cdots + 2hka^{-1}b^{-1}U_{12} + \cdots)]$.

	U_{11}	U_{22}	U_{33}	U_{12}	U_{23}	U_{13}
Se1	443(8)	315(6)	283(6)	0	0	53(5)
Se2	641(7)	276(5)	371(5)	8(4)	9(3)	4(5)
Se3	637(7)	278(4)	314(5)	−11(4)	21(3)	−34(4)
C1	388(51)	345(42)	360(44)	−25(33)	−11(30)	108(38)
N1	437(41)	411(38)	290(33)	−11(29)	−10(27)	−51(30)
C2	874(73)	368(47)	428(49)	−57(42)	−148(36)	76(48)
C3	931(79)	706(58)	328(45)	164(51)	−148(38)	−167(48)
C4	737(60)	563(50)	348(42)	99(47)	−34(38)	−22(41)
C5	763(69)	511(47)	325(45)	64(45)	124(35)	−75(43)
Se4	482(8)	320(6)	312(6)	0	0	49(6)
Se5	600(7)	292(5)	408(5)	23(3)	24(3)	26(5)
Se6	621(7)	301(4)	296(4)	43(4)	13(3)	−2(4)
C6	412(51)	395(44)	292(41)	20(34)	23(30)	16(38)
N2	472(43)	347(37)	416(40)	55(30)	35(28)	87(34)
C7	582(60)	461(49)	338(42)	−31(40)	−134(34)	−72(39)
C8	840(74)	620(55)	476(52)	16(50)	−21(40)	−101(48)
C9	1469(101)	513(53)	357(49)	−221(56)	31(37)	−47(56)
C10	561(59)	537(47)	351(45)	138(40)	137(36)	30(41)

Table 3. Bond lengths in Å with standard deviations in parentheses.

Molecule I		Molecule II	
Se1 – Se2	2.870(1)	Se4 – Se5	2.863(1)
Se1 – Se3	2.449(1)	Se4 – Se6	2.451(1)
Se2 – C1	1.856(6)	Se5 – C6	1.841(6)
Se3 – C1	1.902(6)	Se6 – C6	1.889(6)
C1 – N1	1.283(8)	C6 – N2	1.313(9)
N1 – C2	1.500(9)	N2 – C7	1.499(9)
C2 – C3	1.556(10)	C7 – C8	1.538(10)
C3 – C4	1.505(11)	C8 – C9	1.527(12)
C4 – C5	1.581(10)	C9 – C10	1.591(11)
C5 – N1	1.508(9)	C10 – N2	1.484(9)
Some intramolecular distances			
Se3 – Se3′	3.413(1)	Se6 – Se6′	3.392(1)
Se3 – Se2	3.208(1)	Se5 – Se6	3.209(1)
Se2 – C5	3.148(7)	Se5 – C10	3.187(7)
Se3 – C2	3.062(7)	Se6 – C7	3.023(7)

structure emerged from the output, and was refined by a full matrix least squares program which minimizes the function $\sum w(|F_o| - K|F_c|)^2$, where $w = 1/\sigma_F$ and K is a scale factor. Unobserved reflections with $K|F_c|$ larger than the observable limit were included in the refinement with F_o put equal to the limit. There are two crystallographically independent half molecules in the asymmetric unit, the central selenium atoms of the molecules being located on the twofold axes $(0,y,\frac{1}{4})$ and $(\frac{1}{2},y,\frac{1}{4})$.

After introducing anisotropic temperature factors, the factor $R = \sum||F_o| - |F_c||/\sum|F_o|$, converged to the value 0.041. The parameter shifts at this stage of refinement, were all less than 1/5 of the standard deviations. The hydrogen atom positions were not revealed in the final difference map which contained no spurious peaks.

The final observed and calculated structure factors may be obtained from the author S. H. upon request.

The scattering factors used were taken from the *International Tables for X-Ray Crystallography*,[34] those of selenium were corrected for anomalous dispersion using the $\Delta f'$ and $\Delta f''$ values calculated by Cromer.[35]

The final atomic coordinates are listed in Table 1 and components of atomic vibration tensors in Table 2. Interatomic distances and angles are listed in Tables 3 – 4. Some short intermolecular distances and least squares planes through the molecules are given in Tables 5 – 6.

RESULTS AND DISCUSSION

The two crystallographically independent molecules, with bond lengths and angles indicated, are shown in Fig. 1. There are hardly significant differences between corresponding bond lengths in the two molecules, but several differences in bond angles are significant. The ligands in molecules of type I and II (see Fig.

Table 4. Bond angles in degrees with standard deviations in parentheses.

Molecule I		Molecule II	
Se2 – Se1 – Se3′	161.95(3)	Se5 – Se4 – Se6′	161.37(3)
Se2 – Se1 – Se2′	124.28(3)	Se5 – Se4 – Se5′	124.76(3)
Se3 – Se1 – Se3′	88.34(3)	Se6 – Se4 – Se6′	87.58(3)
Se2 – Se1 – Se3	73.72(3)	Se5 – Se4 – Se6	73.84(3)
Se1 – Se2 – C1	78.8(2)	Se4 – Se5 – C6	78.2(2)
Se1 – Se3 – C1	90.0(2)	Se4 – Se6 – C6	89.1(2)
Se2 – C1 – Se3	117.3(3)	Se5 – C6 – Se6	118.7(3)
Se2 – C1 – N1	124.3(4)	Se5 – C6 – N2	123.7(4)
Se3 – C1 – N1	118.5(4)	Se6 – C6 – N2	117.6(4)
C1 – N1 – C2	124.0(5)	C6 – N2 – C7	122.6(5)
C1 – N1 – C5	122.4(5)	C6 – N2 – C10	124.3(5)
N1 – C2 – C3	101.5(5)	N2 – C7 – C8	104.0(5)
C2 – C3 – C4	107.1(6)	C7 – C8 – C9	105.2(6)
C3 – C4 – C5	103.5(6)	C8 – C9 – C10	103.9(6)
C4 – C5 – N1	102.6(5)	C9 – C10 – N2	102.0(5)
C5 – N1 – C2	113.2(5)	C7 – N2 – C10	112.9(5)

Table 5. Some short intermolecular distances in Å. Standard deviations in parentheses. The distances are calculated from atoms in the original molecules (extreme left) to atoms in molecules whose tranformations are given in the central column of the table.

Se1 – C5	$1-x,1-y,-z$	3.83(1)
Se2 – Se3	$x,1+y,z$	3.591(1)
Se2 – C2	$x,1+y,z$	3.74(1)
Se6 – Se5	$x,1+y,z$	3.594(1)
Se5 – C7	$x,-1+y,z$	3.66(1)
C3 – C8	$x,-1+y,-1+z$	3.64(1)
C4 – C9	$x,y,-1+z$	3.85(1)
C4 – C8	$x,-1+y,-1+z$	3.73(1)
C4 – C6	$x,1-y,-\frac{1}{2}+z$	3.85(1)

1 and Table 6) are both planar within 0.05 Å, except for hydrogen and the two outer carbon atoms of the pyrrolidine rings. The central selenium atom is coordinated to all four ligand selenium atoms in the molecule, resulting in a trapezoid planar structure, quite similar to those found in divalent selenium and tellurium bis(dialkyldithiocarbamates).[1] Thus the selenium bis(1-pyrrolidinecarbodiselenoate) has a class I structure, and not a class II or class III (trichalcogenide) structure.[4] There is no short intermolecular contact from the central selenium atom in a molecule to ligand atoms in neighbour molecules. In this respect, selenium (bis(1-pyrrolidinecarbodiselenoate) is more like the dithiocarbamates of selenium than those of tellurium.[1] For comparison, the coordination around the central atom in the present investigation and in related compounds, is shown in Fig. 2.

Table 6. Least squares planes through the molecules.

Plane

1: Se1, Se2, Se3, Se2′, Se3′
2: Se1, Se2, Se3, C1, N1, C2, C5
3: Se4, Se5, Se6, Se5′, Se6′
4: Se4, Se5, Se6, C6, C7, C10, N2

Equation of planes based on coordinates of the monoclinic cell. Coordinates from Table 1 give distances of atoms from plane in Å.

Plane

1: $14.648\,X+8.086\,Z+5.303=0$
2: $15.052\,X+0.362\,Y-7.013\,Z+5.833=0$
3: $14.737\,X-7.888\,Z-1.972=0$
4: $15.057\,X-0.019\,Y-7.073\,Z-1.695=0$

Interplanar angle

Plane 1 – Plane 3: 0.88°
Atomic distances from planes in Å:
Plane 1. Se1: 0.0, Se2: −0.030, Se3: 0.043, Se2′: 0.030, Se3′: −0.043.
Plane 2. Se1: 0.104, Se2: −0.048, Se3: −0.082, C1: −0.047, N1: −0.035, C2: 0.061, C5: 0.046.
Plane 3. Se4: 0.0, Se5: −0.021, Se6: 0.032, Se5′: 0.021, Se6′: −0.032.
Plane 4. Se4: −0.085, Se5: 0.062, Se6: 0.051, C6: 0.029, N2: 0.022, C7: −0.019, C10: −0.060.
The ligand in molecule I is planar to within 0.042 Å, that in II is planar within 0.028 Å.

In the $SeSe_4$ coordination groups, the stronger central atom to ligand bonds Se1 – Se3 and Se4 – Se6 are 2.449(1) and 2.451(1) Å, respectively. The weaker bonds, Se1 – Se2 and Se4 – Se5 which are *trans* to the strong ones, are 2.870(1) and 2.863(1) Å, respectively. The resulting three-center four-electron bonding systems, consisting of pairs of weak and strong Se – Se bonds *trans* to each other, have an average length of 5.32 Å. This closely corresponds to the length of the analogous three-center systems found in selenium dithiocarbamates, when the difference in covalent radius between sulfur and selenium, 0.13 Å, is taken into consideration.[1–3] It is also exactly equal to the average length of the almost linear three-center Se – Se – Se systems found in triselenocyanate and triselenourea ions.[36,37] The two different $SeSe_4$ groups are nearly planar (Table 6), the planes are nearly parallel with the molecular twofold axes and with each other. The $SeSe_4$ groups deviate less from square geometry than the SeS_4 and TeS_4 groups in the selenium- and tellurium bis(dialkyldithiocarbamates).[1–3,8,9] This is mainly due to sterical factors. When the sulfur atoms in a dithiocarbamate ligand are replaced by the larger selenium atoms, the ligand bite becomes larger, increasing from 2.94 to 3.20 Å. This results in an increase in the intraligand S – Se – S angle of about 3° when sulfur is replaced by selenium. The increased interligand Se3 – Se3′ and Se6 – Se6′ repulsions across the smaller of the two interligand angles are offset by the lengthening of the Se – Se bonds relative to a Se – S bond, so these angles remain close to 87°. As a result of these factors, the larger interligand Se – Se – Se angle have an average

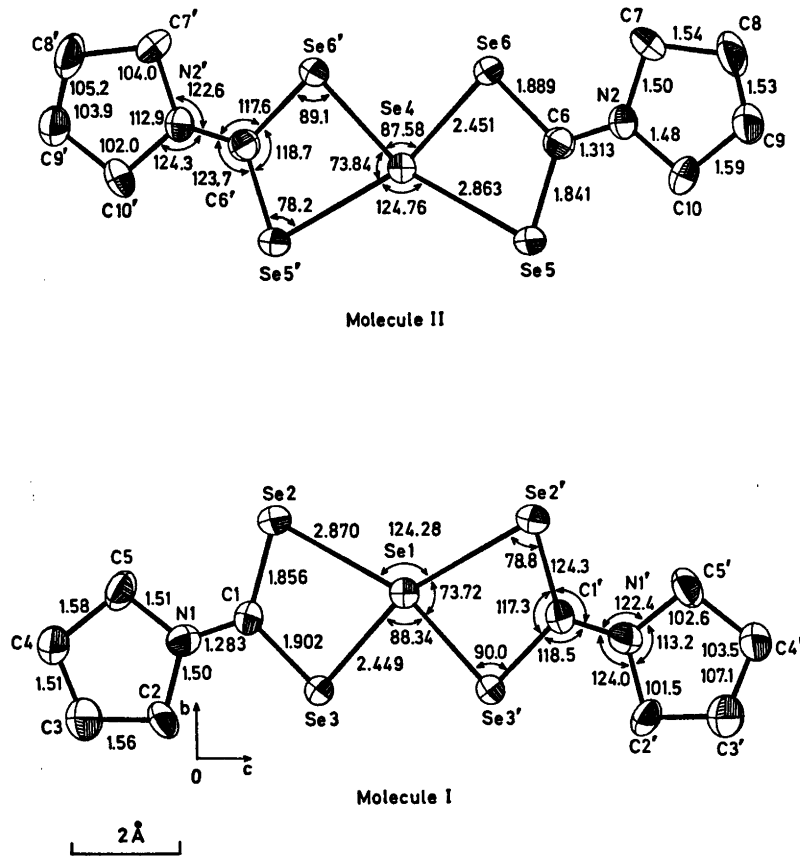

Fig. 1. The two types of molecules in the unit cell as seen along *a*. Molecule II has been moved one unit cell length along *b*, to prevent overlap with molecule I. Primed letters denote atoms in one half of the molecules, related to those in the asymmetric unit by the twofold symmetry axes parallel with *b* through Se1 and Se4. Distances are in Å and angles in degrees.

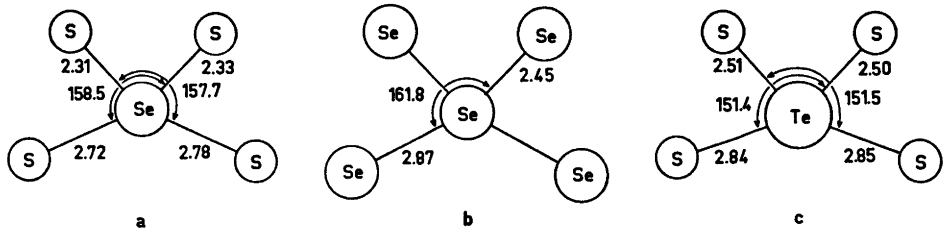

Fig. 2. The coordination around the central atoms in (a) selenium bis(diethyldithiocarbamate), (b) selenium bis(1-pyrrolidinecarbodiselenoate), and (c), tellurium di(methylxanthate). The bond lengths and angles in (b) are average values. All complexes are viewed along the normal to the least squares planes of the atoms shown. Bond lengths are in Å, angles in degrees.

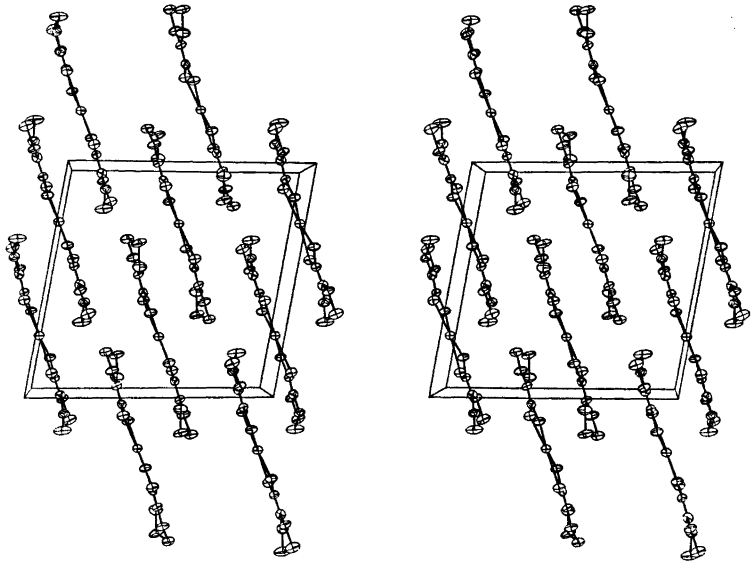

Fig. 3. The unit cell contents as seen along *b*. The *a* axis is horizontal, while *c* is represented by the nearly vertical edge (stereo drawing).

value of only 124.52(3)° in the present investigation. The corresponding angle is larger than 130° in the selenium dithiocarbamates,[2,3] and is found to have values up to 146° in analogous tellurium compounds.[1,5,8,9]

The asymmetry in the selenium-selenium bonds are reflected in the length of the selenium-carbon bonds. To a long selenium-selenium bond there corresponds a short selenium-carbon bond, and *vice versa*. For a short bond, the average length is 1.849(6) Å, for a long one, it is 1.896(6) Å. These values are not significantly different from those found in the diethyldiselenocarbamate of zink,[22] where there is asymmetry in the zink-selenium bonds, and they agree well with values found in other metal diselenocarbamates.[13,22,23,27] The bond lengths are intermediate between the values expected for carbon-selenium single (1.94 Å) and double (1.73 Å) bond lengths.

The average C...N bond length is found to be 1.30(1) Å in the present investigation. This corresponds to a π-bond order of 0.5 based on Paulings bond order/bond length relationship, with parameters used by Merlino.[38] The average π-bond orders for the short and long carbon-selenium bonds are 0.1 and 0.2. In the dithiocarbamates of divalent selenium and tellurium, the average π-bond order for the C...N bond is close to 0.3, while the averages for the short and long C–S bonds are close to 0.5 and 0.1, respectively. This may indicate that the resonance form 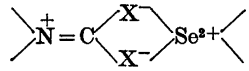 (X = S or Se) contributes more to the structure in a selenium(II) bis(dialkyldiselenocarbamate) than in selenium(II) and tellurium(II) bis(dialkyldithiocarbamates). As in the dithiocarbamates,[1] there is uneven contribution from resonance forms of the types 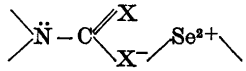 and 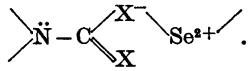 .

This increase in mesomeric shift of electron density from nitrogen to the ligand donor atoms may be part of the explanation why the structure found in the present investigation is that of a selenium(II) complex rather than that of a regular triselenide.

The angles on the CSe_2 carbon atoms and the nitrogen atoms correspond to sp^2 hybridization, in agreement with the suggested resonance forms. However, due to the strain in the pyrrolidine rings, the nitrogen ring angles are

small, only approximately 113°. The other ring angles and the bond lengths in the rings, have normal values.

In Fig. 3, the contents of a unit cell is shown as seen along the *b* axis. It can clearly be seen that the molecules are stacked nearly parallel to each other and that the molecular planes are nearly parallel with the *b* axis. The molecules are packed so that molecules of type I and II with a common *z* coordinate for their central selenium, are rotated about 180° relative to each other through a hypothetical axis lying along the length of each molecule. The central selenium atoms are not involved in any close contacts, but there are short intermolecular Se2···Se3 contacts between molecules of type I and Se5···Se6 contacts between molecules of type II. These contacts are 3.59 Å, which is considerably shorter than two times the van der Waals radius of selenium (4.00 Å). As a result, the molecules are connected into long chains parallel to the *b* axis by these weak Se···Se interactions. The intermolecular Se1–Se3···Se2 and Se4–Se5···Se6 angles are both close to 104°.

REFERENCES

1. Husebye, S. *Compounds of Divalent Selenium and Tellurium with Bidentate Ligands, Their Preparation, Structure and Bonding*, Diss., University of Bergen, Bergen 1969.
2. Husebye, S. and Helland-Madsen, G. *Acta Chem. Scand. 24* (1970) 2273.
3. Anderson, O. P. and Husebye, S. *Acta Chem. Scand. 24* (1970) 3141.
4. Brøndmo, N. J., Esperås, S. and Husebye, S. *Acta Chem. Scand. A 29* (1975) 93.
5. Graver, H. and Husebye, S. *Acta Chem. Scand. A 29* (1975) 14.
6. Husebye, S. and Helland-Madsen, G. *Acta Chem. Scand. 23* (1969) 1398.
7. Husebye, S. *Acta Chem. Scand. 19* (1965) 774.
8. Husebye, S. *Acta Chem. Scand. 24* (1970) 2198.
9. Fabiani, C., Spagna, R., Vaciago, A. and Zambonelli, L. *Acta Crystallogr. B 27* (1971) 1499.
10. Barnard, D. and Woodbridge, D. T. *J. Chem. Soc.* (1961) 2922.
11. Rosenbaum, A., Kirschberg, H. and Leibnitz, E. *J. Prakt. Chem. 19* (1963) 1.
12. Rosenbaum, A. *Chem. Abstr. 62* (1965) 7629h.
13. Bonamico, M. and Dessy, G. *Chem. Commun.* (1967) 1114.
14. Jensen, K. A. and Krishnan, V. *Acta Chem. Scand. 21* (1967) 2904.
15. Furlani, C., Cervone, E. and Diomedi Camassei, F. *Inorg. Chem. 7* (1968) 265.
16. Durgaprasad, G., Sathyanarayana, D. N. and Patel, C. C. *Can. J. Chem. 47* (1969) 631.
17. Kamitani, T., Yamamoto, H. and Tanaka, T. *J. Inorg. Nucl. Chem. 32* (1970) 2621.
18. Lorentz, B., Kirmse, R. and Hoyer, E. *Z. Anorg. Allg. Chem. 378* (1970) 144.
19. Shankaranarayana, M. L. *Acta Chem. Scand. 24* (1970) 351.
20. Jensen, K. A. and Krishnan, V. *Acta Chem. Scand. 24* (1970) 1088.
21. Shankaranarayana, M. L. *Acta Chem. Scand. 24* (1970) 2065.
22. Bonamico, M. and Dessy, G. *J. Chem. Soc. A (1971)* 264.
23. Beurskens, P. T. and Cras, J. A. *J. Cryst. Mol. Struct. 1* (1971) 63.
24. Jensen, K. A., Mynster Dahl, B., Nielsen, P. H. and Borch, G. *Acta Chem. Scand. 25* (1971) 2039.
25. *Organic Selenium Compounds*, Klayman, D. L. and Günther, W. H. J., Eds., Wiley, New York 1973. Chapters by (a) Shine, J. p. 294; (b) Jensen, K. A., Henriksen, L., and Nielsen, P. H., p. 835; (c) Karle, I. L. and Karle, J., p. 989; and (d) Jensen, K. A. and Jørgensen, C. K., p. 1017.
26. Kirmse, R. and Hoyer, E. *Z, Anorg. Allg. Chem. 401* (1973) 295.
27. Noordik, J. H. and Smits, J. M. M. *Cryst. Struct. Commun. 3* (1974) 253.
28. Throughton, P. G. H. *Siemens Rev. XXXVII* (1970), Fourth Special Issue, p. 9.
29. Sletten, J. *Acta Chem. Scand. 27* (1973) 229.
30. Coppens, P., Leiserowitz, L. and Rabinovich, D. *Acta Crystallogr. 18* (1965) 1035.
31. Shiono, R. *Normalized Structure Factors Program*, The Crystallography Laboratory, University of Pittsburgh, Pittsburgh 1966.
32. Main, P. and Woolfson, M. M., Department of Physics, University of York, England, and Germain, G., Laboratorie de Chimie Physique, Université de Leuven, Belgium. *Multan. A Computer Program for Automatic Solution of Crystal Structure*, Dept. of Physics, University of York, York 1971.
33. Germain, G., Main, P. and Woolfson, M. M. *Acta Crystallogr. A 27* (1971) 368.
34. *International Tables for X-Ray Crystallography*, Kynoch Press, Birmingham 1962, Vol. III, p. 204.
35. Cromer, D. T. *Acta Crystallogr. 18* (1965) 17.
36. Hauge, S. *Acta Chem. Scand. 25* (1971) 1134.
37. Hauge, S., Opedal, D. and Aarskog, J. *Acta Chem. Scand. 24* (1970) 1107.
38. Merlino, S. *Acta Crystallogr. B 24* (1968) 1441.

Received February 10, 1975.

Acta Chemica Scandinavica A 29 (1975) 615—622

On the Standard Potential of the Cr(III)—Cr(II) Couple in 1 M NaCl Medium

GEORGE BIEDERMANN and VINCENZO ROMANO *

Department of Inorganic Chemistry, The Royal Institute of Technology, 100 44 Stockholm 70, Sweden

The standard potential for $Cr(III)+e^- \rightleftharpoons Cr(II)$ in the medium 1 M NaCl at 25 °C has been determined; it is -429 ± 1 mV. The data are summarized in Table 1.

Experimental conditions facilitating the employment of the Cr(III) – Cr(II) couple for equilibrium analysis are described in some detail.

This communication summarizes the results of our efforts to find a convenient approach for the study of equilibria in which Cr(III) ions participate by the measurement of the potential of the Cr(III) – Cr(II) couple. The approach has been tested by the determination of the standard potential of this couple in 1 M NaCl medium.

The serious difficulties, encountered when classical methods of preparation, analysis, and emf measurements are applied, may probably be regarded as the main reason that only two systematic attempts seem to have been made to ascertain the magnitude of the Cr(III) – Cr(II) standard potential.

Benefiting from the experience gained by Mazzuchelli [1] in his exploratory work of 1905, Forbes and Richter [2] developed in 1917 an anaerobic technique to prepare solutions of precisely known chromium(II) chloride and chromium(III) chloride content as well as to determine the emf of the cell

$$Hg \mid Cr_t \mid 0.1\ M\ HCl \mid 0.1\ M\ HCl \mid Hg_2Cl_2(s), Hg$$

where Cr_t is the chromium test solution containing 0.1 M HCl. Although due to the initially rapid decomposition of the Cr(II) ions 30 – 40 h were required to attain a constant emf value and a substantial correction had to be introduced for the loss of Cr(II), Forbes and Richter presented evidence [2] for the reversibility of the Cr(III), Cr(II)/Hg half-cell. One can calculate on the basis of their data, comprising the $[Cr(II)][Cr(III)]^{-1}$ range 0.1 to 4.7, a value of -402 ± 5 mV for the standard potential.

Forbes' and Richter's work was extended by Grube and Schlecht,[3] who in 1926 studied at 18 °C the Cr(III) – Cr(II) couple in chloride, sulfate, and acetate solutions. Their conclusions [3] corroborate the results of the previous investigators. Two main complications arose. The log $[H^+]$ range available for the measurements is narrow; at high acidities the chromium(II) ions become rapidly oxidized by H^+ while at low hydrogen ion concentrations the sluggish hydrolysis of Cr(III) must be taken into account. Moreover, the complex formation equilibria of the chromium(III) ions are attained at room temperature so slowly that emf measurements of long duration are required which can be interpreted only if the concurrent oxidation of Cr(II) is prevented throughout.

METHOD OF INVESTIGATION

The experimental approach which has proved to be practical for the $Eu^{3+} - Eu^{2+}$ couple [4,5] has been mainly followed.

We started each series of experiments with a solution of the general *composition*

B Cr(III), H_0 H^+, $(1.000\ M - 3B - H_0)Na^+$, 1.000 M Cl^-

* Present address: Department of General and Inorganic Chemistry, University of Palermo, Palermo, Italy.

which will be denoted in the following discussion by S_0, while the solution arising from S_0 by electrolytic reduction will be represented by S.

The B range 5 to 28 mM has been investigated. In more dilute solutions difficulties were encountered. When, *e.g.*, in a 1 mM test solution the surface of the mercury redox electrode was renewed (see later), the redox potential was found to increase at a diminishing rate for about an hour and then became practically constant. Its starting value was in accord with the data obtained in the higher B range but the steady state value indicated that, because of the accumulation of impurities, the ratio $[Cr(II)][Cr(III)]^{-1}$ was considerably lower in the vicinity of the electrode than in the bulk solution.

With the available current supply the study of more concentrated solutions would require an unpractically long experiment.

In each case, the starting value for the proton excess, H_0, was chosen to equal B. As we have not been able to suppress entirely the reaction

$$Cr(II) + H^+ \rightarrow Cr(III) + 1/2\ H_2 \qquad (1)$$

the hydrogen ion concentration of the test solution, h, diminished slowly in the course of a series of measurements. As glass electrode data indicated, in no case did the value of h drop below 0.1 mM, however. Coulometric alkalification experiments afforded evidence that under the present conditions the hydrolysis of Cr(III) is negligible for $\log h > -4$.

In order to minimize the variation of the activity factors of the reacting species, all the test solutions were made to contain 1 M Cl^- by the addition of NaCl. The standard state has been defined so that the activity factors of the reacting species tend to unity as the composition of the solution tends to 1 M NaCl.

Our attempts to study the $Cr^{3+} - Cr^{2+}$ couple in perchlorate media, which was our original intention, have failed. As soon as an appreciable amount of Cr^{2+} had been generated, the reaction

$$8\ Cr^{2+} + ClO_4^- + 8H^+ \rightarrow 8Cr^{3+} + 4H_2O + Cl^- \qquad (2)$$

started to proceed and within a short time the hydrogen ion concentration decreased so much in the vicinity of the cathode that some chromium(III) hydroxide precipitated.

We have not been able to prepare chloride-free chromium(II) perchlorate solutions by chemical methods either; reduction with the amalgams of zinc and of cadmium, and dissolution of chromium metal of spectrographic purity in perchloric acid were tried.

The *electrolytic generation* of Cr(II) ions was carried out in the circuit

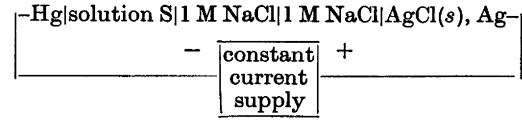

The current supply was synchronized with a digital counter and throughout the electrolysis the current strength was recorded each minute. The number of moles of electrons introduced into S at cathodic reduction, μ, is believed to possess an uncertainty of less than 0.01 %.

Following an electrolysis step a certain period of time was found to be required for the attainment of a steady state.

An excess of Cr(II) ions is built up in the vicinity of the cathode during the electrolysis; its decline was followed by measuring the emf between the cathode pool and one of the other two mercury electrodes placed in the diametrically opposed receptacles of the measuring vessel. Generally about 15 min were needed to reach a uniform concentration throughout the test solution. At this stage each of the mercury electrodes should exhibit the same value for the redox potential and any further variation should be explainable on the basis of reaction (1). This condition entails the validity of the equation

$$[Cr(II)] = \mu/V - (H_0 - h) \qquad (3)$$

where V represents the volume of the test solution and μ the moles of electrons introduced at cathodic reduction. An additional complication has arisen at the highest B levels studied and in the experiments where part of the Cr(II) ions were reoxidized electrolytically. In these cases the redox potential of the test solution was found to change monotonically for a period covering in some instances as much as 12 h, while the hydrogen ion concentration varied only slightly. As the trend in the redox

potential had opposite signs in the reduction and in the oxidation experiments, we ascribe the drift to the slow attainment of the chloride complex formation equilibria which become displaced by electrolysis.

All the data considered for the evaluation of the standard redox potential correspond to the steady state and satisfy eqn (3).

The instantaneous value of *the hydrogen ion concentration, h*, in the chromium test solutions was measured by determining the emf of the cell

$$-\text{glass electrode}|\text{S}|\text{RE}+;$$
$$\text{RE} = |1\text{ M NaCl}|1\text{ M NaCl}|\text{AgCl}(s), \text{Ag} \qquad \text{(G)}$$

The emf of this cell at 25 °C may be expressed by

$$E_G = e_{RE} - e_{G,0} - 59.16 \log h + e_j \qquad (4)$$

In eqn. (4) e_{RE} represents the potential of the reference half-cell RE, e_j is the symbol for the liquid junction potential arising between S and 1 M NaCl and $e_{G,0}$ denotes a term remaining constant in a series of measurements but, due to the uncontrollable changes slowly occurring in the surface layer of the glass electrode, its magnitude has to be determined in each experiment.

For the estimation of *the liquid junction potential*, e_j, the emf of the cell

$$\text{H}_2 \;\; \left| h\text{H}^+, (1.000\text{ M} - h)\text{Na}^+, 1.000\text{ M Cl}^- \right| \text{RE}+ \qquad \text{(H)}$$
glass

was determined as a function of h in the range 0.01 to 0.06 M. The data can be described to within 0.1 mV by the simple equation

$$e_j = (66 \pm 1)h$$

Incidentally these measurements indicated that under the present experimental conditions the glass electrode may be regarded to be equivalent with the hydrogen half-cell to within a few hundreths of a mV.

Assuming a concentration distribution of the Henderson type, this liquid junction potential can be estimated with the conductance values of 1 M HCl and 1 M NaCl solutions as well as with the relevant transport numbers, all taken from Ref. 6, to $e_j = 59.16 \log (1 + 2.87_5 h)$. For the low h values in question this equation may be simplified to $e_j = 74h$. The deviation from the data may be explained by our approximation that the conductance of HCl–NaCl mixtures of 1 M Cl^- is a linear function of the conductances of 1 M HCl and 1 M NaCl solutions.

The potential of the reference half-cell, e_{RE}, was evaluated at regular intervals by measuring the emf of cell (H) with a solution containing 10.00 mM H^+. In accordance with our choice of standard state the potential of the hydrogen half-cell is given by $59.16 \log h p_{H_2}^{-\frac{1}{2}}$.

During the six months when the final measurements were carried out, e_{RE} proved to change by but 0.2 mV, from 235.4 to 235.2 mV, thus no appreciable contamination occurred in RE.

A check on this e_{RE} value may be obtained by recalling that on the scale of the conventional activity factors — reference state 1 M ideal solution in the solvent water — our e_{RE} value equals $e^0(\text{AgCl,Ag}) - 118.32 \log \gamma_{HCl}^{trace}$, where $e^0(\text{AgCl,Ag}) = 222.3_5 \pm 0.1$ mV [7] denotes the standard potential of the Cl^-, AgCl/Ag half-cell, and γ_{HCl}^{trace} is the symbol for the trace activity factor of hydrochloric acid in 1 M NaCl. Neglecting the difference between volume and weight molarities we may take Harned's value [8] for $\log \gamma_{HCl}^{trace}$ (1 m NaCl) $= -0.12_4$, thus e_{RE} can be estimated to be 237.0 mV. The deviation, about 2 mV, may be ascribed to the lattice imperfections in our silver electrodes which were prepared by electrolysis. Another reason might be the difference in the bromide contamination levels.

To obtain the actual value of $e_{G,0}$ the emf of cell (G) was measured in each experiment prior to the generation of Cr(II) ions, thus with $h = H_0$.

The *redox potential* of the Cr(III) – Cr(II) couple was determined by measuring the emf of the cell

$$-\text{Hg}|\text{S}|\text{RE}+ \qquad \text{(R)}$$

Provided that the chloride complex formation equilibria had been reestablished in S after an electrolysis step, the emf of cell (R) may be expressed by the equation

$$E_R = e_{RE} - e_{R,0} - 59.16 \log \frac{[\text{Cr(III)}]}{[\text{Cr(II)}]} + e_j \qquad (5)$$

where $e_{R,0}$ represents the standard potential whose magnitude is sought. As the total chromium concentration was always less than 3 % of the total molarity, the ratio [Cr(III)] ×

$[Cr(II)]^{-1}$ differs from $[Cr^{3+}][Cr^{2+}]^{-1}$ by the constant factor $(1+\sum\beta_n')(1+\sum\beta_n)^{-1}$ where β_n and β_n' denote the formation constants of the n chloride bearing chromium(III) and chromium(II) complex species.

According to eqns. (3) and (5) each pair of simultaneous E_R, E_G data obtained in the steady state, when only reaction (1) proceeds, furnishes a value for $e_{R,0}$

$$e_{R,0} = e_{RE} - Er + e_j - 59.16 \log [(B - \mu/V + H_0 - h)/(\mu/V - H_0 + h)] \quad (6)$$

EXPERIMENTAL

Materials and analysis

Chromium(III) chloride stock solutions were prepared by dissolving chromium pellets, free from spectrographically detectable impurities (supplied by Johnson, Matthey & Co., London), in a small excess of freshly distilled azeotropic hydrochloric acid. At the initial stage some hydrogen sulfide was found to evolve. Probably all the sulfur impurity could be flushed out, however, as H_2S by the vigorous stream of hydrogen generated throughout the dissolution.

The chromium content of the stock solutions, always kept at around 0.1 M, was determined iodometrically after having transformed Cr(III) to Cr(VI) with a hot alkaline hydrogen peroxide solution. The proton excess of the stock, also made to have a value of around 0.1 M, was determined potentiometrically with a glass electrode by coulometric alkalification.

Dust and basic impurities (mainly carbonate ions) were removed from commercial *sodium chloride* batches of *p. a.* quality by preparing first a saturated solution, filtering it through sintered glass and then precipitating at 0 °C by hydrogen chloride finely divided NaCl crystals. The crystals were dried and finally ignited at 360 °C. In an effort to keep bacterial and other contamination at a minimum, the test solutions were prepared *in situ* by introducing into the cell vessel first the chromium stock, then a weighed amount of NaCl and finally the required volume of water. The volume of the test solution was chosen to have a value between 75.0 and 100.0 ml.

Nitrogen was taken from a cylinder and freed from oxygen by passing it in succession through a column of activated copper kept at 170 °C, distilled water, 1 M NaCl, and two solutions containing 0.1 M $CrCl_2$ and 0.8 M NaCl maintained in intimate contact with amalgamated zinc grains. In the last stage of purification the gas stream was lead through sintered glass of porosity G4 to remove floating dust.

To check the purity of this nitrogen, the gas was in the course of a series of emf measurements allowed to build up a small overpressure over the test solution and then the gas stream was stopped. After a period of several hours, while the electrolysis and the emf measurements were continued, the nitrogen flow was reestablished at atmospheric pressure. In no case, even with solutions containing 0.1 mM Cr(II), was the extinguishment or the reintroduction of nitrogen found to cause an appreciable change in the emf value.

Mercury was purified, as usual in this laboratory, by double distillation at a partial pressure of oxygen just insufficient to give rise to the formation of HgO. Dust and other impurities gathering on the surface during preservation were eliminated by filtration through sintered glass immediately before use.

To estimate the trace amount of *oxidizing agents* left in our test solutions, coulometric redox titrations were made with a low current strength, *e.g.* 0.5 mA. It was then observed that while the current was passed for several minutes, E_R remained constant at the starting value of around -20 to -30 mV and then a dramatic increase in E_R ensued. The assumption that the moles of electrons needed to be introduced at cathodic reduction to achieve a monotonic increase in E_R equals the equivalents of oxidizing impurities present, yields a contamination level of 20 μM. As the emf of the cell $-Ag,AgCl(s)|1\ M\ NaCl|Hg_2Cl_2(s),Hg+$ has the value of 45.4 mV [9] and this is not far from the $-E_R$ value found with the Cr(II)-free starting solutions, the contaminant consists probably of calomel not removable from the mercury through simple filtration. For the high B values studied in the present work this amount of impurities may be regarded as negligible.

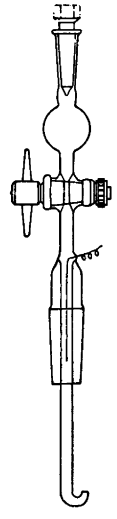

Fig. 1a. Mercury electrode for measurement of the redox potential. The stopcock is made from self-lubricating teflon.

Electrodes and apparatus

In each experiment three *mercury electrodes* were employed. The first, forming a pool in the central receptacle of the vessel, served as the cathode, while the other two were inserted to measure the redox potential of the test solution. One of them was similar to the cathode while the second is illustrated in Fig. 1a. This electrode was designed to make possible the convenient renewal of the mercury surface, the overflow gathered in a receptacle. To avoid contamination with grease a teflon stopcock was built into the electrode vessel.

In the initial stage of every series of measurements all the three electrodes yielded coincident redox potential values, indicating the establishment of a steady state in the test solution. As the experiment proceeded, the electrodes having a stationary surface, the cathode, and the stationary pool, gave emf values increasingly lower than the emf value measured with a fresh mercury surface. At the end of some experiments of several days duration a difference as great as 5 mV was found. Obviously the surface of the stationary electrodes became slowly covered by substances, such as particles originating from filter paper and other dust, catalyzing the oxidation of Cr(II) by H^+. As a consequence in the layers adjacent to the stationary electrode surfaces the ratio $[Cr(II)][Cr(III)]^{-1}$ was smaller than in the bulk.

The emf values measured with the stationary electrodes were ignored as unreliable and for all the $e_{R,0}$ calculations the emf value obtained with a fresh surface was accepted, provided it was found reproducible to within 0.1 mV. In each experiment this degree of reproducibility could be easily attained as soon as the chloride complex formation equilibria had been reestablished after an electrolysis step; the data of Fig. 1b show some typical results.

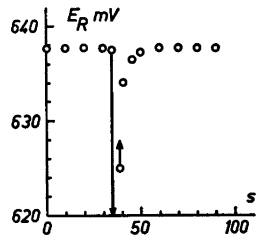

Fig. 1b. Effect of the renewal of mercury surface on the redox potential; E_R as a function of time. The electrode was flushed in the 35th second. The test solution contained 0.72 mM Cr(II), 1.24 mM Cr(III), and 1.75 mM H^+. The E_R *versus* time data were obtained automatically by programming a digital voltmeter to take a reading each second, for clarity only a few points selected at random are shown.

Glass electrodes of Thalamid type supplied by Schott & Gen., Mainz, were used throughout this work. In the acidity range of interest they have often been compared and found to be equivalent to within 0.1 mV with the hydrogen half-cell.

Platinum nets of 2×2 cm size coated cathodically by a thick layer of silver crystals served as electrodes in the coulometric circuit. For each series of emf measurements two Ag,AgCl electrodes, also prepared by electrolysis and covered by a thin AgCl layer, were employed, the emf between them was never found to exceed 0.1 mV.

The cell arrangement and other experimental equipment were similar to that described in a preceding communication of this laboratory.[5]

The experiments were carried out automatically with the programmable data acquisition system constructed for precision potentiometry by Dr. Tom Wallin and one of the present authors. The E_R and E_G data possess a precision of 0.1 mV, the number of ampere-seconds passed through the test solution were measured with an uncertainty not exceeding 0.01 %.

Current levels between 0.5 and 5 mA were chosen, depending on the chromium concentration. Following an electrolysis step, both E_R and E_G were measured at 1 min intervals for at least an hour after the establishment of the steady state. Moreover, in every series of experiments two or three measurement intervals of 12 h duration were inserted. A complete set of measurements took a minimum of three days. The significance of these details is discussed in the Results section.

RESULTS

The standard potential values deduced from the final series of measurements, in which a number of precautions were taken to attain a high precision, are summarized in Table 1. This covers the chromium concentration (and consequently also the approximate hydrogen ion concentration) levels 5, 10, 22, and 27 mM; at each level the ratio $[Cr(III)][Cr(II)]^{-1}$ is seen to have been made to vary considerably, the extreme values being 7 and 0.2.

The data presented in Table 1 appear to afford evidence for the validity of our basic assumptions expressed by eqns. (3) and (5) as the $e_{R,0}$ values do not show appreciable systematic trend with any of the main experimental variables: the total chromium concentration, the ratio $[Cr(III)][Cr(II)]^{-1}$, and the acidity.

To put this conclusion, which represents the

Table 1. Survey of results.

h mM	[Cr(II)] mM	[Cr(III)] mM	$-e_{R,0}$ mV	h mM	[Cr(II)] mM	[Cr(III)] mM	$-e_{R,0}$ mV
28.05	8.81	17.9	428.8	10.64	5.55	4.53	428.1
27.72	9.63	17.1	429.7	10.60	6.30	3.78	428.2
27.60	11.8	14.9	429.7	10.56	7.10	2.99	428.5
27.60	13.2	13.5	429.9	10.28	7.65	2.43	430.5
27.07	16.1	10.6	430.2*	10.32	8.12	1.97	429.6
27.07	13.8	12.9	428.9*	10.16	8.38	1.70	431.0
24.11	2.99	19.3	429.4	9.85	8.18	1.90	428.8*
23.92	2.80	19.4	430.6	9.25	7.80	2.28	429.8*
23.46	4.52	17.7	430.2	10.73	2.69	7.39	431.5
23.38	4.45	17.8	429.6	10.73	3.50	6.58	430.7
22.48	5.74	16.5	431.3	10.16	5.36	4.72	429.5
22.13	7.59	14.7	431.0	10.16	6.16	3.92	428.6
21.87	9.52	12.7	430.5	10.00	6.81	3.27	429.1
21.62	11.5	10.8	431.1	4.96	1.43	3.33	430.0
21.29	13.3	8.90	431.7	4.54	1.83	2.93	429.0
10.89	1.81	8.27	427.9	4.04	2.14	2.62	428.8
10.84	2.24	7.84	427.9	3.62	2.54	2.23	429.0
10.76	2.64	7.44	428.5	3.13	2.87	1.90	428.4
10.76	3.13	6.96	428.4	2.89	3.00	1.76	427.6
10.64	3.80	6.28	428.8	2.71	3.07	1.70	427.8
10.64	4.28	5.80	429.0	1.97	3.25	1.51	428.3
10.64	4.76	5.32	428.1				

chief result of this work, into quantitative terms we may compare the grand average of all the 43 points $e_{R,0} = -429.4$ mV with particular averages. The set of data corresponding to the four chromium concentration levels studied yield the $-e_{R,0}$ values: 429.5 mV (27 mM), 430.6 mV (22 mM), 429.1 mV (10 mM) and 428.6 mV (5 mM). The 23 data found with solutions of $[Cr(III)][Cr(II)]^{-1} > 1$ furnish the average $e_{R,0} = -429.5$ mV, while the 20 points with $[Cr(III)][Cr(II)]^{-1} < 1$ $e_{R,0} = -429.2$ mV. We would therefore propose as the most probable value

$$e_{R,0} = -429.5 \pm 1 \text{ mV}$$

The experiments in which chromium(III) ions were anodically generated in a prereduced solution provide additional support for this estimate. These oxidation experiments, marked with an asterisk in Table 1, are seen to yield $e_{R,0}$ values agreeing closely with the others. Thus we may have little doubt that the potential measured with a fresh mercury surface may be regarded as reversible.

Our value for the standard potential has thus been found to be about 30 mV more negative than the estimates which can be derived on the basis of the work of the previous investigators [2,3] who studied dilute chromium solutions containing some hydrochloric acid. As the formation constants of the chromium(III) chloride complex species are not yet ascertained, the medium effect on the standard potential cannot be exactly calculated.

The following arguments suggest, however, that our result is in accordance with the conclusion of the classical investigators. Ignoring the activity factor variations and neglecting complex formation in the dilute solutions of Forbes [2] and of Grube [3], the assumption $[Cr(II)] = [Cr^{2+}]$ leads to the relationship. -429.5 (standard potential in 1 M NaCl medium) $= -400$ (standard potential in dilute chromium chloride solution) $-59.16 \log (1 + \sum \beta_n)$ where β_n denotes the formation constant of $CrCl_n^{(3-n)+}$. Hence we obtain for $\log (1 + \sum \beta_n)$ a value of around 0.5. This conjecture falls within the limits of the widely different estimates [10] reported for the β_n's.

Finally we have to discuss *the time requirement* for the performance of a complete series of emf measurements.

The E_R data of Table 1 represent the steady state in which exclusively reaction (1) was

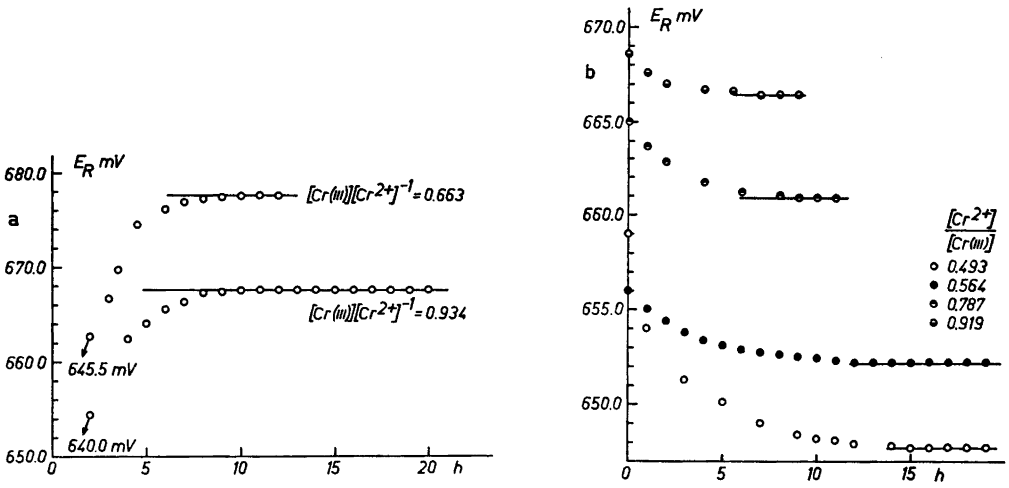

Fig. 2. Illustration of slow equilibration ensuing (a) the generation of Cr(III) ions and (b) the generation of Cr(II) ions; E_R as a function of the time elapsed after the termination of the electrolysis. In each experiment the total chromium concentration was kept at 26.69 mM. The horizontal lines represent the emf values corresponding to the attainment of the complex formation and dissociation equilibria. The emf values below the arrows in Fig. 2a were taken a few seconds after the completion of the oxidation.

found to occur. After each step of electrolysis both E_R and E_G were recorded at least for an hour. Moreover, to test whether the chloride complex formation equilibria were really attained, the reduction was often interrupted for 12 to 20 h but the $e_{R,0}$ value always proved to remain constant to within 0.2 – 0.3 mV. Such long interruptions have a detrimental effect on the precision of the standard potential evaluation since it now involves the unavoidable drift of the glass electrode. A considerable part of the spread in the $e_{R,0}$ values of Table 1 may be ascribed to this source of uncertainty.

Periods exceeding one hour were needed for the attainment of the steady state only in the oxidation experiments and in the reduction steps at the 27 and 22 mM chromium levels with points corresponding to a low $[Cr(II)] \times [Cr(III)]^{-1}$ value. As the generation of Cr(II) proceeded, and the ratio $[Cr(II)][Cr(III)]^{-1}$ approached unity even at these high concentrations the steady state was found to be reached within an hour.

The sluggish equilibration ensuing Cr(III) generation is illustrated in Fig. 2a, while the time dependence of E_R in some typical reduction experiments is shown in Fig. 2b. No appreciable variation in E_G could be detected in the course of these measurements.

We may then conclude that for equilibrium analysis it is practical to build up a $[Cr(II)] \times [Cr(III)]^{-1}$ ratio of around unity before introducing the ligand.

When this and the other precautions described earlier in this work are strictly kept, our experience indicates that for experiments of a duration not exceeding about 12 h the parasitic reaction $Cr^{2+} + H^+ \rightarrow Cr^{3+} + \frac{1}{2}H_2$ may be neglected. Thus complex formation equilibria between Cr(III) and some weak acids might also become accessible to an experimental study with the Cr(III) – Cr(II) couple.

Acknowledgements. We are indebted to Docent Derek Lewis and Dr. Tom Wallin for valuable discussions. We would also like to express our appreciation to our friends Messrs Jan Johansson, Sture Lind and Bo Surtén who constructed and maintained many parts of our equipment.

The present work was financially supported by the Italian National Research Council (Consiglio Nazionale delle Ricerche) and by the Swedish Natural Science Research Council (Statens Naturvetenskapliga Forskningsråd).

REFERENCES

1. Mazzuchelli, A. *Gazz. Chim. Ital. 35* (1905) 417.
2. Forbes, G. S. and Richter, H. W. *J. Amer. Chem. Soc. 39* (1917) 1140.
3. Grube, G. and Schlecht, L. *Z. Elektrochem. 32* (1926) 178.
4. Biedermann, G. and Terjošin, G. *Acta Chem. Scand. 23* (1969) 1896.
5. Biedermann, G. and Silber, H. G. *Acta Chem. Scand. 27* (1973) 3761.
6. Landolt-Börnstein Zahlenwerte und Funktionen, Sechste Auflage, II Band, 7. Teil, Springer Berlin 1960.
7. Bates, R. G. and Bower, V. E. *J. Res. Nat. Bur. Stand. 53* (1954) 283.
8. Harned, H. S. *J. Amer. Chem. Soc. 57* (1935) 1865.
9. Gerke, R. H. *J. Amer. Chem. Soc. 44* (1922) 1684.
10. *Stability Constants of Metal-Ion Complexes*, Compiled by Sillén, L. G. and Martell, A. E., Special Publication No. 17 and No. 25, The Chemical Society, London 1964 and 1970.

Received January 7, 1975.

Acta Chemica Scandinavica A 29 (1975) 623—631

On the Crystal Structures of TiS_3, ZrS_3, $ZrSe_3$, $ZrTe_3$, HfS_3, and $HfSe_3$

SIGRID FURUSETH, LEIF BRATTÅS and ARNE KJEKSHUS

Kjemisk Institutt, Universitetet i Oslo, Blindern, Oslo 3, Norway

Structure determinations of TiS_3, ZrS_3, $ZrSe_3$, $ZrTe_3$, HfS_3, and $HfSe_3$ on the basis of three-dimensional single crystal X-ray data have revealed that the $ZrSe_3$ type structure occurs in two variants, here termed A and B. Variant A matches the earlier found $ZrSe_3$ type, whereas variant B corresponds to a kind of mirror image. Kinetic factors associated with the crystal growth are believed to be responsible for the occurrence of these two variants.

The trichalcogenides of titanium, zirconium, hafnium, thorium, and uranium are believed to be isostructural with $ZrSe_3$, whereas various assignments of this structure type to niobium and tantalum trichalcogenides have proved to be incorrect (*cf. e.g.*, Refs. 1 – 4 and references therein). Except for $ZrSe_3$, the compounds have been classified structurally on the basis of similarities in their X-ray powder patterns. Proper structure determinations of compounds which have previously been only superficially classified need not necessarily be a trivial task, and the present work on the structures of TiS_3, ZrS_3, $ZrSe_3$, $ZrTe_3$, HfS_3, and $HfSe_3$ may serve as an example of this.

EXPERIMENTAL

Single crystals of TiS_3, ZrS_3, $ZrSe_3$, $ZrTe_3$, HfS_3, $HfSe_3$, and $HfTe_3$ were prepared earlier by means of chemical transport reactions.[4] A new compound $TiSe_3$ was prepared similarly [from 99.99 % Ti (A. D. Mackay) and 99.998 % Se (Bolidens Gruvaktiebolag)], using ~350 °C for the cold point and 100 to 150 °C for the temperature difference between the hot and cold regions. Details specifying relevant characteristics for the crystals subject to this study are recorded in Table 1.

Single crystal X-ray data for each compound were collected photographically, using the Weissenberg technique and Zr-filtered Mo$K\alpha$-radiation. The $TiSe_3$ and $HfTe_3$ crystals obtained so far, have proved to be unsuitable for structure determinations. For the other compounds, three-dimensional intensity data were obtained from integrated Weissenberg films. The intensities were measured microphotometrically except for the weakest reflections, which were estimated visually.

A supplementary set of data for TiS_3 was collected with an automatic Picker diffractometer. The $\omega - 2\theta$ scan technique was utilized at a scan speed of 1° min^{-1} up to $\sin\theta/\lambda = 0.8$. The background was measured at each of the scan range limits. The intensities of three selected test reflections, measured for every 50th reflection during the data collection, demonstrated a systematic variation which was corrected for in the sets of observed intensities. A graphite crystal was used for monochromatization, the scan range was $2\theta(\alpha_1) - 0.9$ to $2\theta(\alpha_2) + 0.9°$, and the background was measured for 30 s on each side of the reflections. Reflections with $I_{net.} \leqq 1.5\sigma(I)$ were regarded as unobserved.

As is evident from Table 1, needle shaped crystals are characteristic for compounds belonging to the $ZrSe_3$ family. The monoclinic b axis is always oriented along the needle axis. The actual shapes of the crystals were evaluated with the aid of an optical goniometer in combination with a travelling microscope. Apart from two cases (see Table 1), absorption corrections were carried out in accordance with the actual crystal shapes. (No corrections for dispersion and secondary extinctions were performed.)

The computational work, including corrections, data reductions, scalings, Patterson- and Fourier-syntheses, full matrix least squares refinements of the structure factors, and calculations of interatomic distances and angles was carried out using programmes of Groth.[5]

Atomic scattering factors were taken from

Table 1. Specifications of single crystal specimens (for abreviations A, B, and Tw see text). Data were recorded on Weissenberg films.

Compound [a]	No. of crystals tested	Crystal type (% occurrence)	Crystal dimensions (mm)	Crystal shape for absorption correction	Total No. of reflections (unobserved)	No. of reflections for least squares refinement
TiS_3	8	B(~90 %),Tw(~10 %)	0.010×0.030×0.95 0.015×0.040×0.80 [b]	Cylindrical As observed [b]	382(139) 654(327) [b]	243 316 [b]
ZrS_3	12	A(~85 %),Tw(~15 %)	0.012×0.033×1.87	As observed	604(250)	353
$ZrSe_3$	13	A(~90 %),Tw(~10 %)	See Ref. 1			
$ZrTe_3$	10	B(~90 %),Tw(~10 %)	0.020×0.020×0.305	As observed	622(290)	322
HfS_3	14	A(~90 %),Tw(~10 %)	0.009×0.025×0.294	Cylindrical	581(143)	425
$HfSe_3$	15	B(~70 %),A(~15 %), Tw(~15%)	0.008×0.032×0.312	As observed	593(192)	400

[a] $TiSe_3$ and $HfTe_3$ were unsuitable for structure determination. [b] Data recorded with diffractometer (counter).

Hanson *et al.*[6] Anisotropic thermal motion of the atoms was allowed for according to the expression $\exp[-(\beta_{11}h^2+\beta_{22}k^2+\beta_{33}l^2+\beta_{12}hk+\beta_{13}hl+\beta_{23}kl)]$. The extent of agreement between the observed and calculated structure factor data is judged from the average and weighted reliability factors $R=\sum||F_o|-|F_c||/\sum|F_o|$ and $R^*=[\sum w(|F_o|-|F_c|)^2/\sum w|F_o|^2]^{\frac{1}{2}}$ where w denotes the weight factor. (The observed and calculated structure factor data are available from the authors upon request.)

RESULTS

(i) *Homogeneity ranges and compositions.* Phase analyses by visual and microscopic inspection, X-ray diffraction, and density measurements, as well as chemical analyses of suitable single crystal specimens, have unequivocally showed (*cf.* Ref. 4) that all compounds subject to this study obtain the stoichiometric 1:3 composition without appreciable ranges of homogeneity. The question of non-stoichiometry and homogeneity ranges has been considered for the zirconium and hafnium trichalcogenides in a recent paper by Jellinek *et al.*[7]; they conclude that chalcogen-deficiency (*viz.* TX_{3-x}; where T=Ti, Zr, or Hf, X=S, Se, or Te, and $x>0$) seems likely for these compounds. The inferences of Jellinek *et al.* are apparently based on results reported in Refs. 8 and 9. McTaggart and Wadsley's [8] work cannot be taken as a support for this view, since they state that "there is little chemical evidence to suggest that the trichalcogenides are anything but stoichiometric". Schairer and Shafer,[9] on the other hand, explicitly state that ZrS_3 and HfS_3 both take "a rather large range of stoichiometry (*i.e.* metal-sulfur ratios)". Their deductions are based on quantitative analyses of single crystal specimens of the two compounds, grown under different thermal conditions (by chemical transport reactions). A large number of single crystal batches for most of the compounds subject to this study have been obtained under a variety of different thermal conditions. Careful examinations of these have invariably confirmed a stoichiometric $TX_{3.00\pm0.04}$ composition, where the error limits are imposed by the inherent uncertainties of the experimental techniques.

The unit cell dimensions of the Ti, Zr, and Hf trichalcogenides (as determined by least squares refinements of Guinier powder photographic data) are listed in Table 2. These, together with the observed densities,[4] show that the unit cell content is 2 TX_3 groups for

Table 2. Unit cell dimensions for compounds with the $ZrSe_3$ type structure (variants A and B); values are quoted from Ref. 4.

Compound	a (Å)	b (Å)	c (Å)	β (°)
TiS_3	4.958(2)	3.4006(11)	8.778(4)	97.32(4)
ZrS_3	5.1243(11)	3.6244(10)	8.980(3)	97.28(2)
$ZrSe_3$	5.4109(12)	3.7488(9)	9.444(2)	97.48(2)
$ZrTe_3$	5.8939(14)	3.9259(12)	10.100(2)	97.82(2)
HfS_3	5.0923(11)	3.5952(7)	8.967(2)	97.38(2)
$HfSe_3$	5.388(2)	3.7216(10)	9.428(3)	97.78(3)
$HfTe_3$	5.879(2)	3.9022(9)	10.056(3)	97.98(3)

all compounds.

(ii) *Structure determinations.* The only systematic extinctions in the diffraction data for all crystals subject to this study are of the type $0k0$ absent when $k=2n+1$, leaving a choice between $P2$, $P2_1$, Pm, $P2/m$, and $P2_1/m$ for the space group. In accordance with the results of Krönert and Plieth [1] for $ZrSe_3$, the correct space group proved to be $P2_1/m$.

The clear-cut relationships in composition, crystal shapes, unit cell dimensions, X-ray powder diffraction intensity data, and space group suggested very strongly that all the group IV A trichalcogenides are isostructural with $ZrSe_3$.[1] HfS_3 was more or less arbitrarily chosen as the first object for examination in this programme. The results for this compound (Table 3) indeed confirmed that it adopts the assumed $ZrSe_3$ type structure. This finding further reinforced our presentiments of a plain and unchallenging research programme merely designed to provide values for interatomic distances and angles.

Already the next member of the family studied, TiS_3, gave unexpected results, which forced us to change attitude. The first set of film data for this compound lead to a structure which, although definitely related to that of $ZrSe_3$, differs in such fundamental aspects that the designation isostructural no longer applies. As a consequence, it was considered to be worthwhile to undertake a complete re-examination (by Fourier and difference syntheses as well as numerous least squares refinements starting from different initial coordinates) of the photographic data set, and finally, to collect a set of diffractometer data for another crystal. Evaluation of these data confirmed our earlier findings.

The subsequent structure determinations of ZrS_3, $ZrTe_3$, and $HfSe_3$ showed ZrS_3 to be isostructural with $ZrSe_3$, whereas $ZrTe_3$ and the first sample crystals of $HfSe_3$ turned out to be isostructural with TiS_3. Later on, another crystal of $HfSe_3$ was found that proved to be isostructural with $ZrSe_3$.

The final positional and thermal parameters for the various compounds subject to this study are listed in Table 3. Only the parameters deduced from the diffractometer data are given for TiS_3, and only values for one of the variants of $HfSe_3$.

(iii) *Twinning.* As previously documented,[1,8,10–14] twinning is frequently encountered among these TX_3 crystals. A number of crystals of each compound were examined in order to find a rough estimate for the fraction of twins (tw, see Table 1). It should be pointed out that the actual figures are unreliable since the number of crystals tested is very small. Moreover, only crystals with apparently perfect external shape and of suitable size for single crystal X-ray work were tested. On the background of Krönert and Plieth's [1] suggestions regarding the origin of the twin formation, care was taken to avoid mechanical disturbance of the crystal specimens prior to the X-ray diffraction experiments.

In close connection with the twinning phenomenon comes the observation of two variants of the $ZrSe_3$ type structure. As is evident from Table 1, a certain set of experimental conditions for a given compound results mainly in either the $ZrSe_3$ or TiS_3 form

Table 3. Positional and thermal parameters for compounds with A and B variants of the $ZrSe_3$ type structure. Space group $P2_1/m$, all atoms in position 2(*e*).

Variant		A		B			
Compound		ZrS_3	$ZrSe_3$[a]	HfS_3	TiS_3	$ZrTe_3$	$HfSe_3$
	x	0.2837(3)	0.285	0.2839(2)	0.7152(8)	0.7069(6)	0.7145(3)
	z	0.6553(2)	0.656	0.6548(1)	0.6528(3)	0.6660(4)	0.6563(2)
	β_{11}	0.0033(5)		0.0023(3)	0.0164(18)	0.0084(10)	0.0032(4)
T	β_{22}	0.0065(4)	$B=0.45$ Å^2	0.0062(3)	0.0065(14)	0.0164(8)	0.0006(3)
	β_{33}	0.0014(2)		0.0013(1)	0.0016(4)	0.0046(4)	0.0004(1)
	β_{13}	−0.0016(4)		0.0004(2)	−0.0078(14)	−0.0051(10)	−0.0061(3)
	x	0.7631(7)	0.762	0.7611(2)	0.2392(10)	0.2391(4)	0.2370(7)
	z	0.5543(4)	0.554	0.5546(7)	0.5505(5)	0.5561(3)	0.5533(4)
	β_{11}	0.0007(9)		0.0010(15)	0.0164(24)	0.0034(6)	0.0040(8)
X_I	β_{22}	0.0026(8)		0.0027(14)	0.0084(20)	0.0003(4)	0.0022(7)
	β_{33}	0.0012(3)	$B=0.45$ Å^2	0.0003(5)	0.0022(5)	0.0004(2)	0.0015(3)
	β_{13}	0.0002(8)		−0.0019(14)	−0.0104(16)	−0.0053(5)	−0.0090(9)
	x	0.4725(8)	0.456	0.4642(13)	0.5320(11)	0.5661(4)	0.5455(8)
	z	0.1716(5)	0.174	0.1702(8)	0.1762(5)	0.1676(3)	0.1733(5)
	β_{11}	0.0052(11)		0.0015(16)	0.0238(26)	0.0002(6)	0.0080(11)
X_{II}	β_{22}	0.0061(10)		0.0101(15)	0.0142(20)	0.0059(10)	0.0122(10)
	β_{33}	0.0004(3)	$B=0.45$ Å^2	0.0034(7)	0.0019(5)	0.0026(2)	0.0022(4)
	β_{13}	0.0014(11)		−0.0018(16)	−0.0081(18)	−0.0028(6)	−0.0036(10)
	x	0.8799(7)	0.888	0.8768(13)	0.1205(11)	0.0963(5)	0.1113(7)
	z	0.1699(4)	0.169	0.1697(7)	0.1737(5)	0.1616(3)	0.1673(4)
	β_{11}	0.0013(9)		0.0009(16)	0.0239(24)	0.0075(7)	0.0070(10)
X_{III}	β_{22}	0.0002(8)		0.0051(15)	0.0120(20)	0.0107(6)	0.0050(10)
	β_{33}	0.0005(3)	$B=0.45$ Å^2	0.0016(6)	0.0016(5)	0.0022(2)	0.0019(3)
	β_{13}	−0.0007(9)		0.0013(14)	−0.0121(18)	−0.0081(7)	−0.0101(10)
R		0.076	0.11	0.066	0.070	0.057	0.073
R^*		0.101	–	0.088	0.074	0.076	0.096

[a] Quoted from Krönert and Plieth.[1]

(termed the A and B variants, respectively, in Table 1 and the discussion) admixed with twins. Once again, much significance cannot be placed on the actual percentage figure given. In fact a systematic search for both of the variants was only carried out for $HfSe_3$, and even in this case the search was terminated when the less common A form had been detected for two crystals.

DISCUSSION

For description of the $ZrSe_3$ structure, reference is made to, *e.g.*, Refs. 1, 3, and 4; presently determined interatomic distances and angles (calculated from the unit cell dimensions in Table 2, and the positional parameters in Table 3) being given in Table 4.

The two variants of the $ZrSe_3$ type structure have so far been referred to as the TiS_3 and $ZrSe_3$ types. This nomenclature may serve to distract attention from the main subject by coupling the distinction to concrete members of the $ZrSe_3$ family. The atomic arrangements for both variants are illustrated in Fig. 1, using HfS_3 and $ZrTe_3$ as examples. On comparing A and B of this diagram, it is seen (neglecting the difference in scale) that the two arrangements are a kind of mirror image of each other. Thus, we adopt an alternative designation in the remainder of this paper in which the $ZrSe_3$ and TiS_3 variants are termed A and B, respectively.

Although the A and B variants are indeed almost mirror images, Fig. 1 shows that it is not a question of identity through transforma-

tion of the coordinate system. Examination of the positional parameters in Table 3 reveals that these obey the relations

$$x_A = 1 - x_B,\ y_A = y_B, \text{ and } z_A = z_B \quad (1)$$

to a very good approximation regardless of the actual compound chosen for comparison. The relations are found to hold even better for $HfSe_3$ where both variants have been examined. The results of conversion according to eqn. 1 is to simulate the behaviour of a mirror plane of symmetry parallel to (100) at $x = \frac{1}{2}$.

It is seen that the deviation of β from 90° (actually observed 97 – 98°, *cf.* Table 2) prevents perfect right/left hand identity relations between the A and B variants. This is also brought out in Fig. 2, which shows the connection between A and B in relation to the configuration of near X neighbours around a given T. The (say) A coordination polyhedron has been translated half a unit length in the direction of the a axis. Since the line connecting X_{II} and X_{III} is to a very good approximation parallel to [100], $X_{III,A}$ will then coincide with $X_{II,B}$, and similarly $X_{II,A}$ with $X_{III,B}$ in this diagram. Such an operation does not, on the other hand,

Table 4. Interatomic distances and angles in the structures of TiS_3, ZrS_3, $ZrSe_3$, $ZrTe_3$, HfS_3, and $HfSe_3$. Data referring to variant A are printed in italics.

Interatomic distances (Å) based on data from Tables 2 and 3 (quoted from Ref. 1 for $ZrSe_3$).

Compound	TiS_3	*ZrS_3*	*$ZrSe_3$*	$ZrTe_3$	*HfS_3*	$HfSe_3$
2 $T-X_I$	2.496(4)	*2.602(3)*	*2.71$_7$*	3.030(4)	*2.588(4)*	2.752(3)
1 $T-X_I$	2.416(6)	*2.724(4)*	*2.87$_0$*	2.829(4)	*2.697(6)*	2.624(4)
1 $T-X_I$	2.855(6)	*2.707(4)*	*2.86$_8$*	3.467(4)	*2.698(6)*	3.100(4)
2 $T-X_{II}$	2.667(4)	*2.602(3)*	*2.73$_3$*	3.163(3)	*2.612(5)*	2.935(4)
2 $T-X_{III}$	2.358(4)	*2.605(3)*	*2.74$_3$*	2.771(3)	*2.590(4)*	2.586(3)
$T-X$ average	2.539	*2.631*	*2.76$_6$*	3.028	*2.622*	2.784
$T-X$ scattering	0.497	*0.122*	*0.15$_3$*	0.696	*0.110*	0.514
2 $T-X_m$	2.302(4)	*2.384(3)*	*2.47$_4$*	2.634(3)	*2.379(4)*	2.508(3)
1 $X_{II}-X_{III}$	2.038(7)	*2.090(5)*	*2.34$_4$*	2.761(3)	*2.102(8)*	2.333(5)
$T-X_I$[a]	4.171(3)	*4.534(2)*	*4.72$_1$*	4.839(2)	*4.494(3)*	4.554(2)
$X_{II}-X_{III}$[a]	2.921(7)	*3.035(5)*	*3.06$_7$*	3.134(3)	*2.991(8)*	3.057(5)
$T-T$[a]	3.631(4)	*4.189(2)*	*3.74$_9$*	4.338(5)	*4.166(1)*	3.956(2)

[a] Shortest interatomic distance neglected as bonding.

Interatomic distances (Å) based on data from Tables 2 and 3 (quoted from Ref. 1 for $ZrSe_3$), but with positional parameters transformed according to eqn. 1.

Compound	*TiS_3*	ZrS_3	$ZrSe_3$	*$ZrTe_3$*	HfS_3	*$HfSe_3$*
2 $T-X_I$	*2.454(4)*	2.646(3)	2.76$_5$	*2.965(4)*	2.631(4)	*2.701(3)*
1 $T-X_I$	*2.630(6)*	2.509(4)	2.63$_5$	*3.110(4)*	2.480(6)	*2.870(4)*
1 $T-X_I$	*2.639(6)*	2.925(4)	3.10$_6$	*3.182(4)*	2.917(6)	*2.851(4)*
2 $T-X_{II}$	*2.486(4)*	2.785(3)	2.94$_0$	*2.921(3)*	2.803(5)	*2.720(3)*
2 $T-X_{III}$	*2.488(4)*	2.473(3)	2.59$_2$	*2.963(3)*	2.459(4)	*2.745(3)*
$T-X$ average	*2.516*	2.655	2.79$_2$	*2.999*	2.648	*2.757*
$T-X$ scattering	*0.185*	0.452	0.51$_4$	*0.219*	0.458	*0.169*
2 $T-X_m$	*2.267(3)*	2.418(3)	2.51$_4$	*2.594(3)*	2.418(4)	*2.467(3)*
1 $X_{II}-X_{III}$	*2.043(7)*	2.086(5)	2.33$_2$	*2.778(3)*	2.101(8)	*2.348(5)*
$T-X_I$[a]	*4.299(3)*	4.408(2)	4.58$_2$	*5.008(2)*	4.368(3)	*4.700(2)*
$X_{II}-X_{III}$[a]	*2.915(7)*	3.039(5)	3.08$_0$	*3.117(3)*	2.992(8)	*3.041(5)*
$T-T$[a]	*4.012(4)*	3.796(2)	3.97$_8$	*4.824(5)*	3.770(1)	*4.397(2)*

[a] Shortest interatomic distance neglected as bonding.

Table 4. Continued.

Interatomic angles (°) based on data from Tables 2 and 3 (quoted from Ref. 1 for $ZrSe_3$).

Compound		TiS_3	*ZrS_3*	*$ZrSe_3$*	$ZrTe_3$	*HfS_3*	$HfSe_3$
1	$T-X_I-T$	85.88(15)	*88.29(12)*	*87.3*	80.76(10)	*87.98(17)*	85.07(11)
2	$T-X_I-T$	113.20(15)	*103.83(10)*	*103.9*	115.33(9)	*103.49(16)*	113.79(10)
2	$T-X_I-T$	95.31(16)	*103.68(10)*	*104.0*	95.48(10)	*104.01(16)*	94.71(10)
1	$T-X_I-T$	140.19(20)	*141.30(15)*	*141.1*	138.63(15)	*141.42(22)*	140.41(15)
1	$T-X_{II}-T$	79.20(14)	*88.30(13)*	*86.9*	76.73(8)	*86.98(20)*	78.69(11)
2	$X_{III}-X_{II}-T$	58.32(15)	*66.41(11)*	*64.9*	55.29(8)	*65.63(18)*	57.44(10)
1	$T-X_{III}-T$	92.31(17)	*88.17(11)*	*86.2*	90.19(12)	*87.90(19)*	92.04(12)
2	$X_{II}-X_{III}-T$	74.33(18)	*66.26(11)*	*64.4*	69.73(9)	*66.72(19)*	73.07(12)
1	$T-X_m-T$	95.24(18)	*98.94(13)*	*98.5*	96.38(14)	*98.14(23)*	95.79(13)
2	$X_{II}-X_m-T$	99.56(18)	*89.91(15)*	*89.7*	99.19(14)	*90.65(20)*	99.49(12)
2	$X_{III}-X_m-T$	80.45(18)	*90.09(15)*	*90.3*	80.82(14)	*89.35(20)*	80.51(12)
1	X_I-T-X_I	85.88(13)	*88.29(10)*	*87.3*	80.76(11)	*87.98(12)*	85.07(9)
1	X_I-T-X_I	140.19(17)	*141.30(13)*	*141.1*	138.63(16)	*141.42(16)*	140.41(13)
2	X_I-T-X_{II}	93.33(10)	*86.58(9)*	*87.0*	95.95(6)	*87.06(15)*	93.62(8)
2	X_I-T-X_{III}	85.14(12)	*86.80(8)*	*87.8*	85.94(7)	*87.33(14)*	85.05(9)
1	$X_{II}-T-X_{II}$	79.20(12)	*88.30(10)*	*86.6*	76.73(9)	*86.98(15)*	78.69(8)
2	$X_{II}-T-X_{III}$	47.35(15)	*47.33(10)*	*50.7*	54.99(8)	*47.66(17)*	49.49(10)
1	$X_{III}-T-X_{III}$	92.31(15)	*88.17(9)*	*86.2*	90.19(13)	*87.90(14)*	92.04(10)
1	X_m-T-X_m	95.24(18)	*98.94(14)*	*98.5*	96.38(13)	*98.14(23)*	95.79(13)

Interatomic angles (°) based on data from Tables 2 and 3 (quotes from Ref. 1 for $ZrSe_3$), but with positional parameters transformed according to eqn. 1.

Compound		*TiS_3*	ZrS_3	$ZrSe_3$	*$ZrTe_3$*	HfS_3	*$HfSe_3$*
1	$T-X_I-T$	*87.70(15)*	86.47(11)	85.4	*82.91(11)*	86.21(16)	*87.09(12)*
2	$T-X_I-T$	*104.06(16)*	112.90(10)	113.3	*105.26(9)*	112.74(15)	*104.03(10)*
2	$T-X_I-T$	*104.17(16)*	94.84(10)	94.9	*105.13(9)*	95.02(16)	*104.19(10)*
1	$T-X_I-T$	*140.48(20)*	141.07(15)	140.8	*139.06(14)*	141.16(22)	*140.69(15)*
1	$T-X_{II}-T$	*86.33(16)*	81.21(11)	79.2	*84.45(10)*	79.78(17)	*86.35(13)*
2	$X_{III}-X_{II}-T$	*65.81(16)*	58.98(11)	57.5	*62.60(8)*	58.10(17)	*65.10(11)*
1	$T-X_{III}-T$	*86.22(16)*	94.23(13)	92.6	*82.98(10)*	93.95(21)	*85.38(11)*
2	$X_{II}-X_{III}-T$	*65.68(16)*	74.75(12)	73.1	*61.06(8)*	75.41(20)	*64.01(11)*
1	$T-X_m-T$	*97.17(18)*	97.08(13)	96.4	*98.38(14)*	96.03(22)	*97.92(13)*
2	$X_{II}-X_m-T$	*89.92(18)*	99.33(12)	99.4	*89.01(14)*	100.26(20)	*89.33(12)*
2	$X_{III}-X_m-T$	*90.08(18)*	80.67(12)	80.6	*90.99(14)*	79.74(20)	*90.67(12)*
1	X_I-T-X_I	*87.70(13)*	86.47(9)	85.4	*82.91(12)*	86.21(12)	*87.09(10)*
1	X_I-T-X_I	*140.48(17)*	141.07(13)	140.8	*139.07(16)*	141.16(17)	*140.69(13)*
2	X_I-T-X_{II}	*87.58(11)*	92.23(8)	93.1	*89.11(7)*	92.84(13)	*87.24(10)*
2	X_I-T-X_{III}	*87.97(11)*	84.01(9)	84.7	*89.75(7)*	84.54(14)	*88.23(8)*
1	$X_{II}-T-X_{II}$	*86.33(14)*	81.21(9)	79.2	*84.45(11)*	79.78(12)	*86.35(10)*
2	$X_{II}-T-X_{III}$	*48.51(15)*	46.28(10)	49.4	*56.34(8)*	46.49(17)	*50.89(10)*
1	$X_{III}-T-X_{III}$	*86.22(14)*	94.23(10)	92.6	*82.98(11)*	93.95(15)	*85.38(9)*
1	X_m-T-X_m	*97.17(18)*	97.08(13)	96.4	*98.38(14)*	96.03(22)	*97.92(13)*

bring T_A and T_B or $X_{I,A}$ and $X_{I,B}$ to even partial coincidence.

Fig. 2 also serves to illustrate that variant B has a considerably higher irregularity in the coordination polyhedron than the A variant. Consultation of Table 4 shows that the distinction between the two variants in this respect concerns mainly the scattering of the interatomic $T-X$ distances, whereas the average $T-X$ distances hardly are affected on turning

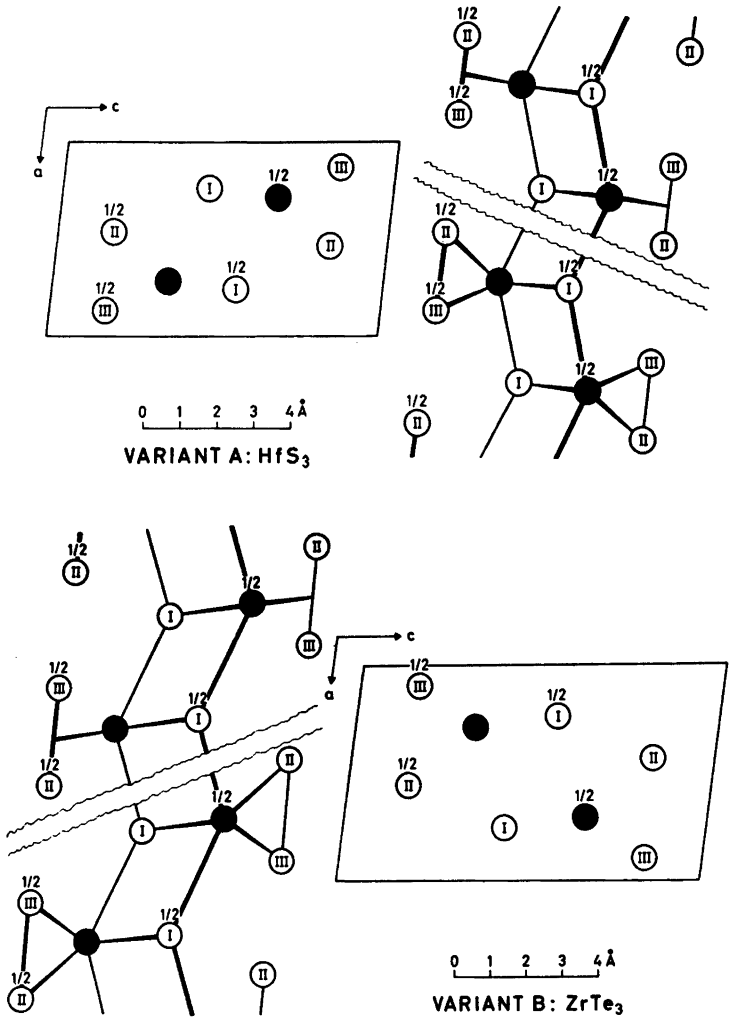

Fig. 1. Variants A and B of the $ZrSe_3$ type structure shown in (010) projection, illustrated by data obtained for HfS_3 and $HfTe_3$, respectively. Numbers give fractions of projection axis, origin being shifted to $0,\frac{1}{4},0$. Filled and open circles represent metal (T) and non-metal (X) atoms, respectively. Possible bonding paths between atoms or pairs of atoms are indicated on the right and left hand sides of the diagrams.

from the one variant to the other. As seen from Fig. 2, the irregularity of the B variant is directly related to the fact that the quasi mirror-plane relating A and B in the superimposed model intersects the line connecting X_{II} and X_{III} at an oblique angle. In the A variant, T and X_I lie approximately in the plane perpendicular to the $X_{II}-X_{III}$ pair through its mid-point X_m. Since the said perpendicular plane and the quasi mirror-plane do not coincide, this can no longer hold for the B coordination polyhedron. It should be emphasized that this merely serves to rationalize the relations between the A and B coordination polyhedra, but does not provide an explanation of the higher irregularity of the latter.

The "symmetry" relations between the A and B variants also lead to a working hypothesis for the mechanism governing the occurrence of two so closely related modifications. Since the

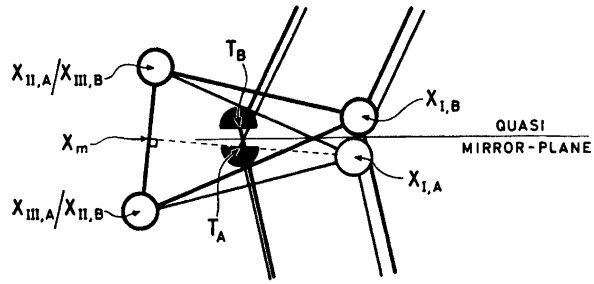

Fig. 2. Configurations of near X neighbours around T in variant A and B; superimposed to emphasize the quasi mirror-plane relationship between them.

crystals of the $ZrSe_3$ family are grown from the vapour phase (see Experimental) where kinetic factors are known to play an important role, it is natural to couple the formation of the A and B modifications to kinetics. The free energy of the two variants must be rather similar (but by no means equal) as evinced by the practically identical average values for the bonding interatomic distances (Table 4) in each case. Growth spirals (believed to be among the key factors in crystal growth) can be either right or left handed. It seems natural to associate one of the variants with a right handed growth spiral and the other with a left handed. In order to explain why this process does not lead to a corresponding rearrangement of the unit cell in relation to the coordination polyhedron, the initial crystal nuclei ought to be replicas. However, soon after nucleation the growth step occurs which initiates and determines the A/B individuality of the crystal. Experimental data over and above those available at present appear to be needed in order to resolve this problem. The future considerations should also aim at incorporating into the same model the apparently related occurrence of twinning.

All attempts [1,3,4,7] to describe the bonding situation in compounds of the $ZrSe_3$ family start with the configuration of eight near X atoms around each T. In Refs. 3 and 4 the generalized (8−N) rule is utilized to give an overall picture. Although details concerning the actual bonds do not enter into these considerations, each of the eight X atoms is apprehended as ligands bonded directly to the central T atom in a configuration described as a distorted bicapped trigonal prism. The arrangement of the bonds according to this approach is illustrated in the bottom right and left parts of Fig. 1, and the nature of all bonds is tentatively assumed to be of σ character. Jellinek *et al.*[7] have recently proposed an alternative model for the bonding in these compounds according to which each of the $X_{II}-X_{III}$ pairs is regarded as bonded to T as a single ligand. As depicted in the upper right and left parts of Fig. 1 the resulting coordination polyhedra around the central T atoms could then be described as distorted octahedra. Molecular orbitals of π symmetry on the $X_{II}-X_{III}$ fragments must in this case be considered as being used in bonding to d_π orbitals on T.

In the most extreme versions, the two models are clearly incompatible, and it is therefore appropriate at this stage to discuss their individual *pro et contra*:

(1) The assumption [1,3,4] of essentially σ bonds for $T-X_{II}$, $T-X_{III}$, and $X_{II}-X_{III}$ leads to a concentration of the valence electrons in a very restricted area of space, as evident from Fig. 1 and from the narrow interatomic angles ($X_{II}-T-X_{III}$, $T-X_{II}-X_{III}$, and $T-X_{III}-X_{II}$) listed in Table 4. This apparent disadvantage of the model in Refs. 1, 3, and 4 is clearly corrected for in the Jellinek *et al.* $X_{II}-X_{III}$ pair bonded model.

(2) Crystals with the (most symmetric) A variant of the $ZrSe_3$ type structure do not show any consistent and clear-cut distinction between the bonding interatomic distances $T-X_I$, $T-X_{II}$, and $T-X_{III}$ (Table 4). With a distinctly different bonding situation for $T-X_I$ and $T-X_m$ the model of Jellinek *et al.* seems to offer no reliable explanation for this conformity in interatomic distances. The consistent trend in the observations for the whole series of compounds can certainly not be attributed to accidental circumstances.

(3) The fact that the $ZrSe_3$ type structure

occurs in two variants appears to be indifferent to the choice between the above bonding models.

(4) The X-ray photoelectron spectra of ZrS_3 and $ZrSe_3$ and their interpretation by Jellinek *et al.* do not provide an unambiguous criterion for a choice between the two bonding models. The reason for this conclusion stems from the fact that both of the models agree on $X_{II}-X_{III}$ pairs with internal bonding, the dispute concerns only the connection between T and the $X_{II}-X_{III}$ fragment.

To summarize the situation, we conclude that both models have attractive features. It is therefore tempting to suggest their combination to a unified model, which perhaps does not make such a clear-cut distinction between symmetry and spatial location of the valence electrons. Moreover, bonding interactions resulting from effective charges may also be of importance. As an outline for future work it may be of value to perform a comparative analysis of all structures containing internally bonded non-metal pairs. Accumulation of more experimental data for the compounds belonging to the $ZrSe_3$ family will also be of utmost importance.

REFERENCES

1. Krönert, W. and Plieth, K. *Z. Anorg. Allg. Chem. 336 (1965)* 207.
2. Selte, K., Bjerkelund, E. and Kjekshus, A. *J. Less-Common Metals 11* (1966) 14.
3. Hulliger, F. *Struct. Bonding (Berlin) 4* (1968) 83.
4. Brattås, L. and Kjekshus, A. *Acta Chem. Scand. 26* (1972) 3441.
5. Groth, P. *Acta Chem. Scand. 27* (1973) 1837.
6. Hanson, H. P., Herman, F., Lea, J. D. and Skillman, S. *Acta Crystallogr. 17* (1964) 1040.
7. Jellinek, F., Pollak, R. A. and Shafer, M. W. *Mater. Res. Bull. 9* (1974) 845.
8. McTaggart, F. K. and Wadsley, A. D. *Aust. J. Chem. 11* (1958) 445.
9. Schairer, W. and Shafer, M. W. *Phys. Status Solidi A 17* (1973) 181.
10. Hahn, H. and Harder, B. *Z. Anorg. Allg. Chem. 288* (1956) 241.
11. Hahn, H. and Ness, P. *Naturwissenschaften 44* (1957) 534.
12. Hahn, H., Harder, B., Mutschke, U. and Ness, P. *Z. Anorg. Allg. Chem. 292* (1957) 82.
13. Hahn, H. and Ness, P. *Z. Anorg. Allg. Chem. 302* (1959) 37, 136.
14. Jellinek, F. *Ark. Kemi 20* (1963) 447.

Received January 27, 1975.

Acta Chemica Scandinavica A 29 (1975) 632—636

Furfuryl Alcohol. Part 1. A Near-infrared Study of the Self- and Heteroassociation of Furfuryl Alcohol in Carbon Tetrachloride

LIISA STRANDMAN

Department of Physical Chemistry, University of Helsinki, Meritullinkatu 1, SF-00170 Helsinki 17, Finland

Self-association of furfuryl alcohol in dilute carbon tetrachloride and cyclohexane solutions was studied by the near-infrared spectrometric method. The tendency of the alcohol to undergo self-association was found to be somewhat less than that of the ordinary simple alcohols. No signs of intramolecular hydrogen bonding could be detected. The heteroassociation of furfuryl alcohol with tetrahydrofuran, acetone, dimethyl sulfoxide, hexamethylphosphoramide, and pyridine was studied. Formation constants, frequency shifts, and thermodynamic parameters are given for these systems. The proton donor strength of furfuryl alcohol was found to be of about the same magnitude as that of the ordinary simple alcohols. The measurements were carried out at five different temperatures. The frequency shifts were found to depend only slightly upon the concentration of the base.

Relatively little is known about the association, complex formation, and molecular vibrations of the industrially important alcohol, furfuryl alcohol (FOH). The present paper is the first one in a series of papers that will deal with the properties of this alcohol. A study of the infrared, matrix infrared, and Raman spectra of furfuryl alcohol is in progress, and for this purpose some knowledge of the intramolecular hydrogen bonding as well as of the proton donor strength of this alcohol will be of value.

EXPERIMENTAL

Chemicals. Furfuryl alcohol (*purissimum* grade, Fluka AG.) was first dried with anhydrous $MgSO_4$ and then distilled under reduced pressure through a 20 cm Vigreux column. The product, a colourless liquid with a refractive index of $n_D^{25} = 1.483$, was stored under nitrogen gas atmosphere. Carbon tetrachloride (spectroscopic grade "Uvasol", E. Merck AG.) was dried with and stored over molecular sieve beads (4A from The British Drug Houses Ltd.). Cyclohexane (spectroscopic grade, E. Merck AG.) was treated with sodium wire and distilled through a 20 cm Vigreux column. The product was stored over molecular sieves. The remaining compounds, all commercially available, were carefully purified by distillation, except dimethyl sulfoxide which was purified by crystallization. The physical constants were checked against those reported in the literature.

Spectrophotometric measurements. The measurements were carried out with a Beckman DK-2A Ratio Recording Spectrophotometer. The scanning region was that of the fundamental OH vibration, from 3100 to 2700 nm. Quartz cells of type 110-QI (Hellma, Müllheim/Baden) with path lengths of 1 to 50 mm were used in pairs of equal path length. In most cases the recordings were first made at 25 °C, then at the other temperatures, and finally a second time at 25 °C to ascertain whether evaporation had occurred. The temperature varied within a few tenths of a degree during a single measurement. The spectrophotometer was purged with nitrogen at a rate of about 25 l/h to prevent moisture from condensing on the cell windows. Each series of measurements was started by scanning a zero absorbance baseline over the region in question. The concentrations were corrected for the variation in density of carbon tetrachloride with temperature. Only carbon tetrachloride (or cyclohexane) was in the reference cell when the self-association was studied, whereas in the heteroassociation studies the reference sample was a base-carbon tetrachloride solution of the same concentration as in the sample studied.

Calculations. The monomer-dimer equilibrium constants for self-association K_c (M^{-1})

were calculated by the method of Liddel and Becker [2] from initial slopes of plots of the apparent molar absorption coefficient ε_m at the maximum of the monomer ν_{OH} absorbance against the concentration.

When calculating equilibrium constants for 1:1 complexes it was assumed that no higher complexes existed. Furthermore, the measurements were carried out at alcohol concentrations so dilute that self-association could be neglected. The equilibrium equation can be written as $A + B \rightleftharpoons AB$, where A indicates the proton donor (the alcohol), B the proton acceptor (the base), and AB the complex formed. The following symbols are used: c_A° = original concentration of the alcohol, c_B° = original concentration of the base, c_A and c_B = equilibrium concentrations of the alcohol and the base, respectively, A° and A = absorbance of the free hydroxyl group before and after the complex formation, ε = molar absorption coefficient of the alcohol, and b = path length. The equilibrium constant can then be written as $K = c_{AB}/c_A c_B$. In dilute solutions, activities can be replaced by the corresponding concentrations. Because $A^\circ = \varepsilon b c_A^\circ$, $A = \varepsilon b c_A$, and $c_{AB} = c_A^\circ - c_A$, the equilibrium constants can be expressed as

$$K = \frac{c_A^\circ - c_A}{c_A c_B} = \frac{A^\circ - A}{A[c_B^\circ - (c_A^\circ - c_A)]} = \frac{1 - A/A^\circ}{(A/A^\circ)[c_B^\circ - c_A^\circ(1 - A/A^\circ)]}$$

The complexation enthalpy ΔH is evaluated by plotting $\ln K$ as a function of $1/T$: $\ln K = -\Delta H/RT + \text{constant}$. $\Delta H \sim \Delta H^\circ$ can be calculated from the slope of the straight line. The equations for calculating ΔG° and ΔS° are $\Delta G^\circ = -RT \ln K$ and $\Delta S^\circ = (\Delta H^\circ - \Delta G^\circ)/T$.

The estimated uncertainty in the shifts $\Delta\nu$ is ± 2 cm^{-1}. The uncertainty limits of the association enthalpy ΔH are of the magnitude 4 – 15 %, the larger figure applying to the heteroassociation studies with tetrahydrofuran and acetone. The uncertainty of the equilibrium constant is about 5 – 10 %; also here the higher percentage relates to tetrahydrofuran and acetone.

RESULTS AND DISCUSSION

The self-association of furfuryl alcohol. Despite a number of investigations, no agreement about the self-association model of the alcohols has been reached. This is apparent in some of the more recent studies (Refs. 3 – 5). In most cases some average characteristic is measured and an attempt is made to accommodate the results obtained with the model considered. The advantage of the infrared method is that concentrations of different species, *i.e.* monomers, dimers, and higher associates, can be estimated. The main problem is why the dimers give lower $\Delta\nu$ values than the higher associates. There are two contradictory views: either the hydrogen bonds in dimers are extraordinarily weak and in the higher polymers normal, or the hydrogen bonds in the dimers are normal and in the higher associates unusually strong.[6]

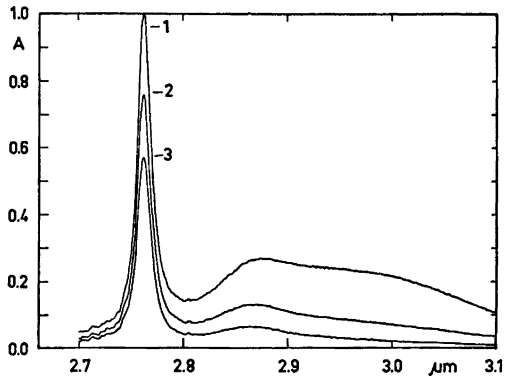

Fig. 1. Illustrative spectra of furfuryl alcohol (fundamental region of the ν_{OH} vibration) in CCl_4 at 25 °C. Concentrations (cell thickness 1 mm) 1. 0.151 M, 2. 0.103 M, 3. 0.072 M.

Fig. 1 presents spectra of furfuryl alcohol at different dilutions. No evidence of intramolecular hydrogen bonding can be seen in the plot. A possible explanation is that because the molecule as a whole is almost planar, the formation of a hydrogen bond between the π-electrons of the ring and the hydrogen in the OH group would lead to a strongly bent C – C bond. More surprising, however, is the fact that no hydrogen bonding to the ring oxygen is apparent. As can be seen in Fig. 2a, such hydrogen bonding would result in an energetically possible ring of five atoms. According to CNDO/2 and INDO calculations the *cis*- and *gauche*-rotamers seem to prevail over the *trans*-conformer (Fig. 2b).[23]

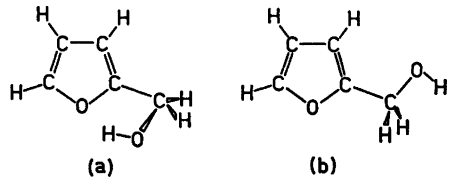

Fig. 2. Two conformers of furfuryl alcohol. (a), *gauche;* (*b*), *trans.*

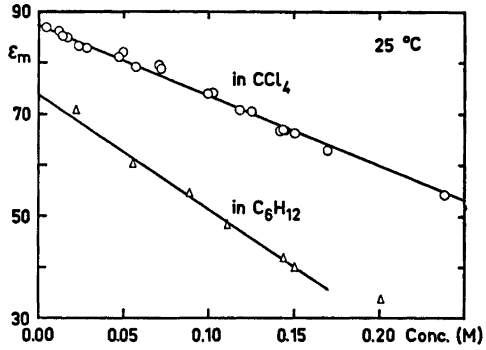

Fig. 3. A plot of the apparent molar absorption coefficient ε_m at the maximum of the monomer ν_{OH} absorbance against the concentration of the alcohol (no base present).

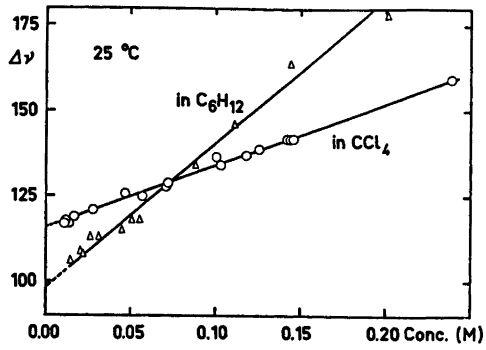

Fig. 4. A plot of the $\Delta\nu$ values of the alcohol dimer against the concentration of the alcohol.

These calculations imply that the interaction between the OH group and the ring oxygen is either very weak or does not exist. Thus the present author concludes that only intermolecular H-bonding can exist.

Calculations by Becker's method give the equilibrium dimerization constants K_2 (CCl_4) = 0.78 M^{-1} and K_2 (C_6H_{12}) = 1.43 M^{-1} for the self-association of furfuryl alcohol at 25 °C. The values of ε_m are plotted against the concentration in Fig. 3. These plots are linear within the limits of experimental accuracy up to concentrations as high as 0.25 M. The non-zero limiting values of the slopes imply that the dimer is stable.[2] Comparison with the literature values for ethanol in carbon tetrachloride solutions, *viz.*, $K = 0.89$ [7] or $K = 0.76$ [8] at 25 °C, shows that furfuryl alcohol may be slightly less associated than this most widely used reference alcohol. The values $K = 0.95$ [9] and $K = 0.64$ [10] at 25 °C have also been reported for the dimerization of ethanol, but the calculation method is not that of Becker and thus the results cannot be compared directly.

The absorption maximum between 2840 nm < λ < 2900 nm (Fig. 1) can be considered as the dimer absorption band. According to Murty,[5] alcohols and phenols generally give values of about 125 cm^{-1} for the monomer-dimer shift $\Delta\nu$. It is obvious that the absorption maximum at lower frequencies is due to the higher associates.

Table 1. Data on hydrogen bonding between furfuryl alcohol (FOH) and various bases in CCl_4 at 25 °C. Some literature values are included for comparison. THF = tetrahydrofuran, DMSO = dimethyl sulfoxide, and HMPA = hexamethylphosphoramide. The alcohol monomer absorbs at 3620 cm^{-1} (CCl_4, 25 °C).

System	$\Delta\nu$/cm^{-1}	K_{11}/M^{-1}	$-\Delta H°$ kJ mol^{-1}	$-\Delta G°$ kJ mol^{-1}	$-\Delta S°$ kJ mol^{-1} K^{-1}
FOH-THF	192	1.98	12.6	1.69	36.5
Phenol-THF[13]	285	13.6	16.7		
FOH-acetone	128	1.58	13.5	1.14	41.5
EtOH-acetone[14]	113	1.14	12.1		
Phenol-acetone[15]	193		13.8		
FOH-DMSO	244	15.2	18.1	6.83	37.7
Phenol-DMSO[16]	350 (20 °C)		33.4		
FOH-HMPA	310	58.3	20.2	10.04	34.0
EtOH-HMPA[17]	271	30.5	19.8		
Phenol-HMPA[17]			29.9		
FOH-pyridine	340	4.46	18.0	3.69	47.9
EtOH-pyridine[18]	276	2.41	15.3		
Phenol-pyridine[19]	492 (20 °C)		29.3		

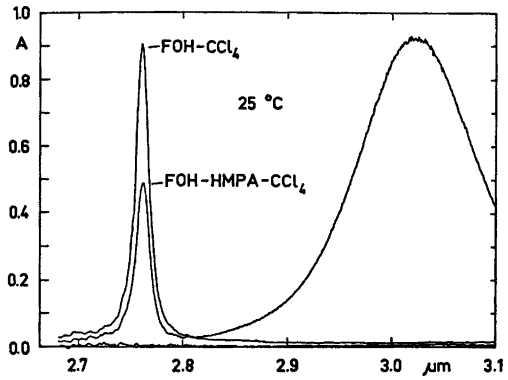

Fig. 5. A spectrum illustrating the contour of the absorption band in the heteroassociation studies. Alcohol concentration 0.0051 M and the concentration of HMPA 0.0170 M (cell thickness 20 mm).

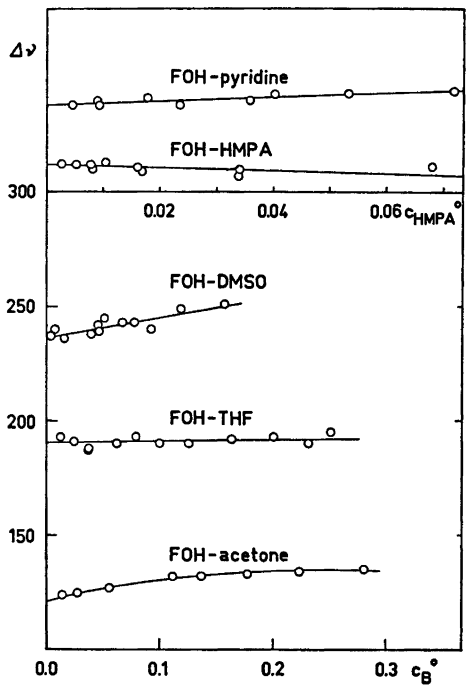

Fig. 6. Influence of the concentration of the base on $\Delta\nu$ of FOH – base complexes in CCl_4 at 25 °C.

The $\Delta\nu$ value of the dimer was found to vary with the alcohol concentration. The results are given in Fig. 4. Kivinen *et al.*[4] have presented a model for the association of alcohols in carbon tetrachloride solutions, which assumes the following sequence: monomer – cyclic dimer – open dimer – open trimer and/or higher linear associates – cyclic trimer and/or tetramer. If only the infrared results are available, it is difficult to say anything definite in this particular case about the structures of the associates. Some preliminary research has been done on the dielectric properties of furfuryl alcohol. In carbon tetrachloride solutions the Kirkwood-Fröhlich correlation factor g (Refs. 11 and 12) seems to exceed unity even in dilute solutions. That could imply a favourably parallel arrangement of the alcohol molecules and thus the linear structures even for dimers would be probable. $\Delta\nu$ (dim) in cyclohexane varies more with the concentration of the alcohol than $\Delta\nu$ (dim) in carbon tetrachloride. Moreover, the association is stronger in the former solvent than in the latter.

Table 2. Temperature dependence of the values of $\Delta\nu$ and $\partial\nu(\text{complex})/\partial T$.

System	T / °C	$\Delta\nu$ / cm^{-1}	$\partial\nu(\text{complex})/\partial T$ / $cm^{-1}\ K^{-1}$
FOH-THF	0.5	197	
	15	193	
	25	192	0.28 (0 – 50 °C)
	35	187	
	50	183	
FOH-acetone	0.5	145	
	15	137	
	25	132	0.57 (0 – 50 °C)
	35	128	
	50	117	
FOH-DMSO	0.7	252	
	15	248	
	25	244	0.43 (0 – 50 °C)
	35	239	
	50	231	
FOH-HMPA	0.5	317	
	15	316	
	25	308	0.24 (0 – 50 °C)
	35	307	
	50	305	
FOH-pyridine	0.3	351	
	15	346	
	25	340	0.40 (0 – 50 °C)
	35	335	
	50	331	

The heteroassociation of furfuryl alcohol. The heteroassociation of furfuryl alcohol was studied by varying the acceptor strength of the proton acceptors employed: one acceptor was reasonably weak (tetrahydrofuran), one was of me-

dium strength (acetone) and three were strong (dimethyl sulfoxide, hexamethylphosphoramide, and pyridine). In all these cases the shape of the ν_{OH} absorption band of the complex was symmetrical; the values of the alcohol monomer-complex shift $\Delta\nu$ were easily estimated (Fig. 5). The results are given in Table 1 together with some literature values for ethanol and phenol. The data in Table 1 imply that the tendency of furfuryl alcohol to form complexes is approximately similar to that of ordinary simple alcohols.

It has been suggested [20] that in the heteroassociation the value of $\Delta\nu$ would vary with the concentration of the base. Therefore different base concentrations were used in measuring values of $\Delta\nu$; the results are given in Fig. 6. It can be seen that the concentration dependence of $\Delta\nu$ is rather small. Joris and Schleyer have studied only the complex formation of methanol. Possibly $\Delta\nu$ of alcohols other than methanol does not vary considerably with the base concentration.

It has been reported in the literature that $\Delta\nu$ varies with temperature. Table 2 gives the results of a study of furfuryl alcohol as a function of temperature. As is seen, the temperature coefficient $\partial\nu$ (complex)/∂T varies considerably for the systems studied. It diminishes with increasing size of the base molecule, from +0.57 for acetone to +0.24 for hexamethylphosphoramide. Zdzienski and Wood [21] have given two alternative explanations of this phenomenon. Either at the lower temperatures the solvent contracts and compresses the complex, thus producing shorter and stronger hydrogen bonds, or the multiplicity of association is increased on cooling. Since the spectra show the existence of higher than 1:1 complexes to be unlikely even at 0 °C, at least the latter of Zdzienski's and Wood's explanations is not applicable. A preferable explanation is a solvent effect on the hydrogen bond.

The suitability of carbon tetrachloride as an inert solvent in hydrogen bond studies has been discussed during the past few years. Although CCl_4 is not as inert as desired, no suitable substitute for it has been found for infrared studies. Arnett and his coworkers [22] have recently discussed this problem, concluding that carbon tetrachloride is quite a good solvent after all.

Acknowledgements. The author wishes to thank Professor Antti Kivinen for his valuable suggestions and critical comments during the course of this work. Support received through a research grant from the Emil Aaltonen Foundation is gratefully acknowledged.

REFERENCES

1. Strandman, L. *Unpublished results.*
2. Liddel, U. and Becker, E. D. *Spectrochim. Acta 10* (1957) 70.
3. Duboc, C. *Spectrochim. Acta 30 A* (1974) 431, 441.
4. Kivinen, A., Murto, J., Korppi-Tommola, J. and Kuopio, R. *Acta Chem. Scand. 26* (1972) 904.
5. Murty, T. S. S. R. *Can. J. Chem. 48* (1970) 184.
6. Bellamy, L. J. *Advances in Infrared Group Frequencies*, Methuen, London 1968, Chapter 8.
7. Kivinen, A. and Murto, J. *Suom. Kemistilehti B 40* (1967) 6.
8. Blanks, R. F. and Prausnitz, J. M. *J. Chem. Phys. 38* (1963) 1500.
9. Ibbitson, D. A. and Moore, L. F. *Chem. Commun.* (1965) 339.
10. Coburn, Jr., W. C. and Grunwald, E. J. *J. Amer. Chem. Soc. 80* (1958) 1318.
11. Kirkwood, J. G. *J. Chem. Phys. 7* (1939) 911.
12. Fröhlich, H. *Theory of Dielectrics*,Clarendon Press, Oxford 1958, p. 36.
13. Singh, S. and Rao, C. N. R. *J. Amer. Chem. Soc. 88* (1966) 2142.
14. Kivinen, A., Murto, J. and Kilpi, L. *Suom. Kemistilehti B 40* (1967) 301.
15. Joesten, M. D. and Drago, R. S. *J. Amer. Chem. Soc. 84* (1962) 3817.
16. Gramstad, T. *Spectrochim. Acta 19* (1963) 829.
17. Kuopio, R. *Personal communication.*
18. Becker, E. D.*Spectrochim. Acta 17* (1961) 436.
19. Gramstad, T. *Acta Chem. Scand. 16* (1962) 807.
20. Joris, L. and von Raguè Schleyer, P. *Tetrahedron 24* (1968) 5991.
21. Zdzienski, H. K. and Wood, J. L. *J. Chem. Soc. Faraday Trans. 2* (1974) 409.
22. Arnett, E. M., Mitchell, E. J. and Murty, T. S. S. R. *J. Amer. Chem. Soc. 96* (1974) 3875.
23. Hasanein, A. A. and Kováč, Š. *Collect. Czech. Chem. Commun. 39* (1974) 3613.

Received February 7, 1975.

Acta Chemica Scandinavica A 29 (1975) 637—640

The Crystal and Molecular Structure of Pyridazine Hydrochloride at —170 °C

T. OTTERSEN

Department of Pharmacy, University of Oslo, Oslo 3, Norway

The crystal and molecular structure of the title compound, $C_4H_5N_2^+Cl^-$, has been determined by X-ray methods using 722 reflections above background level collected by counter methods at −170 °C. The crystals are orthorhombic, space group *Pbcm*, with cell dimensions: $a = 9.664(3)$ Å, $b = 8.800(2)$ Å, $c = 6.629(1)$ Å. There are four molecules per unit cell. The structure model was refined to an R-factor of 0.042. In order to reduce the influence of the valence electrons all reflections with $\sin\theta/\lambda < 0.5$ Å^{-1} were excluded in the last stages of the refinement procedure (leaving 421 F_o' s, $R = 0.045$). There is no indication that the protonation has any effect on the bond lengths in the pyridazine moiety. However, the intraring bond angle at the protonated nitrogen is opened by about 7°, the value found here is 125.8(3)°. There is a short nitrogen-chloride hydrogen bond of 2.996(3) Å, and a close contact of 3.315 Å between the chloride ion and the heterocycle normal to the ring.

The structure determination of pyridazine hydrochloride is part of a series of structure investigations of 3,6-pyridazindiones and related compounds (see Ref. 1 and references therein).

Pyridazine, one of the basic azabenzenes, is not known to occur in nature, but some of its derivatives have been found useful as growth inhibitors and medicinals, and the chemistry of the parent ring and its derivatives has attracted considerable interest. (Refs. 2 and 3 and references therein). Several structure investigations have been carried out for pyridazines (Refs. 1 and 3, and references therein), and a number of theoretical calculations have been performed on pyridazine.[4,5]

An electron diffraction study of 3,6-dichloropyridazine is now in progress,[6] and the present structure investigation was carried out to study the effect of protonation on the aromatic ring. This would give a more complete picture of the structural changes which occur in the pyridazine moiety upon changes in its "environment", and it would be of interest to see if these structural changes are the same as those found upon protonation of other azabenzenes.

EXPERIMENTAL

The compound was crystallized by slow evaporation of a solution of pyridazine in *conc.* hydrochloric acid. Rectangular, colourless plate-shaped crystals were formed.

Oscillation and Weissenberg photographs indicated orthorhombic symmetry. The systematically absent reflections were those characteristic of the space groups $Pca2_1$ and *Pbcm*, and the observed density indicated four formula units of $C_4H_3N_2^+ Cl^-$ in the unit cell. Fourier refinements later applied showed the space group to be the centrosymmetric *Pbcm* with the ions placed in the mirrorplane.

A computer-controlled Syntex-P$\bar{1}$ four-circle diffractometer with graphite-monochromatized Mo$K\alpha$ radiation and equipped with an Enraf-Nonius liquid nitrogen cooling device (modified by H. Hope) was utilized for preliminary experiments and for the measurement of diffraction intensities. The work was carried out using a crystal of dimensions $0.4 \times 0.2 \times 0.1$ mm. Unit cell parameters were determined by a least-squares treatment of the angular coordinates of fifteen symmetry-independent reflections with 2θ-values from 35 to 53°. The temperature at the crystal site was −170 °C.

Three-dimensional intensity data were recorded using the ω-scanning mode with scan speed variable from 2 to 12° min^{-1}, depending on the peak intensity of the reflections. Background counting time was equal to $0.7 \times$ scan time. The variations in the intensities of three standard reflections which were remeasured after every fifty reflections were random and

less than three times their standard deviations. Accordingly no corrections were applied to the intensity data for these variations.

The estimated standard deviations were taken as the square root of the total counts with a 2 % addition for experimental uncertainties. Of the 898 symmetry-independent reflections measured ($2\theta_{max} = 60°$), 722 had intensities larger than twice their standard deviations. These were regarded as "observed" reflections, and the remaining were excluded from further calculations. The intensities were corrected for Lorentz and polarization effects. The computer program used, as well as programs subsequently employed, is part of a local assembly of computer programs for CYBER-74 and is described in Ref. 7.

The atomic scattering factors used were those of Doyle and Turner [8] for C, N, and Cl^-, and of Stewart *et al.*[9] for H.

CRYSTAL DATA

Pyridazine hydrochloride, $C_4H_5N_2^+Cl^-$, orthorhombic. Cell dimensions at −170 °C: a = 9.664(.003) Å, b = 8.800(.002) Å, c = 6.629(.001) Å. Figures in parentheses are estimated standard deviations. V = 563.7 Å^3; M = 116.5 amu; D_{obs} (19 °C) = 1.36 g/cm^3; Z = 4; D_{calc} = 1.373 g/cm^3; $F(000)$ = 240. Absent reflections: ($0kl$) for k odd; ($h0l$) for l odd; space group *Pbcm*.

STRUCTURE DETERMINATION

The x and y coordinates of the chloride ion were derived from the Patterson map. Assuming the centrosymmetric space group, the chloride ion was placed in the mirror plane (z = 1/4). Successive Fourier refinements based on this position revealed the positions of all other non-hydrogen atoms.

The structure model was refined to a conventional R of 0.082. At this point anisotropic temperature factors were introduced for all non-hydrogen atoms and the hydrogen atoms were placed in calculated positions. The location of the proton bonded to a nitrogen atom was derived from both the nitrogen-chloride distances and the intraring bond angles of the nitrogen atoms. Full-matrix least-squares refinement of all x and y coordinates, anisotropic thermal parameters for non-hydrogen atoms and isotropic thermal parameters for hydrogen atoms using all observed reflections converged to a weighted R_W of 0.051 and a conventional R of 0.042.

Earlier structure determinations (see Ref. 1 and references therein) have indicated that structural parameters found for molecules like the present heterocycle are significantly influenced by the asphericity of the valence electrons. In order to reduce this influence all reflections with sin $\theta/\lambda < 0.5$ Å^{-1} were excluded from the refinement. Earlier work (see Ref. 1 and references therein) has shown that this asphericity has little or no effect when this cutoff value in sin θ/λ is used. Least-squares refinement of all parameters (s = 43) involving non-hydrogen atoms using the 421 observed reflections (m) with sin $\theta/\lambda \geq 0.5$ Å^{-1} resulted in a conventional R of 0.045, an R_W of 0.040, and an R-factor for the total data set of 0.043. The "goodness of fit" ($\{|\sum W(F_o - |F_c|)^2/(m-s)\}^{\frac{1}{2}}$) is 1.18. Atomic parameters for nonhydrogen atoms, obtained in this refinement are listed in Table 1, and parameters for hydrogen atoms, from the refinement using all observed reflections, are given in Table 2. A list of observed and cal-

Table 1. Fractional atomic coordinates and thermal parameters with estimated standard deviations (all × 10^5) for non-hydrogen atoms. The z-parameter for all atoms is 1/4. The temperature factor is given by exp $-(B_{11}h^2 + B_{22}k^2 + B_{33}l^2 + B_{12}hk + B_{13}hl + B_{23}kl)$. Results from the refinement using high-angle data only.

Atom	x	y	B_{11}	B_{22}	B_{33}	B_{12}
Cl	19203(8)	5188(8)	528(10)	407(11)	1173(21)	−125(13)
N1	39423(36)	41579(34)	509(27)	534(31)	1703(67)	86(42)
N2	25920(32)	38428(30)	525(27)	421(26)	1156(55)	−16(42)
C3	15851(35)	48467(39)	509(28)	552(36)	1282(66)	−24(43)
C4	19054(44)	64033(34)	605(31)	460(28)	1601(68)	132(58)
C5	32856(37)	67915(34)	634(36)	424(29)	1464(69)	−55(48)
C6	42673(34)	56084(48)	500(25)	638(38)	1910(77)	−189(58)

Table 2. Fractional atomic coordinates (× 10^3) and isotropic thermal parameters with estimated standard deviations for hydrogen atoms. The *z*-parameters are 1/4. Results from the refinement using all observed data.

Atom	*x*	*y*	*B*
H2	234(4)	289(6)	4.2(1.1)
H3	72(4)	449(4)	2.2(.8)
H4	121(4)	707(4)	2.5(.9)
H5	357(4)	784(5)	3.1(1.0)
H6	524(4)	584(4)	2.0(.9)

culated structure factors is available from the author upon request. (May also be obtained from: Department of Chemistry, University of Oslo, Oslo 3, Norway.)

Standard deviations in molecular parameters were calculated from the correlation matrix ignoring standard deviations in cell parameters.

DISCUSSION

Bond lengths and bond angles are given in Fig. 1, where also the numbering of the atoms is indicated.

There is no indication that the protonation of N2 has any effect on the bond lengths of the pyridazine moiety. The two nitrogen-carbon bonds are found to be equal, and the difference in the C3 – C4 and C5 – C6 lengths is only 0.005 Å. The differences between the bond lengths found in this study, and those found in other structure investigations of pyridazine [6,10] are also small (see Table 3).

However, the changes in the intraring bond angles of the pyridazine moiety are large. The angle at N2, which is the protonated nitrogen, increases by about 7° (119° in 3,6-dichloropyridazine,[6] 125.8° in the present study). This increase is about the same as those of ~6° which are found for the corresponding angles in pyrimidine [11,12] and pyrimidine-2-one.[11] The changes in the other intraring angles of the pyridazine moiety are smaller (preliminary results for 3,6-dichloropyridazine [6] are: ∠N2 – C3 – C4: 124°; ∠C3 – C4 – C5: 116°) and are probably caused by the opening of the bond angle at N2.

The molecular arrangement in the crystal is

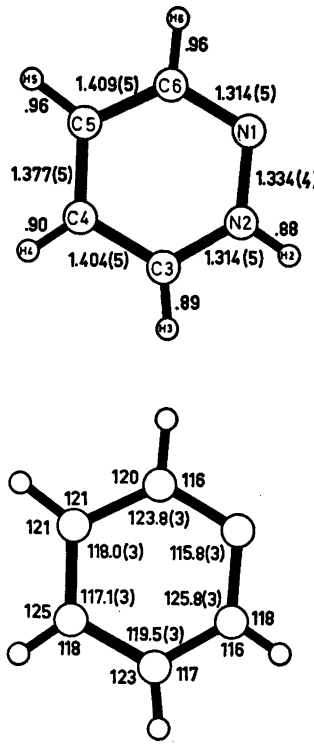

Fig. 1. Bond lengths (Å) and bond angles (°). The estimated standard deviations, in parentheses, are in the last digit given for the corresponding parameter. E.s.d.'s in bond lengths involving hydrogen atoms are about 0.03 Å, and in bond angles involving hydrogen atoms about 2°. Structure model obtained using high-angle data only in the refinement.

Table 3. Bond lengths (Å) found for the pyridazine moiety. Estimated standard deviations are given in parentheses.

Bond	$C_4H_5N_2^+$ (This investigation)	[a]3,6-Dichloropyridazine [6]	[b]pyridazine [10]
N1 – N2	1.334(4)	1.34	1.330
N2 – C3	1.314(5)[c]	1.32	
C3 – C4	1.406(5)[d]	1.39	
C4 – C5	1.377(5)	1.38	1.375

[a] Preliminary results from an electron diffraction study. [b] Gas-phase structure model based on microwave spectra. [c] Mean of the N1 – C6 and the N2 – C3 bond lengths. [d] Mean of the C3 – C4 and the C5 – C6 bond lengths.

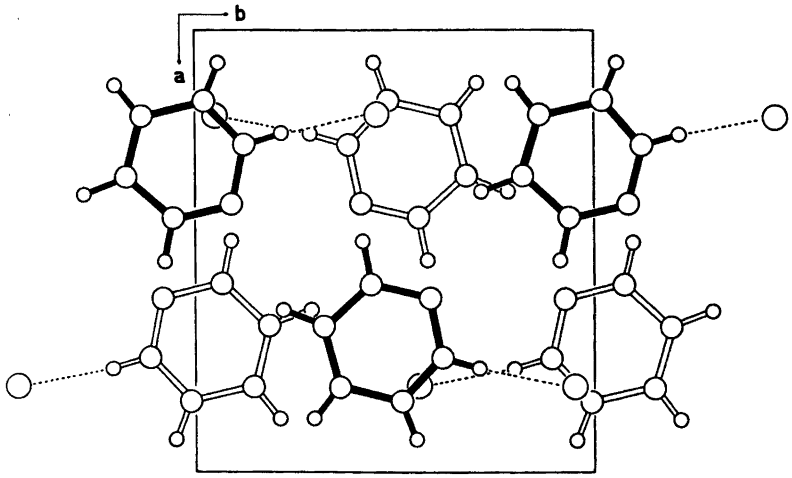

Fig. 2. The crystal structure as seen along the *c*-axis.

visualized in Fig. 2. There is a short hydrogen bond of 2.996(3) Å from N2 to the chloride ion. [The angle at H2 is 175(2)°]. Similar short hydrogen bonds are found in the hydrochlorides of pyridine [13] and pyrimidine.[11] The chloride ion is wedged in between the N2-C3 bonds of the aromatic rings in the layers "above" and "below" [distance: *c*/2, 3.315(1) Å]. This type of packing is also found in both pyrimidine hydrochloride [11] and 1-methylcytosine hydrobromide.[14] Both the shortness of the hydrogen bond and the close contact between the chloride ion and the heterocyclic ring are probably caused by electrostatic attractions.

REFERENCES

1. Ottersen, T. *Acta Chem. Scand. A 28* (1974) 1145.
2. Castle, R., Ed., *Heterocyclic Compounds 28*, Wiley, New York 1973.
3. Ottersen, T. *Acta Chem. Scand. 27* (1973) 797.
4. Gropen, O. and Skancke, P. N. *Acta Chem. Scand. 24* (1970) 1768.
5 Almløf, J., Roos, B., Wahlgren, U. and Johansen, H. *J. Electron Spectrosc. Rel. Phenom. 2* (1973) 51.
6. Almenningen, A., Bjørnsen, B., Ottersen, T., Seip, R. and Strand, T. *To be published.*
7. Groth, P. *Acta Chem. Scand. 27* (1973) 1837.
8. Doyle, P. A. and Turner, P. S. *Acta Crystallogr. A 24* (1968) 390.
9. Stewart, R. F., Davidson, E. R. and Simpson, W. T. *J. Chem. Phys. 42* (1965) 3175.
10. Werner, W., Dreizler, H. and Rudolph, H. D. *Z. Naturforsch. 22 A* (1957) 531.
11. Furberg, S. and Aas, J. B. *To be published.*
12. Wheatley, P. J. *Acta Crystallogr. 13* (1960) 80.
13. Rerat, C. *Acta Crystallogr. 15* (1962) 427.
14. Bryan, R. F. and Tomita, K.-I. *Acta Crystallogr. 15* (1962) 1174.

Received January 31, 1975.

Acta Chemica Scandinavica A 29 (1975) 641—646

Short Communications

A Note on the V—P, V—As and Cr—As Systems

ROLF BERGER

Institute of Chemistry, University of Uppsala, Box 531, S-751 21 Uppsala, Sweden

In previous work on compounds in the V—As and Cr—As systems the samples have generally been synthesized in evacuated silica tubes. This method, however, has to be used with some reservation since the arsenides can readily become contaminated by reaction with the silica. These hazards are particularly serious in the case of the vanadium arsenides, where V_5As_3 and V_3As are isotypic with the corresponding silicides. The author has in fact observed chemical attack on the tube walls, accompanied by considerable variations in unit cell dimensions, during attempts to prepare or anneal metal-rich vanadium arsenides in silica tubes.

The method of arc-melting on a water-cooled copper hearth under a protective atmosphere offers a considerable advantage from the contamination point of view, and in addition provides higher temperatures than those attainable in silica tubes. In the present study, arc-melting has therefore been utilized as a complement to the silica tube technique in a survey on the metal-rich parts of the V—P, V—As and Cr—As systems.

The phase-analytical work was based on powder diffraction investigations performed with a Guinier-Hägg type focusing camera, using $CrK\alpha_1$ radiation ($\lambda = 2.28962$ Å) with silicon ($a = 5.43054$ Å) or germanium ($a = 5.65771$ Å) as internal calibration standards.

The V—P system. The phases VP_2, VP, V_4P_3, $V_{12}P_7$, and V_3P have been characterized in previous work.[1–5] In addition, Boller [3] has reported an intermediate phase of approximate composition $V_{2.4}P$. In the present study the occurrence of a phase between $V_{12}P_7$ and V_3P was confirmed. This phase could be prepared both by silica tube synthesis and arc-melting. The powder photograph could be indexed on the basis of orthorhombic symmetry, yielding the cell parameters $a = 6.204$ Å, $b = 3.307$ Å, $c = 7.536$ Å. The structure is most probably of the Co_2P (anti-$PbCl_2$) type.[6] Intensity calculations using the atomic coordinates of Co_2P as refined by Rundqvist [7] showed a very good agreement with the observed values. A complete structure analysis has been started.

The V—As system. The use of the higher temperatures attainable in the arc furnace has yielded a number of phases which were not obtained in earlier work using the silica tube technique. The occurrence of β-V_4As_3 has already been reported in an earlier communication.[9] In addition, two new orthorhombic phases have been found. Single-crystal diffraction data indicate that both phases crystallize with $Pnma$ or $Pn2_1a$ symmetry. The phase denoted β, which has also been prepared by silica tube syntheses at temperatures above 1000 °C, shows a marked homogeneity range. The unit cell dimensions have been found to vary from $a = 6.437$ Å, $b = 7.673$ Å, $c = 9.280$ Å and $V = 458.4$ Å^3 to $a = 6.414$ Å, $b = 7.628$ Å, $c = 9.299$ Å and $V = 454.9$ Å^3. The other orthorhombic phase, γ, stable only at elevated temperatures has the dimensions $a = 9.463$ Å, $b = 7.519$ Å, $c = 6.471$ Å and $V = 460.5$ Å^3. Intensity calculations strongly suggest that γ is isotypic with β-Yb_5Sb_3 reported by Brunton and Steinfink.[8] It is notable that the cell volumes of β and γ are nearly equal. In fact, the phases might be related by a polymorphic transformation, since, in one experiment β was found after treating γ at 800 °C in a silica tube for four days in the presence of traces of iodine. The occurrence of β at this temperature is thought not to correspond to equilibrium, but can be explained on the basis of a relatively rapid polymorphic transformation followed by a rather sluggish eutectoid decomposition. Heat-treatments of β at 1000 °C for several days support this latter assumption, since, despite a kinetically more favourable situation, only a partial decomposition into tetragonal V_3As_2 [9] and tetragonal V_5As_3 (W_5Si_3 type) [10] occurred. The latter phase is considered to be arsenic deficient[11] and shows a considerable homogeneity range. The phase-analytical data in combination with considerations of atomic volumes suggest a composition of V_5As_3 for both the orthorhombic phases, with four formula units to the cell. A single-crystal structure analysis of β has been made and will soon be reported in this journal. The phase-analytical studies have also indicated the occurrence of a phase with the approximate composition V_2As. No single crystals of this phase have yet been obtained, but powder photographs

indicate a hexagonal unit cell of dimensions $a = 7.6519$ Å, $c = 3.3584$ Å, containing four formula units.

The Cr—As system. Arc-melting of a mixture of CrAs and Cr_4As_3 has yielded a new high-temperature phase, which could be indexed according to orthorhombic symmetry. The comparison of powder photographs and intensity calculations strongly suggested that this new phase – occurring together with CrAs – is isotypic with γ in the V—As system of the β-Yb_5Sb_3 structure type. The cell parameters found were $a = 9.263$ Å, $b = 7.446$ Å, $c = 6.393$ Å and $V = 440.9$ Å^3. In arc-melted alloys no intermediate phase more chromium-rich than Cr_3As was found. The Cr_3As (A15) phase as reported by Yuzuri [12] and Hollan *et al.*[13] was thus not obtained. Arc-melted specimens did not contain the high-temperature polymorph of Cr_3As (Fe_2P type). [14–16] This might be due to insufficiently rapid quenching. One specimen heat-treated in an induction furnace at 1450 °C showed, however, weak lines of the hexagonal phase together with the tetragonal form (Cu_2Sb type).

Acknowledgement. Financial support from the Swedish Natural Science Research Council is gratefully acknowledged.

1. Hulliger, F. *Nature (London) 204* (1964) 775.
2. Schönberg, N. *Acta Chem. Scand. 8* (1954) 226.
3. Boller, H. *Monatsh. Chem. 104* (1973) 48.
4. Olofsson, O. and Ganglberger, E. *Acta Chem. Scand. 24* (1970) 2389.
5. Jawad, H., Lundström, T. and Rundqvist, S. *Phys. Scr. 3* (1971) 43.
6. Nowotny, H. *Z. Anorg. Chem. 254* (1947) 31.
7. Rundqvist, S. *Acta Chem. Scand. 14* (1960) 1961.
8. Brunton, G. D. and Steinfink, H. *Inorg. Chem. 10* (1971) 2301
9. Berger, R. *Acta Chem. Scand. A 28* (1974) 771.
10. Boller, H. and Nowotny, H. *Monatsh. Chem. 97* (1966) 1053.
11. Boller, H. and Nowotny, H. *Monatsh. Chem. 98* (1967) 2127.
12. Yuzuri, M. *J. Phys. Soc. Jap. 15* (1960) 2007.
13. Hollan, L., Lecocq, P. and Michel, A. *C. R. Acad. Sci. 260* (1965) 2233.
14. Wolfsgruber, H., Boller, H. and Nowotny, H. *Monatsh. Chem. 99* (1968) 1230.
15. Baurecht, H.E., Boller, H. and Nowotny, H. *Monatsh. Chem. 102* (1971) 373.
16. Jeitschko, W. and Johnson, V. *Acta Crystallogr. B 28* (1972) 1971.

Received May 12, 1975.

On the Crystal Conformation of 1,3,9,11-Tetraoxacyclohexadecane at Room Temperature

P. GROTH

Department of Chemistry, University of Oslo, Oslo 3, Norway

16-Membered rings have been studied by Dale and co-workers.[1,2] A marked tendency for the saturated ring skeleton to assume the diamond lattice is observed. Semiquantitative calculations of the conformational energies [3] show that the "square" conformation has the lowest enthalpy. This conformation was found in the crystals of 1,1,9,9-tetramethylcyclohexadecane.[4] Ring substitution by hetero atoms (oxygen) may reduce the *gauche* interactions at corner positions of the "square" conformation,[5] which indeed is the preferred crystal conformation of 1,5,9,13-tetraoxacyclohexadecane.[6] The compact "rectangular" conformation has only 5.03 kJ/mol higher enthalpy than the "square".[3] The symmetry number is 4 for both, but since only the "rectangular" form is a *d,l*-pair, it has an entropy term (at 300 K) of 1.7 kJ/mol in its favour, and the free-energy difference is only 3.4 kJ/mol.

The crystals of $C_{12}O_4H_{24}$ belong to the triclinic system with dimensions $a = 5.799(1)$ Å, $b = 7.731(1)$ Å, $c = 7.815(1)$ Å, $\alpha = 70.21(1)°$, $\beta = 82.46(1)°$, $\gamma = 88.19(1)°$ for Dirichlets reduced cell, and one molecule in the unit cell. 527 observed reflections were measured on an automatic four-circle diffractometer at room temperature (Mo$K\alpha$-radiation). Statistical tests strongly indicated the space group $P\bar{1}$. The structure was solved by direct methods [7] and refined by full-matrix least squares technique

Table 1. Final fractional coordinates (multiplied by 10^4) and thermal parameters for carbon and oxygen atoms.

Atom	X	Y	Z	B
O1	1194(43)	5805(29)	2081(29)	4.0(.6)
O2	7586(16)	6774(12)	6604(11)	4.4(.2)
O3	7636(23)	3908(18)	8940(16)	4.6(.3)
O4	4350(31)	3729(20)	2488(23)	4.3(.5)
C1	2131(23)	4551(16)	1652(17)	5.3(.3)
C2	2529(26)	7468(18)	1190(18)	5.8(.3)
C3	1787(29)	8887(21)	2262(24)	3.9(.4)
C4	2366(15)	8103(11)	4199(11)	4.0(.2)
C5	4909(33)	7804(20)	4447(22)	3.6(.4)
C6	5158(16)	6965(13)	6458(12)	5.4(.2)
C7	7899(25)	5940(19)	8379(17)	2.5(.3)
C8	9152(31)	2956(22)	8008(21)	4.7(.4)
C9	8001(22)	1312(15)	8205(16)	3.3(.3)
C10	5789(28)	1430(18)	7277(18)	4.0(.3)
C11	6172(27)	2521(17)	5194(19)	3.4(.3)
C12	3916(16)	2871(11)	4401(12)	3.4(.2)

indicate a hexagonal unit cell of dimensions $a = 7.6519$ Å, $c = 3.3584$ Å, containing four formula units.

The Cr—As system. Arc-melting of a mixture of CrAs and Cr_4As_3 has yielded a new high-temperature phase, which could be indexed according to orthorhombic symmetry. The comparison of powder photographs and intensity calculations strongly suggested that this new phase – occurring together with CrAs – is isotypic with γ in the V—As system of the β-Yb_5Sb_3 structure type. The cell parameters found were $a = 9.263$ Å, $b = 7.446$ Å, $c = 6.393$ Å and $V = 440.9$ Å^3. In arc-melted alloys no intermediate phase more chromium-rich than Cr_3As was found. The Cr_3As (A15) phase as reported by Yuzuri [12] and Hollan *et al.*[13] was thus not obtained. Arc-melted specimens did not contain the high-temperature polymorph of Cr_3As (Fe_2P type). [14–16] This might be due to insufficiently rapid quenching. One specimen heat-treated in an induction furnace at 1450 °C showed, however, weak lines of the hexagonal phase together with the tetragonal form (Cu_2Sb type).

Acknowledgement. Financial support from the Swedish Natural Science Research Council is gratefully acknowledged.

1. Hulliger, F. *Nature (London) 204* (1964) 775.
2. Schönberg, N. *Acta Chem. Scand. 8* (1954) 226.
3. Boller, H. *Monatsh. Chem. 104* (1973) 48.
4. Olofsson, O. and Ganglberger, E. *Acta Chem. Scand. 24* (1970) 2389.
5. Jawad, H., Lundström, T. and Rundqvist, S. *Phys. Scr. 3* (1971) 43.
6. Nowotny, H. *Z. Anorg. Chem. 254* (1947) 31.
7. Rundqvist, S. *Acta Chem. Scand. 14* (1960) 1961.
8. Brunton, G. D. and Steinfink, H. *Inorg. Chem. 10* (1971) 2301
9. Berger, R. *Acta Chem. Scand. A 28* (1974) 771.
10. Boller, H. and Nowotny, H. *Monatsh. Chem. 97* (1966) 1053.
11. Boller, H. and Nowotny, H. *Monatsh. Chem. 98* (1967) 2127.
12. Yuzuri, M. *J. Phys. Soc. Jap. 15* (1960) 2007.
13. Hollan, L., Lecocq, P. and Michel, A. *C. R. Acad. Sci. 260* (1965) 2233.
14. Wolfsgruber, H., Boller, H. and Nowotny, H. *Monatsh. Chem. 99* (1968) 1230.
15. Baurecht, H.E., Boller, H. and Nowotny, H. *Monatsh. Chem. 102* (1971) 373.
16. Jeitschko, W. and Johnson, V. *Acta Crystallogr. B 28* (1972) 1971.

Received May 12, 1975.

On the Crystal Conformation of 1,3,9,11-Tetraoxacyclohexadecane at Room Temperature

P. GROTH

Department of Chemistry, University of Oslo, Oslo 3, Norway

16-Membered rings have been studied by Dale and co-workers.[1,2] A marked tendency for the saturated ring skeleton to assume the diamond lattice is observed. Semiquantitative calculations of the conformational energies [3] show that the "square" conformation has the lowest enthalpy. This conformation was found in the crystals of 1,1,9,9-tetramethylcyclohexadecane.[4] Ring substitution by hetero atoms (oxygen) may reduce the *gauche* interactions at corner positions of the "square" conformation,[5] which indeed is the preferred crystal conformation of 1,5,9,13-tetraoxacyclohexadecane.[6] The compact "rectangular" conformation has only 5.03 kJ/mol higher enthalpy than the "square".[3] The symmetry number is 4 for both, but since only the "rectangular" form is a *d,l*-pair, it has an entropy term (at 300 K) of 1.7 kJ/mol in its favour, and the free-energy difference is only 3.4 kJ/mol.

The crystals of $C_{12}O_4H_{24}$ belong to the triclinic system with dimensions $a = 5.799(1)$ Å, $b = 7.731(1)$ Å, $c = 7.815(1)$ Å, $\alpha = 70.21(1)°$, $\beta = 82.46(1)°$, $\gamma = 88.19(1)°$ for Dirichlets reduced cell, and one molecule in the unit cell. 527 observed reflections were measured on an automatic four-circle diffractometer at room temperature (Mo$K\alpha$-radiation). Statistical tests strongly indicated the space group $P\bar{1}$. The structure was solved by direct methods [7] and refined by full-matrix least squares technique

Table 1. Final fractional coordinates (multiplied by 10^4) and thermal parameters for carbon and oxygen atoms.

Atom	X	Y	Z	B
O1	1194(43)	5805(29)	2081(29)	4.0(.6)
O2	7586(16)	6774(12)	6604(11)	4.4(.2)
O3	7636(23)	3908(18)	8940(16)	4.6(.3)
O4	4350(31)	3729(20)	2488(23)	4.3(.5)
C1	2131(23)	4551(16)	1652(17)	5.3(.3)
C2	2529(26)	7468(18)	1190(18)	5.8(.3)
C3	1787(29)	8887(21)	2262(24)	3.9(.4)
C4	2366(15)	8103(11)	4199(11)	4.0(.2)
C5	4909(33)	7804(20)	4447(22)	3.6(.4)
C6	5158(16)	6965(13)	6458(12)	5.4(.2)
C7	7899(25)	5940(19)	8379(17)	2.5(.3)
C8	9152(31)	2956(22)	8008(21)	4.7(.4)
C9	8001(22)	1312(15)	8205(16)	3.3(.3)
C10	5789(28)	1430(18)	7277(18)	4.0(.3)
C11	6172(27)	2521(17)	5194(19)	3.4(.3)
C12	3916(16)	2871(11)	4401(12)	3.4(.2)

and the minimum residual method.[8]* Hydrogen positions were calculated, but not refined. Final fractional coordinates and thermal parameters for carbon and oxygen atoms are given in Table 1. The R-value arrived at was 11.8 % (weighted value $R_w = 6.8$ %) for 527 observed reflections. Weights in least squares were obtained from the standard deviations in intensities, $\sigma(I)$, taken as

$$\sigma(I) = [C_T + (0.02C_N)^2]^{\frac{1}{2}}$$

where C_T is the total number of counts and C_N the net count.

The structure (shown in Fig. 1) is disordered, with equal amounts of *d*- and *l*-forms (ordered rings with half weight, related by the centre of symmetry in the unit cell. Averaged bond distances and angles of the title compound, (I), may be compared with those of 1,5,9,13-tetraoxacyclohexadecane,[6] (II):

	(I)	(II)
C–O	1.410 Å	1.415 Å
C–C	1.516 Å	1.507 Å
C–C–O	108.1°	108.3°
C–CO–C	112.6°	113.3°
C–C–C	113.3°	112.9°

The average O–C–O angle is 115.0°. Dihedral angles are given in Fig. 2.

A list of observed structure factors is available from the author.

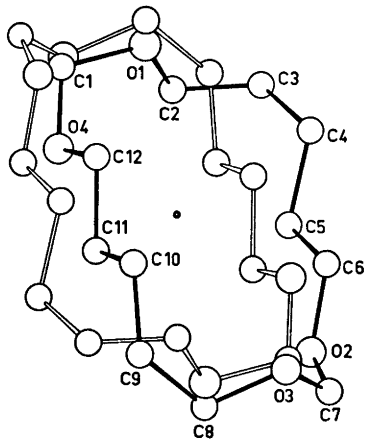

Fig. 1. Schematic drawing showing the statistical disorder in the crystal. The two (ordered) rings (with half weight) related by the centre of symmetry, are situated nearly at a common site in the unit cell.

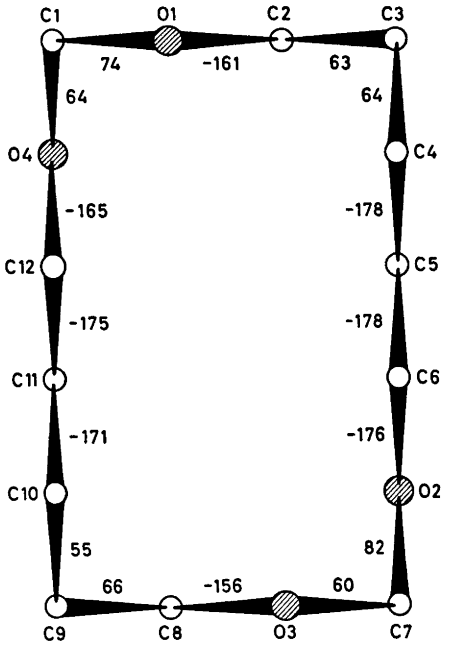

Fig. 2. Schematic drawing showing the dihedral angles.

1. Dale, J. and Borgen, G. *Chem. Commun.* (1970) 1340.
2. Dale, J. and Ekeland, T. *Acta Chem. Scand. 27* (1973) 1519.
3. Dale, J. *Acta Chem. Scand. 27* (1973) 1115.
4. Groth, P. *Acta Chem. Scand. A 28* (1974) 808.
5. Dale, J. *Tetrahedron 30* (1974) 1683.
6. Groth, P. *Acta Chem. Scand. 25* (1971) 725.
7. Germain, G., Main, P. and Woolfson, M. M. *Acta Crystallogr. A 27* (1971) 368.
8. Groth, P. *Acta Chem. Scand. 27* (1973) 1837.

Received April 22, 1975.

* All programs used (except those for phase determination) are included in this reference.

Molecular Structure of Gaseous Bis(dimethylboryl) Disulfane, $(CH_3)_2BSSB(CH_3)_2$

R. JOHANSEN,[a] H. M. SEIP[a] and W. SIEBERT[b]

[a] Department of Chemistry, University of Oslo, Oslo 3, Norway, and [b] Fachbereich Chemie der Philipps-Universität, Marburg/Lahn, Germany

Planar B–S arrangements have been found in a number of compounds by gas electron diffraction (ED).[1–4] The main reason is considerable π-bond character in the B–S bonds as shown by *ab initio* calculations on H_2BSH, which gave a barrier to internal rotation of nearly 20 kcal/mol.[5] The present study of $(CH_3)_4B_2S_2$ was carried out for comparison with the BS compounds studied previously and to find the effect of delocalisation on the SS bond length and the torsional angle about this bond compared to other disulfides.

The compound was synthesised by one of us (W.S.),[6] and the electron-diffraction diagrams recorded with Balzers' eldigraph KD-G2 in Oslo.[7,8] The nozzle temperature was about 65 °C. Three sets of plates were recorded: Set 1 (6 plates, electron wavelength 0.05849 Å, nozzle-to-plate distance 500 mm); Set 2 (4 plates, 0.05858 Å, 250 mm); and Set 3 (1 plate, 0.05839 Å, 250 mm). The plates in set 2 and set 3 were unfortunately too light to give quite satisfactory intensity data. The data were treated in the usual way.[9] A composite intensity curve was computed, and the s-range 1.75–26.0 Å used in the structure determination. The scattering amplitudes and modification function were the same as applied previously.[3]

Least-squares refinements of the structure were carried out assuming C_2 symmetry. We assumed further the methyl groups to have a threefold symmetry axis coinciding with the B–C bond and planar arrangements about the boron atoms. In some calculation free rotation of the methyl groups was simulated and in other cases the torsional angles for the methyl groups were fixed. The results for the most important parameters were nearly the same in these refinements.

Mean amplitudes of vibration (u) were computed as described by Stølevik *et al.*[10] The force constants assumed for the $(CH_3)_2BS$-moieties were essentially the same as used for $(CH_3)_2BSCH_3$.[3] The S–S stretching constant was taken from H_2S_2.[11] Various values were tried for the constant for torsion about the S–S bond. The best agreement between experimental and theoretical ED data was obtained for low torsional constants. The value used in the final calculations, 0.04 mdyn Å rad^{-2}, is less than half of the constant found in H_2S_2.[11]

Table 1. Distances (r_a [20]), angles and mean amplitudes in $(CH_3)_4B_2S_2$. The standard deviations given in parentheses apply to the last digit given.

	r (Å)	u^{ED} (Å)[a]	u^S (Å)[b]
S–B	1.805(5)	0.044(4)	0.055
S–S	2.078(4)	0.040(4)	0.051
C–B	1.573(5)	0.057(4)	0.058
C–H	1.090(5)	0.068(3)	0.078
$C_1\cdots S_1$	2.836(6)	0.083	0.080
$C_2\cdots S_1$	2.976(7)	0.083 (6)[c]	0.076
$C_1\cdots S_2$	4.561(5)	0.095	0.098
$C_2\cdots S_2$	3.293(9)	0.17	0.17
$B_1\cdots S_2$	3.091(5)	0.10	0.10
$C_1\cdots C_2$	2.760(10)	0.076	0.082
$C_1\cdots B_2$	5.599(38)	0.24	0.23
$C_1\cdots C_3$	7.020(34	0.24	0.23
$C_1\cdots C_4$	5.548(40)	0.41	0.39
$C_2\cdots B_2$	4.550(55)	0.39	0.38
$C_2\cdots C_4$	5.174(95)	0.54	0.53
$B_1\cdots B_2$	4.275(30)	0.25	0.24
	Degrees		
$\angle B_1S_1S_2$	105.3(4)		
$\angle S_1B_1C_1$	114.0(6)		
$\angle S_1B_1C_2$	123.4(4)		
$\angle BCH$	109.8(6)		
$\phi(BSSB)$	120(6)		
$\phi(S_2S_1B_1C_1)$	179(4)		

[a] Refined or assumed in the electron-diffraction investigation. [b] Calculated assuming a simple force field as described in the text. [c] The values were assumed equal.

The mean amplitudes for the bond distances were difficult to determine from the ED data because of the short s-range. The geometrical parameters obtained were nearly the same if these amplitudes were refined or kept at the values computed as described above. The results of the investigation given in Table 1 are averages of values obtained in several refinements. The standard deviations include the effect of correlation between the intensity data. Comparison of the experimental and theoretical radial distribution curves is shown in Fig. 1. The difference curve reflects the noise in the experimental data for $s > 20$ Å^{-1}.

As in related molecules the arrangements about the B–S bonds are planar in $(CH_3)_4B_2S_2$, indicating some π-bond character. The torsional angle about the S–S bond is about 120° (0° for the *syn* form). The standard deviation is quite large, but a planar *anti* form can be ruled out.

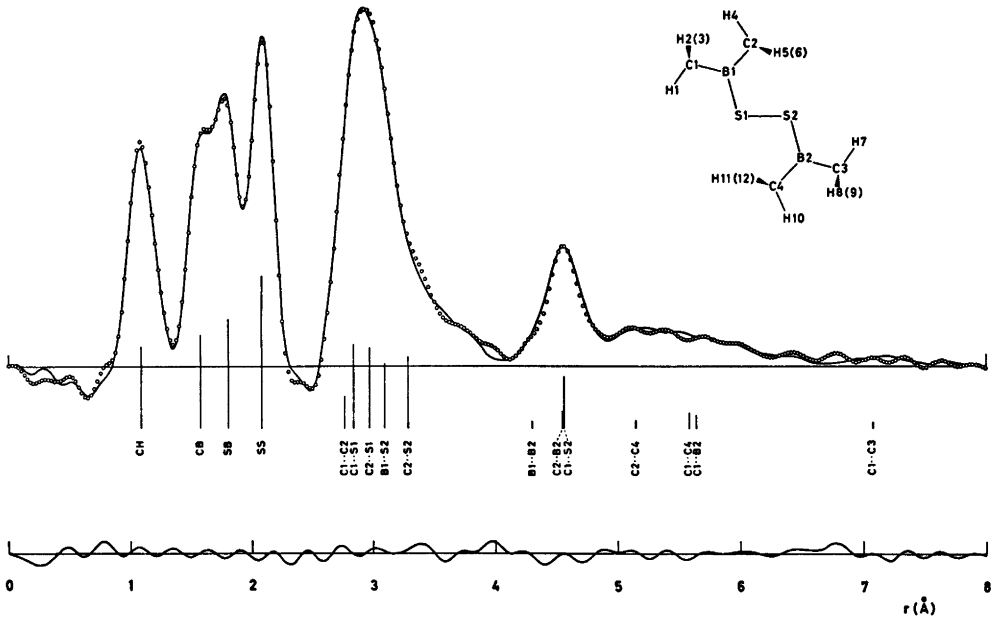

Fig. 1. Experimental (circles) and theoretical radial distribution functions for bis(dimethylboryl) disulfane (artificial damping constant [9] $k = 0.003$ Å^2). The differences between experimental and theoretical values are also shown.

The bond distances are almost identical to those found in dimethyl-1,2,4-trithia-3,5-diborolane [1]

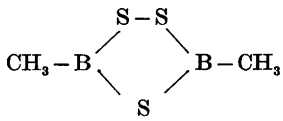

with a rather long S–S bond. In XSSX compounds this bond length varies considerably with the electronegativity of X. In H_2S_2, $(CH_3)_2S_2$, Cl_2S_2, and F_2S_2 the S–S bond lengths are 2.05_5 Å,[12] 2.02_2 Å,[13] 1.93_1 Å,[14] and 1.88_7 Å,[15] respectively. The torsional angle is close to 90° in all these molecules.

No accurate experimental barriers have been reported for H_2S_2, though it seems clear that the *syn* and *anti* barriers are both fairly high;[16] a result also obtained by *ab initio* calculations. Veillard and Demuynck [17] obtained (in kcal/mol) 9.3 and 6.0 for the *syn* and *anti* barriers, respectively. Pappas [18] found 8.4 and 4.2 in H_2S_2 and 16.0 and 9.2 in $(CH_3)_2S_2$. These results may be compared to preliminary values obtained by *ab initio* calculations on H_2BSSBH_2.[19] The equilibrium angle becomes abouth 102° and the barrier in the *anti* form is very low, about 0.7 kcal/mol. It should be noted that while this angle corresponds to the minium in the potential curve, a value averaged over the oscillations is obtained by electron diffraction.

The barriers in X_2S_2 have been described to lone-pair–lone-pair repulsion in the planar forms and hyperconjugation of the type

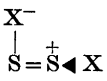

in the orthogonal form.[15,16] The *ab initio* calculations seem to support this hypothesis to some extent.[17,18] The reduced barrier in the *anti* form of $H_4B_2S_2$, and probably also in $(CH_3)_4B_2S_2$, is most likely due to considerable delocalisation in the π-system. However, though the torsional angle becomes somewhat greater than 90°, the reduction is not large enough to give an equilibrium structure with planar skeleton. With considerable deviation from planarity the S–S bond length should depend largely on the electronegativity of the substituents; *i.e.* a bond length similar or slightly longer than found in H_2S_2 is reasonable.

1. Seip, H.M., Seip, R. and Siebert, W. *Acta Chem. Scand. 27* (1973) 15.
2. Almenningen, A., Seip, H. M. and Vassbotn, P. *Acta Chem. Scand. 27* (1973) 21.

3. Brendhaugen, K., Nilssen, E. W. and Seip, H. M. *Acta Chem. Scand. 27* (1973) 2965.
4. Johansen, R., Nilssen, E. W., Seip, H. M. and Siebert, W. *Acta Chem. Scand. 27* (1973) 3015.
5. Gropen, O., Nilssen, E. W. and Seip, H. M. *J. Mol. Struct. 23* (1974) 289.
6. Siebert, W., Gast, E. and Schmidt, J. *Organomet. Chem. 23* (1970) 329.
7. Zeil, W., Haase, J. and Wegmann, L. *Z. Instrumentenk. 74* (1966) 84.
8. Bastiansen, O., Graber, R. and Wegmann, L. *Balzers' High Vacuum Report 25* (1969) 1.
9. Andersen, B., Seip. H. M., Strand, T. G. and Stølevik, R. *Acta Chem. Scand. 23* (1969) 3224.
10. Stølevik, R., Seip, H. M. and Cyvin, S. J. *Chem. Phys. Lett. 15* (1972) 263.
11. Elvebredd, I. and Cyvin, S. J. *Z. Anorg. Allg. Chem. 370* (1969) 310.
12. Winnewisser, M. and Haase, J. *Z. Naturforsch. A 23* (1968) 56.
13. Beagley, B. and McAloon, K. T. *Trans. Faraday Soc. 67* (1971) 3216.
14. Beagley, B., Eckersley, G. H., Brown, D. P. and Tomlinson, D. *Trans. Faraday Soc. 65* (1969) 2300.
15. Kuczkowski, R. L. *J. Amer. Chem. Soc. 86* (1964) 3617.
16. Winnewisser, G., Winnewisser, M. and Gordy, W. *J. Chem. Phys. 49* (1968) 3465.
17. Veillard, A. and Demuynck, J. *Chem. Phys. Lett. 4* (1970) 476.
18. Pappas, J. *To be published.*
19. Gropen, O. *Acta Chem. Scand. To be published.*
20. Kuchitsu, K. and Cyvin, S. J. In Cyvin, S. J., *Molecular Structures and Vibrations*, Elsevier, Amsterdam 1972, Chapter 12.

Received June 18, 1975.

Acta Chemica Scandinavica A 29 (1975) 647—650

The Crystal Structure of 1,3-Dimethyl-4-(1,2,3-triazolio)sulfide

KURT NIELSEN

Chemical Laboratory B, Technical University of Denmark, DK-2800 Lyngby, Denmark

The crystal structure of 1,3-dimethyl-4-(1,2,3-triazolio)sulfide, $C_4H_7N_3S$, has been investigated by X-ray crystallographic methods. The crystals are monoclinic, space group $P2_1/a$, with $a = 7.75 \pm 0.02$ Å, $b = 10.56 \pm 0.03$ Å, $c = 8.30 \pm 0.02$ Å and $\beta = 114.3 \pm 0.2°$. Three-dimensional data were collected using an automatic equi-inclination diffractometer and Mo$K\alpha$-radiation. The structure was refined by the method of least squares to an R-value of 0.034.

The molecular structure of the mesoionic compound 1,3-dimethyl-4-(1,2,3-triazolio)sulfide can be regarded as a resonance hybrid of the forms (A) – (E).

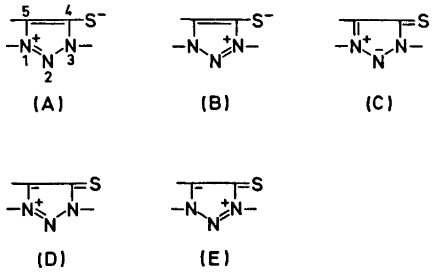

^{13}C-NMR spectra [1] indicate a localization of charge on N1 corresponding to a dominant contribution from either (A), (C), or (D). In order to confirm this result an X-ray investigation was carried out. The preparation and the discussion of the chemical aspects of the compound have been published by Begtrup,[2] who also provided suitable single crystals.

EXPERIMENTAL

Lattice type and space group were established from Weissenberg and precession photographs using Cu- and Mo-radiation. Three-dimensional data between a cylinder of radius $Y = 5.4°$ and a hemisphere with sin $\theta/\lambda < 0.6$ Å^{-1} were measured on an automatic equi-inclination diffractometer (Stoe & Cie, Darmstadt, DBR) using Mo$K\alpha$-radiation from a graphite monochromator and ω-scan technique. Higher order contamination was reduced by means of pulse height discrimination.

The diffractometer output was processed using a program, which takes into account the polarization of the incident beam. This leaves 960 sets of symmetry related reflections with $I > 2\sigma(I)$. No correction for absorption was made.

The remaining calculations were performed using THE X-RAY SYSTEM.[3] All calculations were carried out on the IBM 370/165 at NEUCC, Technical University of Denmark.

CRYSTAL DATA

Crystal system: monoclinic (b unique).

Unit cell: $a = 7.75 \pm 0.02$ Å
$b = 10.56 \pm 0.03$ Å,
$c = 8.30 \pm 0.02$ Å,
$\beta = 114.3 \pm 0.2°$.

$d_{calc} = 1.39$ g/cm^3.
4 mol of $C_4H_7N_3S$ per unit cell.

Systematic absences: $h0l$ for h odd,
$0k0$ for k odd

Space group: $P2_1/a$.

STRUCTURE DETERMINATION

The sulfur atoms were found from the Harker section in the three-dimensional Patterson function, and the remaining atoms, except hydrogen, were then found in a Fourier map phased from these positions. The structure was refined by a full-matrix least squares procedure, using first isotropic and later anisotropic tem-

perature factor parameters. Convergence was reached at $R = 0.055$.

A difference Fourier synthesis was calculated after refinement was ended, and it clearly showed the hydrogen atoms in the expected positions. A few cycles of least squares refinement were computed with the positional parameters and the isotropic temperature factors of the hydrogen atoms included. Agreement factors $R = 0.034$ and $R_w = 0.046$ were obtained. The standard deviations $\sigma(F)$, derived from counting statistics, were modified for use as weights in the least squares refinement. The weighting function used, $w = (0.3 + 2.0\sigma^2(F) + 0.025F + 0.02/F - 0.6 \sin\theta/\lambda)^{-1}$, was found to give an average of $w|F_o - F_c|^2$ which is nearly independent of the magnitude of F and sin θ/λ.

The scattering factors for C, N, and S were taken from *International Tables*.[4] For the hydrogen atoms, the scattering factors calculated by Stewart, Davidson and Simpson [5] were used. No correction for anomalous dispersion was made.

The final positional and thermal parameters and their estimated standard deviations are listed in Tables 1 and 2. A list of observed and calculated structure factors may be obtained from the author on request.

DESCRIPTION AND DISCUSSION OF THE STRUCTURE

Bond lengths and bond angles and their estimated standard deviations are listed in Tables 3 and 4. The standard deviations are

Table 1. Final atomic coordinates and their standard deviations $\times 10^4$. For hydrogen isotropic U-values ($\times 10^2$ Å^2) are given.

Atom	x	$\sigma(x)$	y	$\sigma(y)$	z	$\sigma(z)$	U	$\sigma(U)$
S	0.3490	(1)	0.4108	(1)	0.1585	(1)		
N1	0.3735	(2)	0.2519	(2)	0.5906	(2)		
N2	0.3746	(3)	0.1493	(2)	0.5007	(2)		
N3	0.3673	(2)	0.1951	(2)	0.3472	(2)		
C4	0.3607	(3)	0.3247	(2)	0.3368	(3)		
C5	0.3655	(3)	0.3592	(2)	0.5010	(3)		
C6	0.3848	(4)	0.2380	(3)	0.7718	(3)		
C7	0.3597	(4)	0.1067	(2)	0.2085	(3)		
H1	0.3641	(39)	0.4400	(26)	0.5531	(36)	4.8	(0.7)
H2	0.3299	(65)	0.3129	(44)	0.8013	(57)	10.6	(1.4)
H3	0.5155	(63)	0.2183	(37)	0.8541	(54)	9.1	(1.2)
H4	0.3042	(55)	0.1638	(38)	0.7751	(47)	8.4	(1.1)
H5	0.4456	(62)	0.1388	(40)	0.1580	(54)	9.6	(1.2)
H6	0.2251	(73)	0.0968	(41)	0.1252	(63)	11.2	(1.5)
H7	0.4027	(52)	0.0228	(39)	0.2633	(49)	8.6	(1.1)

Table 2. Anisotropic temperature factor parameters in units of 10^{-4} Å^2 with their estimated standard deviations in parentheses.

Atom	U_{11}	U_{22}	U_{33}	U_{12}	U_{13}	U_{23}
S	649 (4)	386 (3)	318 (3)	−34 (3)	214 (3)	44 (2)
N1	383 (8)	390 (9)	252 (8)	20 (7)	132 (7)	−6 (7)
N2	486 (10)	344 (10)	322 (9)	45 (8)	176 (8)	26 (7)
N3	383 (9)	310 (8)	265 (8)	16 (7)	131 (7)	−14 (7)
C4	348 (10)	320 (10)	303 (10)	−3 (8)	110 (8)	−5 (8)
C5	489 (12)	324 (11)	345 (10)	7 (9)	189 (9)	−25 (8)
C6	557 (13)	666 (16)	285 (11)	−7 (13)	212 (10)	15 (10)
C7	651 (15)	391 (13)	391 (12)	33 (11)	238 (11)	−78 (10)

Table 3. Interatomic distances in Å. Standard deviations $\times 10^3$ in parentheses.

Atoms	Distance	σ
S – C4	1.707	(4)
C4 – C5	1.396	(5)
N1 – C5	1.343	(4)
N3 – C4	1.370	(5)
N1 – C6	1.478	(5)
N3 – C7	1.464	(4)
N1 – N2	1.317	(4)
N2 – N3	1.342	(4)
C5 – H1	0.959	(29)
C6 – H2	0.976	(51)
C6 – H3	0.983	(40)
C6 – H4	1.009	(43)
C7 – H5	0.982	(54)
C7 – H6	0.992	(46)
C7 – H7	0.988	(39)

Table 4. Bond angles in degrees with their estimated standard deviations.

Atoms	Angle	σ
N3 – C4 – C5	102.3	0.2
S – C4 – C5	132.7	0.2
S – C4 – N3	125.0	0.2
C4 – N3 – C7	126.8	0.2
C4 – N3 – N2	113.9	0.2
C7 – N3 – N2	119.3	0.3
N3 – N2 – N1	103.5	0.2
N2 – N1 – C6	118.9	0.2
N2 – N1 – C5	112.9	0.3
C6 – N1 – C5	128.1	0.2
N1 – C5 – C4	107.3	0.2
N1 – C5 – H1	120.5	1.9
C4 – C5 – H1	132.2	1.9
N1 – C6 – H2	109.0	2.8
N1 – C6 – H3	109.9	3.1
N1 – C6 – H4	109.1	2.2
H2 – C6 – H3	115.4	3.3
H2 – C6 – H4	106.5	4.0
H3 – C6 – H4	106.8	3.2
N3 – C7 – H5	107.5	2.5
N3 – C7 – H6	107.8	3.3
N3 – C7 – H7	108.2	2.4
H5 – C7 – H6	116.2	4.0
H5 – C7 – H7	110.3	3.7
H6 – C7 – H7	106.6	3.3

derived from the standard deviations of the cell dimensions and the standard deviations of the coordinates of the atoms in question. An analysis of the planarity of the molecule shows (Table 5) that this is almost planar, the two methyl carbon atoms being significantly out of plane. However, a subsequent calculation shows that the sulfur atom lies 0.011 Å away from the best plane through the triazole ring only, indicating that the sulfur atom is slightly out of plane.

Table 5. Analysis of the planarity in the 1,3-dimethyl-4-(1,2,3-triazolio)-sulfide molecule. The equation for the plane is $m_1x + m_2y + m_3z = d$, where x,y,z are fractional coordinates, and d is the origin to plane distance in Å. Atoms marked with * are those defining the plane.

$m_1 = 7.1637$	$m_1 = 7.1575$
$m_2 = 0.3340$	$m_2 = 0.3197$
$m_3 = -0.2808$	$m_3 = -0.2626$
$d = 2.5957$	$d = 2.5986$

Atom	Distance (Å)	Atom	Distance (Å)
*N1	−0.0019	*N1	0.0000
*N2	−0.0028	*N2	−0.0011
*N3	0.0035	*N3	0.0018
*C4	0.0021	*C4	−0.0016
*C5	0.0022	*C5	0.0010
*S	−0.0030	S	−0.0111
C6	0.0239	C6	0.0292
C7	−0.0416	C7	−0.0445
H1	0.0049	H1	0.0035

The temperature factors of the atoms attached to the ring are strongly anisotropic,

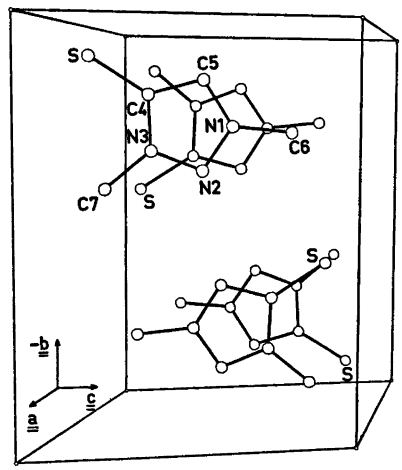

Fig. 1. The content of a unit cell. The numbering of the atoms is shown on one molecule. On the remaining molecules only the sulfur atoms are marked.

with their highest value along the a^*-axis, which is almost perpendicular to the plane of the triazole ring. The angle between the normal to the plane and the a^*-axis is 2.7°. As expected, the temperature factor of the hydrogen atom bonded to C5 is considerably smaller than those of the hydrogen atoms in the methyl groups.

The only interatomic distance less than the van der Waals distance is 3.48 Å, and is found between the methyl carbon atom, C7, and the sulfur atom in molecules related by the operation of the screw axis. The deviations from the plane of the triazole ring of the two atoms are in this direction. The shortest distance between the sulfur atom and the methyl hydrogen atoms is 2.98 Å. The remaining contact distances are approximately equal to the sum of the van der Waals radii of the atoms in question. Several of these are found between the almost parallel molecules related by the operation of the glide plane. The distances range from 3.65 to 3.98 Å, and the average distance between the planes of the molecules is approximately equal to the van der Waals distance between aromatic molecules. The C4–S bond distance of 1.707 Å is a representative of C–S distances found in similar compounds containing the group N–CS–X, where X is either C or N.[6–13] The C–S bond is predominantly a single bond, which is seen from the bond character of 1.28, calculated from the formula given by Pauling [14] with the C–S distance equal to 1.81 Å, corrected by 0.03 Å for the negatively charged sulfur atom.[15] The C=S distance is equal to 1.59 Å. The C4–N3 distance of 1.370 Å is somewhat longer than would be expected from theoretical calculations on 1,2,3-triazole itself.[16] This may be due to the decrease of π-electrons in the ring in presence of the sulfur atom.

In order to distinguish between the canonical forms (A) to (E), the bond characters for the N1–C5, N1–N2, and N2–N3 bonds were calculated, using idealized single bond and double bond distances of 1.46 and 1.26 Å, respectively, for N–N bonds,[17] and 1.475 and 1.265 Å, respectively, for the C–N bonds. From a bond character of 1.36 for the N1–C5 bond and the bond character for the C4–S bond it is concluded that the forms (D) and (E) only give a minor contribution to the total structure. For the N1–N2 bond the bond character is 1.46, and for the N2–N3 bond it is 1.32, leading to the conclusion that the resonance hybrid is made up predominantly of form (A), and almost equal amounts of the forms (B) and (C).

REFERENCES

1. Begtrup, M. *Acta Chem. Scand. B 28* (1974) 61.
2. Begtrup, M. *Acta Chem. Scand. 25* (1971) 3500.
3. Stewart, J. M. *THE X-RAY SYSTEM*, Technical Report TR-192, University of Maryland, College Park, Md.
4. *International Tables for X-Ray Crystallography*, Kynoch Press, Birmingham 1962.
5. Stewart, R. F., Davidson, E. R. and Simpson, W. T. *J. Chem. Phys. 42* (1965) 3175.
6. Ansel, G. B. *J. Chem. Soc. Perkin Trans. 2* (1972) 841.
7. Valle, G., Cojazzi, G., Busetti, V. and Mammi, M. *Acta Crystallogr. B 26* (1970) 468.
8. Sletten, E., Sletten, J. and Jensen, L. H. *Acta Crystallogr. B 25* (1969) 1330.
9. Carlisle, C. H. and Hossian, M. B. *Acta Crystallogr. 21* (1966) 249.
10. Domiano, P., Gasparri, G. F., Nardelli, M. and Sgarabotto, P. *Acta Crystallogr. B 25* (1969) 343.
11. Andreetti, G. D., Domiano, P., Gasparri, G. F., Nardelli, M. and Sgarabotto, P. *Acta Crystallogr. B 26* (1970) 1005.
12. Seccombe, R. C., Tillack, J. V. and Kennard, C. H. L. *J. Chem. Soc. Perkin Trans. 2* (1973) 6.
13. Seccombe, R. C. and Kennard, C. H. L. *J. Chem. Soc. Perkin Trans. 2* (1973) 9.
14. Pauling, L. *The Nature of the Chemical Bond*, Cornell Univ. Press, Ithaca 1948.
15. Hahn, T. *Z. Kristallogr. 109* (1957) 438.
16. Dewar, M. J. S. and Gleicher, G. J. *J. Chem. Phys. 44* (1966) 759.
17. Sabesan, M. N. and Venkatesan, K. *Acta Crystallogr. B 27* (1971) 986.

Received February 25, 1975.

Acta Chemica Scandinavica A 29 (1975) 651—660

Conformational Analysis. X. The Molecular Structure, Torsional Oscillations, and Conformational Equilibria of Gaseous 1,1,2,2,3,3-Hexachloropropane ($CHCl_2CCl_2CHCl_2$) as Determined by Electron Diffraction and Compared with Semi-empirical (Molecular Mechanics) Calculations

LIV FERNHOLT and REIDAR STØLEVIK

Department of Chemistry, University of Oslo, Blindern, Oslo 3, Norway

Gaseous 1,1,2,2,3,3-hexachloropropane has been studied at a nozzle temperature of 112 °C. The abundant conformer (*GG*) is the one without parallel (1:3) Cl···Cl interactions. According to semi-empirical calculations the remaining conformers [*AG*, *GG*(1:3), and *AA*] are from 3.6 to 6.0 kcal/mol less stable than *GG*.

Structural parameters in the *GG* conformer are presented with error limits (2σ). The following values for bond lengths (r_g) and bond angles ($\angle\alpha$) were obtained. Within the $C-CHCl_2$ groups: $r(C-C)=1.558(16)$ Å, $r(C-Cl)=1.780(10)$ Å, $\angle CCCl=111.4°(0.8)$; within the $>CCl_2$ group: $r(C-Cl)=1.752(18)$ Å, $\angle CCCl=108.8°(0.4)$, and $\angle CCC=108.0°(2.0)$. The deviations from a strictly all-staggered (1:2) conformation are quite small.

The torsional force constant has been estimated from the electron-diffraction data, and the values of the fundamental torsional frequencies have been limited to the range 85 – 117 cm^{-1}, with 99 cm^{-1}(A) and 103 cm^{-1}(B) as the most probable values.

To a large extent the structural parameters predicted by the molecular-mechanics calculations reasonably agree with the experimental results.

I. INTRODUCTION

This work is part of a systematic conformational study of halogenated propanes, by electron diffraction in the gas phase. Results for the following molecules have recently been published: $BrH_2C-CHBr-CH_2Br$,[1] $BrH_2C-CH_2-CH_2Br$,[2] $ClH_2C-CHCl-CH_2Cl$,[3] $Cl_3C-CCl_2-CCl_3$,[4] $Cl_2HC-CCl_2-CCl_3$,[5] and $Cl_2HC-CH_2-CCl_3$.[6] Also molecules with $-CH_2X$(X;Cl or H) groups bonded to the central C atom of a $C-C-C$ skeleton were studied: $C(CH_2Cl)_4$,[7] $(CH_3)_2C(CH_2Cl)_2$,[8] and $CH_3-C(CH_2Cl)_3$.[9]

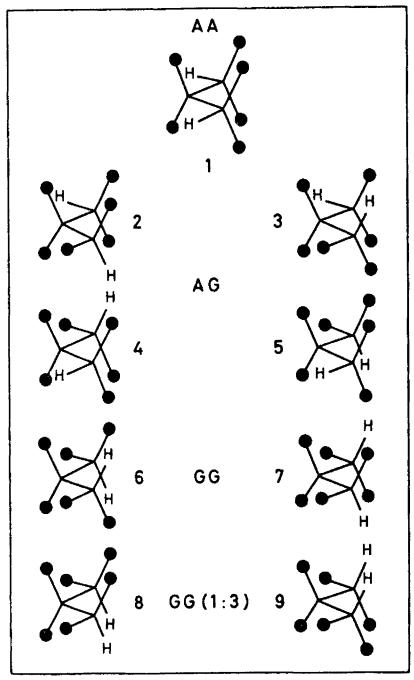

Fig. 1. The staggered conformers in $CHX_2CX_2CHX_2$.

General information [10] relevant to this investigation and to the electron-diffraction method [11] is found in Refs. 10 and 11.

The compound will be referred to as H6. The number of all-staggered (1:2) conformers in H6 is nine, as indicated in Fig. 1. There are four spectroscopically distinguishable conformers, *AA*, *AG*, *GG*, and *GG(1:3)*, with classical multiplicities [2] 1, 4, 2, and 2, respectively. The symbols *A* (*anti*) and *G* (*gauche*), used in conformational names, thus indicate whether the *hydrogen atoms* are *anti* or *gauche* relative to the CCC plane. The symbols (*A* and *G*) are also used in order to indicate *anti/gauche* relations of a Z′···Z″ distance (Z: H, Cl) in a Z′−C−C−C−Z″ fragment, while lower case letters (a and g) indicate whether a Z′···Z″ distance (Z: C, H, Cl) is *anti* or *gauche* in a Z′−C−C−Z″ fragment (see Table 7).

Chlorinated propanes were extensively studied by Sheppard *et al.* using NMR and vibrational spectroscopy. The principal results obtained from such studies in the liquid phase are found in Refs. 12, 13, and 14. In heavily chlorinated propanes many staggered conformers have parallel C−Cl bonds on the same side of the carbon skeleton. Conformers which possess parallel (1:3) Cl···Cl interactions, are energetically less stable than conformers without such interactions.[12] *GG* (Fig. 2) is therefore expected to be the most stable conformer of H6.

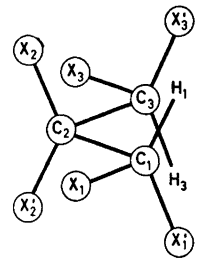

Fig. 2. The numbering of atoms in the *GG* conformer (No. 6 in Fig. 1).

II. CALCULATION OF CONFORMATIONAL ENERGIES, GEOMETRIES, TORSIONAL BARRIERS, AND FORCE CONSTANTS

The semi-empirical energy model corresponds to simple molecular-mechanics calculations, including atom-atom potentials and valence force constants as described in Ref. 1.

Energy parameters (*a*, *b*, *c*, *d*, and V_0) were taken from the paper by Abraham and Parry,[15] and the diagonal force constants of Table 5 were used. In minimizing the energy, the geometry was constrained as described in Sect. V-A.

The values of the structural parameters are shown in Table 1. According to these results

Table 1. Calculated structural parameters for the stable conformers of $CHX_2CX_2CHX_2$, (X=Cl). The projection of the XCX′ angle (in C−CHX_2) on a plane perpendicular to the C−C axis was assumed to be 120°.

Parameter (normal value)	*GG*	*AG*	*AA*	*GG(1:3)*
C−X (1.760 Å) in $-CHX_2$	1.776	1.775	1.772	1.777
C−X (1.760 Å) in $>CX_2$	1.788	1.785	1.781	1.788
C−C (1.513 Å)	1.561	1.568	1.569	1.569
C−H (1.094 Å)	1.094	1.094	1.096	1.094
∠CCC (110.0°)	110.6	115.5	121.1	112.7
∠CCX (109.47°) in $-CHX_2$	113.2	114.2	114.6	114.8
∠CCX (109.47°) in $>CX_2$	109.9	109.1	107.9	109.7
∠CCH (109.47°)	109.6	108.9	108.9	107.4
Torsion angles				
$\phi_{1-2}(60°)^a$	−118.1	+123.7	±0.0	+128.4
	$(-120.0)^b$	$(+120.0)^b$	$(0)^b$	$(+120.0)^b$
$\phi_{2-3}(60°)^a$	−118.1	−10.3	±0.0	−128.4
	$(-120.0)^b$	$(0)^b$	$(0)^b$	$(-120.0)^b$

[a] $\phi_0 = 60°$ in eqn. (1) in Ref. 1. [b] Torsion angles of the all-staggered (1:2) conformers *GG* (No. 6), *AG* (No. 2), *AA* (No. 1), and *GG(1:3)*/(No. 8); see also Fig. 1.

Table 2. Calculated conformational energies (kcal/mol) for $CHX_2CX_2CHX_2$, (X = Cl).

Type of energy[a]	*GG*	*AG*	*AA*	*GG(1:3)*
E (bonded)	4.74	7.67	10.64	8.09
E (van der Waals)	5.66	5.94	4.90	6.72
E (polar: Cl···H)	−6.22	−6.11	−6.02	−5.74
E (polar: Cl···Cl)	24.42	24.74	25.06	24.74
E (total)	28.56	32.24	34.59	33.81
E (total) − *E* (GG) = ΔE^m	0 (min.)	3.66	6.01	5.23

[a] Details about the energy expression are found in Ref. 1. The zero-point vibrational energies of the conformers are not included.

Table 3. Calculated conformational energies and torsional barriers in $CHX_2CX_2CHX_2$, (X = Cl). Details about the conformational minima are given in Tables 1 and 2. The energy values here are relative to the *GG* value. See also Fig. 1 and explanations in the text.

ϕ_{2-3}(°)	ϕ_{1-2}(°) −180 180	−120	−60	0	60	120
180	25.3	14.1	29.3	13.9	29.3	14.1
−180						
120	14.1	*GG(1:3)* 5.2	15.3	*AG* 3.7	15.0	*GG* 0.0
60	29.3	15.3	42.1	17.5	41.9	15.0
0	13.9	*AG* 3.7	17.5	*AA* 6.0	17.5	*AG* 3.7
− 60	29.3	15.0	41.9	17.5	42.1	15.3
−120	14.1	*GG* 0.0	15.0	*AG* 3.7	15.3	*GG(1:3)* 5.2

the value of ∠CCC is very large for *AA* and quite small for *GG*. The greatest deviation from staggered torsion angles is found in the conformer *AG* (*ca.* 10°), while *GG* is nearly staggered, and *AA* is exactly staggered. It is noteworthy that the resulting conformational symmetries are equal to those of the staggered conformers (*AA*: C_{2v}, *AG*: C_1, *GG*: C_2, and *GG(1:3)*: C_s).

Conformational energies are found in Table 2. According to the present energy model, *GG* is the conformer of lowest energy. The destabilizing effects of parallel (1:3) Cl···Cl interactions are clearly demonstrated.

Torsional barriers may be estimated from the energy values in Table 3. Each energy value in Table 3 corresponds to a conformer having all structural parameters adjusted; except for one or two torsion angles (ϕ), corresponding to *eclipsed* conformers, being kept at constant values (ϕ: ± 60, ± 180°). The actual values of the geometry variables are not shown in Table 3, however, the values of the torsion angles ϕ_{1-2} and ϕ_{2-3} are approximately those given in parenthesis. Clearly, the stable conformers correspond to well-defined minima of the potential-energy function. The lowest barrier is as high as *ca.* 9 kcal/mol [*GG(1:3)*→*GG*].

Torsional force constants were computed according to their definitions (Table 4). Derivatives were calculated numerically at the potential-energy minima. Except for *GG*, the interaction constants ($F_{\phi\phi'}$) are quite large in magnitude.

III. CALCULATION OF VIBRATIONAL QUANTITIES

Valence force constants, except for the torsional part of the force field, were taken from

Table 4. Calculated torsional force constants for $CHX_2CX_2CHX_2$, (X = Cl).

Type of force constant [in mdyn Å(rad)$^{-2}$]	*GG*	*AG*	*AA*	*GG(1:3)*
$F_\phi(1-2)^a = \partial^2E/\partial\phi^2_{1-2}$	0.49	0.51	0.45	0.53
$F_\phi(2-3)^a = \partial^2E/\partial\phi^2_{2-3}$	0.49	0.50	0.45	0.53
$F_{\phi\phi}{}^b = \partial^2E/\partial\phi_{1-2}\partial\phi_{2-3}$	−0.08	−0.28	−0.39	−0.31

[a] Diagonal force constant. [b] Interaction force constant (non-diagonal element).

Table 5. Valence force constants for $CHX_2CX_2CHX_2$, (X = Cl).

Stretch (mdyn Å^{-1})	Bend [mdyn Å(rad)$^{-2}$]
C−C: 4.39	CCC: 0.94
	CCX: 1.08
C−X: 3.35	CCH: 0.69
	XCX: 1.13
C−H: 4.89	XCH: 0.83

Stretch/stretch (mdyn Å^{-1}; C is common)
C−X/C−X: 0.49, C−X/C−C: 0.73, C−C/C−C: 0.064

Stretch/bend [mdyn (rad)$^{-1}$]
C−C is common; C−C/CCX: 0.19, C−C/CCH: 0.25, C−C/CCC: 0.35
C−X is common; C−X/CCX: 0.55, C−X/XCH: 0.33, C−X/XCX: 0.40

Bend/bend [mdyn Å (rad)$^{-2}$], bond angles on the same C atom

C−X is common; XCX/CCX: −0.13
C−C is common; CCC/CCH: −0.12
C−H is common; HCX/HCX: 0.09, CCH/HCX: 0.10

C−C is common, but bond angles on adjacent C atoms
CCH/CCX: 0.04 (HCCX anti), CCH/CCX: −0.04 (HCCX gauche)
CCC/CCX: 0.04 (CCCX anti), CCC/CCX: −0.03 (CCCX gauche)
CCX/CCX: −0.09 (XCCX anti), CCX/CCX: 0.07 (XCCX gauche)

Torsion [a] [mdyn Å (rad)$^{-2}$] for the GG conformer
$F_\phi(1\text{-}2) = F_\phi(2\text{-}3) = 0.86$ [b] and $F_{\phi\phi'}(1\text{-}2;\ 2\text{-}3) = 0$

[a] The torsional force constants were defined as follows: each fragment of type A′−C_i−C_2−A″ (A: C, Cl, H) were assigned an equal torsional force constant. The total force constant (F_ϕ) for the torsion coordinate ϕ_{i-2} (i = 1,3) is thus the sum of nine equal contributions. The input to Gwinn's normal-coordinate program demands a separate specification for each of the torsion fragments. [b] This value was estimated from the electron-diffraction data as described in Sect. V−B.

the work [16] by Schachtschneider and Snyder. Certain compromises between force constant values had to be made. The final values selected for H6 are given in Table 5. The diagonal torsional force constants were adjusted (Sect. V-B).

The normal-coordinate program described by Gwinn [17] was used in computing vibrational frequencies (Table 6) for the *GG* conformer of H6. The molecular model possessed C_2 symmetry [A(14) and B (13)].

Mean amplitudes of vibration (u) and vibrational correction terms, $D = r_\alpha - r_a = (u^2/r) - K$, were calculated according to the formulas derived in Ref. 18. Their values are found in Table 7.

According to the semi-empirical model (Table 4), the value of the torsional interaction

Table 6. Fundamental frequencies (ω) in the *GG* conformer of $CHX_2CH_2CHX_2$, (X = Cl and ω in cm^{-1}).
The force constants in Table 5 and the Cartesian coordinates (C_2 sym.) in Table 9 were used. Species (A and B) and approximate interpretations of modes are given: C–H, C–C, and C–X indicate stretching of these types of bonds, while CCC, CCH, CCX, XCX, and HCX indicate bending of these types of bond angles.

90 (A: CCX), 99 (A: torsion + +),[a] 103 (B: torsion + −),[a]
157 (B: CCX), 163 (A: CCX), 172 (B: CCX),
193 (A: CCX+XCX), 253 (A: XCX in $>CX_2$), 274 (B: XCX),
344 (A: XCX), 345 (B: CCX+XCX), 365 (A: CCX+XCX),
561 (B: CCX+C–X), 643 (A: C–X in $>CX_2$), 728 (B: C–X),
776 (B: C–X), 787 (A: C–X), 834 (A: CCC+C–X),
885 (B: C–X in $>CX_2$), 982 (A: C–C), 1169 (B: C–C+CCH),
1257 (A: CCH), 1265 (B: CCH+C–C), 1487 (A: HCX),
1490 (B: HCX), 2933 (A: C–H), 2993 (B: C–H)

[a] The deformations in torsion angles ($\Delta\phi$) are approximately: A($\Delta\phi_{1-2} \simeq +\Delta\phi_{2-3}$) and B($\Delta\phi_{1-2} \simeq -\Delta\phi_{2-3}$).

Table 7. Mean amplitudes of vibration (u) and vibrational correction terms ($-D$) for the *GG* conformer of $CHX_2CX_2CHX_2$ at 112 °C. (X = Cl, see Fig. 2). The force constants in Table 5 and the Cartesian coordinates in Table 9 were used in calculating these quantities. The correction term corresponds to $r_a - r_\alpha = K - (u^2/r) = -D$.

Type of dist. (r)	r (Å)	u (Å)	$K-(u^2/r)$
C–X′ (in–CHX_2)	(1.78)	0.0537	0.00615
C–X (in–CHX_2)	(1.78)	0.0538	0.00722
C–X (in CX_2)	(1.76)	0.0548	0.00295
C–C	(1.57)	0.0542	0.00171
C–H	(1.09)	0.0778	0.01023
$C_2\cdots H_1$	(2.19)	0.1090	0.00413
$C_2\cdots X_1$	(2.74)	0.0758	0.00522
$C_2\cdots X_1'$	(2.74)	0.0758	0.00394
$C_1\cdots C_3$	(2.57)	0.0787	0.00008
$C_1\cdots X$	(2.72)	0.0746	0.00156
$X_1\cdots H_1$	(2.37)	0.1057	0.00973
$X_1'\cdots H_1$	(2.37)	0.1057	0.00779
$X_1\cdots X_1'$	(2.90)	0.0739	0.00851
$X_2\cdots X_2'$	(2.88)	0.0721	0.00294
$H_1\cdots H_3$ (GG)	(3.12)	0.1977	−0.00196
$C_1\cdots H_3$ (g)	(2.79)	0.1544	−0.00170
$H_1\cdots X_2'$ (a)	(3.69)	0.1043	0.00410
$H_1\cdots X_2$ (g)	(2.91)	0.1468	0.00022
$H_1\cdots X_3'$ (GG)	(2.66)	0.2233	−0.00796
$C_1\cdots X_3'$ (g)	(3.12)	0.1372	−0.00159
$C_1\cdots X_3$ (a)	(4.15)	0.0772	0.00179
$X_1\cdots X_2$ (g)	(3.22)	0.1370	0.00019
$X_1\cdots X_2'$ (g)	(3.22)	0.1425	−0.00079
$X_1'\cdots X_2'$ (g)	(3.22)	0.1359	−0.00056
$X_1'\cdots X_2$ (a)	(4.32)	0.0754	0.00242
$X_1\cdots X_3$ (AA)	(5.47)	0.1073	−0.00032
$X_1\cdots X_3'$ (AG)	(4.74)	0.1472	−0.00177
$X_1'\cdots X_3'$ (GG)	(3.87)	0.1942	−0.00580

Table 8. Vibrational quantities in the *GG* conformer of $CHX_2CX_2CHX_2$, calculated with different values of the torsional force constant (F_ϕ). (X = Cl). See also explanations given in Tables 5, 6, 7 and 9.

F_ϕ[mdyn Å(rad)$^{-2}$]	0.63	0.86[a]	1.17
u(X···X)	u (in Å units)[b] at 112 °C		
$X_1'\cdots X_3'$ (GG)	0.2113	0.1942	0.1805
$X_1\cdots X_3'$ (AG)	0.1518	0.1472	0.1434
$X_1\cdots X_2$ (g)	0.1424	0.1370	0.1326
$X_1\cdots X_2'$ (g)	0.1479	0.1425	0.1381
$X_1'\cdots X_2'$ (g)	0.1417	0.1359	0.1310
Low frequencies	ω (in cm^{-1} units)[c]		
Torsion (A)	85	99	112
Torsion (B)	90	103	117
Bending (A)	91	90	91
(B)	153	157	162
(A)	160	163	166
(B)	171	172	173
(A)	193	193	194
(A)	251	253	255
(B)	271	274	279
(A)	341	344	347
(B)	342	345	348
(A)	362	365	369
(B)	558	561	565

[a] The best value as determined in Sect. V–B. [b] Mean amplitude of vibration (u). [c] All frequency values calculated with $F_\phi = 0.86$ are found in Table 6.

Table 9. Cartesian coordinates (x,y,z) of atoms in the *GG* conformer of $CHX_2CX_2CHX_2$.

Atom (X=Cl)	x (Å)[a]	y (Å)[a]	z (Å)[a]
C_3	0[b]	0[b]	0[b]
C_1	1.2829	0.9072	0
X_1	2.7334	−0.1184	0
H_1	1.2829	1.5365	0.8900
X_1'	1.2829	1.9328	−1.4504
C_3	−1.2829	0.9072	0
X_3	−2.7334	−0.1184	0
H_3	−1.2829	1.5356	−0.8900
X_3'	−1.2829	1.9328	1.4504
X_2	0	−1.0165	1.4378
X_2'	0	−1.0165	−1.4378

[a] See Fig. 2. These values of the Cartesian coordinates were used in the calculations of all vibrational quantities (staggered model). [b] The origin of the coordinate system is on the atom C_3.

constant ($F_{\phi\phi'}$) for *GG* is much smaller in magnitude than the diagonal element (F_ϕ). All vibrational quantities were calculated with $F_{\phi\phi'}$ equal to zero. Although the values of the torsional frequencies depend on the value of $F_{\phi\phi'}$ it has been shown [4] that the u and K values are much less dependent on the value of $F_{\phi\phi'}$.

Some of the vibrational quantities are quite sensitive to the value of the torsional element F_ϕ. In Table 8 are shown low vibrational frequencies and mean amplitudes of vibrational corresponding to values of F_ϕ in the range 0.63 − 1.17 mdyn Å (rad)$^{-2}$.

Values of the Cartesian coordinates, which were used in calculations of all vibrational quantities, are found in Table 9.

IV. EXPERIMENTAL AND DATA REDUCTION

H6 was obtained from "K & K" laboratories. The purity of the sample which was used, was better than 98 %.

Electron-diffraction photographs were made at a nozzle temperature of 112 °C in the Oslo apparatus [19] under conditions summarized below.

Nozzle-to-plate distance (mm)	480.7	200.8
Electron wave length (Å)	0.06460	0.06460
Number of plates	4	6

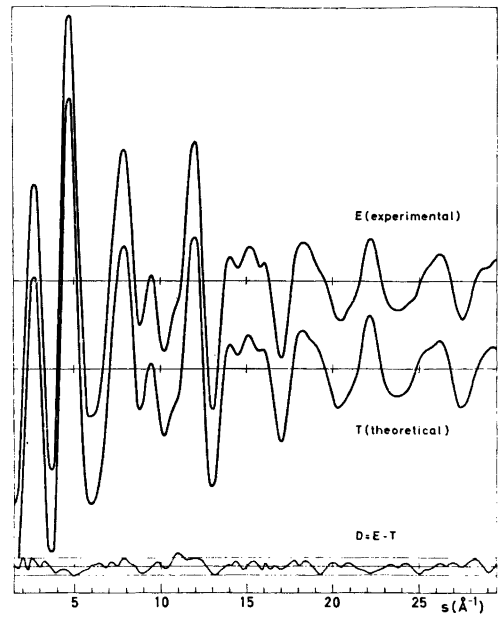

Fig. 3. Experimental (E) and theoretical (T) intensity curves, and $D=E-T$, corresponding to the final least-squares parameters. The straight lines give the experimental uncertainties (±3 times experimental standard deviation).

Range of data, in s (Å^{-1})	1.500 − 19.375	7.25 − 43.25
Data interval, Δs (Å^{-1})	0.125	0.250
Estimated uncertainty in s-scale (%)	0.14	0.14

The electron wave length was determined by calibration against gold and corrected by an experiment with CO_2 giving a correction of +0.1 % in the s-scale. The data were reduced in the usual way [20] to yield an intensity curve for each plate.

Average curves for each set of distances were formed. A composite curve was then made by connecting the two average curves after scaling. The final experimental curve is shown in Fig. 3. The intensities were modified [20] by $s/|f_{Cl}'|^{-2}$. The scattering amplitudes were calculated by the partial-wave method,[21] using Hartree-Foch atomic potentials.[22]

The radial-distribution curve obtained by Fourier [20] transformation of the final experimental intensity curve is shown in Fig. 4.

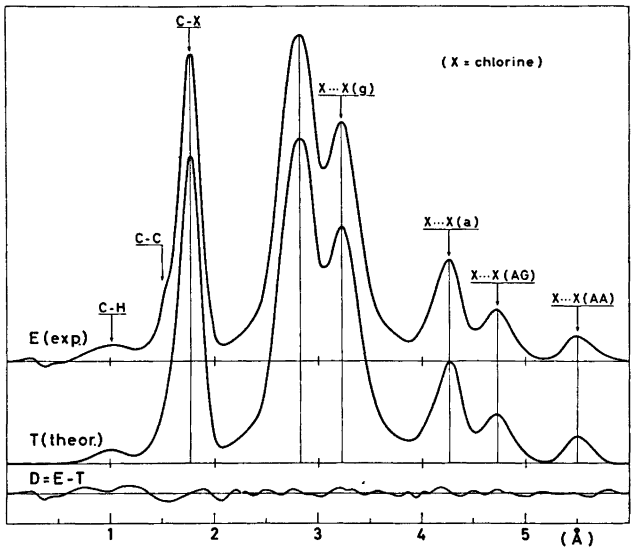

Fig. 4. Experimental (E) and theoretical (T) radial distribution curves, and $D=E-T$. The curves were calculated from the intensity curves in Fig. 3. with an artificial damping constant of 0.0020 Å^2. Some of the peaks corresponding to non-bonded internuclear distances have been indicated; see also Tables 12 and 7.

V. STRUCTURE ANALYSIS

From the experimental RD-curve (Fig. 4) several conclusions can be reached before starting the least-squares refinements. The fact that the peak marked X···X(AA) is present in the experimental curve, shows that the abundant conformer at 112 °C has to be either *GG* or *GG(1:3)*. Only these two conformers possess the very long (*ca.* 5.5 Å) internuclear distance of the type X···X(AA), which corresponds to $X_1\cdots X_3$ in Fig. 2 (see also Fig. 1).

According to the calculated energy values in Table 2, *GG(1:3)* is *ca.* 5 kcal/mol less stable than *GG*. If the semi-emirical results are approximately correct, the percentages of other conformers than *GG* have to be very small (<1 %).

A. Least-squares refinements

In calculating theoretical intensities for the least-squares refinements,[20] it was decided not to consider contributions from other conformers than *GG*.

Several assumptions about bond lengths and bond angles were made in constructing the molecular model, as summarized below (see Fig. 2):

(1) the $>CX_2$ group possess C_{2v} symmetry,

(2) the $C-CHX_2$ groups are equal and possess C_s symmetry.

Models were adjusted in terms of the following structural parameters: $r(C-H)$, $r(C-C)$, $r(C_2-X)$, $r(C_1-X)=r(C_3-X)$, $\angle CCC$, $\angle CCH$, $\angle CC_2X$, $\angle CC_1X)=\angle CC_3X$, $\angle(XC_1X')=\angle(XC_3X')$, and the torsion angles ϕ_{1-2} and ϕ_{2-3}. $\angle(XC_1X')$ is the projection of the XC_1C' angle on a plane perpendicular to the C_1-C_2 axis. For the strictly all-staggered (1:2) *AA* conformation (Fig. 1) the torsion angles ϕ_{1-2} and ϕ_{2-3} are both zero degrees. The atoms $H-C-C-C-H$ are then coplanar. For the strictly all-staggered (1:2) *GG* conformation in Fig. 2, the value is $-120°$ for both ϕ_{1-2} and ϕ_{2-3}, corresponding to a planar arrangement of the atoms $X_1-C_1-C_2-C_3-X_3$.

Non-bonded internuclear distances were computed as dependent quantities, restricted under the constraints of geometrically consistent r_α parameters.[23,24] The bonds C−X and C−X′ in the $-CHX_2$ group are not vibrationally identical, (Table 7), however, this fact was allowed for when D values ($D=r_\alpha-r_a=(u^2/r)-K$) were assigned to the internuclear distances.

B. Determination of torsional force constants

Assuming $F_\phi(1-2)=F_\phi(2-3)=F_\phi$ and $F_{\phi\phi'}=0$, the value of F_ϕ was estimated from the electron-diffraction data as follows: u and K values for different values of F_ϕ were calculated (Sect. III) and then included in the least-squares refinements. The value of F_ϕ which lead to a minimum in the error sum (V'PV), was 0.86 mdyn Å (rad)$^{-2}$, within error limits of *ca.* 30 %. The error limits are subjective to a certain degree, and do not allow for *systematic* [4] errors.

VI. FINAL RESULTS

Parameters from the least-squares refinements and their standard deviations (σ) corrected for correlation [25] in the experimental data, are given in Table 10. The final parameters correspond to refinements with equal weights for all intensities. Data beyond $s=29.5$ Å^{-1} were not included in these refinements.

Parameter-correlation coefficients (ϱ) are shown in Table 11.

The deviation of torsion angles from a strictly all-staggered (1:2) *GG* conformation is small (3.8°), but statistically significant ($\sigma=0.7°$).

Table 10. Structural parameters in the *GG* conformer of $CHX_2CX_2CHX_2$, (X = Cl). Standard deviations are shown in parentheses. The uncertainty (0.14 %) in the s-scale has been included in the standard deviations for bond lengths. An experiment with CO_2 gave a correction of +0.1 % in the s-scale. The bond lengths are therefore 0.1 % longer than the least-squares estimates.

Bond lengths (Å)[a] (r_a-values)	Bond angles (°)[a] ($\angle\alpha$-values)
$r(C-C)=1.556(8)$	$\angle CCC=108.0(1.0)$
$r(C-X)=1.778(5)$ in $-CHX_2$	$\angle CCX=111.4(0.4)$ in $C-CHX_2$
$r(C-X)=1.750(9)$ in $>CX_2$	$\angle CCX=108.8(0.2)$ in $>CX_2$
$r(C-H)=1.02(4)$	$\angle CCH=105.2(4.1)$
$\phi_{1-2}=\phi_{2-3}=-116.2°(0.7)$[b]	$\angle(XCX')$[c] $=120.5(0.8)$

[a] The geometrical assumptions were explained in Sect. V—A. [b] The torsion angles of the *GG* conformer were refined assuming $\phi_{1-2}=\phi_{2-3}$ as suggested by the results in Table 1. $\phi_{1-2}=\phi_{2-3}$ corresponds to C_2 symmetry. [c] The projection of the XCX′ angle in $C-CHX_2$ on a plane perpendicular to the C—C axis of that group.

Table 11. Parameter correlation ($\varrho\times100$).

Parameter[a]		(1)	(2)	(3)	(4)	(5)	(6)	(7)	(8)	(9)	(10)	(11)	(12)
$r(C_1-X)$	(1)	100											
$r(C_2-X)$	(2)	−85	100										
$r(C-C)$	(3)	−1	−8	100									
$r(C-H)$	(4)	−6	9	−7	100								
$\angle CCC$	(5)	−70	78	−7	9	100							
$\angle C_2CX$	(6)	25	−29	−72	19	−23	100						
$\angle CC_2X$	(7)	−24	26	7	−18	1	−52	100					
$\angle CCH$	(8)	27	32	−53	29	−20	63	−40	100				
ϕ[b]	(9)	17	−24	−3	−1	−49	30	17	−3	100			
$\angle(XCX')$[c]	(10)	−74	63	−37	16	61	20	19	−5	6	100		
$u(C-X)$[d]	(11)	−41	46	−41	10	33	21	3	6	−6	45	100	
Scale[e]	(12)	31	−27	−51	8	−33	63	−30	33	18	−2	30	100

[a] The geometrical assumptions were explained in Sect. V—A. [b] Torsion angles: $\phi_{1-2}=\phi$ and $\phi_{2-3}=\phi$. [c] The projection of the XCX′ angle in $C-CHX_2$ on a plane perpendicular to the C—C axis of that group. [d] All $u(C-X)$ values were refined as one parameter. [e] Scale factor between experimental and theoretical intensities.

The fit obtained between theoretical and experimental curves (Figs. 3 and 4) using u and K values calculated with the force constants of Table 5 is quite satisfactory. Moreover, it is important that the large number of u values do not have to be adjusted as individual parameters. However, it ought to be kept in mind that all torsion dependent u and K values have been adjusted *simultaneously* by adjusting the diagonal torsional force constant (Sect. V-B). The vibrationally consistent set of u values in Table 7, which combine information from both vibrational spectroscopy and electron diffraction, are considered the final ones for H6.

The u values of the C – Cl bonds were refined, together with the structural parameters, as one variable. The average value obtained (0.054 Å) is in excellent agreement with the calculated values in Table 7.

VII. DISCUSSION

It has been shown that the abundant conformer, in the gas phase, at 112 °C, is *GG*. Although the percentages of *AA*, *AG*, and *GG(1:3)* were not determined, it is unlikely that the sum of contributions from these conformers is greater than 10 %. The conformational energies predicted by the semiempirical model (Table 2) are thus consistent with the experimental finding. Moreover, if the calculated energies are approximately correct, the contributions from other conformers than *GG* are negligible at 112 °C.

The value of the torsional force constant calculated in Sect. II (Table 4) is too low compared with the experimentally estimated value (Sect. V-B). However, the structural parameter values calculated for the *GG* conformer (Table 1) agree quite well with the corresponding experimental values (Table 10). The largest discrepancies are found for r(C – H) and ∠CCH, however, these parameters are experimentally very uncertain. Although adjustments within the non-torsional force constants and the "normal" reference parameters could remove most of the remaining discrepancies, it was felt that results from additional molecules ought to be included before such corrections were considered.

According to the semi-empirical calculations, all stable conformers of H6 are nearly staggered (Table 1), however, some bond angles are probably quite different within the conformers. The most dramatic difference is expected for the value of ∠CCC, which is quite small in *GG*, while the value in *AA* is *ca.* 10° greater. Such a large ∠CCC value, (121°) for *AA* is consistent with the *experimental* result obtained for octachloropropane (08). In 08 the experimental value is 119° ($\sigma = 2°$). The *AA* conformer of H6 and the all-staggered (1:2) conformer of 08 both have parallel C – Cl bonds on both sides of the carbon skeleton.

The structural parameters of the $\begin{matrix} X \\ X \end{matrix}\!\!>\!C\!<\!\!\begin{matrix} C \\ C \end{matrix}$ group in H6 and 08 have been compared in Table 12. The differences in parameter values between the two molecules are highly significant. The values in Table 12 clearly demonstrate the steric effects of having parallel C – Cl bonds on both sides of the carbon skeleton. It is noteworthy that the deviations from all-staggered (1:2) conformations, are small in both molecules.

Observed vibrational frequencies for H6 were not available, however, the force constants used

Table 12. Comparison of structural parameters in 1,1,2,2,3,3-hexachloropropane (H6) and octachloropropane (08).

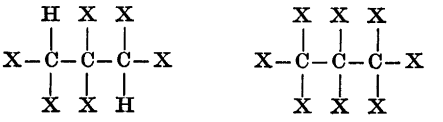

H6 08

Bond lengths and bond angles in the group[a,b]	*GG* conformer of H6[c] (see Fig. 2)	All-staggered (1:2) conformer of 08[d]	Difference (H6 – 08)
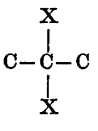			
r_a(C – C) (Å)	1.556(8)	1.655(15)	– 0.099
r_a(C – X) (Å)	1.750(9)	1.810(20)	– 0.060
$\angle_\alpha$CCC (°)	108.0(1.0)	119.0(2.0)	– 11.0
$\angle_\alpha$CCX (°)	108.8(0.2)	104.5(0.5)	+ 4.3

[a] C_{2v} symmetry was assumed for this group. [b] Standard deviations are given in parentheses. [c] The remaining structural parameters are found in Table 10. [d] Further details about 08 are found in Ref. 4.

in this work are consistent with the electron-diffraction data. Moreover, the diagonal element of the torsional force field in the *GG* conformer have been estimated, (Sect. V-B), and the values of the fundamental torsional frequencies [ω_ϕ(A) and ω_ϕ(B)] have been limited to the range 85 – 117 cm^{-1}. The most probable values are 99 and 103 cm^{-1} for ω/(A) and ω/(B), respectively (Table 8). For the *GG* conformer the lowest fundamental is the "CCX bending" frequency at *ca.* 90 cm^{-1}(A).

Acknowledgements. We are grateful to Cand. real. Arne Almenningen for recording the diffraction photographs. Computer programs made available by Dr. H. M. Seip, Prof. W. D. Gwinn, and Cand.real. S. Rustad have been extensively used in this work. Financial support from Norges almenvitenskapelige forskningsråd is gratefully acknowledged.

REFERENCES

1. Stølevik, R. *Acta Chem. Scand. A 28* (1974) 299.
2. Farup, P. E. and Stølevik, R. *Acta Chem. Scand. A 28* (1974) 680.
3. Farup, P. E. and Stølevik, R. *Acta Chem. Scand. A 28* (1974) 871.
4. Fernholt, L. and Stølevik, R. *Acta Chem. Scand. A 28* (1974) 935.
5. Johnsen, J. P. and Stølevik, R. *Acta Chem. Scand. A 29* (1975) 201.
6. Johnsen, J. P. and Stølevik, R. *Acta Chem. Scand. A 29* (1975) 457.
7. Stølevik, R. *Acta Chem. Scand. A 28* (1974) 327.
8. Stølevik, R. *Acta Chem. Scand. A 28* (1974) 455.
9. Stølevik, R. *Acta Chem. Scand. A 28* (1974) 612.
10. Bastiansen, O., Seip, H. M. and Boggs, J. E. *Perspect. Struct. Chem. 4* (1971) 60.
11. Seip, H. M. In Sim, G. A. and Sutton, L. E., Eds., *Molecular Structure by Diffraction Methods*, Specialist Periodical Reports, The Chemical Society, London 1973, Vol. 1, Part 1, Chapter 1.
12. Dempster, A. B., Price, K. and Sheppard, N. *Spectrochim. Acta A 25* (1969) 1381.
13. Dempster, A. B., Price, K. and Sheppard, N. *Spectrochim. Acta A 27* (1971) 1563.
14. Dempster, A. B., Price, K. and Sheppard, N. *Spectrochim. Acta A 27* (1971) 1579.
15. Abraham, R. J. and Parry, K. J. *J. Chem. Soc. B* (1970) 539.
16. Schachtschneider, J. H. and Snyder, R. G. *Vibrational Analysis of Polyatomic Molecules. IV.* (Force constants for the haloparaffins). Project No. 31450, Technical Report No. 122-63 of Shell Development Company.
17. Gwinn, W. D. *J. Chem. Phys. 55* (1971) 477.
18. Stølevik, R., Seip, H. M. and Cyvin, S. J. *Chem. Phys. Lett. 15* (1972) 263.
19. Bastiansen, O., Hassel, O. and Risberg, E. *Acta Chem. Scand. 9* (1955) 232.
20. Andersen, B., Seip, H. M., Strand, T. G. and Stølevik, R. *Acta Chem. Scand. 23* (1969) 3224.
21. Peacher, J. and Willis, J. C. *J. Chem. Phys. 46* (1967) 4809.
22. Strand, T. G. and Bonham, R. A. *J. Chem. Phys. 40* (1964) 1686.
23. Morino, Y., Kuchitsu, K. and Oka, T. *J. Chem. Phys. 36* (1962) 1108.
24. Kuchitsu, K. *J. Chem. Phys. 49* (1968) 4456.
25. Seip, H. M. and Stølevik, R. In Cyvin, S. J., Ed., *Molecular Structures and Vibrations*, Elsevier, Amsterdam 1972.

Received February 10, 1975.

Acta Chemica Scandinavica A 29 (1975) 661—671

The Electrophilic Nature of Triarylmethyl Substrates in Acetonitrile

ARVE MARTINSEN, TOR AUSTAD and JON SONGSTAD

Department of Chemistry, University of Bergen, N-5014 Bergen-Univ., Norway

Through competition experiments between various inorganic pseudohalide ions, the electrophilic nature of some substituted and unsubstituted triphenylmethyl halides and perchlorates in an aprotic solvent, acetonitrile, has been examined. For all substrates examined, the reactivity sequence has been found to be $N_3^- \sim NC^- \sim OCN^- > SCN^-$, suggesting that the so-called azide probe is of limited usefulness toward this class of substrates in acetonitrile.

In the presence of an ionic perchlorate the relative reactivity of the azide ion is increased while the presence of nucleophilic anions levels the reactivities of the applied pseudohalide ions. It is suggested that nucleophilic anions are able to deionize the carbenium ions or separated ion pairs to species of lower charge separation. Since this deionization has been found to be extremely rapid, the reacting species from the triarylmethyl substrates are approximately the same, regardless of whether highly ionized triarylmethyl perchlorates or very weakly dissociated triarylmethyl halides are employed as reactants. The rather similar relative reactivities of the various pseudohalide ions toward triarylmethyl halides and triarylmethyl perchlorates substantiate this conclusion.

Finally, the consequences of the deionization mechanism on salt effects are discussed. It is concluded that the deionization mechanism is the probable cause for the very negative salt effects observed in certain S_N1 reactions. The deionization mechanism appears to be limited to reactions of substrates which give highly delocalized carbenium ions.

The fundamental studies by Winstein and coworkers [1] have resulted in the general acceptance of the fact that the S_N1 mechanism of saturated carbon compounds, RX, is highly complex. A number of species may be the reacting one, depending upon the substrate, the nucleophile, the solvent, the ionic strength *etc.* Several species like those depicted in the Winstein dissociation scheme,[2] in addition to various types of solvent-separated ion-pairs,[3–5] may well give rise to first order kinetics and a racemic product. Since the electrophilic nature of the reacting carbon atom undoubtedly varies greatly with the stretching of the R—X bond, various reactivity sequences may be observed and yet the usual characteristics of an S_N1 mechanism may still apply.

The majority of the reactions of saturated carbon compounds which satisfy the criteria of being S_N1 reactions are solvolysis reactions in protic or mixed solvents. These reactions, however, appear to constitute a special class of S_N1 reactions, probably due to be ability of protic solvents to hydrogen bond to most of the usual leaving groups and thus favour the formation of ionic species. For reactions performed in protic solvents, positive salt effects are in most cases observed,[2,6,7] regardless of whether the increased ionic strength is due to salts of nucleophilic or non-nucleophilic anions, contrary to what is found for reactions performed in dipolar aprotic solvents.[8–10] The exceptional salt effects on S_N1 reactions observed in dipolar aprotic solvents suggest that further knowledge of S_N1-type reactions in aprotic solvents may shed some light upon S_N1 reactions in general. Parker,[11] particularly, has stressed the importance of studying S_N2 reactions in dipolar aprotic solvents, primarily to avoid the effect of solvation of the reacting nucleophile. In the case of studies on substrates exhibiting S_N1 behaviour it appears even more important to do so, due to the additional effect of protic species upon the substrate.

Unfortunately, when examining reactions of substrates reacting by the S_N1 mechanism in dipolar aprotic solvents, there are several experimental difficulties which are not readily

coped with. This is primarily caused by the fact that since the most usual S_N1 reactions are alcoholysis and similar solvolysis reactions which necessarily can not be studied, the actual number of possible reactions available for detailed study is greatly diminished. Furthermore, accurate kinetic studies on S_N1 reactions in dipolar aprotic solvents are in most cases difficult to perform due to the high rates of these reactions, requiring the use of special techniques.[12,13] Several attempts were made during the present study to measure the rates of the reaction between unsubstituted triphenylmethyl halides and perchlorate and various inorganic anions in acetonitrile: the stopped-flow technique was utilised as described in the Experimental Part. The rates of the reactions, however, could not be determined, confirming the previous findings of extremely high rates of reaction.[12,13] The only kinetic study on reactions between carbenium ions [5] and various nucleophiles in dipolar aprotic solvents has been performed on stabilized dyestuff cations,[13] where the high rates of reaction prevented a detailed investigation.

Apart from some isomerizations,[10–14] few reactions are therefore available for studies on S_N1 reactions in aprotic solvents. This leaves the classical competition experiments,[9,15] employing S_N1-type substrates as a natural mode of attacking the problem of obtaining further information on S_N1 reactions in dipolar aprotic solvents. In this work we want to report the results of experiments of this type performed in acetonitrile employing some triarylmethyl compounds as substrates and applying various pseudohalide ions as nucleophiles, eqn. 1.

$$RX + \begin{matrix} N_1 \\ N_2 \end{matrix} \longrightarrow \begin{matrix} RN_1 \\ RN_2 \end{matrix} \qquad (1)$$

$R = Ph_3C$, $X = Cl$, Br and ClO_4.
$R = (4\text{-}MePh)_3C$ and $(4\text{-}MeOPh)_3C$, $X = Cl$
$N = N_3^-$, NC^-, OCN^-, and SCN^-.

The triarylmethyl compounds and the pseudohalide ions are well suited for this type of experiment since, in most cases, both the products and the unreacted pseudohalide ions can be rapidly determined with high accuracy applying solution IR. In Table 1 are listed the absorption frequencies and integrated extinction coefficients in the $2000-2300$ cm^{-1} region of the triphenylmethyl pseudohalides and the pseudohalide ions measured in acetonitrile. (For the sake of brevity, only the constants for unsubstituted triphenylmethyl compounds are listed in Table 1).

In none of the examined reactions could products resulting from *para*-attack, *p*-benzhydrylphenyl pseudohalides (I), be detected. Only the normal products, triphenylmethyl pseudohalides (II) could be isolated. Due to the small steric demands of the applied nucleophiles, products like (I) are not to be expected.[18]

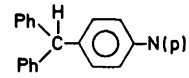

(I)

(II)

Table 1. Absorption frequencies in the $2000-2300$ cm^{-1} range of triphenylmethyl pseudohalides and pseudohalide ions in acetonitrile together with half-band widths and integrated extinction coefficients at 25 °C.

X^-	Ph_3CX	ν cm^{-1}	$\nu_{\frac{1}{2}}$ cm^{-1}	$A \times 10^{-4}$ M^{-1} cm^{-2}
CN^- [a]		2058	14	0.059
	Ph_3CCN [b]	2239	8	0.055
	Ph_3CNC [b]	2126	11	1.0
N_3^- [a]		2005	10	7.2
	Ph_3CN_3 [c]	2102	10	1.4
OCN^- [a]		2140	23	5.2
	Ph_3CNCO [d]	2252	12	9.1
SCN^- [a]		2059	12	4.1
	Ph_3CNCS [d]	2047	100	15

[a] Ref. 16. [b] Ref. 17 (measurements performed in carbon tetrachloride). [c] Ref. 10. [d] This work.

The use of the triarylmethyl compounds as substrates offered an additional advantage due to the fact that these compounds range from very weakly dissociated compounds X = Cl and Br, to extensively dissociated ones, X = ClO_4 (see Experimental Part). Furthermore, as none of the usual inorganic anions, Cl^-, Br^-, ClO_4^-, *etc.*, absorb in the 2000 – 2300 cm^{-1} region, the measurements according to eqn. 1 could be performed at greatly varying ionic strength by addition of the appropriate salts.

Acetonitrile was chosen as solvent, as its low donicity keeps to a minimum the effects of possible reaction between substrate and solvent.[19] Tetraphenylarsonium salts were in all cases used as the source of the nucleophilic anions to ensure a complete dissociation in acetonitrile.

EXPERIMENTAL

Materials. The purification of acetonitrile and the applied tetraphenylarsonium salts was performed as previously reported.[16] Dichloromethane, "Baker Analyzed" reagent, was distilled from phosphorus pentoxide and finally from calcium hydride prior to use. Lithium perchlorate, Fluka *purum* wasserfrei, was used without further purification.

Triphenylmethyl chloride and triphenylmethyl bromide, both Fluka *purum*, were purified as reported.[17] Triphenylmethyl perchlorate was made according to Longworth and Mason.[20] M.p. 148 – 149 °C, (150 °C [20]).

4,4′,4″-Trimethyltriphenylmethyl chloride was prepared from the corresponding alcohol and crystallized several times from acetonitrile. M.p. 176 – 178 °C, (180 °C [21]).

4,4′,4″-Trimethoxytriphenylmethyl chloride, EGA-Chemie KG, was repeatedly crystallized from dry acetonitrile.

Stock solutions of the substrates and the various anhydrous tetraphenylarsonium salts were made prior to use according to a previously described procedure.[17]

The melting points are corrected.

Competition experiments. Assuming the nucleophiles to react with the same species forming the products in first order reactions with respect to the attacking nucleophiles, the relative rates are given by:

$$\frac{kN_1}{kN_2} = \frac{[RN_1]/[N_1]}{[RN_2]/[N_2]} \qquad (2)$$

where $[RN_1]$ and $[RN_2]$ are the concentrations of the products, respectively, and $[N_1]$ and $[N_2]$ are the initial concentrations of the reacting nucleophiles. As the k_{N_1}/k_{N_2} ratios for the majority of the competition reactions examined were found to be close to unity, equal concentrations of the nucleophiles were applied and eqn. 2 reduces to eqn. 3:

$$k_{N1}/k_{N2} = [RN_1]/[RN_2] \qquad (3)$$

Due to the unstable nature of the triarylmethyl isoselenocyanates in acetonitrile, particularly in the presence of cyanide ions,[22] reactions with the selenocyanate ion were not included in this study. In the other reactions studied, the products were found to be stable in the presence of unreacted reactants, at least at our time-scale. (The product composition did not change as judged by the IR spectrum of the reaction mixture immediately after mixing, and after a delay of 15 to 20 minutes). However two exceptions were noted: 4,4′,4″-trimethyltriphenylmethyl isothiocyanate was found to react rather rapidly with ionic cyanide and cyanate causing low accuracy in the k_{CN^-}/k_{SCN^-} and k_{OCN^-}/k_{SCN^-} ratios when 4,4′4,″-trimethyltriphenylmethyl chloride was the substrate. The isothiocyanate from 4,4′,4″-trimethoxytriphenylmethyl chloride was so unstable in the presence of the other ions that the thiocyanate ion could not be included in the competition experiments toward this substrate. The unstable nature of triarylmethyl isothiocyanates has previously been noted.[23]

When the cyanide ion was one of the reacting ions, the yield of triarylmethyl cyanide and the amount of unreacted ionic cyanide were calculated from the peak heights due to the competing anion and the product formed from this anion. This procedure was necessary because of the low extinction coefficients of ionic cyanide and of the triarylmethyl cyanides. No attempt was made to determine the relative amounts of triarylmethyl cyanide and of triarylmethyl isocyanide when cyanide ion was employed as reagent. Concentration of reagents at least one order of magnitude higher than generally applied in this study, $\approx 1 \times 10^{-3}$ M, would have been necessary to obtain reliable information about the ambident nature of the cyanide ion toward the various substrates.[17]

When the thiocyanate ion was one of the reactants, the amount of the organic isothiocyanate formed was not usually estimated due to the broadness of this absorption in the 2050 cm^{-1} region (see Table 1).

The general procedure was to add a 1:1 mixture of the nucleophiles *to* the freshly prepared solution of the triarylmethyl substrate. Each of the nucleophiles was slightly in excess, 3 to 5 %, of the reacting substrate. In the case of the triarylmethyl halides, the product composition was found to be independent of whether the nucleophiles were added to the substrate or *vice versa*. Likewise, the rate of mixing did not appear to cause a significant change in the product composition. When triphenylmethyl perchlorate was the substrate, however, the relative

yields of products appeared to be highly dependent upon how the solutions were mixed.

The results from the competition experiments are listed in Tables 2 to 4. In Tables 5 to 7 are listed the results of competition experiments with 4,4',4''-trimethoxytriphenylmethyl chloride as substrate, performed in the presence of various amounts of lithium perchlorate, tetraphenylarsonium perchlorate and tetraphenylarsonium chloride, respectively.

The competition ratios were calculated from experiments performed at least in duplicate. The differences between parallel determinations were within the experimental error due to the uncertainties in the peak heights. Only in the case where triphenylmethyl perchlorate was the substrate did the discrepancy between the parallel determinations exceed the calculated maximum uncertainty. In the competition experiments where both the products could be determined, the total yield of products was found to be quantitative as calculated from the amount of the reacting substrate.

The IR measurements were performed with a Unicam SP 200 G Infrared Spectrophotometer at 25 ± 1 °C applying 0.1 cm liquid cells.

Dissociation constants of triphenylmethyl compounds in acetonitrile at 25.0 °C. A: Triphenylmethyl perchlorate. A solution of triphenylmethyl perchlorate in dichloromethane showed two peaks of similar intensity in the 400 – 500 nm region. The molar extinction coefficients at 25 °C of the peaks at 434 nm and 410 nm were 3.69×10^4 M^{-1} cm^{-1} and 3.68×10^4 M^{-1} cm^{-1}, respectively, in excellent agreement with published values.[20,24]

In acetonitrile the two peaks were shifted to 430 and 403 nm and the molar extinction coefficients of these peaks ranged from 3.5×10^4 to 3.7×10^4 M^{-1} cm^{-1} and were found to be independent of the concentration of triphenylmethyl perchlorate in the $5 - 20 \times 10^{-4}$ M region, suggesting this compound to be completely dissociated in acetonitrile in this concentration range. The experimentally determined value for the extinction coefficient in acetonitrile is lower than the value reported in the literature, 4×10^4 M^{-1} cm^{-1}.[25,26] For lower concentrations of triphenylmethyl perchlorate than 3×10^{-4} M, a slight but significant reduction of the molar extinction coefficient in acetonitrile was observed. As the observed molar extinction coefficients in dichloromethane were in agreement with the published values, it appears safe to conclude that the lower extinction coefficients observed in acetonitrile on extreme dilution were due to some impurity in the applied solvent, most probably traces of water, and not to impurities in the applied samples of triphenylmethyl perchlorate.

Conductance measurements of freshly prepared solutions of triphenylmethyl perchlorate in acetonitrile at 25.0 °C were performed and the $\Lambda - c^{\frac{1}{2}}$ plots were found to be, within the experimental error, completely linear for concentrations in the $2.5 - 7 \times 10^{-4}$ M range. (On further lowering of the concentration a significant increase in the equivalent conductivity was observed. A deviation from linearity in the $\Lambda - c^{\frac{1}{2}}$ plot at low concentrations is to be expected if traces of water are present in the solvent). On extrapolation to infinite dilution, a limiting equivalent conductivity of 166.0 ohm^{-1} cm^{-2} mol^{-1} for triphenylmethyl perchlorate was calculated.

Conductance measurements on tetraphenylarsonium perchlorate in acetonitrile at 25.0 °C gave conductance parameters for this salt in excellent agreement with those determined by Springer and co-workers.[27] The nearly identical slopes in the $\Lambda - c^{\frac{1}{2}}$ plots for the two examined compounds can be considered as additional evidence for the complete dissociation of triphenylmethyl perchlorate in acetonitrile. From the limiting equivalent conductivity of 166.0 ohm^{-1} cm^{-2} mol^{-1} for triphenylmethyl perchlorate and the literature value for λ_0 (ClO_4),[27] the limiting equivalent conductivity of the triphenylmethyl carbenium ion, λ_0 (Ph_3C^+), was calculated to be 62.3 ohm^{-1} cm^{-2} mol^{-1} in acetonitrile at 25.0 °C.

B. Triphenylmethyl chloride and triphenylmethyl bromide. From UV measurements of 0.02 M solutions of triphenylmethyl chloride and triphenylmethyl bromide, the dissociation constants for these two compounds in acetonitrile at 25.0 °C were found to be 7.0×10^{-11} and 9.6×10^{-10} M, respectively. Calculations based upon conductance measurements in acetonitrile, and applying the calculated limiting equivalent conductivity for the triphenylmethyl carbenium ion and values in the literature for λ_0 (Cl^-) [28] and λ_0 (Br^-),[27] gave dissociation constants for these two substrates in acetonitrile which were generally ten times those determined by the UV method. Since traces of water in the applied solvent will give too low values by the UV method and too high values by the conductance method for the dissociation constants, the observed discrepancy between the two set of measurements is to be expected. The exact values of the dissociation constants of triphenylmethyl chloride and triphenylmethyl bromide are of limited importance to the discussion of the results from the competition experiments.

C. Dissociation of triphenylmethyl substrates in the presence of salts of inorganic anions. Attempted Stopped-Flow measurements. On adding small amounts of various salts of nucleophilic anions to triphenylmethyl perchlorate dissolved in acetonitrile, the colour of the solutions disappeared instantaneously. The reactions between a 5×10^{-5} M solution of triphenylmethyl perchlorate and 1×10^{-3} M solutions of tetraphenylarsonium azide, tetraphenylarsonium bromide, and tetraphenylarsonium iodide, respectively, were studied by a Stopped-Flow Spectrophotometer. The rates of the reactions, however, were extremely rapid and could not be determined by this technique. Assuming

the reactions to be second order, a lower limit of the rate constants of 5×10^6 M^{-1} s^{-1} could be estimated from these measurements.

On adding tetraphenylarsonium perchlorate to a solution of triphenylmethyl bromide a small but significant increase of the colour of the solution due to the triphenylmethyl carbenium ion was observed. (In a saturated solution of tetraphenylarsonium perchlorate in acetonitrile, 1.5×10^{-2} M, the concentration of the triphenylmethyl carbenium ion from a 1×10^{-2} M solution of triphenylmethyl bromide was twice that when this substrate was dissolved in pure acetonitrile). The rate of the increase of the concentration of the triphenylmethyl carbenium ion from triphenylmethyl bromide in acetonitrile upon the addition of various amounts of tetraphenylarsonium perchlorate was extremely high and could not be determined by the stopped-flow technique.

Conductance measurements confirmed the trend in the results from the UV measurements. The conductivity of a solution, 1.005×10^{-2} M in triphenylmethyl bromide and 6.08×10^{-4} M in tetraphenylarsonium perchlorate, was 3.5 % higher than the calculated conductivity if no increase in the ionization had taken place. Similarly, the conductivity of a solution, 1.005×10^{-2} M in triphenylmethyl bromide and 6.18×10^{-4} M in tetraphenylarsonium iodide, was found to be 4.4 % lower than the calculated conductivity if no decrease in the ionization had taken place.

Conductance measurements. The measurements were performed with a Conductivity Meter CDM3 employing an immersion type conductivity cell, CDC 403, with a cell constant of 1.00 cm. The conductivity of the applied acetonitrile was less than 1×10^{-7} ohm^{-1} cm^{-1}.

Stopped-flow measurements. The measurements were performed with a Durrum Stopped-Flow Model D-110.

RESULTS

In Table 2 are listed the k_{N_3}/k_{N_3} ratios for the various triarylmethyl substrates at 25 °C in acetonitrile. (The results in Table 2 and in the following tables refer to experiments in which the mixture of the competing nucleophiles was added *to* the substrate if not otherwise stated).

The results in Table 2 clearly show that the azide ion, being an α-nucleophile, and an often used trapping agent for carbenium ions in solvolysis reactions,[29] is only as reactive as are the cyanate ion and the cyanide ion as viewed from the experimentally determined competition ratios, $k_{N_3^-}/k_{OCN^-}$ and $k_{N_3^-}/k_{CN^-}$, respectively. This suggests that the azide probe is of limited reliability in reactions toward triarylmethyl substrates in acetonitrile, as noted by Darwish and Preston.[15] From Table 2 it can also be seen that the effect of the *para*-substituents in triarylmethyl chlorides is small. Only toward triarylmethyl substrates containing substituents which strongly stabilize the carbenium ion, *i.e.* *p*-dialkylamino substituted derivatives, does the azide ion retain its exceptional reactivity in dipolar aprotic solvents.[13] In the usual S_N2 reactions toward aliphatic carbon compounds in acetonitrile the azide ion does not behave exceptionally and the following reactivity sequences are known:

MeI: $CN^- \gg N_3^- > OCN^- \approx NCS^-$ [30]
MeTos: $CN^- \gg N_3^- > OCN^- > NCS^-$ [31]

The thiocyanate ion appears to be significantly less reactive than the other three ions, as viewed from the competition experiments, and the relative reactivity of this ion toward the triarylmethyl substrates appears to parallel its reactivity in the typical S_N2 reactions. However, the thiocyanate ion may well act as a thionucleophile toward the triarylmethyl substrates and thus form an unstable triarylmethyl

Table 2. k_{N_3}/k_{N_3} ratios for various triarylmethyl sybstrates at 25 °C in acetonitrile.

Substrate	Substrate $\times 10^3$ M	$k_{N_3^-}/k_{CN^-}$	$k_{N_3^-}/k_{OCN^-}$	k_{OCN^-}/k_{CN^-}
Ph_3CCl	1.33	2.17 ± 0.06	1.34 ± 0.06	1.52 ± 0.06
Ph_3CBr	1.33	1.81 ± 0.09	1.25 ± 0.09	1.25 ± 0.06
Ph_3CClO_4	1.34	1.54 ± 0.09	1.98 ± 0.1	0.90 ± 0.06
$(p\text{-MePh})_3CCl$	1.15	1.57 ± 0.09	1.75 ± 0.09	0.85 ± 0.05
$(p\text{-MeOPh})_3CCl$	1.19	1.41 ± 0.08	1.87 ± 0.1	0.71 ± 0.04
		k_{CN^-}/k_{SCN^-}	k_{OCN^-}/k_{SCN^-}	
Ph_3CCl	1.33	6.75 ± 0.1	10.5 ± 0.1	
Ph_3CBr	1.33	4.91 ± 0.06	6.35 ± 0.06	
$(p\text{-MePh})_3CCl$	1.15	$\leq 19 \pm 8$	$\leq 16 \pm 7$	

thiocyanate.[32] During the isomerization of the first formed organic thiocyanate to the corresponding isothiocyanate, the ion competing with the thiocyanate ion for the original triarylmethyl substrate, is allowed once more to compete for the triarylmethyl moiety, eqn. 4.

$$\begin{aligned} RX + \begin{matrix} Y \\ NCS^- \end{matrix} &\longrightarrow \begin{matrix} RY \\ RSCN \end{matrix} \\ RSCN + \begin{matrix} Y \\ SCN^- \end{matrix} &\longrightarrow \begin{matrix} RY \\ RNCS \end{matrix} \end{aligned} \qquad (4)$$

The results from the studies involving the thiocyanate ion may therefore be ambiguous.

The leaving group appears to exert a pronounced influence upon the various competition ratios. Increasing dissociation of the triarylmethyl substrates seems to decrease the relative reactivity of the azide ion, and to increase the relative reactivity of the thiocyanate ion, but the general trend is by no means certain. The effect of the leaving group, however, is for most of the competition ratios significant, and should not be neglected. The dependence of rates of reactions of triphenylmethyl halides upon the displaced halide ion was first recognized by Hill.[33]

Table 3. The effect of concentration of reactants upon k_{OCN^-}/k_{CN^-} and $k_{N_3^-}/k_{CN^-}$.

Substrate	Substrate × 10^3 M	k_{OCN^-}/k_{CN^-}
Ph_3CCl	1.35	1.52 ± 0.06
	13.3	1.56 ± 0.06
Ph_3CBr	1.35	1.25 ± 0.06
	13.3	1.35 ± 0.06
		$k_{N_3^-}/k_{CN^-}$
Ph_3CCl	1.35	2.17 ± 0.06
	4.0	2.14 ± 0.06
Ph_3CClO_4	1.35	1.54 ± 0.09
	4.0	0.32 ± 0.02

In Table 3 are listed the results from some competition experiments performed with various reagent concentrations and in Table 4 are the experimentally determined competition ratios when the mixture of the nucleophiles was added *to* the substrate and *vice versa*.

The results in Tables 3 and 4 suggest that competition experiments toward weakly dissociated substrates may well be performed under differing experimental conditions. However, toward triphenylmethyl perchlorate, a completely dissociated substrate, various results may be obtained depending upon concentrations of reactants and experimental procedure. The significant change in the competition ratios upon a change in the concentration of triphenylmethyl perchlorate suggests that the electrophilic nature of the reacting species for this substrate is concentration dependent, but no explanation for this experimental fact is available at the present stage. In any event, the results in Tables 3 and 4 clearly indicate that detailed discussions based upon a limited number of experiments should be avoided.

In Tables 5, 6 and 7 are listed the results from competition experiments toward 4,4′4″-trimethoxytriphenylmethyl chloride in the presence of various amounts of lithium perchlorate, tetraphenylarsonium perchlorate, and tetraphenylarsonium chloride, respectively.

The results from the competition experiments in the presence of the various salts, Tables 5 to 7, can be summarized as follows:

1. The presence of lithium perchlorate and tetraphenylarsonium perchlorate (both salts increasing the dissociation of the alkyl halide)

Table 4. $k_{N_3^-}/k_{CN^-}$ as a function of mixing.

Substrate		Substrate × 10^3 M	$k_{N_3^-}/k_{CN^-}$
Ph_3CCl	Substrate added to nuc.	1.35	2.17
	Nuc. added to substrate	1.35	2.1
Ph_3CCl	Substrate added to nuc.	4.0	2.1
	Nuc. added to substrate	4.0	2.1
Ph_3CClO_4	Substrate added to nuc.	4.0	0.98
	Nuc. added to substrate	4.0	0.32
	» » » »	1.35	1.54

Table 5. The effect of lithium perchlorate upon $k_{N_3^-}/k_{CN^-}$ and $k_{N_3^-}/k_{OCN^-}$. The substrate is (*p*-MeOPh)$_3$CCl.

(*p*-MeOPh)$_3$CCl × 10^3 M	$LiClO_4$ × 10^4 M	$k_{N_3^-}/k_{CN^-}$	$k_{N_3^-}/k_{OCN^-}$
1.34	0.00	1.41 ± 0.08	1.87 ± 0.1
1.34	0.60	1.43	2.15
1.34	2.00	1.50	2.49
1.31	6.00	1.91	3.23
1.31	16.0	2.32	3.70
1.31	180	3.75	≈12

Table 6. The effect of tetraphenylarsonium perchlorate upon $k_{N_3^-}/k_{CN^-}$ and $k_{N_3^-}/k_{OCN^-}$. The substrate is (*p*-MeOPh)$_3$CCl.

(*p*-MeOPh)$_3$CCl × 10^3 M	Ph_4AsClO_4 × 10^4 M	$k_{N_3^-}/k_{CN^-}$	$k_{N_3^-}/k_{OCN^-}$
1.34	0.00	1.41 ± 0.08	1.87 ± 0.1
1.28	0.33	1.47	2.45
1.28	0.67	1.58	
1.24	3.33	1.82	2.94
1.18	6.00	1.94	
1.23	16.5	2.08	
1.29	29.6	2.23	

Table 7. The effect of tetraphenylarsonium chloride upon $k_{N_3^-}/k_{CN^-}$ and $k_{N_3^-}/k_{OCN^-}$. The substrate is (*p*-MeOPh)$_3$CCl.

(*p*-MeOPh)$_3$CCl × 10^3 M	Ph_4AsCl × 10^4 M	$k_{N_3^-}/k_{CN^-}$	$k_{N_3^-}/k_{OCN^-}$
1.34	0.00	1.41 ± 0.08	1.87 ± 0.1
1.34	0.60	1.42	2.20
1.34	1.74	1.41	2.34
1.34	5.90	1.38	2.59
1.34	11.6	1.31	2.67
1.34	17.4	1.22	2.48
1.34	23.1		2.35
1.24	52.1	0.55	1.98

increases the trapping ability of the azide ion, especially relative to that of the cyanate ion. The effect is noticeable even for concentrations of these two salts considerably smaller than that of the substrate and thus the reacting nucleophiles. The effect of the cation appears to be negligible.

2. The presence of tetraphenylarsonium chloride, a source of the common ion, decreases only to a small extent the $k_{N_3^-}/k_{CN^-}$ ratio. Only for concentrations of tetraphenylarsonium chloride exceeding that of the substrate is this trend significant. The $k_{N_3^-}/k_{OCN^-}$ ratios increase for concentrations of the ionic chloride up to that of the substrate, but then decrease.

DISCUSSION

As has been pointed out by Kovačević and co-workers,[34] the azide probe seems to yield useful mechanistic informations in two extreme cases, *i.e.* direct displacement reactions (S_N2) and when carbenium ions are the only possible reacting species. Since the relative ability of

the various ions to compete for slightly dissociated substrates, like triphenylmethyl chloride and triphenylmethyl bromide, is about the same as when the completely dissociated triphenylmethyl perchlorate is employed as the substrate, the triphenylmethylcarbenium ion can not possibly be the reacting species in the present competition experiments (Table 2). The significant influence of the leaving group in the triphenylmethyl halides upon the competition ratios may be considered as additional evidence againts the triphenylmethylcarbenium ion being the reacting species. According to Kovačević,[34] the azide ion should therefore not show any exceptional preference for the triarylmethyl substrates in acetonitrile as experienced in the present study.

As shown in the Experimental Part, the addition of a salt of a non-nucleophilic anion to a solution of a triphenylmethyl halide in acetonitrile, causes a rapid increase of the concentration of the triphenylmethylcarbenium ion, Ph_3C^+. Salts of nucleophilic ions, on the other hand, cause a rapid reduction in the concentration of the triphenylmethylcarbenium ion. None of the examined reactions was sufficiently slow to be followed by the stopped-flow technique.

These unsuccessful kinetic studies allow one to propose that when ionic species are added to solutions of triphenylmethyl substrates in acetonitrile, the equilibria between the various possible species [2-5] are set up extremely rapidly. This reorganization of the various species may well be the first step in reactions of triarylmethyl substrates in acetonitrile. As a prerequisite for this mechanism, the energy required for the transformation of colourless species, as ion pairs of various types, presumably tetrahedral and thus sp^3 hybridized, to coloured sp^2 hybridized carbenium ions containing coplanar central bonds [35] and *vice versa* must be very low. The facile dissociation of triarylmethyl substrates in a number of solvents suggests this to be the case. The repeatedly documented stability of triarylmethyl carbenium ions which do not contain stabilizing substituents may well be due to an effect of the lattice in the case of crystalline salts of carbenium ions and due to the solvating power of the solvent when the usual protic solvents are employed.[36]

In acetonitrile, these stabilizing effects are largely absent and the stability of the triarylmethylcarbenium ions in this solvent relative to the various ion pairs is probably very low. In a reaction between a triarylmethyl substrate and a nucleophilic anion, the species first formed by the very rapid deionization step may well be the actual electrophilic species in the consecutive reaction (s) by which the final product is formed. Since the species formed through the deionization step are presumably far less selective toward the various nucleophiles than are the free or solvated carbenium ions, the reaction between the weakly separated species formed in the first step and the various nucleophiles is rapid and k_{N_1}/k_{N_2} ratios close to unity are observed. The fact that ion pairs may well be considerably less selective than are free and solvated carbenium ions was first recognized by Ritchie.[37]

The mechanism for the reaction between a completely dissociated triarylmethyl substrate, RX, and a nucleophilic anion N^-, may thus be as depicted in the following scheme.

$$RX \rightleftharpoons R^+ + X^-$$

$$A:\ R^+ + N^- \xrightarrow{k_2} RN$$

$$B:\ R^+ + N^- \xrightarrow{k_b} (R^{\delta+}\cdots N^{\delta-}) \begin{cases} \xrightarrow{k_c} RN \\ \xrightarrow{k_d} N^x \end{cases} RN^x$$

In the case of reactions with triarylmethyl substrates, which yield stabilized carbenium ions as do triarylmethyl substrates containing *p*-dimethylamino substituents, k_b and k_c are negligible compared with k_2. No deionization takes place due to the stability of the carbenium ion and the carbenium ion alone is the electrophilic species. Second order kinetics are observed and the azide ion is at least three orders of magnitude more reactive than is the cyanide ion both in protic and aprotic solvents.[13] For a recent review, see Ref. 36.

In reactions of triarylmethyl substrates which do not contain substituents capable of exerting a stabilizing effect upon the corresponding carbenium ions, as the substrates used in the

present work, k_2 is considerably smaller than k_b and k_c. (The carbenium ions are consumed nearly entirely in the deionization step and will have negligible influence on the product composition.) The last step in B may be either an intramolecular rearrangement from an ion pair to the stable product or, in view of the small selectivity of ion pairs as suggested by Ritchie,[37] k_d is considerably greater than k_c and the final step is thus a displacement reaction. The fact that the trapping ratios when triphenylmethyl perchlorate was the substrate were found to be a function of experimental procedure may be due to varying degree of deionization.

In the case of slightly dissociated substrates, *i.e.* triarylmethyl halides, the deionization of the minute amount of carbenium ions will take place in the first step as for completely dissociated substrates. Ionization of these substrates is actually inhibited by the halide ions prior to the addition of the competing nucleophiles. This effect is the probable reason for the very limited dissociation of these substrates in acetonitrile (see Experimental Part). Since ion pairs of approximately the same type are obtained from completely dissociated substrates in the presence of nucleophilic anions and from slightly dissociated substrates due to the deionizing effect of the nucleophilic counter ions, the same trapping ratios are to be expected for the two classes of substrates, in agreement with the results of the present study.

In Table 8 some experimentally determined k_{N_1}/k_{N_3} ratios are compared with values obtained by multiplying the k_{N_1}/k_{N_3} and k_{N_2}/k_{N_3} ratios. The excellent agreement between the observed and calculated competition ratios may be considered as additional evidence for a common mechanism B in the studied reactions.

Upon the addition of increasing amounts of the ionizing perchlorate, Tables 5 and 6, the $k_{N_3^-}/k_{CN^-}$ ratio and especially the $k_{N_3^-}/k_{OCN^-}$ ratio is seen to increase. This suggests that, in the presence of this non-nucleophilic anion, the deionization due to the competing nucleophilic anions does not completely suppress the carbenium ions and some product may then be formed by mechanism A, *i.e.* through reaction between carbenium ions and the nucleophilic anions. The trend in the competition ratios in Tables 5 and 6 clearly indicate that, when free carbenium ions are available as electrophilic species, the relative reactivity of the anions toward triarylmethylcarbenium ions is $N_3^- > CN^- > OCN^-$, in agreement with the usual reactivity sequence toward carbenium ions.[13] Upon addition of the deionizing chloride ion, Table 7, a small decrease of the $k_{N_3^-}/k_{CN^-}$ ratio is observed, suggesting that the reaction depicted by A is even more depressed.

The finding that the $k_{N_3^-}/k_{CN^-}$ ratios decrease with increasing dissociation constants of the triarylmethyl substrates, Table 2, deserves some further comment. It is highly probable that, due to the extreme reactivity of azide ions toward carbenium ions, the majority of the ion pairs formed from the carbenium ions in the deionization step are ion pairs from the carbenium and azide ions. Less free azide ions will thus be left in the solution and, if the final step in mechanism B is a displacement reaction, the formation of organic cyanides will be favoured.

The deionization mechanism as suggested above for the first step in the reaction between

Table 8. Comparison between k_{N_1}/k_{N_3} determined experimentally and from the product of k_{N_1}/k_{N_3} and k_{N_2}/k_{N_3}.

Substrate	$k_{N_3^-}/k_{CN^-}$ Observed	Calc.[a]	k_{OCN^-}/k_{CN^-} Observed	Calc.[b]
Ph_3CCl	2.17 ± 0.06	2.03 ± 0.18	1.52 ± 0.06	1.56 ± 0.05
Ph_3CBr	1.81 ± 0.09	1.56 ± 0.16	1.25 ± 0.06	1.29 ± 0.04
Ph_3CClO_4	1.54 ± 0.09	1.78 ± 0.18		
$(p\text{-MePH})_3CCl$	1.57 ± 0.09	1.49 ± 0.15		
$(p\text{-MeOPh})_3CCl$	1.41 ± 0.08	1.32 ± 0.12		

[a] $k_{N_3^-}/k_{CN^-}(\text{calc.}) = k_{N_3^-}/k_{OCN^-} \times k_{OCN^-}/k_{CN^-}$ (Table 2).
[b] $k_{OCN^-}/k_{CN^-}(\text{calc.}) = k_{OCN^-}/k_{SCN^-} \times k_{SCN^-}/k_{CN^-}$ (Table 2).

triarylmethyl substrates and nucleophilic anions demands that carbenium ions are destabilized relative to the less dissociated ion pairs in the presence of nucleophilic species. From a purely electrostatic point of view the opposite effect is to be expected. The only possible explanation for the deionization appears to be a stabilization of weakly dissociated species relative to carbenium ions through interaction between the nucleophilic anions and the phenyl groups favouring sp^3 hybridized species at the expence of sp^2 hybridized planar carbenium ions. In protic solvents the nucleophilic anions due to their solvation shell will not exert this effect and the triarylmethylcarbenium ions, stabilized by these solvents, are the electrophilic species favouring the formation of triarylmethyl azides.

Recent magnetic resonance studies on triarylmethylcarbenium ions have revealed that only 25 to 30 % of the positive charge resides on the central carbon atoms, the remaining charge being located in the phenyl groups, notably in the *para*-positions.[38] It is highly possible that in triarylmethylcarbenium ions which do not contain stabilizing substituents, this delocalization of positive charge is sufficient to make the central carbon atom in the ion pair to act as a more attractive electrophilic center for the nucleophilic species than the central carbon atom in the carbenium ion.

The consequences of the suggested deionization mechanism on salt effects in S_N1 reactions are obvious. When carbenium ions or related species are the only possible intermediates in a reaction, and these intermediates are not sufficiently stabilized by the solvent, nucleophilic species may exert very negative salt effects.[8–10] The deionization mechanism may also be the reason why highly erratic salt effects are observed even in protic solvents.[7] In line with the suggestion that the deionizatio mechanism is only operative in reactions of substrates with delocalized charge on the corresponding carbenium ion it is interesting to note that very small and even negative *b*-values in the Winstein equation [1,2,6] are observed only when the reacting substrate contains several phenyl groups.[7,10]

The special effect observed in the present study may be general in aprotic solvents, but since the solvation of the nucleophilic species appears to enter as an important factor, effects of various magnitude may be observed. In this context it is interesting to note that triphenylmethyl halides have greatly varying dissociation constants in the various dipolar aprotic solvents.[20,39] This suggests that trapping ratios, salt effects *etc.* in reactions of triarylmethyl substrates may vary from one dipolar solvent to another.

Acknowledgement. The authors are indebted to Dr. G. W. Francis for valuable comments.

REFERENCES

1. Ritchie, C. D. In Coetzee, J. F. and Ritchie, C. D., Eds., *Solute-Solvent Interactions*, Marcel Dekker, New York and London 1969, p. 272.
2. Winstein, S., Kleindienst, P. E., Jr. and Robinson, G. C. *J. Amer. Chem. Soc. 83* (1961) 885.
3. Eigen, M. *Discuss. Faraday Soc. 24* (1957) 25.
4. Atkinson, G. and Kor, S. K. *J. Phys. Chem. 71* (1967) 673.
5. Olah, G. A. *J. Amer. Chem. Soc. 94* (1972) 808.
6. Winstein, S., Appel, B., Baker, R. and Diaz, A. *Chemical Society (London) Special Publication, 19* (1965) 109.
7. Bunton, C. A., Del Pesco, T. W., Dunlop, A. M. and Yang, K.-U. *J. Org. Chem. 36* (1971) 887.
8. Ceccon, A., Fava, A. and Papa, J. *J. Amer. Chem. Soc. 91* (1969) 5547.
9. Loupy, A. and Seyden-Penne, J. *C. R. Acad. Sci. Ser. C 273* (1971) 1665.
10. Austad, T. and Songstad, J. *Acta Chem. Scand. 26* (1972) 3141.
11. Parker, A. J. *Chem. Rev. 69* (1969) 1.
12. Braunmann, J. I. and Archie, W. C., Jr. *J. Amer. Chem. Soc. 92* (1970) 5891.
13. Ritchie, C. D., Shiner, G. A. and Badding, V. G. *J. Amer. Chem. Soc. 89* (1967) 2063.
14. Fava, A., Iliceto, A., Ceccon, A. and Koch, P. *J. Amer. Chem. Soc. 87* (1965) 1045.
15. Darwish, D. and Preston, E. A. *Tetrahedron Lett.* (1964) 113.
16. Austad, T., Songstad, J. and Åse, K. *Acta Chem. Scand. 25* (1971) 331.
17. Austad, T., Songstad, J. and Stangeland, L. J. *Acta Chem. Scand. 25* (1971) 2327.
18. Lorand, J. P. and Bartlett, P. D. *J. Amer. Chem. Soc. 88* (1966) 3294.
19. Mayer, U. and Gutmann, V. *Monatsh. Chem. 102* (1971) 148.
20. Longworth, W. R. and Mason, C. P. *J. Chem. Soc. A.* (1966) 1164.
21. Davies, G. L., Hay, D. H. and Wilkams, G. H. *J. Chem. Soc.* (1956) 4397.
22. Stangeland, L. J., Austad, T. and Songstad, J. *Acta Chem. Scand. 27* (1973) 3919.

23. Bacon, R. G. R., Köchling, J. and Robinson, T. A. *J. Chem. Soc.* (1964) 5600.
24. Bentley, A., Evans, A. G. and Halpern, J. *Trans. Faraday Soc.* (1951) 711.
25. Zanella, P. and Tagliani, G. *J. Organometal. Chem. 12* (1968) 355.
26. Plazzogna, G., Zanella, P. and Doretti, L. *J. Organometal. Chem. 29* (1971) 169.
27. Springer, C. H., Coetzee, J. G. and Kay, R. L. *J. Phys. Chem. 73* (1969) 471.
28. Popov, A. I. and Humphrey, R. E. *J. Amer. Chem. Soc. 81* (1959) 2043.
29. Raber, D. J., Harris, J. M., Hall, R. E. and v. R. Schleyer, P. *J. Amer. Chem. Soc. 93* (1971) 4821 and 4829.
30. Austad, T., Engemyr, L. B. and Songstad, J. *Acta Chem. Scand. 25* (1971) 3536.
31. Engemyr, L. B. and Songstad, J. *Acta Chem. Scand. 26* (1972) 4179.
32. Miotti, U. and Ceccon, A. *Ann. Chim. (Rome) 54* (1964) 851.
33. Hill, E. A. *Chem. Ind. (London)* (1965) 1696.
34. Kovačević, D., Majerski, Z., Borčić, S. and Sunko, D. E. *Tetrahedron 28* (1972) 2469.
35. Andersen, P. and Klewe, B. *Acta Chem. Scand. 19* (1965) 791.
36. Ritchie, C. D. *Accounts Chem. Res. 5* (1972) 348.
37. Ritchie, C. D. *J. Amer. Chem. Soc. 93* (1971) 7324.
38. Ray, G. J., Kurland, R. J. and Colter, A. K. *Tetrahedron 27* (1971) 735.
39. Pocker, Y. *J. Chem. Soc.* (1958) 240.

Received January 22, 1975.

Acta Chemica Scandinavica A 29 (1975) 672—676

NMR Studies on Cyclic Arsenites. ^{1}H NMR Spectral Analysis and Conformational Studies of 2-Chloro-5-methyl- and 2-Phenyl-5-methyl-1,3,2-oxathiarsolane and 2-Chloro-5-methyl-1,3,2-dithiarsolane and -1,3,2-dioxarsolane

DAGFINN W. AKSNES and MALVIN BJORØY

Department of Chemistry, University of Bergen, Allégaten 70, 5014 Bergen-Univ., Norway

The ^{1}H NMR spectra of the title compounds have been completely analyzed although no separation of the geometrical isomers was achieved. Approximate values of the ring torsional angles have been obtained. The present results demonstrate the tendency of a sulfur atom to increase the puckering of the ring. The NMR data are adequately described on the basis of flexible twist-envelope conformations. In the *cis* isomers the steric requirements of the substituents seem to confine the ring to a particular conformation whereas the *trans* forms get significant contributions from two pseudo-rotamers.

It is generally accepted that the five-membered ring exists in highly flexible puckered conformations where only the more bulky substituents have specific steric interactions.[1,2] NMR spectroscopy has supplied detailed information about five-membered rings although facile interconversions between numerous equi-energy conformers present considerable difficulties.

In preceeding papers the NMR spectra of a series of arsolanes,[3,4] and phospholanes [5,6] have been studied. The NMR spectra were adequately explained on the basis of rapidly interconverting non-planar forms with a stable configuration at arsenic or phosphorus. Our previous results demonstrated the tendency of a sulfur atom to increase the puckering of the ring. Similar observations have also been reported for the 1,3-dithiolane [7,8] and 1,3-oxathiolane [9] rings as compared with the 1,3-dioxolane ring.

2-Substituted 5-methyl-1,3,2-dioxarsolanes and -1,3,2-dithiarsolanes [4] as well as the analogous phospholanes,[5,6,10] have been found to exist as *cis* and *trans* isomers with the latter predominating. In a series of 2,4-dialkyl 1,3-dioxolanes [2] and -1,3-oxathiolanes,[9] however, the *cis* forms are thermodynamically more stable than the *trans* isomers.

In order to obtain more information about externally substituted arsolanes we have prepared compounds I–IV and investigated their ^{1}H NMR spectra. The ^{1}H NMR spectra of the *cis* and *trans* isomers have been fully analyzed for the three latter compounds.

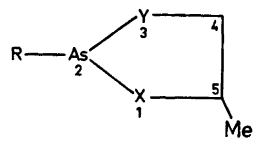

I; R=Cl, X=O, Y=S
II; R=Ph, X=O, Y=S
III; R=Cl, X=Y=S
IV; R=Cl, X=Y=O

EXPERIMENTAL

Compound I was prepared from 3-mercaptopropane-2-ol and trichloroarsine in tetrachloromethane solution under dry N_2 atmosphere; b.p.$_{0.2}$ 70 °C. Compound II was synthesized from 3-mercaptopropane-2-ol and phenyl dichloroarsine in diethyl ether solution using triethylamine as base; b.p.$_{1.0}$ 100 °C. The pre-

paration of III and IV has been described in a previous paper.[4]

The NMR spectra were examined in deuteriochloroform and carbon disulfide solutions (*ca.* 50 % v/v). The NMR samples were prepared as previously described.[3,4]

The 60 MHz and 100 MHz spectra were recorded on JEOL-C-60H and VARIAN HA-100 spectrometers, respectively. Line positions were obtained by averaging the results of four frequency-calibrated spectra at about 50 Hz sweep width (1 – 1.5 Hz/cm).

The NMR spectra were analyzed as $ABCD_3$ spin systems using the computer programs UEANMR II,[11] UEAITR[12] and KOMBIP.[13] The computations were performed on a UNIVAC 1110 computer. The root-mean-square deviations of 63 – 90 experimental and calculated transitions were less than 0.08 for the *trans* isomers and less than 0.10 for the *cis* isomers (except *cis*-IV).

The graphical output was obtained using a Calcomp Plotter.

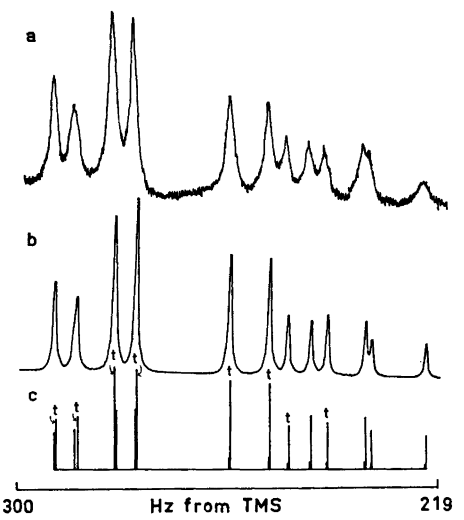

Fig. 1. The BC region of the 100 MHz spectrum of compound II: a, experimental spectrum; b and c, computed spectra for a *cis:trans* distribution of 1:2. Transition lines originating from the *trans* isomer are labelled t.

RESULTS AND DISCUSSION

The spectral analysis of compounds II – IV was tedious owing to partial overlap of spectral lines from pairs of geometrical isomers. The trial

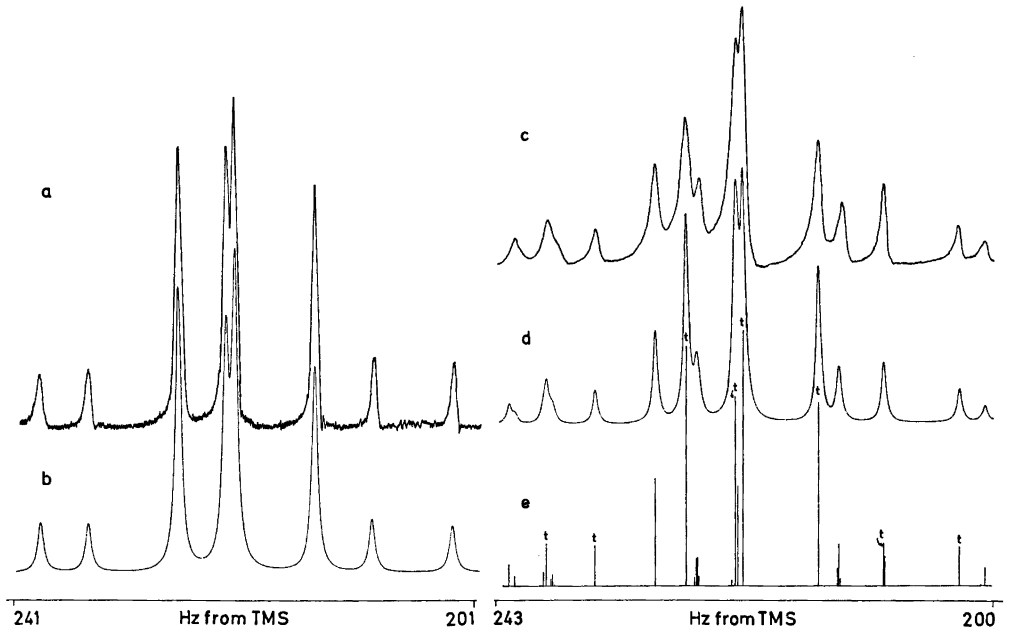

Fig. 2. The BC region of the 60 MHz spectrum of compound III: a and b, experimental and computed exchange-averaged spectra, respectively, resulting from rapid interconversions of the *cis* and *trans* forms (a small amount of tetraphenylarsonium chloride was added to the sample used for spectrum c)[4]; c, experimental spectrum of the individual isomers; d and e, computed spectra for a *cis:trans* distribution of 1:2. Transition lines originating from the *trans* iromer are labelled t.

parameters were obtained by analyzing the spectra as $ABPX_3$ systems on a first-order basis. However, only a lengthy trial-and-error analysis yielded acceptable trial values. The refined parameters resulting from iterative computer-analysis of the $ABCD_3$ spin systems, are listed in Table 1. The contributions from the individual isomers of compounds II and III are shown in Figs. 1 and 2 together with the calculated and experimental total spectra. The effect of rapid exchange of chlorine on the spectrum of III is also demonstrated in Fig. 2.

The methyl spectrum of compounds II – IV consists of two doublets with intensity ratio *ca.* 1:2, that partly overlap as shown in the low-temperature spectrum of compound IV in Fig. 3. The two individual methyl signal groups show that these compounds exist as a mixture of *cis* (A) and *trans* (B) isomers. However, only exchange-averaged NMR spectra resulting from rapid exchange of chlorine [2–5] were observed for I and IV at 30 °C. No significant change in the spectrum of I was observed in the temperature range 30 to −100 °C. For compound IV, however, we were able to "freeze out" both isomers at −90 °C (Fig. 3).

The methyl signals of the major isomers appear at higher field than the corresponding signals of the minor isomers. The low-field methyl signals have been assigned to the *cis* isomers since protons *cis* to the As – R bond should suffer downfield shifts according to the para-

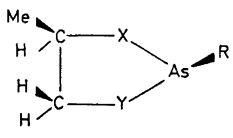

A

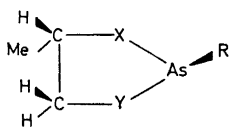

B

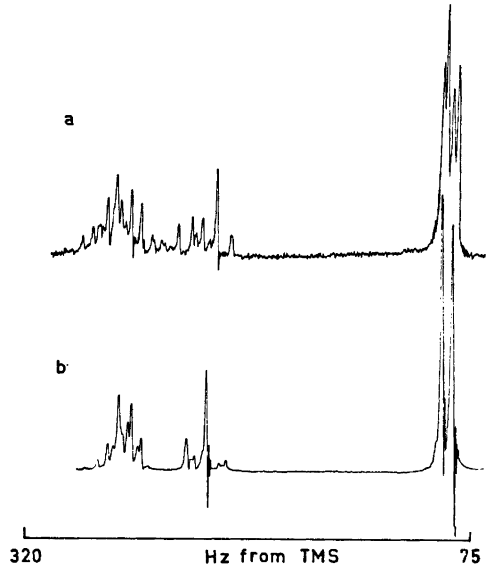

Fig. 3. Experimental 60 MHz spectrum of compound IV in CS_2 solution: a, −90 °C; b, 30 °C

Table 1. 60 MHz NMR parameters and ring torsional angles (ψ) of compounds I – IV.[a]

Compound	I	II[b]		III		IV	
		cis	*trans*	*cis*	*trans*	*cis*	*trans*
Temp. °C	30	34		30		−90	
ν_A[c]	4.78	3.92	4.11	4.22	4.46	4.36	4.49
ν_B	3.41	2.85	2.85	3.86	3.80	4.51	4.36
ν_C	3.01	2.34	2.52	3.57	3.58	3.80	3.55
ν_{Me}	1.49	1.34	1.18	1.63	1.48	1.40	1.36
J_{BC}[d]	−11.39	−11.69	−11.23	−12.70	−12.15	−9.2	−8.74
J_{AB}	4.18	3.77	4.11	3.59	4.13	5.9	5.65
J_{AC}	9.59	10.56	7.69	8.89	6.61	9.2	8.70
J_{AMe}	6.06	5.92	5.90	6.64	6.60	5.8	6.17
J_{BMe}	0.00	0.00	0.00	−0.10	−0.02	0.0	−0.28
J_{CMe}	−0.03	0.05	0.04	−0.05	−0.03	0.0	0.00
R	2.3	2.8	1.9	2.6	1.6	1.6	1.5
ψ(deg.)	59	62	56	61	53	53	52

[a] The methine and methylene protons are labelled A and BC, respectively. [b] Measured at 100 MHz. [c] Chemical shifts in δ-values. [d] Coupling constants in Hz.

magnetic shift effect of chlorine and phenyl substituents.[3-6,14,15] Furthermore, as a result of the stereospecific effect the methine proton signals of the *trans* isomers (H_A *cis* to As–R) appear at lower field than the corresponding signals of the *cis* isomers (H_A *trans* to As–R), The assignment of the methylene signals followed from the spectral analysis. The chemical shifts of the methylene protons indicate that the anisotropy effect of the 5-methyl group rather than 2-R group, dominates.

The observed predominance of the *trans* isomers in the present compounds and related arsolanes [4] and phospholanes,[5,6] in contrast to the situation in 2,4-dialkyl-1,3-dioxolanes [2] and -1,3-oxathiolanes,[9] probably reflects changes in 1,3-steric interactions as a result of replacing carbon 2 by a trivalent group V element.

On the basis of the present NMR studies (*vide infra*) and previous results,[4] we believe that the investigated molecules can be adequately described by the twist-envelope conformations below. Since pseudo-libration is expected to occur in these systems,[1,2] each of these conformations represents the average of

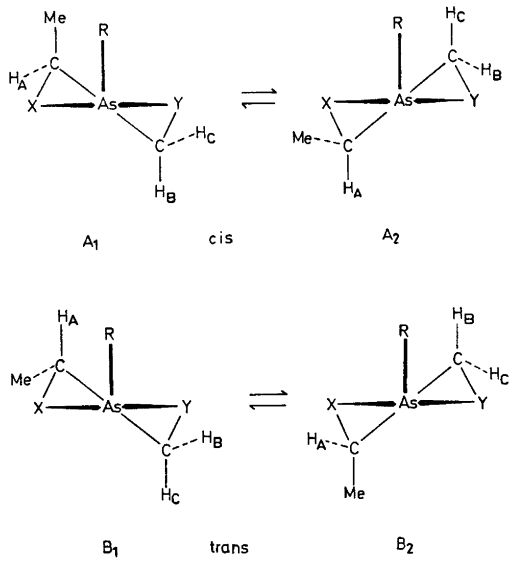

a continuum of conformations of practically equal energy.

The X–C–C–Y torsional angle, ψ, of these ring systems has been calculated from the vicinal coupling constants of the CH_2CHCH_3-moiety using the *R*-value method due to Lambert.[16] However, we wish to emphasize that the calculated torsional angles characterize only the mean geometry of the geometrical isomers. The estimated value of ψ in *cis*-IV is probably too small due to a significant uncertainty in the spectral parameters of that particular isomer.

The results of this study together with those presented earlier [4,6] have demonstrated that replacement of the oxygen atoms by sulfur increases the ring puckering by 3–6°. Similar observations have also been made for 1,3-dithiolanes,[7,8] and 1,3-oxathiolanes.[7]

The J_{AC} coupling constant is 5–7 Hz greater than J_{AB} in the *cis* isomers. This difference is reduced to 2.5–3.5 Hz in the corresponding *trans* forms. Bergesen and Bjorøy [6] have also obtained similar results for 2-substituted 5-methyl-1,3,2-dithiaphospholanes and -1,3,2-oxathiaphospholanes. The large value of J_{AC} in the *cis* forms suggests that this coupling involves the pseudo-axial hydrogens of the A_2 rotamer. A significant contribution from A_1-like rotamers would result in a smaller value of J_{AC} and a corresponding increase in J_{AB}. The equatorial preference of the 5-methyl group probably reflects severe *syn*-axial interactions between the substituents at carbon 5 and arsenic in the A_1 conformer.

In contrast, the reduced difference between J_{AB} and J_{AC} in the *trans* forms indicates comparable contributions from the B_1 and B_2 pseudo-rotamers. This implies that the energy minima of the *trans* isomers are less affected by the steric requirements of the substituents than the *cis* isomers where a particular conformation appears to be strongly favoured.

Since the NMR parameters of compounds III and IV, subjected to rapid exchange of chlorine, have been reported,[4] it is of interest to calculate the corresponding weighted average values from the present data. The following values of the vicinal coupling constants (in Hz) have been obtained by assuming a 1:2 distribution of the *cis* and *trans* isomers, respectively.

Compound III:

$J_{BC} = -12.35$ (−12.04); $J_{AB} = 3.90$ (4.04)
$J_{AC} = 7.39$ (7.18); $J_{AMe} = 6.62$ (6.63)

Compound IV:

$J_{BC} = -8.89$ (−9.14); $J_{AB} = 5.73$ (5.74)
$J_{AC} = 8.87$ (8.88); $J_{AMe} = 6.05$ (6.04)

The agreement with the previously reported values,[4] in parentheses, is better than expected in view of possible solvent and temperature effects.

The measured geminal coupling constants, J_{BC}, are well within the reported ranges for five-membered rings.[1-10,14,15,,17] The magnitude of J_{BC} is seen to increase when passing from 1,3,2-dioxarsolanes to 1,3,2-dithioarsolanes *via* 1,3,2-oxathiarsolanes. This increase in $|J_{BC}|$ is mainly due to the electronegativity difference between oxygen and sulfur and to increased ring puckering.[18]

REFERENCES

1. Altona, C., Buys, H. R. and Havinga, E. *Rec. Trav. Chim. Pays-Bas 85* (1966) 973.
2. Willy, W. E., Binsch, G. and Eliel, E. L. *J. Amer. Chem. Soc. 92* (1970) 5394.
3. Aksnes, D. W. and Vikane O. *Acta Chem. Scand. 26* (1972) 835, 2532.
4. Aksnes, D. W. and Vikane, O. *Acta Chem. Scand. 27* (1973) 1337, 2135.
5. Bergesen, K. and Vikane, T. *Acta Chem. Scand. 26* (1972) 2153.
6. Bergesen, K. and Bjorøy, M. *Acta Chem. Scand. 27* (1973) 1103, 3477.
7. Sternson, L. A., Coviello, D. A. and Egan, R. S. *J. Amer. Chem. Soc. 93* (1971) 6529.
8. Keskinen, R., Nikkilä, A. and Pihlaja, K. *J. Chem. Soc. Perkin Trans. 2* (1973) 1376.
9. Keskinen, R., Nikkilä, A., Pihlaja, K. and Riddell, F. G. *J. Chem. Soc. Perkin Trans. 2* (1974) 466.
10. Goldwhite, H. *Chem. Ind. (London)* (1964) 495.
11. Woodman, C. M. *Personal communication.*
12. Johannesen, R. B., Ferretti, J. A. and Harris, R. K. *J. Magn. Resonance 3* (1970) 84.
13. Aksnes, D. W. *KOMBIP, Progr. No. 205*, Quantum Chemistry Program Exchange, Indiana University, Chemistry Department, Bloomington, Ind.
14. Haake, P. McNeal, J. P. and Goldsmith, E. J. *J. Amer. Chem. Soc. 90* (1968) 715.
15. Peake, S. C., Fild, M., Schmutzler, R., Harris, R. K., Nichols, J. M. and Rees, R. G. *J. Chem. Soc. Perkin Trans 2* (1972) 380.
16. Lambert, J. B. *Accounts Chem. Res. 4* (1971) 87.
17. Cahill, R., Cookson, R. C. and Crabb, T. A. *Tetrahedron 25* (1969) 4681, 4711, and references therein.
18. Anteunis, M., Swaelens, G. and Gelan, J. *Tetrahedron 27* (1971) 1917.

Received February 28, 1975.

Acta Chemica Scandinavica A 29 (1975) 677—689

Multicomponent Polyanions. 14. A Potentiometric and Spectrophotometric Study of Equilibria in the $H^+ - MoO_4^{2-} - HAsO_4^{2-}$ System in 3.0 M $Na(ClO_4)$ Medium Covering the Range $1.5 < -\log[H^+] < 9$

LAGE PETTERSSON

Department of Inorganic Chemistry, University of Umeå, S-901 87 Umeå, Sweden

Equilibria between H^+, MoO_4^{2-} and $HAsO_4^{2-}$ have been studied in 3.0 M $Na(ClO_4)$ medium at 25 °C by means of potentiometric (glass electrode) and to some extent by spectrophotometric measurements. The $-\log[H^+]$ range 1.5 – 9 has been covered. Data have been analysed using the least squares computer program LETAGROPVRID. All data could be explained with two types of species, the colourless $(H^+)_6(MoO_4^{2-})_5(HAsO_4^{2-})_2$, $(H^+)_{10}(MoO_4^{2-})_6(HAsO_4^{2-})_2$, $(H^+)_{11}(MoO_4^{2-})_6(HAsO_4^{2-})_2$, $(H^+)_{12}(MoO_4^{2-})_6(HAsO_4^{2-})_2$ and the "yellow" $(H^+)_{14}(MoO_4^{2-})_9(HAsO_4^{2-})$, $(H^+)_{15}(MoO_4^{2-})_9(HAsO_4^{2-})$, $(H^+)_{16}(MoO_4^{2-})_9(HAsO_4^{2-})$, $(H^+)_{17}(MoO_4^{2-})_9(HAsO_4^{2-})$ with the following formation constants: $\log \beta_{6,5,2} = 60.92 \pm 0.04$, $\log \beta_{10,6,2} = 75.25 \pm 0.04$, $\log \beta_{11,6,2} = 80.73 \pm 0.05$, $\log \beta_{12,6,2} = 84.07 \pm 0.07$, $\log \beta_{14,9,1} = 100.11 \pm 0.02$, $\log \beta_{15,9,1} = 103.81 \pm 0.05$, $\log \beta_{16,9,1} = 106.14 \pm 0.05$, $\log \beta_{17,9,1} = 107.48 \pm 0.05$. The errors given are $3\sigma(\log \beta)$.

The preliminary spectrophotometric data confirm the results from the emf investigation.

Tentative structures of the proposed complexes are given.

In a current project at this department, aqueous three-component polyanion equilibria are systematically investigated using equilibrium as well as structural methods. An equilibrium analysis in the system $H^+ - MoO_4^{2-} - HPO_4^{2-}$ in the range $1.5 < -\log[H^+] < 9$ has shown that there are two series of heteropolyanions formed, one colourless with the complexes $Mo_5P_2O_{23}^{6-}$, $HMo_5P_2O_{23}^{5-}$ and $H_2Mo_5P_2O_{23}^{4-}$ and one, "yellow" with the complexes $H_3Mo_9PO_{34}^{6-}$, $H_4Mo_9PO_{34}^{5-}$, $H_5Mo_9PO_{34}^{4-}$, $H_6Mo_9PO_{34}^{3-}$ and $Mo_{18}P_2O_{62}^{6-}$. The former predominates at Mo/P ratios $\lesssim 2.5$ and the latter at Mo/P ratios $\gtrsim 9$. For a complete survey of the equilibrium results of this system together with structural and other results the reader is referred to Ref. 1.

In order to see whether the same type of complexes are found when phosphate ions are replaced with arsenate ions, we have performed a complete equilibrium analysis covering the range $1.5 < -\log[H^+] < 9$ and it is the result of this investigation that will be reported and discussed in the present paper. The equilibria that will be studied can be written in the general form.

$$p\mathrm{H}^+ + q\mathrm{MoO_4^{2-}} + r\mathrm{HAsO_4^{2-}} \rightleftharpoons (\mathrm{H}^+)_p(\mathrm{MoO_4^{2-}})_q(\mathrm{HAsO_4^{2-}})_r$$

For brevity a complex formed will in the following often be given the notation (p,q,r).

Comments on some previous work. Complex formation between molybdate and arsenate ions in acidified solutions has long been known. As early as 1826 Berzelius [2] reported that arsenic acid with an excess of molybdic acid forms a yellow species. In the decades around 1900 the molybdate-arsenate system was the object of extensive research activity and a large number of crystalline molybdoarsenates were identified. The most frequently found Mo/As ratios in the compounds analysed are 9 and 3 but the ratios 12, 8, 2.5, 2, and 1 have also been proposed. This early, mainly preparative, work is extensively reviewed in Mellor [3] and Gmelin.[4]

While the compositions of many solid phases are known, knowledge of the equilibrium conditions in solution is, on the other hand, incomplete, although many different experi-

mental methods have been used. The previously most thorough investigation on the system in aqueous solutions seems to have been made by Contant and other members of the Paris group.[5–10] They have used spectrophotometric, polarographic, and potentiometric methods and have also prepared and analysed solid phases. They propose that the main complexes in weakly acidified solutions comprise a series of hexamolybdodiarsenates $H_nMo_6As_2O_{26}^{(6-n)-}$ $(n=0,1,2)$. The formation constant for $Mo_6As_2O_{26}^{6-}$ was calculated to be 5×10^{69} and the acidity constants for the protonated species were found to be 5.9 and 2.6 respectively. For molybdenum excess they proposed an $HMo_{17}As_2O_{64}^{11-}$ species whereas the existence of an $HMo_{11}AsO_{39}^{6-}$ complex is more questionable. In acid solutions ($pH\leq 2$) they proposed $Mo_{18}As_2O_{62}^{6-}$ and tetrameric trimolybdoarsenate species. In strongly acidified solutions containing excess of arsenate they found indications for complexes with Mo/As ratios of 2/2 and 1/2.

Contant *et al.* have thus found indications for the existence of many molybdoarsenate species and have also given formation constants for some of them. However, it is clear that a more thorough analysis of the system is necessary. In particular, a greater data range and better data treatment must be presented before the complexes of the system can be identified with certainty.

EXPERIMENTAL

The present study has been carried out in close connection with Parts I [11] and II [1] in this series.

Chemicals and analyses. Solutions of $NaClO_4$ and $HClO_4$ were prepared and analysed as described by Sjöberg [12] and solutions of Na_2MoO_4 as described in Part I.[11] Arsenate stock solutions were prepared by using recrystallized $Na_2HAsO_4.7H_2O$ (Merck *p.a.*) and analysed by gravimetric determination as according to Vogel,[13] these analyses were reproducible within 0.1 %.

Apparatus. The same emf equipment and arrangement as described earlier [11,12] were used. However, in the latest part of the titration series an automat edpotentiometric titrator was used.[14] The spectrophotometer used was a Heath model 721 single beam instrument with an automatic sample-reference changer combined with an automated potentiometric titrator. A detailed description of the automatic potentiometric-spectrophotometric titration system will be given in a forthcoming paper by Ginstrup and Lyhamn. A sample cell, of flow-through type, with a path length of 0.100 mm (HELLMA QS) was employed.

Methods. The emf measurements were carried out as a series of potentiometric titrations (glass electrode) in 3.0 M $Na(ClO_4)$ medium. In every titration the total concentrations of molybdate, B, and arsenate, C, were kept constant and the free hydrogen ion concentration, h, was varied by addition of H^+. The excess concentration of hydrogen ions, H, was calculated over the zero level MoO_4^{2-}, $HAsO_4^{2-}$, H_2O, and the titrations thus give a series of data sets $H(\log h)_{B,C}$.

The combined emf-spectrophotometric measurements were made so that for each titration point the emf was measured until equilibrium was obtained, and then the transmittance, T, was measured at 32 different wavelengths from 205 to 360 nm, mostly with increments of 5 nm. As reference a 3 M $NaClO_4$ solution was used. The spectrophotometric measurements give data $T(\lambda)_{\log h,B,C}$ or $OD(\lambda)_{\log h,B,C}$ (OD stands for absorbance).

The mathematical analysis of emf data was performed with the least squares program LETAGROPVRID [15] version ETITR [16] and the error squares sum $U=\sum(H_{calc}-H)^2$ has been minimized. The standard deviations are defined and calculated according to Sillén.[17,18] The computation was performed on a CD 3300 computer in Umeå.

For some general features of the experimental and computational methods used in the present investigation the reader is referred to Ref. 19.

With regard to the binary equilibria the following assumptions on species and equilibrium constants will be made:

For the $H^+-MoO_4^{2-}$ equilibria we will make use of the results obtained by Sasaki and Sillén,[20] [25 °C, 3.0 M $Na(ClO_4)$]. They report the following species and formation constants (valid for $-\log[H^+]>2.5$): $HMoO_4^-(\log\beta_{1,1}=3.89)$, $H_2MoO_4(\log\beta_{2,1}=7.50)$, $Mo_7O_{24}^{6-}(\log\beta_{8,7}=57.74)$, $HMo_7O_{24}^{5-}(\log\beta_{9,7}=62.14)$, $H_2Mo_7O_{24}^{4-}$ $\log\beta_{10,7}=65.68)$, $H_3Mo_7O_{24}^{3-}(\log\beta_{11,7}=68.21)$. For $-\log[H^+]<2.5$ a larger complex (34,19) with $\log\beta_{34,19}=196.3$ and a cation (5,2) with $\log\beta_{5,2}\approx19$ are proposed. This explanation of the system might not be wholly correct. In a subsequent Letagrop analysis Sillén [21] found that some additional complexes must be present and the most likely ones seemed to be octamolybdates. We have performed some control titrations on the system (partly reported in Ref. 11) and have found that the residuals obtained when using the above mentioned complexes and formation constants are so small compared to the large effects in the molybdoarsenate system, that they will not disturb our search for three-component complexes, and will at the worst, cause some minor changes in the formation constants obtained.

For the $H^+-HAsO_4^{2-}$ equilibria no study reporting formation constants in 3.0 M $Na(ClO_4)$ has been published and it was necessary to make a separate determination. The concentration range $5\leq C\leq160$ mM was covered and the system was found to be mononuclear.

There were, – however, some deviations at the highest concentrations studied which might indicate an incipient dimerisation. These deviations are, however, negligible as 40 mM is the highest arsenate concentration used in the present molybdate-arsenate investigation. In a Letagrop calculation using data with $C \leq 160$ mM we obtained the following formation constants: $\log\beta_{1,0,1} = 6.272 \pm 0.012$ and $\beta_{2,0,1} = 8.474 \pm 0.018$. The errors given are $3\sigma(\log\beta)$.

DATA, CALCULATIONS AND RESULTS

Emf measurements

Data. The data of the present investigation includes 1487 experimental points divided into 92 different titrations. The data covers the range $1.5 < -\log[H^+] < 9$ and the total concentrations have been varied within the limits 5 mM $\leq B \leq$ 160 mM and 1.5 mM $\leq C \leq$ 40 mM. In order to check the reversibility of equilibria both backward (increasing $-\log[H^+]$) and forward (decreasing $-\log[H^+]$) titrations have been carried out and this check has been made for most B,C-combinations. Equilibria are attained rapidly except at $-\log[H^+] \approx 3$ for B/C ratios $\gtrsim 3$. When $C \gtrsim 20$ mM and the B/C ratio is $\gtrsim 3$, a white precipitate, which considerably restricts the available data range, was formed. For instance in a titration with $B = 160$ and $C = 40$ mM (the highest B,C-combination studied) precipitation appeared in the range $4 \lesssim -\log[H^+] \lesssim 7$.

As was the case in our earlier molybdophosphate investigation, it was found, that the present data consists of two main groups, one with data corresponding to colourless solutions and another with data corresponding to yellow solutions. The limit between these two sets of data is rather sharp and easy to detect visually. It was found that colourless solutions were obtained for ratios $B/C \lesssim 3$ whereas for higher ratios yellow solutions were obtained at $-\log[H^+] \lesssim 6$. In order to visualize the emf "effects" arising from the ternary complexes formed, we found it convenient to construct the same type of residual plots $\Delta_0(\log[H^+])_{B,C}$ as in the molybdophosphate investigation. $\Delta_0 = H_{calc} - H$, where H is the total analytical H^+ concentration over the zero level (MoO_4^{2-}, $HAsO_4^{2-}$, H_2O) and H_{calc} is calculated assuming that only the known binary $H^+ - MoO_4^{2-}$ and $H^+ - HAsO_4^{2-}$ complexes are present. Examples of such residual plots for three representative concentrations are given in Fig. 1. We found for all B,C-combinations studied that there was a pit in the plots at $-\log[H^+] \approx 6$. At B/C ratios > 3 there was also another pit and this acid pit was characteristic for yellow solutions.

For treatment and discussion it was found convenient to divide the data into five different sets and the following division was made:

Data I: Experimental data from $-\log[H^+] \approx 8$ to the bottom of the neutral pit. This data range corresponds to a very narrow region and includes such data that will give information of the first formed ternary complexes (colourless solutions).

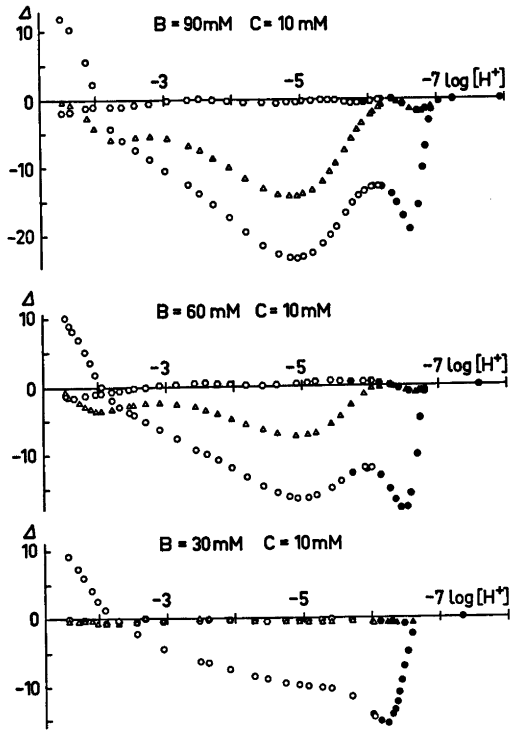

Fig. 1. Residual plots $\Delta = H_{calc} - H$ in mM for three B,C-combinations. For each combination the quantities Δ_0, Δ_{00}, and Δ_1 are plotted with the symbols ○, △ and ◇, respectively. The indices refer to three different assumptions. 0: Only binary complexes. 00: Binary complexes together with (5,2) and (6,2) species. 1: Binary complexes together with (5,2), (6,2) and (9,1) species. Filled symbols are obtained in forward and unfilled in backward titrations.

Table 1. Result from Letagrop calculations performed on the Data I Region.

(p,q,r)	U_{min} $\times 10^{-2}$	$\sigma(H)$ mM	$\log\beta_{p,q,r}$ $\pm 3\sigma(\log\beta)$
4,2,1	29.46	4.52	28.97 ± 0.09
5,2,1	78.45	7.38	35.19 ± 0.17
4,3,1	22.74	3.97	30.37 ± 0.09
5,3,1	8.14	2.38	36.85 ± 0.05
6,3,1	42.80	5.45	43.29 ± 0.13
5,4,1	26.62	4.30	38.14 ± 0.10
6,4,1	7.60	2.30	44.70 ± 0.05
7,4,1	22.45	3.95	51.25 ± 0.10
6,5,1	33.78	4.84	45.95 ± 0.13
7,5,1	15.31	3.26	52.58 ± 0.08
7,4,2	4.98	1.86	53.35 ± 0.06
8,4,2	21.12	3.83	59.87 ± 0.11
7,5,2	14.92	3.22	54.64 ± 0.11
8,5,2	1.65	1.07	61.23 ± 0.03
9,5,2	6.24	2.08	67.77 ± 0.07
10,5,2	27.70	4.39	27.70 ± 0.16
8,6,2	16.49	3.38	62.54 ± 0.12
9,6,2	3.44	1.55	69.10 ± 0.05
10,6,2	2.79	1.39	75.68 ± 0.05
11,6,2	15.90	3.32	82.19 ± 0.12
9,7,2	20.98	3.82	70.39 ± 0.15
10,7,2	7.79	2.33	76.97 ± 0.09
11,7,2	3.78	1.62	83.57 ± 0.06
12,7,2	13.88	3.11	90.17 ± 0.12
11,8,2	13.31	3.04	84.82 ± 0.11
12,8,2	7.24	2.24	91.45 ± 0.09
10,6,3	4,77	1.82	77.79 ± 0.08
11,6,3	7.89	2.34	84.41 ± 0.10
12,6,3	18.75	3.61	90.84 ± 0.16
11,7,3	3.84	1.63	85.67 ± 0.08
12,7,3	2.21	1.24	92.25 ± 0.05
13,7,3	13.28	3.04	98.85 ± 0.14
12,8,3	4.53	1.77	93.63 ± 0.08
13,8,3	1.86	1.13	100.15 ± 0.05
14,8,3	8.34	2.41	106.78 ± 0.10
13,9,3	7.17	2.24	101.49 ± 0.09
14,9,3	3.18	1.49	108.04 ± 0.07
15,9,3	6.51	2.13	114.71 ± 0.11
14,10,3	11.88	2.87	109.30 ± 0.13
15,10,3	5.90	2.02	115.93 ± 0.10
14,8,4	4.57	1.78	108.84 ± 0.10
15,8,4	11.65	2.84	115.48 ± 0.16
14,9,4	6.45	2.12	110.13 ± 0.10
15,9,4	3.04	1.45	116.75 ± 0.08
16,9,4	7.13	2.23	123.41 ± 0.13
15,10,4	6.32	2.10	118.13 ± 0.12
16,10,4	3.20	1.49	124.64 ± 0.08
17,10,4	3.93	1.65	131.23 ± 0.09
16,11,4	8.11	2.37	126.02 ± 0.15
17,11,4	4.51	1.77	132.54 ± 0.11

Table 1. Continued.

8,5,2	1.03	0.85	61.11 ± 0.05
9,5,2			67.13 ± 0.16
8,5,2	1.65	1.07	61.22 ± 0.11
9,6,2			67.48 ± 1.03
8,5,2	0.74	0.72	61.02 ± 0.07
10,6,2			75.28 ± 0.11
12,7,3	1.61	1.06	91.56 ± 0.39
13,8,3			100.05 ± 0.18
13,8,3	1.67	1.08	100.15 ± 0.05
14,9,3			–
15,9,4	2.93	1.43	116.52 ± 0.28
16,10,4			124.23 ± 0.38
16,10,4	2.55	1.34	124.42 ± 0.16
17,10,4			130.80 ± 0.24

Data II: All colourless data with $-\log[H^+] > 2.9$. (Data in the whole neutral pit region and acid data with $B/C \leq 3$.)

Data III: Yellow data ($B/C > 3$) with $-\log[H^+] > 2.9$.

Data IV: Both colourless and yellow data with $-\log[H^+] > 2.9$. (This data set consists of a compilation of suitable data for a covariation of equilibrium constants.)

Data V: Yellow data ($B/C > 3$) with the acidity range extended to $-\log[H^+] \approx 1.5$.

Evaluation of compositions of the complexes. The evaluation was carried out using the same procedure as described earlier.[19] This procedure includes a trial and error search for complexes using the computer program LETAGROPVRID. In the present search we started with a *pqr*-analysis based on the data set denoted Data I. The result of this analysis is given in Table 1 and visualized in Fig. 2. It is seen that the lowest error squares sums are obtained for the complexes (8,5,2) and (13,8,3) with a somewhat lower error squares sum for the (8,5,2) complex. An inspection of the residuals obtained for these best complexes indicated, however, rather large systematic deviations and it was concluded that none of the complexes tested could alone satisfactorily explain the data range in question. We therefore extended our analysis and on the basis of the results obtained we then tested some pairs of complexes. The results of these calculations are collected in Table 1. Apparently, the pair of complexes giving the lowest error squares sum is (8,5,2)+(10,6,2). However, other pairs also give comparable error squares sums. In spite of this we will initially assume

Table 2. Results from Letagrop calculations. In all the calculations the binary complexes and constants given under "EXPERIMENTAL" were used. When no 3σ is given, the constant has not been varied.

Data range	No. of titr./ No. of points	$U \times 10^{-4}$	$\sigma(H)$ mM	$\log\beta_{p,q,r} \pm 3\sigma(\log\beta)$						
				(8,5,2)	(10,6,2)	(11,6,2)	(12,6,2)	(14,9,1)	(15,9,1)	(16,9,1)	(17,9,1)
I	16/145	0.74	0.72	61.02 ± 0.07	75.28 ± 0.11						
II	24/319	0.43	0.37	60.92 ± 0.04	75.25 ± 0.04	80.73 ± 0.05	84.23 ± 0.06				
III	18/319	1.66	0.73	60.92	75.25	80.73	84.23	100.07 ± 0.03	103.81 ± 0.06	106.12 ± 0.12	
IV	25/360	0.71	0.44	60.92	75.25	80.73 ± 0.06	84.07 ± 0.07	100.11 ± 0.02	103.81 ± 0.05	106.11 ± 0.09	
IV[a]	25/360	0.46	0.36	60.92	75.25	80.68 ± 0.07	84.05 ± 0.06	100.10 ± 0.02	103.81 ± 0.03	106.11 ± 0.07	
V	19/369	1.73	0.69	60.92	75.25	80.73	84.07	100.11	103.81	106.14 ± 0.05	107.48 ± 0.05

[a] Alter E_0 var.

Fig. 2. Results of a *pqr*-analysis in the Data I region. Lowest error squares sums ($10^{-1} \times U_{min}$) are plotted as a function of various *pq*-sets for $r = 1$, 2, 3, and 4.

that the complexes (8,5,2) + (10,6,2) are the main complexes in the Data I region and then continue and test these complexes in the Data II region as well. The analysis of the Data II region resulted in a model containing the complexes (8,5,2), (10,6,2), (11,6,2), and (12, 6,2). This model gave a good fit to the data and the residuals showed no systematic deviations and seemed to lie within the experimental errors. Formation constants with corresponding standard deviations are given in Table 2. Attempts to explain this data range solely with a (5,2) or a (6,2) series of complexes were not successful.

In the next step of our search for complexes we analysed the data set denoted Data III and assumed that the colourless complexes found were exactly known. Concerning the remaining residuals, the neutral pit had practically disappeared, but a distinct acid pit still remained (exemplified in Fig. 1, the residuals are denoted Δ_{00}). Inspection of the $\Delta_{00}(\log [H^+])_{B,C}$ plots pointed to an Mo/As ratio in the formed complexes of about nine and Letagrop calculations also confirmed that a model

including the complexes (14,9,1), 15,9,1) and (16,9,1) could best explain our experimental data. Formation constants with corresponding standard deviations are given in Table 2. It might be mentioned that yellow solutions in the previous studied molybdophosphate system also could be explained with an analogous (9,1) series.[1]

Our analysis of experimental data with $-\log[H^+] > 2.9$ thus resulted in a model consisting of two series of complexes, one series of colourless and one series of yellow complexes. In order to confirm these two series further and also to obtain a final set of "best" equilibrium constants and standard deviations we have carried out a calculation on the Data IV set and made a covariation of equilibrium constants of both yellow and colourless species (except (8,5,2) and (10,6,2)). The result of this covariation is given in Table 2. As seen, the equilibrium constants of the complexes came out as much the same as in the separate determinations and the standard deviations obtained were also of satisfactory magnitude. The residuals obtained after this calculation are collected in Table 3 and denoted Δ_1.

In order to test for the influence of an error in E_0 (a constant in the expression for the measured emf) a calculation was carried out where the E_0-values were setwise adjusted and then the ternary constants (except (8,5,2) and (10, 6,2)) were varied. This calculation lowered the error squares sum and the standard deviations, but the values of the formation constants were, as expected, approximately unchanged (See Table 2). The remaining residuals (denoted Δ_2) are given in Table 3.

In order to obtain better confirmation of the (16,9,1) complex and also in order to find additional more acidic complexes, the data range was extended to $-\log[H^+] = 1.5$ for B/C ratios greater than three. Some titrations with B/C ratios less than three were also performed in this extended $-\log[H^+]$-range, but the residuals obtained were so small that we found it meaningless to try to find additional more acidic low B/C ratio species using solely emf data.

Calculations on data with $B/C > 3$ (Data V) strongly confirmed the (16,9,1) complex. However, inspection of the residuals obtained indicated that some additional complex must be present. We assumed that this complex was (17,9,1) and when (16,9,1) and (17,9,1) were varied together we obtained a good fit to the experimental data. Formation constants with corresponding standard deviations are given in Table 2.

In the molybdophosphate system previously studied we found indications of a dimerization of (17,9,1) to (34,18,2),[1] but when, in the present molybdoarsenate system, the monomer was replaced by the dimer in the calculations, the error squares sum was increased from 173 to 205 and when they were allowed to compete against each other the dimer was not accepted at all. However, when concentrated (16,9,1) and (17,9,1) solutions are stored for some days the colour changes from faint-yellow to bright-yellow and in the Raman spectra of such solutions a new peak with high intensity appears indicating the formation of a new species, probably the dimer.

Spectrophotometric measurements

The spectrophotometric measurements are in progress and the main purpose of the study is to confirm the results obtained from the emf investigation. The final results, including calculated molar absorption coefficients of the proposed species at the different wave lengths, will be published in a forthcoming paper by Lyhamn and Pettersson. Here only some preliminary observations will be stated.

Fig. 3 shows some representative curves in a titration where the total molybdenum concentration was kept constant and where the B/C ratio was continuously changed. In addition the free hydrogen ion concentration was kept almost constant in the course of the titration. Curve 1 represents a pure polymolybdate solution and when the B/C ratio is decreased to about nine by the addition of arsenate (curves 2,3 and 4) the absorbance increases over the whole wavelength range studied due to the formation of molybdoarsenate complexes. The binary $H^+ - HAsO_4^{2-}$ system does not absorb in the wavelength range chosen. Further addition of arsenate (curves 5, 6 and 7) causes the curves to intersect at two so-called isosbestic points (at $\lambda \approx 235$ and 274 nm). The B/C ratio in curve 7 is three and

Table 3. Experimental data $H(\log h)_{B,C}$ in the data IV region. For each point the quantities $\log h$, H, Δ_0, Δ_1, and Δ_2 are given (in mM). The quantity Δ is the residual $H_{calc}-H$. The indices 0, 1, and 2 refer to three different assumptions.

0. Only binary $H^+-MoO_4^{2-}$ and $H^+-HAsO_4^{2-}$ complexes with constants given under "EXPERIMENTAL".
1. Binary complexes and constants as in 0 together with proposed ternary complexes with constants given in Table 2.
2. The same complexes as in 1, but with constants obtained after an E_0-variation; see Table 2.

SATS 1. B=0.160 C=0.040

log h	H	Δ_0	Δ_1	Δ_2
-2.916	296.57	-18.22	0.43	-0.03
-3.072	294.00	-21.12	0.64	0.20
-3.216	291.47	-23.27	0.95	0.52
-3.375	288.98	-25.68	0.97	0.55
-3.542	286.54	-28.15	0.89	0.47
-3.725	284.13	-30.96	0.68	0.27
-3.926	281.77	-34.10	0.49	0.09
-4.148	279.45	-37.53	0.43	0.02
-4.381	277.16	-40.82	0.57	0.10

SATS 2. B=0.080 C=0.040

log h	H	Δ_0	Δ_1	Δ_2
-2.956	173.00	-11.07	-0.53	-0.16
-3.092	171.22	-12.47	-0.44	-0.05
-3.366	167.98	-14.74	-0.33	0.06
-3.678	164.79	-16.88	-0.19	0.13
-3.869	163.24	-18.26	-0.16	0.09
-4.199	160.97	-20.67	-0.01	0.10
-4.430	159.49	-22.20	0.15	0.17
-4.623	158.03	-23.12	0.40	0.36
-4.786	156.61	-23.68	0.62	0.52

SATS 3. B=0.040 C=0.040

log h	H	Δ_0	Δ_1	Δ_2
-2.986	110.00	-6.12	-0.69	-0.41
-3.165	107.85	-7.02	-0.66	-0.40
-3.375	105.78	-7.83	-0.60	-0.36
-3.561	104.28	-8.46	-0.54	-0.33
-3.787	102.83	-9.24	-0.47	-0.32
-3.971	101.88	-9.90	-0.43	-0.31
-4.182	100.94	-10.69	-0.36	-0.29
-4.386	100.03	-11.36	-0.23	-0.20
-4.567	99.13	-11.85	-0.08	-0.08
-4.720	98.27	-12.22	0.03	0.01
-4.902	96.95	-12.55	0.20	0.16
-5.042	95.69	-12.80	0.32	0.27
-5.189	94.06	-13.14	0.45	0.40
-5.409	90.96	-14.14	0.56	0.55

SATS 4. B=0.160 C=0.020

log h	H	Δ_0	Δ_1	Δ_2
-2.893	272.84	-16.96	-0.82	-0.60
-3.133	268.94	-20.10	-0.30	-0.07
-3.303	266.40	-22.31	-0.06	0.19
-3.522	263.41	-25.31	0.01	0.27
-3.793	260.25	-29.37	-0.27	-0.03
-4.044	257.87	-33.47	-0.71	-0.51
-4.334	255.54	-38.02	-1.01	-0.86
-4.560	253.70	-40.99	-0.99	-0.87
-4.727	252.11	-42.58	-0.87	-0.75
-4.904	249.88	-43.44	-0.67	-0.54
-5.077	246.60	-43.12	-0.38	-0.21
-5.287	240.30	-40.72	0.12	0.35
-5.572	226.77	-34.48	0.15	0.46

SATS 5. B=0.120 C=0.020

log h	H	Δ_0	Δ_1	Δ_2
-2.955	210.16	-13.59	-0.18	-0.19
-3.117	208.06	-15.33	0.08	0.09
-3.293	206.00	-17.20	0.21	0.23
-3.478	203.99	-19.15	0.24	0.26
-3.684	202.01	-21.40	0.13	0.15
-3.909	200.07	-24.05	-0.06	-0.06
-4.177	198.17	-27.29	-0.26	-0.28
-4.472	196.30	-30.53	-0.28	-0.34
-4.728	194.47	-32.61	-0.08	-0.20
-4.912	192.67	-33.42	0.16	-0.03
-5.043	190.90	-33.54	0.36	0.09
-5.143	189.17	-33.32	0.49	0.15
[illegible]	185.79	-32.46	0.58	0.10
-5.396	182.54	-31.36	0.57	-0.03
-5.481	179.39	-30.24	0.51	-0.20
-5.614	173.42	-28.16	0.35	-0.51

SATS 6. B=0.060 C=0.020

log h	H	Δ_0	Δ_1	Δ_2
-3.111	117.77	-9.89	-0.83	-0.05
-3.517	114.80	-12.25	-0.74	-0.00
-4.026	111.98	-15.07	-0.73	-0.25
-4.606	109.30	-17.92	-0.44	-0.13
-4.974	106.74	-18.75	-0.05	0.39

SATS 7. B=0.020 C=0.020

log h	H	Δ_0	Δ_1	Δ_2
-2.930	56.00	-2.91	-0.38	-0.25
-3.001	55.45	-3.13	-0.39	-0.27
-3.153	54.37	-3.50	-0.36	-0.24
-3.330	53.34	-3.84	-0.32	-0.21
-3.547	52.35	-4.23	-0.29	-0.19
-3.830	51.39	-4.74	-0.26	-0.19
-4.210	50.47	-5.50	-0.21	-0.19
-4.585	49.58	-6.21	-0.12	-0.13
-4.845	48.72	-6.66	-0.03	-0.06
-5.025	47.89	-7.02	0.04	-0.00
-5.160	47.09	-7.38	0.07	0.03
-5.354	45.56	-8.20	0.07	0.05
-5.497	44.13	-9.08	0.06	0.06
-5.602	42.78	-9.98	0.02	0.06
-5.741	39.76	-12.04	-0.08	0.04
-5.876	37.63	-13.30	-0.12	0.05
-6.024	33.18	-15.11	-0.22	0.06
-6.228	25.16	-13.90	-0.64	-0.19

SATS 8. B=0.160 C=0.010

log h	H	Δ_0	Δ_1	Δ_2
-4.342	224.00	-20.62	0.14	-0.05
-4.187	231.36	-18.56	0.21	-0.01
-3.909	234.59	-16.78	0.29	0.06
-3.809	236.16	-15.89	0.40	0.17
-3.634	239.21	-14.44	0.47	0.23
-3.471	242.16	-13.14	0.50	0.25
-3.322	244.99	-12.09	0.38	0.13
-3.181	247.72	-11.12	0.22	-0.03
-2.965	252.91	-9.02	0.06	-0.21

SATS 9. B=0.120 C=0.010

log h	H	Δ_0	Δ_1	Δ_2
-3.020	192.59	-8.90	1.14	1.16
-3.163	190.79	-10.07	1.13	1.16
-3.307	189.03	-11.26	1.10	1.14
-3.454	187.30	-12.47	1.04	1.08
-3.604	185.60	-13.77	0.91	0.96
-3.761	183.93	-15.21	0.72	0.76
-3.924	182.29	-16.74	0.51	0.55
-4.095	180.67	-18.33	0.34	0.37
-4.274	179.09	-19.96	0.25	0.27
-4.464	177.53	-21.55	0.25	0.27
-4.658	176.01	-22.94	0.37	0.38
-4.836	174.50	-23.88	0.58	0.59
-5.088	171.57	-24.29	0.98	0.97
-5.239	168.74	-23.66	1.13	1.09
-5.428	163.35	-21.67	1.05	0.94
-5.613	155.87	-18.78	0.63	0.42
-5.768	147.97	-16.37	0.01	-0.25
-5.967	135.24	-14.13	-0.62	-0.92
-6.125	122.29	-13.63	-1.08	-1.40

SATS 10. B=0.110 C=0.010

log h	H	Δ_0	Δ_1	Δ_2
-2.906	180.69	-9.23	-0.15	0.00
-3.044	179.02	-10.33	-0.10	0.05
-3.263	176.57	-12.08	-0.09	0.07
-3.417	174.98	-13.36	-0.16	0.00
-3.576	173.41	-14.73	-0.29	-0.12
-3.739	171.87	-16.18	-0.45	-0.29
-3.910	170.36	-17.73	-0.62	-0.47
-4.090	168.87	-19.36	-0.75	-0.62
-4.283	167.41	-21.08	-0.82	-0.71
-4.487	165.98	-22.73	-0.78	-0.69
-4.687	164.56	-24.08	-0.63	-0.54
-4.854	163.18	-24.82	-0.41	-0.32
-4.982	161.81	-25.04	-0.25	-0.13
-5.218	157.86	-24.24	-0.06	0.14
-5.401	152.87	-22.33	-0.10	0.17
-5.580	145.95	-19.54	-0.32	-0.01
-5.748	137.65	-16.75	-0.62	-0.25
-5.886	129.37	-14.84	-0.78	-0.35
-6.010	120.51	-13.63	-0.73	-0.18
-6.157	107.47	-12.86	-0.41	0.34

SATS 11. B=0.100 C=0.010

log h	H	Δ_0	Δ_1	Δ_2
[illegible]	167.96	-8.91	-0.64	-0.45
-2.952	166.31	-10.02	-0.56	-0.37
-3.106	164.70	-11.25	-0.52	-0.33
-3.264	163.12	-12.46	-0.46	-0.27
-3.437	161.57	-13.90	-0.53	-0.34
-3.622	160.04	-15.50	-0.69	-0.50
-3.815	158.55	-17.22	-0.88	-0.70
-4.020	157.08	-19.06	-1.03	-0.87
-4.237	155.64	-20.95	-1.08	-0.95
-4.465	154.23	-22.77	-1.01	-0.90
-4.842	151.48	-24.69	-0.71	-0.56
-5.057	148.82	-24.58	-0.53	-0.31
-5.299	143.78	-22.88	-0.41	-0.08
-5.615	132.56	-18.43	-0.69	-0.19
-5.965	112.76	-13.90	-0.92	-0.14
-6.180	94.82	-13.17	-0.65	0.53

SATS 12. B=0.090 C=0.010

log h	H	Δ_0	Δ_1	Δ_2
-3.043	151.01	-10.41	-0.22	-0.11
-3.347	148.16	-12.51	0.11	0.24
-3.521	146.77	-13.84	0.13	0.25
-3.715	145.42	-15.46	0.01	0.14
-3.936	144.08	-17.41	-0.22	-0.10
-4.182	142.77	-19.60	-0.44	-0.34
-4.436	141.49	-21.64	-0.58	-0.50
-4.648	140.22	-22.89	-0.58	-0.50
-4.807	138.98	-23.41	-0.52	-0.43
-4.925	137.76	-23.48	-0.44	-0.34
-5.018	136.57	-23.31	-0.36	-0.25
-5.306	130.88	-21.39	-0.20	-0.03
-5.505	124.65	-18.88	-0.28	-0.09
-5.753	113.81	-15.38	-0.54	-0.30
-5.914	104.71	-13.71	-0.62	-0.29
-6.145	87.26	-12.74	-0.21	0.33

Table 3. Continued.

SATS 13. B=0.080 C=0.010

log h	H	A_0	A_1	A_2
-2.920	136.60	-8.37	-0.11	-0.01
-3.051	135.31	-9.18	0.09	0.19
-3.193	134.05	-10.07	0.25	0.35
-3.346	132.81	-11.07	0.36	0.46
-3.511	131.56	-12.18	0.40	0.51
-3.699	130.40	-13.59	0.32	0.42
-3.905	129.22	-15.17	0.20	0.30
-4.152	128.07	-17.19	0.01	0.09
-4.420	126.94	-19.23	-0.11	-0.05
-4.650	125.83	-20.60	-0.12	-0.07
-4.814	124.73	-21.17	-0.08	-0.03
-5.023	122.60	-21.18	0.03	0.09
-5.260	118.56	-20.01	0.09	0.18
-5.469	112.96	-17.93	-0.03	0.07
-5.720	103.22	-14.93	-0.37	-0.26
-5.924	92.57	-13.25	-0.53	-0.34
-6.110	79.73	-13.00	-0.47	-0.16

SATS 14. B=0.060 C=0.010

log h	H	A_0	A_1	A_2
-2.891	106.01	-6.25	0.02	-0.02
-3.134	104.12	-7.55	0.24	0.23
-3.412	102.30	-8.97	0.37	0.37
-3.569	101.41	-9.81	0.36	0.37
-3.741	100.54	-10.77	0.32	0.33
-3.938	99.68	-11.93	0.24	0.24
-4.165	98.84	-13.31	0.16	0.14
-4.404	98.01	-14.67	0.14	0.10
-4.614	97.19	-15.67	0.19	0.13
-4.897	95.60	-16.42	0.36	0.24
-5.064	94.06	-16.41	0.49	0.31
-5.186	92.57	-16.13	0.57	0.32
-5.401	88.36	-14.96	0.62	0.22
-5.544	84.53	-13.88	0.56	0.04
-5.710	78.82	-12.66	0.43	-0.21
-5.887	71.14	-11.94	0.37	-0.39
-6.005	64.82	-12.01	0.42	-0.43

SATS 15. B=0.040 C=0.010

log h	H	A_0	A_1	A_2
-5.528	60.50	-12.18	-0.40	-0.10
-5.355	63.41	-12.21	-0.16	0.03
-5.188	65.52	-12.24	-0.06	0.04
-4.981	67.13	-12.13	-0.08	-0.03
-4.831	68.00	-11.94	-0.14	-0.11
-4.624	68.86	-11.49	-0.24	-0.20
-4.399	69.57	-10.78	-0.30	-0.25
-4.186	71.08	-8.84	-0.34	-0.22
-3.612	72.03	-7.76	-0.27	-0.11
-3.316	73.38	-6.73	-0.32	-0.13
-3.142	74.87	-5.88	-0.42	-0.23

SATS 16. B=0.040 C=0.010

log h	H	A_0	A_1	A_2
-5.051	67.02	-12.57	-0.44	-0.04
-3.526	72.60	-7.67	-0.49	-0.10
-3.182	74.08	-6.16	-0.28	0.15
-2.752	76.73	-4.21	-0.53	0.02

SATS 17. B=0.030 C=0.010

log h	H	A_0	A_1	A_2
-2.922	60.49	-4.65	-0.73	-0.52
-3.454	58.06	-6.22	-0.67	-0.48
-3.586	57.60	-6.60	-0.69	-0.52
-3.888	56.69	-7.47	-0.71	-0.59
-4.254	55.82	-8.56	-0.71	-0.64
-4.435	55.39	-9.06	-0.68	-0.63
-4.711	54.55	-9.63	-0.56	-0.53
-4.902	53.74	-9.91	-0.46	-0.42
-5.044	52.95	-10.08	-0.40	-0.34
-5.241	51.44	-10.30	-0.33	-0.22
-5.376	50.02	-10.49	-0.31	-0.13
-5.493	45.03	-11.69	-0.46	-0.02
-6.012	36.04	-14.67	-0.80	0.15

SATS 18. B=0.020 C=0.010

log h	H	A_0	A_1	A_2
-3.050	43.50	-2.86	-0.00	0.05
-3.145	43.07	-3.11	0.01	0.06
-3.358	42.24	-3.56	0.02	0.08
-3.619	41.43	-4.06	0.02	0.08
-3.954	40.66	-4.78	0.03	0.06
-4.362	39.92	-5.53	0.08	0.07
-4.547	39.55	-5.88	0.12	0.09
-4.697	39.20	-6.13	0.16	0.11
-4.818	38.85	-6.32	0.21	0.14
-5.002	38.17	-6.63	0.25	0.17
-5.135	37.51	-6.89	0.29	0.19
-5.324	36.26	-7.42	0.31	0.20
-5.455	35.10	-7.95	0.30	0.19
-5.691	32.00	-9.44	0.20	0.10
-5.859	28.64	-10.89	0.06	-0.03
-5.968	25.76	-11.79	-0.08	-0.15
-6.114	20.74	-12.00	-0.29	-0.35

SATS 19. B=0.160 C=0.005

log h	H	A_0	A_1	A_2
-2.882	244.75	-6.06	-1.61	-1.56
-3.477	230.94	-7.33	-0.49	-0.42
-3.608	227.73	-7.47	-0.11	-0.04
-3.839	222.57	-8.17	0.10	0.16
-4.079	217.64	-9.26	0.66	0.12
-4.400	212.01	-10.86	-0.24	-0.19
-4.583	209.30	-11.80	-0.44	-0.40
-4.782	206.66	-12.68	-0.60	-0.57
-4.984	204.08	-13.30	-0.58	-0.55
-5.164	201.57	-13.55	-0.36	-0.33
-5.310	199.12	-13.55	-0.09	-0.06
-5.479	195.16	-13.03	0.37	0.41
-5.638	189.88	-12.05	0.43	0.46
-5.856	178.82	-9.81	-0.05	-0.02
-6.054	163.36	-7.25	0.27	0.33

SATS 20. B=0.120 C=0.005

log h	H	A_0	A_1	A_2
-4.524	161.10	-10.99	0.14	0.06
-4.378	162.67	-10.27	0.26	0.18
-4.253	164.20	-9.71	0.29	0.20
-4.031	167.19	-8.73	0.33	0.24
-3.932	168.64	-8.32	0.33	0.24
-3.742	171.46	-7.51	0.37	0.28
-3.572	174.18	-6.92	0.29	0.19
-3.417	176.80	-6.53	0.08	-0.02
-3.272	179.32	-6.23	-0.19	-0.29
-2.988	184.12	-5.44	-0.56	-0.67

SATS 21. B=0.100 C=0.005

log h	H	A_0	A_1	A_2
-2.826	157.35	-4.36	-0.18	-0.17
-2.933	155.86	-4.82	-0.16	-0.15
-3.040	154.41	-5.21	-0.11	-0.10
-3.144	152.98	-5.55	-0.03	-0.01
-3.246	151.56	-5.84	0.09	0.11
-3.344	150.20	-6.10	0.22	0.24
-3.443	148.85	-6.39	0.32	0.34
-3.544	147.52	-6.72	0.39	0.41
-3.645	146.22	-7.08	0.42	0.45
-3.855	143.68	-7.95	0.38	0.40
-4.077	141.23	-8.99	0.26	0.28
-4.313	138.86	-10.12	0.14	0.15
-4.564	136.56	-11.19	0.11	0.12
-4.696	135.45	-11.68	0.12	0.12
-4.827	134.35	-12.09	0.17	0.17
-5.060	132.20	-12.58	0.35	0.35
-5.233	130.12	-12.65	0.54	0.54
-5.403	127.12	-12.29	0.60	0.57
-5.577	122.42	-11.25	0.31	0.25
-5.798	113.20	-9.19	-0.27	-0.39
-5.977	102.66	-7.73	-0.51	-0.63

SATS 22. B=0.080 C=0.005

log h	H	A_0	A_1	A_2
-2.962	126.95	-5.24	-0.46	-0.36
-3.064	125.83	-5.62	-0.41	-0.31
-3.166	124.74	-5.96	-0.34	-0.24
-3.268	123.67	-6.29	-0.26	-0.16
-3.371	122.61	-6.63	-0.20	-0.09
-3.474	121.57	-6.99	-0.15	-0.05
-3.579	120.55	-7.38	-0.13	-0.02
-3.688	119.55	-7.82	-0.14	-0.04
-3.800	118.56	-8.32	-0.19	-0.09
-3.916	117.59	-8.85	-0.25	-0.16
-4.035	116.64	-9.41	-0.31	-0.22
-4.157	115.70	-9.98	-0.36	-0.28
-4.282	114.77	-10.55	-0.39	-0.32
-4.410	113.86	-11.14	-0.40	-0.33
-4.542	112.97	-11.62	-0.38	-0.32
-4.739	111.65	-12.28	-0.29	-0.24
-4.858	110.79	-12.57	-0.19	-0.13
-5.062	109.11	-12.90	-0.00	0.07
-5.260	106.67	-12.76	0.15	0.27
-5.386	104.35	-12.25	0.14	0.29
-5.582	98.96	-10.73	-0.10	0.11
-5.818	89.13	-8.46	-0.35	-0.07
-5.981	79.73	-7.09	-0.23	0.15

SATS 23. B=0.060 C=0.005

log h	H	A_0	A_1	A_2
-2.853	99.04	-4.45	-0.14	-0.13
-3.170	97.09	-5.68	-0.06	-0.04
-3.327	96.67	-7.14	-0.07	-0.04
-3.789	93.12	-8.27	-0.20	-0.17
-3.927	92.36	-8.93	-0.27	-0.24
-4.068	91.62	-9.54	-0.32	-0.29
-4.217	90.88	-10.21	-0.35	-0.33
-4.367	90.16	-10.86	-0.34	-0.33
-4.518	89.45	-11.44	-0.31	-0.29
-4.660	88.76	-11.91	-0.22	-0.21
-4.788	88.07	-12.24	-0.12	-0.11
-4.895	87.39	-12.43	-0.03	-0.02
-5.055	86.07	-12.47	0.09	0.10
-5.209	84.16	-12.31	0.16	0.15
-5.372	81.15	-11.77	0.17	0.13
-5.484	78.36	-10.23	0.10	0.11
-5.694	71.46	-8.24	0.11	0.02

SATS 24. B=0.040 C=0.005

log h	H	A_0	A_1	A_2
-2.891	69.86	-4.06	-0.08	-0.11
-3.060	68.05	-4.64	0.02	-0.00
-3.251	67.08	-5.26	0.10	0.09
-3.488	66.06	-6.07	0.14	0.14
-3.681	65.38	-6.79	0.09	0.10
-3.834	64.96	-7.38	0.05	0.05
-4.131	64.13	-8.61	-0.08	-0.08
-4.371	63.54	-9.55	-0.15	-0.16
-4.516	63.14	-10.03	-0.16	-0.17
-4.696	62.45	-10.46	-0.08	-0.11
-4.837	61.75	-10.57	-0.05	-0.09
-4.984	60.68	-10.48	0.04	-0.03
-5.135	59.14	-10.09	0.15	0.04
-5.300	56.74	-9.32	0.26	0.08
-5.493	52.89	-8.19	0.22	-0.04
-5.632	49.17	-7.26	0.25	-0.08
-5.716	46.56	-6.82	0.22	-0.15
-5.863	41.09	-6.22	0.33	-0.10
-5.998	34.94	-6.19	0.39	-0.10
-6.129	27.96	-6.57	0.60	0.05

SATS 25. B=0.015 C=0.005

log h	H	A_0	A_1	A_2
-6.317	3.95	-1.56	-0.31	-0.17
-6.208	6.45	-3.55	-0.12	0.10
-6.052	11.19	-6.48	-0.01	0.19
-5.893	15.60	-7.03	-0.09	0.04
-5.632	20.68	-6.17	-0.14	-0.10
-5.490	22.66	-5.81	-0.18	-0.16
-5.184	25.36	-5.48	-0.29	-0.31
-4.602	27.55	-5.02	-0.53	-0.54
-3.353	29.67	-3.18	-0.57	-0.51
-3.072	30.49	-2.71	-0.57	-0.51
-2.864	31.30	-2.27	-0.58	-0.52

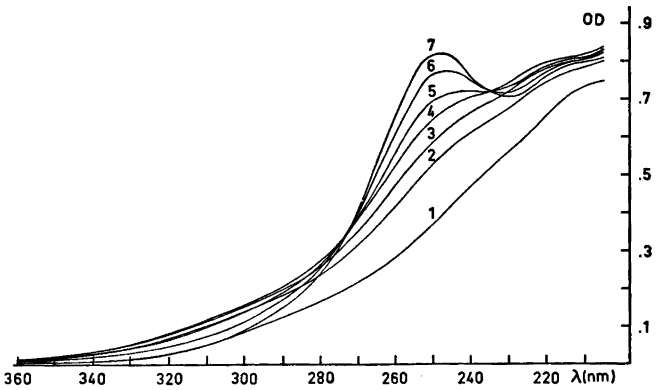

Fig. 3. Absorbance curves $OD(\lambda)_{B,C}$ for solutions with $B = 12.01$ mM at some chosen B/C-ratios. Curve No., B/C, $-\log[H^+]$; 1, ∞, 2.24; 2, 15.3, 2.30; 3, 11.3, 2.32; 4, 8.9, 2.35; 5, 6.0, 2.36; 6, 4.0, 2.39; 7; 3.0, 2.42.

when further decreasing the B/C ratio to one (the last point in the titration) the curves practically coincide. However, they are omitted in the figure for the sake of clarity.

In the hope of obtaining a more accurate estimate of the B/C ratios in predominant complexes, we have plotted the measured absorbance as a function of the B/C ratio at different wavelengths. Two such plots are illustrated in Fig. 4. In Fig. 4a ($\lambda = 235$ nm, one of the two isosbestic points) there is an evident break in the absorbance at $B/C \approx 9$ and in Fig. 4b ($\lambda = 300$, where the "yellow" complexes are the major contributors to the absorbance) there is an equally evident break at $B/C \approx 3$.

In some other titrations both B and C were kept constant and the H^+ concentration was changed. It was found that for B/C ratios where, according to the emf results, the colourless series of complexes should be predominant, absorbance curves almost identical to 7 in Fig. 3, with absorbance peaks at $\lambda \approx 250$ nm, were obtained and the position of this peak changed very little when the H^+ concentration was changed. In titrations where the "yellow" complexes should be predominant, no characteristic peak was obtained (see curve 4 in Fig. 3). However, the shape of the absorbance curve changes very little with the H^+ concentration, an indication for a series of complexes with the same nuclearity.

The spectral behaviour of titrations hitherto performed thus seems to be consistent with the emf result. Some preliminary Letagrop calculations on spectrophotometric data have also confirmed that all data hitherto collected (five titrations) can be completely explained with the complexes and formation constants proposed from the emf measurements.

CONCLUSION AND DISCUSSION

The present investigation has by means of emf, but also by spectrophotometric methods, greatly clarified the equilibrium conditions in molybdoarsenate solutions and has given compositions and equilibrium constants for the main complexes formed in the system. Two series of complexes exist, one colourless with the species (8,5,2), (10,6,2), (11,6,2), (12,6,2) and one "yellow" with the species (14,9,1), (15,9,1), (16,9,1), (17,9,1). The molybdoarsenate system thus shows great similarities with the molybdophosphate system previously studied.[1]

The main "yellow" species in both systems belong to an analogous monomeric (9,1)-series. The emf data in the molybdoarsenate system do not indicate any dimerization to (18,2)-species as is the case in the molybdophosphate system. However, Raman spectra from concentrated (16,9,1) and (17,9,1) solutions showed that a new species was formed and comparison with a solid phase isomorphous to Na_6Mo_{18}-

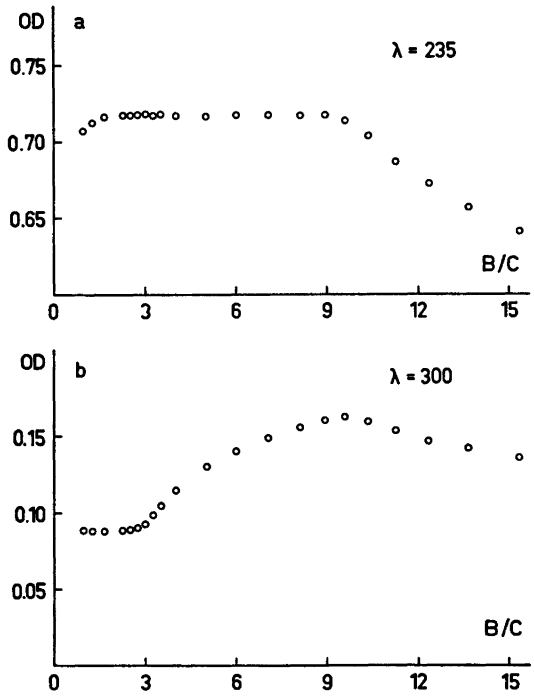

Fig 4. Absorbance values plotted as a function of B/C-ratio for two different wave lengths.

$P_2O_{62}(H_2O)_{24}$ indicated that this species probably is a (34,18,2) species.

The colourless complexes in the molybdophosphate data could be completely explained with a series of the three pentamolybdodiphosphates (8,5,2), (9,5,2), (10, 5,2), whereas in the present system the data could not be explained solely with one series homonuclear in B and C. In addition to the three hexamolybdodiarsenates (10,6,2), (11,6,2), (12,6,2), an (8,5,2) complex also seems to be formed.

Comparisons of the strength of analogous complexes in the two systems are given in Table 4. Apparently (8,5,2) is stronger in the molybdophosphate system, while the (9,1) complexes and especially (14,9,1) are stronger in the molybdoarsenate system.

In order to visualize the equilibrium conditions in the present system we have calculated the concentrations of different species as a function of log[H+]. The calculations have been performed by using a version of the computer program SOLGAS,[22] valid for equilibria in solution and equipped with a plotting procedure (Gunnar Eriksson, to be published). The results, for some representative total concentrations, are illustrated as diagrams in Fig. 5, a–e.

In solutions with an excess of arsenate, for instance at $B/C = 1$ (Fig. 5a), all the molybdenum is bound in the colourless (5,2) and (6,2) complexes. At $B/C = 3$, the same ratio as in the hexamolybdodiarsenate complexes, these are predominating, but there are also small amounts of the (9,1) complexes present (Fig. 5b). At $B/C = 6$ (Fig. 5c) both the colourless and the "yellow" series of complexes are present and as the (9,1) series is built up at higher acidities than the colourless series, there is a space in the log[H+] range where binary $H^+ - MoO_4^{2-}$ species are formed. At $B/C = 9$ (Fig. 5d), the same ratio as in the enneamolybdoarsenate complexes, the (9,1) complexes predominate in the acid range and before they are formed, the first members of the colourless molybdoarsenate series together with binary $H^+ - MoO_4^{2-}$ species are present. Finally, in solutions with molybdenum excess, for instance

Table 4. Formation constants of analogous complexes in the molybdoarsenate and molybdophosphate systems.

(p,q,r)	Proposed formula	$\log \beta_{p,q,r} \pm 3\sigma(\log \beta)$		pK_a	
		X=P	X=As	X=P	X=As
(8,5,2)	$Mo_5X_2O_{23}^{6-}$	61.97 ± 0.02	60.92 ± 0.04	–	–
(14,9,1)	$H_3Mo_9XO_{34}^{6-}$	98.40 ± 0.06	100.11 ± 0.02	–	–
(15,9,1)	$H_4Mo_9XO_{34}^{5-}$	102.81 ± 0.06	103.81 ± 0.05	4.41	3.70
(16,9,1)	$H_5Mo_9XO_{34}^{4-}$	105.84 ± 0.07	106.14 ± 0.05	3.04	2.33
(17,9,1)	$H_6Mo_9XO_{34}^{3-}$	106.85 ± 0.18	107.47 ± 0.06	1.01	1.33

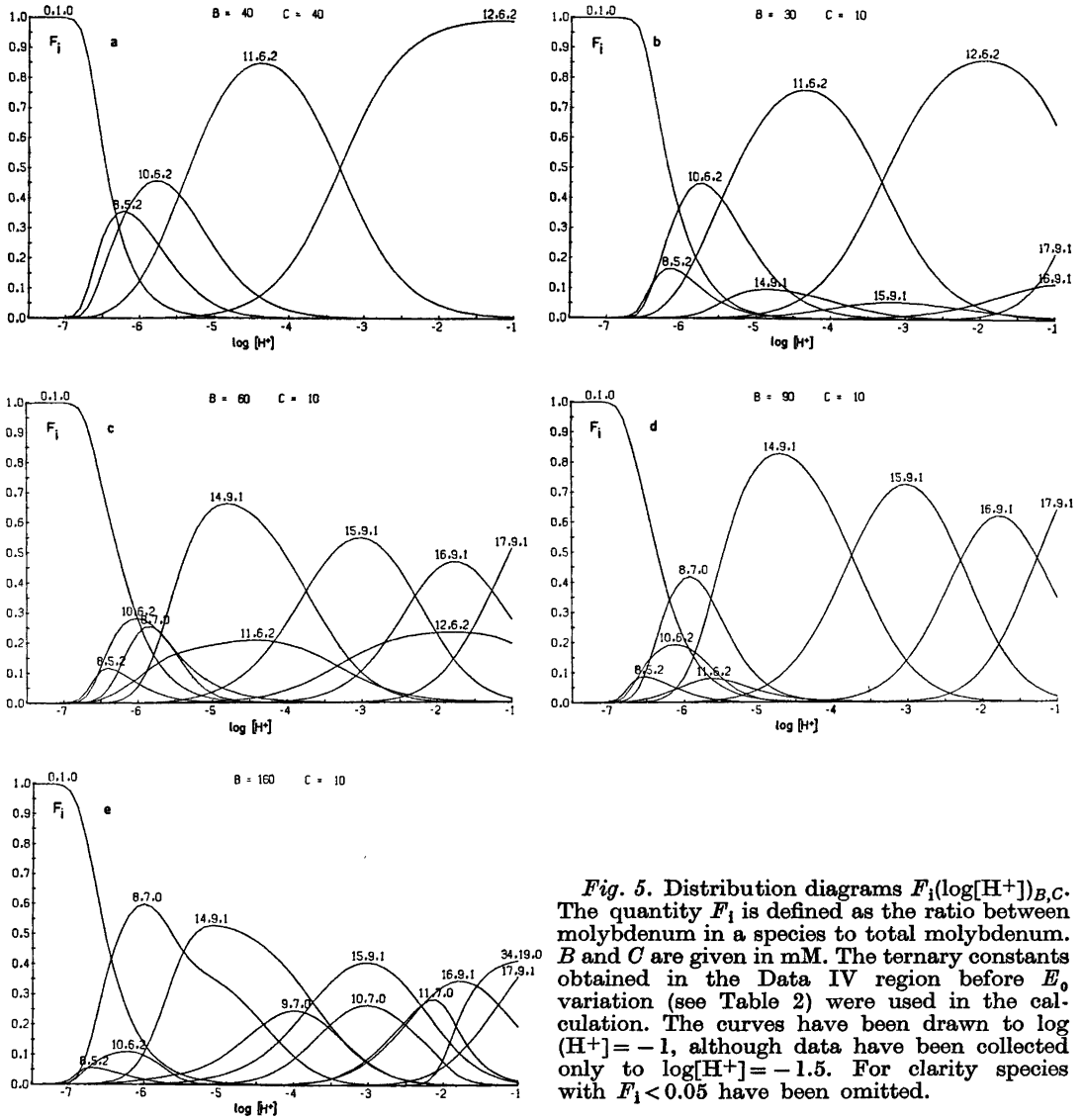

Fig. 5. Distribution diagrams $F_i(\log[H^+])_{B,C}$. The quantity F_i is defined as the ratio between molybdenum in a species to total molybdenum. B and C are given in mM. The ternary constants obtained in the Data IV region before E_0 variation (see Table 2) were used in the calculation. The curves have been drawn to log $(H^+) = -1$, although data have been collected only to $\log[H^+] = -1.5$. For clarity species with $F_i < 0.05$ have been omitted.

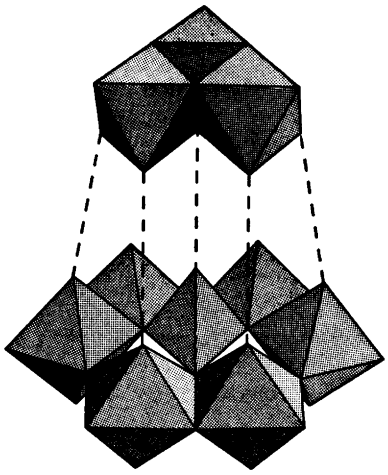

Fig. 6. Proposed structure of the (9,1) unit.

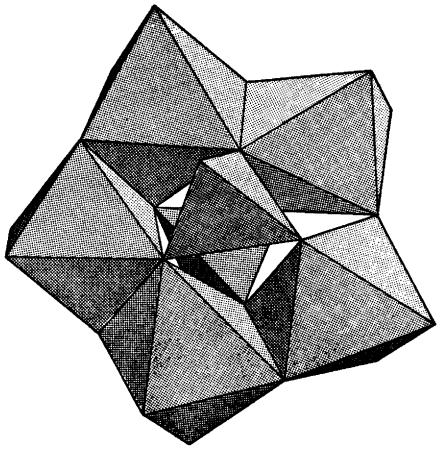

Fig. 7. Proposed structure of the (5,2) unit.

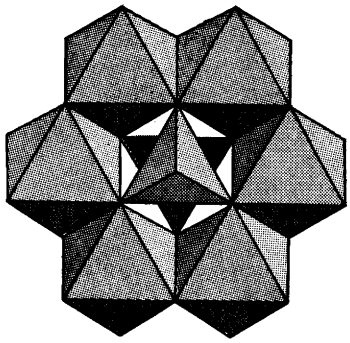

Fig. 8. Proposed structure of the (6,2) unit.

$B/C = 16$ (Fig. 5e), the (9,1) complexes are quite predominant and the molybdenum excess (over the 9/1 ratio) is bound in binary $H^+ - MoO_4^{2-}$ complexes.

Solid phases and possible structures. Through slow evaporation of equilibrium solutions we have tried to obtain crystalline phases of the different complexes proposed. From colourless solutions we have not yet succeeded in preparing crystals large enough for single crystal X-ray work. White microcrystalline powders have been obtained from (8,5,2), (10,6,2) and (11,6,2) solutions and X-ray powder films have shown the powders to be of the same phase. However, from very acid (6,2) solutions (faint yellow), we have obtained two other colourless phases which are under X-ray investigation. The compositions of these colourless phases are not yet known. From (16, 9,1) and (17,9,1) solutions crystals isomorphous to the molybdophosphate phases $Na_3H_6Mo_9PO_{34}(H_2O)_{12}$, corresponding to a (17,9,1) complex, and $Na_6Mo_{18}P_2O_{62}(H_2O)_{24}$, corresponding to a (34,18,2) complex, have been obtained and are under X-ray investigation.

Because of the isomorphism it seems reasonable to assume that the series of (9,1) complexes have the same (9,1) structure unit as has been found in the phosphate case,[23] see Fig. 6. With regard to the structures of the colourless complexes, there is no reason to suspect that the (8,5,2) species would have a structure different from the (5,2) unit (see Fig. 7) found in the molybdophosphate phases $Na_6Mo_5P_2O_{23}(H_2O)_{13}$, corresponding to a (8,5, 2) complex, and $Na_4H_2Mo_5P_2O_{23}(H_2O)_{10}$, corresponding to a (10,5,2) complex, that have been completely structurally determined.[24,25] A plausible structure for the (6,2) structure unit in the three hexamolybdodiarsenate species proposed is given in Fig. 8. Support for this tentative structure can be found from the analogy with the three pentamolybdodiphosphates. The first member of the series $(H^+)_{10}(MoO_4^{2+})_6(HAsO_4^{2-})_2$ should then be given the formula $Mo_6As_2O_{26}^{6-}$ and with the structure proposed the protons in the protonated species (11,6,2) and (12,6,2) can then easily be explained by being attached to the free arsenate oxygens. The reason that the molybdate octahedra in the main colourless molybdoarsenate complexes form a six-ring and not a five-ring

as in the molybdophosphate case may be due to the fact that the arsenate tetrahedron is somewhat larger than the phosphate tetrahedron. (The mean distances P–O and As–O are 1.53 and 1.75 Å, respectively.[36])

Acknowledgements. I thank Professor Nils Ingri for much valuable advice, for his great interest and for all the facilities placed at my disposal. Thanks are also due to Lab.ing. Agneta Nordin for valuable help with the experimental part of the potentiometric measurements. The English of the present paper has been corrected by Dr. Michael Sharp. The work forms part of a program financially supported by the Swedish Natural Science Research Council.

REFERENCES

1. Pettersson, L. *Chem. Scr. 7* (1975) 145.
2. Berzelius, J. J. *Pogg. Ann. 6* (1826) 369, 383.
3. Mellor, J. W. A. *Comprehensive Treatise on Inorganic and Theoretical Chemistry*, Longmans–Green, London 1929, Vol. IX, p. 205.
4. *Gmelins Handbuch der anorganischen Chemie*, 8. Auflage, System number 53, 1935, p. 362.
5. Souchay, P. and Contant, R. *C. R. Acad. Sci. Ser. C 265* (1967) 723.
6. Souchay, P., Contant, R. and Fruchart, J. M. *C. R. Acad. Sci. Ser. C. 264* (1967) 976.
7. Contant, R. *C. R. Acad. Sci. Ser. C 267* (1968) 1479.
8. Contant, R. *Theses*, Université de Paris VI, 1972.
9. Contant, R. *Bull. Soc. Chim. Fr.* (1973) 3277.
10. Souchay, P. and Contant, R. *Bull. Soc. Chim. Fr.* (1973) 3287.
11. Pettersson, L. *Acta Chem. Scand. 25* (1971) 1959.
12. Sjöberg, S. *Acta Chem. Scand. 25* (1971) 2149.
13. Vogel, A. I. *Quantitative Inorganic Analysis*, 3 rd Ed., Longmans–Green, London 1961, p. 500.
14. Ginstrup, O. *Chem. Instrum. 4* (1973) 141.
15. Ingri, N. and Sillén, L. G. *Ark. Kemi 23* (1964) 97.
16. Arnek, R., Sillén, L. G. and Wahlberg, O. *Ark. Kemi 31* (1969) 353; Brauner, P., Sillén, L. G. and Whiteker, R. *Ark. Kemi 31* (1969) 365.
17. Sillén, L. G. *Acta Chem. Scand. 16* (1962) 159.
18. Sillén, L. G. and Warnqvist, B. *Ark. Kemi 31* (1969) 341.
19. Pettersson, L., Andersson, I., Lyhamn, L. and Ingri, N. *Trans. Roy. Inst. Technol., Stockholm 1972*, No 256.
20. Sasaki, Y. and Sillén, L. G. *Acta Chem. Scand. 18* (1964) 1014.
21. Sillén, L. G. *Pure Appl. Chem. 17* (1968) 55.
22. Eriksson, G. *Acta Chem. Scand. 25* (1971) 2651.
23. Strandberg, R. *Acta Chem. Scand. A28* (1974) 217.
24. Strandberg, R *Acta Chem. Scand. 27* (1973) 1004.
25. Hedman, B. *Acta Chem. Scand. 27* (1973) 3335.
26. *International Tables for X-Ray Crystallography*, Kynoch Press, Birmingham 1962, Vol. III.

Received February 3, 1975.

Acta Chemica Scandinavica A 29 (1975) 690—694

The Crystal and Molecular Structure of Hexahydro-3,6-pyridazinedione at —165 °C

T. OTTERSEN

Department of Pharmacy, University of Oslo, Oslo 3, Norway

The crystal and molecular structure of the title compound, $C_4H_6N_2O_2$, has been determined by X-ray methods using 732 reflections above background level collected by counter methods at −165 °C. The crystals are orthorhombic, space group *Ibca*, with cell dimensions: $a = 9.112(2)$ Å, $b = 17.063(3)$ Å, $c = 6.175(1)$ Å, with eight molecules in the unit cell. The structure model was refined to an *R*-factor of 0.039. In order to reduce the influence of the valence electrons all reflections with $\sin\theta/\lambda < 0.5$ Å^{-1} were excluded in the last stages of the refinement procedure (leaving 489 F_o's, $R = 0.031$). The molecule has a "twisted boat" conformation with C_2 symmetry. It is found that substitution at C1 has a significant effect on the molecular parameters.

The structure determination of hexahydro-3,6-pyridazinedione (cyclic succinhydrazide) is part of a series of structure investigations of 3,6-pyridazinediones and related compounds (see Ref. 1 and references therein).

s-Diformylhydrazine has been found [2] to have a planar S-shape (excluding the hydrogen atoms) in the crystal state, and the bond lengths indicate a high degree of conjugation over the entire molecule. Both experimental [3–5] and theoretical [6,7] results imply that the N−C=O fragment is easily altered by both substitution and hydrogen bonding. A study of how changes in conformation and substitution will affect the conjugation in the *s*-diformylhydrazine (O=C−N−N−C=O) fragment is therefore of interest. A structure determination of cyclic succinhydrazide was consequently carried out. This molecule was expected to have a "twisted boat" conformation close to that found for 1,4-cyclohexanedione [8] which gives a nonplanar diformylhydrazine fragment.

EXPERIMENTAL

Cyclic succinhydrazide was synthesized by reduction of 3,6-pyridazinedione (maleic hydrazide) with aluminium amalgam.[9] The crude product was recrystallized in ethyl alcohol. Rhomb-shaped platy crystals were formed.

Oscillation, Weissenberg and precession photographs indicated orthorhombic symmetry. The systematically absent reflections were those characteristic of the space group *Ibca* and the observed density indicated eight molecules in the unit cell (*i.e.* ½ molecule per asymmetric unit).

A computer-controlled Syntex $P\bar{1}$ four-circle diffractometer with graphite-monochromatized Mo$K\alpha$ radiation and equipped with an Enraf-Nonius liquid nitrogen cooling device (modified by H. Hope), was utilized in the determination of unit cell parameters and the collection of intensity data. The work was carried out using a crystal of dimensions 0.3 × 0.2 × 0.05 mm. Cell constants and their standard deviations were determined by a least-squares treatment of the angular coordinates of fifteen symmetry-independent reflections with 2θ-values between 42 and 50°. The temperature at crystal site was −165 °C.

Three-dimensional intensity data were recorded using the $\omega - 2\theta$ scanning mode with scan speed variable from 2 to 8° min^{-1}, depending on the peak intensity of the reflection. Background counting time was equal to 0.7 × scan time. Reflections with 2θ-values larger than 50° which had integrated counts of less than 5 cps, determined in a 2 s scan over the reflection, were not measured. The variations in the intensities of three standard reflections which were remeasured after every fifty reflections were random. Accordingly no corrections were applied to the intensity data for these variations.

The estimated standard deviations were taken as the square root of the total counts with a 2 % addition for experimental uncertainties. Of the 787 symmetry-independent

reflections measured ($2\theta_{max}=70°$), 732 had intensities larger than twice their standard deviations. These were regarded as "observed" reflections, and the remaining were excluded from further calculations. The intensities were corrected for Lorentz and polarization effects. The computer program used, as well as programs subsequently employed, is part of a local assembly of computer programs for CYBER-74 and is described in Ref. 10.

The atomic scattering factors used were those of Doyle and Turner [11] for oxygen, nitrogen, and carbon, and of Stewart *et al.*[12] for hydrogen.

CRYSTAL DATA

Hexahydro-3,6-pyridazinedione (cyclic succinhydrazide), $C_4H_6N_2O_2$, orthorhombic. Cell dimensions at $-165\,°C$: $a=9.112(2)$ Å, $b=17.063\ (3)$ Å, $c=6.175(1)$ Å. Figures in parentheses are estimated standard deviations. $V=960.1$ Å^3; $M=114.1$ amu; D_{obs} (19 °C) $=1.57$ g/cm^3; $Z=8$; $D_{calc}=1.579$ g/cm^3; $F(000)=480$. Absent reflections: $(h\,k\,l)$ for $h+k+l$ odd; $(0kl)$ for k odd and l odd; $(h0l)$ for h odd and l odd; $(hk0)$ for h odd and k odd; space group *Ibca*.

STRUCTURE DETERMINATION AND REFINEMENTS

The phase problem was solved by a computer procedure [13] based on direct methods utilizing tangent refinement.

The structure model was refined to a conventional R of 0.07. At this point the hydrogen atoms were placed in calculated positions and anisotropic thermal parameters for all nonhydrogen atoms were introduced. Full matrix least-squares refinement of all positional parameters, anisotropic thermal parameters for nonhydrogen atoms and isotropic thermal parameters for hydrogen atoms using all observed reflections converged to a weighted R_w of 0.046 and a conventional R of 0.039.

Table 2. Fractional atomic coordinates (x 10^3) and isotropic thermal parameters with estimated standard deviations for hydrogen atoms. Results from the refinement using all observed data.

Atom	x	y	z	B
H1	−127(1)	493(1)	−18(2)	2.1(3)
H2	−115(1)	723(1)	54(2)	1.5(3)
H3	−215(1)	679(1)	226(1)	1.3(3)

Earlier structure determinations [1,2,4,5,14] have indicated that structural parameters found for molecular systems like the present one are significantly influenced by the asphericity of the valence electrons. In order to reduce this influence all reflections with $\sin\theta/\lambda<0.5$ Å^{-1} were excluded from the refinement [leaving 489 F_o's (m)]. Earlier work [2,5,14] has shown that this asphericity has little or no effect when this cutoff value in $\sin\theta/\lambda$ is used. Least-squares refinement of all parameters $(s=37)$ involving nonhydrogen atoms resulted in a conventional R of 0.031, an R_w of 0.034, and an R-factor for the total data-set of 0.042. The "goodness of fit" $(\{\sum W(F_o-|F_c|)^2/(m-s)\}^{\frac{1}{2}})$ is 1.51. Atomic parameters for nonhydrogen atoms, obtained in this refinement are listed in Table 1, and parameters for hydrogen atoms, from the refinement using all observed reflections, are given in Table 2. A list of observed and calculated structure factors is available from the author upon request. (May also be obtained from: Department of Chemistry, University of Oslo, Oslo 3, Norway.)

Standard deviations in molecular parameters

Table 1. Fractional atomic coordinates and thermal parameters with estimated standard deviations (all $\times 10^5$) for nonhydrogen atoms. The temperature factor is given by exp $-(B_{11}h^2+B_{22}k^2+B_{33}l^2+B_{12}hk+B_{13}hl+B_{23}kl)$. Results from the refinement using high-angle data only.

Atom	x	y	z	B_{11}	B_{22}	B_{33}	B_{12}	B_{13}	B_{23}
O	4255(7)	60422(4)	4536(13)	182(6)	84(2)	924(19)	11(4)	−50(14)	−42(9)
N	−17311(7)	54095(4)	2(14)	180(6)	60(2)	865(17)	4(5)	56(13)	−56(9)
C1	− 9418(8)	60567(5)	4046(16)	216(7)	59(2)	620(21)	11(5)	8(15)	−29(9)
C2	−18329(8)	67886(5)	7566(17)	234(7)	60(2)	1017(21)	20(5)	−114(17)	−88(10)

were calculated from the correlation matrix ignoring standard deviations in cell parameters.

The r.m.s. difference between the observed U_{ij}'s (high-angle data refinement) and those calculated from the "rigid body" model [15] is 0.0004 Å², which indicates that the molecule may be regarded as a rigid body. The atomic positions were accordingly corrected for the librational motion. The eigenvallues of T are 0.10, 0.09 and 0.09 Å², and the r.m.s librational amplitudes are 4.3, 1.9 and 1.3°. The major axis is nearly parallel with a line through O – O′.

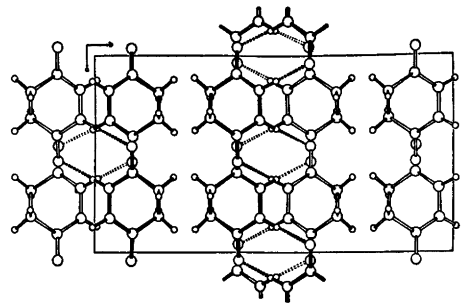

Fig. 1. The crystal structure as seen along the *c*-axis.

DISCUSSION

A view of the molecular packing in the crystal is given in Fig. 1. Hydrogen bonding across the centres of symmetry forms chains along the (101) and ($\bar{1}$01) directions. The N – C = O fragments form hydrogen bonded "dimers" similar to those found for formamide.[16] The length of the hydrogen bonds (2.762 Å) is equal to that found for diformylhydrazine.[2] Overlapping molecules in two chains [one along (101) and one along ($\bar{1}$01)] are separated by $c/2$ (3.088 Å). Between the chains there are only van der Waals contacts in the (010) direction. The closest nonbonding contact (excluding hydrogen atoms) is 3.465 Å [C2···C2 $(-0.5-x,1.5-y,0.5-z)$].

Bond lengths and bond angles are listed in Table 3 and some also in Fig. 2, where the numbering of the atoms is indicated. All three bonds O – C1, C1 – N and N – N are significantly longer than the corresponding bonds of, respectively, 1.234(1), 1.333(1) and 1.383(2) Å found for diformylhydrazine.[2] The results from a series of structure investigations of formamide and substituted formamides in the gas state (see Refs. 3 and 17, and references therein) indicate that both the C1 – O and C1 – N bonds are lengthened by approximately 0.01 Å when a methyl group is introduced at C1. The differences between the results obtained in this investigation and those found for diformylhydrazine are of the same magnitude. The lengthening of the N – N bond may be caused by the twist of 25.5° (see Table 4) around this bond. Also, the configuration around N is slightly nonplanar. This bond length is close

Table 3. Bond lengths (Å) and bond angles (°). The estimated standard deviations are given in the last digit of the corresponding number and are in parentheses. For nonhydrogen atoms are the parameters obtained in the refinement based only on high-angle data, used in the calculations.

	Bond length	E.s.d.	Corrected bond length		Bond angle	E.s.d.
O – C1	1.247	(1)	1.248	O – C1 – N	121.61	(8)
N – C1	1.341	(1)	1.344	O – C1 – C2	123.51	(8)
N – N′	1.401	(1)	1.402	C1 – N – N′	122.43	(5)
C1 – C2	1.506	(1)	1.509	N – C1 – C2	114.88	(6)
C2 – C2′	1.533	(2)	1.535	C1 – C2 – C2′	109.85	(6)
N – H1	0.93	(2)		C1 – N – H1	121	(1)
C2 – H2	0.98	(2)		N′ – N – H1	116	(1)
C2 – H3	0.98	(2)		C1 – C2 – H2	107	(1)
				C1 – C2 – H3	107	(1)
Hydrogen bond length				C2′ – C2 – H2	114	(1)
N – O($-x,1-y,-z$)	2.762(1)			C2′ – C2 – H3	110	(1)
				H2 – C2 – H3	109	(2)

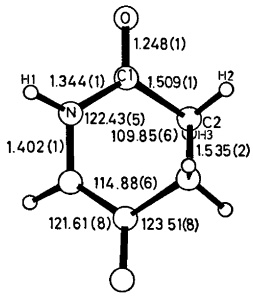

Fig. 2. Bond lengths (Å) (corrected for thermal vibration effects) and bond angles (°) with estimated standard deviations. Structure model obtained using high-angle data only in the refinement.

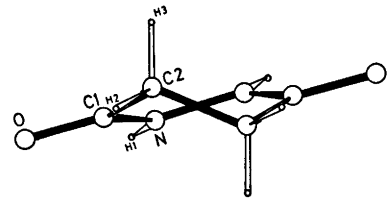

Fig. 3. The molecular conformation as seen along the *b*-axis.

Table 5. Deviations (Å × 10^3) from a least-squares plane through O,N,C1, and C2.

Atom	Deviations	Atom	Deviations
O	1	O′	379
N	1	N′	−43
C1	−4	C1′	394
C2	1	C2′	878
H1	−31	H1′	−335

to that found for 1,2-dimethyl-3,6-pyridazinedione [18] [1.406(1) Å], where the configuration around the N-atoms is about the same as in the present structure. However, a lengthening of this bond caused by the substitution at C1 is indicated by the difference in the N−C (methyl) bonds found in *N*-methylformamide [3] and *N*-methylacetamide.[17] The C2−C2′ bond has a normal $C(sp^3)-C(sp^3)$ bond length,[19] while the C1−C2 bond is about 0.01 Å shorter than the corresponding lengths for *N*-methylacetamide and acetamide.[20] This shortening is probably a result of the increased conjugation over the N−C=O fragment which is caused by the hydrogen bonding. There is a significant lengthening of the C−O bonds and a corresponding shortening of the C−N bonds in the present structure compared with similar non-hydrogen bonded molecules, as has been found earlier (see Refs. 2, 3, and 7 and references therein).

The bond angles around C1 are similar to those found for the corresponding angles in other 3,6-pyridazinediones.[4,5,18] The ∠C1−N−N′ is opened by about 3° compared with diformylhydrazine[2] and is close to the ones found for 1,2-dimethyl-3,6-pyridazinedione.[18]

A drawing of the molecular conformation is given in Fig. 3. The molecule has a "twisted boat" conformation, as has been found for 1,4-cyclohexanedione,[8] with C_2 symmetry. The four atoms O, N, C1, and C2 are planar (see Table 5). The values of the dihedral angles around the C1−N and N−N bonds are much smaller than those found around the C1−C2 and C2−C2 bonds. This is probably caused by conjugation over the entire diformylhydrazine fragment.

Table 4. Dihedral angles (°) with estimated standard deviations. The angles are positive in a right-hand screw.

Dihedral angle	(°)
O−C1−N−N′	178.1(1)
O−C1−C2−C2′	142.2(1)
C2−C1−N−N′	−2.7(2)
N−C1−C2−C2′	−37.0(1)
C1−N−N′−C1′	25.5(2)
C1−C2−C2′−C1′	56.2(1)

REFERENCES

1. Ottersen, T. *Acta Chem. Scand. A 29* (1975) 637.
2. Ottersen, T. *Acta Chem. Scand. A 28* (1974) 1145.
3. Kitano, M. and Kuchitsu, K. *Bull. Chem. Soc. Jap. 47* (1974) 631.
4. Ottersen, T. *Acta Chem. Scand. 27* (1973) 797.
5. Ottersen, T. *Acta Chem. Scand. A 28* (1974) 666.
6. Ottersen, T. and Jensen, H. H. *J. Mol. Struct. 26* (1975) 355.
7. Ottersen, T. *J. Mol. Struct. 26* (1975) 365.

8. Groth, P. and Hassel, O. *Acta Chem. Scand 18* (1964) 923.
9. Feuer, H., Bachman, G. B. and White, E. M. *J. Amer. Chem. Soc. 73* (1951) 4716.
10. Groth, P. *Acta Chem. Scand. 27* (1963) 1837.
11. Doyle, P. A. and Turner, P. S. *Acta Crystallogr. A 24* (1968) 390.
12. Stewart, R. F., Davidson, E. R. and Simpson, W. T. *J. Chem. Phys. 42* (1965) 3175.
13. Germain, G., Main, P. and Woolfson, M. M. *Acta Crystallogr. A 27* (1971) 368.
14. Ottersen, T., Christophersen, C. and Treppendahl, S. *Acta Chem. Scand. A 29* (1975) 45.
15. Shoemaker, V. and Trueblood, K. N. *Acta Crystallogr. B 24* (1968) 63.
16. Ladell, J. and Post, B. *Acta Crystallogr. 7* (1954) 559.
17. Kitano, M., Fekuyama, T. and Kuchitsu, K. *Bull. Chem. Soc. Jap. 46* (1973) 384.
18. Ottersen, T. *Acta Chem. Scand. 27* (1973) 835.
19. Bastiansen, O. and Trætteberg, M. *Tetrahedron 18* (1962) 147.
20. Kitano, M. and Kuchitsu, K. *Bull. Chem. Soc. Jap. 46* (1973) 3048.

Received March 21, 1975.

Acta Chemica Scandinavica A 29 (1975) 695—698

Magnetic Structures and Properties of $CrP_{1-x}As_x$

KARI SELTE,[a] HJALTE HJERSING,[a] ARNE KJEKSHUS,[a] ARNE F. ANDRESEN,[b] and P. FISCHER[c]

[a]Kjemisk Institutt, Universitetet i Oslo, Blindern, Oslo 3, Norway, [b]Institutt for Atomenergi, Kjeller, Norway, and [c]Delegation AF, Eidgenössisches Institut für Reaktorforschung, Würenlingen, Switzerland

X-Ray and neutron diffraction and magnetic susceptibility measurements show that CrP and CrAs exhibit a complete range of solid solubility, with P and As randomly arranged in an MnP type structure. Like CrAs, the As-rich samples undergo a transition from MnP to NiAs type structure at high temperatures. A double, *c* axis helimagnetic ordering is observed for $0.93 \lesssim x \leqq 1$ in $CrP_{1-x}As_x$.

In our systematic investigations of structural and magnetic properties of phases with the MnP type structure, one of the most unexpected results has been the absence of cooperative magnetic behaviour for CrP above 17 K.[1] This finding places CrP in a special position in comparison with CrAs,[2–4] MnP,[5,6] MnAs,[7,8] FeP,[9] and FeAs,[10] which take helimagnetic, ferromagnetic or canted magnetic structures below room temperature. In order to explore this problem further, the examination of CrP was extended down to 1.2 K and pursued into the domain of the ternary $CrP_{1-x}As_x$ phase.

EXPERIMENTAL

The binary compounds CrP and CrAs were prepared by heating stoichiometric quantities of the elements (99.0 % Cr (powder crystals), 99.999 % P, and 99.9999 % As (Koch-Light Laboratories)) in evacuated, sealed silica tubes as described in Refs. 1 and 3. Ternary $CrP_{1-x}As_x$ samples of desired compositions were prepared from appropriate proportions of CrP and CrAs, by means of a series of annealings at 950 – 1100 °C, interrupted by intermediate crushings. The samples were finally cooled to room temperature over a period of two days.

Experimental details concerning X-ray and neutron diffraction and magnetic susceptibility measurements are included in Ref. 10. The neutron diffraction data for CrP at 4.2 and 1.2 K were obtained in Würenlingen using a He bath cryostat and neutrons of wave length 2.319 Å.

RESULTS AND DISCUSSION

As demonstrated by the continuous variations in the orthorhombic unit cell dimensions of $CrP_{1-x}As_x$ with the composition parameter

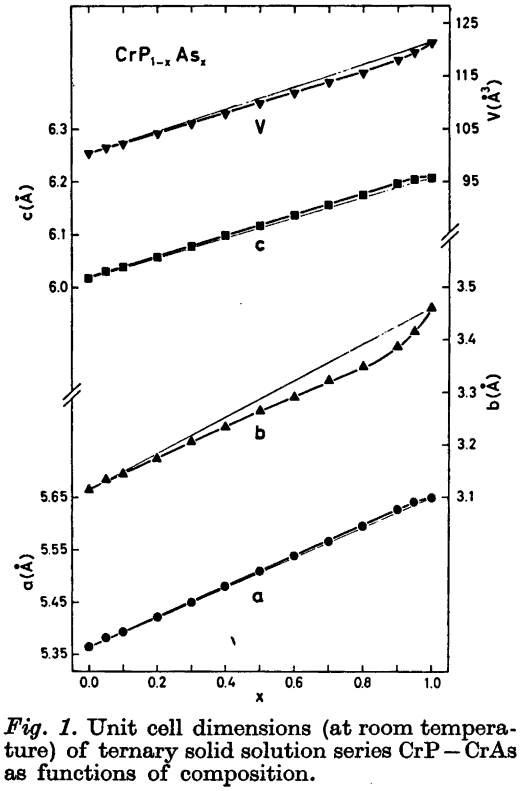

Fig. 1. Unit cell dimensions (at room temperature) of ternary solid solution series CrP – CrAs as functions of composition.

Table 1. Unit cell dimensions and positional parameters with standard deviations for some $CrP_{1-x}As_x$ samples; space group *Pnma*, positions 4(*c*). (Overall profile reliability factors ranging between 0.029 and 0.041.)

x	0			0.90			0.95		
T(K)	1.2	4.2	293	5	80	293	5	80	293
a(Å)	5.346(6)	5.347(6)	5.367(7)	5.597(1)	5.609(1)	5.628(1)	5.581(4)	5.596(4)	5.640(2)
b(Å)	3.107(4)	3.108(4)	3.122(4)	3.350(1)	3.360(1)	3.398(1)	3.360(2)	3.367(2)	3.415(1)
c(Å)	5.999(6)	6.001(6)	6.017(8)	6.178(1)	6.187(1)	6.200(1)	6.188(3)	6.174(3)	6.206(2)
x_T	0.0078(5)	0.0080(5)	0.0068(12)	0.0086(12)	0.0105(14)	0.0101(13)	as for CrAs		
z_T	0.1940(4)	0.1938(4)	0.1930(5)	0.1996(11)	0.1979(10)	0.2006(11)			
x_X	0.1853(3)	0.1852(3)	0.1852(3)	0.1966(6)	0.1971(6)	0.1999(7)			
z_X	0.5648(3)	0.5645(4)	0.5656(3)	0.5737(9)	0.5739(9)	0.5744(7)			

x (Fig. 1), CrP and CrAs exhibit complete, mutual solid solubility. Except for the binary end members [1,3] of the series, a possible extension of the homogeneity range of $CrP_{1-x}As_x$ to metal/non-metal (atomic) ratios different from 1.00 has not been investigated. The X-ray data show that $CrP_{1-x}As_x$ ($0 \leqq x \leqq 1$) takes the MnP type structure with random distribution of the two kinds of non-metal atoms at room temperature.

As evinced by line broadening of reflections on the Guinier photographs, the successive annealings improved considerably the crystalline perfection of the samples. Since the reflections with $k \neq 0$ generally were observed to be more diffuse than those with $k = 0$, the incomplete randomization should occur mainly in the b direction of the crystallites. This problem proved to be rather acute for the large scale, neutron diffraction samples.

The structural data as deduced from neutron diffraction experiments (Table 1) show only minor variations in the unit cell dimensions of CrP and $CrP_{0.10}As_{0.90}$ below room temperature, whereas $CrP_{0.05}As_{0.95}$, which experiences helimagnetic ordering below 246 – 260 K, reveals appreciable changes in the unit cell dimensions associated with its superimposed first and second (or higher) order phase transformation (*cf.* Refs. 2 – 4, 11 – 13). The positional parameters derived for CrP at 4.2 and 1.2 K are only insignificantly different from those reported for 17 K in Ref. 1. Taking into account that CrAs and $CrP_{0.05}As_{0.95}$ undergo cooperative magnetic ordering whereas $CrP_{0.10}As_{0.90}$ does not, the present values for the positional parameters of the ternary samples are consistent with those reported [3] for CrAs.

The fact that CrAs (as opposed to CrP) undergoes a second (or higher) order crystallographic

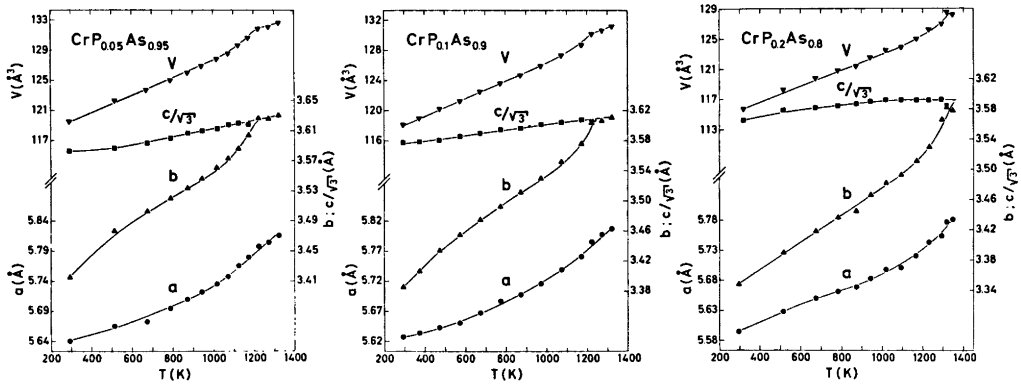

Fig. 2. Unit cell dimensions of three $CrP_{1-x}As_x$ samples as functions of temperature. Average relative expansion coefficients α_a [$= (a_T - a_{T'})/a_{300}(T - T')$], α_b, α_c multiplied by 10^6 K are 24, 54, 9; 27, 59, 9; and 22 ,61, 15 for $CrP_{0.20}As_{0.80}$, $CrP_{0.10}As_{0.90}$, and $CrP_{0.05}As_{0.95}$, respectively.

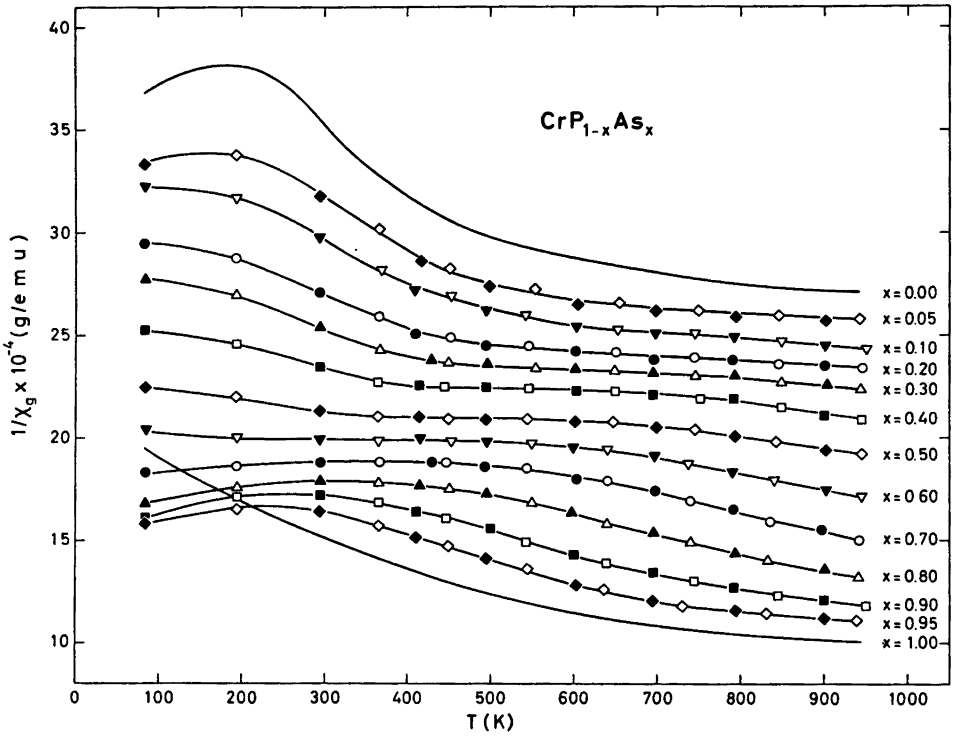

Fig. 3. Reciprocal magnetic susceptibility *versus* temperature for various $CrP_{1-x}As_x$ samples.

transformation to the NiAs type structure at 1173 ± 20 K,[11] has prompted a high temperature X-ray study of the As-rich $CrP_{1-x}As_x$ samples. As evident from Fig. 2, corresponding transitions to that in CrAs were observed at 1230 ± 50, 1270 ± 50, and 1350 ± 50 K for $x = 0.95$, 0.90, and 0.80, respectively. The latter temperature represents, in practice, the upper limit for our high temperature X-ray diffraction camera. Although the trend in the above temperatures suggests that the transformation continues at even higher temperatures in samples with $x < 0.80$, the approaching onset of melting or decomposition leads to little confidence in such an extrapolation.

Fig. 3 shows the gradual changes in the temperature dependence of the reciprocal magnetic susceptibility with the composition parameter x. Field strength dependent susceptibilities were not observed, and as seen from Fig. 3, none of the individual thermomagnetic curves fulfils the Curie-Weiss Law over any range of temperature.

The 4.2 and 1.2 K neutron diffraction diagrams of CrP give no indication of any long range magnetic ordering, thus confirming the conclusion of Ref. 1.

The double, c axis type helimagnetic ordering of CrAs[2-4] extends to a composition $x \approx 0.93$ of the $CrP_{1-x}As_x$ phase. At 80 K negligible changes

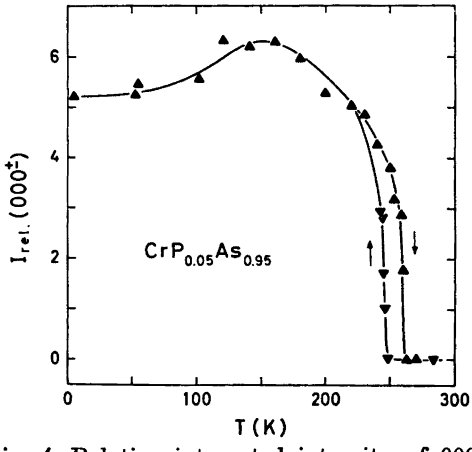

Fig. 4. Relative integrated intensity of $000^{\pm}$ *versus* temperature for $CrP_{0.05}As_{0.95}$.

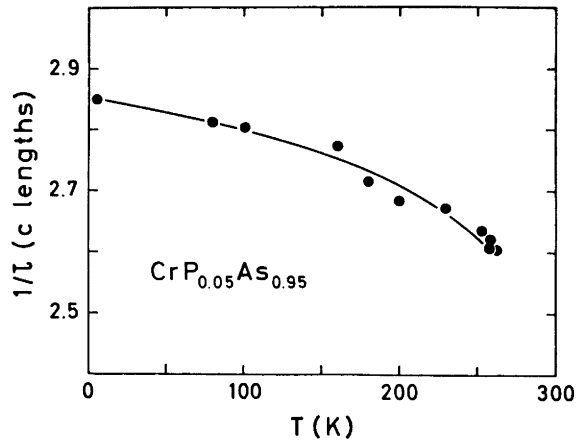

Fig. 5. Spiral periodicity as function of temperature for $CrP_{0.05}As_{0.95}$.

were experienced in all parameters specifying the spirals on going from CrAs to $CrP_{0.05}As_{0.95}$ ($\tau/2\pi c^* = 0.355(2)$, $\mu_T = 1.7(1)$ μ_B, $\phi = -132(3)°$, and β fixed at 90°). As evident from Fig. 4, the onset of the cooperative magnetic phenomenon in $CrP_{0.05}As_{0.95}$ is accompanied by a marked hysteresis, resembling also in this respect CrAs. The 5 % content of P leads to a slight lowering of the Néel temperature (from 261 – 272 K for CrAs to 246 – 260 K). Both the spiral periodicity (Fig. 5) and the phase angle between the independent spirals are somewhat temperature dependent in $CrP_{0.05}As_{0.95}$. (The latter inference provides the only consistent explanation of the peculiar shape of the curve in Fig. 4 below 150K, since $CrP_{0.05}As_{0.95}$ has no ferromagnetic component.)

The results for $Cr_{1-t}V_tAs$ [12] and $CrP_{1-x}As_x$ are consistent in that the helimagnetic ordering in both phases is destroyed at some 5 % substitution of Cr or As with another metal or nonmetal. A brief discussion of possible reasons for the breakdown of the helimagnetic mode in such phases is given in Ref. 12.

Acknowledgement. The assistance of Ing. Stanislav Vratislav (I.A.E.A.-fellow from The Technical University of Prague, Czechoslovakia) in some of the neutron diffraction measurements is greatly appreciated.

REFERENCES

1. Selte, K., Kjekshus, A. and Andresen, A. F. *Acta Chem. Scand. 26* (1972) 4188.
2. Kazama, N. and Watanabe, H. *J. Phys. Soc. Japan 30* (1971) 1319.
3. Selte, K., Kjekshus, A., Jamison, W. E., Andresen, A. F. and Engebretsen, J. E. *Acta Chem. Scand. 25* (1971) 1703.
4. Boller, H. and Kallel, A. *Solid State Commun. 9* (1971) 1699.
5. Felcher, G. P. *J. Appl. Phys. 37* (1966) 1056.
6. Forsyth, J. B., Pickart, S. J. and Brown, P. J. *Proc. Phys. Soc. 88* (1966) 333.
7. Bacon, G. E. and Street, R. *Nature (London) 175* (1955) 518.
8. Schwartz, L. H., Hall, E. L. and Felcher, G. P. *J. Appl. Phys. 42* (1971) 1621.
9. Felcher, G. P., Smith, F. A., Bellavance, D. and Wold, A. *Phys. Rev. B 3* (1971) 3046.
10. Selte, K., Kjekshus, A. and Andresen, A. F. *Acta Chem. Scand. 26* (1972) 3101.
11. Selte, K. and Kjekshus, A. *Acta Chem. Scand. 27* (1973) 3195.
12. Selte, K., Hjersing, H., Kjekshus, A. and Andresen, A. F. *Acta Chem. Scand. A 29* (1975) 312.
13. Selte, K., Kjekshus, A., Aaby, S. and Andresen, A. F. *Acta Chem. Scand. In press.*

Received March 10, 1975.

Acta Chemica Scandinavica A 29 (1975) 699—705

Crystal Structure of the 1:1 Addition Compound Between Durene and Hexafluorobenzene

TOR DAHL

Institute of Mathematical and Physical Sciences, University of Tromsø, Box 790, 9001 Tromsø, Norway

The 1:1 addition compound between durene and hexafluorobenzene crystallizes at +20 °C in the monoclinic space group $C2/m$ with cell parameters $a = 9.478$ Å, $b = 15.771$ Å, $c = 7.232$ Å, $\beta = 133.46°$. The structure is disordered. The partner molecules are stacked alternately in infinite columns and the mean separation between the molecular planes is 3.51 Å. The benzene rings of the partner molecules are twisted 19° relative to each other. At lower temperatures the crystals are triclinic. Analysis of poor intensity data taken at −100 °C shows that the benzene rings of the partner molecules are nearly parallel at this temperature.

The crystal structures of the 1:1 addition compounds of hexafluorobenzene (HFB) with *p*-xylene [1] and mesitylene [2] are quite different from that of its addition compound with hexamethylbenzene.[3,4]

While the two former structures indicate little or no contribution of charge-transfer forces, the latter shows similarity to structures of charge-transfer complexes. To obtain more information about how the number of methyl groups in compounds of this kind affect their structure, the crystal structure of the 1:1 compound between durene and HFB was investigated.

DESCRIPTION OF THE CRYSTALS. CRYSTAL DATA

At +20 °C the crystals are monoclinic and the following cell parameters were found: $a = 9.478 \pm 0.004$ Å, $b = 15.771 \pm 0.003$ Å, $c = 7.232 \pm 0.003$ Å, $\beta = 133.36 \pm 0.03°$. This face-centered cell was chosen in order to have an axis (c) in the direction along which the crystals are elongated. Another face-centered cell with a β-angle of 130.63° in which this direction is along [101] could have been chosen. Assuming two molecules of each kind in the cell the calculated density is 1.36 g/cm³.

Of the reflections hkl those with $h + k = 2n + 1$ are absent, and as both the molecules may have centres of symmetry, the space group was assumed to be $C2/m$.

When the crystals are cooled to −50 °C twins of a triclinic modification are obtained. The twin plane corresponds to (010) in the monoclinic form. No exact determination of the transition point has been made. NMR measurments [5] show a rapid decrease in the proton second moment when the temperature is increased above 250 K indicating that the transition may occur at this temperature. Cell parameters of the triclinic modification have not been determined, but the diagrams indicate no doubling of any axes and only moderate changes of the cell parameters relative to those of the monoclinic cell.

EXPERIMENTAL

The crystals were obtained by evaporating the solvent from an ether solution of the two components at −25 °C. They are unstable on exposure to the atmosphere and were kept in sealed glass capillaries.

The cell parameters and the intensities for the monoclinic form were measured at the University of Bergen on a paper-tape controlled Siemens AED diffractometer using Mo$K\alpha$-radiation. Six reflections were used for the least squares refinement of the cell parameters. The intensity data were collected using a five-value scan technique.[6] 311 reflections whose intensities were more than two times the standard deviations were regarded as observed. The in-

tensities of two standard reflections which were measured at intervals of 50 reflections were approximately constant during the first 70 % of the data collection time, but decreased to less than half of their original values during the rest of the time. The crystals are thus not very stable even in sealed capillaries when exposed to the X-ray beam.

The computer program used for the data reduction has been written at the Weizmann Institute of Science, Rehovoth, and has been modified for Univac 1110 by L. M. Milje and K. Åse. The diffractometer programs have been written by K. Maartmann-Moe. All the other programs used in this work are described in Ref. 7. The atomic form factors are given in Ref. 8. The weight factors used in the least squares refinement are $(I_t-I_b)^2/[I_t+I_b+k^2(I_t-I_b)]$ where k, which is the standard deviation in the scaling curve, was estimated to be 0.015. The dimensions of the crystal were approximately $0.1\times0.2\times0.3$ mm^3 and absorption corrections were found to be unimportant and not performed. The effect of secondary extinction seems to be small and was not corrected for.

For the low-temperature diagrams an ENRAF-NONIUS N_2 gas-flow cooling device was used. A considerable number of crystals were destroyed or moved in the capillary before any diagram could be obtained, and data for a complete structure determination was therefore not taken. A zero-layer Weissenberg diagram was eventually obtained, taken at -100 °C with 30° rotation about the direction corresponding to the c-axis of the monoclinic cell. Using reflections from both individuals of the twin crystal, a rough visual intensity estimation of 29 observed reflections was made. Six low-angle unobserved reflections were also included in the data.

STRUCTURE DETERMINATION OF THE MONOCLINIC FORM

None of the possible ordered structures were found to be correct and disorder had to be introduced. An attempt was made to refine a structure based on a model in which the durene molecule has the orientation shown in Fig. 1A and the HFB molecule has two non-equivalent orientations, each with one of its mirror planes in (010). As the R-value obtained was not below 10 % and the thermal vibration parameters were unreasonably large, this model was assumed to be incorrect.

Satisfactory results were obtained using a model with the durene molecule oriented as in Fig. 1A, and with the HFB molecule in the two equivalent orientations indicated in Fig. 1B.

During the least squares refinement the following restrictions were put on the geometry of the molecules:

Durene: $\angle OC_6C_4=180°$, $C_4-C_6/C_6-O=1.52/1.40$,[9] $C5-O/C6-O'=2$ HBF (for all C–F bonds): $\angle OCF=180°$, $F-C/C-O=1.326/1.394$.[10]

In the last refinement cycles all positional and thermal parameters were varied, giving 65 independent parameters. H-atoms with positions calculated assuming disorder due to rotation of the methyl groups were included in the structure factor calculations. A conventional R-value of 7.9 % was obtained ($R_W=6.8$ %).

Observed and calculated structure factors are given in Table 1, positional and thermal parameters in Table 2, bond distances and angles and intermolecular distances in Table 3 and principal axes of the vibration ellipsoids in Table 4. Sections through a three-dimensional Fourier map along the molecular planes are shown in Fig. 3 and the packing of the molecules is shown in Fig. 4.

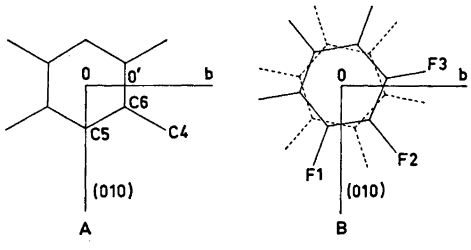

Fig. 1. The orientation of the molecules in the monoclinic form.

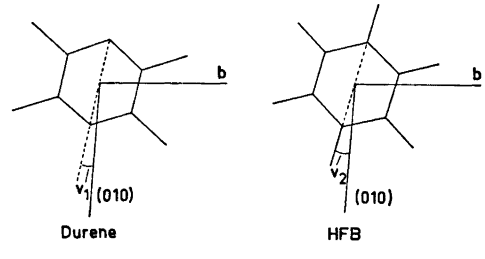

Fig. 2. The orientation of the molecules in the triclinic form.

Table 1. Observed and calculated structure factors, ten times the absolute values. The columns listed are h, k, l, F_o, F_c.

2	0	0	369.	-387.
4	0	0	107.	-107.
6	0	0	32.	34.
1	1	0	640.	646.
3	1	0	26.	- 34.
0	2	0	901.	828.
2	2	0	164.	-164.
4	2	0	115.	-104.
6	2	0	23.	30.
1	3	0	229.	-233.
3	3	0	109.	- 99.
5	3	0	41.	40.
0	4	0	432.	-411.
2	4	0	14.	7.
4	4	0	64.	- 57.
1	5	0	17.	- 16.
3	5	0	176.	-165.
5	5	0	63.	63.
0	6	0	83.	78.
2	6	0	164.	-151.
4	6	0	39.	39.
1	7	0	125.	-117.
3	7	0	74.	- 73.
5	7	0	45.	43.
0	8	0	179.	-168.
2	8	0	141.	-143.
4	8	0	74.	74.
1	9	0	131.	-129.
3	9	0	42.	46.
5	9	0	18.	14.
0	10	0	49.	- 50.
2	10	0	33.	39.
4	10	0	30.	34.
1	11	0	70.	72.
3	11	0	15.	28.
0	12	0	100.	104.
2	12	0	28.	30.
1	13	0	50.	47.
3	13	0	15.	- 14.
0	14	0	36.	32.
2	16	0	14.	- 1.
-6	0	1	37.	- 34.
-4	0	1	168.	-172.
-2	0	1	203.	201.
0	0	1	149.	-147.
2	0	1	272.	-277.
-5	1	1	40.	43.
-3	1	1	163.	-169.
-1	1	1	257.	-260.
1	1	1	122.	128.
3	1	1	34.	- 31.
5	1	1	30.	- 34.
-6	2	1	27.	- 36.
-4	2	1	14.	7.
-2	2	1	296.	283.
0	2	1	50.	- 55.
2	2	1	42.	- 40.
-5	3	1	22.	32.
-3	3	1	68.	65.
-1	3	1	86.	- 81.
1	3	1	219.	201.
3	3	1	51.	65.
-4	4	1	68.	83.
-2	4	1	66.	55.
0	4	1	78.	80.
2	4	1	23.	20.
-7	5	1	16.	16.
-3	5	1	142.	-131.
-1	5	1	145.	145.
1	5	1	190.	-182.
3	5	1	38.	46.
-6	6	1	29.	33.
-4	6	1	56.	51.
-2	6	1	227.	-220.
0	6	1	37.	- 38.
2	6	1	40.	- 42.
-5	7	1	16.	28.
-3	7	1	40.	- 44.
-1	7	1	20.	31.
1	7	1	140.	-140.
3	7	1	39.	43.
5	7	1	19.	25.
-8	8	1	17.	4.
-6	8	1	22.	25.
-4	8	1	38.	44.
-2	8	1	34.	- 38.
2	8	1	44.	43.
4	8	1	16.	15.
-3	9	1	55.	53.
-1	9	1	28.	29.
1	9	1	49.	46.
-4	10	1	38.	- 40.
-2	10	1	40.	38.
0	10	1	41.	37.
-3	11	1	29.	- 27.
-1	11	1	39.	30.
3	11	1	32.	- 39.
-4	12	1	25.	- 38.
0	12	1	17.	22.
2	12	1	32.	- 39.
-3	13	1	20.	- 22.
-1	13	1	32.	39.
0	14	1	19.	28.
-6	0	2	43.	- 42.
-4	0	2	104.	-105.
-2	0	2	1139.	1279
0	0	2	94.	101.
2	0	2	18.	- 19.
-7	1	2	41.	35.
-5	1	2	120.	-120.
-3	1	2	216.	-212.
-1	1	2	1285.	1341
1	1	2	106.	-106.
3	1	2	49.	- 45.
-6	2	2	16.	- 10.
-4	2	2	42.	- 41.
-2	2	2	312.	311.
0	2	2	65.	- 74.
2	2	2	59.	- 58.
4	2	2	23.	19.
-7	3	2	42.	41.
-5	3	2	137.	-131.
-3	3	2	50.	- 64.
-1	3	2	63.	- 61.
1	3	2	71.	- 67.
3	3	2	23.	- 19.
-6	4	2	47.	51.
-4	4	2	93.	- 89.
-2	4	2	195.	-201.
0	4	2	53.	- 64.
2	4	2	86.	- 85.
4	4	2	26.	27.
-7	5	2	31.	31.
-5	5	2	81.	- 76.
-1	5	2	90.	- 85.
1	5	2	68.	- 70.
3	5	2	23.	26.
-6	6	2	81.	82.
-4	6	2	181.	-176.
0	6	2	34.	- 40.
2	6	2	39.	- 36.
4	6	2	24.	20.
-7	7	2	16.	8.
-5	7	2	46.	46.
-3	7	2	167.	-170.
-1	7	2	46.	- 47.
1	7	2	96.	- 94.
3	7	2	43.	43.
-6	8	2	55.	53.
-4	8	2	45.	- 48.
-2	8	2	128.	-130.
0	8	2	116.	-119.
2	8	2	19.	23.
-5	9	2	65.	71.
-3	9	2	58.	- 56.
-1	9	2	109.	-109.
3	9	2	26.	28.
-6	10	2	17.	10.
-4	10	2	40.	50.
-2	10	2	17.	- 12.
2	10	2	29.	30.
-3	11	2	58.	60.
-1	11	2	48.	47.
1	11	2	22.	30.
-2	12	2	77.	77.
4	12	2	49.	46.
-1	13	2	56.	56.
-2	14	2	22.	20.
-4	16	2	18.	- 0.
-8	0	3	17.	- 33.
-6	0	3	19.	16.
-4	0	3	13.	14.
-2	0	3	228.	-228.
0	0	3	24.	- 17.
-7	1	3	24.	- 26.
-5	1	3	108.	-111.
-3	1	3	139.	143.
1	1	3	77.	- 81.
-6	2	3	28.	44.
-4	2	3	40.	34.
-2	2	3	94.	-100.
0	2	3	55.	51.
-7	3	3	23.	- 24.
-3	3	3	108.	94.
-1	3	3	68.	61.
-6	4	3	27.	36.
-4	4	3	42.	- 41.
-2	4	3	28.	41.
2	4	3	21.	23.
-5	5	3	23.	22.
-3	5	3	29.	- 16.
-1	5	3	49.	- 55.
-8	6	3	21.	25.
-4	6	3	97.	-100.
-2	6	3	30.	31.
0	6	3	78.	- 81.
-7	7	3	24.	28.
-5	7	3	26.	28.
-3	7	3	46.	- 53.
-1	7	3	44.	- 49.
-8	8	3	17.	18.
-2	8	3	26.	15.
0	8	3	15.	- 3.
2	8	3	16.	12.
-1	9	3	20.	20.
-2	10	3	19.	17.
-5	11	3	30.	- 33.
-3	11	3	18.	23.
-2	12	3	26.	30.
-5	13	3	16.	- 18.
-2	14	3	23.	26.
-8	0	4	23.	22.
-6	0	4	84.	- 86.
-2	0	4	393.	401.
0	0	4	28.	- 27.
2	0	4	19.	- 8.
-7	1	4	46.	- 43.
-5	1	4	69.	- 69.
-3	1	4	455.	482.
-1	1	4	25.	- 31.
1	1	4	24.	- 23.
-8	2	4	33.	31.
-6	2	4	82.	- 83.
-2	2	4	167.	169.
0	2	4	36.	- 37.
-5	3	4	16.	- 27.
-3	3	4	30.	26.
-1	3	4	39.	- 40.
1	3	4	25.	- 27.
-8	4	4	43.	41.
-6	4	4	86.	- 85.
-4	4	4	23.	- 37.
-2	4	4	35.	- 35.
0	4	4	38.	- 42.
-7	5	4	36.	39.
-5	5	4	74.	- 75.
-3	5	4	61.	- 56.
-1	5	4	29.	- 33.
-8	6	4	31.	33.
-6	6	4	43.	- 41.
-4	6	4	55.	- 56.
-2	6	4	32.	- 34.
0	6	4	34.	- 34.
2	6	4	13.	17.
-9	7	4	17.	- 2.
-7	7	4	65.	64.
-5	7	4	93.	- 95.
-3	7	4	38.	- 44.
-1	7	4	44.	- 49.
-8	8	4	19.	10.
-6	8	4	31.	33.
-4	8	4	67.	- 70.
-2	8	4	49.	- 53.
-7	9	4	29.	34.
-3	9	4	39.	- 39.
-1	9	4	21.	- 21.
-5	11	4	23.	22.
-3	11	4	29.	31.
-1	11	4	19.	15.
-4	12	4	34.	32.
-2	12	4	29.	31.
-3	13	4	31.	32.
-2	14	4	19.	13.
-6	0	5	46.	- 41.
-4	0	5	46.	39.
0	0	5	21.	- 22.
-11	1	5	20.	- 9.
-9	1	5	19.	- 20.
-5	1	5	45.	56.
-3	1	5	44.	- 31.
-6	2	5	21.	- 15.
-4	2	5	30.	29.
-7	3	5	17.	21.
-9	5	5	22.	13.
-7	5	5	18.	12.
-5	5	5	20.	- 27.
-2	6	5	21.	- 29.
-5	7	5	25.	- 28.
-8	0	6	37.	- 31.
-6	0	6	32.	- 24.
-4	0	6	188.	174.
-9	1	6	20.	12.
-7	1	6	51.	- 46.
-5	1	6	67.	67.
-3	1	6	74.	61.
-1	1	6	22.	- 13.
-8	2	6	28.	- 23.
-4	2	6	103.	95.
-9	3	6	24.	22.
-7	3	6	45.	- 40.
-3	3	6	22.	13.
-9	5	6	29.	28.
-7	5	6	46.	- 37.
-5	5	6	22.	- 25.
-3	5	6	22.	- 17.
-8	6	6	24.	23.
-6	6	6	45.	- 44.
-4	6	6	37.	- 22.
-9	7	6	28.	22.
-7	7	6	22.	- 12.
-5	7	6	31.	- 30.
-3	7	6	23.	- 23.
-8	8	6	36.	28.
-9	9	6	27.	6.
-7	9	6	23.	12.
-4	12	6	23.	16.
-3	3	7	24.	- 0.
-8	0	8	27.	- 21.
-6	0	8	30.	38.
-5	1	8	44.	38.
-8	4	8	32.	- 18.

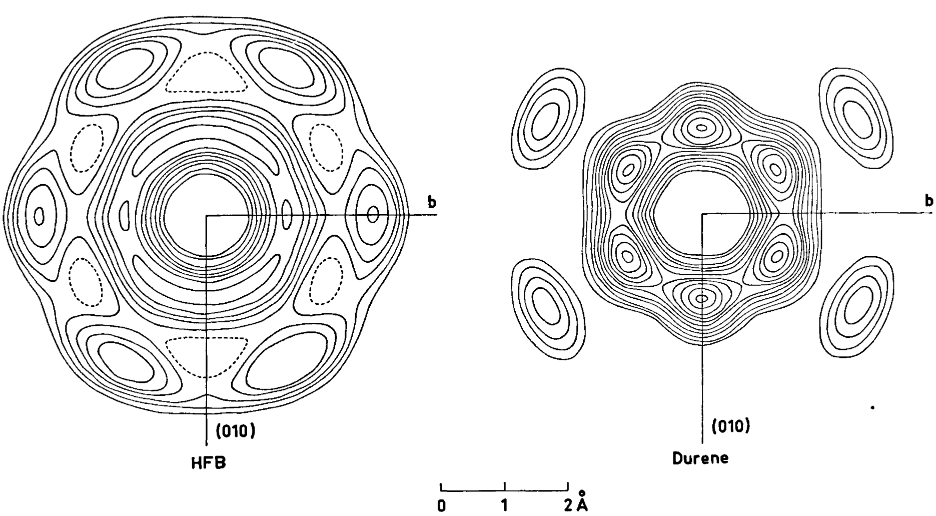

Fig. 3. Sections through a three-dimensional Fourier map along the molecular planes. Contour intervals of 1/4 e/Å^3 and lowest contour at 1 e/Å^3. Broken lines represent contours around the minima.

Table 2. Coordinates and anisotropic thermal parameters according to the expression: $\exp -(B_{11}h^2 + B_{22}k^2 + B_{33}l^2 + B_{12}hk + B_{13}hl + B_{23}kl)$, with estimated standard deviations in parentheses.

	x	y	z	B_{11}	B_{22}	B_{33}	B_{12}	B_{13}	B_{23}
F 1	0.3578(29)	−0.0562(17)	0.7189(43)	0.067(5)	0.0323(33)	0.122(6)	0.031(5)	0.138(10)	0.018(7)
F 2	0.2826(31)	−0.1063(21)	0.6986(44)	0.074(7)	0.0260(22)	0.123(8)	−0.021(6)	0.134(15)	−0.014(7)
F 3	−0.0751(24)	0.1637(5)	0.5365(50)	0.138(12)	0.0117(4)	0.142(13)	0.038(4)	0.177(29)	0.023(6)
C 1	0.1834(15)	−0.0288(9)	0.6122(22)	0.086(8)	0.0175(32)	0.101(12)	0.026(9)	0.166(20)	0.021(9)
C 2	0.1448(16)	0.0544(11)	0.6018(22)	0.016(6)	0.0165(14)	0.063(10)	−0.010(4)	0.039(12)	−0.006(6)
C 3	−0.0386(12)	0.0839(2)	0.5187(26)	0.020(8)	0.0128(12)	0.067(7)	0.003(3)	0.052(14)	0.006(7)
C 4	0.2039(6)	0.1570(4)	0.1399(8)	0.145(4)	0.0148(6)	0.153(5)	−0.053(2)	0.222(8)	−0.027(2)
C 5	0.1955(6)	0	0.1342(7)	0.051(3)	0.0124(5)	0.070(4)	0	0.089(6)	0
C 6	0.0978(3)	0.0753(2)	0.0671(4)	0.066(2)	0.0087(3)	0.073(3)	−0.013(1)	0.108(5)	−0.007(2)

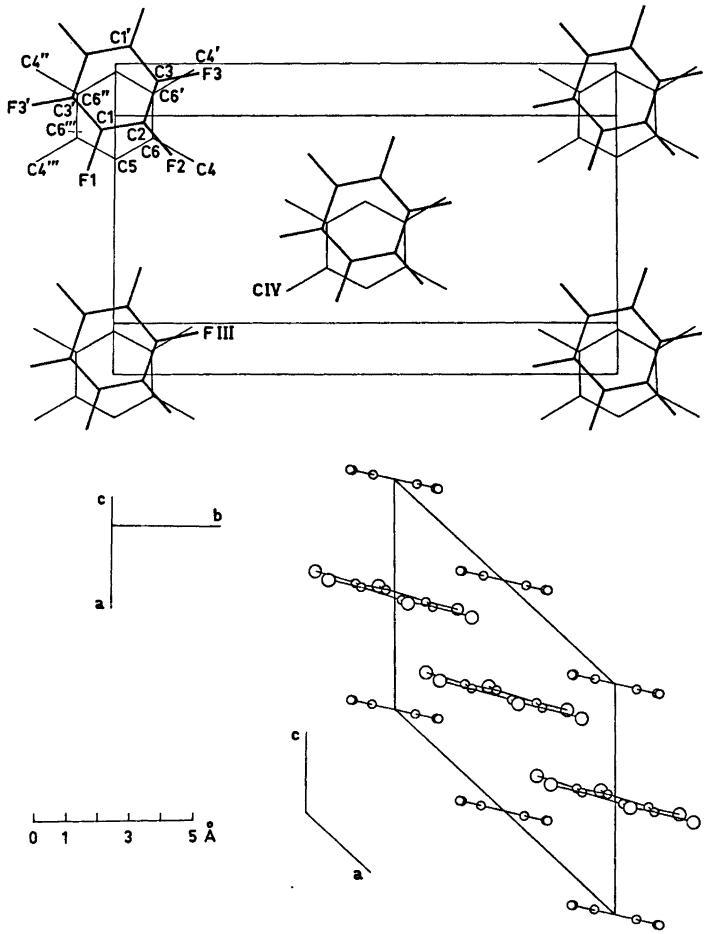

Fig. 4. The packing of the molecules viewed perpendicular to the plane of the durene molecule and perpendicular to (010).
Only one of the equivalent orientations of the HFB-molecule is shown.

THE ORIENTATION OF THE MOLECULES IN THE TRICLINIC FORM

The space group of the triclinic crystals was assumed to be $P\bar{1}$. The axes are denominated as the corresponding axes of the monoclinic cell.

The experimental data obtained for this modification permit only determination of approximate orientations of the molecules projected along [001]. This was done by calculating a series of R-values for structures which were varied systematically by rotation of the molecules independently about their plane normal. Near the minimum value the rotations were made in steps of 3°. For each orientation the coordinates were calculated using a value of 86.3° for α^* (measured on the diagrams) and assuming the values of a^* and b^* to increase by 1.5 % compared with those of the monoclinic cell. The angle between the c-axis and the molecular plane was assumed to be as in the monoclinic form for both molecules. Isotropic B-values, 8 Å^2 for the F-atoms and the methyl C-atoms and 4 Å^2 for the ring C-atoms, were used.

The lowest R-value, 20.9 %, in which both observed and unobserved reflections are included, was obtained for the orientations shown in Fig. 2, the values of v_1 and v_2 being 9 and 12°, respectively. These orientations are be-

Table 3. Bond distances (Å) and angles (°) and intermolecular distances (Å). Values in parentheses are approximate standard deviations.

Distances in HFB (0.01 – 0.02)		Distances in durene (0.004)	
C3′ – C1	1.35	C5 – C6	1.373
C1 – C2	1.35	C6 – C6′	1.379
C2 – C3	1.38	C4 – C6	1.490
C1 – F1	1.33		
C2 – F2	1.27	Angles in durene (0.3)	
C3 – F3	1.29	C6‴ – C5 – C6	119.7
		C5 – C6 – C6′	120.2
Angles in HFB (1.5)		C4 – C6 – C5	119.7
C3′ – C1 – C2	117.1	C4 – C6 – C6′	120.2
C1 – C2 – C3	122.4		
C2 – C3 – C1′	120.2	Intermolecular distances (0.03)	
F1 – C1 – C3′	120.9	F1 – C5	3.48
F1 – C1 – C2	122.0	F1 – C6‴	3.52
F2 – C2 – C1	117.4	F3′ – C4″	3.62
F2 – C2 – C3	120.1	F3 – C4′	3.64
F3 – C3 – C2	121.8	F2 – C4	3.66
F3 – C3 – C1′	117.9	C3′ – C6″	3.48
		C1 – C6‴	3.51
		FIII – CIV	3.33

lieved to be correct within a few degrees. The benzene rings of the molecules are thus twisted ~3° relative to each other about their plane normals.

DISCUSSION

Where nothing else is stated the discussion refers to the structure of the monoclinic form.

Rigid body analysis of the thermal vibrations show the largest r.m.s. angle of libration to be 11.8° for both molecules, which is a slightly higher value than those found for the other addition compounds in this series. The largest axis of libration is nearly parallel to the *c*-axis for both molecules. No correction of the interatomic distances for this effect has been performed.

A distance of 3.33 Å is observed between an F-atom and a methyl C-atom belonging to different stacks. This distance is only 0.09 Å longer than the remarkably short contact of the same kind observed in the addition compound between HFB and mesitylene.[2] The corresponding angle C(ring) – C(methyl)···F is 158.0°.

Table 4. Principal axes of the thermal vibration ellipsoids.

	R.m.s. amplitudes Å	Components of the r.m.s. amplitudes (Å) $U(x)$	$U(y)$	$U(z)$
F 1	0.660	0.268	0.629	0.134
	0.405	0.379	−0.062	0.551
	0.325	0.300	−0.085	−0.019
F 2	0.590	0.256	−0.558	0.132
	0.410	0.264	0.035	0.542
	0.396	0.450	0.124	0.124
F 3	0.655	0.730	0.231	0.194
	0.447	0.244	0.118	0.561
	0.315	0.188	−0.283	0.153
C 1	0.534	0.496	0.395	0.350
	0.379	0.379	−0.253	0.326
	0.232	0.044	−0.024	−0.198
C 2	0.460	0.093	−0.455	0.045
	0.333	0.081	−0.005	0.383
	0.180	0.241	0.027	0.135
C 3	0.406	0.054	0.397	0.111
	0.320	0.135	−0.065	0.390
	0.204	0.266	−0.007	0.118
C 4	0.674	0.763	−0.339	0.345
	0.419	0.217	0.053	0.534
	0.307	0.181	0.262	0.034
C 5	0.395	0	0.395	0
	0.351	0.480	0	0.287
	0.291	0.049	0	0.323
C 6	0.424	0.507	−0.198	0.275
	0.303	0.208	0.252	0.220
	0.270	0.009	−0.083	0.263

Because of the restrictions put on the geometry of the durene molecule, all of its C-atoms are in the same plane. No atoms of the HFB molecule deviate significantly from the least squares plane through this molecule, the largest deviation being 0.038 Å. The angle between the *c*-axis and the plane normal, "the stacking angle", is 12.8° for the durene molecule and 15.4° for the HFB molecule, and the angle between the molecular planes is 3.6°.

The mean distance between the molecular planes is 3.51 Å. The corresponding distances in the addition compounds of HFB with *p*-xylene,[1] mesitylene,[2] and hexamethylbenzene (triclinic form)[4] are 3.55 Å, 3.56 Å, and 3.43 Å, respectively. The standard deviations in these values are 0.005 – 0.01 Å. It seems reasonable to believe that the distance in the disordered trigonal form of the hexamethylbenzene-compound is shorter than 3.51 Å when the HFB molecule has its most probable orientation, although this distance has not been calculated exactly.[3] It

may therefore be concluded that the distance between the molecular planes in the durene-compound is shorter than in the *p*-xylene-compound and the mesitylene-compound, but longer than in both modifications of the hexamethylbenzene-compound.

The calculated angles between (010) and O-F1, O-F2 and O-F3 (Fig. 1 B) are 19.0, 40.2 and 77.7°, respectively. The two equivalent orientations of the HFB molecule are thus ~22° apart, and the benzene ring of this molecule is twisted ~19° relative to that of the durene molecule about its plane normal. During the transition between the monoclinic and the triclinic modification the durene molecule and the HFB molecule are rotated in opposite directions, 9 and 7°, respectively, relative to the mirror plane and twin plane (010). This finding and the large librational amplitudes in the monoclinic modification indicate very low barriers to rotation of the molecules in the crystals. However, the possibility of a more complicated disorder of the monoclinic form than that arrived at in this work should not be disregarded.

The relative orientation of the molecules in both modifications is thus different from that in the *p*-xylene-compound and the mesitylene-compound in which the benzene rings are twisted 30° relative to each other about their plane normals.[1,2] The nearly parallel orientation of the benzene rings in the low-temperature form is similar to that found in the low-temperature form of the hexamethylbenzene-compound.[4] The disordered room-temperature structure of these two compounds differ, however, as the largest proportion of the partner molecules is parallel in the hexamethylbenzene-compound.[3]

This work confirms, thus, that there is a close relationship between interplanar distance, relative orientation of the molecules and number of methyl groups in these addition compounds. In compounds with more than three methyl groups increasing number of such groups favours a short interplanar distance and a parallel orientation of the benzene rings, which overlap with a C–C bond of one ring approximately above the center of the adjacent ring. These are typical features of charge-transfer complexes.[11] Increasing numbers of methyl groups in aromatic hydrocarbons also increase their donor strength in charge-transfer complexes.[12]

The nature of the HFB-compounds with aromatic hydrocarbons have been much discussed and it has been shown that the increased interaction caused by the methyl groups may be due to other factors than charge-transfer forces.[13] The lack of charge-transfer bands in their spectra [14,15] is the most important argument against the existence of charge-transfer forces in solutions of these compounds.

However, the variations in the crystal structures are difficult to explain by considering van der Waals forces only and the direction of the variations makes it reasonable to interprete them as being due to contribution of charge-transfer forces in crystals of compounds with more than three methyl groups.

Acknowledgements. The author wishes to thank professor Asbjørn Hordvik and cand. real Lars Kristian Hansen for doing most of the work with the data collection.

REFERENCES

1. Dahl, T. *Acta Chem. Scand. A 29* (1975) 170.
2. Dahl, T. *Acta Chem. Scand. 25* (1971) 1031.
3. Dahl, T. *Acta Chem. Scand. 26* (1972) 1569.
4. Dahl, T. *Acta Chem. Scand. 27* (1973) 995.
5. Gilson, D. F. R. and McDowell, C. A. *Can. J. Chem. 44* (1966) 945.
6. Troughton, P. G. H. *Siemens Review XXXVII* (1970) *Fourth Special Issue: X-Ray and Electron Microscopy News.*
7. Groth, P. *Acta Chem. Scand. 27* (1973) 1837.
8. Hansen, H. P., Herman, F., Lea, J. D. and Skillman, S. *Acta Crystallogr. 17* (1964) 1040.
9. Baubour, J. L. and Sanquer, M. *Acta Crystallogr. B 30* (1974) 2371.
10. Almenningen, A., Bastiansen, O., Seip, R. and Seip, H. M. *Acta Chem. Scand. 18* (1964) 2115.
11. Herbstein, F. H. *Perspect. Struct. Chem. 4* (1971) 166.
12. Briegleb, G. *Elektronen-Donator-Acceptor-Komplexe*, Springer, Berlin 1961.
13. Swinton, F. L. In *Molecular Complexes*, Elek, London 1974, Vol. 2.
14. Foster, R. and Fyfe, C. A. *Chem. Commun.* (1965) 642.
15. Beaumont, T. G. and Davis, K. M. C. *J. Chem. Soc. B* (1967) 1131.

Received March 20, 1975.

Acta Chemica Scandinavica A 29 (1975) 706—708

Refinement of the Crystal Structure of VP_2

MARGARETA GÖLIN, BERTIL CARLSSON and STIG RUNDQVIST

Institute of Chemistry, University of Uppsala, Box 531, S-751 21 Uppsala, Sweden

Crystals of VP_2 have been prepared by the chemical transport technique, using iodine as the transport agent. The crystal structure has been refined from single crystal diffractometer data to a conventional R-value of 0.03. VP_2 belongs to the $OsGe_2$ ($NbAs_2$)-type structure (space group $C2/m$) and the unit cell dimensions are $a = 8.4641(6)$ Å, $b = 3.1054(4)$ Å, $c = 7.1698(4)$ Å, $\beta = 119.264(7)°$.

The occurrence of VP_2 was first reported by Zumbusch and Biltz.[1] They found by qualitative comparisons of the powder diffraction films that the three phosphides VP_2, NbP_2, and TaP_2 are structurally very similar. This observation was subsequently confirmed by Hulliger,[2] who indexed the powder patterns and concluded that the three diphosphides crystallize with the $NbAs_2$-type structure.[3–6]

According to Furuseth and Kjekshus,[6] $NbAs_2$ crystallizes with the non-centrosymmetric space group symmetry $C2$. The crystal structure of $OsGe_2$ is closely related to the $NbAs_2$ structure, and in discussions of the properties of $NbAs_2$-type compounds, Hulliger,[7] and Andres *et al.*[8] include $OsGe_2$ among the representatives. The structure of $OsGe_2$ was, however, described by Weitz *et al.*[9] in the centrosymmetric space group $C2/m$.

In the course of synthetic studies of transition metal phosphides by chemical transport methods we obtained VP_2 in single crystal form. In view of the space group problem of the $NbAs_2$-type compounds we decided to make an accurate refinement of the VP_2 structure. During this work Jeitschko and Donohue [10] published a report on the structures of the high-pressure phases CrP_2 and $CrAs_2$. Both compounds were found to crystallize with the $OsGe_2$-type structure, and for CrP_2, the space group was shown to be $C2/m$ within the (relatively high) accuracy of the diffraction data.

EXPERIMENTAL DETAILS

Preparation. The starting materials for the synthesis of VP_2 were red phosphorus of purity higher than 99 % and vanadium metal obtained from Materials Research Corporation, USA. The claimed purity was 99.95 % and according to the supplied analysis the major impurities were (in ppm): Fe 200, P 125, Ca 60, Cr 50, and Mn 50. Polycrystalline VP_2 was synthesized by heating red phosphorus and vanadium metal flakes in evacuated and sealed silica tubes at a temperature of 800 °C for 72 h. The product was then used as feedstock material in a chemical transport reaction with iodine as the transport agent. The iodine was introduced into the silica tubes in amounts corresponding to 5 mg I_2/cm^3, using an early version of the gas manipulation system as described by Richardson.[11] The silica tubes were inserted in a four-zone horizontal tube furnace, with the feedstock end at a temperature of about 800 °C and the growth zone at about 700 °C. Needle-shaped crystals, some of them with lengths up to 4 cm, were formed after a period of five days. The crystals were used for the X-ray diffraction work after rinsing in benzene.

X-Ray diffraction. Determination of the unit cell dimensions was carried out by X-ray powder methods using a Hägg-Guinier-type focussing camera with $CrK\alpha_1$ radiation. Silicon ($a = 5.43054$ Å) was used as the internal calibration standard, and the cell dimensions were refined by the least squares method. The single crystal studies were performed with a Stoe four-circle computer-controlled diffractometer with a graphite monochromator and $MoK\alpha$ radiation. The crystal used for the structure determination was in the form of a parallelepiped and bounded by [100], [010], and [001] faces with the approximate dimensions $50 \times 120 \times 20$ μm in the a, b, and c directions, respectively. The intensities were recorded using the ω-2θ

Table 1. Structure data for VP_2. Space group $C2/m$; $a = 8.4641(6)$ Å, $b = 3.1054(4)$ Å, $c = 7.1698(4)$ Å, $\beta = 119.264(7)°$; $U = 164.4$ Å^3; $Z = 4$; all atoms in 4 i positions. The form of the temperature factor is $\exp[-(\beta_{11}h^2 + \cdots + 2\beta_{12}hk + \cdots)]$, $\beta_{12} = \beta_{23} = 0$.

Atom	Positional parameters			Anisotropic thermal parameters $\beta_{ij} \times 10^4$			
	x	y	z	β_{11}	β_{22}	β_{33}	β_{13}
V	0.84301(6)	0	0.30163(7)	15(1)	86(4)	15(1)	8(1)
P(1)	0.59962(11)	0	0.39969(12)	24(1)	117(6)	26(1)	16(1)
P(2)	0.14074(11)	0	0.02893(12)	22(1)	122(6)	19(1)	9(1)

Table 2. Interatomic distances (Å) in VP_2. Distances up to 4 Å are included. When greater than one, the number of equivalent distances from a central atom to its neighbours precedes the notation for the neighbouring atom.

V – 2P(2)	2.427(1)	P(1) – P(1)	2.699(2)	P(2) – P(2)	2.210(2)
P(2)	2.440(1)	2P(1)	2.717(1)	2P(2)	2.599(1)
2P(1)	2.476(1)	2P(1)	3.105(0)	2P(2)	3.105(0)
P(1)	2.481(1)	2P(2)	3.143(1)	2P(2)	3.811(1)
2P(1)	2.493(1)	2P(2)	3.241(1)		
V	2.786(1)	P(2)	3.472(1)		
2V	3.105(0)	P(2)	3.579(1)		
P(2)	3.872(1)				
2P(2)	3.912(1)				
2P(2)	3.949(1)				
2P(1)	3.975(1)				

step scan technique. Within the range of $0° \leq 2\theta \leq 120°$, reflexions were recorded corresponding to $0 \leq h \leq +15$, $0 \leq k \leq +6$ and $-13 \leq l \leq +15$. Measurements of three reference reflexions recorded every 38th reflexion indicated that the diffractometer operated in a stable manner during the whole intensity measurement period.

Numerical calculations. The numerical calculations were performed on an IBM 1800 and an IBM 370/155 computer using standard-type crystallographic programs as described in detail by Lundgren.[12]

STRUCTURE REFINEMENT

609 non-equivalent reflexions were recorded. Absorption corrections were applied, using the value of 76.3 cm^{-1} for the linear absorption coefficient. The minimum and maximum transmission factors were 0.66 and 0.87, respectively.

The structure was refined by the least squares method. The function minimized was $\sum w(|F_o| - |F_c|)^2$. The weights were assigned according to the formula

$w^{-1} = \sigma^2(F_o) + (0.05|F_o|)^2$

with $\sigma(F_o)$ based on counting statistics. 93 reflexions with $|F_o| < 3\sigma(F_o)$ were omitted from the refinements.

The refinement was started assuming $C2$ symmetry with the initial positional parameters taken from the values for $NbAs_2$ as given by Furuseth and Kjekshus.[6] Atomic scattering factors were taken from Hanson *et al.*[13] and corrections for anomalous dispersion from the International Tables.[14] Anisotropic temperature factors and an isotropic extinction correction according to Coppens and Hamilton[15] were included in the refinement.

The non-centrosymmetric refinement converged with the final agreement factors

$$R = \sum||F_o| - |F_c||/\sum|F_o| = 0.0336$$

$$R_w = [\sum w(|F_o| - |F_c|)^2/\sum w|F_o|^2]^{\frac{1}{2}} = 0.0476$$

An inspection of the results of the refinement showed that the deviations from centrosymmetry were negligible, and a final refinement was accordingly made assuming $C2/m$ symmetry. The final agreement factors were $R = 0.0339$ and $R_w = 0.0478$.

The structure data obtained are presented in Table 1. A list of interatomic distances is given in Table 2. In both tables, numbers in parentheses are the estimated standard deviations in the

least significant digits. Lists of observed and calculated structure factors can be obtained from the authors on request.

CONCLUDING REMARKS

In connection with their structure analysis of CrP_2, Jeitschko and Donohue [10] gave a thorough description and discussion of the $NbAs_2$-type structure. Only a few comments on the VP_2 structure are therefore given here.

The atomic arrangements in VP_2 and CrP_2 are very similar. As a consequence of the larger size of the vanadium atoms in comparison with the chromium atoms, the V – V and V – P distances are on an average 0.05 Å larger than the corresponding distances in CrP_2. The P – P distances are also somewhat larger in VP_2, the shortest P(2) – P(2) distance being 2.210(2) Å in VP_2 and 2.189(2) Å in CrP_2.

Concerning the space group symmetry of $NbAs_2$-type compounds we conclude, in agreement with Jeitschko and Donohue, that there is no convincing evidence for the lower space group $C2$. The structures of CrP_2 and VP_2 both conform to the $C2/m$ symmetry to a high degree of accuracy, and for NbP_2 and TaP_2, powder diffractometer data clearly indicate [16] that there can be no major deviation from the higher symmetry.

Acknowledgement. Financial support from the Swedish Natural Science Research Council is gratefully acknowledged.

REFERENCES

1. Zumbusch, M. and Biltz, W. *Z. Anorg. Allg. Chem. 249* (1942) 1.
2. Hulliger, F. *Nature (London) 204* (1964) 775.
3. Saini, G. S., Calvert, L. D. and Taylor, J. B *Can. J. Chem. 42* (1964) 630.
4. Furuseth, S. and Kjekshus, A. *Nature (London) 203* (1964) 512.
5. Furuseth, S. and Kjekshus, A. *Acta Chem. Scand. 18* (1964) 1180.
6. Furuseth, S. and Kjekshus, A. *Acta Crystallogr. 18* (1965) 320.
7. Hulliger, F. *Structure and Bonding*, Springer-Verlag, Berlin-Heidelberg-New York 1968 Vol. 4, p. 123.
8. Andres, K., Hull Jun., G. W. and Hulliger, F. *J. Mater. Sci. 7* (1972) 344.
9. Weitz, G., Born, L. and Hellner, E. *Z. Metallk. 51* (1960) 238.
10. Jeitschko, W. and Donohue, P. C. *Acta Crystallogr. B 29* (1973) 783.
11. Richardson, M. *J. Crystal Growth 21* (1974) 12.
12. Lundgren, J.-O. *Crystallographic Computer Programs*, University of Uppsala, Uppsala, Sweden, UUIC-B13-04-2 (1975).
13. Hanson, H. P., Herman, F., Lea, J. D. and Skilman, S. *Acta Crystallogr. 17* (1964) 1040.
14. *International Tables for X-Ray Crystallography*, Kynoch Press, Birmingham 1962, Vol. III.
15. Coppens, P. and Hamilton, W. C. *Acta Crystallogr. A 26* (1970) 71.
16. Rundqvist, S. (1966). *Unpublished.*

Received March 24, 1975.

Acta Chemica Scandinavica A 29 (1975) 709—712

On the Mechanism of Keto—Enol Tautomerization for Acetylacetone and 2-Carbethoxycyclohexanone

N. C. SØNDERGAARD, P. E. SØRENSEN and J. ULSTRUP

Chemistry Department A, The Technical University of Denmark, Building 207, DK-2800 Lyngby, Denmark

The keto—enol tautomerization reactions of acetylacetone and 2-carbethoxycyclohexanone in mixtures of water and dioxan has been investigated and the rate constants and activation parameters obtained for both the ketonization and enolization reactions. The transition states are found to contain several water molecules. Analysis of the activation parameters on the basis of recent quantum theories of proton transfer reactions in polar media suggests that the proton transfers in the water-substrate chain involve at least one step in which a separate H_3O^+ unit is formed (step-wise mechanism), and that the main contribution to the high negative entropies of activation observed is the loss of translational degrees of freedom.

There is good evidence that the hydration of carbonyl compounds in general proceeds by a "cooperative" mechanism, in which the transition state contains the substrate and several water molecules organized in a ring structure,[1–5] and in which an important step is the synchronous or step-wise transfer of protons in this ring. We present here experimental data, which suggest that also the reversible keto-enol transformation for acetylacetone (*acac*) and 2-carbethoxy-cyclohexanone (*cc*) in water and water/dioxan mixtures probably proceeds by such a mechanism.

EXPERIMENTAL

Materials. Doubly distilled water was used throughout. Acetylacetone, *purum* (E. Merck, Darmstadt) and 2-carbethoxycyclohexanone (kindly supplied by Dr. D. W. Earls, Stirling University, UK) were purified by distillation *in vacuo*, and the middle fraction collected and stored for no longer than one week. Dioxan, *technical* (BASF) was purified according to literature procedures.[6]

Kinetic and equilibrium measurements. The pure substrates are predominantly in the enol form, stabilized by intramolecular hydrogen bonds. In water containing solutions the enol form is partly converted to keto form. The kinetics of the keto—enol conversions were determined in two ways: (a) the equilibration of a solution of substrate (usually 6×10^{-4} M) was followed spectrophotometrically (on a Beckman DB GT spectrophotometer) at 274 nm (*acac*) or 260 nm (*cc*), where the enols have maximum absorption; or (b) the enolization rate was determined by adding excess bromine to a solution of substrate (*acac* only) and following the decay of bromine spectrophotometrically at 410 nm.

Equilibrium constants were determined in several ways: (1) by extrapolation of kinetic plots to zero time. The optical density thus obtained was combined with the one measured at "infinite" time (equilibrium value); (2) by combination of rate constants from bromination and equilibration experiments; (3) by a titration procedure,[7] where added bromine reacts immediately with all enol present in an equilibrated solution, and the excess bromine is quenched rapidly with allyl alcohol.

RESULTS AND DISCUSSION

The equilibration rates were strictly first order in substrate concentration. The measured k_{obs} is a sum of the first order enolization (k_e) and ketonization (k_k) rate constants, and from a knowledge of the equilibrium constant $K_E = k_e/k_k$ the rate constants could be determined separately at each water concentration and temperature. Fig. 1 shows the measured dependence of K_E on the water concentration, and Fig. 2 the dependence of $\log_{10} k_e$ and $\log_{10} k_k$ on $\log_{10}[H_2O]$. The figures also include

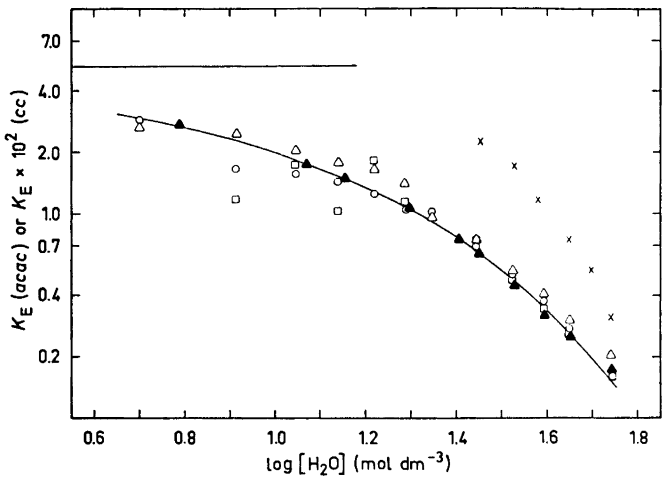

Fig. 1. Dependence of K_E on water concentration in the dioxan mixtures; 298.2 K. The horizontal line shows the value of K_E obtained for pure dioxan.[8] △ Titration (*acac.*) ▲ NMR (*acac*) Ref. 8. ○ Extrapolation (*acac*). □ Bromination (*acac*). × Extrapolation (*cc*).

recent data by Watarai and Suzuki [8] for acetylacetone in water/dioxan mixtures. Reaction orders with respect to water are shown in Table 1, and Table 2 shows the formal activation and thermodynamic parameters determined from equilibration experiments in the temperature interval 15 – 45 °C.

Since K_E for *cc* is very small at the water concentration used (Fig. 1), it could not be obtained with the desired accuracy, but the ketonization activation parameters could be estimated without large error by directly using k_{obs} values for k_k. For *acac* it is seen from Fig. 1 that the agreement between K_E values determined by different experimental techniques is good at high water concentrations but rather poor at lower concentrations. The values obtained by titration are in general too high, which is perhaps not surprising, since it is difficult to quench the excess bromine by allyl alcohol sufficiently rapidly. The K_E values determined by bromination experiments are consistent with the others at the higher water concentrations, even though the kinetic bromination curves are treated as pure first order plots. This has been shown by Bell and Crooks [9] not to be strictly correct, but analysis of the present data showed that the expected deviation is small.

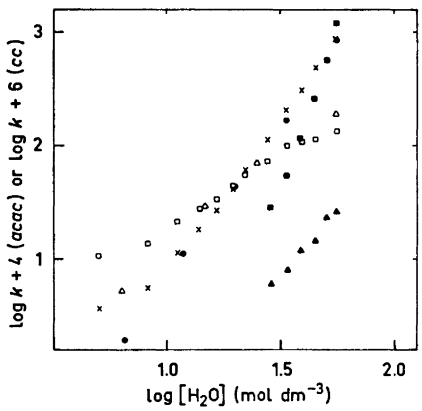

Fig. 2. Dependence of k_e and k_k on water concentration in dioxan mixtures; 298.2 K. △ k_e (*acac*) Ref. 8. ● k_k (*acac*) Ref. 8. □ k_e (*acac*). × k_k (*acac*). ▲ k_e (*cc*). ■ k_k (*cc*).

We believe that the most accurate way of determining K_E is by NMR techniques as done by Watarai and Suzuki.[8] The solid curve in Fig. 1 is an exponential least squares fit using their results, and interpolated values from this curve have been used for separating our k_{obs} into k_e and k_k. K_E values for *acac* in pure water (15.0 %) and dioxan (84.0 %) were also taken from Ref. 8. These values are required in the extrapolation method mentioned earlier. For *cc* only pure dioxan stock solutions were used, and the value 76 % was applied for the equilibrium percentage in this solvent.[9]

Table 1. Reaction orders with respect to water. The numbers in parenthesis refer to the range of water concentration in mol dm^{-3}.

Compound	Acetylacetone		2-Carbethoxy-cyclohexanone
	Ref. 8	This work	This work
Enolization	2.3 – 0.7 (6.4 – 55.5)	1.2 (5.0 – 55.5)	2.3 (28.5 – 55.5)
Ketonization	1.7 – 3.2 (6.4 – 55.5)	1.8 – 2.9 (5.0 – 55.5)	4.0 – 7.9 (28.5 – 55.5)

Table 2. Activation and thermodynamic parameters. $[H_2O]$ in mol dm^{-3}. $\Delta H^{\ddagger}$ and ΔH in kJ mol^{-1}, $\Delta S^{\ddagger}$ and ΔS in J K^{-1} mol^{-1}.

Compound		Acetylacetone Ref. 8[a]				This work				2-Carbethoxy-cyclohexanone This work	
	$[H_2O]$	$\Delta H^{\ddagger}$	$\Delta S^{\ddagger}$	ΔH	ΔS	$\Delta H^{\ddagger}$	$\Delta S^{\ddagger}$	ΔH	ΔS	$\Delta H^{\ddagger}$	$\Delta S^{\ddagger}$
Enolization	55.5					41 ± 2	−143 ± 4	−8 ± 2	−42 ± 6		
Ketonisation						49 ± 2	−101 ± 4	8 ± 2	42 ± 6	53 ± 2	−123 ± 4
Enolization	19.4	40.0	−168	−8.2	−23	42 ± 2	−149 ± 4	−6 ± 2	−21 ± 6		
Ketonization		48.2	−145	8.2	23	48 ± 2	−128 ± 4	6 ± 2	21 ± 6		[b]

[a] Water concentration 9.6 mol dm^{-3}. [b] The reaction was extremely slow at this water concentration.

Our value, $k_{obs} = 1.02 \times 10^{-1}$ s^{-1} for *acac* in pure water at 25 °C is directly comparable and agrees well with that of Watarai and Suzuki, who found $k_{obs} = 1.01 \times 10^{-1}$ s^{-1}. Both values disagree with that estimated by Ahrens *et al.*[11] ($k_{obs} = 2.5 \times 10^{-3}$ s^{-1}), who, however, used an indirect method. The data suggest that the reversible keto-enol conversions can be represented schematically as

$$acac: \text{ketone},[x + (0.6 - 1.7)]H_2O + 1.2H_2O \rightleftharpoons \text{enol},xH_2O + (1.8 - 2.9)H_2O \quad (1)$$

$$cc: \text{ketone},[y + (1.7 - 5.6)]H_2O + 2.3H_2O \rightleftharpoons \text{enol},yH_2O + (4.0 - 7.9)H_2O \quad (2)$$

where x and y are the hydration numbers for the enol forms of *acac* and *cc*, respectively.

Care must of course be exercised in coming to conclusions from rate data, for which the reaction medium is changed as much as in the present (and previous) investigation. However, both the reaction order with respect to water and the large negative activation entropies strongly suggest that several water molecules form part of the activated complex, as also found previously for carbonyl hydration reactions. The difference in the number of water molecules entering the transition state in the two systems and the slightly (numerically) higher values of $\Delta S^{\ddagger}$ for the ketonization of *cc* than for *acac* can be understood, if x is larger than y. This seems reasonable in view of the hydrophobic character of *cc* compared with *acac* and implies that the transition states for the two systems are more similar than suggested by the different reaction orders with respect to water. Previous investigations of the keto-enol conversion of *acac* [8] and of the hydration of 1,3-dichloroacetone [5] furthermore show that the reaction order with respect to water is very little dependent on the nature of the less polar medium component (dioxan or acetonitrile), whereas if alcohols are the second medium component, the reaction order is lower. This is probably due to a partial replacement of water by hydroxylic solvents in the activated complex

The large negative activation entropies for hydration and keto–enol reactions have been ascribed to the formation of a cyclic transition structure,[4,8] *i.e.* to the loss of translational entropy, when water enters the activated complex. In this complex protons are believed to migrate by a Grotthus-like mechanism. However, the relatively small difference in $\Delta S^{\neq}$ for *acac* and *cc*, in spite of the difference in the number of water molecules entering, suggests that intramolecular reorganization entropy might also be of importance.

An estimate of this contribution can be made on the basis of recently developed theories of electron and proton transfer in polar media.[12,13] Since the characteristic proton frequency $\Omega_p \gg kT/\hbar$ at room temperature, the proton movement in the transition complex is of sub-barrier nature, and all proton reorganization terms therefore appear in the pre-exponential factor of the reaction probability. Using 0.35 Å for the proton shift distance [14] and $\Omega_p = 3.8 \times 10^{14}$ s^{-1} [15] a value of -29 J K^{-1} per proton is obtained for a harmonic potential, whereas -8 J K^{-1} mol^{-1} per proton is found, if a Morse potential is used for the proton bond. This suggests that proton reorganization in the water chain is of some importance, but the dominating contribution is the translational entropy.

The proton transfer was previously suggested to proceed by a stepwise mechanism,[16] forming a separate intermediate H_3O^+. This point can be further illustrated in the following way. For reactions of the kind investigated the solvent reorganization energy E_s is quite small, being of the order of 50 kJ mol^{-1}.[17] From the pK values of *acac* (= 9.0) and *cc* (= 11.0) the free energies of formation of H_3O^+ in a step-wise mechanism are found to be 60 kJ mol^{-1} and 75 kJ mol^{-1}, respectively. Within the framework of the theories mentioned this gives 60 kJ mol^{-1} and 75 kJ mol^{-1} for the activation energies for *acac* and *cc*, respectively, corresponding to effectively "barrierless" reactions.[12] This agrees quite well with the experimentally observed $\Delta H^{\neq}$ values (the intrinsic $\Delta S^{\neq}$ was seen to be small). On the other hand, a concerted mechanism has an initial and a final state only and a free energy of reaction given by the keto-enol equilibrium constant. From the reported values of the latter (for pure dioxan) the calculated activation energies for this mechanism would be approximately 10 kJ mol^{-1} and 11 kJ mol^{-1} for *acac* and *cc*, respectively, *i.e.* substantially less than observed experimentally. Since the theoretical energy of activation is only weakly dependent on the equilibrium constant,[12,13] the order of the values estimated would refer to a considerable range of water concentrations. The analysis of the rate data thus suggests that protons migrate in a transition complex chain or ring structure with several water molecules in such a way that the chain is "broken" in at least one link, forming a separate H_3O^+ entity.

Acknowledgement. We thank Mrs. A. M. Kjær for technical assistance.

REFERENCES

1. Eigen, M. *Discuss. Faraday Soc. 39* (1965) 7.
2. Dahn, H. and Aubort, J.-D. *Helv. Chim. Acta 51* (1968) 1348.
3. Bell, R. P. and Critchlow, J. E. *Proc. Roy. Soc. (London) Ser. A 325* (1971) 35.
4. Bell, R. P. and Sørensen, P. E. *J. Chem. Soc. Perkin Trans. 2* (1972) 1740.
5. Bell, R. P., Millington, J. P. and Pink, J. M. *Proc. Roy. Soc. (London) Ser. A 303* (1968) 1.
6. Bell, R. P. and Jensen, M. B. *Proc. Roy. Soc. (London) Ser. A 261* (1961) 38.
7. Bell, R. P. and Lidwell, O. M. *Proc. Roy. Soc. (London) Ser. A 176* (1940) 88.
8. Watarai, H. and Suzuki, N. *J. Inorg. Nucl. Chem. 36* (1974) 1815.
9. Bell, R. P. and Crooks, J. E. *Proc. Roy. Soc. (London) Ser. A 286* (1965) 285.
10. Dieckmann, W. *Ber. Deut. Chem. Ges. 55* (1922) 2470.
11. Ahrens, M.-L., Eigen, M., Kruse, W. and Maass, G. *Ber. Bunsenges. Phys. Chem. 74* (1970) 380.
12. Levich, V. G., Dogonadze, R. R. and Kuznetsov, A. M. *Elektrochim. Acta 13* (1968) 1025.
13. Dogonadze, R. R., Ulstrup, J. and Kharkats, Yu. I. *J. Chem. Soc. Faraday Trans. 2 70* (1974) 64.
14. Conway, B. E. In Bockris, J. O. M. and Conway, B. E., Eds., *Modern Aspects of Electrochemistry*, Butterworths, London 1974, Vol. 3.
15. More O'Ferrall, R. A., Koeppl, G. W. and Kresge, A. J. *J. Amer. Chem. Soc. 93* (1971) 1.
16. Jaffe, M. R., Fay, D. P., Cefola, M. and Sutin, N. *J. Amer. Chem. Soc. 93* (1971) 2878.
17. Kresge, A. J. *Chem. Soc. Rev. 2* (1973) 475.
18. Pearson, R. G. and Dillon, R. L. *J. Amer. Chem. Soc. 75* (1953) 2439.

Received March 20, 1975.

Acta Chemica Scandinavica A 29 (1975) 713—716

Crystal Structures of the Hydrochlorides of Pyrimidine and Pyrimidin-2-one

SVEN FURBERG and JOHAN B. AAS

Department of Chemistry, University of Oslo, Oslo 3, Norway

The crystal structures of the hydrochlorides of pyrimidine and pyrimidin-2-one have been derived from counter measurements and refined to $R = 0.030$ and 0.047, respectively. Standard deviations in bond distances lie in the range 0.003 – 0.004 Å. The main effect of protonation in both compounds is to increase the ring angle at the nitrogen atom by 6°. The ions are linked together by N – H . . . Cl^- hydrogen bonds of lengths 3.00 – 3.06 Å. There are also several close (CH) . . . Cl^- contacts with H . . . Cl^- distances in the range 2.6 – 2.9 Å.

Continuing our investigations of the structure of pyrimidine derivatives [1,2] we have determined the crystal structures of the hydrochlorides of pyrimidine (P.HCl) and pyrimidin-2-one (P-2-one.HCl). The main purpose of the work is to establish the effect of protonation on the molecular structure of the simplest pyrimidines.

EXPERIMENTAL. STRUCTURE ANALYSIS

The compounds were prepared by mixing pyrimidine and pyrimidin-2-one with equivalent amounts of hydrochloric acid in alcoholic solution and recrystallized from alcohol. The space groups were derived from Weissenberg diagrams and unit cell dimensions measured on a diffractometer. The densities were measured by flotation.

Recrystallization of P.HCl ($C_4H_4N_2$.HCl) yielded thin hydroscopic plates (100) elongated along *b*. They had to be kept in glass capillaries during the X-ray exposures. Systematic absences correspond to space groups *Cmca* or *C2ca*, of which the former was chosen, being strongly favoured by the intensity statistics. Unit cell dimensions are $a = 6.747(1)$ Å, $b = 9.222(1)$ Å, $c = 18.651(2)$ Å. The density was found to be 1.35 g/cm³ and there are eight molecules in the unit cell. All atoms must lie in mirror planes.

P-2-one.HCl ($C_4H_4N_2O$.HCl) was obtained as stable needles elongated along *b*. The space group is *Pbca*, with unit cell dimensions $a = 10.204(1)$ Å, $b = 9.180(1)$ Å and $c = 12.898(2)$ Å. The density is 1.46 g/cm³ and there are eight formula units per cell.

The intensity measurements were made on crystals of dimensions 0.2 – 0.4 mm, using an automatic diffractometer and monochromatic Mo$K\alpha$ radiation. The $\omega/2\theta$ scan mode was employed. Reflections with $2\theta < 65°$ and $I > 2\sigma(I)$ were measured, 700 for P.HCl and 1183 for P-2-one.HCl. The intensities were scaled on the basis of measurements of three standard reflections. Corrections for absorption and extinction were not applied. The atomic form factors were those of Hanson *et al.*,[3] except for hydrogen.[4]

The structures were solved by vector methods and refined by full-matrix least squares calculations. The weighting scheme was based on standard deviations from counter statistics and 2 % fluctuations in diffractometer stability. Anisotropic temperature factors were applied to the non-hydrogen atoms, isotropic ones to the hydrogen atoms. The final value of R was 0.030 ($R_w = 0.038$) for P.HCl and 0.047 ($R_w = 0.047$) for P-2-one.HCl. The parameters are given in Tables 1 and 2.

Lists of observed and calculated structure factors will be supplied by the authors on request.

The cations were assumed to be rigid bodies. The r.m.s. difference between the atomic vibration tensor components calculated from Tables 1 and 2 and those derived from the model was 0.0007 Å² for $P.H^+$ and 0.0016 Å² for P-2-one.H^+ Librational corrections to the bond lengths were derived (Table 3). Fig. 1 shows the thermal ellipsoids.

The calculations were carried out on CYBER-74.[4]

Table 1. Positional (x10^5 for non-hydrogens, $\times 10^4$ for hydrogens) and thermal ($\times 10^5$) parameters for P.HCl. E.s.d.'s in parenthesis. The temperature factor is exp $[-B11h^2+B22k^2+B33l^2+B12hk+B13hl+B23kl)]$.

ATOM	x	y	z	B	B11	B22	B33	B12	B13	B23
CL	0(0)	26506(5)	8185(3)		3132(16)	1338(7)	283(1)	0(0)	0(0)	-64(4)
N1	0(0)	75413(16)	7884(8)		2685(42)	1348(21)	192(4)	0(0)	0(0)	-91(17)
N3	0(0)	65428(24)	19223(10)		5914(84)	1738(38)	276(6)	0(0)	0(0)	393(22)
C2	0(0)	64240(23)	12187(12)		4338(81)	1147(27)	316(7)	0(0)	0(0)	32(21)
C4	0(0)	78776(29)	21862(13)		4367(81)	2252(42)	197(6)	0(0)	0(0)	-198(25)
C5	0(0)	90765(27)	17626(12)		4697(90)	1496(31)	309(7)	0(0)	0(0)	-418(23)
C6	0(0)	88651(24)	10427(12)		4197(78)	1176(24)	284(6)	0(0)	0(0)	81(21)
H1	0(0)	7385(28)	343(18)	5.1(.5)						
H2	0(0)	5514(26)	1804(14)	6.2(.6)						
H4	0(0)	7928(28)	2693(18)	7.7(.7)						
H5	0(0)	51(27)	1956(15)	6.2(.7)						
H6	0(0)	9543(29)	728(12)	5.4(.6)						

Table 2. Parameters for P-2-one.HCl. Given as in Table 1.

ATOM	x	y	z	B	B11	B22	B33	B12	B13	B23
CL	21498(6)	4698(6)	11199(5)		897(6)	1819(7)	938(6)	418(11)	-565(9)	-492(18)
N1	53619(20)	36127(21)	48547(15)		883(19)	939(22)	652(15)	-293(36)	-181(27)	-187(29)
N3	48446(19)	17873(22)	46735(16)		746(18)	1168(24)	588(13)	-93(36)	239(25)	64(31)
O2	55568(18)	28587(23)	57275(14)		1846(28)	2488(39)	538(11)	-296(45)	-223(26)	-292(34)
C2	58483(21)	27561(24)	48917(18)		669(18)	1231(30)	518(15)	78(41)	73(30)	-246(36)
C4	34448(23)	16958(28)	37688(20)		733(21)	1245(30)	665(17)	-328(45)	95(34)	-414(48)
C5	37982(26)	25781(33)	29615(21)		1117(29)	1958(43)	585(17)	-719(65)	-327(37)	78(48)
C6	47773(27)	35337(38)	31488(21)		1107(28)	1418(35)	635(18)	-463(54)	-169(38)	438(44)
H1	6954(34)	4228(32)	4128(21)	6.1(.7)						
H3	3794(38)	1196(34)	5172(24)	6.6(.8)						
H4	2738(27)	971(38)	3782(18)	4.7(.6)						
H5	3371(26)	2480(28)	2327(21)	4.7(.6)						
H6	5894(27)	4164(38)	2617(22)	5.9(.7)						

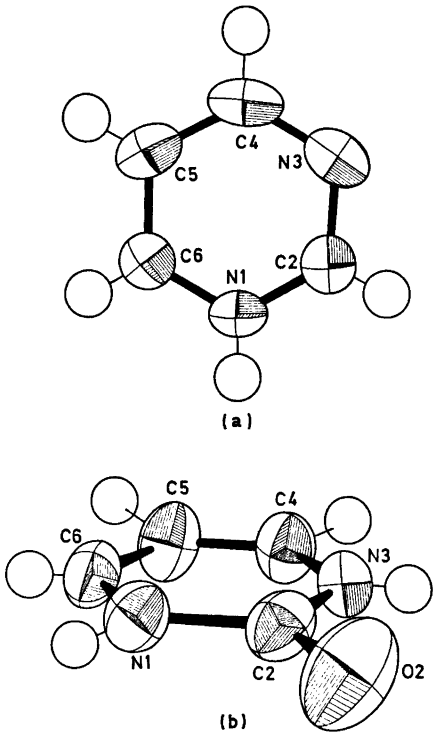

Fig. 1. Thermal ellipsoids plotted at 50 % level. (a) P.H+ viewed along x. (b) P-2-one.H+ viewed along y.

RESULTS AND DISCUSSION

The structure of the cations. The bond lengths (uncorrected and corrected values) and angles in the cations P.H+ and P-2-one.H+ are given in Table 3. For comparison the (corrected) values reported for pyrimidine [6] and pyrimidine-2-one[2] are also included.

It is seen that the main structural effect of protonation is to increase substantially the ring angle at the protonated nitrogen atom (N1 in P.HCl and N3 in P-2-one.HCl). This is in agreement with earlier evidence that bonding of an extraannular atom to a ring nitrogen atom causes the ring angle to increase.[7] The angle is increased by 5.8° in P.H+ and by 5.9° in P-2-one.H+. The interior angles adjacent to the site of addition are correspondingly adjusted.

As for the effect of protonation on bond lengths a comparison of P-2-one and P-2-one.H+ shows that significant changes occur in this case. Ring bonds adjacent to the protonated atom N3 increase in length by about 0.02 Å, whereas C4–C5 becomes shorter by 0.036 Å and C6–N1 by 0.020 Å. In fact, P-2-one.H+ has very nearly *mm* symmetry. Protonation of cytosine produces similar changes both in angles and bonds.[8] On the other hand there are no clearly significant differences in

Table 3. Bond lengths (Å) and angles (°) for P.H+ and P-2-one.H+ with estimated standard deviations. E.s.d.'s in bond lengths for P are 0.007 – 0.008 Å, for P-2-one 0.003 – 0.004 Å.

	P.H+ Uncorr.	P.H+ Corr.	P Corr.	P-2-one.H+ Uncorr.	P-2-one.H+ Corr.	P-2-one Corr.
N1 – C2	1.306(3)	1.331	1.33	1.375(3)	1.387	1.384
C2 – N3	1.317(3)	1.333	1.34	1.379(3)	1.387	1.367
N3 – C4	1.326(3)	1.348	1.35	1.330(3)	1.341	1.320
C4 – C5	1.359(4)	1.384	1.41	1.358(4)	1.367	1.403
C5 – C6	1.357(3)	1.373	1.38	1.355(4)	1.361	1.355
C6 – N1	1.310(3)	1.331	1.36	1.324(3)	1.333	1.353
C2 – O2				1.203(3)	1.208	1.244
N1 – H1	0.84(3)			0.90(3)		
C2 – H2	0.93(3)					
C4 – H4	0.95(3)			0.98(3)		
C5 – H5	0.97(3)			0.93(3)		
C6 – H6	0.87(3)			0.96(3)		
N3 – H3				0.88(3)		
N1 – C2 – N3	123.2(0.2)		128.2	112.6(0.2)		118.3
C2 – N3 – C4	116.6(0.2)		115.1	124.1(0.2)		118.2
N3 – C4 – C5	122.7(0.2)		122.5	120.9(0.2)		124.6
C4 – C5 – C6	117.3(0.2)		116.3	116.8(0.3)		116.8
C5 – C6 – N1	119.5(0.2)		122.7	121.4(0.3)		119.0
C6 – N1 – C2	120.9(0.2)		115.2	124.1(0.2)		123.0
N1 – C2 – O2				123.7(0.2)		119.8
N3 – C2 – O2				123.7(0.2)		121.9

bond lengths between pyrimidine and its hydrochloride. The relatively low accuracy of the pyrimidine analysis, and the thermal effects, make, however, a meaningful comparison difficult. The *mm* symmetry of pyrimidine is lost on protonation and the two ring bonds at N1 become equal, 1.331 Å.

The oxygen atom is engaged in hydrogen bonding in P-2-one, but not in P-2-one.H+ and the C=O bond is accordingly shorter in the latter case.

The cation P.H+ is planar by space group requirement. Some of the atoms in P-2-one.H+ are significantly (up to 0.014 Å) displaced from the least squares plane and this cation is slightly curved in the crystal in the same manner as P-2-one.[2]

Crystal structures. The cations are linked to the chlorine ions by N – H ... Cl^- hydrogen bonds. There is one such bond of length 3.002 Å in P.HCl, two in P-2-one.HCl, of lengths 3.043 and 3.064 Å, respectively. The bonds lie approximately in the pyrimidine planes and are nearly linear, the N – H ... Cl^- angles being 165 – 171°. They are shorter than "normal" N – H ... Cl^- bonds (3.1 – 3.2 Å) but longer

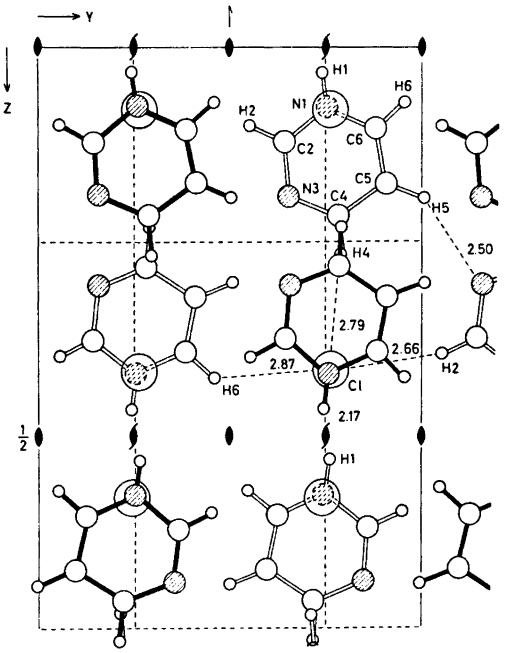

Fig. 2. The structure of P.HCl in *a* projection. Molecules at $x = 0$ in open lines, at $x = 1/2$ in heavy lines. Short contacts in broken lines.

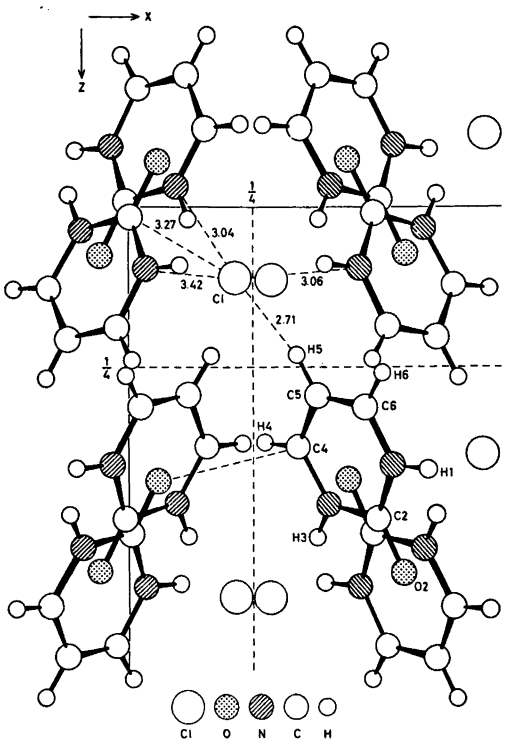

Fig. 3. The structure of P-2-one.HCl in *b* projection. Broken lines indicate contacts.

than, *e.g.*, that of 2.95 Å in pyridine hydrochloride.[9]

The general arrangement of the ions in the two crystals is shown in Figs. 2 and 3.

P.HCl has a layer structure (Fig. 2), with all atoms in mirror planes at $x=0$ and $x=1/2$. Within a layer the chlorine ions have close contacts (2.6 – 2.9 Å) to hydrogen atoms H2, H4, and H6 in different neighbouring cations, in addition to the hydrogen bond involving H1. There is also a rather short distance (2.50 Å) between N3 and H5. The shortest inter-layer contacts (3.38 Å) are between the chlorine ions in one layer and the atoms N1 in the layers above and below. This makes the chlorine ions nearly octahedrally coordinated to atoms in six different cations. There is very little stacking overlap between the cations and the layers appear to be held together mainly by electrostatic $N^+ \ldots Cl^-$ interactions. Similar packing arrangements have been observed in several hydrohalides of nitrogen heteroaromatics.[8,10]

In P-2-one.HCl (Fig. 3) parallel cations inclined 50.6° to the *ac* plane stack in columns in the *b* direction. The shortest $Cl^- \ldots Cl^-$ distance is 4.73 Å. The chlorine ions are linked to N1 and N3 in different cations by the hydrogen bonds, which form an angle of 88° with one another. They also have a short contact (2.7 Å) to H5 and are at approximately van der Waals distance from C2 (3.27 Å) and N1 (3.42 Å) in other neighbouring cations. The oxygen atom is not involved in hydrogen bonding, the nearest atom in another cation being C4 at a distance of 3.04 Å.

REFERENCES

1. Furberg, S. and Solbakk, J. *Acta Chem. Scand. A 28* (1974) 435.
2. Furberg, S. and Solbakk, J. *Acta Chem. Scand. 24* (1970) 3230.
3. Hanson, H. R., Hermann, F., Lea, J. D. and Skillman, S. *Acta Crystallogr. 17* (1964) 1040.
4. Stewart, R. F., Davidson, E. R. and Simpson, W. T. *J. Chem. Phys. 17* (1964) 3175.
5. Groth, P. *Acta Chem. Scand. 27* (1973) 1837.
6. Wheatley, P. J. *Acta Crystallogr. 13* (1960) 80.
7. Singh, C. *Acta Crystallogr. 19* (1965) 861.
8. Trus, B. L. and March, R. H. *Acta Crystallogr. B 28* (1972) 1834.
9. Rerat, C. *Acta Crystallogr. 15* (1962) 427.
10. Bryan, R. F. and Tomita, K. I. *Acta Crystallogr. 15* (1962) 1174.

Received March 10, 1975.

Acta Chemica Scandinavica A 29 (1975) 717—724

An X-Ray Investigation of Ammonium and Thallium(I) *P,P*-Dithiophospha-cyanurates

BENGT AURIVILLIUS and CLAES STÅLHANDSKE

Division of Inorganic Chemistry 2, Chemical Center, The Lund Institute of Technology, P.O. Box 740, S-220 07 Lund 7, Sweden

The crystal and molecular structures for ammonium and thallium(I) *P,P*-dithiophospha-cyanurates, $NH_4^+(C_2H_3N_3PO_2S_2)^-$ and $Tl^+(C_2H_3N_3PO_2S_2)^-$, have been determined from three-dimensional X-ray diffractometer data. The crystal structures are isotypic and the symmetry is monoclinic, space group $P2_1/c$. The cell dimensions are for the ammonium salt $a = 7.204(2)$, $b = 12.222(2)$, $c = 9.348(1)$ Å, $\beta = 102.15(2)°$ and for the thallium salt $a = 7.146(2)$, $b = 12.208(3)$, $c = 9.193(2)$ Å, $\beta = 100.75(2)°$. The NH_4^+ compound has been refined to an *R*-value of 0.022 for 1897 reflections and the Tl^+ compound to an *R*-value of 0.022 for 1443 reflections. The X-ray investigations have confirmed the structural formula earlier suggested for the anion $(C_2H_3N_3PO_2S_2)^-$. The anion contains a non-planer 6-membered ring C_2N_3P. Hydrogen N−H···O join the anions to two endless chains related by $\bar{1}$.

When urea and phosphorus pentasulfide are allowed to react at temperatures about 100 °C and the product is treated with water, large crystals are formed. The first to analyse this reaction product was Kutschig [1] who arrived at the tentative structural formula NH_4^+-$(C_2H_3N_2PO_2S_2)^-$. Subsequently, Hemmelmayr [2] carried out a more elaborate investigation and found the empirical formula $C_2H_7N_4PO_2S_2$. He also concluded that the substance was the ammonium salt of the cyclic anion $(C_2H_3N_3$-$PO_2S_2)^-$, shown in Fig. 1. Hemmelmayr has also described a number of other substances which probably also contain the *P,P*-dithiophospha-cyanurate rest. Thus he synthesized a compound which he gave the empirical formula $C_2H_4N_3PO_2S_2 + 2H_2O$, which may be the *P,P*-dithiophospha-cyanuric acid dihydrate. He also describes two tertiary barium salts, one of which was given the formula $Ba_3[(C_2HN_3$-$PO_2S_2).H_2O]_2 + 8.5H_2O$. Furthermore, Kutschig[1] prepared a primary silver salt of composition $Ag(C_2H_3N_3PO_2S_2)$. Hemmelmayr's results are mentioned in reference works. [3,4] It is stated in Ref. 3, however, that sufficient analytical data have not been given for $C_2H_7N_4PO_2S_2$ to ascertain the cyclic anion in the salt. As far as we are aware, no modern work concerning this anion has been carried out, and we therefore started the present investigation.

EXPERIMENTAL

Crystal preparation and analysis. Crystals of $NH_4(C_2H_3N_3PO_2S_2)$ were prepared according to Hemmelmayr [2] and recrystallized several times from hot water. Elemental analyses made by Messrs. Dornis and Kolbe (Mühlheim a.d. Ruhr) gave the following results: C 11.25 (11.29); H 3.30(3.27); N 26.10(26.17); S 29.86 (29.90); P 14.53(14.48). Calculated values are given in parentheses. The empirical formula given by Hemmelmayr was thus confirmed. Suitable single crystals of the compound Tl-$(C_2H_3N_3PO_2S_2)$ were obtained by mixing solutions of $TlNO_3$ and $NH_4(C_2H_3N_3PO_2S_2)$.

Crystal data. The dimensions of the monoclinic unit cells for the compounds were determined from least-squares analysis of the positions of about 30 reflections for each compound. These reflections were measured on a single crystal diffractometer with Mo$K\alpha$ radiation, the θ-values varying between 17 and 20 °. The following results were obtained: NH_4^+; $a = 7.204(2)$, $b = 12.222(2)$, $c = 9.348(1)$ Å, $\beta = 102.15(2)°$, $V = 804.6$ Å^3. Tl^+; $a = 7.146(2)$, $b = 12.208(3)$, $c = 9.193(2)$ Å, $\beta = 100.75(2)°$, $V = 787.9$ Å^3. The measured density for NH_4-$(C_2H_3N_3PO_2S_2)$, 1.775 g cm^{-3}, was determined by flotation. The calculated densities for four formula units in the unit cell are 1.768 g cm^{-3}

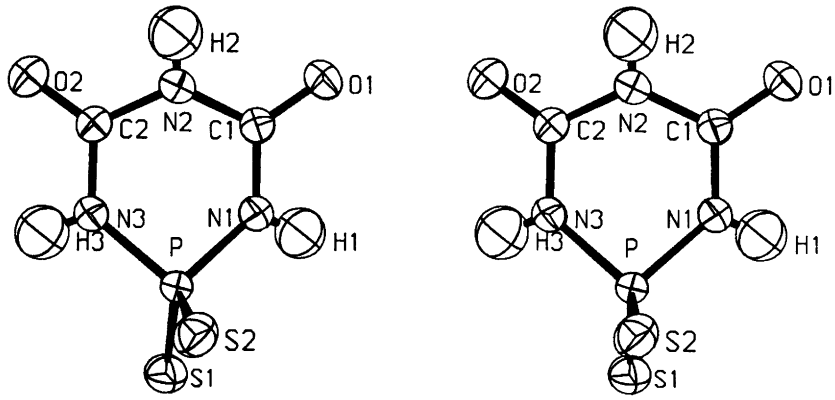

Fig. 1. Stereoscopic pair of drawings showing the anion $(C_2H_3N_3PO_2S_2)^-$ in $NH_4(C_2H_3N_3PO_2S_2)$. Thermal ellipsoids are drawn to enclose 75 % probability.

for the ammonium salt and 3.38 g cm^{-3} for the thallium salt. Systematic absences of the reflections $h0l$ with $l = 2n+1$ and $0k0$ with $k = 2n+1$ are consistent with space group $P2_1/c$.

Single crystal work. For $NH_4(C_2H_3N_3PO_2S_2)$ a prismatic crystal with the dimensions 0.25 × 0.20 × 0.10 mm^3 was mounted with a along the ϕ axis of the diffractometer. Intensity data were collected on a computer-controlled Enraf-Nonius CAD-4 diffractometer with Mo$K\alpha$ radiation and a graphite monochromator. The $\omega - 2\theta$ scan technique was employed with a peak scan interval $\Delta\omega = (0.9 + 0.5 \tan\theta)°$. The scan interval was extended 25 % at both ends for the background measurements. A fast pre-scan was used to calculate the scan speed at which a minium number of counts (3000) was obtained within a maximum measuring time (3 min.). The intensities of 2350 independent reflections were measured in the range $3° < \theta < 30°$. 453 of these were weaker than $3\sigma(I)$, where $\sigma(I)$ is based on counting statistics. The remaining 1897 reflections were corrected for Lorentz, polarization and absorption effects ($\mu_{MoK\alpha} = 8.0$ cm^{-1}). Two standard reflections were measured at regular intervals.

For $Tl(C_2H_3N_3PO_2S_2)$ a crystal with the dimensions 0.12 × 0.08 × 0.06 mm^3 was used and the intensity data were collected and corrected in the same way as for the ammonium compound. 1804 unique reflections were measured in the range $3° < \theta < 27.5°$ and 1443 of these could be considered as observed. The linear absorption coefficient was 213 cm^{-1} in this case and the transmission factors varied from 0.35 to 0.46.

DETERMINATION AND REFINEMENT OF THE STRUCTURES

$NH_4(C_2H_3N_3PO_2S_2)$. The positions of the phosphorus and sulfur atoms were deduced from the three-dimensional Patterson function. All other atoms, including the hydrogen atoms of the NH_4^+ group, were found from successive difference Fourier maps. The resulting positions were refined by means of least-squares calculations using anisotropic temperature factors for the non-hydrogen atoms and isotropic ones for the hydrogens. In the final refinement a parameter was included to correct for isotropic secondary extinction. The weight factor used in the refinement was: $w_i^{-1} = \sigma^2(|F_o|^2)/4|F_o|^2 + 0.00035|F_o|^2 + 0.32$. The conventional R-factor was 0.022 and the weighted one 0.032 for the 1897 observed reflections. The secondary extinction parameter g was found to be 1.4(1) × 10^4, and the value of S defined by $S = [\sum w_i(|F_o| - |F_c|)^2/(m-n)]^{1/2}$, where m and n are the number of observations and the number of parameters varied, respectively, was 1.0. The atomic scattering factors used for the non-hydrogen atoms were those given by Cromer and Mann [5] and for hydrogen those given by Stewart *et al.*[6]

$Tl(C_2H_3N_3PO_2S_2)$. The positional parameters for the ammonium compound were used as starting parameters in a least-squares refinement. The weight factor used in the final refinement was $w_i^{-1} = \sigma^2(|F_o|^2)/4|F_o|^2$. The final agreement factors were $R = 0.022$ and $R_w = 0.028$ for the 1443 observed reflections. The secondary extinction parameter was found to be 0.51(2) × 10^4 and $S = 1.4$. Final positional and thermal parameters for both compounds are given in Tables 1 and 2. Lists of observed and calculated |F|-values are available on request from the Division of Inorganic Chemistry 2. All calcu-

lations were made on the UNIVAC 1108 computer in Lund, using programs briefly described by Stålhandske.[7]

DISCUSSION OF THE STRUCTURE

The ammonium compound

The present structure determination of $NH_4(C_2H_3N_3PO_2S_2)$ has confirmed the structural formula suggested by Hemmelmayr.[2] The compound may thus be denoted ammonium *P,P*-dithiophospha-cyanurate. Fig. 1 shows a stereoscopic illustration of the cyclic anion and Fig. 2 gives the distances and angles within the anion as found in the ammonium salt. Selected distances and angles in the structure with their e.s.d.'s are listed in Table 3. The phosphorus atom is tetrahedrally coordinated. The P–S distances are 1.953(1) and 1.978(1) Å, respectively, and they differ significantly. They fall as expected between the value 1.916 Å for a P–S double bond and that of 2.116 Å for a P–S single bond,[8,9] and they agree with those found in other dithiophosphates (see Table 4). The two P–N distances, 1.697 (2) and 1.700(2) Å agree with the P–N bond length of 1.695(4) Å (mean value) in 1,2,3,4-tetraphenyl-2,4-dithiocyclodiphosphazane $[PhNP(S)Ph]_2$,[14] where the phosphorus atoms

Table 1. Final positional parameters for $NH_4(C_2H_3N_3PO_2S_2)$ and $Tl(C_2H_3N_3PO_2S_2)$. Standard deviations are given in parentheses. The isotropic temperature factors for the hydrogen atoms are also listed.

Atom	*x*	*y*	*z*	*B*
The ammonium compound				
N(4)	.02342(20)	.64603(12)	.91217(17)	
S(1)	.72034(5)	.67618(3)	.52247(4)	
S(2)	.95417(5)	.59720(3)	.26796(4)	
P	.73698(5)	.57509(3)	.36382(4)	
O(1)	.69908(15)	.26132(8)	.36024(13)	
O(2)	.30419(15)	.48904(9)	.06686(12)	
N(1)	.73220(17)	.44240(9)	.41737(13)	
N(2)	.53633(17)	.38417(9)	.20065(13)	
N(3)	.52683(17)	.57191(9)	.24108(14)	
C(1)	.65966(17)	.35775(10)	.33027(14)	
C(2)	.44729(18)	.48422(10)	.16422(14)	
H(1)	.8034(32)	.4261(18)	.4885(25)	2.9(4)
H(2)	.4882(33)	.3360(19)	.1506(25)	3.1(4)
H(3)	.4675(33)	.6290(20)	.2171(23)	3.2(4)
H(4)	.0479(61)	.5886(38)	.8782(48)	9.4(11)
H(5)	−.0802(49)	.6378(27)	.9595(34)	6.5(7)
H(6)	.1132(61)	.6668(33)	.9806(44)	8.3(10)
H(7)	.0041(51)	.6955(30)	.8510(40)	7.0(8)
The thallium compound				
Tl	.01162(3)	.65480(2)	.91680(3)	
S(1)	.72484(21)	.68012(11)	.52047(16)	
S(2)	.96325(19)	.59650(11)	.26276(15)	
P	.74064(19)	.57656(10)	.36010(15)	
O(1)	.69669(55)	.26383(29)	.36429(47)	
O(2)	.30799(52)	.49058(32)	.06694(43)	
N(1)	.73234(66)	.44500(35)	.41824(52)	
N(2)	.53799(67)	.38557(38)	.20194(52)	
N(3)	.53153(63)	.57349(36)	.23841(54)	
C(1)	.65874(75)	.36022(40)	.33212(63)	
C(2)	.45026(72)	.48583(42)	.16374(56)	
H(1)	.8009(90)	.4282(49)	.4984(73)	1.8(13)
H(2)	.4746(113)	.3298(66)	.1492(95)	4.0(18)
H(3)	.4870(102)	.6294(61)	.2115(78)	2.4(15)

Table 2. Anisotropic thermal parameters and their standard deviations. The temperature coefficient is expressed as $\exp[-(h^2\beta_{11}+k^2\beta_{22}+l^2\beta_{33}+2\,hk\beta_{12}+2\,hl\beta_{13}+2\,kl\beta_{23})]$.

Atom	β_{11}	β_{22}	β_{33}	β_{12}	β_{13}	β_{23}
The ammonium compound						
N(4)	.011103(25)	.00309(8)	.00844(16)	.00064(11)	.00069(16)	−.00002(9)
S(1)	.01257(7)	.00303(2)	.00594(4)	−.00072(3)	.00215(4)	−.00121(2)
S(2)	.00908(7)	.00334(2)	.00475(4)	−.00053(3)	.00089(4)	−.00020(2)
P	.00699(6)	.00173(2)	.00437(4)	−.00036(2)	−.00045(3)	−.00008(2)
O(1)	.01124(20)	.00210(6)	.00943(14)	.00025(9)	−.00178(13)	.00049(7)
O(2)	.00891(19)	.00349(6)	.00683(12)	−.00027(9)	−.00221(11)	.00010(7)
N(1)	.00988(22)	.00219(6)	.00549(13)	−.00075(9)	−.00192(13)	.00070(7)
N(2)	.01051(22)	.00201(6)	.00544(12)	−.00009(9)	−.00107(13)	−.00039(7)
N(3)	.00834(21)	.00200(6)	.00700(14)	.00043(9)	−.00197(13)	−.00003(7)
C(1)	.00707(21)	.00223(7)	.00596(14)	−.00017(10)	.00031(14)	.00022(8)
C(2)	.00738(22)	.00247(7)	.00496(13)	−.00021(10)	.00023(13)	.00009(8)
The thallium compound						
Tl	.01052(5)	.00348(2)	.00887(4)	.00045(2)	.00097(3)	−.00039(2)
S(1)	.01134(29)	.00264(9)	.00552(17)	−.00096(12)	.00216(17)	−.00111(9)
S(2)	.00794(28)	.00342(9)	.00425(15)	−.00053(13)	.00105(16)	.00001(10)
P	.00596(24)	.00159(8)	.00387(15)	−.00032(10)	−.00041(15)	.00002(9)
O(1)	.00977(81)	.00153(23)	.00863(57)	.00018(34)	−.00142(53)	.00107(29)
O(2)	.00762(78)	.00352(28)	.00613(53)	−.00038(35)	−.00152(48)	−.00021(30)
N(1)	.00840(91)	.00215(29)	.00453(56)	−.00082(39)	−.00171(57)	.00052(32)
N(2)	.00971(96)	.00199(27)	.00497(58)	.00002(42)	−.00079(58)	.00003(32)
N(3)	.00681(90)	.00163(27)	.00614(59)	.00065(39)	−.00060(56)	.00052(33)
C(1)	.00686(95)	.00190(33)	.00621(65)	−.00024(43)	.00093(62)	−.00017(36)
C(2)	.00744(100)	.00199(32)	.00458(67)	−.00011(43)	.00082(64)	.00009(34)

are tetrahedrally coordinated. As the length of a P−N single bond is 1.77 Å,[15] the actual P−N bonds must have some π bond character. Peterson and Wagner [14] and Bullen, Rutherford and Tucker [16] have discussed the influence of the non-bonded N···N distance on the P−N bond lengths in cyclic P−N compounds, and they state that a short N···N distance will at

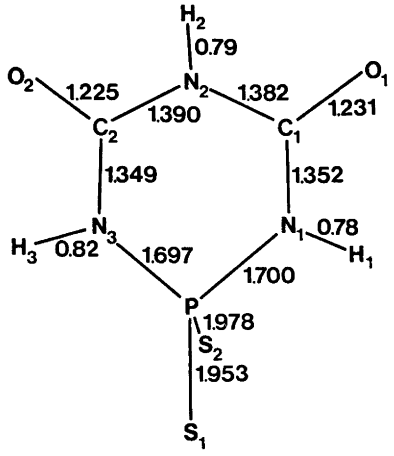

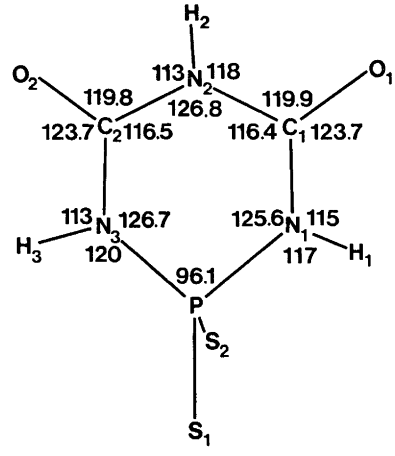

Fig. 2. Bond lengths and angles in the anion in the structure of $NH_4(C_2H_3N_3PO_2S_2)$.

Table 3. Selected distances and angles in the crystal structures of ammonium and thallium(I) *P,P*-dithiophospha-cyanurates.

Distances and angles within the $(C_2H_3N_3PO_2S_2)^-$ion

Atoms	Distances (Å) for the NH_4^+-compound	the Tl^+-compound
P–S(1)	1.953(1)	1.961(2)
P–S(2)	1.978(1)	1.980(2)
P–N(1)	1.700(2)	1.697(5)
P–N(3)	1.697(2)	1.692(5)
N(1)–H(1)	0.78(3)	0.83(7)
N(3)–H(3)	0.82(3)	0.77(8)
N(1)–C(1)	1.352(2)	1.349(7)
N(3)–C(2)	1.349(2)	1.344(7)
C(1)–O(1)	1.231(2)	1.231(7)
C(2)–O(2)	1.225(2)	1.221(7)
N(2)–H(2)	0.79(3)	0.91(9)
N(2)–C(1)	1.382(2)	1.374(8)
N(2)–C(2)	1.390(2)	1.390(7)

Atoms forming angle	Angles (°) for the NH_4^+-compound	the Tl^+-compound
S(1)–P–S(2)	115.99(2)	115.1(1)
S(1)–P–N(1)	111.82(5)	111.3(2)
S(1)–P–N(3)	109.84(5)	110.1(2)
S(2)–P–N(1)	109.31(5)	109.7(2)
S(2)–P–N(3)	112.02(5)	112.9(2)
N(1)–P–N(3)	96.13(6)	96.3(3)
P–N(1)–H(1)	117(2)	118(5)
P–N(3)–H(3)	120(2)	117(6)
P–N(1)–C(1)	125.6(1)	125.0(4)
P–N(3)–C(2)	126.7(1)	126.9(4)
C(1)–N(1)–H(1)	115(2)	116(5)
C(2)–N(3)–H(3)	113(2)	115(6)
N(1)–C(1)–O(1)	123.7(2)	123.2(6)
N(3)–C(2)–O(2)	123.7(2)	123.8(5)
O(1)–C(1)–N(2)	119.9(2)	119.9(5)
O(2)–C(2)–N(2)	119.8(2)	120.1(5)
N(1)–C(1)–N(2)	116.4(2)	116.8(5)
N(3)–C(2)–N(2)	116.5(2)	116.2(5)
C(1)–N(2)–H(2)	118(2)	118(6)
C(2)–N(2)–H(2)	113(2)	112(6)
C(1)–N(2)–C(2)	126.8(2)	126.8(5)

Distances and angles in the NH_4^+-group in $NH_4(C_2H_3N_3PO_2S_2)$.

Atoms	Distance (Å)	Atoms forming angle	Angle(°)
N(4)–H(4)	0.81(5)	H(4)–N(4)–H(5)	110(4)
N(4)–H(5)	0.95(4)	H(4)–N(4)–H(6)	111(5)
N(4)–H(6)	0.85(5)	H(4)–N(4)–H(7)	113(5)
N(4)–H(7)	0.82(4)	H(5)–N(4)–H(6)	103(4)
		H(5)–N(4)–H(7)	112(4)
		H(6)–N(4)–H(7)	107(4)

Table 4. Phosphorus-sulfur distances (Å) and angles S–P–S (°) in selected dithiophosphates.

Compound	Short distance P–S	Long distance P–S	Average	Angle S–P–S	Ref.
$K[S_2P(OCH_3)_2]$	1.960(13)	1.960(13)	1.96	118.2(9)	10
$Pb[S_2P(i-OC_3H_7)_2]_2$	1.93 1.95	1.99 2.03	1.98		11
$Pb[S_2P(OC_2H_5)_2]_2$	1.968(7) 1.969(7)	1.991(9) 1.995(8)	1.98	116.2(4) 115.4(3)	12
$Zn[S_2P(OC_2H_5)_2]_2$	1.973(11) 1.992(7)	1.987(9) 2.001(5)	1.99	109.7(4) 108.0(3)	13
$NH_4(C_2H_3N_3PO_2S_2)$	1.953(1)	1.987(1)	1.97	115.99(2)	present work
$Tl(C_2H_3N_3PO_2S_2)$	1.961(2)	1.980(2)	1.97	115.1(1)	present work

least to some degree lengthen the P – N distance. However, the effect seems to be small, judging from the P–N distances mentioned above and the non-bonded N···N interactions in $C_2H_7N_4PO_2S_2$ and in $[PhNP(S)Ph]_2$ which are 2.53 and 2.22 Å, respectively.

The anion $(C_2H_3N_3PO_2S_2)^-$ may be regarded as a substituted biuret molecule, where N–H bonds of the terminal nitrogen atoms have been replaced by N–P bonds (*cf.* Fig. 1) thus forming the cyclic anion.

The anion $(C_2H_3N_3PO_2S_2)^-$ is not planar (Fig. 1) and the same applies to its biuret part. The N, C, and O atoms of each urea part lie in a plane to within 0.003 Å. The dihedral angle between these parts is 163.8(3) °, whereas the corresponding angle in perdeuterated biuret hydrate is 173.7 °.[17] The 6-membered ring C_2N_3P has a shallow boat form (Fig. 1).

Intermolecular distances and hydrogen bonding. There are two short intermolecular contacts between the anions of the present crystal structure. One, which occurs between S(1) (x,y,z) and C(1) $(-x,-y,-z)$ is found to be 3.340(1) Å. Using the van der Waals radii 1.70 Å for C (*cf.* Pauling [8]) and 1.72 Å for sulfur (Lee and Goodacre [9]) the sum of the radii will be 3.42 Å. The other short contact of 3.338(3) Å occurs between C(2) (x,y,z) and C(2) $(-x,-y,-z)$. All other intermolecular contacts are equal to or longer than the corresponding van der Waals radii.

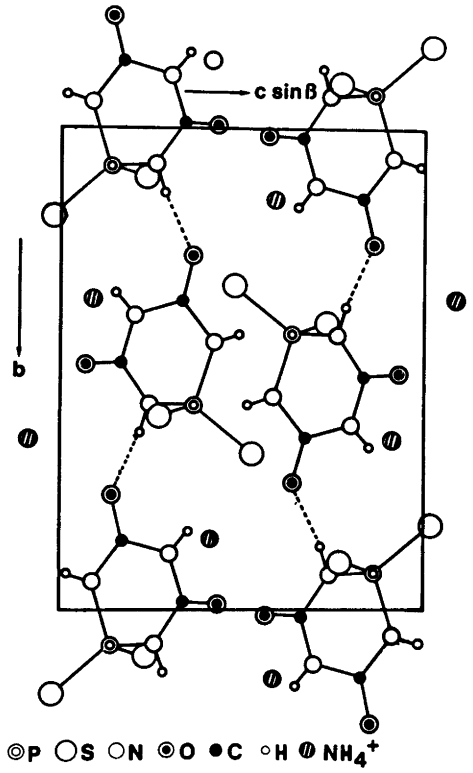

Fig. 3. Projection of the crystal structure of $NH_4(C_2H_3N_3PO_2S_2)$ along the a axis. Supposed hydrogen bonds N(3)–H(3)···O(1) are indicated by dashed lines.

Table 5. Distances less than 3.60 Å from R^+ to other non-hydrogen atoms. R^+ denotes Tl^+ and NH_4^+ and x, y, z refer to the coordinates given in Table 1.

Distance from R^+ (x,y,z) to	Distances (Å) for Tl^+	NH_4^+
S(1) $(x-1,1.5-y,0.5+z)$	3.146(2)	3.391(2)
S(2) $(x-1,y,1+z)$	3.339(1)	3.517(2)
S′(2) $(x-1,1.5-y,0.5+z)$	3.341(2)	3.411(2)
S″(2) $(1-x,1-y,1-z)$	3.504(2)	3.437(2)
Average: $R^+-S(2)$	3.40	3.46
O(1) $(1-x,0.5+y,1.5-z)$	2.933(4)	2.953(2)
O(2) $(-x,1-y,1-z)$	2.918(4)	2.920(2)
O′(2) $(x,y,1+z)$	3.053(4)	2.938(2)
N(2) $(1-x,1-y,1-z)$		3.566(2)
C(1) $(1-x,1-y,1-z)$	3.582(7)	3.540(2)

As the positions of the hydrogen atoms in the ammonium group are determined with low accuracy and a neutron diffraction study is in progress, the discussion of the hydrogen bonding system involving the ammonium group will be made in a forthcoming paper. The distance of 2.874(2) Å may correspond to a $N-H\cdots O$ hydrogen bond between O(1) (x,y,z) and N(3) $(-x,\frac{1}{2}+y,\frac{1}{2}-z)$. By means of this postulated hydrogen bond the anions of the crystal structure are joined to two separate but structurally equivalent endless chains (Fig. 3). The two chains may in turn be linked by hydrogen bonds *via* the ammonium ions.

Coordination of the ammonium ions. Distances less than 3.60 Å between amino nitrogen and other atoms of the crystal structure are listed in Table 5. The seven shortest distances occur to sulfur and oxygen atoms. Using the radii values 1.40, 1.84 and 1.48 Å for O^{2-}, S^{2-} and NH_4^+, respectively, as given in Ref. 8, the expected NH_4-S and NH_4-O distances will be 3.32 and 2.88 Å, respectively. The four NH_4-S distances actually found range between 3.39 and 3.52 Å, and the three NH_4-O distances range between 2.92 and 2.95 Å. The resulting seven-fold coordination around N (NH_4^+) is quite irregular, but may be described as an one-capped trigonal prism (*cf.* Fig. 4). The basal planes of the trigonal prism (O2,S1, S2 and S2″,S2′,O2′) form a dihedral angle of 3°. It may also be mentioned that one of the quadrangular faces of the polyhedron is planar by symmetry and the other is planar within 0.3 Å.

The thallium compound

Table 3 gives corresponding distances and angles in the crystal structures of ammonium

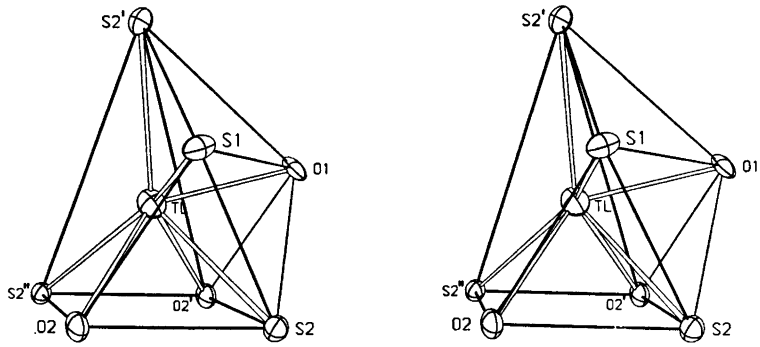

Fig. 4. Stereoscopic illustration of the seven-fold coordination of thallium (I) in $Tl(C_2H_3N_3PO_2S_2)$. For notations and distances, see Table 5. The same illustration applies to the isotypic compound $NH_4(C_2H_3N_3PO_2S_2)$.

and thallium(I) *P,P*-dithiophosphacyanurates. Considering at first only the atoms of the 6-membered ring, C_2N_3P, it is seen that no significant differences occur between the distances and angles. Considering the Tl–S and Tl–O distances less than 3.60 Å, Tl is coordinated to four sulfur atoms and to three oxygen atoms (Table 5). The Tl–S(1) distance is 0.25 Å shorter than the average of the three Tl–S(2) distances. The corresponding difference for the ammonium compound is 0.07 Å. As the ionic radii of Tl^+ and NH_4^+ do not differ very much (see Ref. 8) it may be concluded that Tl^+ is relatively more firmly bonded to the S(1) atom than NH_4^+. This situation is also reflected in the observed P–S(1) distances, 1.961(2) Å for the thallium compound and 1.953(1) Å for the ammonium compound. The sevenfold coordination of thallium (Fig. 4) is almost identical to that found for the ammonium compound. However, a fifth sulfur atom S(1) $(x-1,y,z)$ is situated at a distance of 3.84 Å from the Tl^+ ion and a two-capped trigonal prism results if this atom is included in the coordination polyhedron. These seven and eight coordinations are in good agreement with those found for other thallium(I) compounds. Thus Jennische and Hesse[18] in their study of thallium(I) dimethyldithiocarbamate found that Tl^+ was coordinated to seven sulfur atoms at distances of 2.99–3.74 Å, the coordination polyhedron being a one-capped trigonal prism, less distorted than that given in Fig. 4. As seen from Table 5, four Tl–S distances in the present compound fall in the range 3.146(2) to 3.504(2) Å. These distances may be regarded as mainly ionic, as the sum of the ionic radii[8] is 3.28 Å. The fifth Tl–S distance of 3.84 Å indicates only a weak interaction. A summary of selected Tl(I)–S distances has recently been given by Esperås and Husebye.[19] The distances observed for the present compound fall in the range reported by them. The three Tl–O distances (Table 5) vary between 2.918(4) and 3.053(4) Å, and these interactions are also mainlyionic as the sum of the ionic radii[8] is 2.80 Å.

Conclusion

Two isotypic salts of the hypothetic *P,P*-dithiophosphacyanuric acid have been investigated, *viz.* the ammonium and the thallium(I) salts. No significant differences occur for the $(C_2H_3N_3PO_2S_2)^-$ anions in the two structures. The six-membered ring skeleton C_2N_3P deviates from planarity and has a shallow boat form. The phosphorus atom is tetrahedrally coordinated. In the crystal structures the anions $(C_2H_3N_3PO_2S_2)^-$ are joined by N–H···O hydrogen bonds to two endless chains related by $\bar{1}$. The chains may in turn be joined by hydrogen bonds *via* the ammonium ions to a three-dimensional network.

Acknowledgements. This work received financial support from the Swedish Natural Science Research Council.

REFERENCES

1. v. Kutschig, K. *Sitzungsber. Akad. Wiss. Wien, Math. Naturwiss. Kl. Abt. 2B 97* (1888) 391.
2. Hemmelmayr, F. *Sitzungsber. Akad. Wiss. Wien, Math. Naturwiss. Kl. Abt. 2B 114* (1905) 335.
3. Mann, F. G. *The Heterocyclic Derivatives of Phosphorus, Arsenic, Antimony and Bismuth* in Berger, A. W., Ed., *The Chemistry of Heterocyclic Compounds*, Interscience, New York 1950, p. 21.
4. Kosolapoff, G. M. *Organophosphorus Compounds*, Wiley, New York 1950, p. 310.
5. Cromer, D. T. and Mann, J. B. *Acta Crystallogr. A 24* (1968) 321.
6. Stewart, R. F., Davidson, E. R. and Simpson, W. T. *J. Chem. Phys. 42* (1965) 3175.
7. Stålhandske, C. *Acta Crystallogr. B 30* (1974) 1586.
8. Pauling, W. *The Nature of the Chemical Bond*, 3rd Ed., Cornell University Press, Ithaca, New York 1960.
9 Lee, J. D. and Goodacre, G. W. *Acta Crystallogr. B 27* (1971) 1841.
10. Coppens, P., MacGillavry, C. H., Hovenkamp, S. G. and Douwes, H. *Acta Crystallogr. 15* (1962) 765.
11. Lawton, S. L. and Kokofailo, G. T. *Nature (London) 221* (1969) 550.
12. Ito, T. *Acta Crystallogr. B 28* (1972) 1034.
13. Ito, T., Igarashi, T. and Hagihara, H. *Acta Crystallogr. B 25* (1969) 2303.
14. Peterson, M. B. and Wagner, A. J. *J. Chem. Soc. Dalton Trans.* (1973) 106.
15. Cruickshank, D. W. J. *Acta Crystallogr. 17* (1964) 671.
16. Bullen, G. J., Rutherford, J. S. and Tucker, P. A. *Acta Crystallogr. B 29* (1973) 1439.
17. Craven, B. M. *Acta Crystallogr. B 29* (1973) 1525.
18. Jennische, P. and Hesse, R. *Acta Chem. Scand. 27* (1973) 3531.
19. Esperås, S. and Husebye, S. *Acta Chem. Scand. 27* (1973) 3355.

Received February 20, 1975.

Acta Chemica Scandinavica A 29 (1975) 725—730

Electron-diffraction Studies of Chlorobutatriene and Chlorobutenynes. III. Molecular Structure of Gaseous 2-Chlorobutenyne

ARNE ALMENNINGEN,[a] GRETE GUNDERSEN,[a] MATS GRANBERG[b] and FRED KARLSSON[b]

[a]Department of Chemistry, University of Oslo, Oslo 3, Norway and [b]Department of Physical Chemistry, University of Stockholm, Arrhenius Laboratory, Fack, S-104 05 Stockholm, Sweden

The molecular structure of 2-chlorobuten-3-yne has been investigated by electron diffraction from the vapour. Normal coordinate calculations based upon an assumed force field supplied amplitudes of vibration which could not be determined from the electron-diffraction data, and correction terms which were used in the geometrically consistent r_α-refinements. The structural parameters (r_a-values are given) were found to be: C(sp)–H = 1.078(16) Å, C(sp^2)–H = 1.106(16) Å, C≡C = 1.220(6) Å, C=C = 1.340(5) Å, C–C = 1.422 (5) Å, C–Cl = 1.738(4) Å, ∠C=C–C = 124.7 (0.5)°, ∠C≡C–C = 177.0(5.8)°, ∠C=C–Cl = 119.5(2.4)°, ∠C=C–H = 122.0(3.2)° and ∠C≡C–H = 180.0° (assumed). Parenthesized values are 2σ where systematic uncertainties are included.

This electron-diffraction study of 2-chlorobuten-3-yne was initiated as a part of the determination of the molecular structures of C_4H_3Cl-isomers.[1,2]

EXPERIMENTAL AND CALCULATION PROCEDURES

2-Chlorobuten-3-yne was prepared as described previously.[3] The compound was purified[4] by gas liquid chromatography at a temperature of 50 °C using a column packed with diethylhexyl sebacate (15 %) absorbed on Chromosorb. The substance was prevented from extensive polymerization by storing the sample at low temperatures (−70 °C) and by using hydroquinone as stabilizer. Electron-diffraction photographs were made in the Oslo Apparatus[5] at nozzle-to-plate distances of 48 and 20 cm, keeping the sample reservoir at about −27 °C. The electron wavelength was 0.06464 Å as calibrated against diffraction patterns of gaseous benzene. The scattering functions for the 35 kV electrons were those computed for chlorobutatriene.[1] Four plates made at each of the two camera distances were selected for the structure analysis. The experimental modified intensities and the corresponding radial distribution curve were obtained from the distributions of the scattered intensity recorded on the plates by the usual procedure,[6] and they are shown in Figs. 1 and 2, respectively. The structure analysis and supporting calculations were carried out using the standard computer programs and procedures,[6–8] as described previously.[1]

CALCULATIONS AND REFINEMENTS

A general planar model for 2-chlorobutenyne is described by thirteen geometrical parameters; see Fig. 3. By assuming ∠C≡C–H = 180°, ∠C=C–H_6 = ∠C=C–H_7, $r_{C_1H_6} = r_{C_1H_7} = r_{C_4H_8} + 0.027$ Å $= r_{CH}$, the number of variable parameters was reduced to the following nine: r_{CH}, $r_{C\equiv C}$, $r_{C=C}$, r_{C-C}, r_{C-Cl}, ∠C=C–C, ∠C≡C–C (*trans* to ∠C=C–C), ∠C=C–Cl, and ∠C=C–H.

The diagonal force field given in Table 1 was designed using force constants taken from similar molecules, and it was used in normal coordinate calculations based upon coordinates consistent with the r_a-model given in Table 3. The resulting D- and l-values[8] are also given in Table 3.

The interpretation of the experimental radial distribution curve was straightforward as indicated by the approximate positions for the important interatomic distances shown in Fig. 2 (see Table 3). Least-squares refinements

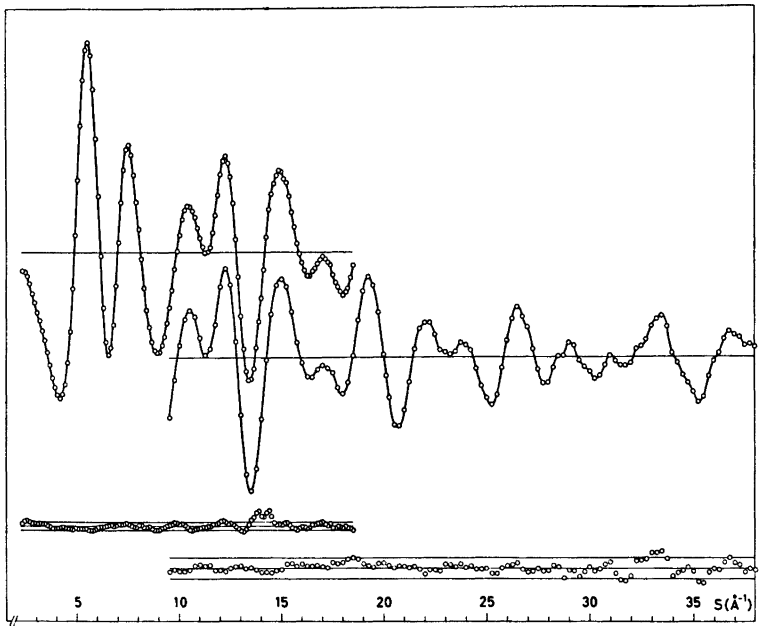

Fig. 1. Experimental intensity data for 2-chlorobutenyne from the 48 cm ($\Delta s = 0.125$ Å^{-1}) and 20 cm ($\Delta s = 0.25$ Å^{-1}) camera distances, and the corresponding difference between the experimental intensities and the theoretical ones computed according to the parameter values of Table 4. The full lines given along with the differences indicate the estimated uncertainties (three standard deviations) of the experimental intensity points.

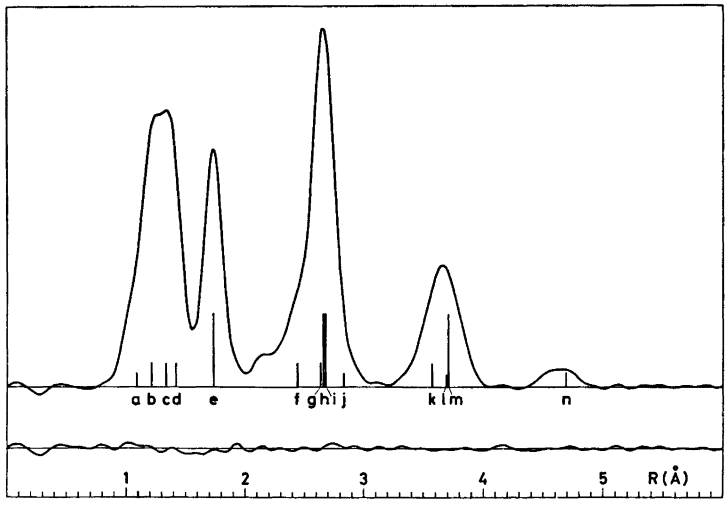

Fig. 2. Experimental radial distribution curve for 2-chlorobutenyne calculated for the artificial dampling constant $k = 0.0015$ Å^2. The approximate positions of the important interatomic distances are indicated: a, C(sp)–H and C(sp^2)–H; b, C≡C; c, C=C; d, C–C; e, C–Cl; f, $C_1 \cdots C_3$; g, $C_2 \cdots C_4$; h, $C_3 \cdots Cl$; i, $C_1 \cdots Cl$; j, $Cl \cdots H_7$; k, $C_1 \cdots C_4$; l, $Cl \cdots H_6$; m, $C_4 \cdots Cl$; n, $Cl \cdots H_5$.
The difference between the experimental and theoretical radial distribution curves calculated according to the parameter values in Table 4 is also given.

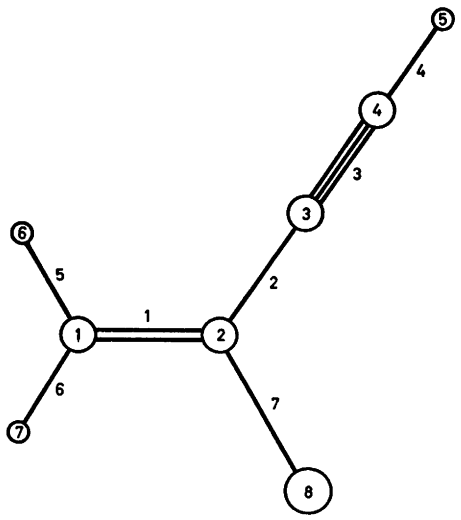

Fig. 3. Numbering of the atoms and bonds in 2-chlorobutenyne, C_4H_3Cl.

Table 1. Force field for 2-chlorobuten-3-yne.[a]

$K_1 = 9.1$	$K_{16} = 0.50$	$\varrho_5^{16} = 0.20$
$K_2 = 4.6$	$K_{15} = 0.50$	$\varrho_6^{15} = 0.20$
$K_3 = 15.7$	$K_{56} = 0.50$	$\varrho_7^{12} = 0.30$
$K_4 = 6.3$	$K_{17} = 0.85$	$\varrho_2^{17} = 0.25$
$K_5 = 5.5$	$K_{12} = 0.84$	$\chi_{12}^{16} = \chi_{15}^{17} = 0.12$
$K_6 = 5.5$	$K_{27} = 1.03$	$\chi_{12}^{15} = \chi_{16}^{17} = 0.14$
$K_7 = 3.9$	$K_{23}^{b} = 0.32$	
	$K_{34}^{b} = 0.23$	

[a] For numbering of the bonds, see Fig. 3. The meaning of the symbols: K_i, stretching of bond i; K_{ij}, bending of angle between bonds i and j; ϱ_k^{ij}, bending of bond k out of ij-plane; χ_{kl}^{ij}, torsion between the ij- and kl-planes. The force constants are given in md/Å and md Å/(rad)². [b] Identical force constants for bending in plane and out of plane are assumed.

were carried out under conditions given in Table 2. The result of a r_a-refinement where the amplitudes of vibration (l-values) were fixed at the calculated values, is given in Table 3. The C≡C−C angle was fixed at 180° since, when allowed to refine, it oscillated about 180° and no improvement of the least-squares fit was observed for deviation from 180°. A corresponding r_α-refinement where the calculated D-values given in Table 3, were used to obtain a geometrically consistent model, was carried out. This did not result in any significant changes in the refined parameter values nor in the least-squares fit. Further r_α-refinements of the structure were carried out including amplitudes of vibration. Amplitudes for overlapping distances were refined in groups. Attempts to refine the group of amplitudes corresponding to the C,C bond distances resulted in unreasonable values, as was also the case for the Cl···H non bonded amplitudes. Adjustments of amplitudes for the C···H and H···H non-bonded distances were never implemented. The simultaneous refinement of the amplitudes did not cause any significant changes in the geometrical parameters. In the r_α-refinements the C≡C−C angle converged to 177.0(2.9)° when allowed to refine. This did not, however, affect the other parameters nor the least-squares fit significantly. The final results are given in Table 4, and Table 5 comprises the elements of the corresponding correlation matrix. The differences between the experimental and theoretical intensities and radial distribution curves calculated according to these results are shown in Figs. 1 and 2, respectively.

The r_a-values given in Table 4 were transformed to the corresponding r_α-values and the

Table 2. Refinement conditions for 2-chlorobuten-3-yne.

Curve Camera distance (cm)	Data range s_{min}	s_{max}	Data interval Δs	Constants of the weightscheme [6,7] s_1	s_2	w_1	w_2	p_1	p_2	W
48	2.25	18.50	0.125	6.00	15.00	0.05	0.01	−0.64	0.146	1.0
20	9.50	38.00	0.25	9.50	24.00	0.05	0.02	−0.60	0.125	0.5

Table 3. Computed *D*- and *l*-values, and r_a-structure for 2-chlorobutenyne.[a]

Parameters[b]		*D*-Values	*l*-Values	r_a-Structure[c]
C–H	4,5	−0.0325	0.072	1.067(7)
	1,6	−0.0121	0.074	1.094(7)
	1,7	−0.0127	0.074	1.094(7)
C≡C	3,4	−0.0099	0.036	1.217(2)
C=C	1,2	−0.0024	0.041	1.336(2)
C–C	2,3	−0.0014	0.048	1.421(2)
C–Cl	2,8	−0.0011	0.046	1.737(1)
C···C	2,4	−0.0024	0.052	2.639(3)
	1,3	−0.0014	0.063	2.440(4)
	1,4	+0.0006	0.083	3.571(5)
C···Cl	1,8	−0.0001	0.064	2.659(4)
	3,8	−0.0004	0.067	2.682(4)
	4,8	+0.0018	0.098	3.709(4)
Cl···H	8,7	+0.0010	0.145	2.832(25)
	8,6	−0.0036	0.096	3.695(9)
	8,5	−0.0047	0.148	4.695(7)
C···H	3,5	−0.0282	0.077	2.284(8)
	2,5	−0.0139	0.085	3.706(8)
	1,5	−0.0068	0.123	4.598(10)
	2,6	−0.0062	0.098	2.108(14)
	3,6	−0.0003	0.139	2.701(24)
	4,6	+0.0044	0.176	3.598(27)
	2,7	−0.0074	0.098	2.108(14)
	3,7	−0.0059	0.097	3.424(11)
	4,7	−0.0021	0.103	4.601(10)
H···H	6,7	−0.0169	0.116	1.894(33)
	5,6	−0.0005	0.226	4.511(27)
	5,7	−0.0067	0.131	5.647(15)
∠C=C–C		–	–	124.7(0.2)
∠C–C≡C		–	–	[180.0]
∠C=C–Cl		–	–	121.0(0.3)
∠C=C–H		–	–	120.1(1.4)
R_w[d](%)		–	–	6.42

[a] Correction terms (*D*-values), amplitudes (*l*-values) and distances (r_a) in Å; angles in degrees. The r_a-structure gives the result of r_a-refinement (no *D*-value correction) using the calculated *l*-values. [b,c,d] See corresponding comments under Table 4.

moments of inertia for the molecule were calculated. The results are given in Table 4 along with those obtained from the microwave data (r_z-values).[4] The uncertainty limits for the values obtained from the electron-diffraction data are probably at least 0.5 % as estimated from calculations based upon parameter values given increments according to their standard deviations.

Table 4. Important parameter values and corresponding moments of inertia for 2-chlorobutenyne.[a]

Parameters[a]		r_a[c]	*l*[c]
C–H	4,5	1.078(8)	0.073(7)′
	1,6	1.106(8)	0.075(7)′
	1,7		
C≡C	3,4	1.220(3)	[0.036]
C=C	1,2	1.340(3)	[0.041]
C–C	2,3	1.422(2)	[0.048]
C–Cl	2,8	1.738(1)	0.049(2)
C···C	2,4	2.634(4)	0.049(2)″
	1,3	2.445(5)	0.059(5)
	1,4	3.584(18)	0.088(16)
C···Cl	1,8	2.663(16)	0.061(2)″
	3,8	2.680(18)	0.064(2)″
	4,8	3.701(12)	0.109(9)
Cl···H	8,7	2.833(34)	[0.145]
	8,6	3.696(15)	[0.096]
	8,5	4.664(21)	[0.148]
∠C=C–C		124.7(0.2)	
∠C–C≡C		177.0(2.9)	
∠C=C–Cl		119.5(1.2)	
∠C=C–H		122.0(1.6)	
R_w[d](%)		5.95	
I_a[e](73.63)[4]		73.5	
I_b(163.41)		163.2	
I_c(237.05)		236.7	

[a] Results of r_α-refinements (the distances given are r_a-values). Distances, r_a, amplitudes, *l*, in Å; angles in degrees; moment of inertia, *I*, in *u* Å^2.
[b] See Fig. 3 for numbering of the atoms.
[c] Parenthesized values are standard deviations obtained from the least-squarer refinement (σ_{LS}) and they refer to the last digits given. For the distance parameters they should be corrected for systematic uncertainties according to $\sigma=[\sigma_{LS}^2+(0.001\ r)^2]^{\frac{1}{2}}$. Quantities in brackets are assumed values and primed amplitudes are refined in groups.
[d] Agreement factor $R_w=[\sum w_i\Delta_i^2/\sum w_i I_i^2(\text{obs})]^{\frac{1}{2}}$ where $\Delta_i=I_i(\text{obs})-I_i(\text{th})$.
[e] Moments of inertia (r_α-values); parenthesized values are microwave results (r_z-values). See text for estimates of uncertainties.

DISCUSSION

The agreement factor ($R_w=5.95$ %) and the difference curves shown in Figs. 1 and 2 demonstrate that the final model (Table 4) is in good agreement with the experimental data. The refined amplitudes of vibration agree well with those calculated from the assumed force field (*see* Tables 3 and 4). The moments of inertia based upon the electron-diffraction

Table 5. Correlation matrix for parameters of 2-chlorobutenyne.

$r_{C\equiv C}$	r_{C-C}	$r_{C=C}$	$\angle C=C-C$	$\angle C\equiv C-C$	r_{C-Cl}	$\angle C=C-Cl$	r_{C-H}	$\angle C=C-H$	l_{CH}	$l_{C_3C_4}$	$l_{C_1C_4}$	$l_{C_1C_3}$	l_{C_4Cl}	l_{C-Cl}	Scales 48 cm	20 cm
1.0																
−0.3	1.0															
0.45	−0.36	1.0														
0.38	0.33	0.26	1.0													
0.04	0.01	0.01	0.10	1.0												
−0.12	−0.14	−0.14	0.40	−0.04	1.0											
0.18	0.10	0.04	0.11	0.90	−0.08	1.0										
0.47	−0.12	0.54	0.26	0.01	−0.02	0.11	1.0									
−0.21	0.20	−0.23	0.04	−0.20	−0.03	−0.18	−0.42	1.0								
−0.62	0.04	−0.09	−0.10	0.02	0.13	−0.09	−0.17	0.09	1.0							
0.19	0.26	−0.12	0.08	0.67	−0.19	0.78	−0.08	−0.05	−0.11	1.0						
0.07	0.15	0.02	0.10	−0.66	0.02	−0.35	0.00	0.21	−0.07	−0.19	1.0					
0.22	0.04	0.15	0.05	0.28	0.04	0.31	0.21	−0.26	−0.17	0.30	−0.16	1.0				
0.17	0.19	0.07	0.18	−0.82	0.01	−0.65	0.06	0.24	−0.11	−0.39	0.72	−0.19	1.0			
−0.13	0.23	−0.24	−0.07	0.01	−0.09	0.06	−0.34	0.32	0.00	0.38	0.13	−0.12	0.12	1.0		
−0.30	0.21	−0.36	−0.19	0.07	−0.12	0.11	−0.49	0.42	0.10	0.34	0.10	−0.14	0.02	0.48	1.0	
−0.17	0.33	−0.31	−0.12	−0.03	−0.17	0.06	−0.41	0.32	0.04	0.49	0.19	−0.06	0.18	0.70	0.53	1.0

data are in good agreement with those obtained from the microwave data [4] as compared with the estimated uncertainty limits.

The carbon, chlorine bond length is found to be 1.738(4) Å; the parenthesized value is 2σ where systematic uncertainties are included (see note *c* in Table 4). This is significantly longer than those found for the $C(sp^2)-Cl$ bond in *cis*- and *trans*-1-chlorobutenyne [1.716 (5) Å, 1.717(4) Å],[2] but within the range usually found for this distance type. In 2-chlorobutenyne the C–Cl bond is adjacent to a conjugated single bond and opposite a relatively large C=C–C angle. Its environment is therefore similar to that of the C–Cl bonds in 2,3-dichlorobutadiene [9] [$\angle C=C-C=126.9(0.2)°$] where also the $C(sp^2)-Cl$ bond is relatively long [$r_{C-Cl}=1.747(2)$ Å].

A slight bend of the C≡C–C chain was observed in butenyne [$\angle C\equiv C-C=177.9$ (1.2)°].[10] A similar value for the C≡C–C angle is found in 2-chlorobutenyne, but due to the lower accuracy of the determination, the deviation from linearity of the C≡C–C chain is not significant in this compound. The chlorine subtitution has resulted in a small opening of the C=C–C angle and a slight shortening of the C–C bond as compared to the unsubstituted hydrocarbon [$\angle C=C-C=123.1(0.5)°$ and $r_{C-C}=1.431(3)$ Å],[10] while the other structural parameters are not significantly different in the two compounds. Comparison of the carbon skeleton in monochloro substituted butenynes will be carried out and related to the unsubstituted hydrocarbon in more detail in the last paper of this series.

Acknowledgements. We are grateful to Professor Otto Bastiansen and Professor Ragnar Vestin for their stimulating interest in this project, and we wish to express our gratitude to Dr. Hans M. Seip for helpful discussions and suggestions regarding the manucript.

REFERENCES

1. Almenningen, A., Gundersen, G., Borg, A., Granberg, M. and Karlsson, F. *Acta Chem. Scand. A 29* (1975) 395.
2. Almenningen, A., Gundersen, G., Borg, A., Granberg, M. and Karlsson, F. *Acta Chem. Scand. A 29* (1975) 545.
3. Vestin, R., Borg, A. and Lindblom, T. *Acta Chem. Scand. 22* (1968) 687.
4. Karlsson, F., Granberg, M. and Vestin, R. *Acta Chem. Scand. A 28* (1974) 206.
5. Bastiansen, O., Hassel, O. and Risberg, E. *Acta Chem. Scand. 9* (1955) 232.
6. Andersen, B., Seip, H. M., Strand, T. G. and Stølevik, R. *Acta Chem. Scand. 23* (1969) 3224.
7. Seip, H. M., Strand, T. G. and Stølevik, R. *Chem. Phys. Lett. 3* (1969) 617.
8. Stølevik, R., Seip, H. M. and Cyvin, S. J. *Chem. Phys. Lett. 15* (1972) 263.
9. Neisses, J. A., Gundersen, G. and Hedberg, K. *To be published.*
10. Fukuyama, T., Kuchitsu, K. and Morino, Y. *Bull. Chem. Soc. Jap. 42* (1969) 379.

Received March 4, 1975.

Acta Chemica Scandinavica A 29 (1975) 731—737

Electron-diffraction Studies of Chlorobutatriene and Chlorobutenynes. IV. Molecular Structure of Gaseous 4-Chlorobutenyne

ARNE ALMENNINGEN,[a] GRETE GUNDERSEN,[a] MATS GRANBERG [b] and FRED KARLSSON [b]

[a] Department of Chemistry, University of Oslo, Oslo 3, Norway and [b] Department of Physical Chemistry, University of Stockholm, Arrhenius Laboratory, Fack, S-104 05 Stockholm, Sweden

The molecular structure of 4-chlorobuten-3-yne has been investigated by electron-diffraction from the vapour. Normal coordinate calculations based upon an assumed force field supplied amplitudes of vibration which could not be determined from the electron-diffraction data, and correction terms which were used in the geometrically consistent r_α-refinement. The structural parameters (r_a-values are given) were found to be: C–H = 1.078(16) Å, C≡C = 1.213(5) Å, C=C = 1.332(7) Å, C–C = 1.429(5) Å, C–Cl = 1.637(4) Å, ∠C=C–C = 125.3(1.2)°, ∠C≡C–C = 181.0(3.8)°, ∠C≡C–Cl = 182.9(5.2)°, ∠C=C$_1$–H = 126.9(5.4)° and ∠C=C$_2$–H = 114.61(5.2)°. Parenthesized values are 2σ where estimates of systematic uncertainties are included.

This electron-diffraction investigation of 4-chlorobuten-3-yne concludes the structural studies of the five isomeric C_4H_3Cl species by this method.[1–3]

EXPERIMENTAL AND CALCULATION PROCEDURES

4-Chlorobuten-3-yne was prepared by adding monovinyl acetylene to a potassium hypochlorite solution.[4,5] The substance was isolated and purified by gas liquid chromatography at a temperature of 100 °C, using a column packed with diethyl-hexyl sebacate (15 %) absorbed on Chromosorb. The compound was prevented from polymerization by storing the sample at −70 °C. Diffraction photographs were made in the Oslo Apparatus [6] at nozzle-to-plate distances of 48 cm and 20 cm, keeping the sample reservoir at about −30 °C. The electron wavelength was 0.06464 Å as calibrated against diffraction patterns of gaseous benzene. The scattering functions for the 35 kV electrons used were those computed for chlorobutatriene.[1] Four plates for each of the two camera distances were selected for the structure analysis. The data reduction, structure analysis, and supporting calculations were carried out in routine fashion [7–9] as described for chlorobutatriene.[1] The modified intensities and radial distribution curves obtained are shown in Figs. 1 and 2, respectively.

CALCULATIONS AND REFINEMENTS

A general planar model of 4-chlorobutenyne is described by thirteen parameters; see Fig. 3. Assuming all C(sp^2)–H bond distances to be equal and ∠C=C$_1$–H$_7$ = ∠C=C$_1$–H$_6$, the number of adjustable parameters was, however, reduced to the following ten: r_{C-H}, $r_{C\equiv C}$, $r_{C=C}$, r_{C-C}, r_{C-Cl}, ∠C=C$_1$–H, ∠C=C$_2$–H, and defined alternately *trans* with respect to each other ∠C=C–C, ∠C–C≡C, and ∠C≡C–Cl.

The diagonal force field given in Table 1 was designed by adopting force constants from similar molecules, and it was used in normal coordinate calculations [9] based upon coordinates consistent with the r_a-model given in Table 3. The resulting D- and l-values are also given in Table 3.

The interpretation of the main features of the radial distribution curve was straightforward as indicated by the approximate positions of the important interatomic distances shown in Fig. 2. Least-squares refinements were carried out under conditions given in Table 2, and the

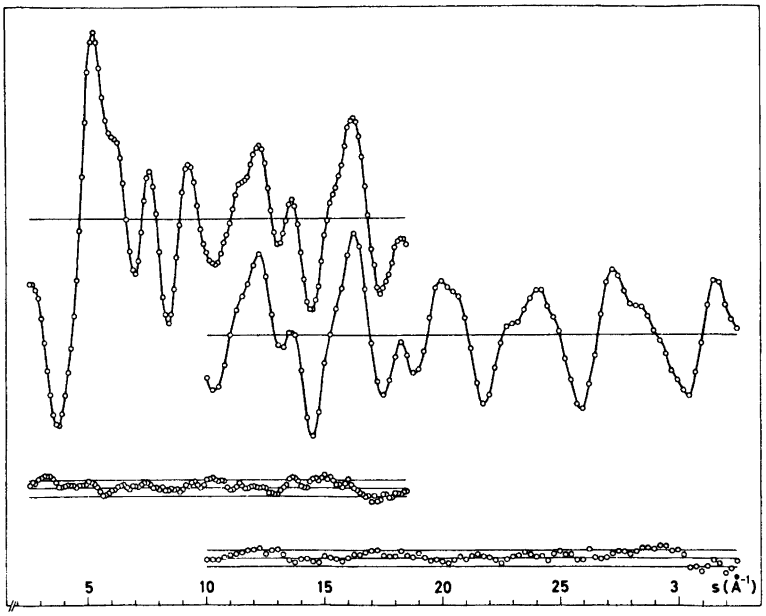

Fig. 1. Experimental intensity data for 4-chlorobutenyne from the 48 cm ($\Delta s = 0.125$ Å^{-1}) and 20 cm ($\Delta s = 0.25$ Å^{-1}) camera distances, and the corresponding differences between experimental and theoretical intensities computed according to the parameter values of Table 4(II) The full lines given along with the differences indicate the estimated uncertainties (three standard deviations) of the experimental intensity points.

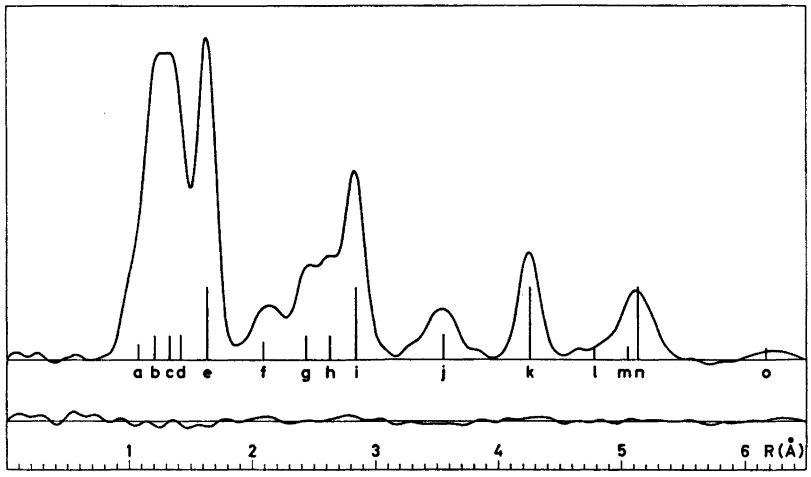

Fig. 2. Experimental radial distribution curve for 4-chlorobutenyne calculated for the artificial damping constant $k = 0.0015$ Å^2. The approximate positions of the important interatomic distances are indicated: a, C–H; b, C≡C; c, C=C; d, C–C; e, C–Cl; f, four C···H; g, $C_1 \cdots C_3$; h, $C_2 \cdots C_4$; i, $C_3 \cdots Cl$; j, $C_1 \cdots C_4$; k, $C_2 \cdots Cl$; l, $Cl \cdots H_5$; m, $Cl \cdots H_6$; n, $C_1 \cdots Cl$; o, $Cl \cdots H_7$. The difference between the experimental and theoretical radial distribution curves calculated according to the parameter values in Table 4 (Model II) is also shown.

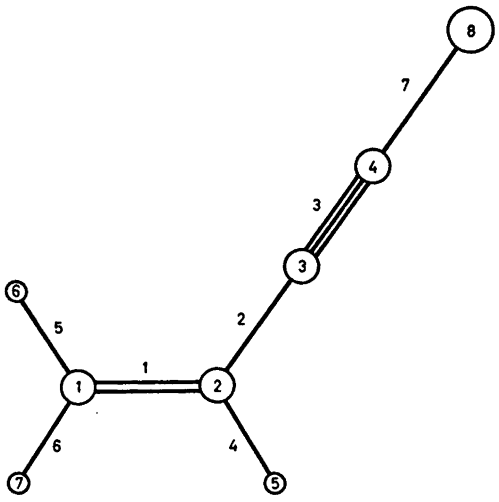

Fig. 3. Numbering of atoms and bonds in 4-chlorobutenyne, C_4H_3Cl.

Table 1. Force field for 4-chlorobuten-3-yne.[a]

$K_1 = 9.10$	$K_{16} = 0.59$	$\varrho_5^{16} = 0.20$
$K_2 = 4.60$	$K_{15} = 0.59$	$\varrho_6^{15} = 0.20$
$K_3 = 15.70$	$K_{56} = 0.25$	$\varrho_4^{11} = 0.20$
$K_4 = 5.40$	$K_{14} = 0.53$	$\varrho_2^{14} = 0.25$
$K_5 = 5.50$	$K_{12} = 0.84$	$\chi_{12}^{16} = \chi_{14}^{15} = 0.16$
$K_6 = 5.50$	$K_{24} = 0.25$	$\chi_{12}^{15} = \chi_{14}^{16} = 0.13$
$K_7 = 5.16$	$K_{23}^{b} = 0.32$	
	$K_{37}^{b} = 0.28$	

[a] For numbering of the bonds, see Fig. 3. The meaning of the symbols: K_i, stretching of bond i; K_{ij}, bending of angle between bonds i and j; ϱ_k^{ij}, bending of bond k out of ij-plane; χ_{kl}^{ij}, torsion between the ij- and kl-planes. The force constants are given in md/Å and md Å/(rad)². [b] Identical force constants are assumed for bending in plane and out of plane.

result of an r_a-refinement where the amplitudes were fixed at the calculated values and all CCH angles at 122.0° is given in Table 3. No changes in the distance parameters were observed when ∠C≡C−C and ∠C≡C−Cl were included in the refinement. The values obtained for the angles were then ∠C=C−C = 124.6(0.3)°, ∠C≡C−C = 177.2(1.6)°, and ∠C≡C−Cl = 176.5(2.1)° and the least-squares fit improved somewhat ($R_w = 9.71$ %). The D-values given in Table 3 were now used to obtain a geometrically consistent model, and the corresponding r_α-refinements were carried out. This resulted in a significantly better least-squares fit as the agreement factors were 8.94 and 8.60 %, respectively, for the models with linear and non-linear Cl−C≡C−C chains. The bond distances in these two models did not differ significantly and the refined valence angles were for the linear one ∠C=C−C = 125.1(1.3)° and for the non-linear one ∠C=C−C = 124.6(0.6)°, ∠C=C−C = 180.1(1.7)°, and ∠C≡C−Cl = 182.5(2.3)°. The r_α-results do not suggest any significant deviation from linearity of the Cl−C≡C−C chain contrary to the implications of the r_a-results. Also, the bond distances from the r_α-refinements are significantly longer than those obtained from the r_a-refinements of the structure (*cf.* values in Table 3 and 4). Comparisons of experimental and theoretical radial distribution curves for the described models revealed that the r_a-results gave poor agreement in the region where the bond distances are located.

The r_α-refinement of the structure was continued by including amplitudes of vibration and the CCH-angles in the refinement. As the values obtained for the CCH-angles seemed somewhat unreasonable, refinements were also carried out

Table 2. Refinements conditions for 4-chlorobuten-3-yne.

Curve	Data range		Data	Constants of the weight scheme [7,8]						
Camera distance (cm)	s_{min}	s_{max}	interval Δs	s_1	s_2	w_1	w_2	p_1	p_2	W
48	2.50	18.50	0.125	6.00	15.00	0.05	0.01	−0.64	0.146	1.0
20	10.00	32.50	0.250	10.00	24.00	0.05	0.02	−0.60	0.125	0.5

Table 3. Computed *D*- and *l*-values, and r_a-structure for 4-chlorobutenyne.[a]

Parameters [b]		*D*-Values	*l*-Values	r_a-Structure [c]
C–H	2,5	−0.0216	0.075	1.070(7)
	1,6	−0.0209	0.074	1.070(7)
	1,7	−0.0211	0.074	1.070(7)
C≡C	3,4	−0.0050	0.036	1.204(2)
C=C	1,2	−0.0058	0.041	1.326(3)
C–C	2,3	−0.0097	0.048	1.417(2)
C–Cl	4,8	−0.0123	0.042	1.635(1)
C···C	2,4	−0.0058	0.051	2.621(2)
	1,3	−0.0089	0.065	2.435(3)
	1,4	−0.0047	0.085	3.553(4)
C···Cl	3,8	−0.0066	0.046	2.838(2)
	2,8	+0.0001	0.056	4.255(2)
	1,8	+0.0023	0.113	5.134(4)
Cl···H	8,5	+0.0003	0.147	4.773(7)
	8,6	+0.0068	0.231	5.047(8)
	8,7	−0.0022	0.120	6.173(8)
C···H	1,5	−0.0150	0.098	2.099(7)
	3,5	−0.0229	0.108	2.081(7)
	4,5	−0.0130	0.126	3.192(7)
	2,6	−0.0154	0.097	2.099(7)
	3,6	−0.0059	0.141	2.720(6)
	4,6	+0.0003	0.179	3.619(7)
	2,7	−0.0151	0.097	2.099(7)
	3,7	−0.0203	0.097	3.407(7)
	4,7	−0.0137	0.104	4.569(8)
H···H	5,6	−0.0281	0.119	3.057(13)
	5,7	−0.0082	0.161	2.460(8)
	6,7	−0.0342	0.122	1.815(11)
∠C=C–C		–	–	125.2(0.3)
∠C–C≡C		–	–	180.0
∠C≡C–Cl		–	–	180.0
∠C=C_1–H		–	–	122.0
C=C_2–H		–	–	122.0
∠R_w [d] (%)		–	–	9.98

[a] Correction terms (*D*-values), amplitudes (*l*-values) and distances (r_a) in Ångströms; angles in degrees. The r_a-structure gives the result of a r_a-refinement (no *D*-value correction) using the calculated *l*-values. [b,c,d] See corresponding comments under Table 4.

keeping these parameters fixed at 122.0°. In both models l_{C-H} and $l_{Cl\cdots H_8}$ were kept at the calculated values given in Table 3 as they refined to unreasonable values with large standard deviations, as was also the case for $l_{Cl\cdots H_8}$ [0.41(27) Å] when the CCH-angles were kept at 122.0°. The results of both refinements are given in Table 4. The differences between the experimental and theoretical intensities and radial distribution curves are given in Figs. 1 and 2, respectively, for the less restricted model (Table 4, II) and Table 5 comprises the elements of the error matrix from the corresponding least-squares refinement.

The r_a-values given in Table 4 were transformed to the corresponding r_α-values and the moments of inertia were calculated for the two models. The results are given in Table 4 together with those obtained from microwave data (r_z-values).[10] The uncertainty limits for the electron-diffraction values are probably at least 0.5 % as estimated from calculations based upon parameter values given increments according to their standard deviations.

DISCUSSION

The failure of the r_a-model to represent the data in a satisfactory manner was not surprising as the location of the heavy chlorine atom at the end of the rather flexible –C≡C-chain should suggest that large shrinkage effects would be encountered for the non-bonded interactions which are responsible for a major contribution to the scattered intensity. In fact, as calculated from the *D*-values used in this investigation, the shrinkage effects for the $C_3\cdots Cl$, $C_2\cdots Cl$, and $C_1\cdots Cl$ distances respectively were 0.010, 0.027, and 0.033 Å. A least-squares r_a-refinement would therefore result in a compromise yielding too short bond distances. The results of the geometrically consistent r_α-refinement should therefore be more reliable, although the correction terms applied originate from an assumed force field. The difference curve in Fig. 2 does not, however, suggest that any serious problems due to shrinkage effects are remaining and the good agreement between calculated and refined amplitudes of vibration is reassuring. On the other hand, the moments of inertia calculated from the electron-diffraction data are smaller than those obtained from the microwave data [10] (*cf.* Table 4), which may suggest that the shrinkage effect is somewhat underestimated. The differences are, however, probably not significant, at least not for the less restricted model. This model exhibits what we at first sight considered to be unreasonable values for the CCH-angles. However, the facts that it seems to conform better to the microwave moments of inertia and also gave amplitudes of

Table 4. Important parameter values and moments of inertia for 4-chlorobutenyne.[a]

Parameters [b]		I r_a [c]	I l [c]	II r_a [c]	II l [c]
C–H	2,5 1,6 1,7	1.086(7)	[0.075]	1.078(8)	[0.075]
C≡C	3,4	1.214(2)	0.038(4)′	1.213(2)	0.036(4)′
C=C	1,2	1.333(3)	0.043(4)′	1.332(3)	0.041(4)′
C–C	2,3	1.428(2)	0.050(4)′	1.429(2)	0.048(4)′
C–Cl	4,8	1.638(1)	0.038(1)	1.637(1)	0.039(3)
C···C	2,4	2.633(3)	0.060(6)	2.632(3)	0.054(6)
	1,3	2.438(6)	0.069(6)	2.447(6)	0.064(6)
	1,4	3.557(8)	0.090(8)	3.558(8)	0.091(8)
C···Cl	3,8	2.840(2)	0.047(3)	2.838(2)	0.047(3)
	2,8	4.251(2)	0.058(3)	4.250(2)	0.058(3)
	1,8	5.133(5)	0.105(4)	5.135(5)	0.104(5)
Cl···H	8,5	4.762(8)	[0.147]	4.861(36)	0.144(48)
	8,6	5.046(10)	[0.231]	5.142(47)	[0.231]
	8,7	6.169(9)	0.137(33)	6.181(41)	0.136(33)
∠C=C–C		124.4(0.6)		125.3(0.6)	
∠C≡C–C		179.7(1.9)		181.0(1.9)	
∠C≡C–Cl		182.1(2.6)		182.9(2.6)	
∠C=C_1–H		[122.0]		126.9(2.7)	
∠C=C_2–H		[122.0]		114.6(2.6)	
R_w [d] (%)		8.51		8.05	
I_a [e] (–)[10]		11.5		11.5	
I_b (358.49)		356.2		357.3	
I_c (370.60)		367.7		368.8	

[a] Results of r_α-refinements (the distances given are r_a-values). Different restrictions are imposed on the two models as indicated by the brackets. Distances, r_a, amplitudes, l, in Å; angles in degrees; moment of inertia, I, in u Å². [b] See Fig. 3 for numbering of the atoms. [c] Parenthesized values are standard deviations obtained from the least-squares refinement (σ_{LS}) and they refer to the last digits given. For the distance parameters they should be corrected for systematic uncertainties according to $\sigma=[\sigma_{LS}^2+(0.001\ r)^2]^{\frac{1}{2}}$. Quantities in brackets are assumed values. Primed amplitudes are refined in groups. [d] Agreement factor $R_w=[\sum w_i \Delta_i^2/\sum w_i I_i^2(\text{obs})]^{\frac{1}{2}}$ where $\Delta_i=I_i(\text{obs})-I_i(\text{th})$. [e] Moments of inertia ($r_\alpha$values); parenthesized values are microwave results (r_z-values). See text for estimates of uncertainties.

vibration in closer agreement with the calculated ones, gives it more credibility than the electron diffraction data alone would have done. In particular we would like to point out that the problems with the Cl···H_5 amplitude of vibration suggested that the position of the H_5-atom was wrong when the C=C–H_5 = 122.0° was assumed, while it refined to a value close to the calculated one when this angle was included in the refinement. We will therefore choose the less restricted model to represent the final structure of 4-chlorobutenyne (Table 4, II). Apart from the location of the hydrogen atoms this has otherwise only minor consequences for the molecular structure as the other structural parameters do not differ significantly in the two models.

The C(sp)–Cl bond in 4-chlorobutenyne is found to be 1.637(2) Å. The parenthesized value corresponds to 2σ where σ is corrected for systematic uncertainties. This bond, as well as the triplebond of 1.213(5) Å, is in agreement with the corresponding bond in *tert*-butylchloroacetylene, $(CH_3)_3C-C\equiv C-Cl$ [1.637(5) and 1.210(5) Å].[11] The C≡C bonds in acetylene and butenyne are 1.212(1) Å and 1.213(1) Å, respectively, which indicate that chlorine substitution does not affect this bond significantly contrary to what seems to be the case for the C(sp^2)=C(sp^2) bond.[12]

The carbon skeleton found for 4-chlorobutenyne is compared to those of the three other chlorobutenynes [2,3] and the unsubstituted hydrocarbon [13] in Table 6. The acetylene chain in

Table 5. Correlation matrix for parameters of 4-chlorobutenyne. (Model II, Table 4).

$r_{C\equiv C}$	r_{C-C}	$r_{C=C}$	$\angle C=C-C$	$\angle C\equiv C-C$	r_{C-Cl}	$\angle C\equiv C-Cl$	r_{C-H}	$\angle C=C_2-H$	$\angle C=C_1-H$	l_{C-C}
1.0										
−0.22	1.0									
0.54	−0.11	1.0								
−0.02	0.02	−0.34	1.0							
0.43	0.16	0.09	0.62	1.0						
−0.37	0.04	−0.13	−0.06	0.01	1.0					
0.50	0.15	0.19	0.28	0.87	0.09	1.0				
0.52	−0.11	0.42	−0.05	0.17	−0.15	0.22	1.0			
0.05	−0.05	−0.03	−0.24	−0.02	0.04	−0.04	0.01	1.0		
−0.15	0.13	−0.23	0.32	0.30	−0.07	0.13	−0.35	0.26	1.0	
0.25	−0.26	0.43	−0.16	0.04	0.19	0.13	0.21	−0.01	−0.24	1.0
0.20	−0.16	0.13	−0.26	−0.22	0.04	−0.16	0.11	0.09	−0.27	0.15
0.00	0.04	0.00	0.09	0.10	0.02	0.07	0.04	−0.01	0.12	0.14
0.09	−0.09	0.12	−0.19	−0.13	0.08	−0.07	0.04	0.05	−0.25	0.14
−0.05	−0.01	−0.05	−0.02	−0.09	−0.19	−0.13	−0.25	−0.05	0.02	−0.05
−0.13	−0.03	0.02	−0.08	−0.10	−0.01	−0.09	−0.19	−0.03	−0.04	0.09
−0.06	0.05	0.00	−0.01	−0.04	−0.09	−0.07	−0.17	−0.04	0.02	0.04
−0.03	0.04	0.07	−0.07	−0.05	−0.01	−0.04	−0.02	−0.01	−0.10	0.05
−0.07	0.02	0.03	−0.08	−0.13	0.08	−0.15	0.07	−0.01	−0.13	0.05
−0.09	0.01	−0.04	0.01	−0.05	0.05	−0.09	−0.03	−0.06	0.01	0.01
−0.27	0.01	−0.07	−0.07	−0.14	0.09	−0.14	−0.40	0.04	0.07	0.03
−0.01	0.11	0.06	−0.03	−0.02	−0.20	−0.03	−0.22	−0.11	−0.04	0.06

Table 5. Continued.

$l_{C_3C_4}$	$l_{C_1C_4}$	$l_{C_1C_3}$	l_{C_3Cl}	l_{C_2Cl}	l_{C_4Cl}	l_{ClH_6}	l_{ClH_5}	l_{ClH_7}	Scales 48 cm	20 cm
1.0										
−0.04	1.0									
0.54	−0.07	1.0								
−0.03	0.04	0.12	1.0							
0.09	0.03	0.08	0.51	1.0						
−0.02	0.05	0.06	0.47	0.36	1.0					
0.03	0.04	0.02	0.26	0.18	0.20	1.0				
0.07	0.01	−0.02	0.03	0.02	0.02	0.58	1.0			
0.00	0.01	−0.03	0.06	0.06	0.04	−0.04	−0.02	1.0		
−0.04	0.05	0.06	0.41	0.33	0.32	0.17	−0.02	0.04	1.0	
−0.02	0.05	0.13	0.78	0.60	0.58	0.29	0.02	0.07	0.38	1.0

Table 6. The carbon skeleton in butenyne and chlorobutenynes.[a]

	C=C	C−C	C≡C	$\angle C=C-C$	$\angle C\equiv C\cdots C$
Butenyne [13]	1.344(4)	1.434(3)	1.215(3)	123.1(0.5)	177.9(1.2)
cis-1-Chlorobytenyne [2]	1.345(7)	1.426(6)	1.212(6)	123.9(0.6)	178.0(2.2)
trans-1-Chlorobytenyne [2]	1.356(7)	1.436(6)	1.220(8)	120.7(1.0)	180.2(2.4)
2-Chlorobutenyne [3]	1.340(5)	1.422(5)	1.220(6)	124.7(0.5)	177.0(5.8)
4-Chlorobutenyne [b]	1.332(7)	1.429(5)	1.213(5)	125.2(1.2)	181.0(3.8)

[a] Distances, r_a, in Å; angles in degrees. Parenthesized values correspond to 2σ where systematic uncertainties are included. [b] This work.

butenyne appears to be slightly bent. The determination of the C–C≡C angle in the chlorobutenynes are associated with large standard deviations which makes it impossible to determine small deviations from linearity, and *cis*-chlorobutenyne seems to be the only chlorobutenyne where a similar trend is observed. The variations of the carbon skeletons in the five butenynes considered are small. The only systematic trend apparent to us is that the average carbon-carbon bond length is longer and the C=C–C angle smaller in *trans*-chlorobutenyne than in the other chlorobutenynes, while the corresponding values for butenyne are intermediate to these.

The chlorine atom should interact with the rest of the molecule both by the inductive effect and by the competing resonance effect as one lone pair of the chlorine atom will participate in the π-electron delocalization in the conjugated system. We can, however, see no obvious ways to relate the structures of the carbon skeletons in the five butenynes to such effects. For example, no systematic lengthening of the C=C bond as compared to butenyne is observed in the three pertinent chlorobutenynes, contrary to what is observed in chloro-substituted ethylenes.[12] A similar lengthening of the C=C bond in ethylenes is, however, also observed by methyl substitution.[14] This suggests that this effect could be rationalized by considering non-bonded repulsions rather than in terms of inductive and resonance effects, which also seems to be consistent with the apparent invariance toward chlorine substitution of the C≡C bond. We feel that the observed variations of the structural parameters for the carbon skeletons in the five butenynes considered are too small to be a subject for extensive discussions about their origins. However, the previous arguments and the notion that these parameters seem to adjust in such a manner as to give C···C and C···Cl non-bonded interactions across one valence angle in the ethylenic groups in narrow ranges (2.42–2.45 Å and 2.67–2.70 Å, respectively) suggest that non-bonded repulsions should be included in any such discussion.

Acknowledgements. We are grateful to Professor Otto Bastiansen and Professor Ragnar Vestin for their stimulating interest in this project and we wish to express our gratitute to Dr. Hans. M. Seip for helpful discussions and suggestions regarding the manuscript.

REFERENCES

1. Almenningen, A., Gundersen, G., Borg, A., Granberg, M. and Karlsson, F. *Acta Chem. Scand. A 29* (1975) 395.
2. Almenningen, A., Gundersen, G., Borg, A., Granberg, M. and Karlsson, F. *Acta Chem. Scand. A 29* (1975) 545.
3. Almenningen, A., Gundersen, G., Granberg, M. and Karlsson, F. *Acta Chem. Scand. A 29* (1975) 725.
4. Jacobson, R. A. and Carothers, W. H. *J. Amer. Chem. Soc. 55* (1933) 4667.
5. Granberg, M., Karlsson, F. and Vestin, R. *Acta Chem. Scand. B 28* (1974) 580.
6. Bastiansen, O., Hassel, O. and Risberg, E. *Acta Chem. Scand. 9* (1955) 232.
7. Andersen, B., Seip, H. M., Strand, T. G. and Stølevik, R. *Acta Chem. Scand. 23* (1969) 3224.
8. Seip, H. M., Strand, T. G. and Stølevik, R. *Chem. Phys. Lett. 3* (1969) 617.
9. Stølevik, R., Seip, H. M. and Cyvin, S. J. *Chem. Phys. Lett. 15* (1972) 263.
10. Karlsson, F., Granberg, M. and Vestin, R. *Acta Chem. Scand. A 29* (1975) 111.
11. Haase, J., Steingross, W. and Zeil, W. *Z. Naturforsch. 22a* (1967) 195.
12. Ivey, R. C. and Davies, M. I. *J. Chem. Phys. 57* (1972) 1909.
13. Fukuyama, T., Kuchitsu, K. and Morino, Y. *Bull. Chem. Soc. Jap. 42* (1969) 379.
14. Tokue, I., Fukuyama, T. and Kuchitsu, K. *J. Mol. Struct. 23* (1973) 33.

Received March 4, 1975.

Acta Chemica Scandinavica A 29 (1975) 738—744

The Structures of Two Crystalline Forms of Bromo-(ethylenethiourea)phenyltellurium(II)

OLAV VIKANE

Department of Chemistry, University of Bergen, N-5014 Bergen-Univ., Norway

The 1:1 complex of benzenetellurenyl bromide with ethylenethiourea, $C_6H_5Te(etu)Br$, crystallizes in two different space groups. One form, I, occurs as yellow monoclinic plates with space group $C2/c$ and $Z=8$; the other form, II, occurs as orange red monoclinic prisms with space group $P2_1/c$ and $Z=4$. The unit cell dimensions for I are: $a=15.5394(11)$ Å, $b=9.0893(9)$ Å, $c=19.0269(18)$ Å, $\beta=114.774(6)°$, and for II: $a=7.0513(6)$ Å, $b=12.7786(11)$ Å, $c=14.4676(12)$ Å, $\beta=102.309(7)°$.

In both structures, the tellurium atom is bonded to one phenyl carbon atom and, in directions nearly perpendicular to the Te–C bond, to one ethylenethiourea sulfur atom and one bromine atom. The three-centre system S–Te–Br is nearly linear, and the Te–C bond nearly bisects the S–Te–Br angle. The bond lengths and angles involving tellurium are: Te–S = 2.5560(15) Å, Te–Br = 2.8348(10) Å, Te–C = 2.116(3) Å, ∠S–Te–Br = 177.22(3)°, ∠S–Te–C = 89.05(10)°, ∠Br–Te–C = 86.46(10)° in I, and Te–S = 2.5231(15) Å, Te–Br = 2.9694(10) Å, Te–C = 2.123(4) Å, ∠S–Te–Br = 175.96(3)°, ∠S–Te–C = 89.45(12)°, ∠Br–Te–C = 87.02(11)° in II.

In the structure of II the fourth position of a square-planar tellurium(II) coordination is approached by a bromine atom of an adjacent molecule, at Te···Br = 3.8313(10) Å, in a direction which makes an angle of 162.29(11)° with the Te–C bond. In the structure of I, this approach of a "fourth ligand" is missing.

The crystal structures of 1:1 complexes between benzenetellurenyl chloride or bromide and thiourea have been determined by Foss and Husebye.[1] The coordination around tellurium was described as based on square-planar four-coordination with one position, *trans* to the phenyl group, vacant.[1,2]

In a recent paper the syntheses of an 1:1 complex between benzenetellurenyl bromide and ethylenethiourea was reported.[3] The complex was found to crystallize in two different space groups. This article reports the structures of the two different crystalline forms of bromo(ethylenethiourea)phenyltellurium(II). As in the structures of chloro- and bromo(phenyl)thioureatellurium(II), the tellurium atoms are three-coordinated, and the coordinations around tellurium are nearly planar. A comparison of the structures in the two different space groups has been made, and the differences are discussed.

EXPERIMENTAL

Methods used for data collection and reductions, and computational procedures are as described previously.[4,5] For the $C2/c$ form, I, the measurements were performed on a crystal with the following dimensions, given as distances from the point of intersection of the crystal faces (001), (110), and ($\bar{1}$10): to (00$\bar{1}$), 0.109 mm; to ($\bar{1}$10), 0.187 mm; and to (1$\bar{1}$0), 0.187 mm. For the $P2_1/c$ form, II, the crystal used had the following dimensions, given as distances from the point of intersection of the crystal faces (0$\bar{1}\bar{1}$), (01$\bar{1}$), (1$\bar{1}\bar{1}$), and (11$\bar{1}$): to (0$\bar{1}$1), 0.155 mm; to (011), 0.148 mm; and to ($\bar{1}$00), 0.187 mm.

The scale factors, based on the reference reflections, varied within 6 % for I, and 8 % for II. 2624 of 3664 independent reflections within $\theta=30°$ were found to be stronger than the lower limit for I. The corresponding numbers for II are 2662 of 3982.

CRYSTAL DATA

The crystals of I are yellow monoclinic plates. Systematic absences are: hkl for $h+k$ odd, $h0l$ for l odd. The space group is either Cc (No. 9) or $C2/c$ (No. 15). Subsequent structure analyses showed the space group to be $C2/c$.

Table 1. Atomic coordinates in fractions of monoclinic cell edges for bromo(ethylenethiourea) phenyltellurium(II) with space group $C2/c$. Origin at a centre of symmetry. Isotropic thermal parameters (Å²) in the form $\exp-[8\pi^2U(\sin^2\theta/\lambda^2)]$. Standard deviations from least squares are given in parentheses.

	x	y	z	U
Te	0.069468(17)	0.19402(3)	0.406262(15)	
Br	−0.09558(3)	0.34897(5)	0.39148(3)	
S	0.21436(7)	0.04273(13)	0.42009(6)	
C(1)	−0.0182(2)	0.0057(4)	0.3697(2)	
C(2)	−0.0910(3)	0.0030(5)	0.2951(2)	
C(3)	−0.1513(3)	−0.1180(5)	0.2718(3)	
C(4)	−0.1379(3)	−0.2353(5)	0.3214(3)	
C(5)	−0.0654(3)	−0.2329(4)	0.3946(2)	
C(6)	−0.0065(3)	−0.1118(4)	0.4185(2)	
C(7)	0.2663(2)	−0.0064(4)	0.5157(2)	
C(8)	0.3767(4)	−0.1105(6)	0.6283(3)	
C(9)	0.2991(3)	−0.0374(6)	0.6450(3)	
N(1)	0.3428(2)	−0.0881(4)	0.5444(2)	
N(2)	0.2385(2)	0.0286(4)	0.5703(2)	
H(2)	−0.089(3)	0.094(4)	0.259(2)	0.053(11)
H(3)	−0.200(3)	−0.111(5)	0.228(3)	0.067(15)
H(4)	−0.177(3)	−0.312(5)	0.308(3)	0.069(15)
H(5)	−0.055(3)	−0.322(5)	0.431(3)	0.066(13)
H(6)	0.042(2)	−0.117(4)	0.473(2)	0.035(9)
H(8A)	0.436(3)	−0.067(5)	0.650(3)	0.077(17)
H(8B)	0.375(4)	−0.224(6)	0.635(3)	0.100(19)
H(9A)	0.262(3)	−0.099(6)	0.661(4)	0.087(18)
H(9B)	0.326(3)	0.049(6)	0.682(3)	0.080(16)
H(N1)	0.372(3)	−0.127(5)	0.516(2)	0.067(14)
H(N2)	0.189(3)	0.087(5)	0.556(3)	0.073(16)

The crystals of II are orange red monoclinic prisms extended along the a axis. Systematic absences are: $h0l$ for l odd, $0k0$ for k odd. The space group is $P2_1/c$ (No. 14).

The unit cell dimensions were determined by measuring, on the diffractometer, the θ-values (all about 20°) of 27 reflections for I and 29 reflections for II, by a method described by Maartmann-Moe.[6] The calculations were done by a least squares procedure. The standard deviation in the λ value is taken into account in the calculation of the standard deviation in the unit cell parameters. The unit cell dimensions for I are: $a=15.5394(11)$ Å, $b=9.0893(9)$ Å, $c=19.0269(18)$ Å, $\beta=114.774(6)°$, $Z=8$, $D_x=2.10$ g/cm³, $D_m=2.11$ g/cm³, $\mu_{(MoK\alpha)}=61.3$ cm⁻¹.

The unit cell dimensions for II are: $a=7.0513(6)$ Å, $b=12.7786(11)$ Å, $c=14.4676(12)$ Å, $\beta=102.309(7)°$, $Z=4$, $D_x=2.01$ g/cm³, $D_m=2.02$ g/cm³, $\mu_{(MoK\alpha)}=58.7$ cm⁻¹.

STRUCTURE DETERMINATION

The structures were solved by Pattersson and Fourier methods and refined to R-values of 0.028 for I and 0.033 for II. Altogether 171 parameters were refined in each structure.

The three-dimensional Fourier difference maps, based on the data of the final refinements, showed no peaks higher than 0.2 e/Å³ in either of the two structures.

Observed and calculated structure factors for the two structures are available from the author.

The atomic coordinates and thermal parameters are listed in Tables 1 – 4.

RESULTS

Bond lengths and angles in the two forms of bromo(ethylenethiourea)phenyltellurium(II), based on the atomic coordinates in Tables 1 and 2, are listed in Table 5. Views of the structures, as seen normal to the plane through the

Table 2. Atomic coordinates in fractions of monoclinic cell edges for bromo(ethylenethiourea)-phenyltellurium(II) with space group $P2_1/c$. Origin at a centre of symmetry. Isotropic thermal parameters (Å²) in the form $\exp-[8\pi^2U(\sin^2\theta/\lambda^2)]$. Standard deviations from least squares are given in parentheses.

	x	y	z	U
Te	0.20656(4)	0.38999(2)	0.46655(2)	
Br	0.27579(7)	0.48648(3)	0.65752(3)	
S	0.17234(19)	0.30383(10)	0.30692(8)	
C(1)	0.4235(6)	0.2785(3)	0.5247(3)	
C(2)	0.6161(7)	0.3003(4)	0.5272(3)	
C(3)	0.7555(7)	0.2269(5)	0.5635(4)	
C(4)	0.7032(10)	0.1320(5)	0.5974(4)	
C(5)	0.5163(11)	0.1110(5)	0.5950(5)	
C(6)	0.3718(9)	0.1840(4)	0.5580(5)	
C(7)	−0.0277(7)	0.2248(3)	0.3014(3)	
C(8)	−0.2307(9)	0.0832(5)	0.2628(5)	
C(9)	−0.3401(8)	0.1698(4)	0.3035(5)	
N(1)	−0.0420(7)	0.1299(3)	0.2650(3)	
N(2)	−0.1882(6)	0.2503(3)	0.3278(3)	
H(2)	0.635(7)	0.379(4)	0.500(3)	0.071(16)
H(3)	0.897(9)	0.235(5)	0.558(4)	0.094(19)
H(4)	0.805(10)	0.074(5)	0.622(5)	0.13(2)
H(5)	0.464(10)	0.035(5)	0.609(4)	0.12(2)
H(6)	0.239(8)	0.163(4)	0.555(4)	0.087(19)
H(8A)	−0.290(7)	0.055(4)	0.203(4)	0.068(17)
H(8B)	−0.221(7)	0.028(4)	0.300(3)	0.060(17)
H(9A)	−0.465(9)	0.193(5)	0.250(4)	0.10(2)
H(9B)	−0.376(8)	0.137(4)	0.363(4)	0.071(17)
H(N1)	0.063(8)	0.098(4)	0.241(4)	0.078(18)
H(N2)	−0.200(8)	0.323(4)	0.353(4)	0.080(17)

Table 3. Anisotropic thermal parameters (Å²) in the form $\exp-[2\pi^2(h^2a^{-2}U_{11}+\cdots+2hka^{-1}b^{-1}U_{12}+\cdots]$, for bromo(ethylenethiourea)phenyltellurium(II) with space group $C2/c$. The values for Te, Br, and S have been multiplied by 10^4 and the values for C and N by 10^3. Standard deviations in parentheses.

	U_{11}	U_{22}	U_{33}	U_{12}	U_{23}	U_{13}
Te	337.2(11)	356.1(13)	398.2(14)	−20.2(11)	−1.9(12)	140.5(10)
Br	409(2)	425(2)	546(3)	151.3(18)	4(2)	154(2)
S	370(5)	683(7)	441(5)	113(5)	−2(6)	192(5)
C(1)	32.1(18)	32.6(19)	33(2)	2.0(15)	−1.5(16)	13.4(16)
C(2)	44(2)	46(2)	34(2)	−6.3(19)	0.9(19)	12.5(19)
C(3)	46(2)	58(3)	39(3)	−8(2)	−2(2)	8(2)
C(4)	51(3)	44(3)	52(3)	−13(2)	−15(2)	27(2)
C(5)	52(2)	35(2)	43(2)	−0.4(18)	−1.2(18)	23(2)
C(6)	41(2)	36(2)	34(2)	4.2(17)	1.6(17)	14.0(18)
C(7)	31.6(19)	38(2)	45(2)	−1.2(16)	−3.3(18)	17.0(18)
C(8)	55(3)	59(3)	61(3)	16(3)	13(3)	24(3)
C(9)	48(3)	67(3)	51(3)	11(2)	8(3)	22(2)
N(1)	47(2)	69(3)	54(2)	21.9(19)	8(2)	25.9(19)
N(2)	44(2)	57(2)	49(2)	15.5(18)	6.8(19)	22.6(18)

Table 4. Anisotropic thermal parameters ($Å^2$) in the form $\exp-[2\pi^2(h^2a^{-2}U_{11}+\cdots+2hka^{-1}b^{-1}U_{12}+\cdots]$, for bromo(ethylenethiourea)phenyltellurium(II) with space group $P2_1/c$. The values for Te, Br, and S have been multiplied by 10^4 and the values for C and N by 10^3. Standard deviations in parentheses.

	U_{11}	U_{22}	U_{33}	U_{12}	U_{23}	U_{13}
Te	430.5(17)	364.3(15)	490.7(17)	−13.7(15)	26.8(14)	78.3(12)
Br	472(3)	371(2)	476(3)	34(2)	−1(2)	130(2)
S	504(7)	620(8)	493(7)	−100(7)	−62(6)	142(6)
C(1)	44(3)	35(2)	45(2)	2(2)	7.2(19)	7(2)
C(2)	47(3)	49(3)	57(3)	0(2)	3(2)	11(2)
C(3)	44(3)	77(4)	67(3)	14(3)	1(3)	16(3)
C(4)	73(4)	70(4)	74(4)	23(4)	19(3)	13(3)
C(5)	81(5)	70(4)	141(6)	8(4)	58(5)	26(4)
C(6)	54(3)	57(4)	120(5)	−2(3)	38(3)	22(4)
C(7)	44(3)	43(3)	40(2)	−1(2)	−2(2)	4(2)
C(8)	55(4)	49(3)	87(4)	−7(3)	−18(3)	21(3)
C(9)	51(3)	51(3)	83(4)	−11(3)	−21(3)	18(3)
N(1)	56(3)	43(2)	81(3)	2(2)	−21(2)	21(2)
N(2)	45(2)	46(2)	72(3)	−1(2)	−20(2)	24(2)

coordination group, are shown in Figs. 1 and 2. Stereoscopic views of the contents of the unit cells of the two forms are shown in Figs. 3 and 4.

In each of the structures, the tellurium atom is bonded to one phenyl carbon atom and, in directions nearly perpendicular to the Te–C bond, to one bromine atom and one ethylenethiourea sulfur atom. The coordination around the tellurium atom is nearly planar in both structures. The largest deviation from a least-squares plane through Te, Br, S, and C(1) is 0.015 Å in I and 0.031 Å in II. The least-squares plane through the coordination group passes 0.010 Å from C(4) in I and 0.016 Å from C(4) in II.

The three-centre system Br–Te–S is nearly linear in both structures. The Br–Te–S bond angle is 177.22(3)° in I and 175.96(3)° in II. A similar deviation from linearity is found in the structure of bromo(phenyl)thioureatellurium(II) where the Br–Te–S bond angle is 174.1°.[1]

The Te–C bond nearly bisects the angle of the three-centre system. The S–Te–C bond angle is 89.05(10)° in I and 89.45(12)° in II, and the Br–Te–C bond angle is 86.46(10)° in I and 87.02(11)° in II.

The Te–S bond length, 2.5560(15) Å in I and 2.5231(15) Å in II, are both longer than the sum of the single-bond radii, 2.41 Å,[7] and also longer than the Te–S bond length, 2.50 Å, found in the structure of chloro- and bromo-(phenyl)thioureatellurium(II).[1] The Te–Br bond length, 2.8348(10) Å in I and 2.9694(10) Å in II, are both shorter than the Te–Br bond length, 3.11 Å, found in the structure of bromo-(phenyl)thioureatellurium(II).[1] The Te–Br bond in I is about 0.135 Å shorter than the Te–Br bond in II, and the Te–S bond in I is about 0.033 Å longer than the Te–S bond in II. It is seen that the shortest Te–S bond has the longest Te–Br bond in *trans* position. However, the rather small difference between the Te–S bond lengths in I and II is not expected to have such a pronounced effect on the length of the *trans*-positioned Te–Br bond. It is therefore believed that differences in the crystal packing in the two different space groups are the main reason for the longer Te–Br bond in II than in I. The sum of the lengths of the *trans*-positioned Te–S and Te–Br bonds is 5.391 Å in I and 5.493 Å in II. The sum of the lengths of the *trans*-positioned Te–S and Te–Br bonds in bromo(phenyl)thioureatellurium(II) is 5.61 Å.[1] In the structure of *cis*-dibromodithioureatellurium(II) [8] where likewise bromine and thiourea are *trans*-positioned, the Te–S bond length is 2.47 Å and the Te–Br bond length is 3.05 Å, and the sum of the lengths of the *trans*-positioned Te–S and Te–Br bonds is 5.52 Å. The structures of two crystalline forms of di-μ-bromobis[diethylenethioureatellurium(II)] di-

Table 5. Bond lengths (Å) and angles (°) in bromo(ethylenethiourea)phenyltellurium(II) with space group $C2/c$, I, and with space group $P2_1/c$, II. A prime denotes an atom in the position $\bar{x}, 1-y, 1-z$, where x, y, z are the coordinates in Table 2. Standard deviations are given in parentheses.

	I	II		I	II
Te – S	2.5560(15)	2.5231(15)	S – Te – Br	177.22(3)	175.96(3)
Te – Br	2.8348(10)	2.9694(10)	S – Te – C(1)	89.05(10)	89.45(12)
Te – Br′		3.8313(10)	C(1) – Te – Br′		162.29(11)
Te – C(1)	2.116(3)	2.123(4)	Br – Te – C(1)	86.46(10)	87.02(11)
C(1) – C(2)	1.396(5)	1.380(7)	Te – C(1) – C(2)	119.0(3)	119.7(3)
C(1) – C(6)	1.377(5)	1.378(8)	Te – C(1) – C(6)	121.3(2)	120.2(3)
C(2) – C(3)	1.391(6)	1.379(7)	C(2) – C(1) – C(6)	119.6(3)	120.0(4)
C(3) – C(4)	1.380(7)	1.387(9)	C(1) – C(2) – C(3)	119.2(3)	119.3(4)
C(4) – C(5)	1.376(5)	1.348(10)	C(2) – C(3) – C(4)	120.3(3)	120.5(5)
C(5) – C(6)	1.381(5)	1.401(9)	C(3) – C(4) – C(5)	120.2(4)	120.1(5)
			C(4) – C(5) – C(6)	119.7(3)	120.6(6)
			C(1) – C(6) – C(5)	120.9(3)	119.5(5)
S – C(7)	1.712(4)	1.723(5)	Te – S – C(7)	104.60(15)	102.49(16)
C(7) – N(1)	1.311(5)	1.317(16)	S – C(7) – N(1)	122.1(3)	123.4(3)
C(7) – N(2)	1.319(7)	1.311(7)	S – C(7) – N(2)	127.6(3)	126.1(3)
N(1) – C(8)	1.471(7)	1.453(8)	N(1) – C(7) – N(2)	110.3(3)	110.4(4)
N(2) – C(9)	1.464(6)	1.473(7)	C(7) – N(1) – C(8)	112.4(4)	112.2(4)
C(8) – C(9)	1.523(9)	1.536(9)	C(7) – N(2) – C(9)	112.1(4)	112.7(4)
			N(1) – C(8) – C(9)	102.2(4)	103.2(4)
			N(2) – C(9) – C(8)	102.7(4)	101.3(4)
C(2) – H(2)	1.08(4)	1.06(5)	C(1) – C(2) – H(2)	114(2)	118(3)
C(3) – H(3)	0.86(4)	1.03(6)	C(3) – C(2) – H(2)	126(2)	123(3)
C(4) – H(4)	0.89(5)	1.04(6)	C(2) – C(3) – H(3)	117(3)	122(3)
C(5) – H(5)	1.03(5)	1.08(7)	C(4) – C(3) – H(3)	122(3)	117(3)
C(6) – H(6)	0.99(3)	0.97(6)	C(3) – C(4) – H(4)	121(3)	122(4)
			C(5) – C(4) – H(4)	119(3)	118(4)
			C(4) – C(5) – H(5)	120(2)	124(4)
			C(6) – C(5) – H(5)	120(2)	116(4)
			C(1) – C(6) – H(6)	125(2)	123(3)
			C(5) – C(6) – H(6)	115(2)	117(3)
C(8) – H(8A)	0.93(5)	0.95(5)	C(7) – N(1) – H(N1)	124(2)	122(3)
C(8) – H(8B)	1.04(6)	0.88(5)	C(8) – N(1) – H(N1)	124(2)	125(3)
C(9) – H(9A)	0.94(6)	1.08(6)	C(7) – N(2) – H(N2)	116(4)	119(3)
C(9) – H(9B)	1.03(5)	1.04(6)	C(9) – N(2) – H(N2)	123(4)	124(3)
N(1) – H(N1)	0.92(5)	0.97(6)	N(1) – C(8) – H(8A)	105(3)	114(3)
N(2) – H(N2)	0.88(5)	1.01(5)	N(1) – C(8) – H(8B)	105(3)	111(3)
			C(9) – C(8) – H(8A)	107(3)	117(3)
			C(9) – C(8) – H(8B)	111(4)	109(4)
			H(8A) – C(8) – H(8B)	116(4)	103(4)
			N(2) – C(9) – H(9A)	109(2)	115(3)
			N(2) – C(9) – H(9B)	105(3)	112(3)
			C(8) – C(9) – H(9A)	116(3)	109(3)
			C(8) – C(9) – H(9B)	111(3)	106(3)
			H(9A) – C(9) – H(9B)	111(5)	113(5)

bromide [9] have Te – S bond lengths of 2.495, 2.491, and 2.481 Å, and the bond lengths of the corresponding *trans*-positioned Te – Br bonds are 3.048, 3.015, and 3.079 Å. The sums of the bond lengths of *trans*-positioned Te – S and Te – Br bonds are 5.543, 5.506, and 5.560 Å. In the structure of centrosymmetric *trans*-dibromobis(ethylenethiourea)tellurium(II),[10] the Te – S bond length is 2.69 Å and the Te – Br bond length is 2.78 Å, and the sum of the Te – S and

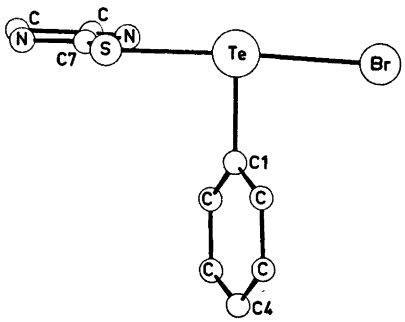

Fig. 1. Bromo(ethylenethiourea)phenyltellurium(II), with space group $C2/c$, as seen normal to the plane through the coordination group.

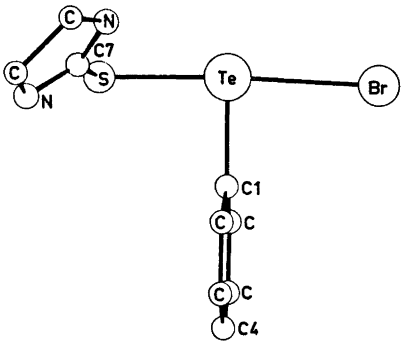

Fig. 2. Bromo(ethylenethiourea)phenyltellurium(II), with space group $P2_1/c$, as seen normal to the plane through the coordination group.

the Te – Br bond lengths is 5.47 Å. Thus, although in tellurium(II) complexes with ethylenethiourea in *trans* position to bromine the Te – S bonds are shorter and the Te – Br bonds are longer than the bonds in centrosymmetric complexes of divalent tellurium, the sum of the Te – S and the Te – Br bond lengths varies only slightly, relative to the sum in centrosymmetric complexes.

The Te – C bond lengths found in the present structures, 2.116(3) Å in I and 2.123(4) Å in II, are equal within the accuracies of the structure determinations. The same Te – C bond length has also been found in the crystal structures of chloro- and bromo(phenyl)thioureatellurium-(II),[1] phenylbis(thiourea)tellurium(II) chloride,[11] and in the phenyldithiocyanato- and phenyldiselenocyanatotellurate(II) anions,[5] indicating that the Te – C bond is nearly a single covalent bond.[5]

The *trans* bond-lengthening effect of the phenyl group is more pronounced than that of thiourea or ethylenethiourea. In the structure of II, as in phenylbis(thiourea)tellurium(II) chloride,[11] and in chloro- and bromo(phenyl)-thioureatellurium(II),[1] the fourth position of a square-planar coordination is virtually vacant. In II, a bromine atom of an adjacent molecule, at a position $\bar{x},1-y,1-z$, where x, y, z are the bromine coordinates in Table 2, lies 3.8313(10) Å from tellurium, in a direction which makes an angle of 162.29(11)° with the direction of the Te – C bond. In the structure of bromo(phenyl)-thioureatellurium(II),[1] a corresponding bromine atom of an adjacent molecule, over a symmetry centre, lies 3.77 Å from tellurium in a direction which makes an angle of 164° with the direction of the Te – C bond. These atoms, although at such a distance as to indicate only very weak bonding interaction with tellurium, approach the fourth coordination site of a square-planar structure. In the structure of I, as in the structures of tetramethylammonium phenyldithiocyanatotellurate(II) and tetramethylammonium phenyldiselenocyanatotellurate(II),[5] there is no

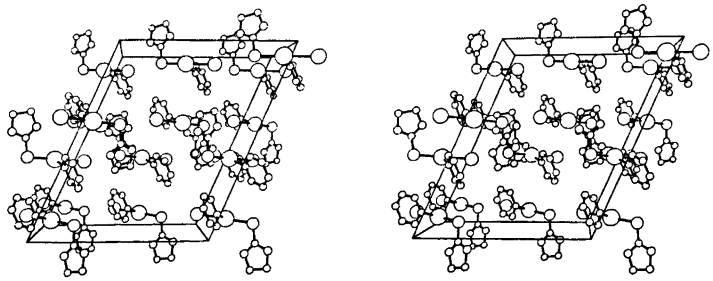

Fig. 3. A stereoscopic view of the cell packing in bromo(ethylenethiourea)phenyltellurium(II), with space group $C2/c$, as seen along the b crystal axis.

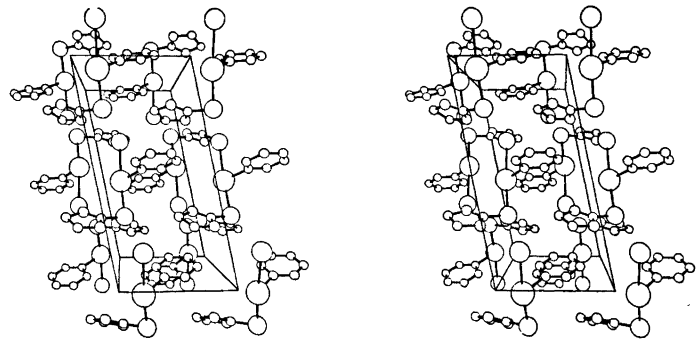

Fig. 4. A stereoscopic view of the cell packing in bromo(ethylenethiourea)phenyltellurium(II), with space group $P2_1/c$, as seen along the b crystal axis.

such approach of a weakly bonded fourth ligand.

The tellurium atom and the carbon atoms of the phenyltellurium group are nearly co-planar in both structures. The largest deviation from a least-squares plane is 0.025 Å in I and 0.015 Å in II. The angle between this plane and the least-squares plane through the coordination group is 64.6° in I and 87.0° in II.

The sulfur atom, the two nitrogen atoms, and the three carbon atoms of the ethylenethiourea group are nearly planar in both structures. The largest deviation from a least-squares plane is 0.036 Å in I and 0.055 Å in II. In the structure of I the plane of the ethylenethiourea group is nearly co-planar with the least-squares plane through Te, S, Br, and C(7). In II the angle between the two corresponding planes is 44.1°. The S – C bond length in the two structures are equal within the accuracies of the structure determinations, the average bond length is 1.718 Å. The Te – S – C bond angle is 104.60(15)° in I and 102.49(16)° in II.

HYDROGEN BONDING

In the structure of I the closest nitrogen-bromine approach occurs between N(1) and the bromine atom at $x+\frac{1}{2},y-\frac{1}{2},z$, where x, y, z are the bromine coordinates in Table 1. The N(1)···Br distance is 3.471(5) Å and the H(N1)···Br distance is 2.62(5) Å. The N(1) – H(N1)···Br angle is 154(2)°, the C(7) – N(1)···Br angle is 105.4(3)°, the C(8) – N(1)···Br angle is 142.0(3)°, the C(7) – N(1) – H(N1) angle is 124(2)°, and the C(8) – N(1) – H(N1) angle is 124(2)°. In the structure of II the closest nitrogen-bromine approach occurs between N(2) and the bromine atom at $\bar{x},1-y,1-z$, where x,y,z are the bromine coordinates in Table 2. The N(2)···Br distance is 3.434(4) Å, and the H(N2)···Br distance is 2.49(5) Å. The N(2) – H(N2)···Br angle is 156(3)°, the C(7) – N(2)···Br angle is 116.1(3)°, the C(9) – N(2)···Br angle is 124.6(3)°, the C(7) – N(2) – H(N2) angle is 119(3)°, and the C(9) – N(2) – H(N2) angle is 128(3)°. This probably represents N – H···Br hydrogen bonds in the two structures. The apparently stronger hydrogen bond in II than in I, as indicated by the shorter N···Br distance, may be one of the effects that cause the longer Te – Br bond in II than in I.

REFERENCES

1. Foss, O. and Husebye, S. *Acta Chem. Scand. 20* (1966) 132.
2. Foss, O. *Pure Appl. Chem. 24* (1970) 31.
3. Vikane, O. *Acta Chem. Scand. A 29* (1975) 150.
4. Åse, K. *Acta Chem. Scand. 25* (1971) 838.
5. Hauge, S. and Vikane, O. *Acta Chem. Scand. A 29* (1975) 755.
6. Maartman-Moe, K. *Siemens Review* XLI (1974) 54.
7. Pauling, L. *The Nature of the Chemical Bond*, 3rd. Ed., Cornell University Press, Ithaca 1960.
8. Foss, O., Johnsen, K., Maartmann-Moe, K. and Marøy, K. *Acta Chem. Scand. 20* (1966) 113.
9. Herland, P., Lundeland, M. and Marøy, K. *Acta Chem. Scand. 26* (1972) 2567.
10. Foss, O., Kjøge, H. M. and Marøy, K. *Acta Chem. Scand. 19* (1965) 2349.
11. Foss, O. and Marøy, K. *Acta Chem. Scand. 20* (1966) 123.

Received February 26, 1975.

Acta Chemica Scandinavica A 29 (1975) 745—748

Ionic Concentrations in Calcium Phosphate Solutions. II. The Solubility of Hydroxylapatite in Water or Salt Solutions at 37 °C

H. E. LUNDAGER MADSEN

Department of Inorganic Chemistry, Royal Veterinary and Agricultural University, Thorvaldsensvej 40, DK-1871 Copenhagen V, Denmark

A table of calcium and phosphate concentrations in solutions saturated with respect to hydroxylapatite [$Ca_5OH(PO_4)_3$] at 37 °C and at various concentrations of an indifferent salt has been computed; pH is the independent variable, with $5 \leq pH \leq 8$. Two different values of the solubility product have been used, one equal to ten times the other, the higher one corresponding to approach to equilibrium from supersaturation. An order-of-magnitude calculation of the surface Helmholtz function of hydroxylapatite has been carried out on the basis of the ratio between the solubility products and a typical value of crystal size, using the Gibbs-Kelvin equation.

The most important compound among the calcium phosphates is hydroxylapatite, $Ca_5OH(PO_4)_3$, mainly because it is the major inorganic constituent of hard tissue in higher animals. Its solubility has been the subject of numerous publications, yet reliable values of its solubility product at ordinary temperatures have not been obtained until recently. Unlike the first paper in this series,[1] the present one does not report new measurements; we shall use Bjerrum's results [2] in the calculations. In addition, we shall discuss some important factors affecting the solubility of hydroxylapatite.

THE SOLUBILITY PRODUCT OF HYDROXYLAPATITE

The process of dissolution of hydroxylapatite in an aqueous system is

$$Ca_5OH(PO_4)_3 \rightarrow 5Ca^{2+} + OH^- + 3PO_4^{3-}$$

and the solubility product is defined as

$$K_{sp} = a(Ca^{2+})^5 a(OH^-) a(PO_4^{3-})^3$$

which may also be written

$$pK_{sp} = 5pCa + pOH + 3pPO_4$$

where $pX = -\log a(X)$ (analogous to pH).

Bjerrum [2] used a different formulation, particularly suitable for salts of weak acids dissolved in acid solutions and originally applied to the solubility of $CaCO_3$.[3] He wrote the dissolution process

$$Ca_5OH(PO_4)_3 + 4H^+ \rightarrow 5Ca^{2+} + 3HPO_4^{2-} + H_2O$$

and determined the quantity

$$pK_{sp}' = 5pCa + 3pHPO_4 - 4pH$$

which is related to pK_{sp} as follows:

$$pK_{sp}' = pK_{sp} - 3pK_3 - pK_w$$

where K_3 is the third dissociation constant of phosphoric acid, and K_w is the dissociation constant of water. The advantage of using pK_{sp}' lies in the fact that it is obtained from the directly measured quantities $[Ca^{2+}]$, [P] (total phosphate contration), and pH with the aid of only one equilibrium constant, *viz.* pK_2 of phosphoric acid; pK_3 is not known with the same precision as pK_2.

Table 1 gives the values found by Bjerrum together with the results of more recent determinations.

Bjerrum's two values represent approach to equilibrium from super- and unsaturated solutions, respectively. The same two different values were invariably found even with an equilibration time of several weeks. The other

Table 1.

T, °C	pK_{sp}'	pK_{sp}	Ref.
37	6.5; 7.5	56.7; 57.7	2
25		54.6; 57.4	4
25		58.3; 60.0	5
37		59.1	6

values in the table correspond to the lower one of Bjerrum's values. Wier, Chien, and Black [5] used a column-elution technique, which may, perhaps, not allow for sufficient time for the establishment of equilibrium. Moreno, Gregory, and Brown [4] stated that the value obtained depended on the treatment of samples prior to the experiment.

We conclude that one value of the solubility product must be used when it is desired to calculate the amount of hydroxylapatite, which may precipitate from a given solution, and another value when dissolution is considered, and that there is a "dead zone" of concentrations at which neither precipitation nor dissolution occurs at a measurable rate. Of course, hydroxylapatite, like any other well-defined sparingly soluble salt, possesses one, and only one, thermodynamic solubility product at any given temperature, but at present we do not know the proper value at, say, 25 °C.

In all the above determinations, calcium-phosphate complexes in solution have been neglected. This does not, however, lead to erroneous results unless the values are used far outside the pH range in which they have been determined, approximately $5 \leq pH \leq 8$.

CALCULATIONS OF ION CONCENTRATIONS

The calcium and total phosphate concentrations as functions of pH in the range $5 \leq pH \leq 8$ were calculated from Bjerrum's values of pK_{sp}' and the value 7.182 for pK_{a2} of phosphoric acid at 37 °C.[7] The set of equations used is:
electroneutrality

$$2[Ca^{+2}] = [H_2PO_4^-] + 2[HPO_4^{2-}] \quad (1)$$

and equilibria

$$[HPO_4^{2-}]a(H^+)/[H_2PO_4^-] = K_{ac2} \quad (2)$$

$$[Ca^{2+}]^5[HPO_4^{2-}]^3/a(H^+)^4 = K_{csp}' \quad (3)$$

The solution for $[Ca^{2+}]$ is

$$[Ca^{2+}] = \left\{\tfrac{1}{8}\left[\frac{a(H^+)}{K_{ac2}} + 2\right]^3 a(H^+)^4 K_{csp}'\right\}^{1/8}$$

from which the other concentrations are easily found. $a(H^+)$ is defined as 10^{-pH}. K_{ac2} and K_{csp}' depend on the ionic strength I of the solution and are found by iteration. For activity coefficients, the Güntelberg [8] (or Guggenheim-Schindler [9]) formula has been used:

$$\log \gamma_i = Az_i^2 I^{\frac{1}{2}}/(1 + I^{\frac{1}{2}})$$

where z_i is the charge of ion species No. i in units of the electronic charge, and A is the constant of the Debye-Hückel equation.

The calculations were carried out on a Hewlett-Packard electronic calculator model 9100A with a model 9101 extended memory, both for solutions in pure water and for solutions containing an indifferent salt contributing to the ionic strength by an amount I_0. The results are given in Table 2 for $I_0 = 0$ and 0.15, respectively, the latter corresponding roughly to isotonic salt solution. Copies of tables for intermediate values of I_0 as well as a copy of the program may be obtained from the author on request.

DISCUSSION

It is evident from a comparison of the present data with those obtained earlier for brushite and tetracalcium monohydrogen phosphate [1] that hydroxylapatite is considerably less soluble than both other compounds throughout the whole pH range investigated. During precipitation of hydroxylapatite the quantity $5[P] - 3[Ca^{2+}]$ is constant, and the pH at saturation as well as the amount precipitated from a given supersaturated solution may be found by interpolation. The direct application of the table is limited to cases, where the condition (1) is fulfilled; however, as the fraction of total phosphate which occurs as HPO_4^{2-} is a function only of pH and I, the product $[Ca^{2+}]^5[P]^3$ also depends on these two parameters only. Hence one may determine whether a given solution is saturated, unsaturated, or supersaturated by calculating this product and comparing it with the value found from the tabulated data for the actual values of pH and I.

Table 2. Calcium and total phosphate concentrations in mmol/l.

I_0 =	0				0.15			
pK_{sp}' =	6.5		7.5		6.5		7.5	
pH	$[Ca^{2+}]$	[P]	$[Ca^{2+}]$	[P]	$[Ca^{+2}]$	[P]	$[Ca^{2+}]$	[P]
5.0	4.797	9.552	3.231	6.431	16.563	33.054	11.838	23.632
5.1	3.634	7.226	2.484	4.938	13.079	26.086	9.438	18.823
5.2	2.784	5.526	1.926	3.822	10.403	20.732	7.564	15.073
5.3	2.153	4.263	1.505	2.979	8.321	16.568	6.087	12.118
5.4	1.678	3.314	1.183	2.336	6.687	13.297	4.914	9.772
5.5	1.317	2.591	.936	1.840	5.393	10.709	3.979	7.900
5.6	1.040	2.037	.744	1.455	4.464	8.648	3.229	6.399
5.7	.826	1.608	.594	1.155	3.540	6.998	2.626	5.191
5.8	.659	1.275	.476	.920	2.878	5.673	2.139	4.216
5.9	.529	1.014	.383	.734	2.344	4.604	1.745	3.428
6.0	.426	.808	.310	.587	1.914	3.741	1.427	2.788
6.1	.345	.646	.252	.471	1.565	3.041	1.168	2.269
6.2	.281	.517	.205	.378	1.282	2.474	.957	1.848
6.3	.229	.415	.168	.304	1.052	2.013	.786	1.504
6.4	.189	.333	.139	.245	.865	1.638	.647	1.225
6.5	.156	.268	.115	.197	.714	1.333	.534	.988
6.6	.129	.216	.095	.160	.590	1.085	.442	.812
6.7	.108	.175	.080	.129	.489	.883	.366	.661
6.8	.091	.142	.067	.105	.407	.719	.305	.539
6.9	.077	.115	.057	.085	.340	.586	.254	.439
7.0	.065	.094	.048	.070	.285	.477	.213	.358
7.1	.056	.078	.041	.058	.240	.389	.180	.292
7.2	.048	.064	.036	.048	.203	.318	.152	.238
7.3	.041	.053	.031	.040	.173	.261	.129	.195
7.4	.036	.045	.027	.033	.148	.214	.111	.161
7.5	.031	.038	.023	.028	.127	.177	.095	.133
7.6	.027	.032	.020	.024	.109	.147	.082	.110
7.7	.024	.027	.018	.020	.095	.123	.071	.092
7.8	.021	.024	.016	.018	.083	.103	.062	.077
7.9	.019	.020	.014	.015	.072	.087	.054	.065
8.0	.016	.018	.012	.013	.063	.074	.047	.056

The difference in solubility resulting from the two values of pK_{sp}' is not so great as it appears at first sight. Consider for instance a solution with $I_0 = 0$, pH = 6.0 and $5pCa + 3pHPO_4 - 4pH = 6.5$. If hydroxylapatite is precipitated from this solution, until the latter quantity attains the value 7.5, then pH will be 5.86, and 1.59 μmol/l $Ca_5OH(PO_4)_3$ will have been precipitated. This amounts to only 1.87 % of the calcium and 0.57 % of the phosphate.

The most plausible explanation of the two different solubility products is that the two ways of approaching equilibrium produce crystals of different size. In an unsaturated solution the smallest crystals are dissolved first, and in this case the crystals will, in general, be larger than in the other case. X-Ray diffractometric investigations show [10] that the crystals obtained by direct precipitation at 37 °C are 500 – 1000 Å long and 100 – 200 Å thick. The solubility of a small crystal is found from the Gibbs-Kelvin equation for solids:

$$\Delta\mu = 2\gamma_j \overline{V}/h_j$$

where $\Delta\mu$ is the excess chemical potential, γ_j is the solid-liquid interfacial Helmholtz function of crystal face No. j, h_j is the perpendicular distance of this face from the center of gravity of the crystal, and $\overline{V}$ is the volume occupied by one formula unit in the crystal. Hydroxylapatite belongs to the hexagonal system, a = 9.432 Å, c = 6.881 Å, and $Z = 2$. The crystals are hexagonal prisms terminated by hexagonal pyramids. We have $\Delta\mu = kT \ln 10 = 9.85 \times 10^{-21}$ J/formula unit, and $\overline{V} = 2.65 \times 10^{-28}$ m³/formula unit; if we put $h_j = 100$ Å for the prismoidal faces, we find $\gamma_j = 0.186$ J/m². Though nothing but a rough estimate, this value is in excellent agreement with the relation between solubility and interfacial Helmholtz function found by

Nielsen and Söhnel [11] from nucleation data.

The persistent supersaturation in solutions in contact with solid hydroxylapatite is explained by assuming that the crystals grow by twodimensional nucleation, in which case there is no observable growth below a certain critical supersaturation. The spiral growth mechanism is ruled out for two reasons: 1° The presence of a screw dislocation in a crystal of the size in question will increase its energy and thereby its solubility to an extent at least as great as the surface effect. 2° Analyses by Wagner [12] and Kahlweit [13] show that if the growth rate is proportional to some power of the supersaturation (1 or 2 in this case), then the latter will decrease steadily with a limiting value of 0.

On the other hand, point defects – vacancies and substitutions – are very frequent in hydroxylapatite, and they cause an increase in solubility, too. Careful preparation and treatment of the samples used for solubility measurements are vital for obtaining a reliable solubility product; results from unspecified commercial products are of no value.

Acknowledgements. The author wishes to thank Professor A. Tovborg Jensen for his interest and valuable advice, and Dr. K. J. Pedersen for critically reading the manuscript.

REFERENCES

1. Madsen, H. E. L. *Acta Chem. Scand. 24* (1970) 1671.
2. Bjerrum, N. *Nordiska (19. skandinaviska) naturforskarmötet*, Helsingfors 1936, p. 344; *Selected Papers*, Copenhagen 1949, p. 245.
3. Bjerrum, N. and Gjaldbæk, J. K. *Kgl. Vet. Landbohøjsk. Årsskr.* (1919) p. 47.
4. Moreno, E. C., Gregory, T. M. and Brown, W. E. *J. Res. Nat. Bur. Stand. Sect. A 72* (1968) 773.
5. Wier, D. R., Chien, S. H. and Black, C. A. *Soil Sci. 111* (1971) 107.
6. Moreno, E. C., Kresak, M. and Zahradnik, R. T. *Nature (London) 247* (1974) 63.
7. Bates, R. G. and Acree, S. F. *J. Res. Nat. Bur. Stand. 30* (1943) 129.
8. Güntelberg, E. *Studier over Elektrolyt-Aktiviteter i vandige Opløsninger*, Copenhagen 1938.
9. Guggenheim, E. A. and Schindler, T. D. *J. Phys. Chem. 38* (1934) 539.
10. Christensson, F. and Jervøe, P., *Unpublished results.*
11. Nielsen, A. E. and Söhnel, O. *J. Crystal Growth 11* (1971) 233.
12. Wagner, C. *Z. Elektrochem. 65* (1961) 581.
13. Kahlweit, M. In Eyring, H., Henderson, C. and Jost, W., Eds., *Precipitation and Ageing, Physical Chemistry X*, New York 1970.

Received January 21, 1975

Acta Chemica Scandinavica A 29 (1975) 749—754

Chromatographic Separation and Optical Activity of Co(III) Complexes with Mixed Ethylenediamine—Trimethylenediamine Coordination Spheres

OLE BANG, ARNE ENGBERG, KJELD RASMUSSEN and FLEMMING WOLDBYE

Chemistry Department A, The Technical University of Denmark, Building 207, DK-2800 Lyngby, Denmark

A paper chromatographic method is developed for separation and purification of [Co en_2tn]$^{3+}$ and [Co en tn_2]$^{3+}$. Both complexes are resolved in the form of their bromides by means of nitro-$(+)_D$-camphor. The less soluble nitrocamphorates yield the $(+)_D$-bromides.

Absorption, circular dichroism and rotatory dispersion spectra are presented, and dipole and rotatory strengths compared to those of [Co en_3]$^{3+}$ and [Co tn_3]$^{3+}$.

It is concluded that the $(+)_D$ enantiomers of the mixed complexes have the same absolute configuration, Λ, as $(+)_D$-[Co en_3]$^{3+}$ and $(-)_D$-[Co tn_3]$^{3+}$.

The "first absorption band" ($450 < \lambda_{max} < 500$ nm) of tris(diamine) chelates of Co(III) and Cr(III), in which the central atom is a member of three identical five-membered rings exhibit rotatory strengths (in aqueous solution), which appear to be only slightly dependent upon the constitution of the diamine. The slight deviation from octahedral symmetry of a tris(diamine) Co(III) chromophore can be well approximated as D_3. Under this point group the $^1T_{1g}$ state is split into ^1E and $^1A_2$ states. The rotatory strength of the $^1A_1 \rightarrow {}^1E$ transition increases in the series 1,2-ethanediamine (en), 1,2-propanediamine (pn), 2.3-butanediamine (2,3-bn) and 2-methyl-1,2-propanediamine (i-bn.[1,2] The rotatory strength of the other component of the first band the $^1A_1 \rightarrow {}^1A_2$ transition, increases on substitution by optically active pn and 2,3-bn, but decreases on substitution by *meso*-2,3-bn and i-bn. An increase in net rotatory strength ($\sum R$) on substitution by an optically inactive diamine is accompanied by an increase in molar extinction so that the dissymmetry factor $g \equiv (\varepsilon_l - \varepsilon_d)/\varepsilon^*$ remains almost unchanged. The average extinction coefficient ε is defined as $\varepsilon^* = (\varepsilon_l + \varepsilon_d)/2$. Note that a substance circularly dichroic at wavelength λ does not obey Lambert's (or Beer's) law for light of wavelength λ polarized otherwise than circularly,[3] and that it is therefore theoretically meaningless to speak of its "extinction coefficient, ε, at λ". In practice, ε as measured without specification of the polarization state of the light is usually a satisfactory approximation[3] to ε^*.

This suggests that changes in degree of "forbiddenness" of the electronic transitions rather than changes in the relative steric disposition of their electric and magnetic dipole moments are responsible for the changes in rotary strengths.

An effect of a different nature could be expected when the diamines of the type mentioned above were replaced by a diamine, the chelation of which results in the formation of a six-membered ring, and this expectation caused us to undertake a study of tris(diamine) chelates involving 1,3-propanediamine ("trimethylenediamine", tn). The most conspicuous effect, a drastic reduction of the rotatory strengths occurring with a coordination sphere consisting of three trimethylenediamine molecules, has been reported earlier by one of us.[4] The present paper deals with our subsequent investigations of the tris(trimethylenediamine)

and the mixed en-tn Co(III) complexes. Among the results are the preparation and resolution of [Co en tn_2]$^{3+}$ and the resolution of [Co en_2tn]$^{3+}$, which are here reported for the first time. Part of our results were presented in a preliminary communication.[5]

After the completion of this work, the methods developed here were used in a study of the analogous Cr(III) complexes.[6]

EXPERIMENTAL

"Pure complexes". $(+)_D$-[Co en_3]$^{3+}$ and $(-)_D$-[Co tn_3]$^{3+}$ were obtained by standard methods, using *d*-tartaric acid and nitro-$(+)_D$- camphor as resolving agents.

"Mixed complexes". According to Bailar and Work [7] [Co en_2tn]Cl_3 may be prepared by the reaction of [Co en_2Cl_2]$^+$ with tn. As we have shown by the chromatographic procedure described below, the products thus prepared are generally contaminated by [Co en_3]$^{3+}$ and/or [Co en tn_2]$^{3+}$, and the mere analytical result corresponding stoichiometrically to the formula [Co en_2tn]$^{3+}$ is therefore no indication of purity. Salts of [Co en tn_2]$^{3+}$ are not easily obtained by an analogous procedure, and we have been able to obtain only rather impure preparations [8] by, *e.g.*, reacting [Co tn_2Cl_2]Cl or [Co tn_2CO_3]$^+$ with en at various acidities in water or dimethylsulfoxide as solvents. Again the impurities in the salts isolated are the different tris(diamine)chelates. In view of the kinetic inertness characteristic of all of these chelates once they are formed this tendency to "randomisation of the sphere of coordination" is a somewhat unexpected feature of the reactions described.

Chromatographic separation. Being unable, *e.g.* by repeated recrystallization and by fractional precipitation, to isolate pure preparations of either of the mixed complexes directly from the mixtures resulting from the above-mentioned substitution reactions, we resorted to develop a preparative chromatographic method capable of separating all of the four possible tris(diamine) complex ions. For the purpose of preparing [Co en tn_2]$^{3+}$ we have chosen to apply this method to the mixtures obtained from the oxidation of solutions of cobalt(II) chloride containing ethylenediamine and trimethylenediamine in amounts sufficient for the complete conversion of the cobalt to tris(diamine)complexes and in a ratio promoting the formation of the desired complex. Such reaction mixtures invariably contain all of the four possible tris(diamine)-complexes (in ratios partly depending upon the initial concentration ratio of en and tn), and when the oxidation is carried out in the presence of activated charcoal these account for almost all of the cobalt present. (In the absence of charcoal varying amounts of unidentified, probably polynuclear species are formed.)

Numerous publications deal with the separation of transition metal complexes by chromatographic methods. Suffice it to mention Jensen *et al.*,[9] Dwyer *et. al.*[10] and Druding and Hagel,[11] who describe separation of luteo complexes, among others, by column, paper and thin-layer chromatography. A paper chromatographic technique was chosen for the present work.

All experiments were carried out using 1 mm thick Whatman 3MM paper. Three techniques were employed: ascending chromatography on 10×140 mm^2 strips, and descending on 155×190 mm^2 and on 460×570 mm^2 sheets. The first-mentioned was used for the initial screening of eluent formulations, the second for further development of the more promising ones, and the third for chromatography on a preparative scale.

After a long series of experiments, the following eluent formation was found satisfactory: 1-butanol – acetone – "liquid phenol" (90 % phenol, 10 % water) – pyridine – benzene – water – 80 % acetic acid(14:14:30:14:14:4:7 by volume).

[Co en_2tn]$^{3+}$ was conveniently obtained as a by-product from the preparation of [Co en tn_2]$^{3+}$. However, for the purpose of isolating solely [Co en_2tn]$^{3+}$ we recommend the application of the chromatographic separation to the mixture obtained by the preparation of [Co en_2tn]Cl_3 according to Bailar and Work,[7] which contains [Co en_2tn]$^{3+}$ in a higher proportion (> *ca.* 60 % of the Co) than any of the mixtures obtainable directly from the oxidation.

Preparation of [*Co en* tn_2]$Cl_3.3\frac{1}{2}H_2O$ and [*Co* en_2*tn*]$Cl_3.3\frac{1}{2}H_2O$. To a solution of 8.0 g $CoCl_2.6H_2O$ (34mmol) in 35 ml 1 M HCl was added 6.0 ml (anhydrous) trimethylenediamine (70 mmol), 2.8 ml ethylenediamine monohydrate (34 mmol) and 1.0 g of activated charcoal (in that order). After oxidation for 17 h by a stream of air sufficiently vigorous to keep the charcoal suspended, the charcoal was removed by filtration and the filtrate condensed to 30 ml by evaporation in a stream of air at room temperature. The precipitate formed by the addition of 150 ml abs. ethanol was recovered by filtration and washed with ethanol. Yield after drying in the air 11.3 g (~80 %) based upon the reaction scheme $CoCl_2.6H_2O + enH_2O + 2\ tn + HCl + \frac{1}{4}O_2 \rightarrow$ [Co en tn_2].$3\frac{1}{2}H_2O + 4H_2O$ The mixture of tris(diamine) complex salts thus obtained was separated by descending paper chromatography as follows. The salt mixture was applied to sheets (460×570 mm^2) in straight lines along the shorter edge (2.5 g of salt to 16 sheets, or approximately 1 mmol per meter).

The chromatograms were developed in glass tanks (Shandon Panglass Chromatank 2192 Model 500 – 20 in., four sheets to a tank)

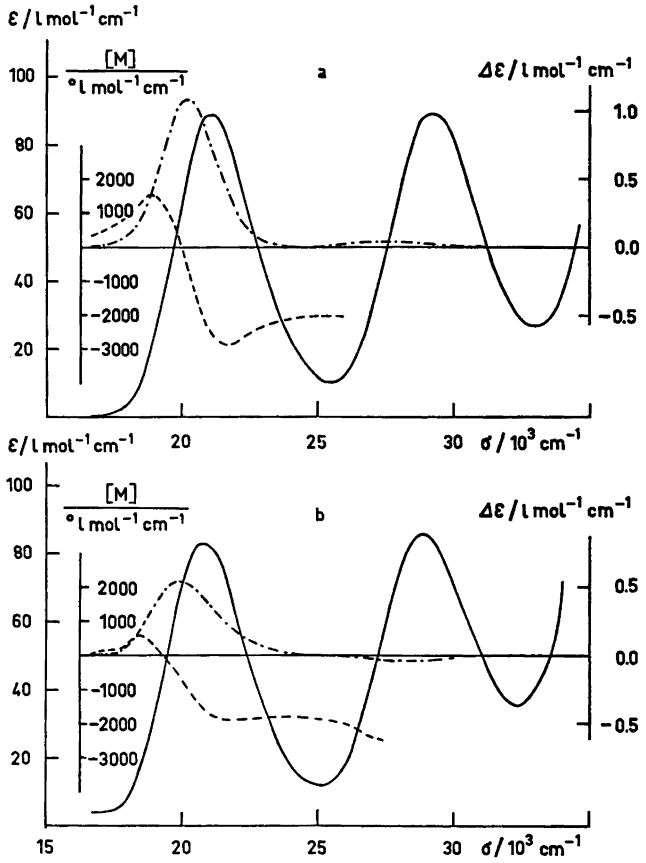

Fig. 1. Absorption (—), rotatory dispersion (---) and circular dichroism (—·—·) spectra of (a) (+)$_D$-[Co en$_2$tn]$^{3+}$ and (b) (+)$_D$-[Co en tn$_2$]$^{3+}$.

at 25 °C for *ca.* 150 h using the final eluent described above in a quantity of *ca.* 0.5 liter per sheet.

The chromatogram consisted of four well separated zones representing from top to bottom the ions [Co en$_3$]$^{3+}$, [Co en$_2$tn]$^{3+}$, [Co en tn$_2$]$^{3+}$, and [Co tn$_3$]$^{3+}$. The (16 times) two zones containing the desired complexes were cut out (cutting along the front of the [Co en tn$_2$]$^{3+}$ and [Co en$_2$tn]$^{3+}$ zones and the tail of the [Co en$_2$tn]$^{3+}$ zone, this zone being separated from the following zone of [Co en$_3$]$^{3+}$ by *ca.* 5 cm of white paper) and extracted each by four successive 200 ml portions of water. The four extracts of each complex were combined, evaporated to dryness in a stream of air at room temperature and the residue dissolved in the smallest possible volume of water (1—2 ml). 130 ml of ethanol: ether (75:25) were added and the chlorides precipitated by subsequent addition of 2.5 ml 4 M HCl. The precipitates were filtered off, rinsed with 96 % ethanol and dried in the air at room temperature. Yields and analyses: [Co en$_2$tn]Cl$_3$.3½H$_2$O 2.42 g (17 %): found C 19.85; H 6.63; N 19.97; Cl 25.38; Co 12.56; calc. C 19.89; H 6.20; N 19.89; Cl 25.16; Co 13.94. [Co en tn$_2$]Cl$_3$.3½H$_2$O 3.68 g (25 %): found C 21.56; H 7.04; N 19.42; Cl 24.22; Co 12.08; calc. C 22.00; H 6.47; N 19.24; Cl 24.36; Co 13.49.

Resolution. Isolation of (+)$_D$-[Co en$_2$tn]Br$_3$ and (+)$_D$-[Co en tn$_2$]Br$_3$.1½H$_2$O. 2.00 g of the complex chloride to be resolved (*ca.* 4.6 mmol) and 1.50 g sodium nitro-(+)$_D$-camphor (6.8 mmol) were dissolved in the smallest sufficient amounts of water at room temperature, and the solutions were mixed. When necessary, a little more water was added in order to obtain a clear solution. The solution was evaporated at room temperature under stirring. A stream of air was applied until the first crystals appeared. The crystallisation was fractionated so that the first fraction of the nitrocamphorate amounted to 1.00—1.20 g (*ca.* 1.3 mmol) after filtration and rinsing with chilled water. (Caution: The nitrocamphorate of [Co en tn$_2$]$^{3+}$

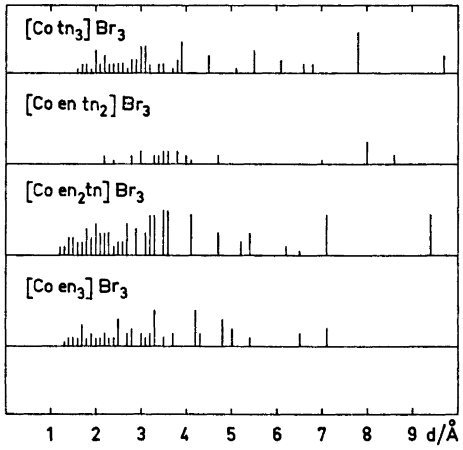

Fig. 2. X-Ray powder diagrams of the bromides. Heights indicate relative intensities.

is considerably more soluble in water than that of [Co en_2tn]$^{3+}$.) Further fractions may be obtained by the addition of 0.5 g sodium nitrocamphor so that the $(+)_D$-enantiomer may in both cases be almost quantitatively isolated.

The first fractions of the nitrocamphorates were converted to bromides. 1.15 g of the [Co en_2tn]$^{3+}$ salt was agitated with 1.5 ml 48 % HBr and 30 ml ethanol for 4 h, filtered, washed with ethanol and air-dried; yield 0.59 g (82 %). 1.00 g of the [Co en tn_2]$^{3+}$ salt was dissolved in 1.5 ml 48 % HBr, precipitated with 250 ml ethanol, centrifuged, washed with ethanol and air-dried; yield 0.53 g (84 %). Analyses: $(+)_D$-[Co en_2tn]Br_3; found C 17.13; H 5.37; N 17.00; Br 48.32; calc. C 17.06; H 5.32; N 17.05; Br 48.63. $(+)_D$-[Co en tn_2]$Br_3.1\frac{1}{2}H_2O$; found C 17.74; H 5.39; N 15.62; Br 44.85; calc. C 17.99; H 5.57, N 15.74; Br 44.90.

Microanalyses for C, H, N and halogens were made by Mr. Preben Hansen, Chemistry Department II, The H. C. Ørsted Institute, University of Copenhagen. Microanalyses for Co were carried out by atomic absorption.[13] Since the completion of our work, similar compounds have been resolved successfully on sephadex resins.[1,2]

Measurements

Absorption spectra were recorded at 25 °C by means of a Cary 14 spectrophotometer. The concentration of the solutions measured was 10^{-2} mol l^{-1} with respect to the complex bromides.

Circular dichroism was recorded at 25 °C by means of a Roussel-Jouan Dichrographe at concentrations of 10^{-2} mol l^{-1}.

Rotatory dispersion was measured with a Perkin-Elmer polarimeter model 141 and was also recorded by means of a Cary 11 spectrophotometer with ORD attachment[19]. All measurements were carried out at a concentration of 10^{-2} mol l^{-1} and at 25 °C.

Optical spectra of $(+)_D$-[Co en_2tn]$^{3+}$ and $(+)_D$-[Co en tn_2]$^{3+}$ are shown in Fig. 1. The data for the maxima of the first band are, with (σ,ε) and $(\sigma,\Delta\varepsilon)$ in ($10^3 cm^{-1}$, 1 $mol^{-1}cm^{-1}$): $(+)_D$-[Co en_2tn]$^{3+}$ ABS (21.10, 89), CD (20.20, 1.09); $(+)_D$-[Co en tn_2]$^{3+}$ ABS (20.79, 83), CD (19.92, 0.54).

^1H NMR spectra were recorded at 25 °C by means of a Varian A 60 spectrometer. Deuteration of the amino groups was accomplished by triple recrystallisation from D_2O (99.8 %). The solutions measured contained (20 ± 1) % of the complex chlorides in D_2O.

The spectra of the four possible tris(diamine)-chelates are individually characteristic so that the spectra of the mixed chelates cannot be reproduced by linear combinations of the pure en and tn complexes. In each of the three spectra of the mixed en-tn and the pure tn complexes the methylene protons give rise to two band systems, one attributable to protons at carbon atoms bonded to one nitrogen (low field), and one attributable to protons at C_2 in tn (high field). The ratios of the areas of these two band systems in each case correspond to the theoretical ratios (12:2, 12:4, and 12:6, respectively).

X-Ray powder photographs were taken using Co$K\alpha$ radiation and are shown in Fig. 2. Crystals of the racemic bromides were prepared by evaporation of a saturated solution at room temperature. The comminuted crystals were washed with ethanol and dried in air. Attempts at preparing large crystals of the active $(+)_D$-[Co en tn_2]-salt have not been successful. The powder diagrams confirm that the prepared compounds are pure, mixed complexes rather than mixtures of pure complexes.

Infrared and far infrared spectra have been reported elsewhere.[15] They also confirm the individuality of the compounds.

DISCUSSION

The absolute configurations of $(+)_D$-[Co en_3]$^{3+}$ and $(-)_D$-[Co tn_3]$^{3+}$ are known from X-ray work [16,17] to be identical and of the type designated Λ. The gradual change in CD observed in the sequence of complexes shown in the figure strongly suggests that $(+)_D$-[Co en_2tn]$^{3+}$ and $(+)_D$-[Co en tn_2]$^{3+}$ both possess same absolute configuration (Λ). This is in accordance with the "solubility criterion" when applied to the nitro-$(+)_D$-camphorates. After this work was carried out, $(+)_D$-[Co en_2tn]$^{3+}$

Table 1. Rotatory and dipole strengths of the first absorption band.

	$S \times 10^{38}$ esu	$S_{act} \times 10^{38}$ esu	$\sum R_{obs}$ Biot	$\chi \times 10^{21}$ esu‡		$\sum R_{calc}$ Biot		
				II	III	I	II	III
(+)$_D$-[Co en$_3$]$^{3+}$ *Λ*-configuration	13.75	4.00	4.68	1.36	0.73			
(+)$_D$-[Co en$_2$tn]$^{3+}$	14.30	4.55	3.17			3.02	3.11	3.07
(+)$_D$-[Co en tn$_2$]$^{3+}$	13.49	3.74	1.87			1.46	1.08	1.36
(−)$_D$-[Co tn$_3$]$^{3+}$ *Λ*-configuration	10.58	0.83	−0.31	−0.20	−0.05			

was found[18] to have the *Λ* configuration.

The lower symmetry of the mixed en-tn complexes as compared to the pure en and tn complexes is probably responsible for the fact that the mixed complexes exhibit relatively large dipole strengths within their "first" absorption band.

It has been suggested [8] that the rotatory strength of the "first" absorption band of a mixed tris(diamine) complex might be approximated by a sum of mutually independent contributions from the three chelate rings. Results of examining this hypothesis are presented in Table 1. The dipole and rotatory strengths S and $\sum R_{obs}$ are obtained in the usual way from the absorption spectra and the dichrograms. The rotatory strengths of the mixed complexes are calculated under three schemes. In column I, $\sum R_{calc}$ is obtained by simple linear interpolation between $\sum R_{obs}$ of the pure complexes. In column II a scheme [19] is used in which the suggestion by Moffitt [20] that only a part, S_{act}, of the observed dipole strength contributes to the optical activity, is combined with an attempt at taking into consideration the nonlinear variation of the dipole strength caused by the stepwise contribution of en and tn. In this scheme

$$S_{act} = S - S_{[Co(NH)_6]^{3+}} = S - 9.75 \times 10^{-38} \text{esu}$$

$$\sum R_{calc} = [(3-x)\chi_{en} + x\chi_{tn}]\sqrt{S_{act}/3}$$

$$\chi = \sum R_{obs}/3\sqrt{S_{act}/3}$$

In column III, the same scheme is used, substituting S for S_{act}, *i.e.* disregarding the suggestion due to Moffitt.

In contrast to what is found for the analogous Cr(III) complexes,[6] the results of the three calculation schemes differ appreciably, particularly for [Co en tn$_2$]$^{3+}$. Under all three schemes it is implicitly assumed that the conformation of a five- and of a six-membered chelate ring either has no influence on the rotatory strength or is unchanged through the series. The disagreement suggests that such assumptions may be invalid.

Acknowledgements. The authors wish to thank Dr. Gunner Borch for assistance in the measurements of circular dichroism, rotatory dispersion and absorption spectra, Mrs. Susanne Refn, Department of Organic Chemistry, The Technical University of Denmark, for assistance with the ^{1}H NMR spectra, and Mrs. Bente Saustrup Kristensen for X-ray powder diagrams. Professor K. Yamasaki is thanked for communicating results prior to publication.

REFERENCES

1. Kojima, M., Funaki, H., Yoshikawa, Y. and Yamasaki, K. *To be published.*
2. Kojima, M, Yoshikawa, Y. and Yamasaki, K. *Bull. Chem. Soc. Jap. 46* (1973) 1687.
3. Woldbye, F. and Bagger, S. *Acta Chem. Scand. 20* (1966) 1145.
4. Woldbye, F. *Proc. 7th ICCC*, Stockholm 1962, p. 41.
5. Bang, O., Engberg, A., Rasmussen, K. and Woldbye, F. *Proc. 3rd Symp. Coord. Chem. Vol. I*, Akadémiai Kiadó, Budapest 1970, p 63.
6. Rancke-Madsen, M. and Woldbye, F. *Acta Chem. Scand. 26* (1972) 3405.
7. Bailar, J. C., Jr. and Work, J. B. *J. Amer. Chem. Soc. 68* (1946) 232.
8. Woldbye, F. In Snatzke, G., Ed., *Optical Rotatory Dispersion and Circular Dichroism in Organic Chemistry*, Heyden, London 1967, p. 101.
9. Jensen, A., Bjerrum, J. and Woldbye, F. *Acta Chem. Scand. 12* (1958) 1202.
10. Dwyer, F. P., MacDermott, T. E. and Sargeson, A. M. *J. Amer. Chem. Soc. 85* (1963) 2913.

11 Druding, L. F. and Hagel, R. B. *Anal. Chem. 38* (1966) 478.
12. MacDermott, T. E. *Chem. Commun.* (1968) 223.
13. Engberg, A. *Anal. Chim. Acta 50* (1970) 531.
14. Woldbye, F. *Acta Chem. Scand. 13* (1959) 2137.
15. Rasmussen, K. *Spectrochim. Acta 30* (1974) 1763.
16. Nakatsu, K., Shiro, M., Saito, Y. and Kuroya, H. *Bull. Chem. Soc. Jap. 30* (1957) 158.
17. Nomura, T., Marumo, F. and Saito, Y. *Bull. Chem. Soc. Jap. 42* (1969) 1016.
18. Schousboe-Jensen, H. V. F. *Acta Chem. Scand. 26* (1972) 3413.
19. Woldbye, F. *Studier over Optisk Aktivitet*, Polyteknisk Forlag, Copenhagen 1969, p. 217 f.
20. Moffitt, W. *J. Chem. Phys. 25* (1956) 1189.

Received February 24, 1975.

Acta Chemica Scandinavica A 29 (1975) 755—762

The Crystal Structures of Tetramethylammonium Phenyldithiocyanatotellurate(II) and Tetramethylammonium Phenyldiselenocyanatotellurate(II)

SVERRE HAUGE and OLAV VIKANE

Department of Chemistry, University of Bergen, N-5014 Bergen-Univ., Norway

The crystal structures of tetramethylammonium phenyldithiocyanatotellurate(II), $[(CH_3)_4N][C_6H_5Te(SCN)_2]$, I, and tetramethylammonium phenyldiselenocyanatotellurate(II), $[(CH_3)_4N][C_6H_5Te(SeCN)_2]$, II, have been determined by three-dimensional X-ray diffraction methods. The crystals of the two compounds are isomorphous, monoclinic, with space group $C2/c$ (No. 15). There are eight formula units per unit cell, and the unit cell dimensions are: $a=15.747(6)$ Å, $b=9.219(3)$ Å, $c=23.153(8)$ Å, $\beta=100.58(5)°$ for I, and $a=15.840(4)$ Å, $b=9.341(2)$ Å, $c=23.384(4)$ Å, $\beta=100.67(2)°$ for II. Intensity data were collected by means of an automatic single-crystal diffractometer, using Nb-filtered Mo$K\alpha$ radiation. Least squares refinement, based on 3464 independent, non-zero reflections for I and 2425 for II, resulted in a conventional R value of 0.064 for I and 0.045 for II.

The structure of the phenyldithiocyanatotellurate(II) ion and the phenyldiselenocyanatotellurate(II) ion may be regarded as based on square-planar coordination with one position, *trans* to the phenyl group, vacant. Each tellurium atom is bonded to a phenyl carbon atom and, in directions approximately perpendicular to the Te–C bond, to two thiocyanate sulfur atoms in I and to two selenocyanate selenium atoms in II. The three-centre systems, S–Te–S and Se–Te–Se, are nearly linear. In the thiocyanato compound the bond lengths and angles involving tellurium are: Te–S(1) = 2.665(2) Å, Te–S(2) = 2.702(2) Å, Te–C(3) = 2.104(5) Å, ∠S(1)–Te–S(2) = 174.94(6)°, ∠S(1)–Te–C(3) = 89.34(17)°, and ∠S(2)–Te–C(3) = 87.35(17)°, In the selenocyanato compound the corresponding bond lengths and angles are: Te–Se(1) = 2.7636(11) Å, Te–Se(2) = 2.8233(12) Å, Te–C(3) = 2.100(6) Å, ∠Se(1)–Te–Se(2) = 175.40(3)°, ∠Se(1)–Te–C(3) = 89.5(2)°, ∠Se(2)–Te–C(3) = 87.9(2)°.

The tetramethylammonium ions are subjected to disorder or extreme thermal motions, with the central nitrogen in a fixed position.

Three-coordinated complexes of divalent tellurium have previously been studied by Foss and co-workers.[1,2] The crystal structures of phenylbis(thiourea)tellurium(II) chloride,[1] and of chloro- and bromo(phenyl)thioureatellurium-(II) [2] have been determined. The structures of these compounds can be regarded as based on square-planar coordination with one position, *trans* to the phenyl group, vacant.[1,2]

The present crystal structures of tetramethylammonium phenyldithiocyanatotellurate(II), I, and tetramethylammonium phenyldiselenocyanatotellurate(II), II, are the first structures of anionic complexes of divalent tellurium. They are three-coordinated, as are the compounds referred to above. The syntheses of the two compounds are described in a previous paper.[3]

EXPERIMENTAL

The X-ray data were collected with Nb-filtered Mo$K\alpha$ radiation ($\lambda_{\alpha_1}=0.70926$ Å), by use of a Siemens automatic, off-line, single-crystal diffractometer AED 1, operated as a three-circle instrument. For the thiocyanato compound, I, the measurements were performed on a crystal with the following dimensions, given as distances from the point of intersection of the crystal faces $(\bar{1}\bar{1}2)$, $(\bar{1}\bar{1}0)$, and $(\bar{1}00)$: to $(\bar{1}10)$, 0.128 mm; to (001), 0.073 mm; to $(00\bar{1})$, 0.067 mm; to (110), 0.330 mm. For the selenocyanato compound, II, the crystal used had the following dimensions, given as distances from the point of

Table 1. Atomic coordinates for tetramethylammonium phenyldithiocyanatotellurate(II), in fractions of monoclinic cell edges. Origin at a centre of symmetry. Isotropic thermal parameters ($Å^2$) in the form exp $-[8\pi^2U(\sin^2\theta/\lambda^2)]$. Standard deviations from least squares are given in parentheses.

	x	*y*	*z*	*U*
Te	0.14619(2)	0.16977(5)	0.45062(2)	
S(1)	0.15468(13)	−0.1142(2)	0.43041(9)	
S(2)	0.13147(15)	0.4605(3)	0.46097(10)	
C(1)	0.1579(4)	−0.0999(8)	0.3593(3)	
N(1)	0.1601(5)	−0.0899(8)	0.3110(3)	
C(2)	0.1327(5)	0.4917(9)	0.3934(5)	
N(2)	0.1323(6)	0.5106(9)	0.3431(4)	
C(3)	0.0167(4)	0.1692(7)	0.4069(3)	
C(4)	−0.0037(5)	0.1739(9)	0.3458(3)	
C(5)	−0.0882(6)	0.1717(9)	0.3176(4)	
C(6)	−0.1545(5)	0.1653(7)	0.3495(4)	
C(7)	−0.1344(5)	0.1624(9)	0.4100(4)	
C(8)	−0.0504(5)	0.1627(9)	0.4377(4)	
N(3)	0.3783(3)	0.1792(6)	0.3368(2)	0.0503(12)
C(9)	0.3763(7)	0.0750(15)	0.2864(6)	0.139 (4)
C(10)	0.3869(7)	0.0884(14)	0.3910(5)	0.122(4)
C(11)	0.2944(7)	0.2573(12)	0.3242(5)	0.106(3)
C(12)	0.4526(9)	0.2763(12)	0.3327(6)	0.143(4)
H(4)	0.032(4)	0.167(7)	0.322(3)	0.058(19)
H(5)	−0.109(5)	0.146(8)	0.280(4)	0.09(3)
H(6)	−0.219(7)	0.163(9)	0.341(4)	0.12(3)
H(7)	−0.185(6)	0.160(9)	0.430(4)	0.12(3)
H(8)	−0.030(6)	0.179(8)	0.481(4)	0.11(3)

Table 2. Atomic coordinates for tetramethylammonium phenyldiselenocyanatotellurate(II), in fractions of monoclinic cell edges. Origin at a centre of symmetry. Isotropic thermal parameters ($Å^2$) in the form exp $-[8\pi^2U(\sin^2\theta/\lambda^2)]$. Standard deviations from least squares are given in parentheses. Of the disordered carbon atoms of the tetramethylammonium ion, C(9) to C(12) are assigned an occupancy factor of 0.6, and C(9′) to C(12′) are assigned an occupancy factor of 0.4.

	x	*y*	*z*	*U*
Te	0.14761(3)	0.16531(6)	0.44920(2)	
Se(1)	0.15855(6)	−0.12681(10)	0.43357(4)	
Se(2)	0.13252(7)	0.46574(11)	0.45537(5)	
C(1)	0.1577(6)	−0.1129(9)	0.3593(4)	
N(1)	0.1570(6)	−0.1025(9)	0.3106(4)	
C(2)	0.1357(6)	0.4829(11)	0.3856(7)	
N(2)	0.1398(8)	0.4902(12)	0.3349(5)	
C(3)	0.0194(4)	0.1603(8)	0.4052(3)	
C(4)	0.0010(5)	0.1683(11)	0.3454(3)	
C(5)	−0.0858(7)	0.1637(12)	0.3170(4)	
C(6)	−0.1513(6)	0.1574(11)	0.3486(4)	
C(7)	−0.1318(5)	0.1533(12)	0.4068(4)	
C(8)	−0.0462(5)	0.1552(11)	0.4352(4)	
N(3)	0.3782(4)	0.1713(7)	0.3392(3)	0.0566(15)
C(9)	0.3811(14)	0.072(2)	0.2923(9)	0.146(8)
C(10)	0.3873(11)	0.097(2)	0.3952(7)	0.097(5)
C(11)	0.2946(11)	0.2486(19)	0.3259(7)	0.089(5)
C(12)	0.4518(14)	0.272(2)	0.3382(9)	0.137(7)
C(9′)	0.381(2)	0.019(3)	0.3634(14)	0.131(11)
C(10′)	0.3977(18)	0.247(3)	0.3947(12)	0.118(9)
C11′)	0.2931(15)	0.182(3)	0.3016(10)	0.080(7)
C(12′)	0.4513(13)	0.204(2)	0.3035(9)	0.067(6)

Table 3. Anisotropic thermal parameters (Å²) for the phenyldithiocyanatotellurate(II) ion, in the form of exp $-[2\pi^2(h^2a^{-2}U_{11}+\cdots+2hka^{-1}b^{-1}U_{12}+\cdots)]$. All values have been multiplied by 10^3. Standard deviation are given in parentheses.

	U_{11}	U_{22}	U_{33}	U_{12}	U_{23}	U_{13}
Te	45.2(2)	69.9(3)	47.3(2)	−1.0(2)	−5.2(2)	6.7(2)
S(1)	75.5(11)	66.4(13)	63.0(10)	7.9(10)	20.0(9)	15.5(9)
S(2)	87.5(14)	76.0(16)	80.7(15)	0.9(12)	−15.0(11)	3.6(11)
C(1)	48(3)	61(5)	70(5)	−2(3)	−9(4)	13(3)
N(1)	102(5)	89(5)	73(4)	1(4)	−15(4)	27(4)
C(2)	59(4)	61(5)	123(8)	1(4)	17(5)	16(5)
N(2)	131(7)	115(7)	115(7)	−2(6)	31(6)	6(6)
C(3)	46(3)	48(4)	48(3)	0(3)	−2(3)	10(2)
C(4)	58(4)	87(6)	53(4)	6(4)	−1(4)	10(3)
C(5)	79(5)	100(7)	62(5)	9(5)	−12(5)	−15(4)
C(6)	52(4)	83(6)	103(7)	5(4)	6(5)	−5(4)
C(7)	48(4)	94(6)	92(6)	8(4)	16(5)	15(4)
C(8)	60(6)	94(6)	64(4)	1(4)	6(5)	24(4)

intersection of the crystal faces (001), ($\bar{1}$01), and (11$\bar{1}$): to (100), 0.113 mm; to ($\bar{1}$00), 0.016 mm; to (10$\bar{1}$), 0.151 mm; to (00$\bar{1}$), 0.141 mm; to (0$\bar{1}$0), 0.244 mm. In each case the crystal was mounted with the *b* axis approximately along the ψ axis of the diffractometer. Intensity data were collected using a "five value" measuring procedure, as described by Åse.[4] Six reference reflections were measured at intervals of 50 reflections. The net intensities were later brought to a common scale by using the intensity variations of the reference reflections.[4] The scale factors varied from 1.00 to 1.08 for I, and from 1.00 to 1.06 for II. The lower limit for observed reflections was set equal to three times the standard deviation in net intensity. The standard deviation was taken as $(I_t+I_b)^{\frac{1}{2}}$, where I_t is the total intensity, and I_b is the background intensity.[4] 3464 of 4983 independent reflections within $\theta=30°$ were found to be stronger than the lower limit for I. The corresponding numbers for II were 2425 of 5135.

The data were corrected for Lorentz and polarization effects according to standard procedures, and for absorption,[5] and secondary extinction.[6]

Least squares refinements were carried out with a full-matrix program which minimizes the function $r=(\sum W(|F_o|-K|F_c|)^2$ where K is a scale factor, and the weight, W, is the inverse of the variance in F_o. The variance in F_o was taken to be

$$\sigma^2(F_o)=F_o^2[I_t+I_b+k^2(I_t-I_b)^2]/4(I_t-I_b)^2$$

where k may be interpreted as the relative standard deviation in the scaling curve. Non-observed reflections for which $K|F_c|$ is greater

Table 4. Anisotropic thermal parameters (Å²) for the phenyldiselenocyanatotellurate(II) ion, in the form of exp $-[2\pi^2(h^2a^{-2}U_{11}+\cdots+2hka^{-1}b^{-1}U_{12}+\cdots)]$. All values have been multiplied by 10^3. Standard deviations are given in parentheses.

	U_{11}	U_{22}	U_{33}	U_{12}	U_{23}	U_{13}
Te	48.5(3)	69.5(4)	58.1(3)	0.8(3)	−6.0(3)	4.8(2)
Se(1)	82.8(7)	58.8(6)	70.3(6)	8.5(5)	2.2(5)	16.0(5)
Se(2)	91.7(8)	61.4(8)	109.4(9)	4.9(6)	−16.5(6)	−14.2(7)
C(1)	75(6)	66(6)	76(6)	−4(5)	−14(5)	26(5)
N(1)	110(7)	101(7)	109(6)	2(5)	−22(6)	29(6)
C(2)	52(6)	52(6)	127(10)	−6(5)	6(9)	21(9)
N(2)	129(9)	123(9)	140(11)	6(7)	15(8)	49(9)
C(3)	49(4)	56(5)	48(4)	2(4)	0(4)	6(3)
C(4)	54(5)	112(8)	59(5)	−5(6)	−6(5)	−1(4)
C(5)	92(7)	132(10)	66(6)	−6(8)	−12(7)	−17(5)
C(6)	55(5)	109(8)	95(7)	4(6)	8(7)	2(5)
C(7)	57(6)	141(10)	90(7)	1(7)	21(7)	16(5)
C(8)	49(5)	116(8)	65(5)	6(6)	0(6)	14(4)

Table 5. Bond lengths (Å) and angles (°) in tetramethylammonium phenyldithiocyanatotellurate(II). Standard deviations are given in parentheses.

Te – S(1)	2.665(2)	S(1) – Te – S(2)	174.94(6)
Te – S(2)	2.702(2)	S(1) – Te – C(3)	89.34(17)
Te – C(3)	2.104(5)	S(2) – Te – C(3)	87.35(17)
S(1) – C(1)	1.663(8)	Te – S(1) – C(1)	96.2(3)
S(2) – C(2)	1.594(11)	Te – S(2) – C(2)	94.3(3)
C(1) – N(1)	1.128(11)	S(1) – C(1) – N(1)	179.8(6)
C(2) – N(2)	1.179(14)	S(2) – C(2) – N(2)	177.8(7)
C(3) – C(4)	1.393(9)	Te – C(3) – C(4)	120.7(4)
C(4) – C(5)	1.370(11)	Te – C(3) – C(8)	121.2(4)
C(5) – C(6)	1.386(14)	C(3) – C(4) – C(5)	120.5(6)
C(6) – C(7)	1.380(13)	C(4) – C(5) – C(6)	120.4(7)
C(7) – C(8)	1.361(10)	C(5) – C(6) – C(7)	119.2(7)
C(8) – C(3)	1.379(10)	C(6) – C(7) – C(8)	120.0(7)
		C(7) – C(8) – C(3)	121.8(7)
		C(8) – C(3) – C(4)	119.0(5)
N(3) – C(9)	1.506(14)	C(9) – N(3) – C(10)	106.2(12)
N(3) – C(10)	1.495(13)	C(9) – N(3) – C(11)	105.4(11)
N(3) – C(11)	1.486(12)	C(9) – N(3) – C(12)	103.8(14)
N(3) – C(12)	1.488(15)	C(10) – N(3) – C(11)	112.1(12)
		C(10) – N(3) – C(12)	115.9(15)
		C(11) – N(3) – C(12)	112.2(13)
C(4) – H(4)	0.86(7)	C(3) – C(4) – H(4)	126(4)
C(5) – H(5)	0.91(8)	C(5) – C(4) – H(4)	122(4)
C(6) – H(6)	1.00(9)	C(4) – C(5) – H(5)	117(5)
C(7) – H(7)	1.00(9)	C(6) – C(5) – H(5)	119(6)
C(8) – H(8)	1.01(9)	C(5) – C(6) – H(6)	117(5)
		C(7) – C(6) – H(6)	123(6)
		C(6) – C(7) – H(7)	115(5)
		C(8) – C(7) – H(7)	124(5)
		C(7) – C(8) – H(8)	123(5)
		C(3) – C(8) – H(8)	118(5)

than the measurement limit were included in the refinement, with $|F_o|$ equal to the limit.

The calculated structure factors were based on the scattering curve of Stewart *et al.*[7] for hydrogen, and the curves listed in *International Tables* (Ref. 8, Table 3.3.1 A and B) for all other atoms. Using the $\Delta f'$ and $\Delta f''$ values given in *International Tables* (Ref. 8, Table 3.3.2 A), the tellurium, selenium, and sulfur scattering curves were corrected for anomalous dispersion by taking the amplitude of f as the corrected value.[4]

The calculations were carried out on a UNIVAC 1110 computer. The programs used in the calculations are described elsewhere.[4] The drawings were made by use of ORTEP.[9]

CRYSTAL DATA

The crystals of I and II are orange red, isomorphous, monoclinic prisms and plates. Systematic absences are: hkl for $h+k$ odd, $h0l$ for l odd. The space group is either Cc (No. 9) or $C2/c$ (No. 15). Subsequent structure analyses showed the space group to be $C2/c$.

The unit cell dimensions, as refined by least squares from diffractometer-measured θ-values (all about 20°) of 18 reflections for I, and 20 reflections for II, are: $[(CH_3)_4N][C_6H_5Te(SCN)_2]$, I, $a = 15.747(6)$ Å, $b = 9.219(3)$ Å, $c = 23.153(8)$ Å, $\beta = 100.58(5)°$, $Z = 8$, $D_x = 1.59$ g/cm³, $D_m = 1.58$ g/cm³, $\mu_{MoK\alpha} = 21.0$ cm⁻¹. $[(CH_3)_4N][C_6H_5Te(SeCN)_2]$, II, $a = 15.840(4)$ Å, $b = 9.341(2)$ Å, $c = 23.384(4)$ Å, $\beta = 100.67(2)°$, $Z = 8$, $D_x = 1.87$ g/cm³, $D_m = 1.86$ g/cm³, $\mu_{MoK\alpha} = 64.1$ cm⁻¹.

STRUCTURE DETERMINATION

The structures were solved by Patterson and Fourier methods, and refined by full-matrix least squares. The Fourier maps of I and II show only one distinct peak from the tetramethylammonium cation. This peak was later shown to be at the position of the nitrogen atom. The maps of II show eight small peaks in the neighbourhood of the position of the nitro-

Table 6. Bond lengths (Å) and angles (°) in tetramethylammonium phenylidselenocyanatotellurate(II). Standard deviations are given in parentheses. Of the disordered carbon atoms of the tetramethylammonium ion, C(9) to C(12) are assigned an occupancy factor of 0.6, and C(9′) to C(12′) are assigned an occupancy factor of 0.4.

Te – Se(1)	2.7636(11)	Se(1) – Te – Se(2)	175.40(3)
Te – Se(2)	2.8233(12)	Se(1) – Te – C(3)	89.5(2)
Te – C(3)	2.100(6)	Se(2) – Te – C(3)	87.9(2)
Se(1) – C(1)	1.735(9)	Te – Se(1) – C(1)	93.9(3)
Se(2) – C(2)	1.749(16)	Te – Se(2) – C(2)	91.7(4)
C(1) – N(1)	1.139(13)	Se(1) – C(1) – N(1)	179.5(7)
C(2) – N(2)	1.181(19)	Se(2) – C(2) – N(2)	177.3(9)
C(3) – C(4)	1.377(10)	Te – C(3) – C(4)	120.0(5)
C(4) – C(5)	1.412(12)	Te – C(3) – C(8)	120.7(4)
C(5) – C(6)	1.387(15)	C(3) – C(4) – C(5)	118.7(7)
C(6) – C(7)	1.351(12)	C(4) – C(5) – C(6)	120.7(7)
C(7) – C(8)	1.396(11)	C(5) – C(6) – C(7)	119.8(8)
C(8) – C(3)	1.365(12)	C(6) – C(7) – C(8)	120.1(8)
		C(7) – C(8) – C(3)	121.0(7)
		C(8) – C(3) – C(4)	120.2(6)
N(3) – C(9)	1.44(2)	C(9) – N(3) – C(10)	111.3(12)
N(3) – C(10)	1.465(19)	C(9) – N(3) – C(11)	107.8(11)
N(3) – C(11)	1.488(18)	C(9) – N(3) – C(12)	104.9(13)
N(3) – C(12)	1.50(2)	C(10) – N(3) – C(11)	110.7(11)
		C(10) – N(3) – C(12)	111.2(11)
		C(11) – N(3) – C(12)	110.8(11)
N(3) – C(9′)	1.53(3)	C(9′) – N(3) – C(10′)	107.9(17)
N(3) – C(10)′	1.48(3)	C(9′) – N(3) – C(11′)	104.1(15)
N(3) – C(11′)	1.47(2)	C(9′) – N(3) – C(12′)	113.5(15)
N(3) – C(12′)	1.51(3)	C(10′) – N(3) – C(11′)	115.2(15)
		C(10′) – N(3) – C(12′)	108.8(14)
		C(11′) – N(3) – C(12′)	110.7(12)

gen atom. Four of these positions were given an occupancy factor 0.6, and the other four an occupancy factor of 0.4. Later refinement of the occupancy factors did not change these values. The Fourier maps of I also show disorder in the positions of the carbon atoms of the tetramethylammonium ion, but not more than four positions for carbon atoms could be picked out with any certainty. These carbon atoms were given unity occupancy factors.

A three-dimensional Fourier difference map, based on all the non-hydrogen atoms, indicated the positions of the phenyl hydrogen atoms in each structure. For I, refinement including the five phenyl hydrogen atoms resulted in reasonable C – H bond lengths and angles. For II, however, refinement including the five phenyl hydrogen atoms did not succeed.

The final refinement converged at an R-value of 0.064 for I, and 0.045 for II. The final Fourier difference maps showed no peaks higher than 0.46 e/Å^3 for I, and 0.34 e/Å^3 for II. The peaks of highest electron density were located in the neighbourhood of the positions of the disordered methyl carbon atoms of the tetramethylammonium ion.

Observed and calculated structure factors are available from the authors.

The final atomic coordinates and thermal parameters are listed in Tables 1 – 4.

THE PHENYLDITHIOCYANATO- AND PHENYLDISELENOCYANATOTELLURATE(II) IONS

Bond lengths and angles in the phenyldithiocyanatotellurate(II) and phenyldiselenocyanatotellurate(II) ions, based on the atomic coordinates in Tables 1 and 2, are listed in Tables 5 and 6. The uncertainties in the cell dimensions are taken into account in the given standard deviations. Views of the structures, as seen normal to the plane through the coordination group, are reproduced in Figs. 1 and 2. A stereoscopic view of the content of the unit cell of the two compounds is shown in Figs. 3 and 4.

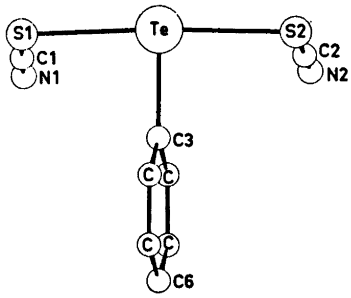

Fig. 1. The phenyldithiocyanatotellurate(II) ion, as seen normal to the plane through the coordination group.

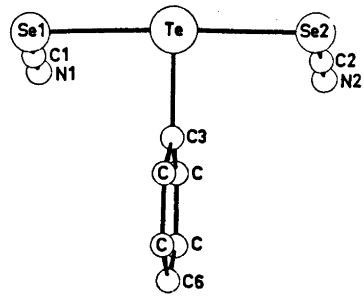

Fig. 2. The phenyldiselenocyanatotellurate(II) ion, as seen normal to the plane through the coordination group.

In the two compounds, each tellurium atom is bonded to a phenyl carbon atom and, in directions approximately perpendicular to the Te – C bond, to two thiocyanate sulfur atoms or to two selenocyanate selenium atoms. The coordination around the tellurium atom is nearly planar in both compounds; the largest deviation from a least-squares plane through Te, S(1), S(2), and C(3) in I is 0.050 Å, and from a least-squares plane through Te, Se(1), Se(2), and C(3) in II, 0.056 Å. These least-squares planes pass 0.036 Å from C(6) in I and 0.030 Å from C(6) in II.

The three-centre systems, S – Te – S and Se – Te – Se, are nearly linear. The S – Te – S bond angle is 174.94(6)° and the Se – Te – Se bond angle is 175.40(3)°. A similar deviation from linearity is found in the crystal structure of phenylbis(thiourea)tellurium(II) chloride where the S – Te – S bond angle is 172.0(4)°.[1]

The Te – C bond nearly bisects the angle of the three-centre system. In I the S – Te – C angles are 89.34(17) and 87.35(17)°, and in II the Se – Te – C angles are 89.5(2) and 87.9(2)°.

In I the S – Te – S bonding system is slightly asymmetric, with Te – S bond lengths of 2.665(2) and 2.702(2) Å. The mean value of the two Te – S bond lengths is 2.684 Å, which is, within the error, equal to the mean Te – S bond length found in the crystals of phenylbis(thiourea)-tellurium(II) chloride,[1] and in the crystals of centrosymmetric square-planar complexes of divalent tellurium.[10] In II the Se – Te – Se bonding system is a little more asymmetric than the S – Te – S bonding system in I. The Te – Se bond lengths are 2.7636(11) and 2.8233(12) Å, and the mean value is 2.794 Å, which is about 0.02 Å shorter than the average Te – Se bond length, 2.816 Å, found in the crystals of centrosymmetric square-planar complexes of divalent tellurium.[11–13]

The Te – C bond lengths found in the two structures, 2.104(5) Å in I and 2.100(6) Å in II, are equal within the accuracy of the structure determinations. They are equal to the Te – C(sp^2) single covalent bond length, 2.107 Å,

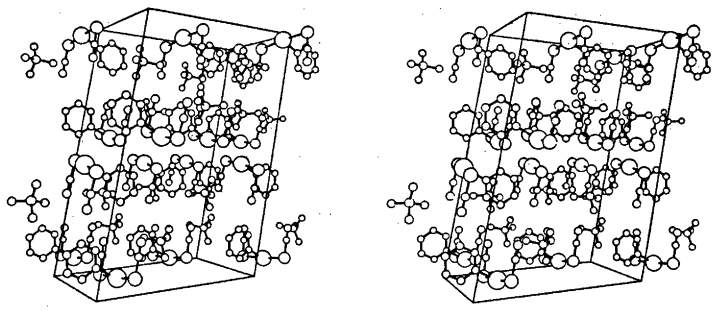

Fig. 3. A stereoscopic view of the cell packing in tetramethylammonium phenyldithiocyanato-tellurate(II), as seen along the *b* crystal axis.

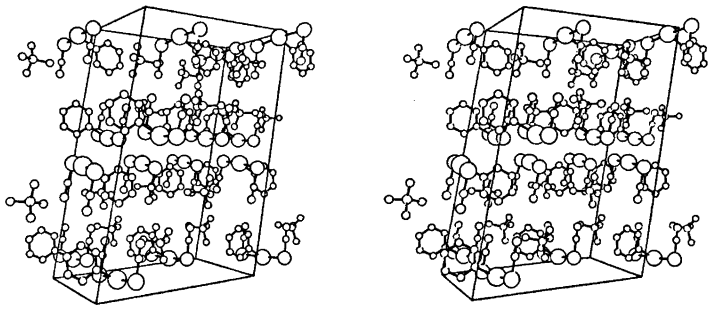

Fig. 4. A stereoscopic view of the cell packing in tetramethylammonium phenyldiselenocyanatotellurate(II), as seen along the *b* crystal axis.

which is the sum of the covalent radii of tellurium, 1.37 Å,[14] and of sp^2-hybridized carbon, 0.737 Å.[15] The same Te–C bond length has also been found in the crystals of phenylbis(thiourea)tellurium(II) chloride,[1] chloro- and bromo(phenyl)thioureatellurium(II),[2] and *o*-formylphenyltellurenyl bromide.[16]

The two thiocyanate groups in I and the two selenocyanate groups in II are linear within the accuracy of the structure determinations. The two S–C bond lengths in I are 1.663(8) and 1.594(11) Å, and the Te–S–C angles are 96.2(3) and 94.3(3)°. The two Se–C bond lengths in II are 1.735(9) and 1.794(16) Å, and the Te–Se–C angles are 93.9(3) and 91.7(4)°. The C–N bond lengths in the two thiocyanate groups in I and the two selenocyanate groups in II are equal within the error. The mean value of the four C–N bond lengths is 1.155 Å. The two thiocyanate groups in I are approximately co-planar, and so are the two selenocyanate groups in II. A least-squares plane through the two groups passes 0.021 Å from tellurium in I and 0.017 Å from tellurium in II. In each compound the plane makes an angle of 73.6° with the least-squares plane through the coordination group.

The tellurium atom and the carbon atoms of the phenyltellurium group are nearly co-planar in both structures, the largest deviation from a least-squares plane being 0.01 Å. The angle between this plane and the least-squares plane through the coordination group is 83.2° in I and 85.7° in II.

Divalent tellurium most often forms four-coordinated square-planar complexes, but when a phenyl group is one of the ligands, the position opposite to the phenyl group is vacant.[1,2,10] In terms of a bonding scheme for divalent tellurium based on *p*-orbitals,[1,2,10,17] the phenyl group engages a tellurium 5*p*-orbital in bonding so effectively that little if any bonding power of this 5*p*-orbital is left for bonding in a direction *trans* to the C–Te bond.

In phenylbis(thiourea)tellurium(II) chloride there is a chloride ion in a direction which makes an angle of 163° with the direction of the Te–C bond, at a distance of 3.61 Å from tellurium.[1] This may be regarded as a fourth, "missing" ligand of a square-planar arrangement. In the two present structures there is no certain approach of a fourth ligand. In II, however, the Se(2) atom of an adjacent molecule located at $\frac{1}{2}-x, \frac{1}{2}-y, 1-z$, where x, y, z are the coordinates of the Se(2) atom in Table 2, lies 3.965(2) Å from tellurium, in a direction which makes an angle of 159.6(2)° with the direction of the Te–C bond. In I the corresponding Te···S distance is larger than 4 Å.

THE TETRAMETHYLAMMONIUM ION

The bond lengths and angles in the tetramethylammonium ions are listed in Tables 5 and 6, and the shapes of the ions appear from Figs.3 and 4.

The four methyl carbon atoms of the tetramethylammonium ion are disordered in both compounds. The large thermal parameters might indicate that the disorder is due to extreme thermal motions, with the ion rotating more or less about the central nitrogen atom. It appears more plausible, however, that there is a statistical distribution of ions in two or more distinct orientations.

The tetramethylammonium ion is nearly tetrahedral. Due to the disorder, the derived bond lengths and angles are rather inaccurate, but the values are within the normal range.

CRYSTAL PACKING

A stereoscopic drawing of the content of the unit cell of the two compounds is shown in Figs. 3 and 4. There are no particular short non-bonding distances in any of the structures with exception of the Te···Se(2) approach mentioned above. Thus, the two structures consist of well separated tetramethylammonium ions and phenyldithiocyanatotellurate(II) ions in I, and tetramethylammonium ions and phenyldiselenocyanatotellurate(II) ions in II.

REFERENCES

1. Foss, O. and Marøy, K. *Acta Chem. Scand. 20* (1966) 123.
2. Foss, O. and Husebye, S. *Acta Chem. Scand. 20* (1966) 132.
3. Hauge, S. and Vikane, O. *Acta Chem. Scand. 27* (1973) 3596.
4. Åse, K. *Acta Chem. Scand. 25* (1971) 838.
5. Coppens, P., Leiserowitz, L. and Rabinovich, D. *Acta Crystallogr. 18* (1965) 1035.
6. Zachariasen, W. H. *Acta Crystallogr. 16* (1963) 1139.
7. Stewart, F., Davidson, E. R. and Simpson, W. T. *J. Chem. Phys. 42* (1965) 3175.
8. *International Tables for X-Ray Crystallography*, Kynoch Press, Birmingham 1962, Vol. III.
9. Johnson, C. K. *ORTEP* Report ORNL 3794, Oak Ridge National Laboratory, Oak Ridge.
10. Foss, O. *Pure Appl. Chem. 24* (1970) 31.
11. Åse, K., Bøyum, K., Foss, O. and Marøy, K. *Acta Chem. Scand. 25* (1971) 2457.
12. Hauge, S. and Tysseland, M. *Acta Chem. Scand. 25* (1971) 3072.
13. Åse, K., Foss, O. and Roti, I. *Acta Chem. Scand. 25* (1971) 3808.
14. Pauling, L. *The Nature of the Chemical Bond*, 3rd. Ed., Cornell University Press, Ithaca 1960.
15. Bastiansen, O. and Tretteberg, M. *Tetrahedron 17* (1962) 147.
16. Baiwir, M., Llabres, G., Dideberg, O., Dupont, L. and Piette, J. L. *Acta Crystallogr. B 30* (1974) 139.
17. Foss, O. *Acta Chem. Scand. 16* (1962) 779.

Received February 26, 1975.

Acta Chemica Scandinavica A 29 (1975) 763—770

The Crystal Structures of Chloro(ethylenethiourea)phenyltellurium(II) and Bromo(ethyleneselenourea)phenyltellurium(II)

OLAV VIKANE

Department of Chemistry, University of Bergen, N-5014 Bergen-Univ., Norway

Chloro(ethylenethiourea)phenyltelluriun(II), $C_6H_5Te(etu)Cl$, I, and bromo(ethyleneselenourea)phenyltellurium(II), $C_6H_5Te(esu)Br$, II, form isomorphous monoclinic crystals with space group $P2_1/c$. The unit cell dimensions for I are: $a = 7.0342(6)$ Å, $b = 12.3808(10)$ Å, $c = 14.3923(11)$ Å, $\beta = 102.252(7)°$, and for II: $a = 7.1968(8)$, $b = 12.8766(10)$ Å, $c = 14.3374(12)$ Å, $\beta = 101.460(9)°$.

In I and II each tellurium atom is primarily three-coordinated, being bonded to one phenyl carbon atom and, in directions nearly perpendicular to the Te – C bond, to one ethylenethiourea sulfur atom and one chlorine atom in I, and to one ethyleneselenourea selenium atom and one bromine atom in II. The three-centre systems S – Te – Cl and Se – Te – Br are nearly linear, and the Te – C bond nearly bisects the angle of the three-centre system. The bond lengths and angles involving tellurium are: Te – S = 2.5211(10) Å, Te – Cl = 2.8486(10) Å, Te – C = 2.120(2) Å, ∠S – Te – Cl = 176.03(2)°, ∠S – Te – C = 89.22(7)°, ∠Cl – Te – C = 87.29(7)° in I, and Te – Se = 2.6160(16) Å, Te – Br = 3.0537(16) Å, Te – C = 2.118(7) Å, ∠Se – Te – Br = 175.62(3)°, ∠Se – Te – C = 89.94(19)°, ∠Br – Te – C = 86.67(19)° in II. The fourth position of a square-planar arrangement around tellurium is approached by a chlorine or bromine atom of an adjacent molecule, at Te···Cl = 3.7401(10) Å in I and at Te···Br = 3.8490(16) Å in II, in directions which make an angle of 162.51(7)° and 163.31(19)° with the direction of the Te – C bond, respectively, for I and II.

Divalent tellurium most often forms four-coordinated square-planar complexes,[1,2] but when a phenyl group is one of the ligands, the position opposite to the phenyl group is vacant.[3–6] The first three-coordinated complexes of divalent tellurium are described by Foss and coworkers, and the crystal structures of chloro- and bromo(phenyl)thioureatellurium(II) have been determined.[3,4] Later, in a recent paper the crystal structures of two different crystalline forms of bromo(ethylenethiourea)phenyltellurium(II) were reported.[6] The syntheses and crystal data of the two present compounds, chloro(ethylenethiourea)phenyltellurium(II), I, and bromo(ethyleneselenourea)phenyltellurium(II), II, are reported earlier.[7,8] They are found to be isomorphous with the $P2_1/c$ form of bromo(ethylenethiourea)phenyltellurium(II).

The scope of the present work is to gain further information about the relative *trans* bond-lengthening effects of ligands in tellurium(II) complexes.

EXPERIMENTAL

Methods used for data collection and reductions, and computational procedures are as described previously.[5,9] For compound I, the measurements were performed on a crystal with the following dimensions, given as distances from the point of intersection of the crystal faces $(01\bar{1})$, $(0\bar{1}\bar{1})$, $(1\bar{1}\bar{1})$, and $(11\bar{1})$: to $(\bar{1}00)$, 0.227 mm; to $(0\bar{1}1)$, 0.141 mm; to(011), 0.125 mm. For compound II, the crystal used had the following dimensions, given as distances from the point of intersection of the crystal faces $(0\bar{1}\bar{1})$, $(01\bar{1})$, and (100): to $(0\bar{1}1)$, 0.078 mm; to (011), 0.047 mm; to $(\bar{1}00)$, 0.180 mm.

The scale factors, based on the reference reflections, varied within 5 % for I, and 4 % for II. 3050 of 3835 independent reflections within $\theta = 30°$ were found to be stronger than the lower limit for I. The corresponding numbers for II are 1842 of 4078.

Table 1. Atomic coordinates in fractions of monoclinic cell edges for chloro(ethylenethiourea)-phenyltellurium(II). Origin at a centre of symmetry. Isotropic thermal parameters (Å²) in the form $\exp - 8\pi^2 U(\sin^2\theta/\lambda^2)$]. Standard deviations from least squares are given in parentheses.

	x	y	z	u
Te	0.20099(2)	0.391455(13)	0.469660(12)	
Cl	0.26387(10)	0.48019(5)	0.65631(5)	
S	0.16956(10)	0.30863(6)	0.30708(5)	
C(1)	0.4176(4)	0.27560(19)	0.52475(17)	
C(2)	0.6097(4)	0.2944(2)	0.5213(2)	
C(3)	0.7502(5)	0.2198(3)	0.5560(2)	
C(4)	0.7029(6)	0.1251(3)	0.5942(3)	
C(5)	0.5153(6)	0.1050(3)	0.5978(4)	
C(6)	0.3708(5)	0.1802(3)	0.5636(3)	
C(7)	−0.0363(4)	0.2295(2)	0.29672(16)	
C(8)	−0.2443(5)	0.0862(3)	0.2548(3)	
C(9)	−0.3504(5)	0.1766(3)	0.2949(3)	
N(1)	−0.0511(4)	0.13223(19)	0.25949(19)	
N(2)	−0.1977(3)	0.25823(19)	0.32176(17)	
H(2)	0.640(4)	0.355(3)	0.491(2)	0.052(9)
H(3)	0.886(5)	0.237(3)	0.547(2)	0.078(11)
H(4)	0.801(5)	0.070(3)	0.617(3)	0.081(11)
H(5)	0.479(7)	0.042(4)	0.621(3)	0.116(16)
H(6)	0.254(5)	0.170(3)	0.567(2)	0.074(11)
H(N1)	0.038(5)	0.104(2)	0.238(2)	0.051(9)
H(N2)	−0.219(5)	0.331(3)	0.343(2)	0.069(10)
H(8A)	−0.289(6)	0.063(3)	0.195(3)	0.093(13)
H(8B)	−0.225(5)	0.022(3)	0.298(2)	0.076(11)
H(9A)	−0.444(5)	0.206(3)	0.251(2)	0.071(11)
H(9B)	−0.403(5)	0.159(3)	0.352(3)	0.083(12)

CRYSTAL DATA

The crystals of I and II are orange red, isomorphous, monoclinic prisms, extended along the a axis. Systematic absences are: $h0l$ for l odd, $0k0$ for k odd. The space group is $P2_1/c$ (No. 14).

The unit cell dimensions were determined as described elsewhere.[5,6] The θ-values (all abouth 20°) of 29 reflections for I and 31 reflections for II, were measured as described by Maartmann-Moe[10] The unit cell dimensions are: $a = 7.0342(6)$ Å, $b = 12.3808(10)$ Å, $c = 14.3923(11)$ Å, $\beta = 102.252(7)°$, $z = 4$, $D_x = 1.87$ g/cm³, $D_m = 1.87$ g/cm³, $\mu_{MoKa} = 28.7$ cm⁻¹, for I, and: $a = 7.1968(8)$ Å, $b = 12.8766(10)$ Å, $c = 14.3374(12)$ Å, $\beta = 101.460(9)°$, $z = 4$, $D_x = 2.23$ g/cm³, $D_m = 2.23$ g/cm³, $\mu_{MoKa} = 86.2$ cm⁻¹, for II.

STRUCTURE DETERMINATION

The structures were solved by Patterson and Fourier methods, and refined to R-values of 0.024 for I and 0.040 for II. Altogether 171 parameters were refined in each structure. The three-dimensional Fourier difference maps, based on the data of the final refinements, showed no peaks higher than 0.2 e/Å³ for I, and 0.3 e/Å³ for II.

Observed and calculated structure factors for the two structures are available from the author.

The atomic coordinates and thermal parameters are listed in Tables 1–4.

RESULTS

Bond lengths and angles in chloro(ethylenethiourea)phenyltellurium(II) and bromo(ethyleneselenourea)phenyltellurium(II), based on the atomic coordinates in Tables 1 and 2, are listed in Tables 5 and 6. The uncertainties in the unit cell dimensions are taken into account in the given standard deviations. Views of the structure of I and II, as seen normal to the plane through the coordination group, are shown in Figs. 1 and 2. Stereoscopic

Table 2. Atomic coordinates in fractions of monoclinic cell edges for bromo(ethyleneselenourea)-phenyltellurium(II). Origin at a centre of symmetry. Isotropic thermal parameters ($Å^2$) in the form $\exp-[8\pi^2U(\sin^2\theta/\lambda^2)]$. Standard deviations from least squares are given in parentheses.

	x	y	z	u
Te	0.20107(8)	0.39012(4)	0.46453(4)	
Br	0.26934(12)	0.48751(6)	0.66261(5)	
Se	0.17065(12)	0.30477(7)	0.29660(5)	
C(1)	0.4167(11)	0.2825(6)	0.5212(5)	
C(2)	0.6045(13)	0.3054(7)	0.5247(6)	
C(3)	0.7484(14)	0.2341(8)	0.5601(6)	
C(4)	0.6964(16)	0.1400(9)	0.5909(6)	
C(5)	0.5111(18)	0.1157(9)	0.5896(8)	
C(6)	0.3686(15)	0.1870(8)	0.5539(7)	
C(7)	−0.0442(11)	0.2220(6)	0.2954(5)	
C(8)	−0.2440(16)	0.0822(8)	0.2660(9)	
C(9)	−0.3463(14)	0.1714(8)	0.3049(9)	
N(1)	−0.0580(10)	0.1264(5)	0.2626(5)	
N(2)	−0.1966(10)	0.2516(5)	0.3228(5)	
H(2)	0.621(12)	0.348(6)	0.486(5)	0.07(3)
H(3)	0.886(16)	0.251(8)	0.562(7)	0.18(4)
H(4)	0.819(10)	0.094(6)	0.620(5)	0.07(2)
H(5)	0.454(15)	0.050(8)	0.596(7)	0.13(4)
H(6)	0.225(11)	0.178(8)	0.547(5)	0.07(2)
H(N1)	0.056(12)	0.093(6)	0.240(6)	0.10(3)
H(N2)	−0.224(11)	0.333(6)	0.338(5)	0.08(3)
H(8A)	−0.289(11)	0.067(6)	0.206(5)	0.06(3)
H(8B)	−0.228(14)	0.028(7)	0.316(6)	0.10(4)
H(9A)	−0.420(11)	0.198(6)	0.260(5)	0.05(3)
H(9B)	−0.432(18)	0.201(10)	0.363(9)	0.14(5)

Table 3. Anisotropic thermal parameters ($Å^2$) in the form $\exp-[2\pi^2(h^2a^{-2}U_{11}+\cdots+2hka^{-1}b^{-1}U_{12}+\cdots]$, for chloro(ethylenethiourea)phenyltellurium(II). The values for Te, Cl, and S have been multiplied by 10^4 and the values for C and N by 10^3. Standard deviations in parentheses.

	U_{11}	U_{22}	U_{33}	U_{12}	U_{23}	U_{13}
Te	389.4(9)	342.9(8)	417.6(9)	−14.1(8)	14.1(8)	81.1(6)
Cl	441(3)	384(3)	439(3)	25(3)	−12(3)	120(3)
S	435(4)	566(4)	423(3)	−86(3)	−62(3)	136(3)
C(1)	38.2(13)	32.9(12)	38.3(13)	−0.7(11)	3.8(10)	10.3(11)
C(2)	43.9(15)	46.5(16)	49.7(16)	−2.3(13)	5.1(13)	12.6(13)
C(3)	40.2(16)	69(2)	65.1(19)	5.9(16)	3.7(17)	15.9(16)
C(4)	64(2)	70(2)	69(2)	25.4(19)	15.1(18)	15.1(18)
C(5)	77(3)	64(2)	127(4)	10(2)	49(3)	31(3)
C(6)	48.7(19)	56.4(19)	110(3)	2.4(17)	37(2)	29(2)
C(7)	40.0(14)	37.1(13)	32.1(12)	2.8(11)	−1.0(10)	6.6(10)
C(8)	53.6(18)	42.9(17)	65(2)	−5.0(14)	−12.5(15)	18.1(17)
C(9)	44.2(17)	48.4(17)	68(2)	−6.4(15)	−16.7(16)	18.6(16)
N(1)	45.2(14)	41.4(13)	63.6(16)	4.6(11)	−12.9(11)	19.5(12)
N(2)	40.7(12)	38.8(12)	59.6(14)	−3.4(10)	−14.8(11)	19.2(11)

Table 4. Anisotropic thermal parameters (Å²) in the form $\exp-[2\pi^2(h^2a^{-2}U_{11}+\cdots+2hka^{-1}b^{-1}U_{12}+\cdots]$, for bromo(ethyleneselenourea)phenyltellurium(II). The values have been multiplied by 10^3. Standard deviations in parentheses.

	U_{11}	U_{22}	U_{33}	U_{12}	U_{23}	U_{13}
Te	48.2(3)	40.6(3)	48.2(3)	−1.9(3)	0.7(3)	7.2(2)
Br	47.8(5)	40.0(5)	46.7(5)	3.4(4)	−1.0(4)	11.6(4)
Se	43.9(5)	60.3(6)	41.7(5)	−8.0(5)	−5.6(4)	11.0(4)
C(1)	48(5)	36(4)	39(4)	−6(4)	−1(4)	9(4)
C(2)	57(6)	54(6)	45(5)	−3(5)	5(5)	14(5)
C(3)	75(7)	75(7)	54(6)	2(6)	5(5)	9(5)
C(4)	70(8)	84(8)	60(6)	34(7)	7(6)	3(6)
C(5)	90(9)	59(7)	104(8)	1(8)	32(7)	23(7)
C(6)	56(6)	62(6)	85(7)	5(6)	19(5)	15(6)
C(7)	48(5)	43(5)	36(4)	3(4)	−2(4)	3(4)
C(8)	73(8)	46(6)	79(8)	−3(6)	−12(6)	17(7)
C(9)	49(6)	56(6)	94(8)	2(6)	−28(6)	15(6)
N(1)	41(4)	51(5)	78(5)	3(4)	−16(4)	17(4)
N(2)	45(4)	44(4)	67(5)	−5(4)	−14(4)	24(4)

Table 5. Bond lengths (Å) and angles (°) in chloro(ethylenethiourea)phenyltellurium(II). A prime denotes an atom in the position $\bar{x},1-y,1-z$, where x,y,z are the coordinates in Table 1. Standard deviations are given in parentheses.

Te−Cl	2.8486(10)	S−Te−Cl	176.03(2)
Te−S	2.5211(10)	S−Te−C(1)	89.22(7)
Te−C(1)	2.120(2)	Cl−Te−C(1)	87.29(7)
Te−Cl′	3.7401(10)	C(1)−Te−Cl′	162.51(7)
C(1)−C(2)	1.383(4)	Te−C(1)−C(2)	120.19(17)
C(1)−C(6)	1.376(5)	Te−C(1)−C(6)	121.2(2)
C(2)−C(3)	1.368(4)	C(2)−C(1)−C(6)	118.6(2)
C(3)−C(4)	1.365(5)	C(1)−C(2)−C(3)	120.6(3)
C(4)−C(5)	1.355(6)	C(2)−C(3)−C(4)	120.6(3)
C(5)−C(6)	1.389(6)	C(3)−C(4)−C(5)	119.7(3)
		C(4)−C(5)−C(6)	120.6(3)
		C(5)−C(6)−C(1)	119.9(3)
S−C(7)	1.728(3)	Te−S−C(7)	102.57(9)
C(7)−N(1)	1.313(3)	S−C(7)−N(1)	123.20(19)
C(7)−N(2)	1.311(4)	S−C(7)−N(2)	125.49(17)
N(1)−C(8)	1.462(4)	N(1)−C(7)−N(2)	111.3(2)
N(2)−C(9)	1.466(4)	N(1)−C(8)−C(9)	102.8(2)
C(8)−C(9)	1.525(5)	N(2)−C(9)−C(8)	102.4(2)
		C(7)−N(1)−C(8)	111.6(2)
		C(7)−N(2)−C(9)	111.7(2)
C(2)−H(2)	0.91(3)	C(1)−C(2)−H(2)	119.1(19)
C(3)−H(3)	1.01(4)	C(3)−C(2)−H(2)	129.2(19)
C(4)−H(4)	0.98(4)	C(2)−C(3)−H(3)	116.8(19)
C(5)−H(5)	0.90(5)	C(4)−C(3)−H(3)	123.5(19)
C(6)−H(6)	0.84(4)	C(3)−C(4)−H(4)	121(2)
		C(5)−C(4)−H(4)	119(2)
		C(4)−C(5)−H(5)	122(3)
		C(6)−C(5)−H(5)	118(3)
		C(5)−C(6)−H(6)	122(2)
		C(1)−C(6)−H(6)	118(2)
C(8)−H(8A)	0.89(4)	N(1)−C(8)−H(8A)	108(3)
C(8)−H(8B)	1.00(3)	N(1)−C(8)−H(8B)	106(2)
C(9)−H(9A)	0.88(3)	H(8A)−C(8)−H(8B)	108(4)
C(9)−H(9B)	0.99(3)	C(9)−C(8)−H(8A)	120(3)

Table 5. Continued.

N(1)–H(N1)	0.83(3)	C(9)–C(8)–H(8B)	112(2)
N(2)–H(N2)	0.97(3)	N(2)–C(9)–H(9A)	107(2)
		N(2)–C(9)–H(9B)	108(2)
		C(8)–C(9)–H(9A)	112(2)
		C(8)–C(9)–H(9B)	117(2)
		H(9A)–C(9)–H(9B)	109(4)
		C(7)–N(1)–H(N1)	122(2)
		C(8)–N(1)–H(N1)	126(3)
		C(7)–N(2)–H(N2)	122(2)
		C(9)–N(2)–H(N2)	125(3)

Table 6. Bond lengths (Å) and angles (°) in bromo(ethyleneselenourea)phenyltellurium(II). A prime denotes an atom in the position, $\bar{x}$,1-y1-z, where x,y,z are the coordinates given in Table 2. Standard deviations are given in parentheses.

Te–Br	3.0537(16)	Se–Te–Br	175.62(3)
Te–Se	2.6160(16)	Se–Te–C(1)	89.94(19)
Te–C(1)	2.118(7)	Br–Te–C(1)	86.67(19)
Te–Br′	3.8490(16)	C(1)–Te–Br′	163.31(19)
C(1)–C(2)	1.374(13)	Te–C(1)–C(2)	121.0(5)
C(1)–C(6)	1.385(13)	Te–C(1)–C(6)	119.8(6)
C(2)–C(3)	1.400(13)	C(1)–C(2)–C(3)	121.6(8)
C(3)–C(4)	1.368(15)	C(2)–C(3)–C(4)	117.9(9)
C(4)–C(5)	1.367(18)	C(3)–C(4)–C(5)	121.8(9)
C(5)–C(6)	1.396(15)	C(4)–C(5)–C(6)	119.9(9)
		C(1)–C(6)–C(5)	119.6(9)
		C(2)–C(1)–C(6)	119.2(7)
Se–C(7)	1.875(8)	Te–Se–C(7)	99.5(2)
C(7)–N(1)	1.315(10)	Se–C(7)–N(1)	122.6(5)
C(7)–N(2)	1.294(11)	Se–C(7)–N(2)	125.3(5)
N(1)–C(8)	1.464(13)	N(1)–C(7)–N(2)	112.1(7)
N(2)–C(9)	1.478(12)	N(1)–C(8)–C(9)	103.3(8)
C(8)–C(9)	1.528(16)	N(2)–C(9)–C(8)	101.6(8)
		C(7)–N(1)–C(8)	110.9(7)
		C(7)–N(2)–C(9)	112.0(7)
C(2)–H(2)	0.81(8)	C(1)–C(2)–H(2)	116(4)
C(3)–H(3)	1.00(11)	C(3)–C(2)–H(2)	119(4)
C(4)–H(4)	1.07(7)	C(2)–C(3)–H(3)	123(4)
C(5)–H(5)	0.96(10)	C(4)–C(3)–H(3)	116(4)
C(6)–H(6)	1.03(8)	C(3)–C(4)–H(4)	118(4)
		C(5)–C(4)–H(4)	123(4)
		C(4)–C(5)–H(5)	119(5)
		C(6)–C(5)–H(5)	118(5)
		C(5)–C(6)–H(6)	117(4)
		C(1)–C(6)–H(6)	122(4)
C(8)–H(8A)	0.87(7)	N(1)–C(8)–H(8A)	103(5)
C(8)–H(8B)	0.94(9)	N(1)–C(8)–H(8B)	109(4)
C(9)–H(9A)	0.92(7)	H(8A)–C(8)–H(8B)	108(6)
C(9)–H(9B)	1.09(12)	C(9)–C(8)–H(8A)	114(4)
N(1)–H(N1)	1.03(9)	C(9)–C(8)–H(8B)	108(4)
N(2)–H(N2)	1.09(8)	N(2)–C(9)–H(9A)	101(4)
		N(2)–C(9)–H(9B)	106(4)
		C(8)–C(9)–H(9A)	108(4)
		C(8)–C(9)–H(9B)	107(4)
		H(9A)–C(9)–H(9B)	110(6)
		C(7)–N(1)–H(N1)	119(4)
		C(8)–N(1)–H(N1)	120(4)
		C(7)–N(2)–H(N2)	122(4)
		C(9)–N(2)–H(N2)	123(4)

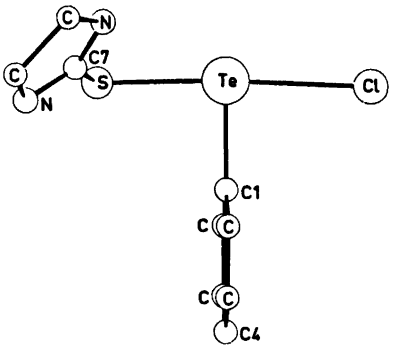

Fig. 1. Chloro(ethylenethiourea)phenyltellurium(II), as seen normal to the plane through the coordination group.

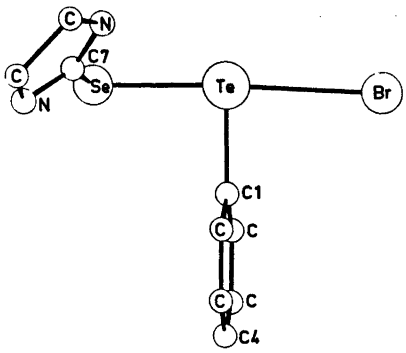

Fig. 2. Bromo(ethyleneselenourea)phenyltellurium(II), as seen normal to the plane through the coordination group.

views of the content of the unit cell of I and II are shown in Figs. 3 and 4.

In each of the structures the tellurium atom is primarily three-coordinated, being bonded to one phenyl carbon atom and, in directions nearly perpendicular to the Te – C bond, to one ethylenethiourea sulfur atom and one chlorine atom in I, and to one ethyleneselenourea selenium atom and one bromine atom in II. Thus, the coordination around the tellurium atoms in I and II are similar to that of the isomorphous form of bromo(ethylenethiourea)-phenyltellurium(II).[6] The coordination around the tellurium atom is nearly planar in both structures. The largest deviation from a least-squares plane through Te, S, Cl, and C(1) is 0.024 Å in I. The largest deviation from the corresponding least-squares plane through Te, Se, Br, and C(1) is 0.041 Å in II. The least-squares plane through the coordination group pass 0.057 Å from C(4) in I and 0.046 Å from C(4) in II.

The three-centre systems, S – Te – Cl, and Se – Te – Br are both nearly linear. The S – Te – Cl bond angle is 176.03(2)° and the Se – Te – Br bond angle is 175.62(3)°. A similar deviation from linearity is also found in the crystals of the isomorphous form of bromo(ethylene-thiourea)phenyltellurium(II), where the S – Te – Br bond angle is 175.96(3)°.[6]

The Te – C bond nearly bisects the angle of the three-centre system in both I and II. The S – Te – C bond angle is 89.22(7)° and the Cl – Te – C bond angle is 87.29(7)° in I. In the structure of II the Se – Te – C bond angle is 89.94(19)° and the Br – Te – C bond angle is 86 67(19)°. In the structure of the isomorphous form of bromo(ethylenethiourea)phenyltellurium(II) the corresponding S – Te – C and Br – Te – C bond angles are 89.45 and 87.02°, respectively.[6]

The Te – S bond length, 2.5211(10) Å in I is, within the error, equal to the Te – S bond length 2.5231(15) Å, found in the crystals of the isomorphous form of bromo(ethylene-thiourea)phenyltellurium(II).[6] This is nearly 0.11 Å longer than the sum of the single bond radii, 2.41 Å,[14] and about 0.02 Å longer than the Te – S bond length, 2.50 Å, found in the crystals of chloro- and bromo(phenyl)thio-ureatellurium(II).[3] In chloro- and bromo-(ethylenethiourea)phenyltellurium(II) as in chloro- and bromo(phenyl)thioureatellurium (II), substitution of bromine for chlorine has, within the error, no effect on the length of the Te – S bond *trans* to chlorine or bromine.

The Te – Cl bond length, 2.8486(10) Å in I, is about 0.49 Å longer than the sum of the single bond radii, 2.36 Å, but considerably shorter than the van der Waals contacts.[11] In the crystals of chloro(phenyl)thioureatel-lurium(II) the Te – Cl bond length, 3.00 Å, is 0.64 Å longer than the sum of the single bond radii.[3] The Te – Cl bond in chloro(ethylene-thiourea)phenyltellurium(II) shorter than in chloro(phenyl)thioureatellurium(II), together with the Te – Br bond in bromo(ethylene-thiourea)phenyltellurium(II) shorter than in bromo(phenyl)thioureatellurium(II),[3,6] indicate a more pronounced *trans* bond-lengthen-

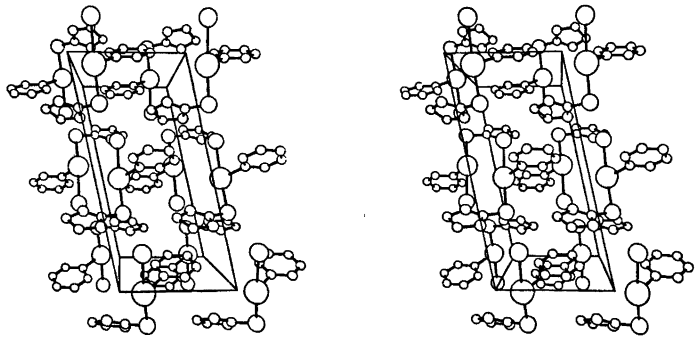

Fig. 3. A stereoscopic view of the cell packing in chloro(ethylenethiourea)phenyltellurium(II), as seen along the *b* crystal axis.

ing effect of thiourea than ethylenethiourea on a Te-halogen bond.

The Te–Se bond length, 2.6160(16) Å, in II, is 0.076 Å longer than the sum of the single bond radii, 2.51 Å.[14] The Te–Br bond length in II, 3.0537(16) Å, is intermediate between the Te–Br bond length, 2.9694 Å, found in the structure of the isomorphous form of bromo(ethylenethiourea)phenyltellurium(II) [6] and the Te–Br bond length 3.11 Å found in the structure of bromo(phenyl)thioureatellurium (II).[3] This indicates a relative *trans* bond lengthening order: thiourea ≥ ethyleneselenourea > ethylenethiourea when *trans* to a Te–Br bond.

The Te–C bond lengths, 2.120(2) Å in I and 2.118(7) Å in II, are equal, within the accuracy of the structure determination. The same Te–C bond length has also been found in the structures of bromo(ethylenethiourea)-phenyltellurium(II),[6] chloro- and bromo(phenyl)thioureatellurium(II),[3] chloro(phenyl)bis-thioureatellurium(II),[4] and in the structures of the phenyldithiocyanato- and phenyldiselenocyanatotellurate(II) anions,[5] indicating that the Te–C bond is nearly a single covalent bond.[5]

As pointed out by Foss *et al.* the coordination around the tellurium atom may be regarded as based on square-planar arrangement.[1–4] In the two present structures, as in the structure of the isomorphous form of bromo(ethylenethiourea)phenyltellurium(II),[6] the fourth coordination site of a square-planar structure, *trans* to the phenyl group is approached by a halogen atom of an adjacent molecule, over a symmetry centre. In I a chlorine atom of an adjacent molecule, in the position $\bar{x},1-y,1-z$, where x,y,z are the chlorine coordinates in Table 1, lies 3.7401(10) Å from tellurium, in a direction which makes an angle of 162.51 (7)° with the direction of the Te–C bond. In II the corresponding bromine atom lies

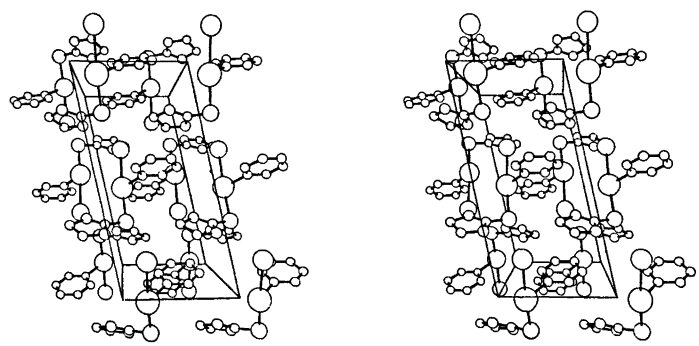

Fig. 4. A stereoscopic view of the cell packing in bromo(ethyleneselenourea)phenyltellurium(II), as seen along the *b* crystal axis.

3.8490(16) Å from tellurium, in a direction which makes an angle of 163.31(19)° with the direction of the Te – C bond.

The tellurium atom and the carbon atoms of the phenyltellurium group are nearly co-planar in both structures. The largest deviation from a least-squares plane being 0.01 Å in I and 0.02 Å in II. The angle between this plane and the least-squares plane through the coordination group is 87.24° in I and 86.25° in II.

The sulfur atom, the two nitrogen atoms, and the three carbon atoms of the ethylene-thiourea group are nearly co-planar. So are the selenium atom, the two nitrogen atoms, and the three carbon atoms in the ethylene-selenourea group. The largest deviation from least-squares plane is 0.048 Å in I and 0.045 Å in II. The angle between this plane and the least-squares plane through Te, S, Cl, and C(7) in I or Te, Se, Br, and C(7) in II, is 44.9 and 45.5°, respectively.

The S – C bond length, 1.728(3) Å, and the Te – S – C bond angle of 102.57(9)° in I are, within the error, equal to the S – C bond length, 1.723 Å and Te – S – C bond angle, 102.49° found in the isomorphous form of bromo-(ethylenethiourea)phenyltellurium(II).[6] The corresponding Se – C bond length in II is 1.875 (8) Å, and the Te – Se – C bond angle is 99.5 (2)°.

HYDROGEN BONDING

In both structures the closest nitrogen-halogen approaches occur between N(2) and the halogen atom at $\bar{x}$,1-y,1-z, where x, y, z are the halogen coordinates in Tables 1 and 2. In I the N(2)···Cl distance is 3.297(2) Å, and the H(N2)···Cl distance is 2.36(3) Å. The N(2) – H(N2)···Cl angle is 162(2)°, the C(7) – N(2)···Cl angle is 116.19(16)°, the C(9) – N(2)···Cl angle is 126.29(16)°, the C(7) – N(2) – H(N2) angle is 122(2)°, and the C(9) – N(2) – H(N2) angle is 125(2)°. In II the N(2)···Br distance is 3.413(7 Å, and the H(N2)···Br distance is 2.33(8) Å. The N(2) – H(N2)···Br angle is 168(4)°, the C(7) – N(2)···Br angle is 117.3(5)°, the C(9) – N (2)···Br angle is 125.7(5)°, the C(7) – N(2) – H(N2) angle is 122(4)°, and the C(9) – N(2) – H(N2) angle is 123(4)°. This probably represent N – H···Cl and N – H···Br hydrogen bonds in I and II.

REFERENCES

1. Foss, O. In Andersen, P., Bastiansen, O. and Furberg, S. *Selected Topics in Structure Chemistry*, Universitetsforlaget, Oslo 1967, p. 145.
2. Foss, O. *Pure Appl. Chem. 24* (1970) 31.
3. Foss, O. and Husebye, S. *Acta Chem. Scand. 20* (1966) 132.
4. Foss, O. and Marøy, K. *Acta Chem. Scand. 20* (1966) 123.
5. Hauge, S. and Vikane, O. *Acta Chem. Scand. A 29* (1975) 755.
6. Vikane, O. *Acta Chem. Scand. A 29* (1975) 738.
7. Vikane, O. *Acta Chem. Scand. A 29* (1975) 150.
8. Vikane, O. *Acta Chem. Scand. A 29.* (1975) 152.
9. Åse, K. *Acta Chem. Scand. 25* (1971) 838.
10. Maartmann-Moe, K. *Siemens Review* XLI (1974) 54.
11. Pauling, L. *The Nature of the Chemical Bond*, 3rd. Ed., Cornell University Press, Ithaca 1960.

Received February 26, 1975.

Acta Chemica Scandinavica A 29 (1975) 771—777

The Crystal Structure of Potassium Seleniumtriselenocyanate Hemihydrate

SVERRE HAUGE

Department of Chemistry, University of Bergen, N-5014 Bergen-Univ., Norway

The crystal structure of potassium seleniumtriselenocyanate hemihydrate, $KSe(SeCN)_3 \cdot \frac{1}{2} H_2O$, has been determined by X-ray methods, and refined by full matrix least squares procedures. The crystals are triclinic, space group $P\bar{1}$ (No. 2), with $a = 9.170(2)$ Å, $b = 13.377(3)$ Å, $c = 9.057(2)$ Å, $\alpha = 106.22(2)°$, $\beta = 100.64(2)°$, $\gamma = 99.07(2)°$, and four formula units per unit cell.

In the crystals, the seleniumtriselenocyanate ions are dimerized. The eight selenium atoms of the dimerized unit are approximately coplanar, and the six cyano groups are located on the same side of the plane. The Se – Se – Se bond angles are in the ranges from 170.58(6) to 174.94(5)° and from 86.13(5) to 98.41(5)°. There are four rather short Se – Se bonds, from 2.395(2) to 2.419(2) Å, and four long ones, from 3.089(2) to 3.255(2) Å. The short ones are significantly longer than the Se – Se single-bond distance, 2.34 Å, and the long ones are shorter than van der Waals approaches. Each long Se – Se bond occurs *trans* to a short Se – Se bond. The total lengths of the rather unsymmetrical, approximately linear three-selenium systems (the sum of the lengths of the two Se – Se bonds) are from 5.508 to 5.647 Å. This is 0.19 to 0.33 Å longer than the total lengths of the more symmetrical linear three-selenium systems of the triselenocyanate ion.

The dimerized unit can be looked upon as built up of two selenium diselenocyanate molecules, $Se(SeCN)_2$, bridged together through the selenium atoms of two selenocyanate ions.

Several rather short Se···Se contacts, from 3.34 Å upwards, occur between eight-selenium units.

In 1884 – 1886 Verneuil [1] isolated and determined the composition of potassium seleniumtriselenocyanate, $KSe(SeCN)_3 \cdot \frac{1}{2} H_2O$, although he described it as a monohydrate. Its crystal structure analysis, reported here, has been carried out as a part of a study of linear three-selenium systems.

CRYSTAL DATA

Preparative and crystallographic data on potassium seleniumtriselenocyanate hemihydrate and other seleniumtriselenocyanates have been reported earlier.[2] A short note on the crystal structure of the potassium salt has also been reported.[3]

The salt, $KSe(SeCN)_3 \cdot \frac{1}{2} H_2O$, forms reddish-brown prisms extended along the short *ac* diagonal, with $a = 9.170(2)$ Å, $b = 13.377(3)$ Å, $c = 9.057(2)$ Å, $\alpha = 106.22(2)°$, $\beta = 100.64(2)°$, and $\gamma = 99.07(2)°$. Collection of X-ray data was done by means of a Siemens AED diffractometer, using Nb-filtered Mo$K\alpha$ radiation, $\lambda(\alpha_1) = 0.70926$ Å. For determination of cell parameters, θ, ϕ, and X settings for 23 reflections with high θ-values were measures and evaluated by means of a least squares program.

There are four formula units per unit cell; density, calc. 2.87, found 2.89 g/cm^3. The space group, from structure analysis is $P\bar{1}$ (No. 2).

The crystal used for data collection had the following dimensions, given as distances to faces from the point of intersections of the crystal faces $(0\bar{1}0)$, $(\bar{1}01)$, and (101): to (010), 0.114 mm; to $(10\bar{1})$, 0.158 mm; to $(\bar{1}0\bar{1})$, 0.336 mm.

Intensity data were collected using a "five value" measuring procedure. The net count of two reference reflections measured at intervals of 50 reflections, fell by about 14 % during the collection period. The lower limit for observed reflections was set equal to three times the standard deviation in net intensity. 3150 out of 4945 reflections with $\theta < 28°$ were found to be stronger than the lower limit. The remaining reflections were judged as unobserved and set equal to the limit. 24 reflections which showed extraordinary high, or erratic, background count were at a later stage omitted from the data.

The intensities were corrected for absorption.[4] The linear absorption coefficient, $\mu = 159.4$ cm^{-1}.

Table 1. Atomic coordinates for potassium selenium triselenocyanate in fractions of triclinic cell edges. Origin at a centre of symmetry. Standard deviations from least squares are given in parentheses.

	x	y	z
Se_1	0.06300(10)	0.13858(7)	−0.06314(10)
Se_2	0.07100(9)	0.12554(7)	0.19737(10)
Se_3	−0.19849(10)	0.10495(8)	0.18396(12)
Se_4	0.72016(9)	0.12574(7)	0.60281(10)
Se_5	0.46001(9)	0.13382(7)	0.60678(9)
Se_6	0.47137(10)	0.13623(8)	0.87409(10)
Se_7	0.41279(11)	0.12399(7)	0.24275(10)
Se_8	0.11004(10)	0.13602(8)	0.56510(11)
C_1	0.1420(10)	0.2862(8)	−0.0010(10)
C_2	−0.1851(10)	0.2454(9)	0.2837(12)
C_4	0.7986(9)	0.2666(8)	0.7337(10)
C_6	0.5298(10)	0.2824(8)	0.9653(10)
C_7	0.4534(9)	0.2685(8)	0.3346(10)
C_8	0.1771(10)	0.2785(8)	0.6131(10)
N_1	0.1809(10)	0.3745(7)	0.0265(10)
N_3	−0.1767(11)	0.3339(8)	0.3434(14)
N_4	0.8458(9)	0.3514(6)	0.8199(10)
N_6	0.5699(11)	0.3725(7)	0.0220(10)
N_7	0.4751(10)	0.3575(7)	0.3941(10)
N_8	0.2201(10)	0.3685(7)	0.6432(10)
O	0.1767(8)	0.4831(6)	0.3874(8)
K_1	0.5560(3)	0.4726(2)	0.7336(3)
K_2	0.9099(3)	0.4773(2)	0.1697(3)

Table 2. Anistropic thermal parameters (Å²) in the form $\exp[-2\pi^2(h^2a^{-2}U_{11}+\cdots+2hka^{-1}b^{-1}U_{12}\cdots)]$. All values have been multiplied by 10^3. Standard deviations from least squares refinement in parentheses.

	U_{11}	U_{22}	U_{33}	U_{12}	U_{23}	U_{13}
Se_1	35.0(5)	29.4(5)	24.8(4)	4.0(4)	9.9(3)	5.0(4)
Se_2	27.9(4)	29.6(4)	25.0(4)	3.7(3)	9.2(3)	5.4(3)
Se_3	35.4(5)	35.8(5)	36.0(5)	3.4(4)	13.4(4)	7.2(4)
Se_4	30.0(5)	44.7(6)	44.2(5)	3.5(4)	9.0(4)	7.9(4)
Se_5	34.2(5)	32.6(5)	34.0(5)	7.7(4)	7.6(4)	4.0(4)
Se_6	26.7(4)	23.8(4)	23.9(4)	5.0(3)	6.5(3)	4.5(3)
Se_7	42.1(5)	35.9(5)	26.0(4)	5.6(4)	11.2(4)	7.6(4)
Se_8	25.3(4)	31.1(5)	33.5(4)	5.9(3)	4.4(3)	5.1(3)
C_1	40(5)	29(5)	33(4)	−2(4)	10(4)	4(4)
C_2	38(5)	35(5)	31(4)	8(4)	8(4)	16(4)
C_4	31(5)	44(6)	61(6)	8(4)	25(5)	18(4)
C_6	30(4)	36(5)	25(4)	8(4)	14(4)	8(3)
C_7	41(5)	42(6)	24(4)	7(4)	7(4)	8(4)
C_8	23(4)	40(6)	38(5)	5(4)	18(4)	1(4)
N_1	74(5)	42(5)	40(4)	−7(4)	12(4)	6(4)
N_3	81(6)	42(5)	50(5)	21(5)	17(4)	27(5)
N_4	68(6)	46(6)	120(9)	17(5)	24(6)	17(5)
N_6	64(6)	37(5)	54(5)	8(4)	11(4)	17(4)
N_7	93(7)	40(6)	43(5)	0(5)	1(4)	24(5)
N_8	38(4)	29(4)	57(5)	0(3)	5(4)	1(4)
O	58(4)	53(4)	52(4)	6(3)	22(3)	9(3)
K_1	47.8(12)	37.6(12)	38.9(11)	4.6(10)	10.2(9)	6.2(9)
K_2	44.6(11)	36.8(12)	43.2(11)	3.5(9)	9.4(9)	11.7(9)

THE STRUCTURE ANALYSIS

The structure was solved by Patterson and Fourier methods and refined to an R-value of 0.042. The three-dimensional Fourier difference map based on the data of the final refinement showed no peak higher than 0.9 e Å^{-3}.

Computational procedures and programs used are described elsewhere.[5]

The final atomic coordinates and temperature parameters are listed in Tables 1 and 2.

The structure factors are available from the author on request.

RESULTS

The di-μ-selenocyanato-bis{diselenocyanatoselenate(II)} anion. Bond lengths, close contacts, and angles in the anion, based on the atomic coordinates of Table 1, are given in Fig. 1 and Tables 3 and 4. Distances from the potassium ions and from the water molecule to neighbouring atoms are given in Table 5. The uncertainties in cell dimensions are taken into account in the given standard deviations. In the tables, superscript I denotes an atom at $(x,y,z-1)$, II at $(1+x,y,z)$, III at $(x-1,y,z)$, IV at $(x,y,1+z)$, V at $(\bar{x},\bar{y},\bar{z})$, VI at $(1-x,\bar{y},1-z)$, VII at $(\bar{x},\bar{y},1-z)$, VIII at $(1-x,1-y,1-z)$, IX at $(1-x,1-y,\bar{z})$, X at $(2-x,1-y,1-z)$, and XI at $(\bar{x},1-y,1-z)$, where x, y, z are the coordinates of Table 1.

In the crystal structure of potassium seleniumtriselenocyanate, layers of selenium atoms occur parallel to the *ac* plane at y approximately 0.128 and −0.128. The selenium atoms of a layer are held together through bonds and through weaker interactions. Two layers, interrelated through symmetry centres at $y=0$, are held together through short Se···Se contacts, making a double layer. The cyano groups are located on the outsides of the double layer, and the potassium ions and the water molecules are located between the double layers.

As seen from Fig. 1, the seleniumtriselenocyanate ions are dimerized in the crystals. The eight selenium atoms of the dimerized unit, *i.e.* the two central atoms, Se_2 and Se_5, the four terminal atoms, Se_1, Se_3, Se_4, and Se_6, and the two bridging atoms, Se_7 and Se_8, are approximately co-planar. The largest deviation of an atom from a least squares plane is −0.21 Å.

Each of the two central selenium atoms, Se_2 and Se_5, has a distorted square-planar environment, with long bonds to bridging selenium atoms *trans* to rather short bonds to terminal selenium atoms. The variation in the lengths of the short Se−Se bonds, from 2.395(2) to 2.419(2) Å, is small, but significant. The short bonds are definitely longer than the Se−Se single bond distance, 2.34 Å. The long bonds are from 3.092(2) to 3.244(2) Å, and thus shorter than van der Waals approaches. The Se−Se−Se angles of the four approximately linear three-selenium systems at each central selenium atoms are from 170.58 to 174.94°. The total lengths of these rather unsymmetrical systems (the sum of the lengths of the two Se−Se bonds) are 5.508 to 5.647 Å, and thus 0.19 to 0.33 Å longer than the more symmetrical linear three-selenium systems of the triselenocyanate ion.[6-8]

Approximately in the plane of the eight-selenium unit, each terminal selenium atom has a close contact to a bridging selenium atom of a neighbouring eight-selenium unit, and each bridging selenium atom has two close contacts to terminal selenium atoms of two neighbouring eight-selenium units (*cf.* Fig. 1). The contacts are from 3.464 Å and upwards. The Se−Se···Se angles are from 164.11 to 172.58°. Each of the linear three-selenium system thereby has short contacts in both ends, of equal length. These short contacts have probably some influence on the bond

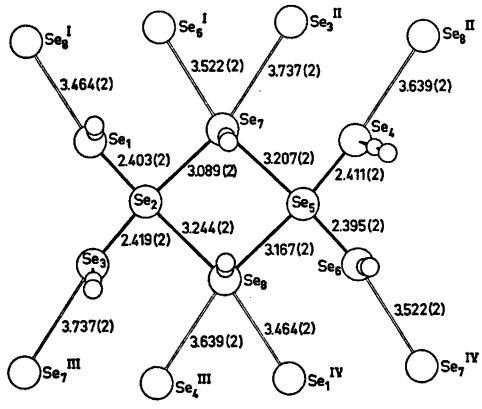

Fig. 1. The di-μ-selenocyanato-bis{diselenocyanatoselenate(II)} anion in $KSe(SeCN)_3 \cdot \frac{1}{2} H_2O$, as seen normal to the *ac* plane.

Table 3. Angles (°) in the plane of the eight selenium unit. Standard deviations in parentheses.

$Se_1-Se_2-Se_3$	97.60(5)	$Se_4-Se_5-Se_6$	98.41(5)
$Se_3-Se_2-Se_8$	86.13(5)	$Se_6-Se_5-Se_8$	88.54(5)
$Se_8-Se_2-Se_7$	87.32(5)	$Se_8-Se_5-Se_7$	86.64(4)
$Se_7-Se_2-Se_1$	89.64(5)	$Se_7-Se_5-Se_4$	83.37(5)
$Se_1-Se_2-Se_8$	173.06(5)	$Se_4-Se_5-Se_8$	172.81(5)
$Se_3-Se_2-Se_7$	170.58(6)	$Se_6-Se_5-Se_7$	174.94(5)
$Se_2-Se_1\cdots Se_6^{I}$	169.29(5)	$Se_2-Se_7\cdots Se_3^{II}$	165.17(4)
$Se_2-Se_3\cdots Se_7^{III}$	167.62(4)	$Se_5-Se_7\cdots Se_6^{I}$	164.11(4)
$Se_5-Se_4\cdots Se_8^{II}$	172.58(5)	$Se_2-Se_8\cdots Se_1^{IV}$	167.03(4)
$Se_5-Se_6\cdots Se_7^{IV}$	169.17(5)	$Se_5-Se_8\cdots Se_4^{III}$	166.88(4)
$Se_5-Se_7\cdots Se_3^{II}$	100.45(4)	$Se_2-Se_8\cdots Se_4^{III}$	100.82(4)
$Se_2-Se_7\cdots Se_6^{I}$	101.03(4)	$Se_5-Se_8\cdots Se_1^{IV}$	100.90(4)
$Se_6\cdots Se_7\cdots Se_3^{II}$	64.74(4)	$Se_4^{III}\cdots Se_8\cdots Se_1^{IV}$	66.27(4)

Table 4. Bond lengths and short distances (Å) and angles (°) out of the plane of the eight selenium unit. Standard deviations in parentheses.

Se_1-C_1	1.876(10)	$\angle Se_1-C_1-N_1$	174.6(7)
C_1-N_1	1.121(13)	$\angle Se_2-Se_1-C_1$	97.2(3)
Se_3-C_3	1.817(11)	$\angle Se_3-C_3-N_3$	178.6(10)
C_3-N_3	1.139(15)	$\angle Se_2-Se_3-C_3$	94.6(3)
Se_4-C_4	1.866(9)	$\angle Se_4-C_4-C_4$	176.8(8)
C_4-N_4	1.145(11)	$\angle Se_5-Se_4-C_4$	93.9(3)
Se_6-C_6	1.843(10)	$\angle Se_6-C_6-N_6$	178.1(8)
C_6-N_6	1.139(13)	$\angle Se_5-Se_6-C_6$	96.5(3)
Se_7-C_7	1.824(10)	$\angle Se_7-C_7-N_7$	177.7(8)
C_7-N_7	1.129(13)	$\angle Se_2-Se_7-C_7$	87.9(3)
		$\angle Se_5-Se_7-C_7$	81.0(3)
Se_8-C_8	1.808(10)	$\angle Se_8-C_8-N_8$	179.7(8)
C_8-N_8	1.144(14)	$\angle Se_2-Se_8-C_8$	86.3(3)
		$\angle Se_5-Se_8-C_8$	83.8(3)
$Se_2\cdots Se_1^{V}$	3.339(2)	$\angle Se_1-Se_2\cdots Se_1^{V}$	93.47(5)
		$\angle Se_3-Se_2\cdots Se_1^{V}$	76.17(5)
		$\angle Se_7-Se_2\cdots Se_1^{V}$	97.47(4)
		$\angle Se_8-Se_2\cdots Se_1^{V}$	93.11(4)
$Se_5\cdots Se_4^{VI}$	3.426(2)	$\angle Se_4-Se_5\cdots Se_4^{VI}$	100.36(4)
		$\angle Se_6-Se_5\cdots Se_4^{VI}$	101.78(5)
		$\angle Se_7-Se_5\cdots Se_4^{VI}$	75.59(4)
		$\angle Se_8-Se_5\cdots Se_4^{VI}$	76.26(4)
$Se_1\cdots Se_2^{V}$	3.339(2)	$\angle Se_2-Se_1\cdots Se_2^{V}$	86.53(5)
		$\angle C_1-Se_1\cdots Se_2^{V}$	176.1(3)
$Se_4\cdots Se_5^{VI}$	3.426(2)	$\angle Se_5-Se_4\cdots Se_5^{VI}$	79.63(4)
		$\angle C_4-Se_4\cdots Se_5^{VI}$	172.1(3)
$Se_8\cdots Se_8^{VII}$	3.621(2)	$\angle Se_2-Se_8\cdots Se_8^{VII}$	89.22(4)
		$\angle Se_5-Se_8\cdots Se_8^{VII}$	109.18(4)
		$\angle C_8-Se_8\cdots Se_8^{VII}$	166.4(3)

Table 5. Distances from the potassium ions and from the water molecule. Bond lengths (Å) and angles (°). Standard deviations are given in parentheses.

$K_1\cdots N_7$	2.920(9)	$\angle N_7\cdots K_1\cdots N_8$	72.7(3)
$K_1\cdots N_8$	3.029(10)		
$K_1\cdots N_1^{VIII}$	2.958(8)	$\angle N_1^{VIII}\cdots K_1\cdots N_6^{VIII}$	72.3(3)
$K_1\cdots N_6^{VIII}$	3.108(11)	$\angle N_1^{VIII}\cdots K_1\cdots N_7^{VIII}$	86.0(3)
$K_1\cdots N_7^{VIII}$	2.854(11)	$\angle N_6^{VIII}\cdots K_1\cdots N_7^{VIII}$	76.3(3)
$K_1\cdots O^{VIII}$	2.909(9)		
$K_2\cdots N_6$	3.084(10)	$\angle N_6\cdots K_2\cdots N_4^{IV}$	67.2(3)
$K_2\cdots N_4^{IV}$	3.039(9)	$\angle N_6\cdots K_2\cdots N_3^{III}$	73.5(3)
$K_2\cdots N_3^{III}$	2.907(14)	$\angle N_4^{IV}\cdots K_2\cdots N_3^{III}$	109.4(3)
$K_2\cdots N_1^{IX}$	3.118(11)	$\angle N_1^{IX}\cdots K_2\cdots N_8^{VII}$	72.5(3)
$K_2\cdots N_8^{VII}$	2.849(10)	$\angle N_1^{IX}\cdots K_2\cdots N_4^{X}$	64.2(3)
$K_2\cdots N_4^{X}$	2.909(9)	$\angle N_8^{VII}\cdots K_2\cdots N_4^{X}$	89.3(3)
$K_2\cdots O^{II}$	2.820(8)		
$O\cdots N_8$	3.116(13)	$\angle N_8\cdots O\cdots N_3^{XI}$	83.6(4)
$O\cdots N_3^{XI}$	2.933(13)	$\angle N_8\cdots O\cdots K_1^{VII}$	114.4(3)
$O\cdots K_1^{VIII}$	2.909(9)	$\angle N_8\cdots O\cdots K_2^{III}$	129.7(3)
$O\cdots K_2^{III}$	2.820(8)	$\angle N_3^{XI}\cdots O\cdots K_1^{VII}$	110.0(3)
		$\angle N_3^{XI}\cdots O\cdots K_2^{III}$	100.8(3)
		$\angle K_1^{VIII}\cdots O\cdots K_2^{III}$	110.9(3)

lengths in the three-selenium system, particularly on the long bonds between central atoms and bridging atoms. Thus, the Se_2-Se_7 bond length is 3.089 Å and the $Se_7\cdots Se_3^{II}$ distance is 3.737 Å. The effect, if any, of Se_3^{II} on the Se_2-Se_7 bond length is probably small. On the other hand, the Se_2-Se_8 bond length is 3.244 Å and the close contact $Se_8\cdots Se_1^{IV}$ is 3.464 Å; the Se_5-Se_7 bond length is 3.207 Å and the contact $Se_7\cdots Se_6^{I}$ is 3.522 Å; the Se_5-Se_8 bond length is 3.167 and the contact $Se_8\cdots Se_4^{III}$ is 3.639 Å.

The close contacts may also have a small influence on the rather short Se–Se bond lengths between the central atoms and the terminal atoms. In the approximately linear

a *b* *c*

system $-Se\cdots Se-Se-Se-$, the short bond length *b* is probably to some degree influenced by the neighbouring atoms on both sides. Since the bond *b* has nearly the strength of a covalent bond and since the difference between *a* and *c* is rather small, from 0.22 Å and upwards, and a relatively short bond *c* occurs together with a relative long *a*, and *vice versa*, the total effect on *b* is expected to be small.

The six cyano groups of the eight-selenium unit are all located at the same side of the least squares plane through the unit, and the Se–C bonds makes angles of 70.3 to 82.7° with the plane. Only one of the selenocyanate groups, $Se_1-C_1-N_1$, has a significant devia-

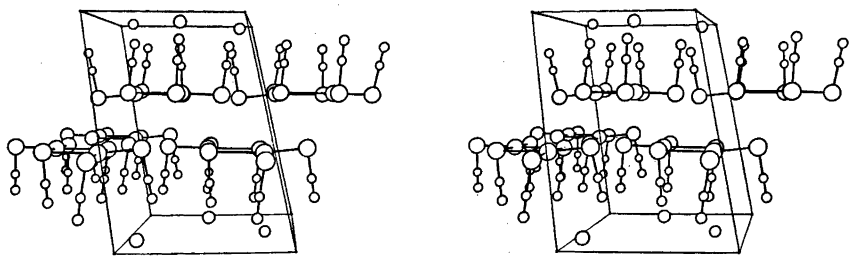

Fig. 2. A stereoscopic pair of drawings of $KSe(SeCN)_3.\frac{1}{2}H_2O$. The cell drawn is along the *a* and *c* axes from 0 to 1 and along *b* axis from $-\frac{1}{2}$ to $\frac{1}{2}$.

tion from linearity, the $Se_1-C_1-N_1$ angle being 174.6(7)°. The Se–C bond lengths are from 1.808(10) to 1.876(10) Å, with mean value 1.839 Å. As seen from Table 4, the two selenium atoms Se_1 and Se_4 with the longest Se–C bond lengths have close contacts to selenium atoms located *trans* to the carbon atoms. Thus, the Se_1-C_1 bond length is 1.876(10) Å, the $Se_1\cdots Se_2^V$ distance is 3.339(2) Å, and the angle $C_1-Se_1\cdots Se_2^V$ is 176.1(3)°. The Se_4-C_4 is 1.866(9) Å, the $Se_4\cdots Se_5^{VI}$ is 3.426(2) Å, and $C_4-Se_4\cdots Se_5^{VI}$ is 172.1(3)°. This tendency of lengthening of the Se–C bond caused by the close contact *trans* to the Se–C bond is uncertain since the standard deviations are rather large.

The C–N bond lengths, from 1.121(13) to 1.145(11) Å, are equal within the accuracy of the structure analysis.

The dimensions of the selenocyanate groups are in the same range as have been found earlier.[6–9]

The close selenium-selenium contacts from atoms in the layer at y approximately 0.128 to atoms in the layer at y approximately −0.128, occur, as mentioned above, from Se_1 to Se_3^V and from Se_4 to Se_5^{VI}. Furthermore, the central selenium atom Se_2 has a close contact to Se_1^V, the distance is 3.339 Å and the angles $Se-Se_2\cdots Se_1^V$ are from 76.17 to 97.47°. The other central selenium atom, Se_5, has a contact to Se_4^{VI}, 3.426 Å; the angles $Se-Se_5\cdots Se_4^{VI}$ are from 75.59 to 101.78°. The distance between the two bridging selenium atoms Se_8 and Se_8^{VII} is 3.621 Å and the angle $C_8-Se_8\cdots Se_8^{VII}$ is 166.4°.

The central selenium atoms, Se_2 and Se_5, have both a square-planar coordination. The tendency of selenium(II) and of tellurium(II) in their complexes toward square-planar coordination is well known.[10] It is therefore likely that the central selenium atoms, in the present structure, are acting as donors in the fifth approaches which are at approximately right angles to the square-planar coordinations.

The eight-selenium unit can be looked upon as built up of two selenium diselenocyanate molecules $Se(SeCN)_2$, bridged together through the selenium atoms of two selenocyanate ions. In the crystals of selenium diselenocyanate,[10–12] the molecules lie across a crystallographic mirror plane, with the middle selenium atom in the plane; the Se–Se bond lengths are 2.33 Å and the Se–Se–Se angle is 103°. Short Se···N contacts occur in directions which indicate a tendency to square-planar coordination at all selenium atoms. The Se···N distances at the central selenium atom are both 3.16 Å, and at each of the terminal selenium atoms, 3.07 and 3.27 Å. In the present adduct with potassium selenocyanate, the selenium diselenocyanate molecules retain their approximate shape. The Se–Se bond is now being approached at approximately 180° by a selenium atom of a selenocyanate group with the CN part of the group at right angle to the approach, instead of by the nitrogen end of a selenocyanate group. The approach is now stronger and the Se–Se bonds, *trans* to the approach, become a little longer.

The tendency to square-planar coordination at the terminal selenium atoms of selenium diselenocyanate are found in the present structure at Se_1 and Se_4. Se_1 is bonded to C_1 and to Se_2. The bond lengths are 1.876 and 2.403 Å, respectively; the $Se_2-Se_1-C_1$ angle is 97.2°. The Se_1-Se_2 bond is approached at 169.29° by Se_8^I, the $Se_1\cdots Se_8^I$ distance is 3.464 Å. The C_1-Se_1 bond is approached at 176.1° by Se_3^V, the $Se_1\cdots Se_3^V$ distance is 3.339 Å. The atoms Se_8^I and Se_3^V are 0.622 and 0.077 Å, respectively, from the plane through $Se_2Se_1C_1$. The surroundings of the terminal selenium atom Se_4, are much the same as for Se_1. Se_4 is bonded to C_4 and to Se_5. The bond lengths are 1.866 and 2.411 Å, respectively; the $Se_5-Se_4-C_4$ angle is 93.9°. The Se_4-Se_5 bond is approached at 172.59° by Se_8^{II}, the $Se_4\cdots Se_8^{II}$ distance is 3.639 Å. The C_4-Se_4 bond is approached at 172.1° by Se_5^{VI}, the $Se_4\cdots Se_5^{VI}$ distance is 3.426 Å. The atoms Se_8^{II} and Se_5^{VI} are −0.442 and 0.273 Å, respectively, out of the plane through $Se_5Se_4C_4$. The terminal selenium atoms Se_3 and Se_6 have close contacts *trans* to Se_3-Se_2 and Se_6-Se_5, respectively, but no close contacts *trans* to the cyano groups.

The environment of the potassium ions and the water molecule. The potassium ions and the water molecule lie at y approximately ½, between double layers of selenium atoms around $y=0$ and 1. The closest contacts of the potassium ions and of the water molecule are listed in Table 5. The water molecule is surrounded by two potassium ions, at distances

of 2.820 and 2.909 Å and K···O···K angle of 110.9°, and by two nitrogen atoms, at distances of 2.933 and 3.116 Å and a N···O···N angle of 83.6°. The latter contacts probably involve weak O–H···N hydrogen bonds. The arrangement around the water molecule is approximately tetrahedral, the K···O···N angles being in the range 105.3 to 129.7°.

The potassium ion K_2 is surrounded by six nitrogen atoms, at distances ranging from 2.849 to 3.118 Å, and by one oxygen atom, at 2.820 Å. The shape of the resulting polyhedron is rather irregular. Three of the nitrogen atoms lie on a plane above and three lie in a plane below the potassium ion; both planes are approximately parallel to the *ac* plane. The oxygen atom lies between the two planes.

The surroundings of the potassium ion K_1 is much the same as of K_2 with the exception that one of the nitrogen atoms below potassium is missing. The distances from K_1 to the nitrogen atoms are in the range 2.854 to 3.108 Å, and the distance from K_1 to oxygen is 2.909 Å.

The K···O distances are in the normal range (*cf.* Ref. 13, p. 258) and so are the K···N distances. The sum of the K···N ionic radii is 3.04 Å. In potassium selenocyanate,[9] the closest K···N distances are 2.89, 2.94, and 3.12 Å; in potassium thiocyanate,[14] 2.97 and 2.89 Å, and in potassium triselenocyanate hemihydrate,[7] in the range 2.86 to 3.04 Å.

REFERENCES

1. Verneuil, A. *Ann. Chim. Phys.* [6] *9* (1886) 289.
2. Hauge, S. *Acta Chem. Scand. 25* (1971) 3081.
3. Hauge, S. *Acta Chem. Scand. 25* (1971) 1135.
4. Coppens, P., Leiserowitz, L. and Rabinovich, D. *Acta Crystallogr. 18* (1965) 1035.
5. Åse, K. *Acta Chem. Scand. 25* (1971) 838.
6. Hauge, S. and Sletten, J. *Acta Chem. Scand. 25* (1971) 3094.
7. Hauge, S. *Acta Chem. Scand. 25* (1971) 3103.
8. Hauge, S. *Acta Chem. Scand. A 29* (1975) 163.
9. Swank, D. D. and Willett, R. D. *Inorg. Chem. 4* (1965) 499.
10. Foss, O. In Andersen, P., Bastiansen, O. and Furberg, S. *Selected Topics in Structure Chemistry*, Oslo 1967, p. 145.
11. Aksnes, O. and Foss, O. *Acta Chem. Scand. 8* (1954) 1787.
12. McDonald, W. S. and Pettit, L. D. *J. Chem. Soc. A* (1970) 2044.
13. *International Tables of X-Ray Crystallography*, Kynoch Press, Birmingham 1962, Vol. III.
14. Akers, C., Peterson, S. W. and Willett, R. D. *Acta Crystallogr. B 24* (1968) 1125.

Received March 17, 1975.

Acta Chemica Scandinavica A 29 (1975) 778—782

The Crystal Structure of Potassium Seleniumtrithiocyanate Hemihydrate

SVERRE HAUGE and PER ARNE HENRIKSEN

Department of Chemistry, University of Bergen, N-5014 Bergen-Univ., Norway

Potassium seleniumtrithiocyanate hemihydrate, $KSe(SCN)_3 \cdot \frac{1}{2}H_2O$, has been prepared from selenium oxidized by bromine and reacted with potassium thiocyanate.

The crystal structure has been determined by X-ray methods, and refined by full-matrix least squares procedures. The crystals are triclinic, space group $P\bar{1}$ (No. 2), with $a = 8.775$ (4) Å, $b = 15.067(5)$ Å, $c = 8.956(4)$ Å, $\alpha = 119.64$ (3)°, $\beta = 101.03(3)°$, $\gamma = 99.62(2)°$, and four formula units per unit cell.

In the crystals, the seleniumtrithiocyanate ions are dimerized. The two selenium atoms and the six sulfur atoms of the dimerized unit are approximately co-planar. The six cyano groups are located on the same side of the plane. Each of the two selenium atoms has an approximately square-planar coordination. The S—Se—S angles are in the range from 168.89 (10) to 176.26(11)° and from 84.24(8) to 98.52 (12)°. There are four rather short Se—S bonds, from 2.252(2) to 2.318(3) Å, and four long ones, from 2.906(3) to 3.112(3) Å. The short ones are significantly longer than Se—S single-bond distance, 2.21 Å, and the long ones are shorter than van der Waals approaches. Each long Se—S bond occurs *trans* to a short Se—S bond. The total lengths of the rather unsymmetrical approximately linear S—Se—S systems (the sums of the lengths of the two Se—S bonds) are from 5.197 to 5.364 Å.

The salt, potassium seleniumtrithionate hemihydrate, $KSe(SCN)_3 \cdot \frac{1}{2}H_2O$, has been isolated from an aqueous solution made by treating a suspension of selenium with bromine and then adding potassium thiocyanate. Without going into details concerning the reaction steps, the net reaction can be written:

$$Se + Br_2 + 3SCN^- = Se(SCN)_3^- + 2Br^-$$

The crystal structure of the analogous selenocyanate compound, potassium triselenocyanate hemihydrate, has been reported earlier.[1]

EXPERIMENTAL

Preparation of potassium seleniumtrithiocyanate hemihydrate. 0.05 mol (4 g) of selenium was suspended in 100 ml water of 50 °C, and 0.046 mol (2.5 ml) of bromine was added under stirring. After the reaction was finished, a solution, heated to 50 °C, of 0.25 mol (24 g) of KSCN in 50 ml water was added. The combined solution was filtered and then stored in a refrigerator for 5 h. The crystals which had deposited were filtered off and dried. Yield, 3.3 g, or 24 % based on the amount of bromine employed. (Found: Se 26.30 Calc. for $KSe(SCN)_3 \cdot \frac{1}{2}H_2O$: 26.24)

The salt can be recrystallized from a solution of 20 g KSCN in 50 ml water. The crystals are yellow triclinic prisms extended along the short *ac* diagonal.

CRYSTAL DATA

Collection of X-ray data was done by use of Nb-filtered Mo$K\alpha$ radiation, $\lambda(\alpha_1) = 0.70926$ Å, by the same methods as for the analogous selenocyanate complex.[1] The cell parameters were evaluated from the θ angle of 11 resolved reflections.

$KSe(SCN)_3 \cdot \frac{1}{2}H_2O$, space group $P\bar{1}$ (No. 2), $a = 8.775(4)$ Å, $b = 15.067(5)$ Å, $c = 8.956(4)$ Å, $\alpha = 119.64(3)°$, $\beta = 101.09(3)°$, $\gamma = 99.62(2)°$, $Z = 4$. $D_x = D_m = 2.08$ g/cm³. Number of reflections recorded with measurable intensities, 2945 out of 5657 possible within $\theta = 30°$. $\mu = 51.8$ cm^{-1}.

The crystal used for data collection had the following dimensions, given as distances from the point of intersection of $(11\bar{1})$, $(12\bar{1})$, and $(1\bar{1}1)$; to (010), 0.034 mm; to $(0\bar{1}0)$, 0.052 mm; to $(\bar{1}\bar{1}1)$, 0.10 mm; and to $(\bar{1}1\bar{1})$ 0.28 mm.

Intensities were corrected for absorption[2] and extinction.[3]

Table 1. Atomic coordinates for potassium seleniumtrithiocyanate hemihydrate in fractions of triclinic cell edges. Origin at a centre of symmetry. Standard deviations from least squares are given in parentheses.

	x	y	z
Se_1	0.22700(8)	0.11774(6)	−0.14168(10)
Se_2	0.63014(7)	0.13601(6)	0.24619(10)
S_1	0.2092(2)	0.1003(2)	−0.4130(3)
S_2	−0.0257(2)	0.1268(2)	−0.1365(3)
S_3	0.9017(2)	0.1552(2)	0.2830(3)
S_4	0.6345(2)	0.1299(2)	0.5005(3)
S_5	0.5981(2)	0.1456(2)	−0.0742(3)
S_6	0.2890(2)	0.1247(2)	0.2005(3)
C_1	0.2756(9)	0.2311(7)	−0.3350(10)
C_2	0.0173(8)	0.2620(6)	−0.0099(10)
C_3	0.9701(8)	0.2905(6)	0.4081(10)
C_4	0.7362(9)	0.2597(7)	0.6513(10)
C_5	0.6281(7)	0.2757(6)	0.0492(10)
C_6	0.3474(8)	0.2574(6)	0.3104(10)
N_1	0.3197(10)	0.3195(6)	−0.2840(10)
N_2	0.0398(7)	0.3530(6)	0.0747(10)
N_3	1.0188(7)	0.3827(6)	0.4949(10)
N_4	0.8096(9)	0.3473(6)	0.7512(9)
N_5	0.6495(8)	0.3669(6)	0.1389(10)
N_6	0.3904(8)	0.3493(6)	0.3867(9)
O	0.4056(6)	0.4902(4)	0.1710(7)
K_1	0.2654(2)	0.52154(14)	0.4509(2)
K_2	0.8293(2)	0.52197(14)	0.1013(2)

Table 2. Anistropic thermal parameters (Å²) in the form $\exp[-2\pi^2(h^2a^{-2}U_{11}+\cdots+2hka^{-1}b^{-1}U_{12}+\cdots)]$. All values have been multiplied by 10^3. Standard deviations from least squares refinement in parentheses.

	U_{11}	U_{22}	U_{33}	U_{12}	U_{23}	U_{13}
Se_1	27.4(3)	17.1(3)	22.1(3)	6.9(2)	8.5(3)	5.4(2)
Se_2	22.7(3)	13.9(3)	20.2(3)	4.4(2)	6.9(2)	3.1(2)
S_1	50.5(9)	25.6(8)	21.5(8)	7.6(7)	9.1(7)	7.1(7)
S_2	25.6(7)	23.5(8)	32.5(8)	4.3(6)	10.0(7)	6.1(6)
S_3	26.6(7)	26.3(8)	36.6(9)	10.3(6)	14.3(7)	8.7(6)
S_4	43.0(9)	28.6(9)	29.0(8)	5.7(7)	17.3(7)	6.0(7)
S_5	37.1(8)	23.6(8)	30.2(8)	9.1(6)	10.2(7)	8.2(6)
S_6	35.2(8)	27.5(8)	30.3(8)	4.4(6)	14.1(7)	7.2(6)
C_1	48(4)	34(4)	24(3)	15(3)	17(3)	14(3)
C_2	28(3)	28(3)	29(3)	9(3)	13(3)	6(2)
C_3	27(3)	27(3)	34(3)	7(2)	17(3)	9(2)
C_4	42(4)	29(3)	24(3)	11(3)	11(3)	9(3)
C_5	23(3)	27(3)	32(3)	7(2)	16(3)	11(2)
C_6	30(3)	28(3)	31(3)	12(3)	17(3)	14(2)
N_1	93(5)	31(3)	38(4)	14(3)	19(3)	26(3)
N_2	38(3)	32(3)	46(3)	12(3)	14(3)	11(3)
N_3	37(3)	34(3)	51(4)	4(2)	23(3)	10(3)
N_4	71(4)	42(4)	27(3)	15(3)	13(3)	11(3)
N_5	51(3)	32(3)	45(4)	12(3)	18(3)	19(3)
N_6	54(3)	34(3)	39(3)	17(3)	17(3)	18(3)
O	42(2)	36(3)	36(2)	12(2)	15(2)	13(2)
K_1	37.3(7)	28.7(7)	33.4(8)	10.5(6)	14.3(6)	11.0(6)
K_2	47.2(8)	30.2(8)	27.6(7)	6.8(6)	11.3(6)	12.9(6)

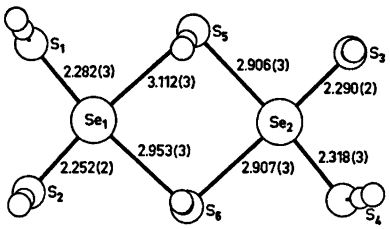

Fig. 1. The di-μ-thiocyanato-bis[dithiocyanatoselenate(II)] anion in $KSe(SCN)_3.\frac{1}{2}H_2O$, as seen normal to the *ac* plane.

THE STRUCTURE ANALYSES

The structure was solved by Patterson and Fourier methods and by reference to the structure of $KSe(SeCN)_3.\frac{1}{2}H_2O$.

The *R*-value in the final full-matrix least squares refinement was 0.046. The Fourier difference map based on these data showed no higher peak than 0.3 e Å^3.

Computational procedure and programs used are described elsewhere.[3] The final atomic coordinates and temperature parameters are listed in Tables 1 and 2.

The structure factors are available from the author on request.

RESULTS

The di-μ-thiocyanato-bis[dithiocyanatoselenate (II)] anion. Bond lengths and angles in the anion, based on the atomic coordinates of Table 1, are given in Fig. 1 and Table 3. Distances from the potassium ions and from the water molecule to neighbouring atoms are given in Table 4. The uncertainties in cell dimensions are taken into account in the given standard deviations.

As seen from Fig. 1, the seleniumtrithiocyanate ions are dimerized in the crystals. The two central atoms, Se_1 and Se_2, the four terminal sulfur atoms, S_1, S_2, S_3, and S_4, and the two bridging sulfur atoms, S_5 and S_6, are approximately co-planar. The largest deviation of an atom from a least squares plane is 0.21 Å.

Each of the selenium atoms has a distorted square-planar environment, with long bonds to bridging sulfur atoms *trans* to rather short bonds to terminal sulfur atoms. The short bonds, from 2.252(2) to 2.318(3) Å, are definitely longer than the Se–S single bond, 2.21 Å. The long bonds are from 2.906(3) to 3.112(3) Å, and thus shorter than van der Waals approaches. The S–Se–S angles of the four approximately linear S–Se–S systems are from 168.89(10) to 176.26(11)°.

The length of a symmetrical linear S–Se–S system (the sum of the lengths of the two Se–S bonds) is unknown. An estimated value can be derived from the length of the symmetrical linear Se–Se–Se system [4–6] by subtracting the difference between the covalent radii of

Table 3. Angles (°) in the dimerized seleniumtrithiocyanate ion and distances (Å) in the thiocyanate groups in the same ion. Standard deviations in parentheses.

$S_1-Se_1-S_2$	98.52(12)	$S_3-Se_2-S_4$	95.50(11)
$S_2-Se_1-S_6$	89.38(11)	$S_4-Se_2-S_6$	86.50(10)
$S_6-Se_1-S_5$	84.24(8)	$S_6-Se_2-S_5$	88.87(9)
$S_5-Se_1-S_1$	88.48(10)	$S_5-Se_2-S_3$	89.09(10)
$S_1-Se_1-S_6$	171.38(10)	$S_3-Se_2-S_6$	176.26(11)
$S_2-Se_1-S_5$	168.89(10)	$S_4-Se_2-S_5$	175.31(9)
S_1-C_1	1.676(10)	$\angle Se_1-S_1-C_1$	97.9(3)
C_1-N_1	1.135(13)	$\angle S_1-C_1-N_1$	179.2(7)
S_2-C_2	1.695(8)	$\angle Se_1-S_2-C_2$	99.0(3)
C_2-N_2	1.148(11)	$\angle S_2-C_2-N_2$	177.2(5)
S_3-C_3	1.685(8)	$\angle Se_2-S_3-C_3$	97.5(3)
C_3-N_3	1.150(10)	$\angle S_3-C_3-N_3$	179.0(6)
S_4-C_4	1.669(7)	$\angle Se_2-S_4-C_4$	95.8(4)
C_4-N_4	1.132(10)	$\angle S_4-C_4-N_4$	177.5(7)
S_5-C_5	1.645(8)	$\angle Se_1-S_5-C_5$	86.9(2)
C_5-N_5	1.156(11)	$\angle Se_2-S_5-C_5$	90.4(4)
		$\angle S_5-C_5-N_5$	178.6(8)
S_6-C_6	1.658(9)	$\angle Se_1-S_6-C_6$	88.0(4)
C_6-N_6	1.147(11)	$\angle Se_2-S_6-C_6$	88.0(3)
		$\angle S_6-C_6-N_6$	178.9(6)

Table 4. Distances from the potassium ions and from the water molecule. Bond lengths (Å) and angles (°). Standard deviations are given in parentheses.[a]

$K_1 \cdots N_2$	3.005(6)	$\angle N_2 \cdots K_1 \cdots N_6$	80.5(2)
$K_1 \cdots N_6$	2.827(9)	$\angle N_2 \cdots K_1 \cdots N_3^{I}$	74.2(3)
$K_1 \cdots N_3^{I}$	2.972(9)	$\angle N_6 \cdots K_1 \cdots N_3^{I}$	77.3(3)
$K_1 \cdots N_3^{II}$	3.089(8)	$\angle N_3^{II} \cdots K_1 \cdots N_5^{II}$	80.7(2)
$K_1 \cdots N_5^{II}$	3.050(8)	$\angle N_3^{II} \cdots K_1 \cdots N_6^{II}$	123.9(2)
$K_1 \cdots N_6^{II}$	2.931(6)	$\angle N_5^{II} \cdots K_1 \cdots N_6^{II}$	72.4(2)
$K_1 \cdots O$	2.868(7)		
$K_2 \cdots N_5$	2.792(10)	$\angle N_5 \cdots K_2 \cdots N_4^{III}$	86.6(3)
$K_2 \cdots N_4^{III}$	2.876(7)		
$K_2 \cdots N_1^{IV}$	2.847(9)	$\angle N_1^{IV} \cdots K_2 \cdots N_3^{V}$	73.7(2)
$K_2 \cdots N_3^{V}$	3.050(8)	$\angle N_1^{IV} \cdots K_2 \cdots N_4^{V}$	102.9(2)
$K_2 \cdots N_4^{V}$	3.069(7)	$\angle N_3^{V} \cdots K_2 \cdots N_4^{V}$	67.0(2)
$K_2 \cdots O^{IV}$	2.783(6)		
$O \cdots N_5$	3.028(10)	$\angle N_5 \cdots O \cdots N_1^{IV}$	87.9(3)
$O \cdots N_1^{IV}$	2.990(10)	$\angle N_5 \cdots O \cdots K_1$	113.9(3)
$O \cdots K_1$	2.868(7)	$\angle N_5 \cdots O \cdots K_2^{IV}$	129.7(2)
$O \cdots K_2^{IV}$	2.783(6)	$\angle N_1^{IV} \cdots O \cdots K_1$	113.2(2)
		$\angle N_1^{IV} \cdots O \cdots K_2^{IV}$	125.3(3)
		$\angle K_1 \cdots O \cdots K_2^{IV}$	106.9(2)

[a] Superscript I denotes an atom at $(x-1,y,z)$, II at $(1-x,1-y,1-z)$, III at $(x,y,z-1)$, IV at $(1-x,1-y,z)$, and V at $(2-x,1-y,1-z)$, where x,y,z are the coordinates of Table 1.

selenium and sulfur, $2(r_{Se}-r_S)$, which give $(5.31-0.26)$ Å $=5.05$ Å. The total lengths of the unsymmetrical approximately linear S–Se–S systems in the present structure are from 5.197 to 5.364 Å, and thus 0.15 to 0.31 Å longer than the estimated value of a symmetrical linear S–Se–S arrangement.

The six cyano groups of the dimerized unit are all located on the same side of the least squares plane through the selenium atoms and the sulfur atoms. The Se–S–C angles are from 86.9(2) to 99.0(3)°. The S–C–N groups have only small, if any, significant deviation from linearity, the S–C–N angles are from 177.2(5) to 179.2(7)°. The mean values of the S–C bond lengths and the C–N bond lengths are 1.671 and 1.145 Å, respectively, and there is no significant deviation from these mean values.

The present crystal structure shows great resemblance with the structures of the corresponding selenocyanate compounds [1,7] with regard to the intra-ionic structure. But while the selenium atoms of the selenocyanate groups have a great tendency of forming interionic Se···Se contacts, to give double layers of selenium atoms, the sulfur atoms of the thiocyanate groups do not form such interionic

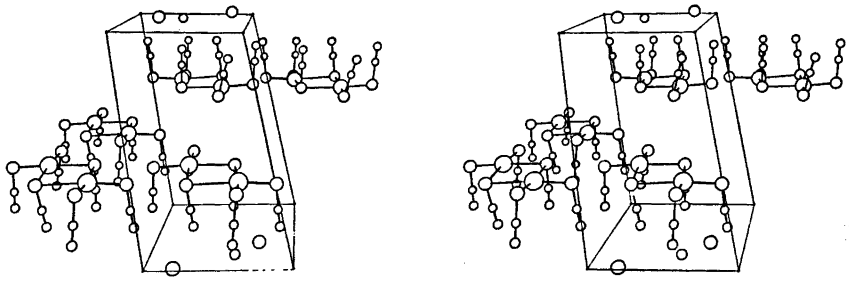

Fig. 2. A stereoscopic pair of drawings of $KSe(SCN)_3.\frac{1}{2}H_2O$. The cell drawn is along the a and c axis from 0 to 1 and along b axis from $-\frac{1}{2}$ to $\frac{1}{2}$.

S···Se or S···S contacts. The shortest interionic S···Se distance in the present structure, between single layers, is 3.542(3) Å, and the shortest S···S distance is 3.486(3) Å.

In the crystal structure of $KSe(SeCN)_3 \cdot \frac{1}{2}H_2O$ [1] and the corresponding rubidium salt [7] the dimerized seleniumtriselenocyanate ion can be looked upon as built up of two selenium diselenocyanate molecules, $Se(SeCN)_2$, bridged together through the selenium atoms of two selenocyanate ions. In the present structure, the dimerized unit of seleniumtrithiocyanate can be looked upon as built up of two selenium dithiocyanate molecules, $Se(SCN)_2$, bridged together through the sulfur atoms of two thiocyanate ions. In the crystals of selenium dithiocyanate,[8] the molecules lie across a crystallographic mirror plane passing through the selenium atom, the Se–S bond lengths are 2.21 Å and the S–Se–S angle is 101°. Short Se–N contacts occur in directions which indicate a tendency to square-planar coordination at the selenium atom. The Se···N distances are 2.98 Å. In the present adduct with potassium thiocyanate, the selenium dithiocyanate molecules retain their approximate shape. The Se–S bond is now being approached at approximately 180° by a sulfur atom of a thiocyanate group instead of by the nitrogen end of a thiocyanate group. The approach is now stronger, resulting in a little longer Se–S bonds *trans* to the approach, and smaller S–Se–S angles. At Se_1 the sum of the two Se–S bond lengths is 4.534 Å and the angle is 98.52(12)°, and at Se_2 the sum is 4.608 Å and the angle is 95.50(11)°.

The environment of the potassium ions and the water molecule. The potassium ions and the water molecule lie at y approximately $\frac{1}{2}$, packed between nitrogen atoms with y about 0.35 and 0.65. The closest contacts of the potassium ions and the water molecule are listed in Table 4. The shapes of the resulting polyhedrons around the water molecule and the potassium ions are very much the same as found in the structure of $KSe(SeCN)_3 \cdot \frac{1}{2}H_2O$.[1]

REFERENCES

1. Hauge, S. *Acta Chem. Scand. A 29* (1975) 771.
2. Coppens, P., Leiserowitz, L. and Rabinovich, D. *Acta Crystallogr. 18* (1965) 1035.
3. Åse, K. *Acta Chem. Scand. 25* (1971) 838.
4. Hauge, S. and Sletten, J. *Acta Chem. Scand. 25* (1971) 3094.
5. Hauge, S. *Acta Chem. Scand. 25* (1971) 3103.
6. Hauge, S. *Acta Chem. Scand. A 29* (1975) 163.
7. Hauge, S. *Acta Chem. Scand. A 29* (1975). *In press.*
8. Ohlberg, S. M. and Vaughan, P. A. *J. Amer. Chem. Soc. 76* (1954) 2649.

Received March 17, 1975.

Acta Chemica Scandinavica A 29 (1975) 783—786

Crystal Structure of 1,1′-Dihydroperoxycyclododecanyl-peroxide-1,1′ at —160 °C

P. GROTH

Department of Chemistry, University of Oslo, Oslo 3, Norway

The crystals are triclinic with dimensions $a = 8.657(6)$ Å, $b = 11.808(4)$ Å, $c = 12.526(5)$ Å, $\alpha = 77.22(3)°$, $\beta = 77.54(4)°$, $\gamma = 81.68(4)°$ for Dirichlet's reduced cell. The space group is $P\bar{1}$ with two molecules in the unit cell. The structure was solved by direct methods and refined by full-matrix least squares technique to an R-value of 5.7 % ($R_w = 4.4$ %) for 2254 observed reflections measured on an automatic four-circle diffractometer. Mean values of C – O, C – O, and C – C bond distances are 1.474, 1.427, and 1.526 Å, respectively. The C – O – O angles of the hydroxyperoxy groups are 110.0 and 109.1°. The corresponding angles of the peroxy bridge are 108.2 and 108.4°. The asymmetric environments of the non-methylene carbon atoms resemble those observed for trimeric acetone peroxide and 1,1′-dihydroperoxycyclohexanyl-peroxide-1,1′. The conformation of the molecule is *cis*, and the dihedral angle C – O – O – C is 124.3°. There are possibly two *intra*-molecular hydrogen bonds of lengths 2.870 and 2.765 Å, respectively.

A crystal structure determination of 1,1′-dihydroperoxycyclododecanylperoxide-1,1′ has

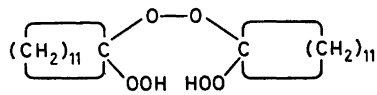

been carried out in order to study the hydroperoxy group, especially its ability to form

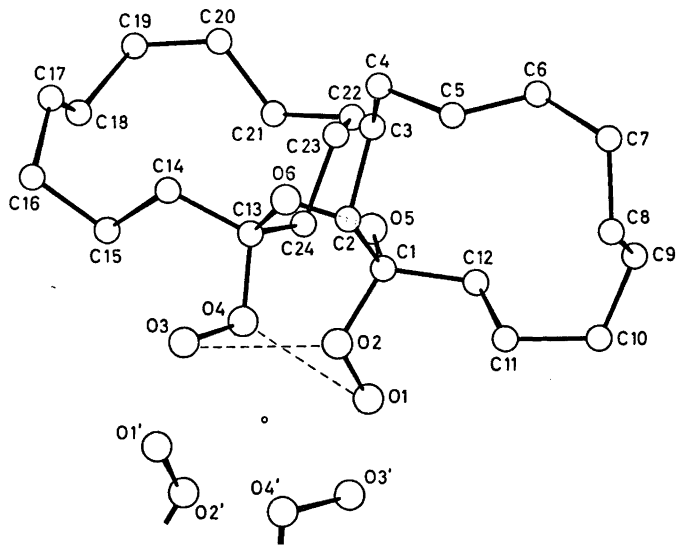

Fig. 1. Schematic drawing of the molecule.

Table 1. Final fractional coordinates and thermal parameters with estimated standard deviations (multiplied by 10^5 for O- and C-atoms and by 10^4 for H-atoms). Hmn is bonded to Cm. The expression for anisotropic vibration is exp $[-(B11h^2+B22k^2+B33l^2+B12hk+B13hl+B23kl)]$.

ATOM	X	Y	Z	B11	B22	B33	B12	B13	B23
O1	112471(32)	49335(22)	16781(28)	1446(53)	586(25)	395(22)	668(58)	-219(55)	-417(38)
O2	99383(31)	52577(20)	25469(19)	1418(51)	388(24)	329(21)	62(54)	-271(53)	-128(35)
O3	77848(34)	49422(21)	13873(21)	1916(58)	369(24)	521(24)	-1015(62)	-454(59)	218(38)
O4	86683(29)	57456(20)	5845(19)	1243(48)	274(23)	342(21)	-217(53)	-356(50)	-88(34)
O5	96782(28)	72242(20)	16628(19)	728(43)	377(23)	318(20)	-126(48)	-398(46)	-19(33)
O6	88086(27)	71896(20)	15862(19)	644(44)	473(24)	383(20)	-173(49)	-355(46)	-224(33)
C1	99919(44)	64287(30)	26462(28)	1846(73)	248(33)	292(31)	77(75)	-464(75)	-81(50)
C2	87277(44)	65545(32)	36812(28)	1831(70)	443(36)	227(29)	-1109(88)	-178(72)	-198(51)
C3	82973(46)	78097(34)	38864(31)	1114(74)	587(38)	488(33)	539(84)	-598(88)	-223(56)
C4	77867(46)	78547(35)	51211(31)	968(73)	666(40)	338(32)	483(86)	-188(78)	-315(58)
C5	89860(46)	74818(33)	58384(29)	1112(73)	447(36)	281(30)	166(82)	-389(75)	-221(52)
C6	102862(48)	82676(33)	55695(31)	1245(77)	398(37)	454(34)	112(85)	-394(83)	-247(56)
C7	117897(49)	77779(36)	61161(33)	1338(81)	667(43)	493(36)	-414(94)	-399(88)	-357(63)
C8	127141(46)	67524(35)	56588(31)	1031(78)	743(43)	349(33)	-115(89)	-583(78)	-88(60)
C9	135895(44)	78962(37)	44451(32)	671(67)	874(46)	422(35)	-562(89)	-394(77)	55(64)
C10	139258(45)	61138(38)	37941(31)	737(71)	1034(58)	331(33)	688(93)	-317(76)	-91(64)
C11	124666(46)	57421(34)	35328(31)	1178(78)	515(38)	487(32)	494(85)	-648(81)	-278(56)
C12	116472(44)	66748(32)	27175(29)	817(65)	436(35)	386(30)	53(75)	-384(71)	-91(50)
C13	79836(42)	69183(30)	5322(28)	853(70)	292(34)	283(30)	-113(75)	-421(71)	-156(49)
C14	62218(44)	71887(33)	4922(30)	842(68)	588(38)	366(31)	-293(88)	-232(73)	-251(54)
C15	57894(45)	66585(33)	-4477(31)	913(71)	543(38)	489(34)	-491(83)	-437(79)	-218(57)
C16	48819(45)	78491(37)	-6877(31)	875(72)	804(46)	485(33)	-673(98)	-292(78)	-331(61)
C17	37263(44)	83553(36)	-9861(32)	694(66)	695(43)	495(35)	-255(83)	-445(77)	-288(58)
C18	45535(48)	88397(38)	-21793(32)	1182(77)	837(47)	419(35)	-601(96)	-687(83)	-182(63)
C19	49888(47)	101828(38)	-23766(32)	944(73)	758(45)	457(35)	178(91)	-429(81)	54(62)
C20	61823(46)	103888(32)	-17895(30)	964(72)	443(36)	399(33)	-15(82)	-332(78)	-98(54)
C21	78465(44)	97785(31)	-22455(29)	1879(72)	364(35)	289(30)	-157(79)	-338(75)	1(51)
C22	98965(44)	97478(31)	-15496(30)	1889(70)	377(35)	426(33)	-386(79)	-466(78)	2(54)
C23	88638(44)	89438(31)	-4819(29)	1141(71)	314(33)	328(31)	-188(77)	-558(75)	-102(50)
C24	99259(41)	76489(30)	-4392(27)	711(63)	355(34)	259(28)	-99(72)	-223(68)	-138(49)

ATOM	X	Y	Z	B	ATOM	X	Y	Z	B
H21	9128(35)	6878(26)	4328(24)	2,9(,7)	H141	5934(35)	7955(27)	432(25)	2,9(,7)
H22	7753(35)	6216(26)	3568(24)	2,7(,7)	H142	5646(35)	6666(26)	1289(25)	2,4(,7)
H31	7483(36)	8173(26)	3491(24)	3,1(,7)	H151	5974(35)	5715(27)	-288(25)	2,8(,7)
H32	9253(36)	8386(26)	3585(25)	2,9(,7)	H152	6553(35)	6857(26)	-1123(24)	2,3(,7)
H41	6768(35)	7335(26)	5439(24)	2,3(,7)	H161	3321(34)	6762(26)	116(24)	2,3(,6)
H42	7287(35)	8783(27)	5178(25)	2,8(,7)	H162	3816(35)	6597(26)	-1148(25)	2,8(,7)
H51	9436(35)	6629(26)	5759(24)	1,3(,7)	H171	4845(35)	8798(26)	-462(25)	2,1(,7)
H52	8454(35)	7346(26)	6651(25)	2,8(,7)	H172	2574(36)	8572(26)	-915(25)	1,7(,7)
H61	9896(35)	9836(26)	5783(25)	2,8(,7)	H181	3889(36)	8729(26)	-2696(24)	3,2(,7)
H62	18661(35)	8496(26)	4722(25)	2,3(,7)	H182	5526(36)	8329(26)	-2376(25)	2,1(,7)
H71	11338(36)	7498(26)	6929(25)	2,7(,7)	H191	3944(36)	10581(26)	-2168(25)	4,3(,7)
H72	12439(35)	8413(26)	5985(24)	2,7(,7)	H192	5269(35)	10356(25)	-3193(25)	3,2(,7)
H81	12873(35)	6153(26)	5697(25)	2,4(,7)	H201	5881(35)	9969(27)	-981(24)	1,2(,7)
H82	13498(35)	6488(26)	6186(24)	3,8(,7)	H202	6247(35)	11168(26)	-1866(25)	1,9(,7)
H91	14888(36)	7357(26)	4468(25)	2,3(,7)	H211	8174(35)	10272(27)	-3829(25)	1,9(,7)
H92	12962(36)	7854(26)	4898(25)	1,8(,7)	H212	7788(35)	8967(27)	-2315(25)	,8(,7)
H101	14546(35)	5377(26)	4229(24)	,8(,7)	H221	9865(35)	18545(26)	-1411(25)	3,1(,7)
H102	14747(35)	6322(26)	3083(24)	2,8(,7)	H222	10251(36)	9488(26)	-1975(25)	2,7(,7)
H111	11663(35)	5580(26)	4239(25)	1,8(,7)	H231	7768(36)	9141(26)	46(24)	1,4(,7)
H112	12782(35)	4968(26)	3211(24)	3,8(,7)	H232	9564(36)	9114(26)	58(24)	1,6(,7)
H121	12354(35)	6786(26)	1909(25)	2,2(,7)	H241	10171(36)	7346(26)	-451(25)	2,1(,7)
H122	11532(35)	7489(26)	2935(24)	1,2(,7)	H242	8793(36)	7567(26)	-1153(24)	,8(,7)

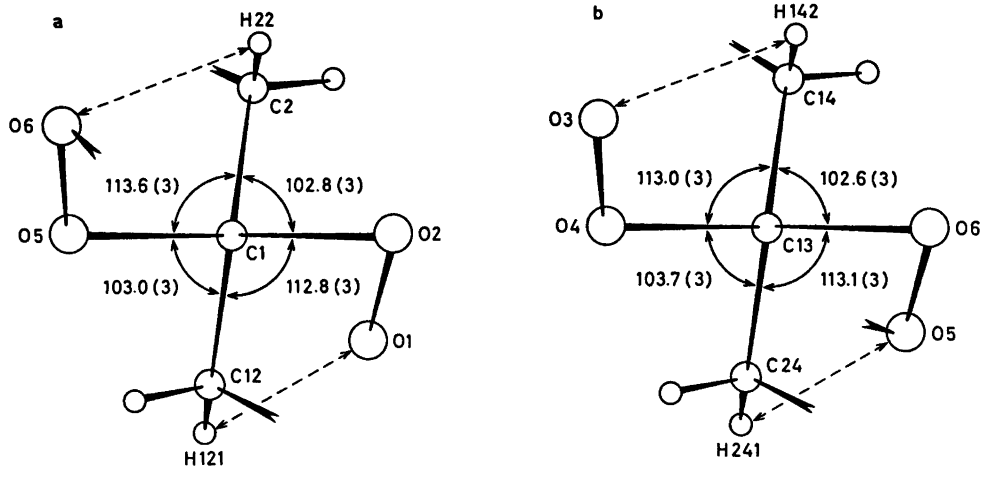

Fig. 2. Schematic drawing showing the asymmetric environments of the carbon atoms C1 and C13.

Table 2. Bond distances and angles and dihedral angles with estimated standard deviations.

Distance	Å	Distance	Å
O1 – O2	1.470(3)	C12 – C1	1.527(5)
O5 – O6	1.476(3)	C13 – C14	1.519(5)
O3 – O4	1.475(3)	C14 – C15	1.528(5)
O2 – C1	1.424(4)	C15 – C16	1.527(5)
O5 – C1	1.426(4)	C16 – C17	1.517(5)
O4 – C13	1.428(4)	C17 – C18	1.532(5)
O6 – C13	1.431(4)	C18 – C19	1.520(6)
C1 – C2	1.525(5)	C19 – C20	1.526(5)
C2 – C3	1.539(5)	C20 – C21	1.525(5)
C3 – C4	1.531(5)	C21 – C22	1.521(5)
C4 – C5	1.531(5)	C22 – C23	1.530(5)
C5 – C6	1.521(5)	C23 – C24	1.532(5)
C6 – C7	1.518(5)	C24 – C13	1.521(5)
C7 – C8	1.529(5)	O1 – O4	2.870(4)
C8 – C9	1.539(5)	O1 – O5	2.845(3)
C9 – C10	1.521(6)	O3 – O2	2.765(4)
C10 – C11	1.515(5)	O3 – O6	2.774(3)
C11 – C12	1.532(5)	O1 – O4′	2.987(3)

Angle	(°)	Angle	(°)
O1 – O2 – C1	110.0(2)	C12 – C1 – O2	114.3(3)
O3 – O4 – C13	109.1(2)	C13 – C14 – C15	114.5(3)
O2 – C1 – O5	110.6(3)	C14 – C15 – C16	113.2(3)
O4 – C13 – O6	109.9(3)	C15 – C16 – C17	114.8(3)
O2 – C1 – O5	113.6(3)	C16 – C17 – C18	114.5(3)
C12 – C1 – O5	105.0(3)	C17 – C18 – C19	114.3(3)
C24 – C13 – O4	105.7(3)	C18 – C19 – C20	114.6(3)
C14 – C13 – O4	113.0(3)	C19 – C20 – C21	114.0(3)
C13 – O6 – O5	108.4(2)	C20 – C21 – C22	115.6(3)
C1 – O5 – O6	108.2(2)	C21 – C22 – C23	114.3(3)
C2 – C1 – O2	102.8(3)	C22 – C23 – C24	114.1(3)
C12 – C1 – O2	112.8(3)	C23 – C24 – C13	113.1(3)
C14 – C13 – O6	102.6(3)	C24 – C13 – C14	114.8(3)
C24 – C13 – O6	113.1(3)	O2 – O1 – O4	76.9(1)
C1 – C2 – C3	114.9(3)	O2 – O1 – O5	55.3(1)
C2 – C3 – C4	112.8(3)	O4 – O3 – O2	80.6(1)
C3 – C4 – C5	114.2(3)	O4 – O3 – O6	57.5(1)
C4 – C5 – C6	113.4(3)	O1 – O4 – O3	87.1(2)
C5 – C6 – C7	114.1(3)	O1 – O4 – C13	115.9(2)
C6 – C7 – C8	114.3(3)	O3 – O2 – O1	91.3(2)
C7 – C8 – C9	113.4(3)	O3 – O2 – C1	115.5(2)
C8 – C9 – C10	114.4(3)	O2 – O1 – O4′	133.0(2)
C9 – C10 – C11	114.8(3)	O1 – O4′ – O3′	107.9(2)
C10 – C11 – C12	113.8(3)	O1 – O4 – C13′	113.0(2)
C11 – C12 – C1	114.3(3)		

Dihedral angle	(°)
C1 – O5 – O6 – C13	−124.3(3)
C1 – C2 – C3 – C4	−152.3(3)
C2 – C3 – C4 – C5	68.0(4)
C3 – C4 – C5 – C6	67.5(4)
C4 – C5 – C6 – C7	−169.4(3)
C5 – C6 – C7 – C8	68.9(4)
C6 – C7 – C8 – C9	67.4(4)
C7 – C8 – C9 – C10	−152.4(3)
C8 – C9 – C10 – C11	69.2(4)
C9 – C10 – C11 – C12	67.0(4)
C10 – C11 – C12 – C1	−167.0(3)
C11 – C12 – C1 – O2	70.6(4)
C12 – C1 – O2 – O3	67.8(4)
C13 – C14 – C15 – C16	−168.9(3)
C14 – C15 – C16 – C17	65.0(4)
C15 – C16 – C17 – C18	68.5(4)
C16 – C17 – C18 – C19	−151.3(3)
C17 – C18 – C19 – C20	69.4(4)
C18 – C19 – C20 – C21	68.0(4)
C19 – C20 – C21 – C22	−168.7(3)
C20 – C21 – C22 – C23	65.7(4)
C21 – C22 – C23 – C24	69.4(4)
C22 – C23 – C24 – C13	−150.3(3)
C23 – C24 – C13 – C14	71.1(4)
C24 – C13 – C14 – C15	68.0(4)

hydrogen bonds, and to establish the cyclododecane ring conformation.

The crystals of $C_{24}H_{46}O_6$ are triclinic. Dimensions for Dirichlet's reduced cell are $a = 8.657(6)$ Å, $b = 11.808(4)$ Å, $c = 12.526(5)$ Å, $\alpha = 77.22(3)°$, $\beta = 77.54(4)°$, $\gamma = 81.68(4)°$. Statistical tests indicate the space group $P\bar{1}$. There are two molecules in the unit cell ($\varrho_c = 1.18$ g/cm³, $\varrho_o = 1.16$ g/cm³). The intensities were measured (at −160 °C) on a Syntex $P\bar{1}$ diffractometer with an Enraf-Nonius liquid-nitrogen cooling device (modified by H. Hope.) With an observed-unobserved cutoff at $1.5\sigma(I)$, 2254 reflections were recorded as observed. The radiation was Mo$K\alpha$ ($\lambda = 0.71069$ Å) and $2\theta_{max} = 45°$. No corrections for absorption or secondary extinction effects have been carried out.

The structure was solved by direct methods [1] and refined by full-matrix least squares techniques.[2*] Anisotropic temperature factors were introduced for oxygen and carbon atoms. Weights in least squares were obtained from the standard deviations in intensities, $\sigma(I)$,

$$\sigma(I) = [C_T + (0.02\ C_N)^2]^{\frac{1}{2}}$$

taken as where C_T is the total number of counts and C_N the net count. The final R-value

* All programs used (except those for phase determination) are included in this reference.

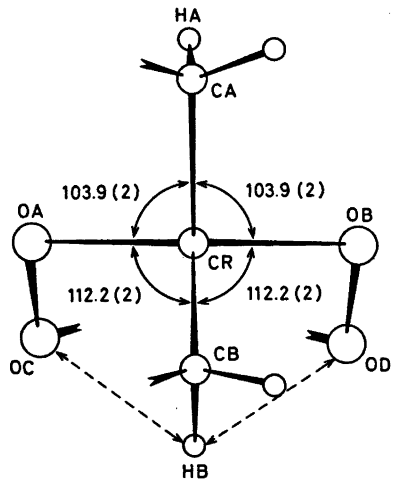

Fig. 3. Schematic drawing showing the asymmetric environment of the spiro carbon atom, CR, of dimeric peroxides. OH, OB, OC, and OD are oxygens of the peroxy bridges.

was $R = 5.7$ % ($R_w = 4.5$ %) for 2254 observed reflections.

Final fractional coordinates and thermal parameters with estimated standard deviations are given in Table 1. The principal axes of the thermal vibration ellipsoids were calculated from the temperature parameters of Table 1. Maximum r.m.s. amplitudes range from 0.177 to 0.262 Å. Due to the size of the molecule, no rigid-body analysis of translational, librational and screw motion has been carried out.

Interatomic distances, bond angles and dihedral angles are listed in Table 2. The standard deviations, in parentheses, are estimated from the correlation matrix of the last least squares refinement cycle. A list of observed structure factors is available from the author.

Fig. 1 shows that the conformation of the molecule with respect to the hydroperoxy group is *cis*. Average bond distances and angles of the hydroperoxy group and the peroxy bridge of the present compound, (I), may be compared with those of 1,1′-dihydroperoxycyclohexanylperoxide-1,1′[3] (II):

	(I)	(II)
O–O	1.474(3) Å	1.477(4) Å
C–O	1.427(4) Å	1.437(5) Å
C–O–O (hydroperoxy)	109.6(3)°	110.4(3)°
C–O–O (peroxy)	108.2(2)°	107.9(3)°

Although no significant differences occur among bond distances and angles, the dihedral angle C–O–O–C is somewhat smaller in I (124.3(3)°) than in II (126.3(3)°).

As in the case of II, the hydroperoxy hydrogen atoms could not be localized in the difference Fourier map. Table 2 indicates that there are two *intra*-molecular hydrogen bonds, O1···O4 (2.870 Å) and O3···O2 (2.765 Å). Since the O–O···O angles are as small as 76.9 and 80.6°, respectively, this cannot, however, be stated with confidence. In II one of the two hydrogen bonds was *inter*-molecular.

The arrangements around the carbon atoms C1 and C13 are asymmetric as shown in Fig. 2 (a) and (b). The angles C12–C1–O5, C2–C1–O2, C24–C13–O4 and C14–C13–O6 have an average value of 103.0°, while the average of C2–C1–O5, C12–C1–O2, C14–C13–O4, and C24–C13–O6 is 113.1°. The distortions may roughly be described as "rotations" (*ca.* 7°) about axes through C1 and C13 normal to the paper plane (Fig. 2). Similar results were obtained for II, and also for trimeric acetone peroxide.[4] In dimeric peroxides [5–7] the corresponding axes of "rotation" are normal to the C–C–C planes (see Fig. 3). It seems reasonable to relate the effects to *intra*-molecular oxygen-hydrogen repulsions (as indicated by the dotted lines in the figures).

Deviations of the 12-membered ring conformation from the idealized "square" model with 422-symmetry (containing eight synclinal and four anti-periplanar partial conformations) are in good agreement with earlier findings. In 2,12-dibromocyclododecanone [8] the average synclinal torsional angle is 68.4°, in azacyclododecane hydrochloride [9] 68.4°, and in the title compound it is 68.2°. Corresponding values for antiperiplanar dihedral angles (°) are

−171.6,	−150.2,	−170.7,	−153.8
−168.6,	−153.4,	−168.2,	−155.1
−169.4,	−152.4,	−167.0,	−152.3
−168.9,	−151.3,	−168.7,	−150.3

The mean value of the C–C–C angles (114.2°) agrees closely with that of 2,12-dibromocyclododecanone (114.1°).

No short *inter*-molecular contacts are observed.

Acknowledgements. The author would like to thank cand.real. T. Ledaal for supplying the compound, and A. Aasen for technical assistance during data collection.

REFERENCES

1. Germain, G., Main, P. and Woolfson, M. M. *Acta Crystallogr. A 27* (1971) 368.
2. Groth, P. *Acta Chem. Scand. 27* (1973) 1837.
3. Groth, P. *Acta Chem. Scand. 23* (1969) 2277.
4. Groth, P. *Acta Chem. Scand. 23* (1969) 1311.
5. Groth, P. *Acta Chem. Scand. 21* (1967) 2608.
6. Groth, P. *Acta Chem. Scand. 21* (1967) 2631.
7. Groth, P. *Acta Chem. Scand. 21* (1967) 2695.
8. Dehli, J. and Groth, P. *Acta Chem. Scand. 23* (1969) 587.
9. Dunitz, J. D. and Weber, H. P. *Helv. Chim. Acta 47* (1964) 1138.

Received April 22, 1975.

Acta Chemica Scandinavica A 29 (1975) 787—793

Syntheses and Crystal Structures of Ethylenethiourea(iodo)-phenyltellurium(II) and Ethyleneselenourea(iodo)phenyl-tellurium(II)

OLAV VIKANE

Department of Chemistry, University of Bergen, N-5014 Bergen-Univ., Norway

The phenyltellurium(II) complexes, C_6H_5Te-(etu)I, I, and C_6H_5Te(esu)I, II, where etu = ethylenethiourea and esu = ethyleneselenourea, have been prepared from the corresponding bromo complexes through ligand exchange with sodium iodide in methanol, and the crystal structures have been determined by three-dimensional X-ray methods.

The crystals of I and II are isomorphous, space group $P2_1/c$ with $Z=4$. The unit cell dimensions are: $a=8.1441(14)$ Å, $b=11.3750(12)$ Å, $c=13.9243(16)$ Å, $\beta=105.181(9)°$ for I, and $a=8.2209(17)$ Å, $b=11.3305(13)$ Å, $c=14.1563(19)$ Å, $\beta=104.816(12)°$ for II.

In the structures, each tellurium atom is three-coordinated, being bonded to one phenyl carbon atom and, in directions nearly perpendicular to the Te–C bond, to one iodine atom and one ethylenethiourea sulfur atom in I, and to one iodine atom and one ethyleneselenourea selenium atom in II. The three-centre systems S–Te–I and Se–Te–I are nearly linear, and the Te–C bond nearly bisects the angle of the three-centre system. The bond lengths and angles involving the tellurium atom are: Te–I = 3.0033(12) Å, Te–S = 2.614(2) Å, Te–C = 2.124(6) Å, ∠S–Te–I = 175.88(4)°, ∠S–Te–C = 88.57(17)°, ∠I–Te–C = 88.24(17)° in I, and Te–I = 3.0951(14) Å, Te–Se = 2.6791(18) Å, Te–C = 2.112(7) Å, ∠Se–Te–I = 177.31(2)°, ∠Se–Te–C = 89.92(17)°, ∠I–Te–C = 88.15(17)° in II.

Structures of three-coordinated tellurium(II) compounds reported recently include those of C_6H_5Te(etu)Br,[1] C_6H_5Te(etu)Cl,[2] C_6H_5Te(esu)Br,[2] and the two anions $[C_6H_5Te(SCN)_2]^-$ and $[C_6H_5Te(SeCN)_2]^-$.[3]

The first complexes of the type ArTe(L)X, where L is thiourea and X is chlorine or bromine, were prepared by Foss and Hauge in 1959,[4] and the crystal structures of C_6H_5Te(tu)Cl, C_6H_5Te(tu)Br, and $C_6H_5Te(tu)_2Cl$ have been determined.[5–8] The tendency of tellurium(II) in its complexes is toward square-planar four-coordination, but when the phenyl group is one of the ligands, the tellurium(II) atom becomes three-coordinated, due to the pronounced *trans* bond-lengthening effect of the phenyl group.

The tellurium(II) complexes may be regarded as models for transition states in nucleophilic displacements at divalent tellurium.[7,9] Bond lengths and angles in the three-coordinated as well as the four-coordinated tellurium(II) complexes indicate linear transition states. Furthermore, in the linear transition state the in- and outgoing groups are bonded, at 180°, through a single p orbital of the central tellurium atom.[7,9]

EXPERIMENTAL

Ethylenethiourea(iodo)phenyltellurium(II), C_6H_5Te(etu)I, was prepared using 1 mmol (0.386 g) of bromo(ethylenethiourea)phenyltellurium(II), C_6H_5Te(etu)Br,[10] dissolved in 10 ml of warm methanol. To the solution was added 2 mmol (0.3 g) of sodium iodide dissolved in 5 ml of warm methanol. During the addition a colour change from orange red to deep red was observed. The solution was filtered while hot, and placed at room temperature for 5 h. Yield: 0.41 g (94 %). M.p. 116–118 °C (dec.). (Found: C 24.93; H 2.57; N 6.39; S 7.36; I 29.21. Calc. for $C_9H_{11}N_2STeI$: C 24.89; H 2.54; N 6.46; S 7.38; I 29.26).

Ethyleneselenourea(iodo)phenyltellurium(II), C_6H_5Te(esu)I, was prepared in the same way

as the ethylenethiourea analogue, using 1 mmol (0.43 g) of bromo(ethyleneselenourea)phenyltellurium(II), $C_6H_5Te(esu)Br$, [11]dissolved in 10 ml of warm methanol, and adding 2 mmol (0.3 g) of sodium iodide dissolved in 5 ml of warm methanol. During the addition the colour of the solution changed from orange red to deep red. The solution was filtered while hot, and placed at room temperature for 3 h. Yield: 0.46 g (95 %). M.p. 137 – 139 °C (dec.). (Found: C 22.51; H 2.32; N 5.79; I 26.42. Calc. for $C_9H_{11}N_2SeTeI$: C 22.47; H 2.29; N 5.83; I 26.40).

Space groups were determined from single-crystal oscillation and Weissenberg photographs.

Methods used for data collection and reductions, and computational procedures are as described previously.[3,12] For ethylenethiourea(iodo)phenyltellurium(II), I, the measurements were performed on a crystal with the following dimensions, given as distances from the point of intersection of the crystal faces $(01\bar{1})$, (100), and $(0\bar{1}1)$: to (011), 0.093 mm; to $(0\bar{1}1)$, 0.062 mm; to $(\bar{1}00)$, 0.156 mm. The crystal used for ethyleneselenourea(iodo)phenyltellurium(II), II, had the following dimensions, given as distances from the point of intersection of the crystal faces $(01\bar{1})$, (100), and $(0\bar{1}1)$: to (011), 0.108 mm; to $(0\bar{1}1)$, 0.061 mm; to $(\bar{1}00)$, 0.266 mm. The scale factors, based on the reference reflections, varied within 7 % for I, and 9 % for II. The lower limit for observed reflections was set equal to two times the standard deviation in net intensity. 2346 of 3211 independent reflections within $\theta = 28°$ were found to be stronger than the lower limit for I. The corresponding numbers for II are 2595 of 3278.

CRYSTAL DATA

The crystals of I and II are brown red, isomorphous, monoclinic prisms, extended along the a axis. Systematic absences are: $h0l$ for l odd, $0k0$ for k odd. The space group is $P2_1/c$ (No. 14).

The unit cell dimensions were determined as described elsewhere.[1,3] The θ-values (all about 20°) of 31 reflections for I, and 36 reflections for II, were measured as described by Maartmann-Moe.[13] The unit cell dimensions are: $a = 8.1441(14)$ Å, $b = 11.3750(12)$ Å, $c = 13.9243(16)$ Å, $\beta = 105.181(9)°$, $Z = 4$, $D_x = 2.32$ g/cm³, $D_m = 2.31$ g/cm³, $\mu_{(MoK\alpha)} = 51.1$ cm⁻¹ for I, and: $a = 8.2209(17)$ Å, $b = 11.3305(13)$ Å, $c = 14.1563(19)$ Å, $\beta = 104.816(12)°$, $Z = 4$, $D_x = 2.50$ g/cm³, $D_m = 2.49$ g/cm³, $\mu_{(MoK\alpha)} = 79.1$ cm⁻¹ for II.

Table 1. Atomic coordinates in fractions of monoclinic cell edges for ethylenethiourea(iodo)-phenyltellurium(II). Origin at a centre of symmetry. Standard deviations from least squares are given in parentheses.

	x	y	z
Te	0.12590(5)	0.54450(4)	0.38028(3)
I	0.22215(6)	0.79411(4)	0.43960(4)
S	0.0653(2)	0.32341(15)	0.33286(13)
C(1)	0.3472(7)	0.5338(5)	0.3248(4)
C(2)	0.3587(8)	0.6067(6)	0.2482(4)
C(3)	0.5043(9)	0.5976(7)	0.2114(5)
C(4)	0.6304(9)	0.5165(7)	0.2493(5)
C(5)	0.6160(8)	0.4418(6)	0.3289(5)
C(6)	0.4733(7)	0.4508(6)	0.3664(5)
C(7)	0.1585(7)	0.2522(5)	0.4426(4)
C(8)	0.2454(11)	0.0929(6)	0.5478(6)
C(9)	0.2970(10)	0.2067(6)	0.6073(5)
N(1)	0.1597(7)	0.1346(5)	0.4472(4)
N(2)	0.2362(7)	0.2985(5)	0.5282(4)

STRUCTURE DETERMINATION

The structures were solved by Patterson and Fourier methods and refined to R-values of 0.037 for I and 0.046 for II. Altogether 127 parameters were refined in each structure. The three-dimensional Fourier difference maps, based on the data of the final refinements, showed no peaks higher than 0.7 e/Å³ in either of the two structures.

Table 2. Atomic coordinates in fractions of monoclinic cell edges for ethyleneselenourea-(iodo)phenyltellurium(II). Origin at a centre of symmetry. Standard deviations from least squares are given in parentheses.

	x	y	z
Te	0.12505(6)	0.53971(4)	0.37574(4)
I	0.21685(7)	0.79818(5)	0.43782(4)
Se	0.06070(10)	0.31321(7)	0.32560(5)
C(1)	0.3441(7)	0.5320(5)	0.3252(5)
C(2)	0.3621(9)	0.6071(6)	0.2501(5)
C(3)	0.5082(10)	0.5994(7)	0.2160(6)
C(4)	0.6331(9)	0.5168(7)	0.2559(6)
C(5)	0.6191(8)	0.4426(7)	0.3322(6)
C(6)	0.4772(9)	0.4503(6)	0.3694(5)
C(7)	0.1646(9)	0.2406(7)	0.4439(5)
C(8)	0.2580(14)	0.0899(8)	0.5555(7)
C(9)	0.3062(10)	0.2065(7)	0.6080(6)
N(1)	0.1728(9)	0.1241(5)	0.4555(5)
N(2)	0.2395(9)	0.2928(6)	0.5280(4)

Table 3. Anisotropic thermal parameters (Å²) in the form $\exp-[2\pi^2(h^2a^{-2}U_{11}+\cdots+2hka^{-1}b^{-1}U_{12}+\cdots)]$, for ethylenethiourea(iodo)phenyltellurium(II). The values have been multiplied by 10^3. Standard deviations in parentheses.

	U_{11}	U_{22}	U_{33}	U_{12}	U_{23}	U_{13}
Te	32.2(2)	40.2(2)	47.3(3)	1.8(2)	2.3(2)	11.3(2)
I	63.0(3)	39.5(2)	56.1(3)	−1.3(2)	−6.1(2)	17.4(2)
S	45.2(10)	44.5(10)	45.7(10)	−9.6(8)	−2.8(8)	7.4(8)
C(1)	30(3)	39(3)	41(3)	−6(3)	−6(3)	7(3)
C(2)	50(4)	51(4)	35(4)	−7(3)	−1(3)	8(3)
C(3)	49(4)	66(5)	42(4)	−15(4)	−1(4)	14(3)
C(4)	45(4)	66(5)	46(4)	−7(4)	−11(4)	13(3)
C(5)	38(4)	52(4)	50(4)	−2(3)	−13(3)	9(3)
C(6)	34(3)	39(3)	51(4)	1(3)	−5(3)	5(3)
C(7)	30(3)	37(3)	40(4)	−4(3)	−2(3)	14(3)
C(8)	92(6)	43(4)	58(5)	7(4)	−1(4)	8(5)
C(9)	75(5)	36(4)	51(4)	−7(4)	11(3)	1(4)
N(1)	54(4)	30(3)	65(4)	0(3)	−3(3)	18(3)
N(2)	50(3)	44(3)	42(3)	−7(3)	−1(3)	10(3)

Observed and calculated structure factors for the two structures are available from the author.

The atomic coordinates and thermal parameters are listed in Tables 1 – 4.

RESULTS

Bond lengths and angles in ethylenethiourea.(iodo)phenyltellurium(II), I, and ethyleneselenourea(iodo)phenyltellurium(II), II, based on the atomic coordinates in Tables 1 and 2, are listed in Tables 5 and 6. The uncertainties in the unit cell dimensions are taken into account in the given standard deviations. Views of the structures of I and II, as seen normal to the plane through the coordination group, are shown in Figs. 1 and 2. Stereoscopic views of the content of the unit cell of I and II are shown in Figs. 3 and 4.

In each of the structures the tellurium atom is three-coordinated, being bonded to one phenyl carbon atom and, in directions nearly perpendicular to the Te – C bond, to one iodine

Table 4. Anisotropic thermal parameters (Å²) in the form $\exp-[2\pi^2(h^2a^{-2}U_{11}+\cdots+2hka^{-1}b^{-1}U_{12}+\cdots)]$, for ethyleneselenourea(iodo)phenyltellurium(II). The values have been multiplied by 10^3. Standard deviations in parentheses.

	U_{11}	U_{22}	U_{33}	U_{12}	U_{23}	U_{13}
Te	33.1(2)	36.7(3)	49.8(3)	1.1(2)	2.4(2)	13.1(2)
I	66.0(4)	37.5(3)	56.4(3)	−1.9(3)	−7.5(3)	18.9(3)
Se	36.9(4)	34.4(4)	40.2(4)	−5.6(4)	−2.3(3)	7.0(3)
C(1)	18(3)	25(3)	47(4)	8(3)	−5(3)	6(3)
C(2)	42(4)	49(4)	55(5)	−6(4)	−10(4)	3(4)
C(3)	45(5)	59(5)	59(5)	−6(4)	−12(4)	10(4)
C(4)	34(4)	57(5)	55(5)	−3(4)	−18(4)	9(4)
C(5)	29(4)	47(5)	56(5)	22(3)	−12(4)	7(4)
C(6)	40(4)	37(4)	50(4)	21(4)	−5(4)	4(3)
C(7)	40(4)	55(5)	36(4)	−5(4)	−7(4)	21(3)
C(8)	117(9)	46(5)	56(6)	−3(6)	−1(5)	−3(6)
C(9)	52(5)	38(4)	54(5)	−3(4)	0(4)	5(4)
N(1)	76(5)	32(3)	51(4)	2(4)	1(3)	15(4)
N(2)	58(4)	46(4)	38(3)	−10(3)	−4(3)	12(3)

Table 5 Bond lengths (Å) and angles (°) in ethylenethiourea(iodo)phenyltellurium(II). Standard deviations are given in parentheses.

Te–I	3.0033(12)	∠S–Te–I	175.88(4)
Te–S	2.614(2)	∠S–Te–C(1)	88.57(17)
Te–C(1)	2.124(6)	∠I–Te–C(1)	88.24(17)
C(1)–C(2)	1.373(9)	∠Te–C(1)–C(2)	118.7(4)
C(1)–C(6)	1.403(8)	∠Te–C(1)–C(6)	118.9(4)
C(2)–C(3)	1.413(11)	∠C(2)–C(1)–C(6)	122.4(5)
C(3)–C(4)	1.378(10)	∠C(1)–C(2)–C(3)	118.1(5)
C(4)–C(5)	1.426(10)	∠C(2)–C(3)–C(4)	121.5(6)
C(5)–C(6)	1.397(10)	∠C(3)–C(4)–C(5)	119.4(6)
		∠C(4)–C(5)–C(6)	119.5(5)
		∠C(5)–C(6)–C(1)	119.0(5)
S–C(7)	1.720(6)	∠Te–S–C(7)	102.6(2)
C(7)–N(1)	1.340(8)	∠S–C(7)–N(1)	120.6(4)
C(7)–N(2)	1.305(7)	∠S–C(7)–N(2)	128.1(4)
N(1)–C(8)	1.470(9)	∠N(1)–C(7)–N(2)	111.3(5)
N(2)–C(9)	1.505(8)	∠C(7)–N(1)–C(8)	111.3(5)
C(8)–C(9)	1.535(10)	∠C(7)–N(2)–C(9)	112.1(5)
		∠N(1)–C(8)–C(9)	103.7(5)
		∠N(2)–C(9)–C(8)	101.4(5)

atom and one ethylenethiourea sulfur atom in I, and to one iodine atom and one ethyleneselenourea selenium atom in II.

The coordination around the tellurium atom is nearly planar in both structures. The largest deviation from a least-squares plane through Te, S, I and C(1) in I is 0.043 Å, and the largest deviation from the corresponding plane through Te, Se, I and C(1) in II is 0.029 Å. The least-squares plane through the coordination group passes 0.011 Å from C(4) in I and 0.032 Å from C(4) in II.

The three-centre systems S–Te–I and Se–Te–I are nearly linear. The S–Te–I bond angle in I is 175.88(4)°, and the Se–Te–I bond angle in II is 177.31(2)°. Similar devia-

Table 6. Bond lengths (Å) and angles (°) in ethyleneselenourea(iodo)phenyltellurium(II). Standard deviations are given in parentheses.

Te–I	3.0951(14)	∠Se–Te–I	177.31(2)
Te–Se	2.6791(18)	∠Se–Te–C(1)	89.92(17)
Te–C(1)	2.112(7)	∠I–Te–C(1)	88.15(17)
C(1)–C(2)	1.399(10)	∠Te–C(1)–C(2)	120.0(4)
C(1)–C(6)	1.448(9)	∠Te–C(1)–C(6)	119.9(5)
C(2)–C(3)	1.407(12)	∠C(2)–C(1)–C(6)	120.1(6)
C(3)–C(4)	1.397(11)	∠C(1)–C(2)–C(3)	119.2(6)
C(4)–C(5)	1.397(12)	∠C(2)–C(3)–C(4)	120.5(7)
C(5)–C(6)	1.399(11)	∠C(3)–C(4)–C(5)	121.2(7)
		∠C(4)–C(5)–C(6)	119.7(6)
		∠C(5)–C(6)–C(1)	119.2(6)
Se–C(7)	1.866(7)	∠Te–Se–C(7)	99.8(2)
C(7)–N(1)	1.329(10)	∠Se–C(7)–N(1)	123.0(5)
C(7)–N(2)	1.330(9)	∠Se–C(7)–N(2)	127.4(5)
N(1)–C(8)	1.462(11)	∠N(1)–C(7)–N(2)	109.5(6)
N(2)–C(9)	1.491(9)	∠C(7)–N(1)–C(8)	112.3(6)
C(8)–C(9)	1.518(11)	∠C(7)–N(2)–C(9)	112.6(6)
		∠N(1)–C(8)–C(9)	104.1(6)
		∠N(2)–C(9)–C(8)	101.5(6)

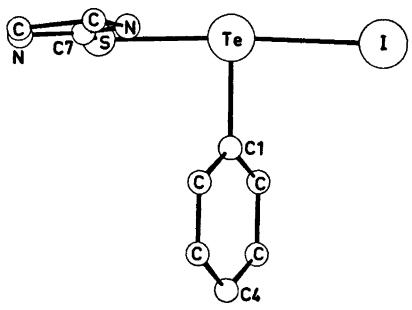

Fig. 1. Ethylenethiourea(iodo)phenyltellurium (II), as seen normal to the plane through the coordination group.

tions from linearity are also found in the crystals of chloro- and bromo(ethylenethiourea)-phenyltellurium(II),[1,2] bromo(ethyleneselenourea)phenyltellurium(II),[2] and chloro- and bromo(phenyl)thioureatellurium(II),[5–7] where the bond angle of the three-centre system varies from 171.9(5) to 177.22(3)°.

The Te–C bond nearly bisects the angle of the three-centre system in both structures. The S–Te–C bond angle is 88.57(17)°, and the Se–Te–C bond angle is 89.92(17)°. The I–Te–C bond angle is 88.24(17)° in I and 88.15(17)° in II.

The Te–S bond length, 2.614(2) Å in I, is about 0.092 Å longer than the mean Te–S bond length, 2.522 Å, found in the crystals of chloro- and bromo(ethylenethiourea)phenyltellurium(II),[1,2] and about 0.204 Å longer than the sum of the single-bond radii.[14] The Te–Se bond length, 2.6791(18) Å in II, is about 0.063 Å longer than the Te–Se bond length, 2.616 Å found in the crystals of bromo(ethyleneselenourea)phenyltellurium(II),[2] and about

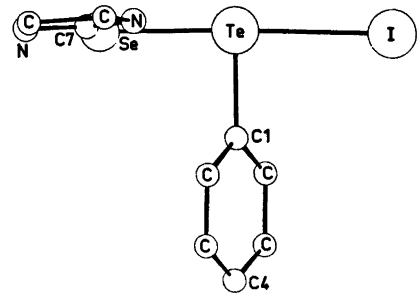

Fig. 2. Ethyleneselenourea(iodo)phenyltellurium(II), as seen normal to the plane through the coordination group.

0.139 Å longer than the sum of the single-bond radii[14] Thus, it is seen that substitution of iodine for chlorine or bromine causes an increase in the length of the *trans*-positioned Te–S or Te–Se bond of 0.092 and 0.063 Å, respectively. Substitution of bromine for chlorine is known to cause no significant lengthening of the *trans*-positioned Te-ligand bond.[1,2,5–7] Thus, the iodine atom appears to have a far more pronounced *trans* bond-lengthening effect on a Te–S or a Te–Se bond than has chlorine or bromine. This indicates the following order of relative *trans* bond-lengthening effect of halogens on a Te–S or a Te–Se bond: I > Br ~ Cl.

The Te–I bond length, 3.0033(12) Å in I, and 3.0951(14) Å in II, is 0.303 and 0.395 Å, respectively, longer than the sum of the single-bond radii.[14] The 0.092 Å shorter Te–I bond length in I as compared with II, indicates a stronger Te–I bond when the *trans*-positioned ligand is ethylenethiourea than when it is ethyleneselenourea. Furthermore, the *trans* bond–lengthening effect of iodine on a Te–S bond is more pronounced than the effect on a Te–Se bond.

As pointed out by Foss,[7,9] the tellurium(II) complexes may be regarded as model substances for transition states in nucleophilic displacements on divalent tellurium. From several works on the preparation of tellurium(II) complexes,[4,6,15,16] it is known that chlorine, bromine, and iodine displace each other in the order mentioned. Nucleophilic reactivity may then relate to the ability of the reagent to engage the *p* orbital of the electrophilic centre in bonding, at the expense of the bond at 180°.[9] This is in accord with the relative *trans* bond-lengthening order of bromine and iodine on a Te–S or a Te–Se bond indicated above. That bromine displaces chlorine is, however, not reflected in the *trans* bond-lengthening effects of chlorine and bromine.

The Te–C bond lengths, 2.124(6) Å in I and 2.112(7) Å in II, are equal within the accuracies of the structure determinations. The same Te–C bond length has been found in the structures of chloro- and bromo(ethylenethiourea)phenyltellurium(II),[1,2] bromo(ethyleneselenourea)phenyltellurium(II),[2] the phenyldithiocyanato- and the phenyldiselenocyanatotellurate(II) ions,[3] chloro- and bromo(phenyl)

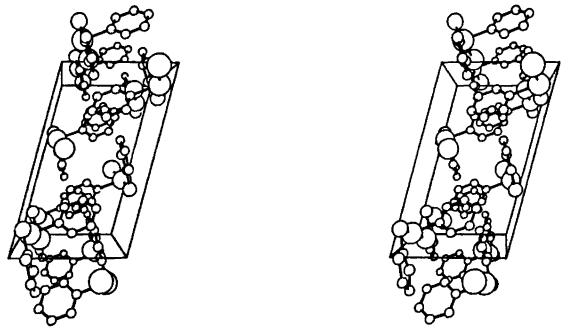

Fig. 3. A stereoscopic view of the cell packing in ethylenethiourea(iodo)phenyltellurium(II), as seen along the *b* crystal axis.

thioureatellurium(II),[5–7] phenylbis(thiourea)-tellurium(II) chloride,[6–8] and *o*-formylphenyltellurenyl bromide,[17] indicating that the Te – C bond is a single covalent bond.[3]

The coordination around the tellurium atom may be regarded as based on a square-planar arrangement.[6,7] In the structures of the isomorphous forms of chloro- and bromo(ethylenethiourea)phenyltellurium(II),[1,2] and in bromo(ethyleneselenourea)phenyltellurium(II),[2] the fourth position of a square-planar coordination, *trans* to the phenyl group, is approached by a halogen atom of an adjacent molecule, over a symmetry centre. In the two present structures, as in the structure of the second form of bromo(ethylenethiourea)phenyltellurium(II),[1] this approach of a fourth ligand is missing.

The tellurium atom and the carbon atoms of the phenyltellurium group are nearly co-planar in both structures, the largest deviation from a least-squares plane being 0.019 Å in I and 0.035 Å in II. The angle between this plane and the least-squares plane through the coordination group is 60.43 ° in I and 61.18 ° in II. In the structure of the *C*2/*c* form of bromo(ethylenethiourea)phenyltellurium(II) [1] the angle between these two least-squares planes is 64.6 °.

The sulfur atom, the two nitrogen atoms and the three carbon atoms of the ethylenethiourea group in I are nearly co-planar. So are the selenium atom, the two nitrogen atoms and the three carbon atoms of the ethyleneselenourea group in II. The largest deviation from the least-squares plane is 0.019 Å in I and 0.009 Å in II. The angle between this plane and a least-squares plane through Te, S, I, and C(7) in I, or through Te, Se, I, and C(7) in II, is 5.37 and 4.28 °, respectively. In the structure of the *C*2/*c* form of bromo(ethylenethiourea)phenyltellurium(II) [1] the atoms of the ethylenethiourea group lie nearly in the plane through Te, S, Br, and C(7). Thus, the ethylenethiourea group in I and the ethyleneselenourea group in II have the same orientation as the ethylenethiourea group in the *C*2/*c*

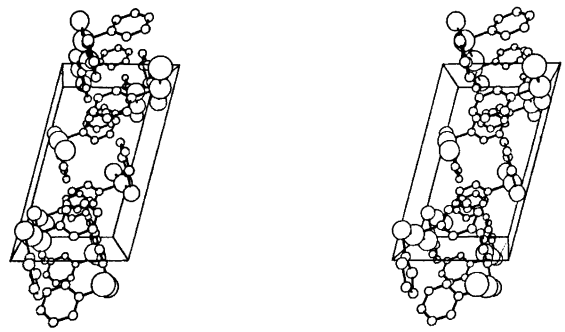

Fig. 4. A stereoscopic view of the cell packing in ethyleneselenourea(iodo)phenyltellurium(II), as seen along the *b* crystal axis.

form of bromo(ethylenethiourea)phenyltellurium(II).[1]

The S–C bond length, 1.720(6) Å, and the Te–S–C bond angle, 102.6(2)°, in I are, within the error, equal to the S–C bond lengths and Te–S–C bond angles found in the structures of chloro- and bromo(ethylenethiourea)phenyltellurium(II).[1,2] The corresponding Se–C bond length, 1.866(7) Å, and Te–Se–C bond angle, 99.8(2)°, in II are, within the error, equal to the Se–C bond length and Te–Se–C bond angle found in the structure of bromo(ethyleneselenourea)-phenyltellurium(II).[2]

CRYSTAL PACKING

Stereoscopic views of the content of the unit cell of I and II are shown in Figs. 3 and 4. In both structures there are no particular short non-bonding distances between the different molecules, Thus, the crystals of I and II consist of well separated ethylenethiourea(iodo)phenyltellurium(II) molecules in I, and ethyleneselenourea(iodo)phenyltellurium-(II) molecules in II.

REFERENCES

1. Vikane, O. *Acta Chem. Scand. A 29* (1975) 738.
2. Vikane, O. *Acta Chem. Scand. A 29* (1975) 763.
3. Hauge, S. and Vikane, O. *Acta Chem. Scand. A 29* (1975) 755.
4. Foss, O. and Hauge, S. *Acta Chem. Scand. 13* (1959) 2155.
5. Foss, O. and Husebye, S. *Acta Chem. Scand. 20* (1966) 132.
6. Foss, O. In Andersen, P., Bastiansen, O. and Furberg, S. *Selected Topics in Structure Chemistry*, Universitetsforlaget, Oslo 1967, 145.
7. Foss, O. *Pure Appl. Chem. 24* (1970) 31.
8. Foss, O. and Marøy, K. *Acta Chem. Scand. 20* (1966) 123.
9. Foss, O. *Acta Chem. Scand. 16* (1962) 779.
10. Vikane, O. *Acta Chem. Scand. A 29* (1975) 150.
11. Vikane, O. *Acta Chem. Scand. A 29* (1975) 152.
12. Åse, K. *Acta Chem. Scand. 25* (1971) 838.
13. Maartman-Moe, K. *Siemens Review* XLI (1974) 54.
14. Pauling, L. *The Nature of the Chemical Bond*, 3rd, Ed., Cornell University Press, Ithaca 1960.
15. Foss, O. and Fossen, S. *Acta Chem. Scand. 15* (1961) 1618.
16. Foss, O. *Personal communication.*
17. Baiwir, M., Llabres, G., Dideberg, O., Dupont, L. and Piette, J. *Acta Crystallogr. B 30* (1974) 139.

Received February 26, 1975.

Acta Chemica Scandinavica A 29 (1975) 794—798

The Molecular Structure of 2,2-Dimethoxypropane, $CH_3—O—C(CH_3)_2—O—CH_3$, in the Gas Phase

E. E. ASTRUP and A. M. AOMAR

Department of Chemistry, University of Oslo, Oslo 3, Norway

The molecular structure of 2,2-dimethoxypropane has been investigated in the gas phase by the electron-diffraction method. The preferred conformation is found to be *gauche,gauche* with a C_2 symmetry. The dihedral angle, α (COCO), is 52.0(1.2)°. The geometric parameters are: r (C−O) = 1.423(6) Å, r(C−C) = 1.513(8) Å, r(C−H) = 1.104(8) Å, ∠COC = 114.0(1.4)°, ∠OCO = 117.4(2.2)°, ∠CCC = 112.2(2.9)°, ∠CCH = 111.6(1.1)°, ∠OCH = 107.8(1.3)°.

The structure of 2,2-dimethoxypropane (Fig. 1) was investigated in order to obtain information about the conformation of what may be looked upon as a unit-brick of larger ring systems, $-(CH_2-O-C(CH_3)_2-O)_n-$. This structure determination is part of a study on cyclic and acyclic ethers.

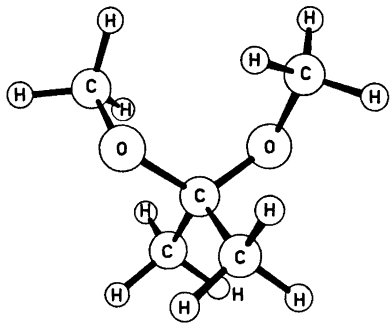

Fig. 1. 2,2 Dimethoxypropane.

Cumper[1–4] and co-workers have investigated a number of different methoxy compounds using electric dipole moment measurements and ultraviolet and NMR spectroscopic investigations. They conclude that in the $(CH_3)_{4-n}C(OCH_3)_n$ derivatives only hindered rotation of the methoxy groups occurs. Calculations of the charge distributions for the mentioned methoxy derivatives have been performed by Nagy and Párkányi [5] and correlated with NMR data.

EXPERIMENTAL

The electron diffraction diagrams of a commercial sample of 2,2-dimethoxypropane were taken on a Balzers Eldigraph KDG2 unit. The sample was kept at about 0 °C during exposure. The background pressure during the experiment was approximately 1.5×10^{-5} Torr. The electron diffraction patterns were recorded at 25.00 and 50.00 cm nozzle-to-plate distances and the electron wavelengths were 0.05850 and 0.05852 Å, respectively. For the structure analysis five plates for the 25 cm distance and four plates for the 50 cm distance were selected. The intensity was recorded on a photometer for each 0.25 mm on the photographic plates. Each plate was oscillated about the center of the diffraction diagrams, and the intensity integrated over the arc. The data were treated the usual way. [6] An experimental background was subtracted on each plate before averaging the intensity data. The molecular intensity curves from the 25 cm and 50 cm nozzle-to-plate distances were scaled and combined to one experimental molecular intensity curve extending from $s = 1.375$ Å^{-1} to $s = 30.00$ Å^{-1} (Fig. 2). The mean values were used in the overlap region. The intensity was modified by $s/|f_C'||f_O'|$, where f' is the complex scattering factor [7,8] for carbon and oxygen, respectively.

The distances and the vibrational amplitudes estimated from the experimental radial distribution (RD) curve were refined by a least-squares procedure. The calculations have been carried out on CDC 3300 and CDC 7400 (CYBER) computers. [6]

STRUCTURE ANALYSIS AND RESULTS

Approximate values for the structure parameters used in the least-squares analysis are determined from the experimental RD curve in Fig. 3.

The bond distances in the molecule are represented by the two first peaks in the RD curve. The first peak at 1.1 Å corresponds to the C–H bond distances. All the C–H distances are assumed to be equal. The peak at 1.5 Å contains both the C–O and C–C bond distances. From the structure of related molecules, dimethoxymethane [9] and tetramethoxymethane,[10] a difference in the central and terminal C–O bond lengths should be expected. Unfortunately, in this investigation the correlations between the C–O and C–C bond distances and the corresponding vibrational amplitudes are so large that these parameters may not be determined with a great accuracy, and consequently only a mean C–O bond distance may be determined. At least two of the four mentioned parameters had to be kept at fixed values to give reasonable results during the refining procedure. Table 1 shows the parameter values from different refinements together with the errors of square residuals.

The next peak in the RD curve, at about 2.4 Å, contains information about the CCO, OCO, COC, and CCC bond angles. The main contributions to this peak are the four C···O distances from the oxygen atoms in the methoxy groups to the methyl carbon atoms (2.36 Å), the O···O distance(2.43 Å), which corresponds to an OCO angle of 117.4°, the two C···C distances from methoxy carbons to the central carbon atom (2.39 Å) (∠COC equal to 114.0°), and the C···C distances between the two methyl group carbon atoms (2.51 Å), corresponding to a CCC angle of 112.2°. The shoulder at about 2.0–2.2 Å shows the O···H distances in the methoxy groups and the C···H distances between the central carbon atom and the methyl hydrogen atoms. It is assumed that the CCC plane formed by the central carbon atom and the methyl carbon atoms is perpendicular to the OCO plane and bisecting the angle OCO.

The maxima determining the conformation of the molecule are the three well-resolved peaks in the outer part of the RD curve at 2.9, 3.3, and 3.7 Å. The first of these represents the C···O distances between non-bonded methoxy carbon and oxygen atoms (2.89 Å), and the two shorter C···C distances between methoxy and methyl carbon atoms (2.89 Å). The next peak corresponds to the C···C distances between the methoxy carbons (3.30 Å), and the last peak the two longer C···C distances between methoxy and methyl carbon atoms (3.67 Å).

The best agreement between experimental and theoretical curves is obtained for a *gauche*, *gauche* conformation of the C–O–C–O–C chain, the dihedral angle being 52.0°. A *gauche*,

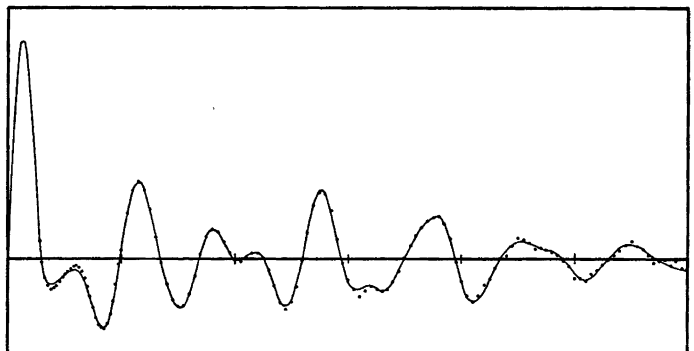

Fig. 2. 2,2-Dimethoxypropane. Theoretical (solid line), experimental (dots), and difference molecular intensity curve.

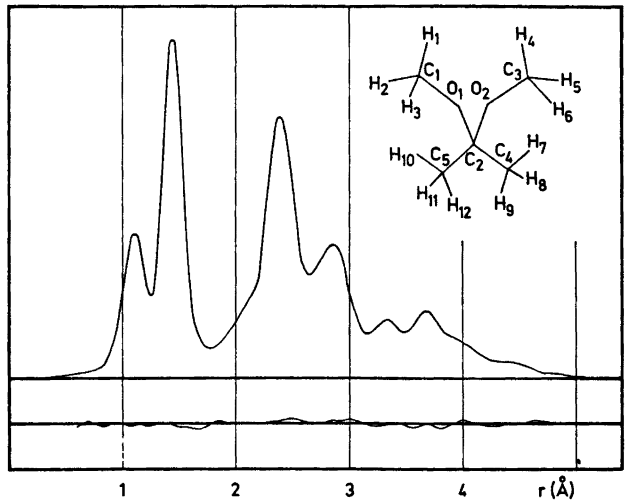

Fig. 3. 2,2-Dimethoxypropane. Theoretical radial distribution curve. The lower curve shows the difference between the experimental and the theoretical values. Artificial damping constant $k = 0.002$ Å.

Table 1. The results of different cycles of least-squares refinement of the parameters for the C–O and C–C bond distances and vibrational amplitudes. $\sum$ shows the errors of square residuals for each cycle. Due to the large correlation of the listed parameters, only two of these could be refined simultaneously.

C–O		C–C		
R	*u*	*R*	u^a	$\sum$
1.41[a]	0.051(7)	1.508(16)	0.050	483.8
1.425(6)	0.048[a]	1.506(9)	0.050	113.0
1.425(6)	0.046[a]	1.510(9)	0.050	111.8
1.424(6)	0.044[a]	1.513(8)	0.050	113.8
1.424(6)	0.046[a]	1.510(8)	0.048	110.9
1.424(6)	0.046[a]	1.510(8)	0.046	110.3
1.423(6)	0.046[a]	1.510(8)	0.044	110.2
1.423(6)	0.045[a]	1.513(8)	0.044	107.2
1.423(6)	0.044[a]	1.514(8)	0.044	109.0

[a] Values kept fixed during the refinement.

gauche conformation could be expected because the lone pair interaction in this conformation should be more favourable than in an all-*anti* conformation. The angle OCO is found to be 117.4° and the angle COC to be 114.0°. The latter is in good agreement with the corresponding angle in the cyclic ether 1,3,5-trimethyltrioxan,[11] and the acyclic dimethoxymethane [9] and tetramethoxymethane.[10] The OCO angle found in this molecule is, however, somewhat larger than those found in the other ethers mentioned above.

In both dimethoxymethane and 2,2-dimethoxypropane are the shortest O···H distances, which extend over more than one angle, fairly small, 2,09 and 2.34 Å, respectively. This is a fact which may indicate an interaction between oxygen and hydrogen atoms. Also the C–C bond distances in this molecule are found to be shorter (1.513 Å) than what is usually found for such bonds. It should be mentioned that a shorter C–C bond distance (1.49 Å) also is found in 1,3,5-trimethyltrioxan.

The twist of the CH_3 groups about the C–C and C–O bonds cannot be determined with great accuracy because of the poor scattering power of hydrogen atoms. It was assumed that the two methyl groups had an equal twist, and the best result was obtained for an ideal staggered conformation. The twist of the methoxy CH_3 groups were also assumed to be equal and refined to 15.9° from an ideal staggered position.

As already mentioned, the refinement of the C–O and C–C bond distances and their vibrational amplitudes may not be carried out simultaneously because of the great correla-

Table 2. Structure parameters for 2,2-dimethoxypropane obtained by least-squares refinement on the intensity data. Distances (r_a-values) and mean amplitudes of vibration (u-values) are given in Å, angles in degrees. The standard deviations given in parentheses have been corrected to take into account data correlation. The uncertainty arising from error in the electron wavelength is included. (For numbering system of the atoms see Fig. 3.)

Distances	r	u
C–O	1.423(6)	0.045
C–C	1.513(8)	0.044
C–H	1.104(8)	0.070(04)
$O_1 \cdots O_2$	2.432(21)	0.064(15)
$C_4 \cdots O_2$	2.359(12)	0.079
$C_1 \cdots O_2$	2.885(12)	0.110(11)
$C_1 \cdots C_2$	2.388(16)	0.073(09)
$C_4 \cdots C_5$	2.512(36)	0.078
$C_1 \cdots C_4$	2.886(18)	0.108
$C_1 \cdots C_3$	3.303(31)	0.120
$C_1 \cdots C_5$	3.671(8)	0.128(12)
$O_1 \cdots H_1$	2.038(16)	0.091(18)
$O_1 \cdots H_6$	2.337(29)	0.120
$O_1 \cdots H_8$	2.611(17)	0.116
$O_1 \cdots H_9$	2.662(24)	
$O_1 \cdots H_7$		
$O_1 \cdots H_4$	3.526(41)	0.122
$O_1 \cdots H_5$	3.705(31)	
$C_2 \cdots H_7$	2.177(14)	0.093
$C_1 \cdots H_6$	2.891(56)	0.148
$C_1 \cdots H_4$	3.510(53)	0.156
$C_1 \cdots H_7$	3.953(28)	0.120
$C_1 \cdots H_8$	3.997(17)	0.120
$C_1 \cdots H_5$	4.336(35)	0.160
$C_1 \cdots H_9$	4.537(16)	0.132
$H_7 \cdots H_8$	1.782(14)	0.094
$H_1 \cdots H_2$	1.831(12)	
$H_1 \cdots H_4$	4.597(48)	0.20
Angles		deg.
∠COC		114.0(1.4)
∠OCO		117.4(2.2)
$\alpha(CH_3O)^a$		52.0(1.2)
∠OCH		107.8(1.3)
$\tau(CH_3)^b$		15.9(2.1)
∠CCC		112.2(2.9)
∠CCH		111.6(1.1)

[a] α is the twist angle of the methoxy groups around the central CO bonds. (Dihedral angle C–O–C–O). [b] τ is the twist angle of the CH_3 in the methoxy groups around the terminal CO bonds.

tions. Two of these parameters were kept at fixed values during the refinements. If the vibrational amplitudes are fixed at reasonable values, the C–C and the C–O distances may be refined simultaneously with the COC, OCO, CCC, OCH, and CCH angles, the twist angles of the CH_3–O– groups and the methoxy CH_3 groups, and the vibrational amplitudes for O···O and the shorter O···H non-bonded distances. As the correlation between the COC and CCC angles is considerable (0.8), the vibrational amplitudes for the C···C and C···O distances have been refined in separate cycles. The remaining vibrational amplitudes have been grouped according to distance type and lengths and refined in separate cycles. Keeping some parameters at fixed values during the refinements results in too small standard deviations for some of the parameters. To compensate for this, the approach proposed by Seip,[15] has been applied to some of the most important parameters. The final parameters are shown in Table 2 and the correlation matrix in Table 3.

CONCLUSION

As expected the conformation of 2,2-dimethoxypropane is found to correspond to that of dimethoxymethane, i.e. *+gauche, +gauche*. Due to substitution of hydrogen atoms by the much larger CH_3 groups the angles in 2,2-dimethoxypropane are generally somewhat larger than the corresponding angles in dimethoxymethane [9] and the dihedral angle of the C–O–C–O–C chain somewhat smaller (52 and 63°, respectively), giving more space to the methyl groups. The bond distances are found to be close to what is usually found for distances of this type. The shortest non-bonded $O_1 \cdots H_6$ distance is, however, found to be somewhat short, and this may indicate that a weak oxygen-hydrogen interaction is present.

Dipole moment measurements show that 2,2-dimethoxypropane possesses a small dipole moment, as is also found for dimethoxymethane (0.61 D[12] and 0.99 D,[9] respectively). By comparison[12] of these moments with that of a compound having a *+gauche, −gauche* conformation of the C–O–C–O–C skeleton (*e.g.* 1.3-dioxan) it is seen that the latter has a considerably greater dipole moment (1.9 D[13]). Dipole moments for the *gauche,anti* and *anti,anti* conformations should be expected to be still larger.

Calculations of dipole moments [1] according to Eyring,[14] has been carried out for different

Table 3. Correlation matrix (× 100) for the parameters. (The coefficients having absolute values less than 20 are not given.)

Parameters		1	2	3	4	5	6	7	8	9	10	11	12
1	$r(C_1-O_1)$	100											
2	∠COC		100										
3	∠OCO		−87	100									
4	$\alpha(CH_3O)^a$			38	100								
5	∠OCH					100							
6	$\tau(CH_3)^b$		42	−27			100						
7	$r(C_2-C_5)$	−24	−34	30			−28	100					
8	∠CCC		86	−86	−28		24		100				
9	∠CCH		−33	39			−31		−43	100			
10	$u(O_1\cdots O_2)$		−30	24			23		−78		100		
11	$u(O_1\cdots H_1)$		37	−53		21		−21	30	−65		100	
12	scale	−24	−22	26		−24	−29	59				−21	100

[a] α is the twist angle of the methoxy groups around the central CO bonds. [b] τ is the twist angle of the CH_3 in the methoxy groups around the terminal CO bonds.

conformers of the molecule. The best agreement with the measured dipole moment is obtained for a dihedral angle of 77°, which is in good agreement with the result of this work.

Ackowledgement. We are grateful to Mr. K. Brendhaugen for his assistance during the experiment.

REFERENCES

1. Cumper, C. W. N., Melnikoff, A. and Vogel, A. I. *J. Chem. Soc. A* (1966) 323.
2. Cumper, C. W. N. and Rossiter, R. F. J. *Phys. Chem. 76* (1972) 525.
3. Cumper, C. W. N., Melnikoff, A. and Vogel, A. I. *J. Chem. Soc. A* (1966) 242.
4. Cumper, C. W. N., Melnikoff, A., Mooney, E. F. and Vogel, A. I. *J. Chem. Soc. B* (1966) 874.
5. Nagy, J. and Párkányi, L. *Acta Chim. (Budapest) 71* (1972) 159.
6. Andersen, B., Seip, H. M., Strand, T. G. and Stølevik, R. *Acta Chem. Scand. 23* (1969) 3224.
7. Peacher, J. and Wills, J. C. *J. Chem. Phys. 46* (1967) 4809.
8. Strand, T. G. and Bonham, R. A. *J. Chem. Phys. 40* (1964) 1686.
9. Astrup, E. E. *Acta Chem. Scand. 27* (1973) 3271.
10. Mijlhoff, F. C., Geise, H. J. and van Schaick, E. J. M. *J. Mol. Struct. 20* (1973) 393.
11. Astrup, E. E. *Acta Chem. Scand. 27* (1973) 1345.
12. Dale, J. and Ekeland, T. *Acta Chem. Scand. 27* (1973) 1519.
13. Arbousow, B. A. *Bull. Soc. Chim. Fr.* (1960) 1311.
14. Eyring, H. *Phys. Rev. 39* (1932) 746.
15. Seip, H. M. *A Specialist Periodical Report: Molecular Structure by Diffraction Methods*, The Chemical Society, London 1973, Vol. 1, p. 53.

Received May 16, 1975.

Acta Chemica Scandinavica A 29 (1975) 799—802

Short Communications

The Structure of *O*-[3-Phenyl-5-(1,2,3,4-oxatriazolio)] Oxide at —165 °C

T. OTTERSEN

Department of Pharmacy, University of Oslo, Oslo 3, Norway

In a recent study [1] the structure of the *meso*-ionic compound *N*-[3-phenyl-5-(1,2,3,4-oxatriazolio]phenylamide was investigated by X-ray diffraction methods. The results obtained for the central five-membered ring showed the same structural features as those found for the isoelectronic sydnones [2] (*i.e.* a planar ring with bond distances indicating a conjugated system, except for a relatively long intra-ring C–O length (1.40 – 1.42 Å), and an exocyclic "pure" double bond). *meso*-Ionic structures have recently attracted considerable interest because of their marked pharmacological activity associated with certain members of this group of organic compounds.[3,4] In order to study this *meso*-ionic oxatriazolio system further and to complement the earlier results, a structure investigation of the title compound was undertaken.

The compound[5,6] was recrystallized from ethanol. The space group was determined as $P2_1/c$ by film methods, and it was found that there are eight molecules in the unit cell, *i.e.* two molecules in the asymmetric unit (in the following denoted A and B, respectively). A computer controlled Syntex-P$\bar{1}$ diffractometer with graphite-monochromatized Mo$K\alpha$ radiation and equipped with an Enraf-Nonius liquid nitrogen cooling device, modified by H. Hope, was utilized for preliminary experiments and for the measurement of diffraction intensities. A crystal of approximate dimensions 0.2 × 0.1 × 0.05 mm was used. Unit cell parameters were determined by a least-squares treatment of the angular coordinates of thirty symmetry-independent reflections with 2θ-values between 17 and 37°. The temperature at the crystal site was −165 °C. The crystal data are: *O*-[3-phenyl-5-(1,2,3,4-oxatriazolio)]oxide, $C_7H_5N_3O_2$, $M = 163.1$ amu, space group $P2_1/c$, $a = 15.160(3)$ Å, $b = 5.030(1)$ Å, $c = 19.769(7)$ Å, $\beta = 111.49°(2)$, $V = 1402.8$ Å^3, $Z = 8$, $D_{calc} = 1.544$ g/cm^3, $F(000) = 672$.

Three-dimensional intensity data were recorded using the ω-2θ scanning mode with scan speed variable from 2 to 8° min^{-1}, depending on the peak intensity of the reflection. Background counting time was equal to 0.7 × (scan time). Reflections with 2θ-values larger than 40°, which had integrated counts of less than 7 cps, determined in a 2 s scan over the reflection were not measured. The variations in the intensities of three standard reflections which were remeasured after every hundred reflections, were random and less than three times their standard deviations. Accordingly no corrections were applied for these varia-

Table 1. Fractional atomic coordinates and thermal parameters with estimated standard deviations for non-hydrogen atoms. The temperature factor is given by exp $[-2\pi^2(u_{11} \times (a^*h)^2 + u_{22}(b^*k)^2 + u_{33}(c^*l)^2 + u_{12}(a^*b^*hk) + u_{13}(a^*c^*hl) + u_{23}(b^*c^*kl))]$.

Atom	x	y	z	u_{11}	u_{22}	u_{33}	u_{12}	u_{13}	u_{23}
O1A	.7787(3)	.3908(10)	.1614(2)	.0257(27)	.0361(34)	.0263(25)	.0076(26)	.0057(22)	-.0016(27)
N2A	.7403(3)	.6007(12)	.1849(2)	.0264(31)	.0313(39)	.0222(28)	.0093(32)	.0057(26)	.0011(30)
N3A	.6583(3)	.6276(11)	.1354(2)	.0165(29)	.0263(34)	.0198(27)	.0010(30)	.0048(24)	.0028(31)
N4A	.6336(3)	.4639(12)	.0782(2)	.0295(34)	.0298(38)	.0193(28)	-.0003(31)	.0088(26)	-.0022(29)
C5A	.7196(5)	.3043(15)	.0930(3)	.0291(42)	.0241(45)	.0290(41)	.0021(39)	.0138(36)	.0046(38)
O6A	.7279(3)	.1186(10)	.0618(2)	.0404(31)	.0300(31)	.0406(29)	.0076(29)	.0262(25)	-.0088(29)
C7A	.5944(4)	.8321(13)	.1421(3)	.0189(34)	.0189(41)	.0187(33)	.0003(33)	.0058(29)	-.0005(33)
C8A	.6217(4)	.9822(14)	.2054(3)	.0201(34)	.0323(44)	.0158(31)	-.0007(34)	.0073(28)	.0009(34)
C9A	.5619(4)	1.1751(14)	.2109(3)	.0357(43)	.0272(44)	.0204(33)	-.0005(38)	.0134(33)	-.0004(36)
C10A	.4749(4)	1.2168(15)	.1555(3)	.0301(42)	.0251(43)	.0321(38)	-.0006(38)	.0174(34)	.0007(36)
C11A	.4466(4)	1.0594(14)	.0923(3)	.0285(39)	.0239(43)	.0228(33)	-.0004(35)	.0072(30)	.0011(34)
C12A	.5092(4)	.8617(14)	.0860(3)	.0263(38)	.0218(40)	.0238(33)	-.0003(36)	.0106(31)	.0011(36)
O1B	.7255(3)	.8958(11)	.4011(2)	.0268(28)	.0438(38)	.0471(33)	-.0067(30)	.0301(25)	-.0019(33)
N2B	.7762(4)	-.0353(13)	.4631(3)	.0282(36)	.0364(45)	.0589(44)	-.0123(35)	.0180(34)	-.0017(38)
N3B	.8521(3)	.1136(12)	.4992(2)	.0252(31)	.0249(36)	.0295(31)	-.0001(32)	.0159(26)	-.0008(32)
N4B	.8577(3)	.3351(12)	.4558(2)	.0217(32)	.0363(41)	.0216(30)	.0004(32)	.0065(26)	.0003(32)
C5B	.7762(5)	.3277(17)	.3958(4)	.0336(46)	.0346(55)	.0337(42)	.0053(44)	.0145(39)	-.0010(43)
O6B	.7433(3)	.4835(12)	.3453(2)	.0429(33)	.0630(44)	.0259(26)	.0138(32)	.0051(25)	.0004(31)
C7B	.9261(5)	.0371(14)	.5585(3)	.0346(41)	.0239(41)	.0265(36)	.0049(38)	.0168(32)	-.0003(36)
C8B	.9119(5)	-.1848(16)	.5955(4)	.0634(58)	.0258(50)	.0514(52)	.0074(47)	.0428(47)	.0003(46)
C9B	.9827(7)	-.2444(18)	.6511(4)	.1000(79)	.0377(56)	.0442(54)	.0128(60)	.0577(57)	.0089(47)
C10B	1.0649(6)	-.0990(19)	.6665(3)	.0748(66)	.0528(65)	.0236(40)	.0277(60)	.0230(45)	.0007(47)
C11B	1.0775(5)	.1189(17)	.6483(3)	.0467(50)	.0451(55)	.0231(38)	.0130(48)	.0122(37)	-.0096(44)
C12B	1.0068(4)	.1853(14)	.5823(3)	.0270(38)	.0309(46)	.0222(34)	.0101(38)	.0108(31)	.0003(37)

tions. The estimated standard deviations were taken as the square root of the total counts with a 2 % addition of the net intensity for experimental uncertainties. Of the 2279 reflections measured ($2\theta_{max} = 60°$), 1422 had intensities larger than twice their standard deviations. These were regarded as "observed" reflections and used in the refinements. The intensities were corrected for Lorentz and polarization effects. The computer program used, as well as programs subsequently employed, is part of a local assembly of computer programs for CYBER-74 and is described in Ref. 7. The atomic scattering factors used were those of Doyle and Turner[8] for carbon, nitrogen and oxygen, and of Stewart *et al.*[9] for hydrogen.

The phase problem was solved by the MULTAN program package.[10] The structure model was refined to a conventional R of 0.15. At this point the hydrogen atoms were placed in calculated positions and given a common isotropic temperature factor of 2.5 Å^2. Anisotropic thermal parameters for all nonhydrogen atoms were introduced. Indications of disorder (*i.e.* large anisotropic thermal parameters, *small* spurious peaks in a Fourier synthesis) were found for both phenyl rings. Full-matrix least-squares refinement of all positional and anisotropic thermal parameters for the nonhydrogen atoms converged to a conventional R of 0.074 and a weighted R_w of 0.072. Final parameters for nonhydrogen atoms are listed in Table 1, and calculated positional parameters used for hydrogen atoms are given in Table 2. A list of observed and calculated structure factors is available from the author upon request. (Also available from Department of Chemistry, University of Oslo, Norway). Standard deviations in molecular parameters were calculated from the correlation matrix ignoring standard deviations in cell parameters.

Mean bond lengths and bond angles are listed in Fig. 1. where the numbering of the atoms is indicated. Deviations from least-squares planes through the five and six-membered rings, respectively, are given in Table 3. The rings are planar and the dihedral angles N2–N3–C7–C8 and N2–N3–C7–C12 are, respectively, −4.6(9) and 176.9° (6) for molecule A, and −4.7(9) and 174.3° (6) for molecule B. The molecular dimensions obtained for the five-membered rings confirm the results found for *N*-[3-phenyl-1,2,3,4-oxatriazolio)]phe-

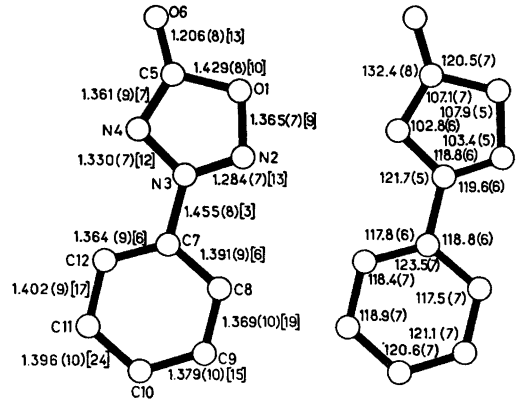

Fig. 1. Mean bond lengths (Å) and bond angles (°) with estimated standard deviations. The numbers in brackets are the differences ($\times 10^3$) in the results obtained for the two molecules.

Table 2. Calculated fractional coordinates used for hydrogen atoms.

Atom	x	y	z
C8HA	0.685	0.949	0.246
C9HA	0.580	1.293	0.255
C10HA	0.430	1.357	0.161
C11HA	0.384	1.092	0.052
C12HA	0.491	0.742	0.041
C8HB	0.853	−0.307	0.575
C9HB	0.947	−0.384	0.694
C10HB	1.118	−0.159	0.732
C11HB	1.137	0.231	0.670
C12HB	1.016	0.342	0.552

Table 3. Deviations (Å $\times 10^3$) from least-squares planes. Those for atoms used to define the plane are given in italicized figures. The first two columns are results for molecule A, the next two for molecule B.

	Plane A1	Plane A2	Plane B1	Plane B2
O1	*−4*	29	*−4*	4
N2	*6*	82	*−2*	64
N3	*−5*	12	*7*	−31
N4	*1*	−63	*−9*	−173
C5	*3*	−53	*9*	−128
O6	−19	−126	−7	219
C7	−27	*10*	6	*−11*
C8	−134	*−11*	−105	*12*
C9	−139	*3*	−143	*−11*
C10	−72	*6*	−15	*7*
C11	2	*−7*	106	*−4*
C12	28	*−1*	134	*6*

Angle between planes A1 and A2: 3.7°
Angle between planes B1 and B2: 5.9°

nylamid,[1] and again indicate the relationship between these *meso*-ionic systems and the isoelectronic sydnones.

1. Ottersen, T., Christophersen, C. and Treppendahl, S. *Acta Chem. Scand. A 29* (1975) 45.
2. Hope, H. and Thiessen, W. *Acta Crystallogr. B 25* (1969) 1237.
3. Thomas, T. L., Fedorchuk, M., Shetty, B. V. and Anderson, F. E. *J. Med. Chem. 13* (1970) 196.
4. Kier, L. B., AL-Shamma, A., Hahn, R. and Tye, A. *J. Pharm. Sci. 55* (1966) 1467.
5. Christophersen, C. and Treppendahl, S. *Acta Chem. Scand. 25* (1971) 625.
6. Cristophersen, C. and Treppendahl, S. *Acta Chem. Scand. 26* (1972) 858.
7. Groth, P. *Acta Chem. Scand. 27* (1973) 1837.
8. Doyle, P. A. and Turner, P. S. *Acta Crystallogr. A 24* (1968) 390.
9. Stewart, R. F., Davidson, E. R. and Simpson, W. T. *J. Chem. Phys. 42* (1965) 3175.
10. Germain, G., Main, P. and Woolfson, M. M. *Acta Crystallogr. A 27* (1971) 368.

Received June 18, 1975.

The Gas Phase Electron Diffraction Pattern of Beryllium Borohydride

KRISTEN BRENDHAUGEN, ARNE HAALAND* and DAVID P. NOVAK

Department of Chemistry, University of Oslo, Blindern, Oslo 3, Norway

Despite extensive investigations by a variety of techniques [1–9] there remain some puzzling aspects to the structure of gaseous beryllium borohydride. These are perhaps most clearly brought out by the electron diffraction experiments [1–4] from which at least two types of intensity curves have been obtained. A possible, but we feel unlikely, explanation for this difference is gross impurities in the solid sample used in one of the studies. A second possibility is that two or more species of gaseous molecule can be obtained from solid BeB_2H_8 in amounts depending on the state of the sample. This explanation gains plausibility from the fact that BeB_2H_8 is known to exist as polymeric chains in the crystal.[10] Indeed one type of diffraction pattern is known to have been obtained from freshly sublimed material kept at liquid N_2 temperature until just before the experiments were performed,[3] another from an aged sample.[4] Moreover, the infrared and Raman spectra of gaseous and matrix isolated BeB_2H_8 have been interpreted as evidence for the presence of two forms of monomeric BeB_2H_8 in equilibrium in the gas phase.[7]

We have carried out experiments designed to test the hypothesis described above. These involve solid samples of different histories and an all-glass nozzle-inlet system to eliminate the possibility of sample decomposition by contact with metal.

The BeB_2H_8 had been prepared by Dr. T. H. Cook at the University of Wyoming from B_2H_6 and $Be(CH_3)_2$. All the material used came from the same preparation and had been carefully purified by sublimation.

An all-glass inlet system was designed for Balzers Eldigraph KD-G2 which permitted the reservoir containing the solid sample to be kept outside the diffraction chamber. The diffraction patterns were recorded with a nozzle-to-plate distance of 327.3 mm and an electron wavelength of 0.0585 Å. Sufficient vapor pressure was obtained by submerging the reservoir in an oil bath maintained at 55 °C. In order to prevent condensation in the inlet system and particularly at the glass nozzle tip the latter was heated to 60 – 70 °C.

First the scattering pattern was recorded with a sample of BeB_2H_8 consisting of large clear colorless crystals. Then crystalline BeB_2H_8 was distilled into a liquid N_2 cooled cold finger and kept in liquid N_2 until 2 or 3 min before the diffraction pattern was recorded. Then

nylamid,[1] and again indicate the relationship between these *meso*-ionic systems and the isoelectronic sydnones.

1. Ottersen, T., Christophersen, C. and Treppendahl, S. *Acta Chem. Scand. A 29* (1975) 45.
2. Hope, H. and Thiessen, W. *Acta Crystallogr. B 25* (1969) 1237.
3. Thomas, T. L., Fedorchuk, M., Shetty, B. V. and Anderson, F. E. *J. Med. Chem. 13* (1970) 196.
4. Kier, L. B., AL-Shamma, A., Hahn, R. and Tye, A. *J. Pharm. Sci. 55* (1966) 1467.
5. Christophersen, C. and Treppendahl, S. *Acta Chem. Scand. 25* (1971) 625.
6. Cristophersen, C. and Treppendahl, S. *Acta Chem. Scand. 26* (1972) 858.
7. Groth, P. *Acta Chem. Scand. 27* (1973) 1837.
8. Doyle, P. A. and Turner, P. S. *Acta Crystallogr. A 24* (1968) 390.
9. Stewart, R. F., Davidson, E. R. and Simpson, W. T. *J. Chem. Phys. 42* (1965) 3175.
10. Germain, G., Main, P. and Woolfson, M. M. *Acta Crystallogr. A 27* (1971) 368.

Received June 18, 1975.

The Gas Phase Electron Diffraction Pattern of Beryllium Borohydride

KRISTEN BRENDHAUGEN, ARNE HAALAND* and DAVID P. NOVAK

Department of Chemistry, University of Oslo, Blindern, Oslo 3, Norway

Despite extensive investigations by a variety of techniques [1–9] there remain some puzzling aspects to the structure of gaseous beryllium borohydride. These are perhaps most clearly brought out by the electron diffraction experiments [1–4] from which at least two types of intensity curves have been obtained. A possible, but we feel unlikely, explanation for this difference is gross impurities in the solid sample used in one of the studies. A second possibility is that two or more species of gaseous molecule can be obtained from solid BeB_2H_8 in amounts depending on the state of the sample. This explanation gains plausibility from the fact that BeB_2H_8 is known to exist as polymeric chains in the crystal.[10] Indeed one type of diffraction pattern is known to have been obtained from freshly sublimed material kept at liquid N_2 temperature until just before the experiments were performed,[3] another from an aged sample.[4] Moreover, the infrared and Raman spectra of gaseous and matrix isolated BeB_2H_8 have been interpreted as evidence for the presence of two forms of monomeric BeB_2H_8 in equilibrium in the gas phase.[7]

We have carried out experiments designed to test the hypothesis described above. These involve solid samples of different histories and an all-glass nozzle-inlet system to eliminate the possibility of sample decomposition by contact with metal.

The BeB_2H_8 had been prepared by Dr. T. H. Cook at the University of Wyoming from B_2H_6 and $Be(CH_3)_2$. All the material used came from the same preparation and had been carefully purified by sublimation.

An all-glass inlet system was designed for Balzers Eldigraph KD-G2 which permitted the reservoir containing the solid sample to be kept outside the diffraction chamber. The diffraction patterns were recorded with a nozzle-to-plate distance of 327.3 mm and an electron wavelength of 0.0585 Å. Sufficient vapor pressure was obtained by submerging the reservoir in an oil bath maintained at 55 °C. In order to prevent condensation in the inlet system and particularly at the glass nozzle tip the latter was heated to 60 – 70 °C.

First the scattering pattern was recorded with a sample of BeB_2H_8 consisting of large clear colorless crystals. Then crystalline BeB_2H_8 was distilled into a liquid N_2 cooled cold finger and kept in liquid N_2 until 2 or 3 min before the diffraction pattern was recorded. Then

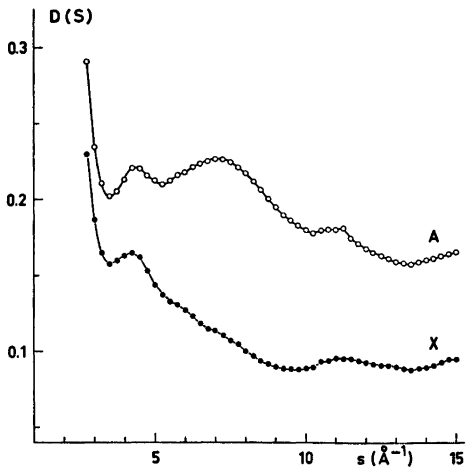

Fig. 1. Gas phase electron scattering patterns of beryllium borohydride. Optical densities obtained with crystalline solid sample (X) and with solid sample condensed at liquid N_2 temperature (A).

the liquid N_2 was withdrawn, the reservoir inserted in the hot oil bath and the data recorded as soon as it warmed up.

The difficulties associated with the recording of the diffraction pattern of BeB_2H_8 have been described.[4] Here we shall only add that the charging effect with the consequent deflection of the primary beam appeared even more pronounced with a glass than a metal nozzle. Nevertheless three reasonably good plates were obtained from each run. The scattering pattern on the three plates obtained in each run were very similar.

The uncorrected optical densities of one plate obtained with the amorphous white solid resulting when gaseous BeB_2H_8 is condensed at liquid N_2 temperature (A) and one plate obtained with a crystalline solid sample (X) are shown in Fig. 1. It is at once clear that the two curves are significantly different. Curve X resembles the intensity curve obtained by Gundersen *et al.*[4] in that it contains one peak with maximum around $s = 5$ and a broad shoulder on the high s side. Curve A resembles the intensity curve obtained by Almenningen *et al.*[3] in that it contains two clearly separated peaks at $s =$ 4 and 7 Å^{-1}, though the latter peak appears to be greater in curve A.

Before proceeding we must point out that there also appears to be a perplexing difference in the "backgrounds" of the two molecular intensity curves in Fig. 1, the background to curve A being higher in the region from about $s = 4$ to about $s = 10$ Å^{-1}. Since the photographs themselves have circular symmetry, it is unlikely that the difference is due to extraneous scattering. The difference could be explained if it is assumed that the gas jet contained different amounts of the constituent atoms, B, Be, and H, in the two experiments leading to a real difference in the atomic intensity. But this appears unlikely since no solid residues indicating decomposition, was observed in either run, and since the plates obtained in each run were consistent. Another possible explanation could be luminiscence from the scattering region during experiment A.

Whatever the reason for the difference in backgrounds, it is clear from the difference in the diffraction patterns obtained that at least two different species of gaseous molecule may be obtained from solid BeB_2H_8 and that their relative amounts depend on the state of the solid sample.

Since it cannot be taken for granted that each of the two or more species have the exact composition "BeB_2H_8", reliable information about the chemical composition of the gas jet is needed before firm conclusions regarding structure can be drawn from the electron diffraction data.

Acknowledgements. We are grateful to Dr. T. H. Cook for the sample of BeB_2H_8, to the Norwegian Research Council for Science and the Humanities for financial support and to Cand.real. Grete Gundersen and Dr. Ken Hedberg for helpful discussions.

1. Silbiger, G. and Bauer, S. H. *J. Amer. Chem. Soc. 68* (1946) 312.
2. Bauer, S. H. *J. Am. Chem. Soc. 72* (1950) 622.
3. Almenningen, A., Gundersen, G. and Haaland, A. *Acta Chem. Scand. 22* (1968) 859.
4. Gundersen, G., Hedberg, L. and Hedberg, K. *J. Chem. Phys. 59* (1973) 3777.
5. Nibler, J. M. and McNabb, J. *Chem. Commun.* (1969) 134.
6. Nibler, J. W. and Dyke, T. *J. Amer. Chem. Soc. 92* (1970) 2920.
7. Nibler, J. W. *J. Amer. Chem. Soc. 94* (1972) 3349.
8. Ahlrichs, R. *Chem. Phys. Lett. 19* (1973) 174.
9. Marynick, D. S. and Lipscomb, W. M. *J. Amer. Chem. Soc. 95* (1973) 7244.
10. Marynick, D. S. and Lipscomb, W. N. *Inorg. Chem. 11* (1972) 820.

Received June 19, 1975.

Acta Chemica Scandinavica A 29 (1975) 803—809

Properties of Sb-compounds with Rutile-like Structures

J. D. DONALDSON,[a] A. KJEKSHUS,[b] D. G. NICHOLSON[b] and T. RAKKE[b]

[a]Department of Chemistry, Chelsea College, University of London, Manresa Road, London S.W.3, England and [b]Department of Chemistry, University of Oslo, Blindern, Oslo 3, Norway

Powder X-ray diffraction, magnetic susceptibility, and ^{121}Sb Mössbauer measurements are reported for the so-called random-rutiles $CrSbO_4$, $FeSbO_4$, $RhSbO_4$, $AlSbO_4$, and $GaSbO_4$, the tri-rutiles $MgSb_2O_6$, $CoSb_2O_6$, $NiSb_2O_6$, and $ZnSb_2O_6$, and the distorted tri-rutile $CuSb_2O_6$.

The rutile (TiO_2-*r*) type structure and its closely related variants are frequently found among binary dioxides,[1] and substitutional TiO_2-*r* type solid solution phases can often be prepared from mixtures of such dioxides. Rutile-like atomic arrangements are also found for apparently well-defined ternary Sb and Te compounds (*cf.*, *e.g.*, Ref. 2): $MSbO_4$ (M = Cr, Fe, Rh, Al, and Ga), MSb_2O_6 (M = Mg, Co, Ni, Cu, and Zn), and M_2TeO_6 (M = Cr, Fe, Al, and Ga). According to current classifications the $MSbO_4$ compounds belong to the random-rutiles, whereas MSb_2O_6 and M_2TeO_6 belong to the tri-rutiles (*cf.* Fig. 1). These series of compounds represent a hitherto little explored source of information on the bonding properties of Sb and Te. Since M_2TeO_6 is better characterized,[3–5] the present work was concentrated on the Sb-compounds. A ^{121}Sb Mössbauer study [6] which includes all but two of these compounds was reported after the experimental part of this investigation was completed.

EXPERIMENTAL

The samples were prepared by mixing appropriate amounts of the materials specified below in open porcelain crucibles (previously fired with Sb_2O_3 at 1000 °C). The temperature was slowly raised to 800 °C where the first heat treatments ranged from 4 h to 3 weeks. The samples were crushed and reannealed at 900–1000 °C for 4 h to 2 weeks, and finally, slowly cooled to room temperature.

For M = Cr and Fe in $MSbO_4$, Cr flakes (99.999 %; Koch-Light Laboratories) and turnings from Fe rods (99.99+ %; Johnson, Matthey & Co.), respectively, and Sb_2O_3 (A. R.; Riedel-de Haën AG) were initially dissolved in hydrochloric acid (G.R.; Merck). After treatment of these solutions with nitric acid (G.R.; Merck), hydrous oxides were precipitated with NH_3(aq) (G. R.; Merck), filtered, washed with NH_4NO_3/NH_3 solution, and dried. ($CrSbO_4$ and $FeSbO_4$ can also be obtained through direct reactions between Cr_2O_3 or Fe_2O_3 and Sb_2O_3, but this procedure requires considerably longer heating periods.) The sources of M = Al, Ga, and Rh in $MSbO_4$ were $NH_4Al(SO_4)_2 \cdot 12H_2O$ (A. R.; Riedel-de Haën AG), $Ga_2(SO_4)_3$, and Rh_2O_3 (G.R.; K. & K. Laboratories, Inc.), respectively, and for M = Mg, Cu, and Zn in MSb_2O_6, MgO, CuO, and ZnO (G.R.; Merck) were used. The previously synthesized [7] products of $CoSb_2$ and $NiSb_2$ were used as starting materials for $CoSb_2O_6$ and $NiSb_2O_6$.

DTA/DTG data were collected with a Mettler Recording Vacuum Thermoanalyzer, using ~50 mg samples and silica (≦900 °C) and Al_2O_3 (> 900 °C) crucibles (Al_2O_3 as reference). Experimental details concerning X-ray diffraction, magnetic susceptibility, and ^{121}Sb Mössbauer measurements with subsequent data reduction are described in Refs. 8–10.

RESULTS AND DISCUSSION

(i) *The samples.* The present study was based on powder samples since attempts to make single crystals (at > 1000 °C) were unsuccessful. Decompositions and/or reactions with the porcelain crucibles were observed in the range 1150–1250 °C. Decomposition temperatures and products could not be determined more accurately (by *e.g.*, DTA/DTG methods) be-

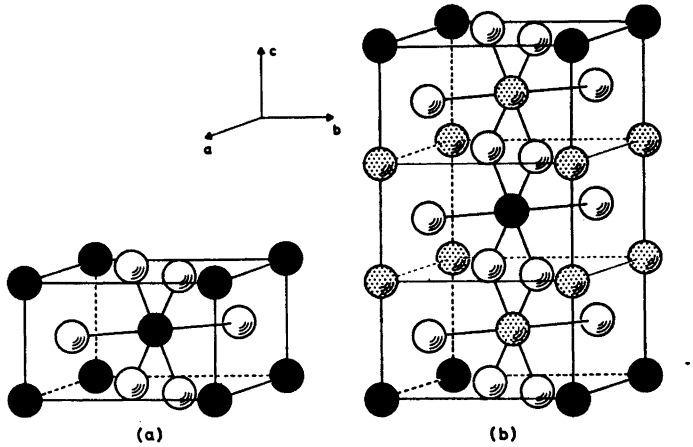

Fig. 1. Models emphasizing the main features of the (a) rutile or so-called random-rutile and (b) tri-rutile type structures.

Table 1. Room temperature tetragonal unit cell dimensions (with standard deviations) for $M\mathrm{SbO_4}$ and $M\mathrm{Sb_2O_6}$.

Random-rutiles			Tri-rutiles		
Compound	a (Å)	c (Å)	Compound	a (Å)	c (Å)
$CrSbO_4$	4.5837(3)	3.0477(4)	$MgSb_2O_6$	4.6489(6)	9.2334(17)
$FeSbO_4$	4.6347(3)	3.0732(3)	$CoSb_2O_6$	4.6535(4)	9.2804(18)
$RhSbO_4$	4.6122(7)	3.1073(6)	$NiSb_2O_6$	4.6417(4)	9.2203(15)
$AlSbO_4$	4.5300(4)	2.9731(4)	$CuSb_2O_6$[a]	4.6353(4)	9.2993(13)
$GaSbO_4$	4.5986(9)	3.0349(10)	$ZnSb_2O_6$	4.6679(5)	9.2676(15)

[a] Monoclinically deformed; $a=b$ (calculated, not fixed) and $\beta=91.15(1)$.

cause of disturbing reactions with all crucible materials tried.

The present samples are conveniently characterized by the unit cell dimensions recorded in Table 1; these data also serve to establish identity with those studied in Refs. 11, 12.

Among the $M\mathrm{SbO_4}$ and $M\mathrm{Sb_2O_6}$ compounds reported earlier, only $M=\mathrm{Fe}$ was claimed in both variants. For this reason considerable efforts were made to duplicate the preparation of $FeSb_2O_6$, using the original recipe,[11] co-precipitation reactions (see Experimental), as well as oxidation experiments on $FeSb_2$. According to Ref. 11, $FeSb_2O_6$ should be obtainable at 1000 °C, but even systematic variation of the reaction and annealing temperatures between 600 and 1100 °C did not result in the desired compound. As a matter of fact, $FeSbO_4$ was invariably obtained, and as the only product at ~1000 °C (more specifically $900 \leqq t \leqq 1100$ °C), where the excess antimony oxide originally present in the crucible was observed to volatilize. These findings do not finally reject $FeSb_2O_6$ as non-existent, since the synthesis of the related $FeTa_2O_6$ could only be obtained[13] through a careful control of the oxygen partial pressure.

Contrary to the suggestion in Ref. 6, no indication of a homogeneity range has been observed for $NiSb_2O_6$. (The distinction between brown and green reaction products consists in different crystallite size, the former being presently observed for roughly amorphous products.)

(ii) *Magnetic susceptibilities.* The sign of the magnetic susceptibilities divides the compounds under consideration into a diamagnetic and a paramagnetic class. The fact that the present

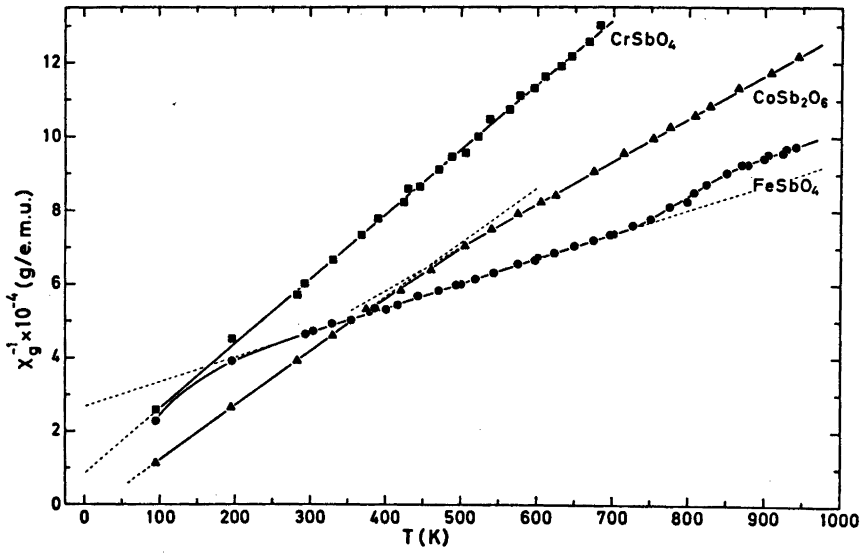

(a)

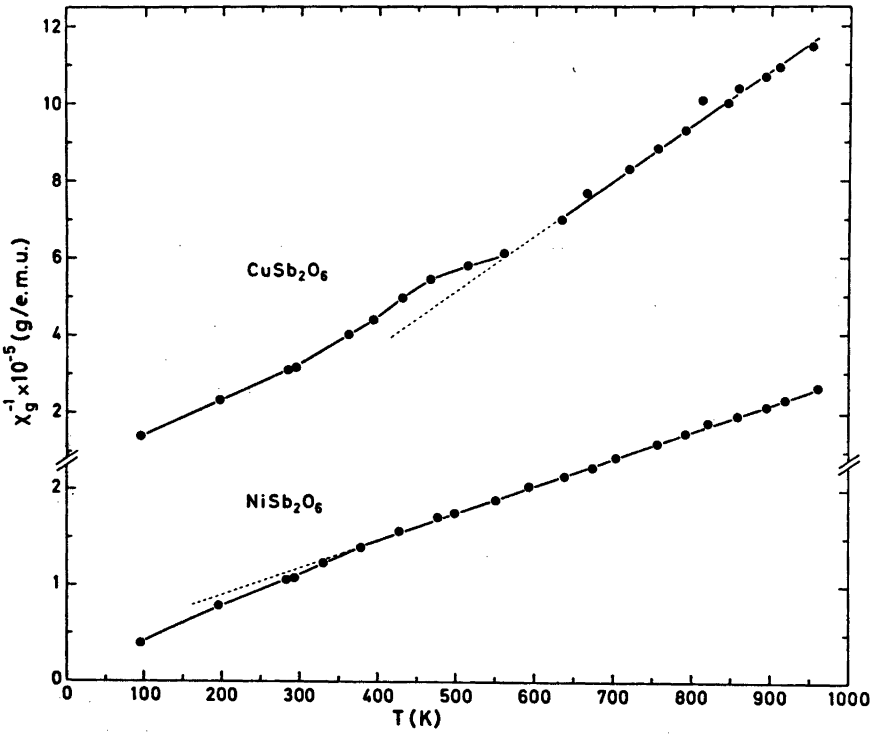

(b)

Fig. 2. The reciprocal magnetic susceptibility of (a) $CrSbO_4$, $FeSbO_4$, and $CoSb_2O_6$ and (b) $NiSb_2O_6$ and $CuSb_2O_6$ as a function of temperature.

Table 2. Susceptibilities of diamagnetic $MSbO_4$ and MSb_2O_6 expressed according to $(1/\chi_g)\times 10^{-6} = AT - B$ $(90 \leqq T \leqq 950$ K).

Compound	$A \times 10^3$ (g/e.m.u.K)	B (g/e.m.u.)
$AlSbO_4$	0.1	3.0
$GaSbO_4$	3.4	5.5
$RhSbO_4$	0.0	8.1
$MgSb_2O_6$	1.5	3.5
$ZnSb_2O_6$	4.3	7.4

Table 3. Evaluated parameters (θ, μ_p, $2S$) for temperature intervals (T_i to T_f) where Curie-Weiss Law is satisfied for $MSbO_4$ and MSb_2O_6. Estimated uncertainties in μ_p are ± 0.1 B.M.; correspondingly in $2S$.

Compound	$T_i - T_f$(K)	θ(K)	μ_p(B.M.)	$2S$	n
$CrSbO_4$	90–950	-50 ± 10	3.3	2.5	3
$FeSbO_4$	250–730	-400 ± 60	5.4	4.5	5
$CoSb_2O_6$	90–375	-20 ± 5	4.6	3.7	3
	500–950	-110 ± 20	5.3	4.4	–
$NiSb_2O_6$	90–375	-15 ± 5	3.0	2.2	2
	375–950	-110 ± 20	3.3	2.5	–
$CuSb_2O_6$	90–300	-50 ± 10	1.9	1.1	1
	560–950	$+140\pm30$	1.5	0.8	–

data are uncorrected for induced diamagnetism (due to the lack of reliable corrections) does not alter this classification.

The reciprocal susceptibility $(1/\chi)$ of the diamagnetic compounds $MgSb_2O_6$, $ZnSb_2O_6$, $AlSbO_4$, $GaSbO_4$ and $RhSbO_4$ show a linear dependence on temperature (T) to a reasonable approximation. These relationships are conveniently used to present our results for the compounds in Table 2.

As illustrated in Fig. 2, the paramagnetic compounds $CrSbO_4$, $FeSbO_4$, $CoSb_2O_6$, $NiSb_2O_6$, and $CuSb_2O_6$ satisfy Curie-Weiss Law [$\chi^{-1} = C^{-1}(T-\theta)$ where C and θ are the Curie and Weiss constants, respectively] over various temperature intervals. The $1/\chi_g$ *versus* T curve for $CrSbO_4$ is linear (90 – 950 K; the part from 650 to 950 K being omitted in order to compress the diagram), that for $NiSb_2O_6$ consists of two linear spans, whereas those for $FeSbO_4$, $CoSb_2O_6$, and $CuSb_2O_6$ reveal additional curved sections. The characteristic magnetic parameters [θ, $\mu_p = \sqrt{8C_{mol}}$ = paramagnetic moment, and S = spin quantum number according to the "spin only" approximation $\mu_p = g\sqrt{S(S+1)}$ with $g = 2$] are listed in Table 3. The last column of the table gives the number of unpaired electrons (n) predicted from ionic models (M^{3+}, Sb^{5+}, $4O^{2-}$ and M^{2+}, $2Sb^{5+}$, $6O^{2-}$) with completely quenched orbital momenta for the M atoms. The discrepancies between these and the "observed" values ($2S$) are no more than one would expect from the crudeness of the models, and the findings concur to that extent with those for other compounds when compared with unrealistic ionic models.

The changes in the "number of unpaired electrons" as functions of temperature, as brought out in Fig. 2 and Table 3, appear to be of different origin. As discussed in section (iii), the thermomagnetic behaviour of $CuSb_2O_6$ below 560 K has its parallel in structural alterations. The deviation from Curie-Weiss Law for $FeSbO_4$ above 725 K may also be correlated with structural features. The changes at 375 – 500 and 375 K (Fig. 2) in $CoSb_2O_6$ and $NiSb_2O_6$, respectively, are, on the other hand, not correlated with observable structural effects.

Concerning the possibility of cooperative magnetic ordering in these compounds at low temperatures, no definite conclusion can be drawn from the present thermomagnetic data. The most interesting candidate for a low temperature neutron diffraction study is $FeSbO_4$, with $\theta = -400$ K and a curved $1/\chi$ *versus* T portion below 250 K.

(iii) *Structural aspects.* The room temperature structures of the compounds under consideration divide into three categories: $MSbO_4$ (tetragonal), MSb_2O_6 (tetragonal), and $CuSb_2O_6$ (monoclinic); *cf.* Table 1.

According to a more detailed description, $MSbO_4$ should belong [12] to the TiO_2-*r* type structure [space group $P4_2/mnm$: M and Sb randomly distributed in 2(*a*), O in 4(*f*)]. As also illustrated in Fig. 1, the tri-rutiles MSb_2O_6 should have [11] an ordered rutile-like atomic arrangement [space group $P4_2/mnm$: M in 2(*a*), Sb in 4(*e*), O_I in 4(*f*), and O_{II} in 8(*j*)] with trebled *c* axis. The structure of $CuSb_2O_6$ at room temperature is registered [11] as a monoclinically distorted variant [space group $P2_1/c$:

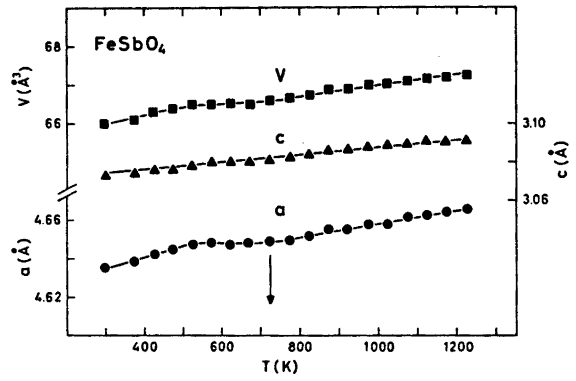

(a)

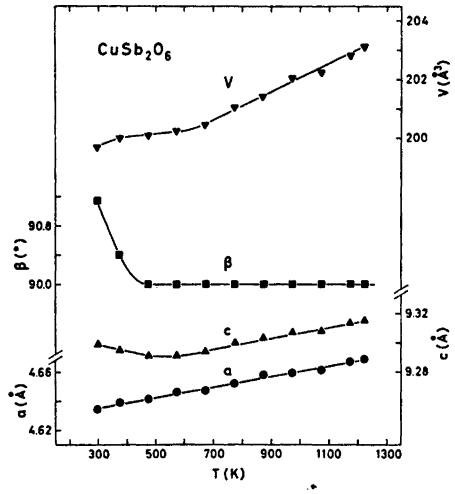

(b)

Fig. 3. Unit cell dimensions of (a) $FeSbO_4$ and (b) $CuSb_2O_6$ *versus* temperature.

Cu in 2(*a*), Sb in 4(*e*), O_I in 4(*e*), O_{II} in 4(*e*), and O_{III} in 4(*e*)] of the tri-rutile type.

Common for all these compounds is that no proper structure determination has been carried out. The structural assignments have merely been done on the basis of rather superficial tests, in which only a selected value (set of values) for the variable positional parameters have been used to calculate X-ray intensities for comparison with visually estimated powder data. For this reason, all these compounds are candidates for structural reinvestigations.

The demand for anewed attention is greater for $MSbO_4$ than for the others since the hitherto assumed complete crystallographic equivalence of *M* and Sb appears difficultly reconcilable. [The situation for $MSbO_4$ may, in many respects, be a parallel to that for TeO_2 prior to 1961 (*cf.* Ref. 14), and the interesting findings for the latter compound should stimulate anewed attention on $MSbO_4$.] In view of the experimental difficulties encountered in attempts to prepare single crystals of $MSbO_4$, the powder neutron diffraction technique lends itself as the most suitable means of investigation.

If one accepts as a working hypothesis that *M* and Sb really are distributed at random in $MSbO_4$, it is pertinent to ask whether randomization of *M* and Sb also occurs in MSb_2O_6 at high temperatures (*viz.* search for a tri-rutile to random-rutile type, order/disorder transformation in the latter class of compounds). For this reason MSb_2O_6 and $MSbO_4$ (for com-

parison purposes) were subjected to differential thermal analysis, high temperature X-ray diffraction, and quenching experiments (see Ref. 15) between room temperature and 1100 °C. None of the MSb_2O_6 compounds showed any sign of an order/disorder transformation. This finding makes the assumed disordered status of $MSbO_4$ even more intriguing.

The thermal expansion curves of $FeSbO_4$ and $CuSb_2O_6$ are presented in Fig. 3, since the thermomagnetic curves (Fig. 2) for these compounds showed somewhat abnormal behaviours. Fig. 3a demonstrates changes in the slopes of a and V at 725 K, which is just the temperature for the commencing anomaly in the magnetic susceptibility. Whereas the significance of the coincidences for $FeSbO_4$ may well be argued, the correlation between structural and magnetic behaviour of $CuSb_2O_6$ appears to be more clear-cut. As evident from Fig. 3b, $CuSb_2O_6$ undergoes a structural alteration above room temperature, where the symmetry changes from monoclinic to tetragonal. The monoclinic angle (β) for the distorted tri-rutile type modification of $CuSb_2O_6$ is not sensitive enough for a stipulation of the temperature for the reversible, second (or higher) order phase transition. The minimum (at ~ 550 K) in the thermal expansion curve for c (Fig. 3b) may provide a better measure for the conversion temperature; it is interesting to note that this matches the upper temperature of the non-linear $\chi^{-1}(T)$ section (Fig. 2b and Table 3).

A detailed structural investigation of $CuSb_2O_6$ at low and high temperatures is highly desirable, but, it is nevertheless tempting to present some naive considerations on the present findings. The distorted tri-rutile type structure for $CuSb_2O_6$ is perhaps not unexpected in view of the fact that high-spin Cu(II) compounds frequently exhibit so-called Jahn-Teller distortions of their octahedral coordination. The situation in low temperature $CuSb_2O_6$ may thus be analogous to that in CuF_2, where the regular TiO_2-r type structure is also monoclinically distorted.[16] However, if a Jahn-Teller mechanism could be held responsible for the distortion in monoclinic $CuSb_2O_6$ relative to tetragonal $CuSb_2O_6$, another mechanism [*e.g.*, (partial) delocalization of the unpaired electron] would have to be invented to account for the occurrence of the latter variant.

Table 4. ^{121}Sb Mössbauer parameters for $CrSbO_4$, $FeSbO_4$, $GaSbO_4$, $MgSb_2O_6$, $CoSb_2O_6$, and $CuSb_2O_6$ at 4.2 K; chemical shifts with respect to $Ba^{121}SnO_3$. Probable experimental errors are ± 0.01 mm/s in δ, ± 1.0 mm/s in eQV_{zz}, and ± 0.05 mm/s in Γ (width at half maximum).

	δ (mm/s)	eQV_{zz} (mm/s)	Γ (mm/s)	η	A (%)
$CrSbO_4$	−0.18	0 (fixed)	4.99	—	14.8
	−0.19	7.8	4.35	0.94	14.8
$FeSbO_4$	−0.07	0 (fixed)	6.59	—	15.3
	−0.06	5.1	3.87	0.90	15.3
$GaSbO_4$	+0.35	0 (fixed)	3.50	—	23.4
	+0.34	1.5	3.35		23.4
$MgSb_2O_6$	+0.17	0 (fixed)	3.00	—	15.1
	+0.15	3.8	2.75		15.1
$CoSb_2O_6$	−0.17	0 (fixed)	3.85	—	15.8
	−0.16	2.7	3.35		15.8
$CuSb_2O_6$	+0.13	0 (fixed)	2.92	—	22.5
	+0.13	1.3	2.89		22.5

(iv) *^{121}Sb Mössbauer spectroscopy.* The ^{121}Sb Mössbauer parameters for $CrSbO_4$, $FeSbO_4$, $GaSbO_4$, $MgSb_2O_6$, $CoSb_2O_6$, and $CuSb_2O_6$ derived from computer fitting of data collected at 4.2 K are contained in Table 4. The chemical shifts (δ) are given with respect to $Ba^{121}SnO_3$ source and when converted to shifts relative to the InSb standard, the present δ values are in excellent agreement with those obtained by Wooten *et al.*[6] at 77 K. The quadrupole interaction (eQV_{zz}) is small for all compounds and is hardly significant for $MgSb_2O_6$ and insignificant for $GaSbO_4$, $CoSb_2O_6$, and $CuSb_2O_6$.

Neither the present results nor those of Wooten *et al.*[6] give any definite indication of spectral line broadening or splitting originating from magnetic coupling between the M atoms in the compounds referred to as paramagnetic in section ii.

There is some correlation between δ and structure, which Wooten *et al.* couple to charges on the M atoms according to a formal ionic model. However, the magnitude of δ appears to be more typical of covalently bonded Sb(V). Other aspects are taken up in Ref. 6.

REFERENCES

1. Rogers, D. B., Shannon, R. D., Sleight, A. W. and Gillson, J. L. *Inorg. Chem.* *8* (1969) 841.
2. Bayer, G. *Ber. Deut. Keram. Ges.* *39* (1962) 535.

3. Kunnmann, W., La Placa, S., Corliss, L. M., Hastings, J. M. and Banks, E. *J. Phys. Chem. Solids 29* (1968) 1359.
4. Montmory, M. C., Belakhovsky, M., Chevalier, R. and Newnham, R. *Solid State Commun. 6* (1968) 317.
5. Montmory, M. C. and Newnham, R. *Solid State Commun. 6* (1968) 323.
6. Wooten, J. B., Long, G. G. and Bowen, L. H. *J. Inorg. Nucl. Chem. 36* (1974) 2177.
7. Kjekshus, A. and Rakke, T. *Acta Chem. Scand. A 28* (1974) 1001.
8. Furuseth, S., Kjekshus, A. and Andresen, A. F. *Acta Chem. Scand. 23* (1969) 2325.
9. Donaldson, J. D., Kjekshus, A., Nicholson, D. G. and Tricker, M. T. *Acta Chem. Scand. 26* (1972) 3215.
10. Kjekshus, A. and Nicholson, D. G. *Acta Chem. Scand. A 28* (1974) 469.
11. Byström, A., Hök, B. and Mason, B. *Arkiv Kemi, Mineral. Geol. 15 B* (1941) No. 4.
12. Brandt, K. *Arkiv Kemi, Mineral. Geol. 17 A* (1943) No. 15.
13. Takano,M. and Takada, T. *Mater. Res. Bull. 5* (1970) 449.
14. Leciejewicz, J. *Z. Kristallogr. 116* (1961) 345.
15. Kjekshus, A. and Rakke, T. *Acta Chem. Scand. A 29* (1975) 443.
16. Billy, C. and Haendler, H. M. *J. Amer. Chem. Soc. 79* (1957) 1049.

Received March 25, 1975.

Acta Chemica Scandinavica A 29 (1975) 810—816

Magnetic Structures and Properties of $Cr_{1-t}Co_tAs$ and $Fe_{1-t}Co_tAs$

KARI SELTE,[a] ARNE KJEKSHUS,[a] STIAN AABY [a] and ARNE F. ANDRESEN [b]

[a] Kjemisk Institutt, Universitetet i Oslo, Blindern, Oslo 3, Norway and [b]Institutt for Atomenergi, Kjeller, Norway

The pseudo-binary CrAs – CoAs and FeAs – CoAs systems have been investigated by X-ray and neutron diffraction and magnetic susceptibility measurements. Both systems are characterized by complete solid solubility, and the structures of the ternary, random solid solution phases are of the MnP type at and below room temperature. Like CrAs and CoAs, all $Cr_{1-t}Co_tAs$ samples and Co-rich $Fe_{1-t}Co_tAs$ samples undergo a transition from MnP to NiAs type structure at high temperatures. The double, *c* axis helimagnetic orderings in CrAs and FeAs extend slightly into the ternary regions ($t \approx 0.07$ in $Cr_{1-t}Co_tAs$ and $t \approx 0.03$ in $Fe_{1-t}Co_tAs$).

The MnP type atomic arrangement has proved to give rise to various interesting cooperative magnetic structures (*viz.* ferromagnetic,[1] antiferromagnetic,[2] and helimagnetic [1–3] modes or varieties [2–10] thereof, depending on composition, temperature, pressure and magnetic field). In order to explore the factors which influence the occurrence of the various modes, attention has recently been focussed on ternary MnP type phases. With the present contribution on $Cr_{1-t}Co_tAs$ and $Fe_{1-t}Co_tAs$, together with forthcoming papers on $V_{1-t}Co_tAs$ and $Cr_{1-t}Fe_tAs$, all possible combinations $TAs-T'As$ [2,7,11–14] of binary compounds with MnP type structure have been examined.

EXPERIMENTAL

Batches of CrAs, FeAs, and CoAs were prepared from the elements [99.5 % Cr (Koch-Light Laboratories; crushed powder from commercial, electrolytic grade material), 99.99 % Fe and 99.99+ % Co (Johnson, Matthey & Co.; turnings from rods), and 99.9999 % As (Koch-Light Laboratories)] as described in Refs. 15–17. Ternary samples of desired compositions were prepared from appropriate proportions of the binary compounds by 3–4 heat treatments of one week's duration at 850 °C, interrupted by intermediate crushings. The samples were finally cooled to room temperature over a period of three days.

Experimental details concerning X-ray and neutron diffraction (including data reduction) and magnetic susceptibility measurements have been reported earlier.[16]

RESULTS AND DISCUSSION

(i) *Chemical crystal structures.* Fig. 1 shows the room temperature unit cell dimensions of $Cr_{1-t}Co_tAs$ and $Fe_{1-t}Co_tAs$ as functions of the composition parameter *t*. The continuous variations in all unit cell dimensions with *t* demonstrate the complete solid solubility in the CrAs – CoAs and FeAs – CoAs systems. The possibility that the homogeneity ranges of $Cr_{1-t}Co_tAs$ and $Fe_{1-t}Co_tAs$ extend to metal/non-metal (atomic) ratios different from 1.00 has not been examined for $t \neq 0$ and 1.[15–17]

X-Ray and neutron diffraction data confirm an MnP type atomic arrangement at and below room temperature for $0 \leq t \leq 1$ in both phases. Moreover, the data show that the substituted atoms are distributed randomly over the metal sub-lattices. The sample $Cr_{0.95}Co_{0.05}As$, which exhibits helimagnetic ordering below 130 – 160 K, reveals appreciable changes in the dimensions of its MnP type unit cell (Table 1) connected with the superimposed first and second (or higher) order phase transformation. This peculiarity, which is typical of CrAs and its slightly substituted ternary derivatives (*cf.* Refs. 7, 12, 15, 18–20), is not observed for $Cr_{0.90}Co_{0.10}As$ and $Fe_{0.95}Co_{0.05}As$. The least

Fig. 1. Orthorhombic unit cell dimensions of ternary, solid solution series (a) CrAs – CoAs and (b) FeAs – CoAs as functions of composition.

Table 1. Unit cell dimensions and positional parameters with standard deviations for $Cr_{0.95}Co_{0.05}As$, $Cr_{0.90}Co_{0.10}As$, and $Fe_{0.95}Co_{0.05}As$; space group *Pnma*, positions 4(*c*). (Overall profile reliability factors ranging between 0.029 and 0.047.)

Sample	$Cr_{0.95}Co_{0.05}As$			$Cr_{0.90}Co_{0.10}As$			$Fe_{0.95}Co_{0.05}As$		
T(K)	4.2	80	293	4.2	80	293	6	80	293
a(Å)	5.565(1)	5.562(1)	5.633(1)	5.594(1)	5.595(1)	5.604(1)	5.421(1)	5.428(1)	5.416(1)
b(Å)	3.555(1)	3.556(1)	3.454(1)	3.384(1)	3.393(1)	3.443(1)	3.328(1)	3.344(1)	3.379(1)
c(Å)	6.114(1)	6.110(1)	6.211(1)	6.187(1)	6.183(1)	6.187(1)	6.002(1)	6.010(1)	6.011(1)
x_T	0.0089(15)	0.0079(11)	0.0047(12)	0.0114(15)	0.0074(9)	0.0077(13)	0.0030(5)	0.0035(5)	0.0042(5)
z_T	0.2015(11)	0.2004(8)	0.2008(9)	0.2000(13)	0.1986(7)	0.2011(10)	0.1994(3)	0.1984(3)	0.1986(3)
x_X	0.2043(5)	0.2036(4)	0.2011(5)	0.1992(7)	0.1990(4)	0.2004(5)	0.2014(5)	0.2014(5)	0.2013(4)
z_X	0.5794(15)	0.5847(10)	0.5773(6)	0.5742(8)	0.5743(5)	0.5771(6)	0.5769(5)	0.5761(5)	0.5792(5)

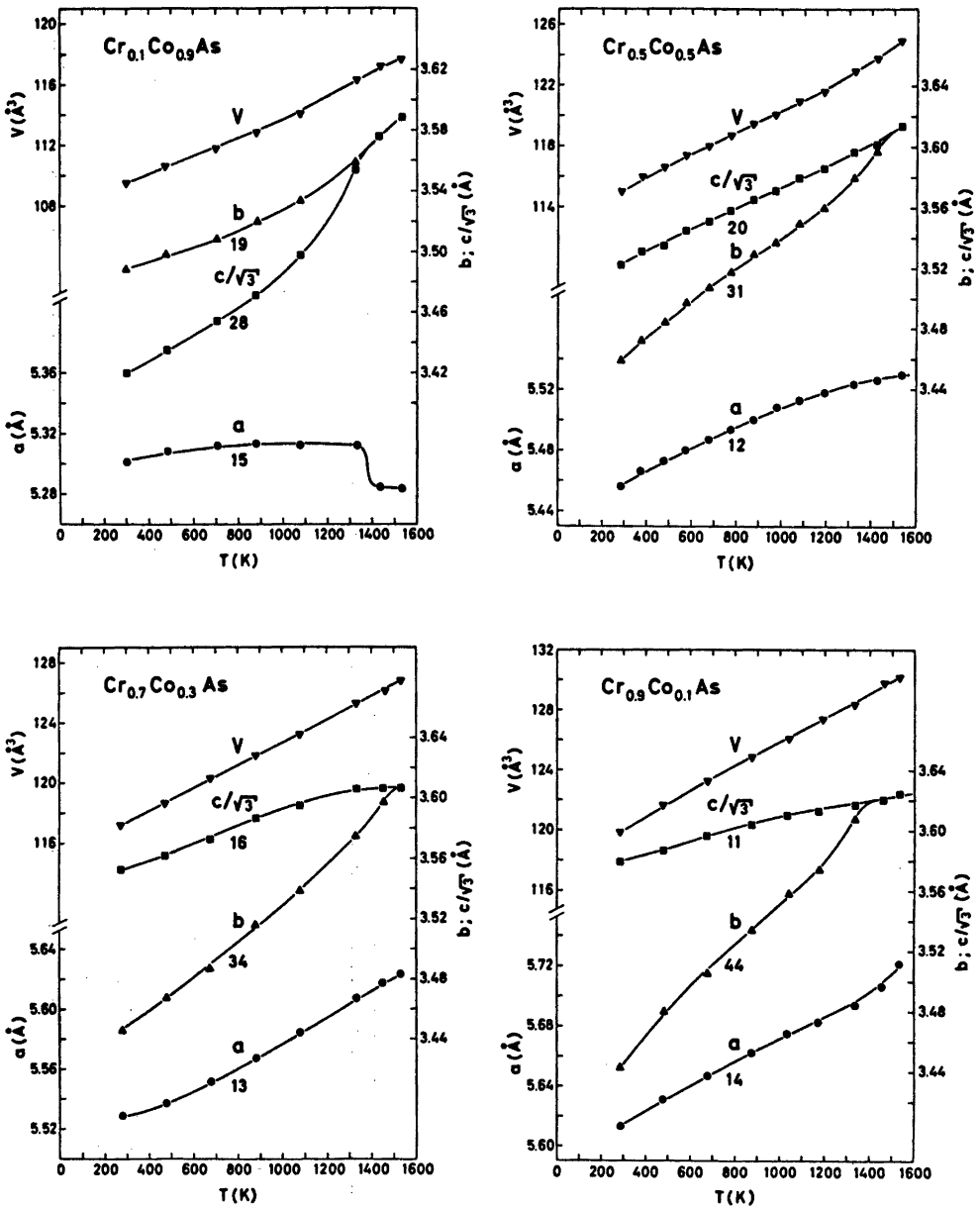

Fig. 2. Unit cell dimensions of representative $Cr_{1-t}Co_tAs$ samples *versus* temperature. Average relative expansion coefficients $\alpha_a(=(a_T-a_{T'})/a_{300}(T-T'))$, α_b, and α_c multiplied by 10^6 K are positioned below the appropriate curves (300 – 1200 K).

squares, profile refined positional parameters (Table 1) derived for $Fe_{0.95}Co_{0.05}As$ at various temperatures fit nicely in with the data for FeAs,[16] those for $Cr_{0.95}Co_{0.05}As$ vary in the same way as for CrAs,[15,18] whereas those for $Cr_{0.90}Co_{0.10}As$ stay virtually constant at values matching CrAs at room temperature.

CrAs and CoAs exhibit second (or higher) order crystallographic transformations to the NiAs type structure at temperatures of 1173 ± 20 and

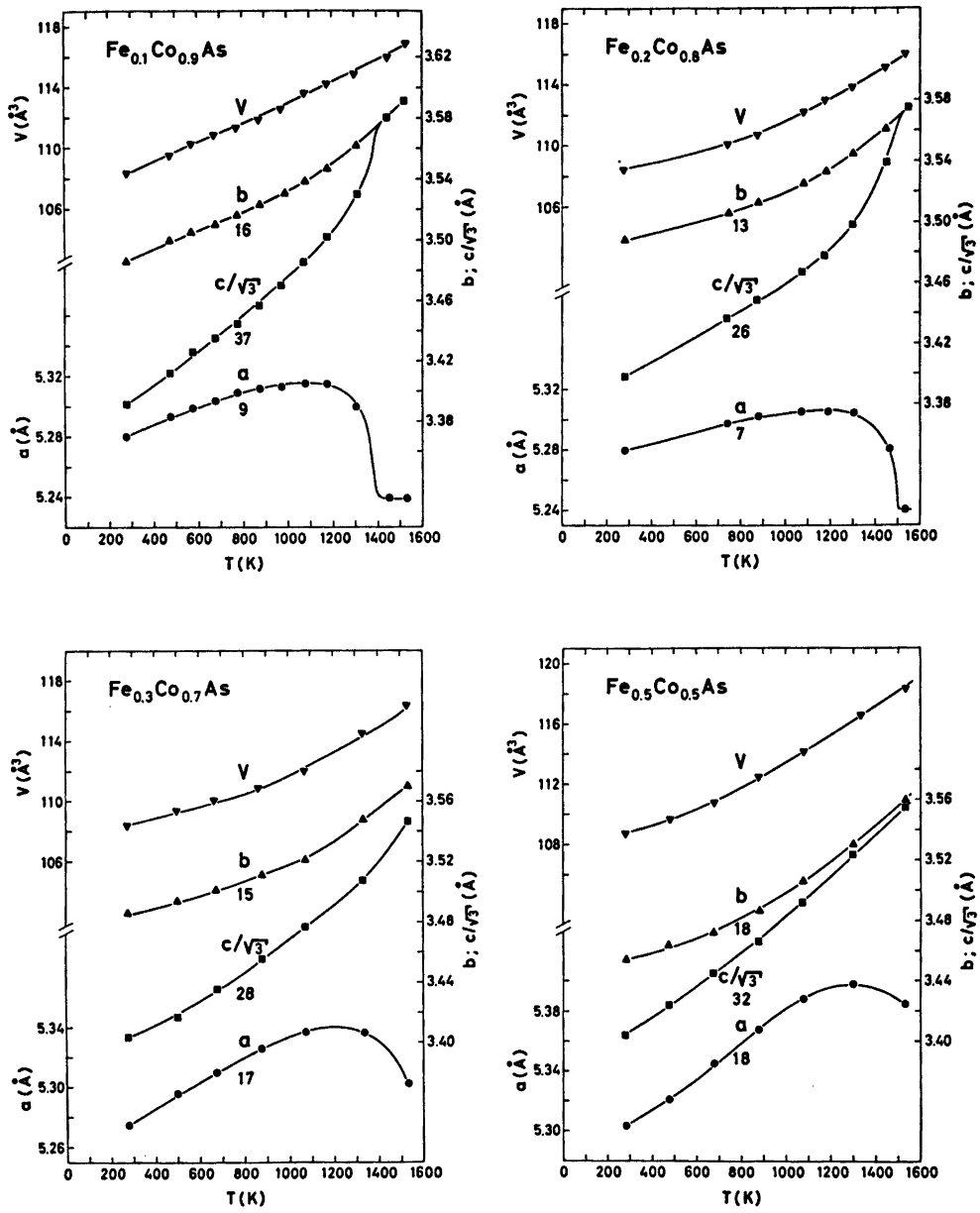

Fig. 3. Unit cell dimensions of $Fe_{1-t}Co_tAs$ samples *versus* temperature. Average relative expansion coefficients α_a, α_b, and α_c ($\times 10^6$ K) are given on the diagrams (300 – 1100 K).

1248 ± 20 K, respectively, whereas no such transformation occurs in FeAs below its melting point of 1343 ± 20 K.[16,21] This distinction is projected into the ternary samples, where $Cr_{1-t}Co_tAs$, as seen from Fig. 2, undergoes transformation at temperatures close to those for CrAs and CoAs. For $Fe_{1-t}Co_tAs$ transformations are only found for $0.8 \leqq t \leqq 1$ (*cf.* Fig. 3).

(ii) *Magnetic susceptibility.* Figs. 4 and 5 show that the temperature dependences of the reciprocal magnetic susceptibility of $Cr_{1-t}Co_tAs$

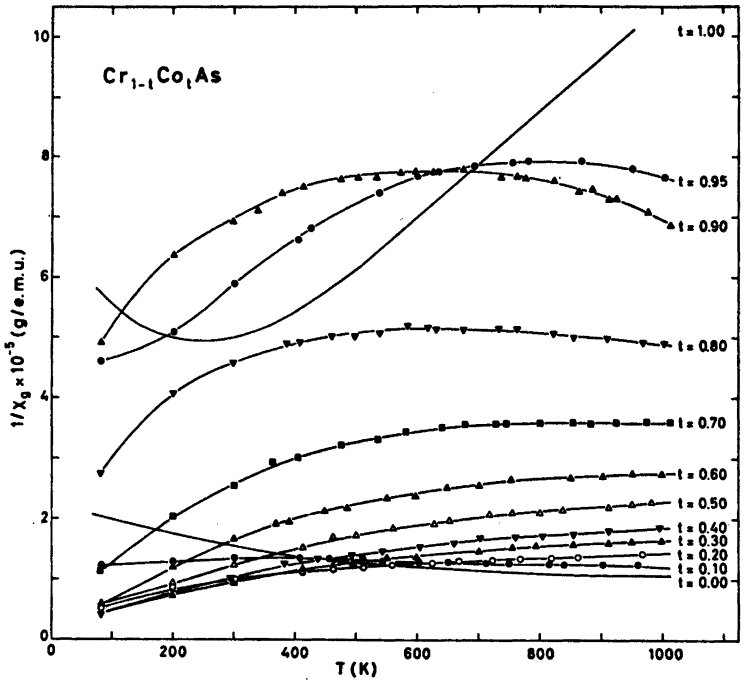

Fig. 4. Reciprocal magnetic susceptibility *versus* temperature for $Cr_{1-t}Co_tAs$ samples.

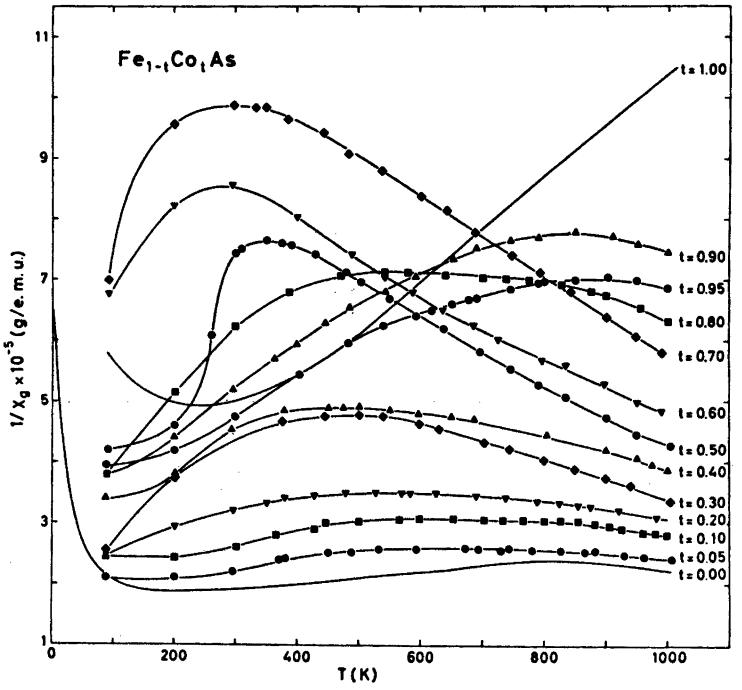

Fig. 5. Thermomagnetic data for $Fe_{1-t}Co_tAs$.

and $Fe_{1-t}Co_tAs$ undergo progressive changes with the composition parameter t. No field strength dependent susceptibilities were observed. The thermomagnetic curves for the binary compounds agree with corresponding data reported in Refs. 12, 16, and 17. Apart from FeAs ($\sim 300 - \sim 650$ K) and CoAs (> 490 K) none of the $Cr_{1-t}Co_tAs$ and $Fe_{1-t}Co_tAs$ samples satisfies the Curie-Weiss Law.

(iii) *Magnetic structures.* Helimagnetism has previously been observed for CrAs [7,15,18] and FeAs,[16] whereas CoAs [17] exhibits no cooperative phenomenon above 4.2 K. The helimagnetic ordering in CrAs and FeAs is of the double, c-axis type, and it extends in both the investigated systems only slightly into the ternary composition ranges ($t \approx 0.07$ for $Cr_{1-t}Co_tAs$ and (say) $t \approx 0.03$ for $Fe_{1-t}Co_tAs$).

Only small changes were experienced in the variable spiral parameters (β fixed at 90°) on going from CrAs (80 K: $\mu_T = 1.70 \pm 0.05$ μ_B, $\tau/2\pi c^* = 0.353(1)$, $\phi = -133 \pm 1°$)[15] to $Cr_{0.95}Co_{0.05}As$ (4.2 K: $\mu_T = 1.65 \pm 0.05$ μ_B, $\tau/2\pi c^* = 0.346(1)$, $\phi = -124 \pm 1°$; 80 K: $\mu_T = 1.65 \pm 0.05$ μ_B, $\tau/2\pi c^* = 0.360(1)$, $\phi = -128 \pm 1°$; 145 K: $\tau/2\pi c^* = 0.373(1)$). However, already a 5 % substitution of CrAs by CoAs leads to a substantial lowering of the Néel temperature (from 261 – 272 K for CrAs to 130 – 160 K). Significant indication of reflections characteristic of the helimagnetic arrangement was not found for $Cr_{0.90}Co_{0.10}As$.

The cooperative magnetism in $Cr_{0.95}Co_{0.05}As$ is associated with a marked hysteresis which involves two distinct MnP type phases. As shown in Fig. 6 the hysteresis is brought out in both nuclear and magnetic reflections of the neutron diffraction diagrams. Similar hystereses are observed for CrAs [7,15,18] and CrAs-rich samples of $V_{1-t}Cr_tAs$,[12] $Cr_{1-t}Mn_tAs$,[7] $Cr_{1-t}Fe_tAs$,[20] and $CrP_{1-x}As_x$.[19] The helimagnetic structures of these phases have also another feature in common in that both the phase angle (ϕ) between the spirals and the spiral turn angle (α) vary little with temperature.

The helimagnetic arrangement in pure FeAs [16] extends slightly into the ternary range of $Fe_{1-t}Co_tAs$. The neutron diffraction diagrams of $Fe_{0.95}Co_{0.05}As$ gave only insignificant indications of magnetic reflections, and the magnetic phase boundary was tentatively positioned at $t = 0.03$.

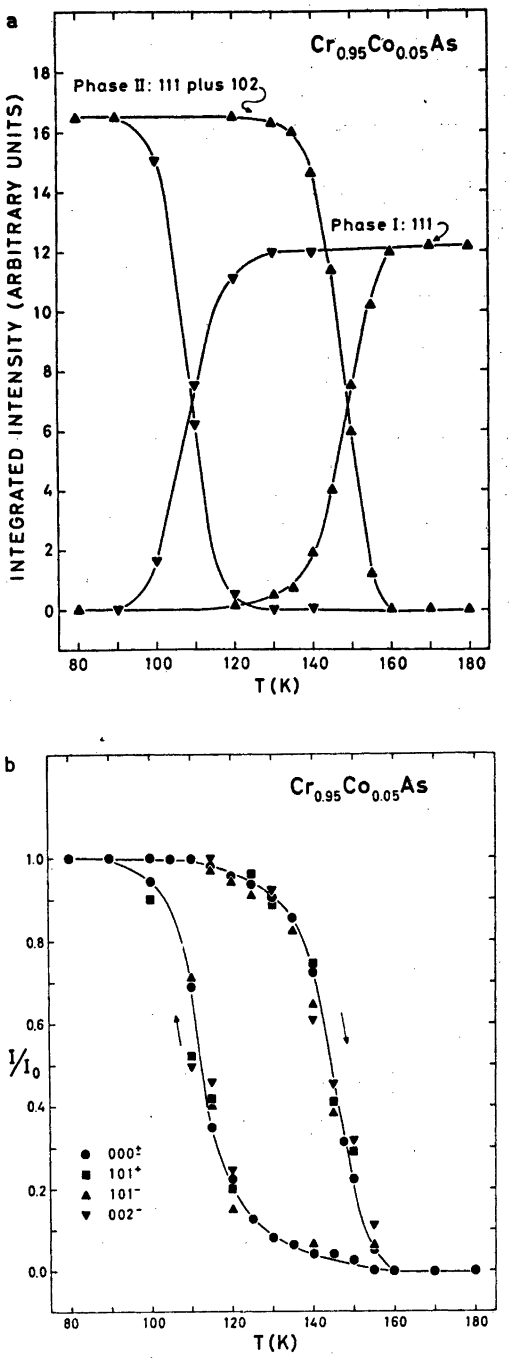

Fig. 6. Integrated intensities *versus* temperature of (a) 111 of paramagnetic, high temperature state (phase I) and 111 plus 102 for helimagnetic, low temperature (phase II) state and (b) 000± 101+, 101−, and 002− of $Cr_{0.95}Co_{0.05}As$.

The data for the cooperative magnetic states of $T_{1-t}T'_tAs$ and $TP_{1-x}As_x$ phases which have been collected hitherto, have revealed the contours of a pattern.[2,7,12–14,19,22] Among the mono-phosphides and -arsenides of the 3*d* series which take the MnP type structure, cooperative magnetic states are found for Cr, Mn, and Fe, but are lacking for V and Co. Appreciable composition regions for cooperative modes in ternary phases are only observed when Mn is one constituent. The cooperative modes in CrAs, FeP, and FeAs are destroyed at some 5 – 10 % substitution with a metal different from Mn or another non-metal.[12,19,22] Possible reasons for the breakdown of the helimagnetic modes in these phases are briefly discussed in Refs. 12 and 22. These considerations, which were based on the findings for $V_{1-t}Cr_tAs$ and $FeP_{1-x}As_x$, are necessarily somewhat speculative, since the parameters specifying the helimagnetic states (μ_T, α, ϕ and T_N) show an almost discontinuous drop at the magnetic phase boundary. Including also the present knowledge concerning $Cr_{1-t}Co_tAs$ and $Fe_{1-t}Co_tAs$ the most likely explanation of the limited extensions of the helimagnetic regions in $Cr_{1-t}T_tAs$, $CrP_{1-x}As_x$, $Fe_{1-t}T_tAs$, and $FeP_{1-x}As_x$ appears to be that the magnetic exchange parameters decrease rapidly with small variations in t or x, thus inducing corresponding decreases in T_N for such phases.

REFERENCES

1. Felcher, G. P. *J. Appl. Phys. 37* (1966) 1056.
2. Selte, K., Kjekshus, A. and Andresen, A. F. *Acta Chem. Scand. A 28* (1974) 61.
3. Forsyth, J. B., Pickart, S. J. and Brown, P. J. *Proc. Phys. Soc. 88* (1966) 333.
4. Nagai, H., Hihara, T. and Hirahara, E. *J. Phys. Soc. Japan 29* (1970) 622.
5. Schwartz, L. H., Hall, E. L. and Felcher, G. P. *J. Appl. Phys. 42* (1971) 1621.
6. Ishizaki, A., Komatsubara, T. and Hirahara, E. *J. Phys. Soc. Japan. 30* (1971) 292.
7. Kazama, N. and Watanabe, H. *J. Phys. Soc. Japan 30* (1971) 1319.
8. Sirota, N. N., Vasilev, E. A. and Govor, G. A. *J. Phys. (Paris) C 32* (1971) 987.
9. Banus, M. D. *J. Solid State Chem. 4* (1972) 391.
10. Kallel, A., Boller, H. and Bertaut, E. F. *J. Phys. Chem. Solids 35* (1974) 1139.
11. Selte, K., Kjekshus, A. and Oftedal, T. A. *Acta Chem. Scand. A 28* (1974) 803.
12. Selte, K., Hjersing, H., Kjekshus, A. and Andresen, A. F. *Acta Chem. Scand. A 29* (1975) 312.
13. Selte, K., Kjekshus, A., Valde, G. and Andresen, A. F. *Acta Chem. Scand. In press.*
14. Selte, K., Kjekshus, A., Valde, G. and Andresen, A. F. *To be published.*
15. Selte, K., Kjekshus, A., Jamison, W. E., Andresen, A. F. and Engebretsen, J. E. *Acta Chem. Scand. 25* (1971) 1703.
16. Selte, K., Kjekshus, A. and Andresen, A. F. *Acta Chem. Scand. 26* (1972) 3101.
17. Selte, K. and Kjekshus, A. *Acta Chem. Scand. 25* (1971) 3277.
18. Boller, H. and Kallel, A. *Solid State Commun. 9* (1971) 1699.
19. Selte, K., Hjersing, H., Kjekshus, A., Andresen, A. F. and Fischer, P. *Acta Chem. Scand. A 29* (1975) 695.
20. Selte, K., Kjekshus, A. and Andresen, A. F. *To be published.*
21. Selte, K. and Kjekshus, A. *Acta Chem. Scand. 27* (1973) 3195.
22. Selte, K., Kjekshus, A., Oftedal, T. A. and Andresen, A. F. *Acta Chem. Scand. A 28* (1974) 957.

Received April 22, 1975.

Acta Chemica Scandinavica A 29 (1975) 817—823

Absorption of Circularly Polarized Light by the $^2E \leftarrow {}^4A_2$ and $^2T_2 \leftarrow {}^4A_2$ Transitions in Ruby in Strong Magnetic Fields. II

I. TRABJERG

Chemical Laboratory IV, H. C. Ørsted Institute, Universitetsparken 5, DK-2100 Copenhagen Ø, Denmark

The longitudinal Zeeman-splitting of the $^2T_2$ (E_b) state of ruby has been measured at 4.2 K and the relative dipole strengths of the components involved were found at 80 K. The results were obtained by combining a pulsed magnet and an optical multichannel analyzer. The g-factor was found to be 4.15 ± 0.09, while the intensity ratio at 20.4 Wb/m^2 (204 kgauss) was 0.7 ± 0.1 for right-, and 0.15 ± 0.09 for left-circularly polarized light. The dipole strength of the most intense component of the B3 line did not vary with the magnetic field.

The electronic transitions of Cr^{3+} in ruby have been subject to investigation for many years, and are now qualitatively very well understood.[1–5] A considerable contribution to this understanding has been obtained by means of data from the spin-forbidden transitions within the t_2^3-configuration. These are all slightly split for all but Kramers degeneracy, and a considerable amount of effort has been devoted to Zeeman-measurements on these lines. This has resulted in determination of the g-factors for the ^2E, the $^2T_2(E_A)$ and $^2T_2(A)$ components.[2,3,5–8] However, the three components of the $^2T_1$ and the E_B component of the $^2T_2$ have not yet been determined. This is mainly because the absorption-lines involved are so broad, that either extremely strong fields or a quite different technique than previously used would be necessary. The purpose of this paper is to report on the determination of the g-factor for the $^2T_2(E_B)$ state and on the relative electronic intensity of its components by a technique using circularly polarized light and a pulsed magnet.

THEORY

The splitting pattern for the transitions to the $^2T_2$ state, called the B-lines is shown in Fig. 1, and those to ^2E, the R-lines, in Fig. 2. The intensity of these lines is due to spin-orbit coupled quartet-character contributions of the wave functions, mainly from the nearby quartets.[1]

Of the B1 and B2 lines of Fig. 1, only the heavily drawn lines have been observed. These lines are so sharp, that they permit a determination of the g-factors. The calculated intensity ratio of the B3 absorption line components is 1:3,[1] the strong ones are shown with heavy lines in Fig. 1. This line is considerably broader, and no separation has been observed for fields up to 230 kgauss. The broadening is due to relaxation to the other components of the same state, with the same spin.[9] The separation in energy is very close to that of a phonon observed in emission as well as in excitation spectra of the R-lines.[10] This has been used to explain the fact that the B3 line is double.[11,12] Further structure of the B3 line could be caused by a localized phonon added to this phonon. This effect has been observed in emission, where a structure with a characteristic vibrational energy of approximately 35 cm^{-1} can be seen in the phonon-line.[13] Assuming now that the B3 line does not hide a vibrational line from any other component, it will be assumed, that its first order moment is practically independent of the phonons. This seems reasonable because the Zeeman-splitting changes the energy differences by about 50 cm^{-1}, while

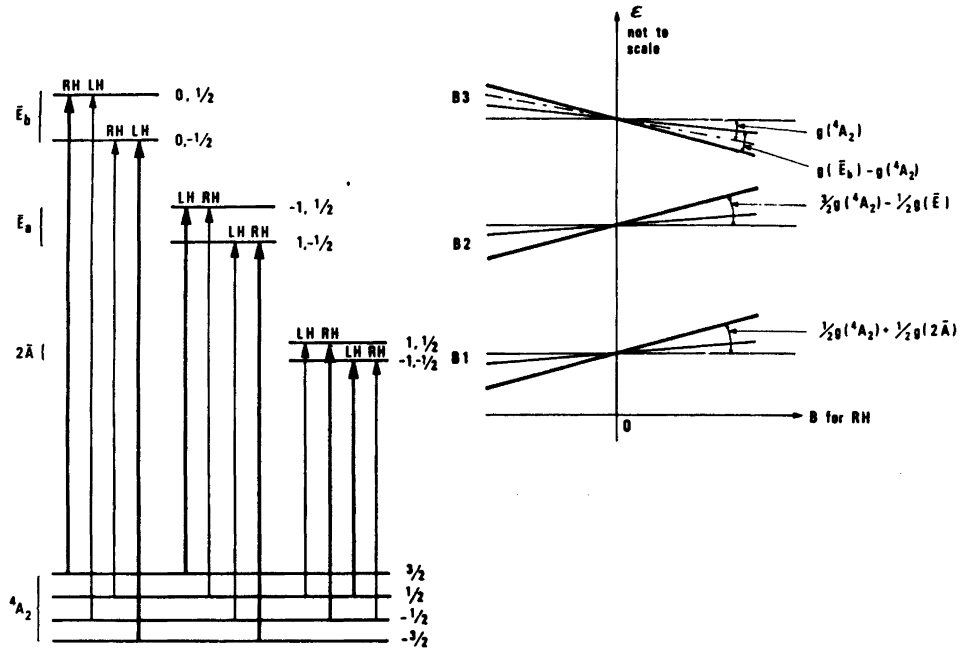

Fig. 1. Transition diagram and splitting pattern of the $^2T_2$ components.

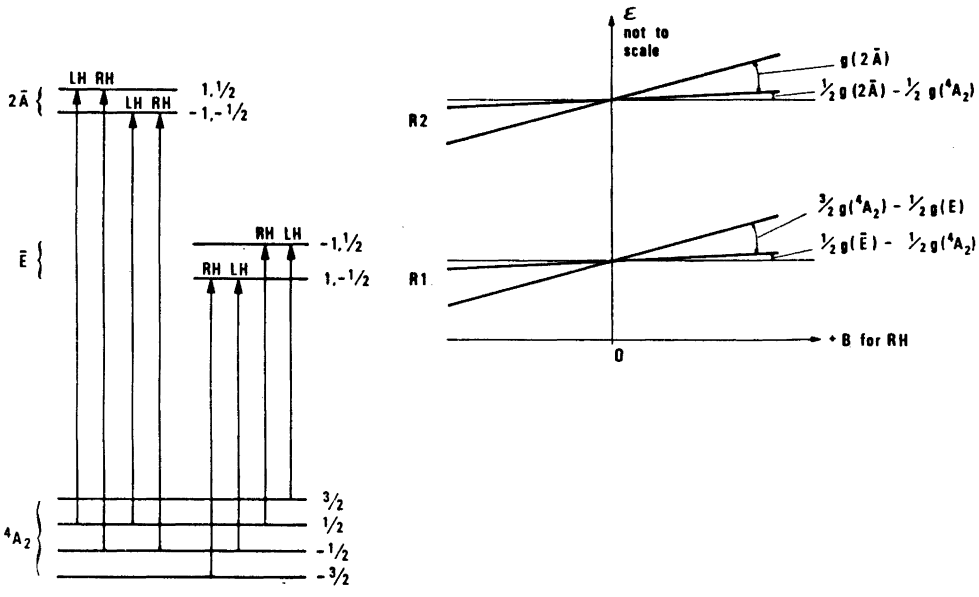

Fig. 2. Transition diagram and splitting pattern of the ^2E components.

resonance effects are expected to be within a few cm^{-1}.

The two components of each of the LH and RH circularly polarized spectra will be split by the amount $g-g_e$, and placed symmetrically with half this value above, and half below the value g. Here g is the ground state splitting, and g_e that of the excited state. The deviation of their common moment from g will therefore give information about their relative intensity and g_e. The intensity ratio is determined only by the electronic transition moment contribution and the ground state population.

EXPERIMENTAL

Two samples of ruby were used, one containing 0.15 mol % Cr^{3+}, and one 0.41 mol %. Only the last one, however, was used for the *B*-lines. The magnetic field was obtained by discharging a loaded capacitor through a small coil in which the sample was placed with its axis parallel to the field.[7] Light from a flash tube timed to fire at the maximum field was focused on the sample. Having passed parallel to the C_3-axis it was again focused through a circular polarizer on the spectrograph slit. The dispersed light was focused on the Videcon tube of an SSR Optical Multichannel Analyzer, where the spectra were stored on one of the two 500-channel digital memories. The other memory was used for dark current subtraction. The resolution at 5000 Å was two channels corresponding to 0.2 Å. Typically, however, a slitwidth of 1 Å was used, due to the limited sensitivety of the Videcon tube. Each spectrum was summed from 10 to 40 shots, and after accumulation, the spectra were transferred to a RC4000 computer. A background spectrum was also tranferred, to divide, channel by channel, into all spectra, before plotting and further data-handeling.

The set-up is shown in Fig. 3. A clock pulse goes to a unit built into the optical multichannel analyzer, OMA and is here stored until the next TV-frame retrace. Then the OMA is activated for one frame time, and a signal is sent to the switch to fire the magnet. When the magnet is fired, a signal goes to the flash-delay. This will fire the flash at the maximum of the field, and a spectrum will be collected. The firing has ended before the frame retrace is over and collection begins. The spectra are inspected on the oscilloscope which is also used to set the flash-delay.

Qualitatively the results are very clear, as seen of Fig. 4. which shows spectra recorded at 77 K for 35 different fields. The intensity variation of the B1 and B2 lines show clearly how the ground-state population changes with the Zeeman-splitting, which in a new way confirms the well-known transition diagram. The displacement of the B3 line goes the opposite way from that of the B1 and B2 lines, and excludes the possibility that the B3 line should be a vibration on one of these. The left circularly-polarized component gains slightly in intensity and remains narrow for higher fields, while the right-hand component

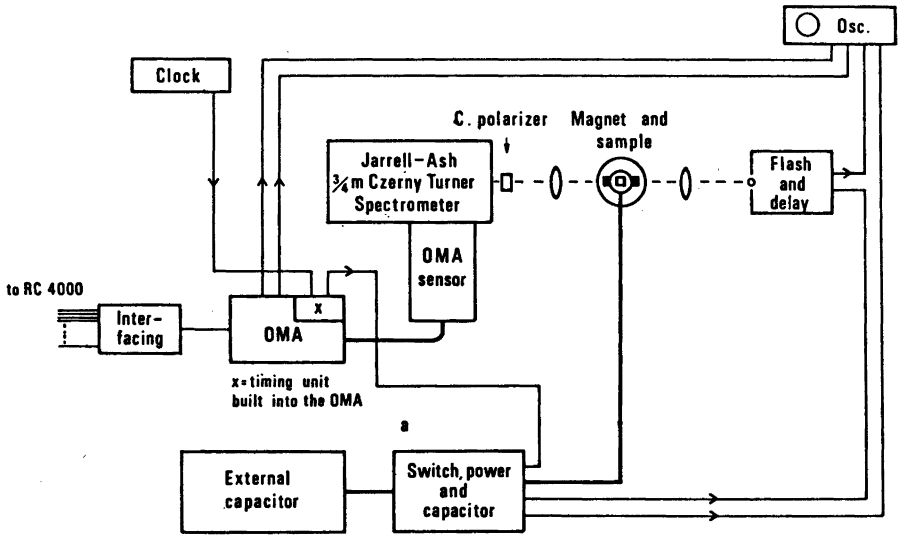

Fig. 3. The experimental set-up for recording pulsed-magnet Zeeman-spectra on an optical multichannel analyzer.

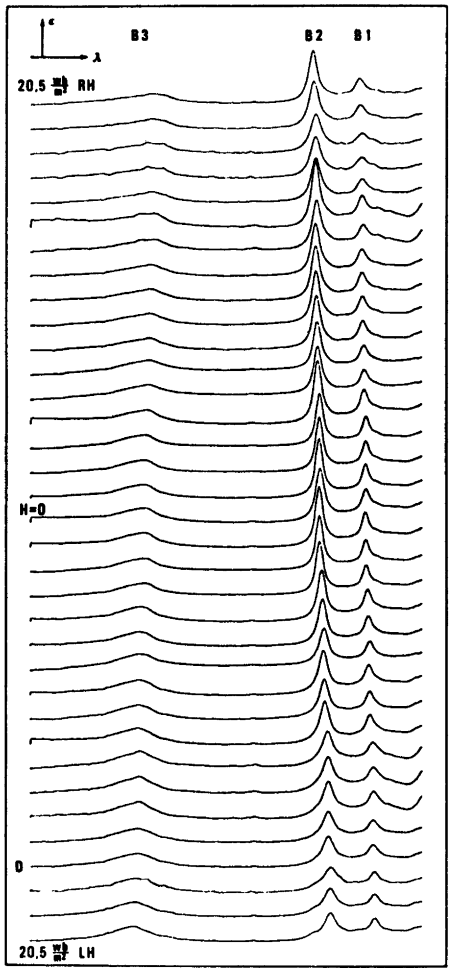

Fig. 4. Extinction coefficient as function of channel number (wavelength) of all three B-lines for 35 values of the magnetic field. One spectrum D was lost during data handling and has been replaced by its neighbour.

broadens and loses intensity. These facts confirm that the LH transition from the microstate with $S=-\frac{3}{2}$ has higher intensity than that from the state with $S=-\frac{1}{2}$, as the line will sharpen when the strongest component gains relatively in intensity, due to the ground state repopulation. Conversely the RH transition will have transferred intensity from the stronger to the weaker component, and a splitting will therefore result in a broadening.

Quantitatively the E_b-g-factor was determined from an experiment performed at 4.2 K, where practically all intensity was concentrated in the strongest LH component of the B3 line, and the RH component of the B2 line. The displacement of this component gave $g(^2T_2,E_b)=4.15\pm0.15$.

Fig. 5 shows a plot of the B3 line position as function of the applied voltage, together with the line whose slope is equal to the ground state splitting g. The spread of the points is considerable, but not enough to blur the apparent inconsistency of these results. The extreme RH end of the plot shows that the points are reasonably close to the line. As its point of gravity is determined by two components with equal distances from this line, the intensities of these components must be practically equal, and the change in dipole strength intensity contribution must therefore just cancel that of the population change. The population contributions were determined from the intensity ratios of the B1 and B2 lines of the same spectra and the zero-field spectrum. This ratio was closer to 1, than the ratio calculated considering a Boltzmann distribution.

The RH-side gave an electronic contribution to the weakest component of 0.7 times that of the strongest one practically independent of the $g(\bar{E}_b)$-factor. Using the liquid He temperature spectrum and the same population ratio, the electronic contribution from the LH spectrum was found to be 0.15, in clear disagreement with both the value found from the RH branch and the calculated electric dipole value of $\frac{1}{3}$.[1]

To check, whether a phonon-contribution could influence the displacement of the point of gravity of the B3 line, a new series of spectra were calculated from a set of original ones. The 35 spectra were added channel by channel after displacing the channel number by a parameter, p, multiplied by the magnetic field. Spectra were plotted for 35 values of p, including those matching the displacements of the B1 and B2 lines, but no special features could be seen at the B3-position for those p-values. This was taken as a strong evidence, that no phonons on the B1 and B2 lines contributed significantly to the B3 line. Further, if the displacement was partly due to the movement of such a contribution, the change of the $^2T_2,\bar{E}_b$-part must have been larger, as all other possible contributions move to the opposite side of that observed. Such a larger

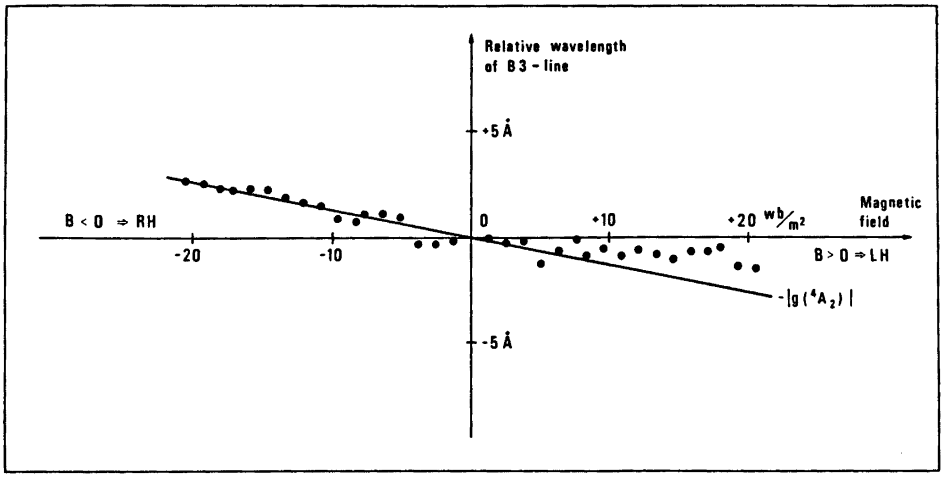

Fig. 5. Relative position of B3 line as a function of the magnetic field (points) compared to the ground state splitting (line).

change would, however, make the discrepancy worse. To check whether it was reasonable to use the B1 and B2 intensities for calculating the population ratio in the ground state, similar studies were made on the R-line spectra. These had to be recorded anyhow to calibrate the magnetic field.

The intensity ratios thus determined were in agreement with those obtained from the B lines for the fields used. For smaller fields, however, there seemed to be a threshold, below which the relaxation time was considerably longer than the firing time. No attempts were made, however, to determine the relaxation times as function of the splitting energy, as this would fall outside the scope of this work, and a modification of the magnet would be desirable to change the time dependence of the field from a cosine to a step-function.[14]

An interesting observation, not yet discussed, was that the two components of both of the R-lines were approaching different intensities when the magnetic field approached zero from either side. For the R1 line, the transitions from the microstates with $S = \pm\frac{1}{2}$ were 10 % higher than those from the states with $S = \pm\frac{1}{2}$, and of the R2 line, the components of the transition to the $1,\frac{1}{2}$-microstate were 10 % higher than those to the $1,-\frac{1}{2}$-microstate. For stronger fields, the Boltzmann distribution takes over, and the differences are

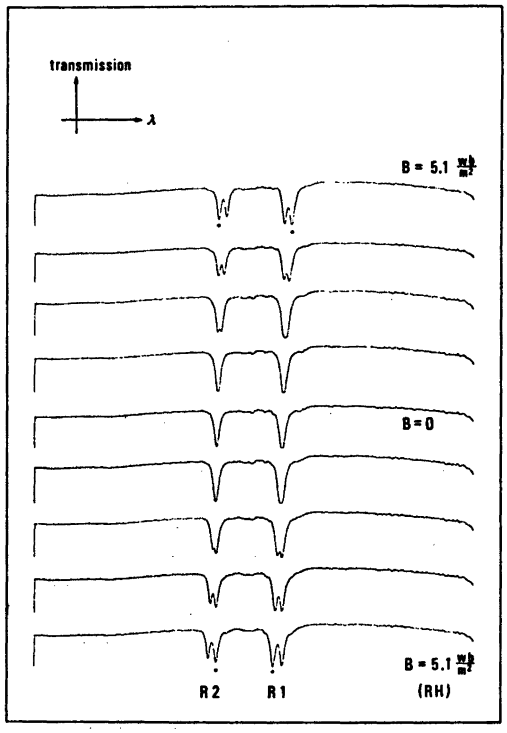

Fig. 6. Transmission of circularly polarized light by the R-lines for medium and small magnetic fields illustrating the intensity ratios between the components for H→0. The lines labeled · are those gaining intensity by ground state repopulation.

Table 1. Values for $g\|\|$ of Ruby doublet states.

	Ours	Ref. 8	Ref. 6	Ref. 4
$g\|\|[\bar{E}(^2E)]$	2.470 ± 0.003	2.56 ± 0.16	2.67	2.59
$g\|\|[2\bar{A}(^2E)]$	1.444 ± 0.003	1.63 ± 0.13	1.21	1.23
$g\|\|[2\bar{A}(^2T_2)]$	0.510 ± 0.005	0.69 ± 0.09	0.65	.96
$g\|\|[\bar{E}_a(^2T_2)]$	2.961 ± 0.005	2.97 ± 0.15	3.39	2.97
$g\|\|[\bar{E}_b{}^2T_2]$	4.15 ± 0.15			

blurred. To illustrate this, some low-field R-line spectra are shown in Fig. 6.

At present it seems hard to find any other explanation of the observed discrepancy, than to say that the dipole contribution to the B3 line components varies strongly with the magnetic field. In that case, however, the B1, B2 and R-line intensities cannot be used with confidence to scale the ground-state population, and this could just as well be considered to be the equilibrium value. But this modification will only lower the RH-result and raise the LH-result by 0.1, which is just the experimental standard deviation. From the intensity variation of the B3 line with the magnetic field, it was found that the dipole contribution to the strongest component was independent of the field within the experimental deviations. The g-values obtained from the experiments are shown in Table 1.

Experimentally the use of an optical multichannel analyzer has proven to be a great success in several aspects compared to the use of film. First the spectra can be observed immediately on an oscilloscope, and a lot of work with test-exposures is saved. Second the camera can be left in the same position through a long series of experiments, and the wavelength is thereby a well defined function of the channel number, facilating calibration considerably. Finally, the spectra are immediately in digital form and linear in intensity, ready for all kinds of combinations. To make CD, MCD or LD combinations however, the two kinds of spectra necessary for each should be made with alternating shots as the baseline might not be well defined. The linearity combined with the circularly polarized-light technique are the features that have made the present determination of the B3 line possible. The most severe draw-back is the lack of sensitivity of the TV videcon, which only in the infrared can compete with fast films. However, at wavelengths where films can be used, there are also image devices available with high quantum yield, which combined with a TV videcon offer the advatages of both.

CONCLUSION

It has been proven that a combination of a pulsed magnet, an optical multichannel analyzer, and the appropriate light polarizer is a powerful tool to obtain qualitative and quantitative information about magnetically active, blended absorption bands of widths up to about 100 cm^{-1}. For the magnetic field parallel to the C_3 axis, the g-factors were determined for the E^2 and $^2T_2$ states of ruby, as well as the relative intensity of the component of the $^2T_2(\bar{E}_b)$ state.

Acknowledgement. The author wishes to thank Professor C. J. Ballhausen for helpful discussions, Dr. J. S. Avery for revising the text of this paper and "Statens naturvidenskabelige Forskningsråd" for making available the optical multichannel analyzer.

REFERENCES

1. Sugano, S. and Tanabe, Y. *J. Phys. Soc. Jap. 13* (1958) 880.
2. Sugano, S. and Tsujikawa, I. *J. Phys. Soc. Jap. 13* (1958) 889.
3. Sugano, S. and Peter, M. *Phys. Rev. 122* (1961) 381.
4. Macfarlane, R. M. *J. Chem. Phys. 39* (1963) 3118.
5. Macfarlane, R. M., *Phys. Rev. B 1* (1970) 989.

6. Aoyagi, K., Kajiura, M. and Uesugi, M. *J. Phys. Soc. Jap. 25* (1968) 1387.
7. Trabjerg, I. and Güdel, H. U. *Acta Chem. Scand. A 28* (1974) 8.
8. Aoyagi, K. and Misu, A. *J. Phys. Soc. Jap. 18* (1963) 1448.
9. Kushida, T. and Kikuchi, M. *J. Phys. Soc. Jap. 23* (1967) 1333.
10. Nelson, D. F. and Sturge, M. D. *Phys. Rev. 137* (1965) A 1117.
11. Forman, R. A. *Bull. Amer. Phys. Soc.* March 1974.
12. Forman, R. A. *Private communication.*
13. Jortner, J. *Private communication.*
14. Dworschak, G., Haberey, F., Hildebran, P., Kneller, E. and Schreiber, D. *Rev. Sci. Instrum., 45* (1974) 243.

Received April 9, 1975.

Acta Chemica Scandinavica A 29 (1975) 824—826

NMR Experiments on Cyclic Sulfites. VI. The Orientation Effect of an S=O Group on the Proton Chemical Shifts in Trimethylene Sulfites

PER ALBRIKTSEN

Chemical Institute, University of Bergen, N-5000 Bergen, Norway *

The shielding of protons in trimethylene sulfites has been discussed in terms of the electrical field effect and the anisotropy effect of the S=O dipol.

Studies on the conformational behaviour of six-membered cyclic sulfites give evidence for the preferential occurrence of chair forms with an axial S=O bond.[1-3] Two heavily substituted sulfites have, however, been reported [4,5] to exist in a chair form with an equatorial S=O bond. Ultransonic experiments [6] suggest an equilibrium between chair forms with an axial (*ca.* 99 %) and an equatorial S=O group as regards the trimethylene sulfite. The nature of the data from ultrasonic measurements is, however, such that one cannot use it to prove any structural assignments. The axial S=O bond is quoted to be 14.7 ± 4 kJ mol^{-1} more stable as compared to the equatorial bond.[7] It is the purpose of this paper to demonstrate the orientation effects of the S=O bond on the proton chemical shifts.

EXPERIMENTAL

The sulfites were prepared from appropriate diols and thionyl chloride according to the methods previously reported.[1] The isomers of 4,6-dimethyl-TM**-sulfite were purified using a preparative gas chromatograph. The isomers of *trans*-1-3-2-dioxathiadecalin-2-oxide were separated by distillation. The distillate containing the isomer with axial S=O bond was purified by GLC. The residue from the distillation was dissolved in ethanol and cooled to -10 °C and the isomer with equatorial S=O bond crystalized then as white needles, m.p. 50 – 50.5 °C.

The NMR spectra were obtained on samples containing 20 % sulfite dissolved in CCl_4, using a Varian Associates HA-100 operating at 98 MHz for proton resonance. The spectra were analysed using the computer programmes LAOCN3 [8] and UEAITR.[9]

The parameters are assumed to be correct to ± 0.2 Hz. The computations are carried out using a UNIVAC 1110 computer.

RESULTS AND DISCUSSION

From X-ray data [10] of TM-sulfite it can be calculated that the internuclear distance between the axial sulfinyl oxygen and the axial 4-hydrogen is *ca.* 2.5 Å, a value within the range of the sum of the van der Waals radii of hydrogen and oxygen. An axial S=O bond is, however, more stable as compared to an equatorial S=O bond.[1] The stability of an axial S=O bond in TM-sulfites has been attributed to an increased rotational barrier about single bonds in system containing adjacent electron pairs and polar bonds.[1,11] Moreover, it is possible that in addition to this effect similar effects as proposed [12] for cyclic sulfoxides contribute; *i.e.*, that attractive terms outweigh repulsions and create a favourable interaction between the axial sulfinyl oxygen and the axial 4 and 6 hydrogens. The difference between the chemical shifts of protons in a cyclic sulfite has been interpreted [13] as being due to the electric field effect and

* Present address: Rafinor A/S & Co., N-5154 Mongstad, Norway.

** Tm = trimethylene.

Table 1. Chemical shifts in ppm from TMS and coupling constants in Hz.

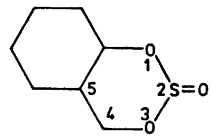

Comp. No.	δ_{4a}	δ_{4e}	δ_{5a}	δ_{5e}	$^2J_4$	$^3J_{4a5e}$	$^3J_{4a5a}$	$^3J_{4e5e}$	$^3J_{4e5a}$	$^2J_5$	$^3J_{CH_3}$
I	4.507	3.630	[a]	–	−11.43	–	11.22	–	4.14	–	
II	4.053	4.187	[a]	–	−11.81	–	11.27	–	5.54	–	
III	5.01	1.25[b]	1.76	1.78	–	2.4	11.6	–	–	−14.1	6.4
IV	4.48	1.40[b]	1.78	1.72	–	2.2	11.5	–	–	−14.1	6.3
V	5.00	1.35[b]	2.08	1.97	–	4.0	9.5	5.5	5.4	−14.1	6.3
	1.55[b]	4.42									

[a] Cannot be measured. [b] The methyl group.

magnetic anisotropy effect of the S=O bond. The shielding region of the S=O bond is assumed to be similar to the −C≡C− bond,[1] *i.e.* a positive shielding cone and a negative area transverse to the bond direction.

Assuming a chair form for the TM-sulfite with an axial S=O bond it can be seen that the protons in the positions 4 and 6 lie within the deshielding region. The *syn* axial 4 and 6 protons relative to the axial S=O bond are exposed to the maximum deshielding. This has, however, been used as evidence for an axially situated S=O bond in TM-sulfites.[1] For TM-sulfites with an equatorial S=O bond it is expected that the chemical shift difference between axial and equatorial 4 (or 6) protons should be small. This is because the axial 4 and 6 protons lie within a similar shielding region. This orientation effect of the S=O bond on the chemical shift difference between the geminal 4 (or 6) protons is easily demonstrated by experiments (Table 1). In compound I, with axial S=O bond, the axial 4 proton is 0.9 ppm more deshielding as compared to the geminal equatorial proton. The data of compound II, with equatorial S=O bond, show, however, that the axial 4 proton is *ca.* 0.15 ppm more shielded compared to the geminal equatorial proton.

The orientation effect of the sulfinyl group can easily be demonstrated from the chemical shift difference of the corresponding 4 (or 6) protons in the two isomers with the S=O bond either axial or equatorial. The chemical shift difference of the axial 4 proton of the isomers I and II, or III and IV is *ca.* 0.5 ppm (Table 1). This difference is due to the difference in both the electrical field effect and the magnetic anisotropy effect of the S=O bond in the two systems. The contribution to the proton shielding of a C−H bond of the electric field effect, due to an axial or an equatorial neighbouring S=O dipol can be obtained from the formula derived by Buckingham [14] and generalized by Pritchard and Lauterbur.[13] The results from such calculations (Table 2) suggest that the change in the electrical field effect,

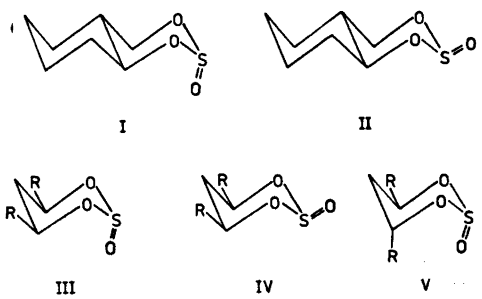

I II III IV V

I: *trans*-1,3,2-Dioxathiadecalin-2a-oxide. II: *trans*-1,3,2-Dioxathiadecalin-2e-oxide. III: 4e-6e-Dimethyl-1,3,2-dioxathiane-2a-oxide. IV: 4e,6e-Dimethyl-1,3,2-dioxathiane-2e-oxide. V: 4e,6a-Dimethyl-1,3,2-dioxathiane-2a-oxide. R=methyl.

Table 2. The effect of the S=O electric field on the chemical shift of ring protons in position 4 and 6.[a]

	Axial proton	Equatorial proton
S=O axial	−0.31	−0.17
S=O equatorial	−0.12	−0.06
$S=O_{ax}-S=O_{eq}$	−0.19	−0.11

[a] Calculated from formula derived by Buckingham.[13] Negative values mean a high frequency shift. The values are in ppm.

caused by changing the S=O dipole from the axial to the equatorial position, is responsible for *ca.* 0.2 ppm of the shift difference between the axial 4 (or 6) protons in compounds I and II, or III and IV. Similar calculations (Table 2) for the equatorial 4 (or 6) protons as regards the different orientations of the S=O dipole suggest that the difference in the field effect is *ca.* 0.1 ppm. The chemical shift differences caused by the field effect of the sulfinyl bond accounts for only 20−30 % of the observed shift difference for the axial and the equatorial 4 (or 6) protons. The shielding effect of the axial S=O bond on the *syn* axial 4 and 6 protons in TM-sulfites appears to be large. Studies on substituted thiane-1-oxides [12] show that an axial S=O bond is 5.4 kJ mol^{-1} more stable as compared to an equatorial S=O bond and this preference was attributed to an attractive interaction between an axial S=O bond and the *syn* axial hydrogens. Such interactions, as regards TM-sulfites, could give rise to an anomalous high frequency shift of the *syn* axial 4 and 6 protons relative to the geminal equatorial protons. CNDO* calculations [16] give, however, no significant difference in the charge density on the two geminal 4 protons. It is apparent that the major contribution to the chemical shift difference of the 4 and 6 protons in cyclic sulfites is due to the anisotropy of the S=O bond. The shift difference of the protons in position 5 is little affected by the change of the S=O dipole from the axial position to the equatorial position.

* CNINDO: CNDO and INDO molecular orbital program including *d* orbitals.[15]

The orientation effect of the S=O dipole on the 4 and 6 protons in compound V is in accordance with findings of compounds III and IV. Compound V is assumed to be twisted [4] with the two "*syn* axial" groups, S=O and axial-4-methyl group, pointing away from each other. Models of a twist conformation of compound V suggest that the "equatorial" 4 proton occupies a similar position relative to the S=O bond as the axial 4 (6) proton in compound IV. The "axial" 6 proton in V has a position similar to the 4 (6) proton in compound III, relative to the S=O bond. This is also in accordance with the observed shift difference, 0.6 ppm, obtained for the 4 and 6 protons of compound V.

REFERENCES

1. Albriktsen, P. *Acta Chem. Scand. 25* (1971) 478; *26* (1972) 1783, 3684.
2. Green, C. H. and Hellier, D. G. *J. Chem. Soc. Perkin Trans 2* (1972) 458.
3. Wood, G., McIntosh, J. M. and Miskow, M. H. *Can. J. Chem. 49* (1971) 1202.
4. Wucherpfennig, W. *Justus Liebigs Ann. Chem. 737* (1970) 144.
5. van Woerden, H. F. and de Vries-Miedema, A. T. *Tetrahedron Lett.* (1971) 1687.
6. Hamblin, P. C., White, R. F. M., Eccleston, G. and Wyn-Johnes, E. *Can. J. Chem. 47* (1967) 2731.
7. van Woerden, H. F. and Havinga, E. *Rec. Trav. Chim. Pays-Bas 86* (1967) 341, 353.
8. Castellano, S. and Bothner-By, A. A. *J. Phys. Chem. 41* (1964) 3863.
9. Johannesen, R. B., Ferretti, J. A. and Harris, R. K. *J. Magn. Resonance 3* (1970) 84.
10. Altona, C., Geise, H. J. and Romers, C. *Rec. Trav. Chim. Pays-Bas 85* (1966) 1197.
11. Wolfe, S., Rauk, A., Tel. L. M. and Csizmadia, J. G. *J. Chem. Soc. B.* (1971) 136.
12. Johanson, C. R. and McCants, Jr., D. *J. Amer. Chem. Soc. 86* (1964) 2935.
13. Pritchard, J. G. and Lauterbur, P. C. *J. Amer. Chem. Soc. 83* (1961) 2105.
14. Buckingham, A. D. *Can. J. Chem. 38* (1960) 300.
15. Dobosh, P. A. *Quantum Chemistry Program Exchange*, QCPE 141, Indiana University.
16. Albriktsen, P. *Unpublished results.*

Received April 17, 1975.

Acta Chemica Scandinavica A 29 (1975) 827—832

Photoelectron Spectra and Molecular Properties. LIII.[1] Methyl-substituent Effects on the Hexatriene π System

E. E. ASTRUP,[a*] H. BOCK,[a] K. WITTEL [a] and P. HEIMBACH [b]

[a] Chemisches Institut der Universität, D-6 Frankfurt, Theodor-Stern-Kai 7, Germany and [b] Max-Planck-Institut für Kohlenforschung, D-433 Mülheim, Kaiser-Wilhelm-Platz 1, Germany

The photoelectron (PE) spectra of *trans*-hexatrienes-1,3,5 with methyl groups in 2, 3, 1/1, 1/2 or 1/6 positions are reported. The first three bands are assigned to π-ionizations according to SPINDO calculations. The shifts caused by methyl substitution are small relative to those observed for butadiene, a finding, that may be explained by assuming a "buffer quality" of larger π systems which obscures the substituent effects. First and second order methyl group perturbations of the hexatriene π system are discussed, considering as well the accuracy of photoelectron spectroscopically determined ionization potentials.

The effect of methyl substituents on π systems has been the subject of many photoelectron spectroscopic investigations.[2–11] The observed lowering of the π ionization energies is best rationalized by first and/or second order perturbations,[2,12] *i.e.* inductive and/or hyperconjugative effects, respectively. Therefore, it has been repeatedly attempted to determine characteristic perturbational parameters. For methyl butadienes a simple LCBO MO approach only considering occupied orbitals proved to be successful: Beez, Bieri, Bock and Heilbronner [2] have shown that ionization energies can be satisfactorily predicted within this model by first order perturbation, and that considerable improvement is achieved by incorporating "through space" interactions [13] between butadiene π orbitals and the pseudo-π methyl group orbitals into the LCBO MO treatment.[2] For illustration, Fig. 1 displays the π-orbital movements for the mono-methyl hexatrienes as predicted by a first order perturbation [2]

$$\delta IE_J = (c_{J\mu})^2 \, \delta A' \quad (\delta A' = 0.8 \text{ eV}) \qquad (1)$$

and, in addition by a "through space" hyperconjugation ($\Delta IE \sim 0.25$ eV).[2] Obviously, only for 2- or 3-methyl hexatriene isomers a further

* Present address: Department of Chemistry, University of Oslo, Oslo 3, Norway.

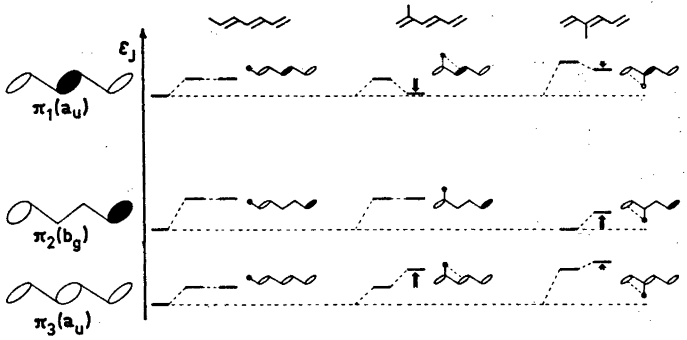

Fig. 1. π Orbital energy differences for mono-methyl hexatrienes as predicted by first and second order perturbations within an LCBO MO model.

Table 1. Vertical ionization potentials, IE_n (eV), and vibrational frequencies $\nu\oplus$ (cm^{-1}) of hexatriene,[2] the mono-methyl hexatrienes and some dimethyl derivatives; as well as SPINDO orbital energies ε_J (eV).

	hexatriene		1-methyl		2-methyl			3-methyl			1,1-dimethyl			1,2-dimethyl			1,6-dimethyl		
	IE_n	ε_J	IE_n	ε_J	IE_n	$\nu\oplus$	ε_J	IE_n	$\nu\oplus$	ε_J	IE_n	$\nu\oplus$	ε_J	IE_n	$\nu\oplus$	ε_J	IE_n	$\nu\oplus$	ε_J
$n=1$	8.45	8.00	8.16	8.05	8.31	1380	8.12	8.28	1370	8.08	7.88	1370	8.12	8.01	1375	8.11	7.95	1370	8.10
$n=2$	10.43	9.70	10.16	9.68	9.95	1180	9.69	10.24	1170	9.79	9.79	1170	9.66	9.78	1200	9.64	9.89	1200	9.64
$n=3$	11.6	10.96	11.5	11.00	11.2		10.89	11.1		10.81	11.2		11.03	11.2		10.89	11.3		11.01

Fig. 2. PE spectra of some mono- and dimethyl hexatrienes.

stabilization or a counteracting destabilization is possible, while for all-*trans* 1-methyl hexatriene structural requirements are not met, which would justify an inclusion of this additional perturbation. To elucidate how well the above specified LCBO MO π model is suited for larger polyenes, the photoelectron spectra of some methyl and dimethyl hexatrienes are investigated.

The PE spectra of 2, 3, 1/1, 1/2 and 1/6 methyl substituted hexatrienes are reproduced in Fig. 2; Table 1 contains the vertical ionization potentials and includes also those of hexatriene [2] and 1-methyl hexatriene.[2]

All the PE spectra exhibit more or less the same overall picture: two isolated bands with one vibrational progression each at lower energies followed by a broad "mountain" of overlapping bands between 11 eV and 16 eV. The spectra of the disubstituted derivatives show even less structure in this region due to the additional σ ionizations caused by the second methyl group. Obviously, only the position of the first two bands can be read off with sufficient accuracy, and therefore will be included in the following discussion.

SPINDO calculations [14] yield the three π orbitals as highest occupied ones (Fig. 2) contrary to the assignment by a comparison of ethylene and hexatriene [2,15] on the basis of an LCBO MO model. But as already pointed out, the third PE bands – π or σ – will not be included in the discussion, due to the poor resolution of the spectra.

The SPINDO orbital energies (Fig. 2) are in reasonable agreement with the experimental ionization potentials, although this semiempirical method is parametrized to reproduce ionization potentials of planar hydrocarbons. Except for the lowest orbital energy $\varepsilon_1^{\text{SPINDO}}$ for disubstituted derivatives, all other π orbital energies are calculated to lie slightly below the experimental ionization energies. This can be traced back to the definition of "vertical IPs" as "weighted mean" of the vibrational progression, which probably deviates from the parametrization using the "highest peak" of each band. Judging from the SPINDO eigenvalues, the orbital sequence for all-*trans*-hexatriene is π_1, π_2, π_3, σ with the latter two nearly degenerate. As pointed out above, bands 3 and 4 overlap strongly in all PE spectra (Fig. 2 and Ref. 2). Therefore, an assignment π_1, π_2, σ, π_3 – in good agreement with the one for the *cis*-isomer and resulting in a nearly symmetrical split for the three π orbitals [2] – cannot be excluded. An unsymmetrical π split, following from the assumption of a π_1, π_2, π_3, σ sequence, may however be understood within an LCAO MO model, since the first unoccupied π^* orbital also belongs to the irreducible representation b_g as does π_2.

Experimentally observed shifts of the π_1 and π_2 ionization potentials on methyl substitution of hexatriene are compared in Fig. 3 to the ones calculated by the LCBO MO model perturbation (*cf.* Fig. 1), *e.g.* for 2-methyl hexatriene

$$\begin{aligned} IE_1(\text{2-Me-C}_6\text{H}_7) &= IE(\text{C}_6\text{H}_8) + c_{23}^2\delta_{A'} \\ &= 8.45 - 0.5^2 \times 0.8 \\ &= 8.24 \text{ eV} \end{aligned} \qquad (2)$$

Fig. 3 shows for example that the observed IE_1 shift of 2-methyl hexatriene relative to hexatriene is slightly smaller than the calculated LCBO MO perturbation (1), in agreement with an assumed stabilization of the π_1 orbital due to a bonding "through space" interaction (Fig. 1). On the contrary, a corresponding split for π_2 expectedly (Fig. 1) can be neglected. More pronounced are the observed differences for 3-methyl hexatriene relative to hexatriene: ΔIE_1 is larger than $\Delta\pi_1$ and ΔIE_2 smaller than $\Delta\pi_2$, the shifts predicted by LCBO MO perturbation; corrections by "through space interactions", *i.e.* bonding stabilization for π_1 and antibonding destabilization for π_2, point in the right direction. Analogous arguments may be used for most π ionizations of the disubstituted derivatives. Obviously, incorporation of "through space" interactions between π orbitals of hexatriene and pseudo π orbitals of the methyl group improve agreement between observed and calculated shifts (Fig. 3 and 1).

Although the extended LCBO MO model seems to allow reasonable rationalization of the π ionization differences on methyl substitution of hexatriene, nevertheless, several limiting remarks are necessary. Thus comparison with methyl substitution effects on smaller polyenes [2,7] demonstrates that the hexatriene

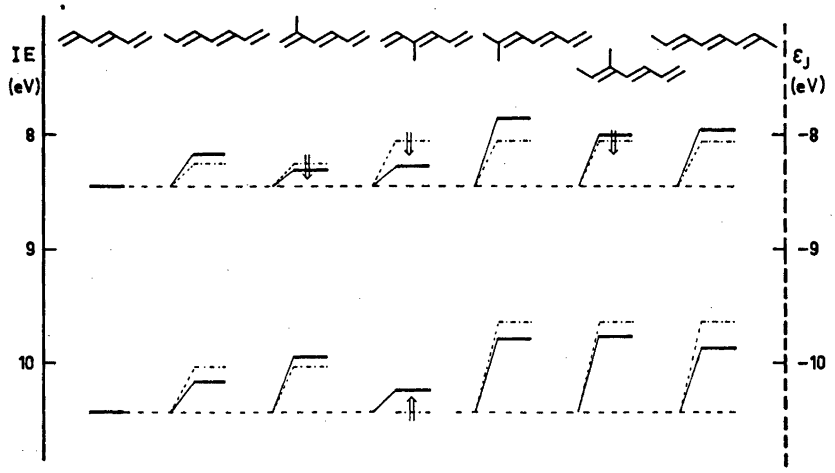

Fig. 3. Comparison of ionization potentials $IE_{1,2}$ of methyl substituted hexatrienes with calculated LCBO MO perturbations of the hexatriene π system (— measurement, —·—·— perturbation calculation).

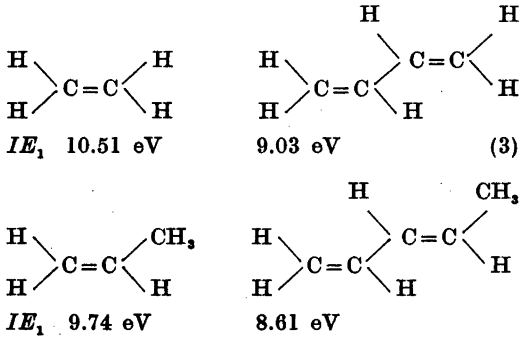

perturbation is only a relatively small one. In addition, a thorough examination of the correlation diagram (Fig. 3) reveals, that a pronounced influence of substituent position cannot be detected. Within the mono-substituted derivatives the experiment shows no differences between the 1-, 2-, or 3-substituents for the π_1 orbital and only a minimal distinction of 0.2 eV between the 1- and 2- substituents for the π_2 orbital. The same applies to the dimethyl hexatrienes, expectedly exhibiting an approximately doubled shift. But on the other hand, the largest difference $\Delta IE_1 \sim 0.15$ eV observed for 1,2- and 1,1-dimethyl isomers, is only a moderate one. Summarizing with respect to the experimental data, and comparing with the "through space" interaction model developed for methyl butadienes, there is mostly agreement, but as the observed effects for methyl hexatrienes are much smaller, an unequivocal support hardly seems possible.

Regarding the experiment, the reproducibility is estimated to be about 0.02 eV.[16] The uncertainty in the reading off is even for sharp peaks at least of the same order of magnitude. The calibration, using xenon and argon (12.13 eV and 15.76 eV) is outside the π ionization region discussed. Furthermore, whether the vertical ionization potentials are determined as the "highest peak" or the "weighed mean" of the fine structure will add to the uncertainty, since the bands do not possess the same shape, and this may amount to one vibrational spacing, *i.e.* to $\sim 0.1-0.2$ eV. All these uncertainties may add up to the same order of magnitude as the observed differences for the hexatriene derivatives investigated. Based on the relatively great number of ionization potentials observed, an attempt has been made to determine a set of optimal parameter values in the expression for the total methyl perturbation:

$$\delta IE_J = (c_{J\mu})^2 \left[\Delta\alpha + \beta^2/(\alpha_{CH_3} - IE_J^\circ)\right] \quad (4)$$

with $\Delta\alpha$ as the inductive parameter, β the resonance integral, and α_{CH_3} the Coulomb integral for the methyl group pseudo π orbital. By use of a least-squares method, the difference between the observed and the calculated perturbation was minimized. Unfortunately, only a very shallow minimum is obtained, and ob-

viously, wrong values for the parameters (4) satisfy the minimum criterion within the limits of errors. The minimum is for HMO eigenfunctions at $\Delta\alpha = -0.5$ eV, $\beta = -3.8$ eV, $\alpha_{CH_3} = -17.6$ eV with $V = \sum(\delta\varepsilon_J^{exp.} - \delta\varepsilon_J^{calc.})^2 = 0.08$, but allowing an only slightly larger $V = 0.095$, a range of $\Delta\alpha$ from -1.0 to $+0.8$ eV is covered. Variation of the method, *i.e.* starting the optimalization from SPINDO or LCBO orbital coefficients $c_{J\mu}$ did not change the overall result. An explanation for this failure is offered by a strong correlation between the calculated parameters (4); thus any values of the "best" parameters would become meaningless.

In conclusion, it should be pointed out, that the methyl substitution effects on the hexatriene π system are in accord with independent investigations concerning compounds of comparable molecular size.[10,17] The dependence of properties on the methyl substitution position is disappointingly small. This observation can be explained by assuming a kind of "buffer" quality for most of the larger π systems, which internally compensates for smaller donor or acceptor perturbations.

SYNTHESES

The *trans*-2- and 3-methyl hexatrienes have been prepared by Hofmann elimination of the corresponding dimethylbenzylhexadienyl ammonium bromide according to literature procedures [19] followed by gaschromatography separation of the two isomers.[20] All *trans*-octatriene-2,4,6 has been obtained by isomerization of octatriene-1,3,5 [21] and purified by recrystallization from ethanol.[20] *trans,trans*-5-Methyl heptatriene-1,3,5 has been synthesized from butadiene and butine-2 using a cobalt catalyst [22] and separated by distillation in a spinning band column.[20] Purity of all compounds has been checked by usual spectroscopic methods.[20]

PE SPECTRA

The PE spectra of methyl substituted hexatrienes (1 to 5) are recorded on a Perkin Elmer PS 16 spectrometer. Argon and xenon have been used for calibration, and the resolution of the apparatus was about 25 mV. Vertical ionization potentials for fine structured bands are quoted as weighed mean,[18] *i.e.*

$$IE_v = \sum_n IE_n I_n / \sum_n I_n.$$

For unstructured bands, the value for the maximum is given.

CALCULATIONS

SPINDO calculations have been performed on the UNIVAC 1108 of the Hochschul-Rechenzentrum at Frankfurt University. We get results for hexatriene slightly different from those in Ref. 2, but cannot offer an explanation. The card deck has been checked against some published calculations.

Acknowledgements. Dr. Lindholm and Dr. Åsbrink (Royal Institute of Technology, Stockholm) kindly supplied the SPINDO program and Miss Pohlenz (University of Frankfurt) helped in recording the spectra. One of us (E. E. A.) wishes to acknowledge a research grant from the Alexander von Humboldt-Stiftung.

REFERENCES

1. Part LII: Stafast, H. and Bock, H. *Tetrahedron. In print.*
2. Beez, M., Bieri, G., Bock, H. and Heilbronner, E. *Helv. Chim. Acta 56* (1973) 1028; *cf.* also Sustmann, R. and Schubert, E. *Tetrahedron Lett.* (1972) 2739.
3. Mollère, P., Bock, H., Becker, G. and Fritz, G. *J. Organomet. Chem. 46* (1972) 89.
4. Klessinger, M. *Angew. Chem. 11* (1972) 544; *Int. Ed. 11* (1972) 525.
5. Weidner, U. and Schweig, A. *J. Organomet. Chem. 39* (1972) 261.
6. Dewar, M. J. S. and Worley, S. D. *J. Chem. Phys. 50* (1969) 654.
7. Frost, D. C. and Sandhu, J. S. *Indian J. Chem. 9* (1971) 1105.
8. Ensslin, W., Bock, H. and Becker, G. *J. Amer. Chem. Soc. 96* (1974) 2757.
9. Brogli, F., Clark, P. A., Heilbronner, E. and Neuenschwander, M. *Angew. Chem. 85* (1973) 414; *Int. Ed. 12* (1973) 422.
10. Turner, D. W., Baker, C., Baker, A. D. and Brundle, C. R. *Molecular Photoelectron Spectroscopy*, Wiley-Interscience, London 1970, p. 281.
11. Bischof, P. K., Dewar, M. J. S., Goodman, D. W. and Jones, T. B. *J. Organomet. Chem. 82* (1974) 89.
12. Libit, L. and Hoffmann, R. *J. Amer. Chem. Soc. 96* (1970) 1370.
13. Hoffmann, R. *Accounts Chem. Res. 4* (1971) 1.
14. Fridh, C., Åsbrink, L. and Lindholm, E. *Chem. Phys. Lett. 15* (1972) 282.
15. Bock, H. and Ramsey, B. G. *Angew. Chem. 85* (1973) 773; *Int. Ed. 12* (1973) 734.
16. Turner, D. W., Baker, C., Baker, A. D. and Brundle, C. R. *Molecular Photoelectron Spectroscopy*, Wiley-Interscience, London 1970.
17. Methyl substituted naphthalenes have been investigated by E. Heilbronner and co-

workers; personal communication E. Heilbronner.
18. Smith, W. L. *Mol. Phys. 26* (1973) 361.
19. Hwa, J. C. H., deBenneville, P. L. and Sims, H. J. *J. Amer. Chem. Soc. 82* (1960) 2537.
20. Scholz, K.-H. *Thesis*, University Bochum 1974.
21. Kloosterziel, A. and van Drunen, I. A. A. *Rec. Trav. Chim. Pays-Bas 88* (1969) 1084.
22. Kopp, W. *Thesis*, University Bochum 1970.

Received March 3, 1975.

Acta Chemica Scandinavica A 29 (1975) 833—839

Characterization of Decaaqua-μ-oxodi-iron(III) by Mössbauer and Vibrational Spectroscopy

J. M. KNUDSEN,[a] ERIK LARSEN,[b] J. E. MOREIRA[a*] and O. FAURSKOV NIELSEN[c]

[a] Physical Laboratory I, [b] Chemistry Department I and [c] Chemistry Department V, The H. C. Ørsted Institute, University of Copenhagen, Universitetsparken 5, DK-2100 Copenhagen, Denmark

Iron(III) nitrate and perchlorate solutions to which 0.5 – 2.0 equivalents of base were added have been investigated by Mössbauer, Raman and IR spectrometry. These methods establish conclusively the existence of the decaaqua-μ-oxodi-iron(III) ion.

The hydrolysis of iron(III) has been studied extensively over many years. Recently, the subject has been reviewed by Sylva [1] and to some degree by Murray.[2] The first systematic investigation of the equilibria involved in the hydrolysis was made by Hedström using electrometric titrations of dilute solutions.[3] The system was described by the following three equilibria involving mono- and binuclear iron-(III) species:

$Fe^{3+} + H_2O \rightleftharpoons Fe(OH)^{2+} + H^+$,

$K_{11} = 9.0 \times 10^{-4}$ M

$Fe^{3+} + 2H_2O \rightleftharpoons Fe(OH)_2^+ + 2H^+$,

$K_{12} = 4.9 \times 10^{-7}$ M^2

$2Fe^{3+} + 2H_2O \rightleftharpoons Fe_2(OH)_2^{4+} + 2H^+$,

$K_{22} = 1.2 \times 10^{-3}$ M

Since the work of Hedström the hydrolysis products of iron(III) at relatively low pH values have usually been considered to be at least the three species $Fe(OH)^{2+}$(1:1), $Fe(OH)_2^+$(1:2), $Fe_2(OH)_2^{4+}$ (2:2). Arnek and Schlyter [4] included also the trinuclear $Fe_3(OH)_4^{5+}$ (3:4). However, the reported equilibrium constants show that the 1:2 and 3:4 species are present in concentrations usually several orders of magnitudes lower than the concentrations of the other species.

Hedström formulated the 2:2 complex as $[(H_2O)_4Fe(OH)_2Fe(H_2O)_4]^{4+}$ but potentiometric measurements cannot distinguish between this and $[(H_2O)_5Fe-O-Fe(H_2O)_5]^{4+}$. However, Mulay and Selwood [5] performed magnetic susceptibility measurements on partly hydrolyzed solutions of iron(III) perchlorate and their results were interpreted by Schäffer [6] in favour of the μ-oxo dimer. These observations and contemplations were not appreciated and instead Schugar *et al.*[7] suggested that the dimer was a di-μ-hydroxodi-iron(III) complex. This point of view was also taken by Murray [8] in spite of the preliminary information then available from the application of the Mössbauer effect to the study of frozen solutions of partly hydrolyzed iron(III).[8]

The present paper is focussing on this controversy and several techniques are used to demonstrate beyond reasonable doubts that the binuclear complex is a nearlinear oxo-bridged species.

EXPERIMENTAL

Mössbauer spectra. Solutions of iron(III) nitrate and perchlorate were made from reagent-grade salts. Weighed amounts of the iron salt and of sodium hydrogen carbonate were dissolved in distilled water in separate flasks and the bicarbonate solution was mixed dropwise to the iron solution while stirring to prevent high local concentration of base. Distilled water was then added to reach the desired volume and the solution was stirred for some minutes to free it

* On leave from Universidade Federal do Ceará, Fortaleza, Brazil.

from carbon dioxide. All reported spectra were taken using freshly prepared frozen solutions. However, it was ascertained that even aged solutions (over weeks) gave identical spectra.

The Mössbauer samples consisted of approximately 2 ml of solution in a plastic cell of 2.0 cm diameter. The cell with the sample was quickly dipped into liquid nitrogen thus freezing with a cooling rate of about 400 K per minute. This cooling rate seems to be high enough to secure the formation of a glass when iron(III) perchlorate is used. With iron(III) nitrate segregation effects appear when the above procedure is followed. The segregation effects may be avoided either by increasing the cooling rate or by the addition of small amounts of a glass former such as ethanol.[9] Apart from differences due to glassforming properties of the nitrate and perchlorate ions there are no differences between the Mössbauer spectra of frozen solutions of $Fe(NO_3)_3$ and $Fe(ClO_4)_3$. Therefore, most of the computational work concerning the Mössbauer spectra was done for solutions made from iron(III) perchlorate.

The Mössbauer spectra were taken with a conventional constant acceleration set-up incorporating a Nuclear Data multichannel analyzer. The source used was ^{57}Co on Pd. The velocity scale was calibrated periodically with metallic iron as a standard. Isomer shifts quoted here are relative to Co on Pd. The source was always at room temperature. The temperature of the absorbers was held constant at 100 K for most runs but results are not very sensitive to temperature from liquid nitrogen temperature to around 160 K for rapidly quenched samples. We have observed that for higher temperatures segregation effects can again be a disturbing factor.

Mössbauer parameters were obtained by an iterative curve fitting procedure in a RC 4000 computer. Estimates of the concentration of the various species based on Mössbauer spectra were made from areas in the fitted spectra.

Vibrational spectra. Raman spectra of solutions in H_2O and D_2O prepared as above in the concentration range 0.4 – 2 M were obtained at room temperature using a Coderg PH1 spectrometer with a cooled PM-tube (EMI 9558) and a photon counting system. The 514.5 nm line of a Spectra-Physics 165 Ar^+-laser (~350 mW) was used as light source. A cylindrical 4 mm i.d. glass tube was used as cell. A 90° scattering was used and the polarization of the laser beam was kept fixed. The depolarization measurements were made by the conventional method of two different analyzer orientations in the scattered beam. Due to sample absorption of the exciting line a rather poor signal-to-noise ratio was obatined making the depolarization measurements less accurate than usual. Raman shifts from 200 to 600 cm^{-1} are reported. The observed lines are rather broad and weak and the Raman shifts are only considered accurate to ± 5 cm^{-1}.

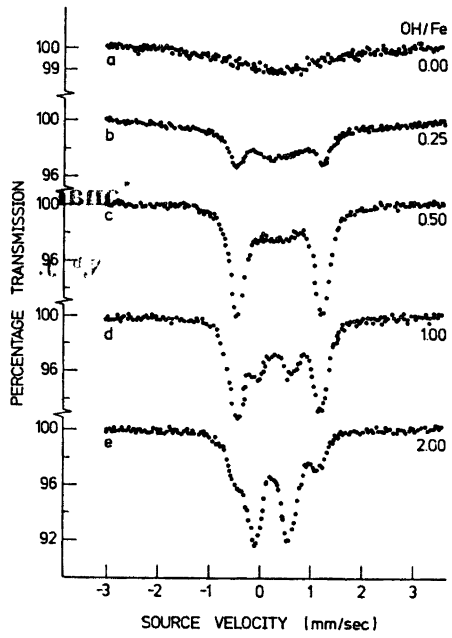

Fig. 1. Mössbauer spectra of rapidly frozen aqueous solutions of $Fe(ClO_4)_3$ for different ratios between the concentration of added base and the total concentration of iron(III). The solutions were 0.67 M in Fe(III). All spectra were recorded at the temperature $T = 100$ K.

Infrared spectra were obtained from D_2O solutions in the concentration range 0.7 – 1.2 M. An RIIC GC-1 silver chloride microcell with 0.025 mm path length was used in a Perkin-Elmer 125 spectrometer. Only the region 700 – 1000 cm^{-1} was studied in detail. The observed line frequencies are considered accurate to ± 3 cm^{-1}.

RESULTS

Mössbauer spectra. In Fig. 1 are shown the Mössbauer spectra of rapidly frozen 0.67 M aqueous solutions of $Fe(ClO_4)_3$ recorded at $T = 100$ K, for different ratios between the concentration of added base, and the total concentration of iron(III) (OH/Fe). Solutions of $Fe(NO_3)_3$ frozen by quenching and at the same concentrations show Mössbauer spectra similar to those seen in Fig. 1 (see Ref. 9, Fig. 1).

Spectrum 1a shows a broad line characteristic of magnetic relaxation effects in the high-spin ferric ion.[10] This spectrum corresponds to a perchlorate solution without any base added. At

room temperature, this solution has pH ~ 0.8 and its colour is light yellow.

Addition of base to the iron(III) solution up to about 0.5 equivalent of base per mol of iron results in the appearing of a quadrupole doublet in the Mössbauer spectra of the frozen solutions.

Fig. 1c shows the Mössbauer spectrum obtained for a 0.67 M iron perchlorate solution with 0.5 equivalent of base added per mol of total iron(III). For this orange solution pH at room temperature is 1.5. In the spectrum in Fig. 1c the broad line dominant in Fig. 1a and b is still visible but now a quadrupole doublet with an isomer shift of 0.31 ± 0.06 mm/s and a quadrupole splitting of 1.67 ± 0.06 mm/s is dominating.

Further addition of base results in a new component with isomer shift 0.25 ± 0.06 mm/s and quadrupole splitting 0.66 ± 0.06 mm/s (Spectra 1d and 1e), while the intensity of the lines for the other components decreases.

The component with quadrupole splitting 0.66 mm/s is practically the only component present when the ratio OH/Fe exceeds 2.0 until no more base can be added without immediate precipitation.

In Fig. 2 are shown the Mössbauer spectra of three binuclear iron(III) species at 100 K and the Mössbauer parameters are collected in Table 1.

Vibrational spectra. In Table 2 are listed the observed infrared absorption frequencies and Raman shifts for hydrolyzed iron(III) complexes of $Fe(NO_3)_3$ and $Fe(ClO_4)_3$ solutions in H_2O and D_2O.

DISCUSSION

In the following we shall discuss the results of the different kinds of spectroscopy to prove that the binuclear iron(III) hydrolysis product is a μ-oxo rather than a di-μ-hydroxo complex.

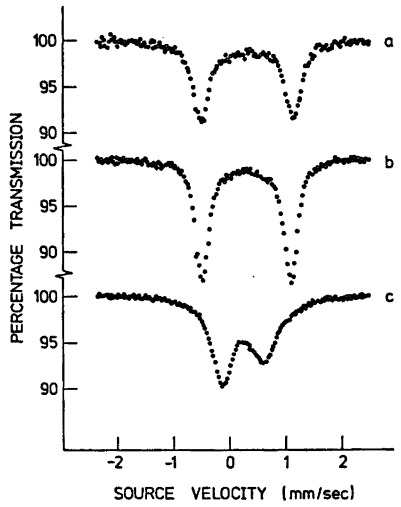

Fig. 2. Mössbauer spectra of: (a) a frozen aqueous solution of $Fe(ClO_4)_3$ with OH/Fe = 0.5; (b) a powder of $Na_3[(Fe\ heedta)_2O]$; (c) a powder of $[Fe(pic)_2OH]_2$. All spectra were recorded at the temperature $T = 100$ K.

Nozik and Kaplan [11] discussed the significance of the Mössbauer spectra of frozen acid solutions of $FeCl_3$ and $Fe(NO_3)_3$. They considered that for the $FeCl_3$ solution, 80 % of the ferric ion was in the form $Fe(H_2O)_5Cl^{2+}$ and that for the $Fe(NO_3)_3$ solution the only species present was the hexahydrated ion $Fe(H_2O)_6^{3+}$. The $Fe(NO_3)_3$ solution showed a Mössbauer spectrum similar to the spectrum seen in Fig. 1a.

Using the hydrolysis equilibrium constants measured by Milburn and Vosburgh,[12] calculations suggest that for the iron(III) perchlorate solution without any addition of base (OH/Fe = 0) most of the iron is present in the form

Table 1. Mössbauer parameters of some iron(III) dimers at 100 K.

δ: isomer shift in mm/s relative to ^{57}Co on Pd. Uncertainty ± 0.06 mm/s.
ΔE_q: quadrupole splitting in mm/s. Uncertainty ± 0.06 mm/s. Γ_1 and Γ_2: linewidth in mm/s at half intensity. Uncertainty ± 0.06 mm/s.
A_1/A_2: Ratio between area of lines in the quadrupole doublets.

Compound	δ	ΔE_q	Γ_1	Γ_2	Γ_1/Γ_2	A_1/A_2
Aqua dimer	0.31	1.67	0.37	0.38	0.97	1.03
$(Fe\ heedta)_2O$	0.26	1.66	0.30	0.29	1.03	1.01
$(Fe\ pic_2OH)_2$	0.23	0.78	0.48	0.67	0.72	0.95

Table 2. Infrared spectra (700 – 1000 cm^{-1}) and Raman spectra (200 – 600 cm^{-1}) of hydrolyzed iron(III) complexes in H_2O and D_2O solutions (0.4 – 2 M) of $Fe(ClO_4)_3$ and $Fe(NO_3)_3$.

$Fe(ClO_4)_3$ in H_2O			$Fe(ClO_4)_3$ in D_2O			$Fe(NO_3)_3$ in H_2O			$Fe(NO_3)_3$ in D_2O			Assignment
Raman			Raman			IR	Raman		Raman			IR
ν	I_{rel}	pol.	ν	I_{rel}	pol.	ν	ν	I_{rel}	pol.	ν	I_{rel}	pol.	ν	
						870							870	Fe – O – Fe antisym. stretch
	[a]			[a]			~501	vw	p					Fe – O stretch in $Fe(H_2O)_6^{3+}$
388	s	p					388	s	p	488	vw	p		Fe – O stretch in $Fe(D_2O)_6^{3+}$
			377	s	p					378	s	p		Fe – O stretch in $-Fe(H_2O)_5$
335sh	w	p?					337sh	w	p?					Fe – O stretch in $-Fe(D_2O)_5$
			324sh	w	p?					325sh	w	p		Fe – O stretch in $-Fe(H_2O)_5$
246?	vw	p	248?	vw	p		250?	vw	p	247?	vw	p		Fe – O – Fe sym. stretch

[a] A weak, broad band may be hidden by the ClO_4^- band at 460 cm^{-1}, s, strong; w, weak; vw, very weak; p, polarized; sh, shoulder.

of the hexahydrated monomer $[Fe(H_2O)_6]^{3+}$.

We shall assume that monomeric species $[Fe(H_2O)_6]^{3+}$ are the species that give rise to the large relaxation broadened line seen in Fig. 1a. The other monomeric and dimeric species are only present in a small proportion and their contribution to the Mössbauer spectrum at this pH can be neglected.

Addition of base to the iron(III) solution up to about 0.5 equivalent OH^- per Fe^{3+} results in the appearing of a quadrupole doublet in the Mössbauer spectra of the respective frozen solutions. This feature is seen in spectra 1b and 1c. In spectrum 1c (OH/Fe = 0.5) the most prominent lines come from a quadrupole doublet with isomer shift of 0.31 mm/s and quadrupole splitting of 1.67 mm/s. The value of this isomer shift is characteristic of a high spin iron(III) state.[13] The quadrupole splitting of 1.67 mm/s is large for a high spin iron(III) species. Mössbauer spectra of high spin iron(III) compounds which show quadrupole splitting in this range (~1.5 mm/s) have been reported by several investigators [14–16] and assigned to iron(III) μ-oxo bridges of the type $LFe-O-FeL$ where L can be different ligands.

Using the equilibrium constants of Milburn and Vosburgh [12] for $Fe(NO_3)_3$ or $Fe(ClO_4)_3$ 0.67 M aqueous solutions with OH/Fe = 0.5 we estimate that *ca.* 50 % of the total iron is in the form of the aqua dimer. Spectrum 1c was by computer fitted to three lorentzians, one lorentzian corresponding to the relaxation broadened spectrum of the ion $Fe(H_2O)_6^{3+}$ and the other two lorentzians corresponding to the quadrupole splitting. Measuring the areas of the lines we may get a rough estimate of the relative amount of each species present in the sample. The ratio between the areas in the Mössbauer spectrum of Fig. 1c corresponding to the monomeric species (broad line) and wide split species (quadrupole doublet) gives a proportion of 60 % of the total area for the species corresponding to the quadrupole splitting of 1.67 mm/s. The χ^2 tests for the computer fitting were excellent. This fact may be taken as a support of the assumption of only two species being present in the sample.

We assign the quadrupole split spectrum ($\Delta E_q = 1.67$ mm/s) to the dimeric species which is one of the hydrolysis products.

The Mössbauer technique is one way of

studying the magnetic interaction between the two high spin ($^6A, t_{2g}^3 e_g^2$) iron(III) ions of the dimer. In this connection it is noteworthy that the lines of the quadrupole doublet are comparatively narrow. This may be explained by assuming a zero magnetic field on the site of the absorbing nucleus and since we know the iron(III) to be in the high spin state this fact is indicative of a strong antiferromagnetic coupling producing a diamagnetic dimer ground state.

The Mössbauer spectrum of $[(\text{Fe heedta})_2\text{O}]^{2-}$ (where heedta $^{3-}$ is the anion of *N*-(2-hydroxyethyl)-ethylene diamine-*N*,*N*′,*N*′-triacetic acid) is shown on Fig. 2 spectrum b. From an X-ray investigation [17] this species is known to be an oxo-bridged dimer. Spectrum 1a is the spectrum of the aqua dimer.

For the purpose of comparison we have in Fig. 2c included the Mössbauer spectrum of the picolinate (pic complex $[(\text{pic})_2\text{Fe(OH)}_2\text{Fe(pic)}_2]$). This complex is reported [18] to be a di-μ-hydroxo complex. While the lines for $[(\text{Fe heedta})_2\text{O}]^{-2}$ and the aqua dimer have line widths less than twice the natural line width and are approximately symmetric, the lines for $[(\text{pic})_2\text{Fe(OH)}_2\text{Fe(pic)}_2]$ are much broader and asymmetric. In Table 1 the relevant parameters obtained at 100 K are given, allowing a quantitative comparison.

Buckley *et al.* studied the relation between the antiferromagnetic coupling and asymmetry of Mössbauer spectra for symmetrical, binuclear iron(III) complexes.[19] For complexes having strong antiferromagnetic coupling with $J \sim -100$ cm^{-1} (J is the constant of the Heisenberg-Dirac-Van Vleck operator $2J\ \mathbf{S}_a \times \mathbf{S}_b$ of the spin-Hamiltonian [20]) the population of the lowest lying, diamagnetic state is close to 100 % even at elevated (*i.e.* room) temperatures, and symmetric quadrupole split lines are observed. For binuclear complexes with weak antiferromagnetic coupling such as $[(\text{Fe salen Cl})_2]$ (salen = ethylenebis(salicylaldimine)) with $J = -7.5$ cm^{-1} the diamagnetic ground state is populated close to 100 % only at very low temperatures (≈liquid He temperatures). At higher temperatures the paramagnetic states are populated and this fact is observed in the Mössbauer spectrum as an asymmetric broadening increasing with increasing temperature.[19]

The observations of Buckely *et al.* are quite similar to our findings for $[(\text{Fe heedta})_2\text{O}]$ (strong coupling) and $[(\text{Fe pic}_2\text{OH})_2]$ (weak coupling) as is evident from Fig. 2. We furthermore conclude that the aqua dimer (spectrum 2a) is an oxobridged dimer with such a value of the antiferromagnetic coupling constant, J, that mainly the ground state is populated at $T = 100$ K.

The Mössbauer spectra in Fig. 1d and e are obtained on frozen solutions where the iron(III) is hydrolyzed beyond the stage of the binuclear species. The narrow-split quadrupole lines seen in Fig. 1d and 1e are similar to the Mössbauer spectrum of the polymer isolated from nitrate solutions by Spiro and co-workers.[21]

As far as they can be detected by the Mössbauer spectra, the polymeric species appear only in solutions containing more than 0.5 equivalent of base added per mol of iron, at the concentration used in this work (0.67 M). This is in concordance with the results obtained from ultracentrifuge experiments.[21]

The Mössbauer spectra of the polymeric species, at $T = 4$ K, as recorded by Spiro *et al.*[21] are six-line, hyperfine split spectra. This rules out the possibility that the spectrum of highly hydrolysed solutions (Spectrum 1e) can be due to an antiferromagnetically coupled dimeric species, for instance $(\text{Fe}-(\text{OH})_2-\text{Fe})^{4+}$, as suggested by Dezsi and co-workers.[22] The quadrupole doublet seen in the spectra of iron nitrate or perchlorate solutions, at moderate values of pH (Spectrum 1c) is not magnetically split at $T = 4$ K, as it can be seen in the spectra recorded by Dezsi *et al.*[22]

From the Mössbauer spectra it is very likely that the high-molecular species which gives rise to spectrum 1e is not formed by the condensation of oxo bridged dimers. This idea elucidates the study of rate of precipitation made by Knight and Sylva [23] who found that the 4+ dimer represents a "trap" for iron(III) when Fe^{3+} is hydrolyzed. They also found that acidified "iron hydroxide" does not form from the 4+ dimer directly but only *via* a monomeric iron(III).

Vibrational spectra

The vibrational spectra seem to corroborate the existence of $[(\text{H}_2\text{O})_5\text{Fe}-\text{O}-\text{Fe}(\text{H}_2\text{O})_5]^{4+}$ in the solutions investigated.

Raman spectra. Within experimental uncertainty the results for the dimer are independent of the anion. However, in the solutions made from iron(III) nitrate, mononitrato iron(III) is expected and Raman lines attributable to this complex are seen at 387 and 338 cm^{-1} in solutions without base added. No corresponding perchlorate complex has been observed. This may appear strange considering that NO_3^- and ClO_4^- carry the same charge but it may be rationalized in terms of the large difference in pK_a for HNO_3 and $HClO_4$. The nitrato iron(III) complex will not be discussed further in this paper. It was convenient to use both iron salts because the Raman lines from the anions overlap lines from the iron complex differently. Thus in the partly hydrolyzed H_2O solution from $Fe(NO_3)_3$ the FeO_6 symmetric stretching mode is observed at 501 cm^{-1},[24] whereas this band is partly covered by the 460 cm^{-1} band from perchlorate in the solutions made from $Fe(ClO_4)_3$. The corresponding FeO_6 stretching vibration for $Fe(NO_3)_3$ in D_2O is observed at 488 cm^{-1}.

The bands observed at 388 cm^{-1} and 335 cm^{-1} in H_2O solutions are found at 377 cm^{-1} and 325 cm^{-1} in D_2O. They are assigned to Fe–O stretching vibrations in $-FeO_6$ since frequency shifts with this order of magnitude between the hydrogen and deuterium compounds are expected for these stretching vibrations.[25]

The band found near 250 cm^{-1} is attributed to the symmetric Fe–O–Fe stretching vibration because it is nearly independent of hydrogen-deuterium exchange. Unfortunately, a very weak grating ghost may be seen at ~245 cm^{-1}, but instrumental conditions under these experiments have been chosen such that the ghost most probably should be considered excluded.

Infrared spectra. Partly hydrolyzed iron(III) nitrate in D_2O exhibits a band at 870 cm^{-1} and a weaker band at 830 cm^{-1} and the partly hydrolyzed perchlorate shows bands at 870 cm^{-1} and 933 cm^{-1}, the latter being weak.

The 830 cm^{-1} band can be assigned to the IR-active $\nu_3(A_2'')$-vibration of the nitrate ion, and the 933 cm^{-1} band can correspondingly be assigned to the $\nu_1(A_1)$-vibration of the perchlorate ion indicating a violation of selection rules for the free ion.[26] The 870 cm^{-1} band cannot be caused by librational modes of the coordinated D_2O molecules because these modes are found at lower frequencies in similar complexes.[25] Furthermore, we expect the corresponding HDO modes at lower frequencies and the H_2O modes, which might be expected at this frequency, should be excluded in D_2O solutions. In accordance with observations[27] on monooxo-bridged systems it seems reasonable to assign the band at 870 cm^{-1} to a Fe–O–Fe *anti*-symmetric stretching vibration.

The assignment of the vibrational spectra is given in Table 2. It is interesting to compare the frequencies for the symmetric (~250 cm^{-1}) and the *anti*-symmetric (~870 cm^{-1}) Fe–O–Fe stretching vibrations found in this work with corresponding frequencies[27] for oxo-bridged compounds with known structures. In dioxo-bridged systems all stretching vibrations are observed at frequencies below 760 cm^{-1} and this is certainly incompatible with the iron dimer. For bent mono oxo-bridged species an *anti*-symmetric stretching vibration is observed in the range 770–835 cm^{-1} and a symmetric vibration falls between 450 and 560 cm^{-1}. The linear μ-oxo dimers exhibit corresponding stretching vibrations between 820 and 950 cm^{-1} (*anti*-sym.) and between 215 and 230 cm^{-1} (symmetric). The observed stretching frequencies for the iron complex not only prove that it is a μ-oxo dimer but also point towards a linear structure. A linear structure is very sensible from a chemical consideration because this geometry maximizes the π-bonding of the system and in this way makes the oxide ion less basic than it would be with a lone pair available for proton attack.

Other measurements. Since the magnetic susceptibility measurements by Selwood[5] also Schugar *et al.*[7] have reported such measurements. The latter authors held the opinion that the 4+ dimer should have a rather low J value infering a di-μ-hydroxo bridge. Such result is not surprising considering the low precision of the technique for the study of solutions containing several paramagnetic species. Broersma[28] observed proton magnetic relaxation rates for iron(III) perchlorate solutions as a function of pH. The results were interpreted in terms of a diamagnetic dimer. A similar conclusion was obtained by Judkins[29] studying the ^{17}O NMR of hydrolyzed ferric perchlorate. These latter results are thus in accordance with the results presented in this paper.

Acknowledgements. J. E. Moreira wants to thank the Danish International Development Agency (DANIDA) for a fellowship.

REFERENCES

1. Sylva, R. N. *Rev. Pure Appl. Chem. 22* (1972) 115.
2. Murray, K. S. *Coord. Chem. Rev. 10* (1974) 1.
3. Hedström, B. O. A. *Ark. Kemi 6* (1953) 1.
4. Arnek, R. and Schlyter, K. *Acta Chem. Scand. 22* (1968) 1327.
5. Mulay, L. N. and Selwood, P. W. *J. Amer. Chem. Soc. 77* (1955) 2693.
6. Schäffer, C. E. *J. Inorg. Nucl. Chem. 19* (1958) 149.
7. Schugar, H., Walling, C., Jones, R. B. and Gray, H. B. *J. Amer. Chem. Soc. 89* (1967) 3712.
8. Knudsen, J. M., Araujo, F. T., Dufresne, A. and Lima, C. G. *Chem. Phys. Lett. 11* (1971) 134.
9. Dufresne, A., Knudsen, J. M., Moreira, J. E. and Neto, K. S., *Chem. Phys. Lett. 20* (1973) 108.
10. Mørup, S. In Seidel, C. W. and Dieterly, D. K., Eds., *Mössbauer Effect Methodology*, Plenum Press, New York 1974.
11. Nozik, A. J. and Kaplan, M., *J. Chem. Phys. 49* (1968) 4141.
12. Milburn, R. M. and Vosburgh, W. C. *J. Amer. Chem. Soc. 77* (1955) 1352.
13. Greenwood, N. N. and Gibb, T. C. *Mössbauer Spectroscopy*, Chapman and Hall, London 1971.
14. Reiff, W. M., Baker, W. A. and Erickson, N. E. *J. Amer. Chem. Soc. 90* (1968) 4794.
15. Reiff, W. M. *J. Chem. Phys. 54* (1971) 4718.
16. Schugar, H. J., Rossman, G. R., Barraclough, C. G. and Gray, H. B. *J. Amer. Chem. Soc. 94* (1972) 2683.
17. Lippard, S. J., Schugar, H. J. and Walling, C. *Inorg. Chem. 6* (1967) 1825.
18. Schugar, H. J., Rossman, G. R. and Gray, H. B. *J. Amer. Chem. Soc. 91* (1969) 4564.
19. Buckley, A. N., Herbert, I. R., Rumbold, B. D., Wilson, G. V. H. and Murray, K. S. *J. Phys. Chem. Solids 31* (1970) 1423.
20. Glerup, J. *Acta Chem. Scand. 26* (1972) 3775.
21. Brady, G. W., Kurkjian, C. R., Lyden, E., Robin, M. B., Saltman, P., Spiro, T. and Terzis, A. *Biochemistry 7* (1968) 2185.
22. Dezsi, I., Gorobchenko, V., Komor, M., Lukashevich, I., Vértes, A. and Tsirskishviei, K. *Acta Chim. Acad. Sci. Hung. 70* (1971) 329.
23. Knight, R. J. and Sylva, R. N. *J. Inorg. Nucl. Chem. 36* (1974) 591.
24. Sharma, S. K. *J. Inorg. Nucl. Chem. 35* (1973) 3831.
25. Nakagawa, I. and Shimanuchi, T. *Spectrochim. Acta 20* (1964) 429.
26. Herzberg, G. *Molecular Spectra and Molecular Structure* II, Van Nostrand, 9th printing, New York 1960.
27. Wing, R. M. and Callahan, K. P. *Inorg. Chem. 8* (1969) 871.
28. Broersma, S. *J. Chem. Phys. 26* (1957) 1405.
29. Judkins, M. R. *Thesis*, University of Calif., Berkeley 1968.

Received May 27, 1975.

Acta Chemica Scandinavica A 29 (1975) 840—842

Crystal Structure of 1,1-Dihydroperoxycyclododecane at —160 °C

P. GROTH

Department of Chemistry, University of Oslo, Oslo 3, Norway

The crystals are orthorhombic with cell dimensions $a = 5.973(1)$ Å, $b = 13.140(4)$ Å, $c = 16.164(4)$ Å, space group $P2_12_12_1$, and four molecules in the unit cell. The structure was solved by direct methods and refined by full-matrix least squares technique to an R-value of 2.4 % ($R_w = 2.3$ %) for 896 observed reflections measured on an automatic four circle diffractometer. The two O—O distances are 1.462 and 1.467 Å. The significant difference between the two C—O bonds (1.442 and 1.410 Å) is probably related to the hydrogen bonding system, consisting of *inter*-molecular bonds only. The average C—C bond distance and C—C—C angle of the cyclododecane ring are 1.524 Å and 114.3°, respectively.

In two earlier attempts to determine the hydrogen bonding systems formed by hydroperoxy groups,[1,2] the hydrogen atoms themselves could not be found in the difference Fourier maps, and the results are therefore somewhat incomplete. In the hope of obtaining a more accurate description, a crystal structure determination of 1,1-dihydroperoxycyclododecane ($C_{12}H_{24}O_4$) has been carried out.

The crystals are orthorhombic with cell dimensions $a = 5.973(1)$ Å, $b = 13.140(4)$, Å, $c = 16.164(4)$ Å. The space group is $P2_12_12_1$ and there are four molecules in the unit cell ($\varrho_o = 1.22$ g/cm³, $\varrho_o = 1.21$ g/cm³). The intensities were measured (at -160 °C) on a Syntex $P\bar{1}$ diffractometer with an Enraf-Nonius liquid nitrogen cooling device (modified by H. Hope). The radiation was Mo$K\alpha$ ($\lambda = 0.71069$ Å) and $2\theta_{max} = 45°$. With an observed-unobserved cutoff at $2.0\sigma(I)$, 896 reflections were recorded as observed. The crystal size was $(0.09 \times 0.16 \times 0.28)$ mm³. No corrections were made for absorption or secondary extinction effects.

Table 1. Final fractional coordinates and thermal parameters with estimated standard deviations. The expression for anisotropic vibration is $\exp[-2\pi^2(h^2a^{*2}U11 + \cdots\cdots + 2klb^*c^*U23)]$. Hmn is bonded to Cm and HOm to Om.

ATOM	X	Y	Z	U11	U22	U33	U12	U13	U23
O1	.02178(28)	.30738(11)	.62916(8)	.0218(9)	.0161(8)	.0230(8)	.0009(8)	-.0057(7)	-.0021(7)
O2	.13981(31)	.22019(12)	.64467(10)	.0239(10)	.0170(9)	.0277(10)	.0034(8)	-.0020(9)	.0009(7)
O3	.31894(25)	.41978(11)	.65853(8)	.0193(10)	.0276(9)	.0154(8)	-.0036(8)	.0023(7)	.0018(7)
O4	.33839(31)	.44408(13)	-.03788(10)	.0332(11)	.0312(10)	.0287(9)	.0073(9)	.0085(8)	.0034(8)
C1	.09283(40)	.39971(17)	.66966(13)	.0171(14)	.0194(13)	.0192(13)	-.0010(12)	-.0018(11)	-.0010(11)
C2	-.06972(47)	.47752(18)	.63451(16)	.0192(16)	.0285(13)	.0211(15)	.0018(13)	.0004(12)	-.0005(11)
C3	-.30992(44)	.58848(17)	.65360(17)	.0229(15)	.0287(14)	.0266(15)	-.0012(13)	-.0038(14)	.0008(12)
C4	-.29885(47)	.66251(18)	.64428(17)	.0302(16)	.0201(15)	.0249(15)	.0003(14)	-.0041(14)	.0004(12)
C5	-.39419(46)	.64617(21)	.10762(15)	.0185(14)	.0213(15)	.0298(15)	.0032(14)	-.0057(12)	-.0005(12)
C6	-.33282(48)	.67751(20)	.19689(15)	.0239(17)	.0211(16)	.0324(16)	.0023(13)	-.0058(14)	-.0018(12)
C7	-.47458(53)	.62888(24)	.26331(17)	.0271(18)	.0285(18)	.0276(16)	.0046(15)	-.0001(14)	-.0018(12)
C8	-.43728(47)	.51476(21)	.27331(18)	.0211(15)	.0326(17)	.0275(16)	-.0026(14)	.0033(14)	-.0007(13)
C9	-.28565(46)	.48536(19)	.33413(17)	.0233(15)	.0314(16)	.0188(15)	.0004(14)	.0015(13)	-.0018(12)
C10	-.14798(54)	.37353(23)	.29152(14)	.0254(16)	.0291(16)	.0283(14)	-.0000(14)	.0029(14)	.0006(12)
C11	-.11516(54)	.34319(23)	.20001(15)	.0262(16)	.0187(16)	.0261(14)	-.0003(14)	.0048(13)	.0008(11)
C12	.09433(45)	.39012(24)	.16386(14)	.0176(14)	.0159(14)	.0215(13)	.0008(13)	-.0001(12)	-.0002(11)

ATOM	X	Y	Z	B	ATOM	X	Y	Z	B
H21	-.2146(41)	.4633(15)	.0575(13)	.7(4)	H22	-.0727(37)	.4679(15)	-.0276(14)	1.3(4)
H31	.1158(42)	.6134(17)	.3138(14)	1.8(5)	H32	.0547(37)	.5929(16)	.1112(14)	1.2(4)
H41	-.2794(45)	.6514(17)	-.0181(15)	2.4(5)	H42	-.1483(37)	.7336(17)	.0481(12)	1.5(4)
H51	-.4468(41)	.5771(20)	.1978(14)	1.8(5)	H52	-.5293(43)	.6875(17)	.0914(13)	1.8(5)
H61	-.3511(40)	.7529(18)	.1978(12)	1.4(5)	H62	-.1772(44)	.6642(18)	.2478(14)	1.2(5)
H71	-.6301(45)	.6424(18)	.2498(13)	1.5(5)	H72	-.4531(54)	.6656(18)	.3171(15)	2.5(6)
H81	-.4718(38)	.4786(15)	.2187(15)	1.2(4)	H82	-.5493(42)	.4948(17)	.3128(14)	1.8(5)
H91	-.1998(36)	.4987(15)	.3651(14)	.9(4)	H92	-.0814(35)	.5317(16)	.2772(13)	.8(4)
H101	-.2757(45)	.3305(18)	.3178(14)	2.4(5)	H102	-.0886(48)	.3528(17)	.3210(14)	1.8(5)
H111	-.2523(38)	.3661(16)	.1698(12)	.5(4)	H112	-.1026(42)	.2705(18)	.1968(12)	.8(4)
H121	.2263(41)	.3484(16)	.1773(12)	.8(4)	H122	.1224(39)	.4578(18)	.1842(12)	1.2(5)
H02	.2584(63)	.2159(24)	.0336(19)	5.5(9)	H04	.4201(55)	.3932(22)	-.0519(19)	4.0(8)

Table 2. Interatomic distances, bond angles and dihedral angles with estimated standard deviations.

Distance	Å	Distance	Å
O1 – O2	1.462(2)	C7 – C8	1.525(4)
O3 – O4	1.467(2)	C8 – C9	1.520(4)
C1 – O1	1.442(3)	C9 – C10	1.523(4)
C1 – O3	1.410(3)	C10 – C11	1.534(4)
C1 – C2	1.520(4)	C11 – C12	1.526(4)
C2 – C3	1.531(3)	C12 – C1	1.516(3)
C3 – C4	1.527(3)	O2 – O1′	2.764(3)
C4 – C5	1.519(4)	O4 – O2′	2.843(3)
C5 – C6	1.532(4)	O2 – HO2	.870(35)
C6 – C7	1.519(4)	O4 – HO4	.858(31)

Angle	(°)	Angle	(°)
C1 – O1 – O2	109.8(1)	C7 – C8 – C9	114.7(2)
C1 – O3 – O4	109.2(2)	C8 – C9 – C10	114.0(2)
O1 – C1 – O3	109.9(2)	C9 – C10 – C11	114.0(2)
O1 – C1 – C2	102.1(2)	C10 – C11 – C12	112.2(2)
O1 – C1 – C12	112.5(2)	C11 – C12 – C1	115.2(2)
O3 – C1 – C2	113.9(2)	O1 – O2 – HO2	102.5(21)
O3 – C1 – C12	103.2(2)	O2 – HO2 – O1	173.9(31)
C12 – C1 – C2	115.6(2)	HO2 – O1′ – O2′	118.9(10)
C1 – C2 – C3	114.6(2)	HO2 – O1′ – C1′	128.5(10)
C2 – C3 – C4	112.9(2)	O3 – O4 – HO4	97.8(21)
C3 – C4 – C5	115.0(2)	O4 – HO4 – O2′	169.2(30)
C4 – C5 – C6	114.9(2)	HO4 – O2′ – O1′	103.1(9)
C5 – C6 – C7	114.9(2)	HO4 – O2′ – HO2′	115.3(24)
C6 – C7 – C8	114.1(2)		

Dihedral angle	(°)
C1 – C2 – C3 – C4	-160.4(2)
C2 – C3 – C4 – C5	67.7(3)
C3 – C4 – C5 – C6	69.4(3)
C4 – C5 – C6 – C7	-158.1(2)
C5 – C6 – C7 – C8	68.6(3)
C6 – C7 – C8 – C9	66.1(3)
C7 – C8 – C9 – C10	-164.0(2)
C8 – C9 – C10 – C11	68.9(3)
C9 – C10 – C11 – C12	69.0(3)
C10 – C11 – C12 – C1	-156.9(2)
C11 – C12 – C1 – C2	69.1(3)
C12 – C1 – C2 – C3	68.4(3)

The structure was solved by direct methods [3] and refined by full-matrix least squares technique.[4]* Anisotropic temperature factors were introduced for oxygen and carbon atoms. Methylene hydrogen atom positions were calculated, while the two H-atoms of the hydroperoxy groups were seen as the largest peaks in the difference Fourier map. Atomic form factors were those of Hanson *et al.*[5] except for hydrogen.[6] Weights used in least squares were obtained from the standard deviations in intensities, $\sigma(I)$, taken as

$$\sigma(I)=[C_T+(0.02C_N)^2]^{\frac{1}{2}}$$

where C_T is the total number of counts and C_N the net count. The final R-value was 2.4 % (R_w = 2.3 %) for 896 observed reflections.

* All programs used (except those for phase determination) are included in this reference.

Final fractional coordinates and thermal parameters with estimated standard deviations are given in Table 1. The principal axes of the thermal vibration ellipsoids were calculated from the temperature parameters of Table 1. Maximum to r.m.s. amplitudes range from 0.149 to 0.211 Å (corresponding B-values of 1.76 and 3.52 Å^2). Because of the size of the molecule, no rigid-body analysis of translational, librational and screw motion has been carried out.

Interatomic distances, bond angles, and dihedral angles are listed in Table 2. The standard deviations, given in parentheses, are estimated from the correlation matrix of the last least squares refinement cycle. A list of observed structure factors is available from the author.

The *inter*-molecular hydrogen bonding system, shown in Fig. 1, forms endless double chains along [100] with O···O distances of 2.764 and 2.843 Å. O2 is an acceptor as well as a donor, while O1 accepts HO4. The fact that O3 is not involved in hydrogen bonding may possibly be related to the significant difference between the bond lengths C1 – O1 (1.442 Å) and C1 – O3 (1.410 Å). A similar, though statistically insignificant, effect was observed in 1,1′-dihydroperoxycyclohexanylperoxide-1,1′,[1] (I). In 1,1′-dihydroperoxycyclododecanylperoxide-1,1′,[2] (II), both oxygens are involved in *intra*-molecular hydrogen bonds, and the C – O bonds are equal. Table 2 shows that bond distances and angles involved in the hydrogen bonding system have normal values. Bond distances and angles of the hydroperoxy groups correspond, within three times e.s.d.'s, to those of (I) and (II).

The arrangement around C1 is asymmetric, with angles C2 – C1 – O1 and C12 – C1 – O3 about 10.5° smaller than C2 – C1 – O3 and C12 – C1 – O1. The effect (described in detail elsewhere [2]) is probably related to *intra*-molecular oxygen-hydrogen repulsions.

Deviations of the 12-membered ring conformation from the idealized "square" model with 422-symmetry (containing eight synclinal and four *anti*-periplanar partial conformations) may be compared with those of (II). The average synclinal torsional angles agree closely (68.4 and 68.2°). However, the anti-periplanar dihedral angles (°) are more nearly equal in the title compound:

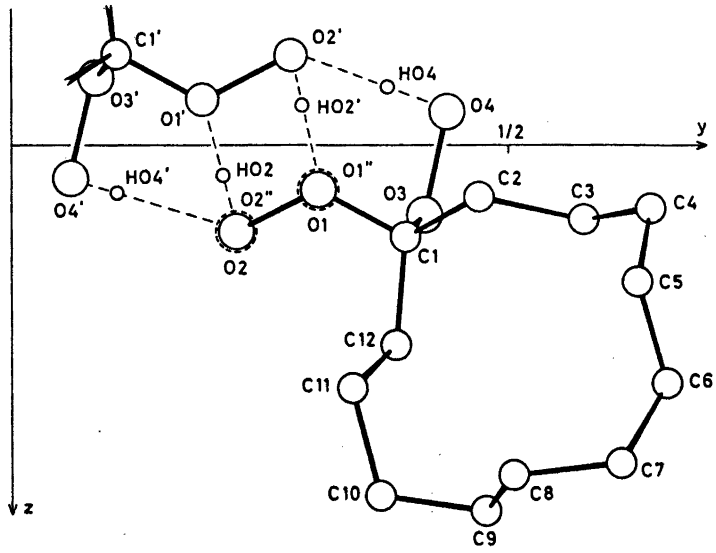

Fig. 1. Schematic drawing of the molecule and the hydrogen bonding system, viewed along [100]. O1″ and O2″ are in the neighbouring cell.

−160.4, −158.1, −164.0, −156.9

than in (II):

−169.4, −152.4, −167.0, −152.3

−168.9, −151.3, −168.7, −150.3

The average C−C bond distance and C−C−C angle (1.524 Å and 114.3°) correspond closely with those of (II) (1.526 Å and 114.1°). Methylene C−H bond distances range from 0.96 to 1.05 Å.

Except for the hydrogen bonds, no short *inter*-molecular contacts are observed.

Acknowledgement. The author would like to thank cand. real. T. Ledaal for supplying the compound, and A. Aasen for technical assistance during data collection.

REFERENCES

1. Groth, P. *Acta Chem. Scand. 23* (1969) 2277.
2. Groth, P. *Acta Chem. Scand. A 29* (1975) 783.
3. Germain, G., Main, P. and Woolfson, M. M. *Acta Crystallogr. A 27* (1971) 368.
4. Groth, P. *Acta Chem. Scand. 27* (1973) 1837.
5. Hanson, P., Herman, F., Lea, J. D. and Skillman, S. *Acta Crystallogr. 17* (1964) 1040.
6. Stewart, R. F., Davidson, E. and Simpson, W. T. *J. Chem. Phys. 42* (1965) 3175.

Received May 12, 1975.

Acta Chemica Scandinavica A 29 (1975) 843—848

The Crystal Structure of Rubidium Seleniumtriselenocyanate Hemihydrate

SVERRE HAUGE

Department of Chemistry, University of Bergen, N-5014 Bergen-Univ., Norway

The crystal structure of rubidium seleniumtriselenocyanate hemihydrate, $RbSe(SeCN)_3 \cdot \frac{1}{2}H_2O$, has been determined by X-ray methods, and refined by full matrix least squares procedures. The crystals are triclinic, space group $P\bar{1}$ (No. 2), with $a = 9.180(2)$ Å, $b = 13.227(3)$ Å, $c = 9.144(2)$ Å, $\alpha = 83.89(2)°$, $\beta = 100.02(2)°$, $\gamma = 74.97(2)°$, and four formula units per unit cell.

In the crystals, the seleniumtriselenocyanate ions are dimerized. The dimensions of the dimerized unit are nearly the same as in the corresponding potassium salt. The eight selenium atoms of the unit are approximately co-planar, and the six cyano groups are located on the same side of the plane.

Each of the two central selenium atoms has a square-planar coordination with two long Se–Se bonds *trans* to two short Se–Se bonds. The four rather short Se–Se bonds are from 2.391(2) to 2.409(2) Å, and the long ones from 3.127(2) to 3.331(2) Å. The short ones are definitely longer than the Se–Se single-bond distance 2.34 Å, and the long ones are shorter than van der Waals approaches. The total lengths of these rather unsymmetrical, approximately linear three-selenium systems (the sum of the length of the two Se–Se bonds) are 5.536 to 5.737 Å which are a little longer than in the corresponding potassium salt.

Short Se···Se contacts, from 3.37 Å upwards, occur between dimerized units.

The seleniumtriselenocyanate ion was first isolated in 1884–1886 in the form of the potassium salt,[1] as one of the oxydation products of aqueous potassium selenocyanate. Later, rubidium seleniumtriselenocyanate hemihydrate, $RbSe(SeCN)_3 \cdot \frac{1}{2}H_2O$, was isolated from the reaction between aqueous rubidium cyanide and selenium diselenocyanate.[2] Its crystal structure, reported here, has been determined as part of a study of asymmetric linear three-selenium systems. The crystal structure of the corresponding potassium salt has been reported earlier.[3]

CRYSTAL DATA

Preparative and crystallographic data on rubidium seleniumtriselenocyanate hemihydrate have been reported earlier.[2] The space group is $P\bar{1}$ (No. 2), $a = 9.180(2)$ Å, $b = 13.227(3)$ Å, $c = 9.144(2)$ Å, $\alpha = 83.89(2)°$, $\beta = 100.02(2)°$, $\gamma = 74.97(2)°$, $z = 4$. $D_x = 3.11$ g/cm³, $D_m = 3.12$ g/cm³. The present cell parameters have been chosen to get a better comparison between this structure and that of the corresponding potassium salt.[3] They are derived, from what has been reported earlier,[3] by interchanging the a and c axes and giving the b axis opposite direction.

Collection of X-ray data was done by the same methods as for the corresponding potassium salt, using Nb-filtered Mo$K\alpha$ radiation, $\lambda(\alpha_1) = 0.70926$ Å. Number of reflections recorded with measurable intensities, 2664 out of 5075 possible within $\theta = 28°$. $\mu = 200$ cm^{-1}. The cell parameters were evaluated from the settings of 21 resolved reflections. The crystals used for data collection had the following dimensions, given as distances to faces from an arbitrarily chosen point; to (001) and (00$\bar{1}$), 0.082 mm; to (010) and (0$\bar{1}$0), 0.065 mm; to (011), 0.077 mm; to (0$\bar{1}\bar{1}$), 0.068 mm; to (01$\bar{1}$), 0.079 mm; to (10$\bar{1}$) and ($\bar{1}$01), 0.086 mm.

There was no decrease in the net count of the reference reflections during the collection period.

Fifteen reflections which showed extraordinarily high, or erratic, background count were at a later stage omitted from the data.

Intensities were corrected for absorption [4] and extinction.[5]

Table 1. Atomic coordinates in fractions of triclinic cell edges. Isotropic thermal parameters (Å²) in the form exp $[-8\pi^2 U(\sin^2\theta/\lambda^2)]$. Standard deviations from the least squares refinement in parentheses.

	x	y	z	U
Se_1	−0.02749(14)	0.13985(9)	−0.14850(13)	
Se_2	−0.01134(14)	0.12233(9)	0.11893(13)	
Se_3	−0.26734(15)	0.10719(11)	0.11809(13)	
Se_4	0.64421(14)	0.11827(9)	0.52315(14)	
Se_5	0.37849(13)	0.13340(8)	0.52197(13)	
Se_6	0.38571(15)	0.12699(10)	0.78550(14)	
Se_7	0.33122(15)	0.12897(10)	0.15988(14)	
Se_8	0.01767(15)	0.13765(10)	0.48366(14)	
C_1	−0.0234(13)	0.2780(9)	−0.1718(13)	0.037(3)
C_3	−0.3497(14)	0.2449(10)	0.1307(14)	0.043(3)
C_4	0.6240(14)	0.2596(9)	0.5293(13)	0.038(3)
C_6	0.3674(14)	0.2682(10)	0.7830(14)	0.040(3)
C_7	0.2480(12)	0.2687(9)	0.1545(12)	0.029(3)
C_8	−0.0189(13)	0.2801(9)	0.4423(13)	0.033(3)
N_1	−0.0145(12)	0.3634(8)	−0.1849(12)	0.051(3)
N_3	−0.3969(14)	0.3298(9)	0.1428(13)	0.064(3)
N_4	0.6105(13)	0.3473(9)	0.5313(12)	0.057(3)
N_6	0.3546(12)	0.3568(9)	0.7814(12)	0.053(3)
N_7	0.1933(11)	0.3574(8)	0.1542(11)	0.042(3)
N_8	−0.0391(11)	0.3700(8)	0.4196(11)	0.044(3)
O	0.6098(10)	0.4735(10)	0.8190(10)	0.059(3)
Rb_1	0.24627(14)	0.46638(9)	0.43210(14)	
Rb_2	0.83597(15)	0.46082(10)	0.09079(14)	

THE STRUCTURE ANALYSES

The structure was solved by Patterson and Fourier methods and by reference to the structure of $KSe(SeCN)_3 \cdot \frac{1}{2}H_2O$.[3] The x and z coordinates of the selenium atoms in the present structure could be derived from the coordinates in the potassium salt by subtracting about 0.08 cell edge in x and z coordinates. The y coordinates are about the same in the two structures. The R-value in the final full-matrix least squares refinement was 0.043. The Fourier difference map based on these data showed no higher peak than 0.9 e/Å³.

Computational procedure and programs used are described elsewhere.[6] The final atomic coordinates and temperature parameters are listed in Tables 1 and 2.

The structure factors are available from the author on request.

Table 2. Anisotropic thermal parameters (Å²) in the form exp $[-2\pi^2(h^2a^{-2}U_{11} + \cdots 2hka^{-1}b^{-1}U_{12} + \cdots)]$. All values have been multiplied by 10^4. Standard deviations from least squares refinement in parentheses.

	U_{11}	U_{22}	U_{33}	U_{12}	U_{23}	U_{13}
Se_1	375(7)	323(7)	253(7)	−148(6)	−51(5)	54(5)
Se_2	315(7)	316(6)	267(7)	−147(5)	−43(5)	74(5)
Se_3	371(8)	487(8)	514(9)	−242(6)	−156(6)	148(6)
Se_4	245(6)	288(6)	426(8)	−86(5)	−103(5)	87(5)
Se_5	248(6)	237(6)	302(7)	−65(5)	−67(5)	68(5)
Se_6	428(8)	326(7)	301(7)	−137(6)	−67(5)	85(6)
Se_7	331(7)	307(6)	366(8)	−76(5)	−76(5)	48(6)
Se_8	342(7)	366(7)	380(8)	−115(6)	−42(6)	74(6)
Rb_1	338(7)	308(6)	319(7)	−80(5)	−63(5)	59(5)
Rb_2	408(7)	374(7)	313(7)	−146(6)	−79(5)	102(6)

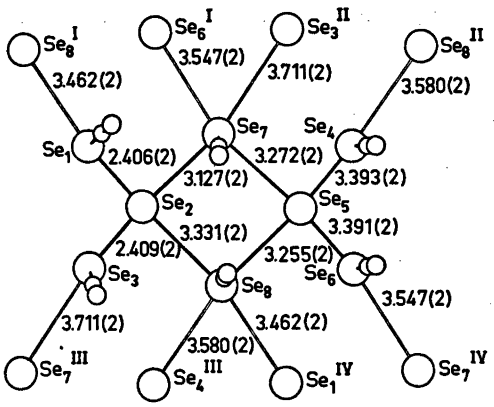

Fig. 1. The di-μ-selenocyanato-bis[diselenocyanatoselenate(II)] anion in $RbSe(SeCN)_3 \frac{1}{2}H_2O$, as seen normal to the *ac* plane.

RESULT

The di-μ-selenocyanato-bis[diselenocyanatoselenate(II)] anion. Bond lengths, close contacts, and angles in the anion, based on the atomic coordinates of Table 1, are given Fig. 1 and Tables 3 and 4. Distances from the rubidium ions and from the water molecule to neighbouring atoms are given in Table 6. The uncertainties in cell dimensions are taken into account in the given standard deviations. In the tables, superscript I denotes an atom at $(x,y,z-1)$, II at $(1+x,y,z)$, III at $(x-1,y,z)$, IV at $(x,y,1+z)$, V at $(\bar{x},\bar{y},\bar{z})$, VI at $(1-x,\bar{y},1-z)$, VII at $(\bar{x},\bar{y},1-z)$, VIII at $(1-x,1-y,1-z)$, IX at $(\bar{x},1-y,\bar{z})$, X at $(1-x,1-y,\bar{z})$, XI at $(\bar{x},1-y,1-z)$, where x, y, z are the coordinates of Table 1.

As in the crystals of the corresponding potassium salt, the selenium atoms occur in layers parallel to the *ac* plane at y approximately 0.127 and -0.127. Two layers, interrelated through symmetry centers at $y=0$, make a double layer. The cyano groups are located on the outsides of the double layer, the rubidium ions and the water oxygen have y approximately $\frac{1}{2}$ and are therefore located between double layers.

To show the resemblance of the layers in the two structures, Table 5, with a monoclinic coordinate system, has been worked out. The double layers in the two structures are almost identical, but from the difference in the direction of the *b* axes it is seen that the stacking of the double layers are different.

Some of the differences in bond lengths, close contacts, and angles will be underlined here. The short selenium-selenium bond lengths at the central selenium atoms, Se_2 and Se_5, are in mean 0.007 Å shorter in the present structure. This difference is uncertain since the standard deviation on the Se–Se bonds is 0.002 Å. The long selenium-selenium bonds at Se_2 and Se_5 are in the mean 0.07 Å longer. In the mean, the total length of the unsymmetrical three-selenium system, the sum of the lengths of the two Se–Se bonds, are 0.06 Å longer. This must mainly be explained as caused by the different packing in the two crystals.

In the structure of the potassium salt, the two Se–C bond lengths in the selenocyanate groups at Se_1 and Se_4 were, with some uncer-

Table 3. Angles (°) in the plane of the eight selenium unit. Standard deviations in parentheses.

$Se_1-Se_2-Se_3$	97.55(7)	$Se_4-Se_5-Se_6$	99.32(7)
$Se_3-Se_2-Se_8$	86.69(6)	$Se_6-Se_5-Se_8$	86.94(6)
$Se_8-Se_2-Se_7$	87.40(5)	$Se_8-Se_5-Se_7$	86.31(5)
$Se_7-Se_2-Se_1$	88.80(6)	$Se_7-Se_5-Se_4$	87.23(6)
$Se_1-Se_2-Se_8$	170.69(6)	$Se_4-Se_5-Se_8$	172.64(6)
$Se_3-Se_2-Se_7$	173.20(6)	$Se_6-Se_5-Se_7$	172.60(6)
$Se_2-Se_1\cdots Se_8^{I}$	169.71(5)	$Se_2-Se_7\cdots Se_3^{II}$	165.28(5)
$Se_2-Se_3\cdots Se_7^{III}$	168.49(6)	$Se_5-Se_7\cdots Se_6^{I}$	164.33(5)
$Se_5-Se_4\cdots Se_8^{II}$	170.35(5)	$Se_2-Se_8\cdots Se_1^{IV}$	167.53(5)
$Se_5-Se_6\cdots Se_7^{IV}$	170.84(5)	$Se_5-Se_8\cdots Se_4^{III}$	167.97(5)
$Se_5-Se_7\cdots Se_3^{II}$	98.79(5)	$Se_2-Se_8\cdots Se_4^{III}$	99.32(5)
$Se_2-Se_7\cdots Se_6^{I}$	100.84(5)	$Se_5-Se_8\cdots Se_1^{II}$	100.73(5)
$Se_6^{I}\cdots Se_7\cdots Se_3^{II}$	65.63(5)	$Se_4^{III}\cdots Se_8\cdots Se_1^{II}$	68.36(5)

Table 4. Bond lengths and short distances (Å) and angles (°) out of th plane of the eight selenium unit. Standard deviations in parentheses.

Se_1-C_1	1.828(13)	$\angle Se_1-C_1-N_1$	177.3(9)
C_1-N_1	1.149(17)	$\angle Se_2-Se_1-C_1$	95.2(4)
Se_3-C_3	1.806(13)	$\angle Se_3-C_3-N_3$	177.6(9)
C_3-N_3	1.120(17)	$\angle Se_2-Se_3-C_3$	95.0(5)
Se_4-C_4	1.838(13)	$\angle Se_4-C_4-N_4$	179.2(8)
C_4-N_4	1.136(17)	$\angle Se_5-Se_4-C_4$	94.5(4)
Se_6-C_6	1.829(13)	$\angle Se_6-C_6-N_6$	179.4(10)
C_6-N_6	1.145(17)	$\angle Se_5-Se_6-C_6$	94.7(4)
Se_7-C_7	1.799(12)	$\angle Se_7-C_7-N_7$	178.3(9)
C_7-N_7	1.149(14)	$\angle Se_2-Se_7-C_7$	83.7(4)
		$\angle Se_5-Se_7-C_7$	81.2(4)
Se_8-C_8	1.812(12)	$\angle Se_8-C_8-N_8$	178.1(8)
C_8-N_8	1.145(16)	$\angle Se_2-Se_8-C_8$	90.2(4)
		$\angle Se_5-Se_8-C_8$	97.0(4)
$Se_2\cdots Se_1^{V}$	3.369(2)	$\angle Se_1-Se_2\cdots Se_1^{V}$	92.09(5)
		$\angle Se_3-Se_2\cdots Se_1^{V}$	75.31(5)
		$\angle Se_7-Se_2\cdots Se_1^{V}$	102.10(5)
		$\angle Se_8-Se_2\cdots Se_1^{V}$	97.02(5)
$Se_5\cdots Se_4^{VI}$	3.452(2)	$\angle Se_4-Se_5\cdots Se_4^{VI}$	102.31(5)
		$\angle Se_6-Se_5\cdots Se_4^{VI}$	100.73(6)
		$\angle Se_7-Se_5\cdots Se_4^{VI}$	74.32(5)
		$\angle Se_8-Se_5\cdots Se_4^{VI}$	72.52(5)
$Se_1\cdots Se_2^{V}$	3.369(2)	$\angle Se_2-Se_1\cdots Se_2^{V}$	87.91(5)
		$\angle C_1-Se_1\cdots Se_2^{V}$	172.3(4)
$Se_4\cdots Se_5^{VI}$	3.452(2)	$\angle Se_5-Se_4\cdots Se_5^{VI}$	77.69(5)
		$\angle C_4-Se_4\cdots Se_5^{VI}$	170.7(4)
$Se_8\cdots Se_8^{VII}$	3.724(2)	$\angle Se_2-Se_8\cdots Se_8^{VII}$	84.41(5)
		$\angle Se_5-Se_8\cdots Se_8^{VII}$	110.17(5)
		$\angle C_8-Se_8\cdots Se_8^{VII}$	164.6(4)

Table 5. A comparison of the coordinates of the selenium atoms in the crystal structure of rubidium seleniumtriselenocyanate hemihydrate with the selenium coordinates in the corresponding potassium salt.[a]

	$KSe(SeCN)_3\cdot\frac{1}{2}H_2O$			$RbSe(SeCN)_3\cdot\frac{1}{2}H_2O$		
	X	*Y*	*Z*	*X*	*Y*	*Z*
Se_1	0.176	1.736	−1.164	0.278	1.764	−1.069
Se_2	0.287	1.572	1.251	0.359	1.543	1.340
Se_3	−2.124	1.315	1.218	−2.048	1.352	1.301
Se_4	6.239	1.575	4.923	6.362	1.492	5.028
Se_5	3.830	1.676	4.924	3.980	1.682	5.049
Se_6	3.928	1.706	7.335	4.022	1.602	7.445
Se_7	3.426	1.553	1.669	3.523	1.627	1.728
Se_8	0.615	1.704	4.537	0.684	1.736	4.707

[a] The reference coordinate system is a monoclinic system where the *a* and *c* axes of the triclinic cells are unchanged and the *b* axis is at right angle to the *a* and *c* axes. The coordinates of the monoclinic system, *X*, *Y*, *Z* in Å, relative to the triclinic cells, are given by:

$X = ax + by(\cos\gamma - \cos\alpha\cos\beta)/\sin^2\beta$

$Y = by(1-\cos^2\alpha-\cos^2\beta-\cos^2\gamma+2\cos\alpha\cos\beta\cos\gamma)^{\frac{1}{2}}/\sin\beta$

$Z = cz + by(\cos\alpha - \cos\beta\cos\gamma)/\sin^2\beta$

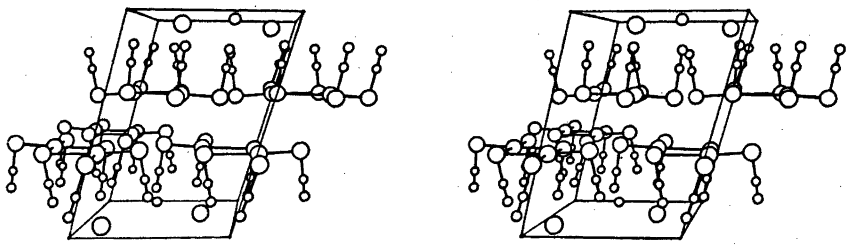

Fig. 2. A stereoscopic pair of drawings of $RbSe(SeCN)_3.\frac{1}{2}H_2O$. The cell drawn is along the *a* and *c* axes from 0 to 1 and along the *b* axis from $-\frac{1}{2}$ to $\frac{1}{2}$.

tainties, found to be a little longer than the others. The lengthening of the bonds was explained by the close Se···Se contacts between single layers, *trans* to the Se–C bonds. The present structure has about the same Se···Se contacts between single layers, but the Se–C bond lengthening is not observed.

A comparison of the crystal structure of the dimerized seleniumtriselenocyanate ion as it occurs in the potassium salt, with the structure of selenium diselenocyanate has been done earlier.[3] In the structure of selenium diselenocyanate [7,8] the Se–Se bond lengths are 2.33 Å and the Se–Se–Se angle is 103 °. Two short Se···N contacts, 3.16 Å, occur in directions indicating a square planar coordination at the central selenium atom. The dimerized seleniumtriselenocyanate as it occurs in the potassium and rubidium salts, can be looked upon as built up of two selenium diselenocyanate molecules bridged together through the selenium atoms of two selenocyanate ions. The Se–Se bonds of the $Se(SeCN)_2$ parts of the anion are approached by the selenium atoms of the selenocyanate ions, resulting in square planar coordinations at the central selenium atoms. In the present structure, the sums of the two Se–Se bond lengths in the $Se(SeCN)_2$ parts of the

Table 6. Distances from the rubidium ions and from the water molecule. Bond lengths (Å) and angles (°). Standard deviations are given in parentheses.

$Rb_1\cdots N_4$	3.224(11)	$\angle N_4\cdots Rb_1\cdots N_6$	66.5(3)
$Rb_1\cdots N_6$	3.233(11)	$\angle N_4\cdots Rb_1\cdots N_7$	95.0(3)
$Rb_1\cdots N_7$	3.080(11)	$\angle N_4\cdots Rb_1\cdots N_8$	129.3(3)
$Rb_1\cdots N_8$	3.187(12)	$\angle N_6\cdots Rb_1\cdots N_7$	127.7(3)
$Rb_1\cdots N_1^{IX}$	3.076(9)	$\angle N_6\cdots Rb_1\cdots N_8$	86.7(3)
$Rb_1\cdots N_4^{VIII}$	3.101(13)	$\angle N_7\cdots Rb_1\cdots N_8$	67.6(3)
$Rb_1\cdots N_8^{XI}$	3.087(11)	$\angle N_1^{IX}\cdots Rb_1\cdots N_4^{VIII}$	80.8(3)
$Rb_1\cdots O^{VIII}$	2.977(11)	$\angle N_1^{IX}\cdots Rb_1\cdots N_8^{XI}$	70.9(3)
		$\angle N_4^{VIII}\cdots Rb\cdots N_8^{XI}$	71.5(3)
$Rb_2\cdots N_1^{II}$	3.298(12)	$\angle N_1^{II}\cdots Rb_2\cdots N_3^{II}$	103.7(3)
$Rb_2\cdots N_3^{II}$	3.146(14)	$\angle N_1^{II}\cdots Rb_2\cdots N_7^{II}$	62.3(3)
$Rb_2\cdots N_7^{II}$	3.132(10)	$\angle N_1^{II}\cdots Rb_2\cdots N_8^{II}$	124.0(3)
$Rb_2\cdots N_8^{II}$	3.019(10)	$\angle N_3^{II}\cdots Rb_2\cdots N_7^{II}$	122.6(3)
$Rb_2\cdots N_1^{X}$	3.277(12)	$\angle N_3^{II}\cdots Rb_2\cdots N_8^{II}$	80.2(3)
$Rb_2\cdots N_6^{VIII}$	3.061(11)	$\angle N_7^{II}\cdots Rb_2\cdots N_8^{II}$	69.1(3)
$Rb_2\cdots N_7^{X}$	3.030(10)	$\angle N_1^{X}\cdots Rb_2\cdots N_6^{VIII}$	65.5(3)
$Rb_2\cdots O'$	2.907(9)	$\angle N_1^{X}\cdots Rb_2\cdots N_7^{X}$	63.5(3)
		$\angle N_6^{VIII}\cdots Rb_2\cdots N_7^{X}$	80.8(3)
$O\cdots N_3^{XI}$	2.916(15)	$\angle N_3^{XI}\cdots O\cdots N_6$	93.0(5)
$O\cdots N_6$	3.114(18)	$\angle N_3^{XI}\cdots O\cdots Rb_1^{VIII}$	105.3(4)
$O\cdots Rb_1^{VIII}$	2.977(11)	$\angle N_3^{XI}\cdots O\cdots Rb_2^{IV}$	95.0(4)
$O\cdots Rb_2^{IV}$	2.907(9)	$\angle N_6\cdots O\cdots Rb_1^{VIII}$	123.0(4)
		$\angle N_6\cdots O\cdots Rb_2^{IV}$	127.0(4)
		$\angle Rb_1^{VIII}\cdots O\cdots Rb_2^{VI}$	104.8(3)

anion are 4.784 and 4.815 Å, and the corresponding angles are 99.32 and 97.55°, respectively. In the structure of the potassium salt, the sums are 4.806 and 4.822 Å and the angles are 98.41 and 97.60°. From the three crystal structures it seems that an increase of 0.02–0.03 Å in the sum of the two Se–Se bond lengths corresponds to a decrease of one degree in the Se–Se–Se angle.

Crystal packing. The rubidium ions and the water molecule lie at y approximately ½, between double layers of selenium atoms around $y=0$ and 1. The closest contacts of the potassium ions and of the water molecule are listed in Table 6. The water molecule is surrounded by two rubidium ions, at distances of 2.907 and 2.977 Å, and by two nitrogen atoms at distances of 2.916 and 3.114 Å. The latter contacts probably involve weak O–H···N hydrogen bonds. The N···O···N angle is 93.3°. The arrangement around the oxygen atom is approximately tetrahedral, the Rb···O···Rb angle is 104.8° and the N···O···Rb angles are in the range 95.0 to 127.0°.

Each of the rubidium ions is surrounded by seven nitrogen atoms and one oxygen atom, with three of the nitrogen atoms in a plane above and four nitrogen atoms approximately in a plane below the rubidium ion; both planes are approximately parallel to the *ac* plane. The oxygen atom lies between the two planes. The Rb···N distances are in the range 3.020 Å to 3.298 Å, and the Rb···O distances are 2.907 and 2.977 Å.

The Rb···O distances are in the normal range (*cf.* Ref. 6, p. 259), and so are the Rb···N distances, the sum of the Rb···N ionic radii being 3.19 Å.[7]

REFERENCES

1. Verneuil, A. *Ann. Chim. Phys.* [6] *9* (1886) 289.
2. Hauge, S. *Acta Chem. Scand. 25* (1971) 3081.
3. Hauge, S. *Acta Chem. Scand. A 29* (1975) 771.
4. Coppens, P., Leiserowitz, L. and Rabinovich, D. *Acta Crystallogr. 18* (1965) 1035.
5. Hauge, S. *Acta Chem. Scand. A 29* (1975) 225.
6. Åse, K. *Acta Chem. Scand. 25* (1971) 838.
7. Aksnes, O. and Foss, O. *Acta Chem. Scand. 8* (1954) 1787.
8. McDonald, W. S. and Pettit, L. D. *J. Chem. Soc. A.* (1970) 2044.
9. *International Tables for X-Ray Crystallography*, Kynoch Press, Birmingham 1962, Vol III.
10. Pauling, L. *The Nature of the Chemical Bond.* 3rd. Ed., Cornell University Press, Ithaca, New York 1960.

Received March 17, 1975.

Acta Chemica Scandinavica A 29 (1975) 849—854

The Complex Formation between Pb^{2+} and the Maleate and Hydrogen Maleate Ions

ÅKE OLIN and PÄR SVANSTRÖM

Institute of Chemistry, University of Uppsala, P.O.B. 531, S-751 21 Uppsala, Sweden

From emf measurements of $[Pb^{2+}]$ and $[H^+]$ at 25 °C the stability constants of the complexes between lead(II) and the maleate and hydrogen maleate ions have been determined in 1 M $NaClO_4$. The species PbA, PbA_2, PbA_3, PbHA, and $Pb(HA)_2$ are formed. No mixed complexes could be detected.

There have been comparatively few studies made on the complex formation between Pb^{2+} and dicarboxylic acids, H_2A. This is probably due to the limited solubility of most lead(II) dicarboxylate salts. Measurements of log $[H^+]$ in buffers, the method generally employed, will then be less accurate. Central ion measurements do not suffer to the same extent from a low solubility and polarographic methods have been used in a number of cases. The more accurate potentiometric technique using a lead amalgam electrode does not seem to have been used to study such systems.

The prime purpose of the present investigation has been to determine which species are formed between Pb^{2+} and a dicarboxylic acid. Maleic acid (*cis*-butenedioic acid) was chosen since its dissociation constants are well separated, which will facilitate the interpretation of the data. Moreover, lead maleate is sufficiently soluble to permit potentiometric measurements with an amalgam electrode. The lead-maleate system has previously been studied by Yasuda, Yamasaki, and Ohtaki [1] using a glass electrode. These authors were interested in the trend in the value of the formation constant of the 1:1 complex for a series of divalent metal ions. The experimental conditions were hence chosen so that this complex could be expected to predominate. No effort was made to find out if other complexes were also formed in the system. Nozaki, Mise, and Higaki [2] using polarographic measurements have reported stability constants for PbA, PbA_2, and PbA_3 in 0.2 M $NaClO_4$. The formation of the last complex is not firmly established since its presence was inferred from data in solutions, where a substantial amount of the perchlorate ions had been exchanged for the ligand. No evidence for protonated species has been presented.

METHOD OF INVESTIGATION

The experiments have been carried out as potentiometric titrations in a 1 M $Na(ClO_4)$ medium containing various total (analytical) concentrations of H^+, H; lead(II), B; and maleate, A. Generally B and the ratio H/A were kept constant in an experiment. A was varied by the addition of a maleate buffer. The hydrogen ion concentration, h, and the concentration of Pb^{2+}, b, were measured at 25 °C with the cells

$$-\ \text{glass} \mid \text{equilibrium solution S} \mid \text{ref} + \quad \text{(I)}$$

$$E_g = E_g^\circ - 59.16(\text{mV}) \log(h/\text{M}) - E_j \quad (1)$$

$$-\ \text{Pb-Hg} \mid \text{equilibrium solution S} \mid \text{ref} + \quad \text{(II)}$$

$$E_{Pb} = E_{Pb}^\circ - 29.58\ (\text{mV})\ \log\ (b/\text{M}) - E_j \quad (2)$$

Solution S had the general composition $B\text{Pb(II)}$, $H\text{H}^+$, 1 MNa^+, $A\text{A}^{2-}$, $(1\text{M} + 2B + H - 2\text{A})\ \text{ClO}_4^-$. The determination of the liquid junction potential, E_j, is described in a later section. The cell parameters, E_g° and E_{Pb}°, were determined in solutions with known h and b values. E_{Pb}° could in most titrations

be determined from the first point in a titration, where $A = 0$ and sufficient acid was present to suppress the hydrolysis of Pb^{2+}. It was not found convenient to add so much acid to the starting solution that E_g^o could also be determined. Instead E_g^o was determined in a separate solution before, and usually also after, a titration. This technique was also used to determine E_{Pb}^o for reverse titrations. The transfer of the glass electrode from the solution used for calibration to S and *vice versa* did not affect the accuracy of the measurements since E_g^o proved to be constant within 0.2 mV for several weeks.

The reversibility of the equilibria was shown by titrations carried out in the reverse direction.

The large difference between the dissociation constants, $pK_1 \simeq 1.6$ and $pK_2 \simeq 5.6$, made it convenient to divide the investigation in the following parts: (i) the proton-maleate system, (ii) the lead-hydrogen maleate system, (iii) the lead-maleate system, (*iv*) the lead-hydrogen maleate-maleate system (mixed complexes). The upper limit for the ligand concentration was set in the vicinity of 0.1 M, since Sandell [3] has shown that if more than about 10 % of the perchlorate ions are exchanged variations in the activity factors become appreciable. The glass electrode measurements have been used only to calculate the HA^- and A^{2-} concentrations in the equilibrium solutions. No attempt was made to determine the ligand number, $\bar{n}$, since this quantity can only be obtained with low accuracy. In system (*ii*) this is caused by the high acidity and the small extent of the complex formation and in system (*iii*) by the limited solubility of lead maleate, which makes measurements at values of B larger than about 0.001 M impossible. The equilibrium analysis has therefore been founded on functions based on the amalgam measurements in conjunction with preliminary values of $[HA^-]$ and $[A^{2-}]$ from the glass electrode potentials.

The liquid junction potential in cells (I) and (II) can be expected to be caused mainly by the presence of H^+, HA^-, and A^{2-} ions in S. The potential E_j defined by eqns. (1) and (2) includes an activity factor, which is generally assumed to be constant. E_j is then identified with the liquid junction potential. It can easily be shown from Henderson's expression for this potential that within the concentration ranges used, E_j can be approximately written as

$$E_j = l[H^+] + m[HA^-] + n[A^{2-}] = E_{j,h} + E_{j,ha} + E_{j,a} \quad (3)$$

where l, m, and n are constants. $E_{j,h}$ was determined from cell (I) with A and $B = 0$ and found to be $-(58 \pm 2)h$ mV for $h < 0.05$ M, which is close to the value calculated from the limiting molar conductivities and to the value reported by Ahrland and Kullberg.[4] From their paper l is found to be -65 mV M^{-1} at constant $[ClO_4^-] = 1$ M. From this value $l = -61$ mV M^{-1} can be estimated from the limiting molar conductivities for constant $[Na^+] = 1$ M. $E_{j,ha}$ and $E_{j,a}$ were found from measurements with the glass electrode in a number of $HA^- - A^{2-}$ buffers, which yielded $m = -13.5$ mV M^{-1} and $n = -9.2$ mV M^{-1}. Similar measurements in $H_2A - HA^-$ buffers yielded $m = -10$ mV M^{-1} for $l = -58$ mV M^{-1}. This is not significantly different from the result obtained in the less acid buffers.

As pointed out by Biedermann and Ohtaki [5] the fact that E_j can be linearized is no proof of constant activity factors. These authors measured the changes in the emf of a probe for hydrogen ions in a 3 M perchlorate medium in which the cationic composition was varied and concluded that the observed changes were mainly due to a variation in the activity factor for H^+. It is likely that similar changes occur in our systems also, but it should be noted that the theoretically estimated values of l, m, and n are of the same magnitude as the experimental values.

EXPERIMENTAL

Chemicals and analysis. Unless otherwise stated all chemicals were of *p.a.* quality. The agreement was 0.1 % or better between different methods of analysis or between replicate determinations when only one method was used.

Sodium perchlorate was prepared by neutralizing Na_2CO_3(Merck) with $HClO_4$ (Merck) following the directions given by Biedermann.[6] The stock solution of the recrystallized product was analysed by evaporating weighed samples to constant weight. Tests for Fe^{3+}, Cl^-, and SO_4^{2-} were negative.

Lead perchlorate was prepared from PbO (Merck) and $HClO_4$ as described by Olin.[7] The lead content of the stock solution was deter-

mined as $PbSO_4$ after evaporation with H_2SO_4, and as $Pb(IO_3)_2$ after precipitation with HIO_3.[8] The analytical hydrogen ion concentration was found from potentiometric titrations with dilute standard $HClO_4$. A Gran extrapolation was used for the equivalence point determination.

Silver perchlorate. A stock solution was prepared from $AgNO_3$ (Merck) and $HClO_4$ *via* Ag_2O. The silver ion concentration was found by a potentiometric titration with standard NaCl.

Perchloric acid solutions were prepared from $HClO_4$ (Merck) by dilution. They were standardized against tris(hydroxymethyl)aminomethane and $KHCO_3$.

Sodium hydroxide solutions were prepared from a 50 % NaOH (EKA Bohus) solution by dilution and standardized against $HClO_4$.

Maleic acid (Merck "zur Synthese") was used as received. A test by thin layer chromatography according to Stahl [9] for the presence of fumaric acid was negative. Separate tests indicated that this method is capable of detecting 0.2 % fumaric acid in a sample of maleic acid. Stock solutions of the acid were standardized by potentiometric titrations with NaOH using the second equivalence point determined by a Gran extrapolation. The formula weight found was 116.1 (calc. 116.1) The various buffers containing H_2A, HA^-, and A^{2-} were prepared by mixing stock solutions of maleic acid and sodium hydroxide. Lead amalgam was prepared by dissolving lead metal (Merck silberfrei) in mercury (Kebo redist.). The amalgam was stored under 0.02 M $HClO_4$ in a N_2 atmosphere and the lead concentration was 0.1 % (weight). An amalgam prepared from mercury purified according to Whitnack and Sasseli [10] gave the same results.

Apparatus. The measurements were performed in an oil thermostat at 25 ± 0.1 °C using the salt bridge described by Forsling, Hietanen and Sillén.[11] The reference half-cell was 1 M $NaClO_4$ | 1 M ClO_4^-, 0.99 M Na^+, 0.01 M Ag^+ | AgCl, Ag. The glass electrode, Beckman type 40498, was checked against the quinhydrone electrode in the acidity range covered by the titrations.

The Ag, AgCl electrode was prepared according to Brown.[12] The emf's of cell (I) were measured to ± 0.1 mV with a Metrohm Herisau compensator E388. The emf's of the amalgam electrode were measured to ± 0.01 mV with a digital voltmeter, Data Precision 2520.

Nitrogen or argon was used for stirring and removal of oxygen from the solutions. The gas was purified by passing it through activated copper, 10 % NaOH, 10 % H_2SO_4 and finally 1 M $NaClO_4$.

The glass electrode showed a constant potential within a few minutes after an addition. The potential of the amalgam electrode took about 20 min to reach a constant value. It was then stable within ± 0.03 mV for at least 12 h. Tests showed that this electrode followed eqn. (2) within 0.2 mV in the B range studied, 0.0003 M $< B <$ 0.01 M.

RESULTS AND CALCULATIONS

The general composition of a complex will be written $H_pB_qA_r$. The stability constant of the complex is defined by

$$\beta_{p,q,r} = [H_pB_qA_r]\, h^{-p} b^{-q} a^{-r} \qquad (4)$$

Preliminary values of the constants were obtained by standard graphical procedures. These values were then refined by the least squares program Letagrop Vrid, version Etitr.[13] $U = \sum(E_{calc} - E_{exp})^2$ was minimized. Anticipating the results we shall in the following for the sake of simplicity set $q = 1$, *i.e.* only mononuclear complexes are formed.

i. The $H^+ - A^{2-}$ system. Since this system has been thoroughly studied by Dellien and Malmsten [14] only a few titrations were performed. A was 0.010 or 0.025 M and $\bar{n}$ was varied between 0.04 and 1.65. The values of the equilibrium constants obtained, *viz.* $\beta_{1,0,1} = 10^{5.63}\mathrm{M}^{-1}$ and $\beta_{2,0,1} = 10^{7.28}\mathrm{M}^{-2}$ are in good agreement with those reported by Dellien and Malmsten.

ii. The $Pb^{2+} - HA^-$ system. It will be convenient to write the complexes H_pBA_r with $p = r$ as $B(HA)_n$ and the stability constants as $\beta_n^{HA} = \beta_{n,1,n}(\beta_{1,0,1})^{-n}$. Titrations were performed at $B = 0.001$, 0.005, and 0.010 M. Provisional values of $[HA^-]$ were calculated from the expression $(A - B + b)h\beta_{1,0,1}/(1 + \beta_{1,0,1} h + \beta_{2,0,1}h^2)$, which is based on the assumption that PbHA and PbA are formed. The graphical treatment indicated that $Pb(HA)_2$ was also present. The numerical calculations, in which allowance for small amounts of PbA_n complexes were made, gave for 165 experimental points in $H_2A - HA^-$ buffers the following values of the equilibrium constants with their estimated standard deviations [15] within parentheses: $\beta_1^{HA} = 3.78(0.02)$ M^{-1}, $\beta_2^{HA} = 5.3(0.3)$ M^{-2}, and $\sigma(E_{Pb}) = 0.03$ mV. E_j (mV) was calculated from eqn. (3) with $l = -58$ mV M^{-1} and $m = -10$ mV M^{-1}. Due to their small values the constants are very sensitive to the choice of l and m. A change of m from -10 mV M^{-1} to -13.5 mV M^{-1}, which value was obtained in $HA^- - A^{2-}$ buffers, altered β_1^{HA} to 3.49(0.02) M^{-1} and

β_2^{HA} to 4.7(0.3) M^{-2}, respectively. $\sigma(E_{Pb})$ remained unchanged.

It may be shown that the change in β_1^{HA}, $\Delta\beta_1^{HA}$, is approximately given by $\Delta\beta_1^{HA} = \Delta m$ ln 10/29.58, where Δm is the change in the coefficient of $[HA^-]$.

Calculations were also performed on the assumption that only PbHA was formed. β_1^{HA} then became 4.09 M^{-1}. Beside increased standard deviations, $E_{calc} - E_{exp}$ showed systematic deviations. Although small, these deviations cannot be removed by simply changing the coefficients in the expression for E_j. Only by the addition of a second degree term in $[HA^-]$ would they dissappear. In order to eliminate a β_2^{HA} value of 5 M^{-2} from the equilibrium model the coefficient of such a $[HA^-]^2$ term would need to be about 60 mV M^{-2}. If present, this term ought to have been detected in the E_j determination. In summary we propose the following equilibrium constants

$\beta_1^{HA} = 3.8 \pm 0.3$ M^{-1} or $\beta_{1,1,1} = (1.6 \pm 0.3) \times 10^6$ M^{-2}

$\beta_2^{HA} = 5$ M^{-2} or $\beta_{2,1,2} = 9 \times 10^{11}$ M^{-4}

The value for β_2^{HA} probably represents an upper limit and no estimate of the uncertainty can be given. A comparison between experimental and calculated values of $\eta = \log(B_c/b)$ where $B_c = B - \sum_1^3 \beta_{0,1,i}\ ba^i$ is made in Fig. 1.

iii. The $Pb^{2+} - A^{2-}$ system. The measurements were carried out in buffers with $[A^{2-}]/[HA^-] = 0.75$ and 2. B was 0.001 M or less on account of the low solubility of lead maleate. a was calculated from $a = (H-h)/(2\ \beta_{2,0,1}h + \beta_{1,0,1} + \beta_{1,1,1}b)h$ and E_j as $-13.5[HA^-] - 9.2[A^{2-}]$. The graphical treatment indicated the formation of PbA, PbA_2, and PbA_3. There are significant deviations from a model with only PbA and PbA_2 when $[A^{2-}] > 0.07$ M, *i.e.* close to its upper limit in the experiments. The presence of PbA_3 might therefore be a bit uncertain. The numerical treatment of 139 experimental points yielded the following values of $\beta(\sigma(\beta))$: $\beta_{0,1,1} = 5.54(0.02) \times 10^2$ M^{-1}, $\beta_{0,1,2} = 1.06(0.01) \times 10^4$ M^{-2}, and $\beta_{0,1,3} = 2.4(0.1) \times 10^4$ M^{-3}. $\sigma(E_{Pb})$ was 0.09 mV. An inspection of $E_{calc} - E_{exp}$ suggests that a main contribution to $\sigma(E_{Pb})$ is errors in E_{Pb}^0, which was determined from only one point in each titration. A calculation in which E_{Pb}^0 was varied individually for each titration gave $\beta_{0,1,1} = 5.60(0.03) \times 10^2$ M^{-1}, $\beta_{0,1,2} = 1.10(0.01) \times 10^4$ M^{-2}, $\beta_{0,1,3} = 2.2(0.1) \times 10^4$ M^{-3}, and $\sigma(E_{Pb}) = 0.04$ mV. The average shift in E_{Pb}^0 was 0.2 mV. In summary we propose the following equilibrium constants

$\beta_{0,1,1} = (5.57 \pm 0.09) \times 10^2$ M^{-1}

$\beta_{0,1,2} = (1.08 \pm 0.03) \times 10^4$ M^{-2}

$\beta_{0,1,3} = (2.3 \pm 0.3) \times 10^4$ M^{-3}

A comparison between experimental and calculated values of $\eta_c = \log(B_c/b)$ where $B_c = B - \sum_1^3 \beta_i^{HA} b[HA^-]^i$ is made in Fig. 2.

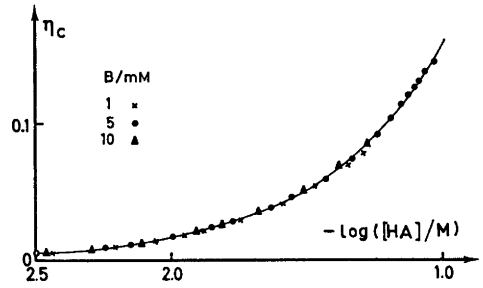

Fig. 1. η_c as a function of $\log[HA^-]$. η_c is calculated from B_c, which is B reduced by the terms for PbA, PbA_2 and PbA_3. Drawn curve is calculated from the stability constants determined in this investigation.

iv. Mixed complexes. The absence of mixed complexes is indicated by the measurements in section (iii), since $\log(B/b) = f(a)$ is independent of the ratio $[A^{2-}]/[HA^-]$ in the buffer. In order to test this point further we have tried to estimate the best experimental conditions for detecting such complexes.

Assume that the mixed complex Pb(HA)A is formed. Then

$$B \simeq b(1 + \beta_1^{HA}[HA^-] + \beta^*\beta_{0,1,1}[HA^-]a + \beta_{0,1,2}a^2) = b\phi \quad (5)$$

where $Pb(HA)_2$ and PbA_3 have been neglected and β^* is the formation constant of the mixed complex from PbA and HA^-. From (2) and (5) one obtains

$$\left(\frac{\partial E}{\partial[HA^-]}\right)_{a,B} = -\frac{RT}{2F}\left(\frac{\partial \ln\phi}{\partial[HA^-]}\right)_{a,B} - \left(\frac{\partial E_j}{\partial[HA^-]}\right)_{a,B} \quad (6)$$

and

$$\left(\frac{\partial \ln\phi}{\partial[HA^-]}\right)_{a,B} = \frac{\beta_1^{HA} + \beta^*\beta_{0,1,1}a}{\phi} \quad (7)$$

The greatest change in E due to the formation of Pb(HA)A on varying $[HA^-]$ is found when

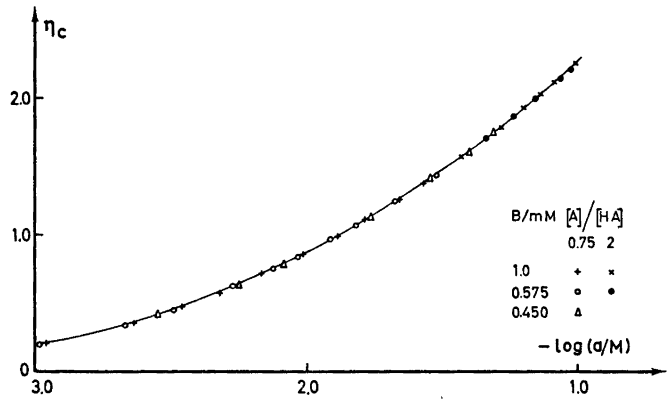

Fig. 2. η_c as a function of log a. In the calculation of η_c terms for $PbHA^+$ and $Pb(HA)_2$ have been subtracted. Drawn curve is calculated from the stability constants determined in this investigation.

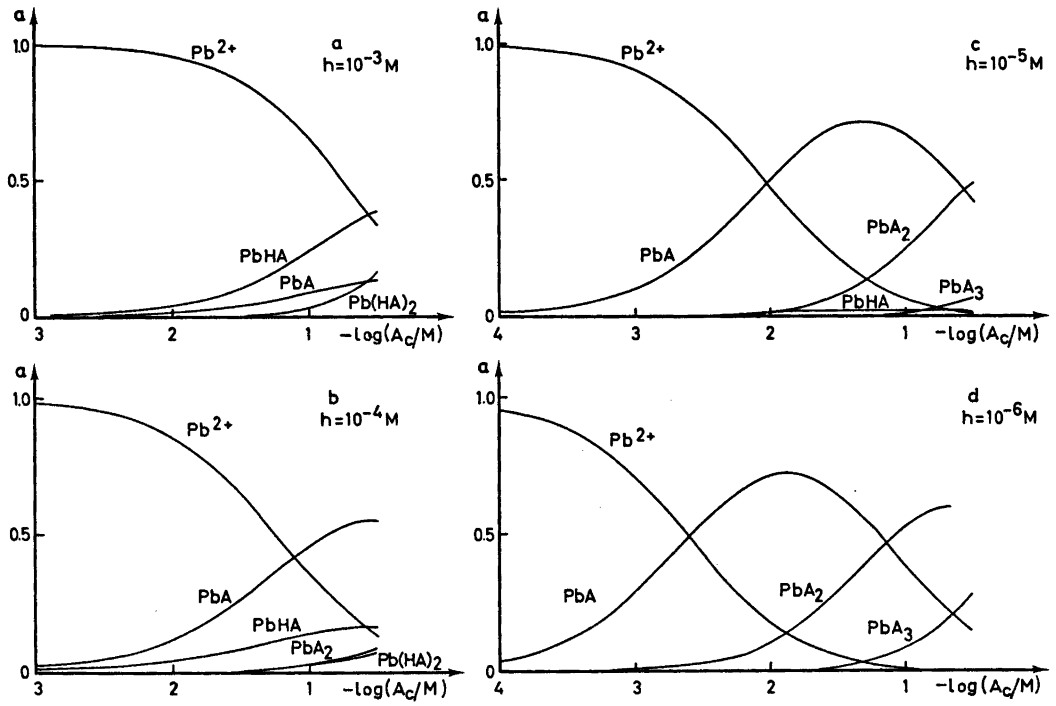

Fig. 3. The relative amounts (α) of the lead maleate complexes, at different values of h, as a function of log A_c. A_c is the total maleate concentration not bound to Pb(II).

$\beta^*\beta_{0,1,1}a/\phi$ is a maximum. This occurs at $a \simeq 0.01$ M for small values of β^*. Data from a titration with HA^- at constant $a = 0.01$ M could, however, be fully explained by the previously proposed complexes. Mixed complexes are thus not formed in detectable amounts.

The distribution of lead(II) on the proposed species as a function of log A_c is shown in Fig. 3 at four selected values of h. A_c is the

total maleate concentration not bound to Pb(II).

The experimental data can be obtained from the authors on request.

DISCUSSION

There is agreement between the present results and those of Nozaki *et al.*[2] on the formation of PbA, PbA_2, and PbA_3. The values of the step stability constants, 550, 20, and 2 M^{-1}, respectively, show that the first complex has considerable strength whereas the stabilities of the higher complexes rapidly decline. A more extensive discussion of these values will be postponed until accurate data have been collected for the complex formation of Pb^{2+} with other simple dicarboxylate ions.

As can be expected from the low basicity of the hydrogen maleate ion the stability constant for PbHA is small and the step stability constant for $Pb(HA)_2$ is only about 1 M^{-1}. This value is so small that the presence of $Pb(HA)_3$ cannot be regarded as fully established. Evidence for the formation of $Pb(HA)A^-$ could not be found. An estimate based on eqn. (6) and the expected accuracy of the amalgam electrode suggests that the equilibrium constant of the reaction $PbA + HA^- = Pb(HA)A^-$, β^*, cannot be larger than about 1 M^{-1}. A small value for β^* is reasonable. A comparison with the constant for the reaction $Pb^{2+} + HA^- = PbHA^+$ suggests that it should be less than β_1^{HA}, *i.e.* < 4 M^{-1}. From the extensive data on the lanthanoid-malonate systems[16] one finds that the value of β^* is about one half of the value of β_1^{HA}. Protonated complexes are not formed in significant amounts in the rare earth-maleate systems,[14] which demonstrates the weakness of the hydrogen maleate ion as ligand.

Acknowledgements. The authors thank Professor Bengt Nygård for the facilities put at their disposal. This work has been supported by a grant from the Swedish Natural Science Research Council.

REFERENCES

1. Yasuda, M., Yamasaki, K. and Ohtaki, H. *Bull. Chem. Soc. Jap. 33* (1960) 1067.
2. Nozaki, T., Mise, T. and Higaki, K. *Nippon Kagaku Zasshi 88* (1967) 1168.
3. Sandell, A. *On the Formation of Alkoxyacetate and (Alkylthio) acetate Complexes with Copper(II) and some other Divalent Metal Ions, Dissertation, Lund 1971.*
4. Ahrland, S. and Kullberg, L. *Acta Chem. Scand. 25* (1971) 3457.
5. Ohtaki, H. and Biedermann, G. *Bull. Chem. Soc. Jap. 44* (1971) 1515.
6. Biedermann, G. *Ark. Kemi 9* (1956) 277.
7. Olin, Å. *Acta Chem. Scand. 14* (1960) 126.
8. Gentry, G. H. R. and Sherrington, L. G. *Analyst 71* (1946) 31.
9. Stahl, E. *Thin-Layer Chromatography*, Academic, New York and London 1965.
10. Whitnack, G. C. and Sasseli, R. *Anal. Chim. Acta 47* (1969) 267.
11. Forsling, W., Hietanen, S. and Sillén L. G. *Acta Chem. Scand. 6* (1952) 901.
12. Brown, A. S. *J. Amer. Chem. Soc. 56* (1934) 646.
13. Brauner, P., Sillén, L. G. and Whiteker, R. *Ark. Kemi 31* (1969) 365.
14. Dellien, I. and Malmsten, L.-Å *Acta Chem. Scand. 27* (1973) 2877.
15. Sillén L. G. *Acta Chem. Scand 18* (1964) 1085.
16. Dellien, I. and Grenthe, I. *Acta Chem. Scand. 25* (1971) 1387.

Received March 24, 1975.

Acta Chemica Scandinavica A 29 (1975) 855—860

Microwave Spectrum, Structural Parameters and Nuclear Quadrupole Coupling of *cis*-1-Chlorobuten-3-yne

FRED KARLSSON, MATS GRANBERG and RAGNAR VESTIN

Department of Physical Chemistry, Arrhenius Laboratory, University of Stockholm, S-104 05 Stockholm, Sweden

The microwave spectra of the two natural isotopic species of *cis*-1-chlorobuten-3-yne: $CH^{35}ClCHCCH$ and $CH^{37}ClCHCCH$ together with the monodeuterated species: $CH^{35}ClCHCCD$, have been measured and assigned in the region 26 500 – 40 000 MHz. The rotational constants A, B and C for the ground state as well as the centrifugal distortion constants Δ_J, Δ_{JK}, Δ_K, δ_J and δ_K were determined.

The distance between the chlorine atom and the ethynyl hydrogen atom was determined to be 4.679 ± 0.005 Å from the change in moments of inertia due to isotopic substitution. The inertial moments corresponding to the average structure of $CH^{35}ClCHCCH$ were calculated from an estimated valence force field to confirm an electron diffraction investigation of the molecular structure. This force field was also used to predict the centrifugal distortion constants.

The nuclear quadrupole coupling constants χ_{aa} and χ_{bb} were calculated for the $CH^{35}ClCHCCH$ and $CH^{37}ClCHCCH$ species and further used to estimate the symmetry of the field gradient around the C – Cl-bond.

In contrast to *trans*-1-chlorobuten-3-yne,[1] which has a very simple microwave spectrum due to the near degeneracy to an almost prolate symmetric rotor, the spectrum of *cis*-1-chlorobuten-3-yne resisted our attempts at interpretation for nearly two years. Two other chemical isomers: 2-chlorobuten-3-yne[2] and 4-chlorobuten-3-yne[3] were successfully interpreted in the meantime although these investigations started later.

The main reason for our interest in the rotational spectrum of *cis*-1-chlorobuten-3-yne as well as its chemical isomers was to supply additional information for a detailed analysis of the molecular structure of these compounds with electron diffraction in the gas phase.[4] In fact it was the first preliminary structure data of *cis*-1-chlorobuten-3-yne from the electron diffraction experiments that made it possible to predict the rotational constants accurately enough for an assignment of the microwave transitions. On the other hand, the moments of inertia obtained from the analysis of the microwave spectrum have been valuable for confirming the structure obtained with electron diffraction.[5]

EXPERIMENTAL

Incomplete dehydrochlorination of 1,4-dichloro-2-butyne by alkali yields small amounts of *trans*- and *cis*-1-chlorobuten-3-yne.[6] These substances can be isolated from the reaction mixture and purified with gas-liquid chromatography. A mixture of the normal and deuterated species is most conveniently prepared by using D_2O and C_2H_5OD instead of normal water and ethanol in the dehydrochlorination reaction. Due to the strong alkaline milieu the hydrogen-deuterium exchange proceeds rapidly for the ethynyl group.

The microwave spectra were recorded on a Hewlett-Packard model 8460 A R-band spectrometer with a phase stabilized source oscillator. The recordings were made at room temperature or -15 °C and at a pressure ranging from 10 to 50 mTorr. The frequency region was 26 500 – 40 000 MHz. The precision of the measured transitions was estimated to be 0.05 MHz.

MICROWAVE SPECTRUM

The region 26 500 – 40 000 MHz was swept at a rate of 1 MHz/s in order to assign the spectral transitions. Early calculations of the

rotational constants from an assumed structure and calculations of the components of the dipole moments with the CNDO method suggested a spectrum mainly composed of Q-branch transitions active through the μ_b dipole moment.[4] These transitions are strong but very sensitive to the structural parameters of the molecule. The R-branch b-type transitions were hidden effectively among the numerous weak transitions of the spectrum. However, a good preliminary structure obtained from electron diffraction measurements [5] made it possible to guess successfully on the two strongest Q-branch b-type transitions in the region 26 500 – 40 000 MHz: $15_{2,13} \rightarrow 15_{3,12}$ and $16_{2,14} \rightarrow 16_{3,13}$. The identification was supported by the characteristic nuclear quadrupole hyperfine splitting into doublets for these two transitions.

Revealing the Q-branch part of the spectrum gave us two relations between the rotational constants: the differences A – C and the asymmetry parameter $\varkappa$.[7] The remaining relation, which is necessary for identifying the R-branch transitions can be obtained by assuming the inertial defect to be zero for a planar molecule. However, due to vibrational effects this is far from being true and we obtained a much closer estimate by calculating the inertial defect from a simple estimated force field.

The strongest Q-branch and R-branch b-type transitions for the two isotopic species $CH^{35}ClCHCCH$ and $CH^{37}ClCHCCH$ were measured with high resolution and, for the most abundant species $CH^{35}ClCHCCH$, the strongest lines of the weak R-branch a-type transitions were also observed and measured with high resolution: see Tables 1 and 2. The lines from

Table 1. The observed rotational transitions for *cis*-1-chlorobuten-3-yne, $CH^{35}ClCHCCH$, are given as $\nu_{obs} = \nu_{center} + \Delta\nu_i$ (in MHz) where ν_{center} is the center of the hypothetical unsplit line and $\Delta\nu_1$, $\Delta\nu_2$, $\Delta\nu_3$, and $\Delta\nu_4$ are the observed nuclear quadrupole hyperfine splitting of the rotational transition.

$CH^{35}ClCHCCH$								ν_{center}	$\Delta\nu_1$	$\Delta\nu_2$	$\Delta\nu_3$	$\Delta\nu_4$
J'	K_{-1}'	K_{+1}'	J	K_{-1}	K_{+1}	μ	$J'_{K_{-1}'K_{+1}'} \leftarrow J_{K_{-1}K_{+1}}$		$F=J+\frac{3}{2}$	$F=J+\frac{1}{2}$	$F=J-\frac{1}{2}$	$F=J-\frac{3}{2}$
7	1	7	6	1	6	a	29 544.85		–	–	–	–
7	0	7	6	0	6	a	30 246.78		0.86	−0.87	−0.87	0.86
8	0	8	7	0	7	a	34 201.40		0.70	−0.70	−0.70	0.70
9	1	9	8	1	8	a	37 722.27		–	–	–	–
9	0	9	8	0	8	a	38 133.61		0.58	−0.59	−0.59	0.58
7	0	7	6	1	6	b	27 724.80		−0.91	1.63	0.84	−1.74
6	1	6	5	0	5	b	28 757.19		2.36	−3.63	−2.22	3.81
7	1	7	6	0	6	b	32 066.76		1.92	−2.71	−1.88	2.82
8	0	8	7	1	7	b	32 381.36		−0.64	0.95	0.56	−0.95
8	1	8	7	0	7	b	35 467.33		1.44	−1.88	−1.39	1.92
9	0	9	8	1	8	b	36 867.61		−0.33	0.32	0.32	−0.33
9	1	9	8	0	8	b	38 988.17		1.22	−1.22	−1.22	1.22
10	3	7	10	2	8	b	26 864.20		1.79	−2.41	−1.82	2.47
15	3	12	15	2	13	b	27 507.74		−1.68	2.05	1.67	−2.08
9	3	6	9	2	7	b	28 098.72		2.25	−3.05	−2.25	3.09
13	2	11	13	1	12	b	29 397.22		−4.42	5.60	4.39	−5.63
16	3	13	16	2	14	b	29 768.30		−2.41	2.85	2.41	−2.87
7	3	4	7	2	5	b	30 634.90		2.55	−3.73	−2.46	3.72
17	3	14	17	2	15	b	32 831.92		−2.95	3.51	3.01	−3.57
18	4	14	18	3	15	b	33 379.66		0.20	−0.20	−0.20	0.20
19	4	15	19	3	16	b	33 640.27		−0.46	0.46	0.46	−0.46
17	4	13	17	3	14	b	33 863.14		0.94	−0.94	−0.94	0.94
20	4	16	20	3	17	b	34 739.56		−1.16	1.16	1.16	−1.16
16	4	12	16	3	13	b	34 955.74		1.56	−1.56	−1.56	1.56
15	4	11	15	3	12	b	36 485.94		1.99	−1.99	−1.99	1.99
18	3	15	18	2	16	b	36 646.13		−3.51	4.00	3.47	−3.98
21	4	17	21	3	18	b	36 731.12		−1.84	1.84	1.84	−1.84
14	4	10	14	3	11	b	38 258.91		2.33	−2.33	−2.33	2.33
15	2	13	15	1	14	b	38 457.29		−4.65	5.80	4.65	−5.81
22	4	18	22	3	19	b	39 622.47		−2.43	2.42	2.42	−2.43

Table 2. The observed rotational transitions for *cis*-1-chlorobuten-3-yne, $CH^{37}ClCHCCH$, given as in Table 1.

$CH^{37}ClCHCCH$							ν_{center}	$\Delta\nu_1$	$\Delta\nu_2$	$\Delta\nu_3$	$\Delta\nu_4$
J'	K_{-1}'	K_{+1}'	J	K_{-1}	K_{+1}	μ	$J'_{K_{-1}'K_{+1}'} \leftarrow J_{K_{-1}K_{+1}}$	$F=J+\frac{3}{2}$	$F=J+\frac{1}{2}$	$F=J-\frac{1}{2}$	$F=J-\frac{3}{2}$
7	0	7	6	1	6	b	27 136.85	−0.71	1.24	0.70	−1.35
7	1	7	6	0	6	b	31 565.52	1.45	−2.18	−1.39	2.23
8	0	8	7	1	7	b	31 724.43	−0.44	0.74	0.41	−0.78
9	0	9	8	1	8	b	36 144.98	−0.28	0.28	0.28	−0.28
9	1	9	8	0	8	b	38 339.32	0.95	−0.95	−0.95	0.95
15	3	12	15	2	13	b	27 029.35	−1.35	1.34	1.34	−1.35
16	3	13	16	2	14	b	29 103.73	−1.94	1.93	1.93	−1.94
17	3	14	17	2	15	b	31 961.42	−2.48	2.48	2.48	−2.48
18	4	14	18	3	15	b	33 226.55	—	—	—	—
19	4	15	19	3	16	b	33 314.06	—	—	—	—
17	4	13	17	3	14	b	33 836.88	0.83	−0.84	−0.84	0.83
20	4	16	20	3	17	b	34 198.86	−0.79	0.78	0.78	−0.79
16	4	12	16	3	13	b	35 007.97	1.27	−1.27	−1.27	1.27
18	3	15	18	2	16	b	35 562.47	−2.74	2.74	2.74	−2.74
21	4	17	21	3	18	b	35 941.44	−1.32	1.31	1.31	−1.32
15	4	11	15	3	12	b	36 569.18	1.68	−1.68	−1.68	1.68
22	4	18	22	3	19	b	38 560.42	−1.79	1.79	1.79	−1.79

Table 3. The observed rotational transitions for *cis*-1-chlorobuten-3-yne, $CH^{35}ClCHCCD$, given as in Table 1.

$CH^{35}ClCHCCD$							ν_{center}	$\Delta\nu_1$	$\Delta\nu_2$	$\Delta\nu_3$	$\Delta\nu_4$
J'	K_{-1}'	K_{+1}'	J	K_{-1}	K_{+1}	μ	$J_{K_{-1}'K_{+1}'} \leftarrow J_{K_{-1}K_{+1}}$	$F=J+\frac{3}{2}$	$F=J+\frac{1}{2}$	$F=J-\frac{1}{2}$	$F=J-\frac{3}{2}$
7	1	7	6	0	6	b	30 631.32	1.97	−2.80	−2.08	3.06
8	0	8	7	1	7	b	30 857.18	−0.84	0.87	0.87	−0.84
8	1	8	7	0	7	b	33 870.41	1.61	−2.05	−1.59	2.12
9	0	9	8	1	8	b	35 144.75	−0.46	0.46	0.46	−0.46
9	1	9	8	0	8	b	37 223.25	1.25	−1.25	−1.25	1.25
10	0	10	9	1	9	b	39 295.14	−0.22	0.22	0.22	−0.22
16	3	13	16	2	14	b	28 333.92	−2.48	2.91	2.49	−2.92
17	3	14	17	2	15	b	31 181.81	−3.05	3.59	3.07	−3.60
18	4	14	18	3	15	b	32 065.09	0.26	−0.27	−0.27	0.26
19	4	15	19	3	16	b	32 229.20	−0.41	0.40	0.40	−0.41
17	4	13	17	3	14	b	32 594.76	1.05	−1.05	−1.05	1.05
20	4	16	20	3	17	b	33 180.50	−1.13	1.13	1.13	−1.13
16	4	12	16	3	13	b	33 686.88	1.65	−1.65	−1.65	1.65
18	3	15	18	2	16	b	34 749.03	−3.80	3.80	3.80	−3.80
21	4	17	21	3	18	b	34 974.17	−1.85	1.84	1.84	−1.85
22	4	18	22	3	19	b	37 623.15	−2.43	2.42	2.42	−2.43
24	5	19	24	4	20	b	39 525.94	—	—	—	—
23	5	18	23	4	19	b	39 856.32	−0.67	0.67	0.67	−0.67

the species $CH^{35}ClCHCCD$ in the spectrum of the deuterated samples were identified and measured with high resolution: see Table 3.

The rotational constants and five centrifugal distortion parameters were fitted to the observed spectrum by the least squares method: see Tables 4 and 5.

CENTRIFUGAL DISTORTION

The five centrifugal distortion parameters Δ_J, Δ_{JK}, Δ_K, δ_J and δ_K were included in the least square fitting process of the rotational constants:[8,9] see Table 5. This was necessary to obtain a good fit. These constants were also calculated from the assumed structure

Table 4. Observed rotational constants in MHz for three isotopic species of *cis*-1-chlorobuten-3-yne.

	A	B	C
$CH^{35}ClCHCCH$	8942.40 ± 0.01	2572.271 ± 0.004	1994.994 ± 0.003
$CH^{37}ClCHCCH$	8857.50 ± 0.02	2519.494 ± 0.005	1958.967 ± 0.005
$CH^{35}ClCHCCD$	8569.43 ± 0.02	2450.872 ± 0.010	1903.284 ± 0.009

Table 5. Measured and calculated centrifugal distortion constants for three isotopic species of *cis*-1-chlorobuten-3-yne in kHz.

	$CH^{35}ClCHCCH$		$CH^{37}ClCHCCH$		$CH^{35}ClCHCCD$	
	obs.	calc.	obs.	calc.	obs.	calc.
Δ_J	2.20 ± 0.02	2.81	2.16 ± 0.05	2.72	2.07 ± 0.05	2.61
Δ_{JK}	−17.8 ± 0.1	−20.9	−17.8 ± 0.2	−20.4	−16.3 ± 0.5	−19.7
Δ_K	53. ± 1.	56.2	56. ± 2.	55.1	45. ± 5.	54.5
δ_J	0.700 ± 0.002	0.893	0.661 ± 0.005	0.859	0.672 ± 0.009	0.832
δ_K	3.3 ± 0.1	4.20	3.7 ± 0.2	4.09	2.3 ± 0.4	3.98

Table 6. The absolute values of the coordinates for the chlorine atom and the ethynyl hydrogen atom calculated with Kraitchman's equations and the distance between these atoms compared with the coordinates and the distance obtained from an electron diffraction investigation of the structure.[5] Conversion factor 505 376 (MHz) (au Å²).

	Microwave spectroscopy (Å)		Electron diffraction (Å)	
Atom	|a|	|b|	|a|	|b|
Cl	1.4493	0.5345	1.454	0.535
H	3.1004	1.6263	3.113	1.627
Distance				
Cl − H	4.679		4.667	

and a simple estimated valence force field with force constants estimated from similar bonds in smaller molecules.[7]

The following symbols are used for the force constants according to Gribov.[10] K_i is the force constant for the stretching of the bond i, K_{ij} is the bending of the angle between the bonds i and j, ϱ_k^{ij} is the bending of the bond k out of the plane spanned by the bonds i and j, χ_{kl}^{ij} finally is the torsion between the planes spanned by the bonds i and j, and k and l, respectively.

The values of the constants are with the bond numbers of Fig. 1: $K_1 = 3.85$, $K_2 = 9.10$, $K_3 = 4.62$, $K_4 = 15.69$, $K_5 = 6.31$, $K_6 = 6.31$, $K_7 = 5.64$, $K_{12} = 0.85$, $K_{23} = 0.84$, $K_{26} = 0.53$, $K_{37} = 0.53$, $K_{34} = 0.32$, $K_{45} = 0.23$, $\varrho_2^{17} = 0.312$, $\varrho_2^{36} = 0.286$ and $\chi_{36}^{17} = 0.512$ in md/Å mdÅ and for stretching and bending constants, respectively. The same force constants were assumed for bending in plane and out of plane for the linear acetylenic group.

The theoretically obtained centrifugal distortion constants were valuable for the identification of the spectral lines. Especially some of the *Q*-branch transitions are strongly displaced by the centrifugal distortion.

MOLECULAR STRUCTURE

Nothing has been found that indicates a deviation from planarity in the molecular structure. The inertial defect for $CH^{35}ClCHCCH$ is 0.34 ± 0.02 au Å² and we obtained 0.39 au Å² with a theoretical calculation assuming planarity and using the previously mentioned force field.

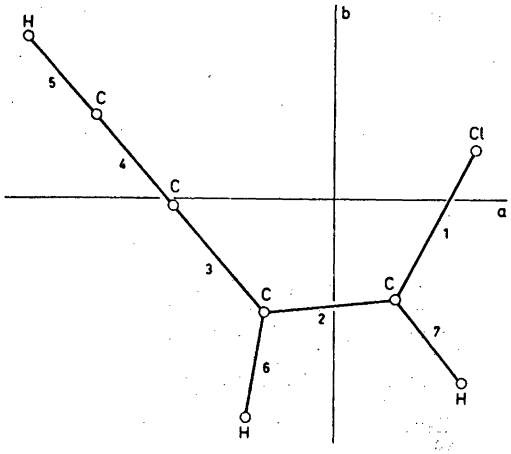

Fig. 1. Assumed structure of *cis*-1-chlorobuten-3-yne with principal axes of inertia.

The Cartesian coordinates for the chlorine atom and the ethynyl hydrogen atom were calculated in the principal axis system of the $CH^{35}ClCHCCH$ molecule from the change in the moments of inertia I_b and I_c on isotopic substitution:[11,12] see Table 6. These coordinates were in good agreement with those calculated from the electron diffraction study of the structure: see Table 6. The chlorine and the ethynyl hydrogen atom are well away from the principal axes and the moments of inertia are accurately determined, so that the main source of uncertainty is in the vibrational effects. Change in inertial defect and the effect of change in effective bond length with isotopic substitution will be most critical for the position of the hydrogen atom.[13] Therefore we expect the error of the hydrogen-chlorine distance to be about ± 0.005 Å.

Throughout the entire investigation of the chlorobutenyne structures we have used the principal moments of inertia obtained from microwave spectroscopy to confirm the electron diffraction measurements.[4] The moments of inertia obtained with microwave spectroscopy derives from the effective rotational structure r_0.[14,15] For $CH^{35}ClCHCCH$: $I_a^0 = 56.514$, $I_b^0 = 196.471$ and $I_c^0 = 253.322$ au Å^2. Using the force field above, these moments were transformed to the corresponding average structure parameters: $I_a^z = 56.604$, $I_b^z = 196.855$ and $I_c^z = 253.405$ au Å^2. This was in good agreement with the values from the electron diffraction structure and this removed some remaining uncertainties there.[5]

QUADRUPOLE COUPLING

The rotational transitions are split into four observable peaks by the interaction of the rotation with the quadrupole moment of the chlorine nucleus.[7] However, in many cases the components overlap partially or completely so that only a doublet or a single line can be distinguished.

A least squares fitting of the quadrupole coupling constants χ_{aa} and χ_{bb} to the observed splittings into quartets or doublets was made with the LETAGROP method.[8,16] In order to avoid systematic errors, only splitting values greater than 0.70 MHz were accepted. The values obtained are for ^{35}Cl in $CH^{35}ClCHCCH$: $\chi_{aa} = 16.3 \pm 0.4$ and $\chi_{bb} = -46.8 \pm 0.2$ MHz and for ^{37}Cl in $CH^{37}ClCHCCH$: $\chi_{aa} = 11.8 \pm 0.8$ and $\chi_{bb} = -36.2 \pm 0.4$ MHz.

These constants can be transformed to the principal axis system of the quadrupole coupling tensor if we assume that one of these tensor axes coincides with the C–Cl bond and if we know the direction of the C–Cl bond in the principal axis system of the inertial moments: see Fig. 1. The coordinates of the chlorine atom could be calculated from the difference in the moments of inertia for the two isotopic species with ^{35}Cl and ^{37}Cl as described above but that was not possible for the carbon atom in the C–Cl bond due to the low natural abundance of the ^{13}C and the high costs of preparing ^{13}C enriched samples. However, since the coordinates of the chlorine and the ethynyl hydrogen atom are so close to the coordinates calculated from the electron diffraction structure it is reasonable to expect that the position of the carbon atom in the C–Cl bond obtained with electron diffraction is significant enough for the transformation of the coupling constants: see Table 6.

With the quadrupole tensor axis z parallel to the C–Cl bond and y perpendicular to the molecular plane we obtained the following principal values for ^{35}Cl in $CH^{35}ClCHCCH$: $\chi_{xx} = 39.3 \pm 0.7$ and $\chi_{yy} = 30.5 \pm 0.7$ MHz. The uncertainty limits are estimated from the measured deviation of the constants χ_{aa} and χ_{bb} and the assumption that the error in the

coordinates of the carbon atom in the C–Cl bond is less than ±0.005 Å.

According to Goldstein et al.[17] the difference $\chi_{xx}-\chi_{yy}$ is related to the numbers of electrons lost from chlorine as a result of double bonding δ, with $\delta=(\chi_{xx}-\chi_{yy})/164.6$. The value δ may be regarded as approximately defining the double bond character of the C–Cl bond. We obtained $\delta=0.05\pm0.01$. This value is comparable with $\delta=0.04$ obtained for vinyl chloride.[18] So the presence of the acetylene group does not seem to have any major effect on the double bond character of the C–Cl bond.

The principal components of the chlorine quadrupole coupling tensor for the $CH^{35}ClCHCCH$ molecule above are of course very uncertain due to the necessary assumptions but we were able to test them to some extent by calculating the χ_{aa} and the χ_{bb}-values for the $CH^{35}ClCHCCD$ molecule. The change in direction of the C–Cl bond in the principal axis system of inertial moments due to the deuterium substitution was estimated from the electron diffraction structure and the transformation yielded: $\chi_{aa}=19.2$ and $\chi_{bb}=-49.7$ MHz. The calculated hyperfine splitting of the rotational transitions for $CH^{35}ClCHCCD$ using the above constants agreed with those observed within the error of measurement.

Acknowledgements. We thank all those who have contributed to this paper and especially Dr. Stig Ljunggren and Mr. Hasse Karlsson for pleasant cooperation and valuable discussions.

REFERENCES

1. Karlsson, F. and Vestin, R. *Acta Chem. Scand. 27* (1973) 3033.
2. Karlsson, F., Granberg, M. and Vestin, R. *Acta Chem. Scand. A 28* (1974) 206.
3. Karlsson, F., Granberg, M. and Vestin, R. *Acta Chem. Scand. A 29* (1975) 111.
4. Karlsson, F. *Chem. Commun Univ. Stockholm* (1974) No. 1.
5. Almenningen, A., Gundersen, G., Borg, A., Granberg, M. and Karlsson, F. *Acta Chem. Scand. A 29* (1975) 395.
6. Vestin, R., Borg, A. and Lindholm, T. *Acta Chem. Scand. 22* (1968) 687.
7. Gordy, W. and Cook, R. L. *Microwave Molecular Spectra*, Interscience, New York 1970.
8. Watson, J. K. G. *J. Chem. Phys. 46* (1967) 1935.
9. Kirchhoff, W. H. *J. Mol. Spectrosc. 41* (1972) 333.
10. Gribov, L. A. *Vvedenie v teoriyu i raschët kolebatelnÿkh spektrov mnogoatomnÿkh molekul*, Istadelstvo Leningradskogo Universita, 1965.
11. Kraitchman, J. *Amer. J. Phys. 21* (1953) 17.
12. Costain, C. C. *J. Chem. Phys. 29* (1958) 864.
13. Laurie, V. W. and Herschbach, D. R. *J. Chem. Phys. 37* (1962) 1687.
14. Herschbach, D. R. and Laurie, V. W. *J. Chem. Phys. 37* (1962) 1668.
15. Morino, Y., Kuchitsu, K. and Oka, T. *J. Chem. Phys. 36* (1962) 1108.
16. Sillén, L. G. *Acta Chem. Scand. 16* (1962) 159.
17. Goldstein, J. H. and Bragg, J. K. *Phys. Rev. 75* (1949) 1453.
18. Gerry, M. C. L. *Can. J. Chem. 49* (1971) 255.

Received April 3, 1975.

Acta Chemica Scandinavica A 29 (1975) 861—865

The Crystal and Molecular Structure of the Copper(II) Complex of 2-Nitroso-1-naphthol: $[Cu(C_{10}H_6NO_2)_2].H_2O$

J. KORVENRANTA and H. SAARINEN

Department of Inorganic Chemistry, University of Helsinki, SF-00100 Helsinki 10, Finland

The crystal and molecular structure of the monohydrate of the copper(II) complex of 2-nitroso-1-naphthol (⇌1,2-naphthoquinone-2-oxime) has been determined by three-dimensional X-ray methods. The monoclinic cell dimensions are: $a = 6.395(4)$ Å, $b = 19.311(23)$ Å, $c = 14.274(24)$ Å, $\beta = 98.2(1)°$. The space group is $P2_1/c$ and $Z = 4$. The structure was solved by conventional Patterson and Fourier methods and refined by least-squares procedures. The final R-value, based on 1473 reflections, is 0.073.

The complex has a distorted square pyramidal geometry with two oxime nitrogen atoms (Cu – N, 1.988(8) and 1.978(9) Å) and two naphtholic oxygen atoms (Cu – O, 1.976(8) and 1.971(7) Å) in an approximately square planar configuration, and the oxygen atom of the water molecule in apical position (Cu – O, 2.195(7) Å).

The dissimilarity in the behaviours of 1-nitroso-2-naphthol (⇌1,2-naphthoquinone-1-oxime) and 2-nitroso-1-naphthol (⇌1,2-naphthoquinone-2-oxime) toward metal ions has been reported by several authors. In solution, 1-nitroso-2-naphthol forms transition metal complexes of considerably higher stability than does 2-nitroso-1-naphthol.[1] This tendency is also valid for several derivatives of the isomers, and it cannot be explained by the different acid strengths of the ligands.[2] The visible, near ultraviolet, and infrared absorption spectra of metal complexes derived from the 1,2-isomers are also markedly different.[3]

It can be expected that the different properties of 1-nitroso-2-naphthol and 2-nitroso-1-naphthol complexes in solution are also reflected in the structures of the compounds in the solid state. In a previous paper, we reported the crystal structure of the diacetone adduct of the copper(II) complex of 1-nitroso-2-naphthol.[4] Our studies on solid copper(II) complexes of 1,2-nitrosonaphthols are now continuing with a 2-nitroso-1-naphthol type of ligand, and in this paper the crystal structure of bis(1,2-naphthoquinone-2-oximato)copper(II) monohydrate is decribed.

EXPERIMENTAL

Crystal preparation and analysis. The copper(II) complex of 2-nitroso-1-naphthol was prepared by a standard method.[5] The precipitated reddish brown monohydrate was washed with water and ethanol and dried in air. The microcrystalline product was dissolved in warm acetone. On gradual cooling, crystals suitable for X-ray analysis formed within a few days. (Found: C 56.57; H 3.43; N 6.58; Cu 15.0. Calc. for $C_{20}H_{14}O_5N_2Cu$: C 56.40; H 3.31; N 6.58; Cu 14.92).

The copper(II) complexes of 1-nitroso-2-naphthol and 2-nitroso-1-naphthol are both precipitated from aqueous solution as their monohydrates. However, on recrystallization from acetone under similar conditions, the complexes behave differently. The crystalline compound obtained from the acetone solution of the 2-nitroso-1-naphthol complex is still monohydrate, whereas the copper(II) complex of 1-nitroso-2-naphthol yields a 1:2 acetone adduct.[4]

Crystal data. Weissenberg photographs showed that crystals of the present complex belong to the monoclinic system. The space group, from systematic absences, is $P2_1/c$.

Unit cell dimensions were obtained by least-squares procedures from a powder photograph taken by use of a Hägg-Guinier camera, Cu$K\alpha$ radiation and calcium fluoride ($a = 5.4630$ Å) as internal standard. Based on four formula units in the cell, the calculated density of

1.621 g cm^{-3} is in agreement with that of 1.61 g cm^{-3} obtained by the flotation method. Crystal data for $[Cu(C_{10}H_6NO_2)_2].H_2O$ are:

a = 6.395(4) Å	V = 1744.9 Å^3
b = 19.311(23) Å	FW = 425.89
c = 14.274(24) Å	Z = 4
β = 98.2(1)°	Space group $P2_1/c$

Intensity data. The crystal selected for data collection had approximate dimensions 0.3 × 0.2 × 0.2 mm. Single-crystal intensity data from levels $0kl - 5kl$ were collected by use of a Stoe-Güttinger diffractometer and Ni-filtered Cu radiation (Cu$K\alpha$, $\lambda = 1.5418$ Å). Of the 2634 recorded reflections, 1473 with $I > 3\sigma(I)$ were used for the structure analysis. The data were corrected for Lorentz and polarization effects. No correction for absorption was applied [μ(Cu$K\alpha$) = 21.3 cm^{-1}].

Structure determination. The structure was solved by the heavy atom method. The approximate position of the copper atom was determined from Harker vectors in a three-dimensional Patterson synthesis. Subsequent Fourier syntheses gave the positions of other non-hydrogen atoms of the complex. The atomic scattering factors for Cu^{2+}, O, N, and C were taken from International Tables for X-Ray Crystallography.[6]

The refinement of the structure was carried out by block-diagonal least-squares procedures. The weighting scheme was $w = 1/(a + |F_o| + b|F_o|^2)$ with $a = 35.0$ and $b = 0.007$. Eight cycles of refinement with isotropic thermal parameters yielded a R-value of 0.087 ($R = \sum||F_o| - |F_c||/\sum|F_o|$). The refinement was then continued with anisotropic thermal parameters. The final R-value was 0.073 for 1473 reflections.

The final atomic coordinates and thermal parameters together with their estimated standard deviations are given in Table 1. A list of the observed and calculated structure factors is obtainable on request from the authors. All calculations were carried out on an Elliott 803 B computer using programmes of Daly, Stephens, and Wheatley.[7]

Table 1. Fractional atomic coordinates (× 10^4) and thermal parameters [a] (× 10^3). Estimated standard deviations are given in parentheses.

Atom	X/a	Y/b	Z/c	U_{11}	U_{22}	U_{33}	$2U_{12}$	$2U_{23}$	$2U_{13}$
C(1)	664(16)	−217(7)	3127(7)	34(7)	41(6)	23(5)	5(9)	1(8)	18(8)
C(2)	−1324(16)	−299(5)	2492(7)	16(6)	46(6)	37(5)	−3(8)	−4(9)	7(8)
C(3)	−3054(17)	−709(6)	2724(8)	39(7)	43(6)	46(6)	3(10)	5(10)	35(11)
C(4)	−2815(19)	−1023(6)	3575(8)	53(8)	42(6)	39(6)	−13(11)	6(10)	34(11)
C(5)	−739(20)	−1286(6)	5136(8)	67(9)	34(6)	51(7)	5(11)	24(10)	58(12)
C(6)	1128(19)	−1214(6)	5771(8)	60(8)	44(7)	40(6)	41(11)	25(10)	14(11)
C(7)	2857(18)	−833(6)	5554(7)	54(8)	42(6)	29(5)	21(11)	17(10)	19(10)
C(8)	2694(19)	−518(6)	4683(7)	63(8)	41(6)	27(5)	7(12)	−12(10)	−21(10)
C(9)	801(16)	−561(5)	4019(6)	37(6)	27(5)	27(5)	19(9)	−1(8)	15(8)
C(10)	−905(17)	−965(5)	4256(7)	44(7)	35(6)	38(6)	5(10)	4(9)	20(10)
C(11)	1967(16)	1399(5)	175(7)	35(6)	36(6)	29(5)	11(9)	−9(8)	20(9)
C(12)	3921(18)	1477(5)	791(7)	48(7)	28(5)	42(6)	−24(9)	−4(9)	39(10)
C(13)	5586(19)	1900(6)	558(8)	48(8)	34(6)	58(7)	−23(11)	−3(11)	21(12)
C(14)	5318(20)	2250(6)	−286(9)	56(9)	45(7)	62(8)	−24(12)	−12(12)	46(13)
C(15)	3124(23)	2562(6)	−1781(9)	87(10)	30(6)	54(8)	−11(13)	15(11)	37(14)
C(16)	1241(27)	2510(6)	−2399(9)	130(13)	37(8)	47(9)	38(15)	34(13)	89(15)
C(17)	−387(22)	2099(6)	−2186(9)	82(10)	43(7)	46(7)	21(13)	36(11)	31(13)
C(18)	−161(19)	1727(5)	−1329(7)	63(8)	36(6)	34(6)	43(11)	12(9)	28(11)
C(19)	1692(18)	1767(5)	−702(7)	52(7)	28(5)	28(5)	9(10)	7(8)	27(9)
C(20)	3375(19)	2184(5)	−931(8)	55(8)	28(5)	45(6)	10(10)	3(10)	25(11)
N(1)	−1257(12)	34(5)	1668(5)	23(5)	51(5)	23(4)	5(8)	16(7)	1(7)
N(11)	3979(14)	1108(4)	1598(6)	51(6)	33(5)	29(5)	−9(8)	−4(8)	5(8)
O(1)	−2795(11)	1(4)	1006(5)	39(5)	60(5)	28(4)	−17(8)	12(7)	−4(7)
O(2)	2175(12)	150(4)	2899(5)	54(5)	48(4)	28(4)	−10(8)	15(7)	10(7)
O(3)	3019(11)	−341(3)	920(4)	42(5)	32(4)	27(3)	2(6)	1(6)	4(6)
O(11)	5574(11)	1148(4)	2227(5)	40(5)	58(5)	38(4)	−10(7)	−19(8)	−18(6)
O(12)	494(11)	1020(4)	423(5)	37(4)	39(4)	33(4)	−6(7)	22(6)	2(6)
Cu	1481(2)	503(1)	1593(1)	44(1)	48(1)	34(1)	−5(2)	8(2)	14(1)

[a] The anisotropic thermal parameters are of the form $\exp[-2\pi^2(h^2a^{*2}U_{11} + k^2b^{*2}U_{22} + l^2c^{*2}U_{33} + 2hka^*b^*U_{12} + 2klb^*c^*U_{23} + 2hla^*c^*U_{13}]$.

Table 2. Equations of mean planes and, in square brackets, deviations (Å) of atoms from these planes. X', Y', and Z' are orthogonal axes related to X, Y, and Z by $X'=X+Z\cos\beta$, $Y'=Y$, and $Z=Z\sin\beta$.

Plane I: N(1), N(11), O(2), O(12)
$-0.4605X'+0.7680Y'+0.4451Z'=1.6513$
[N(1) −0.027, N(11) −0.026, O(2) 0.024, O(12) 0.022,
Cu −0.191, O(1) −0.102, O(11) 0.017]
Plane II: C(1)−C(10)
$-0.4295X'+0.8126Y'+0.3940Z'=1.4836$
[C(1) 0.007, C(2) 0.015, C(3) −0.004, C(4) −0.014,
C(5) 0.008, C(6) 0.017, C(7) −0.001, C(8) −0.022,
C(9) 0.004, C(10) −0.010, Cu −0.076, O(1) −0.068, O(2) 0.020, N(1) −0.012]
Plane III: C(11)−C(20)
$-0.4401X'+0.7778Y'+0.4488Z'=1.6772$
[C(11) −0.004, C(12) 0.009, C(13) 0.008, C(14) −0.002,
C(15) 0.003, C(16) 0.008, C(17) 0.004, C(18) 0.008,
C(19) −0.007, C(20) −0.020, Cu −0.186, O(11) 0.088, O(12) 0.023, N(11) 0.023]

Table 3. Mean bond lengths (Å) of the coordination planes of *o*-nitrosophenol and 1,2-nitrosonaphthol complexes.

Compound	C−O	C−N	N−O	M−O	M−N	Ref.
Ferroverdin [a]	1.30	1.42	1.25	1.95	1.84	9
Bis(4-methyl-1-quinone-2-oximato)Cu, py	1.27	1.35	1.25	1.97	2.00	8
Tris(4-chloro-1-quinone-2-oximato)Ni,K^+.$(CH_3)_2CO$	1.25	1.33	1.27	2.06	2.01	10
Bis(1,2-naphthoquinone-1-oximato)Cu.2$(CH_3)_2CO$	1.30	1.35	1.26	1.95	1.99	4
Bis(1,2-naphthoquinone-2-oximato)Cu.H_2O	1.28	1.35	1.26	1.97	1.98	This work
Diaqua(1,2-naphthoquinone-2-oximato-4-sulfonate)Cu.$3H_2O$	1.26	1.35	1.25	1.95	1.96	11
α-5-(2′-Chloroethoxy)-*o*-quinone-2-oxime	1.25	1.31	1.37			12

[a] $K[Fe(qo)_3]$, where qoH = 4-vinylphenyl ester of 4-hydroxy-3-nitrosobenzoic acid.

RESULTS AND DISCUSSION

The bond lengths and bond angles of the complex with their standard deviations can be seen in Fig. 1. It shows a nearly square planar configuration around Cu^{2+} with two oxime nitrogen atoms and two naphtholic oxygen atoms at the mean distances of 1.98 and 1.97 Å, respectively. The chelate rings are thus five-membered, which is in agreement with the structures recently found for several other similar compounds (*cf.* Table 3). The naphthalene planes are in *trans*-position intersecting at an angle of about 4°, so that the structure of the complex is noticeably planar (Table 2).

The 4+1 coordination around Cu^{2+} is completed by the water oxygen atom at a distance of 2.195(7) Å, which indicates a relatively strong interaction between the atoms. A quite similar 4+1 coordination was observed in the 1:1 pyridine adduct of bis(4-methyl-1-quinone-2-oximato)copper(II) complex.[8]

A projection of the structure of the present complex along the *b*-axis is illustrated in Fig. 2, where the shortest intermolecular distances are also shown. It can be seen that the shortest distances (2.74 and 2.81 Å) are formed between

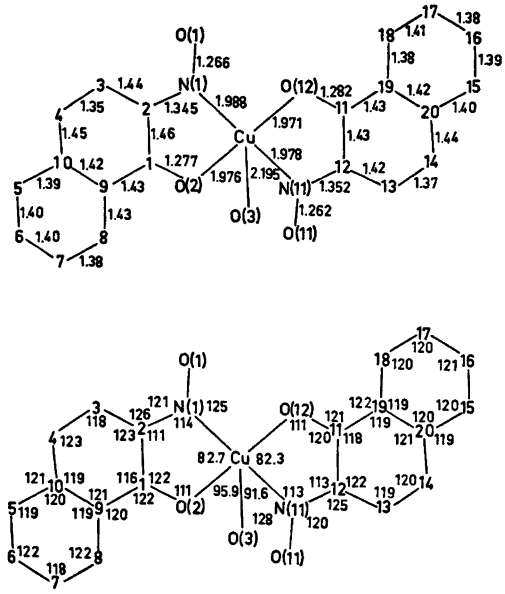

Fig. 1. Schematic representation of the complex showing bond lengths (Å) and angles (°). For the sake of clarity, the angles N(1) – Cu – O(3) and O(12) – Cu – O(3) of 97.9 and 96.6° are not included. The average e.s.d.'s in bond lengths are: Cu – O, 0.007; Cu – N, 0.008; N – O, 0.011; C – O, 0.012; C – N, 0.013; C – C, 0.016. The e.s.d.'s in angles are in the range 0.3 – 1.3 °.

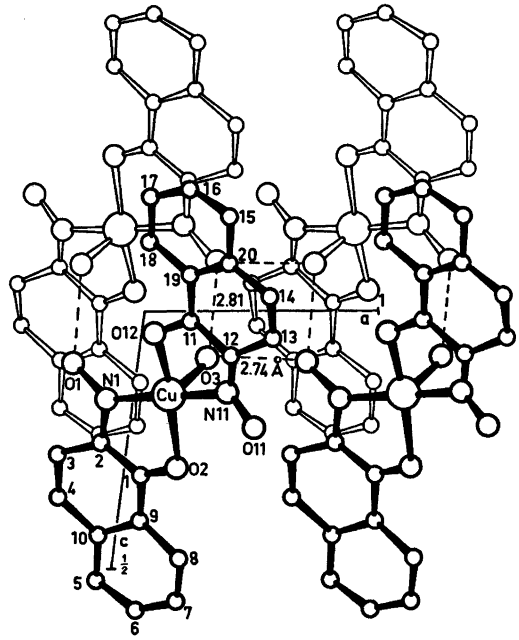

Fig. 2. Partial packing diagram of $[Cu(C_{10}H_6NO_2)_2].H_2O$ as viewed down the *b*-axis. The shortest intermolecular distances are marked with broken lines.

the water oxygen and the oxime oxygen atoms of the two neighbouring complex molecules, which suggests that the structure is stabilized by the presence of hydrogen bonds between these atoms.

The structure of the complex does not differ essentially from the structure of the 1-nitroso-2-naphthol complex studied earlier.[4] In principle the bonding of Cu^{2+} to the chelating groups of the ligands is similar, and the respective bond lengths and angles are nearly equal. Thus the above-mentioned differences in the properties of the complexes in solutions cannot be explained by fundamental differences in the molecular structures in the solid state. Unfortunately, since the 1-nitroso-2-naphthol complex obtained previously was the diacetone adduct and the present complex is the monohydrate, direct comparison of the molecular packings of the compounds is not possible.

The crystal structures of six different complexes derived from *o*-nitrosophenols or 1,2-nitrosonaphthols are now available. The bond lengths in the coordination planes of these chelates are collected in Table 3. For comparison, the corresponding values of an uncoordinated ligand of the same type are also included.

It can be seen that the respective C – O, C – N, and N – O distances in all six complexes are practically equal. The only marked deviation occurs in the C – N bond of ferroverdin, which is lengthened to some extent. However, the difference is not very significant, especially when one takes into account that the results reported for this particular compound are rather tentative. This being the case, the structures of the complexes can be described as essentially similar, and nitrosophenol and nitrosonaphthol ligands can be said to behave analogously.

All the compounds in Table 3 have been named according to the quinone oxime structure. However, as pointed out previously, the bond lengths in the complexes display contributions from the nitrosophenol as well as the quinone oxime structure.[4] The choice made

here has mainly been influenced by the well-established patterns of the short and long C–C bonds in the nitrosophenol complexes.[8,10] These are characteristic for the *o*-quinone molecule. The resemblance of the chelating groupings in the nitrosophenol and nitrosonaphthol complexes and additionally the significantly short C(3)–C(4) bond (1.34(1) to 1.37(2) Å) found in the nitrosonaphthol compounds studied support the equal naming of all the complexes.

Acknowledgements. The financial support of the Jenny and Antti Wihuri Foundation of the Finnish Academy of Sciences and the Finnish National Research Council for Sciences is gratefully acknowledged.

REFERENCES

1. Mäkitie, O. and Saarinen, H. *Suom. Kemistilehti B 44* (1971) 209.
2. Saarinen, H. *Ann. Acad. Sci. Fenn. A II 170* (1973).
3. Gurrieri, S. and Siracusa, G. *Inorg. Chim. Acta 5* (1971) 650.
4. Saarinen, H. and Korvenranta, J. *Acta Chem. Scand. A 29* (1975) 409.
5. Charalambous, J., Frazer, M. J. and Taylor, F. B. *J. Chem. Soc. A* (1969) 2787.
6. *International Tables for X-Ray Crystallography*, Kynoch Press, Birmingham 1962, Vol. III.
7. Daly, J. J., Stephens, F. S. and Wheatley, P. J. *MRSA* Final Report (1963) No. 52.
8. McPartlin, M. *Inorg. Nucl. Chem. Lett. 9* (1973) 1207.
9. Candeloro, S., Grdenic, D., Taylor, N., Thomson, B., Viswamitra, M. and Hodgin, D. C. *Nature (London) 224* (1969) 589.
10. Carreck, P. W., Charalambous, J., Kensett, M. J., McPartlin, M. and Sims, R. *Inorg. Nucl. Chem. Lett. 10* (1974) 749.
11. Korvenranta, J. and Saarinen, H. *Finn. Chem. Lett. In press.*
12. Van Oijen, J. W. L. and Romers, C. *Acta Crystallogr. 17* (1966) 169.

Received April 14, 1975.

Acta Chemica Scandinavica A 29 (1975) 866—872

The Crystal Structure of Scandium Selenate Pentahydrate

JUSSI VALKONEN,[a] LAURI NIINISTÖ,[a] BIRGITTA ERIKSSON,[b] LARS OLOF LARSSON[b] and ULF SKOGLUND[b]

[a]Department of Chemistry, Helsinki University of Technology, SF-02150 Otaniemi, Finland and [b]Departments of Inorganic and Structural Chemistry, Arrhenius Laboratory, University of Stockholm, Fack, S-104 05 Stockholm, Sweden

The crystal structure of $Sc_2(SeO_4)_3.5H_2O$ has been determined by single crystal X-ray diffraction techniques. The compound crystallizes in the space group $P\bar{1}$, with unit cell dimensions $a = 11.225(4)$, $b = 11.804(3)$, $c = 5.766(2)$ Å, $\alpha = 91.35(4)$, $\beta = 100.10(2)$ and $\gamma = 89.03(7)°$. There are two formula units in each cell. Partial solution of the structure was accomplished by direct methods; subsequent electron density calculations revealed the positions of all non-hydrogen atoms. The structure was refined by least-squares calculations to an R value of 0.084 for 1730 significant reflections. The scandium atoms are octahedrally coordinated by oxygen atoms belonging to selenate groups and to water molecules. The mean Sc—O distances in scandium coordination polyhedra vary from 2.08 to 2.10 Å and mean Se—O bond lengths in selenate groups from 1.61 to 1.64 Å.

Our work on scandium sulfates and selenate pentahydrates was initiated as part of an investigation into the structural chemistry of rare earth compounds. Crystal and IR data for these compounds have been given and discussed in a previous report.[1] We are now reporting the results of a three-dimensional X-ray characterization of scandium selenate pentahydrate.

EXPERIMENTAL

Measurement of crystal and intensity data. The crystal data of $Sc_2(SeO_4)_3.5H_2O$ are summarized in Table 1.

Single crystal intensities were collected on a Philips PW 1100 diffractometer, with graphite monochromated Cu$K\alpha$ radiation. A scintillation counter with pulse height discrimination was used to detect the radiation. The dimensions of the crystal were $0.14 \times 0.10 \times 0.08$ mm³. The $\theta - 2\theta$ scan technique was employed, with a scan range of 1.5° and a scan speed of 0.02°/s.

Table 1. Crystal data of scandium selenate pentahydrate.

Formula	$Sc_2(SeO_4)_3.5H_2O$
Formula weight	608.88
Lattice constants	$a = 11.225(4)$ Å
	$b = 11.804(3)$ Å
	$c = 5.766(2)$ Å
	$\alpha = 91.35(4)°$
	$\beta = 100.10(2)°$
	$\gamma = 89.03(7)°$
Cell volume	$V = 751.8$ Å³
Measured density	$D_m = 2.67$ g cm^{-3}
Calculated density	$D_x = 2.69$ g cm^{-3}
Molecules per unit cell	$Z = 2$
Space group	$P\bar{1}$

Three test reflections were measured hourly to check for possible decomposition or misalignment of the crystal in the X-ray beam, but none occurred during the data collection. The background intensities were calculated as averages of the intensities at each end of the scan interval. All reflections with $\theta < 60°$ were recorded and, of these, 1730 reflections were considered to be significant based on the criterion $\sigma(I_{net})/I_{net} < 0.25$. The net intensities were corrected for Lorentz and polarization factors as well as for absorption ($\mu = 170$ cm^{-1}).

Structure determination and refinement. All calculations were carried out using IBM 1800 and 360/75 computers in Stockholm and a UNIVAC 1108 computer in Helsinki; the crystallographic programs have been described elsewhere.[2,3]

Unit cell dimensions indicated the presence of two formula units in each cell, and thus it was not possible to solve the Patterson function owing to the large number of heavy atoms. E-Statistics did not give any clear indication of the presence or absence of a symmetry center. We attempted to solve the structure by direct methods using the symbolic addition

Table 2. Fractional atomic coordinates ($\times 10^4$) and isotropic thermal parameters ($\times 10^2$). Standard deviations are given in parenthesis.

Atom	x	y	z	U
Sc(1)	4732(8)	7634(4)	4822(5)	0.50(6)
Sc(2)	4594(9)	2611(5)	4789(5)	0.64(6)
Sc(3)	8600(7)	34(3)	956(3)	0.71(8)
Sc(4)	626(6)	5129(3)	8677(3)	0.61(7)
Se(1)	6596(4)	2588(2)	2054(2)	0.57(4)
Se(2)	6000(4)	7639(2)	1888(2)	0.71(4)
Se(3)	3279(4)	7605(2)	7738(2)	0.55(4)
Se(4)	2651(4)	2607(2)	7561(2)	0.85(4)
Se(5)	1547(4)	74(2)	3928(2)	1.13(4)
Se(6)	7723(4)	5128(2)	5724(2)	0.77(4)
O(1)	6797(20)	2766(9)	3528(10)	0.01(26)
O(2)	4116(29)	2930(14)	1319(14)	2.15(35)
O(3)	6880(23)	1244(11)	1694(12)	0.94(29)
O(4)	8884(22)	3328(10)	1738(11)	0.32(27)
O(5)	6158(22)	8883(10)	1259(11)	0.15(27)
O(6)	8122(25)	6833(12)	1691(13)	1.48(32)
O(7)	3347(28)	7110(14)	1441(14)	2.63(36)
O(8)	6407(28)	7970(13)	3333(14)	2.22(34)
O(9)	969(30)	8339(14)	7928(16)	3.21(40)
O(10)	5783(24)	8139(12)	8374(13)	1.80(32)
O(11)	3138(29)	6412(14)	8406(15)	2.39(38)
O(12)	3232(26)	7497(13)	6331(13)	1.92(33)
O(13)	2527(32)	2628(16)	6112(16)	3.78(42)
O(14)	817(24)	1714(12)	7977(13)	1.58(31)
O(15)	5283(24)	2251(12)	8193(13)	1.29(32)
O(16)	2058(25)	3929(12)	7803(13)	1.42(32)
O(17)	2694(23)	1319(11)	3868(12)	0.16(27)
O(18)	910(22)	9628(10)	2496(11)	0.70(27)
O(19)	3783(28)	9280(14)	4592(14)	2.85(38)
O(20)	9141(20)	104(10)	4482(11)	0.25(27)
O(21)	9841(25)	5212(13)	4848(13)	1.74(32)
O(22)	8497(30)	5567(15)	7127(15)	3.47(40)
O(23)	6692(31)	3849(15)	5841(15)	2.32(39)
O(24)	5779(25)	5912(13)	5004(13)	2.20(33)
W(1)[a]	2733(26)	5009(13)	376(14)	2.14(35)
W(2)	8652(26)	6346(13)	9473(14)	1.70(32)
W(3)	8586(28)	3836(15)	9359(15)	3.09(39)
W(4)	904(23)	1290(11)	417(12)	1.31(31)
W(5)	442(25)	8779(12)	225(13)	1.62(32)
W(6)	6787(22)	237(10)	9106(11)	0.54(27)
W(7)	7052(24)	1418(11)	5792(11)	0.90(30)
W(8)	2249(28)	3775(14)	3735(14)	2.53(39)
W(9)	1473(21)	7072(10)	3832(11)	0.42(28)
W(10)	7821(27)	8423(13)	5818(14)	2.19(36)

[a] W indicates water oxygen atoms.

procedure [4] and, after several attempts, succeeded in finding a partial solution, giving the positions of four selenium and two scandium atoms. Refinement in the centric space group did not lead to further improvements and therefore the acentric case $P1$ was tested. Calculations revealed that the six atoms found were almost symmetrically located in the cell with respect to each other. An electron density map phased on these six atoms yielded the positions of the remaining non-hydrogen atoms.

Coordinates of the atoms were refined by the

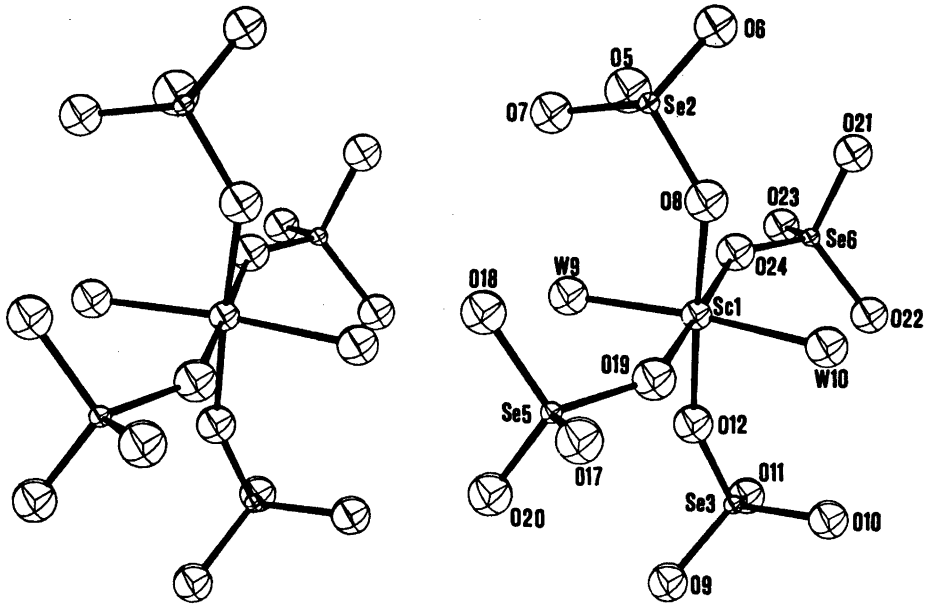

Fig. 1. A stereoscopic view of the coordination about the Sc(1) atom.

method of block-diagonal least-squares calculations with isotropic temperature factors. The scattering factors for the neutral atoms were used.[5] Corrections were made for anomalous dispersion but not for extinction. In the refinement the weighting scheme of Hughes [6] with $|F_{o,min}| = 5.0$ and $h = 4.0$ was used.

The final R value was 0.084 ($R = \sum||F_o| - |F_c||/\sum|F_o|$). It was not possible to locate any of the hydrogen atoms from a difference Fourier map calculated after the final refinement. The goal of this investigation, however, was to study the coordination of the non-hydrogen atoms and for this purpose the intensity data were quite satisfactory in spite of the rather high speed employed in data collection.

The positional and thermal parameters with their estimated standard deviations are given in Table 2. A listing of the observed and calculated structure factors is available from the authors upon request.

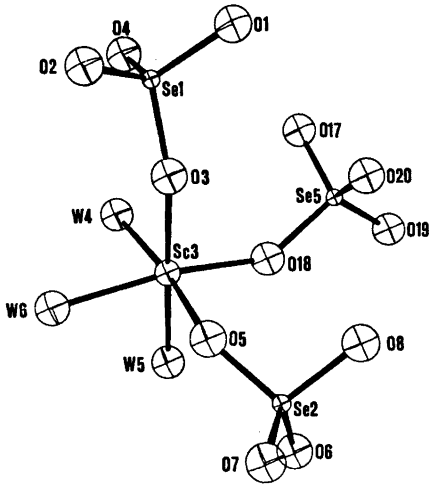

Fig. 2. A perspective drawing showing the coordination about the Sc(3) atom.

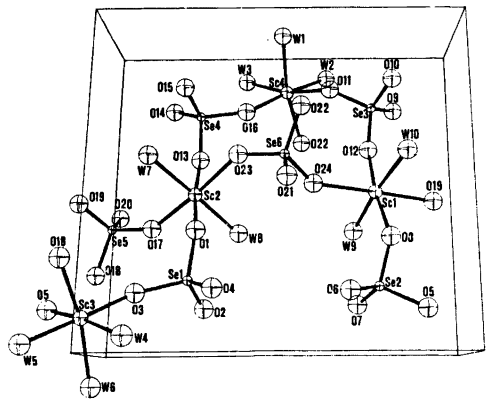

Fig. 3. A perspective drawing of the structure of $Sc_2(SeO_4)_3.5H_2O$ showing the unit cell packing. The a axis is vertical, the b axis is horizontal and the c axis points into the paper.

Table 3. Bond lengths (Å) and selected angles (°) involving Sc.[a] Estimated standard deviations are given in parenthesis.

Sc(1) – O(8)	2.100(18)	Sc(2) – O(1)	2.065(14)
Sc(1) – O(19)	2.031(18)	Sc(2) – O(13)	2.062(21)
Sc(1) – O(12)	2.035(17)	Sc(2) – O(17)	2.045(14)
Sc(1) – O(24)	2.130(16)	Sc(2) – O(23)	2.114(18)
Sc(1) – W(9)	2.106(13)	Sc(2) – W(7)	2.176(14)
Sc(1) – W(10)	2.131(16)	Sc(2) – W(8)	2.141(17)
Sc(3) – O(3)	2.026(15)	Sc(4) – O(11)	2.127(17)
Sc(3) – O(18)	2.045(12)	Sc(4) – O(16)	2.009(16)
Sc(3) – O(5)	2.002(14)	Sc(4) – O(22)	2.012(17)
Sc(3) – W(4)	2.119(15)	Sc(4) – W(1)	2.078(15)
Sc(3) – W(5)	2.101(16)	Sc(4) – W(2)	2.153(16)
Sc(3) – W(6)	2.166(13)	Sc(4) – W(3)	2.120(18)

O(19) – Sc(1) – W(10)	80.7(6)	W(4) – Sc(3) – W(6)	82.8(5)
O(24) – Sc(1) – W(10)	99.3(6)	O(3) – Sc(3) – O(18)	96.7(5)
W(9) – Sc(1) – W(10)	172.2(6)	O(18) – Sc(3) – W(6)	165.4(6)
O(19) – Sc(1) – O(24)	177.9(7)	O(3) – Sc(3) – W(5)	178.7(5)
O(23) – Sc(2) – W(7)	84.5(6)	O(11) – Sc(4) – W(1)	82.8(6)
O(23) – Sc(2) – W(8)	96.1(7)	O(22) – Sc(4) – W(3)	101.5(7)
O(1) – Sc(2) – O(13)	173.8(7)	O(11) – Sc(4) – W(3)	166.7(6)
W(7) – Sc(2) – W(8)	177.5(7)	O(16) – Sc(4) – W(2)	172.5(6)

[a] Only the extreme angle values are listed for each coordination octahedron.

DESCRIPTION AND DISCUSSION OF STRUCTURE

The scandium atoms are octahedrally coordinated by oxygen atoms belonging to selenate groups and to water molecules. Scandium atoms Sc(1) and Sc(2) are coordinated by two water molecules while the remaining scandium atoms are coordinated by three; thus all water molecules are in the inner-coordination sphere of scandium atoms. Figs. 1 and 2 show the coordination about scandium atoms Sc(1) and Sc(3), respectively. The atomic numbering scheme adopted is indicated in these pictures and in Fig. 3 which shows the unit cell viewed down the *c*-axis.

The Sc – O distances vary between 2.00 Å and 2.17 Å, but there are not significant differences between the scandium atoms. The mean Sc – O values for Sc(1) – Sc(4) are 2.09, 2.10, 2.08, and 2.08 Å, respectively; the average of all Sc – O distances is 2.09 Å. This average is in good agreement with the bond lengths reported in recent literature for six-coordinated scandium,[7–9] but is slightly less than the value obtained by combining the suggested ionic radii (1.40 Å for O^{2-} and 0.745 Å for Sc^{3+}).[10,11]

It should be noted that the mean Sc – O(water) distance (2.13 Å) is somewhat longer than the corresponding Sc – O(selenate) distance (2.05 Å); a similar pattern has been observed in several rare earth sulfates.[12–14] This difference leads to slightly more distorted coordination octahedra for Sc(3) and Sc(4), which are coordinated by three water oxygens, as compared to Sc(1) and Sc(2); *cf.* Table 3 for distances and angles.

In the selenate groups the average value of all Se – O bond lengths is 1.63 Å; *cf.* Table 4 for distances and angles involving selenium atoms. The mean values of Se – O distances for selenate groups Se(1) – Se(6) come within the estimated standard deviations from this value. However, the individual bond lengths in some selenate groups vary significantly; *e.g.* in the Se(6) group they range from 1.57 to 1.70 Å. The mean Se – O distances found in this study are comparable to the corresponding bond lengths observed in other selenates. Table 6 lists the selenates whose crystal structures are known, along with their average Se – O bond lengths. The overall average is 1.64 Å and the mean values for different selenate groups do not differ much from this value. A closer look at

Table 4. Bond lengths (Å) and angles (°) in SeO_4 groups. Estimated standard deviations are given in parenthesis.

Se(1) – O(1)	1.654(12)	Se(2) – O(5)	1.626(13)
Se(1) – O(2)	1.578(16)	Se(2) – O(6)	1.614(15)
Se(1) – O(3)	1.663(14)	Se(2) – O(7)	1.636(16)
Se(1) – O(4)	1.652(13)	Se(2) – O(8)	1.650(16)
Se(3) – O(9)	1.652(18)	Se(4) – O(13)	1.614(18)
Se(3) – O(10)	1.613(14)	Se(4) – O(14)	1.599(15)
Se(3) – O(11)	1.591(17)	Se(4) – O(15)	1.619(14)
Se(3) – O(12)	1.581(15)	Se(4) – O(16)	1.643(15)
Se(5) – O(17)	1.603(13)	Se(6) – O(21)	1.696(16)
Se(5) – O(18)	1.676(12)	Se(6) – O(22)	1.649(17)
Se(5) – O(19)	1.670(16)	Se(6) – O(23)	1.622(18)
Se(5) – O(20)	1.618(13)	Se(6) – O(24)	1.571(14)

O(1) – Se(1) – O(2)	112.5(7)	O(13) – Se(4) – O(14)	112.3(8)
O(1) – Se(1) – O(3)	112.8(6)	O(13) – Se(4) – O(15)	108.2(9)
O(1) – Se(1) – O(4)	102.9(6)	O(13) – Se(4) – O(16)	101.2(9)
O(2) – Se(1) – O(3)	104.5(7)	O(14) – Se(4) – O(15)	108.2(7)
O(2) – Se(1) – O(4)	115.8(7)	O(14) – Se(4) – O(16)	113.4(8)
O(3) – Se(1) – O(4)	108.6(7)	O(15) – Se(4) – O(16)	113.3(7)
O(5) – Se(2) – O(6)	112.6(7)	O(17) – Se(5) – O(18)	105.9(6)
O(5) – Se(2) – O(7)	108.3(7)	O(17) – Se(5) – O(19)	104.3(7)
O(5) – Se(2) – O(8)	101.1(7)	O(17) – Se(5) – O(20)	111.3(7)
O(6) – Se(2) – O(7)	115.2(8)	O(18) – Se(5) – O(19)	105.2(7)
O(6) – Se(2) – O(8)	107.9(8)	O(18) – Se(5) – O(20)	109.0(6)
O(7) – Se(2) – O(8)	110.8(8)	O(19) – Se(5) – O(20)	120.2(7)
O(9) – Se(3) – O(10)	114.6(8)	O(21) – Se(6) – O(22)	116.2(8)
O(9) – Se(3) – O(11)	107.9(9)	O(21) – Se(6) – O(23)	112.8(8)
O(9) – Se(3) – O(12)	108.0(8)	O(21) – Se(6) – O(24)	101.9(7)
O(10) – Se(3) – O(11)	103.7(7)	O(22) – Se(6) – O(23)	105.2(8)
O(10) – Se(3) – O(12)	109.6(8)	O(22) – Se(6) – O(24)	110.3(8)
O(11) – Se(3) – O(12)	113.1(8)	O(23) – Se(6) – O(24)	110.7(8)

Table 5. Additional distances less than 3.0 Å. Polyhedral edges are not included. Estimated standard deviations are given in parenthesis.

O(1) – W(7)	2.959(18)	O(13) – W(8)	2.952(25)
O(1) – W(8)	2.952(18)		
		O(14) – W(4)	2.768(20)
O(2) – W(1)	2.735(22)	O(14) – W(7)	2.994(18)
O(2) – W(4)	2.727(20)		
		O(15) – W(3)	2.807(21)
O(3) – W(4)	2.933(20)	O(15) – W(6)	2.675(19)
O(3) – O(5)	2.846(19)		
		O(16) – W(3)	2.879(24)
O(4) – W(8)	2.743(19)		
O(4) – W(3)	2.703(12)	O(17) – W(8)	2.915(21)
O(5) – W(5)	2.914(20)	O(18) – W(5)	2.721(19)
O(5) – W(6)	2.946(18)		
		O(19) – W(9)	2.696(20)
O(6) – W(9)	2.819(18)	O(19) – W(10)	2.697(22)
O(6) – W(2)	2.635(22)		

Table 5. Continued.

		O(20)–W(7)	2.609(20)
O(7)–W(1)	2.759(22)	O(20)–W(10)	2.645(20)
O(7)–W(5)	2.794(21)		
		O(21)–W(8)	2.675(24)
O(8)–W(10)	2.822(22)	O(21)–W(9)	2.685(20)
O(9)–W(5)	2.709(24)	O(22)–W(2)	2.790(24)
O(9)–W(10)	2.720(22)		
		O(23)–W(7)	2.885(22)
O(10)–W(2)	2.844(20)		
O(10)–W(6)	2.642(18)	O(24)–W(9)	2.952(19)
O(11)–W(1)	2.781(23)	W(1)–W(2)	2.887(21)
		W(1)–W(3)	2.807(21)
O(12)–W(9)	2.859(19)	W(2)–W(3)	2.968(23)
O(12)–W(10)	2.985(23)	W(4)–W(5)	2.978(20)
		W(4)–W(6)	2.835(17)
		W(5)–W(6)	2.853(18)

Table 6. Comparison of averaged Se–O distances (Å) found in selenate structures. Vibrationally corrected values are given in parenthesis.

Compound	Mean Se–O distance	E.s.d[a]	Reference
H_2SeO_4	1.61	n.a.	Bailey & Wells [15]
$[Al_2(OH)_2(H_2O)_8](SeO_4)_2.2H_2O$	1.62	n.a.	Johansson [16]
$MnSeO_4$	1.65	0.02	Fuess & Will [17]
$CoSeO_4$	1.64	0.05	Fuess & Will [17]
$NiSeO_4$	1.67	0.02	Fuess & Will [17]
$HgSeO_4$	1.64	0.07	Dorm [18]
$Cu(NH_3)_4SeO_4$	1.635 (1.643)[b]	0.008	Morosin [19]
Na_2SeO_4	1.654	0.021	Kálmán & Cruickshank [20]
K_2SeO_4	(1.648)	0.016	Kálmán, Stephens & Cruickshank [21]
$NiSeO_4.6H_2O$	1.65	0.03	Fuess [22]
$Ce_2(SeO_4)_3.5H_2O$	1.65	0.03	Aslanov, Farag &
	1.65	0.04	Porai-Koshits [23]
	1.65	0.03	
$Na_2Cu(SeO_4)_2.2H_2O$	1.649	0.014	Pentavin & Philippot [24]
$K_2Co(SeO_4)_2.2H_2O$	1.634	0.007	Pentavin
	1.633	0.006	Philippot & Lindqvist [25,26]
$Sc_2(SeO_4)_3.5H_2O$	1.637	0.016	This work
	1.632	0.016	
	1.609	0.018	
	1.619	0.018	
	1.642	0.016	
	1.635	0.018	

[a] The e.s.d column lists the largest deviation in individual bond length (Å) in each crystallographically independent polyhedron. [b] From Ref. 20.

the structures, however, reveals in some cases rather large variations in the individual bond lengths within the same selenate group. For instance, in $CoSeO_4$ the shortest distance is 1.56 ± 0.02 Å while the longest one is 1.69 ± 0.03 Å;[17] a somewhat similar situation is found in H_2SeO_4.[15]

The scandium atoms are cross-linked in the structure by sharing their selenate ions with other scandium atoms, as can be seen in Fig. 3. Linkages approximately parallel to the *b*-axis are formed, joining the Sc(1) and Sc(2) atoms *via* Se(5) and Se(6) selenate groups into continuous chains. To these chains, Sc(3) atoms are linked by Se(1) and Se(2) groups and, on the opposite side, Sc(4) by Se(3) and Se(4) groups; thus a three-dimensional structure is formed. Not all selenate oxygen atoms, however, are bonded to scandium atoms, there are ten oxygen atoms which are exclusively bounded to selenium atoms (*cf.* Table 3).

The structure is further strengthened by hydrogen bonding, which may involve the water molecules and selenate oxygens. The listing of additional distances less than 3.0 Å in Table 5 also includes the possible hydrogen bonds.

Acknowledgements. The authors sincerely thank Professor Peder Kierkegaard and Professor Arne Magnéli for their encouraging and stimulating interest in this work. The work has been financially supported by the Swedish Natural Science Research Council.

REFERENCES

1. Niinistö, L., Valkonen, J. and Larsson, L. O. *Finn. Chem. Lett.* (1975). 45.
2. *The X-Ray System – Version of June 1972*, Technical Report TR-192. Computer Science Center, University of Maryland 1972.
3. Niinistö, L. and Larsson, L. O. *Acta Crystallogr. B 29* (1973) 623.
4. Karle, J. and Karle, I. L. *Acta Crystallogr. 21* (1966) 849.
5. *International Tables of Crystallography* III. Kynoch Press, Birmingham 1962, Table 3.3.1.A.
6. Hughes, E. W. *J. Amer. Chem. Soc. 63* (1941) 1737.
7. Anderson, T. J., Neuman, M. A. and Melson, G. A. *Inorg. Chem. 12* (1973) 927.
8. Hansson, E. *Acta Chem. Scand. 27* (1973) 2841.
9. Anderson, T. J., Neuman, M. A. and Melson, G. A. *Inorg. Chem. 13* (1974) 158.
10. Shannon, R. D. and Prewitt, C. I. *Acta Crystallogr. B 25* (1969) 925.
11. Shannon, R. D. and Prewitt, C. T. *Acta Crystallogr. B 26* (1970) 1046.
12. Aslanov, L. A., Rybakov, V. B., Ionov, V. M., Porai-Koshits, M. A. and Ivanov, V. I. *Dokl. Akad. Nauk SSSR 204* (1972) 1122.
13. Dereigne, A., Manoli, J.-M., Pannetier, G. Herpin, P. *Bull. Soc. Fr. Mineral. Cristallogr. 95* (1972) 269.
14. Larsson, L. O., Linderbrandt, S., Niinistö, L. and Skoglund, U. *Suom. Kemistilehti B 46* (1973) 314.
15. Bailey, M. and Wells, A. F. *J. Chem. Soc. 217* (1951) 968.
16. Johansson, G. *Acta Chem. Scand. 16* (1962) 403.
17. Fuess, H. and Will, G. *Z. Anorg. Allg. Chem. 358* (1968) 125.
18. Dorm, E. *Acta Chem. Scand. 23* (1969) 1607.
19. Morosin, B. *Acta Crystallogr. B 25* (1969) 19.
20. Kálmán, A. and Cruickshank, D. W. J. *Acta Crystallogr. B 26* (1970) 436.
21. Kálmán, A., Stephens, J. S. and Cruickshank, D. W. J. *Acta Crystallogr. B 26* (1970) 1145.
22. Fuess, H. *Z. Anorg. Allg. Chem. 379* (1970) 204.
23. Aslanov, L. A., Farag, I. S. A. and Porai-Koshits, M. A. *Zh. Fiz. Khim. 47* (1973) 1057.
24. Peytavin, S. and Philippot, E. *Cryst. Struct. Commun. 2* (1973) 221.
25. Peytavin, S., Philippot, E. and Lindqvist, O. *Cryst. Struct. Commun. 2* (1973) 163.
26. Peytavin, S., Philippot, E. and Lindqvist, O. *Rev. Chim. Miner. 11* (1974) 37.

Received May 7, 1975.

Acta Chemica Scandinavica A 29 (1975) 873—880

Short Communications

On the Barrier to Internal Rotation in H_2BSSBH_2. An *ab initio* Study

O. GROPEN

Institute of Mathematical and Physical Sciences, Department of Chemistry, University of Tromsø, Tromsø, Norway

Electron diffraction studies have shown that the B—S arrangements are planar in a number of compounds.[1] These results give strong evidences for considerable π-bond orders in the B—S bonds. This conclusion is supported by *ab initio* calculations on H_2BSH.[1] Recently, bis(dimethylboryl)disulfane was studied by electron diffraction.[2] As in related compounds the B—S arrangement is planar. The obtained torsional angle (120° from the *syn* form) is somewhat larger than the corresponding angle found in the compounds XSSX, and the S—S bond distance was found to be almost identical to the similar bond in dimethyl-1,2,4-trithia-3,5-diborolane (2.076 Å).[3]

These rather long S—S bonds (2.05 Å in H_2S_2) and large deviation from the *anti* form give no indication of delocalization in the π-system, but do not exclude a conjugation in the planar state either. In a previous semi-empirical calculation rather high bond orders were found in trithiadiborolanes.[4] The best way to clarify the properties of the S—S bonds in these molecules seems to be by *ab initio* calculations. The bis(boryl)disulfane molecule was chosen as a reasonable test system (see fig. 1). The potential curve for rotation around the S—S bond has been calculated.

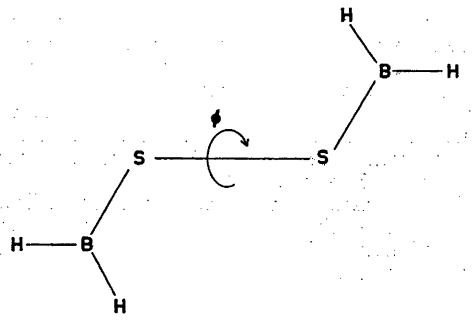

Fig. 1. Geometry of $BH_2S_2BH_2$ and definition of the angle ϕ.

Table 1. Calculated total energies in a.u. and energy differences in kcal/mol.

Dihedral angle (°)	Total energy	Energy differences
180	−845.768687	0
150	−845.768830	−0.08966
120	−845.769442	−0.47339
90	−845.769428	−0.46461
0	−845.739385	+18.37235

The calculations were performed using the program MOLECULE[5] which solves the Roothaan-Hall equations for a Gaussian type of basis. A (10,6,1/7,3/4) basis [6] set contracted to double zeta was applied, and no geometry optimization was performed during the rotation around the disulfide bond. The geometry parameters were put equal to the observed values for bis(dimethylboryl)disulfane, except for the B—H bond length and the angles around boron where the values 1.20 Å and 120° were chosen, respectively.

The total energy was calculated for both *syn* and *anti* form together with 150, 120, and 90° for the dihedral angle (*syn* chosen equal to 0°). The following potential $E = a_0 + a_1 \cos\phi + a_2 \cos 2\phi + a_3 \cos 3\phi + a_4 \cos 4\phi$ was fitted to the obtained results.

The calculated total energies together with energy differences are presented in Table 1 and the potential curve drawn in Fig. 2. The energy minimum is predicted to be at a dihedral angle of 102°, and the barriers to internal rotation around the S—S bond are estimated to 19.1 and 0.7 kcal/mol for *syn* and *anti*, respectively. The *syn* barrier is probably much too high as geometry optimization is important in this form. The *anti* barrier, however, should be fairly reliable. Taking the differences of the compounds into consideration the agreement with the observed value for the dihedral angle in bis(dimethylboryl)disulfane (120°) is rather good, and the shallow minimum and low barrier are consistent with results obtained in the electron diffraction investigation. The energy minimum and the *anti* barrier were also determined excluding the calculated value for the *syn* form and using only four terms. The obtained *anti* barrier and dihedral angle were

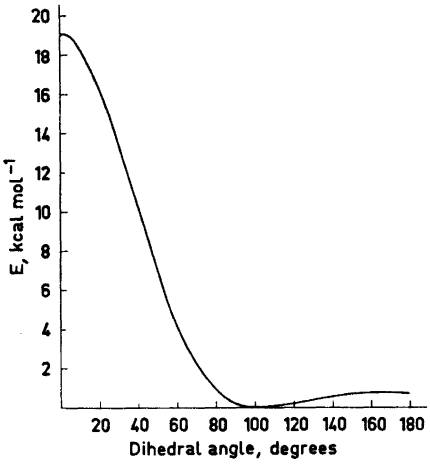

Fig. 2. The total energy as a function of the dihedral angle ϕ.

then found to be 0.6 kcal/mol and 103°, respectively. Compared with hydrogen disulfide the dihedral angle is increased from 90 to 102°, and the *anti* barrier reduced from 4.2 (calculated with same type of basis)[7] to 0.69 kcal/mol.

These reductions of the *anti* barrier and the very shallow minimum compared to hydrogen disulfide supply strong arguments for considerable delocalization in the planar form.

This conjugation is, however, not strong enough to give a planar equilibrium conformation, and with dihedral angle close to 90° the delocalization will not influence the S – S bond length to any extent.

1. Gropen, O., Nilssen, E. W. and Seip, H. M. *J. Mol. Struct. 23* (1974) 289.
2. Johansen, R., Seip, H. M. and Siebert, W. *Acta Chem. Scand. A 29* (1975) 644.
3. Seip, H. M., Seip, R. and Siebert, W. *Acta Chem. Scand. 27* (1973) 15.
4. Gropen, O. and Vassbotn, P. *Acta Chem. Scand. 27* (1973) 3079.
5. Almlöf, J. USIP Report 72-09, University of Stockholm, Stockholm 1972.
6. Roos, B. and Siegbahn, P. *Theor. Chim. Acta 17* (1970) 199.
7. Pappas, J. *Private communications.*

Received June 18, 1975.

Crystal Structure of Methyl 2,3-*O*-Isopropylidene-β-D-allo-hept-6-ynofuranoside

P. GROTH

Department of Chemistry, University of Oslo, Oslo 3, Norway

Methods for the synthesis and separation of epimeric uronic acids have been studied by Kjølberg *et al.*[1] One of the methods used for chain extention has been the ethynylation reaction described by Jones *et al.*[2] Reaction between methyl 2,3-*O*-isopropylidene-β-D-ribo-1,5-dialdopentofuranoside and ethynyl-magnesium bromide gave two isomers (C-5 epimers) in approximately equal amounts.[3] Since configurational assignments based on spectroscopic data were somewhat uncertain, an X-ray crystallographic investigation of the isomer which was supposed to be the methyl-2,3-*O*-isopropylidene-β-D-allo-hept-6-ynofuranoside has been carried out.

The crystals of $C_{11}O_5H_{16}$ are orthorhombic with cell dimensions $a = 5.855(2)$ Å, $b = 11.555(3)$ Å, $c = 18.174(3)$ Å and four molecules in the unit cell ($D_x = 1.23$ g/cm³). The space group is $P2_12_12_1$. The structure was solved by direct methods[4] and refined by full-matrix least squares technique *[5] to an R-value of 3.4 % ($R_w = 4.1$ %) for 971 reflections observed on an automatic four circle diffractometer at room temperature. Anisotropic temperature factors were introduced for oxygen and carbon atoms. The hydroxyl and methyl hydrogen atoms were found in the difference Fourier map. Positional parameters for the remaining hydrogen atoms were calculated. Weights for least squares refinement were obtained from the standard deviations in intensities, $\sigma(I)$, taken as

$$\sigma(I) = [C_T + (0.02C_N)^2]^{\frac{1}{2}}$$

where C_T is the total number of counts and C_N the net count.

Final fractional coordinates and thermal parameters with estimated standard deviations are given in Table 1. The principal axes of thermal vibration ellipsoids for carbon atoms were calculated from the temperature parameters of Table 1. Maximum r.m.s. amplitudes range from 0.220 to 0.331 Å (corresponding B-values 3.80 and 8.63 Å²).

Bond distances and angles are listed in Table 2. Fig. 1 is a schematic drawing of the molecule (viewed along [100]) which shows that it has the D-allo configuration.

* All programs used (except those for phase determination) are included in this reference.

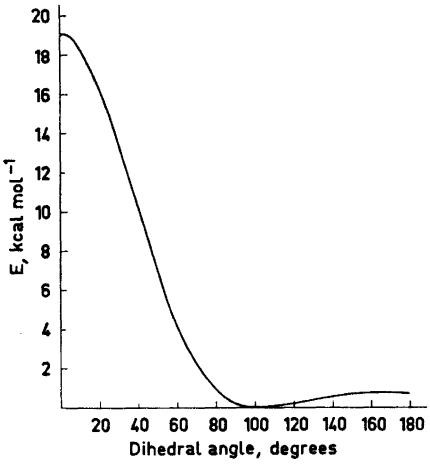

Fig. 2. The total energy as a function of the dihedral angle ϕ.

then found to be 0.6 kcal/mol and 103°, respectively. Compared with hydrogen disulfide the dihedral angle is increased from 90 to 102°, and the *anti* barrier reduced from 4.2 (calculated with same type of basis)[7] to 0.69 kcal/mol.

These reductions of the *anti* barrier and the very shallow minimum compared to hydrogen disulfide supply strong arguments for considerable delocalization in the planar form.

This conjugation is, however, not strong enough to give a planar equilibrium conformation, and with dihedral angle close to 90° the delocalization will not influence the S – S bond length to any extent.

1. Gropen, O., Nilssen, E. W. and Seip, H. M. *J. Mol. Struct. 23* (1974) 289.
2. Johansen, R., Seip, H. M. and Siebert, W. *Acta Chem. Scand. A 29* (1975) 644.
3. Seip, H. M., Seip, R. and Siebert, W. *Acta Chem. Scand. 27* (1973) 15.
4. Gropen, O. and Vassbotn, P. *Acta Chem. Scand. 27* (1973) 3079.
5. Almlöf, J. USIP Report 72-09, University of Stockholm, Stockholm 1972.
6. Roos, B. and Siegbahn, P. *Theor. Chim. Acta 17* (1970) 199.
7. Pappas, J. *Private communications.*

Received June 18, 1975.

Crystal Structure of Methyl 2,3-*O*-Isopropylidene-β-D-allo-hept-6-ynofuranoside

P. GROTH

Department of Chemistry, University of Oslo, Oslo 3, Norway

Methods for the synthesis and separation of epimeric uronic acids have been studied by Kjølberg *et al.*[1] One of the methods used for chain extention has been the ethynylation reaction described by Jones *et al.*[2] Reaction between methyl 2,3-*O*-isopropylidene-β-D-ribo-1,5-dialdopentofuranoside and ethynyl-magnesium bromide gave two isomers (C-5 epimers) in approximately equal amounts.[3] Since configurational assignments based on spectroscopic data were somewhat uncertain, an X-ray crystallographic investigation of the isomer which was supposed to be the methyl-2,3-*O*-isopropylidene-β-D-allo-hept-6-ynofuranoside has been carried out.

The crystals of $C_{11}O_5H_{16}$ are orthorhombic with cell dimensions $a = 5.855(2)$ Å, $b = 11.555(3)$ Å, $c = 18.174(3)$ Å and four molecules in the unit cell ($D_x = 1.23$ g/cm³). The space group is $P2_12_12_1$. The structure was solved by direct methods[4] and refined by full-matrix least squares technique *[5] to an R-value of 3.4 % ($R_w = 4.1$ %) for 971 reflections observed on an automatic four circle diffractometer at room temperature. Anisotropic temperature factors were introduced for oxygen and carbon atoms. The hydroxyl and methyl hydrogen atoms were found in the difference Fourier map. Positional parameters for the remaining hydrogen atoms were calculated. Weights for least squares refinement were obtained from the standard deviations in intensities, $\sigma(I)$, taken as

$$\sigma(I) = [C_T + (0.02C_N)^2]^{\frac{1}{2}}$$

where C_T is the total number of counts and C_N the net count.

Final fractional coordinates and thermal parameters with estimated standard deviations are given in Table 1. The principal axes of thermal vibration ellipsoids for carbon atoms were calculated from the temperature parameters of Table 1. Maximum r.m.s. amplitudes range from 0.220 to 0.331 Å (corresponding B-values 3.80 and 8.63 Å²).

Bond distances and angles are listed in Table 2. Fig. 1 is a schematic drawing of the molecule (viewed along [100]) which shows that it has the D-allo configuration.

* All programs used (except those for phase determination) are included in this reference.

Table 1. Final fractional coordinates and thermal parameters with estimated standard deviations. The expression for anisotropic vibration is $\exp(-2\pi^2(h^2a^{*2}U11 + \cdots + 2klb^*c^*U23))$. Hm is bonded to Cm, HMmn to CMm, and HO to O5.

ATOM	X	Y	Z	U11	U22	U33	U12	U13	U23
O1	1.0680(6)	.2943(3)	.6921(2)	.0464(24)	.0575(23)	.0548(22)	.0021(21)	-.0054(19)	.0121(21)
O2	.7518(8)	.5382(3)	.6343(2)	.0694(27)	.0426(21)	.0684(22)	.0021(22)	-.0197(24)	-.0047(19)
O3	.5082(7)	.4407(3)	.5628(2)	.0569(25)	.0458(21)	.0621(22)	-.0002(22)	-.0171(23)	.0045(19)
O4	.6672(6)	.2944(3)	.6966(2)	.0473(24)	.0508(28)	.0366(17)	-.0058(24)	.0037(18)	-.0005(18)
O5	.6469(8)	.1195(3)	.5248(2)	.0559(26)	.0669(25)	.0464(21)	.0004(26)	.0013(23)	-.0121(19)
C1	.8698(9)	.3619(5)	.6943(3)	.0479(34)	.0511(38)	.0406(29)	-.0033(33)	-.0037(34)	-.0053(28)
C2	.8603(11)	.4285(4)	.6229(3)	.0474(36)	.0417(38)	.0495(38)	-.0062(34)	-.0016(34)	.0036(25)
C3	.6924(9)	.4618(4)	.5751(3)	.0494(36)	.0463(29)	.0398(28)	.0001(31)	.0007(27)	-.0049(26)
C4	.6127(10)	.2612(4)	.6229(3)	.0418(32)	.0468(38)	.0383(27)	.0034(31)	.0051(28)	-.0085(22)
C5	.7266(11)	.1465(5)	.6014(3)	.0481(38)	.0479(32)	.0432(31)	-.0029(32)	.0010(29)	-.0055(24)
C6	.6665(11)	.0534(5)	.6535(3)	.0646(43)	.0461(31)	.0574(31)	.0058(34)	.0049(32)	-.0058(28)
C7	.6145(13)	-.0195(5)	.6949(4)	.0936(52)	.0503(35)	.0783(40)	.0053(39)	.0204(45)	.0111(35)
C8	.5899(11)	.5538(5)	.5775(3)	.0614(42)	.0434(31)	.0634(34)	.0016(34)	-.0117(34)	.0068(28)
CM1	1.1012(16)	.2222(7)	.7554(4)	.0623(59)	.0795(49)	.0723(43)	.0043(53)	-.0130(51)	.0278(39)
CM2	.7019(19)	.6042(8)	.5098(5)	.0938(88)	.0757(54)	.0802(52)	-.0066(54)	.0003(52)	.0301(44)
CM3	.3961(16)	.6256(7)	.6373(5)	.0760(58)	.0541(47)	.0921(55)	.0095(49)	-.0094(54)	.0044(45)

ATOM	X	Y	Z	B	ATOM	X	Y	Z	B
H1	.870(8)	.409(3)	.738(2)	2.6(10)	H2	1.026(10)	.442(4)	.604(2)	3.4(11)
H3	.764(8)	.337(3)	.526(2)	2.3(8)	H4	.432(9)	.253(3)	.621(2)	2.9(9)
H5	.984(8)	.160(3)	.608(2)	3.3(10)	H7	.583(9)	-.086(4)	.734(3)	7.2(15)
HM11	.977(17)	.159(7)	.758(4)	9.7(24)	HM12	1.019(18)	.241(5)	.799(2)	9.4(13)
HM13	1.261(9)	.181(4)	.753(2)	8.2(13)	HM21	.838(13)	.559(5)	.498(3)	8.1(19)
HM22	.568(12)	.616(5)	.476(3)	5.4(19)	HM23	.759(15)	.679(6)	.528(3)	8.6(23)
HM31	.254(15)	.622(6)	.573(4)	8.2(22)	HM32	.448(13)	.699(5)	.613(3)	5.7(17)
HM33	.336(13)	.587(5)	.652(3)	7.3(21)	HO	.771(15)	.397(5)	.499(3)	7.7(19)

Table 2. Bond distances and angles with estimated standard deviations.

DISTANCE	(Å)	DISTANCE	(Å)	DISTANCE	(Å)
C1 - O1	1.399(6)	O1 - CM1	1.433(6)	C1 - O4	1.420(6)
C4 - O4	1.429(6)	C2 - O2	1.432(6)	C3 - O3	1.431(6)
C8 - O2	1.413(6)	C8 - O3	1.418(7)	C5 - O5	1.433(6)
C1 - C2	1.513(7)	C2 - C3	1.519(7)	C3 - C4	1.522(7)
C8 - CM2	1.521(9)	C8 - CM3	1.506(9)	C4 - C5	1.535(8)
C5 - C6	1.476(8)	C6 - C7	1.171(8)	O5 - O3	2.780(5)

ANGLE	(°)	ANGLE	(°)
C1 - O1 - CM1	114.5(5)	C1 - O4 - C4	107.8(4)
C2 - O2 - C8	107.8(4)	C3 - O3 - C8	107.6(4)
O1 - C1 - O4	112.8(4)	O1 - C1 - C2	106.9(4)
O4 - C1 - C2	105.9(4)	C1 - C2 - O2	110.1(4)
C1 - C2 - C3	104.7(4)	O2 - C2 - C3	104.2(5)
C2 - C3 - C4	105.2(4)	C2 - C3 - O3	104.8(4)
O3 - C3 - C4	110.2(4)	C3 - C4 - O4	105.3(4)
C5 - C4 - O4	111.9(4)	C3 - C4 - C5	112.4(4)
O2 - C8 - O3	104.3(4)	O3 - C8 - CM2	110.0(6)
O2 - C8 - CM2	111.1(6)	CM2 - C8 - CM3	113.9(6)
O3 - C8 - CM3	108.7(6)	O2 - C8 - CM3	108.3(5)
C4 - C5 - O5	106.3(5)	C4 - C5 - C6	111.3(4)
C6 - C5 - O5	110.7(4)	C5 - C6 - C7	178.6(7)
C5 - O5 - O3'	111.0(3)	O5 - O3' - C3'	122.6(3)
O5 - O3' - C8'	126.9(3)		

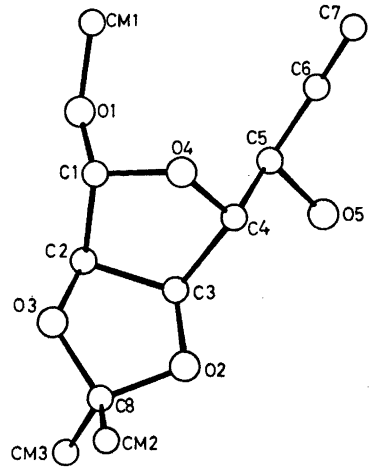

Fig. 1. Schematic drawing of the molecule viewed along [100].

The bond distances and angles do not differ significantly from corresponding ones in methyl-α-D-galactofuranoside.[6] The two five-membered rings have the envelope form with O4 and C8 both 0.47 Å out of the planes (to within 0.01 Å) through C1, C2, C3, C4, and C2, C3, O2, O3, respectively. The angle between the planes is 63.9°. Apart from a hydrogen bond (of length 2.780 Å) between O5 and O3 in a symmetry related molecule, there are no short intermolecular contacts.

A list of observed and calculated structure factors is available from the author.

Acknowledgement. The author would like to thank cand.mag. Nils Berg for preparing the crystals.

1. Kjølberg, O. and Sverreson, T. B. *Acta Chem. Scand. 26* (1972) 3245.
2. Jones, E. R. H., Skattebøl, L. and Whiting, M. C. *J. Chem. Soc.* (1956) 4765.
3. Berg, N. and Kjølberg, O. *Unpublished results.*
4. Germain, G., Main, P. and Wollfson, M. M. *Acta Crystallogr. A 27* (1971) 368.
5. Groth, P. *Acta Chem. Scand. 27* (1973) 1837.
6. Klewe, B. and Reine, A. *Unpublished results.*

Received September 24, 1975.

Counter-ion Quadrupole Splittings in Lyotropic Liquid Crystals. Determination of the Sign of the Order Parameter

G. LINDBLOM, B. LINDMAN and G. J. T. TIDDY*

Lund Institute of Technology, Physical Chemistry 2, Chemical Center, P.O.B. 740, S-220 07 Lund 7, Sweden

Many recent investigations have utilised the occurrence of static effects in nuclear magnetic resonance (NMR) spectra to obtain information on ionic interactions in liquid crystals and model membranes,[1-9] A theoretical approach based on a simple electrostatic model has been used to explain the quadrupole splittings observed for different counter-ions in various liquid crystalline (l.c.) phases.[10] The l.c. phases of the sodium octanoate-decanol-water system have been well documented in the classic studies of Ekwall *et al.*,[11] making this system the obvious starting point for systematic investigations of ion quadrupole splittings. However, ^{23}Na splittings for the lamellar (D) phase were an order of magnitude smaller than predicted by the theory and were temperature dependent,[4,10] decreasing to zero at higher temperatures.[4] Also, the ^{23}Na splittings observed for powder and aligned samples were not in agreement with theoretical equations.[4] In addition, the ^{23}Na splittings were consistent[4] with a non-lamellar structure[11] for the C phase although this appeared to be unlikely from previous NMR studies.[12] These difficulties have been resolved in the present investigation, and the sign of the sodium ion order parameter (S), previously unknown, has been deduced.

Sodium splittings have been determined for C and D phase samples using continuous-wave and spin-echo techniques. Sample preparation and continuous-wave measurements were carried out as described previously.[4,12] Spin-echo measurements were made using a Bruker Bkr 322-S pulsed spectrometer operating at 23.81 MHz, with the splitting being obtained from the modulation of the free induction decay following a $\pi/2$ pulse.

Both aligned and powder samples were examined as a function of temperature and phase structures were checked using a polarising microscope with hot stage attachment.

The quadrupole splittings (Δ) of the sodium resonance in aligned and powder samples are given[10] by equations (1) and (2), respectively.

$$\Delta = |(3\cos^2\theta_{LD} - 1)\ \sum_i P_i \nu_Q{}^i S_i| \quad (1)$$

$$\Delta = |\sum_i P_i \nu_Q{}^i S_i| \quad (2)$$

where $\nu_Q = e^2qQ/4h$ is the effective quadrupole coupling constant; P_i is the fraction of sodium ions in site i;

$S = 1/2\ (3\cos^2\theta_{DM} - 1)$ if the asymmetry parameter is neglected.

θ_{LD} and θ_{DM} are the angles between director and magnetic field and between director and electric field gradient, respectively. Note that in general only the absolute value of S may be obtained from the splitting.

The results can be summarised as follows:

(a) If water evaporation during sample preparation is avoided then values of Δ for powder and aligned samples are related by equations (1) and (2) at all temperatures.

(b) The splittings are a complex function of temperature and composition. (See Figs. 1 and 2; similar results have been obtained elsewhere.[13])

(c) Values of Δ for the C phase are similar to those of adjacent D phase samples.

For the discussion of these data it is important to note that the ^{23}Na splittings of the sodium octanoate-decanol-water system are considerably smaller than those obtained with soaps having a sulfate end-group. If the electrostatic model discussed in Ref. 10 is used in combination with counter-ion association degrees of Ref. 14 the order parameter of the bound sodium ions is obtained to be considerably less than unity for the present system. The

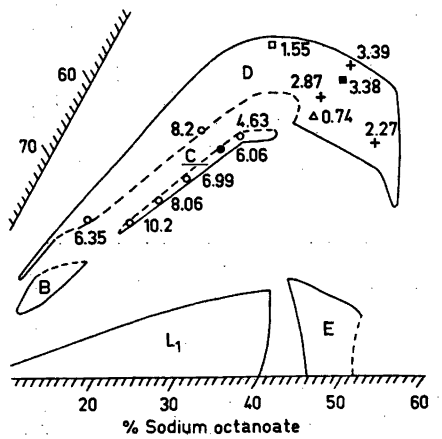

Fig. 1. Partial phase diagram (from Ref. 11) showing sample compositions and measured splittings. Temperatures of measurements were 300 ± 1 K and 294 ± 1 K for D and C phases, respectively. A Δ value of 8.06 kHz was measured at 303 K for the C phase sample indicated by ●.

* Permanent address: Unilever Research Port Sunlight Laboratories, Unilever Ltd., Port Sunlight, Wirral, Merseyside, England L62 4XN

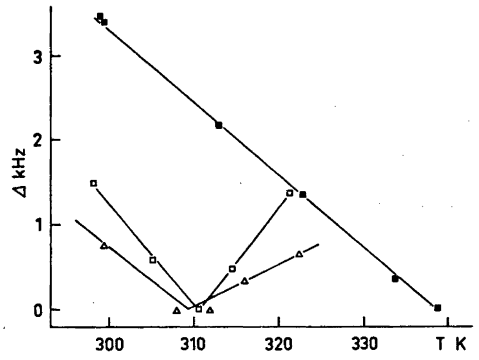

Fig. 2. Temperature dependence of the ^{23}Na quadrupole splitting of three lamellar powder samples in the sodium octanoate-decanol-D_2O system. Symbols refer to sample compositions with the same symbols in Fig. 1. As a result of a finite spin relaxation rate very small splittings are unobservable, and the zero splitting means that no modulation of the free induction decay was discernable. (The lines are drawn merely as an aid to the eye; there is no theoretical justification for a linear temperature dependence of the splittings.)

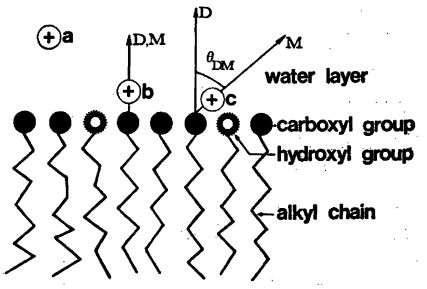

Fig. 3. Schematic drawing of the counter-ion binding at the lamellar surface according to the discussion in the text. The following three possibilities are shown: (a) The counter-ion is moving freely in the water layer. This location is characterized by $S=0$. (b) The counter-ion is located symmetrically with respect to the amphiphile polar end-group. In this case the average angle between the director (D) and the electric field gradient (M) is equal to 0°. (c) The counter-ion is located between amphiphile polar head-groups.

order parameter is zero for $\theta_{DM}=54°\ 44'$, the magic angle. Changes in temperature or composition give rise to changes in θ_{DM}. With an average θ_{DM} value which is close to the magic angle both positive and negative S values may be encountered and that this is so in the present case can be inferred from both the variable temperature and concentrations studies (Figs. 1 and 2). It seems not possible to understand vanishing quadrupole splittings well within the liquid crystal stability ranges in another way. Changes in S cannot be due to fundamental changes in the structure of the l.c. phase since concurrent changes are not observed in alkyl chain proton resonance [12] or water deuteron quadrupole splittings.[15] If increasing temperature or hydration may be assumed to weaken the amphiphile-counter-ion interaction (*cf.* Ref. 16) we have here for the first time a method to obtain the sign of the order parameter. Thus if the counter-ion splitting increases with increasing temperature or water content this indicates that the order parameter is positive while in the opposite case a negative order parameter is indicated.

These considerations open the way for using counter-ion quadrupole splittings to obtain unique information on the detailed location of counter-ions at the surface of an amphiphile aggregate. Except for the highest water contents, our observations suggest that over wide concentration and temperature ranges θ_{DM} takes on large values. A location of bound sodium ions between adjacent carboxyl groups involving hydrogen-bonding between water of counter-ion hydration and surfactant end-group is a plausible model to explain these findings. Our findings with alkyl sulfates or sulfonates correspond to much higher S values and thus small values of θ_{DM}. This is not unexpected in view of the symmetric end-groups and the low tendency of these end-groups to become involved in hydrogen-bonding. An attempt to visualize different locations of counter-ions at a lamellar surface is presented in Fig. 3. It should be noted that S is determined not only by the average value of θ_{DM} but also by its range of variation, and that according to eqs. 1 and 2, a zero splitting may result from exchange between sites having different signs of S or ν_Q. However, the general conclusions appear to be independent of these effects since the temperature dependences are large.

Because alkyl chain resonances were similar in C and D phases, it was proposed [12] that the C phase structure was an emulsion of lamellar phase and a small amount of micellar solution rather than the tetragonal rod structure favoured by Ekwall *et al.* [11] Previous ^{23}Na splittings were consistent with the second structure,[4] but the similarity between values of Δ for C and D phases supports the emulsion structure. Further studies are in progress using other techniques to resolve this problem.

1. Johansson, Å. and Lindman, B. In Gray, G. W. and Winsor, P. A., Eds., *Liquid Crystals and Plastic Crystals*, Ellis Horwood Ltd., Chichester, U. K. 1974, Vol. 2, p.192.

2. Lindblom, G., Wennerström, H. and Lindman, B. *Chem. Phys. Lett. 8* (1971) 489.
3. Lindblom, G. *Acta Chem. Scand. 25* (1971) 2767.
4. Lindblom, G. and Lindman, B. *Mol. Cryst. Liquid. Cryst. 22* (1973) 45.
5. Shporer, M. and Civan, M. M. *Biophys. J. 12* (1972) 114.
6. Chen. D. M. and Reeves, L. W. *J. Amer. Chem. Soc. 94* (1972) 4384.
7. Berendsen, H. J. C. and Edzes, H. T. *Ann. N. Y. Acad. Sci. 204* (1973) 459.
8. Reeves, L. W. and Tracy, A. S. *J. Amer. Chem. Soc. 96* (1974) 365.
9. Lindblom, G., Persson, N.-O., and Arvidson, G. In Friberg, S., Ed., *Lyotropic Liquid Crystals and the Structure of Biomembranes, Advan. Chem. Ser.* (1975), Chapter 9. *In press.*
10. Wennerström, H., Lindblom, G. and Lindman, B. *Chem. Scr. 6* (1974) 97.
11. Ekwall, P., Mandell, L. and Fontell, K. *Acta Polytechnica Scand. 74* (1968) I–III; Ekwall, P. In Brown, G., Ed., *Advances in Liquid Crystals 1* (1975) 1.
12. Tiddy, G. J. T. *J. Chem. Soc. Faraday Trans. 1* (1972) 369.
13. Dijkema, C. and Berendsen, H. J. C. *Personal communication.*
14. Lindman, B. and Brun, B. *J. Colloid Interface Sci. 42* (1973) 388.
15. Lindblom, G., Persson, N.-O. and Lindman, *B. Proceedings of the VIth International Conference on Surface Active Agents*, Sept 1972, Carl Hanser Verlag München, 1973, Vol. II, p. 939; Persson, N.-O. and Lindman, B. *J. Phys. Chem. 79* (1975) 1410.
16. Gustavsson, H., Lindblom, G., Lindman, B., Persson, N.-O. and Wennerström, H. In Johnson, J. F. and Porter, R. S., Eds., *Liquid Crystals and Ordered Fluids*, Plenum, New York 1974, Vol. 2, p. 161.

Received May 27, 1975.

Crystallizations and Transformations of $SrCl_2$-Hydrates in H_2O-Solutions in Quartz Flasks

BJØRN BERGTHORSSON

Chemistry Department B, The Technical University of Denmark, DtH 301, DK-2800 Lyngby, Denmark

The search for materials suitable for energy storage has aroused an interest in the kinetics of nucleation and the growth of salt hydrates.[1] In a previous paper [2] it was shown that $SrCl_2.6H_2O$ can, if properly treated, be heated above 61.3 °C – the temperature of transition for the system $SrCl_2.6H_2O \rightleftharpoons SrCl_2.2H_2O$ + sat. solution – without transforming into dihydrate; $SrCl_2.H_2O$ is formed at approx. 71 °C.

The system, $SrCl_2.H_2O$ + sat. solution, can be supercooled approx. 100 °C in quartz flasks if treated as described below; the temperature of transition for $SrCl_2.2H_2O \rightleftharpoons SrCl_2.H_2O$ + sat. solution is approx. 135 °C. The limit of supercooling – approx. 30 °C where hexahydrate is generated – depends probably on the quartz container used but not on the monohydrate crystals.

The system, $SrCl_2.H_2O$ + sat. solution, can also be supercooled – from 61.3 °C down to approx. 20 °C – and the limit, where hexahydrate is formed, depends probably also on the container used and not on the supercooled system (*cf.* results obtained with $CaCl_2$-hydrates [3]).

Experimental details and results. Sample $SrCl_2$, El-chemical, from Merck, Germany. The analysis of the sample and the experimental arrangement is described earlier.[2] The cleaning of the quartz flasks which contained the $SrCl_2$-system has been modified as follows: the vacuum grease (Apiezone H) was first removed; the last residue was thoroughly washed away by chloroform. Then the flask was washed with alcohol and water and filled with conc. H_2SO_4 which contained 25 g $NaClO_4$ per 1 H_2SO_4 (analysed reagents). The flask was left for 12 h at 100 °C, and then thoroughly washed with distilled water (sp. conductivity less than 5×10^{-7} Ω^{-1} cm^{-1}).

A $SrCl_2$-solution was filtered through a filter, type VSWP 04700, white, plain, pore size 0.025 μm; stainless pressure filter holder, type XX4004700. Filter and filterholder from Millipore Corp. U.S.A.; before use they were washed repeatedly with distilled water until the sp. cond. was less than $10^{-6}\Omega^{-1}$ cm^{-1}. The washing and the filtration of the $SrCl_2$-solution into a quartz flask was performed in a laminar air flow cabinet; the pore sizes of the air filter were less than 0.6 μm.

Before starting an experiment, a $SrCl_2$-solution was heated to 100 °C, cooled and then exhausted four or five times. It proved to be

2. Lindblom, G., Wennerström, H. and Lindman, B. *Chem. Phys. Lett. 8* (1971) 489.
3. Lindblom, G. *Acta Chem. Scand. 25* (1971) 2767.
4. Lindblom, G. and Lindman, B. *Mol. Cryst. Liquid. Cryst. 22* (1973) 45.
5. Shporer, M. and Civan, M. M. *Biophys. J. 12* (1972) 114.
6. Chen. D. M. and Reeves, L. W. *J. Amer. Chem. Soc. 94* (1972) 4384.
7. Berendsen, H. J. C. and Edzes, H. T. *Ann. N. Y. Acad. Sci. 204* (1973) 459.
8. Reeves, L. W. and Tracy, A. S. *J. Amer. Chem. Soc. 96* (1974) 365.
9. Lindblom, G., Persson, N.-O., and Arvidson, G. In Friberg, S., Ed., *Lyotropic Liquid Crystals and the Structure of Biomembranes, Advan. Chem. Ser.* (1975), Chapter 9. *In press.*
10. Wennerström, H., Lindblom, G. and Lindman, B. *Chem. Scr. 6* (1974) 97.
11. Ekwall, P., Mandell, L. and Fontell, K. *Acta Polytechnica Scand. 74* (1968) I–III; Ekwall, P. In Brown, G., Ed., *Advances in Liquid Crystals 1* (1975) 1.
12. Tiddy, G. J. T. *J. Chem. Soc. Faraday Trans. 1* (1972) 369.
13. Dijkema, C. and Berendsen, H. J. C. *Personal communication.*
14. Lindman, B. and Brun, B. *J. Colloid Interface Sci. 42* (1973) 388.
15. Lindblom, G., Persson, N.-O. and Lindman, *B. Proceedings of the VIth International Conference on Surface Active Agents*, Sept 1972, Carl Hanser Verlag München, 1973, Vol. II, p. 939; Persson, N.-O. and Lindman, B. *J. Phys. Chem. 79* (1975) 1410.
16. Gustavsson, H., Lindblom, G., Lindman, B., Persson, N.-O. and Wennerström, H. In Johnson, J. F. and Porter, R. S., Eds., *Liquid Crystals and Ordered Fluids*, Plenum, New York 1974, Vol. 2, p. 161.

Received May 27, 1975.

Crystallizations and Transformations of $SrCl_2$-Hydrates in H_2O-Solutions in Quartz Flasks

BJØRN BERGTHORSSON

Chemistry Department B, The Technical University of Denmark, DtH 301, DK-2800 Lyngby, Denmark

The search for materials suitable for energy storage has aroused an interest in the kinetics of nucleation and the growth of salt hydrates.[1] In a previous paper [2] it was shown that $SrCl_2.6H_2O$ can, if properly treated, be heated above 61.3 °C – the temperature of transition for the system $SrCl_2.6H_2O \rightleftharpoons SrCl_2.2H_2O$ + sat. solution – without transforming into dihydrate; $SrCl_2.H_2O$ is formed at approx. 71 °C.

The system, $SrCl_2.H_2O$ + sat. solution, can be supercooled approx. 100 °C in quartz flasks if treated as described below; the temperature of transition for $SrCl_2.2H_2O \rightleftharpoons SrCl_2.H_2O$ + sat. solution is approx. 135 °C. The limit of supercooling – approx. 30 °C where hexahydrate is generated – depends probably on the quartz container used but not on the monohydrate crystals.

The system, $SrCl_2.H_2O$ + sat. solution, can also be supercooled – from 61.3 °C down to approx. 20 °C – and the limit, where hexahydrate is formed, depends probably also on the container used and not on the supercooled system (*cf.* results obtained with $CaCl_2$-hydrates [3]).

Experimental details and results. Sample $SrCl_2$, El-chemical, from Merck, Germany. The analysis of the sample and the experimental arrangement is described earlier.[2] The cleaning of the quartz flasks which contained the $SrCl_2$-system has been modified as follows: the vacuum grease (Apiezone H) was first removed; the last residue was thoroughly washed away by chloroform. Then the flask was washed with alcohol and water and filled with conc. H_2SO_4 which contained 25 g $NaClO_4$ per 1 H_2SO_4 (analysed reagents). The flask was left for 12 h at 100 °C, and then thoroughly washed with distilled water (sp. conductivity less than 5×10^{-7} Ω^{-1} cm^{-1}).

A $SrCl_2$-solution was filtered through a filter, type VSWP 04700, white, plain, pore size 0.025 μm; stainless pressure filter holder, type XX4004700. Filter and filterholder from Millipore Corp. U.S.A.; before use they were washed repeatedly with distilled water until the sp. cond. was less than $10^{-6}\Omega^{-1}$ cm^{-1}. The washing and the filtration of the $SrCl_2$-solution into a quartz flask was performed in a laminar air flow cabinet; the pore sizes of the air filter were less than 0.6 μm.

Before starting an experiment, a $SrCl_2$-solution was heated to 100 °C, cooled and then exhausted four or five times. It proved to be

advantageous to have a stopcock between a quartz flask and the pyrex glass apparatus; thus it was possible to mount two flasks on each apparatus. Although the system was thoroughly and repeatedly exhausted, a trace of foreign gases was left: small air bubbles could always be seen on the bottom of a flask after having dissolved monohydrate crystals. Foreign gases are, strictly speaking, a part of the system. For further details the reader is referred to the previous paper.[2]

The vapour pressure is indicative of the supersaturation; one notices that the curve for the supersaturated system, $SrCl_2.H_2O$ + sat. solution (above 45 °C), lies below the curve for the system which consists of two solid phases: $SrCl_2.6H_2O + SrCl_2.2H_2O$. By using below mentioned vapour pressure measurements to prolong curve 3, Fig. 2, Ref. 2, the obtained results may be illustrated.

The system, $SrCl_2.H_2O$ + sat. solution, was supercooled down to approx. 30 °C where hexahydrate was formed. The limit of supercooling was reached if and only if the monohydrate crystals were generated and grown as follows: the monohydrate was generated by heating the system, $SrCl_2.6H_2O$ + sat. solution, from 69.5 to 71.2 °C in less than 5 min, then staying for 1 min before the system was cooled (in 2 min) to 70.3 – 70.4 °C. The system was kept at this temperature for 3 – 4 h; then it was slowly cooled (10 min) to 69.9 °C, and thereafter it was slowly heated, 0.02 °C/h, up to 71.0 °C before supercooling.

The procedure has the following background: the temperature of transition for the system, $SrCl_2.6H_2O \rightleftharpoons SrCl_2.H_2O + 5H_2O$ (sat. solution), is 70.2 °C.[2] The first seeds of monohydrate crystals were found to be formed at approx. 70.6 °C; at 70.35° the crystals are slowly growing while the hexahydrate crystals are slowly dissolving; at temperatures below 70.2 °C the process is reversed.

The limit (30 °C) at which hexahydrate was formed depended apparently slightly on the rate of cooling. When the rate was 2 °C/h the hexahydrate was formed at 29 ± 2 °C in eight experimental runs using four different quartz flasks; but when the rate was 0.25 °C/h then hexahydrate was formed at 31 ± 2 °C (four runs).

Monohydrate crystals, not generated and grown as described above but more rapidly, could previously be supercooled only down to a temperature which lay slightly below 70 °C.[2] This phenomenon was now found to be due to the nucleation and growth conditions above 70.2 °C; it was eliminated by following precisely the above described procedure.

The vapour pressure of a solution saturated with respect to the monohydrate has been measured at 33, 40, and 50 °C and found to be 16.85, 24.80, and 42.4 mmHg, respectively. With the aid of the Clausius-Clapeyron equation in the approximate form $\Delta \ln p/(\Delta 1/T) = -Q/R$ it is found that Q is nearly constant between 30 and 70 °C (10.6 kcal). This conforms with the fact that the solubility is practically constant in this interval.[2]

The procedure for determining the limit of supercooling for the system, $SrCl_2.2H_2O$ + sat. solution, has the same basic features as described above: dihydrate crystals are generated from hexahydrate crystals at a temperature slightly (1.5 °C) above the temperature of transition (61.3 °C) for $SrCl_2.6H_2O \rightleftharpoons SrCl_2.2H_2O + 4H_2O$ (sat. solution) – here rapidly grown hexahydrate crystals are suitable only.[2] After having cooled the system to 61.3 °C it was slowly heated, 0.1 °C/h, up to 63 °C, then more rapidly, 0.5 °C/h, up to 67 – 68 °C before supercooling. The system $SrCl_2.2H_2O$ + sat. solution, could be supercooled down to 20 ± 2 °C (in eight experimental runs using four different flasks). The rate of cooling was 0.8 °C/h.

The dihydrate can be generated and grown from the hexahydrate at any temperature between 61.3 and 70.2 °C;[2] it was therefore an easy task to get rapidly generated and grown dihydrate crystals which could not be supercooled down to 20 °C. Experience showed that too much solid substance in a flask (this is valid for all three types of crystals) had to be avoided when working with a thermodynamically instable system: crystals are stressed or even broken if space is lacking, and they may then initiate a process in the thermodynamically instable system.

Fig. 1 shows the results obtained when supersaturated $SrCl_2$-solutions (without contact with crystals) were cooled in three of the four flasks (one broke). The points marked A, B, and C refer to the three flasks; a point shows the temperature and pressure (which is a measure

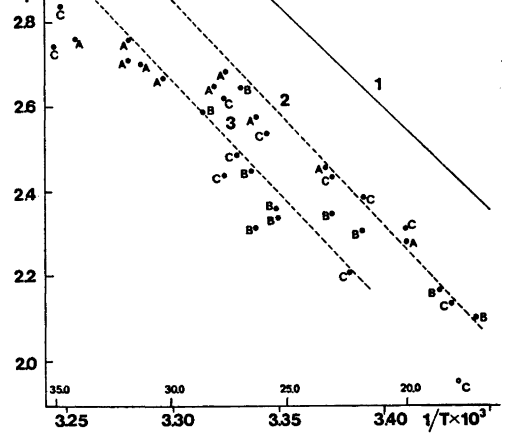

Fig. 1. Vapour pressure curves of saturated solutions of $SrCl_2$-hydrates in comparison with vapour pressures and temperatures at which hexahydrate was formed.

of the $SrCl_2$-concentration) at which hexahydrate is formed in a supercooled solution. The rate of cooling (from 70 °C) was 2 °C/h.

The flasks A and B were mounted on the same apparatus and therefore identically treated; for example, the $SrCl_2$-conc. and the cooling rate were always identical for both during a run. It was always possible to supercool B more than A.

The results show that the nucleation is heterogeneous, not homogeneous. Foreign seeds – probably from the walls of the flasks – act as a catalyst for nucleation of hexahydrate. Fig. 1 shows that these foreign seeds determine most likely also the limits found for the systems represented by the curves 2 and 3 (*cf.* Fig. 2, Ref. 2); as mentioned before these limits were found to be approx. 20 and 30 °C, respectively. The results are analogous to those obtained when $CaCl_2$-hydrates were studied.[3]

The transformation of hexahydrate into dihydrate above 61.3 °C, of dihydrate into hexahydrate below 61.3 °C, and of monohydrate into dihydrate below 135 °C are all found to depend either on foreign seeds or on proper nonequilibrium conditions. The influence of these factors can be minimized so that (1) a solution saturated with respect to and in contact with hexahydrate crystals can be heated above 61.3 °C without giving dihydrate (monohydrate is generated), (2) a solution saturated with respect to and in contact with monohydrate crystals can be supercooled without giving dihydrate, (3) a solution saturated with respect to and in contact with dihydrate crystals can be supercooled approx. 40 °C. Monohydrate or dihydrate crystals do not influence the limit of supercooling.

The $SrCl_2$-systems exhibit large supersaturations as is often the case when salt hydrates are involved. For large supersaturation, the effects of foreign seeds have to be taken into consideration. The experiments indicate that it will be difficult to study homogeneous nucleation or the effect of a hydrate on the nucleation of a higher one: it is necessary to begin by getting the influence of foreign seeds under control, and this may be very difficult to realize. If the aim is to control in practice nucleation and growth of a hydrate exhibiting large supersaturation, it is probably more productive to study the catalytic effect of definite foreign seeds or of non-equilibrium conditions caused by ultrasonic waves.

The following phenomenon – which perhaps can be used to purify $SrCl_2$ – was observed: hexahydrate crystals in a sat. solution (kept on a table) crept rather rapidly up the glass wall. This resulted in a complete spatial separation of the phases. The phenomenon proved to be connected with a temperature radiation from a warm object, the crystals always creeping up the wall which faced the object.

1. Belton, G. and Ajami, F. *Thermochemistry of Salt Hydrates/Conservation and Better Utilization of Electric Power by Means of Thermal Energy*, Report No. NSF/RA/N-73-Ø79, University of Pennsylvania, Philadelphia, U.S.A., 1973.
2. Bergthorsson, B. *Acta Chem. Scand. 24* (1970) 1735.
3. Bergthorsson, B. *Acta Chem. Scand. 26* (1972) 1292.

Received August 27, 1975.

Acta Chemica Scandinavica A 29 (1975) 881—889

Thermodynamics of Metal Complex Formation in Aqueous Solution. IX. A Calorimetric and Potentiometric Study of the Azide Complexes of Nickel(II) and Hydrogen

STEN AHRLAND and EFRAIM AVŞAR*

Inorganic Chemistry 1, Chemical Center, University of Lund, P.O.B. 740, S-220 07 Lund 7, Sweden

The stability constants of the nickel(II) and hydrogen azide complexes in aqueous solution have been determined potentiometrically by glass electrode measurements in different buffer solutions. The enthalpy changes and hence also the entropy changes for the complex formation reactions have been determined by a calorimetric titration technique.

All data refer to 25.00 °C and an aqueous sodium perchlorate medium of ionic strength 1.00 M.

Three fairly weak mononuclear complexes are formed in the nickel(II) system, in slightly exothermic reactions. In the formation of the rather weak hydrazoic acid, the enthalpy and the entropy term contribute about equally to the fairly large decrease of the free energy.

In some preceding papers of this series,[1–3] the thermodynamic functions of the stepwise complex formation of some selenocyanate and thiocyanate complexes have been reported. It is of interest to investigate how these will change for a ligand of analogous electronic structure but containing only one kind of donor atom. Such a ligand is found in the azide ion where bonding can take place only *via* relatively hard N-atoms while in thiocyanate and selenocyanate the acceptor has a choice between the hard N and the soft S or Se. In the following, the results of such studies of the azide complexes of H^+, Ni^{2+}, Zn^{2+}, Fe^{3+}, and Hg^{2+} will be reported, starting with H^+ and Ni^{2+} in the present paper.

A great number of azide complexes of various metal ions have been studied by different methods,[4] while the enthalpy data available for such complexes are scarce.

The present investigation has been performed at 25.00 °C and in an aqueous sodium perchlorate medium of ionic strength 1.00 M. The free energy changes were obtained from potentiometrically determined formation constants according to

$$\Delta G^\circ_j = -RT \ln K_j$$

and the entropy changes, ΔS°_j, were calculated from calorimetrically estimated enthalpy data according to

$$\Delta G^\circ_j = \Delta H^\circ_j - T\Delta S^\circ_j$$

On account of the low stability of nickel(II) azide complexes, their formation would be most accurately studied by potentiometric determination of the free central ion concentration. In the present case, however, no workable electrode is available for this purpose. Therefore, the free ligand concentration [L] has been determined *via* pH measurements in nickel solutions containing azide-hydrazoic acid buffers. In order to evaluate these measurements, the acidity constant of the hydrazoic acid has to be known. It has therefore been determined in separate measurements. For the subsequent determination of ΔH°_j, also the heat of association of the acid has to be known.

The nickel(II) azide system has previously been studied spectrophotometrically by Senise and Godinho [5] ($I = 1.0$ M), and potentiometri-

* Present address: Technical University of Istanbul, Chemical Engineering Faculty, Department of Physical Chemistry, Macka-Istanbul, Turkey.

cally by Maggio *et al.*[6] ($I = 3.0$ M) at 25 °C; but only the first formation constant has been estimated by these authors. Neither the consecutive formation constants nor the enthalpy changes have hitherto been reported.

The proton azide system has, on the other hand, been extensively investigated at various ionic strengths and temperatures.[7–12] No calorimetric determination of $\Delta H°$ under the conditions of this investigation seems to have been carried out so far, however. At $I = 0$ and 25 °C $\Delta H° = -15.05$ kJ mol^{-1} has been found [7] for the association $H^+ + N_3^- \rightarrow HN_3$.

EXPERIMENTAL

Chemicals. Nickel(II) perchlorate was prepared by dissolving nickel(II) carbonate (Merck, *p.a.*) in perchloric acid (Baker *a.r.*) and recrystallized from water. In order to prevent hydrolysis, a small excess of acid was used.[13] The nickel concentration was determined gravimetrically by precipitation with dimethylglyoxime. The free acid concentration in the stock solution was determined by potentiometric titration.

Sodium azide (B.D.H. and/or Merck) was purified by precipitation with absolute alcohol from an almost saturated aqueous solution. After three recrystallisations, the salt was dried at 110 °C. An $\simeq 2$ M standard stock solution was prepared by dissolving a weighed amount of the salt in double distilled water. The concentration was determined by treating samples with an excess of standard sulfuric acid, boiling away the hydrazoic acid and titrating the residual strong acid alkalimetrically.

Sodium perchlorate was prepared and analyzed as before.[3] The Ag,AgCl electrodes were prepared according to Brown.[14]

Procedure. The calorimeter and the measurement technique have been described before.[15] The measurements were performed as a series of titrations of a solution T into a calorimeter solution S. Usually the solution S contained the central ion and T the ligand. In order to reach higher ligand concentrations, however, some titrations have been performed where the central ion has been added to a ligand solution.

The heats of dilution were determined by similar titrations, but with only one of the reactants present.

Every titration was as a rule carried out twice and the reproducibility was generally within 0.04 J.

Values of [H$^+$] have been measured with a glass electrode (Radiometer, Type G 202 C, DP) in conjunction with a Radiometer PHM 52 Digital pH Meter. The measurements were arranged as titrations at constant C_M, or constant C_H in the case of the proton azide system. Equal volumes of the solutions T_1 and T_2 (see Tables 1 and 2) were added to V_0 ml of the solution S. A magnetic stirrer provided efficient mixing. The final emf values were attained within a few minutes. Every titration was repeated four times with a reproducibility within 0.2 mV. Since evaporation of hydrazoic acid affects the measured potentials markedly, the reaction vessel must be tightly closed and the potentials read as quickly as possible. The acid vapour also attacks the metallic parts of the measuring equipment forming corrosion products which even in minute amounts may cause violent explosions.

Table 1. Corresponding values of E_H, h, $C_L - C_H$ and the values of K_a for the proton azide system.

For all series: $V_0 = 10.00$ ml and $V = (V_0 + 2v)$ ml.

S: C_H M $HClO_4$, $C_{NaClO_4} = 1.000$ M
T_1: $2C_H$ M $HClO_4$, $C_{NaClO_4} = 1.000$ M
T_2: $C_L = 0.200$ M NaN_3, $C_{NaClO_4} = 0.800$ M

$C_L - Ca$ (mM)	$-E_H$ (mV)	h (mM)	$K_a \times 10^5$ (M)
$C_H = 0.02500$ M			
19.44	−6.1	0.046	3.59
25.00	0.2	0.036	3.61
29.55	4.5	0.031	3.61
33.33	7.6	0.027	3.61
36.54	9.9	0.025	3.62
39.29	11.8	0.023	3.60
41.67	13.3	0.022	3.61
43.75	14.6	0.021	3.61
45.59	15.7	0.020	3.60
47.22	16.6	0.019	3.59
48.68	17.3	0.019	3.61
50.00	18.0	0.018	3.60
51.19	18.6	0.018	3.61
53.26	19.6	0.017	3.60
55.00	20.4	0.016	3.61
	Average value		3.61
$C_H = 0.05000$ M			
14.29	31.1	0.122	(3.52)
16.67	27.3	0.105	(3.53)
18.75	24.4	0.094	(3.54)
20.59	22.1	0.086	(3.55)
22.22	20.2	0.080	3.56
23.68	18.6	0.075	3.56
25.00	17.3	0.071	3.58
26.19	16.1	0.068	3.57
27.27	15.1	0.065	3.58
28.26	14.2	0.063	3.58
29.17	13.4	0.061	3.58
30.00	12.7	0.060	3.58
31.48	11.5	0.057	3.59
32.76	10.5	0.055	3.59
33.87	9.7	0.053	3.59

Table 2. Data pertaining to the potentiometric measurements on the nickel(II) azide system. The symbols refer to Fig. 1.

For all series: V_0 = 20.00 ml and equal volumes of solutions T_1 and T_2 were added during the titrations.

$C_L - C_H$ (mM)	$-E_H$ (mV)	h (mM)	[L] (mM)	$\bar{n}$	$\bar{n}$/[L] (M^{-1})
○ S: C_M = 30.00 mM, C_H = 50.00 mM, C_{NaClO_4} = 910.0 mM T_1: C_L = 1000 mM T_2: C_M = 60.00 mM, C_H = 100.0 mM, C_{NaClO_4} = 820.0 mM					
33.33	−15.0	0.0651	27.69	0.190	6.86
65.39	2.4	0.0331	54.50	0.364	6.68
92.86	11.5	0.0232	77.77	0.504	6.48
116.7	17.5	0.0184	98.22	0.616	6.27
137.5	21.8	0.0155	116.1	0.713	6.14
155.9	25.2	0.0136	132.6	0.777	5.86
172.2	27.9	0.0123	147.3	0.831	5.64
186.8	30.0	0.0113	159.8	0.900	5.63
200.0	31.8	0.0105	171.4	0.954	5.57
222.7	34.6	0.0094	192.0	1.03	5.34
241.7	36.8	0.0087	207.4	1.14	5.50
257.7	38.5	0.0081	222.8	1.16	5.21
271.4	39.8	0.0077	234.4	1.24	5.29
283.3	40.9	0.0074	243.9	1.32	5.41
□ S: C_M = 50.00 mM, C_H = 50.00 mM, C_{NaClO_4} = 850.0 mM T_1: C_L = 1000 mM T_2: C_M = 100.0 mM, C_H = 100.0 mM, C_{NaClO_4} = 700.0 mM					
33.33	−17.8	0.0726	24.84	0.171	6.88
65.39	−0.2	0.0366	49.31	0.322	6.53
92.86	9.0	0.0256	70.55	0.447	6.34
116.7	15.2	0.0201	89.81	0.538	5.99
137.5	19.6	0.0169	106.6	0.618	5.80
155.9	22.9	0.0149	121.2	0.694	5.73
172.2	25.7	0.0134	135.2	0.741	5.48
186.8	27.8	0.0123	146.7	0.803	5.47
200.0	29.7	0.0114	158.0	0.840	5.32
211.9	31.2	0.0108	167.4	0.890	5.32
222.7	32.5	0.0102	176.2	0.930	5.28
241.7	34.5	0.0095	190.4	1.03	5.41
257.7	36.0	0.0089	202.8	1.10	5.43
271.4	37.3	0.0085	212.3	1.18	5.56
283.3	38.3	0.0082	220.1	1.27	5.77
△ S: C_M = 70.00 mM, C_H = 50.00 mM, C_{NaClO_4} = 790.0 mM T_1: C_L = 1000 mM T_2: C_M = 140.0 mM, C_H = 100.0 mM, C_{NaClO_4} = 580.0 mM					
33.33	−21.0	0.0822	21.92	0.164	7.48
65.39	−3.2	0.0411	43.88	0.308	7.02
92.86	6.2	0.0285	63.30	0.423	6.68
116.7	12.4	0.0224	80.54	0.516	6.41
137.5	16.8	0.0189	95.47	0.601	6.30
155.9	20.3	0.0165	109.4	0.665	6.08
172.2	23.0	0.0148	121.9	0.719	5.90
186.8	25.2	0.0136	132.7	0.774	5.83
200.0	26.9	0.0127	142.1	0.828	5.83
211.9	28.3	0.0121	149.1	0.897	6.01
222.7	29.5	0.0115	156.9	0.940	5.99
241.7	31.4	0.0107	168.7	1.04	6.17

Table 2. Continued.

$C_L - C_H$ (mM)	$-E_H$ (mV)	h (mM)	[L] (mM)	$\bar{n}$	$\bar{n}$/[L] (M^{-1})
257.7	32.9	0.0101	178.7	1.13	6.33
271.4	34.1	0.0096	188.0	1.19	6.33
283.3	35.1	0.0093	194.1	1.28	6.60
■ S: $C_M = 50.00$ mM, $C_H = 100.8$ mM, $C_{NaClO_4} = 850.0$ mM T_1: $C_L = 1000$ mM T_2: $C_M = 100.0$ mM, $C_H = 200.0$ mM, $C_{NaClO_4} = 700.0$ mM					
66.16	−18.1	0.0734	49.40	0.337	6.82
87.03	−10.7	0.0550	65.91	0.423	6.42
105.4	−5.5	0.0450	80.55	0.499	6.20
121.8	−1.7	0.0388	93.40	0.569	6.09
136.4	1.3	0.0345	105.0	0.629	5.99
149.6	3.8	0.0313	115.7	0.678	5.86
161.5	5.9	0.0289	125.3	0.725	5.79
172.4	7.7	0.0269	134.6	0.756	5.62
182.3	9.3	0.0253	143.1	0.784	5.48
191.4	10.6	0.0240	150.9	0.810	5.37
199.7	11.8	0.0229	158.1	0.833	5.27
207.4	12.8	0.0221	163.8	0.873	5.33
221.2	14.4	0.0207	174.8	0.927	5.30
233.1	15.7	0.0197	183.7	0.988	5.38
● S: $C_M = 100.0$ mM, $C_H = 100.0$ mM, $C_{NaClO_4} = 700.0$ mM T_1: $C_L = 1000$ mM T_2: $C_M = 200.0$ mM, $C_H = 200.0$ mM, $C_{NaClO_4} = 400.0$ mM					
42.86	34.4	0.1379	26.14	0.169	6.47
66.67	23.0	0.0888	40.62	0.261	6.43
87.50	15.7	0.0669	53.93	0.336	6.23
105.9	10.7	0.0550	65.60	0.403	6.14
122.2	6.8	0.0473	76.29	0.460	6.03
136.8	3.8	0.0421	85.71	0.512	5.97
150.0	1.3	0.0382	94.47	0.556	5.89
161.9	−0.7	0.0353	102.2	0.597	5.84
172.7	−2.4	0.0331	109.0	0.637	5.84
182.6	−3.7	0.0314	114.9	0.677	5.89
191.7	−4.9	0.0300	120.3	0.714	5.94
207.7	−6.7	0.0280	128.9	0.788	6.11
▲ S: $C_M = 100.0$ mM, $C_H = 27.12$ mM, $C_{NaClO_4} = 700.0$ mM T_1: $C_L = 1000$ mM T_2: $C_M = 200.0$ mM, $C_H = 50.00$ mM, $C_{NaClO_4} = 400.0$ mM					
18.53	−22.9	0.0885	10.95	0.077	7.03
38.57	−4.1	0.0426	22.71	0.157	6.91
56.57	6.3	0.0284	33.99	0.226	6.65
73.30	13.3	0.0216	44.58	0.288	6.46
88.75	18.5	0.0177	54.28	0.345	6.36
103.1	22.7	0.0150	63.91	0.392	6.13
116.3	26.0	0.0132	72.48	0.439	6.06
140.3	31.1	0.0108	88.25	0.520	5.89
161.2	34.9	0.0093	102.2	0.590	5.78
179.6	37.7	0.0084	112.8	0.669	5.93
196.0	39.8	0.0077	122.7	0.734	5.98
210.7	41.4	0.0073	129.1	0.816	6.32
223.9	42.6	0.0069	136.3	0.876	6.43

The slope of the glass electrode used was checked repeatedly and found to be 59.1 ± 0.1 mV.

Potentiometric measurements on the proton azide system. The emfs of cells of the following type are measured.

$$+\text{G.E.}\left|\begin{array}{l} C_H \text{ M } HClO_4 \\ C_L \text{ M } NaN_3 \\ NaClO_4 \text{ to} \\ I = 1.00 \text{ M} \end{array}\right| \begin{array}{l} 1.00 \text{ M} \\ NaClO_4 \end{array} \left|\begin{array}{l} 0.025 \text{ M} \\ NaCl \\ \\ 0.975 \text{ M} \\ NaClO_4 \end{array}\right| \text{Ag,AgCl}-$$

The solutions S, T_1 and T_2 had the following compositions,

$$\text{S: } \begin{cases} C_H \text{ M } HClO_4 \\ C_{NaClO_4} = 1.00 \text{ M} \end{cases}$$

$$T_1: \begin{cases} 2C_H \text{ M } HClO_4 \\ C_{NaClO_4} = 1.00 \text{ M} \end{cases}$$

$$T_2: \begin{cases} C_L \text{ M } NaN_3 \\ (1.00 - C_L) \text{ M } NaClO_4 \end{cases}$$

On mixing of the solutions, practically all the free acid in solutions S will be converted into HN_3. The ionic strength of the resulting solution will then be 1 M.

The emf of the above cell is given (in mV) at 25.00 °C by

$$E_H = E^\circ_H + 59.16 \log h + E_j \quad (1)$$

where h is the free hydrogen ion concentration, E°_H the cell constant and E_j the liquid junction potential. E_j depends almost only on h and can therefore be determined separately.[16]

The dissociation constant of hydrazoic acid is given by

$$K_a = \frac{h(C_L - C_H + h)}{C_H - h} \quad (2)$$

Data pertaining to the potentiometric measurements on the proton azide system and the values of K_a in the medium used are given in Table 1.

In the beginning of the series, the values of K_a are slightly lower for $C_H = 50.00$ mM than

Table 3. Enthalpy data of the proton azide system. For all series: $V_0 = 90.00$ ml. and $V = (V_0 + v)$ ml.

(a) S: $C_H = 20.00$ mM, $C_{NaClO_4} = 980.0$ mM
T: $C_L = 200.0$ mM, $C_{NaClO_4} = 800.0$ mM

v (ml), Q_{corr} (J), δQ_{corr} (J); 2.00, 5.096, −0.003; 4.00, 5.016, 0.067; 6.00, 5.062, −0.010; 8.00, 4.856, 0.020; 10.00, 2.308, 0.203; 12.00, 0.224, −0.004.

S: $C_H = 40.00$ mM, $C_{NaClO_4} = 960.0$ mM
T: $C_L = 200.0$ mM, $C_{NaClO_4} = 800.0$ mM

v (ml), Q_{corr} (J), δQ_{corr} (J): 2.00, 5.180, −0.080; 4.00, 5.163, −0.065; 6.00, 5.135, −0.040; 8.00, 5.113, −0.022; 10.00, 5.104; −0.020; 12.00, 5.112, −0.043; 14.00, 5.022, 0.012; 16.00, 4.912, −0.004; 18.00, 3.806, 0.173; 20.00, 0.920, 0.150; 22.00, 0.201, −0.009.

S: $C_H = 60.00$ mM, $C_{NaClO_4} = 940.0$ mM
T: $C_L = 200.0$ mM, $C_{NaClO_4} = 880.0$ mM

v (ml), Q_{corr} (J), δQ_{corr} (J): 2.00, 5.131, −0.030; 4.00, 5.126, −0.025; 6.00, 5.128, −0.028; 8.00, 5.140, −0.041; 10.00, 5.122, −0.015; 12.00, 5.130, −0.036; 14.00, 5.128, −0.037; 16.00, 5.123; −0.037; 18.00, 5.121, −0.044; 20.00, 5.080, −0.020.

(b) S: $C_L = 25.00$ mM, $C_{NaClO_4} = 975.0$ mM
T: $C_H = 100.0$ mM, $C_{NaClO_4} = 900.0$ mM

v (ml), Q_{corr} (J), δQ_{corr} (J): 2.00, 2.500, 0.048; 4.00, 2.480, 0.067; 6.00, 2.498, 0.048; 8.00, 2.530, 0.014; 10.00, 2.518, 0.023; 12.00, 2.517, 0.019; 14.00, 2.515, 0.013; 16.00, 2.497, 0.016; 18.00, 2.453, 0.026; 20.00, 2.376, 0.008.

S: $C_L = 50.00$ mM, $C_{NaClO_4} = 950.0$ mM
T: $C_H = 100.0$ mM, $C_{NaClO_4} = 900.0$ mM

v (ml), Q_{corr} (J), δQ_{corr} (J): 2.00, 2.494, 0.057; 4.00, 2.485, 0.065; 6.00, 2.499, 0.051; 8.00, 2.551, −0.002; 10.00, 2.545, 0.004; 12.00, 2.570, −0.022, 14.00, 2.536, 0.012, 16.00, 2.534, 0.013, 18.00, 2.540, 0.006, 20.00, 2.535, 0.010.

for $C_H = 25.00$ mM. Since the evaporation of hydrazoic acid may well be noticeable at the high concentrations reached initially for $C_H = 50$ mM, however, the slightly lower values of K_a are not very surprising. At higher values of C_L very much the same values of K_a are found for both values of C_H.

Calorimetric measurements on the proton azide system. Two different titration procedures have been applied. In one of these, sodium azide solutions of $C_L = 0.200$ M and $I = 1.00$ M were added to perchloric acid solutions of varying concentration but of the same $I = 1.00$ M (Table 3, a). In the other procedure, solutions containing varying amounts of sodium azide were titrated with a perchloric acid solution (Table 3, b). The heat change corrected for dilution is Q_{corr}; δQ_{corr} is the difference between the heat change calculated from the values of K ($K = 1/K_a$) and $\Delta H°$ found and that measured experimentally, *i.e.* $\delta Q_{corr} = (Q_{corr,calc} - Q_{corr})$.

The enthalpy change of the formation of hydrazoic acid has been calculated by the least squares computer program "Kalori"[17] which minimizes the error square sum,

$$U(\beta_j, \Delta H°_j) = \sum_{i=1}^{n} (Q_{i,corr} - Q_{i,calc})^2$$

where n is the number of experimental points. This program also allows a simultaneous determination of K and $\Delta H°$ from the calorimetric data. Only slightly different values result from this procedure as compared with a calculation where K is kept at the potentiometrically found value (see below).

Potentiometric measurements on the nickel(II) azide system. The emfs of cells of the following type are measured:

$$+\text{G.E.} \left| \begin{array}{l|l} C_M \text{ M } Ni(ClO_4)_2 & \\ C_H \text{ M } HClO_4 & \\ C_L \text{ M } NaN_3 & 1.00 \text{ M } NaClO_4 \\ NaClO_4 \text{ to} & \\ I = 1.00 \text{ M} & \end{array} \right| \left| \begin{array}{l} \\ \\ \\ \\ \\ \end{array} \right.$$

$$\left| \begin{array}{l} 0.025 \text{ M NaCl} \\ 0.975 \text{ M } NaClO_4 \end{array} \right| \text{Ag,AgCl} -$$

The measurements have been carried out with different buffer ratios. In this case, the solutions S, T_1 and T_2 used to prepare the lefthand cell solutions had the following compositions (see also Table 2):

$$\text{S:} \begin{cases} C_M \text{ M } Ni(ClO_4)_2 \\ C_H \text{ M } HClO_4 \\ (1.00 - 3C_M) \text{ M } NaClO_4 \end{cases}$$

$$T_1\text{: } 1.000 \text{ M } NaN_3$$

$$T_2\text{: } \begin{cases} 2C_M \text{ M } Ni(ClO_4)_2 \\ 2C_H \text{ (or} \sim 2C_H) \text{ M } HClO_4 \\ (1.00 - 6C_M) \text{ M } NaClO_4 \end{cases}$$

On the first addition of equal volumes of solutions T_1 and T_2 a buffer of the ratio $C_H:C_L$ was formed. Apart from the effect of the complex formation, $I = 1$ is maintained.

The free ligand concentration [L] has been calculated from

$$[L] = K_a(C_H - h)/h \quad (3)$$

where h is found according to eqn. (1).

The ligand number $\bar{n}$ is obtained from

$$\bar{n} = (C_L - C_H + h - [L])/C_M \quad (4)$$

From $\bar{n}([L])$, the constants β_j are calculated in the usual manner.

Calorimetric measurements on the nickel(II) azide system. Both buffered and unbuffered solutions were used in the calorimetric measurements. Because of the volatility of hydrazoic acid, a low buffer ratio was used. When ligand was added to a solution of the central ion (Table 4, a–e), deviations were observed for high values of C_M when high ligand concentrations were reached.

These points are not included in the subsequent calculations. In the back titration procedure (see Table 4, f–i), where the central ion was added to a solution of the ligand, the hydrolysis was negligible due to the low central ion concentration, high ligand concentrations and consequently effective complex formation.

The enthalpy changes have been calculated by the least squares computer program "Letagrop Kalle".[18]

RESULTS

The results from the "Kalori" program and the potentiometrically determined formation constant for the proton azide system are given below:

K (M^{-1}) $(2.77 \pm 0.07) \times 10^4$ (pot),
$-\Delta H°$(kJ mol^{-1}) 12.76 ± 0.09,
$(2.58 \pm 0.69) \times 10^4$ (cal.)
12.77 ± 0.09

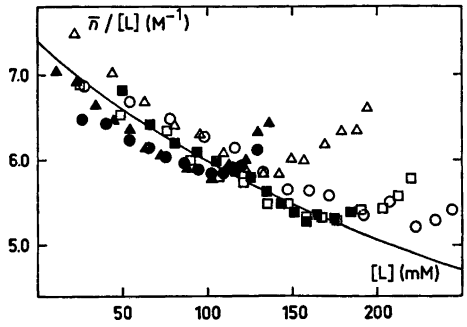

Fig. 1. $\bar{n}/[L]$ *vs.* [L] plot, the integration of which gives the X-functions, *cf.* Table 2. The curve has been computed from the values of β_j.

Table 4. Enthalpy data of the nickel(II) azide system. For all series: $V_0 = 90.00$ ml and $V = (V_0 + v)$ ml.

(a) S: $C_M = 20.00$ mM, $C_H = 0.4$ mM, $C_{NaClO_4} = 939.6$ mM
T: $C_L = 1000$ mM

v (ml), Q_{corr} (J), δQ_{corr} (J): 3.00, 0.816, 0.034; 6.00, 0.416, 0.020; 9.00, 0.399, 0.062; 12.00, 0.428, 0.046; 15.00, 0.388, 0.093; 18.00, 0.403, 0.049; 21.00, 0.390, 0.048; 24.00, 0.356, 0.066; 27.00, 0.347, 0.056.

(b) S: $C_M = 40.00$ mM, $C_H = 0.9$ mM, $C_{NaClO_4} = 879.1$ mM
T: $C_L = 1000$ mM

v (ml), Q_{corr} (J), δQ_{corr} (J): 3.00, 1.634, 0.078; 6.00, 0.792, −0.005; 9.00, 0.799, 0.032; 12.00, 0.801, 0.058; 15.00, 0.840, 0.018; 18.00, 0.819, 0.030; 21.00, 0.816, 0.029; 24.00, 0.807, 0.002; 27.00, 0.817, −0.039.

(c) S: $C_M = 40.00$ mM, $C_H = 0.9$ mM, $C_{NaClO_4} = 879.1$ mM
T: $C^\circ_L = 1000$ mM, $C^\circ_H = 100.0$ mM

v (ml), Q_{corr} (J), δQ_{corr} (J): 3.00, 1.573, 0.061; 6.00, 0.694, −0.004; 9.00, 0.721, 0.009; 12.00, 0.699, 0.053; 15.00, 0.711, 0.047; 18.00, 0.692, 0.061; 21.00, 0.673, 0.066; 24.00, 0.689, 0.030; 27.00, 0.707, −0.011.

(d) S: $C_M = 60.00$ mM, $C_H = 1.3$ mM, $C_{NaClO_4} = 818.7$ mM
T: $C^\circ_L = 1000$ mM, $C^\circ_H = 100.0$ mM

v (ml), Q_{corr} (J), δQ_{corr} (J): 3.00, 2.219, 0.072; 6.00, 0.984, −0.059; 9.00, 0.978, 0.012; 12.00, 0.992, 0.035; 15.00, 1.017, 0.029; 18.00, 1.026, 0.023; 21.00, 1.046, −0.006; 24.00, 1.140, −0.118.

(e) S: $C_M = 100.0$ mM, $C_H = 2.12$ mM, $C_{NaClO_4} = 697.9$ mM
T: $C^\circ_L = 1000$ mM, $C^\circ_H = 100.0$ mM

v (ml), Q_{corr} (J), δQ_{corr} (J): 3.00, 3.495, 0.003; 6.00, 1.405, −0.133; 9.00, 1.426, −0.062; 12.00, 1.467, −0.034; 15.00, 1.532, −0.052; 18.00, 1.598, −0.090.

(f) S: $C_L = 200.0$ mM, $C_{NaClO_4} = 800.0$ mM
T: $C_M = 100.0$ mM, $C_H = 2.12$ mM, $C_{NaClO_4} = 697.9$ mM

v (ml), Q_{corr} (J), δQ_{corr} (J): 3.00, 0.732, −0.064; 6.00, 0.530, 0.059; 9.00, 0.487, 0.054; 12.00, 0.463, 0.035; 15.00, 0.410, 0.049.

(g) S: $C_L = 400.0$ mM, $C_{NaClO_4} = 600.0$ mM
T: $C_M = 100.0$ mM, $C_H = 2.12$ mM, $C_{NaClO_4} = 697.9$ mM

v (ml), Q_{corr} (J), δQ_{corr} (J): 3.00, 1.411, −0.126; 6.00, 1.061, 0.109; 9.00, 0.991, 0.107; 12.00, 0.984, 0.026; 15.00, 0.924, 0.013.

(h) S: $C_L = 600.0$ mM, $C_{NaClO_4} = 400.0$ mM
T: $C_M = 100.0$ mM, $C_H = 2.12$ mM, $C_{NaClO_4} = 697.9$ mM

v (ml), Q_{corr} (J), δQ_{corr} (J): 3.00, 1.850, −0.071; 6.00, 1.529, 0.145; 9.00, 1.509, 0.060; 12.00, 1.543, −0.069; 15.00, 1.586, −0.200.

(i) S: $C_L = 800.0$ mM, $C_{NaClO_4} = 200.0$ mM
T: $C_M = 100.0$ mM, $C_H = 2.12$ mM, $C_{NaClO_4} = 697.9$ mM

v (ml), Q_{corr} (J), δQ_{corr} (J): 3.00, 2.160, 0.006; 6.00, 1.942, 0.115; 9.00, 1.994, −0.040; 12.00, 1.990, −0.133.

Table 5. Calculations, assuming two or three mononuclear complexes.

β_1 (M^{-1})	7.1	7.0	7.5	7.6	7.4	7.4	7.6	7.2	7.4
β_2 (M^{-2})	24	26	18	13	16	16	13	18	18
β_3 (M^{-3})				40	30	25	10	20	20
σ(Ref. 18)	0.216	0.227	0.181	0.077	0.073	0.071	0.068	0.070	0.070
U	2.715	2.980	1.893	0.336	0.300	0.284	0.264	0.280	0.280

Since the potentiometric measurements yield a much more precise value of K, this value is considered to be the "best" one.

The $\bar{n}$/[L] *vs.* [L] plot for the nickel(II) system is shown in Fig. 1. Within the limits of experimental errors, the course of this function up to [L]$\simeq$120 mM is almost the same for the different values of C_M and C_H. Thus, no polynuclear complexes seem to exist in this range. However, at higher free ligand concentrations deviations occur depending on both C_H and, especially, C_M (Fig. 1). These are probably due to the formation of polynuclear hydrolytic species,[19,20] maybe also to changes in the activity coefficients by progressive exchange of ClO_4^- for N_3^-. Similar deviations occur in the calorimetric measurements between series of different C_M.

The potentiometric measurements indicate two mononuclear complexes. A third one is possibly formed but no significant value of β_3 can be calculated. The calorimetric measurements are much better fitted with three mononuclear complexes, however, as is evident from the calculations (Table 5).

With the very last set of constants, a somewhat better fit to the potentiometric data is also achieved. This set has been accepted as the "best" one.

The thermodynamic functions of the nickel(II) and proton azide complexes and collected in Table 6.

DISCUSSION

Only two investigations of the nickel(II) azide system seem to have been performed previously.[5,6] Our value of β_1 agrees fairly well with that reported by Senise and Godinho under the same conditions, $\beta_1 = 6.9 \pm 0.1$ M^{-1}. The value of β_1 reported by Maggio *et al.*[6] ($\beta_1 = 11 \pm 1$ M^{-1}) in a perchlorate medium of $I = 3$ M is also compatible with the present result.

Our value of K for hydrazoic acid agrees excellently with that found potentiometrically by Maggio *et al.*[8] under the same conditions, *viz.* $K = 2.75 \times 10^4$ M^{-1}.

Our value of $\Delta H°$ for the proton azide system, -12.76 kJ mol^{-1}, agrees fairly well with that found calorimetrically at 25 °C and $I = 0$ by Gray and Waddington,[7] -15.05 kJ mol^{-1}. Also the value of Boughton and Keller,[10] -16 kJ mol^{-1}, at 26 °C and $I = 0$, found by means of the temperature coefficient method is well compatible with the calorimetric determinations. This is not unexpected for a system involving only one reaction with a large heat effect.

Table 6. The overall formation constants and the values of $\Delta G°_j$, $\Delta H°_j$ and $\Delta S°_j$ for the consecutive steps of the nickel(II) and hydrogen azide systems at 25.00 °C and $I = 1.00$ M. The errors given correspond to three standard deviations or to estimated errors.

System	j	β_j (M^{-j})	$-\Delta G°_j$ (kJ mol^{-1})	$-\Delta H°_j$ (kJ mol^{-1})	$\Delta S°_j$ (J mol^{-1} K^{-1})
$Ni^{2+} - N_3^-$	1	7.4 ± 0.4	4.96 ± 0.13	0.96 ± 0.14	13.4 ± 0.6
	2	18 ± 6	2.2 ± 0.8	3.3 ± 0.8	-3.7 ± 3.7
	3	20 ± 10	0.3 ± 1.5	10.3 ± 1.7	-34 ± 8
$H^+ - N_3^-$	1	$(2.77 \pm 0.07) \times 10^4$	25.36 ± 0.06	12.76 ± 0.09	42.3 ± 0.4

The value of $\Delta S° = 39.3$ J mol^{-1} K^{-1} at 25 °C that can be calculated from the data of D'Orazio and Wood [12] agrees surprisingly well with our value, 42.3 ± 0.4 J mol^{-1} K^{-1}.

An enthalpy change close to zero is found for the first nickel azide complex, as should be expected for a reaction between a moderately hard acceptor and a moderately hard donor. As the complex formation goes on, the consecutive steps become more and more exothermic, as is also to be expected on account of the progressively weaker hydration. Consequently, the entropy change decreases from its originally positive value to negative ones. While the first complex is entropy stabilized, the following ones are entirely enthalpy stabilized.[21,22]

In the proton azide system, on the other hand, already the coordination of the first, and only, ligand is a strongly exothermic reaction, providing about half of the free energy decrease of the reaction. Certainly the proton must be characterized as a predominantly hard acceptor, since it prefers fluoride ion to the heavier halides, hydroxide ion to hydrogensulfide ion, *etc.* This is readily understood on account of its high charge density which implies strong electrostatic attraction. On the other hand, the bonds formed by the proton are markedly covalent, at least in case of donors which are not very hard. In such cases, the extra bonding energy would tend to make the reaction exothermic. At the same time, the entropy gain is quite high, on account of the strong hydration of the proton. Proton complexes therefore often constitute exceptions from the general rule that the formation of very strong complexes in aqueous solution involves either a large gain of entropy ($\Delta S° \gg 0$) or a large decrease of enthalpy ($\Delta H° \ll 0$) but never both.[22]

Further discussion will be postponed until the results of the following investigations are available.

Acknowledgements. We are much indebted to Dr. Lennart Kullberg for good advice on the execution of the measurements, and for many interesting discussions. These investigations have been supported by Statens naturvetenskapliga forskningsråd (The Swedish Natural Science Research Council). The stay at the University of Lund for one of us (E. Avşar), has been made possible by a generous fellowship from the Scientific and Technical Research Council of Turkey. The support given by these organizations is gratefully acknowledged.

REFERENCES

1. Ahrland, S., Avşar, E. and Kullberg, L. *Acta Chem. Scand. A 28* (1974) 855.
2. Ahrland, S. and Kullberg, L. *Acta Chem. Scand. 25* (1971) 3692.
3. Kullberg, L. *Acta Chem. Scand. A 28* (1974) 897.
4. Sillén, L. G. and Martell, A. E. Eds., *Stability Constants of Metal-Ion Complexes*, Chemical Society, London, Special Publications No. *17*, (1964) and No. *25* (Supplement to No. *17*) (1971).
5. Senise, P. and Godinho, O. E. S. *J. Inorg. Nucl. Chem. 32* (1970) 3641.
6. Maggio, F., Romano, V. and Pellerito, L. *J. Electroanal. Chem. 15* (1967) 227.
7. Gray, P. and Waddington, T. C. *Proc. Roy Soc. A 235* (1956) 106.
8. Maggio, F., Romano, V. and Pellerito, L. *Ann. Chim. (Rome), 57* (1967) 191.
9. Burns, E. A. and Chang, F. D. *J. Phys. Chem. 63* (1959) 1314.
10. Boughton, J. H. and Keller, R. N. *J. Inorg. Nucl. Chem. 28* (1966) 2851.
11. Bunn, D., Dainton, F. S. and Duckworth, S. *Trans. Faraday Soc. 57* (1961) 1131.
12. D'Orazio, L. A. and Wood, R. H. *J. Phys. Chem. 67* (1963) 1435.
13. Bolzán, J. A., Jáuregui, E. A. and Arvia, A. J. *Electrochim. Acta 8* (1963) 841.
14. Brown, A. S. *J. Amer. Chem. Soc. 56* (1934) 646.
15. Ahrland, S. and Kullberg, L. *Acta Chem. Scand. 25* (1971) 3471.
16. Ahrland, S. and Kullberg, L. *Acta Chem. Scand. 25* (1971) 3457.
17. Karlsson, R. and Kullberg, L. *Chemica Scr. In press.*
18. Arnek, R. *Ark. Kemi 32* (1970) 81.
19. Burkov, K. A., Lilič, L. S. and Sillén, L. G. *Acta Chem. Scand. 19* (1965) 14.
20. Arnek, R. *Acta Chem. Scand. 22* (1968) 1102.
21. Schwarzenbach, G. *Pure Appl. Chem. 24* (1970) 307; *Chimia 27* (1973) 1.
22. Ahrland, S. *Struct. Bonding (Berlin) 15* (1973) 167.

Received June 9, 1975.

Acta Chemica Scandinavica A 29 (1975) 890—894

Thermodynamics of Metal Complex Formation in Aqueous Solution. X. A Calorimetric and Potentiometric Study of the Azide Complexes of Zinc(II)

STEN AHRLAND AND EFRAIM AVŞAR*

Inorganic Chemistry 1, Chemical Center, University of Lund, P.O.B. 740, S-220 07 Lund 7, Sweden

The stability constants and the enthalpy changes for the formation of the azide complexes of zinc(II) have been determined in an aqueous medium of unit ionic strength with sodium perchlorate as a supporting electrolyte at 25.00 °C. The constants have been measured potentiometrically by means of an amalgam electrode, while the enthalpy changes were found calorimetrically. Four mononuclear complexes of moderate strength are formed. The first three steps are slightly endothermic, with a positive entropy change while the last step is exothermic, with a negative entropy change.

The studies of the thermodynamics of metal azide systems begun in the previous paper [1] of this series with nickel(II) is now continued with another divalent metal ion of mainly (a)-character, *viz.* zinc(II).

Like the previous investigations in this series,[1] the present one refers to a temperature of 25.00 °C and a medium of an ionic strength $I = 1.00$ M, with sodium perchlorate as the supplementary salt.

For this system, the most favourable method for the determination of the stability of weak complexes can be applied, *viz.* measurement of the free metal ion concentration, by means of the zinc amalgam electrode.

The stability constants have previously been determined potentiometrically by means of the dropping zinc amalgam electrode by Neves and Sant'Agostino [2] (at 25 °C and $I = 2.0$ M) and polarographically by Banerjea and Sing [3] at 25 °C and $I = 2$ M. However, no determination of the enthalpy changes connected with the complex formation seems to be reported so far.

EXPERIMENTAL

Chemicals. Sodium azide (B. D. H. and/or Merck) was purified and analyzed as described before.[1]

Zinc(II) perchlorate, zinc amalgam and sodium perchlorate were prepared and analyzed as before.[4] The Ag,AgCl electrodes were prepared according to Brown.[5]

Calculation of formation constants from potentiometric measurements of the free central ion concentration. The stepwise formation constants have been evaluated both graphically and numerically. The graphical method has been described before.[4] For the numerical calculations the least squares program "EMK" has been used.[6] This program minimizes the error square sum,

$$U(\beta_j) = \sum_{i=1}^{n} w_i (E_{M,i} - E_{M,i,\mathrm{calc}})^2$$

where w_i is the weight of individual observations, n the number of observations and $E_{M,i}$ the pertinent emf as defined before.[7] As the absolute random error in $E_{M,i}$ seems to be much the same for all points, these are given the same weight.

The potentiometric measurements. The emf of the following cell is measured:

$-\mathrm{Zn(Hg)}$	C_M M $\mathrm{Zn(ClO_4)_2}$ C_L M $\mathrm{NaN_3}$ $\mathrm{NaClO_4}$ to $I = 1.00$ M	1.00 M $\mathrm{NaClO_4}$	0.025 M NaCl 0.975 M $\mathrm{NaClO_4}$	Ag,AgCl +

* Present address: Technical University of Istanbul, Chemical Engineering Faculty, Department of Physical Chemistry, Macka-Istanbul, Turkey

A Leeds & Northrup 7555 Type K-5 potentiometer was used. The scale reading was reliable to ± 0.01 mV.

The measurements were arranged as titrations where the solutions in the left-hand half-cell were obtained by adding a known volume v (ml) of a solution T to $V_0 = 15.00$ ml of a solution S. The solutions S and T had the following compositions:

$$\text{S: } \begin{cases} C_M' \text{ M } Zn(ClO_4)_2 \\ (1.00 - 3C_M') \text{ M } NaClO_4 \end{cases} \qquad \text{T: } 1.000 \text{ M } NaN_3$$

Before and during the titrations the solutions were deaerated and mixed by a stream of purified nitrogen. To obtain the correct vapour pressure, the nitrogen was first bubbled through 1.00 M $NaClO_4$ solution. The potentials reached their equilibrium values very quickly, and the reproducibility was in general $\simeq 0.08$ mV for low ligand concentrations and even better for high concentrations.

In the same manner as before [7] it has been checked that the zinc amalgam electrode obeys Nernst's law.

Several difficulties arose in the measurements. First, the rapid dissolution of zinc amalgam in hydrazoic acid even at values of pH as high as $\simeq 5$ prevented the use of a buffered ligand solution. Also in the case of pure $Zn(ClO_4)_2$ solutions, the dissolution of zinc amalgam for low values of C_M was significant at values of pH $\lesssim 4$. For $C_M' = 5$ mM, and even for 10 mM, a steady decrease of emf was observed due to a gradual increase of C_M. At higher C_M' values, the dissolution of zinc amalgam was insignificant.

For this reason, an unbuffered ligand solution was used in the experiments, in spite of the fact that a perceptible hydrolysis of Zn^{2+} then takes place at high values of C_M. Five values of C_M' were used, *viz.* 10, 15, 20, 30 and 40 mM. For all series, the initial value of pH was about 5.

For $C_M' = 10$ mM, the initial pH was varied between 4.86 and 5.19 without any influence on the emf's. Consequently, no hydrolysis occurred.

For $C_M' = 15$ mM, two initial values of pH were used, 4.74 and 5.04. At a certain ligand concentration, hydrolysis set in and the solution became cloudy. At this point, the titrations were interrupted. Higher ligand concentrations could be reached without precipitation if large volumes were added directly and the equilibrium emf's measured before the slow formation of solid phase had had time to occur. Similar procedures were adopted also for all the series of higher C_M'. In order to minimize the errors due to the dissolution of the zinc amalgam electrode, the amalgam was added after the ligand solution and the emf then measured immediately. This could be done as the values of E_0' were very reproducible and therefore easy to determine separately.[7]

Both the graphical procedure and a curve-fitting program, executed by a high-speed computer, indicated four mononuclear complexes. Both methods gave almost the same value of the formation constants. The "EMK" program [6] which uses the directly measured potentials and the corresponding concentrations of metal and ligand as input data gave, on the other hand, slightly different values.

The calorimetric measurements. The calorimeter and the measurement technique have been described before.[8] Every titration series was in general carried out twice and the reproducibility was usually within 0.06 J.

A buffered ligand solution was used, in order to prevent the hydrolysis of zinc [9] during the titration. Although it is *per se* desirable to use high ratios of $C_H:C_I$ in order to suppress the hydrolysis as far as possible, very high ratios cannot be recommended because of the volatility of hydrazoic acid which easily causes the formation of explosive metal azides on various parts of the instrument. A leakage of acid will moreover affect the measured heats of reaction significantly. It is therefore advisable to work with low buffer ratios or preferably no buffer at all, if the hydrolysis is negligible.

In four of the eight titrations series, a buffered ligand solution was added to a solution of zinc perchlorate (Table 1, a–e). In order to reach the high ligand concentrations where the higher complexes are formed, reversed titrations were also performed. In these, zinc perchlorate solution was added to both buffered and unbuffered azide solutions (Table 1, e–h). Here, Q_{corr} is the heat change corrected for dilution, *i.e.* $Q_{corr} = (Q_{exp} - Q_{dil})$ and δQ_{corr} is the difference between the heat change calculated for each point from the ΔH_j and β_j of all the species involved and the experimentally measured heat change, *i.e.* $\delta Q_{corr} = (Q_{corr,calc} - Q_{corr})$.

The enthalpy changes have been calculated by the least squares computer program "Letagrop Kalle".[10]

RESULTS AND DISCUSSION

Data pertaining to the potentiometric measurements on the zinc(II) azide system are collected in Table 2.

The following sets of constants are calculated by the two procedures mentioned above:

Overall constants	Graphical and curve-fitting	"EMK"
β_1 (M^{-1})	5.48 ± 0.15	5.73 ± 0.60
β_2 (M^{-2})	18.0 ± 3.9	21 ± 12
β_3 (M^{-3})	147 ± 26	145 ± 60
β_4 (M^{-4})	254 ± 46	280 ± 90

The errors given correspond to three standard deviations. As can be seen, the errors given by

Table 1. The enthalpy data for the formation of the azide complexes of zinc(II). For all series: $V_0 = 90.00$ ml and $V = (V_0 + v)$ ml.

(a) S: $C_M = 20.00$ mM, $C_{NaClO_4} = 940.0$ mM and pH = 5.01
T: $C^\circ_L = 1000$ mM, $C^\circ_{HClO_4} = 200.0$ mM

v (ml), $-Q_{corr}$ (J), δQ_{corr} (J): 3.00, 0.719, 0.061; 6.00, 0.698, −0.059; 9.00, 0.811, −0.053; 12.00, 0.935, −0.000; 15.00, 0.981, 0.019; 18.00, 1.008, 0.056; 21.00, 0.955, 0.069; 24.00, 0.846, −0.002; 27.00, 0.765, −0.033.

(b) S: $C_M = 20.00$ mM, $C_{NaClO_4} = 940.0$ mM and pH = 4.28
T: $C^\circ_L = 1000$ mM, $C^\circ_{HClO_4} = 200.0$ mM

v (ml), $-Q_{corr}$(J), δQ_{corr} (J): 3.00, 0.595, −0.016; 6.00, 0.658, −0.096; 9,00. 0.796, −0.069; 12.00, 0.889, −0.047; 15.00, 0.896, −0.067; 18.00, 0.901, −0.051; 21.00, 0.875, −0.043; 24.00, 0.808, −0.050; 27.00, 0.738, −0.050.

(c) S: $C_M = 40.00$ mM, $C_{NaClO_4} = 880.0$ mM and pH = 5.04
T: $C^\circ_L = 1000$ mM, $C^\circ_{HClO_4} = 200.0$ mM

v (ml), $-Q_{corr}$ (J), δQ_{corr} (J): 3.00, 1.180, −0.001; 6.00, 1.303, −0.018; 9.00, 1.473, −0.005; 12.00, 1.668, 0.076; 15.00, 1.717, 0.067; 18.00, 1.743, 0.086; 21.00, 1.546, −0.078; 24.00, 1.453, −0.112; 27.00, 1.397, −0.094.

(d) S: $C_M = 60.00$ mM, $C_{NaClO_4} = 820.0$ mM and pH = 4.90
T: $C^\circ_L = 1000$ mM, $C^\circ_{HClO_4} = 200.0$ mM

v (ml), $-Q_{corr}$ (J), δQ_{corr} (J): 3.00, 1.620, 0.010; 6.00, 1.734, −0.026; 9.00, 1.933, −0.006; 12.00, 2.116, 0.038; 15.00, 2.223, 0.063; 18.00, 2.233, 0.045; 21.00, 2.191, 0.019; 24.00, 2.113, −0.017; 27.00, 2.025, −0.023.

(e) S: $C^\circ_L = 500.0$ mM, $C^\circ_{HClO_4} = 100.0$ mM, $C^\circ_{NaClO_4} = 600.0$ mM
T: $C_M = 100.0$ mM, $C_{NaClO_4} = 700.0$ mM and pH = 4.24

v (ml), $-Q_{corr}$ (J), δQ_{corr} (J): 3.00, 2.399, 0.068; 6.00, 2.241, −0.004; 9.00, 2.150, −0.009; 12.00, 2.036, −0.025; 15.00, 1.914, −0.042.

(f) S: $C^\circ_L = 700.0$ mM, $C^\circ_{HClO_4} = 100.0$ mM, $C^\circ_{NaClO_4} = 400.0$ mM
T: $C_M = 100.0$ mM, $C_{NaClO_4} = 700.0$ mM and pH = 4.24

v (ml), $-Q_{corr}$ (J), δQ_{corr} (J): 3.00, 2.545, 0.063; 6.00, 2.483, 0.025; 9.00, 2.468, 0.025; 12.00, 2.427, 0.011; 15.00, 2.382, 0.001.

(g) S: $C_L = 800.0$ mM, $C_{NaClO_4} = 200.0$ mM
T: $C_M = 100.0$ mM, $C_{NaClO_4} = 700.0$ mM and pH = 4.24

v (ml), $-Q_{corr}$ (J), δQ_{corr} (J): 3.00, 2.602, 0.141; 6.00, 2.509, 0.035; 9.00, 2.514, 0.032; 12.00, 2.538, 0.051; 15.00, 2.532, 0.046.

(h) S: $C_L = 1000$ mM
T: $C_M = 100.0$ mM, $C_{NaClO_4} = 700.0$ mM and pH = 4.24

v (ml), $-Q_{corr}$ (J), δQ_{corr} (J): 3.00, 2.380, −0.033; 6.00, 2.423, −0.012; 9.00, 2.312, −0.142; 12.00, 2.378, −0.092; 15.00, 2.429, −0.054.

"EMK" are much larger than the errors of the other set. Since the input data to the curve-fitting procedure consist of the graphically estimated free ligand concentrations and the corresponding values [11] of X, any errors in the evaluation of the free ligand concentrations will not be introduced in the subsequent calculations. Consequently, smaller errors are likely to occur when this procedure is used.

Since a somewhat better fit to the calorimetric data is obtained from the estimates of the "EMK" program, this set of constants is considered as the "best" one.

The heat effects accompanying the complex formation are rather small. Therefore, fairly high Zn^{2+} concentrations have to be used, and the heats of dilution of participating species must moreover be determined very carefully. Further,

Table 2. Corresponding values of v, C_L and E_M for the zinc azide system.

C_M' (mM)→		10.00	15.00	20.00	30.00	40.00
v (ml)	C_L (mM)	E_M (mV)				
0.25	16.39	1.15	1.11	1.09	1.06	1.00
0.50	32.26	2.26	2.21	2.15	2.09	1.99
0.75	47.62	3.38	3.27	3.22	3.12	2.96
1.00	62.50	4.51	4.45	4.36	4.16	3.97
1.25	76.92	5.68	5.57	5.52	5.24	5.03
1.50	90.91	6.98	6.77	6.66	6.32	6.06
1.75	104.5	8.20	7.96	7.81	7.41	7.07
2.00	117.6	9.53	9.15	8.95	8.52	8.07
2.50	142.9	11.91	11.58	11.32	10.62	10.07
3.00	166.7	14.32	13.98	13.54	12.82	12.04
3.50	189.2	16.69	16.26	15.73	14.87	13.99
4.00	210.5	18.90	18.36	17.82	16.89	15.81
4.50	230.8	21.12	20.48	19.90	18.89	17.73
5.00	250.0	23.14	22.52	21.85	20.78	19.63
6.00	285.7	26.90	26.28	25.50	24.39	23.09
7.00	318.2	30.21	29.66	28.88	27.67	26.32
8.00	347.8	33.23	32.69	31.87	30.68	29.22
9.00	375.0	35.96	35.40	34.59	33.53	32.18
10.00	400.0	38.45	37.84	37.06	36.04	34.82
11.00	423.1	40.59	40.04	39.29	38.30	37.11
12.00	444.4	42.51	41.99	41.29	40.35	39.22
13.00	464.3	44.26	43.80	43.06	42.23	41.15
14.00	482.8	45.87	45.45	44.78	43.97	42.92
15.00	500.0	47.35	46.96	46.30	45.56	44.55
16.00	516.1			47.68	47.00	46.05

hydrazoic acid is formed, or dissociated, during the titrations. To correct for this, the values of K and $\Delta H°$ of the proton azide determined in the previous investigation [1] have been applied.

The thermodynamic functions of the azide complexes of zinc(II) are given in Table 3.

In spite of the difference of medium, our values of β_j agree fairly well with those reported by Neves and Sant'Agostino [2] ($\beta_1 = 6.0$ M^{-1}; $\beta_2 = 22$ M^{-2}; $\beta_3 = 220$ M^{-3}; $\beta_4 = 780$ M^{-4} at 25 °C and $I = 2$ M).

The enthalpy changes for the consecutive complexes of the zinc(II) azide system are all slightly endothermic, except the last step which is weakly exothermic. The complex formation between zinc and azide ions, with exception of the last step, is entropy stabilized which should be expected when the donors and the acceptors involved are hard.[12–14]

A striking feature of the azide system of zinc(II) is the abrupt increase of both $\Delta S°_j$ and $\Delta H°_j$ that takes place at the third step, but

Table 3. The overall formation constants and the values of $\Delta G°_j$, $\Delta H°_j$ and $\Delta S°_j$ for the consecutive steps of the azide complexes of zinc(II) at 25.00 °C and $I = 1.00$ M. The errors given correspond to three standard deviations.

j	β_j (M^{-j})	$-\Delta G°_j$ (kJ mol^{-1})	$\Delta H°_j$ (kJ mol^{-1})	$\Delta S°_j$ (J mol^{-1} K^{-1})
1	5.73 ± 0.60	4.33 ± 0.26	2.57 ± 0.30	23.1 ± 1.3
2	21 ± 12	3.2 ± 1.4	2.3 ± 1.7	19 ± 7
3	145 ± 60	4.8 ± 1.7	7.6 ± 2.3	42 ± 9
4	280 ± 90	1.6 ± 1.3	−6.5 ± 3.8	−16 ± 12

remarkably enough not at the second step as is the case for most zinc(II) systems. The reason for the discontinuities is probably changes of co-ordination taking place during the complex formation, so that the increased number of water molecules released will be reflected in the entropies. As the liberation of water is an endothermic process, similar discontinuities, though less marked, also are expected in the enthalpies. At these steps, the value of $\Delta S°_j$ will therefore be particularly high and $\Delta H°_j$ will be less exothermic, or more endothermic, than normally.[14]

Acknowledgement. The support given to these investigations by Statens naturvetenskapliga forskningsråd (The Swedish Natural Science Research Council) and the Scientific and Technical Research Council of Turkey is gratefully acknowledged.

REFERENCES

1. Ahrland, S. and Avsar, E. *Acta Chem. Scand. A 29* (1975) 881.
2. De Almeida Neves, E. F. and Sant'Agostino, L. *Anal. Chim. Acta 49* (1970) 591.
3. Banerjea, D. and Sing, I. P. *J. Indian Chem. Soc. 39* (1962) 353.
4. Ahrland, S. and Kullberg, L. *Acta Chem. Scand. 25* (1971) 3692.
5. Brown, A. S. *J. Amer. Chem. Soc. 56* (1934) 646.
6. Karlsson, R. *Private communication.*
7. Ahrland, S., Avsar, E. and Kullberg, L. *Acta Chem. Scand. A 28* (1974) 855.
8. Ahrland, S. and Kullberg, L. *Acta Chem. Scand. 25* (1971) 3471.
9. Gubeli, A. O. and Ste-Marie, J. *Can. J. Chem. 45* (1967) 827.
10. Arnek, R. *Ark. Kemi 32* (1970) 81.
11. Fronæus, S. In Jonassen, H. B. and Weissberger, A. *Technique of Inorg. Chem.* Interscience, New York, London 1963, Vol. 1, Chapter 1.
12. Ahrland, S. *Helv. Chim. Acta 50* (1967) 306.
13. Ahrland, S. *Struct. Bonding (Berlin) 5* (1968) 118.
14. Ahrland, S. *Struct. Bonding (Berlin) 15* (1973) 167.

Received June 9, 1975.

Acta Chemica Scandinavica A 29 (1975) 895—906

Nucleophilic Substitutions on *o*-Nitrobenzeneselenenyl Halogenides (Cl and Br). A Kinetic Study

TOR AUSTAD

Department of Chemistry, University of Bergen, N-5014 Bergen-Univ., Norway

The rate of reaction between *o*-nitrobenzeneselenenyl halogenides (Cl and Br) and 20 different nucleophiles has been measured in methanol using a stopped-flow spectrophotometer. For each of the nucleophiles examined, the kinetic plots showed the reaction to be of second order, first order in each of the reactants. A linear relationship between log k_2 and E° (oxidation potential) was established for anionic nucleophiles having the same nucleophilic atom. The proton basicity of the nucleophile was found to be negligible in determining the reactivity towards Se^{II}, and within the experimental errors the rate constants were found to be the same when changing the leaving group from bromide to chloride. The mechanism has been discussed in terms of previous studies concerning substitution reactions on *o*-nitrobenzenesulfenyl substrates.

Nucleophilic substitution reactions on divalent selenium are generally believed to be much faster than the analogous reactions on divalent sulfur. Thus, kinetic studies involving nucleophilic substitutions on Se^{II} are far less numerous than those on divalent sulfur. Due to the large decrease in the rate of reaction between two negatively charged ions observed in a dipolar aprotic solvent as compared with a protic solvent,[1] kinetic experiments of the reaction between various polythionates containing divalent selenium atoms in the chain ($^-O_3S-Se-SO_3^-$, $^-O_3S-Se-Se-SO_3^-$, and $^-O_3S-S-Se-S-SO_3^-$) and ionic cyanide have successively been performed in acetonitrile.[2,3] Apart from these studies, no systematic kinetic work concerning nucleophilic attack on Se^{II} has been reported in the literature until now.

However, a number of nucleophilic displacement reactions on divalent selenium are known, and a relative measure of the selenophilicity of various seleno bases has been obtained by studying systems of the type depicted by eqn. 1.[4–6]

$$Nu_1^- + R-Se-Nu_2 \rightleftharpoons R-Se-Nu_1 + Nu_2^- \quad (1)$$

With regard to nucleophilic attack on S^{II}, Foss [7,8] has pointed out that the reactivity of thio nucleophiles increases in the order of increasing oxidation potential of the systems:

$$2Nu^- \rightleftharpoons Nu-Nu + 2e^- \quad E^\circ \quad (2)$$

that is, the nucleophilic reactivity increases with increasing ease of oxidation of the thio anion to the corresponding disulfide. Data from displacement reactions on Se^{II} appear to indicate a similar relationship.[4–6,9]

Sulfenyl sulfur has been characterised as a soft electrophilic centre, comparable to peroxide oxygen.[10] In nucleophilic substitution on the sulfenyl sulfur atom of the trithionate ion, $^-O_3S-S-SO_3^-$, in 50 wt % methanol-water, Ritter and Krueger [11] have pointed out that although polarizability of the nucleophile is the dominant factor, basicity is also important. According to the HSAB principle,[12] divalent selenium is believed to be an even softer electrophilic centre than divalent sulfur. Consequently, the hydrogen basicity of the nucleophile, as a factor determining the reactivity, is supposed to be less important for divalent selenium than for divalent sulfur.

Many equilibrium and kinetic studies concerning nucleophilic attack on S^{II} are available. It therefore appears reasonable to discuss kinetic data involving displacement on Se^{II} in relation to previous studies on S^{II}. The kinetic

data so far [2,3] indicate that nucleophilic substitutions on Se^{II} follow the same mechanism as proposed for nucleophilic attack on S^{II}, which in most cases is believed to fit a synchronous bimolecular mechanism.[13] This is in agreement with the crystal structures of a number of selenium(II) complexes which have been determined.[14–16] The complexes may, according to Foss,[17] be regard as reaction intermediates or models for the transition state in nucleophilic substitution on Se^{II}.

In this paper we wish to report a kinetic study on the reaction between *o*-nitrobenzeneselenenyl halogenides (Br and Cl) and 20 different nucleophiles in methanol. The main purpose of the work is to obtain a quantitative measure for the nucleophilicity of the various seleno bases towards Se^{II}, and to shed further light on the factors determining reactivity. Finally the reaction mechanism will be discussed.

RESULTS

The substrate *o*-nitrobenzeneselenenyl halogenide was chosen because the products are stable and many of them have been synthesised previously.[18] The products of the reaction between the various nucleophiles and the substrate, reaction (3), are listed in Table 1.

$$X-Se-R+Nu^- \xrightarrow{MeOH} Nu-Se-R+X^- \qquad (3)$$

where R = *o*-nitrophenyl and X = Cl or Br

In all cases the reaction 3 showed excellent second order kinetics, first order in each of the reactants. The rate of reaction was followed at 430 nm applying a stopped-flow spectrophotometer. The experimental data on the reaction between *o*-nitrobenzeneselenenyl bromide and the various nucleophiles are tabulated in Table 2.

The nucleophilicity of the dithiocarbamates (Nos. 1 and 2) appears to be very much affected by the organic moiety linked to the nitrogen atom, and it seems to parallel the basicity of the corresponding secondary amines. The pK_a values of piperidine and dimethylamine are 11.12 and 10.73, respectively.

The di-*O*-ethyldithiophosphate ion (No. 8) is more than twice as nucleophilic towards Se^{II} as is the corresponding di-*O*-methyl anion (No.

Table 1. Products of the reaction between various nucleophiles and *o*-nitrobenzeneselenenyl bromide.

No.	Compound (R = *o*-nitrophenyl)	Ref.	M.p. °C [b]
1	R–Se–S–C(S)–(piperidyl)	[a]	148 (lit. 134)[c]
2	R–Se–S–C(S)–$N(Me)_2$	[a]	189
3	R–Se–S–Ph	20	54–55
4	R–Se–CN	21	143
5	R–Se–S_2O_3K	18	*ca.* 190 dec.
6	R–Se–S–$P(S)Me_2$	[a]	117
7	R–Se–S–$P(S)(OMe)_2$	[a]	89
8	R–Se–S–$SP(S)(OEt)_2$	[a]	62
9	R–Se–S–$P(O)(OEt)_2$	18	Oil
10	R–Se–S–$P(O)(O\text{-}iPr)_2$	[a]	Oil
11	R–Se–Se–$P(O)(OMe)_2$	[a]	42
12	R–Se–Se–$P(O)(OEt)_2$	[a]	Oil
13	R–Se–Se–$P(O)(O\text{-}iPr)_2$	[a]	Oil
14	R–Se–S–SO_2–Me	18	96
15	R–Se–S–SO_2–Ph	18	147
16	R–Se–SCN	18	107
17	R–Se–SeCN	22	109–110
18	R–Se–S–$C(NH_2)_2Br$	[a]	199
19	R–Se–Se–$C(NH_2)_2Br$	[a]	216
20	R–Se–SO_2–Ph	18	109

[a] This work. [b] The values of the melting points correspond with those given in the references quoted. [c] Ref. 19.

Table 2. Pseudo-first-order rate constant (k) and second-order rate constant (k_2) for the reaction between *o*-nitrobenzeneselenenyl bromide and different nucleophiles in methanol at 25 °C.

No.	Nucleophile	[Nu] × 10^2 M	k s^{-1}	k_2 M^{-1} s^{-1}	E° [a] (V)
1	(piperidyl)–C(=S)–S^-	0.50 1.00	22.4 41.5	4200	(+0.25)
2	$(Me)_2$–N–C(=S)–S^-	0.399 0.798 1.59 2.40	11.5 22.6 43.9 64.3	2667	(+0.21)
3	Ph–S^-	0.585 1.17 2.33	40.1 76.5 170.2	7000	+0.3 [b]
4	CN^-	0.50 1.00 2.00 3.00	3.58 8.64 18.7 30.0	994	+0.19 [b]
5	$S_2O_3^{2-}$	0.30 0.35 0.40	0.376 0.425 0.505	125	−0.169 [c]
6	$(Me)_2$P(=S)–S^-	0.50 1.00 2.00 3.00	1.75 3.66 7.08 10.43	350	(−0.03)
7	$(MeO)_2$P(=S)–S^-	0.50 1.00 2.00 3.00 4.00	0.0854 0.144 0.293 0.443 0.559	14.5	(−0.37)
8	$(EtO)_2$P(=S)–S^-	0.50 1.00 2.00 3.00 4.00	0.150 0.366 0.682 1.18 1.59	35.3	(−0.28)
9	$(EtO)_2$P(=O)–S^-	1.00 2.00 3.00	0.0207 0.0408 0.0573	1.97	−0.53 [d]
10	$(iPrO)_2$P(=O)–S^-	0.50 1.00 2.00 3.00	0.0247 0.0493 0.0939 0.136	4.57	−0.50 [d]
11	$(MeO)_2$P(=O)–Se^-	0.50 1.00 2.00 3.00	0.439 1.09 2.47 3.56	120	−0.37 [d]
12	$(EtO)_2$P(=O)–Se^-	0.50 1.00 2.00	0.859 1.59 3.12	160	−0.34 [d]

Table 2. Continued.

13	$(iPrO)_2\overset{O}{\overset{\|}{P}}-Se^-$	0.50 1.00 2.00 3.00	1.21 2.21 4.48 6.67	222	-0.31^d
14	$Me-\overset{O}{\overset{\|}{\underset{\|}{S}}}-S^-$ (O)	1.00 2.00 3.00 4.00	0.0305 0.0566 0.0848 0.110	2.82	-0.54^e
15	$Ph-\overset{O}{\overset{\|}{\underset{\|}{S}}}-S^-$ (O)	0.50 2.00	0.0148 0.0683	3.25	-0.49^e
16	SCN^-	1.00 2.00 4.00	0.00158 0.00519 0.00286	0.133	-0.77^f
17	$SeCN^-$	0.50 1.00	0.00887 0.0173	1.73	$\approx -0.57^g$
18	$(NH_2)_2C=S$	0.50 1.00 2.00 3.00	0.313 0.545 1.01 1.61	53.3	-0.42^h
19	$(NH_2)_2C=Se$	0.50 1.00 2.00	11.9 27.8 53.6	2625	-0.24^i
20	$Ph-\overset{O}{\overset{\|}{\underset{\|}{S}}}$ (O)	0.25 0.50 1.00 2.00	0.00487 0.0108 0.0203 0.0407	2.05	

[a] The values in parentheses are estimated from k_2 and Fig. 1. [b] Ref. 11. [c] Ref. 23, [d] Ref. 24, [e] Refs. 8 and 25, [f] Ref. 26, [g] Ref. 27, [h] Ref. 28, [i] Ref. 29.

7), which suggests that the nucleophilic nature of the group $-\overset{S}{\overset{\|}{P}}-S^-$ is very sensitive to electronic effects. The high reactivity of the dimethyldithiophosphinate ion (No. 6) relatively to the above mentioned dithiophosphates, indicates that the inductive effect caused by the oxygen atoms in compounds Nos. 7 and 8 is superior to the mesomeric backbonding effect.

With regard to the reactivity of the di-*O*-alkylmonothiophosphates, Nos. 9 and 10, and the seleno analogues, Nos. 12 and 13, Table 2 shows that the nucleophilicities of these anions are also very sensitive to the organic moiety. The seleno nucleophiles are more powerful nucleophilic agents towards Se^{II} than are the corresponding thio nucleophiles, by a factor of nearly 100.

The difference in the nucleophilic nature of seleno and thio nucleophiles is, however, smaller in the case of the selenocyanate ion (No. 17) and the thiocyanate ion (No. 16). The former is about 13 times more reactive towards Se^{II} than is the latter.

The small difference in the rate constants of the methanethiosulfonate ion (No. 14) and the benzenethiosulfonate ion (No. 15), shows that the electronic arrangement on the thiosulfonate group, $-SO_2-S^-$, is very little affected by the

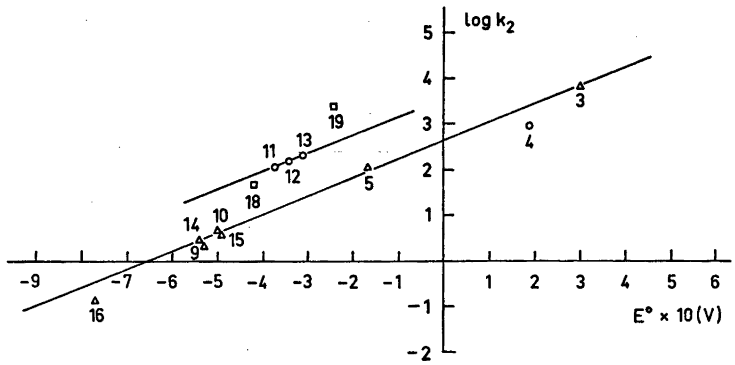

Fig. 1. Logarithm of the rate constants for the reaction of nucleophiles with *o*-nitrobenzeneselenyl bromide as a function of the oxidation potential of the nucleophile. The numbers correspond to those listed in Table 2.

organic group attached to the sulfonyl sulfur atom.

Table 2 further shows that the thiophenolate ion (No. 3) is the strongest nucleophile, and that the cyanide ion is nearly 10 times more nucleophilic than the thiosulfate ion. It is further seen that the rate constants of the benzenesulfinate ion (No. 20) and the selenocyanate ion (No. 17) are nearly identical in methanol.

In the case of the two neutral nucleophiles, *i.e.*, thiourea (No. 18) and selenourea (No. 19), the reaction product is a salt, eqn. 4.

$$\mathrm{Br-Se-R + (NH_2)_2C=X \xrightarrow{MeOH}}$$
$$\mathrm{(NH_2)_2C^+ - X - Se - R + Br^-} \qquad (4)$$

where R = *o*-nitrophenyl and X = S or Se
According to Table 2, selenourea is about 50 times more reactive than thiourea.

The column to the right in Table 2 contains the oxidation potentials for the nucleophiles. The values which are placed in parentheses are estimated by means of the second order rate constants and Fig. 1. In all cases the oxidation potentials are based on the system represented by eqn. 2. In order to verify if there exists any relationship between k_2 and E°, a graphical representation of log k_2 *versus* E° was made, Fig. 1.

The figure shows that the thio nucleophiles $Ph-S^-$, $S_2O_3^{2-}$, $(iPrO)_2P(O)-S^-$, $Me-SO_2-S^-$, and $(EtO)_2P(O)-S^-$ appear to conform to a linear relationship between log k_2 and E°. With regard to the di-*O*-alkylmonoselenophosphates, Fig. 1 clearly shows that these nucleophiles give a relationship different from that found for the thio nucleophiles. The values of the second order rate constants for the seleno nucleophiles are higher than predicted by the oxidation potentials relatively to the thio nucleophiles.

However, all the thio nucleophiles do not lie on the same line in the log $k_2 - E^\circ$ plot. Thiourea has a higher value of k_2 than predicted by the oxidation potential, while k_2 of the thiocyanate ion is lower than expected from the E° value. The same trend is also found for the analogous seleno nucleophiles, *i.e.*, selenourea has a higher reactivity and selenocyanate a lower one than expected from their E° values relatively to the di-*O*-alkylmonoselenophosphates.

The effect on the rate constants when changing the leaving group from bromide to chloride has been studied for some of the nucleophiles. The experimental data for the reaction between *o*-nitrobenzeneselenenyl chloride and five different nucleophiles are listed in Table 3. Table 4 clearly shows that when changing the leaving group from bromide to chloride, the effect on the second order rate constant is rather small. In all cases the ratio $k_2(Br)/k_2(Cl)$ is close to 1.

Second order rate constants for 6 of the nucleophiles have also been determined at different temperatures, 15, 25, 30, and 35 °C, and activation parameters have been calculated, Tables 5 and 6. It is seen that both the enthalpy and entropy of activation change

Table 3. Pseudo-first-order rate constant (k') and second-order rate constant (k_2) for the reaction between *o*-nitrobenzeneselenenyl chloride and different nucleophiles in methanol at 25 °C.

Nucleophile	Nu × 10^2 M	k' S^{-1}	k_2 M^{-1} s^{-1}
$S_2O_3^{2-}$	0.25	0.285	
	0.50	0.643	128
	1.00	1.213	
$(MeO)_2P(O)-Se^-$	0.50	0.392	
	1.00	0.892	90.0
	2.00	0.208	
$(iPrO)_2P(O)-S^-$	0.50	0.0332	
	1.00	0.0522	
	2.00	0.0971	5.0
$(iPrO)_2P(O)-Se^-$	0.50	1.05	
	1.00	2.02	202
	2.00	4.16	
CN^-	0.50	4.00	
	1.00	9.24	1066
	2.00	20.5	

drastically when going from an ionic nucleophile to a neutral one.

Finally some attempts were made to study kinetically the reaction between benzeneselenenyl bromide and the above mentioned nucleophiles in methanol, but in all cases the rate was too high. Even when using the weakest nucleophilic agent of Table 2, SCN^-, the reaction was too fast to be followed by means of the stopped-flow technique.

$$Ph-Se-Br + SCN^- \xrightarrow[MeOH]{k_2} Ph-Se-SCN + Br^- \quad (5)$$

Experimentally we may then conclude that the second order rate constant of reaction 5 is $k_2 > 6 \times 10^4$ M^{-1} s^{-1}. Thus, upon changing the substrate from *o*-nitrobenzeneselenenyl bromide to benzeneselenenyl bromide, the second order rate constant of the thiocyanate ion increases at least by at factor of 10^6.

Table 4. The effect of the leaving group in nucleophilic substitution on *o*-nitrobenzeneselenenyl bromide (chloride) in methanol at 25 °C.

Nucleophile	k_2 (Br) M^{-1} s^{-1}	k_2 (Cl) M^{-1} s^{-1}	k_2 (Br) / k_2 (Cl)
$S_2O_3^{2-}$	125	128	0.97
$(MeO)_2P(O)-Se^-$	120	90	1.33
$(iPro)_2P(O)-S^-$	4.57	5.0	0.91
$(iPro)_2P(O)-Se^-$	160	202	1.10
CN^-	994	1066	0.93

DISCUSSION

The data listed in Table 2 show that the relative order of reactivity of the anionic thio nucleophiles towards *o*-nitrobenzeneselenenyl halogenide is completely consistent with the nucleophilic sequence previously reported on the basis of exchange reactions on S^{II}, Se^{II} and Te^{II} in protic solvents.[4-8] The nucleophilicity progressively increases in the order: $SCN^- < (EtO)_2P(O)-S^- < Me-SO_2-S^- < Ph-SO_2-S^- < (iPrO)_2P(O)-S^- < (MeO)_2P(S)-S^- <$

Table 5. Pseudo-first-order rate constant (k') and second-order rate constant (k_2) for the reaction between *o*-nitrobenzeneselenenyl bromide and various nucleophiles in methanol at different temperatures.

Nucleophile	[Nu] × 10^2 M	15 °C k' s^{-1}	k_2 M^{-1} s^{-1}	25 °C k_2 M^{-1} s^{-1}	30 °C k' s^{-1}	k_2 M^{-1} s^{-1}	35 °C k' s^{-1}	k_2 M^{-1} s^{-1}
$(NH_2)_2C=S$	0.5	0.252			0.333		0.363	
	1.0	0.521	48.9	53.3	0.609	60.5	0.672	66.9
	2.0	0.912			1.14		1.27	
$(iPrO)_2P(O)-S^-$	0.5	0.0151			0.0365		0.0432	
	1.0	0.0313	3.08	4.57	0.0627	6.10	0.0927	8.39
	2.0	0.0608			0.118		0.152	
$(iPrO)_2P(O)-Se^-$	0.5	0.648			1.26		1.49	
	1.0	1.33	133	222	2.52	250	3.00	305
	2.0	2.67			4.85		6.11	
CN^-	0.5	2.29			5.36		6.80	
	1.0	4.60	500	994	11.0	1110	14.6	1460
	2.0	10.8			25.1		33.8	
$(NH_2)_2C=Se$	0.5	9.24			13.7		15.20	
	1.0	19.8	1950	2625	29.7	2820	33.1	3225
	2.0	38.8			55.6		61.5	

$(EtO)_2P(S)-S^- < S_2O_3^{2-} < Me_2P(S)-S^- < Me_2N-C(S)-S^- <$ (piperidyl)$-C(S)-S^- <$ $Ph-S^-$.

Among the thio nucleophiles whose oxidation potentials are known, there appears to be a linear correlation between log k_2 and E°, Fig. 1. On the basis than the proton basicity of these nucleophiles differs widely ($pK_a \approx -6$ and $pK_a = 7.5$ in the case of $Me-SO_2-S^-$ and $Ph-S^-$, respectively), this relationship suggests that the proton basicity of the nucleophiles does not play any role in substitution reactions on Se^{II}.

One may notice that two of the thio nucleophiles, *i.e.*, the thiocyanate ion and especially thiourea do not appear to fit the log $k_2 - E^\circ$ relationship represented by the other thio nucleophiles. Due to the instability of thiocyanogen, $(SCN)_2$, in aqueous solution, the experimental E°-value [26] of the thiocyanate ion may perhaps be too high, and this may explain the discrepancy. Thiourea, being an uncharged nucleophile, probably is far less solvated in methanol than the other anionic thio nucleophiles, and therefore, according to Parker,[30] it may be a relatively stronger nucleophilic reagent towards Se^{II}. However, within these limitations the fit is very good.

The present results are in agreement with the findings of Foss [7-8] that in displacement reactions on divalent sulfur, thio anions of more positive E° will displace thio anions of lower E°.

Oxidation potentials of other thio anions may then be estimated by means of the second order rate constant and Fig. 1. The oxidation potentials of the nucleophiles (piperidyl)$-C(S)-S^-$, $Me_2NC(S)-S^-$, $Me_2P(S)-S^-$, $(MeO)_2P(S)-S^-$, and $(EtO)_2P(S)-S^-$ have been determined in this way, Table 2. The oxidation potential of the diethyldithiocarbamate ion has been measured as +0.33 V in 60 % ethanol by Gregg and Tyler.[31] The estimated E° values of the dithiocarbamates in this work are somewhat lower.

Table 6. Activation parameters for the reaction between *o*-nitrobenzeneselenenyl bromide and various nucleophiles in methanol at 25 °C.

Nucleophile	ΔH^* kcal/mol	ΔS^* cal/mol deg.	ΔF^* kcal/mol
$(NH_2)_2C=S$	3.3	−40	15.2
$(NH_2)_2C=Se$	3.7	−30	12.8
$(iPro)_2P(O)-S^-$	10.4	−21	16.7
$(iPrO)_2P(O)-Se^-$	6.8	−25	14.2
CN^-	8.7	−16	13.4

The relationship between log k_2 and E^o is not a general one that applies for all type of nucleophiles. This is clearly demonstrated by the di-*O*-alkylmonoselenophosphates which appear to make their own correlation, Fig. 1. However, the slopes of the lines that correspond to the thio nucleophiles and the seleno nucleophiles are similar. On the basis that the hydrogen basicity of the nucleophile is negligible in determining the reactivity towards Se^{II}, it is not possible to explain why the thio and the seleno nucleophiles form different log $k_2 - E^o$ plots by discussing the data in terms of the Edwards [32] equation (6).

$$\log (k_{Nu}/k_{H_2O}) = \alpha E_n + \beta H \quad (6)$$

According to Edwards,[32] E_n and H are the nucleophilic and basic constants for the nucleophiles, and α and β are the corresponding substrate constants. In the case of *o*-nitrobenzeneselenenyl bromide the present work gives α and β values of ≈ 3.9 and ≈ 0, respectively. The fact that the anionic thio nucleophiles and the seleno nucleophiles provide different log $k_2 - E^o$ plots, and the deviation of the points that correspond to thiourea and selenourea from these lines, suggests that a general representation of the nucleophilicity towards various substrates should contain at least two more parameters related to the nucleophiles. Concerning Se^{II} as the electrophilic centre, we may then conclude that the Edwards equation is unsuitable for determining the reactivity of the nucleophiles listed in Table 2.

The rate at which a nucleophile attacks a carbon atom sometimes parallels the affinity of the nucleophile for protons. Especially in a series of anions whose reactivity atom is the same, the connection between rate constant and pK_a values of the nucleophiles is well established.[33] Concerning a softer electrophilic centre, *i.e.*, Se^{II}, the present data indicate that there exists an analogous relation between the rate constant and the oxidation potential that changes with the nature of the nucleophilic atom and with the charge on the nucleophile.

The nucleophilic reactivity of the cyanide ion towards Se^{II} in methanol, in terms of its oxidation potential, is more like the reactivity of thio nucleophiles than of the seleno nucleophiles, Fig. 1.

Reaction mechanism

Both structural [14–16] and kinetic [2,3] data point to a nucleophilic attack on Se^{II} *trans* to the leaving group, followed by synchronous bond formation and breaking. Foss [17] has described the bonding in the transition state as a three-centre-four-electron bonding system.

o-Nitrobenzeneselenenyl compounds, like the analogous thio compounds, are usually found to be more stable than the unsubstituted compounds. This property of the ortho-substituted compounds is probably due to the formation of an intramolecular three-centre arrangement containing one of the oxygen atoms of the nitro group, the chalcogen atom, and the atom attached to the latter (I).[34]

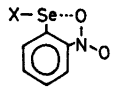

(I)

Thus, in the present substrate the position *trans* to the leaving group is already occupied by an intramolecular interaction between Se and O. In order to attack *trans* to the leaving group, the intramolecular three-centre arrangement of the substrate has to break down in solution, or if the three-centre-system is still maintained in solution, the nucleophile has to push the nitro group aside. In the latter case there will be an additional energy term for the three-centre formation between the nucleophile, the selenium atom, and the leaving group. Thus, the free energy of activation in the case of the *ortho*-nitro substrate should be higher than in the case of the unsubstituted substrate. The present kinetic experiments on the reaction between unsubstituted benzeneselenenyl bromide and ionic thiocyanate, which is believed to follow a synchronous mechanism, are in line with these statements.

On the other hand, a mechanism involving a rate determining break-down of the O···Se–X arrangement first-hand would predict the overall reaction to be of first order (independent of the nucleophile). However, such a mechanism is not in agreement with the kinetic data.

To gain further information about the reaction mechanism, the leaving group has been changed from bromide to chloride. The relative

nucleophilicity of Cl^- and Br^- towards S^{II} in protic medium has been found by Kice and co-workers [35] to have a factor of 35 in favour of Br^-. Considering divalent tellurium as the central atom, a large increase in the *trans* bond-lengthening effect was observed when substituting iodide for bromide.[36] With regard to divalent selenium it is not unreasonable to assume a similar increase in the *trans* bond-lengthening effect when going from chlorine to bromine. Thus, a synchronous mechanism in the present reaction probably should give rise to a marked change in the rate constant upon changing the leaving group from bromide to chloride. However, Table 4 clearly shows that within the experimental errors the rate constants are nearly unaffected by changing the leaving group.

On the assumption that the free energy of activation, ΔF^*, consists of an energy term associated to the break-down of the O···Se–X arrangement, ΔF^* (O···Se–X), and a second energy term associated to the displacement of the leaving group, ΔF^* (X), a synchronous bond formation and bond breaking can probably only take place on either of the following two conditions:

(1) ΔF^* (O···Se–X) has to be much larger than ΔF^* (X), and furthermore, the energy required to break up O···Se–Cl has to be nearly equal to the energy required to break up O···Se–Br. That is, ΔF^* (O···Se–X) $\gg$ ΔF^* (X) and ΔF^* (O···Se–Cl) $\approx$ ΔF^* (O···Se–Br). The high reactivity of benzeneselenenyl bromide relatively to the ortho-nitro substrate accords with the first statement.

(2) The difference in the free energy of activation associated to the break-down of O···Se–Cl and O···Se–Br, $\delta\Delta F^*$ (O···Se–X), must be nearly equal to the difference in the free energy of activation associated to the displacement of the two leaving groups Br and Cl, $\delta\Delta F^*$ (X). That is, $\delta\Delta F^*$ (O···Se–X) $\approx$ $\delta\Delta F^*$ (X). In terms of the *trans* bond-lengthening effect of the ligands,[36] the break-down of O···Se–Cl should require a higher energy than is the case for the break-down of the O···Se–Br arrangement. Moreover, the energy required to displace a bromide ion from Se^{II} is believed to be higher than the energy required to displace a chloride ion.

Alternatively, the present data can be explained by a two-step mechanism, eqn. 7.

$$R-Se-X + Nu^- \xrightarrow{\text{slow}} [\text{Intermediate}]^- \xrightarrow{\text{fast}} R-Se-Nu + X^- \quad (7)$$

The first step, the intermediate formation, is thought to be the rate determining step, and the second step is a fast elimination of the leaving group. Such a two-step addition-elimination process has been labelled S_AN by Kosower.[37] Bond formation thus preceeds bond breaking.

X-Ray crystallographic studies on *o*-nitrobenzeneselenenyl compounds show that the Se–X bond lies in the plane of the nitro group and the benzene ring.[34] Two ways of approach to the Se atom may be considered, *i.e.*, (a) nucleophilic attack *trans* to the phenyl group which appears very unlikely due to the large *trans* bond-lengthening effect of this group commonly observed,[17] and (b) nucleophilic attack normal to the plane of the molecule. The intermediate in the latter case may be represented by the complex (II).

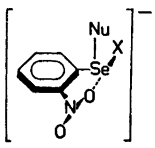

(II)

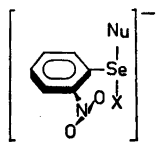

(III)

Concerning divalent selenium, such a configuration is, however, considered to be unlikely. Prior to the elimination of the leaving group, a fast rearrangement to the more energetic favourable form (III) may take place. The interaction between O and Se in (III) is probably smaller.

The overall mechanism may then be represented by eqn. 8.

$$I + Nu^- \xrightarrow[\text{rate det.}]{\text{slow}} [\text{intermediate(II)}] \xrightarrow{\text{fast}} [\text{intermediate(III)}] \xrightarrow{\text{fast}} \text{products} \quad (8)$$

A transition state similar to (III) has been suggested by Givens and Kwart [38] for the reaction between *o*-nitrobenzenesulfenyl chloride and the acetate ion.

Stable salts of phenyldiselenocyanatotellurate(II) and phenyldithiocyanatotellurate(II) have recently been prepared by Hauge and Vikane.[39] The structural geometry of these anions, which may be regarded as models for the transition state in nucleophilic substitution on divalent tellurium, have shown both of the anions to have a linear three-centre arrangement normal to the benzene ring in accordance with the intermediate (III).[40]

Likewise, Wynne and co-workers [41,42] have isolated a number of dihalo(aryl)selenate(II) and dihalo(aryl)tellurate(II) salts which probably have the same configuration around the chalcogen atom. The authors pointed out that 2,4-dinitrophenylselenenyl bromide was unreactive towards tetraorganylphosphonium halides, and the inability to isolate a dibromo(2,4-dinitrophenyl)selenate(II) is probably due to the presence of a coordinated *o*-nitro group and the instability of any higher coordinated species.[42]

No difference in the reaction mechanism has been suggested in the nucleophilic cleavage of unsubstituted and *o*-nitro substituted symmetrical disulfides by triphenylphosphine in aqueous dioxane.[43] The reactivity of these two disulfides towards Ph_3P is reported to be nearly the same. Moreover, the poor correlation in the Hammett plot of the *o*-nitrobenzenesulfenyl substrates suggests that the electronic requirements for these reactions are almost unimportant, and this is in agreement with a synchronous displacement reaction on S^{II}.[38,44]

The $O\cdots S-X$ arrangement of the *o*-nitrobenzenesulfenyl halide probably breaks down in solution, and a rotation about C–S takes place. The large difference in the rate constant between the unsubstituted benzeneselenenyl bromide and the *o*-nitro substituted substrate (a factor $> 10^6$) may indicate that the $O\cdots Se-X$ arrangement is still maintained in solution. Thus, the difference in the electrophilic behaviour of *o*-nitrobenzenesulfenyl and the analogous selenenyl compounds may be interpreted on the basis of the relative ability of the chalcogens to form stable three-centre arrangements, which is believed to follow the order $S \ll Se < Te$.[17]

Due to the difference in the solvation of the various nucleophiles in metanol, it is difficult to discuss the relative values of the activation parameters in Table 6. However, both ΔH^* and ΔS^* of the neutral nucleophiles (thiourea and selenourea) are smaller than for the anionic nucleophiles. The unfavourable entropy of activation of thiourea and selenourea may be explained by a strong solvation of the polar transition state relative to the initial state. It appears that the most strongly solvated nucleophile has the highest ΔS^*, which appears reasonable. The low ΔH^*-values of the neutral nucleophiles suggest that the transition states in these cases are relatively more stable than the transition states of the anionic nucleophiles. With regard to divalent tellurium as the central atom. Foss [17] has pointed out that neutral three-centre arrangements are usually more stable then anionic three-centre systems. Thus, the activation parameters may be related to a transition state of the three-centre type.

With regard to the reaction between *o*-nitrobenzeneselenenyl halogenide and the various nucleophiles, the present data cannot discriminate between the two possible mechanisms described above, *i.e.*, a synchronous bond formation and bond breaking and a two-step addition elimination process probably involving the selenium *d*-orbitals. However, in view of kinetic [2,3] and structural [14–16] data referred to earlier, the former mechanism appears to be the most reasonable one.

EXPERIMENTAL

Solvents. Methanol "Merck" *p.a.* was used without further purification. Acetonitrile was purified as reported previously.[1]

Substrates. *o*-Nitrobenzeneselenenyl bromide was prepared from *o*-nitrophenyl selenocyanate and excess of bromine in dry chloroform.[45] The product was recrystallized three times from light petroleum (40 – 60 °C). M.p. 65 °C (lit.[45] 64 – 65 °C).

o-Nitrobenzeneselenenyl chloride was kindly provided by Mr. R. Eriksen.[46]

Benzeneselenenyl bromide was synthesised from the diselenide and bromine in dry chloroform.[47] The compound was recrystallized three times from light petroleum (40 – 60 °C). M.p. 60 °C (lit.[48] 61 – 62 °C).

Nucleophiles. The following sources of the nucleophiles were employed: (piperidyl)–$CS_2Na.2H_2O$,[49] $Me_2NCS_2Na.2H_2O$,[49] Ph–SNa, Ph_4AsCN,[1] $(Ph_4As)_2S_2O_3$, $Me_2PS_2Na.2H_2O$,[50] $(MeO)_2PS_2K$,[51] $(EtO)_2PS_2NH_4$,[51] $(EtO)_2P(O)$–SNa,[24] $(iPrO)_2P(O)$–SNa,[24] $(MeO)_2P(O)$–SeNa,[24] $(EtO)_2P(O)$–SeNa,[24] $(iPrO)_2P(O)$–SeNa,[24] $MeSO_2SK$,[7] $PhSO_2SPh_4As$,[52] Ph_4AsSCN,[53] $Ph_4AsSeCN$,[53] $(NH_2)_2C=S$ ("Fluka", *puriss.*

p.a.), $(NH_2)_2C=Se$ ("Fluka", *purum*, recrystallized from water), $PhSO_2Na.2H_2O$.[7]

Sodium thiophenolate was prepared *in situ* by dissolving equivalent amounts of thiophenol and sodium in methanol.

$(Ph_4As)_2S_2O_3$ was precipitated from an aqueous solution of Ph_4AsCl and a large excess of $Na_2S_2O_3.5H_2O$. The dry compound was then dissolved in a small volume of absolute ethanol, and the insoluble sodium salts were filtered off. The solvent was removed in vacuum and the procedure was repeated twice. Iodometric analysis showed the compound to contain 97 % $(Ph_4As)_2S_2O_3$. (Found: C 65.61; H 4.83; S 7.21. Calc. for $C_{18}H_{40}O_3S_2As_2$: C 65.57; H 4.56; S 7.29).

Products. Most of the products of Table 1 were synthesised by the general procedure described by Foss.[18]

The dithiocarbamates, Nos. 1 and 2, Table 1, were recrystallized from benzene/light petroleum (40 – 60 °C) and pure benzene, respectively. The di-*O*-alkyldithiophosphates, Nos. 7 and 8, and the dimethyldithiophosphinate, No. 6, were recrystallized from benzene/light petroleum (40 – 60 °C).

The adducts of *o*-nitrobenzeneselenenyl bromide with thiourea and selenourea were isolated from acetonitrile. Equivalent amounts of the selenenyl bromide and the nucleophile were mixed, whereupon the product precipitated. The compounds were recrystallized from boiling acetonitrile. Both products, especially the adduct of selenourea, were slightly soluble in this solvent.

Kinetics. The rate of the reaction between the *o*-nitrobenzeneselenenyl substrates and the various nucleophiles was followed at 430 nm with a Durrum stopped-flow spectrophotometer. The kinetic runs were performed under pseudo-first order conditions applying a large excess of the nucleophile. The substrate concentration was about $1 - 3 \times 10^{-4}$ M. The second order rate constants were obtained by plotting the pseudo-first order constant against the concentration of the nucleophile. In all cases excellent second order kinetics were observed.

The reaction between benzeneselenenyl bromide and ionic thiocyanate was too fast to be followed at 460 nm by means of the stopped-flow technique. The second order rate constant of this reaction was calculated to be greater than 6×10^4 M^{-1} s^{-1}.

Acknowledgement. The author wishes to thank Professor O. Foss for valuable discussion and Dr. S. Husebye for providing samples of the dithiocarbamates and the di-*O*-alkyldithiophosphates.

REFERENCES

1. Austad, T. *Acta Chem. Scand. A 28* (1974) 693.
2. Austad, T. *Acta Chem. Scand. A 29* (1975) 71.
3. Austad, T. *Acta Chem. Scand. A 28* (1974) 935.
4. Foss, O. *Acta Chem. Scand. 3* (1949) 435.
5. Foss, O. *Acta Chem. Scand. 3* (1949) 1385.
6. Foss, O. *Acta Chem. Scand. 6* (1952) 508.
7. Foss, O. *Kgl. Nor. Vitensk. Selsk. Skr.* (1945) No. 2 (1947).
8. Foss, O. *Acta Chem. Scand. 1* (1947) 307.
9. Foss, O. *Abstr. 24th. Intern. Congr. Pure Appl. Chem.*, Hamburg 2 – 8 September Vol. 4, p. 103, Butterworths, London 1974.
10. Kice, J. L. and Large, G. B. *J. Amer. Chem. Soc. 90* (1968) 4069.
11. Ritter, R. D. and Krueger, J. H. *J. Amer. Chem. Soc. 92* (1970) 2316.
12. Pearson, R. G. and Songstad, J. *J. Amer. Chem. Soc. 89* (1967) 1827.
13. Ciuffarin, E. and Fava, A. *Progr. Phys. Org. Chem. 6* (1968) 81.
14. Foss, O. and Hauge, S. *Acta Chem. Scand. 17* (1963) 1807.
15. Hauge, S., Opedal, D. and Aarskog, J. *Acta Chem. Scand. 24* (1969) 1107.
16. Hauge, S. and Sletten, J. *Acta Chem. Scand. 25* (1971) 3094.
17. Foss, O. *Pure Appl. Chem. 24* (1970) 31.
18. Foss, O. *J. Amer. Chem. Soc. 69* (1947) 2236.
19. Twiss, F., Jones, F. A. and Hadley, D. J. *British Patent 441, 653* (1936).
20. Rheinboldt, H. and Giesbrecht, E. *Justus Liebigs Ann. Chem. 568* (1950) 198.
21. Challenger, F. and Peters, A. T. *J. Chem. Soc.* (1928) 1369.
22. Rheinboldt, H. and Giesbrecht, E. *J. Amer. Chem. Soc. 81* (1959) 866.
23. Cobble, J. W., Stephens, H. P., McKinnon, I. R. and Westrum Jr., E. F. *Inorg. Chem. 11* (1972) 1669.
24. Foss, O. *Acta Chem. Scand. 1* (1947) 8.
25. Foss, O. *Acta Chem. Scand. 3* (1949) 986.
26. Bjerrum, N. and Kirschner, A. *Die Rhodanide des Goldes und das freie Rhodan*, Copenhagen 1918.
27. Hauge, S. *Acta Chem. Scand. 25* (1971) 3081.
28. Preisler, P. W. and Berger, L. *J. Amer. Chem. Soc. 69* (1947) 322.
29. Preisler, P. W. and Scortia, T. N. *J. Amer. Chem. Soc. 80* (1958) 2309.
30. Parker, A. J. *Chem. Rev. 69* (1969) 1.
31. Gregg, E. C. and Tyler, W. P. *J. Amer. Chem. Soc. 72* (1950) 4561.
32. Edwards, J. O. *J. Amer. Chem. Soc. 76* (1954) 1540.
33. Leffler, J. E. and Grunwald, E. *Rates and Equilibria of Organic Reactions*, Wiley, New York and London 1963, p. 243.
34. Eriksen, R. and Hauge, S. *Acta Chem. Scand. 26* (1972) 3153.
35. Kice, J. L. and Large, G. B. *J. Amer. Chem. Soc. 90* (1968) 4069.
36. Vikane, O. *Personal communication.*
37. Kosower, E. M. *Introduction to Physical*

Organic Chemistry, Wiley, New York 1968, p. 65.
38. Givens, E. N. and Kwart, H. *J. Amer. Chem. Soc. 90* (1968) 378.
39. Hauge, S. and Vikane, O. *Acta Chem. Scand. 27* (1973) 3596.
40. Hauge, S. and Vikane, O. *Personal communication.*
41. Wynne, K. J. and Pearson, P. S. *Inorg. Chem. 11* (1972) 1196.
42. Petragnani, N., Torres, L., Wynne, K. J. and Williams, D. J. *J. Organometal. Chem. 76* (1974) 241.
43. Overman, L. E., Matzinger, D., O'Connor, E. M. and Overman, J. D. *J. Amer. Chem. Soc. 96* (1974) 6081.
44. Brown, C. and Hogg, D. R. *Chem. Commun.* (1967) 38.
45. Behaghel, O. and Seibert, H. *Ber. Deut. Chem. Ges. 66* (1933) 708.
46. Eriksen, R. *Acta Chem. Scand. 26* (1972) 1274.
47. Rheinboldt, H. In Houben-Weyl, *Methoden der organischen Chemie*, 4th Ed., G. Thieme, Stuttgart 1955, Band IX, p. 1164.
48. Behaghel, O. and Seibert, H. *Ber. Deut. Chem. Ges. 65* (1932) 815.
49. Gleu, K. and Schwab, R. *Angew. Chem. 62* (1950) 320.
50. Kuchen, W., Strolenberg, K. and Metten, J. *Chem. Ber. 96* (1963) 1733.
51. Ketelaar, J. A. A. and Gersmann, H. R. *Rec. Trav. Chim. Pays-Bas 77* (1958) 973.
52. Austad, T. *Acta Chem. Scand. A 29* (1975) 241.
53. Austad, T., Songstad, J. and Åes, K. *Acta Chem. Scand. 25* (1971) 331.

Received May 27, 1975.

Acta Chemica Scandinavica A 29 (1975) 907—910

A Thermochemical Study of Hydrolysed $Bi(ClO_4)_3$ Solutions

ÅKE OLIN

Institute of Chemistry, University of Uppsala, P.O.B. 531, S-751 21 Uppsala, Sweden

The enthalpy and entropy changes of the hydrolysis reactions of Bi^{3+} have been determined by enthalpy titrations with hydrolysed $Bi(ClO_4)_3$ solutions in 3 M $(Na)ClO_4$ at 25 °C. The results were:

$Bi^{3+} + H_2O \rightarrow BiOH^{2+} + H^+$
$\Delta H° = 17 \pm 6$ kJ mol^{-1}; $\Delta S° = 27 \pm 20$ J K^{-1} mol^{-1}
$6Bi^{3+} + 12H_2O \rightarrow Bi_6(OH)_{12}^{6+} + 12H^+$
$\Delta H° = 133 \pm 3$ kJ mol^{-1}; $\Delta S° = 450 \pm 10$ J K^{-1} mol^{-1}

The measurements also indicate that at least one further complex is present in small amounts in addition to the species $Bi_6(OH)_{12}^{6+}$ and $BiOH^{2+}$ found earlier from emf measurements. It is tentatively identified as $Bi_3(OH)_4^{5+}$.

From emf measurements [1] on hydrolysed bismuth(III) perchlorate solutions in 3 M $(Na)ClO_4$ medium the following reactions and equilibrium constants were suggested

$6Bi^{3+} + 12H_2O \rightleftharpoons Bi_6(OH)_{12}^{6+} + 12H^+$;
$\beta_{12,6} = 2.14$ M^7
$Bi^{3+} + H_2O \rightleftharpoons BiOH^{2+} + H^+$; $\beta_{1,1} = 0.026$ M

Some years ago a calorimetric study was made on this system using the titration technique developed by Schlyter.[2] When the enthalpy changes of the above reactions were calculated by the methods described in Ref. 3, it was found that the estimated standard deviation in the heat evolved per addition was somewhat larger than expected from the calorimetric measurement uncertainties. This cast some doubt on the correctness of the hydrolysis scheme proposed from the emf data, particularly as the interpretation of such data is uncertain when high powers are present in the expressions for the equilibria. It was therefore decided to postpone further treatment of the calorimetric data until more evidence had been accumulated to establish the correctness of the formulas of the species present. A bismuth(III) hydroxide perchlorate formed from equilibrium solutions has now been shown from a crystal structure determination [4] to contain discrete hexameric units with the same structure as suggested from X-ray diffraction studies on solutions.[5] With the composition of the main complex now firmly established, the calculations on the data from the enthalpy titrations have been resumed and the results will be presented here.

EXPERIMENTAL

The experiments were carried out in the apparatus described by Schlyter [2] as a series of titrations in which a strongly acid $Bi(ClO_4)_3$ solution, T, was added to a hydrolysed bismuth(III) perchlorate solution, S, in the calorimeter. The compositions of S and T were chosen so that in each titration $[Bi(III)] = B$, and $[ClO_4^-] = 3.000$ M were kept constant. The analytical hydrogen ion concentrations, H, in the solutions were (B, H_S, H_T/mol dm^{-3}); 0.010, −0.01020,2.655; 0.025, −0.02552,2.892; 0.050, −0.05105,2.809; 0.100, −0.1306,2.580; 0,0,2.980.

Two titrations were made for each value of B. The results from the runs with $B = 0$ were used to correct the heat evolved per addition, Q, for the heat of dilution of the perchloric acid in the titrant. The preparation and analysis of the chemicals and stock solutions were made as described in Ref. 1.

CALCULATIONS

The data have been treated with the least squares computer program LETAGROP KALLE,[6] which searches for a set of parameters that minimizes the error square sum $U = \sum(Q_{calc} - Q_{exp})^2$. The parameters to be determined are primarily the enthalpy changes, $l_{p,q}$,

Table 1. Results from the least squares refinements $i-v$. Only parameters followed by the estimated standard deviation within parenthesis have been varied. The values of $l_{p,q}$ are in kJ mol^{-1}, $\sigma(Q)$ and δQ in J, and $\beta_{q,p}$ in $M^{(p-q+1)}$.

Refinement	$\beta_{12,6}$	$l_{12,6}$	$\beta_{1,1}\times 10^2$	$l_{1,1}$	$\sigma(Q)$	δQ	$\beta_{4,3}$	$l_{4,3}$
i	2.14	132	2.60	16	0.29			
		(1)		(2)				
ii	2.1	132	3.0	17	0.28			
	(0.2)	(1)	(0.2)	(3)				
iii	2.14	125	2.60	12	0.23	0.42		
		(1)		(2)		(0.08)		
iv	2.14	133	2.60	17	0.22		0.16	54
		(1)		(2)			(0.02)	(4)
v	2.14	133	2.60	14	0.23		0.16	56
		(0.5)		(2)				(4)

of the hydrolysis reactions $qBi^{3+}+pH_2O \rightleftharpoons Bi_q(OH)_p+pH^+$. For convenience, charges will be omitted on the complex. The equilibrium constants, $\beta_{p,q}$, can also be treated as adjustable parameters by the program as well as (constant) errors in the analyses of the solutions and in the measurement of Q. In order to save computer time only one of the titrations for each value of B was included in the calculations. Moreover, data for $B=0.1$ M were excluded at first, since most of the data for this B value refer to solutions with so high and varying acidities that it appeared doubtful if the basic assumption of constant activity factors was valid. The selected titrations comprise 56 data points (V/cm^3, Q/J). V denotes the volume of titrant added.

The calculations will be reported as a series of refinements ($i-v$) in which the $l_{p,q}$ have been computed under various assumptions. The results are collected in Table 1 for ease of comparison. A number within parenthesis is the estimated standard deviation (esd.) calculated by the program. If the value of a parameter is not followed by an esd. the parameter was kept constant during the refinement. $\sigma(Q)$ is the esd. of $Q_{calc}-Q_{exp}$.

i. $l_{12,6}$ and $l_{1,1}$ were calculated assuming the equilibrium constants from the emf measure-

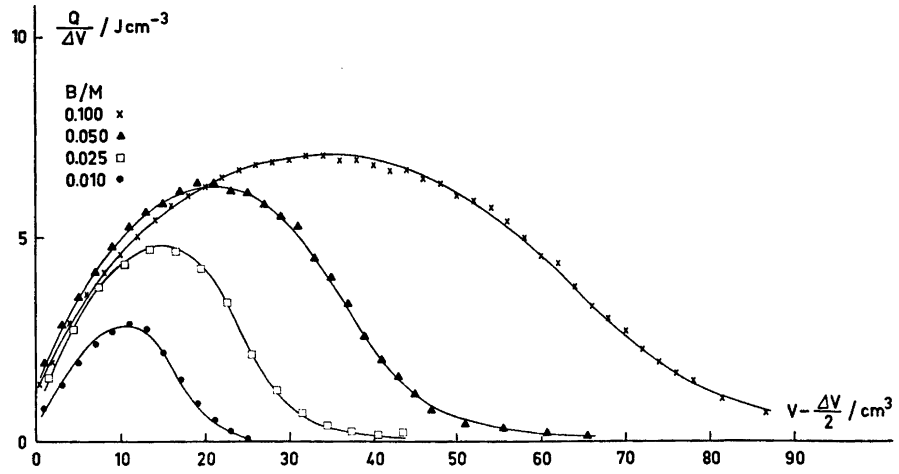

Fig. 1. The heat evolved in an experimental point per cm^3 of titrant added, $Q/\Delta V$, as a function of $V-\Delta V/2$. V is the total volume of titrant. The curves have been drawn through the $Q/\Delta V$ values calculated with the parameters from refinement *v*.

ments to be correct. The $\sigma(Q)$ is larger than the value expected from the calorimeter measurement uncertainties, 0.15 – 0.20 J, and the differences between Q_{calc} and Q_{exp} are systematic at the highest acidities. More heat is evolved than expected from the model. On the whole, however, there is a reasonable agreement between Q_{calc} and Q_{exp} and the fact that the former follows the rather unusual course of Q_{exp} (see Fig. 1) points to the essential correctness of the data and their interpretation. The heats evolved at high acidities moreover confirm that complexes other than $Bi_6(OH)_{12}^{6+}$, *viz.* $BiOH^{2+}$, must also be present. From the emf measurements this was not so easily recognized at high values of B on account of the large liquid junction potentials.

ii. $l_{p,q}$ and $\beta_{p,q}$ were varied simultaneously. The program partly failed to find the minimum in U (see "slumpskott" in LETAGROP program description). The values of the standard deviations are therefore approximate. A recalculation of $\beta_{12,6}$ and $\beta_{1,1}$ from the data given in Ref. 1 was made with the program LETAGROP VRID, version ETITR.[7] The following values were obtained: $\beta_{12,6} = 2.14(0.04)$ M[7] and $\beta_{1,1} = 2.64(0.04) \times 10^{-2}$ M. These values agree very well with those obtained graphically in the original work. $\sigma(E)$ was 0.18 mV for 134 data points (every second was used). The first four points in the 0.0001 M titration and the first point in the 0.0005 M titration showed large deviations between E_{calc} and E_{exp}. If these points were rejected $\sigma(E)$ dropped to 0.13 mV. Since there is good agreement between the equilibrium constants obtained from the emf and the calorimetric measurements the discrepancies in the heat data at high acidities are not likely to be caused by erroneous equilibrium constants. They may rather be caused by the presence of small amounts of additional complexes or systematic errors.

iii. Analytical and systematic errors in the calorimetric measurements. Since $Bi^{3+}(aq)$ is a rather strong acid the deviations at high acidities can not be removed by the introduction of analytical errors of reasonable magnitude. No calculations were therefore made on this assumption. One calculation on the 0.05 and 0.025 M titrations was performed with an assumed, constant error in Q, δQ. Despite the improvement in $\sigma(Q)$ the result is difficult to accept, since, it is hard to find a reasonable explanation for a δQ as large as 0.4 J.

iv. Additional complexes present. In this series of refinements it was assumed that in addition to $Bi_6(OH)_{12}^{6+}$ and $BiOH^{2+}$, $Bi_q(OH)_p$ was present. The following pairs of p and q were tested: (p,q), (2,1), (2,2), (3,2), (4,2), (3,3), (4,3), (5,3), (6,3), (4,4). These pairs include most of the p,q combinations found in the hydroxo complexes of metal ions. $\beta_{p,q}$ was estimated from the deviations between Q_{calc} and Q_{exp} at high acidities on the assumption that $l_{p,q}/p = 12.5$ kJ mol^{-1}. This is a rounded-off value based on $l_{12,6}$ and $l_{1,1}$. The (V,Q) data were next subjected to a least squares treatment in which $\beta_{12,6}$ and $\beta_{1,1}$ were kept constant and the other parameters varied. These calculations ruled out the combinations (2,1), (2,2), (3,3), and (4,4), which either failed to converge or decrease $\sigma(Q)$. The compatibilities of the remaining combinations with the emf data were next tested by calculating $\Delta E = E_{calc} - E_{exp}$ using the β values from the calorimetric data. This test definitely ruled out (4,2) and (6,3) which showed large ΔE. (3,2) showed smaller but systematic deviations and was also rejected, which left (4,3) and (5,3) as possible species. No choice between these alternatives could be made from the error square sums. The value of $l_{5,3} = 38(8)$ kJ mol^{-1} is smaller than expected, since $l_{p,q}/p$ in most systems has been found to be almost constant.[8] With one additional complex, $Bi_3(OH)_4^{5+}$ would hence be the most likely alternative and only data for this complex have been entered in Table 1.

A refinement of the emf data with $Bi_3(OH)_4^{5+}$ included gave $\beta_{12,6} = 2.09(0.04)$ M[7], $\beta_{1,1} = 2.60(0.04) \times 10^{-2}$ M, and $\beta_{4,3} = 0.20(0.07)$ M[2], and $\sigma(E) = 0.11$ mV (five points excluded). $\beta_{12,6}$ and $\beta_{1,1}$ are thus almost unaffected by the introduction of $Bi_3(OH)_4^{5+}$ and within one standard deviation the same value of $\beta_{4,3}$ is obtained from the emf and calorimetric measurements.

v. Data from one titration with $B = 0.1$ M were included in the refinement. $\sigma(Q)$ for 98 data points became 0.23 J, which may be compared with the value 0.32 J if $Bi_3(OH)_4^{5+}$ is left out. The agreement between Q_{calc} and Q_{exp} is shown in Fig. 1.

DISCUSSION

From Table 1 one may conclude that despite the various assumptions made, the values of $l_{12,6}$ and $l_{1,1}$ stay fairly constant. Since the relative amount of $BiOH^{2+}$ increases with decreasing B the value of $l_{1,1}$ obtained from refinements *i*, *ii*, and *iv* will be used. The presence of $Bi_3(OH)_4^{5+}$ is only tentative. The concentration of any additional complex is at most a few percent of B and its presence and composition hence difficult to establish. Further discussion of the data for $Bi_3(OH)_4^{5+}$ will therefore not be made.

Table 2 contains some thermodynamic quantities for $Bi_6(OH)_{12}^{6+}$ and $BiOH^{2+}$ calculated per mol of complex formed. Symbols without a subscript refer to the reaction

$$qBi^{3+} + pH_2O \rightarrow Bi_q(OH)_p + pH^+ \quad (1)$$

Quantities for the reaction

$$qBi^{3+} + pOH^- \rightarrow Bi_q(OH)_p \quad (2)$$

have subscripted symbols. In the calculations of these quantities, $\Delta H°$ for $H_2O \rightarrow H^+ + OH^-$ was taken as 54.8 kJ mol^{-1} and $\Delta S°$ as -88 J K^{-1} mol^{-1}.

The enthalpy and entropy parts of the free energy change for reaction (2) are both favourable. This is also the case for other metal ions. Reckoned per mol of hydroxide, the values of $-\Delta H°$ and $\Delta S°$ are amongst the largest hitherto observed and they make Bi^{3+}(aq) one of the strongest acids of its kind. $-\Delta H°_{OH}/p$ for hydroxo complexes of divalent metal ions are with few exceptions less than 35 kJ mol^{-1},[8] which is considerably less than 44 kJ mol^{-1} found for $Bi_6(OH)_{12}^{6+}$. Although a direct comparison of these figures is somewhat hazardous because of probable variations in the coordination numbers of the oxygen atoms, a larger value for the bismuth complex is reasonable on account of the higher charge of the Bi^{3+} ion. The entropy change, again reckoned per mol of hydroxide, is generally less than 100 J K^{-1} mol^{-1} for divalent metal ions.[8] The corresponding value for $Bi_6(OH)_{12}^{6+}$ is 125 J K^{-1} mol^{-1}. The greater reduction in net charge per metal ion which occurs for the bismuth complex probably causes the increase in $\Delta S°_{OH}/p$. The standard entropy of Bi^{3+}(aq), -190 ± 10 J K^{-1} mol^{-1},[9] is lower than for most divalent ions, which also can be expected to contribute to a higher ligational entropy for Bi^{3+}.

Table 2. Thermochemical data for hydroxo complexes of Bi^{3+}. Unsubscripted quantities refer to the reaction $qBi^{3+} + pH_2O \rightarrow Bi_q(OH)_p + pH^+$ and subscripted, to the reaction $qBi^{3+} + pOH^- \rightarrow Bi_q(OH)_p$. The limits of error correspond to 3σ.

	$Bi_6(OH)_{12}^{6+}$	$BiOH^{2+}$
$\Delta G°$/ kJ mol^{-1}	-1.89 ± 0.14	9.01 ± 0.15
$\Delta H°$/ kJ mol^{-1}	133 ± 3	17 ± 6
$\Delta S°$/ J K^{-1} mol^{-1}	450 ± 10	27 ± 20
$\Delta H°_{OH}$/ kJ mol^{-1}	-525	-38
$\Delta S°_{OH}$/ J K^{-1} mol^{-1}	1500	115

The wide variety of compositions found for the hydrolysis products of metal ions make correlations of the thermodynamic data for hydroxo complexes with such quantities as charge and size difficult to detect and few relationships of this type have been proposed. Messmer and Baes [10] suggested the relation; $\Delta S°_{OH}(corr)/p = 28 + 1.0Z^2$ cal K^{-1} mol^{-1}, where Z is the charge of the uncomplexed metal ion and $\Delta S°_{OH}(corr)$ is the entropy change corrected for the cratic part.[11] For $Bi_6(OH)_{12}^{6+}$ this quantity is 41 cal K^{-1} mol^{-1}, which is larger than predicted. The value of the constant term (28) appears, however, to be somewhat too low to judge from the data presented by Arnek.[8]

REFERENCES

1. Olin, Å. *Acta Chem. Scand. 11* (1957) 1445.
2. Schlyter, K. *Trans. Roy. Inst. Technol. Stockholm* (1959) No. 132.
3. Carell, B. and Olin, Å. *Acta Chem. Scand. 16* (1962) 2357.
4. Sundvall, B. *Acta Chem. Scand. A 28* (1974) 1036.
5. Danforth, M. D., Levy, H. A. and Agron, P. A. *J. Chem. Phys. 31* (1959) 1458.
6. Arnek, R. *Ark. Kemi 32* (1970) 81.
7. Brauner, P., Sillén, L. G. and Whiteker, R. *Ark. Kemi 31* (1969) 365.
8. Arnek, R. *Ark. Kemi 32* (1970) 55.
9. Vasil'ev, V. P. and Ikonnikov, A. A. *Zh. Fiz. Khim. 45* (1971) 292.
10. Mesmer, R. E. and Baes, C. F., Jr. *Inorg. Chem. 6* (1967) 1951.
11. Gurney, R. W. *Ionic Processes in Solution*, McGraw Hill, New York 1953.

Received May 30, 1975.

Acta Chemica Scandinavica A 29 (1975) 911—918

Fluoroalcohols. Part 23. A Near-infrared Study of the Hydrogen Bonding of Trifluoroethanol and Hexafluoro-2-propanol with Pyridine, Diphenyl Sulfoxide and Flavone

ANTTI KIVINEN,[a] JUHANI MURTO,[b] SEIJA LILJEQUIST[b] and SINIKKA VAARA[a]

[a] Department of Pharmacy, University of Helsinki, Fabianinkatu 35, SF-00170 Helsinki 17, Finland and [b] Department of Physical Chemistry, University of Helsinki, Meritullinkatu 1 C, SF-00170 Helsinki 17, Finland

Heteroassociation of 2,2,2-trifluoroethanol and 1,1,1,3,3,3-hexafluoro-2-propanol with pyridine, pyridine-*N*-oxide, flavone, and diphenyl sulfoxide in carbon tetrachloride was studied by near-infrared method, and spectral data for the 1:1 complexes of these acid-base pairs are reported. In the case of pyridine and pyridine-*N*-oxide, the 2:1 alcohol-base complexes were also studied. Results are also reported for the complexation of ethanol and 2-propanol with pyridine. The hydrogen-bonded OH stretching absorptions of hexafluoro-2-propanol–pyridine and hexafluoro-2-propanol–pyridine-*N*-oxide complexes are complicated in form. The reasons for this are discussed.

In our studies on the hydrogen bonding and other properties of fluorinated alcohols we needed a quantitative estimate of the H-bond strengths of some fluoroalcohol–base pairs. Accordingly, we report in this paper spectral measurements for ternary mixtures containing 2,2,2-trifluoro-ethanol (TFE) or 1,1,1,3,3,3-hexafluoro-2-propanol (HFP), and different bases in carbon tetrachloride.

EXPERIMENTAL

Chemicals. Ethanol, 2,2,2-trifluoroethanol, 1,1,1,3,3,3-hexafluoro-2-propanol and carbon tetrachloride were purified as before.[2] 2-Propanol (U.C.B., Belgium) was treated with molecular sieves 4A and distilled at atmospheric pressure, b.p. 82 °C. Pyridine (Noyry-Baker N. V., Deventer, Holland) was distilled at atmospheric pressure, b.p. 115–115.8 °C, and stored over molecular sieves 4A. Pyridine-*N*-oxide (Fluka A. G., Switzerland) was distilled, b.p. 113–116 °C/1 mmHg. Diphenyl sulfoxide (Aldrich Chemicals) was crystallized from light petroleum, m.p. 69–70 °C. Phenol (E. Merck A. G., Darmstadt, chromatographic grade), flavone (Koch-Light Laboratories Ltd., England *purissimum* grade) and pentadeuteriopyridine (E. Merck A. G., Darmstadt) were used as received.

Spectrometric measurements were carried out with a Beckman DK-2A spectrophotometer. The recording of the spectra and the preparation of solutions have been reported previously.[2–4] Concentrations were corrected for the thermal expansion of the solvent. As before, temperature cycling was used in recording the spectra; *i.e.*, before and after recordings at different temperatures the spectra were scanned at 25 °C to ascertain that no alcohol had evaporated. This technique also guarantees that no reaction occurred between carbon tetrachloride and the bases while the spectra were being recorded. (A slow reaction may occur especially in amine-carbon tetrachloride solutions. The presence of phenols or acidic alcohols seems to retard these reactions, however.[5])

The various alcohol-base complexes were scanned at room temperature from 4000 to 400 cm^{-1} with a Perkin-Elmer 337 spectrophotometer equipped with an external recorder. In some cases a Perkin-Elmer 621 spectrophotometer was also employed. Sealed cells equipped with NaCl or KBr windows were used.

Calculations. The values of the formation constants K_{11} of the 1:1 hydrogen-bonded complexes were calculated as described previously.[3]

Estimation of the values of the formation constants K_{21} of the 2:1 alcohol–base complexes was carried out as described previously.[4] Briefly, the method is as follows. The formation constants refer to the following equilibria:

$$A + B \rightleftharpoons AB;\ K_{11} = c_{AB}/c_A c_B \quad (1)$$

$$A + AB \rightleftharpoons A_2B;\ K_{21} = c_{A_2B}/c_A c_{AB} \quad (2)$$

In ternary alcohol – base – carbon tetrachloride mixtures, where the concentration of the alcohol exceeds that of the base, we can assume that the 2:1 alcohol – base complexes are the only higher complexes present in addition to 1:1 complexes. On introducing the auxiliary quantities $x = 1/c_A$ and $y = c_B^\circ/(c_A^\circ - c_A)$ where c_A° and c_B° are the total (formal) concentrations of alcohol and base, respectively, and c_A is the concentration of free alcohol at equilibrium, we obtain the equation

$$y = \left(1 - \frac{2K_{21}}{K_{11}}\right) + \frac{x}{K_{11}} + \frac{K_{21}(4K_{21} - K_{11})}{K_{11}x + 2K_{11}K_{21}} \quad (3)$$

The experimental values of x and y were computed and the parameters K_{11} and K_{21} were varied until the best fit of eqn. (3) to experimental points was found. The calculations were performed on a computer. Thermodynamic quantities were calculated in the usual way.[3]

The $\Delta\nu$OH values are believed to be accurate within $\pm 3-5$ cm^{-1}, ΔH values within $\pm$ 2 kJ mol^{-1} and K_{11} values within 10 %. For the accuracy of the K_{21} values, see Ref. 4.

The non-SI units used were: 1 M = 1 mol dm^{-3}; 1 mmHg = 133.3 Pa.

RESULTS AND DISCUSSION

It can be seen from the data collected in Table 1 that both flavone and diphenyl sulfoxide (DPSO) are almost equally strong as proton acceptors. HFP is a somewhat stronger proton donor than TFE, the formation constants for complexes of the former being about ten times those for the latter with the same base. It has been noted previously that the hydrogen-bonding ability is of the same order of magnitude for TFE and phenol,[3] despite the difference in their pK_a values. Gramstad [6] has reported the values $\Delta\nu$OH = 294 cm^{-1} and $-\Delta H$ = 24.1 kJ mol^{-1} for the phenol – DPSO system. These values do not differ markedly from the respective values for the TFE – DPSO system. The data in Table 1 reveal also that DPSO is a somewhat weaker proton acceptor than DMSO, since the frequency shift for the TFE – DMSO system is 306 cm^{-1} and that for the HFP – DMSO system is 437 cm^{-1}, the respective $-\Delta H$ values being 23.6 kJ mol^{-1} and 29.2 kJ mol^{-1}.[3]

The estimation of the values of $\Delta\nu$OH for alcohol – DPSO systems was straightforward, but the same was not true when flavone was the base (Fig. 1). Hydrogen bonding to the carbonyl oxygen often leads to an unsymmetrical νOH complex absorption band.[7–10] The estimate of $\Delta\nu$OH given in Table 1 for the HFP – flavone system is somewhat inaccurate because of the complex form of the "bonded" νOH bands. Some measurements

Table 1. Spectral data for 1:1 hydrogen-bonded complexes in carbon tetrachloride at 25 °C. Py = pyridine, PyO = pyridine-*N*-oxide, Py-d_5 = pentadeuteriopyridine.

System	K_{11} / M^{-1}	$\Delta\nu$OH / cm^{-1}	$-\Delta H^\circ$ / kJ mol^{-1}	$-\Delta G^\circ$ / kJ mol^{-1}	$-\Delta S^\circ$ / J K^{-1} mol^{-1}
TFE – flavone	43.7	254 [a]	21.7	9.37	41.4
HFP – flavone	352	399 [a]	29.7	14.6	51.0
TFE – $(C_6H_5)_2SO$	43.7	255	21.9	9.37	42.3
HFP – $(C_6H_5)_2SO$	448	378	30.7	15.1	51.9
MeOH – Py	2.63	287			
EtOH – Py	1.97	280	16.7	1.67	50.2
EtOH – Py-d_5	2.13	280			
i-PrOH – Py	1.53	270	16.1	1.05	50.2
t-BuOH – Py	1.25	260			
TFE – Py	35.3	427	26.0	8.83	57.7
TFE – PyO	180	408	27.7	12.9	49.8
HFP – Py	608	> 530 [a]	38.3	15.9	75.3
HFP – Py-d_5	564	552			
HFP – PyO	2485	> 507 [a]	36.9	19.4	59.0
PhOH – Py	46.6	471 [a]			

[a] The band is complex in form; see text.

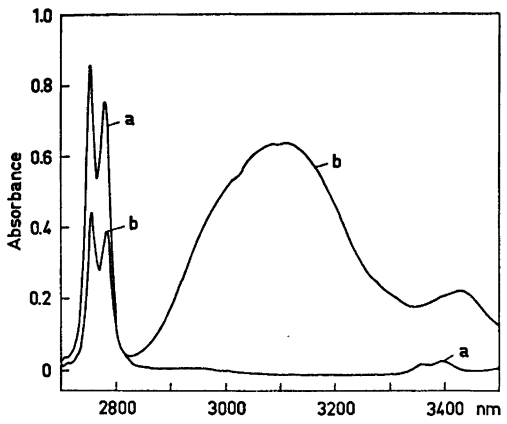

Fig. 1. Illustrative spectra for the system HFP – flavone. Solvent CCl_4, temperature 25 °C, path length 20 mm. Curve a, 0.00448 M HFP; curve b, 0.00448 M HFP + 0.00487 M flavone (0.00487 M flavone as reference).

were also made with hexachloro-2-propanol (HCP) as the acid. The association band of the spectrum of the HCP – flavone system was not symmetric; the frequency shift was estimated as 404 cm^{-1}. Flavone itself has absorptions between 3200 and 3300 cm^{-1} (probably overtones of the C=C and C=O vibrations between 1600 and 1650 cm^{-1}) [11] and incomplete compensation of these absorptions may also affect the spectra. Surprisingly, the bonded OH absorption of the TFE – flavone system seems to be symmetric in form.

The explanation given by Fritzsche [7] and Joris and Schleyer [9] for the existence of two association bands due to hydrogen bonding to carbonyl oxygen, namely, that in the carbonyl group there are two bonding sites (n- and π-electron sites) seems quite reasonable.

The results obtained in this work for hydrogen bonding of various alcohols with pyridine and its N-oxide are presented in Table 1. For comparison, some literature values for fluoroalcohol – pyridine systems are collected in Table 2. In most cases the latter are in good agreement with our values (Table 1). In addition, the ΔH-values reported by Becker [12] for ordinary alcohol – pyridine complexes are almost equal to those obtained here. The value for the complexation enthalpy ($-\Delta H = 25.5$ kJ mol^{-1}) reported by Findlay and Kidman [13] seems to be too large.

The $\Delta\nu$-values reported for methanol – pyridine vary from 267 to 304 cm^{-1} and for phenol – pyridine from 444 to 492 cm^{-1} (see the references given by Joris and Schleyer [9]). The former of these systems has a simple "bonded" νOH band, and the scatter of the literature values of $\Delta\nu$ may in part (but not wholly) be due to the fact that some authors have extrapolated the $\Delta\nu$'s to infinite dilution whereas others have not. The values of $\Delta\nu$OH obtained in this way may be as much as 15 – 20 cm^{-1} smaller than the unextrapolated values. We consider this extrapolation method somewhat arbitrary, however. The values of $\Delta\nu$OH reported in Table 1 are unextrapolated, high dilution values which are practically independent of the concentration of base.

The data in Table 1 reveal that for ordinary

Table 2. Literature values for 1:1 hydrogen-bonded complexes of fluoroalcohols with pyridine. Temperature 25 °C. Methods: infrared for $\Delta\nu$OH, calorimetric for $-\Delta H°$. TFP = 2,2,3,3-tetrafluoro-1-propanol, PFTB = perfluoro-t-butyl alcohol.

System	$\Delta\nu$OH / cm^{-1}	$-\Delta H°$ / kJ mol^{-1}	Solvent	Reference
TFE – Py	370		vapour	17
TFP – Py	370		vapour	17
TFE – Py	425		CCl_4	17
TFP – Py	430		CCl_4	17
TFE – Py	428	27.9	CCl_4	18,19,20
TFE – Py		32.7	hexane	18,19,20
HFP – Py		35.1	CCl_4	21
HFP – Py		41.0	hexane	21
PFTB – Py	835	43.1	CCl_4	22
PFTB – Py		52.3	hexane	22

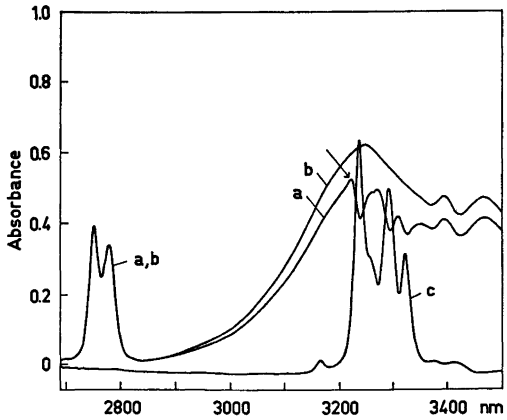

Fig. 2. Illustrative spectra for the system HFP – pyridine. Solvent CCl_4, temperature 25 °C, path length 20 mm. Curve a, 0.00462 M HFP + 0.00438 M Py (reference 0.00438 M Py); curve b, 0.00509 M HFP + 0.00532 M Py-d_5 (reference 0.00532 M Py-d_5); curve c, 0.0110 M Py (reference CCl_4).

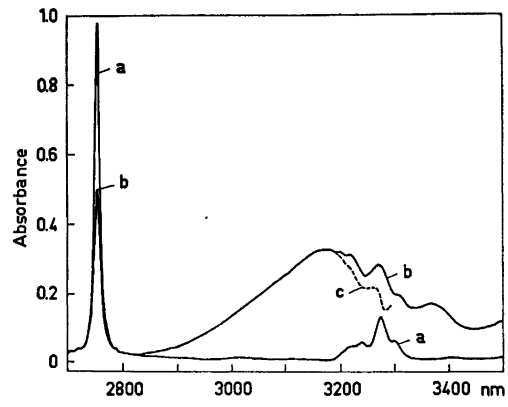

Fig. 3. Illustrative spectra for the system phenol – pyridine. Solvent CCl_4, temperature 25 °C, path length 20 mm. Curve a, 0.00208 M PhOH (reference CCl_4); curve b, 0.00208 M PhOH + 0.0229 M Py (reference 0.0229 M Py); curve c (broken), difference spectrum a – b.

alcohols the tendency to heteroassociation diminishes slightly in the order MeOH > EtOH > i-PrOH > *t*-BuOH. The association bands are symmetric in all cases.

For some systems studied the hydrogen-bonded OH stretching band was complicated in form. For example, the association band of the system HFP – Py (Py = pyridine) comprises several maxima and minima (Fig. 2a) and that of the system HFP – PyO (PyO = pyridine-*N*-oxide) is relatively sharp, not the usual rounded shape (see below).

The association band of the HFP – Py system (Fig. 2) does not allow us to estimate the value of $\Delta\nu$OH. However, it can be concluded from the frequency of the first maximum, indicated by an arrow in Fig. 2, that the value of $\Delta\nu$OH must be above 530 cm^{-1}. The contours of the association bands of various fluoroalcohol – nitrogen-containing base pairs will be discussed in a later paper. However, it may be noted here that the frequency of the first overtone of the OH bending vibration in some cases falls in the region of the "associated" OH band, which may lead to fine structure by means of Fermi resonance.

The deuterination of pyridine does not markedly alter the acceptor ability of the base (*e.g.*, EtOH – Py, Table 1). The association constant is slightly greater for the HFP – pyridine system than for HFP – pyridine-d_5, but the difference does not exceed the experimental error. The association band for HFP – pyridine-d_5 (Fig. 2b) is simpler than the band for HFP – pyridine and allows $\Delta\nu$OH to be estimated as 552 cm^{-1}. The "true" $\Delta\nu$OH for HFP – pyridine is probably close to this value.

Spectra for PhOH – Py in the νOH region are similar to spectra for HFP – Py and comprise several maxima and minima (Fig. 3). Especially in spectra of solutions with relatively high pyridine content the first maximum has the usual round form of an OH association band. The two (or three) submaxima following this first maximum obviously arise from the absorption of the phenol (*cf.* the difference spectrum c in Fig. 3). The present data do not allow us to decide whether the value of $\Delta\nu$OH measured from the first maximum in the spectra of the phenol – pyridine complex is the "true" $\Delta\nu$OH value (which we nevertheless consider probable) or only the lower limit for it, as in the case of the HFP – Py system.

Apart from the effect on the vibration of the proton donor, association also influences vibrations of the proton acceptor.[21–24] This is illustrated by spectrum a in Fig. 2. The νCH vibrations of hydrogen-bonded pyridine molecules

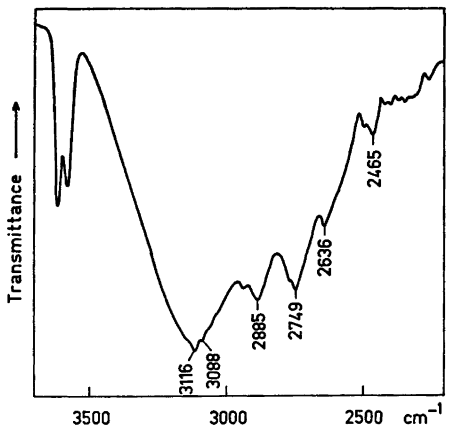

Fig. 4. Illustrative spectra for the system HFP – pyridine-*N*-oxide. Solvent CCl_4, temperature: ambient, path length 2 mm. Curve a, 0.0467 M HFP + 0.0239 M PyO (reference 0.0239 M PyO); curve b, 0.0239 M PyO (reference CCl_4).

are shifted by a few cm^{-1} to higher frequencies, so that the νCH absorption is not completely compensated for despite the fact that the formal concentration of pyridine in the reference cell equals that of the sample cell.

The spectrometric quantities are of the same order of magnitude when TFE or HFP form hydrogen bonds to PyO as when they bond to Py. As the pK_a (pK_{BH^+}) values of pyridine and of its *N*-oxide differ markedly from each other [pK_a(Py) = 5.29; pK_a(PyO) = 0.79 [20]], we may conclude that factors other than basicity affect the strength of hydrogen bonds in these systems. The complexing abilities of Py and PyO are similar also in hydrogen-bonded systems with phenol [26] and in charge-transfer association with iodine.[27] The reason for this is thoroughly discussed by Beggiato *et al.*[27]

The form of the association band in the spectrum of the HFP – PyO system is almost triangular (Fig. 4), in contrast to the usual round form. The two sharp submaxima at about 3080 and 3120 cm^{-1} may in part be due to incomplete compensation of the absorption of PyO in this region. There are, in addition, several other submaxima at lower frequencies. The form of the bonded OH absorption of the HFP – PyO complex thus resembles that found by Huong and Graja [28] for the phenol – MePyO complex.

As mentioned above, the hydrogen-bonding ability of TFE resembles that of phenol. Thus it is interesting to compare data for TFE – Py with those reported for PhOH – Py. The latter is one of the most suitable systems to use as a reference acid-base pair, considering the low volatility of the components, medium hydrogen bond strength and the presence in the proton acceptor of only one lone electron pair with known direction (*cf.* Ref. 29).

Table 3 shows most of the literature values for the phenol – pyridine system in carbon tetrachloride, including enthalpy and entropy values. We can conclude that the "true" value of K_{11} is slightly below 50 M^{-1} at 25°C and that $-\Delta H^\circ$ is about 27 – 30 kJ mol^{-1}. The scatter of the $-\Delta S^\circ$ values is considerable, however. In Fig. 5 the $-\Delta H^\circ$ values are plotted against ΔS° and indicate an apparent linear enthalpy-entropy relationship (*cf.* Ref. 37). It is to be especially emphasized that we are dealing with the same reaction in same conditions

Table 3. Literature values for 1:1 hydrogen-bonded complexes between phenol and pyridine in carbon tetrachloride at 25 °C. Methods: infrared for all except the last line where the dielectric method was used.

K_{11} / M^{-1}	$\Delta\nu$OH / cm^{-1}	$-\Delta H^\circ$ / kJ mol^{-1}	$-\Delta S^\circ$ / J K^{-1} mol^{-1}	Ref.
60 (20 °C)	492	29.3	66.1	30
35.2(30 °C)	465	27.2	62.8	31
59 (20 °C)		27.2	59.0	32
50	473	23.4	46.4	33
49		27.2	60.2	34
41	475	37.7	96.2	35
45		29.3	71.1	36

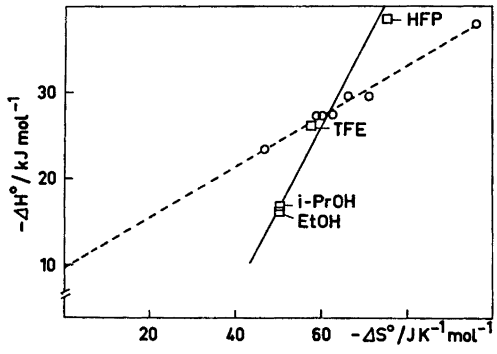

Fig. 5. Plot of $-\Delta H^\circ$ against $-\Delta S^\circ$ for the system phenol – pyridine (broken line, values from Table 4) and for alcohol – pyridine systems (full line).

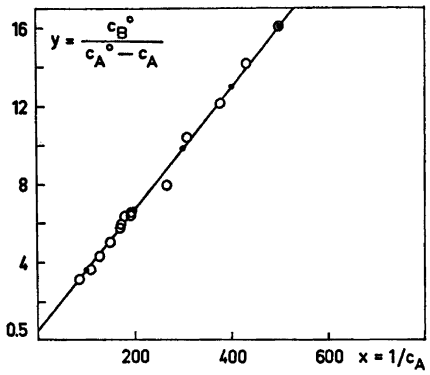

Fig. 6. Experimental (open symbols) and calculated (filled symbols) values of x and y for complex formation by TFE and pyridine at 25 °C. The curve is drawn through the calculated points.

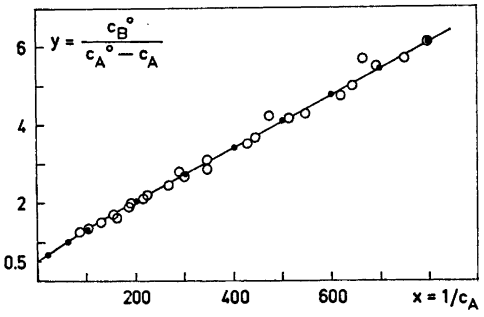

Fig. 7. As in Fig. 6, but for complex formation by TFE and pyridine-*N*-oxide.

and thus care should be taken when the phenol – pyridine system is used as reference. The most probable value for $-\Delta S^\circ$ is about 60 J K^{-1} mol^{-1}. For the hydrogen bonding of EtOH, i-PrOH, TFE or HFP with pyridine the $\Delta H - \Delta S$ relationship is approximately linear (Fig. 5).

In the case of hydrogen bonding of TFE or HFP with pyridine or its *N*-oxide, 2:1 alcohol – base complexation was also studied. As previously,[4,38] the method of Néel *et al.*[39] was used. The curves $y = f(x)$ for the various systems studied are shown in Figs. 6 – 7 and the calculated values of formation constants are collected in Table 4.

The values of K_{11} shown in Table 4 are about 15 % smaller throughout than those obtained directly for 1:1 complexes (Table 1). One may expect greater experimental uncertainty in simultaneous calculation of K_{11} and K_{21}. However, the results indicate that the neglecting of the 2:1 complexes leads to too large values for K_{11}.

For bases with two virtually independent bonding sites, a value of about 4 is expected for the ratio K_{11}/K_{21}, as with dioxan – alcohol complexes.[38] For bases with one bonding site values of K_{11}/K_{21} less than 4 indicate that both alcohol (or phenol) molecules of the 2:1 complexes bond simultaneously to the same acceptor atom. If, on the other hand, the ratio K_{11}/K_{21} is notably greater than 4, the second alcohol molecule bonds to the oxygen of the alcohol molecule already engaged in a 1:1 complex.[39,40] Eqn (4) illustrates this schematically for pyridine complexes.

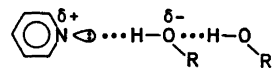

Table 4. Values of K_{11} and K_{21} for 1:1 and 2:1 hydrogen-bonded complexes, respectively, between TFE or HFP and Py or PyO at 25 °C in carbon tetrachloride.

System	$\frac{K_{11}}{M^{-1}}$	$\frac{K_{21}}{M^{-1}}$	$\frac{K_{11}}{K_{21}}$
TFE – Py	31.8	10.4	3.1
TFE – PyO	146	21.6	6.8
HFP – Py	511	9.43	54
HFP – PyO	1870	48.6	38

The formation of a 1:1 complex may lead to some transfer of charge from the nitrogen atom to the oxygen atom of the alcohol, thus enchancing the "basicity" of oxygen [41] and favouring the structure expressed by scheme (4).

The observed ratio K_{11}/K_{21} is considerably greater for HFP than for TFE systems and indicates the "linear" structure of scheme (4) for 2:1 HFP – base systems. Since there is only one free electron pair at the nitrogen atom, one would intuitively assume the same geometry for 2:1 TFE – base complexes, for which the ratio K_{11}/K_{21} is of the order of 4. The assumption being true, we cannot infer the geometry of a 2:1 alcohol – base complex solely on the basis of the magnitude of the ratio K_{11}/K_{21}. We thus prefer a linear structure similar to that proposed for complexes of tetramethylurea with various phenols.[42]

When the hydrogen bonding occurs to oxygen atoms, say to ethers or carbonyl compounds, the situation is somewhat different from bonding to nitrogen because of the two lone pairs of electrons. This was discussed recently by Christian and Keenan.[43]

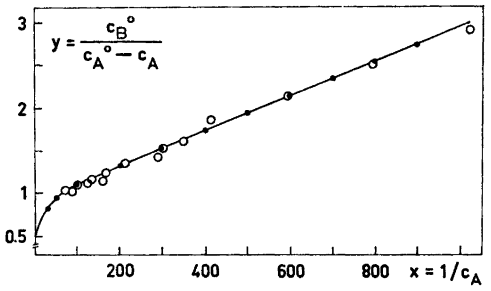

Fig. 8. As in Fig. 6, but for complex formation by HFP and pyridine.

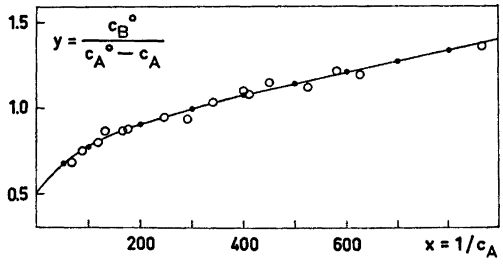

Fig. 9. As in Fig. 6, but for complex formation by HFP and pyridine-*N*-oxide.

The use of carbon tetrachloride as solvent for hydrogen bonding studies has been widely discussed in the literature. It has been claimed that CCl_4 is an unsuitable solvent especially for systems with pyridine as base.[44] At present, however, there is not sufficient evidence to set pyridine systems apart from other common systems.[45]

Acknowledgements. We thank Mrs. Ritva Kuopio, Ph. Lic., for valuable assistance during this work. We gratefully acknowledge financial support from the Jenny and Antti Wihuri Foundation and from the Finnish Academy.

REFERENCES

1. Part 22. Murto, J., Kivinen, A., Manninen, A. and Perttilä, M. *Spectrochim. Acta A 31* (1975) 217.
2. Kivinen, A. and Murto, J. *Suom. Kemistilehti B 40* (1967) 6.
3. Kivinen, A., Murto, J. and Kilpi, L. *Suom. Kemistilehti B 40* (1967) 301.
4. Kivinen, A., Murto, J. and Kilpi, L. *Suom. Kemistilehti B 42* (1969) 19.
5. Ginn, S. W. and Wood, J. *Spectrochim. Acta A 23* (1967) 611, and the references cited.
6. Gramstad, T. *Spectrochim. Acta 19* (1963) 829.
7. Fritzsche, H. *Spectrochim. Acta 21* (1965) 799, and the references cited.
8. Ōsawa, E., Kitamura, K. and Yoshida, Z. *J. Amer. Chem. Soc. 89* (1967) 3813.
9. Joris, L. and Schleyer, P. von R. *J. Amer. Chem. Soc. 90* (1968) 4599.
10. Murthy, A. S. N. and Rao, C. N. R. *Appl. Spectrosc. Rev. 2* (1968) 69.
11. Jose, C. I., Phadke, P. S. and Rama Rao, A. V. *Spectrochim. Acta A 30* (1974) 1199.
12. Becker, E. D. *Spectrochim. Acta 17* (1961) 436.
13. Findlay, T. J. V. and Kidman, A. D. *Aust. J. Chem. 18* (1965) 521.
14. Hall, A. and Wood, J. L. *Spectrochim. Acta A 23* (1967) 1257.
15. Reece, I. H. and Werner, R. L. *Spectrochim. Acta A 24* (1968) 1271.
16. Sherry, A. D. *Ph. D. Thesis*, Kansas State University, 1971; *Diss. Abstr. B 32* (1971) 3288.
17. Sherry, A. D. and Purcell, K. F. *J. Phys. Chem. 74* (1970) 3535.
18. Sherry, A. D. and Purcell, K. F. *J. Amer. Chem. Soc. 92* (1970) 6386.
19. Purcell, K. F., Stikeleather, J. A. and Brunks, S. D. *J. Amer. Chem. Soc. 91* (1969) 4019.

20. Sherry, A. D. and Purcell, K. F. *J. Amer. Chem. Soc. 94* (1972) 1853.
21. Wood, J. L. In Yarwood, J., Ed., *Spectroscopy and Structure of Molecular Complexes*, Plenum Press, London 1973, Chapter 4.
22. Clotman, D., Van Lerberghe, D. and Zeegers-Huyskens, T. *Spectrochim. Acta A 26* (1970) 1621.
23. Dorval, C. and Zeegers-Huyskens, Th. *Spectrochim. Acta A 29* (1973) 1805.
24. Cummings, D. L. and Wood, J. L. *J. Mol. Struct. 20* (1974) 1.
25. Ochiai, E. *Aromatic Amine Oxides*, Elsevier, Amsterdam 1967, p. 97.
26. Kulevsky, N. and Lewis, L. *J. Phys. Chem. 76* (1972) 3502.
27. Beggiato, G., Aloisi, G. G. and Mazzucato, U. *J. Chem. Soc. Faraday Trans. 1.* (1974) 628.
28. Huong, P. V. and Graja, A. *Chem. Phys. Lett. 13* (1972) 162.
29. Joris, L., Mitsky, J. and Taft, R. W. *J. Amer. Chem. Soc. 94* (1972) 3438, and the references cited.
30. Gramstad, T. *Acta Chem. Scand. 16* (1961) 807.
31. Dunken, H. and Fritzsche, H. *Z. Chem. 1* (1961) 249.
32. Rubin, J. and Panson, G. S. *J. Phys. Chem. 69 (1965)* 3089.
33. Zharkov, V. V., Zhitinkina, A. V. and Zhokhova, F. A. *Zh. Fiz. Khim. 44* (1970) 223.
34. Frizsche, H. *Ber. Bunsenges. Phys. Chem. 68* (1964) 459.
35. Singh, S. and Rao, C. N. R. *Can. J. Chem. 44* (1966) 2611.
36. Bishop, R. J. and Sutton, L. E. *J. Chem. Soc.* (1964) 6100.
37. Leffler, J. E. *J. Org. Chem. 31* (1966) 533.
38. Kivinen, A. and Murto, J. *Suom. Kemistilehti B 42* (1969) 190.
39. Néel, J., Pineau, P. and Quivoron, C. *J. Chim. Phys. 62* (1965) 37.
40. Gramstad, T. and Van Binst, G. *Spectrochim. Acta 22* (1966) 1681.
41. Zeegers-Huyskens, T. *Spectre de vibration de complexes à liaison hydrogéne*, Louvain 1969, Chapter 3.
42. Muller, J. P., Vergrusse, G. and Zeegers-Huyskens, T. *J. Chim. Phys. 69* (1972) 1439.
43. Christian, S. D. and Keenan, B. M. *J. Phys. Chem. 78* (1974) 432.
44. Guidry, R. M. and Drago, R. S. *J. Phys. Chem. 78* (1974) 454, and the references cited.
45. Arnett, E. M., Mitchell, E. J. and Murty, T. S. S. R. *J. Amer. Chem. Soc. 96* (1974) 3875.

Received May 12, 1975.

Acta Chemica Scandinavica A 29 (1975) 919—926

The Crystal and Molecular Structure of Sodium *p*-Nitrosophenolate Trihydrate

H. J. TALBERG

Department of Chemistry, University of Oslo, Oslo 3, Norway

The crystal structure of sodium *p*-nitrosophenolate trihydrate has been determined from *X*-ray diffraction data collected at −162 °C and refined by least squares methods. The space group is $P\bar{1}$, with cell dimensions $a = 6.106(2)$ Å, $b = 6.706(2)$ Å, $c = 11.529(3)$ Å, $\alpha = 100.76(2)°$, $\beta = 92.73(2)°$ and $\gamma = 110.14(2)°$ at −162 °C. The final R factor was 3.2 % and the estimated deviations in bond lengths are about 0.001 Å and in angles 0.1°. The nitroso group atoms are acceptors in four hydrogen bonds. The C−N bond length (1.340 Å) is among the shortest and the N−O bond length (1.303 Å) the longest observed for *C*-nitroso compounds. The conjugation in the anion is compared with that in the corresponding acid. The "double" bonds are 0.02−0.04 Å longer and the "single" bonds 0.01−0.07 Å shorter in the anion than in the acid.

The present structure determination of sodium *p*-nitrosophenolate trihydrate (I) is part of a series of structural investigations of monomeric *C*-nitroso compounds and the oximes which are derived from these by protonation or tautomeric proton exchange. So far the crystal structure of *N*,*N*-dimethyl *p*-nitrosoaniline (II), its hydrochloride (III), potassium *p*-nitrosophenolate monohydrate (IV) and quinone 4-oxime (V) have been investigated.[1–4]

In marked contrast to (IV) forming green crystals the title compound forms pale *red* crystals indicating that the quinonoid character in the anion is more pronounced in (I) than in (IV).

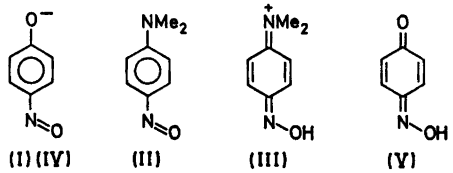

(I) (IV) (II) (III) (V)

EXPERIMENTAL

Pale red needle-shaped crystals were grown by slow evaporation of an alkaline ethanolic solution of quinone 4-oxime. A preliminary film investigation showed that they were triclinic. In Mo$K\alpha$ radiation at 18 °C they decomposed after 24 h.

Unit cell constants at 18 °C were calculated using measurements of seven reflections on a Picker diffractometer with Mo$K\alpha$ radiation.

Three-dimensional data were collected and unit cell constants were determined at low temperature using a crystal of dimensions $0.6 \times 0.2 \times 0.1$ mm. The measurements were made on a Syntex $P\bar{1}$ diffractometer with graphite monochromatized Mo$K\alpha$ radiation and equipped with an Enraf-Nonius liquid nitrogen cooling device (modified by H. Hope). The temperature at the crystal site was −162 °C. Cell constants were determined by least squares treatment of measurements of twelve reflections. Intensity data were collected using the variable $\omega - 2\theta$:scan technique. Prior to each scan the intensity was measured with stationary crystal and counter, and the scan speed accordingly adjusted. The scan speed varied between 2.0 and 6.0 °/min, and the total time for background counts at the scan limits $2\theta(\alpha_1) - 1.2°$ and $2\theta(\alpha_2) + 1.2°$ was 0.7 of the time of integration. A hemisphere of reciprocal space was examined. All reflections having 2θ less than 45 ° were measured; between 45 and 70 ° only reflections having integrated counts of more than a preset value during a 2 s scan over the peak were measured. The intensity of three test reflections measured for every 50 reflections showed no significant change during the measurement. Out of 3076 unique reflections 2419 had intensities larger than $2.5 \times \sigma(I)$. They were regarded as observed. $\sigma(I)$ is the estimated standard deviations of the

Table 1. Fractional atomic coordinates and thermal parameters ($\times 10^5$) for nonhydrogen atoms. Estimated standard deviations in parentheses. The temperature factors are expressed as: $\exp -(B_{11}h^2+B_{22}k^2+B_{33}l^2+B_{12}hk+B_{13}hl+B_{23}kl)$.

Atom	x	y	z	B_{11}	B_{22}	B_{33}	B_{12}	B_{13}	B_{23}
Na	25717(7)	53612(7)	42925(4)	720(12)	896(11)	158(3)	702(19)	76(9)	110(9)
OW1	32090(14)	24807(14)	50470(7)	1110(23)	905(20)	160(5)	805(34)	133(17)	133(17)
OW2	72663(15)	15592(14)	65646(7)	810(22)	1160(21)	206(5)	881(35)	26(18)	222(17)
OW3	83571(14)	34790(14)	37325(7)	841(22)	937(21)	224(6)	800(35)	−17(17)	5(17)
O1	42561(14)	38546(13)	26725(7)	968(22)	1228(21)	134(5)	1053(35)	24(17)	66(16)
O4	26023(14)	9835(13)	−28257(6)	937(21)	978(20)	153(5)	796(33)	184(16)	53(16)
N4	13081(15)	15973(14)	−20756(8)	740(23)	763(21)	157(6)	517(36)	78(18)	72(17)
C1	35871(18)	33209(17)	15724(9)	696(25)	693(23)	160(6)	526(40)	64(20)	110(19)
C2	50131(18)	26370(18)	7300(9)	676(26)	1043(26)	175(7)	956(43)	43(21)	121(21)
C3	43214(18)	20695(17)	−4558(9)	635(25)	901(25)	172(7)	769(41)	117(20)	101(20)
C4	21338(17)	21213(16)	−9185(9)	573(24)	689(23)	150(6)	492(39)	51(20)	98(19)
C5	6897(18)	27658(17)	−1018(9)	569(25)	895(25)	192(7)	652(41)	50(20)	131(20)
C6	13728(18)	33550(18)	10885(9)	669(26)	980(25)	174(7)	801(42)	166(21)	107(20)

net intensity based on counting statistics. A 2 % uncertainty due to experimental fluctuations were included in the estimated standard deviations of the net intensity. The atomic scattering factors for the heavy atoms were those of Doyle and Turner [5] and for hydrogen those of Stewart *et al.*[6] All programs except for the ORTEP program [7] applied during the structure investigation are described in Ref. 8.

CRYSTAL DATA

Sodium *p*-nitrosophenolate trihydrate, $NaC_6H_4O_2N.3H_2O$, triclinic, space group $P\bar{1}$. Dimension of the unit cell at 18 °C: $a=6.144(5)$ Å, $b=6.776(5)$ Å, $c=11.56(1)$ Å, $\alpha=100.87(3)°$, $\beta=93.08(3)$ $\gamma=109.91(4)°$, $V=440.8$ Å^3. At −162 °C: $a=6.106(2)$ Å, $b=6.706(2)$ Å, $c=11.529(3)$ Å, $\alpha=100.76(2)°$, $\beta=92.73(2)°$, $\gamma=110.14(2)°$, $V=432.3$ Å^3. D_{calc} (18 °C) = 1.500 g/cm^3. D_{calc} (−162 °C) = 1.530 g/cm^3.

STRUCTURE DETERMINATION

The structure was determined by the use of a sharpened Patterson synthesis. Positions of peaks forming a hexagon around the third highest peak in the Patterson map gave input parameters to a computer program which translated an anion model in steps and calculated R-values after each step using 91 low order reflections. The resulting R-map showed only one minimum position, reasonable from packing considerations. Subsequent Fourier and least squares refinements reduced the conventional R factor to 0.06. At this stage positional parameters for all hydrogen atoms were calculated from stereochemical considerations. Least squares full matrix refinements of positional and thermal parameters of all atoms converged with a conventional R factor of 0.032, a weighted R_w factor of 0.037 and a goodness of fit S of 1.92. Using 2008 reflections with $\sin\theta/\lambda > 0.45$ the refinement yielded $R=0.035$, $R_w=0.034$, and $S=1.45$. The difference between the scale factors is insignificant (0.140(1) and 0.143(3), respectively.) The only significant difference appears in the NO bond length which is shortened by 0.004 Å or 2.9σ disregarding valence electron scattering. The nitrogen atom is shifted towards the O4 oxygen atom which

Table 2. Fractional atomic coordinates ($\times 10^3$) and isotropic thermal parameters with estimated standard deviations for hydrogen atoms.

Atom	x	y	z	B
H2	645(3)	254(2)	106(1)	1.8(3)
H3	526(3)	163(2)	−99(1)	1.4(3)
H5	−84(3)	274(2)	−45(1)	1.7(3)
H6	41(3)	380(2)	163(1)	1.3(3)
H1W1	276(3)	200(3)	567(2)	2.8(4)
H2W1	306(3)	135(3)	457(1)	2.3(3)
H1W2	610(3)	142(3)	693(2)	3.0(4)
H2W2	832(4)	154(3)	705(2)	4.4(5)
H1W3	729(4)	364(3)	339(2)	4.5(5)
H2W3	820(3)	214(3)	348(2)	2.9(4)

Table 3. Bond lengths (Å) and angles (°). Estimated standard deviations in parentheses. Bond lengths in quinone 4-oxime are also given. Libration corrected bond lengths from the refinement with all observed reflections are given on the second line.

	Anion	Acid		Anion	Acid
O1–C1	1.2586(12)	1.243(3)	C3–C4	1.4286(14)	1.441(4)
	1.2595	1.245		1.4317	1.450
O4–N4	1.3031(11)	1.371(3)	C4–C5	1.4284(14)	1.450(4)
	1.3052	1.377		1.4308	1.460
N4–C4	1.3402(13)	1.302(3)	C5–C6	1.3576(14)	1.330(4)
	1.3412	1.305		1.3586	1.332
C1–C2	1.4494(14)	1.466(4)	C6–C1	1.4471(14)	1.452(4)
	1.4519	1.473		1.4501	1.460
C2–C3	1.3536(14)	1.329(4)			
	1.3547	1.332			

Bond angles in the anion

O1–C1–C2	121.1(1)
O1–C1–C6	122.0(1)
C6–C1–C2	116.9(1)
C1–C2–C3	121.8(1)
C2–C3–C4	120.6(1)
C3–C4–C5	118.5(1)
C4–C5–C6	121.5(1)
C5–C6–C1	120.8(1)
C3–C4–N4	124.8(1)
C5–C4–N4	116.7(1)
C4–N4–O4	117.1(1)

Distances in the polyhedron surrounding the sodium ion

Na··O*W*1(a)	2.3983(9)
Na··O*W*1(b)	2.4791(9)
Na··O*W*2(b)	2.4253(9)
Na··O*W*3(c)	2.4358(9)
Na··O*W*3(b)	2.4241(9)
Na··O1(a)	2.4002(9)
O*W*1··O1(a)	3.0749
O*W*1··O1(b)	3.1510

Distances and angles involving hydrogen atoms.

	O–H	H···O,H···N	O···O,O···N	O–H···O(N)	H–O–H
O*W*1–H1···O4(d)	0.86(2)	1.97(2)	2.812(1)	164.9(1.6)	101.7(1.5)
O*W*1–H2··O*W*2(e)	0.82(2)	2.08(2)	2.899(1)	177.1(1.5)	
O*W*2–H1··O4(d)	0.83(2)	2.09(2)	2.879(1)	163.6(1.3)	105.7(1.7)
O*W*2–H2··N4(f)	0.84(2)	2.03(2)	2.850(1)	167.2(2.0)	
O*W*3–H1··O4(g)	0.86(2)	1.97(2)	2.821(1)	172.1(1.7)	106.0(1.7)
O*W*3–H2··O1(a)	0.80(2)	2.05(2)	2.844(1)	172.0(2.1)	
	C–H		C–C–H		C–C–H
C2–H	0.97(2)	C1–C2–H	116.6(9)	C4–C5–H	116.4(8)
C3–H	0.94(1)	C3–C2–H	121.6(9)	C6–C5–H	122.2(8)
C5–H	0.99(2)	C2–C3–H	120.6(8)	C5–C6–H	120.9(8)
C6–H	0.95(1)	C4–C3–H	118.9(8)	C1–C6–H	118.3(8)

Other intermolecular contacts

O1···O4(a)	3.296
C2···C3(g)	3.279

Dihedral angles in the anion

C3–C4–N4–O4	0.5(2)
C5–C4–N4–O4	−179.2(1)
C4–N4–O4···O*W*1	−137.6(1)
C4–N4–O4···O*W*2	−37.4(2)
C4–N4–O4···O*W*3	98.0(1)
C5–C4–N4···O*W*2	2.8(2)

Symmetry codes

(a): x y z (b): $-x+1$ $-y+1$ $-z+1$ (c): $x-1$ y z
(d): x y $z+1$ (e): $-x+1$ $-y$ $-z+1$ (f): $x+1$ y $z+1$
(g): $-x+1$ $-y$ $-z$

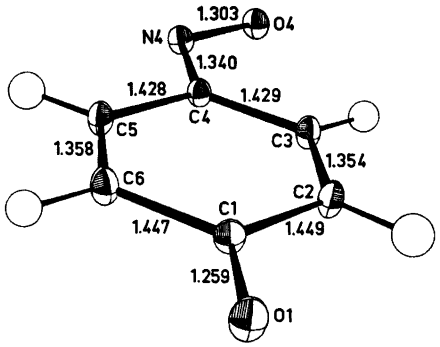

Fig. 1. 50 % probability ellipsoids, bond lengths (Å) and numbering of atoms in the anion.

is not affected. Probably asphericity of the valence electron density causes some of the differences observed.[9] However, only the parameters dependent upon all reflections will be considered in the following, as they are more directly comparable with those of quinone 4-oxime.

A list of structure amplitudes is available from the author upon request. Final parameters are listed in Tables 1 and 2.

An analysis of the thermal parameters in the anion was carried out. Magnitudes and directions of the principal axis of the vibrational ellipsoids are indicated in Fig. 1. The r.m.s. discrepancy between the atomic vibrational tensor component obtained in the structure determination and those calculated from a rigid body analysis was 0.0006 Å². The translational r.m.s. amplitudes of vibration along the principal axes are 0.11, 0.10 and 0.09 Å². The r.m.s. librational amplitudes are 3.8, 1.8, and 1.4°. The largest increase in bond lengths was 2.2σ when adjusting the coordinates according to this libration.

Bond lengths and angles with their estimated standard deviations are given in Table 3. Fig. 1 shows numbering of atoms and distances in the anion. The estimated standard deviations were calculated from the correlation matrix. Deviations from least squares planes are given in Table 4.

DISCUSSION

Interionic structural features. A general view of the structure is shown in Fig. 2. This figure also shows a stereo plot of the structure of the potassium salt, *i.e.* (IV).

The present structure has several features which differ markedly from those of the potassium salt. While in the latter the cation coordinates four anions, the sodium ion in (I) has only one anion contact. The most important difference is, however, in the coordination about the anion terminal atoms. Fig. 3 shows this coordination. As may be seen, the nitroso group atoms are acceptors in four hydrogen bonds in the sodium salt. In the potassium salt the only hydrogen bond is between the water oxygen atom and the *phenoxide* oxygen atom. The latter is also an acceptor in the sodium salt. The coordination around O4 is tetrahedral in (I) and threefold pyramidal in (IV), while O1 has a threefold planar coordination in (I) and a tetrahedral coordination in (IV).

Four hydrogen bonds involving the *W*2 and the *W*3 water molecules are linking together anions while two hydrogen bonds involving the *W*1 water molecule constitute a bridge between the organic layers in (I). Five of six acidic protons are engaged in hydrogen bonds to the anion while the last one is donated from O*W*1 to O*W*2. The hydrogen bond lengths are normal.

The p-*nitrosophenolate ion.* The anion has the same weakly expressed boat form as its corresponding acid, *i.e.* (V). Furthermore, bond angles not involving the N4 and the O4

Table 4. Atomic coordinates and deviations (Å) of atoms from a least-squares plane through the benzene ring atoms C1, C2, C3, C4, C5, and C6.

C1	1.4074	−0.2578	0.0026
C2	0.8776	1.0913	−0.0034
C3	−0.4540	1.3342	−0.0002
C4	−1.3894	0.2543	0.0047
C5	−0.8874	−1.0829	−0.0056
C6	0.4457	−1.3391	0.0019
O1	2.6480	−0.4698	0.0061
O4	−3.1885	1.6131	0.0069
N4	−2.7220	0.3964	0.0130
H2	1.523	1.809	−0.056
H3	−0.778	2.214	−0.008
H5	−1.564	−1.808	−0.027
H6	0.772	−2.234	0.008

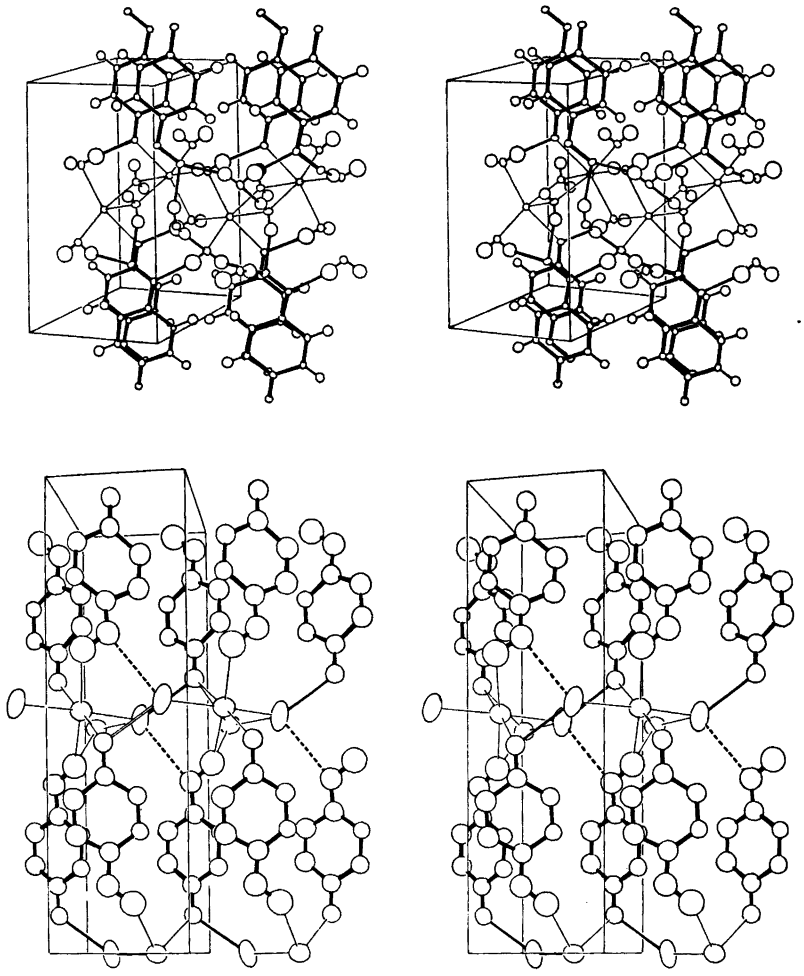

(I)

(IV)

Fig. 2. A stereoscopic illustration of the structure of sodium *p*-nitrosophenolate trihydrate (I) and potassium *p*-nitrosophenolate monohydrate (IV). Thermal ellipsoids and spheres are scaled to 50 % probability.

atom are very similar to corresponding angles in (V).

The angle at N4 is, however, 4.5° wider, the exocyclic angles at C4 are more equal and the nonbonded O4···C3 distance is 0.04 Å longer in (I) than in (V). These differences are probably a result of forming four hydrogen bonds to the nitroso group atoms.

In Table 3 anion bond lengths are compared with those of (V). All differences except that between the C1 – C6 bond lengths are highly significant. As expected an increase in conjugation expressed by lengthening of "double" bonds and shortening of "single" bonds appears upon ionization.

A comparison of the CN and the NO bond length values listed in Table 5 shows that the CN bond in (I) is among the shortest observed and that the NO bond in (I) is the longest observed for *C*-nitroso compounds. The distances resembles those of the violurates [15,16] and are nearly identical to those of the dicyanonitrosomethanidide anion.[17] The CN bond is 0.11 Å shorter and the NO bond 0.03 Å longer than

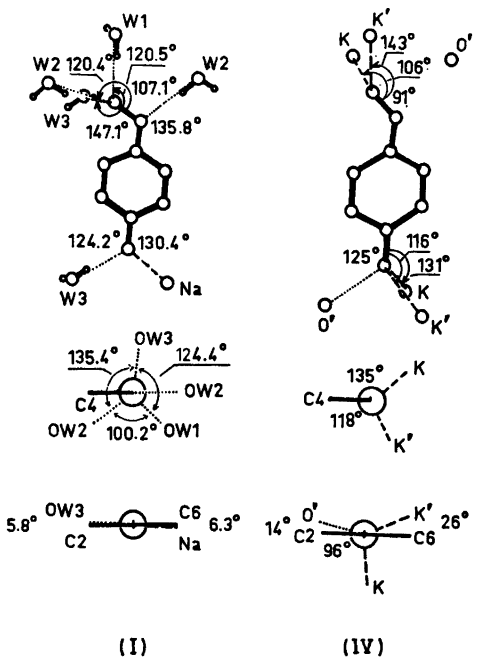

Fig 3. The coordination about the anion in (I) and (IV).

the corresponding bond in the nitrosobenzene dimer [1.454(5) Å and 1.268(4) Å, respectively].[18]

The charge distribution in the anion. The charge distribution in the anion is of considerable interest as it is a transition state when

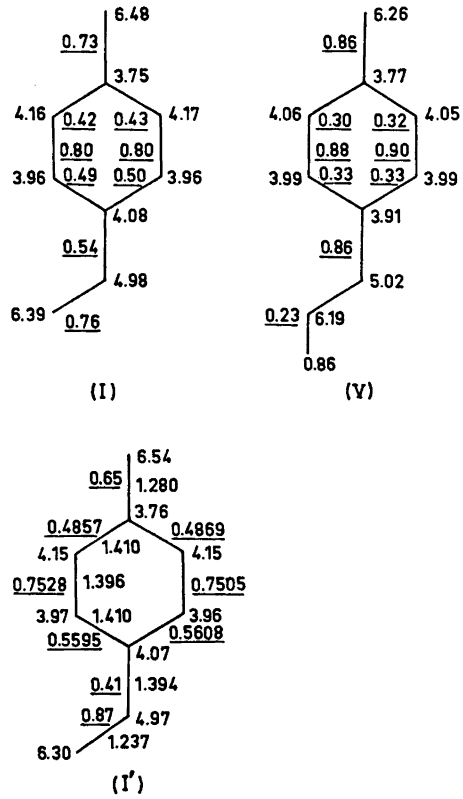

Fig. 4. Results from the CNDO/2 calculations. Underlined figures are the π-bond orders, while the other figures denote the total charge densities. In the anion with *mm* symmetry, (I'), also the "input" bond lengths are shown.

Table 5. Structural parameters in monomeric nitrosocompounds.

Compound[a]	Method[b]	*R* value in X-ray invest.	Bond lengths (Å) C–N	N–O	Bond angle (°) CNO	Ref.
A	e.d.		1.57(2)	1.171(8)	121(2)	10
B	e.d.		1.49(3)	1.22(3)	113(1)	11
	(*ab initio* calculations)		(1.499)	(1.208)	(113.0)	12
C	m.w.		1.401(5)	1.228(5)	115(1)	13
D	x.,c.	0.116	1.358(9)	1.265(8)	116	14
E	x.,f.		1.34(2)	1.26(2)	119	15
F	x.,f.	0.118	1.34(2)	1.27(2)	122	16
G	x.,c.	0.035	1.330(1)	1.285(1)	116.4(1)	17
(I)	x.,c.	0.037	1.340(1)	1.303(1)	117.1(1)	

[a] A, Trifluoro nitrosomethane; B, Nitrosomethane; C, Nitrosyl cyanide; D, 4-Nitroso-5-triphenyl-phosphoranylidene-aminobenzo(1,2-c:3,4-c)difurazan; E, Potassium violurate dihydrate; F, Cupric violurate tetrahydrate; G, Potassium dicyanonitrosomethanidide. [b] e.d., electron diffraction; m.w., microwave; x., X-ray diffraction; c., counting; f., film.

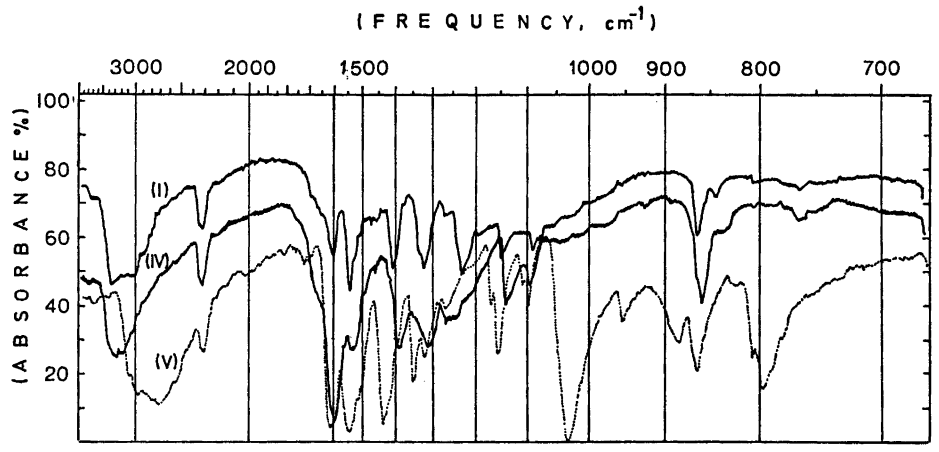

Fig. 5. The IR spectra of (I), (IV) and (V) in KBr recorded on a Perkin-Elmer 137 spectrophotometer. Peak positions:

(IV):	1590	1525	1380	1310		1260		1135	1090		
(I):	1600	1545	1400	1330		1230		1150	1090		
(V):	1620	1550	1440	1350	1325		1170	1155	1100	1030	(ωNO)[22]

quinone 4-oxime converts to *p*-nitrosophenol.[19]

In order to obtain information on this distribution both CNDO/2 [20] and INDO [21] calculations were performed. The atomic coordinates used were those given in Table 4. Also an isolated ion having hypothetical structural parameters expressing a strong benzenoid character and *mm* symmerty in the benzene ring were treated. The results from the CNDO/2 calculations are shown in Fig. 4. The INDO results were nearly identical. The negative charge (*i.e.* 87 %) is predicted to be nearly equally distributed between the two oxygen atoms, and the O1 atom to be slightly more negative than the O4 atom. This is also the case in the π-electron system. These results are rather surprising as the UV studies of the tautomeric equilibrium indicate that 85 % of the species exists as oxime.[19] Simple VB calculations indicate that the O4 atom has twice the charge situated at the O1 atom.

The CNDO/2 calculations indicate that the benzene ring symmetry is less than *mm* as the C1 – C2 bond is predicted to be longer than the C1 – C6 bond, the C2 – C3 bond shorter than the C6 – C5 bond and the C3 – C4 bond longer than the C5 – C4 bond. Actually all these trends are seen in the experiment. The measured differences are, however, not significant (2σ between C2 – C3 and C5 – C6).

The influence of hydrogen bonding on the quinonoid character. Unfortunately the low accuracy of the molecular structure in (IV) does not allow a discussion of this question by a comparison of anions in (I) and (IV). Owing to the differences in the hydrogen bonding it seems, however, reasonable to expect a measurable difference between the two ions as to the quinonoid character.

Two observations indicate that (IV) has less quinonoid character than (I): the green colour of the potassium salt and the red colour of the sodium salt, and the fact that the potassium salt becomes red upon dehydration by heating to 100 °C. Probably the introduction of four hydrogen bonds to the nitroso group or the removal of one hydrogen bond from the phenoxide oxygen atom causes a red shift of a $\pi \rightarrow \pi^*$ transition into the visible region.

The IR spectrum of (IV) in KBr has features which make it markedly different from that of (I). The two spectra are shown in Fig. 5. The band at 1230 cm^{-1} in (I) has previously been assigned to a ωNO frequency by Hadzi.[22] This band is missing in the spectrum of (IV). On the other hand a band at 1260 cm^{-1} in the spectrum of (IV) is missing in the spectrum of (I). This may possibly indicate that the NO bond is shorter in (IV) than in (I).

The IR spectra of (I) and (IV) in nujol mull were also recorded. No differences in peak positions were observed between these spectra and those from the KBr tablets.

REFERENCES

1. Rømming, C. and Talberg, H. J. *Acta Chem. Scand. 27* (1973) 2246.
2. Drangfelt, O. and Rømming, C. *Acta Chem. Scand. A 28* (1974) 1101.
3. Talberg, H. J. *Acta Chem. Scand. A 28* (1974) 593.
4. Talberg, H. J. *Acta Chem. Scand. A 28* (1974) 910.
5. Doyle, P. A. and Turner, P. S. *Acta Crystallogr. A 24* (1970) 2232.
6. Stewart, R. F., Davidson, E. R. and Simpson, W. T. *J. Chem. Phys. 42* (1965) 3175.
7. Johnson, C. K. *ORTEP*, Report ORNL-3795, Oak Ridge National Laboratory, Oak Ridge (1965).
8. Groth, P. *Acta Chem. Scand. 27* (1973) 1837.
9. Coppens, P. *Acta Crystallogr. A 25* (1969) 180.
10. Davis, M. I., Boggs, J. E. Coffey, D. and Hanson, H. P. *J. Phys. Chem. 69* (1965) 3727.
11. Coffey, D., Britt, C. O. and Boggs, J. *J. Chem. Phys. 49* (1968) 591.
12. Talberg, H. J. and Ottersen, T. *J. Mol. Struct. 29* (1975) 225.
13. Dickinson, R., Kirby, G. W., Sweeny, J. G. and Tydler, J. K. *Chem. Commun.* (1973) 241.
14. Cameron, T. S. and Prout, C. K. *J. Chem. Soc. C* (1969) 2285.
15. Gillier, H. *Bull. Soc. Chim. Fr 88* (1965) 2373.
16. Hamelin, M. *Acta Crystallogr. B 28* (1972) 228.
17. Holene, M. R. and Klewe, B. *Acta Chem. Scand. To be published.*
18. Dietrich, D. A., Paul, I. C. and Curtin, D. Y. *J. Amer. Chem. Soc. 96* (1974) 6372.
19. Norris, R. K. and Sternhell, S. *Tetrahedron Lett.* (1967) 97.
20. Pople, J. A. and Segal, G. A. *J. Chem. Phys. 44* (1966) 3289.
21. Pople, J. A., Beveridge and Dobosh, P. A. *J. Chem. Phys. 47* (1967) 2026.
22. Hadzi, D. *J. Chem. Soc.* (1965) 2725.

Received May 27, 1975.

Acta Chemica Scandinavica A 29 (1975) 927—934

Structural Studies on the Rare Earth Carboxylates. 24. The Crystal and Molecular Structure of Hexaaquafumarato-dimaleatodineodymium(III) Hexahydrate

EVA HANSSON and CHRISTINA THÖRNQWIST

Physical and Inorganic Chemistry 1, Chemical Center, University of Lund, P.O.B. 740, S-220 07 Lund 7, Sweden

The crystal and molecular structure of $Nd_2(C_4H_2O_4)_3.12H_2O$ has been determined from three-dimensional photographic X-ray data. One formula unit crystallizes in a triclinic unit cell with dimensions $a = 6.195(1)$ Å, $b = 11.260(3)$ Å, $c = 10.709(2)$ Å, $\alpha = 110.39(2)°$, $\beta = 90.29(2)°$, and $\gamma = 79.32(2)°$. The space group is $P\bar{1}$. The structure contains the maleate ion and the fumarate ion in the ratio 2:1. It is composed of infinite neodymium-maleate-fumarate layers joined together by hydrogen bonds *via* the lattice water molecules. The neodymium ion is coordinated by six carboxylate and three water oxygens forming a distorted monocapped square antiprism. The Nd−O bond distances are in the range 2.43 − 2.62 Å.

Maleate, malonate, and oxalate ions are potential chelating ligands forming chelates with seven, six, and five members, respectively. In solution their complexes with the trivalent lanthanoid ions show the expected decrease in stability with increasing ring size, *i.e.* oxalate > malonate > maleate.[1–3] The decrease in stability between the oxalate and malonate chelates is reflected in the solid state. Thus, while all oxalate ions in $M_2ox_3.nH_2O$ (M = lanthanoid ion) form five-membered chelate rings [4,5] only part of the malonate ions in $M_2mal_3.nH_2O$ form six-membered rings.[6–8] The non-chelated malonate ions are bound to M^{3+} through both oxygens of one carboxylate group. The presence of chelating carboxylate groups in these complexes results in fairly irregular coordination polyhedra.

The present investigation was undertaken in order to determine how the maleate ion is bound to M^{3+} and to study the geometry of the coordination polyhedron formed.

Another point of interest is the conformation of the maleate ion. Two different conformational patterns for the ion have been reported. In Cu-maleate.H_2O, where the maleate ion forms a seven-membered chelate ring, the two carboxylate groups are twisted by 46° out of the carbon chain plane.[9] In Li_2maleate.$2H_2O$, Na_2maleate.H_2O, and Cd-maleate.$2H_2O$, where no chelate is formed, one carboxylate group lies approximately in the carbon chain plane, while the other one is twisted by 61 − 84° out of this plane.[10–12]

EXPERIMENTAL

Preparation and analysis. Water solutions of neodymium nitrate and maleic acid were mixed in the molar ratio 1:3 and the pH was adjusted to 3 with dilute ammonia. Slow evaporation at room temperature resulted in a mixture of prismatic crystals of NMF (the title compound) and aggregates of irregular crystals of another neodymium compound (phase 2). The latter crystals were of very poor quality and could not be used for single crystal work. It was noticed that the crystals of NMF were formed at the initial stage of the precipitation, and pure NMF could be filtered off before the precipitation of phase 2 started. The amount of NMF obtained in this way corresponds to a content of 5 % fumaric acid in the maleic acid used. NMR-spectra of the acid show, however, that the content of fumaric acid is at most 0.5 %. Isomerization of the maleate ion thus seems to occur during the crystallization. (Found: Nd 33.1; C 17.6; H 4.5. Calc for $Nd_2(C_4H_2O_4)_3.12H_2O$ (846.6): Nd 34.1; C 17.0; H 3.5).

X-Ray diffraction work. A prismatic crystal of the dimensions $0.25 \times 0.08 \times 0.11$ mm^3, mounted along the 0.25 mm edge, was used in recording the layers $0kl - 5kl$.

Non-integrated, equi-inclination Weissenberg photographs were taken with Ni-filtered Cu-radiation using the multi-film technique. 2200 independent reflexions were recorded representing about 70 % of the possible number in the investigated reciprocal region. The intensities of the reflexions were measured visually by comparison with a calibrated scale. The data were corrected for the Lorentz, polarization and absorption effects. The linear absorption coefficient is 273 cm^{-1} and the transmission factors, evaluated by numerical integration,[18] were in the range 0.10 – 0.34.

Powder photographs were taken at room temperature with a Guinier-Hägg camera of radius 5.00 cm using Cu$K\alpha$ radiation ($\lambda = 1.5405$ Å). Lead nitrate (cubic, $a = 7.8568$ Å) was used as standard.

NMF crystallizes in the Laue class $\bar{1}$. The possible space groups are thus $P1$(No. 1) and $P\bar{1}$(No. 2).[13] The structure was assumed to be centrosymmetric and the subsequent calculations did not contradict this assumption. The unit cell dimensions were obtained by a least squares treatment of the powder data, minimizing $\sum w(\sin^2\theta_o - \sin^2\theta_c)^2$ with weights $w = 1/\sin^2 2\theta_o$

The unit cell dimensions for $Nd_2(C_4H_2O_4)_3 \cdot 12H_2O$ are,
$a = 6.195(1)$ Å, $b = 11.260(3)$ Å, $c = 10.709(2)$ Å,
$\alpha = 110.39(2)°$, $\beta = 90.29(2)°$, and $\gamma = 79.32(2)°$.

DETERMINATION AND REFINEMENT OF THE STRUCTURE

The position of neodymium was found from a three-dimensional Patterson synthesis. After least-squares refinement of the preliminary atomic parameters of neodymium and the interlayer scale factors, a three-dimensional difference synthesis gave the positions of the oxygen and carbon atoms.

The interlayer scale factors, the atomic coordinates, and the isotropic temperature factors for all atoms were improved by least squares refinement. The quantity $\sum w(|F_o| - |F_c|)^2$ was minimized, with weights w chosen according to Cruickshank.[14] Reflexions not obeying the condition $0.80 \leq |F_o|/|F_c| \leq 1.25$ were given zero weight. An analysis of the weighting scheme used is given in Table 1. The atomic scattering factors for O and C were taken from *International Tables* [15] and that for Nd from Cromer *et al.*[16] After refinement the value of the conventional discrepancy index $R = \sum||F_o| - |F_c||/\sum|F_o|$ was 0.086 and the weighted R-factor $wR = [\sum w(|F_o| - |F_c|)^2/\sum w|F_o|^2]^{\frac{1}{2}}$ was 0.101. Further refinement using anisotropic thermal parameters for Nd resulted in the following R-values: $R = 0.079$ and $wR = 0.094$ and it was considered reasonable to assign anisotropic temperature factors for the neodymium atom. The shifts of all parameters were less than 0.5 % of their estimated standard deviations in the last cycle of refinement. It was not possible to locate the hydrogen atoms.

The final atomic parameters with their estimated standard deviations are given in Table 2. A difference map based on these parameters showed a peak about 5 e/Å^3 at the position of neodymium and spurious peaks about 2 e/Å^3 in other regions. The final structure factor list is available on request.

All computations were performed on the UNIVAC 1108 computer in Lund, Sweden,

Table 1. Analysis of the weighting scheme $w = 1/(1 + |F_o| + 0.03|F_o|^2 + 0.001|F_o|^3)$. The averages $\overline{w\Delta^2}$, where $\Delta = |F_o| - |F_c|$, are normalized.

Interval $\|F_o\|$	Number of reflexions	$\overline{w\Delta^2}$	Interval sin θ	Number of reflexions	$\overline{w\Delta^2}$
0 – 14	197	0.84	0.00 – 0.37	79	1.46
14 – 19	185	1.03	0.37 – 0.47	131	1.11
19 – 24	203	1.02	0.47 – 0.54	139	0.90
24 – 28	208	1.18	0.54 – 0.59	143	0.85
28 – 32	211	0.90	0.59 – 0.64	135	0.91
32 – 37	207	0.87	0.64 – 0.68	139	1.17
37 – 43	208	0.96	0.68 – 0.71	142	0.82
43 – 50	212	1.01	0.71 – 0.74	131	0.81
50 – 62	213	1.10	0.74 – 0.77	120	0.96
62 – 151	197	1.09	0.77 – 0.80	107	1.01

Table 2. Atomic parameters with estimated standard deviation for $Nd_2(H_2C_4O_4)_3.12H_2O$.

Atom	Group	$x \times 10^4$	$y \times 10^4$	$z \times 10^4$	B/Å^2
Nd		42.6(8)	2194.5(4)	1264.8(4)	(1.46)[a]
O(1)	COO^-	3657(13)	757(6)	1462(6)	2.3(1)
O(2)	COO^-	1639(14)	1881(7)	3314(7)	2.9(1)
O(3)	COO^-	8046(14)	−1626(7)	957(7)	2.7(1)
O(4)	COO^-	8940(15)	229(8)	1247(8)	3.2(1)
O(5)	COO^-	−3352(14)	3129(7)	2893(7)	2.7(1)
O(6)	COO^-	−888(15)	4348(8)	3331(8)	3.2(1)
O(7)	H_2O	3132(14)	3420(7)	1498(7)	2.6(1)
O(8)	H_2O	−1325(15)	4053(7)	591(8)	3.1(1)
O(9)	H_2O	−3049(14)	1788(7)	−218(7)	2.8(1)
O(10)	H_2O	−415(17)	6863(9)	4078(9)	3.5(2)
O(11)	H_2O	2798(16)	6032(8)	1929(8)	3.3(1)
O(12)	H_2O	−3126(16)	6642(8)	2029(8)	3.5(2)
C(1)	COO^-	3439(20)	1118(10)	2715(10)	2.5(2)
C(2)	=CH-	5087(23)	705(11)	3534(11)	3.1(2)
C(3)	=CH-	7047(21)	21(11)	3093(10)	2.8(2)
C(4)	COO^-	7997(18)	−489(9)	1655(9)	2.0(1)
C(5)	COO^-	−2667(18)	4125(9)	3621(9)	2.0(1)
C(6)	=CH-	−4071(20)	5072(10)	4832(10)	2.5(2)

[a] The anisotropic thermal parameters for neodymium, calculated from the expression: $\exp[-(h^2\beta_{11}+2hk\beta_{12}+\cdots)]$ are $\beta_{11}=0.00860(95)$, $\beta_{22}=0.00413(7)$, $\beta_{33}=0.00431(6)$, $\beta_{12}=-0.00108(7)$, $\beta_{13}=0.00134(7)$, and $\beta_{23}=0.00195(4)$, resulting in root mean square displacements along the principal axis of the thermal ellipsoid $R_1=0.1621$(Å), $R_2=0.1073$(Å), and $R_3=0.1441$(Å).

using the programmes PIRUM,[17] CELSIU, DRF, DATAP2, LALS, DISTAN, PLANE, and ORTEP.[18]

DESCRIPTION AND DISCUSSION OF THE STRUCTURE

The superscripts (i) – (vii) are used to indicate the following equivalent sites in the structure.

	x,y,z
(i)	$\bar{x}+1,\bar{y},\bar{z}$
(ii)	$x-1,y,z$
(iii)	$\bar{x}-1,\bar{y}+1,\bar{z}+1$
(iv)	$x+1,y,z$
(v)	$\bar{x},\bar{y},\bar{z}$
(vi)	$\bar{x},\bar{y}+1,\bar{z}$
(vii)	$\bar{x},\bar{y}+1,\bar{z}+1$

where x,y,z are the atomic coordinate given in Table 2. The numbering of the atoms constituting the two ligands maleate and fumarate is shown in Fig. 1.

The structure of NMF is shown in Fig. 2. The maleate ion is not chelated. One of its carboxylate groups, O(3) – C(4) – O(4), holds the neodymium ions in pairs, and the oxygens of the other, O(1) – C(1) – O(2), are coordinated to one of the neodymium ions in the next pair along the a-axis. The Nd-maleate chains built in this way are linked together to layers by the fumarate ions. Adjacent layers are joined by hydrogen bonds *via* the lattice water molecules O(10), O(11), and O(12). These water molecules are in turn hydrogen bonded to each other forming chains parallel to a.

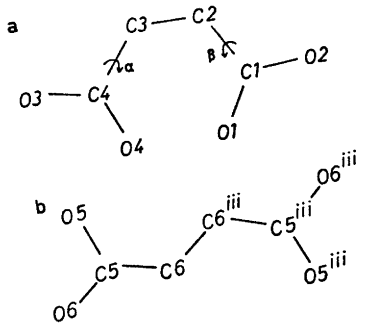

Fig. 1. Designation of the atoms in the two different ligands. a. The maleate ion; b. The fumarate ion.

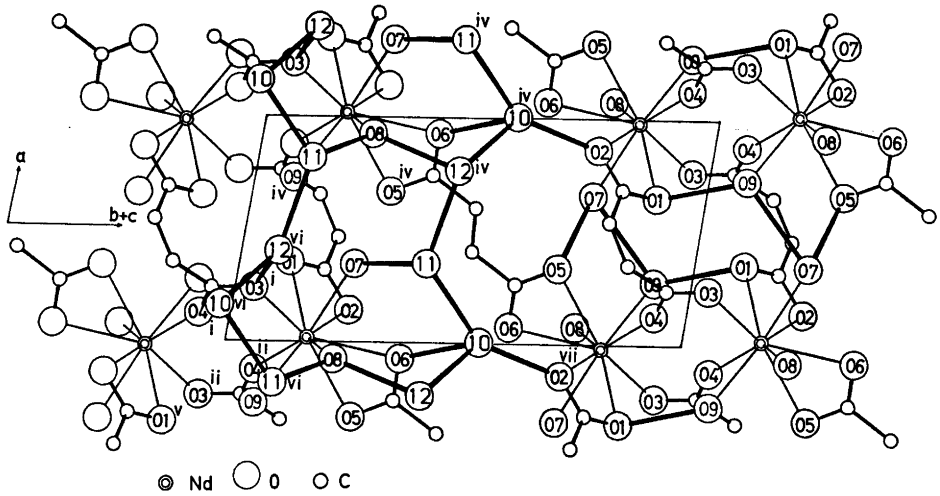

Fig. 2. The Nd-maleate-fumarate layer and the hydrogen bonding. The Nd-maleate chains around $y=z=0$ and $y=z=1$ linked by the fumarate ion at $(\frac{1}{2},\frac{1}{2},\frac{1}{2})$ are projected on $(0,1,\bar{1})$. The lattice water molecules around $y=\frac{1}{2}$, $z=0$ and their hydrogen bonding are shown in the right part of the figure. The hydrogen bonds within the Nd-maleate chain are shown in the left part. Hydrogen bonds are indicated by broad lines.

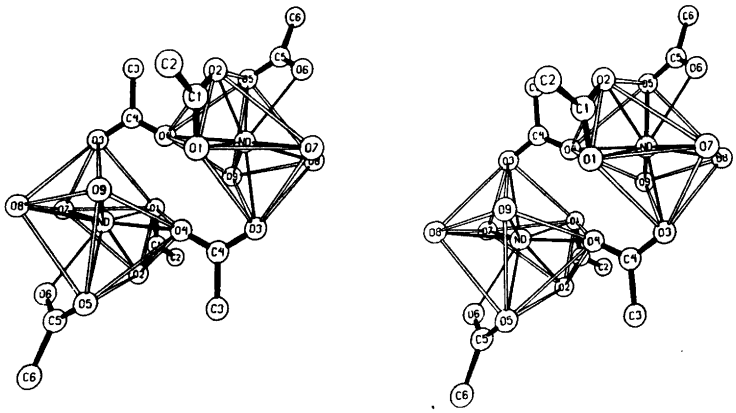

Fig. 3. A stereoscopic pair of drawings showing the coordination polyhedra around Nd and Nd^{v}. The edges of the square antiprism are indicated by open lines.

The coordination polyhedron. There are nine oxygens coordinated to each neodymium ion, *cf.* Fig. 3. The carboxylate groups O(1)–C(1)–O(2) and O(5)–C(5)–O(6) each form a four-membered chelate ring with the metal ion. The carboxylate groups O(3)–C(4)–O(4) are bridging between the two neodymium ions. The remaining three oxygens are the water oxygens O(7), O(8), and O(9). Besides the two carboxylate bridges the two polyhedra are coupled to each other by hydrogen bonds between O(1) and O(9). The Nd–O bond distances are in the range 2.43–2.62 Å, with the average 2.51 Å. The geometry of the bridge $Nd-O(3^{i})-C(4^{i})-O(4^{i})-Nd^{v}$ brings the oxygen $O(4^{i})$ fairly close to Nd, but the distance $Nd-O(4^{i})$, 3.06 Å, seems to be too long to be an bond distance. Moore *et al.*[19] considered a La–O distance of 2.92 Å in a carboxylate bridge of the present type to represent at most a weak lanthanum-oxygen interaction while the corresponding Sm–O

Table 3. Selected distance (Å) and angles (°) with their estimated standard deviations.

A. The coordination polyhedron

Nd – O(1)	2.56(1)	O(2) – O(7)	3.26(1)
Nd – O(2)	2.51(1)	$O(3^{i}) – O(4^{ii})$	3.91(1)
$Nd – O(3^{i})$	2.48(1)	$O(3^{i}) – O(7)$	2.89(1)
$Nd – O(4^{ii})$	2.43(1)	$O(3^{i}) – O(8)$	3.03(1)
Nd – O(5)	2.55(1)	$O(3^{i}) – O(9)$	3.16(1)
Nd – O(6)	2.62(1)	$O(4^{ii}) – O(5)$	3.18(1)
Nd – O(7)	2.52(1)	$O(4^{ii}) – O(9)$	2.86(1)
Nd – O(8)	2.45(1)	O(5) – O(8)	3.32(1)
Nd – O(9)	2.49(1)	O(5) – O(9)	3.13(1)
O(1) – O(2)	2.19(1)	O(6) – O(2)	2.92(1)
$O(1) – O(3^{i})$	3.18(1)	O(6) – O(5)	2.18(1)
$O(1) – O(4^{ii})$	3.08(1)	O(6) – O(7)	2.97(1)
O(1) – O(7)	2.94(1)	O(6) – O(8)	2.85(1)
$O(2) – O(4^{ii})$	3.07(1)	O(7) – O(8)	2.98(1)
O(2) – O(5)	3.25(1)	O(8) – O(9)	2.80(1)

B. The maleate ion

O(1) – O(2)	2.19(1)	O(1) – C(1) – O(2)	118(1)
C(1) – O(1)	1.26(1)	O(1) – C(1) – C(2)	124(1)
C(1) – O(2)	1.29(1)	O(2) – C(1) – C(2)	118(1)
C(1) – C(2)	1.46(2)	C(1) – C(2) – C(3)	125(1)
C(2) – C(3)	1.30(2)	C(2) – C(3) – C(4)	126(1)
C(3) – C(4)	1.52(1)	C(3) – C(4) – O(3)	120(1)
C(4) – O(3)	1.23(1)	C(3) – C(4) – O(4)	119(1)
C(4) – O(4)	1.27(1)	O(3) – C(4) – O(4)	121(1)
O(3) – O(4)	2.18(1)		

C. The fumarate ion

O(5) – O(6)	2.18(1)	O(5) – C(5) – O(6)	121(1)
C(5) – O(6)	1.24(1)	O(5) – C(5) – C(6)	120(1)
C(5) – O(5)	1.27(1)	O(6) – C(5) – C(6)	120(1)
C(5) – C(6)	1.51(1)	$C(5) – C(6) – C(6^{iii})$	123(1)
$C(6) – C(6^{iii})$	1.26(2)		

D. The possible hydrogen bonds

$O(7) – O(5^{iv})$	2.67(1)	$O(5^{iv}) – O(7) – O(11)$	97.8(3)
O(7) – O(11)	2.78(1)	$O(11^{vi}) – O(8) – O(12)$	98.1(4)
$O(8) – O(11^{vi})$	2.82(1)	$O(1^{i}) – O(9^{iv}) – O(7)$	111.8(4)
O(8) – O(12)	2.79(1)	$O(2^{vii}) – O(10) – O(6)$	110.2(4)
$O(9) – O(1^{v})$	2.81(1)	$O(10) – O(11) – O(12^{iv})$	126.3(4)
$O(9^{iv}) – O(7)$	2.90(1)	$O(3^{i}) – O(12^{vi}) – O(10^{vi})$	101.9(4)
$O(10) – O(2^{vii})$	2.69(1)		
O(10) – O(6)	2.73(1)		
O(11) – O(10)	2.83(1)		
$O(11) – O(12^{vi})$	2.73(1)		
$O(12^{vi}) – 0(3^{i})$	2.78(1)		
O(12) – O(10)	2.73(1)		

Table 4. Deviation in Å from least squares planes within the coordination polyhedron and the maleate and fumarate ions. The atoms defining the plane are in each case given above the asterisk.

Atom	Distance	Atom	Distance	Atom	Distance
A. The coordination polyhedron					
O(2)	0.16	O(1)	−0.23		
O(5)	−0.16	O(4^{ii})	0.26		
O(8)	0.17	O(9)	−0.25		
O(7)	−0.18	O(3^{i})	0.22		
*		*			
Nd	1.10	Nd	−1.24		
O(6)	−1.48	O(4^{i})	1.77		
B. The maleate ion					
C(1)	0.00	C(2)	0.00	C(3^{i})	0.01
C(2)	0.00	C(1)	−0.01	C(4^{i})	−0.04
C(3)	0.00	O(1)	0.00	O(3^{i})	0.01
C(4)	0.00	O(2)	0.00	O(4^{i})	0.01
*		*		*	
O(1)	0.12	Nd	−0.20	Nd	0.09
O(2)	−0.11			Nd^{v}	−0.05
O(3)	1.05				
O(4)	−1.11				
C. The fumarate ion					
O(5)	0.00				
O(6)	0.01				
C(5)	−0.01				
C(6)	−0.01				
C(6^{iii})	0.01				
C(5^{iii})	0.01				
O(5^{iii})	−0.01				
O(5^{iii})	−0.00				
*					
Nd	−0.08				

distance of 3.22 Å was regarded as non-bonding. Similar carboxylate bridges were also found in the lanthanoid malonates $N_2mal_3.8H_2O$,[6] $Nd_2mal_3.6H_2O$,[7] and $Eu_2mal_3.8H_2O$.[8] In those structures the distances corresponding to Nd···O(4^{i}) are: Nd−O, 2.72 and 2.61 Å; Eu−O, 2.84 Å and were regarded as bond distances.

The coordination polyhedron is an intermediate between a monocapped square antiprism (CSAP) and a tricapped trigonal prism (TCTP). The "square" faces of the antiprism are O(1)−O(4^{ii})−O(9)−O(3^{i}) and O(2)−O(5)−O(8)−O(7) and the triangular faces of the trigonal prism are O(3^{i})−O(7)−O(8) and O(2)−O(5)−O(4^{ii}). The angle between the "square" faces of the antiprism is 8° while that between the triangular faces of the trigonal prism is 14°. The CSAP is outlined in Fig. 3.

The atoms defining the square base of the cap are coplanar within ±0.2 Å and those defining the square base of the prism are coplanar within ±0.3 Å (Table 4A). The two "squares" are of about the same size with average edge lengths of 3.1 and 3.2 Å. The noncoordinated oxygen O(4^{i}) is situated outside the square base of the prism.

The maleate ion. The conformation of the maleate ion is the same as in the maleate structures containing the non-chelated ion. The

carbon chain, and the two C−COO groups are planar within the limits of error (Table 4B). The torsion angles α and β between each of the C−COO planes and the carbon chain plane (Fig. 1) are $\alpha = -83°$ and $\beta = 6°$. The corresponding angles in Li_2maleate are 81.4 and 7.0°, and in Na_2maleate 66.3 and −16.9°.[20] In Cd-maleate which contains two independent maleate ions these angles are 83.6 and −17.5° in one and 66.6 and −15.6° in the other.[12] Thus, the group C(3)=C(2)−C(1)O(1)O(2) is approximately planar in five different environments. This finding agrees with the fact that R−C−COO groups (R=C−, C=, N−, O−, S−) are as a rule found to be planar.[21] Accordingly one might expect that the second carboxylate group too lies in the plane of the carbons. However, such an arrangement seems impossible due to repulsion between the carboxylate groups.

With the bond distances and angles assumed to represent an unstrained carbon framework of the present type (C=C−C, 121.5°; C=C, 1.34 Å; C−C, 1.49 Å)[22] and a C−COO group unaffected by its environment, (C−C−O, 117.5°; C−O, 1.26 Å)[23] the distance O(1)···O(4) of a completely planar maleate ion would be as short as 1.60 Å.

Bond distances and angles within the maleate ion are given in Table 3B. The standard deviations are too large to permit any detailed discussion of the dimensions of the ion. It should be mentioned that the C=C−C angles are found to be larger than the value 121.5° quoted above, in accordance with the results obtained for the alkali maleates.[20]

The fumarate ion. The fumarate ion has a center of symmetry and is planar within the limits of errors (Table 4C), in agreement with the empirical rule mentioned above. Planar or approximately planar fumarate groups are found also in fumaric acid[24] and in hydrogen fumarates and fumarates.[25–28]

The bond distances and angles in the fumarate ion (Table 3C) agree with those found in other fumarate structures.

The hydrogen bonds. Regarding distances between a water oxygen and other oxygens shorter than 3.20 Å and not constituting coordination polyhedron edges as possible hydrogen bond distances, there is just one suitable distance for each of the water hydrogens. The longest of these distances is 2.90 Å. Thus a reasonable hydrogen bond system can be chosen even though the positions of the hydrogen atoms have not been located. The two hydrogen bond acceptors of each water molecule are given in Table 3D.

The lattice water molecules, O(10), O(11), and O(12) are hydrogen bonded to each other forming infinite chains of the type ···O(12)··· O(10)···O(11)···O(12^{iv})···O(10^{iv})··· parallel to the *a*-axis (Fig. 2), and situated between the metal-ligand layers. Adjacent metal-ligand layers are linked by hydrogen bonds *via* the water molecules of these chains. The carboxylate oxygens O(2), O(3), and O(6) each accept one hydrogen bond from the chains, and the coordinated water molecules O(7) and O(8) donate one and two hydrogen bonds, respectively, to the chains.

Intra layer hydrogen bonds are formed by the water molecules O(7) and O(9). The bonds O(7)···O(5^{iv}) and O(9^{iv})···O(7) link adjacent polyhedra in the *a*-direction and the bond O(9)···O(1^{v}) links the two polyhedra of a pair as mentioned above.

Acknowledgements. This work is part of a research project supported by the Swedish Natural Science Research Council.

REFERENCES

1. Grenthe, I., Gårdhammar, G. and Rundcrantz, E. *Acta Chem. Scand. 23* (1969) 93.
2. Dellien, I. *Acta Chem. Scand. 27* (1973) 733.
3. Dellien, I. and Malmsten, L.-Å. *Acta Chem. Scand. 27* (1973) 2877.
4. Hansson, E. *Acta Chem. Scand. 24* (1970) 2969.
5. Hansson, E. *Acta Chem. Scand. 27* (1973) 823.
6. Hansson, E. *Acta Chem. Scand. 27* (1973) 2441.
7. Hansson, E. *Acta Chem. Scand. 27* (1973) 2813.
8. Hansson, E. *Acta Chem. Scand. 27* (1973) 2827.
9. Prout. C. K., Carruthers, J. R. and Rossotti, F. J. C. *J. Chem. Soc. A* (1971) 3342.
10. Town, W. G. and Small, R. W. H. *Acta Crystallogr. B 29* (1973) 1950.
11. James, M. N. G. and Williams, G. J. B. *Acta Crystallogr. B 30* (1974) 1257.
12. Post, M. L. and Trotter, J. *J. Chem. Soc. Dalton Trans.* (1974) 674.
13. *International Tables for X-Ray Crystallography*, Kynoch Press, Birmingham 1969, Vol. I.

14. Cruickshank, D. W. J. In Rollet, J. S. Ed., *Computing Methods in Crystallography*, Pergamon, Glasgow 1965, pp. 99 – 116.
15. *International Tables for X-Ray Crystallography*, Kynoch Press, Birmingham 1968, Vol. III.
16. Cromer, D. T., Larsson, A. C. and Waber, J. T. *Acta Crystallogr. 17* (1964) 1044.
17. Werner, P. E. *Ark. Kemi 31* (1970) 513.
18. Liminga, R. *Acta Chem. Scand. 21* (1967) 1206.
19. Moore, J. W., Glick, M. D. and Baker, W. A. *J. Amer. Chem. Soc. 94* (1972) 1858.
20. James, M. N. G. and Williams, G. J. B. *Acta Crystallogr. B 30* (1974) 1249.
21. Oskarsson, Å. *Structural Studies on Solid Iminodiacetate Compounds*, Thesis, Lund 1974.
22. Darlow, S. F. *Acta Crystallogr. 14* (1961) 1257.
23. Hahn, T. *Z. Kristallogr. 109* (1957) 4.
24. Bednowitz, A. L. and Post, B. *Acta Crystallogr. 21* (1966) 566.
25. Gupta, M. P. and Sahn, R. G. *Acta Crystallogr. B 26* (1970) 61.
26. Gupta, M. P. and Sahn, R. G. *Acta Crystallogr. B 26* (1970) 1964.
27. Gupta, M. P. and Sahn, B. N. *Acta Crystallogr. B 26* (1970) 1969.
28. Gupta, M. P., Prasad, S. M., Sahn, R. G. and Sahn, B. N. *Acta Crystallogr. B 28* (1972) 135.

Received April 1, 1975.

Acta Chemica Scandinavica A 29 (1975) 935—938

Bromide Ion Quadrupole Relaxation in Non-aqueous Solution

BJÖRN LINDMAN

Division of Physical Chemistry 2, Lund Institute of Technology, Chemical Center, S-220 07 Lund, Sweden

The ^{79}Br quadrupole relaxation of the bromide ion was studied as a function of counterion and concentration in dimethyl sulfoxide and methanol and in water-dioxane mixtures. Whereas alkali and halide ion quadrupole relaxation is generally observed to be rapid in non-aqueous environments, ^{79}Br relaxation in dilute dimethyl sulfoxide solutions was found to be slower than in aqueous solution. The extrapolated infinite dilution $^{79}Br^-$ relaxation rate in dimethyl sulfoxide was found to be in good agreement with that predicted by a theory of Hertz assuming an electrostatic origin of the time-modulated electric field gradients causing relaxation.

Nuclear magnetic resonance has in many different ways been fruitfully applied to elucidate molecular interactions and microdynamic properties of electrolyte solutions.[1–4] Studies based on static or dynamic characteristics of the resonance signal from the solvent's nuclei have, in a number of cases, given quite detailed information on many aspects of solvent-solvent and ion-solvent interactions, such as solvation numbers, life-times of ion-solvent complexes and the effects of ions on solvent-solvent interactions. The NMR signals from the ions in the solution contain complementary information on ion-solvent interactions as well as information on ion-ion interactions. Many simple ions do possess nuclei with manageable NMR sensitivities, but progress in the field has been made more difficult by problems of accounting quantitatively for both shielding and relaxation effects.

Most monoatomic ions have nuclei with electric quadrupole moments and the interactions of these with electric field gradients generally dominate nuclear magnetic relaxation in diamagnetic systems. A quantitative rationalization of an ions's quadrupole relaxation is of great significance in connection with attempts to understand several aspects of electrolyte solutions. However, as regards the origin of the field gradients, the time-modulation of which gives relaxation, there has been considerable controversy. While the early "electrostatic" approach of Hertz [5] and Valiev [6,7] related the field gradients to point charges and dipoles, an alternative model, based on overlap effects, was advanced by Deverell.[8] Whereas Deverell's model is difficult to test quantitatively, Hertz has with a recently improved version [9,10] of his electrostatic theory been able to account [11–13] for ion-ion and ion-solvent contributions to relaxation in a large number of aqueous systems.*

While several systematic studies of ion relaxation in aqueous solution have been reported, the information on non-aqueous or mixed solvent systems is very limited. Halide ion quadrupole relaxation rates have been reported for methanol,[14,15] dimethyl sulfoxide,[14] nitromethane, [16] and for mixtures of acetonitrile,[17] methanol,[15,18] and acetone [18] with water. However, in general, these data do not permit a separation of the relaxation rates into contributions from ion-solvent and ion-ion interactions. Recently, Melendres and Hertz [19] presented the first analysis using the electrostatic theory of ion relaxation rates in non-aqueous solution. An interesting result of theirs is that, in contrast to aqueous solutions, the methanolic solutions show (using the data of Ref. 15) a considerable orientation of the molecules in the first solva-

* Further support for the "electrostatic" origin of the field gradients will be given in a forthcoming review article together with S. Forsén.

tion sphere of Cl^- and Br^- ions.

The approach of Hertz [9,10] appears to be fruitful and its further application to other systems is expected to be helpful in the elucidation of ion-solvent and ion-ion interactions in non-aqueous environments. The present study, concerned with $^{79}Br^-$ relaxation in methanol and dimethyl sulfoxide as well as in dioxane-water mixtures, lends further support to the relevance of the electrostatic approach and gives some new aspects on the variation of the relaxation rate with concentration. The NMR experiments were performed at 26 ± 2 °C essentially as in our previous ^{79}Br NMR investigations.[14,20,21] The experimental concentration dependences for $1/T_2$ of ^{79}Br are given in Fig. 1 for NaBr, KBr, NH_4Br and Bu_4NBr in dimethyl sulfoxide, for NaBr in methanol and for NaBr, KBr and Bu_4NBr in dioxane-water mixed solvent. The value obtained by extrapolation to infinite dilution in methanol, $1/T_{20} \simeq 14\,700$ s^{-1}, agrees closely with that derived by Melendres and Hertz [19] from the ^{81}Br data of Hall *et al.*[15] for LiBr in methanol. For dimethyl sulfoxide solutions, the concentration dependence of Br relaxation is much greater than for water or methanol solutions, thus making the estimation of $1/T_{20}$ quite difficult. With KBr, Bu_4NBr and NaBr the concentration dependence of the relaxation is approximately linear and in all these cases a value of $1/T_{20} = 1050$ s^{-1} is obtained by linear extrapolation to zero concentration. Since it has been emphasized recently by Hertz *et al.*[12] that instrumental broadening may be important in the present type of measurements, attempts were made by reducing field modulation amplitude and frequency and by employing flux stabilizer and field homogeneity coils to obtain an improved value of $1/T_{20}$ in dimethyl sulfoxide. The value then obtained was close to that given above but must, in view of the marked concentration dependence of relaxation, still be considered as rather approximative. This is, however, not critical for the present discussion.

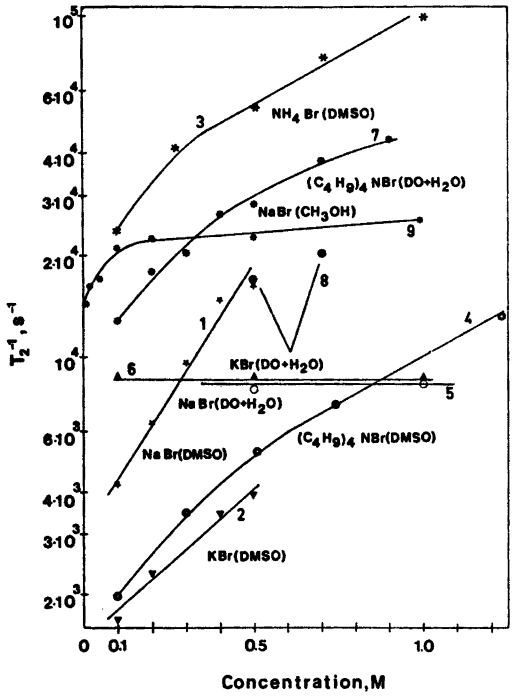

Fig. 1. $^{79}Br^-$ transverse relaxation rates in non-aqueous and mixed solvent systems as a function of electrolyte concentration. Systems studied were

1, NaBr in dimethyl sulfoxide (DMSO); 2, KBr in dimethyl sulfoxide; 3, NH_4Br in dimethyl sulfoxide; 4, $(C_4H_9)_4NBr$ in dimethyl sulfoxide; 5, NaBr in a mixture of dioxane (20 % by weight) and water; 6, KBr in a mixture of dioxane (20 % by weight) and water; 7, $(C_4H_9)_4NBr$ in a mixture of dioxane (20 % by weight) and water; 8, KBr in a mixture of dioxane (40 % by weight) and water; 9, NaBr in methanol.

It is interesting to note that, while in all cases considered by Melendres and Hertz [19] the alkali and halide ion quadrupole relaxation rates were found to be greater in non-aqueous environment than in water, we find the $^{79}Br^-$ relaxation rate in dimethyl sulfoxide to be smaller than in water ($1/T_{10} = 1500$ s^{-1} according to Hertz *et al.*[12] and $1/T_{20} = 1650$ s^{-1} according to our own line width measurements). The implications of this for Br^- ion solvation in dimethyl sulfoxide will now be examined using Hertz' theory [9] and following the procedure of Melendres and Hertz.[19] These authors consider three cases, characterized by different degrees of solvent orientation around the relaxing ion, and give explicit formulae for the infinite dilution relaxation rates. Their "fully random distribution model", which assumes a random orientation and distribution of solvent point dipoles, predicts ($T_1 = T_2$, *i.e.* an extreme narrowing situation, is assumed)

$$\frac{1}{T_{20}} = \frac{24\pi^3}{5} \times \frac{2I+3}{I^2(2I-1)} \left[\frac{PeQ(1+\gamma_\infty)}{h}\right]^2 \times \frac{m^2 c_{solv} \tau_{solv}}{r_0^5} \quad (1)$$

where I is the spin quantum number; P the polarization factor; eQ the nuclear quadrupole moment; $(1+\gamma_\infty)$ the Sternheimer antishielding factor; m is the electric dipole moment of the solvent molecule; c_{solv} the solvent concentration; τ_{solv} is the rotational correlation time of the solvent; r_0 the distance of closest approach between the relaxing nucleus and the solvent point dipoles. For P and $1+\gamma_\infty$ the same values were used as in Ref. 19, for m the gas phase value was used and c_{solv} was calculated from the density.[22] τ_{solv} was taken to be 4.5×10^{-12}s (*cf.* Refs. 2, 23 and 24), a value which is close to that calculated from the Debye equation with the Gierer-Wirtz microviscosity factor.[25] If r_0 is taken as the sum of the solvent molecular radius (calculated from molecular volume, assuming hexagonal closest packing), and the Br^- ionic radius (assumed to be 1.95 Å) one obtains from eqn. (1) $1/T_{20} = 750$ s^{-1}. It can thus be inferred that Hertz' electrostatic theory of ion quadrupole relaxation assuming random solvent distribution and orientation gives a good rationalization of the experimental findings. (Probably the above procedure overestimates r_0; a slightly smaller value would improve agreement between theory and experiment but in view of the considerable uncertainty in some of the quantities in eqn. (1), and in the experimental $1/T_{20}$, more detailed considerations are not presently justified.)

Melendres and Hertz [19] also consider two models characterized by the presence of a distinct first solvation sphere. For their "non-oriented solvation" model we obtain a calculated relaxation rate of $1/T_{20} = 2000$ s^{-1} and for the "fully oriented solvation" model we obtain, assuming random lateral distribution,* $1/T_{20} = 3600$ s^{-1}. In the calculations we have used the same r_0 values as above and assumed the solvation number to be 6. (A more realistic r_0 value may lead to markedly greater calculated relaxation rates.) It can be seen that the two models assuming a distinct solvation sphere predict much higher values of $1/T_{20}$ than given by experiment. On the other hand, the much higher value of $1/T_{20}$ for Br^- in methanol is, as shown by Melendres and Hertz,[19] best described by the "fully oriented solvation" model, which involves a distinct solvation sphere of radially oriented solvent dipoles. Surveying temperature dependence studies of 0.4 M KBr, NaBr, NH_4Br and Bu_4NBr solutions in dimethyl sulfoxide were performed to elucidate these problems further. The Arrhenius' activation energies of Br^- relaxation, which were found to be 11 – 12 kJ/mol for KBr, NaBr, NH_4Br and somewhat higher for Bu_4NBr, are considerably smaller than the activation energy of viscosity (16.7 kJ/mol [22]), *i.e.* the same relation as for aqueous solutions.

The discussion of the infinite dilution relaxation rate of Br^- in dimethyl sulfoxide supports the applicability of Hertz' electrostatic theory of ion quadrupole relaxation. Furthermore, according to our analysis, data are consistent with a bromide ion solvation in dimethyl sulfoxide which does not involve a distinct solvation sphere. This is the same as deduced for water [9] but in contrast to the findings with methanol as solvent.[19] A weak bromide ion solvation in dimethyl sulfoxide correlates well with what Schläfer and Schaffernicht [26] deduced for the chloride ion from conductivity data. These authors refer this observation to the low accessibility of the positive part of the solvent dipole. A weak halide ion solvation in dimethyl sulfoxide has also been inferred recently by Gopal and Jha.[27] By investigating further solvents in the same way and correlating the deduced solvation characteristics with solvent molecular properties a more detailed understanding of the variation in halide ion solvation between different solvents can probably be provided.

While the ion-solvent contribution to an ion's quadrupole relaxation is now fairly well understood, an interpretation of the ion-ion contribution is much more difficult.[10] The data given in Fig. 1 show some interesting features, such as the very strong variation of the $^{79}Br^-$ relaxation with cation in dimethyl sulfoxide,

* One difficulty in this analysis is that the fully random distribution model may predict the same relaxation rate as the fully oriented solvation model with some lateral order. Information from other types of studies which does not seem presently available is required to provide a safe distinction between the two possibilities.

but a detailed discussion of the variable concentration results has to await experimental studies of further systems as well as of the effect of electrolyte on solvent mobility. It appears, however, that the magnitude of the relaxation rate alterations is within a range which can be explained by ion-pair formation,[19] but it is not clear why the ion-pair contribution to Br^- relaxation should vary with the cation in the way indicated. (Another possible interpretation would be in terms of a perturbation by the cation of a symmetrical solvation sphere involving lateral order and thus quenching effects.) The observations for the dioxane-water mixed solvent system resemble those of aqueous systems with a weak concentration dependence for alkali halides but a very strong one for tetraalkylammonium halides.[14,20,21] It is interesting to note that the strong effect of non-polar groups on Br^- relaxation is evident even in the presence of a considerable amount of dioxane. Thus, complete elimination of Br^- ions from the surface of the nonpolar solute is not effected by dioxane.

Note added in proof. The author was recently informed about similar studies in progress in Prof. Hertz' laboratory. Prof. Hertz and Dr. Weingärtner (personal communication) have in agreement with the present findings observed Br^- and I^- quadrupole relaxation at low concentrations to proceed more slowly in dimethyl sulfoxide than in water. Hertz and Weingärtner have also studied halide ion quadrupole relaxation in several other solvents.

Acknowledgements. Lars-Gunnar Torstensson is thanked for performing part of the measurements and Sture Forsén for helpful discussions. Håkan Wennerström and Thomas Bull are thanked for valuable comments on the manuscript.

REFERENCES

1. Hertz, H. G. In Falkenhagen H., Ed., *Theorie der Elektrolyte*, S. Hirzel Verlag, Leipzig 1971, p. 479.
2. Hertz, H. G. *Progr. Nucl. Magn. Resonance Spectrosc. 3* (1967) 157.
3. Hertz, H. G. In Franks, F., Ed., *Water. A Comprehensive Treatise*, Plenum Press, New York 1973, Vol. 3, p. 301.
4. Deverell, C. *Progr. Nucl. Magn. Resonance Spectrosc. 4* (1969) 235.
5. Hertz, H. G. *Z. Electrochem. Ber. Bunsenges. Phys. Chem. 65* (1961) 20.
6. Valiev, K. A. *Sov. Phys. JETP 11* (1960) 883.
7. Valiev, K. A. *Sov. Phys. JETP 10* (1960) 77.
8. Deverell, C. *Mol. Phys. 16* (1969) 491.
9. Hertz H. G. *Ber. Bunsenges. Phys. Chem. 77* (1973) 531.
10. Hertz, H. G. *Ber. Bunsenges. Phys. Chem. 77* (1973) 688.
11. Hertz, H. G., Holz, M., Keller, G., Versmold, H. and Yoon, C. *Ber. Bunsenges. Phys. Chem. 78* (1974) 493.
12. Hertz, H. G., Holz, M., Klute, R., Stalidis, G. and Versmold, H. *Ber. Bunsenges. Phys. Chem. 78* (1974) 24.
13. Hertz, H. G. and Holz, M. *J. Phys. Chem. 78* (1974) 1002.
14. Lindman, B., Forsén, S. and Forslind, E. *J. Phys. Chem. 72* (1968) 2805.
15. Hall, C., Haller, G. L. and Richards, R. E. *Mol. Phys. 16* (1969) 377.
16. Gentzler, R. E., Stengle, T. R. and Langford, C. H. *Chem. Commun.* (1970) 1257.
17. Stengle, T. R., Pan, Y.-C. E. and Langford, C. H. *J. Amer. Chem. Soc. 94* (1972) 9037.
18. Richards, R. E. and Yorke, B. A. *Mol. Phys. 6* (1963) 289.
19. Melendres, C. A. and Hertz, H. G. *J. Chem. Phys. 61* (1974) 4156.
20. Lindman, B., Wennerström, H. and Forsén, S. *J. Phys. Chem. 74* (1970) 754.
21. Wennerström, H., Lindman, B. and Forsén, S. *J. Phys. Chem. 75* (1971) 2936.
22. Lindberg, J. J. *Finska Kemistsamf. Medd. 71* (1962) 77.
23. Zeidler, M. D. *Ber. Bunsenges. Phys. Chem. 69* (1965) 659.
24. Chaughule, R. S. and Gupta L. C. *Proc. Indian Acad. Sci. Sect. A 76* (1972) 153.
25. Gierer, A. and Wirtz, K. *Z. Naturforsch. 8a* (1953) 532.
26. Schläfer, H. L. and Schaffernicht, W. *Angew. Chem. 72* (1960) 618.
27. Gopal, R. and Jha, J. S. *J. Phys. Chem. 78* (1974) 2405.

Received April 11, 1975.

Acta Chemica Scandinavica A 29 (1975) 939—944

On the Structure of the Peptide Linkage. The Structures of Formamide and Acetamide at —165°C and an *ab initio* Study of Formamide, Acetamide, and *N*-Methylformamide

TOR OTTERSEN

Department of Pharmacy, University of Oslo, Oslo 3, Norway

The crystal and molecular structures of formamide and rhombohedral acetamide have been refined using X-ray data sets collected at −165 °C. The principal bond lengths found are, formamide: CO, 1.243(2) Å, CN, 1.319(2) Å; acetamide: CO, 1.243(4) Å, CN, 1.336(4) Å, CC, 1.510(3) Å. The influence of hydrogen bonding on the conjugated N−C=O fragment is evident. A series of *ab initio* calculations has been performed on acetamide and *N*-methylformamide. The results are compared with those obtained earlier for formamide.

In a recent series of theoretical investigations utilizing *ab initio* methods (see Ref. 1 and references therein) the effect of hydrogen bonding has been studied for the conjugated peptide linkage, using formamide as a model compound. The results obtained (*i.e.* an increased conjugation over the N−C=O fragment expressed as a shortening of the N−C bond and a lengthening of the C−O bond) are in good agreement with those found in a series of structure investigations of 3,6-pyridazinediones and related compounds (see Ref. 2 and references therein).

The crystal structure of formamide has been determined earlier by film methods.[3] However, the accuracy of this investigation is relatively poor, and a new structure determination was, therefore, carried out in order to study the effect of hydrogen bonding on the structural parameters. A series of structure investigations in the gaseous state of formamide and related molecules has recently been published.[4–7] In these investigations significant differences were found between the C−N and C−O bond lengths obtained for formamide [6] and acetamide,[5] and between *N*-methylformamide [7] and *N*-methylacetamide.[4] Similar differences (*i.e.* a lengthening of both bonds upon substitution at C) were found between the results obtained in the crystal structure determinations of *N*,*N*′-diformylhydrazine [8] and succinic hydrazide.[2] It was, therefore, decided to carry out a structure investigation of acetamide within the same experimental framework as for formamide (for earlier crystal structure determinations of acetamide see Refs. 9–11).

In order to study changes in electron populations of the N−C=O fragment induced by substitution, a series of *ab initio* calculations was performed on acetamide and *N*-methylformamide to complement earlier calculations on formamide.[1,12] It was further decided to optimize the C−C, C−N and C−O bonds in order to see if the changes found experimentally upon substitution are reflected by the *ab initio* method.

EXPERIMENTAL AND CALCULATIONS

A. X-Ray diffraction

A computer-controlled Syntex P$\bar{1}$ four circle diffractometer (at the Dept. of Chemistry) with graphite monochromatized Mo$K\alpha$ radiation and equipped with an Enraf-Nonius liquid nitrogen cooling device (modified by H. Hope), was utilized in the determination of unit cell parameters and the collection of intensity data. For both data sets the temperature at the crystal site was −165 °C. All computer programs utilized are part of a local assembly of computer

Table 1. Crystal data at −165 °C.

Parameter	Formamide CH_3NO	Acetamide C_2H_5NO
Space group	$P2_1/c$	$R3c$
a (Å)	3.613(3)	11.516(2)
b (Å)	9.053(6)	
c (Å)	8.419(4)	13.091(2)
β (°)	125.39(4)	
V (Å^3)	224.5	1503.4
Z	4	18
M (amu)	45.04	59.07
D_{calc}(g/cm^3)	1.332	1.174
F(000)	96	576

programs which is described in Ref. 13. Atomic scattering factors used were those of Doyle and Turner [14] for oxygen, nitrogen and carbon, and of Stewart *et al.*[15] for hydrogen.

I. Formamide. A crystal of dimensions 0.6 × 0.6 × 0.2 mm, grown by slow evaporation of an ethyl alcohol solution at −30 °C (the air was kept free from water by use of $CaCl_2$), was used for all experiments. Cell constants and their standard deviations were determined by a least-squares treatment of the angular coordinates of fifteen symmetry-independent reflections with 2θ-values between 39 and 55°. Three-dimensional intensity data were recorded using the ω scanning mode with scan speed variable from 2 to 8° min^{-1}, depending on the peak intensity of the reflection. Background counting time was 0.6 × scan time. The variations in the intensities of three standard reflections which were remeasured after every sixty reflections were random and less than three times their standard deviations. Accordingly no corrections were applied for these variations.

The estimated standard deviations were taken as the square root of the total counts with a 2 % addition for experimental uncertainties. Of the 822 symmetry-independent reflections measured ($2\theta_{max} = 60°$) 721 had intensities larger than 2.5 times their standard deviations. These were regarded as "observed" reflections, and the remaining were excluded from further calculations. The intensities were corrected for Lorentz and polarization effects. Crystal data are given in Table 1.

Least-squares refinements, utilizing the positional parameters found by Ladell and Post [3] as starting values, of all positional parameters, anisotropic thermal parameters for nonhydrogen atoms, and isotropic thermal parameters for hydrogen atoms, using all observed data, converged to a weighted R_w of 0.088 and a conventional R of 0.070. In order to reduce the influence of valence electrons on the refined parameters, all reflections with $\sin\theta/\lambda < 0.5$ were excluded from the refinement, leaving 494 F_o's. Least-squares refinement of all parameters involving nonhydrogen atoms resulted in a weighted R_w of 0.071, a conventional R of 0.061 and an R for the total data set of 0.084. Parameters obtained in this refinement for nonhydro-

Table 2. Fractional atomic coordinates and thermal parameters with estimated standard deviations for nonhydrogen atoms. The temperature factor is given by $\exp\{-2\pi^2[U_{11}(a^*h)^2 + U_{22}(b^*k)^2 + U_{33}(c^*l)^2 + U_{12}(a^*b^*)hk + U_{13}(a^*c^*)hl + U_{23}(b^*c^*)kl]\}$

Atom	x	y	z	U_{11}	U_{22}	U_{33}	U_{12}	U_{13}	U_{23}
Formamide									
O	.7173(4)	−.0688(1)	.2484(1)	.0367(6)	.0163(5)	.0365(6)	.0032(3)	.0217(4)	.0053(3)
N	.4208(4)	.1570(1)	.1190(1)	.0342(7)	.0150(5)	.0361(7)	.0030(3)	.0209(5)	.0010(3)
C	.5929(4)	.0568(1)	.2583(1)	.0265(6)	.0176(6)	.0311(6)	−.0013(3)	.0158(5)	−.0008(3)
Acetamide									
O	.2403(2)	−.0024(1)	−.0014(1)	.0230(9)	.0207(8)	.0322(8)	.0097(6)	−.0037(6)	.0032(5)
N	.3328(2)	−.1009(2)	.0915(1)	.0212(9)	.0223(9)	.0262(8)	.0086(6)	−.0015(6)	·0036(6)
C	.4758(2)	.1281(2)	.0350(2)	.0207(9)	.0223(9)	.0269(10)	.0037(6)	−.0010(7)	.0008(7)
C1	.3401(2)	.0024(1)	.0395(2)	.0194(10)	.0189(9)	.0196(7)	.0078(5)	.0008(7)	−.0010(7)

Table 3. Fractional atomic coordinates and isotropic thermal parameters with estimated standard deviations for hydrogen atoms. Results from the refinements using all observed data.

Atom	x	y	z	B
Form-amide				
H1	.398(7)	.140(3)	.007(3)	2.9(4)
H2	.341(7)	.293(3)	.154(3)	3.5(5)
H3	.611(7)	.087(2)	.362(3)	2.4(4)
Acet-amide				
H1	.254(4)	−.173(3)	.100(3)	2.8(6)
H2	.402(3)	−.097(2)	.120(2)	.6(4)
H4	.481(4)	.193(4)	.095(3)	4.1(8)
H5	.544(4)	.108(5)	.047(3)	4.0(8)
H6	.484(4)	.187(4)	−.019(3)	3.5(7)

gen atoms are given in Table 2, and parameters for hydrogen atoms, from the refinement using all observed data, are listed in Table 3. The molecular parameters obtained (Fig. 2) are in agreement with the earlier results.[3]

II. Acetamide. A crystal of dimensions 0.3 × 0.3 × 0.4 mm, grown from the melt, was used for all experiments. The analysis of the angular coordinates of fifteen reflections (the computer program used is part of the diffractometer program library) with 2θ-values between 7 and 25° indicated the rhombohedral space group [9,10] ($R3c$). This is rather surprising since metastable orthorhombic crystals (space group $Pccn$) are usually formed by cooling of the melt.[11] Later, several crystals grown from melts of acetamide were examined, and in all cases the rhombohedral system was found. Cell constants and their standard deviations were determined by a least-squares treatment of fifteen symmetry-independent reflections with 2θ-values between 19 and 38°. Three-dimensional intensity data were recorded using the ω-2θ scanning mode with scan speed variable from 2 to 8° min^{-1}, depending on the peak intensity of the reflections. All reflections which had integrated counts of less than 15 cps, determined in a 2 s scan over the peak, were not measured. The intensities of three standard reflections, which were remeasured after every fifty reflections, showed a small regular decrease (to about 0.97 of their initial value). Accordingly the intensities were corrected for this decrease.

The estimated standard deviations were taken as the square root of the total counts with a 2 % addition for experimental uncertainties. Of the 465 symmetry-independent reflections measured ($2\theta_{max} = 60°$), all had intensities larger than twice their standard deviations and were used in the refinements. The intensities were corrected for Lorentz and polarization effects. Crystal data are given in Table 1.

Least-squares refinements, utilizing the positional parameters found by Denne and Small [10] as starting values, of all positional parameters, anisotropic thermal parameters for nonhydrogen atoms, and isotropic thermal parameters for hydrogen atoms, converged to a weighted R_w of 0.054 and a conventional R of 0.043. In order to reduce the influence of valence electrons on the refined parameters, all reflections with $\sin\theta/\lambda < 0.5$ were excluded from the refinement, leaving 282 F_o's. Least-squares refinement of all parameters involving nonhydrogen atoms resulted in a weighted R_w of 0.044, a conventional R of 0.038 and an R for the total data set of 0.045. Parameters obtained in this refinement for nonhydrogen atoms are given in Table 2, and parameters for the hydrogen atoms, from the refinement using all observed data, are listed in Table 3. The molecular parameters obtained (Fig. 2) are in good agreement with those found earlier.[10] Listings of observed and calculated structure factors for both structure determinations are available upon request from the author or the Department of Chemistry, University of Oslo, Oslo 3, Norway. Standard deviations in molecular parameters were calculated from the correlation matrix ignoring standard deviations in cell parameters.

B. Theoretical calculations

The calculations were carried out using the program MOLECULE [16] which solves the Roothan-Hall equations for a Gaussian type basis. A ($7s3p/4s$) basis set [17] contracted to ($4s2p/2s$) was applied. In all cases a scale factor of 1.2 was applied [18] for the exponents of the hydrogen s functions. This basis set has been used previously for studies like the present one and has turned out to be adequate.[1,12,17] A further discussion of this basis set compared

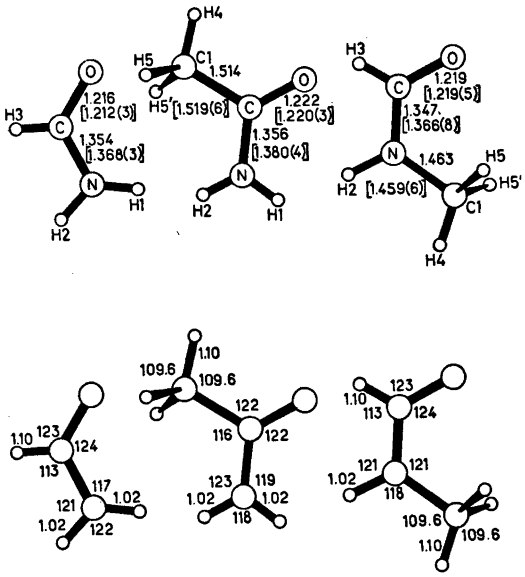

Fig. 1. Optimized (top) and assumed molecular parameters from the *ab initio* calculations. The numbers in brackets are those found in the gaseous state by electron diffraction (see Refs. 5 – 7) with estimated limits or error.

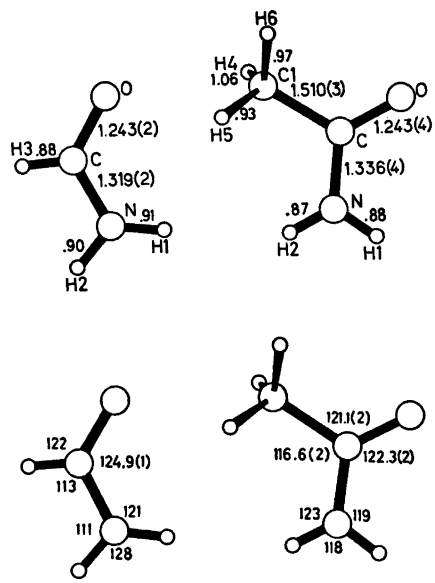

Fig. 2. Bond lengths (Å) and bond angles (°) with estimated standard deviations. Positional parameters used for non-hydrogen atoms are those from the refinement using only high-angle data. Standard deviations in dimensions involving hydrogen atoms (positional parameters used for hydrogen atoms are those from the refinement using all observed reflections) are about 0.03 Å and 2°.

with larger ones may be found in Ref. 12.

The molecules were assumed to have a plane of symmetry according to Fig. 1, where also the labelling of the atoms is indicated, and assumed structural parameters are given. All results from theoretical calculations for formamide are taken from Ref. 12.

The CO (R_{CO}), CN (R_{CN}) and CC (R_{CC}) bonds were optimized simultaneously for acetamide and *N*-methylformamide. The optimized bond lengths are given in Fig. 1, and the optimized total energies obtained are listed in Table 4.

Only small differences are found in the R_{CO} and R_{CN} values of formamide and acetamide. A small lengthening of the CO bond upon introduction of a methyl group at C is indicated, in agreement with the results obtained by electron diffraction studies.[4–7] (see also Fig. 1, where some of these results are given). However, the significant lengthening of the CN bond upon substitution found in a series of structure investigations,[4–6,8] (see also the present results for formamide and acetamide, which are given in Fig. 2), is not reflected by the *ab initio* calculations. Also, the shortening obtained by the optimalization procedure, of the CN bond in *N*-methylformamide compared with that of formamide, is not found in the experimental results.[4–7]

Stretching force constants and some of the interdependencies in the force fields are given in Table 5. Only small differences are found between the three molecules. However, it is interesting to note that for both acetamide and *N*-methylformamide F_{CO} has increased and F_{CN} decreased compared to formamide.

Table 4. Total energies (a.u.) for the optimized molecules.

Molecule	Total energy (a.u.)
Formamide	−168.68145
Acetamide	−207.67915
N-Methyl-formamide	−207.66671

Table 5. Stretching force constants in mdyn/Å, and regression coefficients.[a]

	Form-amide	Acet-amide	M-ethyl-*N* form-amide
F_{CO}	13.0	13.8	13.6
F_{CN}	8.0	7.7	7.6
F_{CC1}		4.4	
F_{NC1}			5.7
$\Delta R^{\circ}_{CO}/\Delta R_{CN}$	−0.100	−0.090	−0.100
$\Delta R^{\circ}_{CO}/\Delta R_{CC1}$		−0.040	
$\Delta R^{\circ}_{CO}/\Delta R_{CN1}$			0
$\Delta R^{\circ}_{CN}/\Delta R_{CO}$	−0.160	−0.170	−0.170
$\Delta R^{\circ}_{CN}/\Delta R_{CC1}$		−0.040	
$\Delta R^{\circ}_{CN}/\Delta R_{NC1}$			−0.010
$\Delta R^{\circ}_{CC1}/\Delta R_{CO}$		−0.125	
$\Delta R^{\circ}_{CC1}/\Delta R_{CN}$		−0.075	
$\Delta R^{\circ}_{NC1}/\Delta R_{CO}$			0
$\Delta R^{\circ}_{NC1}/\Delta R_{CN}$			−0.020

[a] The regression coefficients, $c = \Delta R^{\circ}_{A}/\Delta R_{B}$, are given such that a forced change ΔR_{B} in (each of) the bond length(s) induces a shift $\Delta R^{\circ}_{A} = c\Delta R_{B}$ in the equilibrium value of R_{A}.

DISCUSSION

Bond lengths and bond angles obtained in the X-ray structure analyses are listed in Fig. 2, where the labelling of the atoms is indicated. The molecules are planar (see Table 6, where deviations from least-squares planes are given). When the bond lengths are compared with those obtained in the gaseous state [5,6] (see also Fig. 1, where these bond lengths are listed), the effect of hydrogen bonding on the N−C=O fragment is evident. Both the formamide and acetamide molecules participate in four hydrogen bonds. (Parameters for these bonds are given in Table 7). The C−N bond is shortened by 0.04−0.05 Å and the C−O bond is lengthened by 0.02−0.03 Å upon formation of the hydrogen bonds. This increased conjugation caused by hydrogen bonding from nitrogen to oxygen is generally found for these N−C=O systems.[2,8] The C−N length obtained for formamide in the present work [1.319(2) Å] is very close to those found for pyridazine hydrochloride [19] [1.314(5) Å], and is far shorter than those obtained for 3,6-pyridazinediones (Ref. 2 and references therein). *Ab initio* calculations on formamide [12,20] indicate a significant transfer of electron density from the C−O bond to the C−N bond upon dimerization *via* hydrogen bonding.

Table 6. Deviations from least squares planes through the nonhydrogen atoms.

Atom	Deviation (Å × 10³) Formamide	Acetamide
O	0	−3
N	0	−3
C	0	9
C1		−3
H1	47	−57
H2	−40	9
H3	−8	

However, the ∠NCO is unaffected by this increased conjugation. The values found for this parameter in formamide and acetamide in the present work are the same as those obtained in the gaseous state.[5,6] The anomalous ∠CNH2 in formamide (111°) is probably caused by the hydrogen bond formation.

The lengthening of the C−N bond in acetamide compared to formamide must be caused by the introduction of a methyl group at C, and has been noted earlier.[4–7,2,8] Mulliken type population analyses (see Table 8) indicate that this substitution results in a decreased population at C and increased overlap populations in both the C−O and C−N bonds. The C−C1 bond is about 0.01 Å shorter in the crystal than in the gas [5] probably because of the increased conjugation over the N−C=O fragment caused by the hydrogen bonding. A similar C−C bond is found in cyclic succinhydrazide [2] [1.509(1) Å].

Results from Mulliken type population analyses for formamide, acetamide and *N*-methylformamide are listed in Table 8. It is interesting to note how the overlap population of the C−N bond varies with the optimized bond lengths. For *N*-methylformamide, and also diformylhydrazine [12] (C−N length: 1.341 Å, overlap population 0.165), a decreasing overlap population, as compared with that found for formamide, results in a shortened bond distance, while for acetamide, where a small increase in the C−N bond length is indicated, a larger overlap population is found. However, in the case of the hydrogen bonded formamide structures [1,12,20] which have been studied by *ab initio* calculations, a different situation is found. In these complexes a shortening of the C−N bond, caused by the formation of hydrogen

Table 7. Hydrogen bond parameters. The coordinates of the acceptor atom are related to those given in Table 2 by the symmetry operation given.

Donor	Acceptor	Symmetry operation	N···O (Å)	H···O (Å)	N−H···O (°)	C−O···N (°)
Formamide						
N−H1	O	$1-x,\frac{1}{2}+y,-z$	2.944(2)	2.04	170	118.1(1)
N−H2	O	$1-x,-y,-z$	2.881(2)	1.99	169	127.7(1)
Acetamide						
N−H1	O	$1/3-x,-1/3+y,1/6+z$	2.913(3)	2.06	162	123.8(2)
N−H2	O	$1/3+x,-1/3+x-y,1/6+z$	2.883(3)	2.02	172	128.9(2)

bonds, leads to an increased overlap population. In all structures studied the gross atomic population of O has increased with increasing C−O length, and, except in acetamide, the overlap population of the C−O bond has decreased with increasing C−O length. Also, the gross atomic population of C obtained for acetamide is much smaller (by 0.12−0.15) than those found for the other molecular systems containing the N−C=O linkage which have been studied (Ref. 1 and references therein).

Table 8. Gross atomic populations, overlap populations and dipole moments (D) of the optimized molecules. The geometries may be found in Fig. 1.

Atom	Form-amide	Acet-amide	*N*-Methyl form-amide
Gross atomic populations			
O	8.551	8.560	8.561
C	5.456	5.306	5.436
N	7.863	7.865	7.870
Cl		6.643	6.273
H1	.646	.648	
H2	.655	.659	.653
H3	.829		.825
H4		.755	.810
H5		.782	.786
Overlap populations			
C−O	1.163	1.252	1.145
C−N	.257	.279	.206
C−Cl		.475	
N−Cl			.245
N−H1	.602	.619	
N−H2	.621	.632	.633
C−H3	.795		.809
Cl−H4		.722	.772
Cl−H5		.723	.779
Dipole moments (D)	4.136	4.196	4.221

REFERENCES

1. Ottersen, T., Jensen, H. H., Johansen, R. and Wisløff-Nilssen, E. *J. Mol. Struct. 30* (1976) 379.
2. Ottersen, T. *Acta Chem. Scand. A 29* (1975) 690.
3. Ladell, J. and Post, B. *Acta Crystallogr. 7* (1954) 569.
4. Kitano, M., Fukuyama, T. and Kuchitsu, K., *Bull. Chem. Soc. Jap. 46* (1973) 348.
5. Kitano, M. and Kuchitsu, K. *Bull. Chem. Soc. Jap. 46* (1973) 3048.
6. Kitano, M. and Kuchitsu, K. *Bull. Chem. Soc. Jap. 47* (1974) 67.
7. Kitano, M. and Kuchitsu, K. *Bull. Chem. Soc. Jap. 47* (1974) 631.
8. Ottersen, T. *Acta Chem. Scand. A 28* (1974) 1145.
9. Senti, F. and Harker, D. *J. Amer. Chem. Soc. 62* (1940) 2008.
10. Denne, W. A. and Small, R. W. H. *Acta Crystallogr. B 27* (1971) 1094.
11. Hamilton, W. C. *Acta Crystallogr. 18* (1965) 866.
12. Ottersen, T. and Jensen, H. H. *J. Mol. Struct. 26* (1975) 355.
13. Groth, P. *Acta Chem. Scand. 27* (1973) 1837.
14. Doyle, P. A. and Turner, P. S. *Acta Crystallogr. A 24* (1968) 390.
15. Stewart, R. F., Davidson, E. R. and Simpson, W. T. *J. Chem. Phys. 42* (1965) 3175.
16. Almlöf, J. *USIP Rep. 72−09*, University of Stockholm, September 1972.
17. Roos, B. and Siegbahn, P. *Theoret. Chim. Acta 17* (1970) 209.
18. Dunning, T. H., Jr. *J. Chem. Phys. 53* (1970) 2823.
19. Ottersen, T. *Acta Chem. Scand. A 29* (1975) 637.
20. Ottersen, T. *J. Mol. Struct. 26* (1975) 365.

Received June 4, 1975.

Acta Chemica Scandinavica A 29 (1975) 945—955

Heat Capacity and Thermodynamic Properties of Bismuth in the Range 300 to 950 K. Fusion Characteristics

FREDRIK GRØNVOLD

Department of Chemistry, University of Oslo, Blindern, Oslo 3, Norway

The heat capacity of nominally 99.9999 mass per cent pure bismuth has been studied by adiabatic shield calorimetry in the region 300 to 950 K. Values of enthalpy and entropy increments have been derived and tabulated for selected temperatures. The enthalpy and entropy of fusion at 544.60 K are (11131 ± 11) J mol^{-1} and 20.44 ± 0.02) J K^{-1} mol^{-1}, respectively. The premelting excess heat capacity corresponds to the presence of about 1×10^{-5} M of liquid-soluble/solid-insoluble impurities in the sample. The postmelting (or prefreezing) excess heat capacity is of comparable magnitude and is apparently not caused by impurities. The derived constant volume heat capacity shows excess over the harmonic value for solid bismuth which is attributed to a beginning higher-order transformation. For liquid bismuth C_V decreases from about 26 to 22.6 J K^{-1} mol^{-1} over the region 550 to 900 K.

1. INTRODUCTION

The heat capacity behavior of solid metals in the region just below melting has not yet been thoroughly explored and diverging opinions and results exist with regard to premelting. Thus, in the case of tin, which we have recently studied,[1] the premelting anomaly does not exceed the effect of 3×10^{-6} M of liquid-soluble/solid-insoluble impurities. The anomaly is thus of the order 300 times smaller than indicated by earlier results [2,3] which accordingly had been incorrectly related to heterophase fluctuation premelting.

In order to gain further insight in the premelting phenomenon we have also been studying bismuth, another low-melting element with melting temperature suitably located for exploration under close to equilibrium conditions in our adiabatic shield type calorimeter.

In addition to the many heat capacity results for solid bismuth above room temperature, derived from enthalpy measurements over large temperature intervals,[4–11] data have also been obtained over smaller intervals with a semi-adiabatic technique by Carpenter and Harle.[12] They interpreted the rapidly increasing rise in heat capacity of solid bismuth near the melting point as due to the presence of about 2×10^{-4} M of impurity. According to Hultgren *et al.*[13] both the results by Kubaschewski and Schrag [11] and a single measurement by Umino [10] just below the melting point show an increase in heat capacity which might be preparatory to melting. The cited measurements were performed on samples of unstated or low purity, however, and more accurate measurements on high purity bismuth were therefore desirable.

Both Carpenter and Harle,[12] Bronson and MacHattie,[14] Franzosini and Clusius [15] and others have deduced constant volume heat capacities from their experimental results and concluded that the excess over the harmonic value could not be ascribed to conduction electron contributions, but rather to peculiarities of the lattice vibrations.

The heat capacity determinations on liquid bismuth have been largely diverging.[7,8,10,16] Smoothly decreasing heat capacity values in the molten region were first observed by Carpenter and Harle,[12] and more recently by Bell and Hultgren [17] in the range 545 to 800 K. Preliminary measurements by Brooks [18] showed a similar decrease, but the values were 2 to 3 % higher.

The absence of a pronounced decrease in heat capacity just after melting was seen by Bell

and Hultgren [17] as a disproval of the usual interpretation of the diffraction patterns of liquid bismuth in terms of aggregates of atoms with solid-like structure. Such aggregates should finish breaking up only a few kelvin above the melting point, and the process should thus give much higher heat capacity values in the vicinity of fusion than those observed. The available data seemed more in accord with the theory by Kincaid and Eyring [19] in which the bonding is considered to change into that of a monoatomic gas, with C_p decreasing toward $5R/2$ at high temperatures. Decreasing heat capacities above the melting temperature are common to many metallic liquids, and in a statistical mechanical treatment Chapman [20] showed that this can be related to the pair correlation function behavior. The increase in C_p on further rise in temperature was ascribed mainly to the increasing dilational heat capacity.

The early enthalpy of fusion determinations on bismuth [7–11,21–29] offered a wide choice between 8.95 and 12.3 kJ mol^{-1}. The three most recent sets of determinations [30–32] have narrowed the band to 11.3 ± 0.2 kJ mol^{-1}. This is still discomfortingly wide compared to the presently attainable accuracy, and the results are only partly overlapping within their stated limits from about 0.5 to 1.0 %. Thus, an improved determination of the enthalpy of fusion of bismuth seemed of interest.

2. EXPERIMENTAL

Sample. The zone-refined 99.9999 mass per cent pure bismuth was obtained from Koch-Light Laboratories, Ltd. England. Typical analyses of the impurities present were (in ppm by mass): Ag(0.1), Ca(0.1), Mg(0.1), Pb(0.1), Si(0.1). Of the crushed 12 mm diameter rod 261.124 g was sealed in the calorimetric container together with about 1 m of 3 mm diameter silica cord. The silica cord was coiled spirally in the sample space and its purpose was to prevent breakage of the container on fusion and thermal cycling of the sample.

A mass spectrometric analysis was carried out after the completion of the measurements. It showed the presence of the following impurities (in ppm by atoms): C(4), N(0.6), O(16), F(0.4), Na(17), Mg(1), Al(0.6), Si(3), P(0.1), S(1), Cl(6), K(7), Ca(5), Ti($\leq$0.1), Cr($\leq$0.1), Fe(5), Cu(7), Zn(0.4), Ga(0.7), As($\leq$0.1), Y($\leq$0.1), Ag($\leq$0.2), W($\leq$0.2).

Calorimetric technique. The calorimetric apparatus and measurement technique have been described in detail [33] along with results obtained for the heat capacity of a standard sample of α-Al_2O_3. The calorimeter is operated with adiabatic shields and intermittent energy inputs with temperature equilibration between each input. The 50 cm^3 sample container of silica glass has a well for the heater and platinum resistance thermometer, axially located in the cylindrical silver calorimeter. The calorimeter-sample assembly is suspended inside a double-walled silver shield system with enclosed heaters. Outside the shields is a heated guard system, also of silver. The whole assembly is placed in a vertical tube furnace.

The temperature differences between corresponding parts of calorimeter and shield are measured by means of Pt-to-(Pt + 10 mass per cent Rh)thermopiles. The amplified signals are recorded and also used for automatic control of the shield heaters to maintain quasi-adiabatic conditions during input and drift periods. The temperature of the guard body is kept automatically 0.4 K below that of the shield, while the temperature of the furnace core is kept 10 K lower to secure satisfactory operation of the control units.

Heat-capacity measurements of the empty calorimeter were carried out in a separate series of experiments. They represented from 67 to 72 per cent of the total outside the fusion region. Small corrections were applied for differences in mass of the empty and full containers and for "zero" drift of the calorimeter. The temperature excursions of the shields from the calorimeter temperature were of negligible importance. The thermometer resistance was measured with a Mueller bridge (Leeds & Northrup Model 8072), automated locally with stepping motors and a gated null-detector, operated by a computer (Hewlett-Packard Model 2114 B) in the more recent series of experiments. The derived temperatures are judged to correspond with the IPTS-68 to within 0.01 at 500 K and 0.1 K at 1000 K. Precision is considerably better, and the temperature increments are measured to 0.0003 K. The computer-operated energy inputs from a constant-current supply (John Fluke Current Calibrator Model 382 A in most of the experiments) were measured with an integrating voltmeter (Hewlett-Packard Model 2401 C). The accuracy of the energy inputs is about 0.025 %). Both Mueller-bridge and (potential) × (time) readings are automatically transferred to punch cards (IBM 545) together with time and other relevant information and then processed by a digital computer.

3. RESULTS AND DISCUSSION

Thermodynamic properties. Results of the determinations of the molar heat capacity of bismuth are presented in Table 1 in chronological order. The approximate temperature

Table 1. Heat capacity of bismuth. $M(\mathrm{Bi}) = 208.98$ g mol^{-1}.

$\langle T \rangle$ / K	C_p / J K^{-1} mol^{-1}	$\langle T \rangle$ / K	C_p / J K^{-1} mol^{-1}
Series I		Series VIII	
302.72	26.04	529.93	28.89
317.55	26.08	539.69	32.56
332.38	26.33	544.55	4424.1
347.11	26.52	546.19	3373.9
		550.25	29.89
Series II		555.23	29.80
360.48	26.59	560.22	29.96
375.29	26.77	565.23	29.88
390.06	27.04	570.25	29.80
404.82	27.19	575.38	29.75
419.59	27.38	580.72	29.71
434.37	27.52		
449.16	27.70	Series IX	
464.00	27.85	541.91	1887.9
478.88	28.12	544.60	301 000
		544.60	219 000
Series III		544.60	96 300
489.89	28.40	544.62	12 610
504.76	28.40	545.14	165.30
		547.41	29.96
Series IV		549.92	29.96
516.28	28.88		
521.21	28.94	Series X	
527.79	28.99	311.44	26.11
534.37	29.03	320.44	26.08
538.76	29.17	328.23	26.14
540.93	29.36	337.25	26.40
542.57	29.68	346.25	26.38
543.57	46.94		
544.26	170.22	Series XI	
544.52	1367.0	616.87	29.45
		630.89	29.38
Series V		644.98	29.47
534.56	28.94	659.13	29.37
537.03	29.02	673.38	29.21
539.49	29.29	687.73	29.04
541.94	30.51	702.17	28.90
543.85	91.85	716.72	28.69
544.57	5633	731.36	28.72
544.59	170 400	746.11	28.56
544.60	574 000		
544.60	9 700 000	Series XII	
544.60	1 320 000	756.98	28.42
548.70	109.13	771.95	28.22
560.25	29.80	787.01	28.17
		802.16	28.17
Series VI		817.38	28.30
591.35	29.54	832.67	28.35
606.51	29.60	847.99	28.41
621.75	29.38	863.34	28.55
637.10	29.17	878.78	28.57
		894.35	28.38
Series VII		909.99	28.58
457.68	27.62	925.75	28.65
472.53	27.98	941.66	28.67
487.41	28.36	950.08	28.88
502.32	28.50		
517.27	28.75		

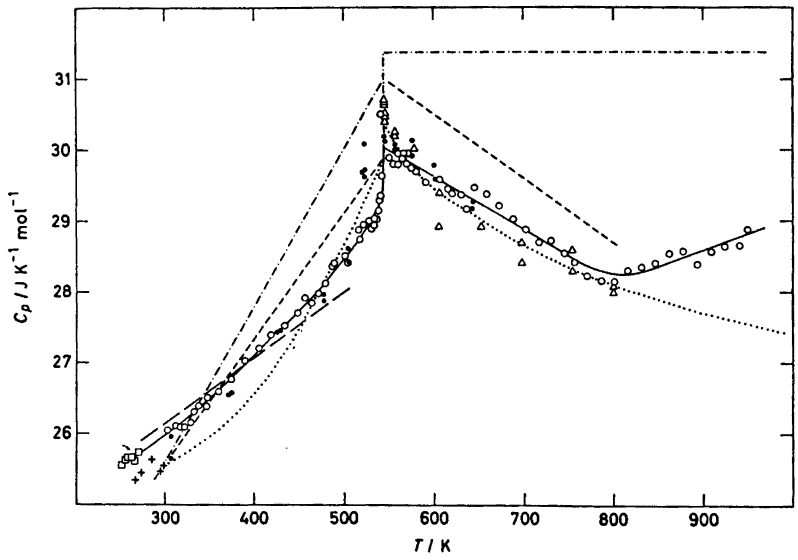

Fig. 1. Heat capacity of bismuth. —○— represents present results, — — — assessment by Kelley,[34] · · · assessment by Hultgren *et al.*[35], □ results by Franzosini and Clusius,[15] + results by Anderson,[36] ● results by Carpenter and Harle,[12] —— —— results by Bronson and McHattie,[14] △ results by Bell and Hultgren,[17] – – – results by Brooks.[18]

increments in the determinations can usually be inferred from the adjacent mean temperatures in the table.

The curve of heat capacity against temperature is shown in Fig. 1 together with the assessed values by Kelley [34] and Hultgren *et al.*[35] and some of the earlier heat capacity determinations. The spread between the assessments is indicative of the divergencies in the earlier multitude of data which will not be discussed in detail here. In the lower temperature region the present results join well with those by Franzosini and Clusius,[15] which are about 1 % higher than those by Anderson [36] in the region 250 to 280 K and 5 % lower than the result by Mikryukov and Tyapunina [37] at 293 K. Excellent agreement with the results by Bronson and MacHattie [14] was obtained over the common region (300 to 400 K), while the observations by Carpenter and Harle [12] are slightly lower than the present below 450 K and rise considerably above as the melting point is approached. The excessive rise was ascribed to impurity premelting by the authors. Recent measurements by Brooks [18] on solid and liquid bismuth coincide with the present ones around 350 K, but diverge negatively below and positively above. At 500 K they are about 2 % higher and likewise at 800 K for liquid bismuth. The results were considered as preliminary, however, due to the larger than usual spread. The results by Carpenter and Harle [12] for liquid bismuth are practically equal to the present ones over the common region (550 to 650 K), while those by Bell and Hultgren [17] are about 0.5 % lower in the region 600 to 800 K.

A steady increase from 29 to 36 J K^{-1} mol^{-1} over the region 550 to 1200 K was claimed by Wüst *et al.*[7] while almost constant values (31 to 33 J K^{-1} mol^{-1}) over the region 550 to 1000 K were reported by Iitaka,[8] Umino,[10] and Förster and Tschentke.[16]

Results of the fractional enthalpy of fusion determinations are found in Table 2. Slight pre- and postmelting contributions above the smoothly extrapolated heat capacities of the solid and liquid phases are included in the enthalpy and entropy of fusion values:

$\Delta H_f = (11131 \pm 11)$ J mol^{-1}, $\Delta S_f = (20.44 \pm 0.02)$ J K^{-1} mol^{-1}

The observed temperature of fusion for about 95 % of the sample fused is at zero pressure $T_f = (544.60 \pm 0.01)$ K from calibrations of the

Table 2. Fractional enthalpy of fusion determinations on bismuth. $M(\mathrm{Bi}) = 208.98$ g mol^{-1}.

$\langle T \rangle$ / K	C_p / J K^{-1} mol^{-1}	ΔT / K	Δt / min	$\sum \Delta H$ / J mol^{-1}	T_{fin} / K	1/F
Series IV, run 7 – 10						
542.480	29.68	1.097	15	0	543.108	
543.573	46.94	0.9286	26	16.3	544.037	683
544.261	170.22	0.4476	44	79.3	544.485	140.4
544.522	1 367.0	0.0742	27	178.5	544.559	62.35
Series V, run 3 – 12						
539.480	29.29	2.4746	45	0	540.718	
541.942	30.51	2.4465	49	2.7	543.165	4 126
543.855	91.85	1.3790	30	88.7	544.544	125.6
544.565	5 633	0.0422	29	325.2	544.586	34.25
544.590	170 400	0.0085	66	1 773	544.594	6.283
544.598	574 000	0.0076	82	6 134	544.602	1.816
544.602	9 700 000	0.0003	120	9 038	544.602	1.232
544.602	1 320 000	0.0011	44	10 490	544.603	1.062
548.701	109.13	8.1972	60	11 139	552.800	1.000
560.245	29.80	14.891	48	11 139	567.691	1.000
Series VIII, run 1 – 5						
529.930	28.89	9.9340	85	0	534.895	
539.693	32.56	9.5958	68	31.5	544.491	353.1
544.545	4 424.1	0.1075	21	503.9	544.599[a]	22.07
546.186	3 373.9	3.1751	158	11 123	547.774	1.000
550.252	29.89	4.9069	30	11 123	552.735	1.000
Series IX, run 1 – 7						
541.905	1 887.9	5.3956	136	10 028	544.601	1.110
544.602	301 000	0.0008	38	10 269	544.602	1.084
544.603	219 000	0.0011	52	10 510	544.603	1.059
544.604	96 300	0.0025	53	10 751	544.605	1.035
544.615	12 610	0.0191	46	10 991	544.624	1.013
545.141	165.30	1.0336	153	11 131	545.657	1.000
547.413	29.96	2.5021	34	11 131	548.159	1.000

$\Delta H_f = (11131 \pm 11)$ J mol^{-1}; $\Delta S_f = (20.44 \pm 0.02)$ J K^{-1} mol^{-1}; $T_f = 544.60$ K.

[a] No wait for complete equilibration.

platinum resistance thermometer at the triple point of water and the melting points of tin and zinc on the International Practical Temperature Scale of 1968.[33] The fusion temperature is in good agreement with the results by McLaren and Murdock [39] [$T_f = 544.525$ K (ITPS 48)] allowing for change to ITPS 68 (+0.067 K) and reduction to zero pressure (+0.004 K).

Earlier determinations of the enthalpy of fusion of bismuth are collected in Table 3. The agreement between the present value and that by Castanet *et al.*[31] is very good. Among the earlier values none is closer than that by Person [22] of 1848; his determination of the enthalpy of fusion of tin was also remarkably good.[1] The estimate by Kelley [34] (10.88 kJ mol^{-1}) and the most recent one by Hultgren *et al.*[35] (11.30 kJ mol^{-1}) are 2.3 % lower, and 1.5 % higher than the present result, respectively.

Values of C_p, $[H^\circ(T) - H^\circ(298.15\ \mathrm{K})]$, and $[S^\circ(T) - S^\circ(298.15\ \mathrm{K})]$ are listed in Table 4 for selected temperatures. The results for solid bismuth up to 542.60 K have been least squares fitted by a polynomial expression, with a standard deviation of 0.32 % for a single

Table 3. Enthalpy of fusion determinations on bismuth.

Authors	Year	ΔH_f/kJ mol^{-1}
Person [21]	1846	10.8
Person [22]	1848	11.05
Mazzotto [23]	1886	10.84
Roos [24]	1916	10.9
Wüst *et al.*[7]	1918	8.95
Iitaka [8]	1919	10.70
Awbery and Griffiths [9]	1926	11.37
Umino [10]	1926	12.33
Kubaschewski and Schrag [11]	1940	11.00
Cavallaro [25]	1944	11.77
Nagasaki and Fujita [26]	1952	11.92
Oelsen *et al.*[26]	1955	11.38
Oelsen [27]	1957	11.21 11.46
Schürmann and Träger [29]	1961	11.42
Chiotti *et al.*[30]	1966	11.527 ± 0.075
Castanet *et al.*[31]	1968	11.125 ± 0.063
Malaspina *et al.*[32]	1971	11.247 ± 0.113
Grønvold	1975	11.131 ± 0.011

measurement. For the liquid region from 547.44 K a similarly fitted expression resulted in a standard deviation of 0.31 %. The accuracy of the integrated thermodynamic function values is estimated to be 0.3 % and of the fusion properties 0.1 %. The present enthalpy values are 0.94 % higher than the assessed values by Hultgren *et al.*[35] for solid bismuth at the melting temperature, 0.57 % lower for liquid bismuth at the same temperature, and only 0.10 % lower at 900 K. The older assessment by Kelley [34] differs considerably more, from + 0.8 to + 2.7 % in the enthalpy of solid bismuth, and from − 0.4 to + 2.8 % for liquid bismuth. It reflects the large inaccuracy in many of the earlier determinations.

Pre- and postmelting. The heat capacity of solid bismuth shows a considerable upwards trend already around 500 K, but the measurement at 543.57 K (Ser. IV, run 8) is the first which deviates markedly from the polynomial curve which reaches 29.49 J K^{-1} mol^{-1} at the temperature of fusion. The excess above this curve is provisionally ascribed to premelting. The observed heat capacity values in the fusion region – uncorrected for curvature – are shown in Fig. 2 on a semi-logarithmic scale. They compare surprisingly well with the excess heat capacity calculated for 1×10^{-5} M of liquid-soluble/solid-insoluble impurities according to the equation:[40]

$$C_i(\text{prem}) = x_2{}^+ RT_f^2/[(T_f - T_i)^2 - (\Delta T/2)^2]$$

Here $x_2{}^+$ is the total mol fraction of impurities, T_i the temperature, and ΔT the temperature interval to which C(prem) refers.

For comparison the results of Carpenter and Harle [12] in this region are also shown in Fig. 2. They indicate that the presence of 3×10^{-4} M of liquid-soluble/solid-insoluble impurities might explain the high heat capacities observed. Even such a moderate amount of impurity is seen to have an enormous influence on the observed heat capacities as melting is approached, and causes 2 % of the bismuth to be in the molten state 3 K below the ideal fusion temperature. In the present case only 0.1 % of the bismuth is molten 1 K below the ideal fusion temperature.

According to the mass spectrometric analysis several elements are present in the sample in amounts sufficient to cause the observed excess heat capacity below the fusion temperature provided they are less soluble in solid bismuth than in liquid. This is no doubt the case with oxygen, which presumably is present in form of oxides in the grain boundaries of solid bismuth. Based upon the results by Griffith and Mallett [41]

Table 4. Thermodynamic properties of bismuth. $M(\mathrm{Bi}) = 208.92$ g mol^{-1}.

T / K	C_p / J K^{-1} mol^{-1}	$H°(T) - H°(298.15\ \mathrm{K})$ / J mol^{-1}	$S°(T) - S°(298.15\ \mathrm{K})$ / J K^{-1} mol^{-1}
298.15	25.90	0	0
300	25.92	47.9	0.160
320	26.15	568.9	1.840
340	26.39	1094	3.431
360	26.63	1624	4.947
380	26.86	2159	6.393
400	27.09	2698	7.777
420	27.33	3242	9.104
440	27.60	3792	10.381
460	27.89	4346	11.614
480	28.18	4907	12.807
500	28.47	5474	13.964
520	28.77	6046	15.085
540	29.30	6626	16.180
544.60(s)	(29.49)	6761	16.429
544.60(l)	(30.06)	17892	36.867
560	29.83	18353	37.702
580	29.67	18947	38.745
600	29.58	19540	39.750
620	29.50	20131	40.718
640	29.39	20720	41.653
660	29.24	21306	42.555
680	29.07	21889	43.426
700	28.88	22469	44.266
720	28.70	23045	45.077
740	28.54	23617	45.861
760	28.41	24186	46.620
780	28.32	24754	47.357
800	28.28	25320	48.074
820	28.28	25885	48.772
840	28.32	26451	49.454
860	28.39	27018	50.121
880	28.47	27587	50.774
900	28.56	28157	51.415
920	28.65	28729	52.044
940	28.74	29303	52.661

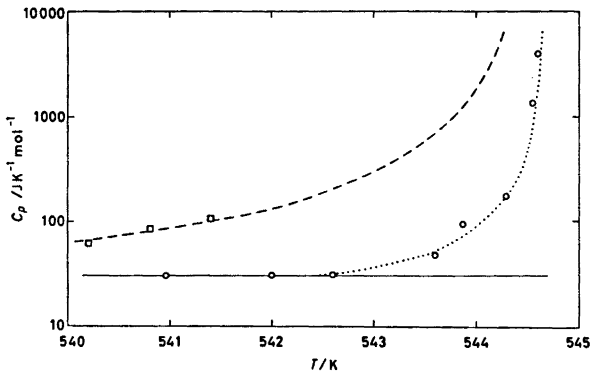

Fig. 2. Premelting heat capacity of bismuth. O represents present results, □ results by Carpenter and Harle,[12] · · · and — — — calculated values for 1×10^{-5} M and 3×10^{-4} M of liquid-soluble/solid-insoluble impurities.

in the region 400 to 750 °C the oxygen equilibrium concentration is only 3×10^{-6} M in liquid at the temperature of fusion. The observed oxygen content is therefore mainly assumed to be due to oxides of sodium, potassium, calcium, iron, and copper. If part of these oxides go into solution, sufficient impurities are at hand. In the case of sodium, the bismuth-rich binary eutectic temperature is 491 K,[42] and of potassium it is 538 K.[42] These two elements are thus suspected as responsible for the premelting behavior. While iron is known for its insolubility in solid and liquid bismuth, both calcium and copper show binary eutectics close to pure bismuth at 543 K.[42] Thus, the premelting seems to have been caused by the solid-insoluble/liquid-soluble impurities present in the sample, and the study of even purer samples and also of samples with addition of suitably controlled impurities is desirable in order that a more definite answer to the question be provided.

Solid-soluble/liquid-soluble impurities will in general cause interval melting. Under equilibrium conditions the heat capacity will then rise rather sharply, but not become infinite, and fall rapidly again at a higher temperature. From Series V it appears that 89 % of the enthalpy of fusion occurs within 0.017 K, but again it is not possible to relate this interval unambiguously to the impurities present, even though calcium and copper are likely candidates. The width is evidently not caused by temperature gradients in the calorimeter, since 26 % of the enthalpy of fusion falls within a temperature interval of 0.0003 K (Series V, run 9).

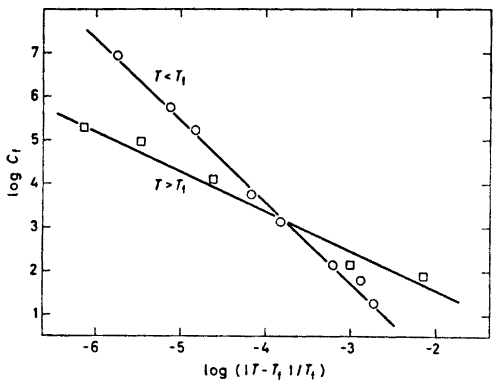

Fig. 3. Log-log plot of estimated pre- and postmelting heat capacity of bismuth against $|T-T_f|/T_f$ where T_f is the fusion temperature. Circles for $T < T_f$, squares for $T > T_f$.

As can be seen from the runs of Series V and IX, the postmelting heat capacity is of considerable magnitude. About 3.5 % of the fusion enthalpy remains to be acquired 0.002 K above the temperature at which the heat capacity starts to decrease, and 1.3 % still remains at a temperature 0.021 K higher.

In order to compare the pre- and postmelting behavior of the bismuth sample the logarithm of the excess heat capacity is plotted against the logarithm of ($|T-T_f|/T_f$), see Fig. 3. A constant slope indicates that the results can be described in terms of a critical index α according to the equation:

$$C_f = a(|T-T_f|/T_f)^{-\alpha} + b$$

Below the temperature of the maximum – taken as the fusion temperature – the critical exponent $\alpha \approx 1.9$, or close to the value expected for a liquid-soluble/solid-insoluble impurity. Above the maximum $\alpha \approx 0.6$. This change is not unexpected, since the behavior above the liquidus line is principally different from that in the solidus/liquidus region. The presence of an exponent value of the same magnitude as for other critical phenomena is therefore pleasing. The problem of delayed equilibration, especially with regard to solution of impurities and its influence on the derived critical exponent, has not yet been explored in detail.

Heat capacity of bismuth at constant volume. The molar heat capacity of bismuth at constant volume can be derived from that at constant pressure by the thermodynamic relationship:

$$C_V = C_p - (\alpha^2/\varkappa)VT$$

where α is the volume expansion coefficient, $\varkappa$ the isothermal compressibility and V the molar volume.

The thermal expansivity of solid bismuth has been measured in the low-temperature region and up to temperatures approaching the melting point by several authors.[43] The discontinuities reported in the range 250 to 350 K by Jay and Jacobs [44] and Goetz [45] were not supported by more recent work of Cave and Holroyd [46] and others. Over the region 150 to 540 K the expansion coefficient of the hexagonal a-axis increases from 11.5 to 11.8×10^{-6} K^{-1}, and of the

c-axis from 17.3 to 17.6×10^{-6} K^{-1}. These results agree with those by White [47] at 283 K ($\alpha_a = 11.63 \times 10^{-6}$ K^{-1}, $\alpha_c = 17.05 \times 10^{-6}$ K^{-1}) and are taken as representative. The molar volume of the solid is calculated from the lattice constant data, while that for liquid bismuth and also the expansivity of the liquid, are taken from the extensive investigation by Lucas.[48]

The isothermal compressibility ($\varkappa_T$) is 2.9 10^{-12} Pa^{-1} at room temperature.[43] Its value for solid bismuth at the fusion temperature ($\varkappa_T = 3.7 \times 10^{-12}$ Pa^{-1}) is derived from the value for liquid bismuth at the same temperature (4.25×10^{-12} Pa^{-1} by Kleppa [49] and 4.38×10^{-12} Pa^{-1} by Filippov *et al.*[50]) and the difference in compressibility between liquid and solid bismuth ($\varkappa_T = 0.58 \times 10^{-12}$ Pa^{-1} according to Bridgman.[51] From the increase in the adiabatic compressibility ($\varkappa_S$) of liquid bismuth with temperature, as derived by Filippov *et al.*[50] from ultrasonic velocity measurements, the isothermal compressibility ($\varkappa_T = \varkappa_S + \alpha^2 VT/C_B$) rises to 5.2×10^{-12} Pa^{-1} at 900 K.

The derived dilation contribution and heat capacity at constant volume are given in Table 5 for selected temperatures. The unusually small dilation contribution for solid bismuth compared to the liquid is mainly caused by the small thermal expansivity of the solid. This results in a notable rise in the constant volume heat capacity of solid bismuth above the classical limit $3R$ or 24.76 J K^{-1} mol^{-1}, see Fig. 4. Such a large increase in C_V over the harmonic value in the solid state does not seem to be a general prerequisite to fusion, and was not observed in our related study of the fusion of tin.[1] For liquid bismuth a pronounced decrease in C_V to 22.6 J K^{-1} mol^{-1} at 900 K is noted.

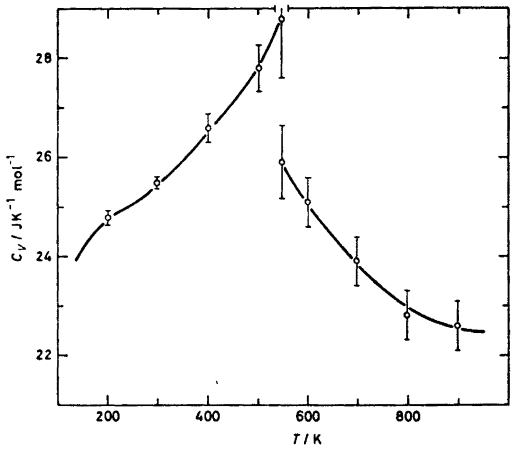

Fig. 4. Estimated constant volume heat capacity of solid and liquid bismuth.

Earlier authors [12,14,15] who have deduced constant volume heat capacities of solid bismuth, have generally attributed the observed excess over the harmonic value to peculiarities of the lattice vibrations. There are presently no firm indications, however, that the excess is due to further anharmonic contributions. It view of the low temperature of fusion, the excess heat capacity from structural disorder in the solid is presumably small. It seems therefore more tempting to attribute the excess heat capacity mainly to a beginning higher-order transformation into a more metallic phase with a smaller molar volume. Thereby the small expansivity

Table 5. Tentative resolution of the heat capacity of bismuth into components. $M(\mathrm{Bi}) = 208.98$ g mol^{-1}.

T / K	C_p(obs) / J K^{-1} mol^{-1}	C(d) / J K^{-1} mol^{-1}	C_V / J K^{-1} mol^{-1}
200	(25.0)	0.2	(24.8)
300	25.92	0.4	25.5
400	27.09	0.5	26.6
500	28.47	0.6[5]	27.8
544.60(s)	(29.5)	0.7	(28.8)
544.60(l)	(30.1)	4.2	(25.9)
600	29.58	4.5	25.1
700	28.88	5.0	23.9
800	28.28	5.5	22.8
900	28.56	6.0	22.6

might be accounted for, and the possible presence of such a phase finds further support in the actual existence of four allotropic modifications of solid bismuth [43] at pressures below 40 000 atm.

Inferences about the structure of liquid bismuth have been derived from many diffraction studies.[43] According to Danilova *et al.*[43] the structure is close-packed with some face-centered character. The same conclusion was arrived at by Sharrah and Smith.[53] The face-centered component is reported to decrease with increasing temperature by Richter *et al.*[54] Further X-ray diffraction evidence for the existence of two types of structures in liquid bismuth have recently been presented by Richter.[55] The spherical close-packing (structure I) and the other structure (II) both show up as straight chains with shortest neighbour distances of 3.17 and 3.35 Å, respectively. (These results have not been correlated with the previously reported changes in structure with temperature and thermal data.)

The statistical theory of fluids which allows for high mobility of the short-range ordered particles and is utilizing the radial distribution function behavior [20,56,57] seems appropriate for deriving the thermal properties. Very precise diffraction data are required, however, in order that the radial distribution function might show further structural effects than those associated with the repulsive part of the interatomic potential. The considerable drop in C_V for liquid bismuth signals important changes in the radial distribution over the region 545 to 800 K which might ultimately be detected.

The heat capacity at constant volume at 900 K is far above the value $3R/2$, which supposedly is the high-temperature limit in the usual statistical approach, and is equally far below the values derived in the collective moment approach by Eisenschitz and Wilford [58] and by Bratby *et al.*[59] An intermediate limiting value for $C_V = 2R$ was derived by Brillouin [60] who assumed that the two transverse wave motions for a monoatomic liquid degenerate into a whirl system for which there is no potential energy. The estimated C_V for liquid bismuth at 900 K is closest to the latter value.

Acknowledgements. The author thanks Olav H. J. Christie and Arne S. Stabel for carrying out the mass spectrometric analyses. Bjørn Lyng Nielsen kindly assisted with the experimental work.

REFERENCES

1. Grønvold, F. *Rev. Chim. Minér. 11* (1974) 568.
2. Bartenev, G. M. *Zh. Tekh. Fiz. 17* (1947) 1321, 1325; *Zh. Fiz. Khim. 22* (1948) 57; *Zh. Eksp. Teor. Fiz. 20* (1950) 218.
3. Khomyakov, K. G., Kholler, V. A. and Zhvanko, S. A. *Vestn. Mosk. Gos. Univ. 7* No. 3, *Ser. Fiz-Mat. i Estestven. Nauk.* No. 2 (1952) 41; *cf. Chem. Abstr. 46* (1952) 9404g.
4. Stücker, N. *Sitz. ber. Akad. Wiss. Wien 114* IIa (1905) 657.
5. John, H. *Vierteljahresschr. Naturforsch. Ges. Zürich 53* (1908) 186.
6. Schübel, P. *Z. Anorg. Chem. 87* (1914) 81.
7. Wüst, F., Meuthen, A. and Durrer, R. *Forschungsarb. Ver. deutsch. Ing.* Heft 204 (1918).
8. Iitaka, I. *Sci. Repts. Tohoku Imp. Univ. 8* (1919) 99.
9. Awbery, J. H. and Griffiths, E. *Proc. Roy. Soc. (London) 38* (1926) 378.
10. Umino, S. *Sci. Repts. Tohoku Imp. Univ. 15* (1926) 597.
11. Kubaschewski, O. and Schrag, G. *Z. Elektrochem. 46* (1940) 675.
12. Carpenter, L. G. and Harle, T. F. *Proc. Roy. Soc. (London) A 136* (1932) 243.
13. Hultgren, R., Orr, R. L., Anderson, P. D. and Kelley, K. K. *Selected Values of Thermodynamic Properties of Metals and Alloys*, Wiley, New York 1963.
14. Bronson, H. L. and MacHattie, L. E. *Can. J. Res. A 16* (1938) 177.
15. Franzosini, P. and Clusius, K. *Z. Naturforsch. A 19* (1964) 1430.
16. Förster, F. and Tschentke, G. *Z. Metallk. 32* (1940) 191.
17. Bell, H. and Hultgren, R. *Met. Trans. 2* (1971) 3230.
18. Brooks, C. *III. International Conference on Chemical Thermodynamics etc.*, Baden near Vienna, Austria, 3–7 Sept. 1973, Vol. II p. 72.
19. Kincaid, J. F. and Eyring, H. *J. Chem. Phys. 5* (1937) 587; *6* (1938) 620.
20. Chapman, T. W. *Mater. Sci. Eng. 1* (1966) 65.
21. Person, C. C. *C. R. Acad. Sci. 23* (1846) 163.
22. Person, C. C. *Ann. Chim. Phys. 24* (1848) 128; see also (Poggend.) *Ann. Physik. 76* (1849) 432.
23. Mazzotto, D. *Mem. Reale Ist. Lombardo Cl. Sci. Mat. Nat. 16* (1886) 1.
24. Roos, *Z. Anorg. Allg. Chem. 94* (1916) 329.
25. Cavallaro, U. *Atti Reale Accad. Ital. Rend. Cl. Sci. Fiz. Mat. Nat. 4* (1943) 520.
26. Nagasaki, S. and Fujita, E. *Nippon Kinzoku Gakkai-shi 16* (1952) 313.

27. Oelsen, W., Rieskamp, K. H. and Oelsen, O. *Arch. Eisenhüttenw. 26* (1955) 253.
28. Oelsen, W. *Arch. Eisenhüttenw. 28* (1957) 1.
29. Schürmann, E. and Träger, H. *Arch. Eisenhüttenw. 32* (1961) 397.
30. Chiotti, P., Gartner, G. J., Stevens, E. R. and Saito, Y. *J. Chem. Eng. Data 11* (1966) 571.
31. Castanet, R. Bros, J.-P. and Laffitte, M. *C. R. Acad. Sci. 267* (1968) 669.
32. Malaspina, L., Gigli, R. and Piacente, V. *Rev. Int. Hautes Temp. Réfract. 8* (1971) 211.
33. Grønvold, F. *Acta Chem. Scand. 21* (1967) 1695.
34. Kelley, K. K. *Contributions to the Data on Theoretical Metallurgy.* XIII. U.X. Bureau of Mines Bull. *584*, Wash. D. C. 1960.
35. Hultgren, R., Desai, P. D., Hawkins, D. T., Gleiser, M., Kelley, K. K. and Wagman, D. D. *Selected Values of the Thermodynamic Properties of the Elements*, Amer. Soc. Metals, Ohio, 1973.
36. Anderson, C. T. *J. Amer. Chem. Soc. 52* (1930) 2720.
37. Mikryukov, V. E. and Tyapunina, N. A. *Fiz. Met. Metalloved. 3* (1956) 31.
38. The International Practical Temperature Scale of 1968. *Metrologia 5* (1969) 35.
39. McLaren, E. H. and Murdock, E. G. *Can. J. Phys. 41* (1963) 95.
40. Westrum, E. F., Jr., Furukawa, G. T. and McCullough, J. P. in *Experimental Thermodynamics*, Butterworths, London 1968, Vol. 1, p. 189.
41. Griffith, C. B. and Mallett, M. W. *J. Amer. Chem. Soc. 75* (1953) 1832.
42. Hultgren, R., Desai, P. D., Hawkins, D. T., Gleiser, M. and Kelley, K. K. *Selected Values of the Thermodynamic Properties of Binary Alloys*, Amer. Soc. Metals, Ohio, 1973.
43. *Gmelins Handbuch der anorganischen Chemie*, 8th Ed. Wismuth, Ergänzungsband, Verlag Chemie 1964.
44. Jay, A. H. *Proc. Roy. Soc. (London) A 143* (1934) 465.
45. Jacobs, R. B. and Goetz, A. *Phys. Rev. 51* (1937) 159.
46. Cave, E. R. and Holroyd, L. V. *J. Appl. Phys. 31* (1960) 1357.
47. White, G. K. *J. Phys. C 2* (1969) 573.
48. Lucas, L.-D. *Mém. Sci. Rev. Mét. 61* (1964) 1.
49. Kleppa, O. J. *J. Chem. Phys. 18* (1950) 1331.
50. Filippov, S. I., Kazakov, N. B. and Pronin, A. *Izv. Vysshikh Uchebn. Zaveedini Chernya Met. 9* (1966) 8.
51. Bridgman, P. W. *Phys. Rev. 38* (1931) 182.
52. Danilova, I. A., Danilov, V. I. and Spektor, E. Z. *Dokl. Akad. Nauk. SSSR 82* (1952) 561.
53. Sharrah, P. C. and Smith, G. P. *J. Chem. Phys. 21* (1953) 228.
54. Richter, H., Breitling, G. and Hesse, F. *Z. Naturforsch. 12a* (1957) 896; see also *Naturwissenschaften 44* (1957) 109.
55. Richter, H. In Takeuchi, S., Ed., *The Properties of Liquid Metals*, Prof of the II. International Conference, Tokyo, 3 – 8 Sept. 1972, Taylor & Francis Ltd., London 1973.
56. Hirschfelder, J. O., Curtis, C. F. and Bird, R. B. *Molecular Theory of Gases and Liquids*, Wiley, New York 1954.
57. Rice, S. A. In Hughel, T. J., Ed., *Liquids; Structural Properties; Solid Interactions*, Proc. of Symp. G. M. Res. Lab., Michigan 1963, Elsevier, Amsterdam 1965.
58. Eisenschitz, R. and Wilford, M. J. *Proc. Phys. Soc. (London) 80* (1962) 1078.
59. Bratby, P., Gaskell, T. and March, N. H. *Phys. Chem. Liquids 2* (1970) 53.
60. Brillouin, L. *Trans. Faraday Soc. 33* (1937) 54.

Received April 4, 1975.

Acta Chemica Scandinavica A 29 (1975) 956—958

Short Communications

On the Crystal Structure of Tin(II) Bromide

JAN ANDERSSON

Department of Inorganic Chemistry, Chalmers University of Technology and the University of Göteborg, P.O.Box, S-40220 Göteborg 5, Sweden

A compound with the stoichiometric formula $SnBr_2$ was prepared by heating metallic tin with hydrobromic acid under reflux and then distilling off the constant boiling mixture of $HBr-H_2O$. The remaining dark brown liquid gave colourless transparent needles on cooling.

X-Ray diffraction data were collected with Weissenberg techniques. The crystals have orthorhombic symmetry and belong to space group No. 62, *Pnma*, or No. 33, $Pna2_1$.[1] The cell dimensions, as determined from Guinier powder diffraction data, are:

$a=8.384(3)$ Å, $b=4.233(2)$ Å, $c=10.516(4)$ Å, $V=373.2$ Å^3

The unit cell contains 4 formula units.

A three-dimensional Patterson synthesis was calculated from *h0l* and *h1l* Weissenberg data. Assuming all the atoms to occupy the point position *Pnma:* 4(*c*), *i.e.* $\pm(x,\frac{1}{4},z),\pm(\frac{1}{2}-x,\frac{3}{4},\frac{1}{2}+z)$ it was possible to explain all the peaks in the Patterson synthesis and to determine the x and z parameters of the atoms. A least squares refinement based on 138 *h0l* and *h1l* reflections yielded an R-value of 8.2 %. More data are to be collected.

Fig. 1. shows a projection of the structure of $SnBr_2$ on the xz plane. Each tin is surrounded by eight bromine, six of which lie at the apices of a trigonal prism while the remaining two lie outside prism faces. The configuration of bromine around tin in $SnBr_2$ is thus similar to that in $2SnBr_2.H_2O$,[2] $6SnBr_2.5H_2O$,[3] and $3SnBr_2.H_2O$.[4]

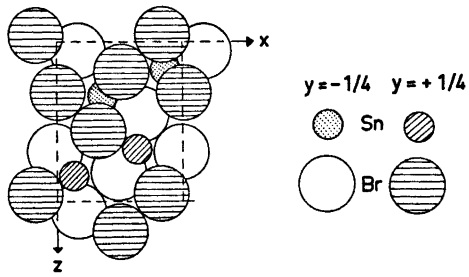

Fig. 1. A projection of the structure of $SnBr_2$ on the xz plane.

Table 1. Approximate atomic parameters for $SnBr_2$.

Atom	x	y	z
Sn	0.1336	0.2500	0.8350
Br(1)	0.3305	0.2500	0.5506
Br(2)	0.5117	0.2500	0.1855

Since $SnCl_2$ is isomorphous with $PbBr_2$ it might be expected that $SnBr_2$ was also isomorphous with $PbBr_2$. The tin and lead coordination polyhedra are fairly similar in $SnCl_2$, $SnBr_2$ and $PbBr_2$, *i.e.*, trigonal prisms with anions outside the centers of prism faces, but Sn is eight-coordinated in $SnBr_2$ whereas Sn and Pb are nine-coordinated in $SnCl_2$ and $PbBr_2$.

In $SnBr_2$ the five bromine nearest to tin are at 2.81, 2.90, 2.90, 3.11, 3.11 Å. These five bromine form a polyhedron similar to the tetragonal pyramide of bromine around tin in $NH_4SnBr_3.H_2O$.[5]

This work has been supported financially by the Swedish Natural Science Research Council, Contract No. 2318.

1. *International Tables for X-Ray Crystallography*, 2nd Ed., Kynoch Press, Birmingham 1952, Vol. I.
2. Andersson, J. *Acta Chem. Scand. 26* (1972) 1730.
3. Andersson, J. *Acta Chem. Scand. 26* (1972) 2543.
4. Andersson, J. *Acta Chem. Scand. 26* (1972) 3813.
5. Andersson, J. *To be published.*

Received August 25, 1975.

A Mössbauer Investigation of Some Iron Carbonyl Compounds

HANS MOSBÆK

Chemistry Department A, The Technical University of Denmark, DK-2800 Lyngby, Denmark

In recent years, the structure and Mössbauer spectra of iron carbonyl compounds have attracted much interest.[1–3] Also in this laboratory, work has been carried out in order to elucidate the relative strength of σ- and π-bonds in iron carbonyl compounds; this has involved the same assumptions as in the investigation of substituted dinitrosyl dicarbonyl iron compounds.[4] The investigated compounds of the general formula $Fe(CO)_3L_2$ are all assumed to have the structure of a rigid trigonal bipyramid with the substituents in the axial positions. This structure is based on IR and X-ray crystal investigations.[5,6] The non rigid structure obtained by NMR [1,7,8] is assumed to exist only in solutions. The Mössbauer parameters were determined by Elron Mössbauer equipment on the solid compounds wafered between polyethylene at approximately 80 K and a commercial source of ^{57}Co in platinum was used. All the investigated compounds were prepared according to literature methods.

From the experimental data summarized in Table 1 it follows that there is a rather great variation in the quadrupole splitting, whereas the variation in the isomer shift is very small (as normal for similar iron compounds).

As the investigated compounds are all uncharged, the variation in the quadrupole splitting should be explained by differences in the bonding properties of the ligands. Furthermore the L-ligands will give the greatest contribution to this variation. The contribution from the carbonyl groups is rather small judging from the variation in the force constants for the CO-group where the discrepancies are almost within the accuracy of the applied force field.[9] Moreover, the variation in the bonding of the carbonyl groups will be levelled to some extent since both the bonding and the antibonding E'-orbitals are filled. (The notation used here is consistent with the character table given by F. A. Cotton [20]). Using the normally accepted assumptions for approximate calculations of the electric field gradient (EFG) for transition elements, only the $3d$ electrons are considered, as the overwhelming contribution to EFG comes from these orbitals.[10] In such cases we have for the quadrupole splitting:

$$\Delta E_Q \propto n(d_{x^2-y^2}) + n(d_{xy}) - n(d_{z^2}) - \tfrac{1}{2}[n(d_{xz}) + n(d_{yz})] \quad (1)$$

where n represents the orbital occupancy. In the compounds $[Fe(CO)_3L_2]$ with constant bonding to the "$(CO_3$"-moiety this expression can be rewritten

$$\Delta E_Q \propto K' - \sigma_L - \tfrac{1}{2}(K'' - \tfrac{1}{2}\pi_L + K'' - \tfrac{1}{2}\pi_L) = K - \sigma_L + \tfrac{1}{2}\pi_L \quad (2)$$

where σ_L represents the amount of charge transferred to the d_{z^2} orbital by σ-bonding (to L) and π_L represents the amount of charge transferred to the ligand π-orbitals (on L) from the E''-orbitals (i.e. d_{xz} and d_{yz}).

In the following discussion it will be assumed that $\Delta E_Q > 0$ for all compounds in Table 1;[2] referring to eqn. (2), this means that $K > 0$.

As we only have one equation to characterize the σ- and π-bonding properties of the ligands, it is necessary to incorporate earlier results regarding the ligands [11–15] in order to achieve some qualitative values for the bond strengths (bond strength will refer to the magnitude of the MO coefficient in LCAO description).

The ligands triphenylarsine and triphenylstibine are characterized by the greatest quadrupole splittings and these ligands must [following eqn. (2)] have the weakest σ-bond or/and the strongest π-bond. These ligands have been investigated by IR-spectroscopy and ^{121}Sb-Mössbauer spectroscopy and the results are interpreted in that way that the two ligands have rather poor π-acceptor capacities and therefore they must be characterized by a very weak σ-donor capacity (at least regarding donation to the d_{z^2}-orbital). The ligands triphenylphosphite and -phosphine are situated in the middle of the observed quadrupole splitting scale and have very close values of the quadrupole splitting. We must therefore suspect that these ligands have stronger σ-bonds than the arsine and stibine homologues and further more that values of $(\sigma_L - \frac{1}{2}\pi_L)$ for the two ligands must also be close.

Table 1. Data for $Fe(CO)_3L_2$-compounds.

L	$\sigma^{a,b}$ mm/S	$\Delta E_Q{}^{b,d}$ mm/S	$k_{COeq}{}^{c,e}$ mdyn/Å
$As\phi_3$	0.20	3.20	14.5
$Sb\phi_3$	0.19	3.16	14.5
$P\phi_3$	0.16	2.63	14.3
$P(O\phi)_3$	0.15	2.61	15.1
$P(C_4H_9)_3$	0.15	2.31	14.2
$P(OCH_3)_3$	0.12	2.28	14.8
$P[N(CH_3)_2]_3$	0.15	2.27	14.4
$CN\phi$	0.16	2.03	14.8

[a] Isomer shift relative to sodium nitroprusside. [b] Quadrupole splitting. [c] Calculated as in Ref. 9. [d] ±0.02 mm/S. [e] ±0.2 mdyn/Å.

As it is known from IR-[15] and Mössbauer-spectroscopy [4] that $P(OC_6H_5)_3$ has stronger π-bonds than $P(C_6H_5)_3$, $P(OC_6H_5)_3$ must also have stronger σ-bonds in order to fulfill eqn. (2).

Also, the ligands tributylphosphine, trimetylphosphite, and tris(metylamino)phosphine have close quadrupole splitting values and must [according to eqn. (2)] have the same value of $(\sigma_L - \frac{1}{2}\pi_L)$. According to IR-spectroscopy [15] the π-strengths should vary in the order $P(OCH_3)_3 > P(C_4H_9)_3 > P(N(CH_3)_2)_3$ and the σ-strength should show a similar variation. This variation is confirmed for $P(C_4H_9)_3$ and $P(N(CH_3)_2)_3$, since the aminophosphine has the smaller basicity [17] and therefore should exhibit the weakest σ-bonding. The relative strong σ- and π-bonding of trimetylphosphite is confirmed by Mössbauer-spectroscopy of other iron compounds.[18] The last compound in Table 1, CNC_6H_5, is characterized by a pronounced low quadrupole splitting and must according to eqn. (2) have very strong σ-bonding and/or weak π-bonding. The smallness of the quadrupole splitting suggests that both mechanisms are in work. This is confirmed by IR-spectroscopic investigations [19] which reveal that the C–N stretching frequency of the complexed isocyanide ligand is higher than the frequency of the uncomplexed ligands. This suggests that the σ-bonding is stronger than the π-bonding as σ-bonding will tend to raise and π-bonding to lower the frequency.

In conclusion, it is found that the σ-bond strength decreases in the following sequences:

$$CNC_6H_5 > P(OCH_3)_3 > P(C_4H_9)_3 > P(N(CH_3)_2)_3$$

and $P(OC_6H_5)_3 > P(C_6H_5)_3 > As(C_6H_5)_3 \simeq Sb(C_6H_5)_3$.

The π-bond strength shows also variations but in general it has not been possible to calculate qualitative values for π-bond strengths.

It is generally assumed [3,11,12,21] that there is a correlation between σ-donor and π-acceptor properties of ligands. From the present work it follows that this is not always the case.

1. Cullen, W. R., Harbourne, D. A., Liengme, B. V. and Sams, J. R. *Inorg. Chem. 8* (1969) 1464.
2. Clark, M. G., Cullen, W. R., Garrod, R. E. B., Maddock, A. G. and Sams, J. R. *Inorg. Chem. 12* (1973) 1045.
3. Carroll, W. E., Deeney, F. A., Delawey, J. A. and Lalor, F. J. *J. Chem. Soc. Dalton Trans.* (1973) 718.
4. Mosbæk, H. and Poulsen, K. G. *Acta Chem. Scand. A 28* (1974) 157.
5. Cotton, F. A. and Parish, R. V. *J. Chem. Soc.* (1960) 1440.
6. Kelbourn, B. T., Raebum, V. A. and Thompson, D. T. *J. Chem. Soc. A* (1969) 1960.
7. Mann, B. E. *Chem. Commun.* (1971) 1173.
8. Akhtar, M., Ellis, P. E., MacDiarmid, A. G. and Odom, J. D. *Inorg. Chem. 11* (1972) 2917.
9. Dalton, J., Paul, I., Smith, C. and Stone, F. G. A. *J. Chem. Soc. A* (1968) 1199.
10. Harris, C. B. *Inorg. Chem. 7* (1968) 1517.
11. Graham, W. A. G. *Inorg. Chem. 7* (1968) 315.
12. Angelici, R. J. and Malone, M. D. *Inorg. Chem. 6* (1967) 1731.
13. Stewart, R. P. and Freichel, P. M. *Inorg. Chem. 7* (1968) 1942.
14. Delbeke, F. T., Claeys, E. G. and van der Kelen, G. P. *J. Organometal Chem. 28* (1971) 391.
15. Horrocks, W. D. and Taylor, R. C. *Inorg. Chem. 2* (1963) 723.
16. Bowen, L. H., Garrou, P. E. and Long, G. G. *Inorg. Chem. 11* (1972) 182.
17. Thorsteinson, E. M. and Basolo, F. *J. Amer. Chem. Soc. 88* (1966) 3929.
18. Libbey, E. T. and Bancroft, G. M. *J. Chem. Soc. Dalton Trans.* (1974) 87.
19. Cotton, F. A. and Zingales, F. *J. Amer. Chem. Soc. 83* (1961) 351.
20. Cotton, F. A. *Chemical Applications of Group Theory*, Interscience, New York 1965.
21. Bigorgne, M. *J. Inorg. Nucl. Chem. 26* (1964) 107.

Received August 6, 1975.